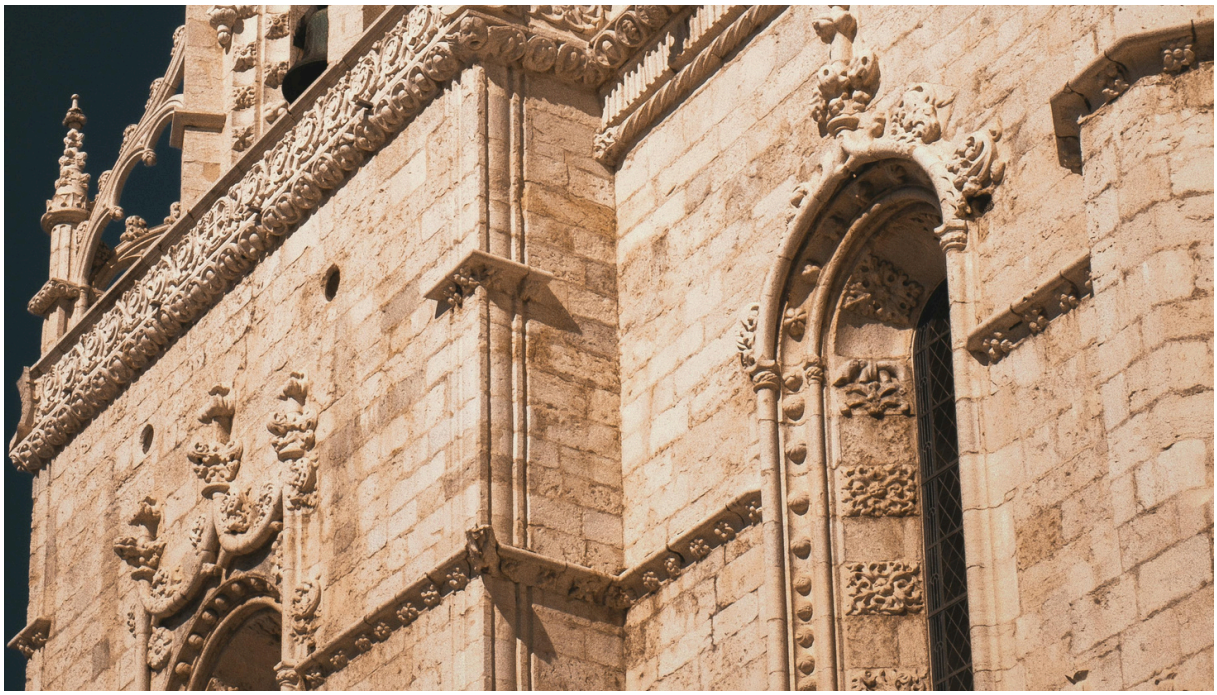
cinpar2026

XIII International Conference on Building Pathology and Constructions Repair

15th to 17th July 2026 - Lisboa, Portugal



BOOK OF PROCEEDINGS



COPYRIGHT PAGE

Title

XXII International Conference on Building Pathology and Construction Repair (CINPAR2026) - Book of Proceedings

Editors

Tiago Miguel Ferreira
Esequiel Mesquita
Humberto Varum

Graphic Design

Carolina Silvestre

Edition

1st Edition, July 2026

ISBN

978-989-35910-2-4

DOI

10.57859/ulisboa-istceris.000065

Preface

Continuing a tradition established in 2003, the XXII International Conference on Building Pathology and Construction Repair (CINPAR 2026) brought the international community together at Instituto Superior Técnico, University of Lisbon, Portugal, from 15 to 17 July 2026. This volume contains the scientific and technical contributions presented at the conference.

Over its first 21 editions, CINPAR grew into an international meeting place for researchers, engineers, architects, construction professionals, public authorities, and students. Its in-person and virtual editions have been hosted in Brazil, Argentina, Portugal, Chile, Italy, and Türkiye. This history bears witness to the strength of the CINPAR community and to the lasting importance of the questions that led to the conference's creation more than two decades ago.

Those questions are, if anything, more urgent today. Urbanisation and population growth continue to increase the demand for buildings and infrastructure. At the same time, much of the existing built environment is ageing and needs to be assessed, maintained, adapted, and strengthened. Natural and human-induced hazards place further pressure on structures and communities, often revealing vulnerabilities that have developed over many years.

There are also compelling environmental, economic, and cultural reasons to make better use of what has already been built. Extending the service life of existing assets can reduce the consumption of materials and other resources, while the conservation of historic buildings protects values that cannot be replaced. In many cases, demolition and reconstruction are neither economically realistic nor environmentally or culturally acceptable.

The future of the construction sector will therefore depend as much on how we care for existing buildings and infrastructure as on what we build anew. Successful intervention requires a sound understanding of materials, structural systems, deterioration processes, and the methods available for inspection, testing, and assessment. It also requires repair and strengthening solutions that are effective, durable, and compatible with the original construction. Technical knowledge alone is not enough: appropriate standards, responsible management, and close cooperation between research and practice are equally important.

It was within this context that CINPAR 2026 received 212 abstracts, resulting in the acceptance of 154 full papers. The scientific programme comprised 42 sessions: 32 general sessions, three technical sessions, four keynote sessions, and three thematic sessions. These figures are a clear indication of the scale of the conference and of the range of work currently being undertaken in building pathology, rehabilitation, and construction repair.

The papers in these proceedings are organised under eight themes: Inspection and Defects; Materials and Techniques; Natural Hazards; Infrastructure; Design Projects and Rehabilitation Works; Built Heritage; Management and Standards; and Research and Recent Developments. The contributions cover a wide field. They examine diagnostic and non-destructive testing methods, the behaviour and characterisation of construction materials, structural assessment, hazard mitigation, and the conservation of historic buildings. They also present new repair technologies, case studies of rehabilitation projects, and research on the management and long-term performance of the built environment.

The keynote lectures and thematic sessions gave particular attention to questions that are likely to shape the field in the coming years. These included automated and large-scale non-destructive testing, integrated methods for assessing existing and historic structures, the seismic behaviour and strengthening of traditional construction, and the use of digital technologies in the diagnosis of building pathology. The discussions showed the value of bringing scientific research, professional experience, and technological development into closer contact. They also reminded us that interventions must respond not only to questions of safety and durability, but also to the character and cultural significance of the buildings concerned.

These proceedings are the result of the work of a broad international community. We hope they will be useful to researchers, practitioners, students, asset owners, public authorities, and others responsible for the care of buildings, infrastructure, and built heritage. Beyond recording the work presented in Lisbon, we hope the volume will encourage further discussion, research, and cooperation.

We sincerely thank the authors for choosing CINPAR 2026 as the forum in which to present their work. We are also grateful to the members of the Scientific Committee for the time, care, and expertise they devoted to evaluating the submitted contributions. Our thanks extend to the keynote speakers, thematic-session organisers, session chairs, and participants, whose involvement gave substance and energy to the scientific programme.

The conference would not have been possible without the commitment of the International Organising Committee, the Local Organising Committee, and the Honorary Committee, together with the work of many colleagues and volunteers. We are deeply grateful to our sponsors—hci, Instituto Nova Engenharia, Kerakoll, JETSJ, Imperalum, OZ, and STAP—whose generous support played an essential part in making CINPAR 2026 possible. We also thank our institutional supporters for their valued cooperation, and our media partners for helping to extend the reach of the conference.

We hope that the discussions begun at CINPAR 2026 will continue long after the conference itself. May these proceedings support new research, encourage lasting cooperation, and help advance the thoughtful and responsible care of our built environment.

Tiago Miguel Ferreira

Chair of CINPAR 2026

On behalf of the Organising Committee



COMMITTEES

International Organising Committee

Tiago Miguel Ferreira, IST, Portugal (Chairman)
Ana Mafalda Matos, FEUP, Portugal
Esequiel Mesquita, UFC, Brazil
Humberto Varum, FEUP, Portugal
Lais Costa, UFC, Brazil
Monica Garcez, UFRGS, Brazil
Mylene Vieira, UFC, Brazil

Honorary Committee

The Honorary Committee of CINPAR consists of distinguished individuals who have made substantial contributions to the development and continuation of the congress over the years. Their inclusion acknowledges the dedication and efforts of those who have helped shape the history and standing of CINPAR.

Francisco Carvalho, UVA, Brazil (Founder of CINPAR)
Alexandre Bertini, UFC, Brazil
Ángel Oshiro (in memoriam), UTN, Argentina
Eduardo Ballán, UCJC, Spain
Esequiel Mesquita, UFC, Brazil
Gibson Meira, IFPB, Brazil
Hector Cardozo, USalta, Argentina
Humberto Varum, FEUP, Portugal
Jeferson Marinho, URCA, Brazil
Jorge Sota, UTN, Argentina
María Positieri, UTN, Argentina
María Soledad Gómez, PUC, Chile
Monica Garcez, UFRGS, Brazil
Petr Stepánek, BRNO, Czech Republic



Local Organising Committee

Tiago Miguel Ferreira, IST, Portugal
Rita Bento, IST, Portugal
Inês Flores-Colen, IST, Portugal
Elaine Gregório, IST, Portugal
Eloísa Castilho, IST, Portugal
Giovanna Schafer, IST, Portugal
Jessica Bersch, IST, Portugal
Maria Paula Mendes, IST, Portugal
Iran Segundo, IST, Portugal



Scientific Committee

Adrià Sánchez Calvillo, UMICH, Mexico
Alejandro Jimenez Rios, Bath, UK
Alexandre A. Costa, NCREP, Portugal
Ana Cecilia Vasconcelos, UFC, Brazil
Ana Sofia Guimarães, FEUP, Portugal
Ana Velosa, UA, Portugal
André R. Barbosa, OSU, USA
António Arêde, FEUP, Portugal
Bartolomeo Pantò, Durham, UK
Bruno Silva, NCREP, Portugal
Cristian Sandoval Mandujano, PUC, Chile
Beatriz Zapico Blanco, USE, Spain
Cristoforo Demartino, Roma Tre, Italy
Daniel V. Oliveira, UM, Portugal
Davi Teixeira, IFCE, Brazil
Daniel Ribeiro Cardoso, UFC, Brazil
Diego Ricca, UFC, Brazil
Dulce Henriques, ISEL, Portugal
Elena Kapogianni, NTUA, Greece
Eduardo Júlio, IST, Portugal
Enrico Quagliarini, UNIPVM, Italy
Enrico Spacone, Ud'A, Italy
Eugênio Moreira, UFC, Brazil
Eva Barreira, FEUP, Portugal
Federica Del Carlo, UNIPI, Italy
Fernando Pinho, UNL, Portugal
Genevieve Foray, INSA Lyon, France
Gabriele Bernardini, UNIPVM, Italy
Gibson Meira, IFPB, Brazil
Giuseppe Brando, Ud'A, Italy
Graça Vasconcelos, UM, Portugal
Hugo Rodrigues, UA, Portugal
Humberto Varum, FEUP, Portugal
Ignacio Lombillo, UNICAN, Spain
Ilaria Venanzi, UNIPG, Italy
Inês Flores-Colen, IST, Portugal
Isabel Torres, UC, Portugal
J.A.R. Mendes da Silva, UC, Portugal
Javier Ortega, CSIC, Spain
João Pantoja, UNB, Brazil
João H. Negrão, UC, Portugal
João Luiz Calmon, UFES, Brazil
João Miranda Guedes, FEUP, Portugal
João Ramôa Correia, IST, Portugal
Jonathas Iohanathan de Oliveira, UFC, Brazil
Jorge de Brito, IST, Portugal
José Jara, UMSNH, Mexico
Jose M. Adam, UPV, Spain
Luca Pelà, UPC, Spain
Leonardo Inojosa, UNB, Brazil
Luís Paulo Mourão, UFC, Brazil
Luiz Melgaço, UFMG, Brazil
Manuela Almeida, UM, Portugal
Maria Giovanna Masciotta, Ud'A, Italy
Mariapaola Riggio, OSU, USA
Mehmet Emiroglu, SAU, Turkey
Miguel Azenha, UM, Portugal
Mislav Stepinac, UNIZG, Croatia
Nicola Tarque, UPM, Spain
Nuno Mendes, UM, Portugal
Paulo B. Lourenço, UM, Portugal
Paulo Miranda, IFCE, Brazil
Pedro Delgado, IPVC, Portugal
Nuria Chiara Palazzi, UNAB, Chile
Nuno Valentim, FAUP, Portugal
Paulina Faria, UNL, Portugal
Pere Roca, UPC, Spain
Pilar Baquedano Julià, USM, Chile
Rafel Ramírez Eudave, Delft, Netherlands
Ricardo Almeida, IPV, Portugal
Ricardo Paiva, UFC, Brazil
Rita Bento, IST, Portugal
Romain Sousa, Vigobloco, Portugal
Romeu Vicente, UA, Portugal
Rui Silva, UM, Portugal
Sandra Lucas, TU/e, Netherlands
Savvas Saloustros, EPFL, Switzerland
Serena Cattari, UniGe, Italy
Sergio Lagomarsino, UniGe, Italy
Sofia Araújo Lima Bessa, UFMG, Brazil
Valentina Marincioni, UCL, United Kingdom
Vasco P. de Freitas, FEUP, Portugal
Xavier Romão, FEUP, Portugal



Cinpar 2026
XXII International Conference on Building Pathology and Constructions Repair
15th to 17th July 2026 - Lisboa, Portugal

Institutional Support

FUNDEC | CERIS | TÉCNICO UNIVERSIDADE DE LISBOA | ICS | ORDEM DOS ENGENHEIROS | ORDEM DOS ARQUITECTOS

cib student chapter | UNIVERSIDADE ESTADUAL VALE DO ACARAÚ | GECoRPA GRÉMIO DO PATRIMÓNIO | ALCONPAT BRASIL | rilem

Media Partners

CONSTRUÇÃOMAGAZINE | rpee revista portuguesa de engenharia de estruturas | Pedra & Cal | infrastructures

Proudly Sponsored By

Gold Sponsor

hcl CONSTRUÇÕES

Silver Sponsors

NOVA ENGENHARIA | kerakoll

Bronze Sponsors

JET SJ | imperalum | Diagnóstico, Levantamento e Controlo de Qualidade em Estruturas e Fundações, Lda. | stap

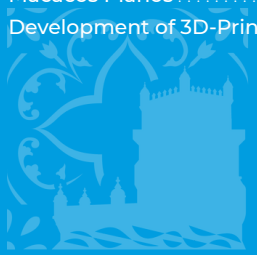
Indice

Copyright Page 2
Preface 3
Commitees 5
Supports, Partners and Sponsors 7
Inspection and Defects 13
Towards an Automatic Defect Detection on Historical Surfaces Based on Hyperspectral Imaging Data: A Hierarchical Classification Framework 14
Pathological Manifestations in Residential Construction: Warranty Assessment in Fortaleza – CE 25
A 3D Tomographic GPR Inspection Using a Self-Constructed Cable-Driven Robot of the Torre de la Vela in La Alhambra (Granada, Spain) 33
Corrosion in Exposed Concrete Structures of Modern Architecture: A Case Study of the Failure of the Roof Slab of the Water Tank at the University Restaurant of UnB 42
Análise de Dados de Patologias Higrotérmicas: Estudo Estatístico de Relatórios Técnicos de Edifícios 54
Building Inspection As A Technical Tool For Risk Management: A Case Study–Based Methodology For Intervention Prioritization In Residential Buildings 66
Automated large-scale sonic inspection of the northern façade of the Torre de la Vela in the Alhambra (Granada, Spain) 78
Comportamiento Sísmico de Estructuras Prefabricadas Existentes 88
Analysis of Pathological Manifestations in a Public School in The Municipality of Juazeiro do Norte, Ceará: A Case Study 98
Análise das manifestações patológicas nas edificações do Centro Turístico Igreja do Céu no Município de Viçosa do Ceará 110
Use of the Cut Matrix in the Analysis of Pathological Manifestations in Housing Units of the Minha Casa Minha Vida Program: A Case Study 122
Análise dos Defeitos em Pavimento Rodoviário Flexível sob Diferentes Condições Climáticas 134
Building Pathologies in the Rehabilitation of Substandard Housing: Technical Assessment of Housing Improvement Works 146
Investigation of Ultrasonic Propagation Angles for the Identification of Wood Elastic Properties 158
Progressive Failure Analysis in Elevated Swimming Pool Waterproofing Systems: A Diagnostic Framework for Correlating Executive Non-conformities and Watertightness Loss Mechanisms 169
Pathology of Ceramic Tile Systems in Brazil: Investigating Moisture Expansion in BIIb Tiles through a Multi-Analytical Case Study 182
Rehabilitation of Waterproofing Systems in Large-Span Precast Hollow Core Slabs, with crack treatment applied under adverse conditions: Methodology with Flexible Thermoplastic Polyolefin (PO-F) Waterproofing Membranes 194
Vision-based Structural Health Monitoring for Detection and Characterization of Cracks in Concrete: A Systematic Review 214
Diagnostic Analysis of Differential Settlement Using the Berberian Method and Foundation Reinforcement with Mega Piles in a Residential Structure: A Case Study in Goiânia, Brazil 226
Systematic cataloging of information for the semantic enrichment of the HBIM model of the Almofala Church 238
Diagnóstico de Manifestações Patológicas em uma Edificação Comercial de Múltiplos Pavimentos: Estudo de Caso no Centro Histórico de Porto Alegre 249

Inspeção Predial e Diagnóstico de Manifestações Patológicas em uma Edificação de Múltiplos Pavimentos: Estudo de Caso em Porto Alegre ... 259
Characterisation and Assessment of Structural Timber Elements of a Building in the Historic Centre of Viseu, Portugal ... 267
Impacts of Deficient Maintenance on the Integrity and Durability of Reinforced Concrete Reservoirs ... 279
Advanced Resilience Techniques for Historical and Understudied Sacral Architecture – The ARTHUR Project ... 291
Mapping Façade Soiling Patterns through Image Processing ... 298
Impactos da Manutenção Baseada na Condição no Desempenho da Envolvente dos Edifícios ... 310
Avaliação da Conservação de Edificações Públicas com Base em Ordens de Serviço e Classificação de Criticidade pel Matric GUT ... 321

Materials and Techniques ... 334

Low-Carbon Cements and Construction Durability: A Systematic Review ... 335
Effects of Limestone Filler, Metakaolin, and Polypropylene Fibers on the Flow Properties and Buildability of Cementitious Mixtures for 3D Concrete Printing (3DCP) ... 356
Hipocarbonic Concretes: A Brazilian Overview of SCMs Used in the Repair of Reinforced Concrete Structures ... 369
Origem e Interferência dos Teores de Cálcio de Fragmentos Cerâmicos do Século XVIII em Pernambuco ... 381
Avaliação da Substituição Parcial de Cimento por Pó Reciclado: Influência na Resistência à Compressão de Pastas Cimentícias ... 390
Control of Fresh Concrete's Composition Through Non-intrusive Microwave Electrical Impedance Spectroscopy ... 400
Linking Fabrication Route, Microstructure, and Fire Performance in Mycelium-Based Insulation Composites ... 412
Durability Assessment of Sargassum-Based Compressed Earth Blocks Under Abrasion Cycles ... 425
Experimental Study of Microbial Biomineralization in Carbonated and Precracked Cementitious Matrices ... 436
On the Seismic and Energy Retrofit of Masonry Buildings Using Inorganic Matrix Composites ... 448
Mortar with Steelmaking Slag for Repairs of Historic Buildings ... 459
Cementitious Composites With Steel Industry Residues and Interaction with Atmospheric CO_2 ... 471
Modified Masonry Triplets for the Shear Characterisation and Numerical Modelling of NFRCM-Strengthened Masonry ... 480
Compressive Behaviour of Masonry Columns Strengthened with PBO-FRCM Systems: Experimental and DEM Numerical Investigation ... 490
Alkaline Durability of AR-glass FRCM Systems: Tensile Behaviour of Bare Fibres and Cement-Based Composites Under Direct and Accelerated Conditioning ... 502
Betão Branco de Elevado Desempenho Eco-eficiente com Incorporação de Pó de Vidro para Aplicações Arquitetónicas ... 511
Enhancing the Tensile Performance of Natural Fibers for Inorganic Matrix Composites in Masonry Strengthening ... 523
An Investigation on the Mechanical Response of Composite-Reinforced Mortar for Masonry Strengthening ... 524
Energy Efficiency and Sustainable Materials in Façade Rehabilitation: Challenges of Thermal Insulation in the Azores ... 525
Caracterização Mecânica da Alvenaria Ordinária de Lisboa através de Ensaios com Macacos Planos ... 536
Development of 3D-Printed Conductive Mortar Electrodes for Smart Bricks ... 548



Natural Hazards 558

The Use of Aerial Surveying for Land Regularization Purposes and the Right to The City: The Case of Dorothy Stang in the Federal District 559
Monitoring of Geological Risk Areas Using UAVs with High-Precision Aerial Photogrammetry Support: The Case of Sol Nascente, Section 3, Federal District, Brazil 570
From Risk Assessment to Mitigation and Emergency Planning for Multiple Natural Hazards in Urban Built Environments: A Mesoscale, User-Dynamicsbased Framework 584
Physical Vulnerability to Floods in Historic Urban Areas: A Building-Scale Assessment Approach 596
Watershed as a Basis for Heritage Vulnerability Assessment of Historic Urban Landscapes 605
A Structured Methodology for Post-Fire Structural Assessment and Rehabilitation of Unreinforced Masonry Housing in Seismic Regions 617
Assessment of the Impact of Mining Activities with Particular Focus on Mining Tremors Affecting Masonry Structures 629
Seismic Vulnerability Assessment of a Heritage Unreinforced Masonry Building: Pushover Analysis 630
Análise da Reconstrução da Infraestrutura Escolar do Rio Grande do Sul Decorrente dos Efeitos do Desastre Climático Ocorrido em 2024 641
GeoAI Resilience-Based Approach for Critical Assets Under Natural Hazards 653
Climate Resilience Skills for Cultural Heritage Buildings: A European Educational Framework Developed through the ECOHERITAGE Project 664

Infrastructure 677

Surface Distress Evaluation of Interlocking Concrete Block Pavements Using the Pavement Condition Index (PCI): A Case Study in Brazil 678
A Computational Tool Based on Artificial Neural Networks for Supporting PCI Evaluation in Interlocking Concrete Block Pavements 690
Analysis of the Influence of Rainfall Variability on Asphalt Pavement Deterioration: A Case Study Based on Functional Condition Surveys 700
Impact of Structural Pathologies on Property Market Value 712
Failure Mechanisms of the Partial Collapse of the South Road Axis (Eixo Rodoviário Sul) in Brasilia 723
Procedure for Assessing the Dynamic Resistance of Existing Bridge Structures Located in Seismically Active Mining Areas 733
Thermal Behavior of Urban Pavements Under the Influence of Tree Shading: Implications for Pavement Performance and Durability 734
Classes de Agressividade do Concreto no Brasil: Influência Regional, Patologias e Implicações em Projeto 746
Impact of Defects on the Deflection Response of Interlocking Pavements 757
Infrastructure, Architecture, and Tourism Urbanization: Digital Modeling of the Impacts of the Sabiaguaba Environmental and Gastronomic Complex, Fortaleza, Ceará, Brazil 766
Pathological Manifestations in Building Structures: Evaluation of Causes, Impacts on Durability, and Intervention Costs 778
Analysis of Pathological Manifestations Resulting from Prolonged Work Stoppage in Public Educational Construction: Impacts on the Execution of Coatings 788
Análise da Expansão da Infraestrutura Urbana de Brasília. Aspectos da Reabilitação de Viadutos no Trevo de Triagem Norte 799
Avaliação de Vulnerabilidade Sísmica de Escolas de Lisboa: Da Priorização à Escala Urbana à Análise Estrutural Detalhada 810

Design Projects and Rehabilitation Works 822

Decarbonizing Built Heritage: A Technical-Qualitative Assessment of Integrated Retrofit Strategies at the BMCC 823
Improving Daylight and Energy Efficiency in University Buildings: A Study of the Darcy Ribeiro Campus at the University of Brasilia - Brazil 835
A Resilience Clock for Residential Buildings: Age- and Hazard-Conditioned Fragility and Functional Loss via SFD(t) × UHS(TR) 847
Seismic Assessment and Strengthening of the Church of Santo Tomás de Aquino in Rondocan, Peru 859
Integration of an HBIM Model with Thermographic and Damage Image Analysis Based on Computer Vision 870

Built Heritage 882

Structural Fire Risk in Historic Urban Districts: A Component-Based Analysis of its Relationship with Multidimensional Poverty 883
Análise Patológica de Edificação Histórica com Proposta de Reabilitação: Um estudo de caso no Estado do Ceará, Brasil 884
Desafios na Reabilitação de Edificações no Brasil: A Formação Acadêmica como Elemento-Chave para a Qualidade das Intervenções 893
Semantic Structuring of Generic HBIM Elements for Building Systems 902
Caracterização de Chacotas Históricas a Partir de Classificação Análoga de Rochas Sedimentares Através de Microscopia por Luz Polarizada 914
Argumentación en Contra del Uso de Revoques Texturados Plásticos en Fachadas Patrimoniales. El Caso del Museo Provincial de Bellas Artes de Santa Fe (Argentina) 926
HBIM-Driven Management of Diagnostic Information: A Proof of Concept 938
Challenges in Data Collection for the Development of Maintenance Plans for Historic Buildings for Cultural use Integrated with HBIM Models 951
Residual Mechanical Properties of Masonry Materials After Exposure to High Temperatures 963
From Theory to Practice: Expert Views on Vulnerability of URM Buildings 975
Integration of an HBIM Digital Model with GPR Data Interpreted Using Machine Learning 986
Lime Mortars with Fibres and Residues for the Sustainable Rehabilitation of Wattle and Daub Walls 998
O Sítio Histórico de Sobral, Brasil: A Importância do Tombamento pelo IPHAN na Requalificação de Edificações e Espaços Urbanos 1010
Componentes Pré-Fabricados de Argamassa Armada: Quadro Analítico dos Danos em um CAIC em Goiânia 1022
Architectural Documentation of the San Sebastian Church 1034
Integração entre Tradição e Inovação: Desafios para Aplicação da Madeira Laminada Colada em Patrimônios Edificados 1046
Benchmarking Traditional Earthen Construction Technologies for Sustainable and Affordable Housing in Tanzania 1058
Underground Intervention in a Historic Building: Structural Compatibility and Heritage Preservation at the Museu Paulista 1070
Modelagem Digital do Museu da Imagem e do Som a Partir de Nuvem de Pontos 1082
Social Tourism and Modern Heritage: Digital Documentation and Conservation of the SESC Garanhuns Holiday Camp (1956), Brazil 1092
Integrating Computer Vision and Machine Learning for Detection of Damage in Historic Buildings 1102
Electromechanical Self-Sensing Behavior of Lime Mortars with Carbon Nanotubes and Microfibers 1114
Geophysical Characterization of Historic Masonry Using Ground-Penetrating Radar (GPR) 1127

Damage Mapping of a 50's Building as a Strategy for Maintenance ... 1138
Digital Documentation of Cultural Heritage Based on High-Resolution Scanning ... 1150
Point Clouds Beyond BIM: Aesthetic Composition and Montage Techniques for Immersive Room Films in Heritage Education ... 1160
Adaptive vs. Uniform Decimation: A Quantitative Analysis of 3D Mesh Optimization for HBIM ... 1172
HBIM for Modeling a Cultural Heritage Asset Using a Hybrid Scan-to-BIM Workflow: Challenges and Insights from the Pinacoteca do Ceará ... 1182
A Multi-Sensor Acquisition Framework for Built Heritage Documentation: Application at the Church of Nossa Senhora da Conceição de Almofala ... 1193
Wattle and daub (tabique) mortars in Northern Portugal ... 1206
Framework for Assessing and Mapping Degradation Risks in Historic Building Facades ... 1214
Incorporation of Eggshell Residues in Lime Mortars for Rehabilitation of Wattle and Daub Walls ... 1224
Mapping Technical Façade Elements Under Low-intensity Seismicity to Support Risk-informed Urban Decision-Making ... 1233
Large-Scale Seismic Vulnerability Assessment of Masonry Buildings: A Critical Appraisal of Index-based Methods ... 1245
Retrofitting Techniques Applied to Chilean Masonry Towers: A Preliminary Typological Survey of Four Case Studies ... 1257
Material Parameter updating Based on Operational Modal Analysis (OMA): Application to the Sciri Tower ... 1268
Metodologia Digital Integrada para a Conservação do Património Construído: da Reconstrução Virtual ao Fabrico Aditivo ... 1279
Porto Historical Heritage - Digital Twins and Underground Excavation Works ... 1287
Unveiling hybrid two-way out-of-plane response of existing unreinforced masonry structures through extensive shake-table testing ... 1299

Management and Standards ... 1311

Conceptual Model of Resilient Decision-Making for PDHR in Critical Zones ... 1312
Heritage Management and the Progressive Deterioration of an Earthen Troje in Mexico City ... 1325
Proposed Adaptation of the GUT Criticality Matrix for the Maintenance Management of Concrete Pavements in Fuel Stations: A Comparative Approach between Mechanical Damage and Chemical Attack ... 1337
Data Structuring and Systemic Failure Analysis in Built Asset Management: Application to Fire Detection and Suppression System Maintenance ... 1349
Leveraging Data Analytics to Manage Visitor Flows in Heritage Sites ... 1361
Study of Strategies for the Evaluation of Metal Structures Under Fire Action ... 1373

Research and Recent Developments ... 1383

Corrosion Assessment for Prestressed Steel Strands Based on Experimental Data and Numerical Analysis ... 1384
Optimising Resource Value Extraction in Demolition and Rehabilitation: A Digital Twin-Transition Approach - EU Horizon DISCOVER project ... 1396
Análise Química por Fluorescência de Raios X Portátil em Metal do Passado ... 1408
Proposal for an Optimal Timing for Maintenance and Rehabilitation Strategies on Interlocking Pavements ... 1420
Influence of Construction and Demolition Waste as Fine Aggregate Replacement on the Performance of Self-Compacting Mortars ... 1431
Durabilidade da Cor em Concretos Pigmentados Pretos: Avaliação do Comportamento Cromático sob Envelhecimento Acelerado ... 1439
Band Gap Tuning of 1D Phononic Crystals for Subway Vibration Mitigation: A Parametric Study of Periodic Foundations and Barriers ... 1453
Discrete Element-based Particle Modelling Optimization for Stone Masonry Wall's Structural Assessment ... 1465
The Role of the CIB Student Chapter IST/UL: Perspectives on Research and Cooperation ... 1477



INSPECTION AND DEFECTS



Cinpar 2026
XXII International Conference on Building Pathology and Constructions Repair
15th to 17th July 2026 - Lisboa, Portugal

Towards an Automatic Defect Detection on Historical Surfaces Based on Hyperspectral Imaging Data: a Hierarchical Classification Framework

Maria Francesca MUCCIOLI[1], Marco D'ORAZIO[2], Elisa DI GIUSEPPE[3]

[1] DICEA Dept., Università Politecnica delle Marche, Ancona, Italy, m.muccioli@pm.univpm.it
[2] DICEA Dept., Università Politecnica delle Marche, Ancona, Italy, m.dorazio@staff.univpm.it
[3] DICEA Dept., Università Politecnica delle Marche, Ancona, Italy, e.digiuseppe@staff.it

Abstract: Continuous and systematic monitoring of built heritage surfaces is essential for effective conservation, as it enables the early detection of defects and timely interventions, resulting not only in improved preservation outcomes but also in a more efficient management of resources. However, current inspection techniques are often time-consuming and strongly dependent on the professional expertise, especially when invasive quantitative analyses are not feasible and assessments rely primarily on qualitative observations. In this context, Hyperspectral (HS) Imaging is gaining increasing relevance in the heritage field, as it allows physicochemical information to be associated with each image pixel of a surface. This study proposes a hierarchical and hybrid methodology that combines statistical analysis, Deep Learning (DL), and Machine Learning (ML) techniques applied to HS imaging data for the automatic classification of heritage surface alterations and defects. First, Independent Component Analysis (ICA) is employed as a statistical dimensionality reduction technique to enhance informative spectral patterns related to surface degradation. A selected ICA component is then used as input to a U-Net Convolutional Neural Network (CNN), which is trained to identify and segment macro-scale degraded areas on historical surfaces. Subsequently, a Random Forest (RF) classifier is applied to the original HS data, restricted to the regions detected by the U-Net, to discriminate specific degradation typologies. This multi-stage strategy enables the spatial identification of surface alterations and defects, and the workflow is further extended to the metric quantification of the detected areas by exploiting the Ground Sampling Distance (GSD). Although the classification is currently restricted to a single material and two specific types of degradation, and notwithstanding challenges posed by surface roughness and cast shadows, preliminary results are promising and suggest that the proposed approach has the potential to support conservation professionals in the rapid detection and quantification of built heritage surface alterations and defects.

Keywords: Built Heritage, Defect Detection, Automatic Inspection, Remote Sensing, Hyperspectral Imaging

1. Introduction

The proper conservation of built heritage relies on the effective management of restoration processes. Restoration should not be regarded as a last-resort intervention to prevent the loss of an asset, but rather, it should form part of a continuous maintenance strategy that is as minimally invasive as possible. To enable this approach, continuous maintenance must be supported by equally continuous monitoring. A preventive rather than curative approach to conservation contributes to a more efficient allocation and management of resources, as it allows for timely interventions and reduces the need for extensive and costly restoration actions (A Vandesande and Van Balen 2018; ICOMOS 2011; Aziliz Vandesande et al. 2018; Della Torre 2021).

However, such an approach is not always feasible, as monitoring entails time-consuming procedures conducted by specialised professionals. Furthermore, techniques aimed at obtaining precise quantitative data (e.g., destructive analyses) may be invasive and therefore unsuitable for historic built surfaces (Valença, Gonçalves, and Júlio 2013).

For these reasons, the development of new methods and procedures that allow these analyses to be conducted in a highly automated manner is of primary importance.

The widespread adoption of Artificial Intelligence (AI) has enabled the development of automatic classification procedures, such as the classification of image data through Machine Learning (ML) and Deep Learning (DL) techniques, which are now employed across a broad range of fields. These include, for instance, medicine (Cai, Gao, and Zhao 2020) and food quality control processes (Liu et al. 2025), as well as the building sector and the field of restoration, where they support the automatic mapping of decay phenomena.

The application of AI models to the classification of alterations on heritage surfaces via images is increasingly becoming a consolidated practice. This approach is progressively extending beyond purely research contexts toward operational applications and has been the subject of several review studies (Giannuzzi and Fatiguso 2024; Mishra 2021; Fiorucci et al. 2020).

However, recent advancements do not rely solely on traditional imaging approaches based on RGB data, but increasingly exploit additional spectral wavelengths extending beyond the visible range, such as MultiSpectral (MS) and HyperSpectral (HS) imagery. By investigating further portions of the electromagnetic spectrum, these techniques enable the detection of features that are not discernible to the naked eye and allow the extraction of relevant physicochemical information, thus providing quantitative data acquired through non-contact measurements (Mukhtar, Arbabi, and Viegas 2025).

The acquisition of these additional spectral channels, which in the case of HS imaging can reach hundreds of wavelengths, generates high-dimensional datasets whose management and interpretation through conventional manual procedures become practically unfeasible (Donoho 2000). In this context, AI-based methodologies emerge not merely as supportive tools, but as essential frameworks for the effective processing and interpretation of high-dimensional spectral information (Datta et al. 2022).

Examples of advanced imaging techniques combined with AI-based pipelines for the detection of alterations and decay on heritage surfaces are reported in the literature. For instance, González Manich et al. (González Manich et al. 2016) employed HS imaging to acquire data from a portion of the façade of Glasgow Cathedral (UK). In their study, small Regions Of Interest (ROIs) corresponding to different types of decay were selected to train a Support Vector Machine (SVM) classifier for the automatic segmentation of the acquired image. The results were compared with a manual mapping procedure which, although slightly more accurate, required significantly longer processing times (hours versus minutes). Similarly, Zahiri et al. (Zahiri et al. 2022) classified materials on the façade of a historic building in Bergen (Norway) using a supervised ML algorithm based on Partial Least Squares Discriminant Analysis (PLSDA). The study compared the performance of MS and HS acquisitions, demonstrating the superiority of HS data due to the higher spectral resolution and richer spectral information recorded. Another contribution is provided by Li et al. (Li et al. 2024), who acquired HS imaging data from the Dazu Rock Carvings (China) and processed the dataset using four different supervised ML algorithms to automatically classify and segment decay phenomena such as delamination, efflorescence, crust formation, and biological colonisation, achieving classification accuracies of up to 98%.

Although previous studies have demonstrated that HS imaging combined with AI techniques can detect even millimetric alterations with promising results, they frequently focus on the application and comparison of distinct models, treating them as separate analytical solutions. Moreover, most contributions conclude with the identification and segmentation of decay phenomena, without further translating these results into operationally meaningful outputs.

In this perspective, the present study proposes a hierarchical multi-step framework that integrates statistical approaches, ML and DL techniques within a unified workflow aimed at enhancing the classification of decay phenomena basing on HS images. Furthermore, it introduces a methodological procedure for converting pixel-based outputs into dimensional data, thereby enabling the quantitative estimation of degraded surface areas and supporting more practical decision-making processes.

The present study does not aim to deliver a universally applicable model but introduces a hybrid, hierarchical methodological framework for classifying surface degradation phenomena. To demonstrate the proposed workflow, an experimental heritage case study is presented: although the current application focuses on a specific surface material and two distinct types of degradation, it serves to validate the feasibility of the hierarchical approach and the on-site acquisition procedure. This initial implementation establishes a framework that can be further scaled and adapted to more complex heritage scenarios in future research. Thus, given the limited dataset, the proposed approach is not intended for immediate general use, but rather as a methodological foundation that can be refined and expanded in future work.

The manuscript is structured as follows: *Section 2* presents the selected case study for data acquisition, along with a description of the data collection procedures. *Section 3* describes the proposed methodological framework, providing a preliminary overview in *Section 3.1* and a detailed description of each step from *Sections 3.2* to *3.5*. *Section 4* reports the results of applying the methodology to the case study data, and finally, *Section 5* is dedicated to conclusions.

2. Case study and data acquisition

The selected heritage site for this study is the façade of one of the most important Christian sites in Italy, the *Basilica of the Holy House* in Loreto, in the Marche Region (central Italy). Commissioned in the XVI century by the Archbishop of the nearby city of Recanati, the Basilica houses a smaller inner structure traditionally believed to be the house of the Virgin, brought from Nazareth by flying angels (Santarelli 2014, 1999). The façade is constructed of Istrian stone and is divided into three sections by pairs of pillars (Fig. 1a). The HS images used in this study were acquired on the base of one of these pillar pairs, specifically the third from the left (Fig. 1b), which exhibits several forms of decay, the most evident being cracks and incoherent patching with cement mortar.



Figure 1 – The façade of the Basilica of the Holy House of Loreto (left) and the selected stone base chosen for analysis (right)

HS images acquisition was performed using a Cubert ULTRIS X20 Plus camera (Cubert n.d.), featuring 164 spectral bands with a spectral sampling of 4 nm over a range from 350 to 1000 nm, thus covering part of the UV-A region as well as the entire visible and near-infrared (NIR) spectrum. Owing to the integration of a panchromatic camera, the instrument enables a pansharpening procedure that upscales the spectral images from a spatial resolution of 410 × 410 px to 1886 × 1886 px, allowing the capture of sub-millimetre details.

Since HS acquisition requires stable radiometric conditions and thus consistent illumination, measurements were conducted on a clear-sky day when direct sunlight did not strike the façade in order to avoid cast shadows and localised dark areas.

Images were acquired at close range to ensure high spatial definition. The HS camera was positioned at a distance of 155 cm from the selected area and moved horizontally on a line by 50 cm between successive acquisitions. Vertically, the acquisition started from a height of 70 cm and proceeded upward (120, 170 cm), resulting in a total of 24 HS images.

Prior to acquisition, the camera was calibrated through white, dark, and distance calibration procedures (Shaikh et al. 2021; Hugemann 2010; Del Pozo et al. 2017). White calibration consisted of acquiring a full-frame image of a 50 × 50 cm reference panel with 99% reflectance, used to convert the arbitrary digital numbers recorded by the instrument into reflectance values. Dark calibration accounts for the dark current noise internally generated by the sensor and was performed by covering the camera lenses. Finally, distance calibration corrects the parallax effect caused by the multi-array configuration of the instrument. This procedure was carried out using an asymmetric checkerboard panel, whose black–white intersections are detected by an integrated image registration algorithm to spatially align the images recorded by the different lenses.

The acquisition setup is pictured in Figure 2.

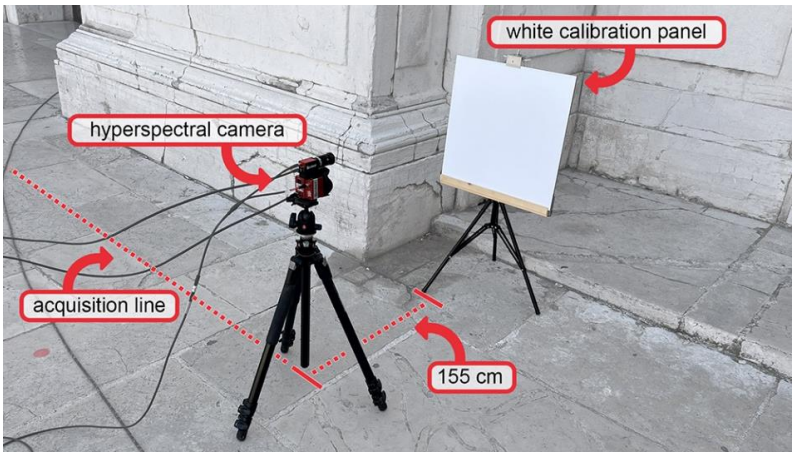


Figure 2 – Hyperspectral images acquisition setup

3. Materials and methods

3.1 Method overview

The present chapter is devoted to the description of the procedures underlying the proposed method for classifying decay phenomena within the collected HS image dataset. This subsection, in particular, provides an overview of the methodological framework, which is described in detail in the following subsections (Fig. 3).

The first step (*Section 3.2*) involves image preprocessing through a statistical technique, namely Independent Component Analysis (ICA), aimed at reducing data complexity and enhancing relevant features associated with macro-scale decay patterns. The second step (*Section 3.3*) consists of identifying the macro-area to be analysed in greater detail through a DL approach based on a Convolutional Neural Network (CNN). Subsequently (*Section 3.4*), the selected area is further investigated using a supervised ML procedure, specifically a Random Forest (RF) classifier. Finally (*Section 3.5*), the resulting image-based outputs are converted into dimensional data by exploiting the Ground Sampling Distance (GSD), thereby providing a practical tool to support professionals in the quantitative assessment of detailed decay areas.

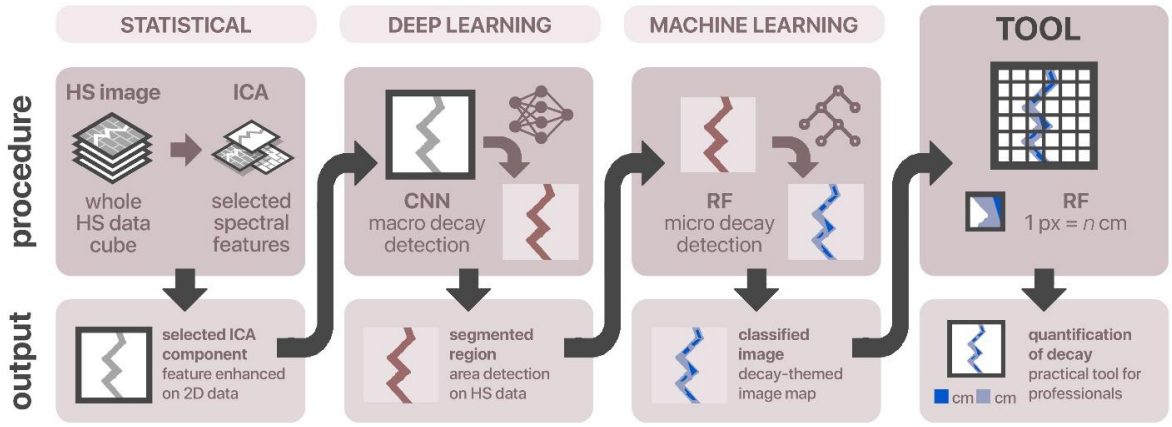


Figure 3 – Schematic overview of the proposed methodology for decay detection

3.2 Preprocessing: dimensionality reduction

HS imaging data are intrinsically information-rich, as each pixel is represented by a reflectance value for every wavelength recorded by the sensor (164 spectral bands in the present case). Consequently, each pixel can be interpreted as a high-dimensional vector in spectral space. While this constitutes a valuable source of information, it also results in a high-dimensional dataset characterised by strong inter-band correlation and substantial redundancy. Such characteristics increase computational burden and may hinder classification performance, even when advanced AI-based methods are employed (Donoho 2000; Pei, Huang, and Zhou 2023). Therefore, a preliminary dimensionality reduction step is typically required, either through projection onto a reduced set of components or through the selection of the most informative transformed features.

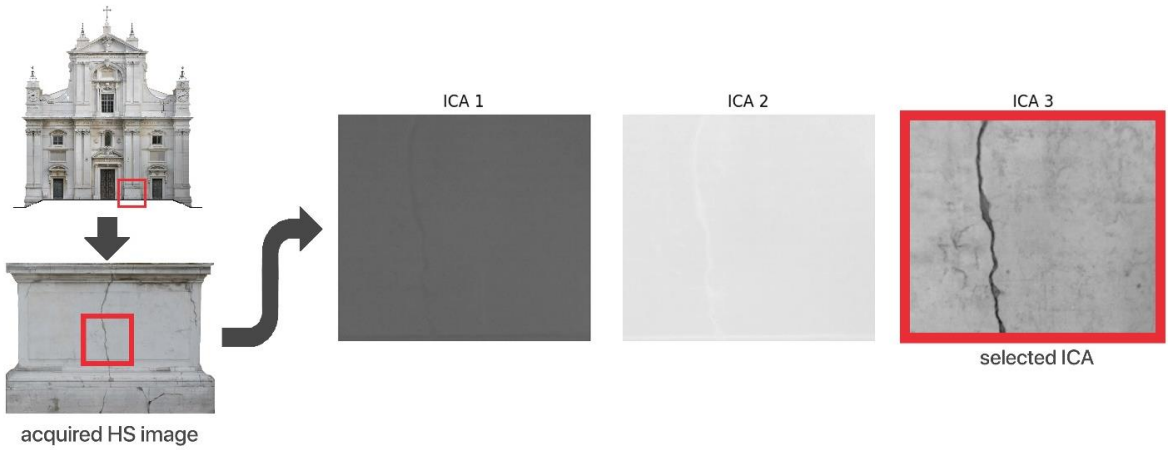
In HS analysis, widely adopted mathematical approaches for dimensionality reduction include Principal Component Analysis (PCA) and ICA (Kuras et al. 2021; Kale et al. 2017). Both methods treat each pixel as a spectral vector and aim to transform the original correlated space into a more compact representation. PCA identifies orthogonal directions (*principal components*) along which the variance of the data is maximised. By projecting the data onto these directions, PCA removes linear correlation between spectral bands while preserving most of the overall variance. The resulting components are uncorrelated linear combinations of the original bands (Kale et al. 2017; Greenacre et al. 2022). ICA, by contrast, seeks statistically independent and non-Gaussian components under the assumption of linear mixing. Rather than merely decorrelating the data, ICA attempts to separate the observed signals into underlying independent sources (Kale et al. 2017; Naik and Kumar 2011). Consequently, ICA may provide a representation that is more interpretable when the spectral signal arises from the combination of distinct physical or material contributions.

In the present study, ICA was applied to HS images with the aim of distinguishing macro-scale decay areas from non-degraded regions. The algorithm was used to extract three independent components, corresponding to statistically independent spectral sources. These components were subsequently reshaped into 2D spatial maps, i.e., grayscale images where each pixel represents the intensity of the corresponding component, highlighting areas where it is most discriminative (Fig. 4). Prior to ICA execution, a normalisation step was performed to minimise the influence of varying illumination conditions. Among them, the component exhibiting the highest spatial contrast between degraded and non-degraded areas was selected as input for the subsequent stage (*Section 3.3*). This choice was guided by interpretability and spatial discriminative capability rather than by purely statistical criteria. The adoption of a single ICA-derived image enabled a

substantial reduction of spectral dimensionality while preserving the spatial patterns most relevant for macro-scale degradation segmentation.

Figure 4 –ICA-elaborated images extracted from one of the acquired hyperspectral images

3.3 Where? Macro-scale decay detection



ICA preprocessing allowed for data simplification and the separation of the acquired image into a 2D map of altered and non-altered areas. The next step involves defining a method for the automatic identification of these macroareas, without human intervention. CNNs are DL-based tools commonly employed for this purpose, performing image segmentation by extracting hierarchical features and comparing them with a labeled training set to classify image regions (Courville, Goodfellow, and Bengio 2016).

For this study, a pre-trained U-Net for crack detection was selected for macro-decay identification due to its ability to preserve fine details through its encoder-decoder architecture (Jiangtao, Ruhaiyem, and Panpan 2025). Applied to the ICA-processed 2D image, the U-Net enabled the automatic spatial segmentation of the macro-altered area (Fig. 5), providing spatial context on which to perform the subsequen step (*Section 3.4*).

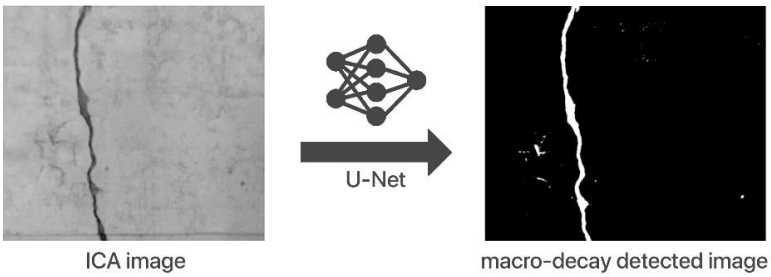


Figure 5 –Segmented area of macro-decay detected by the U-Net on the ICA-elaborated image

3.4 What? Supervised classification of micro-scale decay

The previous section enabled the identification of the area for detailed classification of smaller-scale decay on the original HS images. This step was useful to limit the investigation to a well-defined region, reducing computational effort while providing more precise information regarding the location and type of decay.

Decay classification within the detected area was performed using a supervised ML algorithm. In particular, RF was chosen due to its simplicity, low computational requirements, and robustness with small datasets. In RF, the training dataset (in this case, HS pixels) is split into subsets that are randomly assigned to individual decision trees. Each tree casts a vote for the classification, and the final category is determined by majority vote (Ilehag et al. 2017).

For this purpose, a representative HS image of micro-decay (incoherent patching with cement mortar inside cracks) was selected, and ROIs were labeled as "patch" or "crack" (unpatched areas). This labeled dataset of HS pixels was then used for training the classifier, whose results and performance are described in *Section 4*.

3.5 How much? Quantification of decay

Up to this point, the procedure allowed for the automatic detection and classification of decay, but its quantification remains challenging. Raw HS images lack an intrinsic scale, and irregularly shaped areas are not easily measurable without approximation. However, since the HS camera functions like a standard camera with additional spectral channels, it is possible to compute the real-world dimensions of the detected regions using the GDS.

GSD is a common concept in remote sensing that defines the actual size of a single pixel in metres (Felipe-García, Hernández-López, and Lerma 2012). For a camera with a given Field Of View (FOV) and a known distance (D) from an object, the physical size of the scene along one axis can be estimated as (Eq. 1):

$$\text{Scene size} = 2 \cdot D \cdot \tan(\frac{FOV}{2}) \quad (1)$$

The GSD, i.e., the real-world size of a single pixel, is then obtained by dividing the scene size by the number of pixels (N_{pixels}) along that axis (Eq. 2) and finally, the area of a given decay type can be calculated by multiplying the number of pixels in the corresponding mask ($N_{pixels,mask}$) by the area of a single pixel given by its GDS on the x and y directions (Eq. 3):

$$\text{GDS} = \frac{GDS}{N_{pixels}} \quad (2)$$

$$\text{Decay area} = N_{pixels,mask} \cdot GDS_x \cdot GDS_y \quad (3)$$

This approach allows for the quantification of micro-decay regions in real-world units, providing a reliable estimate of the altered surface.

4. Results

The application of the proposed workflow to the collected dataset produced results consistent with those shown in Fig. 6. Macro-scale decay features (major cracks) were successfully detected in the HS images, and micro-scale decay patterns (incoherent cement mortar patches) were accurately classified. In addition to the segmented images, a legend reporting the identified decay forms and their quantitative measurements was generated.

The RF model, trained on a representative image including both forms of decay, was subsequently tested on the remaining 23 acquired images after masking the macro-scale areas of interest using the U-Net. When compared with ground truth decay masks, the model achieved accuracy values up to 74% for the detection of cracks and 83% for patches under favourable illumination conditions.

However, this performance was primarily observed in the central portion of the stone base, where illumination was relatively uniform. In the upper and lower areas, classification performance heavily decreased (Fig. 7).

In these regions, the presence of mouldings introduces variations in illumination, resulting in cast shadows, which, although limited in intensity, negatively affect both macro-scale detection through the U-Net and the subsequent micro-scale classification. Although HS acquisitions were conducted under carefully controlled lighting conditions and a normalisation step was applied prior to ICA processing to mitigate illumination variability, residual lighting heterogeneity influenced the final classification results.

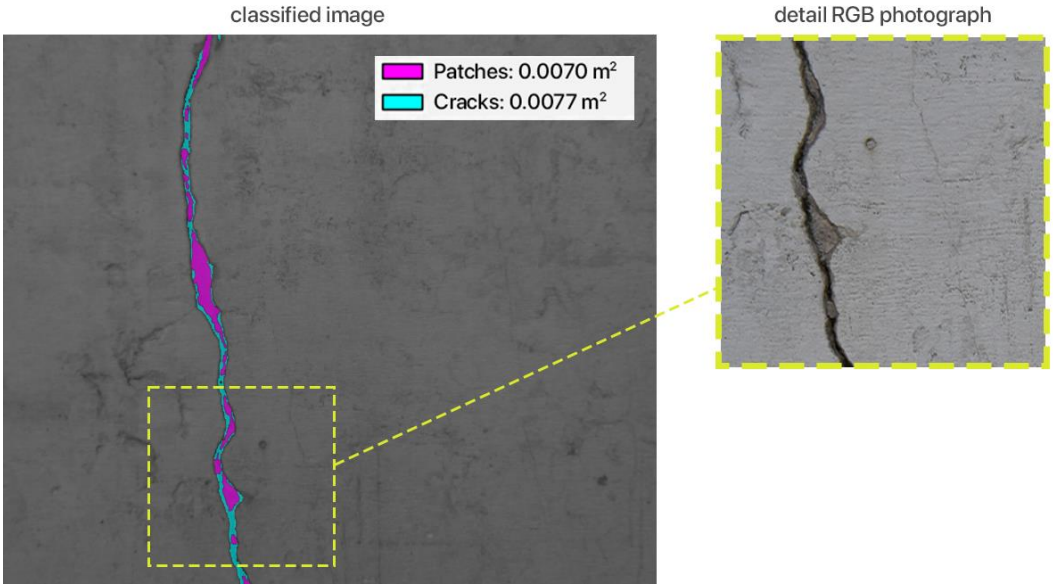


Figure 6 – Classified hyperspectral image obtained through the proposed procedure. The yellow box highlights a detail of the crack with incoherent patches to improve visual clarity

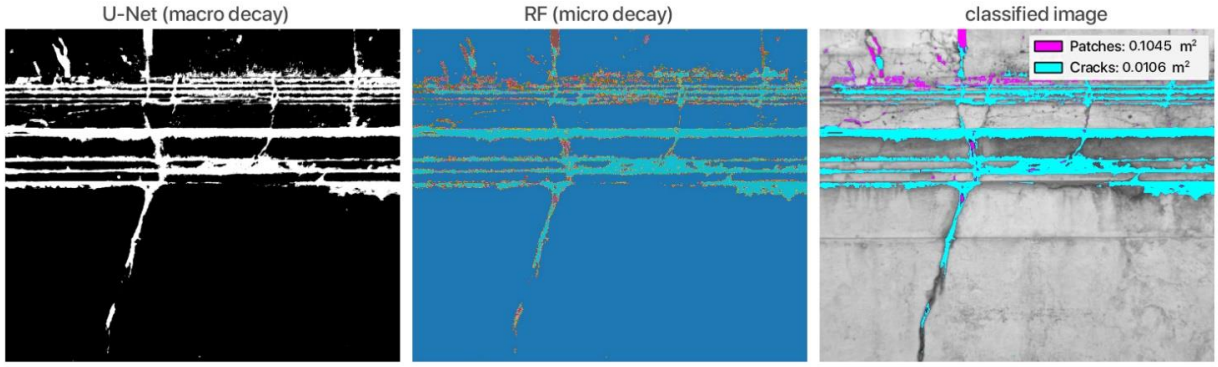


Figure 7 – Macro-scale decay classification using the U-Net, micro-scale classification using the RF classifier, and final classified image including quantitative measurement of decay areas on an image affected by shadows

5. Conclusion

Effective monitoring strategies, both in terms of accuracy and time-efficiency, are of paramount importance to guarantee the early detection of criticalities on built heritage surfaces, thus enabling timely interventions and the avoidance of invasive and costly operations. In this perspective, AI-based automated pipelines for the classification of heritage surface images are currently a hot topic in the literature. Within this context, the application of these pipelines to advanced imagery, such as HS imaging data, is of great interest and is currently under development.

This study aimed to contribute to this field of research by proposing a hierachical methodological framework that combines different approaches: prior statistical pre-processing through ICA, the identification of macro-decay areas through a U-Net segmentation and the detailed classification of alterations within these areas using supervised RF classification. The proposed workflow also includes a method for the metric quantification of the classified surfaces exploiting the concept of GDS, thus providing professionals with a tool capable of

quantifying the extent of alterations, useful when such measurements are required for restoration material estimation or administrative documentation.

Although the first results are promising, they remain moderate, and the procedure shows limitations when dealing with noisy datasets or suboptimal illumination conditions, which is a critical issue widely reported in the literature, particularly for on-field applications (Themistocleous et al. 2020; Hemmleb et al. 2006; McCoy 2005). Future work could evaluate the impact of different solar angles on classification accuracy and investigate whether preliminary surface cleaning, such as dust removal, reduces light scattering. Additionally, approaches to enhance illumination conditions through the use of supportive artificial lighting could be explored. However, implementing lighting conditions in the field presents significant logistical challenges, including complex architectural and urban contexts that hinder the acquisition setup, or the portability of heavy equipment. Furthermore, specific lamp types like halogen sources, which are essential for collecting reliable HS imaging data due to their continuous spectrum, are increasingly difficult to source, as they have been largely phased out of the market due to energy efficiency regulations.

Moreover, since the present study aimed primarily at proposing a methodological framework rather than achieving a perfect solution, the experimental dataset was very limited, constrained to only two types of decay (cracks and patches) on a single material (Istrian stone). Future studies should expand this framework to a broader range of material and degradation patterns. Indeed comprehensive material and decay spectral libraries of heritage surfaces are currently lacking and are required and need to enhance models' generalisaiton (Zahiri et al. 2022). Additionally, U-Net performance was limited in detecting cracks, but procedures focusing on the identification of different macro-decay types (e.g., stains) could be explored.

Despite these limitations, the present study represents a valuable contribution towards the automatic classification of decay on heritage surfaces through HS imaging.

Acknowledgments

The authors would like to express their gratitude to the Superintendence for Archaeology, Fine Arts and Landscape for the Provinces of Ancona and Pesaro e Urbino and to the Pontifical Sanctuary of the Holy House of Loreto for their valuable cooperation and for providing access for data collection. This research received no external funding.

References

Cai, Lei, Jingyang Gao, and Di Zhao. 2020. "A Review of the Application of Deep Learning in Medical Image Classification and Segmentation." *Annals of Translational Medicine* 8 (11): 713–713. https://doi.org/10.21037/atm.2020.02.44.

Courville, Aaron, Ian Goodfellow, and Yoshua Bengio. 2016. *Deep Learning*. *Nature*. Vol. 29.

Cubert. n.d. "Ultris X20 Plus." Cubert. Accessed January 14, 2025. https://cubert-hyperspectral.com/en/ultris-x20-plus/.

Datta, Debaleena, Pradeep Kumar Mallick, Akash Kumar Bhoi, Muhammad Fazal Ijaz, Jana Shafi, and Jaeyoung Choi. 2022. "Hyperspectral Image Classification: Potentials, Challenges, and Future Directions." *Computational Intelligence and Neuroscience*. Hindawi Limited. https://doi.org/10.1155/2022/3854635.

Donoho, David L. 2000. "The Curses and Blessings of Dimensionality." *American Math. Society Lecture-Math Challenges of the 21st Century*, 1–33. https://doi.org/10.1.1.329.3392.

Felipe-García, Beatriz, David Hernández-López, and José Luis Lerma. 2012. "Analysis of the Ground Sample Distance on Large Photogrammetric Surveys." *Applied Geomatics* 4 (4): 231–44. https://doi.org/10.1007/s12518-012-0084-2.

Fiorucci, Marco, Marina Khoroshiltseva, Massimiliano Pontil, Arianna Traviglia, Alessio Del Bue, and Stuart James. 2020. "Machine Learning for Cultural Heritage: A Survey." *Pattern Recognition Letters* 133 (May): 102–8. https://doi.org/10.1016/J.PATREC.2020.02.017.

Giannuzzi, Valeria, and Fabio Fatiguso. 2024. "Historic Built Environment Assessment and Management by

Deep Learning Techniques: A Scoping Review." *Applied Sciences (Switzerland)* 14 (16). https://doi.org/10.3390/app14167116.

González Manich, C., T. Kelman, F. Coutts, B. Qiu, P. Murray, C. González-Longo, and S. Marshall. 2016. "Exploring the Use of Image Processing to Survey and Quantitatively Assess Historic Buildings." *Structural Analysis of Historical Constructions: Anamnesis, Diagnosis, Therapy, Controls - Proceedings of the 10th International Conference on Structural Analysis of Historical Constructions, SAHC 2016*, 125–32. https://doi.org/10.1201/9781315616995-15.

Greenacre, Michael, Patrick J. F. Groenen, Trevor Hastie, Alfonso Iodice D'Enza, Angelos Markos, and Elena Tuzhilina. 2022. "Principal Component Analysis." *Nature Reviews Methods Primers* 2 (1): 100. https://doi.org/10.1038/s43586-022-00184-w.

Hemmleb, M, F Weritz, a Schiemenz, a Grote, C Maierhofer, and Laser Scanning. 2006. "Multi-Spectral Data Acquisition and Processing Techniques for Damage Detection on Building Surfaces." *Ievm*, 1–6.

Hugemann, Wolfgang. 2010. "Correcting Lens Distortions in Digital Photographs."

ICOMOS, UNESCO. 2011. "The Valletta Principles for the Safeguarding and Management of Historic Cities, Towns and Urban Areas." *Principles, as Adopted by the 17th ICOMOS General Assembly*.

Ilehag, R., M. Weinmann, A. Schenk, S. Keller, B. Jutzi, and S. Hinz. 2017. "Revisiting Existing Classification Approaches for Building Materials Based on Hyperspectral Data." *International Archives of the Photogrammetry, Remote Sensing and Spatial Information Sciences - ISPRS Archives* 42 (3W3): 65–71. https://doi.org/10.5194/isprs-archives-XLII-3-W3-65-2017.

Jiangtao, Wang, Nur Intan Raihana Ruhaiyem, and Fu Panpan. 2025. "A Comprehensive Review of U-Net and Its Variants: Advances and Applications in Medical Image Segmentation." *IET Image Processing* 19 (1): 1–36. https://doi.org/10.1049/ipr2.70019.

Kale, Karbhari V., Mahesh M. Solankar, Dhananjay B. Nalawade, Rajesh K. Dhumal, and Hanumant R. Gite. 2017. "A Research Review on Hyperspectral Data Processing and Analysis Algorithms." *Proceedings of the National Academy of Sciences India Section A - Physical Sciences* 87 (4): 541–55. https://doi.org/10.1007/s40010-017-0433-y.

Kuras, Agnieszka, Maximilian Brell, Jonathan Rizzi, and Ingunn Burud. 2021. "Hyperspectral and Lidar Data Applied to the Urban Land Cover Machine Learning and Neural-Network-Based Classification: A Review." *Remote Sensing* 13 (17): 3393. https://doi.org/10.3390/rs13173393.

Li, Xingyue, Haiqing Yang, Chiwei Chen, Gang Zhao, and Jianghua Ni. 2024. "Deterioration Identification of Stone Cultural Heritage Based on Hyperspectral Image Texture Features." *Journal of Cultural Heritage* 69 (September): 57–66. https://doi.org/10.1016/j.culher.2024.07.011.

Liu, Detianjun, Enguang Zuo, Dingding Wang, Liang He, Liujing Dong, and Xinyao Lu. 2025. "Deep Learning in Food Image Recognition: A Comprehensive Review." *Applied Sciences* 15 (14): 7626. https://doi.org/10.3390/app15147626.

McCoy, Roger M. 2005. *Field Methods in Remote Sensing*. *Canadian Geographer / Le Géographe Canadien*. Vol. 50. http://doi.wiley.com/10.1111/j.1541-0064.2006.00161_2.x.

Mishra, Mayank. 2021. "Machine Learning Techniques for Structural Health Monitoring of Heritage Buildings: A State-of-the-Art Review and Case Studies." *Journal of Cultural Heritage* 47 (January): 227–45. https://doi.org/10.1016/j.culher.2020.09.005.

Mukhtar, Sani, Amir Arbabi, and Jaime Viegas. 2025. "Advances in Spectral Imaging: A Review of Techniques and Technologies." *IEEE Access* 13 (February): 35848–902. https://doi.org/10.1109/ACCESS.2025.3544476.

Naik, G R, and Dinesh K Kumar. 2011. "An Overview of Independent Component Analysis and Its Applications." *Informatica* 35 (1). https://www.informatica.si/index.php/informatica/article/view/334.

Pei, Zhongming, Yong Mao Huang, and Ting Zhou. 2023. "Review on Analysis Methods Enabled by Hyperspectral Imaging for Cultural Relic Conservation." *Photonics* 10 (10). https://doi.org/10.3390/photonics10101104.

Pozo, S. Del, P. Rodríguez-Gonzálvez, L. J. Sánchez-Aparicio, A. Muñoz-Nieto, D. Hernández-López, B. Felipe-García, and D. González-Aguilera. 2017. "Multispectral Imaging in Cultural Heritage Conservation." *International Archives of the Photogrammetry, Remote Sensing and Spatial Information Sciences - ISPRS Archives* 42 (2W5): 155–62. https://doi.org/10.5194/isprs-archives-XLII-2-W5-155-2017.

Santarelli, Giuseppe. 1999. *La Santa Casa Di Loreto*. Edited by Mondadori.

———. 2014. *L'Arte a Loreto*. Edited by Edizioni Santa Casa. Loreto.

Shaikh, Muhammad Saad, Keyvan Jaferzadeh, Benny Thörnberg, and Johan Casselgren. 2021. "Calibration of a Hyper-Spectral Imaging System Using a Low-Cost Reference." *Sensors (Basel, Switzerland)* 21 (11). https://doi.org/10.3390/S21113738.

Themistocleous, Kyriacos, Evagoras Evagorou, Christodoulos Mettas, Maria Prodromou, and Diofantos G. Hadjimitsis. 2020. "The Documentation of Cultural Heritage Sites in Cyprus Using Integrated Techniques: The Case Study of the Church of Agios Athanasios and Kyrillos." In *Eighth International Conference on Remote Sensing and Geoinformation of the Environment (RSCy2020)*, edited by Kyriacos Themistocleous, Silas Michaelides, Vincent Ambrosia, Diofantos G. Hadjimitsis, and Giorgos Papadavid, 73. SPIE. https://doi.org/10.1117/12.2571640.

Torre, Stefano Della. 2021. "Italian Perspective on the Planned Preventive Conservation of Architectural Heritage." *Frontiers of Architectural Research* 10 (1): 108–16. https://doi.org/10.1016/j.foar.2020.07.008.

Valença, J., L.M.S. Gonçalves, and E. Júlio. 2013. "Damage Assessment on Concrete Surfaces Using Multi-Spectral Image Analysis." *Construction and Building Materials* 40 (March): 971–81. https://doi.org/10.1016/j.conbuildmat.2012.11.061.

Vandesande, A, and K Van Balen. 2018. "Preventive Conservation Applied to Built Heritage: A Working Definition and Influencing Factors." In *Innovative Built Heritage Models*, 63–72. CRC Press.

Vandesande, Aziliz, Koenraad van Balen, Stefano Della Torre, and Fausto Cardoso. 2018. "Preventive and Planned Conservation as a New Management Approach for Built Heritage: From a Physical Health Check to Empowering Communities and Activating (Lost) Traditions for Local Sustainable Development." *Journal of Cultural Heritage Management and Sustainable Development* 8 (2): 78–81. https://doi.org/10.1108/JCHMSD-05-2018-076.

Zahiri, Zohreh, Debra F. Laefer, Tobias Kurz, Simon Buckley, and Aoife Gowen. 2022. "A Comparison of Ground-Based Hyperspectral Imaging and Red-Edge Multispectral Imaging for Façade Material Classification." *Automation in Construction* 136 (April): 104164. https://doi.org/10.1016/J.AUTCON.2022.104164.

cinpar2026
XXII International Conference on Building Pathology and Constructions Repair
15th to 17th July 2026 - Lisboa, Portugal

Pathological Manifestations in Residential Construction: Warranty Assessment in Fortaleza – CE.

Allefy Teles SAMPAIO[1], Willlames DE ALBUQUERQUE[2], Eliana BARRETO[3]

[1] Universidade de Pernambuco, Recife, Brasil, ats1@poli.br
[2] Universidade de Pernambuco, Recife, Brasil, was@poli.br2
[3] Universidade de Pernambuco / Universidade Católica de Pernambuco, Recife, Brasil, eliana@poli.brl3

Abstract: This article analyzes the pathological manifestations identified in a vertical condominium development located in Fortaleza, Ceará, focusing on the technical assessment of construction warranty periods and conditions. The methodology employed is based on systematic building inspection, the application of non-destructive testing, and documentary analysis of design drawings and owner's manuals, with ABNT NBR 16747:2020 as the central normative support. The results highlight the prevalence of cracks in ribbed slabs, infiltration in basements, and failures in anchoring systems, raising the technical-legal debate between construction defects and loss of warranty due to absence of preventive maintenance. The climatic context of Fortaleza — bioclimatic zone 8, high humidity, and coastal environmental aggressiveness — is identified as a factor that accelerates the progression of pathologies. The conclusion points to the need for systematized inspection protocols and greater rigor in construction site supervision as instruments for prevention and mitigation of damage.

Keywords: Building pathology; Building inspection; Construction warranty; Pathological manifestations.

1. Introduction

Brazilian residential housing production in recent decades has been marked by cycles of accelerated expansion, driven by federal financing programs and by the growth in demand for vertical condominium units in major urban centers. This intense pace of production, often associated with compressed timelines and the adoption of lower-cost construction solutions, created favorable conditions for the early emergence of pathological manifestations in buildings delivered to the market. Recent studies have demonstrated that the incidence of anomalies in residential buildings in Brazil is high and that much of these occurrences originate from verifiable failures in the design and execution phases (Bauer; Pavon; Oliveira, 2019).

The relevance of this topic transcends the technical dimension and reaches the legal field, since Brazilian law — through the Civil Code (art. 618) and the Consumer Protection Code — imposes objective liability on construction companies and developers for the soundness, safety, and habitability of delivered works. The interface between these legal provisions and the technical criteria established by ABNT NBR 15575:2013 — Performance Standard for Residential Buildings — configures a field of permanent tension between the interests of users and those of construction companies, making the technical assessment of warranties an instrument of growing importance in the context of national diagnostic engineering (Pujadas; Oliveira; Neto, 2021).

In this scenario, building inspection emerges as a central methodology for the identification, classification, and diagnosis of pathological manifestations, allowing the technical distinction between construction defects — for which the builder is responsible — and deterioration resulting from the absence of preventive maintenance — for which the user or the condominium is responsible. This distinction, apparently simple in its conceptual formulation, proves to be complex in practice, requiring the qualified

professional to master rigorous investigation methods and possess in-depth knowledge of the degradation mechanisms of construction systems (Bauer; Pavon; Oliveira, 2019).

Fortaleza, capital of the state of Ceará, presents climatic characteristics that confer singularity to the behavior of buildings in its territory and that justify the conduct of specific studies on building pathology in this context. The city is located in bioclimatic zone 8, according to ABNT NBR 15220:2005, being marked by average annual temperatures exceeding 26°C, average relative air humidity around 78%, intense solar radiation, and a rainfall regime concentrated in the first half of the year. These climatic factors act synergistically as potentiating agents of pathological manifestations, especially those related to moisture, concrete carbonation, and degradation of waterproofing systems (Silva; Brito; Gaspar, 2020).

The environmental aggressiveness of the northeastern coast, characterized by high concentration of chloride ions in the marine atmosphere, represents an additional risk factor for the durability of reinforced concrete structures. The penetration of chlorides through concrete, accelerated by the presence of cracks and by the low quality of rebar coverage, triggers electrochemical corrosion processes that compromise the structural integrity of buildings within periods shorter than the service life established by current technical standards (Medeiros; Helene; Grochoski, 2021). This situation is aggravated by the combination of high temperature and high relative humidity, conditions that intensify the deterioration reactions of concrete and coating materials (Carasek; Cascudo; Scartezini, 2019).

Given this context, the present work aims to identify and analyze the pathological manifestations present in a vertical condominium development in Fortaleza-CE, evaluating their origin, degree of risk, and classification within the warranty periods established by applicable legislation and technical standards. The research seeks to contribute to the advancement of knowledge on building pathology in the northeastern climatic context and to the improvement of building inspection processes as an instrument of asset management and conflict resolution within the scope of construction warranties.

2. Methodology

This research is configured as a case study of applied nature, with qualitative and quantitative approach, of descriptive and analytical character. The object of analysis is a vertical condominium development for residential use, located in the municipality of Fortaleza, Ceará, delivered less than five years before the inspection date. The development comprises multiple towers, with basement intended for parking, ground floor with common use areas, and typical floors with residential units.

The inspection constitutes the central method of this research, understood as the set of technical procedures intended for the assessment of the conditions of use, maintenance, and performance of a building, with a view to identifying anomalies, diagnosing their causes, and formulating technical recommendations. As highlighted by Bauer, Pavon, and Oliveira (2019), systematized building inspection represents a significant methodological advance over traditional inspections, as it incorporates objective criteria for risk classification and requires the responsible professional to adopt a multidisciplinary approach that integrates knowledge of structures, installations, coatings, and maintenance management.

The inspection process was structured in four sequential and interdependent stages. The first consisted of documentary research, with analysis of architectural, structural, hydrosanitary, and waterproofing projects, verification of the Owner's Manual and Common Areas Manual delivered by the construction company, and consultation of the work's Descriptive Memorial. Documentary analysis prior to field inspection is pointed out by Pujadas, Oliveira, and Neto (2021) as an indispensable stage for the correct interpretation of identified anomalies, as it allows comparison between what was executed and what was designed, and identification of conformity deviations that might otherwise be erroneously attributed to use or maintenance.

The second stage corresponded to systematic visual inspection, conducted by a qualified civil engineer in all common areas of the development — basement, ground floor, roofs, facades, and circulation areas — with standardized photographic recording of all identified anomalies. Visual inspection, although it is the

primary method for diagnosing anomalies, should be complemented by specific tests when the complexity or severity of anomalies so requires (Carasek; Cascudo; Scartezini, 2019). This complementation was carried out in the third stage, dedicated to the application of non-destructive testing (NDT), which included: percussion with rubber hammer to identify detachment in ceramic and mortar coatings; surface moisture measurement with digital hygrometer; thermographic analysis by infrared camera for mapping of hidden infiltrations; and measurement of crack opening with fissurometer and graduated magnifying glass. Infrared thermography, in particular, has been highlighted by recent literature as a highly effective tool in the diagnosis of hidden infiltrations and coating detachment on facades, allowing the identification of anomalies not visible to the naked eye with precision and without destructive intervention in the building (Bauer; Pavon; Oliveira, 2019).

The fourth and final stage consisted of the classification and assessment of anomalies, conducted according to two complementary criteria. Regarding origin, pathological manifestations were classified as endogenous (design, materials, or execution), exogenous (external agents), or functional (inadequate use or absence of maintenance), following the taxonomy widely adopted in national technical literature (Pujadas; Oliveira; Neto, 2021). Regarding the degree of risk, anomalies were classified as critical, regular, or minimal, based on the assessment of the potential for damage to safety, habitability, and functionality of the building. This dual classification is fundamental for warranty assessment, as it allows identification, with objective technical basis, of which manifestations constitute construction defects for which the builder is responsible and which result from maintenance failures attributable to the condominium (Medeiros; Helene; Grochoski, 2021).

It is pertinent to note that the adopted methodology is in compliance with ABNT NBR 16747:2020 — Building Inspection: Guidelines, Concepts, Terminology, and Procedure — a standard that, by systematizing building inspection procedures in Brazil, consolidated the state of the art of methodological practices developed and discussed by the national technical-scientific community over the last decade.

3. Results and Discussion

The building inspection conducted in the condominium development that is the object of this study resulted in the identification of an expressive set of pathological manifestations distributed across different construction systems and areas of the building. The anomalies were grouped into four main categories: manifestations in reinforced concrete structures; infiltrations and waterproofing failures; anomalies in anchoring and fastening systems; and manifestations in coatings and sealing systems. This distribution pattern is consistent with the incidence profile reported by recent studies on anomalies in Brazilian residential buildings, in which manifestations related to moisture and structural cracking consistently rank among the most frequent and have the greatest impact on the quality of use and durability of buildings (Carasek; Cascudo; Scartezini, 2019; Silva; Brito; Gaspar, 2020).

The pathological manifestation of greatest recurrence and severity identified in the development was the presence of cracks in ribbed slabs, located predominantly in the basement — parking area — and in the roof slabs. The measured openings ranged between 0.2 mm and 1.8 mm, with numerous occurrences exceeding the control limits established by ABNT NBR 6118:2014 for structures in environmental aggressiveness class II. Cracking in reinforced concrete structures can originate from multiple mechanisms, including plastic and drying shrinkage, excessive loads, differential settlement of foundations, dimensioning errors, and execution failures in reinforcement placement (Medeiros; Helene; Grochoski, 2021).

In the case under analysis, the distribution pattern of cracks, predominantly in regions of rib support and with orientation transverse to the main ribs, is indicative of bending stresses higher than those foreseen in the design or of insufficient reinforcement in the region of negative moments, suggesting possible execution error in the assembly of the reinforcement. This type of anomaly is classified by Bauer, Pavon, and Oliveira (2019) as of endogenous origin, with cause in the execution phase, constituting a construction defect whose diagnosis should be based on the joint analysis of the cracking pattern, the geometric characteristics

of the structure, and the records of technological control of the concrete. In Figure 01, it is possible to visualize the cracks in the ribbed slab.

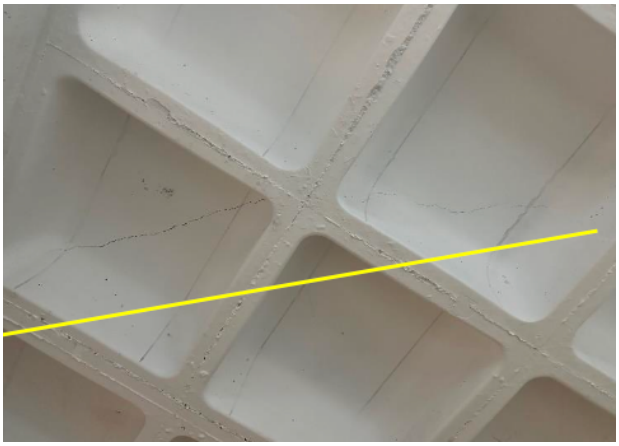


Figure 1 – Authors, 2026

The severity of this manifestation is potentiated by the climatic and environmental context of Fortaleza. Silva, Brito, and Gaspar (2020) demonstrated that the degradation rate of reinforced concrete structures in environments of high relative humidity and temperature is significantly higher than that observed in regions of temperate climate, due to the greater speed of carbonation reactions and the penetration of aggressive agents. On the northeastern coast, the combination of structural cracking with the high concentration of chlorides in the marine atmosphere creates particularly favorable conditions for the depassivation of steel and the development of electrochemical corrosion, compromising the service life of the structure within periods shorter than the design service life (Medeiros; Helene; Grochoski, 2021). This scenario reinforces the classification of these cracks as critical-degree anomalies, with potential for evolution toward compromise of the structural safety of the building.

Monitoring of fissures with fissurometers over thirty days revealed that approximately 60% of the identified cracks exhibited active behavior, with measurable variation in opening throughout the observation period. The distinction between active and passive fissures is methodologically relevant for warranty assessment, as active fissures indicate that the degradation process is ongoing, which, associated with the distribution pattern described, points to a construction defect originating in the execution phase. According to Pujadas, Oliveira, and Neto (2021), the activity of a fissure is one of the central technical criteria for the classification of risk degree and for the definition of responsibilities within the scope of construction warranties, since active fissures in reinforced concrete structures rarely originate exclusively from absence of maintenance, being, in most cases, a symptom of design or execution failure.

Infiltrations constituted the second category of greatest incidence in the development, with occurrences recorded in the basement, in the roof slabs, and in the interfaces between different construction systems. Carasek, Cascudo, and Scartezini (2019) identified, in a survey on pathological manifestations in Brazilian residential buildings, that manifestations related to moisture represent the largest portion of pathological occurrences in buildings, being responsible for significant secondary damage to coatings, electrical installations, and structures, in addition to direct impact on the quality of life of users.

In the basement of the development, infiltrations of groundwater through the retaining walls and floor slab were identified, with formation of efflorescence, moisture stains, and, in some points, emergence of free water. This situation is indicative of failure in the waterproofing system of the buried structures, either due to absence of adequate waterproofing or due to failure in the execution of the system specified in the design. Analysis of the waterproofing designs revealed that the specified system was technically compatible with normative requirements; however, visual inspection indicated failures in execution, particularly at the interfaces between the floor slab and the retaining walls, regions of greatest vulnerability in basement

waterproofing systems (Silva; Brito; Gaspar, 2020). In Figure 2 it is possible to identify points of soiling, caused by the presence of water.



Figure 3 – Authors, 2026

Infiltrations in the basement piping deserve specific analysis, as they presented a distinct pattern from infiltrations due to waterproofing failure. Visual inspection and thermographic analysis revealed moisture concentrated in the regions of connection between piping and structure, suggesting failure in the sealing of pipe passages through the slab and retaining walls, an anomaly of endogenous origin, with cause in the execution phase, which constitutes a construction defect regardless of the time elapsed since the delivery of the development. In Figure 3, it is possible to identify points with failure of watertightness between slab and piping.

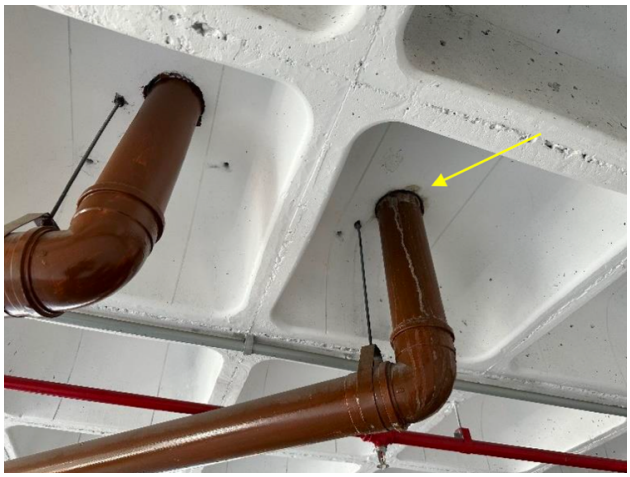


Figure 3 – Authors, 2026

Infiltrations in the roof slabs presented a distinct pattern, with moisture stains on the underside of the slabs and signs of deterioration of the waterproofing coating on the upper surface. The analysis of exposure conditions, flat slab with insufficient slope in some sections, forming ponding, and the condition of the waterproofing coating suggests the concurrence of design failure (inadequate slope) and absence of periodic maintenance of the waterproofing system. This situation exemplifies the complexity of warranty assessment in buildings, in which responsibility may be shared between the builder and the condominium, requiring individualized analysis of each manifestation for the correct attribution of responsibilities (Pujadas; Oliveira; Neto, 2021).

In this sense, it is fundamental to consider that ABNT NBR 5674:2012 establishes minimum periodicities for the maintenance of waterproofing systems, and that the absence of records of preventive maintenance by the condominium may constitute partial loss of warranty. However, as warned by Medeiros, Helene, and Grochoski (2021), the absence of maintenance does not exempt the builder from responsibility when the pathological manifestation has proven origin in execution or design failure, being necessary the analysis of the causal nexus for the correct attribution of responsibilities in each concrete case.

One of the pathological manifestations of greatest technical severity identified in the inspection was the presence of a non-standardized anchoring system in a structural element of the basement, executed with untreated steel rebar, without adequate anchor bolt and without any conformity with design specifications or applicable technical standards. This anomaly represents a serious deviation from good construction practices, constituting potential risk to the structural safety of the building and, consequently, to the physical integrity of the users. In Figure 4, it is possible to visualize the anchoring system executed.



Figure 4 – Authors, 2026

The use of steel rebar as an anchoring element, without structural dimensioning, without corrosion protection, and without conformity with applicable normative prescriptions, is classified as a critical-degree anomaly, in the technical sense of the term, by combining two simultaneous risk factors: the mechanical inadequacy of the element — not dimensioned for the stresses to which it is subjected — and vulnerability to corrosion accelerated by the basement environment, characterized by high humidity and, in the coastal context of Fortaleza, by potential presence of chlorides in groundwater (Carasek; Cascudo; Scartezini, 2019). Bauer, Pavon, and Oliveira (2019) emphasize that anomalies originating from execution failures that compromise the structural safety of the building fall into the category of serious redhibitory defects, for which the builder's responsibility subsists regardless of the user's maintenance conduct, since the defect originates prior to the delivery of the work.

The analysis of pathological manifestations identified in the development evidences the complexity of the technical-legal classification of responsibilities within the scope of construction warranties. The distinction between construction defect — for which the builder is responsible — and deterioration resulting from absence of preventive maintenance — for which the condominium is responsible — is, frequently, the central point of disputes between condominium residents and builders, and its resolution requires the engineer responsible for the inspection to master rigorous investigation methodologies and the ability to technically substantiate their conclusions (Pujadas; Oliveira; Neto, 2021).

ABNT NBR 15575:2013 introduced a significant advance in this debate by establishing, explicitly, that the design service life of construction systems is conditioned to the performance of preventive maintenance according to the minimum periodicities established and by the Manual of Use, Operation, and Maintenance of the building. However, Silva, Brito, and Gaspar (2020) demonstrated that the application of this principle

cannot be done mechanically, being necessary to verify, in each case, whether the pathological manifestation would have occurred even with regular performance of preventive maintenance. When the answer is affirmative — that is, when the anomaly has proven origin in design or execution failure — the builder's responsibility subsists, regardless of the user's conduct.

In the development that is the object of this study, the individualized analysis of each pathological manifestation, based on the causal nexus methodology, allowed the identification of three distinct categories of classification: manifestations of exclusive builder responsibility (active cracks in slabs, non-standardized anchoring system, infiltrations due to execution failure of basement waterproofing); manifestations of shared responsibility (roof infiltrations with concurrence of design failure and absence of maintenance); and manifestations of condominium responsibility (deterioration of coatings due to absence of cleaning and documented periodic maintenance). This tripartite categorization is consistent with the approach proposed by Medeiros, Helene, and Grochoski (2021), who recommend causal nexus analysis as a central methodological instrument in the assessment of responsibilities in building inspections, avoiding both undue imputation of responsibility to the builder and unjust transfer of burden to the condominium.

The climatic context of Fortaleza introduces an additional variable in this debate. Carasek, Cascudo, and Scartezini (2019) demonstrated that the conditions of high temperature, relative humidity, and environmental aggressiveness characteristic of the northeastern coast accelerate the degradation processes of construction systems, effectively reducing the service life of waterproofing systems, coatings, and concrete structures in relation to the reference values established by national technical standards, calibrated for average climatic conditions of Brazilian territory. This finding has direct implications for warranty assessment in Fortaleza, as it suggests that the periodicities of preventive maintenance established by standards and owner's manuals may be insufficient for the local climatic context, which, in turn, may constitute inadequacy of the product delivered to the use environment, responsibility that falls on the builder, not on the user.

4. Conclusion

The inspection identified critical anomalies, such as cracks in ribbed slabs, infiltrations in the basement, and anchoring systems outside normative standards. These failures are classified as construction defects for which the builder is responsible, as they compromise the structural safety and habitability of the condominium. In the case of roof infiltrations, responsibility is shared, requiring individualized expertise to determine the causal nexus of each occurrence.

The climate of Fortaleza, with high salinity and humidity, accelerates degradation, requiring that builders adapt designs and condominiums implement rigorous preventive maintenance plans. The absence of maintenance by the condominium manager does not exempt the builder from responsibility if the origin of the pathology is proven to be endogenous. It is recommended to strengthen quality control during execution and maintain detailed documentary records to substantiate technical decisions and prevent litigation.

References

BRAZILIAN ASSOCIATION OF TECHNICAL STANDARDS. NBR 6118: Design of concrete structures — Procedure. Rio de Janeiro: ABNT, 2014. 238 p.

BRAZILIAN ASSOCIATION OF TECHNICAL STANDARDS. NBR 15575: Residential buildings: performance. Rio de Janeiro: ABNT, 2013. 6 parts.

BRAZILIAN ASSOCIATION OF TECHNICAL STANDARDS. NBR 16747: Building inspection: guidelines, concepts, terminology and procedure. Rio de Janeiro: ABNT, 2020.

BAUER, Elton; PAVON, Eliane; OLIVEIRA, Ercília Hitomi. Analysis of building facade inspection methods. Built Environment, Porto Alegre, v. 19, n. 1, p. 203–224, Jan./Mar. 2019.

CARASEK, Helena; CASCUDO, Oswaldo; SCARTEZINI, Luiz Marcelo Bessa. Importance of substrate in mortar coating adhesion and associated pathologies. Built Environment, Porto Alegre, v. 19, n. 3, p. 7–28, Jul./Sep. 2019.

MEDEIROS, Marcelo Henrique Farias de; HELENE, Paulo Roberto do Lago; GROCHOSKI, Marcos. Durability and service life of reinforced concrete structures: critical review of prediction models and Brazilian normative prescriptions. Matéria, Rio de Janeiro, v. 26, n. 2, e13003, 2021.

PUJADAS, Flávio Zanetti de Arruda; OLIVEIRA, Dênio Ramam Carvalho de; NETO, João da Costa Faria. Building inspection and performance assessment of buildings: methodological foundations and practical applications. Built Environment, Porto Alegre, v. 21, n. 4, p. 45–62, Oct./Dec. 2021.

SILVA, Armando; BRITO, Jorge de; GASPAR, Pedro Lima. Degradation models and service life of building facades: application to the Brazilian context of high humidity and temperature. Built Environment, Porto Alegre, v. 20, n. 2, p. 117–138, Apr./Jun. 2020.

Cinpar 2026
XXII International Conference on Building Pathology and Constructions Repair
15th to 17th July 2026 - Lisboa, Portugal

A 3d tomographic GPR inspection using a self-constructed cable-driven robot of the Torre de la Vela in La Alhambra (Granada, Spain)

Miguel Ángel GARCIA[1], Mar ELIZO[1], Fernando RAMONET[2], Sofía APARICIO[2], Juan Carlos LIÉBANA[2], Antonio DE LA CRUZ[2], Pablo SANZ-HONRADO[2], Javier ORTEGA[2], Margarita GONZÁLEZ[2], José Javier ANAYA[2]

[1] Information Processing and Telecommunication center. ETSIT. UPM. Madrid, Spain, {miguelangel.garcia.izquierdo, mar.ealonso}@upm.es
[2] Institute for Physical and Information Technologies (ITEFI), Spanish National Research Council (CSIC), Madrid, Spain, {fernando.ramonet; sofia.aparicio; juancarlos.liebana, antonio.cruz, pablo.sanz, javier.ortega, m.g.hernandez, jj.anaya}@csic.es

Abstract: Ground Penetrating Radar is a non-destructive technique that involves emitting high-frequency electromagnetic waves that travels through a physical medium. Changes in the electromagnetic properties, voids or discontinuities produce reflections that allow the characterization of its internal structure. This technology is widely used for detecting buildings pathologies in both modern and historical built heritage. However, GPR inspection is usually performed manually. This makes the process time-consuming if large areas of a building need to be evaluated. Additionally, manual inspections are restricted to areas accessible by hand, which increase the difficulties in the inspection of the building's upper areas without easy external access.

In this work, a 3d tomographic reconstruction from internal and external GPR inspections of the upper part of the northern facade of the Torre de la Vela is presented. The area analysed is located 20 meters high above the ground and presents visible cracks and deterioration. The wall is made of rammed earth and brick masonry and an external area of 20 m^2 has been studied using a mounted GPR in a self-constructed cable driven robot, while the internal corresponding area has been analysed by manual inspections. Results reveal structural details, cracks depth as well as the level of deterioration that would be difficult to observe without the external inspection.

This case study shows the possibility of conducting complete, quick and efficient inspections in difficult access parts of facades with applications in both historical heritage and modern built structures without the need of installing additional structures such as scaffolding. During the inspection, the inspected façade has remained visible the entire time, allowing the visitors to access areas that might have been restricted using traditional inspection methods. Finally, this application highlights the capability of automated systems in architectural heritage inspection and validation of structural diagnosis.

Keywords: Built heritage; non-destructive testing (NDT); GPR; cable-driven robotic drone; rammed earth.

1. Introduction

The structural diagnosis of architectural heritage has increasingly relied on non-destructive testing (NDT) technologies capable of revealing internal features without compromising the integrity of historic materials. Among these methods, Ground Penetrating Radar (GPR) has emerged as one of the most versatile tools for investigating subsurface conditions due to its ability to detect anomalies such as voids, moisture, cracks,

inhomogeneities, and concealed architectural elements within masonry, stone, and composite historic structures.

GPR involves emitting high-frequency electromagnetic waves into the material being inspected. When these waves travel through the material and encounter material changes, discontinuities, voids, or inclusions, part of the energy is reflected due to changes in electromagnetic properties, allowing the internal structure to be characterized and visualized.

A GPR equipment usually has separate transmitting and receiving antennas operating in pulse-echo mode. The received signal is called a radargram and represents the reflections of the electromagnetic waves as they pass through the material. The radargram is a 2D false-color (B-Scan) representation where the X-axis shows the distance travelled by the antenna and the Y-axis the wave's propagation time through the material or structure. The colors indicate the intensity of the reflections, and any lines, patches, or hyperbolas that appear suggest objects, stratified materials, or anomalies. Generally, strong reflections have bright tones (white, if on a black/gray scale, or very dark); while weak reflections have intermediate tones, and areas without contrast are uniform.

Apart from two-dimensional (B-scan) GPR can provide three-dimensional (C-scan) reconstructions of structural components, allowing a more comprehensive understanding of the physical state of heritage assets. However, despite its proven diagnostic potential, the traditional implementation of GPR remains constrained by practical challenges inherent to build heritage: limited accessibility, fragile surfaces, steep vertical geometries, and safety risks for operators, particularly in elevated or deteriorated areas. [1, 2]

To overcome these limitations, recent research has focused on integrating GPR sensors into robotic and aerial platforms, enabling more systematic, safe, and efficient inspection strategies. Robotic ground systems equipped with GPR, such as omnidirectional platforms combining radar, impact-echo, and vision-based localization, have demonstrated considerable improvements in the speed, accuracy, and spatial consistency of subsurface data acquisition, [3, 4, 5]. These systems also support multimodal data fusion, enabling the correlation of mechanical and electromagnetic indicators of structural health for enhanced decision-making.

A major technological breakthrough has been the integration of GPR into unmanned aerial systems (UAS), enabling airborne, non-contact inspection of vertical and overhead surfaces. Drone-mounted GPR addresses key challenges encountered in heritage environments, notably accessibility and operator safety, by acquiring radar data without physical contact with sensitive surfaces. Although operating GPR in non-contact mode introduces complexities, such as increased signal attenuation and geometric distortion, recent experimental studies employing microwave tomography (MWT) based inverse scattering techniques have demonstrated that contactless UAS-GPR can achieve imaging performance comparable to traditional ground-coupled surveys when properly processed [6].

Hybrid robotic-aerial systems further expand the operational possibilities of GPR in heritage conservation. Platforms such as EASEEbot, which combine free-flight remote sensing with wall-climbing capabilities, allow drones to alternately collect thermal, RGB, and GPR data by transitioning between aerial and contact modes. These systems contribute to the creation of digitally enriched 3D models or digital twins integrating surface and subsurface information to support comprehensive envelope diagnostics. Although originally designed for energy-efficiency assessment, the underlying technology directly translates to the needs of cultural heritage, where multi-sensor integration and precise spatial mapping offer substantial advantages for conservation planning [7].

Advances in electromagnetic modelling and GPR data processing have been crucial to enabling these robotic and drone-based approaches. Developments in linear inverse scattering, clutter mitigation, signal enhancement, and tomographic reconstruction provide the mathematical foundation required to interpret data collected under non-ideal conditions where antenna motion, distance variation, and material heterogeneity introduce significant noise. Such algorithms are essential for analysing complex masonry structures typical of historic buildings, particularly when using mobile platforms that record radar signals

from varying geometries and offsets. Additional refinement through adaptive filtering, edge detection, and thresholding has achieved high accuracy in detecting voids and defects in ancient walls and composite masonry, including large-scale field applications such as the Ming Great Wall [8, 9].

Taken together, these developments illustrate a field undergoing rapid transformation. The integration of GPR into robotic and aerial systems offers a new paradigm for heritage diagnosis, enabling safer, faster, and more comprehensive inspection of culturally significant structures. As research continues to advance in platform design, sensor miniaturization, and inverse modelling, robotic and UAS-based GPR methods are poised to become central tools for preventive conservation, structural monitoring, and long-term documentation of built heritage.

This paper presents a case study inspection carried out using a cable-driven robot, of a section of the Vela tower's external wall located 20 meters high. Section 2 describes the cable-driven robot and the used GPR device. In section 3 the description of the campaign and the experimental setup are presented. Results are shown in section 4 and finally, several conclusions are presented related with this work. This advancement confirms the feasibility of using GPR-equipped robotic to inspect historic walls, façades, and other vertical elements where ground access is restricted

2. The cable-driven robot

For the external façade inspection, a cable-driven robot has been specifically designed and constructed for the automated inspection of large planar structures such as historic masonry facades as is the case of the Torre de la Vela in La Alhambra (Granada). This system allows precise, repetitive and reproducible positioning, an essential requirement for surface GPR inspection.

The Proceq GP8800 equipment, shown in Figure 1, was used in the inspections carried out at the Alhambra. The main advantage of this model is its portability, since its antenna is wireless and the control and processing equipment is located on a tablet (iPad). Furthermore, its weight, including the battery, of less than 800 grams facilitates its integration into robotic applications. This GPR emits an electromagnetic signal in a continuous frequency range between 400 and 6000 MHz, which allows for high-resolution imaging, but has the drawback of a limited penetration depth, approximately 65 cm, depending on the material.



Figure 1 – Proceq GP8800 used in the inspections

The primary objective of the robot is to enable a controlled movement of the frame along the surface of the building. The motion is constrained to a single plane, allowing the system to operate within a two-dimensional workspace. The mechanical part of the robot is composed by a rigid frame suspended by two

cables, and using pulleys as shown in Figure 2 (left). The positioning system is controlled using an Arduino microcontroller, two stepper motors with its transmission components and its control electronics.



Figure 2 – Cable-driven robot deployment in the façade (left) and photograph of the frame carrying the GPR antenna (right).

To maintain stable contact with the façade, the mobile unit employs two propellers mounted parallel to the wall, generating thrust toward the surface. This approach mechanism ensures consistent coupling between the GPR device and the wall while compensating for external disturbances such as wind. Figure 3 shows details of the real-time inspection of the exterior façade.

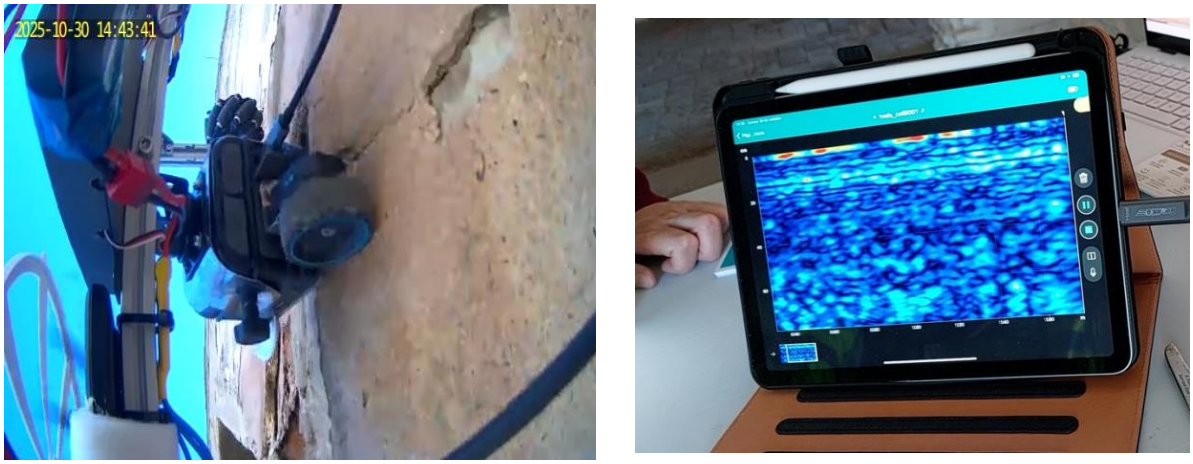


Figure 3 – Real-time inspection of the façade of the Vela tower using the cable-driven robot and the corresponding result shown in a tablet

3. Experimental campaign. Torre de la Vela. La Alhambra (Granada)

The GPR inspections in La Torre de la Vela correspond to the experimental campaign carried out in October 2025. The participating entities are: CSIC (Spanish Research Council) and, UPM (Technical University of Madrid). The central zone of the north façade has been inspected, both the interior and the exterior.

In the Torre de la Vela only the central part, internal and external, has been inspected. The external zone is 20m high from the floor and has been inspected by the cable driven robot. An important aspect for this inspection methodology is that, thanks to the incorporation of the robot, it is not necessary to install external elements as scaffolding. These elements do not allow the complete vision of the monument by the visitors. In this way, the inspections have been carried out to study the state of the monument, while at the same time, the visitor can observe it completely, without any kind of visual obstacle.

3.1 Torre de la Vela. Exterior assessment.

The exterior wall has been assessed using the cable-driven robot. Figure 4 presents the setup used for this inspection. The photograph on the left shows the Torre de la Vela with superimposed elements. Robot, marked in yellow, is suspended by two cables. The two motors that control the movement of the system are located inside the window. Outside, specifically on both sides of the roof, are the set of pulleys, that transmits the tension produced by the motors to the frame, allowing robot's positioning. Inside the tower, near the window, are the operators. It is necessary to both, monitor the robot's positioning, and manage the GPR data received from the inspection in real time.

Finally, since the robot's positioning is not visible to the operator inside, it was necessary to install two cameras, both using WiFi communication, which are essential for the proper operation of the robot. The first is an onboard camera, located in the frame that allows real-time visualization of the GPR, particularly its contact with the inspected wall. The second, located at the base of the tower, allows real-time visualization of the frame position on the facade. This is achieved by using the corrected image to generate an orthophoto overlaid with a mesh that, after initial calibration, indicates the robot's intended position and trajectory, Figure 4.

The inspected exterior area is located at 20 meters high and presents visible cracks and deterioration. The wall is made of rammed earth and, in some areas, brick masonry and the inspected area is 20 m^2.

Figure 4b shows the inspected exterior area, overlaid with a mesh for identifying the vertical lines. For the external measurements, the GPR has been installed on the cable-driven robot described in section 2. In this case, lineal inspections were taken every 25 cm, from vertical references 4 to 10 and from 14 to 21. Vertical lines start at A and ends at H.

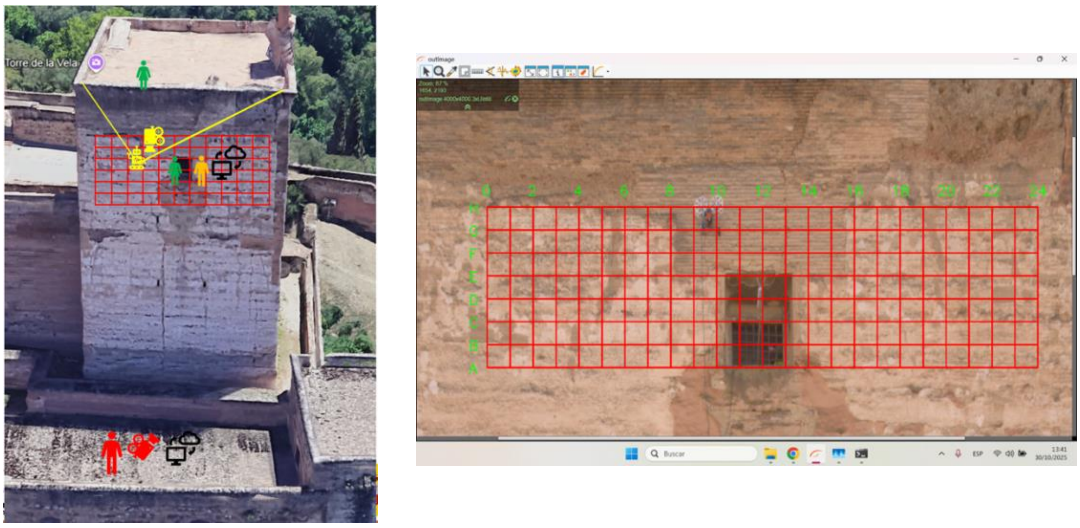


Figure 4 – Vela tower. Inspection setup

3.2 Torre de la Vela. Interior assessment

The interior area, which is accessible, has been manually inspected. The explores areas are located at left and the right of the window. The area at the right of the window is 5x2.8 m, and the area at the left is 2x3.6 m, in both cases an area inspection has been carried out each 10cm, both horizontal and vertical, Figure 5.



Figure 5 – Vela tower. Internal view of the inspected area

4. Experimental results

This section shows some of the most relevant results that were obtained during inspections. Between the selected results are the images that show the different types of material (bricks, rammed earth), cracks or holes and internal elements of high reflectivity.

4.1 External inspection

The exterior area was inspected using a cable-guided robot tracing vertical line. As shown in Figure 4, a grid was defined to reference the position. Each square represents approximately 0.5 meters. Two vertical radargrams were taken per grid in two zones. The first zone is located to the left of the window, between vertical references 6 and 9, while the second zone is located to the right of the window, between vertical references 14 and 21.

Figure 6 shows two vertical radargrams located at references 8.5 and 14. The path of the radargrams has been carried out from bottom to top and are represented by red arrows superimposed on the high-resolution image generated by a point cloud.

The radargram on the left corresponds to the vertical path referenced as 8.5 (left of the window). The most notable feature of this image is the appearance of a high-reflectivity zone at a height of 2 meters, coinciding with the brick wall. These reflections occur at a depth of 50 cm, which likely corresponds to the interface zone between the masonry and the rammed earth wall.

The radargram on the right corresponds to the vertical path referenced as 14 (right of the window). Two aspects stand out in this image: first, the confirmation of the masonry depth on both sides of the window as approximately 50 cm; second, the appearance of reflections at heights of 30 and 90 cm. These reflections correspond to cracks present in the wall, and their depth can be observed to be greater than 70 cm.

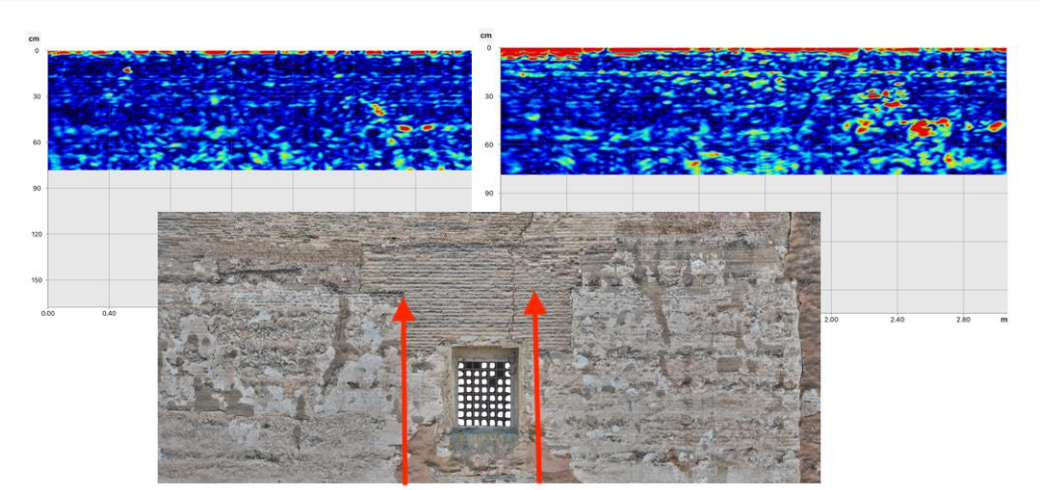


Figure 6 – Vela tower. External radargrams to the left and right of the window. Superimposed to the image are the corresponding red lines of the inspections

4.2 Internal inspection

The inspection of the interior area is a manual area inspection. The inspected portion of the wall is shown in Figure 7. It has been divided into six zones. The three lower zones extend from 20 cm to 1.80 meters in height. The first of these is located to the left of the window, while the remaining two are to the right. The three upper zones extend the inspected area by an additional 1 meter in height, from 1.80 to 2.60 meters. In terms of width, the zones to the left of the window are 2 meters wide, and those to the right are 2.40 and 2 meters wide, respectively.

The most significant results in this inspection were those from the upper zones, with similar results obtained in all three areas. Figure 5 shows, for example, the area near the top right of the window, marked with a red

rectangle. The C-Scan integrates reflectivity between 53 and 67 cm deep. From this, the presence of two materials with different densities and compaction can be deduced. Furthermore, they are separated at a height that coincides with the position of the wooden beam. The same phenomenon can be observed in the inspections of the other zones. The figure also includes two radargrams corresponding to vertical trace 4 and horizontal trace 37.

The vertical trace shows reflections at depths of 20 to 30 cm, indicating the presence of layers of rammed earth from the interior, likely added during a restoration after the original construction. The horizontal trace shows reflections at 1.20, 1.80, and 2.20 meters, originating from cracks that reach depths exceeding 60 cm.

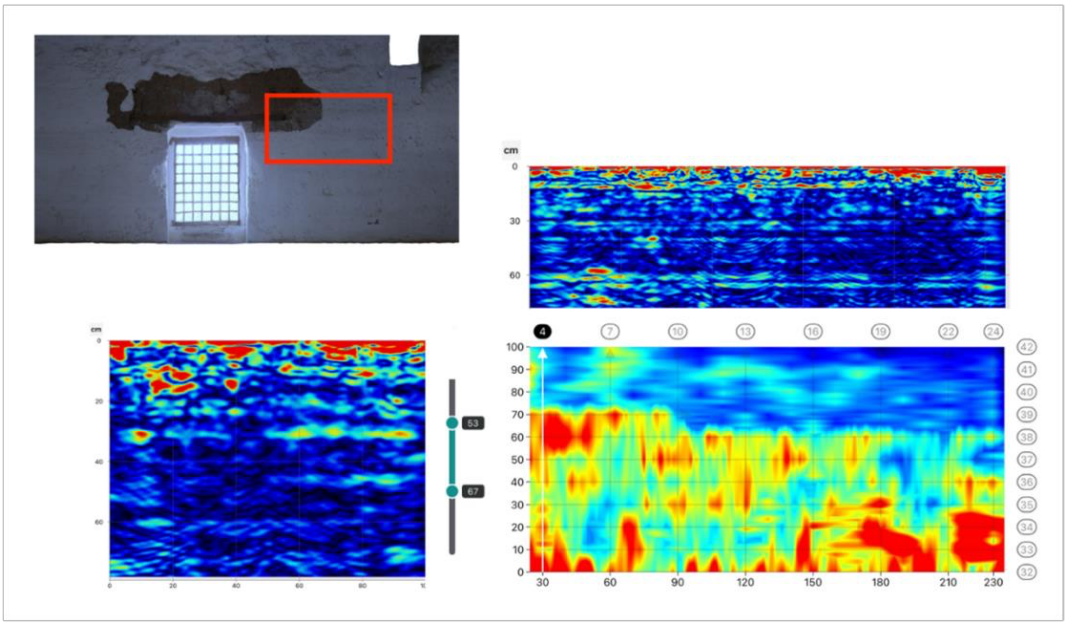


Figure 7 – Vela tower. Internal radargrams and C-Scan of the are marked with a red rectangle

5. Conclusions

This paper presents some of the ground-penetrating radar (GPR) inspections carried out at the Alhambra complex, specifically at the Vela tower. These inspections have analyzed the internal structure of the walls of the building, revealing layers of different materials, cavities, and cracks. A particularly noteworthy aspect of this work is the inspection, using a cable-driven robot, of a section of the Vela tower's external wall located 20 meters high. This inspection did not obstruct the view of the monument, as it did not require the installation of external elements such as scaffolding.

Ground-penetrating radar (GPR) inspections have revealed the internal structure of the walls in the inspected buildings, showing different layers of material, voids, and heterogeneities. Automated inspections using a cabled robot have allowed access to previously uninspected areas and the identification of cracks and their depths within the walls.

Acknowledgments

This work has been supported by the projects PID2022-140071OB-C22 and PID2024-159276OB-C43. The authors gratefully acknowledge the financial support provided by these two projects for the development of this research.

References

[1] Catapano, Ilaria, Giorgio Gennarelli, Giovanni Ludeno, y Francesco Soldovieri. “Applying Ground Penetrating Radar and Microwave Tomography Data Processing in Cultural Heritage: State of the Art and Future Trends.” IEEE Signal Processing Magazine (2019). https://doi.org/10.1109/msp.2019.2895121.

[2] Solla Carracelas, Mercedes, María de la Vega Pérez Gracia, Susana Lagüela, y Susana Fontul. “Applications of the Ground Penetrating Radar Technique to Heritage Buildings: Case Studies and Combination with Other Non Destructive Testing.” En Diagnosis of Heritage Buildings by Non Destructive Techniques, editado por Blanca Tejedor Herrán y Daniel Bienvenido Huertas, 575–624. Elsevier, 2024. https://doi.org/10.1016/B978-0-443-16001-1.00022-X.

[3] Hoxha, E., J. Feng, D. Sanakov, y J. Xiao. “Robotic Inspection and Subsurface Defect Mapping Using Impact Echo and Ground Penetrating Radar.” IEEE Robotics and Automation Letters 8, n.° 8 (agosto de 2023): 4943–4950. https://doi.org/10.1109/LRA.2023.3290386.

[4] Baikovitz, Alexander, Paloma Sodhi, Michael Dille, y Michael Kaess. “CMU GPR Dataset: Ground Penetrating Radar Dataset for Robot Localization and Mapping.” arXiv (15 de julio de 2021). https://arxiv.org/abs/2107.07606.

[5] Fang, Y., F. Yang, X. Qiao, M. Xu, L. Fang, J. Liu, y F. Li. “Cross Line Fusion of Ground Penetrating Radar for Full Space Localization of External Defects in Drainage Pipelines.” Remote Sensing 17, n.° 194 (2025). https://doi.org/10.3390/rs17020194.

[6] Esposito, G., G. Gennarelli, G. Ludeno, A. Salari, D. Erricolo, F. Soldovieri, e I. Catapano. “Assessing Contactless versus Contact GPR for Vertical Structure Inspection.” IEEE Geoscience and Remote Sensing Letters 22 (2025): 3003605.

[7] Chen, Guanbo, Beyza Kiper, Xuchu Xu, Bilal Sher, Semiha Ergan, y Chen Feng. “EASEEbot: A Robotic Envelope Assessment for Energy Efficiency.” 2022. https://doi.org/10.22260/ICRA2022/0012.

[8] Pérez Gracia, Vega, Ramón González Drigo, y Roger Sala. “Ground Penetrating Radar Resolution in Cultural Heritage Applications.” Near Surface Geophysics 10 (2012): 77–87. https://doi.org/10.3997/1873 0604.2011015.

[9] Qian, Wei, Wenjing Tian, Tao Zhang, Xujun Zhu, y Ning Li. “Advanced GPR Signal Processing for Void Detection in Historic Masonry Structures: Application to the Ming Great Wall.” Measurement 268 (2026): 120629.

cinpar2026
XXII International Conference on Building Pathology and Constructions Repair
15th to 17th July 2026 - Lisboa, Portugal

Corrosion in Exposed Concrete Structures of Modern Architecture: A Case Study of the Failure of the Roof Slab of the Water Tank at the University Restaurant of UnB

Matheus Gregorio KAMINSKI[1], Vanda Alice Garcia ZANONI[2],
Valdirene Maria Silva CAPUZZO[3], Andressa Tainara Campelo de JESUS[4]

[1] University of Brasília, Brasília, Brazil, matheuskaminski@unb.br
[2] University of Brasília, Brasília, Brazil, vandazanoni@unb.br
[3] University of Brasília, Brasília, Brazil, valdirenemaria@unb.br
[4] University of Brasília, Brasília, Brazil, andressa.jesus@unb.br

Abstract: This paper presents a case study of the collapse of the water tank roof slab at the University of Brasília (UnB) Student Restaurant (RU), an iconic modern architectural building constructed with exposed concrete in the 1970s. The failure was primarily driven by advanced corrosion of the steel reinforcements on the internal face of the slab (tank lid), exacerbated by the tank's high relative humidity and lack of internal waterproofing. The investigation identified the root causes, characterized the degradation state post-collapse, and documented the adopted reconstruction solution, balancing structural safety, durability, and heritage preservation. Preliminary findings revealed permanent saturation from vapor transport via gaseous diffusion and capillary action through the porous concrete matrix, leading to interstitial (within pores) and surface condensations on the internal face — a more aggressive mechanism than the external wet-dry cycle from rainfall. This caused concrete cover spalling, diffuse cracking, deep carbonation exceeding rebar depth, and up to 100% cross-section loss in steel bars, progressively reducing load-bearing capacity under constant humid exposure. Visual inspections, technical surveys, and non-destructive tests confirmed that construction detailing typical of the 1970s, combined with absent waterproofing on both faces, accelerated internal corrosion beyond external influences. Due to irreversible damage, the slab was fully removed and replaced with a lighter steel frame and acoustic steel roofing sheets, minimizing permanent loads on tank walls, enhancing inspectability, and preventing recurrence while preserving the building's volumetric and architectural expression. The study emphasizes continuous monitoring of aging exposed concrete structures, particularly reservoir lids vulnerable to internal vapor/condensation, and contributes to discussions on corrosion mechanisms, risk assessment, intervention strategies, and maintenance for modern Brazilian heritage.

Keywords: Pathological manifestations, exposed concrete, waterproofing, modern heritage, preventive maintenance.

1. Introduction

The degradation of reinforced concrete structures represents one of the main challenges in contemporary civil engineering, particularly when involving buildings of cultural value. The corrosion of steel reinforcements, a complex electrochemical phenomenon, constitutes one of the most frequent causes of structural collapse in aged constructions, compromising the safety, durability, and material integrity of buildings that often hold cultural significance (Tuutti, 1982; Broomfield, 2007; Neville, 2011). In contexts where exposed concrete serves both as a defining element of architectural language and a structural component — as occurs in Brazilian modern architecture — degradation assumes dimensions that transcend purely

technical aspects, posing dilemmas between material preservation and structural adequacy (Prudon, 2008; Jonge and Doolaar, 1998; Kühl, 2008).

The University Restaurant (RU) of the University of Brasília, designed and built in the 1970s, paradigmatically exemplifies this tension. An emblematic edifice of modern architecture, characterized by the expressive use of exposed concrete and innovative structural solutions for its time (Schlee, 2014), the RU recently experienced the rupture of the water tank roof slab, an event that triggered a more in-depth technical investigation into the conservation state of its structure. The collapse, preceded by advanced corrosive processes in the reinforcements, revealed the vulnerability of structural elements exposed to permanent humidity conditions and the absence of adequate protection systems—factors that combined with typical constructive characteristics of the period to accelerate deterioration (Helene, 1992a; Cascudo, 1997; Bolina, Tutikian, and Helene, 2019).

The investigation of this case presents scientific and practical relevance across multiple dimensions. First, the study contributes to understanding corrosion mechanisms in reinforced concrete structures subjected to constant humidity, a common context in water tanks, reservoirs, and roof elements (Macdonald, 2003). Second, the research documents and analyzes pathological manifestations resulting from advanced corrosive processes, providing subsidies for diagnosing similar cases in other buildings (American Concrete Institute, 2016b; Morais et al., 2020). Third, and no less importantly, the investigation records the technical solution adopted for recomposing the element, highlighting the choices and compromises necessary when seeking to reconcile structural safety with patrimonial preservation (Feilden, 2003; Canziani and Quist, 2025).

The preliminary analysis of the case revealed intense moisture penetration, absence of effective waterproofing, detachment of concrete cover, diffuse cracking, and significant loss of cross-section in the steel bars. Mechanisms associated with concrete carbonation and constructive detailing typical of the era resulted in the progressive reduction of the slab's load-bearing capacity until its collapse (Ekolu, 2020; Ribeiro, 2018). Given the high degree of deterioration and the technical and economic unfeasibility of recovering the slab, the decision was made to completely remove the collapsed element and replace it with a lighter roofing structural system, composed of a metal framework and steel tiles—a solution that sought to balance safety, durability, and preservation of architectural volumetry requirements (American Concrete Institute, 2016a).

The present investigation had the following objectives: (i) to identify and characterize the causes of the reinforced concrete roof slab collapse; (ii) to document the degradation state and analyze the failure mode of the element; (iii) to assess the contribution of factors such as carbonation, recurrent infiltrations, and constructive detailing to accelerating the corrosive process; (iv) to document the technical solution adopted for reconstruction; and (v) to contribute to the debate on corrosion mechanisms, risk assessment, intervention strategies, and maintenance in aged reinforced concrete structures, particularly those with patrimonial value (Mehta and Monteiro, 2014; Souza and Ripper, 1998).

The study reinforces the relevance of continuous monitoring of aged structures and highlights the ongoing challenge of reconciling technically adequate solutions with the conservation of formal and material attributes of Brazilian modern architecture's heritage (Croft and Macdonald, 2019; Dyer, 2015). In this sense, the UnB RU case offers significant contributions to the interdisciplinary debate among engineering, architecture, and patrimonial conservation fields. Although these fields often operate with distinct logics, real case studies prove to be opportunities for dialogue and knowledge interaction.

2. Case Contextualization and Building Characterization

The RU/UnB is a landmark of modern architecture on the Darcy Ribeiro Campus. Designed by architect José Galbinski and built in the 1970s, the building reflects Brazilian modernism, characterized by the expressive use of exposed concrete and the integration between structure and form (Prudon, 2008; Jonge and Doolaar,

1998). The edifice is not merely a functional facility supporting academic life, but an exemplar of built heritage that embodies the visual and technical identity of its era (Kühl, 2008).

2.1 The architectural concept and constructive system

The structural conception of the RU is based on the robustness of reinforced concrete, a material that enabled the execution of large spans and cantilevers typical of the period (Neville, 2011). The water tank of the complex was designed as a prominent volume, executed in cast-in-place concrete (Figure 1). The original roof slab, the object of this study, consisted of a solid inclined reinforced concrete slab, whose primary function was the top closure of the reservoir, ensuring the protection of the stored water and the integrity of the architectural volume.



Figure 1 – Aerial photograph of the exposed concrete water tank, highlighting the inclined slab of the tower integrated into the main RU/UnB building. Source: Authors, 2025.

In the 1970s, constructive detailing did not consider cover thickness as a determining parameter for the service life of the reinforcements; mechanical strength was prioritized as the primary factor to ensure the durability of reinforced concrete. At that time, standards were less rigorous regarding watertightness and environmental aggressiveness as factors accelerating the onset of pathological manifestations (Helene, 1992a; Mehta and Monteiro, 2014).

2.2 Exposure conditions

The water tank roof slab, without a waterproofing or protection system, was exposed to climatic variations and rainfall action (Figures 2 and 3):

- Internal Environment: The underside of the slab, lacking a waterproofing or protection system, was subject to moisture from evaporation and condensation of the stored water, maintaining the concrete at high moisture content; and

- External Environment: The upper face was exposed to cyclic variations in temperature, solar radiation, relative humidity, and rain—factors that promote wetting and drying cycles, the opening of microcracks, and the penetration of aggressive agents.



Figure 2 – Illustrative image of the water tank's exposure during a rainy period, showing surface runoff and water penetration through cracks in the roof slab. Source: Authors, 2026.

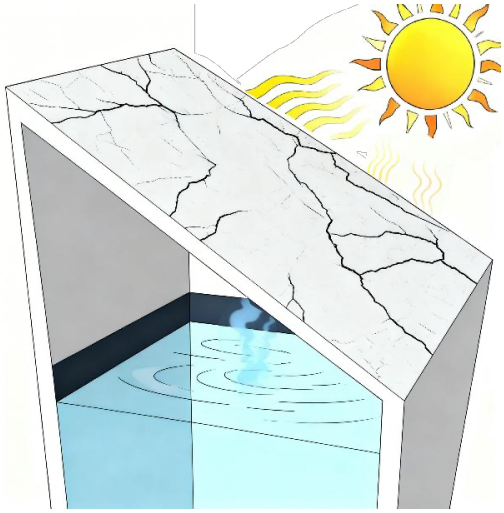


Figure 3 – Illustrative image of the water tank's exposure during a hot and dry period, showing water vapor passage from the internal to the external environment through the roof slab. Source: Authors, 2026.

The presence of an aged waterproofing system at the end of its service life, combined with the absence of periodic maintenance, allowed moisture and carbon dioxide (CO_2) to penetrate the concrete's porous matrix. This scenario is critical for exposed concrete structures, where the aesthetic expression of the exposed material may be compromised by protective coatings that could mitigate the carbonation front and, consequently, corrosion (Broomfield, 2007; Ekolu, 2020).

2.3 The Slab Rupture Event

Throughout its service life, no inspections of the water tank detected excessive deformations or cracks compromising watertightness. Therefore, it cannot be confirmed that the slab collapse occurred suddenly, although the degradation process was progressive over decades. The rupture revealed that the element's load-bearing capacity had been severely compromised by reinforcement cross-section loss, preventing stress redistribution and leading to structural failure (Bolina, Tutikian, and Helene, 2019). The event underscores the need to reconcile preservation of the RU's original volumetry with the adoption of contemporary technological solutions that ensure user safety and heritage longevity (Cascudo, 1997; Croft and Macdonald, 2019).

3. Methodological Procedures for Inspection and Analysis

The investigation of the roof slab collapse in the water tank was conducted through an approach combining visual inspections, technical surveys, and documentation analysis. The objective was to establish a preliminary diagnosis of the rupture causes, document the element's degradation state, and technically substantiate the adopted reconstruction solution (American Concrete Institute, 2016b).

3.1 Visual Inspections and Photographic Documentation

Visual inspections were performed in two stages: the first immediately after the collapse, when the element was still in situ; the second after partial debris removal, allowing access to the underside of the slab and constructive details. During these inspections, visible pathological manifestations were documented, including:

- Cracking: visualization of the distribution, orientation, and width of cracks;
- Spalling: identification of areas with loss of bond between concrete and reinforcement;
- Reinforcement corrosion: visual assessment of the oxidation degree in exposed steel bars;
- Moisture: verification of stains, efflorescences, and signs of recurrent infiltration; and
- Structural integrity: analysis of concrete continuity and identification of weakened zones (Bolina, Tutikian, and Helene, 2019; Morais et al., 2020).

Photographic documentation was carried out using a high-resolution digital camera, capturing details at multiple scales: general views of the element, crack and corrosion details, and close-ups of critical areas. This visual documentation served as the basis for subsequent analysis and communication with project teams involved in the reconstruction (Macdonald, 2003).

3.2 Technical Survey and Geometric Characterization

A metric survey was conducted to characterize the slab's original dimensions, including thickness, spans, and reinforcement detailing. This survey was performed through:

- Direct measurements with tape measure and level, establishing the element's main elevations;
- Consultation of original design documentation for comparison between design and execution; and
- Analysis of concrete cross-sections, allowing estimation of cover thickness and steel bar positions (Neville, 2011).

These data were necessary to determine whether the original constructive detailing complied with executive designs and to assess if design deficiencies contributed to accelerating the corrosion process (Helene, 1992a, 1992b).

3.3 Concrete Degradation Analysis

Characterization of the concrete degradation state was performed through procedures combining visual observation with non-destructive investigation techniques:

- Sclerometry: measurement of surface concrete hardness at multiple points, providing an indication of strength; and
- Carbonation depth: determination of the carbonation front advancement depth through phenolphthalein assays, an indicator that changes color in the presence of alkaline pH (Mehta and Monteiro, 2014; Ekolu, 2020).

These procedures provided quantitative data on the material's deterioration degree and the degradation mechanisms in action.

3.4 Reinforcement Investigation and Corrosion Quantification

Reinforcement corrosion was investigated through procedures that assessed both the extent and severity of the phenomenon:

- Observation of residual diameters: to quantify cross-section loss in bars at multiple points along their length; and
- Adhesion analysis: qualitative assessment of the concrete-steel bond, checking for detachment and anchorage loss (Ribeiro, 2018; Broomfield, 2007).

Quantification of cross-section loss was fundamental to estimate the reduction in the slab's load-bearing capacity and justify the unfeasibility of recovering the original element (Tuutti, 1982).

3.5 Analysis of Exposure Conditions and Moisture

The exposure conditions investigation included:

- Waterproofing system verification: inspection of the presence or absence of protective layers on the upper and lower faces of the slab, highlighting the lack of internal protection that allowed continuous water vapor penetration and surface/interstitial condensations; and
- Drainage assessment: analysis of rainwater runoff capacity on the external face and identification of moisture accumulation or water penetration points.

These data enabled understanding of the element's exposure regime: externally, wet-dry cycles with pluviometric infiltrations accelerating microcracks; internally, high relative humidity (~100%) in the reservoir promoting vapor transport by diffusion and capillarity in porous concrete, with interstitial (in pores) and surface (on the underside) condensations maintaining permanent saturation. This internal mechanism was the main accelerator of underside reinforcement corrosion, surpassing external impact by preventing drying cycles that limit electrochemical corrosion (Ekolu, 2020; Mehta and Monteiro, 2014).

3.6 Consultation of Documentation and Constructive Detailing Analysis

The investigation included consultation of the building's original designs to:

- Verify reinforcement detailing: compare design with actual execution, identifying possible deviations;
- Assess specified cover: compare design requirements with standards in force at the time against current standards and practices;
- Understand constructive solutions: analyze how critical details such as joints, anchorages, and reinforcement protection were resolved; and
- Contextualize the construction era: understand the technological and normative limitations of the 1970s, which may explain design deficiencies (Souza and Ripper, 1998; Associação Brasileira de Normas Técnicas, 2024).

This analysis was important to understand that the collapse resulted not only from maintenance neglect but also from period-typical constructive characteristics that made the element vulnerable to long-term degradation.

3.7 Methodological Framework

The approach enabled constructing a diagnosis by associating data collected from each procedure. Visual inspections provided the general overview; technical surveys established geometry and detailing; concrete and reinforcement analyses quantified degradation; and documentation consultation contextualized findings. This joint and complementary analysis of evidence provided a more comprehensive diagnosis for assessing the situation and decision-making.

4. Diagnosis of the Degradation Mechanisms and Causes of the Slab Rupture

The results obtained from inspections and technical surveys confirmed a critical degradation state of the roof slab, with irreversible damage compromising the structural safety of the element. The collapse of the University of Brasília University Restaurant roof slab indicates a synergy of degradation processes accumulated over five decades. The technical diagnosis indicates that the failure resulted from the combination of the aggressiveness of the reservoir's internal microclimate, the absence of effective protective barriers, and the constructive detailing typical of the 1970s.

4.1 Pathological Manifestations and Conservation State

The investigation revealed that the slab exhibited an advanced deterioration condition, characterized by moisture transport mechanisms of aggressive agents well-recognized in the literature. The collected data pointed to:

- Diffuse cracking: Presence of cracks on both faces of the slab, with openings facilitating direct entry of oxygen and water;
- Spalling: Loss of bond in extensive areas of the underside, exposing reinforcements to the humid reservoir environment;
- Loss of bar cross-section: Drastic reduction in the original diameter of steel reinforcements, reaching levels that made load support unfeasible; and
- Deep carbonation: The carbonation front reached and exceeded the reinforcement depth across nearly the entire slab length, eliminating the steel's natural chemical protection. .

4.2 Determining Factors for the Collapse

The results indicated that the rupture was the outcome of a combination of technical failures. The absence of effective waterproofing was the catalyzing factor, allowing moisture to remain trapped in the concrete matrix for decades.

Inspections confirmed that the 1970s constructive detailing, although common for the era, did not foresee the durability requirements necessary for a high-humidity environment, such as the interior of a water reservoir. The synergy between carbonation and recurrent infiltrations exponentially accelerated the corrosion process in the years leading up to failure.

4.3 Watertightness Failure and Vapor Transport

The primary cause of degradation was intense moisture penetration into the slab, with emphasis on the underside exposed to internal water vapor, exacerbated by the reservoir's high relative humidity microclimate. The absence of waterproofing on the upper and lower faces facilitated vapor transport through diffusion and capillarity in the concrete's porous matrix, generating interstitial condensations (in pores) and surface condensations (on the internal face) that favored steel corrosion reactions (Dyer, 2015; Mehta and Monteiro, 2014).

The internal face of the slab, acting as a reservoir lid, is subjected to a continuous cycle of condensation. According to Cincotto and Helene (1984), the presence of aggressive free CO2 in the condensed water accelerates the leaching of calcium hydroxide (portlandite), increasing the porosity of the cement paste and facilitating the depassivation of the reinforcement. Constant moisture from evaporation and condensation of stored water accelerated underside reinforcement corrosion, surpassing external impact by preventing drying cycles. Externally (Figure 4), pluviometric infiltrations penetrated microcracks, but the wetting-drying cycle made the action less aggressive.



Figure 4 – Original condition of the upper external face of the collapsed slab, highlighting multiple cracks and pronounced wear of the protective mortar layer. Source: Authors, 2025.

4.4 Carbonation and Reinforcement Depassivation

Phenolphthalein tests confirmed the carbonation front advancement not only to the reinforcement level but through the entire slab thickness. The reaction of atmospheric CO_2 with cement hydration products reduced the concrete's pH — originally alkaline (pH > 12.5) — to values below 9.

This phenomenon caused steel depassivation, breaking the protective oxide layer naturally surrounding bars in a basic environment. In 1970s exposed concrete structures, nominal cover was often thin or irregular, advancing the carbonation front's contact with reinforcement and initiating corrosion propagation across its entire area.

4.5 Advanced Corrosion and Cross-Sectional Loss

Once depassivated and in the presence of electrolyte and oxygen, reinforcements initiated accelerated oxidation. The diagnosis identified two critical effects from corrosion:

1. Volumetric expansion: Corrosion products (rust) occupy up to six times the original steel volume. This expansion generated internal tensile stresses in the concrete, resulting in longitudinal cracking and, ultimately, cover detachment (spalling), splitting the slab at half its thickness (Figure 5); and

2. Metallic cross-section reduction: Analysis of bars post-rupture revealed 100% cross-sectional loss at critical points (Figure 5). This drastic reduction compromised tensile stress absorption capacity, essential for the solid slab's equilibrium.



Figure 5 – Internal face of the collapsed slab: exposed corroded reinforcements. Highlighting steel bar cross-section total loss. Source: Authors, 2025.

4.6 Final Rupture Mechanism

The conjunction of the above factors culminated in reducing the slab's load-bearing capacity below service loads (self-weight and occasional overloads). As explained by Souza and Ripper (1998), the era's constructive detailing lacked sufficient safety reserve to withstand such material degradation.

Collapse occurred when the residual steel bar section could no longer support tensile stresses from bending moment. Loss of bond between corroded steel and carbonated concrete also contributed to failure, preventing effective stress transfer and leading to abrupt element rupture.

4.7 Definition of the Intervention

Given the technical unfeasibility of recovering the original solid slab, risk analysis results substantiated complete element removal. The adopted solution consisted of replacement with a lightweight roofing system formed by steel purlins fixed to reservoir walls and closure with thermoacoustic steel tiles.

The main objective of the adopted technological solution for reconstruction was reducing self-weight on reservoir walls and eliminating new corrosion risks in reinforced concrete roofing elements. This intervention restored water tank functionality, ensuring watertightness and safety, without affecting the exposed reinforced concrete tower walls (Figures 6, 7, and 8).



Figure 6 – RU water tank at the start of inspection services. Source: Authors, 2026.



Figure 7 – RU water tank during reconstruction. Source: Authors, 2026.



Figure 8 – RU water tank after roof reconstruction. Source: Authors, 2026.

5. Discussion on the Adopted Solution and Its Structural and Architectural Implications

The adopted solution for the studied case highlights a recurring issue in interventions on modern architecture buildings: the need to reconcile structural safety, durability, and preservation of architectural attributes. In the case of the University of Brasília University Restaurant water tank roof slab, the high degree of degradation of the original element—particularly the advanced corrosion of the reinforcements on the internal face—ruled out a conservative approach based on localized repairs and recovery of the original element. The extent of pathological manifestations, significant loss of reinforcement cross-section, and global compromise of load-bearing capacity indicated that maintaining the original system would pose a risk incompatible with usage and minimum structural performance criteria required for the building, as established by Brazilian standards and the American Concrete Institute (2016b).

From a strictly technical standpoint, the complete removal of the collapsed slab and its replacement with a lighter system—composed of a metal framework and steel tiles—proved to be a solution with lower self-weight, reducing permanent loads transmitted to the reservoir and decreasing demands on existing supports, thereby contributing to overall safety. Additionally, replacing a solid reinforced concrete element with a lighter and more easily inspectable constructive system tends to facilitate future maintenance routines, allowing better control over infiltration points, watertightness failures, and early deterioration processes (Helene, 1992a).

From a durability perspective, by introducing materials and systems more compatible with performance demands in humid environments, the intervention sought not only to recompose the roofing function but also to reduce the likelihood of recurrence of similar pathological mechanisms—such as vapor transport through gaseous diffusion and capillarity in the concrete's porous matrix, with interstitial (in pores) and surface condensations on the internal face. In this sense, the design decision should be understood not merely as an emergency response to the collapse, but as a long-term risk mitigation strategy, aligned with contemporary principles of structural durability management (Dyer, 2015; Mehta and Monteiro, 2014). Thus, the integrity of the exposed concrete walls composing the tower's volumetry was ensured.

In modern buildings constructed with exposed concrete, the original materiality holds intrinsic value. According to the theoretical principles of Kühl (2008) and Prudon (2008), the constructive system often integrates the building's formal language itself, and therefore, the removal of an original element implies a material loss that cannot be considered irrelevant, even if the component is volumetrically recompensed.

In the analyzed case, the technical unfeasibility of reconstituting the original slab—exacerbated by the high internal relative humidity that promoted constant condensations on the underside, accelerating reinforcement corrosion—led to a pragmatic stance, focusing preservation efforts on conserving the volumetry, architectural reading, and integrity of the built ensemble.

The conducted study highlights bottlenecks in conservation practices, where durability required by technical standards proves insufficient after decades of building exposure to the internal vapor

transport/condensation phenomenon without proactive maintenance. The challenge, therefore, is not only to conserve existing matter but to establish criteria for intervening without altering the architectural intent of the asset.

Another important aspect concerns the role of preventive maintenance. The studied case demonstrates that the collapse did not result from a single isolated factor, but from the progressive combination of ineffective waterproofing on internal and external faces, recurrent infiltrations, carbonation, and advanced reinforcement corrosion. In other words, it is a cumulative process that could, at least in part, have been identified and controlled before reaching a critical stage — especially the internal vapor transport that maintained permanent saturation on the underside. This reinforces the need for systematic inspection programs in aged structures, particularly those associated with continuous use and patrimonial value.

6. Conclusion

The investigation into the rupture of the University Restaurant (RU/UnB) water tank roof slab led to the conclusion that the structural collapse was the inevitable outcome of a prolonged degradation process, dominated by advanced corrosion of the reinforcements on the internal face of the reinforced concrete cover. The technical analysis revealed that this phenomenon was accelerated by the absence of waterproofing on the underside, enabling vapor transport through gaseous diffusion and capillarity in the concrete's porous matrix, with constant interstitial (in pores) and surface condensations maintaining permanent saturation due to the high relative humidity in the reservoir—a mechanism that proved more aggressive than the external wetting-drying cycle.

The study demonstrated that the constructive characteristics of the 1970s, although representative of Brazilian modernism, exhibited intrinsic vulnerabilities regarding durability in permanent humid environments. The deep carbonation of the concrete and the loss of steel bar cross-section—up to 100% at nodal points—confirmed the technical and economic unfeasibility of localized repairs, justifying complete replacement with a lightweight metal system. The intervention prioritized structural safety and maintainability, while preserving the building's volumetry, architectural expression, and the reversibility of the adopted technological solution.

Finally, this case underscores the need for preventive maintenance programs and continuous monitoring in aged exposed concrete structures, particularly internal elements exposed to vapor and condensations, such as reservoir covers. The challenge of preserving Brazilian modern heritage lies in the ability to diagnose these internal degradation mechanisms early on, implementing solutions that integrate engineering's technical rigor with the architectural attributes of the patrimonial asset.

Acknowledgments

The authors thank the Brazilian National Council for Scientific and Technological Development (CNPq), the Coordination for the Improvement of Higher Education Personnel (PROAP/CAPES), and the Deanship of Research and Innovation (DPI) of the University of Brasília (UnB) for financial support. They also thank the Infrastructure Secretariat (INFRA/UnB), the Oscar Niemeyer Planning Center (CEPLAN/UnB) for technical support and documentary data, and the Materials Testing Laboratory of the Faculty of Technology at UnB for laboratory analyses.

References

American Concrete Institute. 2016a. *ACI 201.2R-16: Guide to Durable Concrete*. Farmington Hills: ACI.

American Concrete Institute. 2016b. *ACI 562-16: Code Requirements for Assessment, Repair, and Rehabilitation of Existing Concrete Structures and Commentary*. Farmington Hills: ACI.

Associação Brasileira de Normas Técnicas. 2024. *NBR 6118: Projeto de Estruturas de Concreto*. Versão Corrigida 2:2024. Rio de Janeiro: ABNT.

Bolina, F. L., B. F. Tutikian, and P. Helene. 2019. *Patologia de Estruturas*. São Paulo: Oficina de Textos.

Broomfield, J. P. 2007. *Corrosion of Steel in Concrete: Understanding, Investigation and Repair*. 2nd ed. London: Taylor & Francis.

Canziani, Andrea, and Wido Quist. 2025. *CONCRETO Code Book: Study on Historic Concrete Conservation*. Delft: DOCOMOMO International; Delft University of Technology.

Cascudo, O. 1997. *O controle da corrosão de armaduras de concreto: Inspeção e técnicas eletroquímicas*. São Paulo: PINI.

Cincotto, M. A.; and P. R. do L. Helene. Patologia de estrutura de concreto armado. In: REUNIÃO ANUAL DO IBRACON, 26., 1984, São Paulo. Anais... São Paulo: IBRACON, 1984. p. 593-596.

Croft, Catherine;, and Susan Macdonald. 2019. *Concrete: Case Studies in Conservation Practice*. Los Angeles: Getty Conservation Institute.

Jonge, de Wessel, and Arjan Doolaar. 1998. *The Fair Face of Concrete: Conservation and Repair of Exposed Concrete*. Eindhoven: DOCOMOMO International / Eindhoven University of Technology.

Dyer, Thomas. 2015. *A Durabilidade do Concreto*. Rio de Janeiro: Editora Ciência Moderna.

Ekolu, S. O. 2020. Implications of global CO2 emissions on natural carbonation and service lifespan of concrete infrastructures—Reliability analysis. *Cement and Concrete Composites* 114: 103744.

Feilden, B. M. 2003. *Conservation of Historic Buildings*. 3rd ed. Oxford: Butterworth-Heinemann.

Helene, Paulo R. L. 1992a. *Manual para Reparo, Reforço e Proteção de Estruturas de Concreto*. 2nd ed. São Paulo: PINI.

Helene, P. R. L. 1992b. *Corrosão em armaduras para concreto armado*. São Paulo: PINI.

Kühl, B. M. 2008. *Preservação da arquitetura moderna: Discussões, experiências, perspectivas*. São Paulo: Annablume; FAPESP.

Macdonald, Susan. 2003. *Concrete: Building Pathology*. Oxford: Blackwell Science.

Mehta, P. K., and Monteiro, P. J. M. 2014. *Concrete: Microstructure, Properties, and Materials*. 4. th ed. New York: McGraw-Hill Education.

Morais, J. M. P. de, A. M. da Silva, E. N. Barboza, E. M. da Silva, and B. B. de Oliveira. 2020. "Análise de manifestações patológicas em estruturas de concreto armado: uma revisão." *Research, Society and Development* 9, no. 7: e759974964.

Neville, Adam M. 2011. *Properties of Concrete*. 5th ed. Harlow: Pearson.

Prudon, Theodore H. M. 2008. *Preservation of Modern Architecture*. Hoboken, NJ: John Wiley & Sons.

Ribeiro, Daniel. 2018. *Corrosão e Degradação em Estruturas de Concreto*. 2nd ed. Rio de Janeiro: LTC.

Schlee, André Rosenthal *et al.* 2014. *Registro arquitetônico da Universidade de Brasília*. Brasília: Editora Universidade de Brasília.

Souza, Vicente Custódio de, and Thomaz Ripper. 1998. *Patologia, Recuperação e Reforço de Estruturas de Concreto*. São Paulo: Pini.

Tuutti, K. 1982. *Corrosion of Steel in Concrete*. Stockholm: Swedish Cement and Concrete Research Institute.

Cinpar 2026
XXII International Conference on Building Pathology and Constructions Repair
15th to 17th July 2026 - Lisboa, Portugal

Análise de dados de patologias higrotérmicas: estudo estatístico de relatórios técnicos de edifícios

Mariana NADAIS[1], Rui P. CUNHA[2], João M. P. Q. DELGADO[3], Ana S. GUIMARÃES[4], Pedro F. PEREIRA[5]

[1] CONSTRUCT, Faculdade de Engenharia (FEUP), Universidade do Porto, Rua Dr. Roberto Frias s/n, Porto, 4200-465, Portugal, mariana.nadais@fe.up.pt
[2] CONSTRUCT, Faculdade de Engenharia (FEUP), Universidade do Porto, Rua Dr. Roberto Frias s/n, Porto, 4200-465, Portugal, up200502062@edu.fe.up.pt
[3] CONSTRUCT, Faculdade de Engenharia (FEUP), Universidade do Porto, Rua Dr. Roberto Frias s/n, Porto, 4200-465, Portugal, jdelgado@fe.up.pt
[4] CONSTRUCT, Faculdade de Engenharia (FEUP), Universidade do Porto, Rua Dr. Roberto Frias s/n, Porto, 4200-465, Portugal, anasofia@fe.up.pt
[5] CONSTRUCT, Faculdade de Engenharia (FEUP), Universidade do Porto, Rua Dr. Roberto Frias s/n, Porto, 4200-465, Portugal, fpfp@fe.up.pt

Resumo: As patologias higrotérmicas constituem um dos principais fatores de degradação do ambiente construído, afetando a integridade física dos materiais, a durabilidade dos elementos construtivos e o desempenho higrotérmico dos edifícios. O seu aparecimento resulta de interações complexas entre a exposição climática, características dos materiais, práticas construtivas, processos de envelhecimento e fenómenos relacionados com a humidade, que assumem um papel central na avaliação da patologia e na definição de estratégias de reabilitação. A diversidade de soluções construtivas e de condições de exposição observadas em edifícios existentes torna particularmente relevante o estudo da manifestação e da evolução destas patologias.

Este trabalho caracteriza as patologias higrotérmicas com base na análise de 103 relatórios técnicos de inspeção do Instituto da Construção Sustentável (ICS) da Universidade do Porto. A análise estatística permitiu identificar a distribuição das patologias por tipologia, elementos construtivos e causas, bem como avaliar a existência de associações significativas entre estas variáveis. Os resultados destacam a infiltração de água como a patologia mais frequente, seguida da degradação de revestimentos e da degradação biológica. Verificaram-se ainda padrões consistentes entre patologias, mecanismos e elementos da envolvente. Identificam-se dois grandes grupos de mecanismos: patologias associadas à entrada de água devido à falta de estanquidade e patologias decorrentes de condições higrotérmicas interiores inadequadas. Os resultados reforçam a necessidade de estratégias de reabilitação integradas e preventivas centradas no controlo das fontes de humidade.

Palavras-chave: Patologias higrotérmicas, edifícios, humidade.

1. Introdução

As patologias da construção representam um desafio significativo para a durabilidade, a funcionalidade e a sustentabilidade do ambiente construído. Entre os diversos processos de degradação que afetam os edifícios, as patologias higrotérmicas assumem particular relevância, uma vez que decorrem de interações complexas entre os fluxos de calor, de ar e de humidade nos elementos construtivos (Bayat Pour et al., 2024; Hajdukiewicz et al., 2015). Estes fenómenos desenvolvem-se frequentemente em camadas ocultas da envolvente do edifício, podendo permanecer indetectáveis até que a deterioração visível se torne evidente,

momento em que danos materiais significativos e problemas na qualidade do ambiente interior já podem ter ocorrido (Dias Pereira et al., 2023; Mattsson et al., 2024; Palani et al., 2023).

Os fenómenos relacionados com a humidade são amplamente reconhecidos como um dos principais motores de degradação dos edifícios. Os seus efeitos vão além dos danos estéticos, afetando a integridade estrutural dos materiais, o desempenho térmico dos sistemas envolventes e a saúde e o conforto dos ocupantes (Heracleous et al., 2025; Schroderus et al., 2025). A exposição prolongada à humidade pode desencadear uma cadeia de mecanismos de degradação, incluindo a degradação de revestimentos, o desenvolvimento biológico, a cristalização de sais e a corrosão de elementos metálicos. Assim, a compreensão dos mecanismos que regem o comportamento higrotérmico é essencial para um diagnóstico fiável e para o desenvolvimento de estratégias eficazes de manutenção e reabilitação.

A relevância destas patologias tem sido amplamente evidenciada em estudos europeus. O sistema SYCODÉS, uma das bases de dados mais completas de relatórios periciais em França, demonstra que as falhas de estanquidade representam mais de 60% dos defeitos registados, o que sublinha o papel dominante dos fenómenos de humidade na degradação dos edifícios (AQC, 2016; CIB, 2013). Tendências semelhantes são observadas em outros contextos europeus, nos quais as patologias da envolvente representam uma parcela significativa dos sinistros reportados (CIB, 2013).

No contexto português, estudos sobre edifícios históricos demonstram igualmente a prevalência de processos de degradação associados à humidade, que afetam uma ampla gama de materiais e sistemas construtivos. Problemas como infiltrações, humidade ascensional, condensação e eflorescência são recorrentes em paredes de alvenaria e em sistemas de revestimento, podendo estender-se a elementos de madeira e de metal (Branco & Torres, 2009).

Apesar do reconhecimento generalizado da importância dos fenómenos higrotérmicos, a investigação existente tende a focar-se em casos específicos ou em análises numéricas, sendo ainda limitada pela disponibilidade de estudos baseados em conjuntos de dados reais provenientes de inspeções técnicas. Estes conjuntos de dados são essenciais para identificar padrões de ocorrência, caracterizar mecanismos subjacentes e compreender a relação entre causas e manifestações.

Neste contexto, o presente estudo analisa uma amostra de relatórios de inspeção técnica do Instituto da Construção Sustentável (ICS) da Universidade do Porto, com o objetivo de caracterizar as patologias higrotérmicas mais frequentes e explorar as suas relações com elementos construtivos específicos por meio de métodos estatísticos. Através da integração de uma tipologia estruturada de patologias com análises descritivas e de associação, o estudo procura identificar padrões consistentes de degradação e apoiar o desenvolvimento de estratégias de diagnóstico e de reabilitação mais eficazes.

Este estudo distingue-se por recorrer a um conjunto alargado de dados empíricos provenientes de relatórios reais de inspeção, permitindo uma abordagem estatística ainda pouco explorada na literatura sobre patologia da construção. A sistematização das patologias, dos elementos construtivos afetados e das suas causas contribui para uma melhor compreensão dos mecanismos de degradação higrotérmica e para o apoio à tomada de decisão em contexto de manutenção e reabilitação de edifícios.

2. Metodologia

2.1 Enquadramento do Estudo

O enquadramento metodológico adotado neste estudo baseia-se na classificação sistemática das patologias higrotérmicas de acordo com os seus mecanismos subjacentes de transporte de humidade e as suas manifestações materiais observáveis. Os processos de degradação higrotérmica são amplamente reconhecidos como decorrentes de interações complexas entre os fluxos de calor, ar e humidade na envolvente dos edifícios, influenciando tanto a durabilidade dos materiais quanto a qualidade do ambiente interior (Bayat Pour et al., 2024; Hajdukiewicz et al., 2015).

Para apoiar a interpretação diagnóstica, as patologias foram organizadas em fenómenos primários, correspondentes aos mecanismos físicos que promovem o transporte e a acumulação de humidade, e em efeitos secundários, que representam os processos de degradação material decorrentes da presença prolongada dessas condições. Esta estrutura de classificação segue abordagens amplamente consolidadas na literatura sobre patologia da construção (Freitas Vasco Peixoto & Almeida, 2012; Palani et al., 2023).

Os fenómenos primários considerados incluem as principais vias de entrada ou mobilização de água nos edifícios: humidade por condensação, quando a temperatura desce abaixo do ponto de orvalho (Freitas Vasco Peixoto & Almeida, 2012; Rohsenow et al., 1998); humidade por infiltração, associada à entrada de água da chuva por meio de fissuras, juntas ou de sistemas de impermeabilização defeituosos (Freitas Vasco Peixoto & Almeida, 2012); humidade ascensional, resultante do transporte capilar a partir do solo (Boinas et al., 2016; Delgado et al., 2015; Guimarães et al., 2016); e fugas em redes técnicas (Freitas Vasco Peixoto & Almeida, 2012). Os efeitos secundários correspondem às manifestações materiais associadas à presença prolongada de humidade, tais como degradação de revestimentos, eflorescências, degradação biológica e corrosão.

Esta organização tipológica permite analisar, de forma estruturada, as relações entre causas e manifestações, fornecendo um quadro consistente para a interpretação dos resultados estatísticos e a compreensão dos padrões observados no parque edificado estudado.

2.2 Aquisição de Dados

A base empírica do estudo consiste numa revisão sistemática de relatórios de inspeção e de diagnóstico produzidos pelo Instituto da Construção Sustentável (ICS) da Universidade do Porto, no âmbito da sua atividade técnico-científica, no período compreendido entre 1995 e a atualidade. Estes relatórios documentam avaliações diagnósticas realizadas em edifícios com diferentes tipos de patologias construtivas.

O processo de seleção da amostra foi desenvolvido em duas etapas sequenciais. Numa primeira fase, foi analisado um conjunto inicial de 384 relatórios técnicos disponíveis na base de dados do ICS. Esta etapa teve como objetivo identificar a totalidade dos casos potencialmente relevantes para fenómenos de natureza higrotérmica.

Numa segunda fase, procedeu-se à aplicação de critérios de inclusão e exclusão previamente definidos, com o objetivo de garantir a consistência da amostra e a sua adequação ao objetivo do estudo. Foram incluídos apenas os relatórios que apresentavam patologias higrotérmicas com manifestação em elementos interiores dos edifícios e informação suficiente para a identificação de causas e mecanismos associados.

Foram excluídos os documentos que não apresentavam patologias higrotérmicas relevantes ou cuja incidência se restringia exclusivamente a outros tipos de problemas, nomeadamente patologias estruturais, questões de acessibilidade ou degradações exteriores sem impacto no ambiente interior.

Após a aplicação destes critérios, obteve-se uma amostra final de 103 relatórios considerados adequados ao âmbito do estudo.

A amostra resultante abrange edifícios habitacionais, de serviços, industriais e de uso misto, representando diferentes períodos construtivos e soluções técnicas.

Para cada caso selecionado, a informação foi sistematizada de forma estruturada em folha de cálculo, tendo sido construída uma grelha de codificação própria para registo consistente das variáveis em análise, nomeadamente: tipologia do edifício, localização, subtipo de patologia, elemento construtivo afetado, causas identificadas e recomendações de intervenção. A codificação foi realizada integralmente pelo autor, com base na leitura sistemática de todos os relatórios e na aplicação de critérios de classificação previamente definidos, garantindo uniformidade na atribuição das categorias.

3. Resultados

3.1 Distribuição de Patologias Higrotérmicas

A análise dos 103 relatórios de inspeção técnica revela uma forte concentração geográfica dos casos: o distrito do Porto é responsável por 73,7% das ocorrências, seguido de Aveiro (17,8%) e de Braga (4,8%). Os restantes distritos representam, em conjunto, 3,7% dos casos (Figura 1). Importa, no entanto, referir que a amostra analisada tem origem predominantemente na área de atuação do ICS, sediado no Porto, o que contribui para a concentração observada nesta região.

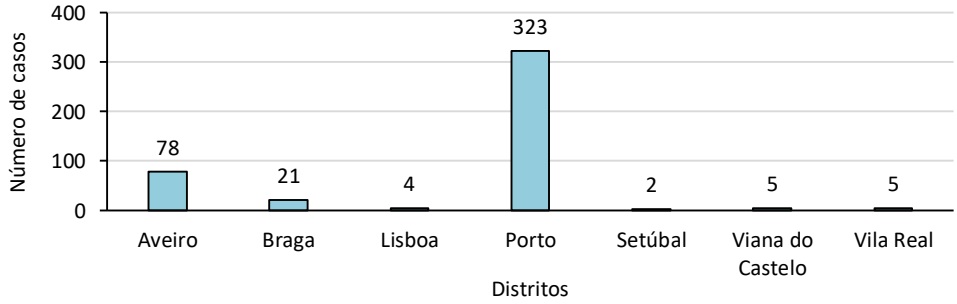


Figura 1 – Distribuição geográfica dos casos (número de ocorrências)

No total, foram identificadas 438 ocorrências patológicas, distribuídas nas oito categorias higrotérmicas definidas na Secção 2.1. A distribuição dos diferentes tipos de patologias encontra-se apresentada na Figura 2.

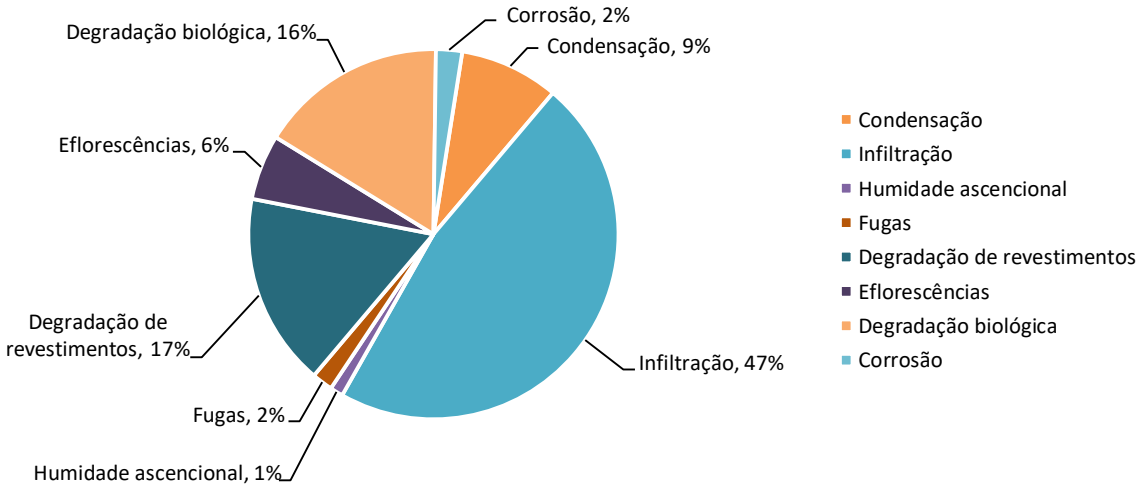


Figura 2 – Distribuição das patologias higrotérmicas (%)

A infiltração de água é a patologia mais prevalente, responsável por 47% das ocorrências totais (206 casos). Este resultado evidencia o papel dominante da infiltração de água na degradação dos elementos da envolvente dos edifícios.

A segunda categoria mais frequente corresponde à degradação de revestimentos, com 74 ocorrências (17%), seguida de perto pela degradação biológica, com 72 ocorrências (16%).

A condensação representa 9% das ocorrências, indicando uma presença moderada, porém relevante, de desequilíbrios de humidade no interior, frequentemente associados à ventilação e aquecimento deficientes. A eflorescência corresponde a 6% dos casos e geralmente está associada à migração de humidade por meio de materiais porosos.

As restantes patologias apresentam frequências comparativamente reduzidas: a humidade ascensional representa 1% das ocorrências, as fugas, 2%, e a corrosão, 2%.

De forma geral, os resultados indicam que a maioria das patologias observadas está diretamente associada a mecanismos de entrada e retenção de humidade, reforçando o papel central dos processos higrotérmicos na degradação dos edifícios.

3.2 Distribuição de Patologias pelos Elementos Construtivos

Foi realizada uma análise estatística, com recurso ao software IBM SPSS Statistics, com o objetivo de avaliar a existência de associações entre: (i) os elementos construtivos e os tipos de patologias; e (ii) as causas e as patologias identificadas. Para o efeito, aplicou-se o teste do qui-quadrado de independência.

A hipótese nula (H_0) pressupõe a inexistência de associação entre as variáveis em análise. Em ambos os casos, os resultados obtidos apresentaram valores de p inferiores a 5% ($p < 0,05$), o que levou à rejeição da hipótese nula. Estes resultados evidenciam associações estatisticamente significativas entre as variáveis analisadas, indicando que a ocorrência das patologias não é aleatória, mas depende tanto das características dos elementos construtivos quanto dos mecanismos causais subjacentes.

3.2.1 Elementos Construtivos vs Tipos de Patologias

A distribuição das patologias entre os diferentes elementos construtivos revela padrões consistentes, como ilustrado na Figura 3.

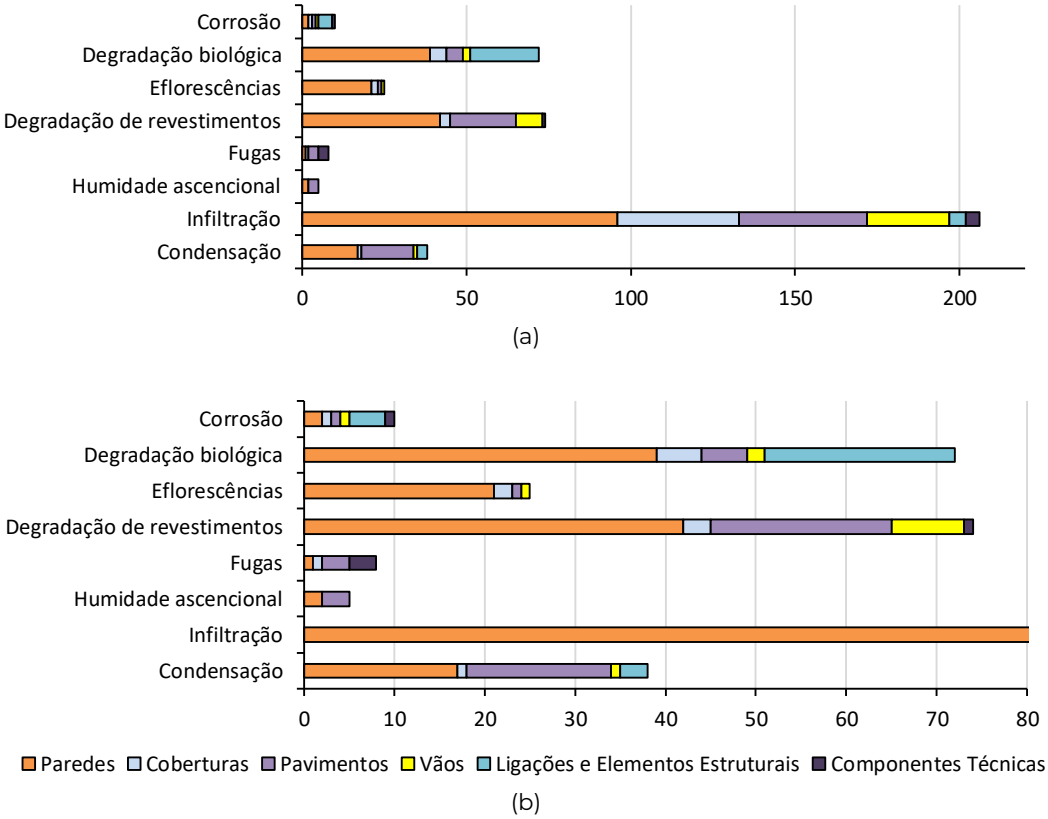


Figura 3 – (a) Distribuição das patologias por elementos construtivos; (b) detalhe ampliado

Verifica-se uma concentração significativa de ocorrências nos elementos da envolvente, com particular destaque para as paredes, que apresentam o maior número de patologias registadas. Este resultado

confirma a elevada exposição destes elementos às ações climáticas, nomeadamente à precipitação e ao vento.

A infiltração de água destaca-se como a patologia mais frequente, ocorrendo predominantemente em paredes, mas também com expressão relevante em coberturas, pavimentos e vãos. A condensação apresenta incidência significativa, sobretudo em paredes e pavimentos, o que reflete problemas associados à ventilação e ao desempenho térmico.

A degradação biológica e a degradação de revestimentos apresentam igualmente um número elevado de ocorrências, distribuídas por diversos elementos. A primeira ocorre predominantemente em paredes, ligações e elementos estruturais, enquanto a segunda se manifesta sobretudo em paredes e pavimentos.

A eflorescência surge principalmente em paredes, associada à migração de humidade por meio de materiais porosos. As fugas apresentam baixa incidência e estão essencialmente associadas a componentes técnicos. A corrosão ocorre de forma pontual, sobretudo em elementos estruturais e em ligações metálicas. Por fim, a humidade ascensional afeta quase exclusivamente paredes, devido ao contacto direto com o solo.

De forma geral, conclui-se que as paredes constituem o elemento mais vulnerável à ocorrência de patologias higrotérmicas, seguidas por pavimentos, coberturas e vãos.

3.2.2 Causas vs Tipos de Patologias

Para a análise das causas associadas às patologias higrotérmicas, adotou-se um sistema de codificação, apresentado na Tabela 1, que identifica e descreve os diferentes mecanismos de origem considerados neste estudo.

Tabela 1 – Codificação das causas das patologias higrotérmicas

Causa	Descrição
1	Ventilação insuficiente ou inexistente; aquecimento insuficiente
2	Ausência ou insuficiência de isolamento térmico
3	Presença de pontes térmicas
4	Falta de estanquidade da envolvente
5	Dimensionamento inadequado da rede de drenagem de águas pluviais
6	Envelhecimento e degradação de materiais
7	Deslocação ou fissuração de telhas
8	Humidade ascensional proveniente do solo
9	Fugas em redes de canalização
10	Utilização de materiais inadequados ou com elevada porosidade
11	Deficiências de conceção construtiva
12	Humidade de construção
13	Migração de sais solúveis
14	Proteção inadequada de elementos metálicos

Com base nesta classificação, foi analisada a relação entre as causas identificadas e os diferentes tipos de patologias, conforme apresentado na Figura 4.

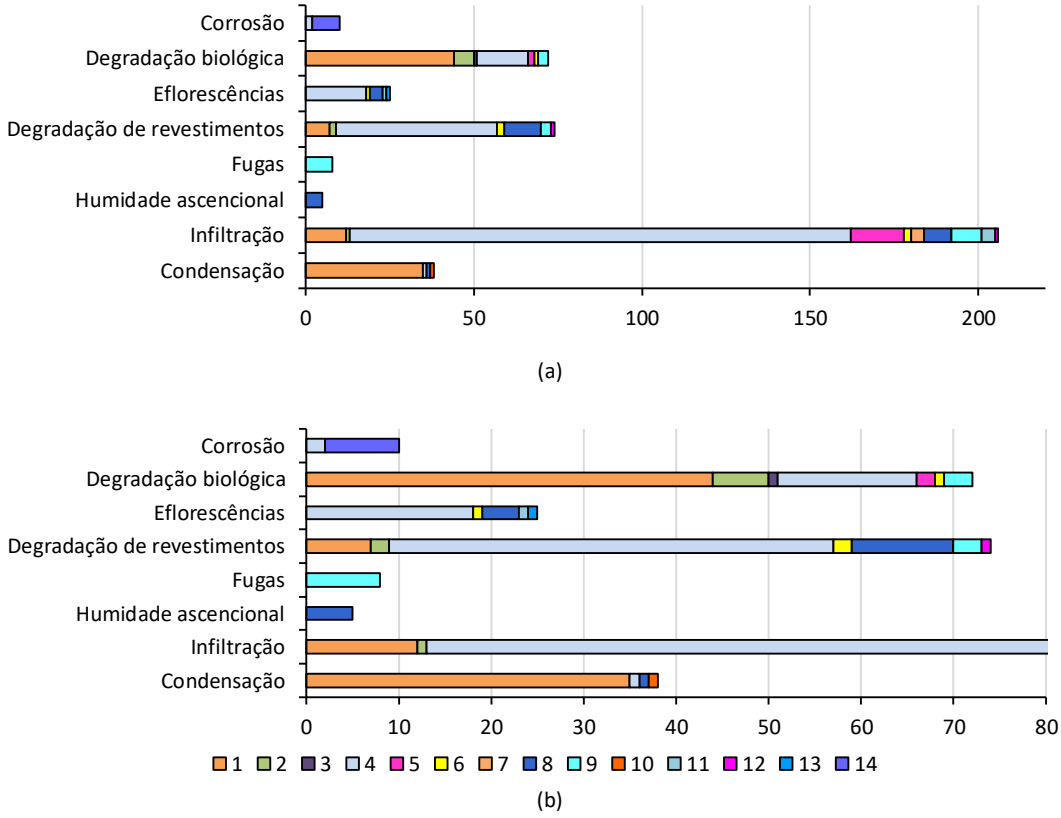


Figura 4 – (a) Distribuição das patologias por causas; (b) detalhe ampliado

A análise evidencia padrões claros de associação entre patologias e mecanismos causais, permitindo identificar as principais origens dos processos de degradação higrotérmica.

A condensação encontra-se quase exclusivamente associada à causa 1, correspondente a condições interiores inadequadas, nomeadamente ventilação insuficiente, renovação de ar fraca, produção elevada de vapor e/ou aquecimento insuficiente. As restantes causas surgem de forma residual, confirmando a forte dependência desta patologia das condições higrotérmicas interiores.

As infiltrações são predominantemente explicadas pela causa 4, relacionada à falta de estanquidade da envolvente e às deficiências de impermeabilização, as quais são responsáveis pela maioria dos casos. Verificam-se ainda contributos secundários associados à drenagem inadequada, à humidade do solo, a fugas e, pontualmente, a condições interiores desfavoráveis.

A humidade ascensional apresenta uma correspondência direta e exclusiva com a causa 8, associada à ascensão de humidade proveniente do solo, não sendo identificadas outras causas relevantes. De forma semelhante, as patologias classificadas como fugas estão exclusivamente associadas à causa 9, correspondente a roturas ou deficiências nas redes de canalização.

A degradação de revestimentos é predominantemente associada à causa 4, evidenciando o impacto da entrada de água na envolvente. Registam-se ainda contributos relevantes da humidade ascensional (causa 8) e das condições interiores (causa 1), bem como ocorrências menos expressivas relacionadas com envelhecimento dos materiais, deficiências de conceção e variações do teor de humidade.

As eflorescências estão sobretudo associadas à causa 4 e também são influenciadas pela humidade ascensional (causa 8). As restantes causas, como a migração de sais ou deficiências de conceção, apresentam expressão residual.

A degradação biológica ocorre predominantemente devido a condições de humidade elevada no interior (causa 1), com contribuição significativa da entrada de água na envolvente (causa 4). Outras causas, como envelhecimento, fugas ou drenagem deficiente, têm impacto reduzido.

Por sua vez, a corrosão está principalmente associada à causa 14, relacionada à proteção inadequada de elementos metálicos, sendo complementada por ocorrências pontuais associadas a deficiências de estanquidade.

De forma geral, identificam-se dois grandes grupos de mecanismos dominantes. Por um lado, as patologias associadas à entrada e circulação de água na envolvente, tais como infiltrações, degradação de revestimentos, eflorescências e parte dos fenómenos de corrosão, estão maioritariamente relacionadas com a causa 4, que se destaca como o principal fator de degradação. Por outro lado, as patologias dependentes das condições higrotérmicas interiores, nomeadamente a condensação e a degradação biológica, encontram-se fortemente associadas à causa 1.

Adicionalmente, verificam-se associações unívocas entre determinados mecanismos físicos e causas específicas, destacando-se a humidade ascensional (causa 8) e as fugas (causa 9). As restantes causas identificadas apresentam contributos residuais, sem impacto significativo no total de ocorrências.

4. Discussão

4.1 Interpretação dos mecanismos de degradação

Os resultados obtidos evidenciam o papel dominante da humidade como principal agente de degradação do desempenho dos edifícios, confirmando tendências amplamente reportadas na literatura europeia (AQC, 2016; CIB, 2013). No entanto, mais do que uma simples prevalência de patologias associadas à água, os dados sugerem a existência de um sistema de degradação estruturalmente dependente de falhas persistentes na gestão da humidade ao longo do ciclo de vida dos edifícios.

A elevada incidência de infiltrações não deve ser interpretada apenas como um problema pontual de estanquidade, mas como um indicador de vulnerabilidades sistémicas associadas ao projeto, execução e envelhecimento da envolvente. A concentração destes casos em elementos como fachadas, coberturas e vãos sugere que os pontos singulares da construção continuam a constituir fragilidades recorrentes, frequentemente subestimadas em fases de projeto e manutenção. Esta tendência é consistente com resultados de outros levantamentos europeus, nos quais as interfaces entre fachadas e vãos são frequentemente identificadas como pontos críticos de entrada de humidade (AQC, 2016).

Adicionalmente, a associação entre infiltração de água, degradação de revestimentos e eflorescências evidencia a natureza progressiva dos processos de degradação. Em vez de fenómenos independentes, estas manifestações representam diferentes estágios de um mesmo mecanismo físico, no qual a entrada de água desencadeia alterações químicas e físicas cumulativas nos materiais. Esta leitura reforça a necessidade de abordagens diagnósticas que considerem cadeias de degradação e não apenas sintomas isolados (Freitas Vasco Peixoto & Almeida, 2012; Palani et al., 2023).

Por outro lado, as patologias associadas a condições higrotérmicas interiores, como condensação e degradação biológica, revelam um segundo regime de comportamento, fortemente dependente das condições de utilização e de ventilação. Este resultado sugere que uma parte significativa das patologias não pode ser explicada apenas por deficiências construtivas, mas também por padrões de ocupação e desempenho dos sistemas de ventilação e aquecimento. Assim, a fronteira entre patologia construtiva e comportamento de utilização torna-se difusa, exigindo abordagens integradas de análise.

A análise das causas permite distinguir dois grandes grupos de mecanismos de degradação. O primeiro está associado à entrada e circulação de água na envolvente e é dominado por falhas de estanquidade e impermeabilização. Este grupo concentra a maioria das patologias mais frequentes, evidenciando que o controlo da água líquida constitui o aspeto mais crítico na prevenção da degradação higrotérmica. O

segundo grupo está relacionado com as condições higrotérmicas interiores, sendo dominado por problemas de ventilação e controlo de vapor, que conduzem a fenómenos de condensação e crescimento biológico.

Adicionalmente, a existência de associações diretas e exclusivas entre determinadas patologias e causas específicas, como a humidade ascensional e o contacto com o solo, ou as fugas e as redes de canalização, demonstra que alguns mecanismos apresentam uma relação física bem definida e previsível. Em contraste, outras patologias resultam da combinação de múltiplos fatores, o que reflete a natureza multifatorial dos processos de degradação em edifícios.

De forma geral, os resultados evidenciam que a degradação higrotérmica resulta da interação entre condições ambientais, características construtivas e fatores de utilização, sendo essencial uma abordagem integrada para sua compreensão e mitigação.

4.2 Implicações e Estratégias de Intervenção

Os padrões estatísticos identificados evidenciam a necessidade de estratégias de intervenção que atuem sobre os mecanismos subjacentes à acumulação de humidade na envolvente dos edifícios. Em particular, a predominância de defeitos associados à infiltração e a sua relação com patologias secundárias indicam que as estratégias de reabilitação devem priorizar o controlo da entrada de água antes da correção das manifestações secundárias.

A elevada incidência de patologias em paredes, coberturas e interfaces com vãos reforça igualmente a necessidade de intervenções direcionadas para os elementos mais expostos às ações climáticas e às falhas de impermeabilização.

4.2.1 Intervenções em fenómenos primários

A infiltração de água, identificada como a patologia mais frequente da amostra, deve ser tratada por meio da correção dos pormenores construtivos em fachadas e vãos, incluindo a aplicação de selantes elásticos, pingadeiras e remates adequados. Em interfaces porosas, podem ser aplicadas barreiras localizadas ou argamassas impermeabilizantes. Em paredes enterradas, deve-se proceder à renovação das membranas impermeáveis e à instalação de sistemas de drenagem eficazes. Em coberturas planas e terraços, é essencial garantir a continuidade das membranas, a correta pendente e o funcionamento adequado dos sistemas de escoamento. Nos pavimentos em contacto com o solo, devem ser adotadas soluções de impermeabilização contínua ou caixas de ar ventiladas.

Os resultados obtidos demonstram igualmente uma associação significativa entre condensação, degradação biológica e condições higrotérmicas interiores inadequadas. Assim, a mitigação destes fenómenos deve passar pela melhoria da ventilação (natural, híbrida ou mecânica), garantindo uma renovação adequada de ar, bem como o reforço do isolamento térmico, assegurando a continuidade nos pontos singulares. A manutenção de temperaturas interiores adequadas e, quando necessário, o recurso à desumidificação são igualmente medidas relevantes.

A humidade ascensional, embora menos frequente, apresentou uma associação direta com o contacto com o solo, justificando intervenções centradas na interrupção da ascensão capilar e na melhoria da drenagem periférica, recorrendo a diferentes técnicas, como, por exemplo, a criação de barreiras químicas ou físicas ou a implementação de soluções de ventilação na base das paredes. Os revestimentos contaminados por sais devem ser removidos e substituídos por soluções compatíveis e permeáveis ao vapor.

As fugas identificadas nos relatórios analisados exigem intervenções localizadas de deteção e reparação das redes de canalização.

4.2.2 Remediação de efeitos secundários

A degradação biológica deve ser tratada com limpeza, desinfeção e aplicação de fungicidas apropriados, seguida da utilização de revestimentos permeáveis ao vapor. As eflorescências podem ser removidas por escovagem ou lavagem controlada, sendo recomendada a aplicação de materiais compatíveis com ambientes sujeitos à migração de sais. A corrosão exige limpeza, passivação e proteção dos elementos metálicos, enquanto a degradação de revestimentos implica a sua substituição após estabilização das condições higrotérmicas.

4.3 Limitações do Estudo

Apesar dos contributos relevantes do conjunto de dados analisado, importa reconhecer algumas limitações do estudo. A análise baseia-se em relatórios de inspeção provenientes de uma única entidade, localizada no Norte de Portugal, o que resulta numa maior concentração de casos nesta região. Consequentemente, a amostra não reflete integralmente a diversidade do parque edificado português, limitando a generalização dos resultados à escala nacional.

A identificação das patologias e respetivas causas depende da interpretação técnica realizada nos relatórios de inspeção, podendo introduzir algum grau de subjetividade. Além disso, a análise das relações entre patologias e causas assenta nessa mesma informação interpretativa, o que pode gerar alguma dependência entre as variáveis consideradas e deve ser tido em conta na interpretação dos resultados.

Embora a base de dados apresente elevada riqueza de informação, variáveis como a idade dos edifícios, o tipo de utilização ou os sistemas construtivos não foram exploradas em profundidade. A inclusão destas dimensões em trabalhos futuros poderá contribuir para uma compreensão mais abrangente da variabilidade das patologias higrotérmicas.

Investigações futuras poderão igualmente alargar o conjunto de dados, integrando informação proveniente de outras instituições ou combinando relatórios de inspeção com a monitorização contínua de parâmetros higrotérmicos, como temperatura e humidade.

De forma global, os resultados obtidos contribuem para uma melhor compreensão das inter-relações entre os mecanismos de transporte de humidade, os processos de degradação dos materiais e os elementos construtivos. Este conhecimento revela-se fundamental para o desenvolvimento de metodologias de diagnóstico mais robustas e de estratégias de manutenção e reabilitação mais eficazes.

5. Conclusões

O presente estudo permitiu analisar, de forma sistemática, a ocorrência de patologias higrotérmicas em edifícios, com base numa amostra de 103 relatórios de inspeção e de diagnóstico, contribuindo para uma melhor compreensão dos mecanismos de degradação associados à humidade.

Os resultados evidenciam que a infiltração de água constitui o principal fator de degradação da envolvente dos edifícios, sendo a patologia mais frequente e associada à maioria dos processos de deterioração observados. Este facto confirma a elevada vulnerabilidade dos elementos construtivos às falhas de estanquidade e à ação da água da chuva, particularmente em fachadas e nas interfaces com vãos.

Verificou-se ainda que as patologias higrotérmicas não ocorrem de forma isolada, mas sim integradas em cadeias de degradação inter-relacionadas. Destaca-se a associação entre infiltração, degradação de revestimentos e eflorescências, bem como entre condensação e degradação biológica, evidenciando a existência de mecanismos físicos distintos associados, respetivamente, à envolvente exterior e às condições higrotérmicas interiores.

A análise por elementos construtivos demonstrou que as paredes constituem o elemento mais vulnerável, devido à sua exposição às ações climáticas e à sua função como principal interface entre o ambiente exterior

e interior. Pavimentos e coberturas apresentam igualmente relevância, sobretudo em situações de contacto com o solo ou exposição direta à precipitação.

Do ponto de vista estatístico, foram identificadas associações significativas entre patologias, elementos construtivos e causas, confirmando a existência de padrões consistentes de ocorrência e reforçando a natureza não aleatória dos processos de degradação higrotérmica. Em particular, distinguem-se dois grandes grupos de mecanismos dominantes: (i) patologias associadas à entrada de água na envolvente, relacionadas sobretudo com deficiências de estanquidade; e (ii) patologias associadas às condições higrotérmicas interiores, resultantes de ventilação insuficiente e desempenho térmico inadequado.

Do ponto de vista aplicado, os resultados evidenciam a necessidade de estratégias de diagnóstico e reabilitação centradas nas causas dos fenómenos e não apenas nas suas manifestações visíveis. A correção de patologias superficiais sem eliminação dos mecanismos subjacentes tende a conduzir à recorrência dos problemas ao longo do tempo.

Em termos gerais, este estudo contribui para o conhecimento dos mecanismos de degradação higrotérmica em edifícios, através da sistematização de um conjunto alargado de dados empíricos provenientes de relatórios técnicos reais. A abordagem estatística adotada permite identificar padrões consistentes entre patologias, elementos construtivos e causas, fornecendo uma base útil para o desenvolvimento de metodologias de diagnóstico mais robustas e estratégias de reabilitação mais eficazes.

Como trabalho futuro, recomenda-se o alargamento da base de dados a outras regiões e instituições, bem como a integração de variáveis contextuais e de monitorização higrotérmica contínua, de forma a aprofundar a compreensão dos mecanismos de degradação e aumentar a capacidade preditiva das análises.

Agradecimentos

Esta publicação resulta do projeto RETIME - Urban Adaptation and Alert Solutions for a TIMEly (re)Action, cofinanciado pela União Europeia ao abrigo do Acordo de Subvenção n.º 101147113. O conteúdo e os resultados aqui apresentados são da exclusiva responsabilidade dos autores e não refletem necessariamente as opiniões da Comissão Europeia ou da Agência Executiva Europeia para o Clima, Infraestruturas e Ambiente (CINEA). Nem a União Europeia nem a entidade financiadora podem ser responsabilizadas pelo mesmo.

Este trabalho foi financiado por: UID/04708/2025 e https://doi.org/10.54499/UID/04708/2025, da Unidade de Investigação CONSTRUCT - Instituto de I&D em Estruturas e Construções - financiada pela Fundação para a Ciência e a Tecnologia, I.P./ MECI, através de fundos nacionais.

O autor João M.P.Q. Delgado agradece o apoio da FCT – Fundação para a Ciência e a Tecnologia através do contrato de Estímulo ao Emprego Científico Individual 2020.00828.CEECIND/CP1590/CT0004.

Referências

AQC. (2016). *SYCODÉS pathologies*.

Bayat Pour, M., Niklewski, J., Naghibi, A., & Frühwald Hansson, E. (2024). A literature review of probabilistic hygrothermal assessment for building envelopes. *Building and Environment*, *261*, 111756. https://doi.org/10.1016/j.buildenv.2024.111756

Boinas, R., Guimarães, A. S., & Delgado, J. M. P. Q. (2016). Rising damp in Portuguese cultural heritage – a flood risk map. *Structural Survey*, *34*(1), 43-56. https://doi.org/10.1108/ss-07-2015-0034

Branco, D., & Torres, I. (2009). Humidade em Construções Históricas. In *PATORREB* (pp. 583–588).

CIB. (2013). A state-of-the-art report on building pathology. *VP (ed) CIB–W086-building pathology*

Delgado, J. M. P. Q., Guimarães, A. S., & de Freitas, V. P. (2015). Numerical Simulations Applied to Drying Out Buildings with Rising Damp Problems. In J. M. P. Q. Delgado, A. S. Guimarães, & V. P. de Freitas (Eds.), *Hygrothermal Risk on Building Heritage: A Methodology for a Risk Map* (pp. 33-41). Springer International Publishing. https://doi.org/10.1007/978-3-319-19114-0_3

Dias Pereira, L., Saraiva, N. B., & Soares, N. (2023). Hygrothermal Behavior of Cultural Heritage Buildings and Climate Change: Status and Main Challenges. *Applied Sciences*, *13*(6).

Freitas Vasco Peixoto, d., & Almeida, A. M. d. (2012). *Manual de apoio ao projecto de reabilitação de edifícios antigos / coord. Vasco Peixoto de Freitas ; pref. A. Matos de Almeida*. Ordem dos Engenheiros. Região Norte.

Guimarães, A. S., Delgado, J. M. P. Q., & de Freitas, V. P. (2016). Treatment of rising damp in historic buildings: Experimental campaign of wall base ventilation and interface effect analysis. *Journal of Cultural Heritage*, *20*, 733-738. https://doi.org/10.1016/j.culher.2016.02.012

Hajdukiewicz, M., Byrne, D., Keane, M. M., & Goggins, J. (2015). Real-time monitoring framework to investigate the environmental and structural performance of buildings. *Building and Environment*, *86*, 1-16. https://doi.org/10.1016/j.buildenv.2014.12.012

Heracleous, C., Panagiotou, R., Ioannou, I., Michael, A., & Philokyprou, M. (2025). Hygrothermal performance monitoring and indoor thermal evaluation in adobe structures. *Energy and Buildings*, *346*, 116049. https://doi.org/10.1016/j.enbuild.2025.116049

Mattsson, C., Nordquist, B., Johansson, D., Bagge, H., & Wallentén, P. (2024). A quantitative and qualitative literature review of water damage in buildings occurring in building service systems, appliances and wet rooms. *Indoor and Built Environment*, *33*(7), 1173-1189. https://doi.org/10.1177/1420326X241248331

Palani, H., Khaleghi, H., Salehi, P., & Karatas, A. (2023). Assessing Hygrothermal Performance in Building Walls Engineered for Extreme Cold Climate Environments. *Sustainability*, *15*(24).

Rohsenow, W. M., Hartnett, J. P., & Cho, Y. I. (1998). *Handbook of heat transfer* (Vol. 3). Mcgraw-hill New York.

Schroderus, S., Havelka, J., Kouch, A., Illikainen, K., Alitalo, S., & Fedorik, F. (2025). Hygrothermal performance of hybrid multi-storey buildings under future climate scenarios. *Applied Thermal Engineering*, *259*, 124917. https://doi.org/10.1016/j.applthermaleng.2024.124917

XXII International Conference on Building Pathology and Constructions Repair
15th to 17th July 2026 - Lisboa, Portugal

Building Inspection As A Technical Tool For Risk Management: A Case Study–Based Methodology For Intervention Prioritization In Residential Buildings

Mariana GOMES SCHAEFER[1], Elisangela SOUZA RIBEIRO SILVA[2]

[1] Instituto Nova Engenharia, Porto Maua, Brasil, marianaschaefer@hotmail.com1

[2]Pindamonhangaba, Brasil, elisaeng.civil@gmail.com2

Abstract: The aging of the existing building stock, combined with the absence of systematic maintenance plans, has increased the occurrence of pathological manifestations and risk situations in multifamily residential buildings. In this context, building inspection plays a strategic role, enabling not only the diagnosis of existing defects but also supporting technical decision-making based on risk criteria. This article aims to present and discuss the application of a structured building inspection methodology using a multifamily residential condominium as a case study and to evaluate its potential as a risk management and intervention prioritization tool. The adopted methodology is based on systematic visual technical inspections, the classification of defects according to building systems, the analysis of their origin and criticality, and the prioritization of interventions according to the associated risk level. The analyzed data were obtained from a technical inspection report, allowing the identification of the most critical systems and the assessment of the impacts resulting from the lack of preventive maintenance. The results indicate that the methodological application of building inspections makes it possible to transform technical information into objective support for decision-making, contributing to risk mitigation, resource optimization, and the extension of the building's service life. It is concluded that building inspection, when guided by technical criteria and risk analysis, constitutes an essential tool for the technical management of residential buildings, with a high potential for replication in different construction contexts.

Keywords: Building inspection; risk management; maintenance management; service life; multifamily residential buildings.

1. Introduction

When dealing with engineering works, they are commonly associated with characteristics such as safety, strength, durability, and versatility. However, constructions cannot be considered permanently durable, as they are subject to deformation and deterioration processes resulting from physical and chemical phenomena inherent to materials over time.

According to IBAPE (2005), pathological manifestations correspond to defects that occur in civil constructions as a result of multiple factors. Building pathology can be understood as the set of manifestations that arise during construction or throughout the service life of a building, compromising the expected performance of the structure and its constituent systems.

The term "pathology" originates from the Greek words *pathos* (disease) and *logos* (study), meaning the study of diseases. In the context of civil engineering, it refers to the analysis of building degradation mechanisms. Pathological analysis also involves fundamental aspects such as the time of occurrence and the exposure conditions of building components, making concepts such as durability, service life, and performance particularly relevant (ALVES and SIMEÃO, 2022).

The safety, performance, and durability of residential buildings are central concerns in contemporary civil engineering. The aging of the building stock, combined with the absence of systematic maintenance practices, has significantly contributed to the emergence of pathological manifestations, premature degradation of building systems, and, in more critical situations, risks to the physical integrity of occupants.

Pathological problems may originate from several factors, including unforeseen overloads, the use of inadequate or low-quality materials, insufficient knowledge of material properties, noncompliance with technical standards, design flaws, construction errors, lack of maintenance, and the natural aging of buildings. Furthermore, environmental conditions exert a direct influence on the degradation processes of building systems (FARIAS and MARINHO, 2021).

For the proper intervention of identified pathologies, a detailed study of their causes and formation mechanisms is indispensable. Knowledge of the different types of pathological manifestations contributes significantly to an accurate diagnosis. Through this process, combined with technical inspection and proper management, it is possible to identify the symptoms, causes, and origins of anomalies (TUTIKIAN and PACHECO, 2013).

Following the stages of inspection, diagnosis, and prognosis, it is the responsibility of the professional in charge to define the interventions necessary to correct the identified problems. The set of actions aimed at the recovery, repair, or strengthening of structures is referred to as therapy. Considering that each type of anomaly presents specific characteristics, the careful selection of the most appropriate techniques and materials for each situation becomes essential (ARAÚJO, 2021).

Traditionally, building maintenance in residential structures is carried out reactively, motivated by the occurrence of visible failures or emergency situations. This approach, besides being economically inefficient, tends to increase risk levels and reduce the service life of the building. In this context, building inspection stands out as a fundamental technical tool, capable of providing structured information regarding the condition of building systems and supporting decision-making based on technical and risk-related criteria (HELENE, BOLINA, and TUTIKIAN, 2019).

For professionals in the field, the correct identification and classification of anomalies present in a building are essential. These manifestations may be associated with both construction defects and performance deficiencies related to the building system, as well as defects that pose risks to the safety and health of occupants. A proper understanding of these occurrences contributes significantly to technical analysis and to the development of effective maintenance and intervention plans.

Given this context, the relevance of studying building pathologies becomes evident, both from preventive and corrective perspectives. Therefore, this article aims to demonstrate how building inspection, when conducted systematically and guided by risk analysis, can be used as a management tool for prioritizing interventions in multifamily residential buildings. To this end, the application of a building inspection methodology in a residential condominium is presented, based on real data obtained from a technical report, with the additional objective of contributing to the development of practical guidelines to assist professionals in decision-making processes.

2. Theoretical Framework

2.1. Building Maintenance

Building maintenance constitutes an essential component of contemporary civil engineering, being directly responsible for preserving the performance, safety, functionality, and durability of buildings throughout their life cycle. According to ABNT NBR 5674:2012, maintenance is defined as the "set of activities to be carried out in order to preserve or restore the functional capacity of a building and its constituent systems."

This definition broadens the traditional concept of maintenance, which is no longer viewed as exclusively corrective but rather as a continuous, preventive, and strategic process. This perspective is aligned with ABNT NBR 15575:2013 (Performance Standard), which introduces the concept of Design Service Life (DSL), conditioning building performance on the proper execution of maintenance activities throughout its lifespan.

ABNT NBR 5674:2012 establishes three main types of maintenance: Corrective maintenance: performed after the occurrence of failures; Preventive maintenance: based on scheduled interventions; Predictive maintenance: based on performance monitoring.

Within the context of the case study, there is a predominance of failures resulting from the absence of preventive maintenance, as evidenced by the presence of pathologies such as water infiltration, cracking, and coating degradation.

Authors such as Helene (2005) emphasize that every building is subject to natural degradation processes resulting from physical, chemical, and biological actions, including concrete carbonation, reinforcement corrosion, thermal variations, and the action of aggressive environmental agents.

Building maintenance should be understood as an organized management system involving the planning, execution, control, and documentation of interventions. Furthermore, the standard highlights the importance of the User, Operation, and Maintenance Manual, as established by ABNT NBR 14037:2011, an essential document for guiding users and facility managers.

According to Sena (2020), the absence of a structured maintenance system is one of the main causes of premature building deterioration, resulting in accelerated degradation, exponential increases in maintenance costs, reduced service life, and safety risks, among numerous other consequences. Studies in the field of building pathology indicate that intervention costs increase exponentially over time and may be up to five times higher when repairs are carried out during advanced stages of deterioration.

In this context, maintenance acts as a fundamental mechanism for controlling deterioration through periodic inspections and planned interventions, contributing to delaying the progression of pathological manifestations and ensuring compliance with performance requirements throughout the building's service life.

2.2. Building Inspection

Building inspection constitutes an important technical tool for the identification, analysis, and classification of anomalies and defects in buildings. However, it is still not widely adopted by condominium managers and facility administrators, which compromises its preventive and predictive role, limiting its application primarily to corrective situations.

Building inspection differs from isolated surveys due to its comprehensive, structured nature and its focus on identifying anomalies, defects, and nonconformities across the various building systems.

According to ABNT NBR 16747 (ABNT, 2020), building inspections must follow specific guidelines, emphasizing the importance of adopting an appropriate methodology, systematically documenting evidence, and conducting a technical analysis of the identified pathological manifestations. When performed rigorously, inspection enables not only the diagnosis of the current condition of a building but also an understanding of the degradation mechanisms that are developing over time.

Deutsch (2016) highlights that the early identification of construction-related problems significantly facilitates their resolution and reduces intervention costs. The analysis and understanding of deterioration symptoms, whether in structural elements or finishing components, help prevent or minimize the progression of damage over time. In this regard, periodic inspections become essential for the continuous monitoring of building conditions.

The absence of inspection and, consequently, adequate maintenance tends to generate progressive problems in buildings, leading to premature obsolescence and the emergence of construction deficiencies. A lack of awareness regarding the importance of building inspection contributes to making necessary interventions more complex and economically burdensome.

Building maintenance is not limited to preserving property assets; it also aims to ensure that performance levels remain within acceptable standards, preventing user discomfort and restrictions on building use. Through appropriate inspection and maintenance practices, it is possible to extend the service life of a building and ensure improved conditions of safety and habitability (Farias and Marinho, 2021).

In this context, building inspection in structures exhibiting pathological manifestations has become an increasingly relevant topic in civil engineering, particularly in response to growing demands for safety and performance in buildings (Sena et al., 2020). Problems resulting from such manifestations may range from minor defects to situations that compromise structural stability and, in extreme cases, may lead to building collapse.

2.3. Risk Management

Risk management applied to buildings involves the systematic identification, analysis, and assessment of events that may compromise the safety, performance, and functionality of building systems. In this context, risk-based maintenance emerges as a strategic approach in which interventions are prioritized according to the probability of failure occurrence and the severity of their consequences throughout the building's life cycle.

Approaches aligned with international standards, such as ISO 31000, reinforce the need for decision-making processes based on technical criteria and structured methodologies, reducing subjectivity in assessments and promoting a more efficient allocation of resources. The integration of building inspection and risk management makes it possible to transform technical data into strategic information, contributing to the development of more effective, performance-oriented maintenance plans.

In the context of residential buildings, risk can be understood as the combination of the probability of failure occurrence and the magnitude of its consequences. Risk management in civil engineering involves stages such as hazard identification, vulnerability analysis of building systems, and the definition of appropriate mitigation measures, considering technical, operational, and economic aspects.

Based on the technical literature and building inspection practices, risks in buildings can be classified into different categories. Structural risk is related to the stability of the building and includes situations such as loss of load-bearing capacity, excessive cracking, and, in extreme cases, partial or total collapse. Functional risk refers to the impairment of building system performance, including failures in installations, water infiltration, and degradation of enclosure components. Health risk is associated with conditions that affect indoor environmental quality, such as the presence of moisture, mold, and biological agents. Economic risk is linked to the progressive increase in intervention costs resulting from the absence of preventive maintenance and the advancement of pathological manifestations (MARTINS and CAVALCANTE, 2022).

In addition to these classifications, risk assessment in buildings should also consider the concept of criticality, which relates the importance of the affected system to the consequences of its failure. Essential systems, such as structural and safety-related systems, require greater rigor in analysis and intervention prioritization. In this regard, the adoption of risk matrices and prioritization tools enables a more objective and transparent approach to defining corrective and preventive actions (Carraro, 2020).

Another relevant aspect concerns the integration of risk management with the principles of durability and service life of buildings. The degradation of materials and building components occurs progressively and, when not monitored, may lead to significant performance loss. The incorporation of risk-based maintenance strategies allows failures to be anticipated, reduces the need for emergency interventions, and increases the overall efficiency of building management, aligning with regulatory requirements and international best practices.

Therefore, it is essential to understand that risk management should be directly integrated into maintenance practices, constituting a continuous and dynamic cycle composed of inspection, diagnosis, intervention, and monitoring stages. This process enables the systematic monitoring of building conditions, supporting more accurate and sustainable decision-making over time.

In summary, the application of risk management in conjunction with building inspection represents a consistent technical approach for improving building performance and safety. By enabling the rational prioritization of interventions and the optimization of available resources, this integration contributes significantly to extending the service life of buildings, reducing long-term costs, and mitigating risks to occupants, thereby establishing itself as an essential practice in contemporary civil engineering (Antunes, 2010).

3. Methodology

This study is characterized as applied research of an exploratory nature, conducted through a case study using both qualitative and quantitative approaches, based on the implementation of a technical building inspection and risk analysis. The adopted methodology consists of the application of a systematic visual building inspection in multifamily residential buildings, aiming to identify and evaluate the performance conditions of building systems.

Initially, a literature review on building inspection and risk management was conducted to provide the theoretical foundation for the study. Sources such as books, scientific articles, technical standards, and specialized publications, both in print and electronic formats, were consulted to ensure the necessary basis and consistency for the research development.

The inspection covered the main building systems of the analyzed properties, including structural systems, façades, roofing systems, electrical installations, plumbing and sanitary systems, and common areas. The identified anomalies were classified according to their origin, nature, and level of criticality, considering criteria related to safety, performance, and potential impact on occupants.

The prioritization of interventions was carried out using a risk-based analysis approach, associating the severity of consequences with the probability of progression of the pathological manifestations. The analyzed data were obtained from a technical building inspection report prepared by a qualified professional, ensuring the reliability of the information used.

As a complementary outcome of the research, a set of technical guidelines was developed and structured in the form of a guidance manual, with the objective of assisting professionals in the identification, analysis, and prioritization of interventions in buildings affected by pathological manifestations.

3.1 Description of the Case Study

The case study refers to a medium-sized multifamily residential building, more than a decade old, constructed using a conventional reinforced concrete structural system. The building is in continuous use and lacks a documented history of systematic preventive maintenance. The inspected areas included façades, common areas, exposed structural systems, roofing systems, and accessible building installations. No destructive testing or laboratory evaluations were conducted, characterizing the inspection as predominantly visual in nature.

3.2 Results

The analysis of the pathological manifestations identified during the inspections revealed a predominance of problems related to water infiltration, accounting for 35% of the recorded occurrences. This was followed by cracking, representing 25% of the observed anomalies, corrosion processes, accounting for 15% of the occurrences, and other pathological manifestations, which represented the remaining 25%.

The most affected building systems were the façades, with 12 recorded anomalies classified as having high criticality, followed by roofing systems, with 8 occurrences classified as medium criticality, and structural systems, with 5 occurrences classified as critical.

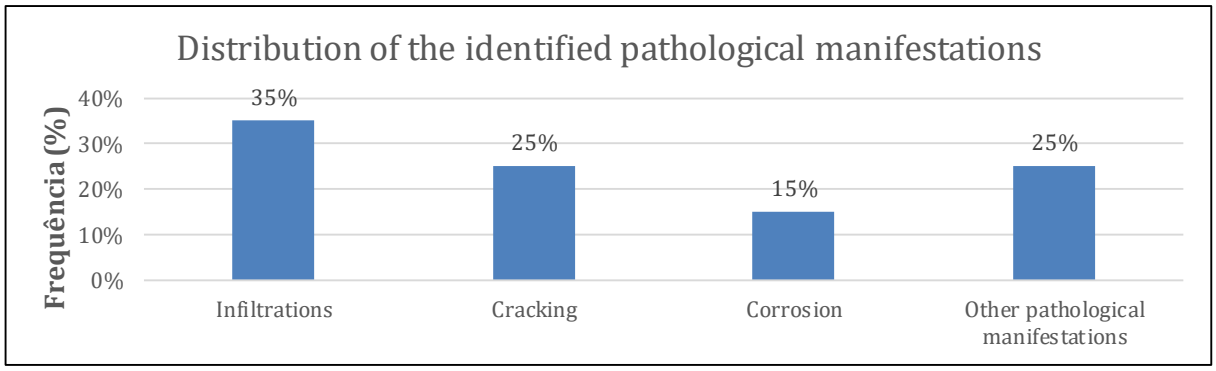
Based on the pathological manifestations identified during the building inspection, and considering that a significant proportion of buildings lack formal inspection records or systematic maintenance plans, a practical guide was developed for engineering and building inspection professionals. The purpose of this material is to assist in the technical diagnosis of anomalies, risk management, maintenance control, and decision-making support.

The practical building inspection guide was structured based on the analysis of technical reports and the recurrence of pathological manifestations observed in buildings, enabling the systematization of the main occurrences and their implications for the performance of building systems. This approach makes it possible to transform empirical data into technical guidelines applicable to professional practice.

Consequently, the guide contributes to the standardization of inspection and maintenance practices, promoting greater efficiency, safety, and reliability in interventions carried out on buildings.

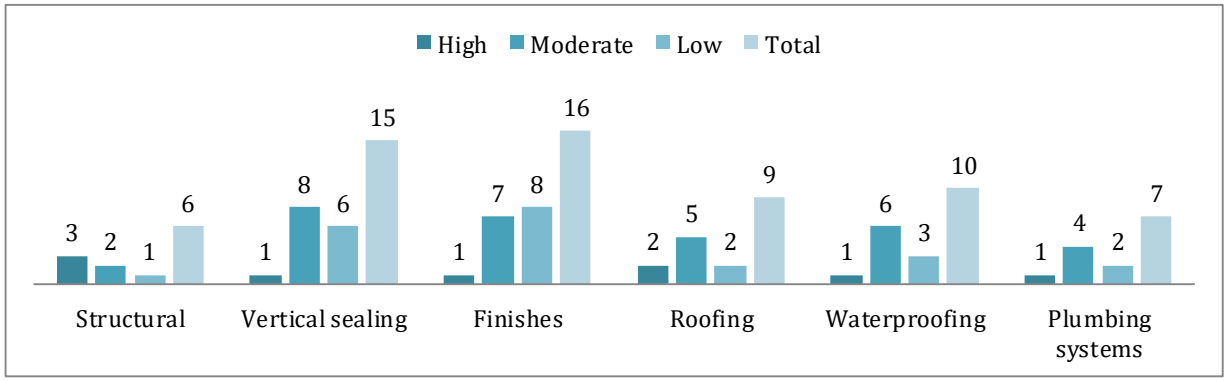
3.2.1 Analysis of Building Defects Identified in the Residential Building

Figure 1 – Percentage Distribution of Building Defects Identified During the Building Inspection



Water infiltration was identified as the most prevalent defect, accounting for 35% of the recorded occurrences, followed by cracking (25%) and corrosion-related deterioration (15%). The remaining defects collectively represented 25% of the anomalies identified during the inspection process.

Figure 2 – Distribution of Anomalies by Building System and Criticality Level



The analysis of the building inspection results revealed a predominance of pathological manifestations classified as having moderate criticality, accounting for 50.0% of the total recorded anomalies (34 occurrences). Low-criticality anomalies represented 33.8% of the occurrences (23 records), while those classified as high criticality corresponded to 16.2% of the total (11 occurrences).

It was observed that façade cladding and vertical enclosure systems exhibited the highest incidence of pathological manifestations, highlighting the need for both corrective and preventive maintenance actions in these components. On the other hand, although the structural and roofing systems presented a lower number of occurrences, they accounted for the majority of the anomalies classified as highly critical due to their potential risks to occupant safety, building stability, and the performance of building systems.

The results demonstrate that evaluating criticality in conjunction with the frequency of pathological manifestations constitutes a valuable tool for establishing intervention priorities. This approach enables maintenance resources to be directed toward the systems with the greatest potential impact on building safety, functionality, and durability..

3.2.2 Technical Guide for Residential Building Inspection

This manual aims to guide professionals in conducting comprehensive building inspections of existing residential buildings, enabling them to identify construction defects, assess the condition of building components, classify risks, propose technical interventions, and support the development of maintenance plans.

Table 1 – Stage 1: Inspection Planning

Scope definition	
Inspection Type (NBR 16747)	**Description**
Simple Visual Inspection Level (1)	It is a preliminary inspection based on visual observation and photographic records, conducted without the use of diagnostic equipment or destructive and non-destructive testing methods.
Detailed Visual Inspection Level (2)	It involves a more detailed visual inspection and may include the use of basic diagnostic equipment (such as moisture meters, crack gauges, and similar devices), as well as the analysis of technical documentation, including drawings, specifications, and operation and maintenance manuals.
Comprehensive Inspection Level (3)	It is the most comprehensive level of inspection, involving non-destructive testing, laboratory analyses, the use of advanced diagnostic equipment, and, when necessary, consultation with specialized experts.
Inspection Areas	Common Areas; Residential Units; Technical Areas.
Objective	General Diagnosis; Risk Assessment; Support for Rehabilitation Planning..
Documentary Review	
Documents	Design documents (architectural, structural, and building services drawings); Building operation and maintenance manual (ABNT NBR 14037); Maintenance history records (ABNT NBR 5674); Previous inspection reports or technical assessments; Building age.
Logistical Planning	
Description	Schedule access to residential units; Verify personal protective equipment (PPE) requirements (hard hat, gloves, safety boots, safety glasses, etc.); Prepare inspection equipment, including a camera, moisture meter, thermal imaging camera, measuring tape, crack gauge, level, and other necessary tools.

Table 2 – Stage 2: External Building Inspection

Areas	Inspect	Observations
Facade	Cracking (vertical, horizontal, and diagonal); Detachment of cladding or finishing materials; Efflorescence; Presence of vegetation; Condition of expansion joints; Deterioration of stonework elements.	Common Defects: Water infiltration through cracking; Concrete carbonation; Coating system failure.
Roof	Type (flat or pitched); Waterproofing condition; Presence of water ponding; Drains and drainage system; Cracks; Metal elements (corrosion).	Critical Attention: Water infiltration; Drainage system failures; Connections to vertical service risers.
Terraces and Balconies	Cracking; Improper slope (insufficient drainage gradient); Deterioration of flooring surfaces; Water infiltration; Guardrail systems.	
External Structural Elements	Exposed reinforcing steel; Reinforcement corrosion; Concrete spalling/delamination; Structural deformations.	

Table 3 – Stage 3: Internal Inspection of Common Areas

Areas	Inspect	Observations
Stairwell	Walls (moisture and cracking); Ceilings; ventilation and lighting conditions; Condition of surface finishes.	
Basements and Garages	Rising damp; Moisture ingress / water infiltration; Mold growth; Drainage system performance; Ventilation conditions.	
Technical Areas	Mechanical room; Water storage tanks; Electrical distribution boards; Service risers (vertical shafts).	

Table 4 – Stage 4 – Inspection of residential units

Areas	Inspect	Observations
Walls and Ceilings	Cracking; Moisture staining; Mold growth; Paint delamination/peeling..	
Kitchens and Sanitary Installations	Water infiltration; leakage; Ventilation and condensation; Condition of surface finishes.	
Openings (doors and windows)	Sealing performance; Water ingress; Degradation of window/door frames; Thermal bridging.	
Flooring	Detachment (or peeling) Cracking Deformations Moisture / Dampness	

Table 5 – Stage 5 – Inspection of building systems

Areas	Inspect	Observations
Structural system	Structural cracks; Deformations; Reinforcement corrosion	
Waterproofing system	Roof defects (or roofing failures); Infiltrations / Water ingress; Membrane deterioration	
Hydraulic system	Leaks; Inadequate pressure; Infiltrations / Water ingress	
Electrical system	Overloads; Electrical panels (distribution boards); Exposed wiring	

Table 6 – Stage 6 – use of instrumentation

Areas	Inspect	Observations
Thermography	Identify thermal bridges; Detect hidden infiltrations / concealed; water ingress.	
Moisture measurement	Identify rising damp; Assess critical levels.	
Crack gauge	Measure crack progression / crack development over time	
Other equipment	Level; Measuring tape; Lux meter (optional)	

Table 7 – Stage 7 – Identification and classification of pathologies

Type	Origin	Severity classification
Cracking; Infiltration / Water ingress; Corrosion	Design; Execution / Construction; Maintenance	Light; Moderate; Severe

Table 8 – Stage 8 – Analysis of causes

Type	Analysis	Observations
Relate the pathologies	Construction defects; Lack of Maintenance; Environmental factors; Improper use / Inadequate use.	

Table 9 – Stage 9 – Prioritization of interventions

Time for action	Classification and criteria	Priority level	Weight	Action
Immediate	Manifestations with an imminent risk to the physical integrity of users, to the structural stability of the building, or to the continuity of operation of essential systems.	Critical	5	Immediate intervention
Short term	Structural problems, severe infiltrations, detachment of materials, and safety risks.	High	4	Short-term intervention
Medium term	Non-structural cracks, deterioration of finishes, waterproofing failures, and localized infiltrations.	Moderate	3	Monitoring and scheduled corrective action
Long term	Aesthetic manifestations or low-progress defects, with no significant impact on safety or functionality.	Low	1	Preventive maintenance

Table 10 – Stage 10 – Explicit weighting criteria

Criticality Index (CI)	**Rating Scale**	
IC= P x I x U	Note	Description
Where: • P = Probability of progression; • I = Functional/structural impact; • U = Urgency of intervention.	1 2 3	Low Moderate High

Table 11 – Stage 11 – Preparation of the technical report

To be presented in the report	Property identification; Construction description; Methodology; Photographic record; Identified pathologies; Diagnosis; Risk analysis; Recommendations	**Observations**

Table 12 – Stage 12 – Maintenance plan

Proposed Maintenance	Preventive Maintenance; Corrective Maintenance; Schedule; Monitoring.	**Observations**

Table 13 – Stage 13 – Professional best practices

Guidelines	Comply with technical standards; Document all evidence; Use clear technical language; Maintain impartiality; Ensure safety during inspection.	**Observations**

Table 14 – Stage 14 – Practical checklist (operational summary)

CheckList	Planning; Document review; External inspection; Internal inspection; Systems assessment; Use of instruments; Diagnosis; Risk analysis; Prioritization; Report preparation.	**Observations**
Simplified Inspection Flow	Plan → Inspect → Diagnose → Classify risk → Intervene → Monitor	

From a practical perspective, the results contribute to the work of engineers, facility managers, and condominium administrators by providing a technical basis for the development of maintenance plans. The methodology presented can be replicated in other buildings, provided that their specific construction characteristics are taken into consideration. An effective building inspection requires a systematic, technical, and integrated approach that considers all building components and systems. Building pathology professionals should not only identify defects but, more importantly, interpret their underlying causes and implement measures to prevent risks, thereby ensuring safety, durability, and performance throughout the building's life cycle.

4. Conclusion

This study aimed to present and systematize the main stages of building inspection in existing buildings, highlighting its relevance as a technical tool for performance assessment. The objective was to demonstrate to building inspectors, facility managers, and other professionals in the construction industry that building inspection constitutes a fundamental instrument for analyzing risk factors associated with building safety, encompassing activities ranging from data collection and document verification to the technical responsibilities related to building maintenance management.

The results obtained corroborate previous studies that identify water infiltration as one of the most recurrent pathological manifestations in multifamily residential buildings, generally associated with waterproofing failures, sealant degradation, inadequate drainage systems, lack of preventive maintenance, and deficiencies in cladding systems. The high incidence of these occurrences in façades and roofing systems reinforces the need for periodic inspections and preventive maintenance programs focused on building enclosure and protection systems.

Furthermore, although the structural system exhibited a lower number of anomalies, its classification as critical demonstrates that risk assessment should not be based solely on the frequency of occurrences but also on their potential consequences for building safety and durability.

The findings presented are limited to the analysis of a single case study and therefore do not allow for absolute generalizations to other building typologies. Nevertheless, the proposed methodology demonstrates potential for replication in different contexts. The main contribution of this study lies in the development of a simplified methodology for prioritizing interventions based on building inspection and risk analysis.

The analysis clearly demonstrated that building safety is a cross-cutting issue involving all stakeholders in the construction process, from the design phase to maintenance management throughout the building's service life. In this regard, the importance of raising awareness and providing training for managers of multifamily residential buildings regarding the need for periodic inspections and the implementation of structured maintenance plans should be emphasized.

Building conservation represents an essential strategy for ensuring the proper functioning of building systems and minimizing the occurrence of defects. Building safety is directly related to the adoption of appropriate practices in design, construction, operation, and maintenance. Consequently, preventive action proves to be more effective than reactive approaches, making it inadequate to wait for pathological manifestations to appear before taking corrective measures. Therefore, periodic inspections, technical assessments, and continuous monitoring of building conditions are indispensable.

The adoption of a structured maintenance plan, combined with proper document management and systematic monitoring of building conditions, contributes significantly to the prevention of failures, the reduction of corrective intervention costs, and the extension of the service life of building systems.

In conclusion, when conducted through a structured methodology and guided by risk-analysis criteria, building inspection constitutes a strategic tool for the technical management of multifamily residential buildings, promoting greater safety, performance, and durability throughout their life cycle.

Bibliographic References

HELENE, Paulo; BOLINA, Fabricio L.; TUTIKIAN, Bernardo F. Patologia de estruturas. São Paulo: Oficina de Textos, 2019.

HELENE, P. Manual para reparo, reforço e proteção de estruturas de concreto. 2ed, São Paulo: Pini, 1992.

IBAPE/SP - Instituto Brasileiro de Avaliações e Perícias de Engenharia de São Paulo. Inspeção Predial /Checkup Predial: Guia da boa manutenção. 3ª ed. Editora Leud, São Paulo, 2005.

ASSOCIAÇÃO BRASILEIRA DE NORMAS TÉCNICAS. NBR 5674: Manutenção de edificações – Requisitos para o sistema de gestão de manutenção. Rio de Janeiro: ABNT, 2012.

ASSOCIAÇÃO BRASILEIRA DE NORMAS TÉCNICAS. NBR 15575: Edificações habitacionais – Desempenho. Rio de Janeiro: ABNT, 2013.

ASSOCIAÇÃO BRASILEIRA DE NORMAS TÉCNICAS. NBR 14037: Diretrizes para elaboração de manuais de uso, operação e manutenção das edificações — Requisitos para elaboração e apresentação dos conteúdos. Rio de Janeiro: ABNT, 2011.

SENA, G. O. et al. Patologia das Construções. 1ª ed. Editora 2B educação, Salvador, 2020.

ASSOCIAÇÃO BRASILEIRA DE NORMAS TÉCNICAS. ABNT NBR 16747: Inspeção predial — Diretrizes, conceitos, terminologia e procedimento. Rio de Janeiro: ABNT, 2020.

DEUTSCH, S. F. Perícias de Engenharia: A apuração dos fatos. 3ª ed. Editora Leud, São Paulo, 2016.

FARIAS, LMDE; MARINHO, JLA. Inspeção predial em edificações com manifestações patológicas: anamnese, diagnóstico, prognóstico e responsabilidades. In: XVII Congresso Internacional sobre Patologia e Reabilitação das Construções. Anais...Fortaleza: CINPAR. (2021).

MARTINS, Fabiano Battemarco da Silva; CAVALCANTE, João Carlos da Silva. Manifestações patológicas na construção civil: estudo de caso. Revista Tecnológica da UniversidadeSanta Úrsula, v. 5, n. 2, p. 79-100, (2022).

CARRARO, Carolina Lemos; DIAS, João Fernando. Diretrizes para prevenção de manifestações patológicas em Habitações de Interesse Social. Ambiente Construído, v. 14, p. 125-139, (2014).

ANTUNES, Giselle Reis. Estudo de manifestações patológicas em revestimento de fachada em Brasília-sistematização da incidência de casos. Diss. Mestrado, UnB, Brasília, (2010).

CARRARO, Carolina Lemos; DIAS, João Fernando. Diretrizes para prevenção de manifestações patológicas em Habitações de Interesse Social. Ambiente Construído, v. 14, p. 125-139, (2014).

ARAÚJO, Mariana Arruda. Perícia de engenharia na construção civil: análise patológica. Monografia (Especialização em Construção Civil) Universidade Federal de Minas Gerais, Belo Horizonte, (2021).

ASSOCIAÇÃO BRASILEIRA DE NORMAS TÉCNICAS. ABNT NBR 16636: elaboração e desenvolvimento de serviços técnicos especializados de projetos arquitetônicos e urbanísticos. Rio de Janeiro: ABNT, 2016.

ALVES, Victor F.; SIMEÃO, Gustavo D. S. Análise e viabilidade dos sistemas de impermeabilização rígido e flexível em edificações. Gama: UNICEPLAC, (2022).

IBAPE/SP – INSTITUTO BRASILEIRO DE AVALIAÇÕES E PERÍCIAS DE ENGENHARIA DE SÃO PAULO. Inspeção predial: check-up predial – guia da boa manutenção. 3. ed. São Paulo: Leud, (2005).

FARIAS, LMDE; MARINHO, JLA. Inspeção predial em edificações com manifestações patológicas: anamnese, diagnóstico, prognóstico e responsabilidades. In: XVII Congresso Internacional sobre Patologia e Reabilitação das Construções. Anais... Fortaleza: CINPAR. (2021).

TUTIKAN, B.; PACHECO, M. Inspeção, diagnóstico e prognóstico na construção civil. Boletim Técnico. ALCONPAT. México (2013).

cinpar2026
XXII International Conference on Building Pathology and Constructions Repair
15th to 17th July 2026 - Lisboa, Portugal

Automated large-scale sonic inspection of the northern façade of the Torre de la Vela in the Alhambra (Granada, Spain)

Javier ORTEGA[1], Fernando RAMONET[1], Pablo SANZ-HONRADO[1], Juan Carlos LIÉBANA[1], Sofía APARICIO[1], Javier SUÁREZ[2], Margarita GONZÁLEZ[1], José Javier ANAYA[1]

[1] Institute for Physical and Information Technologies (ITEFI), Spanish National Research Council (CSIC), Madrid, Spain, {javier.ortega; fernando.ramonet; pablo.sanz; juancarlos.liebana; sofia.aparicio; m.g.hernandez; jj.anaya}@csic.es
[2] Departamento de Mecánica de Estructuras e Ingeniería Hidráulica, Universidad de Granada, Granada, Spain, fjsuarez@ugr.es

Abstract: Sonic testing provides essential information about the internal condition of historical construction systems and materials, such as masonry and rammed earth walls. The method is fully non-destructive and is based on the emission of low frequency acoustic waves that are able to penetrate through thick construction elements. The analysis of the propagation characteristics of the sonic wave through a wall, e.g., sonic velocity, allows differentiating sound areas from deteriorated ones, or identifying inner voids. Nevertheless, sonic inspection is commonly carried out manually, which turns the process highly time consuming if the objective is to evaluate large areas of a building. Moreover, manual inspections are also limited to areas of the buildings that are accessible by hand, preventing the inspection of upper areas of the building with no access from the exterior.

The present paper shows the result of a large-scale sonic inspection of the upper part of the northern façade of the Torre de la Vela, in the Alhambra. The wall is made of rammed earth with visible cracks and alterations done with brick masonry. A Cable-Driven Parallel Robot was fabricated to automate the sonic emission from the exterior part of the tower. The sonic wave was received with accelerometers placed in the interior. An area of 13 m x 4 m, at a height of around 20 m above ground, was inspected. Automating the inspection resulted in a total of 168 emission points and 368 reception points, separated approximately 0.5 m between them, thus obtaining a dense coverage of the inspected area. The results illustrate the large variability in the inner conditions of the earthen wall in different areas of the façade. The presented on-site application and validation shows the potential of using highly automated systems for the inspection and structural diagnosis of the architectural heritage.

Keywords: Built heritage; non-destructive testing (NDT); sonic testing; cable-driven parallel robot; rammed earth.

1. Introduction

Non-Destructive Testing (NDT) is a fundamental tool for the on-site structural diagnosis of construction elements that guarantees their integrity without disrupting their functioning. This is particularly important for historical constructions, as there is a need to avoid any possible harm to the original material during inspection. Among NDT techniques, sonic testing is particularly widespread for historical masonry elements. The propagation of sonic waves through, for example, thick masonry walls, varies according to their internal condition. Thus, the analysis of sonic wave propagation characteristics, e.g., velocity, through a wall, allows detecting deteriorated areas, identifying inner voids or cracks or evaluating their inner morphology (Leucci *et al.* 2011; Valluzzi *et al.* 2018; Luchin *et al.* 2020).

However, most NDT techniques, including sonic testing, usually have an important limitation. They were initially conceived for localized inspections and are carried out manually. As a result, enlarging the scale of inspection to large areas of a building, such as a full façade, becomes impossible in practical terms due to time constraints. More so, if the aim is to evaluate upper areas of the building that are out of reach for manual inspections, unless considering the use of supplementary structures like scaffolding.

This limitation can be addressed through the development of robotic systems. These systems require automating the robot movement, precise positioning and ensuring good quality signal emission. The present paper aims to show the results obtained with a novel Cable-Driven Parallel Robot (CDPR) system developed to carry out sonic testing in large vertical surfaces, such as building façades. Its functioning (movement, repetition, speed, signal emission quality, etc.) was tested at the *Torre de la Vela*, the tallest and most emblematic rammed earth tower in the *Alcazaba* of the *Alhambra*, in Granada (Spain).

The upper part of the northern façade was inspected using the CDPR. The wall is made of rammed earth and shows cracks and alterations done with brick masonry. The automated system allowed inspecting an area of approximately 13 m x 4 m (length x height), at a height of 20 m above the ground. The objective was to collect enough data to carry out the tomographic reconstruction of the portion of the façade inspected, which requires a dense coverage of the inspected area with multiple emission and reception positions.

The present paper first introduces the concept and principles of tomographic reconstruction based on sonic data. Then, the test method and setup are presented, including a brief introduction of the CDPR and its development. Finally, the results obtained are shown and discussed, which include 3D tomographic images and illustrate the high spatial variability in the inner conditions of the earthen wall across the portion of the façade evaluated.

2. Principles of tomographic reconstruction

The procedure used for sonic inspection is based on the transmission method. Sonic waves propagate from one surface of the wall to the opposite one. In practical terms, the test consists of introducing mechanical energy into the solid by means of an impact generated on one of its surfaces. The energy propagates through the solid as elastic waves, and a receiver, e.g., an accelerometer located at another point in the solid, records the signal. For each emitter (impact) and receiver position, i.e., each emitter-receiver pair, the time of flight can be calculated, and, since the distance between them is known, the velocity of propagation can also be estimated. This velocity depends on the physical and mechanical properties of the solid, such as density and modulus of elasticity. However, the velocity estimated by this method also depends on the internal condition of the solid. The existence of cracks or voids within a solid will cause the wave path to deviate from the straight line between the emission and reception coordinates assumed for the calculation, which means that the estimated velocity decreases. Lower velocities are thus generally associated with material deterioration and the presence of cracks or material discontinuities within the structure. That is why sonic tests are particularly useful for evaluating the degree of homogeneity of historic structures, such as the rammed earth walls of the *Torre de la Vela*.

When sonic tests are performed manually, the inspection is usually focused on specific areas. Localized measurements can detect isolated internal defects, but they are not always representative of the highly heterogeneous cross-sections that characterize historic building elements. Sonic tomography can be used to obtain a more detailed graphic representation of the interior, but it requires multiple emitter-receiver pairs to generate a large number of intersecting sonic rays that penetrate the material from different angles.

The results of a tomographic inspection are *N* sonic rays that intersect at different angles, covering a volume defined by the inspection window. There are various tomographic reconstruction methods that allow obtaining images of the interior of masonry elements based on acoustic (sonic or ultrasonic) wave propagation data (Fais and Casula 2010; Zielińska and Rucka 2018; Matías *et al.* 2021). Most methods are based on discretizing the inspected volume into a specific number of voxels. Each voxel is traversed by a

varying number of rays. A value of velocity is assigned to each voxel based on the information from the traversing rays. For example, the Simultaneous Iterative Reconstruction Technique (SIRT) (Kaks and Slaney 2001), estimates the velocity by solving iteratively a system of equations constituted by as many equations as rays resulting from the inspection. Each equation multiplies a slowness value (defined as the inverse of the velocity) in each voxel by the distance traversed by the ray within this voxel. The sum of all the times computed for all voxels traversed by the ray should be equal to the total time of flight of this ray. The iterative process followed to solve such system of equations continues until convergence is reached, i.e., when the calculated times of flight of all rays match the measured times within a predefined margin of error.

In the present paper, the reconstruction method adopted involves assigning to each voxel a value of velocity that is the median of the estimated velocities of all sonic rays passing through that voxel. To minimize the impact of outliers, the median value is used instead of the average. Given the significant variability in the distances between emitters and receivers used for this calculation, the median is weighted, giving greater weight to the velocities calculated for rays traveling shorter distances. The aim is to minimize the greater uncertainty in calculating the velocity for longer rays. It should be noted that, in the present case study, some emitter-receiver distances can exceed 5 m, while the wall thickness is approximately 1.6 m. Finally, to smooth the transition between voxels, the values are adjusted by averaging them with neighbouring voxels.

Obtaining a velocity value for each voxel within the volume, allows reconstructing tomographic images in 3D and obtaining a point cloud of velocity values within the volume, i.e., an inner 3D point cloud. This point cloud can be combined with the 3D point cloud obtained, for example, from a photogrammetric reconstruction, i.e., the exterior 3D point cloud. The integration of both point clouds can help in the interpretation of the results by associating superficial and inner information of the inspected element.

The resolution of the tomographic reconstruction depends on the number of rays. A greater number of rays allows for a smaller voxel size, as there will be more intersecting rays per voxel. Consequently, the resolution of the reconstructed image will be higher. This effect is illustrated by the diagram in Figure 1, representing a 1 x 1 x 1 m inspected volume. Aiming for a tomographic reconstruction, there is a need for intersecting rays that a direct sonic test inspection cannot provide (Figure 1a). Increasing the number of emission and reception points, and, therefore, the number of rays, allows obtaining a denser coverage of the inspected volume, resulting in a higher-resolution tomographic image. For example, if the same voxel size division was used for the two cases displayed in Figure 1b and 1c, the low-resolution case (Figure 1b) could contain voxels with no information (with no rays traversing them).

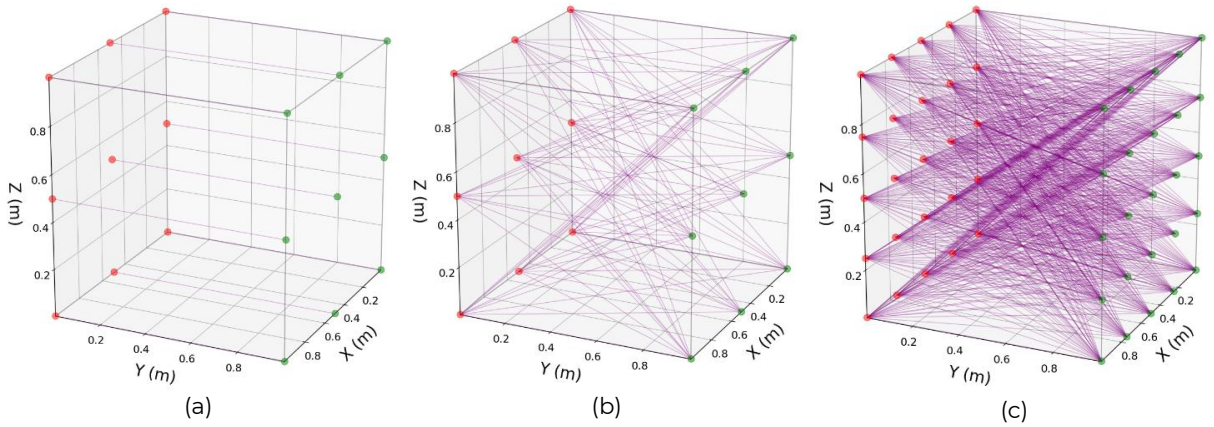


Figure 1 – Tomographic resolution based on the number of rays: (a) only direct transmission rays; (b) low resolution grid (c) high resolution grid

The preceding graphs demonstrate that generating a tomographic image requires a large number of rays to adequately cover a representative volume of the wall. For this reason, sonic inspection for tomographic imaging is difficult to implement in practice if it is done manually, as it becomes highly time-consuming.

For this technique to be viable, automated systems are necessary. Automating sonic tomography inspections allows to increase the resolution in a region of interest simply by increasing the number of sampling points in the area where a relevant structural anomaly or irregularity has been detected. Furthermore, automating the inspection also allows increasing the scale of inspection, moving from local inspections to large areas (e.g., an entire facade).

3. Inspection methodology

The robotic inspection system was tested at the *Torre de la Vela*. Figure 2 shows the inspection area over an orthophoto of the north façade, obtained from a photogrammetric survey. The tower has a square floor plan measuring 16 meters on each side and is 26.8 meters high. The elevation of the north façade shows that it is constructed with two materials: rammed earth as the original material and brick masonry, likely used for repairs. The interior of the wall is whitewashed. The inspection area has a total extent of 12.7 m wide x 3.5 m high (marked in red in Figure 2). Within this area, there are repair patches made with brick masonry, specifically the entire area above the window, and several vertical cracks visible from the exterior.

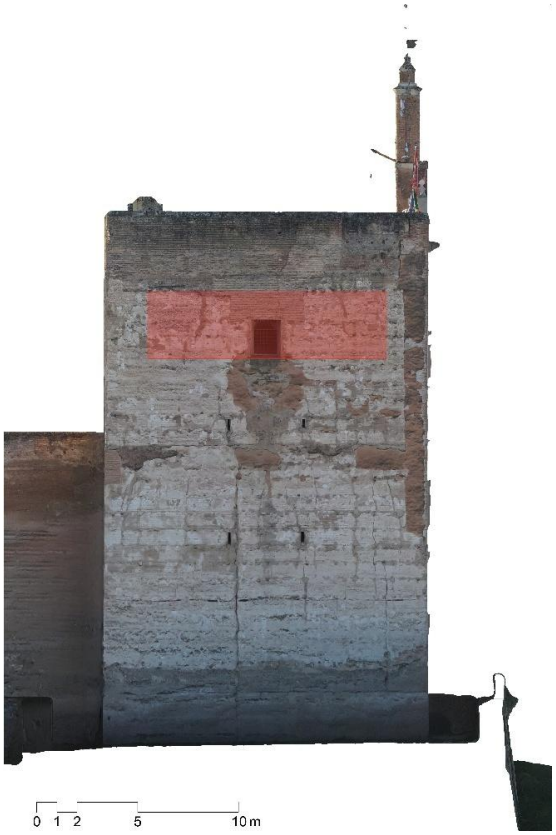


Figure 2 – Orthophoto of the north façade of the *Torre de la Vela* with the inspection area marked in red.

3.1 Robotic system

The system is a CDPR that allows moving an automatic mechanical hitting device, capable of generating controlled acoustic waves, throughout a large area using pulleys, cables and motors. A detailed description of the system can be found in Ramonet *et al.* (2026). In summary, the hitting system is a solenoid with a vibration sensor that records the emission signal (see details in Ortega *et al.* 2024). The system (Figure 3a) is installed on a vertical frame suspended by cables and pulleys that are placed on the top corners of the façade. To ensure contact of the hitting system with the wall during operation, the system incorporates two drone propellers that, when activated, push the frame against the surface (Figure 3b).



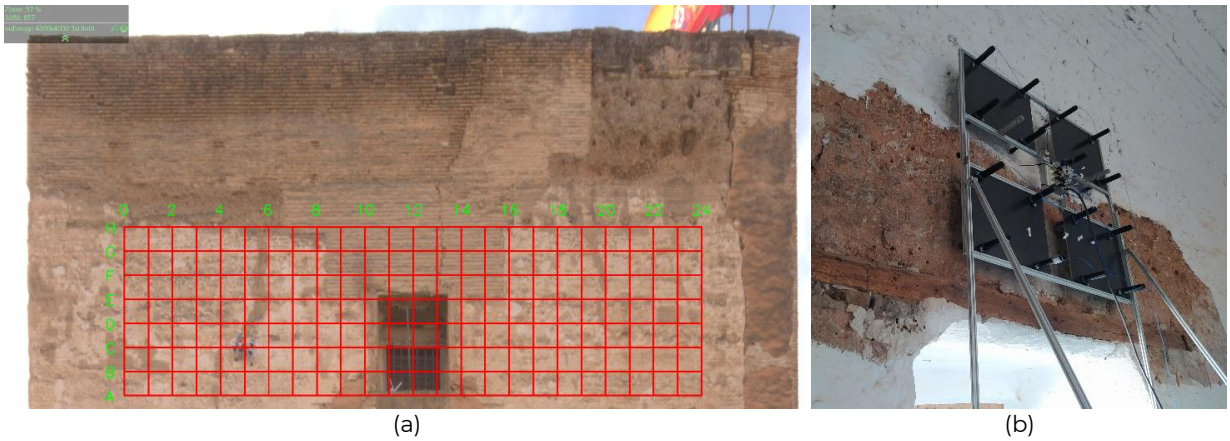
(a) (b)

Figure 3 – (a) CDPR suspended at *Torre de la Vela*; and (b) close view of the suspended frame with hitting system

3.2 Test setup

The reception system is a matrix of 16 accelerometers that is placed in the interior of the tower, at the opposite surface of the inspected wall. The testing procedure involved the CDPR going through a predefined inspection grid while the reception system is kept at a fixed position. The reception system is then manually moved to a different position, and the CDPR robot moves through the inspection grid again. This process was repeated as many times as positions are defined for the reception system.

The emission grid is shown in Figure 4a and consists of a uniform reticular grid with a spacing of 0.5 m. The grid has a total of 25 columns and 8 rows. The emission system can move automatically throughout all points defined by the grid. For remote control and monitoring, a camera was installed outside the tower that transmitted video via videoconference. A code was developed for real-time correction of the image perspective, eliminating distortion, creating parallel lines, and enabling measurements by superimposing the reference grid shown in Figure 4a to the video. The code was developed using Adaptive Vision Studio 5.1 software, based on OpenCV. This system allowed for real-time visualization of the robot's movement and the recording of its exact position during each phase of the inspection and at the exact moment of impact, which is essential for CDPR control and subsequent tomographic reconstruction. This system guaranteed a full control of all emission and reception coordinates at all times during the inspection.



(a) (b)

Figure 4 – (a) Emission grid with CDPR placed on point 5C; and (b) example of positioning of reception system

The reception system was placed in 23 different positions to cover a similar area on the opposite wall surface. Figure 4b shows an example of the reception system, positioned in the area above the façade window. The 16 accelerometers can measure simultaneously. Thus, the total number of reception points is 368 (23 x 16). It is noted that, for each position of the reception system, the emission system did not go through all columns defined in the grid of Figure 4a. Depending on the position of the reception system, only a number of columns on either side of that position were inspected, with the aim of ensuring that no distance between the emitter and the receiver exceeded 5 m. For example, for the receiving positions closest to column 24, only columns 16-24 were inspected.

The total number of transmitter-receiver pairs resulting from this inspection setup was 22,384. For each pair, 10 sonic signals were emitted (10 hits per emission point), so the number of measurements taken was 223,840. These numbers again demonstrate the impossibility of carrying out this inspection without automated systems. The inspection took approximately 12.5 hours, spread over three mornings. System setup and testing took another morning (approximately 5 hours), while the removal of the system, clean up and pick up of all devices took approximately 2 hours on the last day of the inspection. The large amount of data generated also highlights the importance of automating signal processing to obtain the results that will be shown in the next section. It is also important to note that not all transmitter-receiver pairs resulted in signals of sufficient quality. Occasionally, due to possible decoupling between the accelerometers and the wall surface, impact failure, or lack of transmission between the emitter and receiver points, some sonic waves were not received or the noise was greater than the signals. After eliminating those signals that could not be processed, the total number of valid emitter-receiver pairs for processing was 16,076. Figure 5 shows the rays coverage of the inspected area (the figure shows only 5,000 of the 16,076 total rays for readability). The reception points are marked in green and correspond to the 23 positions of the system. The emission points are marked in red. These points varied slightly with respect to the position of the grid. The use of the camera, capable of recording the exact position of the system in real time, allowed for obtaining the exact coordinates of each emitter point.

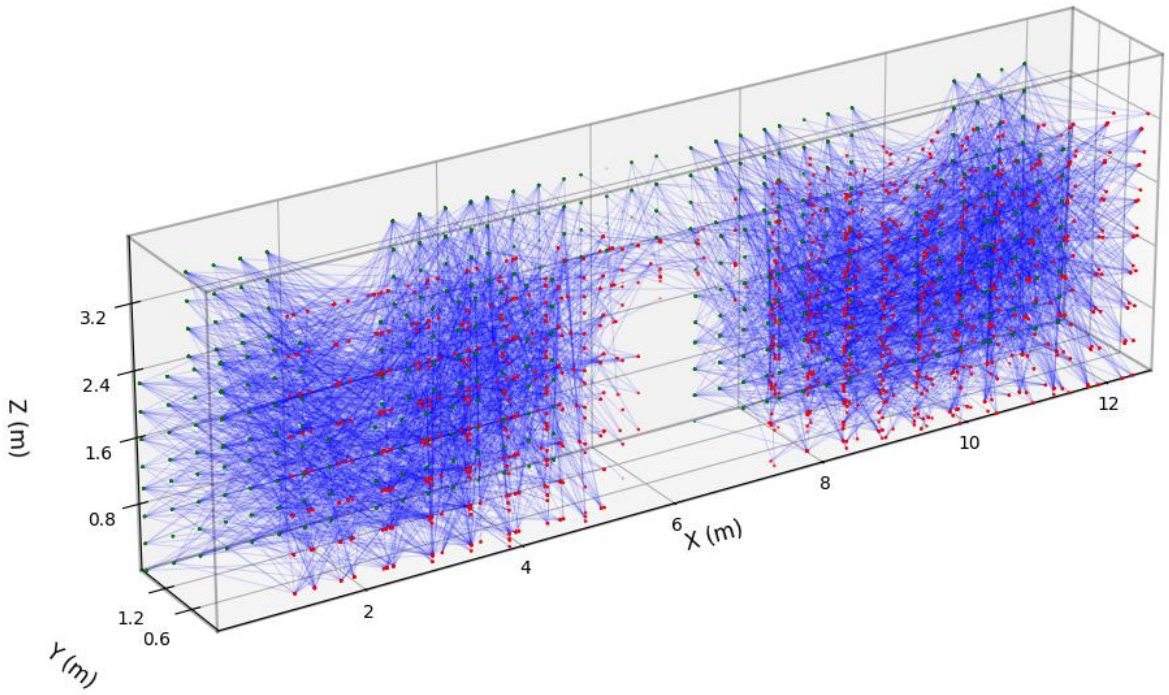


Figure 5 – Sonic rays (selection of 5,000 out of the total of 16,076) generated during the inspection at *Torre de la Vela*. Emission points at the exterior are marked in red while reception points in the interior are marked in green

As previously mentioned, the resolution of a tomographic image depends largely on the number of rays passing through each voxel. Figure 6 shows a 3D representation of the ray coverage density per voxel, for a voxel size of 0.2 m. Each voxel is marked with a sphere at its centroid, and the colour indicates the number of rays passing through it. There is a high number of rays per voxel in the two central areas at both sides of the window, consistently above 10, and in some cases exceeding 20 rays per voxel. In those areas near the perimeter of the inspection area, the density decreases. Nevertheless, most voxels are traversed by a minimum of 5 rays.

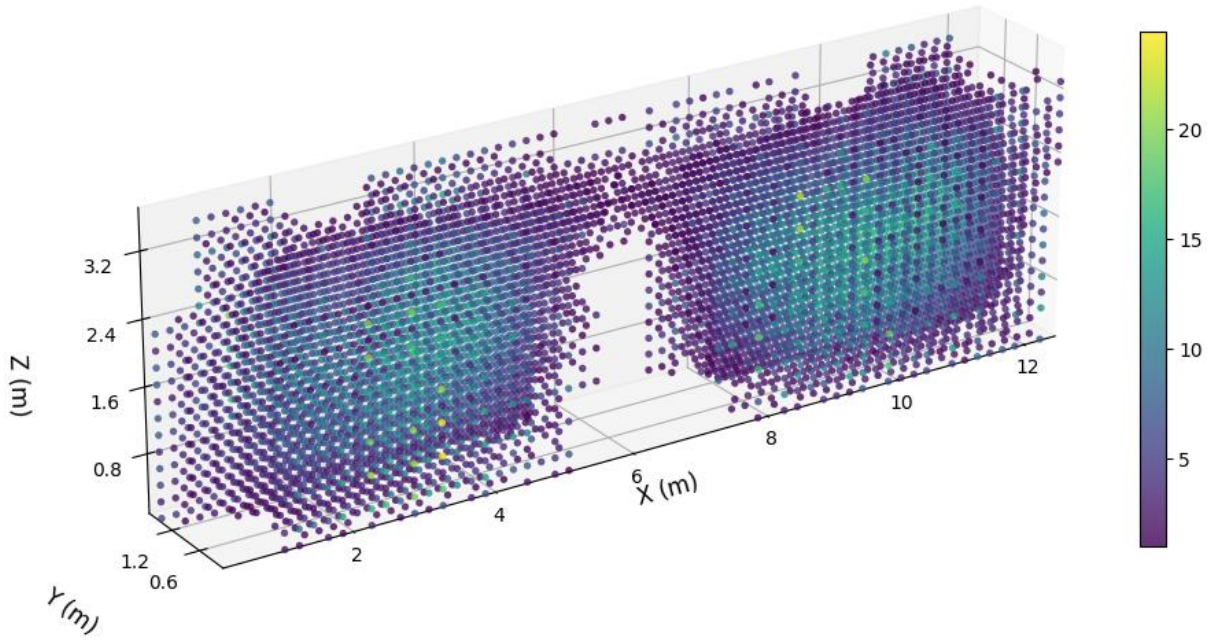


Figure 6 – Ray coverage density per voxel (scale indicates the number or rays per voxel)

4. Results and discussion

Using the tomographic reconstruction procedures described previously, 3D images of the inspected area in the tower were generated. The reconstructions provide a smeared (and smoothed) spatial distribution of velocities across the inspected volume. Voxels with constant velocity values can be joined in the visualization to form iso-surfaces, delimiting homogeneous areas. The iso-surfaces represent velocity variations throughout the volume, offering valuable information about the interior of the structure by dividing the volume into areas with poor or good sound transmission.

The tomographic reconstruction of the inspected volume in the Torre de la Vela is shown in Figure 7, using a velocity range between 500 (red) and 1,400 m/s (blue). The reconstructed volume shows areas of significant variability in terms of velocity. The lowest recorded velocities (< 500 m/s) are found in the upper central section (above the window). This area coincides with the brick masonry patch visible from the exterior. In the interior of the tower, this area is constructed of rammed earth, thus indicating that the repair must have an unknown thickness within the wall. The inner interface between rammed earth and brick masonry is likely the reason for the poor sonic transmission in this area.

On both sides of the window, greater homogeneity is observed, with less extreme variations. The highest velocities are recorded in the lower half of both areas, reaching up to 1,700 m/s in some localized zones. Velocities decrease in the upper half. In particular, there is a vertical band in the middle of the left panel where velocities drop below 1,000 m/s. Similarly, almost symmetrically, in the middle part of the right panel, estimated velocities decrease in the upper half.

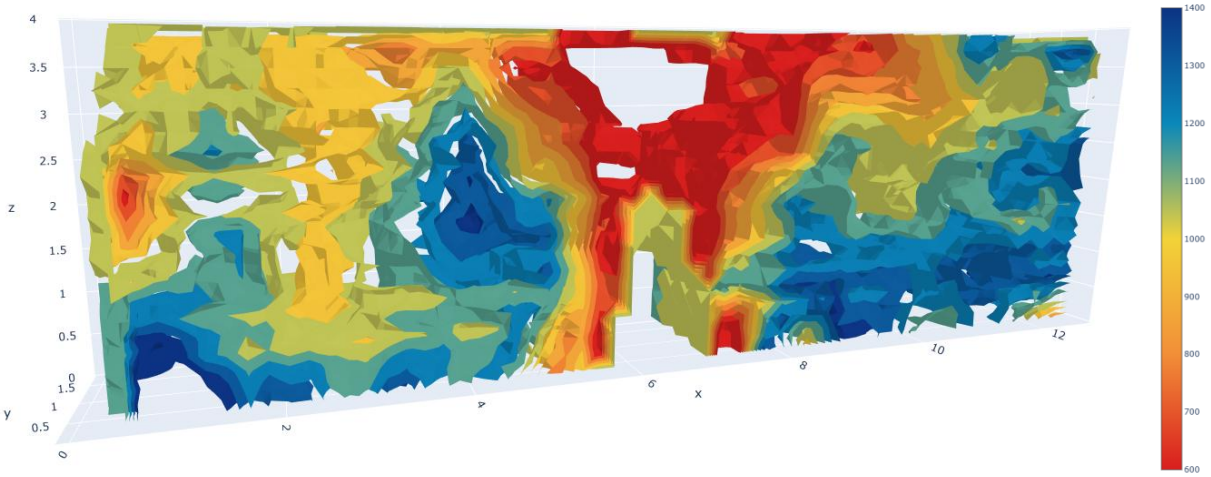


Figure 7 – 3D tomographic reconstruction of the interior of the inspected area at *Torre de la Vela*, based on iso-surfaces (dimensions in m and values of velocity in m/s)

Overlaying the tomographic reconstruction with the photogrammetric 3D point cloud of the Torre de la Vela helps to validate the observations made. Figure 8 shows the combination of the tower's exterior point cloud, the interior point cloud (both obtained by photogrammetry), and the inner point cloud of the inspected wall, resulting from the sonic tomography.

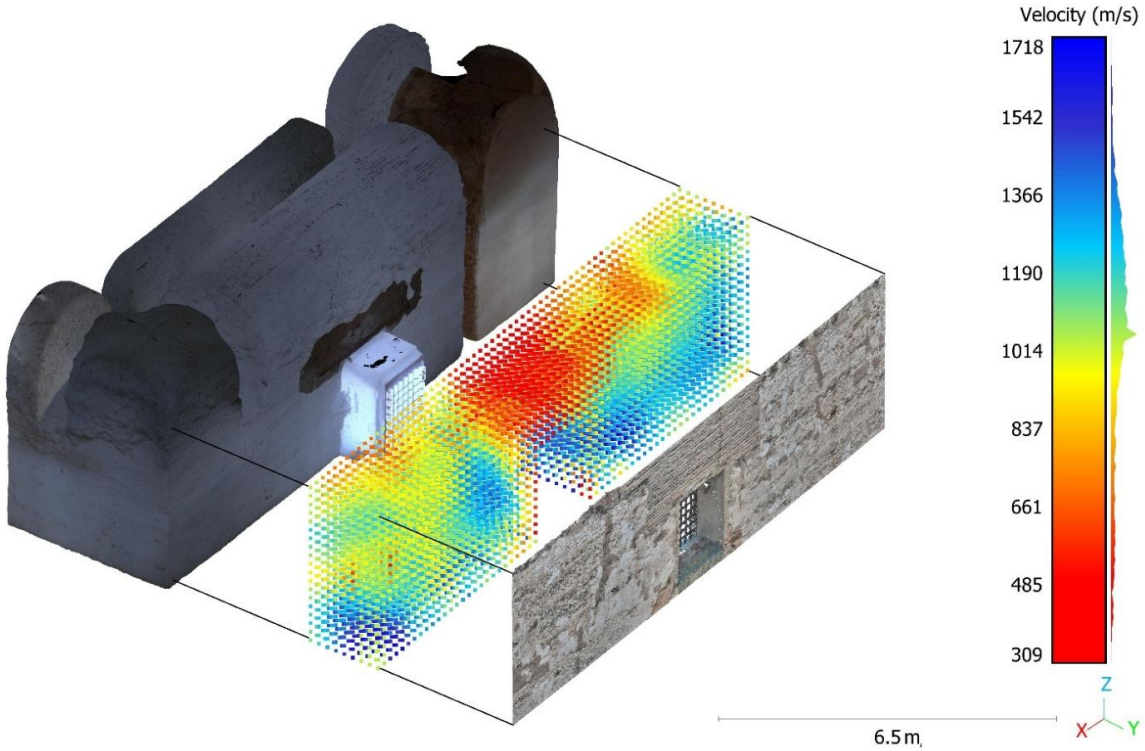


Figure 8 – Combination of the 3D point cloud obtained from the photogrammetric survey and the inner point cloud obtained from the tomographic reconstruction of the inspected area at the *Torre de la Vela*

Regarding the velocities obtained, the average velocity within the inspected area was 970 m/s, the median was 925 m/s, and the standard deviation was 350 m/s (coefficient of variation of 36%). Results show high heterogeneity, revealing variations in terms of material, but also in terms of internal conditions, such as the presence of cracks running through the wall.

Figure 9 shows a detail of the 3D point cloud, with a perspective view of the tower's north elevation from the outside. The first image shows the photogrammetric point cloud. The second image shows also the inner point cloud obtained from the tomographic reconstruction, but only displaying (in red) those points with a velocity lower than the median velocity (970 m/s). These points correspond to areas with poor sound transmission and may correspond to deteriorated areas or highlight the presence of structural discontinuities (e.g., cracks). The images show good correlation between both point clouds, between the areas with lower velocities and the damage (or alterations) visible from the outside. As previously mentioned, a high density of low-velocity points is observed above the window, which is made of a different material and exhibits vertical cracks. On both sides of the window, at x = 3 m and x = 10 m (according to the coordinate system used in Figure 7), there are two vertical cracks in the rammed earth wall that correspond well to the decrease in velocities observed in those areas. The 3D reconstruction indicates that these cracks are not superficial and extend through the wall. These results aim to demonstrate the potential of combining both techniques to aid in the interpretation of the findings.



Figure 9 – Perspective view of a detail of the façade comparing the point cloud obtained from the photogrammetry (left) and adding the point cloud from the tomographic reconstruction, showing (in red) only those points with velocities lower than the median (v < 970 m/s) (right)

5. Conclusions

The results of the sonic inspection carried out at the *Torre de la Vela* of the *Alhambra* demonstrate the potential of automating inspection systems for the characterization of historical buildings. The large amount of data that can be collected using these systems allows for the creation of 3D tomographic images of the interior of the rammed earth walls. These images provide qualitative information about large structural elements, locating and delimiting deteriorated areas, identifying potential cracks and their extent, and distinguishing between different building materials.

The inspections carried out covered an area of approximately 13 x 4 meters. The results showed that, for this type of historical constructions, variations in the internal condition of the wall can be significant. Assuming that the material properties are uniform throughout the wall can lead to a conservative analysis (if material properties are based on the results obtained in the most deteriorated areas, for example), which may result in a more invasive intervention on the heritage site than necessary. Conversely, assuming average or upper-range properties could lead to overlooking potentially more deteriorated areas and overestimating the structural capacity of the building. Scaling up the inspection to the entire building or large elements, such as the façade, allows for more detailed structural analyses that can inform localized interventions targeted at specific areas.

Overlaying tomographic images with point clouds obtained from photogrammetry aids in the interpretation of the results. Combining both techniques allow for the precise location and delimitation of the most deteriorated areas, as well as the correlation of internal information with surface data visible from the outside.

Acknowledgments

The team acknowledges the '*Patronato de La Alhambra y Generalife*', for the access granted to the Alhambra and the active collaboration during the project. The publication is part of the MeDeAH project PID2022-140071OB-C21, funded by MCIN/AEI/10.13039/501100011033/FEDER, EU. Pablo Sanz's pre-doctoral contract is funded by MCIN/AEI/10.13039/501100011033/FEDER, EU and ESF+. Project supported by a 2024 Leonardo Grant for Scientific Research and Cultural Creation from the BBVA Foundation (The BBVA Foundation accepts no responsibility for the opinions, statements and contents included in the project and/or the results thereof, which are entirely the responsibility of the authors).

References

Fais, Silvana, and Giuseppe Casula. 2010. "Application of acoustic techniques in the evaluation of heterogeneous building materials." NDT & E International 43 (2): 62–69. https://doi.org/10.1016/j.ndteint.2009.10.004.

Kaks, Avinash C., and Malcolm Slaney. 2001. "Principles of Computerized Tomographic Imaging." Classics in Applied Mathematics 33. Society for Industrial and Applied Mathematics (SIAM), Philadelphia, USA. https://doi.org/10.1137/1.9780898719277.

Leucci, Giovanni, Nicola Masini, Raffaele Persico, and Francesco Soldovieri. 2011. "GPR and sonic tomography for structural restoration: the case of the cathedral of Tricarico." Journal of Geophysics and Engineering 8 (3): S76–S92. https://doi.org/10.1088/1742-2132/8/3/S08.

Luchin, Guillermo, Luís F. Ramos, and Michele D'Amato. 2020. "Sonic Tomography for Masonry Walls Characterization." International Journal of Architectural Heritage 14 (4): 589–604. https://doi.org/10.1080/15583058.2018.1554723.

Matias, Manuel, Fernando Almeida, Rui Moura, and Nuno Barraca. 2021. "High resolution NDT in the characterization of the inner structure and materials of heritage buildings walls and columns." Construction and Building Materials 267, 121726. https://doi.org/10.1016/j.conbuildmat.2020.121726.

Ortega, Javier, Marnix F.L. Meersman, Sofía Aparicio, Juan Carlos Liébana, Rodrigo Martín, José Javier Anaya, and Margarita González. 2023. "An automated sonic tomography system for the inspection of historical masonry walls." Open Research Europe 3 (60). https://doi.org/10.12688/openreseurope.15769.1.

Ramonet, Fernando, Javier Ortega, Pablo Sanz-Honrado, Sofía Aparicio, Margarita González, Francisco Javier Suárez, Juan Carlos Liébana, and José Javier Anaya. 2026. "Automated Sonic Inspections for Heritage Infrastructures Using a Cable-Driven Robotic System." In: Saloustros, S., Beyer, K. (eds) Structural Analysis of Historical Constructions. SAHC 2025. RILEM Bookseries, vol 68. Springer, Cham: 936-947. https://doi.org/10.1007/978-3-032-16767-5_74.

Valluzzi, Maria Rosa, Elvis Cescatti, Giuliana Cardani, Lorenzo Cantini, Luigi Zanzi, Camilla Colla, and Filippo Casarin. 2018. "Calibration of sonic pulse velocity tests for detection of variable conditions in masonry walls." Construction and Building Materials 192: 272–286. https://doi.org/10.1016/j.conbuildmat.2018.10.073.

Zielińska, Monika, and Magdalena Rucka. 2018. "Non-destructive assessment of masonry pillars using ultrasonic tomography." Materials 11 (12), 2543. https://doi.org/10.3390/ma11122543.

COMPORTAMIENTO SÍSMICO DE ESTRUCTURAS PREFABRICADAS EXISTENTES

Estrella Torres García[1], Bertha Alejandra Olmos Navarrete[2], José Manuel Jara Guerrero[3], Guillermo Martínez Ruiz[4]

[1]Universidad Michoacana de San Nicolás de Hidalgo, Michoacán, México, 1612397c@umich.mx
[2]Universidad Michoacana de San Nicolás de Hidalgo, Michoacán, México, bertha.olmos@umich.mx
[3]Universidad Michoacana de San Nicolás de Hidalgo, Michoacán, México, jose.jara@umich.mx
[4]Universidad Michoacana de San Nicolás de Hidalgo, Michoacán, México, guillermo.martinez@umich.mx

Abstracto: Las estructuras prefabricadas de concreto han experimentado un crecimiento significativo a nivel mundial debido a sus ventajas constructivas y económicas, especialmente en edificaciones industriales, comerciales y residenciales; sin embargo, su desempeño sísmico ha mostrado una respuesta variable a lo largo de la historia. Eventos como el terremoto de Tangshan, China (1976), evidenciaron colapsos masivos del orden del 85% en zonas de máxima intensidad, lo que reveló la alta vulnerabilidad de sistemas con detalles sísmicos deficientes. Posteriormente, sismos como Armenia (1988), Northridge (1994), Wenchuan (2008), L'Aquila (2009), Turquía (2011), Emilia (2012) y Kaikoura (2016) confirmaron que las principales fallas en edificios prefabricados existentes se concentran en las conexiones entre los elementos. Entre las deficiencias más recurrentes se identifican las losas alveolares simplemente apoyadas sin anclaje adecuado, la ausencia de capa de compresión colada en sitio, la falta de continuidad del refuerzo y las conexiones incapaces de transmitir momento o fuerzas cíclicas significativas. Estas condiciones han provocado comportamientos frágiles, pérdida del apoyo de los elementos horizontales y, en algunos casos, colapsos progresivos. Por otro lado, la evidencia también muestra casos de desempeño satisfactorio cuando existen detalles estructurales adecuados. Durante la secuencia sísmica de Canterbury (2010–2011), varios edificios prefabricados presentaron un comportamiento satisfactorio; de igual manera, las estructuras prefabricadas presforzadas mostraron un desempeño sobresaliente durante el sismo de Kobe (1995). Estos antecedentes sugieren que el comportamiento sísmico no depende del sistema prefabricado, sino del diseño adecuado de las conexiones y de la continuidad estructural. El presente trabajo investiga y analiza la evidencia documentada del comportamiento sísmico de estructuras prefabricadas existentes. Las conclusiones explican con claridad las principales vulnerabilidades de las estructuras prefabricadas y los factores que han tenido mayor influencia en su respuesta sísmica, con un enfoque especial en el desempeño sísmico de las conexiones empleadas en los casos analizados.

Keywords: Concreto prefabricado, comportamiento sísmico, conexiones prefabricadas, estructuras existentes.

1. Introducción

Las estructuras prefabricadas de concreto han sido ampliamente utilizadas desde mediados del siglo XX debido a sus ventajas en rapidez constructiva, control de calidad y eficiencia económica, Fib (2003). No obstante, su desempeño sísmico ha sido objeto de debate, en particular en edificaciones existentes diseñadas sin criterios específicos para acciones sísmicas.

Diversos terremotos han evidenciado que las fallas en estas estructuras se concentran principalmente en las conexiones entre elementos, más que en los propios elementos prefabricados, Karuma *et al.* (2018). En

este contexto, estudios posteriores han señalado que la falta de continuidad estructural y la incapacidad de las conexiones para transmitir fuerzas cíclicas constituyen las principales fuentes de vulnerabilidad, *Wood et al. (1993).*

El objetivo del presente trabajo es realizar un análisis crítico del comportamiento sísmico de estructuras prefabricadas existentes, identificando patrones comunes de falla y los factores estructurales que rigen su respuesta.

2. Evidencia sísmica y evolución del comportamiento estructural

Las estructuras prefabricadas de concreto han sido ampliamente utilizadas desde mediados del siglo XX en países como Japón, China, Nueva Zelanda, Italia y Estados Unidos, debido a sus ventajas constructivas y de control de calidad. Sin embargo, su desempeño sísmico ha sido históricamente cuestionado, principalmente por deficiencias en el diseño y la ejecución de las conexiones (Fib 2003).

En los primeros eventos sísmicos relevantes, como el terremoto de Tangshan (Ms 7.8, 1976), se registraron colapsos generalizados en edificaciones que incorporaban elementos prefabricados, en particular sistemas de losas de concreto apoyadas sobre muros con escasa o nula conexión entre los elementos. La ciudad se ubicaba en una zona donde no se requería diseño sísmico, por lo que estas estructuras fueron concebidas únicamente para resistir cargas gravitacionales (Housner *et al.* 2002).

En consecuencia, los elementos horizontales dependían del apoyo por contacto, sin garantizar la transferencia de fuerzas laterales ni la continuidad estructural. Durante el sismo, la ausencia de conexión entre diafragmas y elementos verticales provocó la pérdida de soporte de las losas y fallas frágiles en los muros, lo que activó mecanismos de colapso progresivos. Este evento marcó un punto de partida al impulsar la investigación sobre las conexiones en sistemas prefabricados.

Posteriormente, el sismo de Armenia (1988) mostró colapsos en edificaciones prefabricadas de mediana altura, conformadas por muros prefabricados que actuaban como elementos principales tanto para cargas verticales como para cargas laterales, junto con losas prefabricadas que formaban los diafragmas de piso. A pesar de esta configuración, el sistema no logró adoptar un comportamiento monolítico debido a la deficiente capacidad de sus conexiones. Las uniones entre muros presentaban baja resistencia y escasa ductilidad, lo que impedía la adecuada transmisión de las fuerzas sísmicas (Wood *et al.* 1993).

En Northridge (Mw 6.8, 1994), a pesar de existir normativa sísmica avanzada, se observaron fallas importantes en estacionamientos prefabricados. Estas fallas no se debieron a la resistencia de los elementos, sino a la incompatibilidad entre el sistema de gravedad y el sistema lateral, así como a la falta de continuidad en el diafragma, como se muestra en la Figura 1. Estas fallas se manifestaron en colapsos parciales de estructuras de estacionamiento (Iverson *et al.* 1994; Mitchell *et al.* 1995).



Figura 1 – Daños en el estacionamiento de la Universidad Estatal de California en Northridge tras el sismo de 1994: (a) separación entre elementos prefabricados y pérdida de continuidad del sistema de piso; (b) falla de columnas del sistema de gravedad y pérdida de soporte en vigas y losas. Fuente: Iverson *et al.* (1994).

En contraste, en Japón, tras la actualización de la normativa de 1981, las estructuras prefabricadas presforzadas mostraron un desempeño sobresaliente durante el sismo de Kobe (Mw 7.2, 1995), las estructuras prefabricadas presforzadas correspondían principalmente a edificaciones con comportamiento tipo marco, en las que vigas presforzadas y columnas de concreto reforzado conformaban sistemas estructurales continuos capaces de transmitir fuerzas laterales y momentos. A diferencia de sistemas prefabricados basados en apoyos simples, la evidencia de formación de articulaciones plásticas, de interacción viga-columna y de ocurrencia de fallas en columnas antes que en vigas sugiere que las conexiones proporcionaban continuidad estructural, probablemente mediante detalles de tipo monolítico o conexiones húmedas coladas en sitio. Esta configuración favoreció un comportamiento dúctil y estable, lo que permitió el desarrollo de mecanismos resistentes y controlados. El buen desempeño observado se atribuye, además, al uso de criterios de diseño sísmico más conservadores, a la regularidad estructural en planta y en elevación, al empleo de materiales de alta calidad y a la supervisión de los procesos constructivos de las edificaciones (Muguruma *et al.* 1995).

Asimismo, en Nueva Zelanda, la evolución normativa y el desarrollo de tecnologías como PRESSS (Precast Seismic Structural Systems) permitieron mejorar significativamente el desempeño sísmico de estructuras prefabricadas, como se evidenció en la secuencia sísmica de Canterbury (2010–2011) (Fleischman *et al.,* 2014). Este avance fue el resultado de una transición en el diseño sísmico, que incorporó criterios de diseño por capacidad y de diseño detallado dúctil.

A partir de la actualización de la norma NZS 3101, se introdujeron requisitos específicos para sistemas de piso prefabricados, reconociendo dos problemas fundamentales antes ignorados: 1) el alargamiento de vigas asociado a la formación de articulaciones plásticas, que induce pérdidas de apoyo en elementos prefabricados, y 2) la incompatibilidad de deformaciones entre sistemas de piso y sistemas laterales (marcos o muros), lo que compromete la transferencia de cargas (Fleischman *et al.* 2014).

La evidencia observada en los edificios de Christchurch confirma la efectividad de estos enfoques. En estructuras con marcos prefabricados emulativos que empleaban conexiones coladas en sitio (Figura 2), se observó la formación controlada de articulaciones plásticas en las vigas, mientras que las columnas permanecieron esencialmente en el rango elástico, en concordancia con los principios de diseño por capacidad. Sin embargo, aun en estos sistemas se identificaron vulnerabilidades en los sistemas de piso prefabricados. Se registraron agrietamientos longitudinales, fractura de la malla electrosoldada y una reducción de la capacidad de transferencia de fuerzas, asociados principalmente a la incompatibilidad de deformaciones y al alargamiento de las vigas.

Aunque no se produjo el colapso del sistema de piso, estas requirieron apuntalamiento temporal y fueron evaluadas como cercanas al estado límite de colapso, evidenciando que los efectos acumulados de la deformación del sistema estructural pueden comprometer el desempeño de los elementos prefabricados aun cuando el sistema principal mantiene su estabilidad.



Figura 2 – a) Conexión de esquina en marco prefabricado; b) Colado de cierre (stitch joint) entre vigas prefabricadas. Fuente: Fleischman *et al.* (2014).

En contraste, estructuras que incorporaron tecnologías avanzadas como aislamiento sísmico en la base o sistemas desarrollados bajo el programa PRESSS tales como marcos postensados no adheridos (PT) con comportamiento auto-centrante y sistemas de muros acoplados tipo “rocking” con disipadores de energía UFPs, mostraron un desempeño sísmico sobresaliente, con daño estructural prácticamente nulo y rápida recuperación funcional (Fleischman *et al.* 2014).

En el caso del edificio Southern Cross Medical Building, su sistema estructural consistía en el uso combinado de marcos postensados en una dirección y muros “rocking” en la otra, lo que permitía controlar la respuesta sísmica mediante mecanismos de recentrado y de disipación de energía localizados. Asimismo, el detalle de la conexión viga–columna de la Figura 3 confirma la efectividad del sistema postensado no adherido (PT), donde la ausencia de daños y fisuraciones en la zona de conexión refleja la capacidad del sistema para acomodar deformaciones sin provocar daños permanentes.



Figura 3 – Detalle de la conexión viga–columna en un marco postensado no adherido (PT). Fuente: Pampanin *et al.* (2011) y Fleischman *et al.* (2014).

Por otro lado, en el edificio con aislamiento sísmico en la base, mostrado en la Figura 4, el excelente desempeño observado se atribuye a la reducción significativa de las demandas sísmicas transmitidas a la superestructura, lo que permite desplazamientos controlados y una respuesta esencialmente elástica.

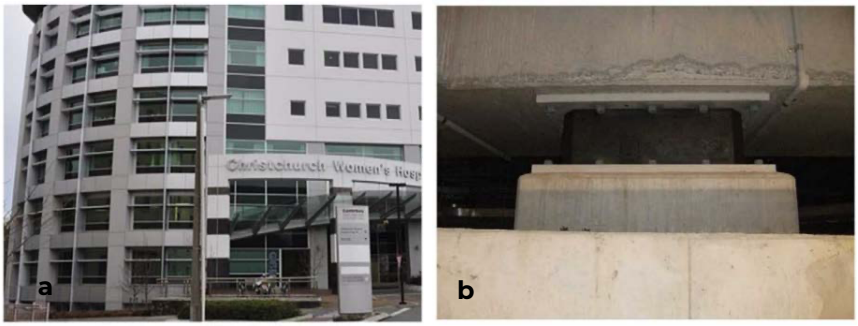


Figura 4 – a) Fachada principal del Christchurch Women’s Hospital (Christchurch, Nueva Zelanda); b) disposición del aislamiento sísmico tipo LRB en la losa de cimentación. Fuente: Kam *et al.* (2011).

Estos sistemas logran controlar la respuesta sísmica mediante dos estrategias distintas pero complementarias: 1) reducción de la demanda sísmica mediante el aislamiento en la base, y 2) control de la no linealidad estructural mediante mecanismos de recentrado y disipación de energía en las conexiones PRESSS. Este enfoque representa un cambio fundamental respecto a los sistemas tradicionales, en los que el daño se distribuye de manera no controlada entre los elementos estructurales.

A diferencia de lo observado en Tangshan (1976), en China el terremoto de Wenchuan (Mw 7.9, 2008) evidenció un comportamiento significativamente más favorable en edificaciones industriales prefabricadas, donde las conexiones tipo ménsula no presentaron fallas, y solo mostraron agrietamientos locales, sin

pérdida de soporte. Este comportamiento sugiere la existencia de mecanismos de conexión mecánica capaces de garantizar la continuidad estructural (Zhao *et al.* 2009).

En el terremoto de L'Aquila (Mw 6.3, 2009), se evidenciaron nuevamente deficiencias críticas en estructuras prefabricadas industriales. La mayoría de las estructuras afectadas correspondían a naves industriales de un solo nivel y edificios comerciales de hasta tres niveles, diseñados conforme a normativas que, en muchos casos, carecían de disposiciones específicas para el diseño sísmico de conexiones prefabricadas. Las conexiones viga–columna, diseñadas principalmente para cargas gravitacionales, fallaron por pérdida de apoyo debido a su dependencia de la fricción. Las altas aceleraciones verticales registradas redujeron la fuerza normal en los apoyos, lo que disminuyó la capacidad de fricción y provocó el deslizamiento de las vigas (Toniolo y Colombo 2012). Este mecanismo se ilustra en la Figura 5, donde se observa la pérdida de apoyo de una viga prefabricada.



Figura 5 – Falla por pérdida de apoyo en la conexión viga-columna de la estructura prefabricada. Fuente: Toniolo y Colombo (2012).

Asimismo, se documentó la falla de los conectores metálicos utilizados para la fijación de muros prefabricados, que presentaron deformaciones plásticas y desgarramiento bajo la acción de fuerzas laterales inducidas por el sismo, como se observa en la Figura 6. Estas fuerzas no fueron consideradas en el diseño original, ya que los muros fueron idealizados como elementos no estructurales. Sin embargo, durante el evento sísmico, los muros interactuaron con el sistema estructural principal, lo que modificó la distribución de fuerzas e indujo demandas no previstas en las conexiones.



Figura 6 – Falla de conectores metálicos en muros prefabricados sometidos a fuerzas laterales en su plano. Fuente: Toniolo y Colombo (2012).

En el terremoto de Van, Turquía (Mw 7.2, 2011), se observaron comportamientos contrastantes en estructuras prefabricadas. Ozden *et al.* (2014) realizaron investigaciones de campo en doce estructuras prefabricadas, incluyendo edificios residenciales de varios niveles, edificaciones públicas y naves industriales de un nivel,

con el objetivo de identificar mecanismos de daño, niveles de desempeño y deficiencias asociadas al diseño, al detallado y a la construcción.

Una de las estructuras evaluadas fue un edificio residencial prefabricado de siete niveles con conexiones viga–columna postensadas resistentes a momento, que mostró un comportamiento sísmico sobresaliente.

No se observaron daños estructurales en los elementos prefabricados ni en las conexiones (Figura 3(a–c)), y el sistema permaneció esencialmente en el rango elástico. Únicamente se registraron grietas diagonales en muros divisorios no estructurales (Figura 3(d)), atribuibles a incompatibilidad de deformaciones.

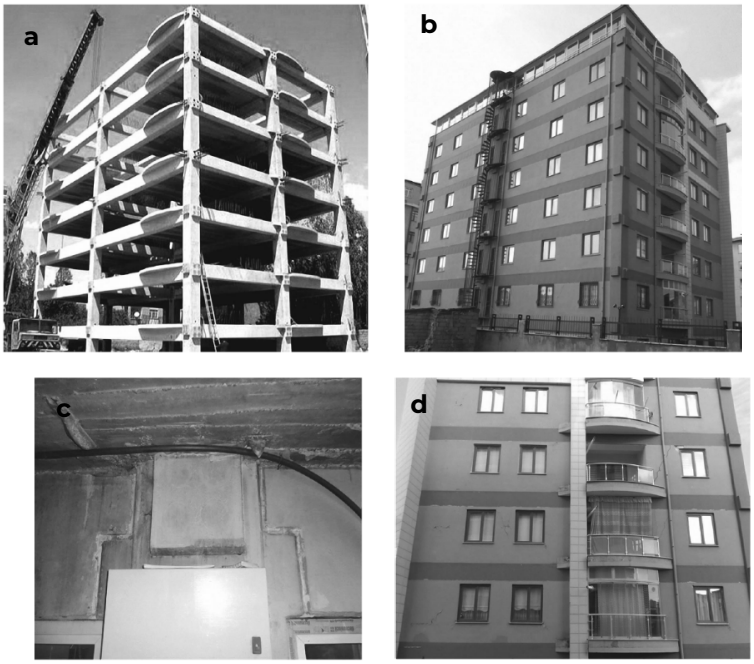


Figura 7 – Edificio residencial prefabricado de siete niveles con conexiones viga-columna postensadas resistentes a momento. (a) Etapa de construcción previa al sismo (b); vista del edificio después del sismo; (c) vista de la conexión postensada sin daños y (d) grietas diagonales en muros divisorios no estructurales. Fuente: Ozden *et al.* (2014).

Asimismo, un gimnasio prefabricado de dos niveles, que incorporaba muros de cortante de concreto colado en sitio como sistema resistente a cargas laterales, presentó daños insignificantes (Figuras 4(b) y 4(c)), a pesar de que estructuras cercanas sufrieron daños considerables. Este comportamiento favorable se atribuyó a la rigidez lateral adecuada proporcionada por los muros de cortante y al efecto de diafragma del sistema de entrepiso.



Figura 8 – Vista exterior del gimnasio prefabricado de dos niveles que incorpora muros de cortante de concreto colado en sitio como sistema principal de resistencia lateral. a) Vista de la primera planta; b) Vista de la segunda planta. Fuente: Ozden *et al*. (2014).

En contraste, se observaron daños severos y colapsos parciales en estructuras en procesos de construcción que carecían de muros perimetrales y sistemas de cubierta. En estos casos, la falla se asoció principalmente a la pérdida de soporte de las vigas debido a deficiencias en las conexiones, como la ausencia o mala calidad del grout y la falta de elementos de fijación Figura 7(a–b).

La caída de las vigas generó demandas adicionales no consideradas en el diseño, provocando la formación de articulaciones plásticas en la base de las columnas, la fluencia y ruptura del refuerzo longitudinal y, finalmente, el colapso estructural Figura 7(c–f).

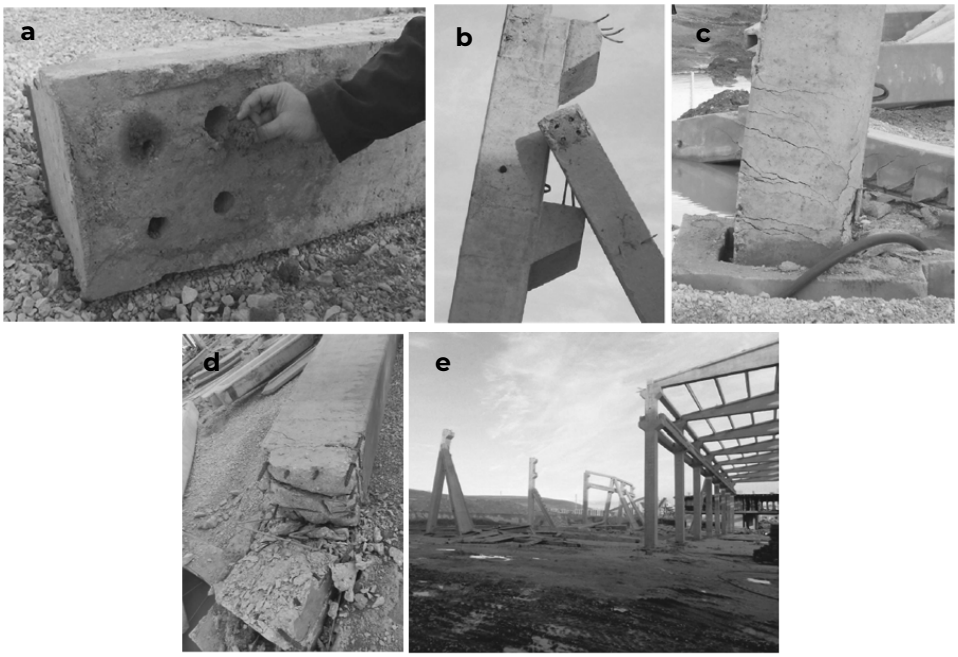


Figura 9 – Falla en la conexión viga-columna y pérdida de apoyo de las vigas de cubierta en la estructura industrial. a) Mala calidad del grout; b) desplazamiento y pérdida parcial del apoyo de la viga; c) formación de una articulación plástica en la columna; d) fluencia y ruptura del acero longitudinal de la columna; y e) colapso de la estructura. Fuente: Ozden *et al.* (2014).

Adicionalmente, se identificaron deficiencias en la calidad de los materiales y en la ejecución constructiva, incluyendo cuantías de refuerzo insuficientes, dimensiones menores a las de diseño y propiedades mecánicas del acero fuera de especificación.

El sismo de Emilia (Mw 6.1**,** 2012) constituye uno de los casos más representativos del comportamiento sísmico deficiente de estructuras prefabricadas existentes, en el que más del 60% de los edificios prefabricados industriales colapsaron o sufrieron daños severos. El mecanismo dominante fue la pérdida de apoyo de las vigas y los elementos de cubierta, debido al uso de conexiones basadas únicamente en fricción y a la ausencia de anclajes mecánicos (Magliulo *et al.* 2013).

Desde un punto de vista mecánico, la resistencia por fricción ($\mu \approx 0.09–0.13$), resultó insuficiente frente a las demandas sísmicas, provocando el deslizamiento de las vigas sobre las columnas y la consecuente pérdida de soporte (Magliulo *et al.* 2013). Este mecanismo se casos, lo que facilitó la caída de los elementos de cubierta y desencadenó colapsos progresivos. Como se observa en la Figura 10, el deslizamiento de las vigas sobre las columnas provocó el colapso de los sistemas de cubierta.

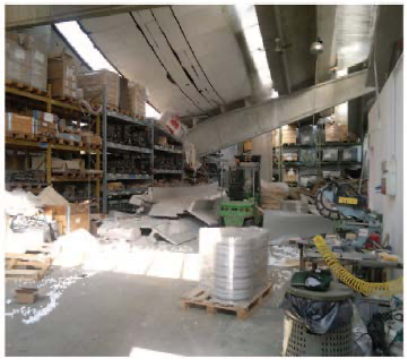


Figura 10 – Pérdida de apoyo de vigas sobre columnas en estructuras prefabricadas, lo que provoca el colapso de los elementos de cubierta. Fuente: Magliulo *et al*. (2013).

Cabe destacar que una gran proporción de las edificaciones afectadas fue diseñada antes de que la región de Emilia fuese clasificada como zona sísmica. Aunque el mapa de peligro sísmico se actualizó en 2003, su aplicación obligatoria en el diseño estructural no se implementó hasta 2008, por lo que muchas estructuras existentes no incorporaban criterios sismorresistentes (Savoia *et al*., 2017). Sin embargo, la evidencia observada en este evento, junto con estudios posteriores, ha llevado a modificaciones normativas significativas. En particular, la normativa italiana DM 14/01/2008 y el Eurocódigo 8 establecen que la resistencia por fricción no debe considerarse como mecanismo principal para resistir acciones sísmicas, y requieren, en su lugar, conexiones capaces de transmitir fuerzas laterales y resistir cargas cíclicas.

En Nueva Zelanda, más recientemente, el sismo de Kaikoura (Mw 7.8, 2016) permitió reevaluar el comportamiento sísmico de estructuras prefabricadas, evidenciando mecanismos de daño asociados a la compatibilidad de deformaciones que no habían sido plenamente identificados en la secuencia sísmica de Canterbury (2010–2011), de acuerdo con Henry *et al*. (2017).

Se registraron demandas sísmicas que excedieron los niveles de diseño en edificaciones con periodos del orden de 1 a 2 segundos, correspondientes principalmente a edificios de marcos de concreto reforzado de entre 5 y 15 niveles, muchos de ellos construidos a partir de la década de 1980 e incorporando sistemas de piso prefabricados, particularmente losas alveolares y unidades tipo doble “tee”. A pesar de que no se observaron colapsos generalizados, aproximadamente el 52% de los edificios evaluados presentaron algún nivel de daño estructural, destacándose las afectaciones en los sistemas de piso. Un fenómeno particularmente significativo fue la elongación residual de las vigas, producto de la acumulación de deformaciones inelásticas en las regiones de articulación plástica, lo que generó rotaciones en las vigas de apoyo y una reducción del apoyo efectivo de las unidades prefabricadas.

Este mecanismo evidenció la vulnerabilidad de conexiones típicamente diseñadas como apoyos simples, lo que provocó daños por desprendimiento del concreto, pérdida de longitud de apoyo y, en otros casos, pérdida de soporte en unidades tipo doble “tee”. Adicionalmente, se identificaron daños significativos en diafragmas de piso, especialmente en sistemas con losas alveolares, donde se observaron agrietamientos concentrados en las esquinas debido a incompatibilidades de deformación, así como grietas transversales cercanas a los apoyos, asociadas a posibles fallas a cortante.

3. Análisis comparativo

El análisis comparativo de los eventos sísmicos estudiados permite establecer que el comportamiento de las estructuras prefabricadas ha estado históricamente dominado por el desempeño de sus conexiones, más que por las propiedades de los elementos estructurales en sí.

En los sistemas prefabricados tradicionales, como los observados en Tangshan (1976), Armenia (1988), L'Aquila (2009) y Emilia (2012), el daño estuvo dominado por la falta de continuidad estructural y por el uso de conexiones incapaces de transmitir fuerzas laterales. En estos casos, las conexiones basadas en fricción o apoyos simples mostraron un comportamiento altamente vulnerable, caracterizado por la pérdida del soporte de los elementos horizontales y el desarrollo de mecanismos de colapso progresivo. Este patrón se repite independientemente de la ubicación geográfica, lo que evidencia una deficiencia conceptual en el diseño estructural.

En contraste, en sistemas cuyas conexiones fueron diseñadas para proporcionar continuidad estructural, como en Kobe (1995), Wenchuan (2008), Canterbury (2010–2011) y en algunas edificaciones evaluadas en Van (2011), se observó un comportamiento sísmico significativamente más favorable. En estos casos, el uso de conexiones húmedas, conexiones postensadas no adheridas, desarrolladas bajo el enfoque PRESSS o mediante dispositivos mecánicos permitió desarrollar mecanismos dúctiles y evitar la pérdida de estabilidad global. Estos resultados indican que el buen desempeño no depende únicamente del tipo de sistema prefabricado, sino también de la existencia de mecanismos de conexión capaces de proporcionar resistencia, ductilidad y capacidad de transmisión de esfuerzos.

El sismo de Kaikoura (2016) introduce un cambio significativo en la interpretación del comportamiento sísmico de las estructuras prefabricadas. A diferencia de eventos como L'Aquila (2009) y Emilia (2012), donde el daño estuvo asociado a la incapacidad de las conexiones para transmitir fuerzas laterales y garantizar la estabilidad del sistema, en Kaikoura se observó que, aun con normativas detalladas, los sistemas de piso prefabricados no estuvieron exentos de daño.

Si bien las normas vigentes hasta ese momento contribuyeron a prevenir el colapso de los sistemas de piso, se registraron daños importantes, incluyendo la reducción del apoyo, el agrietamiento longitudinal y transversal en las losas alveolares, así como afectaciones en la capacidad de transferencia de fuerzas del diafragma. Estos resultados indican que, aunque el nivel de seguridad estructural ha mejorado, el desempeño funcional y la integridad de los sistemas siguen siendo vulnerables ante demandas sísmicas elevadas.

4. Conclusiones

El análisis de la evidencia sísmica documentada permite establecer que el comportamiento sísmico de las estructuras prefabricadas existentes no depende del sistema constructivo en sí, sino del diseño, del detallado y del desempeño de sus conexiones. Los casos estudiados muestran que las fallas más severas se presentan en sistemas en los que las conexiones no garantizan la transmisión de fuerzas laterales ni la continuidad estructural, particularmente en configuraciones basadas en apoyos simples o en mecanismos de fricción.

Asimismo, la evidencia recopilada documenta casos de desempeño satisfactorio. En particular, los sistemas prefabricados que emplean conexiones postensadas desadheridas y conexiones húmedas coladas en sitio han mostrado un comportamiento sísmico favorable, al permitir la transmisión efectiva de las fuerzas, la continuidad estructural y una respuesta más dúctil. Estos sistemas destacan por su capacidad para acomodar deformaciones inelásticas y limitar mecanismos de falla frágil, lo que respalda su implementación como estrategia para mejorar el desempeño sísmico de estructuras prefabricadas.

En este sentido, en los últimos años se han propuesto diversas soluciones de conexión para sistemas prefabricados, particularmente en uniones viga–columna, muros y sistemas de piso orientadas a mejorar su desempeño sísmico. Sin embargo, más allá del desarrollo tecnológico, el desafío actual radica en incrementar la confiabilidad y adopción en zonas sísmicas, lo cual requiere no solo validar su comportamiento mediante evidencia experimental, sino también desarrollar herramientas de análisis y diseño que permitan su aplicación consistente en la práctica profesional.

Referencias

Fédération Internationale du Béton (fib). 2003. Seismic Design of Precast Concrete Buildings. Bulletin No. 27. Lausanne, Switzerland: Fédération Internationale du Béton.

Fleischman, Richard B., José I. Restrepo, Stefano Pampanin, John Maffei, Kurt Seeber, and Frank Zahn. 2014. "Damage Evaluation of Precast Concrete Structures in the 2010–2011 Canterbury Earthquake Sequence." PCI Journal 59 (4): 38–71.

Henry, Richard S., Dmytro Dizhur, Keith J. Elwood, John Hare, and David Brunsdon. 2017. "Damage to Concrete Buildings with Precast Floors during the 2016 Kaikōura Earthquake." Bulletin of the New Zealand Society for Earthquake Engineering 50 (2): 174–86.

Housner, George W., and X. Lili. 2002. The Great Tangshan Earthquake of 1976: Overview Volume. Pasadena, CA: Earthquake Engineering Research Laboratory, California Institute of Technology.

Iverson, James K., and Neil M. Hawkins. 1994. "Performance of Precast/Prestressed Concrete Building Structures during Northridge Earthquake." PCI Journal 39 (2): 38–55. https://www.pci.org/PCI_Docs/Publications/PCI%20Journal/1994/March%20April/Performance%20of%20Precast%20Prestressed%20Concrete%20Building%20Structures%20During%20Northridge%20Earthquake.pdf

Magliulo, Gian Michele, Marco Ercolino, Chiara Petrone, Ornella Coppola, and Gaetano Manfredi. 2014. "The Emilia Earthquake: Seismic Performance of Precast Reinforced Concrete Buildings." Earthquake Spectra 30 (3): 891–912.

Mitchell, Denis, Robert H. Devall, Murat Saatcioglu, Robert Simpson, Riad Tinawi, and Robert Tremblay. 1995. "Damage to Concrete Structures Due to the 1994 Northridge Earthquake." Canadian Journal of Civil Engineering 22 (2): 361–77.

Muguruma, Hideo, Masanori Nishiyama, and Fumio Watanabe. 1995. "Lessons Learned from the Kobe Earthquake: A Japanese Perspective." PCI Journal: 28–42.

Ozden, Sukru, Erman Akpinar, Hakan Erdogan, and Hasan Murat Atalay. 2014. "Performance of Precast Concrete Structures in October 2011 Van Earthquake, Turkey." Magazine of Concrete Research 66 (11): 543–52.

Savoia, Marco, Nicola Buratti, and Luca Vincenzi. 2017. "Damage and Collapses in Industrial Precast Buildings after the 2012 Emilia Earthquake." Engineering Structures 137: 162–80. https://doi.org/10.1016/j.engstruct.2017.01.059.

Toniolo, Giandomenico, and Andrea Colombo. 2012. "Precast Concrete Structures: The Lessons Learned from the L'Aquila Earthquake." Structural Concrete 13 (2): 73–83. https://doi.org/10.1002/suco.201100052.

Wood, Peter R., John B. Berrill, Neil R. Gillon, and Peter J. North. 1993. "Earthquake of 7 December 1988, Spitak, Armenia: Report of the NZNSEE Team Visit of 1989." Bulletin of the New Zealand Society for Earthquake Engineering 26 (3): 253–83. https://doi.org/10.5459/bnzsee.26.3.253-283.

Zhao, Bin, Fabio Taucer, and Tiziana Rossetto. 2009. "Field Investigation on the Performance of Building Structures during the 12 May 2008 Wenchuan Earthquake in China." Engineering Structures 31 (8): 1707–23. https://doi.org/10.1016/j.engstruct.2009.02.039.

cinpar 2026
XXII International Conference on Building Pathology and Constructions Repair
15th to 17th July 2026 - Lisboa, Portugal

ANALYSIS OF PATHOLOGICAL MANIFESTATIONS IN A PUBLIC SCHOOL IN THE MUNICIPALITY OF JUAZEIRO DO NORTE, CEARÁ: A CASE STUDY

Lucas Menezes de FARIAS[1], Lindomar Faustino da SILVA[2], **Jefferson Luiz Alves MARINHO**[3]

[1] Universidad Regional do Cariri – URCA, Juazeiro do Norte-CE, Brazil, lucasmenezes547@gmail.com
[2] Universidad Regional do Cariri – URCA, Juazeiro do Norte-CE, Brazil, lindomar.silva@urca.br
[3] Universidad Regional do Cariri – URCA, Juazeiro do Norte-CE, Brazil, jeff.marinho@urca.br

Abstract: The main requirements of a building are structural safety, watertightness, thermal and acoustic comfort, as well as durability, which can be compromised by pathological manifestations. After anomalies occur, repairs must be carried out promptly to avoid further deterioration. To provide effective solutions, it is essential to properly identify the causes of the anomalies. This study aims to survey pathological manifestations in a public school in the municipality of Juazeiro do Norte-CE. The data were obtained through an on-site visual inspection. The inspection covered both internal and external areas, with photographic records taken in panoramic and detailed form. To determine the dimensions of the openings, a crack gauge was used. Horizontal cracks and fissures were identified in the wall coatings of the classrooms, as well as cracks in different directions and inclined gaps. In addition, cracks were found at the junctions between columns, beams, and slabs. Cracks and detachment in the ceramic flooring were observed, along with diagonal gaps in coatings of wet areas. Furthermore, disintegration of coatings, detachment of PVC ceiling panels, and water/moisture infiltration associated with mold growth were noted. Horizontal and diagonal cracks near window frames, peeling paint on the wall, as well as vertical cracks and detachment in the external masonry were also identified. Finally, dark stains, fissures, and mapped cracks were found on the floor. Thus, the existence of pathological manifestations may be related to failures in some construction phase, lack of maintenance, or design flaws. Correct construction practices, use of quality materials, and preventive maintenance, along with proper care in the use of the building as outlined in the Building Use, Operation, and Maintenance Manual, constitute effective measures not only to mitigate the emergence of pathological manifestations but also to resolve them when already present.

Keywords: Pathological Manifestations. Structural Damage. Maintenance.

1. Introduction

In many countries, the construction sector strongly contributes to economic growth (Chellappa et al., 2020). Globally, with an annual budget of US$ 10 trillion, the sector accounts for 13% of the Gross Domestic Product (GDP) (Barbosa et al., 2017). The sector provides employment to many people and solutions for the growing needs of the world's population (Chellappa; Srivastava, 2024).

However, despite the growth of the construction industry and investments in technologies to improve materials, techniques, and construction systems, a portion of buildings continues to show unsatisfactory performance over time. These construction anomalies, ranging from design flaws and material defects to poor execution, often compromise the longevity and structural integrity of buildings (Lima Júnior et al., 2025).

Among these anomalies are endogenous factors originating from design, materials, or execution, as well as exogenous factors resulting from external influences, natural phenomena, or functional issues that arise after the expected service life of a building. These deficiencies can be attributed to several factors, such as design flaws, execution problems, or the quality of materials used.

Sena et al. (2020) state that pathological manifestations are degradations identified in the building, which may be generated during the construction period (whether using inappropriate construction methods or materials), in the project design itself, or may arise over time due to misuse or inadequate use of the building.

Construction failures are a serious problem by all project stakeholders. This occurs because they can happen at any point in the project life cycle and have a significant effect on project cost and time due to rework, potentially compromising trust among stakeholders (Awasho; Alemu, 2023). Supporting this understanding, Alomari (2022) states that repairing construction failures costs between 2.4% and 3.15% of the total building cost.

Problems arising from pathological manifestations range from minor damage to compromising the safety of buildings, which may culminate in structural collapse (Marinho, Mesquita; 2022). In this regard, Aguiar et al. (2022) argue that knowledge and treatment of building failures contribute to increasing its service life, while also providing notable safety to users. Supporting this understanding, Resende et al. (2022) affirm that by investigating and understanding these manifestations, it is possible to identify the causes of deterioration and take measures to prevent further damage to the building and financial losses to owners.

In this context, pathological manifestations may be related to inadequate use of the building, lack of maintenance, natural wear of materials, exposure to adverse weather conditions, or even design or execution errors (Santos Júnior; Santos; Santos, 2023).

Furthermore, the lack of preventive maintenance and improper use of the building may also compromise its service life. It is important to emphasize that the service life of a building is an important aspect to be considered in civil construction, as it is related to its sustainability and the environmental and economic impact that its premature replacement or repair may generate (Santos Júnior; Santos; Santos, 2023).

In this sense, the main objective of this study is to survey the pathological manifestations in a public school located in the municipality of Juazeiro do Norte-CE.

2. Material and Methods

2.1 Choice of the Study Object

The research carried out was a case study, and for this purpose, the educational institution of interest in this article was the João Alencar de Figueiredo Public Elementary School, one of the largest in the municipal public-school network in Juazeiro do Norte-CE, located on Avenue President Castelo Branco, Romeirão neighborhood, with the following geographic coordinates: 7°13'25.60" S Latitude and 39°18'56.99" W Longitude. It is situated in an urban area, on one of the main avenues of the neighborhood, approximately 80m from Arena Romeirão and 1km from Cariri Shopping, among other high-standard developments nearby. Figure 1 shows the front view of the school, which is surrounded by railings.

Figure 1 – Escola de Ensino Fundamental João Alencar de Figueiredo in Juazeiro do Norte – CE



Currently, the school is closed due to its critical structural condition, with risk of collapse in certain areas. The main justification for choosing the school was the compromised state of its structure, which shows advanced levels of pathological manifestations. In addition, the ease of access for inspection was a determining factor.

It is a building from the 1970s and currently belongs to the State of Ceará. The building has a single floor and about 29 rooms, including classrooms, library, covered sports court, reading room, bathrooms, auditorium, kitchen, and storage room.

Its structure consists of reinforced concrete columns, beams, and slab, with internal and external masonry made of ceramic brick. The facades are coated with mortar and finished with paint. The finishing standard is considered normal/low, with industrial flooring in circulation areas, while other rooms have commercial ceramic flooring. Wet areas also have internal walls coated with commercial ceramic. Most rooms have a slab ceiling, while others are finished with PVC panels, and the roof is covered with ceramic tiles. The internal environments have wood/glass windows, while the doors no longer exist, as they were removed by vandals. The building occupies an entire block, with approximately 60% of the total area built. The dimensions/area of the property were estimated using Google Earth: front – 63.00m, left side – 90.00m, right side – 65.00m, back – 57.00m. The total land area is estimated at 4,569m^2.

The inspection covered the internal and external areas of the school and was carried out on February 15, 2025, using the non-destructive technique of visual inspection of the surface of the structures, aiming to identify signs of failures or damage to confirm the presence of pathological manifestations in the building.

In addition, each photographic record was properly documented with the inclusion of date, time, and geographic coordinates.

To determine the classification of cracks (fissures, cracks, fractures, gaps, and breaches), the methodology of Oliveira (2012) was used, as shown in Table 1, determined through visual inspection using a crack gauge to measure the openings.

Table 1 – Classification of Cracks

Anomalies	Openings (mm)
Fissure	Up to 0,5
Crack	0,5 to 1,5
Fracture	1,5 to 5,0
Gap	5,0 to 10,0
Breach	Above 10,0

According to Table 1, the classification of anomaly openings serves to assess the degree of severity of this type of pathological manifestation and to evaluate the type of maintenance to be applied for the solution of each case.

3. Results and Discussion

During the inspection carried out at the school to assess conditions and identify pathological manifestations, some internal classrooms were selected for photographic records, since most of them presented identical manifestations with the same degree of deterioration. Despite the school's critical structural condition, some environments were in good conservation state, requiring only minor repairs. Below, the pathological problems found only in the internal classrooms of the school are presented (Figures 2 to 14). Subsequently, the pathological manifestations found only in the external areas and internal circulation of the school are presented (Figures 15 to 23).



Figure 2 – Access wall to the classroom

(a) Horizontal fissure (opening of 0,25mm)

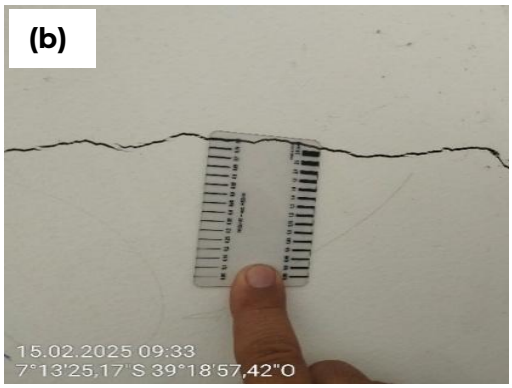


Figure 3 – Corner of the classroom wall

(b) Horizontal crack (opening of 0,8mm)

Regarding the fissures and cracks, these were found in most areas of the school, considering that their presence progressively turned into fractures, as this evolution becomes noticeable throughout the development of this work. From the analysis of Figures 02 and 03, it is possible to identify the potential causes of the anomaly, since according to Caporrino (2018), the main possible causes of horizontal fissures are the expansion of the bedding mortar due to delayed hydration of the magnesium oxide in lime. In addition, another factor would be the expansion of the bedding mortar caused by the cement-sulfate reaction or by the presence of expansive clay minerals in the aggregate. Caporrino (2018) further states that any expansion of the mortar results in horizontal fissures. When expansion occurs and there is no space, the bedding mortar ruptures.

Supporting this understanding, Carneiro, D'Ávila, and Luís (2018) emphasize that fissures, in many situations, are not easily identified, thus requiring extensive knowledge in the field for the application of appropriate correction procedures.



Figure 4 - Fracture located in the central part of the classroom wall

Opening of 1,6mm

As presented in Figure 4, it is possible to identify the potential causes of the pathological manifestation, with the occurrence of the crack located in the central part of the classroom wall being attributed to the lack of proper bonding between the existing masonry and the area where a window had previously been located, later removed during renovations. The absence of bonding mesh during the execution of the masonry contributed to the emergence of this pathological manifestation, since there was no effective connection between the structural elements, leading to the appearance of straight cracks in the region.

In line with this reasoning, Sena et al. (2020) argues that in interface regions between masonry walls and concrete columns, it is also recommended to execute bonding with mesh. These bonds should be applied in the marking masonry (first course) and every two courses along the masonry/column interface. For fixing the mesh, the use of a pin gun is recommended, and a special precaution to be taken is that the pin must be fixed exactly at the mesh fold to prevent possible movements. One way to facilitate this is by employing a metal angle that helps fold the mesh in the correct place and fix the pin. If the pin is not fixed at the fold, interface fissures may occur even with the use of this solution (Sena et al., 2020).



Figure 5 - Inclined fracture near the classroom blackboard

Opening of 2,0mm

As observed in Figure 5, the probable factors contributing to the crack include low soil compaction, which made the building susceptible to structural movements that ultimately compromised it. The likely causes are differential settlements of the foundation, with Caporrino (2018) stating that cracks in structural masonry predominantly develop diagonally from the corners of openings, where stress concentrations are greatest. The author also notes that the main possible causes include aquifer drawdown, settlements caused by neighboring buildings, excavations, vibrations, inadequately designed foundations, and soil alterations.

When, for any reason, foundations undergo differential settlements, the superstructure becomes subject to loads not anticipated in the design. These loads can generate tensile and shear stresses that, consequently, may cause cracks in structural masonry that was not calculated to withstand such forces (Caporrino, 2018).

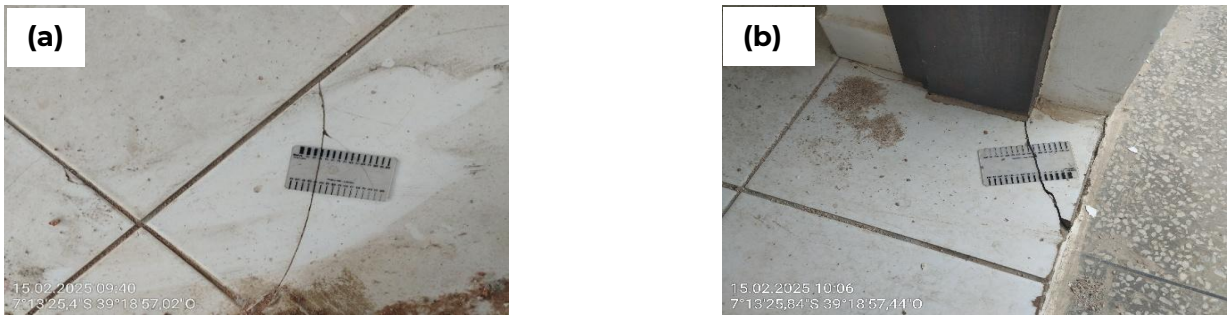


Figure 6 - Crack in ceramic flooring at classroom entrance

(a) Opening of 0,6mm (b) Opening of 1,4mm

Cracks measuring approximately 0.6 mm and 1.4 mm in width were found at the entrance of the school's classrooms (Figure 6). As observed, the probable causes are the lack of adequate negative reinforcement to connect two slab compartments. In this context, Accetti (1998) states that negative reinforcements act in the load flow to prevent stress concentrations, with the purpose of avoiding the possible appearance of cracks over the supports. Since the characteristics of the cracks are not "active," Morais et al. (2020) argue that no major precautions are necessary, as this is a pathological manifestation with only aesthetic effects.

Supporting this understanding, Thomaz (2020) points out that regarding coatings, another pathology resulting from the deformability of structures is the cracking or detachment of ceramic floors or even rigid flooring, because of excessive deformation of the slabs on which they are laid. The author reinforces that when significant slab deflection occurs, the flooring begins to act as its compression layer, producing cracks, chipping, and detachment in the coating. This mainly occurs in cases of "zero slabs" (without screed, with the coating directly bonded to the upper surface).



Figure 7 – Ceramic detachment

Figure 7 shows the detachment of the ceramic coating tile. Detachments are considered when the ceramic tile or the final layer has already fallen off. Sena et al. (2020) state that the main causes of detachments are execution problems that lead to adhesion failure, the lack of an adequate design that considers the variables and materials to be used, as well as the climatic variations to which the coating is subjected, which cause daily temperature differences. The authors further emphasize that another quite common practice that causes detachment is the lack of proper filling and spreading of the adhesive mortar during application.

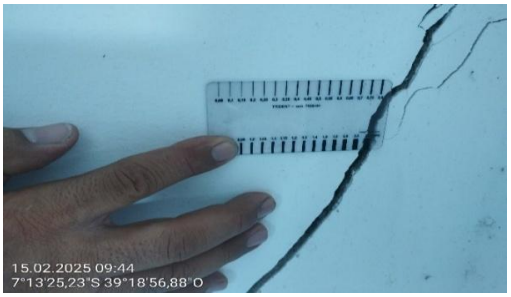


Figure 8 – Inclined gap near classroom entrance
Opening of approximately 6,0mm



Figure 09 – Crack below the classroom blackboard

(a) Opening of approximately 5,0mm



Figure 10 – Crack at the junction of the living room wall

(b) Opening of approximately 3,0mm

As shown in Figures 08, 09, and 10, the probable causes are differential foundation settlement, as previously described in Figure 05 and later in Figure 14.





Figure 11 - Disintegration of wall coating

The presence of disaggregating coating (Figure 11), according to Caporrino (2018), may occur due to the presence of uncarbonated lime and may also be caused by moisture. Possible repairs include eliminating moisture infiltration, drying the coating, brushing the surface, repairing the coating when it becomes powdery, and washing with a hypochlorite solution. All loose material must be removed through brushing and washing, and the coating must be completely dried (Caporrino, 2018).

It is worth noting that the presence of clayey nuclei, with excess fines in the sand or a considerable amount of mica, can lead to coating disaggregation. Mica may also reduce the adhesion of the coating, both to the substrate and between two layers (Cincotto, 1988).





Figure 12 - PVC ceiling panels detaching

As observed in Figure 12, the finishes with functions of waterproofing, weather protection, and improvement of thermoacoustic conditions presented problems in the ceiling, with PVC panels coming loose. According to Carraro (2010), irregularities in the finish, such as poorly executed repairs, are mainly related to the lack of material quality or poor workmanship.

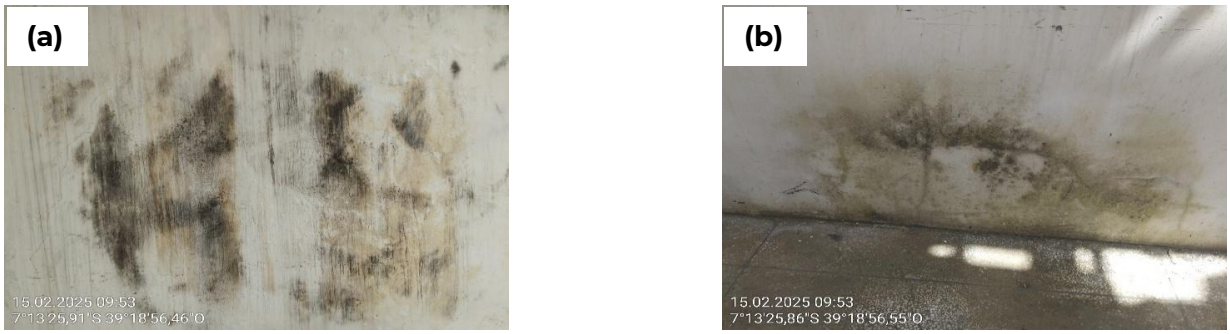


Figure 13 - Infiltration and mold formation

From the analysis of Figure 13, the presence of fungi on the classroom wall can be noted, representing a biological risk. Molds can be prevented during the design phase by adding fungicide to the coating exposed to high humidity, as well as by maintaining environments with natural ventilation and solar radiation to prevent fungal growth (Alucci, Flauzino; Milano, 1988).

Supporting this understanding, Brochado (2016) states that in addition to being a concerning factor for the building, fungi can lead to structural deterioration and affect the performance of certain materials.

The occurrence of fungi may be related to the lack of proper maintenance or repairs in the roofing, hydraulic systems, or waterproofing. Another possible cause of rising damp could be triggered by moisture capillarity in the soil, which is transferred through failures or the absence of adequate waterproofing in the foundation footing or beam (Lima et al., 2018).

This pathological manifestation can generate others, which in turn may lead to plaster detachment. Beyond compromising the aesthetics of the environment, the presence of fungi can negatively impact human health, making the space unhealthy and unsuitable for occupation.



Figure 14 - Diagonal gap above and below window
Opening of approximately 7,0mm

As shown in Figure 14, the cracks are active and have a strong tendency to propagate from the window openings, where there is a considerable reduction in the wall section. To prevent such anomalies, the probable causes are examined, and it is likely that they occurred due to differential foundation settlement, since, in general, the openings are inclined and usually larger, “leaning” toward the point where the greatest settlement occurred (Thomaz, 2020). In this context, another characteristic of cracks caused by settlement is the frequent presence of localized crushing in the form of scales, indicating the shear stresses that produced them. Furthermore, when settlements are significant, a clear variation in crack width can be observed (Thomaz, 2020).

Thomaz (2020) also mentions that differential settlements may result from unbalanced loads; in practice, this can be perfectly identified by cracks starting from the windowsill, approximately at mid-span of the opening.

Still in the analysis of Figure 14, probable causes can also be attributed to the absence of lintels and sills at the lower and upper parts of the window, or possibly the lack of interlocking (bonding) of the blocks. The application of concentrated loads on masonry without the use of lintels and sills to redistribute stresses can lead to the appearance of cracks (Ferreira, 2016).

Cracks may also occur when, even with adequate reinforcement, the imposed load exceeds that anticipated in the structural masonry design.

The following sections will present the pathological manifestations found only in the external areas and internal circulation spaces of the school.



Figure 15 - Crack at the junction between beam and slab

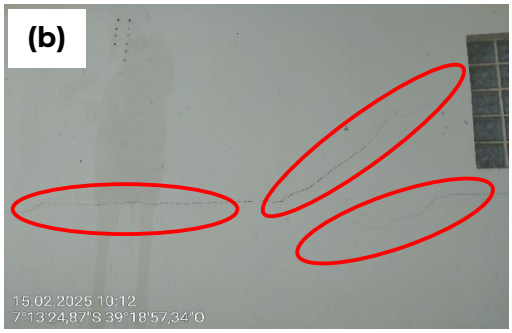


Figure 16 - Horizontal/diagonal cracks

As shown in Figures 15 and 16, the probable causes are also differential foundation settlement, as described in Figures 05 and 14.

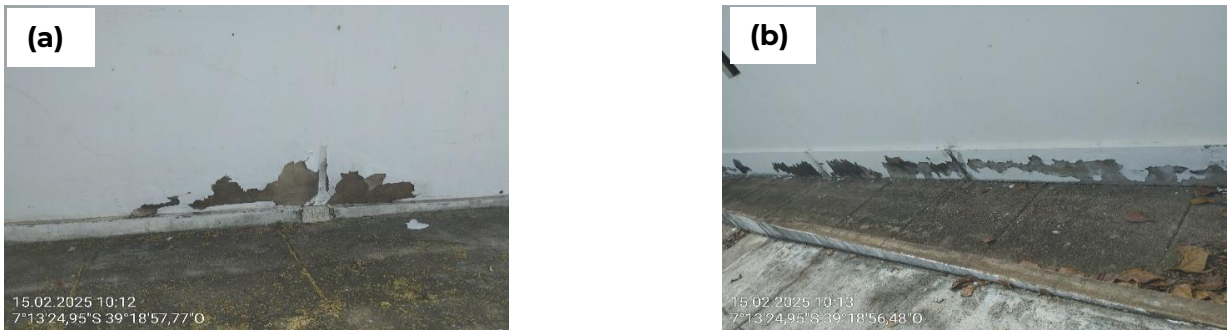


Figure 17 - Paint peeling on the front recess



Figure 18 - Paint peeling on the side wall

The peeling of the paint film, observed in Figures 17 and 18, may result from poor adhesion between the paint film and the mortar coating, solar exposure, and the presence of moisture from rainfall. Polito (2006) states that climatic conditions can contribute to the appearance of paint pathologies caused by relative humidity.

According to Fagundes Neto (2008), paint film peeling may occur when painting is applied over limewash, gypsum, cement, or improperly cured concrete without proper surface preparation. The author also notes that peeling can occur when, in the first painting over plaster, the paint was not properly diluted or there was excess dust on the surface.

Fazenda (1995) comments that another cause of peeling is painting over a heated surface or the reaction of the paint with the substrate, resulting in water-soluble compounds. Peeling may also occur when paint is applied to smooth substrates, such as concrete with release agents or ceramic coatings.

Thomaz (2020) states that in the case of awfully long walls without upper protections such as flashings or coping, detachment of the coating at the top of the wall is common due to water pooling/hygroscopic

expansion of the mortar coating. Detachment of the mortar is also common due to thermal expansion, which is much greater than the expansion of the wall body itself.



Figure 19 - Vertical cracks



Figure 20 - Detachment of the masonry

From the analysis of Figures 19 and 20, the probable causes can be identified. Due to the tensile strength of the bedding mortar and masonry components, as well as the adhesion developed between them, cracks caused by thermal movements may follow the vertical mortar joints or even extend through the masonry components (Thomaz, 2020). As mentioned earlier in this work (Figure 05), in the interface regions between masonry walls and concrete columns, it is recommended to execute bonding with mesh.

In cases where mesh is not available, reinforcements can be placed in the columns using a drill and epoxy-based adhesive to create bonds between the structure and the infill, maintaining the same recommendation of fixing every two courses (Sena et al., 2020).

Caporrino (2018) further states that vertical cracks may also occur at masonry junctions, sections where thickness changes, or regions weakened by the presence of pipes.





Figure 21 – Cracks at the junction of structural elements of columns, beams, and slabs

As observed in Figure 21, the structural framework of the building is likely to be subject to thermal movements, especially in exposed concrete structures. Thomaz (2020) states that the regions most affected are usually the junctions between beams during thermal movements, where internal cracks may appear within the concrete elements and therefore remain undetectable. However, the thermal movement of beams can cause visible cracking in columns; this occurs mainly when the structure lacks expansion joints or when they are poorly designed (openings and spacing). According to Fabiani (1975), the thermal expansion of beams can cause slightly inclined cracks at the ends of columns.

It should also be considered that significant differences in movement occur between the upper and lower surfaces of roof slabs, with the upper surfaces generally subjected to more abrupt and intense movements (Thomaz, 2020).

For solid slabs with large spans, torsional moments that develop near the slab corners can produce diagonal cracks, forming approximately isosceles triangles with the corners. Another type of crack may appear when there is no negative reinforcement between constructively continuous slab panels designed as simply supported, or when the negative reinforcement was undersized or displaced during concreting; in such cases, cracks appear on the upper surface of the slab, approximately following its contour (Thomaz, 2020).

Cracks in beams, as shown in Figure 21, may arise due to the following factors: thermal movement, overloads, excessive structural deformations, foundation settlements, and chemical alterations of materials, such as reinforcement corrosion, for example (Carneiro, D'Ávila; Luís, 2018).

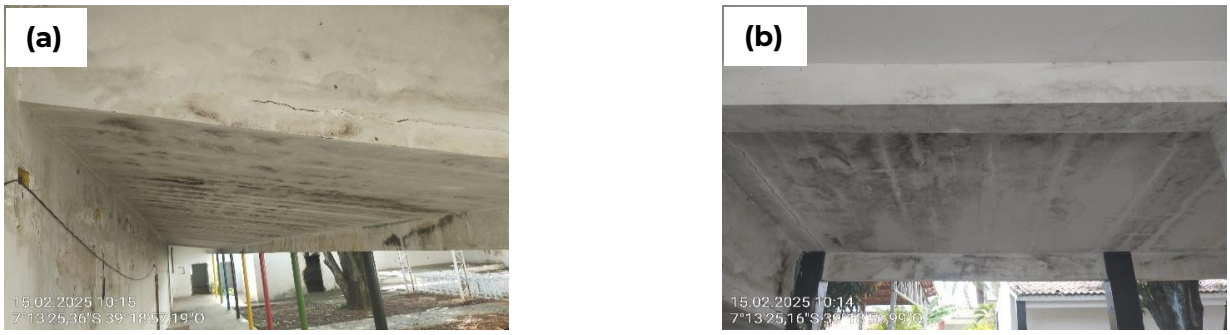


Figure 22 – Dark Spots

The presence of dark stains on the surface, as shown in Figure 22, originates from a group of living organisms (fungi) that proliferate under favorable climatic conditions, such as humid, poorly ventilated, or shaded environments (Fagundes Neto, 2008).

According to Fazenda (1995), the main causes of stain formation are high humidity associated with the presence of decomposing organic materials or plant parasites (vegetation). Ambient temperatures between 0°C and 40°C, relative humidity above 70%, and the presence of oxygen favor the development of fungi and the formation of algae, which invariably occurs in outdoor environments near coastal areas and/or dense vegetation (Fazenda, 1995).

The presence of cracks facilitates fungal growth; moreover, the occurrence of fungi increases dust retention and moisture persistence. This combination of factors constitutes an additional element for fungal proliferation (Fagundes Neto, 2008).



Figure 23 - Mapped fissures and cracks

The cracks and fissures mapped have varied shapes and are distributed across the entire surface, as shown in Figure 23. A possible cause is the shrinkage of the base mortar. The relationship between the probable cause and the anomaly lies in the fact that the mapped cracks/fissures result from an excess of fines in the mortar, that is, a rich mortar, thus causing cracking due to shrinkage. This damage also does not allow for repair, except through the complete removal of the coating (Caporrino, 2018).

Still regarding the mapped cracks, the main originating sources can be cited: mortar shrinkage due to excess fines in the mix, rapid drying, and excessive troweling. They are given this designation because they manifest in a map-like pattern. Many times, they are superficial and can be accentuated by thermal shock, especially on sun-exposed façades (Cincotto, 1989).

4. Conclusion

The main objective of this study was to survey the pathological manifestations in a public school located in the municipality of Juazeiro do Norte-CE, considering both the internal and external areas of the building.

Based on the analyses carried out, it was found that the structural safety of the building is compromised, presenting a series of construction pathologies. Among the main problems identified are cracks, fissures, and fractures of different types, masonry detachment, and advanced-stage gaps. The possible causes of these pathological manifestations include failures in soil compaction, differential foundation settlement, thermal movements, absence of lintels and counter-lintels in windows, lack of maintenance, as well as inadequate execution of previously performed renovations, as evidenced throughout the study.

In addition, cracks and detachment were found in the ceramic coating, as well as fissures and mapped cracks in the industrial flooring. Other problems identified include disintegration of coatings, peeling paint,

detachment of PVC ceiling panels, dark stains, and infiltrations accompanied by mold formation. Given the severity of these manifestations, the fact that the building is interdicted is justified.

Regarding the use of the crack gauge, it was possible to determine the classification of the openings of the anomalies to assess the degree of criticality of the pathological manifestations.

During the development of this study, some limitations were identified. These include the scarcity of information about the renovations carried out throughout the life of the structure, as well as uncertainty regarding the existence or nonexistence of design projects for the building.

Thus, the visual inspection for an initial diagnosis of the problems was effective in identifying damages, although during the analysis of the collected data there may be uncertainty regarding the probable causes, origin, or behavior of the anomalies in order to define the diagnosis. In this sense, to support this diagnosis it is essential to complement with non-destructive tests (ultrasound, radiography—X-rays or gamma rays, rebar detection, among others). As a suggestion for future work, it is recommended to include strategies for structural reinforcement, detailed analyses of the presence and effects of moisture, as well as continuous monitoring of the progression of cracks. These actions may support decision-making regarding the feasibility of use or rehabilitation of the building.

References

AGUIAR, A, A. et. al (2022). Utilização da Matriz GUT na análise das manifestações patológicas em edificações. In: MARINHO, J. L. A; MESQUITA, E. F, T. (org.). Patologia das edificações: Manifestações nas edificações e no patrimônio histórico. 2ª ed. São Paulo: Editora Leud, cap. 1, p. 38-49.

AWASHO, T. T., ALEMU, S. K (2023). Assessment of public building defects and maintenance practices: Cases in Mettu town, Ethiopia. Heliyon, v. 09, n. 04, p. 1-13. https://doi.org/10.1016/j.heliyon.2023.e15052.

ALOMARI, O. M (2022). Identification and Categorization of Building Defects. Civil Engineering and Architecture, v. 10, n. 02, p. 438-446. 10.13189/cea.2022.100204.

ALUCCI, M., FLAUZINO, W., & MILANO, S (1988). Bolor em edifícios: causas e recomendações. Pini, IPT-Instituto de Pesquisas Tecnológicas de São Paulo: São Paulo, 1, 565.

ACCETTI, K. M (1998). Contribuições ao projeto estrutural de edifícios em alvenaria. Dissertação, Universidade de São Paulo, São Carlos.

BROCHADO, J. P. E. R (2016). Desenvolvimento de bolores em edifícios de habitação-Análise de sensibilidade. (Doctoral dissertation, Dissertação (Mestrado em Engenharia Civil) – Universidade do Porto).

BARBOSA, F. et al (2017). Reinventing Construction: A Route to Higher Productivity. Mckinsey Global Institute, in Collaboration with Mckinsey's Capital Projects & Infrastructure Practice.

CARNEIRO, B. M. C., D'ÁVILA, C. A. C., LUÍS, L. L (2018). Influência da NBR 15575:2013 na mudança de abordagem das manifestações patológicas em edificações habitacionais. *In*: MARINHO, J. L. A; COELHO, F. C, A. (org.). Manifestações Patológicas e Reabilitação de Estruturas: Contribuições Relevantes para a melhoria da qualidade e durabilidade das estruturas. 1ª ed. Curitiba: Editora Íthala, Cap. 9, p. 163-177.

CAPORRINO, C. F (2018). Patologias em Alvenarias. 2ª ed. São Paulo: Oficina de Textos. 96 p., ISBN 978-85-7975-304-6.

CINCOTTO, M. A (1988). Patologia das argamassas de revestimento: análise e recomendações in: Tecnologia de Edificações. São Paulo: Ed. Pini. p.549-554.

CINCOTTO, M. A (1989). Patologias das argamassas de revestimento. São Paulo, instituto de Pesquisas Tecnológicas - IPT, 13p., publicação IPT/SP 1801.

CARRARO, C. L (2010). Análise Pós-Obra de Habitações de Interesse Social Visando a Identificação de Manifestações Patologicas. Dissertação de Mestrado. Faculdade de Engenharia Civil, Uberlândia-MG.

CHELLAPPA, V. et al (2020). A knowledge-based approach for enhancing fall prevention in the construction industry. Journal of Statistics and Management Systems, v. 23, n. 2, p. 373- 378. https://doi.org/10.1080/09720510.2020.1736320.

CHELLAPPA, V., SRIVASTAVA, V (2024). Science mapping approach-based review of thermal comfort studies in Indian residential buildings. Journal of Engineering, Design and Technology, v. 22, n. 2, p. 297-315. https://doi.org/10.1108/JEDT-09-2021-0491.

FABIANI, B (1975). Lesões nas edificações. São Paulo. Apostila da disciplina Técnicas da Construção de edifícios, da escola politécnica da universidade de São Paulo, Departamento de engenharia urbana e de construções civis.

FERREIRA, C. R. A (2016). Análise de fissuras e trincas nas alvenarias de vedação: construção de casas em Minas Gerais. (Doctoral dissertation, Monografia – Especialização em Construção Civil, Universidade Federal de Minas Gerais.

FAGUNDES NETO, J. C. P (2008). Perícias de Fachadas em Edificações: Pintura. 1. ed. São Paulo: Editora Leud.

FAZENDA, J. M. R (1995). Aplicações arquitetônicas. In: Tintas e vernizes – ciência e tecnologia, São Paulo, SP: ABARFATI, 2ª ed, p. 855-879.

LIMA JÚNIOR, H. C. et al (2025). Diagnosis of pathological manifestations in popular housing of COHAB in Caruaru, Pernambuco: a forensic approach. Journal of Building Pathology and Rehabilitation, v. 10, n. 68, p. 1-17. 10.1007/s41024-025-00570-3.

LIMA, A. R., D'ÁVILA, C. A. C., KURUSSU, D. T., FERRARI, M. A (2018). Metodologia para realização de perícias em edificações residenciais com manifestações patológicas e elaboração de laudos técnicos. *In*: MARINHO, J. L. A; COELHO, F. C, A. (org.). Manifestações Patológicas e Reabilitação de Estruturas: Contribuições Relevantes para a melhoria da qualidade e durabilidade das estruturas. 1ª ed. Curitiba: Editora Íthala, Cap. 15, p. 269-301.

MARINHO, J. L. A; MESQUITA, E. F, T (2022). Patologia das edificações: Manifestações nas edificações e no patrimônio histórico. 2ª ed. São Paulo: Editora Leud, 296 p., 16x23cm, ISBN 978-85-7456-423-4.

MORAIS, J. M. P. et al (2020). Análises das patologias construtivas: Estudo de caso em uma escola na cidade de Juazeiro do Norte, Ceará, Brasil. Research, Society and Development, v. 09, n. 7, p. 1-25. https://doi.org/10.33448/rsd-v9i7.4421.

OLIVEIRA, A. M (2012). Fissuras, trincas e rachaduras causadas por recalque diferencial de fundações. 2012. Trabalho de Conclusão de Curso (Especialização em Construção Civil) – Universidade Federal de Minas Gerais, Minas Gerais, Belo Horizonte.

POLITO, G (2006). Principais sistemas de pinturas e suas patologias. Apostila Técnica, Universidade Federal de Minas Gerais, Belo Horizonte, março, 1-62.

RESENDE, M. M. et al (2022). Infrared thermal imaging to inspect pathologies on façades of historical buildings: A case study on the Municipal Market of São Paulo, Brazil. Case Studies in Construction Materials, v. 16, p. 1-12. https://doi.org/10.1016/j.cscm.2022.e01122.

SENA, G. O. et al (2020). Patologia das construções. 1ª ed. Salvador: Editora 2B. 256 p., 16x23cm, ISBN 978-85-54815-83-7.

SANTOS JÚNIOR, J. C., SANTOS, J. M. A., SANTOS, M. R. A (2023). Parametric modeling using the BIM methodology for the process of pathology identification in buildings. Journal of Building Pathology and Rehabilitation, v. 8, n. 62, p. 1-12. https://doi.org/10.1007/s41024-023-00311-4.

THOMAZ, E (2020). Trincas em edifícios: causas, prevenção e recuperação. 2ª ed. São Paulo: Oficina de Textos.

Análise das manifestações patológicas nas edificações do Centro Turístico Igreja do Céu no Município de Viçosa do Ceará

Analysis of pathological manifestations in the buildings of the Igreja do Céu Tourist Center in the Municipality of Viçosa do Ceará

Eder Paulus Moraes GUERRA[1] Eduardo de Pádua Araújo de OLIVEIRA[2]

[1] Prof. Me. Universidade Estadual Vale do Acaraú, Sobral, Brasil, eder_paulus@uvanet.br

[2] Eng. Civil Sobral, Brasil, eduardodepadua0202@hotmail.com

Resumo: A conservação e manutenção de edificações históricas são fundamentais para a preservação do patrimônio cultural e arquitetônico de uma sociedade. A importância de manter essas estruturas em bom estado não apenas resguarda o valor histórico e estético, mas também contribui para o desenvolvimento socioeconômico das regiões em que estão inseridas, promovendo o turismo e a identidade cultural local. O presente trabalho tem como objetivo diagnosticar as manifestações patológicas presentes nas edificações do Polo Turístico da Igreja do Céu em Viçosa do Ceará, priorizar as intervenções necessárias para sua conservação e manutenção. Este Polo Turístico abriga a Capela de Nossa Senhora das Vitórias, que é o ponto mais alto da cidade, situada a 900 metros de altitude, no topo do morro que rodeia a cidade. No alto do templo, destaca-se a imagem do Cristo Redentor A metodologia empregada utiliza a Matriz GUT para a priorização das ações de intervenção com base nos dados coletados e analisados considerando a gravidade, urgência e tendência de cada patologia. A preservação do patrimônio histórico tem um impacto significativo no turismo e na economia local. Inicialmente, foi realizada uma inspeção visual detalhada das edificações, identificando as patologias existentes. Este processo facilitou a alocação de recursos e a programação de intervenções com base na criticidade e no potencial de risco para a segurança, funcionalidade e conservação das edificações. Esta metodologia proporciona um framework detalhado para o diagnóstico e planejamento de ações de conservação no Polo Turístico da Igreja do Céu. A abordagem integrada e fundamentada em normas técnicas e ferramentas analíticas estratégicas permitem uma avaliação precisa das condições das edificações, assegurando intervenções eficazes que respeitam e preservam o valor histórico e cultural do local. A implementação de um plano de ação bem fundamentado é importante para a manutenção de sua integridade estrutural.

Palavras-chave: Inspeção predial; Manifestações patológicas; Matriz GUT.

Abstract: The conservation and maintenance of historical buildings are fundamental for the preservation of a society's cultural and specialized heritage. Maintaining these structures in good condition not only safeguards their historical and aesthetic value but also contributes to the socioeconomic development of the regions in which they are located, promoting tourism and local cultural identity. This work aims to diagnose the pathological manifestations present in the buildings of the Igreja do Céu Tourist Center in Viçosa do Ceará, prioritizing the necessary interventions for their conservation and maintenance. This Tourist Center houses the Chapel of Nossa Senhora das Vitórias, which is the highest point in the city, situated at 900 meters altitude, on the top of the hill surrounding the city. At the top of the temple, the image of Christ the Redeemer stands out. The methodology employed uses the GUT Matrix to prioritize intervention actions based on the data found and detailed, considering the severity, urgency, and trend of each pathology. The preservation of historical heritage has a significant impact on tourism and the local

economy. Initially, a detailed visual inspection of the buildings was carried out, identifying existing pathologies. This process facilitated the allocation of resources and the scheduling of interventions based on the criticality and potential risk to the safety, functionality, and conservation of the buildings. This methodology provides a detailed framework for the diagnosis and planning of conservation actions in the Igreja do Céu Tourist Area. The integrated approach, grounded in technical standards and strategic analytical tools, allows for a precise assessment of the buildings' conditions, ensuring effective interventions that respect and preserve the historical and cultural value of the site. The implementation of a well-founded action plan is important for maintaining its structural integrity.

Keywords: Building inspection; Pathological manifestations; GUT matrix.

1. Introdução

A conservação e manutenção de edificações históricas são fundamentais para a preservação do patrimônio cultural e arquitetônico de uma sociedade. A importância de manter essas estruturas em bom estado não apenas resguarda o valor histórico e estético, mas também contribui para o desenvolvimento socioeconômico das regiões em que estão inseridas, promovendo o turismo e a identidade cultural local (Lourenço; Oliveira 2004; Avelino, 2013). Nesse contexto, o diagnóstico preciso das manifestações patológicas presentes nessas edificações e a priorização de intervenções são essenciais para assegurar sua longevidade e funcionalidade, preservando seu valor histórico.

O Polo Turístico da Igreja do Céu, localizado em Viçosa do Ceará, constitui um exemplo notável de patrimônio histórico que necessita de intervenções constantes para a sua preservação. Com edificações que datam do século XIX, como a Igreja Nossa Senhora das Vitorias, fundada em 1938, a manutenção dessas estruturas envolve desafios significativos devido à idade, aos materiais utilizados e às técnicas construtivas da época (Luz 2015). A falta de intervenções regulares pode resultar na deterioração acelerada dessas edificações, comprometendo sua integridade estrutural e valor histórico (Rodrigues 2012; Silva 2017).

O presente trabalho tem como objetivo diagnosticar as patologias presentes nas edificações do Polo Turístico da Igreja do Céu e estabelecer uma priorização para as intervenções necessárias. A abordagem metodológica integra inspeções visuais detalhadas, análises técnicas e a aplicação da Matriz GUT, oferecendo um framework robusto para o planejamento e execução de ações de conservação (Carvalho 1994; Hédis et al., 2013). Este Polo Turístico abriga a Capela de Nossa Senhora das Vitórias, fundada por Monsenhor José Carneiro da Cunha e dedicada a Nossa Senhora das Vitórias. A capela é o ponto mais alto da cidade, situada a 900 metros de altitude, no topo do morro que rodeia a cidade. No alto do templo, destaca-se a imagem do Cristo Redentor, esculpida pelo italiano Agostinho Odísio Balmes em 1937 e inaugurada pelo Bispo José Tupinambá da Frota, da Diocese de Sobral, em 14 de agosto de 1938.

A igreja passou por duas reformas significativas em menos de 20 anos. A primeira, em 1998, resultou na criação do Polo Turístico, Artesanal e Cultural Igreja do Céu, o qual é o foco deste estudo. A segunda reforma, ocorrida em 2016, incluiu a construção de áreas de lazer, estacionamento, restaurantes e uma área de eventos.

As manifestações patológicas presentes em edificações mais antigas causam sérios problemas à vida útil e à durabilidade das estruturas, manifestando-se em diversos tipos e quantidades. No Polo Turístico Igreja do Céu em Viçosa do Ceará, existem edificações recentes, reformadas em 2019, e outras antigas do século XX, como a Igreja de Nossa Senhora das Vitórias. Esta última, apesar de sua importância histórica, passou por uma reforma entre 2019 e 2020 após a queda de sua torre, um evento que despertou maior interesse pela inspeção do local.

A inspeção predial auxilia na identificação, na classificação e nas recomendações de soluções para essas patologias. Já a análise GUT (Gravidade, Urgência e Tendência) prioriza as ações em termos de gravidade, urgência e tendência, sendo de fácil implementação e baixo custo. Este trabalho tem como objetivo mapear e classificar as patologias presentes nas edificações do Polo Turístico Igreja do Céu através da matriz GUT, visando garantir a preservação e a segurança das estruturas, em um local turístico echistórico.

1.1 Matriz de GUT na construção civil: definição, funcionamento e importância

De acordo com Fávere e Silva (2016) foi frente à necessidade de obter resolução para problemas complexos dentro da indústria americana e também da japonesa, no século XX, mais especificamente por volta de 1980, que Charles H. Kepner e Benjamin B. Trego desenvolveram uma ferramenta que ficou conhecida pela nomenclatura “matriz GUT” com o objetivo de fornecer às indústrias uma forma de apresentar solução ao seus problemas.

Gravidade (G):

Avalia o impacto do problema caso ele não seja resolvido. Um problema é considerado grave se causar danos ou comprometer a segurança e o funcionamento de processos ou sistemas. A gravidade é geralmente avaliada em uma escala de 1 a 5, onde 1 representa um impacto mínimo e 5 indica um impacto extremamente severo.

Urgência (U):

Mede o tempo disponível para resolver o problema antes que ele cause consequências mais graves. Um problema é urgente se exigir uma solução imediata para evitar que a situação se agrave. A urgência também é avaliada em uma escala de 1 a 5, onde 1 significa que o problema pode esperar e 5 indica que precisa ser resolvido imediatamente.

Tendência (T):

Avaliar a probabilidade de o problema piorar com o passar do tempo não for solucionado. Um problema com uma tendência alta pode se agravar rapidamente, aumentando seu impacto e urgência. A tendência é medida em uma escala de 1 a 5, onde 1 representa uma tendência de piora mínima e 5 indica uma tendência de agravamento muito rápida.

Figura 1- Referência de valores da Matriz de GUT

MATRIZ GUT				
Ptos	**G** **Gravidade** Consequências se nada for feito.	**U** **Urgência** Prazo para tomada de decisão.	**T** **Tendência** Proporção do problema no futuro.	**G x U x T**
5	Os prejuízos ou dificuldades são extremamente graves.	É necessária uma ação imediata.	Se nada for feito, o agravamento da situação será imediato.	5 x 5 x 5 **125**
4	Muito graves.	Com alguma urgência.	Vai piorar em curto prazo.	4 x 4 x 4 **64**
3	Graves.	O mais cedo possível.	Vai piorar em médio prazo.	3 x 3 x 3 **27**
2	Pouco graves.	Pode esperar um pouco.	Vai piorar em longo prazo.	2 x 2 x 2 **8**
1	Sem gravidade.	Não tem pressa.	Não vai piorar ou pode até melhorar.	1 x 1 x 1 **1**

Fonte: Daychoum (2018)

1.2 Patologias em edificações históricas

As manifestações patológicas em edificações são problemas construtivos que surgem devido a diversas falhas ao longo das etapas do ciclo de vida da construção. Essas falhas podem ocorrer em diferentes fases, incluindo projeto, fabricação, execução, uso e manutenção. Com base em normas e estudos, como a NBR 15575 e outras literaturas especializadas, é possível identificar e compreender melhor as causas das patologias mais comuns.

Em 2012, o Instituto Brasileiro de Avaliações e Perícias de Engenharia (IBAPE), disponibilizou a Norma de Inspeção Predial Nacional, pela qual é possível se obter diretrizes e critérios para a análise de manifestações patológicas através de vistorias.

A partir desta norma, podemos classificar as patologias quanto à sua natureza, nível e grau. De acordo com o grau de risco, as falhas patológicas são classificadas como:

- Grau crítico, que gera riscos à saúde e segurança, com perda de funcionalidade, desempenho e de vida útil - das estruturas.
- Grau médio, que gera perda precoce do desempenho e funcionamento das estruturas; e,
- Grau mínimo, verificada por pequenas falhas, que não comprometem o desempenho das estruturas, por hora.

Para aplicabilidade das vistorias, o IBAPE também as dividiu em 3 níveis, que são:

- Nível 1: Aplicável às vistorias de grandes canteiros, quando o número de imóveis existentes na área de influência da obra seja muito elevado.
- Nível 2: Que deve contemplar uma descrição básica e objetiva do objeto vistoriado, das anomalias e falhas constatadas e uma ilustração fotográfica suficiente para caracterizar sua tipologia, padrão construtivo, estado de conservação, anomalias e falhas existentes.
- Nível 3: Que contempla todos os elementos relacionados no Nível 2 e apresenta uma completa caracterização de revestimentos de piso, parede e forro, esquadrias e elementos aderidos que sejam significativos, além de todos os elementos construtivos que possam ser relevantes para uma completa descrição do imóvel.

1.3 Classificação das anomalias

De acordo com a NBR 16747:2020, as anomalias podem ser classificadas em diversas categorias, tais como:

- Fissuras e Trincas: São aberturas ou separações na estrutura do edifício que podem indicar problemas estruturais graves.

- Infiltrações: Indicam a presença de água nas superfícies, o que pode levar à degradação dos materiais de construção.

- Corrosão: Degradação de elementos metálicos, geralmente causada por exposição à umidade e agentes corrosivos.

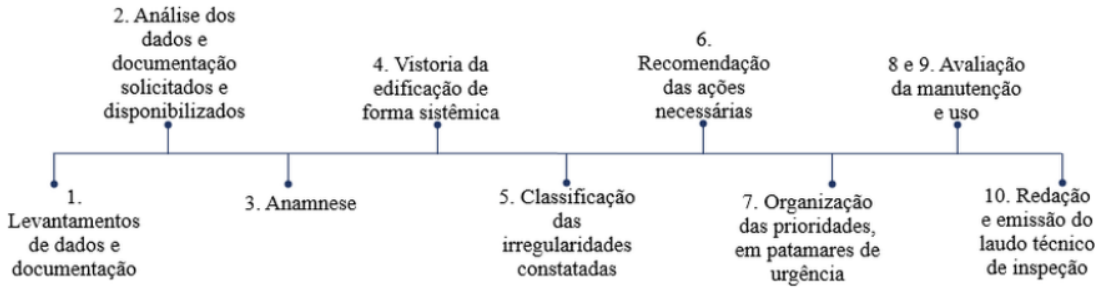
- Destacamento de Revestimentos: Separação de camadas de revestimento das superfícies subjacentes, muitas vezes devido à má aderência ou umidade.

Segundo a NBR 15575 (ABNT, 2013), a vida útil de projeto (VUP) é o período estimado para o qual a construção foi projetada, atendendo aos requisitos de desempenho. Este período pode ser prolongado mediante manutenções corretivas apropriadas. A norma enfatiza que é crucial que os usuários realizem

todas as ações de manutenção para assegurar que a vida útil projetada seja alcançada. Algumas manifestações patológicas podem surgir devido ao uso inadequado ou à falta de manutenção.

A Associação Brasileira de Normas Técnicas (ABNT) estabelece diversas diretrizes para a inspeção e manutenção de edificações. A NBR 16747:2020, por exemplo, detalha os procedimentos para inspeção predial, incluindo conceitos, terminologia e métodos de avaliação (ABNT, 2020). Esta norma é fundamental para assegurar que as inspeções sejam realizadas de forma sistemática e padronizada, garantindo a identificação correta das patologias e a implementação de medidas corretivas eficazes.

Figura 2-Etapas metodológicas da inspeção predial, conforme NBR 16747



Fonte: ABNT (2020)

A NBR 15575:2013 da ABNT estabelece critérios de desempenho para edificações habitacionais, abordando aspectos como segurança, habitabilidade e sustentabilidade. Esta norma é fundamental para a classificação de anomalias e definição de intervenções necessárias para manter o desempenho adequado das edificações ao longo de sua vida útil de projeto (VUP). A adoção dessas diretrizes é especialmente importante em edificações históricas, onde a preservação das características originais deve ser balanceada com a necessidade de garantir segurança e funcionalidade.

1.3.1 Importância na construção civil

A construção civil se beneficia enormemente da Matriz GUT, pois ela permite gerenciar eficientemente os riscos e assegura que os recursos sejam alocados onde mais forem necessários. Ela é utilizada para priorizar reparos em defeitos de construção como fissuras ou infiltrações, decidir sobre atualizações de segurança em edifícios antigos, e programar manutenções preventivas, garantindo que problemas críticos sejam tratados primeiro, conforme sugerido por Meireles (2001) e Sotille (2014) ao discutirem a integração da Matriz GUT com outras metodologias de gestão.

Os principais benefícios da Matriz GUT incluem a capacidade de priorizar de forma objetiva as ações de intervenção, garantindo que os recursos sejam direcionados para as áreas de maior necessidade. A ferramenta também facilita a comunicação entre os diferentes stakeholders envolvidos na preservação das edificações históricas, proporcionando uma base clara e racional para a tomada de decisões. (Scartezini, 2009).

1.4 Técnicas de conservação e restauro

1.4.1 Técnicas invasivas e não invasivas

As técnicas de conservação e restauro podem ser classificadas como invasivas ou não invasivas, dependendo do grau de intervenção necessário. Rodrigues (2012) e Avelino (2013) enfatizam que as

intervenções devem ser minimamente invasivas e, sempre que possível, reversíveis, para preservar as características históricas e arquitetônicas das edificações. Técnicas não invasivas incluem limpeza superficial e reparos menores, enquanto técnicas invasivas podem envolver a substituição de elementos estruturais.

1.4.2 Materiais e métodos compatíveis

A escolha dos materiais e métodos de restauro deve ser compatível com os originais utilizados na construção da edificação. Isso é crucial para manter a integridade histórica e estrutural do edifício. Estudos de caso demonstram que a utilização de materiais inadequados pode levar a novas patologias, agravando os problemas existentes (Silva 2017).

2. Metodologia

Para avaliação das patologias nas edificações do Polo Turístico da Igreja do Céu, foi realizada integração das diretrizes da ABNT NBR 16747:2020 (ABNT 2020) e utilização da Matriz GUT, conforme descrito por Kepner e Tregoe (1981), para a priorização das ações de intervenção. O processo metodológico inclui técnicas de inspeção visual e análise técnica detalhada, objetivando elaborar um plano de ação que atenda às necessidades de conservação, restauro e manutenção das edificações, assegurando a preservação de sua integridade estrutural e valor histórico.

O diagnóstico das condições atuais das edificações e a subsequente priorização das intervenções são divididos nas seguintes etapas:

Inspeção Visual Detalhada: constitui a etapa inicial do diagnóstico, sendo crucial para a identificação preliminar de manifestações patológicas. Esta fase segue recomendações de especialistas (Carvalho 2009; Meireles 2001), adaptadas às peculiaridades das edificações históricas, enfatizando a necessidade de um olhar atento e sistematizado para capturar detalhes que possam indicar a presença de deterioração ou falhas estruturais;

Análise Técnica e Diagnóstico das Patologias: a identificação das causas das patologias é apoiada por uma revisão bibliográfica abrangente, incluindo referências como a NBR 15575 (ABNT 2013), que oferece diretrizes sobre desempenho de edificações habitacionais e critérios para a classificação de anomalias.

E com base nos dados coletados e analisados, as patologias são classificadas e priorizadas utilizando a Matriz GUT. A implementação das ações de intervenção é planejada com base nas prioridades estabelecidas, levando em consideração as melhores práticas em conservação de edificações históricas e as especificidades do patrimônio em estudo. A seleção de técnicas de restauro e reparo é guiada tanto pela eficácia em resolver as patologias identificadas quanto pela compatibilidade com os materiais e métodos construtivos originais das edificações, seguindo princípios de preservação histórica e sustentabilidade.

Esta metodologia proporciona um framework detalhado para o diagnóstico e planejamento de ações de conservação no Polo Turístico da Igreja do Céu. A abordagem integrada e fundamentada em normas técnicas e ferramentas analíticas estratégicas permite uma avaliação precisa das condições das edificações, assegurando intervenções eficazes que respeitam e preservam o valor histórico e cultural do local. A implementação de um plano de ação bem fundamentado e priorizado é crucial para a manutenção da integridade estrutural das edificações e para a continuidade da sua utilização e apreciação por gerações futuras.

3. Resultados e Discussões

Durante a inspeção realizada, foi possível identificar diversas patologias que se repetem em diferentes áreas do Polo Turístico Igreja do Céu.

Tabela 1- Resumo das principais patologias encontradas e suas localizações específicas.

MAPEAMENTO DAS MANIFESTAÇÕES PATOLOGICAS																					
MANIFESTAÇAO PATOLOGICA	AMBIENTE																				AMBIENTES PRESENTES
	1	2	3	4	5	6	7	8	9	10	11	12	13	14	15	16	17	18	19	20	21	
FISSURA			X				X	X	X	X	X	X				X				X	X	10
TRINCA			X					X	X	X	X	X				X				X	X	9
RACHADURA		X				X											X		X			4
FENDA		X															X					2
BRECHA																	X					1
AFUNDAMENTO		X			X					X			X		X							5
DESLIZAMENTO	X																					1
EFLORECENCIA			X	X								X						X				4
MANCHA DE HUMINDADE	X			X		X	X	X	X	X	X	X	X	X	X	X	X	X	X		X	17
DESTACAMENTO DA PINTURA				X												X		X				3

Fonte: Autor (2024)

Figura 3-Localização dos pontos do polo turístico igreja do céu

LEGENDA	
1	ESTACIONAMENTO
2	RAMPA DE ACESSO 01
3	ESCADARIA DE ACESSO AS LOJAS
4	PALCO DE EVENTOS
5	RAMPA DE ACESSO PRINCIPAL
6	LOJA DE ARTESANATO 01
7	LOJA DE ARTESANATO '02
8	BANHEIRO MASCULINO 01
9	BANHEIRO FEMININO, INFANTIL E FRALDARIO 01
10	LANCHONETE 01
11	LANCHONETE 02
12	BANHEIROS FEMININO E MASCULINO 02
13	PLAYGROUD
14	CALÇADÃO 01
15	CALÇADÃO 02
16	IGREJA NOSSA SENHORA
17	ESCADARIA PRINCIPAL
18	SECRETARIA DE TURISMO
19	AREA DE EVENTOS
20	PISTA DE SKATE
21	RESTAURANTE

Fonte: Autor (2024)

3.1 Manifestações patológicas identificadas

3.1.1 Manchas de Umidade

Presentes em quase todos os ambientes do polo, essas manchas indicam problemas de infiltração e falta de impermeabilização adequada. A umidade constante pode levar à contaminação por fungos, comprometendo a saúde dos frequentadores e a durabilidade das construções.

Figura 4-Manchas de umidade na fachada Sudeste do palco de eventos



Fonte: Autor (2024)

3.1.2 Infiltrações

Devido à falta de acesso às partes internas das lojas e restaurantes na praça de alimentação, as infiltrações foram observadas apenas na Igreja Nossa Senhora das Vitórias. Essas infiltrações podem levar a problemas estruturais e estéticos ao longo do tempo.

3.1.3 Fissuras

Encontradas em 10 ambientes diferentes do polo, incluindo paredes externas e internas de diferentes edificações. Essas fissuras podem ser causadas por manuseio do solo, variações térmicas ou falhas na execução e uso de materiais inadequados.

3.1.4 Trincas

Apresentadas em 9 ambientes, as trincas são um tipo de fissura mais profunda e podem indicar problemas estruturais mais graves que devem ser tratados para evitar maiores danos.

3.1.5 Rachaduras

Identificadas em 4 ambientes, as rachaduras podem comprometer a integridade das edificações, necessitando de atenção mais elevada para evitar riscos maiores.

Figura 5-Rachadura no topo do muro de contenção



Fonte: Autor (2024)

3.1.6 Fendas

As fendas, apresentadas em 2 ambientes, possuem maior dimensão e representam uma preocupação significativa. Encontradas no muro de contenção próximo à pista de skate e na escadaria principal, essas falhas indicam problemas graves e devem ser monitoradas de perto para evitar danos maiores.

3.1.7 Brechas

Apresentada em 1 ambiente, as brechas são aberturas muito grandes que indicam sérios problemas estruturais ou colapsos parciais. Essas brechas representam um risco significativo à integridade estrutural e à segurança dos ocupantes e requerem intervenção. A presença dessas brechas em elementos estruturais e não estruturais pode permitir a infiltração de água, agravando problemas de umidade e comprometendo a durabilidade das construções.

3.1.8 Fundamentos

Apresentados em 5 ambientes, os achados foram identificados em diversas áreas das calçadas ao longo do polo. Esses fundamentos são sinais de problemas no subsolo ou má compactação do solo, que podem comprometer a segurança e acessibilidade do local.

3.1.9 Deslizamentos

Correndo em 1 ambiente, as ameaças indicam instabilidade do solo que pode afetar a segurança das construções e dos visitantes, necessitando de intervenções imediatas quando em áreas de grande movimentação.

3.1.10 Eflorescência

Presente em 4 ambientes, a eflorescência é um sinal de infiltração de água nas paredes, causando o aparecimento de depósitos de sais que comprometem a estética e a integridade dos revestimentos.

3.1.11 Descascamento da pintura

Identificado em 3 ambientes, o descascamento da pintura indica problemas de umidade e infiltração, além de possíveis falhas na qualidade da pintura e revestimento, necessitando de reparos para preservar a aparência e proteção das superfícies.

Figura 6-Descascamento de pintura e eflorescência no palco de evento



Fonte: Autor, (2024)

Para priorizar as ações corretivas e de manutenção no Polo Turístico Igreja do Céu, será utilizada a matriz GUT, uma ferramenta eficaz para a avaliação e classificação de problemas com base em três critérios principais: Gravidade, Urgência e Tendência. A aplicação da matriz GUT permite uma análise sistemática das patologias identificadas, auxiliando na determinação das intervenções mais críticas e imediatas.

- Gravidade (G): Avalia o impacto potencial da patologia, considerando os danos que ela pode causar à estrutura, à funcionalidade e à segurança dos usuários.

- Urgência (U): Determina o tempo disponível para a tomada de ações corretivas, priorizando as patologias que requerem intervenções imediatas.

- Tendência (T): Analisa a probabilidade de agravamento da patologia ao longo do tempo, considerando a velocidade com que o problema pode se tornar mais sério.

A seguir, será apresentada a classificação das principais patologias encontradas no Polo Turístico Igreja do Céu através da matriz GUT, proporcionando uma visão clara das prioridades de manutenção e reparo necessárias para garantir a integridade e segurança do local:

Figura 7-Manifestações Patológicas Identificadas no Pólo Turístico Igreja do Céu

MPI 01	Infiltrações e Marcas de Umidade no Palco de shows
MPI 02	Descascamento de Pintura e Eflorescência no Palco de Eventos
MPI 03	Deslizamentos de Terra e Desplacamento do Talude no Estacionamento
MPI 04	Afundamento e Acúmulo de Água em Bloquetes Intertravados na Rampa de acesso
MPI 05	Rachaduras e Fendas em Muro de Contenção de Pedra
MPI 06	Rachaduras nas Lojas de Artesanato
MPI 07	Afundamento do Solo no Jardim Acima do Muro de Contenção
MPI 08	Fissuras, Trincas e Rachaduras nas Paredes Externas do Primeiro Conjunto de Banheiros
MPI 09	Trincas e Fissuras na Igreja de Nossa Senhora das Vitórias
MPI 10	Rachaduras e Fendas na Escadaria
MPI 11	Afundamento do Calçamento em Frente à Escadaria
MPI 12	Manchas de Umidade e Infiltrações na Igreja Nossa Senhora das Vitórias

Fonte: Autor (2024).

Para tratar as trincas e fissuras identificadas, recomenda-se:

-Monitoramento Regular: Acompanhar o desenvolvimento das trincas e fissuras com inspeções periódicas e utilizar técnicas de monitoramento, como marcadores de trinca, para avaliar a evolução e identificar a necessidade de intervenções imediatas.

-Ensaios Não Destrutivos: Realizar ensaios não destrutivos, como ultrassom e termografia, para avaliar o estado interno da estrutura sem causar danos adicionais.

-Reparos Estruturais: Onde necessário, executar reparos estruturais, incluindo a selagem das trincas com materiais adequados e a aplicação de reforços para estabilizar a estrutura.

-Reforço da Fundação: Em caso de movimentação da fundação, pode ser necessário reforçar a fundação da igreja para evitar novas movimentações e assegurar a estabilidade da edificação.

Para as rachaduras e brechas na escadaria, deve-se proceder com:

- A investigação Geotécnica: Realizar um estudo geotécnico para avaliar as condições do solo e identificar a extensão do problema.

- Recompactação do Solo: Caso a compactação inadequada seja confirmada, proceder à recompactação do solo com técnicas apropriadas.
- Melhoria da Drenagem: Implementar um sistema de drenagem eficiente para evitar a acumulação de água e a subsequente desestabilização do solo.
- Reparo da escadaria: Reconstruir as áreas afetadas do piso e muretas, assegurando que a fundação e o solo subjacente estejam adequadamente tratados.
E para correção do afundamento do solo, deve-se recompactar o solo, reforçar o muro de contenção e melhorar a drenagem.

4. Conclusão

Este trabalho apresentou um diagnóstico detalhado das patologias presentes nas edificações do Polo Turístico da Igreja do Céu, em Viçosa do Ceará, utilizando uma metodologia integrada que incluiu inspeções visuais detalhadas e a aplicação da Matriz GUT para a priorização das intervenções necessárias. A pesquisa evidenciou a importância de uma abordagem sistemática e fundamentada em normas técnicas para garantir a conservação e manutenção eficazes de edificações históricas, assegurando a preservação do valor cultural e arquitetônico do local.
Os resultados obtidos destacaram a necessidade de intervenções urgentes em algumas áreas críticas, devido à gravidade das patologias identificadas, como infiltrações, fissuras e destacamento de revestimentos. A aplicação da Matriz GUT foi fundamental para facilitar a alocação de recursos e a programação de ações corretivas, assegurando que as intervenções fossem realizadas de maneira eficiente e direcionada, priorizando a segurança, funcionalidade e preservação das edificações.
As principais intervenções prioritárias são as fendas presentes no muro de contenção, que apresentam o maior grau de risco devido ao seu potencial de comprometimento estrutural significativo. Em seguida, vêm as brechas presentes na escadaria, que também geram riscos graves à segurança dos usuários. É igualmente crucial dar atenção às rachaduras presentes na Igreja Nossa Senhora das Vitórias, pois este é um local onde já ocorreu um incidente de desabamento, ressaltando a necessidade de medidas preventivas rigorosas.
A recuperação de revestimentos deteriorados é importante para manter a integridade estética e histórica das edificações, garantindo a compatibilidade dos novos materiais com os originais. A prevenção de eflorescências e bolores requer a aplicação de tratamentos antifúngicos e hidrofóbicos, a fim de reduzir a umidade e prevenir a formação de bolores e eflorescências.
A manutenção contínua e a inspeção regular das edificações são igualmente importantes para monitorar a eficácia das intervenções e prevenir o surgimento de novas patologias. A adoção de um plano de manutenção preventiva é essencial para prolongar a vida útil das construções e evitar a deterioração acelerada.
Portanto, a execução de um plano de ação bem fundamentado e priorizado é crucial para a manutenção da integridade estrutural das edificações do Polo Turístico da Igreja do Céu e para a continuidade de sua utilização e apreciação pelas gerações futuras. A preservação eficaz das edificações históricas não só garante a proteção de um legado arquitetônico inestimável, mas também fortalece o vínculo da comunidade com sua herança cultural, impulsionando o turismo e o desenvolvimento socioeconômico da área.

Referências

ABNT. NBR 15575: Edificações Habitacionais – Desempenho. Associação Brasileira de Normas Técnicas, 2013.

ABNT. NBR 5674: Manutenção de edificações – Requisitos para o sistema de gestão de manutenção. Associação Brasileira de Normas Técnicas, 2012.

Anais da XXIX semana de história da Universidade de Juiz de Fora-2012.

Andrade, R. T., & Henrique, R. C. 2012. Mapeamento de danos como ferramenta na manutenção do patrimônio arquitetônico: o caso do Mercado Eufrásio Barbosa.

Associação Brasileira de Normas Técnicas. ABNT NBR 15575: Edificações habitacionais — Desempenho. Rio de Janeiro, 2013.

Associação Brasileira de Normas Técnicas. ABNT NBR 16747: Inspeção predial — Diretrizes, conceitos, terminologia e procedimento. Rio de Janeiro, 2020.

Associação Brasileira de Normas Técnicas. 2012. NBR 5674 – Manutenção de edificações – Requisitos para o sistema de gestão de manutenção. Rio de Janeiro.

Associação Brasileira de Normas Técnicas. 2013. NBR 15575 – Edificações habitacionais – Desempenho. Rio de Janeiro.

Brandão, JC Patologia das Construções. Editora ABC, 2007.

Carvalho, E.K. de. Desenvolvimento de Metodologia para Manutenção de

Carvalho, E.K. de. Desenvolvimento de Metodologia para Manutenção de Estruturas de Concreto Armado. Dissertação (Mestrado em Engenharia Civil) – Universidade de Brasília, Brasília, 1994.

Carvalho, E.K. de. Inspeção de edifícios: abordagem prática das patogenias. São Paulo: Pini, 2009.

Estruturas de Concreto Armado. Dissertação (Mestrado em Engenharia Civil) – Universidade de Brasília, Brasília, 1994.

FÁVERI, Rafael; SILVA, Alexandre. MÉTODO GUT APLICADO À GESTÃO DE RISCO DE DESASTRES: UMA FERRAMENTA DE AUXÍLIO PARA HIERARQUIZAÇÃO DE RISCOS. Revista Ordem Pública. p 93 – 107. v. 9, n. 1, jan./jun., 2016

França, F. C. et al. Diagnóstico e prevenção de patologias em edifícios. Revista Engenharia Civil, v. 8, n. 3, p. 54-67, 2011.

Fernandes, J.; Amaral, K.; Brandão, F.; Betti, M.; Silva, M.; Mesquita, E. Caracterização dos danos da Igreja de Nossa Senhora das Vitórias. In: Congresso Brasileiro de Patologia das Construções (CBPAT), 2018, Fortaleza. Anais [...]. Fortaleza: CBPAT, 2018.

Grandiski, P. 2004. Olhar de perito. Revista Téchne, São Paulo, edição 87, ano 12, junho de 2004. p. 24-26.

Hédis, H.R. et al. 2013. Análise GUT e a gestão da informação para tomada de decisão em uma empresa de produtos orgânicos do Rio Grande do Norte. Revista Tecnologia.

Helene, P. 1981. Patologia em Estruturas de Concreto Armado. Editora Pini.

Helene, P. 1981. Quantificação das Origens das Patologias em Edificações. In: Revista de Engenharia Civil.

Kepner, C.H.; Tregoe, B.B. 1981. The New Rational Manager. Princeton, NJ: Princeton Research Press.

Lourenço, Paulo B.; Oliveira, Daniel V. 2004. Recomendações para a análise, conservação e restauro estrutural do património arquitectónico. Guimarães: Universidade do Minho.

Luz, John Kennedy Ferreira da. 2015. A face popular da arquitetura do espetáculo: O Ecletismo como símbolo de transformações sociais no Cabo de Santo Agostinho/PE (1900-1935).

Meira, G. 2017.Corrosão em Estruturas de Concreto Armado: Causas e Efeitos. In: Manual de Patologia das Construções.

cinpar2026
XXII International Conference on Building Pathology and Constructions Repair
15th to 17th July 2026 - Lisboa, Portugal

USE OF THE GUT MATRIX IN THE ANALYSIS OF PATHOLOGICAL MANIFESTATIONS IN HOUSING UNITS OF THE MINHA CASA MINHA VIDA PROGRAM: A CASE STUDY

Lucas Menezes de FARIAS[1], **Jefferson Luiz Alves MARINHO**[2]

[1] Universidad Regional do Cariri – URCA, Juazeiro do Norte-CE, Brazil, lucasmenezes547@gmail.com
[2] Universidad Regional do Cariri – URCA, Juazeiro do Norte-CE, Brazil, jeff.marinho@urca.br

Abstract: In Brazil, the production of social housing is highly concentrated in the *Minha Casa Minha Vida* Program (PMCMV), aimed at low-income families. This Federal Government Program is part of a broad housing policy designed to eradicate the housing deficit, which, according to the João Pinheiro Foundation (2023), amounts to 5.97 million homes, with the Southeast and Northeast regions concentrating most of this deficit. Various pathological manifestations are frequently identified in these housing units, such as cracks, fractures, fissures, and leaks, often occurring in the early stages of use. This study aims to apply the GUT Matrix methodology (Gravity, Urgency, and Trend) in the analysis of pathological manifestations, using a sample of 7 (seven) data points from a total of 37 (thirty-seven) housing units in the Manoel Raimundo de Santana Filho Residential Complex of the PMCMV, located in Juazeiro do Norte - CE. The data were obtained through a company outsourced by *Caixa Econômica Federal*, and a documentary analysis was conducted on the residential unit projects (floor plan and subdivision plan), technical reports, inspection reports, recovery budgets, as well as photographic records of the inspected units. After the analysis, the pathological manifestations were classified and quantified through visual inspection, and based on this, a priority chart was prepared using the GUT method. It was observed that the pathological manifestation related to differential foundation settlement has the highest priority level, and that cracks, fractures, and leaks are the most frequent manifestations. It was possible to conclude the effectiveness of the GUT matrix as a tool for developing an efficient recovery plan, considering the degree of priority for repairing the affected units, especially those that compromise the safety of the building, its users, third parties, as well as its aesthetics.
Keywords: Pathological Manifestations. GUT Matrix. *Minha Casa Minha Vida* Program.

1. Introduction

The construction sector plays a crucial role in the country's economic development, as it generates a significant number of jobs, contributing to the reduction of unemployment and helping to address the housing deficit.

The *Minha Casa Minha Vida* Program (PMCMV) is a housing initiative created by the Federal Government in March 2009, managed by the Ministry of Cities with the participation of collegiate bodies responsible for the program's financing funds. These entities provide subsidies and reduced interest rates for housing loans in both urban and rural areas, targeting low-income families and aiming to reduce Brazil's housing deficit (Brazil, 2023).

Beyond the financial support conditions offered by PMCMV, it is crucial to emphasize that housing quality plays a fundamental role in making the investment worthwhile. Although engineering technologies and the construction materials industry have evolved, various types of pathological manifestations are still observed in PMCMV buildings, and their early appearance is the focus of this research.

The emergence of pathological manifestations within a short period of use in social housing has motivated several academic studies on the subject, given that PMCMV has significant representation in the country's economy, driving both the real estate sector and the construction industry itself, and generating numerous direct and indirect jobs.

In this context, the implementation of the program has been consolidated as a public policy to reduce Brazil's housing deficit. Currently, in the city of Juazeiro do Norte-CE, for example, projects under construction include the Residencial Mirante da Serra I and II, located in the Pedrinhas neighborhood, totaling 384 housing units, and the Residencial Beata Maria de Araújo I and II, located in the São José neighborhood, with 424 units. Together, these two developments comprise 808 housing units under construction in Juazeiro do Norte, scheduled to be delivered to the population this year.

According to Sena *et al*. (2020), pathological manifestations are understood as degradations identified in buildings, which may arise during the construction phase (due to the use of inappropriate methods or materials), during project design, or over time because of misuse or inadequate use of the building.

In general, Marinho and Mesquita (2022) state that the results converge toward the finding that problems arising from pathological manifestations range from minor damage to compromising the safety of buildings, potentially culminating in structural collapse. In this regard, Aguiar *et al*. (2022) argue that knowledge and treatment of building failures contribute to extending its service life, while also providing significant safety for users. Supporting this view, Resende *et al*. (2022) affirm that by investigating and understanding these manifestations, it is possible to identify the causes of deterioration and take measures to prevent further damage to the building and financial losses to owners.

Within this context, pathological manifestations may be related to improper use of the building, lack of maintenance, natural material wear, exposure to adverse weather conditions, or design and construction errors. These manifestations can affect the stability, safety, and functionality of the building, as well as reduce its durability (Santos Júnior; Santos; Santos, 2023).

There are several processes and methods for identifying pathological manifestations in construction, ranging from visual analysis—consisting of inspecting the surface of structures for signs of failures or damage—to more complex tests such as ultrasonography, thermography, and chemical analyses (Santos Júnior; Santos; Santos, 2023).

In this regard, Camargo and Ferrari (2021) state that non-destructive testing (NDT) techniques allow for the evaluation of the quality and integrity of a building without compromising its structure and are widely used for various purposes in the construction industry.

Thus, risk management of anomalies and pathologies is applied when it becomes necessary to prioritize actions among a range of alternatives. From the inspection of a structure, anomalies, failures, and defects are identified, but corrective actions must be prioritized (Knapp; Olivan, 2021).

A methodology that establishes a risk criterion for anomalies and pathologies, translating qualitative assessment into a quantitative indicator of building performance, enables comparative, uniform, and impartial classification. Standardized evaluation criteria based on pre-established parameters make it possible to systematize risk analyses in an analytical manner (Knapp; Olivan, 2021).

Accordingly, the authors further state that the application of the GUT method (Gravity, Urgency, and Trend) makes it possible to compare the performance of the same structure throughout its service life (maintenance management) and/or to compare multiple structures (investment prioritization criteria).

The GUT Matrix methodology aligns with the objectives of NBR 15575-1:2024 – Residential Buildings – Performance – Part 1: General Requirements (ABNT, 2024) and reinforces the importance of disseminating best engineering practices and their role in defending housing quality in Brazil.

Therefore, the application of the GUT Matrix is essential for recognizing the priority of resolving damages found in a building, identifying the most critical item and the need for urgent repairs. Conversely, failure to carry out maintenance may result in more severe damage, leading to higher costs and greater technical demands (Aguiar *et al*., 2022).

In this sense, the main objective of this study is to apply the GUT Matrix methodology as a management tool in the analysis of pathological manifestations, using a sample of 7 (seven) data points from a total of 37 (thirty-seven) housing units in the *Conjunto Residencial Manoel Raimundo de Santana Filho* of the PMCMV, in the city of Juazeiro do Norte - CE.

2. Materials and Methods

2.1 Methodological Procedures

The methodological steps applied in this study were carried out using data provided by a company outsourced by *Caixa Econômica Federal*. These included: residential unit projects (floor plans and subdivision plans), technical reports, inspection reports, and photographic records of the analyzed housing units.

During the inspections, the cell phone camera was used to capture panoramic and detailed photographs of the pathological manifestations under study. A crack gauge, a rubber hammer, and a clipboard were also used to assist with the necessary notes.

The remaining methodological steps were subdivided into two stages. After data analysis, the pathological manifestations were classified and quantified through visual inspection, and based on this, a priority chart

of pathological manifestations was prepared using the GUT method. Following the analysis, the results—whose specific details will be presented in the Results and Discussion section—were consolidated.

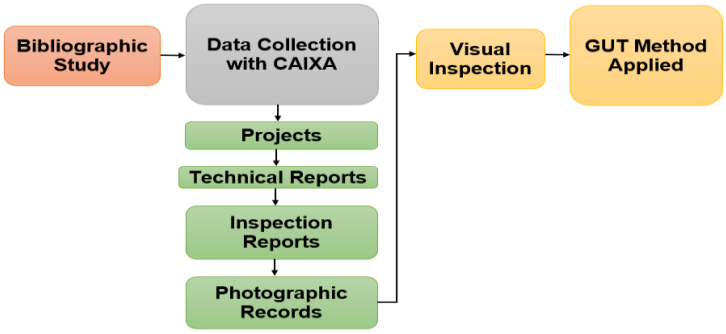


Figure 1 – Flowchart of the Research Stages

2.2 Specification of the GUT Method

The method basically consists of listing anomalies and failures in columns and then assigning each item a score from 1 to 10, depending on the degree of Gravity, Urgency, and Trend. In this study, 1 represents the lowest index for the parameters adopted in the matrix, while 10 represents the highest. Aguiar *et al*. (2022) state that, at the end of the scoring process, it becomes necessary to calculate a number that represents the verification result, thereby determining the priority level for solving the problem. In other words, the item with the highest score will have the greatest priority in addressing the issue.

Through easily interpretable tables, Verzola, Marchiori, and Aragon (2014) established characteristics as parameters for assigning weights to each anomaly, considering both criteria and degree. Based on Tables 1, 2, and 3, it is possible to visualize the main definitions, according to the authors, for the elements of Gravity, Urgency, and Trend in the GUT Matrix.

When classifying **Gravity**, one must consider the possible risks and losses to users. The definition of a problem considered critical was assigned to the levels: Total and High; the designation of a problem considered regular was assigned to the level: Medium; and the definition of a problem considered minimal was assigned to the levels: Low and None, as illustrated in Table 1.

Table 1 – GUT Classification for Gravity

Degree	Degree definition	Note
TOTAL	Risk of death, irreversible impact with excessive loss of performance, extremely high financial loss.	10
TALL	Risk of harm to users, recoverable damage to the environment and the building.	8
MÉDIUM	Health risk to users caused by system degradation, reversible environmental damage, average financial loss.	6
LOW	No risk to users' health, low environmental degradation, need to replace some systems, low financial loss.	3
NONE	No risk to health or physical well-being, minimal environmental deterioration, no damage of value.	1

Regarding **Urgency**, the definition of each level was based on how significant the manifestation is, the time required for the problem to be resolved, and the speed with which the issue must undergo intervention. Accordingly, Table 2 represents the situation described.

Table 2 – GUT Classification for Urgency

Degree	Degree definition	Note
TOTAL	Immediate event, need for property interdiction without extra deadlines.	10
TALL	Imminent event, urgent intervention.	8
MÉDIUM	Adversity expected soon, need to intervene quickly.	6
LOW	Initialization of an incident, intervention still in the form of plans.	3
NONE	Unexpected adversity, but monitoring is necessary for future maintenance.	1

For the topic of **Trend**, the level was defined according to the likelihood of the problem worsening, as well as the possibility of its reduction or disappearance over time, as shown in Table 3.

Table 3 – GUT Classification for Trend

Degree	Degree definition	Note
TOTAL	Progress of the condition immediately, with possible worsening at any time.	10
TALL	Evolution of the situation about to occur.	8
MÉDIUM	Medium-term evolution.	6
LOW	Possible long-term evolution. It may occur. Delayed situation.	3
NONE	Stabilized situation, with no progression of the case.	1

After assigning weights (from 1 to 10) to each item (**Gravity, Urgency, and Trend**), the level of each problem was classified across the three functions, and the product of their respective values was calculated (**G × U × T**). Subsequently, at the end of the scoring process, it becomes necessary to determine a number that represents the verification result, thereby establishing the priority level of the problem. In other words, the item with the highest score will have the greatest priority in resolving the issue.

2.3 Selection of the Residential Development

The research conducted was a case study, for which the *Conjunto Residencial Manoel Raimundo de Santana Filho* (intended for families with incomes up to R$ 1,600 – Range I) was selected. It is in the *Betolândia* neighborhood in the municipality of Juazeiro do Norte-CE. The development has the following geographic coordinates: 7° 12’ 47” South latitude (S) and 39° 18’ 55” West longitude (W). The main justification for choosing this development was the availability of data from *Caixa Econômica Federal – CAIXA*. In addition, the selection criteria included a project that, at the time, had been built less than five (5) years earlier and had been occupied for more than one (1) year, meaning it was still covered by Civil, Professional,

and Material Liability Insurance (RCPM). The housing units were delivered to residents in the beginning of the second semester of 2014.

The development consists of 18 blocks, within which 713 residential units are distributed. Of these, 36 units were adapted for Persons with Disabilities (PWD). The houses are single-story, built with raft foundations, ceramic brick masonry, and roofs made of wooden structures with ceramic tiles. Regarding finishing standards, the houses were delivered with commercial-grade ceramic flooring, latex-painted walls, PVC panel ceilings (without slabs), ceramic wall coverings in bathrooms and kitchens up to 1.80 m in height, aluminum exterior doors, semi-hollow wooden interior doors, and aluminum/glass windows.

Each housing unit (HU) has a built area of 43.85 m², situated on lots measuring 6 m in width by 20 m in depth, totaling 120 m². The internal layout includes: a porch, living/dining room, two bedrooms, a social bathroom, and a kitchen, as shown in Figure 2 below.

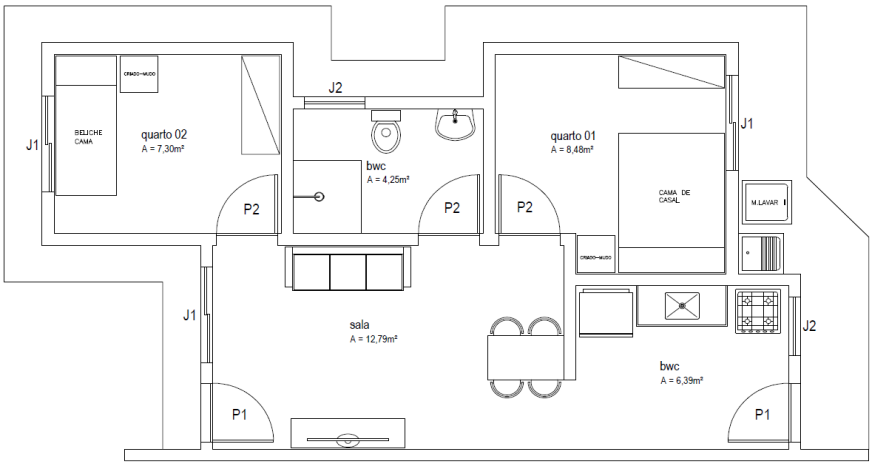


Figure 2 – Floor plan of a housing unit

Given this, the selection of the housing units used in the sample was based on the number of residents who filed Reports of Pathological Manifestations (BOMP) with *Caixa Econômica Federal* in 2017. According to the PMCMV owners' rights and duties handbook, responsibility for construction defects lies with the developer, not with *CAIXA*. However, if the developer fails to respond, residents may seek assistance from *Caixa Econômica Federal*, the Consumer Protection and Defense Program (PROCON), or through legal action.

In this context, of the 713 units in the development, only 37 filed reports with the financing institution due to the presence of pathological manifestations in their units. As a result, *CAIXA's* technical team visited the site to conduct technical inspections of the units, which later produced data through inspection reports for the preparation of the GUT Matrix.

The inspections covered both the internal and external areas of the housing units and were carried out between December 2017 and February 2018. A non-destructive technique of visual inspection was used to verify the presence of pathological manifestations in the units, collecting data and photographic records of each one.

During the inspections, some basic interviews were also conducted with the residents regarding the state of conservation, maintenance, and occurrence of pathological manifestations.

To determine the classification of openings (cracks, splits, fractures, gaps, and breaches), the methodology of Oliveira (2012) was applied, as presented in Table 4, and determined through visual inspection using a crack gauge.

Table 4 – Classification of Cracks

Anomalies	Openings (mm)
Fissure	Up to 0,5
Crack	0,5 to 1,5
Fracture	1,5 to 5,0
Gap	5,0 to 10,0
Breach	Above 10,0

A total of 37 housing units were inspected, from which a subsample of 7 data points was selected, considering the repetition of damages. In this way, the sample set was drawn from different streets and blocks to ensure representation of the pathological manifestations, as presented in Table 5.

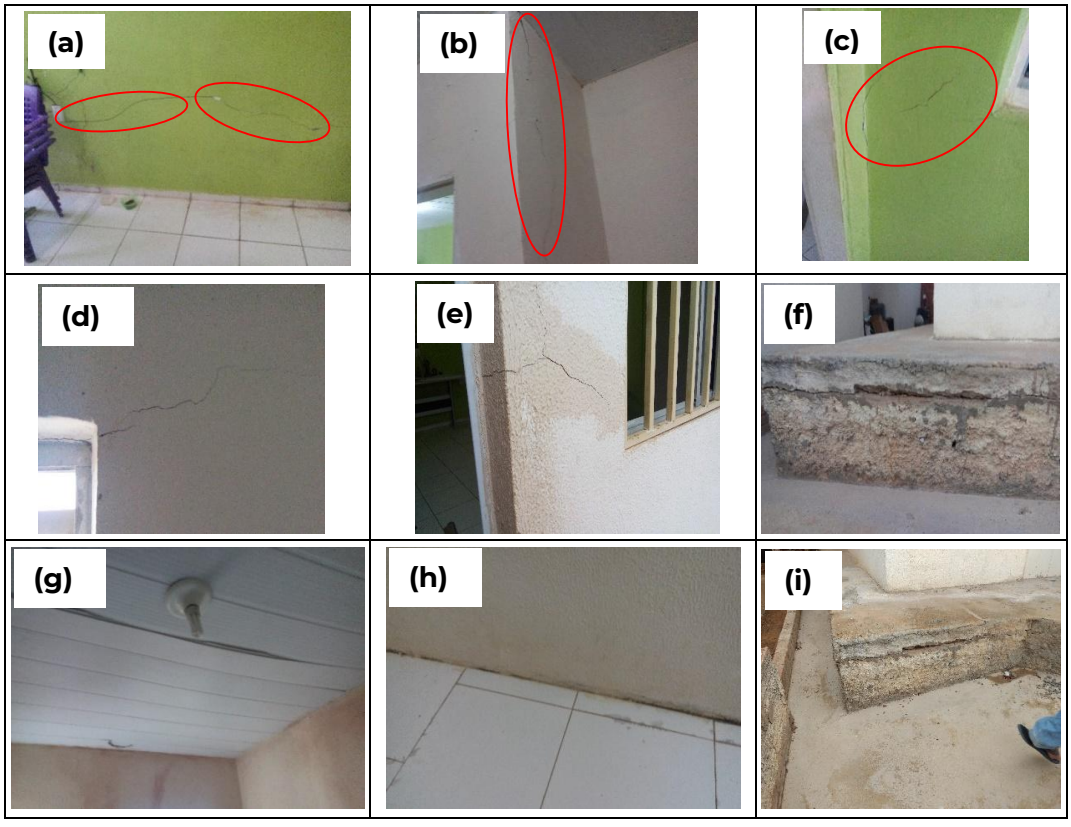
Table 5 – Determination of the Research Sample

ADDRESS	BLOCKS	UNITS	ESTIMATED AGE
Street 1	A	3	4
Street 2	B	2	4
Street 3	C	2	4
Street 5	E	4	4
Street 7	G	2	4
TOTAL	-	**13**	-

After data collection, the records were organized for tabulation and subsequent analysis. For tabulation, Excel was used to create tables, facilitating the analysis and interpretation of the results. All documentary data and photographic records were provided by *ENGEAP – Avaliações e Perícias Ltda.*, a company outsourced by *Caixa Econômica Federal*.

3 Results and Discussion

After inspections carried out in 37 housing units, 7 samples were taken to verify the conditions and identify pathological manifestations, with photographic records made of each one, as shown in the following Figures. Subsequently, Tables 6 and 7 were prepared, containing the application and prioritization matrix for repairing the manifestations using the GUT method. It is worth noting that pathological problems not clearly visible in the photographs were highlighted with circular shapes to indicate the exact location of the anomaly.



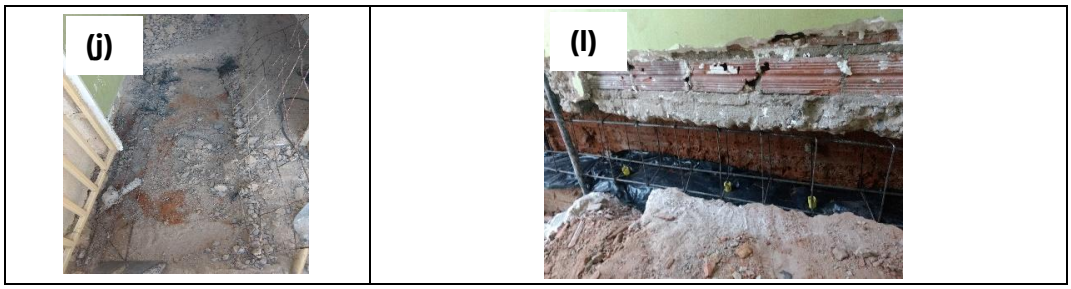


Figure 3 – Pathological Manifestations Identified at Street 2, n°. 30

(a, b) Cracks; (c, d, e) Fissures; (f, i) Differential settlement of the foundation masonry; (g) Deformation of the PVC ceiling; (h) Detachment of the ceramic coating and stains; (j) Inconsistency of the raft foundation; (l) Execution of structural reinforcement in the foundation.

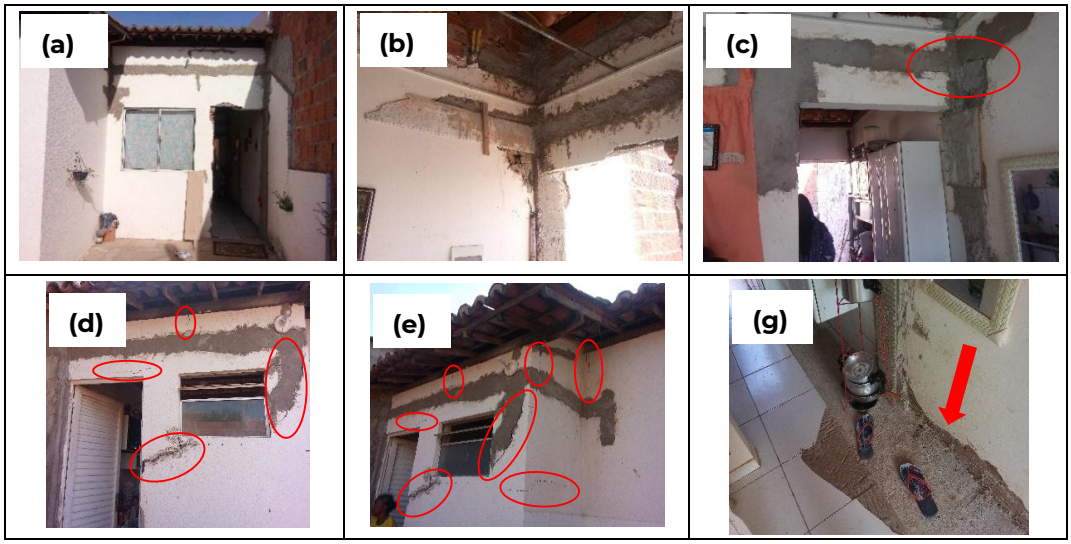


Figure 4 – Pathological Manifestations Identified at Street 5, n° 7

(a, b, c, d, e) Cracks; (g) Ceramic tiles fractured because of structural foundation repair.

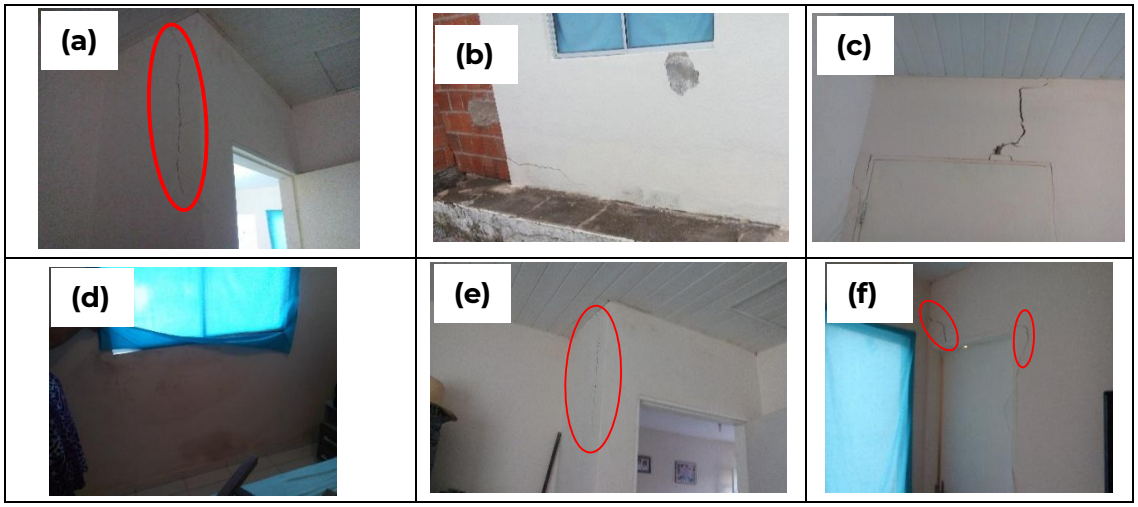


Figure 5 – Pathological Manifestations Identified at Street 2, n°. 24

(a, b, c, e, f) Cracks; (d) Damp stains from wall infiltration.

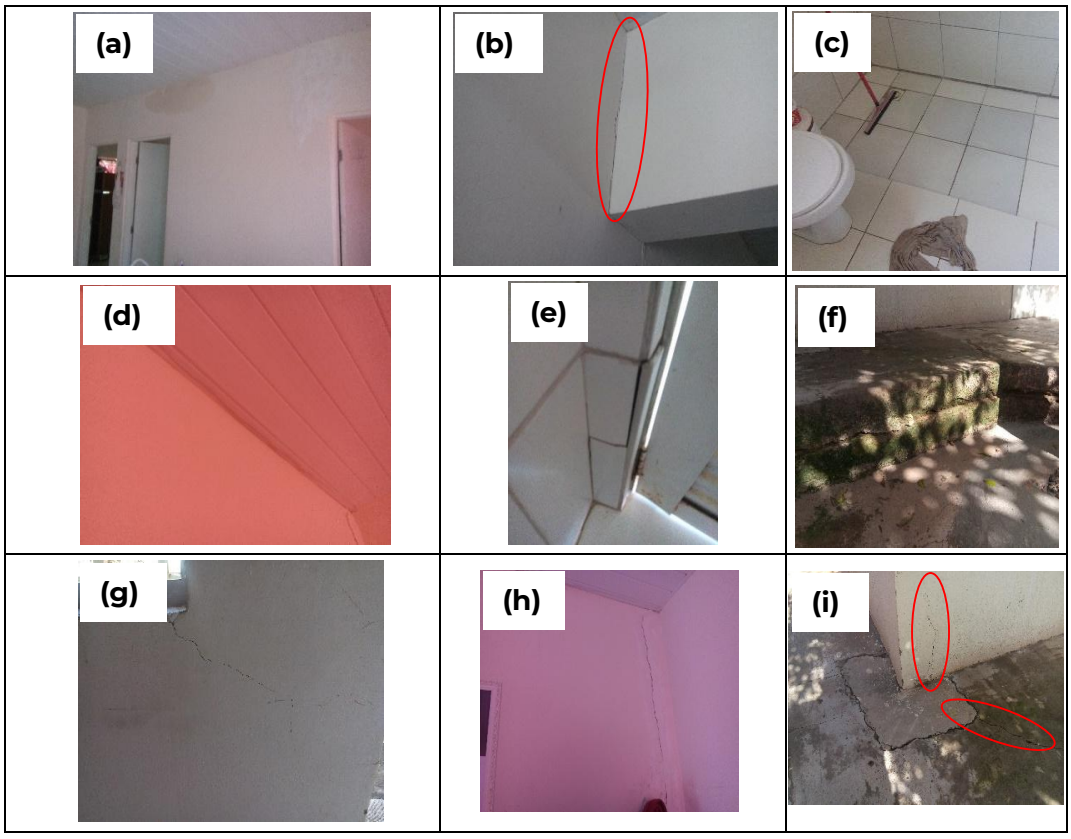


Figure 6 – Pathological Manifestations Identified at Street 3, n°. 18

(a) Infiltration in the interior walls (living room and bedrooms); (b, f, h, i) Cracks; (c) Infiltration and discoloration of the bathroom coating (floor and wall); (d) PVC ceiling in the bedroom with misaligned panels; (e) Detachment of ceramic wall covering in the kitchen; (g) Fissures.



Figure 7 – Pathological Manifestations Identified at Street 1, n°. 31

(a, b) Cracks; (c) Paint deterioration caused by infiltration; (d) Deformation of the PVC ceiling.



Figure 8 – Pathological Manifestations Identified at Street 5, n°. 19

(a, b, c, e) Wall infiltration; (d) Damaged PVC ceiling in Bedroom 1; (f) Leakage from the shower valve.

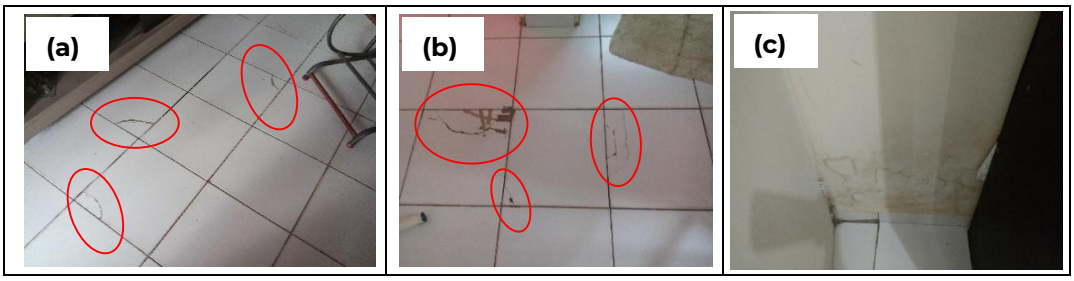


Figure 9 – Pathological Manifestations Identified at Street 7, n°. 61

(a, b) Cracked and worn ceramic flooring; (c) Wall infiltration.

Based on the data collected and the analysis performed, the GUT chart was prepared, indicating the incidence of the diagnosed pathological manifestations, and assigning scores for the method's criteria, along with the resulting product. Finally, the repair priority was established according to the value obtained from the product G×U×T, as shown in Table 6.

Table 6 – Application Matrix of the GUT Method

Item	Housing Unit	Incidence	Gravity	Urgency	Trend	GxUxT	Priority
1	STREET 2, N° 30	High	8	10	8	640	1
2	STREET 5, N° 07	High	8	8	8	512	2
3	STREET 2, N° 24	High	6	8	8	384	3
4	STREET 3, N° 18	High	6	8	8	384	3
8	STREET 1, N° 31	High	6	6	8	288	4
12	STREET 5, N° 19	Medium	6	6	6	216	5
34	STREET 7, N° 61	Low	3	3	3	27	6

Regarding the classification of the incidence level in Table 6, it was established according to the total score in the priority chart, which was based on each level presented in Tables 1 to 3 of subsection 2.2, while also considering the pathological manifestations with the highest incidence in each unit and those requiring greater attention for damage repair/control.

Therefore, the units that presented a higher number of pathological problems compared to the others were classified as *high incidence*. These included: fissures, cracks, fractures, damp stains from wall infiltration,

leaks/infiltration, discoloration of bathroom floors and/or ceramic wall coverings, worn ceramic flooring, fractured ceramic tiles with broken/cracked plates, and rust stains. The other units, which presented fewer pathological problems among those cited, along with isolated issues that were not recurrent in each unit, were classified as *medium* and *low incidence*.

As can still be observed in Table 6, some pathological manifestations have the same degree of priority. For this reason, Table 7 was prepared, in which the manifestations were grouped with their respective diagnoses, in order of priority.

Table 7 – Prioritization for Repair of Pathological Manifestations

Degree of Priority	Identification	Main Pathological Manifestations Identified
1°	STREET 2, N° 30	Structural inconsistency of the raft foundation and differential settlement of the base masonry, medium incidence of cracks, high incidence of fissures. PVC ceiling deformations.
2°	STREET 5, N° 07	High incidence of severe cracks.
3°	STREET 2, N° 24	High incidence of cracks (2 severe) and medium incidence of fissures.
	STREET 3, N° 18	High incidence of cracks (new appearances after the property's repair) and medium incidence of fissures.
4°	STREET 1, N° 31	Medium incidence of cracks, fissures, and hairline fractures.
5°	STREET 5, N° 19	High incidence of damp stains from wall infiltration.
6°	STREET 7, N° 61	High incidence of cracked and worn ceramic flooring.

According to the data from Tables 6 and 7, the pathological manifestations with the highest incidence are wall infiltrations, cracks, fissures, and fractures of various types (inclined, vertical, and horizontal). Regarding the foundations, specifically the raft foundation used in the construction of the PMCMV houses, it is inferred that the manifestations related to the inconsistency of the raft and the differential settlement of the base masonry (Street 2, No. 30) must be addressed first, as they demand greater attention for damage repair and pathology control. These are the most serious issues, precisely because they obtained the highest scores in the GUT Matrix calculation.

There are numerous occurrences of cracks, fissures, and fractures identified in the study area. In this sense, occupying second place in the corrective maintenance priority order is the unit at Street 5, No. 7, which is in a critical condition, presenting many severe cracks. In third place, the units at Street 2, No. 24 and Street 3, No. 18, showed the highest number of cracks (9 and 11, respectively), in addition to a medium incidence of fissures and other pathological manifestations.

The other units with cracks, fissures, and fractures were classified in fourth place, as they generally presented a higher frequency of occurrences, and consequently, a medium incidence. These anomalies were predominantly identified in living rooms and bedrooms. The greatest occurrences were observed in sections with openings, such as wall corners and door frames. This type of fissure may be caused by the absence of reinforcement and the abrupt closing of doors, which can generate stress levels above the wall's admissible limit.

In fifth place in the priority order are infiltrations in internal and external walls, as well as leaks/infiltrations and discoloration of bathroom floors/ceramic coverings, classified as medium damage. Lower-priority damages, which do not require immediate treatment, included cracked, broken, and worn ceramic flooring. In the subsystem of coverings, pathological manifestations (5th and 6th places) were also observed, such as paint stains, damaged PVC ceiling panels, detached ceramic tiles, and color changes.

According to Carraro (2010), irregularities in finishing, such as paint stains and poorly executed repairs, are mainly associated with low-quality materials or inadequate workmanship.

By analyzing the studied sample, it was possible to identify that within four years after the delivery of the houses to their owners (end of the second semester of 2014), all units analyzed presented some type of

pathological manifestation. Since the units were still covered by the Civil, Professional, and Material Liability Insurance (RCPM) at the time the damages appeared, the construction company repaired the residences that presented problems within the five-year warranty period after delivery.

From these results, visual inspection proved to provide valuable data, becoming an extremely useful tool in the evaluation and recognition of pathological manifestations in the studied development. However, integrating other control tools beyond visual assessment, such as the GUT Matrix, was fundamental to complement the results and increase the reliability of this study.

4 Conclusion

The main objective of this study was to apply the GUT Matrix methodology as a management tool in the analysis of pathological manifestations, using a sample of 7 cases from a total of 37 housing units in the Manoel Raimundo de Santana Filho Residential Complex of the PMCMV program, located in Juazeiro do Norte, Ceará.

It was found that the most frequent pathological manifestations in the units were cracks (some of them severe and occurring at high frequency), followed by fissures and fractures, which also showed a significant incidence. The absence of lintels and counter-lintels contributed to the appearance of diagonal fissures/cracks in the walls. The lack of these structural elements over time intensifies the opening of fissures/cracks, which, depending on the material, can cause significant damage due to overloads.

Several infiltrations in internal and external walls, as well as leaks and discoloration of bathroom floors/ceramic coverings, were also identified. Such damages may worsen and compromise the stability of the units if corrective measures are not implemented. It is essential that these problems be identified and treated as quickly as possible to avoid further structural damage and financial losses for the owners. Cracked, broken, and worn ceramic floors were also highly visible. Their recovery requires complete replacement of the material, highlighting the low quality of the materials used and resulting in high additional costs for replacement within a short period.

Regarding the use of the GUT method to rank manifestations by priority level, it was possible to establish a hierarchy of risks, inferring that pathologies related to raft foundation inconsistency and differential settlement of the base masonry demand the greatest urgency for corrective maintenance.

Overall, the pathological problems in the housing units of the analyzed PMCMV residential complex show similarities regardless of the different regions of Brazil. Although the PMCMV provides affordable housing, long-term quality has proven deficient. Proper identification not only assists in solving problems but can also prevent their recurrence in the future, thereby ensuring durability and safety of the constructed structures.

Based on the results obtained in this study, it is possible to establish a strategic plan for correcting the most critical pathological manifestations first, followed by those with the highest incidence, which deteriorate materials and structural elements in terms of both aesthetics and functionality.

It can be concluded that the GUT Matrix is a valuable strategic planning tool that, through visual inspections, supports decision-making regarding possible interventions to repair structural damages. However, the evaluation of structural conditions is a complex subject, and since this tool relies on visual inspection, it has limitations. It is crucial that professionals conducting and analyzing inspections possess knowledge and experience in building pathology to ensure coherent evaluations that reflect the reality of the observed damages.

Thus, visual inspection combined with the GUT Matrix for an initial diagnosis of problems is effective in identifying damages, although during data analysis there may be uncertainty regarding probable causes, origins, or the behavior of anomalies. In this sense, complementary non-destructive tests (such as ultrasound, radiography—X-ray or gamma rays—, and rebar detection) are fundamental to support diagnosis.

References

ASSOCIAÇÃO BRASILEIRA DE NORMAS TÉCNICAS. ABNT NBR 15575-1: Edificações Habitacionais – Desempenho. Rio de Janeiro: ABNT, 2024.

AGUIAR, A, A. et. al. Utilização da Matriz GUT na análise das manifestações patológicas em edificações. In: MARINHO, J. L. A; MESQUITA, E. F, T. (org.). Patologia das edificações: Manifestações nas edificações e no patrimônio histórico. 2. ed. São Paulo: Editora Leud, 2022, cap. 1, p. 38-49.

BRASIL. Ministério das Cidades. Conheça o programa Minha Casa, Minha Vida. 2023. Disponível em: https://www.gov.br/cidades/pt-br/assuntos/noticias-1/conheca-o-programa-minha-casa-minha-vida. Acesso em: 10 jan. 2026.

CAMARGO, M. V., FERRARI, V. J. Compressive strength, and elasticity module of concrete using non-destructive techniques (NDT). Revista Matéria, v. 26, n. 3, p. 1-16, 2021. DOI: https://doi.org/10.1590/S1517-7076202100003.13047.

CAIXA ECONÔMICA FEDERAL. Cartilha do Minha Casa Minha Vida: Direitos e deveres do Contrato. Brasília, 2011. Disponível em: https://www.caixa.gov.br/Downloads/habitacao-minha-casa-minha-vida/Cartilha_Direitos_e_Deveres_Anexo_I_minutas.pdf. Acesso em: 10 jan. 2026.

MARINHO, J. L. A; MESQUITA, E. F, T. Patologia das edificações: Manifestações nas edificações e no patrimônio histórico. 2. ed. São Paulo: Editora Leud, 2022. 296 p., 16x23cm, ISBN 978-85-7456-423-4.

KNAPP, L. M., OLIVAN, L. I. Método GUT: aplicado as estruturas metálicas e estruturas de concreto. 1. ed. São Paulo: Editora Leud, 2021. 144 p., 16x23cm, ISBN 978-85-7456-394-7.

OLIVEIRA, A. M. Fissuras, trincas e rachaduras causadas por recalque diferencial de fundações. 2012. Trabalho de Conclusão de Curso (Especialização em Construção Civil) – Universidade Federal de Minas Gerais, Minas Gerais, Belo Horizonte, 2012.

RESENDE, M. M. *et al*. Infrared thermal imaging to inspect pathologies on façades of historical buildings: A case study on the Municipal Market of São Paulo, Brazil. Case Studies in Construction Materials, v. 16, p. 1-12, 2022. DOI: https://doi.org/10.1016/j.cscm.2022.e01122.

SENA, G. O. *et al.* Patologia das construções. 1. ed. Salvador: Editora 2B, 2020. 256 p., 16x23cm, ISBN 978-85-54815-83-7.

SANTOS JÚNIOR, J. C., SANTOS, J. M. A., SANTOS, M. R. A. Parametric modeling using the BIM methodology for the process of pathology identification in buildings. Journal of Building Pathology and Rehabilitation, v. 8, n. 62, p. 1-12, 2023. DOI: https://doi.org/10.1007/s41024-023-00311-4.

VERZOLA, S. N., MARCHIORI, F. F., ARAGON, J. O. Proposta de lista de verificação para inspeção predial x urgência das manutenções. In: Encontro Nacional de Tecnologia do Ambiente Construído, 15., 2014, Maceió. Anais. [...]. Alagoas, 2014. p. 1226-1235.

Cinpar 2026
XXII International Conference on Building Pathology and Constructions Repair
15th to 17th July 2026 - Lisboa, Portugal

Análise dos defeitos em pavimento rodoviário flexível sob diferentes condições climáticas

José Wémenson Rabelo Chaves[1], Antônio Alves Barbosa Neto[2], Francisco Heber Lacerda de Oliveira[3]

[1] Programa de Pós-Graduação em Engenharia de Transportes - PETRAN / UFC - Universidade Federal do Ceará - UFC, R. Prof. Armando Farias, 703, Fortaleza - CE, 60020-181, Brasil, wemenson.chaves@det.ufc.br
[2] Curso de Engenharia Civil - Universidade Federal do Ceará - UFC, 708 - Campus do Pici, Fortaleza - CE, 60020-181, Brasil, antonio.neto342710@hotmail.com
[3] Programa de Pós-Graduação em Engenharia de Transportes - PETRAN / UFC - Universidade Federal do Ceará - UFC, R. Prof. Armando Farias, 703, Fortaleza - CE, 60020-181, Brasil, heber@det.ufc.br

Resumo: Diversos fatores podem influenciar a degradação dos pavimentos rodoviários, entre eles as condições climáticas e a ausência de manutenção. A ocorrência de chuvas pode favorecer o surgimento de defeitos, pois contribui para a formação de buracos e compromete a resistência à derrapagem, elevando o risco de aquaplanagem e acidentes. Para que as manutenções sejam realizadas no período adequado, torna-se necessário conhecer os defeitos existentes e compreender como estes impactam as condições de trafegabilidade e segurança dos usuários, possibilitando a escolha de intervenções que assegurem níveis satisfatórios de serventia do pavimento. Diante disso, o presente trabalho tem o objetivo de caracterizar os defeitos de um pavimento rodoviário flexível nas estações seca e chuvosa e o impacto na variação do conforto ao rolamento em função dessas condições sazonais. Para tanto, foram realizados registros por vídeomonitoramento de três trechos rodoviários, totalizando 88 km, que permitiram uma análise comparativa das condições superficiais entre as estações seca e chuvosa. Adicionalmente, realizou-se uma avaliação subjetiva por meio do Valor de Serventia Atual (VSA). Verificaram-se 140 ocorrências de defeitos, entre buracos, trincas e fissuras. Observou-se que os remendos evoluíram para buracos devido ao acúmulo de água pluvial e as trincas existentes no período seco tornaram-se buracos em cinco meses, pois a infiltração de água acelerou o desgaste da estrutura. Quanto ao VSA, a rodovia apresentou condições funcionais boas ou ótimas na estação seca, degradando-se para níveis regulares ou péssimos no período chuvoso. Concluiu-se que o maior surgimento de defeitos, principalmente buracos, ocorreu durante o período chuvoso. O VSA evidenciou a evolução dos defeitos e as condições de rolamento dos trechos inspecionados. Por fim, a sazonalidade climática contribuiu para a redução do nível de serventia funcional dos pavimentos flexíveis, acompanhando o aumento da incidência de defeitos.

Palavras-Chaves: Condição de rolamento; Avaliação funcional; Condições sazonais; Valor de Serventia Atual.

1. Introdução

O clima e a ausência de manutenção são fatores que podem influenciar a degradação dos pavimentos rodoviários. Variações extremas de temperatura e de chuvas exercem um impacto na resistência dos pavimentos, uma vez que podem alterar as características de rigidez das camadas e do subleito. A água penetra na interface entre o asfalto e o agregado, e a membrana asfáltica começa a se desprender dos agregados, que então se soltam e formam defeitos na superfície.

Essas variações ambientais têm contribuído para a deterioração prematura dos pavimentos flexíveis, resultando em fissuras, buracos, trilhas de rodas e desagregação. A combinação de fatores climáticos e de tráfego cria um ambiente desafiador para a preservação da condição funcional e estrutural do pavimento (Castro, Silva e Lange, 2014; Jaafar, 2019). Esse quadro exige intervenções cada vez mais frequentes, o que não apenas aumenta os custos de manutenção, mas também prejudica o fluxo de tráfego e compromete a segurança dos usuários (Al-Samahi *et al*., 2024).

A ocorrência desses defeitos na superfície de um pavimento é um indicativo de ineficiência funcional ou estrutural. Dessa forma, os pavimentos precisam ser monitorados continuamente, a fim de gerar informações que subsidiem os Sistemas de Gerência de Pavimentos (SGP), orientando as intervenções na rodovia e suporte para a implantação de novas tecnologias de projeto, construção, manutenção e reabilitação (Haas, Hudson e Zaniewski, 1994).

A avaliação de pavimentos constitui uma etapa fundamental para identificar as intervenções necessárias à melhoria do conforto e da segurança dos usuários. Um dos métodos empregados para essa finalidade é o Levantamento Visual Contínuo – LVC (DNIT, 2003a). Como exemplo, tem-se a rodovia federal brasileira analisada neste estudo, que apresenta trechos que, durante a quadra chuvosa, manifestam diversos defeitos, como buracos e trincas. Após esse período, observa-se que são realizadas intervenções de remendo e recapeamento, como forma de manutenção corretiva. No entanto, sabe-se que a definição de intervenções capazes de garantir níveis satisfatórios de serventia requer a compreensão dos mecanismos de surgimento dos defeitos e de seu comportamento frente às condições ambientais. Nesse contexto, o presente trabalho tem o objetivo de caracterizar os defeitos de um pavimento rodoviário flexível nas estações seca e chuvosa e o impacto na variação do conforto ao rolamento em função dessas condições sazonais.

2. Fundamentação teórica

O principal objetivo da pavimentação é garantir a trafegabilidade em qualquer época do ano e em quaisquer condições climáticas, e proporcionar conforto e segurança aos usuários. Quando o solo natural não é resistente o suficiente para suportar a repetição das cargas das rodas sem sofrer deformações significativas, torna-se necessário construir uma estrutura chamada pavimento. Ela é, portanto, construída sobre o subleito para suportar as cargas dos veículos e distribuir as solicitações em suas diversas camadas, limitando as tensões e deformações, a fim de garantir um desempenho adequado do pavimento por um longo período (Bernucci *et al*., 2022).

Entretanto, ao longo da vida útil, os pavimentos estão sujeitos a um processo de deterioração que reduz suas capacidades estrutural e funcional, em decorrência da ação combinada do tráfego e de fatores ambientais (Antunes, Guimarães e Rocha, 2021; Bernucci et al., 2022). Nesse contexto, torna-se importante compreender a origem, os tipos e os mecanismos de evolução dessas falhas, de modo a subsidiar a adoção de estratégias eficazes de prevenção, correção e manutenção (Santana *et al*., 2025).

As condições ambientais adversas representam desafios para a manutenção de pavimentos flexíveis. As temperaturas extremas do ar ou as chuvas extensas em determinadas regiões, causam a degradação estrutural e funcional das camadas asfálticas levando ao aparecimento de buracos, de fissuras e de trilhas de roda (Wu, Pang e Zhu, 2024). Sabe-se que o número de irregularidades e defeitos varia entre as estações do ano (sazonalidade climática), sendo mais intenso nos períodos chuvosos, quando o pavimento se torna mais suscetível a esse tipo de ocorrência (Castro, Silva e Lange, 2014).

As precipitações, associadas a uma drenagem deficiente dos pavimentos, influenciam o surgimento de danos, a redução da resistência estrutural, o aumento da rugosidade e o aparecimento de defeitos o que

resulta na diminuição da vida útil do pavimento e no aumento dos custos de reabilitação (Abdollahi, Kutay e Lanotte, 2024). Dessa forma, é possível perceber que uma drenagem deficiente na rodovia causa problemas, prejudicando o tráfego e diminuindo a segurança.

Os principais defeitos superficiais encontrados em pavimentos flexíveis incluem exsudação, desgaste, fissuramento e trincamento de fadiga, transversal, longitudinal, em bloco e por propagação de juntas (Domingues, 1993; Bernucci *et al*., 2022). Além disso, também são recorrentes defeitos como remendos, panelas, depressões e o afundamento em trilha de roda, que comprometem as condições funcionais e estruturais do pavimento.

A previsão dos defeitos, das irregularidades e dos custos a longo prazo das atividades de manutenção e reabilitação é difícil devido à complexa interação de fatores tráfego, material e as variabilidades climáticas. Dadas essas limitações, existe uma necessidade de mais coleta de dados *in situ* e pesquisas para melhorar a precisão das avaliações de deterioração de pavimentos e aprimorar o planejamento de resiliência (Hong e Prozzi, 2024. Peng *et al*., 2025).

A localização, a escala, a severidade e o mapeamento das deteriorações constituem aspectos cruciais para os Sistemas de Gerenciamento de Pavimentos (SGP) (Hosseini e Smadi, 2021). Devido ao tempo e aos recursos necessários, as inspeções vêm sendo substituídas por abordagens mecanizadas, que incluem desde sensores a laser de alta velocidade, sem contato, até equipamentos capazes de capturar imagens em vídeo da superfície do pavimento (Choi, 2020).

Uma das alternativas de aferir a condição superficial (funcional) do pavimento é por meio do Valor da Serventia Atual (VSA) um parâmetro subjetivo de avaliação. Esse método indica o grau de conforto e suavidade de rolamento proporcionado pelo pavimento. Para isso, atribui-se uma numeração de 0 a 5, resultante da média de notas de avaliadores em um determinado trecho, em um dado momento da vida do pavimento (DNIT, 2003a). Esse método apresenta como limite de aceitabilidade a nota 2,5 para as vias de alto volume de tráfego e 2,0 para as demais. Quando o VSA atinge nota abaixo desse patamar, uma intervenção de manutenção corretiva deve ser realizada, de modo a transformar o índice em um valor superior. Por outro lado, quando o pavimento apresenta o VSA acima deste valor, deve-se realizar manutenção preventiva periódica para manter a condição de rolamento em níveis adequados (DNIT, 2003a).

3. Método de pesquisa

O presente estudo foi dividido nas seguintes etapas: (i) escolha dos trechos a serem inspecionados; (ii) realização de videomonitoramento nos segmentos em dois períodos distintos; (iii) obtenção de dados climáticos (pluviométricos) dos trechos; (iv) detecção dos defeitos a partir das imagens obtidas; (v) determinação do Valor de Serventia Atual (VSA), conforme o DNIT (2003a); e (vi) comparação dos defeitos identificados e da condição funcional do pavimento entre os períodos analisados. A Figura 1 apresenta o fluxograma das etapas realizadas.

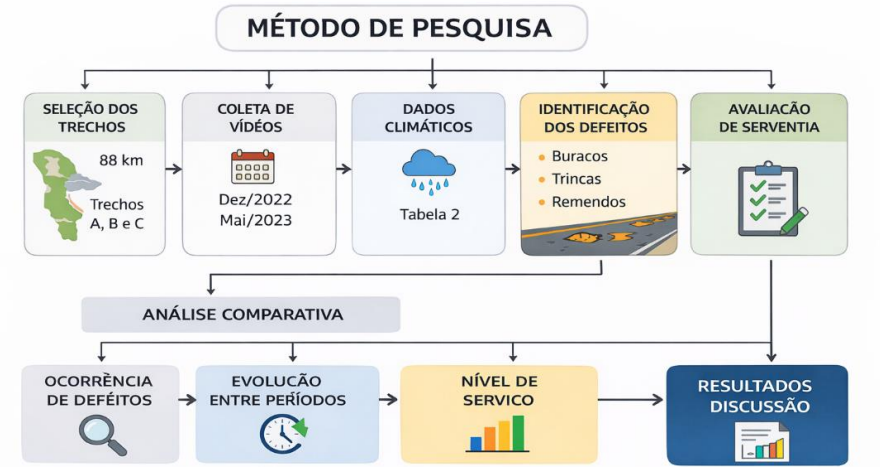


Figura 1 – Fluxograma das etapas realizadas

Escolheu-se um trecho de uma rodovia federal localizada no estado do Ceará, nordeste do Brasil, entre o município de Boa Viagem e de Fortaleza, com extensão de 200 Km. O trecho foi escolhido por ser uma importante rota de integração inter-regional e escoamento industrial e agropecuário. O trecho foi divido em 3 (três) segmentos, denominados de A, B e C (Tabela 1).

Tabela 1 – Trechos que foram analisados da rodovia federal – Ceará

Segmento	Km inicial	Km Final	Distância percorrida (Km)
A	365	333	32
B	301	265	36
C	233	213	20

A pesquisa teve início com a coleta de vídeos nos segmentos no mês de dezembro de 2022 e em maio de 2023 (nos mesmos segmentos da rodovia). A escolha do mês de dezembro corresponde ao período de o final da estação seca e o final da estação chuvosa. Por sua vez, o mês de maio marca o término do período chuvoso na região (Tabela 2). Buscando identificar diferenças relacionadas à sazonalidade climática. A partir dos dados apresentados na Tabela 2, buscou-se correlacionar as condições climáticas observadas nos respectivos períodos com a ocorrência e a evolução dos defeitos no pavimento.

Tabela 2 - Dados pluviométricos de municípios passados pela rodovia federal em estudo

Segmento	2022	2023					
	Dezembro	Janeiro	Fevereiro	Março	Abril	Maio	Total
A	21,5	295,3	167,5	469,7	468	271,2	1693,2
	17,6	208,1	148,2	290,8	206	148,5	1019,2
B	16,2	174	133,3	119,5	178,	92,6	713,6
C	33,5	182	0	147,5	120,5	14	464
	22	153	12	181	144,2	54,2	566,4

(Fonte: FUNCEME, 2023).

Os vídeos foram obtidos por meio de uma câmera de smartphone acoplado no painel de um veículo, com o auxílio de um suporte, ao longo de uma faixa da pista de rolamento da rodovia. Neste estudo, desconsideraram-se os defeitos presentes no acostamento. Nas análises, foram considerados defeitos do tipo trincas, fissuras, buracos, ondulações e escorregamento.

No caso dos defeitos de buracos, foi realizada uma distinção própria envolvendo os buracos, devido ao seu impacto causado na rodovia como também a sua quantidade de vezes apresentado, que serão: evolução da trinca para buraco, crescimento dos buracos, surgimento de buraco no remendo, surgimento de buraco em pavimento estável e trincas severas;

Esses cinco tipos de defeitos relacionados a buracos foram registrados em uma ficha, a fim de quantificar a frequência com que ocorrem, além do registro fotográfico. A partir disso, foi possível identificar os defeitos mais comuns e as fases em que os buracos se manifestam.

Além da análise de defeitos específicos, foi realizada uma avaliação abrangente da rodovia com base no Valor de Serventia Atual (VSA) conforme DNIT (2003a). Durante essa análise, dois avaliadores, presentes no veículo durante a obtenção dos vídeos, atribuíram notas (Tabela 3) a trechos a cada 2 km. Essa abordagem permitiu não apenas avaliar defeitos específicos, mas também obter uma visão geral da qualidade funcional da rodovia.

Tabela 3 – VSA e conceito funcional da condição superficial do pavimento (DNIT, 2003a)

VSA	Conceito	Cor
≥ 4,0	Ótimo	
3,0 – 3,9	Bom	
2,0 – 2,9	Regular	
1,0 – 1,9	Ruim	
< 1,0	Péssimo	

A partir dos resultados obtidos, foram realizadas três análises entre os dois períodos (dezembro de 2022 e maio de 2023): (i) verificação e comparação da ocorrência de defeitos; (ii) análise das condições de rolamento

do pavimento (VSA) e comparação entre os períodos; e (iii) avaliação da influência das condições climáticas na condição funcional do pavimento. Por meio do videomonitoramento, buscou-se identificar as mudanças ocorridas ao longo desse intervalo, especialmente quanto à evolução dos defeitos, ao aumento de severidade e ao surgimento de novas manifestações.

Em seguida, com base nos valores de VSA, aplicou-se o teste t pareado de Student, adotando-se como hipótese nula (H_0) a inexistência de diferença entre os valores observados nos meses de dezembro e maio, e como hipótese alternativa (H_1) a existência de diferença entre esses períodos, considerando um nível de significância de 5% ($\alpha = 0,05$).

Por fim, analisou-se a relação entre a precipitação registrada no mês de dezembro e os valores de VSA nos trechos A, B e C. Para isso, foi elaborado um gráfico de dispersão com base nas médias por agrupamento, sendo o coeficiente de correlação (r) utilizado como medida de associação entre a precipitação e o VSA.

4. Resultados e discussão

Após análise dos vídeos registrados em dezembro de 2022 e maio de 2023, torna-se evidente a ocorrência de mudanças na pavimentação entre as inspeções, com uma variedade de defeitos em todo o trecho. Foi observado ao menos um caso de cada tipo de defeito (DNIT, 2003b) nos vídeos analisados. Esses defeitos englobam trincas, fissuras, buracos, ondulações e escorregamentos. Além disso, há particularidades nos defeitos, como questões relacionadas à drenagem e problemas específicos com os remendos. Os buracos destacam-se como os mais frequentes.

No segmento A, observou-se, no primeiro levantamento realizado em dezembro de 2022, a presença de um defeito do tipo remendo, decorrente de uma manutenção anterior (Figura 2A). Nota-se que uma possível má execução resultou em uma superfície ligeiramente mais elevada, o que comprometeu o escoamento da água em direção ao acostamento, favorecendo seu acúmulo sobre a área remendada. Em decorrência dessa condição, verificou-se que, no levantamento realizado em maio de 2023 (Figura 2B), parte do remendo apresentou desagregação, ocasionando o surgimento de buracos e trincas.



Figura 2 - (A) Ocorrência de remendo e problemas de drenagem na faixa de rolamento (dezembro/2022). (B) Ocorrência de buracos e trincas (maio/2023).

Situação semelhante foi observada no segmento B (Figura 3A), no qual um remendo executado em dezembro de 2022, voltou a apresentar buracos e trincas (Figura 3B). Esse comportamento indica que a intervenção realizada atuou apenas como uma solução temporária, sendo insuficiente para eliminar a causa do defeito e impedir sua reincidência. Ainda no segmento B, observa-se que buracos de baixa severidade acumula água após a ocorrência de precipitação (Figura 4A), favorecendo a infiltração e sua evolução para defeitos mais severos, como evidenciado na Figura 4B.



Figura 3 - (A) Ocorrência de remendo (dezembro/2022). (B) Ocorrência de buracos e trincas (maio/2023).

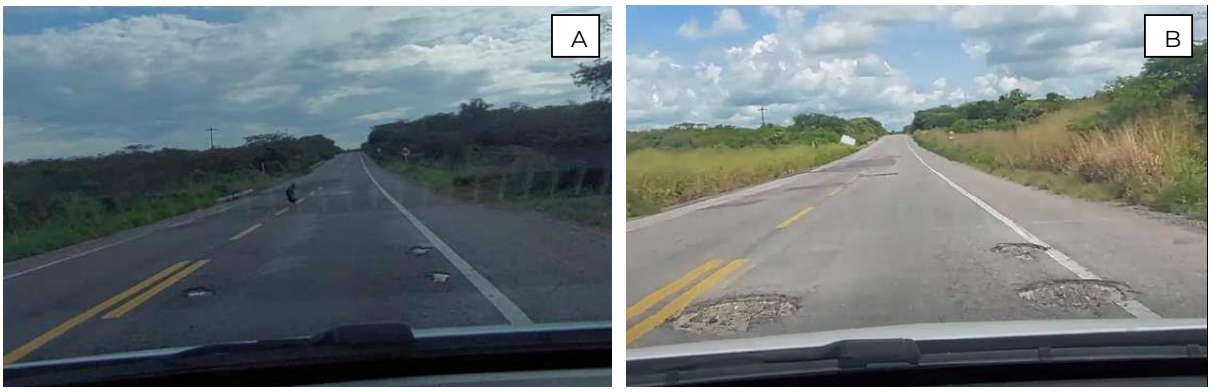


Figura 4 - (A) Ocorrência de buracos (dezembro/2022). (B) Crescimento dos buracos (maio/2023).

Outro defeito frequente nos segmentos inspecionados foram as trincas. Observou-se que algumas dessas trincas (Figura 5A), ao início das precipitações, evoluíram para defeitos do tipo buraco (Figura 5B). Isso ocorre porque a água da chuva infiltra-se nas camadas do pavimento, iniciando pelo revestimento, com o desprendimento de agregados, e avançando para as camadas inferiores. Notou-se que todos os locais da rodovia que possuía trincas se transformaram em buracos.



Figura 5 - (A) Ocorrência de trinca (dezembro/2022). B) Ocorrência de buracos e trincas (maio/2023).

Sabe-se que os remendos nem sempre evoluem para buracos (Barbosa Neto, 2023). No entanto, observou-se que, em cinco meses, um remendo em condições regulares (Figura 6A) se deteriorou, dando origem a buracos (Figura 6B), o que compromete o conforto e a segurança dos usuários. Ressalta-se que os buracos

não se restringiram às áreas remendadas, ocorrendo também em regiões adjacentes, o que indica suscetibilidade a problemas nessas zonas (Figura 6B).

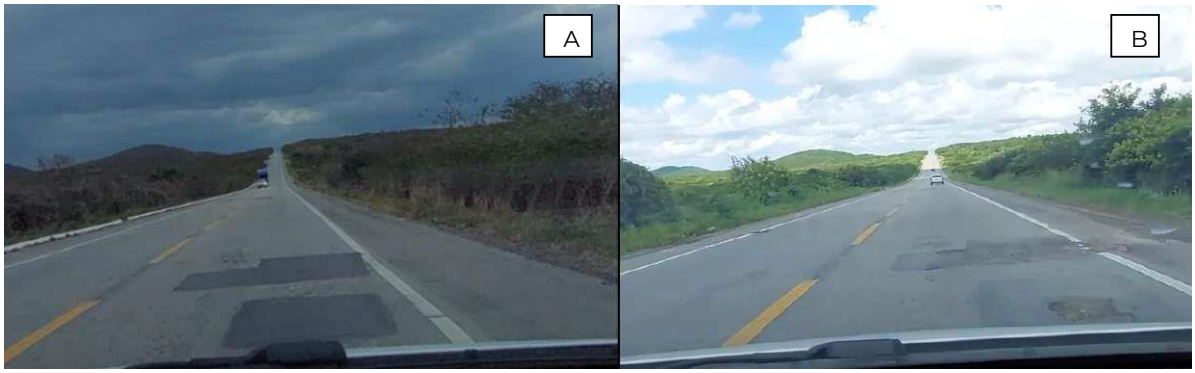


Figura 6 - (A) Ocorrência de Remendo (dezembro/2022). B) Ocorrência de surgimento de buracos (maio/2023).

Na inspeção realizada em maio de 2023, término do período chuvoso, foram observados 21, 65 e 54 defeitos nos segmentos A, B e C, respectivamente. Registram-se poucos intervalos de quilometragem que não apresentaram defeitos. Em alguns trechos, registraram-se mais de 10 defeitos relacionados a buracos (defeito predominante após a quadra chuvosa). Como exemplo, o Segmento C apresentou 2,70 defeitos por quilômetro (Tabela 4).

Tabela 4 - Relação entre o número de defeitos de cada trecho por km em maio

Segmento	Defeito / Km
A	0,66
B	1,81
C	2,70

Na Tabela 5, apresenta-se o total de defeitos registrados nos três segmentos, ao longo dos 88 km analisados. Observa-se uma discrepância do defeito buraco a partir do remendo em relação aos demais, indicando a necessidade de maior atenção quanto à necessidade de manutenção corretiva. Sua elevada ocorrência está associada ao caráter temporário dos remendos, que demandam intervenções frequentes.

Tabela 5 - Evolução dos defeitos do tipo buraco entre dezembro (2022) e maio (2023)

Tipo de defeito	Total de ocorrência
Crescimento de buraco	13
Buracos a partir de trincas	29
Buracos a partir de remendos	63
Surgimentos de buracos	22
Trinca severa	13
Total	**140**

As Tabelas 6, 7 e 8 apresentam os VSA referentes à condição superficial dos trechos avaliados por meio do método subjetivo nos dois períodos distintos. Ao comparar dezembro de 2022 com maio de 2023, observa-se uma redução geral nas médias, indicando diminuição do nível de conforto funcional segundo a percepção dos avaliadores. Essa queda está associada ao aumento do número de defeitos ao longo do período. No Segmento A, a variação média foi de 0,4 pontos, enquanto nos segmentos B e C as reduções foram de 1,9 e 1,1 pontos, respectivamente. Dessa forma, o Segmento A manteve sua condição funcional, enquanto os segmentos B e C apresentaram maior presença de defeitos e menor conforto ao rolamento, com possível redução do nível de desempenho.

Tabela 6 - Nota do VSA em relação ao Segmento A

Entre os Km		Segmento A							
		Dezembro de 2022				Março de 2023			
		Avaliador 1	Avaliador 2	Média	Conceito	Avaliador 1	Avaliador 2	Média	Conceito
365	363	3,3	3,1	3,2	Bom	2,7	2,9	2,8	Regular
363	361	3,5	3,8	3,7	Bom	3,4	3,0	3,2	Bom
361	359	4,1	4,0	4,1	Ótimo	3,6	3,1	3,4	Bom
359	357	4,1	4,4	4,3	Ótimo	2,5	2,7	2,6	Regular
357	355	3,5	4,0	3,8	Bom	3,5	3,3	3,4	Bom
355	353	4,0	4,1	4,1	Ótimo	4,0	3,9	4,0	Ótimo
353	351	3,9	4,2	4,1	Ótimo	3,5	3,5	3,5	Bom
351	349	3,6	4,0	3,8	Bom	3,8	3,7	3,8	Bom
349	347	3,5	3,8	3,7	Bom	3,2	3,1	3,2	Bom
347	345	3,8	4,1	4,0	Ótimo	3,5	3,5	3,5	Bom
345	343	4,4	4,5	4,5	Ótimo	4,3	4,5	4,4	Ótimo
343	341	4,0	4,1	4,1	Ótimo	3,3	3,1	3,2	Bom
341	339	4,2	4,3	4,3	Ótimo	4,0	4,0	4,0	Ótimo
339	337	4,4	4,3	4,4	Ótimo	3,9	4,2	4,1	Ótimo
337	335	4,4	4,4	4,4	Ótimo	4,1	4,3	4,2	Ótimo
335	333	4,5	4,5	4,5	Ótimo	4,4	4,5	4,5	Ótimo

Tabela 7 - Nota do VSA em relação ao Segmento B

Entre os Km		Segmento B							
		Dezembro de 2022				Março de 2023			
		Avaliador 1	Avaliador 2	Média	Conceito	Avaliador 1	Avaliador 2	Média	Conceito
301	299	4,4	4,4	4,4	Ótimo	3,9	4,0	4,0	Ótimo
299	297	3,3	3,3	3,3	Bom	1,7	2,1	1,9	Ruim
297	295	4,5	4,5	4,5	Ótimo	4,0	4,1	4,1	Ótimo
295	293	2,7	3,0	2,9	Regular	0,5	0,9	0,7	Péssimo
293	291	2,6	3,2	2,9	Regular	0,7	0,5	0,6	Péssimo
291	289	3,5	4,0	3,8	Bom	1,0	1,2	1,1	Ruim
289	287	4,2	4,3	4,3	Ótimo	2,0	1,5	1,8	Ruim
287	285	3,5	4,0	3,8	Bom	3,0	1,9	2,4	Regular
285	283	3,7	3,7	3,7	Bom	1,4	2,0	1,7	Ruim
283	281	4,0	4,3	4,2	Ótimo	3,5	3,0	3,3	Bom
281	279	3,7	3,1	3,4	Bom	2,8	2,5	2,7	Regular
279	277	3,9	4,0	4,0	Ótimo	2,9	3,0	3,0	Bom
277	275	3,8	4,1	4,0	Ótimo	2,8	2,5	2,7	Regular
275	273	3,1	3,1	4,1	Ótimo	1,4	0,9	1,2	Ruim
273	271	3,3	3,2	3,1	Bom	1,0	1,5	1,3	Ruim
271	269	3,3	3,1	3,2	Bom	0,5	0,8	0,7	Péssimo
269	267	3,4	3,6	3,5	Bom	1,0	0,7	0,9	Péssimo
267	265	3,5	3,7	3,6	Bom	2,0	1,6	1,8	Ruim

Tabela 8 - Nota do VSA em relação ao Segmento C

Entre os Km		Segmento C							
		Dezembro de 2022				Março de 2023			
		Avaliador 1	Avaliador 2	Média	Conceito	Avaliador 1	Avaliador 2	Média	Conceito
233	231	3,0	3,0	3,0	Bom	3,7	4,1	3,9	Bom
231	229	3,5	3,5	3,5	Bom	4,5	4,8	4,7	Ótimo
229	227	3,1	3,7	3,4	Bom	4,8	4,8	4,8	Ótimo
227	225	4,8	4,8	4,8	Ótimo	3,3	4,0	3,7	Bom
225	223	3,7	4,5	4,1	Ótimo	2,5	3,8	3,2	Bom
223	221	4,2	4,7	4,5	Ótimo	1,0	2,1	1,6	Ruim
221	219	4,5	4,8	4,7	Ótimo	3,0	4,0	3,5	Bom
219	217	5,0	4,9	5,0	Ótimo	4,3	4,8	4,6	Ótimo
217	215	3,6	4,2	3,9	Bom	0,4	2,2	1,3	Ruim
215	213	4,0	4,4	4,2	Ótimo	0,5	0,3	0,4	Péssimo

De acordo com Tabela 6, em dezembro de 2022 as médias variaram entre 3 e 4, correspondendo a conceitos entre bom (31,25%) e ótimo (68,75%), refletindo a baixa incidência de defeitos. Predominavam remendos, fissuras e trincas isoladas, sem impactos na dirigibilidade. Por sua vez, em maio de 2023, as médias variaram entre 2 e 4, com trechos classificados como regular (12,50%), indicando agravamento das condições funcionais. Verificou-se que a presença de buracos impactou diretamente a redução das notas. Ainda assim, o Segmento A manteve, em geral, desempenho satisfatório, com predominância de conceitos bom (50,00%) e ótimo (37,50%).

Por outro lado, nos Segmentos B e C (Tabelas 7 e 8) observou-se maior incidência de defeitos após o período chuvoso, com consequente aumento das classificações ruim e péssimo, evidenciando redução do conforto de trafegabilidade. Destaca-se o segmento B, que apresentou os maiores percentuais de trechos com nível funcional ruim (33,33%). Em determinados locais (entre os km 289 e 287), o nível de serviço reduziu de ótimo para ruim (Tabela 7). Essa queda pode ser explicada pelo maior volume de tráfego e pela condição prévia do pavimento (dezembro/2022), com presença de fissuras e trincas, cuja infiltração de água acelerou a degradação da trafegabilidade no segmento (surgimento de buracos e remendos realizados na manutenção).

No segmento C (Tabela 8), destaca-se uma exceção entre os km 233 e 227, onde houve aumento nas médias em função de um recapeamento asfáltico. Apesar da melhoria local, essa intervenção foi pontual e insuficiente frente à extensão total analisada. Nos demais trechos, manteve-se a tendência de queda nas médias entre os meses de dezembro e maio, indicando a necessidade de intervenções mais abrangentes.

A Tabela 9 apresenta o resumo dos resultados obtidos para os segmentos A, B e C, considerando os valores médios de VSA nos períodos de dezembro/2022 e maio/2023, bem como a variação observada e a significância estatística (p-valor). O Segmento A apresentou uma diminuição de -0,45, indicando menor sensibilidade às variações sazonais. Em contrapartida, o segmento B apresentou a maior queda (-1,72), evidenciando maior quantidade de defeitos ou irregularidades provocadas pelas precipitações e problema de drenagem. Por sua vez, o segmento C apresentou redução de -0,94, presença de locais críticos surgidos no período chuvoso.

Tabela 9 - Síntese dos resultados estatísticos e funcionais

Segmento	VSA Dezembro /2022	VSA Maio /2023	Variação	p-valor	Decisão
A	4,06	3,61	-0,45	0,003	Rejeita H_0
B	3,73	2,01	-1,74	0,0001	Rejeita H_0
C	4,11	3,17	-0,94	0,01	Rejeita H_0

Ainda de acordo com a Tabela 9, verificou-se que todos os segmentos apresentaram redução do VSA no período chuvoso (maio/2023), sendo essa diferença estatisticamente significativa, com p-valores inferiores a 0,05 em todos os casos. Dessa forma, rejeita-se a hipótese nula, concluindo-se que há diferença significativa entre os períodos analisados, evidenciando a influência da sazonalidade na condição funcional dos pavimentos.

Em seguida, ao correlacionar valores de precipitação e os valores de VSA dos segmentos em dois períodos (dezembro/2022 e acumulado de maio/2023), obteve-se os gráficos das Figuras 7 e 8. A correlação entre a precipitação de dezembro e o VSA foi igual a r = 0,83. Por sua vez, a correlação entre a precipitação acumulada até maio/2023 e o VSA foi r = 0,47, caracterizando uma relação positiva moderada. Esses resultados sugerem que maiores volumes de precipitação não implicam, necessariamente, em menores valores de VSA, evidenciando que o desempenho funcional do pavimento também é influenciado por outros fatores, como condições estruturais, qualidade dos materiais e intervenções de manutenção.

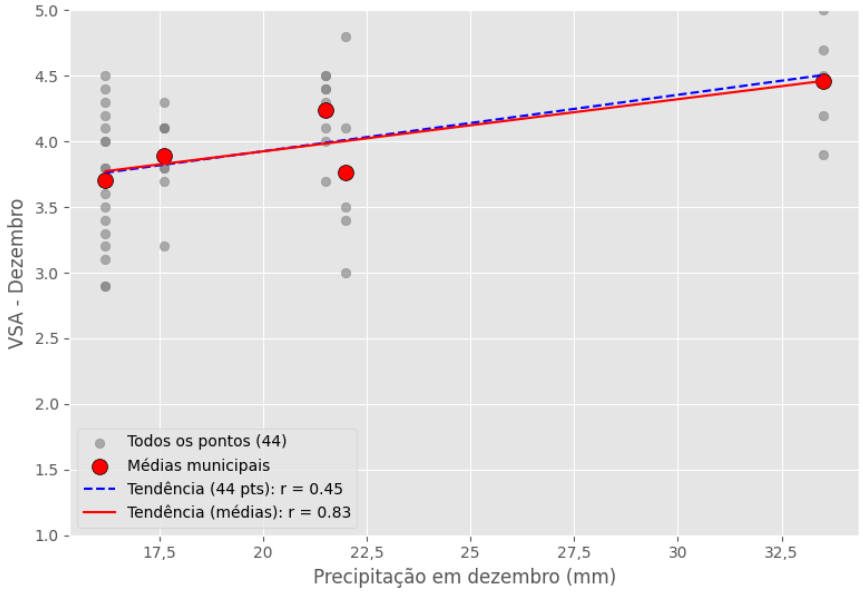


Figura 7 - Relação entre precipitação de dezembro/2022 e VSA

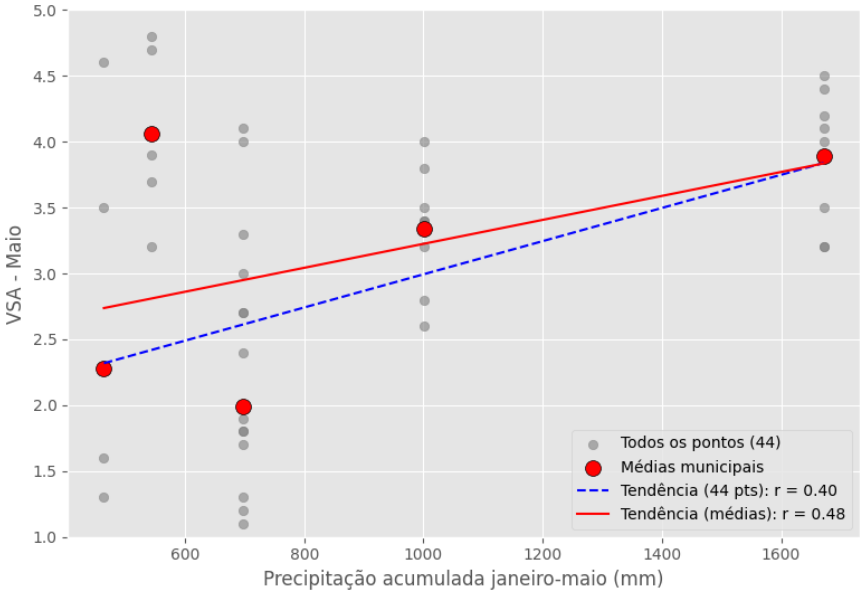


Figura 8 - Relação entre precipitação acumulada de janeiro/2023 a maio/2023 e VSA

De forma geral, os resultados indicam que a sazonalidade, especificamente as precipitações, exerce influência na condição funcional dos pavimentos, promovendo a redução do conforto ao rolamento devido ao aumento de defeitos e irregularidades superficiais, corroborando com os estudos realizados por Castro, Silva e Lange (2014). Além disso, a variabilidade entre os trechos analisados evidencia a necessidade de estratégias de manutenção diferenciadas, considerando as características estruturais e condições locais de drenagem.

5. Conclusão

No contexto da caracterização dos defeitos de um pavimento rodoviário flexível em dois períodos distintos, os resultados evidenciaram a presença de defeitos independentemente da época de inspeção. Constata-se que esses defeitos não estão associados apenas a um período específico. Ao longo do intervalo de tempo

analisado (cinco meses), observa-se a evolução da severidade e o surgimento de novos defeitos, associados à infiltração de água e à recorrente deterioração dos remendos, o que evidencia o caráter, muitas vezes, temporário dessas intervenções. Esse cenário indica a necessidade de incorporar a variabilidade sazonal nas estratégias de manutenção e reabilitação.

A sazonalidade climática contribuiu para a redução do nível de serventia funcional dos pavimentos flexíveis, acompanhando o aumento da incidência de defeitos. Embora tenha sido observada correlação entre precipitação e a serventia ao longo dos períodos analisados, o desempenho funcional do pavimento não depende exclusivamente dos índices pluviométricos das estações seca e chuvosa, sendo também influenciado por fatores como eficiência das ações de manutenção. Assim, concluiu-se que a variabilidade dos defeitos e da condição funcional evidencia a necessidade de adoção de estratégias de manutenção mais adequadas ao período do ano, bem como maior atenção aos sistemas de drenagem e à execução correta de intervenções corretivas, especialmente os remendos.

Agradecimento

O primeiro autor agradece a Coordenação de Aperfeiçoamento de Pessoal de Nível Superior - Brasil (CAPES) pela bolsa concedida que contribuiu para a elaboração deste trabalho.

Referencias

Abdollahi, S. F., M. E. Kutay, and M. Lanotte. 2024. “UPDAPS-Flood: A Mechanistic-Empirical Flexible Pavement Analysis Tool to Evaluate the Effect of Flooding Events on Flexible Pavement Performance.” International Journal of Pavement Engineering 25: 2387743.

Al-Samahi, S., W. Zeiada, G. G. Al-Khateeb, K. Hamad, and A. Alnaqbi. 2024. “A Comparative Study of Pavement Roughness Prediction Models under Different Climatic Conditions.” Infrastructures 9 (167). https://doi.org/10.3390/infrastructures9090167

Antunes, M. A. G., A. C. R. Guimarães, and M. L. Rocha. 2021. “Desempenho funcional, estrutural e de segurança viária de um pavimento rodoviário construído com resíduos reciclados de ardósia ao longo de três anos.” Revista Ibero-Americana de Ciências Ambientais 12 (4): 364–381. https://doi.org/10.6008/CBPC2179-6858.2021.004.0029.

Barbosa Neto, Antônio Alves. "Variações na pavimentação da rodovia BR-020/CE: um estudo das mudanças após a estação chuvosa". 2023. Trabalho de Conclusão de Curso (Bacharelado em Engenharia Civil) – Centro de Tecnologia, Universidade Federal do Ceará, Fortaleza, 2023.

Bernucci, L. B., L. M. G. Motta, J. A. P. Ceratti, and J. B. Soares. 2022. Pavimentação asfáltica: formação básica para engenheiros. 2nd ed. Rio de Janeiro: Petrobras; ABEDA.

Castro, S. R., P. J. Silva, and L. C. Lange. 2014. “Statistical Analysis of Climatic Seasonality on the Paving Conditions of a Brazilian Highway.” Journal of Civil & Environmental Engineering 4 (1): 1–5. https://doi.org/10.4172/2165-784X.1000133.

Choi, S. 2020. “Development of the Road Pavement Deterioration Model Based on the Deep Learning Method.” Electronics 9 (3). https://doi.org/10.3390/electronics9010003.

DNIT. Departamento Nacional de Infraestrutura de Transportes. 2003. DNIT 008/2003 – PRO: Levantamento Visual Contínuo para Avaliação da Superfície de Pavimentos Flexíveis e Semi-Rígidos – Procedimento. Rio de Janeiro: DNIT, 2003a.

DNIT. Departamento Nacional de Infraestrutura De Transportes. 2003. DNIT 005/2003 - TER: Defeitos nos pavimentos flexíveis e semi-rígidos: terminologia. Norma DNIT 005/2003-TER. Rio de Janeiro: DNIT, 2003b.

Domingues, F. A. A. 1993. MID – Manual de Identificação de Defeitos de Revestimento Asfáltico de Pavimentos. São Paulo.

FUNCEME. Desenvolvido Por Fundação Cearense de Meteorologia e Recursos Hídricos (Funceme). Postos Pluviométricos. Ceará. 2023.

Haas, R., Hudson, W. and Zaniewski, J. (1994) Modern Pavement Management. Krieger Publishing Company, Malabar.

Hong, F., and J. Prozzi. 2024. “Assessment of Flooding Impact on Thin Pavement Structure in Texas Coastal Region.” International Journal of Transportation Science and Technology. In press.

Hosseini, S. A., and O. Smadi. 2021. “How Prediction Accuracy Can Affect the Decision-Making Process in Pavement Management System.” Infrastructures 6 (28). https://doi.org/10.3390/infrastructures6020028

Jaafar, M, Z. F. B. 2019. Computational Modeling and Simulations of Condition Deterioration to Enhance Asphalt Highway Pavement Design and Asset Management. PhD diss., University of Mississippi.

Peng, L., L. Gao, F. Hong, and J. Sun. 2025. “Evaluating Pavement Deterioration Rates Due to Flooding Events Using Explainable AI.” Buildings 15 (1452). https://doi.org/10.3390/buildings15091452

Santana, Heloisa Oliveira, and Maria Clara Lacerda de Queiroz. 2025. “Avaliação de patologias em pavimento flexível pelo método VIZIR.” Interfaces do Conhecimento 7 (1).

Wu, Yanan, Yafeng Pang, and Xingyi Zhu. 2024. “Evolution of Prediction Models for Road Surface Irregularity: Trends, Methods and Future.” Construction and Building Materials 449: 138316. https://doi.org/10.1016/j.conbuildmat.2024.138316.

Cinpar 2026
XXII International Conference on Building Pathology and Constructions Repair
15th to 17th July 2026 - Lisboa, Portugal

Building Pathologies in the Rehabilitation of Substandard Housing: Technical Assessment of Housing Improvement Works

Rafael MORAIS[1,2], Ana Carolina RIBEIRO[3], Helena XIMENES[4], **João PANTOJA[5]**

[1] Universidade de Brasília, Brasília, Brazil, rafaelsgam@gmail.com
[2] Companhia de Desenvolvimento Habitacional do Distrito Federal, Brasília, Brazil
[3] Universidade de Brasília, Brasília, Brazil, anacbftribeiro@gmail.com
[4] Universidade de Brasília, Brasília, Brazil, helena.cubas@outlook.com
[5] Universidade de Brasília, Brasília, Brazil, joaocpantoja@gmail.com

Abstract: Substandard housing is often characterised by construction deficiencies, lack of technical assistance and the presence of recurring pathological manifestations that compromise the safety, durability and habitability of buildings. In this context, housing improvement programmes focused on rehabilitation represent a relevant strategy for mitigating processes of deterioration and extending the service life of existing buildings. This article analyses the main pathological manifestations identified in substandard housing and evaluates the effectiveness of the rehabilitation measures adopted under the Housing Improvement Programme of the Companhia de Desenvolvimento Habitacional do Distrito Federal, Brazil. This is an applied and descriptive study, with a mixed-methods approach, developed through multiple instrumental case studies of completed works. Technical diagnoses, detailed designs, specifications, budget spreadsheets, photographic reports and records of on-site inspections were analysed. The pathological manifestations were classified into technical categories, related to the rehabilitation measures adopted, and assessed in terms of occurrence, coverage, cost and criticality. To this end, a condition scale based on the Dutch standard NEN 2767 was used, and a Pathological Criticality Index (PCI) was developed, enabling the identified damage to be ranked. The results highlight the predominance of moisture-related pathologies, which presented the highest levels of criticality and constituted the main mechanism of degradation in the analysed units. The integrated analysis of manifestations, interventions and costs demonstrated that the most critical defects also account for significant investment demands, reinforcing the importance of technical prioritisation strategies. It is concluded that interventions guided by technical diagnosis contribute to mitigating pathologies, improving performance conditions and extending the service life of buildings, consolidating housing improvement works as a strategic tool for the rehabilitation of the substandard housing stock.

Keywords: Building pathology; housing rehabilitation; social housing; building deterioration; service life of buildings.

1. Introduction

Housing precarity in Brazil constitutes a persistent problem, associated with historical processes of exclusionary urbanisation, informal construction and the insufficiency of comprehensive public policies. Although Technical Assistance in Social Housing (Athis) programmes, provided for by Federal Law No. 11,888/2008 (Brazil, 2008), have expanded access to design and technical guidance for low-income families, the qualitative deficit in housing remains significant, particularly with regard to structural safety, sanitary conditions, minimum performance and the durability of buildings.

A large proportion of substandard housing exhibits pathological defects resulting from informal construction, inappropriate use of materials, lack of waterproofing, structural deficiencies, makeshift

building services and successive alterations carried out without technical supervision. These defects compromise habitability, accelerate deterioration processes, reduce the service life of building systems and increase risks to residents' health and safety.

In this context, the rehabilitation of the existing housing stock, through housing improvement programmes, is a key strategy for mitigating damage, restoring minimum performance standards and extending the service life of buildings. In the Distrito Federal, these initiatives are carried out by the Diretoria de Assistência Técnica (Diate) of the Companhia de Desenvolvimento Habitacional do Distrito Federal (Codhab-DF), particularly through the Housing Improvements Programme (Codhab-DF, 2025). This work is aligned with the guidelines of the District Plan for Social Housing (Plandhis), which recognises housing quality as a dimension that goes beyond the physical condition of the building, also encompassing infrastructure, urban integration, services and residents' living conditions (GDF, 2023).

Recent literature on building pathology highlights the importance of technical inspections, databases and systematic records for identifying recurring patterns of defects throughout the life cycle of buildings. Review studies indicate that moisture consistently features among the most frequent categories of pathological manifestations, associated with problems of stability, cracking and component degradation (Berg Oppedal; Kvande, 2024). Reviews of residential buildings also demonstrate that defects result from the interaction between technical, human and environmental factors, requiring analyses that go beyond the description of symptoms and consider the building system, the context of use and the mechanisms of degradation (Mésároš *et al*., 2024).

In the field of social housing, studies on post-occupancy evaluation, co-production and maintenance indicate that technical diagnosis must be linked to an understanding of usage and residents' needs, helping to guide more effective interventions, extend the service life of buildings and inform public housing policies (Garrefa *et al*., 2021; Villa *et al*., 2022; Petersen; Silva; González, 2023). In Brazilian social housing, the presence of moisture and the poor quality of the building envelope are associated with environmental discomfort, health risks and the worsening of inadequate living conditions, reinforcing the need to treat moisture as a central mechanism from diagnosis through to the definition of solutions (Simões; Labaki; Leder, 2025; Simões; Leder; Labaki, 2021).

Despite these advances, there are still few studies that integrate, within a single analytical procedure, the identification of pathological manifestations, their technical classification, the correspondence with rehabilitation measures, the severity of the damage, and the costs associated with interventions in public housing improvement programmes. This gap is particularly relevant in contexts of substandard housing, where decision-making requires technical criteria capable of supporting the prioritisation of actions, the efficient allocation of resources, and the evaluation of the effectiveness of the solutions adopted.

In light of this, this article aims to analyse the main defects identified in substandard housing prior to interventions and to assess, from a technical perspective, the effectiveness of the rehabilitation measures adopted under the Codhab-DF Housing Improvement Programme. The study's contribution lies in systematising the relationship between diagnosis, intervention and cost, based on six case studies, using a condition rating scale based on the Dutch Standard for the Assessment of the Condition of the Built Environment (NEN 2767), coding of the manifestations and measures adopted, and the proposal of a Pathological Criticality Index (PCI) designed to support technical prioritisation in housing programmes.

2. Methodology

This research is characterised as applied, descriptive in nature, with a mixed-methods approach and a qualitative focus, supported by documentary analysis, technical inspections and quantitative systematisation of the pathological manifestations observed. The study was conducted through multiple instrumental case studies, selected from completed projects under the Housing Improvement Programme of the Companhia de Desenvolvimento Habitacional do Distrito Federal (Codhab-DF).

Six housing units located in Região Administrativa XXV – Cidade Estrutural, Distrito Federal, were analysed. The units were identified as Case 1 to Case 6, in order to preserve the residents' identity. The selection criteria included: completion of the works; availability of complete technical documentation; existence of a pre-intervention assessment; photographic records; budget spreadsheets; and technical supervision of the interventions by the lead author during execution.

The documentary basis comprised pre-intervention technical assessments, detailed design drawings, descriptive specifications, calculation reports, budget spreadsheets, and technical and photographic reports produced throughout the works. These documents made it possible to characterise the initial construction conditions, identify pathological manifestations, relate them to the affected areas, verify the solutions adopted, and estimate the costs associated with the categories of intervention.

The technical inspections were guided by the principles of ABNT NBR 16747:2020, which establishes guidelines, concepts, terminology and procedures for building inspection, based on sensory analysis carried out by a qualified professional (ABNT, 2020). In this study, the standard was used as a reference to organise the survey, guide the systematic assessment of building elements and identify the irregularities observed. The inspections took place during the term of the works contracts, through weekly technical visits, involving visual inspection of rooms, building systems and services, photographic documentation of the defects and monitoring of the rehabilitation measures.

The pathological manifestations were classified into four technical categories: structural, moisture, building services and materials, taking into account the predominantly affected construction system and the main mechanism of degradation. To enable systematic cross-referencing between diagnosis and intervention, each defect was assigned a specific code, comprising the category abbreviation and sequential numbering: STR for structural defects, MOI for moisture-related defects, SER for building services, and MAT for materials. The rehabilitation measures were also coded according to the same logic, allowing the creation of a correspondence matrix between defect, technical solution, and intervention category.

The classification of the condition of the manifestations was carried out with the support of NEN 2767, the Dutch standard for assessing the condition of the built environment, which proposes a methodology for the objective determination of the technical condition of building components, based on the identification and classification of defects (NEN, 2019). In this study, the six-level condition scale provided for by the standard was adopted, in which grade 1 corresponds to excellent condition, grade 2 to good condition, grade 3 to reasonable condition, grade 4 to poor condition, grade 5 to severe condition and grade 6 to very poor condition. The assignment of grades took into account photographic records, technical reports and field observations, assessing the apparent severity of the defect, its extent within the environment and its potential impact on safety, habitability, performance and durability.

The overall occurrence of defects was calculated by considering the number of rooms affected in relation to the total number of rooms analysed in the six case studies, according to Equation (1):

$$o = \frac{N}{T} \times 100\ [\%] \tag{1}$$

where "o" corresponds to the occurrence of the defect; "N" corresponds to the number of affected rooms; and "T" corresponds to the total number of rooms analysed.

In addition to the overall occurrence, the prevalence of pathological categories in each case study was calculated, considering the number of rooms affected by a given category in relation to the total number of rooms in the respective housing unit. The prevalence, expressed as a percentage, was calculated using Equation (2):

$$a = \frac{n}{t} \times 100\ [\%] \tag{2}$$

where "a" corresponds to the coverage of the category in the analysed case; "n" corresponds to the number of rooms affected; and "t" corresponds to the total number of rooms in the housing unit.

To assess the technical relevance of the defects, a Pathological Criticality Index (PCI) was developed, calculated by weighting the occurrence of the defect by the technical weight assigned to the corresponding category. The weights were defined based on the potential impact of each category on the building's safety, habitability, operation and durability. Thus, the following weights were adopted: structural = 4; moisture = 4; building services = 3; and materials = 2. The PCI was normalised by dividing by 4, so as to produce values between 0 and 1, as per Equation (3):

$$ICP = \frac{o \times w_c}{4} \quad (3)$$

where "PCI" corresponds to the Pathological Criticality Index; "o" corresponds to the occurrence of the manifestation in decimal form; and "w_c" corresponds to the technical weighting of the category.

The economic analysis was carried out using the project budget spreadsheets, with the works grouped according to the previously defined pathology and intervention categories. The costs were linked to the corresponding rehabilitation measures, allowing the percentage share of each category in the total cost of the works to be estimated. This stage made it possible to relate technical criticality and economic impact, contributing to the identification of the categories with the greatest weight in decision-making and resource allocation.

The effectiveness of the interventions was assessed by comparing the pre-intervention conditions, as recorded in the initial technical assessments and photographic reports, with the post-intervention conditions, as verified from the final records and the documentation certifying completion of the works. The following were considered as evidence of effectiveness: mitigation or elimination of the identified pathological manifestations; restoration of deteriorated elements; improvement in safety, sanitary conditions and functionality; upgrading of building services; and potential contribution to extending the service life of the buildings.

Methodological validation was achieved through triangulation of three sources of evidence: technical documentation of the works, field inspections with photographic records, and budget spreadsheets. The convergence of these sources made it possible to verify the correspondence between diagnosis, the technical solution implemented and the associated cost. Furthermore, the combined use of ABNT NBR 16747 as a reference for building inspection and NEN 2767 as a condition scale contributed to greater standardisation, traceability and reproducibility of the analytical procedure.

3. Results

3.1 Characterisation of the housing units and interventions

Table 1 presents the characterisation of the six case studies, including area, number of occupants, existing rooms before and after the interventions, and total cost of the works. The units analysed are single-family, single-storey dwellings located in Cidade Estrutural, in the Distrito Federal, and exhibit conditions typical of urban substandard housing, characterised by informal extensions, a lack of ongoing technical support, makeshift construction solutions and the progressive deterioration of building systems.

The costs of the interventions ranged from R$ 39,220.04 to R$ 68,831.35, indicating varying levels of complexity in the works. Whilst some cases involved predominantly specific repairs, such as the restoration of cladding, the upgrading of building services and moisture control, others required more extensive interventions, including spatial reconfiguration, the enlargement of rooms, roof repairs and the restoration of structural elements.

Table 1 – Characterisation of the case studies analysed

Case	Description / Total area	Rooms (description / total)		Cost of intervention (R$)
		Pre-intervention	Post-intervention	
1	Single-family detached house, 4 occupants (46.22 m²)	Living room, kitchen, bathroom, hallway, 2 bedrooms, outdoor area (7)	Living room, kitchen, bathroom, hallway, 2 bedrooms, utility room, outdoor area (8)	41,644.84
2	Single-family detached house, 2 occupants (41.35 m²)	Living room, kitchen, bathroom, hallway, 2 bedrooms, outdoor area (7)	Living room, kitchen, bathroom, hallway, 2 bedrooms, outdoor area (7)	39,220.04
3	Single-family detached house, 5 occupants (67.00 m²)	Living room, kitchen, bathroom, hallway, 2 bedrooms, outdoor area (7)	Living room, kitchen, bathroom, hallway, 2 bedrooms, outdoor area (8)	49,561.03
4	Single-family detached house, 4 occupants (70.73 m²)	Living room, kitchen, bathroom, hallway, 2 bedrooms, outdoor area (7)	Living room, kitchen, bathroom, hallway, 2 bedrooms, garage, outdoor area (8)	50,724.85
5	Single-family detached house, 2 occupants (52.97 m²)	Living room, kitchen, bathroom, bedroom, outdoor area (5)	Living room, kitchen, bathroom, 2 bedrooms, hallway, ventilation shaft, outdoor area (8)	68,831.35
6	Single-family detached house, 9 occupants (56.64 m²)	Living room, kitchen, bathroom, hallway, 2 bedrooms, outdoor area (7)	Living room, kitchen, bathroom, hallway, 3 bedrooms, utility room, outdoor area (9)	54,422.13

Source: Authors.

A comparison of conditions before and after the intervention shows that the housing improvements were not limited to repairing structural damage. In some cases, the works also promoted functional adaptations, such as the creation of new spaces, the reorganisation of utility areas, improved circulation, and an expansion of the dwelling's usable capacity. Thus, the interventions served a dual purpose: mitigating pathological manifestations and enhancing the functional quality of the housing units.

3.2 Recurring pathological manifestations prior to the intervention

Analysis of pre-intervention conditions revealed the presence of recurring pathological manifestations in all cases analysed. These defects reflect both the ageing and natural degradation of materials and the lack of technical expertise in the original construction process, in successive extensions, and in maintenance work over time.

The observed defects were grouped into four technical categories: structural deficiencies, moisture-related pathologies, inadequacies in building services, and progressive material degradation. This classification enabled the damage to be organised according to the affected construction system and the predominant mechanism of degradation, facilitating the subsequent relationship between diagnosis, rehabilitation measures and intervention costs. Figure 1 presents examples of the manifestations observed.

Structural and construction defects included cracks and fissures in masonry, deformations in structural and roofing elements, inadequate gutters and flashings, and improvised or undersized elements. Although not all occurrences posed an immediate risk, they indicated degradation processes with the potential to worsen.

Moisture-related defects constituted the most common and technically most significant category. Mould, mildew, stains, water ingress, waterproofing failures, rising damp, paint saponification, corrosion of window frames and displacement of cladding were observed. This damage was associated with the absence or inadequacy of waterproofing, deterioration of roofing and makeshift construction solutions.

Deficiencies in building services involved electrical, plumbing and sanitary installations carried out in an improvised manner, with exposed wiring, a lack of protective devices, precarious networks and deteriorated pipework. Such conditions compromise functional performance and increase safety risks for residents.

The progressive degradation of materials included disintegration, deterioration of components, corrosion of metal elements and displacement of cladding. In many cases, these manifestations were associated with the combined effects of moisture, ageing of materials, exposure to the elements and lack of maintenance.

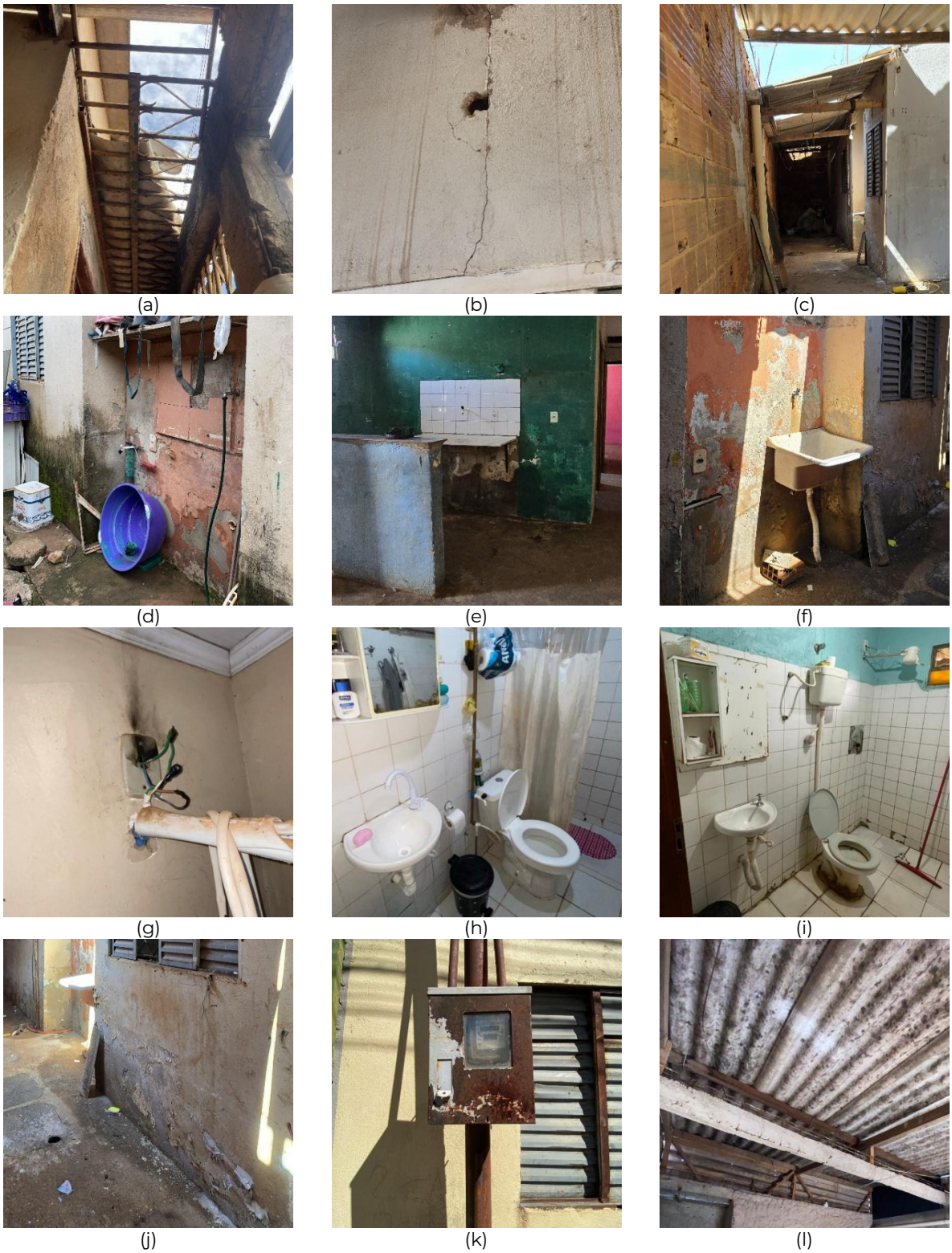


Figure 1 – Examples of pathological manifestations identified in the dwellings analysed: (a–c) structural deficiencies; (d–f) moisture-related pathologies; (g–i) inadequate building services; (j–l) progressive degradation of materials

Considering the occurrence of these defects in the analysed spaces, it was observed that the most frequent damage was associated with moisture and building services. The most common manifestations were mould and mildew, paint saponification, makeshift or inadequate electrical installations, corrosion of metal window frames and rising damp due to capillary action. This pattern indicates that moisture is the main source of damage in the units analysed, acting as the primary mechanism associated with leaks, roof failures, capillary action, deterioration of cladding, corrosion, rotting of window frames and degradation of paintwork.

3.3 Rehabilitation measures adopted in the analysed projects

The rehabilitation measures adopted were defined based on the technical diagnosis of the existing structural conditions and sought to directly address the identified pathological manifestations. To enable a systematic analysis of this relationship, the manifestations and solutions were coded according to their technical nature, maintaining correspondence between the categories of structure, moisture, building services, and materials.

Table 2 presents the correspondence matrix between observed defects and the rehabilitation measures adopted. This matrix demonstrates that the interventions were not treated as isolated actions, but as technical responses tailored to the degradation mechanisms identified in each case.

Table 2 – Pathological manifestations observed and respective rehabilitation measures

Observed manifestations			Rehabilitation measures adopted	
Category	**Description**	**Code**	**Description**	**Code**
Structural	Inadequate gutters, flashings and copings	STR1	Repair/replacement of gutters, flashings and downpipes	STR-S1
Structural	Inadequate roofing (slope, pitch)	STR2	Repair/replacement of roof components	STR-S2
Structural	Deformation of structural elements	STR3	Repair of damaged structural elements	STR-S3
Structural	Cracks and fissures	STR4	Repair of damage to masonry and sealing with repair mortar	STR-S4
Structural	Structural instability	STR5	Repair of damaged structural elements or reinforcement	STR-S5
Moisture	Rotting of wooden window frames	MOI1	Replacement of damaged window and door frames	MAT-S1
Moisture	Corrosion of reinforcement	MOI2	Cleaning, treatment and repair with structural mortar	MAT-S2
Moisture	Corrosion of metal window frames	MOI3	Cleaning and painting or replacement of damaged window and door frames	MAT-S3
Moisture	Peeling of finishes due to moisture	MOI4	Cleaning, waterproofing and restoration of finishes	MOI-S1
Moisture	Fungi, mould and mildew	MOI5	Cleaning, waterproofing and restoration of finishes	MOI-S1
Moisture	Water ingress (rainwater or leaks)	MOI6	Waterproofing and roof repair	MOI-S2
Moisture	Paint saponification	MOI7	Finish restoration	MOI-S3
Moisture	Rising damp (capillary action)	MOI8	Wall waterproofing and capillary barrier	MOI-S4
Building services	Makeshift or inadequate electrical installations	SER1	Inspection and replacement of electrical installations	SER-S1
Building services	Improvised or inadequate plumbing installations	SER2	Inspection and replacement of plumbing components	SER-S2
Building services	Improvised or inadequate sanitary installations	SER3	Inspection and replacement of sanitary components	SER-S3
Materials	Disaggregation	MAT1	Reconstruction of structural elements and cladding	MAT-S5
Materials	Detachment of finishes due to material degradation	MAT2	Finish restoration	MAT-S6
Materials	Deterioration	MAT3	Repair of damaged structural elements or replacement	MAT-S7

Source: Authors.

Analysis of the matrix shows that a significant proportion of the solutions adopted focused on moisture control measures, restoration of cladding, roof repairs, replacement of damaged window and door frames, and upgrading of building services. These measures indicate that the rehabilitation of the units required integrated interventions across different building systems, confirming that the observed damage resulted from combined degradation processes rather than isolated incidents.

3.4 Coverage of categories, measures adopted and intervention costs

Table 3 lists, for each case study, the categories of pathology, the identified manifestations, the coverage of the categories within the environments, the rehabilitation measures adopted and the estimated cost of these measures in relation to the total cost of the works.

Table 3 – Relationship between pathological manifestations, rehabilitation measures and cost

Case	Pathology category	Manifestations	Coverage (a)	Rehabilitation measures adopted	Estimated cost of the measures adopted	
					(R$)	% of total cost
1	Structural	STR1	14.29%	STR-S1	4,100.00	9.85%
	Moisture	MOI3, MOI5, MOI7, MOI8	85.71%	MAT-S3, MOI-S1, MOI-S3, MOI-S4	12,500.00	30.02%
	Building services	SER1, SER2	85.71%	SER-S1, SER-S2	8,200.00	19.69%
	Materials	MAT1, MAT3	14.29%	MAT-S5, MAT-S7	14,300.00	34.34%
2	Structural	STR1	14.29%	STR-S1	3,900.00	9.94%
	Moisture	MOI1, MOI2, MOI3, MOI4, MOI5, MOI6, MOI7, MOI8	85.71%	MAT-S1, MAT-S2, MAT-S3, MOI-S1, MOI-S2, MOI-S3, MOI-S4	11,800.00	30.09%
	Building services	SER1, SER2, SER3	85.71%	SER-S1, SER-S2, SER-S3	7,800.00	19.89%
	Materials	MAT1, MAT2, MAT3	42.86%	MAT-S5, MAT-S6, MAT-S7	13,700.00	34.93%
3	Structural	STR1, STR2, STR3, STR4, STR5	14.29%	STR-S1, STR-S2, STR-S3, STR-S4, STR-S5	6,000.00	12.11%
	Moisture	MOI1, MOI2, MOI3, MOI4, MOI5, MOI6, MOI7, MOI8	100.00%	MAT-S1, MAT-S2, MAT-S3, MOI-S1, MOI-S2, MOI-S3, MOI-S4	14,900.00	30.06%
	Building services	SER1, SER2, SER3	57.14%	SER-S1, SER-S2, SER-S3	9,000.00	18.16%
	Materials	MAT1, MAT2, MAT3	28.57%	MAT-S5, MAT-S6, MAT-S7	14,900.00	30.06%
4	Structural	STR1, STR2	85.71%	STR-S1, STR-S2	5,100.00	10.05%
	Moisture	MOI1, MOI3, MOI4, MOI5, MOI6, MOI7, MOI8	85.71%	MAT-S1, MAT-S3, MOI-S1, MOI-S2, MOI-S3, MOI-S4	15,200.00	29.97%
	Building services	SER1, SER2, SER3	85.71%	SER-S1, SER-S2, SER-S3	10,100.00	19.91%
	Materials	MAT1, MAT2, MAT3	42.86%	MAT-S5, MAT-S6, MAT-S7	17,800.00	35.09%
5	Structural	STR1, STR2, STR3, STR4, STR5	60.00%	STR-S1, STR-S2, STR-S3, STR-S4, STR-S5	9,600.00	13.95%
	Moisture	MOI2, MOI3, MOI4, MOI5, MOI6, MOI7, MOI8	60.00%	MAT-S2, MAT-S3, MOI-S1, MOI-S2, MOI-S3, MOI-S4	19,100.00	27.75%
	Building services	SER1, SER2, SER3	80.00%	SER-S1, SER-S2, SER-S3	12,700.00	18.45%
	Materials	MAT1, MAT2, MAT3	60.00%	MAT-S5, MAT-S6, MAT-S7	15,900.00	23.10%
6	Structural	STR1, STR2, STR3, STR4, STR5	85.71%	STR-S1, STR-S2, STR-S3, STR-S4, STR-S5	9,800.00	18.01%
	Moisture	MOI1, MOI2, MOI3, MOI4, MOI5, MOI7, MOI8	85.71%	MAT-S1, MAT-S2, MAT-S3, MOI-S1, MOI-S3, MOI-S4	16,400.00	30.13%
	Building services	SER1, SER2, SER3	57.14%	SER-S1, SER-S2, SER-S3	9,600.00	17.64%
	Materials	MAT1, MAT2, MAT3	42.86%	MAT-S5, MAT-S6, MAT-S7	10,900.00	20.03%

Source: Authors.

The cost analysis shows that interventions related to moisture accounted for a significant proportion of the investment in all cases, with figures close to 30% of the total cost of the works. This result confirms that moisture was not only the most common category from a technical point of view, but also one of the most significant from an economic perspective.

Interventions in building services also accounted for a significant share of the costs, mainly due to the need to overhaul and replace electrical, plumbing and sanitary systems. Costs associated with structural categories, however, varied more markedly between cases, indicating different levels of complexity in the interventions. In cases involving extensions, more extensive roof repairs or restoration of structural elements, the proportion of this category was higher.

These results allow us to distinguish two main patterns of intervention. The first corresponds to specific rehabilitation measures, focused mainly on moisture control, restoration of finishes, replacement of window frames and upgrading of building services. The second corresponds to more extensive interventions, involving spatial reconfiguration, the enlargement of rooms, structural review and a broader restoration of building systems. This distinction is relevant for public housing improvement programmes, as it indicates that the prioritisation of works should consider not only the frequency of damage, but also the technical complexity and economic impact of the solutions.

3.5 Pathological Criticality Index

Based on the systematisation of occurrences by room and the technical weighting of the categories, the Pathological Criticality Index (PCI) was developed, with the aim of ranking the manifestations according to their relevance to the performance, safety, habitability and durability of buildings.

Table 4 presents the PCI calculated for each identified manifestation, ordered from highest to lowest value.

Table 4 – Pathological Criticality Index (PCI)

Manifestations observed	Category	Weight	Occurrence	PCI
Fungi, mould and mildew	Moisture	4	82.5%	0.83
Saponification in paint	Moisture	4	75.0%	0.75
Corrosion of metal window frames	Moisture	4	57.5%	0.58
Makeshift or inadequate electrical installations	Building services	3	75.0%	0.56
Rising damp (by capillary action)	Moisture	4	55.0%	0.55
Inadequate roofing (slope, pitch)	Structural	4	40.0%	0.40
Rotting of wooden window frames	Moisture	4	30.0%	0.30
Displacement of cladding (due to moisture)	Moisture	4	30.0%	0.30
Improvised or inadequate plumbing installations	Building services	3	37.5%	0.28
Inadequate gutters, flashings and downpipes	Structural	4	22.5%	0.23
Water ingress (rainwater or leaks)	Moisture	4	22.5%	0.23
Cracks and fissures	Structural	4	17.5%	0.18
Displacement of coatings (due to material degradation)	Materials	2	35.0%	0.18
Improvised or inadequate sanitary installations	Building services	3	22.5%	0.17
Deformation of structural elements	Structural	4	12.5%	0.13
Structural instability	Structural	4	10.0%	0.10
Reinforcement corrosion	Moisture	4	10.0%	0.10
Deterioration	Materials	2	20.0%	0.10
Disaggregation	Materials	2	15.0%	0.08

Source: Authors.

Application of the index showed that the most critical defects are strongly associated with moisture. Fungi, mould and mildew; paint saponification; corrosion of metal window frames; and rising damp feature among the most critical defects, confirming that moisture acts as the dominant mechanism of degradation in the units analysed. Furthermore, makeshift or inadequate electrical installations also presented a high level of criticality, due to their high frequency of occurrence and the risk associated with residents' safety.

The PCI made it possible to go beyond simply counting occurrences, providing a technical hierarchy of the manifestations. This prioritisation aids decision-making in housing improvement programmes, as it helps

identify which defects should be prioritised according to their recurrence, severity and potential impact on the safety and durability of buildings.

Taken together, the results indicate that the precarious construction conditions of the analysed units are expressed through recurrent, interdependent and cumulative damage. Moisture stood out as the main mechanism of degradation, both due to the frequency of associated manifestations and its influence on other categories of damage, as well as its impact on the costs of interventions. The association between occurrence, extent, cost and criticality enabled the technical survey to be transformed into a prioritisation tool, with potential for application in public housing improvement programmes.

4. Discussion

The results show that the pathological manifestations observed in the dwellings analysed are not isolated occurrences, but reflect cumulative processes of deterioration associated with informal construction, a lack of technical assistance and insufficient preventive maintenance. This pattern reinforces the need for rehabilitation approaches based on systematic technical diagnosis, particularly in contexts of substandard housing, where different building systems tend to exhibit simultaneous failures.

Among the categories analysed, moisture stood out as the primary mechanism of degradation. Its recurrence and association with secondary manifestations, such as mould, mildew, paint saponification, corrosion of window frames, displacement of cladding and rising damp, indicate that this phenomenon should not be treated as an isolated pathology, but as an underlying driver of deterioration. This finding is consistent with recent literature, which identifies moisture as one of the most frequent categories of defects in residential buildings, associated with failures in design, construction, waterproofing, ventilation and maintenance.

The concentration of these manifestations in kitchens, bathrooms and outdoor areas reinforces this interpretation, indicating the influence of exposure to water, plumbing and sanitary installations, insufficient ventilation and direct exposure to weathering. Thus, the analysis of these defects must consider not only their overall frequency, but also their location within the domestic space and their relationship to the day-to-day use of the dwelling.

The analysis of rehabilitation measures demonstrated that the interventions carried out addressed different aspects of deterioration, encompassing roof repairs, waterproofing, restoration of cladding, replacement of window frames, upgrading of building services and, in some cases, structural restoration and spatial reconfiguration. This set of actions demonstrates that housing improvement, when guided by technical diagnosis, goes beyond the logic of superficial repair and constitutes a strategy for the rehabilitation of the built stock.

The incorporation of cost analysis enhanced the study's contribution by demonstrating that the most recurrent and critical defects are also associated with significant portions of the construction investment. Interventions related to moisture accounted for a significant share of the costs, indicating that the prevention and appropriate treatment of this issue can directly impact the efficiency of public resource allocation.

In this regard, the Pathological Criticality Index (PCI) proved useful as a tool to support technical prioritisation. By combining the occurrence and technical weight of the categories, the index allows defects to be ranked not only by frequency but also by their potential impact on safety, habitability, functionality and durability. The triangulation of technical documentation, field inspections, photographic records and budget spreadsheets lent greater consistency to the procedure, whilst the combined use of ABNT NBR 16747 and NEN 2767 contributed to greater standardisation and traceability of the analysis.

Finally, the results reinforce the role of housing improvements as a strategic public policy tool. By intervening in existing units, these programmes contribute to risk mitigation, the improvement of

habitability conditions, the extension of the service life of buildings and the upgrading of substandard housing stock.

5. Conclusions

This study demonstrated that the substandard dwellings analysed exhibit recurring pathological manifestations, associated mainly with moisture, material degradation, inadequacies in building services and, to a lesser extent, structural deficiencies. Among these categories, moisture stood out as the primary mechanism of degradation, both due to the frequency of associated manifestations and its capacity to trigger secondary damage to finishes, window frames, paintwork, structural elements and living conditions.

The rehabilitation measures proved effective in mitigating the identified pathologies, especially when guided by technical diagnosis and tailored to different building systems. The interventions involved waterproofing, roof inspections, upgrading of building services, replacement of deteriorated components, restoration of cladding and, in some cases, spatial reconfiguration and structural repair.

The main contribution of the study lies in the integrated systematisation of pathological manifestations, rehabilitation measures, condition ratings, coverage, costs and criticality. The combined use of ABNT NBR 16747, NEN 2767 and the Pathological Criticality Index (PCI) enabled the development of an analytical procedure applicable to the technical prioritisation of interventions in public housing improvement programmes.

The cost analysis showed that the most critical pathologies are also associated with significant investment requirements, particularly those related to moisture and building services. Thus, the incorporation of criteria regarding occurrence, coverage, criticality and cost can contribute to greater efficiency in the allocation of public resources and to more informed decisions in contexts of budgetary constraints.

From a public policy perspective, the results confirm the potential of housing improvements as a strategy for rehabilitating the existing building stock, contributing to extending the service life of buildings, improving safety, sanitary conditions and functionality, and reducing housing inadequacy. Limitations include the limited number of cases, the geographical focus on Cidade Estrutural, and the absence of longitudinal monitoring. Future studies could expand the sample and incorporate post-occupancy assessments at different time intervals.

References

ABNT – Associação Brasileira de Normas Técnicas. NBR 16747:2020 – Building inspection: guidelines, concepts, terminology and procedures. Rio de Janeiro, 2020. https://www.abntcatalogo.com.br/pnm.aspx?Q=T3hialA0NENOalJXOWNxMFN1V0ZTNXlTd0hpY2lkMnlCTUFjcWxoMFh5UT0=

Berg Oppedal, L.; Kvande, T. Lessons Learned from Information Sources on Building Defect Studies. Buildings, Basel, vol. 14, no. 5, art. 1231, 2024. https://doi.org/10.3390/buildings14051231

Brazil. Law No. 11,888, of 24 December 2008. Ensures that low-income families receive free public technical assistance for the design and construction of social housing. Diário Oficial da União, Brasília, DF, 26 Dec. 2008. Available at: http://www.planalto.gov.br/ccivil_03/_ato2007-2010/2008/lei/l11888.htm. Accessed on: 11 Aug. 2025.

Codhab-DF – Companhia de Desenvolvimento Habitacional do Distrito Federal. Housing Improvements Programme. Available at: https://www.codhab.df.gov.br/pagina/473. Accessed on: 17 Sept. 2025.

Garrefa, F.; Villa, S. B.; Bortoli, K. C. R.; Stevenson, F.; Vasconcellos, P. B. Resilience in social housing developments through post-occupancy evaluation and co-production. Ambiente Construído, Porto Alegre, vol. 21, no. 2, pp. 151–175, Apr./Jun. 2021. https://doi.org/10.1590/s1678-86212021000200519

GDF - Governo do Distrito Federal. District Plan for Social Housing (PLANDHIS). Brasília: SEDUH, 2023. https://projetos.seduh.df.gov.br/plandhis

ISO - International Organization for Standardization. ISO 15686-1:2011: Buildings and constructed assets - Service life planning - Part 1: General principles and framework. Geneva: ISO, 2011. https://www.iso.org/obp/ui/#iso:std:iso:15686:-1:ed-2:v1:en

Mésároš, P.; Chellappa, V.; Spišáková, M.; Kaleja, P.; Špak, M. Factors influencing defects in residential buildings. Journal of Building Pathology and Rehabilitation, [s.l.], vol. 9, no. 1, art. 31, 2024. https://doi.org/10.1007/s41024-023-00381-4

NEN - Royal Netherlands Standardization Institute. NEN 2767-1+C1:2019 - Condition assessment of the built environment: Part 1: Methodology. Amsterdam: NEN, 2019. https://www.nen.nl/en/nen-2767-1-2017-en-247818

Nunes, O. V. R.; Sousa, I. G. Post-occupancy evaluation of single-family homes renovated with technical assistance in social housing in the Distrito Federal. Brasília: IESB; CAU/DF, 2023.

Petersen, A.; Silva, A.; González, M. Service Life Prediction of Painted Renderings Using Maintenance Data through Regression Techniques. Buildings, Basel, vol. 13, no. 3, art. 785, 2023. https://doi.org/10.3390/buildings13030785

Simões, G. M. F.; Labaki, L. C.; Leder, S. M. Thermal discomfort and adaptation strategies in Brazilian social housing. Building and Environment, [s.l.], vol. 269, art. 112368, 2025. https://doi.org/10.1016/j.buildenv.2024.112368

Simões, G. M. F.; Leder, S. M.; Labaki, L. C. How uncomfortable and unhealthy can social (low-cost) housing in Brazil become with use? Building and Environment, [s.l.], vol. 205, art. 108218, 2021. https://doi.org/10.1016/j.buildenv.2021.108218

STRAUB, A. Dutch standard for condition assessment of buildings. Structural Survey, Bradford, vol. 27, no. 1, pp. 23–35, 2009. https://doi.org/10.1108/02630800910941665

Villa, S. B.; Vasconcellos, P. B.; Bortoli, K. C. R.; Araujo, L. B. Lack of adaptability in Brazilian social housing: impacts on residents. Buildings and Cities, [s.l.], vol. 3, no. 1, pp. 376–397, 2022. https://doi.org/10.5334/bc.180

Cinpar 2026
XXII International Conference on Building Pathology and Constructions Repair
15th to 17th July 2026 - Lisboa, Portugal

Investigation of ultrasonic propagation angles for the identification of wood elastic properties

Sonagnon Jérôme AFOUTOU[1], Omar DOUZANE[1], Anh Dung TRAN LE[1], Laurent LAHOCHE[1], Geoffrey PROMIS[1]

[1] Laboratoire des Technologies Innovantes, EA 3899 – Université de Picardie Jules Verne, Avenue des Facultés – Le Bailly, 80025 Amiens Cedex 1, France, sonagnon.jerome.afoutou@u-picardie.fr ; omar.douzane@u-picardie.fr; anh.dung.tran.le@u-picardie.fr; laurent.lahoche@u-picardie.fr; geoffrey.promis@u-picardie.fr

Abstract: Assessing the structural integrity of old timber structures, which requires reliable estimates of their elastic properties, remains a major challenge for in situ inspection. Current non-destructive techniques generally focus on identifying only the elastic moduli associated with the principal orthotropic directions, without enabling a full determination of the stiffness matrix components. This study proposes an ultrasound-based identification strategy aimed at estimating the complete set of elastic properties of wood under realistic inspection constraints. In an ideal configuration, ultrasonic wave velocities are measured along multiple propagation directions within the three principal orthotropy planes (LR, LT and RT), enabling full mechanical characterization. However, such configurations are rarely achievable in practice due to limited access to timber elements. To address this issue, a complete and well-distributed data set is first considered as a reference, and then progressively degraded to emulate realistic in situ inspection conditions. All available data are subsequently incorporated into an optimization procedure using the Direct algorithm to estimate the elastic properties of wood. The algorithm seeks to minimize the gaps between theoretical wave velocities, computed using Christoffel's equation, and experimental velocities estimated using Hankinson's formula. The sensitivity of the identified properties to the number and orientation of the measurement points is analyzed systematically. The results showed that reducing the measurement angle from 3° to 30° can induce deviations ranging from 0.1% to 4.6% for longitudinal moduli and from 2% to 24% for shear moduli in the RT plane. The study also revealed critical propagation angles that significantly impact the identifiability and reliability of elastic properties. These findings provide practical guidance on optimizing ultrasonic measurement strategies for estimating the mechanical properties of timber structures under in situ conditions.

Keywords: Timber structures, ultrasound, inspection conditions, elastic properties, optimization

1. Introduction

In the past, wood was extensively used in the construction of buildings and engineering structures that now constitute a valuable cultural and historical heritage. Preserving this heritage requires regular inspection and, when necessary, repair or replacement of damaged structural elements that may compromise structural safety. In this context, in-situ assessment of timber structures has become increasingly important, requiring reliable estimation of the physical and mechanical properties of wood without causing damage to the structure. Wood is a natural material characterized by anisotropy and hygroscopic behaviour. Its physical, thermal, and mechanical properties depend significantly on environmental conditions, particularly moisture content, Forest Products Laboratory (2010). Due to its cellular structure, wood is defined by three principal material directions: longitudinal (L), radial (R), and tangential (T). The orthotropic elastic behaviour of wood is described by twelve elastic constants, of which nine are independent. These nine parameters

include the three moduli of elasticity (E_L, E_R, E_T) in the principal directions, the three shear moduli (G_{LR}, G_{LT}, G_{RT}), and the three Poisson's ratios (v_{LR}, v_{LT}, v_{RT}), in the planes of orthotropic symmetry.

Accurate determination of these elastic constants is essential for predicting structural behaviour and assessing structural integrity. However, traditional mechanical testing methods are destructive and therefore unsuitable for in-situ applications. Consequently, non-destructive technique (NDT) techniques have been widely investigated for timber characterization. Several methods have been proposed in the literature, including measurements of density, moisture content, and degradation level, Bahrami *et al.* (2025); Kasal and Anthony (2004); Jaskowska-Lemańska and Wałach (2023); Wang *et al.* (2021); Vössing and Niederleithinger (2018).

Among non-destructive techniques, ultrasonic methods have proven particularly effective for evaluating elastic properties of wood. These methods rely on measuring wave propagation velocities, which can be related to material stiffness and density. Due to the orthotropic nature of wood, wave propagation velocities depend on the direction of propagation. This directional dependence has been described using empirical relationships, such as Hankinson (1921) and more recent two-dimensional models proposed by van Wijk *et al.* (2019), as well as three-dimensional empirical formulations proposed by Afoutou *et al.* (2023). Christoffel (1877) established some equations which give a relationship between the elastic stiffness tensor, density and direction of propagation, on the one hand, and wave velocities, on the other. Solving the Christoffel's equations yields three wave velocities corresponding to quasi-longitudinal and quasi-transverse waves. In an anisotropic medium, these solutions correspond to phase velocities and must be converted to group velocities before being compared with the experimental velocities as demonstrated in Abedi *et al.* (2019). This combination of analytical and empirical approaches is particularly well suited to inverse stiffness matrix determination.

Despite its theoretical robustness, the practical implementation of the Christoffel-based approach under in situ conditions remains challenging. In practice, current in-situ measurements often focus on determining elastic moduli along the principal orthotropic directions. However, such measurements do not allow full determination of the stiffness matrix. Laboratory-based techniques such as resonant ultrasonic spectroscopy used by Longo *et al.* (2012) and immersion methods in Bucur and Rasolofosaon (1998) enable complete characterization of elastic constants. Nevertheless, these methods require controlled laboratory conditions and cannot be applied to existing structures. To overcome these limitations, a novel approach was proposed for identifying the complete stiffness matrix using compression waves measured in multiple directions by Afoutou *et al.* (2024). The ideal characterization would be based on regular measurements of ultrasonic wave propagation velocities in multiple directions, covering the full range of mechanical properties. However, in real inspection scenarios, access to all surfaces of timber elements is often limited. Furthermore, several factors such as moisture gradients, heterogeneity, geometric irregularities, and measurement uncertainties influence wave velocities and complicate parameter identification. Therefore, it is essential to investigate the influence of measurement configuration and directional coverage on the accuracy of identified elastic properties. In particular, the number and distribution of measurement angles may significantly affect the stability of inverse identification methods based on the Christoffel model.

The present study aims to evaluate in-situ inspection strategies for identifying the complete set of mechanical properties of timber structures, with particular emphasis on the influence of measurement angles. The study first assumes an ideal dataset with an identical number of measurements in each principal orthotropic plane (LR, LT, and RT). Subsequently, the dataset is progressively degraded to simulate realistic inspection conditions and evaluate the robustness of the identification method. The paper is organized as follows. Section II presents the theoretical background of wave propagation in anisotropic elastic media and introduces the Christoffel formulation. Section III describes the methodology used for elastic property identification and optimization. Section IV presents and discusses the results obtained under different configurations.

2. Wave propagation in an elastic medium

The propagation of waves is defined by the following equation, Royer and Dieulesaint (1996):

$$\rho \cdot \frac{\partial^2 u_i}{\partial t^2} = C_{ijkl} \cdot \frac{\partial^2 u_l}{\partial x_j \partial x_k} \tag{1}$$

where u_i and u_l denote the displacement components of a materiel point M defined by its coordinates x_j in a Cartesian reference. ρ is the material density, assumed to be homogeneous like C_{ijkl}, which represents the components of elastic stiffness tensor C, in accordance with the following Hooke's law:

$$\underline{\sigma} = C \cdot \underline{\varepsilon} \text{ or } \sigma_{ij} = C_{ijkl} \cdot \varepsilon_{kl} \text{ with } (i,j,k,l) \in \{1,2,3\}^4 \tag{2}$$

σ_{ij} and ε_{kl} are the components of the stress and strain tensors, $\underline{\sigma}$ and $\underline{\varepsilon}$, respectively. The solution to Equation (1) actually takes the form of a progressive plane wave, as exhibited in the following expression, Cuxac (1991):

$$\vec{u}(\overrightarrow{OM}, t) = \vec{U} \cdot g\left(\omega \cdot t - \vec{k} \cdot \overrightarrow{OM}\right) \tag{3}$$

$\vec{U}$ is the maximum displacement vector corrected by function g. $\vec{k}$ designates the wave vector, which is dependent on wave type (compression or shear waves); it is oriented by the unit propagation direction vector $\vec{n}$, hence:

$$\vec{k} = k_\phi \cdot \vec{n} \tag{4}$$

k_ϕ is the unit wave vector and can be written as:

$$k_\phi = \frac{2\pi}{\lambda} = \frac{\omega}{V_\phi} \tag{5}$$

Where, ω is the wave pulsation, V_ϕ phase velocity for compression waves ($\phi = p$) and for either horizontal or vertical shear waves ($\phi = S_h$ or $\phi = S_v$, respectively) and λ is the wavelength associated, as defined in the local reference shown in Figure 1.

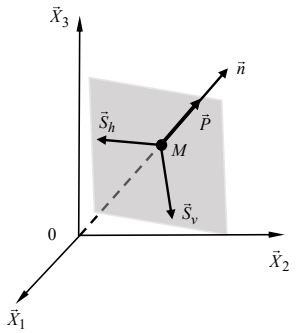


Figure 1 – Local reference Afoutou *et al*. (2024)

The solution to the dynamic wave propagation equation (3) assumes he typical indicial form below:

$$u_i = U_i \cdot exp\left(\omega \cdot t - k_\phi \cdot n_j \cdot x_j\right) \tag{6}$$

Introducing expression (6) into the left-hand term of (1) yields:

$$\rho \cdot \frac{\partial^2 u_i}{\partial t^2} = \rho \cdot \omega^2 \cdot \left[U_i \cdot exp\left(\omega \cdot t - k_\phi \cdot n_j \cdot x_j\right)\right] \tag{7}$$

Similarly, the right-hand term of (1) becomes:

$$\frac{\partial^2 u_l}{\partial x_j \partial x_k} = k_\phi^2 \cdot n_j \cdot n_k \cdot \left[U_l \cdot exp\left(\omega \cdot t - k_\phi \cdot n_j \cdot x_j\right)\right] \tag{8}$$

By combining expressions (7) and (8), relation (1) is replaced by:

$$\rho \cdot \omega^2 \cdot U_i = C_{ijkl} \cdot k_\phi^2 \cdot n_j \cdot n_k \cdot U_l \tag{9}$$

As described in (Bucur 2023), the expression (9) can be rewritten according to Christoffel's notations:

$$\begin{bmatrix} \Gamma_{11} - \rho \cdot V_\phi^2 & \Gamma_{12} & \Gamma_{13} \\ \Gamma_{12} & \Gamma_{22} - \rho \cdot V_\phi^2 & \Gamma_{23} \\ \Gamma_{13} & \Gamma_{23} & \Gamma_{33} - \rho \cdot V_\phi^2 \end{bmatrix} \cdot \begin{pmatrix} U_1 \\ U_2 \\ U_3 \end{pmatrix} = \begin{pmatrix} 0 \\ 0 \\ 0 \end{pmatrix} \tag{10}$$

According to the general case, the solution to the system in (10) is obtained by calculating the eigenvalues of the matrix system. In this case, three values or V_ϕ, corresponding to one compressive and two shear wave velocities, are deduced from solving the characteristic polynomial given by the following expression:

$$det \begin{bmatrix} \Gamma_{11} - \rho V_\phi & \Gamma_{12} & \Gamma_{13} \\ \Gamma_{12} & \Gamma_{22} - \rho V_\phi & \Gamma_{23} \\ \Gamma_{13} & \Gamma_{23} & \Gamma_{33} - \rho V_\phi \end{bmatrix} = 0 \tag{11}$$

For anisotropic materials, it has been demonstrated that wave polarisation is related to phase velocity, propagation direction and stiffness constants. For a pure longitudinal wave, the angle between the displacement vector and the normal to the wave is 0°, whereas for pure shear waves, the angle between the propagation and polarisation vectors is $\pi/2$. This angle varies when the propagation direction deviates from the material's principal directions, Bucur (2023). Knowing the phase velocities and directions of the phase velocity vectors makes it possible to deduce the slowness surface of the group velocities. However, since measurements used to derive elastic constants are taken in assumed planes of symmetry, the angle between group and phase velocities remains confined to that plane. The two-dimensional relationship between the group velocity V_g, and the phase velocity V_Φ, in these planes of symmetry can be found in Postma (1955) and in Abedi *et al.* (2019) as follows:

$$V_g = \sqrt{V_\emptyset^2 + \frac{\partial V_\emptyset}{\partial \emptyset}} \tag{12}$$

where $\emptyset$ represents the angle of the phase vector V in the plane of symmetry. The group angle θ in this plane is given by:

$$\theta = \emptyset + \tanh^{-1}\left[\frac{\partial V_\emptyset / \partial \emptyset}{V_\emptyset}\right] \tag{13}$$

3. Procedure for elastic property determination

3.1. Material and selection of experimental velocities

To illustrate the tree's growth, we identify three principal directions (L, R, and T) and three orthotropic planes (LR, LT, and RT), as shown in Figure 2.

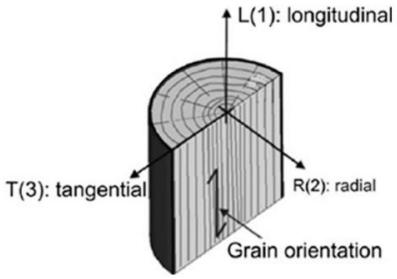


Figure 2 – Principal directions of wood Bucur (2023)

For the rest of the study, Let's define the symmetry axes of wood L, R and T as axes 1, 2 and 3. The velocities and the corresponding stiffnesses are noted as:

$V_L=V_{LL}= V_{11}$, $V_R=V_{RR}= V_{22}$, $V_T=V_{TT}= V_{33}$, $V_{TR}= V_{44}$, $V_{LT}= V_{55}$, $V_{LR} = V_{66}$ and $C_{LL} = C_{11}$, $C_{RR}= C_{22}$, $C_{TT}= C_{33}$, $C_{TR} = C_{44}$, $C_{LT} = C_{55}$, $C_{LR}= C_{66}$.

Since working with the elastic constants (E, v, and G) is most convenient, we will present the compliance matrix, the inverse of the stiffness matrix.

The components of the compliance matrix, [S] = [C] $^{-1}$, are derived as follows:

$$[S] = \begin{bmatrix} \frac{1}{E_L} & -\frac{\nu_{RL}}{E_R} & -\frac{\nu_{TL}}{E_T} & 0 & 0 & 0 \\ -\frac{\nu_{RL}}{E_R} & \frac{1}{E_R} & -\frac{\nu_{TR}}{E_T} & 0 & 0 & 0 \\ -\frac{\nu_{TL}}{E_T} & -\frac{\nu_{TR}}{E_T} & \frac{1}{E_T} & 0 & 0 & 0 \\ 0 & 0 & 0 & \frac{1}{G_{RT}} & 0 & 0 \\ 0 & 0 & 0 & 0 & \frac{1}{G_{LT}} & 0 \\ 0 & 0 & 0 & 0 & 0 & \frac{1}{G_{LR}} \end{bmatrix} \quad (14)$$

We considered the material to be homogeneous and orthotropic, with a constant and homogeneous density throughout the region of interest. The density is assumed to be 450 kg/m³. The elastic properties of interest are summarized in Table 1.

Table 1 – Material properties of softwood, Guitard (1987).

E_L (GPa)	E_R (GPa)	E_T (GPa)	ν_{LR}	ν_{RT}	ν_{TL}	G_{LR} (GPa)	G_{RT} (GPa)	G_{TL} (GPa)
13.1	1	0.636	0.39	0.51	0.02	0.861	0.084	0.745

The elastic property values in the above table will serve as a reference for interpreting the optimization results.

As mentioned in Section 2, our approach involves working systematically within orthotropic planes to optimize the elastic properties.

We used Hankinson's empirical model to generate experimental velocities as a function of propagation angles in each of the three orthotropic planes (LR, LT, and RT). Hankinson's 2D model in an xy plane is expressed as follows:

$$V_{Hank}^{xy} = \frac{V_x \cdot V_y}{V_x \cdot (\sin \alpha_{xy})^{n_{xy}} + V_y \cdot (\cos \alpha_{xy})^{n_{xy}}} \quad (15)$$

V_x and V_y designate the wave velocities in the x and y directions, respectively, and n_{xy} is Hankinson's empirical exponent.

To determine V_L, V_R, V_T, and the three calibration coefficients, we first performed an optimization between the analytical group velocities derived from Christoffel and the velocities derived from Hankinson's empirical model. The values obtained are 5550 m/s, 1650 m/s, and 1310 m/s for the longitudinal velocity V_L, radial velocity V_R, and tangential velocity V_T, respectively. The scaling coefficients for n_{RT}, n_{LT}, and n_{LR} are 1.55, 1.38, and 1.41, respectively. However, this approach generates measurement noise, as the equivalent isotropic theoretical velocities using $V_i = \sqrt{E_i/\rho}$ would yield values of 5395 m/s, 1490 m/s, and 1190 m/s, respectively for the longitudinal, radial, and tangential directions.

Given that equation (15) is continuous, the velocities at defined angular increments are extracted from the empirical velocities obtained to reflect in situ conditions. We have considered six configurations based on the extraction angle increments of the empirical velocities, as summarized in Table 2.

Table 2 – Different configurations tested as function of angle

Configurations	Angles increments	Number of data per plane
C1	3°	61
C2	10°	19
C3	15°	13
C4	30°	7
C5	45°	5
C6	15° without V_L	11 in LR and LT; 13 in RT

Taking the C5 configuration as an example, the velocities used in the elastic property optimization process are summarized in Table 3.

Table 3 – Examples of empirical velocities

Angles (°)	Velocity (m/s) in LR plane	Velocity (m/s) in LT plane	Velocity (m/s) in RT plane
0	5500	5500	1650
45	2069	1707	1250
90	1650	1310	1310
135	2069	1707	1250
180	5500	5500	1650

3.2. Cost Function and Optimization Algorithm

The flowchart in Figure 3 describes the steps used to determine the elastic properties. In short, the cost function deviation defined in following equation was minimized. This function aims to minimize the average deviation across all three planes. The DIRECT algorithm was employed.

$$\overline{f} = \frac{1}{nb}\left(\sum_{i=1}^{nb}\left(V_p^{xy}(\alpha,\theta) - V_{Hank}^{xy}(\alpha,\theta)\right)\right) \quad (16)$$

Where nb is the number of angular combinations chosen in the process of optimizing the elastic properties. For example, for an angular step of 45°, nb = 15.

The dividing rectangles (DIRECT) is a global optimization algorithm designed to solve complex problems where the aim is to minimize a function without knowing its exact form. It is especially useful when precise variable boundaries must be met. Further details can be found in Jones and Martins (2021). A threshold value of 10^{-4} was set for the convergence.

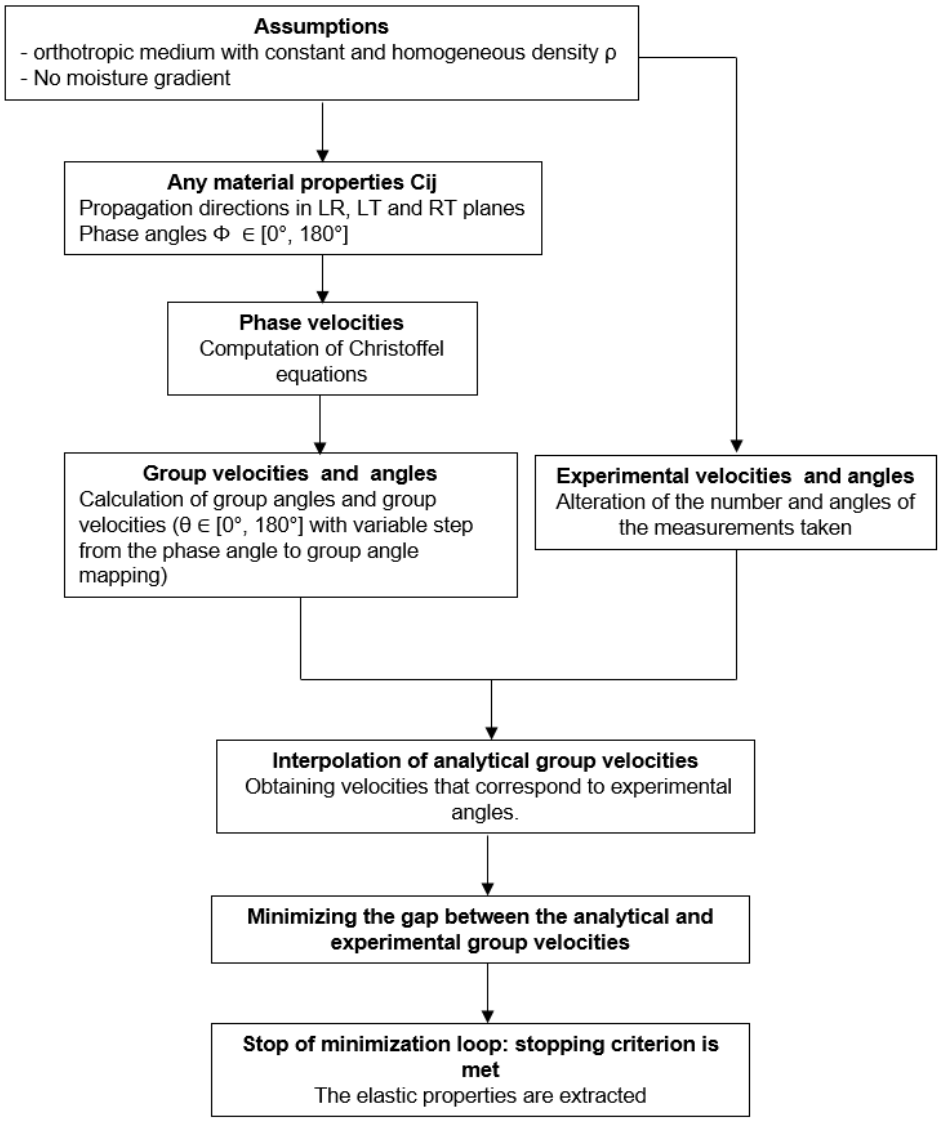


Figure 3 – Flowchart of elastic properties determination

4. Results and Discussion

Figure 4 shows the optimized velocities for the configuration C5 that yield the best values for the desired parameters. These velocities are plotted alongside the analytical Christoffel velocities (Vg_target), which are

calculated using the reference properties from Table 1. The velocities (Vg_C5) represent the experimental velocities. We found that the optimized velocities are in line with the reference velocities with a value of $\overline{f}$ equal to 15 (m/s), indicating correct optimization.

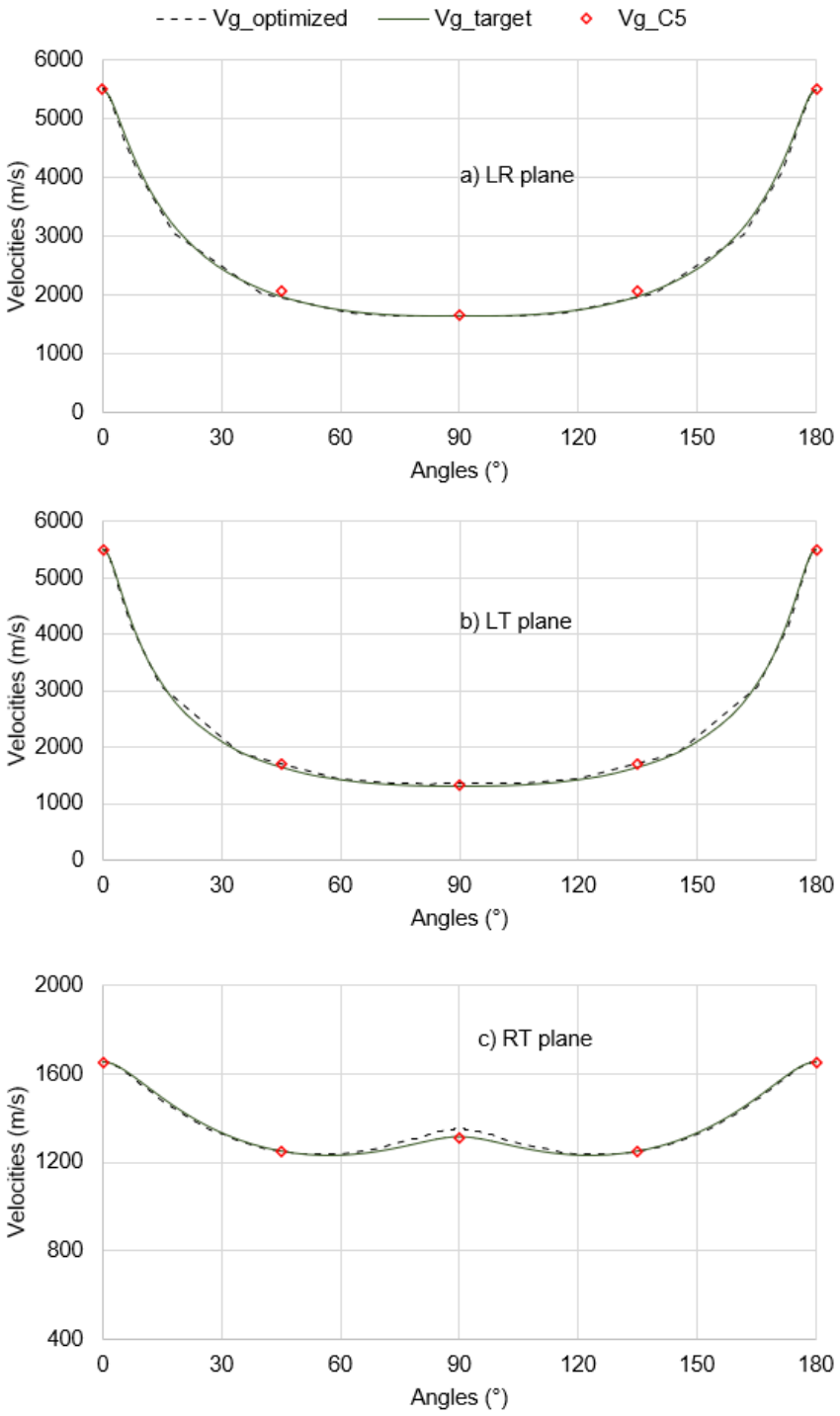


Figure 4 – Example of combination C5 velocities, displayed alongside the optimized and analytical references velocities.

Table 4 summarizes the corresponding elastic properties and the complete set of results for the other configurations.

The results showed that reducing the measurement angle from 3° to 30° (configurations C1 and C4) can lead to relative deviations ranging from 0.1% to 4.6% for longitudinal modules and from 2% to 24% for shear modules in the RT plane.

Specifically, relative deviations of E_L remain below 5%, regardless of the angle increment, except for configuration C6, which yields a relative deviation of 14.2%. This is expected, as no values are provided in the input data along the longitudinal direction (V_L). Regarding the radial modulus (E_R), all configurations except C2 and C6 (with angle increments of 10° and 45°, respectively) yield relative deviations of around 10%. For the modulus in the tangential direction (E_T), configuration C1 (3° pitch) is the best, and configuration C6 yielded the largest relative deviation.

Table 4 –Optimized elastic property values

Configurations	E_L (GPa)	E_R (GPa)	E_T (GPa)	ν_{LR}	ν_{RT}	ν_{TL}	G_{LR} (GPa)	G_{RT} (GPa)	G_{TL} (GPa)
C1	13.111	1.093	0.656	0.498	0.422	0.040	0.998	0.085	0.848
C2	13.037	0.938	0.567	0.409	0.570	0.039	0.998	0.061	0.842
C3	13.037	1.110	0.695	0.498	0.400	0.030	0.998	0.099	0.842
C4	13.704	1.102	0.680	0.102	0.459	0.005	0.708	0.064	0.676
C5	13.556	1.050	0.700	0.102	0.467	0.010	0.885	0.063	0.747
C6	14.963	0.894	0.537	0.483	0.593	0.040	0.998	0.070	0.833

Regarding the Poisson's ratios, it is best to verify all inequalities in the following equation described in Bucur and Najafi (2003), to ensure the stiffness matrix is non-negative.

$$\begin{cases} 1 - \nu_{ij}\nu_{ji} > 0 \ \text{ with } \ i \neq j \text{ and } i,j \in \{L,R,T\}^2 \\ |\nu_{ij}| < \sqrt{\dfrac{E_i}{E_j}} \ \text{ with } \ i \neq j \text{ and } i,j \in \{L,R,T\}^2 \\ 1 - \nu_{LR}\nu_{RL} - \nu_{LT}\nu_{TL} - \nu_{RT}\nu_{TR} - 2\nu_{LR}\nu_{RT}\nu_{TL} > 0 \end{cases} \quad (17)$$

We found that all optimized values satisfy these inequalities, indicating the robustness of the optimization procedure.

Finally, the relative deviations for the shear moduli are large, except for the G_{LR} (2.8%), G_{TL} (0.2%), and G_{RT} (1.7%) configurations, respectively, for C5, C5, and C1. These large deviations explain why it is difficult to obtain shear moduli with a single configuration. However, the C5 configuration appears to be the most suitable. However, the order ($G_{LR} > G_{LT} >> G_{RT}$) holds true for all optimized values.

The study also identified critical propagation angles that significantly impact the identifiability and reliability of elastic properties. This is the case for the 45° angle. These results provide practical recommendations for optimizing ultrasonic measurement strategies aimed at estimating the mechanical properties of timber structures under in situ conditions. While the overall behavior of the nine parameters combined is very interesting (see the curves in Figure 4), optimizing nine parameters is risky due to the potential for local minima, even when a global algorithm is used.

5. Conclusion

This study examined an ultrasonic-based approach for determining the complete stiffness matrix of wood. The study began with an ideal dataset in which propagation directions were uniformly distributed. The

measurement configurations were then progressively degraded to evaluate their influence on the robustness of the identified elastic properties. The findings indicated that augmenting the angular increment from 3° to 30° results in relative deviations ranging from 0.1% to 4.6% for longitudinal moduli and from 2% to 24% for shear moduli in the RT plane. While the longitudinal elastic moduli demonstrated relative stability, the shear moduli exhibited greater sensitivity to measurement configuration. This observation underscores the challenge of accurately identifying these parameters using limited directional data.

The analysis further demonstrated that specific propagation angles, notably around 45°, significantly influence the identifiability and reliability of elastic properties. Despite these limitations, the optimization procedure based on the Direct algorithm and Christoffel's equation demonstrated good robustness, as confirmed by the preservation of expected stiffness relationships. In consideration of the findings, the results provide practical recommendations for optimizing ultrasonic measurement strategies in in-situ timber inspection.

Subsequent research will concentrate on enhancing the robustness of the inverse identification procedure, particularly in the context of estimating multiple parameters concurrently. Furthermore, extending the methodology to surface wave measurements has the potential to improve accessibility in real structures and enhance the reliability of shear modulus estimation. Finally, experimental validation on real timber structures and the integration of measurement uncertainties will be essential steps toward practical field applications.

References

Abedi, Mohammad Mahdi, Alexey Stovas, and Yuriy Ivanov. 2019. “Acoustic Wave Propagation in Orthorhombic Media: Phase Velocity, Group Velocity, and Moveout Approximations.” GEOPHYSICS 84 (6): C269–79. https://doi.org/10.1190/geo2019-0085.1.

Afoutou, Jérôme S., Xi Zhang, and Frédéric Dubois. 2024. “Full Elastic Properties Characterization of Wood by Ultrasound Using a Single Sample.” Wood Science and Technology 58 (1): 403–22. https://doi.org/10.1007/s00226-023-01525-y.

Afoutou, Jérôme Sonagnon, Frédéric Dubois, Nicolas Sauvat, and Mokhfi Takarli. 2023. “A Novel Three-Dimensional Model for the Prediction of Ultrasonic Velocity in Wood Considering Its Orthotropy.” Wood Science and Technology 57: 605–23. https://doi.org/10.1007/s00226-023-01470-w.

Bahrami, Neda, Himadri Rajput, Rahil Changotra, Gordon Murray, and Quan (Sophia) He. 2025. “Review of Non-Destructive Testing for Quality Evaluation of in-Service Timber Utility Poles.” Structures 79 (September): 109484. https://doi.org/10.1016/j.istruc.2025.109484.

Bucur, Voichita. 2023. “A Review on Acoustics of Wood as a Tool for Quality Assessment.” Forests 14 (8). https://doi.org/10.3390/f14081545.

Bucur, V., and S. Kazemi Najafi. 2003. “Negative Poisson Ratios in Wood and Particleboard with Ultrasonic Technique.” In Nondestructive Characterization of Materials XI, edited by Robert E. Green, B. Boro Djordjevic, and Manfred P. Hentschel. Advances in the Statistical Sciences. Springer. https://doi.org/10.1007/978-3-642-55859-7_8.

Bucur, Voichita, and Patrick N. J. Rasolofosaon. 1998. “Dynamic Elastic Anisotropy and Nonlinearity in Wood and Rock.” Ultrasonics 36 (7): 813–24. https://doi.org/10.1016/S0041-624X(98)00004-3.

Christoffel, E. B. 1877. “Ueber die Fortpflanzung von Stössen durch elastische feste Körper.” Annali di Matematica Pura ed Applicata (1867-1897) 8 (1): 193–243. https://doi.org/10.1007/BF02420789.

Cuxac, P. 1991. “Propagation et Atténuation Des Ondes Ultrasoniques Dans Des Roches Fissurées et Anisotropes (Propagation and Attenuation of Ultrasonic Waves in Fissured and Anisotropic Rocks).” Phdthesis, Université de Lorraine.

Forest Products Laboratory. 2010. Wood Handbook: Wood as an Engineering Material. Department of Agriculture Forest Service, Madison, Wisconsin, USA.

Guitard, Daniel. 1987. Mécanique Du Matériau Bois et Composites. Cépaduès-Edition.

Hankinson, R. L. 1921. “Investigation of Crushing Strength of Spruce at Varying Angles of Grain.” Air Service Information Circular 259 (3): 130.

Jaskowska-Lemańska, Justyna, and Daniel Wałach. 2023. “Assessment of the Technical Condition of Timber Structural Elements Using Sclerometric Tests.” Materials 16 (18). https://doi.org/10.3390/ma16186152.

Jones, Donald R., and Joaquim R. R. A. Martins. 2021. “The DIRECT Algorithm: 25 Years Later.” Journal of Global Optimization 79 (3): 521–66. https://doi.org/10.1007/s10898-020-00952-6.

Kasal, Bo, and Ronald W. Anthony. 2004. “Advances in in Situ Evaluation of Timber Structures.” Progress in Structural Engineering and Materials 6 (2): 94–103. https://doi.org/10.1002/pse.170.

Longo, R., T. Delaunay, D. Laux, M. El Mouridi, O. Arnould, and E. Le Clézio. 2012. “Wood Elastic Characterization from a Single Sample by Resonant Ultrasound Spectroscopy.” Ultrasonics 52 (8): 971–74. https://doi.org/10.1016/j.ultras.2012.08.006.

Postma, G. W. 1955. “Wave Propagation in a Stratified Medium.” Geophysics 20 (4): 780–806. https://doi.org/10.1190/1.1438187.

Royer, Daniel, and Eugène Dieulesaint. 1996. Ondes Élastiques Dans Les Solides-Tome 1: Propagation Libre et Guidée-Tome 1. Masson.

Vössing, Konrad J., and Ernst Niederleithinger. 2018. “Nondestructive Assessment and Imaging Methods for Internal Inspection of Timber. A Review.” Holzforschung 72 (6): 467–76. https://doi.org/10.1515/hf-2017-0122.

Wang, Peixuan, Shengcai Li, Nicola Macchioni, Sabrina Palanti, and Gabriele Milani. 2021. “Comprehensive Evaluation Method of Historical Timber Structural Building Taking Fujiu Zhou House as an Example.” Forests 12 (9). https://doi.org/10.3390/f12091172.

Wijk, Kasper van, Jonathan Simpson, and Sam Hitchman. 2019. “A Modified Hankinson Equation for the Wave Speed of Laser Ultrasound in Radiata Pine.” Wave Motion 89 (June): 57–64. https://doi.org/10.1016/j.wavemoti.2019.03.005.

Cinpar 2026
XXII International Conference on Building Pathology and Constructions Repair
15th to 17th July 2026 - Lisboa, Portugal

PROGRESSIVE FAILURE ANALYSIS IN ELEVATED SWIMMING POOL WATERPROOFING SYSTEMS: A DIAGNOSTIC FRAMEWORK FOR CORRELATING EXECUTIVE NON-CONFORMITIES AND WATERTIGHTNESS LOSS MECHANISMS

Micaéle Brandão Silva[1], Marília Araujo[2]

[1] Instituto Nova Engenharia, São Paulo, Brasil, (engenharia@innovapredial.com.br)

[2] Instituto Nova Engenharia, São Paulo, Brasil, (marilia_carla10@hotmail.com)

Abstract: Elevated swimming pools represent a particularly demanding construction typology, in which the interaction between reinforced concrete structures, waterproofing membranes and mechanical protection layers creates a complex multi-layer system that is highly sensitive to execution deviations. Despite the recognised importance of execution quality on waterproofing performance, the technical literature lacks field-documented case studies that systematically correlate quantified executive non-conformities such as mechanical protection layer thickness deviation and reinforcement omission with progressive watertightness loss mechanisms in this specific construction typology. This study presents a forensic diagnostic investigation of a recurrent waterproofing failure in an elevated swimming pool, applying an integrated methodology comprising technical anamnesis, analysis of architectural and waterproofing designs, design-to-execution comparison, systematic visual survey, percussion-based non-destructive testing, inspection window opening and damage mapping. The investigation identified that the mechanical protection layer was executed at 5 cm instead of the 3 cm specified, generating an estimated interfacial overload of 80 to 130 kg/m² calculated from the mortar unit weight of 2,100 kg/m³ and amplified by the complete absence of the reinforcing plastic mesh required by the design. Combined with inadequate treatment of singular points, absence of mandatory watertightness testing records and lack of specialised technical supervision, these deviations triggered a progressive degradation mechanism leading to generalised loss of adhesion, coating detachment and structural impacts extending to the basement level. The original contribution of this study is a replicable forensic diagnostic framework specifically structured for elevated swimming pool waterproofing systems, integrating causal chain analysis; amage mapping and a preventive technical protocol grounded in normative criteria. The findings demonstrate that the waterproofing failure in this case originated not from material inadequacy but from a systemic breakdown in execution quality control, and that technical supervision at the initial stages would have prevented the observed pathological progression.

Keywords: building pathology; waterproofing systems; swimming pools; watertightness loss; failure analysis; construction process.

1. Introduction

The waterproofing system consists of a set of construction operations and techniques (services), comprising one or more layers, whose purpose is to protect buildings against the deleterious action of fluids, vapours and moisture (ABNT NBR 9575, 2010). In this context, watertightness constitutes an essential habitability requirement in buildings, with direct effects on the durability and functionality of construction systems, as addressed in NBR 15575 (2024) through criteria applicable to façades, roofs, floors of wet areas and hydraulic sanitary installations (ABNT NBR 15575, 2024). Water acts as a transport vehicle and electrolyte in concrete. Its uncontrolled presence accelerates chloride and sulphate diffusion; promoting reinforcement depassivation and expansive reactions that drastically compromise structural service life, as detailed in the technical literature of Neville (2011). Despite technological advances in waterproofing materials and systems, failure occurrence remains recurrent in civil construction. The incidence of cracks and early failures in buildings is closely related to deficiencies in technological control and operational errors during the execution phase, frequently surpassing failures originating in the design stages. (Thomaz, 2002). The effectiveness of a waterproofing system is conditioned on the perfect harmony between design guidelines and rigour in the technical detailing in the field (Storte, 1989). Picchi (1986) further states that waterproofing

is considered a specialised service within civil construction, requiring considerable experience, in which details play an important role and where even minimal localised failures can compromise the entire system. The selection of the waterproofing system is conditioned by a set of variables involving substrate characteristics, the type and regime of water action by percolation, positive or negative pressure and the susceptibility of the constructive element to movement and cracking, being determined according to the load imposed by the fluid on the construction parts requiring watertightness (ABNT NBR 9575, 2010, item 5). Pirondi (1992) had already warned of the need to adapt materials and techniques to the specific conditions of each structure, distinguishing situations subject to counter-pressure from those with free drainage. Even when the specified solution is technically adequate, its effectiveness is directly conditioned on correct execution, adequate treatment of critical points and watertightness testing (ABNT NBR 9574, 2008). From the perspective of building pathology, watertightness loss results from a multifactorial process involving design, execution and technological control failures (Thomaz, 2002), acting as a triggering agent for leaching, efflorescence, loss of interlayer adhesion and reinforcement corrosion (Neville, 2011). Diagnostic engineering, integrating technical inspection, historical survey and field investigation, is therefore essential for distinguishing apparent symptoms from underlying degradation mechanisms and defining effective intervention strategies (ABNT NBR 16747, 2020). Although executive deficiencies as the primary origin of waterproofing failures are well established in the literature (Thomaz, 2002; Picchi, 1986), and Carretero-Ayuso & de Brito (2016) have numerically demonstrated the importance of prior supervision in bituminous membrane systems, existing studies focus on roofs and façades. To the authors knowledge, no field-documented study has established a quantified causal chain with measured layer thicknesses, calculated interfacial overloads and non-destructive test results correlating executive non-conformities with progressive watertightness loss specifically in elevated swimming pool systems, a typology subject to permanent hydrostatic pressure and multi-layer mechanical constraints not present in roofing applications. The present study addresses this gap. In this context, the present study presents a case study of recurrent failures in an elevated swimming pool waterproofing system, focusing on root cause analysis associated with execution stages. The research seeks to correlate the observed non-conformities with deviations in the construction process, highlighting the influence of execution on system performance. As a contribution, it proposes preventive technical guidelines grounded in the integration of design, execution and technological control, with a view to reducing the incidence of pathological manifestations and improving the durability and performance of waterproofing systems in swimming pools.

2. Literature Review

In civil construction, waterproofing carried out correctly represents approximately 3% of the construction cost; when executed incorrectly, this percentage can rise to 10%; due to the need to remove finishing coatings to correct failures (Granato, 2002). Satisfactory or perfect guarantee and the absolute performance of a waterproofing product are not linked solely to standardisation guaranteed by bodies and institutions Pirondi (1992). Surveys carried out in Brazil show that approximately 40% of pathological manifestations found in inspections could have been avoided during design elaboration; most design failures are not identified during construction execution, and the most common errors are consequences of the lack of information; description and explanation in the design (Grandiski, 2004). However good the materials used in waterproofing an area, if applied by non-specialised teams, the usefulness of the system will be compromised Mello (2005). Observing that the majority of pathological manifestations in buildings are caused by moisture problems, it is of paramount importance to address this topic, with a view to drawing attention to or even raising awareness, not only among construction companies but also among academics, of the importance of this type of service throughout construction (Bernhoeft; Melhado, 2009).

2.1 Pathology of waterproofing systems

The technical literature shows that executive deficiencies constitute the primary origin of failures in waterproofing systems, with pathological manifestations resulting from the interaction between execution

failures, environmental exposure and structural behaviour (Thomaz, 2002; Bértolo, 2001). The continuous presence of moisture in concrete activates chloride and sulphate ion transport mechanisms that intensify deterioration and compromise structural service life Neville (2011). In elevated swimming pool systems, this mechanism operates under permanently saturated conditions, making the consequences of watertightness loss disproportionately severe compared to intermittently exposed systems. As established by Souza & Ripper (2009), inadequate waterproofing execution is directly linked to progressive structural degradation through reinforcement corrosion, leaching and loss of interlayer adhesion a causal chain fully confirmed in the present case study. Silva & Oliveira (2018) demonstrated that accurate identification of pathological manifestations is a prerequisite for effective system selection and service life extension a finding that underscores the diagnostic value of the forensic methodology applied in this study. Geometric discontinuities in waterproofing systems interfaces, penetrations and joints concentrate stresses and represent the primary loci of pathological initiation, as established by ABNT NBR 9575 (2010) and widely documented by Thomaz (2002), a pattern consistently confirmed in field investigations, including the present case study. The technical criteria established by ABNT NBR 9574 (2008) for the execution of waterproofing systems substrate preparation, layer thickness control, singular point treatment and mandatory watertightness testing represent not merely regulatory requirements but minimum conditions for system performance. Non-conformity with any of these criteria does not simply reduce performance margins; it initiates the degradation chain described above. The critical implication, confirmed by this case study, is that the technical adequacy of the specified materials is rendered irrelevant by executive non-conformity: a technically correct design executed incorrectly performs no better than an inadequate one.

3. Methodology

3.1 Anamnesis and historical survey

Structured technical anamnesis conducted through direct interviews with the building manager, maintenance team and responsible engineer reconstructed the pathological history prior to physical inspection. The pool presented an infiltration history since post-delivery, having been subjected to multiple palliative repair attempts without specialised technical supervision, including localised membrane patching and partial coating replacement, without achieving definitive resolution. This recurrence pattern is consistent with the absence of root cause identification in previous interventions, since palliative repairs applied over a systemically compromised waterproofing layer cannot restore watertightness capacity (IBI, 2023). Critically, the anamnesis confirmed the complete absence of specialised technical supervision (conformity assessment) during original execution a primary risk factor for executive non-conformity, as active quality control at each critical stage is required by ABNT NBR 9574 (2008) and highlighted by Picchi (1986).

3.2 Documentary analysis and design-to-execution comparison

The second stage comprised systematic analysis of all available technical documentation, including architectural, structural and hydraulic designs, and most critically, the waterproofing design prepared in accordance with ABNT NBR 9575 (2010). Documentary analysis served a dual purpose: to establish the technical baseline against which field conditions would be compared, and to identify the design intent regarding layer thicknesses, reinforcement specification, singular point detailing and testing requirements. The waterproofing design specified a double asphalt membrane system a technically appropriate solution for elevated swimming pools given its flexibility under structural movement with a mechanical protection layer of 3 cm thickness, reinforced with plastic mesh positioned at every 1.5 cm within the layer. The design-to-execution comparison methodology followed the criteria established by ABNT NBR 16747 (2020) and the normative guidelines of ABNT NBR 9574 (2008), identifying deviations across four critical parameters: layer thickness; reinforcement specification compliance, singular point detailing and testing documentation.

Each deviation was classified by type, magnitude and potential consequence, enabling the construction of a causal matrix linking executive non-conformities to observed pathological manifestations.

3.3 Field inspection and non-destructive testing

Field inspection followed a pre-defined protocol covering all accessible surfaces vertical walls, horizontal slab, wall–slab interfaces, drain and pipe penetrations, movement joints and adjacent basement elements integrating three complementary methods:

(a) Systematic visual survey across 100% of accessible surfaces, with photographic documentation. Manifestations were classified by type (efflorescence, detachment, hollow sound, cracking, corrosion), location, extent and severity, following ABNT NBR 16747 (2020) and IBI (2023).
(b) Percussion-based non-destructive testing across all accessible wall and floor surfaces to identify adhesion loss regions. Hollow sound response was confirmed across more than 60% of the tested vertical wall surfaces.

(c) Inspection window opening at three locations on vertical walls and one at the wall–slab interface, enabling direct measurement of layer thicknesses, confirmation of reinforcing mesh positioning and examination of the membrane condition beneath the protection layer. Moisture presence was assessed through indirect indicators efflorescence deposits, moisture staining on basement ceiling elements and corrosion product staining at reinforcement locations given that the pool was already dewatered at the time of inspection.

3.4 Damage mapping and causal chain reconstruction

Field findings were organised into a damage mapping framework correlating each anomaly with its location, probable cause, affected element and estimated extent. Causal chain reconstruction followed root cause analysis methodology, distinguishing between: primary causes executive deviations that initiated degradation; secondary causes conditions that amplified or accelerated it; and resulting manifestations observable symptoms constituting the physical evidence of failure.

3.5 Singular point analysis

Singular points where membrane continuity is interrupted by structural elements, penetrations or geometric transitions received specific investigative attention, as they represent the primary loci of waterproofing failure in elevated swimming pool systems (ABNT NBR 9575, 2010; Picchi, 1986). Points evaluated included: wall–slab interfaces; drain and sump penetrations; pipe penetrations; movement joints (three locations); and pool border transitions. Each was assessed for compliance with design detailing, localised reinforcement condition, membrane continuity quality and evidence of preferential infiltration paths since localised failures at these junctions are sufficient to cause generalised watertightness loss, even when the membrane field area remains intact.

3.6 Anomaly classification and diagnostic synthesis

The integrated analysis produced a structured diagnostic synthesis comprising three outputs: anomaly classification by type, location, extent and criticality; root cause hierarchy; and intervention recommendations grounded in the identified causal structure. All anomalies were classified as high criticality per ABNT NBR 16747 (2020) and IBI (2023), given their direct association with structural integrity risk, active moisture infiltration and evidence of reinforcement corrosion conditions that preclude continued use without immediate intervention

Figure 1: Methodology flowchart – Author



The proposed diagnostic framework has a replicable character for wet and damp areas of any buildings, being applicable to different types of waterproofing systems including membranes and sheets, in bonded or unbonded configurations.

4. Results and Discussion

The field investigation revealed progressive adhesion failure with visual evidence of exposed primer layers driven by interfacial overload from executive deviation, compounded by omission of the structural mesh reinforcement in the mechanical protection layer, inadequate singular point treatment and absence of system validation. The identified manifestations constitute sequential stages of a single progressive degradation mechanism, as demonstrated in the following subsections.



Figure 2: Detachment and efflorescence – Author



Figure 3: Efflorescence and hollow sound – Author

4.1 Correlation between design and execution

The comparative analysis between design specifications and field execution conditions identified four critical non-conformities, each with direct causal implication for system performance. The most significant deviation involved the mechanical protection layer thickness: the executed 5 cm exceeded the specified 3 cm by 67%, generating a direct gravitational overload of 42 kg/m² on horizontal surfaces calculated from the 2 cm additional thickness at a mortar unit weight of 2,100 kg/m³ (Neville, 2011; Souza & Ripper, 2009). On vertical surfaces, this additional mass generates shear and tensile stresses at the waterproofing-to-substrate interface that, in the absence of the reinforcing mesh specified in the design, are transferred directly and unevenly to the bonding interface, amplifying the effective overload to an estimated range of 80–130 kg/m². The structural reinforcing mesh specified at every 1.5 cm within the mechanical protection layer was entirely absent in the executed system, eliminating the stress redistribution mechanism and concentrating tensile forces at discrete interface points, accelerating adhesion loss under thermal and structural cycling. The singular points including wall–slab interfaces, poorly executed movement joints and drain penetrations were executed without the localised reinforcement and specific detailing required by the design, creating preferential infiltration paths that bypass the membrane field area entirely.

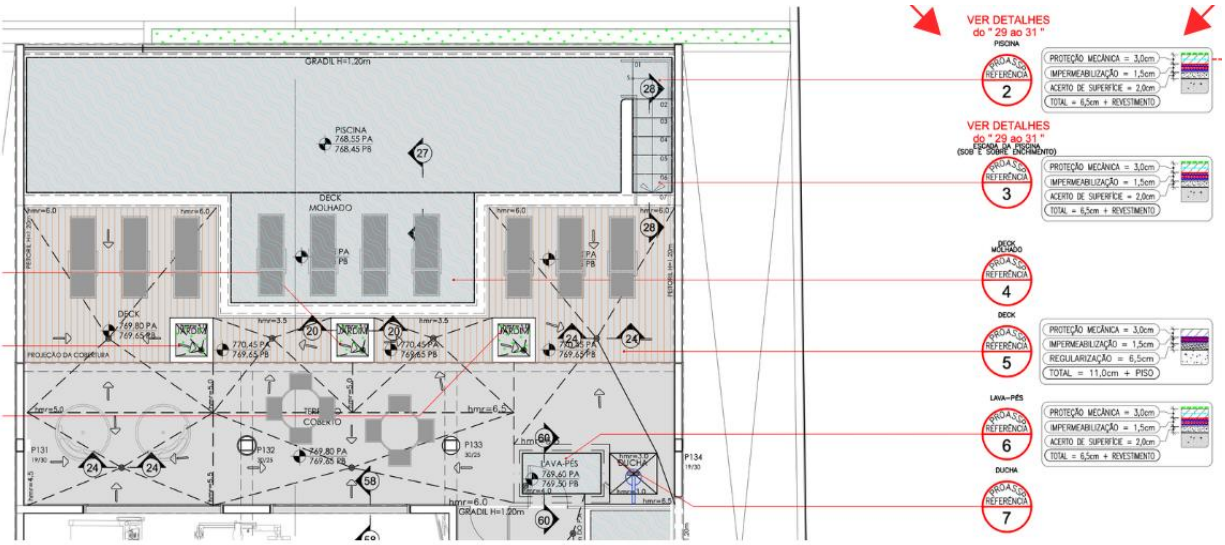


Figure 4: Analyzed waterproofing design – Swimming pool

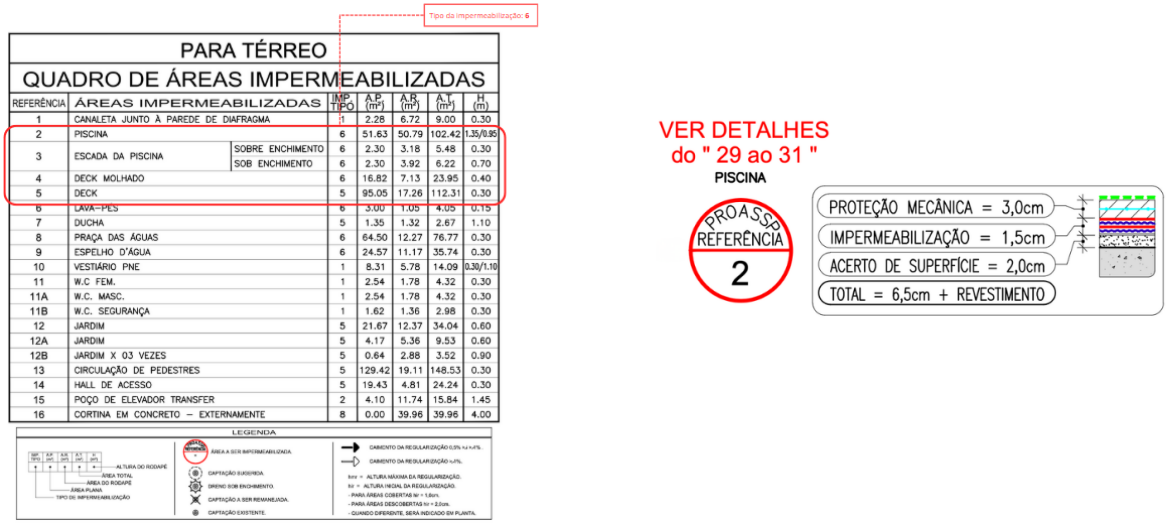


Figure 5: Area and waterproofing type chart

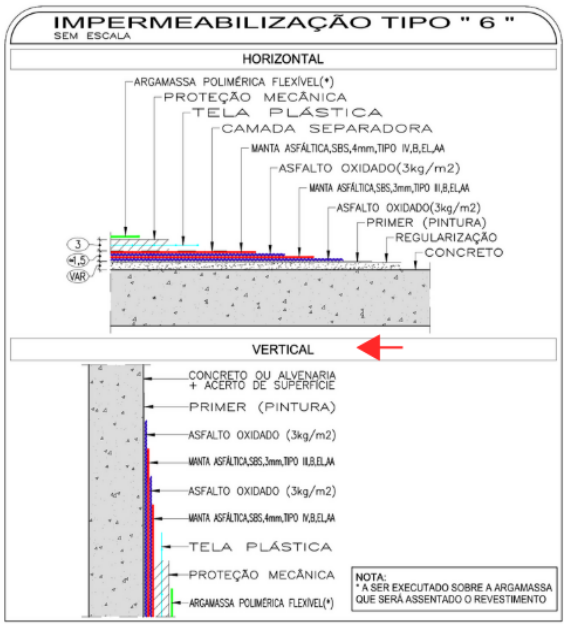


Figure 6: Thickness and layers – Author



Figure 7: Reinforcing plastic mesh – Author



Figure 8: Mechanical protection thickness – Author



Figure 9: Mesh and mechanical protection – Author

4.2 Degradation mechanism and progressive failure analysis

The degradation mechanism follows a four-stage progressive failure sequence initiated by the mechanical overload condition identified in section 4.1. This sequence is essential for distinguishing primary causes from secondary manifestations and for designing interventions that address root causes rather than symptoms.

Stage 1 — Interfacial stress initiation: the 67% thickness excess generated sustained interfacial stresses exceeding the adhesion capacity of the asphalt membrane-to-substrate bond, particularly on vertical surfaces where the additional layer mass acts as a sustained shear force. The absence of the reinforcing mesh eliminated the stress redistribution mechanism, concentrating stress at the weakest interface points. **Stage 2** — Microcracking and initial adhesion loss: sustained interfacial stress combined with thermal cycling and structural movement initiated microcracking at the membrane-to-substrate interface. This stage is typically invisible to visual inspection but produces the hollow sound response detected by percussion testing across more than 60% of the vertical wall area.

Stage 3 — Progressive detachment and membrane exposure: as microcracks coalesce, adhesion loss extends laterally; producing the macroscopic detachment visible in figures 2, 3, 8 and 9. The waterproofing membrane becomes directly exposed to mechanical stress and thermal variation, and at inadequately detailed singular points, to water penetration.

Stage 4 — Watertightness loss and structural propagation: water penetrating through singular points and exposed membrane areas migrates through the structural concrete, producing the efflorescence, moisture staining, horizontal cracking and reinforcement corrosion observed in basement elements (Figure 10). This stage represents the transition from waterproofing failure to structural durability risk, as chloride and sulphate ion transport in saturated concrete activates the reinforcement corrosion mechanism (Neville, 2011). The basement impacts were not the consequence of a single failure event but the terminal stage of a degradation process initiated by executive deviations that remained undetected due to the absence of conformity assessment and watertightness testing at the time of execution.

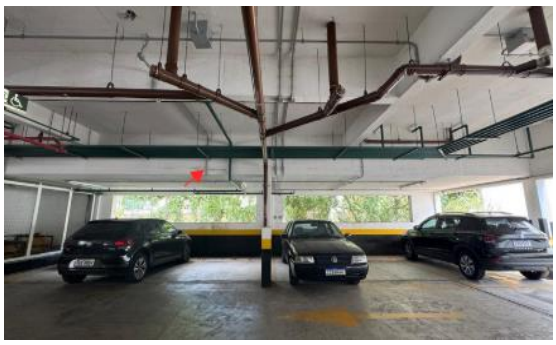


Figure 10: Horizontal crack and presence of moisture – Author

4.3 Design-to-execution synthesis

Tables 1 and 2 confirm that all identified anomalies are attributable exclusively to executive non-conformities, not to design inadequacy the specified double asphalt membrane system is technically appropriate for this typology.

Table 1: Planned vs. Executed Framework — Mechanical protection

Element	Design	Execution	Consequence
Mechanical protection	3 cm	5 cm	Overload
Reinforcement	As per design	Inadequate	Cracking and displacement
Singular points	Detailed	Poorly executed	Infiltration and displacement
Testing	Mandatory	No execution records	Watertightness failure

Table 2: Non-destructive inspection results — damage mapping and criticality classification

Localização / Element	Anomaly identified	Inspection method	Result	Criticality
Full pool perimeter wall–slab interface	Efflorescence along entire perimeter at slab level	Visual survey	Active moisture migration confirmed	High
Vertical walls — pool perimeter	Detachment and displacement of coating and mechanical protection	Visual survey + percussion	Displacement confirmed; 5 cm layer exceeds specified 3 cm; hollow sound across >60% of area	High
Mechanical protection layer — exposed section	Reinforcing mesh after 2 cm of protection	Direct measurement + visual inspection	Mesh at 2 cm; design deviation confirmed	High

Pool border strip	Mesh without galvanic coating in advanced corrosion	Visual survey + inspection window	Active corrosion identified	High
Movement joints — 3 locations	Inadequate execution of joint detailing	Visual survey	Singular points without specified detailing; preferential paths identified	High
Slab and walls — multiple locations	Efflorescence and hollow sound	Visual survey + percussion	Adhesion loss at 7 distinct locations	High

Note: Criticality classification follows ABNT NBR 16747 (2020) and IBI (2023) criteria. Percussion testing performed systematically across all accessible surfaces. Photo references correspond to field inspection records documented in the technical diagnostic report prepared for this building.

4.4 Technical Analysis and Critical Discussion

The results support a critical discussion of three technical dimensions with implications beyond the specific case. First, the interaction between mechanical protection layer overload and membrane adhesion loss. In elevated swimming pool systems, the mechanical protection layer serves a dual function: protecting the asphalt membrane from mechanical damage and distributing loads from the finishing layer. When its thickness exceeds design specification, it transitions from a protective element to a loading element, imposing stresses that the adhesion system was not designed to resist. The 67% thickness excess generated an estimated interfacial overload of 80–130 kg/m² substantially exceeding the adhesion capacity of asphalt membrane systems under sustained and cyclic loading. The progressive nature of the observed detachment is consistent with a mechanism of interfacial degradation by fatigue under cyclic thermal and structural loading. Movements of thermal origin differential expansion and contraction between system layers occur cyclically and introduce shear stresses at the interface between the impermeable layer and its substrate, which can result over time in fatigue of the bonds and, consequently, in progressive loss of adhesion (ASTM C1472, 2006; BS 5385-2, BSI, 2006). According to ASTM C1472 and DTU 44.1 (AFNOR, 2002), thermal movement is the predominant effect in dimensional variations of building components, being a determining factor for the dimensioning of movement accommodation systems. In the new study of the Brazilian normative plan, ABNT/CB-022 CE-22:0001.01 — Study Commission on Design and Execution of Waterproofing, currently under analysis for public consultation as Draft Standard ABNT NBR 9575-1 (2025), defines debonding of the impermeable layer as the loss of adhesion of the impermeable layer to the substrate in bonded systems (item 3.1.42), and establishes as a performance requirement that the impermeable layer must resist the effects caused by hygrothermal variations, such as cracking or crazing through excessive bending or rigidity (item 6.4), as well as debonding caused by total or partial adhesion loss (item 6.3.5). The same draft standard further defines degradation of the impermeable layer as the alteration of initial properties by physical and chemical aspects, caused by agents such as heat and UV rays, generating changes in flexibility, porosity and crazing (item 3.1.41). Experimental records demonstrate that concrete creep over 20 years can reach 1.5 to 3.0 times the value measured in the first two months of loading (Neville; Dilger; Brooks, 1983; ABNT NBR 6118, 2023; Sabbatini, 2005; Thomaz, 2002), evidencing the cumulative nature of this loading on non-structural systems. Second, the amplifying role of reinforcing mesh omission. The mesh serves not only as structural reinforcement but as a stress redistribution mechanism within the protection layer. Its omission transfers all tensile stresses generated by thermal contraction, structural movement and self-weight directly to the membrane interface. This concentration effect explains why adhesion loss was generalised exceeding 60% of the vertical wall area rather than localised, as would be expected if the failure had originated exclusively from singular point deficiencies. Third, the systemic nature of the failure. The convergence of three simultaneous non-conformities thickness excess, reinforcement omission and inadequate executive detailing of singular points suggests not isolated execution errors but a systemic absence of quality control, as recommended in Draft Standard ABNT/CB-022 CE-22:0001.01 — Study Commission on Design and Execution of Waterproofing. Corroborating

Madureira (2017), who proposes a systematic three-stage methodology detailed inspection, post-inspection actions and proactive planning precisely because the absence of formalised inspection procedures is the main gap identified in buildings.".

5. Rehabilitation Guidelines

The rehabilitation protocol prioritises root cause elimination. Given the generalised adhesion loss confirmed across more than 60% of the vertical surface area, palliative approaches are technically contraindicated, as they cannot restore watertightness capacity in a system with compromised membrane interface integrity (IBI, 2023). Complete removal of the existing waterproofing system is therefore required, including potentially affected adjacent areas, to allow full system exposure and identification of hidden failures, for the substrate treatment which, after removal of waterproofing layers, must be subjected to detailed inspection with identification and treatment of structural and non-structural cracks, removal of loose or deteriorated materials through high-pressure water jetting up to 250 bar, and surface regularisation with 1% slope towards the drain. Crack treatment must be performed according to its classification, which may involve resin injection or flexible sealing, in conformity with the criteria of ABNT NBR 6118 (2023). Subsequently, based on Draft Standard ABNT NBR 9575-1 — Waterproofing, Part 1 (ABNT/CB-022 CE-22:0001.01 — Study Commission. Rio de Janeiro: ABNT, 2023–2026. Draft Technical Standard under National Public Consultation), the waterproofing designer must present: preliminary report of waterproofing systems compatible with the structure; preliminary budget and technical-economic feasibility analysis; pre-executive design; detail booklet; descriptive specification; and quantitative material spreadsheet with estimated costs. Table 3 describes the deliverable documents established by Draft Standard ABNT/CB-022 CE-22:0001.01 — Study Commission on Design and Execution of Waterproofing.

Table 3: Deliverable documents of the Pre-Executive Design — Draft Standard ABNT/CB-022 CE-22:0001.01 — Study Commission on Design and Execution of Waterproofing

	Document	Minimum content	Normative basis
1	Floor plans of areas to be waterproofed	Graphic identification of all areas subject to waterproofing	4.5.2
2	Typical section of designed systems	Representation of layers composing each system in each area	4.5.2
3	System specification with Design Service Life (DSL) study	Identification of areas, Design Service Life of systems (DSL.i) and technical specifications	4.5.2 and ISO 15686
4	Area quantitative survey spreadsheet	Quantification in m² by type of area and planned system	4.5.2

Table 4: Deliverable documents of the Executive Design — Draft Standard ABNT/CB-022 CE-22:0001.01 — Study Commission on Design and Execution of Waterproofing

Graphic document / drawing	Essential content	Normative basis
Descriptive Specification	Systems, standards, layers, executive procedures, DSL_i	4.6.2-a
Location plans and system identification	Area demarcation, system codes, slopes; drainage	4.6.2-b
Slope diagram	Graphic representation of inclinations, elevations and drainage points	3.2.13

Executive details	All solutions and layers at adequate scale	4.6.2-c
Quantitative spreadsheet	Materials and services quantified by area and system	4.6.2-d
Technical data sheets (TDS) and Safety Data Sheets (SDS)	Physicochemical characteristics, performance, reference standards, storage, disposal	3.2.20 — NR-18
Guidelines for Operation and Maintenance Manual (OMM)	DSL_i, maintenance periodicity, aggressive agents; prohibited conduct	4.6.2-e · NBR 5674 · NBR 14037
Specification of ABNT standards complied with	Complete list of standards by material, system and service	IBI Scope Manual 3rd Ed. — IMP-D002

Table 5: Conformity assessment — Draft Standard ABNT/CB-022 — CE-22:0001.01 — Study Commission on Design and Execution of Waterproofing

	Document	Purpose	Norm. basis
a	Descriptive Specification (complete)	Technical reference base for verification	9.2.1-a
b	Location plans and system identification	Spatial reference of areas to be verified	9.2.1-b
c	Executive details	Verification of conformity of finishing and layers	9.2.1-c
d	Material and service quantitative spreadsheet	Consumption control and area coverage	9.2.1-d
e	Guidelines for use, maintenance, performance definition and DSL_i expectation	Performance parameter to be verified and maintained	9.2.1-e

5.1 Quality control and acceptance plan

If Draft Standard ABNT/CB-022 CE-22:0001.01 — Study Commission on Design and Execution of Waterproofing is approved after public consultation, technical criteria for conformity assessment must be defined in advance (item 9.2.2, Draft Standard ABNT NBR 9575-1:2025): Technological Control Plan for Materials (TCPM_i): verification of classification, certification or qualification in PSQ/PBQPH of purchased products, Area Acceptance Plan for Service Release: substrate conditions (strength, moisture, temperature, flatness, absence of contaminants), Area Acceptance Plan for Waterproofed Areas with visual; dimensional and watertightness testing inspection by area; chronological photographic reports with identification of the person responsible for acceptance of each stage; construction diary with records of climatic conditions, team, materials used (brand, batch and consumption).

5.2 Technical responsibilities for conformity assessment

If Draft Standard ABNT/CB-022 CE-22:0001.01 — Study Commission on Design and Execution of Waterproofing is approved after public consultation: conformity assessment must be carried out by qualified professionals in architecture and civil engineering, qualified in waterproofing. For these technical services, an ART or RRT must be issued (item 9.3, Draft Standard ABNT NBR 9575-1:2025). Assessment must be performed by the designer or by an independent specialised company without conflict of interest, it cannot be performed by the applicator company, must be contracted by the owner/employer of the works and must be registered with an ART (CREA) or RRT (CAU).

Table 6: Mandatory delivery documents — Item 8.11, Table 22 of Draft Standard ABNT/CB-022 CE-22:0001.01 — Study Commission on Design and Execution of Waterproofing, after public consultation

Document	Mandatory content	Norm. basis
Service Delivery Certificate	· Date of inspection and area handover · Report of services executed and completed · Breakdown of areas with services · Notes on scope changes or impediments · List of products used (brand, batch and consumption) · Watertightness test report · Reference to technical responsibility ART or RRT · Acceptance signature by the employer	8.11 Table 22
Operation and Maintenance Manual	· Periodic_PLACEHOLDER with schedule · Preventive and corrective maintenance procedures · List of aggressive agents · Conduct prohibited by the user	8.11 · NBR 14037 · NBR 5674
Warranty Certificate	Warranty period by system and area · Conditions for warranty lapse · Conditions for possible interventions	8.11 ABNT · NBR 17170
ART / RRT of services	· ART (CREA) or RRT (CAU) for design, execution and conformity assessment · Must be issued for each phase contracted separately	Item 9.3

5.3 As-Built — As Constructed

If Draft Standard ABNT/CB-022 CE-22:0001.01 — Study Commission on Design and Execution of Waterproofing is approved after public consultation: this is a mandatory technical record prepared after execution, faithfully representing the waterproofing design as constructed, including all changes made on site (Draft Standard ABNT NBR 9575-1:2025, item 4.7). It must contain updated plans and details with the systems effectively executed, technical justifications and photographic records of changes, list of products used with technical data sheets, watertightness test results and chronological history of stages (Draft Standard ABNT NBR 9575-1:2025, item 4.7.2). Its preparation is the responsibility of the builder or employer and must be carried out by the designer or qualified professional who technically supervised the execution, with issuance of ART or RRT (Draft Standard ABNT NBR 9575-1:2025, item 4.7.3). The document must be delivered to the employer and filed together with the Building Operation and Maintenance Manual (Draft Standard ABNT NBR 9575-1:2025, item 4.7.4).

6. CONCLUSION

This study demonstrated that the progressive watertightness loss in the investigated elevated swimming pool originated from a systemic breakdown in execution quality control, not from material inadequacy or design failure. The forensic diagnostic investigation identified three simultaneous executive non-conformities 67% mechanical protection layer thickness excess (5 cm vs. 3 cm specified), complete absence of reinforcing plastic mesh and inadequate singular point detailing whose convergence triggered a progressive failure mechanism, culminating in generalised adhesion loss across more than 60% of the vertical wall surface area and structural impacts at basement level. The quantified causal analysis demonstrated that the 2 cm thickness excess generated an estimated interfacial overload of 80–130 kg/m² on vertical surfaces calculated from the mortar unit weight of 2,100 kg/m³ and amplified by the complete absence of the reinforcing mesh that would have redistributed tensile stresses across the bonding interface. Sustained under thermal cycling and structural movement typical of elevated swimming pool systems, this overload initiated an adhesion fatigue failure mechanism consistent with progressive detachment patterns documented in analogous bituminous membrane systems by Carretero-Ayuso & de Brito (2016). The six-stage forensic methodology technical anamnesis, design-to-execution comparison, systematic field inspection with non-destructive testing, damage mapping, singular point analysis and causal chain reconstruction produced three structured outputs: anomaly classification, root cause hierarchy and intervention protocol. This replicable diagnostic framework, applicable to any waterproofing system in wet areas, provides practitioners with a systematic methodology for distinguishing primary failure triggers from secondary manifestations and designing interventions that address root causes rather than symptoms. The Draft Standard ABNT NBR 9575-1 — Waterproofing, Part 1 (ABNT/CB-022 CE-22:0001.01 — Study Commission. Rio de Janeiro: ABNT, 2023–2026), referenced throughout this study, reinforces the importance of specialised design, conformity assessment and construction supervision as essential instruments for execution excellence and end-consumer protection. Diagnostic engineering combined with specialised waterproofing

methodology are essential tools for understanding progressive degradation mechanisms, supporting technically grounded decision-making in rehabilitation and contributing to the durability, safety and performance of buildings in critical systems such as elevated swimming pools.

REFERENCES

A. M. Neville, “Properties of Concrete”, 5th ed. London: Pearson, 2011.

Associação Brasileira de Normas Técnicas (abnt), “NBR 9574: Waterproofing execution”, Rio de Janeiro, 2008.

Associação Brasileira de Normas Técnicas (abnt), “NBR 15575: Residential buildings – Performance”, Rio de Janeiro, 2024.

Associação Brasileira de Normas Técnicas (abnt), “NBR 16747: Building inspection – Guidelines, concepts terminology and procedure”, Rio de Janeiro, 2020.

Associação Brasileira de Normas Técnicas (abnt), “NBR 6118: Design of concrete structures – Procedure”, Rio de Janeiro, 2023.

Associação Brasileira de Normas Técnicas (abnt), “NBR 9575: Waterproofing – Selection and design”, Rio de Janeiro, 2010.

Association Française de Normalisation, "DTU 44.1: Étanchéité des joints de façade par mise en œuvre de mastics". Paris: AFNOR, 2002.

ASTM International, "ASTM C1472: Standard guide for calculating movement and other effects when establishing sealant joint width". West Conshohocken: ASTM International, 2006.

Bernhoeft, L. F.; Melhado, S. B. “A importância dos sistemas de impermeabilização na durabilidade das estruturas”. Jornada de Técnicas de Restauración y Conservación del Patrimonio, v. 1, 2009.

Bértolo, T. “Waterproof testing”. Téchne, São Paulo, n. 51, . 20-23, mar/abr. 2001.

British Standards Institution, "BS 5385 Part 2: Wall and floor tiling” — Design and installation of external ceramic and mosaic wall tiling in normal conditions. Code of practice". London: BSI Standards, 2006.

Carretero-Ayuso, M.J. & de Brito, J. "Analysis of the execution deficiencies of flat roofs with bituminous membranes". Journal of Performance of Constructed Facilities, vol. 30, n. 6, 04016049, 2016.

E. Thomaz, “Cracks in buildings: causes; prevention and repair”. São Paulo: PINI, 2002.

GRANDISKI, P. “Olhar de perito”. Revista Téchne, São Paulo, edição 87, 2004.

IBI – Instituto Brasileiro de Impermeabilização, “Guideline for performance of waterproofing systems”, 2ª ed. 2023.

F. L. Silva and M. do P. S. L. Oliveira, “Pathological manifestations caused by absence or failure of waterproofing ”, Revista Científica Multidisciplinar Núcleo do Conhecimento”, ano 3, ed. 11, vol. 1, p. 76–95, Nov. 2018.

M. Storte, “Waterproofing – Prevention and protection”, 2° RRegional Meeting on Waterproofing of Minas Gerais”, FUMEC, 1989.

Mello, L.S. “Waterproofing – Materials, Procedures and Performance”. São Paulo, Brasil, 2005.

NEVILLE, A.M.; DILGER, W.H.; BROOKS, J.J. “Creep of Plain and Structural Concrete.” London; New York: Construction Press, 1983. 361 p.

Sabbatini, F. H. “Tecnologia de execução de revestimentos de argamassa”. São Paulo: EPUSP, 2005.

Picchi, F.A. “Waterproofing of roofs”. São Paulo: Editora Pini, 1986. 220p.

Pirondi, Zeno. "Practical Manual of Waterproofing and Thermal Insulation". IBI/PINI, 2nd ed. São Paulo, Brasil, 1992. Granato, José Eduardo. "Building Pathologies". Brasil, 2002.

Madureira, S., Flores-Colen, I.; and Brito, J. & Pereira, C. "Maintenance planning of facades in current buildings". *Construction and Building Materials*, vol. 147, p. 790–802, 2017.

Souza, V.C.M. & Ripper, T. *"Patologia, recuperação e reforço de estruturas de concreto"*. São Paulo: PINI, 2009.

cinpar2026
XXII International Conference on Building Pathology and Constructions Repair
15th to 17th July 2026 - Lisboa, Portugal

Pathology of Ceramic Tile Systems in Brazil: Investigating Moisture Expansion in BIIb Tiles through a Multi-Analytical Case Study

Renato Freua SAHADE[1], Carlos Roberto Camello LIMA [2]

[1] Mackenzie Presbyterian University, São Paulo, Brazil, sahaderenato@gmail.com,
[2]Mackenzie Presbyterian University, São Paulo, Brazil carlos.lima@mackenzie.br

Abstract: The intensified occurrence of detachment failures in Brazilian indoor ceramic tile systems (CTS) is frequently associated with the moisture expansion (ME) of BIIb dry-pressed ceramic tiles. This study investigates the influence of ME on CTS durability through a comprehensive characterization of materials from a real-world failure case. The methodology involved a comparative analysis of detached ceramic tiles (CT-D) and unused reference tiles (CT-U) using integrated microstructural Scanning Electron Microscopy (SEM), chemical X-ray fluorescence (XRF), and mineralogical X-ray diffraction (XRD) with Rietveld refinement analysis. Forced expansion tests were conducted to comprehend the mechanisms driving interface failure. Results revealed a critical discrepancy between testing methods: while the standard boiling test yielded low ME values between 0.28 mm/m and 0.33 mm/m, falling below the 0.6 mm/m normative limit, the accelerated autoclave test exposed severe instability with values ranging from 0.84 mm/m to 0.99 mm/m. This represents an increase of over 200%. XRD quantification explained this behavior by revealing a microstructure dominated by a high amorphous phase (53.4%–58.3%) and residual quartz (37.7%–40.7%), with no detected mullite. Chemical analysis confirmed matrix vulnerability with low Al_2O_3/SiO_2 ratios (0.16–0.18) and total alkalis (K_2O + Na_2O ≈ 4.5%), confirming the presence of potentially expansive phases. The combination of autoclave testing with SEM imaging identified the root cause: unlike stable reference tiles which exhibited closed spherical porosity, detached tiles showed high interconnected porosity and phyllosilicates with preserved foliation, confirming incomplete sintering. It is concluded that the irreversible expansion creates shear stresses at the interface, acting as the primary mechanism for detachment. This study's primary contribution is to provide quantitative parameters for the diagnosis, prevention, and future standardization of CTS durability.

Keywords: Ceramic tile system; moisture expansion; detachment; microstructural analysis; durability.

1. Introduction

Ceramic Tile Systems (CTS) play a fundamental role in the Brazilian construction industry due to their durability, mechanical resistance, and aesthetic versatility. However, the sector has experienced significant technical and economic impacts associated with premature failures, particularly tile detachment (Silva *et al.* 2024). Since 2012, the occurrence of detachment in indoor applications has increased substantially, with forensic investigations indicating that up to 80% of BIIb dry-pressed ceramic tiles in surveyed developments exhibited failure within two years of completion (Barboza 2016; Klavdianos 2019).

BIIb ceramic tiles represent a significant portion of the Brazilian market, accounting for approximately 72% of national production due to their cost effectiveness and compatibility with large-scale housing demands (CCB 2024). These tiles are typically produced from a triaxial composition of clay, feldspar, and quartz, balancing plasticity, fluxing behavior, and dimensional stability. The manufacturing process involves three main stages: initial solid-state sintering below 1000 °C, characterized by particle rearrangement and the onset of mullite formation; partial melting between 1000 °C and 1100 °C, driven by feldspathic fluxes and resulting in progressive densification; and a final maturation stage, where optimal vitrification is achieved

without structural collapse (Conte *et al.* 2024; Cruz *et al.* 2022; Silva *et al.* 2018). The resulting microstructure is typically semi porous, composed of a glassy matrix with dispersed crystalline phases, including residual quartz and mullite, and water absorption values ranging from 6% to 10%.

This study is based on the hypothesis that moisture expansion (ME), defined as an irreversible dimensional increase caused by water adsorption into the ceramic body, is the primary mechanism driving these failures (Kayaci 2021; Sahade *et al.* 2025). This time-dependent expansion is understood to generate cumulative shear stresses at the tile adhesive interface (Nastri *et al.* 2015; Feldfogel and Rabinovitch 2021). Once these stresses exceed the adhesive bond strength, detachment occurs, often resulting in a clean separation between the ceramic tile and the adhesive mortar (Figure 1).

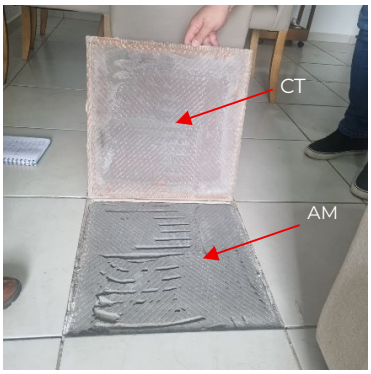


Figure 1 – Detail of the ceramic tile (CT) detached "clean" from the adhesive mortar (AM)

Accordingly, this study adopts an evidence-based approach, in which samples collected from areas exhibiting severe detachment were investigated through a multi-analytical framework. Detached tiles were compared with unused reference samples of similar classification to establish performance benchmarks and to reconstruct the failure mechanisms at the tile–adhesive interface.

Despite extensive research on ceramic tile systems, the limitations of standardized moisture expansion tests in predicting long-term performance remain insufficiently addressed. This study addresses this gap by integrating accelerated testing with microstructural, chemical, and mineralogical analyses, establishing a direct relationship between material characteristics and detachment behavior.

2. Methodology

This section describes the experimental program developed to investigate the relationship between moisture expansion and detachment in ceramic tile systems. The methodology integrates complementary analytical techniques to establish a direct link between material characteristics and failure mechanisms at the tile–adhesive interface.

2.1 Materials

The materials analyzed in this study were collected from a residential development completed in 2017, located in Jaraguá do Sul, southern Brazil. The project consists of eight residential towers, each with seven floors and a total of 448 housing units, comprising approximately 13,000 m² of ceramic tile coverings applied to indoor floors and walls. Shortly after occupancy, the building exhibited widespread and premature tile detachment affecting a significant portion of the system.

Technical data provided by the construction company indicated that the observed failures were independent of typical influencing factors, including solar orientation, floor level, unit location, adhesive mortar type, application method, substrate condition, and the presence of movement joints. Structural

assessments ruled out deformations in slabs and masonry. In addition, corrective actions such as workforce training and changes in application procedures did not mitigate the problem. Although pull-off tests performed according to NBR 13753 indicated adhesion values consistent with normative requirements in unaffected areas, the persistence and generalization of detachment suggest that the root cause is not related to execution or structural behavior, but rather to intrinsic material characteristics.

Two groups of ceramic tile samples were defined for comparative analysis:

- **Detached Ceramic Tiles (CT-D),** removed from areas affected by detachment, identified as samples D1 to D5;
- **Unused Ceramic Tiles (CT-U),** reference tiles of the same classification, sourced from different manufacturers and not installed, were used as a baseline for comparative analysis, comprising samples U1 to U5, including one sample from the same batch as the detached tiles (U2) and from four additional manufacturers (U1, U3, U4, and U5).

All adhesive mortars associated with the detached samples were classified according to NBR 14081 (ABNT 2012) as AC II and AC III (Brazilian classification), corresponding to types C1 and C2 according to EN 12004-1 (CEN 2017).

2.2 Experimental Program

A comprehensive characterization program was carried out to evaluate the physical, mechanical, chemical, mineralogical, and microstructural properties of the ceramic tiles. The objective was to establish a consistent relationship between material characteristics and detachment behavior at the tile-adhesive interface.

2.2.1 Physical and Mechanical Characterization

Water absorption and crazing resistance were determined in accordance with ISO 10545-3 (ISO 2018a) and ISO 10545-11 (ISO 2018b), respectively, for both detached and unused samples. In addition, in situ tensile adhesion tests were performed according to NBR 13753 (ABNT 1996) to evaluate the adhesion strength of the system prior to detachment. It is important to note that once hollow sound was detected by percussion, the test became no longer applicable due to the loss of adhesion.

2.2.2 Moisture Expansion (ME) Determination

Moisture expansion was determined using two procedures applied to both sample groups: the standard boiling method, in accordance with ISO 10545-10 (ISO 2021), and an accelerated procedure combining boiling followed by autoclave conditioning.

Prior to testing, all specimens were subjected to a refiring procedure to establish the reference length, as prescribed by ISO 10545-10 (ISO 2021). This procedure consists of heating the specimens to 550 ± 15 °C for 2 hours followed by controlled cooling. The initial length is then measured relative to a reference bar.

In the standard method, moisture expansion is determined after immersion in boiling water for 24 hours. In the accelerated procedure, the specimens are first subjected to the same boiling stage and subsequently exposed to autoclave conditions for 5 hours at 500 ± 20 kPa and 159 ± 1 °C.

The autoclave procedure was based on an internal method developed by the Materials Laboratory for Construction Products of IPT, established with reference to ISO 10545-3 (ISO 2018a) and ASTM C370 (ASTM 2012).

In both procedures, moisture expansion is calculated as the increase in specimen length relative to the reference length obtained after refiring.

2.2.3 Chemical and Mineralogical Analysis:

X-ray fluorescence (XRF) was used to determine the chemical composition of the ceramic tiles. X-ray diffraction (XRD) with Rietveld refinement was used to quantify the mineralogical composition, including both crystalline phases and amorphous content.

2.2.4 Microstructural Analysis:

Scanning electron microscopy (SEM) was performed on fracture surfaces to evaluate microstructural features, including porosity, morphology of the glassy phase, and the presence of residual mineral phases such as phyllosilicates. These features are directly related to moisture interaction and expansion behavior.

The tests executed, the number of samples tested and their identification are shown in Table 1.

Table 1 - Identification of the tested samples and the tests carried out

Group	Sample	Situation	Ev/ME/ CR	XRD	XRF	SEM
CT-D	1 to 5	Detached	X	X	X	X
CT-U	1 to 5	Unused	X	---	---	X

Key: Ev: Water Absorption. ME: Moisture Expansion. CR: Crazing Resistance. X: Carried out. ---: Not carried out.

The findings from this integrated experimental program are presented and discussed in the following section.

3. Results and Discussion

This section presents the integrated results of the experimental program, establishing a direct relationship between material characteristics, moisture expansion behavior, and the detachment mechanism at the tile-adhesive interface.

3.1 Tensile Adhesion Strength

Table 2 and Figure 2 show the results of in situ tensile adhesion tests performed on adhesive mortars classified as C1 and C2, according to NBR 13753 (ABNT 1996). All measured values exceeded the minimum requirement of 0.30 MPa (dashed red line), indicating adequate initial adhesion performance of the system.

Table 2 - Summary of tensile adhesion strength (pull-off) results by tower, floor level, sun exposure, and adhesive mortar classification (C1/C2), including coefficient of variation (C.V.)

Tower	Floor	Sun Path	Adesive Mortar	Adhesion Strength (MPa)	C.V. (%)
1	1	N	C1	0.50	28
1	6	S	C1	0.42	17
1	7	W	C1	0.36	14
2	1	W	C1	0.38	16
3	1	E	C2	0.54	13
4	1	S	C2	0.44	11
5	5	S	C2	0.55	20
6	6	E	C2	0.58	17

Sun Path refers to the facade orientation (N = North, S = South, E = East and W = West), adopted to represent different solar exposure conditions

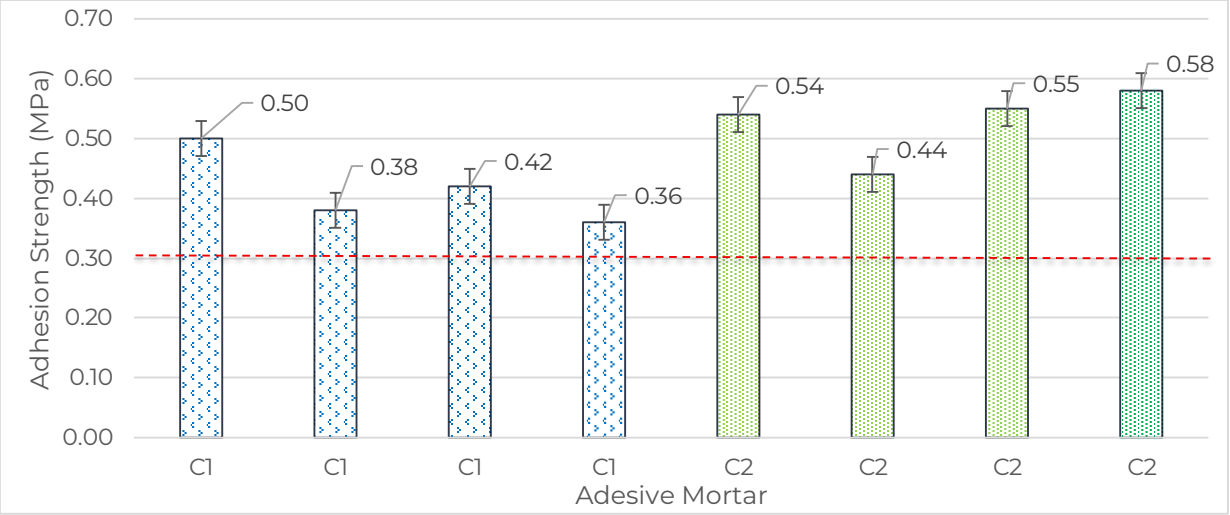


Figure 2 - Tensile adhesion strength (pull-off) results for adhesive mortars C1 and C2, including coefficients of variation

C1 mortars presented values ranging from 0.36 MPa to 0.50 MPa, while C2 mortars ranged from 0.44 MPa to 0.58 MPa. The coefficients of variation varied between 11% and 28%, reflecting typical execution variability without compromising compliance.

No significant influence of parameters such as tower, floor level, or solar orientation was observed, indicating homogeneous behavior across the evaluated conditions.

These results demonstrate that the tile system initially satisfied normative requirements. However, as the pull-off test represents a point-in-time assessment, it does not capture time-dependent degradation mechanisms. The subsequent widespread detachment therefore indicates the action of mechanisms not detectable by this test, particularly those associated with moisture expansion and stress development at the tile-adhesive interface.

3.2 Water Absorption Analysis

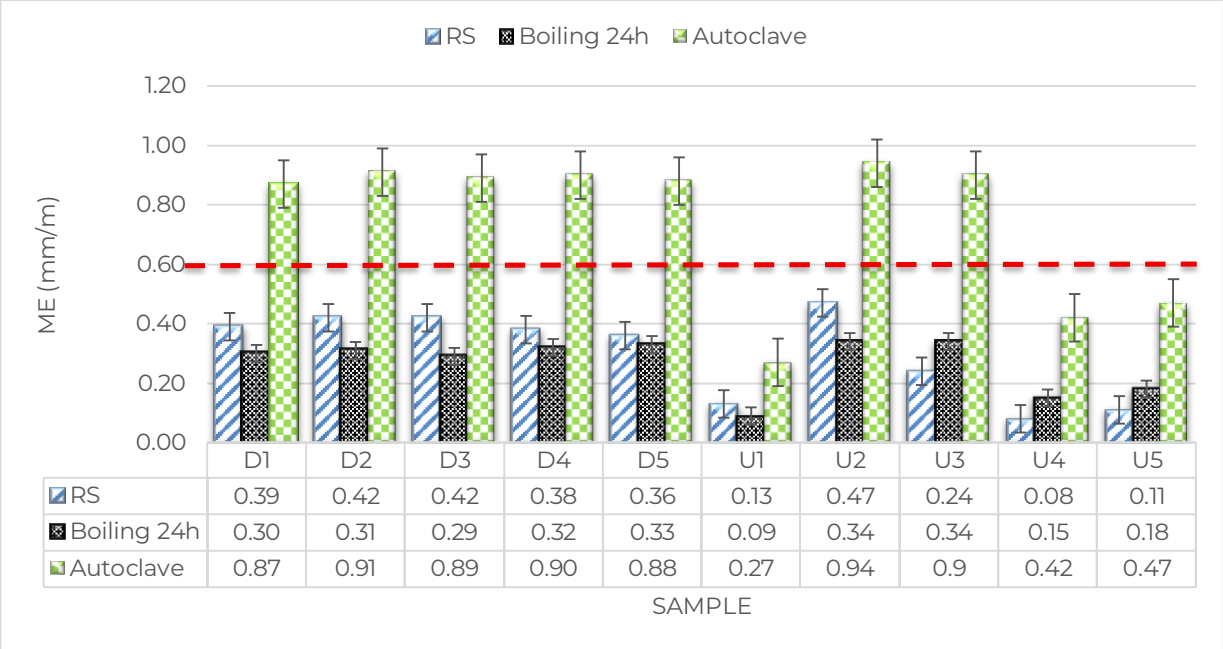
Water absorption values for detached samples ranged from 7.3% to 7.7%, with an average of 7.5%. Unused reference samples ranged from 6.6% to 8.2%, with an average of 7.4%.

All samples were classified as BIIb according to ISO 13006 (ISO 2018c), confirming that both detached and reference tiles belong to the same absorption group.

These results indicate that water absorption alone is not a distinguishing parameter for the observed detachment, reinforcing the need to investigate other mechanisms, particularly moisture expansion.

3.3 Moisture Expansion Analysis

Figure 3 presents the moisture expansion results obtained by refiring, standard boiling, and autoclave testing for both detached and reference samples. The dashed red line in Figure 3 refers to the limit suggested by the ISO 10545-10 (ISO 2021) standard of 0.06% or 0.6 mm/m.



	D1	D2	D3	D4	D5	U1	U2	U3	U4	U5
RS	0.39	0.42	0.42	0.38	0.36	0.13	0.47	0.24	0.08	0.11
Boiling 24h	0.30	0.31	0.29	0.32	0.33	0.09	0.34	0.34	0.15	0.18
Autoclave	0.87	0.91	0.89	0.90	0.88	0.27	0.94	0.9	0.42	0.47

Figure 3 - Graph of the moisture expansion test results for the detached (D) and unused (U) ceramic tile samples

A consistent increase in expansion was observed with increasing test severity. The lowest values were obtained by the boiling method, ranging from 0.28 mm/m to 0.33 mm/m, while autoclave results ranged from 0.87 mm/m to 0.91 mm/m for detached samples. Refiring results were intermediate, between 0.36 mm/m and 0.42 mm/m.

This behavior is consistent with the thermomechanical assumptions of each method and with previous studies (Menezes 2001; Antunes 2019). The boiling method, although standardized, presents well documented limitations in capturing the full expansion potential of partially sintered materials (Menezes 2001; Antunes 2019). In contrast, the autoclave method revealed significantly higher expansion values, exceeding boiling results by more than 200%, as also discussed by Martin (2019).

The low dispersion of autoclave results indicates a consistent and systemic behavior among detached samples, suggesting a common origin related to material formulation and firing conditions. X ray diffraction results confirmed similar phase assemblages among samples, reinforcing this interpretation.

Among the reference samples, three distinct behaviors were identified. Samples U1, U4, and U5 exhibited stable behavior, with autoclave expansion below 0.50 mm/m. In contrast, samples U2 and U3 showed high expansion, reaching values up to 0.94 mm/m, despite complying with normative limits under the boiling method.

Sample U2, representative of the detached tiles, confirms the causal relationship between high moisture expansion and in service detachment. Although compliant under standard testing, the material exhibited critical expansion when subjected to more severe conditions.

These findings reinforce that moisture expansion must be evaluated using accelerated methods to reveal latent instability, as also supported by ASTM C370 (ASTM 2012).

Furthermore, as shown in Figure 3, sample U3 presents behavior comparable to the detached tiles. This relationship is reinforced by the microstructural features illustrated in Figure 4, where both D1 and U3 exhibit preserved phyllosilicates within a porous matrix, indicative of incomplete sintering. Among the reference samples, U3 is the one that most closely resembles the detached tiles in morphological terms, as discussed in the Section 3.6.

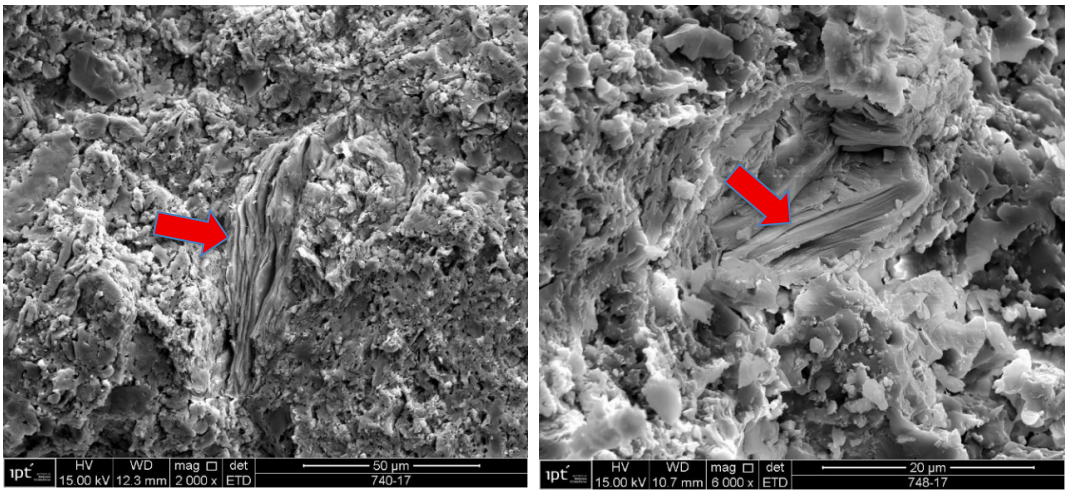


Figure 4 - Fracture surfaces of samples D1 (left) and U3 (right). SEM micrographs obtained using secondary electrons, indicating the presence of preserved phyllosilicates within a porous matrix in both samples

3.4Crazing Resistance

The crazing resistance results, summarized in Table 3, indicate that glaze cracking is not governed solely by moisture expansion (ME), but rather by a combination of factors related to the ceramic body–glaze system.

Table 3 - Summary of Crazing Occurrence vs. EPU and Sample Condition

Sample	Condition	Crazing (Before)	Crazing (Autoclave)	ME Autoclave (mm/m)	Interpretation
D1–D5	Detached	Partial/No	Yes (all)	0.87–0.91	Critical behavior
U2	Reference	No	Yes	0.94	Similar to detached
U3	Reference	No	No	0.90	High ME no crazing
U1, U4, U5	Reference	No	No	0.27–0.47	Stable behavior

All detached samples exhibited crazing after autoclave testing, consistent with their high expansion values and in agreement with observations reported by Kayaci (2021). However, sample U3 did not show crazing despite exhibiting similar expansion levels. This behavior indicates that moisture expansion acts as an aggravating factor rather than a direct cause of crazing. Other parameters, such as thermal compatibility and microstructural characteristics, play a determining role, as discussed by Dvořáková *et al.* (2021).

3.5 Chemical and Mineralogical Analysis

The XRF and XRD analyses provided a detailed understanding of the tile composition, which is fundamental to its susceptibility to ME. The chemical analysis reveals critical molar ratios when compared to the correlations established by Young and Brownell (1959), as illustrated in the graphs of Figures 5 and 6. The Al_2O_3/SiO_2 ratio ranged from 0.164 to 0.185 for samples D1 to D5, with values significantly below the trend line. In parallel, the $(Na_2O + K_2O)/Al_2O_3$ ratio for all samples lies above the historical trend line, varying from 0.328 to 0.429.

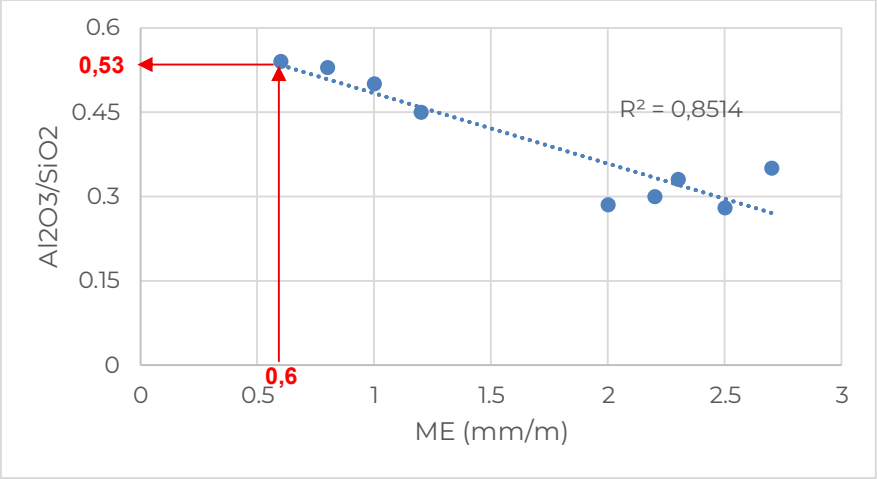


Figure 5 - Al_2O_3/SiO_2 ratio versus ME (8% water absorption). The red-highlighted region indicates the minimum ratio of 0.53 recommended for ceramic tiles with the maximum moisture expansion (ME) suggested by standards (0.6 mm/m)

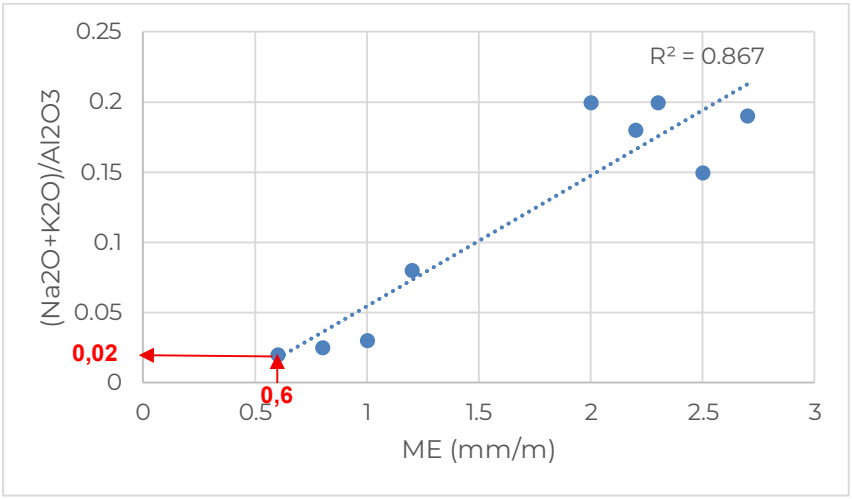


Figure 6 - $(Na_2O + K_2O)/Al_2O_3$ ratio versus ME (8% water absorption). The red-highlighted region indicates the maximum limit recommended by standards for ceramic tiles (0.6 mm/m)

The high quartz content (SiO_2) tends to modify the pore structure of the material (amorphous silica), allowing moisture to penetrate more easily and thereby increasing moisture expansion (ME), as shown in Figure 5 (Cole 1962; Mendonça *et al.* 2012).

Moisture expansion increases with the presence of an alkaline glassy phase, particularly Na and K, and an amorphous phase containing alkaline oxides (Na_2O and K_2O) in the fired ceramic body, as illustrated in Figure 6 (Kayaci 2021). Conversely, it generally decreases with increasing crystalline phases and with higher alkaline-earth content (Ca and Mg) in the structure (Dvořáková *et al.* 2021; Hosseiny *et al.* 2023).

According to Sahade *et al.* (2025), when combined with pressure and temperature determination tests (autoclave), these parameters may represent a more accessible and cost-effective alternative for predicting future expansion.

The mineralogical findings from the XRD analysis with Rietveld refinement confirmed this (Figure 7). The most significant finding was the predominance of a high amorphous phase content, consistently greater than 50% across the samples. The primary crystalline phase was residual quartz (≈37–41%), with minor phases

including hematite-proto and goethite. This highly amorphous microstructure (≈53–58%) is a key contributing factor to the tiles' dimensional instability, as the disordered glassy network provides numerous reactive sites for chemical bonding with water molecules over time (Hosseiny *et al.* 2023).

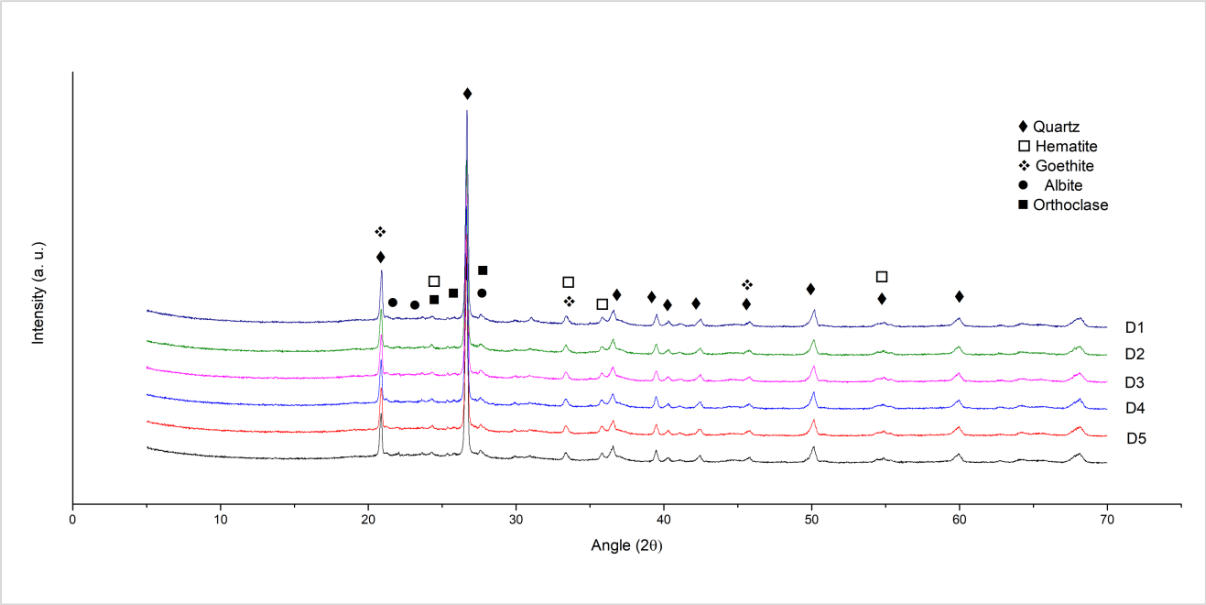


Figure 7 - X-ray diffraction (XRD) patterns of the CT-D samples. The amorphous content was quantified from the halo in the 18°–29° 2θ region

3.6 Microstructural Characteristics

Scanning electron microscopy (SEM) analysis, performed on fracture surfaces, revealed significant differences between detached and reference samples.

Detached samples exhibit a heterogeneous microstructure, characterized by a predominantly porous matrix (Figure 8a), the presence of phyllosilicates with partially preserved foliation, and isolated glassy phase clusters (Figure 8b). This arrangement indicates incomplete and non-uniform sintering, resulting in high open porosity and increased susceptibility to moisture adsorption, which contributes to higher ME values.

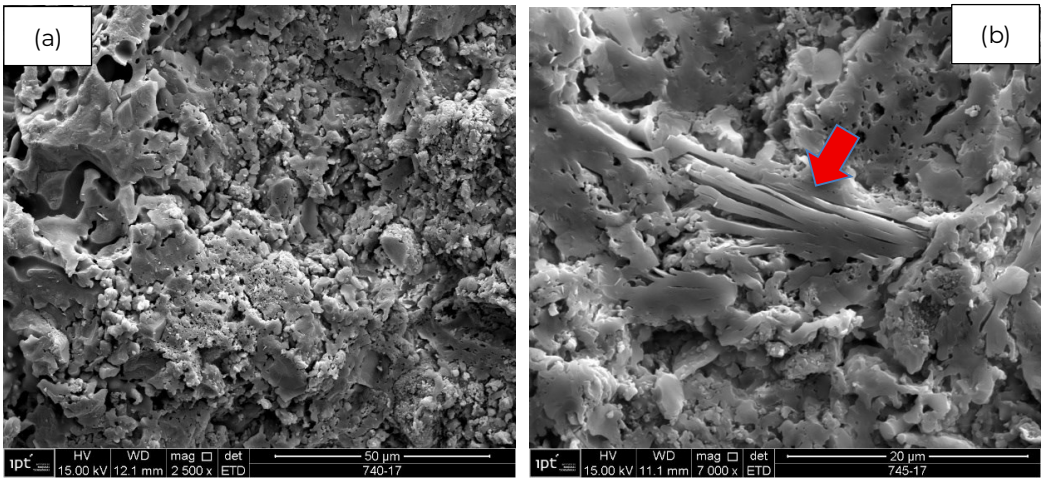


Figure 8 - (a) Porous mass arranging itself as a matrix - mag. 2,500×. (b) Fragments of phyllosilicates with preserved foliation in the middle of the porous mass and isolated glassy clusters - mag. 7000×

In contrast, the unused reference samples present a more homogeneous microstructure, with predominantly closed, sub-spherical pores (Figure 9a) and a continuous glassy matrix (Figure 9b), typical of more effective sintering. This configuration reduces permeability and limits water interaction, being consistent with greater dimensional stability.

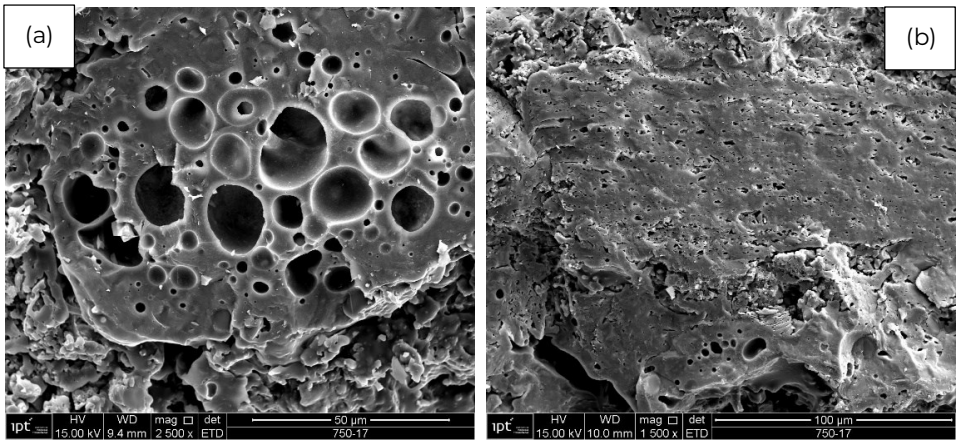


Figure 9 – (a) Closed and sub-spherical pores - mag. 2,500×. (b) Continuous glassy matrix - mag. 1,500×

4. Conclusions

This study demonstrated that the premature detachment of indoor ceramic tile systems is primarily governed by the intrinsic dimensional instability of BIIb ceramic tiles subjected to moisture expansion.

The results establish a direct relationship between material characteristics, moisture expansion, and failure at the tile-adhesive interface. Tiles with high amorphous content, unfavorable chemical ratios, residual quartz, and porous microstructures resulting from incomplete sintering exhibit increased susceptibility to moisture interaction. This leads to progressive and irreversible expansion, generating cumulative shear stresses that ultimately exceed the adhesive bond strength and cause detachment.

From a diagnostic perspective, the findings confirm that moisture expansion must be treated as a primary durability parameter. The observed failures were not associated with execution deficiencies or insufficient initial adhesion, as confirmed by pull-off results in accordance with NBR 13753 (ABNT 1996), but rather with a time-dependent degradation process driven by the ceramic material itself.

A central contribution of this study is the critical assessment of current standardized testing methods. The boiling method defined in ISO 10545-10 (ISO 2021) proved insufficient to represent the actual expansion potential of the tiles, consistently underestimating their behavior. In contrast, the autoclave-based procedure demonstrated higher sensitivity, revealing expansion levels more than twice those obtained by the standard method and identifying latent instability not detectable under conventional testing conditions.

The results further indicate that expansion levels around 0.40 mm/m, below the current normative threshold, are sufficient to induce detachment. This finding highlights the need for a critical reassessment of both limit values and testing methodologies currently adopted in international standards.

Finally, the integration of microstructural, chemical, mineralogical, and accelerated expansion analyses provides a robust framework for understanding detachment mechanisms and improving diagnostic practices. The proposed approach contributes to more reliable material specification and supports future revisions of technical standards aimed at ensuring the durability and long-term performance of ceramic tile systems.

Acknowledgments

The authors acknowledge the financial support provided by Mackenzie Presbyterian University through research grant No. 509. This study is based on the doctoral thesis entitled *"Influence of Moisture Expansion of Ceramic Tiles on the Durability of Ceramic Tile Systems"*, developed within the Graduate Program in Materials Engineering and Nanotechnology at Mackenzie Presbyterian University.

References

Antunes, Elaine Guglielmi Pavei. 2019. Avaliação dos efeitos da expansão por umidade (EPU) das placas cerâmicas na durabilidade dos sistemas de revestimentos cerâmicos internos. PhD diss - Universidade Federal de Santa Catarina.

Associação Brasileira de Normas Técnicas (ABNT). 1996. NBR 13753: Revestimento de paredes internas com placas cerâmicas e com utilização de argamassa colante – Procedimento. Rio de Janeiro: ABNT.

———. 2012. NBR 14081-1: Argamassa colante industrializada para assentamento de placas cerâmicas - Requisitos. Rio de Janeiro: ABNT.

ASTM International. 2012. ASTM C370-12: Standard Test Method for Moisture Expansion of Fired Whiteware Products. West Conshohocken, PA: ASTM.

Barboza, Nathalia, Bruno Loturco, Maurício Besana, and Eder Santin. 2016. "Construtoras de todo o Brasil se mobilizam para encontrar saídas para o descolamento cerâmico." Téchne: A Revista do Engenheiro Civil, no. 234: 18–26.

CCB – Centro Cerâmico do Brasil. 2024. Programa Setorial da Qualidade de Placas Cerâmicas para Revestimento: Relatório Setorial n.° 050/2024. Santa Gertrudes: CCB. https://pbqp-h.mdr.gov.br/psq/placas-ceramicas-para-revestimento/.

Cole, W. F. 1962. "Moisture Expansion of a Ceramic Body and Its Internal Surface Area." Nature 196 (4850): 127–28. https://doi.org/10.1038/196127a0

Conte, S., C. Molinari, M. Ardit, L. Mantovani, M. Tribaudino, G. Cruciani, M. Dondi, C. Zanelli. 2024. "Hazardous Element Inertisation in Vitrified Silicate Ceramics: Effect of Different Matrices." Journal of Hazardous Materials 474: 134657. https://doi.org/10.1016/j.jhazmat.2024.134657.

Cruz, Ricardo Thomé da, Jaime Pedrassani, and Saulo Roca Bragança. 2022. Faianças, grês e porcelanas: matérias-primas, moagem, conformação, secagem, queima, esmaltação, decoração, defeitos e propriedades gerais. Porto Alegre. https://doi.org/10.29327/564493.

Dvořáková, P., A Kloužková, M Kohoutková and M Kolářová. 2021. "Moisture Expansion of Ca-Rich Ceramic Body." In IOP Conference Series: Materials Science and Engineering, 012004. Bristol: IOP Publishing. https://doi.org/10.1088/1757-899X/1050/1/012004

European Committee for Standardization (CEN). 2007. EN 1348: Adhesives for Tiles—Determination of Tensile Adhesion Strength for Cementitious Adhesives. Brussels: CEN.

———. 2017. EN 12004-1: Adhesives for Tiles—Requirements, Evaluation of Conformity, Classification and Designation. Brussels: CEN.

Feldfogel, Shai, and Oded Rabinovitch. 2021. "Evolution and Stability of Tile Detachment: Experiments and Modeling." International Journal of Solids and Structures 210–211: 145–61. https://doi.org/10.1016/j.ijsolstr.2020.11.001

Hosseiny, Amir Hossein Mahmoud, Abolhassan Najafi, and Gholamreza Khalaj. 2023. "Investigation of CaO/MgO on the Formation of Anorthite, Diopside, Wollastonite and Gehlenite Phases in the Fabrication of Fast Firing Ceramic Tiles." Construction and Building Materials 394: 132022. https://doi.org/10.1016/j.conbuildmat.2023.132022

International Organization for Standardization (ISO). 2018a. ISO 10545-3: Ceramic Tiles—Part 3: Determination of Water Absorption, Apparent Porosity, Apparent Relative Density and Bulk Density. Geneva: ISO.

———. 2018b. ISO 10545-11: Ceramic Tiles—Part 11: Determination of Crazing Resistance for Glazed Tiles. Geneva: ISO.

———. 2018c. ISO 13006: Ceramic Tiles—Definitions, Classification, Characteristics and Marking. Geneva: ISO.

———. 2021. ISO 10545-10: Ceramic Tiles—Part 10: Determination of Moisture Expansion. Geneva: ISO.

Kayaci, Kagan. 2021. "Effect of Fluxing Raw Materials on Moisture Expansion of Monoporosa Wall Tile Bodies." Journal of Thermal Analysis and Calorimetry 146 (4): 1603–11. https://doi.org/10.1007/s10973-020-10378-7

Klavdianos, Dionyzio Antonio Martins. 2019. "Entrevista: Desplacamento cerâmico – Construção civil defende rápida resolução." https://cbic.org.br/entrevista-desplacamento-ceramico-construcao-civil-defende-rapida-resolucao/.

Martin, Duncan. 2019. Moisture Expansion in Ceramics. MSc diss., New York State College of Ceramics at Alfred University.

Mendonça, A. M. G. D., J. M. Cartaxo, R. R. Menezes, L. N. L. Santana, G. A. Neves, H. C. Ferreira. 2012. "Expansão por umidade de revestimentos cerâmicos incorporados com resíduos de granito e caulim." Cerâmica 58 (346): 216–24. https://doi.org/10.1590/S0366-69132012000200012

Menezes, Romualdo Rodrigues. 2001. Estudo da expansão por umidade e de características cerâmicas correlatas de placas cerâmicas para revestimento. MSc diss., Universidade Federal da Paraíba.

Nastri, Suelen, Lisandra R. dos S. Conserva, Fabio G. Melchiades, Anselmo O. Boschi. 2015. "A expansão por umidade (EPU) revisitada 20 anos depois: convivendo com a inevitabilidade da EPU." Cerâmica Industrial 20 (1): 24–29. http://doi.org/10.4322/cerind.2015.010

Sahade, Renato Freua, Priscila R. M. Leal, Sérgio S. Lima, Paulo Sérgio da Silva, and Carlos R. C. Lima. 2025. "Investigating the Detachment of Glazed Ceramic Tiles Used in Buildings: A Brazilian Case Study." Materials 18(2), 465. https://doi.org/10.3390/ma18020465.

Silva, Janaina Salustio da, Sandro M. Torres, Ângelo J. Costa e Silva, Fernando A. N. Silva, António C. Azevedo and João M. P. Q. Delgado. 2024. "Adhesion Analysis of Adhesive Mortar Joints in Ceramic Tiles under Static Loading." Buildings 14, no. 3: 670. https://doi.org/10.3390/buildings14030670.

Silva, Karina Ruiz, Liszandra Fernanda Araújo Campos, and Lisiane Navarro de Lima Santana. 2018. "Use of Experimental Design to Evaluate the Effect of the Incorporation of Quartzite Residues in Ceramic Mass for Porcelain Tile Production." Materials Research 22 (1): e20180388. https://doi.org/10.1590/1980-5373-MR-2018-0388

Young, James E., and Wayne E. Brownell. 1959. "Moisture Expansion of Clay Products." Journal of the American Ceramic Society 42 (12): 571–81. https://doi.org/10.1111/j.1151-2916.1959.tb13577.x

Cinpar 2026
XXII International Conference on Building Pathology and Constructions Repair
15th to 17th July 2026 - Lisboa, Portugal

Rehabilitation of Waterproofing Systems in Large-Span Precast Hollow Core Slabs, with crack treatment applied under adverse conditions: Methodology with Flexible Thermoplastic Polyolefin (PO-F) Waterproofing Membranes.

Reabilitação de Sistemas de Impermeabilização em Lajes Alveolares Pré-Fabricadas de Grande Extensão, com tratamento de trincas aplicadas sob condições adversas: Metodologia com Lâminas de Impermeabilização Flexível de Poliolefinas Termoplásticas (PO-F).

Juliana Oliveira ALVES, Marília Carla Araújo

Mendonça de ALENCAR

[1] Instituto Nova Engenharia, Belo Horizonte, Brasil, juliana@jdengdiagnostica.com.br
[2]Instituto Nova Engenharia, Fortaleza, Brasil, marilia@construpat.com.br

Abstract: The rehabilitation of waterproofing systems in large-scale buildings, especially those with precast systems and hollow-core slabs, is critical due to the complex differential structural and thermal movements exhibited by these structures. This behavior is inherent to the structural concept, characterized by a large number of joints and semi-rigid connections. The slenderness of hollow-core slabs, designed for large spans and significant flexural demands, amplifies vertical displacements, differential movements between elements, and thermal expansion, requiring more rigorous expansion-joint and waterproofing designs than those typically used in reinforced concrete structures. Failure of the waterproofing system to accommodate this structural behavior leads to pathological manifestations such as infiltrations, leaks, and efflorescence, classified as critical risk, with serious implications for structural durability, maintenance costs, and the healthfulness of indoor environments. This article presents a case study of the 1,560 m² slab at the Brumadinho/MG Administrative Center, where severe pathological manifestations appeared after one year of use. The methodology, based on standards and guidelines, employed on-site diagnostic investigations with systematic visual inspections, thermography for moisture mapping, and pull-off tests. The failures were attributed to the incompatibility of the original system with structural movement, the absence of a detailed waterproofing design, and inadequate joint execution, resulting in cracks of up to 1.3 mm. The rehabilitation proposal involves flexible thermoplastic polyolefin waterproofing membranes (PO-F). This system was selected for its exceptional structural flexibility, weather resistance, and suitability for application during the rainy season, sealing cracks of up to 3.6 mm without prior treatment and optimizing the intervention. The study contributes to building pathology by demonstrating the technical feasibility and effectiveness of advanced solutions for the rehabilitation of complex waterproofing systems. It aims to improve diagnosis, decision-making, and the application of technologies that enhance the longevity and safety of large roof slabs, mitigating risks. The study concludes that the use of high-performance, flexible systems, with specific bond-breaker detailing over the joints, offers a robust and durable solution, mitigating the risks associated with material fatigue and adhesion failures.
Keywords: Waterproofing, Building Pathology, Precast Structure, Thermography, Thermoplastic Polyolefins.

Resumo: A reabilitação de sistemas de impermeabilização em edificações de grande porte, especialmente aquelas com sistemas pré-fabricados e lajes alveolares, é crítica devido às complexas movimentações estruturais e térmicas diferenciais que estas estruturas apresentam. Este comportamento é inerente ao conceito estrutural, caracterizado pelo grande número de juntas e ligações semirrígidas. A esbeltez das lajes alveolares, projetadas para grandes vãos e forte flexão, amplifica deslocamentos verticais, movimentações diferenciais entre elementos e dilatação térmica, exigindo projetos de juntas de dilatação e de

impermeabilização mais rigorosos que em estruturas de concreto armado. A falha do sistema de impermeabilização em atender a essa dinâmica estrutural acarreta manifestações de patologia como infiltrações, vazamentos e eflorescência, classificadas como risco crítico, com sérias implicações para a durabilidade da estrutura, custos de manutenção e a salubridade dos ambientes. Este artigo apresenta um estudo de caso da laje de 1560m² do Centro Administrativo de Brumadinho/MG, com manifestações de patologia severas após um ano de uso. A metodologia, pautada em normas e diretrizes, empregou investigações diagnósticas *in loco* com inspeções visuais sistemáticas, termografia para mapeamento de umidade e ensaios de arrancamento. As falhas foram atribuídas à incompatibilidade do sistema original com a movimentação estrutural, à ausência de projeto detalhado de impermeabilização e à execução inadequada de juntas, resultando em trincas de até 1,3 mm. A reabilitação propõe lâminas de impermeabilização flexível de poliolefinas termoplásticas (PO-F). Este sistema foi escolhido pela excepcional flexibilidade estrutural, resistência a intempéries e aplicabilidade em período chuvoso, estancando trincas de até 3,6mm sem prévio tratamento, otimizando a intervenção. O estudo contribui para a patologia das construções, demonstrando a viabilidade técnica e a eficácia de soluções avançadas na reabilitação de impermeabilizações complexas. Visa aprimorar diagnóstico, decisão e aplicação de tecnologias para longevidade e segurança de grandes lajes de cobertura, mitigando riscos. O estudo conclui que a utilização de sistemas de alto desempenho, flexíveis, com detalhamento específico de "bond-breakers" sobre as juntas, oferece uma solução robusta e durável, mitigando os riscos associados à fadiga do material e falhas de aderência.
Palavras-chave: Impermeabilização, Patologia da Construção, Estrutura Pré-fabricada, Termografia, Poliolefinas Termoplásticas.

1. Introdução

A degradação de sistemas de impermeabilização em coberturas de grande porte representa um problema recorrente na construção civil, com impactos diretos na durabilidade, no desempenho em serviço e na salubridade das edificações (ABNT, 9575; ABNT, 15575). Em estruturas pré-fabricadas, especialmente aquelas compostas por lajes alveolares de grandes vãos, esse problema é agravado pela ocorrência de movimentações estruturais diferenciais, variações térmicas significativas e elevada incidência de juntas e interfaces construtivas (PCA, 1992; PEREIRA; HELENE, 2007). Esses fatores, quando não devidamente considerados em projeto e execução, favorecem o surgimento de manifestações patológicas como infiltrações, fissuração, eflorescência e perda de aderência dos sistemas impermeabilizantes (ABNT. NBR 9574, HELENE, 1992).

Para garantir o desempenho e a integridade desses sistemas, torna-se essencial a realização de diagnósticos precoces e tecnicamente fundamentados. Nesse contexto, a engenharia diagnóstica se destaca como ferramenta fundamental, integrando inspeções visuais, análise documental e métodos complementares de investigação (ABNT. 16747). Dentre esses métodos, a termografia infravermelha apresenta papel relevante por possibilitar a identificação não destrutiva de variações térmicas associadas à presença de umidade e falhas no sistema de impermeabilização, contribuindo para uma leitura mais abrangente do comportamento da cobertura (TOMITA; CHEW, 2022 MALHOTRA; CARINO, 2004).

A termografia infravermelha baseia-se na detecção da radiação térmica emitida pelos materiais, permitindo mapear anomalias que não são visíveis a olho nu (TOMITA; CHEW, 2022) Quando associada a ensaios mecânicos, como o ensaio de arrancamento (pull-off), e à inspeção visual sistemática, essa técnica amplia significativamente a confiabilidade do diagnóstico, possibilitando a distinção entre sintomas aparentes e mecanismos de degradação subjacentes (ASTM, 2020; MALHOTRA; CARINO, 2004). No estudo em questão, essa abordagem integrada foi aplicada para investigar uma laje alveolar pré-fabricada de grande extensão, onde manifestações patológicas severas foram identificadas em curto período de uso.

Apesar dos avanços nas técnicas de inspeção e diagnóstico, ainda existem desafios importantes relacionados à interpretação dos dados obtidos e à definição de soluções compatíveis com o comportamento estrutural das edificações. Em muitos casos, intervenções inadequadas decorrem da ausência de uma análise sistêmica, que considere simultaneamente projeto, execução, materiais e condições de exposição (ABNT. 15575, HELENE, 1992). Essa lacuna evidencia a necessidade de metodologias mais robustas, capazes de correlacionar causas, mecanismos e manifestações patológicas de forma integrada.

Diante desse cenário, o presente trabalho tem como objetivo analisar as causas das falhas no sistema de impermeabilização de uma cobertura em laje alveolar pré-fabricada e propor uma metodologia de reabilitação tecnicamente compatível com sua dinâmica estrutural. A solução adotada baseia-se na aplicação de lâminas flexíveis de poliolefinas termoplásticas (PO-F), selecionadas por sua elevada capacidade de acomodação de deformações, resistência a intempéries e adequação a condições adversas de execução, conforme discutido na literatura técnica (ABNT. 9574, PERIOTTO, PINHEIRO, FERREIRA. 2014).

2. Revisão Bibliográfica

A literatura técnica sobre impermeabilização evidencia que esse sistema ocupa posição central na proteção das edificações contra a ação da água, sobretudo em elementos expostos de forma contínua à umidade e a variações de temperatura. As normas ABNT NBR 9575 e ABNT NBR 9574 estabelecem, respectivamente, diretrizes para seleção, projeto e execução dos sistemas impermeabilizantes, reforçando que o desempenho da solução depende da articulação entre material, substrato, condições de exposição e detalhamento construtivo (ABNT, 2010; ABNT, 2008). Nesse contexto, Helene (1992; 2003) destaca que a durabilidade do concreto está intrinsecamente associada ao controle da penetração de agentes agressivos e à adoção de medidas preventivas desde a concepção do sistema construtivo.

A relação entre impermeabilização e desempenho em serviço é reforçada pela ABNT NBR 15575, ao estabelecer requisitos mínimos de estanqueidade, manutenção e vida útil de projeto para as edificações habitacionais (ABNT, 2013). Mehta e Monteiro (2014) demonstram que a presença de água em elementos de concreto intensifica mecanismos de degradação, favorecendo processos como fissuração, destacamento, perda de aderência e comprometimento da integridade física do sistema. Assim, a impermeabilização deixa de ser entendida como um recurso acessório e passa a integrar o conjunto de estratégias essenciais à preservação do desempenho global da edificação.

No caso das estruturas pré-fabricadas, a literatura aponta que a eficiência do sistema depende não apenas da resistência dos elementos isolados, mas da qualidade da concepção global, da montagem e do tratamento das interfaces. O PCA (1992) assinala que sistemas pré-fabricados, embora apresentem vantagens de racionalização construtiva e agilidade executiva, exigem projeto rigoroso e detalhamento preciso para assegurar o comportamento esperado em serviço. Periotto, Pinheiro e Ferreira (2014) demonstram que o desempenho das lajes alveolares está condicionado à interação entre os elementos estruturais, capeamentos, apoios e regiões de transferência de esforços. Em complementação, Pereira e Helene (2007) observam que a incompatibilização entre componentes estruturais e sistemas complementares figura entre as principais origens de manifestações patológicas em coberturas de grande área.

A literatura de patologia das construções descreve que sistemas de impermeabilização mal concebidos ou mal executados tendem a manifestar infiltrações, manchas de umidade, eflorescências, bolhas, destacamentos e degradação localizada de revestimentos. Contudo, a interpretação desses sinais requer cautela, uma vez que o sintoma visível pode decorrer da combinação de múltiplos fatores, incluindo insuficiências de projeto, falhas de execução, envelhecimento dos materiais e incompatibilidades entre camadas. A ABNT NBR 16747 orienta a inspeção predial como procedimento técnico estruturado de levantamento, análise e diagnóstico, fundamentado em evidências observáveis e documentação

apropriada (ABNT, 2020). Nessa perspectiva, a engenharia diagnóstica consolida-se como ferramenta indispensável para a distinção entre manifestação aparente e mecanismo de degradação subjacente.

Entre os métodos complementares de investigação, a termografia infravermelha consolidou-se como recurso relevante para a identificação de descontinuidades, variações térmicas anômalas e áreas potencialmente associadas à presença de umidade ou perda de aderência. Tomita e Chew (2022) demonstram que a técnica apresenta elevado potencial para a detecção não destrutiva de delaminações em infraestruturas e edificações, particularmente em superfícies extensas e de acesso restrito. De modo complementar, o ensaio de arrancamento (pull-off) é amplamente empregado para a avaliação da resistência de aderência entre camadas e substratos, permitindo verificar a integridade de interfaces e a compatibilidade entre sistemas aplicados sobre concreto (ASTM, 2020; MALHOTRA; CARINO, 2004). A associação entre inspeção visual, termografia e ensaios mecânicos tem sido amplamente reconhecida como estratégia capaz de ampliar a confiabilidade diagnóstica e reduzir a subjetividade associada às avaliações exclusivamente perceptivas.

No âmbito das soluções de reabilitação, a literatura técnica indica que sistemas flexíveis apresentam maior compatibilidade com estruturas submetidas a deformações, deslocamentos diferenciais e variações dimensionais. Em coberturas de grande extensão, a capacidade de acomodar movimentações sem perda de estanqueidade é frequentemente apontada como um dos critérios decisivos para a seleção da tecnologia de impermeabilização. Nesse cenário, as membranas de poliolefinas termoplásticas (PO-F) surgem na literatura como alternativa de interesse técnico por reunirem flexibilidade, resistência e boa adaptação ao substrato, sobretudo em situações nas quais a solução precisa responder simultaneamente a exigências de continuidade, deformabilidade e desempenho durável em serviço.

Dessa forma, o conjunto de estudos consultados evidência que falhas em sistemas de impermeabilização de lajes pré-fabricadas de grande extensão decorrem, em grande parte, da interação entre insuficiências de projeto, incompatibilidades entre sistemas e comportamento estrutural, além de deficiências executivas em pontos singulares. A literatura também demonstra que a investigação dessas anomalias é fortalecida pela combinação entre inspeção visual e métodos complementares, em especial termografia e ensaios de aderência, como apoio à formulação de diagnósticos tecnicamente mais consistentes. Nesse contexto, soluções flexíveis como as membranas de PO-F representam uma possibilidade tecnológica promissora para coberturas extensas sujeitas a movimentações relevantes, sem que isso configure uma conclusão generalizável, mas sim uma tendência identificada na literatura especializada.

3. Metodologia

A pesquisa adotou abordagem de estudo de caso com finalidade diagnóstica e prescritiva, conforme as diretrizes aplicáveis à inspeção predial e às perícias de engenharia. O objetivo metodológico foi identificar as causas das manifestações patológicas observadas na cobertura, avaliar a extensão dos danos e fundamentar tecnicamente a solução de reabilitação mais compatível com o comportamento da estrutura.

Inicialmente, foi realizado levantamento documental com análise dos projetos disponíveis, registros fotográficos, informações de manutenção e dados do empreendimento. Essa etapa permitiu compreender o sistema construtivo, identificar limitações de informação técnica e reconhecer a ausência de projeto específico de impermeabilização, aspecto relevante para a interpretação das falhas observadas.

Na sequência, procedeu-se à inspeção visual sistemática in loco, com registro das manifestações patológicas por meio de documentação fotográfica e mapeamento das áreas afetadas. Foram observadas infiltrações, umidade localizada, eflorescências, fissuras e descontinuidades em regiões críticas, com maior incidência em juntas, encontros com elementos verticais e pontos de drenagem. A inspeção foi conduzida de modo a relacionar os sintomas visíveis às possíveis causas estruturais, executivas e funcionais.

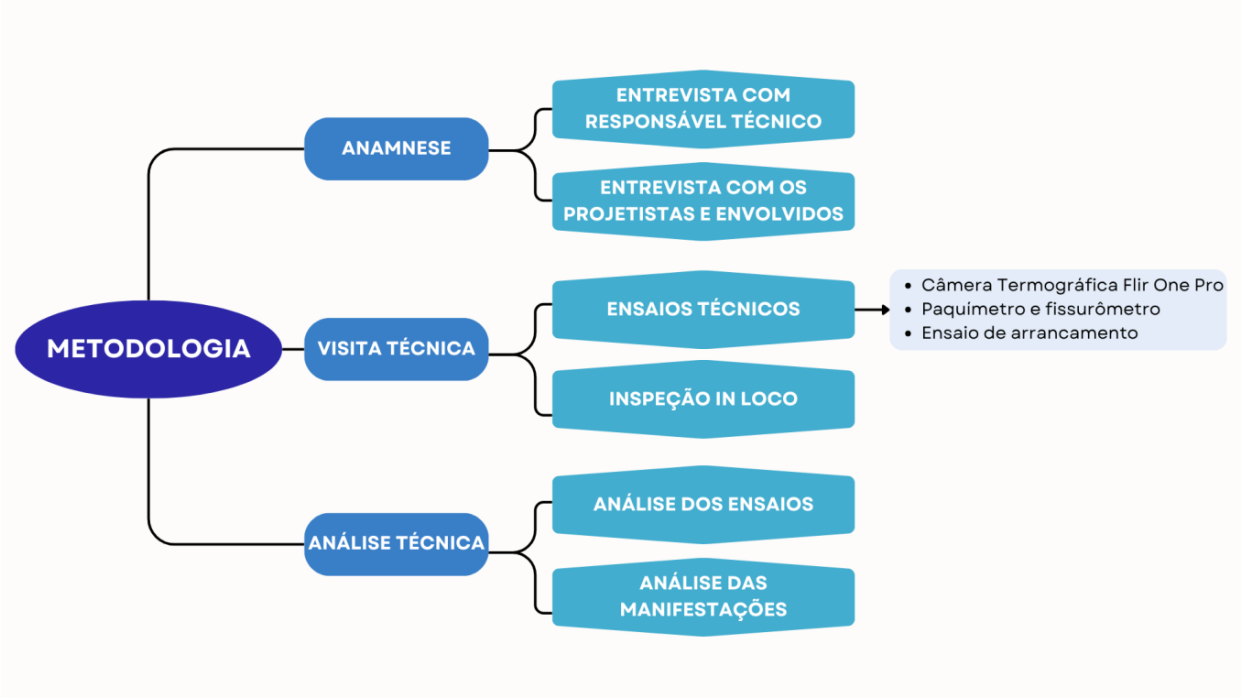


Figura 1 - Fluxograma de metodologia

Como complemento à análise visual, foram empregados ensaios não destrutivos, com destaque para a termografia infravermelha, utilizada para identificar variações térmicas compatíveis com acúmulo de umidade e possíveis falhas no sistema impermeabilizante. Também foram realizados ensaios de arrancamento em pontos estratégicos, com o objetivo de avaliar a aderência do sistema existente e sua compatibilidade com eventual reabilitação por sobreposição.

A interpretação dos resultados foi orientada por uma lógica de causalidade técnica, buscando distinguir sintomas, mecanismos de degradação e agentes agravantes. Em vez de restringir a análise à constatação das manifestações aparentes, a metodologia priorizou a compreensão do comportamento do sistema como um todo, considerando a interação entre estrutura, substrato, movimentação diferencial e desempenho da camada impermeabilizante. A partir dessa leitura, foi possível formular a proposta de intervenção mais adequada ao caso.

4. Resultados e Discussões

As inspeções realizadas na cobertura evidenciaram um quadro patológico expressivo, com infiltrações recorrentes, pontos de umidade persistente, eflorescências e fissuração em áreas variadas da laje. A manifestação dos danos em curto intervalo de uso indicou que o problema não se limitava ao desgaste natural dos materiais, mas resultava de incompatibilidade entre o sistema de impermeabilização adotado e as solicitações reais impostas pela estrutura.

A análise técnica mostrou que o comportamento da laje alveolar pré-fabricada, caracterizado por movimentações diferenciais e deformações associadas à esbeltez do elemento, exigia um sistema impermeabilizante com maior capacidade de adaptação. O desempenho insuficiente do sistema original sugere que a solução empregada apresentava limitação frente às deformações do suporte, especialmente em pontos singulares, como juntas estruturais, transições de plano, encontros com elementos verticais e regiões de drenagem.

Outro fator determinante foi a ausência de projeto detalhado de impermeabilização. Sem diretrizes específicas para regularização de base, tratamento de juntas, caimentos, reforços e pontos singulares, a

execução tende a reproduzir soluções genéricas, pouco adequadas à complexidade do sistema. Em coberturas de grande extensão, essa lacuna pode gerar falhas localizadas que evoluem rapidamente para danos generalizados.

A leitura crítica das anomalias observadas indica que a degradação não decorre apenas da presença de água, mas da combinação entre falhas de concepção, falhas de execução e insuficiente compatibilização entre material e suporte. Em termos técnicos, trata-se de um caso em que a patologia não é apenas sintoma de desgaste, mas resultado da inadequação sistêmica da solução originalmente adotada. Essa interpretação é essencial para evitar diagnósticos simplificados e intervenções meramente corretivas, sem enfrentamento das causas raiz.

A ausência de um projeto detalhado de impermeabilização, a execução inadequada da regularização da base sem o caimento de 2% e pontos de empossamento provocaram a degradação precoce da membrana acrílica, assim como a aplicação com pontos de falhas como falta de aderência e enrugamento da tela de poliéster que apodreceu devido aos intemperes, as viradas de rodapés, tubulações e ralos fora de padrões normativos.



Figura 2: Empossamento



Figura 3: Tela de poliéster sem cobrimento da membrana acrílica



Figura 4: Acabamento em tubo fora de norma

A execução inadequada das juntas estruturais agravou o problema. As juntas de dilatação e as interfaces entre os painéis pré-fabricados, que são pontos críticos de concentração de tensões, não foram tratadas com o devido rigor técnico. A falta de limitadores e de elementos flexíveis nessas regiões permitiu que as movimentações estruturais se transmitissem diretamente ao sistema de impermeabilização, o que permitu

o surgimento de trincas e fissuras na estrutura e no sistema de impermeabilização, causando sua falha prematura.

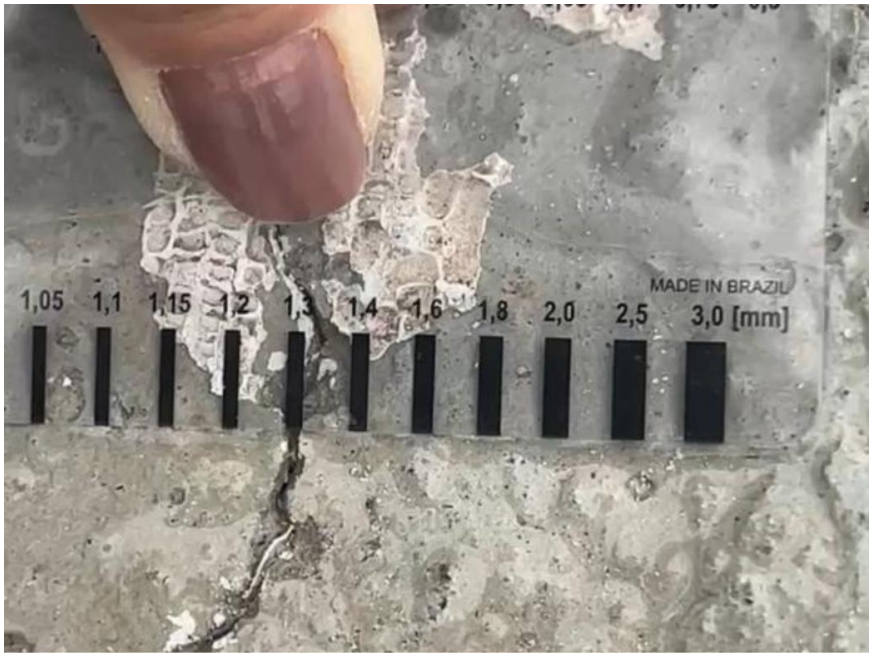


Figura 5: Fissura na laje de 1,3mm



Figura 6: fissura na laje de 1,1mm

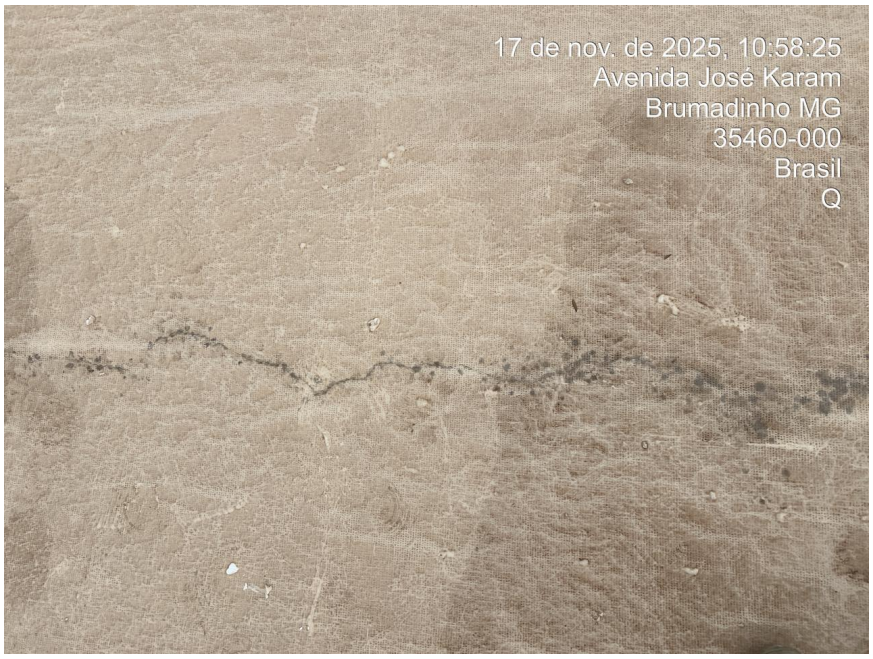


Figura 7: Fissura no sistema de impermeabilização

A termografia confirmou a presença de umidade e infiltrações em áreas extensas da laje, muitas delas não visíveis a olho nu. Os padrões térmicos anômalos indicavam a presença de água na laje alveolar, contribuindo para a degradação do sistema e do substrato. Os ensaios de arrancamento revelaram que, embora a aderência em algumas áreas fosse aceitável, a integridade geral do sistema estava comprometida pelas trincas e pela fadiga do material.

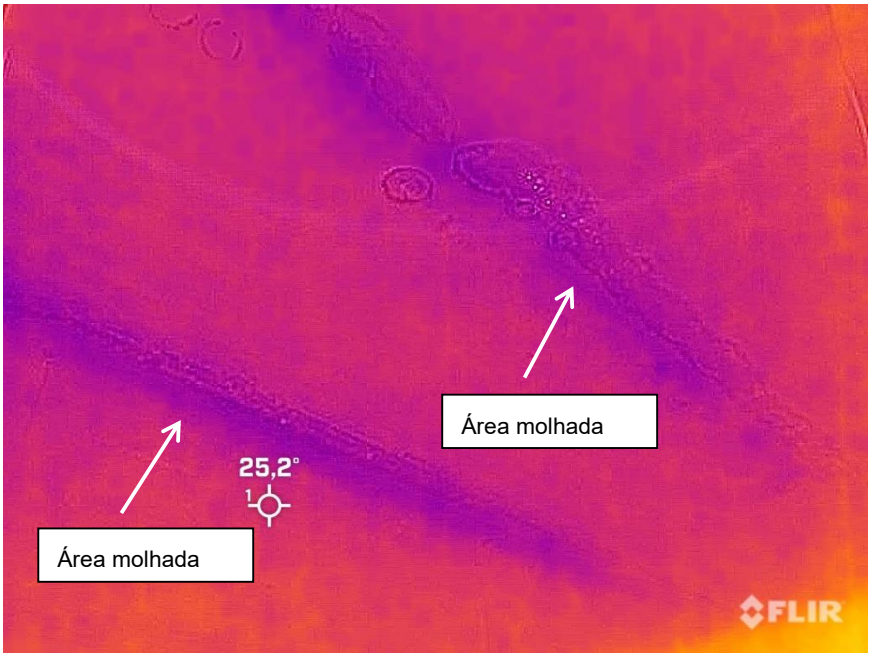


Figura 8: Umidade nos encontros da laje alveolar

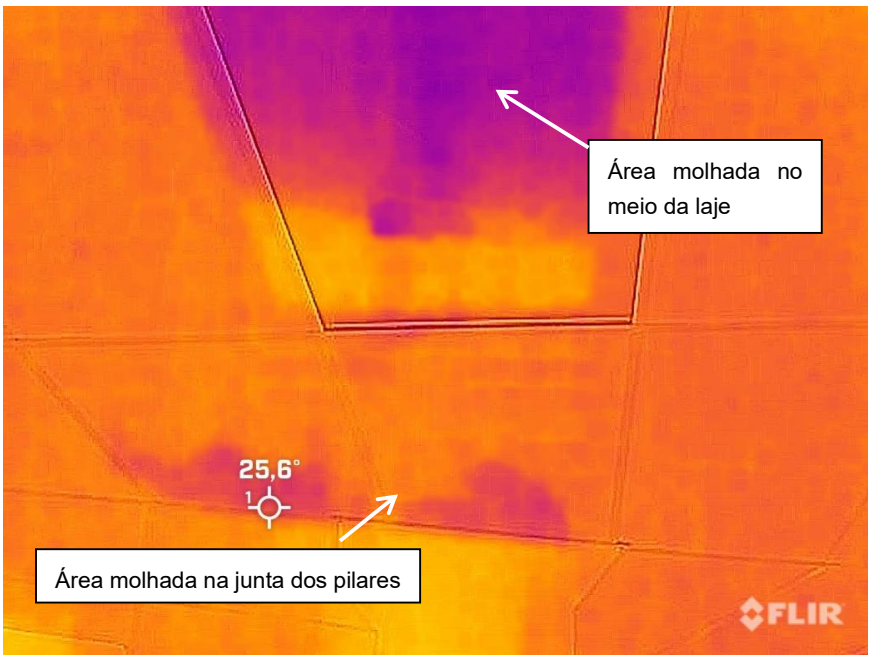


Figura 9: Áreas com umidade

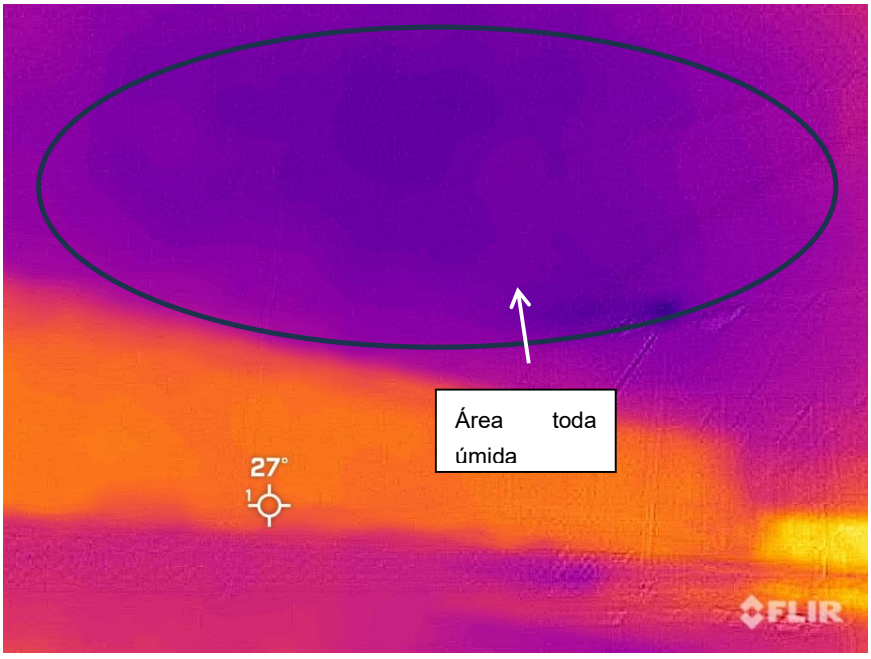


Figura 10 : Áreas com umidade

Diante desse cenário, a discussão se concentrou na busca por uma solução de reabilitação que não apenas corrigisse as manifestações patológicas existentes, mas que também fosse capaz de se adaptar à dinâmica estrutural da laje a longo prazo. A escolha de lâminas de impermeabilização flexível de poliolefinas termoplásticas (PO-F) foi fundamentada em suas propriedades intrínsecas, que se alinham perfeitamente às necessidades do caso.

Diante desse cenário, a comparação entre sistemas mostrou que soluções de natureza mais flexível apresentam vantagens claras em coberturas sujeitas a movimentação estrutural. Nesse contexto, o PO-F se diferencia por oferecer maior capacidade de acomodação deformacional e melhor resposta às fissuras e juntas quando comparado a sistemas mais rígidos ou menos tolerantes ao movimento. Essa característica justifica tecnicamente sua seleção para o caso estudado, especialmente diante da necessidade de durabilidade, estanqueidade e compatibilidade com a estrutura.

Em comparação com membranas acrílicas, o PO-F apresenta vantagem significativa em situações de maior movimentação estrutural, uma vez que sistemas acrílicos tendem a depender de substrato mais estável e apresentam limitação em pontes de fissura mais críticas. Em relação às mantas asfálticas, o PO-F oferece melhor desempenho em detalhes complexos e menor sensibilidade a determinadas condições de aplicação, embora ambas possam ser tecnicamente adequadas em cenários distintos. Já em comparação com poliuretanos, o PO-F se destaca pela combinação entre flexibilidade, estabilidade dimensional e capacidade de execução em condições adversas, desde que o detalhamento das juntas e da superfície seja corretamente executado.

Assim, a escolha do PO-F não se justifica por superioridade absoluta em todos os contextos, mas por sua maior compatibilidade com o mecanismo de falha identificado no presente caso. Esse ponto é importante porque demonstra critério técnico na seleção do sistema, e não preferência aleatória por um produto de mercado.

Tabela 1 – Comparativo de desempenho entre o sistema de impermeabilização original e o sistema PO-F proposto.

Critério de Desempenho	**Sistema de Impermeabilização Original**	**Sistema PO-F Proposto**
Flexibilidade Estrutural	Baixa (não acomoda movimentações)	Excepcional (acomoda grandes deformações)
Capacidade de Ponte de Trincas	Limitada (falha em trincas 0,5mm)	Alta (estanca trincas de até 3,6mm sem pré-tratamento)
Resistência a Intempéries	Moderada (degradação precoce)	Alta (resistência a UV, ozônio, variações térmicas)
Aplicabilidade em Condições Adversas	Restrita (exige tempo seco)	Permite aplicação em período chuvoso
Vantagem Principal	Não há vantagem	Compatibilidade com a dinâmica estrutural da laje

Fonte: Elaborado pelas autoras (2026).

5. Justificativa Econômica da Solução Adotada

Para justificar a escolha da metodologia de reabilitação, procedeu-se a uma análise comparativa de custos diretos e ciclo de vida entre o sistema proposto (Lâminas PO-F) e três alternativas de mercado: manta asfáltica dupla, membrana de poliureia e manta de PVC (Tabela 2).

A análise demonstra que, embora o custo de aquisição dos materiais do sistema PO-F seja superior ao da manta asfáltica dupla, a dispensa das etapas de proteção mecânica e a não exigência de tratamento prévio

para trincas de até 3,6 mm otimizam o escopo da obra. O custo total de intervenção da manta asfáltica dupla apresentou-se inicialmente inferior (R$ 265,80/m² contra R$ 255,00/m² da PO-F). Contudo, a avaliação puramente baseada no custo de implantação é insuficiente para obras de grande magnitude e complexidade estrutural.

Ao incorporar a Vida Útil de Projeto (VUP) na matriz de decisão, o sistema PO-F evidencia sua superioridade financeira. O Custo Anualizado da Lâmina PO-F (R$ 8.292,96/ano) representa uma redução de aproximadamente 38,70% em relação à manta asfáltica dupla (R$ 13.531,44/ano), justificada pela sua longevidade estimada de 50 anos. Conclui-se que a capacidade do material de acomodar as severas movimentações térmicas e estruturais das lajes alveolares mitiga os riscos de falhas precoces, traduzindo-se na alternativa mais econômica e segura ao longo do ciclo de vida da edificação.

Tabela 2 – Análise Comparativa de Custos e Vida Útil dos Sistemas de Impermeabilização Viáveis

Etapas / Parâmetros de Custo	**Lâmina PO-F (CPE)**	**Manta Asfáltica Dupla**	**Membrana Poliureia**	**Manta PVC**
Custo de Material (R$/m²)	R$ 110,00	R$ 17,12	R$ 120,00	R$ 130,00
Custo de materiais de aplicação	R$ 45,00	R$ 15,93	R$ 80,00	R$ 45,00
Custo de Mão de Obra (R$/m²)	R$ 80,00	R$ 40,00	R$ 300,00	R$ 168,00
Regularização / Contrapiso (R$/m²)	R$ 20,00	R$ 80,00	R$ 106,20	45
Proteção Mecânica / Acabamento(R$/m²)	R$ 10,80	R$ 60,00	R$ 40,00	Não se aplica
Tratamento de Trincas de até 3,6mm (R$/m²)	Não se aplica	R$ 3,80	R$ 3,80	Não se aplica
Custo Total de Intervenção (R$/m²)	R$ 265,80	R$ 216,85	R$ 650,00	R$ 388,00
Custo Total de Intervenção Área Total	R$ 414.648,00	R$ 338.286,00	R$ 1.014.000,00	R$ 605.280,00
Vida Útil de Projeto - VUP (anos)	50	25	25	30
Custo Ano (R$/ano)	**R$ 8.292,96**	**R$ 13.531,44**	**R$ 40.560,00**	**R$ 20.176,00**

Fonte: Elaborado pelas autoras (2026).

6. Proposta de Intervenção / Prescrição Técnica

A reabilitação do sistema de impermeabilização da laje do Centro Administrativo de Brumadinho/MG foi concebida para superar as deficiências do sistema original, garantindo estanqueidade duradoura e compatibilidade com as movimentações estruturais da laje alveolar pré-fabricada. A solução proposta baseia-se na aplicação de lâminas de impermeabilização flexível de poliolefinas termoplásticas (PO-F), por ser um material que oferece características superiores para este tipo de desafio devido a sua maior capacidade de acomodar movimentações diferenciais e manter o desempenho de estanqueidade em coberturas de grande extensão.

A metodologia de intervenção compreendeu as seguintes etapas:

1. Preparação da Base: Limpeza rigorosa da superfície da laje, remoção de detritos, regularização de pequenas imperfeições e tratamento de pontos de umidade remanescentes. A aderência do novo sistema depende criticamente de uma base limpa e coesa.



Figura 11: Limpeza da laje



Figura 12: Laje limpa para assentamento da lâmina

2. Tratamento de Trincas e Fissuras: Embora o sistema PO-F tenha alta capacidade de ponte de fissuras (até 3,6mm sem pré-tratamento), as trincas existentes foram avaliadas para garantir a máxima eficácia. Em casos de trincas ativas ou de maior dimensão, foram considerados tratamentos localizados antes da aplicação da manta.

3. Aplicação de Limitadores e Reforço de Juntas: Nas regiões das juntas de dilatação e de encontro entre os painéis pré-fabricados, foram aplicados "bond-breakers" (elementos que impedem a aderência da manta diretamente sobre a junta, permitindo sua movimentação livre) e reforços específicos com a própria manta PO-F. Este detalhe é crucial para absorver as movimentações diferenciais sem comprometer a estanqueidade.



Figura 13: Tratamento de junta de dilatação

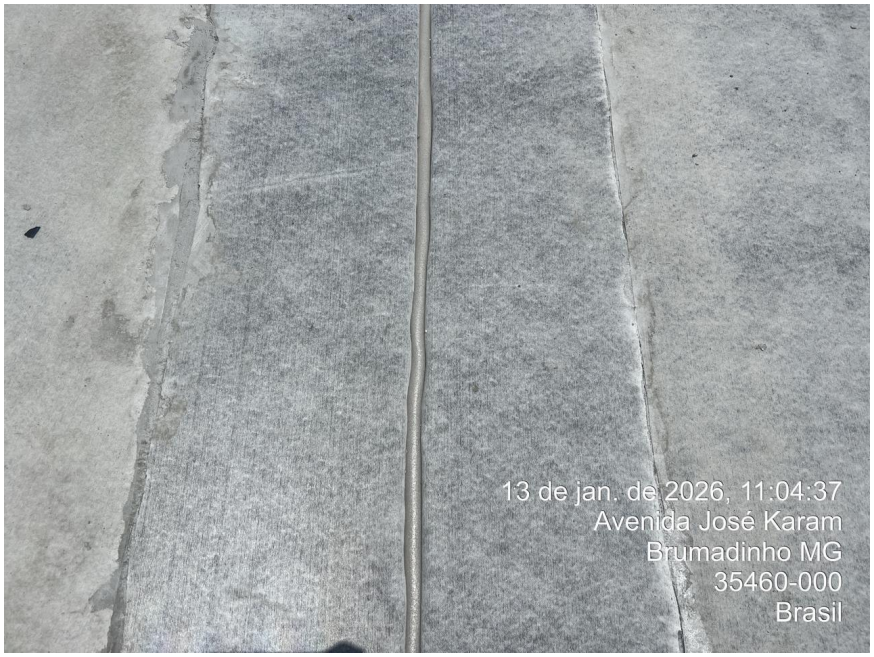


Figura 14: Execução da junta estrutural

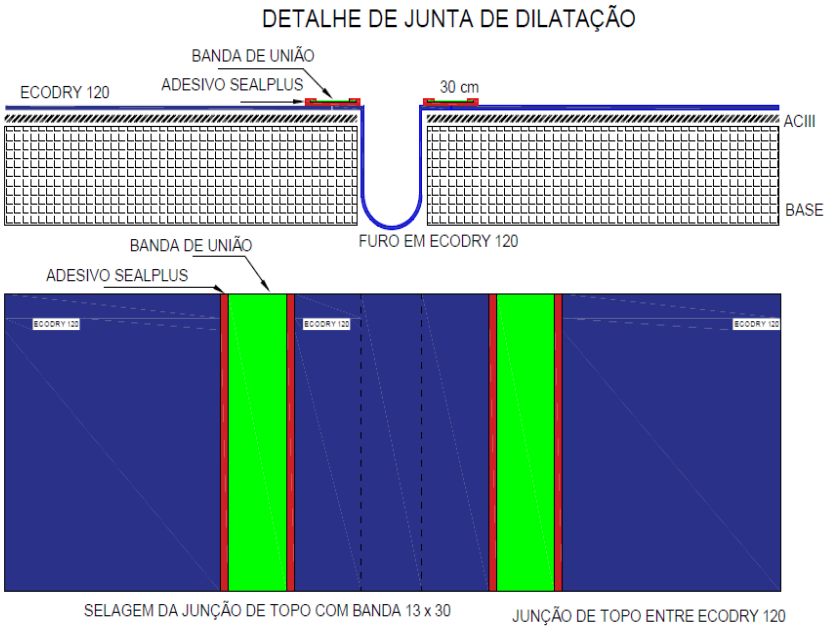


Figura 15: Detalhe da junta estrutural

4. Aplicação das Lâminas PO-F: As lâminas de poliolefinas termoplásticas foram aplicadas com ACIII de alta performance, suas emendas foram realizadas com uma banda do mesmo material de PO-F aderidas com selante fornecido pelo próprio fabricante formando uma membrana contínua e flexível sobre toda a superfície da laje. A técnica de aplicação permite a formação de soldas homogêneas e resistentes, garantindo a integridade do sistema.



Figura 16: Aplicação da lâmina



Figura 17: Lâmina aplicada

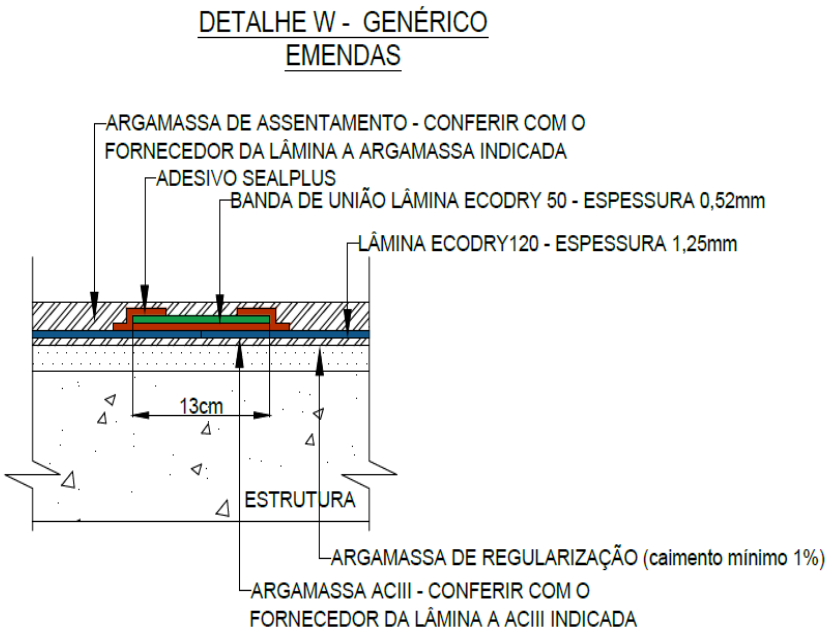


Figura 18: Detalhe da emenda da lâmina

5. Detalhes Construtivos: Cuidados especiais foram dedicados aos detalhes construtivos, como ralos, calhas, encontros com paredes e elementos emergentes. Nestes pontos, foram utilizados reforços e peças moldadas para garantir a continuidade da impermeabilização e evitar pontos de falha.



Figura 19: Acessório pré fabricado para ralo

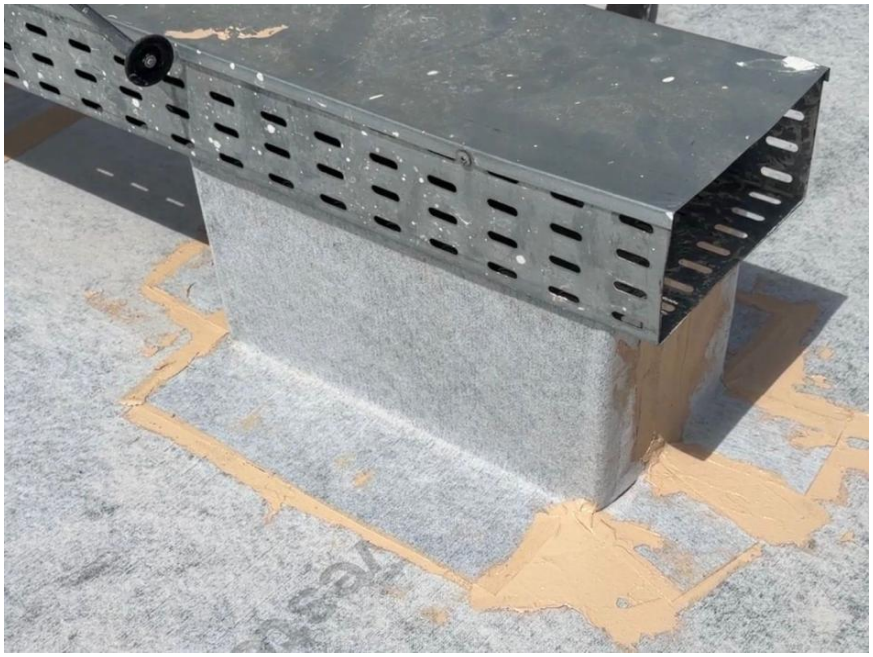


Figura 20: Acabamento dos apoios de acessórios

6. Teste de Holiday: Após a instalação da membrana, foi realizado o Holiday Test (teste de faísca elétrica). Este ensaio não destrutivo utiliza uma sonda de alta voltagem para detectar microfuros, falhas ou descontinuidades na membrana, garantindo que a superfície esteja 100% estanque antes da liberação da área. Este rigoroso controle de qualidade é fundamental para a eficácia a longo prazo do sistema reabilitado.

7. Testes de Estanqueidade: Após a conclusão das emendas realizadas após a identificação de falhas com o aparelho de Holiday Teste, foram realizados testes de estanqueidade por lâmina d'água para verificar a eficácia do novo sistema.



Figura 21: Lâmina de água para teste de estanqueidade

8. Aplicação de membrana acrílica: Antes da liberação da área, para garantir a eficácia e prolongar a vida útil das lâminas de PO-F foi aplicada uma camada de membrana acrílica, para promover uma blindagem superficial e proteger da ação dos raios UV no material impermeabilizante.



Figura 22: Menbrana acrilica aplicada para proteção UV

A escolha do sistema PO-F foi estratégica devido à sua excepcional flexibilidade estrutural, resistência a intempéries (incluindo raios UV e ozônio) e a possibilidade de aplicação em período chuvoso, o que otimizou o cronograma da intervenção em um ambiente de condições adversas. A capacidade de estancar trincas de até 3,6mm sem prévio tratamento simplificou o processo e reduziu os custos de mão de obra e materiais.

7. Conclusão

O estudo de caso evidencia que o desempenho de sistemas de impermeabilização em coberturas pré-fabricadas de grande extensão depende de maneira decisiva da compatibilidade entre a solução adotada e o comportamento estrutural da edificação. No caso analisado, a ocorrência precoce de infiltrações, umidade persistente, fissuração e eflorescência demonstrou que o sistema original não possuía capacidade suficiente para acomodar as movimentações diferenciais da laje alveolar, especialmente em regiões de junta e pontos singulares.

A investigação reforça que a falha da impermeabilização não pode ser interpretada apenas como defeito do material, mas como resultado de uma cadeia de incompatibilidades entre projeto, execução e comportamento estrutural. Esse entendimento é relevante porque desloca a discussão de uma abordagem meramente corretiva para uma visão sistêmica da patologia, na qual a solução precisa ser coerente com a causa raiz do problema.

A proposta de reabilitação com lâminas flexíveis de poliolefinas termoplásticas (PO-F) mostrou-se tecnicamente adequada ao caso por reunir flexibilidade, resistência às intempéries e capacidade de acomodação deformacional superior a sistemas menos adaptáveis. A comparação com outras soluções reforça que a seleção do sistema impermeabilizante deve considerar o mecanismo de falha, o grau de movimentação da estrutura e as condições reais de exposição, e não apenas critérios genéricos de aplicabilidade.

Do ponto de vista científico e prático, o artigo contribui para a engenharia diagnóstica ao demonstrar a importância da associação entre inspeção visual, termografia, ensaios de aderência e análise documental na formulação de um diagnóstico consistente. Contribui também para a engenharia de reabilitação ao mostrar que soluções flexíveis, quando corretamente detalhadas, podem oferecer desempenho mais robusto em coberturas de grande porte submetidas a movimentação estrutural. Assim, o trabalho reforça a necessidade de projetos de impermeabilização específicos, compatibilizados com a estrutura e orientados por critérios de desempenho, durabilidade e manutenção.

7. Referências

ABNT. NBR 9574: Execução de impermeabilização. Rio de Janeiro: ABNT, 2008.

ABNT. NBR 9575: Impermeabilização — Seleção e projeto. Rio de Janeiro: ABNT, 2010.

ABNT. NBR 13752: Perícias de engenharia na construção civil. Rio de Janeiro: ABNT, 1996.

ABNT. NBR 16747: Inspeção predial — Diretrizes, conceitos, terminologia e procedimento. Rio de Janeiro: ABNT, 2020.

ABNT. NBR 5674: Manutenção de edificações — Requisitos para o sistema de gestão de manutenção. Rio de Janeiro: ABNT, 2024.

ABNT. NBR 15575: Edificações habitacionais — Desempenho. Rio de Janeiro: ABNT, 2013.

ASTM. Standard Test Method for Pull-Off Strength of Coatings Using Portable Adhesion Testers. ASTM D4541. West Conshohocken: ASTM International, 2020.

HELENE, P. R. L. Manual para reparo, reforço e proteção de estruturas de concreto. São Paulo: Pini, 1992.

HELENE, P. R. L. Manual para reparo, reforço e proteção de estruturas de concreto. São Paulo: Red Rehabilitar, 2003.

MALHOTRA, V. M.; CARINO, N. J. Handbook on nondestructive testing of concrete. 2. ed. Boca Raton: CRC Press, 2004.

MEHTA, P. K.; MONTEIRO, P. J. M. Concreto: microestrutura, propriedades e materiais. 2. ed. São Paulo: IBRACON, 2014.

PCA. Precast/Prestressed Concrete Institute Manual. Chicago: PCI, 1992.

HELENE, Paulo; PEREIRA, Fernanda. Rehabilitación y mantenimiento de estructuras de concreto. 1. ed. São Paulo: [editora não confirmada], 2007

PERIOTTO, Bruna Catoia; PINHEIRO, Libânio Miranda; FERREIRA, Marcelo de Araújo. Emprego do capeamento estrutural para melhoria do desempenho de lajes alveolares protendidas. REEC - Revista Eletrônica de Engenharia Civil, Goiânia, v. 8, n. 2, 2014. DOI: 10.5216/reec.v8i2.27557.

TOMITA, Ko; CHEW, Michael Yit Lin. A review of infrared thermography for delamination detection on infrastructures and buildings. Sensors, v. 22, n. 11, 2022.

Cinpar 2026
XXII International Conference on Building Pathology and Constructions Repair
15th to 17th July 2026 - Lisboa, Portugal

Vision-based structural health monitoring for detection and characterization of cracks in concrete: A systematic review

Daiane Oliveira da SILVA[1], Luís Paulo Mourão dos SANTOS[2], Rosineide Fernando da PAZ[3].

[1] UFC, Russas, Brasil, daianeoliveira@alu.ufc.br
[2] UFC,Russas, Brasil, msantos@ufc.br
[3] UFC, Russas, Brasil, rfdapaz@ufc.br

Abstract: Structural Health Monitoring (SHM) has evolved significantly over recent decades, driven by the need for more accurate, objective, and continuous methods for assessing the integrity of concrete structures. In this context, computer vision has emerged as a promising tool by enabling the automated detection and quantitative characterization of cracks from images, reducing reliance on subjective visual inspections and complex instrumented systems. This paper presents a systematic literature review aimed at analyzing how computer vision techniques have been applied to structural health monitoring, with emphasis on the detection and characterization of cracks in concrete structures. The bibliographic survey covers methods based on digital image processing, machine learning, and deep learning, discussing their capabilities, limitations, and accuracy levels reported in recent studies. The review was conducted through searches in the Scopus (Elsevier) and Web of Science (Clarivate Analytics) databases, selected for their relevance and comprehensive coverage in the fields of civil engineering and computational sciences. The search strategies involved combinations of keywords related to structural monitoring, computer vision, and concrete cracking. Inclusion and exclusion criteria were established considering thematic scope, type of structural application, publication period, and methodological clarity of the studies. The selected works were analyzed with respect to the techniques employed, computational approaches adopted, and parameters extracted for crack characterization. Comparative analysis allowed the identification of trends, recent advances, and limitations of existing approaches. The reviewed studies indicate that the integration of computer vision and SHM results in innovative, non-invasive, and potentially scalable techniques capable of supporting decision-making in structural inspection and maintenance programs. Thus, this work contributes to the systematization of the state of the art and to the consolidation of image-based structural monitoring as a viable and complementary alternative to traditional structural diagnostic techniques.

Keywords: Structural health monitoring; Computer vision; Concrete cracks; Artificial intelligence; Mobile devices; Systematic Review

1. Introduction

The durability and safety of reinforced concrete structures have become central concerns in contemporary civil engineering, particularly in light of aging infrastructure and increasing performance demands throughout the lifecycle of buildings. Although widely used, concrete exhibits heterogeneous behavior and low tensile strength, which favors the development of cracks under mechanical loading and environmental actions. These cracks not only compromise structural durability but also serve as relevant indicators of structural integrity, being widely used as parameters for structural assessment (Narayanan and Subramaniam, 2017).

The evolution of cracks is directly associated with damage mechanisms in concrete, ranging from the nucleation of microcracks to their propagation and coalescence at macroscopic levels (Shahin et al., 2024). Geometric parameters such as width, length, and orientation are fundamental for damage characterization and structural behavior analysis, enabling inferences regarding loading conditions, degradation processes,

and potential failures (Qingguo et al., 2019; Wei, Makhloof and Ren, 2022). In this context, accurate crack detection and quantification become essential steps for effective monitoring and maintenance strategies.

Traditionally, crack identification has been performed through visual inspections and conventional methods, which are highly dependent on the evaluator's experience. Despite their widespread use, these approaches present significant limitations, including subjectivity, low repeatability, and difficulty in large-scale application (Wan et al., 2023). These constraints have driven the development of more advanced approaches capable of providing quantitative and continuous diagnostics of structural conditions (Jayaraju et al., 2022).

In this scenario, Structural Health Monitoring (SHM) emerges as a promising approach for the continuous assessment of structural integrity. SHM integrates sensors, data acquisition systems, and analytical techniques to detect, locate, and quantify damage over time, supporting data-driven decision-making (Xu et al., 2024). With advancements in sensor networks and embedded systems, SHM has evolved significantly, expanding its applicability across different structural contexts (Yao et al., 2024).

More recently, the incorporation of artificial intelligence techniques has transformed the SHM field, particularly regarding automated damage detection (Reis et al., 2025). Machine learning and deep learning methods have been widely explored for processing large volumes of data, with particular emphasis on computer vision-based applications (Sofi et al., 2022). Convolutional neural networks (CNNs), such as U-Net and Mask R-CNN, have demonstrated high performance in crack detection and segmentation on concrete surface images, enabling more robust and automated analyses (Meng et al., 2023).

Semantic segmentation represents a significant advancement in this context, as it allows detailed crack identification at the pixel level, enabling the extraction of essential geometric parameters for structural assessment (Zeng et al., 2024; Wu et al., 2024). This approach contributes to transforming visual inspection into a quantitative process aligned with the demands of modern monitoring systems.

At the same time, there has been a growing use of mobile devices as platforms for structural data acquisition and processing. Smartphones, equipped with high-resolution cameras and embedded sensors, have been explored as low-cost alternatives for SHM applications, expanding access to monitoring technologies (Sarmadi et al., 2023; Kromanis, 2020). This trend reinforces the potential for scalable and accessible solutions, particularly in resource-constrained environments.

Despite these advances, the literature remains fragmented regarding the integration of artificial intelligence, computer vision, mobile devices, and SHM applications. Studies often address these elements in isolation, making it difficult to identify trends, gaps, and research opportunities. Furthermore, there is a lack of systematic analyses that consolidate the main advances, methodologies, datasets, and limitations of the proposed models (Wu et al., 2025).

Given this context, a structured and comprehensive analysis of the literature is required to synthesize the state of the art and identify future research directions. Systematic literature reviews play a fundamental role in this process by applying rigorous methods for the selection, analysis, and interpretation of scientific studies, ensuring greater reliability and reproducibility of results.

Thus, the present study aims to conduct a systematic literature review on the use of artificial intelligence and computer vision for crack detection in concrete structures, with emphasis on integration with structural health monitoring systems and the use of mobile devices. The objective is to identify the main scientific advances, technological trends, adopted methodologies, and existing gaps, contributing to the direction of future research and the development of more efficient and accessible solutions in the field of civil engineering.

2. Methodology

2.1 Search Strategy and Review Design

This study adopts a Systematic Literature Review (SLR) approach with the objective of identifying, analyzing, and synthesizing the most recent contributions related to the use of computer vision and artificial intelligence for crack detection and characterization in concrete structures. The choice of an SLR is justified by the need to ensure a structured, transparent, and reproducible process, enabling the consolidation of the state of the art within the context of SHM.

The review was conducted based on four main axes: (i) computational methods and algorithms employed, (ii) image acquisition techniques, (iii) performance evaluation metrics, and (iv) emerging technological trends. In this way, the study aims not only to map existing approaches but also to understand the evolution of techniques over time and their inherent limitations. Figure 1 schematically illustrates the intersection between the main thematic criteria adopted in the systematic review.

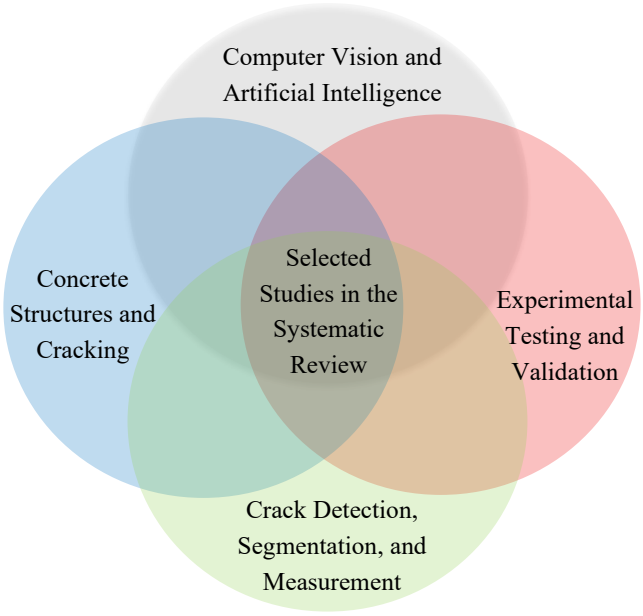


Figure 1 – Venn diagram of search strategies applied in the Scopus and Web of Science databases.

The literature search was carried out in the Scopus (Elsevier) and Web of Science (Clarivate Analytics) databases, selected due to their broad coverage and relevance in the fields of civil engineering, materials science, and applied computing. Articles indexed in Scopus were accessed in full through the ScienceDirect platform. In addition, the adopted time frame spans from 2015 to 2025, justified by the significant growth of deep learning techniques and the consolidation of architectures such as convolutional neural networks (CNNs), as well as the emergence of widely used frameworks such as TensorFlow and PyTorch. This period represents a phase of technological transformation in the field of computer vision applied to engineering.

2.2 Search Strategy and Study Selection Criteria

The search strategy was structured based on the combination of technical keywords and Boolean operators, with specific adaptations for each database according to their indexing characteristics. The objective was to retrieve studies addressing, simultaneously: (i) crack detection, segmentation, and measurement in concrete; (ii) the application of machine learning and deep learning techniques; (iii) the use of computer vision in experimental contexts; and (iv) image acquisition using digital cameras or mobile devices.

The search strings were organized into three main thematic groups: crack detection, segmentation, and measurement, also incorporating terms related to the use of mobile devices. Table 1 presents the main search strings applied across the selected databases.

Table 1 – Search strategies adopted in the systematic review, including identification codes, databases, and corresponding search strings.

Code	Database	Search String
SD-1	ScienceDirect	("concrete" AND "crack detection" AND ("crack width" OR "crack length") AND "deep learning")
SD-2	ScienceDirect	("concrete specimen" AND "crack" AND ("image segmentation" OR "computer vision") AND "laboratory")
SD-3	ScienceDirect	("smartphone" AND "crack" AND "concrete" AND ("measurement" OR "image analysis"))
SC-1	Scopus	TITLE-ABS-KEY("crack detection" AND concrete AND "deep learning")
SC-2	Scopus	TITLE-ABS-KEY("crack segmentation" AND concrete AND "machine learning")
SC-3	Scopus	TITLE-ABS-KEY("crack measurement" AND concrete AND "computer vision")
WOS-1	Web of Science	TS=("crack detection" AND concrete AND ("machine learning" OR "deep learning"))
WOS-2	Web of Science	TS=("crack segmentation" AND concrete AND ("computer vision" OR CNN))
WOS-3	Web of Science	TS=("crack measurement" AND concrete AND ("smartphone" OR "mobile imaging"))

After executing the searches, all retrieved records were exported in .ris format and imported into the Rayyan platform, a tool widely used in systematic reviews (Ouzzani et al., 2016). This step enabled the organization of the dataset and the identification of duplicate records. The study selection process followed the guidelines of the PRISMA (Preferred Reporting Items for Systematic Reviews and Meta-Analyses) protocol, ensuring transparency and reproducibility throughout the review process (Page et al., 2021).

As illustrated in Figure 2, a total of 1,931 records were initially identified from the selected databases. After the removal of 413 duplicate records, 1,518 unique studies remained for title and abstract screening. The potentially relevant articles were subsequently assessed through full-text reading according to the predefined eligibility criteria, resulting in a final corpus of 95 studies included in the qualitative analysis.

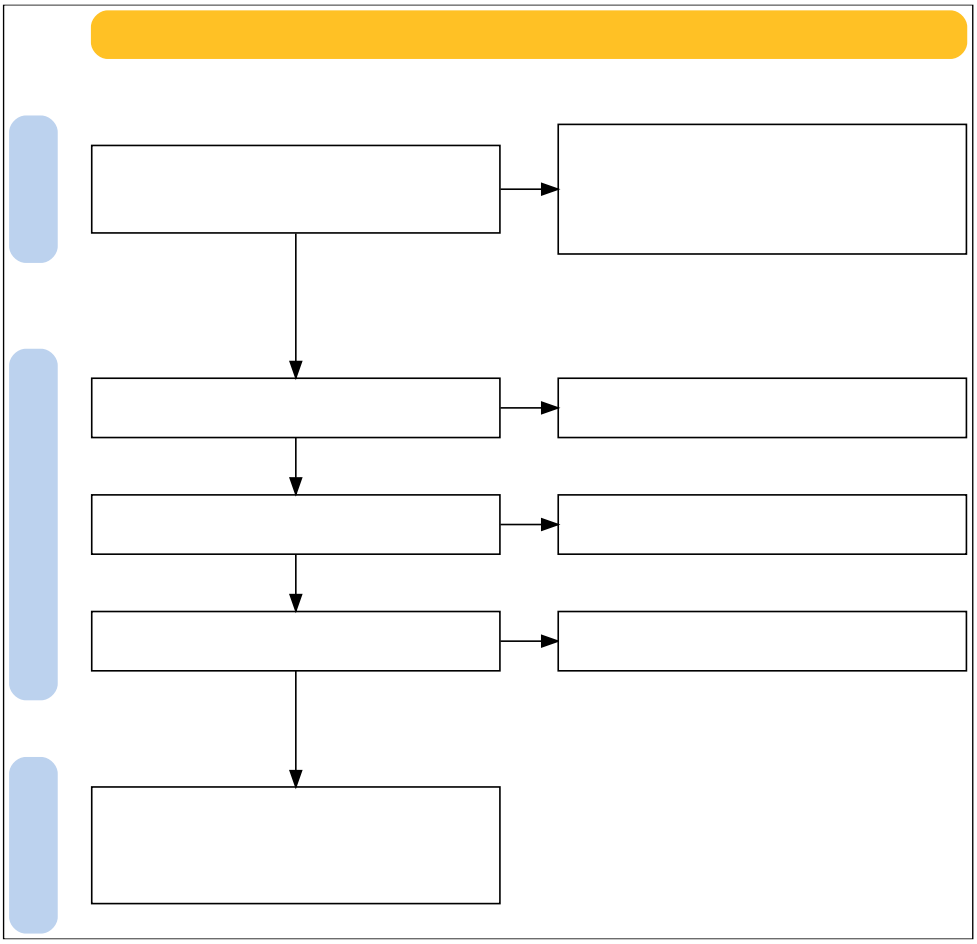


Figure 2 – Flowchart of the identification, screening, eligibility, and inclusion process of studies in the systematic review, developed according to PRISMA guidelines. Source: Authors.

To ensure consistency, transparency, and reproducibility, clear inclusion and exclusion criteria were established. Eligible studies were those addressing crack detection, segmentation, or measurement in concrete, applying computer vision, machine learning, or deep learning techniques, published in peer-reviewed journals between 2015 and 2025, and presenting clear methodological descriptions.

Conversely, studies were excluded if they were not related to structural engineering, lacked adequate methodological description, consisted only of abstracts without full-text availability, were duplicated across databases, or did not involve image-based analysis. This process ensured the selection of a robust set of studies aligned with the research objectives.

2.3 Data Extraction and Analysis

After defining the final set of studies, a systematic data extraction process was conducted to standardize the information and enable comparative analyses among the selected works. For each article, the following information was collected: (i) type of computational approach (image processing, machine learning, or deep learning); (ii) architecture or algorithm used (e.g., CNN, U-Net, YOLO); (iii) application context (laboratory or field); (iv) data acquisition method (cameras, smartphones, sensors); (v) crack-related parameters analyzed (width, length, area); and (vi) performance metrics (accuracy, precision, recall, IoU).

The extracted data were organized and comparatively analyzed, allowing the identification of: (i) prevailing technological trends; (ii) the evolution of algorithms over time; (iii) key methodological limitations; and (iv) existing research gaps.

This analysis provides the foundation for the next section of the paper, in which the results of the systematic review are presented and discussed, focusing on the evolution of techniques, performance of methods, and opportunities for advancement in computer vision-based SHM.

3. Results and Discussion

3.1 Overview of Publications and Evolution of the Field

The analysis of the selected studies reveals a well-defined technological evolution in crack detection in concrete structures, strongly driven by advances in artificial intelligence and computer vision over the past decade. In general, a transition is observed from methods based on digital image processing and classical machine learning to approaches grounded in deep learning, particularly convolutional neural networks.

As these techniques matured, the field evolved from classification and object detection strategies toward pixel-level semantic segmentation approaches, enabling higher accuracy in crack representation and allowing for precise geometric quantification. More recently, the incorporation of attention mechanisms, transformer-based architectures, and generative artificial intelligence has emerged, indicating a new technological frontier focused on automation, robustness, and advanced data interpretation. Table 2 summarizes this evolution, highlighting the main technological phases, seminal works, and their contributions to the advancement of the field.

Table 2 –Summary of the main studies and the temporal evolution of crack detection techniques in concrete.

Period	Technological Phase	Key Studies	Main Contribution
Pre-2015	Image Processing and Classical ML	Yamaguchi & Hashimoto (2010); Jahanshahi & Masri (2012)	Use of edge detection filters, thresholding, and morphological operations; low robustness
2015–2017	Deep Learning (Classification)	Ronneberger et al. (2015); Cha et al. (2017)	Introduction of CNNs and U-Net; crack classification
2017–2018	Object Detection	Cha et al. (2018); Zhang et al. (2018)	Use of Faster R-CNN; detection of multiple types of damage
2018–2020	Semantic Segmentation	Dung & Anh (2019); Liu et al. (2019)	Pixel-level classification; crack measurement
2021–2022	Attention Mechanisms and Transformers	Liu et al. (2021); Wang & Su (2022)	Improved detection of fine and complex cracks
2023–2025	Generative AI and Foundation Models	Li et al. (2025); Duan et al. (2025)	Use of GANs, SAM, and LLMs; data generation and automated reporting

Although the systematic search was restricted to publications between 2015 and 2025, seminal studies published before 2015 were included exclusively for historical contextualization of the technological evolution of crack detection methods.

Recent publications (2023–2025) indicate an advanced stage of maturity in the field, characterized by the adoption of more complex, efficient, and hybrid models. There is a notable increase in the use of architectures based on attention mechanisms, such as Vision Transformers and Swin Transformers, which aim to overcome the limitations of CNNs in capturing global context (Xiong et al., 2024). In parallel, emerging approaches based on generative artificial intelligence, diffusion models, and large language models (LLMs) point to a new frontier focused on data synthesis, mitigation of sample scarcity, and support for automated decision-making (Duan et al., 2025; Farahzadi et al., 2025).

From a quantitative perspective, the scientific production in this field has grown steadily over the last decade, with a marked increase after 2020, reflecting the rapid advancement of deep learning techniques and the increasing availability of computational resources. Although recent publications have accumulated fewer citations due to their recency, studies published between 2017 and 2020 remain highly influential and played a key role in establishing the foundations of AI-based crack detection.

The geographical distribution of publications, shown in Figure 3, reveals a strong concentration of research activity in Asia. China clearly dominates the field, accounting for 280 publications, which represents nearly half of the scientific production identified in this review. India (88 publications), the United States (60 publications), and South Korea (50 publications) also demonstrate significant contributions. This distribution highlights the leading role of these countries in the development of artificial intelligence, computer vision, and structural health monitoring technologies. Furthermore, the concentration of publications in a limited number of countries suggests the existence of well-established research hubs, while indicating opportunities for broader international collaboration and technology transfer to regions with lower scientific output.

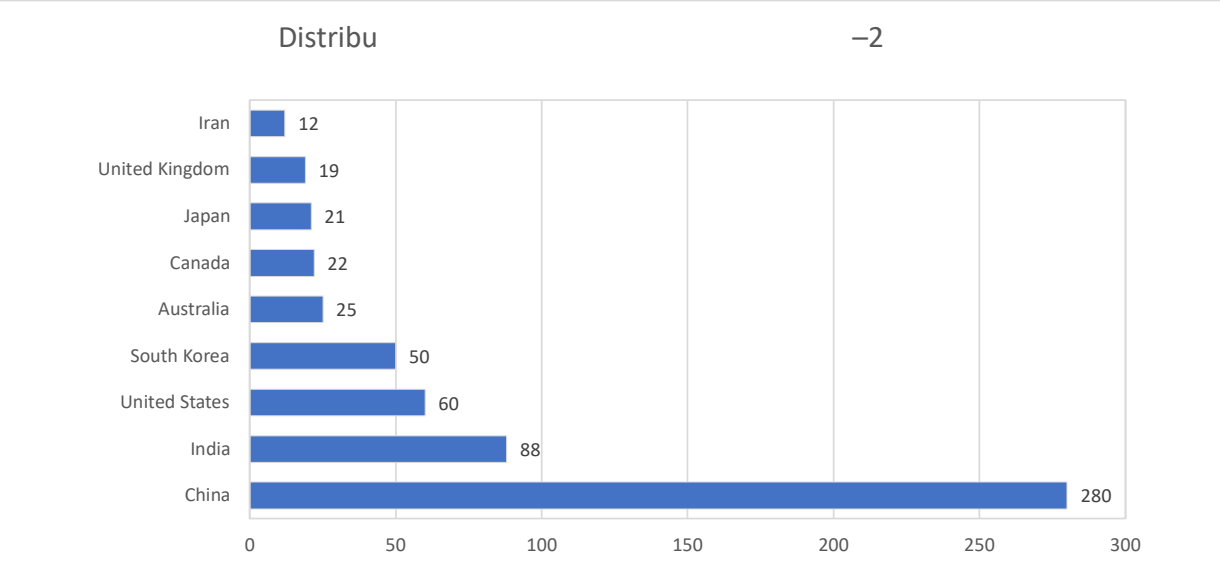


Figure 3 – Distribution of publications by country identified in the systematic review. Source: Authors' elaboration based on Scopus and Web of Science databases.

The predominance of Asian countries in the publication landscape is consistent with their substantial investments in artificial intelligence research, smart infrastructure, and digital transformation. This trend suggests that future advances in AI-based structural inspection are likely to continue being driven by research groups from these regions, particularly in the development of scalable and real-time monitoring solutions.

3.2 Methods, Approaches, and Evaluation Metrics

The analysis of the selected studies reveals a consistent evolution of computational approaches applied to crack detection and quantification in concrete structures. Initially, methods based on digital image

processing and classical machine learning predominated, in which feature extraction was manually designed through edge detection, thresholding, and texture analysis techniques. Although widely used in early applications, these approaches presented limited robustness to noise, illumination variations, and complex surface conditions.

From 2015 onwards, the consolidation of convolutional neural networks (CNNs) marked a significant methodological shift, enabling automatic feature extraction directly from image data. Early applications focused primarily on crack classification tasks and subsequently evolved toward object detection frameworks based on bounding boxes, improving the localization of structural damage. As the field matured, semantic segmentation emerged as the dominant paradigm, allowing pixel-level crack identification and the extraction of geometric parameters such as crack width, length, and affected area.

A quantitative assessment of the 65 studies included in this review highlights the predominance of deep learning-based approaches. Approximately 95% of the analyzed studies employed CNN-based architectures as their primary computational framework. Among them, U-Net and its variants—including Attention U-Net, R2U-Net, CrackUnet, and TransUNet—were identified in approximately 35% of the publications, confirming their widespread adoption for crack segmentation tasks. More recently, hybrid CNN–Transformer architectures have gained prominence, representing nearly 15% of the reviewed studies. These models combine the efficient local feature extraction capability of CNNs with the global contextual representation provided by attention mechanisms, resulting in improved performance for thin, discontinuous, and complex crack patterns.

A critical comparison of the reviewed methods indicates that Fully Convolutional Networks (FCNs) played a pioneering role in semantic segmentation but often suffered from loss of fine crack details and discontinuities. U-Net-based architectures significantly improved segmentation accuracy and robustness, becoming the most widely adopted framework in the literature. Attention-enhanced models further increased performance by selectively emphasizing crack regions and suppressing background noise. More recently, Transformer-based and hybrid architectures have demonstrated superior capability in capturing long-range spatial dependencies and global contextual information, particularly in challenging inspection scenarios. However, these gains are generally accompanied by increased computational complexity, higher training costs, and greater hardware requirements, which may limit their deployment in real-time applications and embedded systems.

Regarding model evaluation, Accuracy, Precision, Recall, F1-score, and Intersection over Union (IoU) were the most frequently reported performance metrics. Although these indicators provide a robust assessment of image-based detection performance, relatively few studies investigated metrics directly associated with structural assessment or maintenance decision-making. Furthermore, most validation procedures were conducted using laboratory datasets or controlled image collections, while a smaller number of studies evaluated model performance under real inspection conditions. This limitation highlights the persistent challenge of domain shift, where variations in lighting conditions, surface textures, environmental noise, shadows, and image acquisition procedures can significantly reduce model generalization and practical applicability in structural health monitoring programs.

From an engineering perspective, the transition from crack classification to pixel-level segmentation represents an important advancement for structural inspection practice. Detailed crack characterization enables more reliable condition assessment, supports maintenance planning, and provides valuable information for structural health monitoring systems. Nevertheless, the limited number of studies validated under real field conditions indicates that further efforts are still required to bridge the gap between laboratory performance and practical implementation in infrastructure inspection and maintenance. The table 3 presents a comparative summary of the main architectures used for crack segmentation, highlighting their characteristics, performance, and applicability.

Table 3 –Comparison of segmentation architectures applied to crack detection in concrete.

Architecture	Segmentation Accuracy	Efficiency / Speed	Key Characteristics
FCN	Moderate	High	Pioneering architecture, with loss of fine details and crack connectivity
U-Net	High	Moderate	Good edge and detail capture; robust with limited datasets
Attention U-Net	Very high	Moderate to low	Improved focus on cracks and better noise suppression
Lightweight U-Net (MobileNet)	High	Very high	High performance with low computational cost; suitable for mobile devices
CNN + Transformer	Very high	Variable	Captures both global and local context; effective for complex crack patterns

3.3 Gaps and Trends in the Application of AI for Crack Detection

The integrated analysis of the literature, combined with the bibliometric mapping performed using VOSviewer (Van Eck & Waltman, 2010), provides insights into the current maturity level of AI-based crack detection research in concrete structures. Figure 4 presents the keyword co-occurrence network, revealing four major thematic clusters that characterize the field. The green cluster is centered on semantic segmentation and crack quantification, emphasizing pixel-level analysis for the extraction of geometric parameters relevant to structural assessment. The yellow cluster is associated with UAV-based inspection and remote sensing technologies, highlighting the growing use of automated data acquisition systems for large-scale infrastructure monitoring. The red cluster connects BIM, Digital Twins, durability assessment, and non-destructive testing, reflecting the integration of crack detection results into digital asset management and predictive maintenance frameworks. Finally, the blue cluster encompasses attention mechanisms and transformer-based architectures, representing recent advances in feature extraction and segmentation performance. Together, these clusters demonstrate the evolution of crack detection from isolated computer vision tasks toward integrated Structural Health Monitoring (SHM) ecosystems.

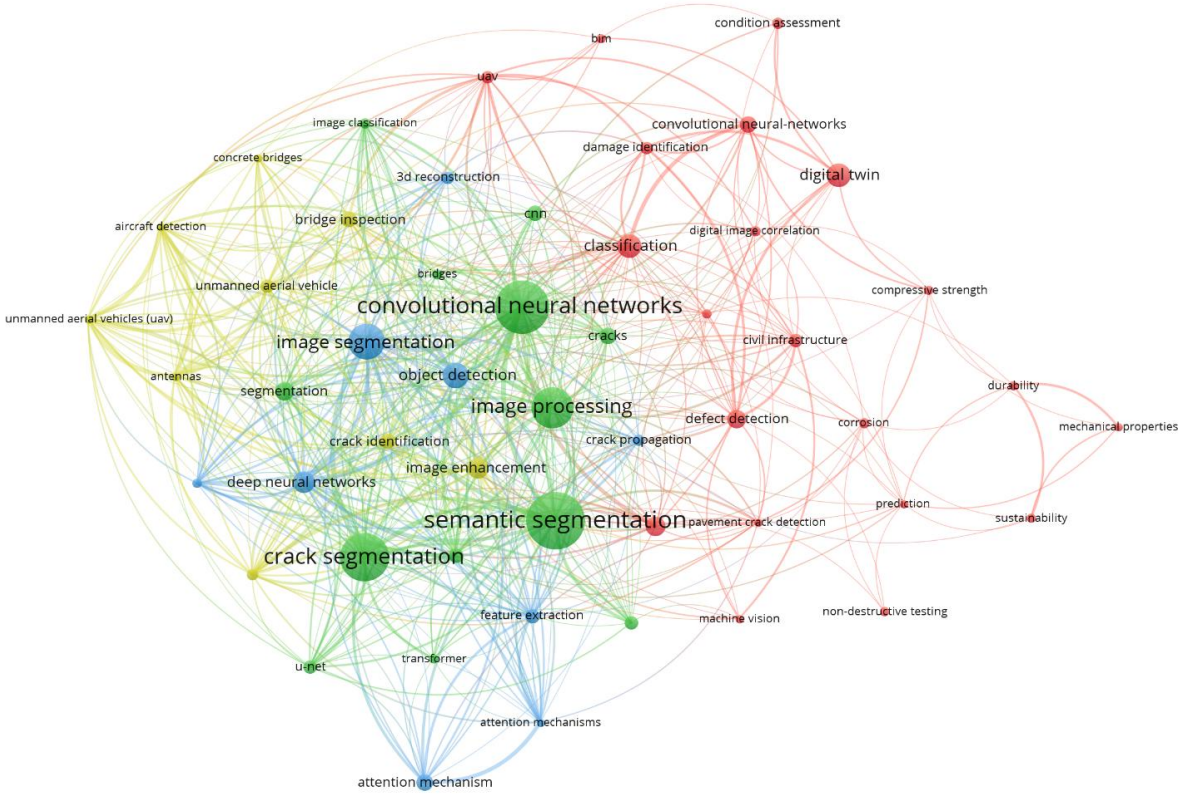


Figure 4 – Keyword co-occurrence map, illustrating the thematic organization of the analyzed literature.

Despite the significant progress achieved during the last decade, several research gaps remain. The most recurrent challenge is the scarcity of large-scale annotated datasets, as most publicly available databases are acquired under controlled laboratory conditions. Consequently, models that achieve excellent results on benchmark datasets often exhibit reduced performance in real inspection environments affected by lighting variations, shadows, surface contamination, weathering effects, and heterogeneous concrete textures.

Another important limitation concerns the restricted validation of proposed methods under practical operating conditions. Although approximately 95% of the reviewed studies employed deep learning-based approaches, only a limited number evaluated their models in real infrastructure inspection scenarios. Furthermore, the increasing computational complexity of state-of-the-art architectures, particularly Transformer-based and hybrid CNN–Transformer models, may restrict their deployment on mobile devices, drones, and edge-computing platforms commonly used in structural inspections.

To address these limitations, several emerging trends can be identified. Generative artificial intelligence, including Generative Adversarial Networks (GANs) and diffusion models, has been increasingly explored to generate synthetic crack images and mitigate data scarcity. At the same time, transformer-based architectures continue to gain prominence due to their ability to model long-range spatial dependencies and improve segmentation accuracy in complex crack patterns.

Recent studies also point toward multimodal and integrated SHM frameworks, combining image data with information obtained from sensors, laser scanners, and unmanned aerial vehicles (UAVs). Advances in edge computing, lightweight neural networks, foundation models, and large language models indicate a future in which crack detection systems become more autonomous, interpretable, and suitable for field deployment. The integration of these technologies with BIM, Digital Twins, and predictive maintenance strategies represents a promising pathway toward intelligent infrastructure management.

4. Conclusions

This study, conducted through a Systematic Literature Review, provided a comprehensive and up-to-date overview of the application of artificial intelligence to crack detection in concrete structures. The findings reveal a clear technological evolution from traditional digital image processing techniques to deep learning-based approaches, particularly convolutional neural networks applied to semantic segmentation. The bibliometric analysis further confirms this trend, highlighting the central role of deep learning and the consolidation of the field within the broader context of Structural Health Monitoring (SHM), characterized by strong interactions between computer vision, artificial intelligence, and engineering applications.

From a methodological perspective, the reviewed studies demonstrate a continuous progression toward more accurate, robust, and automated solutions, especially through the incorporation of attention mechanisms and transformer-based architectures capable of modeling complex spatial relationships. Despite these advances, important challenges remain, including the scarcity of annotated datasets, limited model generalization under real inspection conditions, and the high computational requirements associated with state-of-the-art architectures, all of which restrict their large-scale implementation in engineering practice.

The identified research trends indicate a new phase of development driven by generative AI, multimodal sensing, edge computing, and intelligent decision-support systems. The integration of these technologies with digital environments such as BIM and Digital Twins creates new opportunities for automated inspection, condition assessment, and predictive maintenance of infrastructure assets. Future research should therefore prioritize field validation, computational optimization, and model interpretability, contributing to the transition from laboratory-oriented research toward robust and scalable solutions suitable for real-world structural inspection and maintenance programs.

References

Duan, S., Tan, X., Guo, P., Guo, Y., & Bao, Y. (2025). The transformative roles of generative artificial intelligence in vision techniques for structural health monitoring: A state-of-the-art review. In *Advanced Engineering Informatics* (Vol. 68). Elsevier Ltd. https://doi.org/10.1016/j.aei.2025.103719

Dung, C. V., & Anh, L. D. (2019). Autonomous concrete crack detection using deep fully convolutional neural network. *Automation in Construction*, *99*, 52–58. https://doi.org/10.1016/j.autcon.2018.11.028

Farahzadi, L., Odeh, I., Kioumarsi, M., & Shafei, B. (2025). Automated image-based condition assessment of the built environment: A state-of-the-art investigation of damage characteristics and detection requirements. In *Results in Engineering* (Vol. 26). Elsevier B.V. https://doi.org/10.1016/j.rineng.2025.104978

Jayaraju, P., Somasundaram, K., Suprakash, A. S., & Muthusamy, S. (2022). A Deep Learning- Image Based Approach for Detecting Cracks in Buildings. *Traitement Du Signal*, *39*(4), 1429–1434. https://doi.org/10.18280/ts.390437

Kromanis, R. (2020). Health monitoring of bridges. In *Start-Up Creation* (pp. 369–389). Elsevier. https://doi.org/10.1016/B978-0-12-819946-6.00014-X

Li, S., Yan, F., Li, Z., Hu, Q., Xu, S., & Liu, S. (2025). TCI-Net: Structural Feature Enhancement and Multi-Level Constrained Network for Reliable Thin Crack Identification on Concrete Surfaces. *IEEE Access*, *13*, 65604–65616. https://doi.org/10.1109/ACCESS.2025.3558409

Meng, Q., Hu, L., Wan, D., Li, M., Wu, H., Qi, X., & Tian, Y. (2023). Image-based Concrete Cracks Identification under Complex Background with Lightweight Convolutional Neural Network. *KSCE Journal of Civil Engineering*, *27*(12), 5231–5242. https://doi.org/10.1007/s12205-023-0923-1

Narayanan, A., & Subramaniam, K. V. L. (2017). Damage assessment in concrete structures using piezoelectric based sensors. *Revista ALCONPAT*, *7*(1), 25–35. https://doi.org/10.21041/ra.v7i1.173

Ouzzani, M., Hammady, H., Fedorowicz, Z., & Elmagarmid, A. (2016). Rayyan—a web and mobile app for systematic reviews. Systematic Reviews, 5, 210. https://doi.org/10.1186/s13643-016-0384-4

Page, M. J., McKenzie, J. E., Bossuyt, P. M., Boutron, I., Hoffmann, T. C., Mulrow, C. D., et al. (2021). The PRISMA 2020 statement: An updated guideline for reporting systematic reviews. BMJ, 372, n71. https://doi.org/10.1136/bmj.n71

Qingguo, T., Qijun, L., Ge, B., & Li, Y. (2019). A methodology framework for retrieval of concrete surface crack's image properties based on hybrid model. *Optik*, *180*, 199–214. https://doi.org/10.1016/j.ijleo.2018.11.013

Reis, H. C., Turk, V., Kaya Yildiz, C. M., Bozkurt, M. F., Karagoz, S. N., & Ustuner, M. (2025). A deep neural network combined with a two-stage ensemble model for detecting cracks in concrete structures. *Frontiers of Structural and Civil Engineering*, *19*(7), 1091–1109. https://doi.org/10.1007/s11709-025-1199-y

Sarmadi, H., Entezami, A., Yuen, K.-V., & Behkamal, B. (2023). Review on smartphone sensing technology for structural health monitoring. *Measurement*, *223*, 113716. https://doi.org/10.1016/j.measurement.2023.113716

Shahin, M., Chen, F. F., Maghanaki, M., Hosseinzadeh, A., Zand, N., & Khodadadi Koodiani, H. (2024). Improving the Concrete Crack Detection Process via a Hybrid Visual Transformer Algorithm. *Sensors*, *24*(10). https://doi.org/10.3390/s24103247

Sofi, A., Jane Regita, J., Rane, B., & Lau, H. H. (2022). Structural health monitoring using wireless smart sensor network – An overview. *Mechanical Systems and Signal Processing*, *163*, 108113. https://doi.org/10.1016/j.ymssp.2021.108113

Van Eck, N. J., & Waltman, L. (2010). Software survey: VOSviewer, a computer program for bibliometric mapping. Scientometrics, 84(2), 523–538. https://doi.org/10.1007/s11192-009-0146-3

Wan, S., Guan, S., & Tang, Y. (2023). Advancing Bridge Structural Health Monitoring: Insights into Knowledge-Driven and Data-Driven Approaches. *Journal of Data Science and Intelligent Systems*, *2*(3), 129–140. https://doi.org/10.47852/bonviewJDSIS3202964

Wei, X., Makhloof, D. A., & Ren, X. (2022). Analytical Models of Concrete Fatigue: A State-of-the-Art Review. In *CMES - Computer Modeling in Engineering and Sciences* (Vol. 131, Number 2). Tech Science Press. https://doi.org/10.32604/cmes.2022.020160

Wu, Y., Li, S., Li, J., Yu, Y., Li, J., & Li, Y. (2025). Deep learning in crack detection: A comprehensive scientometric review. In *Journal of Infrastructure Intelligence and Resilience* (Vol. 4, Number 3). Elsevier B.V. https://doi.org/10.1016/j.iintel.2025.100144

Wu, Y., Li, S., Zhang, J., Li, Y., Li, Y., & Zhang, Y. (2024). Dual attention transformer network for pixel-level concrete crack segmentation considering camera placement. *Automation in Construction*, *157*. https://doi.org/10.1016/j.autcon.2023.105166

Xiong, B., Hong, R., Wang, J., Li, W., Zhang, J., Lv, S., & Ge, D. (2024). DefNet: A multi-scale dual-encoding fusion network aggregating Transformer and CNN for crack segmentation. *Construction and Building Materials*, *448*. https://doi.org/10.1016/j.conbuildmat.2024.138206

Xu, W., Zheng, X., Shen, Y., & Luo, Y. (2024). Dynamic wireless sensor network-based structural health monitoring system for retractable roof structure. *Journal of Building Engineering*, *98*, 111302. https://doi.org/10.1016/j.jobe.2024.111302

Yao, W., Li, H., & Li, Y. (2024). Integrated Machine Learning and Region Growing Algorithms for Enhanced Concrete Crack Detection: A Novel Approach. *Applied Sciences (Switzerland)*, *14*(21). https://doi.org/10.3390/app14219745

Zeng, Q., Fan, G., Wang, D., Tao, W., & Liu, A. (2024). A systematic approach to pixel-level crack detection and localization with a feature fusion attention network and 3D reconstruction. Engineering Structures, 300. https://doi.org/10.1016/j.engstruct.2023.117219

Cinpar 2026
XXII International Conference on Building Pathology and Constructions Repair
15th to 17th July 2026 - Lisboa, Portugal

Diagnostic analysis of differential settlement using the Berberian Method and foundation reinforcement with Mega Piles in a residential structure: A case study in Goiânia, Brazil

Beatriz GALVÃO[1], Marília ALENCAR[2], Arthur RODRIGUES[3], Gabryella NUNES[4], Sibely NUNES[5]

[1]Construpat, Fortaleza, Brazil, beatrizgalvao.eng@gmail.com
[2]Instituto Nova Engenharia, Fortaleza, Brazil, marilia@construpat.com.br
[3]Construpat, Fortaleza, Brazil, arthurnascimentorodrigues@gmail.com
[4]Instituto Nova Engenharia, Fortaleza, Brazil, mouraagabryella@gmail.com
[5]Construpat, Fortaleza, Brazil, sibelymoura@alu.ufc.br

Abstract: In small-scale residential construction, inadequate soil preparation is still frequent, despite the fact that it constitutes the main support element of the building and one of the most recurrent causes of pathological manifestations, such as differential settlement. In this context, this study focuses on the diagnostic analysis of active differential settlement and the discussion of the applicability of foundation reinforcement through Mega Piles in existing buildings. This article presents a case study of a single-family residence located in Goiânia, GO, built ten years ago, which exhibited recurrent cracks and fissures associated with active differential settlement. The diagnosis was based on a technical inspection and the application of Berberian's Perpendicular Bisector Theorem to the observed fissures, enabling the identification of three critical settlement points related to soil heterogeneity and the loss of its load-bearing capacity. The crack openings ranged from 0.30 mm to 1.8 mm, with a predominance of diagonal patterns, characteristic of differential ground movements. The study highlights the ineffectiveness of previous superficial corrective interventions, such as metallic stitching, as they did not address the primary cause of the problem. As a solution, foundation reinforcement using Mega Piles was proposed as the recommended intervention, consisting of pressed reaction piles whose application is suitable for existing buildings and sites with restricted access. This technique uses the structure itself as a reaction element, allowing immediate wedging and controlled load transfer. The work presents the diagnostic methodology, the recommended intervention methodology, and concludes that geotechnical stabilization is an indispensable condition for subsequent structural rehabilitation.

Keywords: Differential settlement, Berberian Method, Mega Piles, Fissure.

1. Introduction

The construction industry plays a fundamental role in the socioeconomic development of any country. It is responsible not only for job creation and economic growth, but also for producing the built environment in which people live [1]. Within this sector, single-family residential buildings represent one of the most significant building typologies in terms of construction volume, reflecting a continuous and widespread demand worldwide [2]. For these buildings to perform their function safely and durably, it is essential that their structural elements, including columns, beams, slabs, and walls, be properly designed and executed in order to ensure the integrity of the system over time [3]. However, none of these elements can perform adequately without a solid base to support them. In this context, the foundation stands out as the most critical element of a building, since it is responsible for safely transferring structural loads to the ground and directly conditioning the performance and stability of the entire construction throughout its service life [4].

The selection of an appropriate foundation system depends on geotechnical and structural investigations, taking into account factors such as soil type, groundwater level, and climatic conditions, while also

complying with local building regulations to ensure structural safety and stability [5]. Although these criteria are well established in technical literature and standards, negligence during the preliminary stages, particularly in geotechnical investigation and in the proper preparation of the foundation soil, remains a recurring problem. From this perspective, soil, although it is the primary supporting element of any structure, is often treated inadequately in construction practice due to the involvement of professionals who are not specialized in foundations, the presence of unusual unidentified materials, and the lack of accurate information on local conditions [4]. This compromises the load-bearing capacity of the foundation and creates conditions for the development of structural pathologies.

Among the most critical anomalies observed in the superstructures of residential buildings, differential settlement stands out because of its diagnostic complexity and its potential to cause progressive damage. Since most buildings undergo settlements of only a few tens of millimeters, which are generally imperceptible to the naked eye, estimating these deformations should be part of routine foundation design practice, so that the predicted values remain below admissible limits [6]. According to ABNT NBR 6122:2022, Sections 6.1 and 6.2, foundation design must account for soil deformations, since heterogeneity in the underlying layers and construction failures may lead to non-uniform settlements [7]. These movements may become visually apparent through fissures and cracks, which, when properly interpreted using appropriate diagnostic methods, provide evidence capable of revealing both the location and the nature of the ongoing settlement, as observed in the case study presented herein.

In 1970, the Brazilian professor Dickran Berberian proposed a technique known as the Perpendicular Bisector Rule to determine the causative factor of a crack. According to this method, when the perpendicular bisectors of the cracks observed in the walls of a building are traced, the point at which these lines converge indicates the region of greatest foundation subsidence. This makes the method a diagnostic tool of considerable practical value for identifying points of differential settlement in residential buildings [8] [9]. In the present study, this procedure was applied as an auxiliary tool in the diagnostic investigation of a single-family dwelling in Goiânia, state of Goiás, Brazil, making it possible to map the zones of subsoil instability on the basis of the recorded pathological manifestations and to support the definition of the structural intervention adopted.

Given that differential settlement was identified as the cause of the fissures and cracks in the building located in Goiânia, foundation underpinning using mega piles, also known as reaction piles or jacked piles, emerges as a high-performance technological solution for existing buildings, as it is a non-destructive and low-impact technique. Among its main advantages is the immediate transfer of load by using the structure's own weight as the reaction force. This makes it possible to stabilize the settlement without requiring extensive demolition and without interrupting the use of the building, which is especially relevant in situations involving restricted access [10].

Therefore, considering that the safety of the built environment depends directly on the integrity of the foundations that support it, the relevance of investigating and disseminating effective methodologies for structural diagnosis and rehabilitation becomes evident. In view of the limited consolidated technical and scientific literature on both the Perpendicular Bisector Rule and mega piles, this article presents a diagnostic analysis of a real case of active differential settlement in a single-family residence and discusses the technical effectiveness of mega piles as a solution for definitive structural stabilization.

2. Methodology

This study was characterized as an applied case study, with a qualitative approach and descriptive objectives, focused on diagnostic investigation and on proposing a solution for structural pathological manifestations.

The object of study was a single-family residence with a floor area of 226.77 m², approximately ten years old, located in Condomínio do Lago, in Goiânia, GO, Brazil (Figures 1 and 2).



Figure 1 - Front View (on site).



Figure 2 - Location (Google Maps, 2025).

As described in the technical report supporting this case study, the investigation was divided into three main stages: document review and anamnesis, on-site technical inspection, and definition of the geotechnical rehabilitation methodology. In the initial stage, a technical anamnesis was conducted through interviews with the owner in order to reconstruct the history of the building and previous interventions. It was found that the structure had already undergone superficial repairs, such as the "Z-shaped metal stitching" technique, which had not been successful in remediating the cracks. At the same time, the available architectural drawings were analyzed, and the absence of structural, foundation, and soil investigation documents was confirmed, reinforcing the need for a diagnosis based on the observed damage patterns. For anomaly mapping, the supporting tools included a millimeter-graduated steel measuring tape for measuring crack openings and a Bosch GMS 120 wall scanner, used to identify the presence of embedded metallic elements and piping in the affected areas. The field procedure consisted of a detailed inspection of all areas of the residence, with photographic documentation and classification of the cracks according to their morphology, including direction, width, and extent, as well as their location, ranging from the perimeter wall to interior spaces such as the suite and living room.

During the inspection, atypical structural behavior was identified with respect to the building's position on the site. As illustrated in the cross section (Figure 3), part of the structure was founded directly on natural ground at the higher elevation, whereas other areas, including the living room, bedrooms, and part of the

sanitary installations, were built over partially filled zones in order to level the internal platforms. According to Milititsky et al. (2015), the lack of quality control in fill placement creates zones of heterogeneity that are classic sources of differential settlement, since such materials may be poorly compacted and may settle unevenly relative to the adjacent natural ground. Thus, although conventional engineering judgment would normally indicate the fill area as the zone of greatest risk, the inspection revealed that the most severe damage manifestations, characterized by diagonal cracks and clear signs of differential settlement, were predominantly concentrated in the upper part of the site, affecting the main suite, the kitchen, the area near the swimming pool, and the side wall adjoining these spaces.

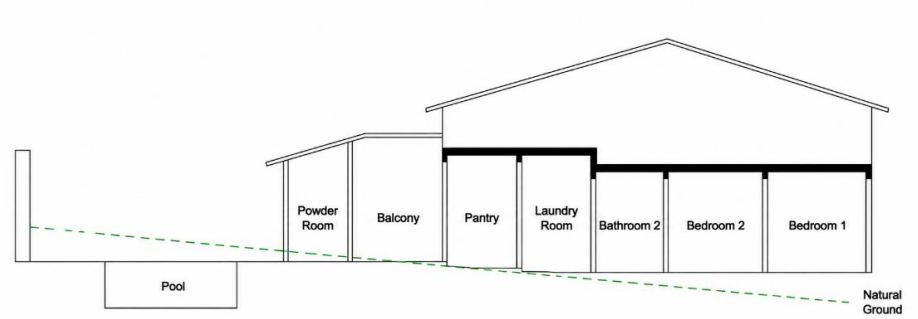


Figure 3 - Cross Section of the Building.

This spatial distribution of the cracks suggests that the instability mechanism is not limited to the densification of the fill material, but rather involves differential movements within the natural ground itself. Visual analysis indicates that the foundation at the higher elevation may not have a bearing capacity compatible with moisture variations and the local stresses imposed by the wall, resulting in loss of support that is expressed as vertical displacements, that is, differential settlement, and in the development of the observed pathological manifestations from the side wall to the interior of the residence.

The mapping of the cracks identified in the plan shown in Figure 4 made it possible to correlate the location of the anomalies with the different ground levels and structural elements. This analysis is essential for identifying the compartments most susceptible to stress variations and differential settlement.

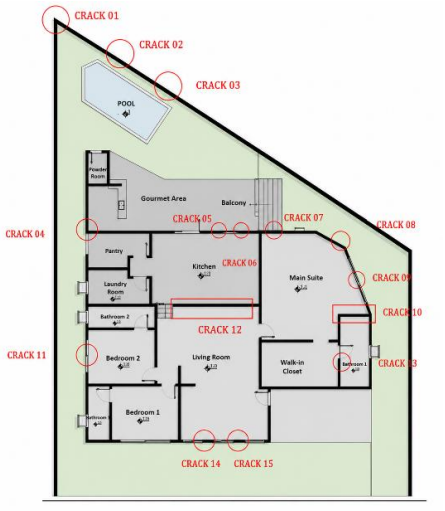


Figure 4 - Mapping of the Identified Cracks

2.1. Perpendicular Bisector Method

For data analysis and confirmation of active differential settlement, Berberian's Perpendicular Bisector Rule was applied to the mapping of the identified diagonal and horizontal cracks. This method consists of a widely used technique for identifying the agent or mechanism responsible for the appearance of cracks in building elements. The technique consists of drawing lines perpendicular to the axis of the diagonal cracks identified during the inspection. Since these openings occur perpendicular to tensile stresses, the convergence of the traced lines directly indicates the support point that underwent the greatest vertical displacement, as shown in Figure 5 (Quirino, 2023; Silva, 2019).

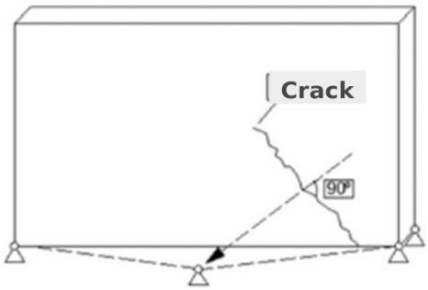


Figure 5 - Perpendicular Bisector Method (Source: Silva & Rodrigues, 2019).

To illustrate the application of Berberian's Perpendicular Bisector Rule to the present case study, Figure 6 shows the projection of the perpendicular bisector from a representative diagonal crack identified during the inspection. The same procedure was subsequently applied to all representative diagonal cracks, and the convergence of the projected lines enabled the identification of the three differential settlement zones presented in Figure 7.

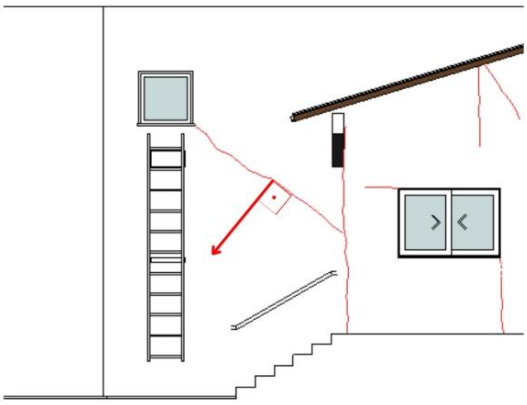


Figure 6 - Application of Berberian's Perpendicular Bisector Rule

3. Diagnostic Analysis and Proposed Rehabilitation Strategy

The application of the Perpendicular Bisector Rule (Silva, 2019) to the mapped cracks made it possible to isolate the geotechnical origin of the structural movements. By projecting orthogonal lines perpendicular to the axis of each diagonal crack, a convergence of vectors was obtained, pointing to three critical points of vertical displacement: the external corner of the kitchen, the end of the suite, and the angular section of the perimeter wall. This geometric triangulation confirms that the differential settlement is not widespread, but

rather concentrated at specific foundation points where there is a transition in levels or a variation in the bearing capacity of the natural ground, as shown in Figure 7.



Figure 7 - Mapping of the Observed Differential Settlements.

During the inspection, the measured crack openings ranged from 0.3 mm to 1.80 mm, with the largest openings observed in the kitchen corner and in the main suite. Most of the observed cracks exhibited a diagonal orientation, which is consistent with differential settlement mechanisms. Representative examples are presented in Figures 8, 9 and 10.

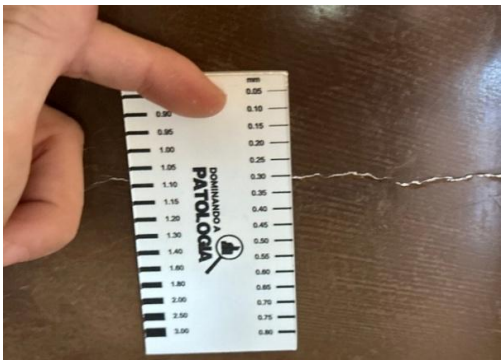


Figure 8 - Crack (opening = 0.30 mm)



Figure 9 – Diagonal crack (opening = 1.80 mm)



Figure 10 - Diagonal crack observed in the kitchen corner

3.1. Proposed Therapy – Mega Piles

Given the diagnosis of differential settlement concentrated in transition zones and in the elevated portion founded on natural ground, foundation underpinning using the Mega Pile technique was proposed. Mega piles, also known as reaction piles or jacked piles, differ from other driven piles because they are installed statically through the reaction force generated by a hydraulic jack acting against a reaction frame or against the existing structure itself, provided that the structure can withstand the applied loads (Teixeira et al., 2020). The selection of this intervention is justified by the nature of the identified problem, since the technique allows direct control of the applied load through manometric readings and can be executed in confined spaces. This is essential for the rapid stabilization of structures at risk, without the need for additional deformations for the underpinning system to begin carrying load effectively.

According to ABNT NBR 6122:2022, reaction piles, referred to as mega piles or jacked piles, consist of concrete or steel elements introduced into the ground by means of a hydraulic jack reacting against a pre-existing structure or against a structure specifically created for that purpose. The installation of each segment proceeds until one of the following limits is reached: the reaction capacity of the structure itself, when it begins to show signs of uplift, cracking, or deformation; the structural limit of the pile, corresponding to the maximum resistance of the steel or concrete element; or the resistance of the soil, when the element reaches a sufficiently stiff layer capable of preventing further penetration.

According to ABNT NBR 6122:2022, Annex Q (normative), item Q.4, the jacking and wedging loads for reaction piles must be specified in design and shall be at least 1.5 times the working load. In the context of underpinning existing structures, the working load at each intervention point is not predetermined by theoretical calculation, but is defined during execution by the actual reaction capacity of the building, monitored continuously through manometric readings until structural response signs such as uplift, cracking, or deformation are observed. The wedging load is subsequently applied in accordance with item Q.4, respecting the structural limits identified during jacking. This empirical load control procedure is inherent to the mega pile technique when applied to existing buildings and does not exempt the intervention from compliance with the normative requirements of ABNT NBR 6122:2022.

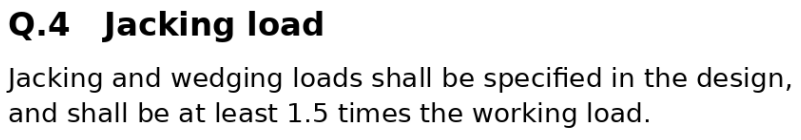


Figure 11 - Jacking Load (ABNT, adapted by the author).

The use of mega piles is therefore intended to stabilize the settlement observed in the existing foundation, redistribute stresses to levels compatible with the bearing capacity of both the soil and the structure, provide additional and immediate support, mitigate differential displacements, and eliminate or reduce the progression of cracks and deformations, thereby restoring the load-bearing capacity of the foundation and extending the building's service life. Prior to any intervention, SPT or CPTu soundings are strongly recommended in the vicinity of the affected areas in order to determine the depth required for pile support and to characterize the competent bearing strata of the subsoil. In the case study presented herein, such geotechnical investigations were not carried out, which constitutes a limitation of the present study. Their execution prior to the proposed intervention is considered essential for the accurate design and safe implementation of the mega pile underpinning.

Should the proposed intervention be carried out, the execution procedure is recommended to follow the stages described below, based on established practice for mega pile underpinning:

3.1.1. Area preparation and excavation of the working pit

Initially, the pile installation point is defined according to the structural analysis. Next, a pit approximately 1.0 m × 1.0 m is manually excavated to a depth of about 1.0 m below the support base of the structure, thereby ensuring safe shoring conditions and adequate access for the crew. Finally, the bearing surface is cleaned and leveled to allow the proper positioning of the hydraulic jack.

3.1.2. Installation of the reaction system

The hydraulic jack is positioned against the grade beam, footing block, or previously assessed structural element. The hydraulic power unit, equipped with a calibrated pressure gauge, is then installed, allowing accurate pressure readings during the operation. Before jacking begins, the vertical alignment of the equipment is adjusted in order to ensure the proper insertion of the segments into the ground.

3.1.3. Installation of the segments (repetitive procedure)

Segment installation consists of a repetitive procedure in which the initial segment, whether a concrete pipe or a threaded steel tube, is first positioned, after which the hydraulic jack is activated, thereby driving the segment into the ground by reaction. The maximum pressure recorded on the gauge is immediately converted into the corresponding applied load (tf), while the structural response is continuously monitored by observing any local uplift, opening or closing of cracks, audible structural responses, and deformations in the supporting beams. Once the maximum stroke is reached, the equipment is retracted and a new segment is coupled, either by direct bearing in the case of concrete, or by threading in the case of the steel tube, and the process is repeated until one of the termination criteria is met: unacceptable structural reaction, maximum system capacity, or refusal due to soil resistance.

For determining the loads involved in the process, it is necessary to understand the operating principle of mega piles, which is based on the interaction of three main components: the hydraulic jack, whose piston has a given area (A) and is responsible for applying the force (F); the hydraulic power unit, which functions as a pump that delivers pressurized oil to the jack; and the pressure gauge, which measures the oil pressure (p) and, consequently, allows the determination of the force applied to the system.

The force applied during installation is obtained from Equation (1) below, in which F represents the force, p the pressure measured by the gauge, and A the internal area of the hydraulic jack piston.

$$F = p \times A \tag{1}$$

This equation allows the load applied to the pile at each stage of installation to be accurately determined. Each segment is jacked into the ground until a predefined pressure limit is reached, at which point the jack is retracted and a new segment is added, with the cycle repeated as many times as necessary. In this way, the pile is progressively built from the bottom up, using the existing structure itself as the reaction system.

3.1.4. Determination of the final pile load

The final pile load corresponds to the value recorded during the last jacking cycle prior to reaching the limit imposed by the structure, the soil, or the pile itself. This value represents the actual and effective capacity of the element at that specific intervention point and is used as the basis for determining the total number of piles required for foundation underpinning.

3.1.5. Wedging and preloading

Wedging is the stage that ensures the effective transfer of load from the structure to the mega pile after jacking. It is the process that brings the pile into an active load-bearing condition, allowing it to contribute

immediately to structural support. Proper execution of wedging is essential because it distinguishes the behavior of mega piles from that of other foundation strengthening techniques that depend on additional settlement to mobilize their bearing capacity.

3.1.5.1. Load transfer and level adjustment

After jacking, the hydraulic jack may be used to apply a controlled preload in order to ensure firm contact between the structure and the pile and to correct minor level differences, whenever technically feasible and safe, thereby promoting partial crack closure and stabilization of the structural condition. This adjustment must always be limited and carefully monitored in order to avoid overloading the existing structure.

3.1.5.2. Installation of the head block

Once the final load achieved during jacking has been established, the head block is installed. It may be precast or cast in place using concrete with strength compatible with the applied demands, serving as the intermediate element between the pile and the structural support point.

3.1.5.3. Repositioning of the jack and application of the preload

With the head block in place, the hydraulic jack is positioned once again between the top of the pile and the underside of the head block, making it possible to apply the preload required for final locking. This load, which is lower than the maximum jacking load, is intended to ensure continuous and firm contact between the pile and the structure, guarantee that the pile enters an active load-bearing condition without depending on subsequent settlements, stabilize residual deformations prior to locking, and allow fine level adjustment whenever applicable. The value of this load must be compatible with the local structural capacity and with the behavior observed during jacking.

3.1.5.4. Locking with wedges

With the load applied, locking is carried out by means of steel wedges placed on either side of the jack or between the top of the pile and the head block, depending on the system adopted. The wedges prevent load release after the jack is removed, ensure the immediate transfer of forces to the pile, and maintain the stability of the assembly until the infill materials have fully cured.

3.1.5.5. Final wedging and completion of the head block

After the initial locking, final wedging of the space between the top of the pile and the original foundation or intermediate structural element is carried out. The most commonly used methods include constructing the head block in high-strength reinforced concrete, using bearing pieces, steel wedges, and final concreting to ensure composite action, which is the traditional procedure widely adopted in underpinning with mega piles, or injecting microconcrete, structural mortar, or high-strength grout in order to ensure full bonding and continuity of load transfer. Finally, the jack is removed under controlled gradual release, the load remains active in the system, and the pile immediately begins to act as a load-bearing element, thereby confirming the effectiveness of the wedging process and the stability of the assembly.

3.1.6. Injection, when applicable:

When applicable to steel mega piles or concrete mega piles using injection techniques, cement grout is introduced through the interior of the pile after jacking, ensuring that the grout exits through the tip and is distributed along the shaft. During the process, the injected volume, pressure, and return behavior are recorded, and curing is then allowed in accordance with the technical specification.

3.1.7. Structural reconditioning and monitoring

Once the installation of all piles has been completed, settlement stabilization should be verified and cracks and levels monitored for a minimum period of 30 days after underpinning. The necessary structural repairs should then be carried out, including masonry, beams, and finishes, concluding with the issuance of a technical compliance report after stabilization has been confirmed. It is noted that the execution of this intervention and the subsequent monitoring fall outside the scope of the present study, and their documentation is recommended as the subject of future work.

Figures 12 to 15 below illustrate the execution process of the mega pile system:



Figure 12 - Installation of the Hydraulic Jack. Source: Reproduced from the Geotecnia Brasil YouTube channel (2022).



Figure 13 - Hydraulic Jack Head Block.Source: Reproduced from the Geotecnia Brasil YouTube channel (2022).



Figure 14 - Locking of the Wedging System Using Steel Wedges. Source: Reproduced from the Geotecnia Brasil YouTube channel (2022).



Figure 15 - Structural Reconditioning and Post-Intervention Monitoring. Source: Reproduced from the Geotecnia Brasil YouTube channel (2022).

The mega pile solution is technically well suited to settlement-related problems, as it acts directly beneath the existing structure and provides immediate load-bearing capacity after wedging, with a level of load control that is distinctive among foundation methods. In addition, it eliminates the need for deep excavations, extensive drilling, or vibration, and can be executed even under extremely restricted access conditions, making it a safe and effective solution for emergency stabilization and structural rehabilitation.

4. Conclusions

The present study demonstrated that the application of Berberian's Perpendicular Bisector Rule to a real case of active differential settlement was considered an effective and practical diagnostic tool. By mapping the observed fissures and projecting orthogonal lines to their axes, it was possible to precisely identify three critical points of vertical displacement, located at the external corner of the kitchen, the end of the suite, and the angular section of the perimeter wall, all concentrated in the highest portion of the site over natural ground. This geometric method allowed the diagnosis to be grounded in the observed pattern of structural distress rather than in assumptions, which is particularly relevant in contexts where geotechnical investigation documents and structural drawings are unavailable, as was the case in this study.

The case also revealed important lessons regarding the conditions that led to the pathological manifestations. The absence of prior geotechnical investigation, the presence of fill placed without adequate quality control, and the heterogeneity of the natural ground were identified as the primary factors responsible for the differential settlement. Furthermore, the ineffectiveness of the superficial corrective measures previously adopted, such as metallic stitching, reinforces that surface-level interventions are insufficient when the root cause lies in foundation instability. These findings serve as a practical warning for professionals involved in small-scale residential construction, where geotechnical investigation is frequently omitted.

Based on the diagnosis, foundation underpinning with Mega Piles was proposed as the recommended intervention. This technique presents itself as technically suitable for the case studied, given its capacity for direct load control through manometric readings, its compatibility with restricted-access conditions, and its ability to provide immediate load-bearing capacity after wedging without requiring additional settlements. The proposed approach is based on the guidelines of ABNT NBR 6122:2022 and geotechnical stabilization is identified as an indispensable prerequisite for any subsequent structural rehabilitation. The execution of the proposed intervention and its monitoring fall outside the scope of the present study, and their documentation is recommended as the subject of future work.

References

[1] ASSOCIAÇÃO BRASILEIRA DE NORMAS TÉCNICAS. ABNT NBR 6.122:2022: Projeto e execução de fundações. 1 ed. Rio de Janeiro: ABNT, 2022.

[2] CINTRA, J. C. A.; AOKI, N.; ALBIERO, J. H. Fundações diretas: projeto geotécnico. São Paulo, Oficina de Textos, 2011.

[3] GEOTECNIA BRASIL Estaca Mega Prática Atual e Desafios de Execução YouTube 3 novembro 2022 Disponível em https://www.youtube.com/watch?v=E4p-nLPCUOg Acesso em 15 abril 2026

[4] MEDEIROS, M. H. F.; ANDRADE, J. J. O.; HELENE, P. Durabilidade e vida útil das estruturas de concreto. In: ISAIA, G. C. (org.). Concreto: Ciência e Tecnologia. 1. ed. v. 2. São Paulo: IBRACON, 2011. Cap. 22.

[5] MILITITSKY, Jarbas; CONSOLI, Nilo César; SCHNAID, Fernando. Patologia das Fundações. 2. ed. São Paulo: Oficina de Textos, 2005.

[6] QUIRINO, J. R. A. et al. Regra da mediatriz para a elucidação de patologias nas edificações. Revista FT, v. 27, n. 128, nov. 2023. DOI: 10.5281/zenodo.10183224.

[7] Ribeiro, Julia Cândido, Ana Carolina Pereira de Oliveira, e Claudio Bonfante de Oliveira. 2023. “ANÁLISE E PROJETO DE FUNDAÇÕES E SUA IMPORTÂNCIA PARA SEGURANÇA E ECONOMIA NAS OBRAS: ESTRATÉGIAS AVANÇADAS DE ANÁLISE E PROJETO DE FUNDAÇÕES”. Revista Ibero-Americana De Humanidades, Ciências E Educação 9 (11):2612-50. https://doi.org/10.51891/rease.v9i11.11969.

[8] SANTOS, Rômulo Bernardo. Construção civil e economia brasileira: potencialidades e evolução do mercado de trabalho do setor nos anos recentes. 2020. 132 f. Dissertação (Mestrado Acadêmico em Economia) - Faculdade de Economia, Universidade Federal Fluminense, Niterói, 2020.

[9] SILVA, Daniel Rodrigues da; RODRIGUES, Fernando Teixeira Leite. Patologias em estruturas de concreto: estudo de caso em uma instituição pública de ensino. 2019. 72 p. Trabalho de Conclusão de Curso (Bacharel em Engenharia Civil) – UniEvangélica, Anápolis, 2019. Disponível em: http://repositorio.aee.edu.br/bitstream/aee/8696/1/Daniel%20Rodrigues%20e%20Fernando%20Teixeira.pdf. Acesso em: 20 mar. 2026.

[10] TEIXEIRA, André Tavares et al. Análise de reforço de fundação com estaca mega metálica. 2020. Trabalho de Conclusão de Curso (Graduação em Engenharia Civil) – Universidade Presbiteriana Mackenzie, São Paulo, 2020.

[11] UNITED NATIONS HUMAN SETTLEMENTS PROGRAMME (UN-Habitat). Housing. Nairobi: UN-Habitat, 2023. Disponível em: https://unhabitat.org/topic/housing. Acesso em: 20 mar. 2026.

Cinpar 2026
XXII International Conference on Building Pathology and Constructions Repair
15th to 17th July 2026 - Lisboa, Portugal

Systematic cataloging of information for the semantic enrichment of the HBIM model of the Almofala Church.

Guilherme L. DE OLIVEIRA[1], José L. G. MENDES[2], Carlos E. M. DE SOUSA[3], Renan N. PAULO[4], Jesus E. M. MACHADO[5], Davi RAMALHO[6],**Esequiel F. T. MESQUITA[7]**

[1] Federal University of Ceará, Fortaleza - CE, Brazil, guilhermeoliveira@arquitetura.ufc.br

[2]Federal University of Ceará, Fortaleza - CE, Brazil, lucasmendes@arquitetura.ufc.br

[3]Federal University of Ceará, Fortaleza - CE, Brazil,eugeniomoreira@iaud.ufc.br

[4] Federal University of Ceará, Fortaleza - CE, Brazil, renanpaulo2712@gmail.com

[5] Federal University of Ceará, Fortaleza - CE, Brazil, enzomachado16@gmail.com

[6] Federal University of Ceará, Fortaleza - CE, Brazil, daviramalho@arquitetura.ufc.br

[7] Federal University of Ceará, Fortaleza - CE, Brazil, emesquita@ufc.br

Summary: The preservation and management of built cultural heritage require documentation strategies that integrate construction data, historical information, and essential data for preventive conservation and continuous monitoring. In this context, Heritage Building Information Modeling (HBIM) emerges, aiming to transpose the Building Information Modeling methodology to the context of historical assets, allowing the creation of digital representations that unify geometry with its semantic database. However, it is common for digital models to still emphasize only geometric information while dissociating technical information, resulting in visually accurate but semantically empty models. In this context, this study focuses on the Church of Our Lady of the Conception of Almofala, a historical heritage site in Ceará state listed by IPHAN (National Institute of Historic and Artistic Heritage), which, despite its relevance, lacks systematized technical records capable of supporting future restoration interventions. Therefore, this work aims to collect, identify, and categorize historical and constructive information necessary for the semantic enrichment of the future HBIM model of the building, using forms developed within the Documenta-CE project, specifically designed for cataloging heritage attributes. To this end, a bibliographic review of vernacular techniques applied in the region and the mechanical properties of the materials used was conducted. Following this, a technical visit to the church was carried out to collect visual and material information, which was then used to complete the technical form. As a result, a hierarchical and categorized database was created according to BIM standards, to be applied in future HBIM models of the church. Finally, this work attests to the applicability of the developed form in the collection and cataloging of heritage information, while contributing to the preservation and management of Ceará's built heritage.

1. Introduction

The safeguarding of historical built heritage demands, in contemporary engineering and architecture, a methodological transition from purely reactive interventions to preventive conservation strategies. For the diagnosis of structural vulnerabilities and the mitigation of pathological processes to be effective, the consolidation of geometric, historical, and physicochemical data in a centralized, auditable, and continuously updatable technical repository is imperative (Lourenço 2006; ICOMOS 2017).

In this context, Heritage Building Information Modeling (HBIM) has established itself as the main technological response in the sector, proposing the adaptation of Building Information Modeling (BIM) principles to the complexities of pre-existing structures (Murphy, McGovern, and Pavia 2009). However, the specialized literature points to a recurring methodological mismatch in the practice of heritage digitization: driven by advances in reality capture sensors (such as laser scanning and aerial photogrammetry), projects often restrict themselves to geometric hyper-representation. This methodological asymmetry generates three-dimensional models with high visual precision, but which are

"semantically empty," lacking essential non-geometric parameters—such as the stratigraphy of materials, the mapping of degradations, and the mechanical properties of the substrate. This deficiency makes it impossible to fully utilize these tools for structural simulations and for managing the life cycle of buildings (Bruno et al. 2018; Pocobelli et al. 2018).

Overcoming this informational gap proves particularly critical in the context of vernacular architecture, whose construction systems are highly susceptible to harsh microclimates. The Church of Our Lady of the Conception of Almofala, a heritage site listed by the National Institute of Historic and Artistic Heritage (IPHAN) on the coast of Ceará, is a paradigmatic case. Subjected to a prolonged historical process of burial by shifting dunes, the building embodies a complex pathological condition (marked by intense salt crystallization and capillary rise) that requires much more than visual records to support future rehabilitation projects.

Given this analytical and documentary gap, this research aims to propose and apply a methodological protocol for the systematic collection and categorization of constructive and pathological attributes aimed at semantic enrichment in HBIM (Historical Building Information Modeling). Through the implementation of Characterization Sheets developed within the Documenta-CE project, the study establishes a workflow that converts field technical inspection into a relational and parameterizable database. By structuring this information under an object-oriented architecture (compatible with BIM platforms), this work aims to demonstrate the feasibility of providing digital models with the informational rigor required by diagnostic engineering, directly contributing to the safeguarding of Ceará's historical heritage.

2. The Role of HBIM in Structural Conservation

2.1. Semantic enrichment and pathology management:

The BIM model, by definition, transcends traditional graphic representation by integrating parametric information into each of its virtual elements. In the context of built heritage (HBIM), the process of inserting non-geometric data is known as semantic enrichment. This procedure consists of linking specific metadata—such as the physical-chemical properties of materials, history of interventions, state of conservation, and levels of degradation—to the three-dimensional components of the model (Brumana et al. 2018).

For rehabilitation engineering and restoration architecture, this parameterization is a determining factor for the success of structural damage diagnosis. Traditionally, the mapping of pathologies (such as cracks, mortar disintegration, and rising damp) is carried out in a two-dimensional way or in decentralized textual reports, which hinders spatial visualization and systemic understanding of degradation (Bruno et al. 2018). By incorporating this data directly into the HBIM model, professionals have a unified and three-dimensional environment for pathology management.

Semantic enrichment allows, for example, a finite element model (FEM) for structural simulation to be fed with the real properties of degraded materials, extracted directly from the BIM database (Oreni et al. 2014). Furthermore, the systematic categorization of pathological manifestations in the virtual environment enables advanced spatial analyses, such as the identification of fault propagation patterns and the correlation between structural damage and external agents.

In this way, the insertion of non-geometric data transforms HBIM from a simple static repository into an active management tool. It begins to act as a digital twin (digital twin) focused on preventive conservation, allowing technical teams to perform scenario simulations, plan interventions with greater precision, and monitor the behavior of the structure throughout its life cycle (Pocobelli et al. 2018).

2.2. Vernacular techniques and regional materials:

Colonial and vernacular-influenced architecture is often characterized by the use of self-supporting mixed masonry and historical lime and sand-based mortars. Understanding the mix and mechanical behavior of these traditional mortars is the first step for any compatible intervention. The introduction of Portland cement in historical masonry restorations, for example, can accelerate degradation processes due to the incompatibility of stiffness and permeability (Veiga 2017).

For diagnostic engineering, the analysis of monuments located in coastal microclimates requires an understanding of aggressive vulnerabilities, which combine high salinity, abrasion, and humidity. Established conservation literature demonstrates that capillary rise combined with contamination by marine chlorides and sulfates is one of the main causes of collapse in historical masonry (Goudie and Viles 1997). The crystallization and hydration cycles of these salts within the pores (cryptoflorescence) generate expansive mechanical stresses that exceed the tensile strength of mortars and bricks, resulting in powdery disintegration and severe loss of resistant section over time (Scherer 2004; Binda, Saisi and Tiraboschi 2000).

In the context of advanced digital documentation, historical buildings present additional technical and methodological challenges. Traditional surfaces, such as those coated with whitewash, exhibit high albedo and high reflectance. Studies indicate that excessively light or reflective surfaces can scatter the light beam.*Laser Scanner*(TLS), generating noise in the point cloud or data gaps (*data voids*) that require hybrid capture strategies integrated with photogrammetry (Hichri et al. 2013).

In this sense, the semantic enrichment of HBIM models transcends the aesthetic register. By parameterizing physical properties (such as porosity and compressive strength) and mapping weathering damage directly onto BIM objects, a vital information model is created for seismic or gravitational vulnerability assessments. The insertion of this non-geometric data into the virtual environment is what allows the transition from a simple 3D model to a digital twin capable of feeding finite element (FEM) simulations and guiding precise structural reinforcement designs (Angelini et al. 2017).

3. Acquisition and Cataloging Methodology

3.1. Methodological Protocol for On-Site Data Acquisition

To ensure that the three-dimensional model (HBIM) transcends mere aesthetic representation and is effectively applicable to diagnostic engineering, it was necessary to establish a rigorous reality capture protocol. The methodology developed by the Documenta-CE project team aims to standardize the pre-field, multisensor acquisition, and information organization stages, ensuring the technical reliability and traceability of the collected data for subsequent geometric and semantic modeling.

The core of this protocol is based on a hybrid digitization strategy, combining active and passive surveying techniques to overcome the individual operational limitations of each piece of equipment. Laser Scanning (Terrestrial - TLS and Mobile - SLAM) is employed as the primary method for obtaining millimeter-precision point clouds of internal surfaces and facades accessible at ground level. Simultaneously, Digital Photogrammetry, performed with the support of Unmanned Aerial Vehicles (UAVs), is applied for mapping roofs, inaccessible vertical elements, and for capturing high-resolution photorealistic textures. Data fusion is essential in structural diagnosis, as it eliminates traditional shadow zones and spatial gaps (data voids), resulting in a continuous and metrically reliable digital skeleton of the building.

Beyond spatial capture, the protocol innovates by requiring the simultaneous structuring of non-geometric documentation directly on the construction site. During laser scanning, the technical team performs a rigorous visual and tactile inspection, based on standardized survey forms. At this stage, the construction typologies are identified, cracking patterns are mapped, the level of degradation of historical mortars is recorded, and pathological manifestations are noted, such as areas affected by moisture or salt crystallization.

Finally, the methodology establishes the mandatory registration of metadata and paradata (detailed information about the data acquisition and processing process). The developed protocol requires the systematic recording of specifications and calibrations of the equipment used, environmental lighting conditions, and grid density profiles at the time of on-site operation. For conservation engineering, this archival rigor ensures that the generated point cloud and the future HBIM model are not interpreted as mere static visual products, but rather as traceable, scientifically reproducible databases capable of supporting structural analyses with perfectly known and documented margins of error..

3.2. Structuring and systematic approach to the attribute characterization form

The digitization of built heritage has historically faced the structural challenge of the "semantic void": the generation of highly precise three-dimensional geometric models that, however, lack data on the materiality, history, and structural degradation embedded in their components. Assuming the mitigation of this semantic void as the fundamental element for defining our protocol, the on-site inspection stage was implemented through the application of HBIMPath (Magalhães et al. 2025). This is a characterization form specifically designed to address the ontology of Ceará's built heritage.

The logical structure of this tool transcends purely descriptive functionality, being based on an object-oriented data architecture designed to fill informational gaps. This premise ensures direct compatibility with the hierarchy of classes and families inherent in parametric modeling platforms (such as Revit and Archicad).

The documentary protocol organizes data acquisition into constructive macro-categories (masonry, window and door frames, and structural elements, among others), as illustrated in Figure 2, proceeding to the decomposition of each architectural component into three systematic informational dimensions created to address the shortcomings of the digital model:

1. Stratigraphic Decomposition: In contrast to traditional two-dimensional documentation—which often conceives of sealing elements in a monolithic way—this instrument requires detailed discrimination of the constituent layers (structural core, successive mortar substrates, and finishing coatings). By feeding the geometric model with this stratification, the internal data gap is filled, which proves imperative for rehabilitation engineering, as it enables the association of mechanical properties and specific degradation states to each stratum. Consequently, the detection of physical-chemical incompatibilities between vernacular materials and subsequent contemporary interventions is optimized.
2. Morphological and Aesthetic Parameterization: To combat the absence of computable properties, the form promotes the conversion of qualitative attributes into classificatory and quantifiable data. This processing encompasses the detailing of articulation mechanisms, sealing typologies, and the exhaustive cataloging of finishes (textures, reflectance indices, and standardized colorimetry systems, such as Pantone and RGB). The insertion of this metadata ensures that the HBIM model achieves a high Level of Information (LOI), an indispensable criterion for scientific restoration projects that require rigor in chromatic and textural reintegration.
3. Traceability and Metadata Anchoring: The definitive mitigation of the semantic void requires that textual information be intrinsically tied to spatial geometry. The document establishes the "Final Modeling Code," functionally operating as a globally unique identifier (GUID). This code establishes a one-to-one relationship between the inspected physical element and its respective digital representative in the model. Additionally, the form includes variables for the insertion of paradata, encompassing correlation with historical documentary sources, geometric detail sketches, and the mandatory verification of the associated photographic collection.

2 FLOOR SPECIFICATIONS				
2.1 Floor Identification				
Final Modeling Code				
Attachment No.:				
Layers	Identification	Thickness	Materials	Composition
Structure				
Substrate 1				
Substrate 1				
Finish 1				
Finish 2				
FINISHES				
Finish pattern	☐	Smooth	☐	Stencil
	☐	Stencil		
Surface finish	☐	Matte	☐	Semi-Gloss
	☐	Satin	☐	Glossy
Ornamentation level of the finish layer	☐	Low	☐	High
	☐	Medium		
Number of colors present	☐	1	☐	3
	☐	2	☐	Polychromatic
Color system	☐	Pantone	☐	CMYK
	☐	RGB	☐	Hexadeciamal
Application of diverse ornaments	☐	YES	☐	NO
ADDITIONAL DATA				
Is there historical documentation?	☐	YES	☐	NO
If yes, describe the applied ornament (material, ornamentation level, functionality). Were the mandatory photographic records taken?				
Were the mandatory photographic records taken?	☐	YES	☐	NO
Attachment No.:				
Observations:				

Figure 1– Systematic approach to in-situ data collection via the HBIMPath protocol: parameterization of morphological, stratigraphic, and structured degradation attributes for integration into parametric models (HBIM).

In summary, HBIMPath structures its informational dimensions in such a way that combating the "semantic void," which represents the greatest methodological challenge in digital preservation—since models limited to geometric hyper-representation act as inert visual shells that induce diagnostic paralysis—acts as the generating principle of the entire survey, converting the subjectivity inherent in empirical visual inspections into a relational and structured database. Thus, the characterization form is consolidated as the exact translation protocol between the materiality of historical buildings and the digital interface, providing the necessary data infrastructure for future structural behavior simulations and for the optimized lifecycle management of built heritage.

4. Results

4.1. On-site survey and data collection

The practical application of the methodological protocol at the Almofala Church occurred through a field campaign that integrated high-precision geometric capture with systematic technical inspection. Documenting this monument required specific strategies due to its unique material and environmental conditions: the building bears the physical marks of its history of being buried by mobile dunes (between 1897 and the 1940s) and features facades entirely covered in whitewash, whose high albedo effect challenges the reading of laser and photogrammetric sensors (Figure 1). To overcome this complexity, the acquisition process was subdivided into two simultaneous and complementary fronts: three-dimensional digital reconstruction and semantic cataloging of constructive attributes.

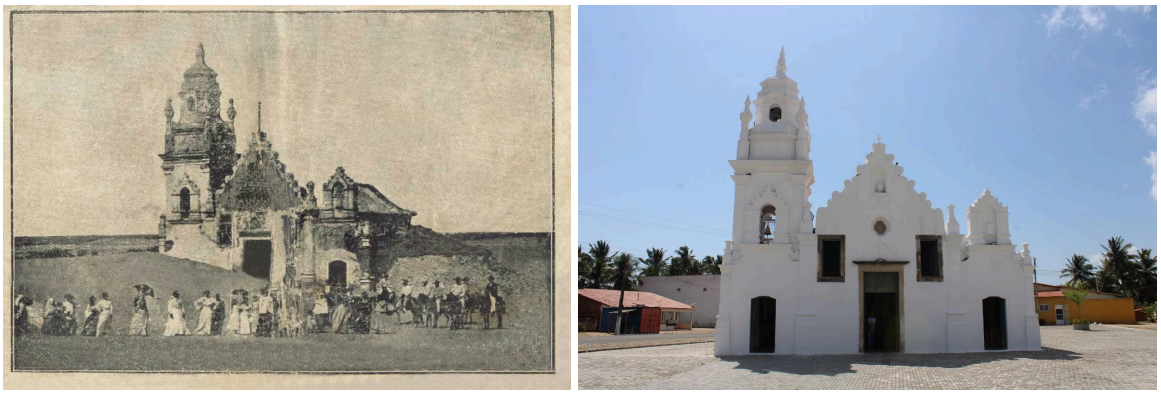


Figure 2– Church of Our Lady of the Conception of Almofala: (a) Historical record of burial by shifting dunes; (b) Current view highlighting the high-albedo whitewash.

4.1.1. Three-Dimensional Geometric Survey

The geometry capture followed a data fusion strategy. For mapping the internal surfaces and facades at ground level, Terrestrial Laser Scanning (TLS) and SLAM (Simultaneous Localization and Mapping) technology were used. The use of the Leica BLK2GO sensor allowed for agile navigation through the interior of the nave and sacristy in journeys of approximately 15 minutes, ensuring the continuity of the point cloud in spaces with complex geometry. Complementarily, the Leica BLK360 static sensor was positioned at 26 strategic stations to ensure maximum density in areas with a high level of ornamental detail, such as the main altar.

PFor the documentation of the roof and upper areas of the bell tower—historically inaccessible areas prone to data voids—aerial photogrammetry was employed using the DJI Mavic 3T Enterprise model. The flight plan (with approximate durations of 30 minutes) followed an 80% overlap pattern and generated a total of 470 images from converging nadir and orbital trajectories. These images were essential for generating high-resolution orthophotos that supported texture mapping and the visual identification of cracks and pathologies in the ceramic tile and the tower's crowning.

Processing the ground scans (26 TLS stations and 2 SLAM paths) in Leica Cyclone REGISTER 360 software resulted in a unified point cloud with an average overlap of 69%. This consolidated model is composed of approximately 430 million points and has a maximum registration error of 0.003 m (3 mm). Subsequently, global alignment between the laser base and the 288 million vertices generated by photogrammetric processing was performed in the CloudCompare environment, resulting in a single, gap-free geometric product (Figure 3).

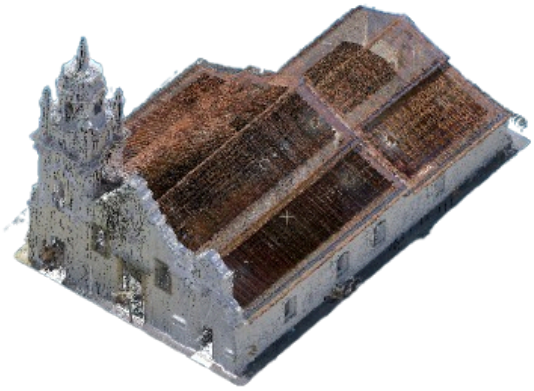


Figure 3 -Unified point cloud resulting from multisensor integration (UAV and TLS), demonstrating the suppression of spatial gaps in global volumetry.

4.1.2. Semantic Inspection and Cataloging

In parallel with geometric digitization, non-geometric data was collected using the HBIMPath protocol (Magalhães et al. 2025), developed within the scope of the Documenta-CE project.The inspection focused on identifying the constituent layers of the masonry and window and door frames, as well as identifying the main pathologies manifested in these elements (Figure 4), translating physical reality into the logic of BIM objects. Each inspected element received a "Final Modeling Code," ensuring traceability between the real item and its future digital representation.



Figure 4 -Semantic survey of pathological manifestations associated with the marine microclimate: (a) Salt crystallization in mixed masonry; (b) Degradation by wood-boring insects/humidity; (c) Severe oxidation in metallic components.

Semantic data collection prioritized the stratigraphy of materials, identifying lime mortar substrates and different levels of finish. Aesthetic characterization included color measurement using standardized systems (RGB and Pantone), fundamental for recording the whitewash of the church, whose high albedo represents a technical challenge for the calibration of optical sensors. Additionally, the state of conservation of each component was recorded, documenting the presence of saline efflorescence and material disintegration; this data was linked to the record through mandatory photographic records and detailed sketches. This approach ensured that the survey resulted not only in a geometric "shell," but in a structured technical inventory, ready to feed the semantic enrichment of the HBIM model.

4.2. Structuring the semantic database in the HBIM environment

Structuring the collected information*in loco*This constitutes the critical preparatory phase for the future semantic enrichment of the virtual environment. Although three-dimensional geometric modeling (HBIM) has not been completed at the time of publication of this work, the data consolidated in the Characterization Sheets — generated from the processing of more than one hundred high-resolution photographic records and visual inspections — are already fully tabulated to be transposed to parametric software in the form of customized metadata.



Figure 5 -Isometric perspective of the three-dimensional model (HBIM) of the Church of Our Lady of the Conception of Almofala, Ceará.

To ensure interoperability and traceability of information in this pre-modeling stage, the "Final Modeling Code" (e.g., ALV_INT_NAVE_01 for masonry or ESQ_POR_PRINCIPAL_01 for window and door frames) was adopted as the primary key (GUID -*Globally Unique Identifier*This code acts as a one-to-one link, connecting the cataloged physical evidence to its future three-dimensional representation, establishing a rigorous relational data flow, as illustrated in the figure.Figure6.

The semantic cataloging of the masonry of the Almofala Church illustrates the effectiveness of this method. Instead of predicting the modeling of the walls as mere homogeneous solids, the data scope dictates that the future HBIM model be parameterized to reflect the actual stratigraphic decomposition: a core structure of mixed masonry (stone and brick), covered with historical lime-rich mortars and finished with whitewash. From a diagnostic engineering perspective, the pathologies identified in the photographs were organized as future instance attributes of the elements. The schematic record of "rising damp by capillarity" and "saline efflorescence" at the bases of the internal walls unequivocally documents the impact of the history of burial by dunes. Once inserted into the BIM environment, this parameterization will cease to be a textual report, enabling the automatic extraction of quantities (e.g., exact calculation of the area of plaster to be replaced) and the generation of thematic degradation maps.

A similar procedure was applied to the inventory of architectural elements and joinery. The main door of the temple, for example, had its materials (solid wood and wrought iron hardware) and its state of conservation rigorously documented. The planned inclusion of parameters regarding "severe oxidation of the hardware by salt spray" and "mechanical abrasion" by wind agents will computationally translate the material's behavior in the face of the coastal microclimate. Additionally, the preliminary tabulation of aesthetic attributes, such as the color system (e.g., RGB: 242, 240, 235 for whitewash with dirt), already ensures a high Level of Information (LOI), an essential methodological requirement for future studies of chromatic reintegration.

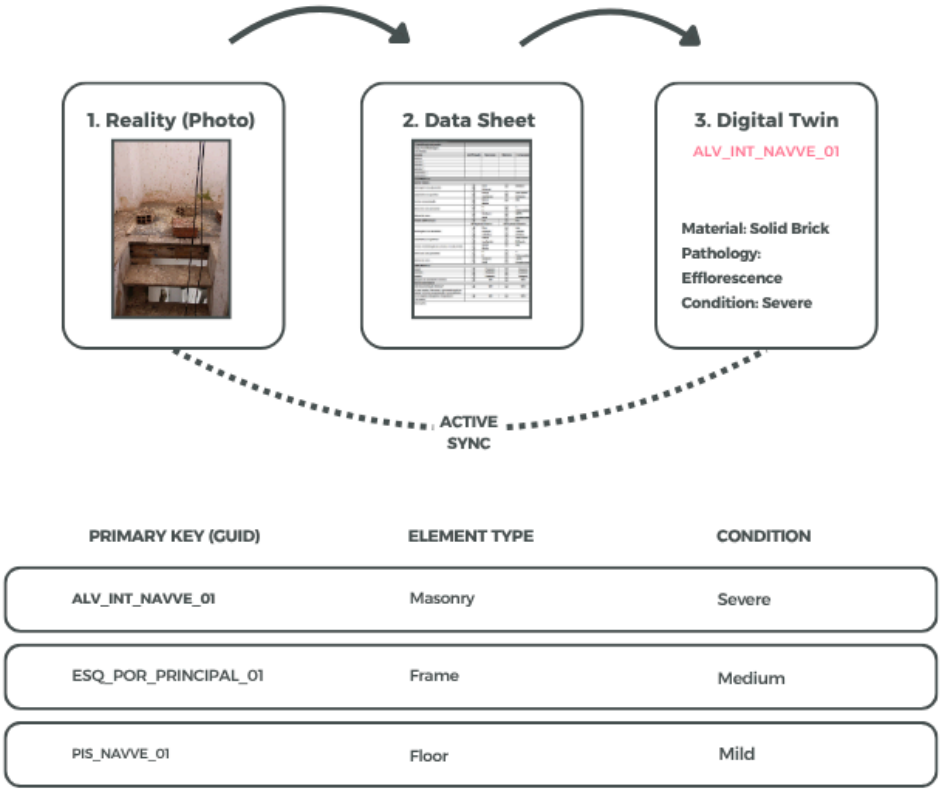


Figure 6– Information transition flowchart: from empirical inspection to the consolidation of the parameterized relational database (GUID) for future application in HBIM.

In this way, the structured semantic database for the Church of Almofala paves the way for the consolidation of an authentic digital twin (*digital twin*By organizing pathological and constructive information in advance under a logical and object-oriented architecture, restoration engineers and architects are provided with the centralized database necessary for the future modeling stage to reach its analytical fullness, enabling the planning of preventive interventions based on quantifiable and historically grounded data.

5. Conclusions

This study demonstrated that the transition from traditional documentation methods to the HBIM (Heritage Building Information Modelling) environment represents a paradigm shift in diagnostic engineering and the conservation of historical heritage. The application of the methodological protocol developed within the scope of the Documenta-CE project, validated at the Church of Our Lady of the Conception of Almofala, proved the technical feasibility of integrating highly accurate reality capture with rigorous semantic cataloging.

For professionals and researchers seeking to replicate this approach in other heritage sites, the study demonstrates that the hybrid digitization strategy does not depend exclusively on a rigid equipment setup, but on a principle of technical complementarity. The integration of laser scanning (either TLS or SLAM) with photogrammetry via UAV constitutes a workflow adaptable to the reality and resources of different teams. This arrangement proved to be the definitive method for suppressing spatial gaps (data voids) and recording the totality of geometric complexity in buildings with accessibility restrictions.

However, the main contribution to methodological replicability lies in the systematization of on-site data collection through Attribute Characterization Sheets (HBIMPath). Replicators can adopt this instrument as

a universal vector for translation between empirical inspection and digital parameterization, regardless of the target BIM modeling platform. By decomposing pre-existing conditions stratigraphically and linking each pathology and material to a Final Modeling Code (GUID), the protocol definitively solves the critical problem of the "semantic void" inherent in traditional point clouds.

From the perspective of structural pathology, the semantic enrichment guided by this method transforms the graphical representation into an active management tool. The documented vulnerabilities—such as the severe degradation due to saline efflorescence in Almofala—feed a relational database that acts as a genuine digital twin. For future architecture and engineering teams, this centralized infrastructure enables the automated extraction of quantities of degraded areas and the precise dimensioning of physically and chemically compatible preventive interventions.

Finally, the results attest to the structuring impact of the support provided by the Chief Scientist of Culture program of the Government of the State of Ceará and the Federal University of Ceará. The workflow validated here transcends the local case study, delivering to the technical-scientific community and public managers a modular, auditable, and high-Level of Information (LOI) methodological protocol. Its systematic adoption by other institutions is the fundamental step for the transition from a merely reactive conservation model to the predictive and continuous safeguarding of Brazilian heritage.

Acknowledgments

The authors express their gratitude to the Government of the State of Ceará and the Ceará Foundation for Support of Scientific and Technological Development (FUNCAP) for the essential support for research through the Chief Scientist of Culture Program. Special thanks are extended to the entire technical and scientific team of the Documenta-CE project, with particular emphasis on the researchers responsible for the preparation of the...*Technical Notebook No. 01 - Reality Capture*(Eugênio Moreira, Renan Nogueira Paulo, Lucas Mendes, Guilherme Lopes de Oliveira, Mylene Melo and Esequiel Mesquita). The methodological rigor established by this team during the digitization campaigns.*in loco*It was the fundamental basis for structuring the semantic database presented in this study.

References

Angelini, Andrea, Corrado Chisari and Antonio Macaluso. 2017. “HBIM for the preservation of a historic infrastructure: The Carlo III bridge of the Carolino Aqueduct.” Applied Geomatics 9(4): 275–288. https://doi.org/10.1007/s12518-017-0196-3

Binda, Luigia, Antonella Saisi e Carmassi Tiraboschi. 2000. “Investigation procedures for the diagnosis of historic masonries.” Construction and Building Materials 14 (4): 199–233. https://doi.org/10.1016/S0950-0618(00)00018-0.

Brumana, Raffaella, Daniela Oreni, Luigi Barazzetti, Fabrizio Banfi, and Mattia Previtali. 2018. “HBIM for the Privilege of Historical Built Environments: From LOD to LOI.” Sensors 18 (3): 900. https://doi.org/10.3390/s18030900.

Bruno, Silvia, N. Bruno, e R. Roncella. 2018. “HBIM for Conservation: A New Proposal for Information Modeling.” Remote Sensing 10 (11): 1751. https://doi.org/10.3390/rs10111751.

Goudie, Andrew S., e Heather A. Viles. 1997. Salt Weathering Hazards. Chichester: John Wiley & Sons.

Hichri, N., C. Stefani, L. De Luca e P. Veron. 2013. “Review of the ‘As-Built’ BIM Approaches.” ISPRS Annals of the Photogrammetry, Remote Sensing and Spatial Information Sciences II-5/W1: 107–112. https://doi.org/10.5194/isprsannals-II-5-W1-107-2013.

ICOMOS. 2017. Principles for the Recording of Monuments, Groups of Buildings and Sites. Paris: International Council on Monuments and Sites.

Lourenço, Paulo B. 2006. “Recommendations for restoration of ancient buildings and the survival of a masonry chimney.” Construction and Building Materials 20 (4): 239–251. https://doi.org/10.1016/j.conbuildmat.2005.08.026.

Murphy, Maurice, Eugene McGovern e Sara Pavia. 2009. “Historic building information modelling (HBIM).” Structural Survey 27 (4): 311–327. https://doi.org/10.1108/02630800910985108.

Oreni, Daniela, Raffaella Brumana, Stefano Della Torre, Fabrizio Banfi, and Luigi Barazzetti. 2014. “Survey turned into HBIM: The restoration and the work involved concerning the Basilica di Collemaggio after the earthquake (L'Aquila).” ISPRS Annals of the Photogrammetry, Remote Sensing and Spatial Information Sciences II-5: 267–273. https://doi.org/10.5194/isprsannals-II-5-267-2014.

Pocobelli, D. P., H. A. Boehm, P. Bryan, J. Hare e J. Kennedy. 2018. “BIM for heritage science: a review.” Heritage Science 6 (1): 30. https://doi.org/10.1186/s40494-018-0191-4.

Scherer, George W. 2004. “Stress from crystallization of salt.” Cement and Concrete Research 34 (9): 1613–1624. https://doi.org/10.1016/j.cemconres.2003.12.034.

Veiga, Rosário. 2017. “Historic mortars: characterization, assessment and repair: A review.” Advances in Materials Science and Engineering 2017: 8183036. https://doi.org/10.1155/2017/8183036.

Magalhães, Brendda Karen Oliveira, Gabriel Souza Duarte, Alice Brasil de Matos Galvão, Ana Cecília Serpa Braga Vasconcelos, and Laís Cristina Barbosa Costa. 2025. "Documentation strategies for parameterization of HBIM models: A case study of the José de Alencar Theater." Digital Applications in Archaeology and Cultural Heritage 38: e00443. https://doi.org/10.1016/j.daach.2025.e00443.

cinpar2026
XXII International Conference on Building Pathology and Constructions Repair
15th to 17th July 2026 - Lisboa, Portugal

Diagnóstico de manifestações patológicas em uma edificação comercial de múltiplos pavimentos: estudo de caso no centro histórico de Porto Alegre

Maria Eduarda da Silva DEMBOGURSKI[1]*, Daniel Thomaz FARINA[1]; José Maria de MOURA JUNIOR[1], Angela Borges MASUERO[1] e Denise DAL MOLIN[1]

[1] Laboratório de materiais e ambiente construído, Universidade Federal do Rio Grande do Sul, Porto Alegre, Brasil, mariae.dembogurski@gmail.com

Abstract: O presente trabalho tem como objetivo identificar e analisar as manifestações patológicas presentes em uma edificação de múltiplos pavimentos localizada no município de Porto Alegre. A inspeção teve por finalidade avaliar as condições técnicas, de uso e de manutenção da edificação, de modo a subsidiar a elaboração de um plano de manutenção e a definição de ações corretivas e preventivas, priorizadas de acordo com o grau de risco associado às anomalias identificadas. A metodologia adotada fundamentou-se na norma básica para perícia de engenharia do IBAPE/SP, abrangendo a definição do nível e do tipo de inspeção, a análise da documentação disponível, a coleta de informações junto ao síndico, o estabelecimento de orientações técnicas, a hierarquização das intervenções e o registro fotográfico das ocorrências. Foram realizadas inspeções visuais em todas as áreas de uso comum da edificação, desde a cobertura das caixas d'água até os subsolos, com a devida caracterização das anomalias e a indicação das recomendações técnicas pertinentes. A priorização das intervenções foi efetuada por meio da adaptação da matriz G.U.T (Gravidade, Urgência e Tendência). Os resultados evidenciam a predominância de fissuras e trincas em paredes e lajes, degradação dos revestimentos de fachadas, bem como a presença recorrente de umidade e bolor, condições estas agravadas pela idade da edificação, pela porosidade dos materiais e pela ausência de manutenção sistemática. Conclui-se que as manifestações patológicas identificadas comprometem o desempenho e a vida útil dos sistemas construtivos, além de afetarem as condições de saúde, segurança e habitabilidade, tornando indispensável a implementação de medidas corretivas conforme as recomendações técnicas apresentadas.

Keywords: inspeção predial, manifestações patológicas, patologia, matriz GUT.

1. Introdução

As manifestações patológicas na construção civil correspondem a um conjunto de anomalias que provocam danos às estruturas, aos elementos não estruturais e de vedação, podendo se manifestar de forma superficial ou profunda (Silva *et al.,* 2023). A degradação das edificações ao longo de sua vida útil está associada a diversos fatores, entre eles: à ação de agentes ambientais, deficiências de projeto, falhas executivas, má qualidade dos materiais ou o emprego inadequado dos mesmos, mudança de finalidade construtiva e à ausência ou inadequação de manutenção (Ferreira; Lobão, 2018; Silva *et al*., 2022). Tais fatores contribuem para o surgimento de manifestações patológicas, as quais comprometem o desempenho, a durabilidade e a segurança das construções. Essas manifestações podem se originar devido as ações externas, como variações térmicas, precipitação e radiação solar, mas também devido a condições internas, relacionadas à umidade, ventilação e processos de condensação (Oliveira, 2021; Silva *et al.,* 2023).

A identificação e análise dessas anomalias constituem etapa fundamental para a determinação de suas causas e mecanismos de degradação. A correta caracterização das manifestações patológicas permite a definição de estratégias de intervenção mais assertivas, contribuindo para a recuperação do desempenho e

para a mitigação dos problemas (Bertolini, 2010). Segundo Ferreira e Oliveira (2021), muitas dessas manifestações patológicas poderiam ser evitadas mediante maior rigor nas etapas de concepção, especificação de materiais, execução e planejamento de manutenção. A discrepância entre as condições de projeto e a execução se destaca como fator crítico na redução da vida útil das edificações (Bezerra, 2018).
Diante desse contexto, observa-se a necessidade de estudos aplicados que permitam a caracterização e o diagnóstico de manifestações patológicas em edificações existentes, especialmente em áreas urbanas consolidadas e de relevância histórica. Assim, o presente trabalho tem como objetivo realizar o diagnóstico de manifestações patológicas em uma edificação comercial de múltiplos pavimentos, localizada no centro histórico de Porto Alegre, visando à identificação de suas causas e à geração de subsídios técnicos para intervenções que promovam a recuperação do desempenho e a ampliação da vida útil da edificação.

2. Delimitação do entorno

A edificação em estudo configura o objeto central desta análise, demandando a compreensão do contexto em que se insere no meio urbano. O imóvel, de uso comercial, está localizado no bairro Centro Histórico, na cidade de Porto Alegre, Rio Grande do Sul. Trata-se de uma obra de múltiplos pavimentos com aproximadamente 70 anos de idade, constituída por um pavimento térreo e sete pavimentos tipo, englobando uma área construída superior a 5.500 m².

Sob a ótica construtiva, a edificação foi executada segundo os padrões convencionais de sua época, sendo sustentada por uma estrutura principal em concreto armado com fechamentos externos e internos em alvenaria convencional. O sistema de cobertura apresenta configuração mista, empregando telhas de fibrocimento e lajes com impermeabilização na região dos reservatórios. A consolidação destas características físicas e estruturais evidencia a longevidade da obra, estabelecendo o cenário fundamental para a avaliação do esgotamento natural da vida útil de seus componentes originais.

A dinâmica ambiental e climática do entorno exerce influência contínua e decisiva sobre a preservação e a durabilidade do envoltório da edificação. O ambiente em que o prédio está situado enquadra-se na classe de agressividade 2 (moderada), conforme os parâmetros da NBR 6118:2026 para zonas urbanas. Somado a isso, a cidade de Porto Alegre caracteriza-se por um clima subtropical úmido, com variações extremas de temperatura ao longo do ano e uma umidade relativa do ar que se mantém elevada. A exposição ininterrupta a essas intempéries ao longo de sete décadas atua como o principal agente acelerador do desgaste dos materiais de fachada e dos sistemas de impermeabilização das lajes de cobertura, criando as condições ambientais ideais para a deflagração e o agravamento das manifestações patológicas mapeadas.
A Figura 1, apresenta a fachada da edificação em estudo e a sua localização.

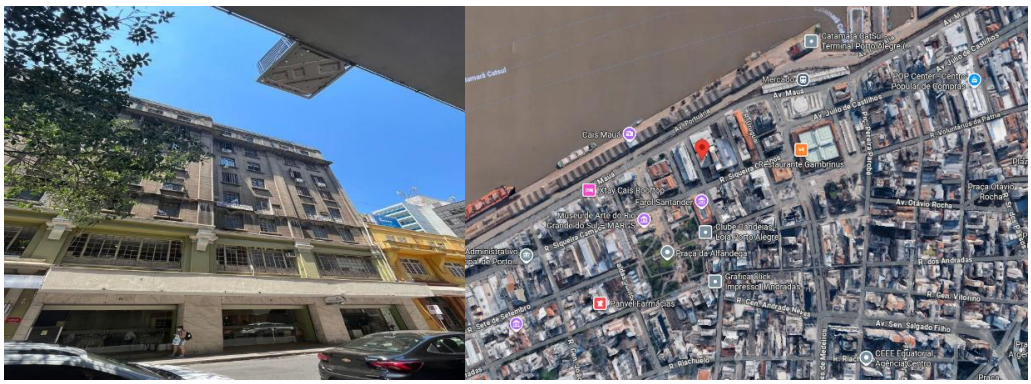


Figura 1 – Fachada da edificação em estudo e sua localização.

3. Metodologia

A condução deste estudo fundamentou-se numa abordagem qualitativa, estruturada a partir de uma inspeção predial embasada nas diretrizes do Instituto Brasileiro de Avaliações e Perícias de Engenharia (IBAPE) e nos procedimentos estabelecidos pela ABNT NBR 16747:2020. A classificação da inspeção como Nível 2 fundamentou-se nos critérios propostos pelo IBAPE/SP, sendo esta caracterizada pela realização de vistoria técnica detalhada em edificações de média complexidade, associada à análise documental, levantamento fotográfico e coleta de informações junto à gestão predial. A adoção deste escopo normativo assegura a padronização na recolha de dados, permitindo a identificação de anomalias construtivas e falhas de manutenção que afetam o desempenho do edifício.

O levantamento patológico concentrou-se no mapeamento das manifestações que comprometem diretamente a estanqueidade, a estabilidade e a durabilidade da envoltória. Durante a etapa de campo, os sistemas construtivos (principalmente o revestimento das fachadas, caixilharias, lajes impermeabilizadas e estruturas em balanço) foram inspecionados para correlacionar as manifestações patológicas visíveis (como fissuras, eflorescências e corrosão) com os seus respetivos mecanismos de degradação e causas primárias. Essa investigação transforma o registo visual num diagnóstico técnico do estado de conservação atual, isolando as variáveis necessárias para a posterior quantificação do risco.

Para o tratamento e hierarquização dos dados recolhidos, aplicou-se o método de análise de criticidade adaptado da Matriz GUT (Gravidade, Urgência e Tendência). Cada manifestação patológica mapeada foi avaliada num sistema de pesos (variando de 1 a 10) que quantifica o impacto na saúde e segurança (Gravidade), o tempo disponível para evitar o colapso da função (Urgência) e o potencial de evolução geométrica do dano (Tendência), resultando numa classificação de risco estratificada em níveis Crítico, Regular e Mínimo. A aplicação desta matriz converte as observações qualitativas num índice de priorização numérico e objetivo, estruturando a base para a apresentação e discussão na secção de resultados. A metodologia utilizada para classificação da ordem de prioridades dos vícios construtivos encontrados foi desenvolvida com as funções de criticidade e pesos seguintes (Quadro 1):

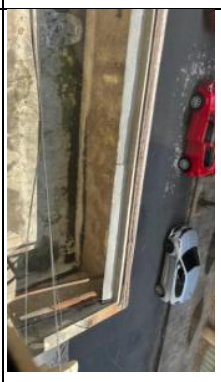
Quadro 1 - Parâmetros de avaliação de criticidade aplicados à matriz GUT

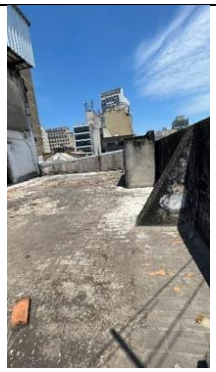
GRAU	GRAVIDADE	TENDÊNCIA	QUADRO EVOLUTIVO	PESO
Total	Perda de vidas humanas, falhas graves de concepção e/ou execução de projeto, danos ao meio ambiente ou defeito grave na própria edificação, além de despesas extras com eletricidade, água ou gás no condomínio	Eventos em ocorrência	Evolução imediata	10
Alta	Possibilidade de ferimento em pessoas, danos ao meio ambiente ou à própria edificação	Evento prestes a ocorrer	Evolução em curto prazo	8
Média	Desconfortos, deterioração do meio ambiente e outras anomalias construtivas existentes na edificação	Evento prognosticado para breve	Evolução em médio prazo	6
Baixa	Pequenos incômodos ou pequenos prejuízos financeiros	Evento prognosticado para adiante	Evolução em longo prazo	3
Nenhuma	-	Evento imprevisto	Não vai evoluir	1

4. Resultados

A partir do levantamento de dados e da inspeção visual detalhada da edificação em estudo, procedeu-se ao mapeamento e diagnóstico das manifestações patológicas, culminando na elaboração da matriz de diagnóstico e definição de conduta. O Quadro 2 sistematiza as evidências empíricas coletadas, focando estritamente nos sistemas de envoltória, estruturas e impermeabilização, que apresentaram os níveis mais agudos de degradação. A matriz correlaciona a manifestação patológica observada ao seu mecanismo de ação e provável causa, fornecendo a base técnica necessária para a proposição das terapêuticas adequadas à recuperação e preservação do imóvel.

Quadro 2 – Matriz de diagnóstico e definição de conduta

Manifestação patológica	Registro visual	Local	Manifestação patológica	Mecanismo	Terapêutica adequada
Degradação de Revestimento Externo		Fachadas externas em geral	Bolor extremo, manchas escuras, umidade generalizada e eflorescências	Exposição ininterrupta às intempéries, alta porosidade do material original (argamassa tipo pó de pedra/Cirex) e total ausência de limpeza preventiva	Hidrojateamento com solução fungicida, remoção de áreas desagregadas, aplicação de selador e repintura com tinta acrílica elastomérica
Sobrecarga e Empoçamento		Marquise da fachada principal	Acúmulo de água, vegetação aparente e peso não previsto de múltiplos equipamentos	Subdimensionamento ou obstrução de ralos, falha de impermeabilização e instalação irregular de dezenas de condensadoras de ar-condicionado	Desobstrução do escoamento, refazimento da impermeabilização e elaboração de laudo estrutural para redistribuição ou remoção das cargas térmicas
Corrosão de Armaduras		Laje da casa de máquinas e pilares do 9º andar	Fissuras orientadas no sentido das barras de aço, desplacamento do betão e manchas de oxidação	Infiltração crônica de umidade que rompeu a passivação do concreto, agravada por reparações paliativas anteriores que apenas mascararam o dano	Escarificação do concreto contaminado, limpeza mecânica das barras, aplicação de inibidor de corrosão e recomposição com argamassa polimérica estrutural

Manifestação patológica	Registro visual	Local	Manifestação patológica	Mecanismo	Terapêutica adequada
Perda de Estanqueidade		Terraços descobertos e lajes de cobertura	Infiltrações severas, manchas e mofo nos tetos e paredes dos andares inferiores (ex: restaurante)	Fim da vida útil do sistema de impermeabilização (manta asfáltica antiga), falhas em ralos e ausência de manutenção periódica	Remoção do sistema antigo, regularização do caimento e execução de nova impermeabilização asfáltica com proteção mecânica e revestimento
Oxidação e Falha de Vedação		Esquadrias de ferro em diversos andares	Ferrugem avançada, dificuldade de fechamento e entrada de águas pluviais	Exaustão da proteção anticorrosiva, falta de manutenção lubrificante e ausência de pingadeiras nas fachadas	Lixamento profundo, aplicação de fundo convertedor de ferrugem, pintura adequada e calafetação com selante PU no perímetro da esquadria
Deterioração Biológica		Esquadrias de madeira	Caixilhos empenados, apodrecimento da madeira e furos na estrutura	Exposição contínua à umidade sem renovação de vernizes protetores e ataque ativo de insetos xilófagos (cupins)	Substituição das peças estruturalmente comprometidas, execução de descupinização, aplicação de verniz protetor e selagem das frestas
Fissuras e Trincas		Paredes de fachada e interfaces estruturais	Aberturas lineares no revestimento argamassado	Variações de temperatura intensas nas fachadas leste/norte, dilatação diferencial entre materiais e desgaste do revestimento rígido	Abertura da trinca em perfil "V", limpeza, aplicação de selante elastomérico, estruturação com tela de poliéster e nivelamento superficial

Proliferação de Flora Parasitária		Peitoris de janelas e frestas na fachada	Vegetação invasiva no revestimento	Acúmulo de sujidade atuando como substrato orgânico, retenção crônica de umidade e ausência de higienização da fachada	Remoção manual cuidadosa da raiz, aplicação de herbicida específico, limpeza profunda da área e vedação da fresta original com selante

Deste modo, as anomalias, desconformidades e falhas constatadas na vistoria realizada no local de estudo, com suas respectivas siglas (Quadro 3), foram as seguintes:

Quadro 3 – siglas utilizadas para categorizar as anomalias encontradas

Sigla	Descrição
(FTR)	Tratamento de trincas, fissuras e restauração dos danos nos revestimentos de argamassa das fachadas, paredes e muros, incluindo repintura.
(IMP)	Impermeabilizações nas áreas descobertas.
(ESQ)	Revisão de esquadrias, pingadeiras e vedações.
(UAC)	Uniformização, restauração e disposição dos aparelhos de ar condicionado em locais corretos.
(MEF)	Manutenção e estanqueidade da fachada.
(PPC)	Regularização de itens referentes ao PPCI.
(RSC)	Reparos no sistema de cobertura.
(EQP)	Substituição de equipamentos que estão em más condições e pontos de corrosão (proteções, escadas e guarda-corpos).
(RIE)	Revisão das instalações Elétricas.
(RIH)	Revisão das Instalações Hidráulicas.
(EST)	Análise, parecer técnico de engenharia, monitoramento e recuperação de estruturas (marquise, laje da casa de máquinas e estruturas com corrosão).

De acordo com a metodologia proposta, a priorização das manifestações patológicas foi realizada por meio da aplicação da matriz GUT (Tabela 1), sendo o índice final obtido pelo produto entre os parâmetros de gravidade, urgência e tendência (G × U × T).

Tabela 1 – matriz Gravidade x Urgência x Tendência

SIGLAS	GRAVIDADE	URGÊNCIA	TENDÊNCIA	NÚMERO DE PONTOS	PRIORIDADE
FTR	6	8	6	288	7º
IMP	10	10	10	1000	2º

ESQ	6	8	8	384	6º
UAC	6	8	3	144	9º
MEF	8	10	10	800	4º
PPC	3	6	1	18	11º
RSC	6	6	3	108	10º
EQP	10	10	8	800	3º
RIE	8	6	8	384	5º
RIH	6	6	6	216	8º
EST	10	10	10	1000	1º

Embora os itens relacionados ao PPCI possuam elevada relevância normativa no contexto atual das exigências de segurança contra incêndio, a baixa priorização atribuída na matriz GUT decorre da ausência de inconformidades críticas iminentes identificadas durante a vistoria. Dessa forma, as pontuações mais elevadas foram direcionadas às manifestações patológicas que apresentavam risco estrutural e funcional imediato, como infiltrações severas, corrosão de armaduras e sobrecargas estruturais.

Assim sendo, a ordem de prioridades dos serviços de reparos das anomalias e falhas, com suas respectivas recomendações técnicas é apresentada no Quadro 4

Quadro 4 – Prioridades segundo pontuação

PRIORIDADE	SIGLA	DESCRIÇÃO	PONTOS
1º	EST	Análise, parecer técnico de engenharia, monitoramento e recuperação de estruturas (marquise, laje da casa de máquinas e estruturas com corrosão).	1000
2º	IMP	Impermeabilizações nas áreas descobertas.	1000
3º	EQP	Substituição de equipamentos que estão em más condições e pontos de corrosão (proteções, escadas e guarda-corpos).	800
4º	MEF	Manutenção e estanqueidade da fachada.	800
5º	RIE	Revisão das instalações elétricas.	384
6º	ESQ	Revisão de esquadrias, pingadeiras e vedações.	384
7º	FTR	Tratamento de trincas, fissuras e restauração dos danos nos revestimentos de argamassa das fachadas, paredes e muros.	288
8º	RIH	Revisão das instalações hidráulicas.	216
9º	UAC	Uniformização, restauração e disposição dos aparelhos de ar condicionado em locais corretos.	144
10º	RSC	Reparos no sistema de cobertura.	108
11º	PPC	Regularização de itens referentes ao PPCI.	18

Embora os itens EST e IMP tenham apresentado pontuações equivalentes na matriz GUT, a prioridade superior atribuída ao item EST fundamentou-se no maior potencial de comprometimento da estabilidade estrutural e da segurança dos usuários, especialmente devido à presença de corrosão de armaduras, degradação de elementos estruturais e sobrecargas identificadas na edificação.

O panorama diagnóstico evidencia que a edificação encontra-se num estado crítico de conservação, causado primariamente pelo esgotamento da vida útil da sua envoltória. O revestimento original das fachadas, executado em argamassa porosa (tipo pó de pedra/Cirex), perdeu a sua capacidade devido, principalmente, à ausência de manutenções e limpezas ao longo de décadas. Essa negligência transformou as paredes externas em uma superfície altamente absorvente, catalisando a proliferação severa de bolor, algas e a formação de fissuras generalizadas. Como consequência, a falência desta barreira primária permitiu o ingresso contínuo de umidade para os ambientes internos, degradando acabamentos, esquadrias e comprometendo a salubridade das salas comerciais.

Cabe salientar que o município de Porto Alegre possui legislação específica voltada à obrigatoriedade de inspeções prediais periódicas, instituída pela Lei Complementar nº 806/2016. Entretanto, mesmo diante da existência deste instrumento normativo, a edificação analisada apresentou elevado grau de deterioração, evidenciando que a obrigatoriedade legal, isoladamente, não garante a adequada conservação das construções. Fatores como a ausência de manutenção preventiva sistemática, a postergação de reparos e o acúmulo de degradações ao longo das décadas contribuíram significativamente para a evolução das manifestações patológicas identificadas.

Paralelamente à degradação da fachada, o colapso dos sistemas de impermeabilização atua como o segundo vetor de maior impacto na edificação. A inspeção constatou que os terraços descobertos e as lajes de cobertura perderam integralmente a sua estanqueidade, resultando em infiltrações descendentes agressivas que danificaram severamente os tetos e lajes dos pavimentos inferiores, como observado no restaurante do andar térreo, situação indicada na Figura 2. A incapacidade das coberturas em gerir o escoamento das águas pluviais gera um ciclo de deterioração constante, exigindo a demolição e o refazimento integral dos sistemas de manta asfáltica para que se estanque a origem do dano antes de qualquer intervenção estética nos ambientes internos.



Figura 2 – Ações resultantes de infiltrações localizadas.

Por fim, a sinergia entre a umidade crônica e a sobrecarga não prevista culminou no surgimento de anomalias estruturais de risco elevado. O estudo identificou indícios claros de corrosão de armaduras na laje da casa de máquinas e em pilares. Este risco é drasticamente agravado na marquise principal, que, além de sofrer com o empoçamento de águas pluviais, foi indevidamente convertida numa área técnica para suportar dezenas de condensadoras de ar-condicionado. A combinação de oxidação das armaduras com a imposição de cargas para as quais a estrutura não foi originalmente dimensionada configura um cenário de risco iminente, exigindo ações corretivas imediatas e análises estruturais aprofundados para garantir a segurança dos usuários.

5. Conclusão

O diagnóstico técnico da edificação comercial demonstra que o imóvel atingiu um estado crítico de degradação, resultante da combinação direta entre o esgotamento natural da vida útil dos seus materiais e a ausência histórica de manutenções preventivas. O mapeamento patológico evidenciou que a porosidade do revestimento de fachada altamente degrado, aliada ao colapso crônico dos sistemas de impermeabilização nas coberturas, afetou a estanqueidade da edificação e isso resultou em anomalias estruturais severas, como a oxidação de armaduras. Deste modo, conclui-se que o cenário não se resume a desgastes estéticos pontuais, mas a uma falência sistêmica que exige intervenções corretivas profundas para restabelecer a capacidade de resposta da obra às ações externas de intemperismo.

As consequências desta deterioração vão além do prejuízo puramente material, impondo riscos físicos diretos e imediatos aos usuários. A inspeção in loco constatou que a marquise da fachada principal atua sob sobrecarga não prevista de equipamentos de climatização e empoçamento de água, enquanto lajes e pilares apresentam expansão por corrosão com iminência de desprendimento de fragmentos de concreto. A manutenção do uso diário comum como edificação comercial, com estas vulnerabilidades apresentadas, configura um risco contínuo à vida, justificando a nota máxima de criticidade atribuída a estes elementos e transmitindo a grande importância de reparos focados na estabilidade global.

A matriz de diagnóstico e definição de conduta ilustra com clareza os impactos severos da gestão reativa sobre o custo global de manutenção em edificações longevas. A literatura técnica e a prática pericial demonstram que a omissão de rotinas preventivas simples, como a lavagem periódica das fachadas e a desobstrução de ralos pluviais, acelera a falência dos sistemas constituintes da obra. No caso analisado, essa negligência forçou a necessidade atual de substituição integral das mantas asfálticas, escarificação profunda do concreto armado e repintura total do edifício. Desta forma, evidencia-se que a economia inicial gerada pela ausência de manutenções preventivas culmina em despesas financeiras acumuladas e altamente onerosos para a administração atual do condomínio.

A reversão definitiva deste cenário de degradação demanda uma transição estruturada para a cultura da engenharia de manutenção preventiva. A garantia da durabilidade pós-reforma exige que a gestão predial implemente um programa de revisões periódicas rigorosamente alinhado às diretrizes da ABNT NBR 5674:2024 (Manutenção de edificações - Requisitos para o sistema de gestão de manutenção), monitorando a integridade da envoltória e controlando a inserção de novas cargas estruturais. Ao programar as recuperações imediatas com mão de obra especializada e adotar um controle contínuo dos sistemas construtivos, a instituição não apenas resolverá os problemas atuais, mas assegurará a resiliência do patrimônio e a preservação de um ambiente seguro e plenamente funcional para as suas atividades comerciais.

Referências

Associação Brasileira de Normas Técnicas (ABNT). 2020. ABNT NBR 16747: Inspeção Predial — Diretrizes, Conceitos, Terminologia e Procedimento. Rio de Janeiro: ABNT.

Associação Brasileira de Normas Técnicas (ABNT). 2024. ABNT NBR 5674: Manutenção de Edificações — Requisitos para o Sistema de Gestão de Manutenção. Rio de Janeiro: ABNT.

Associação Brasileira de Normas Técnicas (ABNT). 2026. ABNT NBR 6118: Projeto de Estruturas de Concreto — Procedimento. Rio de Janeiro: ABNT.

Bertolini, Luca. 2010. Materiais de Construção: Patologia, Reabilitação, Prevenção. São Paulo: Oficina de Textos.

Bezerra, J. M. B. 2018. “Caracterização da Formação Barreiras na Cidade de João Pessoa com Base em Sondagens SPT e Estudo Geotécnico de uma Encosta com Alto Risco de Deslizamento.” Master’s thesis, Universidade Federal de Pernambuco.

Ferreira, A. R., and R. F. Oliveira. 2021. “Patologias na Construção Civil: Estudo de Caso em Duas Residências na Cidade de Iraí de Minas – MG.” GETEC 10 (26): 1–16. https://revistas.fucamp.edu.br/index.php/getec/article/view/2362.

Ferreira, J. B., and V. W. N. Lobão. 2018. “Manifestações Patológicas na Construção Civil.” Caderno de Graduação – Ciências Exatas e Tecnológicas – UNIT-SERGIPE 5 (1): 71–80.

Oliveira, P. R. 2021. “Levantamento das Manifestações Patológicas: Estudo de Caso de Manifestações Patológicas em Condomínio de Paredes de Concreto Moldadas in Loco.” CIPPUS 9 (1). https://doi.org/10.18316/cippus.v9i1.8110.

Silva, A. J. F., P. C. P. Feitosa, A. J. F. Silva, and J. C. Sales. 2023. “Analysis of Pathological Manifestations in the Municipal Public Market of the City of Frecheirinha – CE: Case Study.” In Anais do Congresso Internacional sobre Patologia e Reabilitação das Construções (CINPAR). Sobral: Universidade Estadual Vale do Acaraú. https://doi.org/10.4322/CINPAR.2023.002.

Silva, E., et al. 2022. “Recuperação das Fachadas de um Edifício da Cidade do Recife/PE – Estudo de Caso.” In Anais do Congresso Internacional sobre Patologia e Recuperação de Estruturas (CINPAR). Lisboa. https://doi.org/10.4322/CINPAR.2022.021.

cinpar2026
XXII International Conference on Building Pathology and Constructions Repair
15th to 17th July 2026 - Lisboa, Portugal

Inspeção predial e diagnóstico de manifestações patológicas em uma edificação de múltiplos pavimentos: estudo de caso em Porto Alegre

Maria Eduarda da Silva DEMBOGURSKI[1]*, Daniel Thomaz FARINA[1]; José Maria de MOURA JUNIOR[1], Angela Borges MASUERO[1] e Denise DAL MOLIN[1]

[1] Laboratório de materiais e ambiente construído, Universidade Federal do Rio Grande do Sul, Porto Alegre, Brasil, mariae.dembogurski@gmail.com

Abstract: O presente artigo tem como objetivo identificar e analisar as manifestações patológicas existentes em uma edificação residencial de múltiplos pavimentos, visando à avaliação de suas condições técnicas, de uso e de manutenção. A partir dessa análise, busca-se subsidiar a elaboração de um plano de manutenção e a definição de ações corretivas e preventivas nos sistemas construtivos, priorizadas conforme o grau de risco associado. A metodologia adotada consistiu na realização de inspeção visual para identificação das anomalias, seguida da aplicação da matriz G.U.T. (Gravidade, Urgência e Tendência), com o intuito de estabelecer a hierarquização das intervenções necessárias. Os resultados indicam que as manifestações patológicas observadas estão predominantemente relacionadas a falhas ou inexistência de manutenção adequada ao longo da vida útil da edificação. As anomalias identificadas comprometem o desempenho e a durabilidade dos componentes dos sistemas construtivos, além de impactarem negativamente as condições de saúde, segurança e habitabilidade dos usuários. Conclui-se que a adoção de um plano de manutenção estruturado e baseado em critérios técnicos é fundamental para a mitigação dos danos identificados e para a preservação da vida útil da edificação.

Keywords: manifestações patológicas, patologia, matriz GUT.

1. Introdução

As edificações, ao longo de sua vida útil, estão sujeitas a processos de degradação que comprometem seu desempenho, segurança e durabilidade. Nesse contexto, as manifestações patológicas na construção civil constituem um campo de estudo essencial, sendo compreendidas como anomalias ou falhas que afetam os sistemas construtivos, podendo ter origem em erros de projeto, execução, materiais inadequados ou ações externas ao longo do tempo (Cavalcanti, 2022; Caporrino, 2015).

A durabilidade das estruturas está diretamente associada à sua capacidade de resistir às ações ambientais e às condições de uso previstas em projeto (Santos *et al.*, 2023). No entanto, a ausência de manutenção adequada favorece o surgimento e a evolução de manifestações patológicas, comprometendo o desempenho estrutural e funcional das edificações (Dutra, 2023). Dessa forma, práticas de manutenção preventiva tornam-se fundamentais para assegurar a vida útil e a segurança das construções (Santos et al., 2018).

Para mitigar os riscos técnicos e econômicos associados à perda de desempenho, a NBR 16747 (2020) estabelece a inspeção predial periódica como ferramenta fundamental. A inspeção leva em conta as características construtivas do edifício, a idade de seus sistemas e componentes, sua vida útil projetada, a exposição ambiental, a presença de agentes e processos de degradação e uma avaliação geral de seu desempenho durante o uso (Reginato *et al.*, 2025). Embora pareça simples, constitui o ponto de partida crítico para qualquer investigação, permitindo identificar causas de danos e facilitar a tomada de decisão

sobre intervenções e programas de manutenção. A inspeção visual, em particular, é amplamente reconhecida como o ponto de partida para investigações de danos, permitindo a identificação preliminar de sintomas, suas possíveis causas e a definição de estratégias de intervenção (Azevedo *et al.; 2023;* Vargas e Torres, 2025). A correta interpretação das manifestações patológicas é, portanto, indispensável para compreender os mecanismos de degradação, identificar suas causas e propor soluções adequadas, assegurando não apenas a recuperação dos danos existentes, mas também a prevenção de ocorrências futuras.

Diante desse contexto, o presente trabalho tem como objetivo realizar o diagnóstico de manifestações patológicas em uma edificação residencial de múltiplos pavimentos, localizada no centro histórico de Porto Alegre, contribuindo para a compreensão dos processos de degradação em edificações inseridas em ambientes urbanos consolidados e fornecendo subsídios técnicos para intervenções adequadas.

2. Delimitação do entorno

O objeto de estudo desta pesquisa consiste em uma edificação de uso residencial localizada no bairro Azenha, na cidade de Porto Alegre, Rio Grande do Sul. Trata-se de uma obra de múltiplos pavimentos com aproximadamente 45 anos de idade, estruturada por um pavimento térreo, cinco pavimentos tipo que abrigam 30 unidades habitacionais, além de um reservatório superior e casa de máquinas. Sob a ótica construtiva, o edifício foi erguido segundo os padrões convencionais de sua época, sustentado por uma estrutura principal em concreto armado, com vedações externas e internas em alvenaria e sistema de cobertura composto por telhas de fibrocimento. A consolidação destas características físicas e estruturais estabelece o cenário técnico para a avaliação do estado de conservação do imóvel, evidenciando o grau de solicitação imposto aos materiais ao longo de mais de quatro décadas de uso contínuo. A Figura 1, a seguir, apresenta a fachada principal da edificação em estudo.



Figura 1 – Fachada principal da edificação em estudo e localização da edificação.

A preservação e a durabilidade desta edificação são diretamente influenciadas pela dinâmica climática e ambiental do seu entorno. O ambiente urbano no qual o prédio está inserido enquadra-se na classe de agressividade 2 (moderada), conforme os parâmetros da NBR 6118:2026. Somado a isso, a cidade de Porto Alegre caracteriza-se por um clima subtropical úmido, marcado por variações térmicas rigorosas ao longo do ano e uma umidade relativa do ar consistentemente elevada. A exposição ininterrupta a essas

intempéries atua como o principal agente acelerador do desgaste mecânico e higrotérmico dos materiais de fachada e dos sistemas de cobertura, criando o ambiente propício para a deflagração das manifestações patológicas que comprometem a estanqueidade da obra.

3. Metodologia

A condução desta pesquisa pautou-se em uma abordagem principalmente quantitativa, estruturada a partir de uma inspeção predial rigorosa fundamentada nas diretrizes do Instituto Brasileiro de Avaliações e Perícias de Engenharia (IBAPE). O levantamento técnico enquadrou-se no Nível 2 de complexidade, caracterizado pela vistoria tátil-visual minuciosa das áreas comuns, aliada ao registro fotográfico e à anamnese com a gestão predial, dispensando a execução de ensaios destrutivos. A adoção dessa metodologia normativa garante a padronização na coleta dos dados, viabilizando a identificação das anomalias construtivas e falhas de manutenção que comprometem o desempenho geral do edifício.

O mapeamento das manifestações patológicas foi direcionado especificamente para os sistemas que afetam a estanqueidade, a estabilidade estrutural e a integridade da envoltória da edificação. Durante as investigações de campo, os componentes construtivos, com destaque para os revestimentos argamassados de fachada, esquadrias, lajes de cobertura e elementos de concreto armado nas áreas de garagem, foram avaliados para correlacionar os sintomas visíveis (como trincas, eflorescências, umidade e bolor) aos seus respectivos mecanismos de degradação. Essa investigação converte a mera observação visual em um diagnóstico técnico, isolando as variáveis necessárias para a etapa subsequente de quantificação e priorização de riscos.

Para o tratamento e a hierarquização das necessidades de intervenção, empregou-se o método de criticidade adaptado da Matriz GUT (Gravidade, Urgência e Tendência). Cada manifestação patológica catalogada recebeu uma pontuação em uma escala de pesos (variando de 1 a 10) que mensura o risco à saúde e segurança dos usuários (Gravidade), o prazo limite para evitar a falência funcional do elemento (Urgência) e o potencial de progressão física do dano (Tendência), categorizando os resultados finais em graus de risco Crítico, Regular e Mínimo. A aplicação desta ferramenta consolida as constatações qualitativas em índices numéricos objetivos, estabelecendo a base estrutural indispensável para a apresentação da matriz de diagnóstico e discussão das condutas terapêuticas na seção de resultados. A metodologia utilizada para classificação da ordem de prioridades dos vícios construtivos encontrados foi desenvolvida com as funções de criticidade e pesos seguintes, segundo Quadro 1.

Quadro 1 – Parâmetros de avaliação de criticidade (Gravidade, Urgência e Tendência) aplicados à matriz GUT

GRAU	GRAVIDADE	PESO
Total	Perda de vidas humanas, falhas graves de concepção e/ou execução de projeto, danos ao meio ambiente ou defeito grave na própria edificação, além de despesas extras com eletricidade, água ou gás no condomínio	10
Alta	Possibilidade de ferimento em pessoas, danos ao meio ambiente ou à própria edificação	8
Média	Desconfortos, deterioração do meio ambiente e outras anomalias construtivas existentes na edificação	6
Baixa	Pequenos incômodos ou pequenos prejuízos financeiros	3
Nenhuma	-	1
GRAU	**URGÊNCIA**	**PESO**
Total	Eventos em ocorrência	10
Alta	Evento prestes a ocorrer	8

Média	Evento prognosticado para breve	6
Baixa	Evento prognosticado para adiante	3
Nenhuma	Evento imprevisto	1
GRAU	**TENDÊNCIA**	**PESO**
Total	Evolução imediata	10
Alta	Evolução em curto prazo	8
Média	Evolução em médio prazo	6
Baixa	Evolução em longo prazo	3
Nenhuma	Não vai evoluir	1

4. Resultados

A consolidação dos dados recolhidos durante a inspeção predial permitiu o mapeamento e o diagnóstico preciso das manifestações patológicas que acometem a edificação. O Quadro 1 sintetiza as principais anomalias construtivas identificadas, focando estritamente nos sistemas de envoltória (fachadas e esquadrias), cobertura e estruturas de concreto armado, que concentram os danos de maior severidade. A estruturação desta matriz correlaciona diretamente o sintoma visual ao seu mecanismo de degradação, estabelecendo a base necessária para a definição das condutas corretivas.

Quadro 1 – Matriz de diagnóstico e definição de conduta

Manifestação patológica	Registro visual	Sintoma	Mecanismo	Causas prováveis	Terapêutica Adequada
Corrosão de Armaduras e Fissuras Estruturais		Fissuras longitudinais no concreto, destacamento do cobrimento e armaduras expostas com oxidação avançada.	Expansão volumétrica eletroquímica do aço (corrosão) por perda de passivação.	Infiltração crônica de umidade no concreto armado e falhas históricas de manutenção corretiva.	Escarificação do concreto contaminado, limpeza mecânica das barras, aplicação de inibidor de corrosão e recomposição com argamassa polimérica.
Degradação do Revestimento de Fachada		Descascamento da pintura, fissuras generalizadas, manchas escuras e proliferação de microorganismos.	Absorção capilar de água e biodeterioração.	Exposição contínua às intempéries climáticas associada à total ausência de lavagem e manutenção periódica.	Lavagem técnica (hidrojateamento), tratamento perimetral de trincas com selante PU, aplicação de fundo preparador e repintura com tinta acrílica Premium (com biocidas).

Perda de Estanqueidade da Cobertura		Infiltrações severas no forro e paredes dos apartamentos do último pavimento (6º andar).	Infiltração descendente de águas pluviais por gravidade.	Deficiências no capeamento e na vedação das telhas de fibrocimento, além de obstrução por falta de limpeza nas calhas.	Revisão integral das vedações, substituição de telhas danificadas, desobstrução e limpeza do sistema de calhas pluviais.
Recalque de Piso de Garagem (Placas Bailarinas)		Fissuras ramificadas, desagregação do concreto e afundamento irregular das placas do piso sob tráfego.	Perda de suporte de fundação combinada com fadiga mecânica por compressão.	Fuga de material do subsolo (provavelmente lavagem do solo por vazamento em tubulações enterradas) e carga de veículos.	Investigação do subsolo para correção de possíveis vazamentos tubulares, recompactação do subleito e concretagem de nova placa estrutural.
Umidade e Bolor em Áreas Internas		Estufamento do forro de gesso, bolhas na pintura e colônias de fungos (mofo) nas paredes.	Saturação higroscópica e deficiência de trocas de ar.	Falha na estanqueidade da fachada externa, infiltrações oriundas de pavimentos superiores e ventilação mecânica/natural insuficiente.	Correção da infiltração na origem (fachada/tubulação), remoção do material contaminado, instalação de exaustores mecânicos e pintura antimofo.
Oxidação e Falha de Esquadrias		Ferrugem aguda nos perfis metálicos, perda de funcionalidade (fechamento) e ingresso de água da chuva.	Corrosão metálica e desgaste de elementos de vedação.	Esgotamento da película anticorrosiva original, exposição à umidade e ausência de pingadeiras nos peitoris.	Lixamento agressivo do metal, aplicação de fundo convertedor de ferrugem, repintura, calafetação do perímetro com selante e instalação de pingadeiras.

A análise qualitativa da matriz evidencia que a perda de estanqueidade da envoltória atua como o principal vetor de degradação do edifício, desencadeando um efeito dominó sobre os demais sistemas. A falência da

pintura e do revestimento das fachadas, impulsionada por décadas sem manutenção preventiva, permitiu que a umidade constante penetrasse na alvenaria, gerando os quadros severos de insalubridade (mofo e bolor) no interior dos apartamentos e acelerando a oxidação das esquadrias metálicas. Conclui-se que o tratamento isolado das anomalias internas será ineficaz se a barreira primária de proteção do edifício (fachada e telhado) não for integralmente restaurada, comprovando a interdependência sistêmica das falhas construtivas mapeadas.

Para transpor esta avaliação qualitativa para um modelo objetivo de tomada de decisão, as manifestações patológicas foram submetidas à análise de criticidade por meio da Matriz GUT (Gravidade, Urgência e Tendência). O Quadro 2 apresenta o índice de priorização extraído da inspeção técnica, filtrado para os sistemas estruturais e de envoltória que compõem o escopo desta pesquisa. A quantificação dessas variáveis permite hierarquizar os reparos não apenas pelo incômodo estético, mas pelo risco real de colapso ou dano à vida humana, orientando o plano de manutenção do condomínio de forma técnica.

Quadro 2 – Avaliação de prioridades pelo método GUT

Sistema / Manifestação	Gravidade (G)	Urgência (U)	Tendência (T)	Pontuação (G x U x T)	Risco Global
Tratamento de trincas e corrosão estrutural	10	10	10	1000	Crítico (1º)
Manutenção e estanqueidade da fachada	6	10	8	480	Regular (5º)
Reparos no sistema de cobertura (telhado)	6	10	8	480	Regular (6º)
Umidade e bolor interno	6	10	8	480	Regular (7º)
Manutenção do piso de concreto (garagem)	10	8	8	480	Crítico (4º)
Revisão de esquadrias e vedações	6	10	6	360	Mínimo (10º)

A interpretação da Matriz GUT comprova que os danos com potencial de ruína mecânica exigem intervenção em caráter emergencial. O tratamento de trincas e da corrosão estrutural atingiu a pontuação máxima possível (1000 pontos), refletindo o perigo iminente de desprendimento de blocos de concreto armado e o risco de perda de estabilidade, caracterizando um cenário de urgência e tendência de evolução gravíssimas. Por outro lado, a recuperação da fachada, cobertura e contenção de umidade apesar de apresentarem menor risco imediato de colapso (Gravidade 6), receberam nota máxima em Urgência (10), pois a sua negligência contínua atua como o combustível para a degradação dos elementos estruturais. Fica evidente que a priorização deve focar primariamente na integridade física do suporte de concreto para, no mesmo plano de ação, restaurar o envoltório que impede a entrada de novos agentes agressivos.

5. Conclusão

A avaliação pericial do imóvel evidencia um nível avançado de deterioração, provocado pela combinação entre o fim da vida útil dos componentes e a ausência contínua de conservação preventiva. As inspeções identificaram falhas graves, como a alta permeabilidade do revestimento externo, a inoperância da impermeabilização da cobertura e o recalque do piso da garagem, anomalias que comprometeram diretamente a proteção contra umidade e a solidez da edificação. Portanto, a situação atual ultrapassa o mero envelhecimento visual e caracteriza um colapso sistêmico, o que demanda obras de recuperação urgentes para devolver a segurança e a habitabilidade à estrutura diante das condições climáticas.

As consequências dessa deterioração impõem riscos físicos e sanitários diretos aos moradores da edificação. A inspeção constatou a oxidação avançada de armaduras em elementos portantes e o recalque de placas de concreto na garagem, anomalias classificadas com o grau máximo de criticidade devido ao perigo de colapso mecânico, além de quadros de insalubridade gerados pela proliferação de fungos no interior das unidades. A permanência dessas vulnerabilidades compromete a segurança global do condomínio, necessitando uma priorização absoluta das recuperações estruturais e da restauração da envoltória.

O Quadro 1 observado no artigo ilustra o impacto negativo da gestão estritamente reativa sobre o custo global de edificações longevas. A omissão de rotinas preventivas básicas, como a lavagem da fachada, a desobstrução de calhas e a investigação precoce de vazamentos no subsolo, atuou como acelerador para a ruína dos sistemas; na prática, essa negligência forçou a necessidade atual de escarificação do concreto armado, reconstrução da laje de piso da garagem e repintura integral do prédio. Evidencia-se, portanto, que a aparente economia gerada pela falta de manutenção preventiva resultou na transferência de passivos financeiros onerosos para a administração atual.

A reversão definitiva deste cenário de degradação exige a transição para uma cultura da engenharia de manutenção contínua. A garantia da durabilidade pós-reforma demanda que a gestão condominial adote um programa de revisões periódicas rigorosamente alinhado às diretrizes da ABNT NBR 5674, monitorando a integridade da envoltória e a estabilidade das estruturas de concreto. Ao executar os reparos críticos priorizados pela matriz de risco utilizando mão de obra especializada e ao instituir o controle preventivo dos sistemas, o condomínio não apenas sanará as falhas existentes, mas assegurará a durabilidade do patrimônio e a preservação de um ambiente habitacional seguro e salubre.

References

Associação Brasileira de Normas Técnicas (ABNT). 2020. NBR 16747: Inspeção Predial – Diretrizes, Conceitos, Terminologia e Procedimento. Rio de Janeiro: ABNT.

Azevedo, V. F. B., et al. 2023. “Analysis of Pathological Manifestations through Damage Map: Case Study in Buildings I and K of the Polytechnic School of Pernambuco.” In Anais do XIX International Conference on Building Pathology and Constructions Repair (CINPAR 2023). Sobral: CINPAR. https://doi.org/10.4322/CINPAR.2023.003.

Caporrino, C. F. 2015. Patologia das Anomalias em Alvenarias e Revestimentos Argamassados. São Paulo: Pini.

Cavalcanti, L. R. 2022. “Manifestações Patológicas e Mapa de Danos: Um Olhar sobre a Preservação do Patrimônio Histórico da Cidade do Recife/PE.” Master’s thesis, Universidade de Pernambuco.

Dutra, A. P., et al. 2023. “Diagnóstico na Fachada da Igreja de São José.” In Memorias del XVII Congreso Latinoamericano de Patología de la Construcción y XIX Congreso de Control de Calidad en la Construcción (CONPAT 2023), edited by Álvaro G. Sánchez Bellido, Juan Carlos Rojas Vidovic, Alan J. Aparicio Ortubé, Enio J. Pazini Figueiredo, and Pedro Castro Borges. Santa Cruz de la Sierra, Bolivia. https://doi.org/10.21041/CONPAT2023/PC6652.

Reginato, L. A., et al. 2025. “Technical Assessment of Pathological Manifestations and Maintenance Conditions in External Facade Cladding with Fiber-Cement Panels.” In Memorias del XVIII Congreso Iberoamericano de Patología de la Construcción y XX Congreso de Control de Calidad en la Construcción (CONPAT 2025), edited by Ángel Castillo Talavera, José Luis García Calvo, Enio J. Pazini Figueiredo, and Pedro Castro Borges, 555–570. Madrid, España. https://doi.org/10.21041/CONPAT2025/V2PC4.

Santos, D. G. dos, et al. 2018. “Mensuração e Distribuição de Patologias na Degradação em Argamassa.” Gestão e Gerenciamento, no. 8: 12–18. https://nppg.org.br/revistas/gestaoegerenciamento/article/view/9.

Santos, C. S., J. R. de A. Quirino, L. M. dos S. Reis, G. J. da C. Gomes, and A. A. Fonseca. 2023. “A Patologia Estrutural no Domínio da Engenharia Civil.” Revista Pesquisa e Educação a Distância 1 (30): 1–2.

Vargas, F., and J. Torres. 2025. “El Poder de la Inspección Visual Dentro de la Investigación de Daños en Estructuras.” In Memorias del XVIII Congreso Iberoamericano de Patología de la Construcción y XX Congreso de Control de Calidad en la Construcción (CONPAT 2025), edited by Ángel Castillo Talavera, José Luis García Calvo, Enio J. Pazini Figueiredo, and Pedro Castro Borges, 684–696. Madrid, España. https://doi.org/10.21041/CONPAT2025/V2PC38.

CINPAR 2026
XXII International Conference on Building Pathology and Constructions Repair
15th to 17th July 2026 - Lisboa, Portugal

For Peer Review Only

Characterisation and Assessment of Structural Timber Elements of a Building in the Historic Centre of Viseu, Portugal

Mônica NICOLAU [1], Paulo COSTEIRA[2], Esequiel MESQUITA[3], José PADRÃO[4]

[1] Centro Universitário Cidade Verde, Maringá, Brasil, monicanicolau.engenharia@gmail.com
[2] Instituto Politécnico de Viseu, Viseu, Portugal, pcosteira@estgv.ipv.pt
[3] Federal University of Ceara, Fortaleza, Brasil, emesquita@ufc.br
[4] Instituto Politécnico de Viseu, Viseu, Portugal, jpadrao@estgv.ipv.pt

Abstract: This study is part of a body of research on the historic built heritage of the city of Viseu, Portugal, and presents a detailed characterisation of a building located in its historic centre. The aim is to advance technical and scientific knowledge of timber structures in Portuguese-built heritage, with particular emphasis on tabique walls and timber floors. The methodology included an architectural and structural survey of the building, complemented by in situ inspections and non-destructive testing, including measurements using the Resistograph® and the determination of natural vibration frequencies in the timber floors through environmental vibration analysis using a seismograph. These procedures made it possible to assess the state of conservation of the timber elements, identify potential pathologies and obtain relevant parameters for structural analysis. The environmental vibration tests made it possible to identify the frequencies of the first vertical vibration modes of the floors, which ranged from 16.97 to 23.32 Hz. These results allowed for an indirect estimation of the floors' stiffness and revealed that whether or not the floorboards are included is relevant to the analytical calculation of the floor frequencies. It was also observed that the average Resistograph® values are consistent with the vibration frequencies of the floors, that is, the floor with the lowest frequency also has the lowest Resistograph® value. The study thus contributes to more informed and sustainable rehabilitation interventions.

Keywords: Tabique walls, Inspection, Timber floors, Stiffness of the floors, Resistograph®

1. Introdução

A reabilitação do património exige compreensão aprofundada do comportamento estrutural dos sistemas tradicionais. No contexto português, as paredes de tabique e os pavimentos de madeira maciça constituem soluções amplamente difundidas até o início do século XX. Apesar da sua relevância histórica e estrutural, estes elementos são frequentemente substituídos por desconhecimento do seu desempenho mecânico. A ausência de diagnóstico baseado em dados experimentais conduz a intervenções excessivamente intrusivas.

Esta investigação tem por objetivo complementar um conjunto de estudos conduzidos no Departamento de Engenharia Civil da ESTGV/IPV sobre o edificado histórico do centro urbano de Viseu (Fernandes, 2015; Padrão et al., 2021a; Padrão et al., 2021b). Esses estudos evidenciam que a substituição indiscriminada de paredes de tabique e pavimentos de madeira decorre, sobretudo, da ausência de caracterização experimental sistemática do seu desempenho estrutural, contrariamente à perceção recorrente de que tais elementos desempenham uma função meramente construtiva ou de compartimentação. Padrão et al. (2021a; 2021b) demonstra que as paredes de tabique podem contribuir para a segurança estrutural, quando estão sujeitas a ações gravíticas, bem como para o contraventamento global da estrutura.

Os pavimentos de madeira assumem um papel essencial na distribuição de esforços verticais e na estabilização do conjunto estrutural, como demonstrou Ilharco et al. (2018). Neste tipo de construções,

também é comum a existência de paredes de alvenaria de pedra ao nível do rés-do-chão. Estes elementos de elevada rigidez são capazes de dissipar as cargas gravíticas existentes na zona central do edifício e provenientes dos pisos superiores, conduzidas pelas paredes interiores de tabique que se apoiam diretamente nos elementos horizontais de madeira. Esta interação entre paredes de alvenaria de granito e as estruturas de madeira maciça configuram um sistema híbrido tradicional com comportamento integrado.

O edifício aqui estudado possui um sistema construtivo comum ao património construtivo da zona onde está inserido, isto é, paredes exteriores e em contacto com o solo em alvenaria de granito, paredes interiores (e algumas paredes exteriores situadas em pisos superiores) em tabique e pavimentos e cobertura em estrutura de madeira maciça. Na região de Viseu e em diversas regiões de Portugal, há uma grande presença das paredes de tabique no património edificado.

Com este estudo pretende-se contribuir para um melhor conhecimento dos sistemas construtivos usados neste tipo de edifícios, combinando ensaios semi-destrutivos e não destrutivos, realizados em elementos de madeira, com a análise e discussão dos resultados. A informação obtida poderá vir a ser relevante e contribuir para futuros trabalhos de conservação e/ou reabilitação de edifícios situados em centros históricos, em particular os da cidade de Viseu.

2. Caracterização Construtiva do Edifício

O edifício, objeto de estudo (Nicolau, 2023), localiza-se na Rua do Gonçalinho, n.º 33, na cidade de Viseu. O edifício em estudo é uma habitação multifamiliar do século XIX, com 4 pisos elevados e cobertura (ver Figura 1). Trata-se de uma construção com paredes de alvenaria de granito (situadas nas fachadas e no arranque de paredes interiores em contacto com o solo), com paredes interiores em tabique (encontrando-se, também, em algumas paredes exteriores elevadas, fruto de ampliações posteriores) e pavimentos e cobertura em madeira maciça. Foi observada a presença pontual de alvenaria de tijolo maciço em paredes exteriores situadas em pisos superiores (sobretudo na fachada principal). Foram identificadas variações geométricas entre pisos, associadas a diferentes fases construtivas. A cobertura era revestida em telha cerâmica tradicional. Observou-se que existiam paredes de tabique simples, paredes de tabique com tábuas diagonais incorporadas, todas com fasquio de secção retangular. Foi verificada grande variabilidade dimensional, característica desta técnica artesanal tradicional, tábuas verticais com secção retangular ou costaneira, espaçamento irregular entre elementos e espessuras variáveis de argamassa (Figura 2a).



a) Alçado principal do edifício b) Materiais existentes na fachada

Figura 1 – Edifício objeto de estudo

Os conetores metálicos eram constituídos por pregos forjados de secção variável, característica de edifícios mais antigos. Na ligação entre as paredes de tabique e as paredes de alvenaria resistentes foram encontrados ligadores metálicos em chapa, chumbados na alvenaria de granito e pregados na parede de tabique, também característicos deste sistema construtivo, como ilustrado na Figura 2b. Essas ligações influenciam diretamente a rigidez global, a transferência de esforços horizontais e o comportamento sob ações dinâmicas. A inspeção visual permitiu identificar que se tratava de um edifício com um sistema construtivo idêntico aos descritos e estudados no centro histórico de Viseu (Fernandes, 2025; Padrão et al., 2020).



a) Janela de inspeção da parede de tabique PT 4.2



b) Ligação com 1 ligador metálico

Figura 2 – Paredes de tabique com tábuas costaneiras e diagonais, de secção variável, e ligadores metálicos

3. Metodologia Experimental

A metodologia experimental adotada envolveu o levantamento arquitetónico e estrutural do edifício e a sua inspeção e diagnóstico com recurso a ensaios não destrutivos: com um Resistograph®, para aferir o estado de conservação das madeiras e de vibração ambiental em pavimentos de madeira, através de sismógrafo.

3.1 Levantamento Arquitetónico e Estrutural

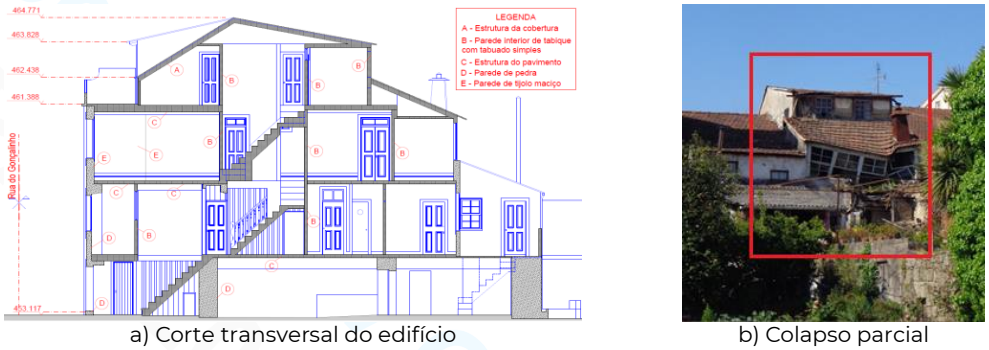
O levantamento arquitetónico e estrutural foi desenvolvido através de uma inspeção visual sistematizada, medições diretas, abertura de janelas de inspeção e registo fotográfico detalhado. Inicialmente, procedeu-se ao levantamento métrico completo do edifício, incluindo a determinação das dimensões globais, alturas piso a piso, espessuras de paredes, geometrias de vãos e caracterização volumétrica geral. Estas medições foram auxiliadas pela confrontação com plantas, cortes e alçados de arquitetura recentes, permitindo identificar a organização estrutural e a distribuição dos sistemas construtivos por piso. No corte transversal representado na Figura 3a é possível observar que as paredes exteriores do alçado principal são em alvenaria de pedra (piso 0) e tijolo maciço (pisos superiores, no alçado principal), enquanto as paredes exteriores da envolvente do edifício e as divisórias interiores são em tabique. No momento da primeira inspeção, o edifício encontrava-se desocupado e com elevado grau de deterioração, incluindo o colapso parcial da estrutura posterior (Figura 3b), circunstância que condicionou a seleção das áreas passíveis de inspeção segura.

3.1.1 Levantamento das Paredes de Tabique

Com o objetivo de caracterizar a tipologia das paredes de tabique, foi implementada uma metodologia baseada na abertura controlada de janelas de inspeção, com dimensões aproximadas de 1,00 m x 0,50 m. Cada parede foi identificada segundo nomenclatura específica por piso (ex.: PT.4.13) (ver Figura 4a), permitindo rastreabilidade /e organização dos dados recolhidos.

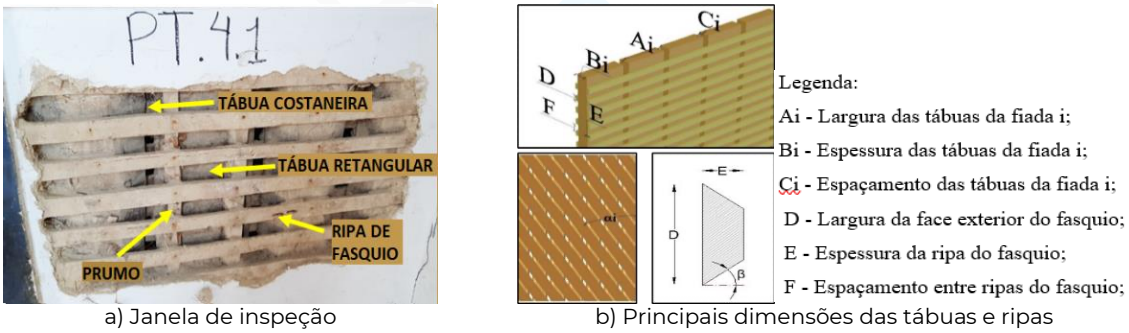
A abertura das janelas de inspeção possibilitou a identificação da constituição interna das paredes, tábuas verticais (incluindo costaneiras), ripas horizontais (fasquio), eventuais tábuas diagonais associadas a zonas com vãos, contribuindo para maior rigidez local e elementos de ligação e apoios às estruturas adjacentes. Observou-se predominância de paredes simples com tábuas verticais (Padrão et al., 2020). Foram ainda

recolhidos dados dimensionais médios das tábuas verticais e das ripas de fasquio, abrangendo largura, espessura e espaçamento, de acordo com o esquema geral ilustrado na Figura 4b. Os dados obtidos são apresentados na Tabela 1, permitindo posterior comparação com valores da bibliografia (Padrão et al, 2021a; Padrão et al., 2021b). A dimensão dos elementos constituintes, nomeadamente os elementos resistentes em madeira de pinho bravo, revela-se adequada e dentro daquilo que são as características típicas das paredes de tabique inseridas nos edifícios típicos do centro histórico de Viseu (Padrão et al, 2020).



a) Corte transversal do edifício b) Colapso parcial

Figura 3 – Levantamento arquitetónico e estrutural do edifício



a) Janela de inspeção b) Principais dimensões das tábuas e ripas

Figura 4 – Levantamento das paredes de tabique

Tabela 1 – Resumo das dimensões das tábuas verticais e das ripas de fasquio das PT interiores e exteriores

Nível	Modelo	Piso	Tábuas Verticais - valores médios (cm)			Ripas de Fasquio - valores médios (cm)		
			Largura A	Espessura B	Espaçamento C	Largura D	Espessura E	Espaçamento F
0	T2S	1	12,84	4,22	2,75	3,34	1,31	3,66
1	T2S	2	16,34	4,00	3,13	3,17	1,06	3,40
2	T2S	3	17,16	3,51	2,53	3,13	1,10	3,72
Valor médio (cm)			16,40	3,82	2,77	3,14	1,12	3,57
Desvio padrão (cm)			3,86	0,69	1,43	0,47	0,57	0,64
Coef. de variação (%)			23,52	17,93	51,71	15,03	50,99	17,82

3.1.2 Levantamento dos Pavimentos de Madeira

Os pavimentos eram constituídos por soalho de madeira, com uma espessura média de 2,5 cm, apoiados em vigas secundárias, igualmente de madeira pinheiro-bravo (Pinus pinaster). O pavimento possuía um forro de teto, em tabuado de madeira, com uma espessura média de 2,0 cm, que se desenvolvia perpendicularmente às fachadas principal e posterior, sendo que ao longo do edifício eram apoiadas nas vigas secundárias, paralelas à fachada principal que conjuntamente com os frechais das paredes de tabique

constituíam o pavimento. A inspeção permitiu identificar a orientação dos vigamentos e a disposição das paredes de tabique, paralelas e perpendiculares às vigas principais, influenciando o seu comportamento como elementos de compartimentação, ver as plantas ilustradas nas Figuras 5, 6 e 7.

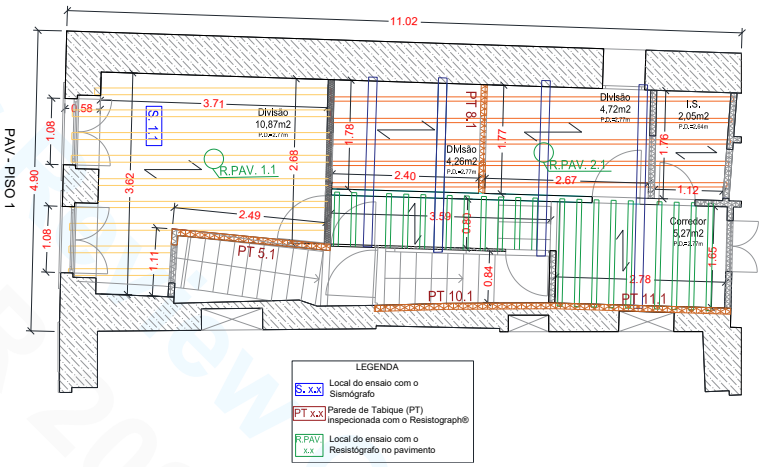


Figura 5 – Planta estrutural do piso 1

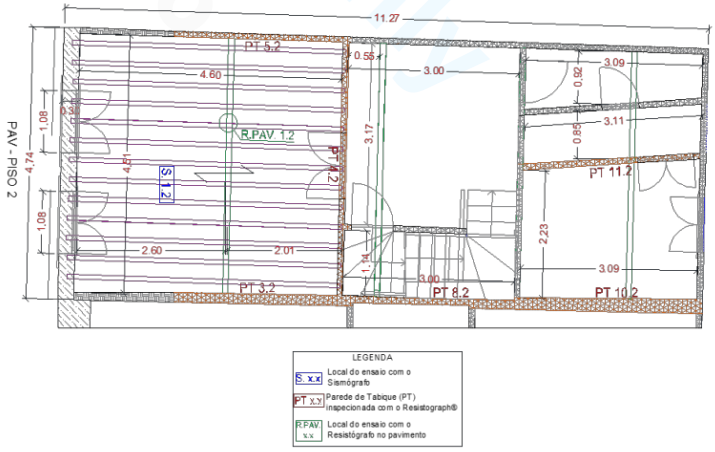


Figura 6 – Planta estrutural do piso 2

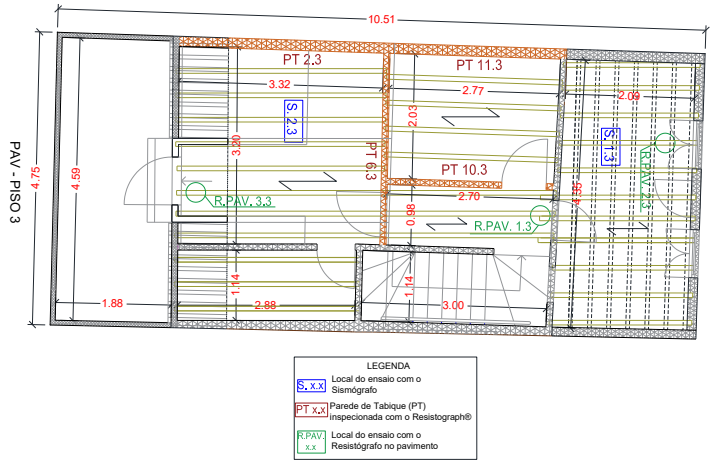


Figura 7 – Planta estrutural do piso 3

Na Figura 8 apresentam-se, em corte, as secções médias dos pavimentos dos pisos 1, 2 e 3. Na Tabela 2 apresentam-se as dimensões médias dos elementos de madeira que compõem essas secções. Identificaram-se diferenças entre pisos, tanto em termos dimensionais como no estado de conservação. Observou-se que algumas vigas apresentavam degradação superficial, devido a ataque de caruncho e de fungos de podridão (ver Tabela 2).

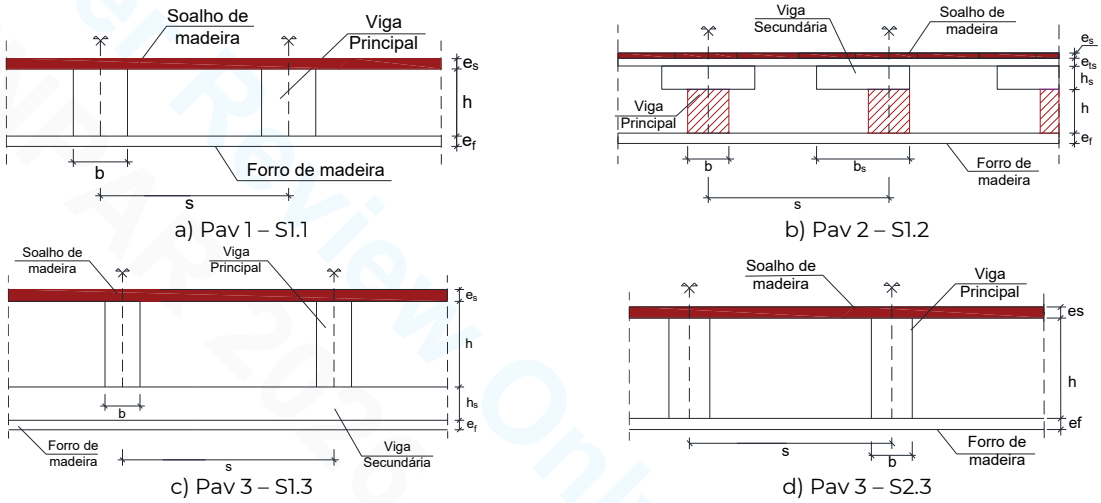


Figura 8 – Secção média dos elementos de madeira que compõem os pavimentos dos pisos 1, 2 e 3

Tabela 2 – Características geométricas médias das secções dos elementos de madeira dos pavimentos

Pavimento	Características geométricas médias (m)										
	Vigas Principais					Soalho	Tabuado Superior	Forro	Vigas Secundárias		
	b	h	h'	s	L	e_s	e_{ts}	e_f	b_s	h_s	s
Pav. 1 – S1.1	0,110	0,130	0,085	0,370	3,71	0,025	0,000	0,020	0,000	0,000	0,000
Pav. 2 – S1.2	0,080	0,080	0,080	0,350	2,60	0,015	0,020	0,020	0,180	0,045	0,350
Pav. 3 – S1.3	0,075	0,180	0,155	0,445	2,09	0,025	0,000	0,020	0,060	0,070	0,310
Pav. 3 – S2.3	0,075	0,180	0,170	0,390	3,32	0,025	0,000	0,020	0,000	0,000	0,000

Nota: h' representa a altura da viga principal desprezando a área degradada.

3.2 Inspeção e Diagnóstico

Como referido anteriormente, a campanha de ensaios experimentais *in situ* pretendia avaliar o estado de conservação de alguns elementos de madeira, designadamente nos pavimentos e nas paredes de tabique. Para tal, foram realizados dois tipos de ensaios: de vibração ambiental e com o Resistograph®.

3.2.1 Ensaios de Vibração Ambiental

O procedimento utilizado no ensaio de vibração ambiental dos pavimentos, envolveu a utilização de um sismógrafo, para a medição das acelerações verticais dos pavimentos e/ou das vigas dos pavimentos submetidas à vibração ambiente e à aplicação de impulsos verticais espaçados no tempo. Nos ensaios foram utilizados sismógrafos constituídos por acelerómetros triaxiais (GeoSIG GSR-18bit), com uma frequência de aquisição de 250 Hz, tendo os mesmos sido posicionados em pontos de maior deslocamento modal, conforme os modos de vibração com interesse em identificar. Efetuados os registos temporais em aceleração, os resultados são decompostos em frequências através da utilização de algoritmos clássicos de

For Peer Review Only

FFT (Transformada Rápida de Fourier). Neste caso os registos foram analisados através do programa GeoDAS. Posteriormente, estes resultados foram comparados com valores estimados através de um método analítico, considerando diferentes hipóteses para quantificar a rigidez. Neste estudo, o sismógrafo foi posicionado nos pisos 1, 2 e 3 e foram feitos, na totalidade, 4 ensaios em locais diferentes (ver localizações nas Figuras 5, 6 e 7).

3.2.2 Ensaios com Resistograph®

Para avaliar o estado de conservação dos elementos de madeira, foi tida em conta a variação do estado de conservação em profundidade das zonas de madeira da secção de perfuração. O equipamento funciona através da introdução forçada de uma agulha metálica de aproximadamente 1,5 mm no fuste e 3 mm na extremidade de corte, que penetra no elemento de madeira maciça a uma velocidade linear e de rotação constantes. O equipamento apresenta controlo automático da velocidade de avanço e de rotação, sendo a duração típica de uma perfuração da ordem de 1 a 2 minutos para profundidades até cerca de 44 cm (22 a 44 cm/min de velocidade média). O aparelho mede e regista continuamente a resistência à perfuração (energia despendida para avançar através do material), gerando um resistograma (gráfico detalhado).

O estado de conservação das zonas de uma secção de madeira é classificado em função da leitura do Resistograph®, quando comparada com o valor médio:

- **Bom estado de conservação**: quando a leitura é superior a 50% do valor médio, sendo estas zonas assinaladas a verde na barra de abscissas do gráfico (ver Figura 12);
- **Ligeiro estado de degradação**: quando a leitura se encontra entre 25% e 50% do valor médio, sendo estas zonas assinaladas a amarelo na barra de abscissas do gráfico (ver Figura 12);
- **Estado de degradação avançado**: quando a leitura é inferior a 25% do valor médio, sendo estas zonas assinaladas a vermelho na barra de abscissas do gráfico (ver Figura 12).

Refira-se que o valor médio corresponde à média dos valores da ordenada, entre o início e o fim do elemento ensaiado.

A sondagem com o Resistograph® nos pavimentos foi efetuada mediante o possível acesso às vigas dos pavimentos (Figura 9a). Executou-se o ensaio em 6 vigas do pavimento do edifício, 2 vigas do pavimento do piso 1 (ver localização na Figura 5), 1 viga do pavimento do piso 2 (ver localização na Figura 6) e 3 vigas do pavimento do piso 3 (ver localização na Figura 7). A realização do ensaio em paredes de tabique é semelhante (Figura 9b). Executou-se o ensaio em 12 paredes de tabique, 2 paredes do piso 1, 6 paredes do piso 2 e 4 paredes do piso 3. As localizações destes ensaios estão representadas nas Figuras 5, 6 e 7.



a) Vigas b) Paredes de tabique

Figura 9 – Realização do ensaio com Resistograph®

4. Análise e Discussão dos Resultados Obtidos

Inicialmente, são apresentados os resultados dos ensaios realizados nos pavimentos, que são: ensaio de vibração ambiental e o ensaio com a utilização do Resistograph®. Posteriormente, apresentar-se-ão os resultados com o Resistograph® nas paredes de tabique.

4.1 Ensaios nos Pavimentos de Madeira

Os resultados experimentais do ensaio de vibração ambiental dos pavimentos serão comparados com os valores estimados das frequências dos pavimentos. Também se procurou correlacionar os resultados dos ensaios com Resistograph® com os resultados do ensaio de vibração ambiental, de modo a avaliar a influência da degradação dos elementos de madeira na rigidez dos pavimentos.

4.1.1 Ensaio de vibração ambiental

Os ensaios de vibração ambiental permitiram identificar as frequências dos primeiros modos de vibração nas direções longitudinal, transversal e vertical. A Tabela 3 apresenta os resultados referentes ao modo vertical, considerado o mais relevante para este estudo. Estes valores encontram-se na gama de frequência previsível para este tipo de pavimento, de acordo com a bibliografia de referência (Ilharco et al., 2018). Os valores obtidos, afastam-se dos valores da frequência associada às sobrecargas, resultando numa situação de conforto na utilização do pavimento.

Tabela 3 – Registo dos resultados com o Sismógrafo (modo de vibração na direção vertical)

Ensaio	Localização	Vão (m)	Frequência (Hz)
Pav. 1 - S1.1	Teto do piso 0	3,71	16,97
Pav. 2 - S1.2	Teto do piso 1	2,60	22,83
Pav. 3 - S1.3	Teto do piso 2	2,09	20,14
Pav. 3 - S2.3	Teto do piso 2	3,32	23,32

4.1.2 Valores estimados das frequências dos pavimentos

Para se estimar analiticamente os valores das frequências dos pavimentos ensaiados é necessário quantificar as ações permanentes atuantes, estimar a rigidez das secções dos pavimentos e caracterizar as propriedades da madeira. Estimou-se que todos os elementos constituintes dos pavimentos são da madeira de classe de resistência C18 (Espécies coníferas) de acordo com a NP EN 338 (2003). O valor médio do módulo de elasticidade (E_{mean}) admitido foi 9,0 GPa e para a massa volúmica (ρ_{mean}) assumiu-se 380 Kg/m^3.

Os cálculos foram efetuados segundo o Eurocódigo 5 (2022), através do procedimento usado em Ilharco et al (2018) na identificação dinâmica dos pavimentos. Para um pavimento simplesmente apoiado em duas faces opostas, a frequência fundamental *f* pode ser calculada usando a Equação 1.

$$f = \left(\frac{\pi}{2 \times L^2}\right) \times \sqrt{\frac{EI_l}{m}} \quad (1)$$

Em que: *L* - vão do pavimento (m); *m* - massa por unidade de área (Kg/m^2); EI_l - rigidez equivalente de flexão (N.m^2/m). A rigidez equivalente de flexão, EI_l, é calculada através da Equação 2, considerando o valor médio do módulo de elasticidade e as características geométricas médias das vigas desses pavimentos.

$$EI_l = \left(E_{mean} \times \frac{I_l}{s}\right) \quad (2)$$

Em que: E_{mean} - valor médio do módulo de elasticidade (GPa); I_l – momento de inércia da secção das vigas (m^4); s – espaçamento entre vigas, medido entre eixos (m).

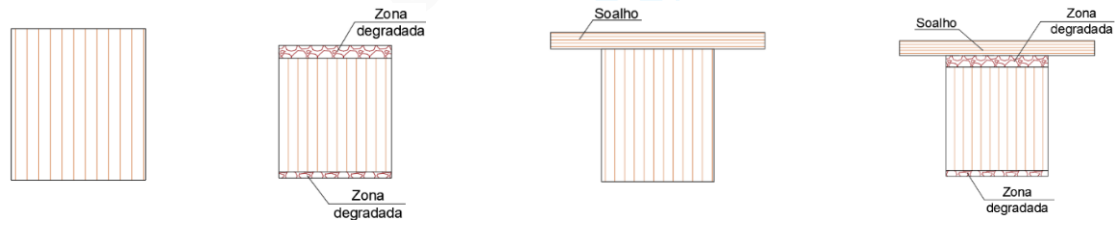
As secções médias dos pavimentos encontram-se ilustradas na Figura 8 e as características geométricas

estão resumidas na Tabela 2. Na Tabela 4 apresentam-se os valores das ações permanentes adotadas.

Na cálculo das frequências dos pavimentos foram consideradas 4 hipóteses: Hip 1- considerou-se a secção total das vigas principais; Hip 2 - considerou-se a secção das vigas principais, desprezando a área degradada, medida com o Resistograph®; Hip 3 - considerou-se a secção das vigas principais com a contribuição do soalho (secção em T); Hip 4 - considerou-se a secção das vigas principais com a contribuição do soalho (secção em T), desprezando a área degradada das vigas, medida com o Resistograph®. Na Figura 10 representam-se esquematicamente, as 4 hipóteses consideradas, com as devidas adaptações às secções médias dos pavimentos. Na Tabela 5 apresentam-se os valores estimados das frequências dos pavimentos.

Tabela 4 – Valores das ações permanentes utilizados no cálculo das frequências

Ações	Pav. 1 – S1.1	Pav. 2 – S1.2	Pav. 3 – S1.3	Pav. 3 – S2.3
Peso Próprio da Viga Principal (kN/m)	0,054	0,024	0,051	0,051
Peso Próprio do Soalho (kN/m)	0,035	0,020	0,042	0,037
Peso Próprio do Tabuado Superior (kN/m)	0,000	0,027	0,000	0,000
Peso Próprio das Vigas Secundárias (kN/m)	0,000	0,031	0,024	0,000
Peso Próprio do Forro (kN/m)	0,028	0,027	0,034	0,030
Total (kN/m)	0,118	0,128	0,151	0,118



a) Hip 1 -secção média da viga principal

b) Hip 2 - secção média da viga principal, desprezando a área degradada

c) Hip 3 – secção da viga principal com a contribuição do soalho

d) Hip 4 - secção da viga principal com a contribuição do soalho, desprezando a área degradada

Figura 10 – Esquema, em corte, das 4 hipóteses consideradas no cálculo das frequências dos 3 pavimentos

Tabela 5 – Valores estimados das frequências dos pavimentos

Pavimento	Vão (m)	Massa (Kg/m²)	Hip 1		Hip 2		Hip 3		Hip 4	
			EI_l (Nm²/m)	*f* (Hz)	EI_l (Nm²/m)	*f* (Hz)	EI_l (Nm²/m)	*f* (Hz)	EI_l (Nm²/m)	*f* (Hz)
Pav. 1 - S1.1	3,71	32,51	489871,62	14,01	136933,28	7,41	1322189,50	23,02	490794,16	14,02
Pav. 2 - S1.2	2,60	37,28	87771,43	11,27	-	-	1256640,69	42,66	1256640,69	-
Pav. 3 - S1.3	2,09	43,98	737191,01	46,56	470714,54	37,20	1950406,06	75,73	1137460,32	57,83
Pav. 3 - S2.3	3,32	30,84	841153,85	23,53	708605,77	21,60	2333235,83	39,20	1183197,25	27,91

Nota: Não existem resultados para o Pav. 2 – S1.2 (Hip 2 e Hip 4) porque a viga principal não apresentava degradação.

De uma forma geral, os valores obtidos no cálculo das frequências são consistentes com as 4 hipóteses estudadas, isto é, a frequência cresce com o aumento da rigidez da secção. Observa-se que as frequências obtidas *in situ* são normalmente superiores às obtidas pela utilização da Equação 1.

Na Hip 1, o valor obtido para as frequências é mais baixo porque se desprezou a contribuição do soalho, o que mostra que a rigidez real do sistema é superior.

Na análise dos resultados obtidos na Hip 3 (contribuição do soalho) observa-se que eles são consideravelmente superiores, o que leva a concluir que efetivamente a ligação entre o soalho e a viga principal não é tão eficaz como no modelo analítico. A rigidez real encontra-se entre a Hip 1 e a Hip 3. Ao considerar-se a degradação (Hip 2), os resultados analíticos aproximam-se dos experimentais nos Pav. 1 - S1.1 e Pav. 3 - S2.3, evidenciando a relevância para o estado de conservação do material na avaliação estrutural.

No caso particular do ensaio Pav. 3 - S1.3, os valores teóricos obtidos na Hip 1 são muito superiores (mais do dobro) quando comparados com o valor experimental. Como esta frequência está dentro dos valores obtidos para os outros pavimentos, crê-se que pode existe algum aspeto na parte da inspeção que não tenha sido bem aferido e que condiciona todo o cálculo subsequente.

De referir, ainda, que as incertezas existentes sobre o tipo de apoios (podem não ter a rotação totalmente livre), podem justificar, em parte, as diferenças entre os valores estimados e os experimentais.

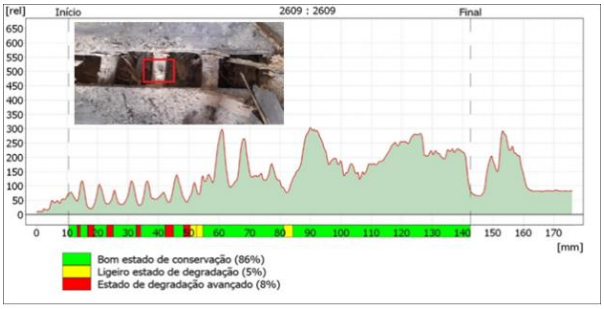
De forma global, conclui-se que a rigidez, o estado de conservação e a interação entre elementos são determinantes no comportamento dinâmico, sendo indispensável a validação experimental dos modelos teóricos.

4.1.3 Ensaios com Resistograph®

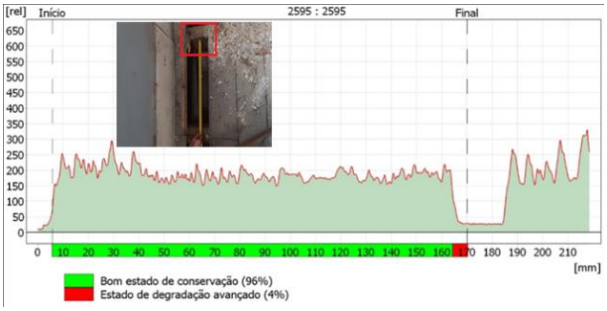
As sondagens com o Resistograph® nos pavimentos foram efetuadas, quer a partir da face superior do elemento, quer a partir da face inferior, mediante a acessibilidade às vigas. Foram ensaiadas 2 vigas de suporte dos pavimentos (localizações R.PAV.2.1 e R.PAV.1.2) e 4 vigas principais das secções dos pavimentos. Na Tabela 6 resumem-se, apenas, os resultados dos 4 ensaios nas vigas principais dos pavimentos e na Figura 11 ilustram-se dois exemplos dos resistogramas obtidos.

Tabela 6 – Dimensões das vigas e resultados do Resistograph®

Pavimento	Localização	Dimensões – b x h (cm)	Valor médio
Pav. 1	R. PAV.1.1	11,0 x 13,0	149
Pav. 3	R. PAV.1.3	8,0 x 18,0	212
	R. PAV.2.3	7,5 x 18,0	183
	R. PAV.3.3	7,5 x 18,0	229



a) R.PAV.1.1 (b=11cm; h=13cm) - Valor médio = 149



b) R.PAV.2.3 (b=7,5cm; h=18cm) - Valor médio = 183

Figura 11 – Gráficos dos ensaios do Resistograph® realizado em vigas principais dos Pisos 1 e 3

Na Figura 11ª observa-se o gráfico do ensaio efetuado numa viga principal do piso 1 (R.PAV. 1.1), onde se realizou o ensaio de vibração ambiental, assim como, as características do elemento ensaiado (tipo de elemento e respetiva dimensão). Este ensaio foi efetuado a partir da face superior do elemento, atingindo um comprimento de 140 mm, tendo-se verificado que o elemento possui grande heterogeneidade em profundidade, com uma acentuada variação nos primeiros 50 mm do elemento, que indica um estado de degradação avançado, observado visualmente. Na Figura 11b, ilustra-se o gráfico do ensaio efetuado numa

viga principal do piso 3 (R.PAV.2.3), Este ensaio foi efetuado a partir da face superior da viga principal, atingindo um comprimento de 170 mm. O resultado mostra que o elemento é homogéneo em profundidade, com um estado avançado de deterioração na face inferior, que visualmente não se observou. As localizações em planta destes ensaios podem ser visualizadas nas Figuras 5 e 6.

Em quase todos os elementos, constatou-se alguma homogeneidade de valores (estado de conservação). Com efeito, os picos nos gráficos das vigas ensaiadas corresponderam à penetração da agulha nas fibras (situadas na direção perpendicular), nomeadamente nos anéis de Primavera e de Outono. No início e no final da secção, verificaram-se valores de resistência à penetração menores, o que corresponde a alguma degradação superficial. O comprimento de sondagem (perfuração), em quase todos os casos, atingiu a distância face a face do elemento ensaiado (na direção da perfuração).

4.1.4 Efeito aproximado da degradação na madeira na frequência dos pavimentos

Um aspeto que se procurou analisar foi a correlação dos ensaios de vibração ambiental e do Resistograph®. Na Tabela 7 comparam-se os resultados desses dois ensaios. Como o número de ensaios é insuficiente para se estabelecer uma correlação, procurou-se analisar estes resultados na tentativa de se identificar alguma tendência entre eles. Observa-se uma correspondência entre os dois resultados, isto é, o pavimento que tem a menor frequência, também tem o menor "valor de Resistograph®", mostrando, o comportamento esperado, que a perda de resistência de um elemento de madeira provoca uma redução da rigidez do pavimento e, naturalmente, da sua frequência.

Tabela 7 – Registo dos resultados com o Sismógrafo (modo de vibração na direção vertical)

Pavimento	Resistograph® (valor médio)	Frequência Experimental (Hz)
Pav. 1 - S1.1	149	16,97
Pav. 3 - S1.3	183	20,14
Pav. 3 - S2.3	229	23,32

4.2 Ensaios nas Paredes de Tabique

Como referido na secção 3.2.1, executou-se o ensaio com Resistograph® em 12 paredes de tabique do edifício. No Tabela 8 apresentam-se os resultados obtidos, assim como a identificação de todas as paredes de tabique ensaiadas e as espessuras das respetivas tábuas.

Da análise dos resultados, concluiu-se que as tábuas das paredes de tabique ensaiadas (exteriores e interiores, em cada piso) apresentaram um bom estado de conservação, com degradação superficial num número reduzido de elementos.

5. Considerações Finais

A fase de inspeção e diagnóstico demonstrou ser fundamental para a compreensão e preparação, bem como para a escolha dos locais e dos ensaios experimentais a realizar. Neste tipo de edifícios, em que os sistemas construtivos são muitas vezes adaptados a situações específicas que não podem ser previstas é necessário realizar uma inspeção o mais detalhada possível para mitigar as dúvidas que possam existir sobre os materiais utilizados e o sistema construtivo existente.

Através do ensaio de vibração ambiental, constatou-se que as frequências para o primeiro modo de vibração na direção vertical, encontram-se dentro da gama de frequências previsível para este tipo de pavimentos. Este ensaio foi útil para aferir indiretamente a rigidez dos pavimentos de madeira.

Os resultados obtidos com o Resistograph® mostraram que as vigas de madeira dos pavimentos apresentaram um bom estado de conservação, ainda que algumas apresentem degradação superficial

ligeira. As tábuas das paredes de tabique ensaiadas (exteriores e interiores, em cada piso) também apresentaram um bom estado de conservação, com degradação superficial num número reduzido de elementos.

O estudo demonstrou que as soluções construtivas seguem um padrão regional coerente e que a madeira mantém uma capacidade resistente adequada.

Tabela 8 – Resultados com o Resistograph® nas Paredes de Tabique

Localização	Identificação	Espessura das tábuas (cm)	Valor médio
Piso 1	PT 5.1	4,54	157
	PT 8.1	4,10	224
Piso 2	PT 3.2	3,36	82
	PT 4.2	3,99	200
	PT 5.2	4,33	151
	PT 8.2	4,73	182
	PT 10.2	4,25	170
	PT 11.2	4,20	172
Piso 3	PT 2.3	4,34	180
	PT 6.3	3,45	219
	PT 10.3	3,00	237
	PT 11.3	4,20	171

6. Referências

Eurocódigo 5. (2022) NP EN 1995-1-1: Projeto de Estruturas de Madeira - Parte 1-1: Regras gerais – Regras comuns e regras para edifícios. IPQ.

Fernandes, C. R. 2015. "Avaliação Experimental do Comportamento Mecânico de Paredes de Tabique." Dissertação de Mestrado. Instituto Politécnico de Viseu. Portugal.

Ilharco, T., [et al.] (2018). "Caracterização de pavimentos antigos de madeira através de identificação dinâmica." Revista Portuguesa de Engenharia de Estruturas. Ed. LNEC. Série III. n.º 8. ISSN 2183- 8488. pp. 83-91.

Nicolau, M. (2023). "Caracterização *in situ* dos elementos estruturais em madeira de um edifício situado no centro histórico de Viseu." Dissertação de Mestrado. Instituto Politécnico de Viseu. Portugal.

NP EN 338. (2003). "Madeira para Estruturas – Classes de Resistência." IPQ.

Padrão, J. Guedes, J., Pinto, J., Arêde, A. (2020). "As paredes de tabique em Viseu – Detalhes construtivos e caracterização material." Revista Portuguesa de Engenharia de Estruturas. Ed. LNEC. Série III. n. º14. ISSN 2183-8488. pp.71-84.

Padrão, J., Guedes, J., Pinto, J., Arêde A. 2021a. "Tabique walls, a light timber structure – constructive details and material characterization." Architecture, Structures and Construction Journal. Ed. Springer Nature. https://doi.org/10.1007/s44150-021-00010-z.

Padrão, J., Silva, R., Arêde, A., Guedes, J. 2021b. "Paredes de tabique submetidas à compressão vertical – proposta de ensaio *in situ* e interpretação dos resultados obtidos." Revista Portuguesa de Engenharia de Estruturas. Ed. LNEC. Série III. n.º 17. ISSN 2183-8488 pp. 39-48.

For Peer Review Only CINPAR 2024

CINPAR 2026
XXII International Conference on Building Pathology and Constructions Repair
15th to 17th July 2026 - Lisboa, Portugal

Impacts of Deficient Maintenance on the Integrity and Durability of Reinforced Concrete Reservoirs

Amanda Ávila de **SOUZA**, Marília Carla Araújo Mendonça de ALENCAR

[1] Instituto Nova Engenharia, São Paulo, Brasil, amanda@construpat.com.br
[2] Instituto Nova Engenharia, Fortaleza, Brasil, marilia@construpat.com.br

Abstract: Reinforced concrete reservoirs are widely used in condominiums, industrial facilities, commercial buildings, logistics warehouses, and residential buildings, being intended for the storage of potable water for human consumption and non-potable water for technical uses, such as fire prevention and firefighting systems. These structures play a fundamental role in building water supply systems; however, the absence or insufficiency of systematic technical inspection and maintenance programs is recurrently observed, a condition that favors the progression of deterioration mechanisms throughout their service life.

Cracking constitutes an inherent manifestation in reinforced concrete structures and may be associated with factors such as shrinkage, thermal variations, structural actions, design conditions, and execution-related aspects. In the absence of adequate corrective measures and waterproofing systems with compatible performance, these cracks begin to act as preferential pathways for the ingress of water and aggressive agents into the concrete, favoring the occurrence of persistent infiltration, the advancement of carbonation processes, and, consequently, the depassivation of the reinforcement.

The depassivation of steel triggers corrosive processes characterized by the volumetric expansion of the steel itself, which induces internal stresses in the concrete, promoting cover spalling and the progressive reduction of the effective steel cross-sectional area. These phenomena result in a gradual loss of load-bearing capacity, compromising the structural integrity, durability, and functional performance of the reservoirs. In more severe situations, the evolution of these processes may culminate in localized or generalized structural collapse, in addition to risks associated with contamination of the stored water.

In this context, this article presents and discusses the main pathological manifestations associated with deficient maintenance in reinforced concrete reservoirs, such as efflorescence and failures in waterproofing systems, as well as the risks resulting from this scenario, reinforcing the importance of preventive maintenance as a fundamental strategy for preserving the structural integrity and durability of these structures.

Keywords: Water reservoir; Building maintenance; Concrete degradation; Corrosion; Waterproofing.

1. Introduction

Reinforced concrete reservoirs constitute fundamental elements for the functional performance of buildings, as they ensure water storage and supply regulation, while also meeting, in many cases, demands related to human consumption, technical reserves, and fire prevention and firefighting systems. Due to their function, such structures remain continuously subjected to the action of water, to stresses resulting from hydrostatic pressure, and to exposure conditions that require adequate performance in terms of watertightness, safety, and durability throughout their service life.

Although reinforced concrete is widely recognized for its versatility and robustness, its performance should not be interpreted as inherent or permanent, but rather as the result of the interaction among design, execution, conditions of use, and, above all, maintenance. In this regard, Helene (1992) emphasizes that the durability of concrete structures depends directly on the control of deterioration mechanisms and on the adoption of preventive measures compatible with the exposure conditions, while Souza and Ripper (1998) observe that pathological manifestations should be understood as symptoms of ongoing degradation processes, whose origin is often associated with failures accumulated throughout the structure's service life.

In the case of reservoirs, maintenance assumes an even more critical role, since the constant presence of water and the requirement for watertightness make these structures particularly sensitive to the evolution of construction anomalies, the wear of protective coatings, the deterioration of joints, the onset of cracks, and the progressive loss of performance of surface protection systems. When there is no periodic inspection, monitoring of service conditions, and preventive or corrective interventions in a timely manner, minor nonconformities tend to evolve into more complex pathological conditions, compromising not only the functionality of the reservoir, but also its integrity and durability.

From this perspective, deficient maintenance should not be understood merely as the absence of visible repairs, but rather as the insufficiency of systematic actions of control, conservation, and technical monitoring. This condition favors the onset and intensification of recurrent pathological manifestations in reinforced concrete reservoirs, such as infiltration, persistent moisture, efflorescence, leaching, cracking, carbonation, reinforcement corrosion, concrete cover spalling in relation to the reinforcement, degradation of coatings, and deterioration of waterproofing systems. In structures intended for water storage, such manifestations rarely occur in isolation, and it is more appropriate to interpret them as part of a progressive deterioration process, in which maintenance failures contribute to the acceleration of degradation mechanisms.

This understanding is reinforced by studies applied to reinforced concrete reservoirs. Torres et al. (2016), when analyzing elevated reservoirs constructed in reinforced concrete in the urban area of the city of Pelotas, RS, identified the recurrent occurrence of manifestations such as cracks, dirt accumulation, spalling, reinforcement corrosion, and efflorescence, associating these findings, to a large extent, with execution failures, inadequacies in relation to the design, and the absence of periodic maintenance. The results show that the impairment of the performance of these structures does not arise exclusively from a single pathological mechanism, but from the interaction among construction-related factors, due to design and execution failures, continuous exposure to moisture, and neglect of preventive conservation practices.

Additionally, the degradation of protection and waterproofing systems in reservoirs, when not identified and addressed early, favors the loss of watertightness and intensifies the action of moisture on structural elements, contributing to the onset and progression of pathological manifestations such as efflorescence, moisture stains, reinforcement corrosion, cover spalling, and structural degradation, thereby compromising the performance, watertightness, and durability of the structure (Santos, Silva, and Florian 2022).

Thus, analyzing the impacts of deficient maintenance on reinforced concrete reservoirs implies understanding that the loss of performance of these structures results from a chain of factors, in which the absence of inspection, the postponement of interventions, neglect regarding watertightness, and the progressive degradation of construction systems favor the onset and aggravation of pathological manifestations. More than identifying isolated symptoms, it becomes necessary to recognize maintenance

as a determining variable for the preservation of the structural integrity, functionality, and service life of these structures.

In this context, the present article analyzes the impacts of deficient maintenance on the integrity, durability, and performance of elevated reinforced concrete reservoirs, addressing the main pathological manifestations associated with this scenario and the risks resulting from their progression. It seeks to demonstrate that preventive maintenance, associated with proper technical diagnosis and the adoption of corrective measures in a timely manner, constitutes an essential strategy to contain the evolution of damage, mitigate risks, and preserve the functionality, safety, and service life of these structures.

2. Theoretical Framework

Understanding the impacts of deficient maintenance on reinforced concrete reservoirs requires an integrated analysis of the factors that influence their durability, performance, and behavior when exposed to degradation agents throughout their service life. As pointed out by Torres et al. (2016), the pathological manifestations observed in this type of structure may result from multiple factors, whether isolated or combined, including execution failures, construction deficiencies, exposure conditions, and the absence of adequate maintenance. In this context, the following theoretical framework brings together the main concepts necessary to demonstrate how the insufficiency of preventive actions, periodic inspections, and corrective interventions favors the onset and aggravation of damage in reinforced concrete reservoirs, as well as the technical and functional risks associated with the progression of these manifestations. In order to understand this relationship in a sequential manner, the discussion begins with maintenance and conservation, followed by watertightness, degradation mechanisms, pathological manifestations, and, finally, the risks resulting from performance loss.

2.1 Maintenance and Conservation of Reinforced Concrete Reservoir

The maintenance of reinforced concrete reservoirs comprises the set of technical actions intended to preserve watertightness, durability, functional performance, and structural integrity throughout their service life. Due to continuous exposure to moisture, contact with stored water, and service conditions, these structures require periodic inspections and preventive interventions capable of identifying failures at an early stage and containing the progression of degradation processes.

The absence of periodic maintenance is directly related to the progressive worsening of pathological manifestations, since failures that are initially superficial or localized tend to evolve when not identified and corrected in a timely manner. In this regard, Torres et al. (2016) highlight a high incidence of cracks, reinforcement corrosion, concrete spalling, leaks, efflorescence, and leaching in elevated reinforced concrete reservoirs, associating such occurrences primarily with the absence of periodic maintenance.

Thus, the proper conservation of these structures is not limited to the correction of already established damage, but involves the continuous observation of cracks, signs of infiltration, loss of waterproofing performance, surface manifestations, and other indications of deterioration, in order to prevent initially localized anomalies from evolving into more complex and costly rehabilitation conditions (Torres et al. 2016). Among the most relevant aspects of this conservation process, the preservation of watertightness and the performance of waterproofing systems stands out, since the loss of these conditions favors water ingress and the intensification of deterioration processes.

2.1.1 Watertightness, Waterproofing, and Functional Performance

Watertightness constitutes an essential requirement for the functional performance of reservoirs, since the structure must ensure water storage without losses, infiltration, or undesirable exchange with the external environment. In this context, waterproofing acts as a complementary protection system, contributing to the

reduction of permeability, the preservation of surfaces, and the maintenance of service conditions over time (Sampaio, Silva, and Florian 2021).

When execution failures, construction discontinuities, material aging, or degradation of protective coatings occur, watertightness is lost, favoring the infiltration and percolation of water through structural elements. This process simultaneously compromises the durability of the concrete, the protection of the reinforcement, and the operational efficiency of the system, and may result in leaks, increased internal moisture, and the progressive evolution of damage associated with the continuous presence of water in the structure (Sampaio, Silva, and Florian 2021).

Capraro et al. (2019) emphasize that the recurrent presence of moisture and the loss of protective barriers favor the action of degradation mechanisms that reduce the service life of the structure, especially when associated with insufficient concrete cover, carbonation, and reinforcement depassivation. Thus, watertightness should not be understood merely as a requirement for hydraulic operation, but as a condition directly linked to the durability, conservation, and safety of the reservoir. Once this condition is compromised, a favorable scenario is created for the development of degradation mechanisms that begin to act progressively on both the concrete and the reinforcement.

2.1.1.1 Degradation Mechanisms in Reinforced Concrete Reservoirs

With the loss of watertightness and the intensification of water ingress into structural elements, degradation mechanisms begin to develop progressively. These processes are directly related to the reduction of the natural protection provided by the concrete cover and by the high alkalinity of the solution present in the pores of the concrete. As highlighted by Helene (1992), the concrete cover acts simultaneously as a physical barrier against the ingress of external agents and as a means of chemical protection for the reinforcement.

When this protection is compromised by cracking, failures in watertightness, wetting and drying cycles, aging of protection systems, or other construction discontinuities, favorable conditions are established for the ingress of water and aggressive agents into the structural element. In this context, cracking assumes a relevant role not only as an initial manifestation, but also as a preferential pathway for the penetration of moisture and deleterious substances.

The continuity of this process favors the advancement of carbonation in the concrete cover, with the progressive reduction of the alkalinity of the medium and the consequent loss of the passive condition of the steel. When the carbonation front reaches the depth of the reinforcement, depassivation occurs, creating a favorable environment for the onset of the corrosion process, especially in structures subjected to the recurrent presence of water (Helene 1992).

Once initiated, reinforcement corrosion tends to progress continuously, producing expansive compounds that generate internal stresses in the adjacent concrete. This volumetric increase induces additional cracking, loss of bond between steel and concrete, and subsequently, spalling or detachment of the concrete cover, with exposure of the reinforcement and worsening of the deterioration process. It is, therefore, a self-accelerating mechanism, in which corrosion reduces the effective steel cross-sectional area and simultaneously compromises the durability, integrity, and functional performance of the structure (Helene 1993).

At the same time, the continuous percolation of water through the concrete may promote leaching processes, characterized by the dissolution and transport of soluble compounds from the cementitious matrix. This phenomenon contributes to increased permeability, material weakening, and the transport of salts to the surface, where visible crystalline deposits may occur, often associated with efflorescence. Thus, degradation mechanisms do not act in isolation, but rather in an interdependent manner, composing a progressive deterioration scenario that becomes perceptible through visible manifestations in the structure (Helene 1992).

2.1.1.2 Main Pathological Manifestations in Reinforced Concrete Reservoirs

As a result of the continuous action of these degradation mechanisms, visible pathological manifestations begin to appear, reflecting on the surface the progression of internal damage already established within the structure. Among the most recurrent occurrences in reinforced concrete reservoirs subjected to deficient maintenance are cracking and fissures, infiltration and leaks, concrete spalling and detachment, reinforcement corrosion, efflorescence, moisture stains, waterproofing failures, and biological contamination, among others.

In structures with more advanced deterioration, loss of concrete cover over the reinforcement, exposed reinforcement, concrete spalling, and, in severe cases, reduction of the steel bar cross-sectional area may also be observed. These manifestations are among the most frequent occurrences in elevated reinforced concrete reservoirs, reflecting the direct impact of the absence of preventive and corrective maintenance on the functional performance, durability, and structural integrity of the system (Torres et al. 2016).

The identification of these manifestations makes it possible to understand not only the conservation condition of the reservoir, but also the potential worsening of the pathological condition when damage remains active. In this way, the progression of these manifestations no longer represents merely a localized loss of performance, but becomes directly related to structural, functional, and sanitary risks associated with the continuity of deterioration.

3. Risks Associated with Deterioration and Performance Loss

When pathological manifestations remain uncorrected and degradation mechanisms continue to act, the effects of deficient maintenance are no longer limited to the appearance or superficial performance of the structure and begin to compromise its overall behavior. The continued ingress of water, associated with the persistence of active cracks and the insufficiency of waterproofing systems, keeps the concrete exposed to percolation and favors the progression of carbonation, creating conditions conducive to reinforcement depassivation and the advancement of the corrosion process (Helene 1992).

As corrosion progresses, the expansive products formed around the reinforcement generate internal stresses that intensify cracking, promote cover spalling, and further increase the exposure of the steel to water and oxygen. As a consequence, there is a progressive reduction in the effective cross-sectional area of the bars, loss of bond between steel and concrete, and a decrease in the load-bearing capacity of structural elements. In more severe situations, when this process develops without adequate corrective interventions, the stability of the structure may be compromised, with the possibility of localized or even generalized collapse (Helene 1993).

In addition to structural risks, deficient maintenance also directly compromises the functional performance of the reservoir. The persistence of watertightness failures, infiltration, and leaks reduces the operational reliability of the storage system, which may result in continuous water waste, reduced supply efficiency, and the need for shutdowns for emergency interventions. In public or collective-use reservoirs, this condition goes beyond the material dimension of pathology and directly interferes with the continuity of the service provided and with the operational safety of the building (Torres et al. 2016).

Added to this are the risks related to the persistence of moisture and the continuity of chemical processes within the structure. Continuous leaching promotes the dissolution and transport of compounds from the cement paste, contributing to increased permeability, loss of surface cohesion, and worsening of concrete degradation. In parallel, the formation of efflorescence indicates the existence of water movement within the material and the presence of soluble salts, showing that conditions favorable to the continuity of deterioration remain active. When this condition persists without correction of the source of water ingress,

the tendency is for the conservation state to progressively worsen and for the extent of damage to increase (Menezes et al. 2006).

Finally, the impacts of performance loss in water reservoirs also extend to the sanitary dimension. The continuous presence of moisture, sealing failures, surface deterioration, biofilms, and biological contamination compromises the proper conservation conditions of the system, which may affect the quality of the stored water and increase users' exposure to inadequate sanitary conditions. Thus, the effects of deficient maintenance are not limited to material degradation, but simultaneously affect durability, structural safety, system functionality, and the sanitary reliability of the structure in service.

4. Methodology

Based on the theoretical framework presented, which demonstrated the relationship between deficient maintenance, degradation mechanisms, and the occurrence of pathological manifestations in reinforced concrete reservoirs, the methodology of this study was defined with the purpose of verifying, in a real-world situation, how such phenomena manifest in the field and how they can be technically analyzed.

For the development of this study, an approach based on bibliographic research and a case study was adopted. The bibliographic research was used to provide the theoretical basis for degradation mechanisms, pathological manifestations, and the impacts of deficient maintenance in reinforced concrete reservoirs, based on previously published technical and scientific references.

Based on this conceptual foundation, the next stage consisted of the practical application of these references through the analysis of a real case, in order to establish a correspondence between the phenomena described in the literature and the conditions effectively observed in the evaluated structure.

Additionally, a case study was carried out with the objective of correlating the concepts addressed in the theoretical framework with the pathological manifestations observed in the field. The analysis was conducted through the damage mapping method, used for the graphical recording and identification of pathological manifestations, associated with the technical anamnesis of the structure.

In this context, the object of study was selected for presenting conditions representative of the degradation scenario discussed in the previous sections, allowing an integrated analysis between theory and practice. The object of study consists of a reinforced concrete reservoir located in an industrial area in the municipality of Sorocaba/SP, whose evaluation was carried out through on-site inspection, photographic records, and mapping of the pathological manifestations observed.

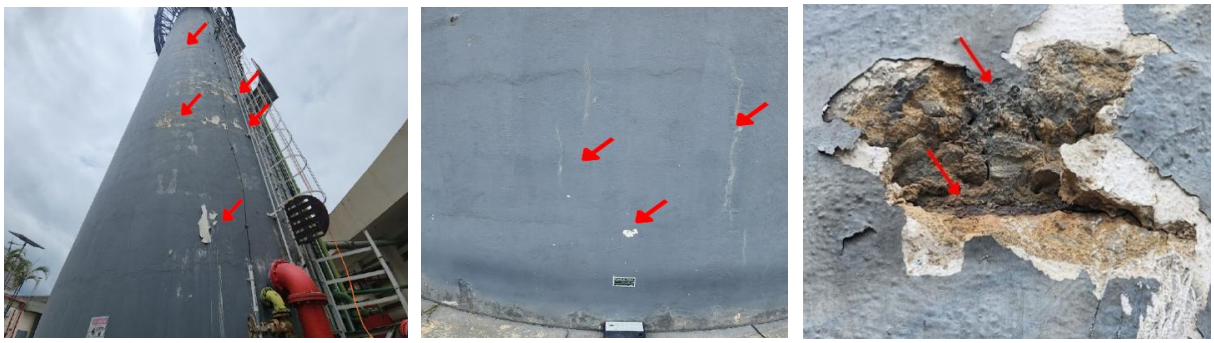
The adoption of these methodological procedures made it possible not only to characterize the identified anomalies, but also to understand their evolution and their possible links with maintenance failures, loss of functional performance, and impairment of watertightness, in line with the approach developed throughout the theoretical framework.

These inspection and anamnesis stages provided sufficient technical support for the diagnosis of the identified pathological manifestations, allowing the analysis of their probable causes and origins, as well as the preparation of the prognosis of the condition and the definition of the applicable therapeutic and repair measures.

Based on these procedures, photographic records and mapping elements were obtained to support the presentation of the anomalies observed in the field, which are presented and discussed in the following section.



Figure 1 – General view of the inspected reservoir, Author's archive (2026)



(a) (b) (c)

Figure 2 – Inspected reservoir, showing paint peeling in (a) and (b), concrete spalling and reinforcement corrosion in (c), Author's archive (2026)

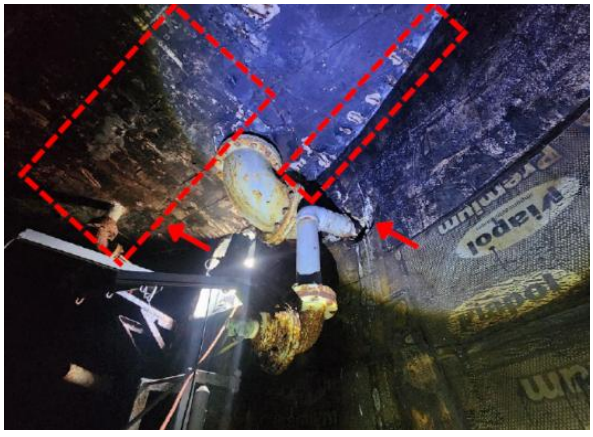


Figure 3 - Presence of reinforcement corrosion, Author's archive (2026)



Figure 4 - Presence of efflorescence, Author's archive (2026)



Figure 5 – Presence of reinforcement corrosion

Author's archive (2026)

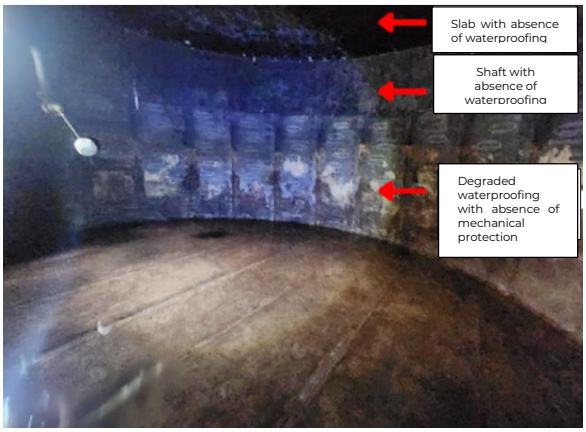


Figure 6 – Inspected reservoir, internal area, absence of slab waterproofing and mechanical protection

Author's archive (2026)

5. Results and Discussion

5.1. Characterization of the Observed Pathological Manifestations

Based on the methodological procedures adopted, the main anomalies identified during the inspection of the elevated reinforced concrete reservoir under study are presented below. Initially, the aim is to visually characterize the structure and highlight the general conditions observed in the field, in order to contextualize the pathological manifestations identified and establish the relationship between the records obtained and the degradation scenario discussed in the theoretical framework.

The visual inspection and photographic survey revealed a set of pathological manifestations compatible with a progressive deterioration process associated with deficient maintenance and the loss of performance of surface protection and watertightness systems. figure 1 presents the general view of the inspected structure, allowing the object of study and its overall conservation condition to be contextualized.

On the external surfaces, manifestations such as coating degradation, surface defects, fissures and cracks, as well as localized spalling, were identified, as illustrated in figure 2. These occurrences indicate a reduction in the performance of the surface protection system and favor the exposure of the substrate to environmental actions, in addition to constituting potential pathways for the ingress of moisture and aggressive agents.

In addition to the manifestations observed externally, the internal inspection revealed more critical conditions related to the loss of watertightness and the continuous action of moisture in regions directly exposed to contact with water. Inside the reservoir, evidence of degradation and localized absence of waterproofing, deposits compatible with leaching and efflorescence, the presence of reinforcement corrosion and pipe corrosion, as well as concrete spalling and deterioration in critical regions, especially at interfaces and pipe penetrations, were observed, as shown in figures 3 to 7.

Taken together, the records indicate that the observed manifestations do not occur in isolation, but rather constitute an interdependent pathological condition, in which the absence of preventive and corrective maintenance contributes to the continuity and worsening of damage. This finding leads to the need for a technical interpretation of the identified anomalies, seeking to relate the signs observed in the field to the degradation mechanisms and impacts discussed in the theoretical framework.

5.1.1 Technical Analysis of the Identified Anomalies and Their Relationship with Degradation Mechanisms

The analysis of the photographic survey reveals a pathological condition directly associated with deficient maintenance and the loss of performance of the reservoir's surface protection and watertightness systems. The observed manifestations, such as coating degradation, cracking, efflorescence, failures in the waterproofing system, concrete spalling, and reinforcement corrosion, demonstrate that deterioration occurs in a progressive and interdependent manner.

In general, the presence of cracks and discontinuities favors the ingress of water and aggressive agents into the concrete, intensifying mechanisms such as carbonation, reinforcement depassivation, corrosion, and subsequent cover spalling. At the same time, the continuity of water percolation contributes to leaching processes and the formation of efflorescence, indicating loss of watertightness and reduction in the functional performance of the structure.

On the external surfaces, paint peeling and the observed spalling areas indicate impairment of surface protection and progressive exposure of the substrate to environmental actions, which accelerates material aging and increases the vulnerability of the concrete to moisture ingress. In more advanced areas, exposed reinforcement and signs of corrosion reveal that the degradation process has already gone beyond the coating layer, reaching structural elements with potential impairment of durability.

Inside the structure, stains, efflorescence, and areas with waterproofing failures reinforce the occurrence of watertightness loss over time. These identified anomalies are technically compatible with continuous percolation processes, dissolution and transport of compounds from the cementitious matrix, characterizing phenomena associated with leaching and efflorescence, while also favoring the worsening of degradation at construction interfaces and pipe penetrations.

It is therefore observed that the pathological manifestations identified in the field corroborate the theoretical framework previously developed, especially regarding the relationship between deficient maintenance, loss of watertightness, progression of degradation mechanisms, and the emergence of interdependent pathological manifestations. In this sense, the records obtained not only confirm the presence of visible damage, but also demonstrate a continuous process of performance loss with structural, functional, and sanitary implications.

5.2.Summary of the Identified Pathological Manifestations

In order to systematize the findings observed in the field and to establish an integrated interpretation between the identified evidence, the associated mechanisms, and their predominant technical impacts, Table 1 was developed, presenting a summary of the main pathological manifestations identified in the studied reservoir.

The organization of these data demonstrates that the observed manifestations are not limited to isolated or punctual occurrences, but rather constitute a pathological condition consistent with the progressive loss of structural performance. The correlation between observed evidence, associated mechanisms, and technical impacts reinforces that the absence of preventive and corrective maintenance has favored not only the onset of damage, but also its evolution and interdependence over time.

Table 1 – Summary of the pathological manifestations identified in the studied reservoir

Pathological manifestation	Evidence observed in the field	Associated mechanism / relation to deficient maintenance	Predominant technical impact
Paint peeling	Loss of adhesion, detachments and surface defects on the shaft	Lack of maintenance and loss of performance of surface protection	Increased exposure of the substrate to weathering and moisture
Cracking and fissures	Visible cracks on external and internal surfaces	Lack of monitoring and treatment, allowing ingress of water and aggressive agents	Loss of watertightness and intensification of deterioration
Infiltration and leakage	Persistent moisture, percolation and water flow marks	Continuity of uncorrected defects and degradation of interfaces	Compromised functional performance, worsening of the pathological condition and potential acceleration of carbonation
Waterproofing system failures	Areas with discontinuities, adhesion failures, degradation and loss of performance	Absence of preventive and corrective maintenance of the watertightness system	Reduced watertightness and increased vulnerability of the concrete
Efflorescence	Whitish deposits, stains and runoff with compound transport	Continuous water percolation and dissolution of compounds from the cementitious matrix	Indication of loss of watertightness and progressive substrate degradation
Reinforcement corrosion	Exposed reinforcement, oxidation signs and deterioration of structural elements	Continuous ingress of moisture and aggressive agents, without repair of affected areas	Reduction of steel cross-section and compromise of structural durability
Concrete cover spalling	Localized material loss, detachment and exposure of reinforcement	Expansion of corrosion products and progression of damage without intervention	Direct exposure of reinforcement and aggravation of structural deterioration
Corrosion in metallic components	Oxidation signs in pipes and internal metallic elements	Humid environment and lack of component maintenance	Loss of performance of elements and indication of environmental aggressiveness

Source: Prepared by the author, 2026.

5.3. Impacts of Deficient Maintenance on the Structure, Service Life, and Associated Risks

The analysis of the real case demonstrates that the absence or insufficiency of maintenance in elevated reinforced concrete reservoirs contributes decisively to the progressive loss of structural performance, promoting the worsening of the observed pathological manifestations and increasing the risks associated with their continued operation. In the studied reservoir, it was verified that the identified degradation does not result from an isolated event, but rather from a continuous process of exposure to moisture, associated with the loss of watertightness, deterioration of surface protection and waterproofing systems, and discontinuity of conservation actions over time.

In this context, manifestations such as paint peeling, fissures and cracks, infiltration, failures in the waterproofing system, spalling, and signs of moisture should not be understood merely as localized anomalies, but as indicators of performance loss and progressive worsening of the pathological condition. The persistence of these occurrences without systematic technical monitoring and without the adoption of appropriate corrective measures favors the evolution of damage, increases the extent of affected areas, and enhances the occurrence of more severe degradation mechanisms, gradually compromising the integrity of structural elements and reducing the service life of the structure.

From a risk perspective, deficient maintenance simultaneously compromises the functionality, durability, and structural safety of the reservoir. At an initial level, the damage affects watertightness and the operational performance of the structure, potentially leading to water loss through leakage, reduced reliability of the storage system, the need for emergency interventions, and increased rehabilitation costs. At more advanced stages, the progression of pathological manifestations may compromise the conservation condition of structural elements, accelerate the overall deterioration of the structure, and increase the risk of performance loss in service and localized instability (Torres, Silva, and Paliga 2016).

In addition to structural and functional effects, deficient maintenance in water reservoirs may also lead to significant sanitary implications. The continuous presence of moisture, sealing failures, surface degradation, and possible biological contamination processes compromise the adequate conservation conditions of the system, potentially affecting the quality of the stored water and increasing users' exposure to inadequate sanitary conditions. Thus, the impacts of deficient maintenance in reinforced concrete reservoirs are not limited to material degradation, but simultaneously affect structural durability, structural safety, system functionality, operational reliability, and sanitary conditions in service (Torres, Silva, and Paliga 2016).

From a maintenance management perspective, the results obtained reinforce that periodic and technically guided inspection constitutes an essential tool for the early identification of anomalies and for the adoption of appropriate interventions before damage evolves into more severe stages with higher recovery costs. Therefore, maintenance should be understood not only as a corrective practice, but as an indispensable strategy for preserving the service life, safety, performance, and reliability of elevated reinforced concrete reservoirs throughout their operation.

6. Conclusions

The present study demonstrated that deficient maintenance in elevated reinforced concrete reservoirs has a direct influence on the evolution of deterioration mechanisms and the progressive loss of structural performance. The pathological manifestations identified, such as cracks, infiltration, waterproofing system failures, efflorescence, reinforcement corrosion, concrete cover spalling, and coating degradation, should not be interpreted merely as isolated occurrences, but rather as part of a continuous and interdependent deterioration process favored by the absence of periodic inspections and adequate preventive maintenance actions.

In the analyzed case study, evidence of loss of watertightness was observed, including degradation and localized absence of waterproofing, signs of leaching, efflorescence, reinforcement corrosion, corrosion of

metallic components, and concrete spalling. These manifestations indicate the simultaneous action of mechanisms associated with continuous water percolation, transport of compounds from the cementitious matrix, reduction of the protection provided by the concrete cover, and the progression of corrosion processes, demonstrating that the observed deterioration already affects elements directly related to durability and structural performance.

The results obtained reinforce that the loss of performance of waterproofing systems is one of the main triggering factors of pathological processes in reinforced concrete reservoirs. The continuous ingress of water through cracks, construction interfaces, and sealing failures promotes carbonation, reinforcement depassivation, corrosion, leaching, and efflorescence formation, establishing a progressive deterioration cycle capable of significantly accelerating the reduction of the structure's service life.

The application of technical inspection combined with damage mapping proved effective for the characterization of the identified pathological manifestations and for correlating the symptoms observed in the field with the deterioration mechanisms described in the literature, contributing to the diagnosis of the structure's conservation condition and to the definition of appropriate corrective interventions.

Therefore, it is concluded that the adoption of systematic inspection, monitoring, and preventive maintenance programs is essential to preserve the structural integrity, extend the service life of elevated reinforced concrete reservoirs, and minimize operational and structural risks. The findings of this study practically demonstrate the impacts of deficient maintenance on the integrity and durability of these structures, showing that the absence of technical monitoring favors the progression of damage, increases rehabilitation costs, and raises risks related to structural safety, operational functionality, and the sanitary conditions of water storage systems. In this context, maintenance should be regarded not as a cost, but as an essential investment for preserving built assets, mitigating risks, and ensuring the safety, reliability, and durability of reinforced concrete reservoirs throughout their service life.

References

Capraro, H. F., M. F. Souza, A. L. Silva, and R. T. Mendes. 2019. "Manifestações patológicas em estruturas de concreto armado: causas e mecanismos." Revista IBRACON de Estruturas e Materiais 12 (5): 987–1005.

Helene, Paulo. 1992. Corrosão em Armaduras para Concreto Armado. São Paulo: Pini.

Helene, Paulo. 1993. "Contribuição ao estudo da corrosão em armaduras de concreto armado." São Paulo: Escola Politécnica da Universidade de São Paulo.

Menezes, R. R., H. N. L. Lira, L. N. L. Santana, and G. A. Neves. 2006. "Eflorescência em materiais à base de cimento." Cerâmica 52 (324): 388–394.

Sampaio, J. P. S., V. M. B. Silva, and J. B. Florian. 2021. "Manifestações patológicas em reservatórios de concreto armado: causas e implicações." Revista ALCONPAT 11 (3): 450–468.

Santos, F. R., V. M. B. Silva, and J. B. Florian. 2022. "Degradação de sistemas de impermeabilização e sua influência na durabilidade do concreto armado." Revista Engenharia Civil 68: 45–60.

Torres, Ariela da Silva, Vívian Michele Bandeira da Silva, and Charlei Marcelo Paliga. 2016. "Patologias em reservatórios elevados de concreto armado." Revista IBRACON de Estruturas e Materiais 9 (4): 565–582.

Souza, Vicente Custódio Moreira de, and Thomaz Ripper. 1998. Patologia, Recuperação e Reforço de Estruturas de Concreto. São Paulo: Pini.

Advanced Resilience Techniques for Historical and Understudied Sacral Architecture – The ARTHUR Project

Mislav STEPINAC[1]

[1] Faculty of Civil Engineering, University of Zagreb, Croatia, mislav.stepinac@grad.unizg.hr

Abstract: This paper presents an ongoing research framework aimed at improving the seismic resilience of historical and understudied sacral architecture through an explicitly multidisciplinary approach. The study focuses on unreinforced masonry churches, which represent a significant portion of the European cultural heritage yet remain insufficiently characterized in terms of structural behaviour, material properties, and vulnerability under seismic loading. The research integrates structural engineering, material characterization, social science perspectives, and digital technologies into a unified methodological framework. Building upon these findings, an expeditious seismic vulnerability assessment method is being developed to enable rapid yet sufficiently reliable evaluation at regional scale. At the current stage, the results are preliminary, as data collection and analysis are ongoing. The expected outcomes include improved assessment methodologies, enhanced understanding of URM behaviour, and transferable strategies for the preservation and strengthening of sacral architecture in seismic regions.

Keywords: church, sacral architecture, URM, earthquake, masonry

1. Introduction

Stone and masonry have been predominant construction materials in Mediterranean regions for centuries, shaping the architectural identity of the area. For monumental structures such as urban churches and cathedrals, stone was carefully cut and laid in courses to ensure stability and durability. In contrast, more modest buildings, including small regional churches, were often constructed using rubble and irregular stones. Over time, these structures incorporated brick masonry as well, creating a distinctive hybrid construction method that blended traditional and evolving techniques. This is particularly evident in sacral traditional (and vernacular) buildings in Croatia, especially in continental regions. While cathedrals and central religious institutions were constructed following the best practices of their time, smaller to medium sacral buildings often adhered to local traditions, using available materials and the limited knowledge of local craftsmen. These types of structures represent a significant portion of sacral buildings worldwide and are important from engineering, architectural, and conservation perspectives. They also hold considerable social and ethnographic significance.

The ARTHUR project, funded by Croatian Science Foundation (HRZZ) will focus on these smaller, understudied but very important sacral buildings. The proposed research aims to address existing gaps by integrating structural, social, and technological approaches into a unified framework for resilience assessment. As these buildings have a profound influence on their communities but are particularly vulnerable to earthquakes, the project will address several critical aspects often overlooked in societal development.

2. State-of-the-art

Historic masonry is a generic term and does not result from industrial or controlled processes; rather, it is an artisan product, influenced by factors such as the availability of materials, the period of construction, the

building's importance, and the skills of the masons (Borri *et al.*, 2018). The seismic vulnerability of historical stone masonry and unreinforced (URM) buildings has been extensively demonstrated by recent earthquakes worldwide (Turkey (Günaydin *et al.*, 2021), Italy (Penna *et al.*, 2019), Greece (Vlachakis, Vlachaki and Lourenço, 2020) and Croatia (Stepinac *et al.*, 2021)). Focusing just on 2nd earthquake in Croatia, more than 57,000 buildings were damaged. Many historical and cultural buildings partially collapsed and/or were severely damaged. The region which suffered the most is characterized by small historical settlements with important parish churches, chapels and isolated noble residences with palaces (Salaman *et al.*, 2022). In the affected region, 308 immovable cultural assets with 4,416 heritage buildings were damaged. According to the World Bank report (*World Bank Report: Croatia Earthquake – Rapid Damage And Needs Assessment, 2020, June 2020, Government of Croatia*) and HCPI (*The Database of Usability Classification, Croatian Centre of Earthquake Engineering (HCPI—Hrvatski Centar za Potresno Inženjerstvo); Faculty of Civil Engineering, University of Zagreb: Zagreb, Croatia, 2020.*), 206 religious heritage buildings were damaged, 52 were severely damaged or demolished. In addition, 50 more churches were damaged but are not under heritage protection. In total, damage to churches is estimated to be 406,7 million euros. When accounting for the Zagreb earthquake, which affected an additional 100 religious buildings with an estimated damage of €778 million, the financial significance of investigating this topic becomes even more evident. Two common types of damage to such churches are shown in Figure 1.



Figure 1 – Damages to traditional churches after Petrinja earthquake in 2020

A comprehensive literature review reveals that sacral architecture is particularly vulnerable to earthquake damage due to its distinctive geometry, construction materials, building techniques, etc. This issue is evident worldwide, with numerous case studies from Italy providing clear evidence of the widespread impact of seismic activity on these structures. Analysis of damage patterns was done by numerous research groups (Casolo *et al.*, 2000; Lagomarsino and Podestà, 2004a, 2004b; Olivito *et al.*, 2019; Uva *et al.*, 2019; Fuentes *et al.*, 2021; Formisano *et al.*, 2022; Imperatore, Lignola and Ferracuti, 2023). The preliminary assessment and damage classification of Croatian sacral architecture was already done by the author and supported with the private company (Studio Arhing) (Anđić, Stepinac and Pojatina, 2024) and will be done extensively by established research group of ARTHUR project. Structural damage is only one of many critical factors; understanding the composition and quality of construction materials is equally essential. If the masonry material is particularly poor, the primary failure mechanism may not be a large-scale structural collapse, but rather the progressive disintegration or crumbling of the masonry itself. Furthermore, the building's overall seismic response depends on the stiffness and interaction of all structural components, including horizontal elements such as floors, vaults, and roof systems. Churches, for instance, often lack

intermediate floors, which distinguishes them from ordinary buildings and renders them more vulnerable to seismic forces. In many cases, churches do not exhibit a unified global behaviour under seismic actions but instead respond as assemblages of macro-elements with autonomous responses. Beyond these considerations, numerous other factors, such as construction techniques, material degradation, and previous modifications must be carefully evaluated. Consequently, earthquakes pose significant risks not only to human life and property but also to heritage. This project will focus on heritage-protected buildings, with a particular emphasis on the understudied sacral architecture of continental Croatia. However, the developed methodology, with appropriate adaptations, has the potential for broader application across the entire Mediterranean region. In addition to engineering perspectives, interdisciplinary studies emphasize the integration of social factors in resilience strategies. The studies on post-disaster social vulnerability assessments (Lo Monaco *et al.*, 2023; Onescu *et al.*, 2024) illustrate how community engagement and ethnographic data enhance understanding of cultural risks. This approach will be mirrored in the Croatian context, ensuring that the proposed methodologies are culturally sensitive and community-focused. Preserving the existing building stock addresses also social challenges, environmental protection, and resource efficiency, and represents a complex engineering process. Sustainable development, a long-term goal of global policy, aims to extend the lifespan of existing buildings. The general concept of building renovation processes emphasizes the principle of "build back better" to retrofit and strengthen damaged buildings, aiming to reduce earthquake risks and improve quality of life.

3. Research group and methodology

The ARTHUR project will diverge by focusing on classifying stone and mixed stone-brick masonry structures and developing a database of their mechanical properties. The proposed research will systematically collect and categorize material properties from approximately 50 churches, incorporating data from existing renovation projects and new on-site investigations. ISCARSAH guidelines will be applied to ensure consistency. The locations of the churches are shown in Figure 2.

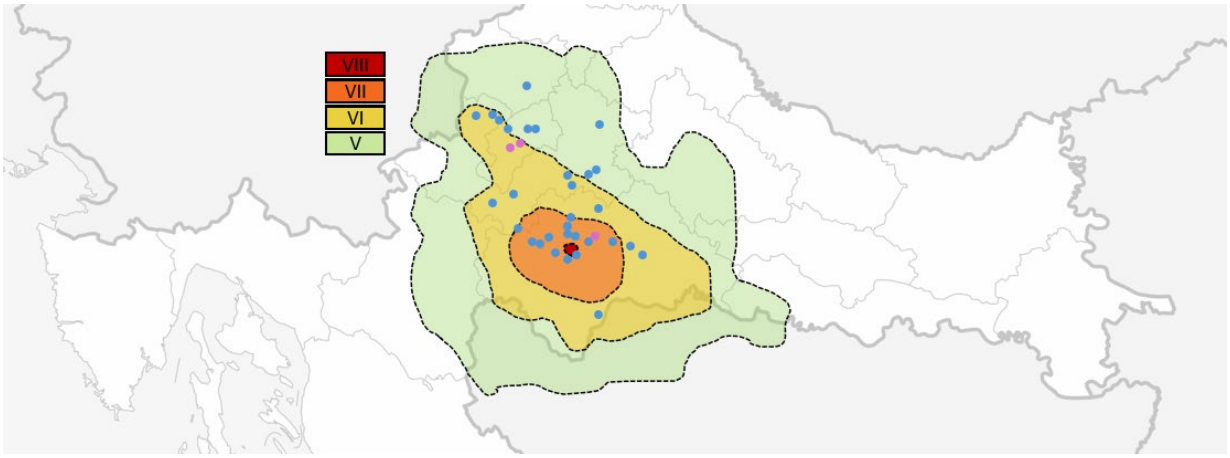


Figure 2 – The distribution of churches to be investigated within the project. Rural churches are marked in blue, while urban city churches are marked in purple, overlaid on the EMS-98 [38] intensity map of Petrinja earthquake

The final step of the project will involve digitalization, representation, and dissemination. Churches will be scanned by laser scanner and/or LiDAR, modelled in 3D and produced as scaled physical models through 3D printing. The project objectives align with several guidelines and global initiatives:

- Venice Charter (1964) and all other International Charters for the Conservation and Restoration of Monuments and Sites.

- Sendai Framework for Disaster Risk Reduction 2015–2030 and United Nations Office for Disaster Risk Reduction to prevent new disaster risks, reduce existing ones, and strengthen resilience through multi-hazard disaster risk management.
- The UN Sustainable Development Goals, particularly Goals 9, 11, and 12, which focus on building resilient infrastructure, making cities inclusive and sustainable, and ensuring responsible consumption and construction patterns.
- UNESCO's Recommendation such as the Recommendation concerning the Preservation of, and Access to, Documentary Heritage Including in Digital Form (2015) and the Recommendation on Science and Scientific Researchers (2017) which underscore the significance of preserving cultural heritage and supporting scientific research in this domain.
- The Kyoto Protocol (1997), Paris Agreement (2015) and all World Climate Summits related to existing buildings and engineering works.
- The European Education Agenda guidelines for actively contributing to improving skills in the construction sector and promoting innovation and sustainability.
- The European Commission's Investment Plan acknowledges that the renovation and maintenance of buildings are fundamental to achieving numerous political objectives, including economic growth, social inclusion, and cultural preservation.
- The New European Bauhaus aims at three fundamental values: sustainability, aesthetics, and inclusion, with a focus on maintaining existing buildings.
- ICOMOS-IFLA Principles (2017): These principles address the preservation of rural landscapes, recognizing their cultural, natural, and historical significance.
- The Smart Specialization Strategy of the Republic of Croatia until 2029 and EU Digital Decade Policy Programme by 2030, setting specific targets in areas like digital skills, infrastructure, and public engagement.

The proposed research is highly interdisciplinary as it involves many fields of technical sciences (civil engineering, fundamental technical sciences, architecture and urban planning, environmental engineering, material science, geodesy, etc.). The multidisciplinary approach is evident in the use and implementation of data from natural sciences (seismology, applied mathematics, and mathematical modelling) and their impact on social (economics, law) and humanities (heritage protection, sociology, ethnology) sciences.

The ARTHUR project's research methodology is designed to provide a comprehensive understanding of the resilience of sacral architecture by integrating structural, social, and technological analyses. The project will be divided into four working groups shown in Figure 3. The project is led by University of Zagreb and supported with numerous scientists from European universities and professionals from Croatian design and architectural offices highly involved in the post-earthquake(s) renovations (also shown in Figure 3).

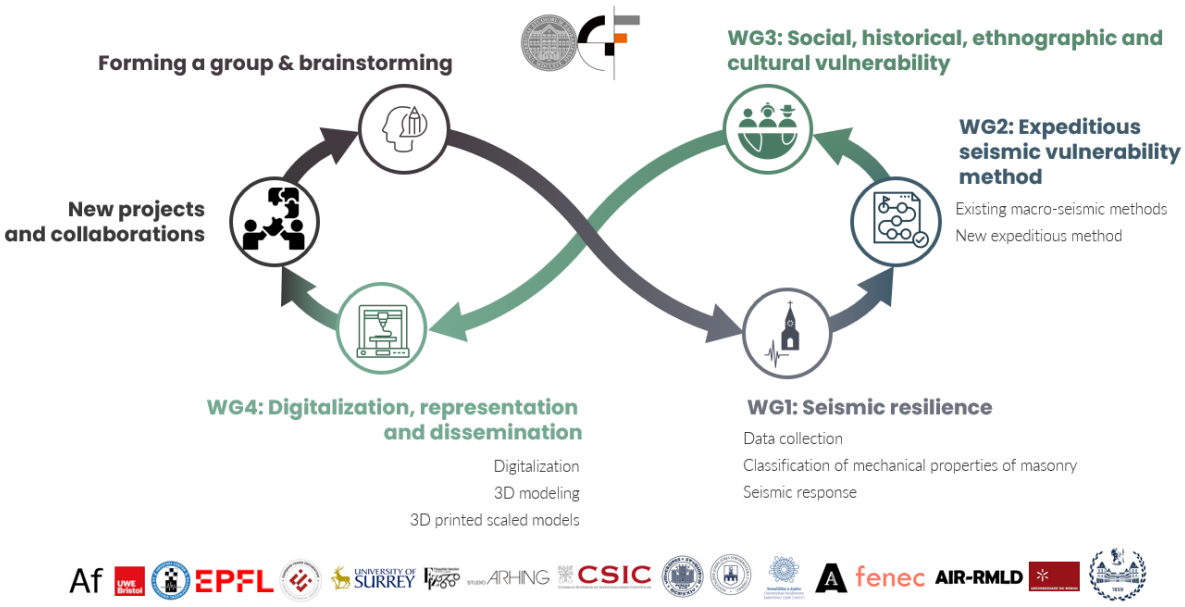


Figure 3 – Working groups of ARTHUR project

4. Conclusion

The presented research establishes a structured and explicitly multidisciplinary framework for addressing the seismic resilience of historical and insufficiently investigated sacral architecture. The approach deliberately moves beyond purely structural considerations by integrating engineering analysis with social-science perspectives and advanced digital technologies, thereby aligning technical performance with cultural significance and community relevance. The ARTHUR project consolidates these dimensions into a coherent methodology that combines seismic vulnerability assessment, detailed structural evaluation, historical and ethnographic interpretation, and digital representation.

At the current stage, the results remain preliminary and should be interpreted as part of an ongoing and progressively expanding research process. A substantial body of documentation is being systematically collected, including data from approximately seventy professional projects, field surveys, and in-situ investigations. This dataset will be further analysed to establish statistically and mechanically consistent classifications of material properties and structural typologies. Particular attention is directed toward the characterization of masonry behaviour through a combination of semi-destructive testing, laboratory analysis, and numerical modelling.

The research is structured through a sequence of interrelated objectives. The initial phase is dedicated to a comprehensive state-of-the-art review and preliminary investigations (O1), ensuring a critical positioning within existing scientific and professional knowledge. This is followed by systematic on-site testing and material classification (O2), which directly inform the development and calibration of numerical models used to simulate seismic response (O3). Building upon these validated models, an expeditious vulnerability assessment method (O4) is being developed to enable rapid yet sufficiently accurate evaluations applicable at regional scale. The final objective (O5) focuses on digitalization, dissemination, and representation, where 3D modelling and additive manufacturing are employed to translate analytical findings into accessible visual and physical formats, supporting both expert interpretation and broader communication.

The integration of digital tools is not treated as a representational afterthought but as an analytical and communicative extension of the research itself. Three-dimensional models, parametric representations, and

scaled printed elements facilitate the exploration of intervention strategies, enabling iterative testing of strengthening approaches while preserving architectural authenticity. In parallel, the inclusion of ethnographic inquiry and stakeholder engagement introduces a dimension that is frequently absent in engineering-driven studies. By systematically incorporating local knowledge, perceptions of risk, and cultural narratives, the project expands the definition of resilience beyond structural capacity toward a more comprehensive socio-cultural construct.

Although definitive conclusions cannot yet be drawn, the anticipated contribution of this research lies in the development of a validated, scalable, and interdisciplinary framework for the assessment and enhancement of sacral architecture. The ongoing expansion and analysis of the dataset are expected to significantly improve the reliability of vulnerability assessments and to bridge the persistent gap between advanced analytical methods and their practical application in heritage contexts.

Acknowledgments

This research was funded by the Croatian Science Foundation, grant number IP-2025-02-4892 (ARTHUR project - Advanced Resilience Techniques for Historical and Understudied Sacral Architecture), project leader: Mislav Stepinac.

References

Anđić, D., Stepinac, M. and Pojatina, J. (2024) "Damage Classification of Sacral Architecture After the Earthquakes in Croatia," RILEM Bookseries, 47, pp. 1065–1076. Available at: https://doi.org/10.1007/978-3-031-39603-8_85.

Borri, A. et al. (2018) "Calibration of a visual method for the analysis of the mechanical properties of historic masonry," Procedia Structural Integrity, 11, pp. 418–427. Available at: https://doi.org/https://doi.org/10.1016/j.prostr.2018.11.054.

Casolo, S. et al. (2000) "Analysis of seismic damage patterns in old masonry church facades," Earthquake Spectra, 16(4), pp. 757–773. Available at: https://doi.org/10.1193/1.1586138.

Formisano, A. et al. (2022) "Seismic vulnerability assessment of two territorial case studies of Italian ancient churches: comparison between simplified and refined numerical models," International Journal of Masonry Research and Innovation, 7(1–2), pp. 172–216. Available at: https://doi.org/10.1504/IJMRI.2022.119890.

Fuentes, D.D. et al. (2021) "Preliminary Seismic Damage Assessment of Mexican Churches after September 2017 Earthquakes," International Journal of Architectural Heritage, 15(4), pp. 505–525. Available at: https://doi.org/10.1080/15583058.2019.1628323.

Günaydin, M. et al. (2021) "Seismic damage assessment of masonry buildings in Elazığ and Malatya following the 2020 Elazığ-Sivrice earthquake, Turkey," Bulletin of Earthquake Engineering [Preprint]. Available at: https://doi.org/10.1007/s10518-021-01073-5.

Imperatore, S., Lignola, G.P. and Ferracuti, B. (2023) "SEISMIC VULNERABILITY ASSESSMENT OF AN ITALIAN ANCIENT CHURCH ACCORDING TO CONVENTIONAL APPROACHES," COMPDYN Proceedings [Preprint]. Available at: https://doi.org/10.7712/120123.10575.21313.

Lagomarsino, S. and Podestà, S. (2004a) "Seismic vulnerability of ancient churches: I. Damage assessment and emergency planning," Earthquake Spectra, 20(2), pp. 377–394. Available at: https://doi.org/10.1193/1.1737735.

Lagomarsino, S. and Podestà, S. (2004b) "Seismic vulnerability of ancient churches: II. Statistical analysis of surveyed data and methods for risk analysis," Earthquake Spectra, 20(2), pp. 395–412. Available at: https://doi.org/10.1193/1.1737736.

Lo Monaco, A. et al. (2023) “Seismic assessment of Romanian Orthodox masonry churches in the Banat area through a multi-level analysis framework,” Engineering Failure Analysis, 153, p. 107539. Available at: https://doi.org/10.1016/J.ENGFAILANAL.2023.107539.

Olivito, R.S. et al. (2019) “Seismic vulnerability of ancient masonry buildings: The case study of low-rise towers,” AIP Conference Proceedings, 2116. Available at: https://doi.org/10.1063/1.5114434.

Onescu, I. et al. (2024) “Simplified Vulnerability Assessment of Historical Churches in Banat Seismic Region, Romania,” International Journal of Architectural Heritage [Preprint]. Available at: https://doi.org/10.1080/15583058.2024.2341054.

Penna, A. et al. (2019) “Damage to churches in the 2016 central Italy earthquakes,” Bulletin of Earthquake Engineering, 17(10), pp. 5763–5790. Available at: https://doi.org/10.1007/S10518-019-00594-4.

Salaman, A. et al. (2022) “Post-Earthquake Condition Assessment and Seismic Upgrading Strategies for a Heritage-Protected School in Petrinja, Croatia,” Buildings 2022, Vol. 12, Page 2263, 12(12), p. 2263. Available at: https://doi.org/10.3390/BUILDINGS12122263.

Stepinac, M. et al. (2021) “Damage classification of residential buildings in historical downtown after the ML5.5 earthquake in Zagreb, Croatia in 2020,” International Journal of Disaster Risk Reduction, 56, p. 102140. Available at: https://doi.org/https://doi.org/10.1016/j.ijdrr.2021.102140.

The Database of Usability Classification, Croatian Centre of Earthquake Engineering (HCPI—Hrvatski Centar za Potresno Inženjerstvo); Faculty of Civil Engineering, University of Zagreb: Zagreb, Croatia, 2020. (no date).

Uva, G. et al. (2019) “Structural vulnerability assessment of masonry churches supported by user-reported data and modern Internet of Things (IoT),” Measurement: Journal of the International Measurement Confederation, 131, pp. 183–192. Available at: https://doi.org/10.1016/J.MEASUREMENT.2018.08.014.

Vlachakis, G., Vlachaki, E. and Lourenço, P.B. (2020) “Learning from failure: Damage and failure of masonry structures, after the 2017 Lesvos earthquake (Greece),” Engineering Failure Analysis, 117. Available at: https://doi.org/10.1016/j.engfailanal.2020.104803.

World Bank Report: Croatia Earthquake – Rapid Damage And Needs Assessment, 2020, June 2020, Government of Croatia (no date).

XXII International Conference on Building Pathology and Constructions Repair
15th to 17th July 2026 - Lisboa, Portugal

Mapping Façade Soiling Patterns through Image Processing

Gabriela LENKIEWICZ[1], Jéssica BERSCH[2], Philippe SOUBRIER[3], Nathan VAN DEN BOSSCHE[4], Inês FLORES-COLEN[5]

[1] Ghent University, Ghent, Belgium, gabriela.lenkiewicz@ugent.be
[2] CERIS, Instituto Superior Técnico, Universidade de Lisboa, Av. Rovisco Pais 1, 1049-001, Lisboa, Portugal, jessica.d.bersch@tecnico.ulisboa.pt
[3] Building Physics Group, Department of Architecture and Urban Planning, Ghent University, Ghent, Belgium, philippe.soubrier@ugent.be
[4] Building Physics Group, Department of Architecture and Urban Planning, Ghent University, Ghent, Belgium, nathan.vandenbossche@ugent.be
[5] CERIS, Instituto Superior Técnico, Universidade de Lisboa, Av. Rovisco Pais 1, 1049-001, Lisboa, Portugal, ines.flores.colen@tecnico.ulisboa.pt

Abstract: Soiling is one of the most prevalent pathologies affecting building façades. While often dismissed as an aesthetic issue, soiling patterns serve as critical indicators of how surfaces interact with moisture, rainfall and environmental degradation agents. Typifying these patterns is essential for understanding the relationship between constructive details, material properties and environmental orientation. However, manual classification is subjective and time-consuming. This paper presents an automated approach to translate digital images of rendered façades in Lisbon, Portugal, into quantified soiling maps using a custom Python-based tool. The framework assigns a Soiling Index to each façade pixel and derives zone-based dirty fractions following the literature. It extracts CIELAB colour metrics and anisotropy indicators. Two case studies with contrasting soiling mechanisms were analysed: Case Study 1 exhibits simultaneous dirt washing and white washing driven by floor-level cornices, with an anisotropy of 3.63 confirming horizontal band dominance, dirt washing producing a strongly achromatic darkening ($\Delta L^* = -14.2$; $\Delta E = 14.3$) and white washing a chromatic yellowing shift ($\Delta b^* = +4.7$; $\Delta E = 4.9$) reflecting the re-emergence of the warm-yellow substrate. Case Study 2 exhibits detail-drip dominated dirt washing with the highest colourimetric contrast in the dataset ($\Delta L^* = -39.8$; $\Delta E = 42.0$) concentrated beneath protruding balconies while the broad panel areas remain clean. The results demonstrate that the proposed image-based method can objectively distinguish and co-locate multiple soiling mechanisms and generate physically interpretable indicators for comparative assessment of façade pathology and for future runoff modelling and predictive maintenance strategies.

Keywords: Façade Pathology, Soiling Patterns, Runoff, Image Processing

1. Introduction

The maintenance and monitoring of building façades represent a persistent challenge in construction management as surfaces age and accumulate soiling driven by runoff, atmospheric deposition and biological colonisation. Façade soiling is more than an aesthetic concern: the spatial distribution of dirt records how surfaces interact with moisture and environmental agents over time (Blocken et al. 2013; Dorsey et al. 1996).

Traditional assessment methods rely on manual visual inspection and established pathology atlases and classification schemes, such as the one proposed by Pereira et al. (2021) in the CIB W86 Report regarding New Trends on Building Pathology. Although widely used in practice, manual surveys are inherently

subjective, labour-intensive and difficult to reproduce across observers or building typologies. Developing systematic, repeatable image-based procedures for classifying and quantifying soiling patterns would substantially accelerate and standardise the assessment of façade soiling. In this context, image processing offers a compelling pathway, as digital façade photographs encode both spatial and chromatic information that can be exploited to distinguish between soiled and unsoiled surface areas and to characterise the nature, extent and distribution of soiling typologies.

This paper presents a custom Python-based image analysis framework for observing and interpreting soiling patterns on rendered building façades. The tool assigns a Soiling Index (SI) to each façade pixel based on its Euclidean distance to empirically defined clean and dirty colour prototypes and derives spatial indicators such as zone-level dirty coverage based on Gaspar and de Brito (2005), which are then interpreted considering existing façade pathology classifications. Two case studies in Lisbon, Portugal, are examined to illustrate how the framework helps distinguish between white washing and dirt washing and to derive physically meaningful quantitative descriptors that form a basis for further analysis.

2. Literature review

2.1 Runoff mechanics

Façade soiling can be interpreted as the visible outcome of rainwater runoff interacting with deposited pollutants, material properties and architectural detailing. On vertical envelopes, wind-driven rain (WDR) is the dominant moisture source because, in still air, façades receive virtually no rainwater apart from local splashback near ground level or at projecting elements (Snape and Atkinson 1999). After impact, each raindrop's mass is partitioned between splashing, bouncing, adhesion, evaporation, absorption and runoff, so only a fraction of the impinging water contributes to surface flow (Abuku et al. 2009; Blocken et al. 2013). Runoff develops once the WDR intensity exceeds the material's instantaneous absorption rate or when the outer zone approaches capillary saturation, marking a transition from inward moisture transport to continuous surface films capable of mobilising and redistributing contaminants (Dorsey et al. 1996; Hens 2010).

Both WDR and the resulting runoff are highly non-uniform in space. Their distribution is governed by building geometry, façade orientation, surrounding topography, wind speed and direction, rainfall intensity and raindrop-size distribution, which together generate strong wetting gradients over façades (Blocken and Carmeliet 2006; Chen et al. 2022; Kubilay et al. 2013). At the material and detail scale, parameters such as surface roughness, contact angle and capillary absorptivity, as well as elements like drips, ledges, joints and projections, further control how water films form, break up and re-attach (Dorsey et al. 1996; Robinson and Baker 1975; Park et al. 2018). Smooth or lightly textured surfaces promote concentrated streams and sharp streaks, while rougher textures induce "broken flow" and more diffuse wetting (Dorsey et al. 1996). Hydrophilic surfaces slow films through strong adhesion, whereas hydrophobic ones favour fast, narrow streams (Park et al. 2018).

2.2 Soiling Typologies

Blocken et al. (2013) distinguish three principal outcomes of repeated runoff over contaminated surfaces: white washing (WW), dirt washing (DW) and dirt accumulation (DA). In white washing, frequent or rapid runoff on exposed surfaces removes deposited particles, leaving zones that appear comparatively clean or lighter than their surroundings. In dirt washing, the same water film concentrates and deposits particles at specific locations, particularly at the runoff termination line where the water film loses momentum or evaporates (Dorsey et al. 1996). Dirt accumulation occurs in sheltered zones where particles settle in the absence of significant surface flow (Blocken et al. 2013).

Architectural details strongly amplify these effects. Horizontal ledges, recessed returns, window perimeters, misaligned joints and protruding fixtures create locally concentrated flow paths and recurring stain

signatures (Chew and Tan 2003; Robinson and Baker 1975). Where vertical flow encounters panel breaks or horizontal joints, part of the water is diverted laterally, producing characteristic vertical streaks below the discontinuity (Chew and Tan 2003). The absence of adequate drip details increases the risk that surface tension causes water to wrap around edges and continue along adjacent surfaces, increasing both wetting duration and staining extent (Robinson and Baker 1975). In rendered façades, prolonged and uneven wetting can also produce ghost-like stains in which non-uniform dust deposition makes the underlying structural grid visible at the surface (Flores-Colen et al. 2008).

2.3 Image Processing

Because soiling mechanisms are visually expressed, image processing provides a logical tool for façade assessment. Manual mapping of stains remains labour-intensive and subjective, whereas image-based analysis can detect localised discoloration in a more systematic and repeatable manner (Torres-Gonzáles et al. 2023). Analysis benefits from segmenting the façade into physically meaningful zones associated with specific runoff and deposition mechanisms (Gaspar and de Brito 2005). This allows image processing results to be interpreted in relation to geometry and moisture exposure rather than as isolated colour variation.

Colour-space selection is therefore critical. In principle, CIELAB is better aligned with human perception, because it separates lightness from chromatic variation and supports ΔE-based thresholds such as the just noticeable difference at $\Delta E \approx 2.3$ (Torres-Gonzáles et al. 2023; Muratbekova et al. 2025). However, exploratory tests in this research showed substantial overlap between clean and soiled areas in the a* and b* channels, so that meaningful separation could only be achieved through the L* component, which is highly sensitive to shadowing and illumination changes. By contrast, all three RGB channels exhibited relatively low overlap between classes, and the discriminative signal was distributed in a similar way across R, G and B, allowing the classifier to exploit both chromatic differences and overall brightness variations without relying exclusively on a lightness-like dimension. For this reason, despite its known perceptual limitations, the RGB colour space was ultimately adopted as the primary working space for the façade image analysis in this study.

3. Methodology

3.1 Case Study Selection and Location

Two buildings with rendered façades in Lisbon, Portugal, were selected to evaluate the image processing framework. The selected buildings exhibit contrasting soiling typologies under comparable urban conditions. Both buildings are situated in areas characterised by high population density, which is associated with elevated atmospheric particulate concentrations and restricted airflow, conditions known to intensify façade soiling (D'Orazio et al. 2023).

Case Study 1, located at R. Dona Filipa de Vilhena 7 (Figure 1), presents an east-oriented coating mortar façade showing evidence of white washing across exposed surface zones. Case Study 2, situated at Av. de António José de Almeida 46 (Figure 1), presents a south-oriented façade with pronounced dirt washing concentrated below architectural details. The contrasting soiling mechanisms of the two buildings (Figure 2) provide a suitable basis for evaluating the discriminative capacity of the image processing tool across different physical conditions.



Figure 1 - Geographic context and location of the selected case study buildings in Lisbon, Portugal. Case Study 1 is indicated in blue (R. Dona Filipa de Vilhena 7) and Case Study 2 in green (Av. de António José de Almeida 46).



Figure 2 - Ground-level views of the façades of Case Study 1 (left) and Case Study 2 (right).

3.2 Image acquisition and Preprocessing

Façade images were captured at ground level using a smartphone camera. To enhance chromatic consistency across the image dataset, a colour calibration procedure was applied using a ColorChecker reference chart. The ColorChecker comprises colour patches with known spectral properties. When present in an image, recorded colours can be compared with their reference values to generate a correction profile that addresses white balance, exposure, and sensor response deviations.

Prior to analysis, each image was manually masked in Photoshop to exclude non-façade elements such as windows, balconies, pipes and sky. All excluded regions were replaced with uniform white pixels (RGB values ≥ 245 across all three channels). This masking step ensures that the classifier operates exclusively on exposed façade material and is not influenced by architectural elements or background (Figure 3).

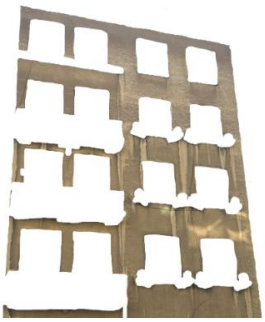


Figure 3 - Overview of the façade of Case Study 1 after manual removal of non-façade elements with Photoshop.

3.3 Image Processing Framework

The analysis tool was implemented in Python and comprises eight processing steps. The framework proceeds from image loading through prototype selection, classification, spatial analysis and cross-case export. The accompanying Figure 4 provides a flowchart illustrating the overall process.

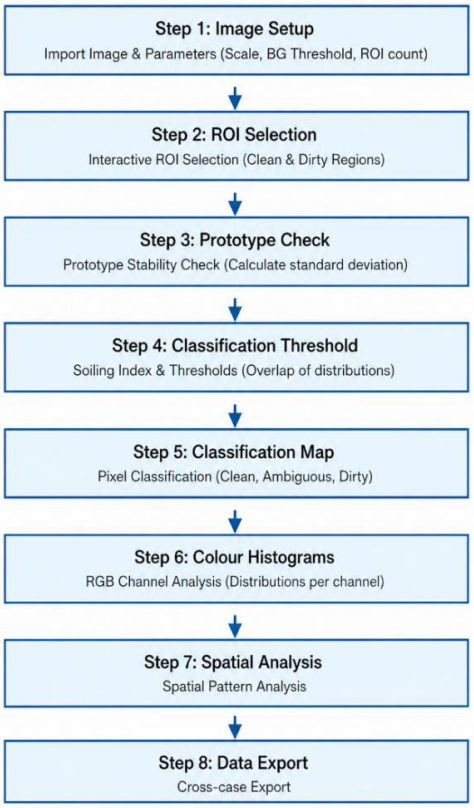


Figure 4 - Overview of the methodological workflow adopted in this study.

Step 1, “Settings and Image Loading”, is where the image is imported, the scale of the picture is chosen, the threshold to delete the background (BG_TRESH) is set and the amount of Region of Interests (ROIs) that the user wants to select for dirty and clean are defined. The background mask removes white sky or border pixels above BG_THRESH = 245, so only real facade pixels are analysed.

Step 2, “Multi ROI-selection”, selects the ROIs of clean and dirty regions on the façade depending on the amount chosen in step 1. The user varies the position of each ROI on the façade so that the prototypes represent the full range of clean and dirty zones, not just one localised spot. Each selected rectangle is cropped from the image and stored as a flat array of RGB pixel values. The coordinates are also saved for later visualisation.

Step 3, “Prototype stability check”, verifies whether the selected ROIs are consistent for R, G and B using the standard deviation (std) across the ROI means:

- std < 10: stable;
- std 10–20: moderate;
- std > 20: unstable.

Step 4, “Soiling index and thresholds”, calculates the Soiling Index (SI) for every ROI pixel and determines the classification threshold from the histogram overlap of the two ROI distributions (clean and dirty), with Equation (1).

$$Soiling\ index\ (SI) = \frac{d_{clean}}{d_{clean} + d_{dirty}} \tag{1}$$

Where:

$$d_{clean} = \sqrt{\left(R_{pixel} - R_{mean,\ clean}\right)^2 + \left(G_{pixel} - G_{mean,\ clean}\right)^2 + \left(B_{pixel} - B_{mean,\ clean}\right)^2} \tag{2}$$

$$d_{dirty} = \sqrt{\left(R_{pixel} - R_{mean,\ dirty}\right)^2 + \left(G_{pixel} - G_{mean,\ dirty}\right)^2 + \left(B_{pixel} - B_{mean,\ dirty}\right)^2} \tag{3}$$

A histogram with 50 bins is constructed for the clean and dirty SI distributions. A bin counts as overlap only if both distributions have at least 5% of their own peak density in that bin, preventing tail pixels from inflating the ambiguous zone. The lower and upper bounds of this overlap define the classification thresholds, with THRESH_CLEAN set to the lower bound and THRESH_DIRTY to the upper bound:

- Overlap found: THRESH_CLEAN to THRESH_DIRTY forms the ambiguous zone;
- No overlap: single boundary at SI = 0.5, classification is fully reliable.

Step 5, “Classification and visualization”, classifies every façade pixel using the thresholds from step 4 and produces a 3-panel figure: original image, colour-coded segmentation map and SI heatmap. Each pixel receives one of three labels:

- Clean (green): SI < THRESH_CLEAN;
- Ambiguous (yellow): THRESH_CLEAN ≤ SI ≤ THRESH_DIRTY;
- Dirty (red): SI > THRESH_DIRTY.

If no overlap is found in step 4, THRESH_CLEAN = THRESH_DIRTY = 0.5, and there is no ambiguous zone. Coverage is computed by counting pixels per class and dividing by the total, ensuring the three percentages always sum to exactly 100%.

Step 6, “RGB channel histograms”, show the distribution of raw R, G and B pixel values from the clean and dirty ROIs separately, one panel per channel. For each channel the overlap area between the two distributions is calculated. A lower overlap means that channel alone can better separate the two classes. These plots help to understand which colour channel carries the most discriminative information.

Step 7, “Spatial Pattern Analysis”, assesses the spatial distribution of soiling across the façade to identify where soiling concentrates through zone-based analysis and to detect directional patterns in soiling distribution, known as anisotropy. The façade is divided into four analytical zones adapted from the framework proposed by Gaspar and de Brito (2005), who originally developed six zones for comprehensive assessment of façade degradation: (1) at or near floor level, (2) on continuous walls, (3) around openings, (4) at parapets, below copings and eaves, (5) below balconies or soffits and (6) in the corners and edges. The adapted zones for this research are summarized in Table 1.

Table 1 - Façade zones used in the spatial analysis.

Zone	Position	Physical significance
Z1	v < 0.15 (roof edge / parapet)	Highest wind-driven rain catch ratio
Z2	0.15 ≤ v < 0.70 (central façade plane)	Main exposed surface, presence of architectural elements
Z3	0.70 ≤ v < 1.00 (lower façade plane)	Main exposed surface, presence of architectural elements
Z4	u < 0.05 or u > 0.95 (vertical edges and corners)	Streamline compression and runoff concentration

For each of the four zones (Z1–Z4), the percentage of dirty pixels is extracted from the classification map generated in the previous step. The zone with the highest percentage is identified as the most affected zone, indicating where soiling is most concentrated on that façade.

Step 8, "Cross-case export", exports all key results to a cross-case CSV file, allowing multiple façades and case studies to be compared in a single table. For each façade, the following metrics are saved:

- Coverage: % clean, % ambiguous, % dirty;
- SI statistics: mean, std;
- Thresholds: THRESH_CLEAN, THRESH_DIRTY, separability gap;
- Colour prototypes: mean R, G, B for clean and dirty;
- Pattern metrics: anisotropy;
- Zone analysis.

A new script (detail_analysis) performs a zoom-level analysis of façade images to inspect local soiling patterns in more detail. It computes ΔE and ΔL*, Δa*, Δb*, as well as RGB values for clean and dirty reference regions and for each identified soiling type and appends these results to the same cross-case CSV file generated in step 8.

3.4 Spatial and Colour metrics

3.4.1 ΔE and ΔL*, Δa*, Δb*

Colour characterisation at the soiling-type level is performed on detailed photographs analysed separately from the full-façade classification. For each soiling zone, mean CIELAB values are extracted for both the soiled area and an adjacent unsoiled reference area on the same façade. The total perceptual colour difference ΔE (CIE76) is computed as the Euclidean distance between the two mean Lab vectors, in Equation (4):

$$E = \sqrt{\Delta L^2 + \Delta a^2 + \Delta b^2} \tag{4}$$

Perception thresholds follow those of Torres-Gonzáles et al. (2023):

- ΔE ≤ 1.0 is imperceptible;
- 1.0 < ΔE < 2.3 is perceptible only upon close inspection;
- ΔE = 2.3 defines the just noticeable difference (JND);
- ΔE > 5.0 is clearly visible to an average observer.

The lightness component ΔL* indicates whether the soiled zone is darker (ΔL* < 0) or lighter (ΔL* > 0) than the unsoiled reference. The chromatic components Δa* and Δb* describe shifts along the red–green and

yellow–blue axes, respectively. A negative Δa* indicates a shift toward green, which can be associated with biological colonisation such as algae or moss growth.

3.4.2 Anisotropy

The anisotropy ratio is defined as the variance of the vertical dirt profile divided by the variance of the horizontal dirt profile. Values exceeding 2.0 indicate that dirtiness varies predominantly with height, consistent with horizontal banding. Values below 0.5 indicate that dirtiness varies predominantly with horizontal position, consistent with vertical streaks. Values close to 1 indicate a diffuse spatial pattern.

4. Results

4.1 Case Study 1

Case Study 1 presents an east-oriented façade exhibiting the highest mean soiling index in the dataset (SI = 0.615) and a clear progressive increase in runoff concentration from top to bottom. The soiling index heatmap (Figure 5) reveals strongly banded soiling organised in persistent horizontal bands at each floor level, driven by the protruding cornices that act as runoff concentrators. The anisotropy value of 3.63 confirms that soiling is directionally organised horizontally, consistent with runoff-dominated deposition rather than a diffuse or vertically streaked pattern.

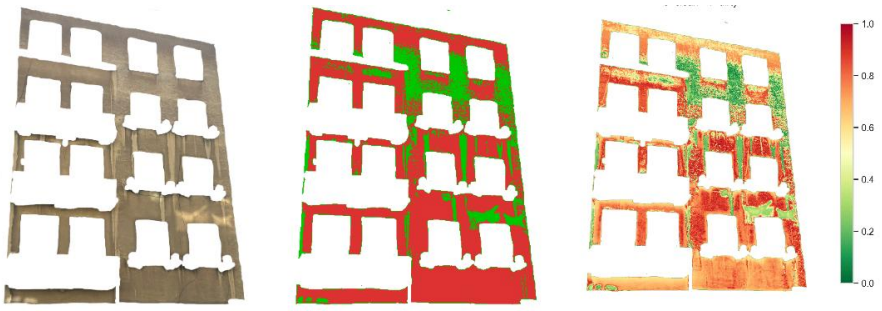


Figure 5 - Classification output for Case Study 1. Left: original image, centre: segmentation map (green = clean, red = dirty), right: Soiling Index heatmap (0 = clean, 1 = dirty).

Table 2 - Summary of zone-level soiling metrics for Case Study 1.

Case study	% dirty per zone			Anisotropy
	Z1	Z2	Z3	
1	62.24	57.19	86.28	3.63

The zone-level results (Table 2) confirm a progressive floor-by-floor soiling gradient: the lower zone Z3 registers 86.28% dirty surface, substantially higher than the upper zone Z1 at 62.24%. This vertical gradient results from the cumulative superimposition of runoff streams from successive upper floors. At each cornice, particle-laden water intercepted from the panel above is channelled along the underside until it detaches at the drip edge and impacts the panel below, depositing a concentrated runoff termination line. Because each lower floor receives contributions from all floors above, the particle load increases progressively toward the façade base (Chew and Tan 2003; Blocken et al. 2013).

The detailed colourimetric analysis (Table 3) reveals that two mechanisms operate simultaneously on the same runoff bands in zone Z2 and are colourimetrically distinguishable. Dirt washing produces a strongly achromatic darkening: ΔE = 14.3 is almost entirely carried by ΔL* = −14.2, with negligible chromatic shifts (Δa*

= 0.0; Δb* = −1.1), consistent with the deposition of spectrally neutral urban particulates. White washing, understood as light streaks and bands produced where frequent or rapid runoff on exposed surfaces removes previously deposited particles, results in a smaller but clearly perceptible colour difference (ΔE = 4.9), dominated by a shift towards yellow (Δb* = +4.7) with modest lightening (ΔL* = +1.2). This behaviour is consistent with flow-based weathering models in which runoff selectively washes out fine particulate deposits along preferential flow paths, leaving locally cleaner, lighter zones adjacent to darker, particle-laden runoff bands (Dorsey et al. 1996; Blocken et al. 2013). In the present case, the observed yellow shift most likely reflects the re-emergence of the façade's inherent warm-yellow substrate colour in these lighter bands, which appears muted in the adjacent dirt-washed zones. The easterly orientation of the façade promotes frequent wetting–drying cycles after rain events, which is known to intensify moisture-related degradation and soiling by increasing the number of cycles over which particles and dissolved material can be redistributed and fixed along runoff paths (Robinson and Baker 1975; Blocken et al. 2013).

Table 3 - CIELAB colorimetric shifts for dirt washing and white washing in zone Z2 of Case Study 1.

Soiling type	ΔE	ΔL*	Δa*	Δb*
Dirt washing	14.3	−14.2	0.0	−1.1
White washing	4.9	+1.2	0.5	+4.7

4.2 Case Study 2

Case Study 2 presents a rendered south-facing façade that illustrates the detail-drip mechanism with exceptional clarity. Despite an overall Moderate soiling level of 16.65%, the soiling index heatmap (Figure 6) concentrates soiling almost exclusively beneath protruding architectural details, balconies and window sills, leaving the broad panel areas between them comparatively clean. This binary contrast is consistent with the runoff termination mechanism described by Dorsey et al. (1996).

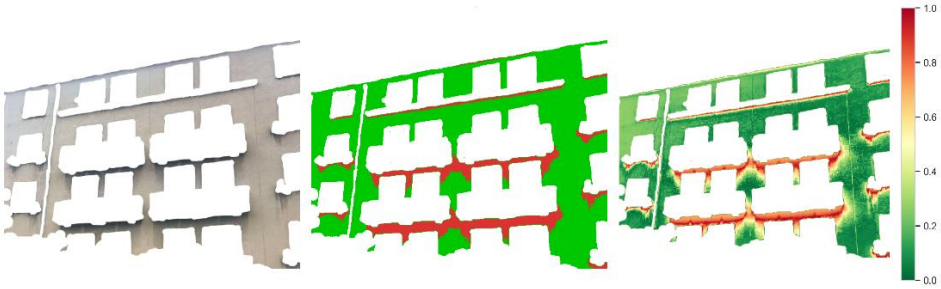


Figure 6 - Classification output for Case Study 2. Left: original image, centre: segmentation map (green = clean, red = dirty), right: Soiling Index heatmap (0 = clean, 1 = dirty).

Table 4 - Summary of zone-level soiling metrics for Case Study 2. % dirty per zone, anisotropy and CIELAB colour metrics for the dominant dirt washing mechanism (detail-drip).

Case study	% dirty per zone			Anisotropy	ΔE	ΔL*
	Z1	Z2	Z3			
2	0.69	11.40	29.52	1.03	42.0	-39.8

The zone-level results (Table 4) confirm the spatial localisation of soiling. The lower façade zone (Z3) carries the highest dirty fraction (29.52%), whereas the roof edge (Z1) remains largely unaffected. The central zone

(Z2) and lower façade zone (Z3) reflect partial staining from detail elements in the mid-height range. This pattern is mechanistically explained by a three-phase runoff sequence operating at each protruding balcony. First, the balcony intercepts the downward-moving water film and concentrates it along its upper surface. Second, once the flow intensity exceeds the surface tension, the water detaches at the outer edge and falls as a narrow-concentrated jet. Third, this jet impacts the wall directly below, depositing a dense particle band — the runoff termination line, that dries out and progressively fades with distance from the balcony edge (Robinson and Baker 1975; Blocken et al. 2013). This repetitive motif reappears identically at each architectural element, confirming that the detailed geometry is the primary organiser of soiling on this façade.

The colourimetric analysis confirms the extreme contrast between the clean panels and the soiled drip zones. The lightness shift $\Delta L^* = -39.8$ and the total colour distance $\Delta E = 42.0$ are the highest values in the dataset, substantially exceeding the clearly visible threshold ($\Delta E > 5.0$). The strongly negative ΔL^* confirms that soiling manifests as an intense, purely achromatic darkening consistent with concentrated atmospheric particulate deposition. The anisotropy of 1.03 indicates a diffuse spatial pattern at the whole-façade scale, reflecting that the individual dark bands beneath details occupy only a small fraction of the total surface and do not dominate the directional statistics. Because the south-facing orientation receives significant wind-driven rain loading only during limited intense rainfall episodes, the large panel areas remain dry between events, while the zones beneath the details are recharged and re-stained at each event (Blocken et al. 2013).

5. Conclusion

This study demonstrates that image processing can classify and quantify façade soiling patterns in a systematic and physically interpretable manner. The nearest-prototype Soiling Index classifier, operating in RGB colour space with reference prototypes derived from user-selected regions of interest and thresholds determined by histogram overlap of ROI distributions, successfully differentiates between soiled and unsoiled surface areas across two case studies exhibiting contrasting soiling mechanisms.

Case Study 1 showed a progressive, floor-by-floor runoff-concentration along the cornices, with two antagonistic processes acting on the same cornice-driven bands. Dirt washing is dominant, producing a strong achromatic darkening ($\Delta L^* = -14.2$; $\Delta E = 14.3$) with an almost neutral chromatic shift ($\Delta b^* = -1.1$). White washing, understood as light streaks and bands produced where frequent or rapid runoff on exposed surfaces removes previously deposited particles, results in a smaller but clearly perceptible colour difference ($\Delta E = 4.9$), dominated by a shift towards yellow ($\Delta b^* = +4.7$), indicating renewed visibility of the façade's warm-yellow substrate in these lighter bands (Dorsey et al. 1996). An anisotropy of 3.63 confirms the dominance of horizontally aligned bands.

Case Study 2 confirmed a detail-drip soiling regime in which protruding balconies and sills function as runoff concentrators, producing the highest colourimetric contrast in the dataset ($\Delta E = 42.0$; $\Delta L^* = -39.8$) while leaving the broad panel areas clean. The method successfully resolved the co-occurrence of two colourimetrically distinct mechanisms in Case Study 1 and identified the governing architectural detail in Case Study 2, demonstrating its capacity to generate physically interpretable indicators beyond simple classification. The quantitative outputs of the framework, SI coverage by class, zone-level dirty fractions, anisotropy and CIELAB colour metrics are mutually consistent and align with the physical mechanisms documented in the literature.

The key innovation of the approach lies in bridging visual observation and quantitative assessment: the soiling index heatmap functions as a structured visual support that guides and validates the observer's interpretation, while the extracted metrics provide an objective, reproducible basis for drawing conclusions that would otherwise depend on subjective judgment. This combination allows soiling typologies, their spatial organisation and their colourimetric signatures to be characterised from standard digital

photographs without specialised equipment, making the method accessible for practical inspection workflows. The framework, therefore, provides a reproducible basis for comparative façade degradation assessment that is not dependent on the subjectivity of manual visual inspection.

Key limitations include sensitivity to ROI selection, variable image quality under field conditions, and the inability to correct for spatially structured illumination differences such as shadows or surface reflections, which can introduce systematic bias into the soiling index.

Several directions for future research emerge from these findings. Extending the method to a larger and more diverse building stock would allow the relationship between architectural typology, material properties, orientation and soiling severity to be systematically characterised across different urban contexts. At the methodological level, automating ROI selection through supervised or self-supervised learning would reduce observer dependency and improve reproducibility across operators. Finally, coupling the image-based soiling index with runoff modelling frameworks would enable the observed spatial patterns to serve as validation data for physically based simulations, closing the loop between field observations and predictive modelling of façade weathering.

Acknowledgments

This research was funded by the Foundation for Science and Technology (FCT) (FCT, https://ror.org/00snfqn58) under the funding UID/6438/2025 (https://doi.org/10.54499/UID/06438/2025) of the CERIS research unit, the scholarship 2023.05316.BD (https://doi.org/10.54499/2023.05316.BD), and the FCT funding ReCoveRing project (https://doi.org/10.54499/2023.17249.ICDT).

References

Abuku, M, B Blocken, and S Roels. 2009. "Moisture response of building facades to wind-driven rain: Field measurements compared with numerical simulations." *JOURNAL OF WIND ENGINEERING AND INDUSTRIAL AERODYNAMICS* 97 (5-6): 197–207. https://doi.org/10.1016/j.jweia.2009.06.006.

Blocken, B, and J Carmeliet. 2006. "The influence of the wind-blocking effect by a building on its wind-driven rain exposure." *JOURNAL OF WIND ENGINEERING AND INDUSTRIAL AERODYNAMICS* 94 (2): 101–127. https://doi.org/10.1016/j.jweia.2005.11.001.

Blocken, B, D Derome, and J Carmeliet. 2013. "Rainwater runoff from building facades: A review." *BUILDING AND ENVIRONMENT* 60: 339–361. https://doi.org/10.1016/j.buildenv.2012.10.008.

Burambekova, Aruzhan, and Pakizar Shamoi. 2024. COMPARATIVE ANALYSIS OF COLOR MODELS FOR HUMAN PERCEPTION AND VISUAL COLOR DIFFERENCE.

Chen, C, HB Zhang, C Feng, YL Xuan, TD Qian, and JC Xie. 2022. "Analysis of wind-driven rain characteristics acting on building surfaces in Shanghai based on long-term measurements." *JOURNAL OF BUILDING ENGINEERING* 45. https://doi.org/10.1016/j.jobe.2021.103572.

Chew, MYL, and PP Tan. 2003. "Facade staining arising from design features." *CONSTRUCTION AND BUILDING MATERIALS* 17 (3): 181–187. https://doi.org/10.1016/S0950-0618(02)00102-2.

D'Orazio, M, E Quagliarini, and A Gianangeli. 2023. "Influence of the rain on algae growth on building facades. A predictive model based on neural networks." *BUILDING AND ENVIRONMENT* 246. https://doi.org/10.1016/j.buildenv.2023.110990.

Dorsey, Julie, Hans Køhling Pedersen, and Pat Hanrahan. 1996. Flow and Changes in Appearance.

Flores-Colen, I, J de Brito, and VP de Freitas. 2008. "Stains in facades' rendering - Diagnosis and maintenance techniques' classification." *CONSTRUCTION AND BUILDING MATERIALS* 22 (3): 211–221. https://doi.org/10.1016/j.conbuildmat.2006.08.023.

Gaspar, P, and J de Brito. 2005. "Mapping defect sensitivity in external mortar renders." *CONSTRUCTION AND BUILDING MATERIALS* 19 (8): 571–578. https://doi.org/10.1016/j.conbuildmat.2005.01.014.

Hens, Hugo. 2010. Wind-Driven Rain: From Theory to Reality. University of Leuven (K.U. Leuven), Leuven, Belgium.

Kubilay, A, D Derome, B Blocken, and J Carmeliet. 2013. "CFD simulation and validation of wind-driven rain on a building facade with an Eulerian multiphase model." *BUILDING AND ENVIRONMENT* 61: 69–81. https://doi.org/10.1016/j.buildenv.2012.12.005.

Muratbekova, Muragul, Nuray Toganas, Ayan Igali, Maksat Shagyrov, Elnara Kadyrgali, Adilet Yerkin, and Pakizar Shamoi. 2025. Color Models in Image Processing: A Review and Experimental Comparison. School of Information Technology and Engineering, Kazakh-British Technical University, Almaty, Kazakhstan.

Park, CW, J Park, N Kim, and Y Kim. 2018. "Modeling water flow on Facade." *AUTOMATION IN CONSTRUCTION* 93: 265–279. https://doi.org/10.1016/j.autcon.2018.05.021.

Pereira, C, J de Brito, I Flores-Colen, and J.D. Silvestre. 2021. *Atlas of defects within Inspection Systems in New Trends on Building Pathology*. Edited by J de Brito and I Flores-Colen.*CIB W086 Report*: International Council for Research and Innovation in Building and Construction (CIB).

Robinson, G., and M. C. Baker. 1975. Wind-driven rain and buildings. Technical Paper (National Research Council Canada. Division of Building Research).

Snape, P, and B Atkinson. 1999. "Mapping rainfall distribution characteristics on facades using surface deposit geometry." DURABILITY OF BUILDING MATERIALS AND COMPONENTS 8, VOLS 1-4, PROCEEDINGS, BUILDING M-55, OTTAWA, ON KIA OR6, CANADA, 1999–01–01.

Torres-Gonzáles, M, J Valença, BO Santos, A Silva, and MP Mendes. 2023. "StainView: A Fast and Reliable Method for Mapping Stains in Facades Using Image Classification in HSV and CIELab Colour Space." *REMOTE SENSING* 15 (11). https://doi.org/10.3390/rs15112895.

Cinpar 2026
XXII International Conference on Building Pathology and Constructions Repair
15th to 17th July 2026 - Lisboa, Portugal

Impactos da Manutenção Baseada na Condição no Desempenho da Envolvente dos Edifícios

Ilídio DIAS[1], **Giovanna BARTELS[2]**, Inês FLORES-COLEN[3], Ana SILVA[4]

[1] CERIS, Civil Engineering Research and Innovation for Sustainability, Instituto Superior Técnico, Universidade de Lisboa, Av. Rovisco Pais, 1049-001 Lisboa, Portugal, ilidio.dias@tecnico.ulisboa.pt
[2] CERIS, Civil Engineering Research and Innovation for Sustainability, Instituto Superior Técnico, Universidade de Lisboa, Av. Rovisco Pais, 1049-001 Lisboa, Portugal, giovanna.schafer@tecnico.ulisboa.pt
[3] CERIS, Civil Engineering Research and Innovation for Sustainability, Instituto Superior Técnico, Universidade de Lisboa, Av. Rovisco Pais, 1049-001 Lisboa, Portugal, ines.flores.colen@tecnico.ulisboa.pt
[4] CERIS, Civil Engineering Research and Innovation for Sustainability, Universidade Lusófona, Campo Grande 376, 1749-024 Lisboa, Portugal, ana.silva.matos@ulusofona.pt

Abstract: The building envelope significantly influences the durability, safety, and functional performance of buildings throughout their service life. However, maintenance is frequently managed reactively, limiting its potential to mitigate degradation and optimize life-cycle costs. While predictive models have been developed and applied in different fields of maintenance in engineering, their alignment with observed in-situ performance remains insufficiently explored.

This study discusses how maintenance affects the durability, costs, and safety of building-envelope elements by integrating empirical inspection data with a stochastic condition-based maintenance model. The analysis is based on nineteen case studies located in Portugal, comprising different building typologies and envelope systems.

Fieldwork inspections were conducted before and after maintenance interventions. Degradation was documented through visual assessment and software-assisted quantification. A stochastic condition-based maintenance framework was applied to simulate degradation progression and intervention strategies. Corrective maintenance was incorporated when elements reached unacceptable degradation levels. This approach made it possible to evaluate how well the model reflected real in-situ performance and to assess how different maintenance strategies affect the claddings' service life and related maintenance costs.

The results reveal that maintenance actions have a measurable impact on service life. The stochastic model was slightly conservative compared with *in situ* observations, but it adequately reproduced overall degradation patterns. The findings demonstrate that maintenance, when strategically planned and condition-based, can be quantified in terms of durability gains and cost implications, supporting its integration as a structured decision-making component in building life-cycle management.

Keywords: Manutenção baseada na condição, envolvente dos edifícios, durabilidade, modelação de degradação.

1. Introdução

A envolvente de um edifício pode ser entendida como a sua "pele", uma vez que estabelece a interface entre os espaços interiores e os agentes externos de degradação (Derakhshi 2020). Através desta função, garantindo níveis contribui para garantir condições adequadas de conforto interior, segurança, e capacidade de adaptação a novas exigências ao longo da vida útil do edifício. Assim, o seu desempenho

assume um papel decisivo na durabilidade e na qualidade global do edifício (Brito et al. 2020; Silva, De Brito, and Gaspar 2016; Watt 2007).

Apesar da sua relevância, a envolvente está particularmente exposta a processos de envelhecimento e deterioração, frequentemente agravados pela ausência de manutenção adequada(Brito et al. 2020; Silva, De Brito, and Gaspar 2016; Watt 2007). Na Europa, e em particular em Portugal, as estratégias de manutenção são maioritariamente corretivas, onde as reparações são realizadas após a ocorrência da "falha", ou no caso dos revestimentos, após presença de anomalias que comprometem o desempenho do revestimento (Jernberg et al. 2004; Long, Henderson, and Montgomery 2001). Esta prática contribui para uma deterioração mais rápida, custos de ciclo de vida mais elevados, redução da vida útil e comprometem o desempenho a longo prazo dos edifícios (Brito et al. 2020; Lopes 2011; Mouratidis 2021; Sandak 2019; Sarja 2002).

Em contrapartida, a manutenção baseada na condição concilia a monitorização ou inspeção do elemento com a análise do seu estado e a subsequente execução de intervenções (CEN 2021). Esta metodologia permite correlacionar o desempenho dos elementos construtivos com a sua probabilidade de falha, promovendo uma recolha sistemática de informação (Cláudia Ferreira et al. 2023). Adicionalmente, esta abordagem prolonga o patamar mínimo de desempenho do edifício e otimiza os custos face à manutenção preventiva predeterminada, enquanto prioriza a redução do risco de falha em comparação com a estratégia corretiva (Lind and Muyingo 2012).

Este estudo combina inspeções in situ com um modelo estocástico de manutenção baseada na condição para examinar a sua influência no desempenho da envolvente do edifício. Embora investigações anteriores neste domínio tenham recorrido a redes de Petri, as suas aplicações assumem pressupostos teóricos com base em dados empíricos, ou seja, com base em vários dados de inspeções a edifícios in situ, anos após a sua aplicação (Dias 2025). O contributo deste trabalho consiste na validação empírica de modelos através da comparação entre as condições reais observadas imediatamente antes e após intervenções. A partir da avaliação de dezanove casos de estudo antes e depois das intervenções de manutenção, esta investigação propõe uma abordagem baseada em evidência empírica que vai além da aplicação isolada de modelos preditivos ou de estratégias corretivas. A recolha de dados in situ permite quantificar a melhoria no estado de conservação dos revestimentos associada às intervenções, avaliar a adequação das transições estocásticas previstas pelos modelos e analisar os seus impactes nos custos e na segurança. Desenvolvida no âmbito do projeto BestMaintenance-LowerRisks (Cláudia Ferreira et al. 2023), esta abordagem integrada contribui para uma calibração mais fiável dos efeitos da manutenção e para uma representação mais rigorosa do desempenho observado em condições reais de serviço.

2. Metodologia

Para avaliar a influência da manutenção na durabilidade, nos custos e na segurança, implementou-se uma metodologia baseada em inspeções nos dezanove casos de estudo selecionados. As inspeções foram realizadas antes e após as intervenções de manutenção, permitindo a comparação direta dos estados de degradação e da evolução do desempenho. Posteriormente, analisaram-se os custos, o estado de degradação e a segurança através de uma matriz de risco de queda de revestimentos em pedra natural aplicados em fachadas.

O estado de degradação dos elementos foi determinado com base no índice de severidade da degradação (S_w). Este índice quantifica o estado global de degradação de um elemento através da razão entre a área degradada, ponderada em função do nível de degradação e da gravidade das anomalias identificadas, e uma área de referência, que corresponde à superfície total do elemento no estado de degradação mais grave possível (Equação 1).

$$S_w = \frac{\Sigma\left(A_n \times k_n \times k_{a,n}\right)}{A \times \Sigma k_{max}} \quad (1)$$

A severidade de degradação S_w correspondente a ação do elemento considera A_n como a área afetada pela anomalia n (m^2), k_n como o fator multiplicador associado à anomalia *n*, de acordo com o seu nível de degradação (variando entre 0 e 4), $k_{a,n}$ como o coeficiente de ponderação que expressa a importância relativa da anomalia *n* (igual a 1 quando não é definida uma ponderação específica), *A* como a área total do elemento m^2 e Σk_{max} representa a soma dos fatores de ponderação correspondente ao nível de degradação mais elevado para um elemento de área *A* (Silva, De Brito, and Gaspar 2016; Cláudia Ferreira et al. 2023; Pedro L. Gaspar and De Brito 2008; Pedro Lima Gaspar 2009).

As estratégias de manutenção foram definidas através de um modelo estocástico de manutenção baseada na condição, no qual uma determinada ação é executada quando o elemento atinge um estado de degradação específico. Neste âmbito, as redes de Petri são utilizadas para representar a dinâmica de degradação e a lógica de intervenção, servindo de apoio ao planeamento da manutenção e à tomada de decisão. Em contraste com os modelos convencionais baseados na avaliação por peritos, esta abordagem é calibrada com dados empíricos de inspeção, o que garante um maior alinhamento entre as trajetórias de degradação simuladas e as condições reais observadas *in situ*, aumentando a robustez e a transferibilidade dos resultados. A aplicação prática deste modelo fundamentou-se na análise comparativa de indicadores de desempenho antes e após as ações de manutenção. Os dados recolhidos permitiram quantificar o impacto imediato de cada intervenção através da redução direta do índice S_w. Adicionalmente, a modelação por redes de Petri possibilitou a simulação de diferentes cenários de manutenção a longo prazo, avaliando o impacto das intervenções tanto na extensão do ciclo de vida dos elementos quanto na mitigação dos custos acumulados. Este processo de calibração contínua reduz a incerteza intrínseca aos modelos de previsão de vida útil, fornecendo uma base matemática sólida para a transição de políticas de manutenção puramente reativas para estratégias proativas e otimizadas (Cláudia Ferreira et al. 2023).

2.1 Casos de Estudo e Modelação Avançada

Foram analisados dezanove casos de estudo em oito edifícios localizados em Portugal. O trabalho *in situ* decorreu entre julho de 2020 e janeiro de 2023, tendo a sua duração alargada, resultado das restrições associadas à pandemia de COVID-19. Durante este período, foram contactadas 42 entidades, das quais 12 aceitaram colaborar. Os edifícios analisados compreenderam imóveis de uso misto (com pisos superiores residenciais e pisos térreos comerciais ou de serviços), edifícios exclusivamente de serviços, edifícios residenciais e instalações industriais. Os elementos da envolvente avaliados incluíram rebocos correntes (63%), caixilharias em alumínio (16%), revestimentos cerâmicos aderentes (11%), revestimentos em pedra natural (5%), e revestimentos cerâmicos em coberturas inclinadas (5%). Para apresentar uma visão global e detalhada dos casos analisados, a Tabela 1 sistematiza o resumo dos casos de estudo em análise, categorizados por edifício (B) e elemento (E), bem como a sua utilização específica e o tipo de elemento da envolvente.

As inspeções foram realizadas em dois momentos distintos: primeiro, para avaliar o estado de conservação atual dos edifícios e, segundo, após as intervenções. O procedimento de levantamento incluiu a utilização de câmara fotográfica, fita métrica, fissurómetro, fichas de inspeção normalizadas, um sistema de classificação do estado de degradação e peças desenhadas dos elementos inspecionados para o mapeamento esquemático de anomalias (Dias 2025).

Para efeitos de modelação, foi necessária a obtenção dos desenhos digitais de cada elemento, preferencialmente em formato CAD, o que em alguns casos exigiu um levantamento dimensional (Dias, Flores-Colen, and Silva 2021).

Tabela 1. Resumo dos casos de estudo.

Casos de Estudo	Tipo de Uso	Elemento da Envolvente
B1-E1	Habitação e Comercial	Reboco corrente
B1-E2		Reboco corrente
B2-E1	Serviços	Reboco corrente
B3-E1	Habitação e Comercial	Reboco corrente
B3-E2		Reboco corrente
B3-E3		Reboco corrente
B4-E1	Serviços	Revestimento Cerâmico em Coberturas Inclinadas
B4-E2		Reboco corrente
B4-E3		Caixilharias em Alumínio
B4-E4		Caixilharias em Alumínio
B4-E5		Caixilharias em Alumínio
B5-E1	Instalação Industrial	Reboco corrente
B5-E2		Reboco corrente
B5-E3		Reboco corrente
B5-E4		Reboco corrente
B6-E1	Habitação e Serviços	Reboco corrente
B7-E1	Habitação e Serviços	Revestimentos Cerâmicos Aderentes
B7-E2		Revestimentos Cerâmicos Aderentes
B8-E1	Habitação e Serviços	Revestimentos em Pedra Natural

As fotografias recolhidas durante as inspeções foram processadas para corrigir distorções geométricas, sendo as imagens retificadas posteriormente importadas para o software *AutoCAD*, onde as anomalias identificadas foram modeladas e representadas espacialmente (*Figura 1*).



Figura 1. Sobreposição do desenho CAD e da fotografia da fachada para posterior identificação espacial e representação esquemática das anomalias observadas. Fonte: Dias (2025).

A fase subsequente consistiu na inspeção visual, que integrou a avaliação da condição do elemento e a identificação de anomalias. Este diagnóstico serviu de base para o mapeamento esquemático de anomalias, conforme ilustrado na **Error! Reference source not found.**.

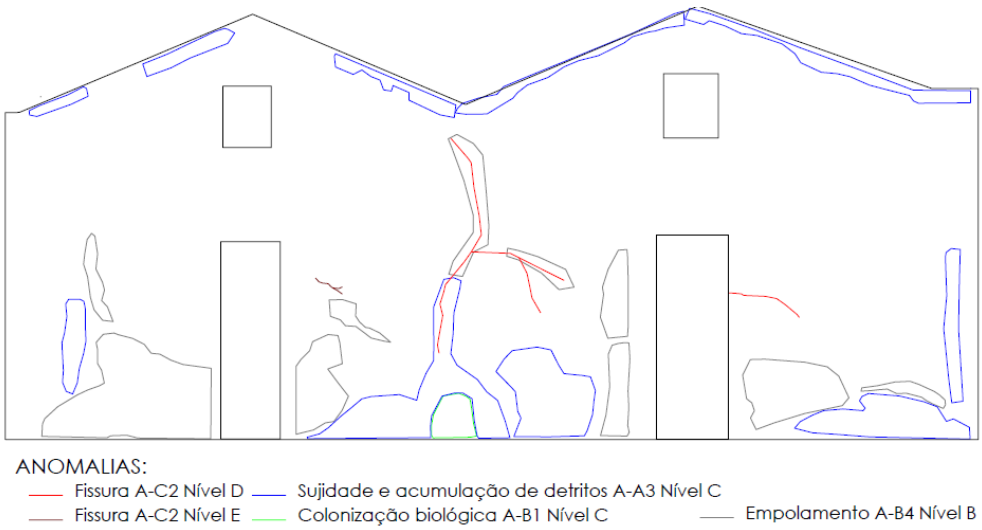


Figura 2. Mapeamento esquemático de anomalias do caso de estudo. Fonte: (Dias 2025)

2.2 Manutenção baseada na condição

A manutenção baseada na condição foi adotada neste estudo para evitar calendários de manutenção excessivamente conservadores, comummente associados a estratégias preventivas predeterminadas que priorizam a redução do risco de falha em detrimento da otimização de custos (Lind and Muyingo 2012). O modelo proposto assume, portanto, a manutenção baseada na condição, onde uma ação é desencadeada sempre que um elemento atinge um nível de degradação específico (C. Ferreira et al. 2021) (por exemplo, ações de limpeza para estados de degradação ligeira ou a substituição total no fim da vida útil).

As redes de Petri foram utilizadas como abordagem de modelação para representar o fluxo de informação e de controlo em sistemas dinâmicos, através de um formalismo matemático com componente gráfica. Este método adequa-se a sistemas nos quais as interações entre componentes são concorrentes, assíncronas, distribuídas, paralelas e estocásticas (Dias 2025; Cláudia Ferreira et al. 2023; Petri 1962; Murata 1989; Ajmone Marsan 1995; C. Ferreira et al. 2018). Uma rede de Petri é definida como um grafo orientado bipartido ponderado com um estado inicial, designado por marcação inicial, composto por lugares e transições interligados por arcos orientados (Peterson 1977; Schneeweiss 2006). Os lugares, as ações e os recursos encontram-se representados na lógica de interação entre a degradação e a manutenção, implementada no modelo estocástico de redes de Petri.

2.3 Custos e segurança pós-intervenção

Uma vez definidos o estado de degradação de cada caso de estudo e a modelação estocástica da manutenção baseada na condição, foram escolhidas as estratégias de intervenção a aplicar nos edifícios, dando continuidade à quantificação dos custos despendidos. Além disso, apresenta-se a matriz que estabelece o risco de queda de revestimentos em pedra natural nas fachadas dos edifícios, como auxílio para identificar as ações necessárias para garantir a segurança dos utilizadores e transeuntes da região onde estão localizados.

2.3.1 Custos

A estrutura económica da metodologia proposta considera os encargos financeiros associados aos custos de manutenção decorrentes da execução das intervenções. A estimativa dos encargos com materiais, mão de obra e equipamentos para cada intervenção baseou-se na plataforma digital *Gerador de Preços* (CYPE 2019). Os custos de intervenção foram expressos por unidade de área (€/m²) para permitir a comparação entre os diferentes casos de estudo.

No presente estudo, as operações de limpeza focam-se na mitigação de anomalias visuais e de superfície na envolvente. O orçamento desta ação contempla a montagem de andaimes ou de sistemas de ancoragem; no caso específico de coberturas, a lavagem com jato de água sob pressão; e a aplicação de biocidas para a erradicação de colonizações biológicas. As intervenções ligeiras caracterizam-se por reparações localizadas, combinando trabalhos de limpeza, correções pontuais e a substituição parcial de componentes danificados, cujas especificidades dependem do elemento construtivo em questão. À semelhança da operação anterior, este custo engloba as estruturas de acesso e de proteção necessárias (andaimes ou linhas de vida em coberturas).

Por fim, o custo de substituição total reflete a renovação integral do elemento, cenário que ocorre tipicamente quando este atinge o fim da sua vida útil. Este encargo inclui o aluguer de meios de acesso, o desmonte e a demolição da solução degradada, o transporte, a gestão e o depósito de resíduos de construção e demolição (RCD), bem como a instalação do novo elemento da envolvente. Excluem-se desta regra as caixilharias em alumínio, cujo custo associado aos meios de acesso não foi contabilizado de forma sistemática em todas as ações.

2.3.2 Segurança

Para avaliar a segurança dos edifícios, foi aplicada uma matriz de risco para fachadas com Revestimento em Pedra Natural (RPN) desenvolvida por Dias (2025). Os parâmetros de cálculo baseiam-se no histórico de anomalias do RPN, no impacto da sua queda e no fluxo de peões na envolvente do edifício. A matriz cruza a probabilidade de queda (*PQ*) com a consequência da queda (*IQ*), definindo o Risco de Queda (*RQ*) através da Equação (2):

$$RQ_{percentual} = PQ \times IQ \times {}^{1}/_{25} \times 100 \quad (2)$$

O valor obtido determina a prioridade da intervenção de manutenção. A probabilidade de queda (*PQ*) é definida em cinco níveis ordenados em função do tempo de serviço do revestimento: o nível 1 corresponde a uma probabilidade de 0% a 10%; o nível 2 abrange o intervalo de 10% a 30%; o nível 3 situa-se entre 30% e 50%; o nível 4 compreende o intervalo de 50% a 70%; e o nível 5 representa uma probabilidade de 70% a 100%.

Por sua vez, o nível de impacto da queda (*IQ*) é calculado através do fluxo diário de transeuntes na envolvente da fachada, sendo categorizado em cinco intervalos de circulação: nível 1 (muito baixa, com menos de 20 pessoas por dia); nível 2 (baixa, de 20 a 100 pessoas por dia); nível 3 (moderada, de 100 a 400 pessoas por dia); nível 4 (alta, de 400 a 1000 pessoas por dia); e nível 5 (muito alta, com mais de 1000 pessoas por dia).

A Matriz de Risco de Queda (Tabela 2) correlaciona a probabilidade de queda (*PQ*) com o nível de impacto (*IQ*). Através desta associação, quanto maior for o valor obtido, mais elevado é o risco e, por conseguinte, maior é a prioridade de intervenção. A matriz categoriza o risco em três níveis de severidade operacional através de um código de cores: baixo (0% a 20%, sinalizado a verde), médio (20% a 50%, sinalizado a amarelo) e alto (50% a 100%, sinalizado a vermelho).

A integração das variáveis anteriormente descritas permitiu o desenvolvimento do Indicador de Risco de Queda (*IRQ*) para o RPN, calculado através da multiplicação do Risco de Queda (*RQ*), obtido na Equação (2),

pelos fatores de majoração: Exposição do Elemento (*E*), Altura do Revestimento (*H*), Área da Placa (*AP*) e Espessura da Placa (*EP*), conforme estabelecido na Equação (3):

$$IRQ = RQ \times E \times H \times AP \times EP \quad (3)$$

Tabela 2. Matriz de Risco de Queda. Fonte: Dias (2025).

		Impacto da Queda *(IQ)*				
		Nível 1	**Nível 2**	**Nível 3**	**Nível 4**	**Nível 5**
Probabilidade da Queda *(PQ)*	**Nível 1**	4%	8%	12%	16%	20%
	Nível 2	8%	16%	24%	32%	40%
	Nível 3	12%	24%	36%	48%	60%
	Nível 4	16%	32%	48%	64%	80%
	Nível 5	20%	40%	60%	80%	100%

Os parâmetros de ponderação para cada uma das variáveis são definidos analiticamente em função das características físicas e funcionais da fachada. A Exposição do Elemento (*E*) é classificada como baixa (1) se existir proteção contra queda em toda a extensão da fachada, média (2) se a proteção for parcial, e alta (3) na ausência de qualquer dispositivo de proteção. A Altura do Revestimento (*H*) é categorizada como baixa (1) até 2 pisos de altura, corrente (2) até 4 pisos, e alta (3) para fachadas com mais de 4 pisos. A Área da Placa (*AP*) assume o valor 1 para pequenas dimensões (áreas inferiores a 0,1 m^2), 2 para médias dimensões (entre 0,1 m^2 e 0,4 m^2) e 3 para grandes dimensões (placas com área superior a 0,4 m^2). Por fim, a Espessura da Placa (EP) é definida como corrente (1) para espessuras até 2,5 cm e alta (2) para valores superiores.

O valor final do IRQ determina o nível de urgência e os prazos limite para as ações de manutenção. Para valores de IRQ entre 0 e 25, a intervenção é considerada não urgente, recomendando-se apenas a monitorização anual do elemento. No intervalo de 26 a 50, torna-se necessária uma intervenção num prazo máximo de 2 anos, reduzindo-se este limite para 1 ano caso o indicador se situe entre 51 e 100. Valores de IRQ entre 101 e 150 exigem uma intervenção imediata num prazo máximo de 6 meses. Por último, um resultado entre 151 e 1350 sinaliza um perigo iminente, exigindo a aplicação imediata de medidas de contingência e a execução da intervenção num prazo limite de 1 mês.

3. Resultados e Discussão

Com base na totalidade dos dados recolhidos, determinou-se a estratégia de intervenção através da modelação estocástica por redes Petri. Nos casos de estudo analisados, as soluções adotadas compreenderam intervenções ligeiras (IL) ou a substituição total (ST) dos elementos, de acordo com o sistematizado na **Tabela *3***.

As estratégias de intervenção foram definidas pelos proprietários e visaram a reabilitação geral ou pontual do edifício, alteração funcional (mudança de uso), modernização, renovação motivada por um estado elevado de degradação ou cumprimento de critérios estéticos. Após a aplicação das respetivas estratégias de intervenção, realizou-se uma nova inspeção com o objetivo de verificar a eventual persistência de anomalias nos elementos da envolvente.

Baseando-se nestas inspeções, o impacto quantitativo da manutenção traduziu-se numa redução do índice de severidade da degradação (ΔS_w) de 26,10% nas caixilharias de alumínio, 9,80% nos rebocos correntes e 2,03% nos revestimentos em pedra natural. Este valor empírico apresenta um elevado alinhamento com a previsão do modelo estocástico do reboco corrente, que estimou uma redução de 8,94% para o nível de intervenção correspondente. Nas caixilharias, o decréscimo médio de ΔS_w obtido *in situ* foi significativamente superior ao previsto, atingindo 26,10% face aos 2,99% estimados pelo modelo estocástico.

Em sentido inverso, o ΔS_w do RPN registado em campo (2,03%) revelou-se inferior ao valor estimado pelo modelo (7,06%).

Tabela 3. Síntese das intervenções dos casos de estudo recolhidos.

Casos de Estudo	Tipo de intervenção	Elemento da Envolvente
B1-E1	Substituição Total	Reboco corrente
B1-E2	Substituição Total	Reboco corrente
B2-E1	Intervenção Ligeira	Reboco corrente
B3-E1	Substituição Total	Reboco corrente
B3-E2	Substituição Total	Reboco corrente
B3-E3	Substituição Total	Reboco corrente
B4-E1	Substituição Total	Revestimento Cerâmico em Coberturas Inclinadas
B4-E2	Intervenção Ligeira	Reboco corrente
B4-E3	Intervenção Ligeira	Caixilharias em Alumínio
B4-E4	Intervenção Ligeira	Caixilharias em Alumínio
B4-E5	Intervenção Ligeira	Caixilharias em Alumínio
B5-E1	Substituição Total	Reboco corrente
B5-E2	Substituição Total	Reboco corrente
B5-E3	Substituição Total	Reboco corrente
B5-E4	Substituição Total	Reboco corrente
B6-E1	Intervenção Ligeira	Reboco corrente
B7-E1	Substituição Total	Revestimentos Cerâmicos Aderentes
B7-E2	Substituição Total	Revestimentos Cerâmicos Aderentes
B8-E1	Intervenção Ligeira	Revestimentos em Pedra Natural

De uma forma geral, a diferença relativa entre os valores observados e previstos evidencia a capacidade do modelo para reproduzir o efeito das intervenções de manutenção, sendo a sua influência maior do que a estimada nos modelos, exceto em RPN. O desvio para um valor inferior ao expectável no RPN pode dever-se ao facto de as intervenções não terem sido integralmente realizadas no estado de condição previsto pelo modelo teórico de manutenção. Os rebocos correntes, que constituíram a amostra maior e estatisticamente mais significativa, serviram de base principal para esta comparação. Embora tenha sido encontrada uma forte correlação entre as observações *in situ* e o modelo teórico, o valor ligeiramente superior registado *in situ* sugere que a parametrização teórica permanece conservadora para os rebocos de fachada. Adicionalmente, as caixilharias em alumínio exibiram uma resposta significativa às intervenções de manutenção, com melhorias de desempenho que frequentemente superaram as previsões teóricas.

Este comportamento conservador pode ser considerado favorável do ponto de vista da gestão da manutenção, uma vez que reduz a possibilidade de sobrestimar o desempenho dos elementos do edifício. A adoção de previsões conservadoras, portanto, pode ser considerada um contributo para minimizar riscos.

Relativamente à eficiência económica, as ações de limpeza resultaram em custos mais baixos, compreendidos entre 14,00 €/m² e 31,37 €/m². As reparações ligeiras apresentaram custos entre 24,14 €/m² e 68,80 €/m², enquanto as substituições totais oscilaram entre 36,68 €/m² e 149,51 €/m². Destaca-se que os limites superiores destes intervalos estiveram consistentemente associados aos revestimentos em pedra natural, refletindo os custos mais elevados de mão de obra especializada e materiais pétreos inerentes a

este elemento e os requisitos adicionais de segurança e acessibilidade normalmente exigidos durante a execução das intervenções.

A monitorização dos revestimentos em pedra natural revelou que a ação de manutenção foi realizada quando o revestimento ainda apresentava um nível de degradação reduzido. Isto ocorreu porque o revestimento exibia defeitos críticos, designadamente o descolamento de elementos pétreos, o que constitui uma anomalia grave e um risco imediato para a segurança e a aptidão ao uso. Perante a presença deste defeito, as decisões de manutenção passam a ser orientadas pelo risco, e não pela progressão da degradação: a prioridade inverte-se da otimização da vida útil para a prevenção do risco de queda de elementos e da perda rápida de funcionalidade. Neste sentido, uma intervenção motivada pelo desprendimento traduz-se tipicamente numa substituição localizada, podendo não resultar numa redução global expressiva da gravidade da degradação quando captada por um índice ponderado pela área, como o S_w. Por outras palavras, a intervenção é motivada por um mecanismo de falha crítico que não é necessariamente proporcional à extensão global da degradação visível.

Sob o ponto de vista da modelação, este cenário evidencia uma condição de fronteira: o modelo estocástico teórico de manutenção foi concebido essencialmente para prever um comportamento de degradação gradual ao longo do tempo, no qual as intervenções são acionadas quando se atinge um limiar de condição predefinido e convencional. O modelo não está estruturado para representar eventos associados a falhas abruptas e críticas à segurança. Os resultados demonstram, portanto, que a avaliação da condição por si só pode não ser suficiente para basear as ações de manutenção em determinados elementos construtivos, como o caso do RPN. Nestes elementos suscetíveis a falhas abruptas, a integração simultânea de indicadores, como o Indicador de Risco de Queda (IRQ), assegura a utilização mais segura da edificação, preservando tanto os utilizadores e transeuntes quanto os ativos construídos.

Em síntese, as evidências *in situ* indicam que a prática real da manutenção integra critérios dinâmicos de gestão do risco que complementam os pressupostos integrados em modelos estocásticos puramente baseados na condição física dos modelos estocásticos. Para o setor industrial e profissional, estas conclusões confirmam a utilidade dos modelos estocásticos como ferramentas de apoio à decisão para o planeamento e orçamentação da manutenção de rotina, mas também sublinham os benefícios de integrar indicadores de riscos para defeitos críticos, refletindo a forma como as intervenções são priorizadas na prática. Esta perspetiva integrada pode auxiliar os *stakeholders* na definição de políticas de manutenção mais realistas, mitigando incertezas e otimizando a fiabilidade do planeamento dos custos do ciclo de vida de sistemas de fachada.

4. Conclusão

Este estudo implementou uma metodologia que combina inspeções *in situ* e modelação estocástica de manutenção baseada na condição, com processos definidos de inspeção pré-intervenção e pós-intervenção, mapeamento esquemático de anomalias, e acompanhamento das estratégias de ações definidas pelos proprietários. Assim, foi possível avaliar o estado de degradação dos elementos da envolvente antes e após as intervenções de manutenção. A viabilidade operacional desta abordagem foi demonstrada através de dezanove casos de estudo, permitindo quantificar os ganhos de desempenho associados a diferentes estratégias de intervenção, avaliar os custos e compreender o papel da manutenção na segurança dos edifícios.

Os resultados indicam que os modelos estocásticos de degradação tendem a ser conservadores na previsão da vida útil. A comparação entre as condições observadas pós-intervenção e as trajetórias de degradação previstas demonstra que os efeitos da manutenção podem ser quantificados e que o seu impacto na durabilidade e no desempenho é frequentemente subestimado.

A integração de dados recolhidos *in situ* na estrutura estocástica de redes de Petri reduziu as discrepâncias entre as curvas teóricas de degradação e o desempenho real observado, aumentando a fiabilidade do

planeamento da manutenção. Demonstrou-se também que os ajustes nas técnicas de intervenção e nas estratégias de acesso *in situ* influenciam a eficiência de custos sem comprometer o desempenho ou a segurança.

O trabalho desenvolvido demonstra a complementaridade entre a modelação estocástica da degradação e a análise de risco proposta. Enquanto os modelos estocásticos fundamentam o planeamento a longo prazo, as ações de manutenção do Revestimento em Pedra Natural (RPN) devem incorporar, em paralelo, os indicadores de risco de queda, mesmo na ausência de degradação superficial avançada. Situações em que anomalias graves afetam o sistema de fixação oculta configuram eventos que, embora discretos, apresentam elevada severidade e urgência. Nestes cenários, torna-se essencial a aplicação conjunta de ferramentas de diagnóstico adequadas, tais como a Matriz de Risco de Queda ou o Indicador de Risco de Queda, salvaguardando a segurança, bem como a validade dos modelos estocásticos.

Em suma, as conclusões validam o posicionamento da manutenção como uma componente estruturada de tomada de decisão ao longo do ciclo de vida do edifício, com implicações mensuráveis na durabilidade, no controlo de custos e na gestão da segurança da envolvente. Os resultados obtidos demonstram que a manutenção baseada na condição é uma metodologia eficaz para apoiar a fase de uso dos edifícios. A integração de dados reais permite visualizar a incerteza associada a esse tipo de manutenção e reforça a sua fiabilidade. Isto contribui para o aumento da durabilidade dos elementos da envolvente e para a utilização mais eficiente de recursos financeiros.

Assim, a manutenção baseada na condição em conjunto com o indicador de risco de queda de RPN se afirmam como ferramentas multifuncionais para a utilização dos edifícios conciliando desempenho, custo e segurança.

Agradecimentos

Os autores agradecem à Fundação para a Ciência e a Tecnologia (FCT), através do projeto BestMaintenance-LowerRisks (PTDC/ECI-CON/29286/2017) e das bolsas de doutoramento (UI/BD/151150/2021 e 2025.02906.BDANA), bem como à unidade de investigação Civil Engineering Research and Innovation for Sustainability (CERIS - FCT-UID/6438/2025, https://doi.org/10.54499/UID/06438/2025), que tornaram possível a realização desta investigação.

Referências

Ajmone Marsan, Marco. 1995. *Modelling with generalized stochastic Petri nets.Wiley series in parallel computing*. Chichester New York Brisbane [etc.]: J. Wiley and sons.

Brito, Jorge, Clara Pereira, José D. Silvestre, and Inês Flores-Colen. 2020. *Expert Knowledge-Based Inspection Systems: Inspection, Diagnosis, and Repair of the Building Envelope*. Cham: Springer International Publishing AG.

CEN, European Commission for Standardization -. 2021. *EN 13306:2021 – Maintenance – Maintenance Terminology.* Brussels: CEN.

CYPE. 2019. "CYPE – Gerador de preços." http://www.geradordeprecos.info/.

Derakhshi, Sareh Saeidi. 2020. "Inhabiting the Architectural Envelope: A Design-based Research on Redefining the Climatic and Atmospheric Performances of Architectural Envelope." PhD Thesis 103 PhD Thesis, Oslo School of Architecture and Design.

Dias, Ilídio. 2025. "Influência da manutenção na durabilidade e custo do ciclo de vida dos elementos da envolvente dos edifícios." PhD Thesis, Instituto Superior Técnico.

Dias, Ilídio, Inês Flores-Colen, and Ana Silva. 2021. "Critical Analysis about Emerging Technologies for Building's Façade Inspection." *Buildings* 11 (2): 53. https://doi.org/10.3390/buildings11020053. https://www.mdpi.com/2075-5309/11/2/53.

Ferreira, C., L. Canhoto Neves, A. Silva, and J. De Brito. 2018. "Stochastic Petri net-based modelling of the durability of renderings." *Automation in Construction* 87: 96-105. https://doi.org/10.1016/j.autcon.2017.12.007. https://linkinghub.elsevier.com/retrieve/pii/S0926580517310889.

Ferreira, C., A. Silva, J. De Brito, I. S. Dias, and I. Flores-Colen. 2021. "The impact of imperfect maintenance actions on the degradation of buildings' envelope components." *Journal of Building Engineering* 33: 101571. https://doi.org/10.1016/j.jobe.2020.101571. https://linkinghub.elsevier.com/retrieve/pii/S2352710220303958.

Ferreira, Cláudia, Ana Silva, Jorge de Brito, and Inês Flores-Colen. 2023. *Maintainability of building envelope elements: optimizing predictive condition-based maintenance decisions.Springer series in reliability engineering*. Cham: Springer.

Gaspar, Pedro L., and Jorge De Brito. 2008. "Service life estimation of cement-rendered facades." *Building Research & Information* 36 (1): 44-55. https://doi.org/10.1080/09613210701434164. https://www.tandfonline.com/doi/full/10.1080/09613210701434164.

Gaspar, Pedro Lima. 2009. "Service life of constructions: development of a method to estimate the durability of construction elements. Application to renderings of current buildings." PhD Thesis, Instituto Superior Técnico.

Jernberg, P., Michael Lacasse, S. Haagenrud, and Christer Sjöström. 2004. *Guide and Bibliography to Service Life and Durability Research for Buildings and Components*.

Lind, Hans, and Henry Muyingo. 2012. "Building maintenance strategies: planning under uncertainty." *Property Management* 30 (1): 14-28. https://doi.org/10.1108/02637471211198152. http://www.emerald.com/pm/article/30/1/14-28/319623.

Long, A. E., G. D. Henderson, and F. R. Montgomery. 2001. "Why assess the properties of near-surface concrete?" *Construction and Building Materials* 15 (2-3): 65-79. https://doi.org/10.1016/S0950-0618(00)00056-8. https://linkinghub.elsevier.com/retrieve/pii/S0950061800000568.

Lopes, Daniel Oliveira. 2011. "A Reabilitação Urbana em Portugal: Importância Estratégica para as Empresas do Setor da Construção Civil e Obras Públicas " MSc Dissertation, Universidade do Porto.

Mouratidis, Kostas. 2021. "Urban planning and quality of life: A review of pathways linking the built environment to subjective well-being." *Cities* 115: 103229. https://doi.org/10.1016/j.cities.2021.103229. https://linkinghub.elsevier.com/retrieve/pii/S0264275121001293.

Murata, T. 1989. "Petri nets: Properties, analysis and applications." *Proceedings of the IEEE* 77 (4): 541-580. https://doi.org/10.1109/5.24143. http://ieeexplore.ieee.org/document/24143/.

Peterson, James L. 1977. "Petri Nets." *ACM Computing Surveys* 9 (3): 223-252. https://doi.org/10.1145/356698.356702. https://dl.acm.org/doi/10.1145/356698.356702.

Petri, Carl Adam. 1962. "Kommunikation mit Automaten." PhD Thesis, University of Hamburg.

Sandak, Anna. 2019. *Bio-Based Building Skin*. 1st ed.*Environmental Footprints and Eco-Design of Products and Processes Series*. Singapore: Springer Singapore Pte. Limited.

Sarja, Asko. 2002. "Reliability based life cycle design and maintenance planning." Workshop on Reliability Based Code Calibration, ETH Zurich.

Schneeweiss, W. G. 2006. "“Review of Petri Net Picture Book” and “Petri Nets for Reliability Modeling”." *IEEE Transactions on Reliability* 55 (2): 391-392. https://doi.org/10.1109/TR.2006.874908. http://ieeexplore.ieee.org/document/1638423/.

Silva, Ana, Jorge De Brito, and Pedro Lima Gaspar. 2016. *Methodologies for Service Life Prediction of Buildings.Green Energy and Technology*. Cham: Springer International Publishing.

Watt, David. 2007. *Building pathology: principles and practice*. 2nd ed. Oxford ; Malden, MA: Blackwell Pub.

XXII International Conference on Building Pathology and Constructions Repair
15th to 17th July 2026 - Lisboa, Portugal

Avaliação da conservação de edificações públicas com base em ordens de serviço e classificação de criticidade pela matriz GUT

Mariana Silva Pires[1], Jessica Siqueira de Souza[1]

[1] Civil and Environmental Engineering Department, PECC—University of Brasília, Campus Darcy Ribeiro, Asa Norte, Brasília 70910-900, Brazil; mari_pires09@hotmail.com

Resumo: A manutenção predial é essencial para preservar o desempenho, a durabilidade e a vida útil dos sistemas construtivos, especialmente em edificações públicas submetidas ao uso contínuo e a restrições de recursos para intervenção. O monitoramento das falhas em operação permite compreender o comportamento das edificações em uso e subsidiar avaliações mais consistentes de seu estado de conservação. Entretanto, embora as ordens de serviço (OS) constituam uma fonte relevante de informação sobre essas falhas, seus registros são frequentemente utilizados apenas para fins operacionais, sendo pouco explorados em análises técnicas sistematizadas. Este trabalho objetiva analisar as ordens de serviço como instrumento de apoio à avaliação da conservação de edificações públicas, por meio de estudo de caso em blocos residenciais pertencentes a uma instituição pública. A metodologia baseia-se na análise de 308 ordens de serviço, das quais foram extraídas e classificadas ocorrências técnicas segundo bloco, sistema construtivo e nível de prioridade, com avaliação da criticidade pela matriz GUT. Os resultados permitiram identificar padrões recorrentes de solicitação, sistemas mais suscetíveis à degradação e diferentes prioridades de intervenção, com destaque para os sistemas hidrossanitário e de vedação e revestimentos. Verificou-se, ainda, que a edificação mais antiga não apresentou o maior número de registros, indicando que fatores como histórico de manutenção, intensidade de uso, condições de exposição e particularidades construtivas também influenciam o estado de conservação. Conclui-se que a análise sistematizada das OS contribui para transformar registros operacionais em indicadores técnicos, subsidiando o diagnóstico e a priorização das ações de manutenção.

Palavras-chave: manutenção predial; durabilidade; ordens de serviço; matriz GUT; conservação de edificações.

1. Introdução

A manutenção das edificações constitui um requisito essencial para a preservação do desempenho ao longo da vida útil. Em consonância com a ABNT NBR 15575 (2024), sua função está associada à conservação das condições de uso, segurança, habitabilidade e durabilidade dos sistemas construtivos, de modo a assegurar que a edificação mantenha, ao longo do tempo, o desempenho previsto em projeto. Além de sua relevância técnica, a manutenção apresenta impacto econômico expressivo no ciclo de vida das edificações. Em edifícios com vida útil de 50 anos, os custos de operação e manutenção podem representar cerca de 75% a 80% do custo total, evidenciando que o adequado planejamento das intervenções é determinante tanto para a conservação do ativo quanto para a racionalização dos recursos empregados (Mahpour, 2023).

Quanto à forma de intervenção, a manutenção das edificações pode ser classificada em três tipos: preventiva, corretiva e preditiva. A ABNT NBR 5674 (2024) trata a manutenção como um conjunto de ações voltadas a prevenir ou corrigir a perda de desempenho da edificação, o que evidência, no âmbito normativo, a centralidade das abordagens preventiva e corretiva. Flores *et al.* (2022) classificam a manutenção

preventiva como aquela realizada de forma planejada, antes da ocorrência da falha, e a manutenção corretiva como a intervenção executada após a identificação de anomalias ou perda de desempenho. Bouabdallaoui *et al.* (2021), por sua vez, incluem a manutenção preditiva como uma estratégia baseada no monitoramento da condição do sistema, permitindo definir o momento mais adequado para a intervenção. Embora essa modalidade não seja apresentada de forma explícita na ABNT NBR 5674 (2024), sua relevância é amplamente reconhecida na literatura, uma vez que possibilita intervenções fundamentadas no estado real dos elementos, contribuindo para a redução de falhas inesperadas, para o melhor planejamento das ações de manutenção e para o uso mais eficiente dos recursos ao longo da vida útil da edificação.

A elaboração de um plano de manutenção adequado é fundamental para orientar as intervenções ao longo da vida útil da edificação. Nesse contexto, o monitoramento de dados históricos, como os registros de ordens de serviço, representa uma importante fonte de informação para a tomada de decisão, pois permite identificar padrões de ocorrência, recorrências e sistemas mais suscetíveis a falhas (D'Orazio et al., 2022; Chelaru et al., 2024; Salzano et al., 2023).Em contrapartida, a literatura aponta que a avaliação das necessidades de manutenção ainda é frequentemente baseada em inspeções visuais e em julgamentos técnicos, o que pode tornar o processo decisório mais subjetivo (Begić *et al*., 2024). Assim, o uso integrado de dados históricos e critérios técnicos contribui para decisões mais consistentes na priorização das intervenções e na definição de ações compatíveis com as condições reais da edificação (Salzano *et al*., 2023).

A insuficiência ou ausência de manutenção favorece o aparecimento e a progressão de diferentes anomalias construtivas, com destaque para problemas relacionados à umidade e infiltração, fissuração, corrosão de elementos metálicos ou armaduras, destacamento de revestimentos e desplacamento de componentes superficiais. Na análise de defeitos em áreas molhadas, Chew (2005) observou elevada ocorrência de vazamentos, corrosão de tubulações e desplacamento de concreto, associando parte desses problemas a falhas de manutenção. Em revisão recente sobre fontes de informação para defeitos em edificações, Berg Oppedal *et al.* (2024) também destacam como recorrentes manifestações como vazamentos em tubulações, falhas no sistema de abastecimento, fissuras em paredes de concreto e umidade em superfícies internas. De forma convergente, Resende *et al.* (2022), ao avaliarem uma edificação histórica, identificaram umidade, fissuras e regiões com destacamento de argamassa como danos que comprometem a integridade e a vida útil do edifício. Em conjunto, esses estudos indicam que a falta de manutenção não apenas intensifica a frequência dessas anomalias, mas também acelera a perda das condições de conservação e desempenho das edificações.

Dessa forma, a padronização dos registros de ordens de serviço e sua conversão em métricas analíticas emergem como uma estratégia promissora para a análise da conservação das edificações ao longo do tempo. A sistematização dessas informações permite identificar recorrências, reconhecer sistemas com maior incidência de falhas, estabelecer ordens de intervenção e produzir indicativos acerca do nível de conservação dos edifícios, ampliando o uso de registros históricos como base empírica para a avaliação das condições construtivas (Alavi *et al*., 2022; Chelaru *et al.,* 2024). Além disso, ao transformar dados operacionais dispersos em informações comparáveis, essa abordagem contribui para reduzir a dependência exclusiva de inspeções visuais e julgamentos subjetivos, frequentemente apontados na literatura como limitações dos

processos convencionais de avaliação da condição predial (Begić e Krstić, 2024; Tan *et al*. 2024; Valença *et al*. 2024).

Diante desse contexto, o presente estudo tem como objetivo analisar os registros de ordens de serviço como fonte de informação para a avaliação da conservação de edificações públicas, buscando identificar padrões de ocorrência, recorrências de falhas, sistemas construtivos mais críticos e parâmetros que subsidiem a definição de prioridades de intervenção a partir de dados históricos reais.

2. Metodologia

O presente estudo desenvolve um estudo de caso a partir da análise de ordens de serviço (OS) relacionadas à manutenção predial de edificações públicas, visando investigar sua aplicabilidade como base empírica para a análise da conservação dos edifícios. Para isso, busca-se compreender a distribuição das demandas de manutenção em função dos blocos, dos sistemas construtivos e das prioridades de atendimento. A análise foi realizada com base em 308 ordens de serviço referentes a doze edificações públicas situadas em Brasília, Distrito Federal, considerando o recorte temporal do ano de 2024. O procedimento metodológico foi organizado em três etapas principais: estruturação da base de dados, definição das prioridades de execução e avaliação do nível de conservação das edificações analisadas, conforme apresentado na Figura 1.

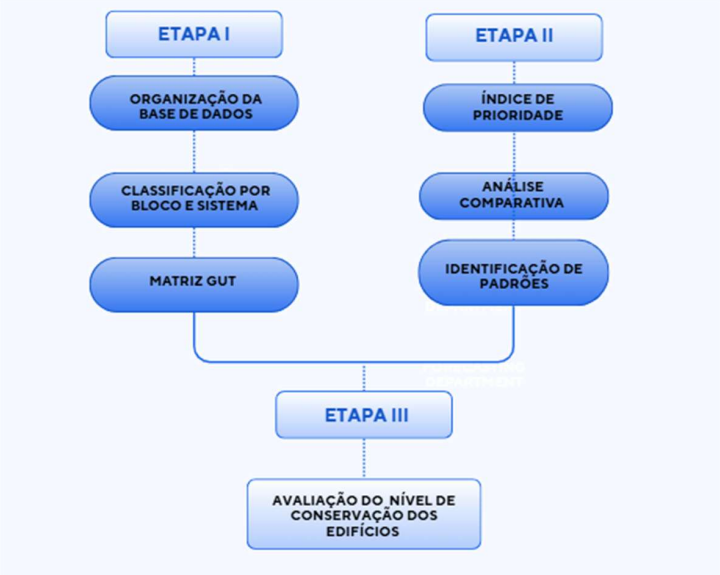


Figura 1 – Fluxograma metodológico

A metodologia foi organizada em três etapas sucessivas.

2.1 Etapa I

Na Etapa I, realizou-se a estruturação da base de dados a partir dos registros de Ordens de Serviço (OS), os quais reúnem informações sobre o bloco, a natureza da ocorrência e o sistema construtivo envolvido. Para viabilizar a análise, as demandas foram padronizadas e agrupadas em oito sistemas construtivos: hidrossanitário, elétrico, estrutural, vedações e revestimentos, áreas sociais, cobertura, comunicação e redes e proteção contra incêndio. Posteriormente, as ocorrências foram avaliadas segundo os critérios de Gravidade, Urgência e Tendência, por meio da matriz GUT. Essa etapa permitiu consolidar e classificar os dados de forma sistemática, possibilitando sua análise segundo os edifícios e os sistemas mais recorrentes. Ressalta-se que as edificações consideradas na amostra foram construídas entre as décadas de 1977 e 2001.

2.2 Etapa II

Na Etapa II, a definição do índice de prioridade das ocorrências foi realizada por meio da matriz GUT, método desenvolvido por Kepner e Tregoe (1981) com o objetivo de apoiar a hierarquização de problemas segundo os critérios de gravidade, urgência e tendência. Em estudos aplicados às edificações, sua utilização tem se mostrado útil na classificação de manifestações patológicas e no direcionamento das ações de manutenção conforme a criticidade observada (Holanda *et al*., 2022 e Braga *et al*., 2019). Para cada ordem de serviço, foram atribuídos valores inteiros de 1 a 5 para cada critério, em que os valores mais elevados correspondem às situações de maior criticidade. A gravidade expressa o impacto da anomalia sobre o desempenho, a segurança e a habitabilidade; a urgência representa a necessidade temporal de intervenção; e a tendência indica a possibilidade de agravamento da ocorrência. Os critérios utilizados para atribuição das pontuações da matriz GUT foram padronizados conforme apresentado na Tabela 1, de modo a reduzir a subjetividade da classificação e permitir maior consistência na avaliação das ordens de serviço.

Tabela 1 – Critérios de pontuação para avaliação da Gravidade, Urgência e Tendência

Pontuação	Gravidade	Urgência	Tendência
1	Impacto insignificante sobre o desempenho ou sobre os usuários.	Não há necessidade imediata de intervenção.	Condição estável, sem expectativa de agravamento.
2	Impacto localizado de baixa intensidade.	A intervenção pode ser postergada sem consequências relevantes.	Espera-se progressão lenta da ocorrência.
3	Impacto funcional moderado ou desconforto aos usuários.	A intervenção deve ser realizada em prazo razoável.	Espera-se agravamento gradual da ocorrência.
4	Impacto significativo sobre o desempenho, o uso ou as condições de segurança.	Requer intervenção em curto prazo.	Há probabilidade de agravamento rápido.
5	Impacto crítico sobre a segurança, a habitabilidade ou a continuidade do serviço.	Requer intervenção imediata.	Há agravamento severo ou acelerado da ocorrência.

Após a atribuição das pontuações de Gravidade, Urgência e Tendência, foi calculado o Índice de Prioridade (IP) de cada ordem de serviço. O IP foi obtido pelo produto entre os três critérios avaliados, conforme apresentado na Equação 1.

$$IP = G \times U \times T \quad (1)$$

em que IP corresponde ao Índice de Prioridade, G à Gravidade, U à Urgência e T à Tendência. Considerando a escala adotada, com pontuações variando de 1 a 5 para cada critério, o valor mínimo possível do índice é 1, correspondente à menor condição de criticidade, e o valor máximo possível é 125, correspondente à condição de maior criticidade.

A utilização do produto entre os critérios permite evidenciar ocorrências em que há simultaneamente maior impacto técnico, maior necessidade temporal de intervenção e maior potencial de agravamento. Dessa forma, o índice não considera apenas a frequência das ordens de serviço, mas também o grau de criticidade associado a cada ocorrência, contribuindo para uma priorização mais consistente das ações de manutenção. A classificação das ocorrências segundo o IP foi organizada em três faixas de prioridade, conforme apresentado na Tabela 2.

Tabela 2 – Classificação das ocorrências segundo as faixas do Índice de Prioridade

Faixa do IP	Nível de prioridade	Interpretação técnica
1 a 41	Médio prazo	Ocorrências de menor criticidade, com impacto limitado e possibilidade de programação da intervenção em horizonte mais amplo.
42 a 83	Curto prazo	Ocorrências de criticidade intermediária, que exigem intervenção programada para evitar agravamento da anomalia ou perda progressiva de desempenho.
84 a 125	Ação imediata	Ocorrências de alta criticidade, associadas a impacto relevante sobre segurança, habitabilidade, funcionalidade ou continuidade do serviço, demandando intervenção prioritária.

Para fins de classificação, os valores obtidos foram agrupados em três níveis de prioridade: médio prazo, curto prazo e ação imediata. A divisão das faixas considerou a amplitude total possível do índice, permitindo organizar as ocorrências em classes progressivas de criticidade. Assim, as demandas enquadradas como ação imediata correspondem às situações de maior relevância técnica, enquanto as classificadas como curto e médio prazo representam ocorrências que podem ser planejadas de acordo com sua evolução, impacto e disponibilidade de recursos.

Diversos autores têm proposto métodos para padronizar dados históricos de manutenção e convertê-los em informações analíticas. Madureira *et al.* (2017) e Flores-Colen, Gomide e Della Flora (2022), utilizaram uma abordagem multicritério para apoiar a priorização de intervenções em fachadas. D'Orazio *et al.*(2022) aplicaram uma abordagem orientada por dados para analisar registros de manutenção e identificar padrões de ocorrência em edifícios. De forma complementar, Chelaru *et al.* (2024) integraram registros históricos, dados de inspeção e informações geométricas em ambiente HBIM para apoiar a avaliação das condições construtivas. Em conjunto, esses estudos demonstram que diferentes métodos podem ser empregados para estruturar dados históricos e ampliar seu uso na análise da conservação das edificações.

2.3 Etapa III

Na Etapa III, procedeu-se à análise integrada dos resultados obtidos a partir da base de ordens de serviço classificada. A avaliação considerou a distribuição das ocorrências por conjunto habitacional, bloco, sistema construtivo e nível de prioridade, permitindo identificar padrões de recorrência, concentração espacial das demandas e sistemas com maior incidência de falhas.

Inicialmente, foram quantificadas as ordens de serviço por sistema construtivo e por bloco, com o objetivo de reconhecer os subsistemas mais suscetíveis à degradação e os setores com maior demanda de manutenção. Em seguida, os resultados do Índice de Prioridade foram agrupados em três classes de intervenção, médio prazo, curto prazo e ação imediata, possibilitando avaliar não apenas a frequência das ocorrências, mas também seu grau de criticidade.

A análise comparativa entre os conjuntos edificados considerou ainda o ano de construção, o número total de ordens de serviço, a distribuição das ocorrências por sistema e a concentração das demandas prioritárias. Essa abordagem permitiu verificar se a idade da edificação apresentava relação direta com o volume e a criticidade das manifestações registradas, bem como identificar possíveis influências de outros fatores, como condições de uso, histórico de manutenção, intervenções anteriores e particularidades construtivas de cada bloco.

Dessa forma, a Etapa III buscou transformar os registros operacionais de manutenção em indicadores técnicos de conservação, subsidiando uma leitura comparativa entre os edifícios avaliados e permitindo a identificação dos sistemas e blocos que demandam maior atenção no planejamento das ações de manutenção.

3. Resultados e Discussões

A análise comparativa das Ordens de Serviço (OS) permitiu avaliar a distribuição das demandas de manutenção entre conjuntos edificados com diferentes períodos de construção. Entre as edificações analisadas, a SQN 206, construída em 1977, corresponde ao conjunto mais antigo, seguida pela SQN 205, de 1981, e pela SQN 109, de 2001, que representa o conjunto mais recente da amostra. De modo geral, os resultados indicam que a idade da edificação constitui um fator relevante para a compreensão das demandas de manutenção, especialmente em sistemas sujeitos ao uso contínuo, à exposição à umidade e ao envelhecimento natural dos componentes, como os sistemas hidrossanitário e de vedação e revestimentos. Entretanto, a distribuição das ocorrências não se mostrou estritamente proporcional ao tempo de construção, indicando que a conservação predial também é influenciada por fatores como histórico de manutenção, intervenções anteriores, intensidade de uso, condições de exposição e particularidades construtivas de cada bloco.

A Tabela 3 apresenta a síntese dos principais indicadores obtidos a partir das ordens de serviço analisadas, considerando o ano de construção, o número total de registros, o bloco com maior concentração de ocorrências, o sistema predominante e a classificação das intervenções segundo o Índice de Prioridade. Essa organização permite uma leitura comparativa inicial dos conjuntos avaliados e contribui para relacionar frequência de ocorrências, criticidade das demandas e estado de conservação das edificações.

Tabela 3 – Síntese dos indicadores obtidos a partir das ordens de serviço analisadas

Conjunto	Ano de construção	Total de OS analisadas	Bloco com maior nº de OS	Sistema predominante	Ocorrências de Ação imediata	Ocorrências de Curto prazo	Ocorrências de Médio prazo
SQN 205	1981	132	Bloco H	Hidrossanitário	24	60	58
SQN 206	1977	102	Bloco K	Hidrossanitário	12	37	54
SQN 109	2001	74	Bloco J	Hidrossanitário	5	25	47

Ressalta-se que o total de ordens de serviço analisadas corresponde ao número de registros administrativos existentes na base de dados. As categorias de prioridade, por sua vez, referem-se às ocorrências técnicas classificadas pelo Índice de Prioridade, uma vez que uma mesma ordem de serviço pode envolver mais de uma manifestação patológica, demanda de manutenção ou sistema construtivo. Assim, a soma das ocorrências classificadas por prioridade pode diferir do número total de ordens de serviço, pois a análise buscou representar tecnicamente as manifestações identificadas em cada registro, e não apenas contabilizar os documentos administrativos de solicitação.

Na SQN 205, construída em 1981, foi observado o maior número total de ordens de serviço entre os conjuntos analisados, com 132 registros. A distribuição interna das ocorrências indicou maior concentração no Bloco H, com 44 OS, correspondente a 33,3% do total, seguido pelo Bloco C, com 34 OS (25,8%), pelo Bloco G, com 29 OS (22,0%), e pelo Bloco L, com 25 OS (18,9%), conforme apresentado na Figura 2. A predominância de registros no sistema hidrossanitário e em vedação e revestimentos indica maior suscetibilidade desses subsistemas a manifestações associadas ao uso contínuo, à umidade, ao envelhecimento dos componentes e à perda progressiva de desempenho.

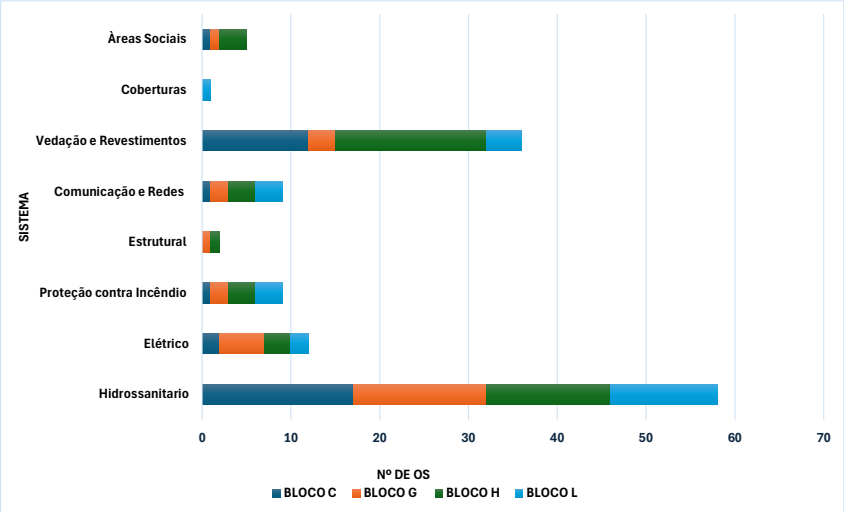


Figura 2 – Distribuição das Ordens de Serviço por sistema e por bloco na SQN 205

Na SQN 206, construída em 1977, foram contabilizadas 102 ordens de serviço. Embora esse conjunto corresponda à edificação mais antiga da amostra, o número total de ocorrências foi inferior ao observado na SQN 205. A maior concentração de registros ocorreu no Bloco K, com 30 OS (29,4%), seguido pelo Bloco B, com 27 OS (26,5%). Os Blocos A e F apresentaram 17 ocorrências cada, equivalentes a 16,7%, enquanto o Bloco J registrou 11 OS, correspondente a 10,8% do total, conforme ilustrado na Figura 3. Esses resultados indicam que a antiguidade da edificação contribui para a intensificação das demandas de manutenção, mas não determina isoladamente sua distribuição nem seu nível de criticidade.

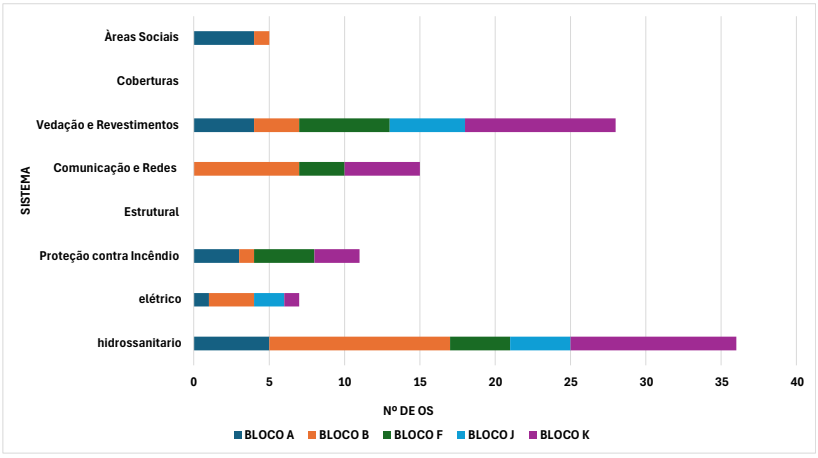


Figura 3 – Distribuição das Ordens de Serviço por sistema e por bloco na SQN 206

Na SQN 109, construída em 2001, foi registrado o menor quantitativo total de ordens de serviço, com 74 registros administrativos. A distribuição interna, entretanto, revelou elevada concentração no Bloco J, responsável por 46 registros, equivalentes a 62,2% do total do conjunto, enquanto o Bloco I concentrou 20 OS (27,0%) e o Bloco H apresentou 8 OS (10,8%), conforme demonstrado na Figura 4. Apesar de se tratar do conjunto mais recente, a concentração das demandas em um único bloco evidencia que a conservação predial deve ser analisada também em escala local, considerando as particularidades de uso, manutenção e desempenho de cada setor da edificação.

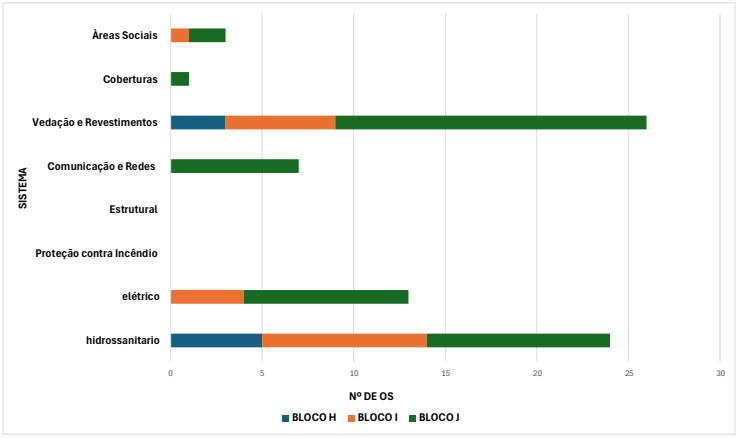


Figura 4 – Distribuição das Ordens de Serviço por sistema e por bloco na SQN 109

A comparação entre os três conjuntos demonstra que as demandas de manutenção não se distribuem de forma homogênea entre as edificações nem entre os blocos pertencentes ao mesmo conjunto. A SQN 205 apresentou o maior número total de ocorrências, embora não seja a edificação mais antiga, enquanto a SQN 109, mesmo sendo a mais recente, apresentou forte concentração de registros em um único bloco. Esses resultados indicam que a idade cronológica é um fator relevante, mas insuficiente para explicar isoladamente o comportamento das manifestações registradas. Assim, a avaliação da conservação deve considerar, de forma integrada, a idade da edificação, o histórico de manutenção, a intensidade de uso, a concentração espacial das ocorrências e os sistemas construtivos mais afetados.

Alguns estudos recentes confirmam que os sistemas hidrossanitários e os sistemas de vedação e revestimentos figuram entre os componentes mais suscetíveis à degradação e, consequentemente, entre os mais recorrentes nas demandas de manutenção predial. Berg Oppedal *et al.* (2024), ao revisarem diferentes fontes de informação sobre defeitos em edifícios, observaram a elevada frequência de ocorrências associadas a erros em tubulações, danos por água, vazamentos internos e fissuração de paredes, evidenciando a relevância das instalações hidrossanitárias e dos elementos de fechamento e acabamento no quadro geral de falhas construtivas. De modo convergente, Gurmu *et al.* (2025), em revisão sistemática sobre defeitos induzidos por ingresso de água, identificaram como componentes mais vulneráveis paredes internas e externas, fachadas, áreas molhadas e sistemas de tubulação, destacando que falhas de impermeabilização, juntas e conexões favorecem manifestações com impactos estruturais, funcionais e estéticos. Essas evidências indicam que os resultados obtidos no presente estudo não representam um comportamento isolado do caso analisado, mas se alinham a tendências observadas em diferentes contextos internacionais, nos quais falhas relacionadas à água, tubulações, vedações e revestimentos figuram entre os principais vetores de degradação e demanda de manutenção em edificações em uso.

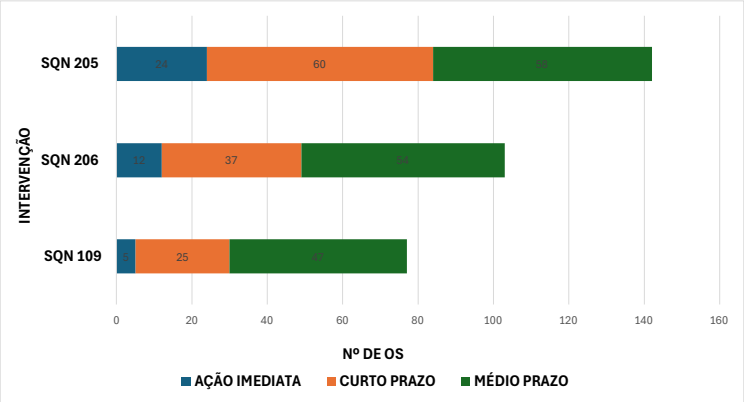


Figura 5 – Classificação das ocorrências segundo o Índice de Prioridade

Conforme apresentado na Figura 5, a classificação das ocorrências pelo Índice de Prioridade permitiu diferenciar as demandas de manutenção segundo seu horizonte de intervenção. Na SQN 205, foram identificadas 24 ocorrências de ação imediata, 60 de curto prazo e 58 de médio prazo. Na SQN 206, registraram-se 12 ocorrências de ação imediata, 37 de curto prazo e 54 de médio prazo. Já na SQN 109, observaram-se 5 ocorrências de ação imediata, 25 de curto prazo e 47 de médio prazo.

Esses resultados indicam que, nos três conjuntos, predominam demandas classificadas como curto e médio prazo, sugerindo que parte significativa das manifestações identificadas ainda pode ser incorporada ao planejamento técnico da manutenção. Entretanto, a presença de ocorrências de ação imediata, especialmente na SQN 205, evidencia a existência de situações com maior impacto potencial sobre o desempenho, a habitabilidade, a segurança ou a continuidade de uso dos sistemas construtivos.

A comparação entre frequência e criticidade demonstra que o volume absoluto de ordens de serviço deve ser interpretado em conjunto com o nível de prioridade das ocorrências. Dessa forma, a classificação pelo IP contribui para uma avaliação mais consistente da conservação predial, evitando que a definição das prioridades de intervenção seja baseada exclusivamente na quantidade de solicitações registradas.

4. Conclusão

Os resultados obtidos demonstram que os registros de ordens de serviço constituem uma fonte empírica relevante para a avaliação da conservação de edificações públicas, pois permitem identificar padrões de recorrência, sistemas construtivos mais suscetíveis à degradação e diferentes níveis de prioridade de intervenção. A análise das ordens de serviço evidenciou maior incidência de ocorrências nos sistemas hidrossanitário e de vedação e revestimentos, confirmando a relevância desses subsistemas nas demandas de manutenção predial e sua maior vulnerabilidade a manifestações como vazamentos, infiltrações, umidade, fissuração, destacamento e perda de desempenho funcional.

A aplicação da matriz GUT mostrou-se adequada para qualificar essa análise, uma vez que possibilitou classificar as ocorrências com base nos critérios de gravidade, urgência e tendência. Ao considerar não apenas a frequência dos registros, mas também o potencial de agravamento e os impactos associados a cada manifestação, o Índice de Prioridade permitiu diferenciar ocorrências que demandam intervenção imediata daquelas que podem ser tratadas no curto ou médio prazo. Dessa forma, a metodologia contribuiu para uma priorização mais racional das ações de manutenção, apoiando a tomada de decisão técnica em contextos de limitação de recursos e necessidade de planejamento das intervenções.

Os resultados também demonstraram que a idade das edificações, embora relevante, não explica isoladamente o comportamento das demandas de manutenção. A edificação mais antiga da amostra não foi aquela que apresentou o maior número de ordens de serviço, indicando que o estado de conservação está relacionado a um conjunto mais amplo de variáveis, como histórico de manutenção, intensidade de uso, qualidade das intervenções anteriores, condições de exposição, desempenho residual dos sistemas e particularidades construtivas de cada bloco. Esse achado reforça a necessidade de avaliar a conservação predial por meio de uma abordagem integrada, que considere simultaneamente a frequência das ocorrências, sua distribuição espacial, os sistemas afetados e o nível de criticidade das manifestações.

Dessa forma, conclui-se que a associação entre dados históricos de manutenção e a matriz GUT representa uma estratégia aplicável para o diagnóstico da conservação predial em edificações públicas. A sistematização das ordens de serviço permite transformar registros administrativos, frequentemente utilizados apenas para fins operacionais, em indicadores técnicos capazes de subsidiar o planejamento da manutenção, a definição de prioridades de intervenção e a identificação de sistemas e setores com maior demanda de atenção.

Como limitação, destaca-se que o estudo foi desenvolvido em um único contexto institucional e geográfico, considerando edificações públicas residenciais vinculadas a uma mesma instituição e registros referentes a um recorte temporal específico. Além disso, embora a matriz GUT tenha permitido estruturar tecnicamente a classificação das ocorrências, a análise estatística das relações entre idade, sistema construtivo, frequência de registros e nível de criticidade ainda pode ser aprofundada. Recomenda-se, portanto, que estudos futuros ampliem a amostra analisada, incorporem séries históricas mais longas e associem os registros de ordens de serviço a inspeções técnicas em campo, de modo a validar os indicadores obtidos a partir dos dados operacionais de manutenção e ampliar sua aplicabilidade em processos de diagnóstico, conservação e planejamento de intervenções em edificações públicas.

Referências

Alavi, Hamed, Rafaela Bortolini, and Núria Forcada. 2022. “BIM-Based Decision Support for Building Condition Assessment.” Automation in Construction 135: 104117. https://doi.org/10.1016/j.autcon.2021.104117.

Associação Brasileira de Normas Técnicas. 2024. NBR 5674: Manutenção de edificações — Requisitos para o sistema de gestão de manutenção. São Paulo: ABNT.

Associação Brasileira de Normas Técnicas. 2024. NBR 15575-1: Edificações habitacionais — Desempenho — Parte 1: Requisitos gerais. Rio de Janeiro: ABNT.

Begić, Haris, and Hrvoje Krstić. 2024. “Comprehensive Review and Comparative Analysis of Building Condition Assessment Models.” Results in Engineering 22: 102176. https://doi.org/10.1016/j.rineng.2024.102176.

Berg Oppedal, Lisa, and Tore Kvande. 2024. “Lessons Learned from Information Sources on Building Defect Studies.” Buildings 14 (5): 1231. https://doi.org/10.3390/buildings14051231.

Bouabdallaoui, Yassine, Zoubir Lafhaj, Patrick Yim, Léo Ducoulombier, and Boumediene Bennadji. 2021. “Predictive Maintenance in Building Facilities: A Machine Learning-Based Approach.” Sensors 21 (4): 1044. https://doi.org/10.3390/s21041044.

Braga, I. C., F. S. Brandão, F. R. C. Ribeiro, and A. G. Diógenes. 2019. “Aplicação da Matriz GUT na análise de manifestações patológicas em construções históricas.” Revista ALCONPAT 9 (3): 320–35. https://doi.org/10.21041/ra.v9i3.400.

Chelaru, B., C. Onuțu, G. Ungureanu, and A. A. Șerbănoiu. 2024. “Integration of Point Cloud, Historical Records, and Condition Assessment Data in HBIM.” Automation in Construction 161: 105347. https://doi.org/10.1016/j.autcon.2024.105347.

Chew, Michael Y. L. 2005. “Defect Analysis in Wet Areas of Buildings.” Construction and Building Materials 19 (3): 233–48. https://doi.org/10.1016/j.conbuildmat.2004.07.005.

D’Orazio, Marco, Elisa Di Giuseppe, and Gabriele Bernardini. 2022. “Occupant Density Impact on Building Maintenance: Data-Driven Approach for University Buildings.” Automation in Construction 141: 104451. https://doi.org/10.1016/j.autcon.2022.104451.

Flores-Colen, Inês, Tito Lívio Ferreira Gomide, and Simone Machado Della Flora. 2022. Manual de manutenção em edificações: estudos, técnicas e aplicações. São Paulo: LEUD.

Flores-Colen, Inês, and Jorge de Brito. 2010. “A Systematic Approach for Maintenance Budgeting of Buildings Facades Based on Proactive and Preventive Strategies.” Construction and Building Materials 24 (9): 1718–29. https://doi.org/10.1016/j.conbuildmat.2010.02.017.

Gurmu, A., D. Denipitiya, and P. U. Wijeratne. 2025. “Causes, Detection and Remediation of Water-Induced Building Defects: A Systematic Review.” In Proceedings of the 13th World Construction Symposium, 385–96. Sri Lanka.

Holanda, Rafael, Sandoval Rodrigues, and Luciana Queiroz. 2022. “Aplicação da Matriz GUT na análise de degradação de fachadas: estudo de caso em prédio de educação superior.” In Congresso Brasileiro de Patologia das Construções — CBPAT 2022, 607–16. https://doi.org/10.4322/CBPAT.2022.053.

Kepner, Charles H., and Benjamin B. Tregoe. 1981. The New Rational Manager. Princeton, NJ: Princeton Research Press.

Madureira, Sara, Inês Flores-Colen, Jorge de Brito, and Cristina Pereira. 2017. “Maintenance Planning of Facades in Current Buildings.” Construction and Building Materials 147: 790–802. https://doi.org/10.1016/j.conbuildmat.2017.04.195.

Mahpour, Amirreza. 2023. “Building Maintenance Cost Estimation and Circular Economy: The Role of Machine-Learning.” Sustainable Materials and Technologies 37: e00679. https://doi.org/10.1016/j.susmat.2023.e00679.

.

Salzano, Antonio, Claudia Maria Parisi, Giovanna Acampa, and Mariangela Nicolella. 2023. “Existing Assets Maintenance Management: Optimizing Maintenance Procedures and Costs through BIM Tools.” Automation in Construction 149: 104788. https://doi.org/10.1016/j.autcon.2023.104788.

Tan, Yu, Guoqiang Li, Ruoyu Cai, Jiaqi Ma, and Ming Wang. 2024. “Building Defect Inspection and Data Management Using Computer Vision, Augmented Reality and BIM Technology.” Automation in Construction 161: 105299. https://doi.org/10.1016/j.autcon.2024.105299.



MATERIALS AND TECHNIQUES



Cinpar 2026
XXII International Conference on Building Pathology and Constructions Repair
15th to 17th July 2026 - Lisboa, Portugal

Low-Carbon Cements and Construction Durability: A Systematic Review

Juliana Gaio Somer[1]; Gersson F. B. Sandoval [2]; **Edna Possan[3]**

[1] Federal University of Latin American Integration, Foz do Iguaçu, Paraná, Brazil, julianagaiosomer@gmail.com
[2] Universidad Pedagógica y Tecnológica de Colombia, Colombia, gersson.barreto@uptc.edu.co
[3] Federal University of Latin American Integration, Foz do Iguaçu, Paraná, Brazil, epossan@gmail.com

Abstract: Reducing clinker content in low-carbon cements and developing alternative binders are essential strategies for mitigating emissions from the cement industry, which accounts for approximately 7% of global anthropogenic CO_2 emissions. Implementing cement decarbonization solutions requires adjustments to the material's physicochemical properties and reactivity. Partial clinker substitution affects cement hydration, C-S-H formation, and portlandite release, thereby highlighting the need for a deeper understanding of the implications of these changes for durability and the life-cycle performance of structures, topics that remain insufficiently addressed in an integrated manner in the literature. From this perspective, this paper presents a systematic review, based on the Methodi Ordinatio approach, of studies published over the last decade in indexed databases, using keyword combinations to critically examine the relationship between low-emission cements, durability, and the service life of structures incorporating them. A total of 48 articles were selected, with the primary focus on quantifying the CO_2 avoidance during cement production, primarily through clinker reduction, without comprehensively addressing the use phase with respect to durability and service life. Durability assessment is typically conducted in a fragmented manner, particularly in studies of novel binders such as LC3 (limestone calcined clay cement) and geopolymers. Compressive and tensile strength tests predominate in evaluating mechanical properties, while resistance to chloride ingress and carbonation are commonly used as indicators of durability. Microstructural and physicochemical analyses are used to evaluate morphology, hydration products, and pore structure. The reviewed studies indicate a tendency for low-emission cements to exhibit higher fineness, in some cases increased C3S and C3A contents, and a lower alkali reserve. Establishing correlations between these parameters and durability, from application through the end of the life cycle, is fundamental to simultaneously ensuring resource-use efficiency, sustainability, and the long-term performance of structures incorporating low-carbon cements.

Keywords: Service life; Clinker; Concrete; Net zero; Decarbonization.

1. Introduction

The civil construction sector is responsible for a significant share of global anthropogenic atmospheric emissions – Portland Cement (PC) production alone accounts for approximately 7% of global carbon emissions. This necessitates technical and scientific strategies on the path toward carbon neutrality, projected for 2050 (Soldado et al. 2021; IEA, WBCSD, and CSI 2018; GCCA 2021). To mitigate environmental impacts, the cement sector has implemented various strategies to reduce CO_2 emissions from its products and processes. Among these, the strategies that contribute most significantly to reaching climate targets at a low cost, in order of implementation, are: reducing the use of clinker in PC manufacturing by substituting it with supplementary materials (SNIC and ABCP 2019; Van Deventer et al. 2015; Griffiths et al. 2023); increasing energy efficiency in the cement production process (Beguedou et al. 2023; Scrivener, John, and Gartner 2018; Chew et al. 2025) and carbon capture, storage and utilization (CCUS) (GCCA 2021; Amran et al. 2022), which possess distinct characteristics and technological maturity levels (Sun et al. 2025).

Cements categorized as "low-emission" generally achieve this status by reducing clinker content, as the clinker production process accounts for 55% to 70% of total process emissions (Y. Wang et al. 2024; Z. Li et al. 2024; Thorne et al. 2024). In this context, the international outlook is for the clinker/cement ratio to reach between 0.52 and 0.57 by 2050 (GCCA 2021; IEA 2023), while in Brazil, this ratio is currently 0.66, with emissions of around 564 kg of CO_2 for every ton of cement produced (SNIC and ABCP 2019), as illustrated in

. On the other hand, despite the efforts, global cement production is still expected to grow slightly over the next decade, with a small decline starting in 2035. In Brazil, consumption is projected to continue growing until 2050 (

).

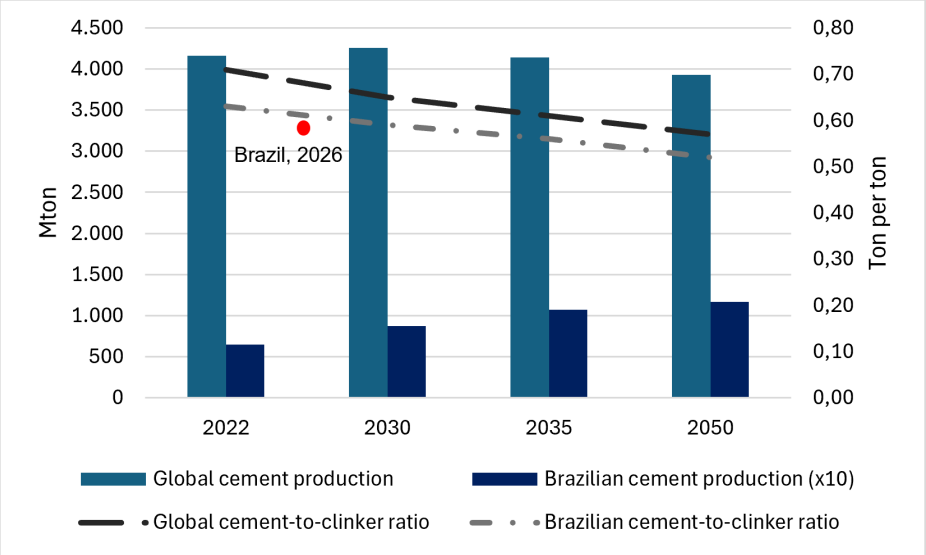


Figure 1 – Correlation between global and Brazilian production outlooks and the clinker factor in cement.

Source: Adapted from IEA, 2023 and SNIC; ABCP, 2019.

Among the partial clinker substitutions in low-emission cements, supplementary cementitious materials (SCMs) such as pozzolans, slag, fly ash, and carbonate materials stand out, as they have well-established technical performance and are widely used commercially (H. Chen and Yang 2023; Z. Li et al. 2024; Scrivener, John, and Gartner 2018). In parallel, research on new SCMs and alternative binders, such as construction and demolition waste (CDW), biomass ash, as well as low-emission geopolymer cements, supersulfated cements, and LC3 (limestone calcined clay cement), for example, has demonstrated significant potential for mitigating atmospheric emissions, reaching up to 40% when compared to PC (Z. Lei and Pavia 2024; Snellings, Suraneni, and Skibsted 2023; Barbhuiya et al. 2025). Conversely, despite scientific advances associated with such materials, their global market penetration remains limited. Recent studies have expanded the discussion to also consider emissions associated with the maintenance and rehabilitation of concrete structures and the use of alternative materials, such as natural fibers (Kasuga 2023; Helaili and Chafra 2023).

The incorporation of SCMs modifies the material's physicochemical characteristics and, consequently, its chemical reactions (kinetics), resulting in a product with distinct properties for application in cement-based materials (Aïtcin, Wilson, and Mindess 2018; Kipkemboi et al. 2020; Bramha Chari and Ranga Rao 2022). In many cases, these changes in cement characteristics can yield benefits, such as promoting void reduction (pore structure refinement) through the addition of finer materials, thereby increasing the concrete's initial strength (Oliveira et al. 2023). On the other hand, a reduction in the most reactive phases, primarily C_3S and

C_3A, is observed. When the added SCM is silica-rich, changes in hydration kinetics, C-S-H formation, and portlandite consumption may result in lower alkali content and reduced concrete pH, directly influencing the durability of construction (Lothenbach, Scrivener, and Hooton 2011; Mehta and Monteiro 2006; K. Zhang et al. 2024).

Regarding the large-scale application of low-carbon cements and binders under development, the barriers to be overcome include the scarcity of clinker substitutes, logistics, adaptations in industrial processes, and the fact that many scientific studies are conducted in isolation, making it difficult to understand the full scope of the studied material's applicability (Biernacki et al. 2017; Possan, Dal Molin, and Andrade 2018). Additionally, other challenges to be overcome include associated costs, potential difficulties in use and application due to the chemical changes the materials present, and evidence regarding durability and the product's life cycle (Hafez et al. 2022; K. Zhang et al. 2024).

Durability can be defined as the structure's capacity to resist physical, chemical, and mechanical degradation mechanisms, thereby maintaining performance throughout its service life (Mehta and Monteiro 2006; Dyer 2014). The traditional model for this purpose consists of standardized laboratory tests such as carbonation, permeability, sulfate attack, freeze-thaw cycles, chloride penetration, and, in some cases, accelerated tests that simulate long-term use (Ali, Naganathan, and Mahalingam 2021; ASTM 2022). Additionally, compliance monitoring is conducted through longitudinal data collection spanning decades. Both types of information enable the development of predictive models that, in addition to serving as a reference for the structure under study, also support standards published by respected regulatory bodies (Van Deventer et al. 2015; Possan, Dal Molin, and Andrade 2018). Increased concrete durability is associated with adjustments in the formulation of cementitious materials and structural elements (C. Li et al. 2023; Huang et al. 2025); this may be a direction for concentrating efforts aimed at updating current standards, including those focused on alternative binders (Perez Villa et al. 2021; Provis 2025) and to understand if the proposed tests and modeling still meet the products currently offered to the market.

In reinforced concrete structures, corrosion of steel reinforcement corrosion is the most common cause of structural deterioration (Soldado et al. 2021; Ranasinghe and De Silva 2022; Bras et al. 2021; J. J. O. Andrade, Possan, and Dal Molin 2017). Simplistically, this occurs because the concrete covering the reinforcement fails to fulfill its function of adequately protecting it from corrosion-promoting elements, allowing the entry of aggressive agents present in the environment that penetrate and diffuse through the cement paste (C. Li et al. 2023; Soldado et al. 2021; J. Shi et al. 2018; J. J. O. Andrade, Possan, and Dal Molin 2017). The number and size of pores and the chemistry composing the cement matrix structure, associated with the building's exposure environment, are examples of factors linked to material durability (X.-Y. Wang 2019; Dyer 2014) that are not yet fully understood in concretes made with low-emission cements (Doussang 2023; Rathnarajan and Pillai 2025).

Cracking and shrinkage are also common problems in concrete, often caused by delayed ettringite formation (DEF), alkali-aggregate reaction (AAR), or sulfate attack. DEF is associated with high curing temperatures, which can be exacerbated by the type or fineness of the clinker substitute material (Franke Portella et al. 2021; Gu et al. 2020; Dyer 2014). AAR is characterized by the formation of an alkali gel that, due to its expansive properties, exerts internal stress on the concrete, leading to cracks (Pan et al. 2012), which can be even more common in concrete with a high water/cement ratio (Dyer 2014). In low-emission cements, alkali-rich SCMs in clinker substitution can drive AAR formation, whereas silica fume rich materials can mitigate this phenomenon (Dyer 2014; Mehta and Monteiro 2006). Attacks by the presence of sulfur (sulfates and sulfites) can be favored by a mechanism like AAR: if the material added for decarbonization is sulfur-rich (Johansson et al. 2024), and is aggravated in more permeable concretes (Dyer 2014).

What all potential problems in low-emission cements that could lead to premature structural degradation have in common is that the state of the art for these types of materials has not yet been reached, and the recovery of structures with these pathological manifestations is usually difficult, often costly, and may limit the acceptance of new products (Barbhuiya et al. 2025). In research on various types of low-carbon cements, in general, not all durability tests associated with traditional PC are performed (Escalante-Garcia, Cabrera-

Luna, and Castillo-Sanchez 2024; Doussang 2023; Hasheminezhad et al. 2024; Robalo et al. 2020). In other cases, it is questioned whether traditional methodology can be applied to low-emission cements (Ali, Naganathan, and Mahalingam 2021; Doussang 2023; Liang et al. 2024), and there are still situations where the product under study shows excellent results in some aspects but does not meet the minimum requirements in others, especially depending on the clinker substitution percentage (Barbhuiya et al. 2025; Hasheminezhad et al. 2024; Robalo et al. 2020).

Recognizing the need for technological advances to decarbonize the PC chain and considering that the service life of concrete structures is a central premise of sustainability, this article presents a systematic literature review that correlates these variables and investigates how building durability has guided the development of low-carbon cements.

2. Methodology

The systematic literature review was based on the *Methodi Ordinatio* framework, which consists of selecting and classifying articles based on their scientific relevance, measured by the result of an *InOrdinatio* equation. This equation combines the journal's impact factor, the number of citations, and the year of publication (Pagani, Kovaleski, and Resende 2015). The research was conducted across the indexed scientific databases Scopus and Web of Science (WoS), which were selected for their large number of publications in engineering, construction technologies, materials science, and sustainability. A series of keyword combinations was used, with the inclusion of new terms at each refinement step, supplemented by Boolean operators "OR" and "AND" and the wildcard character "*" to retrieve the maximum number of publications on the subject. The timeframe was delimited to 2014-2025, which received the maximum weight of 10 in the *InOrdinatio* equation, since technological advancement is a critical factor for this research. The search focused on English-language scientific journal articles. Finally, the terms combined in each stage of the search, along with the number of returned publications, were required to appear in the title, keywords, or abstract of the publication. Regarding the number of publications associated with the year, the information is correlated in **Figure 1a**, while the most frequently occurring words (a minimum of three times) are grouped in **Figure 1b**.

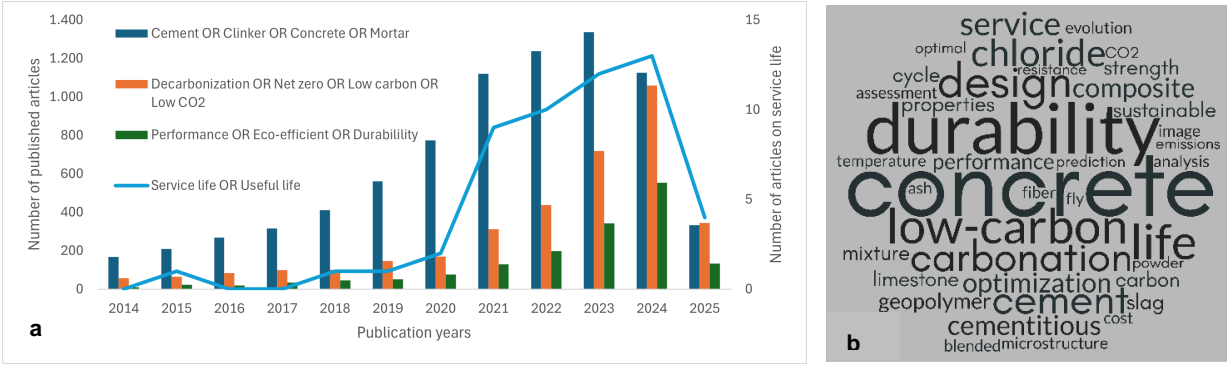


Figure 1: a) Comparison of the number of publications and year as a function of keyword refinement; **b)** word cloud.

In accordance with the eligibility criteria, it was essential that the terms used appeared in all articles. The initial strategy yielded 95 articles, which were added to the Mendeley free reference manager and reduced to 51 after duplicates were removed. Upon implementing a new screening for thematic relevance, the count was further reduced to 48 articles. The *InOrdinatio* equation was applied to these remaining articles using an Excel spreadsheet that considers each journal's impact factor, the year of publication, and the number of citations (Pagani, Kovaleski, and Resende 2015) obtained from Google Scholar. At the end of this process, the 48 selected articles were ranked according to their relevance, based on the established premises and the

method used. In addition to the references obtained through this methodology, other relevant publications on the subject were used during the review to inform the approach and exploration of the topic.

3. Results and discussion

Among the selected articles, it can be observed that, rather than evaluating the durability of existing low-emission PC-based materials, the primary focus of the publications is on assessing the durability of low-carbon materials under development (new materials), particularly under aggressive environmental conditions. Regarding the methods for obtaining results, the main division lies between simulations, models, and/or applied testing. The possibilities for decarbonizing the cement industry range from cement manufacturing to concrete use, as detailed below.

3.1 Geopolymers

In the analyzed publications, the focus is primarily on evaluating mechanical performance and resistance to aggressive environments. While one group of researchers (Cheng et al. 2024) focused on structural improvement through the incorporation of steel fibers (0.5%), another (Liu et al. 2024) considered the reuse of geopolymer concretes as coarse aggregates in environments subject to freeze-thaw cycles. The evidence pertains to the influence of the precursor type and curing conditions on mechanical strength and durability; aggregates derived from fly ash concrete did not perform well in the evaluation, whereas the best results were found in the recyclability of concretes made with metakaolin, red mud, and slag, which was associated with the density and chemical properties of these materials. Two other groups focused on the effects of corrosive environments on geopolymer concrete. In one study involving steel-reinforced geopolymer concrete, the applied tests, modeling, and neural network algorithms led to the conclusion that when observing chloride content, humidity, and temperature, the latter was the most relevant factor in inducing reinforcement corrosion, followed by humidity and chloride content (Wasim, Ngo, and Law 2021). The other study reported positive results on the use of fibers and nanomaterials to enhance the mechanical resistance of geopolymer concrete to chloride attack, thereby increasing its durability (H. Li et al. 2024).

The full replacement of PC with geopolymer binders has been explored in coating applications, focusing on contact angle, surface energy, mechanical properties, and microstructure (A. Wang et al. 2022). The results indicate that the substituents under study have hydrophilic properties like PC and that the test results were positive regarding material porosity, with the advantage of reducing environmental impacts by 50% to 80% in the highest-impact categories, according to the Life Cycle Assessment (LCA) performed (A. Wang et al. 2022). Although this research is relevant to the development and application of technology, none of the studies systematically observe the use and service life of the construction.

3.2 Limestone Calcined Clay Cement (LC3)

As an alternative to PC, ternary cement, also known as LC3, is named for the addition of two other components - generally blast furnace slag and fly ash. Reported benefits include a reduction in atmospheric emissions by replacing a portion of the clinker (Tsivilis et al. 2002; Kim et al. 2018), a decrease in concrete porosity (Kim et al. 2018; Thorne et al. 2024; Du et al. 2023), a reduction in carbonation depth, and consequently, reinforcement protection (Tsivilis et al. 2002), as well as improved clinker reactivity (Tsivilis et al. 2002). Due to these positive characteristics, it has been a subject of study, with results demonstrating a delay in the development of expected compressive strength and greater carbonation depth, which can be detrimental to reinforced concrete due to the increased risk of reinforcement corrosion (Rivera et al. 2021). However, since carbonation is a naturally occurring reaction in concrete, it also contributes to the carbon neutrality goal, provided it does not impair the structure's service life. Therefore, concrete produced with the cements reported in this article can be highly useful in applications where initial strength is not a primary requirement or where there is low exposure to air, such as foundations, pipelines, and similar structures.

Additional research has sought to determine the optimal clinker substitution level in LC3 systems, balancing mechanical performance and carbonation control (Thorne et al. 2024; X.-Y. Wang 2020). Findings indicate that the criteria for using LC3 differ between low-strength concretes (25 MPa), where carbonation must be considered, and high-strength concretes (45 MPa), where mechanical strength predominates (X.-Y. Wang 2020). Mixtures combining PC with fly ash showed strength increments of approximately 20.5% and a 21.1% reduction in CO_2 emissions compared to concrete produced with PC and filler (Thorne et al. 2024). Complementary strategies, such as the incorporation of microcapsules for self-healing, demonstrated the potential for sealing surface cracks with widths exceeding 0.4 mm within 72 hours (Du et al. 2023). However, in studies with high-strength concrete, results indicated that, even after healing, the hydration products formed were brittle, making them prone to re-cracking under load (L. Wang et al. 2023).

3.3 Cements with pozzolanic additions

The use of SCMs, specifically off-specification fly ash and glass spheres, for lightweight concrete, was evaluated in high-performance concrete under flexural load tests to assess mechanical behavior and LCA (Ghahsareh et al. 2025). The mechanical test results were satisfactory, with crack widths remaining below standardized limits. Atmospheric emissions were reduced by up to 20%, the largest fraction of which stems from clinker substitution (Thorne et al. 2024), and by up to 58% due to reduced maintenance requirements (Ghahsareh et al. 2025). However, the LCA is limited to concrete production and does not account for the service life or maintenance requirements of a construction project using this low-carbon cement.

Nanosilica is another SCM that has been explored, particularly because small additions can significantly improve concrete's mechanical properties, especially in aggressive environments, due to its high resistance to sulfate attack (L. Zhang et al. 2023; Xu et al. 2023). Beyond environmental sustainability benefits, some properties of nanosilica are analogous to those of limestone powder: reducing concrete pores through particle packing and assisting reinforcement preservation. Regarding the challenges for large-scale application of this material, the lack of long-term durability studies, dosage standardization, and application systematization stand out (L. Zhang et al. 2023). For the full range of SCMs, microstructure and macroscopic properties need to be evaluated in detail, including extreme situations such as high temperatures (Y. Li, Liu, and Jiang 2024). Natural pozzolans are emerging as an alternative SCM to fly ash, with satisfactory results in workability, strength, water absorption, and chloride diffusion (Robalo et al. 2021).

Focusing on material durability, studies on concrete made with low-carbon cement incorporating 30% fly ash or 50% slag found that resistance to chloride attack is higher than in PC concrete at the same water/cement ratio (Sirivivatnanon, Xue, and Khatri 2022). Although the research focus is on the durability of low-emission cements, there is a stated concern regarding the lack of standardization in codes for certain types of potential clinker substitutes, especially construction waste rich in compounds that remain poorly understood (Liang et al. 2024; Sirivivatnanon, Xue, and Khatri 2022).

3.4 Other solutions

In the line of new product development, studies were conducted to improve the freeze-thaw performance of expanded polystyrene (EPS) concrete, which possesses excellent thermal insulation but unsatisfactory freeze-thaw performance. In this regard, EPS beads were coated with different materials; testing and modeling found that EPS concrete with beads coated with water-based polyurethane and high-performance concrete showed a 60% increase in freeze-thaw resistance compared to uncoated EPS (Yuan et al. 2022). Although the authors cite its use in low-rise buildings and certain engineering applications, they also note that studies on its durability are scarce (Yuan et al. 2022), which may act as a strong deterrent to the popularization of this low-carbon material.

Low-heat expansive cement (LHEC) is presented as a material with the potential for wide use in humid environments, such as dams, as a replacement for PC. Beyond lower CO_2 emissions, since it is primarily composed of granulated blast-furnace slag, its main advantages include high strength, low heat of hydration, and micro-expansion performance (Jin et al. 2024). A challenge still to be overcome with this

material is delayed ettringite formation (DEF), which can cause structural cracking (Dyer 2014); gypsum was added to address this. Promising results indicate the need to not only add gypsum but also to control curing temperatures to minimize DEF formation (Jin et al. 2024).

The use of carbon fiber reinforcement to enhance mechanical performance in low-emission concretes was conducted by two research groups (Diao et al. 2024; Cecen, Aktas, and Ozbayrak 2023). In the first study, the focus was on cement paste with an extremely low water/cement ratio, leading to the conclusion that compressive and tensile strength, freeze-thaw resistance, and drying shrinkage were increased, while freeze-thaw resistance was reduced. Based on these findings, an increase in the service life of structures with these characteristics was inferred (Diao et al. 2024). In a specific application for railway sleeper production, a niche market requiring high early strength, prestressing, and mandatory reinforcement, pieces were produced using low-emission concretes. These were evaluated for both partial PC replacement and reinforcement with polyurethane and carbon fiber (Cecen, Aktas, and Ozbayrak 2023). The highly detailed decarbonization potential assessment indicates that good mechanical performance can be achieved with cements featuring up to 50% clinker substitution by natural pozzolans, resulting in up to 54% fewer atmospheric emissions in the sleepers. However, this reduction will only be achieved if the production of carbon fibers and polyurethane also follows a decarbonization trend; otherwise, the environmental benefits of cement substitution may be progressively lost (Cecen, Aktas, and Ozbayrak 2023). Although this application is focused on the railway market, the author's conclusion addresses a point seldom discussed in other articles: the evaluation of real reduction potential must be comprehensive.

Regarding coarse aggregates but within the decarbonization line, one study indicates the use of bamboo as an aggregate and focuses on mechanisms to overcome material segregation in concrete (X. Chen et al. 2024). While the research is relevant, it brings little contribution regarding zeroing emissions or observing product service life. Similarly, a study was retrieved on grouting materials with additives that increase durability in aggressive environments, with an average carbon emission of 84.86 kg/ton, compared with 280-767 kg/ton in similar studies, significantly reducing atmospheric emissions (Y. Chen et al. 2025).

Also focusing on durability and, in a very particular report, on accelerated carbonation caused by leaked stored CO_2 (Xue et al. 2022), which, with the advent of CCUS technology, may become commonplace. The study was motivated by an incident recorded during tunnel construction in China. A CO_2 leak was detected, and it was observed that the high gas concentration, coupled with elevated pressure, caused rapid and deep carbonation of the concrete, resulting in structural damage and loss of strength due to reinforcement corrosion (Xue et al. 2022). The research focused on evaluating concrete under various CO_2 concentrations and pressures, with different relative humidities. Results showed that although a carbonation front can be beneficial to concrete's compressive strength (Dyer 2014), when the CO_2 partial pressure reaches 1,000 kPa, severe structural damage can occur due to induced carbonation (Xue et al. 2022). The approach in this article points toward an issue surrounding the advancement of CCUS and its potential leaks.

In this stage of the analysis, it was observed that there is a lack of standardization for minimum criteria in conducting research, which often makes literary comparison impractical. Although authors strive for durability in their research, in most cases, it is not possible to compare measurements between the conventional product and the one under study. This is a point of attention that must be addressed for the integration of low-carbon cements into the market, as integrating decarbonization and durability is strategic for all stakeholders in the PC chain, from production to application (Possan 2026).

3.5 Predictive Modeling and Simulation

Although the development of modeling is not new for predicting the durability of cementitious materials (W. Shi, Yu, and Kuang 2012; Zheng, Miao, and Zheng 2023), the subject has been extensively explored by research groups, especially with the advent of Artificial Intelligence algorithms and the use of varied and combined SCMs. However, one question is whether traditional durability models remain applicable to cements with reduced clinker content (Doussang 2023; Liang et al. 2024). Conversely, the use of digital tools and neural networks can accelerate the development of decarbonized products.

Selected publications report simulations for the strength of concrete produced with low-carbon cement (using different SCMs) based on carbonation time (X.-Y. Wang 2022; X. Wang 2022; X.-Y. Wang 2023). The conclusions indicate that for concretes with strength up to 40 MPa, carbonation durability is the criterion for service life, whereas compressive strength is the decisive factor in concretes with strength exceeding 50 MPa (X.-Y. Wang 2022, 2023). In simulations where metakaolin was the SCM used, establishing premises for concrete strength and carbonation service life, alongside optimal mix criteria combining emission reduction and product cost, it was concluded that to meet the requirements, SCM use was minimal because the cost of metakaolin is higher than that of PC (X. Wang 2022). In turn, simulations combining SCMs (metakaolin, fly ash, limestone powder) indicate that a blend of these SCMs can lead to better outcomes in controlling maximum atmospheric emissions, maximum heat of hydration, and concrete electrical resistivity (Lin, Han, and Wang 2021).

In other research, a modeling study aimed to identify the optimal SCM use and water/cement ratio, using compressive strength, additive use, and atmospheric emissions as parameters (Yang, Dong, and Wang 2025). The results indicate that a lower water/cement ratio with fly ash addition increases compressive strength and CO_2 emissions; the application of the models enabled a detailed combination of these variables (Yang, Dong, and Wang 2025).

With a more integrated perspective, one simulation simultaneously considered economic, environmental, mechanical, and durability factors (DeRousseau, Kasprzyk, and Srubar III 2021). The authors highlight a gap in most published models, to the rigidity of input parameters such as costs, availability, and the environmental sustainability of materials. The presented case studies indicate that the most relevant factors in achieving concretes with optimal characteristics are the cost of each component, including SCMs, and the environmental aggressiveness class of the application (DeRousseau, Kasprzyk, and Srubar III 2021). Furthermore, the proposed simulations appear highly useful, particularly by enabling regionalized solutions, an extremely important factor for SCMs.

The proposal for hybrid steel-concrete prefabricated modular buildings was the starting point for a study that modeled the service life of such construction, using PC with partial clinker replacement by SCMs, ultra-lightweight cement, and foam concrete (L. Chen et al. 2024). In addition to evaluating the behavior of the construction material itself, the authors advocate for design-related concepts, such as using concrete with thermal performance that reduces users' electricity consumption during the building's occupancy. This concern is highly relevant and has been noted by other researchers who support the application of engineering concepts as mechanisms for decarbonization (Miller et al. 2025; Watari et al. 2022), given that data indicates that up to 38% of energy-associated CO_2 emissions stem from the built environment (UNEP 2024). Thus, the prefabricated modular structure was studied with respect to cost requirements, carbon emissions, and energy consumption throughout its service life, alongside the effects of extending service life and overall performance. The authors provided comprehensive and important conclusions on atmospheric emission reductions, circular economy, and construction efficiency (L. Chen et al. 2024). One aspect not clearly addressed in other studies but defended as a premise in this one is that durability is key to the circular economy; in this regard, researchers further simulated scenarios to extend the service life of buildings to 100 and 150 years. The main findings include reductions of up to 17% in energy consumption during occupancy and up to 14% in CO_2 emissions, with a service life extended to 150 years (L. Chen et al. 2024).

Regarding concrete durability requirements, there is the concept of "designed concrete," which features a defined standard for minimum strength class, required consistency, water/cement ratio limits, minimum content, and permitted cement types, linked to chemical aspects, in addition to factors such as aggregates, additives, and concrete curing (Dyer 2014). Assuming these truths, modeling or propositional scenarios should, at a minimum, consider these variables to evaluate product quality.

3.6 Life Cycle Assessment (LCA) and Durability

Although LCA constitutes a central tool for measuring environmental impacts throughout the life cycle of products from a sustainability perspective (Rocha and Caldeira-Pires 2019), until the last decade, the influence of the durability of low-carbon concrete structures on the results of this type of analysis was not clear (C. Li et al. 2023). The primary effect has been the development of divergent assessment approaches, which consequently yield very distinct results, ranging from 84 to 612 kg of CO_2 equivalent per m^3 of low-emission concrete (Hafez et al. 2019; D. Lei et al. 2025).

The main durability indicators of a structure stem from the project acceptance requirements, either prescriptive or associated with verified performance (C. Li et al. 2023), and both are governed by relevant standards (Müller, Haist, and Vogel 2014). Prescriptive requirements are linked to the type of environment, or exposure class, for which there are indications regarding materials and concrete cover thickness; for example, it is assumed that meeting these prescriptions will achieve the design service life. In contrast, performance requirements focus on meeting given conditions before reaching a limit state, such as carbonation depth, resistance to chemical attacks, and the natural chemical reactions of concrete. For these, testing and modeling are typically conducted to predict the service life of materials (C. Li et al. 2023; Juenger, Snellings, and Bernal 2019).

Among the analyzed articles, 27 involved testing related to the durability and performance of concrete or mortar (**Table 1**). In six of these, only one parameter was measured, usually a mechanical property. In five others, mechanical, chemical, and microstructural property tests were conducted simultaneously, representing a more comprehensive analysis. Furthermore, among the analyzed article, only three evaluated the studied parameters for more than one year. In thirteen studies, the analysis period was up to 28 days, which is considered a short timeframe when addressing durability. This information highlights the insufficient data to correlate LCA studies with the durability perspective of materials and structures made with low-carbon cement, underscoring the need for further progress in this direction.

Table 1 - Summary of the tests performed, and properties observed in the literature studies analyzed

Material used	Properties				Test time	Ref.
	Physical and Rheologycal	Mechanical	Chemical	Microstructural		

Reinforced concrete (PC with pozzolan and slag)	-	-	Chloride resistance	-	9 Years	(Sirivivatnanon, Xue, and Khatri 2022)
Mortar (PC and Low-heat expansive cement)	-	Compressive Strength Deformation	-	Hydration morphology Hydration products Crystalline structure	120 Days	(Jin et al. 2024)
Reinforced concrete (PC with pozzolan)	Density Water absorption Electrical resistivity Workability	Compressive Strength Deformation Tensile	Carbonation Chloride resistance	-	90 Days	(Robalo et al. 2021)
Ternary Portland cements and Mortar	-	Compressive Strength	Carbonation	-	20 Months	(Rivera et al. 2021)
Reinforced waste-based geopolymer foam concrete	-	Tensile	-	-	90 Days	(Wasim, Ngo, and Law 2021)
Concrete (PC)	-	Compressive Strength	Carbonation	Hydration morphology	28 Days	(Xue et al. 2022)
Mortar (LC3)	-	Compressive Strength	Chloride resistance	Pore size	28 Days	(Du et al. 2023)
Expanded polystyrene (EPS) concrete	-	Compressive Strength Freeze–thaw	-	Pore structure	275 freeze-thaw cycles	(Yuan et al. 2022)
Fiber-reinforced (CP) and LC3 concrete	-	Freeze–thaw	-	Hydration products Pore size	48 Days	(L. Wang et al. 2023)
Pastes and mortar (PC with fly ash and slag)	-	-	Carbonation	Depth and direction of carbonation	3 Months	(K. Zhang et al. 2024)
Reinforced concrete (PC with fly ash and slag)	Humidity	-	-	-	10 Months	(Huang et al. 2025)

Cement Pastes (PC with fly ash, limestone and metakaolin)	Electrical resistivity	Compressive Strength	Heat of hydration CO_2 emission	Crystalline structure	28 Days	(Lin, Han, and Wang 2021)
Concrete (PC)	-	-	-	Phase distribution	28 Days	(X. Chen et al. 2024)
Cement Paste (PC with Colloidal nano-silica)	Workability	Compressive Strength	-	Hydration morphology Hydration products Pore structure	28 Days	(Xu et al. 2023)
Geopolymer Paste (with Steel fiber and ceramsite)	-	Compressive Strength Deformation	-	-	28 Days	(Cheng et al. 2024)
Cement Paste (PC with limestone powder)	Workability	Compressive Strength	Carbonation	-	540 Days	(X.-Y. Wang 2020)
Cement Paste (PC with slag)	Workability	Compressive Strength Freeze–thaw	-	-	28 Days	(X.-Y. Wang and Lee 2021)
Cement Paste (Coal slag and steel slag)	Workability Setting time	Compressive Strength Deformation	-	Phase distribution Hydration products	28 Days	(Y. Chen et al. 2025)
Geopolymer concrete (with fly ash, red mud and slag)	-	Compressive Strength Freeze–thaw	-	Phase distribution Pore structure	28 Days	(Liu et al. 2024)
Geopolymer mortars (with slag, red mud, metakaolin and fly ash)	-	Interfacial adhesive strength	Hardness	Functional Group	1 Year	(A. Wang et al. 2022)
Reinforced concrete (PC with pozzolan)	-	Compressive Strength Deformation Tensile	-	-	28 Days	(Cecen, Aktas, and Ozbayrak 2023)
Cement Paste (PC) reinforced with carbon fiber	Density Water absorption	Compressive Strength Deformation Tensile Freeze–thaw	Drying shrinkage	-	150 Days	(Diao et al. 2024)

Ultra-high-performance concrete (PC with slag) reinforced with fibers	-	Deformation	-	-	28 Days	(Ghahsareh et al. 2025)
Natural fibers in epoxy base	-	Tensile	-	-	1 Day	(Helaili and Chafra 2023)
Mortars (PC with fly ash, limetone filler, pozzolan and slag)	Water absorption Electrical resistivity	Compressive Strength Deformation	Chloride resistance Carbonation	-	90 Days	(Soldado et al. 2021)
Concretes (PC with fly ash and slag)	Water absorption	Compressive Strength	Chloride resistance	Crystalline structure Hydration products Hydration morphology	90 Days	(Van Deventer et al. 2015)
Concretes (PC with silica, calcined clay and limestone)	Density	Compressive Strength Deformation	Carbonation Thermal conductivity	-	28 Days	(L. Chen et al. 2024)

The lack of standardization for LCAs that collectively encompass concrete structures, combined with the fact that current standards do not necessarily cover low-carbon cements, underscores the existing gap in the field. Furthermore, the absence of a clear approach connecting durability with the LCA of low-carbon concretes can lead to contradictory and biased conclusions (D. Lei et al. 2025; C. Li et al. 2023; Hasheminezhad et al. 2024). In the research conducted by (Jiang et al. 2024), the authors report on the difficulties in obtaining experimental data to account for the increased mechanical strength and durability of alternative materials compared to PC concrete. This raises doubts about real decarbonization, as the environmental and economic performance of materials is directly linked to the properties that determine the structure's service life (Jiang et al. 2024).

4. Trends, research gaps and perspectives

The main pathways of the cement sector, whether currently implemented or under implementation to reach Net Zero, include plant energy efficiency, co-processing, the replacement of fossil fuels, and the reduction of clinker content in cement. However, due to issues inherent to the raw material, especially the limestone decarbonation process, the cement industry will depend on carbon capture actions to achieve the neutrality goal. Estimates across various Roadmaps (SNIC and ABCP 2019; IEA, WBCSD, and CSI 2018) suggest that approximately 40% of the decarbonization target is linked to CCUS; however, implementing the necessary carbon capture technologies poses a significant challenge due to associated costs.

Portland cement undergoes decarbonization showing trends in its physicochemical characteristics, particularly increases in fineness, C_3S, and C_3A, and a reduction in alkaline reserve, consequences of

alterations in clinker and cement production. Published works primarily focus on new cementitious materials and alternative binders, such as LC3 and geopolymers, and lack studies on Portland cement with lower clinker content, particularly regarding its effects on the durability of cement-based materials.

The current outlook demands innovation, scientific-technological development, stakeholder training across in the cement and concrete chain, financial investment in research and companies, and local and global regulatory standards and public policies to support the achievement of the sector's zero-emission objective. Significant progress is required in conducting systemic and networked research focused on the durability and service life of products derived from decarbonized Portland cement (**Figure 3**). The use of Machine Learning tools and computational intelligence is of great interest for data analysis, correlation, and system modeling.

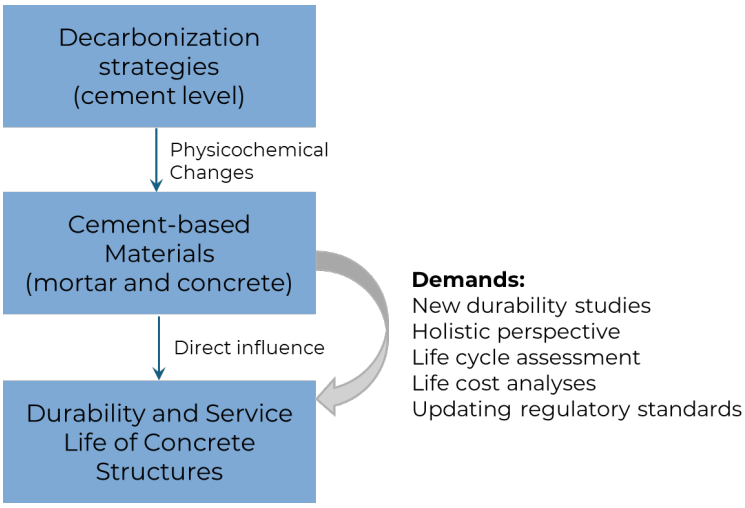


Figure 3 - Summary of the implications of decarbonization in cement and the demands generated.

The main decarbonization pathways focus on cement, the basic raw material of the construction chain, but pay little attention to potential implications in the material's application processes, such as optimizing cement consumption in concrete manufacturing and extending the service life of elements and structures (Watari et al. 2022; GCCA 2021; C. Li et al. 2023; Müller, Haist, and Vogel 2014). Some studies demonstrate that extending the service life of construction can contribute to meeting the sector's global emission targets by 4%-15% (C. Li et al. 2023; Watari et al. 2022); this is a vital agenda for the effective decarbonization of Portland cement sector. Systematic studies are needed to address the trade-off between CO2 reduction and durability throughout the life cycle of concrete structures (Possan 2026), to avoid shifting the problem from cement to concrete, which would result in indirect emissions associated with frequent maintenance or premature reconstruction.

5. Conclusions

The considered literature predominantly addresses the reduction of emissions associated with cement production, yet it comprehensively quantifies, in a comprehensive manner, the actual contribution of materials to decarbonization throughout their life cycle. Methodological fragmentation is evident, with isolated assessments of mechanical or environmental performance failing to consistently correlate with durability, service life, and commercial-scale viability. This gap compromises the robustness of conclusions and limits a safe transition to cement with lower clinker content. Part of this scenario stems from experimental constraints, high costs, and pressure to deliver rapid, novel results.

For the expected environmental gains to be effectively achieved, the implementation of low-carbon cements must be deepened, with durability requirements integrated into the process through holistic Life Cycle Assessment (cradle-to-cradle) studies. Otherwise, the undeclared systemic risk to the chain is a "trade-off": a low-carbon cement that may compromise the durability of the elements and structures produced.

For these reasons, conducting comprehensive interlaboratory studies is recommended to re-evaluate the durability implications of elements and structures manufactured with cement undergoing decarbonization. The results of this process will serve as a basis for updating regulatory standards for low-emission materials, which have direct implications for the carbon market. In parallel, technical qualifications, guidance, and monitoring for professionals working in the cement-based materials and construction chain are fundamental to ensuring specifications, applications, and controls that are compatible with the new performance requirements.

Acknowledgments

This study was financed in part by the Coordenação de Aperfeiçoamento de Pessoal de Nível Superior – Brasil (CAPES), under Call n° 08/2024 – PPGIES/ ILATIT.

References

Aïtcin, Pierre Claude, William Wilson, and Sidney Mindess. 2018. “Concrete in Canada: 50 Years of Progress — Present Concerns.” *Canadian Journal of Civil Engineering* 45 (2). Canadian Science Publishing: 117–24. doi:10.1139/cjce-2016-0343.

Ali, Salid, Sivakumar Naganathan, and B. Mahalingam. 2021. “State of the Art Review on Prescriptive & Performance Based Approaches for Concrete Durability.” *International Journal of Sustainable Construction Engineering and Technology* 12 (2). Penerbit UTHM: 80–88. doi:10.30880/ijscet.2021.12.02.007.

Amran, Mugahed, Natt Makul, Roman Fediuk, Yeong Huei Lee, Nikolai Ivanovich Vatin, Yee Yong Lee, and Kachalla Mohammed. 2022. “Global Carbon Recoverability Experiences from the Cement Industry.” *Case Studies in Construction Materials* 17 (December). Elsevier Ltd. doi:10.1016/j.cscm.2022.e01439.

Andrade, Carmen, Ana Martínez-Serrano, Miguel Ángel Sanjuán, and José A. Tenorio. 2023. “Strength and Resistance to Sulfates, Carbonation and Chlorides Ingress by Substitution of Binder by Hydrotalcite in Several Cement Types.” *Construction Materials* 3 (3). Multidisciplinary Digital Publishing Institute (MDPI): 305–19. doi:10.3390/constrmater3030020.

Andrade, J. J.O., E. Possan, and D. C.C. Dal Molin. 2017. “Considerations about the Service Life Prediction of Reinforced Concrete Structures Inserted in Chloride Environments.” *Journal of Building Pathology and Rehabilitation* 2 (1). Springer Science and Business Media B.V. doi:10.1007/s41024-017-0025-x.

ASTM. 2022. “ASTM C1202 - Test Method for Electrical Indication of Concretes Ability to Resist Chloride Ion Penetration.” West Conshohocken, PA: ASTM International. doi:10.1520/C1202-22.

Barbhuiya, Salim, Bibhuti Bhusan Das, Dibyendu Adak, Kanish Kapoor, and Mohammad Tabish. 2025. “Low Carbon Concrete: Advancements, Challenges and Future Directions in Sustainable Construction.” *Discover Concrete and Cement* 1 (1): 3. doi:10.1007/s44416-025-00002-y.

Beguedou, Essossinam, Satyanarayana Narra, Ekua Afrakoma Armoo, Komi Agboka, and Mani Kongnine Damgou. 2023. “Alternative Fuels Substitution in Cement Industries for Improved Energy Efficiency and Sustainability.” *Energies* 16 (8). MDPI. doi:10.3390/en16083533.

Biernacki, Joseph J., Jeffrey W. Bullard, Gaurav Sant, Kevin Brown, Fredrik P Glasser, Scott Jones, Tyler Ley, et al. 2017. “Cements in the 21st Century: Challenges, Perspectives, and Opportunities.” *Journal of the American Ceramic Society* 100 (7). Blackwell Publishing Inc.: 2746–73. doi:10.1111/jace.14948.

Bramha Chari, K. J., and V. Ranga Rao. 2022. “Durability and Microstructure Characteristics of Concrete with Supplementary Cementitious Materials.” *Civil Engineering Journal (Iran)* 8 (4). Salehan Institute of Higher Education: 683–94. doi:10.28991/CEJ-2022-08-04-05.

Bras, Ana, John Milan van der Bergh, Hazha Mohammed, and Ismini Nakouti. 2021. “Design Service Life of RC Structures with Self-Healing Behaviour to Increase Infrastructure Carbon Savings.” *MATERIALS* 14 (12). ST ALBAN-ANLAGE 66, CH-4052 BASEL, SWITZERLAND: MDPI. doi:10.3390/ma14123154.

Cecen, F, B Aktas, and A Ozbayrak. 2023. “Decarbonization of the Concrete Railway Sleeper Production: Bringing the Low-Dosage Pozzolanic Cement Usage in the Sleeper Production via Novel Laminated CFRPU Reinforcement Technique.” *MATERIALS TODAY SUSTAINABILITY* 23 (September). RADARWEG 29, 1043 NX AMSTERDAM, NETHERLANDS: ELSEVIER. doi:10.1016/j.mtsust.2023.100455.

Chen, Huaguo, and Jianjun Yang. 2023. “A New Supplementary Cementitious Material: Walnut Shell Ash.” *Construction and Building Materials* 408 (December). Elsevier Ltd. doi:10.1016/j.conbuildmat.2023.133852.

Chen, Lijie, Zhenyu Huang, Wei Pan, Ray K L Su, Ying Zhong, and Yi Zhang. 2024. “Low Carbon Concrete for Prefabricated Modular Construction in Circular Economy: An Integrated Approach towards Sustainability, Durability, Cost, and Mechanical Performances.” *JOURNAL OF BUILDING ENGINEERING* 90 (August). RADARWEG 29, 1043 NX AMSTERDAM, NETHERLANDS: ELSEVIER. doi:10.1016/j.jobe.2024.109368.

Chen, Xiang, Hongzhou Zhu, Xuyuan Yang, and Chunxiang Huang. 2024. “Development of Anti-Segregation Device and Uniformity Evaluation for all-Bamboo Aggregate Concrete.” *CONSTRUCTION AND BUILDING MATERIALS* 425 (April). 125 London Wall, London, ENGLAND: ELSEVIER SCI LTD. doi:10.1016/j.conbuildmat.2024.135974.

Chen, Yongquan, Zhonghu Wu, Chi Zeng, Yuan Liu, Shaoyun Pu, Hui Zhang, Zheng Feng, Kun Xu, and Deliang Ni. 2025. “Study on the Workability, Strength, Durability and Environmental of Alkali-Activated Electrolytic Manganese Slag-Fly Ash-Slag Grouting Materials.” *CASE STUDIES IN CONSTRUCTION MATERIALS* 22 (July). RADARWEG 29, 1043 NX AMSTERDAM, NETHERLANDS: ELSEVIER. doi:10.1016/j.cscm.2024.e04199.

Cheng, Zhijun, Zhe Wang, Zhenzhen Liu, and Shan Li. 2024. “Multiple Impact Dynamic Compression Properties of Lightweight Engineered Composites Containing Ceramsite under Different Initial Damages.” *CONSTRUCTION AND BUILDING MATERIALS* 436 (July). 125 London Wall, London, ENGLAND: ELSEVIER SCI LTD. doi:10.1016/j.conbuildmat.2024.136807.

Chew, Yick Eu, Bing Shen How, Jaka Sunarso, Irene Moser, and Viknesh Andiappan. 2025. “Decarbonization of Energy Operations for Hard-to-Abate Industries Through Smart Energy System Optimization.” *Process Integration and Optimization for Sustainability*. Springer. doi:10.1007/s41660-025-00494-y.

DeRousseau, M A, J R Kasprzyk, and W V Srubar III. 2021. “Multi-Objective Optimization Methods for Designing Low-Carbon Concrete.” *FRONTIERS IN MATERIALS* 8 (July). AVENUE DU TRIBUNAL FEDERAL 34, LAUSANNE, CH-1015, SWITZERLAND: FRONTIERS MEDIA SA. doi:10.3389/fmats.2021.680895.

Deventer, Jannie S. J. Van, Rackel San Nicolas, Susan A. Ismail Idawatiand Bernal, David G. Brice, and John L. Provis. 2015. “Microstructure and Durability of Alkali-Activated Materials as Key for Standardization.” *JOURNAL OF SUSTAINABLE CEMENT-BASED MATERIALS* 4 (2, SI). 2-4 PARK SQUARE, MILTON PARK, ABINGDON OR14 4RN, OXON, ENGLAND: TAYLOR & FRANCIS LTD: 116–28. doi:10.1080/21650373.2014.979265.

Diao, Zhaoxu, Xingyu Gan, Jun Xu, Yuan Jin, Haiming Zhang, Laibo Li, Lingchao Lu, and Xin Cheng. 2024. “Enhancement of Mechanical Properties, Durability and Service Life of Low Carbon Cement Paste with Super Low w/c Ratio by Incorporating Carbon Fiber.” *CONSTRUCTION AND BUILDING MATERIALS* 438 (August). 125 London Wall, London, ENGLAND: ELSEVIER SCI LTD. doi:10.1016/j.conbuildmat.2024.137035.

Doussang, Lola. 2023. “Durability of Reinforcement in Low-Carbon Concretes (Low Clinker, Alkali-Activated Slag, Supersulfated Cement).” Toulouse: TOULOUSE University.

Du, Wei, Bo Liu, Danying Zuo, Mingli Wu, Hongjun Li, Mingfang Ba, Junzhe Liu, Runsheng Lin, and Quantao Liu. 2023. “Effect of Microcapsules on the Self-Repairing Ability of Limestone Clay Cement (LC3) Mortar at Different Temperatures.” *CONSTRUCTION AND BUILDING MATERIALS* 400 (October). 125 London Wall, London, ENGLAND: ELSEVIER SCI LTD. doi:10.1016/j.conbuildmat.2023.132718.

Dyer, Thomas. 2014. *Concrete Durability*. 1st ed. Boca Raton: CRC Press. Taylor & Francis Group.

Escalante-Garcia, J. Ivan, Karina Cabrera-Luna, and Yesica B. Castillo-Sanchez. 2024. “Blast Furnace Slag Supersulfated Cements: Composition Optimization, Microstructures, and Environmental Impact.” *Journal of Sustainable Cement-Based Materials*. Taylor and Francis Ltd. doi:10.1080/21650373.2024.2428991.

Franke Portella, Kleber, Nicole Pagan Hasparyk, Mariana D’Orey Gaivão Portella Bragança, Jeferson Luís Bronholo, Bruna Gomes Dias, and Leonardo Evangelista Lagoeiro. 2021. “Multiple Techniques of Microstructural Characterization of DEF: Case of Study with High Early Strength Portland Cement Composites.” *Construction and Building Materials* 311 (December). Elsevier Ltd. doi:10.1016/j.conbuildmat.2021.125341.

GCCA. 2021. *Concrete Future: The GCCA 2050 Cement and Concrete Industry Roadmap for Net Zero Concrete*. London.

Ghahsareh, Fatemeh Mohammadi, Qinghua Zhang, Sina Poorghasem, Hammad Ahmed Shah, Pengwei Guo, Christos Christodoulatos, Weina Meng, and Yi Bao. 2025. “Cradle-to-Grave Life-Cycle Assessment of Ultra-High-Performance Concrete(UHPC) Beams Based on Real-Time Monitoring Data.” *JOURNAL OF CLEANER PRODUCTION* 495 (March). 125 London Wall, London, ENGLAND: ELSEVIER SCI LTD. doi:10.1016/j.jclepro.2025.145098.

Griffiths, Steve, Benjamin K. Sovacool, Dylan D. Furszyfer Del Rio, Aoife M. Foley, Morgan D. Bazilian, Jinsoo Kim, and Joao M. Uratani. 2023. “Decarbonizing the Cement and Concrete Industry: A Systematic Review of Socio-Technical Systems, Technological Innovations, and Policy Options.” *Renewable and Sustainable Energy Reviews* 180 (July). Elsevier Ltd. doi:10.1016/j.rser.2023.113291.

Gu, Yushan, Othman Omikrine Metalssi, Renaud Pierre Martin, Teddy Fen-Chong, and Patrick Dangla. 2020. “Locating Ettringite Due to DEF at the Pore Scale of Cement Paste by Heat-Based Dissolution Tests.” *Construction and Building Materials* 258 (October). Elsevier Ltd. doi:10.1016/j.conbuildmat.2020.120000.

Hafez, Hisham, Rawaz Kurda, Wai Ming Cheung, and Brabha Nagaratnam. 2019. “A Systematic Review of the Discrepancies in Life Cycle Assessments of Green Concrete.” *Applied Sciences (Switzerland)*. MDPI AG. doi:10.3390/app9224803.

Hafez, Hisham, Ahmed Teirelbar, Rawaz Kurda, and Albert Tosic Nikola and de la Fuente. 2022. “Pre-Bcc: A Novel Integrated Machine Learning Framework for predicting Mechanical and Durability Properties of Blended Cement.” *CONSTRUCTION AND BUILDING MATERIALS* 352 (October). 125 London Wall, London, ENGLAND: ELSEVIER SCI LTD. doi:10.1016/j.conbuildmat.2022.129019.

Hasheminezhad, Araz, Daniel King, Halil Ceylan, and Sunghwan Kim. 2024. “Comparative Life Cycle Assessment of Natural and Recycled Aggregate Concrete: A Review.” *Science of the Total Environment*. Elsevier B.V. doi:10.1016/j.scitotenv.2024.175310.

Helaili, Sofiene, and Moez Chafra. 2023. “Identification of Mechanical Properties of a Braided Alfa Stem (Stipa Tenacissima L.) by an Inverse Method.” *JOURNAL OF COMPOSITE MATERIALS* 57 (3). 1 OLIVERS YARD, 55 CITY ROAD, LONDON EC1Y 1SP, ENGLAND: SAGE PUBLICATIONS LTD: 443–50. doi:10.1177/00219983221147685.

Huang, Zhe, Jiazhang Cao, Yiping Yang, Fuyuan Gong, Bin Zeng, Yuxi Zhao, and Koichi Maekawa. 2025. “Long-Term Deformation and Prestress Loss of PRC Beam under Vari-Humidity Environment:

Preliminary Experiments and Multi-Scale Simulations." *ENGINEERING STRUCTURES* 322 (A). 125 London Wall, London, ENGLAND: ELSEVIER SCI LTD. doi:10.1016/j.engstruct.2024.119122.

IEA. 2023. *Net Zero Roadmap: A Global Pathway to Keep the 1.5 °C Goal in Reach*. Paris.

IEA, WBCSD, and CSI. 2018. *Technology Roadmap: Low-Carbon Transition in the Cement Industry*. *International Energy Agency*.

Jiang, Zhangfan, Osman E Ozbulut, Gabriel Arce, and Lisa M Colosi. 2024. "Accounting for Decarbonization Impacts across the Full Life Cycle of Alternative Concrete Materials: A Case-Study for Graphene-Amended Cementitious Composites." *Journal of Cleaner Production* 482. Elsevier Ltd. doi:10.1016/j.jclepro.2024.144186.

Jin, Bingxin, Shuanglei Wu, Shujing Fan, Fafu Hang, and Huxing Chen. 2024. "Strength and Expansion of LHEC with Different Gypsum Contents Under Thermal Curing." *Materials* 17 (23). Multidisciplinary Digital Publishing Institute (MDPI). doi:10.3390/ma17235766.

Johansson, Lisen, Alireza Bahrami, Marita Wallhagen, and Mathias Cehlin. 2024. "A Comprehensive Review on Properties of Tailings-Based Low-Carbon Concrete: Mechanical, Environmental, and Toxicological Performances." *Developments in the Built Environment*. Elsevier Ltd. doi:10.1016/j.dibe.2024.100428.

Kasuga, Akio. 2023. "Evolution of Fib Model Codes: Mastering Challenges and Encountering New Ones." *Structural Concrete* 24 (4). John Wiley and Sons Inc: 4336 – 4340. doi:10.1002/suco.202201073.

Kim, Yoo Jae, Ryno van Leeuwen, Bum Yean Cho, Vedaraman Sriraman, and Anthony Torres. 2018. "Evaluation of the Efficiency of Limestone Powder in Concrete and the Effects on the Environment." *Sustainability (Switzerland)* 10 (2). MDPI. doi:10.3390/su10020550.

Kipkemboi, Benson, Teng Zhao, Shingo Miyazawa, Etsuo Sakai, Nobukazu Nito, and Hiroshi Hirao. 2020. "Effect of C3S Content of Clinker on Properties of Fly Ash Cement Concrete." *Construction and Building Materials* 240 (April). Elsevier Ltd. doi:10.1016/j.conbuildmat.2019.117840.

Lei, Dongyi, Haoxuan Jia, Long Yu, Ying Li, Zhiying Wu, Bing Wang, Ao Zhou, et al. 2025. "Recent Developments in Low-Carbon Engineered Cementitious Composites (ECC)." *Journal of Building Engineering* 100. Elsevier Ltd. doi:10.1016/j.jobe.2024.111734.

Lei, Zehao, and Sara Pavia. 2024. "Biomass Ash (BA) Waste as an Activator to Produce Carbon-Negative Cement." *CEMENT* 18 (December): 100112. doi:10.1016/j.cement.2024.100112.

Li, Chen, Jiaqi Li, Qiaomu Zheng, Qiang Ren, and Zhengwu Jiang. 2023. "Durability of Concrete Coupled with Life Cycle Assessment: Review And." *CEMENT & CONCRETE COMPOSITES* 139 (May). THE BOULEVARD, LANGFORD LANE, KIDLINGTON, OXFORD OX5 1GB, OXON, ENGLAND: ELSEVIER SCI LTD. doi:10.1016/j.cemconcomp.2023.105041.

Li, Heng, Zuhua Zhang, Yulin Deng, Fang Xu, Jie Hu, Deju Zhu, Qijun Yu, and Caijun Shi. 2024. "Geopolymer Composites for Marine Application: Structural Properties And." *CEMENT & CONCRETE COMPOSITES* 152 (September). 125 London Wall, London, ENGLAND: ELSEVIER SCI LTD. doi:10.1016/j.cemconcomp.2024.105647.

Li, Yang, Zhi-yong Liu, and Jin-yang Jiang. 2024. "Microstructure and Macroscopic Properties of Low-Carbon Concrete to Elevated Temperature: State-of-the-Art Review." *JOURNAL OF BUILDING ENGINEERING* 86 (June). RADARWEG 29, 1043 NX AMSTERDAM, NETHERLANDS: ELSEVIER. doi:10.1016/j.jobe.2024.108731.

Li, Zhaoling, Lu Sun, Runsen Zhang, and Tatsuya Hanaoka. 2024. "Decarbonization Pathways Promote Improvements in Cement Quality and Reduce the Environmental Impact of China's Cement Industry." *Communications Earth and Environment* 5 (1). Nature Publishing Group. doi:10.1038/s43247-024-01929-z.

Liang, Qiushuang, Xinlu Huang, Lanfang Zhang, and Haiyan Yang. 2024. "A Review on Research Progress of Corrosion Resistance Of-Activated Slag Cement Concrete." *MATERIALS* 17 (20). MDPI AG, Grosspeteranlage 5, CH-4052 BASEL, SWITZERLAND: MDPI. doi:10.3390/ma17205065.

Lin, Run-Sheng, Yi Han, and Xiao-Yong Wang. 2021. “Experimental Study on Optimum Proportioning of Portland Cements, Limestone, Metakaolin, and Fly Ash for Obtaining Quaternary Cementitious.” *CASE STUDIES IN CONSTRUCTION MATERIALS* 15 (December). RADARWEG 29, 1043 NX AMSTERDAM, NETHERLANDS: ELSEVIER. doi:10.1016/j.cscm.2021.e00691.

Liu, Mengtong, Hui Liu, Pinghua Zhu, Chunhong Chen, Xinjie Wang, and Lingjie Xu. 2024. “Recycling Potential Evaluation of Geopolymer Concrete with Different System Used in Freeze-Thaw Environment.” *CASE STUDIES IN CONSTRUCTION MATERIALS* 21 (December). RADARWEG 29, 1043 NX AMSTERDAM, NETHERLANDS: ELSEVIER. doi:10.1016/j.cscm.2024.e03535.

Lothenbach, Barbara, Karen Scrivener, and R. D. Hooton. 2011. “Supplementary Cementitious Materials.” *Cement and Concrete Research*. doi:10.1016/j.cemconres.2010.12.001.

Mehta, P. Kumar, and Paulo J. M. Monteiro. 2006. *Concrete: Microstructure, Properties and Materials*. 3rd ed. McGraw-Hill. doi:10.1036/0071462899.

Miller, Sabbie A, Maria Juenger, Kimberly E Kurtis, and Jason Weiss. 2025. “Annual Review of Environment and Resources Cement and Alternatives in the Anthropocene,” 59. doi:10.1146/annurev-environ-112621.

Müller, Harald S., Michael Haist, and Michael Vogel. 2014. “Assessment of the Sustainability Potential of Concrete and Concrete Structures Considering Their Environmental Impact, Performance and Lifetime.” *Construction and Building Materials* 67 (PART C). Elsevier Ltd: 321–37. doi:10.1016/j.conbuildmat.2014.01.039.

Oliveira, Dayana Ruth Bola, Gabriela Leite, Edna Possan, and José Marques Filho. 2023. “Concrete Powder Waste as a Substitution for Portland Cement for Environment-Friendly Cement Production.” *Construction and Building Materials* 397 (July): 1–12. doi:10.1016/j.conbuildmat.2023.132382.

Pagani, Regina Negri, João Luiz Kovaleski, and Luis Mauricio Resende. 2015. “Methodi Ordinatio: A Proposed Methodology to Select and Rank Relevant Scientific Papers Encompassing the Impact Factor, Number of Citation, and Year of Publication.” *Scientometrics* 105 (3). Springer Netherlands: 2109–35. doi:10.1007/s11192-015-1744-x.

Pan, J. W., Y. T. Feng, J. T. Wang, Q. C. Sun, C. H. Zhang, and D. R.J. Owen. 2012. “Modeling of Alkali-Silica Reaction in Concrete: A Review.” *Frontiers of Structural and Civil Engineering* 6 (1). Higher Education Press: 1–18. doi:10.1007/S11709-012-0141-2/METRICS.

Perez Villa, Maria, Shayne Oster, Yuchen Liu, Michelle Kim Cao, Indroneil Ganguly, Jeremy Gregory, Hongmei Gu, et al. 2021. *Decarbonizing Concrete Deep Decarbonization Pathways for the Cement and Concrete Cycle in the United*.

Possan, Edna. 2026. “Between Green and Gray: Decarbonization of Portland Cement and Durability of Concrete – a Critical Review.” *Revista ALCONPAT* 16 (1). Alconpat Internacional: 42–59. doi:10.21041/ra.v16i1.978.

Possan, Edna, D. C.C. Dal Molin, and J. J.O. Andrade. 2018. “A Conceptual Framework for Service Life Prediction of Reinforced Concrete Structures.” *Journal of Building Pathology and Rehabilitation* 3 (1). Springer Science and Business Media B.V. doi:10.1007/s41024-018-0031-7.

Provis, John L. 2025. “Perspectives on Research Directions in Cement and Concrete.” *Journal of Asian Concrete Federation* 11 (4): 1–13. doi:10.18702/acf.2025.11.4.1.

Ranasinghe, K, and S De Silva. 2022. *Combined Use of Non-Destructive Tests, Visual Inspection and Service Life Prediction to Ensure the Reliability of Reinforced Concrete*. *J.Natn.Sci.Foundation Sri Lanka*. Vol. 50.

Rathnarajan, Sundar, and Radhakrishna G. Pillai. 2025. “Carbonation Models Using Mix-Design Parameters for Concretes with Supplementary Cementitious Materials.” *Journal of Building Engineering* 104 (June). Elsevier Ltd. doi:10.1016/j.jobe.2025.112392.

Rivera, Rosa Abnelia, Miguel Angel Sanjuan, Domingo Alfonso Martin, and Jorge Luis Costafreda. 2021. “Performance of Ground Granulated Blast-Furnace Slag and Coal Fly Ash Portland Cements Exposed

to Natural Carbonation." *MATERIALS* 14 (12). ST ALBAN-ANLAGE 66, CH-4052 BASEL, SWITZERLAND: MDPI. doi:10.3390/ma14123239.

Robalo, Keila, Hugo Costa, Ricardo do Carmo, and Eduardo Júlio. 2021. "Enhanced Mechanical and Durability Performances of Low Cement Concrete with Natural Pozzolan Addition." *Journal of Advanced Concrete Technology* 19 (5). Japan Concrete Institute: 519 – 535. doi:10.3151/jact.19.519.

Robalo, Keila, Eliana Soldado, Hugo Costa, Luís Carvalho, Ricardo do Carmo, and Eduardo Júlio. 2020. "Durability and Time-Dependent Properties of Low-Cement Concrete." *Materials* 13 (16). MDPI AG. doi:10.3390/MA13163583.

Rocha, Marina Santa Rosa, and Armando Caldeira-Pires. 2019. "Environmental Product Declaration Promotion in Brazil: SWOT Analysis and Strategies." *Journal of Cleaner Production* 235 (October). Elsevier Ltd: 1061–72. doi:10.1016/j.jclepro.2019.06.266.

Scrivener, Karen L., Vanderley M. John, and Ellis M. Gartner. 2018. "Eco-Efficient Cements: Potential Economically Viable Solutions for a Low-CO2 Cement-Based Materials Industry." *Cement and Concrete Research* 114 (December). Elsevier Ltd: 2–26. doi:10.1016/j.cemconres.2018.03.015.

Shi, Jinjie, Danqian Wang, Jing Ming, and Wei Sun. 2018. "Passivation and Pitting Corrosion Behavior of a Novel Alloy Steel (00Cr10MoV) in Simulated Concrete Pore Solution." *Journal of Materials in Civil Engineering* 30 (10). American Society of Civil Engineers: 04018232. doi:10.1061/(asce)mt.1943-5533.0002455.

Shi, Weihua, Zhiwu Yu, and Yachuan Kuang. 2012. "A Probabilistic-Based Durability Analysis of Concrete Structures Exposed to Chloride Containing Environment." *Applied Mechanics and Materials* 204–208. Trans Tech Publications Ltd: 3282–86. doi:10.4028/WWW.SCIENTIFIC.NET/AMM.204-208.3282.

Sirivivatnanon, Vute, Caihong Xue, and Radhe Khatri. 2022. "Service-Life Design of Low-Carbon Concrete Containing Fly Ash and Slag under Marine Tidal Conditions." *ACI MATERIALS JOURNAL* 119 (6). 38800 COUNTRY CLUB DR, FARMINGTON HILLS, MI 48331 USA: AMER CONCRETE INST: 149–64. doi:10.14359/51737226.

Snellings, Ruben, Prannoy Suraneni, and Jørgen Skibsted. 2023. "Future and Emerging Supplementary Cementitious Materials." *Cement and Concrete Research* 171 (September). Elsevier Ltd. doi:10.1016/j.cemconres.2023.107199.

SNIC, and ABCP. 2019. *Roadmap tecnológico do cimento: potencial de redução das emissões de carbono da indústria do cimento brasileira até 2050*. Rio de Janeiro.

Soldado, Eliana, Ana Antunes, Hugo Costa, and Eduardo do Carmo Ricardo and Julio. 2021. "Durability of Mortar Matrices of Low-Cement Concrete with Specific." *CONSTRUCTION AND BUILDING MATERIALS* 309 (November). THE BOULEVARD, LANGFORD LANE, KIDLINGTON, OXFORD OX5 1GB, OXON, ENGLAND: ELSEVIER SCI LTD. doi:10.1016/j.conbuildmat.2021.125060.

Sun, Minmin, Keliang Pang, Siwei Shao, and Donghui Liu. 2025. "Application, Challenges, and Prospects of CCUS Technology in Steel Industry." *Journal of Sustainable Metallurgy*. Springer Science and Business Media Deutschland GmbH. doi:10.1007/s40831-024-00997-x.

Thorne, J, D V Bompa, M F Funari, and N Garcia-Troncoso. 2024. "Environmental Impact Evaluation of Low-Carbon Concrete Incorporating Fly and Limestone." *CLEANER MATERIALS* 12 (June). RADARWEG 29, 1043 NX AMSTERDAM, NETHERLANDS: ELSEVIER. doi:10.1016/j.clema.2024.100242.

Tsivilis, S, E Chaniotakis, G Kakali, and G Batis. 2002. "An Analysis of the Properties of Portland Limestone Cements and Concrete." *Cement & Concrete Composites* 24 (June): 371–78. doi:10.1016/S0958-9465(01)00089-0.

UNEP. 2024. *Global Status Report for Buildings and Construction: Beyond Foundations: Mainstreaming Sustainable Solutions to Cut Emissions from the Buildings Sector*. Nairobi. doi:10.59117/20.500.11822/45095.

Wang, Aoxuan, Yuan Fang, Yingwu Zhou, Chenman Wang, Biqin Dong, and Cheng Chen. 2022. “Green Protective Geopolymer Coatings: Interface Characterization, Modification and Life-Cycle Analysis.” *MATERIALS* 15 (11). ST ALBAN-ANLAGE 66, CH-4052 BASEL, SWITZERLAND: MDPI. doi:10.3390/ma15113767.

Wang, Lei, Zhou Zhu, Ameer Hamza Ahmed, Marco Liebscher, Xiaohong Zhu, and Viktor Mechtcherine. 2023. “Self-Healing Behavior of High-Strength Strain-Hardening Cement-Based (HS-SHCC) Blended with Limestone Calcined Clay Cement(LC3).” *CONSTRUCTION AND BUILDING MATERIALS* 370 (March). 125 London Wall, London, ENGLAND: ELSEVIER SCI LTD. doi:10.1016/j.conbuildmat.2023.130633.

Wang, Xiao-Yong. 2019. “Simulation for Optimal Mixture Design of Low-CO2 High-Volume Ash Concrete Considering Climate Change and CO2 Uptake.” *CEMENT & CONCRETE COMPOSITES* 104 (November). THE BOULEVARD, LANGFORD LANE, KIDLINGTON, OXFORD OX5 1GB, OXON, ENGLAND: ELSEVIER SCI LTD. doi:10.1016/j.cemconcomp.2019.103408.

———. 2020. “Optimal Mix Design of Low-CO2 Blended Concrete with Limestone.” *CONSTRUCTION AND BUILDING MATERIALS* 263 (December). THE BOULEVARD, LANGFORD LANE, KIDLINGTON, OXFORD OX5 1GB, OXON, ENGLAND: ELSEVIER SCI LTD. doi:10.1016/j.conbuildmat.2020.121006.

Wang, Xiaoyong. 2022. “CO2 and Cost-Based Optimum Design of Sustainable Metakaolin-Modified Concrete.” *JOURNAL OF RENEWABLE MATERIALS* 10 (9). 871 CORONADO CENTER DR, SUTE 200, HENDERSON, NV 89052 USA: TECH SCIENCE PRESS: 2431–50. doi:10.32604/jrm.2022.020829.

Wang, Xiao-Yong. 2022. “Optimal Design of Low-Carbon Concrete Containing Fly Ash and Limestone.” *CERAMICS-SILIKATY* 66 (2). TECHNICKA 5, PRAGUE 6, DEJVICE 166 28, CZECH REPUBLIC: UNIV CHEMISTRY & TECHNOLOGY, PRAGUE: 202–10. doi:10.13168/cs.2022.0014.

———. 2023. “Optimization Design of Low-Carbon Hybrid Concrete Containing Slag and Limestone Powder.” *Environmental Science and Pollution Research* 30 (4). Springer Science and Business Media Deutschland GmbH: 10613 – 10623. doi:10.1007/s11356-022-22918-9.

Wang, Xiao-Yong, and Han-Seung Lee. 2021. “Optimal Mix Design of Air-Entrained Slag Blended Concrete Considering and Sustainability.” *ADVANCES IN CONCRETE CONSTRUCTION* 11 (2). PO BOX 33, YUSEONG, DAEJEON 305-600, SOUTH KOREA: TECHNO-PRESS: 99–109. doi:10.12989/acc.2021.11.2.099.

Wang, Yan, Zhifeng Wang, Dongqiang Lei, Chuncheng Zang, and Dong Guo. 2024. “Technology Verification of Portland Cement Clinker Production Driven by Concentrated Solar Energy Directly.” *Renewable Energy* 232 (October). Pergamon: 121064. doi:10.1016/J.RENENE.2024.121064.

Wasim, Muhammad, Tuan Duc Ngo, and David Law. 2021. “Durability Performance of Reinforced Waste-Based Geopolymer Foam under Exposure to Various Corrosive Environments.” *CASE STUDIES IN CONSTRUCTION MATERIALS* 15 (December). RADARWEG 29, 1043 NX AMSTERDAM, NETHERLANDS: ELSEVIER. doi:10.1016/j.cscm.2021.e00703.

Watari, Takuma, Zhi Cao, Sho Hata, and Keisuke Nansai. 2022. “Efficient Use of Cement and Concrete to Reduce Reliance on Supply-Side Technologies for Net-Zero Emissions.” *Nature Communications* 13 (1). Nature Research. doi:10.1038/s41467-022-31806-2.

Xu, Jun, Bo Liu, Qiyong Zhang, Laibo Li, Yali Li, Lingchao Lu, and Xin Cheng. 2023. “Hydration Characteristics, Structure Evolution of Marine Cement with High Durability Modified by Colloidal Nano-Silica for low Carbon Footprints.” *JOURNAL OF BUILDING ENGINEERING* 75 (September). RADARWEG 29, 1043 NX AMSTERDAM, NETHERLANDS: ELSEVIER. doi:10.1016/j.jobe.2023.106981.

Xue, Quan, Liwei Zhang, Kaiyuan Mei, Lin Wang, Xiaochun Wang Yan and Li, Xiaowei Cheng, and Hejuan Liu. 2022. “Evolution of Structural and Mechanical Properties of Concrete Exposed to High Concentration CO2.” *CONSTRUCTION AND BUILDING MATERIALS* 343 (August). 125 London Wall, London, ENGLAND: ELSEVIER SCI LTD. doi:10.1016/j.conbuildmat.2022.128077.

Yang, Bo, Yu Dong, and Xiao-Yong Wang. 2025. “Analysis of the Strength Development, CO2 Emissions, and Optimized Low-Carbon Design of Fly-Ash-Enhanced Composite Concrete.” *BUILDINGS* 15 (4). MDPI AG, Grosspeteranlage 5, CH-4052 BASEL, SWITZERLAND: MDPI. doi:10.3390/buildings15040532.

Yuan, Ji, Dongbin Li, Weilong Li, Hailu Yang, Wenhua Zhang, Linbing Wang, Jianjun Wang, and Zhenzhen Xiong. 2022. “Study on Frost Resistance of EPS Concrete Based on EPS Beads Wrapping Modification.” *CONSTRUCTION AND BUILDING MATERIALS* 345 (August). 125 London Wall, London, ENGLAND: ELSEVIER SCI LTD. doi:10.1016/j.conbuildmat.2022.128400.

Zhang, Kai, Marcus Yio, Hong Wong, and Nick Buenfeld. 2024. “Development of More Accurate Methods for Determining Carbonation Depth in Cement-Based Materials.” *CEMENT AND CONCRETE RESEARCH* 175 (January). THE BOULEVARD, LANGFORD LANE, KIDLINGTON, OXFORD OX5 1GB, ENGLAND: PERGAMON-ELSEVIER SCIENCE LTD. doi:10.1016/j.cemconres.2023.107358.

Zhang, Liqing, Mingqiang Bian, Zhenrong Xiao, and Baoguo Wang Xinyue and Han. 2023. “A Comprehensive Review of Cementitious Composites Modified with Nano: Fabrication, Microstructures, Properties and Applications.” *CONSTRUCTION AND BUILDING MATERIALS* 409 (December). 125 London Wall, London, ENGLAND: ELSEVIER SCI LTD. doi:10.1016/j.conbuildmat.2023.133922.

Zheng, Zhanzhan, Pu Miao, and Lina Zheng. 2023. “Bayesian-Based Durability Life Prediction Method of Nano-Modified Concrete.” *International Journal of Materials and Product Technology* 67 (1). Inderscience Publishers: 26–37. doi:10.1504/IJMPT.2023.132192.

Cinpar 2026
XXII International Conference on Building Pathology and Constructions Repair
15th to 17th July 2026 - Lisboa, Portugal

Effects of Limestone Filler, Metakaolin, and Polypropylene Fibers on the Flow Properties and Buildability of Cementitious Mixtures for 3D Concrete Printing (3DCP)

Ana Beatriz Smith Melo LINS [1], Marcos Alyssandro Soares dos ANJOS [1,2,3], Gabrielly da Mota NUNES [3], **Ana Mafalda MATOS** [4]

[1] Federal Institute of Education, Science and Technology of Paraíba, João Pessoa, Brazil, beatriz.smith@academico.ifpb.edu.br

[2] Graduate Program in Civil and Environmental Engineering, Federal University of Paraíba, João Pessoa, Brazil, marcos.anjos@ifpb.edu.br

[3] Graduate Program in Materials Science and Engineering, Federal University of Paraíba, João Pessoa, Brazil, enggabriellymota@gmail.com

[4] CONSTRUCT-Labest, Faculty of Engineering of the University of Porto, Porto, Portugal, anamatos@fe.up.pt

Abstract: 3D Concrete Printing (3DCP) is an Industry 4.0 technology with the potential to improve productivity and reduce costs in the construction sector. However, the rheological and early-age mechanical requirements imposed by extrusion-based printing systems often necessitate mixtures with high Portland cement content to ensure pumpability, extrudability, and buildability. In this study, an alternative strategy is proposed by assessing the combined use of limestone filler (LF), metakaolin (MK), and polypropylene fibers (PF) as partial cement replacements, aiming to reduce cement consumption while preserving essential fresh-state performance. Binary and ternary mixtures containing up to 50% LF and 10% MK were evaluated through viscosity, flowability, consistency, and buildability tests tailored to the printing system.

The results show that LF improves fluidity but may reduce printing stability, whereas MK increases viscosity and promotes structural build-up. When used together, LF and MK produced mixtures with enhanced performance, especially the FC30MK10 composition, which exhibited an optimal balance between viscosity, spread, and layer stability. In contrast, the inclusion of 1% polypropylene fibers sharply increased viscosity and consistency, rendering the mixture unsuitable for extrusion. These findings help establish a performance window for printable cementitious mixtures and demonstrate that LF and MK are effective, sustainable alternatives for reducing cement usage in 3DCP applications.

Keywords: 3D printing; limestone filler; metakaolin; viscosity; flowability; buildability.

1. Introduction

3D Concrete Printing (3DCP) is a rapidly developing technology that has the potential to transform conventional construction practices through automation and digital fabrication. The main advantages of 3DCP are the architectural design flexibility, higher productivity, reduced material consumption, and the elimination of conventional formwork (Akhlaghi *et al*., 2017; Paul *et al*., 2018; Zhang *et al*., 2019; Olsson *et al*., 2021). Additionally, it can reduce labour costs (50–80%), construction waste (30–60%), and production time (50–70%) (Zhang *et al*., 2019).

However, the successful application of this construction method requires the control of several interdependent parameters—both rheological and equipment-related—particularly the development of mixtures that can be easily extruded while maintaining their geometry after deposition. The ability of the mixtures to retain their shape is related to the buildability of the 3DCP, defined as the capacity of freshly

printed layers to resist vertical and lateral deformation during stacking without collapse (ISO/ASTM 52939, 2023).

The rheological properties of 3DCP mixtures in the fresh state that most strongly influence printing performanceare viscosity, flowability, and buildability, and they are related to the dosage of the compositions, as well as the morphology and gradation of aggregates, water-to-cement ratio, the presence of admixtures, and the incorporation of Supplementary Cementitious Materials (SCMs) (Marchon *et al*., 2018; Chen *et al*., 2020).

For a mixture to be considered pumpable and extrudable, it must have sufficiently low plastic viscosity and adequate flow stress to allow uninterrupted transport through hoses and uniform material delivery at the nozzle. At the same time, the lower layers must exhibit enough structural build-up to support the weight of subsequent layers without excessive deformation (Zhang *et al*., 2021).

Due to the mixture for 3D printing sufficient structuration and rapid gain of early-age stiffness, many studies employ high cement contents. According to Wangler *et al*. (2019), the incorporation of this high cement content is mainly required to satisfy the strict rheological criteria associated with pumping, extrusion stability and buildability.

However, Portland cement is a widely used construction material whose production is responsible for approximately 5–7% of global CO_2 emissions (Shanks *et al*., 2019). Since 3DCP printing has a greater focus on sustainability, it is essential to adopt measures to reduce cement consumption and develop mixtures that are both printable and environmentally sustainable (Chen *et al*., 2019).

According to Chen *et al*. (2019) and Shanks *et al*. (2019), one measure to make 3DCP printing more sustainable is the partial replacement of Portland cement with SCMs such as silica fume, metakaolin, limestone filler, fly ash and blast furnace slag. However, some of these materials have limitations for use, as active silica and slag are scarce worldwide and cannot be used on a large scale (Bhattacherjee *et al*., 2021). Therefore, it is necessary to use other materials, such as limestone filler and metakaolin, in the mixes, because they are regionally accessible and calcined clays have a lower carbon footprint compared to Portland cement (Chen *et al*., 2019). Additionally, a study conducted in the United Kingdom showed that replacing cement with calcined clays and limestone can reduce cement consumption by 13–40% and CO_2 emissions by 10–27% (Shanks *et al*., 2019).

Thus, although research on 3DCP has grown significantly over the last two decades, important knowledge gaps remain, particularly regarding how SCMs and fibers influence fresh-state properties across different printing systems (Bos *et al*., 2016). Therefore, this research aims to examine the effects of varying contents of limestone filler and metakaolin, with and without polypropylene fibers, on the rheological behavior and buildability of cementitious mixtures for extrusion-based 3DCP.

2. Materials and Methods

2.1 Materials

For the production of the 3DCP mixtures, Portland cement CP-V ARI (equivalent to ASTM C150 Type III OPC and CEM I from EN 197-1) was used, a high-early-strength cement without mineral additions. The mixtures also incorporated screened natural river sand passing through a 2.36 mm sieve, metakaolin (MK), limestone filler (LF), 12 mm polypropylene fibers (PF), and laboratory-supplied water. A polycarboxylate-based superplasticizer (SP) and a hydroxypropyl methylcellulose (HPMC) viscosity-modifying agent were also included. Table 1 summarises the physical properties of the materials, and Figure 1 presents the morphology of the fine constituents.

Table 1 – Constituents raw materials characterisation

Propriety	Material	Value
Density (kg/m³)	CP-V	3040
	LF	2710
	MK	2490
	Sand	2610
Compact unit mass (kg/m³)	Sand	1,71
Loose unit mass (kg/m³)	Sand	1,58
Maximum characteristic diameter (mm)	Sand	1,18
Fineness module	Sand	1,42
Maximum particle diameter (µm)	CP-V	8,04
	MK	11,69
	LF	27,71
Specific Surface area – BET (m²/g)	CP-V	1,70
	MK	10,93
	LF	2,75
Total pore volume (cm³/g)	CP-V	$0{,}35 \times 10^{-2}$
	MK	$3{,}22 \times 10^{-2}$
	LF	$4{,}24 \times 10^{-3}$

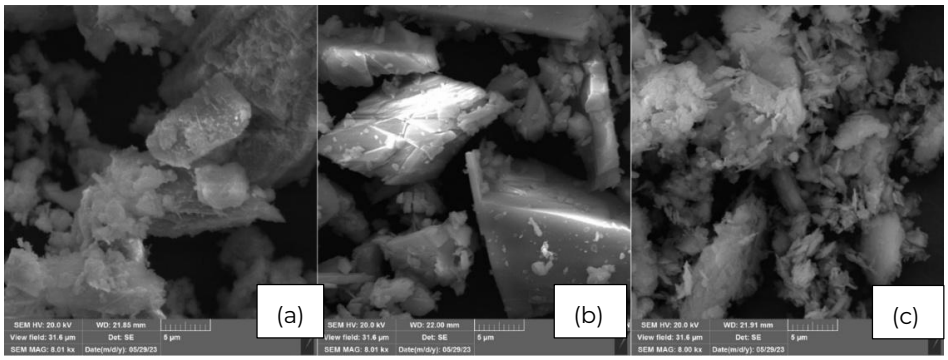


Figure 1 - Scanning Electron Microscopy (SEM) photos of, in secondary electrons mode: (a) CP-V, (b) LF, and (c) MK

2.2 Dosage of the mixtures and printing process

For the preparation of the 3DCP mixtures, a cement-to-sand mass ratio of 1:2 was adopted as the reference proportion. Portland cement was partially replaced by limestone filler and metakaolin in order to reduce cement consumption while maintaining suitable fresh-state performance. The water-to-total-dry-materials ratio was kept constant at 12% for all mixtures. The compositions evaluated in this study are presented in Table 3.

Table 3 – Mix design of 3DCP mixtures developed in the current study

Mixture	CP-V (kg/m³)	LF (kg/m³)	MK (kg/m³)	Sand (kg/m³)	SP (%)	HPMC (%)	w/c (kg/kg)	FP (%)
REF	689,94	-	-	1379,88	0,79	0,15	0,36	-
FC30	478,50	205,75	-	1368,51	0,79	0,15	0,51	-
FC40	409,77	272,91	-	1364,54	0,79	0,15	0,60	-
FC50	340,27	340,27	-	1361,07	0,75	0,15	0,72	-
FC30MK10	408,52	204,26	69,45	1360,36	1,30	0,15	0,60	-

FC30MK10-0,5%FP	350	175	59,5	1165,5	1,30	0,15	0,60	0,5
FC30MK10-1%FP	350	175	59,5	1165,5	1,30	0,15	0,60	1,0
MK10	615,39	-	68,38	1367,52	1,15	0,15	0,36	-
*w/c = water/cement (water to cement mass ratio)								

For the mixing process, the materials were first weighed using a precision scale with 0.1-gram accuracy. The components were then mixed following a defined sequence: homogenization of the dry materials, addition of 75% of the mixing water, incorporation of the superplasticizer, addition of the remaining 25% of water, and finally the introduction of the viscosity-modifying agent. Each mixing stage lasted 2 minutes and was conducted in an inclined-shaft mixer.

To produce the elements used in the buildability assessment, a 3D printer assembled by students from the LABIMACC laboratory (UFPB/IFPB) was employed. The printer features a portal-type structure and is capable of manufacturing components with a volume of up to 1.0 m³ using an extrusion-based system. The printing process consisted of producing block-shaped parts measuring 180 mm × 440 mm × 190 mm (width, length, and height, respectively), using a 25 mm-diameter extrusion nozzle with a deposition height of 20 mm. Printing was performed at a constant speed of 2500 mm/min and an extrusion rate of 1.69 L/min.

2.3 Properties in the fresh state

2.3.1 Viscosity

The viscosity of the compositions was analyzed using a rotational viscometer (model Rotavisc hi-vi I, IKA®). For the test, a spindle (104 mm long) with a geometry composed of 4 blades (25.4 mm long and 12.7 mm in diameter) was used, along with a 600 ml beaker in which the mixture was placed. The angular velocity values were first varied in increasing order and then decreasing, in the following sequence: 8 rpm, 12 rpm, 15 rpm, 17 rpm, 20 rpm, 30 rpm, 40 rpm, 50 rpm, 84 rpm (Nunes *et al*., 2023).

2.3.2 Flowability

The flowability of the mixtures was analyzed through the consistency table test, according to standard NBR 13276 (ABNT, 2016). For this test, a cone-shaped mold and the consistency table were used, and the test was conducted in accordance with the standard's procedures.

2.3.3 Consistency

To measure the consistency of 3DCP compositions, the procedure described in NBR 16606 (ABNT, 2018) was followed, which establishes a method for determining the normal consistency of Portland cement paste using the Vicat apparatus in conjunction with the Tetmajer needle. The analysis of consistency through this test is based on the weight of the needle that penetrates the mixture at rest.

2.3.4 Buildability

ISO/ASTM 52939 (2023) specifies that buildability is evaluated based on the layers' ability to remain stable without collapsing or significant deformation of the printed element. The test was evaluated according to the methodology adapted from Nunes *et al*. (2023), which considered the number of layers needed to print a 3DCP block approximately 190 mm in height. This involved approximately 16 overlapping layers. The buildability was analyzed only for fiber-free mixtures, and its calculation was performed using Equation 1.

$$B = \frac{H_a}{H_P} \qquad \text{(Equation 1)}$$

Where:

B = buildability;

H_a = actual height, in mm;

H_p = total predicted height, in mm (Equation 2).

Where:

H_1 = height of the first layer, in mm;

n = number of stacked layers.

$$H_P = H_1 \times n \qquad \text{(Equation 2)}$$

3. Results and discussion

3.1 Viscosity

Viscosity is a key rheological property for 3D concrete printing, as it reflects the resistance of the mixture to flow under the action of shear stress. Lower viscosity values indicate reduced resistance and greater ease of flow. Figure 2 illustrates the relationship between viscosity and angular velocity for 3DPC mixtures developed (see Table 3), showing that all 3DCP mixtures display pseudoplastic and thixotropic behaviour: viscosity decreases with increasing shear rate, and the mixtures gradually recover their viscosity when left at rest.

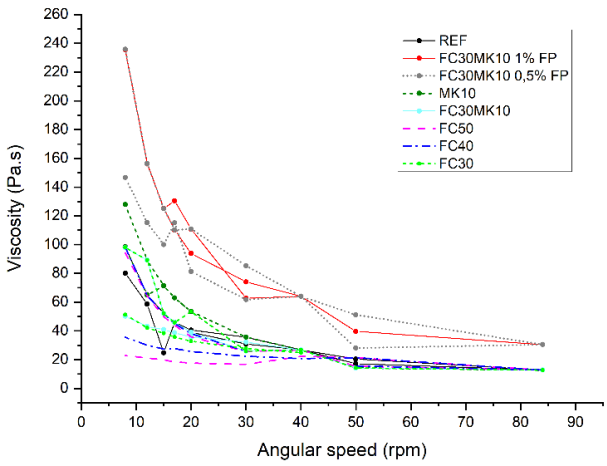


Figure 2 - Viscosity of 3DCP compositions under study

High viscosity implies greater resistance to deformation, limiting the mixture's ability to move smoothly through the pumping system and be extruded without interruption. For this reason, viscosity values at 30 rpm—where the measurements were most stable—were used for comparison, as shown in Figure 3.

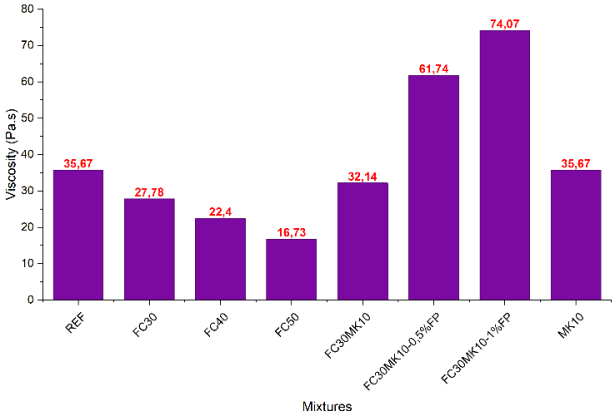


Figure 3 - Viscosity of 3DCP compositions under study

The progressive incorporation of limestone filler (LF) reduced the viscosity of the mixtures, as observed in FC30, FC40 and FC50. This reduction is consistent with the rounded and smooth particle morphology of LF, which decreases flocculation and facilitates internal lubrication, thereby improving flowability. In contrast, the addition of metakaolin (MK) led to an increase in viscosity in the MK10 mixture. This behaviour is attributed to the irregular, plate-like morphology and higher surface area of MK, which increases water demand and enhances resistance to the breakdown of particle agglomerates during shear. These microstructural characteristics are supported by the pore structure and BET surface area data presented in Table 1 and the morphologies observed in Figure 1. (Rojo-López *et al*., 2022).

Viscosity values obtained in this study are comparable to those reported in the literature. Kondepudi *et al*. (2022) documented viscosity ranges of 16–38 Pa·s, while Nunes *et al*. (2023) using the same printing system as in this work, reported values between 21.8 and 53.5 Pa·s. All mixtures in the present study fall within these ranges, except FC30MK10-0.5%FP and FC30MK10-1%FP, which exhibited substantially higher viscosities. These elevated values result from the combined effects of MK—whose high surface area offsets the fluidifying effect of LF—and the presence of polypropylene fibres, which increase internal friction and act as flow barriers, thereby restricting particle movement and raising shear resistance (Rojo-López *et al*., 2022).

3.2 Flowability

Flowability was evaluated using the flow table test in accordance with NBR 13276 (ABNT, 2016), immediately after mixing. Figure 4 presents the spread values obtained for each mix composition presented in Table 3. As can be perceived, values obtained in this research range from 153.3 mm to 257 mm. Previous studies of Ma *et al*. (2018), Kaszyńska *et al*. (2020), and Barbosa *et al*. (2022) suggest that spread diameters between 160 mm and 210 mm generally indicate adequate extrudability for 3D printing systems.

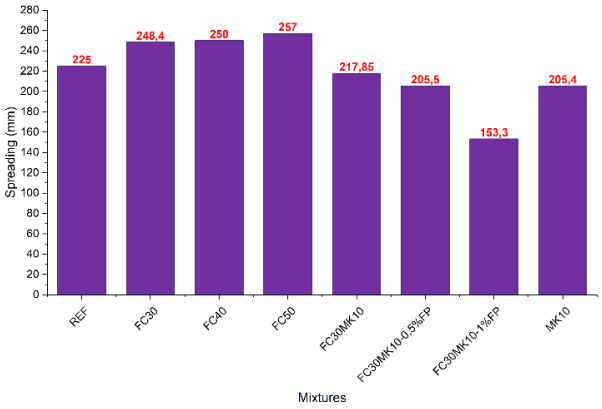


Figure 4 - Spreading of 3DCP compositions

Mixtures FC30, FC40, and FC50 exhibited increases in spread of 10.4%, 11.1%, and 14.2%, respectively, relative to the reference (REF) mixture. This behaviour is consistent with the limestone filler incorporation, whose smooth particle morphology enhances lubrication and reduces internal friction, thereby increasing flowability. Conversely, the MK10 mixture showed an 8.7% reduction in spread compared to REF. This reduction is attributed to the porous microstructure and higher water demand of metakaolin, which increases viscosity and limits the mixture's ability to deform under its own weight (Duan *et al*., 2022).

The FC30MK10-1%FP mixture presented the lowest spread value among the compositions, falling outside the range typically associated with printable mixtures. Although buildability was not evaluated for fibre-containing mixtures, the combination of high viscosity and restricted spread suggests that this mixture would likely present extrusion difficulties. Its rheological behaviour is consistent with the increased resistance induced by fibres, which may compromise particle rearrangement and decrease flowability.

The mixtures that successfully produced printed elements showed spread values between 205.4 mm and 257 mm, reinforcing the idea that both the intrinsic rheological behaviour and the characteristics of the printing system influence the necessary flowability window for extrusion-based 3D concrete printing.

3.3 Consistency

Consistency was assessed using the Tetmajer probe method in accordance with NBR 16606 (ABNT, 2018). The results are presented in Figure 5. Overall, mixtures containing metakaolin (MK) or polypropylene fibres (PF) exhibited greater resistance to penetration, indicating higher stiffness in the fresh state. This increased resistance is associated with the higher surface area and water demand of MK, as well as the internal friction generated by fibres (Tran *et al*., 2021).

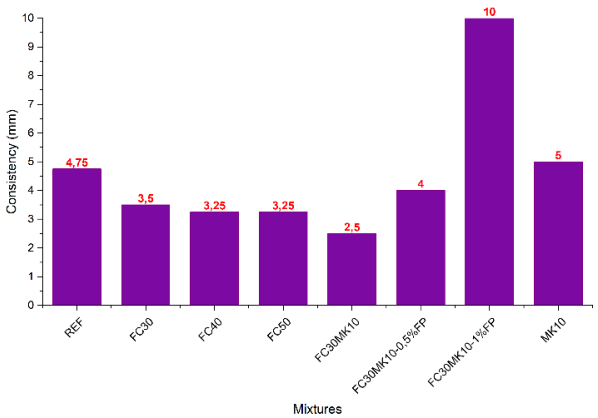


Figure 5 - Consistency of 3DCP compositions

The FC30MK10-1%FP mixture displayed the highest consistency among all formulations. The presence of 1% fibres contributes to a denser internal network, increasing interparticle friction and restricting deformation under the applied load. This behaviour aligns with the role of fibres as micro-reinforcing elements that impede the movement of the paste and aggregate particles, thereby increasing penetration resistance.

In contrast, mixtures containing increasing proportions of limestone filler showed substantial reductions in consistency relative to the reference mixture (REF). The FC30, FC40, and FC50 mixtures exhibited decreases of 26.3%, 31.6%, and 31.6%, respectively. These reductions can be attributed to the fluidifying effect of LF, whose smoother particle morphology reduces mechanical interlocking and allows the probe to penetrate more easily. The behaviour of the FC30MK10 mixture is noteworthy. Despite its higher superplasticizer demand, the mixture exhibited lower penetration resistance than expected for MK-containing systems. This may result from decreased interparticle forces associated with superplasticizer action, which promotes laminar flow and reduces resistance to localized deformation. Similar observations were reported by Gu and Khayat (2024) who found that higher superplasticizer dosages increase fluidity and reduce consistency measurements.

It is worth mentioning that consistency measured with the Tetmajer probe does not fully replicate the structural build-up that occurs during layer deposition in 3D printing. While the probe measures local resistance to penetration under shear, printed layers undergo thixotropic recovery when at rest, allowing viscosity to rebuild and support the weight of subsequent layers. Thus, consistency data should be interpreted alongside viscosity and buildability measurements to fully assess printability.

3.4 Buildability

Buildability was evaluated by printing block-shaped elements and comparing the actual height achieved with the theoretical height predicted by Equation 1, following the methodology adapted from Nunes et al. (2023) and aligned with ISO/ASTM 52939 (2023). This assessment reflects the ability of freshly deposited layers to maintain their geometry without excessive deformation or collapse. Only fibre-free mixtures were considered for this test, as fibre-containing mixtures exhibited viscosity and flowability values outside the printable range and were therefore excluded from extrusion trials.

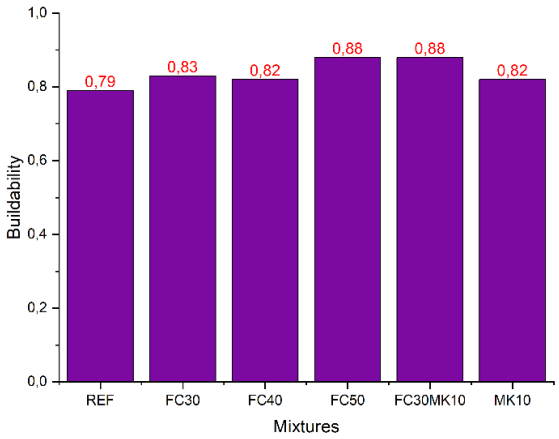


Figure 6 - Buildability of 3DCP compositions

Buildability was evaluated by printing block-shaped elements and comparing the actual height achieved with the theoretical height predicted by Equation 1, following the methodology adapted from Nunes et al. (2023) and aligned with ISO/ASTM 52939 (2023). This assessment reflects the ability of freshly deposited layers to maintain their geometry without excessive deformation or collapse. Only fibre-free mixtures were

considered for this test, as fibre-containing mixtures exhibited viscosity and flowability values outside the printable range and were therefore excluded from extrusion trials.

Although some mixtures achieved similar numerical buildability values, their printed quality differed significantly when visually inspected. The mixtures FC40 and FC50, which contain higher proportions of limestone filler (LF), showed pronounced deformation—particularly on external faces not supported by the internal truss. This behaviour is attributed to the increased flowability induced by LF, which, while beneficial for extrusion, can compromise geometric stability after deposition. By contrast, the MK10 mixture presented improved printing characteristics, with more uniform layer stacking and reduced lateral deformation. This effect is associated with the higher viscosity and structural build-up promoted by metakaolin.

Among all evaluated formulations, the FC30MK10 mixture delivered the most favourable performance, combining adequate viscosity, controlled flowability, and high layer stability. Its printed blocks exhibited minimal deformation and clean stratification. While the FC50 mixture attained one of the highest buildability indices numerically, achieving this required reducing the superplasticizer dosage. Despite the adjustment, the printed element remained more susceptible to deformation compared to MK-containing formulations. This suggests that buildability is influenced not only by viscosity and flowability but also by the restructuring kinetics associated with admixture content (Harbouz et al., 2022).

Overall, the results demonstrate that mixtures incorporating MK tend to enhance buildability and print quality, while excessive LF content increases the likelihood of deformation despite favourable flow properties. This highlights the need for balancing fluidity and structural build-up to achieve stable multi-layer deposition in extrusion-based 3D printing.

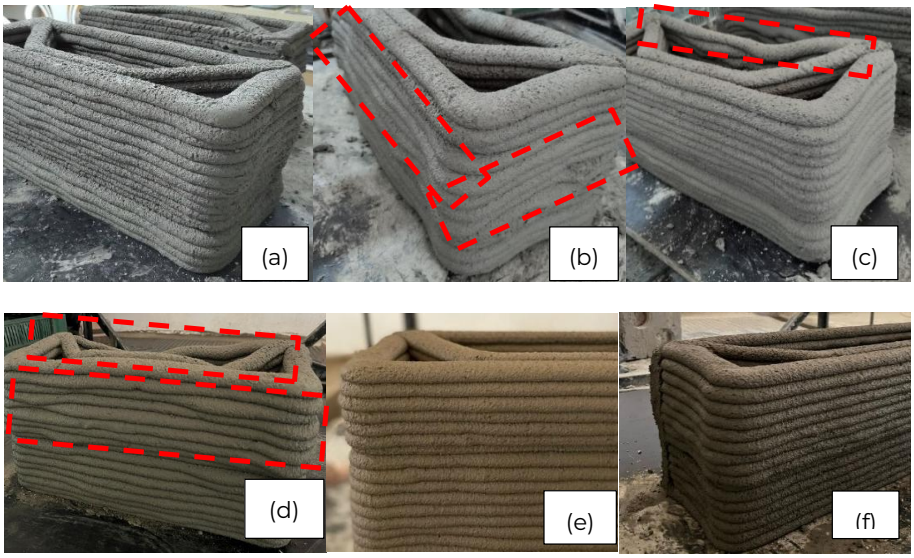


Figure 7 - 3DCP Blocks with mixes under study: (a) REF, (b) FC30, (c) FC40, (d) FC50, (e) FC30MK10, (f) MK10

3.5 Results summary, main trends and interactions

Figure 8 summarizes the fresh properties of the mixtures, highlighting an increase in viscosity, which is correlated with lower fluidity and greater consistency. Notably, in Figure 8, the dotted lines represent the printed mixtures. It is observed that the FC30, FC40, and FC50 mixtures are more deformable, which is attributed to the higher fluidity imparted by the limestone filler. Conversely, mixtures with MK tend to reduce deformation. Therefore, there is an indication that mixtures with viscosities between 32 and 36 Pa·s, spreads between 205 and 225 mm, and Tetmajer probe consistencies between 2.5 and 5 mm can be considered as ideal printing parameters. These are the properties of the REF, MK10, and FC30MK10 mixtures, which demonstrated the best printing capability.

From the combined rheological assessment, mixtures with viscosities between 32 and 36 Pa·s, spreads between 205 and 225 mm, and Tetmajer consistency values between 2.5 and 5 mm can be considered optimal for extrusion-based printing. These ranges correspond to the REF, MK10 and FC30MK10 mixtures, all of which demonstrated the most favourable printing performance and produced elements with superior geometric stability.

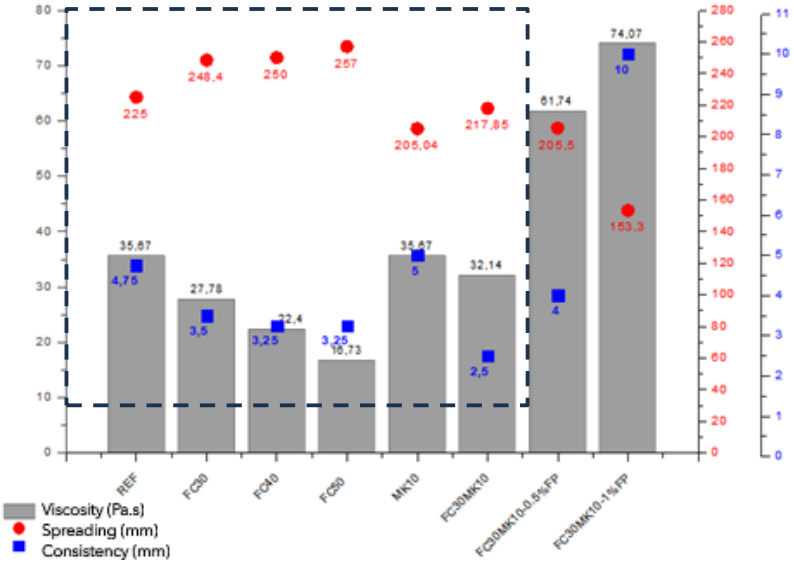


Figure 8 – Fresh properties results overview of the 3DCP compositions under study

4. Conclusions

Based on the experimental results and the adopted methodology, it was possible to develop and evaluate 3D-printable cementitious mixtures incorporating different proportions of limestone filler (LF), metakaolin (MK) and polypropylene fibres (PF). The study enabled a systematic assessment of how these additions influence fresh-state behaviour and printability. The main conclusions are as follows:

- Cement consumption between 340.27 kg/m³ and 478.50 kg/m³ was achieved through binary mixtures containing cement and LF (FC30, FC40 and FC50) and ternary mixtures incorporating cement, LF and MK (FC30MK10 and FC30MK10 with fibres).
- Regarding the reference mixture, the incorporation of limestone filler reduced viscosity by 22.1%, 37.2% and 53.1% in the FC30, FC40 and FC50 mixtures, respectively. In contrast, the MK10 mixture exhibited higher viscosity due to the greater specific surface area and porosity of MK.
- The FC30MK10-1%FP mixture presented the highest viscosity and lowest spread, resulting from the combined effects of MK and polypropylene fibres, which increase internal friction and restrict flow.
- Optimal fresh-state properties for printing in the employed system were associated with spreads between 205 mm and 250 mm, viscosities between 22.5 and 35.67 Pa·s, and Tetmajer probe consistencies between 3.25 mm and 5 mm. Mixtures within these ranges achieved stable layer deposition.
- The FC30MK10-1%FP mixture showed a 100% increase in consistency compared with MK10, attributed to the significant rise in internal friction and shear resistance caused by fibre incorporation.
- Among all evaluated mixtures, FC30MK10 demonstrated the best balance between viscosity, flowability and buildability, meeting the printing criteria and producing high-quality printed elements.

Overall, the results indicate that the combined use of limestone filler and metakaolin can effectively tailor the rheological behaviour required for extrusion-based 3D concrete printing and may therefore represent a technically viable solution for achieving significant partial replacement of Portland cement in printable mixtures.

5. Acknowledgements

This work was financially supported by the National Council for Scientific and Technological Development - CNPQ, Paraiba Research Support Foundation - FAPESQ/PB, Coordenação de Aperfeiçoamento de Pessoal de Nível Superior - Brasil (CAPES) - Finance Code 001, Federal University of Paraíba (UFPB), Federal Institute of Paraíba (IFPB), and Ministry of Education (MEC/SETEC). It was also supported by Base Funding - UIDB/04708/2020 and Programmatic Funding - UIDP/04708/2020 of the CONSTRUCT - Instituto de I&D em Estruturas e Construções - funded by national funds through the FCT/MCTES (PIDDAC); and by FCT – Fundação para a Ciência e a Tecnologia through the individual Scientific Employment Stimulus 2021.01765.CEECIND.

References

Akhlaghi, O., T. Aytas, B. Tatli, D. Sezer, A. Hodaei, A. Favier, K. Scrivener, Y. Z. Menceloglu, and O. Akbulut. 2017. “Modified Poly(carboxylate Ether)-Based Superplasticizer for Enhanced Flowability of Calcined Clay-Limestone-Gypsum Blended Portland Cement.” Cement and Concrete Research 101: 114–22. https://doi.org/10.1016/j.cemconres.2017.08.028.

Associação Brasileira de Normas Técnicas (ABNT). 2016. NBR 13276: Argamassa para assentamento e revestimento de paredes e tetos – Preparo da mistura e determinação do índice de consistência. Rio de Janeiro.

Associação Brasileira de Normas Técnicas (ABNT). 2018. NBR 16606: Cimento Portland – Determinação da pasta de consistência normal. Rio de Janeiro.

Barbosa, M. S., M. A. S. Anjos, K. C. Cabral, and L. S. Dias. 2022. “Development of Composites for 3D Printing with Reduced Cement Consumption.” Construction and Building Materials 341: 127775. https://doi.org/10.1016/j.conbuildmat.2022.127775.

Bhattacherjee, S., A. S. Basavaraj, A. V. Rahul, M. Santhanam, R. Gettu, B. Panda, E. Schlangen, *et al*. 2021. “Sustainable Materials for 3D Concrete Printing.” Cement and Concrete Composites 122: 104156. https://doi.org/10.1016/j.cemconcomp.2021.104156.

Bos, F., R. Wolfs, Z. Ahmed, and T. Salet. 2016. “Additive Manufacturing of Concrete in Construction: Potentials and Challenges of 3D Concrete Printing.” Virtual and Physical Prototyping 11: 209–25. https://doi.org/10.1080/17452759.2016.1209867.

Chen, Y., Z. Li, S. C. Figueiredo, O. Çopuroğlu, F. Veer, and E. Schlangen. 2019. “Limestone and Calcined Clay-Based Sustainable Cementitious Materials for 3D Concrete Printing: A Fundamental Study of Extrudability and Early-Age Strength Development.” Applied Sciences 9 (9): 1809. https://doi.org/10.3390/app9091809.

Chen, Y., S. C. Figueiredo, Z. Li, Z. Chang, K. Jansen, O. Çopuroğlu, and E. Schlangen. 2020. “Improving Printability of Limestone-Calcined Clay-Based Cementitious Materials by Using Viscosity-Modifying Admixture.” Cement and Concrete Research 132: 106040. https://doi.org/10.1016/j.cemconres.2020.106040.

Duan, Z., L. Li, Q. Yao, S. Zou, A. Singh, and H. Yang. 2022. “Effect of Metakaolin on the Fresh and Hardened Properties of 3D Printed Cementitious Composite.” Construction and Building Materials 350: 128808. https://doi.org/10.1016/j.conbuildmat.2022.128808.

Gu, Y., and K. H. Khayat. 2024. “Extrudability Window and Offline Test Methods to Predict Buildability of 3D Printing Concrete.” Cement and Concrete Research 182: 107552. https://doi.org/10.1016/j.cemconres.2024.107552.

ISO/ASTM. 2023. ISO/ASTM 52939: Additive Manufacturing for Construction—Qualification Principles—Structural and Infrastructure Elements. West Conshohocken, PA. https://doi.org/10.1520/F3630-23.

Kaszyńska, M., S. Skibicki, and M. Hoffmann. 2020. “3D Concrete Printing for Sustainable Construction.” Energies 13: 6351. https://doi.org/10.3390/en13236351.

Kondepudi, K., K. V. L. Subramaniam, B. Nematollahi, S. H. Bong, and J. Sanjayan. 2022. “Study of Particle Packing and Paste Rheology in Alkali Activated Mixtures to Meet the Rheology Demands of 3D Concrete Printing.” Cement and Concrete Composites 131: 104581. https://doi.org/10.1016/j.cemconcomp.2022.104581.

Ma, G., Z. Li, and L. Wang. 2018. “Printable Properties of Cementitious Material Containing Copper Tailings for Extrusion Based 3D Printing.” Construction and Building Materials 162: 613–27. https://doi.org/10.1016/j.conbuildmat.2017.12.051.

Marchon, D., S. Kawashima, H. Bessaies-Bey, S. Mantellato, and S. Ng. 2018. “Hydration and Rheology Control of Concrete for Digital Fabrication: Potential Admixtures and Cement Chemistry.” Cement and Concrete Research 112: 96–110. https://doi.org/10.1016/j.cemconres.2018.05.014.

Matos, P. R., T. Zat, M. M. Lima, J. S. A. Neto, M. T. Souza, and E. D. Rodríguez. 2023. “Effect of the Superplasticizer Addition Time on the Fresh Properties of 3D Printed Limestone Calcined Clay Cement (LC3) Concrete.” Case Studies in Construction Materials 19: e02419. https://doi.org/10.1016/j.cscm.2023.e02419.

Nunes, G. M., M. A. S. Anjos, A. B. S. M. Lins, A. M. S. Negreiros, and L. R. Pessoa. 2023. “Evaluation of the Mechanical Behaviour of Representative Volumetric Elements of 3DCP Masonry Mixtures.” Journal of Building Engineering 78: 107650. https://doi.org/10.1016/j.jobe.2023.107650.

Olsson, N. O. E., E. Arica, R. Woods, and J. A. Madrid. 2021. “Industry 4.0 in a Project Context: Introducing 3D Printing in Construction Projects.” Project Leadership and Society 2: 100033. https://doi.org/10.1016/j.plas.2021.100033.

Paul, S. C., G. V. Zijl, M. J. Tan, and I. Gibson. 2018. “A Review of 3D Concrete Printing Systems and Materials Properties.” Rapid Prototyping Journal 24 (4): 784–98. https://doi.org/10.1108/RPJ-09-2016-0154.

Rojo-López, G., B. González-Fonteboa, F. Martínez-Abella, and I. González-Taboada. 2022. “Rheology, Durability, and Mechanical Performance of Sustainable Self-Compacting Concrete.” Case Studies in Construction Materials 17: e01143. https://doi.org/10.1016/j.cscm.2022.e01143.

Shanks, W., C. F. Dunant, M. P. Drewniok, R. C. Lupton, A. Serrenho, and J. M. Allwood. 2019. “How Much Cement Can We Do Without?” Resources, Conservation and Recycling 141: 441–54. https://doi.org/10.1016/j.resconrec.2018.11.002.

Tran, M. V., Y. T. H. Cu, and C. V. H. Le. 2021. “Rheology and Shrinkage of Concrete Using Polypropylene Fiber.” Journal of Building Engineering 44: 103400. https://doi.org/10.1016/j.jobe.2021.103400.

Wangler, T., N. Roussel, F. P. Bos, T. A. M. Salet, and R. J. Flatt. 2019. “Digital Concrete: A Review.” Cement and Concrete Research 123: 105780. https://doi.org/10.1016/j.cemconres.2019.105780.

Zhang, Y., Y. Zhang, W. She, L. Yang, G. Liu, and Y. Yang. 2019. “Rheological and Harden Properties of the High-Thixotropy 3D Printing Concrete.” Construction and Building Materials 201: 278–85. https://doi.org/10.1016/j.conbuildmat.2018.12.061.

Zhang, J., J. Wang, S. Dong, X. Yu, and B. Han. 2019. “A Review of the Current Progress and Application of 3D Printed Concrete.” Composites Part A 125: 105533. https://doi.org/10.1016/j.compositesa.2019.105533.

Zhang, C., V. N. Nerella, A. Krishna, S. Wang, Y. Zhang, V. Mechtcherine, and N. Banthia. 2021. “Mix Design Concepts for 3D Printable Concrete: A Review.” Cement and Concrete Composites 122: 104155. https://doi.org/10.1016/j.cemconcomp.2021.104155.

Zhao, Z., C. Ji, J. Xiao, L. Yao, C. Lin, T. Ding, and T. Ye. 2023. “A Critical Review on Reducing the Environmental Impact of 3D Printing Concrete.” Construction and Building Materials 409: 133887. https://doi.org/10.1016/j.conbuildmat.2023.133887.

Cinpar 2026
XXII International Conference on Building Pathology and Constructions Repair
15th to 17th July 2026 - Lisboa, Portugal

Hipocarbonic concretes: a Brazilian overview of SCMs used in the repair of reinforced concrete structures

Mayara Carelli de Paula COSTA[1], Maria Fernanda PEREIRA[2], Alexandra PEREIRA[3], Maria Teresa Gomes BARBOSA[3]

[1] Federal University of Juiz de Fora, Juiz de For a (MG), Brazil, eng.mayaracarelli@gmail.com

[2] Federal University of Juiz de Fora, Juiz de For a (MG), Brazil, mariafernanda.pereira@estudante.ufjf.br

[3] Federal University of Juiz de Fora, Juiz de For a (MG), Brazil, alexandra.pereira@estudante.ufjf.br

[4] Federal University of Juiz de Fora, Juiz de For a (MG), Brazil, teresa.barbosa@ufjf.br

Abstract: The contemporary concept aims at decarbonization in the Brazilian civil construction industry, emphasizing the importance of using waste materials as supplementary cementitious materials, since cement-based inputs represent a significant fraction of greenhouse gas emissions. Therefore, the objective of this study is to identify, considering the diversity of the Brazilian territory, which waste materials offer the best balance between mechanical performance and environmental benefit at cost-effective levels in cementitious mixtures. The methodology is organized into three stages: a systematic literature review on the use of waste materials as SCMs, covering the period from 2015 to 2025, identifying their origin and application in cementitious matrices. Subsequently, a standardized data extraction was carried out, including technical and economic indicators; the selection criteria were based on the availability of consistent data that allow effective comparison between studies. Thus, studies presenting the following were considered: minimum compressive strength of 20 MPa at 28 days, material consumption (kg/m³), or, when not directly available, values estimated from mix proportions and material densities, as well as concrete density. Finally, embodied CO_2 emissions were estimated for each mixture. The results provided a national overview of the use of waste as SCMs for the development of eco-efficient materials, integrating economic, environmental, and technical aspects related to performance and durability. However, many studies lacked essential information for the proposed analysis, and a concentration of research in the Southeast region of Brazil was observed. Among the analyzed materials, São Tomé stone waste, mining tailings sand, and recycled glass powder showed the best overall performance, combining mechanical adequacy with reductions in embodied CO_2.

Keywords: Low-carbon concrete. Waste. Supplementary cementitious materials. Performance. Structural recovery.

1. Introduction

Decarbonization strategies in the construction industry are part of a broader process aimed at mitigating the effects of climate change and achieving the Sustainable Development Goals (SDGs) (Hafez et al., 2024). The production of traditional structural materials used in Brazil, i.e., reinforced concrete, is associated with significant CO_2 emissions, estimated at approximately 7% of global emissions. (Sbahieh *et al.* (2023)).

Therefore, efforts towards the structural sustainability of buildings have focused on two dimensions: their efficiency, associated with project design, and the reduction of the carbon emissions of the materials produced and marketed. In the first case, the focus is on rationalizing the use of resources, with emphasis on choosing more efficient structural systems that are better suited to the required performance. Recent research shows that design decisions can reduce CO_2 emissions up to 76%, through the appropriate

selection of parameters such as the concrete mechanical strength and the reinforcement ratio. (Olsson *et al.* (2023)).

The second dimension, which refers to decarbonization, focuses on technological innovation, since optimized projects are still dependent on composites with lower carbon intensity, highlighting: the partial replacement of clinker with supplementary cementitious materials (SCMs), such as LC_3 cement, and the development of alternative binders, such as geopolymers (Sbahieh *et al.* (2023); Hafez *et al.,* (2024)), whose potential varies with the regional availability of raw materials.

In line with the circular economy, recent research demonstrates the potential to transform high-impact environmental waste into solutions for the built environment. A notable example is the recycling of marine plastics, such as high-density polyethylene (HDPE) recovered from the oceans, to create new composites with thermal insulation and mechanical strength properties, mitigating the disposal problem and adding value to these materials (Almeida *et al*., 2025).

However, decarbonizing the sector is not limited to new buildings. A significant part of the challenge lies in increasing the life cycle and providing sustainable maintenance services for existing infrastructure, which represents a huge embodied carbon liability (EKN Engineering (2023)). In the case of reinforced concrete structures, deterioration shows itself progressively, compromising integrity and safety. This process results from multiple factors, such as the natural aging of materials, changes in the function or use of buildings (changed loads), design or execution errors, as well as exposure to aggressive environments or extreme events.

Experimentals research demonstrates that the use of combined reinforcement systems in reinforced concrete elements is capable of restoring, and in some cases increasing, the structural capacity and extending the building life cycle (Attia *et al*., (2023)). Researchers indicate that sustainable strategies for the preservation and retrofit of structural systems include techniques such as the use of hypocarbon binders, fiber-reinforced polymer (FRP) systems, self-repair techniques, and the use of computational tools for optimizing the proportioning of cementitious mixtures (Rusnak (2025)). Although promising, these solutions face challenges regarding performance variability, economic viability, and regulatory standardization, which requires joint efforts from researchers, the productive sector, and regulatory sectors.

Given the above, this paper proposes the identification and analysis of the main waste and by-products used in Brazil as supplementary cementitious materials in composites intended for the structural repair of reinforced concrete elements. Aspects related to regional availability, compliance with standards, mechanical performance, and environmental impacts are examined, aiming to support the selection of technically viable, environmentally efficient solutions with an adequate cost-benefit ratio.

1.1 Motivations and paper contributions

Brazil, due to its continental size and socioeconomic diversity, presents significant disparities in the generation, management, and utilization of construction waste (Doussolin and Bittencourt, 2022). In this context, the transition to practices combined with the circular economy, which value the reuse of byproducts and waste as a partial replacement for conventional inputs, becomes strategic for the decarbonization of the Brazilian building industry. Therefore, central motivation of this work lies in the need to understand how different regions of the country, with varying waste generation profiles, can adopt the incorporation of supplementary materials in cementitious matrices. Territorial heterogeneity demands adapted approaches capable of reconciling cost, performance, and environmental impact, ensuring greater practical viability, and local relevance.

The highlight of this study can be summarized as follows:

i. Mapping of waste and by-products currently available in each region of Brazil for use in concrete as additions/supplementary materials;
ii. Comparative evaluation of the technical properties of cementitious mixtures, as well as the carbon footprint of these materials in association with costs and availability, promoting a sustainability analysis;
iii. Identification of the inputs with the best cost-benefit ratio in the Brazilian context, considering technical, economic and environmental viability;

iv. Provision of technical and scientific subsidies to support public policies, standardization and engineering practices aimed at the circular economy and increasing the lifespan of buildings.

1.2 Brazilian territory

Brazil has a territory of 8,515,758.7 km² and is divided into 27 Federative Units, 26 States and the Federal District, grouped into five major Geographic Regions: North, Northeast, Southeast, South and Midwest, considered for planning and management purposes (Figure 1) (EMBRAPA (2020); IBGE (2021)).



.**Figure 1 -** Regions and states of Brazil.

The Brazilian territory presents striking contrasts in its physical and productive space, a direct reflection of its territorial vastness, bioclimatic diversity, and the distribution of industrial and agro-extractive chains (EMBRAPA (2020)). This configuration defines the profile of solid waste generated in each macro-region, determining its potential for reuse as supplementary cementitious admixtures (SCMs). It is observed that the country encompasses macro-territories with distinct productive vocations, which are reflected in the nature and volume of by-products that can be integrated into the low-carbon construction chain

Table 1 presents, by region, the biomes, the main production chains and the generating activities, and summarizes the national scenario, highlighting the regional availability of waste that can guide strategies for decarbonization, circularity and optimization of cementitious matrices.

Table 1 – Summary about macroregion and main characteristics.

Macroregion	Characteristics	Main economics activities	Reference
North	Amazon Florest; equatorial climate (hot and wet)	Plant extration (açaí); bauxite, iron, manganese, gold	IBGE (2024a); IBGE (2023); ANM (2023); MMA (2023); Rocha *et al.* (2022)
Northeast	Caatinga e Atlantica forest; semi-arid and tropical wet climate	Agroindustry; plaster; ceramics; ornamental rocks	IBGE (2024b); ANM (2023); IBGE (2024a); Cruz *et al.* (2023); SEBRAE (2024)
Midweast	Tropical savana climate	Agroindustry; biofuels; mining	MME (2024); MAPA (2024); IBGE (2024b); IBGE (2023); MME/EPE (2024)
Southeast	Atlantica forest; tropical wet climate	Steel industry; iron and limestone mining; petrochemicals; cement plant.	IBGE (2024a); IBGE (2024b); IBGE (2023); DNPM (2023); ANM (2023); ABCP, ABECE e ABCIC (2023)
South	Atlantica forest and Pampa; subtropical climate	Agroindustry; coal; pape rand cellulose	MME/EPE (2024); ANM (2023); IBGE (2024a); Tashima *et al.* (2012)

2. Experimental procedure

The study is based on a systematic literature review and systematic data extraction, focusing on the application of supplementary cementitious materials (SCMs) in concrete and mortars intended for structural repair in the Brazilian macro-regional context. The research protocol is shown in Figure 2.

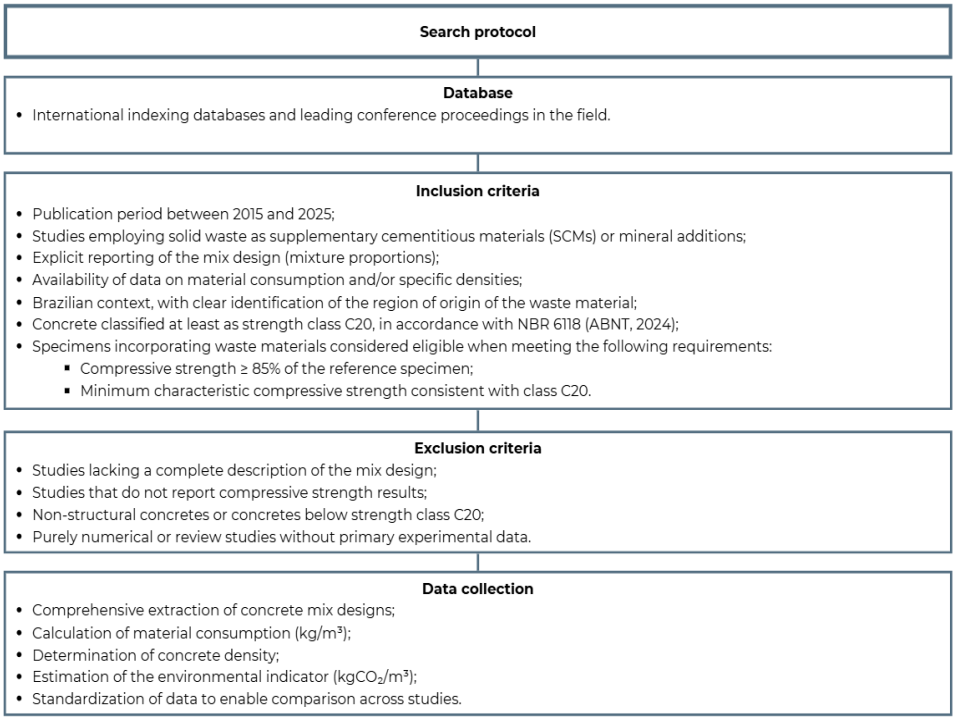


Figure 2 - Search protocol.

2.1 Database

A survey was conducted of the main waste and by-products used as supplementary cementitious materials/additives in cement-based composites with structural characteristics in each Brazil macro-region (Figure 1). For each identified waste, information was compiled regarding its main physical, chemical, and mechanical properties.

2.2 Environmental impact: Calculation method

The environmental impact was determined from the estimation of embodied carbon dioxide (embodied CO_2), adopting the principles of Life Cycle Assessment (LCA), as established by NBR ISO 14040 (ABNT, 2009a) and the requirements defined in NBR ISO 14040 (ABNT, 2009b), as well as the methodological guidelines of the Technical Bulletin "Quantification of embodied CO_2 emission

s in cementitious materials and concrete structures" (ABCP (2023))

To determine the amount of embodied CO_2, attributional LCA was used (IBRACON (2023)), adopting stages A1–A3 (cradle to gate) as the main boundary. The functional unit adopted is 1 m^3 of concrete or mortar, with the inventory modeled from the unit mix. Embodied CO_2 is calculated by summing the emissions associated with each constituent material, obtained by multiplying the unit consumption by the respective emission factor. Emission data are obtained from technical literature and national databases (SIDAC (2026); IBRACON (2023); Ecoinvent (2026)).

The procedure adopted compares the incorporated CO_2, expressed in $kgCO_2/m^3$, between conventional mixtures and mixtures with residues or SCM with equivalent mechanical performance, according to Equation (1).

$$CO_{2,inc} = \sum_{i=1}^{n}(q_i \times FE_i) \quad (1)$$

Being:

$CO_{2,inc}$: CO_2 emissions incorporated from concrete or mortar ($\frac{kgCO_2}{m^3}$);

q_i: consumption of material i in the unit mix ($\frac{kg}{m^3}$);

FE_i: CO_2 emission factor of material i, considering the A1-A3 boundary ($kg\ CO_2/kg$);

i: constituent materials of the mix design (cement, aggregates, water, mineral additions, SCM, additives).

The emission factor for conventional materials:

$$FEi\ =\ FE_{i_{A1-A3}} \quad (2)$$

The emission factor for waste SCM;

$$FEi\ =\ FE_{processing\ +\ transport} \quad (3)$$

3. Results and discussions

3.1 Characterization of SCM materials by macroregion

After applying the methodological selection protocol, the waste materials were organized according to the Brazilian macro-regions (Table 2), considering their origin, regional availability, physicochemical characteristics, and required processing stages. This regional approach highlights the dependence between local productive chains and the availability of supplementary cementitious materials (SCMs), reinforcing the importance of territorial context in the development of low-carbon strategies.

Most residues present high silica contents (SiO_2), either in amorphous or crystalline form, which directly influences their behavior as pozzolanic materials or inert fillers. Agro-industrial ashes (e.g., rice husk ash and sugarcane bagasse ash) exhibit pronounced pozzolanic activity, whereas mining and ornamental rock

residues tend to act predominantly through filler effects, contributing to particle packing and matrix densification.

Table 2 - Compilation of residues used as SCM by region.

Waste	Highlights	Performance
North		
CA: Acai seed ash (Cordeiro *et al*., 2019).	% SiO_2 ≈ 88–92%; pozzolanic activity. Processing: sieving and grinding.	Reduction of porosity. Optimal content ≈ 10%.
BP: Pal Biomas (Percy *et al*., 2021)	% SiO ≈ 63–71%; filler effect. Processing: sieving and grinding.	Reduction of porosity. 7.5% ≤ optimal contente ≤ 15%.
MU: Murumuru bark ash (Souza *et al*., 2024).	% SiO_2 ≈ 66%; partially amorphous. Processing: grinding and calcining.	Reduction of porosity. Optimal content ≈ 6%.
Northeast		
CT: Thermoelectric mineral coal ash (Jacinto, Oliveira e Oliveira, 2025).	% SiO_2≈ 80%; pozzolanic activity. Processing: grinding and sieving (< 75 µm).	Reduction of porosity. Optimal content ≈ 30%.
LV: Red mud (Degen *et al*. 2013).	% SiO_2≈ 74,4–77,7%; amorphous, filler effect + low pozzolanic activity. Processing: grinding	Reduction of porosity. Optimal content ≈ 5 a 15 %.
CB: Biomass ash from ceramic kilns (Mendonça *et al*. 2025).	Variable composition depending on the type of wood; filler effect. Processing: drying and sieving.	Reduction of porosity. Optimal content ≈ 5 a 10%.
Southeast		
CB: Sugarcane bagasse ash (Dias *et al*., 2025; Siqueira e Cordeiro, 2022).	% SiO_2 ≈ 70 - 80%; pozzolanic activity. Processing: grinding.	Reduction of porosity. 7% ≤ optimal contente ≤ 14%.
PV: Glass powder (Soares *et al*., 2022; Sales *et al*., 2017)	% SiO_2 ≈ 70%; filler effect + low pozzolanic activity. Processing: grinding.	Reduction of porosity 10% ≤ optimal contente ≤ 20%.
AR: Mining waste sand and ornamental rock waste (Figueiredo *et al*., 2024).	% SiO_2 ≈ 78%; filler effect. Processing: sieving.	Reduction of porosity 5% ≤ optimal contente ≤ 10%.
PS: São Tomé rock waste (Scalabrini *et al*., 2025).	% SiO_2 ≈ 90–95%;. filler effect Processing: sieving.	Reduction of porosity 10% ≤ optimal contente ≤ 15%.
South		
CZ: Rice Husk Ash (Mourão *et al*., 2025).	% SiO_2 ≈ 85–95%; pozzolanic activity Processing: burning and grinding.	Redução da porosidade. Optimal content ≈ 10%

Nevertheless, this approach represents a simplification, particularly in the context of structural repair, where additional parameters such as durability, compatibility with the existing substrate, shrinkage, and long-term performance are critical. The absence of these indicators in a significant portion of the reviewed literature limits a more comprehensive assessment and should be addressed in future studies.

Figure 3 shows that ornamental rock waste (AS), used primarily as a filler (Figueiredo et al. (2024)), when incorporated into cementitious mixtures, results in an increase in compressive strength of approximately 10% to 25% compared to reference mixtures, with absolute values reaching 52 MPa, while enabling reductions of up to approximately 45% in $kgCO_2/m^3$. São Tomé stone residue (PS) shows even more significant behavior, with a strength increase of approximately 29%, from 52 to 67 MPa, associated with a reduction of about 6% in CO_2 emissions (Scalabrini et al., 2025).

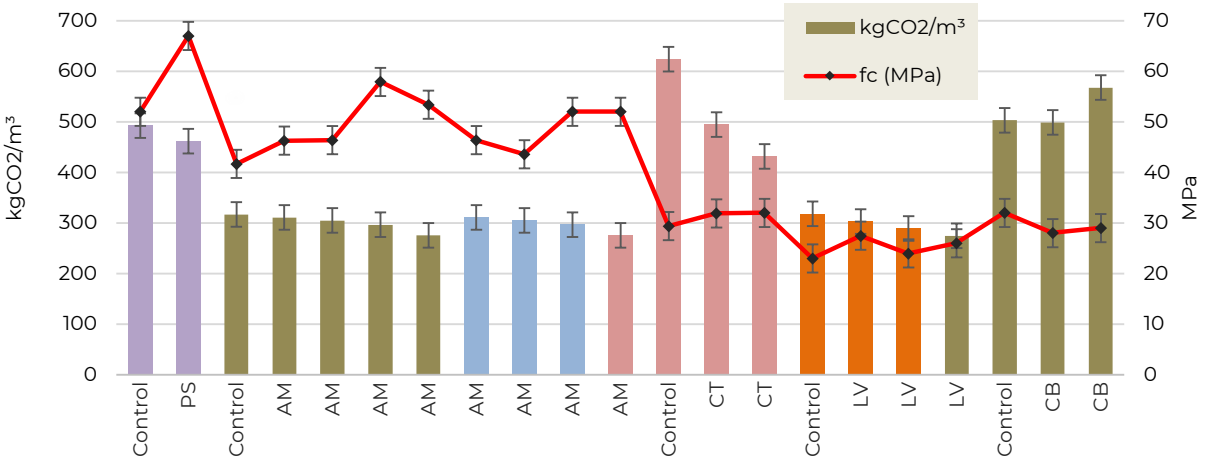


Figure 3 - $kgCO_2/m^3$ versus fc (MPa) graph for reference samples and residues incorporated without processing.

Regarding thermoeletric mineral coal ash (CT) and red mud (LV) (Jacinto, Oliveira and Oliveira (2025); Degen *et al.* (2013)), an intermediate behavior is observed, in which physical and chemical effects act in a complementary way, such as:

i) CT showed low increases in compressive strength, on the order of 2% to 9%, concomitantly with emission reductions ranging from 21% to 31% when compared to reference concretes. This performance is consistent with the composition rich in SiO_2, Al_2O_3 and Fe_2O_3, which confers pozzolanic potential with a more pronounced manifestation at later ages.

ii) LV showed strength gains of approximately 4% to 20% in moderate substitutions, associated with reductions of 5% to 14% in $kgCO_2/m^3$, resulting from its high fineness, high specific surface area, and residual alkalinity, which favor its action as an active filler and the densification of the matrix.

In the case of waste that undergoes grinding (Figure 4), the results indicate that the fineness achieved in processing plays a decisive role in mechanical performance and emission reduction. Recycled glass powder stands out, showing strength increases of around 5% to 10% in conventional concretes and maintenance in high-strength concretes, associated with reductions of up to approximately 20% in incorporated CO_2, depending on the substitution rate (Costa et al. (2026); Soares et al. (2022); Sales et al. (2017)). This behavior is associated with the amorphous vitreous nature of the material, rich in SiO_2, which favors slow pozzolanic reactivity combined with a pronounced filler effect.

Despite these advantages, grinding represents an additional energy demand, and its environmental benefit depends on the balance between improved performance and the emissions associated with comminution processes. This trade-off is not consistently quantified in the literature and represents an important gap for future research.

For calcined residues (CB and MU) (Figure 5) (Souza et al. (2024); Siqueira and Cordeiro (2022)), a compensatory relationship is pointed between the thermal activation of the material and the increased environmental impact associated with processing. Although additional calcination promotes increased fineness, partial amorphization of silica, and improved granular packing, the increases in compressive

strength at 28 days are low, on the order of 1% and 5% when compared to the reference mixtures. This behavior indicates that the mechanical gains resulting from thermal activation should be evaluated in light of the increased energy and the potential increase in CO_2 incorporated into the material.

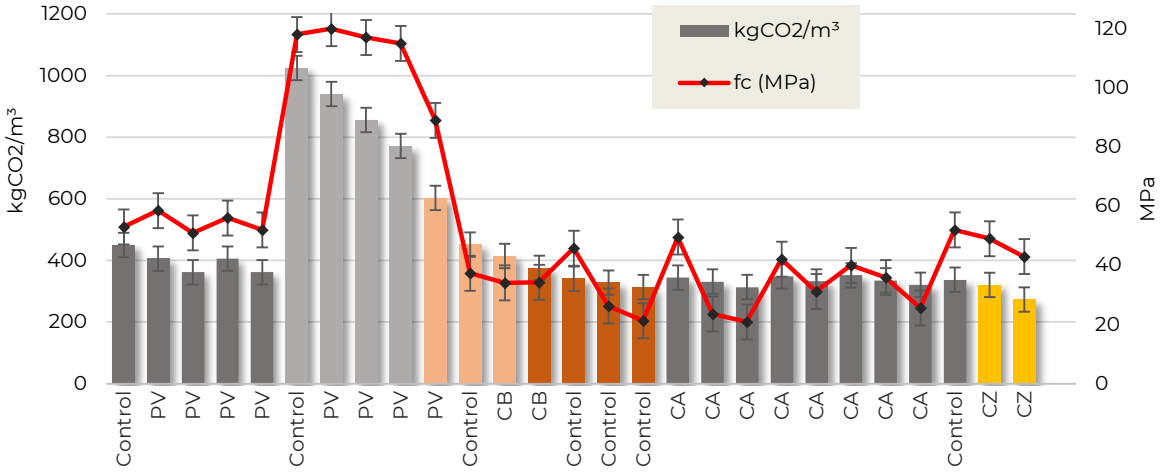


Figure 4 - $kgCO_2/m^3$ versus fc (MPa) graph for reference samples and residues incorporated without processing.

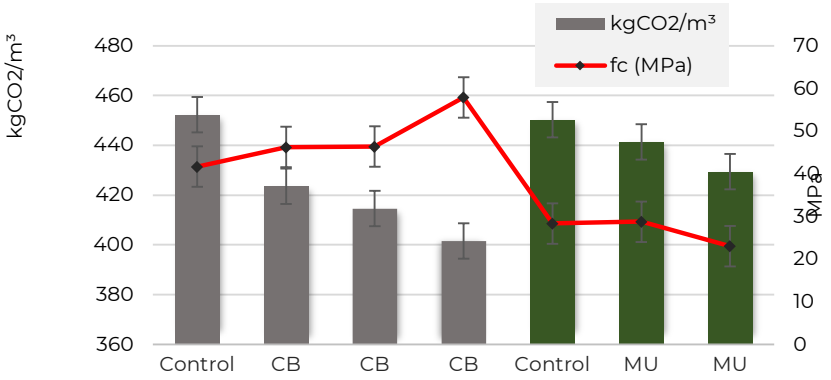


Figure 5 - $kgCO_2/m^3$ versus fc (MPa) graph for reference samples and residues incorporated after calcination.

In summary, Figure 6 correlates the variation in compressive strength at 28 days with the variation in emboidied CO_2, relative to the control of its respective study, for all mixtures analyzed, allowing the identification of the alternatives with the best technical-environmental performance. It can be observed that the most optimized solution corresponds to the São Tomé Stone residue, which combines a significant increase in strength, on the order of 29%, with a reduction of approximately 6% in incorporated CO_2, positioning itself more favorably in the quadrant of greatest mechanical gain associated with reduced emissions.

From a critical perspective, three main trends can be identified: (i) SCMs requiring little or no processing tend to present the best balance between mechanical performance and emission reduction; (ii) highly processed materials, particularly calcined ones, tend to show diminishing environmental returns; and (iii) the relationship between compressive strength gain and CO_2 reduction is not linear, indicating the presence of trade-offs that must be considered in material selection.

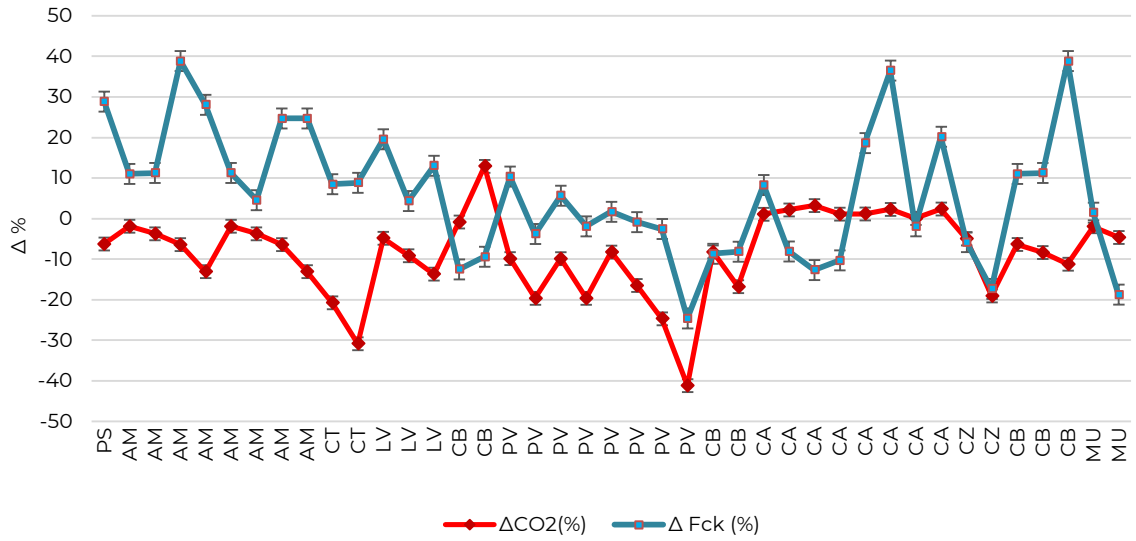


Figure 6 - Graph of variation in compressive strength and embodied CO_2.

3.2 Critical analysis and trade-offs

The combined interpretation of Figures 3 to 6 reveals that the best-performing SCMs are not necessarily those with the highest reactivity, but those that achieve a balance between processing requirements, mechanical performance, and environmental impact. Materials requiring minimal processing (Figure 3) consistently occupy the most favorable regions of the graphs, demonstrating that low-energy strategies can simultaneously enhance strength and reduce embodied CO_2. In contrast, SCMs subjected to grinding (Figure 4) or calcination (Figure 5) tend to shift this balance, often achieving either environmental gains or mechanical improvements, but rarely both. An important aspect emerging from this analysis is the behavior of SCMs that preserve, rather than significantly increase, compressive strength while still reducing CO_2 emissions. This trend is particularly evident for recycled glass powder (PV), which shows a predominantly horizontal shift in Figure 4 and clusters near the region of $\Delta fck \approx 0$ and $\Delta CO_2 < 0$ in Figure 6. From an engineering perspective, this response is especially relevant in structural repair contexts, where maintaining mechanical performance is often more critical than increasing strength. These findings highlight a fundamental trade-off: although increased processing enhances reactivity, it also raises embodied CO_2, potentially offsetting environmental benefits. Therefore, SCM selection should be based on a multi-criteria evaluation that considers not only strength but also processing intensity, regional availability, and overall environmental efficiency.

3.3 Limitations and implications for structural repair

The results should be interpreted considering the limitations inherent to the adopted methodology. The analyzed studies present significant heterogeneity in mix design, curing conditions, and characterization methods, which affects the comparability of results and contributes to the dispersion observed in Figure 6. Furthermore, the estimation of embodied CO_2 is based on emission factors obtained from the literature and national databases, which may not fully capture regional variations in production processes and logistics. This limitation is consistent with broader challenges in national data production, as highlighted by IBGE (2025), which emphasizes the need for standardized, disaggregated, and regionally representative datasets to support reliable indicator development. The strict inclusion criteria adopted in this study, although necessary to ensure consistency, reduced the number of eligible studies and may have affected the representativeness of the dataset.

Moreover, although compressive strength was adopted as the primary comparison parameter, it does not fully represent the performance of materials used in structural repair. Durability-related properties, such as permeability, shrinkage, and compatibility with existing substrates, are critical for long-term performance and were not consistently reported in the analyzed studies. This limitation restricts a more comprehensive assessment and highlights the need for future research integrating mechanical, environmental, and durability indicators to support more robust and application-oriented decision-making.

4. Conclusion

This study aimed to identify the main waste materials that were studied as supplementary cementitious materials for cementitious mixtures between 2015 and 2025, considering the macro-regions of the Brazilian territory and their potential.

In the literature review procedure on the subject, the following criteria were adopted: minimum compressive strength of the mixture of 20 MPa, the specific mass of the constituent materials of the mixtures, the complete description of the mixtures studied (experimental program), the consumption of materials used in the mixtures (kg/m^3), and the determination of the density of the concrete.

In this sense, the literature analysis reveals, however, recurring limitations related to the absence of fundamental information, such as specific mass, detailed granulometric characterization, and complete data on the proportioning of cementitious mixtures, which compromises the thorough comparison between the studies and the consistent evaluation of the environmental impact per unit volume of concrete. Research was found to be concentrated in the Southeast region of Brazil, in contrast to the limited number of studies in other regions. This imbalance reflects broader structural disparities in data production and availability across the country, as highlighted by IBGE (2025), reinforcing the need for regionally disaggregated studies and the valorization of locally available residues.However, the results obtained demonstrate that the incorporation of waste as supplementary cementitious materials can result in structurally adequate and environmentally more efficient concretes, even when the materials have a chemically inert character. In these cases, the microstructural improvement associated with the filler effect and granular packing proved sufficient to maintain or increase compressive strength, as well as to promote gains in the properties analyzed in the studies described in this work. The waste from São Tomé Stone (PS), certain compositions with mining tailings sand (AM), coal ash from thermal power plants (CT), and recycled glass powder (PV) stand out as solutions with the best overall performance, which combined relevant mechanical increases with significant reductions in incorporated CO_2, especially when used without additional processing or subjected only to grinding. In this context, the integration of technical, environmental, and regionally disaggregated data is essential to support more consistent decision-making and to provide technical and scientific basis for public policies, regulatory improvements, and engineering practices aligned with circular economy principles, CO_2 emission reduction, and the extension of the service life of concrete structures.

Acknowledgments

The authors wish to thank the Brazilian National Council for Scientific and Technological Development (CNPq), Coordination of Higher Education Personnel Improvement (CAPES), Foundation for Support and Development of Education Science and Technology of Minas Gerais (FAPEMIG), and Federal University of Juiz de Fora (UFJF).

Barbosa, M.T.G. - Bolsista FAPEMIG - CNPq – Brasil (processo BDT-00007-25).

Reference

Almeida, Manuela, Fabrizio Ascione, Anna Iaccheo, Teresa Iovane, and Margherita Mastellone. 2025. Towards the Necessary Decarbonization of Historic Buildings: A Review. *Energies* 18 (3): 502. https://doi.org/10.3390/en18030502.

Attia, Tamer, Ahmed Abdelrahman, Mohamed Zarzour, and Emad El-Zanati. 2023. Flexural Behavior of Strengthened Concrete Beams with Multiple Retrofitting Systems. *Structures* 58: 1795–1807. https://doi.org/10.1016/j.cscm.2023.e01862.

Barbosa, Maria Teresa Gomes, Mayara Carelli de Paula Costa, and Nelson Luis Gonçalves Dias de Souza. 2026. A Hipocarbonic Binder Strategy through the Reuse of Crushed Tempered Glass. *Applied Sciences* 16 (4): 1483. https://doi.org/10.3390/app16031483.

Brazil. Brazilian Agricultural Research Company (EMBRAPA). 2020. *Atlas of Brazilian rural space*. Brasília.

Brazil. Ministry of Agriculture and Livestock (MAPA). 2024. *Market projections for 2024*. Brasília.

Brazil. Ministry of Mines and Energy (MME). 2024. *Monthly monitoring bulletin for the Brazilian Electric System*. Brasília.

Brazil. Ministry of Mines and Energy (MME) and Energy Research Company (EPE). 2024. *Electrical energy statistical yearbook 2024*. Brasília.

Brazil. Ministry of Environment and Climate Change (MMA). 2023. *Continental biomes of Brazil*. Brasília.

Brazilian Institute of Geography and Statistics (IBGE). 2023. *Brazil's economic indicators: Regional and sectoral overview 2023*. Rio de Janeiro: IBGE.

Brazilian Institute of Geography and Statistics (IBGE). 2024a. *Systematic survey of agricultural production – LSPA 2024*. Rio de Janeiro: IBGE.

Brazilian Institute of Geography and Statistics (IBGE). 2024b. *PEVS – Production of plant extraction and forestry. 2024*. Rio de Janeiro: IBGE.

Brazilian Institute Of Geography And Statistics (IBGE).2025. *Sustainable Development Indicators: Brazil 2025*. Rio de Janeiro: IBGE.

Brazilian Portland Cement Association (ABCP). 2023. *Concrete CO_2 Bulletin: Guidelines for quantifying carbon dioxide emissions associated with concrete production in Brazil*. São Paulo: ABCP.

Brazilian Standartization (ABNT). 2009a. *NBR ISO 14040: Environmental management — Life cycle assessment — Principles and framework*. Rio de Janeiro: ABNT.

Brazilian Standartization (ABNT). 2009b. *NBR ISO 14044: Environmental management — Life cycle assessment — Requirements*. Rio de Janeiro: ABNT.

Brazilian Standartization (ABNT). 2014. *NBR 12653: Pozolanic materials — Requeriments*. Rio de Janeiro.

Brazilian Standartization (ABNT). 2024. *NBR* 2024. *NBR 6118: Design of concrete structures — Procedure*. Rio de Janeiro.

Cordeiro, Luciana de Nazaré; Pinheiro, Isaura Nazaré Lobato; Paes, Paulo Sérgio Lima Souza, and Carlos Menezes Azevedo. 2019. Characterization of Residual Açaí Seed Ash for Addition to Concrete. *Ambiente Construído* 19 (1): 45–55. https://doi.org/10.1590/s1678-86212019000100292

Degen, Maxwell K., Thiago C. Cardoso, Rayara P. Costa, Ângela Borges Masuero, and Denise Carpena Coitinho Dal Molin. 2013. Study of Red Mud as Filler in Cementitious Matrices. In *Congresso Brasileiro do Concreto. Proceedings*....São Paulo: IBRACON.

Dias, Bernardo Fonseca, André Barroso Mourão, Ivan Batista Morais, Lucas Thadeu da Silva Ramos, and Rogério Cabral de Azevedo. 2025. Comparative Study of Mortars Produced with Sugarcane Bagasse Ash. In *ENARC, 2025*. Proceedings... Belo Horizonte.

Doussolin, Jean Pierre, and Mariana Bittencourt. 2022. "How Effective Is the Construction Sector in Promoting the Circular Economy in Brazil and France? A Waste Input–Output Analysis." *Structural Change and Economic Dynamics* 60: 47–58. https://doi.org/10.1016/j.strueco.2021.10.009.

Ecoinvent. 2026. "Cut-off Approach — Allocation Procedures in Life Cycle Assessment." Accessed January 12, 2026. https://support.ecoinvent.org/system-models.

Figueiredo, Aline Santana, Augusto Cesar da Silva Bezerra, Laís Cristina Barbosa Costa, Douglas Mol Resende, Luana Drago Kuster, and Ricardo André Fiorotti Peixoto. 2024. “Sand Mining Tailings as Supplementary Cementitious Material.” *Buildings* 14 (8): 2408. https://doi.org/10.3390/buildings14082408.

Hafez, Hisham, Petar Bajić, Stanislav Aidarov, Xhemsi Malija, Michal Drewniok, Phil Purnell, and Nikola Tošić. 2024. “Parametric Study on the Decarbonization Potential of Structural System and Concrete Mix Design Choices for Mid-Rise Concrete Buildings.” *Materials and Structures* 57 (85): 1–15. https://doi.org/10.1617/s11527-024-02367-1.

Hafez, Hisham; Malchiodi, Beatrice; Tošić, Nikola; Drewniok, Michal; Purnell, Phil; de la Fuente, Albert. 2024. “Decarbonization Potential of Steel Fibre-Reinforced Limestone Calcined Clay Cement Concrete One-Way Slabs.” *Construction and Building Materials* 376: 131144. https://doi.org/10.1016/j.conbuildmat.2024.136847.

Institute for Applied Economic Research (IPEA). 2022. *Regional Development Report: Productive Structure and Spatial Inequalities in Brazil*. Brasília: IPEA.

Jacinto, Victoria Caroline Fernandes, Andreza Giselle de Oliveira, and Marilia Pereira de Oliveira. 2025. “Use of Coal Ash from Thermal Power Plants as a Substitute for Portland Cement in Mortar.” In *66° Congresso Brasileiro do Concreto*. Proceedings...São Paulo: IBRACON.

MEHTA, P. Kumar; MONTEIRO, Paulo J. M. 2014. *Concrete: Microstructure, Properties, and Materials*. 4. ed. New York: McGraw-Hill.

Mendonça, Iuri Veríssimo, Caio Siebra Alcântara, Ana Jéssica Farias da Silva, Marcella Maria Gomes Damasceno, and Lucas Feitosa de Albuquerque Lima Babadopulos. 2025. Experimental Investigation of Concretes Based on Residual Biomass Ash from Ceramic Industry Kilns In *ENARC 2025*. Proceedings...Fortaleza.

National Mining Agency (ANM). 2023. *Sumário mineral brasileiro 2023*. Brasília: ANM.

Neville, A. M. 2011. *Properties of Concrete*. 5th ed. Harlow: Pearson.

Olsson, J. A., S. A. Miller, and M. G. Alexander. 2023. “Near-Term Pathways for Decarbonizing Global Concrete Production.” *Nature Communications* 14: 4574. https://doi.org/10.1038/s41467-023-40302-0.

Percy, Brenno Pires, Camila Pereira de Oliveira, Luciana Carvalho Queiroz, Isaura Nazaré Lobato Paes, Luciana de Nazaré Pinheiro Cordeiro, and Paulo Sérgio Lima Souza. 2021. Study of Palm Biomass Ash as a Supplementary Cementitious Material in Concrete Production. *Research, Society and Development* 10 (10): e425101018590. https://doi.org/10.33448/rsd-v10i10.18590.

Rusnak, C. R. 2025. “Sustainable Strategies for Concrete Infrastructure Preservation: A Comprehensive Review and Perspective.” *Infrastructures* 10 (4): 99. https://doi.org/10.3390/infrastructures10040099.

Scrivener, Karen L., Vanderley M. John, and Ellis M. Gartner. 2018. “Eco-Efficient Cements: Potential Economically Viable Solutions for a Low-CO_2 Cement-Based Materials Industry.” *Cement and Concrete Research* 114: 2–26. https://doi.org/10.1016/j.cemconres.2018.03.015.

Scalabrini, Camila Maria Pereira, Catarina Emmerich Santana, Maria Teresa Paulino Aguilar, and White José dos Santos. 2025. Study of the Addition of São Tomé Stone Waste in High-Strength Cementitious Composites. In *ENARC+ 2025*. Proceedings... Belo Horizonte.

Siqueira, Andréia Arenari, and Guilherme Chagas Cordeiro. 2022. “Sustainable Cements Containing Sugarcane Bagasse Ash and Limestone: Effects on Compressive Strength and Acid Attack of Mortar.” *Sustainability* 14 (9): 5683. https://doi.org/10.3390/su14095683.

Soares, Silvio Maria, Tales Oliveira Gonçalves Freitas, Adilberto Oliveira Júnior, Fernando Giacomini da Silva Ferreira, and José Américo Alves Salvador Filho. 2022. “Assessment of Properties of Ultra-High Performance Cementitious Composites with Glass Powder Waste.” *IBRACON Structures and Materials Journal* 15 (6): e15612. https://doi.org/10.1590/S1983-41952022000600012.

Souza, M. R., *et al*. 2024. “Study of the Potentiality of Murumuru Husk Ash, an Amazonian Agroindustrial Waste, as a Filler to Structural Concrete.” *Revista IBRACON de Estruturas e Materiais* 17 (3): e17307.

Tashima, M. M., *et al*. 2012. Highly Reactive Rice Husk Ash (RHA): Production Method and Evaluation of Pozzolanic Activity *Ambiente Construído* 12 (2): 181–194. https://doi.org/10.1590/S1678-86212012000200009.

Cinpar 2026
XXII International Conference on Building Pathology and Constructions Repair
15th to 17th July 2026 - Lisboa, Portugal

Origem e interferência dos teores de cálcio de fragmentos cerâmicos do século XVIII em Pernambuco

Origin and interference of calcium in ceramic tiles from the 18th centuries in Pernambuco

Pablo GÓES[1], **Eudes ROCHA[2]**, Maurílio MORAES [3], Anne Marie PESSIS[4], Paulo MARTIN [5]

[1] Universidade Federal de Permanbucos /UFPE, PE, Brasil, e-mail: pablo.goes@ufpe.br

[2] Universidade de Pernambuco /UPE, PE, Brasil, e-mail: eudes.rocha@upe.br

[3] Universidade Federal de Permanbucos /UFPE, PE, Brasil, e-mail: maurilio.moraes@ufpe.br

[4] Universidade Federal de Pernambuco /UFPE, PE, Brasil, e-mail: annepessis@gmail.com

[4] Universidade Federal de Pernambuco /UFPE, PE, Brasil, e-mail: paulo.maior@ufpe.br

Resumo: O estudo analisou a origem dos elevados teores de cálcio (Ca) identificados em fragmentos de azulejos históricos portugueses presentes em uma edificação religiosa de Pernambuco, datados da primeira metade do século XVIII. Os valores encontrados foram considerados elevados quando comparados a parâmetros ideais para desempenho mecânico. Situações semelhantes foram observadas em outros estudos sugerindo tanto a utilização de argilas calcárias na fabricação quanto possíveis alterações pós-produção. Diante disso, investigou-se a hipótese de contribuição externa de cálcio por meio da percolação de compostos provenientes das argamassas de assentamento à base de cal. As análises de FRX dessas argamassas indicaram teores superiores a 40% de Ca, evidenciando um potencial significativo de migração. A análise petrográfica por microscopia de luz polarizada confirmou a presença de material esbranquiçado preenchendo microfissuras na matriz cerâmica, indicando processos de infiltração. Para validar experimentalmente essa hipótese, amostras cerâmicas com baixo teor de cálcio foram submetidas à imersão em solução de hidróxido de cálcio. Após o ensaio, verificou-se aumento significativo no teor de Ca, além da deposição do elemento em microfissuras, observada por microscopia eletrônica de varredura (MEV) e análise EDS. Os resultados indicam que os elevados teores de cálcio nos azulejos históricos são decorrentes de uma combinação entre a composição original da matéria-prima e processos de percolação ao longo do tempo. Além disso, a presença de cálcio contribui para a fissuração e degradação das peças, sugerindo que os valores atuais são superiores aos originais de fabricação.

Palavras-chave: Azulejos históricos portugueses; Microscopia; Índice de cálcio, Argamassa.

Abstract: *The study analyzed the origin of the high calcium (Ca) contents identified in fragments of historical Portuguese tiles from a religious building in Pernambuco, dating to the first half of the 18th century. The values found were considered high when compared to ideal parameters for mechanical performance. Similar situations have been reported in other studies, suggesting both the use of calcareous clays in manufacturing and possible post-production alterations. In this context, the hypothesis of external calcium contribution through the percolation of compounds from lime-based setting mortars was investigated. X-ray fluorescence (XRF) analyses of these mortars indicated Ca contents exceeding 40%, highlighting a significant potential for migration. Petrographic analysis*

using polarized light microscopy confirmed the presence of whitish material filling microcracks in the ceramic matrix, indicating infiltration processes. To experimentally validate this hypothesis, ceramic samples with low calcium content were immersed in a calcium hydroxide solution. After the test, a significant increase in Ca content was observed, along with the deposition of the element in microcracks, as evidenced by scanning electron microscopy (SEM) and EDS analysis. The results indicate that the high calcium contents in historical tiles result from a combination of the original raw material composition and long-term percolation processes. Furthermore, the presence of calcium contributes to cracking and degradation of the pieces, suggesting that current values are higher than those at the time of manufacture

Keywords: *Portuguese historical tiles; Microscopy; Technological profile; Ca index; Mortar.*

1. Introdução

Uma das diversas utilizações de materiais cerâmicos é na produção de azulejos para o revestimento de fachadas em edificações. No Brasil colonial os interiores de algumas capelas, igrejas e conventos, costumavam ser revestidos com azulejos importados de Portugal.

A documentação sobre a importação de azulejos no período colonial é escassa. Em função dessa circunstância uma das formas para se definir o período de importação é através dos padrões estéticos.

Nesse contexto, os azulejos importados existentes em 18 edificações religiosas em Pernambuco são classificados cronologicamente a partir dos padrões estéticos em três fases: A primeira, do final do século XVII ao início século XVIII, corresponde a azulejos com temas geométricos e policrômicos produzidos em oficinas, mais por artífices de formação prática do que artística (Santos, 1957) e (Simões, 1965). A segunda, da 1ª metade do século XVIII, a temática concentra-se em cenas religiosas com as cores azul e branco e foram produzidos por artífices organizados em corporações de ofícios (Pileggi, 1958). A terceira, que corresponde a 2ª metade e Século XVIII, foi um período em que, após o terremoto que abalou Lisboa em 1755, a produção tornou-se mais seriada, principalmente associada à Fábrica Real de Cerâmica do Rato, criada em 1767, em resposta a um crescimento da demanda, (Terol, 2021).

Foram coletadas 7 amostras de fragmentos azulejares do Convento e Igreja de Santo Antônio, em Igarassu da 1ª metade do século XVIII, Figura 1. A análise de fluorescência de raio X (FRX) do material chamou atenção o fato de que os fragmentos históricos apresentaram altos teores de cálcio (Ca). Os valores encontrados nas amostras analisadas variam de 24,53% até 29,36% conforme a Tabela 1.

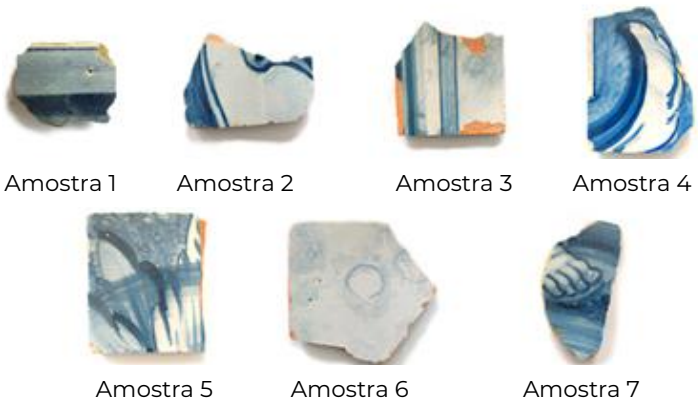


Figura 1 – Fragmentos azulejares da primeira metade do século XVIII, recolhidos do Convento e Igreja de Santo Antônio, em Igarassu.

Tabela 1 – Fluorescência por raio X das amostras da primeira metade do século XVIII, provenientes do Convento de Santo Antônio.

Amostra	Ca	Si	Al	Fe	K	Ti	Pb	Sr	Mn	Zr	Rb	Sn	Zn
Amostra 1	24,53%	45,20%	17,41%	8,81%	2,42%	1,07%	0,40%	0,07%	0,00%	0,04%	0,03%	0,00%	0,01%
Amostra 2	24,25%	42,43%	16,86%	8,94%	5,71%	1,05%	0,54%	0,08%	0,00%	0,04%	0,04%	0,03%	0,02%
Amostra 3	25,16%	42,87%	17,63%	8,11%	4,91%	0,99%	0,16%	0,09%	0,00%	0,04%	0,03%	0,00%	0,01%
Amostra 4	26,15%	42,72%	16,75%	8,23%	4,99%	0,99%	0,00%	0,07%	0,00%	0,04%	0,04%	0,03%	0,00%
Amostra 5	27,08%	43,16%	16,96%	7,97%	3,49%	0,95%	0,25%	0,06%	0,00%	0,04%	0,03%	0,00%	0,01%
Amostra 6	29,00%	42,14%	15,40%	7,63%	4,30%	0,95%	0,28%	0,21%	0,00%	0,04%	0,03%	0,03%	0,00%
Amostra 7	29,36%	40,74%	16,23%	8,38%	3,56%	0,99%	0,50%	0,09%	0,03%	0,04%	0,03%	0,04%	0,01%

Porém, estes altos valores em peças cerâmicas históricas não são um caso isolado. Em uma pesquisa realizada em 50 amostras de diversos tipos de materiais cerâmicos históricos italianos, fabricados entre os séculos XIII e o início do século XVII d.C., as peças estudadas apresentaram altos teores de cálcio, sendo constituídas de argilas calcárias com teores de cal entre 14% e 25% (CaO) (M.S. Tite, 2009). Outro caso foi a análise realizada em azulejos do monastério de San Lorenzo, na Espanha, provenientes do Escorial, e que também apresentou percentuais altos de cal, que variaram entre 22% e 25.5 % de CaO (Agua *et al.*, 2022).

Com base nos dados obtidos nas análises dos fragmentos de azulejos históricos de Pernambuco e, a partir desses dois estudo citados anteriormente, debruçou-se sobre quais as causas desse alto teor de cálcio nos materiais cerâmicos, uma vez que é conhecida sua interferência na modelagem de peças cerâmicas. Além do mais questionou-se que parte dos índices de cálcio dos biscoitos azulejares históricos poderiam ser provenientes das argamassas de assentamento.

Cabe advertir que o teor de cal pode ser proveniente da própria matéria prima utilizada na fabricação das peças cerâmicas. As composições de silício, cálcio e magnésio nas cerâmicas portuguesas estudadas indicaram a utilização de argilas ricas em carbonatos, ou mesmo a adição de materiais carbonáticos à pasta cerâmica. Tais materiais, durante o processo de queima, podem ser responsáveis pela formação de poros ou vazios na placa cerâmica, uma vez que durante a queima ocorre a liberação do CO_2 (Costa *et al*., 2013).

Porém a presença de produtos cálcicos também pode ser originada de mecanismos externos ao azulejo. É possível que certos minerais, como a calcita, podem se formar a partir do processo de carbonatação do hidróxido de cálcio existente nas argamassas de cal utilizadas no assentamento dos azulejos, que podem migrar para o biscoito cerâmico através dos poros existentes no material (Sanjad *et al*., 2004).

Também é possível que ao longo do tempo os ciclos contínuos de umedecimento pelas chuvas e pela umidade do solo, que é absorvida pelas alvenarias, e posterior secagem provoquem a dissolução e precipitação do carbonato de cálcio presente na argamassa, que se deposita nas microfissuras da estrutura interna dos materiais e atua na sua recristalização, produzindo um material rico em cal (Kanan, 2008).

As indústrias cerâmicas tendem a evitar o uso de carbonatos e resíduos de mármore, (calcita ou dolomita), como aditivo para a massa cerâmica, pois esse material pode apresentar grãos isolados de carbonato e que durante a queima se transformam em óxidos de cálcio e magnésio. Além do mais esses óxidos podem sofrer hidratação e expansão com a presença da umidade, provocando fissuração na cerâmica (Alexandre *et al*., 2004). Baixos teores de carbonatos na massa de conformação da cerâmica podem induzir a bons resultados mecânicos. Isso indica que baixos teores de calcita, ou de cal, implicam em maiores percentuais de módulos de rupturas formando peças azulejares mais resistentes (Darweesh, 2000) (Oliveira *et al*., 2001) (Goulart *et al*., 2000).

Assim, indagou-se que o teor de cálcio, identificado através da FRX, nos fragmentos históricos poderia não ser o original totalmente da produção das peças do século XVIII.

2. Questionamentos sobre o cálcio

Como as análises de FRX identificaram um alto teor de cálcio nos azulejos históricos surgiu o questionamento se esses os altos teores de cálcio seriam ou não provenientes da matéria prima utilizada na fabricação azulejos históricos, conforme também visto em outros estudos (Sanjad *et al*., 2004) e (Kanan, 2008).

Entretanto, ao considerar que os azulejos estudados foram assentados com argamassas a base da cal com espessuras que variam entre 0,50 e 1 cm em paredes com tijolos maciços, porosos e que absorvem muita umidade, (com características de elevada higroscopicidade), questionou-se se o cálcio encontrado nas amostras históricas era proveniente da percolação do contato entre a peça e o substrato onde ela se encontrava assentada. Sendo assim, foi realizada a análise da lâmina delgada, juntamente com a FRX da argamassa de assentamento.

Alguns dos fragmentos de azulejos possuía argamassa de assentamento encrustadas nas faces posteriores dos azulejos, essa argamassa foi analisada através de FRX e identificaram-se os percentuais do cálcio. E de fato, os teores identificados foram maiores de 40%, Tabela 2 e Figura 2 . Se considerarmos as paredes das igrejas com espessura que variam ente 0,5 e 1 metro de espessura e úmidas ao longo de mais de 200 anos é factível a existência de processos de percolação do substrato nos biscoitos históricos.

Tabela 2 – FRX das argamassas de assentamento do painel azulejar na qual se identificou altos teores de cálcio, conforme 0.

Ca	Si	Al	Fe	K	Ti	Pb	Sr	Zr	Rb	Ba
43,85%	35,08%	11,98%	5,54%	1,87%	0,73%	0,65%	0,25%	0,04%	0,02%	0,00%
67,38%	17,55%	4,08%	1,79%	3,31%	0,36%	4,99%	0,42%	0,05%	0,05%	0,00%
66,38%	20,16%	4,19%	1,86%	3,44%	0,35%	3,01%	0,46%	0,08%	0,07%	0,00%
53,21%	36,22%	4,88%	2,00%	1,86%	1,46%	0,00%	0,12%	0,03%	0,01%	0,19%



Figura 2 – Face posterior de biscoitos azulejares com fragmentos da argamassa de assentamento de origem histórica e das quais se obtiveram os índices de cálcio, através da FRX.

Uma vez constatado os altos teores de cal da argamassa de assentamento pesquisaram-se quais os efeitos na chacota. Para isso preparou-se uma seção delgada, para análise por microscopia por luz polarizada (MLP), e registrou-se um material argiloso de coloração esbranquiçada envolto pela matriz argilosa avermelhada. A porção esbranquiçada preenche as áreas de fissuras que se prolongam por toda a matriz. Isso é um indício que corrobora os altos teores de cálcio identificados nas análises por FRX como consequência da percolação de hidróxido de cálcio oriundo dos substratos de assentamento na chacota histórica 0.

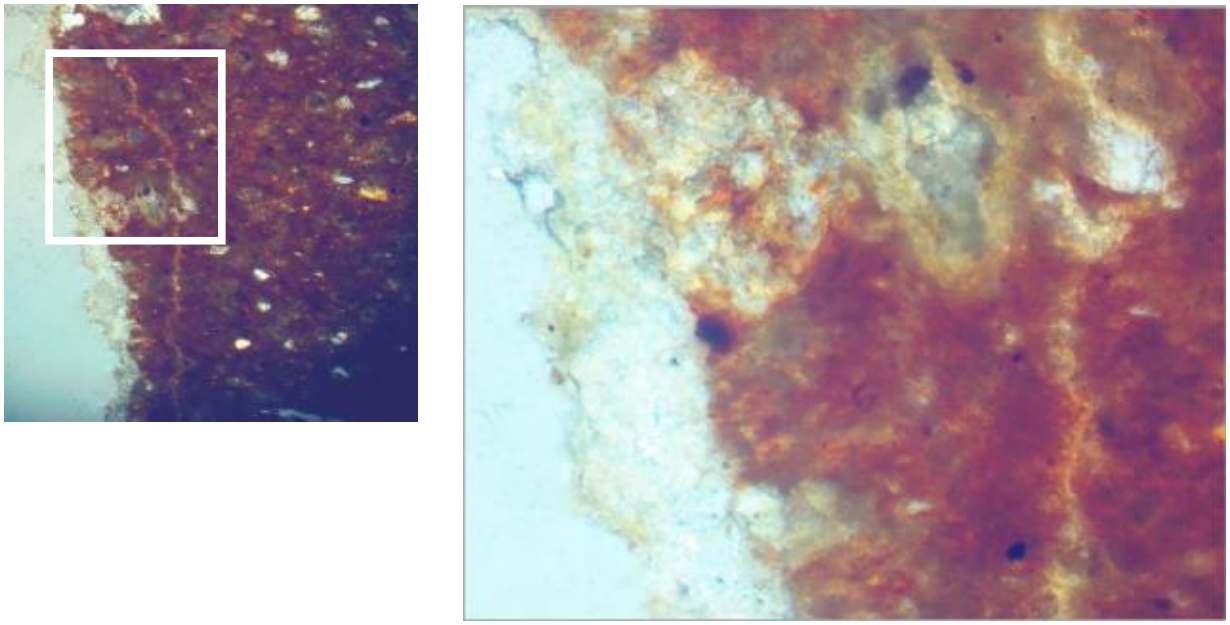


Figura 3 – Identificação do processo de percolação de cal no substrato de assentamento do biscoito do fragmento histórico através das microfissuras. A direita da imagem, no detalhe, a face posterior do biscoito azulejar e que estava em contato com a argamassa na qual ocorreu o processo percolação pelo cálcio da argamassa através de fissura.

Em relação aos teores de cálcio, a análise petrográfica mostrou A percolação através das microfissuras existentes nos fragmentos dos azulejos portugueses. Esta hipótese pode ser corroborada a partir da análise da lâmina delgada obtida na amostra histórica, 0.

A fim de comprovar o processo de percolação do óxido de cálcio da argamassa de assentamento na cerâmica, foram selecionadas amostras cerâmicas com baixo teor de cálcio. Essas amostras foram colocadas em uma solução de cal hidratada [$Ca(OH)_2$]. Após essa exposição selecionou-se uma amostra com maior evidência de percolação, através da observação em uma lupa binocular.

Da amostra selecionada, foram realizadas as FRX, antes e após a imersão, para confirmar o aumento para 9,77 do teor de Ca. Com essa comprovação da contaminação pela Ca foi então preparado um corpo de prova e levado a um microscópio eletrônico de varredura (MEV) onde foram produzidas imagens em escala de ampliação de 1000 vezes. A região selecionada para análise apresentava uma microfissura onde foi verificada a deposição de óxido de cálcio nas regiões de fissura 0 a 0.

Esse processo pode ser desencadeado devido a presença de umidade, sais solúveis e variações térmicas. A água, seja através da chuva, umidade ascendente ou condensação, pode atuar como um meio de transporte para íons dissolvidos. Os íons Ca^{2+} presentes em materiais adjacentes (como uma argamassa rica em cal) pode migrar para zonas de menor concentração como os azulejos. Ao longo

de décadas ou séculos essas exposições podem promover substituição iônica parcial dos íons Fe^{2+}/Fe^{3+} por Ca^{2+}, ou seja, a precipitação de compostos de cálcio nas áreas originalmente ricas em ferro. Nesse processo a composição original dos azulejos é lentamente alterada, e pode comprometer sua integridade estrutural bem como suas propriedades físicas e químicas.

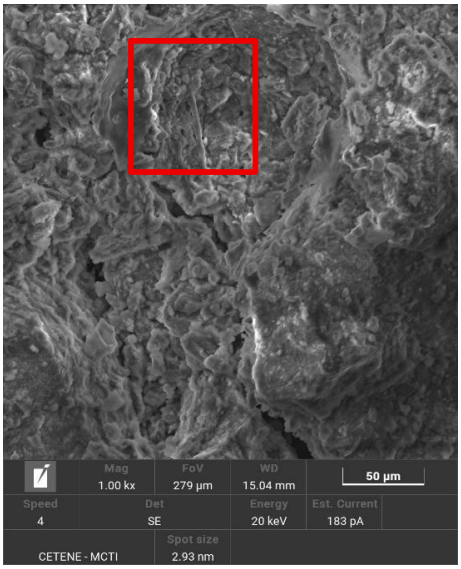


Figura 4 – Detalhe com ampliação x 1000 da região onde a fissura apresenta a deposição de partículas de Ca (partículas brancas) nas microfissuras presentes na amostra da chacota cerâmica produzida em laboratório e submersa em uma solução com 10% de hidróxido de cal (CaOH) durante dois anos a temperatura ambiente (30°). Em vermelho a área onde se realizou o mapeamento dos elementos químicos através de EDS.

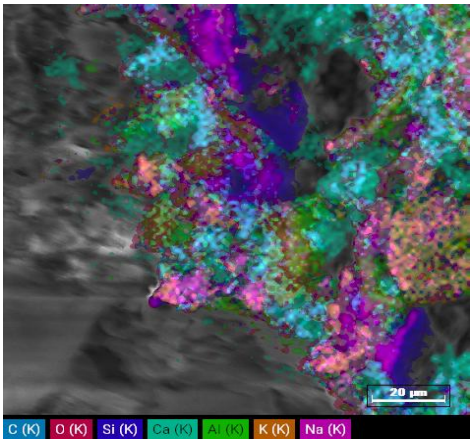


Figura 5 – Mapa de elementos químicos (x 3000) da amostra de chacota cerâmica produzida em laboratório e submersa em uma solução com 10% de hidróxido de cal (CaOH) durante dois anos a temperatura ambiente (30°). Foram detectados carbono (C) na área azul claro, sílica (Si) na área azul escura, oxigênio (O) na área rosa, alumínio (Al) na área verde escuro, cálcio (Ca) na área verde claro, potássio (K) na área marrom e sódio (Na) na área roxa. Para o estudo em questão identificou-se grande quantidade de Ca (0) sem a presença de Fe na região das fissuras.

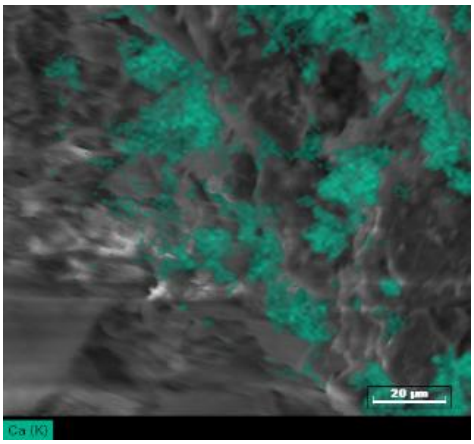


Figura 6 – Mapa de elementos químicos (x 3000) da amostra de chacota cerâmica produzida em laboratório e submersa em uma solução com 10% de hidróxido de cal (CaOH) durante dois anos a temperatura ambiente (30°). Em destaque (verde) da presença de cal nas regiões com microfissuras e poros. Não foi registrada a presença de Fe nessa região de microfissura.

Os dados desse experimento, em conjunto as FRX realizadas nos fragmentos históricos, indicam que os altos teores de cálcio das amostras históricas são provenientes de uma combinação entre a matéria prima, (argila rica em calcita), e a percolação da argamassa de assentamento a base de cal. Cabe destacar que a cal atua na fissuração dos biscoitos históricos, fundamentalmente aquela porção que percola e acelera a degradação dos azulejos. Isso indica que os teores de cálcio identificados atualmente nos azulejos históricos importados de Portugal para o Brasil são superiores aos de quando os biscoitos foram produzidos.

3. Conclusões

Os resultados obtidos permitem concluir que os elevados teores de cálcio (Ca) identificados em algumas amostras de azulejos históricos podem não ser condizentes com as proporções de matéria prima empregada originalmente nas suas manufaturas. Ao considerarmos que esses azulejos estão assentados em paredes com tijolos maciços, em um modelo construtivo com alta higroscopicidade, a análise petrográfica confirmou a presença de material esbranquiçado preenchendo microfissuras na matriz cerâmica, indicando a migração e deposição de cálcio ao longo do tempo.

Esse comportamento foi corroborado experimentalmente por meio da imersão de amostras cerâmicas em solução de hidróxido de cálcio, que resultou no aumento do teor de Ca e na sua deposição preferencial em regiões fissuradas, conforme observado em análises por MEV e EDS.

Dessa forma, conclui-se que os teores atuais de cálcio nos azulejos históricos são resultado de um processo combinado: a composição original da pasta cerâmica e a incorporação progressiva de cálcio ao longo dos séculos, favorecida por condições ambientais como umidade, presença de sais solúveis e variações térmicas. Esse processo implica alterações na composição química original das peças, com possível substituição iônica e recristalização em zonas fragilizadas.

Além disso, a presença e migração de cálcio desempenham papel relevante na degradação dos azulejos, contribuindo para a formação e propagação de fissuras, o que compromete sua integridade estrutural e durabilidade. Assim, os resultados indicam que os valores atualmente medidos podem ser superiores aos originais de fabricação, aspecto fundamental a ser considerado em estudos de caracterização, conservação e restauro de revestimentos azulejares históricos.

Os resultados obtidos neste estudo embora pertencente a uma pequena quantidade de amostras pode servir de ponto de partida para a análise em outros conjuntos azulejares maiores, especialmente aqueles assentados com argamassas à base de cal e submetidos, ao longo de séculos, a condições de elevada umidade e intensa interação com substratos porosos. As constatações desse estudo podem ser relevantes para trabalhos na área de conservação, uma vez que interpretações composicionais baseadas apenas nas análises químicas podem superestimar o teor original de Ca das peças e levar a conclusões equivocadas sobre a tecnologia de fabricação, procedência ou qualidade das argilas utilizadas. Dessa forma, o estudo reforça a necessidade de considerar as interações entre os azulejos, a argamassa e ambiente nas estratégias de preservação, sobretudo em edificações históricas sujeitas à umidade ascendente, infiltrações e ciclos de dissolução e precipitação de sais.

Agradecimentos

Gostaríamos de expressar nossos agradecimentos ao INAPAS (Instituto Nacional de Arqueologia, Paleontologia e Ambiente do Semiárido) pelo financiamento deste projeto, sem o qual esta pesquisa não teria sido possível. Agradecemos também a UFPE (Universidade Federal de Pernambuco) pela disponibilidade da utilização dos laboratórios e equipamentos utilizados nesta pesquisa, cuja contribuição foi essencial para o desenvolvimento e a conclusão deste estudo.

Referências bibliográficas

Agua, F., Sánchez-cabezudo, A., de tudela, A. P., Villegas, M. Á.; García-heras, M. 2022. “Archaeometric case-study of tiles of different dates from the Royal Monastery of San Lorenzo de El Escorial (Spain).” Boletín de la Sociedad Española de Cerámica y Vidrio, Volume 61, Issue 2, , Pages 84-97, ISSN 0366-3175. https://doi.org/10.1016/j.bsecv.2020.09.001.

Alexandre, j.; Xavier, G. C.; Manhães, A. L. F.; Vieira, C. M. F**.** 2004. “Incorporação da cal na massa de conformação de cerâmica vermelha”. Anais do 48° CONGRESSO BRASILEIRO DE CERÂMICA. Curitiba – PR. 10p.,.

Costa, M. L.; Sanjad, T. A. B. C.; Paiva, R. 2013. “The mineralogy and chemistry of the German and Portuguese tiles used to face a historic building in the Amazon region and their natural susceptibility to tropical weathering”**.** In: Acta Amazonica, vol. 43 (3), 323 – 330 p. https://doi.org/10.1590/S0044-59672013000300008

Darweesh, H. H. M. 2000. “Building materials from siliceous clay and low grade dolomite rocks. Ceramics International” (Elsevier). Cairo – Egypt. 8p. Doi: https://doi.org/10.1016/S0272-8842(00)00040-7

Goulart, E. P.; Ribeiro, E. P.; Portela, J.C.S. 2000. “Efeitos da adição de carbonatos à massa cerâmica de revestimento de queima vermelha**”**. Anais do 45° CONGRESSO BRASILEIRO DE CERÂMICA. São Pedro – SP.

Kanan, M. I. 2008. Manual de conservação e intervenção em argamassas e revestimentos à base de cal. Cadernos técnicos n°8. Brasília: IPHAN/ Programa Monumenta,. 172p.

Tite, M.S.. 2009. “The production technology of Italian maiolica: a reassessment”**.** Journal of Archaeological Science 36 - 2065–2080, p 2071. https://doi.org/10.1016/j.jas.2009.07.006

Oliveira, H. A.; Rabelo, E. J. C. 2001. “Análise microestrutural de revestimento cerâmico tipo semi grés com diferentes teores de $CaCO_3$.” Anais do 44° CONGRESSO BRASILEIRO DE CERÂMICA. Florianópolis – SC,

Pileggi, Aristides. 1958. “Cerâmica no Brasil e no Mundo**”**. Ed. Livraria Martins, São Paulo,

Santos, Reynaldo dos. 1957. “O Azulejo em Portugal”, Ed. Lisboa, Lisboa.

Sanjad, T. A. B. C.; Angélica, R. S.; Oliveira, M. M. ; Costa, W. A. M. 2004. **"**Caracterização mineralógica de azulejos de Salvador e Belém dos séculos XVI, XVII e XIX**."** *REM: Revista Escola de Minas* 57: 255-260. https://doi.org/10.1590/S0370-44672004000400007

Simões, J. M. dos Santos. 1965. ”Azulejaria Portuguesa no Brasil (1500-1822)”**.** Ed. Fundação Calouste Gulbenkian, Lisboa,

Terol, Marylène. 2021. “Azulejos em Lisboa”. Ed. Hervas, Paris.

Cinpar 2026
XXII International Conference on Building Pathology and Constructions Repair
15th to 17th July 2026 - Lisboa, Portugal

Avaliação da substituição parcial de cimento por Pó reciclado: Influência na Resistência à Compressão de Pastas Cimentícias

Evaluation of Partial Cement Replacement with Recycled Powder: Influence on the Compressive Strength of Cementitious Pastes

Pablo GÓES[1], Eudes ROCHA[2], Adolpho ARAUJO [3], Yane COUTINHO [1]Arnaldo CARNEIRO [4] Paulo MARTIN [5]

[1] Universidade Federal de Permanbucos /UFPE, PE, Brasil. e-mail: pablo.goes@ufpe.br

[2] Universidade de Pernambuco /UPE, PE, Brasil. e-mail: eudes.rocha@upe.br

[3] Universidade de Pernambuco /UPE, PE, Brasil. e-mail: adolpho.guido@upe.br

[4] Universidade Federal de Pernambuco /UFPE, PE, Brasil. e-mail: arnaldo.carneiro@ufpe.br

[5] Universidade Federal de Pernambuco /UFPE, PE, Brasil. e-mail: paulo.maior@ufpe.br

Resumo: O estudo avaliou a substituição parcial de cimento por pó reciclado (PRH) em pastas cimentícias, focando na resistência à compressão aos 7 e 56 dias de cura. Foram produzidas 13 misturas, sendo uma de referência e 12 com substituição parcial do cimento por pó reciclado híbrido (PRH), nos teores de 10%, 20% e 30%, e com diferentes níveis de finura obtidos por moagem. O PRH foi caracterizado quanto à composição química, granulometria, morfologia e mineralogia, evidenciando predominância de SiO_2, além de partículas irregulares e angulosas com ampla faixa granulométrica. Ensaios de resistência à compressão foram realizados aos 7 e 56 dias. Os resultados mostraram que a finura do PRH não influenciou significativamente a resistência, mas o aumento do teor de substituição reduziu a resistência mecânica. Substituições de 10%, 20% e 30% apresentaram quedas progressivas na resistência, sendo mais acentuadas aos 56 dias. Substituições acima de 30% foram desfavoráveis, comprometendo a hidratação. Embora baixas proporções possam melhorar a microestrutura, a eficácia do PRH como substituto se limita a teores reduzidos.

Palavras-chave: Pastas cimentícias, Pó reciclado, Reutilização de resíduos de construção.

Abstract: *The study evaluated the partial replacement of cement with recycled powder (HRP) in cementitious pastes, focusing on compressive strength at 7 and 56 days of curing. A total of 13 mixtures were produced, including one reference mixture and 12 with partial replacement of cement by hybrid recycled powder (HRP) at levels of 10%, 20%, and 30%, with different fineness levels obtained through grinding. The HRP was characterized in terms of chemical composition, particle size distribution, morphology, and mineralogy, showing a predominance of SiO_2, as well as irregular and angular particles with a wide granulometric range. Compressive strength tests were carried out at 7 and 56 days. The results showed that the fineness of HRP did not significantly influence strength; however, increasing the replacement level reduced mechanical strength. Substitutions of 10%, 20%, and 30% resulted in progressive decreases in strength, more pronounced at 56 days. Replacement levels above 30% were unfavorable, impairing hydration. Although low replacement levels may improve the microstructure, the effectiveness of HRP as a cement substitute is limited to reduced proportions.*

Keywords: *Cementitious pastes, Recycled powder, Reuse of construction waste.*

.1. Introdução

A reciclagem de resíduos da construção e demolição (RCD) pode reduzir a quantidade de resíduos destinados a aterros sanitários, diminuindo os impactos ambientais causados e promovendo uma gestão mais sustentável dos recursos naturais. Segundo a Associação Brasileira de Empresas de Limpeza Pública e Resíduos Especiais (ABRELPE), foram geradas mais de 81 milhões de toneladas de resíduos sólidos no Brasil em 2024. A Secretaria Nacional de Saneamento Ambiental estima que os RCD correspondem a 51% a 70% dos resíduos sólidos urbanos gerados no país.

A disposição inadequada desses resíduos causa problemas socioambientais, como ocupação irregular de áreas urbanas, esgotamento da capacidade dos aterros sanitários, assoreamento de córregos e rios, obstrução das redes de drenagem, proliferação de vetores de doenças e degradação das paisagens rurais e urbanas (Oliveira, 2007).

Um levantamento realizado em cidades brasileiras entre 2010 e 2019 indicou que a geração de RCD aumentou 25%, passando de 33,4 milhões de toneladas/ano em 2010 para 44,5 milhões de toneladas/ano em 2019. A produção per capita aumentou de 174,3 kg/ano em 2010 para 213,5 kg/ano em 2019 (Hendges, 2021).

A produção de agregados reciclados é uma boa alternativa para a destinação dos RCD. Contudo, esse processo gera uma quantidade considerável de partículas finas, que podem apresentar até 35% do volume total de agregados produzidos. Segundo Heinz e Schubert (2007), o tamanho das partículas geradas varia da escala submicrométrica até a milimétrica.

Essas partículas finas geralmente apresentam uma distribuição granulométrica contínua, porém o tamanho médio das partículas varia consideravelmente de acordo com a origem do resíduo, conforme indicado em diversos estudos. Por exemplo, Zhu et al. (2016) estudaram resíduos de tijolos cerâmicos e cimento e encontraram um tamanho médio de partícula de 31,40 μm, enquanto Topic et al. (2017) e Sun et al. (2017) analisaram resíduos de concreto e determinaram tamanhos médios de 12,00 μm e 14,38 μm, respectivamente. Em geral, essas partículas apresentam formato irregular e bordas angulosas (Liu et al., 2014; Zhu et al., 2016).

Com base no tamanho e na composição granulométrica desse material, uma possível aplicação é como adição do tipo fíler. Materiais fíler podem reduzir a porosidade do concreto, minimizando o consumo de pasta de cimento (De Larrard, 2010). Esse efeito resulta do empacotamento das partículas, no qual vazios maiores no concreto podem ser preenchidos pela seleção adequada da proporção e do tamanho das partículas de resíduo (Hunger, 2010), deixando um espaço mínimo para a água, o que é conhecido como efeito microfíler.

Os fíleres são partículas inertes, ou seja, não interagem quimicamente com os produtos de hidratação, embora formem núcleos que favorecem a hidratação do silicato tricálcico (C_3S) e do silicato dicálcico (C_2S) (Ye et al., 2007).

Os materiais fíler comumente utilizados para substituição parcial do cimento são predominantemente de origem calcária. Diversos estudos têm se concentrado na influência de fíleres naturais na hidratação do cimento. Wolf (2010) avaliou o efeito do calcário calcítico no cimento branco. Jordani (2020) analisou a hidratação do cimento Portland com elevados teores de fíler dolomítico com diferentes finuras. No entanto, ainda existem lacunas quanto ao uso de fíleres provenientes de materiais alternativos, como os finos gerados durante a reciclagem de RCD.

Diante da necessidade de melhor compreender o efeito dos finos de RCD em pastas cimentícias e na hidratação do cimento, este estudo teve como objetivo analisar a influência desse material, em diferentes proporções e valores de finura, nas reações de hidratação do cimento.

2. Materiais e métodos

Para os experimentos, foram produzidas 13 combinações: uma pasta de cimento de referência e 12 pastas com substituição do cimento por pó reciclado híbrido (PRH), em volume, nos teores de 10%, 20% e 30%, e com diferentes valores de finura. A nomenclatura utilizada foi M1H10, em que 1H se refere ao tempo de moagem e 10 corresponde ao percentual de substituição empregado. As proporções das pastas produzidas estão detalhadas na Tabela 1.

Tabela 1 – Proporções das pastas produzidas.

Combinações	Cimento (%)	PRH (%)	Tempo de moagem	D50 do PRH
Referência	100	0	–	–
M1H10	90	10	1 h	18.39
M1H20	80	20		
M1H30	70	30		
M2H10	90	10	2 h	15.70
M2H20	80	20		
M2H30	70	30		
M4H10	90	10	4 h	15.27
M4H20	80	20		
M4H30	70	30		
M8H10	90	10	8 h	10.16
M8H20	80	20		
M8H30	70	30		

Para todas as análises realizadas, amostras foram moldadas em corpos de prova cilíndricos de 5 × 10 cm, produzidos com pastas de cimento e de cimento + HRP. Em seguida, as amostras foram preparadas de acordo com cada ensaio.

2.1 Caracterização dos materiais

O cimento utilizado foi o CPV-ARI – alta resistência inicial (equivalente ao cimento Tipo III especificado pela norma ASTM C150/C150M). Esse cimento foi empregado devido à menor quantidade de adições normalmente presentes nos cimentos comerciais, permitindo melhor compreensão da influência dos resíduos da construção e demolição (RCD) nas pastas cimentícias.

O pó reciclado híbrido (PRH) foi obtido como subproduto do processo de produção de agregados reciclados em uma usina de reciclagem. Durante a britagem dos RCD, as partículas finas geradas são separadas por aspiração no britador. O pó reciclado coletado na usina foi peneirado em peneira com abertura de 2,4 mm, a fim de remover partículas maiores e impurezas, como folhas e fragmentos plásticos. Em seguida, realizou-se a moagem em moinho de bolas rotativo por períodos de 1 h, 2 h, 4 h e 8 h. A carga de esferas de alumina, em três diferentes diâmetros, foi de 7900 g. A rotação do moinho foi de 50 rpm, e o tempo de moagem variou de 1 a 8 h. Em cada moagem, foram utilizados 1,5 kg de PRH.

As composições químicas do cimento, fornecidas pelo fabricante, e do PRH estão apresentadas na Tabela 2.

Tabela 2 – Caracterização química do cimento e do PRH.

Óxidos	Cimento	PRH
CaO	59.97	3.28
SiO_2	18.66	80.86
Na_2O	0.17	0.92
Al_2O_3	4.34	5.95
MgO	5.73	0.50
K_2O	0.88	1.05
Fe_2O_3	2.37	1.80
SO_3	4.28	0.28
TiO_2	–	0.30
Insolúvel resíduo	0.79	–
Perda ao fogo (LOI)	3.59	5.06

Com base na caracterização química, os componentes do PRH são semelhantes aos encontrados em materiais de construção usuais, como concreto, argamassa e tijolos, com exceção do TiO_2, comumente utilizado como pigmento branco presente em revestimentos, tintas e azulejos. Além disso, SiO_2, Al_2O_3 e CaO representam cerca de 90% da composição do PRH, sendo o SiO_2 provavelmente proveniente da areia presente no concreto e nas argamassas.

As distribuições granulométricas das partículas de cimento e do PRH são apresentadas na Figura 1. O diâmetro característico das partículas de cimento (D_{50}) foi de 10,5 µm, e a área superficial específica foi de 1250 m²/kg.

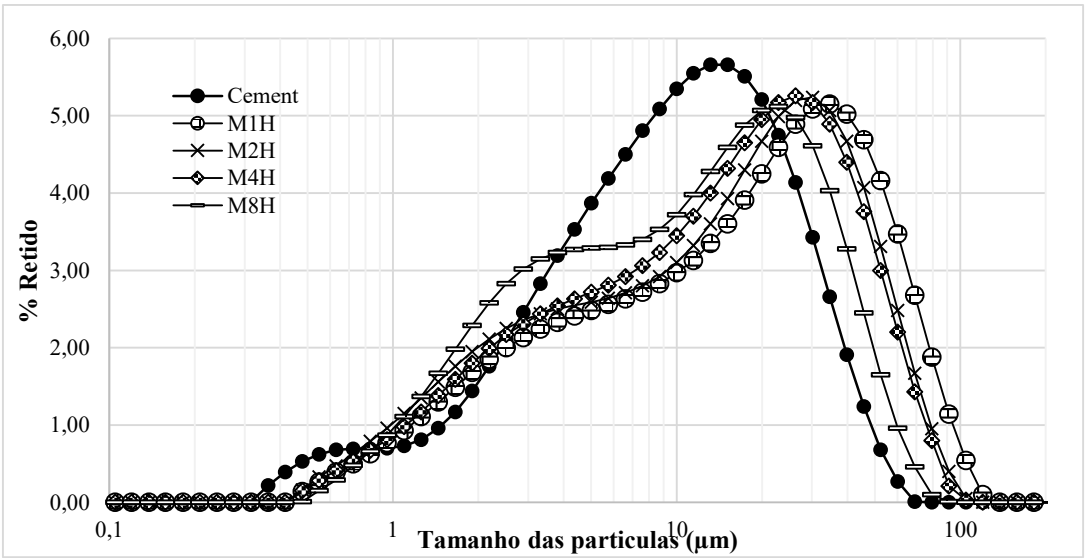
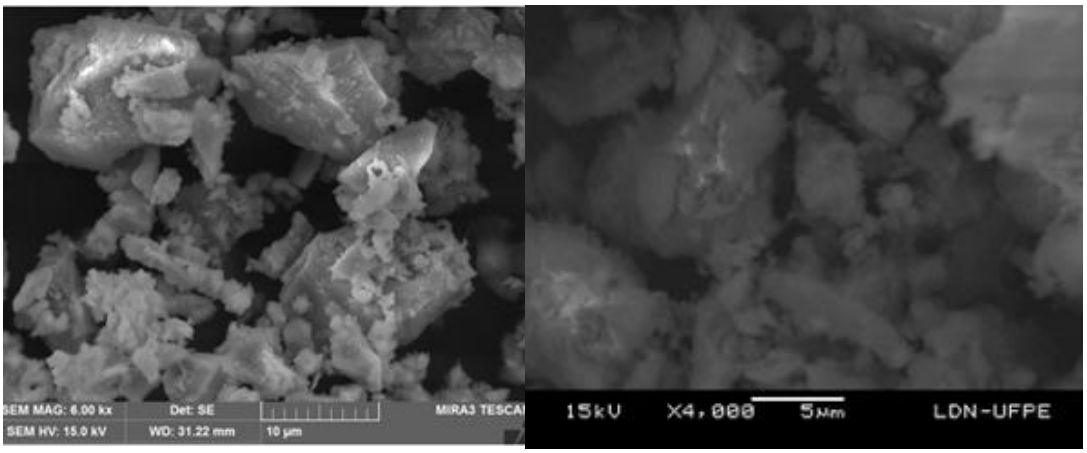


Figura 1 – Distribuição granulométrica das partículas de cimento.

Conforme observado, a distribuição granulométrica do PRH é bem graduada e contínua. O PRH moído por 1 h apresenta partículas de maiores dimensões quando comparado ao material moído por

8 h. Além disso, as dimensões das partículas de PRH variam entre 0,5 e 100 μm, concentrando-se majoritariamente na faixa entre 5 e 50 μm.

As Figuras 2(a) e 2(b) apresentam as micrografias obtidas por microscopia eletrônica de varredura (MEV) do cimento e do PRH, respectivamente.

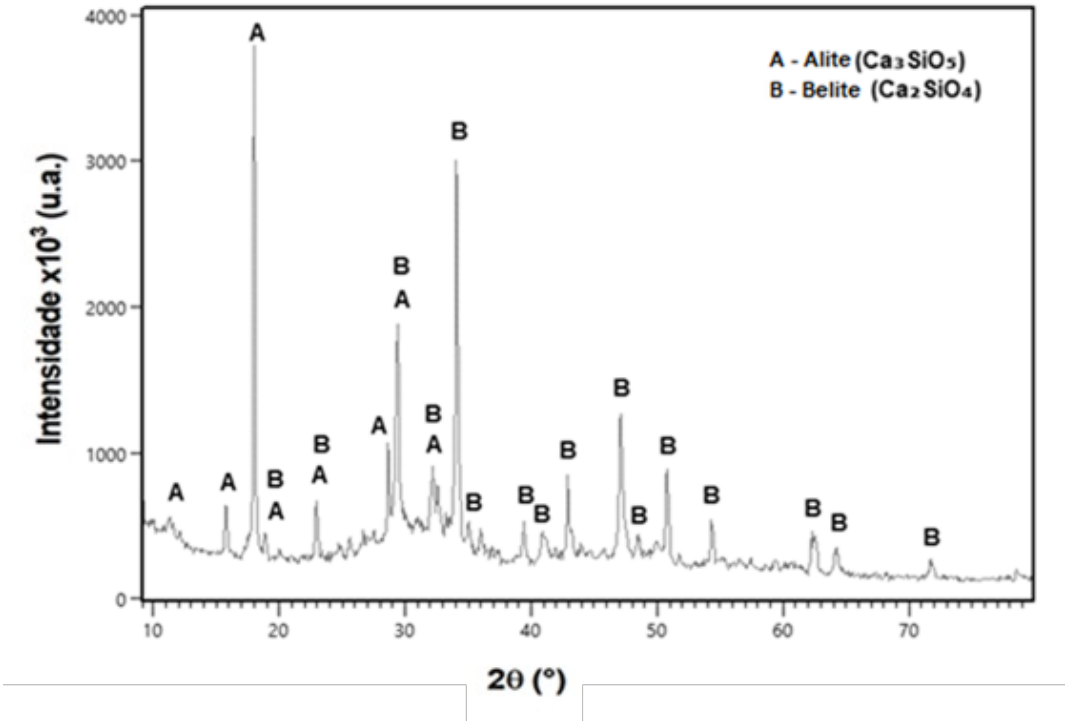


(a) (b)

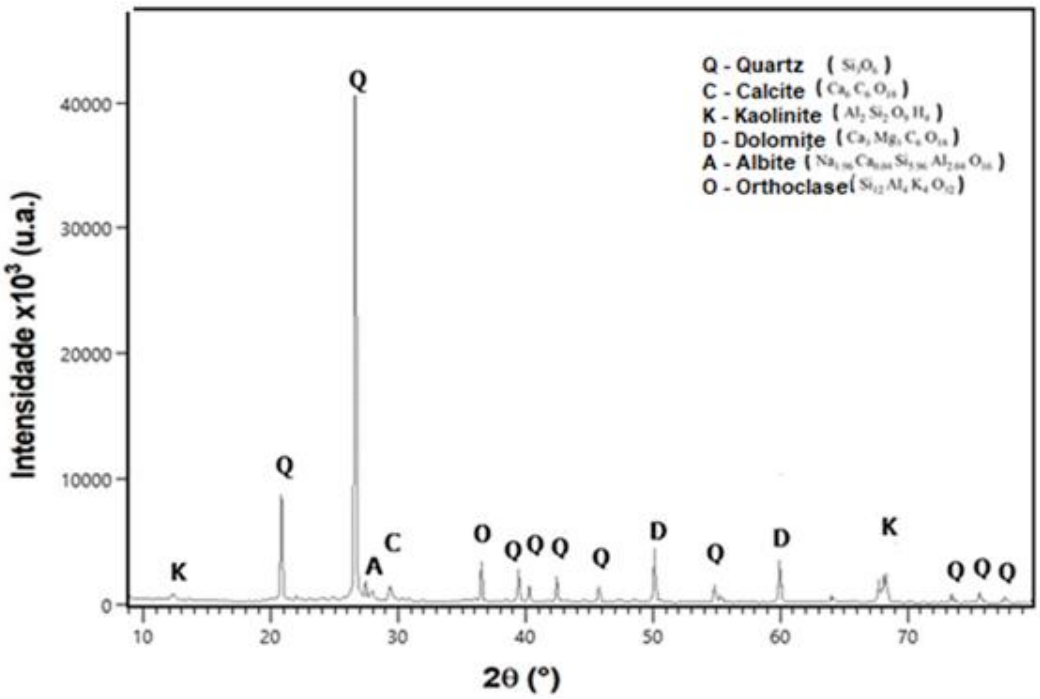
Figura 2 – MEV imagens do (a) cimento (× 6000) e (b) PRH partículas (× 4000).

A imagem de MEV do cimento indica a predominância de partículas angulares e de tamanhos variados. Quanto ao PRH, a imagem mostra algumas partículas de quartzo recobertas por resíduos de materiais cimentícios que aderiram à sua superfície. Conforme observado, as partículas de PRH apresentam bordas afiadas e irregulares, que formam reentrâncias em formato de V. A forma irregular das partículas também foi observada em outros estudos, como o de Liu *et al*. (2014).

Figuras 3(a) e (b) apresentam os difratogramas de DRX do cimento e das partículas de PRH, respectivamente.



(a)



(b)

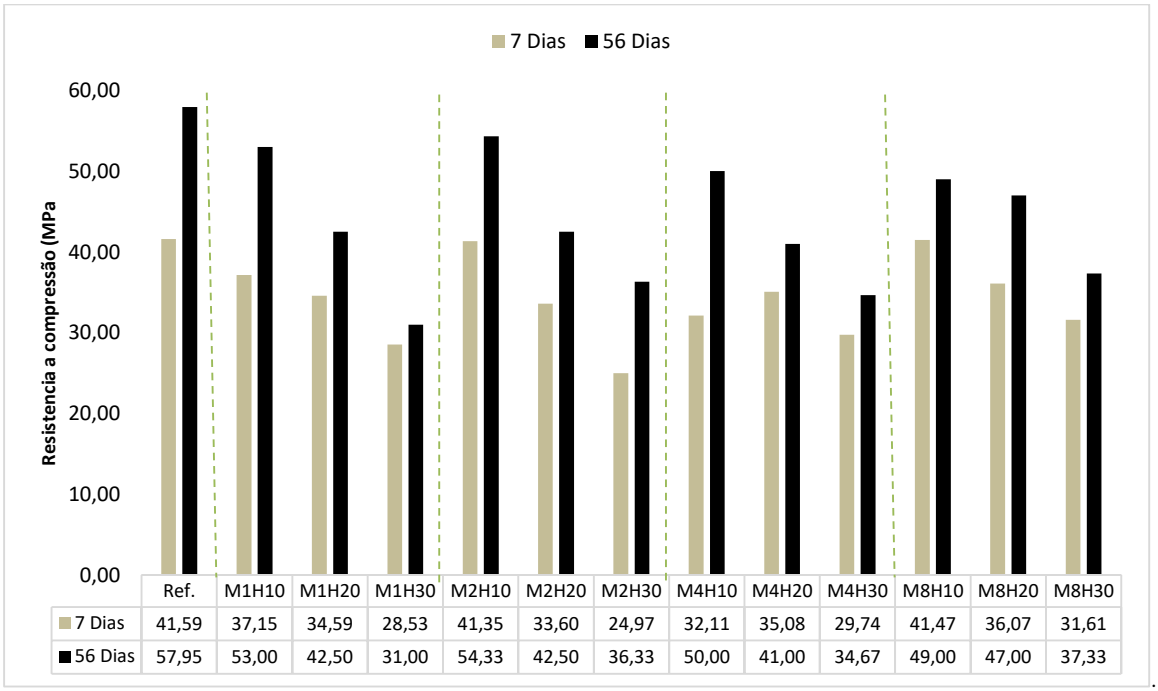
Figura 3 – DRX difratogramas de (a) cimento e (b) partículas de PRH.

O difratograma do cimento apresenta picos característicos de alita e belita, com intensidades variadas. O difratograma do HRP exibe diversos picos, uma vez que se trata de um material de composição bastante heterogênea. A composição química do HRP indica que ele é majoritariamente composto por SiO_2, o que também foi confirmado pelos picos de quartzo, possivelmente provenientes da areia presente no concreto e na argamassa que deram origem ao HRP.

Os demais picos identificados foram determinados com base nas fichas do sistema JCPDS, registradas no International Center for Diffraction Data, sendo eles: quartzo (Si_3O_6), calcita ($Ca_6C_6O_{18}$), caulinita ($Al_2Si_2O_9H_4$), dolomita ($Ca_3Mg_3C_6O_{18}$), albita ($Na_{1.96}Ca_{0.04}Si_{5.96}Al_{2.04}O_{16}$) e ortoclásio ($Si_{12}Al_4K_4O_{32}$), minerais presentes na cal (calcita), no cimento (calcita, caulinita, dolomita e albita), nos agregados e em outros materiais utilizados na construção civil. Além disso, não foi observado halo amorfo.

3. Resultados

Os resultados de resistência à compressão das pastas aos 7 e 56 dias são apresentados na Figura 4.



	Ref.	M1H10	M1H20	M1H30	M2H10	M2H20	M2H30	M4H10	M4H20	M4H30	M8H10	M8H20	M8H30
7 Dias	41,59	37,15	34,59	28,53	41,35	33,60	24,97	32,11	35,08	29,74	41,47	36,07	31,61
56 Dias	57,95	53,00	42,50	31,00	54,33	42,50	36,33	50,00	41,00	34,67	49,00	47,00	37,33

Figura 4 – Resistência à compressão aos 7 e 56 dias das pastas produzidas

Conforme observado na Figura 4, não foi verificada uma tendência clara em relação à redução do tamanho das partículas do PRH e os resultados de resistência à compressão. Em contrapartida, a redução do teor de cimento exerceu influência significativa nos resultados obtidos.

As pastas aos 7 dias, com 10% de substituição do cimento por PRH, apresentaram valores de resistência à compressão variando entre 32,11 e 41,47 MPa, com reduções de 10,7%, 0,58%, 22,8% e 0,29% para M1H10, M2H10, M4H10 e M8H10, respectivamente.

Para a substituição de 20%, os valores variaram entre 24,97 e 35,08 MPa, com reduções de 16,8%, 19,2%, 15,6% e 13,3%. Para 30% de substituição, os valores ficaram entre 24,97 e 31,61 MPa, com reduções de 31,4%, 40,0%, 28,5% e 24,0%.

Aos 56 dias, as pastas com 10% de substituição apresentaram resistências entre 49,00 e 54,33 MPa, com reduções entre 6,2% e 15,4%. Para 20% de substituição, as reduções variaram entre 18,9% e 29,2%, enquanto para 30% variaram entre 35,6% e 46,5%.

Os resultados indicam que a substituição de 30% do cimento por PRH não é vantajosa, resultando em perda significativa da resistência à compressão. A substituição do ligante por um material inerte em baixos teores pode trazer benefícios, como refinamento da porosidade, modificação microestrutural da zona de transição interfacial (redução da espessura da ZTI e interferência no crescimento cristalino), redução da exsudação e aumento da densidade da mistura devido ao preenchimento dos vazios por partículas finas (Fonseca, 2010).

Entretanto, em teores elevados, a redução significativa do ligante afeta negativamente a formação de produtos de hidratação. Na versão anterior da norma brasileira para cimentos comerciais, o limite de fíler calcário no cimento CP II-F era de 10%; a norma atual NBR 16697 (2018) elevou esse limite para 25%. No caso do PRH analisado, a substituição de 30% não se mostrou viável.

Resultado semelhante também foi obtido por Topic *et al.* (2017). Os autores substituíram o cimento por partículas finas provenientes da reciclagem de concreto em proporções de 10%, 20%, 30%, 40% e 50% e verificaram uma redução considerável da resistência à compressão a partir de 30% de substituição, atingindo uma redução de 38% em comparação com a amostra de referência. Além disso, Zhu et al. (2016) também observaram uma diminuição das resistências à compressão e à flexão com o aumento dos teores de substituição. Outro aspecto importante é que, devido ao cimento utilizado, CP V, apresentar elevada resistência inicial, o ganho de resistência entre 7 e 56 dias não foi significativo, permanecendo abaixo de 25%.

4. Conclusão

A resistência à compressão das pastas foi analisada para diferentes teores de substituição do cimento por PRH. Os resultados indicaram que, embora o tamanho de partícula do PRH não tenha influenciado de maneira significativa a resistência das pastas, o percentual de substituição exerceu influência relevante. A partir de 30% de substituição, observou-se uma queda acentuada da resistência à compressão, indicando que elevados teores de substituição podem não ser viáveis, uma vez que afetam negativamente essa propriedade.

Os resultados sugerem que o uso de PRH em substituição ao cimento, em baixos percentuais, pode ser benéfico, contribuindo para a redução da fissuração e para a densificação da matriz cimentícia. Entretanto, teores elevados (a partir de 30%) não são recomendados, pois podem resultar em reduções significativas da resistência à compressão das pastas. Dessa forma, o percentual de PRH a ser utilizado nas misturas deve ser cuidadosamente avaliado, a fim de garantir um desempenho adequado das pastas no estado endurecido.

Agradecimentos

Gostaríamos de expressar nossos agradecimentos ao INAPAS (Instituto Nacional de Arqueologia, Paleontologia e Ambiente do Semiárido) pelo financiamento deste projeto, sem o qual esta pesquisa não teria sido possível. Agradecemos também a UFPE (Universidade Federal de Pernambuco) pela disponibilidade da utilização dos laboratórios e equipamentos utilizados nesta pesquisa, cuja contribuição foi essencial para o desenvolvimento e a conclusão deste estudo.

Referências

ABNT NBR 16697:2018. Cimento Portland – Requisitos

Abrelpe - Associação Brasileira de Empresas de Limpeza Pública e Resíduos. 2025. ”PANORAMA DOS RESÍDUOS SÓLIDOS NO BRASIL 2025**”**. São Paulo: [S.l].

DE LARRARD, F. “Concrete optimisation with regard to packing density and rheology”. 2010. In: 3 RILEM International Symposium on Rheology of Cement Suspensions such as Fresh Concrete, France, v. 1.

FONSECA, Gustavo. 2010. “Adições minerais e as disposições normativas relativas à produção de concreto no brasil: uma abordagem epistêmica”. Dissertação (Mestrado). Universidade federal de Minas gerais. Belo Horizonte

JORDANI, B. 2020. “Hidratação do cimento portland na presença de elevados Teores de fíler dolomito com diferentes finuras”. Tese de Doutorado (Doutorado em Engenharia) – Pós-Graduação em Engenharia Civil da Universidade do Vale do Rio dos Sinos, UNISINOS, São Leopoldo.

HENDGES, A. S. 2021. “VII Congresso Nacional de Educação Ambiental e IX Encontro Nordestino de Biogeografia”.

HEINZ, D., SCHUBERT, J. 2007. “Finely Ground Sand Fraction of Concrete Rubble as a Supplementary Cementitious Material”. In: Grosse, C.U. (eds) Advances in Construction Materials 2007. Springer, Berlin, Heidelberg. https://doi.org/10.1007/978-3-540-72448-3_67

HUNGER, M. 2010. “An integral Design Concept for Ecological Self-Compacting Concrete”. Bouwkunde. PhD Thesis. Eindhoven: Eindhoven University of Technology.

LIU, Q., TONG, T., LIU, S., YANG, D., and YU, Q. 2014. “Investigation of using hybrid recycled powder from demolished concrete solids and clay bricks as a pozzolanic supplement for cement”. Construction and Building Materials, Volume 73,2014, Pages 754-763,ISSN 0950-0618, https://doi.org/10.1016/j.conbuildmat..09.066.

OLIVEIRA, JOÃO CARLOS. 2007. “Indicadores de Potencialidades e Desempenho de Agregados Reciclados de Resíduos Sólidos da Construção Civil em Pavimentos Flexíveis”, Tese de Doutorado. Brasília.

ZHU, P., MAO, X., QU, W., LI, Z., ZHONGGUO J. M. 2016. “Investigation of using recycled powder from waste of clay bricks and cement solids in reactive powder concrete”. Constr. Build. Mater., 133, 246–254.

TOPIC, JAROSLAV; PROSEK, ZNEDEK; PLACHY, TOMAS. 2017. ”Influence of increasing amount of recycled concrete powder on mechanical properties of cement paste”. MATERIALS SCIENCE & ENGINEERING. A, STRUCTURAL MATERIALS: PROPERTIES, MICROSTRUCTURE AND PROCESSING. Czech.

WOLF, J**.** 2010. “Influência do calcário na carbonatação de argamassa de cimento branco”. Tese de Doutorado (Doutorado em Engenharia) – Escola de Engenharia, Programa de Pós-Graduação em Engenharia Civil, UFRGS, Porto Alegre.

SUN, Z.; LIU, F.; TONG, T.; QI, C. 2017. “Hydration of Concrete Containing Hybrid Recycled Demolition Powders”. Journal of Materials in Civil Engineering Vol. 29, Issue 7.

Cinpar 2026
XXII International Conference on Building Pathology and Constructions Repair
15th to 17th July 2026 - Lisboa, Portugal

Control of fresh concrete's composition through non-intrusive microwave electrical impedance spectroscopy

Marcos Roberto FORTULAN[1], Denise de S. SILVA[2], Guilherme HIDACA[3], Francisco J. do NASCIMENTO[4]

[1] CSense Tecnologia Ltda., Rua Alfredo Lopes, 1717, Vila Elizabeth, São Carlos-SP, Brazil, marcos.fortulan@alumni.usp.br
[2] Federal University of São Carlos (UFSCar), Department of Materials Engineering (DEMa), Rodovia Washington Luís, km 235, 13565-905, São Carlos-SP, Brazil, denisesousa@estudante.ufscar.br
[3] University of São Paulo (USP), Department of Mechanical Engineering, São Carlos School of Engineering (EESC), Avenida Trabalhador São Carlense, 400, 13566-970, São Carlos-SP, Brazil, ghidaca@usp.br
[4] Federal University of São Paulo (UNIFESP), Institute of Marine Science (IMar), Rua Carvalho de Mendonça, 144, Encruzilhada, Santos-SP, Brazil, fjnascimento@unifesp.br

Abstract: Understanding the fresh-state behavior of cement-based materials is essential for ensuring performance, durability, and efficient resource use in concrete production. As traditional fresh-state tests often provide indirect or delayed information, non-intrusive electrical impedance sensing emerges as a promising alternative for fast-response, quantitative, and non-destructive characterization. This study aims to evaluate how the electrical properties of fresh concrete are influenced by water content, cement content, and water-to-cement ratio (w/c), using non-intrusive impedance measurements to support mixture characterization and composition control. The w/c ratio was intentionally varied from 0.39 to 0.73. The aggregates were characterized and their granulometry determined; the specific mass of the cement was determined and a slump test was performed. For mechanical characterization, 30 compositions were tested to determine their compressive strength at 7 and 28 days. The electrical data were analyzed to assess influence and correlations between impedance behavior and mixture parameters. The results demonstrate the feasibility of using non-intrusive microwave impedance measurements to characterize the dielectric behavior of fresh concrete. Using the custom 2.4 GHz patch antenna, impedance magnitude and phase spectra were acquired between 1 to 3 GHz, revealing that each mixture exhibited a distinct spectral signature closely associated with variations in water content, cement content and w/c ratio. Materials with low moisture content exhibited higher impedance magnitudes and stable phase responses, whereas mortars and fresh concretes showed significantly lower impedance values, ranging from 7.2 to 40.7 ohms along with noticeable phase-shift variations due to the contribution of free water, dissolved ions, and pore connectivity. These differences confirm that spectral responses are governed by water and cement content and, therefore, by w/c ratio, enabling each mixture to be distinguished by a unique dielectric signature. The patch antenna proved its potential for non-intrusive, composition-dependent influence of fresh concrete.

Keywords: Water-to-Cement Ratio (w/c), Fresh Concrete Composition, Microwave Electrical Impedance, Non-intrusive Measurement, Concrete Quality Control.

1. Introduction

Concrete is the most widely used material in civil construction due to its high mechanical strength, durability, and adaptability to different structural applications (Fortulan *et al.*, 2023). However, the final performance of concrete structures is strongly influenced by the properties of concrete in the fresh state. In particular, the water-to-cement ratio (w/c) directly affects compressive strength, porosity, permeability, durability, and service life (Park *et al.*, 2022). Small variations in this parameter can lead to significant changes in both mechanical behavior and long-term performance, especially in high-performance concrete.

Traditionally, the control of concrete properties relies on standardized laboratory tests, such as the slump test (ABNT NBR 16889) and the axial compressive strength test (ABNT NBR 5739). Although widely accepted, these methods present important limitations. The slump test provides only a qualitative indication of workability and is strongly influenced by admixtures, aggregate grading, and mixture composition. Compressive strength testing, in turn, is destructive, time-consuming, and does not allow immediate corrective actions during production or placement (Fortulan *et al.*, 2023). These limitations are particularly critical when rapid decision-making and real-time quality control are required.

In addition to operational constraints, destructive testing methods present intrinsic uncertainties. Compressive strength exhibits significant spatial variability due to concrete heterogeneity, curing conditions, moisture gradients, and compositional variations, making it difficult to obtain representative results from a limited number of specimens or cores (Breysse *et al.*, 2019; Malhotra and Carino, 2003). As a result, conventional approaches may fail to accurately represent in-situ conditions, especially in large or complex structural elements.

In this context, non-destructive testing (NDT) techniques, such as the Schmidt rebound hammer, ultrasonic pulse velocity (UPV), and combined methods, have been extensively investigated for strength estimation both in laboratory conditions and in situ. However, their reliability when used independently remains limited, as results are strongly influenced by surface conditions, degree of saturation, carbonation, age, and environmental exposure (Breysse *et al.*, 2019; Malhotra and Carino, 2003). Consequently, international recommendations, such as RILEM TC 249-ISC, emphasize the need for statistical analysis, local calibration with destructive tests, and appropriate sampling strategies.

Beyond mechanical wave-based methods, the electrical, electromagnetic, and dielectric properties of concrete are highly sensitive to composition, moisture content, pore structure, and hydration degree. Early studies by Gjørv *et al.* (1977) showed that electrical resistivity decreases with increasing water-to-cement ratio, particularly at intermediate saturation levels, highlighting the influence of pore solution and free water. These findings support the use of electrical and electromagnetic parameters as indirect indicators of concrete quality.

Recent studies have expanded this approach by investigating dielectric properties over a wide frequency range, showing strong correlations between dielectric permittivity, water content, pore volume, and compressive strength (Dinh *et al.*, 2021). Measurements in radiofrequency and microwave ranges are particularly sensitive to free and bound water, which dominates the electromagnetic response of cement-based materials. Since water has significantly higher permittivity than solid phases, changes in moisture state and microstructure during hydration directly affect dielectric parameters.

Experimental evidence also indicates that dielectric properties can be used not only to monitor hydration and moisture evolution but also to predict mechanical performance. Studies on early-age concrete show that complex permittivity enables accurate strength prediction models, offering an alternative to traditional curing-time-dependent tests (Gao *et al.*, 2021). Similarly, correlations between dielectric behavior and compressive strength have been reported for different aggregate sizes and mixture proportions (Zhong *et al.*, 2024).

Furthermore, low-cost electrical sensors originally developed for soil moisture monitoring have been successfully adapted to fresh concrete, enabling continuous and non-destructive assessment of water availability during early hydration. These techniques offer advantages in simplicity, speed, and field applicability, making them suitable for real-time quality control and process optimization.

Overall, the demand for improved production efficiency, reduced cement consumption, and enhanced reliability in technological control has driven the development of advanced non-destructive and non-intrusive techniques. The integration of electrical, dielectric, and mechanical methods, combined with proper calibration and data interpretation, represents a promising approach to overcome the limitations of conventional tests and improve the control of concrete properties from the fresh to the hardened state.

2. Theoretical Background

2.1 Basic concepts of electrical impedance and dielectric properties of cementitious materials

Electrical impedance is a complex quantity that describes the overall opposition that a material or system offers to the flow of an alternating electric current. It can be expressed as:

$$Z(\omega)=R(\omega)+jX(\omega), \text{ with } \omega = 2\pi f \quad (1)$$

where R is the resistance (real component, associated with current conduction) and X is the reactance (imaginary component, related to energy storage and phase lag in the electric field). The angular frequency ω defines the excitation regime (Barsoukov and Macdonald, 2005). As shown in Equation 1, impedance is represented as a complex quantity composed of resistive and reactive contributions.

Analyzing impedance as a function of frequency, known as electrical impedance spectroscopy (EIS), makes it possible to distinguish different physical transport and polarization mechanisms occurring within a material. At low frequencies, ionic conduction and interfacial polarization (Maxwell–Wagner) effects dominate. At higher frequencies, the response is increasingly influenced by polarization mechanisms, particularly the dipolar contribution associated with water, in addition to electronic and atomic contributions (Dinh *et al.*, 2021).

The shape and magnitude of these responses depend on the internal structure, composition, and water content of the material, making impedance a sensitive tool for characterizing complex media such as fresh concrete (Hu *et al.*, 2019). At radiofrequency and microwave frequencies, the analysis is commonly expressed in terms of dielectric properties and scattering parameters.

In cementitious materials, alternating current follows heterogeneous paths through solid phases (hydrated cement and aggregates), pores filled with an aqueous solution, and interfaces between these phases. This heterogeneity gives concrete a multiphase electrical response. Electrical resistance is linked to the connectivity and conductivity of the pore solution, while the dielectric response is strongly sensitive to water content and to microstructural evolution during hydration (Gallardo and Provis, 2021; Dinh *et al.*, 2021).

Dielectric behavior can be described by the complex permittivity, which incorporates energy storage and losses:

$$\varepsilon^*(\omega) = \varepsilon'(\omega) - j\varepsilon''(\omega) \quad (2)$$

where ε' is the real part (ability to store energy in the electric field) and ε'' is the imaginary part (dielectric losses, including contributions from relaxation and conduction). A common way to express the conductive contribution is to incorporate it into ε'' via $\sigma/(\omega\varepsilon 0)$ (Nelson, 1991). According to Equation 2, the dielectric response can be interpreted in terms of energy storage and loss mechanisms.

In RF/microwave techniques without direct electrical contact with the sample, electrode–material interface effects observed in contact EIS are avoided. Nevertheless, the conductivity of the pore solution contributes to ε'' (losses), and the dielectric response is strongly influenced by the water present in the pores (Nelson, 1991; Hu *et al.*, 2019; Dinh *et al.*, 2021).

Microwave dielectric characterization studies show that the dielectric properties of concrete vary with moisture content and curing or hydration time, particularly due to the contribution of water to the effective permittivity (Dinh *et al.*, 2021). In parallel, contact electrical measurements indicate that electrical conductivity (or resistivity) evolves with hydration and tends to reflect the loss of connectivity of the liquid phase (depercolation) and changes in ionic strength over time (Gallardo and Provis, 2021).

Therefore, measuring impedance and/or complex permittivity over a frequency range can provide quantitative information about the physicochemical state of the material, including water content and microstructural evolution (Dinh *et al.*, 2021; Hu *et al.*, 2019).

2.2 Comparison between intrusive and non-intrusive methods: limitations due to ionic conduction, electrode polarization, and sample disturbance

Electrical measurements in cementitious materials are generally classified as intrusive or non-intrusive, depending on how the sensor interacts with the material under analysis.

In intrusive methods, metallic electrodes are in direct contact with the sample, establishing an electrode–material interface through which the alternating current flows. In non-intrusive methods, coupling occurs without direct electrical contact, for example via capacitive or inductive coupling, or via RF/microwave techniques based on transmission lines, resonators, or antennas (Hu *et al.*, 2019; Islam *et al.*, 2024).

Fresh concrete contains a conductive liquid phase (pore solution), whose ionic composition results from the dissolution of soluble cement species and evolves with hydration (Gallardo and Provis, 2021). When an alternating electric field is applied between two electrodes in contact with this matrix, charged species can accumulate at the interfaces, forming charge layers (electric double layer). This process, known as electrode polarization, introduces an additional (typically capacitive) component and can distort the measured response at low frequencies (Barsoukov and Macdonald, 2005).

As a first approximation, the total measured impedance (Z_{med}) can be interpreted as the contribution of the material (Z_{med}) in series with an interfacial contribution (Z_{int}):

$$Z_{med} \approx Z_{mat} + Z_{int} \tag{3}$$

where Z_{int} depends on the surface state of the electrodes, the effective contact geometry and area, and local interface conditions, which can compromise reproducibility and comparability between samples (Hu *et al.*, 2019; Park *et al.*, 2022). In this simplified interpretation, Equation 3 highlights that the measured response includes both material and interfacial contributions. In addition, variations in positioning and in contact or immersion conditions between successive measurements can introduce systematic assembly errors and result dispersion (Park *et al.*, 2022; Hu *et al.*, 2019).

Another relevant factor is the physical disturbance of the sample. In fresh concrete, inserting probes may locally rearrange paste and aggregates and alter the local electric field, reducing the representativeness of the measured volume. These effects tend to be more critical as material heterogeneity increases and as the sensing region becomes more localized.

In non-intrusive RF/microwave approaches, coupling can occur through planar structures (e.g., microstrip) or resonant structures (e.g., patch), in which fringing or evanescent fields interact with the material. The response is often analyzed through variations in parameters such as center frequency, return loss, and phase (S-parameters), which are related to the effective complex permittivity of the medium (Pozar, 2012; Balanis, 2016; Islam *et al.*, 2024).

In addition to avoiding electrode polarization typical of contact measurements, non-contact methods can eliminate interfacial elements in equivalent circuit models and increase temporal stability (Hu *et al.*, 2019).

The feasibility of non-intrusive RF/microwave measurements is linked to frequency selection, which simultaneously affects penetration depth and sensitivity. In non-metallic media, electromagnetic penetration is frequency dependent, with lower frequencies tending to penetrate more deeply. This behavior can be described by quantities such as skin depth, which increases with the resistivity of the medium (Islam *et al.*, 2024). At the same time, conductive losses contribute to ε'' and $\tan(\delta)$, and the water present in pores remains a dominant factor in the effective dielectric response (Nelson, 1991; Dinh *et al.*, 2021).

2.3 Microstrip and patch antenna applied to dielectric characterization of cementitious materials

Microstrip lines and patch antennas are widely used in the RF/microwave range to measure dielectric properties and to sense materials. Both structures rely on the propagation of guided electromagnetic waves over a dielectric substrate and are sensitive to variations in the medium interacting with the electric field (Pozar, 2012; Balanis, 2016; Islam *et al.*, 2024).

A microstrip line consists of a metallic conducting strip deposited on a dielectric substrate, with a metallic ground plane on the opposite side (Figure 1). This configuration supports a quasi-TEM propagation mode. The fields are distributed partly in the substrate and partly in the adjacent medium, motivating the use of an effective permittivity (ε_{eff}) to describe propagation (Pozar, 2012).

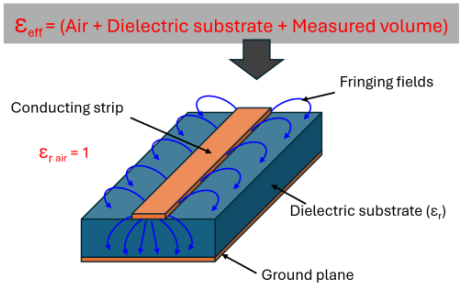


Figure 1 – Conceptual scheme of a microstrip line

However, when applied to the characterization of heterogeneous and conductive materials such as fresh concrete, microstrip lines may present limitations related to the effective interaction depth of fringing fields. Depending on the sensor geometry and material losses, the interaction may be more sensitive to near-surface layers. In general, higher resistivity and lower frequencies favor deeper penetration, whereas lossier materials reduce the effective field reach (Islam *et al.*, 2024).

To increase measurement representativeness and explore a regime with greater spectral selectivity, microstrip patch antennas can be employed. These are resonant structures that share the same construction principle but operate at resonance at a specific frequency.

A patch antenna is composed of a metallic patch over a dielectric substrate and a ground plane under this substrate, forming an open resonant cavity. In this configuration, fringing fields extend beyond the edges and interact with the adjacent medium (Balanis, 2016) (see Figure 2).

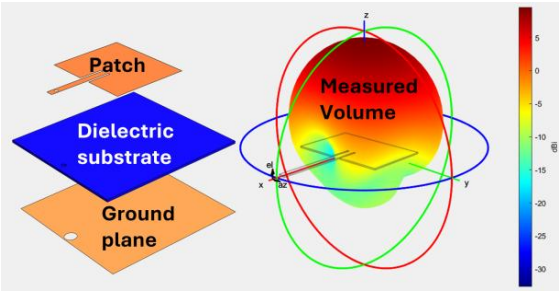


Figure 2 – Microstrip Patch Antenna: schematic (left) and evanescent electric field simulations (right)

The resonance frequency (fundamental mode) can be approximated by:

$$f_r = \frac{c}{2L\sqrt{\varepsilon_{eff}}} \tag{4}$$

Changes in the permittivity and losses of the coupled material modify ε_{eff}, shifting the resonance frequency and the magnitude of the reflection response (S11), or the apparent impedance. As indicated by Equation 4, the resonant response is directly affected by changes in the effective permittivity of the coupled medium. This is the basis of passive antenna sensors, in which sensing is achieved through variations in center frequency, return loss, phase, and reflected or received intensity (Islam *et al.*, 2024).

In the context of this study, the transition from a linear microstrip geometry to a patch antenna was adopted to increase the volumetric representativeness of coupling, reducing the dominance of a very thin surface layer; to reduce sensitivity to micro-roughness and highly localized heterogeneities at the interface, seeking

more stable spectral responses; and to exploit a resonant response (in terms of frequency and return loss) that is easier to track over time for monitoring changes in moisture and composition.

The antenna sensor literature reports high sensitivity to variations in the permittivity of the surrounding medium, with several applications in moisture detection and in diverse dielectric materials (Islam *et al.*, 2024). For cementitious materials, because effective permittivity depends strongly on water content and curing or hydration time, shifts in the resonant response can be exploited for non-intrusive monitoring (Dinh *et al.*, 2021).

According to Islam *et al.* (2024), microstrip antennas are popular for sensing applications because they are conformal, robust, compact, relatively inexpensive, and sensitive to dielectric variations in the substrate or coupled medium. These features are particularly relevant for non-intrusive monitoring of heterogeneous materials. In addition, frequency selection should consider the trade-off between penetration and medium losses. Lower frequencies tend to increase penetration depth in non-metallic materials, while conductive and dielectric losses reduce the effective field reach (Islam *et al.*, 2024; Nelson, 1991).

3. Experimental work

The experimental program was designed to investigate the influence of water content, cement content, and water-to-cement ratio (w/c) on the electrical behavior of fresh concrete using non-intrusive impedance measurements. The methodology combined material characterization, controlled concrete production, fresh-state and hardened-state testing, and the systematic acquisition and processing of electrical data. All experimental procedures were carried out under controlled laboratory conditions and in compliance with applicable Brazilian standards.

3.1 Materials

The cement used in this study was Portland blast-furnace cement CP II. The fine aggregate consisted of medium sand with a maximum particle size (Dmax) of 2 mm, while the coarse aggregate was crushed stone classified as “brita 1”, with a maximum particle size of 19 mm.

The water-to-cement ratio (w/c) was varied over a wide range, from 0.39 to 0.73, to evaluate the influence of mixture composition on the electrical properties of fresh concrete. Aggregate characterization included granulometric analysis and the determination of physical properties, and the specific gravity of the cement was also measured.

Prior to characterization, the aggregates were oven-dried at 110 ± 5 °C for 24 h to eliminate residual moisture. Mixing water was obtained from the local public water supply. All characterization procedures followed relevant Brazilian standards, including ABNT NBR 7211, NBR 17054, NBR 16916, and NBR 16917 for aggregates, and ABNT NBR 16605 for cement specific gravity determination.

3.2 Test Procedure

The experimental methodology was developed and conducted in a university research laboratory at the University of São Paulo (USP), São Carlos campus, specifically at the Laboratory of Industrial Multiphase Flow (LEMI), which operates under a development agreement with the startup coordinating the project. The study was based on planned experimental campaigns aimed at validating a non-intrusive method for measuring the electrical impedance of fresh concrete.

Concrete mixtures were prepared in accordance with ABNT standards, including NBR 12821 for laboratory concrete production and NBR 7212 for batching tolerances. Each mixture was produced in a commercial drum mixer with a nominal capacity of 120 L and a useful batch volume of 30 L. Materials were weighed using digital scales with nominal capacities of 6 kg and 30 kg and respective resolutions of 2 g and 10 g.

Fresh concrete consistency was evaluated using the slump test, in accordance with ABNT NBR 16889. For mechanical characterization, cylindrical specimens were molded and cured in accordance with ABNT NBR 5738, and compressive strength tests were performed at 7 and 28 days following ABNT NBR 5739. A total of 30 different concrete compositions were prepared and electrically characterized. All mixing, molding, and testing procedures were conducted under controlled laboratory conditions to minimize variability between batches and ensure reproducibility.

3.3 Data acquisition and processing

Electrical measurements were performed using a high-precision impedance analyzer, Hioki IM7587-01 (1 MHz–3 GHz), equipped with automatic range control and standard open–short–load calibration. The experimental database was developed exclusively from controlled laboratory measurements.

Impedance measurements were carried out in the frequency range from 1 GHz to 3 GHz, where the electrical behavior of fresh concrete was predominantly dielectric and governed mainly by dipolar polarization mechanisms. The analyzer was configured to record 801 frequency points per sweep, simultaneously acquiring impedance magnitude (Z), phase (PH), resistance (R), and reactance (X).

A microstrip patch antenna designed to resonate at 2.4 GHz was used as the sensing element. This antenna type was selected due to its dielectric sensitivity, non-intrusive operation, design simplicity, and robustness. Its applicability to concrete-related moisture measurements has been demonstrated by Teng *et al.* (2019), and the same physical principle—variations in dielectric permittivity—supports its use for estimating water content, cement content, and the water-to-cement ratio.

The experimental campaign, with the setup shown in Figure 3, generated a dataset from 30 fresh concrete compositions molded into cylindrical specimens with dimensions of 100 × 200 mm, in accordance with ABNT NBR 5738. For each composition, 16 distinct measurements were performed, resulting from the combination of four probe positions on the specimen surface (with 90° rotation between positions), two independent replicas molded from the same batch, and two consecutive measurements at each position to evaluate repeatability.

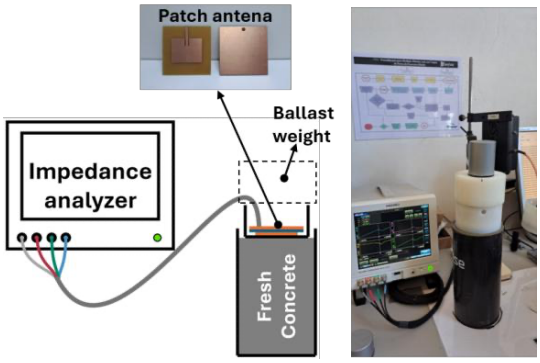


Figure 3 – The experimental setup for data collection: schematic (left) and photographic record (right)

This protocol ensured statistically representative sampling and enabled the assessment of repeatability between replicas, the influence of probe positioning, and the temporal stability of the dielectric response.

The target variables used as outputs for machine learning modeling were the water content (w, kg/m^3), cement content (c, kg/m^3), and water-to-cement ratio (w/c). These parameters were defined from the controlled mixture proportions and served as reference values for training predictive models.

All electrical measurements were conducted within a time window of 30 to 50 minutes after water addition, avoiding the very early hydration stage and remaining sufficiently distant from the initial setting period. The experimental campaign produced approximately 1.54 × 10^6 elementary observations in the raw dataset. For

supervised learning, however, each spectral sweep was treated as a single sample, resulting in 480 complete spectra used for regression modeling.

Data analysis focused on repeatability assessment using the coefficient of variation, sensitivity to changes in mixture parameters, and the ability to discriminate between different concrete compositions. Spectral interpretation emphasized the identification of frequency regions with higher dielectric contrast and improved signal-to-noise ratio, forming the basis for subsequent inverse modeling using machine learning techniques.

4. Results and Discussion

The experiments carried out in this study confirmed the feasibility of non-intrusive microwave measurements for the dielectric characterization of fresh concrete. Measurements were conducted using a patch antenna designed to operate at 2.4 GHz, with acquisition of complete impedance and phase spectra over the 1 GHz to 3 GHz range.

4.1 Spectral Response of Basic Materials

The impedance magnitude and phase responses of basic materials (air, sand, and cement) provide a reference for understanding the dielectric behavior of more complex systems. As shown in Figure 4, these dry materials exhibit high impedance values and stable phase responses across the entire frequency range, indicating predominantly insulating behavior.

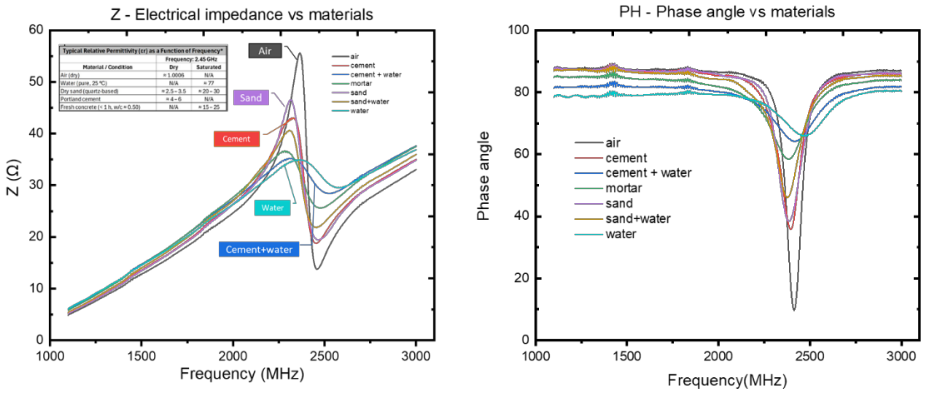


Figure 4 – Impedance spectra measured by Hioki (1–3 GHz) in basic materials, showing sensitivity to water

In contrast, in mortars and fresh concretes, the presence of free water and dissolved ions significantly reduces the impedance magnitude and alters the slope of the phase curve. This behavior evidences the dielectric contribution of the liquid phase and pore connectivity.

These observations confirm that the spectral response is governed by water content, phase distribution, and degree of hydration, establishing the physical basis for interpreting the electrical behavior of fresh concrete.

4.2 Spectral Signature and Material Differentiation

Building on the fundamental behavior of individual materials, the results obtained for concrete mixtures demonstrate that each composition exhibits a distinct spectral signature. Figure 5 shows that the measured dielectric spectrum is sensitive to variations in mixture composition, particularly water content, cement content, and the water-to-cement ratio.

The impedance magnitude and phase curves obtained for different concrete compositions exhibit distinct spectral patterns, confirming the method's ability to differentiate materials with different dielectric

characteristics. The specific spectral signature obtained for each mixture therefore represents a unique dielectric identifier, capable of distinguishing compositions from different mix designs.

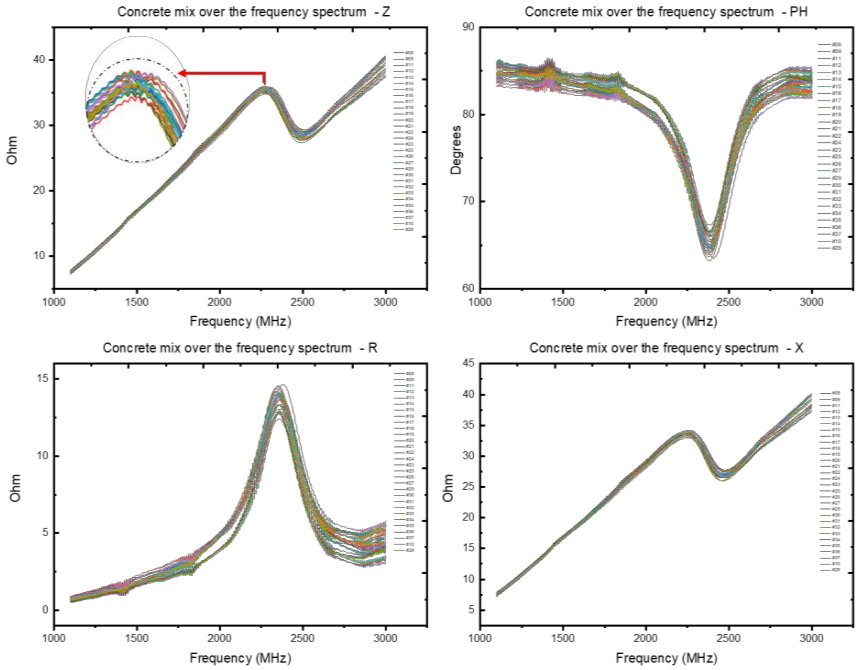


Figure 5 – Z, PH, R, and X spectra obtained with Hioki for the 30 compositions

4.3 Sensitivity of the Patch Antenna to Water Content

The microstrip patch antenna demonstrated high sensitivity to variations in moisture and concrete composition. In measurements where the water content increased, a systematic shift in the resonance frequency and a corresponding change in impedance magnitude were observed.

This behavior results from changes in the effective dielectric permittivity (ε_{eff}) of the medium beneath the antenna: as the water content increases, (ε_{eff}) also increases, modifying the electromagnetic coupling between the patch and the fresh concrete.

This direct relationship between water content and electrical response reinforces the hypothesis that microwave measurements enable non-intrusive characterization of concrete composition, providing a representative volumetric response and minimizing contact-related effects.

4.4 Patch Antenna Structure and Characteristics

Preliminary tests with conventional microstrip lines indicated that the penetration depth of the evanescent field was limited to a few millimeters, restricting sensing to the superficial region of the sample (so-called “wall effect”). To overcome this limitation, a resonant microstrip patch antenna operating around 2.4 GHz was adopted, and its geometry was optimized through electromagnetic simulation.

The final structure consisted of an FR-4 substrate (thickness 1.6 mm; $\varepsilon_r \approx 4.4$), a rectangular metallic patch with dimensions adjusted for resonance at 2.4 GHz (within the ISM band—Industrial, Scientific and Medical), a continuous ground plane on the opposite side, and an insulating dielectric encapsulation in nylon to prevent direct contact between the antenna and the measured material (concrete).

This configuration concentrated the electric field beneath the patch region, generating deeper and more stable fringing fields with greater penetration capability into the sample. The higher volumetric representativeness and lower sensitivity to surface irregularities justified the adoption of the patch antenna as the sensing element for the experimental campaign.

4.5 Future Work

Based on the experimental results obtained in this study, further improvements are proposed for the next stages of methodology development aimed at measuring concrete composition in the fresh state. These include replacing nylon as the probe housing material with a more electrically suitable and preferably hydrophobic material, such as polypropylene (PP) or polytetrafluoroethylene (PTFE), as well as redesigning the patch antenna while explicitly considering the dielectric properties of both the new housing material (PP or PTFE) and the material under test (MUT), with the objective of maximizing electromagnetic coupling and signal transfer.

Additionally, the reflection coefficient S11 is proposed as the primary measurement parameter instead of complex impedance, as it is well established in the literature as the main performance metric for microstrip antennas fed by a 50 Ω line and is widely used for analysis and optimization in recent designs (Galleto and Africa, 2025; Hasan *et al*., 2015; Naidu *et al*., 2023). Further developments include reviewing the sampling procedure to improve repeatability and reproducibility, defined as the ability to obtain similar results for identical compositions produced in different batches, and applying Principal Component Analysis (PCA) to the spectral signatures of new datasets. This approach will be combined with modern machine learning techniques, such as Support Vector Regression (SVR), Random Forest Regression (RFR), XGBoost, and Multilayer Perceptron artificial neural networks (ANN/MLP), aiming to enhance regression performance by exploiting the principal components of each spectral signature.

5. Conclusions

The experimental investigations confirmed the feasibility of non-intrusive microwave electrical impedance spectroscopy for the dielectric characterization of fresh concrete. Measurements performed using a microstrip patch antenna operating around 2.4 GHz, with spectral acquisition over the 1 GHz to 3 GHz range, demonstrated that each concrete mixture exhibits a distinct dielectric signature. This response was shown to be sensitive to variations in water content, cement content, and the water-to-cement (w/c) ratio.

The results demonstrated clear spectral differentiation between materials. Dry materials such as air, sand, and cement exhibited high impedance values and stable phase behavior, consistent with their insulating nature. In contrast, mortars and fresh concrete presented lower impedance magnitudes and altered phase responses due to the presence of free water and dissolved ions. These findings confirm that the dielectric response is primarily governed by water content, phase distribution, and pore connectivity, enabling the association of spectral features with the physical and chemical properties of fresh concrete.

The microstrip patch antenna showed high sensitivity to moisture variations, with increases in water content producing systematic shifts in resonance frequency and corresponding changes in impedance magnitude. This behavior is associated with variations in the effective dielectric permittivity of the medium and the resulting changes in electromagnetic coupling. These results reinforce the potential of microwave-based measurements as a reliable, non-intrusive technique for volumetric characterization of fresh concrete, with reduced sensitivity to contact effects.

From a sensing perspective, the adoption of the resonant patch antenna was essential to overcome the limitations of conventional microstrip lines, particularly the restricted penetration depth of the evanescent field. The optimized antenna configuration enabled deeper electromagnetic field penetration and improved volumetric representativeness, while reducing sensitivity to surface irregularities.

Overall, the results demonstrate that the dielectric spectral signature obtained from microwave impedance measurements can serve as a unique identifier for different concrete mixtures, enabling reliable differentiation between compositions. This capability highlights the potential of the proposed method as a non-destructive and non-intrusive tool for monitoring concrete composition in the fresh state.

Future developments will focus on improving the robustness and accuracy of the methodology. Planned efforts include replacing the nylon probe housing with electrically suitable and hydrophobic materials such

as polypropylene (PP) or polytetrafluoroethylene (PTFE), redesigning the patch antenna considering the dielectric properties of both the housing and the material under test, and adopting the reflection coefficient S11 as the primary measurement parameter. Additional work will address improvements in sampling repeatability and reproducibility, as well as the application of advanced data analysis techniques, including Principal Component Analysis (PCA) combined with machine learning models such as Support Vector Regression, Random Forest Regression, XGBoost, and artificial neural networks (ANN/MLP), to enhance the predictive capability of the spectral data.

Acknowledgments

The authors would like to acknowledge the Laboratory of Industrial Multiphase Flow (LEMI) at the São Carlos School of Engineering, University of São Paulo (EESC-USP), for its valuable support and collaboration in the development of this research. The authors also acknowledge Votorantim Cimentos do Brasil for the provision of materials and technical support.

This work was supported by the São Paulo Research Foundation (FAPESP), Brazil, under Grant No. 2023/15495-7.

References

Associação Brasileira de Normas Técnicas (ABNT). 2009. NBR 12821: Preparação de concreto em laboratório – Procedimento. Rio de Janeiro: ABNT.

Associação Brasileira de Normas Técnicas (ABNT). 2012. NBR 7212: Concreto dosado em central – Preparo, fornecimento e controle. Rio de Janeiro: ABNT.

Associação Brasileira de Normas Técnicas (ABNT). 2015. NBR 5738: Concreto – Procedimento para moldagem e cura de corpos de prova. Rio de Janeiro: ABNT.

Associação Brasileira de Normas Técnicas (ABNT). 2017. NBR 16605: Cimento Portland e outros materiais em pó – Determinação da massa específica. Rio de Janeiro: ABNT.

Associação Brasileira de Normas Técnicas (ABNT). 2018. NBR 5739: Concreto – Ensaio de compressão de corpos de prova cilíndricos. Rio de Janeiro: ABNT.

Associação Brasileira de Normas Técnicas (ABNT). 2019. NBR 7211: Agregados para concreto – Especificação. Rio de Janeiro: ABNT.

Associação Brasileira de Normas Técnicas (ABNT). 2020. NBR 16889: Concreto – Determinação da consistência pelo abatimento do tronco de cone. Rio de Janeiro: ABNT.

Associação Brasileira de Normas Técnicas (ABNT). 2021. NBR 16916: Agregado miúdo – Determinação da densidade e da absorção de água. Rio de Janeiro: ABNT.

Associação Brasileira de Normas Técnicas (ABNT). 2021. NBR 16917: Agregado graúdo – Determinação da massa específica, massa específica aparente e absorção de água. Rio de Janeiro: ABNT.

Associação Brasileira de Normas Técnicas (ABNT). 2024. NBR 17054: Agregados – Determinação da composição granulométrica – Método de ensaio. Rio de Janeiro: ABNT.

Balanis, Constantine A. 2016. Antenna Theory: Analysis and Design. 4th ed. Hoboken: Wiley.

Barsoukov, Evgenij, and J. Ross Macdonald. 2005. Impedance Spectroscopy: Theory, Experiment, and Applications. 2nd ed. Hoboken: Wiley.

Breysse Denys, Jean-Paul Balayssac, Samuele Biondi, David Corbett, Arlindo Goncalves, Michael Grantham, Vincenza A. M. Luprano, Angelo Masi, Andre Valente Monteiro, and Zoubir Mehdi Sbartai. 2019. “Recommendation of RILEM TC 249-ISC on Non-Destructive In Situ Strength Assessment of Concrete.” Materials and Structures 52: 71. https://doi.org/10.1617/s11527-019-1369-2.

Dinh, T. T., S. Hegler, M. Liebscher, I. Navarro de Sosa, H. Li, D. Plettemeier, W. G. Drossel, and V. Mechtcherine. 2021. “Dielectric Material Characterization of Concrete in GHz Range in Dependence on Pore Volume and Water Content.” Construction and Building Materials 311: 125234.

Fortulan, Marcos Roberto, Oscar Mauricio Hernandez Rodriguez, and Francisco Júlio do Nascimento. 2023. “Measurement of Fresh Concrete Components Using Electrical Impedance.” In Proceedings of the 27th International Congress of Mechanical Engineering (COBEM). Rio de Janeiro: ABCM.

Galleto Jr., Fredelino A., and Aaron Don M. Africa. 2025. “Optimization of Microstrip Antenna S11 Gain Using Fuzzy Rough Set-Based Pseudocode Algorithm.” e-Prime: Advances in Electrical Engineering, Electronics and Energy 13: 101061.

Gallardo, Aldo F. Sosa, and John L. Provis. 2021. “Electrochemical Cell Design and Impedance Spectroscopy of Cement Hydration.” Journal of Materials Science 56: 1203–1220. https://doi.org/10.1007/s10853-020-05397-6.

Gao, Song, Kwok L. Chung, Aiqi Cui, Mohamed Ghannam, Jianlin Luo, Lingling Wang, Mingliang Ma, and Zijian Liao. 2021. “Accurate Strength Prediction Models of Ordinary Concrete Using Early-Age Complex Permittivity.” Materials and Structures 54: 172. https://doi.org/10.1617/s11527-021-01765-z.

Gjørv, Odd E., Øystein Vennesland, and A. H. S. El-Busaidy. 1977. “Electrical Resistivity of Concrete in the Oceans.” In Proceedings of the 9th Annual Offshore Technology Conference (OTC), 581–588. Houston, TX. https://doi.org/10.4043/2803-MS.

Hasan, Rashidul Hasan, Md. Moidul Islam, Kazi Saiful Islam, Md. Mostafizur Rahman, and Md. Tanvir Hasan. 2015. “Designing and Analysis of Microstrip Patch Antenna for Wi-Fi Communication System Using Different Dielectric Materials.” American Journal of Engineering Research 4 (10): 118–126.

Hu, Xiang, Caijun Shi, Xiaojin Liu, Jiake Zhang, and Geert de Schutter. 2019. “A Review on Microstructural Characterization of Cement-Based Materials by AC Impedance Spectroscopy.” Cement and Concrete Composites 100: 1–14. https://doi.org/10.1016/j.cemconcomp.2019.03.018.

Islam, Zain Ul, Amine Bermak, and Bo Wang. 2024. “A Review of Microstrip Patch Antenna-Based Passive Sensors.” Sensors 24 (19): 6355. https://doi.org/10.3390/s24196355.

Malhotra, V. M., and Nicholas J. Carino. 2003. Handbook on Nondestructive Testing of Concrete. 2nd ed. Boca Raton: CRC Press. https://doi.org/10.1201/9781420040050.

Naidu, M Lakshmu, K Amrutha, U Gnaneswari, Ch Sridevi, G Sahasra, and M Kalyan. 2023. “Performance Analysis of Rectangular Microstrip Patch Antenna with Partial Ground Plane.” International Journal of Scholarly Research in Engineering and Technology 2 (2). https://doi.org/10.56781/ijsret.2023.2.2.0029.

Nelson, Stuart O. 1991. “Dielectric properties of agricultural products—Measurements and applications.” IEEE Transactions on Electrical Insulation 26 (5): 845–869.

Park, Joohye, Homin Song, and Hajin Choi. 2022. “Estimation of Water-to-Cement Ratio in Cementitious Materials Using Electrochemical Impedance Spectroscopy and Artificial Neural Networks.” Construction and Building Materials 350: 128843.

Pozar, David M. 2012. Microwave Engineering. 4th ed. Hoboken: Wiley.

Teng, Kah Hou, Patryk Kot, Magomed Muradov, Andy Shaw, Khalid Hashim, Michaela Gkantou, and Ahmed Al-Shamma’a. 2019. “Embedded Smart Antenna for Non-Destructive Testing and Evaluation (NDT&E) of Moisture Content and Deterioration in Concrete.” Sensors 19 (3): 547. https://doi.org/10.3390/s19030547.

Zhong, Y., Y. Wang, and B. Zhang. 2024. “Research on Correlation between Dielectric Properties and Compressive Strength of Concrete Based on Aggregate Particle Size.” Journal of Building Engineering 97: 110844.

cinpar2026
XXII International Conference on Building Pathology and Constructions Repair
15th to 17th July 2026 - Lisboa, Portugal

Linking Fabrication Route, Microstructure, and Fire Performance in Mycelium-Based Insulation Composites

Neuza VALADAS[1], Ana Mafalda MATOS[2], Jukka HEINONEN[3]

[1,3] University of Iceland, Hjarðarhagi 2-6, 107, Reykjavik, Iceland, neuza@hi.is
[2] CONSTRUCT-Labest, Faculty of Engineering, University of Porto, Porto, Portugal, anamatos@fe.up.pt

Abstract: The construction industry remains a major emitter of CO_2 (~37% globally), demanding insulation solutions that reduce embodied carbon while maintaining performance. This work investigates mycelium-based composites (MBCs) grown on birch woodchips and modified through targeted additives (sheep wool, silica) and fabrication scales (block-grown vs. mold-grown). The goal is to identify how these parameters influence key functional properties.

MBCs exhibited densities of 140–200 kg/m³ and thermal conductivities of 0.059–0.066 W/m·K, comparable to conventional insulation. Mechanical tests yielded compressive strengths of 0.13–0.47 MPa, suitable for lightweight, non-structural applications. Fire resistance varied markedly: wool-reinforced composites exceeded 2100 s under direct flame exposure, while silica-modified specimens failed after ~720 s. Microstructural analysis revealed that wool promotes continuous hyphal networks and cohesive char formation, whereas silica disrupts filament interconnectivity.

These results confirm that microstructure—governed by additive type and fabrication method—is central to optimizing performance. MBCs thus represent a regenerative, carbon-storing material class capable of meeting future low-carbon insulation demands.

Keywords: mycelium-based composites; bio-based insulation; fire-resistant biocomposites; microstructure–property relationships

1. Introduction

The building and construction sector is responsible for a substantial share of global greenhouse gas emissions, contributing approximately 37% of total global CO_2 emissions (Dyson, 2023). This combined contribution from operational and embodied energy highlights the urgent need to shift towards materials and systems that reduce both energy consumption and the carbon intensity of construction. Conventional insulation materials—such as expanded and extruded polystyrene (EPS, XPS), polyurethane foams (PUR/PIR), mineral wool, and fiberglass—play an essential role in improving building energy efficiency. However, these products have significant environmental drawbacks: their manufacturing is energy-intensive, relies on non-renewable resources, and often involves chemicals that can lead to toxic emissions during production, use, and end-of-life disposal (Alaneme *et al.*, 2023). Their limited recyclability and long-term persistence in landfills further exacerbate environmental impacts.

In response, there is growing interest in bio-based insulation materials derived from renewable resources, which typically exhibit lower embodied energy and can store biogenic carbon during their service life. Materials such as hemp, straw, sheep wool, cork, and cellulose offer promising thermal properties comparable to mineral wool, while simultaneously valorizing agricultural by-products and reducing environmental burdens) (Hetimy *et al.*, 2025). (Babenko *et al.*, 2024). Beyond thermal performance, natural insulation materials avoid hazardous additives, support healthier indoor environments, and align well with circular-economy principles due to their biodegradability or recyclability. Their performance, however, can be sensitive to moisture content, density, and fiber distribution, requiring careful characterization and standardized production methods (Motamedi et al, 2025).

Among these emerging alternatives, mycelium-based composites (MBCs) have gained increasing attention due to their combination of low density, biodegradability, thermal efficiency, and carbon-negative production potential(Fellah *et al.*, 2024). MBCs are produced through fungal colonization of lignocellulosic substrates—such as agricultural residues or woodchips—resulting in a lightweight, porous network where fungal hyphae act as a natural binder. Reported thermal conductivity values typically fall in the range of 0.036–0.06 W/m·K, placing these composites within the performance range of common insulation materials while requiring minimal energy input during fabrication. The growth process itself takes place at near-ambient conditions and relies on biological mechanisms rather than synthetic binders, substantially reducing embodied energy and environmental impacts (Motamedi et al., 2025; Alaneme *et al.*, 2023). Beyond their insulating capacity, MBCs also demonstrate advantageous fire behavior. A common limitation of many organic insulation materials is their flammability—while materials such as mineral wool and fiberglass are non-combustible (Euroclass A1), most bio-based insulations fall into combustible categories such as Euroclass C, D, or E. Mycelium-based materials, however, tend to char instead of igniting easily (Gezer and Kuştaş, 2024). This charring behavior slows flame propagation and reduces heat release during combustion. Research has shown that fungal mycelia are less flammable than several widely used polymers, including PMMA and PLA, and that applying mycelium layers to organic substrates can enhance their fire resistance (Alaneme *et al.*, 2023). In numerous experimental tests, mycelium composites have demonstrated self-extinguishing behavior after the removal of a flame source, while simultaneously forming a protective char layer that improves their fire performance compared with untreated bio-based materials.

However, like other organic materials, they usually achieve only moderate Euroclass fire ratings. For reference, typical foam insulation panels have thermal conductivities of approximately 0.03–0.04 W/m·K, while glass wool typically ranges from about 0.035 to 0.045 W/m·K. MBCs can achieve thermal performance levels comparable to conventional insulation materials while offering additional benefits, including biodegradability and carbon sequestration (Gezer and Kuştaş, 2024). Nevertheless, because they remain

combustible lignocellulosic materials, their fire classification is typically limited, and improvements in fire safety often require specific additives or post-treatments to enhance flame retardancy.

Recent research has explored the potential benefits of mycelium-based composites (MBCs). For example, Zhang et al. produced fungal fibers with added silica that reduced the peak heat release rate by up to 66% while maintaining structural stability under flame exposure (Zhang *et al.*, 2022). Similarly, Chulikavit et al. studied deacetylated mycelium composites and found improved thermal stability and fire resistance, suggesting their use in fire-resistant cladding (Chulikavit *et al.*, 2023). Although mycelium insulation is still a combustible organic material (typically around Euroclass E), it often self-extinguishes once the ignition source is removed, which improves safety (De *et al.*, 2025). This indicates that mycelium has natural flame-retardant potential, especially when combined with small amounts of inorganic additives or protective coatings. Current research is therefore examining mycelium coatings and hybrid composites to further improve fire performance in sustainable construction (Yang, Park and Qin, 2021).

MBCs also offer environmental advantages. During growth, the fungus stores carbon from its substrate, meaning the final material can temporarily act as a carbon sink. Production typically occurs at ambient temperatures and uses agricultural waste, resulting in low energy demand. Life-cycle studies suggest that mycelium insulation can have a smaller carbon footprint than fiberglass or petroleum-based foams (Motamedi et al, 2025). Despite these environmental and functional benefits, significant knowledge gaps remain regarding the standardization of MBC performance. Reviews note that thermal and fire properties remain insufficiently studied (Jones, Bhat, Kandare, *et al.*, 2018). Most work reports only density and thermal conductivity for a few substrate–fungus combinations. Data on specific heat capacity—critical for understanding thermal inertia and fire development—are still scarce, and comprehensive fire testing (e.g., cone calorimetry or limiting oxygen index) is seldom reported. As a result, standardized formulations and testing methods for MBC insulation have not yet been established (Alaneme *et al.*, 2023).

Given these gaps, this study investigates the combined effects of substrate composition, additive type, and fabrication method on the microstructure, thermal behaviour, mechanical properties, and fire resistance of mycelium-based composites grown on birch woodchips using Ganoderma lucidum. Additives—namely, sheep wool and silica—were selected for their potential to influence porosity, thermal response, and flame retardancy. Two fabrication approaches (block-grown and mold-grown) were compared to examine how growth confinement and specimen scale affect density, surface development, and hyphal network continuity. By systematically evaluating these variables, the study aims to clarify structure–property relationships and identify composite formulations with improved performance for sustainable, low-carbon insulation applications.

2. Materials and Methods

2.1 Mycelium Composite Fabrication

Specimens examined in this study were fabricated using a multi-stage process. First, a lignocellulosic substrate was selected and prepared for colonization. Two different fabrication methods were used to produce specimens for mechanical, thermal, and fire performance testing. All samples were grown using the fungal species *Ganoderma lucidum* on sterilized birch woodchips, a locally available forestry by-product in Iceland.

Three substrate formulations were developed to identify the influence of additives

MBC^{s}: Default substrate with silica additive

MBC^{w}: Default substrate with natural wool additive

MBC: Default substrate with no additive (control group)

The additives (wool and silica) were selected for their potential to modify the porosity, thermal resistance, and fire behavior of the composite. All additives were blended with the sterilized substrate before fungal inoculation. After inoculation, the substrate was incubated under controlled environmental conditions (22–25°C, ~70% RH) for 10–14 days, depending on growth progression.

To ensure compatibility with various standardized testing protocols, two distinct fabrication methods were used for growing the mycelium specimens:

- Method I – Block-Grown Samples (Large Scale)

In this method, the mycelium was cultivated in free-form blocks (about 400 × 300 × 350 mm) without the use of molds. After the material was fully colonized and dried, test specimens were cut to the required sizes for each experiment. This technique was mainly applied for tests needing larger samples, such as stiffness and thermal conductivity measurements. These specimens are referred to as **MBCI**.

- Method II – Mold-Grown Samples (Standardized Scale)

For smaller and more precise tests, particularly fire-related experiments, the mycelium was grown directly inside 3D-printed molds. The molds measured 75 × 75 × 12.3 mm and were designed to match the dimensions specified in international testing standards. This minimized the need for additional cutting and ensured consistent sample geometry. These samples are labeled **MBCII**.

Both fabrication methods used the same fungal species, substrate composition, growth conditions, and post-processing steps, including drying and the inactivation of fungal activity. Using two parallel manufacturing approaches enabled the evaluation of scale-dependent effects, facilitated comparison with previous studies employing standardized specimen sizes, and provided insight into how growth confinement and sample geometry influence the final material properties. This framework supports reproducibility, reliable comparison between tests, and relevance for both laboratory research and potential industrial production. The procedures were developed based on a review of previous studies on mycelium-based composites (Dias, Jayasinghe, and Waldmann, 2021; Pelletier et al., 2013; Fellah et al., 2024; Barta et al., 2024; Aiduang, Suwannarach, et al., 2022).

2.2 Specimen production

In **Method I**, the mycelial mixture was placed directly into sealed plastic bags, where it formed compact, dense blocks. In **Method II**, the same mixture was filled into 3D-printed molds. These molds were designed in Fusion 360 and printed with GreenTEC Pro 160 °C PLA filament, selected for its ability to withstand autoclave sterilization at 120 °C. The fungal inoculation was carried out using *Ganoderma lucidum* (reishi) grain spawn.

Both methods followed the same initial preparation steps. First, the substrate materials were selected and mixed, then the mixture was placed either in molds or sealed plastic bags. When molds were used, they were placed inside sterilization bags so they could be autoclaved while maintaining their shape. After sterilization, the substrate was inoculated with fungal spawn under sterile conditions. Once the mycelium had fully colonized the substrate, all samples were dried under controlled conditions to stop biological growth. The drying process consisted of two 12-hour cycles at 40 °C, followed by a 24-hour light compression step to improve dimensional stability. For Method II, the samples were removed from the molds before drying to ensure even moisture removal. This workflow ensured consistent growth conditions across both

fabrication methods while allowing a systematic evaluation of how mold confinement and sample size influence the structural development and performance of the resulting composites.



a) b)

Figure 1 – Block-grown mycelium composites specimens, Method I.

2.3 Test Methods

2.3.1 Density

In this study, density was measured to describe the physical structure of the composites and to allow comparison with typical insulation materials. The density of each specimen (ρ, kg/m³) was calculated using:

$\rho = m / V$

where **m** represents the dry mass (kg), and **V** is the geometric volume (m³). Before measurement, the samples were oven-dried at 60 °C until a constant mass was reached. All measurements were performed under standard laboratory ambient conditions. This procedure ensured consistent moisture removal before weighing, reducing variability and allowing reliable comparison between formulations and fabrication methods.

2.3.2 Thermal conductivity

In this study, measurements were carried out on two MBCI samples produced using Method I, each measuring 100 × 100 × 350 mm. Testing was performed using a FOX 314 Heat Flow Meter in accordance with ASTM C518 and ISO 8301.

During the test, the specimens were positioned between calibrated hot and cold plates to establish steady-state heat transfer. The thermal conductivity (λ) was then determined from the measured heat flux and the temperature difference across the sample. The obtained λ values were used to assess the insulating capability of the composites and to compare their performance with that of conventional insulation materials. This setup allowed precise quantification of steady-state heat transfer and ensured compliance with widely recognized thermal testing standards.

2.3.3 Compressive strength

The compressive strength of the mycelium-based composites was tested using an Instron 8503 universal testing machine. MBCI specimens measuring 95 × 100 × 350 mm^3 were subjected to uniaxial compression in accordance with ASTM C165-07. A constant crosshead speed of 1.27 mm/min was applied until the samples failed (Figure 4). The recorded stress–strain data were used to characterize the compressive behavior of the composites. This evaluation provides important information on the mechanical stability of mycelium composites, supporting their potential use as non-structural insulation or lightweight panels and offering a biodegradable alternative to conventional polymer foams.

2.3.4 Fire Resistance

The fire performance of the mycelium-based composites was assessed using controlled laboratory flame exposure tests in accordance with EN 13501-2. All sample types—including MBCs, MBC^{W}, and both MBC^{I} and MBC^{II}, produced via Method I and Method II—were tested, with each group containing two to four specimens (Figure 5a). During testing, samples were placed 5–7 cm above a burner fueled with a propanol-based gas mixture, resulting in flame temperatures exceeding 660 °C. Surface temperatures and thermal evolution were monitored using an FLIR T640 thermal camera.

Following the approach adapted from Dias et al. (2021), a Kemper burner was used instead of a standard Bunsen burner to achieve higher and more consistent flame temperatures (Dias, Jayasinghe, and Waldmann, 2021). A layer of cotton wool was positioned atop each specimen to act as a visual ignition indicator. Tests were concluded when the cotton ignited, structural failure occurred (e.g., visible perforation), or the mycelium material itself began to burn.

2.3.5 Microstructural observation

Cross-sectional specimens were manually taken from the interior of representative samples produced by each fabrication method described in Section 3.1. The pieces were mounted on metal stubs using conductive carbon adhesive tape for scanning electron microscopy (SEM) analysis. High-resolution Environmental SEM (ESEM) was performed in backscattered electron (BSE) mode and combined with Energy Dispersive X-ray Spectroscopy (EDS) using a FEI Quanta 400 FEG ESEM/EDAX Genesis X4M system. Before imaging, all samples were sputter-coated with a thin Au/Pd layer to improve signal quality and reduce surface charging effects.

3. Results and Discussion

The findings show that Ganoderma lucidum mycelium composites offer a high-performance, bio-based insulation solution, combining low density with excellent thermal efficiency. Measured thermal conductivities ranged from 0.050 to 0.062 $W \cdot m^{-1} \cdot K^{-1}$, comparable to those of high-end synthetic foams. Wool-reinforced variants (MBCW) demonstrated improved fire resistance, retaining structural integrity at temperatures up to 660 °C, making this hybrid configuration the most promising for flame-retardant applications. With a high biogenic carbon content (62.96–73.68 wt%), these composites also act as carbon sinks, potentially contributing to net-negative emissions over a building's lifecycle. Overall, these combined properties—low density, strong thermal performance, enhanced fire resilience, and intrinsic carbon storage—reinforce the potential of mycelium-based composites as next-generation regenerative materials for low-carbon construction. Table 1 highlights the general results of the study. The following sections examine each result property in detail.

Table 1 –Test results summary

Substrates	Density (kg/m³)	Thermal Conductivity (W/m·K)	Compression (MPa)	Fire Resistance (Seconds)
MBC^{S}	150 kg/m³			720
MBC^{W}	140 kg/m³			>2100
MBC^{I}	200 kg/m³	0.05–0.06W/m.K.	0.13–0.47MPa	1020
MBC^{II} (control group)	140 kg/m³			1200

3.1 Density

Low bulk density is a key feature of insulation materials, reducing structural load, easing handling, and providing good thermal resistance per unit mass, which has historically made synthetic foams popular (EPS: 15–35 kg/m³; PU: 30–50 kg/m³).

In this study, large MBCI samples (Method I) had a density (ρ) of 200 kg/m³, whereas smaller MBCII specimens (Method II) had a density of 140 kg/m³. Wool- and straw-modified composites (MBCW, MBCS) ranged from 140–150 kg/m³, giving an overall range of ~120–210 kg/m³. Notably, wool-reinforced composites attained densities ≤140 kg/m³, comparable to mineral wool insulation (80–150 kg/m³), while offering the added advantages of full biodegradability and intrinsic carbon sequestration. This density envelope validates the potential of mycelium composites as viable drop-in replacements within non-structural insulation systems, balancing mechanical integrity with low embodied mass.

Density affects thermal performance by controlling air entrapment, though conductivity and porosity also play a role. The observed densities align with reported mycelium composites (100–390 kg/m³) (Appels *et al.*, 2019), with heat-pressed samples showing higher values due to pore collapse. Scale effects were clear: large MBCI blocks were denser than small MBCII molds, likely due to edge compaction and preservation of microporosity. Wool additives helped maintain a lower density while optimizing void fraction.

Compared to standard building materials, mycelium composites are over three times lighter than MDF (500–1000 kg/m³) and gypsum board (410–950 kg/m³), slightly denser than rock wool (118 kg/m³) (Rajendran, 2022), and denser than polystyrene foams (11–50 kg/m³). Their porous, fungal-bound structure reduces convective heat transfer, enhancing insulation.

Compressive strength is relatively low, limiting structural use. Still, their density and microstructure make them suitable for non-load-bearing applications such as insulation panels, acoustic tiles, partition walls, door cores, or cladding. Overall, mycelium composites offer a sustainable, low-density alternative for high-performance insulation, reducing reliance on synthetic foams and associated environmental impacts.

3.2 Thermal conductivity

The mycelium-based composites showed strong thermal insulation, with thermal conductivity (λ) values between 0.059 and 0.066 W/m·K, comparable to many conventional insulation materials. For reference, EPS typically ranges from 0.036 to 0.046 W/m·K (Saini *et al.*, 2025).

Literature reports a wide range for mycelium composites: Rejeesh (Rajendran, 2022) noted ~0.070 W/m·K, while Alaneme et al. (Alaneme *et al.*, 2023) observed 0.088–0.104 W/m·K. The improved performance in this study likely reflects the choice of fibers and the fabrication method. Surface roughness may slightly influence measurements, with smoother specimens expected to show lower conductivity.

High porosity, low density, and significant internal air volume give mycelium composites their insulating capability. Values reported here align with prior studies (Yang et al., 2017; Schnabel, 2019) showing 0.05–0.07 W/m·K, like glass wool (0.04 W/m·K), extruded polystyrene (0.03 W/m·K), sheep wool (0.05 W/m·K), and kenaf (0.04 W/m·K) (Alaneme *et al.*, 2023). Other studies (Dias, Jayasinghe, and Waldmann, 2021) report 0.088–0.104 W/m·K, comparable to straw, hemp concrete, softwoods, and gypsum. Rock wool has a thermal conductivity of ~0.035 W/m·K for comparison.

Overall, these results confirm that mycelium composites have low thermal conductivity, low density, and a biogenic origin, making them strong candidates for sustainable insulation and energy-efficient construction.

3.3 Compressive strength

Specimens withstood forces from 0.47 to 4.19 kN, corresponding to strengths of 0.13–0.47 MPa, with a standard deviation of 0.16 MPa. Samples with dense, uniformly colonized fungal biomass showed the highest strength. The generally low values reflect the material's lightweight, highly porous nature, typical of insulating or fibrous composites. Variations between samples likely stem from differences in fiber distribution, porosity, or binder content. Despite this, the composites provide adequate stability for non-structural applications, such as thermal or acoustic insulation, rather than load-bearing use, consistent with previous reports highlighting the trade-off between low density and mechanical strength.

While compressive strength is not the main factor for insulation performance, it remains a key material property. Mycelium-based composites typically range from 0.36 to 0.52 MPa, with larger blocks in this study reaching 0.47 MPa, higher than smaller specimens (0.13–0.3 MPa).

Previous research shows mechanical performance depends strongly on substrate type, fiber condition, and processing. For example, 3D-printed mycelial blocks can reach 0.06–0.5 MPa (Soh et al., 2023; Soh and Le Ferrand, 2023), and adding fillers such as sand or chitin nanofibers can significantly increase strength and stiffness (Jones, Bhat, Huynh, et al., 2018; Jin et al., 2013). Post-processing techniques, especially hot pressing, can dramatically boost the elastic modulus—from ~9 MPa cold-pressed to ~97 MPa hot-pressed (Appels *et al.*, 2019).

Overall, the mechanical properties of mycelium composites are largely dictated by substrate composition, additive inclusion, and fabrication method rather than chemical makeup, highlighting the potential to tailor compressive strength and stiffness for specific non-structural applications.

3.4 Fire Resistance

The fire behaviour of the mycelium composites was assessed under controlled conditions using direct flame exposure at approximately 660 °C, with surface temperatures monitored through infrared thermography. The objective of the test was to compare how different formulations responded to the same heat conditions; the procedure was not intended to assign formal fire classifications.

Across all samples, the primary response involved surface charring followed by gradual thermal degradation, with no sustained flaming. The test concluded when one of three conditions occurred: ignition of the cotton indicator layer, visible structural perforation, or sustained combustion of the composite material. Wool-reinforced composites (MBCW) showed the longest resistance to flame exposure, maintaining structural integrity for more than 2100 seconds. Block-grown (MBCI) and mold-grown (MBCII) control specimens resisted between 1020 and 1200 seconds, while silica-modified composites (MBCS) reached only about 720 seconds. The improved behaviour of the wool-based samples is consistent with their more continuous hyphal networks, which support the formation of a cohesive char layer that slows heat penetration.

All formulations were combustible but did not sustain flames once the heat source was removed and produced little smoke. Cotton ignition occurred only in some of the thicker specimens, likely due to slower heat dissipation. These trends are consistent with results reported in earlier studies (Dias, Jayasinghe, and Waldmann, 2021; Liu et al., 2019; Sharma and Sumbria, 2022), which also noted that mycelium tends to char rather than burn, leading to reduced flame spread and lower heat release than is typical for synthetic foams. When compared with the flame spread index referenced in EN 13501-1:2018, the composites fall within Class B (0–25), indicating comparatively good resistance to flame propagation under the test conditions used. Wool-reinforced specimens again performed the best, followed by the control samples, while silica-containing composites consistently showed weaker performance. Taken together, the results indicate that combining mycelium with natural fibres such as wool can improve fire resistance relative to untreated mycelium and silica-modified variants.

These observations are in line with previous research by Jones et al. (2018), which reported that mycelium composites exhibit inherent resistance to ignition due to their charring behaviour. Future studies should include standardized fire testing protocols, explore additional additive combinations, and examine how these materials could be integrated into insulation or panel systems to improve overall fire performance. Table 1 summarises the comparative results obtained under the direct-flame conditions used in this study.

Table 1 –Comparative flame exposure performance of mycelium-based composites under direct flame conditions

Specimen Group	Fabrication Method	Scale	Observations regarding fire exposure	Time to endpoint (seconds)
MBC^{S}	Method II (mold-grown)	Small-scale	Rapid structural breakdown; reduced char cohesion	720
MBC^{W}	Method II (mold-grown)	Small-scale	Maintained integrity; stable char formation	>2100
MBC^{I}	Method I (block-grown)	Large-scale	Developed external char; delayed failure	1020

MBC^{II} (control group)	Method II (mold-grown)	Small-scale	Progressive charring; no sustained flaming	1200

3.5 Microstructural Observation.

SEM analysis showed mycelium uniformly coating all composites (Figure 2). Silica-containing samples had a sparser mycelial network (a), while wool-enhanced and block-grown specimens displayed dense, well-developed mycelial filaments (b, c). Sparse networks in silica samples likely contributed to their lower fire resistance, suggesting that silica should be added after filament establishment.

Block-grown specimens promoted better mycelial skin development (d), though thicker samples may reduce fire performance. Core regions generally had lower hyphal density, limiting mechanical strength, which could be improved via extended colonization or forced airflow. Fiber orientation was irregular, with average hyphae ~1.3 µm in diameter, consistent with previous studies (Appels et al., 2019; Gou et al., 2021; Aiduang et al., 2022; Islam et al., 2017).

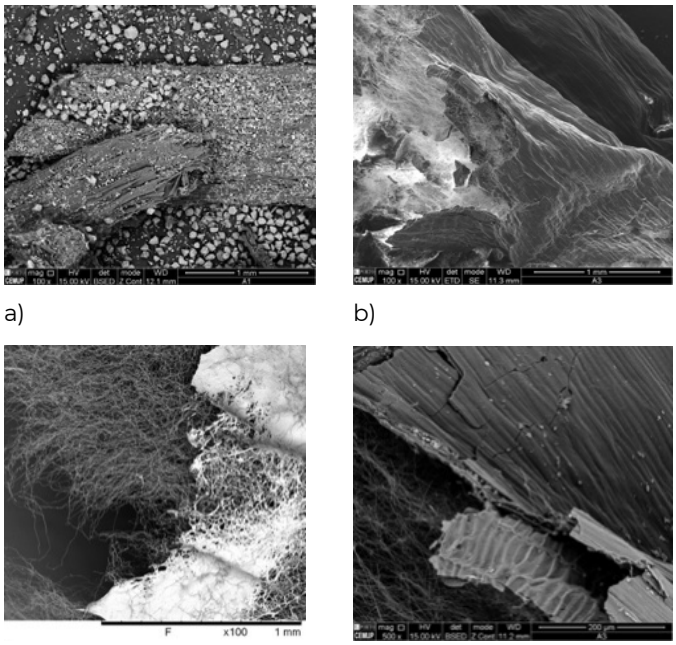


Figure 2 –SEM analyses of mycelium utilizing silica (a), wool (b) as additives, and default mycelium.

4. Conclusions

This study examined how sheep wool, silica, and fabrication method influence the performance of mycelium-based composites produced from Ganoderma lucidum grown on birch woodchips. The results show that variations in additives and growth conditions lead to clear differences in density, microstructure, thermal behaviour, mechanical strength, and fire resistance. Block-grown samples (Method I) reached higher densities (around 200 kg/m^3) and developed a continuous external mycelial layer, while mold-grown

samples (Method II) were lighter (around 140 kg/m³) and showed less developed surfaces, indicating that growth scale and confinement affect hyphal network formation.

Thermal conductivity values between 0.059 and 0.066 W/m·K confirm suitability for non-structural insulation applications. As expected for low-density porous composites, compressive strengths remained modest (0.13–0.47 MPa), appropriate for lightweight interior panels or insulation boards rather than load-bearing uses. Fire behaviour showed the most pronounced differences: wool-reinforced specimens resisted direct flame exposure for more than 2100 seconds, while silica-modified composites lasted about 720 seconds. These results suggest that natural fibres support more cohesive char formation and more stable thermal degradation. SEM images confirmed this difference, showing continuous hyphal networks in wool-based composites and disrupted filaments in silica variants.

To sum up, the findings demonstrate that both additive type and fabrication method play a significant role in determining the structural development and performance of mycelium-based composites. Wool proved to be the most effective additive for improving fire resistance, and block-grown samples offered advantages in surface consolidation and mechanical uniformity. Future studies should include standardized fire classification tests, more extensive thermal characterization—particularly specific heat capacity—and refinements to the growth process to improve internal colonization and reduce sample-to-sample variability.

Acknowledgments

This work was financially supported by: University of Iceland and HSM Askur research fund 202411259 (Neuza Valadas); UID/04708 of the CONSTRUCT - Instituto de I&D em Estruturas e Construções - funded by Fundação para a Ciência e a Tecnologia, I.P./ MCTES through the national funds; and by FCT - Fundação para a Ciência e a Tecnologia through the individual Scientific Employment Stimulus 2021.01765.CEECIND (Ana Mafalda Matos).

References

Aiduang, W., Kumla, J., *et al.* (2022) “Mechanical, Physical, and Chemical Properties of Mycelium-Based Composites Produced from Various Lignocellulosic Residues and Fungal Species,” *Journal of Fungi*, 8(11). Available at: https://doi.org/10.3390/jof8111125.

Aiduang, W., Suwannarach, N., *et al.* (2022) “Valorization of agricultural waste to produce myco-composite materials from mushroom mycelia and their physical properties,” *Agriculture and Natural Resources*, 56(6). Available at: https://doi.org/10.34044/j.anres.2022.56.6.03.

Alaneme, K.K. *et al.* (2023) “Mycelium based composites: A review of their bio-fabrication procedures, material properties and potential for green building and construction applications,” *Alexandria Engineering Journal*. Available at: https://doi.org/10.1016/j.aej.2023.10.012.

Appels, F.V.W. *et al.* (2019) “Fabrication factors influencing mechanical, moisture- and water-related properties of mycelium-based composites,” *Materials and Design*, 161. Available at: https://doi.org/10.1016/j.matdes.2018.11.027.

Babenko, M. *et al.* (2024) “Perspectives of Insulating Biodegradable Composites Derived from Agricultural Lignocellulosic Biomass and Fungal Mycelium: A Comprehensive Study of Thermal Conductivity and Density Characteristics,” *Biomimetics*, 9(11). Available at: https://doi.org/10.3390/biomimetics9110707.

Barta, D.G. *et al.* (2024) “Mycelium-Based Composites as a Sustainable Solution for Waste Management and Circular Economy,” *Materials*, 17(2). Available at: https://doi.org/10.3390/ma17020404.

Chulikavit, N. *et al.* (2023) “Thermal degradation and flame spread characteristics of epoxy polymer composites incorporating mycelium,” *Scientific Reports*, 13(1). Available at: https://doi.org/10.1038/s41598-023-45097-0.

De, G. *et al.* (2025) “Mycelium-coir-based composites for sustainable building insulation,” *Journal of Materials Chemistry A*, 13(14). Available at: https://doi.org/10.1039/d4ta07869a.

Dias, P.P., Jayasinghe, L.B. and Waldmann, D. (2021) “Investigation of Mycelium-Miscanthus composites as building insulation material,” *Results in Materials*, 10. Available at: https://doi.org/10.1016/j.rinma.2021.100189.

Dyson, A., K.N., L.M.L., R.B.K., C.C., D.J., . . . & A.V. (2023). B. materials and the climate: constructing a new future. U.N.E.Programme. (2023) *Building Material and the Climate: Constructing a New Future*, *Building Material and the Climate: Constructing a New Future*. Available at: https://doi.org/10.59117/20.500.11822/43293.

Fellah, M. *et al.* (2024) “Thermal insulation and energy performance’s assessment of a mycelium-based composite wall for sustainable buildings,” *Case Studies in Construction Materials*, 20. Available at: https://doi.org/10.1016/j.cscm.2023.e02786.

Gezer, E.D. and Kuştaş, S. (2024) “Acoustic and Thermal Properties of Mycelium-based Insulation Materials Produced from Desilicated Wheat Straw-Part B,” *BioResources*, 19(1). Available at: https://doi.org/10.15376/biores.19.1.1348-1364.

Gou, L. *et al.* (2021) “Morphological and physico-mechanical properties of mycelium biocomposites with natural reinforcement particles,” *Construction and Building Materials*, 304, p. 124656. Available at: https://doi.org/10.1016/J.CONBUILDMAT.2021.124656.

Grazieschi, G., Asdrubali, F. and Thomas, G. (2021) “Embodied energy and carbon of building insulating materials: A critical review,” *Cleaner Environmental Systems*, 2. Available at: https://doi.org/10.1016/j.cesys.2021.100032.

Hetimy, S. *et al.* (2025) “Assessment of sheep wool as a sustainable building insulation material in hot climate zones,” *Architectural Engineering and Design Management* [Preprint]. Available at: https://doi.org/10.1080/17452007.2025.2560472.

Islam, M.R. *et al.* (2017) “Morphology and mechanics of fungal mycelium,” *Scientific Reports*, 7(1). Available at: https://doi.org/10.1038/s41598-017-13295-2.

Jin, J. *et al.* (2013) “A biomimetic composite from solution self-assembly of chitin nanofibers in a silk fibroin matrix,” *Advanced Materials*, 25(32). Available at: https://doi.org/10.1002/adma.201301429.

Jones, M., Bhat, T., Kandare, E., *et al.* (2018) “Thermal Degradation and Fire Properties of Fungal Mycelium and Mycelium - Biomass Composite Materials,” *Scientific Reports*, 8(1). Available at: https://doi.org/10.1038/s41598-018-36032-9.

Jones, M., Bhat, T., Huynh, T., *et al.* (2018) “Waste-derived low-cost mycelium composite construction materials with improved fire safety,” *Fire and Materials*, 42(7). Available at: https://doi.org/10.1002/fam.2637.

Liu, R. *et al.* (2019) “Preparation of a kind of novel sustainable mycelium/cotton stalk composites and effects of pressing temperature on the properties,” *Industrial Crops and Products*, 141. Available at: https://doi.org/10.1016/j.indcrop.2019.111732.

Motamedi et al (2025) “A Review of Mycelium Bio-Composites as Energy-Efficient Sustainable Building Materials,” *energies*, 18.

Pelletier, M.G. *et al.* (2013) “An evaluation study of mycelium based acoustic absorbers grown on agricultural by-product substrates,” *Industrial Crops and Products*, 51. Available at: https://doi.org/10.1016/j.indcrop.2013.09.008.

Rajendran, R.C. (2022) “Packaging Applications of Fungal Mycelium-Based Biodegradable Composites,” *Fungal Biopolymers and Biocomposites: Prospects and Avenues*. Available at: https://doi.org/10.1007/978-981-19-1000-5_11.

Saini, R. *et al.* (2025) “Critical review of ultra-lightweight foam materials,” *Next Nanotechnology*, 7, p. 100138. Available at: https://doi.org/10.1016/J.NXNANO.2025.100138.

Schnabel, H. (2019) “Analysis of plant materials pretreated by steam explosion technology for their usability as insulating materials,” *Agron. Res., 17 (1)* , 17, pp. 1191–1198.

Sharma, R. and Sumbria, R. (2022) “Mycelium bricks and composites for sustainable construction industry: a state-of-the-art review,” *Innovative Infrastructure Solutions*, 7(5). Available at: https://doi.org/10.1007/s41062-022-00903-y.

Soh, E. *et al.* (2023) “3D printing of mycelium engineered living materials using a waste-based ink and non-sterile conditions,” *Materials and Design*, 236. Available at: https://doi.org/10.1016/j.matdes.2023.112481.

Soh, E. and Le Ferrand, H. (2023) “Woodpile structural designs to increase the stiffness of mycelium-bound composites,” *Materials and Design*, 225. Available at: https://doi.org/10.1016/j.matdes.2022.111530.

Yang, L., Park, D. and Qin, Z. (2021) “Material Function of Mycelium-Based Bio-Composite: A Review,” *Frontiers in Materials*. Available at: https://doi.org/10.3389/fmats.2021.737377.

Yang, Z. (Joey) *et al.* (2017) “Physical and Mechanical Properties of Fungal Mycelium-Based Biofoam,” *Journal of Materials in Civil Engineering*, 29(7). Available at: https://doi.org/10.1061/(asce)mt.1943-5533.0001866.

Zhang, X. *et al.* (2022) “Naturally grown mycelium-composite as sustainable building insulation materials,” *Journal of Cleaner Production*, 342. Available at: https://doi.org/10.1016/j.jclepro.2022.130784.

Zuiderveen, E.A.R. *et al.* (2023) “The potential of emerging bio-based products to reduce environmental impacts,” *Nature Communications*, 14(1). Available at: https://doi.org/10.1038/s41467-023-43797-9.

Cinpar 2026
XXII International Conference on Building Pathology and Constructions Repair
15th to 17th July 2026 - Lisboa, Portugal

Durability assessment of sargassum-based compressed earth blocks under abrasion cycles

Jhade VIMIEIRO[1], Giulia NASCIMENTO[1], Carolina ANDRADE[1], Sofia BESSA[2], João Adriano ROSSIGNOLO[1]

[1] University of São Paulo, Pirassununga-SP, Brazil, jhade@usp.br; giulia.russo@usp.br; caroldaehn@usp.br; rossignolo@usp.br.
[2] Universidade Federal de Minas Gerais (UFMG), Belo Horizonte-MG, Brazil; sofiabessa@ufmg.br.

Abstract: *Sargassum* is a marine macroalgae that, despite its photosynthetic capacity, has exhibited excessive proliferation and recurrent strandings along the Brazilian coastline, leading to significant environmental, social, and economic impacts. This scenario has intensified the search for sustainable strategies to valorise this biomass. In this context, Compressed Earth Blocks (CEB) stand out as a low-impact construction material, closely associated with circular economy principles and the reduction of CO_2 emissions. The incorporation of Sargassum into CEB emerges as a promising pathway for biomass reuse, with potential for carbon sequestration and waste reduction. This study aims to analyse the impact of adding *Sargassum* on the durability of CEB stabilised with different Portland cement contents (5%, 7%, and 10%, by mass), and to assess the technical feasibility of incorporating 2.5%, 5%, 7.5%, and 10% *Sargassum* by volume. The experimental programme involved moulding CEB with various formulations and assessing durability using the wire brush test, a method widely employed to simulate surface degradation by abrasion. Throughout the test cycles, moisture variation and cumulative mass loss were monitored. The results demonstrated that cement stabilisation is essential for incorporating *Sargassum*. In mixtures containing 5% cement, the maximum viable *Sargassum* content was 2.5%, whereas mixtures with 10% cement allowed incorporation of up to 7.5% biomass while maintaining satisfactory durability. Increasing cement content significantly reduced mass loss and volumetric instability, thereby enabling *Sargassum* valorisation without compromising CEB performance. Future work will include mechanical testing, microstructural analyses, and life cycle assessment to support ecodesign decisions and evaluate the environmental impact of each formulation.

Keywords: *Sargassum* biomass, Algae, CEB, Wire brush test.

1. Introduction

In 2015, the United Nations established the Sustainable Development Goals (SDGs), including a target to significantly reduce greenhouse gas emissions by 2030 (United Nations, 2015). In this context, the Intergovernmental Panel on Climate Change (IPCC) highlights urban systems as key actors in achieving this objective. The construction sector, responsible for approximately 37% of global operational energy consumption and CO_2 emissions, plays a particularly critical role. Significant reductions can be achieved throughout the building life cycle, including the design, construction, retrofit, use, and end-of-life stages (IPCC, 2023).

Within the design and construction phases, a promising strategy is the incorporation of locally available residues, by-products, and biomass into construction materials, taking advantage of the sector's high capacity to absorb large volumes of raw materials (Fagundo-Mollineda et al., 2026).

In the Brazilian Amazon coastal region, for instance, *Sargassum* represents an abundant seasonal biomass. *Sargassum* (C. Agardh) is a pelagic macroalga belonging to the class of brown algae (Rosado-Espinosa et

al., 2020). While it contributes to marine biodiversity and carbon dioxide (CO_2) sequestration during its growth (Gouvêa et al., 2020), its biomass has increased significantly in recent decades (Xiao et al., 2020).

The causes of this proliferation remain debated in the scientific literature. Nutrient enrichment is among the most frequently cited hypotheses; however, no definitive consensus has been reached regarding the factors driving this phenomenon (Wang et al., 2019). The decomposition of *Sargassum* in coastal zones increases the concentration of organic matter in the water, reducing light penetration and oxygen levels, and potentially releasing toxic gases such as hydrogen sulphide and ammonia (López-Contreras et al., 2022), as well as heavy metals such as arsenic (Fagundo-Mollineda et al., 2026). In addition, the accumulation of biomass on beaches negatively affects tourism and fisheries, generating socio-economic impacts and substantial public costs for its removal. For these reasons, *Sargassum* proliferation and beach stranding have been considered a new type of natural disaster (Robledo et al., 2021).

Despite these challenges, *Sargassum* remains a largely underutilised biomass with potential for value-added applications, circular economy strategies, and long-term CO_2 sequestration. Investigating valorisation pathways for this biomass is therefore essential to support effective management strategies and public policies and to strengthen the resilience of coastal communities affected by this phenomenon.

The incorporation of *Sargassum* into low-impact construction materials, particularly earthen construction systems, represents a promising approach to both reducing the environmental impacts of the construction sector and promoting sustainable biomass utilisation. Earthen construction techniques have gained renewed scientific interest in recent decades (Beckett et al., 2020) and are increasingly being adopted in contemporary building projects (Gharbage et al., 2025). Among these techniques, compressed earth block (CEB) represents a technological advancement over traditional adobe, as it is produced by compacting a mixture of soil, stabilisers, and water under pressure.

Despite their environmental advantages and favourable thermal and acoustic performance, the wider adoption of earthen construction remains limited due to susceptibility to water absorption and reduced long-term durability, particularly under aggressive environmental conditions (Turco et al., 2025). Failures in earthen architecture are therefore often associated with durability issues when materials are exposed to water (Morel et al., 2012).

Although the exposure of masonry to water can be mitigated through design strategies (such as wide eaves, raised foundations, protective coatings, waterproofing, and physical barriers) the durability of the material must still be ensured (ABNT, 2022; NZS, 2020). In this context, the assessment of the durability of CEB is essential, particularly in regions with high rainfall (Elahi et al., 2020).

Beckett, Jaquin and Morel (2020), in a literature review, present various tests used to assess the durability of earthen materials based on their interaction with water. Complementarily, Panagiotou et al. (2022) analyse water–material interaction mechanisms throughout the service life and the associated quantification methods.

Both studies highlight that climate-induced phenomena play a decisive role in the degradation of earthen masonry. The main durability assessment methods identified include accelerated erosion test, the wire brush test, and the ratio between dry and wet strength. Among these, the wire brush test stands out as a widely adopted method, standardised by several norms, including ASTM D559 (ASTM, 2012), IS 4332-4(IS, 1968), and NBR 13554 (ABNT, 2012).

In this context, incorporating biomass such as *Sargassum* into CEB requires technical validation to ensure that composite performance is not compromised. Improving the engineering properties of CEBs is thus essential to guarantee adequate structural performance, enhanced durability, and practical applicability. Accordingly, this study aims to evaluate the effect of *Sargassum* incorporation on the abrasion resistance of cement-stabilised CEBs using the wire brush test as an indicator of material durability. In addition, the study seeks to contribute to the optimisation of the product's ecodesign and to anticipate potential implications for its application in masonry systems.

2. Materials

2.1 Soils

For this study, a mixture of two soils was used, as neither soil alone exhibited a suitable particle-size distribution to produce CEB. The soils were collected from a site in a tropical region of Brazil, characterised by the presence of both the Atlantic Forest and *Cerrado* biomes (Figure 1). The soils mixtures were characterised in accordance with applicable Brazilian standards. As shown in Table 1, the particle size distribution exhibited a sand content slightly above the range recommended by CRATerre (2000), while the liquid limit was slightly lower. Nevertheless, both parameters remain within the limits established by national standards. X-ray diffraction analysis indicated that quartz is the predominant mineral in the soil mixture, with kaolinite identified as the main clay mineral.

Table 1 - Summary of soil mixture characterisation.

Sample	Granulometry		Specific Gravity (g/cm^3)	Atterberg Limits			Proctor Test		CS (MPa)
	Clay+Silt (%)	Sand (%)		LL (%)	PL (%)	PI (%)	MDD (kg/m^3)	OMC (%)	
Soil mixture	25.3	74.7	2,678	20	15	5	1979	12.46	1.58
Methodology	NBR 7181		Helium gas intrusion	NBR 6459 and 7180			NBR 12023		Axial compression
NBR 8492 and 10833 Limits	10-50	-	-	≤45	-	≤18	-	-	≥2
CRATerre Limits	10-30	≤70	-	25-50	-	03-10	1700-2200	≤15	≥2

Legend: LL = Liquid Limit, PL = Plastic Limit and PI = Plasticity Index, MDD = Maximum dry density, OMC = Optimum moisture content, CS = compressive strength

2.2 Cement

The Brazilian CPII-F 32 Portland cement (equivalent to ASTM Type I/II) was used as a stabiliser for CEB. Composed of Portland clinker, gypsum, and 6–10% limestone filler, it enhances workability and dimensional stability while reducing clinker content and CO_2 emissions. With a 28-day strength class of 32 MPa and a specific gravity of 3050 kg/m^3, it was selected due to its availability in the Amazon coastal region.

2.3 Sargassum

The Sargassum used in this study was collected in March 2025 from the Brazilian Amazon coastal region. The collected biomass was composed of about 10% *S. fluitans*, 15% *S. natans I*, and 80% *S. natans VIII*. Following collection, the biomass samples were washed with seawater to remove sand and subsequently

air-dried under tarpaulins with sun exposure. After drying, the material was shredded and stored under moisture-controlled conditions.

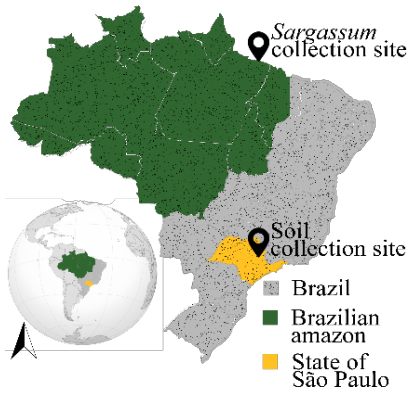


Figure 1 - Brazil and collection site.

It is important to note that fresh *Sargassum* found on beaches typically contains approximately 85% water by mass, owing to its high-water absorption capacity. For this reason, the drying stage was essential to prevent biomass degradation, preserve its integrity, and enable its use in construction applications.

To assess the toxicity of *Sargassum*, a sample was subjected to leaching and solubilisation tests in accordance with NBR 10005 and NBR 10006 (ABNT, 2004c, 2004b), and classified according to NBR 10004 (ABNT, 2004a). The results indicate that the biomass acts as a bioaccumulator of metals and organic compounds, reflecting marine environmental conditions and potential anthropogenic influences. No parameters exceeding regulatory limits were detected in the leachate extract.

In contrast, the solubilised extract exhibited a predominance of inorganic ions, including fluoride (11.3 mg/L), chloride (730 mg/L), sulphate (207 mg/L), and sodium (221 mg/L), characterising a highly saline solution. Notably, dissolved arsenic was detected at 0.453 mg/L, exceeding the drinking water limit (0.01 mg/L), indicating a potential toxicological risk, acording to NBR 10004 (ABNT, 2004a). The elevated concentrations of arsenic and sodium resulted in the classification of the material as Class II-A – Non-inert, corroborating studies reporting high arsenic contents in *Sargassum* (Fagundo-Mollineda et al., 2026).

The fact that only the solubilised extract exceeded regulatory limits suggests that these compounds may be released under prolonged contact with water, without exhibiting the typical behaviour of hazardous waste under more aggressive leaching conditions.

3. Experimental program

3.1 Mix composition and moulding process

In this study, to assess the impact of *Sargassum* incorporation on the durability of stabilised CEB, three control formulations without biomass addition were analysed, containing different cement contents (5%, 7%, and 10% by mass). The addition of cement aimed to enhance the material's durability and enable higher levels of *Sargassum* incorporation. For standardisation purposes, these formulations were designated as C5, C7, and C10.

In addition, four *Sargassum* contents (2.5%, 5%, 7.5%, and 10% by volume) were evaluated. The biomass was incorporated on a volumetric basis due to its significantly lower density compared to the soils. The nomenclature of the formulations was defined based on the cement content, followed by the letter "S" and the corresponding volumetric percentage of *Sargassum*.

For clarity, Table 2 - Formulation compositions and material contents.Table 2, summarises the compositions and materials considered in this study.

Table 2 - Formulation compositions and material contents.

	Materials		
Formulations	**Soil mixture (%)**	**Cement (%)**	***Sargassum* (%)**
C5	100	5	0
C5S2.5	100	5	2.5
C5S5	100	5	5
C5S7.5	100	5	7.5
C5S10	100	5	10
C7	100	7	0
C7S2.5	100	7	2.5
C7S5	100	7	5
C7S7.5	100	7	7.5
C7S10	100	7	10
C10	100	10	0
C10S2.5	100	10	2.5
C10S5	100	10	5
C10S7.5	100	10	7.5
C10S10	100	10	10

To mould the specimens, the oven-dried and disaggregated soils were mixed with cement. The *Sargassum* was pre-wetted to prevent water absorption from the mixture during moulding, owing to its high-water absorption capacity, and was subsequently incorporated into the blend. The mixture was mixed for 3 minutes with the gradual addition of water. The water content was adjusted to 2.5% below the optimum moisture content (OMC).

The specimens were moulded by mechanical compaction in three layers in a cylindrical mould (⌀ 5 cm × 10 cm), with scarification between layers to ensure proper bonding (Figure 2). The mass of each layer, as well as of each specimen, was measured to maintain the maximum dry density (MDD) obtained from the Proctor test.

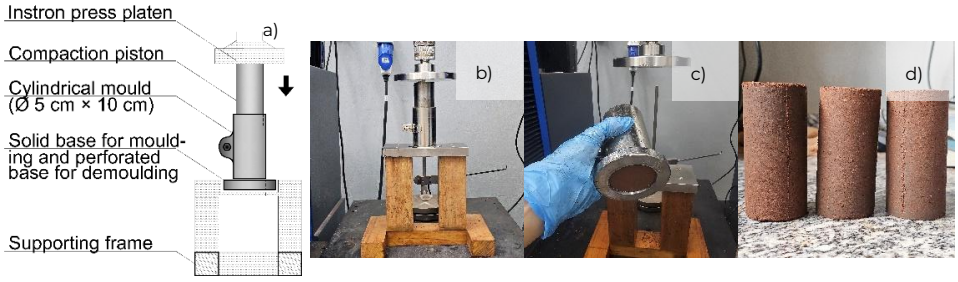


Figure 2 - Moulding process: (a) schematic of the system; (b) compaction; (c) perforated base for demoulding; (d) specimens.

After moulding, the specimens were cured for 28 days in sealed plastic bags to preserve moisture and promote cement hydration. Subsequently, they were oven-dried at 35 °C for 48 hours to reduce residual moisture.

3.2 Wire brush test

The wetting and drying test was conducted in accordance with NBR 13554 (ABNT, 2012), which is similar to ASTM D559 (ASTM, 2012), differing only in the number of wetting–drying cycles. While ASTM D559 specifies 12 cycles, NBR 13554 requires six. Minor adjustments to specimen dimensions were made due to laboratory constraints.

Cylindrical specimens measuring 5 cm in diameter and 10 cm in height were used, instead of the standard dimensions of 10 cm in diameter and 12.7 cm in height. The specimens were immersed in water for 5 hours and subsequently oven-dried at 71 °C for 42 hours. The lateral surfaces were brushed using a steel wire brush, ensuring that the entire surface was covered once (approximately 1.5 kg of applied force, 15 strokes), while the top and bottom faces received four additional strokes (Figure 3).

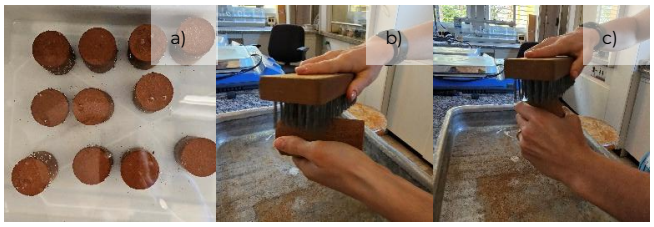


Figure 3 - Wire brush test procedure: (a) immersion in water; (b) lateral surface brushing; (c) top surface brushing.

The cycle was repeated six times. Moisture variation was calculated according to Equation 1.

$$Mv = \frac{(im - ms)}{im} x100 \quad (1)$$

Where: *Mv* is the moisture variation, expressed as a percentage (%);

im is the initial moisture content of the specimen, expressed in grams (g);

ms is the moisture content of the specimen at each stage, expressed in grams (g).

Mass loss was calculated according to Equation 2.

$$Ml = \frac{(idm - \mathrm{fdm})}{idm} x100 \quad (2)$$

Where: *Ml* is the mass loss, expressed as a percentage (%);

idm is the initial dry mass, expressed in grams (g);

fdm is the final dry mass, expressed in grams (g).

4. Results

The moisture variation of formulations containing 5% cement over six wetting–drying cycles is shown in Figure 4. Overall, there was a notable reduction in moisture variation after the first cycle. However, only formulations C5 and C5S2.5 remained stable in subsequent cycles, indicating a strong ability to release the moisture absorbed during the immersion stage.

In contrast, formulation C5S5 showed inconsistent adsorption and desorption values throughout the cycles, although similar values were observed between both stages in the final cycle. Formulations C5S7.5 and C5S10 did not complete the test, failing during the third and second cycles, respectively.

The inability of these formulations to complete all cycles is due to material degradation during the adsorption, desorption, and brushing stages, reflecting their lower resistance to moisture fluctuations and abrasion. This behaviour is a key finding in the assessment of the hygroscopic durability of the studied formulations.

In fact, the high-water retention capacity of earthen materials depends on the porous and microporous structure of the soils, as well as on the physic-chemical affinity between clays and water (Champiré et al., 2016; Giuffrida et al., 2019). In this case, kaolinite, which exhibits lower affinity compared to other clay minerals, is predominant. However, the results suggest that *Sargassum* also plays a role in this water retention capacity.

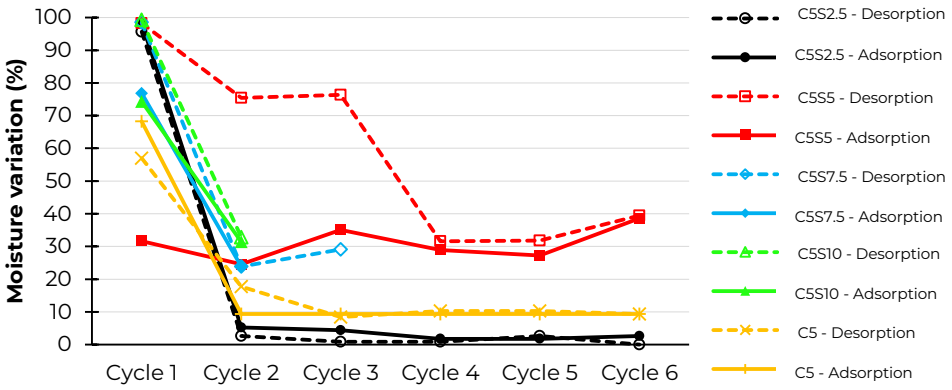


Figure 4 - Moisture variation: formulations with 5% cement.

For formulations containing 7% cement (Figure 5), all formulations exhibited relatively similar behaviour throughout the cycles, with an initial reduction in moisture variation followed by stabilisation in subsequent cycles. Notably, the formulation incorporating 2.5% *Sargassum* (C7S2.5) showed a lower final moisture variation than the reference mixture without biomass addition (C7), suggesting that a low *Sargassum* content may help reduce the hygroscopic variation of the composite.

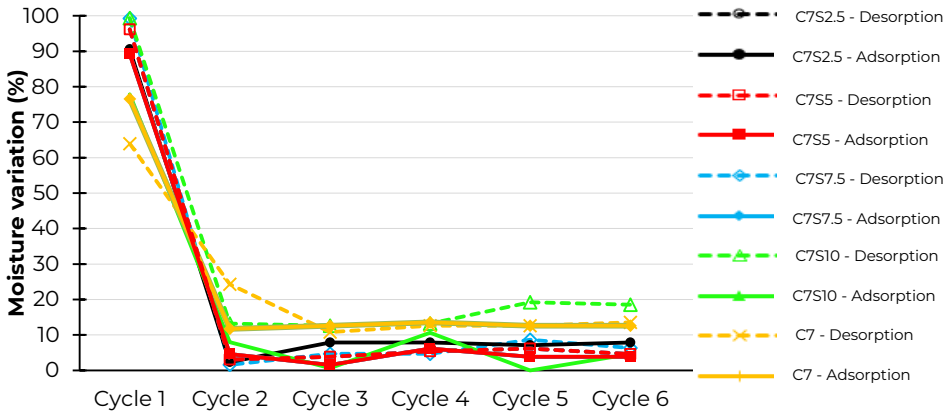


Figure 5 - Moisture variation: formulations with 7% cement.

For 10% cement (Figure 6), the formulations incorporating *Sargassum* did not exhibit significantly greater instability than the reference mixture (C10). Even at higher biomass contents (7.5% and 10%), the high content of cement proved to be effective in controlling water absorption and maintaining material integrity throughout the cycles.

These results indicate that stabilisation with 10% cement can effectively mitigate the impact of *Sargassum* incorporation on the hygroscopic durability of CEB, enabling biomass addition without compromising performance under repeated wetting–drying cycles. However, it should be noted that further durability tests should be conducted to deepen the understanding of the long-term behaviour of these materials.

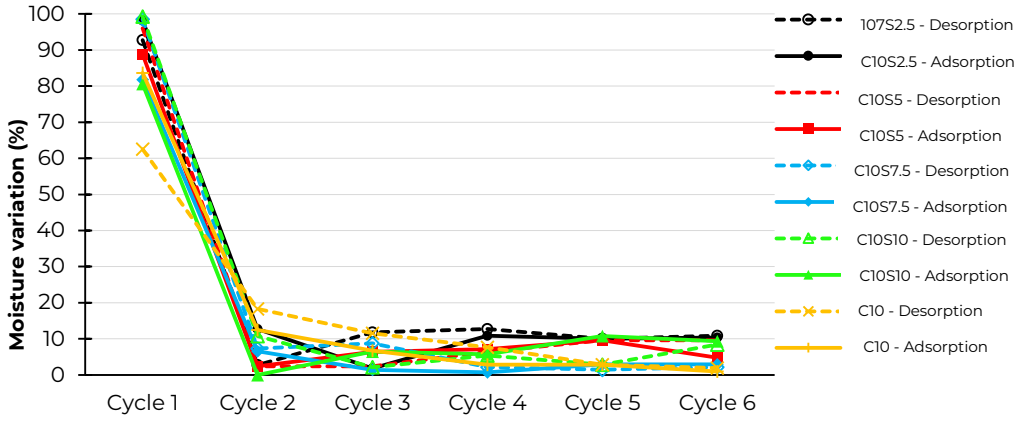


Figure 6 - Moisture variation: formulations with 10% cement.

During the immersion stage (5 hours), bubble formation was observed in the water (Figure 7). This behaviour, associated with the release of air entrapped within the pore structure, was more pronounced in formulations with higher *Sargassum* incorporation.

A possible explanation is the increase in material porosity due to the volumetric shrinkage of *Sargassum* during drying. This shrinkage may generate additional voids within the matrix, facilitating water ingress and the subsequent expulsion of air during immersion. This phenomenon may also help to explain the higher water absorption observed in mixtures containing *Sargassum*, in addition to the inherent hydrophilicity of the biomass, as previously discussed.



Figure 7 - Bubble formation during specimen immersion.

With regard to mass loss after six wetting–drying cycles, according to NBR 13553 (ABNT, 20012) and as also reported in the literature (Beckett et al., 2020), formulations are considered acceptable when mass loss remains below 14%. As shown in Table 3, formulations C5S5, C5S7.5, C5S10, C7S7.5, and C7S10 exceeded this threshold and are therefore not considered suitable. In contrast, all formulations containing 10% cement exhibited mass loss values below the specified limit.

Table 3 - Formulations and mass loss results.

Mass loss (%)					
C5	1.83 ± 0.5	**C7**	0.97 ± 0.2	**C10**	0.97 ± 0.4
C5S2.5	6.56 ± 0.7	**C7S2.5**	4.35 ± 1.0	**C10S2.5**	1.00 ± 0.3
C5S5	-	**C7S5**	13.41 ± 3.1	**C10S5**	6.02 ± 1.4
C5S7.5	-	**C7S7.5**	23.40 ± 3.1	**C10S7.5**	7.05 ± 2.3
C5S10	-	**C7S10**	31.24 ± 2.8	**C10S10**	10.38 ± 2.1

However, it is important to note that NBR 13554 (ABNT, 2012) specifies only half the number of cycles established in international standards, as previously discussed. In this context, there is evidence that some formulations with higher *Sargassum* contents, although exhibiting satisfactory performance after six cycles, may not maintain this behaviour over twelve cycles. These findings are consistent with previous studies that have also adopted six-cycle testing protocols (Bessa et al., 2018; Oliveira et al., 2025).

5. Conclusions

This study investigated the influence of incorporating *Sargassum* on the hygroscopic durability of cement-stabilised CEB using wetting-drying-brush cycles and mass-loss analysis. The results demonstrate that *Sargassum* significantly affects the moisture behaviour and durability of the material, primarily due to its hygroscopic nature and its contribution to increased porosity within the matrix.

Formulations with low cement content (5%) exhibited poor durability performance, particularly at higher *Sargassum* contents, with some formulations failing to complete the test cycles. Intermediate cement content (7%) led to more stable behaviour, although durability remained sensitive to increasing biomass content. In contrast, formulations containing 10% cement showed consistent performance across all *Sargassum* contents, with mass loss values remaining below the normative threshold and no significant instability observed during cyclic exposure.

These findings highlight a clear trade-off between environmental benefits and technical performance. While *Sargassum* represents a promising bio-based resource for sustainable construction, its incorporation must be carefully optimised to avoid compromising durability. The results indicate that adequate cement stabilisation plays a critical role in mitigating the adverse effects of biomass addition, particularly regarding moisture resistance and structural integrity.

Furthermore, the observation that some formulations performed satisfactorily under six wetting–drying cycles but may not withstand more severe conditions suggests that current testing standards may not fully capture long-term durability behaviour. Therefore, further investigations, including extended durability testing and life cycle assessment, are essential to support the development of robust and environmentally optimised CEB formulations.

In real construction scenarios, formulations with low cement content and high biomass incorporation are likely to exhibit poor resistance to moisture exposure, making them unsuitable for external applications or humid climates. Conversely, higher cement contents (e.g., 10%) enable the incorporation of *Sargassum* without compromising durability, allowing for its application in load-bearing or non-load-bearing masonry under typical environmental conditions, particularly when combined with basic protective design measures such as adequate roof overhangs and surface treatments.

The adoption of optimised Sargassum-based CEB may contribute to reducing environmental impacts, promoting circular economy practices, and supporting the valorisation of coastal biomass, especially in regions affected by large-scale Sargassum accumulation.

Acknowledgments

This study was supported by the Government of Canada's New Frontiers in Research Fund (NFRF, NFRF I-2023-00653); National Council for Scientific and Technological Development (CNPq), Brazil (Process 303850/2024-8); São Paulo Research Foundation (FAPESP), grants 2023/12355-0 and 2024/20536-7; Pró-reitoria de Pesquisa (PRPq), UFMG; Rede Mineira de Pesquisa, Desenvolvimento Científico, Tecnológico e Inovação (FAPEMIG RED-00191-23); and Coordenação de Aperfeiçoamento de Pessoal de Nível Superior – Brasil (CAPES) – Finance Code 001.

References

Intergovernmental Panel on Climate Change (IPCC). Climate Change 2023: Synthesis Report. Contribution of Working Groups I, II and III to the Sixth Assessment Report of the Intergovernmental Panel on Climate Change. Edited by Core Writing Team, H. Lee, and J. Romero. Geneva: IPCC, 2023. https://doi.org/10.59327/IPCC/AR6-9789291691647.

United Nations. Transforming Our World: The 2030 Agenda for Sustainable Development. New York: United Nations, 2015. https://sdgs.un.org/2030agenda.

CRAterre. Compressed earth blocks: standards. Grenoble: CRAterre, 2000.

ABNT. (2004a). *NBR 10004 (2004): Resíduos sólidos: Classificação* .

ABNT. (2004b). *NBR 10005 (2004): Procedimento para obtenção de extrato lixiviado de resíduos sólidos*.

ABNT. (2004c). *NBR 10006 (2004): Procedimento para obtenção de extrato solubilizado de resíduos sólidos*.

ABNT. (2012). *ABNT 13554 (2012): Solo-cimento — Ensaio de durabilidade por molhagem e secagem — Método de ensaio*.

ABNT. (2022). *NBR 17014 (2022): Taipa de pilão: Requisitos, procedimentos e controle*.

ABNT. (20012). *ABNT 13553:Materiais para emprego em parede monolítica de solo-cimento sem função estrutural - Requisitos*.

ASTM. (2012). *ASTM D559-03:Standard Test Methods for Wetting and Drying Compacted Soil-Cement Mixtures*.

Beckett, C. T. S., Jaquin, P. A., & Morel, J. C. (2020). Weathering the storm: A framework to assess the resistance of earthen structures to water damage. *Construction and Building Materials*, *242*, 1–12. https://doi.org/10.1016/j.conbuildmat.2020.118098

Bessa, S., Mello, T., & Belo, B. (2018). *ANÁLISE DE DURABILIDADE DE BLOCOS DE SOLO CIMENTO*.

Champiré, F., Fabbri, A., Morel, J. C., Wong, H., & McGregor, F. (2016). Impact of relative humidity on the mechanical behavior of compacted earth as a building material. *Construction and Building Materials*, *110*, 70–78. https://doi.org/10.1016/j.conbuildmat.2016.01.027

Elahi, T. E., Shahriar, A. R., Alam, M. K., & Abedin, M. Z. (2020). Effectiveness of saw dust ash and cement for fabrication of compressed stabilized earth blocks. *Construction and Building Materials*, *259*. https://doi.org/10.1016/j.conbuildmat.2020.120568

Fagundo-Mollineda, A., Freile-Pelegrín, Y., Vásquez-Elizondo, R. M., Vázquez-Delfín, E., & Robledo, D. (2026). Sargassum: Turning Coastal Challenge into a Valuable Resource. *Biomass*, *6*(1), 9. https://doi.org/10.3390/biomass6010009

Gharbage, I., Benmahiddine, F., & Sebaibi, N. (2025). *Mechanical, thermal and hydric properties of compressed earth blocks: A review* (Vol. 104). https://doi.org/10.1016/j.jobe.2025.112387

Giuffrida, G., Caponetto, R., & Nocera, F. (2019). Hygrothermal properties of raw earth materials: A literature review. Em *Sustainability (Switzerland)* (Vol. 11, Número 19). MDPI. https://doi.org/10.3390/su11195342

Gouvêa, L. P., Assis, J., Gurgel, C. F. D., Serrão, E. A., Silveira, T. C. L., Santos, R., Duarte, C. M., Peres, L. M. C., Carvalho, V. F., Batista, M., Bastos, E., Sissini, M. N., & Horta, P. A. (2020). Golden carbon of Sargassum forests revealed as an opportunity for climate change mitigation. *Science of the Total Environment*, *729*. https://doi.org/10.1016/j.scitotenv.2020.138745

IS. (1968). *IS 4332-4: Methods of test for stabilized soils, Part 4: Wetting and drying, and freezing and thawing tests for compacted soil-cement mixtures*.

López-Contreras, A. M., Núñez Valenzuela, P., Celis Garcîa, B., Driegen, J., Huerta Lwanga, E., Domin, P., Polett Gurrola, M., Rosas-Luis, R., Verde Gómez, Y., & de Vrije, T. (2022). *Sargassum in Mexico: from environmental problem to valuable resource*. https://doi.org/10.18174/574423

Morel, J.-C., Bui, Q. B., & Hamard, I. (2012). *Weathering and durability of earthen material and structures*.

NZS. (2020). *Earth buildings not requiring specific engineering design*.

Oliveira, H. A. de, Silva, I. D. V. da, Júnior, C. M. M., Santos, C. P., Carvalho, M. C., & Melo, F. M. C. de. (2025). Durabilidade de tijolo de solo-cimento em soluções agressivas. *OBSERVATÓRIO DE LA ECONOMÍA LATINOAMERICANA*, *23*(3), e9258. https://doi.org/10.55905/oelv23n3-055

Panagiotou, R., Kyriakides, M. A., Illampas, R., & Ioannou, I. (2022). An experimental approach for the investigation of the performance of non-stabilized Compressed Earth Blocks (CEBs) against water-mediated weathering. *Journal of Cultural Heritage*, *57*, 184–193. https://doi.org/10.1016/j.culher.2022.08.009

Robledo, D., Vázquez-Delfín, E., Freile-Pelegrín, Y., Vásquez-Elizondo, R. M., Qui-Minet, Z. N., & Salazar-Garibay, A. (2021). Challenges and Opportunities in Relation to Sargassum Events Along the Caribbean Sea. *Frontiers in Marine Science*, *8*. https://doi.org/10.3389/fmars.2021.699664

Rosado-Espinosa, L. A., Freile-Pelegrín, Y., Hernández-Nuñez, E., & Robledo, D. (2020). A comparative study of Sargassum species from the Yucatan Peninsula coast: morphological and chemical characterisation. *Phycologia*, *59*(3), 261–271. https://doi.org/10.1080/00318884.2020.1738194

Turco, C., Teixeira, M. O., Teixeira, E., & Mateus, R. (2025). Mechanical properties and durability of compressed earth blocks incorporating natural materials. *Journal of Building Engineering*, *111*. https://doi.org/10.1016/j.jobe.2025.113386

Wang, M., Hu, C., Barnes, B. B., Mitchum, G., Lapointe, B., & Montoya, J. P. (2019). *The great Atlantic Sargassum belt*. https://www.science.org

Xiao, J., Wang, Z., Song, H., Fan, S., Yuan, C., Fu, M., Miao, X., Zhang, X., Su, R., & Hu, C. (2020). An anomalous bi-macroalgal bloom caused by Ulva and Sargassum seaweeds during spring to summer of 2017 in the western Yellow Sea, China. *Harmful Algae*, *93*, 101760. https://doi.org/10.1016/J.HAL.2020.101760

Cinpar 2026
XXII International Conference on Building Pathology and Constructions Repair
15th to 17th July 2026 - Lisboa, Portugal

Experimental study of microbial biomineralization in carbonated and pre-cracked cementitious matrices

Ítalo CARVALHO SOUZA[1], Jacinta VELOSO DE CARVALHO[2], Laércio MESQUITA JÚNIOR[1], Gabrielle AVELAR SILVA[3], Maria ALVES FERREIRA[3], Daniela SALES ALVIANO[4], Nahum CAYO[5], Romildo DIAS TOLEDO FILHO[5], Saulo ROCHA FERREIRA[1]

[1] Universidade Federal de Lavras, Departamento de Engenharia Civil, Brasil
[2] Universidade Federal de Lavras, Programa de Ciência e Tecnologia da Madeira, Brasil
[3] Universidade Federal de Lavras, Departamento de Fitopatologia, Brasil
[4] Universidade Federal do Rio de Janeiro, Instituto de Microbiologia Paulo de Góes, Brasil
[5] Universidade Federal do Rio de Janeiro, Programa de Engenharia Civil, Brasil, nahum.chileno@coc.ufrj.br

Abstract: Concrete is widely used in the construction industry due to its advantages in terms of workability, strength, and durability. However, its brittle nature favors the formation of cracks, compromising performance and reducing the service life of structures. As an alternative to conventional repair methods, often associated with high environmental impact, microbially induced calcium carbonate ($CaCO_3$) precipitation has emerged as a sustainable strategy. In this context, the present study aimed to evaluate the influence of the oomycete *Pythium aphanidermatum* on the surface treatment of cracks in previously carbonated concrete matrices. Specimens with a characteristic compressive strength of 25 MPa were cast, including natural samples and others artificially carbonated through 30 wetting–drying cycles. Subsequently, pre-cracks corresponding to 85% of the maximum strength were induced in the carbonated specimens. The specimens were subjected to three treatments: T1 (reference), T2 (surface application of water), and T3 (biological surface application), with a dosage of 2.50 mL/cm of crack. Mechanical strength was evaluated 28 days after treatment. The results did not indicate statistically significant differences among the treatments, suggesting that a single application is not sufficient to promote relevant mechanical recovery. However, microstructural analyses by SEM-EDS evidenced microbial development and the formation of hyphal structures in specimens treated with T3, indicating potential activity as nucleation sites for $CaCO_3$. Although no significant recovery in strength was observed, the study demonstrates advances in the use of biological approaches for crack treatment, highlighting the need to optimize the number of applications to enhance the sealing effect and mechanical recovery.

Keywords: Biological repair, concrete, accelerated carbonation, *Pythium aphanidermatum*.

1. Introduction

In recent years, advances achieved through biotechnology have enabled innovation across different fields, including the construction industry (Meyer et al. 2020). Studies have shown that the use of microorganisms presents potential in sustainable construction, being applicable in soil stabilization, wastewater treatment, and the development of new materials (Majib et al. 2025). These advances have also demonstrated the possibility of applying biotechnology in repair processes and/or crack sealing in cementitious matrices (Van Wylick et al. 2021).

Currently, a variety of products are available for the surface repair of concrete structures, commonly petroleum-derived epoxies and chemical compounds, whose application entails a certain negative impact on the environment and human health (Jonkers et al. 2010; Vijay et al. 2017; Tyagi et al. 2024). This effect can be reduced through the application of microorganisms, since the natural metabolic processes of certain species lead to the precipitation of specific crystals that can act as crack sealants in cementitious matrices. For crack closure, the basic principle consists of incorporating microorganisms capable of promoting the formation of calcium carbonate ($CaCO_3$). The technique commonly applied for this process is known as Microbial Induced Carbonate Precipitation (MICP) (Zhang et al. 2024; Sun et al. 2021), which typically achieves this precipitation of $CaCO_3$ crystals through a ureolytic mechanism. This mechanism involves the use of urea, which is decomposed by the microorganism, producing ammonia and carbonate; the latter is capable of reacting with free calcium ions in an alkaline medium, resulting in the formation of $CaCO_3$. Finally, the formed crystals are deposited on the walls of microbial cells or hyphae due to the nucleation effect (Ojha et al. 2025).

The literature reports various microorganisms, such as bacteria, fungi, microalgae, and some oomycetes, that exhibit potential for application in cementitious matrices, promoting crack closure through $CaCO_3$ precipitation (Khushnood et al. 2022; Van Wylick et al. 2024; Cayo Chileno et al. 2025). Despite the advances achieved, there are still challenges that limit their application. Among the main ones are the conditions of cementitious matrices, which represent a hostile environment for microbial development, as nutrients are not available, moisture is low, and the medium is generally highly alkaline (Jonkers et al. 2010; Ivaškė et al. 2023). However, many structures exposed to the natural environment undergo carbonation processes, in which the penetration of carbon dioxide (CO_2) through the water present in the pores reduces the alkalinity levels of the cementitious matrix (Talukdar et al. 2012; Cui et al. 2015). This effect allows the evaluation of microorganisms capable of developing in media with alkalinity levels below pH 10.

The company Basilisk is one of the leading promoters of the application of microorganisms for surface crack treatment. Through its commercial products, such as Basilisk Self-Healing Repair Mortar MR3 and Basilisk Liquid Repair System ER7, the repair of cracks of approximately 2 mm has been demonstrated (Wiktor and Jonkers 2016). Other studies also report results related to crack closure (~1.5 mm) through surface treatments based on microorganisms, especially when evaluated under controlled laboratory conditions (Li et al. 2024; Sun et al. 2020). However, despite the advances and positive results reported in the scientific literature, further investigation is still required. In this regard, the present study aims to evaluate the mechanical recovery behavior of previously cracked concrete specimens treated with surface repair. The selected microorganism corresponds to an oomycete of the genus *Pythium* and species *aphanidermatum*, which has demonstrated potential for $CaCO_3$ precipitation (calcite and vaterite) through the ureolytic mechanism (Adl et al. 2012; Mesquita Júnior 2022; Cayo Chileno et al. 2025; Chileno et al. 2026). Concrete specimens were used as test samples, which were carbonated in order to simulate aged concrete and reduce the alkalinity level, thereby enabling microbial development as a surface treatment.

2. Methodology

2.1 Material characterization

2.1.1 Concrete components

A pozzolanic cement of type CP V-AR was used, whose properties comply with the requirements established in ASTM C595 (ASTM 2025). In order to determine its chemical composition, an X-ray fluorescence (XRF) analysis was performed. The main oxides identified are presented in Table 1.

Table 1 – Chemical properties of the cement

Parameter	CaO	SiO_2	Al_2O_3	Fe_2O_3	SO_3	MgO	K_2O	TiO_2	SrO	MnO	P_2O_5	ZnO
Cement	43.62	30.32	8.48	4.61	5.71	2.95	1.99	0.78	0.73	0.56	0.20	0.05

The particle size distribution of both aggregates was obtained through sieve analysis, following the procedure described in ASTM C136 (ASTM 2006). The results corresponding to the gradation curves of the fine and coarse aggregates are presented in Figure 1.

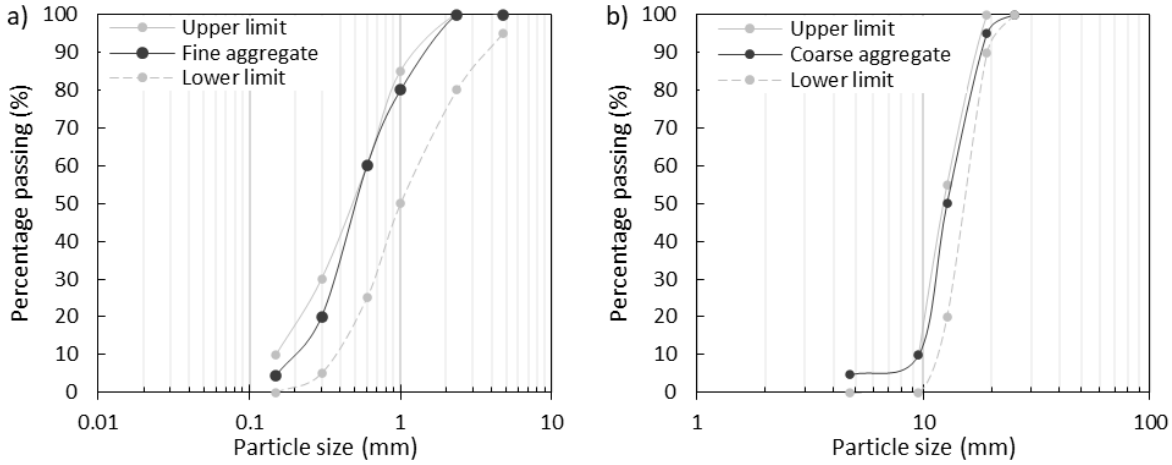


Figure 1 – Particle size distribution: (a) fine aggregate and (b) coarse aggregate

2.1.2 Microbial solution for surface treatment

The biological solution used to evaluate the self-healing process was prepared following the methodology reported in a previous study (Cayo Chileno et al. 2025; Chileno et al. 2026). The species *Pythium aphanidermatum* was employed, which was previously isolated to obtain spores with an approximate concentration of 10^{-5} cells/mL, suspended in a sterile saline solution.

Calcium acetate was used as the calcium source at a final concentration of 100 mM, while urea at 2% was used as the nitrogen source. Both compounds were dissolved in Potato Dextrose Broth (PDB), which acted as a nutrient medium for microbial development.

The spore concentration was determined by counting in a Neubauer chamber. Subsequently, microbial viability was verified through optical microscopy, evaluating active hyphal growth and the cytoplasmic integrity of the cells (Figure 2).

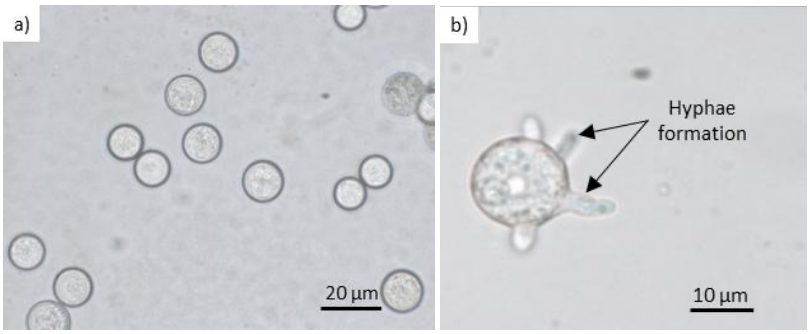


Figure 2 – Optical micrographs of *Pythium aphanidermatum*: (a) spores and (b) germination and hyphal formation

2.2 Composition of the concrete matrix

The concrete mix design was established with the aim of achieving a characteristic compressive strength of 25 MPa at 28 days. The preparation of the mixtures was carried out following the recommendations established by the Brazilian Association of Technical Standards (ABNT), particularly NBR 6118:2003 (ABNT 2023a) and NBR 14931:2004 (ABNT 2023b). The material proportions used for the concrete are presented in Table 2.

Table 2 – Concrete mix proportions with CP V-AR cement

Cement (kg)	Fine aggregate (kg)	Coarse aggregate (kg)	Water (L)	w/c
306	895	912	199	0.65

With this mix design, 16 cubic specimens with dimensions of 100 × 100 × 100 mm were cast. After completing the curing process for 28 days, the samples were classified into three experimental groups: non-carbonated (NC), carbonated (C), and carbonated for phenolphthalein control (F).

2.3 Experimental method

2.3.1 Compressive strength test

The mechanical properties of the specimens were evaluated through compressive strength tests conducted at 28 days of curing, following the procedure established in ASTM C39 (ASTM 2023).

The NC group was used to determine the maximum strength of the produced concrete and to verify whether the average strength obtained corresponded to the design value of approximately 25 MPa.

2.3.2 Carbonation process

After determining the initial strength, the remaining specimens were subjected to an accelerated aging process in order to induce carbonation of the cementitious matrix. The applied methodology was an adaptation of the procedure proposed in the literature (Toledo Filho et al. 2009). For this purpose, 12 specimens from group F were exposed to repeated cycles of water immersion for 24 hours followed by oven drying at 28 °C for 48 hours. A total of 30 cycles were performed to promote a significant level of carbonation in the specimens.

To determine the degree of carbonation of the specimens, a phenolphthalein test using a 2% solution was carried out. This procedure consists of cutting the specimen transversely and applying the reagent to the exposed surface.

2.3.3 Crack induction and repair treatments

Once the carbonation level was determined, three specimens from the NC group were again subjected to compressive testing to evaluate the residual strength of the carbonated concrete.

The remaining specimens were loaded up to approximately 85% of the recorded ultimate load in order to induce controlled crack formation. Subsequently, the pre-cracked specimens were divided into three experimental groups (n = 3): T1 (reference group, maintained under ambient conditions without treatment); T2 (samples subjected to surface application of water); and T3 (samples treated with the microbial solution). The T2 and T3 solutions were applied at a dosage of 2.50 mL per linear centimeter of crack.

2.3.4 Evaluation of mechanical recovery capacity

The efficiency of the repair process was evaluated through the percent regain in compression (PRC), calculated according to the methodology proposed in the literature (Khan et al. 2023), using Equation (1).

$$PRC = 1 - \left(\frac{S_u - S_{28}}{S_u}\right) x\ 100 \quad (1)$$

Where S_u corresponds to the compressive strength, and S_{28} corresponds to the compressive strength after the repair process.

3. Results

After 28 days of curing, the average compressive strength of the reference specimens (NC) was 24.12 ± 0.67 MPa, which is close to the design strength. Subsequently, the carbonation process was initiated. Figure 3a presents the degree of carbonation evaluated through the application of a phenolphthalein solution. Although the samples were subjected to a prolonged treatment of approximately 90 days (30 cycles), the designed concrete exhibited low permeability, which limited the diffusion of CO_2 into the matrix. As a consequence, a carbonation depth not exceeding 3.08 mm from the external surface toward the interior of the specimen was observed (Figure 3b).

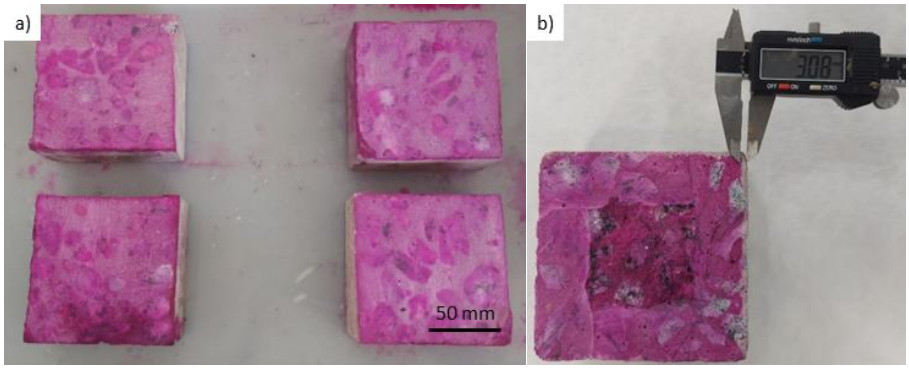


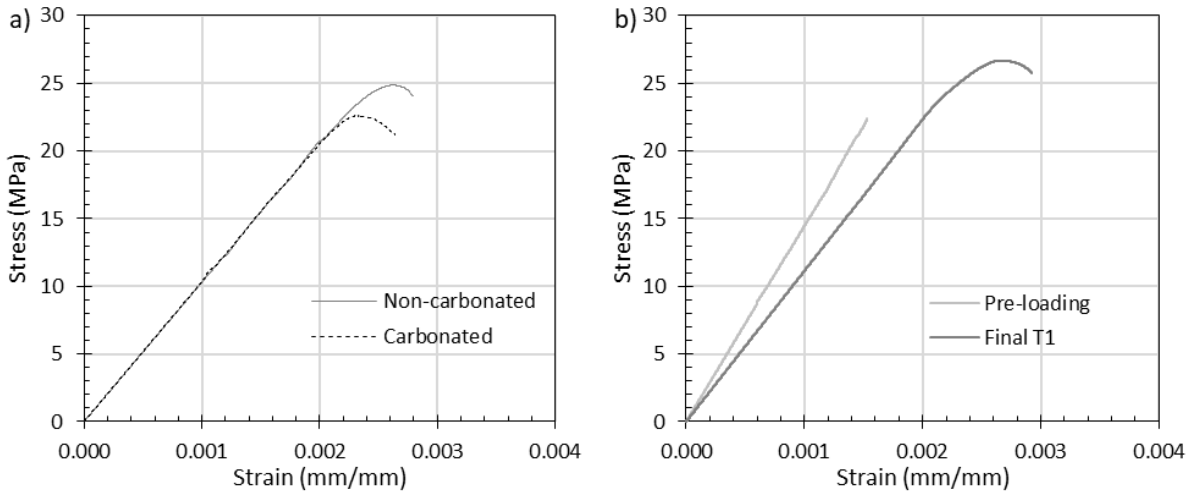
Figure 3 – Carbonation process: (a) control samples and (b) carbonation after 30 cycles

In the literature, this type of test is widely used to evaluate the durability performance of cementitious matrices. The application of a phenolphthalein solution allows the alkalinity level of the material to be visually identified: pigmented regions indicate pH values above 9–10, whereas non-pigmented zones reveal the penetration of external agents that have reacted with the cement hydration products. This phenomenon is mainly associated with the carbonation process, in which atmospheric CO_2 is transported through the water present in the pore structure, reacting with calcium-rich compounds and resulting in the formation of calcium carbonate ($CaCO_3$) (Rocha et al. 2025). These results indicate that matrices with higher porosity facilitate the ingress of aggressive agents, which may compromise the durability of cementitious systems. In particular, in the case of reinforced concrete, the reduction in pH associated with carbonation

may compromise the service life of the reinforcing steel; in the presence of hydrogen ions and oxygen, this condition promotes the initiation of corrosion processes, progressively affecting the structural integrity of the material (Chen et al. 2015).

Studies have reported that the carbonation process may induce an increase in the compressive strength of cementitious matrices (Rocha et al. 2025). This behavior was also observed in the present investigation (Figure 4), where the carbonated specimens (C) exhibited an increase in average strength from 24.12 to 25.06 MPa, corresponding to an approximate increase of 3.87%. However, this increase was not statistically significant (p-value = 0.7188). Despite this, the specimens were subsequently subjected to a pre-load corresponding to 85% of the average strength of group C (approximately 21.30 MPa). The incorporation of the carbonation process at this stage not only allows the simulation of aging conditions of the cementitious matrix but also enables the study of surface treatments based on microorganisms, which exhibit tolerance to pH ranges below 10. In particular, *Pythium aphanidermatum* has been reported to grow under alkaline conditions (pH between 9 and 11), in addition to showing potential to induce calcium carbonate ($CaCO_3$) precipitation (Cayo Chileno et al. 2025).

Figure 4a presents the stress–strain curves. It can be observed that, since the effect of carbonation was not significantly pronounced, the mechanical responses are concentrated within a narrow range of values, without showing relevant increases in either deformation capacity or strength. For the treated specimens, pre-load values close to 22 MPa were recorded, consistent with the mechanical behavior observed in the final curves. In the case of sample T1 (Figure 4b), a slightly more elastic behavior is identified compared to the pre-load condition, whereas in samples T2 and T3 (Figures 4c and 4d), the deformation capacity is similar to that initially induced. This behavior suggests that the combined effect of hydration, promoted by the different solutions used in T2 and T3, together with the exposure time, favored the rehydration of previously unreacted cement particles or those exposed during pre-loading. As a result, a deformational response comparable to the initial loading condition is obtained. Although no significant increase in load-bearing capacity relative to the reference state was observed, the results indicate the possible activation of hydration processes within the concrete matrix. This effect is reported in the literature as the autogenous self-healing process of cementitious matrices, in which cement particles may react upon contact with water (De Rooij et al. 2013; Mohamed et al. 2023).



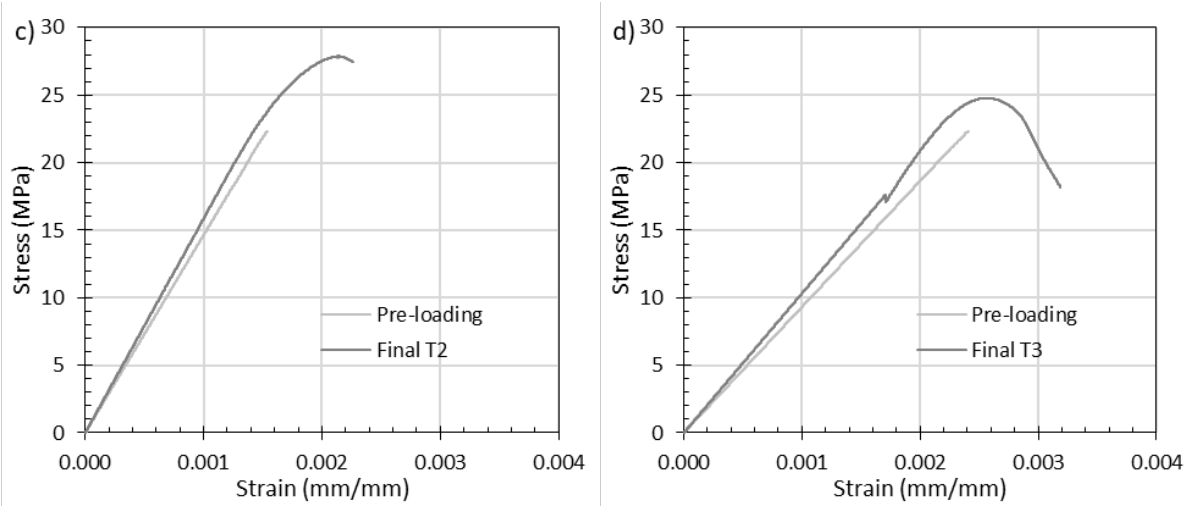


Figure 4 – Stress–strain curves obtained from compression tests: (a) reference matrix before and after carbonation; (b), (c), and (d) matrices treated with T1, T2, and T3, respectively

Figure 5 presents the percent regain in compression, considering as reference the average load of the carbonated specimens. The values corresponding to the pre-load (PT1, PT2, and PT3) are slightly above the projected level, indicating adequate consistency in the application of the loading protocol. Regarding the post-treatment recovery results (PRC), specimens T1 and T3 show values below 100%, evidencing the absence of effective mechanical recovery. On the other hand, treatment T2 reaches values slightly above 100%, suggesting the possible occurrence of a recovery effect in load-bearing capacity. However, the dispersion observed in the data indicates that this behavior was not uniform across all specimens and may have occurred in a localized manner. Finally, the ANOVA statistical analysis did not reveal a statistically significant difference (p-value = 0.3186 > 0.05).

In this context, the results suggest that a single application of 2.50 mL/cm of solution, used in treatments T2 and T3, is not sufficient to ensure consistent recovery of mechanical capacity. Therefore, there is still a need to optimize the application frequency of the treatment in order to achieve surface sealing effects and, consequently, significant load recovery.

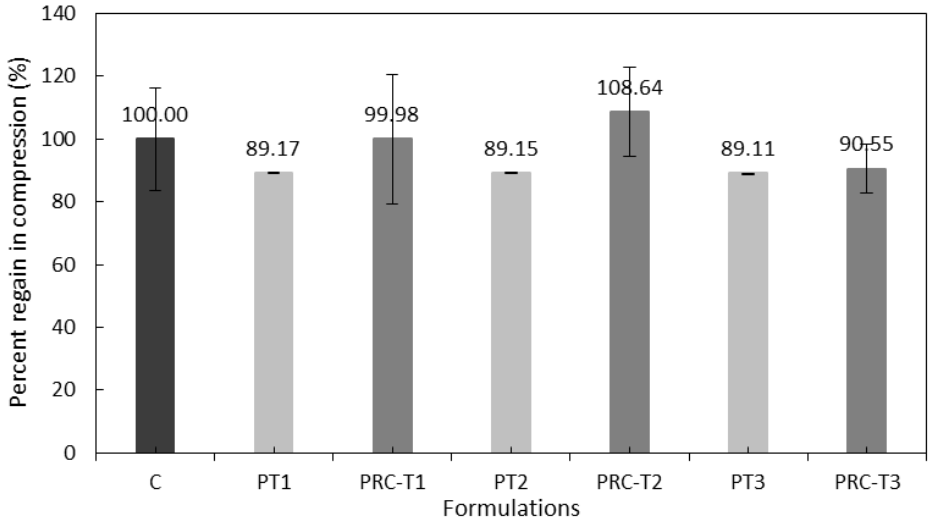


Figure 5 – Percent regain in compressive strength for the different formulations

At the microstructural level, *Pythium aphanidermatum* demonstrated not only its ability to induce $CaCO_3$ precipitation in the forms of calcite and vaterite, but also its capacity to develop within cracks in previously carbonated mortar matrices (Cayo Chileno et al. 2025). However, when evaluated in cement paste matrices, its development was null. Despite these pastes having been subjected to carbonation processes, no perceptible microbial growth was observed. This behavior may be attributed, on the one hand, to the greater difficulty of carbonation in cement pastes, which implies the maintenance of high alkalinity levels, and, on the other hand, to their lower porosity and higher impermeability, conditions that limit spore retention and, consequently, subsequent germination (Chileno et al. 2026).

In the case of the concrete analyzed in the present study, it is observed that the microstructure of the non-carbonated matrix (Figure 6a) is similar to that of treatments T1 and T2 (Figures 6b and 6c), being characterized by a typical cementitious matrix with the presence of hydration products, voids, and aggregates. In contrast, treatment T3 showed a microstructural modification associated with the formation of hyphae (Figure 6d), confirming the ability of the microorganism to develop in treated regions of previously carbonated specimens.

Although high degrees of carbonation, with extensive zones of pH below 9–10, were not achieved, *Pythium aphanidermatum* was able to develop from its spores, suggesting significant tolerance to moderately alkaline conditions and reinforcing its potential application in biomineralization strategies in cementitious matrices.

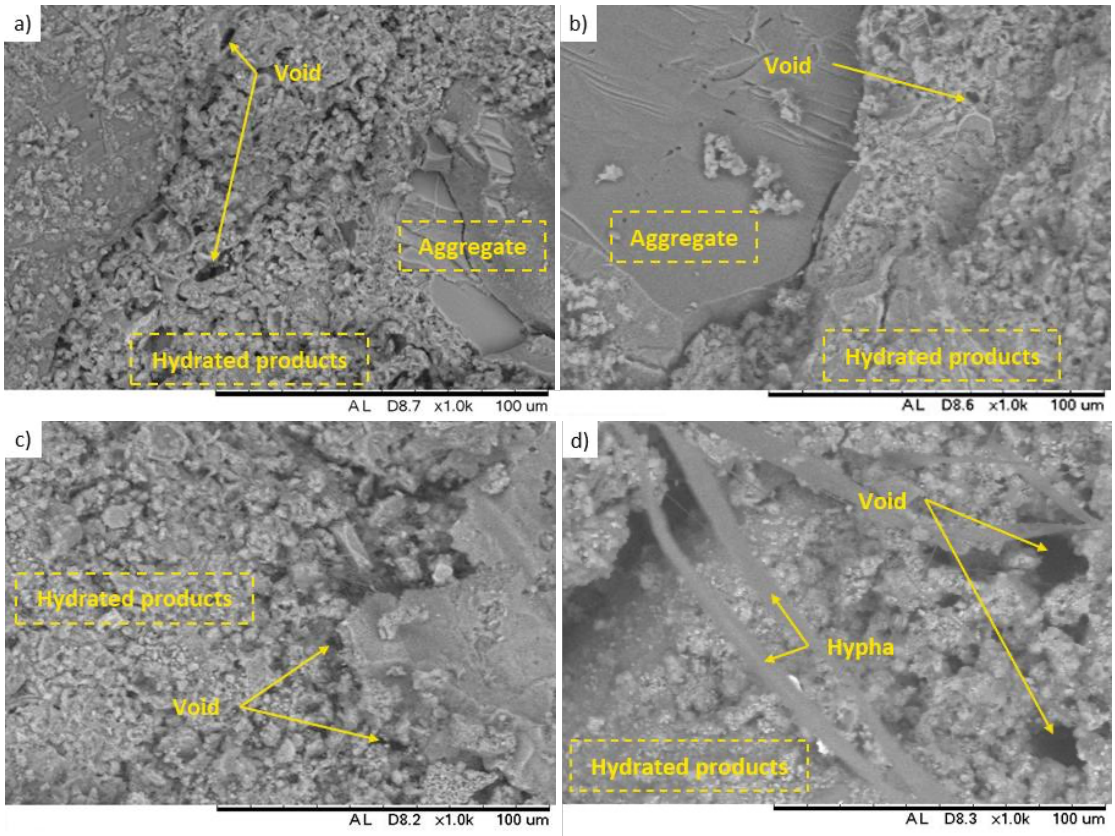


Figure 6 – SEM micrographs at 1,000× magnification: (a) carbonated matrix and (b), (c), and (d) matrix treated with T1, T2, and T3

In other regions of the specimens, the presence of a well-defined mycelial network was identified (Figure 7a), a growth pattern not observed in the matrices corresponding to treatments T1 and T2, which allows this behavior to be attributed to the activity of *Pythium aphanidermatum*. Similarly, in Figure 7b, spores located in porous zones of the matrix are observed, suggesting that these regions favor spore retention and

subsequent microbial development. This effect has also been reported in recycled aggregates, which, due to their high porosity and absorption capacity, enabled the immobilization of fungal spores (Khan et al. 2023).

These findings support the proposal, indicating that the microorganism is capable of developing in cementitious matrices that exhibit a certain degree of porosity and carbonation. However, it is still not possible to precisely establish the number of applications required to achieve effective sealing based on $CaCO_3$ precipitation, highlighting the need for further studies focused on optimizing application conditions and maximizing treatment efficiency.

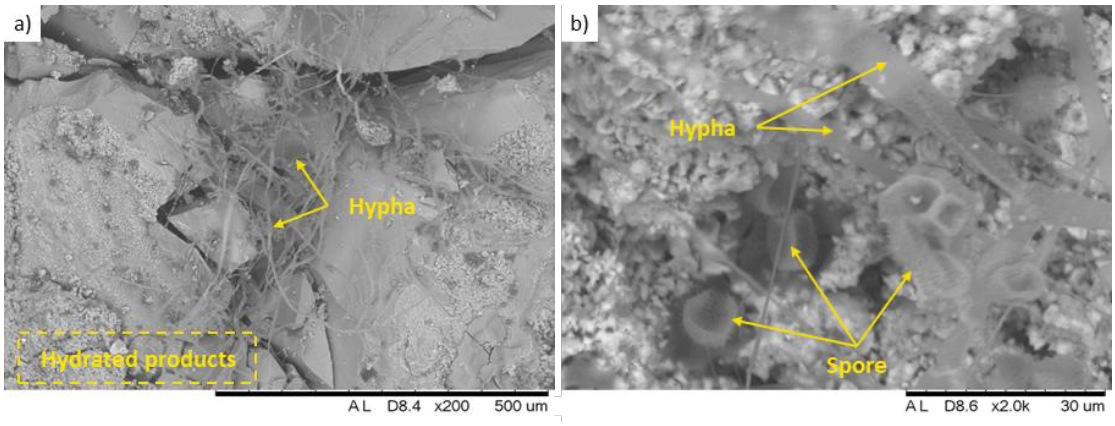
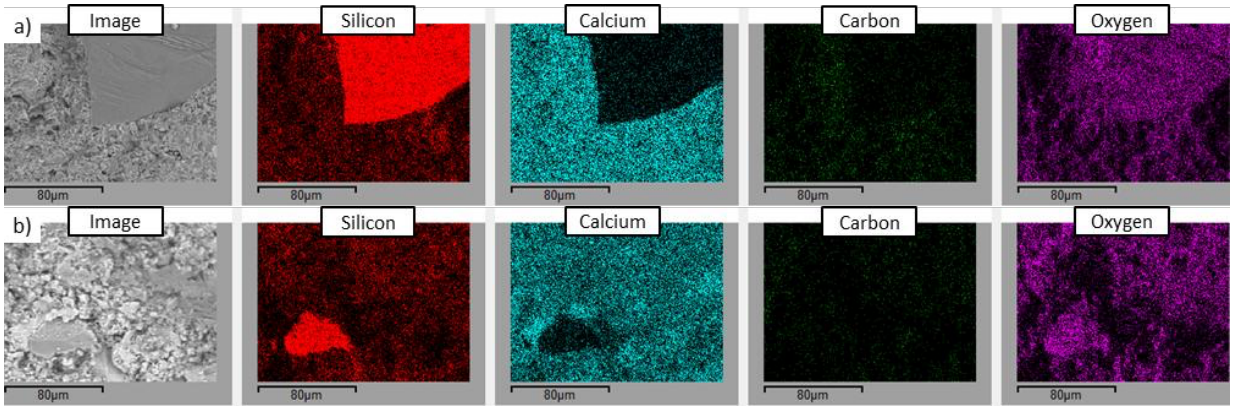


Figure 7 – SEM micrographs of matrix treated with T3: (a) 200× magnification and (b) 2,000× magnification

Additionally, an energy-dispersive spectroscopy (EDS) analysis was performed in order to identify the chemical elements present in the different samples. The carbonated reference matrix, as well as those corresponding to treatments T1 and T2 (Figures 8a, 8b, and 8c), show predominant signals of silicon, associated with aggregates, and calcium, corresponding to cement-derived compounds.

In contrast, in the matrix treated with T3 (Figure 8d), where the presence of hyphae was evidenced, a localized concentration of calcium is observed on their surface, with a slightly defined distribution. This behavior suggests that the composition of the microbial cell wall, rich in cellulose, acts as a nucleation site for calcium carbonate ($CaCO_3$) precipitation, favored by the availability of free calcium in the medium (Cayo Chileno et al. 2025; Ojha et al. 2025).



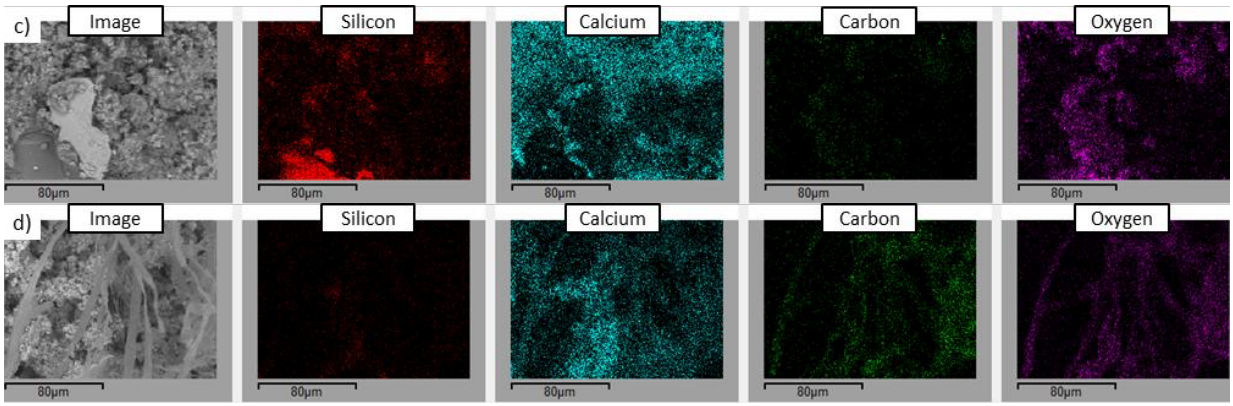


Figure 8 – SEM-EDS elemental mapping of the carbonated matrix (a) and matrices treated with T1 (b), T2 (c), and T3 (d), highlighting the spatial distribution of Si, Ca, C, and O across the microstructure

4. Conclusions

The present study evaluated the surface application of *Pythium aphanidermatum* as a $CaCO_3$ precipitation agent in previously carbonated and pre-cracked concrete matrices. The results of the carbonation process, verified through the application of phenolphthalein, demonstrated that the adopted method, based on 30 cycles, was not sufficient to generate a matrix with extensive carbonated zones. In this regard, to ensure greater depth and uniformity in surface carbonation, future studies should consider the use of controlled-scale accelerated carbonation chambers.

In terms of compressive mechanical response, the stress–strain curves showed that treatments T2 and T3 exhibited behavior similar to the pre-cracking condition, suggesting the possible occurrence of rehydration processes of residual cement particles within the matrix, a phenomenon previously reported in the literature. In turn, the results of the percent regain in compression (PRC) did not show statistically significant improvements, indicating that a single application of the treatment, under the evaluated conditions, is not sufficient to induce relevant changes in the mechanical capacity of the material. However, the microstructural analysis by SEM-EDS confirmed the deposition of spores and the development of hyphal networks, which act as potential nucleation sites for $CaCO_3$ precipitation.

Consequently, although a significant sealing effect was not achieved, the obtained results suggest that optimizing the number of applications and treatment conditions may promote the formation of biomineral products capable of improving matrix performance. Furthermore, *Pythium aphanidermatum* demonstrated its ability to develop in cementitious matrices that still exhibit relatively high alkalinity levels, highlighting its potential as an innovative and environmentally sustainable alternative for self-healing applications, despite its pathogenic nature in certain plant systems.

Acknowledgments

The authors would like to acknowledge CAPES (Coordenação de Aperfeiçoamento de Pessoal de Nível Superior – Brasil, Finance Code 001), FAPEMIG (Research Support Foundation of Minas Gerais), and the Brazilian National Council for Scientific and Technological Development (CNPq) for their financial support.

References

ABNT. 2023a. “Target Normas: ABNT NBR 6118 NBR6118 Projeto de estruturas concreto”. https://www.normas.com.br/visualizar/abnt-nbr-nm/5211/abnt-nbr6118-projeto-de-estruturas-de-concreto.

ABNT. 2023b. “Target Normas: ABNT NBR 14931 NBR14931 Execução de estruturas”. https://www.normas.com.br/visualizar/abnt-nbr-nm/22627/abnt-nbr14931-execucao-de-estruturas-de-concreto-armado-protendido-e-com-fibras-requisitos.

Adl, Sina M., Alastair G. B. Simpson, Christopher E. Lane, et al. 2012. “The Revised Classification of Eukaryotes”. *Journal of Eukaryotic Microbiology* 59 (5): 429-514. https://doi.org/10.1111/j.1550-7408.2012.00644.x.

ASTM. 2006. *ASTM C136: Test Method for Sieve Analysis of Fine and Coarse Aggregates*. ASTM International. https://doi.org/10.1520/C0136-06.

ASTM. 2023. *ASTM C-39: Test Method for Compressive Strength of Cylindrical Concrete Specimens*. ASTM International. https://doi.org/10.1520/C0039_C0039M-21.

ASTM. 2025. *ASTM C595/C595M-25: Specification for Blended Hydraulic Cements*. ASTM International. https://doi.org/10.1520/C0595_C0595M-25.

Cayo Chileno, Nahúm G., Daniela Sales Alviano, Celuta Sales Alviano, et al. 2025. “An Exploratory Study on Crack Healing in Cementitious Matrices Induced by Pythium Aphanidermatum”. *Fungal Biology* 129 (7): 101658. https://doi.org/10.1016/j.funbio.2025.101658.

Chen, Gang, Muhammad N. S. Hadi, Danying Gao, y Liangping Zhao. 2015. “Experimental Study on the Properties of Corroded Steel Fibres”. *Construction and Building Materials* 79 (marzo): 165-72. https://doi.org/10.1016/j.conbuildmat.2014.12.082.

Chileno, Nahúm Gamalier Cayo, Daniela Sales Alviano, Joaquin Humberto Aquino Rocha, et al. 2026. “Surface biomineralization with Pythium aphanidermatum in cracked cement pastes: Limitations and perspectives”. *Matéria (Rio de Janeiro)* 31: e20250555. https://doi.org/10.1590/1517-7076-rmat-2025-0555.

Cui, Hongzhi, Waiching Tang, Wei Liu, Zhijun Dong, y Feng Xing. 2015. “Experimental Study on Effects of CO2 Concentrations on Concrete Carbonation and Diffusion Mechanisms”. *Construction and Building Materials* 93 (septiembre): 522-27. https://doi.org/10.1016/j.conbuildmat.2015.06.007.

De Rooij, Mario, Kim Van Tittelboom, Nele De Belie, y Erik Schlangen, eds. 2013. *Self-Healing Phenomena in Cement-Based Materials: State-of-the-Art Report of RILEM Technical Committee 221-SHC: Self-Healing Phenomena in Cement-Based Materials*. Vol. 11. RILEM State-of-the-Art Reports. Springer Netherlands. https://doi.org/10.1007/978-94-007-6624-2.

Ivaškė, Augusta, Viktor Gribniak, Ronaldas Jakubovskis, y Jaunius Urbonavičius. 2023. “Bacterial Viability in Self-Healing Concrete: A Case Study of Non-Ureolytic Bacillus Species”. *Microorganisms* 11 (10): 2402. https://doi.org/10.3390/microorganisms11102402.

Jonkers, Henk M., Arjan Thijssen, Gerard Muyzer, Oguzhan Copuroglu, y Erik Schlangen. 2010. “Application of bacteria as self-healing agent for the development of sustainable concrete”. *Ecological Engineering*, Special Issue: BioGeoCivil Engineering, vol. 36 (2): 230-35. https://doi.org/10.1016/j.ecoleng.2008.12.036.

Khan, Nangyaley, Hammad Anis Khan, Rao Arsalan Khushnood, Muhammad Faraz Bhatti, y Danish Ilyas Baig. 2023. “Self-Healing of Recycled Aggregate Fungi Concrete Using Fusarium Oxysporum and Trichoderma Longibrachiatum”. *Construction and Building Materials* 392 (agosto): 131910. https://doi.org/10.1016/j.conbuildmat.2023.131910.

Khushnood, Rao Arsalan, Ateeb Muhammad Ali, Muhammad Faraz Bhatti, y Haris Ahmed Khan. 2022. “Self-Healing Fungi Concrete Using Potential Strains Rhizopus Oryzae and Trichoderma Longibrachiatum”. *Journal of Building Engineering* 50 (junio): 104155. https://doi.org/10.1016/j.jobe.2022.104155.

Li, Huayun, Yangfan Wu, Anxiang Zhou, Chenxi Zhao, Lai Deng, y Feng Lu. 2024. “Experimental Study on Self-Healing Performance of Tunnel Lining Concrete Based on Response Surface Methodology”. *Construction and Building Materials* 425 (abril): 136105. https://doi.org/10.1016/j.conbuildmat.2024.136105.

Majib, Nur Mawaddah, Noorulnajwa Diyana Yaacob, Sam Sung Ting, Nor Munirah Rohaizad, y Athirah Marsya Azizul Rashidi. 2025. “Fungal Mycelium-Based Biofoam Composite: A Review in Growth, Properties and

Application". *Progress in Rubber, Plastics and Recycling Technology* 41 (1): 91-123. https://doi.org/10.1177/14777606241252702.

Mesquita Júnior, Laércio. 2022. "Desenvolvimento de agente biológico para autocicatrização em matrizes cimentícias". Tese de Doutoramento, Universidade Federal de Lavras.

Meyer, Vera, Evelina Y. Basenko, J. Philipp Benz, et al. 2020. "Growing a Circular Economy with Fungal Biotechnology: A White Paper". *Fungal Biology and Biotechnology* 7 (1): 5. https://doi.org/10.1186/s40694-020-00095-z.

Mohamed, Abdulahi, Yonghui Zhou, Elisa Bertolesi, Mengmei Liu, Feiyu Liao, y Mizi Fan. 2023. "Factors Influencing Self-Healing Mechanisms of Cementitious Materials: A Review". *Construction and Building Materials* 393 (agosto): 131550. https://doi.org/10.1016/j.conbuildmat.2023.131550.

Ojha, Amiya, Tarun Kanti Bandyopadhyay, Deeplina Das, y Palash Dey. 2025. "Microbial Carbonate Mineralization: A Comprehensive Review of Mechanisms, Applications, and Recent Advancements". *Molecular Biotechnology*, advance online publication, mayo 8. https://doi.org/10.1007/s12033-025-01433-5.

Rocha, Joaquin Humberto Aquino, Nahúm Gamalier Cayo Chileno, y Romildo Dias Toledo Filho. 2025. "Mechanical and Durability Performance of Mortars with Portland Cement, Recycled Concrete Powder, and Metakaolin under Accelerated Carbonation Conditions". *Powder Technology* 453 (marzo): 120616. https://doi.org/10.1016/j.powtec.2025.120616.

Sun, Xiaohao, Linchang Miao, Linyu Wu, Chengcheng Wang, y Runfa Chen. 2020. "The Method of Repairing Microcracks Based on Microbiologically Induced Calcium Carbonate Precipitation". *Advances in Cement Research* 32 (6): 262-72. https://doi.org/10.1680/jadcr.18.00121.

Sun, Xiaohao, Linchang Miao, Linyu Wu, y Hengxing Wang. 2021. "Theoretical Quantification for Cracks Repair Based on Microbially Induced Carbonate Precipitation (MICP) Method". *Cement and Concrete Composites* 118 (abril): 103950. https://doi.org/10.1016/j.cemconcomp.2021.103950.

Talukdar, S., N. Banthia, y J. R. Grace. 2012. "Carbonation in Concrete Infrastructure in the Context of Global Climate Change – Part 1: Experimental Results and Model Development". *Cement and Concrete Composites* 34 (8): 924-30. https://doi.org/10.1016/j.cemconcomp.2012.04.011.

Toledo Filho, Romildo Dias, Flávio De Andrade Silva, E. M. R. Fairbairn, y João De Almeida Melo Filho. 2009. "Durability of Compression Molded Sisal Fiber Reinforced Mortar Laminates". *Construction and Building Materials* 23 (6): 2409-20. https://doi.org/10.1016/j.conbuildmat.2008.10.012.

Tyagi, Gaurav, Mukund Lahoti, Anshuman Srivastava, Deeksha Patil, Umesh U. Jadhav, y Aniruddha S. Purekar. 2024. "Bioconcrete-Enabled Resilient Construction: A Review". *Applied Biochemistry and Biotechnology* 196 (5): 2901-27. https://doi.org/10.1007/s12010-023-04427-8.

Van Wylick, Aurélie, Antonielle Vieira Monclaro, Elise Elsacker, et al. 2021. "A Review on the Potential of Filamentous Fungi for Microbial Self-Healing of Concrete". *Fungal Biology and Biotechnology* 8 (1): 16. https://doi.org/10.1186/s40694-021-00122-7.

Van Wylick, Aurélie, Hubert Rahier, Lars De Laet, y Eveline Peeters. 2024. "Conditions for $CaCO_3$ Biomineralization by *Trichoderma Reesei* with the Perspective of Developing Fungi-Mediated Self-Healing Concrete". *Global Challenges* 8 (1): 2300160. https://doi.org/10.1002/gch2.202300160.

Vijay, Kunamineni, Meena Murmu, y Shirish V. Deo. 2017. "Bacteria based self healing concrete – A review". *Construction and Building Materials* 152 (octubre): 1008-14. https://doi.org/10.1016/j.conbuildmat.2017.07.040.

Wiktor, V., and H. M. Jonkers. 2016. "Bacteria-based concrete: from concept to market". *Smart Materials and Structures* 25 (8): 084006. https://doi.org/10.1088/0964-1726/25/8/084006.

Zhang, Y. S., Y. Liu, X. D. Sun, et al. 2024. "Application of Microbially Induced Calcium Carbonate Precipitation (MICP) Technique in Concrete Crack Repair: A Review". *Construction and Building Materials* 411 (enero): 134313. https://doi.org/10.1016/j.conbuildmat.2023.134313.

cinpar2026
XXII International Conference on Building Pathology and Constructions Repair
15th to 17th July 2026 - Lisboa, Portugal

On the Seismic and Energy Retrofit of Masonry Buildings Using Inorganic Matrix Composites

Ardalan A. HASSAN[1], Senhorinha TEIXEIRA[2], Daniel V. OLIVEIRA[3]

[1] University of Minho, ISISE, ARISE, Guimarães, Portugal, id11790@alunos.uminho.pt
[2] University of Minho, ALGORITMI, Guimarães, Portugal, st@dps.uminho.pt
[3] University of Minho, ISISE, ARISE, Guimarães, Portugal, danvco@civil.uminho.pt

Abstract: The upgrading of the building stock is one of the main objectives of the European Commission's strategy to achieve climate neutrality. Around 85% of buildings in Europe were constructed before 2001, with approximately 50% of them built before 1970. These structures often fall outside the scope of modern seismic and energy regulations, creating a complex challenge in balancing between preservation and modernisation, particularly as they may require significant retrofitting to meet current standards while also maintaining their historical value.

The use of inorganic matrix composite materials has gained increasing attention in recent decades for construction sector applications. A promising solution for concurrent seismic and energy retrofitting is the Textile-Reinforced Mortar (TRM) system, which has demonstrated promising performance in seismic strengthening. However, a key challenge of conventional TRM systems is their reliance on unsustainable insulation materials for energy upgrades in masonry buildings. While these products are affordable, they often entail a high environmental impact. Therefore, to align with European and international objectives for decarbonisation and climate change mitigation, it is relevant to consider eco-friendly, bio-based composite systems, which can significantly reduce carbon emissions and promote sustainability in product development.

In this study, inorganic matrix composites enabling the integrated seismic strengthening and energy upgrading of masonry buildings are reviewed, with particular attention paid to sustainable alternatives to conventional TRM-based insulation systems.

Keywords: Masonry, Seismic and Energy Retrofitting, Textile-Reinforced Mortar (TRM), Inorganic Matrix Composites (IMCs), Sustainable Construction, Bio-based Materials

1. Introduction

The existing building stock in Europe is currently facing a challenge derived from the urgency of climate change and the persistent threat of seismic hazard. A large proportion of residential and public buildings were built without modern seismic and energy provisions, resulting in high structural vulnerability and operational energy demand (Ademovic et al. 2022; Pohoryles and Bournas 2021). This stock is dominated by unreinforced masonry (URM) buildings, which are characterised by a low tensile strength, brittle failure mechanisms, and poor energy efficiency caused by uninsulated envelopes and air leakage. Typically, seismic retrofitting and energy efficiency improvements were applied as independent and uncoordinated interventions. These interventions were frequently governed by disparate regulatory frameworks. However, investigations of damages from recent earthquake events indicated that pure energy retrofits are substantially vulnerable to seismic actions and may completely lose their functions following structural damages (Belleri and Marini 2016).

Applying energy-only retrofits to seismically vulnerable masonry structures can impede energy retrofit investment when the structure experiences earthquake damage (Bournas 2018). On the other hand, purely seismic interventions may limit improvement of long-term building performance by neglecting thermal transmittance, airtightness, and hygrothermal comfort. These investigations lead to a transformation from independent retrofits to integrated retrofit strategies that simultaneously fulfil the requirements of structural safety and thermal performance. However, implementing integrated retrofit approaches requires the development and validation of multifunctional materials presenting enhancement of mechanical and thermal performance and environmental sustainability, which can include materials that are both energy-efficient and capable of reducing carbon emissions throughout their lifecycle. In response to these needs, inorganic matrix composites (IMCs) have emerged as a key solution to enable such integration. These innovative composites enable discreet, externally applied interventions, which reduce the impact on existing structures and their inhabitants and keep their heritage value, such as minimising structural alterations and maintaining historical aesthetics.

IMCs, which are also known in the literature as Textile Reinforced Mortar (TRM), Fabric Reinforced Cementitious Matrix (FRCM), or Composite Reinforced Mortar (CRM), have become a preferred solution for the URM intervention (Papanicolaou et al. 2011). The conventional IMCs consist of high-strength fibre textiles, which are typically made of carbon, glass, basalt, or steel, embedded within a cementitious or lime-based mortar matrix, as seen in Figure 1a. The latter is often convenient for application to existing masonry and historical structures because it provides superior mechanical and hygrothermal compatibility. The transition from organic-based composites, such as Fibre Reinforced Polymers (FRP), to IMCs is motivated by several technical advancements for masonry applications. Epoxy resins, used in the application of FRPs, suffer from low fire resistance and poor vapour permeability, while the inorganic matrices used in TRM are non-combustible and allow the masonry substrate to "breathe", thus preventing the moisture trap that can lead to material degradation (Parisi et al. 2013).

This paper reviews the transition from traditional IMCs to improved solutions with enhanced structural performance, thermal efficiency, durability, constructability, and environmental properties for integrated seismic and energy retrofitting of masonry buildings. In addition, the study highlights advantages, limitations, and research gaps relevant to materials and structural engineering practice.

2. The Combination of Inorganic Matrix Composites with Thermal Insulation Systems

The mechanical properties of IMCs are highly influenced by matrix composition; therefore, the choice of matrix binder is counted as an important parameter governing both mechanical and durability performance. Cement-based matrices provide high compressive strength, but they do not always work well with traditional masonry due to stiffness incompatibility resulting in stress concentrations and cracking at the interface (Angiolilli et al. 2020). Alternatively, lime-based matrices, particularly those made with natural hydraulic lime (NHL), have lower stiffness but are more compatible, ductile, and vapour permeable. This makes them more suitable for weak or historic substrates (Pugliese et al. 2023). Other rapidly developing alternatives are alkali-activated and geopolymer matrices, which offer reduced embodied carbon and, in some cases, significantly lower thermal conductivity than traditional binders (Longo et al. 2020). However, their performance remains sensitive to precursor chemistry, activator composition, and curing conditions, which poses challenges for reproducibility and standardisation.

Experimental studies indicated the synergy between the textile reinforcement and the mortar matrix, which enables stress redistribution through multiple cracking and progressive load transfer rather than sudden brittle failure. Investigations on URM walls strengthened with TRM systems demonstrated a significant increase in shear strength, stiffness retention, and deformation capacity under cyclic horizontal loading (Kouris et al. 2024). In-plane shear capacity is reported to be increased typically from 60% to over 130%, depending on textile type, anchorage detailing, and matrix properties (Azdejkovic et al. 2025). In addition,

TRM strengthening has been shown to substantially increase out-of-plane and deformation capacity, especially when reinforcement is placed eccentrically with respect to the wall thickness (Karlos et al. 2020). Nevertheless, IMCs exhibit improved fire resistance and better compatibility with weak or historic masonry compared to their counterpart FRP systems, hence reducing the risk of substrate damage and enabling application in conservation-sensitive contexts (Triantafillou et al. 2017; Pugliese et al. 2023).

The integration of thermal insulation into the structural TRM layer can be achieved through various configurations (Triantafillou et al. 2017). Depending on structural and construction requirements, the TRM layer may be applied directly on the masonry substrate, on the external face of the insulation, or on both sides of the insulation layer (Figure 1b). In this arrangement, the insulation layer reduces thermal transmittance while the TRM provides seismic resistance through its tensile capacity.

Experimental investigations indicated that placing IMC over the insulation layer substantially improves the out-of-plane capacity by 200–340% compared to an unreinforced wall (Karlos et al. 2020) due to the increased lever arm between the textile reinforcement and masonry compression zone (Triantafillou et al. 2017). Also, further experimental studies demonstrated that such systems maintain residual stiffness and energy dissipation capacity even after cracking, which is critical for seismic intervention. From a thermal perspective, the insulation layer provides conventional U-value reductions in line with current energy regulations; in parallel, the IMC layer improves airtightness, reducing air infiltration by up to 78%, and protects the insulation layer from mechanical damage (Kallioras et al. 2024).

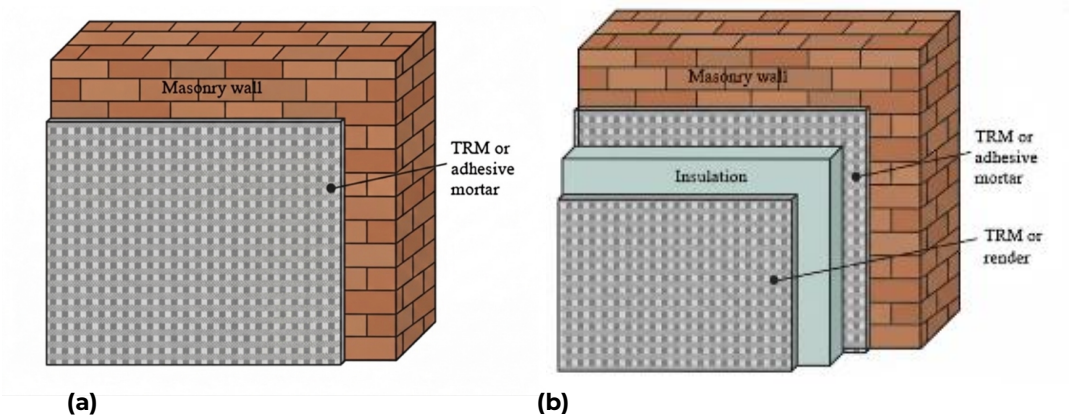


Figure 1 – Schematic view of (a) IMCs and (b) a combination of IMCs with thermal insulation systems on one side of the masonry wall (adapted from (Triantafillou et al. 2017))

Despite the abovementioned advantages, layered systems have several technical challenges. Potential weak planes resulting from multiple interfaces, such as substrate, insulation, and IMC, are vulnerable to debonding under cyclic loading (Figure 2). The associated failure modes were frequently reported from experimental studies when no mechanical anchorage is provided (Triantafillou et al. 2017; Kallioras et al. 2024). On the other hand, the connectors or anchors may present localised thermal bridges and complicate the hygrothermal behaviour, especially if metallic anchors are used without thermal breaks (Valluzzi et al. 2021).

Increased overall thickness of envelopes is another limitation of layered systems, which can be problematic in urban environments with strict façade alignment constraints or in heritage buildings where visual impact must be kept to a minimum. In addition to the above-mentioned mechanical weaknesses, the insulation layer, especially petrochemical-based products such as EPS and XPS, has high embodied carbon and exhibits poor fire performance, thus raising concerns regarding overall sustainability (Pohoryles et al. 2022). Alternatively, to these insulation layers, mineral wool and bio-based insulation materials offer improved fire and environmental performance, but mineral wool production remains highly energy-intensive. Also,

incorporating bio-based materials may need more complicated detailing to guarantee durability and moisture control. Furthermore, Life Cycle Assessment (LCA) indicates that the "carbon payback period", the duration needed for operational energy savings to offset the carbon emitted during the production and installation of these synthetic insulation systems, is much longer than for bio-based alternatives (Kallioras et al. 2024).

Another drawback of layered systems is the limited contribution of material recovery or recycling to the circular economy. In this system, monolithic integration between the layers is required, which often involves strong mechanical or chemical bonding; as a result, separating the synthetic insulation from the IMC layer becomes extremely difficult at the end of the building's service life.

In response to the abovementioned limitations, a limited number of studies have explored the development of multi-purpose composite mortars, in which IMCs are mechanically, thermally, and environmentally enhanced to provide both seismic and energy retrofitting. This methodology seeks to eliminate discrete insulation layers by reducing system thickness, minimising interfaces, and simplifying construction.



Figure 2 – Debonding failure of the composite system on (a), (b) a building prototype scale (Kallioras et al. 2024), and (c) a wallet-scale (Triantafillou et al. 2017) in the laboratory

3. Enhanced Inorganic Matrix Composites

In response to the limitations of layered systems, recent research has focused on developing multi-purpose IMCs in which the matrix itself contributes to thermal insulation. This approach aims to reduce system thickness, eliminate weak interfaces, and enhance sustainability by integrating structural and thermal functions within a single material layer. Several strategies have been proposed to enhance inorganic matrices thermally by replacing standard cement with geopolymer binders and incorporating mineral and lightweight aggregates (e.g., perlite, expanded glass), bio-based aggregates (e.g., rice husk, coffee biochar), phase change materials, and natural fibres (Longo et al. 2020).

Geopolymer binders, derived from precursors such as fly ash or metakaolin, are part of the broader family of alkali-activated materials (AAM) and are particularly suitable for multipurpose composites because of their ability to incorporate a large volume of lightweight or recycled aggregates and their lower embodied carbon compared with ordinary Portland cement (Coppola et al. 2019). Recent experimental investigations indicated that geopolymer-based IMC systems can significantly reduce thermal conductivity by up to 50%

compared to NHL-based IMC while simultaneously keeping sufficient mechanical strength for seismic retrofit (Longo et al. 2020).

The interaction between the matrix and fibre reinforcement for NHL-based and geopolymer-based IMCs was investigated from micrographs, as shown in Figure 3a and Figure 3b, respectively. It is found that in the NHL-based composite, the fabric and the matrix appeared as two distinct phases with minimal contact area, which was restricted primarily to the outer surface of the yarns (Figure 3a). In contrast, the matrix in the geopolymer-based composite effectively penetrates the yarns (Figure 3b). This leads to a significantly larger contact area, with the matrix enveloping the entire lateral surface of the external filaments, a feature likely driven by the fine particle size of the fly ash (Longo et al. 2021). Because of this penetration, the stress distribution and filament tensioning behaved differently between the two composites. The geopolymer-based IMC facilitated a more uniform distribution of stress across the filaments (Figure 3b), meaning that even after matrix cracking occurred, the geopolymer retrofitting often presents higher ductility and energy dissipation, which can partially compensate for lower peak strength.

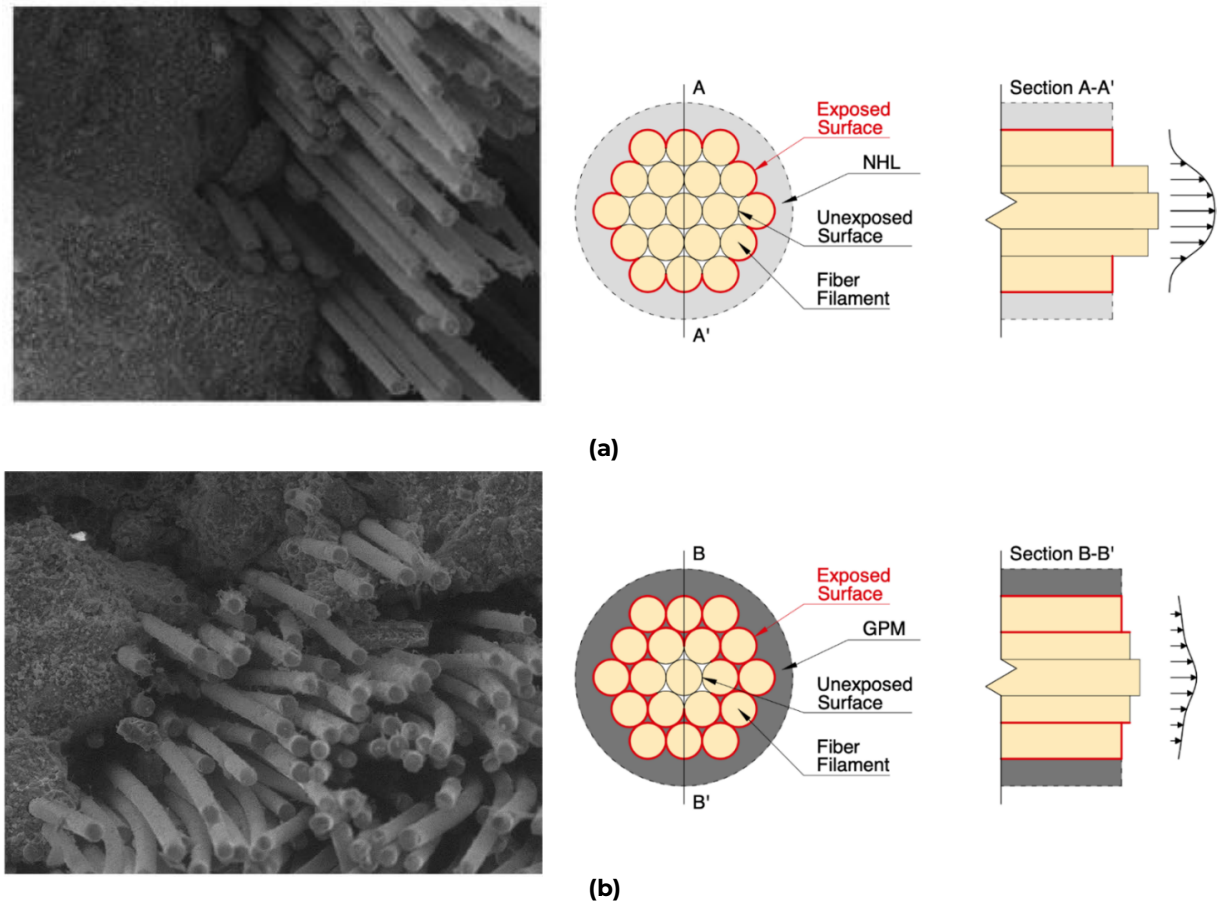


Figure 3 – Micrographs illustrating matrix/fibre interactions in (a) an NHL-based IMC and (b) a geopolymer-based IMC (Longo et al. 2021)

The incorporation of natural fibres into IMC, either as textiles (NTRM) or as dispersed reinforcement, further improves the environmental and thermal profile of multi-purpose composites. Natural fibres such as jute, hemp, and flax have low embodied energy and are renewable materials. They contribute to both crack control and thermal resistance. Recent studies showed that masonry wallets reinforced with NTRM systems achieved substantial increases in lateral load capacity alongside meaningful reductions in thermal transmittance, thus demonstrating their high potential as an integrated retrofit approach (Majumder et al. 2025).

Nevertheless, multi-purpose composites are still constrained by a pronounced thermo-mechanical trade-off. Enhancing thermal insulation of IMCs typically requires increased porosity or incorporation of low-density aggregates. These modifications reduce compressive strength, elastic modulus, and in some cases, bond strength (Ferrández et al. 2024). According to the Scanning Electron Microscope (SEM) images of rice husk ash (RHA)-based mortar, the number and size of pores increased with the RHA-based mortar. Incorporating 30% RHA by weight into the mortar shows a higher number and larger voids, which generates lower conductivity in the mortar and improves its thermal performance by reducing thermal conductivity by up to 62% while maintaining the acceptable compressive strength (Selvaranjan et al. 2021).

While many thermally enhanced mortars still meet minimum strength requirements for masonry strengthening, their reduced stiffness may change load-sharing mechanisms between the fibres and the matrix and cracking behaviour under seismic loading.

3.1 Aggregate Modification for Thermo-Mechanical Enhancement of IMC Systems

The mortar matrix has a major influence on the thermal performance of inorganic matrix composites (IMCs) used in masonry retrofitting. According to European standards (CEN 2020), conventional cement- and lime-based mortars exhibit thermal conductivity values typically in the range of approximately 0.6–1.2 W/m·K, depending on their dry density. These values are considerably higher than those of typical thermal insulation materials. Therefore, aggregate modification has been taken into consideration from recent research as an innovative approach to reduce thermal conductivity while preserving sufficient mechanical performance for seismic retrofit.

Thermal insulation can be incorporated directly into the strengthening layer by replacing natural sand with lightweight or porous aggregates. This reduces density, decreases system thickness and eliminates the need for extra interfaces. This method is especially useful for integrated seismic and energy retrofitting. However, as lightweight aggregates improve thermal properties of the matrix through reducing density and heat transfer, they may also decrease compressive strength, stiffness, and bond capacity. For example, among mineral lightweight aggregates, expanded perlite has been widely investigated due to its highly porous microstructure. The study from Fenoglio et al. (2018) indicates a reduction of thermal conductivity by 50–55% when natural sand was partially substituted by expanded perlite depending on the substitution ratio (Fenoglio et al. 2018).

Significant modifications were also offered by expanded glass aggregates, which usually achieve greater than 50% reductions in thermal conductivity and compressive strengths greater than 8 MPa (Longo et al. 2020). Because of improving matrix–aggregate bonding, natural volcanic aggregates like pumice preserve relatively strong mechanical performance while providing moderate insulating benefits.

In addition to mineral aggregates, recycled and industrial waste materials have been explored as sustainable alternatives. Crushed ceramic waste aggregates provide smaller reductions in thermal conductivity but preserve mechanical properties comparable to conventional mortars.

Recently, bio-based aggregates such as rice husk, cork granules, wood particles, and coffee biochar have been explored due to their low embodied carbon and very low thermal conductivity, frequently below 0.31 W/m·K (Roychand et al. 2023; Selvaranjan et al. 2021). It was observed that rice husk-based mortars can reduce thermal conductivity by up to 59–68%, although high water absorption may affect workability and durability. Furthermore, the mechanical strength was found to be highly dependent on the dosage ratio (Penazzato, Sakhizada, et al. 2024). Similarly, coffee biochar enhances insulation performance and reduces embodied carbon, but a high substitution rate may weaken the matrix (La Scalia et al. 2021; Penazzato, Illampas, et al. 2024). Table 1 presents a comparative overview of various IMC systems in terms of thermal conductivity, compressive strength, and test scale.

The mechanical compatibility of modified mortars is still a challenge for IMC systems. The mortar matrix must guarantee adequate compressive strength and bond capacity to allow efficient stress transfer

between the textile and the masonry substrate, even if textile reinforcement mostly transfers tensile stresses. However, excessive stiffness reductions may limit out-of-plane capacity, highlighting the need for a balanced mix design when integrating thermal and structural retrofit objectives (Majumder et al. 2025; Longo et al. 2021).

Table 1 – Comparative overview of selected IMC systems: thermal conductivity, compressive strength, and test scale

IMC System	Thermal conductivity λ (W/m·K)	Compressive strength fc (MPa)	Test scale	Key reference
Lime-/cement-based mortar	0.6–1.2 W/m·K	N/A	Material	CEN 2020
NHL + expanded perlite	~0.059–0.118 (↓50–55%)	N/A	Material	Fenoglio et al. 2018
Geopolymer + expanded glass	~0.16–0.25 (↓> 50)	>8	Material	Longo et al. 2020
Ordinary Portland Cement (OPC) + burnt rice husk ash	~0.31(↓62%)	>7	Material	Selvaranjan et al. 2021
NHL + rice husk (untreated RH-U or grounded RH-G)	0.28-0.37 (↓59–68%)	~1 (highly rate-dependent)	Material	Penazzato, Sakhizada, et al. 2024
NHL + coffee biochar (bio-aggregate)	<0.3 (↓66–77%)	~5–10 (rate-dependent)	Material	Penazzato, Illampas, et al. 2024)

Note: λ values are approximate ranges from reported mix designs; N/A = data not quantified in reviewed sources. Embodied carbon data was not consistently reported across the reviewed sources and is therefore excluded from this comparison.

3.2 Environmental Impact and Long-Term Performance

From an environmental perspective, integrated seismic-energy retrofit strategies offer clear advantages over separated interventions when assessed on a life-cycle basis. Reducing binder-related embodied carbon is a crucial goal in sustainable construction since cement production contributes significantly to global CO_2 emissions. Compared to traditional cement-based mortars, alkali-activated and geopolymer mortars can contribute to a reduction in embodied carbon, particularly when industrial by-products such as fly ash or slag are used as precursors (Coppola et al. 2019).

Aggregate substitution further influences the environmental performance of thermally enhanced matrix composites. Lightweight, recycled, and bio-based aggregates can reduce material density, embodied energy, and the need for virgin resources. Life-cycle assessment (LCA) studies indicate that aggregate substitution with lightweight or bio-based materials can contribute to reductions in embodied carbon compared to conventional cement-based mortars. For instance, perlite-based plasters have demonstrated significant reductions in embodied carbon when assessed on a cradle-to-site basis, and bio-based aggregates such as spent coffee grounds offer additional sustainability benefits through waste valorisation and reduced reliance on virgin materials (Fenoglio et al. 2018; La Scalia et al. 2021).

Despite their environmental benefits, long-term performance is still a major issue for integrated retrofit systems. The service life of retrofitted systems can be greatly impacted by the degradation of the embedded reinforcement and mortar matrix. For instance, uncoated natural fibres used in NTRM systems are vulnerable to biological deterioration, moisture absorption, and alkaline attack from the surrounding matrix. If the fibres are not appropriately treated, this could eventually result in a significant loss of strength. Surface treatments, mineral coatings, and hybrid reinforcement strategies have been proposed to mitigate these effects, although long-term experimental evidence remains limited. Similarly, compared to conventional binders, alkali-activated matrices may show more shrinkage and efflorescence, which may impact bond performance and durability (Coppola et al. 2019).

In general, performance evaluation and design implementation are becoming more difficult due to the lack of standardised durability testing procedures for integrated seismic-energy retrofit systems. The majority of existing research concentrates on short-term mechanical behaviour, underscoring the necessity of long-term studies that address the interrelated effects of environmental degradation, thermal exposure, and mechanical stress.

4. Discussion and Research Gaps

Comparing layered systems and thermally enhanced composites reveals that neither strategy is superior. Layered systems benefit from technical maturity, predictable structural performance, and compatibility with established insulation technologies, but they suffer from interface-related vulnerabilities and increased thickness. On the other hand, multipurpose composites present strong benefits in terms of material efficiency, decreased thickness, and decreased embodied carbon, but they encounter difficulties with durability, thermo-mechanical trade-offs, and a lack of standardisation.

Critical gaps remain for thermally enhanced IMCs, including the need for standardised mix designs that address thermal, mechanical, and durability aspects. Most studies focus on short-term material performance, neglecting real-world long-term effects. Additionally, while small-scale successes are documented, full-scale system behaviours under various conditions are still missing, particularly in terms of how these systems perform over extended periods and in diverse environmental scenarios. There is also a lack of a numerical approach to evaluate the efficiency of the enhanced system for different climate and seismic regions. Furthermore, sustainability assessments often only cover early lifecycle stages, with methodological inconsistencies impacting robust evaluations of lifecycle implications, which can lead to an incomplete understanding of the long-term environmental impacts of the system across various climate and seismic regions.

5. Conclusions

This study has examined advances in thermally enhanced Inorganic Matrix Composites (IMCs) for the integrated seismic and energy retrofitting of masonry buildings, with particular emphasis on the role of alternative aggregates in replacing natural sand, as well as on sustainability and durability. The investigation demonstrates that lightweight mineral, waste-derived, and agricultural bio-based aggregates offer advantages in reducing thermal conductivity and environmental impact, although they have varying performance in terms of mechanical strength and long-term stability.

While mineral lightweight aggregates currently provide the most balanced combination of thermal and mechanical performance, bio-aggregates present substantial opportunities for reducing embodied carbon and promoting circular economy principles. However, their widespread adoption is constrained by durability concerns and performance variability. Overcoming these limitations through performance-based mix design, interface engineering, long-term and numerical validation is essential.

Thermally enhanced IMC systems offer a promising approach toward multipurpose retrofit solutions that can concurrently enhance environmental sustainability, energy efficiency, and structural safety. To enable the utilisation of this solution in the rehabilitation of the stock of masonry buildings, more research on durability, standardisation, and full-scale system validation are essential.

Acknowledgements

This work was supported by FCT/MCTES under the R&D Unit Institute for Sustainability and Innovation in Structural Engineering (ISISE), under the references UID/4029/2025, UID/PRR/04029/2025 and UID/PRR2/04029/2025, and under the Associate Laboratory Advanced Production and Intelligent Systems ARISE under reference LA/P/0112/2020. This research was also co-financed by the European Regional Development Fund (FEDER), through the Northern Regional Program 2021-2027 (NORTE 2030), Portugal 2030 and by national funds through the R&D project "EcoRehabPanel: Development of prefabricated panels with functional and mechanical gradation towards a more efficient and sustainable rehabilitation of the built environment", project no. 42689, operation code NORTE2030-FEDER-02718000.

References

Ademovic, Naida, Antonio Formisano, Luca Penazzato, and Daniel V. Oliveira. 2022. "Seismic and Energy Integrated Retrofit of Buildings: A Critical Review." *Frontiers in Built Environment* 8 (November). https://doi.org/10.3389/fbuil.2022.963337.

Angiolilli, Michele, Amedeo Gregori, Madura Pathirage, and Gianluca Cusatis. 2020. "Fiber Reinforced Cementitious Matrix (FRCM) for Strengthening Historical Stone Masonry Structures: Experiments and Computations." *Engineering Structures* 224 (December). https://doi.org/10.1016/j.engstruct.2020.111102.

Azdejkovic, Lazar D., T. C. Triantafillou, Catherine Papanicolaou, and Luiz Miranda de Lima. 2025. "Application of Alkali-Activated Materials (AAM) in Seismic and Combined Energy and Seismic Retrofitting of Beam-Type Masonry Walls: In- and out-of-Plane Behavior." *Engineering Structures* 334 (July). https://doi.org/10.1016/j.engstruct.2025.120207.

Belleri, Andrea, and Alessandra Marini. 2016. "Does Seismic Risk Affect the Environmental Impact of Existing Buildings?" *Energy and Buildings* 110 (January): 149–58. https://doi.org/10.1016/j.enbuild.2015.10.048.

Bournas, Dionysios A. 2018. "Concurrent Seismic and Energy Retrofitting of RC and Masonry Building Envelopes Using Inorganic Textile-Based Composites Combined with Insulation Materials: A New Concept." *Composites Part B: Engineering* 148 (September): 166–79. https://doi.org/10.1016/j.compositesb.2018.04.002.

CEN, European Committee for Standardization. 2020. *EN 1745:2020 Masonry and Masonry Products - Methods for Determining Thermal Properties*.

Coppola, L., D. Coffetti, E. Crotti, A. Marini, C. Passoni, and T. Pastore. 2019. "Lightweight Cement-Free Alkali-Activated Slag Plaster for the Structural Retrofit and Energy Upgrading of Poor Quality Masonry Walls." *Cement and Concrete Composites* 104 (November). https://doi.org/10.1016/j.cemconcomp.2019.103341.

Fenoglio, Elisa, Stefano Fantucci, Valentina Serra, Corrado Carbonaro, and Riccardo Pollo. 2018. "Hygrothermal and Environmental Performance of a Perlite-Based Insulating Plaster for the Energy Retrofit of Buildings." *Energy and Buildings* 179 (November): 26–38. https://doi.org/10.1016/j.enbuild.2018.08.017.

Ferrández, Daniel, Alicia Zaragoza-Benzal, Rocío Pastor Lamberto, Paulo Santos, and Jacek Michalak. 2024. "Optimizing Masonry Mortar: Experimental Insights into Physico-Mechanical Properties Using

Recycled Aggregates and Natural Fibers." *Applied Sciences (Switzerland)* 14 (14). https://doi.org/10.3390/app14146226.

Kallioras, Stylianos, Dionysios Bournas, Lampros Koutas, and Francisco Javier Molina. 2024. "Integrated Seismic and Energy Retrofitting of Masonry-Infilled RC Buildings with Textile-Reinforced Mortar and Thermal Insulation: Full-Scale Tests on a Five-Story Prototype." *Journal of Building Engineering* 98 (December). https://doi.org/10.1016/j.jobe.2024.111006.

Karlos, Kyriakos, Aristomenis Tsantilis, and T. C. Triantafillou. 2020. "Integrated Seismic and Energy Retrofitting System for Masonry Walls Using Textile-Reinforced Mortars Combined with Thermal Insulation: Experimental, Analytical, and Numerical Study." *Journal of Composites Science* 4 (4). https://doi.org/10.3390/jcs4040189.

Kouris, L., D. A. Bournas, D. A. Pohoryles, G. Valsamos, T. Savvas, and C. Maduta. 2024. "Seismic plus Energy Upgrading of Masonry Buildings Using Advanced Materials." (Luxembourg). https://doi.org/10.2760/66556.

La Scalia, Giada, Manfredi Saeli, Pier Paolo Miglietta, and Rosa Micale. 2021. "Coffee Biowaste Valorization within Circular Economy: An Evaluation Method of Spent Coffee Grounds Potentials for Mortar Production." *International Journal of Life Cycle Assessment* 26 (9): 1805–15. https://doi.org/10.1007/s11367-021-01968-0.

Longo, Fabio, Alessio Cascardi, Paola Lassandro, and Maria Antonietta Aiello. 2021. "Energy and Seismic Drawbacks of Masonry: A Unified Retrofitting Solution." *Journal of Building Pathology and Rehabilitation* 6 (1). https://doi.org/10.1007/s41024-021-00121-6.

Longo, Fabio, Paola Lassandro, Amir Moshiri, Tejasree Phatak, Maria A. Aiello, and Konrad J. Krakowiak. 2020. "Lightweight Geopolymer-Based Mortars for the Structural and Energy Retrofit of Buildings." *Energy and Buildings* 225 (October). https://doi.org/10.1016/j.enbuild.2020.110352.

Majumder, Arnas, Flavio Stochino, Monica Valdes, Giovanna Concu, Marco Pepe, and Enzo Martinelli. 2025. "Sustainable Masonry Retrofitting and Upgrading Techniques: A Review." *Fibers* 13 (6). https://doi.org/10.3390/fib13060068.

Papanicolaou, Catherine, T. C. Triantafillou, and Maria Lekka. 2011. "Externally Bonded Grids as Strengthening and Seismic Retrofitting Materials of Masonry Panels." *Construction and Building Materials* 25 (2): 504–14. https://doi.org/10.1016/j.conbuildmat.2010.07.018.

Parisi, Fulvio, Ivano Iovinella, Alberto Balsamo, Nicola Augenti, and Andrea Prota. 2013. "In-Plane Behaviour of Tuff Masonry Strengthened with Inorganic Matrix-Grid Composites." *Composites Part B: Engineering* 45 (1): 1657–66. https://doi.org/10.1016/j.compositesb.2012.09.068.

Penazzato, Luca, Rogiros; Illampas, José C.;. Teixeira, and Daniel V.;. Oliveira. 2024. "Development and Characterisation of Lime-Based Mortars Incorporating Coffee-Based Products for Integrated Seismic and Energy Retrofitting." *MATEC Web of Conferences* 403: 03005–03005. https://doi.org/10.1051/matecconf/202440303005.

Penazzato, Luca, Mirwais Sakhizada, Rogiros Illampas, José C. Teixeira, Maura Imbimbo, and Daniel V. Oliveira. 2024. *DEVELOPMENT OF AN ECO-FRIENDLY LIME-BASED MORTAR SUITABLE FOR INTEGRATED RETROFITTING: THERMOPHYSICAL AND MECHANICAL CHARACTERIZATION*. www.isise.net.

Pohoryles, D. A., and D. A. Bournas. 2021. *iRESIST+ Innovative Seismic and Energy Retrofitting of the Existing Building Stock*. https://doi.org/10.2760/496388.

Pohoryles, D. A., D. A. Bournas, F. Da Porto, A. Caprino, G. Santarsiero, and T. C. Triantafillou. 2022. “Integrated Seismic and Energy Retrofitting of Existing Buildings: A State-of-the-Art Review.” *Journal of Building Engineering* 61 (December). https://doi.org/10.1016/j.jobe.2022.105274.

Pugliese, Dora, Valerio Alecci, Rosa Romano, Gianfranco Stipo, Mario De Stefano, and Antonio Nanni. 2023. “Innovative and Sustainable Composite Material for the Seismic and Energetic Upgrade of Historic Masonry Buildings.” *Fibers* 11 (9). https://doi.org/10.3390/fib11090076.

Roychand, Rajeev, Shannon Kilmartin-Lynch, Mohammad Saberian, Jie Li, Guomin Zhang, and Chun Qing Li. 2023. “Transforming Spent Coffee Grounds into a Valuable Resource for the Enhancement of Concrete Strength.” *Journal of Cleaner Production* 419 (September). https://doi.org/10.1016/j.jclepro.2023.138205.

Selvaranjan, Kajanan, J. C. P. H. Gamage, G. I. P. De Silva, and Satheeskumar Navaratnam. 2021. “Development of Sustainable Mortar Using Waste Rice Husk Ash from Rice Mill Plant: Physical and Thermal Properties.” *Journal of Building Engineering* 43 (November). https://doi.org/10.1016/j.jobe.2021.102614.

Triantafillou, T. C., Kyriakos Karlos, Kalliopi Kefalou, and Eirini Argyropoulou. 2017. “An Innovative Structural and Energy Retrofitting System for URM Walls Using Textile Reinforced Mortars Combined with Thermal Insulation: Mechanical and Fire Behavior.” *Construction and Building Materials* 133 (February): 1–13. https://doi.org/10.1016/j.conbuildmat.2016.12.032.

Valluzzi, M. R., Elisa Saler, Alberto Vignato, et al. 2021. “Nested Buildings: An Innovative Strategy for the Integrated Seismic and Energy Retrofit of Existing Masonry Buildings with CLT Panels.” *Sustainability (Switzerland)* 13 (3): 1–19. https://doi.org/10.3390/su13031188.

XXII International Conference on Building Pathology and Constructions Repair
15th to 17th July 2026 - Lisboa, Portugal

Mortar with Steelmaking Slag for Repairs of Historic Buildings

Elói SOUZA[1], Magna BOCAGE[2], Brendda MAGALHÃES[3], **Laís COSTA[4]**

[1] Sustainable Construction and Innovation Laboratory, Federal University of Ceará, Russas, Brazil, eloirsouza@alu.ufc.br
[2] Sustainable Construction and Innovation Laboratory, Federal University of Ceará, Russas, Brazil, magnabocage@alu.ufc.br
[3] Sustainable Construction and Innovation Laboratory, Federal University of Ceará, Russas, Brazil, brendda@alu.ufc.br
[4] Sustainable Construction and Innovation LaboratoryFederal University of Ceará, Russas, Brazil, laiscosta@ufc.br

Abstract: Historic buildings are subject to natural deterioration processes over time, compromising their construction systems. In this context, the use of compatible repair mortars is essential for the preservation of built heritage. Therefore, this study aimed to develop low environmental impact mortars for repair interventions in historic buildings. The mixtures were produced with a 1:5 ratio (binder:aggregate), respecting the typical composition of historic mortars from the state of Ceará, Brazil. Cement and lime were used as binders, with steelmaking slag employed as a full replacement for natural sand. The mortars were characterized in both fresh and hardened states, evaluating their physical and mechanical performance. The results indicated higher apparent density, lower void index and water absorption, as well as superior mechanical performance for the slag-containing mortars compared to historic mortars. Although the use of residues from the steelmaking industry is applicable in mortars, the results demonstrate that their application in interventions on historic buildings should be carried out with caution, particularly due to the increase in mechanical performance, which may compromise material compatibility and the long-term behavior of the construction system.

Keywords: Repair mortars. Historic buildings. Steelmaking slag. Sustainability.

1. Introduction

Historic buildings hold significant cultural and scientific value, serving as testimonies to past construction technologies and architectural expressions (Longobardi and Formisano, 2022). Their preservation safeguards heritage and contributes to the advancement of technical knowledge, as established in the Venice Charter (1964), which guides interventions toward maintaining the historical and aesthetic values of such constructions.

Restoration consists of reintegrating damaged parts of a cultural asset using original or equivalent materials, while preserving its heritage value (Lin et al., 2024). This procedure is essential due to the ageing of historic buildings and their consequent deterioration (Pescari, Budau and Vilceanu, 2023). To achieve this, interventions must reconcile authenticity and functionality, minimal intervention and safety, material compatibility and durability, as well as legibility and aesthetic integration (Vysvaril et al., 2020; Papayianni, Pachta and Stefanidou, 2013).

Despite these well-established conservation principles, the selection of repair materials remains a challenge. The application of mortars incompatible with historic substrates may lead to mechanical decoupling, moisture accumulation, cracking, and long-term accelerated deterioration (Nogueira, Pinto and Gomes, 2020; Loureiro, 2019; Aggelakopoulou et al., 2011). In this context, the characterization of composition, mechanical and hygroscopic parameters is essential to ensure compatibility and the long-term performance of repair interventions in historic buildings (Pavlik et al., 2023).

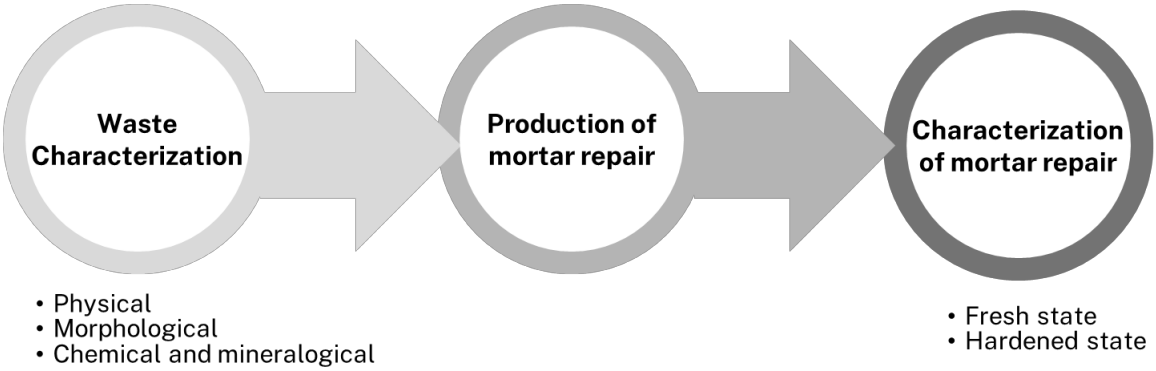
In parallel, the incorporation of industrial by-products into construction materials has been widely explored as a sustainable strategy for construction sector (Salles, 2017; Magalhães, 2018; Loureiro, 2019). However, in heritage applications, such materials must exhibit adequate mechanical performance and ensure physicomechanical compatibility with the original substrate (Groot & Gunneweg, 2019; Veiga, 2017; Posani, Veiga and Freitas, 2022), since not all by-products are compatible with historic constructions. Thus, their use requires careful evaluation prior to application in repair mortars (Gonzalez-Sanchez et al., 2021).

In this context, steelmaking slag emerges as an industrial by-product with potential application in repair mortars, due to its physical and chemical characteristics that may contribute to both mechanical performance and material sustainability. However, its feasibility in heritage interventions still requires investigation regarding its compatibility with historic substrates. Therefore, this study evaluated the performance of repair mortars incorporating steelmaking slag, with emphasis on mechanical and physical parameters relevant to applications in historic buildings.

2. Methodology

Figure 1 presents the experimental flowchart of the research procedure. Initially, the residue used in the production of the repair mortars was characterized. Simultaneously, a sample of the original mortar from the historic building under study was analyzed. Based on these results, the proposed mortar mixtures were produced and subsequently evaluated in fresh and hardened states.

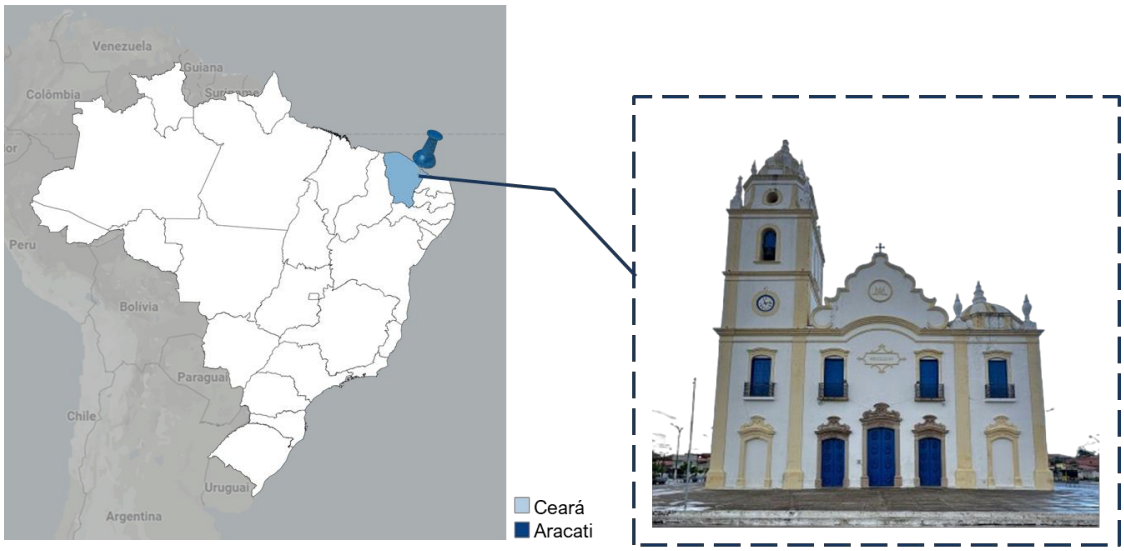
Figure 1 - Flowchart of the research stages.



2.1 Reference historical mortar

The reference historic mortar considered in this study was previously characterized by Souza et al. (2026), based on samples collected from the Church of Nossa Senhora do Rosário (Figure 2). This mortar served as the basis for the development of a repair mortar compatible with the original construction system of the building. The church is located in the municipality of Aracati, in eastern Ceará, Brazil.

Figure 2 – The Church Matriz of Nossa Senhora of Rosário and location in Aracati, Ceará.



The Church of Nossa Senhora do Rosário represents a significant example of Ceará's regional religious architecture constructed using traditional materials and techniques. Originally built in the early 18th century as a small chapel, it underwent successive expansions and was completed in the second half of the 19th century. It is currently designated as the main parish church (Matriz de Nossa Senhora do Rosário).

In the study by Souza et al (2026), a representative mortar sample was extracted from the left lateral façade of the building. The sample was taken from an area that already exhibited signs of deterioration, thereby minimizing intervention in well-preserved regions. The collected material was subjected to physical, chemical, and morphological characterization. The historic mortar exhibited a maximum aggregate size of 2.4 mm and a binder-to-aggregate ratio of approximately 1:5, indicating a composition consistent with traditional construction practices. These characteristics were used as the basis for the formulation and compatibility assessment of the proposed repair mixtures.

2.2 Waste Characterization

The residue selected for this research was a steelmaking slag (SS), generated from the refining process (Figure 3). The material was supplied by an integrated steelmaking facility in Ceará. Its selection was motivated by the economic relevance of the steelmaking sector in the state.

Figure 3 – Steelmaking slag used in this study.



SS was investigated as a full replacement for natural fine aggregate in the proposed repair mortars. The material was reduced by quartering to obtain a representative sample and oven-dried at 105 °C for 24 h prior to use. Particles larger than 4.75 mm were crushed in a jaw crusher (I-4198, Contenco) and sieved to meet the particle size limits for fine aggregates established by NBR 7211 (ABNT, 2019) and to ensure compatibility with

the particle size distribution of the historic mortar (Souza et al, 2026). The materials were then physically characterized, as summarized in Table 1.

Table 1 - List of physical characterization tests performed on the waste.

Property	Principle	Standard
Particle size distribution	Sieving	NBR 17054 (2022)
Specific gravity	Chapman flask	NBR 16916 (2021)
Bulk density	Weighing in a graduated container	NBR 16972 (2021)
Fines contente (material under 75µm)	Washing through sieves	NBR 16973 (2021)

The elemental composition of the SS was determined by X-ray fluorescence (XRF) analysis using a PANalytical Epsilon 3X spectrometer. For this purpose, the sample was previously milled to pass the 75 µm sieve. Mineralogical aspects were discussed based on data available in the literature for steelmaking slags with comparable origin and production process.

2.3 Production and characterization of mortar repair

Based on the reference mix proportion determined through the reconstruction method (Souza et al 2026), repair mortars compatible with the historic build were formulated with a binder-to-aggregate ratio of 1:5. The integration of mix reconstruction and performance analysis enabled the development of mortars with improved physical behaviour, contributing to restoration strategies for historic buildings.

Two binders were used: hydrated lime (CH-I) and Portland cement (CP II-F), allowing evaluation of the influence of binder type on physical and mechanical performance. Natural quartz river sand from Russas, Ceará, Brazil, was adopted as the reference fine aggregate, and potable water supplied by the local utility company was used in all mixtures. After grinding, SS presented a suitable particle size distribution, enabling its use as a full replacement for natural sand. Mixtures were identified using the format XX–YYY, where XX denotes the binder (CP for cement and CH for lime) and YYY indicates the fine aggregate: (REF: conventional aggregate; SSA: steelmaking slag aggregate).

The water-to-binder ratio (w/b) was adjusted to achieve a consistency index of 260 ± 5 mm, in accordance with NBR 16541 (ABNT, 2016). The mortars were evaluated in both fresh and hardened states, and their physical and chemical properties were determined according to the procedures summarized in Table 2.

Table 2 - Experimental program for fresh and hardened mortars.

Test	State	Age (days)	n.	Standard
Consistency index	Fresh	–	–	NBR 13276
Bulk density	Fresh	–	–	NBR 13278
Compressive & flexural strength	Hardened	7 and 28	3	NBR 13279
Void index and specific gravity	Hardened	28	3	NBR 9778

The adopted methodology enabled a systematic assessment of the proposed repair mortars, encompassing material characterization and performance evaluation in both fresh and hardened states. The experimental program provided a consistent basis for comparing conventional and SSA-based mixtures, supporting the development of compatible repair solutions for heritage conservation.

3. Results and Discussion

3.1 Waste Characterization

Table 3 presents the chemical composition of the SS. The slag is characterized by a high content of iron (III) oxide (Fe_2O_3), as expected for a steelmaking by-product. This feature is directly related to the steelmaking refining process, resulting in a material rich in metallic oxides and high-density phases (Baeza et al., 2018). Additionally, considerable amounts of SiO_2 were identified, a compound commonly found in natural sands, along with CaO, a major constituent typically observed in steel slags (Dias et al., 2020; Wang and Chen, 2015).

Table 3 - Chemical composition of the SS.

Component	CaO	Fe_2O_3	SiO_2	MgO	Al_2O_3	MnO	P_2O_5	NaO_2	SO_3	Cr2O3	CO_2
Content (%)	38.45	30.66	12.27	4.96	3.36	3.44	1.88	0.44	0.19	0.48	2.91

Regarding the mineralogical characteristics, Amancio et al. (2020) identified the presence of crystalline phases such as wustite (FeO) and magnetite (Fe_3O_4) in SS. The occurrence of these iron-rich phases confirms that the material was subjected to intense thermal processes typical of steelmaking furnaces. These mineralogical features are consistent with the steelmaking origin of the residue and reflect the high-temperature conditions involved in its production.

The physical properties of the studied materials are presented in Table 4. The SS exhibited the highest specific gravity, approximately 40.15% greater than natural quartz river sand (REF). This result is consistent with chemical composition of SS and its high iron oxide content.

Table 4 - Physical properties of the materials used.

Propriety	**SSA**	**REF**	**Lime**	**Cement**
Specific mass (g/cm³)	3.63	2.61	2.24	3.10
Unit mass (g/cm³)	1.78	1.42	0.43	1.20
Fineness modulus	2.02	1.83	-	-

The fineness modulus of SS indicates a relatively coarse particle size distribution compared to conventional fine aggregates (REF). Figure 4 provides an overview of the granulometric distribution of the studied materials. Both aggregates exhibit a particle size distribution curve within the usable range established by ABNT NBR 7211 (2022), indicating the effectiveness of SS processing to achieve a distribution closer to that of natural sand.

Figure 4 - Particle size distribution curves of the materials used in the research.

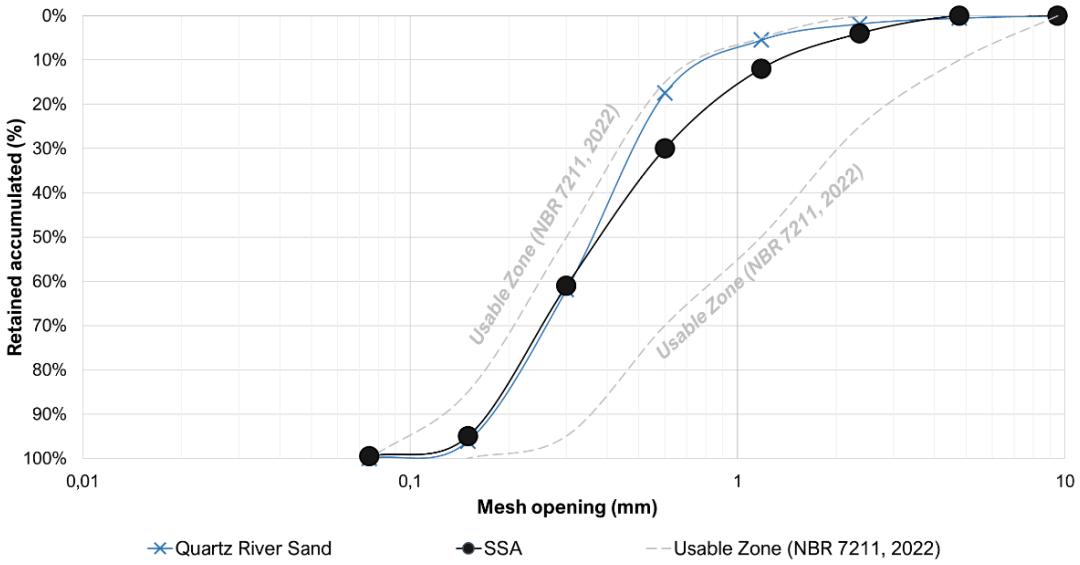
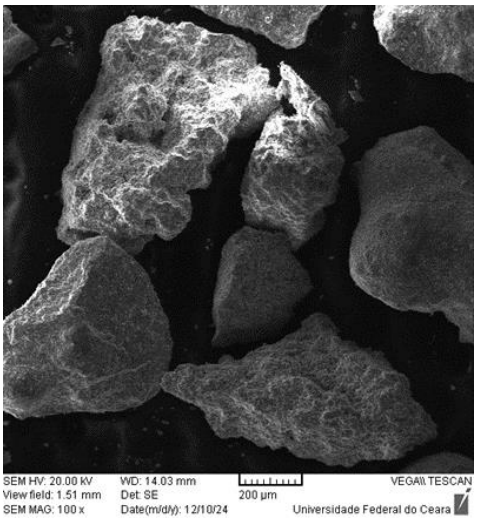


Figure 5 presents the morphological characterization of the SSA, revealing that its particles exhibit an angular morphology. This characteristic is commonly observed in materials subjected to rapid cooling and subsequent mechanical fragmentation processes.

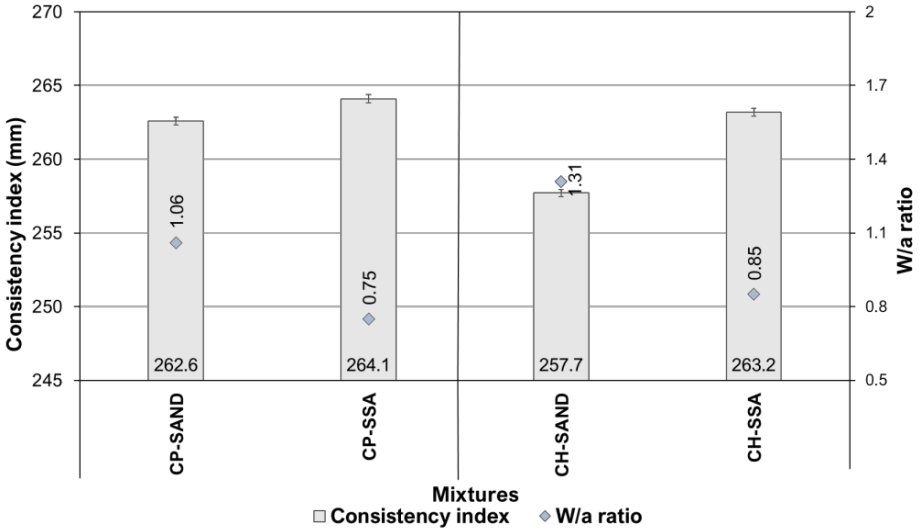
Figure 5 - Morphology of SSA particles obtained with SEM at 100x magnification.



3.3 Characterization of repair mortars in the fresh state

Figure 6 presents the consistency index and corresponding water-to-binder (w/b) ratios of the proposed mortars. Binder type and SSA incorporation significantly affected water demand. Cement-based mortar required a w/b ratio of 1.06, reduced to 0.75 with SSA. Lime-based mortar showed higher water demand, with w/b ratios of 1.31 and 0.85 for the conventional and SSA-modified mixtures, respectively.

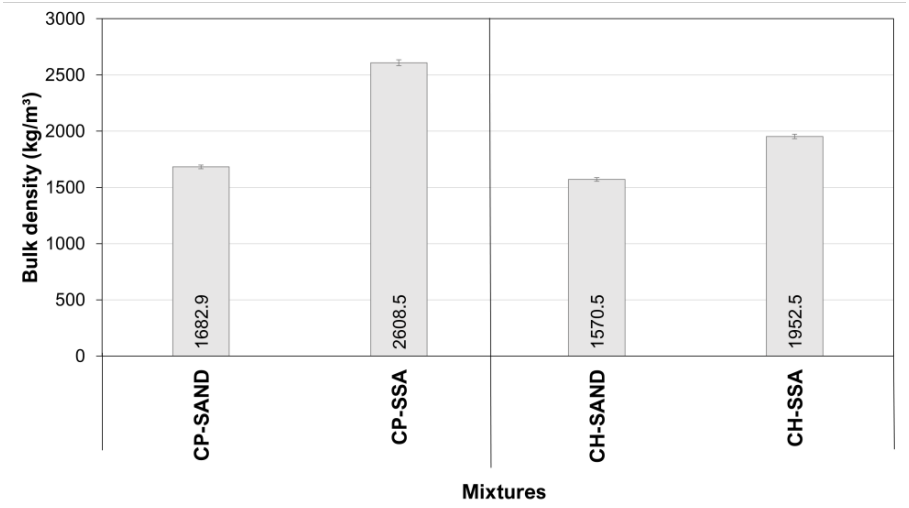
Figure 6 - Consistency index and water/binder ratio of the proposed mortars.



The incorporation of SSA promoted increased flowability despite the lower water content. This behavior is related to its higher specific gravity, which reduces the volumetric proportion occupied by the solid particles and, consequently, the amount of water required in the mixture (Ripardo et al., 2025). Furthermore, because the consistency test is based on impact spreading, denser mixtures tend to disperse more easily under repeated drops, resulting in greater apparent fluidity.

Figure 7 shows the bulk density values of the mortars in the fresh state. This property is directly influenced by the specific gravity of the constituent materials and the volumetric proportions within the mixture.

Figure 7 - Bulk density of the mortars in the fresh state.



The incorporation of SSA led to a substantial increase in fresh bulk density. In cement-based mortars, the replacement of natural sand with SSA resulted in an increase of approximately 55%, which is consistent with the fact that the slag presents a specific gravity about 41% higher than that of the conventional aggregate.

For lime-based mixtures, the lower specific gravity of hydrated lime compared to Portland cement, combined with the higher water demand previously observed, contributed to reduced density values, a behavior also reported by Malathy et al. (2022). Nevertheless, when SSA was incorporated into lime mortars, an increase of approximately 24% in bulk density was observed, highlighting the significant influence of the residue's higher specific gravity when used as a full replacement for natural aggregate. Regarding the fresh-state properties,

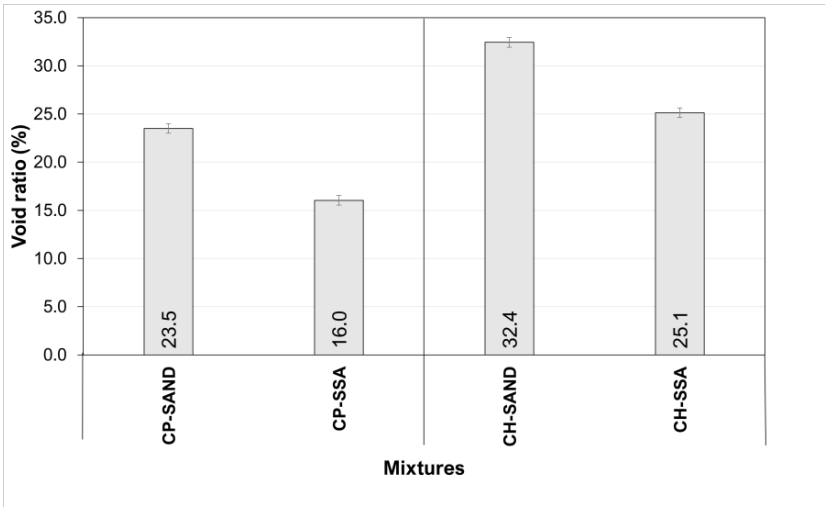
the incorporation of SSA affects the bulk density, primarily due to the intrinsic characteristics of the material; however, it does not significantly impair the workability when compared to the reference historical mortar.

3.4 Characterization of repair mortars in the hardened state

3.4.1 Void ratio and specify mass

Figure 8 presents the void index of the mortars. Lime-based mixtures exhibited higher void index values compared to cement-based mortars, a result consistent with the inherently more porous microstructure of lime-based systems, as widely reported in the literature (Silva, Guerreiro and Duarte, 2025; Gonzalez-Sanchez et al., 2021).

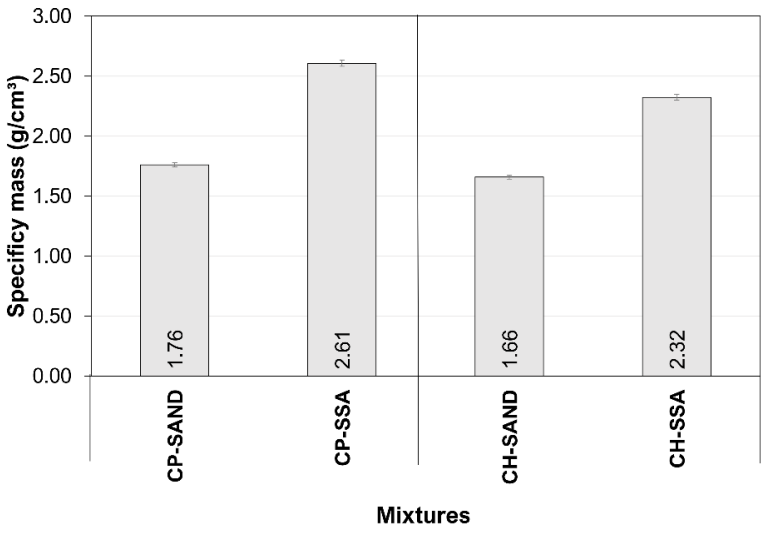
Figure 8 - Void index of the mortars in the hardened state.



Among the mixtures incorporating SSA, the lowest void index values were observed across all studied formulations. The slag presents angular particles and a relatively coarse particle size distribution, characteristics that enhance particle interlocking and packing efficiency, leading to a denser and more compact matrix. This densification effect has also been reported in the literature (Miah et al., 2020).

Figure 9 presents the specific gravity results of the mortars in the hardened state. In general, this property is strongly influenced by the density of the constituent materials, particularly the aggregate, which represents the largest volumetric fraction of the mixture.

Figure 9 - Specific gravity of the mortars in the hardened state.



In cement-based composites, the incorporation of SSA resulted in the highest specific gravity values. This increase is primarily attributed to the elevated density of the steelmaking residue, which is approximately 39% greater than that of the conventional fine aggregate (Table 5), a trend also observed by Amancio et al. (2020).

For lime-based mixtures, the specific gravity values were generally lower than those of cementitious systems. This behavior is associated with the lower density of hydrated lime, approximately 28% lower than that of Portland cement, as well as the higher void index previously observed. Nevertheless, within the lime-based group, the mixture containing SSA exhibited the highest specific gravity, consistent with the greater density of the incorporated residue.

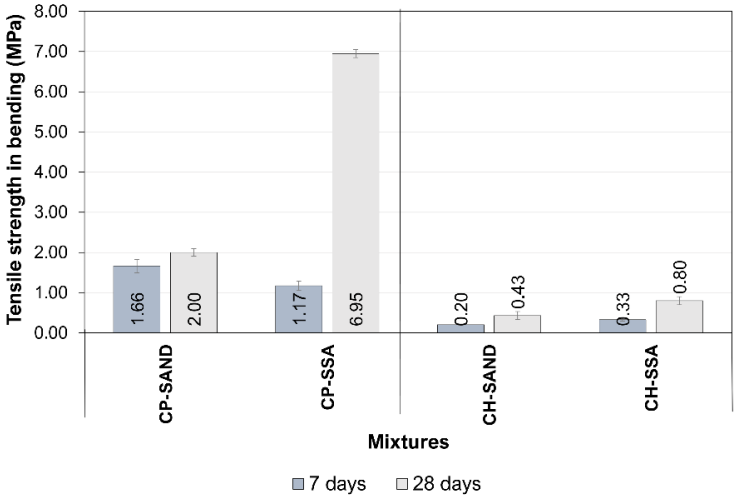
As observed in the fresh state, the incorporation of SSA leads to an increase in the bulk density of the mortar. Nevertheless, this is accompanied by matrix densification and a reduction in pore volume, which may adversely affect the historical substrate.

3.3.2 Mechanical performance of repair mortar

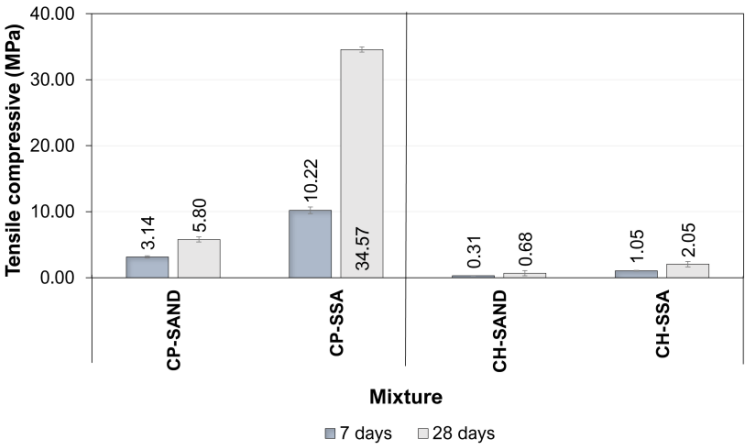
Figure 10 presents the mechanical performance of the mortars at 7 and 28 days, including flexural tensile strength (a) and compressive strength (b). These properties are essential for evaluating the structural behavior of the material, as they reflect its capacity to withstand stresses, control crack propagation, and ensure durability under service conditions.

Figure 10 – (a) Flexural tensile strength and (b) Compressive strength of mortars.

a)



b)



The incorporation of SSA produced mortars with a more resistant and denser matrix, increasing their capacity to withstand internal stresses generated by structural movements. This behavior is associated with the high

density of the residue, the angular morphology of its particles, and its greater hardness compared to conventional aggregates such as quartz and granite (Motz and Geiseler, 2001; Amancio et al., 2020), contributing to better compaction efficiency, lower porosity, and improved mechanical performance.

As a result, the incorporation of SSA led to an increase in both compressive and tensile strength, reflecting the densification of the matrix and the improvement in particle interlocking. These mechanisms also contribute to better stress distribution and resistance to cracking under tensile stresses. As reported in the literature (Liang et al., 2025; Yu et al., 2026), mechanical strength is closely associated with the void ratio, with denser and more compact matrices exhibiting superior performance, while higher porosity levels promote microcracking and reduce structural efficiency.

In lime-based mortars, the incorporation of SSA contributed, albeit slightly, to mechanical performance. However, this improvement was not sufficient to compensate for the lower reactivity of the lime binder, and the mechanical strength values remained significantly lower than those observed in cement-based mixtures.

From a restoration perspective, however, the increased strength associated with the incorporation of SSA can promote mechanical incompatibility with the historical substrate, concentrating stresses at the interface and increasing the risk of localized cracking (Silva, Pinto and Gomes, 2015). Therefore, although SSA contributes to matrix densification and increased strength, ensuring mechanical compatibility remains essential for long-lasting and adequate conservation performance.

Overall, the results show that SSA markedly improves the mechanical performance of cement-based mortars, although this may compromise compatibility with historic substrates. For lime-based mortars, all mixtures, including those with SSA, remain within a low and comparable range, preserving a similar mechanical behavior to the reference mortar. These findings indicate that SSA may have potential for use in lime-based mortars for historic rendering and repair applications, provided that mix proportions are appropriately adjusted to ensure compatibility with the substrate.

4. Conclusions

The use of SSA as a total replacement for natural fine aggregate significantly influenced the behavior of repair mortars in both fresh and hardened states, mainly due to its high specific gravity, angular morphology, and mechanical hardness. Therefore, it can be concluded that:

- The residue reduces water demand while increasing bulk density and apparent fluidity, as a result of its high specific gravity and particle hardness.
- The angular morphology of SSA particles promotes matrix densification, leading to a lower void index and reduced capillary absorption, as well as improved mechanical strength, particularly in cement-based mixtures.
- In lime-based mortars, although strength gains were observed due to enhanced particle interlocking, the intrinsic characteristics of the aerial binder continued to control porosity and overall mechanical performance.

From a conservation perspective, the design of sustainable repair mortars for historic buildings requires careful assessment. Although the incorporation of industrial residues such as SSA is technically viable and may enhance certain properties, not all by-products will be compatible with historic substrates. Ensuring mechanical and physical compatibility remains essential to guarantee durable and appropriate heritage interventions.

Acknowledgments

The authors gratefully acknowledge the funding agencies Coordination for the Improvement of Higher Education Personnel (CAPES), the National Council for Scientific and Technological Development (CNPq), and

the Ceará Foundation for Support to Scientific and Technological Development (FUNCAP) for their financial support. The authors also thank the laboratories of the Federal University of Ceará (UFC), Russas campus, whose infrastructure and staff were essential to the success of this research.

References

Aggelakopoulou, E.; Bakolas, A.; Moropoulou, A. Properties of lime-metakaolin mortars for the restoration of historic masonries. Applied Clay Science, v. 53, n. 1, p. 15–19, 2011.

Amancio, F. A.; Dias, A. R. O.; Lima, D. A.; Cabral, A. E. B. Estudo do comportamento no estado fresco e endurecido de argamassa com escória de aciaria BSSF. Matéria (Rio de Janeiro), v. 26, n. 3, 2021.

Baeza, F. J. Et Al. Influence of recycled slag aggregates on the conductivity and strain sensing capacity of carbon fiber reinforced cement mortars. Construction and Building Materials, v. 184, p. 311–319, 2018.

Brazilian Association of Technical Standards. ABNT NBR 17054: Aggregates – Determination of Particle Size Distribution. Rio de Janeiro, 2022.

Brazilian Association of Technical Standards. ABNT NBR 16916: Fine Aggregate – Determination of Density and Water Absorption. Rio de Janeiro, 2021.

Brazilian Association of Technical Standards. ABNT NBR 16972: Aggregates – Determination of Bulk Density and Voids Index. Rio de Janeiro, 2021.

Brazilian Association of Technical Standards. ABNT NBR 16973: Aggregates – Determination of Fine Material Passing the 75 µm Sieve by Washing. Rio de Janeiro, 2021.

Brazilian Association of Technical Standards. ABNT NBR 13276: Mortar for Laying and Rendering of Walls and Ceilings – Determination of Consistency Index. Rio de Janeiro, 2016.

Brazilian Association of Technical Standards. ABNT NBR 13278: Mortar for Laying and Rendering of Walls and Ceilings – Determination of Bulk Density and Entrained Air Content. Rio de Janeiro, 2005.

Brazilian Association of Technical Standards. ABNT NBR 13279: Mortar for Laying and Rendering of Walls and Ceilings – Determination of Flexural Tensile Strength and Compressive Strength. Rio de Janeiro, 2005.

Brazilian Association of Technical Standards. ABNT NBR 7211: Aggregates for Concrete – Requirements. Rio de Janeiro, 2022.

Brazilian Association of Technical Standards. ABNT NBR 9778: Determination of Water Absorption by Immersion, Voids Index, and Specific Gravity. Rio de Janeiro, 2009.

Dias, A. R. O. Et Al. Efeito da substituição do cimento Portland por escória de aciaria BSSF nas propriedades físicas e mecânicas do concreto. Matéria (Rio de Janeiro), v. 25, n. 4, 2020.

Carta de Veneza. Carta internacional sobre a conservação e o restauro de monumentos e sítios. In: II Congresso Internacional de Arquitetos e Técnicos dos Monumentos Históricos, 1964. http://portal.iphan.gov.br/portal/baixaFcdAnexo.do?id=236.

Liang, H., Qiao, J., Lu, Y., Wang, J., & Zhou, C. Relationships between compressive strength of cement mortars and pore structure characteristics at water-saturation. Journal of the Chinese Ceramic Society, 53(2), 304–312, 2025.

Lin, M.; Roders, A. P.; Nevzgodin, I. Atenção à diversidade: definindo conceitos de intervenção do patrimônio construído em documentos doutrinários internacionais. Patrimônio Construído, v. 8, p. 24, 2024.

Liu, J.; Guo, D.; Zhu, J. Status and development of the comprehensive utilization of steel slag at Baosteel. Baosteel Technical Research, v. 5, n. 2, 2011.

Longobardi, G.; Formisano, A. Seismic vulnerability assessment and consolidation techniques of ancient masonry buildings: the case study of a Neapolitan Masseria. Engineering Failure Analysis, v. 138, 2022.

Loureiro, A. M. Argamassas históricas de Belém do Pará. 2019. Tese (Doutorado em Geologia e Geoquímica) – Universidade Federal do Pará, Belém, 2019.

Malathy, R., Shanmugam, R., Chung, I.-M., Kim, S.-H., & Prabakaran, M. Mechanical and Microstructural Properties of Composite Mortars with Lime, Silica Fume and Rice Husk Ash. Processes, 10 (7), 1424, 2022.

Magalhães, A. C. A. Argamassa de cal com adições pozolânicas: contribuição para o desenvolvimento de formulações para o restauro. 2018. Tese (Doutorado em Arquitetura e Urbanismo) – Universidade Federal da Bahia, Salvador, 2018.

Miah, M. J. et al. Enhancement of mechanical properties and porosity of concrete using steel slag coarse aggregate. Materials, v. 13, n. 12, p. 2865, 2020.

Motz, H.; Geiseler, J. Products of steel slags: An opportunity to save natural resources. Waste Management, 21(3), 285–293, 2001.

Nogueira, R.; Pinto, A. P. F.; Gomes, A. Artificial ageing by salt crystallization: test protocol and salt distribution patterns in lime-based rendering mortars. Journal of Cultural Heritage, v. 45, p. 180–192, 2020.

Pavlik, Z. Et Al. Lightweight thermal efficient repair mortars with expanded glass (EG) for repairing historical buildings: the effect of binder type and EG aggregate dosage on their performance. Energy and Buildings, art. 112526, 2022.

Posani, M.; Veiga, R.; Freitas, V. P. Thermal mortar-based insulation solutions for historic walls: an extensive hygrothermal characterization of materials and systems. Construction and Building Materials, v. 315, art. 125640, 2020.

Ripardo, T. Da S. N.; Torres, E. M. M.; Garcia, P. H. N.; Cabral, A. E. B.; Costa, H. N. Da; Bezerra, I. F. Análise da consistência de argamassas com escória de aciaria BSSF. In: SIMPÓSIO BRASILEIRO DE TECNOLOGIA DAS ARGAMASSAS, 15., 2025. Anais [...]. 2025.

Salles, G. S. Argamassas de substituição em edifícios históricos: estudo da compatibilidade através das propriedades mecânicas e do comportamento à água. 2017. Dissertação (Mestrado) – Universidade Federal do Pará, Belém, 2017.

Silva, B. A.; Guerreiro, E.; Duarte, A. P. C. Comparative study of lime-based mortars for conservation and restoration interventions. Construction and Building Materials, v. 499, 2025.

Wang, H. Y.; Chen, K. Y. A study of the engineering properties of CLSM with a new type of slag. Construction and Building Materials, v. 102, n. 1, p. 422–427, 2016.

Yu, J., Li, W., Bandara, K. M. V. A. U., Wang, S., Xu, X., & Gao, Y. Porosity–strength relationships in cement pastes incorporating GO-modified recycled concrete powder: A data-driven approach. Buildings, 16(1), 46, 2026.

Veiga, R. Air lime mortars: what else do we need to know to apply them in conservation and rehabilitation interventions? A review. Construction and Building Materials, v. 157, p. 132–140, 2017.

Vysvaril, M. Et Al. Non-hydrophobized perlite renders for repair and thermal insulation purposes: influence of different binders on their properties and durability. Construction and Building Materials, v. 263, 2020.

cinpar2026
XXII International Conference on Building Pathology and Constructions Repair
15th to 17th July 2026 - Lisboa, Portugal

Cementitious Composites with Steel Industry Residues and Interaction with Atmospheric CO_2

Pedro SANTOS[1], Karoline CARVALHO[2], Elói SOUZA[3], **Laís COSTA[4]**

[1] Sustainable Construction and Innovation Laboratory, Federal University of Ceará, Russas, Brazil, pedrohenriquesoares@alu.ufc.br
[2] Sustainable Construction and Innovation Laboratory, Federal University of Ceará, Russas, Brazil, carvalhokaroline@alu.ufc.br
[3] Sustainable Construction and Innovation Laboratory, Federal University of Ceará, Russas, Brazil, eloirsouza@alu.ufc.br
[4] Sustainable Construction and Innovation Laboratory, Federal University of Ceará, Russas, Brazil, laiscosta@ufc.br

Abstract: The current climate crisis, driven by high carbon dioxide (CO_2) emissions, has intensified the occurrence of extreme events on the planet. In this context, the construction industry stands out both for its high environmental impact and for its potential to contribute to mitigation solutions, especially through the development of more sustainable materials. Among these solutions, those incorporating waste materials, such as those from the steel industry, stand out. Thus, this research aims to use steelmaking waste as a component in the production of cementitious composites. The composites were developed with total replacement of conventional aggregates by steelmaking waste, Basic Oxygen Furnace (BOF) steel slag, and Kambara Reactor (KR) slag. For comparative purposes, a reference mix was also produced with conventional materials. The composites were characterized in terms of water absorption by capillarity, compressive strength, and their interaction with atmospheric CO_2 using TGA and SEM/EDS. Composites containing steelmaking waste showed compressive strengths similar to those of the reference elements, without compromising mechanical performance. Analyses also revealed high water absorption and the presence of carbon incorporated into the matrix after environmental exposure. Mixtures containing KR and BOF, and KR alone, showed the highest water absorption rates. Regarding carbonation, the reference composites showed lower incorporated carbon content compared to composites with steelmaking waste, with differences of 2.9% and 2.4%, respectively, indicating a lower occurrence of carbonation processes. Therefore, the use of these residues proves to be a viable alternative, without compromising mechanical properties, contributing to the reduction of environmental impacts and the development of more sustainable solutions in civil construction. However, further studies are needed to evaluate in more depth the potential of these materials in CO_2 capture.

Keywords: Climate crisis. CO_2 sequestration. Steelmaking waste. Composite. Sustainable civil construction.

1. Introduction

The global climate crisis has been widely associated with the increase in greenhouse gas emissions, particularly carbon dioxide (CO_2). The growth of carbon emissions over recent decades has intensified extreme climatic events, making it necessary to adopt strategies to mitigate these impacts. Among the various sectors contributing to global emissions, the construction industry stands out, mainly due to concrete production. Currently, it is estimated that Portland cement manufacturing is responsible for approximately 7 to 8% of global CO_2 emissions (Lehne & Preston, 2018; Kajaste & Hurme, 2016).

Other inputs used in the production of cementitious matrices also contribute indirectly to this environmental impact. Mineral extraction for aggregate production affects water and energy consumption, resulting in

indirect CO_2 emissions (Alexander & Mindness, 2005; Padmalal et al., 2008). Considering that concrete is the most widely used construction material in the world, the search for alternatives that progressively reduce the environmental impact associated with its production has become a priority in sustainability-oriented research in civil engineering.

In this context, solutions based on the circular economy have gained significant attention by proposing the reintegration of industrial waste into new production cycles, thereby reducing the need for extracting new natural resources and minimizing associated impacts. A promising approach that has emerged is the use of waste materials as raw materials in construction. Among these, residues from the steel industry stand out. These include basic oxygen furnace (BOF) slag, generated during pig iron refining, and KR slag, originating from the desulfurization process of pig iron (Kambara Reactor). BOF slag is generally composed of calcium, iron and silicon oxides (He, Yang & Guo, 2024), while KR slag is characterized by high contents of calcium compounds, magnesium oxide and residual desulfurizing agents (Pires et al., 2019). The steel industry is characterized by a production route with high embedded CO_2 emissions, while also playing a significant economic role (IABR, 2018).

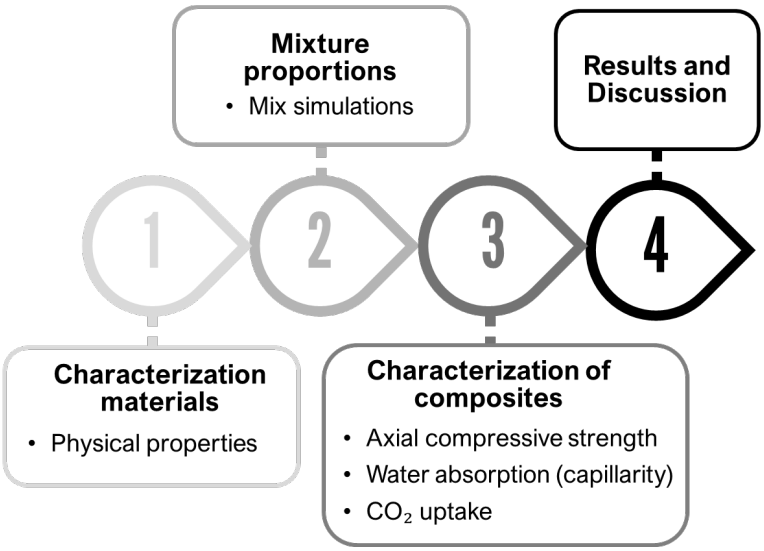
Steel industry residues present chemical and physical characteristics that allow their incorporation into cementitious matrices and have been widely investigated for applications in construction (Guo et al., 2019; Monosi et al., 2016; San-José et al., 2014; Pellegrino & Gaddo, 2009; Lai et al., 2021). In addition to their viability as substitutes for conventional aggregates, studies indicate that steelmaking residues exhibit relevant behavior with respect to carbonation, particularly regarding their durability in CO_2-exposed environments. However, most of these studies focus on specific types of residues, such as BOF slag, while materials like KR slag remain less explored, especially in combined applications. Furthermore, there is a lack of studies that investigate, in an integrated manner, the microstructural changes associated with this process, particularly under real environmental exposure conditions.

Given this scenario, this study aims to evaluate the mechanical performance and behavior under atmospheric CO_2 exposure of cementitious composites produced with the total replacement of conventional aggregates by waste from the steel industry, specifically steelmaking slag (BOF) and annealing slag (KR). To this end, compressive strength tests were performed, along with physical characterizations through capillary water absorption and microstructural characterizations using thermogravimetric analysis (TGA) and scanning electron microscopy coupled with energy dispersive spectroscopy (SEM/EDS), in order to investigate possible evidence of carbonation after environmental exposure, thus contributing to the advancement of sustainable building materials.

2. Methodology

Figure 1 presents the experimental flowchart of the research procedure. The methodology began with the characterization of the raw materials, including steel industry waste and conventional aggregates. Based on the characterization results, the mixture proportions were defined through optimization, aiming to obtain an adequate particle size distribution. Subsequently, the test specimens were molded and evaluated through mechanical, physical, and CO2 interaction tests.

Figure 1 - Flowchart of the research stages.

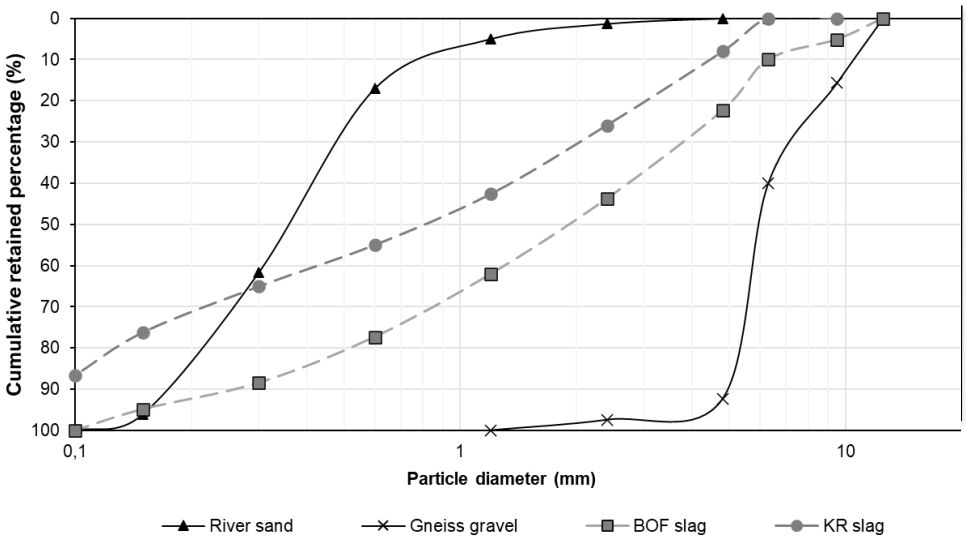


2.1 Materials

For the development of this study, steel industry residues from an integrated steel plant located in the state of Ceará, Brazil, were used, namely basic oxygen furnace (BOF) slag (maximum particle size of 9.5 mm) and KR slag (maximum particle size of 6.3 mm), originating from the pig iron desulfurization process (Kambara Reactor). These materials exhibit physical and granulometric characteristics suitable for their use as substitutes for natural aggregates in cementitious composites.

For comparison purposes, conventional aggregates widely used in the construction industry were employed, namely river sand (maximum particle size of 2.4 mm) and gneiss crushed stone (maximum particle size of 9.5 mm). The particle size distribution of all materials was determined according to ABNT NBR 17054 (2022) and is presented in Figure 2.

Figure 2 – Particle size distribution curve of the materials used in the study.



The main physical properties of the materials and the standards followed for their determination are presented in Table 1. The characterization of the materials ensures an adequate comparison between conventional aggregates and waste from the steel industry, contributing to a better understanding of their behavior in cementitious composites.

Table 1 - List of physical characterization tests performed on the waste.

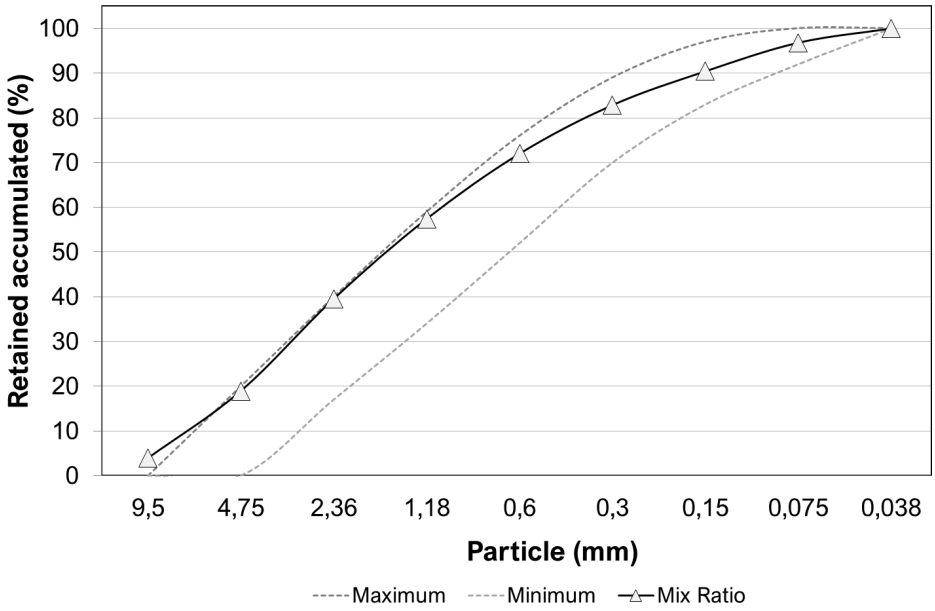
Porperty	Standard	BOF slag	KR slag	River sand	Gneiss gravel
Specific gravity (g/cm^3)	NBR 16916 (2021)	2.95	3.28	2.62	2.63
Bulk density (g/cm^3)	NBR 16972 (2021)	1.80	1.16	1.56	1.37
Fines contente (%)	NBR 16973 (2021)	1.64	1.16	4.70	0.56
Fineness modulus	NBR 17054 (2022)	3.93	2.79	1.81	5.90

The binder used was Type V Portland cement, selected due to its low content of mineral additions and its high early-age compressive strength (ABNT NBR 16665, 2018). The mixing water was potable water supplied by the Water and Sewage Company of Ceará (CAGECE), responsible for the region's water supply.

2.2 Mixture proportioning

The mixture proportions were defined based on particle packing principles. The objective was to develop compositions with a significant content of steel industry waste, without the need for prior processing, adapting the particle size distributions of the materials. To this end, the dosage method proposed by Fernandes (2012) was adopted. This method consists of adjusting the proportions of aggregates so that the resulting particle size distribution approximates as closely as possible an ideal target curve. In this way, the method improves particle packing, reduces void content, and contributes to better mechanical performance of the material. The curve adopted for all mixes produced in the study is shown in Figure 2.

Figure 2 - Curve adjusted for the production of the studied traits.



Using the data obtained in the material characterization stage, mixture simulations were performed to define compositions that presented an adequate particle size distribution. These simulations resulted in different experimental mixtures, including a reference mixture composed entirely of conventional materials and others with partial or total replacement of natural aggregates by steel industry waste.

The experimental mixtures include compositions with replacement of coarse aggregate by KR slag, partial replacement of sand by BOF slag, as well as mixtures that combine different steelmaking residues, aiming at

their direct use without prior processing. These variations allowed for the evaluation of the behavior and performance of the composites under different mixture configurations. All mixture compositions are presented in Table 2.

Table 2 - Composition of the composite mixtures with replacement of natural aggregates by steel industry.

Mixture	Cement	River sand	Gneiss gravel	BOF slag (BF)	KR slag (KR)	Water
REF	1	2.5	3	0	0	0.5
T-BF	1	1.75	3	0.75	0	
T-KR	1	2.5	1.5	0	1.5	
T-BF-KR	1	1.25	1.5	0.75	0.75	

2.3 Characterization of composites

The produced mixtures were analyzed in their hardened state, with their physical and chemical properties evaluated according to the tests presented in Table 3. The composites were cast into cylindrical specimens with dimensions of ø5x10 cm. The specimens remained in the molds for 24 ± 2 hours under controlled environmental conditions (23 ± 2 °C and relative humidity above 90%), followed by demolding.

Table 3 - Experimental tests performed on the hardened composites.

Test	**Standard / Method**	**Age of testing**
Axial compressive strength	ABNT NBR 13279 (2015)	28
Water absorption by capillarity	NBR 9779 (2012)	28
CO_2 uptake	Thermogravimetric analysis (TGA)	28

Regarding the interaction of the produced composites with atmospheric CO_2, samples were collected before and after exposure to a CO_2-rich environment for 20 days.

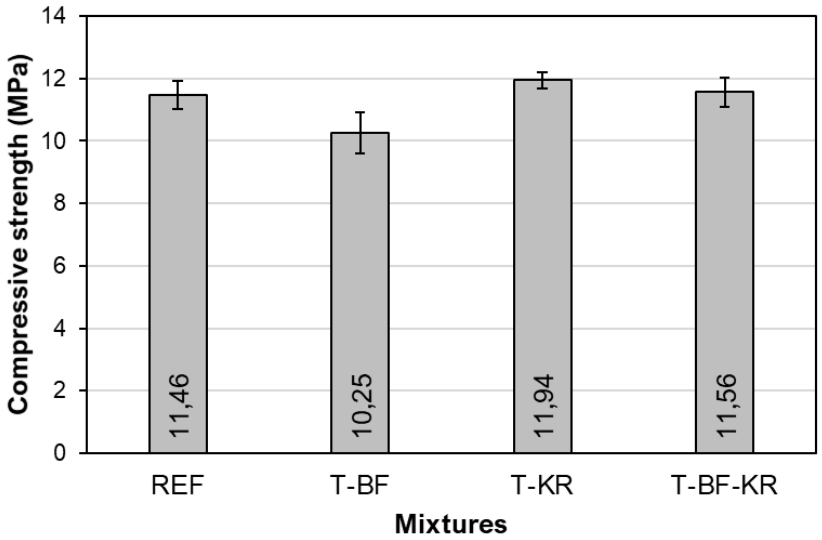
Thermogravimetric analysis (TGA) was employed to evaluate the mass variation as a function of temperature, allowing the identification of thermal decomposition stages and mass changes associated with the release or absorption of gases, such as CO_2. Samples were ground to a particle size of 75 µm before testing. This procedure allowed the comparison of samples under different exposure conditions, providing information on potential CO_2-related reactions over time. CO_2 absorption was indirectly quantified through the mass variations observed during thermal analysis.

Additionally, the point chemical composition was also investigated using energy-dispersive X-ray spectroscopy (EDS) coupled to a TESCAN Vega XMU scanning electron microscope. For this analysis, samples with an approximate diameter of 1 cm were prepared for each mixture.

3. Results and Discussion

Figure 4 presents the compressive strength results of the produced composites. The T-BF-KR mixture exhibited the highest mechanical performance, whereas the T-BF mixture showed the lowest compressive strength values. This behavior may be associated with the irregular particle size distribution of BOF slag, which could have affected particle packing and the interfacial bonding between the cement paste and the aggregates (Chang et al., 2021). However, the observed reduction was not significant, indicating comparable mechanical performance among the mixtures.

Figure 4 – Compressive strength of composites.

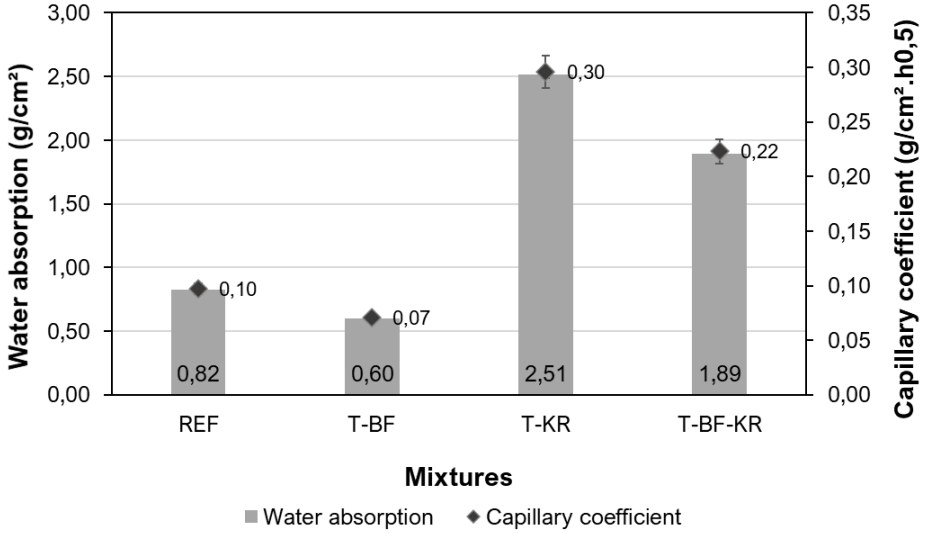


In general, the literature reports that the incorporation of steel industry residues can lead to improvements in mechanical performance on the order of 30 to 50% (Andrade et al., 2021; Costa et al., 2021). However, these results are often associated with the use of previously processed materials, involving strict control of particle size distribution and optimized particle packing.

In the present study, the direct use of these residues was adopted, without prior processing, prioritizing the compatibility of particle size distributions among the available materials. Although the strength gains were less pronounced than those reported in the literature, the results indicate that the replacement of conventional aggregates with steel slags did not impair the mechanical performance of the composites. These findings demonstrate the feasibility of using such residues under simplified application conditions, with potential benefits in terms of cost reduction and lower environmental impact associated with material processing.

Figure 5 presents the results of capillary water absorption of the evaluated mortars. In general, the incorporation of steel industry waste led to distinct behaviors, depending on the mixture.

Figure 5 – Water absorption and Capillary coefficient of mixtures.

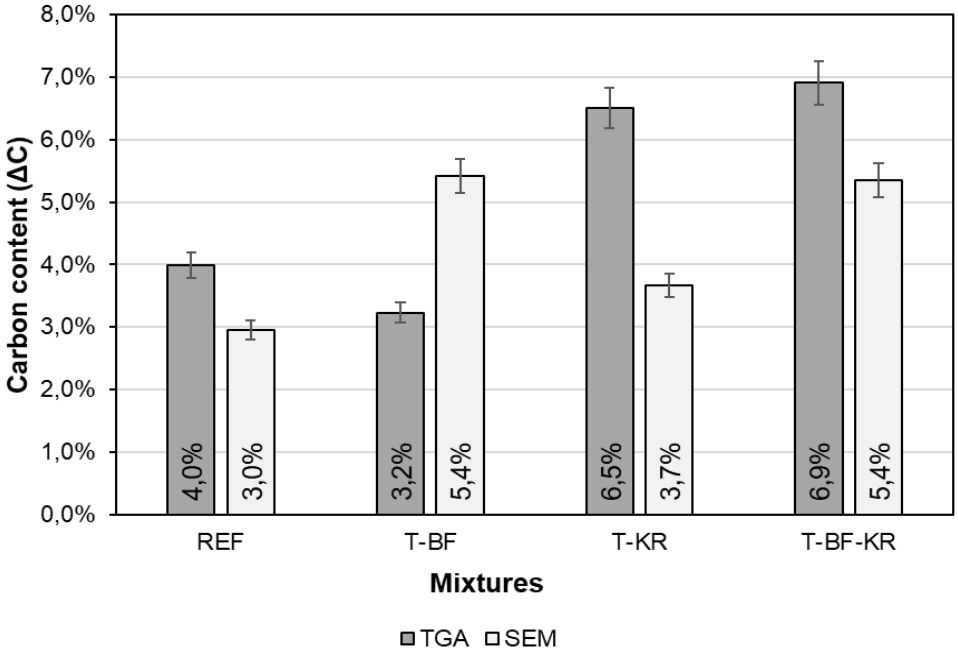


The incorporation of BOF contributed to a reduction in water absorption, indicating a possible refinement of the pore structure and a decrease in the connectivity of capillary pores. In contrast, the presence of KR

resulted in a significant increase in capillary absorption, suggesting the development of a more open pore network. The combined mixture showed an interaction between the wastes, in which the BOF partially mitigated the effects associated with the KR. These results indicate that the nature and reactivity of the incorporated materials directly influence the microstructure of the mortars, leading to changes in their capillary absorption behavior, which is consistent with findings reported in the literature (Monosi et al., 2016; Guo et al., 2019). Despite the increase in capillary absorption associated with the KR, no reduction in mechanical strength was observed, which can be considered a positive outcome for its potential application.

Figure 6 presents the absolute variation in carbon content for the different mixtures, as obtained by TGA and SEM/EDS analyses. In general, all mixtures exhibited an increase in carbon content after exposure, indicating the occurrence of carbonation processes. The observed increase in carbon content after 20 days of environmental exposure suggests the interaction between the composites and atmospheric CO_2, evidencing the occurrence of carbonation reactions.

Figure 6 - Absolute variation in the carbon content of the composites by TGA and SEM/EDS analyses.



The composites incorporating steel industry residues exhibited greater variations in carbon content compared to the reference mixture, indicating a higher tendency for the formation of carbonated compounds. Overall, the results suggest that both BOF and KR slags influence the interaction of the composites with CO_2, although exhibiting distinct behaviors.

The differences observed between the results obtained by TGA and SEM/EDS can be attributed to the specific characteristics of each technique. Thermogravimetric analysis provides a higher level of experimental control, whereas SEM/EDS, applied in an adapted manner, may be influenced by sample heterogeneity and limited representativeness. Nevertheless, both methods indicate consistent trends regarding the increase in carbon content after environmental exposure.

Thus, TGA results suggest a stronger contribution of KR to the increase in carbon content, SEM/EDS measurements indicate a more pronounced effect associated with BOF containing mixtures. These differences suggest that carbonation is not spatially homogeneous within the matrix and is influenced by the heterogeneity of the composites. Although both techniques show an overall increase in carbon content for some mixtures compared to reference, the magnitude and significance of these changes vary depending on

the measurement approach, highlighting the importance of combining bulk and localized analyses to interpret carbonation behavior.

4. Conclusions

This study aimed to evaluate the mechanical performance and the interaction with atmospheric CO_2 of cementitious composites produced with the replacement of natural aggregates by steel industry residues. The main conclusions are as follows:

- The results demonstrated that the use of steel industry residues as a replacement for natural aggregates in cementitious composites is technically feasible, without significant impairment of mechanical performance.
- The incorporation of steelmaking waste directly influences the microstructure and capillary absorption behavior of mortars, with distinct effects observed depending on the type of waste used, without compromising mechanical performance. This highlights the potential application of these materials in sustainable cementitious composites.
- Even without prior material processing, the composites exhibited compressive strength comparable to the reference mixture, highlighting the potential application of these residues under simpler and more cost-effective conditions.
- Regarding interaction with atmospheric CO_2, an increase in carbon content was observed in all samples after the exposure period, indicating the occurrence of carbonation processes.
- The composites incorporating steel industry residues showed greater variations in carbon content, suggesting a higher tendency for the formation of carbonated compounds compared to the conventional material.

Overall, the findings indicate that the use of steel residues may contribute to the reduction of natural resource consumption and support the development of materials with potential interaction with CO_2. Further studies are recommended to investigate the CO_2 uptake potential of these composites in greater depth, including evaluations under controlled conditions and different exposure scenarios.

Acknowledgments

The authors gratefully acknowledge the funding agencies Coordination for the Improvement of Higher Education Personnel (CAPES), the National Council for Scientific and Technological Development (CNPq), and the Ceará Foundation for Support to Scientific and Technological Development (FUNCAP) for their financial support. The authors also thank the laboratories of the Federal University of Ceará (UFC), Russas campus, whose infrastructure and staff were essential to the success of this research.

References

Alexander, M.; Mindness, S. Aggregates in concrete. New York: CRC Press, 2005.

Andrade, H.; et al. Mechanical performance and resistance to carbonation of steel slag reinforced concrete. Construction and Building Materials, v. 298, p. 123910, 2021.

Brazilian Association of Technical Standards. ABNT NBR 17054: Aggregates – Determination of Particle Size Distribution. Rio de Janeiro, 2022.

Brazilian Association of Technical Standards. ABNT NBR 16916: Fine Aggregate – Determination of Density and Water Absorption. Rio de Janeiro, 2021.

Brazilian Association of Technical Standards. ABNT NBR 16972: Aggregates – Determination of Bulk Density and Voids Index. Rio de Janeiro, 2021.

Brazilian Association of Technical Standards. ABNT NBR 16973: Aggregates – Determination of Fine Material Passing the 75 µm Sieve by Washing. Rio de Janeiro, 2021.

Brazilian Association of Technical Standards. ABNT NBR 13276: Mortar for Laying and Rendering of Walls and Ceilings – Determination of Consistency Index. Rio de Janeiro, 2016.

Brazilian Association of Technical Standards. ABNT NBR 13279: Mortar for Laying and Rendering of Walls and Ceilings – Determination of Flexural Tensile Strength and Compressive Strength. Rio de Janeiro, 2005.

Brazilian Association of Technical Standards. ABNT NBR 7211: Aggregates for Concrete – Requirements. Rio de Janeiro, 2022.

Brazilian Association of Technical Standards. ABNT. NBR 5738: Concrete — Procedure for molding and curing test specimens. Rio de Janeiro: Brazilian Association of Technical Standards, 2015.

Brazilian Association of Technical Standards. ABNT. NBR 16665: Portland cement — Requirements. Rio de Janeiro: Brazilian Association of Technical Standards, 2018.

Brazilian Association of Technical Standards. ABNT NBR 9779: Hardened mortar and concrete — Determination of water absorption by capillarity. Rio de Janeiro: Brazilian Association of Technical Standards, 2012.

Costa, L. C. B.; et al. Eco-efficient steel slag concretes: an alternative to achieve circular economy. Revista IBRACON de Estruturas e Materiais, v. 15, p. 15201, 2021.

Fernandes, I. Blocks and pavers: production and quality control. Jaraguá do Sul: Editora Treino Assessoria e Treinamentos Empresariais Ltda., 2012.

Guo, Y.; Xie, J.; Zhao, J.; Zuo, K. Utilization of unprocessed steel slag as fine aggregate in normal- and high-strength concrete. Construction and Building Materials, v. 204, p. 41–49, 2019.

He, D.; Yang, L.; Guo, J. Effect of Carbonation Degree on Mineral Composition, Microstructure, and Cementitious Properties of BOF Slag. Journal of Sustainable Metallurgy, v. 10, p. 2267-2281, 2024.

IABR. Sustainability report 2016–2017. Rio de Janeiro: Instituto Aço Brasil, 2018.

Kajaste, R.; Hurme, M. Cement industry greenhouse gas emissions – management options and abatement cost. Journal of Cleaner Production, v. 112, n. 5, p. 4041–4052, 2016.

Lai, M. H.; et al. Improving mechanical behavior and microstructure of concrete by using BOF steel slag aggregate. Construction and Building Materials, v. 277, p. 122269, 2021.

Lehne, J.; Preston, F. Making concrete change: innovation in low-carbon cement and concrete. London: Chatham House: The Royal Institute of International Affairs, 2018.

Monosi, S.; Ruello, M.; Sani, D. Electric arc furnace slag as natural aggregate replacement in concrete production. Cement and Concrete Composites, v. 66, p. 66–72, 2016.

Padmalal, D.; Maya, K.; Sreebha, S.; Sreeja, R. Environmental effects of river sand mining: a case from the river catchments of Vembanad Lake, southwest coast of India. Environmental Geology, v. 54, p. 879–889, 2008.

Pellegrino, C.; Gaddo, V. Mechanical and durability characteristics of concrete containing EAF slag as aggregates. Cement and Concrete Composites, v. 31, p. 663–671, 2009.

Pires, P. M. et al. Laboratory and Field Evaluation of KR slag-Stabilized Soil for Paving Applications. Journal of Materials in Civil Engineering, v. 31, n.9, p. 04019182, 2019.

San-José, J.; Vegas, I.; Arribas, I.; Marcos, I. The performance of steel-making slag concretes in the hardened state. Materials and Design, v. 60, p. 612–619, 2014.

cinpar2026
XXII International Conference on Building Pathology and Constructions Repair
15th to 17th July 2026 - Lisboa, Portugal

Modified masonry triplets for the shear characterisation and numerical modelling of NFRCM-strengthened masonry

Nandini Priya THATIKONDA[1], Daniele BARALDI[2], Antonella CECCHI[3]

[1] [1] Dipartimento di Culture del Progetto, IUAV University of Venice, Venice, Italy, npthatikonda@iuav.it
[2] Dipartimento di Culture del Progetto, IUAV University of Venice, Venice, Italy, danielebaraldi@iuav.it
[3] Dipartimento di Culture del Progetto, IUAV University of Venice, Venice, Italy, cecchi@iuav.it

Abstract:

The evaluation of shear performance of masonry strengthened with Natural Fiber Reinforced Cementitious Matrix (NFRCM), adopting "modified" triplet specimens, derived from the Representative Elementary Volume (REV) of the running bond masonry texture, is presented in this research. Diagonal Compression Tests (DCT) were conducted, and an adapted Digital Image Correlation (DIC) technique was adopted to capture the deformation at the microstructural level.

Two specimen configurations were studied: an unreinforced triplet and a triplet strengthened with bi-directional jute mesh-reinforced NFRCM. The results demonstrate an improvement in the shear resistance and deformation capacity in the strengthened specimens. Further, a Finite Element (FE) model based on a multi-leaf homogenization technique was also adopted and was validated based on the experimental outcomes.

With this, the research presented, aims at combining novel small-scale specimen derived from a REV where the microstructure is significant, with the well-established shear identification with DCT, to demonstrate an accessible and sustainable testing methodology for masonry, advancing the understanding of micro-mechanical interactions in strengthened masonry.

Keywords: Masonry, Shear characterization, Modified Triplets, Jute-NFRCM.

1. Introduction

Masonry remains one of the most widely used construction system, particularly in historic and vernacular structures. Despite being advantageous due to its ease of construction and load bearing capacity, masonry is inherently weak in resisting tensile and shear stresses. Shear failure represents one of the most critical and recurrent collapse mechanisms, especially under seismic or lateral loading conditions. Improving this shear performance of masonry, therefore, continues to be a major focus of research, both for the preservation of existing structures and the development of more resilient construction systems (Corradi and Borri, 2018).

In recent years, strengthening techniques have gained significant attention as effective strategies to improve the in-plane performance of masonry, especially to resist lateral actions (Alecci *et al.* 2019; Cheng *et al.* 2020). Among these, composite-based solutions such as Fiber Reinforced Cementitious Matrix (FRCM) systems have emerged as a compatible method for masonry strengthening. Unlike Fiber Reinforced Polymers (FRP) (Mazzotti *et al.* 2016), FRCM systems or more commonly Textile Reinforced Mortars (TRM) employ fiber matrices, which allow loads to be distributed more evenly, while also retaining compatibility with the masonry (Garcia-Ramonda *et al.* 2020; Libre *et al.* 2023), a key consideration in conservation engineering and while intervening with built heritage (Valluzzi et al. 2014).

A sustainable evolution of this approach is represented by Natural Fiber Reinforced Cementitious Matrix (NFRCM) systems, which replace synthetic fibers with organic alternatives such as jute, flax, hemp, or sisal (Li *et al.* 2020). Natural fibers have long been a key aspect in improving the flexural and ductile strength of mortars and plasters in traditional constructions, with several examples of short or shredded fibres introduced to the admixtures. While offering several advantages, including low environmental impact, cost-effectiveness, and wide availability, the fiber mesh matrix allows for a high degree of adaptability in tailoring the reinforcement system to specific applications (Codispoti *et al.* 2015; Li *et al.* 2020). As a result, NFRCM systems are increasingly the focus of investigations into sustainable strengthening solutions for masonry structures. Despite their potential, several challenges remain in fully understanding and optimizing the performance of NFRCM-strengthened masonry.

The current research focuses on jute fibers, a widely available and cost-effective natural fiber exhibiting good tensile strength, ductility, and adequate moisture resilience (Majumder *et al.* 2022). These properties make jute particularly suitable for enhancing the mechanical performance of masonry when embedded in a lime-based inorganic matrix. Consequently, experimental investigations evaluating the performance of NFRCM systems applied to masonry, particularly under stresses that are representative of real structural behaviour, are essential (Trochoutsou *et al.* 2021).

With this context established, the research revisits the experimental characterization of masonry shear behaviour which is essential for a reliable and scalable application of such systems. Tests on masonry, both un-strengthened and strengthened, are typically conducted by adopting scaled masonry specimens tested in diagonal compression or shear compression, as outlined in the ASTM standards and RILEM recommendations (ASTM E519/E519M-22; RILEM T. C. LUM B6: 1994). While such tests provide valuable insights into the global response of masonry system, the testing scales with large 1m X 1m masonry wallets present practical challenges, primarily due to the quasi-brittle nature of masonry, making the setups often impractical. These constraints become particularly significant when investigating the performance, with respect to a diverse set of parameters, such as masonry textures and material properties, textile configuration and matrix composition or even durability and resistance (Boem 2022).

With an aim to address these limitations, the current research, proposes a redefinition of the specimen scale. Derived from the Representative Elementary Volume (REV) of the running bond masonry, a 'modified' masonry triplet specimen is adopted. This small-scale configuration improves the ease of experimentation drastically, while retaining prominent microstructural definition of the overall masonry typology adopted (Thatikonda *et al.* 2024). In Section 2.1, the two modified triplet specimen configurations are presented: an unreinforced triplet and a symmetrically strengthened triplet with jute-NFRCM. The diagonal compression test conducted, and the deformations captured with the aid of an adapted Digital Image Correlation (DIC) technique are then presented in Section 2.2. Section 3 presents the proposed multi-leaf homogenization based Finite Element (FE) model, validated with the experimental data, following a discussion of the outcomes and conclusions.

2. Experimental Campaign Modified Masonry Triplet Specimens

2.1 Specimen choice and configurations

Considering the primary aim to revisit the experiment scale, particularly in the context of strengthened specimens, it is essential to rationalize the choice of specimen. The ASTM standards and RILEM recommendations (ASTM E519/E519M-22; RILEM T. C. LUM B6: 1994) outline the Diagonal Compression Test (DCT) to evaluate the shear strength of masonry, with axial force applied along one diagonal to introduce orthogonal tensile stresses. As noted, the proposed specimen is a scaled masonry wall, with dimensions about 1m x 1m, rotated at an angle of 45°, while the load is introduced along one diagonal of the specimen. This specimen scale and test setup are both accompanied with their own set of challenges. Researchers have attempted to address this through redefinition of the test setup, where specimens remain in horizontal

configuration and the force along one diagonal (de Carvalho Bello *et al.* 2021). The quasi-brittle nature of masonry further complicates the interpretation of results, as the measured shear response or crack initiation and propagation are highly sensitive to boundary conditions, loading configuration, and specimen size. This often raises questions regarding the representativeness and scalability of the test outcomes, particularly when extended to strengthened configurations. Further, within these strengthened configurations, recent studies have attempted reducing the specimen scale (Libre *et al.* 2023; Thatikonda *et al.* 2025b).

To redefine the specimen scale, the current research considers the Representative Elementary Volume (REV), fundamental for the micro-mechanical analysis of periodic media such as masonry. A REV together with its neighbouring elements, incorporates the heterogeneity associated with the masonry texture, capturing the overall mechanical response while also accounting for the material micro-structure and stress–strain distributions (Cecchi and Sab, 2002). To practically realize the REV, the masonry triplet defined in the standard EN 1052-3 (2002) is taken as the reference configuration and subsequently modified, by introducing a head joint to better represent the running bond masonry texture, as shown in Figure 1a,b. The specimens are constructed with brick units of length b= 250 mm and height a= 55 mm and depth t= 120 mm, and with mortar joints both bed and head joints with a thickness of e_h = e_v = 10 mm. This specimen configuration can be considered the smallest representative masonry assemblage capable of capturing the governing microstructural characteristics and interactions of the material. In fact, the proposed tests try to avoid capturing the simple mortar joint sliding that can typically be obtained with standard triplet tests (EN 1052-3 (2002)) and aims to activate a more complex shear behaviour involving both the blocks and the mortar joints.

Further, the strengthened specimen, hereby referred to as reinforced specimens, adopts a jute-fibre NFRCM embedded in an inorganic hydraulic lime composite matrix. The reinforcement is provided by a jute fibre mesh with bidirectional yarns arranged in a grid of approximately 10 × 10 mm^2. The mechanical properties of the jute and composite are presented in Table 2. An effective thickness of s=15 mm on each face was achieved, see Figure 1c,d, where the mesh was approximately placed at the mid-thickness of the matrix, as seen constructed in Figure 1e. A coordinate system is introduced, with axes x_1 and x_2 along the horizontal and vertical in-plane directions, respectively, and the x_3 axis along the thickness of the specimen, in the out of plane direction.

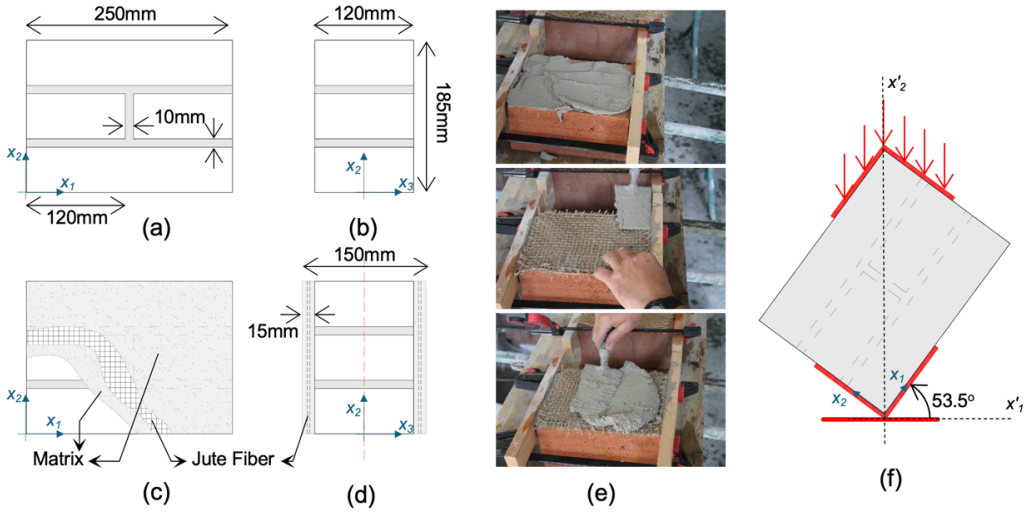


Figure 1 – (a, b) Modified masonry triplet specimen in the unreinforced configuration, (c, d) Triplet symmetrically strengthened with jute-NFRCM, (e) construction of the specimen (f) test setup for DCT

2.2 Test setup and DIC technique

To simulate the diagonal compression and the indirect tension along the orthogonal direction, the specimens were rotated about the x_3 axis at an angle of 53.5°, rotating axes x_1 and x_2 of the original reference system of the triplet to x'_1 and x'_2. The applied load is along the new vertical x'_2 and is aligned with the diagonal of the triplet, as shown in Figure 1f. Using loading and footing shoes of 100 mm each, to minimize local stress concentrations at the contact and to ensure a uniform stress distribution, the load was applied under displacement control, at a rate of 0.1mm/sec. The deformation presented was captured with the aid of an adapted Digital Image Correlation (DIC), outlined in Thatikonda *et al.* (2024). The specimens were equipped with high-contrast targets, and a sequence of high-resolution images captured their motion through the test. Processing this motion with respect to the undeformed state, the deformations and strains were computed by creating a system of virtual extensometers. In this method, the resolution of the images captured impacts the accuracy of these extensometers, allowing a displacement precision to track 10^{-2} pixels and derive a 0.02% strain accuracy.

2.3 Experimental outcomes

A total of eight specimens were tested, four in the unreinforced configuration: URM 04, 05, 06, 07 and four in the strengthened configuration: RM01, 02, 03, 04. Although the DIC technique captured a range of deformations, two of these were considered for the current research; the vertical deformation along the x'_2 axis and along the applied force (Δv), and the deformation presented orthogonally (Δh) along the x'_1 axis. The force-deformations for the unreinforced specimens and the reinforced specimens are plotted in Figures 2 and 3, respectively.

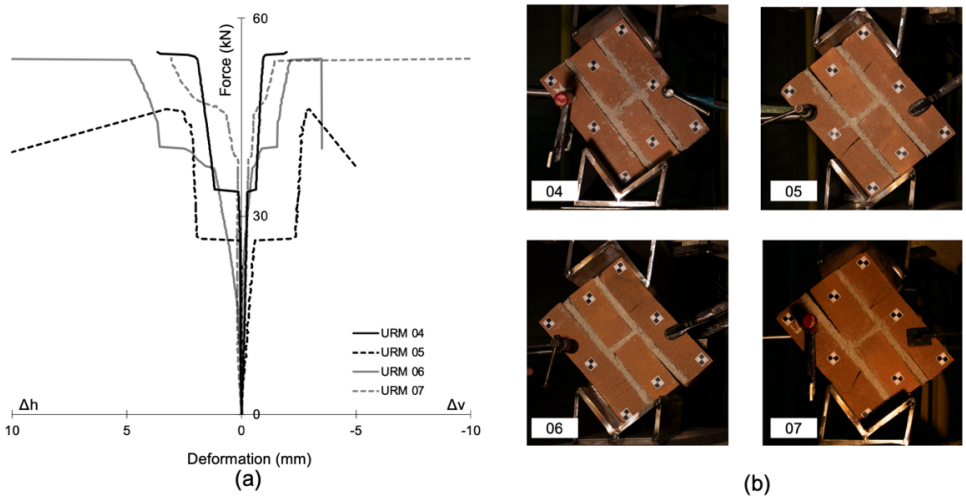


Figure 2 – Unreinforced specimens (a) Applied force and deformation Δv and Δh captured, (b) Failures presented at critical load

Despite some variation in deformation capacities of the specimens, the shear resistance and the ultimate strength of among the tested specimens remains comparable. The unreinforced specimens reached maximum loads of approximately 50–55 kN, whereas the reinforced specimens exhibited higher load capacities, reaching 60–95 kN approximately.

Following crack initiation, the specimens maintained an almost constant shear resistance over a finite displacement range, indicating stable post-cracking behaviour. The unreinforced specimens exhibited an initially brittle response, followed by progressive crack propagation and degradation of the resisting mechanism, governed by a combination of shear and bending actions. In contrast, the reinforced specimens demonstrated improved ductility, evidenced by both the more distributed crack patterns and the post-peak

defamations observed in the force–deformation curves. Further, the reinforced specimens sustained larger deformations before significant loss in the resistance, while a sharp drops in the post crack behaviour was seen is the unreinforced specimens indicate.

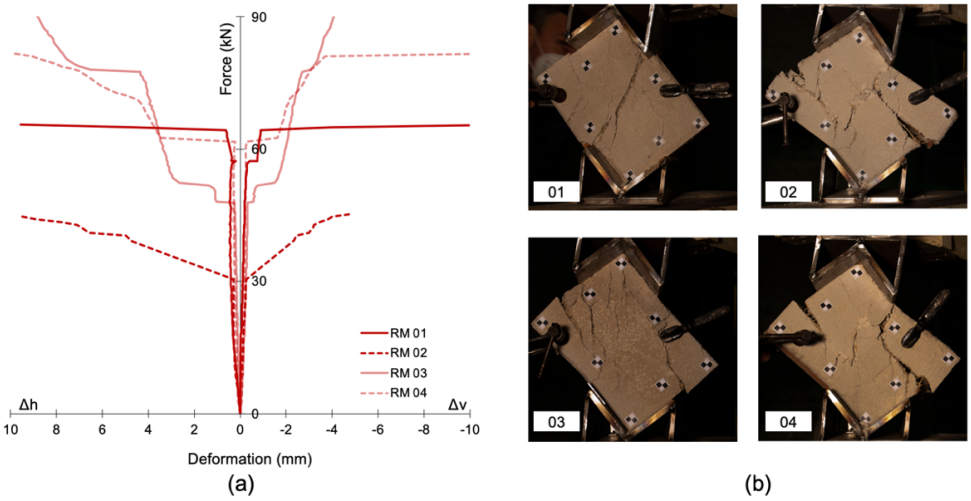


Figure 3– Jute-NFRCM strengthened reinforced specimens (a) Applied force and deformation Δv and Δh captured, (b) Failures presented at critical load

Further, to evaluate the shear stiffness (G) of the specimens, the initial slope of the force displacement curves is considered, the shear stress (τ). shear stain (γ) are calculated as presented in Equation 1, where F is the applied load and A is the normalized cross-sectional area, v_0 and h_0 are the initial lengths in the orthogonal directions.

$$G = \frac{\tau}{\gamma} \; ; \quad \tau = \frac{F}{A} \; ; \quad \gamma = \frac{\Delta v}{v_o} + \frac{\Delta h}{h_o} \tag{1}$$

The shear stiffness computed experimentally are presented in Table 1. The experimental outcome highlights a clear distinction between the unreinforced and strengthened specimens. While the unreinforced masonry exhibits a brittle response with limited deformation capacity, seen in Figure 2a, the strengthened specimens show improved load-carrying capacity, with higher deformation, of about more than 10mm in the orthogonal direction, improved ductility and delayed failure indicating the effectiveness of the reinforcement system, seen in Figure 3a. The average stiffness of the unreinforced and reinforced specimens presented in Table 1 also indicates about 50% increase in the performance of masonry in the presence of jute-NFRCM strengthening.

Table 1 – Initial stiffnesses presented in the specimens, computed according to Equation 1

Unreinforced triplets		**Reinforced triplets**	
URM 04	537.65 MPa	RM 01	655.45 MPa
URM 05	405.16 MPa	RM 02	737.50 MPa
URM 06	622.87 MPa	RM 03	703.15 MPa
URM 07	496.57 MPa	RM 04	979.11 MPa
Average	**515.56 MPa**	*Average*	**768.80 MPa**

3. Finite Element Modelling

The finite element model adopted in this study builds upon the multi-leaf homogenization framework developed by Cecchi (2006) initially introduced for the analysis of CFRP-strengthened masonry walls subjected to both in-plane and out-of-plane loading in the elastic range. The application of this model for NFRCM matrix is elaborated in Thatikonda *et al.* (2025b). Here a two-step homogenization is adopted for deriving the equivalent mechanical characteristics of the elastic continua.

First the NFRCM system and masonry are modelled separately. The NFRCM is modelled as a 3D orthotropic continuum, accounting for the bidirectional fiber mesh embedded mid-width of the composite matrix, following the nomenclature presented in Cecchi (2006) and modelling approach proposed in Thatikonda *et al.* (2025b). The 3D equivalent elastic properties of the strengthening applied is given by the tenor $\mathbf{A}^{\mathbf{NFRCM}}$ or A_{ijkl}^{NFRCM}, where *i,j,k,l* = {1,2,3}, see Table 2.

Table 2 – Mechanical properties of jute-NFRCM constituents and 3D homogenized tensor $\mathbf{A}^{\mathbf{NFRCM}}$

Jute - NFRCM	**Homogenized properties**		
Jute fiber mesh E = 524 MPa ν = 0.2	A_{1111} = 1289.52 MPa	A_{1122} = 231.88 MPa	A_{1133} = 230.45 MPa
	A_{2211} = 231.87 MPa	A_{2222} = 1289.51 MPa	A_{2233} = 230.45 MPa
Mortar matrix E = 1300 MPa ν = 0.2	A_{3311} = 232.22 MPa	A_{3322} = 232.23 MPa	A_{3333} = 1258.39 MPa
	A_{1212} = 525.35 MPa	A_{2323} = 4870.12 MPa	A_{3131} = 4870.37 MPa

For the masonry triplet, a 2D homogenization is adopted and the equivalent elastic continua is presented in the tensor $\mathbf{A}^{\mathbf{M}}$ or A_{ijkl}^{M}, in Table 3.

Table 3– Mechanical properties of masonry constituents and 2D homogenized tensor $\mathbf{A}^{\mathbf{M}}$

Masonry Constituents	**Homogenized properties**		
Brick units E = 4387 MPa ν = 0.2	A_{1111} = 3312.49 MPa	A_{1122} = 261.66 MPa	-
	A_{2211} = 271.51 MPa	A_{2222} = 1119.37 MPa	-
Mortar Joints E = 128 MPa ν = 0.2	-	-	A_{3333} = 3508.55 MPa
	A_{1212} = 398.34 MPa	-	-

In the second step of the homogenization, the previously homogenized jute NFRCM matrix (A_{ijkl}^{NFRCM}) and the masonry (A_{ijkl}^{M}) are integrated following the Equation 2, where t is the masonry thickness, and s is the thickness of each of the NFRCM strengthening layers. The equivalent elastic properties of the reinforced specimen A_{ijkl}^{H}, as presented in Table 4.

$$A_{ijkl}^{H} = \frac{1}{t+2s}\left(tA_{ijkl}^{M} + 2sA_{ijkl}^{NFRCM}\right) \tag{2}$$

Table 4 – Homogenized mechanical properties of the reinforced specimen $\mathbf{A^H}$

Reinforced specimen - Homogenized properties		
A_{1111} = 2907.89 MPa	A_{1122} = 255.7 MPa	-
A_{2211} = 263.58 MPa	A_{2222} = 1153.39 MPa	-
-	-	A_{3333} = 3058.52MPa
A_{1212} = 423.74 MPa	-	-

The triplet specimens are modelled in the commercial software Straus7, where the Finite Element (FE) model adopts anisotropic quadrilateral deformable elements under 2D plain stress hypothesis, aimed at capturing the elastic response and initial shear stiffness, providing a basis for the validation with the experimental results. To establish a comparison between the unreinforced, and the reinforced specimens and to evaluate the reliability of the homogenization method adopted at this scale and heterogeneity, three FE models are proposed.

The first two models consider the unreinforced specimen, with the first one (Model 1) modelling the masonry texture, with brick and mortar discretely defined (see Table 3 for masonry constituent properties adopted), to present a heterogenous model, and the second as a homogeneous FE model (Model 2) with the unreinforced masonry homogenized properties (A_{ijkl}^M). The third model (Model 3) adopts the homogenized properties of the reinforced masonry specimen (A_{ijkl}^H). To simulate the specimen geometry, test setup and boundary condition the FE models were also rotated, and a unit displacement was introduced along the x'_2 axis, and the vertical (Δv) and horizontal (Δh) deformations computed along the x'_2 and x'_1 axes respectively. The deformation distribution of three FE models is presented in Figure 4. For each of these models the resultant force was recorded, along with the orthogonal deformation presented and a comparison with these force-displacement outcomes with that of the experimental data is presented in Figure 5.

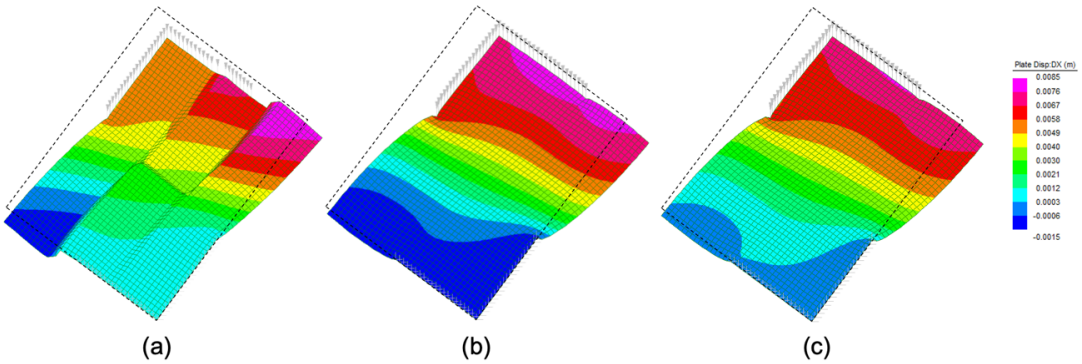


Figure 4 – FE deformations distribution (a) Model 1 - heterogeneous unreinforced triplet model (b) Model 2 - homogenised unreinforced triplet model and (c) Model 3 - reinforced homogenised model

Further adopting the formulation presented in Equation 1, the initial shear stiffness (G) is computed for each of these FE models. The unreinforced specimen models 1 and 2 present an initial stiffness of 678 MPa and 660 MPa, respectively, whereas the reinforced specimen model 3 presents an initial stiffness of 864 MPa. Although the distribution of the deformation is distinguishable in the two unreinforced models presented,

the stiffness computed is alike. The heterogeneous model, similar to the experimental outcomes, shows an improved stiffness with the presence of the jute-NFRCM reinforcement.

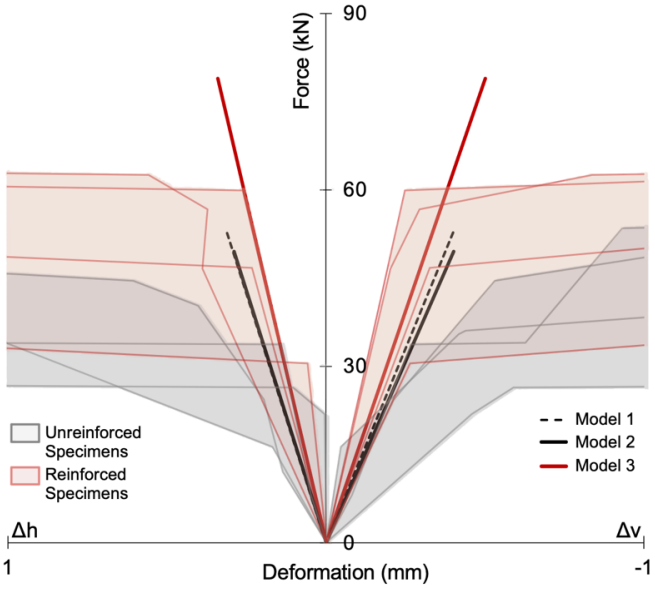


Figure 5 – Initial stiffness computed from the FE model outcomes - compared to the experimental data

4. Conclusion

The current research aims at demonstrating that the proposed modified masonry triplet provides an effective and practical alternative to conventional large-scale specimens for the shear characterization of masonry. The experimental results show that jute-NFRCM strengthening enhances both shear resistance and deformation capacity, with an average improvement of approximately 50% in shear stiffness when compared to unreinforced specimen. The finite element models, particularly based on the multi-leaf homogenization approach, are comparable with experimental results, both in terms of the deformations predicted and the initial stiffness computed, supporting the validity of the adopted modelling strategy.

Further, the manageable specimen scale provides a good foundation for the research within the framework of innovative composites, evaluating various parameters of the NFRCM strengthening, such as textile architecture, durability, and resilience under different mechanical and environmental conditions, amongst others. Furthermore, the FE models present a simple and efficient tool to estimate the performance, and this could be taken forward to introduce non-linear parameters, evaluating ductility and the post peak behaviours of reinforced specimens.

Acknowledgments

The authors acknowledge the Construction Science Laboratory of the University IUAV of Venice (LabsCo) for the support provided in conducting the experiments. The work was partly financed by the National Recovery and Resilience Plan (NRRP), Mission 4, Component 2, Investment 1.1, Call for tender No. 104 published on 2.2.2022 by the Italian Ministry of University and Research (MUR), funded by the European Union - NextGenerationEU - Project Title 'New Insights in the Mechanical Modeling of Cultural Heritage for Sustainable Restoration: Green Composites and Nano-Technologies (GreNaTe)' - CUP: F53D23002060006, PRJ-0191' - Grant Assignment Decree No. 742-2023 adopted on 30.05.2023 by the Italian Ministry of University and Research (MUR).

References

Alecci, Valerio, Sara Barducci, Angelo D'Ambrisi, Mario De Stefano, Francesco Focacci, Raimondo Luciano, and Rosa Penna. "Shear capacity of masonry panels repaired with composite materials: Experimental and analytical investigations." Composites Part B: Engineering 171 (2019): 61-69.

ASTM, “ASTM E519 Standard Test Method for Diagonal Tension (Shear) in Masonry Assemblages”, American Society for Testing Materials (1981): pp. 1–17 (Updated 2022).

Boem, Ingrid. "Masonry elements strengthened with TRM: A review of experimental, design and numerical methods." Buildings 12, no. 9 (2022): 1307.

Cecchi, Antonella, and Karam Sab. "A multi-parameter homogenization study for modeling elastic masonry." European Journal of Mechanics-A/Solids 21, no. 2 (2002): 249-268.

Cecchi, Antonella. "CFRP reinforced masonry walls: analytical and numerical homogenised models." In WSEAS International conferences: 2nd WSEAS Int. Conf. on Applied and Theoretical Mechanics (2006).

Cheng, Shuaian, Shiping Yin, and Lei Jing. "Comparative experimental analysis on the in-plane shear performance of brick masonry walls strengthened with different fiber reinforced materials." Construction and Building Materials 259 (2020): 120387.

Codispoti, Rosamaria, Daniel V. Oliveira, Renato S. Olivito, Paulo B. Lourenço, and Raul Fangueiro. "Mechanical performance of natural fiber-reinforced composites for the strengthening of masonry." Composites Part B: Engineering 77 (2015): 74-83.

Corradi, Marco, and Antonio Borri. "A database of the structural behavior of masonry in shear." Bulletin of Earthquake Engineering 16, no. 9 (2018): 3905-3930.

de Carvalho Bello, Claudia Brito, Daniele Baraldi, Antonella Cecchi, and Daniel V. Oliveira. "Experimental characterization of masonry panels strengthened with NFRCM." Key Engineering Materials 898 (2021): 43-48.

EN 1052-3:2002, “EN 1052-3 Method of test for masonry - Part 3: Determination of initial shear strength”, European Standards, (2002).

Garcia-Ramonda, Larisa, Luca Pela, Pere Roca, and Guido Camata. "In-plane shear behaviour by diagonal compression testing of brick masonry walls strengthened with basalt and steel textile reinforced mortars." Construction and Building Materials 240 (2020): 117905.

Li, Mi, Yunqiao Pu, Valerie M. Thomas, Chang Geun Yoo, Soydan Ozcan, Yulin Deng, Kim Nelson, and Arthur J. Ragauskas. "Recent advancements of plant-based natural fiber–reinforced composites and their applications." Composites Part B: Engineering 200 (2020): 108254.

Libre Jr, Roneh Glenn D., Julius L. Leaño Jr, Luis Felipe Lopez, Carlo Joseph D. Cacanando, Michael Angelo B. Promentilla, Ernesto J. Guades, Lessandro Estelito O. Garciano, and Jason Maximino C. Ongpeng. "In-plane shear behavior of unreinforced masonry wall strengthened with bamboo fiber textile-reinforced geopolymer mortar." Buildings 13, no. 2 (2023): 538.

Majumder, Arnas, Flavio Stochino, Ilenia Farina, Monica Valdes, Fernando Fraternali, and Enzo Martinelli. "Physical and mechanical characteristics of raw jute fibers, threads and diatons." Construction and Building Materials 326 (2022): 126903.

Mazzotti, Claudio, Francesca Ferretti, Barbara Ferracuti, and Andrea Incerti. "Diagonal compression tests on masonry panels strengthened by FRP and FRCM." In Structural analysis of historical constructions: Anamnesis, diagnosis, therapy, controls, pp. 1069-1076. CRC Press (2016).

RILEM "RILEM T. C. LUM B6 - Diagonal tensile strength tests of small wall specimens, 1991." RILEM Recommendations for the testing and use of constructions materials (1994): 488-489.

Thatikonda, Nandini Priya, Daniele Baraldi, Giosue Boscato, and Antonella Cecchi. "Experimental evaluation of elastic shear components for masonry in a Cosserat Continuum." International Journal of Solids and Structures 292 (2024): 112715.

Thatikonda, Nandini Priya, Daniele Baraldi, Giosuè Boscato, and Antonella Cecchi. "Specimen size sensitivity on diagonal compression tests for masonry." In Multiscale and Multiphysics Modelling for Advanced and Sustainable Materials: Euromech Colloquium 642, pp. 405-416. Cham: Springer Nature Switzerland (2025).

Thatikonda, Nandini Priya, Daniele Baraldi, Giosuè Boscato, and Antonella Cecchi. "Adaptation of DIC technique for simplified applications in experimental mechanics." In Journal of Physics: Conference Series, vol. 2802, no. 1, p. 012008. IOP Publishing (2024).

Thatikonda, Nandini Priya, Daniele Baraldi, Giosuè Boscato, and Antonella Cecchi. "Experimental Characterization and Numerical Validation of NFRCM for Strengthening Masonry." In International Conference Mechanics of Masonry Structures Strengthened with Composite Materials, pp. 89-99. Cham: Springer Nature Switzerland (2025).

Trochoutsou, Niki, Matteo Di Benedetti, Kypros Pilakoutas, and Maurizio Guadagnini. "Mechanical characterisation of flax and jute textile-reinforced mortars." Construction and Building Materials 271 (2021): 121564.

Valluzzi, Maria Rosa, Claudio Modena, and Gianmarco de Felice. "Current practice and open issues in strengthening historical buildings with composites." Materials and structures 47, no. 12 (2014): 1971-1985.

Cinpar 2026
XXII International Conference on Building Pathology and Constructions Repair
15th to 17th July 2026 - Lisboa, Portugal

Compressive Behaviour of Masonry Columns Strengthened with PBO-FRCM Systems: Experimental and DEM Numerical Investigation

Matteo MAURO[1], Madalena PONTE[2], José V. LEMOS[3], Pietro MAZZUCA[4], Luciano OMBRES[5]

[1] Department of Civil Engineering, University of Calabria (UNICAL), Rende, Italy, matteo.mauro@unical.it
[2] National Laboratory for Civil Engineering (LNEC), Lisbon, Portugal, mponte@lnec.pt
[3] National Laboratory for Civil Engineering (LNEC), Lisbon, Portugal, vlemos@lnec.pt
[4] Department of Civil Engineering, University of Calabria (UNICAL), Rende, Italy, pietro.mazzuca@unical.it
[5] Department of Civil Engineering, University of Calabria (UNICAL), Rende, Italy, luciano.ombres@unical.it

Abstract: Historic masonry structures, widely distributed in seismic-prone regions, are characterised by low tensile strength, limited deformation capacity, and brittle failure mechanisms under cyclic loading and combined axial–bending actions. Improving their structural performance while preserving material compatibility and architectural integrity remains a major challenge in the seismic rehabilitation of built heritage. In this context, Fibre-Reinforced Cementitious Matrix (FRCM) systems have emerged as effective strengthening solutions due to their compatibility with masonry substrates and reduced invasiveness. Among them, PBO-FRCM composites—consisting of polyparaphenylene benzobisoxazole (PBO) fibre meshes embedded in inorganic matrices—have shown significant potential for confinement of masonry elements. This study investigates the compressive behaviour of masonry columns confined with PBO-FRCM systems through a combined experimental and numerical approach. Square masonry columns were tested under monotonic axial compression loading, including unconfined reference specimens and confined specimens strengthened with a PBO-FRCM system, in order to assess the effectiveness of the confinement. The experimental results confirmed that FRCM confinement enhances both compressive strength and deformation capacity. These results were subsequently used to evaluate the accuracy of the numerical modelling strategy in reproducing the compressive behaviour of both confined and unconfined specimens. To this end, a three-dimensional (3D) numerical model based on the Discrete Element Method (DEM) was developed using 3DEC software, in which the masonry column was represented as an assemblage of deformable blocks interacting through contact interfaces. The model was first calibrated against the experimental response of unconfined columns and then extended to confined configurations through liner elements, adapted to simulate an external FRCM jacketing within a discontinuum framework. The proposed modelling strategy captures the interaction between the masonry substrate and the strengthening system in terms of stress transfer and confinement mechanisms. In particular, the numerical results show good agreement with the experimental response in terms of peak compressive strength, with differences of approximately 6,84 % and 1,36 % for the unconfined and confined configurations, respectively. These results provide quantitative insight into the role of interface behaviour and lateral dilation in the activation of the confinement mechanism, confirming the potential of DEM-based approaches for the simulation of FRCM-strengthened masonry elements.

Keywords: Masonry structures, Columns, FRCM confinement, Discrete Element Method.

1. Introduction

1.1 Literature review

The reuse and rehabilitation of existing buildings represent one of the most effective strategies for reducing the environmental impact associated with the construction sector (Aigwi *et al.* (2023)). Across Europe, a large

portion of the built heritage consists of existing structures, many of which are currently abandoned or affected by various levels of structural degradation. A considerable portion of this stock is composed of masonry constructions, often characterised by significant historical and cultural value.

From a mechanical standpoint, masonry is a quasi-brittle material exhibiting low tensile strength, limited deformation capacity and sudden failure mechanisms. Such behaviour is inherently incompatible with modern seismic design philosophies, which promote ductile structural responses to ensure adequate energy dissipation during earthquake events. For this reason, the development of strengthening techniques capable of enhancing deformability and damage tolerance, while preserving material compatibility and architectural integrity, has become a central topic in structural engineering research.

Among the available solutions, Fabric-Reinforced Cementitious Matrix (FRCM) systems have progressively gained attention (Kouris and Triantafillou (2018)). These systems consist of high-strength fibre meshes embedded in inorganic matrices and have proven particularly suitable for strengthening masonry substrates. Compared with Fibre-Reinforced Polymer (FRP) systems, which were developed earlier, FRCM solutions offer several advantages, including improved compatibility with masonry substrate, vapour permeability and enhanced reversibility of the intervention (Di Tommaso *et al.* (2017)). These characteristics make them particularly attractive for applications involving historical masonry structures.

Extensive experimental research demonstrated the effectiveness of FRCM systems in improving the structural performance of masonry elements (Aiello *et al.* (2021); Ponte *et al.* (2023)), showing their ability to modify typical brittle failure modes and promote a more gradual damage evolution.

Among structural elements, masonry columns have attracted particular attention due to their primary role in load transfer and their vulnerability to brittle failure under combined compression and bending, often induced by seismic actions or load eccentricities. For this reason, they represent an ideal benchmark for evaluating FRCM-strengthening techniques.

Several studies investigated the influence of fibre type in FRCM systems. In addition to steel-based systems, commonly referred to as Steel-Reinforced Grout (SRG) composites (De Santis *et al.* (2017)), other fibres such as glass, carbon, basalt and polyparaphenylene benzobisoxazole (PBO) have been widely employed (Di Ludovico *et al.* (2020); Jing *et al.* (2021)). Among these, PBO fibres have attracted increasing interest due to their high tensile strength and elastic modulus, which enhance the load-carrying capacity of strengthened elements. The increase in ductility is instead primarily related to the interaction between the fibre mesh and the inorganic matrix, as well as to the progressive activation of the reinforcement (Ombres and Verre (2020)).

The role of the inorganic matrix was also extensively investigated, as it represents a key parameter governing the overall response of the composite system (Cascardi *et al.* (2018)). Additional factors influencing performance include load eccentricity (Ombres (2015)), discontinuous reinforcement configuration (Campolongo *et al*. (2023)), and geometric features such as corner rounding (Sneed *et al.* (2017)).

Despite the considerable experimental effort, several uncertainties still affect the design and assessment of FRCM-strengthened masonry columns. Existing analytical models for FRCM-strengthened masonry are typically calibrated on experimental datasets (Ameli *et al.* (2022); Napoli and Realfonzo (2022)), and their reliability is therefore strongly dependent on the representativeness of the available data. In addition, design-oriented formulations have been proposed in international guidelines, such as those provided by the CNR (2020) recommendations, which offer practical approaches for estimating the strength of FRCM-retrofitted masonry elements.

Although the prediction of strength enhancement has been extensively addressed in the literature, greater uncertainty still exists in the quantification of the deformation capacity of strengthened masonry, particularly under complex loading conditions. In this context, axial compression tests play a fundamental role in the mechanical characterisation of the material and in the calibration of numerical models, providing a necessary basis for more advanced investigations involving cyclic or dynamic loading, where post-peak behaviour and damage evolution become critical.

The inherent variability of masonry materials further complicates this issue, as specimens with similar geometry and strengthening configurations may exhibit significantly different mechanical responses. As a result, large experimental datasets would be required to ensure robust and generalisable predictions.

1.2 Numerical approaches

Several numerical modelling approaches have been developed to investigate the mechanical behaviour of masonry structures. Owing to the composite and heterogeneous nature of masonry, governed by the interaction between units and mortar joints, two main strategies are generally adopted: equivalent continuum approaches and discontinuum approaches (Lourenço (2002); Lemos (2007)).

Within continuum frameworks, masonry is typically represented as an equivalent homogeneous material through suitable constitutive relationships capable of reproducing its global response. In this context, modelling strategies are commonly classified into macro-modelling, where masonry is treated as a homogenised continuum, and micro-modelling approaches, in which units and mortar joints are explicitly represented through interface elements. Continuum-based approaches, most commonly implemented through the Finite Element Method (FEM), are widely used due to their versatility and their ability to capture the global structural behaviour of masonry systems. In addition, simplified modelling strategies such as the Equivalent Frame Modelling (EFM) approach are also widely adopted for structural analysis, particularly when reduced computational effort is required.

However, the response of masonry is strongly governed by discontinuities associated with mortar joints, which may undergo opening, sliding and progressive detachment under increasing load levels. The accurate representation of these mechanisms, particularly in the presence of crack propagation and large displacements, may be difficult to achieve within purely continuum-based formulations.

For this reason, discontinuum-based approaches have gained increasing attention in the analysis of masonry structures (Lemos (2007)). In these approaches, masonry is modelled as an assemblage of distinct interacting bodies, where the global response emerges from the interaction between units and their contact interfaces. Among these methods, the Discrete Element Method (DEM) has proven particularly suitable for materials characterised by a block-like structure, such as masonry (Bui *et al.* (2017); Lemos and Costa (2017); Sarhosis *et al.* (2016)).

Originally introduced by Cundall (1971), DEM was developed to simulate the mechanical behaviour of systems composed of interacting discrete bodies. Within this framework, masonry is represented as an assembly of blocks connected through contact laws governing normal and tangential interactions. This approach naturally allows key mechanisms observed in masonry structures to be captured, including joint opening, sliding, block separation and large displacement effects, which play a fundamental role in the structural response and failure modes.

Despite the increasing use of DEM approaches for the analysis of unreinforced masonry structures, their application to FRCM-strengthened systems remains very limited. To the authors' knowledge, no studies are currently available in the literature addressing the modelling of FRCM reinforcement within a three-dimensional (3D) DEM framework such as 3DEC (Itasca Consulting Group (2024)). Only limited contributions can be found for simplified two-dimensional (2D) cases. For instance, Gobbin *et al.* (2020) recently studied the structural behaviour of masonry arches strengthened with externally bonded reinforcement using a 2D DEM approach, where the masonry was modelled as an assemblage of rigid blocks and the reinforcement was represented through truss elements connected to the substrate by means of non-linear springs. This highlights a clear research gap in the numerical modelling of FRCM-strengthened masonry within a discontinuum framework, particularly in 3D analyses.

In this context, the present study proposes a 3D DEM-based strategy for simulating the compressive behaviour of square masonry columns, both unconfined and confined with PBO-FRCM systems. The adopted methodology includes: (i) the experimental characterisation of the constituent materials, FRCM

coupons and masonry columns; (ii) the calibration of the DEM model through the experimental response of the unconfined specimens; (iii) the extension of the modelling framework to FRCM-confined configurations; and (iv) the validation of the proposed approach through comparison between numerical and experimental results in terms of axial stress–strain response and failure mechanisms.

2. Resume of the Experimental Campaign

This section provides an overview of the experimental campaign carried out in Mauro *et al.* (2026), from the characterisation of the constituent materials to the assessment of the FRCM-strengthening system applied to masonry columns. The mechanical properties of the mortars were determined through standard flexural and compressive tests, while the behaviour of the PBO fibre mesh was characterised by means of direct tensile (DT) tests in order to evaluate its tensile strength and stiffness. Subsequently, the mechanical response of the FRCM-strengthening system was investigated through uniaxial DT tests performed on FRCM coupons, allowing the interaction between the fibre mesh and the mortar matrix to be assessed. The strengthening system (Figure 1) was then applied to masonry columns, and its effectiveness was evaluated through axial compression tests carried out on both unconfined reference specimens and confined columns strengthened with FRCM system. All columns had a square cross-section of 250 × 250 mm² and an overall height of 485 mm. Each specimen was constructed using seven courses of two solid clay bricks (250 × 125 × 55 mm³), separated by mortar joints approximately 10 mm thick. The bedding mortar was classified as type M5 in accordance with EN 1996-1-1 (CEN 2005). To ensure uniform load transfer during testing, 20 mm-thick mortar capping layers were applied to the top and bottom surfaces of each specimen.



(a) (b) (c)

Figure 1 – Strengthening procedure: (a) first mortar layer, (b) PBO mesh application, and (c) final mortar layer

For the FRCM reinforcement system, a balanced bidirectional PBO fibre mesh was adopted, characterised by equal fibre densities in both warp and weft directions (22 g/m²) and an equivalent thickness of 0,014 mm in both directions. The mesh exhibited an average tensile strength of 3160 MPa and an elastic modulus of 212 GPa. The matrix consisted of a commercial inorganic lime-based mortar, which exhibited an average compressive strength of 17 MPa and a flexural strength of 5,8 MPa. The FRCM coupons exhibited an average tensile strength of 1325 MPa.

Regarding the columns response, unconfined specimens exhibited a brittle failure mode, characterised by vertical cracks propagating through mortar joints and bricks up to crushing (Figure 2.a). In contrast, confined specimens showed distributed cracking along the FRCM jacket (Figure 2.b), mainly concentrated at the

corners (Figure 2.c), followed by crushing of the masonry core. Further details on the experimental setup, testing procedures, and complete results are provided in the dedicated study (Mauro *et al.* (2026)).



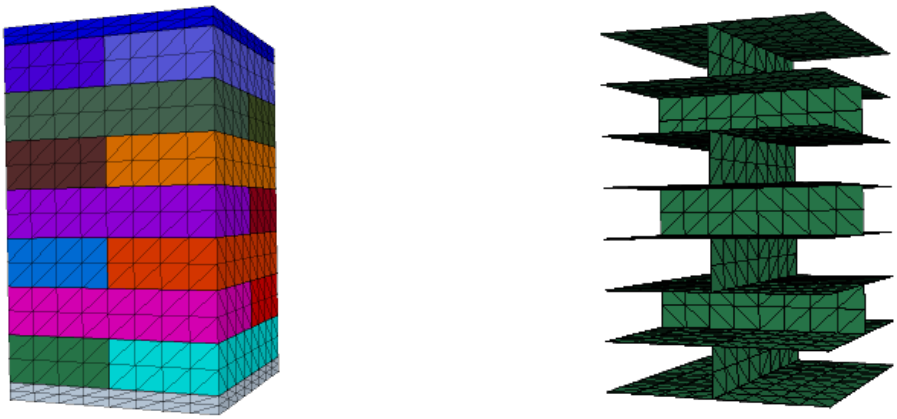
(a) (b) (c)

Figure 2 – Failure modes: (a) crushing of the unconfined column, (b) distributed vertical cracking along the PBO-FRCM jacket, and (c) dominant corner crack propagation

3. DEM Modelling Approach

3.1 Brick Masonry

The numerical analyses were carried out using the 3D distinct element code 3DEC (Itasca Consulting Group (2024)), based on DEM, which represents masonry as an assemblage of interacting blocks (Figure 3.a) separated by both horizontal and vertical contact-joint interfaces (Figure 3.b). Within this framework, the mechanical response of the masonry column results from the interaction between individual units and the constitutive laws governing their interfaces, making this approach suitable for materials characterised by a discontinuous internal structure (Lemos (2007)).

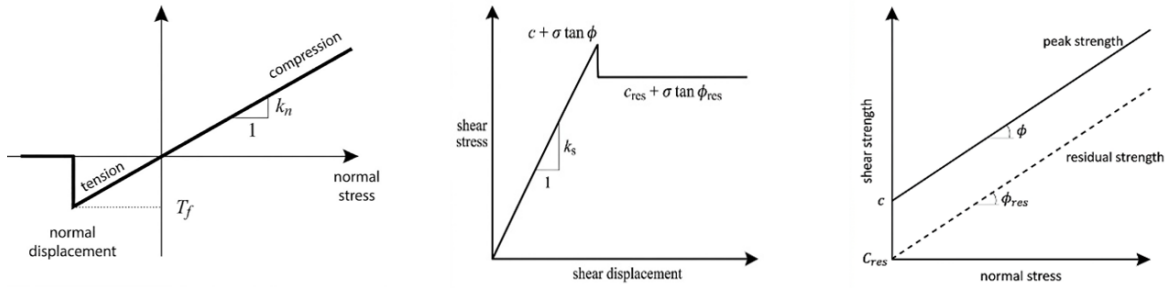


(a) (b)

Figure 3 – DEM model of the unconfined masonry column: (a) geometric configuration and (b) joint arrangement

The masonry units were modelled as deformable blocks discretised using hexahedral zones, with a mesh defined by 2 × 4 × 8 divisions for the masonry units and 2 × 8 × 8 divisions for two steel plates used at the top and bottom of the specimen to simulate the application of a uniform axial load. Large-strain conditions were activated in order to account for the evolution of displacements during loading.

The mechanical behaviour of the masonry units was described using a Mohr–Coulomb constitutive model. The tensile strength was assumed equal to 5 % of the compressive strength, reflecting the brittle behaviour of masonry in tension. The interaction between adjacent units was represented through zero-thickness contact interfaces governed by a Mohr-type contact model (Figure 4), capable of reproducing opening, sliding and inelastic behaviour along the mortar joints. The interface strength parameters were defined based on the mortar properties. Consistently with the assumption adopted for the masonry units, the tensile strength was assumed to be equal to 5 % of the compressive strength. In addition, residual values of cohesion and friction angle were introduced to account for the post-peak degradation of the joint behaviour, as permitted by the adopted contact model.



(a) (b) (c)

Figure 4 – Mohr-Coulomb Joint Model: (a) normal stress vs normal displacement behaviour, (b) shear stress vs shear displacement behaviour, and (c) shear failure criterion (adapted from Itasca Consulting Group (2024))

The contact stiffness parameters were defined according to classical formulations commonly adopted in discrete element modelling of masonry joints. In particular, the normal and shear stiffness, k_n and k_s respectively, were expressed as:

$$k_n = \frac{E_m}{t}, \tag{1}$$

and

$$k_s = \frac{G_m}{t}, \tag{2}$$

where E_m is the Young's modulus of the mortar, t is the average real joint thickness, and G_m is the shear modulus defined as:

$$G_m = \frac{E_m}{2(1+\nu)}. \tag{3}$$

The cohesion parameter of the interface was derived from the compressive strength of the mortar according to the Mohr–Coulomb relationship:

$$c = \frac{f_c(1-\sin\,\phi)}{2\cos\,\phi}. \tag{4}$$

These relations were adopted as a theoretical reference for defining the contact properties, which were then calibrated to reproduce the experimental response of the specimens, with particular reference to the initial stiffness and peak compressive strength. Table 1 summarises the main mechanical parameters adopted in the DEM model, whereas Table 2 presents the key interface properties of the joints.

Regarding the boundary conditions, the bottom steel plate was fully constrained, whereas the top one was restrained in the horizontal directions and allowed to move vertically.

Table 1 - Mechanical parameters adopted for the materials considered in the DEM numerical model

Part	Density (kg/m³)	Young modulus (GPa)	Poisson ratio (-)	Compressive strength (MPa)	Tensile strength (MPa)	Friction angle (°)
Plate	7850,0	210,0	0,30	-	-	-
Brick	1700,0	9,8	0,20	6,60	0,33	32
Mortar	-	4,9	0,20	5,00	0,25	30

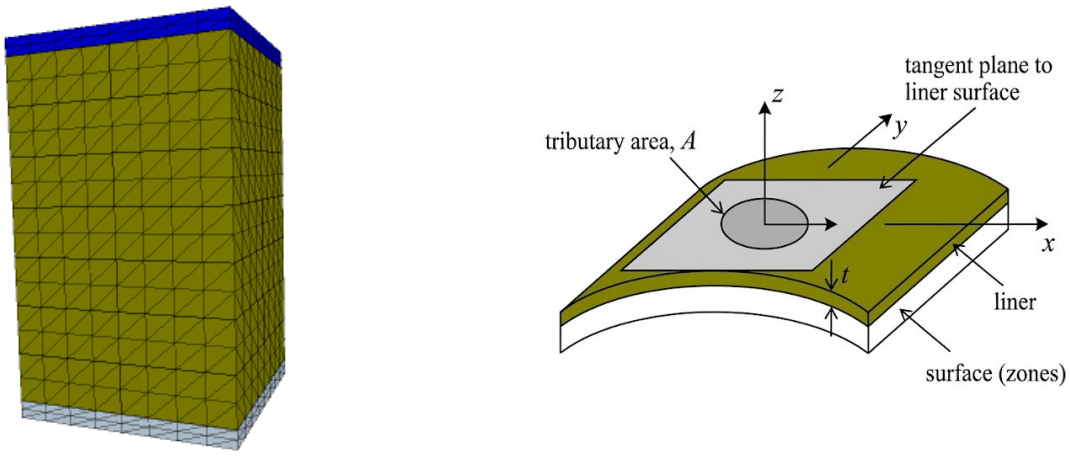
Table 2 – Joint interface properties adopted in the DEM numerical model

	t (m)	K_n (MPa/m)	K_s (MPa/m)	G_m (GPa)	c (MPa)
Joint	0,01	4900	2040	2,04	1,44

A displacement-controlled loading condition was applied by imposing a constant vertical velocity to the top plate. A global numerical damping coefficient equal to 0,3 was introduced to ensure quasi-static conditions and dissipate kinetic energy, while gravity was included to account for the self-weight of the masonry assemblage. The global compressive stress was evaluated by dividing the total reaction force at the loading plate by the cross-sectional area of the column, enabling direct comparison with the experimental stress–strain response.

3.2 FRCM retrofit

The modelling framework was extended to FRCM-confined masonry columns by introducing an external strengthening system through the use of structure liner elements available in 3DEC (Figure 5). In this study, the liner elements, formulated as shell-type structural elements capable of representing thin continuous layers, were employed to represent an equivalent continuous FRCM jacket, following approaches commonly adopted in geomechanics for modelling surface support systems (Chen and Teng (2024); Itasca Consulting Group (2024); Zhang and Nordlund (2021)).



(a) (b)

Figure 5 – DEM model of the FRCM-confined masonry column: (a) geometric configuration and (b) Idealization of interface behaviour at a liner node (adapted from Itasca Consulting Group (2024))

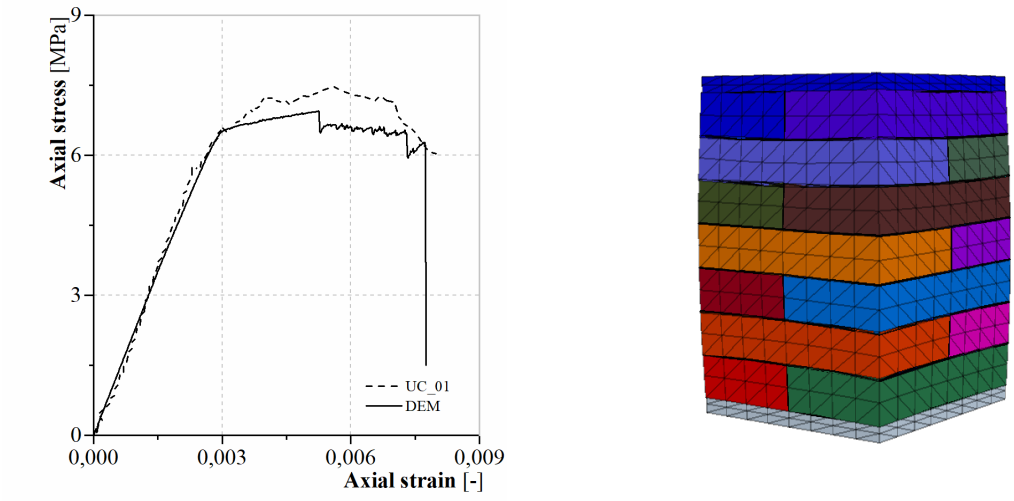
The liner elements were mechanically coupled to the masonry substrate through interface laws governing the transfer of normal and shear stresses, allowing the interaction between the strengthening system and the underlying masonry to be captured (Figure 5.b). The interface behaviour was defined by means of normal and shear coupling stiffness, cohesion and friction parameters, including residual values to account for progressive degradation. Within this framework, the FRCM system was modelled as an equivalent homogeneous membrane characterised by linear elastic behaviour, defined by an assigned Young's modulus, Poisson's ratio and thickness. It should be noted that this approach does not explicitly account for the internal interaction between fibre and matrix, which is inherently simplified into an equivalent constitutive response of the composite system.

The onset of damage in the strengthening system is governed by the interface behaviour between the liner and the masonry substrate, through the definition of strength and residual parameters controlling debonding and sliding mechanisms. Therefore, the adopted modelling strategy aims to capture the global confinement effect rather than the detailed meso-scale behaviour of the FRCM composite.

4. Preliminary results and discussion

The experimental and numerical results are presented in terms of axial stress–strain response for both unconfined and FRCM-confined masonry columns. The calibrated numerical model was first validated against the experimental response of the unconfined specimen.

Although the model does not explicitly incorporate a strain-softening constitutive law, the introduction of residual parameters at the contact level allows the degradation of the masonry response to be effectively captured, resulting in an overall satisfactory agreement with the experimental behaviour. This is confirmed by the comparison between numerical and experimental stress–strain curves, which shows good agreement in terms of initial stiffness, peak compressive strength and overall deformation capacity. Figure 6 presents the experimental–numerical comparison of the axial stress–strain response for the unconfined column, as well as with the corresponding deformed configuration at failure. With reference to the peak strength, the numerical model provided a close estimation of the experimental value, with a difference of approximately 6,84 % (7,46 MPa experimentally versus 6,95 MPa numerically). In terms of axial strain, evaluated by normalising the vertical displacement with respect to the column height, the ultimate value was 0,0081 experimentally and 0,0077 numerically, corresponding to a difference of approximately 4,94 %, as summarised in Table 3.



(a) (b)

Figure 6 – Unconfined masonry column: (a) experimental vs DEM axial stress–strain response and (b) deformed configuration at failure

Table 3 – Comparison between experimental and numerical results for the unconfined masonry column

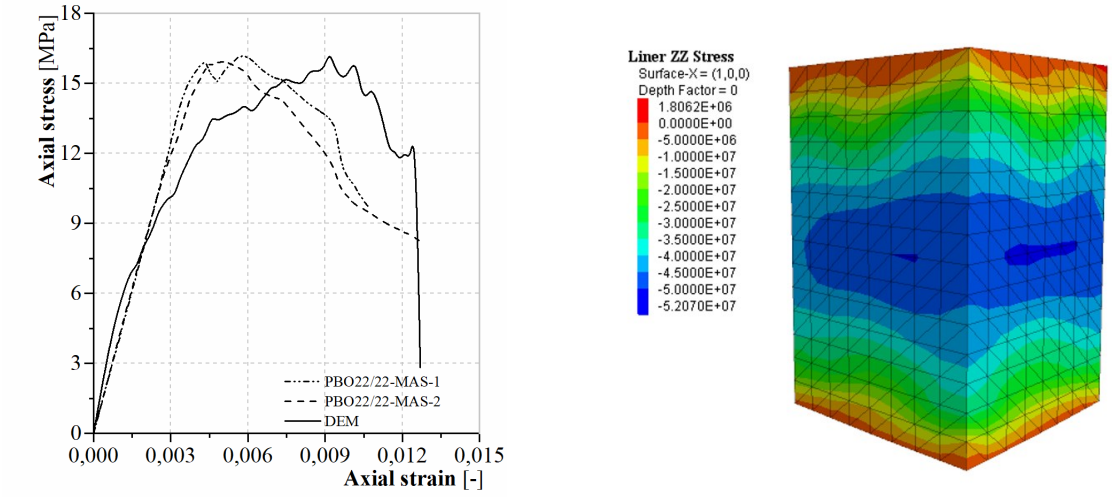
Unconfined Column	Maximum axial stress (MPa)	Ultimate axial strain (-)
Experimental	7,46	0,0081
DEM	6,95	0,0077
Error (%)	6,84	4,94

This validation step provides confidence in the adopted modelling strategy and is subsequently employed for the simulation of the confined configurations.

The comparison between experimental and numerical results (Figure 7.a) highlights the effect of external confinement on the global response of the column. An increase in peak compressive strength is observed, together with a modification of the stress–strain behaviour, characterised by a more gradual evolution of deformation prior to failure. The numerical curves show good agreement with the experimental results in terms of strength enhancement and overall response. However, some discrepancies can be observed in the initial stiffness, particularly after the activation of the reinforcement, leading to differences in the slope of the pre-peak branch. This behaviour can be attributed to the adopted modelling strategy for the external reinforcement.

With reference to the peak strength, the numerical model provided a close estimation of the experimental value, presenting a difference of approximately 1,36 % (16,16 MPa experimentally versus 16,38 MPa numerically). In terms of ultimate axial strain, the experimental value was 0,0118, while the numerical prediction was 0,0125, corresponding to a difference of approximately 5,93 %, as summarised in Table 4.

Moreover, the stress distribution within the liner elements confirms the effectiveness of the confinement provided by the strengthening system (Figure 7.b). The results show a well-distributed compressive stress field, indicating that the jacket actively contributes to the lateral confinement of the column. This indicates that the activation of the confinement mechanism is associated with the progressive dilation of the masonry assemblage, which mobilises the tensile capacity of the external FRCM reinforcement. Moreover, crushing of the masonry core is observed in the numerical model after the activation of the confinement mechanism induced by the external reinforcement, in agreement with the experimental evidence.



(a) (b)

Figure 7 – FRCM-confined masonry column: (a) comparison between experimental and DEM axial stress–strain responses, and (b) stress distribution in the FRCM jacket at peak

Table 4 - Comparison between experimental and numerical results for the FRCM-confined masonry column

Confined Column	Maximum axial stress (MPa)	Ultimate axial strain (-)
Experimental	16,16	0,0118
DEM	16,38	0,0125
Error (%)	1,36	5,93

5. Conclusions

This study investigated the compressive behaviour of masonry columns strengthened with PBO-FRCM systems through a combined experimental and DEM-based numerical approach. From an experimental perspective, the results confirmed that FRCM confinement enhances both the compressive strength and the deformation capacity of masonry columns.

From a numerical standpoint, a DEM-based modelling framework was developed and proposed to simulate the behaviour of both unconfined and confined masonry columns. The model, based on the representation of masonry as an assemblage of deformable blocks interacting through contact interfaces, proved capable of reproducing the global compressive response of unconfined specimens with satisfactory accuracy. In particular, differences of approximately 6,84 % and 4,94 % were obtained for peak compressive strength and ultimate axial strain, respectively.

The modelling strategy was extended to FRCM-confined configurations through the introduction of structure liner elements, enabling the interaction between the masonry substrate and an external reinforcement to be represented within a discontinuum framework. The comparison with experimental results for confined columns showed a very good agreement in terms of peak compressive strength and ultimate deformation capacity, with differences of approximately 1,36 % and 5,93 %, respectively.

The numerical results highlighted that the confinement effect is governed by the dilation of the masonry core and by the interface behaviour between the FRCM reinforcement and the substrate, confirming the capability of the proposed approach to reproduce the main features of the confined response.

The proposed DEM-based modelling strategy provides a robust initial framework for the analysis of FRCM-confined masonry elements and establishes a basis for further developments aimed at improving the modelling of interface behaviour and of the strengthening system. In this perspective, the adoption of advanced constitutive laws, such as strain-softening formulations, is expected to enable a more accurate representation of damage evolution and post-peak response.

Acknowledgments

The authors gratefully acknowledge the TEACH (Technology Applied to Cultural Heritage) Doctoral School of the University of Calabria for the financial support provided through the doctoral scholarship that contributed to this research. The authors also acknowledge the NESDE unit (Seismic Engineering and Structural Dynamics) at the National Laboratory for Civil Engineering (LNEC), Lisbon, Portugal, for hosting the research stay and for the valuable scientific guidance provided during the development of this study.

References

Aiello, Maria Antonietta, Francesco Bencardino, Alessio Cascardi, et al. 2021. “Masonry Columns Confined with Fabric Reinforced Cementitious Matrix (FRCM) Systems: A Round Robin Test.” *Construction and Building Materials* 298 (September). https://doi.org/10.1016/j.conbuildmat.2021.123816.

Aigwi, Itohan Esther, Ahmed Duberia, and Amarachukwu Nnadozie Nwadike. 2023. “Adaptive Reuse of Existing Buildings as a Sustainable Tool for Climate Change Mitigation within the Built Environment.” *Sustainable Energy Technologies and Assessments* 56: 102945. https://doi.org/10.1016/j.seta.2022.102945

Ameli, Zahra, Tommaso D’Antino, and Christian Carloni. 2022. “A New Predictive Model for FRCM-Confined Columns: A Reflection on the Composite Behavior at Peak Stress.” *Construction and Building Materials* 337 (June). https://doi.org/10.1016/j.conbuildmat.2022.127534.

Bui, Tan-Trung, Ali Limam, Vasilis Sarhosis, and Mohammed Hjiaj. 2017. “Discrete Element Modelling of the In-Plane and Out-of-Plane Behaviour of Dry-Joint Masonry Wall Constructions.” *Engineering Structures* 136: 277–294. https://doi.org/10.1016/j.engstruct.2017.01.020.

Campolongo, Francesco, Alessio Cascardi, and Luciano Ombres. 2023. “Prediction of the Additional Compressive Strength Due to PBO-FRCM-Confinement of Brick-Masonry Depending on the Stiffening Effect Caused by Different Discontinuous Wrappings: New Design-Oriented Perspective.” *Structures* 57: 105124. https://doi.org/10.1016/j.istruc.2023.105124.

Cascardi, Alessio, Francesco Micelli, and Maria Antonietta Aiello. 2018. “FRCM-Confined Masonry Columns: Experimental Investigation on the Effect of the Inorganic Matrix Properties.” *Construction and Building Materials* 186: 811–825. https://doi.org/10.1016/j.conbuildmat.2018.08.020.

Consiglio Nazionale delle Ricerche (CNR). 2018. *CNR-DT 215/2018. Istruzioni per la progettazione, l’esecuzione ed il controllo di interventi di consolidamento statico mediante l’utilizzo di compositi fibrorinforzati a matrice inorganica (FRCM).* Roma.

Cundall, Peter A. 1971. “A Computer Model for Simulating Progressive Large-Scale Movements in Blocky Rock Systems.” In *Proceedings of the International Symposium on Rock Fracture*, Nancy, France, paper II-8.

Chen, Yulong, and Junyang Teng. 2024. “3DEC Numerical Analysis of Failure Characteristics for Tunnel in Stratified Rock Masses.” *KSCE Journal of Civil Engineering* 28 (6): 2420–2426. https://doi.org/10.1007/s12205-024-1318-7.

De Santis, Stefano, Gianmarco de Felice, Bahman Ghiassi, Gian Piero Lignola, and Maria Rosa Valluzzi. 2021. “Round Robin Test on Tensile and Bond Behaviour of Steel Reinforced Grout Systems.” In *Structural Analysis of Historical Constructions (SAHC 2020)*, edited by Paulo B. Lourenço and Pere Roca, 290–298. Barcelona: CIMNE. https://doi.org/10.23967/sahc.2021.290.

Di Ludovico, Marco, Alessio Cascardi, Alberto Balsamo, and Maria Antonietta Aiello. 2020. “Uniaxial Experimental Tests on Full-Scale Limestone Masonry Columns Confined with Glass and Basalt FRCM Systems.” *Journal of Composites for Construction* 24 (5). https://doi.org/10.1061/(asce)cc.1943-5614.0001061.

Di Tommaso, Angelo, Francesco Focacci and Francesco Micelli. “Strengthening Historical Masonry with FRP or FRCM: Trends in Design Approach.” *Key Engineering Materials* 747 (2017): 166 - 173. https://doi.org/10.4028/www.scientific.net%2FKEM.747.166.

European Committee for Standardization (CEN). 2005. *EN 1996-1-1: Eurocode 6—Design of Masonry Structures—Part 1-1: General Rules for Reinforced and Unreinforced Masonry Structures.* Brussels.

Gobbin, Francesca, Gianmarco de Felice, and José V. Lemos. 2020. “A Discrete Element Model for Masonry Vaults Strengthened with Externally Bonded Reinforcement.” *International Journal of Architectural Heritage*. https://doi.org/10.1080/15583058.2020.1743792.

Itasca Consulting Group, Inc. 2024. “Background — the 3D Distinct Element Method.” *3DEC Theory and Background*. Accessed March 25, 2026. https://docs.itascacg.com/3dec700/3dec/docproject/source/theory/3dectheory/theory_background.html.

Jing, Lei, Shiping Yin, and Farhad Aslani. 2021. “Experimental Investigation on Compressive Performance of Masonry Columns Confined with Textile-Reinforced Concrete.” *Construction and Building Materials* 269 (February). https://doi.org/10.1016/j.conbuildmat.2020.121270.

Kouris, Leonidas Alexandros S., and Triantafillou, Thanasis C.. 2018. “State-of-the-Art on Strengthening of Masonry Structures with Textile Reinforced Mortar (TRM).” *Construction and Building Materials*, vol. 188. Preprint, Elsevier Ltd, November 10. https://doi.org/10.1016/j.conbuildmat.2018.08.039.

Lemos, José V. 2007. “Discrete Element Modeling of Masonry Structures.” *International Journal of Architectural Heritage* 1 (2): 190–213. https://doi.org/10.1080/15583050601176868.

Lemos, José V., and Alfredo Campos Costa. 2017. “Simulation of Shake Table Tests on Out-of-Plane Masonry Buildings. Part (V): Discrete Element Approach.” *International Journal of Architectural Heritage* 11 (1): 117–124. https://doi.org/10.1080/15583058.2016.1237587.

Lourenço, Paulo B. 2002. “Computations on Historic Masonry Structures.” *Progress in Structural Engineering and Materials* 4 (3): 301–319. https://doi.org/10.1002/pse.120.

Mauro, Matteo, Francesco Campolongo, Alfredo Micieli, Pietro Mazzuca, and Luciano Ombres. 2026. “Influence of Fibre Density and Matrix Properties on the Structural Performance of PBO-FRCM Confined Masonry Columns.” In *Proceedings of REHABEND 2026: Construction Pathology, Rehabilitation Technology and Heritage Management*, Bilbao, Spain, May 26–29, 2026.

Napoli, Annalisa, and Roberto Realfonzo. 2022. “Compressive Behavior of Masonry Columns Confined with FRCM Systems: Research Overview and Analytical Proposals.” *Journal of Composites for Construction* 26 (3). https://doi.org/10.1061/(asce)cc.1943-5614.0001200.

Ombres, Luciano. 2015. “Confinement Effectiveness in Eccentrically Loaded Masonry Columns Strengthened by Fiber Reinforced Cementitious Matrix (FRCM) Jackets.” *Key Engineering Materials* 624: 551–558. https://doi.org/10.4028/www.scientific.net/KEM.624.551.

Ombres, Luciano, and Salvatore Verre. 2020. “Analysis of the Behavior of FRCM Confined Clay Brick Masonry Columns.” *Fibers* 8 (2). https://doi.org/10.3390/fib8020011.

Ponte, Madalena, Andrea Penna, and Rita Bento. 2023. “In-Plane Cyclic Tests of Strengthened Rubble Stone Masonry.” *Materials and Structures/Materiaux et Constructions* 56 (2). https://doi.org/10.1617/s11527-023-02126-8.

Sarhosis, Vasilis, and José V. Lemos. 2018.“A Detailed Micro-Modelling Approach for the Structural Analysis of Masonry Assemblages.” *Computers & Structures* 206: 66–81. https://doi.org/10.1016/j.compstruc.2018.06.003.

Sneed, Lesley H., Christian Carloni, Giulia Baietti, and Giacomo Fraioli. 2017. “Confinement of Clay Masonry Columns with SRG.” *Key Engineering Materials* 747: 350–357. https://doi.org/10.4028/www.scientific.net/KEM.747.350.

Zhang, Ping, and Ering Nordlund. 2021. “A 3DEC Numerical Analysis of the Interaction Between an Uneven Rock Surface and Shotcrete Lining.” *Rock Mechanics and Rock Engineering* 54: 2267–2289. https://doi.org/10.1007/s00603-021-02399-x.

Cinpar 2026
XXII International Conference on Building Pathology and Constructions Repair
15th to 17th July 2026 - Lisboa, Portugal

Alkaline durability of AR-glass FRCM systems: tensile behaviour of bare fibres and cement-based composites under direct and accelerated conditioning

Matteo MAURO[1], Salvatore PRETE[2], Pietro MAZZUCA[3]

[1]Department of Civil Engineering, University of Calabria (UNICAL), Rende, Italy, matteo.mauro@unical.it
[2]Department of Civil Engineering, University of Calabria (UNICAL), Rende, Italy, salvatore.prete@unical.it
[3]Department of Civil Engineering, University of Calabria (UNICAL), Rende, Italy, pietro.mazzuca@unical.it

Abstract: This study investigates the alkaline durability of a Fabric-Reinforced Cementitious Matrix (FRCM) system reinforced with alkali-resistant (AR) glass textiles embedded in a cement-based matrix. The experimental programme was designed to assess the influence of alkaline exposure on both bare fibres and composite coupons, considering different conditioning scenarios. Direct tensile tests were performed on dry AR-glass fibres after 1000 h, 2000 h and 3000 h of alkaline conditioning, as well as on FRCM coupons directly immersed in the same alkaline environment for the same durations. In addition, a further series of FRCM coupons was manufactured using pre-conditioned textiles, in order to evaluate the feasibility of an accelerated ageing procedure based on pre-exposed reinforcement. The results showed that alkaline exposure caused a severe deterioration of the bare fibres, with average tensile strength losses of approximately 61%, 64% and 65% after 1000 h, 2000 h and 3000 h, respectively, whereas the corresponding reduction in elastic modulus remained more limited. By contrast, the tensile performance of the FRCM coupons was less affected. Specimens directly exposed to the alkaline solution exhibited average strength reductions of about 5%, 24% and 14%, while those manufactured with pre-conditioned textiles showed more regular decreases of about 1%, 15% and 16%. Despite this degradation, the composite response was primarily governed by the poor fibre–matrix interaction. All FRCM specimens exhibited a brittle behaviour, characterised by the formation of a first and only crack followed by immediate failure, without the development of an effective multi-cracking stage.

Keywords: AR-glass; FRCM; Alkaline Conditioning; Tensile Behaviour.

1. Introduction

FRCM (Fabric-Reinforced Cementitious Matrix) systems, also referred to as TRM (Textile-Reinforced Mortar), are now widely recognised as effective solutions for the strengthening of existing masonry and reinforced concrete structures, owing to their high compatibility with mineral substrates, vapour permeability, and favourable application-related features. Over the last decade, a substantial body of experimental research has confirmed the structural effectiveness of these systems in various strengthening and rehabilitation applications, highlighting their potential in terms of increased load-carrying capacity, improved deformational response, and control of cracking phenomena (Kouris and Triantafillou (2018); D'Antino (2025); Cascardi *et al.* (2026)). Despite the well-established effectiveness of FRCM systems, their long-term reliability still represents a critical issue, which has not yet been fully clarified from a scientific standpoint nor adequately incorporated into design procedures. Among the potentially aggressive environmental conditions most widely investigated in the literature, alkaline exposure, elevated service temperatures, freeze–thaw cycles, and saline environments are particularly relevant to civil engineering applications (D'Antino (2025)). With regard to the alkaline durability of such systems, the available literature is still limited and fragmented. Basalt fibres have shown marked sensitivity to alkaline attack already at the level of dry

fibres and unembedded textiles, with strength losses increasing significantly with exposure duration and temperature (Micelli and Aiello (2017); Williams Portal *et al.* (2016); Canestri *et al.* (2023)). Subsequent evidence obtained at composite level has confirmed that this vulnerability is also reflected in the mechanical response of FRCM systems, with appreciable reductions in tensile strength, post-cracking stiffness and, in more recent studies, bond capacity to the substrate (Signorini and Nobili (2021); Canestri *et al.* (2025)). By contrast, carbon-based systems have generally shown greater chemical stability in alkaline environments. The available experimental investigations indicate that carbon fibres, considered both in the dry state and within the composite, do not undergo significant reductions in strength under the most commonly investigated exposure conditions (Nobili and Signorini (2017); Signorini *et al.* (2018)). In such systems, the most influential variables appear to be not so much the intrinsic degradation of the fibre itself, but rather the curing conditions, surface treatments, and fibre–matrix interaction mechanisms, which may modify the composite response in terms of bond and stress transfer (Bompadre and Donnini (2022)). The case of glass-based systems is more complex, and the distinction between E-glass and AR-glass plays an essential role. E-glass is known for its high susceptibility to strongly alkaline environments, and the available studies, although still limited in number, show rapid and pronounced degradation of its mechanical properties, observed mainly at yarn and textile level (De Santis and de Felice (2014); Micelli and Aiello (2017)). By contrast, AR-glass fibres exhibit significantly slower degradation kinetics and a greater ability to retain residual strength over time (Canestri *et al.* (2023); Butler *et al.* (2010)). Nevertheless, even in the case of AR-glass, its combination with highly alkaline cement-based matrices still requires further investigation, since microstructural transformations at the fibre–matrix interface may significantly affect the mechanical response of the composite (Butler *et al.* (2009); Butler *et al.* (2010); Donnini *et al.* (2020); Cascardi *et al.* (2025)).

In light of these considerations, the present study is aimed at systematically investigating the durability of FRCM systems exposed to alkaline environments. In particular, attention is focused on the assessment of the behaviour of composites reinforced with AR-glass textiles combined with cement-based matrices; on the evaluation of the influence of curing conditions in terms of duration; and, finally, on the possibility of employing specimens manufactured with pre-aged textiles as an accelerated procedure to simulate the long-term effects of alkaline attack. The results obtained are expected to contribute to a clearer understanding of the degradation mechanisms and residual mechanical response of FRCM systems, providing useful indications both for the updating of accelerated ageing protocols and qualification procedures, and for the development of more reliable design formulations and the technological improvement of inorganic-matrix composite materials intended for the strengthening of the existing built heritage.

2. Materials and methods

2.1 FRCM constituent materials

The FRCM system investigated in the present study consisted of dry alkali-resistant glass (AR-glass) fibres arranged in a uniformly distributed mesh with an areal density of 200 g/m². The bundle spacing was 12 × 12 mm², while the equivalent thickness was 0,040 mm (Figure 1). The tensile properties at ambient temperature were determined by the authors according to the methodology reported in Section 2.2. In particular, the textile exhibited a tensile strength of 1200 MPa, an elastic modulus E_f of 65 GPa, and an ultimate strain of 0,015. As regards the cement-based mortar, the average compressive strength f_{cm} and flexural strength f_{fm}, taken from Cascardi *et al.* (2025), were equal to 14,5 MPa and 3,2 MPa, respectively.



Figure 1 – AR-glass reinforcing textile used in the investigated FRCM system

2.2 Test set-up

The experimental campaign on the FRCM systems was carried out in accordance with the testing protocols defined by RILEM TC 290-IMC. In particular, the specimens were subjected to different exposure conditions in order to assess the influence of the alkaline environment and of curing duration on the tensile response of the composite. With regard to alkaline exposure, both FRCM specimens and dry fibres were immersed in an environment consisting of distilled water containing 0,16% $Ca(OH)_2$, 1% NaOH, and 1,4% KOH. The exposure durations considered were 1000 h, 2000 h, and 3000 h (Figure 2). At the end of each conditioning period, the specimens were removed from the solution, dried, prepared, and then tested in tension according to the set-up and specifications reported later in the text.



Figure 2 –FRCM specimens during curing/conditioning in an alkaline solution bath

Finally, a portion of the previously conditioned textiles was used to manufacture new FRCM coupons, in order to verify the feasibility of an accelerated ageing procedure based on the use of pre-exposed reinforcements. In these cases, the overall curing duration of the coupons was assumed to be equal to the conditioning time undergone by the aged textiles used for their manufacture, namely 1000 h, 2000 h, and 3000 h. All FRCM coupons investigated in the experimental campaign were subsequently dried for 7 days before tensile testing. For comparative purposes, an additional group of reference specimens was also

prepared, left to cure in water for 21 days, and then used as a benchmark for the direct comparison of the obtained results.

Direct tensile (DT) tests were carried out on both the textiles and the FRCM specimens. In particular, the textiles had dimensions of 50 × 500 × 0,04 mm^3 (width × length × thickness), whereas the FRCM specimens were characterised by a cross-section of 50 × 10 mm^2 and a length of 500 mm. As regards the preparation of the FRCM specimens, a single layer of textile (consisting of 5 yarns) was placed between two layers of inorganic matrix, each having a thickness of 5 mm, defined in accordance with the manufacturer's instructions. Before testing, PVC tabs were bonded to the ends of both fibres and composites by means of a conventional epoxy adhesive. This procedure was necessary to improve the gripping of the samples during testing and to ensure proper load transfer from the testing machine to the specimens.

The tests were performed by applying a monotonic load up to failure under displacement control, at a rate of 0,5 mm/min for the textile tests and 0,2 mm/min for the FRCM composites. The tensile strains of both the textiles and the FRCM specimens were measured by means of a video extensometer, which monitored the position of target points arranged along different longitudinal alignments (Figure 3).

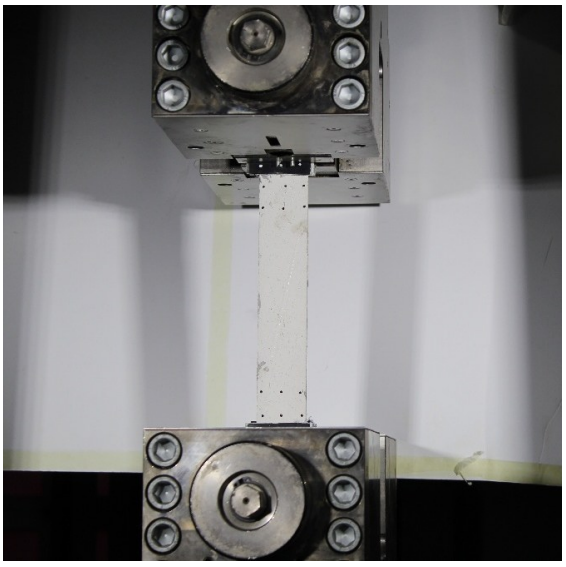


Figure 3 – Tensile test setup for FRCM specimens

3. Experimental results

3.1 Dry fibres

As shown in Figure 4, the results for the dry fibres highlight a marked reduction in tensile strength after conditioning, accompanied by a more limited decrease in elastic modulus. For the unconditioned specimens (NC), the average tensile strength was approximately 801 MPa, with an average elastic modulus of 73 GPa. After 1000 h of conditioning, the average tensile strength decreased to 310 MPa, whereas the average elastic modulus dropped to 66 GPa. For exposure durations of 2000 h and 3000 h, the average tensile strength was equal to 291 MPa and 282 MPa, respectively, while the average elastic modulus reached values of 60 GPa and 59 GPa. Overall, the results show that conditioning produced a severe reduction in tensile strength, with a very pronounced decrease already after the first 1000 h, followed by more limited reductions with increasing exposure duration. In percentage terms, the average residual tensile strength was about 39% of the initial value after 1000 h and decreased to approximately 35% after 3000 h (Figure 5). By contrast, the elastic modulus exhibited a more gradual and less severe decrease, from about 73 GPa to

59 GPa, corresponding to an overall loss of approximately 19% at the end of the maximum conditioning period.

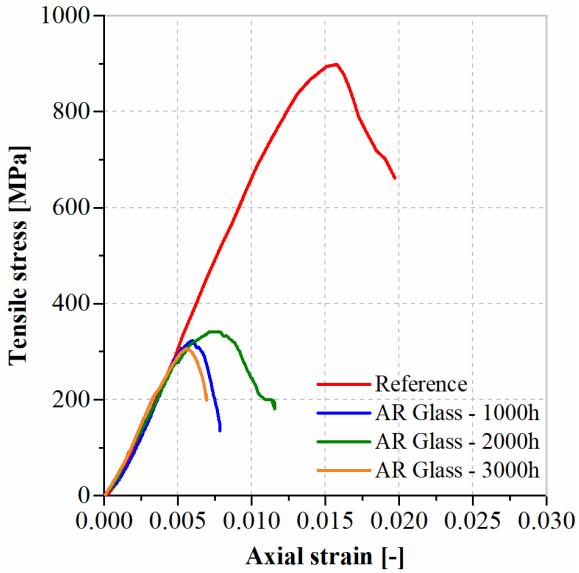


Figure 4 – Tensile stress vs axial strain curves for both unconditioned and conditioned specimens

These results indicate that the effect of conditioning was particularly severe on the load-carrying capacity of the fibres, whereas stiffness was compromised to a comparatively smaller extent.

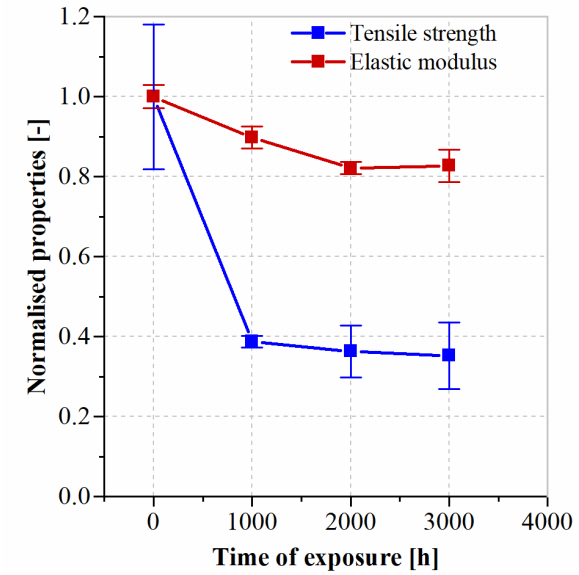


Figure 5 – Normalised properties vs time of exposure

The marked reduction in average tensile strength may be attributed to the fact that the alkaline environment acted directly on the elementary filaments, progressively altering their surface. Although AR-glass exhibits higher alkali resistance than E-glass owing to its zirconia content, this protection does not make the material completely immune to alkaline attack. The strength loss should therefore be interpreted as a consequence of the progressive surface damage of the individual filaments, with the development of local weak points, surface irregularities, and a gradual reduction in filament integrity (Figure 6). In this light, the sharp drop in average tensile strength already observed after 1000 h can plausibly be attributed to the rapid degradation of the most vulnerable filaments, namely those characterised by surface defects more

sensitive to the alkaline environment. The more limited reduction observed between 1000 h and 3000 h suggests instead that, once the weakest fraction of the material had been compromised, degradation proceeded with slower kinetics in the remaining material. The smaller decrease in average elastic modulus may be interpreted by considering that stiffness is less sensitive than strength to the presence of surface-localised defects affecting only part of the filaments. In other words, localised surface damage may severely impair the ultimate tensile capacity, while affecting the global elastic response to a relatively smaller extent, at least until degradation becomes more widespread. This interpretation is plausible, although direct confirmation would require morphological observations on the conditioned filaments.

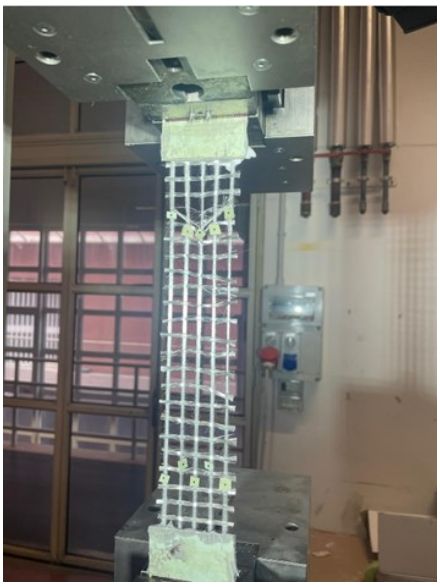


Figure 6 –Failure mode observed in the tensile tests on AR glass specimens

3.2 FRCM composites

For the FRCM specimens exposed to the alkaline environment, the obtained results showed a reduction in tensile capacity with respect to the unconditioned samples, although to an extent significantly smaller than that observed for the dry fibres. Under reference conditions (NC), the average tensile strength was approximately 406 MPa. After 1000 h of alkaline exposure, this value decreased to about 385 MPa, corresponding to a reduction of approximately 5% relative to the initial value (Figure 7). After 2000 h, a more marked decrease was observed, down to approximately 310 MPa, corresponding to a reduction of about 24%, whereas after 3000 h the average tensile strength increased again to approximately 350 MPa, remaining nevertheless lower than the reference value, with an overall loss of about 14%.

Overall, these results indicate that alkaline exposure produced a detrimental effect on the tensile response of the composite, although to a lesser extent than that observed at dry-fibre level. The non-monotonic trend, with the minimum value recorded after 2000 h and a subsequent increase after 3000 h, nevertheless suggests that the results should be interpreted with caution, since this apparent recovery may reasonably be attributed to experimental scatter, the limited number of specimens, and the possible competition between reinforcement degradation and matrix evolution.

By contrast, for the FRCM specimens manufactured with textiles previously conditioned in the alkaline environment and subsequently used for coupon fabrication, the average results showed a more regular and substantially monotonic decay in tensile response with increasing pre-conditioning time of the reinforcement. In particular, for the specimens manufactured with textiles pre-conditioned for 1000 h, the average tensile strength was approximately 402 MPa, showing a very limited reduction, below 1%, with respect to the reference specimens. As the pre-exposure duration increased, the detrimental effect became more evident: after 2000 h, the average tensile strength decreased to approximately 347 MPa,

corresponding to a reduction of about 14%, whereas after 3000 h it decreased further to approximately 340 MPa, corresponding to an overall loss of about 16%.

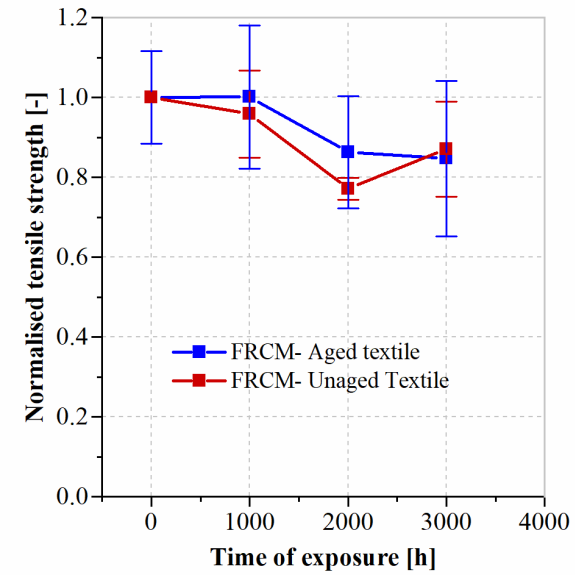


Figure 7 – Reduction of tensile strength observed in the tensile tests on AR glass specimens

The overall interpretation of these results must, however, take into account the peculiar response mechanism of the investigated system. The stress–strain curves in fact showed a substantially similar behaviour for all the examined configurations: the absence of a surface treatment on the textile led to a markedly brittle response of the composite. In particular, the response was characterised by an almost linear initial branch, followed by the formation of a first and only crack (Figure 8), beyond which the specimen rapidly underwent collapse. Once this crack had formed, stress transfer between matrix and textile became highly ineffective; consequently, the system was unable to develop an effective multi-cracking stage or any significant stress redistribution along the reinforcement. Failure therefore occurred almost immediately after first cracking, followed by telescopic rupture of the filaments, according to a mechanism fully consistent with that also observed in the conditioned textiles.

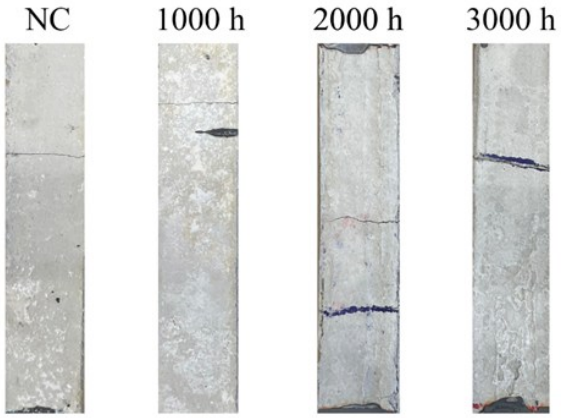


Figure 8 – Failure mode observed in the tensile tests on AR glass specimens

In light of this, the apparently smaller influence of alkaline conditioning on the response of the composite compared with that observed for the dry fibres may reasonably be attributed to the fact that, in this specific FRCM system, the global performance was already strongly limited, from the outset, by the poor quality of the fibre–matrix interaction. In other words, since coupon failure was governed mainly by the early loss of

effectiveness of stress transfer after first cracking, the further degradation induced by the alkaline treatment on the fibres played a relatively less significant role in the overall mechanical response of the composite. As a result, the behaviour of the system appears to be governed more by the intrinsic weaknesses of the stress-transfer mechanism between dry textile and matrix than by reinforcement degradation due solely to the alkaline environment.

4. Conclusions

The present study investigated the alkaline durability of inorganic-matrix FRCM systems, with particular focus on composites reinforced with AR-glass textiles embedded in a cement-based matrix, considering both bare fibres and FRCM coupons subjected to different conditioning procedures. The results showed that alkaline exposure had a markedly detrimental effect on the dry fibres, causing a severe re-duction in tensile strength already after the first 1000 h of conditioning, whereas the elastic modulus exhibited a more limited decrease. This behaviour suggests that degradation was mainly associated with the progressive alteration of the surface of the elementary filaments, leading to a loss of fibre integrity and a rapid reduction in tensile capacity. At the composite level, the effect of alkaline conditioning was significantly less pronounced. FRCM specimens directly immersed in the alkaline solution exhibited smaller reductions in tensile strength than those observed for the bare fibres, although with some experimental scatter and a non-monotonic trend. Similarly, coupons manufactured with previously conditioned textiles showed a progressive decrease in tensile performance with increasing pre-conditioning time, but the overall strength loss remained lower than that recorded for the isolated reinforcement. The overall interpretation of the results indicates that, in the investigated FRCM system, the global mechanical response was not governed exclusively by fibre degradation, but also by the quality of the fibre–matrix interaction. In particular, the absence of a surface treatment in the Glass textile led to a markedly brittle response, characterised by the formation of a first and only crack followed by almost immediate failure, without the development of an effective multi-cracking stage. Consequently, the limited stress-transfer capability after first cracking appears to be the main factor controlling the composite response, thus reducing the apparent influence of alkaline-induced fibre degradation on the overall behaviour of the coupon. Overall, the results confirm the relevance of alkaline environments as a degradation agent for FRCM systems, while also showing that the composite response must be interpreted by jointly considering reinforcement durability and the effectiveness of the fibre–matrix stress-transfer mechanism. In this perspective, the findings contribute to a clearer understanding of the limits and potential of accelerated ageing procedures and provide useful indications for the development of more reliable FRCM systems, characterised by improved internal bond and greater robustness under aggressive environmental conditions.

Acknowledgments

The authors gratefully acknowledge the TEACH (Technology Applied to Cultural Heritage) Doctoral School of the University of Calabria for the financial support provided through the doctoral scholarship that contributed to this research.

References

Bompadre, F. and Donnini, J. 2022. Fabric-Reinforced Cementitious Matrix (FRCM) Carbon Yarns with Different Surface Treatments Embedded in a Cementitious Mortar: Mechanical and Durability Studies. Materials, 15(11): 3927.

Butler, M., Mechtcherine, V. and Hempel, S. 2009. Experimental investigations on the durability of fibre–matrix interfaces in textile-reinforced concrete. Cement and Concrete Composites, 31(4): 221-231.

Butler, M., Mechtcherine, V. and Hempel, S. 2010. Durability of textile reinforced concrete made with AR glass fibre: effect of the matrix composition. Materials and Structures, 43(10): 1351-1368.

Canestri, M., Ferretti, F., Mazzotti, C. 2025. Long-Term Effects of Alkaline Environments on Basalt Fibres. In: Castellazzi, G. and Gentilini, C. (eds) Mechanics of Masonry Structures Strengthened with Composite Materials. Cham: Springer, 43-52.

Canestri, M., Ferretti, F., Sassoni, E. and Mazzotti, C. 2023. On the behaviour of FRCM fibres in saturated alkaline solution. In: Biondini, F. and Frangopol, D.M. (eds) Life-Cycle of Structures and Infrastructure Systems. Abingdon: CRC Press/Balkema - Taylor and Francis Group, 2812-2819.

Cascardi, A., Koutas, L.N., De Santis, S., Ghiassi, B., Micelli, F., Aiello, M.A. and Triantafillou, T. 2026. Textile-Reinforced Mortar (TRM) for retrofitting masonry structures: advantages, challenges and future potential. Materials and Structures, 59: 38.

Cascardi, A., Verre, S., Micelli, F. and Aiello, M.A. 2025. Durability-aimed performance of glass FRCM-confined concrete cylinders: experimental insights into alkali environmental effects. Materials and Structures, 58(10): 329.

D'Antino, T. 2025. Advances and open issues in the use of fiber-reinforced composites as reinforcement of existing and new constructions. Materials and Structures, 58: 312.

De Santis, S. and De Felice, G. 2014. Tensile Behaviour and Durability of Mortar-Based Strengthening Systems with Glass-Aramid Textiles. Key Engineering Materials, 624: 346-353.

Donnini, J., Bompadre, F. and Corinaldesi, V. 2020. Tensile Behavior of a Glass FRCM System after Different Environmental Exposures. Processes, 8(9): 1074.

Kouris, L.A.S. and Triantafillou, T.C. 2018. State-of-the-art on strengthening of masonry structures with textile reinforced mortar (TRM). Construction and Building Materials, 188: 1221-1233.

Micelli, F. and Aiello, M.A. 2019. Residual tensile strength of dry and impregnated reinforcement fibres after exposure to alkaline environments. Composites Part B: Engineering, 159: 490-501.

Nobili, A. and Signorini, C. 2017. On the effect of curing time and aggressive environmental exposure on impregnated Carbon Fabric Reinforced Cementitious Matrix (CFRCM) composite with design considerations. Composites Part B: Engineering, 112: 300-313.

Signorini, C. And Nobili, A. 2021. Comparing durability of steel reinforced grout (SRG) and textile reinforced mortar (TRM) for structural retrofitting. Materials and Structures, 54(3).

Signorini, C., Nobili, A. and Falope, F.O. 2018. Mechanical performance and crack pattern analysis of aged Carbon Fabric Cementitious Matrix (CFRCM) composites. Composite Structures, 202: 1114-1120.

Verre, S. 2021. Effect of Different Environments' Conditioning on the Debonding Phenomenon in Fiber-Reinforced Cementitious Matrix-Concrete Joints. Materials, 14(24): 7566.

Williams Portal, N., Flansbjer, M., Johannesson, P., Malaga, K. and Lundgren, K. 2016. Tensile behaviour of textile reinforcement under accelerated ageing conditions. Journal of Building Engineering, 5: 57-66.

Cinpar 2026
XXII International Conference on Building Pathology and Constructions Repair
15th to 17th July 2026 - Lisboa, Portugal

Betão branco de elevado desempenho eco-eficiente com incorporação de pó de vidro para aplicações arquitetónicas

Sofia RIBEIRO-PINTO[1], Ana Mafalda MATOS[2], Paula MILHEIRO-OLIVEIRA[3], Mário PIMENTEL[4]

[1] DECG, Faculdade de Engenharia, Universidade do Porto, Portugal, up202105717@up.pt
[2] CONSTRUCT, Faculdade de Engenharia, Universidade do Porto, Portugal, anamatos@up.pt
[3] CMUP, Universidade do Porto, Portugal, poliv@up.pt
[4] CONSTRUCT, Faculdade de Engenharia, Universidade do Porto, Portugal, mjsp@reit.up.pt

Resumo: O betão branco de elevado desempenho (HPC) é amplamente utilizado em aplicações arquitetónicas contemporâneas, sobretudo em elementos esbeltos, onde são exigidos elevados níveis de resistência mecânica, durabilidade e qualidade estética. No entanto, o elevado teor de cimento associado a este tipo de materiais levanta preocupações ambientais relevantes, tornando necessária a otimização das matrizes cimentícias utilizadas em aplicações arquitetónicas exigentes.

Este estudo apresenta o desenvolvimento de um HPC branco eco-eficiente, baseado na otimização da matriz cimentícia através da substituição parcial do cimento Portland por adições minerais convencionais, como o fíler calcário, e não convencionais, como o pó de vidro finamente moído. Esta abordagem permite reduzir o consumo de cimento e o impacto ambiental associado, promovendo simultaneamente a valorização de resíduos industriais, sem comprometer o desempenho global do material.

A matriz foi formulada sem agregado grosso e com reduzidas relações água/ligante, visando a obtenção de uma argamassa compacta e adequada a elementos arquitetónicos expostos. A caracterização experimental incluiu ensaios no estado fresco, resistência mecânica à compressão e à flexão e resistividade elétrica, permitindo avaliar o comportamento das misturas em termos de trabalhabilidade, desempenho mecânico e durabilidade potencial.

Os resultados obtidos evidenciam o potencial do HPC branco desenvolvido como material para aplicações arquitetónicas exigentes, conciliando elevados níveis de desempenho mecânico e propriedades associadas à durabilidade com uma abordagem mais sustentável no desenho das matrizes cimentícias.

Palavras-Chave: Betão de elevado desempenho, sustentabilidade, pó de vidro, cimento branco, durabilidade.

1. Introdução

O desenvolvimento de novas matrizes cimentícias tem sido impulsionado pela crescente procura mundial de habitação e infraestruturas, bem como pela evolução da estética arquitetónica, que privilegia estruturas cada vez mais esbeltas e estruturalmente eficientes. Em contrapartida, diversos estudos demonstram que a produção de cimento Portland liberta para a atmosfera uma quantidade de dióxido de carbono (CO_2) e de outros gases com efeito de estufa (GEE) aproximadamente equivalente à massa de ligante produzido, contribuindo de forma significativa para as alterações climáticas globais [1].

Neste contexto, o betão de elevado desempenho (HPC) e o betão de ultraelevado desempenho (UHPC) afirmam-se como soluções de engenharia particularmente promissoras. Estes materiais distinguem-se pelos elevados níveis de resistência à compressão e pela sua fluidez, aliados a uma elevada durabilidade, permitindo assegurar a longevidade das estruturas por períodos superiores a um século [2]. Paralelamente, a redução do impacto ambiental associado a estes materiais pode ser significativamente otimizada através da substituição parcial do cimento Portland por materiais cimentícios suplementares, nomeadamente pó

de vidro finamente moído [3]. Esta solução permite valorizar resíduos de vidro, que representam uma fração relevante dos resíduos sólidos produzidos a nível mundial e que, devido à complexidade técnica dos processos de reciclagem, são frequentemente encaminhados para aterro [4]. A incorporação deste tipo de resíduos no HPC contribui, assim, para a redução do consumo de matérias-primas convencionais e dos custos logísticos associados ao seu transporte, promovendo simultaneamente princípios de economia circular e o desenvolvimento de novos modelos de negócio [5].

Os resíduos industriais de vidro finamente moído devem apresentar dimensões de partículas similares ou inferiores às do cimento, de modo a garantir uma maior reatividade. Embora seja classificado como material pozolânico de acordo com os requisitos químicos definidos pelas normas ASTM C618 e NP 4220, o seu teor de álcalis (Na_2O) tem suscitado preocupações relacionadas com o potencial desenvolvimento de reações álcalis-sílica [6], [7]. Mais recentemente, o pó de vidro foi formalmente reconhecido como adição para betão nos Estados Unidos da América e no Canadá, através das normas ASTM C1866 e CSA A3000, respetivamente.

Contudo, a literatura indica que a reação pozolânica do pó de vidro ocorre de forma mais precoce do que a reação álcalis-sílica, o que limita a disponibilidade de álcalis livres necessários ao desenvolvimento de efeitos deletérios expansivos [4], [7]. Neste contexto, a dimensão das partículas assume um papel crucial na mitigação de eventuais efeitos adversos [7], [8]. Embora sejam geralmente recomendadas partículas com dimensão inferior a 300 µm, estudos demonstram que partículas inferiores a 38 µm apresentam um comportamento pozolânico mais acentuado, enquanto partículas no intervalo entre 38 µm e 75 µm evidenciam uma atividade significativamente reduzida [9]. Adicionalmente, diversos trabalhos reportam melhorias consistentes da durabilidade das matrizes quando o pó de vidro substitui parcialmente o cimento Portland, promovendo igualmente ganhos de resistência em idades mais avançadas e garantindo a estabilidade dimensional do material [10], [11]. Assim, o presente trabalho tem como objetivo principal o desenvolvimento e a otimização de misturas ternárias de betão branco de elevado desempenho (HPC), incorporando materiais cimentícios suplementares, nomeadamente pó de vidro e fíler calcário, como substituição parcial do cimento Portland branco. Pretende-se avaliar de forma sistemática a influência das principais proporções da mistura no comportamento no estado fresco, no desempenho mecânico e nas propriedades associadas à durabilidade, recorrendo a uma metodologia de Desenho de Experiências. O estudo visa, em particular, identificar combinações de parâmetros de mistura que permitam conciliar elevados níveis de fluidez, resistência mecânica e resistividade elétrica, contribuindo para o desenvolvimento de soluções estruturalmente eficientes e mais sustentáveis para elementos arquitetónicos esbeltos sujeitos a flexão moderada.

2. Metodologia da investigação

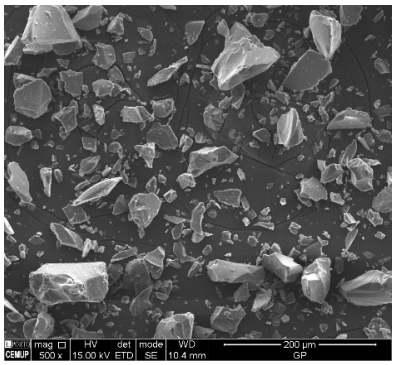
2.1 Materiais constituintes

Para desenvolvimento de HPC, foi produzido em laboratório um ligante ternário constituído por cimento Portland branco CEM II-AL 52,5 N br, fíler calcário de origem, com dimensão máxima de 20 µm e massa volúmica de 2750 kg/m^3, e pó de vidro, com máxima dimensão de 80 µm e massa volúmica de 2600 kg/m^3. Este material, obtido através de resíduos industriais portugueses, e revela-se uma adição promissora para o HPC devido ao elevado teor de sílica amorfa e pozolanicidade. Para a produção deste HPC foi utilizada uma areia natural de quartzo de grãos arredondados, com dimensões entre 0 mm e 1 mm e absorção de 0,5%. Para assegurar a fluidez da mistura face à reduzida relação água/ligante, utilizou-se um superplastificante à base de éteres de policarboxilato (PCE), em conformidade com a norma NP EN 934-2.

A Figura 1 retrata o pó de vidro e a morfologia das partículas através do microscópio eletrónico de varrimento (MEV), respetivamente.



a)



b)

Figura 1 – a) Pó de vidro; b) fotografia das partículas do pó de vidro obtida por microscopia eletrónica de varrimento.

2.2 Planeamento de Experiências

Foi implementado um desenho experimental do tipo superfície de resposta, utilizando um plano fatorial fracionado (uma metade do plano fatorial 2^5) construído a partir de um plano fatorial a dois níveis com cinco fatores quantitativos (as proporções da mistura), complementado com seis pontos centrais (designados Ci) e dez pontos axiais (designados CCi). O plano perfaz um total de 31 ensaios. Para garantir a rotatividade do desenho, os níveis dos fatores foram codificados como −2 (pontos axiais), −1, 0, +1 e +2 (pontos axiais) para cada uma das variáveis [4], [12]. A Tabela 1 apresenta a correspondência entre os níveis codificados e os valores reais de todos os parâmetros da mistura, nomeadamente, a relação volume de água/finos (Vw/Vp), em que os finos são o cimento, o fíler e o pó de vidro; relação em massa água/cimento (w/c); relação em massa superplastificante/finos (Sp/p); relação em massa pó de vidro/cimento (GP/c); relação volume de areia/argamassa (Vs/Vm). Os intervalos dos fatores foram definidos com base na literatura relevante [4], [12] e em ensaios preliminares, uma vez que se trata de uma tarefa não trivial. Foram selecionados intervalos de modo a gerar respostas informativas sem produzir misturas impraticáveis e em regiões onde seria expectável encontrar materiais com desempenho mais próximo do alvo. Nos ensaios preliminares foi adotada uma banda de espalhamento alvo de 100 a 350 mm (Tabela 2). Para calcular as composições, utilizou-se a equação abaixo:

$$Vs + Vp + Vw + Vsp + Va = 1{,}0m^3 \quad (1)$$

em que Vs representa o volume de areia, Vp é o volume de finos (cimento, fíler calcário e pó de vidro), Vw é o volume de água, Vsp é o volume de superplastificante e Va é o volume de ar. Conhecendo as massas volúmicas dos materiais constituintes, apresentadas na secção 2.1, e os rácios apresentados na Tabela 1, é possível determinar as quantidades de cada constituinte em kg/m^3.

Tabela 1 – Identificação das variáveis independentes, níveis e valores codificados e valores reais.

Fatores de design	Unidades	Axial (-2)	Fatorial (-1)	Central 0	Fatorial (+1)	Axial (+2)
Vw/Vp	-	0,42	0,44	0,46	0,48	0,50
w/c	-	0,33	0,36	0,38	0,41	0,43
Sp/p	%	3,45	3,48	3,50	3,53	3,55
GP/c	-	0,20	0,25	0,30	0,35	0,40
Vs/Vm	-	0,35	0,40	0,45	0,50	0,55

2.3 Medição das respostas (variáveis dependentes)

Neste estudo foram produzidas 31 amassaduras de betão branco de elevado desempenho (HPC), procedendo-se à moldagem de provetes prismáticos com dimensões de 40 × 40 × 160 mm³. O procedimento de mistura adotado para a produção das diferentes composições encontra-se esquematizado na Figura 2. As amassaduras foram realizadas recorrendo a uma misturadora normalizada, em conformidade com a norma NP EN 196-1, garantindo a repetibilidade e a uniformidade do processo experimental.

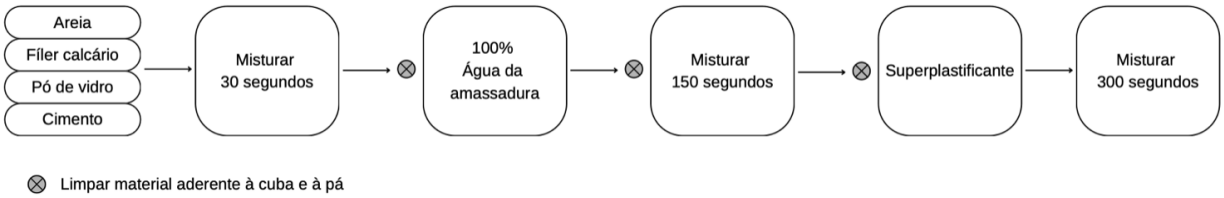


Figura 2 – Procedimento para produção de HPC em laboratório.

A caracterização no estado fresco teve como objetivo a avaliação da trabalhabilidade das matrizes imediatamente após a mistura, assegurando níveis adequados de fluidez, conforme ilustrado na Figura 3. Esta caracterização foi efetuada através do ensaio de espalhamento, de acordo com as recomendações da EFNARC. O valor do espalhamento foi determinado a partir da medição de dois diâmetros perpendiculares, sendo considerado como resultado final o valor médio obtido.

A resistividade elétrica do HPC foi monitorizada como um parâmetro indicativo da compacidade da matriz e da durabilidade potencial do material, recorrendo ao método dos dois elétrodos. Neste procedimento, duas redes de aço inoxidável foram embebidas nas extremidades dos provetes ainda no estado fresco, garantindo o contacto elétrico com a superfície do material. Nas idades estabelecidas, foi aplicada uma corrente elétrica com uma frequência de 100 Hz, medindo-se a diferença de potencial, conforme exemplificado na Figura 4. Este ensaio foi realizado em três provetes por composição do plano experimental, sendo o acompanhamento efetuado até aos 90 dias de idade.

O desempenho mecânico das misturas foi avaliado através de ensaios de resistência à flexão e à compressão, realizados de acordo com a norma NP EN 196-1, aos 28 e aos 90 dias de idade. Os ensaios de compressão foram efetuados sobre os meios provetes resultantes do ensaio de flexão, permitindo uma caracterização consistente e comparável do comportamento mecânico das diferentes composições.

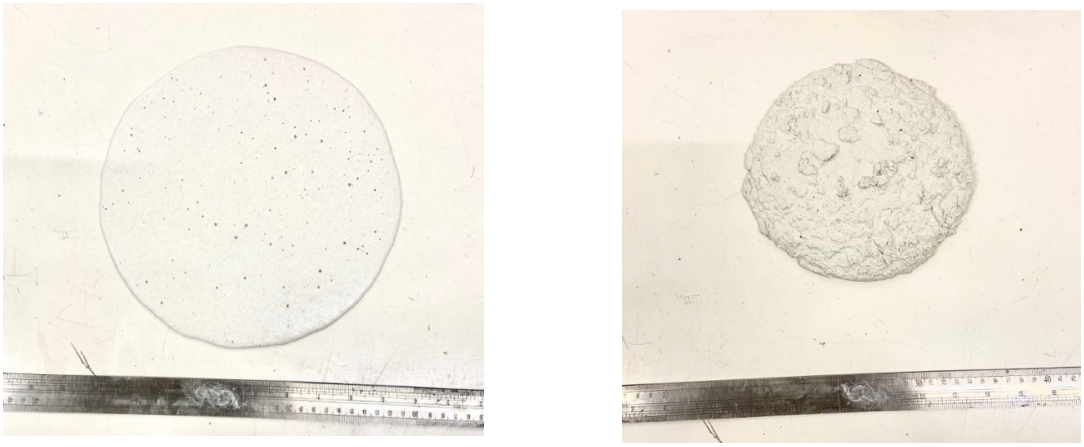


Figura 3 – Espalhamento de duas composições distintas.

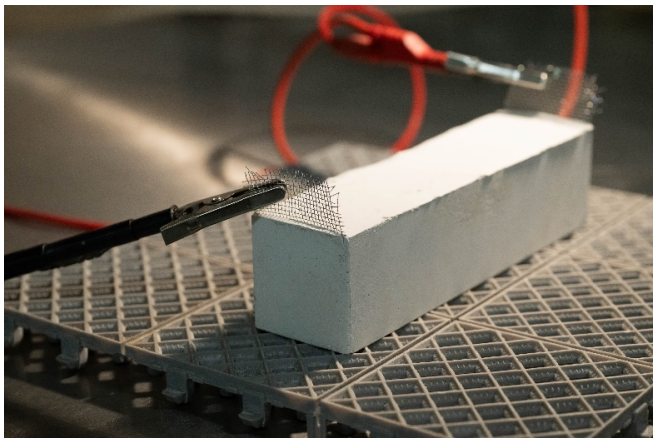


Figura 4 – Ensaio de resistividade elétrica (método dos 2 elétrodos) num provete de HPC.

3. Resultados e Discussão

3.1 Sumário dos resultados experimentais

Os resultados correspondentes ao conjunto integral das 31 misturas, bem como ao subconjunto dos pontos centrais (cinco misturas), encontram-se sumarizados de forma estatística na Tabela 2. Segue-se uma análise sucinta dos principais resultados experimentais obtidos.

As misturas evidenciam valores de fluidez compreendidos entre 100 mm e 321 mm, cobrindo um intervalo alargado de espalhamento. Ao longo do estudo observa-se que, como seria expectável, a diminuição da razão entre o volume de areia e o volume de argamassa (Vs/Vm), bem como o aumento da razão volume de água/volume de pasta (Vw/Vp), resultam em maiores diâmetros de espalhamento. A análise da variabilidade do ensaio de espalhamento (Dflow) mostra que os seis ensaios realizados no ponto central do plano experimental apresentam um coeficiente de variação (CV) de apenas 1,9 %, evidenciando uma variabilidade muito reduzida nessa região do espaço experimental. Em contraste, o coeficiente de variação calculado para o conjunto global das 31 misturas é significativamente superior (24,0 %), conforme indicado na Tabela 2, refletindo a maior dispersão associada às composições localizadas fora da região central, o que pode introduzir desafios adicionais no processo de ajuste de modelos estatísticos.

Relativamente à resistividade elétrica aos 28 dias de idade, os valores observados variam entre 50,85 Ω·m e 97,93 Ω·m, evidenciando diferenças na compacidade da matriz e na conectividade da rede porosa em função das proporções da mistura.

Quanto à resistência à compressão aos 28 dias, os resultados situam-se entre 59,58 MPa e 84,05 MPa, demonstrando que diferentes níveis de desempenho mecânico podem ser alcançados. Estes resultados indicam um adequado desenvolvimento da estrutura resistente da matriz cimentícia, compatível com os requisitos associados a betões de elevado desempenho.

Para além da análise do resumo estatístico da resistividade e da resistência à compressão, nas Figuras 5 e 6 é possível analisar os valores das 31 amassaduras em diferentes idades.

Tabela 2 – Resumo estatístico dos resultados para os pontos centrais e para o conjunto de todas as misturas do plano experimental fracionário.

		Dflow (mm)	Resist_28d (ohm)	Rc_28d (MPa)
Pontos centrais	Média	254,88	68,96	74,94
	Máximo	258,00	71,59	75,94
	Mínimo	251,50	66,76	73,78
	Desvio Padrão	2,66	2,14	1,10
	Coef. Variação (%)	1,04	3,10	1,47
Todos os pontos do plano fatorial	Média	246,29	68,47	74,65
	Máximo	321,00	97,93	84,05
	Mínimo	100,00	50,85	59,58
	Desvio Padrão	53,84	10,17	5,84
	Coef. Variação (%)	21,86	14,86	7,83

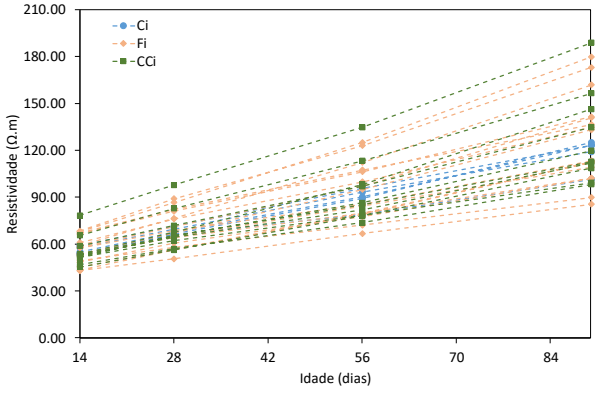


Figura 5 – Resistividade elétrica das diferentes amassaduras aos 14, 28, 56 e 90 dias de idade.

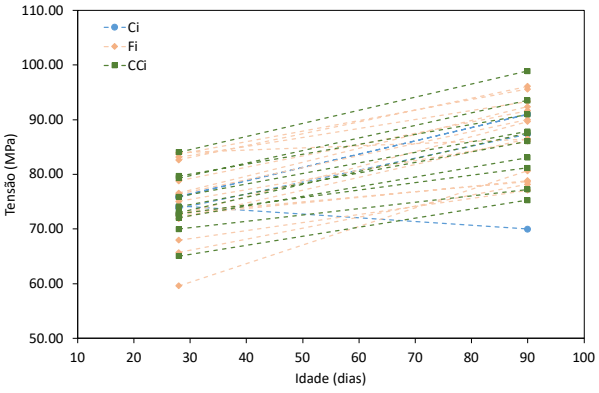


Figura 6 – Valores da resistência à compressão aos 28 e 90 dias de idade.

3.2 Ajuste dos modelos

Com base no desenho fatorial (fracionário) definido neste trabalho, a cada variável de resposta, foi ajustado um modelo de superfície de resposta polinomial de segunda ordem (quadrático), conforme expresso na equação (2):

$$Y = \beta_0 + \sum_{i=1}^{k} \beta_i X_1 + \sum_{i=1}^{k} \beta_{ii} x {X_i}^2 + \sum_{i<j} \sum \beta_{ij} X_i X_j + \varepsilon \quad (2)$$

em que y representa a resposta analisada, x_i representa a i-ésima variável independente, β_0 é o termo constante, β_i, β_{ii} e β_{ij} são os coeficientes associados, respetivamente, aos efeitos lineares, quadráticos e de interação entre dois fatores, e ε designa o termo de erro aleatório.

Os modelos foram ajustados com a ajuda do software Design Expert. O enquadramento metodológico do Desenho de Experiências (Design of Experiments, DoE) permite proceder a uma análise simultânea dos efeitos individuais dos diferentes fatores e das suas interações sobre cada resposta, apoiando a tomada de decisões no desenho de misturas e reduzindo o número de ensaios laboratoriais necessários para alcançar níveis de desempenho predefinidos [13]. Na avaliação da significância estatística foi considerado um nível de significância de 5 %. Foram efetuados diagnósticos aos resíduos e uma avaliação da adequação dos modelos. Usaram-se critérios como o coeficiente de determinação ajustado, BIC, AICc, PRESS e -ln L. Informações adicionais sobre a abordagem metodológica adotada encontram-se descritas em trabalhos anteriores dos autores [12], [14], bem como em referências especializadas sobre DoE [15].

Os modelos estatísticos obtidos para todas as variáveis de resposta estão sintetizados na Tabela 3, formulados com base em fatores codificados. Para cada resposta, os dois coeficientes dos termos com maior impacto são destacados a negrito, enquanto o coeficiente dominante é igualmente sublinhado. Os termos estatisticamente não significativos aparecem identificados pela sigla “NS”.

3.2.1 Modelo de espalhamento (Dflow)

A análise dos coeficientes do modelo evidencia que a razão entre o volume de areia e o volume de argamassa (Vs/Vm) é o parâmetro da mistura mais influente em termos de fluidez da argamassa, com impacto negativo e não linear. Logo a seguir, em termos de importância do efeito, vem a razão volume de água/volume de pasta (Vw/Vp), que atua no sentido oposto. Consequentemente, podemos dizer que o aumento de Vw/Vp promove a fluidez, ao passo que incrementos de Vs/Vm conduzem a uma redução acentuada do espalhamento. Foi igualmente identificada uma interação negativa estatisticamente significativa entre Vw/Vp e Vs/Vm. Quando Vw/Vp e Vs/Vm assumem valores elevados em simultâneo, verifica-se uma diminuição da fluidez relativamente ao efeito positivo esperado do aumento isolado de Vw/Vp.

O modelo de melhor ajuste para o *Slump* (reportado na Tabela 3 em termos de variáveis codificadas), apresenta um coeficiente de determinação ajustado de 94,4%. O modelo correspondente em valores reais é dado por:

$$\text{Slump} = -3340{,}3 + 3568{,}2\ \text{Vw/Vp} + 6568{,}7\ \text{w/c} - 123{,}7\ \text{GP/c} + 7226{,}5\ \text{Vs/Vm} - 6468{,}7\ \text{Vw/Vp} * \text{Vs/Vm} - 8242{,}9\ (\text{w/c})^2 - 6060{,}7 * (\text{Vs/Vm})^2 \quad (2)$$

As curvas de nível da superfície de resposta (Figura 7) identificam uma região operacional em que se atingem os valores desejados de *Slump*, aproximadamente definida pelos intervalos Vw/Vp ∈ [0,44, 0,48] e Vs/Vm ∈ [0,40, 0,50].

Tabela 3 – Modelos ajustados em termos de fatores codificados.

	Dflow (mm)	**1/√Resist_28d (√Ωm)**	**Rc_28d (MPa)**
Intercept	255,38	0,1223	74,27
Vw/Vp	13,15	0,0018	1,44
w/c	7,60	**0,0057**	**-4,99**
sp/p	NS	NS	0,45
GP/c	-6,19	-0,0022	NS
Vs/Vm	**-60,19**	**-0,0074**	**-3,98**
Vw/Vp x Vs/Vm	-6,47	NS	NS
w/c x sp/p	NS	NS	1,05
$(w/c)^2$	-5,15	NS	NS
$(Vs/Vm)^2$	**-15,15**	-0,0013	NS
R^2	0,96	0,9440	0,91
R^2 ajustado	0,94	0,9330	0,89
excluídos (outliers)	nenhum	nenhum	run 29

* A designação NS identifica os fatores que não apresentam significância estatística no modelo, considerando um nível de significância α = 0,05.

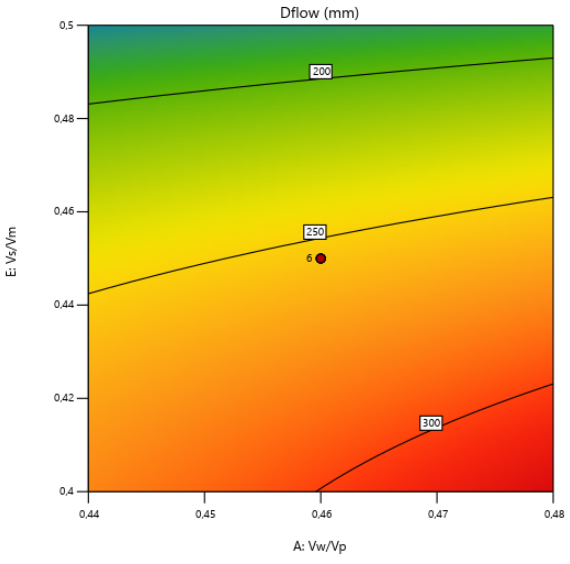


Figura 7 – O espalhamento em função de Vw/Vp e Vs/Vm.

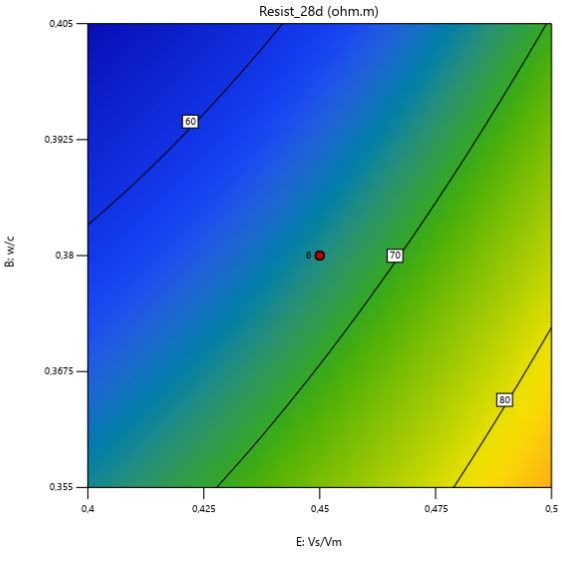


Figura 8 – Resistividade aos 28 dias em função de Vs/Vm e w/c.

3.2.2 Modelo de resistividade elétrica

A análise dos coeficientes do modelo ajustado para 1/Resist_28d evidencia que a razão (Vs/Vm) é o parâmetro da mistura mais influente na resposta em termos de resistividade do material, exercendo um efeito negativo pronunciado. Segue-se, em termos de importância, a razão água/cimento (w/c), que apresenta um efeito positivo significativo. Uma vez que a resposta foi modelada em termos do inverso da raiz quadrada da resistividade, estes resultados indicam que um aumento de Vs/Vm conduz a um acréscimo da resistividade elétrica, enquanto que o aumento de w/c promove uma redução da resistividade aos 28 dias. Para além destes efeitos, a razão volume de água/volume de pasta (Vw/Vp) apresenta um contributo positivo significativo, embora de menor magnitude, sugerindo que níveis mais elevados deste parâmetro da mistura tendem igualmente a reduzir a sua resistividade. O teor de pó de vidro (GP/c) surge com um efeito negativo significativo, indicando um aumento da resistividade associado ao aumento do teor de pó de vidro. Verifica-se ainda a presença de um termo quadrático significativo associado a Vs/Vm, revelando um efeito não linear deste fator na resposta em termos de resistividade. Não foram identificadas interações estatisticamente significativas entre os fatores considerados.

O modelo que melhor se ajusta à resistividade aos 28 dias (apresentado na Tabela 6 em termos de variáveis codificadas) exibe um coeficiente de determinação ajustado elevado (r_{adj}^2=93,3 %), indicando uma boa capacidade explicativa do modelo, sem necessidade de exclusão de ensaios experimentais. Em termos dos valores originais, o modelo é descrito pela equação (3):

$$1/\sqrt{(\text{Resist_28d})} = \text{-0,02798} + 0{,}08890\ \text{Vw/Vp} + 0{,}22917\ \text{w/c} - 0{,}04397\ \text{GP/c} + 0{,}30519\ \text{Vs/Vm} - 0{,}50300\ \text{Vs/Vm}^2 \quad (3)$$

As curvas de nível da superfície de resposta (Figura 8) permitem identificar regiões do espaço experimental associadas a valores mais elevados de resistividade elétrica, correspondendo tipicamente a combinações de valores mais elevados de Vs/Vm e mais reduzidos de w/c. Estas tendências estão em consonância com resultados previamente reportados na literatura, os quais sustentam que a resistividade elétrica é fortemente influenciada pela compacidade da matriz e pela conectividade da rede porosa [16], [17].

3.2.3 Modelo de resistência à compressão

A análise dos coeficientes do modelo ajustado para a resistência à compressão aos 28 dias evidencia que a razão água/cimento (w/c) é o fator mais influente, exercendo um efeito negativo pronunciado, estatisticamente significativo. Este resultado confirma que o aumento de w/c conduz a uma redução significativa da resistência mecânica, em linha com o comportamento para materiais cimentícios. A razão (Vs/Vm) surge igualmente como um parâmetro relevante, apresentando igualmente um efeito significativo negativo sobre Rc_28d. Este efeito sugere que incrementos excessivos de teor de agregado relativamente à fração argamassa conduzem a uma diminuição da resistência mecânica.

Contrastando com estas constatações, a razão volume de água/volume de pasta (Vw/Vp) apresenta um efeito positivo mais moderado na resistência aos 28 dias, embora estatisticamente significativo, indicando que, dentro do intervalo estudado, níveis mais elevados deste parâmetro da mistura podem favorecer uma hidratação mais eficiente ou uma melhor dispersão dos constituintes, sem penalizar significativamente o desempenho mecânico. O teor de superplastificante (sp/p) surge igualmente com um contributo positivo significativo, embora de menor magnitude, refletindo o papel deste adjuvante na melhoria da trabalhabilidade e da homogeneidade da mistura, com impacto indireto na resistência final.

Foi ainda identificada uma interação positiva estatisticamente significativa entre w/c e sp/p, o que revela que a presença de superplastificante pode mitigar parcialmente o efeito negativo do aumento de w/c sobre a resistência mecânica. Não foram observados termos quadráticos significativos para esta resposta, sugerindo um comportamento essencialmente linear da resistência à compressão no intervalo de variação considerado.

O modelo de melhor ajuste para Rc_28d (apresentado na Tabela 3 em termos de variáveis codificadas), apresenta um coeficiente de determinação ajustado de 89,0 %, após exclusão de um ensaio considerado atípico (run 29), revelando ter uma capacidade explicativa adequada para descrever matematicamente esta resposta mecânica. Em termos dos valores originais, o modelo é descrito pela equação (4):

$$Rc_28d = +2332{,}9 + 71{,}93750\ Vw/Vp - 6104{,}2\ w/c - 622{,}88\ sp/p - 79{,}508\ Vs/Vm + 1687{,}0\ w/c * sp/p \quad (4)$$

As curvas de nível da superfície de resposta para a resistência à compressão aos 28 dias (Figura 9) evidenciam a influência dominante da razão água/cimento (w/c) e da razão sólido/argamassa (Vs/Vm). Valores mais elevados de resistência são obtidos para combinações caracterizadas por baixos valores de w/c, sendo este efeito particularmente marcado em todo o domínio experimental analisado. Para um dado valor de w/c, incrementos de Vs/Vm conduzem a uma redução progressiva da resistência, em consonância com o efeito negativo identificado para este parâmetro da mistura. O efeito positivo do superplastificante (sp/p) manifesta-se sobretudo para níveis intermédios a elevados de w/c, refletindo a interação positiva significativa w/c × sp/p identificada no modelo, a qual permite atenuar parcialmente a perda de resistência associada ao aumento do teor de água. Em contraste, a razão Vw/Vp apresenta um impacto mais moderado na configuração das curvas de nível, não alterando significativamente a tendência global da resposta. De um modo geral, as superfícies de resposta indicam que o domínio de maiores resistências mecânicas se encontra associado a misturas com baixa razão água/cimento e valores controlados de Vs/Vm, sendo este resultado coerente com o comportamento clássico de materiais cimentícios e com observações previamente reportadas na literatura [4], [12], [14].

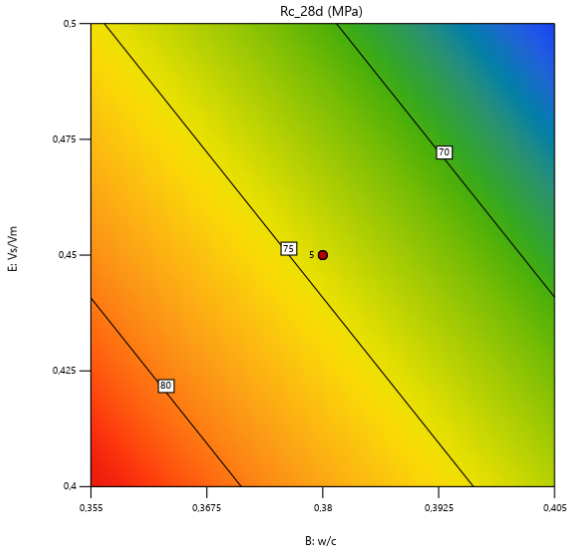


Figura 9 – Resistência à compressão aos 28 dias em função de Vs/Vm e w/c.

3.3 Consequências para o design de misturas

Em síntese, as razões sólido/argamassa (Vs/Vm) e volume de água/volume de pasta (Vw/Vp) assumem-se como os principais parâmetros de controlo do comportamento no estado fresco, devendo ser consideradas de forma integrada no processo de otimização da mistura, de modo a assegurar a fluidez requerida, preferencialmente entre 280 e 300 mm. Em particular, o aumento de Vw/Vp promove a fluidez, enquanto incrementos de Vs/Vm conduzem a uma redução acentuada do espalhamento, sendo ainda identificada uma interação negativa entre estes dois parâmetros.

No que respeita ao comportamento no estado endurecido, avaliado através da resistividade elétrica aos 28 dias, os resultados indicam que a razão sólido/argamassa (Vs/Vm) emerge igualmente como um parâmetro de elevada influência, embora com um efeito de sinal oposto ao observado para a fluidez. Em particular,

valores mais elevados de Vs/Vm conduzem a um aumento da resistividade elétrica aos 28 dias, sugerindo uma matriz mais compacta e uma menor conectividade da rede porosa, mas estão simultaneamente associados a uma redução da resistência à compressão. Este comportamento evidencia que o aumento do teor relativo de sólidos, embora benéfico do ponto de vista da durabilidade potencial, pode penalizar o desempenho mecânico quando excede determinados limiares.

A razão água/cimento (w/c) emerge como o principal parâmetro de controlo da resistência mecânica, apresentando um efeito negativo pronunciado sobre a resistência à compressão aos 28 dias, em linha com o comportamento clássico de materiais cimentícios. Adicionalmente, valores mais elevados de w/c conduzem a uma redução da resistividade elétrica, refletindo uma microestrutura mais permeável. A interação positiva identificada entre w/c e o teor de superplastificante (sp/p) indica, no entanto, que o uso adequado de adjuvantes pode mitigar parcialmente a perda de resistência associada ao aumento do teor de água.

De um modo geral, os resultados obtidos evidenciam a existência de compromissos claros entre desempenho no estado fresco, resistência mecânica e propriedades associadas à durabilidade. Parâmetros da mistura que favorecem a fluidez tendem a penalizar a resistividade e a resistência, enquanto misturas mais ricas em sólidos promovem o desempenho elétrico à custa da trabalhabilidade e, em certos casos, da resistência mecânica. Assim, o desenho de misturas deve assentar numa otimização conjunta de Vs/Vm, Vw/Vp e w/c, explorando o espaço de projeto identificado através das superfícies de resposta, de forma a satisfazer simultaneamente os requisitos no estado fresco e desempenho no estado endurecido.

4. Conclusões

A metodologia baseada em Desenho de Experiências permitiu avaliar de forma sistemática a influência das principais proporções da mistura no comportamento no estado fresco, no desempenho mecânico e nas propriedades associadas à durabilidade potencial. Os resultados evidenciaram que a fluidez das misturas é fortemente condicionada pelas razões volume de areia/volume de argamassa (Vs/Vm) e volume de água/volume de pasta (Vw/Vp), enquanto a razão água/cimento (w/c) assume um papel determinante na resistência à compressão aos 28 dias. A resistividade elétrica mostrou-se igualmente sensível às variações das proporções da mistura, refletindo diferenças na compacidade da matriz e na conectividade da rede porosa.

Os níveis de resistência à compressão obtidos, compreendidos entre aproximadamente 60 MPa e 84 MPa aos 28 dias, confirmam a adequação das matrizes desenvolvidas para aplicações em elementos arquitetónicos esbeltos sujeitos a flexão moderada, para o que será necessário introduzir fibras numa fase posterior deste estudo. Paralelamente, os valores de fluidez alcançados demonstram que é possível compatibilizar elevados requisitos de trabalhabilidade com elevados níveis de desempenho mecânico, através de uma seleção adequada dos parâmetros de mistura.

De um modo geral, os resultados evidenciam a existência de compromissos claros entre desempenho no estado fresco, resistência mecânica e propriedades associadas à durabilidade, reforçando a importância de uma abordagem integrada no dimensionamento das composições. As matrizes ternárias de HPC branco desenvolvidas apresentam, assim, um elevado potencial para aplicações arquitetónicas avançadas, conciliando desempenho mecânico, durabilidade potencial e sustentabilidade ambiental.

Agradecimentos

Este trabalho foi financiado por: UID/04708 da Unidade de Investigação CONSTRUCT - Instituto de I&D em Estruturas e Construções - financiada pela Fundação para a Ciência e a Tecnologia, I.P./ MCTES, através de fundos nacionais; e pela FCT-Fundação para a Ciência e a Tecnologia através do Estímulo ao Emprego Científico 2021.01765.CEECIND (chamada individual). Os autores agradecem às empresas Secil, Omya, Sika, FibreXL e Chryso Portugal. Os autores gostariam também de agradecer o apoio do Laboratório de Estruturas do DECG-FEUP, nomeadamente, à Engenheira Paula Silva e ao Técnico Cláudio Ferraz.

Referências

[1] T. R. Naik, “SUSTAINABLE CONSTRUCTION MATERIALS AND TECHNOLOGIES,” 2007.

[2] A. Camões, “Betões de elevado desempenho,” Sep. 2006, Accessed: Mar. 15, 2026. [Online]. Available: https://hdl.handle.net/1822/6140

[3] L. M. Federico and S. E. Chidiac, “Waste glass as a supplementary cementitious material in concrete – Critical review of treatment methods,” *Cem. Concr. Compos.*, vol. 31, no. 8, pp. 606–610, Sep. 2009, doi: 10.1016/J.CEMCONCOMP.2009.02.001.

[4] S. Nunes, A. M. Matos, T. Duarte, H. Figueiras, and J. Sousa-Coutinho, “Mixture design of self-compacting glass mortar,” *Cem. Concr. Compos.*, vol. 43, pp. 1–11, Oct. 2013, doi: 10.1016/J.CEMCONCOMP.2013.05.009.

[5] N. A. Soliman and A. Tagnit-Hamou, “Development of ultra-high-performance concrete using glass powder – Towards ecofriendly concrete,” *Constr. Build. Mater.*, vol. 125, pp. 600–612, Oct. 2016, doi: 10.1016/J.CONBUILDMAT.2016.08.073.

[6] A. M. Matos and S. C. Joana, “Waste glass powder in cement: Macro and micro scale study,” *Advances in Cement Research*, vol. 28, no. 7, pp. 423–432, Jul. 2016, doi: 10.1680/jadcr.14.00025.

[7] A. M. Matos and J. Sousa-Coutinho, “Durability of mortar using waste glass powder as cement replacement,” *Constr. Build. Mater.*, vol. 36, pp. 205–215, Nov. 2012, doi: 10.1016/j.conbuildmat.2012.04.027.

[8] N. Schwarz, H. Cam, and N. Neithalath, “Influence of a fine glass powder on the durability characteristics of concrete and its comparison to fly ash,” *Cem. Concr. Compos.*, vol. 30, no. 6, pp. 486–496, Jul. 2008, doi: 10.1016/j.cemconcomp.2008.02.001.

[9] M. C. Bignozzi, A. Saccani, L. Barbieri, and I. Lancellotti, “Glass waste as supplementary cementing materials: The effects of glass chemical composition,” *Cem. Concr. Compos.*, vol. 55, pp. 45–52, 2015, doi: 10.1016/j.cemconcomp.2014.07.020.

[10] M. Liu, “Incorporating ground glass in self-compacting concrete,” *Constr. Build. Mater.*, vol. 25, no. 2, pp. 919–925, Feb. 2011, doi: 10.1016/J.CONBUILDMAT.2010.06.092.

[11] C. Shi, Y. Wu, C. Riefler, and H. Wang, “Characteristics and pozzolanic reactivity of glass powders,” *Cem. Concr. Res.*, vol. 35, no. 5, pp. 987–993, May 2005, doi: 10.1016/J.CEMCONRES.2004.05.015.

[12] A. M. Matos, L. Maia, S. Nunes, and P. Milheiro-Oliveira, “Design of self-compacting high-performance concrete: Study of mortar phase,” *Constr. Build. Mater.*, vol. 167, pp. 617–630, Apr. 2018, doi: 10.1016/j.conbuildmat.2018.02.053.

[13] A. M. Matos, P. Milheiro-Oliveira, and M. Pimentel, “Eco-efficient high performance white concrete incorporating waste glass powder,” *Constr. Build. Mater.*, vol. 411, p. 134556, Jan. 2024, doi: 10.1016/J.CONBUILDMAT.2023.134556.

[14] N. Cangussu, A. M. Matos, P. Milheiro-Oliveira, and L. Maia, “Numerical Design and Optimisation of Self-Compacting High Early-Strength Cement-Based Mortars,” *Applied Sciences (Switzerland)*, vol. 13, no. 7, 2023, doi: 10.3390/app13074142.

[15] D. C. Montgomery, G. C. Runger, and N. F. Hubele, *Engineering Statistics, 5th Edition*. John Wiley & Sons, Inc., 2010. Accessed: Nov. 26, 2023. [Online]. Available: https://www.wiley.com/en-us/Engineering+Statistics%2C+5th+Edition-p-9780470631478

[16] O. Sengul, “Use of electrical resistivity as an indicator for durability,” *Constr. Build. Mater.*, vol. 73, pp. 434–441, Dec. 2014, doi: 10.1016/j.conbuildmat.2014.09.077.

[17] P. Azarsa and R. Gupta, “Electrical Resistivity of Concrete for Durability Evaluation: A Review,” *Advances in Materials Science and Engineering*, vol. 2017, pp. 1–30, May 2017, doi: 10.1155/2017/8453095.

cinpar2026
XXII International Conference on Building Pathology and Constructions Repair
15th to 17th July 2026 - Lisboa, Portugal

Enhancing the tensile performance of natural fibers for inorganic matrix composites in masonry strengthening

Mehdi Zahedi [1], Ali Abbass [2], Daniel V. Oliveira [3]

[1] University of Minho, ISISE, ARISE, Department of Civil Engineering, Guimarães, Portugal, mehdi.zhd1993@gmail.com
[2] Technological University Dublin, Built Environment Research and Innovation Centre, Dublin, Ireland, alyabbass11@gmail.com
[3] University of Minho, ISISE, ARISE, Department of Civil Engineering, Guimarães, Portugal, danvco@civil.uminho.pt

Abstract: The construction sector consumes a substantial share of global resources and contributes significantly to greenhouse gas emissions. Therefore, more sustainable approaches are needed not only in new construction, but also in the repair of existing buildings. In this context, natural-fiber-based composites represent a promising alternative for strengthening brick masonry buildings, offering the potential to reduce environmental impact while improving structural performance. This paper explores the modification of natural fiber reinforcements via a graphene/polyurethane coating protocol for as-received hemp intended for use in inorganic matrix composite manufacturing for the structural strengthening of masonry walls. The aim is to improve the tensile behavior of hemp fibers with different diameters, particularly their strength and elastic modulus. Finally, the implementation of this coating protocol resulted in an approximately 500% increase in the initial elastic modulus.

Keywords: Natural fibers, Fiber's coating, Masonry strengthening, Elastic modulus, Tensile strength

cinpar2026
XXII International Conference on Building Pathology and Constructions Repair
15th to 17th July 2026 - Lisboa, Portugal

An Investigation on the Mechanical Response of Composite-Reinforced Mortar for Masonry Strengthening

Mehdi Zahedi[1], Nima Azimi[2], Ali Abbass [3], Daniel V. Oliveira [4]

[1] University of Minho, ISISE, ARISE, Department of Civil Engineering, Guimarães, Portugal, mehdi.zhd1993@gmail.com
[2] Riga Technical University, Faculty of Civil and Mechanical Engineering, Institute of Sustainable Building Materials and Engineering Systems, Kipsalas 6A, LV-1048 Riga, Latvia, nimaa32@gmail.com
[3] Technological University Dublin, Built Environment Research and Innovation Centre, Dublin, Ireland, alyabbass11@gmail.com
[4] University of Minho, ISISE, ARISE, Department of Civil Engineering, Guimarães, Portugal, danvco@civil.uminho.pt.

Abstract: Composite-reinforced mortar (CRM) systems are increasingly adopted for the strengthening of masonry structures; however, their reliable design and implementation remain constrained by the limited availability of systematic mechanical data and insufficient understanding of their interaction with masonry substrates. This challenge is particularly critical, as many masonry structures require repair or strengthening due to ageing and deterioration, as well as extreme actions such as earthquakes, necessitating strengthening solutions that extend service life while preserving structural integrity and architectural value. Within this context, CRM systems have emerged as a promising externally bonded technique, with previous studies reporting improvements in both load-bearing capacity and deformation performance. Nevertheless, CRM remains a relatively recent technology, and the available literature still lacks comprehensive, multi-scale experimental evidence addressing the mechanical response of its constituent components and the structural behavior of strengthened masonry assemblies. To address this gap, the present study employs an experimental program to characterize the tensile response of bare fiber grids and to evaluate the structural effectiveness of CRM strengthening through tensile coupon tests. The results provide a consistent multi-scale mechanical characterization of the CRM system, contributing to a more reliable basis for assessment, design, and implementation of CRM strengthening interventions in masonry structures.

Keywords: Composite-Reinforced Mortar (CRM); Tensile behavior; Mechanical Properties; Strengthening Techniques; Masonry.

XXII International Conference on Building Pathology and Constructions Repair
15th to 17th July 2026 - Lisboa, Portugal

Energy Efficiency and Sustainable Materials in Façade Rehabilitation: Challenges of Thermal Insulation in the Azores

Leo Chaves SOARES[1], Poliana BELLEI[2], Inês FLORES-COLEN[3], **Maria Paula MENDES**[2]

[1] Instituto Superior Técnico, University of Lisbon, Lisbon, Portugal, 1049-001, leo.soares@tecnico.ulisboa.pt

[2] CERENA, Instituto Superior Técnico, University of Lisbon, Lisbon, Portugal, 1049-001, poliana.bellei@tecnico.ulisboa.pt; mpaulamendes@tecnico.ulisboa.pt

[3] CERIS, Instituto Superior Técnico, University of Lisbon, Lisbon, Portugal, 1049-001, ines.flores.colen@tecnico.ulisboa.pt

Abstract: Since the beginning of the 21st century, the European Union has focused on reducing greenhouse gas (GHG) emissions and improving energy efficiency, with buildings accounting for 36% of these emissions. Portugal has committed to achieving carbon neutrality by 2050, focusing on urban rehabilitation and reducing energy poverty, supported by the Recovery and Resilience Plan. This study characterizes the construction sector in the European Union and Portugal, with emphasis on the Autonomous Region of the Azores, by analysing energy consumption and measures to mitigate energy poverty and climate change. The research included a survey targeting architects, engineers, and contractors from the islands of São Miguel, Terceira, Pico, and Faial. The results indicate that the lack of financial resources was the main barrier to energy rehabilitation (reported by 60% of respondents). Priority interventions include external thermal insulation (19%) and improvements in rainwater drainage systems (23%). Expanded polystyrene (EPS) was identified as the most widely used, followed by mineral wool and extruded polystyrene (XPS). All respondents reported experiencing climate change-related events, and 53% expressed confidence in the feasibility of implementing mitigation measures, with recycling the most frequently cited action (70%). Regarding the importance assigned to reducing environmental impact, the production and end-of-life phases were considered the most relevant. Given the region's geographical location, the use of local materials is highlighted as essential to minimize the environmental impact associated with the production of construction materials. It is concluded that the implementation of thermal insulation solutions in the region will enhance the energy efficiency of buildings, contributing to the reduction of energy poverty and the mitigation of construction pathology (reported by 84% of respondents).

Keywords: Sustainability, insulation materials, alternative materials, climate change, autonomous regions

1. Introduction

Since the early 21st century, the EU has set goals to reduce Greenhouse Gas Emissions (GGE) and improve energy efficiency, and promote the use of renewable energy as part of its broader commitment to environmental sustainability (Parlamento Europeu e do Conselho 2018). In alignment with the Paris agreement and related policy frameworks, Portugal has committed to achieving carbon neutrality by 2050. To support this objective, the country implemented the National Energy and Climate Plan 2021-2030.

In the residential sector, improving thermal comfort, particularly through passive measures such as thermal insulation, has been identified as a priority. However, the current housing stock presents significant challenges: approximately 80% of dwellings have low energy performance ratings, and around 75% lack adequate thermal insulation (Ogut, 2023). Although the adoption of insulation solutions has increased since the 1990s, largely driven by European legislation and technological advancements (Resolução do Conselho de Ministros n.º 53/2020), substantial gaps remain.

European policies, such as the Energy Performance of Buildings Directive (EPBD), have played a central role in promoting building rehabilitation. These policies aim to reduce energy consumption, address energy poverty, and accelerate the transition to renewable energy, with the overarching goal of achieving a decarbonized building stock by 2050. In Portugal, urban rehabilitation efforts have focused on enhancing thermal comfort and indoor air quality, with an emphasis on thermal insulation (ADENE 2024).

This regulatory framework has evolved progressively. Directive 2002/91/EC introduced the energy certification system, which was transposed into Portuguese legislation in 2006 through the creation of the National Energy Certification System and Indoor Air Quality (SCE) (Decreto-Lei n.º 78/2006; Freire, 2015). Subsequent updates, including Directive 2010/31/EU and its transposition via Decree-Law n.º 118/2013, reinforced energy efficiency requirements and introduced stricter standards for building systems. More recently, Decree-Law n.º 101-D/2020, transposing Directive (EU) 2018/844, established the current regulatory framework governing the energy performance of buildings in Portugal, including specific adaptations for the Autonomous Region of the Azores.

According to the 2021 Census (INE, 2021), the Azores and Algarve regions experienced growth in their housing stock, with increases in the number of buildings and dwellings. The Azores, with a population of approximately 250,000, face distinct challenges due to their geographical isolation and strong dependence on imported energy (around 60%) (European Commission n. d.). To reduce this dependency, the region has invested in renewable energy sources, particularly geothermal energy, which accounted for 20.5% of electricity generation in 2022, mainly on the islands of São Miguel and Terceira (DRAAC, 2023).

The residential sector in the Azores is particularly significant, representing 20% of total energy consumption and constituting the largest source of CO_2 emissions (European Commission n. d.). As an autonomous region, the Azores must adapt national energy policies to its specific socio-economic and geographic context. Consequently, emission-reduction targets differ from those of mainland Portugal, reflecting regional characteristics, such as the prominence of the agricultural sector (Furtado et al., 2023).

Energy poverty remains a pressing issue in the region. According to Eurostat (2024), 31.4% of the population is at risk of poverty or social exclusion, exceeding the national average. This situation is exacerbated by the age and inefficiency of the housing stock, with a large proportion of buildings constructed before 2000. In response, the Recovery and Resilience Plan (RRP) allocates €67.5 million to improve housing conditions, focusing on both new energy-efficient construction and the renovation of existing buildings.

These initiatives include demonstration projects and financial support mechanisms to increase energy efficiency, reduce energy consumption, and mitigate energy poverty. Among the available solutions, façade thermal insulation is particularly relevant, as it improves building performance, reduces emissions, and enhances indoor comfort (Governo dos Açores, 2024).

The Azorean climate highlights the need for appropriate building design. Mild temperatures, high humidity, and frequent precipitation challenge thermal comfort and durability. With an average annual temperature of 17.5 °C, low thermal variation, and relative humidity around 80%, context-specific solutions such as bioclimatic design and effective insulation are essential (Governo dos Açores, 2019; Azevedo, 2002).

Climate change mitigation is a priority under the Regional Programme for Climate Change (PRAC), which promotes renewable energy, efficiency, and sustainable mobility, emphasizing adaptation and mitigation measures in residential and service sectors to reduce energy demand and environmental impacts (Decreto Legislativo Regional n.º 30/2019/A).In this context, this study analyses energy consumption patterns and thermal insulation solutions in the Azores, based on a survey of stakeholders in the architecture, engineering, and construction (AEC) sector. The objective is to understand professionals' perceptions and contribute to developing more effective communication strategies to improve thermal comfort and overall well-being.

2. Methodology

The present study was conducted by disseminating a structured survey to a range of stakeholders, including professionals from the AEC sector and residents of the Autonomous Region of the Azores. A total of 19 valid responses were collected. The statistical population comprises residents and sector-related stakeholders within the Azores region.

The survey is organized into several thematic sections. It begins with the characterization of respondents, gathering information on their sector of activity, geographic location, and personal and professional profiles. This is followed by a section on housing characteristics, covering ownership status, building condition, renovation history, thermal insulation, and ventilation practices. Subsequently, the survey explores participants' perceptions of energy performance, including the perceived need for energy rehabilitation, awareness of governmental support programs, and familiarity with tools for assessing energy consumption.

A dedicated section on thermal insulation examines respondents' knowledge of available solutions and their preferences between passive and active strategies for achieving thermal comfort. It also evaluates perceptions of insulation materials across multiple dimensions, technical, environmental, economic, and safety-related, with particular emphasis on durability, sustainability, and fire performance.

Finally, the survey addresses respondents' views on climate change and the environmental impact of insulation solutions, considering a life-cycle perspective and their potential contribution to climate change mitigation.

3. Results

3.1 Characterization of Respondents

The survey for this study was conducted in the Autonomous Region of the Azores, involving participants residing on the islands of São Miguel, Terceira, Pico, and Faial in 2023. Data collection was primarily conducted through face-to-face interviews (14 respondents), while the remaining participants responded via email (19 participants). Of the participants, 89% are men, and 11% are women, all residing in coastal areas. Most of the respondents work in the AEC sector, and generally have an intermediate level of professional experience, with the majority falling within the 25 to 49-age range.

3.2 Characterization of the Respondents´ Homes

Of the participants, 11 are homeowners, and eight are tenants. Out of the 19 respondents, only three reported no visible presence of mold inside their homes. Around 42% of respondents live in buildings constructed after 2006 (Figure 1), with 89% confirming the presence of thermal insulation.

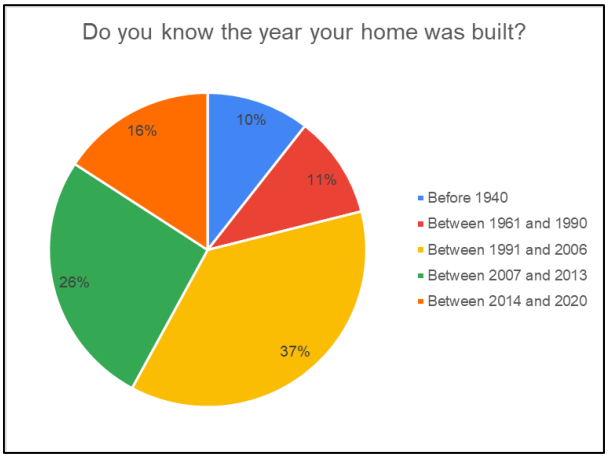


Figure 1 – Distribution of construction year classes of respondents' homes

Among those who reported not having insulation or were unsure, mold and dampness were the most cited reasons for needing energy rehabilitation (Figure 2). However, 92% of those identifying these issues had never carried out rehabilitation works, primarily due to a lack of financial resources.

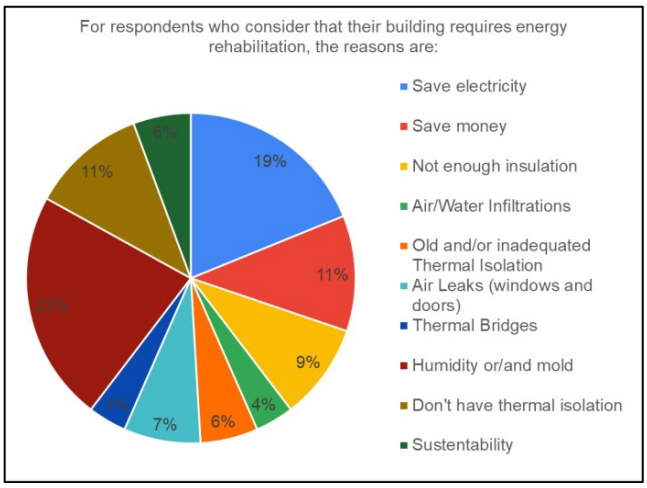


Figure 2 – Selected reasons justifying the need for energy rehabilitation in their respective homes

Approximately 89% of respondents stated they would seek government financial support for energy rehabilitation, aligning with the objectives of the RRP. All participants agreed that investing in rehabilitation is worthwhile, with a focus on improving energy efficiency ratings. Investment in rainwater drainage systems was identified as the top priority due to the region’s climatic conditions, followed by the application of insulation material on walls (Figure 3).

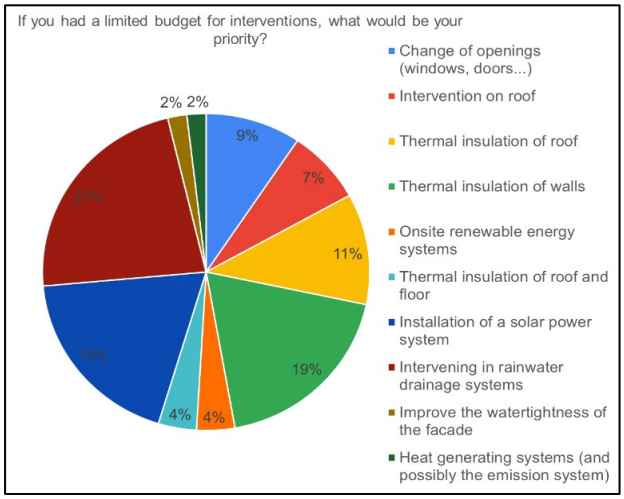


Figure 3 – Type of intervention selected, which respondents would prioritize if they had the available budget

Poor ventilation was not identified as the main cause of mold, as most respondents regularly ventilate their homes (Figure 4). Finally, 63% of participants stated they had no clear understanding of the costs involved in maintaining environmental comfort in their homes.

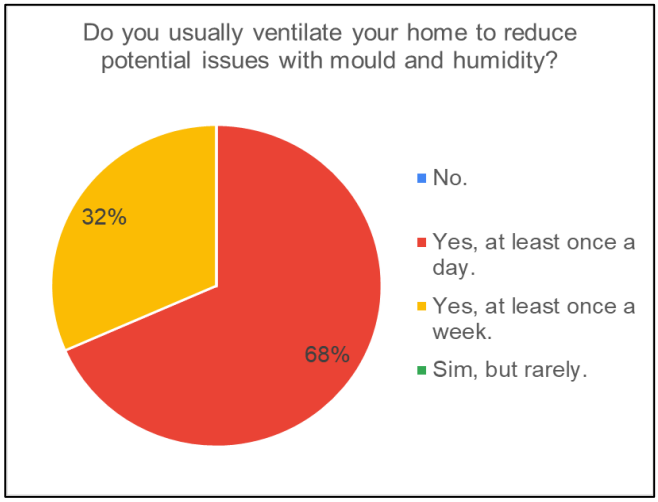


Figure 4 – Frequency with which respondents ventilate their homes to reduce potential issues with mould and humidity

3.3 Characterization of Thermal Insulation

The survey revealed that 15 out of the 19 respondents were knowledgeable about the criteria for selecting and classifying thermal insulation materials (Figure 5), adding credibility to their responses. All respondents stated that expanded polystyrene (EPS) is the most widely used and longest-applied insulation material in the region, which explains the regional perception of its “superior” durability compared to other insulation materials. On the other hand, tenants reported having low knowledge regarding green façades and natural fiber solutions, which are rarely used in the region. The greater commercialization of EPS in the region, compared to other insulation materials, also justifies the fact that it has the lowest market price, followed by mineral wool and extruded polystyrene (XPS), which, according to the respondents, are also among the most commercially available insulation materials.

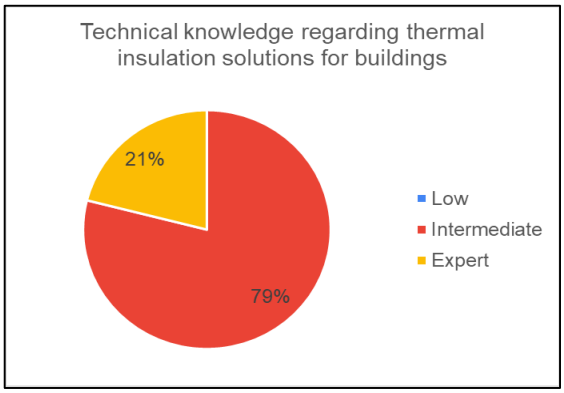


Figure 5 – Percentage of respondents by level of technical knowledge of thermal insulation solutions

The respondents' perception regarding the materials with the greatest maintenance needs, the highest potential for biological growth and the lowest CO_2 emissions converges towards natural materials, such as natural fibers and green façades.

In Figure 6, average values of the classifications obtained for synthetic-origin materials are presented, in Figure 7, for natural-origin insulation materials, and in Figure 8, for mineral wool.

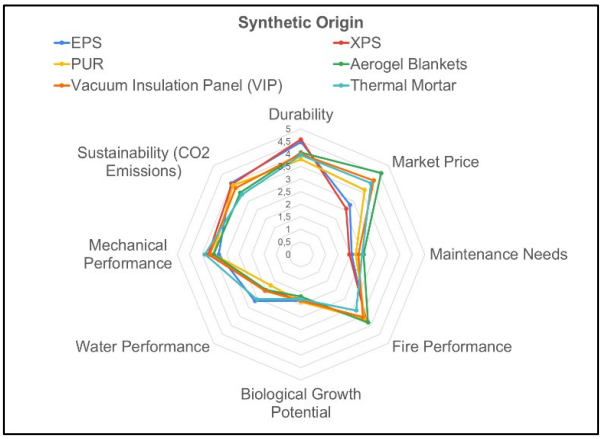


Figure 6 – Average values of the classifications obtained for the various synthetic-origin insulation materials, relative to the criteria under study

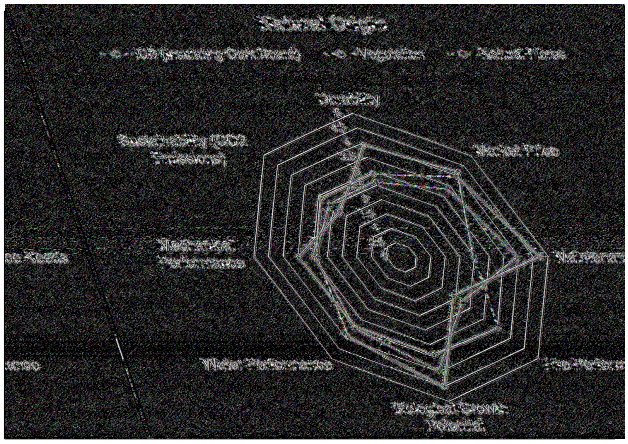


Figure 7 – Average values of the classifications obtained for the various natural-origin insulation materials, relative to the criteria under study

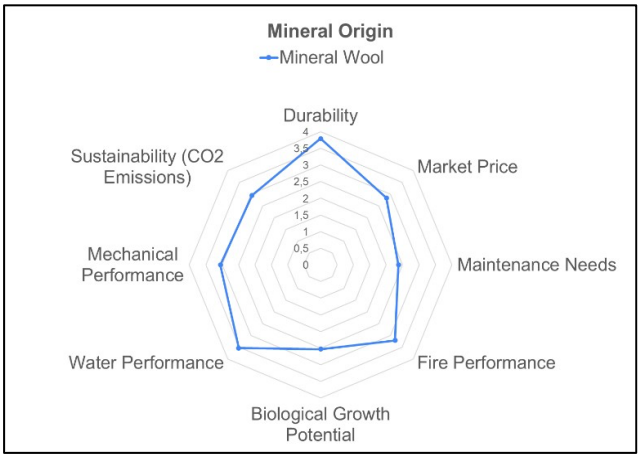


Figure 8 – Average values of the classifications obtained for the various mineral-origin insulation materials, relative to the criteria under study

By analyzing Figures 6 to 8, it can be observed that synthetic-origin materials, compared to materials of other origins, are generally perceived as having better characteristics in various aspects, such as: greater durability, lower maintenance needs, reduced potential for biological growth, and better performance in relation to water, i.e., less water retention. On the other hand, based on the respondents' answers, natural-origin materials stand out for their superior characteristics in terms of fire behavior and sustainability, with lower CO_2 emissions.

Regarding the constructive characteristics that can influence the choice of thermal insulation materials, the most prominent feature was the application of thermal insulation on the exterior of the façade. This solution was perceived by the respondents as a rapidly growing option in the region (proving to be very competitive when compared to other common solutions), associated with quick installation and homes that provide a high level of environmental comfort.

Passive solutions, the balance between these and active solutions, and heating and cooling systems were the options that received the highest percentage of responses as the most suitable for achieving indoor thermal comfort.

Heat pump systems were the solution with the highest response rate. According to the respondents' explanations, this high percentage is due to an incentive system for the production and storage of energy from renewable sources, promoted by the Regional Directorate of Energy. This system allows the investment in heat pumps, both for climate control and Domestic Hot Water (DHW), to be subsidized as a non-repayable grant by the government of the Azores (Direção Regional da Energia 2024).

Approximately 84% of respondents expressed a willingness to choose more sustainable solutions, even if they are more expensive, to reduce CO_2 emissions. The production and end-of-life phases of materials were considered the most important for reducing environmental impact, particularly due to logistical challenges in the Autonomous Region of the Azores. Key environmental goals highlighted by respondents include promoting the circular economy, increasing the use of green energy, and reducing CO_2 emissions. The data collected will be further analyzed in relation to the socioeconomic and environmental context of the Azores.

4. Discussion

All the rehabilitation of the housing stock is a pressing issue in the European Union and Portugal, with energy inefficiency exacerbating energy poverty. Approximately 40 million Europeans, including 17.5% of

the Portuguese population, are unable to adequately heat their homes. The European Union and Portugal have committed to reducing GHG emissions and increasing energy efficiency by 2030 and 2050, with various initiatives underway, such as the RRP (Resolução do Conselho de Ministros n.º 53/2020).

In the Azores, the RRP allocates €67.5 million to improving housing conditions, with a focus on energy efficiency and combating energy poverty (Governo dos Açores 2024). The study's respondents, primarily residents of homes without thermal insulation, identified mold and humidity as critical problems, exacerbated by the region's climatic conditions. Financial constraints were cited as the main barrier to carrying out energy rehabilitation, but 89% of respondents indicated that they would undertake these interventions with government support.

Respondents prioritized the installation of external thermal insulation on façades and improving rainwater drainage systems to address the effects of climate change, which include extreme weather events and rising temperatures, particularly in summer.

Comparative analysis of the results from the present study (Soares, 2023) and those obtained from surveys conducted as part of the EFFICACY project (Bartels et al. 2023) on the use of thermal insulation solutions in building façades on mainland Portugal, reveals several key findings. The EFFICACY data were based on a sample of 127 respondents collected between November 2022 and February 2023 (Parracha et al. 2024; Loura, 2023), and provide a useful benchmark for contextualizing the results presented here.

- In both studies, most of the respondents work in the sector of AEC, allowing for a similar validation of responses.
- In the present study, 63% of respondents reported being satisfied with the comfort level of their homes, compared to 80% on mainland Portugal.
- In both studies, over 62% of respondents, aware of government incentives for energy rehabilitation of homes, deemed these supports inadequate, suggesting that, as in mainland Portugal, the support measures planned for the Azores region should be reassessed to better meet the population's needs.
- Both in the Azores and mainland Portugal, the percentage of respondents indicating the need for additional equipment/devices to improve indoor comfort exceeds 76%, revealing that, in the respondents' view, passive solutions are insufficient to ensure adequate environmental comfort in homes. This high percentage in both studies may explain why most respondents consider investing in an energy rehabilitation intervention worthwhile (as noted by more than 79% of respondents in the mainland Portugal study and all respondents in the present study).
- Reviewing the results from mainland Portugal, 58% of respondents indicated that they either do not believe in climate change or chose not to respond. This contrasts with the present study, in which all respondents reported believing in climate change and having already perceived its effects.
- All Azorean respondents agreed that climate change can influence indoor comfort in buildings and, consequently, affect energy consumption. There was also unanimous agreement that summer is the season most likely to be impacted by climate change. Additionally, they were asked about the approach they would adopt in response to this issue. The predominant response was a reaction/action approach. Respondents justified this choice by stating that climate change is an inevitability whose effects are likely to worsen soon, making it essential for populations to take measures to help reduce its impacts.
- The use of locally sourced Azorean materials was identified as a solution to reduce environmental impacts, considering the significant role the production phase plays in the life cycle of imported materials. Respondents expressed particular concern about the production phase, noting that the region's geographical location logistically constrains the acquisition of products and materials, as a considerable portion depends on long- distance transport (by sea and air).

- Among construction characteristics influencing insulation material choice, external façade insulation was the most frequently chosen option. This preference aligns with the high commercialization of EPS in the Azores region and may reflect the growing trend towards external insulation in Portugal in recent years.
- For solutions considered most effective in improving thermal comfort at home, Azorean respondents highlighted passive façade solutions and a balance of active and passive solutions. Lower percentages associated with heating and cooling systems may be due to the mild temperatures in the region during the whole year. Among active solutions, heat pump systems were favored. In addition to being supported by government incentives in the Azores, their popularity may be linked to increased availability in recent years.

The results presented in Table 1 reflect respondents' perceptions of insulation material performance rather than measured or experimentally validated properties. As such, the findings should be interpreted as indicative of market preferences and professional judgment.

- XPS and polyurethane-based materials (PUR/PUX) are perceived as advantageous in maintenance needs, water resistance, and resistance to biological growth, suggesting that respondents associate these materials with reliability in moisture-prone conditions.
- Thermal insulating mortars are consistently rated highest for fire resistance and mechanical performance in both regions. This may reflect confidence in their compliance with safety regulations and structural robustness.
- The identification of aerogel blankets in the Azores for biological growth resistance suggests awareness of high-performance materials among respondents, although their limited market penetration indicates that such perceptions may not be based on widespread practical application.
- For the sustainability criterion (CO_2 emissions), responses diverge between regions. In the Azores, insulation cork board is perceived as the most sustainable option, likely due to its natural origin and association with low environmental impact. In mainland Portugal, vegetation systems (green walls) are perceived as the most sustainable

Table 1 – Thermal insulation materials with the highest average rating, by performance criterion, for the Azores Autonomous Region (RAA) and mainland Portugal , derived from survey-based studies (Parracha et al. 2024; Parracha et al. 2023: Loura 2023)

Performance Criterion	Best-Rated Insulation Material (Azores)	Best-Rated Insulation Material (Mainland Portugal)
Durability	EPS	Cork insulation board
Market Price	EPS	EPS
Maintenance Needs	XPS	Insulation corkboard
Fire Resistance	Thermal insulating mortars	Thermal insulating mortars
Biological Growth Resistance	Aerogel blankets	PUX/XPS/EPS
Water Resistance	Polyurethane foam (PUR)	XPS
Mechanical Performance	Thermal insulating mortars	Thermal insulating mortars
Sustainability (CO_2 Emissions)	Insulation cork board	Vegetation – green walls

In addition to the information presented in the previous table, respondents indicated that EPS, followed by mineral wool and XPS, are the most widely marketed and applied insulation materials in the Azores. XPS is used for both internal insulation of façades within simple masonry combined with light cladding and in air gaps of double walls and external applications (ETICS). This widespread use makes it more competitively priced compared to other insulation solutions.

5. Conclusion

The results highlight that material selection is influenced by perception, familiarity, and market presence, and may not fully align with quantitative performance data or life-cycle assessments. Considering the results of this study and its scope, the following developments are proposed:

- Conduct a similar study periodically to keep the information in the database promoted by the EFFICACY project up to date.
- Expand the dissemination and development of the survey used in this study to reach a larger number of respondents, making the sample more representative and thus enhancing statistical validity.
- Compare the results of this work with other studies conducted in regions with geographic characteristics like those of the Azores to understand the extent to which the impact of climate change is perceived similarly by respondents and to assess their perspectives on this phenomenon.
- Monitor the use of endogenous materials from the autonomous region of Azores in the construction industry to gather feedback on the classification criteria used in this study.

Acknowledgments

The authors are grateful to the Fundação para a Ciência e a Tecnologia, I.P. (FCT, https://ror.org/00snfqn58) under Grant TWIST Project (https://doi.org/10.54499/2023.16868.ICDT), CERENA (through FCT project UID/04028/2025 (https://doi.org/10.54499/UID/04028/2025), and CERIS (https://doi.org/10.54499/UID/6438/2025). MPM acknowledges the FCT for the individual project 2023.08653.CEECIND. The authors also acknowledge the support of FCT through the ReCoveRing project (https://doi.org/10.54499/2023.17249.ICDT).

References

ADENE. 2024. Eficiencia Energética. https://www.adene.pt/area-tematica/eficiencia-energetica/.

Azevedo, E. B. 2002. “Clima.” Enciclopédia Açoriana. https://www.culturacores.azores.gov.pt/ea/pesquisa/Default.aspx?id=190%203#:~:text=Humidade%20relativa%20do%20ar%20A,m%C3%A9dios%2%200mensais%20pr%C3%B3ximos%20dos%2080%25

Bartels, Giovanna, Beatrice Bartolucci, Chiara Bertolin, Giulia Boccacci, Inês Flores-Colen, Francesca Frasca, Maria Paula Mendes, Ozge Ogut, João Luís Parracha, and Anna Maria Siani. 2023. “EFFICACY Handbook Energy EFFiciency Bullding and CirculAr EConomY for Thermal Insulation Solutions.”

Decreto Legislativo Regional n.º 30/2019/A, de 28 de Novembro. Diário da República n.º 229/2019, Série I de 2019-11-28.

Decreto-lei n.º 78/2006, de 4 de Abril. Diário da República n.º 67/2006, Série I-A de 2006-04-04.

Decreto-Lei n.º 101-D/2020, de 7 de dezembro Diário da República n.º 237/2020, 1º Suplemento, Série I de 2020-12-07: 21-45.

Decreto-Lei n.º 118/2013, de de 20 de agosto. Diário da República n.º 159/2013, Série I de 2013-08-20: 4988-5005.

Direção Regional da Energia. 2024. “Proenergia.“ https://portaldaenergia.azores.gov.pt/portal/Servicos/Proenergia.

DRAAC. 2023. “Energia e Transportes - Relatório do Estado do Ambiente dos Açores 2020-2022.” Governo dos Açores. Secretaria Regional do Ambiente e Ação Climática. 275 pp. https://rea.azores.gov.pt/store/REAA-2022.pdf.

Governo dos Açores. 2019. “Relatório sobre o Estado do Ambiente dos Açores 2017 – 2019.” Secretaria Regional do Ambiente e Ação Climática. 836 pp. https://rea.azores.gov.pt/store/REAA-2019.pdf.

Governo dos Açores. 2024. “PRR - Plano de Recuperação e Resiliência.” https://portal.azores.gov.pt/documents/36649/1e31565c-077b-45af-3833-bb0fe773e702.

Eurostat, E. U. 2024. “People at risk of poverty or social Exclusion in 2024.” https://ec.europa.eu/eurostat/web/products-eurostat-news/w/ddn-20250430-2.

EC. n. d. "Azores." https://clean-energy-islands.ec.europa.eu/countries/portugal/azores

Freire, A. M. 2015. “Reabilitação térmica de fachadas de edifícios com sistemas de isolamento pelo exterior.” Dissertação de Mestrado em Construção e Reabilitação. 142 pp. Instituto Superior Técnico, Lisboa, Portugal.

Furtado, António, Carlos Martins, Filipe Mendonça, Paulo Bermonte, Tarcísio Silva. 2023. ”D2.12 - IANOS Islands Decarbonisation Master Plan.” https://ianos.eu/wp-content/uploads/2024/01/D2.12_IANOS.pdf.

INE. 2021. “Censos.” https://censos.ine.pt/xportal/xmain?xpgid=censos21_main&xpid=CENSOS21&xlang=pt.

Loura B. 2023. “Estudo exploratório sobre as necessidades de informação relacionadas com o isolamento térmico de fachadas em Portugal”. Dissertação de Mestrado em Engenharia Civil. 107 pp. Instituto Superior Técnico, Lisboa, Portugal.

Ogut, I. C. 2023. “Energy poverty in Portugal, Italy, and Norway: awareness, short-term driving forces, and barriers in built environment.” Conf. Series: Earth and Environmental Science, 1176 012023, doi:10.1088/1755-1315/1176/1/012023.

Parlamento Europeu e do Conselho, d. 3. 2018, May 30. “Documento 32018L0844 - Diretiva (UE) 2018/844 do Parlamento Europeu e do Conselho, de 30 de maio de 2018, que altera a Diretiva 2010/31/UE relativa ao desempenho energético dos edifícios e a Diretiva 2012/27/UE sobre a eficiência energética.” Jornal Oficial da União Europeia, 19.06.2018: 75-91.

Parracha, J. L., B. Bartolucci, O. Ogut, G. Boccacci, B. Loura, M. P. Mendes, A. M. Siani, F. Frasca, C. Bertolin, and I. Flores-Colen. 2024. “Questionnaire Survey on the Use of Thermal Insulation Solutions in Building Facades of Portugal, Italy and Norway.” *Procedia Structural Integrity* 55 (2023): 119–26. https://doi.org/10.1016/j.prostr.2024.02.016.

Parracha, João Luís; Bartolucci, Beatrice; Boccacci, Giulia; Ogut, Ozge; Bartels, Giovanna; Siani, Anna Maria; Frasca, Francesca; Bertolin, Chiara; Mendes, Maria Paula; Flores-Colen, Inês. 2023. “The EFFICACY Project Database”, Mendeley Data, V2, doi: 10.17632/z8sphs8vvv.2

Soares C. L. 2024. " Desafios e usos do isolamento térmico em fachadas nos Açores". Dissertação de Mestrado em Engenharia Civil. 117 pp. Instituto Superior Técnico, Lisboa, Portugal.

Cinpar 2026
XXII International Conference on Building Pathology and Constructions Repair
15th to 17th July 2026 - Lisboa, Portugal

Caracterização Mecânica da Alvenaria Ordinária de Lisboa através de Ensaios com Macacos Planos

Jorge FONSECA[1], Hugo RODRIGUES[2], Aníbal COSTA[3]

[1] CERIS-Aveiro, Departamento de Engenharia Civil, Universidade de Aveiro, Portugal, jfonseca@ua.pt
[2] CERIS-Aveiro, Departamento de Engenharia Civil, Universidade de Aveiro, Portugal, hrodrigues@ua.pt
[3] CERIS-Aveiro, Departamento de Engenharia Civil, Universidade de Aveiro, Portugal, agc@ua.pt

Abstract: A preservação de edifícios antigos é essencial para a manutenção do património histórico e cultural. Estas estruturas evidenciam estilos arquitetónicos únicos, promovem a sustentabilidade através da reutilização de materiais e permitem a melhoria do desempenho e do valor dos edifícios pela integração de tecnologias modernas e energeticamente eficientes. A caracterização mecânica da alvenaria resistente em Portugal apresenta desafios significativos devido à elevada heterogeneidade dos métodos construtivos e dos materiais utilizados ao longo do tempo. Nos últimos anos, foram realizados numerosos ensaios com macacos planos em todo o país, com especial incidência no centro histórico de Lisboa, abrangendo edifícios civis e monumentos históricos. De acordo com a tipologia de alvenaria apresentada no EC8-3, a alvenaria ensaiada foi classificada e a determinação das propriedades mecânicas da alvenaria, nomeadamente a tensão de compressão, o módulo de elasticidade e o módulo de distorção, foi obtida através de 83 ensaios in situ com macacos planos. Os resultados indicaram valores médios de resistência à compressão de 1,6 MPa, módulo de elasticidade secante entre 1170 MPa e 2404 MPa e módulo de distorção de 375 MPa. De forma geral, os resultados apresentam boa concordância com os intervalos propostos por referências internacionais e estudos anteriores, embora evidenciem valores de rigidez superiores aos recomendados pelo Código Italiano e pelo projeto de revisão do EC8-3. Estes resultados contribuem para o estabelecimento de valores de referência para a alvenaria tradicional portuguesa e fornecem informação relevante para a avaliação sísmica e calibração de modelos numéricos de edifícios existentes.

Keywords: Ensaios de Macacos Planos, Alvenaria Ordinária, Ensaios In Situ, Caracterização Mecânica

1. Introdução

A preservação dos edifícios antigos é essencial para manter vivo o nosso património histórico e cultural. Estes edifícios apresentam frequentemente estilos arquitetónicos únicos e técnicas construtivas tradicionais que testemunham diferentes épocas da história. A conservação destas estruturas permite não só preservar a autenticidade arquitetónica e estética, mas também promover práticas sustentáveis através da reutilização dos edifícios existentes. A reutilização de materiais de construção já incorporados reduz a necessidade de novos recursos e minimiza o impacto ambiental associado à extração e produção de novos materiais. Além disso, a reabilitação de edifícios antigos possibilita a integração de tecnologias modernas e soluções energeticamente eficientes, melhorando o desempenho e o conforto sem comprometer o seu valor histórico. A preservação e valorização do património arquitetónico antigo contribuem para a sustentabilidade ambiental e para a valorização cultural, garantindo que as gerações futuras possam continuar a usufruir da riqueza do património arquitetónico nacional.

A história do património edificado em Portugal é rica e diversificada, refletindo séculos de influências arquitetónicas e culturais. Desde a Antiguidade até à época contemporânea, as construções existentes no território português testemunham a evolução das técnicas construtivas e da expressão estilística de diferentes períodos históricos. O património arquitetónico português integra uma grande variedade de estilos, desde estruturas da época romana até influências mouriscas e, posteriormente, o desenvolvimento dos estilos gótico, renascentista, barroco e neoclássico.

Embora Portugal continental não tenha sido afetado por sismos de grande magnitude nos últimos anos, a sua localização geográfica torna-o suscetível à ocorrência destes fenómenos, como demonstram acontecimentos históricos marcantes, tais como o terramoto de Lisboa de 1755 (Mw = 8.5), o sismo de Benavente de 1909 (Mw = 6.3) e o sismo do Algarve de 1969 (Mw = 7.8) (Salvalaggio et al. 2024). Estes eventos sísmicos provocaram danos extensos, particularmente nas construções em alvenaria (Correia et al. 2015), sendo que uma parte significativa do edificado existente foi construída antes da introdução dos modernos regulamentos de dimensionamento sísmico, apresentando, por isso, deficiências estruturais relativamente ao desempenho sísmico. O Decreto-Lei n.º 235/83 (República 1983), de 31 de maio, classifica a cidade de Lisboa como zona de elevada sismicidade, enquanto a entrada em vigor do Decreto-Lei n.º 95/2019 (República 2019), de 18 de julho, veio incentivar a avaliação das condições de segurança estrutural nos processos de reabilitação urbana, especialmente em zonas de risco sísmico.

Contudo, a caracterização mecânica da alvenaria resistente em Portugal apresenta desafios significativos devido à elevada heterogeneidade dos métodos construtivos e dos materiais utilizados ao longo do tempo. Nos últimos anos, foram realizados numerosos ensaios com macacos planos em todo o país, com especial incidência no centro histórico de Lisboa, abrangendo desde edifícios correntes até monumentos históricos (ver Figura 1). Estes ensaios têm sido desenvolvidos no âmbito de iniciativas dedicadas à conservação e reabilitação do património edificado.

Adotando a tipologia proposta por Candeias et al. 2020 para a alvenaria portuguesa, as estruturas ensaiadas foram classificadas de acordo com os tipos de alvenaria descritos no referido trabalho, acrescentando-se ainda as alvenarias correntes de tijolo furado e as construções em terra (adobe e taipa) (Fonseca et al. 2025).

Face à escassez de informação experimental sobre as propriedades mecânicas das alvenarias tradicionais portuguesas e à necessidade de dados fiáveis para a avaliação sísmica de edifícios existentes, este estudo tem como principal objetivo caracterizar mecanicamente diferentes tipologias de alvenaria através da análise de resultados obtidos em ensaios in situ com macacos planos. Em particular, pretende-se determinar a resistência à compressão, o módulo de elasticidade e o módulo de distorção das alvenarias ensaiadas, analisar a variabilidade destes parâmetros em função da tipologia construtiva e comparar os resultados obtidos com valores de referência propostos por regulamentos e estudos anteriores. Os resultados apresentados visam contribuir para a definição de valores representativos para a alvenaria portuguesa e apoiar futuras avaliações sísmicas e modelos numéricos de edifícios existentes.



Figura 1 - Fachadas de alguns dos edifícios ensaiados

2. Amostra de dados

A determinação das propriedades mecânicas da alvenaria, nomeadamente a resistência à compressão (f_m), os módulos de elasticidade correspondentes a 10%, 30% e entre 30–60% da tensão máxima (ver Figura 2), o módulo de distorção (G), entre outros parâmetros, foi obtida através da realização de 83 ensaios com macacos planos para a tipologia de alvenaria descrita como "alvenaria de pedra irregular, com seixos rolados e unidades pétreas erráticas e irregulares" (Candeias et al. 2020; Italian Building Code 2019; Vanin et al. 2017; CEN 2019; Fonseca et al. 2025).

Esta tipologia encontra-se presente nas paredes dos edifícios ensaiados no município de Lisboa, com especial incidência na Baixa Pombalina e zonas adjacentes, sendo que muitas destas paredes remontam ao período compreendido entre meados do século XVIII e finais do século XIX.

A presente análise pretende contribuir para um melhor conhecimento das propriedades mecânicas deste tipo de alvenaria portuguesa, facilitar a sua classificação e fornecer uma base sólida para as atuais intervenções de conservação e reabilitação, garantindo a preservação do valioso património arquitetónico de Lisboa para as gerações futuras.

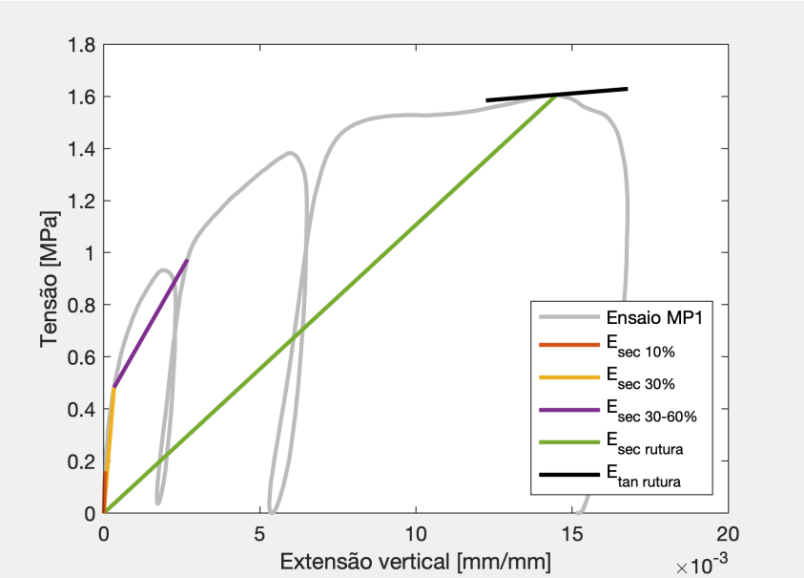


Figura 2 - Módulo de elasticidade determinado através de ensaios com macacos planos

3. Ensaios de macacos planos

Foram realizados ensaios duplos com macacos planos (ver Figura 3), utilizando macacos planos semicirculares com uma área total de 78100 mm², apresentando um valor médio de $k_a$de 0.79 (*DP* = 0.05; *CoV* = 6%) e um valor médio de k_m de 0.79 (*DP* = 0.06; *CoV* = 7.6%), em que *DP* é o desvio padrão e *CoV* o coeficiente de variação. As paredes ensaiadas apresentavam uma espessura média de 0.90 m (*DP* = 039.; *CoV*= 43%).

Para a medição das deformações durante a realização dos ensaios duplos, foram utilizados quatro transdutores de deslocamento: três posicionados verticalmente e um transdutor colocado horizontalmente, conforme ilustrado na Figura 4. A deformação vertical foi calculada considerando a média dos deslocamentos registados pelos três transdutores verticais, traduzindo-se no valor da extensão vertical (ϵ_v).

Para todos os ensaios foram executados ciclos de carga e descarga, tendo estes sido concluídos após a observação, no gráfico Tensão vs. Extensão, da formação de um patamar horizontal, o que indica a capacidade resistente máxima da alvenaria.

A literatura destaca frequentemente o posicionamento dos macacos planos como uma fonte de incerteza, particularmente em alvenarias heterogéneas ou degradadas. Neste estudo, essa limitação foi mitigada através da adoção de uma estratégia sistemática de posicionamento, baseada na configuração geométrica definida na Figura 4. Nas alvenarias correntes, quando as juntas horizontais ou verticais não se encontravam claramente definidas, o posicionamento dos macacos foi sempre determinado de acordo com as dimensões e proporções estabelecidas na Figura 4, privilegiando a repetibilidade do procedimento. Os requisitos de ortogonalidade e espaçamento foram rigorosamente respeitados, assegurando condições consistentes entre diferentes tipologias de parede e configurações de ensaio.

Em alguns casos ocorre a rotura frágil da zona entre macacos planos e, na maioria dos ensaios, é possível observar a abertura de fissuras nessa zona e na região envolvente aos macacos planos (Fonseca et al. 2025). Na presença de argamassas antigas, verifica-se o esmagamento destas na zona envolvente aos macacos, como é exemplo as imagens da Figuras 3c), d) e e).

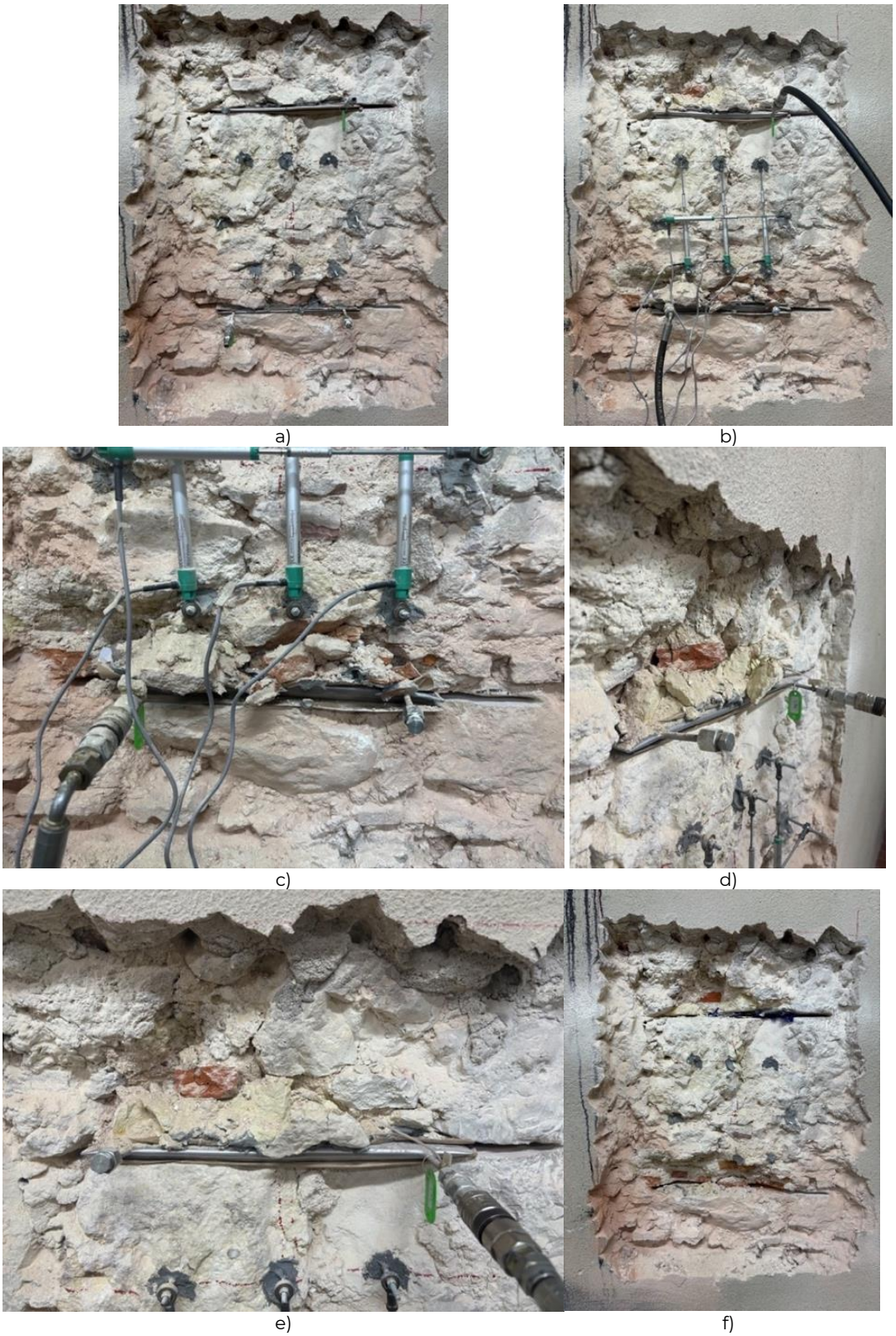


Figura 3 - Ensaio duplo com macacos planos: a) alvenaria após a inserção dos macacos planos; b) alvenaria após a conclusão do ensaio; c) esmagamento da argamassa junto ao macaco inferior; d) e e) esmagamento da argamassa acima do macaco superior; f) alvenaria após a remoção dos macacos.

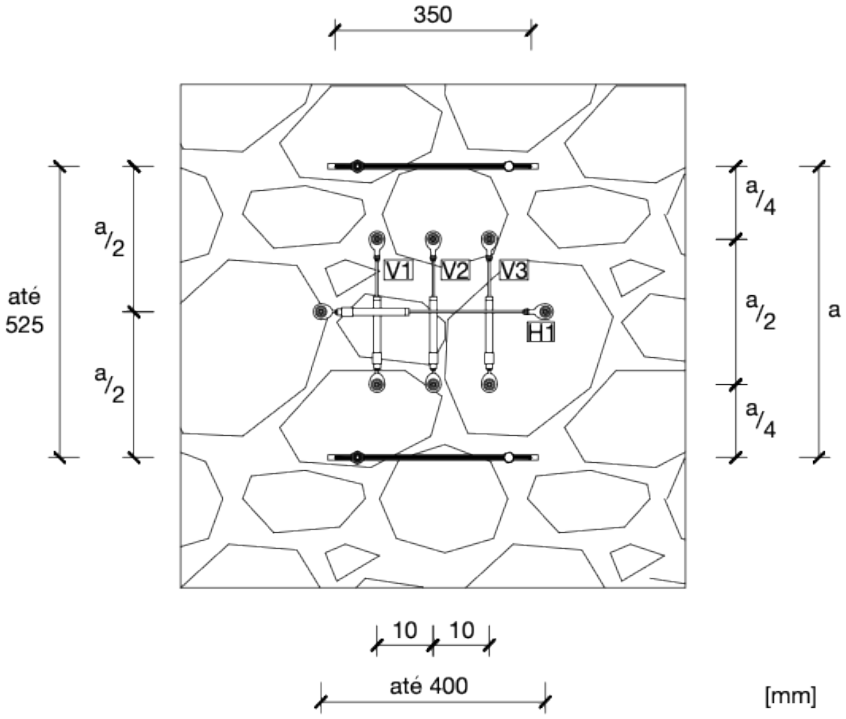


Figura 4 - Configuração geométrica adotada para os ensaios de macacos planos e para os transdutores de deslocamento

4. Caracterização da alvenaria de Lisboa

Para os valores obtidos de resistência à compressão, módulo de elasticidade e módulo de distorção, foram realizados modelos de regressão linear entre as diferentes variáveis determinadas, conforme apresentado na Figura 5.

As regressões entre a resistência à compressão e os diferentes módulos de elasticidade (Figuras 5a), b), c) e d)) apresentaram coeficientes de regressão médios da ordem de 0.65, com exceção da regressão entre f_m e $E_{\text{sec }30-60\%}$. Este modelo foi influenciado pela presença de um valor extremo correspondente a um módulo de elasticidade entre 30% e 60% da tensão máxima significativamente superior aos restantes valores obtidos, claramente identificável na Figura 5c).

A ocorrência destes valores extremos está associada à elevada heterogeneidade da alvenaria, a qual conduz a curvas tensão-extensão atípicas durante os ensaios, originando valores anómalos que podem influenciar os resultados globais das regressões.

A mesma análise pode ser realizada para as relações lineares entre os diferentes módulos de elasticidade, apresentadas na Figura 6. Em particular, nas Figuras 6b) e 6c) identificam-se duas observações extremas associadas a valores elevados de $E_{sec\,30\%}$ e $E_{\text{sec }30-60\%}$, respetivamente. Estas observações refletem a variabilidade inerente às alvenarias tradicionais e estão associadas a diagramas tensão-extensão atípicos obtidos durante os ensaios com macacos planos. Consequentemente, a sua presença afeta o ajuste das regressões lineares e conduz à diminuição dos coeficientes de correlação observados.

Antes do ajuste das distribuições estatísticas, foi realizada uma análise de valores atípicos (outliers) através de diagramas de caixa (boxplots) para cada variável. Foram considerados valores atípicos os resultados situados abaixo de Q1 − 1,5×IQR ou acima de Q3 + 1,5×IQR, sendo Q1 e Q3 o primeiro e terceiro quartis, respetivamente, e IQR a amplitude interquartil. Estes valores foram excluídos apenas da análise das

distribuições estatísticas, de forma a evitar que observações extremas influenciassem significativamente a estimação dos parâmetros das distribuições ajustadas. O número de amostras considerado em cada ajuste estatístico, após a remoção dos valores atípicos, encontra-se indicado nos respetivos gráficos da Figura 7 através do parâmetro N.

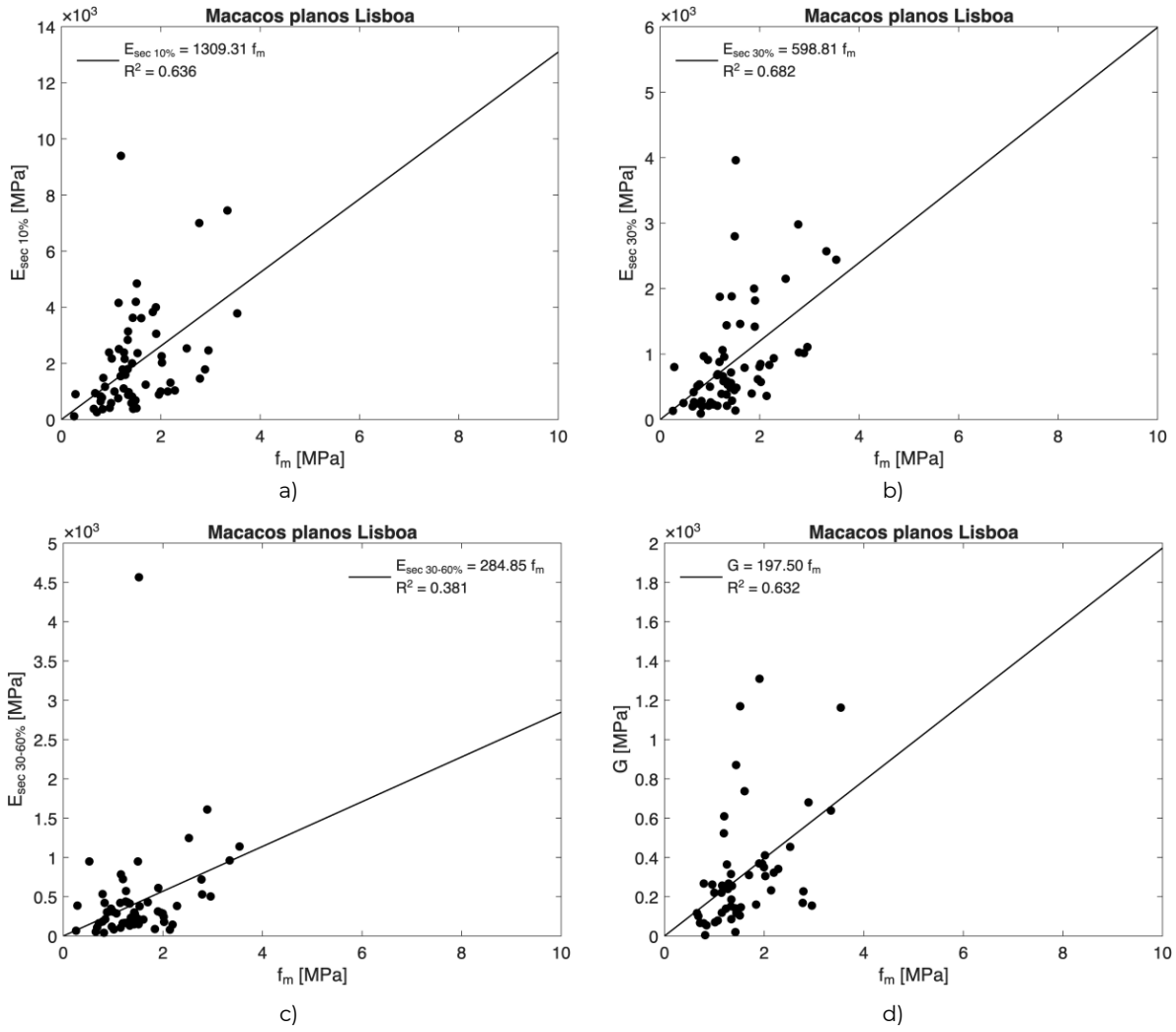


Figura 5 - Análise da rigidez da alvenaria – modelos de regressão linear para: a) $f_m vs. E_{\text{sec } 10\%}$; b) $f_m vs. E_{\text{sec } 30\%}$; c) $f_m vs. E_{\text{sec } 30-60\%}$; e d) $f_m vs. G$.

As distribuições normal e lognormal (ver Figura 7) das variáveis obtidas a partir dos resultados dos ensaios com macacos planos realizados no centro de Lisboa foram determinadas após a exclusão dos valores atípicos identificados através da análise por diagramas de caixa (boxplot), utilizando o critério de 1,5×IQR para cada variável. Entre as cinco variáveis analisadas, a distribuição lognormal apresentou o melhor ajustamento aos histogramas obtidos.

A resistência à compressão (Figura 7a) apresentou uma distribuição aproximadamente normal, indicando uma boa consistência dos resultados obtidos nos ensaios com macacos planos e reforçando a validade desta metodologia para a caracterização da alvenaria. Para os módulos de elasticidade (Figuras 7b), c) e d)) e módulo de distorção (Figura 7e), o melhor ajustamento da distribuição lognormal é explicado pela assimetria positiva dos dados.

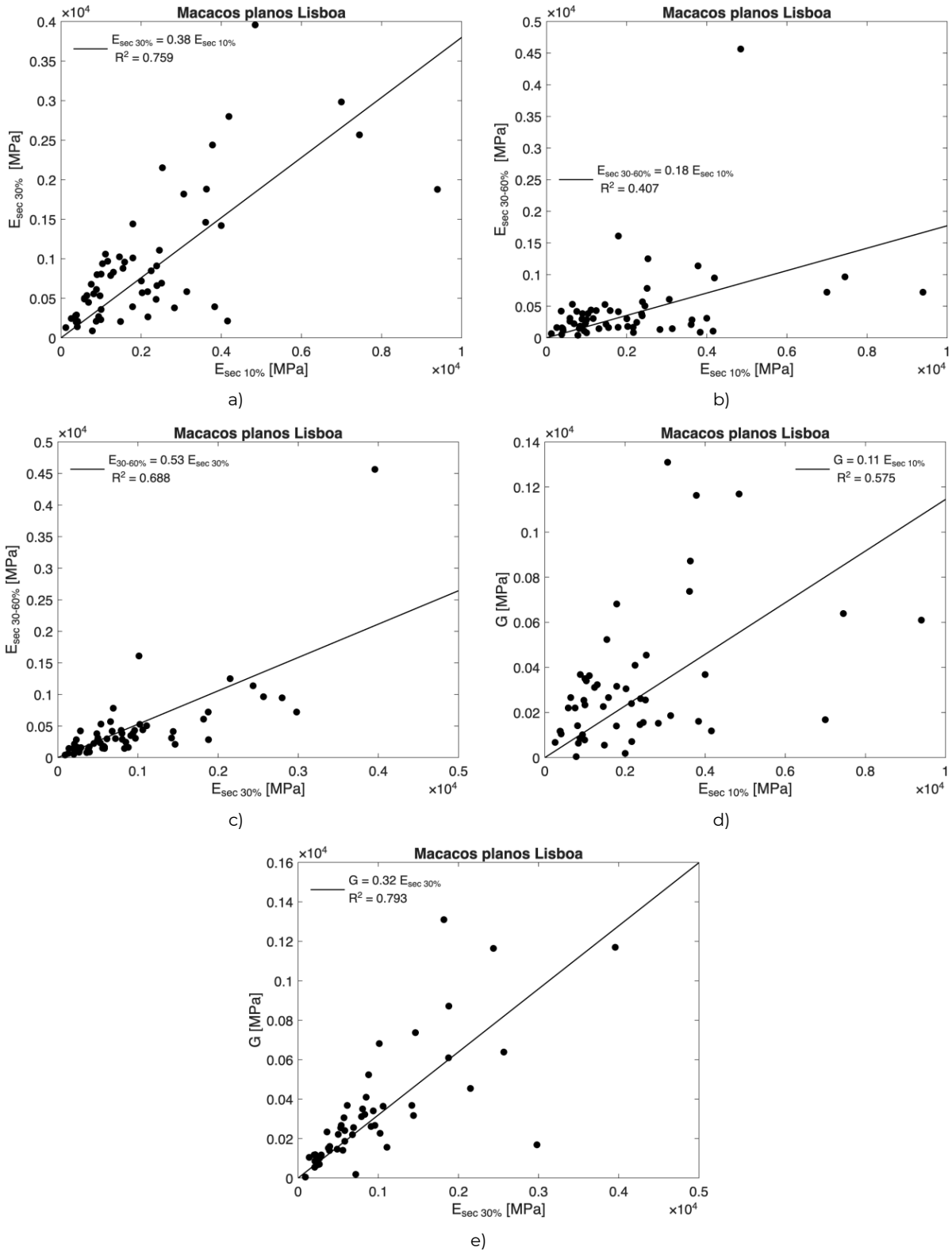


Figura 6 - Modelos de regressão linear dos módulos de elasticidade para diferentes níveis de tensão: a) $E_{\text{sec }10\%}\ vs. E_{\text{sec }30\%}$; b) $E_{\text{sec }10\%-30\%}\ vs. E_{\text{sec }30-60\%}$; c) $E_{\text{sec }30\%}\ vs.\ E_{\text{sec }30-60\%}$; d) $G\ vs. E_{\text{sec }10\%}$; e e) $G\ vs. E_{\text{sec }30\%}$.

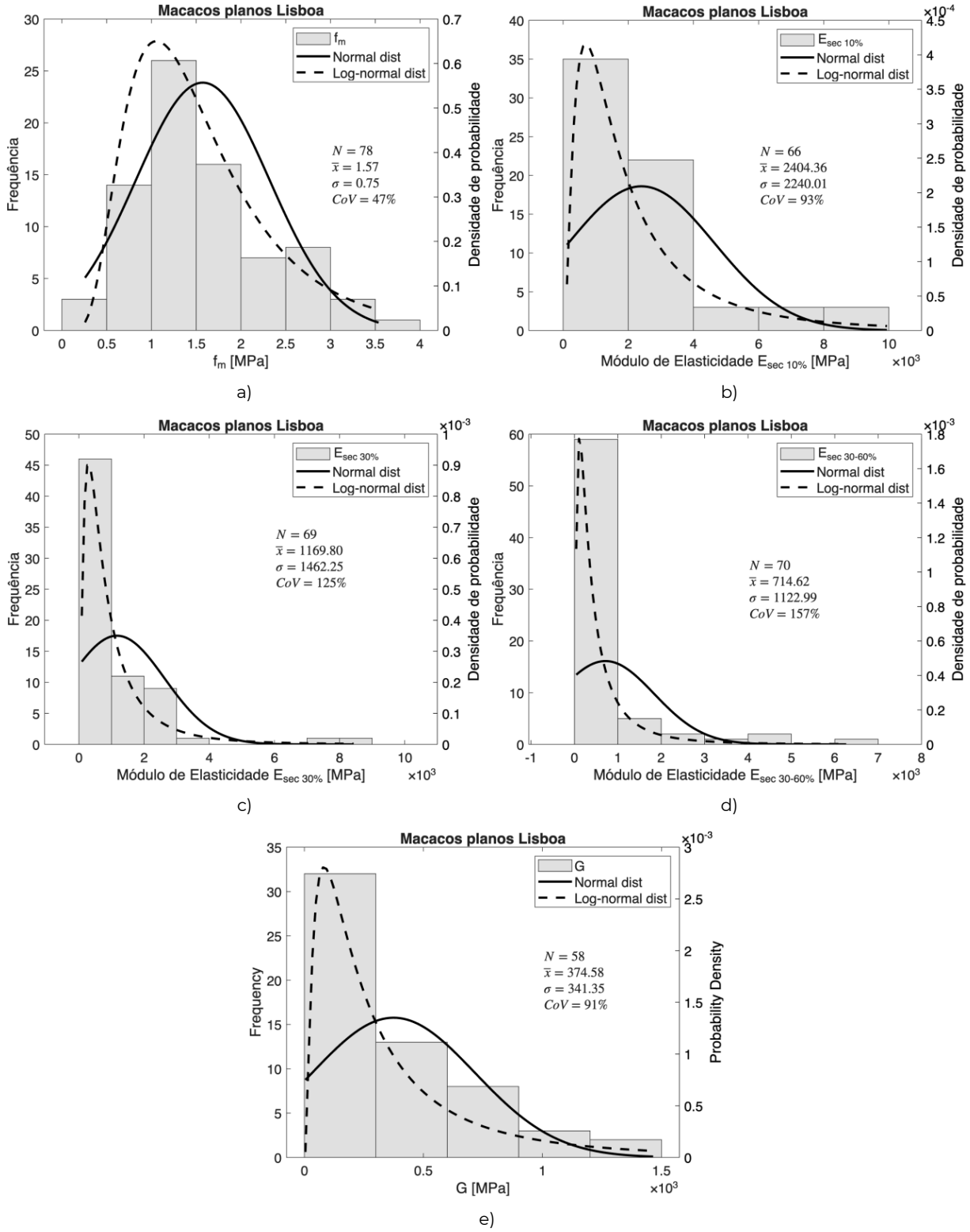


Figura 7 - Histogramas e distribuições de probabilidade de: a) resistência à compressão; b) módulo de elasticidade a 10% da tensão máxima; c) módulo de elasticidade a 30% da tensão máxima; d) módulo de elasticidade entre 30% e 60% da tensão máxima; e e) módulo de distorção.

A Tabela 1 apresenta uma comparação entre os valores médios obtidos através dos ensaios com macacos planos e os valores reportados na literatura para o mesmo tipo de alvenaria considerado neste estudo. Para esta comparação, foram considerados os valores do módulo de elasticidade correspondentes a 10% e 30% da tensão máxima obtidos nos ensaios com macacos planos, tendo em conta a variabilidade ainda existente e o debate em curso relativamente ao valor mais adequado a adotar para o módulo de elasticidade da alvenaria.

Tabela 1 - Comparação das propriedades mecânicas obtidas através dos ensaios com macacos planos no centro histórico de Lisboa com os valores reportados por outros autores.

	f_m **[MPa]**	***E*** **[MPa]**	***G*** **[MPa]**
Macacos planos	1.6	-	375
Macacos planos ($E_{sec10\%}$)	-	2404	-
Macacos planos ($E_{sec30\%}$)	-	1170	-
Candeias et al. 2020	1.1 - 1.9	900	300
Italian Building Code 2019	1.0 - 2.0	690 - 1050	230-350
CEN 2019	1.5	870	290

Os valores obtidos nos ensaios com macacos planos para as propriedades mecânicas da "alvenaria de pedra irregular, com seixos rolados e unidades pétreas erráticas e irregulares" (Candeias et al. 2020; Italian Building Code 2019; Vanin et al. 2017; CEN 2019; Fonseca et al. 2025), presente nos edifícios ensaiados, apresentam resultados médios muito próximos dos reportados por outros autores e dos valores indicados nos regulamentos considerados.

Os valores médios de resistência à compressão obtidos encontram-se dentro dos intervalos propostos na literatura e em documentos normativos. No entanto, os módulos de elasticidade determinados, em particular $E_{\sec 10\%}$, apresentam valores superiores aos valores de referência considerados, evidenciando a importância da caracterização experimental in situ para a definição de parâmetros mecânicos representativos da alvenaria tradicional portuguesa.

5. Conclusões

Os resultados deste estudo evidenciam não apenas a importância da reabilitação dos edifícios antigos em alvenaria, mas também reforçam que as técnicas construtivas tradicionais continuam atuais, constituindo uma abordagem válida e sustentável para a construção contemporânea. A preservação e valorização das estruturas históricas permitem não só salvaguardar o património cultural, mas também reconhecer a relevância contínua destas práticas construtivas. A utilização de materiais naturais, renováveis e recicláveis, como a terra, o adobe, a taipa e o tijolo, reduz a pegada ambiental e promove a sustentabilidade nas novas construções. A integração destas técnicas ancestrais em projetos contemporâneos representa não apenas uma solução eficiente, mas também um compromisso com os princípios ecológicos, contribuindo para um ambiente construído mais resiliente e ambientalmente responsável. Em última análise, a adoção de práticas construtivas tradicionais constitui um contributo relevante para a construção sustentável e para a preservação do planeta para as gerações futuras.

Os resultados obtidos a partir dos 83 ensaios com macacos planos permitiram determinar valores médios de resistência à compressão da ordem de 1,6 MPa, módulos de elasticidade secantes compreendidos entre 1170 MPa e 2404 MPa e módulo de distorção de 375 MPa. De forma geral, estes valores apresentam boa concordância com os intervalos propostos na literatura e em documentos normativos, contribuindo para o estabelecimento de valores de referência para a caracterização da alvenaria tradicional portuguesa.

Por outro lado, o ensaio com macacos planos permite o estudo *in situ* da alvenaria, possibilitando a sua caracterização mecânica sem introduzir danos excessivos nos elementos estruturais. Quando combinado com outras técnicas menos intrusivas, como os ensaios sónicos, os resultados podem ser otimizados, permitindo a determinação das propriedades mecânicas e a calibração de modelos numéricos mais eficientes e representativos das estruturas de alvenaria existentes. Os resultados obtidos nos ensaios evidenciam a importância deste tipo de metodologia na caracterização da alvenaria, demonstrando um excelente desempenho na avaliação do seu comportamento mecânico.

A dispersão observada nas propriedades mecânicas determinadas é consistente com a elevada heterogeneidade característica das alvenarias tradicionais portuguesas. Esta variabilidade pode ser atribuída a diferenças nos materiais constituintes, técnicas construtivas, épocas de construção, estado de conservação e intervenções de reabilitação realizadas ao longo da vida útil dos edifícios. Adicionalmente, a natureza local dos ensaios com macacos planos e a irregularidade geométrica das alvenarias históricas contribuem para a variabilidade observada nos resultados experimentais.

Do ponto de vista prático, os resultados apresentados constituem uma base de referência para a caracterização mecânica de alvenarias tradicionais portuguesas, podendo apoiar engenheiros e técnicos de conservação na avaliação da segurança estrutural de edifícios existentes. Os valores obtidos podem ser utilizados na definição de parâmetros mecânicos para modelos numéricos e em análises de vulnerabilidade sísmica, contribuindo para reduzir a dependência de valores de referência provenientes de regulamentos e estudos realizados noutros países. Adicionalmente, os resultados reforçam a importância da realização de ensaios in situ como suporte aos processos de diagnóstico e à definição de estratégias de reabilitação mais adequadas e fundamentadas.

Agradecimentos

Os autores agradecem o apoio financeiro da Fundação para a Ciência e a Tecnologia, através do projeto UID/6438/2025 da unidade de investigação CERIS.

Jorge Fonseca manifesta o seu agradecimento à Fundação para a Ciência e a Tecnologia (FCT) pelo apoio concedido através da bolsa de doutoramento com a referência 2022.13794.BD, "Influência do nível de conhecimento na avaliação e reforço de edifícios tradicionais de alvenaria de acordo com o Eurocódigo 8", a qual recebeu o DOI https://doi.org/10.54499/2022.13794.BD.

Referências

Candeias, Paulo, António Correia, Alfredo Campos Costa, et al. 2020. «Aspetos gerais da aplicação em Portugal do Eurocódigo 8 – Parte 3 – Anexo C (Informativo) – Edifícios de alvenaria». *rpee | Série III | nº12 |março 2020*.

CEN. 2019. *TC 250/SC8 N855 de 09/10/2010. Eurocode 8: Earthquake resistance design of structures*. Part 3: Assessment and retrofitting of buildings and bridges (WORKING DRAFT). Comite Européen de Normalisation, Bruxelas, Bélgica.

Correia, Mariana R., Paulo B. Lourenco, e Humberto Varum, eds. 2015. *Seismic Retrofitting: Learning from Vernacular Architecture*. CRC Press. https://doi.org/10.1201/b18856.

Fonseca, Jorge, Aníbal Costa, e Hugo Rodrigues. 2025. «Characterization of Portuguese Masonry Walls: Insights from Flat-Jack Tests». *International Journal of Architectural Heritage* 0 (0): 1–34. https://doi.org/10.1080/15583058.2025.2557397.

Italian Building Code. 2019. *Norme tecniche per le costruzioni*.

República, Diário da. 1983. *Decreto-Lei n.º 235/83 -Regulamento de Segurança e Acções para Estruturas de Edifícios e Pontes*. https://diariodarepublica.pt/dr/detalhe/decreto-lei/235-1983-451672.

República, Diário da. 2019. *Decreto-Lei n.º 95/2019 - Regime aplicável à reabilitação de edifícios ou frações autónomas*. Diário da República n.º 136/2019, Série I de 2019-07-18. https://data.dre.pt/eli/dec-lei/95/2019/07/18/p/dre.

Salvalaggio, Matteo, Vasco Bernardo, e Paulo B. Lourenço. 2024. «Exploring Seismic Fragility and Strengthening of Masonry Built Heritage in Lisbon (Portugal) via the Applied Element Method». *Engineering Structures* 320 (dezembro): 118890. https://doi.org/10.1016/j.engstruct.2024.118890.

Vanin, Francesco, Dario Zaganelli, Andrea Penna, e Katrin Beyer. 2017. «Estimates for the Stiffness, Strength and Drift Capacity of Stone Masonry Walls Based on 123 Quasi-Static Cyclic Tests Reported in the Literature». *Bulletin of Earthquake Engineering* 15 (12): 5435–79. https://doi.org/10.1007/s10518-017-0188-5.

XXII International Conference on Building Pathology and Constructions Repair
15th to 17th July 2026 - Lisboa, Portugal

Development of 3D-Printed Conductive Mortar Electrodes for smart bricks

Israel Sousa[1], Antonella D'Alessandro[1,*], Simon Laflamme[2,3], Filippo Ubertini[1]

[1] I Department of Civil and Environmental Engineering, University of Perugia, Via G. Duranti, 93 06125 Perugia (PG) Italy
[2] Department of Civil, Construction, and Environmental Engineering, Iowa State University, Ames, IA, 50010, USA
[3] Department of Electrical and Computer Engineering, Iowa State University, Ames, IA, 50010, USA
Correspondence: antonella.dalessandro@unipg.it

Abstract: Advances in Structural Health Monitoring (SHM) have led to the development of self-sensing composites capable of strain monitoring through piezoresistive behavior. Traditional applications of these smart composites rely on metallic components, such as copper electrodes, to perform electrical measurements. However, integrating metallic elements into cementitious or clay matrices poses architectural and mechanical challenges. This paper introduces a novel approach utilizing a 3D-printed highly conductive cementitious mortar to form embedded electrodes for smart bricks. The fabrication process involved the incorporation of chopped carbon microfibers (CCMF) into the printed cementitious matrix to establish a highly conductive material. Electromechanical cyclic compression tests were conducted to evaluate and compare the performance of the proposed 3D-printed electrodes against conventional copper tape configurations and a combined electrode approach. The results demonstrate an high sensitivity of all the configurations: while the copper tape yielded a higher overall sensitivity compared to the printed electrodes, the standard size smart brick with both 3D-printed electrode and copper tape achieved an intermediate gauge factor of around 215 and the highest linearity among all configurations, reaching a coefficient of determination of 0.84. This approach demonstrates the feasibility of utilizing highly conductive 3D-printed cement mortar as effective electrodes, providing enhanced linearity in smart brick elements.

Keywords: 3D-printed concrete, smart bricks, electrodes, conductive cement mortar, additive manufacturing.

1. Introduction

Damage assessment is a fundamental objective of Structural Health Monitoring (SHM) (Puncello and Caprili, 2023; Rossi and Bournas, 2023), particularly for mitigating the impact of severe hazards such as earthquakes (H. Zhang *et al.*, 2024). Masonry structures are highly vulnerable to seismic events due to their non-homogeneous composition and brittle failure mechanisms (Formisano *et al.*, 2018; Nazimi *et al.*, 2024). Consequently, continuous and systematic monitoring is essential for early damage detection in these structures (Soleymani, Jahangir and Nehdi, 2023). Although well established, traditional SHM systems typically rely on discrete, surface-attached sensors, which can be expensive when deployed in large numbers and may provide only indirect information about the internal condition of structural elements (Laflamme *et al.*, 2023).

To address these limitations, self-sensing construction materials have emerged as a promising alternative for SHM, as they integrate both structural and sensing functions within the constructed element (Wang *et al.*, 2024). These composites can be lime-based (Drougkas *et al.*, 2023), cement-based (J. Zhang *et al.*, 2024; Wang *et al.*, 2024), clay-based (Meoni, Triana Camacho and Ubertini, 2026), among others, and are typically fabricated by incorporating conductive fillers, such as carbon fibers, carbon nanotubes, graphite, or steel fibers into the matrix [(Frąc and Pichór, 2020; Ding *et al.*, 2023; Hao *et al.*, 2023; Li *et al.*, 2023; Rama *et al.*, 2024). The sensing capability of these materials relies on their piezoresistive behavior, which is enhanced near the electrical percolation threshold (D'Alessandro *et al.*, 2016). In contrast, for overpercolated systems, this piezoresistive sensitivity reduces and is replaced by high electrical conductivity, driven by the formation of a dense, continuous network of conductive pathways within the matrix (Laflamme *et al.*, 2023).

Within the framework described above, smart bricks function as masonry-compatible sensing units designed to replicate conventional clay bricks (Meoni, D'Alessandro and Ubertini, 2020). These advanced units possess enhanced piezoresistive capabilities that allow strain characterization through changes in their electrical properties. As embedded sensors, they offer improved structural integration compared to externally attached sensing systems. Typically, copper plates or tapes are utilized as electrodes for electrical measurements (Meoni, D'Alessandro and Ubertini, 2020; Meoni, Triana Camacho and Ubertini, 2026). However, their installation presents distinct technical and architectonic challenges. For instance, Meoni et al. (Meoni *et al.*, 2023) reported unexpected mechanical behavior during testing, which they attributed to mechanical weaknesses developing at the contact interfaces between the mortar layers and the insulating tape used to secure the copper plates.

To overcome these limitations, additive manufacturing technologies, such as 3D concrete printing (3DCP), have emerged as a promising alternative, with advantages in terms of standardization and scalability (Liu *et al.*, 2025; Zhang *et al.*, 2025). Consequently, extruding a highly conductive cementitious mortar directly above the smart brick presents a potential solution for achieving structurally compatible electrode integration, with a good mechanical interface resulting in sensing systems suitable for an easier application in masonry. This paper introduces this novel approach utilizing 3D-printed conductive mortar as an embedded electrode. The study evaluates the electromechanical performance under cyclic compressive loading, comparing the sensitivity and linearity against conventional copper tape configurations and a combination between both types of electrodes in smart bricks.

2. Background

2.1 Smart bricks

Two types of samples were fabricated for this study: a small-sized smart brick with nominal dimensions of 70 × 50 × 50 mm^3, and a standard size smart brick measuring 260 × 120 × 55 mm^3. The composite material was prepared by manually mixing fresh clay with R.STAT/S conductive stainless-steel microfibers at a concentration of 0.25% by mass of the clay. To ensure uniform fiber dispersion, the procedure involved repeatedly flattening the clay matrix, adding the steel microfibers, and folding the mixture ten times. The samples were then cast into wooden molds, pre-sprinkled with sand to prevent clay adhesion, and subsequently demolded. After an initial resting period of 24 h, the bricks underwent a two-stage thermal treatment: a drying phase (2.5 h at 50 °C, followed by 6.5 h at 90 °C) and a subsequent firing phase at 900 °C for 6 h. For the electromechanical characterization, copper tape electrodes were applied to opposite faces of the bricks, and copper wires were soldered to ensure reliable metallic contact. Figure 1 illustrates the small smart brick with copper tape electrodes.

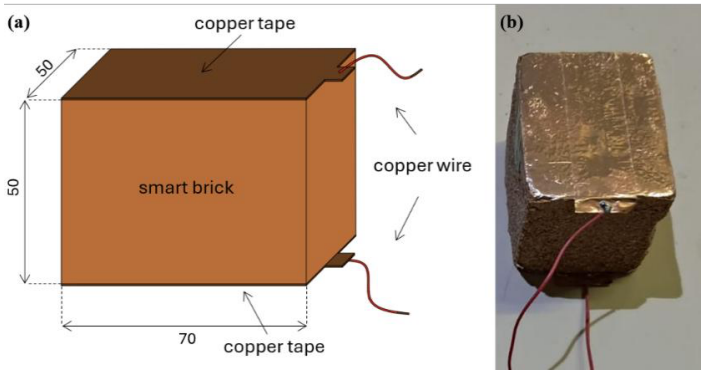


Figure 1 – Schematic representation of the small smart bricks with (a) copper tape electrodes; (b) sample with copper tape electrodes. Units in mm.

2.2 Printed electrodes

A highly conductive cement-based mortar was developed for 3D printing applications. The mix consisted of Portland cement CEM II/B-M (P-LL) 42.5R, siliceous river sand (maximum particle size of 1 mm), and tap water. To induce electrical conductivity, chopped carbon microfibers (CCMF), supplied by SIGRAFIL®, were incorporated at a dosage of 0.4% by mass of cement. To improve printability, based on previous studies, the sand-to-cement and water-to-cement ratios were fixed at 1:1 and 0.55, respectively. Sample fabrication was performed using a WASP 40100 LDM 3D printer equipped with a manually fed extruder. The mixture was designed to ensure that the electrical resistance of the hardened printed electrode remained below 1.0 kΩ. Properties of the utilized CCMF are presented in Table 1.

Table 1 – Properties of chopped carbon-microfibers.

Typical properties	**C C6-4.0/240-G100**
Density	1.80 g/cm³
Mean fiber length milled	6 mm
Filament diameter	7 μm
Tensile strength	4.0 GPa
Tensile modulus	240 GPa
Elongation at break	1.70%
Single filament resistivity	15 μΩm
Bulk density	-
Sizing type	glycerin
Sizing mass content	4.0 %
Compatible with	water-based systems

The mixing procedure started with the manual dry mixing of all solid materials: cement, sand, and CCMF. Subsequently, water was introduced in two distinct stages: initially, 60% of the total volume was added, followed by the remaining 40%. After achieving a homogeneous consistency, the mixture was transferred into the continuous manual-feeding extruder, as illustrated in Figure 2. The printing process involved the extrusion of the fresh conductive mortar at a printing speed of 25 mm/s and an extrusion rate of 864 mm³/s, maintaining a standoff distance of approximately 4 mm. The layers were deposited using an 8 mm nozzle, producing a layer thickness and width of approximately 6 mm. At this stage, the copper tape was removed to enable the printing of the cementitious material in the same region. Prior to printing, the sample was immersed in water to enhance the adhesion between the mortar and the brick surface.

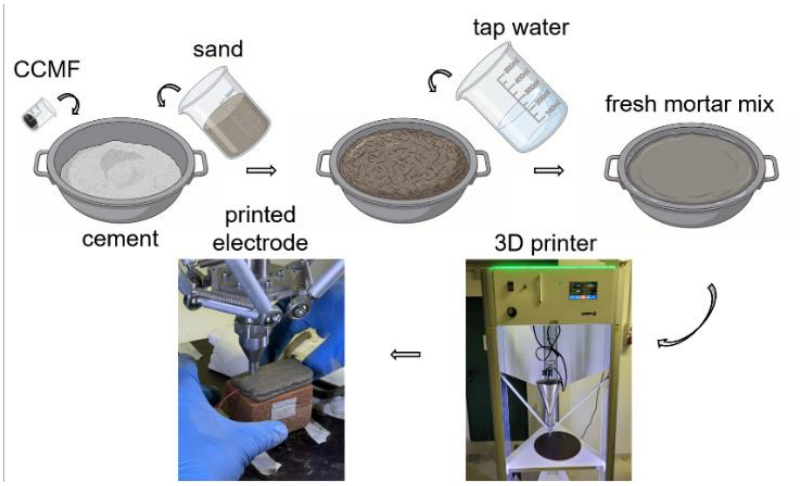


Figure 2 – Fabrication process of the conductive cement-based mortar

Figure 3(a) displays the scheme of the sample with printed electrodes, where copper wires were embedded between the mortar layers during the printing process to establish a reliable electrical connection with the internal conductive networks. Figure 3(b) presents the actual printed electrodes on the fabricated sample. Figure 4(a) illustrates the schematic representation of the standard size smart brick. The different surface configuration is displayed in Figure 4(b), which shows the copper tape electrodes, and Figure 4(c), which presents the printed electrode layers on the smart brick surface.

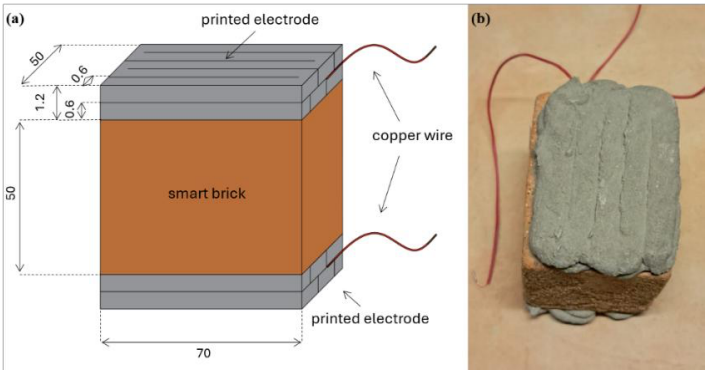


Figure 3 – Schematic representation of the small smart bricks with (a) printed electrodes. (b) Photo evidence of a smart brick sample with printed electrodes. Units in mm.

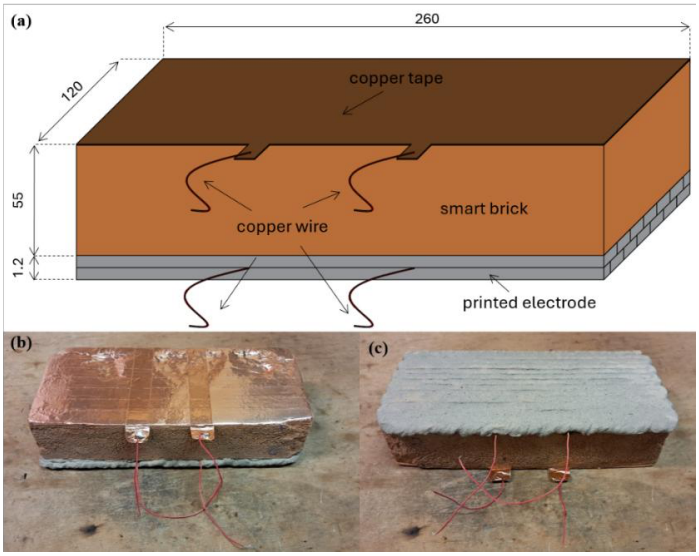


Figure 4 – (a) Representation of the regular size smart bricks sample; (b) view of the top region of the smart brick, with copper tape electrodes; and (c) view of the bottom region of the smart brick, with printed electrodes. Units in mm.

3. Instruments and tests

Electrical measurements were conducted using an NI PXIe-1071 DAQ system equipped with an NI PXIe-4313 module utilizing two channels. A RIGOL DG-1022 function generator supplied a ±10 V square wave input at a frequency of 1 Hz (Downey *et al.*, 2017). A shunt resistor was connected in series with the samples, and the voltage drops across both the resistor and the sample were recorded. The electrical current (i) was calculated using Ohm's law (Equation 1), enabling the estimation of the sample's electrical resistance (R). For the small sample, two-electrode measurements were performed. In contrast, a four-electrode configuration was deployed for the standard size brick due to its geometric scale.

$$R = \frac{V(t)}{i} \tag{1}$$

where, R is the resistance of the sample, i is the current, and $V(t)$ is the voltage.

Electromechanical tests were conducted on two samples to evaluate the piezoresistive performance of the material: (i) a small smart brick, which was tested first with copper tape and subsequently with 3D-printed electrodes; and (ii) a standard size brick, which featured a combined configuration of both printed and copper tape electrodes. Uniaxial cyclic compression tests were performed using an Instron 68TM-50 Universal Testing Machine under load control at a rate of 200 N/s. The experimental setup is presented in Figure 5.

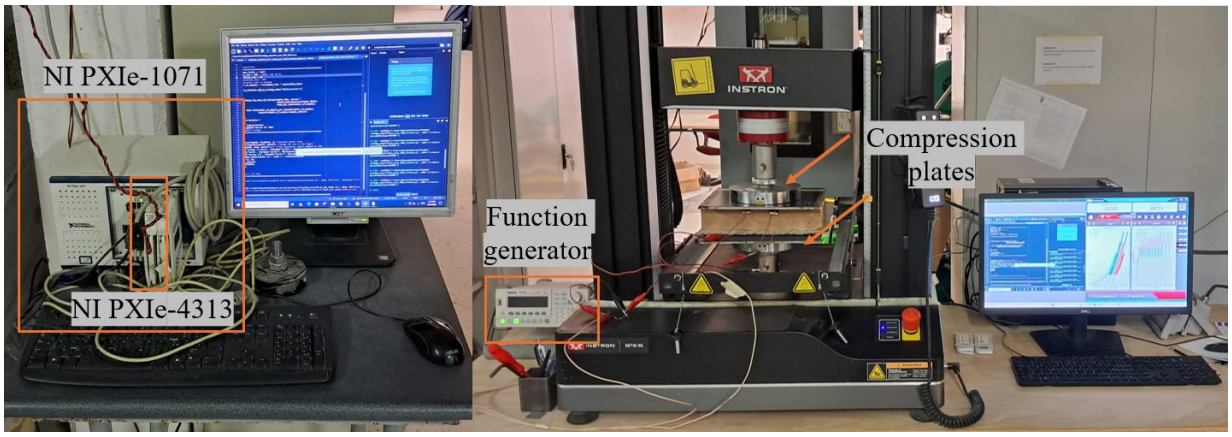


Figure 5 – Test setup for the electromechanical test.

The test initiated with a preliminary 1 kN step ramp followed by a 10-second constant load period as a pre-load phase. Subsequently, the cyclic loading protocol was applied, consisting of 12 cycles divided into three stages of 4 cycles each, with peak loads of 3 kN, 4 kN, and 5 kN, respectively. To ensure uniform load distribution on the standard size brick, an additional metallic platen was placed, which was not required for the small samples. Electrical insulation between the samples and the machine platens was achieved by applying a Kapton layer. Finally, fractional change in resistance (*FCR*) was estimated using Equation 2, following the loading profile illustrated in Figure 6, while the Instron machine displacement data were utilized to determine the axial strain (ε) through Equation 3.

$$FCR = \frac{R - R_0}{R_0} \tag{2}$$

where R_0 is the initial measured resistance, with

$$\varepsilon = \frac{L - L_0}{L_0} \tag{3}$$

where, L is the deformed length of the sample, and L_0 is the initial measured length.

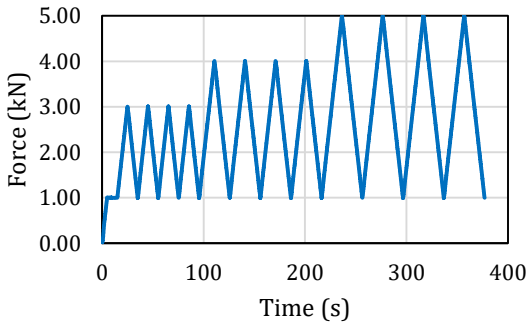


Figure 6 – Applied loading method

The gauge factor (λ), which quantifies the sensitivity of the material, was defined by the relationship between the *FCR* and axial strain, as expressed in Equation 4. To mitigate experimental noise, the gauge factor was determined as the slope of the linear regression computed using the data from the final four loading cycles.

$$\lambda = \frac{FCR}{\varepsilon} \tag{4}$$

4. Results and discussion

Electromechanical testing was first performed on the small brick samples equipped with copper tape electrodes. Figure 7(a) illustrates the applied cyclic load alongside the time-domain correlation between the axial strain and the FCR, plotted starting from the 15th second from the initiation of the test. The FCR trend inversely mirrors the strain profile, indicating that an increase in compressive strain induces a reduction in FCR. This behavior is attributed to the reduction in distance between conductive fibers and the consequently enhanced formation of conductive networks within the smart brick matrix. Within this stabilized region, the magnitude of the FCR changes proportionally with the applied strain. At the maximum peak load of 5 kN, the sample reached a maximum strain of approximately 0.00065 mm/mm, corresponding to a maximum *FCR* drop of around -58%. Figure 7(b) displays the direct correlation between FCR and strain during the final four loading cycles at 5 kN. The linear regression yields a λ of 522.61 and a coefficient of determination (R^2) of 0.72.

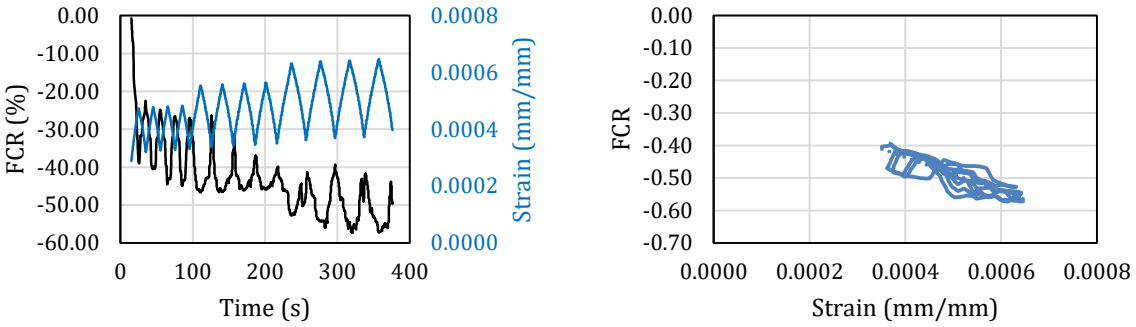


Figure 7 – Electromechanical response of small brick sample dopes with 0.25% with copper tape electrodes: (a) variation of FCR and strain in the time domain; (b) relationship between FCR and strain.

Figure 8(a) presents the time-domain correlation between FCR and axial strain for the small smart brick incorporated with 0.25% steel microfibers and utilizing printed electrodes. As initially expected, the measured strain was slightly higher than that of the reference brick with copper tape electrodes, reflecting an alteration in the overall system stiffness due to the deformability of the new interface configuration. Additionally, a lower FCR magnitude was observed compared to the sample with copper tape, indicating a reduced electrical output. This however came a much better time stability and improved sensing linearity compared to copper tape electrodes. Figure 8(b) displays the FCR and strain relationship during the final four cycles, the linear regression yields a λ of 68.33 and a R^2 of 0.81.

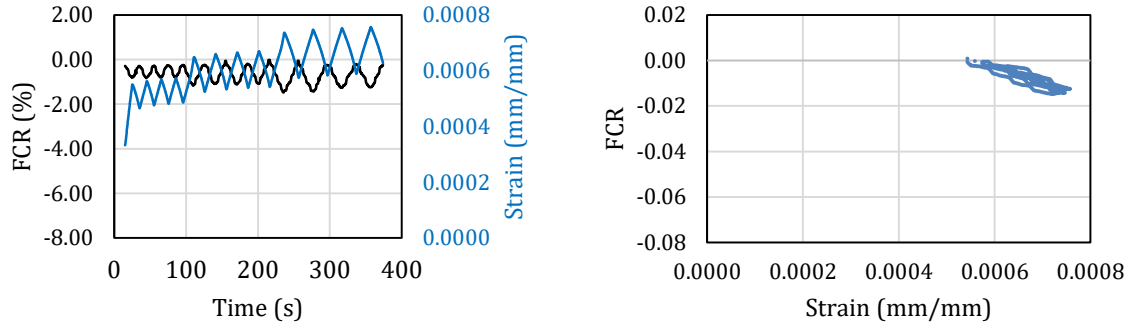


Figure 8 – Electromechanical response of small brick sample doped with 0.25% steel fibers with 3D printed cementitious electrodes: (a) variation of FCR and strain in the time domain; (b) relationship between FCR and strain.

Figure 9(a) presents the time-domain variation of the FCR and axial strain for the standard size brick instrumented with both printed and copper tape electrodes on its surfaces. The electromechanical characterization revealed a maximum peak strain of approximately 0.0004 mm/mm, corresponding to a maximum FCR drop of around -6%. Figure 9(b) illustrates the direct correlation between the FCR and axial

strain during the four final loading stages. The linear regression analysis demonstrates a strong correlation, yielding a gauge factor (λ) of 214.77 and a R^2 of 0.85.

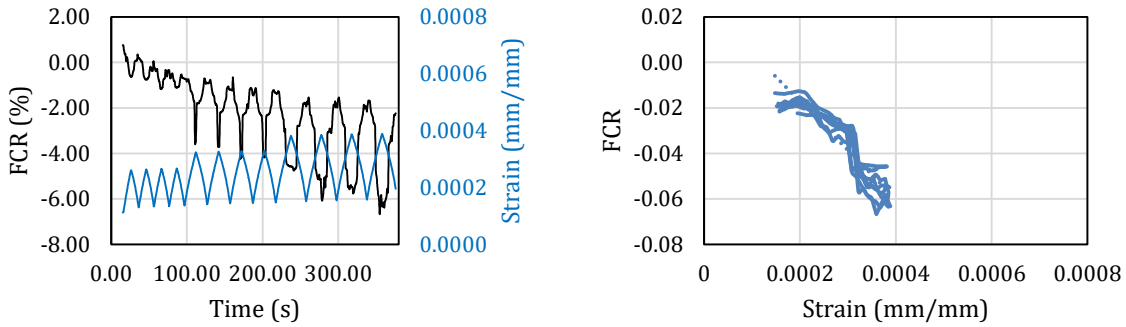


Figure 9 – Electromechanical response of the standard size smart brick sample doped with 0.25% steel fibers and using both 3D printed and copper tape electrodes: (a) variation of FCR and strain in the time domain; (b) relationship between FCR and strain.

The results from the electromechanical tests are summarized in Table 2. For the small smart brick sample, the configuration with copper tape electrodes exhibited a gauge factor 7.6 times higher than the one with printed electrodes, while presenting an 11% lower R^2. On the other hand, the standard size smart brick achieved a gauge factor of 214.77, which is 3.1 times higher than the small brick with printed electrodes but 2.4 times lower than the one with copper tape. Despite this intermediate sensitivity, this larger sample demonstrated the highest linearity among all configurations, with an R^2 of 0.84, representing a 3.7 % increase compared to the small brick utilizing printed electrodes.

Table 2 – Summary of the electromechanical responses for the tested smart bricks (where SSB is small smart brick and StSB represents standard-sized smart brick)

Sample	Type of electrode	λ	R^2
SSB	CT	522.61	0.72
	PE	68.33	0.81
StSB	PE + CT	214.77	0.84

5. Conclusions

This study presented a novel approach for integrating embedded 3D-printed cementitious mortar electrodes into smart bricks. This was achieved by formulating a highly conductive mortar matrix through the incorporation of CCMF. Electromechanical characterizations were performed on small and standard size smart bricks to compare traditional copper tape, the proposed 3D-printed electrodes, and a combination of both.

Electromechanical tests were conducted to evaluate the sensitivity of the smart brick and the performance of the 3D-printed electrodes. For the comparative analysis, the results highlighted a clear trade-off between peak sensitivity and signal reliability. Although the copper tape configuration yielded a higher overall sensitivity, the small-sized smart bricks equipped with 3D-printed electrodes achieved a higher linearity (R^2 = 0.81) and an improved time stability (reduced drift) in comparison to the copper tape. An intermediate gauge factor λ of 214.77 was observed for the standard size sample with copper tape on one face and a printed electrode on the opposite face, while delivering the highest linearity among all tested setups (R^2 =

0.84). Overall, these findings demonstrate that 3D-printed conductive mortar is a viable and structurally cohesive alternative to metallic electrodes, ensuring reliable measurements in smart bricks.

Acknowledgments

The authors would like to gratefully acknowledge the support of the Italian Ministry of University and Research (MUR) via the FIS2021 Advanced Grant "SMS-SAFEST - Smart Masonry enabling SAFEty-assessing STructures after earthquakes" (FIS00001797) on the topic of self-sensing cementitious composites, as well as the European Union - NextGenerationEU under the Italian Ministry of University and Research (MUR) National Innovation Ecosystem grant ECS00000041 – VITALITY, on the topic of 3D concrete printing.

References

D'Alessandro, A. *et al.* (2016) "Investigations on scalable fabrication procedures for self-sensing carbon nanotube cement-matrix composites for SHM applications," *Cement and Concrete Composites*, 65, pp. 200–213. Available at: https://doi.org/10.1016/j.cemconcomp.2015.11.001.

Ding, S. *et al.* (2023) "Self-Sensing Cementitious Composites with Hierarchical Carbon Fiber-Carbon Nanotube Composite Fillers for Crack Development Monitoring of a Maglev Girder," *Small*, 19(9). Available at: https://doi.org/10.1002/smll.202206258.

Downey, A. *et al.* (2017) "Biphasic DC measurement approach for enhanced measurement stability and multi-channel sampling of self-sensing multi-functional structural materials doped with carbon-based additives," *Smart Materials and Structures*, 26(6). Available at: https://doi.org/10.1088/1361-665X/aa6b66.

Drougkas, A. *et al.* (2023) "Design of a smart lime mortar with conductive micro and nano fillers for structural health monitoring," *Construction and Building Materials*, 367, p. 130024. Available at: https://doi.org/10.1016/j.conbuildmat.2022.130024.

Formisano, A. *et al.* (2018) "Seismic vulnerability of Italian masonry churches: The case of the Nativity of Blessed Virgin Mary in Stellata of Bondeno," *Journal of Building Engineering*, 20, pp. 179–200. Available at: https://doi.org/10.1016/j.jobe.2018.07.017.

Frąc, M. and Pichór, W. (2020) "Piezoresistive properties of cement composites with expanded graphite," *Composites Communications*, 19, pp. 99–102. Available at: https://doi.org/10.1016/j.coco.2020.03.005.

Hao, Y. *et al.* (2023) "Recent Advances in Properties and Applications of Carbon Fiber-Reinforced Smart Cement-Based Composites," *Materials*. MDPI. Available at: https://doi.org/10.3390/ma16072552.

Laflamme, S. *et al.* (2023) "Roadmap on measurement technologies for next generation structural health monitoring systems," *Measurement Science and Technology*, 34(9). Available at: https://doi.org/10.1088/1361-6501/acd135.

Li, L. *et al.* (2023) "Carbon nanotube (CNT) reinforced cementitious composites for structural self-sensing purpose: A review," *Construction and Building Materials*. Elsevier Ltd. Available at: https://doi.org/10.1016/j.conbuildmat.2023.131384.

Liu, H. *et al.* (2025) "Embedment of 3D Printed Self-Sensing Composites for Smart Cementitious Components," *Sensors*, 25(19), p. 6005. Available at: https://doi.org/10.3390/s25196005.

Meoni, A. *et al.* (2023) "Strain Monitoring and Crack Detection in Masonry Walls under In-Plane Shear Loading Using Smart Bricks: First Results from Experimental Tests and Numerical Simulations," *Sensors*, 23(4), p. 2211. Available at: https://doi.org/10.3390/s23042211.

Meoni, A., D'Alessandro, A. and Ubertini, F. (2020) "Characterization of the strain-sensing behavior of smart bricks: A new theoretical model and its application for monitoring of masonry structural elements," *Construction and Building Materials*, 250, p. 118907. Available at: https://doi.org/10.1016/j.conbuildmat.2020.118907.

Meoni, A., Triana Camacho, D.A. and Ubertini, F. (2026) “A novel carbon-based smart brick formulation for advanced structural health monitoring of masonry structures,” in C.T. Ng, D. Ozevin, and F. Ubertini (eds.) *Sensors and Smart Structures Technologies for Civil, Mechanical, and Aerospace Systems 2026*. SPIE, p. 19. Available at: https://doi.org/10.1117/12.3090632.

Nazimi, K. *et al.* (2024) “Proposal of Empirical Equations for Masonry Compressive Strength: Considering the Compressive Strength Difference between Bricks and Mortar,” *Buildings*, 14(4), p. 1138. Available at: https://doi.org/10.3390/buildings14041138.

Puncello, I. and Caprili, S. (2023) “Seismic Assessment of Historical Masonry Buildings at Different Scale Levels: A Review,” *Applied Sciences*, 13(3), p. 1941. Available at: https://doi.org/10.3390/app13031941.

Rama, M. *et al.* (2024) “Behavioral assessment of intrinsically formed smart concrete using steel fibre and carbon black composite,” *Heliyon*, 10(5). Available at: https://doi.org/10.1016/j.heliyon.2024.e26948.

Rossi, M. and Bournas, D. (2023) “Structural Health Monitoring and Management of Cultural Heritage Structures: A State-of-the-Art Review,” *Applied Sciences*, 13(11), p. 6450. Available at: https://doi.org/10.3390/app13116450.

Soleymani, A., Jahangir, H. and Nehdi, M.L. (2023) “Damage detection and monitoring in heritage masonry structures: Systematic review,” *Construction and Building Materials*, 397, p. 132402. Available at: https://doi.org/10.1016/j.conbuildmat.2023.132402.

Wang, Y. *et al.* (2024) “Advances in self-sensing cement-based composites containing nano materials for smart civil infrastructures,” *Measurement*, 230, p. 114514. Available at: https://doi.org/10.1016/j.measurement.2024.114514.

Zhang, H. *et al.* (2024) “Post-earthquake structural damage assessment and damage state evaluation for RC structures with experimental validation,” *Engineering Structures*, 304, p. 117591. Available at: https://doi.org/10.1016/j.engstruct.2024.117591.

Zhang, J. *et al.* (2024) “Piezoresistivity and piezopermittivity of cement-based sensors under quasi-static stress and changing moisture,” *Construction and Building Materials*, 425. Available at: https://doi.org/10.1016/j.conbuildmat.2024.136052.

Zhang, Yuying *et al.* (2025) “3D printing technology in concrete construction,” *Nature Reviews Clean Technology*, 1(4), pp. 288–303. Available at: https://doi.org/10.1038/s44359-025-00047-z.



NATURAL HAZARDS



XXII International Conference on Building Pathology and Constructions Repair
15th to 17th July 2026 - Lisboa, Portugal

The use of aerial surveying for land regularization purposes and the right to the city: the case of Dorothy Stang in the Federal District

Valmor Cerqueira PAZOS1, Marta Adriana Bustos ROMERO2, Liza Maria Souza de ANDRADE3, Lenildo Santos da SILVA4, João da Costa PANTOJA5, Juliette Anna Fanny LENOIR6, Vânia Raquel Teles LOUREIRO7 Mafalda Fabiene Ferreira PANTOJA[8]

[1] University of Brasilia, Brasilia-DF, Brazil, pazos@unb.br
[2] University of Brasilia, Brasília-DF, Brazil, romero@unb.br
[3] University of Brasilia, Brasília-DF, Brazil, liza@unb.br
[4] University of Brasilia, Brasilia-DF, Brazil, lenildo@unb.br
[5] University of Brasilia, Brasilia-DF, Brazil, joaopantoja@unb.br
[6] University of Brasilia, Brasilia-DF, Brazil, juliette.lenoir@aluno.unb.br
[7] University of Brasilia, Brasília-DF, Brazil, vanialoureiro@unb.br
[8] Brazilian Institute of Teaching, Development and Research, Brasília-DF, Brazil, mafalda.pantoja@idp.edu.br

Abstract: This article analyzes the use of aerial surveying as a technical instrument articulated with participatory practices in the process of land regularization and in the affirmation of the right to the city in the Dorothy Stang Occupation, in the Federal District. The research associates aerial photogrammetry procedures conducted in accordance with ABNT NBR 17047:2022 with critical university extension actions, which involved the local community in the processes of reading, validating and interpreting territorial data. The surveying was carried out from fifty-nine control points, registered with the Brazilian Institute of Geography and Statistics (IBGE) and obtained through GNSS RTK, enabling the generation of orthomosaics and digital terrain and surface models with a level of precision compatible with the technical requirements of the formal land regularization processes. The analysis of the results shows that the articulation between technical methods and the knowledge produced by the residents expanded the understanding of the socio-spatial dynamics of the settlement, gave greater visibility to the territorial demands and strengthened the technical bases for dialogue with the public authorities. It is observed that the use of aerial surveying, when associated with inclusive and participatory methodologies, contributes to the reduction of information asymmetries and to the strengthening of collective processes of urban rights claims. It is concluded that this approach expands the reach of aerial surveying beyond its strictly instrumental function, consolidating it as a technical and methodological support for the formulation of urban policies guided by criteria of social justice and territorial recognition.

Keywords**:** Favelas and urban communities; Technical advice; Critical university extension; Solidarity technoscience; Social cartography.

1. Introduction

Urban land regularization in Brazil occurs in a context marked by historical inequalities, territorial disputes, and recurrent processes of invisibility of peripheral populations. In informal territories, such as the Dorothy Stang Occupation, located in the region of Sobradinho in the Federal District, the legal recognition of housing is intertwined with the struggle for dignity, permanence, and active citizenship. Such territories express, in an emblematic way, what Andrade and colleagues call the "struggle against socio-environmental injustice in the search for the right to the city" (Andrade *et al*., 2019, p. 207). In this scenario, aerial surveying emerges not only as a technical tool, but as a strategic instrument for the production of socially oriented

knowledge. The incorporation of drones, GNSS RTK receivers and advanced photogrammetry techniques allows for the expansion of community access to spatial information and the strengthening of processes of solidarity technoscience.

In the case of Dorothy Stang, the aerial photogrammetric surveying followed the guidelines of ABNT NBR 17047:2022, which defines the procedures for cadastral surveys for public registration. The implementation of fifty-nine control points with RTK receivers ensured an average accuracy of eight millimeters, meeting the accuracy parameters established by the standard and enabling their future use in administrative regularization processes.

In addition to the technical dimension, aerial surveying is articulated with participatory practices inspired by critical university extension. Andrade and Loureiro (2020) highlight that the role of the citizen university involves bringing together technical knowledge and popular knowledge, forming socio-technical networks that sustain processes of resistance and emancipation. In the same perspective, Periférico, Sociotechnical Advisory Laboratory has been working in informal occupations and settlements in the Federal District to produce shared diagnoses, strengthen community organizations, and develop mapping methodologies sensitive to the realities experienced by residents (Andrade *et al*., 2022). Thus, this article discusses how the application of aerial surveying, articulated with participatory socio-technical processes and based on technical reference standards, contributes to strengthening the right to the city in the Dorothy Stang Occupation.

2. Historical and territorial contextualization of the Dorothy Stang Occupation

The Dorothy Stang Occupation is located in the administrative region of Sobradinho, in the Federal District, Brazil (Figure 1), in an area marked by strong real estate pressure, land disputes, and discontinuity of housing policies. Its territorial conformation is the result of simultaneous processes of social vulnerability and community resistance, expressing dynamics common to the Brazilian urban peripheries (Caldeira, 2000; Maricato, 2011; Rolnik; Klink, 2011). The occupation was named Dorothy Stang in honor of the missionary murdered in 2005, whose trajectory became a symbol of the struggle for socio-environmental justice, dialoguing with the very history of resistance built by the residents of the settlement.

Figure 1 – Location of the Dorothy Stang Occupation, Sobradinho, Federal District



The territorial expansion of the occupation occurred in 2015 by 544 low-income families initially linked to the National Front of Struggle (Costa, 2017), who sought decent housing conditions amid the absence of effective housing policies in the Federal District. As in other informal settlements in the region, its formation is directly linked to inequalities in access to urban land, real estate speculation and the fragmentation of territorial planning policies (Bringel; Domingues, 2011; Paviani, 2010). The absence of basic infrastructure, adequate public services and legal recognition of the subdivision intensified conflicts with inspection agencies and intensified conditions of socio-spatial precariousness.

In this scenario, the occupation was also consolidated as a space for social mobilization, in which community associations, local collectives and support networks acted in the claim of fundamental rights, including access to housing, land regularization and the implementation of public facilities. This process is in line with analyses of social housing movements in Brazil, which highlight the centrality of popular organization for the achievement of urban rights (Gohn, 2017). The territoriality constructed by the residents articulates material dimensions such as self-construction, opening of roads and conformation of collective spaces and symbolic dimensions, which include bonds of solidarity, narratives of belonging and practices of daily resistance (Caldeira, 2000; Paviani, 2010). Dorothy Stang stands out for the organization in sectors or blocks with local representatives, giving its residents a strong identity that remains to this day in the addresses of the houses.

The inclusion of the occupation in the debate on the Regularization of Social Interest (Reurb-S) in the Federal District reinforces the relevance of socio-technical approaches capable of articulating technical knowledge and community practices. Bearing in mind that the accelerated and disorderly urbanization that has characterized the process of occupation of the territory of the Federal District is synonymous with the environmental degradation of the Cerrado biome, Romero *et al*., (2019), the disputes around the characterization of the area, the limits of the subdivision and the identification of lots and buildings demonstrate the need for high-precision technical instruments, but they also show that regularization processes depend on social legitimacy and the participation of residents. The literature on land policies points out that the security of tenure and the production of well-located housing require joint actions between the State, the community, and civil society (Rolnik; Klink, 2011).

Thus, understanding the origin, context and territorial dynamics of the Dorothy Stang Occupation is fundamental to situate the role of aerial surveying as a sociopolitical instrument in the search for the right to the city. In this territory, the technique does not act in isolation: it interacts with practices of resistance, produces narratives and becomes a strategic element for the recognition and permanence of families in the place they have built.

3. Theoretical foundation

The right to the city, as discussed by Harvey (2003) and Rolnik (2015), transcends physical access to urban territory, translating into the effective ability to participate in decisions that shape the production of space. It is a political, collective and procedural right, permanently stressed, in the Brazilian case, by real estate speculation, by the retraction of the regulatory role of the State and by the advance of neoliberal rationalities that weaken legal instruments aimed at territorial protection and urban justice (Jatobá, 2016). In view of this scenario, critical university extension asserts itself as a transformative practice, capable of repositioning the university as an active agent in the dispute for rights. Andrade and Loureiro (2020) argue that the citizen university should contribute to the political organization of social groups, creating emancipatory conditions for intervention in reality" (Andrade; Loureiro, 2020, p. 293), bringing together scientific production, community action, and decision-making processes.

This perspective converges with the approach of the Law Found on the Street, formulated by Roberto Lyra Filho, according to which the law originates in social practices, in concrete struggles and in the collective action of historically oppressed subjects. In this sense, the right to the city is not only declared; it is built in

the territory, in conflicts and mobilizations that demand recognition and permanence. Similarly, Romero *et al*. (2019) state that pronounced environmental problems require complementary design strategies, in order to minimize certain conflicting features.

The experiences of the Peripheral Laboratory materialize this articulation between technical knowledge and emancipatory praxis. As argued by Andrade *et al*. (2019), working in informal territories requires conflict mediation, strengthening community autonomy, and "reconciling knowledge as the foundation of the territorial transformation process" (p. 192). In the case of the Dorothy Stang Occupation, the authors highlight that socio-technical advice, which began in 2016, played a central role in the preparation of urban proposals later incorporated into Complementary Bill No. 986, of June 30, 2021, which defined the Social Interest Regularization Area, ARIS Dorothy Stang, showing how technical production, when constructed in a participatory way, it directly influences institutional agendas (Figure 2). The advisory also contributed to the community being one of the pilot territories of the public policies of the National Secretariat of Peripheries of the Ministry of Cities with the Periferia Viva Program in 2024 and 2025 and with the Land Regularization Program in 2026 (Figure 3).

Figure 2 – Ceremony of inclusion of Dorothy Stang in the Master Plan of the Federal District



Figure 3 – Periodic participatory technical advisory workshops since 2016



Social and environmental issues are inseparable and are presented as a basic and essential concept for sustainable urban development. The pressure of urban occupation and the increasing impermeabilization of the soil compromise the surroundings, especially the vegetation, lead to the extinction of riparian forests and recharge areas, the contamination of the water table and the reduction of biodiversity in the Cerrado, Romero *et al*. (2019). Pronounced environmental problems require complementary design strategies in order to minimize certain conflicting features.

This theoretical set shows that technologies such as drones, GPS RTK receivers and orthomosaics are not neutral tools. Its emancipatory or excluding potential depends on the political, methodological and community orientation that guides its use. The aerial survey can, therefore, both reproduce inequalities when appropriated in a vertical and technocratic way and subvert them when mobilized in participatory processes that expand territorial visibility, strengthen local autonomy and sustain claims for rights.

4. Methodology of cadastral planialtimetric survey with drone and photogrammetric processing

4.1 Background and objective

The methodology adopted was structured to carry out a planialtimetric cadastral survey in the Dorothy Stang Settlement, located in the Administrative Region of Sobradinho (RA V), Brasília-DF. The main objective was to generate high-resolution cartographic products to support the technical registration of buildings, the road system, infrastructure and land limits in the area. The method integrated aerial survey technologies with remotely piloted aircraft (RPAs), high-precision GNSS tracking and digital photogrammetric processing, ensuring geometric accuracy compatible with urban surveys of a cadastral nature.

4.2 General structure of the methodology

The methodology was organized in three main stages: field survey, geodetic processing of the support points and photogrammetric processing for the generation of cartographic products. These steps were designed in an integrated way, in order to ensure strict geometric control, traceability of the data collected and minimization of operational errors. The articulation between field and office allowed the raw data captured to be converted into structured and technically validated cartographic information.

4.3 Field survey

The field survey began with the implementation of 24 targets strategically distributed throughout the study area, configuring the Ground Control Points (GCPs). These points are fundamental for the geometric control of the photogrammetric model, as they allow linking the three-dimensional model to an official geodetic system, ensuring positional accuracy.

Figure 4 shows the spatial distribution of the control and validation points implemented in the study area. The points were positioned in order to ensure homogeneous coverage of the territory, contemplating the peripheral and central portions of the occupation. This configuration allows to reduce geometric distortions in the photogrammetric process and ensure greater reliability in the generation of the orthomosaic and the digital terrain and surface models.

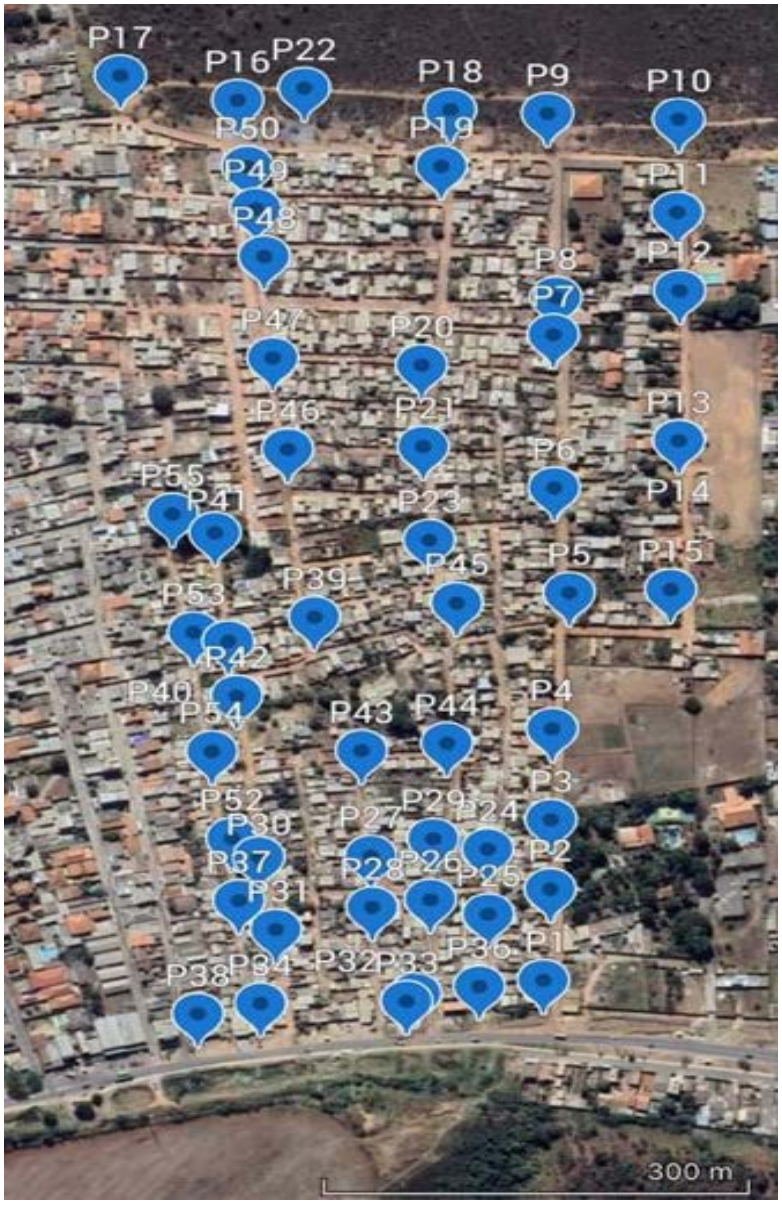


Figure 4 - Spatial distribution of the control and validation points used in the aerial photogrammetric survey in the Dorothy Stang Occupation.

Coordinate tracking was performed with a DJI D-RTK 2 GNSS receiver, compatible with GPS, GLONASS, BeiDou and Galileo systems, with horizontal accuracy of 1 cm + 1 ppm and vertical accuracy of 2 cm + 1 ppm. The observations were later processed by the Precise Point Positioning (PPP) method at the Brazilian Institute of Geography and Statistics (IBGE), using as reference the BRAZ station of the Brazilian Network of Continuous Monitoring (RBMC), in the SIRGAS2000 system (Época 2000.4). This procedure ensured the linkage of the survey to an official and nationally recognized geodetic reference.

The aerial survey was carried out with the DJI Mavic 3 Enterprise Multispectral drone, in a flight carried out on November 13, 2025. The flight planning considered longitudinal and transverse overlap parameters suitable for three-dimensional reconstruction, ensuring that each point of the terrain was recorded in at least six different images. This geometric redundancy is essential for the robustness of the photogrammetric adjustment and for the reliability of the three-dimensional model generated. All data was stored digitally in the equipment, being transferred directly to the computer environment, and thereby eliminating manual transcription steps and reducing potential sources of error.

4.4. Geodetic reference system

The survey was referenced to the Datum SIRGAS2000, adopting geocentric planimetric coordinates and altitudes referred to the Imbituba datum, with a central meridian of 45° WGr., according to the UTM system corresponding to the region. The use of the SIRGAS2000 ensures compatibility with the National Cartographic System and with official cartographic bases, in addition to meeting the technical guidelines applicable to the territory of the Federal District. The link to the RBMC station reinforces the consistency and geodetic traceability of the results obtained.

4.5. Photogrammetric processing

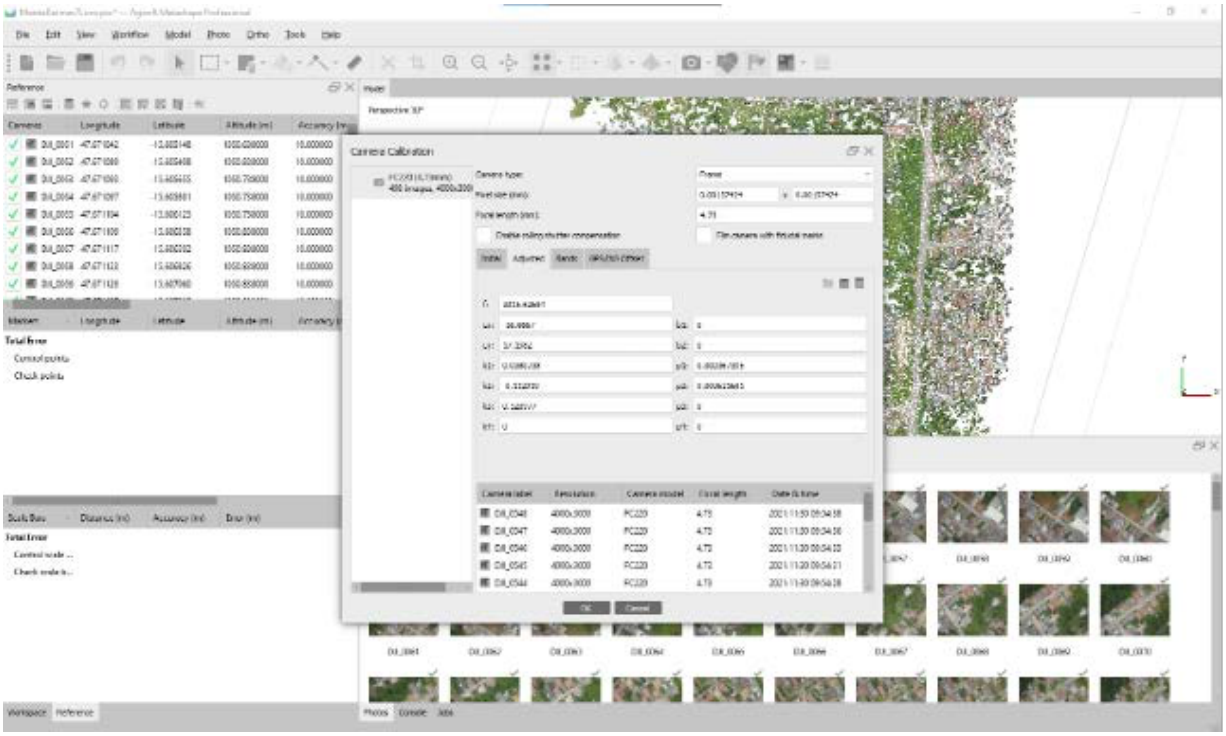
The image processing was performed in the Agisoft Metashape V2.1.2 software, following a structured and sequential workflow. Initially, the photographs were imported with automatic recognition of EXIF metadata, including approximate geographic coordinates. The quality of the images was evaluated, discarding those with an index lower than 0.5, in order to avoid degradation of the final model and optimize the computational performance.

The alignment of the images consisted of determining the position and orientation of the cameras in three-dimensional space. For this, computer vision algorithms were used based on the identification of homologous points (keypoints) and the automatic correspondence between images. The triangulation of these points resulted in the generation of the sparse point cloud, which represents the initial geometric structure of the model. After the preliminary alignment, the internal calibration of the camera was optimized by means of self-calibration, refining the geometric parameters of the adjustment (Figure 4).

Then, the coordinates of the 24 support points processed via PPP were entered. Each point was manually identified in multiple images, ensuring the minimum recommended redundancy of six observations per point. The model was then reprocessed incorporating these controls, significantly increasing the overall geometric accuracy.

From the refined positions of the cameras, the dense point cloud was generated through stereoscopic matching algorithms. Filtering procedures were applied to remove noise and outliers, especially relevant in land surveys. Based on the dense cloud, the Digital Elevation Model (DEM), the Digital Terrain Model (DTM), the three-dimensional grid and the georeferenced orthomosaic were derived. The texture construction was carried out in orthophoto mode, suitable for topographic applications, using mosaic-type blending to maximize sharpness.

Figure 5 – Self-calibration used in Agisoft software



4.6. Precision results

The processing resulted in a Ground Sample Distance (GSD) of 3.48 cm, a reprojection error of 1.25 pixels, and an estimated planimetric error of around 4.35 cm. The photographic coverage demonstrated that all points of the raised polygonal were imaged by at least six photographs, ensuring adequate redundancy for robust three-dimensional reconstruction. The values obtained are compatible with the technical requirements of urban planialtimetric surveys of cadastral character.

4.7. Preparation of the planialtimetric survey

Based on the photogrammetric products generated, the vectorization of the elements of interest in the CAD environment (AutoCAD) was carried out, contemplating buildings, curbs, blocks, walls, fences, lot boundaries and other elements of urban infrastructure. The final survey was organized on boards in A0 format, following the SICAD articulation and the technical guidelines of the competent Secretariat. The set of products generated allowed the consolidation of a detailed and georeferenced cartographic base, able to subsidize land regularization and urban planning actions.

4.8. Methodological considerations

The methodology adopted demonstrated high efficiency by integrating official geodetic control, high-resolution aerial survey and structured photogrammetric processing. The use of support points tracked with high precision, associated with automated digital processing and linking to the SIRGAS2000 system, ensured geometric reliability, technical standardization and data traceability. The method proved to be suitable for applications in land regularization, multipurpose technical cadastre and territorial planning, reconciling precision, operational productivity and scientific consistency.

5. Preliminary results and discussion

The preliminary results demonstrate that the aerial survey contributed decisively to increase the territorial visibility of the community, producing an accurate and socially legitimized spatial representation. As Andrade et al. (2022) point out, the graphic materialization of the territory operates as a device for political affirmation, as it provides residents with concrete instruments to claim presence, institutional recognition, and participation in decision-making processes. In the case of the Dorothy Stang Occupation, the orthomosaic and the derived models worked as mediators capable of revealing the complexity of the settlement before public agencies and external actors.

It is also important to highlight the role of aerial survey tools, especially drone flights, in providing a significant amount of spatial data to support the land regularization process in Dorothy Stang and its related urban planning project. The data produced through the methodology presented in this study serve as the basis for developing urban planning scenarios focused on improving infrastructure in streets and public open spaces, while also supporting in situ surveys of existing housing conditions.In this context, documenting the actual conditions of the area is a fundamental legal step in the land regularization process, as it organizes and consolidates information for each lot and dwelling through identification codes and detailed spatial representation. Moreover, drone flights carried out according to the standards described here provide a reliable and legally compliant database, helping to ensure that the following stages of the regularization process can be conducted more efficiently and securely.

The collective reading of the images allowed the residents to identify elements that would not be captured by isolated technical interpretation, such as informal passages, living areas, conflict zones and symbolic limits that structure the daily life of the occupation. This intersection between the technical knowledge generated by the aerial survey and the territorial knowledge produced by the community experience confirms the dialectic between technical knowledge and social practices described by Andrade et al. (2019). Such articulation proved to be essential to build urban analyses that are more sensitive to the real dynamics of the territory and, therefore, more aligned with emancipatory perspectives.

In addition, the high precision obtained in the survey resulting from the implementation of control points and the application of the parameters defined by ABNT NBR 17047, gives technical robustness to the products generated, making them suitable to support formal stages of land regularization. The reliability of the material reinforces its credibility before public agencies, expanding the potential for using the data both in administrative processes and in political negotiations that involve the recognition and permanence of the community.

6. Final considerations

The experience developed in the Dorothy Stang Occupation shows that the aerial surveying, when articulated with critical university extension practices, is configured as a strategic instrument for the realization of the right to the city. Compliance with the technical parameters defined by NBR 17047 ensures precision and reliability to the products generated, while the active participation of the community confers political legitimacy and expands the transformative reach of the process. This convergence between technical rigor and the collective construction of knowledge is fundamental to face historical inequalities that mark informal territories.

The team of authors of this article, linked to the Peripheral Laboratory of the University of Brasilia, understands the university as a strategic agent in the construction of democratic alternatives for the production of space, acting as a mediator between specialized technical knowledge, social practices and the formulation of public policies. The experience developed in the Dorothy Stang territory evidences this understanding by demonstrating that the use of geospatial technologies, when guided by sensitive,

inclusive and socially committed methodologies, goes beyond the merely instrumental character and consolidates itself as a tool for community strengthening. In this context, the cartography produced ceases to be just a physical record of the territory and begins to assume the role of support for social claims, the construction of collective memory and the practices of territorial resistance.In reality, It contributes to making public policy actions, such as land regularization processes, more democratic by broadening access to technology and ensuring the generation of physical data. As a result for this, experience confirms that the map, far from representing a neutral reality, becomes a political element capable of influencing metropolitan expansion, sustaining struggles for recognition and contributing to the consolidation of fairer territories. In Dorothy Stang, the combination of aerial surveys and active community involvement highlights both the importance and the potential of integrating science, technology, and public participation in the construction of more inclusive and democratically developed cities.

7. Limitations and Future Prospects

Although the results obtained show the relevance of aerial survey associated with participatory socio-technical practices, it is important to recognize some limitations inherent to the process. First, the execution of the survey depends on adequate climatic conditions and specific logistics, which may restrict the frequency of cartographic updates in territories subject to rapid transformations. In addition, the accuracy of the data, although high, does not eliminate the need for continuous validation in the field, especially in areas where the dynamics of occupancy are accelerated and marked by daily changes. It is also worth noting the data processing time, which can take weeks, depending on the power of the computer used.

Another challenge is the sustainability of participatory processes over time. The shared production of territorial knowledge requires continuous involvement of residents, institutional availability of the university and political support for the actions to continue. The absence of permanent public policies that recognize and incorporate socio-technical methodologies hinders the institutionalization of the results and, in certain cases, limits their impact on the administrative processes of land regularization.

Despite these limitations, the study opens up important avenues for future research. The replication of the methodology in other informal territories of the Federal District can contribute to the construction of a collection of social practices and technologies applied to land regularization. From a technical point of view, the advancement of embedded sensors, processing algorithms, and artificial intelligence techniques offers the potential to improve the accuracy of models and automate territorial classification steps. In turn, the expansion of community participation, through continuous training processes, can strengthen local autonomy in the management of spatial data and expand the political impact of social cartography.

Thus, the limitations pointed out here should be understood as opportunities for methodological deepening and expansion of the social and institutional reach of the research, reinforcing the role of the aerial surveying as a strategic instrument in the promotion of the right to the city.

8. Acknowledgments

This work has the support of the National Secretariat of Peripheries, of the Ministry of Cities, in partnership with Fiotec – Fiocruz Support Foundation, FUNAPE – Research Support Foundation and the University of Brasília (UnB), through a public notice of the Deanery of Research and Innovation (DPI).

References

ABNT. 2022. "NBR 17047: Levantamento cadastral territorial para registro público — Procedimento". Rio de Janeiro.

Andrade, Liza Maria Souza de. 2014. "O direito à cidade na construção de territórios insurgentes". Thesis (PhD in Architecture and Urbanism), University of Brasilia, Brasilia. https://repositorio.unb.br/jspui/handle/10482/18042

Andrade, L. M. S.; Loureiro, V.; Lemos, N.; Lenoir, J. 2019. "Extensão e tecnociência solidária: periférico no DF e entorno". Cadernos de Arquitetura e Urbanismo, Belo Horizonte, v. 26, n. 38, p. 189–234. https://www.perifericounb.com/artigos

Andrade, L. M. S.; Loureiro, V. 2022. "Pesquisa e extensão e a universidade cidadã". In: Gordilho-Souza, A. *et al*. (org.). Research in design and extension. Salvador: EDUFBA, 2020. p. 287–305. https://repositorio.ufba.br/bitstream/ri/33427/1/pesquisa-projeto-e-extensao-pos-graduacao-arquitetura-urbanismo.pdf

Andrade, L. M. S. Loureiro, V.; Lemos, N.; Lenoir, J. "Assessoria sociotécnica da resistência do Grupo Periférico no contexto da Reurb-S no DF". In: Campos, M. et al. (ed.). Another social architecture. Vitória: EDUFES, 2022. p. 155–178. https://edufes.ufes.br/items/show/647

Bringel, Breno; Domingues, Viviane. 2011. "Territórios em disputa no Distrito Federal: conflitos, movimentos sociais e ação coletiva". Cadernos Metrópole, São Paulo, n. 25, p. 263–284.

Caldeira, Teresa Pires do Rio. 2000. "Cidade de muros: crime, segregação e cidadania em São Paulo". São Paulo: Edusp.

Costa, Ártemis Sandra Borges Nunes. 2017. "Urbanismo participativo, regularização fundiária e práxis popular diante da lei n° 13.465/2017: o caso da ocupação Dorothy Stang". Dissertation (Master's Degree in Architecture and Urbanism), University of Brasilia, Brasilia. http://repositorio.unb.br/handle/10482/35758

Gohn, Maria da Glória. 2017. "Movimentos sociais e luta pela moradia" São Paulo: Cortez.

Harvey, David. 2003. "O Novo Imperialismo". São Paulo: Loyola.

Jatobá, Sérgio Ulisses. 2016. "Informalidade territorial e mercado de terras urbanas no Distrito Federal". Codeplan, Text for Discussion n°18, Brasília. https://www.codeplan.df.gov.br/wp-content/uploads/2018/02/TD_18_Informalidade_Territorial_Urbana-Mercado_Terras_Urbanas_DF_2016.pdf

Maricato, Ermínia. 2011. "Informalidade territorial e mercado de terras urbanas no Distrito Federal". Petrópolis: Vozes.

Paviani, Aldo. 2010. "Brasília: a metrópole em crise". Brasília: Editora Universidade de Brasília.

Rolnik, Raquel. 2015. "Guerra dos lugares: a colonização da terra e da moradia na era das finanças". São Paulo: Boitempo.

Rolnik, Raquel; Klink, Jeroen. 2011. "Como produzir moradia bem localizada com recursos públicos? Gestão fundiária e justiça social". São Paulo: Instituto Pólis. https://www.mprs.mp.br/media/areas/urbanistico/arquivos/manuais_orientacao/pmcmv.pdf

Romero, M. A. B.; Baptista, G. M. de M.; Lima, E. A. de; Werneck, D. R.; Vianna, E. O.; Sales, G. de L. 2019. "Mudanças climáticas e ilhas de calor urbanas". 1. ed. Brasília: University of Brasilia. v. 1. 151p. http://repositorio.unb.br/handle/10482/34661

Cinpar 2026
XXII International Conference on Building Pathology and Constructions Repair
15th to 17th July 2026 - Lisboa, Portugal

Monitoring of Geological Risk Areas Using UAVs with High-Precision Aerial Photogrammetry Support: The Case of Sol Nascente, Section 3, Federal District, Brazil

João da Costa PANTOJA[1], Valmor Cerqueira PAZOS[2], Mafalda Fabiene Ferreira PANTOJA[3], Lenildo Santos DA SILVA[4], Ana Luiza Alves DE OLIVEIRA[5], Nathaly Sarasty NARVÁEZ[6], Pedro Gomes CARDOSO[7], Helena Cubas XIMENES[8]

[1] Universidade de Brasília, Distrito Federal, Brazil,joaopantoja@unb.br
[2] Universidade de Brasília, Distrito Federal, Brazil,pazos@unb.br
[3] Instituto Brasileiro de Ensino, Desenvolvimento e Pesquisa, Distrito Federal, Brazil, mafalda.pantoja@idp.edu.br
[4] Universidade de Brasília, Distrito Federal, Brazil,lenildo@unb.br
[5] Universidade de Brasília, Distrito Federal, Brazil,ana.luiza@unb.br
[6] Universidade de Brasília, Distrito Federal, Brazil,nathaly.sarasty@unb.br
[7] Universidade de Brasília, Distrito Federal, Brazil,222001082@aluno.unb.br
[8] Universidade de Brasília, Distrito Federal, Brazil,222008771@aluno.unb.br

Abstract:

The accelerated growth of informal urban settlements in environmentally fragile areas has intensified the occurrence of erosive processes and mass movements, increasing the demand for monitoring methodologies capable of providing rapid, accurate, and technically reliable information for risk management. This article presents the results of the monitoring of a gully located in Block 3 of Sol Nascente, Federal District, Brazil. The goal was carried out within the scope of a geotechnological surveillance project aimed at proposing a methodology for the classification and monitoring of geological risk areas. The adopted methodology was based on the use of an Unmanned Aerial Vehicle (UAV), integrated with aerial photogrammetry corrected by Real-Time Kinematic (RTK), enabling the generation of orthomosaics, digital elevation models, topographic profiles, and three-dimensional visualizations from successive flight campaigns conducted throughout 2024. The comparative analysis of the surveys allowed the identification of distinct phases of the erosive process, including periods of reduction in the degraded area associated with landfilling interventions, as well as phases of erosion reactivation related to increased rainfall rates, resulting in the measured expansion of the gully area. The results demonstrated the robustness of the proposed methodology for the temporal monitoring of geological risk areas, contributing to decision-making by civil defense agencies and to the planning of preventive and corrective actions in vulnerable urban contexts.

Keywords: Risk Areas; Gully Erosion; UAV; Aerial Photogrammetry; Geotechnical Monitoring.

1. Introduction

Risk management is a process conducted by multidisciplinary teams with the objective of identifying, analyzing, evaluating, prioritizing, treating, and monitoring risks that may affect the objectives, processes, and outcomes of a project.

According to ISO 31000 (ABNT, 2009), risk is defined as the effect of uncertainty on objectives, that is, possible events that may or may not occur and that, if materialized, may hinder or delay the achievement of the intended results. This topic is directly related to the Desafio DF Program, launched in 2023 by FAP-DF, whose objective is to map environmental risk areas in the Federal District.

Peripheral urban areas of the Federal District present recurrent processes of environmental degradation associated with disordered land occupation, suppression of vegetation cover, and the absence of adequate surface drainage systems. In this context, the occurrence of gullies constitutes one of the main geological

risk factors, with direct impacts on public safety, urban infrastructure, and adjacent environmental systems. These processes tend to intensify in areas characterized by erosion-susceptible soils, rugged topography, and high levels of soil impermeabilization. According to Osterkamp (2008), a gully is defined as a cavity or channel excavated in the soil or in unconsolidated material, generally on slopes, by the action of running water, through which water predominantly flows after rainfall or snowmelt events.

In the Federal District, this investigation becomes particularly relevant, since in 2009 a total of 1,094 ravines and gullies were mapped, occupying a total area of 64.88 hectares, corresponding to approximately 0.01% of the study area (see Figure 1). In addition, processes associated with regional population growth and ongoing climate change have contributed to the intensification and expansion of these erosive features (Oliveira et al., 2009).

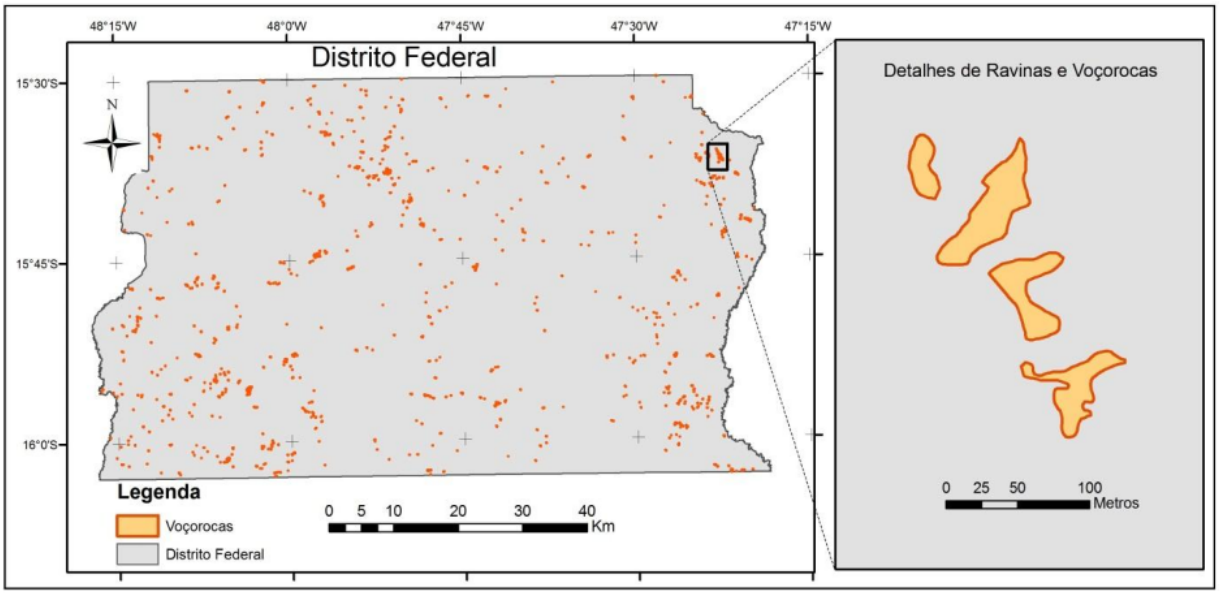


Figure 1: Spatial distribution of ravines and gullies in the Federal District (Oliveira et al., 2009).

Although UAV-based photogrammetry offers numerous advantages, its application in complex terrains also presents challenges. The geometric complexity of areas with steep ravines, dense forests, rocky hills, and intricate urban environments generates a high level of occlusions, variations in lighting and shadows, as well as difficulties in ensuring sufficient image overlap and consistent scale across the surveyed area (Liao, 2025).

As a case study, Chácaras 36 and 74, located in the Administrative Region RA XXXII – Sol Nascente e Pôr do Sol, were selected. These areas were chosen due to their high degree of vulnerability to phenomena such as surface runoff and erosion, as well as their proximity to gullies (SGB, 2022). Furthermore, they present distinct socio-environmental characteristics that require specific mitigation and monitoring approaches (Oliveira et al., 2025). Sol Nascente is part of this context as a territory marked by rapid urban expansion and high socio-environmental vulnerability. The erosive dynamics observed in different sectors of the area highlight the need for continuous monitoring strategies capable of early identification of terrain instability processes and of supporting risk mitigation actions.

Given this context, the present research aims to present and discuss the results of the geotechnological monitoring of a gully located in Block 3 of Sol Nascente, based on successive surveys carried out using UAVs, emphasizing the methodology employed, the products generated, and the comparative analysis of the morphological evolution of the terrain over time.

2. Study Area

The study area corresponds to Block 3 of Sol Nascente, in the Federal District, where a gully has developed associated with the concentration of surface runoff, the exposure of erosion-susceptible soils, and the immediate proximity to densely occupied areas. The erosive process advances toward residential buildings and areas of remaining vegetation, configuring a significant geological risk situation, with potential impacts on the safety of housing and the local population, as presented in Figure 2.

The gully exhibits an irregular geometry, with steep slopes and progressive deepening of the erosive channel, evidencing the combined action of water erosion processes and mass movements. The area is influenced by intense rainfall events, which contribute to the acceleration of erosive dynamics, especially during the rainy season.

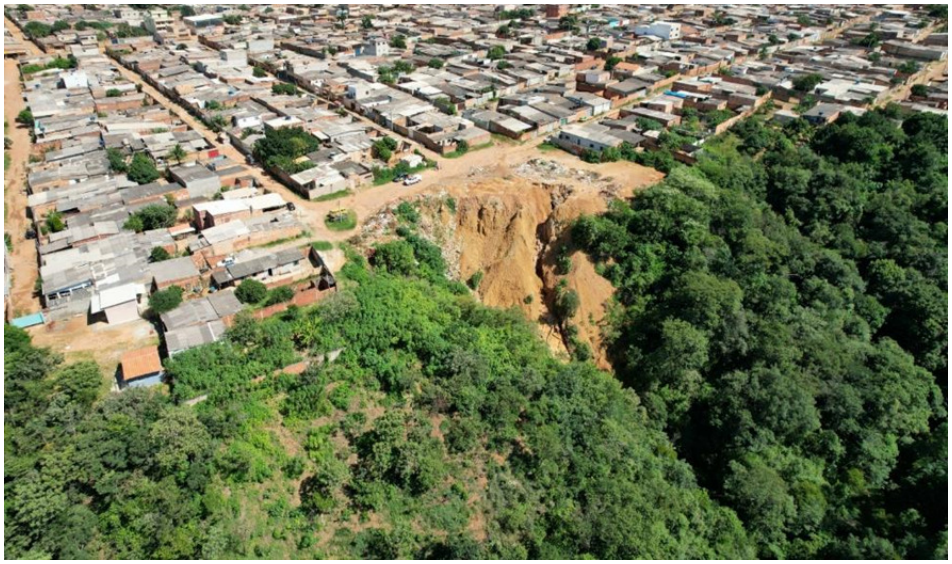


Figure 1: Aerial view from Google

3. Methodology

Once formed, gullies may progressively increase in scale over time. This expansion intensifies hydrological and sediment connectivity, resulting in increased sediment transport and the silting of rivers and reservoirs (Castillo & Gómez, 2016; Poesen, 2018). Due to these changes, continuous monitoring of gullies is necessary to assess the progression of their dimensions and the implications for nearby populations.

The monitoring of the area was carried out through aerial photogrammetry using an Unmanned Aerial Vehicle (UAV), a technique that enables the systematic acquisition of aerial images with high spatial resolution, allowing detailed analyses of terrain morphology and the temporal evolution of erosive processes. The adopted methodological strategy was based on successive flight campaigns, ensuring data comparability over time. Scientific studies, such as the one conducted by Hugenholtz et al. (2013), have demonstrated the effectiveness of using drones in the detection and analysis of gullies.

Throughout 2024, eight flight campaigns were conducted between the months of January and December. For the purposes of analysis in this article, priority was given to the data obtained from the flights carried out in March, August, November, and December, representing different phases of the erosive process observed during the monitoring period. The dates of each field visit are presented in the table below.

Dates of the visits:

1° Field Visits:	31/01/2024
2°Field Visits:	02/29/2024
3°Field Visits:	25/03/2024
4° Field Visits:	25/05/2024
5° Field Visits:	20/07/2024
6° Field Visits:	31/08/2024
7°Field Visits:	09/11/2024
8° Field Visits:	19/12/2024

Table 01: Dates of the visits



Figure 2: High-precision DJI D-RTK 2 GNSS mobile station (compatible with Inspire 3 / Phantom 4 RTK / Matrice 300 RTK and 350 RTK) BR – DJI310



Figure 3: Drone DJI Mavic 3 Thermal

The accuracy of the surveys was significantly improved through the use of a real-time mobile positioning station and an onboard RTK module integrated into the UAV, ensuring higher precision in image georeferencing and in the generation of derived cartographic products (Ekaso et al., 2020). This approach reduced metric uncertainties and provided greater reliability in the analysis of the detected morphological variations.

From the collected aerial images, georeferenced orthomosaics, digital elevation models, contour lines (Figure 06), longitudinal and transverse topographic profiles (Figure 05), as well as three-dimensional models of the monitored area (Figure 07) were generated. For the detailed analysis of the gully, four reference cross-sections were defined and distributed to represent different sectors of the erosive process.

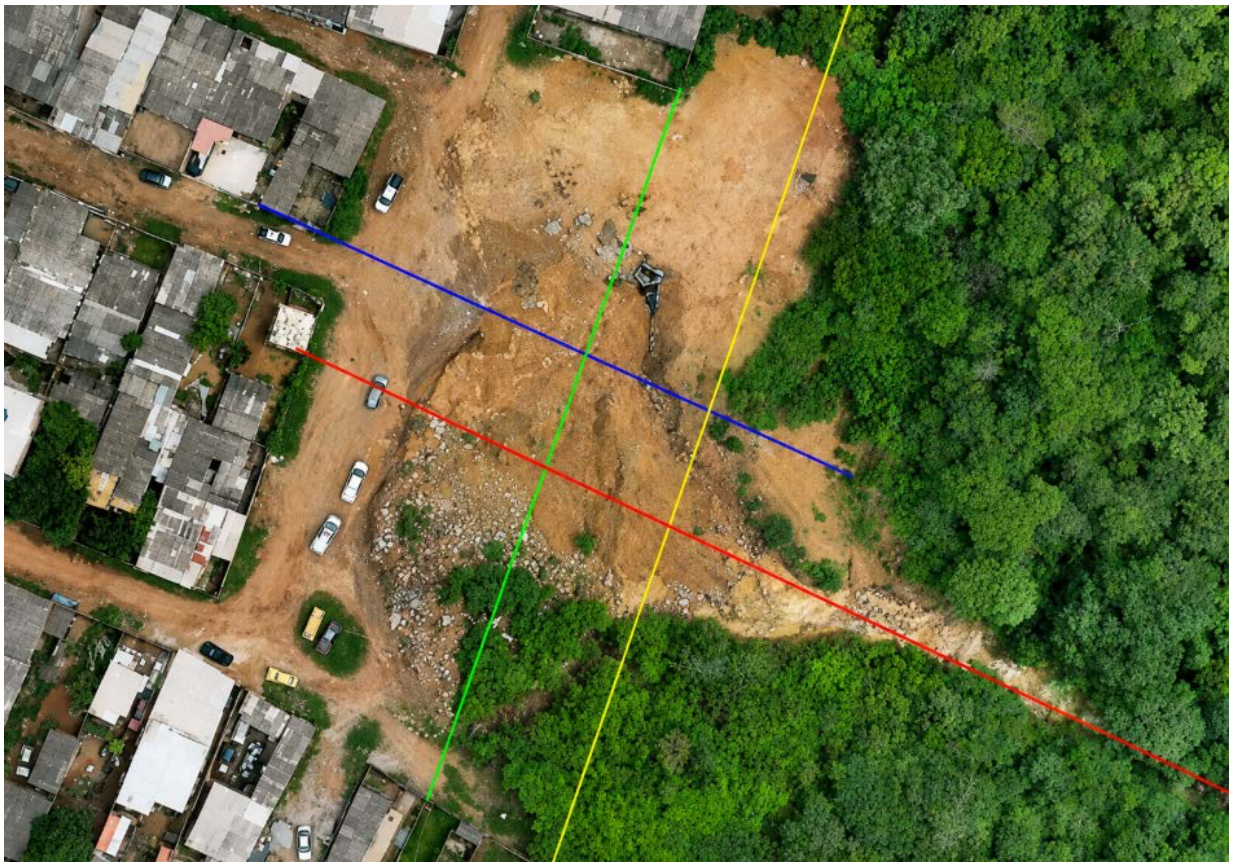


Figure 4: Longitudinal profiles for erosive movement analysis

The results obtained from these cross-sections were organized and graphically represented in Excel spreadsheets, allowing for a comparative visualization of the variations observed between different flight periods. Based on these graphs, it was possible to analyze earth movement over time, identifying changes associated with both erosion and sediment deposition processes.

As a complement to this initial analysis, contour lines with a one-meter interval were also generated for each flight campaign, enabling a more detailed interpretation of the topography of the studied area. In the resulting map, different shades of gray represent the altimetric variation of the terrain, where darker tones indicate greater gully depth. This representation facilitates the understanding of the relief morphology and contributes to the identification of areas with a higher concentration of erosive processes throughout the analyzed period.

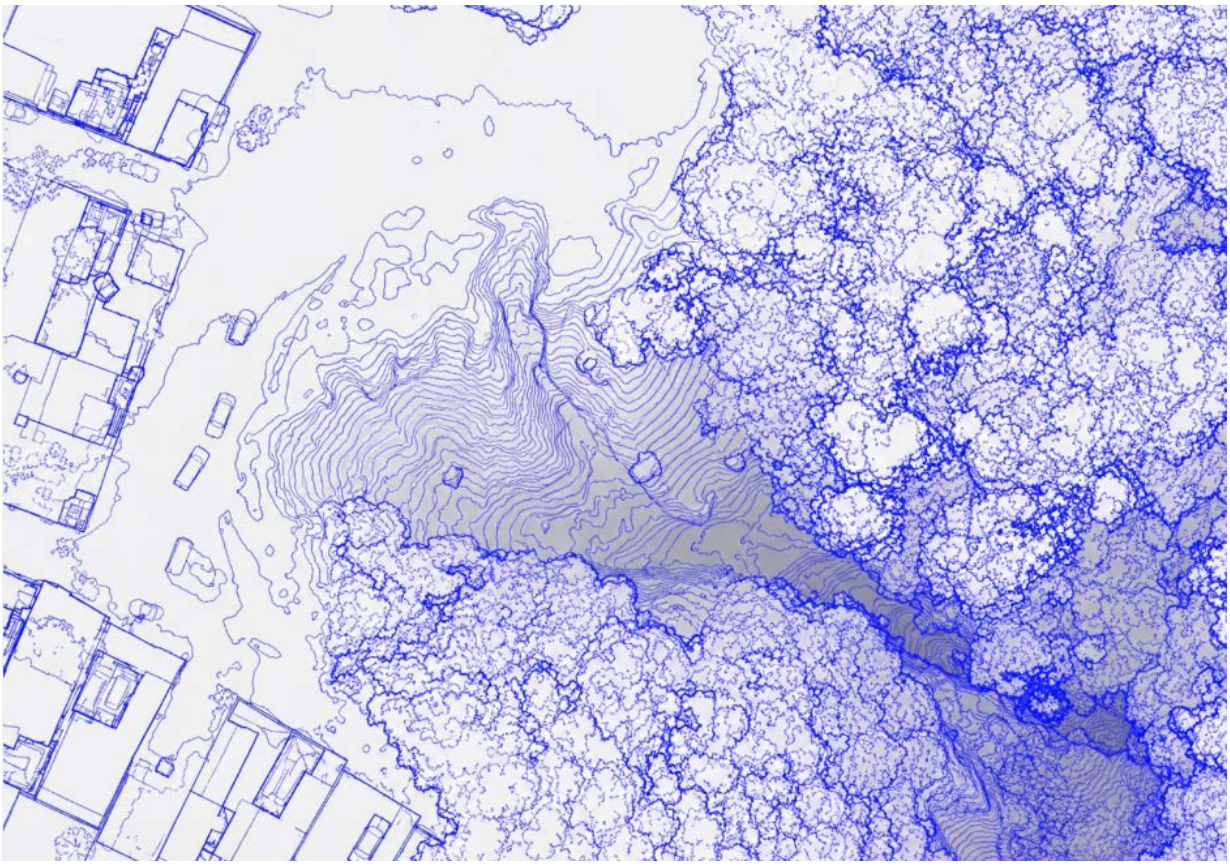


Figure 5: Digital contour model from the survey campaign

The three-dimensional representation images were produced from rectangular cross-sections defined over the terrain, in which the altimetric values extracted from the orthomosaic generated in each flight campaign were applied. This procedure enabled the digital reconstruction of the terrain surface and provided a clearer visualization of height variations and the morphology of the gully throughout the monitoring period.

The comparison between the different 3D models made it possible to identify changes in the terrain, highlighting both deepening processes associated with erosion and modifications resulting from anthropogenic interventions, such as the earth filling carried out in the area. A clear difference can be observed between the first and the fifth field visits, particularly after the execution of the filling process, which resulted in significant modifications to the site's topographic configuration.

These three-dimensional representations contribute to a more intuitive understanding of the gully's evolution, allowing the spatial visualization of the areas with the greatest terrain changes, as illustrated in Figures 07 and 08.



Figure 6 and 8: 3D visualization of the survey campaign

4. Results

The products generated from the flight campaigns clearly demonstrate the spatial and temporal evolution of the gully in Quadra 3 of Sol Nascente. The orthorectified aerial images and digital elevation models made it possible to identify significant changes in the terrain morphology, both in terms of the affected area and the depth of the erosive process.

The comparison between the surveys conducted in March and August indicates a reduction in the eroded area observed in plan view. This decrease is associated with an increase in the volume of material deposited within the gully, characterizing a filling phase. The corresponding topographic profiles reveal the partial infilling of the erosive channel and the temporary smoothing of the slopes, reflecting anthropogenic interference in the natural dynamics of the process.



Figure 9 and 10: Comparative erosion analysis between March (right) and August (left)

In contrast, the comparative analysis between the surveys conducted in August and November reveals the reactivation of the erosive process. During this period, an expansion of the gully area of approximately 461.6 m² was observed, mainly associated with increased precipitation. The topographic profiles indicate a deepening of the channel and a retreat of the slopes, confirming the reactivation of mass movement processes and terrain instability.



Figure 11 and 12: Comparative erosion analysis between August (right) and November (left)

The analysis of the reference cross-sections demonstrates that the morphological variations do not occur uniformly along the gully. Instead, it is possible to identify sectors that are more susceptible to erosion and slope collapse. This heterogeneity highlights the complexity of the erosive dynamics and reinforces the need for detailed monitoring methods capable of capturing the local specificities of the process and understanding the different responses of the terrain to anthropogenic actions and natural conditions.

In this context, the comparative analysis was conducted through the overlay of the gully boundaries obtained from different flight campaigns (Figure 8), combined with the evaluation of variations in planimetric area and the comparison of topographic profiles along the previously defined sections. This integrated approach enabled the identification of changes in slope geometry, as well as the deepening of the erosive channel and the lateral expansion of the degraded area, allowing for a more accurate interpretation of the spatial evolution of the erosive process over time.

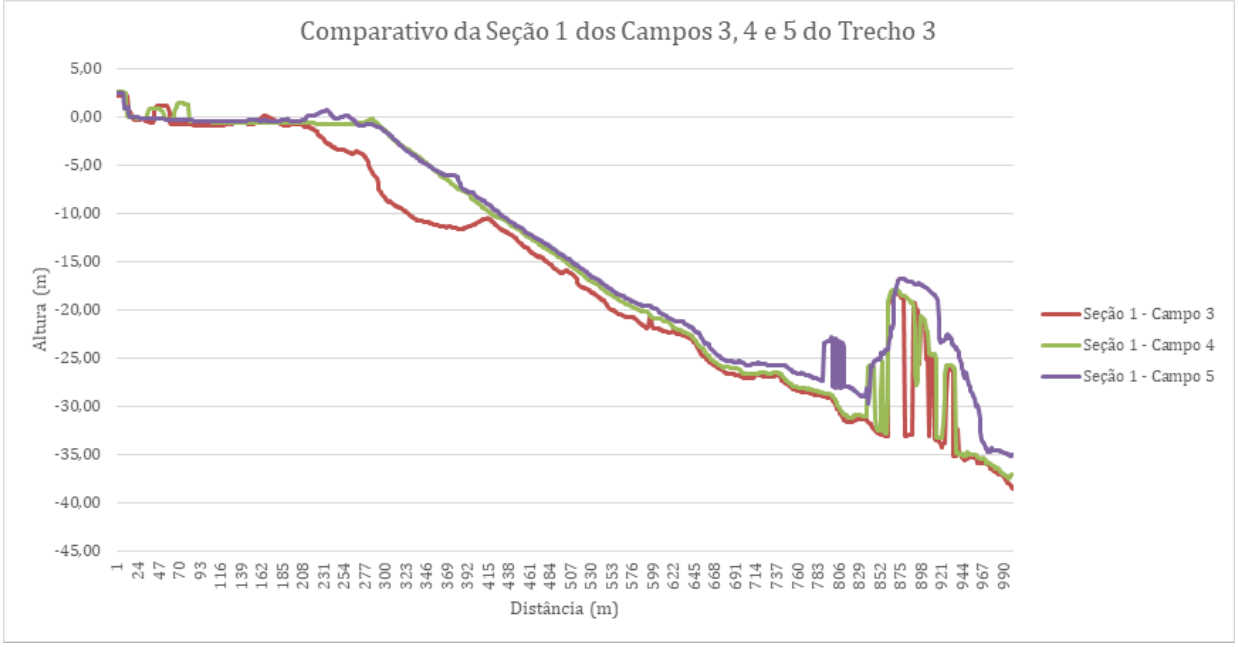


Figure 13: Comparative table of cross-sections from surveys 3, 4, and 5

Another comparative method adopted was the development of maps based on the drone flights, focusing on two main analyses. The first consisted of estimating the expansion of the gully in square meters, visually represented through the overlay of the contours obtained in flights 7 and 8 with those from flights 3 and 6, highlighting the changes that occurred after the onset of the rainy season and following the earth-filling process.

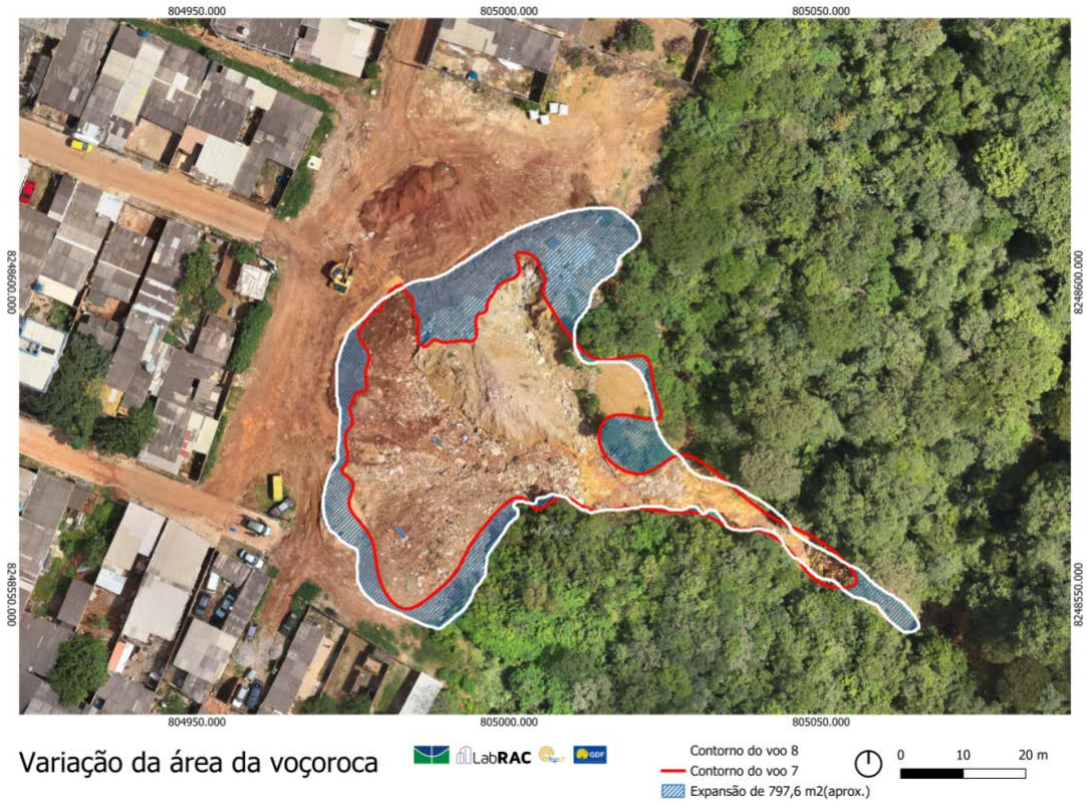


Figure 14: Area variation map from flights 7 and 8

In these comparative maps, the contour corresponding to the most recent flight is shown in red, while the contour from the previous flight is indicated in white, allowing a clearer visualization of the areas where modifications in the gully morphology occurred. The areas highlighted in red represent mass gain resulting from the earth-filling process carried out in the area, whereas the regions shown in blue indicate material loss caused by rainfall and surface runoff. The overlay of these boundaries makes it possible to identify the most dynamic sections of the erosive process, highlighting zones where edge retreat or material deposition occurred. The spatial analysis of these data allowed for the estimation of an approximate variation of 797.6 m^2 in the gully area, demonstrating the significant morphological change that occurred during the analyzed period. Therefore, the comparative maps contribute to understanding the evolution of the erosive process and to identifying the areas most susceptible to continued soil degradation, as illustrated in Figures 09 and 10.

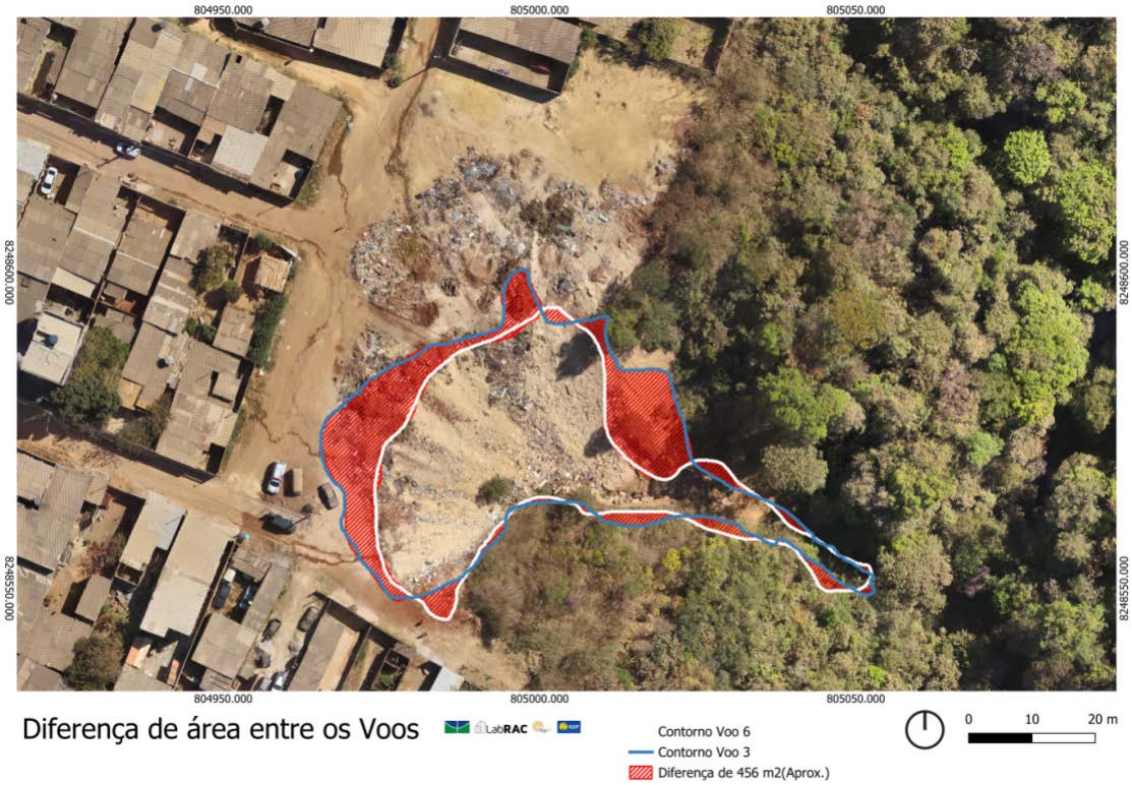


Figure 15: Area variation map from flights 3 and 6

The second analysis refers to the distance between the crater and the surrounding residences, considering the gully boundary and the terrain contour lines, which makes it possible to assess the risk of advancement toward occupied areas, as presented in Figures 11 and 12. For this analysis, measurement axes were drawn perpendicular to the gully boundary toward the nearest buildings, allowing the identification of the shortest distances between the edge of the erosion feature and the residences.



Figure 16: Analysis map – flight 1

The measurements indicate that the proximity of the gully in certain sections represents a potential risk to nearby residences, especially in areas where the topography favors surface water runoff toward the crater. The contour lines included in the map contribute to understanding the relief dynamics by indicating preferential drainage directions and the points most susceptible to the continuation of erosive processes. Thus, the intersection between the gully boundary, the measured distances, and the local topography enables a more accurate assessment of the areas that may be impacted in the event of further advancement of the erosive process.

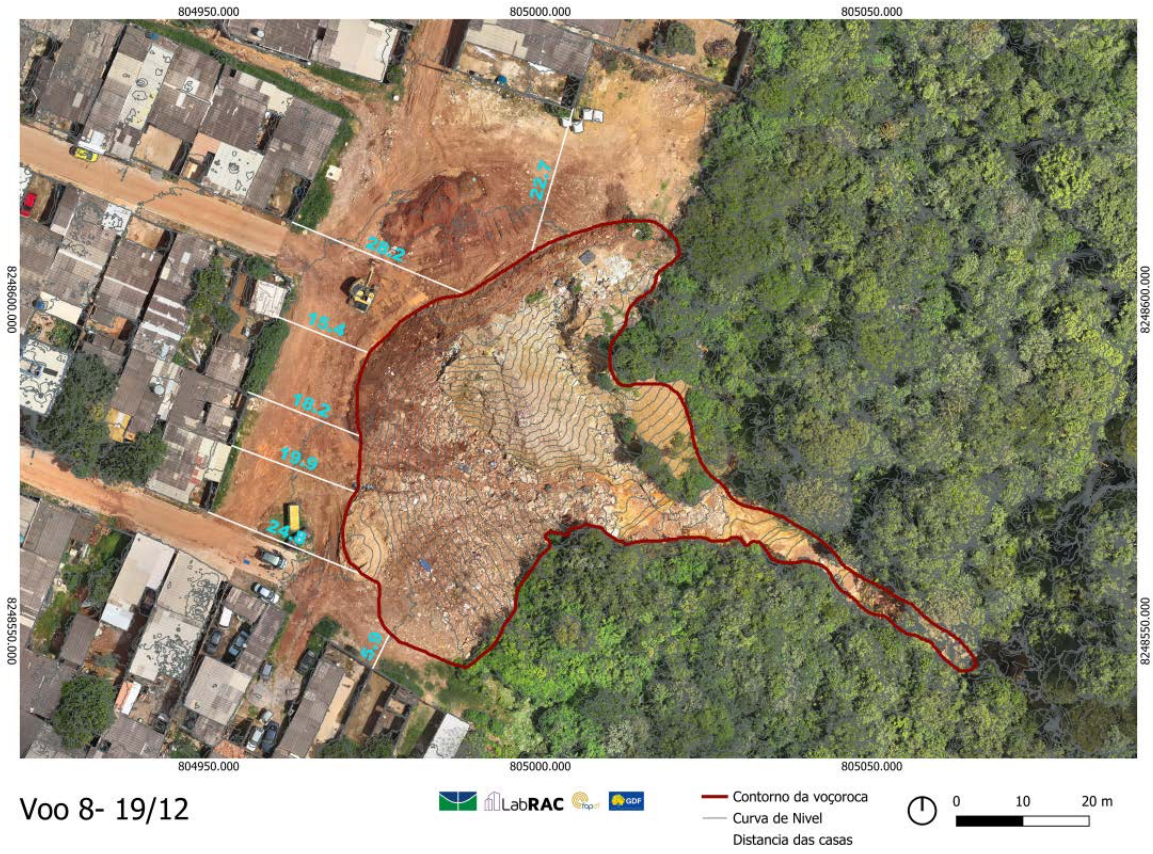


Figure 77: Analysis map – flight 8

The comparison between the first aerial survey (Figure 13) and the most recent monitoring (Figure 14) highlights significant changes in the morphology of the gully throughout the analyzed period. In the first record, a deeper and more continuous configuration of the erosive channel can be observed, with a greater concentration of contour lines within the feature, indicating areas of steeper slopes and deeper terrain incision. In the most recent survey, however, it is possible to identify topographic changes mainly associated with interventions carried out in the area, such as the earth-filling process and the redistribution of material. These modifications resulted in a partial reconfiguration of the internal relief of the gully, reducing its depth in certain sections and altering the surface runoff dynamics.

Furthermore, the comparison between the measured distances from the gully boundary to nearby residences shows minor variations throughout the monitoring period, indicating that although internal modifications occurred within the erosive feature, the lateral advance toward urbanized areas remained relatively limited during the analyzed interval. Therefore, the integrated analysis of the orthomosaics, contour lines, and distance measurements enabled a broader understanding of the spatial evolution of the gully, highlighting both the effects of natural erosive processes and the anthropogenic interventions carried out in the area. This approach contributes to risk assessment and supports the continuous monitoring of the studied site.

5. Discussion

The results obtained highlight the highly dynamic nature of erosive processes in vulnerable urban areas, where localized interventions may produce temporary stabilization effects but do not necessarily interrupt the progression of the phenomenon. The erosive reactivation observed after the filling phase demonstrates the strong influence of climatic conditions—particularly precipitation—on the stability of slopes and the erosive channel.

The use of UAVs combined with RTK correction proved to be fundamental for the accurate detection of these variations, enabling consistent comparative analyses between successive monitoring campaigns. The high spatial resolution of the generated products allowed the identification of subtle morphological changes that would be difficult to detect through traditional field survey methods.

The adopted methodology presents strong potential for application in geotechnological monitoring programs, supporting civil defense agencies, urban planning, and the development of risk mitigation strategies. In contexts of informal settlements and areas with limited accessibility, the use of UAVs represents an efficient, safe, and low-impact alternative for the continuous monitoring of risk-prone areas.

6. Conclusions

The present study aimed to map and monitor geological risk areas in the Federal District. Through the developed methodology, it was possible to identify and characterize risk areas using geological monitoring techniques. The results obtained so far highlight the complexity of the geological and hydrological challenges faced in the region, emphasizing the presence of significant gullies, susceptibility to water erosion, and the direct impact on the safety and well-being of local communities. In the studied areas, anthropogenic factors that aggravate the risks were also identified, such as inadequate waste disposal and the lack of proper drainage infrastructure.

This project contributes to scientific advancement in the field of geotechnological monitoring by providing a replicable methodology for the effective mapping of geological risk areas. Furthermore, the results reinforce the need for integrated public policies that address both the immediate mitigation of identified risks and the prevention of future environmental disasters in the Federal District.

The findings of this study present significant practical implications for the Civil Defense of the Federal District, urban managers, and the scientific community, providing a solid basis for the development of risk mitigation strategies and sustainable urban planning. The applied methodology and the generated data contribute to the development of a geological risk management model adaptable to different urban contexts, promoting community resilience to natural hazards.

The monitoring of the gully located in Quadra 3 of Sol Nascente demonstrated the effectiveness of UAV-based aerial photogrammetry associated with real-time positioning technology as a geotechnological monitoring tool for geological risk areas. The applied methodology enabled the precise identification of different phases of the erosive process, the quantification of area variations, and the understanding of the morphological evolution of the terrain over time.

The results reinforce the importance of continuous monitoring as a tool to support risk management, highlighting the need to integrate this information into public policies aimed at prevention, erosion control, and land-use planning in vulnerable urban areas. The approach presented is replicable in other similar contexts, contributing to the improvement of geological risk management practices in urban environments.

References

ASSOCIAÇÃO BRASILEIRA DE NORMAS TÉCNICAS (ABNT). ISO 31000: Risk management — Principles and guidelines. Rio de Janeiro: ABNT, 2009.

CASTILLO, C.; GÓMEZ, J. A. A century of gully erosion research: Urgency, complexity and study approaches. Earth-Science Reviews, v. 160, p. 300–319, 2016.

EKASO, D.; NEX, F.; KERLE, N. Accuracy assessment of real-time kinematics (RTK) measurements on unmanned aerial vehicles (UAV) for direct geo-referencing. Geocarto International, v. 35, n. 2, p. 165–181, 2020. DOI: https://doi.org/10.1080/10095020.2019.171043.

HUGENHOLTZ, C. H. et al. Geomorphological mapping with a small unmanned aircraft system (sUAS): Feature detection and accuracy assessment of a photogrammetrically derived digital terrain model. Geomorphology, 2013. DOI: https://doi.org/10.1016/j.geomorph.2013.09.02.

LIAO, G. Accuracy optimization and engineering applications of 3D modeling for complex terrains based on UAV oblique photogrammetry. International Core Journal of Engineering, v. 11, n. 11, 2025. DOI: https://doi.org/10.6919/ICJE.202511_11(11).000874.

OLIVEIRA, A. L. A.; NARVÁEZ, N. S.; PANTOJA, J. C. MAIS Method for gully's risk analysis. In: INTERNATIONAL CONFERENCE INTEGRITU–RELIABILITY–FAILURE IN ENGINEERING, MATERIALS, MANUFACTURING AND BIOMECHANICS, 8., 2025, Porto. Proceedings... Porto, 2025.

OLIVEIRA, B. E. N. et al. Identificação dos processos erosivos lineares no Distrito Federal através de fotografias aéreas e geoprocessamento. Geociências (São Paulo), v. 32, n. 1, p. 152–165, 2013.

OSTERKAMP, W. R. Annotated definitions of selected geomorphic terms and related terms of hydrology, sedimentology, soil science and ecology. Reston, VA: U.S. Geological Survey, 2008. Open-File Report 2008–1217.

POESEN, J. Soil erosion in the Anthropocene: Research needs. Earth Surface Processes and Landforms, v. 43, n. 1, p. 64–84, 2018.

SERVIÇO GEOLÓGICO DO BRASIL (SGB). Geological Risk Area Zoning in Brasília – Federal District. Brasília: SGB, 2022.

cinpar2026
XXII International Conference on Building Pathology and Constructions Repair
15th to 17th July 2026 - Lisboa, Portugal

From risk assessment to mitigation and emergency planning for multiple natural hazards in urban built environments: a mesoscale, user-dynamics-based framework

Gabriele BERNARDINI[1], Caterina ALIGHIERI[2], Maud NATALUCCI[3], **Alessia FREDDO[4]**, Enrico QUAGLIARINI[5]

[1] Università Politecnica delle Marche, Ancona, Italy, g.bernardini@staff.univpm.it
[2] Università Politecnica delle Marche, Ancona, Italy, c.alighieri@pm.univpm.it
[3] Università Politecnica delle Marche, Ancona, Italy, maud.natalucci@gmail.com
[4] Università di Catania, Catania, Italy, alessia.freddo@phd.unict.it
[5] Università Politecnica delle Marche, Ancona, Italy, e.quagliarini@staff.univpm.it

Abstract: The mitigation of impacts due to natural hazards (such as floods and earthquakes) on Urban Built Environments (UBEs) should take into account disaster risk assessment tasks as the fundamental steps to build on reliable, comprehensive and effective emergency scenarios. Assessment should hence integrate hazard conditions and urban-use dynamics, as these together determine the spatio-temporal variability of user exposure and vulnerability. To address these interactions, a multiscale approach is essential, enabling the representation of complex relationships among UBE subsystems and supporting the construction of alternative risk scenarios. In this perspective, building-scale information is aggregated at the level of urban public open spaces (e.g., streets and squares), which act as key elements in everyday activities and as critical assets during emergencies. This study proposes a novel framework using dynamic single-risk assessment in UBEs to provide insights into possible mitigation and emergency planning strategies. It integrates the main components influencing risk (hazard, physical vulnerability, user exposure, and user vulnerability), and is applied to floods and earthquakes as relevant disasters in UBEs. Leveraging the microscale level, data are then aggregated into open-space-level risk indices, allowing the identification of scenario-sensitive hotspots under different spatio-temporal user configurations. The application to the historical UBE of Senigallia (Italy) highlights how variations in urban use significantly influence risk distribution and severity, confirming the relevance of integrating behavioural dynamics within urban-scale assessments. The results provide an operational basis for advancing risk mitigation and emergency planning. The identification of recurrent and scenario-specific hotspots supports the prioritisation of interventions, the optimisation of resource allocation, and the development of targeted, context-specific strategies. In this sense, the proposed framework acts as a bridge between risk diagnosis and risk management, providing decision-makers with actionable evidence to customise mitigation measures and emergency response plans according to specific natural hazard scenarios and user dynamics.

Keywords: Multi-Risk Assessment, Flood Risk, Earthquake Risk, Urban Built Environment, Emergency Planning

1. Introduction

Disasters such as earthquakes and floods represent major threats to Urban Built Environments (UBEs), affecting territories due to both their intrinsic natural and geological characteristics, as in the case of seismic hazards, and the increasing influence of climate change, which is exacerbating extreme precipitation events (Davis et al. 2023; Giuliani, De Falco, and Cutini 2021). These phenomena belong to the category of Sudden Onset Disasters (SUODs), characterised by limited warning times and the rapid escalation of impacts in densely populated urban areas (UNDRR 2019). Their effects on urban systems depend not only on hazard intensity but also on the intrinsic vulnerability of UBEs, which involves both its physical characteristics and the users who inhabit and interact with these spaces. User-related factors, including age, mobility, environmental familiarity, and emergency awareness, significantly influence evacuation processes, behavioural responses, and potential casualty levels (Bernardini et al. 2024; Quagliarini et al. 2023; 2025). UBEs should therefore be understood as complex socio-spatial systems where buildings, infrastructures, public spaces, and users interact dynamically (Sharifi 2023), highlighting the need for disaster risk management approaches that address both structural vulnerability and the spatio-temporal distribution of urban populations.

Disaster risk management encompasses mitigation measures, preparedness strategies, and emergency planning actions (Kelman and Glantz 2015), and relies on disaster risk assessment as a key analytical foundation. However, both assessment and management approaches must move beyond static representations of exposure and vulnerability, since the impacts of many hazards are strongly influenced by the spatial and temporal distribution of people, which varies according to daily mobility patterns, tourism flows, and seasonal fluctuations. Neglecting such heterogeneity may lead to substantial misestimations of urban risk (Guo et al. 2025; Dabbeek et al. 2025; Duan and Fei 2025). At the mesoscale, Public Open Spaces (POSs) - such as streets and squares - represent key elements connecting building-level and urban-fabric scales within UBEs (Sharifi 2019). During emergencies, these spaces become critical interfaces where exposure, vulnerability, and behavioural responses concentrate, particularly during evacuation and early response phases. Defining plausible POS-use scenarios is therefore essential to estimate exposed users and their time-varying vulnerabilities (Frigerio et al. 2016; Romano, Bernardini, and Quagliarini 2025). When integrated with hazard and physical vulnerability parameters, this information enables the identification of critical urban hotspots and supports targeted mitigation and emergency planning strategies within disaster risk management frameworks.

In this context, the present study aims to support disaster risk mitigation, with particular reference to flood and seismic hazards. Applying a multi-layer, single-risk assessment methodology to a real case study (the historic UBE of Senigallia, Italy), the research identifies the most critical hotspots exposed to flood and earthquake risks. Based on these results, hazard-specific mitigation strategies and emergency planning measures are developed. The proposed approach integrates physical and user-related components under dynamic conditions through a POS-centred mesoscale framework, capturing interactions between hazard intensity, physical vulnerability, and spatio-temporal variations in exposure.

2. Methods

The method applied in this study is structured into five main phases, which collectively form an integrated workflow (illustrated in "**Error! Reference source not found.**"). This workflow enables the single-risk assessment for flood and earthquake hazards (Phases 1-4), and subsequently supports the development of risk mitigation strategies (Phase 5). The method is finally applied to a real case study, represented by the city of Senigallia, in order to demonstrate the validity and applicability of the proposed approach.

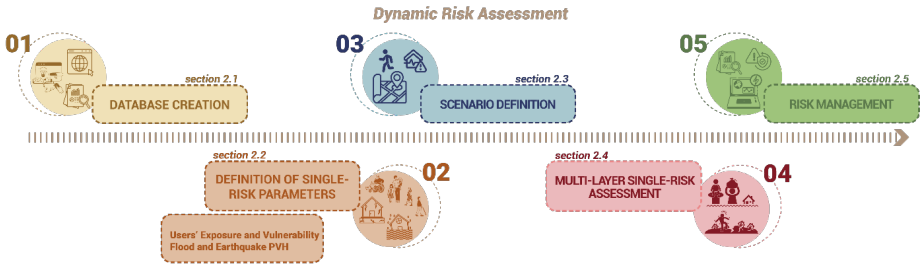


Figure 1 – Workflow

The five phases of the methodology are detailed as follows:

1. *Database creation*. Mesoscale assessment units are represented by POSs linking adjacent buildings and urban functions. A dataset including urban morphology, land use, building features, and hazard parameters supports the risk assessment process (Section **Error! Reference source not found.**);
2. *Definition of Single-Risk Parameters*. The key parameters, hazard, exposure and vulnerability, are assessed at the POS scale for both users and the built environment, including spatio-temporal user dynamics and building characteristics (Section **Error! Reference source not found.**);
3. *Definition of Risk Scenarios.* Single-risk scenarios are defined by combining hazard and vulnerability conditions for floods and earthquakes with shared spatio-temporal user patterns (seasonality, crowding levels, and daily time slots) across risk typologies (Section 2.3);
4. *Multi-layer single-risk assessment*. User exposure, user vulnerability, and *PVH* are integrated into multi-layer single-risk matrices to derive final risk levels for each POS, time period, and scenario. The results are represented as risk maps highlighting worst-case conditions (Section 2.4);
5. *Risk management*. Risk maps identify scenario-sensitive hotspots among the POSs in the UBE; they are compared with current emergency plans to detect conflicts between escape routes and critical areas within the city. Once weaknesses are detected, intervention planning is developed through the identification of new safe routes (Section 2.5).

A real case study was selected to apply the developed method. The city of Senigallia (Ancona, Italy) represents a suitable case study: characterised by significant cultural heritage, it developed along the Misa River and has been affected over time by both riverine floods (major events recorded in 2014 and 2022) and earthquakes (a severe seismic swarm in 1930 and a less intense one in 2022), which in both cases caused extensive damage to buildings, POSs and riverfront areas, compromising urban functionality. Therefore, the city's layout, the high presence of POSs, multi-hazard conditions, and dynamic exposure patterns related to recurrent mass-gathering events hosted in the UBE[1], make Senigallia a suitable case study for analysis, with the ultimate objective of supporting risk mitigation and emergency planning.

2.1 Database creation

A georeferenced database was developed to support the mesoscale POS-centred assessment. The dataset integrates building-level information with open-space characteristics and user-related parameters, enabling the aggregation of micro-scale data to streets and squares.

Building data include construction period, structural typology, number of storeys, and ground-floor use. These attributes were derived from municipal technical cartography[2] and publicly available sources, complemented, where necessary, by field verification and digital platforms (e.g., Google Street View). POSs were mapped and classified according to their geometric configuration, accessibility, and functional role within the urban fabric. Seasonal variability is explicitly considered by distinguishing winter (October-May) and summer (June-September) periods, characterised by differences in tourist presence, opening hours, outdoor uses, and mass-gatherings conditions. Demographic data from the Italian National Institute of

[1] https://www.feelsenigallia.it/en/ (last access: 20.02.2026)
[2] https://www.comune.senigallia.an.it/documento_pubblico/p-p-c-s-senigallia/ (last access: 20.02.2026)

Statistics (ISTAT, 2023 census database[3]) are used to define age-based user categories for exposure and vulnerability assessment. Occupancy loads [persons/m^2] are derived from fire safety regulations for both indoor and outdoor main functions (Ministero dell'Interno 2015). In addition, the theory of pedestrian Levels of Service (LOS) is adopted to model seasonal conditions in outdoor pedestrian areas and mass-gathering scenarios in open spaces (Bloomberg and Burden 2006). This framework was adopted to define the spatio-temporal characterisation of users across the different scenarios, as it has already been validated in previous studies, despite its conservative nature (Quagliarini et al. 2023).

All data were harmonised within a GIS environment to ensure spatial consistency and enable indicator normalisation at the POS scale.

2.2 Definition of single-risk parameters

This study builds upon consolidated approaches for computing hazard, exposure and vulnerability, integrating spatio-temporal urban use patterns with building characteristics (Ferreira and Santos 2020; Bernabei et al. 2021; Quagliarini et al. 2023). These components are expressed through the User Exposure and Vulnerability indices (Section 2.2.1) and the Physical Vulnerability and Hazard indices for flood and earthquake (Section 2.2.2). The response of the built environment to risks is therefore evaluated by combining user-related parameters (exposure and vulnerability), the physical vulnerability of buildings facing each POS, and hazard severity, ultimately describing the effects of flood and earthquake scenarios on public open spaces within the UBE. In detail, Physical Vulnerability (*PV*) reflects intrinsic building characteristics, such as materials, structural configuration, geometry, and conservation state, and is assumed invariant across hazard scenarios. Hazard (*H*) depends on the intensity of the selected event and varies according to the specific flood or earthquake scenario. *PV* and *H* are combined through a matrix-based procedure to derive a synthetic Physical Vulnerability-Hazard (*PVH*) index, which expresses the expected level of damage and its potential effects on adjacent open spaces (Ferreira and Santos 2020).

All indices are finally normalised on a scale from 0 (minimum risk, excluded according to general criteria for risk assessment) to 1 (maximum risk), ensuring mutual comparability and enabling their integration within the multi-layer single-risk assessment framework (see Section 2.4).

2.2.1 Users' Exposure and Vulnerability

User-related indices are derived by combining spatial information on urban functions with time-dependent occupancy assumptions. Users are classified according to their location (indoor or outdoor), type of activity, familiarity with the UBE, and age-related characteristics. Temporal variations in user presence are reconstructed through the intersection of functional schedules and behavioural assumptions, enabling the estimation of the spatio-temporal distribution of users and its aggregation at the POS scale. On this basis, User Exposure (*E*) and User Vulnerability (*UV*) indices are computed as time-dependent factors reflecting both the number of users and their susceptibility under emergency conditions. In detail, four time-dependent parameters are introduced to represent user presence and vulnerability under emergency conditions: Users' Exposure, Age-based User Vulnerability, Familiarity-based User Vulnerability, and Position-based User Vulnerability. These are computed following the methodology described in (Quagliarini et al. 2023; Bernardini et al. 2024). In particular:

- Users' Exposure, *E*, represents crowding levels in POSs under emergency conditions, considering both indoor and outdoor users. It is calculated by aggregating all users associated with a POS and normalising their density against a reference maximum outdoor occupant load;
- Age-based User Vulnerability, *Uva*, reflects the reduced autonomy and emergency response capacity of specific population groups due to age. It is computed as the proportion of age-vulnerable users with respect to the total number of users associated with each open space;

[3] https://demo.istat.it/app/?l=it&a=2023&i=POS (last access 20.02.2026)

- Familiarity-based User Vulnerability, *Uvf*, reflects the limited knowledge of the UBE and its associated risks among non-regular users (e.g., visitors, tourists and occasional users). The indicator is computed as the proportion of low-familiarity users associated with each POS;
- Position-based User Vulnerability, *Uvp*, reflects the location of users within the UBE at the onset of an emergency, which directly influences their exposure to hazard effects. The indicator is hazard-specific: in flood scenarios, vulnerability mainly affects users located outdoors or at ground-floor level due to rising water and flow conditions (Davis et al. 2023), whereas in earthquake scenarios it is primarily associated with users inside buildings because of potential structural damage and falling elements (He et al. 2025).

2.2.2 Flood and Earthquake Physical Vulnerability and Hazard

For both flood and earthquake scenarios, the Physical Vulnerability and Hazard components are combined to quantify the potential impact of hazards on buildings surrounding a POS and the resulting effects on public open spaces.

For flood scenarios, the Flood Physical Vulnerability Index (PV_f) reflects the susceptibility of buildings to flood impact and water ingress, accounting for architectural and structural features with respect to floodwater spreading direction (Miranda and Ferreira 2019). The index is assumed to remain constant across scenarios. The Flood Hazard Index (H_f) represents hazard intensity based on water depth and flow velocity (Davis et al. 2023). PV_f and H_f are combined into the PVH_f index using a matrix-based approach, subdivided into five normalised classes (from negligible to extreme), with numerical values ranging from 0.20 to 1.00 ("**Error!**

Flood PVH_f			Hazard [H = H_f]				
			Negligible [H ≤ 0.75]	Low [0.75 < H ≤ 1.25]	Moderate [1.25 < H ≤ 2.5]	High [2.5 < H ≤ 7.0]	Extreme [H > 7.0]
Flood Physical Vulnerability Index PV_f	Extreme	75 < PV_f ≤ 100	Moderate	High	Extreme	Extreme	Extreme
	High	50 < PV_f ≤ 75	Low	Moderate	High	Extreme	Extreme
	Moderate	25 < PV_f ≤ 50	Low	Low	Moderate	High	Extreme
	Low	PV_f ≤ 25	Negligibile	Low	Low	Moderate	High

Figure 2 - Flood Physical Vulnerability and Hazard matrix

Reference source not found.").

In seismic scenarios, the Earthquake Physical Vulnerability Index (PV_e) is calculated at the building scale by integrating structural and geometrical parameters, conservation state, and the presence of anti-seismic devices (Bernabei et al. 2021). The Earthquake Hazard Index (H_e) is derived from seismic return periods and Peak Ground Acceleration levels, according to national seismic hazard maps and the Limit States of the Italian Building Code (NTC18 Ministero delle Infrastrutture e dei Trasporti 2018). PV_e and H_e are combined into the PVH_e index through a matrix-based procedure linking vulnerability classes to EMS-98 damage grades. PVH_e is normalized from 0 (no damage) to 1 (collapse), representing both structural and non-structural damage potential for buildings facing a POS ("**Error! Reference source not found.**").

2.3 Scenario definition

According to Section 2.1 and Section 2.2 methods for the characterization of user-related factors, different mass-gatherings conditions and spatio-temporal patterns of UBE use can be identified. Nevertheless, for application and demonstration purposes, this study limits the analysis to single-risk assessment (for both flood and earthquake) performed for the most recurring annual scenario, corresponding to a winter working

Earthquake PVH_e			Hazard [Return Periods (years)]			
			[50]	[101]	[475]	[975]
Seismic Physical	Low	PV_e < 0.55	D0	D1	D2	D3

Figure 3 – Earthquake Physical Vulnerability and Hazard matrix

day with outdoors low crowding condition: no mass-gatherings and a density of 0.2 pp/m^2 in the pedestrian areas, corresponding to the condition of LOS A. This scenario was selected for exploratory purposes, as it represents the most frequent typical day, accounting for approximately 66% of the occurrences observed over a year, and it represents an intermediate critical state for both Exposure (*E*) and User Vulnerability (*UV*). To stress the reliability of the framework in capturing daytime variability of risks (i.e., via the user factors), this scenario is analysed across five daily time slots (night-time NT, early morning EM, noon N, afternoon A, evening E) enabling the assessment of temporal risk dynamics. Then, hazard- and vulnerability-specific conditions are selected to derive the indices, that are:

- for flood: moderate hazard level (1.25 $m^2/s < H_f < 2.5$ m^2/s) combined with a PV_f condition of floodwater flowing perpendicularly to the river (conservative assessment);
- for earthquake: moderate hazard level (H_e corresponds to 475-years return period) combined with a PV_e condition of pushing sloped/pitched roof, and anti-seismic devices with poor performance levels (conservative assessment).

These hazard conditions are selected as they represent the most critical situations in which outdoor evacuation process could still be performed by hosted users under both flood and earthquake emergencies (Davis et al. 2023; Bernabei et al. 2021).

2.4 Multi-layer single-risk assessment

The single-risk (*R*) quantifies disaster risk at POSs' scale as a weighted linear aggregation of the indicators described in Section 2.2. For each hazard scenario, risk is computed as in Eq. (1):

$$R = I_{PVH}*PVH + I_{UVp}*UVp + I_{UVa}*UVa + I_{UVf}*UVf + I_E*E \quad (1)$$

where I_i represents the relative importance of each risk factor. These weights are assessed using the Analytic Hierarchy Process (AHP), with distinct schemes for flood and earthquake (Goepel 2013). Experts from the Polytechnical University of Marche (11 for floods, 8 for earthquakes) performed pairwise comparisons of the risk components on a linear 1-9 scale, and the resulting judgments were aggregated into a consensus matrix. Relative priorities were calculated using the Row Geometric Mean Method (RGMM), ensuring that the weights sum to one and that the Consistency Ratio (CR) remains below 10%, validating the comparisons.

The equation is applied separately for flood and earthquake scenarios, producing two single-risk metrics according to the adopted multi-layer single-risk approach. User-related parameters remain consistent across scenarios, whereas *PVH* and *UVp* are hazard-specific. Finally, maps-over-time (MOTs) of the multi-layer single-risk are generated to provide an immediate visualisation of daily risk patterns. Risk levels are classified into five categories: Negligible (0 < index < 0.2), Low (0.2 ≤ index < 0.4), Moderate (0.4 ≤ index < 0.6), High (0.6 ≤ index < 0.8) and Extreme (0.8 ≤ index ≤ 1). This allows the temporal variation of risk across different public open spaces and hazard scenarios to be analysed.

2.5 Risk management: hotspots identification and emergency planning

The multi-layer single-risk assessment introduced in Section 2.4 is employed as an operational tool to support risk management, with specific reference to the evaluation and enhancement of existing emergency planning strategies. In particular, single-risk (*R*) and MOTs are used to investigate the effectiveness of current evacuation layouts by analysing their spatial and temporal consistency with flood and earthquake risk conditions. The procedure is based on the systematic comparison between the official emergency plans and the single-risk MOTs obtained for flood and earthquake hazard scenarios.

Emergency plans identify a set of POSs as designated evacuation paths and safe areas, which essentially do not change over time depending on the use dynamics. These elements are spatially overlaid onto the corresponding risk maps, enabling a direct evaluation of the risk levels associated with the planned evacuation network under different hazard conditions. Through this overlay analysis, hotspots are identified as POSs that are currently designated as evacuation routes or gathering areas but exhibit high risk levels

according to the proposed risk assessment framework. In these locations, relevant levels of potential physical damage, user exposure, or user vulnerability may compromise evacuation safety and emergency response, particularly during daily peak occupancy periods or under unfavourable hazard conditions. As such, hotspots represent critical mismatches between planned emergency functions and risk conditions. The identification of hotspots is performed consistently for both flood and earthquake hazard scenarios, allowing the distinction between recurrent hotspots, which remain critical regardless of time of day, and scenario-sensitive hotspots, whose risk level varies significantly with user dynamics and hazard-specific factors. This distinction is particularly relevant for design-oriented planning, as it supports both long-term mitigation strategies and scenario-dependent emergency measures. Building upon the identification of hotspots, the subsequent step consists of the development of a design-oriented proposal aimed at redefining and integrating alternative evacuation routes within existing emergency plans. These alternative routes are conceived to ensure safer evacuation conditions for the exposed population under both flood and earthquake hazard scenarios.

3. Results and Discussion of the Application to the Case Study of the City of Senigallia

The proposed framework is applied to a representative portion of the historical centre of Senigallia (represented in "Figure 4 – A, B, C").



Figure 4 - Discretization of the historic UBE of Senigallia into buildings, open spaces, links and nodes for the implementation of the proposed framework (A); urban views of Via Portici Ercolani (B, Street View: Google Maps. (2025). [Street View of via Portici Ercolani, Senigallia, Italy]. Retrieved March 9, 2026, from [https://maps.app.goo.gl/ce1wEYEvoKheeJPk8]) and Piazza Roma (C, Street View: Google Maps. (2025). [Street View of Piazza Roma, Senigallia, Italy]. Retrieved March 9, 2026, from [https://maps.app.goo.gl/k9pcztPovTeQVLZy9])

The study area is discretised into a mesoscale urban system ("**Error! Reference source not found.** – A") composed of: (i) POSs (squares and widened street sections), adopted as assessment units; (ii) buildings; (iii) links (street segments); and (iv) nodes (intersections between streets and squares). This representation enables the aggregation of building-scale vulnerability and hazard parameters to the POS level and supports the integration of user-related indices across the urban network. The application of the multi-layer model produces time-dependent single-risk MOTs for both flood and earthquake scenarios, classified into the five risk levels (negligible to extreme). The obtained results are subsequently presented and discussed. Specifically, "**Error! Reference source not found.**" shows flood single-risk MOTs, whereas "**Error! Reference source not found.**" presents the earthquake single-risk MOTs.

In the flood case, risk distribution appears relatively stable across time slots, with low and moderate levels mainly concentrated in POSs located along the riverfront and in its immediate proximity. EM and NT are predominantly low, while N and A are characterized by low-to-moderate risk areas, particularly along the main east-west street axes. This increase corresponds to higher outdoor presence during working hours, amplifying the contribution of users' exposure and vulnerability to the final index. During E, the pattern remains similar to the afternoon configuration, with low-to-moderate risk concentrated along the riverfront and in central connecting links, but without extreme peaks. Overall, the flood MOTs highlight a risk structure strongly influenced by hazard proximity to the river, with temporal variations mainly affecting intensity rather than spatial hierarchy.

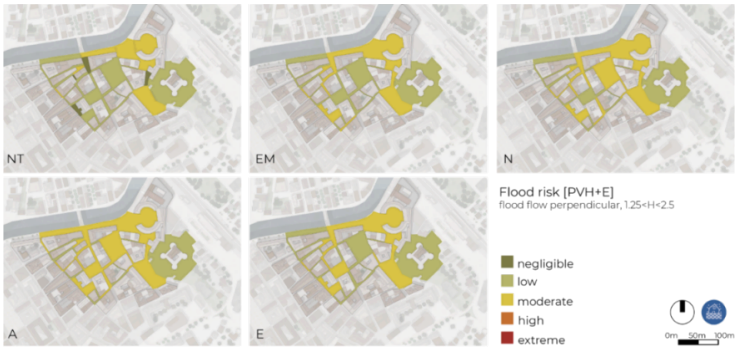


Figure 5 - Maps-over-time of flood risk in moderate H condition (1.25<H<2.5)

In contrast, the seismic MOTs reveal a stronger influence of functional schedules and indoor occupancy, producing sharper temporal fluctuations and localized hotspots with relevant single-risk values. The earthquake maps hence show a more pronounced spatial and temporal variability compared to the flood case, with the emergence of moderate and high-risk values in specific street segments. EM and NT are characterized by elevated risk levels; they appear along the northern riverfront axis and in central street links. Moderate and locally high values are visible even under reduced occupancy, indicating the dominant role of PVH_e. N and A show the most critical configurations. Several central links shift to moderate and high classes, forming a continuous high-risk corridor across the historical fabric. The increase reflects the combined effect of indoor occupancy and position-based user vulnerability under seismic conditions. During E, the spatial pattern becomes more fragmented, also in view of the position of public intended uses (e.g., restaurants, bars, other entertainment buildings) in the UBE, but persistent high-risk segments remain along structurally vulnerable fronts.

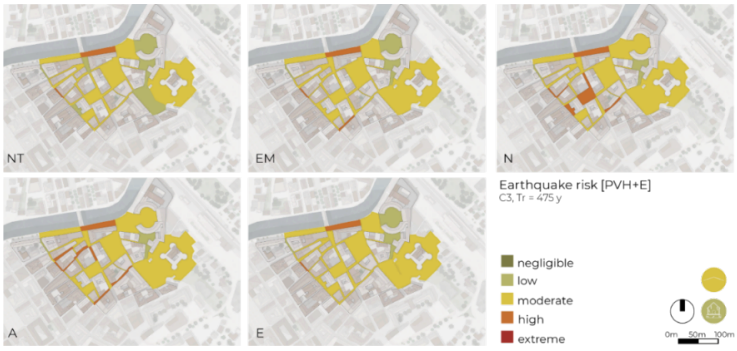


Figure 6 - Maps-over-time of earthquake risk in moderate H condition (H=475 years) and PV condition C3

The MOTs allow the identification of:

- POSs with recurrent high-risk values, mainly corresponding to wider POSs perpendicular to the river (see "Figure 4 – B, C") characterised by large pedestrian spaces, the presence of dehors, and their role as key nodes for daily activities and user flows;

- Time-sensitive high-risk values, emerging primarily in the earthquake scenario during peak occupancy hours.

Then, according to Section 2.4, hotspots are identified through the spatial overlay between the official flood and seismic emergency plans of Senigallia and the most critical daily single-risk configurations derived from the MOTs. Adopting a conservative approach, the reference time slots correspond to the highest *R* values within the recurring winter working-day scenario: A for floods and N for earthquake. Hotspots are defined as all POSs designated as main evacuation routes or gathering areas in the emergency plans that exhibit *R* ≥ Moderate in the selected scenario. The resulting overlay ("**Error! Reference source not found.**") highlights spatial mismatches between evacuation functions defined in the current Civil Protection emergency plans and actual risk conditions (Protezione Civile 2023).

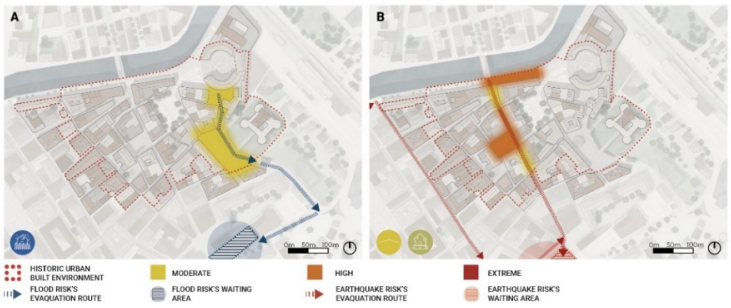


Figure 7 - Hotspots identified in the UBE of Senigallia. Panel (A) shows hotspots for flood in afternoon scenarios, while panel (B) shows hotspots for earthquake in noon scenarios

In the flood scenario, hotspots are mainly concentrated along the riverfront and near the Misa River. Although extreme values do not emerge under the selected moderate hazard level, all the evacuation segments fall within moderate risk classes, potentially affecting accessibility and walkability. In the earthquake scenario, criticalities are more pronounced. The main evacuation route within the study area intersects multiple Moderate and High-risk POSs. Elevated PVH_e values combined with peak indoor occupancy may hinder evacuation due to debris, façade failures, or falling elements. Moreover, several connecting streets show comparable risk levels, reducing the robustness of the evacuation network. Overall, the analysis reveals that: (i) the current evacuation network includes a limited number of main routes and few alternative safe paths, some of which may be exposed to potential risk-increasing conditions according to the assessed factors; (ii) routes are relatively long, particularly for users located near the riverfront.

Based on the identified hotspots, a design-oriented proposal is developed to revise and strengthen the existing emergency layouts. The approach is guided by principles of flexibility and adaptability, aiming to improve safety levels in emergency and evacuation conditions under both flood and earthquake events. The proposal is structured around three main actions, and is shown in "**Error! Reference source not found.**":

- *Identification of temporary safe waiting areas*. Selected central squares are designed as temporary safe areas, provided that they satisfy minimum safety requirements (Davis et al. 2023; Bernabei et al. 2021): (i) adequate capacity (maximum density < 3 persons/m^2, considering only unobstructed space); (ii) absence of significant exposure to falling elements in the seismic case; (iii) suitability under flood conditions, potentially supported by elevated or flood-adapted urban furniture; (iv) clear recognisability through dedicated emergency signage. Some areas are considered suitable for both hazards, while others are retained only for seismic scenarios due to their proximity to the river corridor.
- *Redefinition and integration of evacuation routes*. Alternative evacuation paths are proposed to bypass POSs identified as hotspots and to reduce dependence on a limited number of critical segments. In the seismic case, structurally compliant crossing points over the Misa River are considered as strategic alternatives, whereas in flood conditions river crossings are treated more

cautiously due to hydraulic risk. The revised layout aims to shorten evacuation distances, improve network redundancy, and enhance accessibility toward temporary safe areas.

- *Targeted building assessment along strategic segments*. For evacuation paths and temporary safe areas that remain essential within the revised layout, a more detailed seismic assessment of adjacent buildings is recommended to better characterise the expected damage patterns and their potential local impacts, particularly in terms of debris generation and possible obstructions along evacuation corridors caused by structural or non-structural failures. Priority may be assigned to public buildings, while structural improvement of private ones can be promoted through incentive-based strategies.

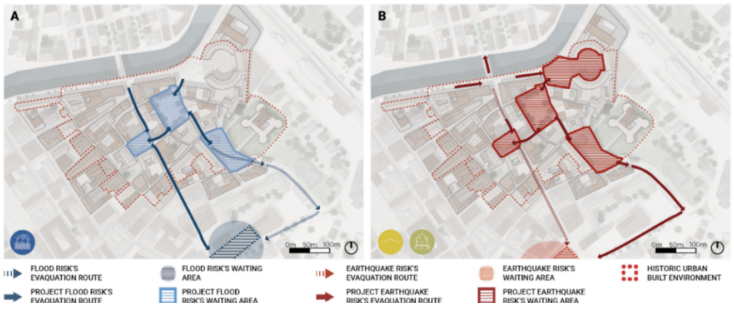


Figure 8 - Proposed implementations for the emergency plans for flood (A) and earthquake (B)

It should be noted that the present application refers to the most recurrent annual crowding condition and does not explicitly include mass-gathering scenarios. Under high-occupancy events, exposure levels would significantly increase, potentially altering the suitability of some temporary safe areas and evacuation paths. Therefore, the emergency plan should be further adapted and stress-tested for event-related overcrowding conditions, with specific attention to reversible uses of public spaces and compatibility between event layouts and emergency functions.

4. Conclusion

This study proposes a design-oriented framework that links single-risk assessment with emergency planning to support the identification of mitigation strategies in UBEs. By comparing risk maps with existing emergency plans, the approach enables the identification of evacuation routes and assembly areas whose risk conditions may compromise safe evacuation. Based on this evidence, the framework supports the definition of alternative evacuation layouts and temporary safe areas, contributing to more adaptable and hazard-consistent emergency strategies.

The methodology integrates hazard characteristics, physical vulnerability and dynamic user-related factors within a POS-centred approach. By aggregating building-scale information to the level of streets and squares, the framework captures spatio-temporal variations in exposure and vulnerability that are often neglected in conventional urban risk assessments. The application to the historical UBE of Senigallia highlights the importance of user dynamics for both flood and earthquake scenarios. Results show that risk distribution depends not only on hazard proximity or building vulnerability, but also on temporal variations in user exposure and vulnerability. Multi-layer single-risk MOTs identify recurrent and scenario-sensitive hotspots, providing a clear spatial and temporal understanding of critical areas. From a design-oriented perspective, the methodology allows authorities to evaluate emergency strategies under recurring use conditions. The scenario-based approach facilitates testing alternative “what-if” configurations, supporting prioritisation of interventions, optimisation of resources, and context-sensitive mitigation strategies.

Despite its contributions, the proposed approach presents some limitations. First, regarding the methodological approach, the assessment of the risk indicators through the AHP method should be extended to additional experts from different university research groups, with diverse backgrounds in flood

and earthquake risk, urban planning, and social vulnerability. Furthermore, the analysis should be complemented by a sensitivity analysis aimed at varying each weight and evaluating its impact on the POS classification. Second, the framework is conceived as a rapid and diagnostic tool to identify critical areas and support preliminary evacuation planning. For operational implementation, the proposed solutions should be complemented by more detailed analyses, including building-scale assessment of seismic and flood damage and evacuation simulations. Such analyses would allow the dynamic performance of evacuation routes to be evaluated under different crowding and behavioural conditions, providing more reliable estimates of potential obstructions, congestion points, and clearance times. Third, the proposed methodology should be applied to a wider range of case studies in order to further validate its feasibility. In particular, it should be tested on case studies for which information on past disaster events and the resulting damages is available, thereby enabling a more comprehensive characterization of impacts and supporting the integration of the proposed strategic framework.

Overall, the proposed methodology provides an operational and transferable tool to support design-oriented risk mitigation and emergency planning in multi-hazard urban contexts, offering decision-makers actionable evidence to prioritise interventions and enhance urban resilience.

Acknowledgments

This research has received funding under the project ReACT ("(planning) Resilient urban and metropolitAn built environments through inClusive mulTi-risk behavioural-based models and simulations", project code PE0000005, CUP E63C22002000002 – funded under the National Recovery and Resilience Plan (NRRP), Mission 4 Component 2 Investment 1.3 ('Partenariati estesi alle università, ai centri di ricerca, alle aziende per il finanziamento di progetti di ricerca di base') funded by the European Union – NextGenerationEU, Italian Ministry of University, according to the Call for tender "Decreto Direttoriale No. 341 of 15/3/2022", Project "Multi-Risk sciEnce for resilienT commUnities undeR a changiNg climate (RETURN)", code PE0000005 – CUP, Concession Decree (Decreto Direttoriale) No. 1552 of 11/10/2022, within the "BANDO a CASCATA" of Spoke 5 TS1 "Insediamenti Urbani e Metropolitani", with relation to the ReACT Concession Decree (Decreto Rettorale di concessione del finanziamento) DR/2025/107 of 13/01/2025 from Università Federico II di Napoli as Spoke.

References

Bernabei, L., G. Mochi, G. Bernardini, and E. Quagliarini. 2021. "Seismic Risk of Open Spaces in Historic Built Environments: A Matrix-Based Approach for Emergency Management and Disaster Response." *International Journal of Disaster Risk Reduction* 65 (August): 102552. https://doi.org/10.1016/j.ijdrr.2021.102552.

Bernardini, Gabriele, Tiago Miguel Ferreira, Pilar Baquedano Julià, Rafael Ramírez Eudave, and Enrico Quagliarini. 2024. "Assessing the Spatiotemporal Impact of Users' Exposure and Vulnerability to Flood Risk in Urban Built Environments." *Sustainable Cities and Society* 100 (July 2023). https://doi.org/10.1016/j.scs.2023.105043.

Bloomberg, Michael R., and Amanda M Burden. 2006. "New York City Pedestrian Level of Service Study Phase I," 1–167.

Dabbeek, Jamal, Helen Crowley, Vitor Silva, and Sevgi Ozcebe. 2025. "Impact of Population Spatiotemporal Patterns on Earthquake Human Losses." *International Journal of Disaster Risk Reduction* 122 (May):105455. https://doi.org/10.1016/j.ijdrr.2025.105455.

Davis, Lucy, Tatiana Larionova, Dhairya Patel, Demiana Tse, Pilar Baquedano Juliá, Pedro Pinto Santos, and Tiago Miguel Ferreira. 2023. "Flood Vulnerability and Risk Assessment of Historic Urban Areas: Vulnerability Evaluation, Derivation of Depth-damage Curves and Cost–Benefit Analysis of Flood Adaptation Measures Applied to the Historic City Centre of Tomar, Portugal." *Journal of Flood Risk Management* 16 (3). https://doi.org/10.1111/jfr3.12908.

Duan, Xiaotong, and Wenjun Fei. 2025. "Assessment of the Impact of Temporal and Spatial Factors on the

Emergency Evacuation Capacity of External Spaces in High-Density Urban Communities during Earthquake Disasters." *International Journal of Disaster Risk Reduction* 129 (October):105760. https://doi.org/10.1016/j.ijdrr.2025.105760.

Ferreira, Tiago M., and Pedro P. Santos. 2020. "An Integrated Approach for Assessing Flood Risk in Historic City Centres." *Water (Switzerland)* 12 (6). https://doi.org/10.3390/w12061648.

Frigerio, Ivan, Stefania Ventura, Daniele Strigaro, Matteo Mattavelli, Mattia De Amicis, Silvia Mugnano, and Mario Boffi. 2016. "A GIS-Based Approach to Identify the Spatial Variability of Social Vulnerability to Seismic Hazard in Italy." *Applied Geography* 74 (September):12–22. https://doi.org/10.1016/j.apgeog.2016.06.014.

Giuliani, Francesca, Anna De Falco, and Valerio Cutini. 2021. "Unpacking Seismic Risk in Italian Historic Centres: A Critical Overview for Disaster Risk Reduction." *International Journal of Disaster Risk Reduction* 59 (June):102260. https://doi.org/10.1016/j.ijdrr.2021.102260.

Goepel, Klaus D. 2013. "Implementing the Analytic Hierarchy Process as a Standard Method for Multi-Criteria Decision Making in Corporate Enterprises – a New AHP Excel Template with Multiple Inputs." In . https://doi.org/10.13033/isahp.y2013.047.

Guo, Qichen, Sheng Jiao, Yuchen Yang, Yan Yu, and Yuqi Pan. 2025. "Assessment of Urban Flood Disaster Responses and Causal Analysis at Different Temporal Scales Based on Social Media Data and Machine Learning Algorithms." *International Journal of Disaster Risk Reduction* 117 (February):105170. https://doi.org/10.1016/j.ijdrr.2024.105170.

He, Pan, Dongqing Zhang, Wei Chen, and Bowen Jia. 2025. "Spatio-Temporal Distribution Estimation and Analysis of Post-Earthquake Casualties in Urban Areas: A Case Study in Chenghua District, Chengdu." *International Journal of Disaster Risk Reduction* 123 (June):105477. https://doi.org/10.1016/j.ijdrr.2025.105477.

Kelman, Ilan, and Michael H. Glantz. 2015. "Analyzing the Sendai Framework for Disaster Risk Reduction." *International Journal of Disaster Risk Science* 6 (2): 105–6. https://doi.org/10.1007/s13753-015-0056-3.

Ministero dell'Interno. 2015. *D.M. 03-08-15, Approvazione Di Norme Tecniche Di Prevenzione Incendi, Ai Sensi Dell'articolo 15 Del Decreto Legislativo 8 Marzo 2006, n. 139.* https://www.gazzettaufficiale.it/eli/id/2015/08/20/15A06189/sg.

Miranda, Fabiana Navia, and Tiago Miguel Ferreira. 2019. "A Simplified Approach for Flood Vulnerability Assessment of Historic Sites." *Natural Hazards*. https://doi.org/10.1007/s11069-018-03565-1.

NTC18 Ministero delle Infrastrutture e dei Trasporti. 2018. "Aggiornamento Delle Norme Tecniche per Le Costruzioni (in Italian); Https://Www.Gazzettaufficiale.It/Eli/Gu/2018/02/20/42/so/8/Sg/Pdf," 1–198. https://www.gazzettaufficiale.it/eli/gu/2018/02/20/42/so/8/sg/pdf.

Protezione Civile, Comune di Senigallia. 2023. "Piani Di Emergenza." 2023. https://www.protezionecivilesenigallia.it/piani-di-emergenza/.

Quagliarini, Enrico, Gabriele Bernardini, Luca Domenella, and Giovanni Marinelli. 2025. "Supporting 'Build Back Better' in Historical Towns: A Novel Methodology to Include Users' Exposure and Vulnerability in Strategic Function Relocation Assessment." *International Journal of Disaster Risk Reduction* 127 (September):105700. https://doi.org/10.1016/j.ijdrr.2025.105700.

Quagliarini, Enrico, Gabriele Bernardini, Guido Romano, and Marco D'Orazio. 2023. "Users' Vulnerability and Exposure in Public Open Spaces (Squares): A Novel Way for Accounting Them in Multi-Risk Scenarios." *Cities* 133 (February):104160. https://doi.org/10.1016/j.cities.2022.104160.

Romano, Guido, Gabriele Bernardini, and Enrico Quagliarini. 2025. "Evaluation of 'Hot Spots' for Pedestrian Risk Assessment and Mitigation in Flood Prone Historic Built Environments." In , 674–85. https://doi.org/10.1007/978-3-032-06978-8_36.

Sharifi, Ayyoob. 2023. "Resilience of Urban Social-Ecological-Technological Systems (SETS): A Review." *Sustainable Cities and Society* 99 (December):104910. https://doi.org/10.1016/j.scs.2023.104910.

UNDRR. 2019. *United Nations Office for Disaster Risk Reduction To Download the Full Report Visit : Https://Gar.Unisdr.Org To Share Your Comments and News on the GAR on Twitter and Facebook , Please Use # GAR2019*.

cinpar2026
XXII International Conference on Building Pathology and Constructions Repair
15th to 17th July 2026 - Lisboa, Portugal

Physical Vulnerability to Floods in Historic Urban Areas: A Building-Scale Assessment Approach

Gabriele BERNARDINI[1], Tiago Miguel FERREIRA[2], **Gessica SPARVOLI**[1], Elena BOSI[3], Enrico QUAGLIARINI[1]

[1] Dipartimento di Ingegneria Civile, Edile e Architettura, Università Politecnica delle Marche, Ancona, IT
[2] CERIS, Department of Civil Engineering, Architecture and Environment, Instituto Superior Técnico (Técnico Lisbon), University of Lisbon, Lisbon, PT
[3] Dipartimento di Architettura e Studi Urbani (DAStU), Politecnico di Milano, Milano, IT

Abstract: Flood Risk Assessment in Historic Urban Areas requires vulnerability models capable of capturing the intrinsic susceptibility of built heritage at the building scale. The present study focuses on the assessment of physical vulnerability, focusing on the impact of building characteristics. Physical vulnerability is defined as the susceptibility of historic buildings to floods, influenced by their construction typology, materials, structural characteristics and ground-floor configuration. A series of physical vulnerability indicators are derived from the existing literature and adapted to heritage-sensitive contexts, with particular attention to data availability and survey feasibility in historic urban fabrics. The indicators are aggregated through a weighted system based on expert judgement to obtain a synthetic physical vulnerability index intended to support building-scale screening and prioritisation. The methodology is applied to the historic centre of Bagnacavallo (Italy), a flood-prone urban area characterised by a dense and heterogeneous built heritage. Results reveal a significant spatial variability of physical vulnerability across the study area, reflecting differences in construction periods, architectural layouts and material properties. The building-scale analysis enables the identification of highly vulnerable heritage structures. The proposed approach offers insights into the intrinsic weaknesses of historic buildings by addressing physical vulnerability independently from hazard intensity and damage-probability modelling. The results support the heritage-oriented prioritisation of preventive conservation and retrofit interventions and demonstrate the value of physical vulnerability as a distinctive analytical dimension in flood risk studies for Historic Urban Areas.

Keywords: Flood Risk Assessment, Physical Vulnerability, Historic Urban Areas, Building-scale Analysis

1. Introduction

Historic Urban Areas are increasingly exposed to flood events driven by climatic changes, fluvial regulation, and progressive urban transformation (Chiara Arrighi et al. 2018; C Arrighi et al. 2023). In these contexts, flooding represents not only a hydrological hazard but also a critical threat to architectural heritage, where structural integrity, material authenticity and cultural value are interconnected. The compact morphology of historic fabrics, combined with ageing construction systems and conservation constraints, increases the potential for damage and complicates post-event resilience (Vojinovic et al. 2016).

The susceptibility of historic buildings to flood effects is influenced by their construction and architectural characteristics (Ferreira and Santos 2020; Vojinovic et al. 2016). Traditional buildings often exhibit increased sensitivity to water infiltration and prolonged water exposure. Ground-floor configurations, which are often aligned with street level and characterised by direct openings, facilitate water penetration and capillary rise. Furthermore, the coexistence of different construction phases and typological adaptations within historic urban fabrics contributes to differentiated structural behaviours under flood conditions. These factors underline the importance of considering vulnerability as an inherent characteristic of individual buildings, rather than a common feature of the overall urban fabric (Ferreira and Santos 2020).

Although flood risk is generally conceptualised as the interaction between hazard, exposure and vulnerability, operational assessments in historic environments often prioritise hydraulic modelling and scenario-based damage estimation (Chiara Arrighi et al. 2018; C Arrighi et al. 2023). Within these approaches, the structural dimension of building vulnerability is often simplified, aggregated at broad scales, or derived from standardised damage functions (Vojinovic et al. 2016). While these approaches provide valuable insights at the territorial or urban scale, they often fail to effectively characterise the inherent vulnerability of heritage structures.

Recent research has increasingly adopted indicator-based models to capture urban vulnerability patterns, integrating parameters related to structural typology, materials and conservation state (Agliata, Bortone, and Mollo 2021; Ferreira and Santos 2020). However, applications in historic contexts still face methodological challenges (Vojinovic et al. 2016). Indicators must be carefully calibrated to reflect heritage-specific characteristics while ensuring compatibility with available datasets and feasible survey procedures (Ferreira and Santos 2020; C Arrighi et al. 2023). Moreover, most existing indicator-based approaches focus on physical attributes of buildings, whereas parameters related to urban form and street-network configuration are less frequently incorporated into physical vulnerability assessments. Nevertheless, research on urban flood modelling highlights the role of street geometry, flow pathways, and local conditions in influencing flood propagation and exposure within cities (Mignot, Li, and Dewals 2019).

A focused assessment of intrinsic physical vulnerability provides a clearer interpretation of structural susceptibility within Historic Urban Areas (Ferreira and Santos 2020). By focusing on measurable architectural and structural attributes, it becomes possible to identify buildings' predisposition to flood damage, regardless of the hazard magnitude. This perspective is particularly relevant for heritage conservation plans, where mitigation/risk-reduction measures and retrofitting strategies can be prioritised according to structural fragility, also in view of their impacts on exposure factors, including population (Bernardini et al. 2025; Chiara Arrighi et al. 2018).

Within this framework, the present study proposes a methodology for assessing the physical vulnerability of historic buildings to flood at the building scale. A structured set of architectural and structural indicators is identified and refined for heritage contexts, ensuring consistency with existing spatial data and survey methods commonly used in Historic Urban Areas. These indicators are combined through a weighted aggregation procedure to determine a vulnerability index. This approach is then applied to the historic centre of Bagnacavallo (Italy), characterised by typological heterogeneity and flood-prone conditions. By focusing on the structural aspect of vulnerability, the present study aims to improve the understanding of the intrinsic fragility of buildings and to support preliminary prioritisation within heritage-oriented flood risk assessment in Historic Urban Areas.

2. Methodology

2.1 Case Study and Data Collection

The historic centre of Bagnacavallo, located in the province of Ravenna within the Emilia-Romagna region (Italy), represents a well-preserved medieval settlement in the Po Valley, the largest alluvial plain in Italy (Figure 1). The area is characterised by geomorphological conditions associated with flood susceptibility, as acknowledged by regional planning documents. According to the Emilia-Romagna Flood Risk Management Plan, the historic urban fabric is located within medium-hazard flood areas, thus confirming its relevance for vulnerability-oriented assessment (Piano di Gestione del Rischio da Alluvione - PGRA). Despite the historic centre not being directly affected by floods during the 2023 Emilia-Romagna event, flood extent maps show inundation in the surrounding areas (Perimetrazione aree allagate eventi 2023-2024). These findings emphasise the need for a structural susceptibility assessment aimed at mitigating potential future damage.

The analysis focuses on 468 buildings belonging to the pre-nineteenth-century core, which is representative of the consolidated historic fabric in terms of urban density, aggregation patterns and typological stratification. The individual building is adopted as the elementary spatial unit of analysis, enabling the direct evaluation of intrinsic architectural and structural characteristics influencing flood susceptibility. This micro-scale analytical perspective allows for differentiated structural configurations within a compact and historically stratified urban context. The built environment comprises a variety of structures, including



Figure 1 - Geographical location of the historic centre of Bagnacavallo and spatial distribution of the main building typologies within the analysed pre-nineteenth-century core.

traditional terraced houses, aggregated residential units, and larger palatial structures. This heterogeneity reflects the constructive and morphological characteristics typical of historic centres in the Po Valley, as shown in Figure 1 (Cantatore 2023).

Data acquisition is structured in order to ensure methodological transparency and reproducibility within a GIS environment (da Silva et al. 2020). Spatial datasets, including building footprints, road networks and urban blocks, are retrieved from regional and municipal geoportals. Building-level attributes relevant to physical vulnerability, including construction period, structural typology, primary materials, number of storeys, ground-floor configuration and conservation condition, were derived from the municipal Historic Centre Survey Plan and verified through targeted field inspections (Piano Particolareggiato del Centro Storico - PPCS 2023). The required attributes were compiled for all 468 buildings included in the analysis and harmonised within the GIS geodatabase. When inconsistencies between documentary sources, cartographic data and field observations were detected, the most recent field evidence was used to update the attribute record.

All spatial and descriptive information is integrated into a structured geodatabase. In the interest of ensuring internal consistency and enabling meaningful comparison across the building stock, the decision is taken

to standardise the attributes. This GIS-based database constitutes the analytical foundation for the subsequent definition and weighted aggregation of physical vulnerability indicators at the building scale.

2.2 Modelling intrinsic physical vulnerability

The intrinsic physical vulnerability of the built environment is assessed using three static indicators that describe building characteristics and stable morphological features at the building scale. The Flood Vulnerability Index (FVI) is derived from existing indicator-based approaches in the literature, while Flood Direction Exposure (FDE) and Road Width (RW) introduce morphology-related information based on street-network configuration, building orientation and spatial layout. These indicators are intended to capture relative differences in physical susceptibility within the historic fabric, rather than to reproduce event-specific hydraulic conditions.

The Flood Vulnerability Index (FVI), derived from the methodology proposed by (Davis et al. 2023; Miranda and Ferreira 2019), represents the central component of the proposed approach. This method is adopted due to its compatibility with detailed building survey data and its suitability for systematic GIS-based implementation at microscale. The FVI is defined as the product of Sensitivity Index (SI) and an Exposure Index (EI), normalised by the maximum theoretical value within the study area (Equation 1):

$$FVI = SI \times EI / FVI_{max} \quad (1)$$

SI captures intrinsic structural susceptibility to flood damage, and is calculated using seven parameters that describe material, structural and geometric characteristics. These include: (S1) state of conservation, evaluated according to the extent of deterioration and cracking; (S2) structural material, distinguishing among reinforced concrete or steel frames, masonry, timber and earthen constructions; (S3) facade finishing material, reflecting the resistance of envelope surfaces to water exposure; (S4) window/door frames' type and condition; (S5) number and configuration of ground-floor openings, representing potential water entry points; (S6) basement configuration, differentiating between absence of sub-grade spaces and direct-access basements; and (S7) entrance threshold height relative to street level. EI accounts for contextual characteristics that influence potential loss, including economic relevance, physical impact potential, and cultural value. It comprises three parameters: (E1) building use, reflecting functional and economic significance; (E2) surrounding surface morphology, describing configurations that may favour or limit water accumulation; and (E3) heritage designation level, representing increasing degrees of cultural value. Each parameter is classified into four vulnerability classes (A–D), associated with increasing weights: 10, 40, 70, and 100. The lowest class is intentionally assigned a non-zero weight to reflect the inherent baseline vulnerability of historic constructions due to ageing materials and traditional building systems. The SI and EI are obtained as weighted sums of their respective parameters prior to aggregation into the final FVI (Davis et al. 2023; Miranda and Ferreira 2019).

The Flood Direction Exposure (FDE) indicator describes the geometric exposure of building façades to potential flood flow directions using the street network as a morphological proxy. The street network is modelled as a parametric graph composed of nodes, defined at intersections, profile changes or width variations, and links, corresponding to road segments between nodes. Each building is associated with the corresponding street link within the GIS database. For each street link, two opposite directions are considered, representing a simplified approximation of possible flow alignment along the street axis. Building classification is determined by the angle between the façade orientation and each assumed direction, resulting in three exposure categories: parallel impact, oblique impact and perpendicular impact. The classifications obtained for the two opposite directions are combined using a 3 × 3 matrix, producing an FDE value ranging from 1 to 5. A value of 1 corresponds to parallel orientations in both directions, while a value of 5 corresponds to perpendicular orientations in both directions. Intermediate values reflect mixed alignments. The index is then normalised by dividing by the maximum possible value, resulting in a dimensionless indicator [-].

This formulation is not intended to represent hydraulic routing or simulated flood dynamics. It does not account for local flow concentration, obstruction effects, water depth, velocity, duration or return period. Its role is instead to introduce, within a preliminary vulnerability screening, a morphology-based descriptor of the potential directional exposure of façades.

The Road Width (RW) indicator represents a morphology-based proxy for the potential influence of road geometry on local flood propagation conditions (Balaian, Sanders, and Abdolhosseini Qomi 2024; Mignot, Li, and Dewals 2019). In compact historic fabrics, street width may affect flow confinement and the spatial distribution of water along the street network, although it cannot directly estimate hydraulic variables such as water depth, velocity or pressure. The index is calculated as the ratio between the width of each street and the maximum street width within the study area, ranging from 0 (excluded) to 1 (for the maximum road width in the considered Historic Urban Areas). This approach aims to identify the roads and buildings along them that are more susceptible to such effects than others.

It is important to note that FVI, FDE and RW are derived from intrinsic structural attributes and stable morphological characteristics of the historic fabric. Therefore, the parameters remain constant within the temporal limits of the analysis, and collectively provide a building-scale representation of intrinsic physical vulnerability within the Historic Urban Areas.

2.3 Index Construction and Weighting Approach

The Physical Vulnerability (PV) index is derived through the weighted aggregation of the three static indicators defined in the previous section. The relative importance of each parameter is determined using the Analytic Hierarchy Process (AHP), a multi-criteria decision-making method that ensures transparent and consistent integration of heterogeneous factors (Goepel 2018; Agliata, Bortone, and Mollo 2022).

Pairwise comparisons among the PV parameters are independently performed by six experts from university research groups, with different backgrounds in flood risk, urban planning, and built heritage conservation. Evaluations employed a linear integer scale from 1 (equal importance) to 9 (maximum importance) within the AHP Excel system (Goepel 2018). The final priorities are calculated through the row geometric mean method (RGMM) and normalised to ensure that their sum is equal to 1. The logical coherence of the pairwise judgments is verified through the Consistency Ratio (CR), with values below 10 % considered acceptable. For the PV index, the aggregated CR was 2.1 %, thereby confirming the reliability and the internal consistency of the comparisons.

The degree of agreement among experts was assessed using the AHP consensus indicator S*, a homogeneity index based on Shannon entropy (Goepel 2018). Six experts with different backgrounds in structural engineering, historic building conservation, and urban planning provided the pairwise comparisons, resulting in a high consensus levelof S* = 98 % for PV . This high level of consensus supports the internal coherence of the weighting scheme within the expert-based AHP procedure. Each parameter is then multiplied by its corresponding weight, and the weighted values are summed to produce the PV index. According to the derived AHP priorities, the PV index for each building is calculated as shown in Equation 2:

$$PV = 0.66 \cdot FVI + 0.235 \cdot FDE + 0.105 \cdot RW \quad (2)$$

This formulation results in a dimensionless measure ranging from 0 to 1, thereby ensuring comparability across the entire built environment.

The PV index is subsequently discretised into five ordered categories: negligible (0.0–0.2), low (0.2–0.4), moderate (0.4–0.6), high (0.6–0.8), and extreme (0.8–1.0). This classification facilitates interpretation, comparability, and GIS-based visualisation, enabling the spatial identification of vulnerable buildings and critical clusters within the historic fabric. The resulting maps support decision-making in flood risk management and heritage conservation by providing a spatially explicit representation of building-scale physical vulnerability (Evans et al. 2024; Taramelli et al. 2022).

3. Results

This section presents the spatial distribution of intrinsic physical vulnerability across the historic centre of Bagnacavallo, examining both the component indicators (FVI, FDE and RW) and the aggregated PV index (Figure 2). The class-based distribution confirms the predominance of low-to-moderate PV values, with 76% buildings classified as low and 17% as moderate. Negligible and high PV classes account for 4% and 3% of the building stock, respectively, while no buildings fall within the extreme class.



Figure 2 - Spatial distribution of the component indicators and PV, according to the general classification ranges adopted for the indicators in this work: (a) Flood Vulnerability Index (FVI), (b) Flood Direction Exposure (FDE), (c) Road Width (RW), (d) aggregated PV index derived from the weighted combination of the three indicators.

FVI map (Figure 2.a) highlights the intrinsic structural susceptibility of the built environment. A higher density of FVI values is observed along the primary roads within the historic core, suggesting a significant correlation between vulnerability and urban hierarchy. Buildings with a large ground-floor opening and complex structural configuration, particularly those located along main roads, show a higher level of vulnerability. Conversely, smaller terraced and row houses located along secondary and narrower streets tend to exhibit lower FVI values, reflecting simplified typologies and more compact façades. The buildings

surrounding the main square show high FVI values, due to the influence of heritage constraints and non-residential ground-floor uses. These uses may increase exposure and limit structural adaptability.

FDE map (Figure 2.b) provides a representation of exposure variations associated with building orientation concerning potential flood flow directions. The majority of buildings fall within parallel or oblique configuration with respect to the street layout, resulting in moderate exposure conditions. Conversely, buildings positioned perpendicularly at street intersections are more directly exposed to incoming water flow, increasing their susceptibility. The irregular and curvilinear layout of the historic street network locally modifies these geometric relationship, contributing to spatial variability in exposure across the urban fabric. Although slope plays a limited role in the present case study due to the flat morphology of the floodplain, the overall orientation of the urban layout remains a relevant factor in shaping potential impact conditions. It should be noted that FDE represents a morphological proxy derived from the geometric relationship between buildings and the street network, rather than from hydraulic flood simulations.

As shown in Figure 2.c, RW reflects the influence of road width on vulnerability. Buildings located along narrow streets generally exhibit higher RW-related vulnerability values, while those facing wider streets or open spaces, such as squares, show lower values. Within the analysed street network, narrow street sections represent a significant proportion of the historic core, reflecting the compact morphology typical of historic settlements in Po Valley. This distribution contributes to the higher RW values observed across the case study.

Finally, the aggregated PV index (Figure 2.d), derived from the weighted combination of FVI, FDE, and RW (Eq. 2), synthesises these spatial patterns. Consistently with the class-based distribution reported above, PV values are predominantly concentrated in the low-to-moderate range (0.2–0.6). This indicates that most buildings present limited to intermediate intrinsic physical susceptibility according to the adopted indicator-based classification. Nevertheless, there is a clear spatial correlation between areas of higher vulnerability and specific geographical locations, particularly along the main roads and primary squares. These areas correspond to buildings in which intrinsic structural susceptibility and adverse exposure conditions converge. The results demonstrate that physical vulnerability is not arbitrary but is closely associated with architectural typology, construction characteristics, and urban morphology. The strong correlation between the component indicators and the aggregated PV index confirms the robustness of the adopted weighting scheme and highlights the dominant influence of intrinsic structural features in shaping vulnerability patterns.

4. Discussion and Final Remarks

The application of the proposed methodology to the historic centre of Bagnacavallo highlights the analytical value of considering intrinsic physical vulnerability as a distinctive dimension within flood risk assessment for Historic Urban Areas. By focusing on structural and morphology-related characteristics at the building scale, the method supports the identification of spatially differentiated susceptibility profiles that may otherwise remain hidden in hazard-centred or macro-scale assessments. In this sense, the PV index should be interpreted as a screening and prioritisation tool, rather than as a direct predictor of flood damage.

The results demonstrate that physical vulnerability is strongly influenced by the interaction between architectural typology and urban morphology. Higher PV values are concentrated along the main roads and around the square, where larger buildings with wider ground-floor openings and more articulated structural configurations prevail. Conversely, smaller terraced and row houses located along secondary streets generally show lower vulnerability levels. These observations indicate that, even within a compact and historically homogeneous urban fabric, intrinsic structural variability significantly influences the spatial distribution of physical susceptibility to flooding.

The aggregated PV index shows broad spatial consistency with the distribution observed in the individual indicators, particularly with the FVI, which has the highest AHP-derived weight. This suggests that the

aggregation procedure preserves the main vulnerability patterns emerging from the component indicators, although the quantitative robustness of the adopted weights should be further examined through dedicated sensitivity analyses. As also observed in the results section, most buildings fall within low-to-moderate vulnerability ranges, while comparatively higher PV values identify spatial clusters where intrinsic structural susceptibility and adverse morphological conditions converge. In this context, the PV index operates as a screening and prioritisation instrument rather than a direct damage predictor, thereby facilitating preventive planning and targeted building-scale assessments.

The building-level resolution represents a key contribution of the study. By capturing the heterogeneity of the urban environment and enabling micro-spatial analysis, the approach provides a detailed understanding of vulnerability drivers and an operational basis for risk-informed decision-making. The translation of architectural and morphological attributes into spatially explicit metrics can also facilitate integration with planning instruments and conservation-oriented risk mitigation strategies.

Nevertheless, some methodological limitations should be acknowledged. The proposed PV index is based on intrinsic building attributes and stable morphological descriptors and therefore does not include event-specific hydraulic variables such as water depth, velocity, duration, flow concentration, obstruction effects or return period. Similarly, the FDE indicator is derived from the geometric relationship between façades and the street network and should be interpreted as a simplified morphological proxy rather than as an output of hydraulic flood modelling. The index has not been calibrated or validated against observed flood damage, measured inundation levels or independent expert classifications of damage susceptibility. These aspects do not undermine its use as a preliminary screening tool, but they limit its interpretation as a predictive damage model. Future research should combine the proposed building-scale vulnerability assessment with hydrodynamic simulations, post-event damage observations and sensitivity analyses on weights and class thresholds.

In conclusion, the study demonstrates that the systematic assessment of intrinsic physical vulnerability at the building scale provides a robust and transferable methodological framework for flood risk analysis in Historic Urban Areas. By revealing spatially structured patterns of susceptibility, the approach supports evidence-based prioritisation and contributes to advancing heritage-sensitive risk mitigation strategies.

References

Agliata, Rosa, Antonio Bortone, and Luigi Mollo. 2021. “Indicator-Based Approach for the Assessment of Intrinsic Physical Vulnerability of the Built Environment to Hydro-Meteorological Hazards: Review of Indicators and Example of Parameters Selection for a Sample Area.” *International Journal of Disaster Risk Reduction* 58 (May): 102199. https://doi.org/10.1016/j.ijdrr.2021.102199.

———. 2022. “The Impact of the Aggregation Formula on Indicator-Based Method for the Assessment of Building Susceptibility to Hydro-Meteorological Hazards.” *International Journal of Disaster Risk Reduction* 72 (April): 102850. https://doi.org/10.1016/j.ijdrr.2022.102850.

Arrighi, C, M Tanganelli, M T Cristofaro, V Cardinali, A Marra, F Castelli, and M De Stefano. 2023. “Multi-Risk Assessment in a Historical City.” *Natural Hazards* 119 (2): 1041–72. https://doi.org/10.1007/s11069-021-05125-6.

Arrighi, Chiara, Lauro Rossi, Eva Trasforini, Roberto Rudari, Luca Ferraris, Marcello Brugioni, Serena Franceschini, and Fabio Castelli. 2018. “Quantification of Flood Risk Mitigation Benefits: A Building-Scale Damage Assessment through the RASOR Platform.” *Journal of Environmental Management* 207 (February): 92–104. https://doi.org/10.1016/j.jenvman.2017.11.017.

Balaian, Sarah K., Brett F. Sanders, and Mohammad Javad Abdolhosseini Qomi. 2024. “How Urban Form Impacts Flooding.” *Nature Communications* 15 (1): 6911. https://doi.org/10.1038/s41467-024-50347-4.

Bernardini, Gabriele, Gessica Sparvoli, Elena Cantatore, Silvana Bruno, Fabio Fatiguso, Ilaria Isacco, Graziano Salvalai, and Enrico Quagliarini. 2025. “From Single to Multi-Risk Perspective: How Heatwaves Risk Mitigation Solutions Can Reduce Terrorist Risk in Historic Outdoor Open Areas.” *Sustainable Cities and Society*, May, 106412. https://doi.org/10.1016/j.scs.2025.106412.

Cantatore, M. F. A. 2023. *DA PLACENTIA A PLACENCIA. Trasformazione Della Morfologia Urbana Di Piacenza Dall'età Tardoantica All'alto Medioevo.*

Davis, Lucy, Tatiana Larionova, Dhairya Patel, Demiana Tse, Pilar Baquedano Juliá, Pedro Pinto Santos, and Tiago Miguel Ferreira. 2023. "Flood Vulnerability and Risk Assessment of Historic Urban Areas: Vulnerability Evaluation, Derivation of Depth-Damage Curves and Cost–Benefit Analysis of Flood Adaptation Measures Applied to the Historic City Centre of Tomar, Portugal." *Journal of Flood Risk Management* 16 (3): 1–18. https://doi.org/10.1111/jfr3.12908.

Evans, Barry, Arthur Lam, Charles West, Reza Ahmadian, Slobodan Djordjević, Albert Chen, and Maria Pregnolato. 2024. "A Combined Stability Function to Quantify Flood Risks to Pedestrians and Vehicle Occupants." *Science of The Total Environment* 908 (January): 168237. https://doi.org/10.1016/j.scitotenv.2023.168237.

Ferreira, Tiago M., and Pedro P. Santos. 2020. "An Integrated Approach for Assessing Flood Risk in Historic City Centres." *Water* 12 (6): 1648. https://doi.org/10.3390/w12061648.

Goepel, Klaus D. 2018. "Implementation of an Online Software Tool for the Analytic Hierarchy Process (AHP-OS)." *International Journal of the Analytic Hierarchy Process* 10 (3). https://doi.org/10.13033/ijahp.v10i3.590.

Mignot, Emmanuel, Xuefang Li, and Benjamin Dewals. 2019. "Experimental Modelling of Urban Flooding: A Review." *Journal of Hydrology* 568 (November 2018): 334–42. https://doi.org/10.1016/j.jhydrol.2018.11.001.

Miranda, Fabiana Navia, and Tiago Miguel Ferreira. 2019. "A Simplified Approach for Flood Vulnerability Assessment of Historic Sites." *Natural Hazards*. https://doi.org/10.1007/s11069-018-03565-1.

Perimetrazione aree allagate eventi 2023-2024. Accessed October 17, 2025. https://servizimoka.regione.emilia-romagna.it/mokaApp/apps/allagam_202305/index.html.

Piano di Gestione del Rischio da Alluvione - PGRA. Accessed October 17, 2025. https://ambiente.regione.emilia-romagna.it/it/suolo-bacino/sezioni/piano-di-gestione-del-rischio-alluvioni.

Piano Particolareggiato del Centro Storico - PPCS. 2023. Accessed October 17, 2025. https://www.labassaromagna.it/Documenti-e-dati/Documenti-tecnici-di-supporto/Piano-Particolareggiato-del-Centro-Storico-PPCS.

Silva, Lucas Borges Leal da, Júlia Santos Humberto, Marcelo Hazin Alencar, Rodrigo José Pires Ferreira, and Adiel Teixeira de Almeida. 2020. "GIS-Based Multidimensional Decision Model for Enhancing Flood Risk Prioritization in Urban Areas." *International Journal of Disaster Risk Reduction* 48 (September): 101582. https://doi.org/10.1016/j.ijdrr.2020.101582.

Taramelli, Andrea, Margherita Righini, Emiliana Valentini, Lorenzo Alfieri, Ignacio Gatti, and Simone Gabellani. 2022. "Building-Scale Flood Loss Estimation through Vulnerability Pattern Characterization: Application to an Urban Flood in Milan, Italy." *Natural Hazards and Earth System Sciences* 22 (11): 3543–69. https://doi.org/10.5194/nhess-22-3543-2022.

Vojinovic, Zoran, Michael Hammond, Daria Golub, Sianee Hirunsalee, Sutat Weesakul, Vorawit Meesuk, Neiler Medina, Arlex Sanchez, Sisira Kumara, and Michael Abbott. 2016. "Holistic Approach to Flood Risk Assessment in Areas with Cultural Heritage: A Practical Application in Ayutthaya, Thailand." *Natural Hazards* 81 (1): 589–616. https://doi.org/10.1007/s11069-015-2098-7.

Cinpar 2026
XXII International Conference on Building Pathology and Constructions Repair
15th to 17th July 2026 - Lisboa, Portugal

Watershed as a Basis for Heritage Vulnerability Assessment of Historic Urban Landscapes

Joana GUEDES[1], João ALEXANDRINO[2], Esequiel MESQUITA[3], Tiago Miguel FERREIRA[4]

[1] Institute of Architecture and Urbanism and Design, Federal University of Ceara, Fortaleza, Brazil, joanapguedes@arquitetura@ufc.br
[2] Institute of Architecture and Urbanism and Design, Federal University of Ceara, Fortaleza, Brazil, joaoalexandrino@arquitetura.ufc.br
[3] Institute of Architecture and Urbanism and Design, Federal University of Ceara, Fortaleza, Brazil, emesquita@ufc.br
[4]Instituto Superior Técnico, University of Lisbon, Lisbon, Portugal, tiago.miguel.ferreira@tecnico.ulisboa.pt

Abstract: Water serves as a primary integrating resource and, since hydrological processes are influenced by the physical urban form, it should be used as the backbone of territorial planning. This work proposes the operationalization of the watershed as a land unit in assessing the sensitivity of urban built heritage to flood events from the perspective of climate change. To determine the area of study, the ottocoded watershed database updated in 2026 was employed. Then, the landscape layers relevant to the characterization of the land unit were selected. Morphological, socioeconomic, and environmental analyses were performed using the open-source software QGIS and the Hand Model application. The results were reclassified and overlaid to identify the most vulnerable elements in flood occurrence. The watershed lens enabled the observation that infrastructure and occupation patterns remodeled the site's characteristics, influencing the vulnerability of the heritage landscape and its asset ensemble to water-related events. This uncovers its potential as an interface between climate risk assessment, urban planning, and historic urban landscape management. In this sense, adopting the watershed drainage area as a land unit allowed interpreting the section as a complex system of interconnected elements within its larger context, enabling a deeper understanding of the landscape and encouraging a truly holistic approach.

Keywords: Built heritage, Watershed, Vulnerability Assessment, Historic Urban Landscape, Climate change.

1. Introduction

Urban heritage, understood as the set of tangible and intangible elements within a city, is an important factor of identity and social cohesion, representing a valuable resource for maintaining well-being in urban areas (Taylor 2023; Y. Wang et al. 2024; UNESCO 2011). From the HUL perspective, cities are the product of a continuous and historical overlapping of layers that manifest both natural and cultural attributes (Ji, Shao, and Du 2020). One of the main drivers of this constant state of transformation is urbanization processes that, when poorly planned, can weaken urban centers and their inhabitants, making them particularly vulnerable to the negative impacts of climate change and other anthropogenic phenomena (United Nations 2017)—a condition that becomes especially critical when it involves built heritage (Adetunji and Daly 2024).

Climate change undermines the sustainable development of communities, posing multiple risks to cultural heritage (Graus et al. 2024; Lankester and Knight 2024; Gallina et al. 2016). It continuously challenges conservation efforts, with severe impacts on the social and economic spheres, highlighting the need to integrate heritage management into the development of adaptation and mitigation actions (Quesada-Ganuza et al. 2021). This integration aligns with the Historic Urban Landscape (HUL) approach, which includes, among other fundamental steps, the assessment of heritage vulnerability to the effects of climate change for consideration in urban planning (World Heritage Training and Research Institute for the Asia and the Pacific Region et al. 2016). Vulnerability assessments are increasingly used to identify critical

points and to provide informational support for the development of solutions across different scales (Fritzsche et al. 2017). According to the IPCC (2022), assessing vulnerability means assessing “The propensity or predisposition to be adversely affected. Vulnerability encompasses a variety of concepts and elements, including sensitivity or susceptibility to harm and lack of capacity to cope and adapt”.

Recognized as the main driver of material degradation of heritage, much of the research combining climate change and preservation focuses on water-related events (Sesana et al. 2021; Salazar, Figueiredo, and Romão 2024; Quesada-Ganuza et al. 2021; Figueiredo, Romão, and Paupério 2020). Most of these studies address the impact of floods on specific elements (Figueiredo, Romão, and Paupério 2020), using object-related indices. This pattern reinforces a gap in the literature, emphasized by Quesada-Ganuza et al. (2021), related to the use of holistic approaches capable of considering the complexity of the context in which the heritage object is embedded. From this perspective, landscape characteristics represented through spatial data form a new dimension of importance for vulnerability assessments, since land use and occupation patterns influence the dynamics and impact of the event (S. Wang, Chen, and Gao 2022; Hassan Rashid, Manzoor, and Mukhtar 2018; Mendonça and Medeiros Leitão 2009; Ferreira, Walsh, and Ferreira 2018).

As a topographic area that collects precipitation toward a common drainage axis, the watershed is a territorial unit that interacts directly with climatic vectors and with land use and occupation (Arshed et al. 2023; Fox 2009, chap. 06). Therefore, this work proposes the operationalization of the watershed as a working scale for a flood vulnerability analysis capable of being reflected in heritage, enabling the guidance of integrated management and planning actions. This proposal's feasibility was tested in a watershed of the city of Fortaleza (Ceará, Brazil) significant for containing the greatest portion of the built heritage portfolio. The vulnerability calculation employed a set of GIS tools to conduct map algebra, based on georeferenced data collected from different governmental repositories. The approach can guide the distribution of conservation efforts through the identification of buildings in more critical situations, proving to be a valuable tool for heritage management.

2. Case Study

Fortaleza, capital of Ceará state (Figure 1, presents a current estimated population of 2.5 million inhabitants, the city has its origins in the 17th century around Forte Schoonenborch, later named Forte Nossa Senhora da Assunção. From the 20th century onward, Fortaleza experienced rapid urban and population growth based on investment in infrastructure and the strengthening of tourism, without, however, having planning policies. This resulted in occupation driven by economic and real estate agents that radically transformed the territory, erasing part of the local memory through heritage demolitions under the “demolish to build” discourse (Raimundo Freitas Aragão, Marcos da Silva Rocha, and Helania Martins de Souza 2019).

Fortaleza's vegetation is typically coastal, with mangrove and restinga areas, a pluviometric index of 1,378 mm/year, and a heterogeneous rainfall regime concentrated in the first quarter of the year. Climate is classified as tropical semi-humid, with an average annual temperature ranging from 26°C to 28°C. The main hydrography of the municipality recognizes four major watersheds: the Cocó River, Maranguapinho River, Pacoti River, and the coastal watershed (IPECE 2026; Prefeitura Municipal de Fortaleza, Secretaria Municipal de Urbanismo e Meio Ambiente, and ICLEI 2020; SEUMA 2015).

Urban occupation patterns associated with climate change have exposed the city to 4 major risks: increase in temperature, extreme rains, prolonged droughts, and sea level rise. According to the Digital Atlas of Disasters in Brazil, between 2001 and 2023, 6 hydrological events were recorded that resulted in 11 deaths, 70,31 million people left homeless, and 116.11 million people directly affected. This meant R$ 189,03 million in material damages and R$ 23,03 million in public losses. (Ministério da Integração e do Desenvolvimento Regional, n.d.; Prefeitura Municipal de Fortaleza, Secretaria Municipal de Urbanismo e Meio Ambiente, and ICLEI 2020).

The analysis scope adopts an Ottocoded level 6 watershed, which represents the smallest drainage area delimited for the region (Figure 1). The Ottocoded hydrographic base is a representation form proposed by Otto Pfafstetter that depicts river flow, connected sections, and water displacement direction. Originating from the Brazilian Systematic Mapping, version 6 follows the hydrographic delimitation proposed by the HydroSHEDS project, a global database containing publicly accessible hydroecological information, associating the water resource management efforts by the National Water Agency with a broader scale (Ana Paula Fiorezi, Alexandre de Amorim Teixeira, and Diana Leite Cavalcanti 2024). The study area, of 21,4 km², on the north coast of the municipality, encompasses 76 (72%) of the 106 listed heritage assets, highlighting the importance of the area for local historical development.

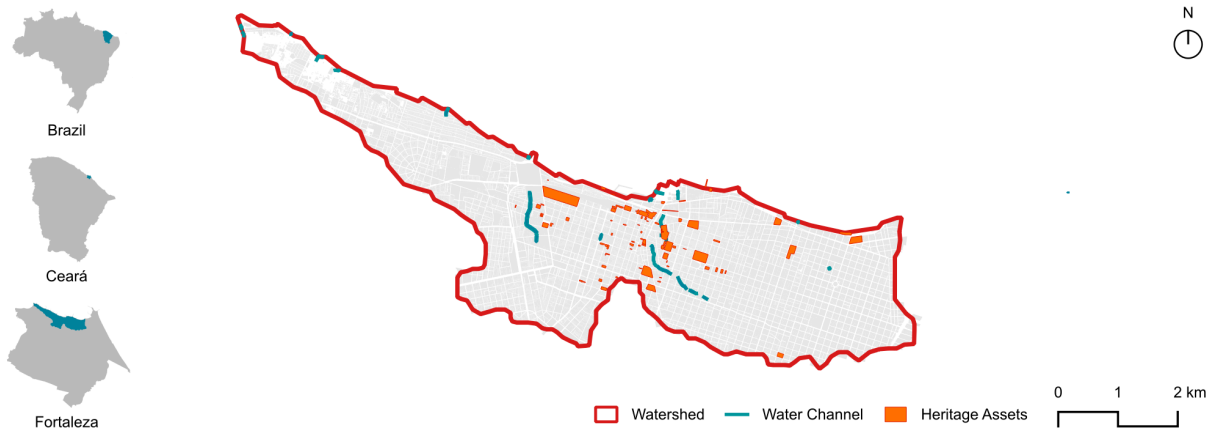


Figure 1 – Location of the study area and delineation of the basin containing the heritage resources of interest.

3. Methodology

For the selection of layers relevant to the vulnerability analysis, this study examined peer-reviewed publications on multi-criteria flood analyses. The authors consulted ScienceDirect, Scopus, and Web of Science databases to select Open Access works published between 2020 and 2025, using the combination of keywords ("flood vulnerability" OR "flood risk") AND ("multi-criteria analysis" OR "multi-criteria evaluation" OR "multi-criteria decision analysis") AND "climate change". A refinement of the initial set, comprising 368 articles, excluded duplicates and removed publications that did not mention, in the title, abstract, or keywords, all topics of interest: "flood risk" or "flood vulnerability"; "multi-criteria" or "multicriteria"; and "climate change". After screening 33 filtered items, 21 publications reported the layers used and formed the basis for the informational selection in this study (Table 1). The primary factor for including layers in the list of interest was their occurrence. A substantial portion of publications utilized common physical and socioeconomic layers, yet many singular occurrences were also noted. This suggests a lack of consistency in how vulnerability is characterized. The authors added new layers during the process to bridge informational gaps in vulnerability characterization.

Table 1 – Amount of layers (by type) incorporated into the reference publications.

Author	Topographic Layers	Infrastructure Layers	Climatic Layers	Socioeconomic Layers
Ahmad et al. (2025)	4	3	1	2
Al-Rjoub and Ibrahim (2025)	9	1	1	0
Broekman, Coetzee, and Cilliers (2025)	4	2	1	0
Chaulagain et al. (2023)	2	3	1	0

Edamo, Bushira, and Ukumo (2022)	13	3	1	1
Faruk et al. (2025)	5	4	1	1
Ghanem and Zaifoglu (2024)	11	3	2	1
Hadipour, Vafaie, and Deilami (2020)	1	0	0	7
Hagos et al. (2022)	3	3	1	0
Leeonis et al. (2024)	2	4	1	2
Merga et al. (2023)	4	1	1	0
Mokhtari et al. (2023)	6	5	1	2
Nahin et al. (2023)	3	4	1	5
Sousa et al. (2025)	3	1	0	0
Sukri et al. (2025)	3	3	0	0
Tang et al. (2021)	5	8	2	5
Vojtek et al. (2021)	6	3	0	0
M. Wang et al. (2025)	3	10	0	2
Weday, Tabor, and Gemeda (2023)	3	2	0	0
Wongthongtham et al. (2023)	6	1	1	0
Zahid et al. (2025)	5	3	1	2

The vulnerability assessment of the study area was carried out through map algebra. The application of the method involved the operationalization of selected geo-referenced spatial layers, provided by sources at different governance scales, resulting in a physical and social characterization of the area (Table 2). To produce analyses tailored to the study area, the layers were clipped to the boundaries of the selected watershed using the free software QGIS (version 3.40.15 - Bratislava) (QGIS Development Team 2024). The HAND Model software (version 1.0) (Antonio Donato Nobre et al. 2016) was used for obtaining the HAND, drainage, and Flow Accumulation layers, enhancing the identification of local hydrological characteristics. All geographic layers were converted to raster format to ensure faster operations.

To perform the map algebra operation, the values of each rasterized attribute were classified according to their influence on the vulnerability to flooding within the study extent, always recognizing five value classes to standardize the investigations; subsequently, these classes were reclassified through a normalization from 1 to 5, from least to most influential. The definition of the threshold values for these classes was carried out in three ways: (i) when the layer data were continuous and not uniformly distributed, the natural breaks (Jenks) classification was used; (ii) when the data had a large range and were predominantly concentrated in low values, a logarithmic scale classification was applied; and (iii) when the data were categorical, a correspondence was established with the values already in use. Thus, 19 layers were reclassified (Table 2), and their average was computed to represent the overall flooding vulnerability of the analyzed territory.

Table 2 – Description of the layers employed by the authors to support the vulnerability analysis.

Feature	Layer	Interpretation	Source
Physical	Elevation	Low elevation areas receive run off from higher regions	SEFIN (2020)
Physical	Slope	Low-slope areas drain water poorly, creating potential for accumulation.	SEFIN (2020)

Physical	Terrain Ruggedness Index (TRI)	Flat areas drain water poorly, creating potential for water accumulation.	SEFIN (2020)
Physical	Flow accumulation (ACC)	Higher values indicate higher water accumulation.	SEFIN (2020)
Physical	HAND	Low HAND shows the closest vertical distance from the nearest river, indicating lower altitude areas more susceptible to flooding.	SEFIN (2020)
Physical	NDVI	Low NDVI indicates urbanized areas.	INPE (2025)
Physical	Soil type	High porosity indicates fast absorption.	SGB/CPRM (2026)
Climatic	Mean annual precipitation	High precipitation values are related to flooding, increasing the likelihood of inundations.	Funceme (2017)
Climatic	Annual frequency of precipitation > = 50 mm	Intense rainfall (>50 mm) corresponds to large water volumes, associated with flooding and inundations.	Funceme (2017)
Climatic	Average maximum precipitation	Areas with a higher number of rainy days exceeding 50 mm are less favorable.	Funceme (2017)
Infrastructure	Drainage density	Areas with a higher density are less favorable.	SEFIN (2020)
Infrastructure	Road density	High road density indicates soil sealing, creating artificial channels that direct urban runoff.	SEFIN (2020)
Infrastructure	Construction sites, foundations, and ruins	Areas near buildings under development, in ruins, or in poor condition are more sensitive.	SEFIN (2020)
Socioeconomic	Population density	A greater number of people are exposed to flooding.	IBGE (2017)
Socioeconomic	Age < 4 years old	Children up to 4 years old have reduced mobility, associated with high dependence due to cognitive limitations.	IBGE (2017)
Socioeconomic	Age > 60 years old	Elder people may face mobility issues, reduced fitness to handle extreme situations, and reluctance to abandon their homes.	IBGE (2017)
Socioeconomic	Female demographics	Sociocultural norms prevent women from engaging in some activities, exposing them more to the effects of adverse events.	IBGE (2017)
Socioeconomic	Total nominal monthly household income	People with lower incomes face difficulty to recover from flooding events.	IBGE (2017)
Socioeconomic	Household density	A greater number of homes are exposed to flooding.	IBGE (2017)

4. Results and Discussion

4.1 Landscape characterization

The reclassification of the layers enabled the spatial interpretation of data through maps (Figure 2) and quantitative analyses (Figure 3) capable of supporting the characterization of the territory and interpreting cultural heritage sensitivity within the scope. The assessment of physical characteristics showed that, despite having high porosity throughout the extent of the scope, there is a predominance of high-sensitivity physical factors (Figure 3). The combination of large areas with high Slope indices (57,4% class 5), TRI (58,5% class 5), HAND (54,8% class 5), in a region mostly with low Flow Accumulation (62,4% class 1), defines the watershed with high water accumulation potential, low drainage capacity, and isolated from adjacent drainage areas. Considering these characteristics, floods are mainly related to rainfall accumulation, reinforcing the need to incorporate information about the distribution of climatic events in the territory—areas with higher maximum averages, annual averages, and amounts of days with rainfall above 50 mm were interpreted as more sensitive.

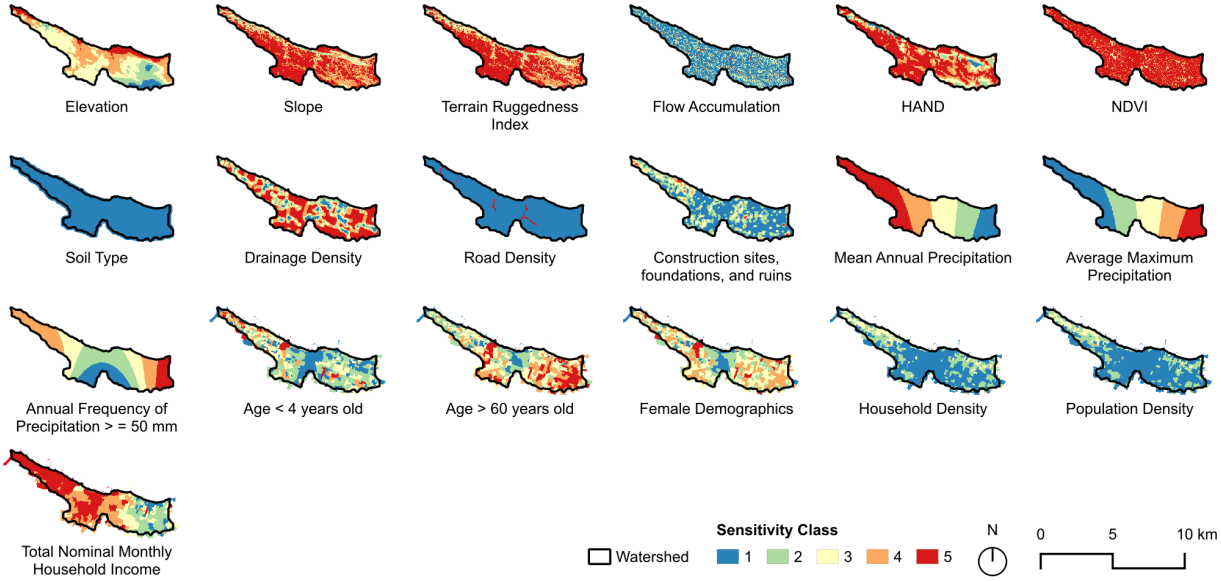


Figure 2 – Layers reclassification. Classes vary from the least influential (class 1) to most influential (class 5) according to their respective interpretations of the sensitivity/ability to cope represented by the layer.

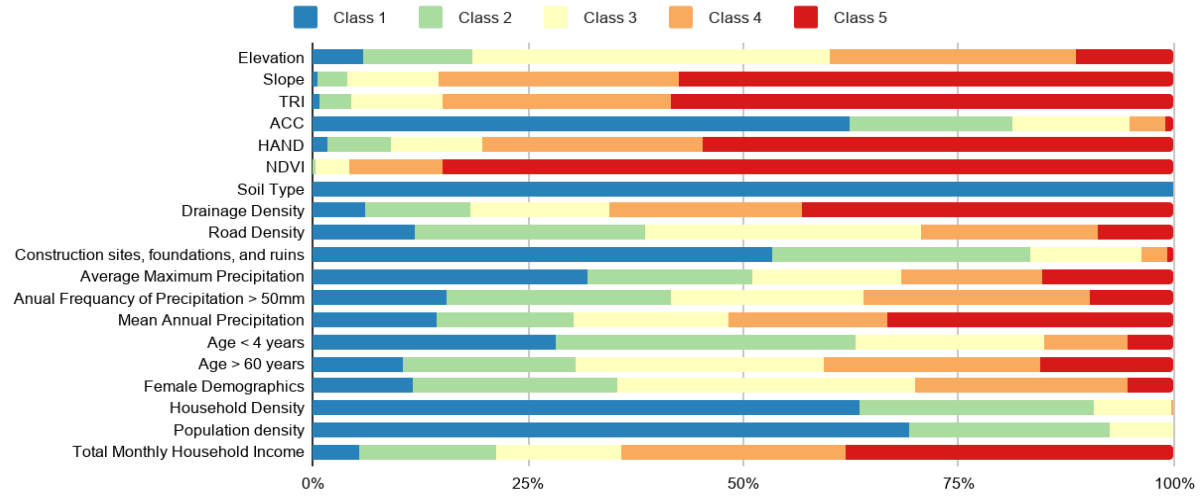


Figure 3 – Area distribution of reclassified layers by class. Classes vary from the least (class 1) to most influential (class 5) according to their respective interpretations of the sensitivity/ability to cope represented by the layer.

The high predominance of non-vegetated areas (84,9% class 5) shown on the NDVI map contributes significantly to the territory's sensitivity and reinforces the need to include analyses of infrastructure and urban morphology layers. Association of low gray drainage densities (43% in class 5 and 22% in class 4) and road density (check other index) evidences high infrastructural sensitivity. The presence of constructions, foundations, and ruins in a few points of the scope (53% in class 1) revealed low structural sensitivity of the surroundings. The dataset confirmed a developed urbanized area, marked by soil imperviousness and inefficient gray infrastructure to deal with the repercussions caused by water-related events.

The population and housing densities found (class 1 in 70% and 63% of the area, respectively) demonstrated a lower number of people and households affected, with it being possible to note low concentration in the central portion of the scope. To incorporate the diversity of impacts on the population, sensitivity associated with differential vulnerability (Zebisch et al. 2023) was assessed through income and demography layers, whose distribution preserved the observed low centrality. Lower income was the greatest sensitivity factor found, with 38% in class 5 and 26% in class 4, exposing that a significant portion of families have lower income. The distribution of the number of elderly people (over 60 years) is balanced, with it being possible to note concentrations in levels 3 and 4 that require attention. Women and children (from 0 to 4 years) classification predominate in levels 2 and 3. Despite the observed urbanization, the data showed the concentration of socioeconomic aspects in regions neighbouring the central portion of the scope. The economic condition of the population is not homogeneous and can affect recovery and adaptation capacity. In this scenario, the older population is the demographic group most prone to sensitizing the scope, demanding more specific and targeted recovery and adaptation actions.

4.2 Land and heritage sensitivity

Results calculated from the average of the reclassified maps (equation 1) comprise a short interval, from 2.05 to 3.95, showing that the combination of the multiple sensitivities and the abilities to cope resulted in a moderate vulnerable territory, with the absence of totally safe or critically vulnerable areas. Despite the homogeneity, the spatial distribution of these values allowed observing that the western zone of the watershed is the most vulnerable area to flooding (Figure 4). This result is mainly influenced by the socioeconomic and infrastructure layers with more critical classifications, which could be the focus of planning actions. The central portion proved less vulnerable because of lower demographic classes and population, and housing density. This may delineate an urban void in the region, reinforcing the need for informational enrichment to characterize territorial dynamics related to aspects such as land use and occupation. This landscape composition affects the heritage under analysis, which is mostly concentrated in the region, reducing connection with the cultural asset and weakening local identity and social memory.

$$\frac{\sum \text{class layers}}{n \text{ layers}} \quad (1)$$

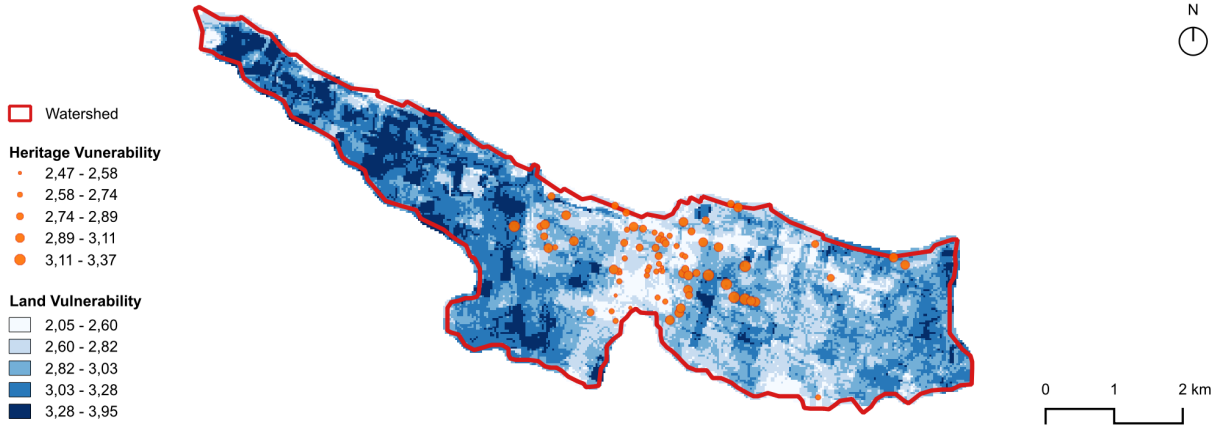


Figure 4 – Landscape and urban heritage vulnerability, assessed using map algebra.

The layer containing the lot boundaries geometries that encompass the heritage buildings assets was overlaid on the landscape vulnerability map, and the index calculated for the territory was transposed to heritage buildings through the QGIS zonal statistics tool, further reducing the found interval (2.47 - 3.37). Taken together, this scenario shows that contextual factors—physical, infrastructural, and socioeconomic—influence the vulnerability of real estate assets, suggesting that this assessment cannot be limited to structural attributes. The quantitative approach used made it possible to establish a hierarchy based on the calculated level of vulnerability, objectively identifying not only the location but also the criticality of the assets. This approach focuses necessary efforts on developing more effective conservation measures, tailored not only to the physical characteristics of the object but also to the environment in which it is situated.

5. Conclusions

Built heritage faces threats related to increasingly frequent extreme climate events. Preservation actions that integrate climate risks require an understanding of both the conservation state of the built heritage and the characteristics of its location. The present work proposes the operationalization of the watershed as the unit of analysis for assessing the vulnerability of built heritage to flooding from the landscape perspective. Adopting the watershed defined an analytical unit with predominantly homogeneous physical characteristics, reinforcing the need to include attributes related to other systems, such as the social, economic, and urban infrastructure systems.

The adoption of a working scale operating at the ecological dimension—the same as that of the natural phenomenon under study—enabled the selection of a concise and efficient territorial subset for the assessment of potential climate impacts. As a working scale, the watershed can allow investigations related to other hazards relevant to the context—particularly when they interact with the occurrence of flooding. It can also enable the proposal of mitigation, adaptation, and response actions for the administrative regions contained within it, engaging with traditional planning and management strategies.

This approach considered 19 layers collected from governmental databases for the characterization of the territory. The reclassification process created dimensionless values across layers with different metrics and enabled the map algebra operation. Interpreting the results operationalized maps and statistics, revealing a territory that, despite being heterogeneous, exhibited moderate vulnerability. The need to visualize the data spatially shaped the reclassification of the layers: classification strategies, such as Jenks natural breaks or the logarithmic scale, were chosen to facilitate the perception of the layers on the GIS map, producing clear representations. This methodological choice may imply a loss of informational detail, since the tool automates the distribution of data into classes, and the process can mask nuances. Therefore, future investigations may adopt a more analytical and mathematical approach, better equipped to handle the mathematical particularities involved in data processing for the definition of vulnerability classes. The multiple datasets used in the literature to characterize the territory and to ground the authors' analyses reinforce that knowledge of the territory is essential for more accurate assessments. This condition highlights the need to incorporate information-enrichment strategies through community participation, combining technical and local knowledge, in order to better support methodological developments like the attribution of weights that represent the relevance of the landscape layers.

The projection of vulnerability relative to the territory onto the dimension of heritage assets revealed the need for more careful consideration. The vulnerability assessment showed that the adverse effects of climate hazards are not limited to the constructed dimension of built heritage, which is influenced by the physical, climatic, urban infrastructure, and socioeconomic dimensions that contextualize them and are shared across distinct assets. Therefore, incorporating this holistic, landscape-centred view can inform and raise awareness among stakeholders involved in heritage conservation, guide decision-making, and support a more integrated and strategic management of portfolios.

Acknowledgments

This work was financially supported by FUNCAP, Project 01172921/2022 – Cientista Chefe Cultura; by the National Council for Scientific and Technological Development (CNPq), Project 131902/2025-3 and Project 140754/2026-1; and by Brazilian Federal Agency for Support and Evaluation of Graduate Education (CAPES), Project 88887.978186/2024-00

References

Adetunji, Olufemi, and Cathy Daly. 2024. “Climate Risk Management in Cultural Heritage for Inclusive Adaptation Actions in Nigeria.” *Heritage* 7 (3): 1237–64. A65. https://doi.org/10.3390/heritage7030060.

Ahmad, Imtiaz, Wang Ping, Sajid Ullah, Khadeijah Yahya Faqeih, Somayah Moshrif Alamri, Eman Rafi Alamery, Asma Abdulaziz Abdullah Abalkhail, and Haji Muhammad Bilal Jan. 2025. “Spatiotemporal Mapping of Urban Flood Susceptibility: A Multi-Criteria GIS-Based Assessment in Nangarhar, Afghanistan.” *Land* 14 (12): 2376. https://doi.org/10.3390/land14122376.

Al-Rjoub, Emad, and Majed Ibrahim. 2025. “Multi-Criteria Analysis to Assess the Area’s Vulnerability to Instantaneous Flood Risk Using GIS in Amman City, Jordan.” *Water Science & Technology*, December 24, 2025, wst2025189. https://doi.org/10.2166/wst.2025.189.

Ana Paula Fiorezi, Alexandre de Amorim Teixeira, and Diana Leite Cavalcanti. 2024. *Base Hidrográfica Ottocodificada Multiescalas Versão 6*. Nota Técnica 5/2024/CCOGI/SHE. Agência Nacional de Águas e Saneamento Básico (ANA). D42. https://metadados.snirh.gov.br/geonetwork/srv/api/records/32e309da-a8c1-443f-90ac-0cd79ce6a33d/attachments/Nota%20técnica%20ANA_SHE_CCOGI%20-%2005_2024.pdf.

Antonio Donato Nobre, Luz Adriana Cuartas, Martin Hodnet, and Jeison P. Santiago. 2016. “HAND Model.” Software. HAND Model - CCST/INPE, São José dos Campos, SP: INPE. https://handmodel.ccst.inpe.br.

Arshed, Abu Bakar, Mohammad Masood, Muhammad Awais Zafar, Ghulam Nabi, and Mudassar Iqbal. 2023. “Effective Management of the Watershed in Response to Historical Climate Change Using a GIS-Based Multi-Criteria Decision Analysis (MCDA).” *Journal of Water and Climate Change* 14 (9): 3178–202. A162. https://doi.org/10.2166/wcc.2023.215.

Broekman, Charl, Christo Coetzee, and Dirk Cilliers. 2025. “Mapping Pluralistic Future Flood Risk Scenarios for Informal Settlements in the eThekwini Metropolitan Municipality, South Africa.” *Natural Hazards* 121 (18): 20949–83. https://doi.org/10.1007/s11069-025-07581-w.

Chaulagain, Deepak, Parshu Ram Rimal, Same Noel Ngando, Benyoh Emmanuel Kigha Nsafon, Dongjun Suh, and Jeung-Soo Huh. 2023. “Flood Susceptibility Mapping of Kathmandu Metropolitan City Using GIS-Based Multi-Criteria Decision Analysis.” *Ecological Indicators* 154 (October 2023): 110653. https://doi.org/10.1016/j.ecolind.2023.110653.

Edamo, Muluneh Legesse, Kedir Bushira, and Tigistu Yisihak Ukumo. 2022. “Flood Susceptibility Mapping in the Bilate Catchment, Ethiopia.” *H2Open Journal* 5 (4): 691–712. https://doi.org/10.2166/h2oj.2022.128.

Faruk, Md. Omar, Irteja Hasan, Joyjit Dey, Mehedi Hasan Ovi, Zarin Tasnim Katha, and Md. Osman Goni. 2025. “Nature-Based Solutions to Combat Flooding in Coastal Region of Bangladesh Using Spatial Multi-Criteria Analysis and Remote Sensing Techniques.” *Nature-Based Solutions* 8 (December 2025): 100279. https://doi.org/10.1016/j.nbsj.2025.100279.

Ferreira, Carla S. S., Rory P. D. Walsh, and António J. D. Ferreira. 2018. “Degradation in Urban Areas.” *Current Opinion in Environmental Science & Health* 5 (October 2018): 19–25. A09. https://doi.org/10.1016/j.coesh.2018.04.001.

Figueiredo, Rui, Xavier Romão, and Esmeralda Paupério. 2020. “Flood Risk Assessment of Cultural Heritage at Large Spatial Scales: Framework and Application to Mainland Portugal.” *Journal of Cultural Heritage* 43 (May 2020): 163–74. A96. https://doi.org/10.1016/j.culher.2019.11.007.

Fox, C. 2009. “River Basin Development.” In *International Encyclopedia of Human Geography*, 414–22. Elsevier. C06. https://doi.org/10.1016/B978-008044910-4.00879-8.

Fritzsche, Kerstin, Stefan Schneiderbauer, Philip Bubeck, Stefan Kienberger, Mareike Buth, Marc Zebisch, and Walter Kahlenborn. 2017. *The Vulnerability Sourcebook - Concept and Guidelines for Standardized Vulnerability Assessments*. Bonn: GIZ.

Funceme. 2017. "Postos Pluviométricos." Government Portal. Funceme, Fortaleza, CE. http://www.funceme.br/?page_id=2694.

Gallina, Valentina, Silvia Torresan, Andrea Critto, Anna Sperotto, Thomas Glade, and Antonio Marcomini. 2016. "A Review of Multi-Risk Methodologies for Natural Hazards: Consequences and Challenges for a Climate Change Impact Assessment." *Journal of Environmental Management* 168 (2016): 123–32. RL. https://doi.org/https://doi.org/10.1016/j.jenvman.2015.11.011.

Ghanem, Ma'in Abed Alhakim Naser, and Hasan Zaifoglu. 2024. "A Geospatial Analysis of Flood Risk Zones in Cyprus: Insights from Statistical and Multi-Criteria Decision Analysis Methods." *Environmental Science and Pollution Research* 31 (22): 32875–900. https://doi.org/10.1007/s11356-024-33391-x.

Graus, Sandra, Tiago Miguel Ferreira, Graça Vasconcelos, and Javier Ortega. 2024. "Changing Conditions: Global Warming-Related Hazards and Vulnerable Rural Populations in Mediterranean Europe." *Urban Science* 8 (2): 42. A70. https://doi.org/10.3390/urbansci8020042.

Hadipour, Vahid, Freydoon Vafaie, and Kaveh Deilami. 2020. "Coastal Flooding Risk Assessment Using a GIS-Based Spatial Multi-Criteria Decision Analysis Approach." *Water* 12 (9): 2379. https://doi.org/10.3390/w12092379.

Hagos, Yonas Gebresilasie, Tesfa Gebrie Andualem, Mesenbet Yibeltal, and Mequanent Abathun Mengie. 2022. "Flood Hazard Assessment and Mapping Using GIS Integrated with Multi-Criteria Decision Analysis in Upper Awash River Basin, Ethiopia." *Applied Water Science* 12 (7): 148. https://doi.org/10.1007/s13201-022-01674-8.

Hassan Rashid, Muhammad Abo Ul, Malik Maliha Manzoor, and Sana Mukhtar. 2018. "Urbanization and Its Effects on Water Resources: An Exploratory Analysis." *Asian Journal of Water, Environment and Pollution* 15 (1): 67–74. A33. https://doi.org/10.3233/AJW-180007.

IBGE. 2017. "Downloads." Government Portal. IBGE, Rio de Janeiro, RJ. https://www.ibge.gov.br/estatisticas/downloads-estatisticas.html.

INPE. 2025. "BIG – Base de Informações Georeferenciadas." Government Portal. Portal de Dados Geoespaciais Do INPE, São José dos Campos, SP. https://data.inpe.br.

IPCC. 2022. "IPCC 2018: Annex I: Glossary." In *Global Warming of 1.5°C: IPCC Special Report on Impacts of Global Warming of 1.5°C above Pre-Industrial Levels in Context of Strengthening Response to Climate Change, Sustainable Development, and Efforts to Eradicate Poverty*, 1st ed. Cambridge University Press. D22. https://doi.org/10.1017/9781009157940.

IPECE. 2026. "Perfil Municipal." Portal de Dados Estatísticos. IPECE Data - Perfil Municipal, Fortaleza, March 15. http://ipecedata.ipece.ce.gov.br/ipece-data-web/module/perfil-municipal.xhtml.

Ji, Xian, Long Shao, and Yu Du. 2020. "Collaborating with Local Communities to Identify Improvement Priorities for Historic Urban Landscape Based on Residents' Satisfaction: An Application of Asymmetric Impact-Performance Analysis in Dandong, China." *Sustainability* 12 (4): 1463. A134. https://doi.org/10.3390/su12041463.

Lankester, Paul, and Ruth Knight. 2024. "Towards a National Heritage Climate Change Risk Assessment Hacia Una Evaluación Del Riesgo de Cambio Climático Del Patrimonio Nacional." *STUDIES IN CONSERVATION* (2-4 PARK SQUARE, MILTON PARK, ABINGDON OX14 4RN, OXON, ENGLAND) 69 (SUP1, SI): 176–89. M. https://doi.org/10.1080/00393630.2024.2375160.

Leeonis, Adam Narashman, Minhaz Farid Ahmed, Bijay Halder, Mazlin Bin Mokhtar, Chen Kim Lim, Liew Juneng, and Rd Puteri Khairani Khirotdin. 2024. "Mitigating Flood Risk at Shah Alam, Malaysia for Sustainable Development." *Discover Sustainability* 5 (1): 352. https://doi.org/10.1007/s43621-024-00504-y.

Mendonça, Francisco, and Sanderson Alberto Medeiros Leitão. 2009. "Riscos e Vulnerabilidade Socioambiental Urbana: Uma Perspectiva a Partir Dos Recursos Hídricos." *GeoTextos* 4 (March 2009). A23. https://doi.org/10.9771/1984-5537geo.v4i0.3300.

Merga, Biratu Bobo, Feye Lama Mamo, Mitiku Badasa Moisa, Firdisa Sadeta Tiye, and Dessalen Obsi Gemeda. 2023. “Assessment of Flood Risk by Using Geospatial Techniques in Wabi Shebele River Sub-Basin, West Hararghe Zone, Southeastern Ethiopia.” *Applied Water Science* 13 (11): 214. https://doi.org/10.1007/s13201-023-02019-9.

Ministério da Integração e do Desenvolvimento Regional. n.d. “Atlas Digital de Desastres No Brasil.” Plataforma de Dados Interativos. With Centro de Estudos e Pesquisas em Engenharia e Defesa Civil(Ceped/UFSC). Tlas Digital - Ministério Da Integração e Do Desenvolvimento Regional (MDR), Secretaria Nacional de Proteção e Defesa Civil (Sedec/MDR. Accessed March 15, 2026. https://atlasdigital.mdr.gov.br/paginas/index.xhtml.

Mokhtari, Elhadj, Farouk Mezali, Brahim Abdelkebir, and Bernard Engel. 2023. “Flood Risk Assessment Using Analytical Hierarchy Process: A Case Study from the Cheliff-Ghrib Watershed, Algeria.” *Journal of Water and Climate Change* 14 (3): 694–711. https://doi.org/10.2166/wcc.2023.316.

Nahin, Khadiza Tul Kobra, Sumaiya Binte Islam, Safat Mahmud, and Irfan Hossain. 2023. “Flood Vulnerability Assessment in the Jamuna River Floodplain Using Multi-Criteria Decision Analysis: A Case Study in Jamalpur District, Bangladesh.” *Heliyon* 9 (3): e14520. https://doi.org/10.1016/j.heliyon.2023.e14520.

Prefeitura Municipal de Fortaleza, Secretaria Municipal de Urbanismo e Meio Ambiente, and ICLEI. 2020. *Plano Local de Ação Climática de Fortaleza (PLAC)*. Plano de Ação Climática. Fortaleza: Secretaria Municipal de Urbanismo e Meio Ambiente (SEUMA).

QGIS Development Team. 2024. “QGIS.” Software. QGIS Project, [S.l.]. https://qgis.org.

Quesada-Ganuza, Laura, Leire Garmendia, Eduardo Roji, and Alessandra Gandini. 2021. “Do We Know How Urban Heritage Is Being Endangered by Climate Change? A Systematic and Critical Review.” *International Journal of Disaster Risk Reduction* 65 (November 2021): 102551. A84. https://doi.org/10.1016/j.ijdrr.2021.102551.

Salazar, L. Gerardo F., Rui Figueiredo, and Xavier Romão. 2024. “Flood Vulnerability Assessment of Built Cultural Heritage: Literature Review and Identification of Indicators.” *International Journal of Disaster Risk Reduction* 111 (September 2024): 104666. A79. https://doi.org/10.1016/j.ijdrr.2024.104666.

SEFIN. 2020. “IDE SEFIN.” Government Portal. Infraestrutura de Dados Espaciais da SEFIN, Fortaleza, CE. https://ide.sefin.fortaleza.ce.gov.br.

Sesana, Elena, Alexandre S. Gagnon, Chiara Ciantelli, JoAnn Cassar, and John J. Hughes. 2021. “Climate Change Impacts on Cultural Heritage: A Literature Review.” *WIREs Climate Change* 12 (4): e710. A182. https://doi.org/10.1002/wcc.710.

SEUMA. 2015. *Drenagem e Manejo Das Águas Pluviais Urbanas Do Município de Fortaleza*. Plano Municipal de Drenagem. Fortaleza: Prefeitura Municipal de Fortaleza. L06. https://urbanismoemeioambiente.fortaleza.ce.gov.br/images/urbanismo-e-meio-ambiente/infocidade/plano_municipal_de_drenagem.pdf.

SGB/CPRM. 2026. “GeoSGB.” Government Portal. GeoSGB - SGB/CPRM, Brasília, DF. https://geoportal.sgb.gov.br/geosgb/.

Sousa, Fernanda Oliveira De, Victor Andre Ariza Flores, Christhian Santana Cunha, Sandra Oda, and Hostilio Xavier Ratton Neto. 2025. “Multi-Criteria Assessment of Flood Risk on Railroads Using a Machine Learning Approach: A Case Study of Railroads in Minas Gerais.” *Infrastructures* 10 (1): 12. https://doi.org/10.3390/infrastructures10010012.

Sukri, Nur Syakila Muhammad, Khairul Nizam Abdul Maulud, Syed Ahmad Fadhli Syed Abdul Rahman, Wan Shafrina Wan Mohd Jaafar, Wan Hanna Melini Wan Mohtar, Rasyikah Md Khalid, Ahmad Shakir Mohd Saudi, and Mohd Nazish Khan. 2025. “Enhancing Urban Flood Vulnerability Mapping with Multi-Criteria Decision Analysis.” *Jurnal Kejuruteraan* 37 (7): 3641–54. https://doi.org/10.17576/jkukm-2025-37(7)-40.

Tang, Jianxiong, Yanmin Li, Shenghui Cui, Lilai Xu, Yuanchao Hu, Shengping Ding, and Vilas Nitivattananon. 2021. “Analyzing the Spatiotemporal Dynamics of Flood Risk and Its Driving Factors in a Coastal Watershed of Southeastern China.” *Ecological Indicators* 121 (February 2021): 107134. https://doi.org/10.1016/j.ecolind.2020.107134.

Taylor, Ken. 2023. “Historic Urban Landscape Paradigm - A Tool for Balancing Values and Changes in the Urban Conservation Process.” *Landscape Architecture Frontiers* 11 (3): 96. A116. https://doi.org/10.15302/J-LAF-1-030043.

UNESCO. 2011. “Recommendation on the Historic Urban Landscape.” Paper presented at General Conference. November 10, 2011.

United Nations. 2017. *New Urban Agenda: H III : Habitat III : Quito 17-20 October 2016*. Nairobi: United Nations.

Vojtek, Matej, Jana Vojteková, Romulus Costache, Quoc Bao Pham, Sunmin Lee, Arfan Arshad, Satiprasad Sahoo, Nguyen Thi Thuy Linh, and Duong Tran Anh. 2021. “Comparison of Multi-Criteria-Analytical Hierarchy Process and Machine Learning-Boosted Tree Models for Regional Flood Susceptibility Mapping: A Case Study from Slovakia.” *Geomatics, Natural Hazards and Risk* 12 (1): 1153–80. https://doi.org/10.1080/19475705.2021.1912835.

Wang, Mo, Jiayu Zhao, Ziheng Xiong, Menghan Zhang, Lie Wang, and Soon Keat Tan. 2025. “Strategic Deployment of Nature-Based Solutions for Urban Flood Management in High-Density Urban Landscapes.” *Ecological Indicators* 176 (July 2025): 113681. https://doi.org/10.1016/j.ecolind.2025.113681.

Wang, Siyou, Shaotao Chen, and Wei Gao. 2022. “Information Services as a Method to Evaluate the Sustainability of Intangible Dimensions of a Historic Urban Landscape: A Case Study in Guangzhou, China.” *Sustainability* 15 (1): 8. A120. https://doi.org/10.3390/su15010008.

Wang, Yuan, Chengxie Jin, Danyang Xu, Tiebo Wang, and Baoxi Wang. 2024. “Analysis of Multi-Dimensional Layers in Historic Districts Based on Theory of the Historic Urban Landscape: Taking Shenyang Fangcheng as an Example.” *Land* 13 (11): 1736. A111. https://doi.org/10.3390/land13111736.

Weday, Mohammed Abdella, Kenate Worku Tabor, and Dessalegn Obsi Gemeda. 2023. “Flood Hazards and Risk Mapping Using Geospatial Technologies in Jimma City, Southwestern Ethiopia.” *Heliyon* 9 (4): e14617. https://doi.org/10.1016/j.heliyon.2023.e14617.

Wongthongtham, Pornpit, Bilal Abu-Salih, Jeff Huang, Hemixa Patel, and Komsun Siripun. 2023. “A Multi-Criteria Analysis Approach to Identify Flood Risk Asset Damage Hotspots in Western Australia.” *Sustainability* 15 (7): 5669. https://doi.org/10.3390/su15075669.

World Heritage Training and Research Institute for the Asia and the Pacific Region, Australian City of Ballarat, Tongji University, and Federation University Australia. 2016. *The HUL Guidebook: Managing Heritage in Dynamic and Constantly Changing Urban Environments; a Practical Guide to UNESCO’s Recommendation on the Historic Urban Landscape*.

Zahid, Aqsa, Hamna Hasan, Shahrukh Khan, Muhammad Ahmed, and Syed Imran Ahmed. 2025. “Flood Risk Assessment for Kunhar River Basin Using GIS-Based Multi-Criteria Decision Analysis (MCDA).” *Journal of Water and Climate Change* 16 (12): 3586–609. https://doi.org/10.2166/wcc.2025.711.

Zebisch, Marc, Kathrin Renner, Massimiliano Pittore, Uta Fritsch, Sophie Rose Fruchter, Stefan Kienberger, Thomas Schinko, et al. 2023. *Climate Risk Sourcebook*. Bonn: Deutsche Gesellschaft für Internationale Zusammenarbeit (GIZ) GmbH.

cinpar2026
XXII International Conference on Building Pathology and Constructions Repair
15th to 17th July 2026 - Lisboa, Portugal

A structured methodology for post-fire structural assessment and rehabilitation of unreinforced masonry housing in seismic regions

Rodrigo CHIPOCO.[1], Denisse GONZALEZ [2]

[1] AEI Smart Build Solutions Ltda., Viña del Mar, Chile, rodrigo@aeismart.cl
[2] AEI Smart Build Solutions Ltda., Viña del Mar, Chile, denisse@aeismart.cl

Abstract: Structural fires in unreinforced masonry housing represent a critical challenge in seismic regions, particularly when thermal exposure does not cause immediate collapse but induces cumulative damage that may compromise future structural performance. In such scenarios, decision-making between total demolition and structural rehabilitation often lacks clear and reproducible technical criteria adapted to local construction practices.

This paper proposes a structured methodology for post-fire structural assessment and rehabilitation of unreinforced masonry housing, oriented toward supporting technical decision-making between demolition and rehabilitation. The methodological framework integrates specialized visual inspection, qualitative classification of thermal damage based on recognized post-fire indicators, consideration of expected structural behavior under seismic demand, and the definition of intervention criteria grounded on material compatibility, minimal intervention, and improvement of shear structural behavior. The proposed approach is consistent with the general principles of formal post-fire inspection protocols, while being adapted to the specific characteristics of masonry structures and post-disaster contexts.

The methodology is applied through the comparative analysis of two real post-fire reconstruction cases in Chile, corresponding to single-story unreinforced masonry dwellings exposed to estimated temperatures below 400 °C. The assessment allowed severe thermal damage scenarios to be ruled out and localized reductions in structural continuity and stiffness to be identified, which were addressed through compatible strengthening strategies, including reinforcement meshes, structural mortars, and upper confinement elements.

The results indicate that, under conditions of moderate thermal damage, structural rehabilitation of post-fire unreinforced masonry housing is technically feasible, avoiding unnecessary demolitions and promoting resilient reconstruction solutions. The proposed methodology may be applicable to similar post-fire scenarios involving unreinforced masonry housing in seismic regions and provides a preliminary basis for future standardization of assessment and intervention criteria in post-disaster contexts.

Keywords: *structural fire; unreinforced masonry; post-fire structural assessment; post-disaster rehabilitation; seismic regions.*

1. Introduction

Large-scale urban fires generate complex scenarios for the structural assessment of existing buildings. Unlike other extreme events, fire does not necessarily cause immediate collapse but induces progressive material degradation that may compromise future structural performance (Ingham 2009; ACI 2021). This condition is particularly critical in unreinforced masonry (URM) housing located in seismic regions, where the assessment must consider not only the post-fire condition but also the expected structural response under seismic demand.

In buildings constructed under standards preceding modern seismic design codes, thermal exposure may affect both the integrity of structural elements and the global continuity of the load-resisting system. Masonry degradation, deterioration of mortars and concrete, and loss of upper confinement generate a

condition of technical uncertainty, especially in the absence of instrumental testing capable of quantifying the reduction in mechanical properties (RILEM 2000; ACI 2021).

In practice, these scenarios are often addressed through conservative decisions, frequently oriented toward total demolition. However, this approach does not always reflect a rigorous structural assessment and may be inefficient from a technical, economic, and social perspective, particularly in attached or continuous housing, where partial demolition may adversely affect the overall structural behavior (fib 2017).

In this context, a structured methodology is required to link observed damage with explicit technical criteria for decision-making and intervention. This study proposes a methodology for the post-fire structural assessment and rehabilitation of unreinforced masonry housing in seismic regions, organized into three levels: damage assessment, structural decision-making, and intervention definition. Its application to real reconstruction cases in the Valparaíso region not only validates its technical relevance but also establishes a systematic, replicable, and traceable process for decision-making in post-fire scenarios within seismic contexts.

2. Context and Case Studies

The analyzed cases correspond to residential buildings affected by the February 2024 wildfire in the Valparaíso Region, Chile, within the framework of an ongoing post-disaster reconstruction process. The dwellings were constructed in the 1970s and correspond to low-rise unreinforced masonry (URM) typologies, including attached, semi-detached, and continuous row configurations, located in the Canal Beagle and Canal Chacao sectors, in the municipalities of Viña del Mar and Quilpué, respectively. This condition is particularly relevant, as the interaction between adjacent units influences both the structural assessment and the feasibility of partial demolition.

During the initial assessment process, a portion of the dwellings were classified for demolition. However, subsequent technical evaluations identified that many of them did not present a risk of collapse, although they required structural repair and strengthening to meet current safety and regulatory requirements. This situation highlighted the need for more precise criteria to distinguish between repairable and non-repairable damage.

The dwellings consist of load-bearing solid clay brick masonry walls, continuous concrete strip footings, and the absence of upper confinement elements prior to the fire. The compressive strength of the base material was estimated at approximately 5 MPa. At the time of inspection, the roof structures were completely destroyed; therefore, the assessment focused on the remaining visible load-resisting elements. **Figure 1** presents the geometric configuration of the dwellings, while **Figure 2** illustrates their grouping within the Canal Beagle sector.

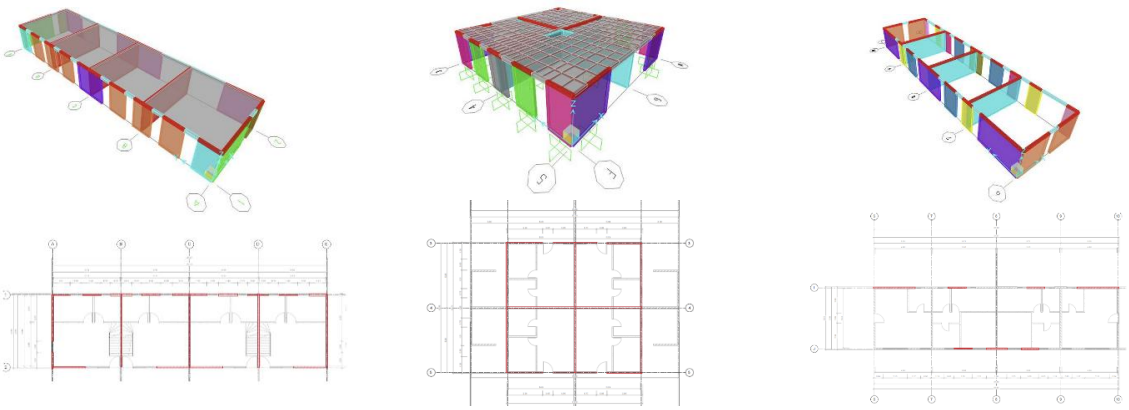


Figure 1 - General typological characteristics of the analyzed dwellings

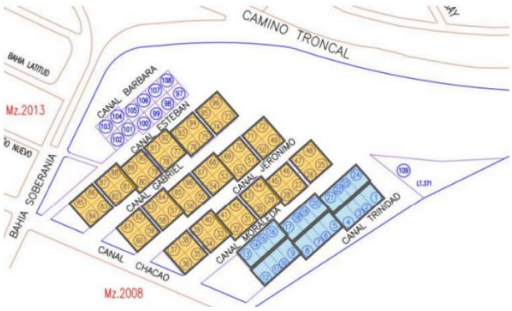


Figure 2 - Spatial configuration of housing units in the study area (MZ 2007 cadastral plan, Municipal Works Department, Viña del Mar)

2.1. Thermal Exposure Conditions and Inspection Timeline

In both cases, the post-fire assessment suggested thermal exposure below 400 °C, based on widely recognized damage indicators, such as the absence of brick vitrification, partial preservation of mortar joints, lack of widespread spalling, and the absence of critical deformations in steel elements.

Although the estimated thermal exposure remained below 400 °C based on observable indicators, this estimation involves uncertainty due to the absence of direct measurements. Nevertheless, the adopted qualitative–rational approach is consistent with post-fire assessment methodologies reported in the literature (RILEM 2000; Ingham 2009; ACI 2019).

The post-fire structural inspection was conducted after complete thermal stabilization of the structures. In the Canal Beagle sector, the detailed inspection was carried out approximately 20 days after the fire, while in Canal Chacao it was conducted after 14 days. These timeframes helped avoid premature diagnoses associated with transient thermal conditions and ensured a reliable assessment of residual structural damage.

3. Structured Methodology for Post-Fire Structural Assessment

The proposed methodology is conceived as a structured decision-making framework, consistent with the general principles of formal post-fire inspection protocols, yet specifically adapted to unreinforced masonry (URM) typologies and to the constraints inherent to post-disaster reconstruction contexts.

The methodology is organized into three sequential and interrelated levels:

- Level I: damage assessment,
- Level II: structural decision-making,
- Level III: structural intervention definition.

This approach transforms conventional inspection and design practices into a structured procedure with explicit criteria, defined outputs, and full traceability, enabling a consistent and reproducible decision-making process.

3.1. Level I: damage assessment

3.1.1. Field Survey

The first stage consisted of a systematic and specialized visual inspection, applied to each dwelling using a post-fire inspection record sheet, as shown in **Figure 3**. This instrument enabled the structured

documentation of both general building characteristics and observed structural conditions, including the spatial localization of damage.

The inspection covered all visible structural elements, including load-bearing walls, wall intersections, openings, upper wall elements (bond beam level), remaining steel structural components, visible damage in reinforced concrete elements, and the overall condition of the structural system after the loss of the roof.

Foundations were not included in the direct visual survey, as they were generally not exposed.

The collected information was documented through; an individual inspection record for each dwelling, damage sketches indicating the spatial distribution of cracks and affected areas, and a photographic record used for subsequent validation, as illustrated in **Figure 4**.

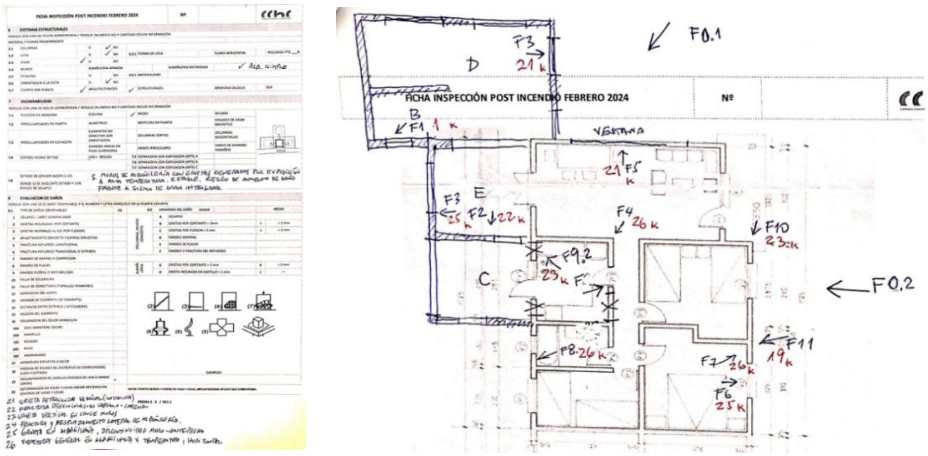


Figure 3 - Field inspection sheet and damage recording diagram

This procedure not only enabled the recording of field observations but also allowed the development of a traceable documentation framework, supporting the verification of on-site data against subsequent structural analysis, design development, and municipal submission processes.

3.1.2. Thermal Damage Indicators



Figure 4 - Representative photographic record of observed damage

Thermal damage assessment was conducted based on observable field indicators, considering visual criteria commonly recognized in post-fire evaluation practice (Ingham 2009; ACI 562-19). The indicators considered included masonry cracking, color changes in concrete and masonry elements, loss of material cohesion, surface disintegration, spalling in concrete elements, mortar deterioration, deformation of residual steel elements, and the presence of combustion-related residues in specific areas associated with prolonged fire exposure due to localized combustible loads, such as furniture or other interior contents.

The interpretation of these indicators enabled the development of a qualitative assessment of thermal damage levels, not based on direct temperature measurements but on observable pathological evidence

consistent with post-fire behavior reported in the literature (ACI 2021; fib 2017; RILEM 2000). The damage evaluation considered crack orientation, continuity, width, and spatial distribution, as well as their relationship with structurally critical zones such as corners, wall intersections, and upper wall regions.

3.1.3. Damage Classification

Based on the field survey, damage was systematically classified into three levels, as defined in Table 1.

Table 1 - Damage Classification

Damage Level	Description	Structural Condition	Recommended Decision
Minor	Superficial cracking, mainly affecting finishes. Structural walls without significant damage.	Structural performance not compromised	Direct rehabilitation
Moderate	Presence of cracks and fissures in walls, with localized material deterioration and evidence of higher thermal exposure.	Possible reduction in structural capacity	Rehabilitation with strengthening
Severe	Wall displacement, loss of masonry unit integrity, large cracks, and extensive damage.	Loss of structural stability	Demolition

In the cases analyzed using this methodology, all evaluated dwellings were classified within the minor and moderate damage categories. No severe damage conditions were identified that would imply a loss of global structural stability or an imminent risk of collapse.

3.1.4. Level I Outputs

The outputs of this stage were not limited to a narrative description of the observed damage but consisted of specific evaluation products, as summarized in Table 2.

Table 2 - Outputs of Level I: Field Assessment and Damage Documentation

Output	Description	Objective
Inspection technical sheet	Structured record of housing characteristics and observed damage	Systematize field data
Photographic record	Visual evidence of observed damage	Validation and traceability
Damage sketch	Spatial identification of cracks, fissures, and affected areas	Relate damage to structural geometry
Damage classification	Determination of damage level: minor, moderate, or severe	Basis for decision-making
Technical observations	Qualitative comments from the evaluator	Complement structural analysis

3.2. Level II: Structural Decision-Making Methodology

3.2.1. Decision Criteria

Structural decision-making was based on determining the feasibility of rehabilitation versus the need for demolition of the affected dwellings. Given the practical constraints associated with post-emergency reconstruction, where destructive testing or advanced instrumental assessments are not feasible, a qualitative–rational approach was adopted for thermal damage classification. This approach was based on the correlation between observed visual indicators and temperature ranges reported in the specialized literature (Ingham 2009; ACI 2021; fib 2017).

The decision process relied on an integrated structural interpretation of the observed damage, considering the continuity of load-bearing walls, the integrity of wall intersections, the global stability of the system, and

the extent of damage affecting structural elements. A dwelling was considered rehabilitable if it maintained structural continuity, showed no evidence of out-of-plane failure or wall displacement, and presented non-predominant damage, even in the presence of localized deterioration or damage to upper confinement elements that could be repaired.

In contrast, demolition was considered when there was loss of structural continuity, global instability, or predominant damage affecting the load-resisting system. These criteria were applied using a technical–rational approach rather than a strictly numerical threshold.

The criteria considered are summarized in **Table 3.**

Table 3 - Decision Criteria

Primary Criterion	Evaluated Condition	Recommended Decision
Structural continuity	Walls and connections maintain integrity	Rehabilitation
Global stability	No out-of-plane failures or wall tilting observed	Rehabilitation
Damage extent	Damage is not predominant in the structural system	Rehabilitation
Recoverability of elements	Bond beams and damaged areas are repairable	Rehabilitation
Loss of continuity	Disconnection of walls or failure at wall intersections	Demolition
Structural instability	Presence of wall tilting or risk of collapse	Demolition
Predominant damage	Significant damage affecting the structural system	Demolition

Note: Criteria are applied through integrated structural interpretation rather than fixed numerical thresholds.

3.2.2. Regulatory and Administrative Criteria

In addition to the residual structural condition, rehabilitation had to be compatible with the applicable regulatory framework. For this purpose, the following aspects were considered: the feasibility of developing a formal architectural and structural design project, compliance with minimum habitability requirements, submission of the project to the local Municipal Works Department (Dirección de Obras Municipales, DOM), the existence of prior municipal approval of the original dwelling, and structural validation through a calculation report and external review.

In this context, the decision to rehabilitate was not based solely on a visual or qualitative assessment, but on the actual feasibility of formalizing a reconstruction permit and obtaining subsequent municipal approval in accordance with current regulations.

Additionally, the proposed rehabilitation strategies were developed and verified through formal structural design projects in accordance with current Chilean regulations, considering criteria related to strength, stability, and expected structural behavior under seismic demand. These verifications supported the technical feasibility of the adopted solutions. However, the objective of this study is not to develop a detailed quantitative seismic analysis, but rather to propose a structured methodology for assessment and decision-making in post-fire scenarios.

3.2.3. Level II Outputs

The output of this stage corresponds to a technical determination of structural feasibility, classifying each dwelling as: rehabilitable, requiring demolition, or rehabilitable subject to a specific strengthening strategy.

In the cases studied, the field survey and subsequent analysis allowed the initially proposed total demolition to be ruled out and replaced with a structural rehabilitation and/or strengthening strategy.

3.3. Level III: Structural Intervention Methodology

The third stage consisted of linking the observed damage and the rehabilitation decision with a specific structural intervention strategy.

A key aspect of this methodology is that the intervention is not defined based on observed in-service failure, but rather on the expected structural behavior under seismic demand.

3.3.1. Identification of Structural Deficits

Based on the field survey and structural analysis, three main structural deficits associated with thermal damage were identified, as summarized in Table 4:

a) Mechanical degradation of masonry: evidenced by cracking, color changes, loss of material cohesion, and surface disintegration. This condition results in a reduction of load-bearing capacity and increased uncertainty in structural behavior under seismic loading (Ramirez et al. 2023).

b) Loss of structural continuity in upper bond beams: associated with concrete degradation, cracking, and spalling, compromising load transfer and wall confinement (Ramirez et al. 2023; Hernández-Montes et al. 2023).

c) Reduction in system ductility: thermal exposure induces more brittle behavior in masonry, reducing its energy dissipation capacity and increasing vulnerability to lateral actions (Li and Purkiss 2005).

Table 4 - Correlation between Observed Damage, Structural Deficits, and Intervention Strategies

Observed Damage	Structural Interpretation	Identified Deficit	Intervention Strategy
Cracking in masonry walls	Mechanical degradation due to thermal effects	Reduction in load-bearing capacity	Strengthening with welded wire mesh and shotcrete
Superficial material disintegration	Loss of material cohesion	Local reduction in strength	Application of bonded structural coating
Discoloration of concrete	Moderate thermal exposure	Possible reduction in mechanical properties	Evaluation and complementary strengthening
Spalling in concrete elements	Loss of cover and cross-section	Reduction in load-bearing capacity	Repair or replacement of the affected element
Damage in upper bond beams	Loss of structural continuity	Deficient load transfer	Rehabilitation or reconstruction of bond beams
Absence or deterioration of upper confinement	Lack of confinement	Reduced global stability of the system	Incorporation of upper confinement elements
General system degradation	Increased brittle behavior	Reduction in ductility	Global strengthening using a composite system

3.3.2. Structural Performance Objectives of the Intervention

The intervention was defined based on structural performance objectives, as summarized in Table 5.

Table 5 - Structural Performance Objectives of the Intervention

Objective	Description
Restore structural continuity	Ensure effective connection between load-bearing elements
Improve shear resistance	Increase resistance to expected seismic demand
Enhance ductility	Promote controlled inelastic behavior
Improve confinement	Improve integrity and stability of load-bearing walls
Ensure load transfer	Guarantee structural load path from roof to walls
Material compatibility	Integrate strengthening elements without construction incompatibilities

3.3.3. Intervention Strategies

The intervention strategies were defined based on the identified structural deficits, aiming not only to repair the observed damage but also to improve expected structural behavior under seismic demand.

Wall strengthening: the adopted solution consisted of applying a structural shotcrete layer reinforced with welded wire mesh, mechanically anchored to the existing substrate to ensure composite action between the remaining masonry, existing concrete elements, and the strengthening layer, as illustrated in Figure 5. This strategy aimed to restore or replace deteriorated areas, increase the load-bearing capacity of the system, improve its expected seismic behavior, and reduce the risk of brittle failure.

Rehabilitation or replacement of upper bond beams: in areas where damage to upper tie beams was identified, their rehabilitation or full replacement was defined, with the aim of restoring the load-bearing capacity of the element, recovering the perimeter confinement, and ensuring proper load transfer from the roof to the load-bearing walls. The strengthening solution is illustrated in Figure 6.

Global ductility enhancement: the incorporation of continuous reinforcement using welded wire mesh and shotcrete was also conceived as a strategy to enhance the overall ductility of the structural system, improving its capacity for stress redistribution and promoting a more stable structural response under seismic demand.

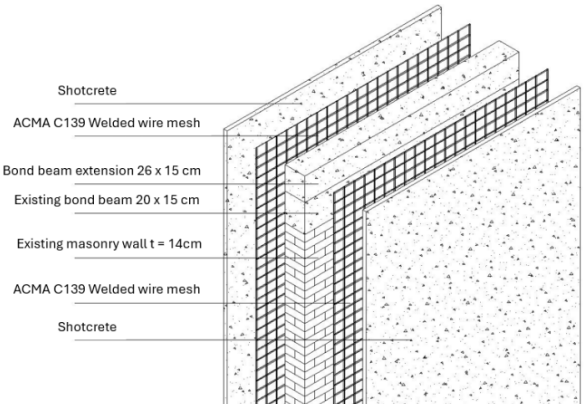


Figure 6 - Wall reinforcement scheme with welded wire mesh and shotcrete

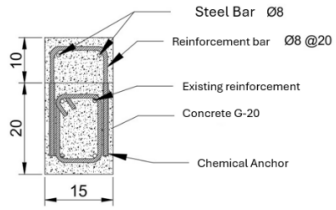


Figure 5 - Schematic detail of upper bond beam rehabilitation

3.3.4. Methodology Synthesis

The overall methodology is summarized in Table 6.

Table 6 - Summary of the Proposed Post-Fire Assessment Methodology

Methodological Level	Input	Process	Output
Level I: Assessment	Field inspection	Data collection using inspection sheets, damage sketches, and photographic records	Damage classification
Level II: Decision	Damage classification and structural assessment	Application of criteria based on structural continuity and damage extent	Definition: rehabilitation or demolition
Level III: Intervention	Rehabilitation decision	Identification of structural deficits and strengthening design	Structural intervention strategy

4. Implemented Structural Rehabilitation Strategies

Based on the identification of structural deficits associated with thermal damage and considering the expected structural behavior under seismic demand, structural rehabilitation strategies were defined and implemented to restore load-bearing capacity, improve structural continuity, and enhance the global ductility of the evaluated dwellings.

The adopted solutions were consistently applied across the analyzed cases, responding to criteria of constructability, feasibility under post-emergency conditions, and coherence with the structural performance objectives defined in the proposed methodology.

4.1 Shear Strengthening of Masonry Walls

The strengthening of masonry walls was aimed at increasing their load-bearing capacity under lateral actions, considering the potential degradation of mechanical properties due to thermal exposure.

The adopted solution consisted of installing welded wire mesh (ACMA C139 type), mechanically anchored to the existing substrate, followed by the application of a structural mortar layer approximately 3 cm thick on the interior face of the walls. This system improved shear resistance, controlled crack propagation, and promoted a more stable structural response.

Additionally, a fiberglass mesh embedded in a compatible mortar was applied on the exterior face, primarily intended for crack control and durability, without a primary structural function.

Overall, the intervention transformed the original system into a composite structural system with improved expected behavior under seismic demand.

4.2 Incorporation of Upper Bond Beam

To restore the structural continuity of the system, a continuous reinforced concrete bond beam was incorporated at the top of the load-bearing walls.

This element, approximately 30 cm in height, acts as an upper confinement system, integrating the walls structurally, improving the redistribution of horizontal forces, and providing an effective connection with the roof.

Its incorporation increased the global stability of the system, reduced vulnerability to out-of-plane failure, and ensured proper load transfer from the roof to the load-bearing walls.

5. Results

The application of the proposed methodology enabled a systematic and structured assessment of fire-damaged unreinforced masonry dwellings, ensuring traceability between field data collection, structural decision-making, and the definition of intervention strategies.

5.1 Characterization of Observed Damage

Field inspections revealed that, despite the scale of the fire, the dwellings did not exhibit collapse conditions or global structural instability. The observed damage was primarily characterized by cracking masonry walls, discoloration of concrete elements associated with thermal exposure, superficial material degradation, and damage to upper bond elements.

In addition, the total loss of the roof was observed in most cases, resulting in direct thermal exposure of load-bearing walls. No indicators of severe thermal damage were identified, such as brick vitrification, massive material loss, or critical deformation of structural elements.

Based on these observations, the damage was classified as either minor or moderate, with no cases identified as severe in terms of global structural stability.

5.2 Technical Validation of Structural Condition

The qualitative damage assessment, based on observable indicators, provided a consistent basis for interpreting the residual structural condition of the dwellings.

Available technical data included compressive strength testing of concrete core samples extracted from existing slabs in representative dwellings, with the purpose of verifying whether the existing structural elements could be retained and incorporated into the proposed rehabilitation strategy. Six valid test results yielded equivalent cylindrical compressive strengths ranging from 20.6 MPa to 25.9 MPa, while two additional core samples could not be tested due to damage sustained during the extraction process. These results provided quantitative information regarding the residual condition of the existing concrete elements and supported the technical decision to retain and incorporate the existing structural components within the proposed rehabilitation strategy.

These findings allowed severe damage scenarios to be ruled out and supported the technical feasibility of structural rehabilitation.

5.3 Adopted Structural Decision

Based on the application of the defined methodological criteria—particularly those related to structural continuity, global stability, and damage extent, the viability of rehabilitation was confirmed for all analyzed cases (100%), and total demolition initially considered during the preliminary assessment was discarded.

Accordingly, a structural rehabilitation strategy was adopted, compatible with the development of formal architectural and structural design projects, their submission to the local municipal authority, and subsequent approval in compliance with current regulations.

This result represents a significant finding, demonstrating that initial demolition decisions can be revised and reversed through a structured technical evaluation process based on explicit and traceable criteria.

5.4 Implementation of Rehabilitation Strategies

The structural intervention strategies defined in Level III were implemented consistently with the identified structural deficits, as illustrated in Figure 7. In particular, the incorporation of shear strengthening in

masonry walls and the construction of upper bond beams restored structural continuity, improved load-bearing capacity, and enhanced expected global stability under seismic demand.

5.5 Comparative Analysis of Case Studies

The comparative analysis of the Canal Beagle and Canal Chacao cases showed that, although both typologies presented similar structural conditions and levels of thermal exposure, differences were observed in the spatial distribution of damage.

In Canal Beagle, damage was more localized, whereas in Canal Chacao a more distributed cracking pattern was identified, associated with the combined effects of thermal damage and prior seismic actions.

These differences did not affect the overall structural decision; however, they required localized adjustments in the extent and configuration of the strengthening strategies, while maintaining a consistent methodological approach in both cases.



Figure 7 - Example of implemented structural strengthening solution in the field

6. Discussion

The results demonstrate that, under conditions of moderate thermal damage, total demolition of unreinforced masonry dwellings is not necessarily a technically justified solution.

The main contribution of this study lies in the application of a structured methodology that translates damage observation into explicit criteria for assessment, decision-making, and intervention, reducing reliance on non-systematic conservative judgments. In this context, the adopted qualitative–rational approach proves appropriate for post-emergency scenarios, where advanced testing is not feasible (fib 2017; ACI 2021), enabling a consistent technical basis derived from observable indicators.

The comparative analysis suggests that the methodology can be adapted to different damage configurations while maintaining consistency in decision-making. Variations between localized and distributed damage are reflected in adjustments to strengthening strategies without altering the overall structural logic (fib 2017; Ingham 2009).

Additionally, the results highlight the importance of considering system-level behavior in attached or continuous housing, where the demolition of a single unit may compromise the global stability of the structure.

From a practical perspective, the validation of the proposed solutions through their development as formal design projects, submission to municipal authorities, and subsequent approval represents a relevant verification of their technical and regulatory feasibility.

A key limitation of the study is the absence of instrumental testing to quantify material degradation, which introduces a degree of uncertainty associated with expert judgment. However, this condition reflects the constraints of real post-fire reconstruction contexts. Therefore, the proposed methodology should be understood as a decision-support framework integrated with subsequent structural verification processes, rather than as a standalone quantitative seismic performance assessment methodology.

These findings are consistent with previous studies indicating that, under moderate thermal exposure, masonry structures may retain sufficient residual load-bearing capacity, provided that appropriate strengthening strategies are implemented.

7. Conclusions

This study demonstrates that the structural rehabilitation of unreinforced masonry dwellings affected by low to moderate thermal severity fires is technically feasible when a structured post-fire assessment methodology is applied.

The proposed methodology integrates field data collection, damage interpretation, and intervention design into a coherent, traceable, and reproducible process, supporting technically sound decision-making.

A key finding is the ability to revise and reverse initial demolition decisions through the application of explicit technical criteria based on structural continuity, global stability, and damage extent. Furthermore, defining interventions based on identified structural deficits and expected structural behavior under seismic demand —rather than solely on observable damage— enhances the expected structural behavior of rehabilitated dwellings under future seismic demand and incorporates resilience criteria into the reconstruction process.

The methodology may be applicable to post-fire reconstruction scenarios involving similar unreinforced masonry typologies and comparable levels of thermal damage. Although additional validation under different building configurations and fire exposure conditions is required, the proposed framework provides a preliminary basis for future standardization of assessment and intervention criteria in post-fire scenarios in seismic regions, as well as a practical tool for decision-making in post-disaster reconstruction processes.

8. References

American Concrete Institute (ACI). 2019. *Code Requirements for Assessment, Repair, and Rehabilitation of Existing Concrete Structures (ACI 562-19).* Farmington Hills, MI: American Concrete Institute.

American Concrete Institute (ACI). 2021. *Guide for Determining Fire Resistance of Concrete Members (ACI 216.1-21).* Farmington Hills, MI: American Concrete Institute.

Fédération Internationale du Béton (fib). 2017. *Fire Design of Concrete Structures – Materials, Structures and Modelling.* fib Bulletin. Lausanne, Switzerland: Fédération Internationale du Béton.

Hernández-Montes, E., L. Hdz-Gil, C. Coletti, S. Dilaria, L. Germinario, and C. Mazzoli. 2023. "Prediction Model for the Evolution of the Deterioration of Bricks in Heritage Buildings in Venice Caused by Climate Change." *Heritage* 6(1): 483–491. https://doi.org/10.3390/heritage6010025

Ingham, J. P. 2009. "Application of Structural Masonry in New Zealand after Fire Exposure." *Journal of Structural Fire Engineering* 1 (1): 39–52.

Li, L. Y., and J. Purkiss, 2005. "Stress–strain constitutive equations of concrete material at elevated temperatures." *Fire Safety Journal*, 40(7), 669–686. DOI: 10.1016/j.firesaf.2005.06.003.

Ramirez, R., B. Ghiassi, P. Pineda, and P. B. Lourenço. 2023. "Hygro-Thermo-Mechanical Analysis of Brick Masonry Walls Subjected to Environmental Actions." *Applied Sciences* 13(7): 4514. https://doi.org/10.3390/app13074514

RILEM TC 129-MHT. 2000. "Test Methods for Mechanical Properties of Concrete at High Temperatures." *Materials and Structures* 33 (1): 6–16.

cinpar2026
XXII International Conference on Building Pathology and Constructions Repair
15th to 17th July 2026 - Lisboa, Portugal

Assessment of the impact of mining activities with particular focus on mining tremors affecting masonry structures

Leszek SŁOWIK[1], Janusz RUSEK[2], **Leszek CHOMACKI**[1], Piotr KNYZIAK[3]

[1] Building Research Institute, Warsaw, Poland, l.slowik@itb.pl, l.chomacki@itb.pl
[2] AGH University of Science and Technology, Krakow, rusek@agh.edu.pl
[3] Warsaw University of Technology, Warsaw, piotr.knyziak@pw.edu.pl

Abstract: The dynamic and static effects associated with underground mining cause damage to buildings within the affected area. Underground mining induces continuous and discontinuous deformations in the mining area, as well as mining-induced tremors, which pose a serious threat to building structures. Underground mining operations can also cause changes in the groundwater level, leading to the flooding. This article concerns the assessment of the impact of mining tremors on masonry buildings. The paper presents an example of structural protections during the construction phase. The strengthening counteracts the negative effects of mining tremors. The main part of the paper consists of an example of the reinforcement of a church attic under mining tremors excitation. The article presents the stability analysis of the church attic structure, which was ultimately reinforced due to the effects of mining. The example highlights the importance of the technique of reinforcing masonry structures using carbon fibre meshes, used to reduces damages caused by mining underground exploitation. The example cited in the article serves as inspiration for the effective use of this type of solution in tensile stress zones within masonry structures. This has been verified in practice following the reinforcement of the structure. The article emphasises the need to apply solutions designed to specific local conditions in order to ensure structural integrity in regions affected by mining operations and to maintain the safety of their structures. The example described may serve as inspiration for an individual and modern approach to the subject of building reinforcement and modernisation.

Keywords: mining tremors, building structures, masonry, structural reinforcement.

cinpar2026
XXII International Conference on Building Pathology and Constructions Repair
15th to 17th July 2026 - Lisboa, Portugal

Seismic Vulnerability Assessment of a Heritage Unreinforced Masonry Building: Pushover Analysis

Helena Arias Lara LEITE[1,2,3], Gustavo Henrique SIQUEIRA[4]

[1] Universidade Estadual de Campinas, Campinas, SP, Brazil, h081593@dac.unicamp.br
[2] Centro Universitário de Jaguariúna (UniFAJ), Jaguariúna, SP, Brazil, helena.arias@prof.unieduk.com.br
[3] Centro Universitário Max Planck (UniMAX), Indaiatuba, SP, Brazil
[4] Universidade Estadual de Campinas, Campinas, SP, Brazil, ghsiq02@unicamp.br

Abstract: Cultural heritage buildings are structures that hold historical, artistic, or cultural significance and are often recognized and protected due to their value to a particular society or culture. Many of these buildings are built with unreinforced masonry (URM). For this type of structure, lateral loads — particularly seismic forces — pose the greatest risk. In this context, this paper conducted a pushover analysis (using the N2 method) of a URM heritage building in northeast Brazil to derive its fragility and capacity curves. The façade of the building was idealized with the equivalent frame (EF) method, and modelled with the OpenSees opensource software framework, using 'Concrete02' material to simulate the flexural behavior of the panel and 'pinching4' to account for shear. Several load patterns were considered in this analysis, among which the most representative ones should have been the modal and the triangular if the building studied vibrated primarily in the fundamental mode. The modal analysis, however, showed that the former affirmation is untrue, and a Modal Pushover Analysis should have been conducted instead. This is a limitation of the present work. The capacity and fragility curves were generated and, according to them, the building studied will most likely reach the first damage level (DL1 - slight damage), and has a 20% likelihood of reaching the second one (DL2 - moderate damage).

Keywords: N2 Method, Equivalent Frame Method, Seismic Vulnerability, Unreinforced Masonry Building, Pushover Analysis

1. Introduction

Despite being located in the center of the South American Plate, Brazil is not completely free from earthquakes. According to Associação Brasileira de Normas Técnicas (2023), its territory can be divided into 5 zones, ranging from 0 to 4. The less hazardous zone, which contemplates most of the country, is zone 0, and the most hazardous one is zone 4.

Hazard, however, is not the only aspect that should be taken into account when assessing seismic risk, as reminded by Liu et al. (2024): "accurate prediction of seismic risk mandates comprehensive data encompassing ground shaking intensity, demographic and socio-economic indicators, as well as the vulnerability of exposed buildings and infrastructure".

Since the colonization of Brazil took part from the Atlantic Ocean inward, coastal states hold many buildings that date back to the late 16th century, whereas western states, such as those that are home to the Amazon rainforest or the Pantanal wetland, do not. When looking at the seismic acceleration map that divides the country into 5 zones, one can notice that zones 2, 3 and 4 coincide with the Amazon rainforest and/or the Pantanal wetland; whereas three coastal states located in the northeast of Brazil - Paraíba, Rio Grande do Norte and Ceará - are classified into zone 1.

Most of these early settlements' buildings were built with unreinforced masonry (URM), a type of construction especially vulnerable to lateral loads, such as seismic loads, according to Como (2013). Several of such buildings are registered as heritage buildings, defined by UNESCO (2013 apud Leite et al., 2025) as "buildings ... that have a diversity of values including symbolic, historic, artistic, aesthetic, ethnological or anthropological scientific and social significance". Therefore, the preservation of these buildings is in our collective interest.

One way of assessing the vulnerability of a building is via its fragility curve: "a graphical representation that shows the probability of a structure experiencing different levels of damage or performance deterioration at varying intensities of ground shaking" (Camayang et al., 2024).

In this context, this paper focuses on the seismic performance assessment of the oldest church in the city of Natal (the capital city of the state of Rio Grande do Norte), an URM building registered as heritage, using nonlinear static methods. The main façade of the building was modeled using the Equivalent Frame (EF) approach (Lagomarsino et al., 2013) with distributed plasticity (DP) through OpenSees (McKenna, 2011), and its seismic performance was evaluated through the N2 Method (Fajfar, 2000).

2. Literature Review

2.1 Pushover-based Analysis

When affected by strong earthquakes, most buildings experience significant inelastic deformations. "A truly realistic assessment of structural behavior in the inelastic range can be made only through nonlinear analysis." There are different types of nonlinear analyses, among which are pushover-based methods, such as the N2 method, which are less demanding and require less data. "Pushover-based methods combine nonlinear static (i.e., pushover) analysis with the response spectrum approach". A multi-degree-of-freedom (MDOF) system is transformed into an equivalent single-degree-of-freedom (SDOF) one, and seismic demand can be obtained from this equivalent SDOF system. This transformation, however, represents the main limitation of the pushover-based methods, because it is an approximation. Despite the aforementioned limitation, if compared to traditional elastic analyses, a pushover-based analysis provides important additional information about the expected structural response, such as data on the strength and ductility of structures and design weaknesses. (Fajfar, 2021)

According to European Committee for Standardization (2004), in order to perform a pushover analysis, "at least two vertical distributions of the lateral load should be applied": a uniform one, proportional to mass; and a modal one, with forces proportional to the lateral force distribution from elastic analysis, i.e., proportional to the first mode shape. For regular buildings, this is well approximated by the triangular pattern.

2.2 The N2 Method

The N2 method was proposed by Fajfar and Gašperšič (1996) as a way of connecting pushover analysis with the response spectrum approach and "for structures that vibrate primarily in the fundamental mode", it will likely "provide reasonably reliable estimates of global seismic demand" (Fajfar and Gašperšič, 1996).

This method can be divided in several steps, according to Fajfar (2000). The first step consists on gathering the data from the structure and the elastic acceleration spectrum, from which it is possible to determine the inelastic spectra in acceleration-displacement (AD) format. After that, a pushover analysis is performed on the MDOF model, under increasing lateral load, and considering different load patterns. The subsequent step consists on the transformation of the MDOF quantities (Q) to equivalent SDOF quantities ($Q*$), as represented on eq. 1, where Γ is the transformation factor, determined by the mass of the equivalent SDOF system ($m*$) and the mass of the MDOF system (m_i) and the displacement shape (ϕ_i), as represented on eq. 2. Then, it is possible to determine the seismic demand for the equivalent SDOF system, from which it is

possible to obtain the global and local seismic demands for the MDOF model. Finally, a performance evaluation can be made, and damage can be analyzed.

$$Q^* = \frac{Q}{\Gamma} \tag{1}$$

$$\Gamma = \frac{m^*}{\sum m_i \phi_i^2} \tag{2}$$

2.3 The Equivalent Frame (EF) Method

In the EF method, the masonry building is represented by an equivalent nonlinear frame structure. “Each resistant masonry wall is subdivided into a set of deformable masonry panels, in which the deformation and the nonlinear response are concentrated, and rigid portions, which connect the deformable ones”. Whereas piers are the main vertical resistant elements (and they carry both vertical and lateral loads), spandrels are the lintels, i.e., the parts of the wall above openings, and they are “secondary horizontal elements (for what concerns vertical loads), which couple the response of adjacent piers in the case of lateral loads”. Lagomarsino et al., 2013).

The definition of the macro-elements geometry is extremely influential on the result of the analysis. A special attention must be paid to the piers, because they represent the main resisting elements of the EF scheme (Siano et al., 2018). After the definition of the macro-elements’ geometry, they must be modeled so that their behavior can be assessed. According to Siano et al. (2018), the non-linearity of the material can be taken into account by two different approaches: lumped plasticity (LP) and distributed plasticity (DP) models. According to Requena-Garcia-Cruz et al. (2023), masonry pears can have flexural or shear failure. The first “can be captured by simulating the axial load-bending moment (N-M) response”, whereas the second “is linked to the diagonal cracking failure and it can be simulated through shear force - deformation / displacement (V-γ) or (V-d) laws”.

3. Methodology

The church that is the object of study in this paper was initially built in 1601, demolished and rebuilt twice. The construction that still stands these days dates back to 1694, according to Araújo (2018). It is made of stone masonry. Its main façade is represented at Figure 1a. It was registered as a heritage building in 1992 (Fundação José Augusto, 2025). This church is located in the city of Natal, which is situated into the seismic zone 1, as highlighted in Figure 1b.

The dimensions of the frontal façade are: width = 12 meters, height of the bell tower = 13 meters, height of the cross’ support = 10 meters, height of the left part = 6 meters. The only information regarding the wall thickness that could be found is that, when the bell tower was rebuilt, it was done so as a load bearing wall with a thickness of 2 meters (Araújo, 2018). Since this information is only pertinent to the bell tower (right part of the façade), a decision was made to consider an overall thickness of 1.30 meters, which is also considerable, albeit a bit more conservative than the bell tower thickness.

In order to apply the EF Method on the church, the spandrels, piers and rigid nodes must be defined before the EF idealization, which is represented on Figure 2. The geometry of the cross section of the pier and spandrel elements was taken as an average for all elements, i.e., since the height of each element should be taken as its in plane dimension, instead of each pier and spandrel having a different height, an average was made and, for piers, the height considered was 0.60 meters, whereas for spandrels the height considered was 1.00 meter. The base considered was the out of plane dimension, i.e., the aforementioned overall thickness of 1.30 meters.



Figure 1 – a) Façade of the church studied: Igreja Matriz de Nossa Senhora da Apresentação (Arquidiocese de Natal, 2025) and b) Location of the city where the church is built according to the brazilian seismic zoning map (Associação Brasileira de Normas Técnicas, 2023; Dlubal Software GmbH, 2024)

In a similar manner as Rodrigues et al. (2024) and inspired by Requena-Garcia-Cruz et al. (2023), OpenSees was used. The materials considered were 'Concrete02' to simulate the flexural behavior of the URM panel and 'pinching4' to simulate shear. Regarding the adoption of 'Concrete02' for simulating URM, Rodrigues et al. (2024) used 'Concrete02' to simulate the flexural behavior of a URM panel of a similar church as the one studied in this paper, whereas Requena-Garcia-Cruz et al. (2023) used 'Concrete06'. Although the latter material "was originally proposed for concrete, it has been proved to satisfactorily capture the masonry behavior" (Sepe et al., 2014, apud Requena-Garcia-Cruz et al., 2023). The same justification was made by Rodrigues et al. (2024) regarding the former material.

The piers and spandrels were also implemented as a displacement-based element with fiber cross-section. Distributed plasticity was adopted for all pier and spandrel elements, modelled as displacement-based beam-column elements ('dispBeamColumn') with 5-point Gauss-Lobatto integration and fiber cross-sections. This formulation, known as DP-DI, allows inelastic deformations to spread along the element length as the analysis progresses, capturing the gradual degradation of stiffness and strength characteristic of unreinforced masonry. The nodal intersection regions were modelled as linear elastic rigid zones, consistent with the equivalent frame idealization. The nonlinear behavior of the masonry is captured by the constitutive laws assigned to the fibers for the axial-flexural response ('Concrete02' material), while the nonlinear shear response is modelled by a separate uniaxial material ('pinching4') coupled to the fiber section through an aggregated section formulation. (Rodrigues et al., 2024).

Several parameters are needed for the correct description of the shear force-deformation curve. As specified by Rodrigues et al. (2024), the ultimate shear strength follows the Turnšek and Čačovič failure criteria; the initial deformation $\gamma 1$ was taken as V3/Ke, with the initial elastic shear stiffness $K_e = GA_s$, where G is the shear modulus and A_s the cross section of the wall (and therefore different for piers and spandrels). The ultimate deformation γ_3 was specified as 0.4%, according to the recommendations of Ministero delle Infrastrutture e dei Trasporti (2019), and γ_4 was specified as 1%, according to Federal Emergency Management Agency (2000).

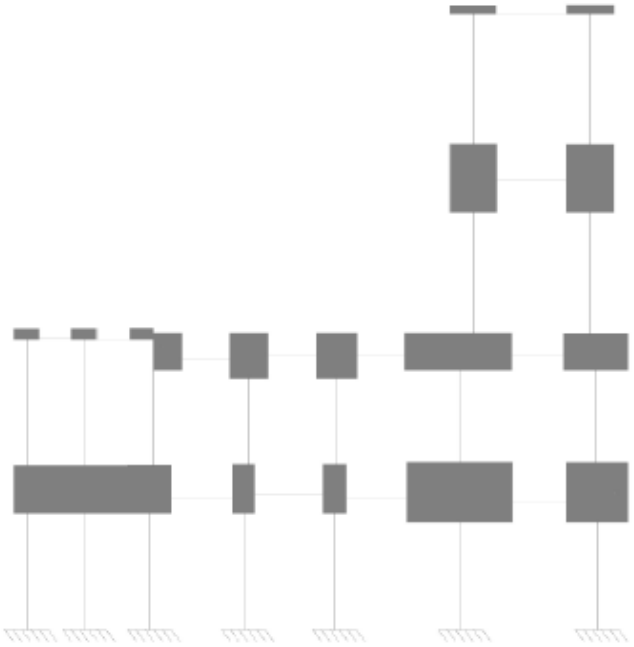


Figure 2 – Equivalent frame idealization

The parameter γ_2 was taken as the average of γ_1 and γ_3. The shear strength of the unreinforced masonry walls is given by eq. 3, where σ_0 is the average compression stress (taken as 0.10 MPa), τ_{0d} is the diagonal cracking strength (taken as 0.20 MPa), l and t are the width and the thickness of the wall section, respectively, and β is a coefficient dependent of the slenderness of the pier and spandrel elements. The residual shear strength V_4 was taken as 20% of the ultimate shear strength V_3, and V_1, V_2 and V_3 were all taken as equal to V_t.

$$V_t = 1.5\tau_{0d} lt\beta \sqrt{1 + \frac{\sigma_0}{1.5\tau_{0d}}} \tag{3}$$

The other material properties considered are shown on Table 1, where γ is the specific weight of the masonry, E is the modulus of elasticity, G is the shear modulus, f_{pc} is the compressive strength, f_t the tensile strength, ε_{c0} is the strain at peak and ε_u is the ultimate strain.

Table 1 – Mechanical properties considered for the constitutive law (Ministero delle Infrastrutture e dei Trasporti, 2019; Requena-Garcia-Cruz et al., 2023; Rodrigues et al., 2024)

γ (kN/m³)	E (MPa)	G (MPa)	f_{pc} (MPA)	f_t (MPa)	ε_{c0}	ε_u
18	1490	490	-6.2	0.18	-0.00832	-0.025

The N2 method was used, and several load patterns were considered. The patterns considered in this study are uniform (UN), mass-proportional (MASS), modal (MODAL) and triangular (TR). Roof displacement was controlled in all patterns.

Lagomarsino and Giovinazzi (2006) established a damage threshold criteria using a κ fraction of peak base shear on the ascending and descending branches of the pushover curve. The damage levels are DL1 (slight damage), DL2 (moderate damage), DL3 (extensive damage) and DL4 (collapse). κ is the total base shear divided by the maximum base shear of the pushover curve. After deriving the capacity curves for a structure and the damage thresholds for all patterns considered, the following step of this analysis is to generate the fragility curves, which represent the answer to the question "given that the seismic demand is $S_{d,pp}$, what is

the probability that the displacement exceeds each damage threshold"? According to the approach of Lagomarsino and Giovinazzi (2006), the fragility curves can be generated by, at first, identifying the displacement thresholds (MDOF) and converting them to SDOF, according to eq. 1. Then, for each damage state, the probability of exceedance given a spectral displacement S_d is calculated using a standard normal cumulative distribution function and a total dispersion $\beta = 0.50$, which accounts for both demand uncertainty (β_D) and capacity uncertainty (β_C).

3.1 An important limitation of the present study

As mentioned on the first paragraph of section 2.2, this analysis will provide reliable results "for structures that vibrate primarily in the fundamental mode" (Fajfar and Gašperšič, 1996). As the analysis progressed, the authors noticed that this structure does not have a clear dominant mode and, therefore, the results achieved have more limitations than initially predicted and a different analysis should have been conducted. A decision was made, however, to proceed with the present study, which represents an initial investigation intended to evaluate the limitations and applicability of the adopted approach, and a suggestion was given on section 5.1 for an improved analysis in order to obtain more reliable results.

4. Results and discussion

4.1 Pushover analysis and performance points

The elastic response spectrum was obtained from the brazilian standard (Associação Brasileira de Normas Técnicas, 2023) for a return period (TR) of 475 years and a soil type E with SPT N ≤ 15 in the first 30 meters. It is represented on Figure 3a. According to Associação Brasileira de Normas Técnicas (2023), Rio Grande do Norte (the state in which the heritage building is located) can be considered at zone 1, with a maximum horizontal seismic acceleration of 0.05g (g being the acceleration due to gravity), for soil type B (rocky).

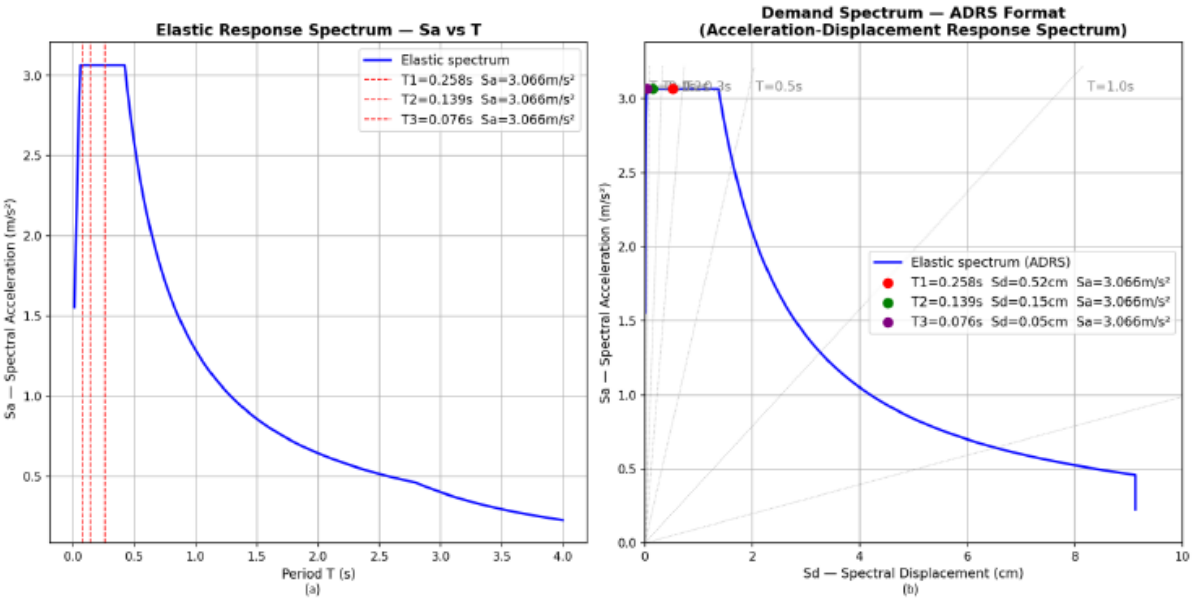


Figure 3 – (a) Response Spectrum (Sa vs T) and (b) Demand spectrum (ADRS format)

In order to convert the elastic response spectrum to the Acceleration-Displacement Response Spectrum (ADRS) format, one must calculate the spectral displacement (Sd) according to eq. 4. The ADRS is represented on Figure 3b. T1, T2 and T3 represent the modal periods of the structure, obtained from the

eigenvalue analysis of the MDOF model. In this same eigenvalue analysis, aside from the modal periods, the fraction of the total mass participating in the horizontal (direction of loading) direction for each mode (U_1), the fraction of the total mass participating in the vertical direction for each mode (U_2) and the cumulative sum ($\sum U_1$) after 3 modes were also computed, and they are shown on Table 2. It is shown that the modes are almost purely X-direction modes, which is consistent for a planar masonry wall pushed horizontally. The cumulative $\sum U_1$ = 98.2% after 3 modes means that the analysis captures almost all the seismically relevant mass in X. However, the limitation mentioned on section 3.1 can also be seen, because it is clear that modes 1 and 2 are equally dominant in this structure.

$$S_d(T) = S_a(T) \times \left(\frac{T}{2\pi}\right)^2 \tag{4}$$

Table 2 – Modal properties - First 3 modes

Mode	T (s)	U_1 (%)	U_2 (%)	$\sum U_1$ (%)
1	0.2580	49.89	0.01	49.89
2	0.1391	47.30	0.01	97.19
3	0.0763	1.00	0.00	98.20

For each load pattern, the pushover analysis is made and the N2 method is run with the objective of computing the performance point (the target displacement, i.e., the expected roof displacement under the design earthquake), the base shear at the performance point (V_t) and the spectral displacement at the performance point ($S_{d,pp}$), which is simply the SDOF target displacement. These results are all plotted on Figure 4.

4.2 Capacity and Fragility curves

The capacity curve was generated for each load pattern. The performance point and the 4 damage threshold markers were added to each curve, and they were all plotted together, as shown of Figure 4.

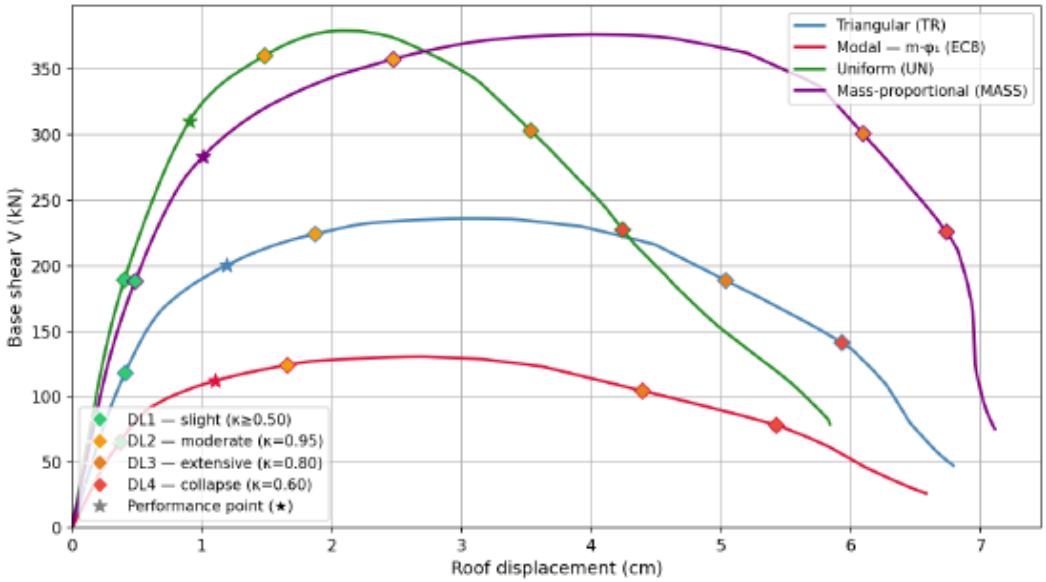


Figure 4 – Capacity curves for each load pattern, with damage threshold markers

Figure 4 shows that the uniform and mass-proportional load patterns have the highest peak base shears (379.4 kN and 376.6 kN, respectively). Additionally, the mass-proportional pattern has also the largest displacement at peak, at around 4 cm and the uniform one is the most different shape-wise. These two patterns, however, are generally considered less representative because they apply more force to lower storeys compared to triangular pattern and they tend to overestimate capacity by not capturing the whipping (or whiplash) effect of upper storeys. In the structure that is the object of this study, this effect is somewhat limited because it is a low-rise structure, therefore the height amplification is not as dramatic as it would be in a tall building.

The lowest peak base shear occurs with the modal pattern, a pattern that should be the most representative one for structures that have the first mode as a clear dominant one. Since the object of this study does not have this clear domination of one mode, as previously pointed, this is also not very representative. The triangular pattern, that should not differ much from the modal one (for regular structures), shows the second lowest peak base shear. This pattern resulted in a pushover curve similar in shape with the pushover curves generated by the modal and the mass-proportional patterns. However, European Committee for Standardization (2004) recommends it as the primary load pattern for structures where the first mode is dominant, which is not true for the structure studied in this paper, as seen on Table 2.

The fragility function was calculated for each pattern and each damage level, as shown on Table 3, and the fragility curves were generated, as shown on Figure 5.

According to these fragility curves, and considering all load patterns studied, for the response spectrum given by Associação Brasileira de Normas Técnicas (2023), the heritage building studied will most likely exceed DL1, will have a fair chance of exceeding DL2 and will most likely not exceed DL3 and DL4. From a preservation point of view, this can be viewed as positive, because the likelihood of the occurrence of moderate damaging is less than 25 %, and, therefore, no big intervention will be needed as a retrofitting strategy.

Table 3 – Fragility - Exceedance Probabilities at Performance Point (logonormal, β = 0.50)

Pattern	$S_{d,pp}$ (cm)	P(DL1) (%)	P(DL2) (%)	P(DL3) (%)	P(DL4) (%)
TR	0.665	98.4	18.2	0.2	0.1
MODAL	0.596	98.6	20.9	0.3	0.1
UN	0.905	94.6	16.1	0.3	0.1
MASS	0.847	92.8	3.7	0.0	0.0

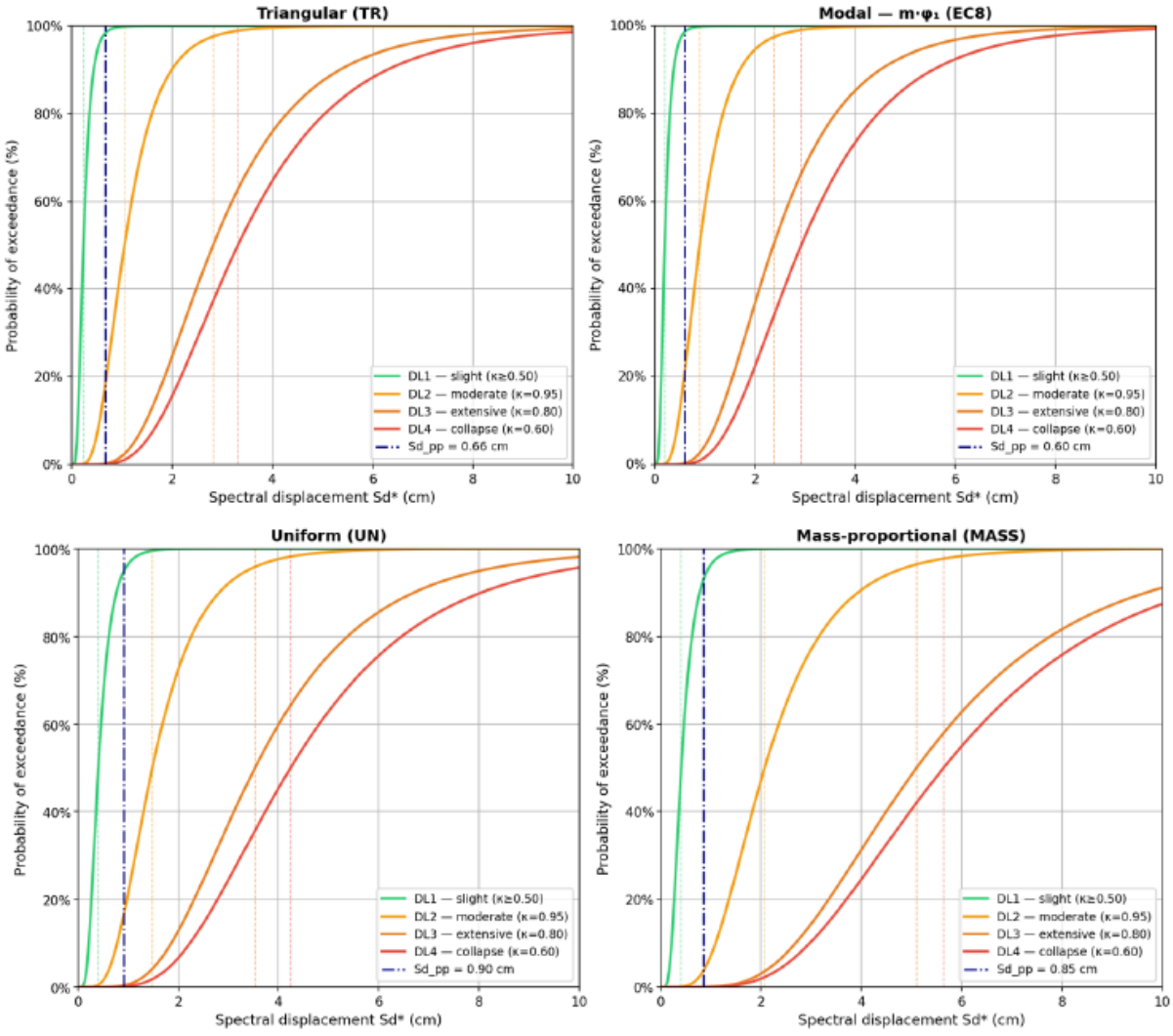


Figure 5 – Fragility curves

5. Conclusions

Despite not being on the most hazardous earthquake zone in Brazil, heritage buildings located on zone 1, such as the church 'Matriz de Nossa Senhora da Apresentação' (object of the present study) are particularly vulnerable to these types of loading. This is due to the fact that colonial or heritage buildings were built with unreinforced masonry, which can be especially susceptible to horizontal loads.

A pushover analysis is a relatively simple method that can provide reliable estimates of the seismic response of buildings. The present study derived the in-plane capacity and fragility curves of the oldest church in the Brazilian city of Natal using pushover analysis to assess its seismic vulnerability. As previously noted, although the uniform and mass proportional load patterns resulted on the highest peak base shear and the lowest probabilities of damage level exceedance, they are the least representative load patterns, because they apply more force to lower storeys compared to triangular pattern and they tend to overestimate capacity by not capturing the whipping (or whiplash) effect of upper storeys.

The patterns that resulted in the highest vulnerability and the lowest peak base shears were the triangular and the modal ones. The latter should have been the pattern that best represented the church studied, and

the former should have been the second best one; however, since the first mode is not clearly dominant, this entire analysis has more limitations than expected, and a different analysis, such as a Modal Pushover Analysis, should be conducted in order to obtain more reliable results.

After deriving the fragility curves, it was possible to ascertain that the building study will likely achieve the threshold for DL2, which results in moderate damage, but will most likely not exceed DL3 and DL4. From a preservation point of view, this can be viewed as positive, because, due to the level of damage achieved, no big intervention will be needed as a retrofitting strategy.

5.1 Suggestion for an improved study

This study was conducted with the objective of assessing the structural vulnerability of a heritage building in Brazil by deriving its capacity and fragility curves. The concept of this pushover analysis was based on the assumption that either the triangular or the modal load patterns would be a good representation of the dynamic inertia force distribution for this structure. This would be true for structures that have a clear dominant mode. In this case, the nearly equal participation of the first two modes is likely a consequence of the structural irregularity. A single pushover analysis with any fixed load pattern is questionable when two modes have nearly equal participation, because no single static load distribution can adequately represent the dynamic response, and, therefore, further studies about this particular structure, in order to improve the quality of the representation of the resulting pushover curve, are necessary. A more rigorous approach would be a Modal Pushover Analysis (MPA), as suggested by Chopra and Goel (2002), which runs separate pushovers for each significant modes and combines the results.

Acknowledgments

The author(s) would like to acknowledge CNPq (Conselho Nacional de Desenvolvimento Científico e Tecnológico) for the financial support provided through a PhD Grant (Process No. 141004/2025-8) and for other Grants (Processes 308040/2021-0 and 308783/2025-5).

References

Araújo, A. T. d. O. (2018). Estudo das alvenarias de edificações históricas: arquitetura religiosa do período colonial no Rio Grande do Norte, com ênfase no sistema construtivo, manifestações patológicas e aplicação da matriz GUT. Master's thesis, Universidade Federal do Rio Grande do Norte, Natal, Brasil.

Arquidiocese de Natal (2025). Arquidiocese de Natal. Available at https://www.arquidiocesedenatal.org.br/post/par%C3%B3quia-de-nossa-senhora-da-apresenta%C3%A7%C3%A3o-cidade-alta-natal. Accessed on July 28, 2025.

Associação Brasileira de Normas Técnicas (2023). NBR 15421: Projeto de estruturas resistentes a sismos. Technical report, ABNT.

Camayang, J. P., O. Dela Cruz, and R. Grutas (2024). Integrating building-and site-specific and generic fragility curves into seismic risk assessment: A prisma-based analysis of methodologies and applications. CivilEng 5(4), 1011–1041.

Chopra, A. K. and R. K. Goel (2002). A modal pushover analysis procedure for estimating seismic demands for buildings. Earthquake engineering & structural dynamics 31(3), 561–582.

Como, M. (2013). Statics of historic masonry constructions, Volume 1. Springer.

Dlubal Software GmbH (2024). Zonas Sísmicas do Brasil Segundo a ABNT NBR 15421:2023. https://www.dlubal.com/pt/zonas-de-carga-para-neve-vento-e-sismos/sismo-abnt-nbr-154212023.html. Accessed on June 3, 2026.

European Committee for Standardization (2004). Eurocode 8: Design of Structures for Earthquake Resistance. Part 1: General Rules, Seismic Actions and Rules for Buildings. Technical Report EN 1998-1, CEN.

Fajfar, P. (2000). A nonlinear analysis method for performance-based seismic design. Earthquake spectra 16(3), 573–592.

Fajfar, P. (2021). The story of the N2 method. International association for earthquake engineering.

Fajfar, P. and P. Gašperšič (1996). The n2 method for the seismic damage analysis of RC buildings. Earthquake engineering & structural dynamics 25(1), 31–46.

Federal Emergency Management Agency (2000). Prestandard and Commentary for the Seismic Rehabilitation of Buildings. Technical Report FEMA 356, FEMA,Washington, D.C.

Fundação José Augusto (2025). Fundação José Augusto. Available at http://www.cultura.rn.gov.br/Index.asp. Accessed on August 5, 2025.

Lagomarsino, S. and S. Giovinazzi (2006). Macroseismic and mechanical models for the vulnerability and damage assessment of current buildings. Bulletin of Earthquake Engineering 4(4), 415–443.

Lagomarsino, S., A. Penna, A. Galasco, and S. Cattari (2013). Tremuri program: an equivalent frame model for the nonlinear seismic analysis of masonry buildings. Engineering structures 56, 1787–1799.

Leite, H. A. L., P. Q. Rodrigues, and G. H. Siqueira (2025). Collapse mechanisms in heritage structures under seismic loads and retrofitting strategies: A literature review. In XXI International Conference on Building Pathology and Constructions Repair (Cinpar).

Liu, Y., Y. Gu, and H. Zhang (2024). Seismic risk assessment and damage analysis: emerging trends and new developments. Journal of Safety Science and Resilience 5(3), 365–381.

McKenna, F. (2011). Opensees: a framework for earthquake engineering simulation. Computing in Science & Engineering 13(4), 58–66.

Ministero delle Infrastrutture e dei Trasporti (2019). Circolare n.7: Istruzioni per l'applicazione dell'Aggiornamento delle Norme Tecniche per le Costruzioni di cui al Decreto Ministeriale 17 Gennaio 2018. Technical report, Gazzetta Ufficiale della Repubblica Italiana, Roma.

Requena-Garcia-Cruz, M., S. Cattari, R. Bento, and A. Morales-Esteban (2023). Comparative study of alternative equivalent frame approaches for the seismic assessment of masonry buildings in OpenSees. Journal of Building Engineering 66, 105877.

Rodrigues, P. Q., E. M. V. Pereira, F. F. Leitão, R. B. Andrade, H. L. Oliveira, and G. H. Siqueira (2024). Seismic performance assessment of an unreinforced masonry historical building using nonlinear static methods. In Ibero-Latin American Congress on Computational Methods in Engineering (CILAMCE).

Siano, R., P. Roca, G. Camata, L. Pelà, V. Sepe, E. Spacone, and M. Petracca (2018). Numerical investigation of non-linear equivalent-frame models for regular masonry walls. Engineering Structures 173, 512–529.

Cinpar 2026
XXII International Conference on Building Pathology and Constructions Repair
15th to 17th July 2026 - Lisboa, Portugal

Análise da Reconstrução da Infraestrutura Escolar do Rio Grande do Sul Decorrente dos Efeitos do Desastre Climático Ocorrido em 2024.

Pedro Jader Antony LINHARES[1], Marcio Augusto Roma BUZAR[2], Fernanda M. de O. M. C. PACOBAHYBA[3], Carlos H. B. Nitão LOUREIRO[4], Amilton FIGUEIREDO[5].

[1] FNDE, Brasília, Brasil, pedro.linhares@fnde.gov.br
[2] FNDE, Brasília, Brasil, marcio.buzar@gmail.com
[3] FNDE, Brasília, Brasil, fernanda.pacobahyba@fnde.gov.br
[4]FNDE, Brasília, Brasil, carlos.nitao@fnde.gov.br
[5]FNDE, Brasília, Brasil, amiltonfigueiredo@mec.gov.br

Resumo:

Os eventos climáticos extremos ocorridos no Rio Grande do Sul em 2024 produziram danos extensivos à infraestrutura pública e comprometeram, de modo particularmente severo, a rede de educação básica. Em resposta, o Governo Federal estruturou, no âmbito do Fundo Nacional de Desenvolvimento da Educação (FNDE) e do Ministério da Educação (MEC), um programa emergencial destinado à recomposição integral de escolas e creches atingidas, com base em critérios técnicos, normativos e orçamentários. O presente artigo analisa o processo de seleção de 28 propostas de reconstrução, com apoio em laudos técnicos padronizados de engenharia, nos projetos referenciais do FNDE e na sistematização dos dados constantes de base de dados estruturada, com ênfase nos aspectos técnico-patológicos, locacionais e financeiros. Os resultados, na análise da infraestrutura, evidenciam predominância de grau de risco crítico, recorrência de patologias associadas à ação da água, comprometimento estrutural e funcional de diversos sistemas construtivos e recomendação majoritária de mudança de local para implantação de novas unidades em localidades mais seguras. No plano financeiro, verificou-se investimento total de R$ 191.167.583,92, distribuído entre creches e escolas padronizadas, com destaque para o Município de Estrela/RS, que concentrou seis propostas e adotou solução construtiva industrializada. Conclui-se que o Programa Emergencial se configura como instrumento essencial para a recomposição plena da rede física educacional, reforçando a diretriz de reconstrução total — e não de reformas paliativas — como resposta adequada aos danos decorrentes dos desastres climáticos.

Palavras-chave: Reconstrução escolar; Patologia das construções; Desastres climáticos; Infraestrutura educacional; FNDE.

1. Introdução

A intensificação dos eventos climáticos extremos tem imposto desafios crescentes à infraestrutura pública brasileira, especialmente nos territórios sujeitos a enchentes, enxurradas, alagamentos recorrentes e instabilidades geomorfológicas. No Rio Grande do Sul, os eventos de 2024 produziram efeitos devastadores sobre a rede pública de ensino, comprometendo edifícios escolares, equipamentos, instalações, acessos e condições mínimas de segurança para o funcionamento das atividades educacionais.

No âmbito da resposta federal, o Programa Reconstrução Emergencial do RS foi estruturado a partir de um desenho técnico-administrativo que condicionou o repasse de recursos à apresentação de laudos de engenharia capazes de demonstrar, com evidências objetivas, a extensão dos danos, a criticidade dos sistemas construtivos e a inviabilidade de recuperação da infraestrutura existente. Tal desenho permitiu qualificar a seleção das propostas com base em parâmetros uniformes de avaliação, ancorados em modelo padronizado de laudo disponibilizado aos proponentes.

Este artigo tem por objetivo examinar, em perspectiva técnico-acadêmica, o processo de seleção das propostas, a função dos laudos técnicos padronizados, os critérios de enquadramento em reconstrução, os principais achados patológicos identificados e a distribuição financeira dos investimentos realizados nas 28 propostas aprovadas. Para robustecer a análise, são tomados como casos ilustrativos os laudos da EMEI Amiguinhos da Natureza, no Município de Relvado/RS, e da EMEI Criança Feliz, no Município de Estrela/RS, ambos emblemáticos quanto à relação entre dano construtivo, vulnerabilidade locacional e decisão pela reconstrução integral em novo local.

2. Metodologia

A pesquisa caracteriza-se como documental, descritiva e analítica, com base em documentação técnica oficial produzida no âmbito do Programa Emergencial de Reconstrução da infraestrutura educacional do Rio Grande do Sul. O corpus documental foi composto por quatro eixos de evidência: (i) o Modelo de Laudo Técnico Comprobatório de Comprometimento da Infraestrutura Escolar, disponibilizado pelo FNDE aos entes proponentes; (ii) os laudos técnicos individuais elaborados pelos municípios; (iii) Base de dados consolidados dos laudos e das propostas, com ênfase na caracterização e sistematização dos danos evidenciados; e (iv) as consolidações financeiras por município e por tipologia de projeto padronizado.

O modelo de laudo foi concebido para padronizar o levantamento dos danos e organizar a análise por sistemas construtivos — cobertura, vedações, instalações hidrossanitárias, instalações elétricas, pisos, estrutura e paisagismo — classificando-os segundo graus de risco e impacto de recuperabilidade, em conformidade com a terminologia da inspeção predial adotada pelo documento.

No tratamento dos dados, procedeu-se à leitura técnica dos laudos e à extração sistemática das variáveis constantes da planilha consolidada: localização anterior e atual, recomendação de novo local, vulnerabilidade da área, recorrência de sinistros, classificação dos subsistemas, grau de risco, impacto, proposta indicada, valor de investimento, valor pago e estágio de execução. O cruzamento desses dados permitiu analisar conjuntamente os aspectos patológicos, locacionais, institucionais e financeiros do processo.

Como estudos de caso ilustrativos, foram mobilizados dois laudos. O primeiro, referente à EMEI Amiguinhos da Natureza, registra que a unidade foi atingida pela enxurrada, situa-se em área vulnerável, possui arroio nas proximidades e teve expressa recomendação de mudança de local, culminando com conclusão pela reconstrução total da escola em outro espaço fora da área de risco. O segundo, referente à EMEI Criança Feliz, registra exposição de 87 horas à enchente, implantação em área alagável, recorrência de agravos ambientais, comprometimento de múltiplos sistemas e conclusão pela reconstrução total em outro local, com demolição do imóvel atual e limpeza final do lote.

3. Desenvolvimento do tema

3.1. Procedimentos para seleção das propostas do Programa Reconstrução Emergencial do RS.

O processo de seleção das propostas foi estruturado com base na Medida Provisória nº 1.248/2024 e na Resolução FNDE nº 12/2024, que estabeleceram critérios técnicos e administrativos para o repasse de recursos federais destinados à reconstrução de unidades escolares.

Foram selecionadas 28 propostas, abrangendo escolas de ensino fundamental e creches, cujos imóveis apresentaram danos classificados como severos ou irrecuperáveis. Entre os principais critérios adotados destacam-se: a comprovação de comprometimento estrutural, a exposição recorrente a riscos ambientais e a inviabilidade técnica ou econômica de recuperação das edificações existentes. Recursos disponibilizados aos municípios nas ações de reforma

A seleção das propostas de reconstrução foi estruturada a partir de um fluxo técnico-administrativo orientado por comprovação documental, laudo técnico mais ART, do comprometimento da unidade escolar atingida. O ingresso no programa exigiu laudo técnico formal subscrito por profissional habilitado, contendo caracterização do imóvel, identificação dos danos, classificação dos sistemas construtivos, análise do grau de risco e conclusão objetiva quanto à necessidade de reconstrução.

No conjunto examinado, foram contemplados 16 municípios, consolidadas 28 propostas de reconstrução, distribuídas entre as tipologias Creche Tipo 1 (7 propostas), Creche Tipo 2 (9 propostas), Escola 13 Salas (1 proposta), Escola 5 Salas (8 propostas) e Escola 9 Salas (3 propostas), totalizando R$ 191.167.583,92 em valor de investimento previsto.

A seleção evidenciou que o programa federal foi concebido para recompor integralmente a capacidade física da rede de ensino afetada, e não para financiar intervenções pontuais de reparo. A base de dados consolidada registra, para as 28 propostas, indicação de solução correspondente à reconstrução, inclusive nos casos em que o impacto foi classificado como “recuperável”, uma vez que a exposição recorrente ao risco e o custo técnico-social de permanência no local justificaram a substituição integral da infraestrutura. As Figuras 1 e 2 ilustram, de forma sucinta, os danos registrados nos 16 municípios mais afetados, os quais foram contemplados com novas infraestruturas de ensino.



Figura 1 – Imagens dos danos causados nas enchentes do Rio Grande do Sul (A).



Figura 2– Imagens dos danos causados nas enchentes do Rio Grande do Sul (B).

3.2. O modelo de laudo técnico como instrumento de padronização e decisão

O Modelo de Laudo Técnico Comprobatório de Comprometimento da Infraestrutura Escolar disponibilizado pelo FNDE cumpriu função estruturante no processo de seleção, ao padronizar os níveis de inspeção, os subsistemas a serem observados, a classificação do grau de risco e a formulação da conclusão final. O documento orienta a vistoria por métodos não destrutivos e inspeção visual, além de exigir registro fotográfico e análise segmentada dos sistemas prediais, em consonância com a lógica da inspeção predial e da patologia das construções.

O modelo organiza a avaliação segundo três níveis de resposta: grau de risco crítico, associado a impacto irrecuperável ou a custo excessivo de recuperação; grau de risco regular, associado a perda parcial de desempenho; e grau de risco satisfatório, quando não há anomalias significativas. Tal arquitetura metodológica permitiu que os dados dos laudos fossem transpostos para a planilha de sistematização, formando uma base comparável entre municípios e unidades escolares distintas.

A relevância desse instrumento pode ser observada tanto no laudo da EMEI Amiguinhos da Natureza quanto no da EMEI Criança Feliz, que reproduzem a lógica do modelo: caracterização da unidade, definição do nível de inspeção, classificação por sistemas, discussão dos danos, análise do risco e conclusão pela reconstrução. Em ambos os casos, a decisão final não decorre apenas de avarias localizadas, mas da combinação entre dano físico, recorrência de agravos ambientais e risco futuro de reocupação do mesmo sítio.

3.3. Projetos padronizados do FNDE e sistemas construtivos industrializados

As propostas aprovadas tomaram por referência os projetos padronizados do FNDE, abrangendo creches Tipo 1 e Tipo 2, figura 3, bem como escolas de 5, 9 e 13 salas, figura 4. A base de dados consolidada demonstra que a recomposição da rede foi estruturada por meio dessas tipologias, o que assegurou padronização orçamentária, compatibilidade entre demandas e projetos e maior racionalidade na instrução das propostas.



Figura 3 – Detalhes dos projetos padronizados – Creches Tipo 1 e Tipo 2



Figura 4 – Detalhes dos projetos padronizados – Escolas 5, 9 e 13 Salas

Do ponto de vista estratégico, a adoção de projetos padronizados facilita não apenas a seleção das propostas, mas também a análise técnica posterior, a contratação, o acompanhamento e a fiscalização. No contexto emergencial, tal opção reduz incertezas de escopo, encurta o tempo de maturação dos empreendimentos e favorece a previsibilidade do custo público necessário para recomposição da oferta educacional.

Além disso, estudo indica a adoção de solução industrializada em propostas do Município de Estrela/RS, aspecto que se associa à estratégia de imprimir maior celeridade à execução das obras. Esse recorte é particularmente relevante porque o município de Estrela concentrou seis propostas, todas registradas com a indicação para solução industrializada, evidenciando o uso do mecanismo como instrumento de resposta mais rápida à emergência.

3.4. Sistematização dos dados e metodologia de análise dos laudos

O procedimento metodológico envolveu: (i) leitura individualizada dos laudos técnicos; (ii) extração padronizada das informações relativas aos sistemas construtivos; (iii) classificação das manifestações patológicas e do grau de risco; (iv) análise cruzada entre recorrência de sinistros, localização e conclusão técnica; e (v) a sistematização dos dados para avaliação do enquadramento das propostas no Programa Emergencial.

A análise foi orientada por referências do campo da patologia das construções, normas técnicas brasileiras e diretrizes institucionais do FNDE.

A base de dados sistematizada, em formato matricial, sintetiza os dados extraídos dos laudos e organiza a análise por eixos: características do terreno e da localização, vulnerabilidade ambiental, recorrência de sinistros, estado dos sistemas construtivos, correlações patológicas, grau de risco, impacto, proposta de solução, indicação de novo local, valores de investimento e estágio de execução. Essa estrutura viabiliza uma leitura sistêmica do conjunto das 28 propostas.

A sistematização demonstra que a avaliação não se limitou a uma percepção impressionista do dano, mas foi composta por uma cadeia lógica: identificação dos agravos; classificação de cada sistema; consolidação do risco global; verificação da possibilidade de permanência ou realocação; e definição da resposta pública adequada. Tal metodologia é especialmente relevante em cenários de desastre, nos quais a pressão por rapidez pode comprometer a qualidade da decisão se não houver um protocolo técnico claro.

No caso da EMEI Amiguinhos da Natureza, por exemplo, o laudo registrou danos severos em esquadrias, cercamentos, instalações elétricas e componentes diversos, além da localização em área alagável próxima ao arroio, concluindo pela reconstrução total em novo local. Já no caso da EMEI Criança Feliz, o laudo documentou que a escola, edificada em concreto armado e com dois pavimentos, permaneceu exposta por 87 horas à enchente, encontrava-se em área vulnerável e alagável, e teve cobertura, forro, instalações, vedações e partes estruturais severamente comprometidos, culminando com recomendação de reconstrução em outro local e demolição do imóvel existente.

3.5. Recursos disponibilizados aos municípios nas ações de Reconstrução

No plano financeiro, a política de reconstrução foi estruturada a partir de valores de referência vinculados às tipologias padronizadas do FNDE. A consolidação da planilha demonstra que, entre as 28 propostas, os investimentos variaram de R$ 3.461.389,15, correspondente ao menor valor registrado para Creche Tipo 2, até R$ 13.413.560,69, referente à proposta de Escola 13 Salas contemplada no Município de Estrela/RS, totalizando R$ 191.167.583,92 em investimentos previstos para recomposição da rede escolar.

A distribuição por tipologia revela concentração em unidades de educação infantil e escolas de porte intermediário: 9 Creches Tipo 2, somando R$ 38.678.824,66; 8 Escolas 5 Salas, somando R$ 67.133.356,88; 7 Creches Tipo 1, com R$ 41.926.925,66; 3 Escolas 9 Salas, com R$ 30.014.916,03; e 1 Escola 13 Salas, com R$ 13.413.560,69. Esse perfil mostra que a recomposição se concentrou na educação infantil e na oferta de escolas padronizadas de menor e médio porte, compatíveis com a distribuição territorial dos danos.

Sob a ótica territorial, os maiores volumes financeiros se concentraram em Estrela/RS (R$ 35.944.701,09), Cruzeiro do Sul/RS (R$ 30.921.748,24), Rio Grande/RS (R$ 16.783.339,22), Lajeado/RS (R$ 15.751.711,42), Marques de Souza/RS (R$ 13.466.361,16) e Relvado/RS (R$ 11.853.058,76). Em Estrela, o montante representa aproximadamente 18,8% de todo o volume previsto para as 28 propostas, o que reforça a centralidade do município no recorte empírico do estudo.

A base de dados também registra R$ 18.964.477,70 como valor pago até o estágio de consolidação apresentado, o que corresponde a cerca de 9,9% do investimento total previsto, revelando que o programa se encontrava em fase inicial ou intermediária de implementação no momento do registro. Esse dado é compatível com a presença, na base, de empreendimentos “em licitação” e “em execução”, com percentuais físicos ainda reduzidos em várias propostas.

Do ponto de vista do desenho da política pública, é importante enfatizar que esses recursos não se destinam à simples reforma da infraestrutura atingida, mas à reconstrução integral da unidade escolar, com base em um novo projeto, nova implantação ou redefinição segura do local, assegurando apoio financeiro suficiente para recompor plenamente a capacidade instalada da rede educacional. A coerência entre a lógica financeira e a lógica técnica aparece no estudo com o indicativo de solução “RECONSTRUÇÃO” para todas as propostas analisadas.

3.6. Descrição dos dados nos municípios mais atingidos (estrela/RS)

Para aprofundar o estudo, elegeu-se o Município de Estrela/RS como recorte analítico específico, por duas razões principais: (i) trata-se do município com maior volume financeiro entre as propostas analisadas, totalizando **R$ 35.944.701,09**; e (ii) foi o município que, no conjunto observado, aparece associado à adoção de solução construtiva industrializada em todas as suas seis propostas.

Em Estrela, as seis propostas distribuíram-se da seguinte forma: 1 Escola 13 Salas (EMEF Leo Joas) no valor de **R$ 13.413.560,69**; 4 Creches Tipo 2 — EMEI Arroio do Ouro, EMEI Cantinho do Lar, EMEI Criança Feliz e EMEI Pingo de Gente — cada uma com valor de **R$ 3.980.597,52**; e 1 Creche Tipo 1 (EMEI Raio de Sol) no valor de **R$ 6.608.750,32**. O conjunto revela um desenho de recomposição que combina grande unidade escolar com forte presença de equipamentos de educação infantil.

A base consolidada registra, para as propostas de Estrela, predominância de área vulnerável, recorrência de sinistros e recomendação de novo local, com exceção de algumas especificidades de classificação de impacto e estado dos sistemas. Também registra, de maneira expressa, a opção por solução industrializada, associada à necessidade de maior rapidez na execução das obras diante da magnitude do desastre e da urgência da retomada do atendimento educacional.

O laudo da EMEI Criança Feliz oferece importante densidade qualitativa para interpretar esse conjunto. A escola foi descrita como edificação de concreto armado, dois pavimentos, com 547,58 m² de área construída, implantada em terreno plano, porém localizada em área vulnerável, com recorrência de agravos ambientais, em área alagável, e com recomendação de mudança de local. O documento registra ainda que a escola permaneceu 87 horas exposta à enchente e que a cota do terreno era de 24,00 m, abaixo da condição considerada adequada para novas construções no município.

Do ponto de vista dos sistemas construtivos, o laudo da Criança Feliz é particularmente elucidativo: classificou como críticos os subsistemas de cobertura (estrutura de suporte, calhas e telhas), as vedações (pintura, alvenaria, esquadrias, revestimentos e forro), as instalações hidrossanitárias, as instalações elétricas, o piso interno e os elementos de paisagismo; na estrutura, registrou vigas em condição crítica e lajes e pilares em condição regular, com observação de percolação excessiva e danos decorrentes do impacto de objetos arrastados pela enchente, inclusive árvores e silos oriundos de indústria vizinha.

O laudo também consignou perda de seção em vigas, armaduras expostas, trechos de alvenaria em ruínas, destruição quase integral das telhas e da estrutura do telhado, comprometimento total da entrada de energia e previsão de obstrução generalizada das instalações hidrossanitárias. Ao final, concluiu pela reconstrução total em outro local, acompanhada de demolição do imóvel atual e limpeza final do lote, por considerar excessivo o custo de recuperação e inadequada a permanência da escola em área sujeita a novas enchentes.

Esse quadro aproxima-se, em essência, da situação registrada no laudo da EMEI Amiguinhos da Natureza, figura 5, também classificada em área vulnerável, com proximidade de curso d'água, danos severos e recomendação de mudança de local. Em ambos os casos, o programa federal opera não como mecanismo de restauração pontual, mas como instrumento de recomposição definitiva da rede, ancorado na retirada das unidades de contextos territoriais reiteradamente inseguros.



Figura 5 – Detalhes dos danos evidenciados nos laudos da EMEI Criança Feliz, no município de Estrela, RS

3.7. Principais achados técnicos e visão sistêmica dos dados

A leitura sistêmica das 28 propostas evidencia uma predominância de diagnósticos associados à umidade excessiva, fissuração, arrancamento, obstrução, oxidação, desplacamento, instabilidade estrutural, entulhamento e, em alguns casos, ataque biológico. Esses descritores aparecem consolidados na planilha

como correlações patológicas dos diversos sistemas construtivos, demonstrando que os danos não se restringiram a acabamentos, mas afetaram o desempenho global das edificações.

No campo locacional, a base de dados consolidada aponta que 25 das 28 propostas apresentam recomendação de novo local, enquanto apenas 3 permanecem associadas à não recomendação de mudança. Esse dado reforça a centralidade da variável territorial na decisão administrativa: o problema não era apenas o dano construtivo pretérito, mas a forte probabilidade de sua recorrência caso a unidade permanecesse implantada no mesmo sítio de risco.

Os dois laudos de caso são ilustrativos desse raciocínio. Na EMEI Amiguinhos da Natureza, o laudo conclui pela reconstrução total em outro espaço fora da área de risco de alagamentos, sublinhando a vulnerabilidade locacional da unidade. Na EMEI Criança Feliz, figura 6, embora alguns elementos estruturais ainda apresentassem classificações intermediárias, o laudo é categórico ao apontar que o custo excessivo de recuperação, aliado à permanência em área alagável e abaixo da cota considerada adequada, inviabiliza a recuperação e justifica a reconstrução em novo local.



Figura 6 – Detalhes dos danos evidenciados nos laudos da EMEI Criança Feliz, no município de Estrela, RS

Esses achados demonstram que, no âmbito do Programa Emergencial, a noção de "reconstrução" deve ser compreendida em sentido amplo: trata-se da recomposição total e segura da capacidade física da unidade escolar, inclusive com redefinição de implantação territorial, e não de mera reposição de componentes danificados.

3.1. Gargalos institucionais na fase licitatória dos empreendimentos

No debate brasileiro sobre implementação de políticas públicas, a noção de capacidade estatal remete ao conjunto de recursos burocrático-institucionais, organizacionais e políticos que permitem ao Estado formular, coordenar e executar políticas de forma efetiva; mais do que um estoque abstrato de recursos, tais capacidades precisam ser ativadas por arranjos de implementação capazes de articular atores, instrumentos e processos em contextos concretos de ação governamental. No campo das contratações públicas, essa discussão ganha densidade específica porque a Lei nº 14.133/2021 elevou o planejamento à condição de princípio e estruturou o processo licitatório como um fluxo que abrange fase preparatória, análise de riscos, definição do modelo de gestão contratual, critérios de medição e pagamento, controle jurídico e posterior acompanhamento da execução.

À luz desse referencial, os dados das 28 propostas indicam que o principal gargalo da fase licitatória não está mais na ausência de projetos, uma vez que todos os empreendimentos constam com estudo ou projeto finalizado, mas na incapacidade de converter essa maturidade técnica em contratação efetiva. Metade da carteira permanece em licitação e, nesse subconjunto, predominam pendências relacionadas à revisão da

documentação técnico-financeira, à liberação de etapas formais para início da obra e ao não encaminhamento de documentos para análise, o que revela fragilidades no arranjo de implementação que conecta município, mandatária e instâncias de validação. Em termos analíticos, isso sugere que a existência de suporte procedimental da Caixa Econômica não elimina, por si só, os custos de coordenação, saneamento técnico e gestão de riscos que a literatura e o TCU reconhecem como centrais na fase preparatória das contratações.

3.2. Gargalos institucionais na fase de execução dos empreendimentos

Na etapa de execução, o problema assume outra feição. A literatura técnico-institucional brasileira sobre obras públicas enfatiza que o êxito do empreendimento depende de um ciclo que começa antes da licitação e prossegue com contratação, fiscalização, medição, pagamento e prestação de contas; por isso, a simples formalização contratual não assegura a entrega do objeto. Esse padrão aparece de forma nítida na carteira analisada: embora 14 propostas estejam classificadas como “em execução”, o montante efetivamente pago corresponde a apenas 9,92% do total empenhado, e parcela expressiva dos casos ainda depende da primeira medição, do desbloqueio de conta ou da regularização do fluxo de repasses para avançar fisicamente. À luz da Lei nº 14.133/2021 e das orientações do TCU, isso indica um deslocamento do gargalo da licitação para a gestão contratual, isto é, para o acompanhamento da execução, a atualização dos riscos, a fiscalização do objeto e a liberação tempestiva dos pagamentos. Observa-se que a escassez de equipes técnicas em municípios de pequeno porte, muitas vezes carentes de especialistas em arquitetura e engenharia, compromete a celeridade dos processos administrativos.

Desse modo, o caso analisado reforça uma hipótese recorrente na literatura brasileira: em políticas intensivas em coordenação federativa e contratação de obras, a efetividade não depende apenas de autorização formal para contratar, mas da capacidade de sustentar, ao longo do ciclo, mecanismos de planejamento, controle, fiscalização e articulação entre os atores envolvidos. No plano empírico, isso significa que os atrasos observados decorrem menos de um déficit isolado de projeto e mais de uma combinação entre fragilidade de planejamento operacional, morosidade no saneamento das pendências licitatórias e baixa conversão da execução contratual em avanço físico-financeiro, com impacto direto sobre o prazo de entrega das unidades. Na figura 7 mostra-se a obra mais avançada do programa de reconstrução, localizada no município de Encantado/RS.



Figura 7 – Detalhes da Construção da Creche – EMEI Lago Azul, Encantado/RS.

3.3. Análise crítica do processo: da seleção das propostas à implementação dos empreendimentos

A análise do processo de reconstrução da infraestrutura escolar do Rio Grande do Sul revela um desenho institucional consistente na identificação do problema e na seleção das intervenções, mas com limitações relevantes na capacidade de implementação. O programa demonstrou elevada robustez na fase de

diagnóstico técnico, ancorada em laudos padronizados e critérios homogêneos de classificação do dano, mas encontrou maiores dificuldades na transição entre aprovação, licitação, execução e entrega das unidades. Essa assimetria entre qualidade do diagnóstico e morosidade da implementação é compatível com a literatura brasileira sobre capacidades estatais, que aponta que instrumentos e normas, por si sós, não asseguram efetividade sem arranjos operacionais capazes de ativá-los ao longo de todo o ciclo da política pública.

Entre os pontos fortes, destaca-se a forma de seleção das propostas, baseada em laudos técnicos padronizados, que conferiram objetividade à tomada de decisão e reduziram a discricionariedade. A análise não se restringiu ao dano construtivo imediato, mas incorporou de maneira sistemática a variável territorial, especialmente a recorrência de alagamentos e a permanência das unidades em áreas vulneráveis. O fato de 25 das 28 propostas apresentarem recomendação de novo local evidencia que a política foi orientada por uma lógica de reconstrução segura, voltada à mitigação do risco futuro e não apenas à reposição física da edificação perdida.

Outro aspecto positivo foi a adoção dos projetos padronizados do FNDE, que assegurou coerência técnica, previsibilidade orçamentária e maior racionalidade à carteira de investimentos. Essa estratégia reduziu incertezas de escopo, facilitou a análise das propostas e favoreceu a compatibilização entre demandas municipais e soluções previamente consolidadas. No caso de Estrela/RS, a adoção de sistemas construtivos industrializados sinaliza tentativa de acelerar a resposta pública em contexto emergencial, sem abdicar de parâmetros mínimos de padronização e controle. O programa, portanto, acertou ao combinar padronização técnica, financiamento integral e diretriz de reconstrução total, afastando soluções paliativas.

Não obstante, os dados evidenciam gargalos relevantes na fase licitatória. Embora todos os empreendimentos possuíssem projetos finalizados, metade da carteira permanecia em licitação, com pendências concentradas na revisão técnico-documental, na liberação de etapas formais e, em alguns casos, na ausência de documentos enviados para análise. Esse quadro indica que o problema deixa de ser técnico-construtivo e passa a ser técnico-administrativo, revelando fragilidades na coordenação entre municípios, mandatária e instâncias de validação. A atuação da Caixa Econômica reforça controles e regularidade procedimental, mas não elimina as assimetrias de capacidade administrativa entre os entes subnacionais, o que contribui para a lentidão do fluxo.

Em síntese, o programa apresenta força seletiva e fragilidade implementacional. Sua robustez reside no diagnóstico técnico, na incorporação do risco territorial e na padronização das soluções; sua limitação está na conversão dessas decisões em execução físico-financeira tempestiva. O caso evidencia que políticas de reconstrução pós-desastre exigem não apenas projetos e orçamento, mas capacidade estatal continuada para articular seleção, licitação, gestão contratual e execução de forma integrada e célere.

Na figura 8 mostra-se o itinerário ao longo do tempo das principais fases da reconstrução das escolas no Rio Grande do Sul.



Figura 8 – Etapas Técnico-Administrativa da Reconstrução de Escolas e Creches no Rio Grande do Sul.

3.4. Plano de ação estruturado p/ ser atendido às recorrentes catástrofes

A experiência do Rio Grande do Sul evidencia que a resposta pública à destruição da infraestrutura escolar não pode depender, a cada evento extremo, da criação de medidas casuísticas e de novos atos normativos, pois esse modelo tende a ampliar o intervalo entre o desastre e a implementação das soluções educacionais. Nesse contexto, mostra-se necessária a instituição de um plano de ação estruturado e permanente, capaz de ser acionado automaticamente quando houver reconhecimento federal de situação de emergência ou estado de calamidade pública.

Essa formulação encontra respaldo em proposta institucional recente voltada ao aperfeiçoamento dos instrumentos de resposta do FNDE em contextos de emergência e calamidade pública, a qual defende a criação de mecanismo normativo prévio capaz de acionar automaticamente procedimentos excepcionais sempre que houver reconhecimento federal da situação de crise, sem necessidade de edição de novos atos a cada ocorrência. Em termos operacionais, esse protocolo deve prever a habilitação imediata dos entes federativos atingidos, a simplificação dos fluxos de adesão e análise técnica, a priorização administrativa das demandas emergenciais e a utilização de modelos e parâmetros previamente aprovados para a reconstrução da infraestrutura escolar.

Os achados do estudo reforçam a pertinência dessa proposta, uma vez que o principal entrave observado não esteve na ausência de solução técnica, mas na dificuldade de converter, com rapidez, propostas já estruturadas em contratação e execução efetiva. Assim, um plano de ação estruturado permitiria reduzir etapas redundantes, conferir maior celeridade à resposta institucional e aproximar o tempo da política pública da urgência imposta pelos desastres climáticos, preservando os mecanismos de controle e prestação de contas.

Desse modo, a institucionalização de um protocolo permanente de resposta educacional a calamidades públicas representa avanço na capacidade estatal de garantir continuidade ao serviço público de educação em contextos de crise. Mais do que medida administrativa, trata-se de converter a experiência acumulada no caso gaúcho em referência para futuros programas emergenciais, tornando a reconstrução da infraestrutura escolar menos contingente e mais célere, previsível e coordenada.

4. Conclusões

O presente artigo analisou o processo de reconstrução da infraestrutura escolar do Rio Grande do Sul após o desastre climático de 2024, com foco na seleção de 28 propostas, no papel dos laudos técnicos padronizados, na adoção de projetos referenciais do FNDE e nos desafios institucionais observados nas fases licitatória e executiva. Os resultados demonstram que o Programa Emergencial foi eficaz na identificação do dano, na qualificação técnica das decisões e na orientação pela reconstrução integral e segura das unidades escolares, especialmente ao incorporar a variável territorial e a recorrência do risco como elementos centrais da tomada de decisão.

Entretanto, a análise crítica evidencia que a robustez do diagnóstico e da seleção não se converteu, com a mesma intensidade, em capacidade de implementação. A permanência de parcela significativa da carteira em licitação, a baixa conversão do valor empenhado em execução física e a dependência de medições iniciais para liberação de recursos revelam limites estruturais na travessia entre aprovação e entrega das obras. Esse descompasso confirma que, em políticas públicas intensivas em coordenação federativa e contratação de obras, a efetividade depende menos da autorização formal e mais da capacidade de sustentar, ao longo do ciclo, mecanismos integrados de planejamento, gestão contratual, fiscalização e pagamento.

À luz desse diagnóstico, a conclusão central do artigo é que a reconstrução pós-desastre demanda a institucionalização de instrumentos permanentes de resposta emergencial, capazes de serem

automaticamente acionados a partir do reconhecimento federal de situação de emergência ou calamidade pública. A proposta de um Protocolo FNDE de Resposta Educacional a Calamidades Públicas, com habilitação automática dos entes afetados, simplificação dos fluxos de adesão e análise, priorização administrativa e uso de parâmetros e modelos previamente aprovados, emerge como desdobramento lógico das evidências analisadas. Tal mecanismo permitiria reduzir etapas administrativas, conferir maior celeridade à atuação institucional e alinhar o tempo da política pública à urgência imposta pelos desastres climáticos, sem prejuízo do controle, da transparência e da prestação de contas.

Conclui-se, portanto, que o principal legado do programa analisado não se restringe à recomposição física das 28 unidades escolares, mas à demonstração de que a resposta pública a eventos climáticos extremos exige arranjos institucionais mais ágeis, previamente regulamentados e orientados à continuidade do serviço educacional. Ao evidenciar simultaneamente os acertos do modelo de seleção e as limitações da implementação, o estudo contribui para o aperfeiçoamento de futuras políticas emergenciais, apontando que a reconstrução segura da infraestrutura educacional deve ser acompanhada de uma governança excepcional de implementação, capaz de transformar diagnóstico qualificado em entrega efetiva no tempo exigido pela emergência.

É fundamental otimizar o fluxo administrativo para viabilizar as contratações por dispensa de licitação em casos emergenciais. Como a legislação impõe prazos rigorosos para essa modalidade, a elaboração dos projetos e a instrução processual devem ser céleres, garantindo que o município aproveite a prerrogativa legal dentro do tempo permitido.

Agradecimentos

Ao corpo técnico do FNDE e Secretarias Municipais de Educação do RS.

Referências

ASSOCIAÇÃO BRASILEIRA DE NORMAS TÉCNICAS. NBR 16747: Inspeção predial — Diretrizes, conceitos, terminologia e procedimento. Rio de Janeiro, 2020.

FUNDO NACIONAL DE DESENVOLVIMENTO DA EDUCAÇÃO. Resolução FNDE nº 12, de 6 de agosto de 2024. Brasília, 2024.

FUNDO NACIONAL DE DESENVOLVIMENTO DA EDUCAÇÃO. Projetos padronizados de escolas e creches. Disponível em: https://www.gov.br/fnde/pt-br/acesso-a-informacao/acoes-e-programas/acoes/obras-projetos-padronizados/ensino-fundamental/ensino-fundamental. Acesso em: 2026.

IBAPE. Norma de Inspeção Predial Nacional. São Paulo, 2012.

BRASIL. Medida Provisória nº 1.248, de 2024. Institui medidas emergenciais em decorrência de desastres climáticos. Diário Oficial da União, Brasília, 2024.

PREFEITURA MUNICIPAL DE RELVADO. Laudo técnico conforme Resolução nº 12 de 2024 do FNDE para escolas com necessidade de reconstrução: EMEI Amiguinhos da Natureza. Relvado, 2024.

PREFEITURA MUNICIPAL DE ESTRELA. Laudo técnico: EMEI Criança Feliz (Reconstrução – Meta 02). Estrela, 2024.

cinpar2026
XXII International Conference on Building Pathology and Constructions Repair
15th to 17th July 2026 - Lisboa, Portugal

GeoAI Resilience-Based approach for critical assets under natural hazards

Maria João FALCÃO SILVA[1], Maria Paula MENDES[2], Filipa SALVADO[3], Ana SILVA[4], Filipe RIBEIRO[5], Mónica AMARAL FERREIRA[6], António ARAÚJO CORREIA[7], Seyed REZVANI[8], Nuno MARQUES ALMEIDA[9], Miguel INÁCIO[10], Liliana OLIVEIRA[11], Cláudia PINTO[12]

[1] LNEC, Lisboa, Portugal, mjoaofalcao@lnec.pt
[2] CERENA-IST, Lisboa, Portugal, mpaulamendes@tecnico.ulisboa.pt
[3] LNEC, Lisboa, Portugal, asalvado@lnec.pt
[4] CERIS-IST, Lisboa, Portugal, ana.ferreira.silva@tecnico.ulisboa.pt
[5] LNEC, Lisboa, Portugal, flribeiro@lnec.pt
[6] CERIS-IST, Lisboa, Portugal, monica.ferreira@tecnico.ulisboa.pt
[7] LNEC, Lisboa, Portugal, aacorreia@lnec.pt
[8] LNEC, Lisboa, Portugal , seyedi.rezvani@tecnico.ulisboa.pt
[9] CERIS-IST, Lisboa, Portugal, nunomarquesalmeida@tecnico.ulisboa.pt
[10] CML, Lisboa, Portugal, miguel.inacio@cm-lisboa.pt
[11] CML, Lisboa, Portugal, ext.liliana.oliveira@cm-lisboa.pt
[12] CML, Lisboa, Portugal, claudia.pinto@cm-lisboa.pt

Abstract: The increasing frequency and intensity of natural hazards associated with climate change and environmental degradation have progressively challenged traditional approaches to building pathology and construction repair, traditionally focused on resistance and post-damage intervention. In this context, the resilience concept has progressively evolved from a predominantly structural and resistance-based paradigm to a multidimensional framework encompassing robustness, redundancy, adaptability, rapid recovery, and learning capacity of the built environment. This work reviews the resilience concept through history as well as the main natural hazards relevant to the built environment, highlighting their impacts on critical assets. Emphasis is placed on infrastructures and building stocks exhibiting heightened vulnerability, including aging residential and industrial buildings, transport and utility networks, cultural heritage assets, and urban areas characterized by high exposure and interdependency among systems. Despite progress in resilience science, major gaps persist in multi-hazard modelling and GEOAI-enabled diagnostics for the built environment. Existing assessments remain largely static and hazard-specific, failing to represent dynamic, interacting risks across different hazards and interlinked infrastructure networks. Although GEOAI has accelerated hazard detection, its broader application is constrained by data inequity, limited ground truth, computational demands, and model drift, which hinder its integration into operational resilience frameworks. A further gap persists between engineering-focused hazard modelling and socio-technical resilience planning, limiting the representation of cascading events and systemic vulnerabilities within decision-support tools. The paper discusses the assessment of infrastructure response under hazard scenarios through the integration of resilience principles supported by the growing capabilities of GeoArtificial Intelligence (GEOAI). By combining engineering assessment with data-driven intelligence and strategic planning, the proposed approach frames resilience as a measurable, actionable, and governance-relevant objective. This contribution highlights the role of GEOAI as a key enabler for advancing resilient construction practices and for supporting policy frameworks aimed at safeguarding critical assets and infrastructures against natural hazards.

Keywords: Extreme events, Urban resilience, Multi-hazard resilience assessment, GEOAI

1. Introduction

Climate change and environmental degradation are increasing both the frequency and intensity of natural hazards, placing growing pressure on the built environment. Floods, storms, and heatwaves are occurring within increasingly complex multi-hazard scenarios, threatening the performance, durability, and continuity of buildings and infrastructure. Projections indicate that, by 2050, average annual losses to infrastructure from riverine flooding could rise by 5% under low-emission scenarios (RCP 2.6) and up to 13% under high-emission scenarios (RCP 8.5), reaching approximately €375–405 billion globally (Ando et al., 2022).

In addition to climate-related hazards, seismic events and other geophysical risks, such as volcanic activity, landslides, and tsunamis, remain significant sources of concern, particularly as nearly half of the world's population lives in areas exposed to these hazards. In Europe, seismic risk is unevenly distributed, with the highest levels concentrated in the Euro-Mediterranean region, especially in countries such as Italy, Greece, and Romania, where high hazard coincides with dense and often vulnerable building stocks. Moderate-risk regions, including the Iberian Peninsula and parts of Central Europe, are characterised by lower seismicity but may still experience significant impacts due to exposure, while Northern Europe exhibits comparatively low hazard levels (UNDRR, 2025; Silva et al, 2023).

Traditionally, engineering has emphasized the capacity of structures to resist predefined loads and hazard levels through deterministic safety factors and hazard-specific design rules. Although these methods have improved structural safety, they often fail to capture the dynamic, systemic, and interdependent character of risk in urban environments. Increasing evidence of cascading failures, infrastructure interdependencies, and prolonged disruptions has therefore shifted attention toward resilience-based frameworks (Rezvani et. al, 2022).

Resilience has progressively shifted from a narrow engineering paradigm centred on rapid recovery towards a more comprehensive and systemic framework encompassing robustness, redundancy, adaptability, recovery, and learning. This perspective recognizes that infrastructure must not only withstand and absorb shocks but also adjust to changing conditions and restore functionality efficiently. Such an approach (Figure 1) is particularly critical for systems and assets characterized by high exposure and vulnerability, including aging buildings, transport and utility networks, cultural heritage, and densely populated urban areas, , where disruptions can propagate across interconnected systems and amplify cascading impacts (Rezvani et. al, 2022; Rezvani et. al, 2023).



Figure 1 – Conceptual diagram of the Need for resilience + GEOAI

Despite recent advances, significant gaps remain. Many resilience assessment methods are still static and hazard-specific, limiting their ability to capture temporal risk dynamics, multi-hazard interactions, cascading

effects, and systemic vulnerabilities. For instance, conventional flood risk assessments often treat hazard and vulnerability as independent components, overlooking how changes in flood frequency or magnitude may inadvertently increase exposure and vulnerability over time (Di Baldassarre, 2014). A well-known example of cascading effects is the 2011 Fukushima Daiichi nuclear disaster, where an earthquake-induced tsunami triggered failures in multiple interconnected systems (Batikh et al., 2025).

A further limitation is the disconnection between engineering models and socio-technical resilience planning, reflecting the inadequate integration of human and technical dimensions (Thomas et al., 2019). GEOAI offers promising tools for hazard detection, monitoring, and analysis through remote sensing, geospatial processing, and machine learning (Figure 1). For example, recent GEOAI-based approaches integrating Geographical Information System (GIS), probabilistic seismic hazard analysis, and spatial modelling tools have been used to identify high-risk areas and assess the resilience of lifeline infrastructure networks under earthquake scenarios, supporting more targeted risk mitigation and planning strategies (Tehrani et al., 2025).

This paper contributes by synthesising resilience concepts, hazard impacts, and GEOAI capabilities into an integrated perspective for assessing and improving resilience in the built environment under multi-hazard conditions.

2. Evolution of the resilience concept

“Building resilience is increasingly recognized not just as a humanitarian or environmental imperative, but as a fundamental pillar of sustainable economic development.” (UNDRR, 2025).

The concept of resilience has evolved significantly across disciplines, expanding in meaning and application. It originated in the physical sciences and engineering, where it described the ability of a material or system to absorb disturbance and quickly return to its original state (Figure 2). This engineering resilience emphasizes stability, resistance, and rapid recovery after disruption. In the built environment, it traditionally guided design practices focused on strength, safety factors, and the capacity of structures to withstand predefined loads and hazard intensities (Castaño-Rosa et. al, 2022; Rezvani et. al, 2023b).

In the 1970s, ecology broadened the concept by defining resilience as the capacity of ecosystems to absorb disturbance while maintaining essential functions, structures, and feedback. This ecological perspective introduced the idea of multiple equilibrium states and highlighted adaptation and reorganization as equally important as resistance. Unlike engineering resilience, it recognizes uncertainty, nonlinearity, and the risk of irreversible change when critical thresholds are crossed (Holling, 1973; Sánchez-Pinillos, 2024).

Resilience later expanded into socio-technical systems, incorporating perspectives from social sciences, economics, and urban studies. In this view, resilience includes not only the physical robustness of infrastructure but also the adaptive capacity of communities, institutions, and governance systems. It reflects the understanding that the built environment is shaped by interactions between physical structures, human behaviour, organizational processes, and policy frameworks (Sharifi, 2023; Rezvani et. al, 2023).



Figure 2 – Timeline for the evolution of resilience concept

This evolution has led to multidimensional resilience frameworks for the built environment, including robustness, redundancy, adaptability, recovery, and learning. These dimensions provide a more comprehensive basis for evaluating how buildings and infrastructure perform under hazard conditions (Al-Humaiqani and Al-Ghamdi, 2022).

Overall, resilience marks a shift from static, deterministic design toward dynamic, systems-based thinking. Instead of only preventing failure, resilience-based approaches seek to maintain essential functions during and after disruption. Although applying resilience in practice remains challenging due to differing definitions, metrics, and data limitations, it remains a key framework for addressing the interconnected challenges of natural hazards, climate change, and urbanization, and for supporting more adaptive, robust, and sustainable infrastructure systems (Tanguay and Amor. 2024).

3. Natural hazards and impacts on the built environment

Natural hazards are a major source of risk for the built environment, and their frequency, intensity, and distribution are increasingly shaped by climate change and environmental degradation (Table 1). They include both climate-related and geophysical events, each with different mechanisms and consequences for buildings and infrastructure. Understanding these impacts is essential for assessing vulnerability and improving the resilience of critical assets (Tanguay and Amor. 2024).

Climate-related hazards include floods, storms, heatwaves, droughts, and wildfires. Many of these events are becoming more frequent, intense, and prolonged in several regions, with growing spatial extent, as evidenced by recent assessments. At the same time, an additional 2.5 billion people are projected to live in urban areas by 2050, further increasing exposure to these hazards (Dodman et. al., 2022). Floods can cause structural damage through hydrostatic and hydrodynamic forces, erosion, and foundation instability, while also damaging non-structural elements and contents. Heatwaves can degrade materials, reduce cooling efficiency, and increase thermal stress, especially in dense urban areas affected by the heat island effect. Storms and strong winds can damage roofs and façades and disrupt power and communication systems, often producing cascading effects (Cheval et. al, 2024; Mendes et. al., 2024).

Geophysical hazards such as earthquakes, landslides, and volcanic activity are generally less frequent but can be highly destructive. Earthquakes threaten structural integrity through dynamic loading and may lead to collapse, especially in buildings not designed to seismic standards. Landslides can damage foundations, transport routes, and access corridors, particularly where unstable slopes, poor drainage, or weak construction practices already exist (Harle et. al, 2024).

Hazard impacts go beyond direct physical damage. Disruptions to transport, water, energy, and telecommunications can impair essential services and trigger cascading failures across interconnected systems (Figure 3). Long-term effects may include accelerated material deterioration, shortened asset lifespan, and rising maintenance and repair costs. Cultural heritage structures are especially vulnerable because of their fragility and historical value (Brunner et. al, 2024)



Figure 3 – Hazard-impact chain

An additional challenge is the rise of multi-hazard and compound events, where hazards occur together or in sequence and intensify one another. These dynamics expose the limits of single-hazard assessments and reinforce the need for integrated approaches that consider physical damage, system interdependencies, functionality, and long-term resilience (Trogrlić et al., 2024).

4. Vulnerability of infrastructure, and gaps in resilience assessment

Within ISO 14091 (2021), climate risk assessment follows a structured framework aligned with the IPCC, with a stronger operational focus, where risk is defined by the interaction between hazard, exposure, and vulnerability. Hazards comprise climate-related events or trends (e.g., floods, heatwaves, sea-level rise) characterised by their intensity, frequency, duration, and spatial extent, while exposure refers to the presence of people, infrastructure, and assets in areas at risk. Vulnerability captures the susceptibility of these systems, typically expressed through sensitivity and limited coping capacity, while adaptive capacity is treated as a distinct but related component reflecting the ability of systems to adjust and reduce potential impacts (Figure 4). These components are interdependent and context-specific, requiring assessment under current and future conditions while accounting for temporal dynamics and uncertainty. Within this framework, resilience is not explicitly defined but can be understood as the ability of a system to anticipate, absorb, and recover from climate-related impacts through risk-informed adaptation strategies. In applied approaches, such as the Resilient Built Environment – Central Europe (RBE-CE) system, these components are operationalised through normalised indicators and combined to quantify climate risk across building and neighbourhood scales (Moro et. al., 2025).

In the built environment, vulnerability is shaped by a combination of physical, functional, and systemic characteristics, including structural condition, design standards, material properties, maintenance levels, and hazard exposure. In many regions, a significant proportion of the building stock consists of aging structures not designed to withstand current hazard intensities or meet modern performance-based standards, making them particularly susceptible to physical damage and functional disruption during hazard events (Tanguay and Amor, 2024).

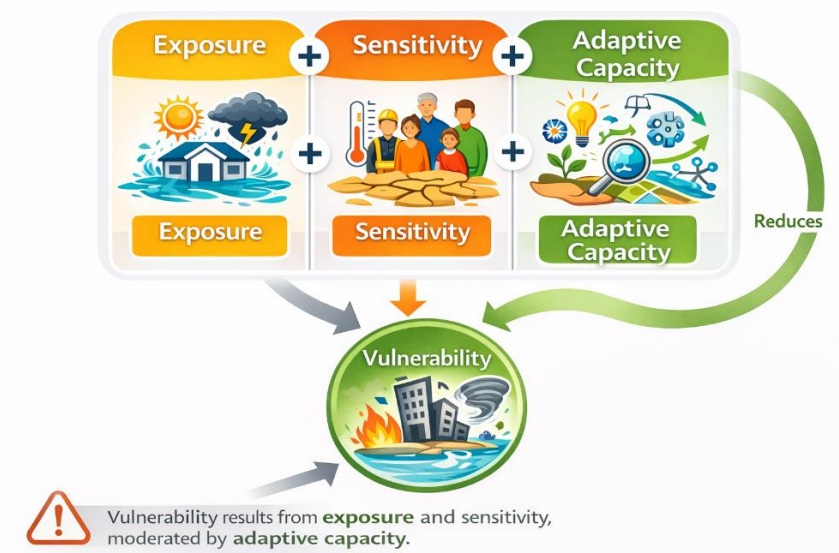


Figure 4 – Vulnerability framework diagram

Aging residential and industrial buildings are especially vulnerable. Many suffer from material deterioration, outdated construction methods, and inadequate maintenance, which reduce their ability to resist or adapt to hazards. Informal and non-engineered buildings, common in rapidly urbanizing areas, further increase vulnerability because they often lack regulatory oversight, technical design, and quality control (Rezvani et. al, 2022).

Critical infrastructure systems, such as transport networks, energy grids, water supply, and telecommunications, also face substantial risk. Their vulnerability is heightened by strong interdependence: failure in one system can trigger disruptions in others. For example, a power outage may affect water distribution, transport operations, and emergency response, amplifying overall hazard impacts. In addition, the spatially distributed and linear nature of infrastructure networks makes them highly exposed, since damage at key nodes or links can reduce the functionality of entire systems (Brunner et. al, 2024).

Cultural heritage assets form another highly vulnerable category. These structures often combine physical fragility with significant historical, architectural, and social value. Their preservation is particularly challenging because interventions must strengthen the asset while maintaining its authenticity. Many heritage buildings also rely on traditional materials and construction techniques that may perform poorly under extreme hazard conditions (Rezvani et. al, 2022).

Dense urban areas are especially exposed to multi-hazard impacts. The concentration of people, buildings, and infrastructure, together with strong interdependence, increases the likelihood of systemic failure. Vulnerability is further influenced by land-use patterns, inadequate drainage, limited open space, and socio-economic inequalities, which affect both exposure and recovery capacity. Therefore, vulnerability is not only a property of individual assets but also of the wider system in which they operate, highlighting the need for integrated assessments that address both component fragility and system interactions (Sharifi, 2023).

Despite progress in resilience research, current assessment methods still have major limitations. Many remain static, relying on predefined scenarios and fixed system conditions, and therefore fail to capture the changing nature of hazards, infrastructure performance, and recovery over time. Another weakness is the continued reliance on single-hazard approaches, which overlook interactions between hazards and the potential for compound and cascading events, leading to underestimation of real risk (Trogrlić et al., 2024).

A further challenge is the gap between engineering-based models and broader socio-technical resilience frameworks. Engineering approaches focus on structural performance, reliability, and failure probability, while socio-technical perspectives include governance, institutional capacity, community preparedness, and economic resilience. Limited integration between these views weakens holistic decision-making (Sharifi, 2023). Data limitations also constrain resilience assessments, especially where reliable, high-resolution information is scarce. Uncertainties in climate projections, hazard models, and infrastructure response add further complexity.

5. Integrating Resilience Principles with GEOAI

The rapid development of GEOAI has created important new opportunities for improving resilience assessment in the built environment (Figure 6). By combining geospatial technologies, remote sensing, and machine learning, GEOAI makes it possible to process large and diverse datasets and to support more dynamic evaluations of hazard exposure, infrastructure condition, and system performance (Rezvani et. al, 2023b)

A key strength of GEOAI lies in hazard detection and monitoring. Satellite imagery, unmanned aerial systems, and ground sensors can be integrated with machine learning models to detect and track hazards such as floods, wildfires, landslides, and storm damage in near real time. These capabilities improve situational awareness and support rapid response, especially in inaccessible or data-scarce regions. Time-series analysis of geospatial information also helps identify long-term trends and patterns, contributing to a better understanding of hazard evolution and changing risk conditions (Padgett et. al., 2024).

GEOAI is also valuable for vulnerability and damage assessment. Advanced image analysis can extract information on building characteristics, structural condition, and land use, enabling large-scale mapping of exposed assets. After hazard events, machine-learning algorithms (MLA) can support damage classification and loss estimation, helping decision-makers prioritize recovery actions. These approaches complement

conventional engineering assessments, which are often slower and limited in spatial scope (Rezvani et. al, 2023b).

Another important contribution is predictive and scenario-based modelling. By integrating climatic, environmental, infrastructural, and socio-economic datasets, GEOAI enables the representation of complex system interactions and supports the analysis of multi-hazard scenarios, including cascading effects and infrastructure interdependencies. Compared with static, single-hazard approaches, this provides a more realistic understanding of temporal variability and system interdependencies (Brunner et. al, 2024).

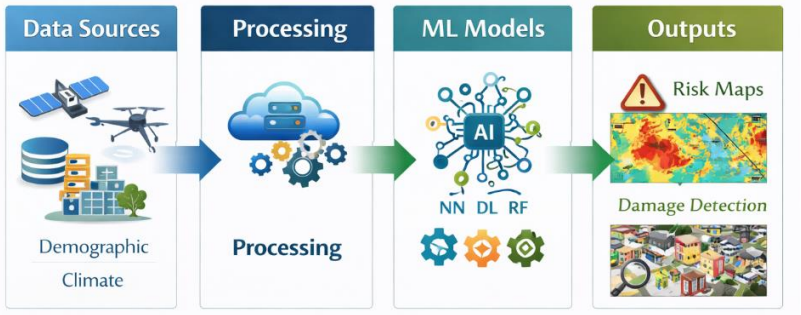


Figure 6 – GEOAI workflow

However, the effective application of GEOAI depends on overcoming key technical and organisational challenges. The integration of heterogeneous geospatial data remains a major barrier, as datasets often differ in structure, scale, and format. Frameworks such as AtlasHDF, which leverages HDF5 for efficient data integration, and PlaniSphere, which aggregates geospatial data through Web Map Service (WMS) protocols, illustrate emerging solutions for managing complex data environments. Nevertheless, the lack of standardised data models continues to hinder interoperability. Efforts such as Geographic Markup Language (GML), fuzzy spatial data models, and emerging Open Geospatial Consortium (OGC) standards, including Training Data Markup Language for AI (TrainingDML-AI), aim to address these limitations by improving data consistency, uncertainty representation, and interoperability.

Cyberinfrastructure (CI) and Geospatial Cyberinfrastructure (GCI) frameworks further support GEOAI applications by integrating data resources, computational tools, and network protocols, enabling scalable and interoperable geospatial analysis (Di and Deng, 2010).

Despite these advances, GEOAI faces persistent limitations. Data availability and quality remain critical challenges, particularly in regions with sparse or inconsistent geospatial information. The lack of reliable ground-truth data constrains model training and validation, affecting accuracy and generalisability. High computational demands and model drift further limit scalability and long-term performance. In addition, GEOAI models often show limited transferability across geographic contexts, requiring continuous recalibration (Padgett et al., 2024; Rezvani et. al., 2023b).

Finally, translating GEOAI outputs into actionable policies remains a significant challenge. Addressing this requires improved interoperability, standardisation, transparency, and governance, as well as stronger coordination among data sources, models, institutions, and stakeholders.

The integration of GEOAI with engineering-based models offers a promising pathway toward hybrid resilience frameworks. While engineering models provide detailed insights into structural behaviour, GEOAI contributes dynamic, data-driven understanding of hazards and system interactions. Together, these approaches enable more realistic multi-hazard modelling, improved assessment of infrastructure interdependencies, and more effective decision-support tools, such as interactive risk maps and scenario-based planning platforms (Figure 7).

Overall, the convergence of resilience theory and GEOAI supports a transition toward dynamic, data-informed, and system-oriented approaches, enabling more proactive and adaptive resilience planning in the built environment.

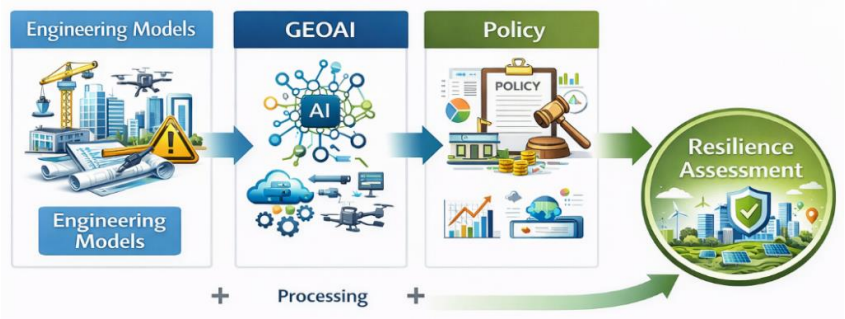


Figure 7 – Integrated framework

6. Implications for Policy and Construction Practice

The growing importance of resilience in the built environment has major implications for both policy and construction practice. As natural hazards become more frequent, severe, and interconnected, conventional risk reduction strategies are no longer enough. Instead, resilience must be embedded across the full lifecycle of buildings and infrastructure, from planning and design to operation, maintenance, and recovery (Rezvani et. al, 2024)

From a policy perspective, a central challenge is turning resilience into a measurable and enforceable objective. This requires standardized metrics, indicators, and assessment methods that can be applied consistently across sectors and scales. Existing regulations are largely based on prescriptive codes that focus on safety and minimum performance under specific hazard scenarios. Although these remain necessary, they do not fully address broader issues such as system functionality, recovery time, and adaptability. Integrating resilience into codes and standards therefore requires a shift toward performance-based and risk-informed approaches, where acceptable levels of service continuity, downtime, and recovery are clearly defined (Al-Humaiqani and Al-Ghamdi, 2022).

Policy frameworks must also reflect the multi-hazard and systemic nature of risk. This means improving coordination across sectors and governance levels, while promoting integrated planning that considers infrastructure interdependencies. Urban planning is especially important, as land-use regulation, zoning, and the protection of critical assets can reduce exposure and vulnerability and help avoid concentrating risk in highly exposed areas. (Trogrlić et. al, 2024).

GEOAI further strengthens evidence-based policymaking by enabling real-time monitoring, dynamic risk assessment, and scenario analysis. These tools can improve early warning systems, emergency response, and investment prioritization. However, their use depends on strong data governance, including data quality, standardization, sharing protocols, and privacy protection (Padgett et. al, 2024).

In the construction sector, resilience requires more holistic design, construction, and maintenance practices. Engineers must consider not only structural safety, but also functionality, adaptability, and lifecycle performance. This includes resilient design measures such as redundancy in critical systems, modular construction for easier repair, and materials suited to changing environmental conditions. Digital tools such as GEOAI, BIM, and digital twins can support simulation, monitoring, predictive maintenance, and resource efficiency (Al-Humaiqani and Al-Ghamdi, 2022).



Figure 9 – Decision-making flowchart

Successful implementation also depends on training, interdisciplinary collaboration, and knowledge transfer. Although resilience may involve higher initial costs, it can reduce long-term damage and recovery expenses. With supportive incentives and lifecycle-based investment thinking, resilience can become a practical foundation for safer, more adaptable, and more sustainable built environments (Tanguay, and Amor, 2024).

7. Conclusions

This study highlights the growing complexity of assessing and managing risks in the built environment under changing natural hazard conditions. The shift from traditional resistance-based approaches toward multidimensional resilience frameworks represents an essential change in both theory and practice, yet remains incomplete due to persistent conceptual, methodological, and operational challenges. Current assessment methods often fail to capture the dynamic, interconnected nature of infrastructure systems, particularly under multi-hazard and cascading scenarios, underscoring the need for integrated, system-level approaches.

In this context, GEOAI offers significant potential by enabling large-scale, data-driven, and near real-time analysis. When combined with engineering models, it supports hybrid approaches that can better represent both physical processes and system interactions. However, its effectiveness depends on data quality, validation, and integration within decision-making frameworks.

A persistent gap remains between technical assessments and policy implementation, driven by the lack of standardised metrics, difficulties in communicating complex results, and institutional fragmentation. Addressing this requires stronger alignment between scientific research, policy, and practice.

Resilience must be understood as a systemic property emerging from the interaction between infrastructure, institutions, users, and environmental conditions. Accordingly, assessment approaches should integrate engineering, environmental, and socio-technical dimensions.

Advancing resilience requires dynamic, data-informed, and system-oriented frameworks that move beyond traditional resistance-based models. Embedding these approaches into policy and practice will depend on technological innovation, institutional coordination, and the development of standardised, user-oriented tools.

Acknowledgments

This work is part of the research being carried out at Civil Engineering Research and Innovation for Sustainability (CERIS), National Laboratory of Civil Engineering (LNEC) and Municipality of Lisbon (CML) and was funded by Fundação para a Ciência e a Tecnologia (FCT) in the framework of project UIDB/04625/2020 and FCT grant GeoARMUR: Geospatial AI for Resilience Management and Urban Recovery (https://doi.org/10.54499/2023.17276.ICDT).

Maria Paula Mendes acknowledges the Portuguese Foundation for Science and Technology (FCT) for strategic funding of CERENA (UIDB/04028/2020) and through the individual project 2023.08653.CEECIND.

References

Al-Humaiqani, M., S. Al-Ghamdi, 2022. “The built environment resilience qualities to climate change impact: Concepts, frameworks, and directions for future research”, Sustainable Cities and Society, Volume 80, https://doi.org/10.1016/j.scs.2022.103797.

Ando, S. C. Fu, F. Roch, U. Wiriadinata. 2022. Sovereign Climate Debt Instruments: An Overview of the Green and Catastrophe Bond Markets. Staff Climate Notes 2022, 004. Washington, DC: International Monetary Fund. https://doi.org/10.5089/9798400210006.066.

Batikh A.S., Alzahrani Y.A., Diaconeasa M.A. (2025) Evaluation of Recent Advances in Multi-Hazard Risk Assessment. Proceedings of the 19th International Conference on Probabilistic Safety Assessment and Analysis, PSA 2025, pp. 600 – 609, DOI: 10.13182/PSA2025-46534.

Brunner, L.G., R. Peer, C. Zorn, R. Paulik, T. Logan. (2024). “Understanding cascading risks through real-world interdependent urban infrastructure”. Reliability Engineering & System Safety, Volume 241, https://doi.org/10.1016/j.ress.2023.109653.

Castaño-Rosa, Raul, Sofie Pelsmakers, Heini Järventausta, Jenni Poutanen, Lassi Tähtinen, Anahita Rashidfarokhi, Saija Toivonen. 2022. “Resilience in the built environment: Key characteristics for solutions to multiple crises”. Sustainable Cities and Society, 87, 104259. https://doi.org/10.1016/j.scs.2022.104259

Cheval, S., Vlad-Alexandru Amihăesei, Zenaida Chitu, Alexandru Dumitrescu, Vladut Falcescu, Adrian Irașoc, Dana Magdalena Micu, Eugen Mihulet, Irina Ontel, Monica-Gabriela Paraschiv, Nicu Constantin Tudose. 2024. “A systematic review of urban heat island and heat waves research (1991–2022)”. Climate Risk Management, Volume 44, https://doi.org/10.1016/j.crm.2024.100603.

Di Baldassarre G., Kemerink J.S., Kooy M., Brandimarte L. (2014). Floods and societies: the spatial distribution of water-related disaster risk and its dynamics (2014) Wiley Interdisciplinary Reviews: Water, 1 (2), pp. 133 - 139, DOI: 10.1002/wat2.1015.

Di, L., & Deng, M. (2010). Enhancing remote sensing education with GeoBrain cyberinfrastructure. In Proceedings of the IEEE International Geoscience and Remote Sensing Symposium (IGARSS) (pp. 98 - 101). IEEE. DOI: 10.1109/IGARSS.2010.5650462.

Dodman, D., B. Hayward, M. Pelling, V. Castan Broto, W. Chow, E. Chu, R. Dawson, L. Khirfan, T. McPhearson, A. Prakash, Y. Zheng, and G. Ziervogel, 2022: Cities, Settlements and Key Infrastructure. In: Climate Change 2022: Impacts, Adaptation and Vulnerability. Contribution of Working Group II to the Sixth Assessment Report of the Intergovernmental Panel on Climate Change [H.-O. Pörtner, D.C. Roberts, M. Tignor, E.S. Poloczanska, K. Mintenbeck, A. Alegría, M. Craig, S. Langsdorf, S. Löschke, V. Möller, A. Okem, B. Rama (eds.)]. Cambridge University Press, Cambridge, UK and New York, NY, USA, pp. 907–1040, doi:10.1017/9781009325844.008.

Harle, Shrikant, Samruddhi Sagane, Nilesh Zanjad, P.K.S. Bhadauria, Harshwardhan P. Nistane. 2024. “Advancing seismic resilience: Focus on building design techniques”. Structures, Volume 66, https://doi.org/10.1016/j.istruc.2024.106432.

Holling, C.S. 1973. “Resilience and Stability of Ecological Systems”. Annual Review of Ecology and Systematics Vol. 4 (1973), pp. 1-23 (23 pages). Published By: Annual Reviews.

ISO 14091 (2021). Adaptation to climate change — Guidelines on vulnerability, impacts and risk assessment. International Organization for Standardization.

Mendes M.P., Flores Colen I. (2024) Greening the Deal: Climate Change Adaption Through Circularity and Energy Efficiency in Buildings. Green Energy and Technology, Part F3728, pp. 3 - 23, DOI: 10.1007/978-3-031-70851-0_1

Moro A., Koja A., Felicioni L., Drmac I., Bazzan E., Hejtmanková B., Prar I. (2025) RBE-CE: A Cross-Scale Assessment System for Climate Adaptation in Central European Built Environment. IOP Conference Series: Earth and Environmental Science, 1546 (1), art. no. 012063, DOI: 10.1088/1755-1315/1546/1/012063

Padgett, J., R. Rincon, P. Panakkal. 2024. “Future cities demand smart and equitable infrastructure resilience modeling perspectives”. npj Nat. Hazards 1, 28 (2024). https://doi.org/10.1038/s44304-024-00028-5.

Rezvani, S. M. H. S., Nuno Marques de Almeida, Maria João Falcão Silva. 2022, Marta Duarte. “Enhancing urban resilience evaluation systems through integrating asset and disaster risk management models and geospatial information tools”. Sustainable Cities and Society, 80, 103814. https://doi.org/10.1016/j.scs.2021.103612.

Rezvani, S. M. H. S., Nuno Marques de Almeida, Maria João Falcão Silva. 2023a. “Climate adaptation measures for enhancing urban resilience”. Buildings, 13(9), 2163. https://doi.org/10.3390/buildings13092163

Rezvani, S. M.H.S, Maria João Falcão Silva, Komljenovic, D., Nuno Marques de Almeida. 2023b. “A Systematic Literature Review on Urban Resilience Enabled with Asset and Disaster Risk Management Approaches and GIS-Based Decision Support Tools”. Applied Sciences, 13(4), 2223. https://doi.org/10.3390/app13042223.

Rezvani, S. M. H. S., Maria João Falcão Silva, Nuno Marques de Almeida. 2024.” The Risk-Informed Asset-Centric (RIACT) Urban Resilience Enhancement Process: An Outline and Pilot-Case Demonstrator for Earthquake Risk Mitigation in Portuguese Municipalities”. Applied Sciences, 14(2), 634. https://doi.org/10.3390/app14020634.

Sánchez-Pinillos, M., V. Dakos, V., S. Kéfi, 2024. “Ecological dynamic regimes: A key concept for assessing ecological resilience”. Biological Conservation, 289, https://doi.org/10.1016/j.biocon.2023.110409.

Sharifi, A. 2023. “Resilience of urban social-ecological-technological systems (SETS): A review”, Sustainable Cities and Society, Volume 99, https://doi.org/10.1016/j.scs.2023.104910.

Silva, V., A. Calderon, M. Caruso, C. Costa, J. Dabbeek, M.C. Hoyos, Z. Karimzadeh, L. Martins, N. Paul, A. Rao, M. Simionato, C. Yepes-Estrada, H. Crowley, K. Jaiswal (2023). Global Earthquake Model (GEM) Seismic Risk Map (version 2023.1), https://doi.org/10.5281/zenodo.8409623.

Tanguay, X. Ben Amor. 2024. “Assessing the sustainability of a resilient built environment: Research challenges and opportunities”. Journal of Cleaner Production, Volume 458, https://doi.org/10.1016/j.jclepro.2024.142437.

Tehrani Z.M., Tehrani G.M., Dorostian A., Akashe B., Almasian M. (2025) Analyzing safety and resilience of the lifeline networks during the earthquake sequence. Natural Hazards, 121 (7), pp. 8091 – 8109. DOI: 10.1007/s11069-024-07047-5.

Thomas J.E., Eisenberg D.A., Seager T.P., Fisher E. (2019) A resilience engineering approach to integrating human and socio-technical system capacities and processes for national infrastructure resilience. Journal of Homeland Security and Emergency Management, 16 (2), art. no. 20170019, DOI: 10.1515/jhsem-2017-0019.

Trogrlić, Robert Šakić , Karina Reiter, Roxana L. Ciurean, Stefania Gottardo, Silvia Torresan, Anne Sophie Daloz, Lin Ma, Noemi Padrón Fumero, Sharon Tatman, Stefan Hochrainer-Stigler, Marleen C. de Ruiter, Julius Schlumberger, Remi Harris, Sara Garcia-Gonzalez, María García-Vaquero, Tamara Lucía Febles Arévalo, Raul Hernandez-Martin, Javier Mendoza-Jimenez, Davide Mauro Ferrario, David Geurts, Dana Stuparu, Timothy Tiggeloven, Melanie J. Duncan, Philip J. Ward. 2024. “Challenges in assessing and managing multi-hazard risks: A European stakeholder’s perspective”. Environmental Science & Policy, Volume 157, https://doi.org/10.1016/j.envsci.2024.103774.

United Nations Office for Disaster Risk Reduction (2025). Global Assessment Report on Disaster Risk Reduction 2025: Resilience Pays: Financing and Investing for our Future. Geneva.

XXII International Conference on Building Pathology and Constructions Repair
15th to 17th July 2026 - Lisboa, Portugal

Climate Resilience Skills for Cultural Heritage Buildings: A European Educational Framework Developed through the ECOHERITAGE Project

Inês FLORES-COLEN[1], Maria KAROGLOU[2], Rose Nangah MANKAA[3], Monu G. VARGHESE[3], Michail DELAGRAMMATIKAS[4], Suzana K. GEORGIEVA[5], Pande P. ANTOSKA[5], M. Alejandro PEDREÑO-ROJAS[6], Paola VILLORIA-SÁEZ[6], César PORRAS-AMORES[6], Emmanuel MANOS VAKONDIOS[4], Vasiliki TSIOURI[2], Giovanna BARTELS[1], Marzia TRAVERSO[3], Maria P. MENDES[7],

[1] CERIS, Instituto Superior Técnico, Universidade de Lisboa, Portugal, ines.flores.colen@tecnico.ulisboa.pt; giovanna.schafer@tecnico.ulisboa.pt

[2] Ethnicon Metsovion Polytechnion (NTUA), Greece, margo@mail.ntua.gr, tsiouriv@mail.ntua.gr

[3] Institute of Sustainability (InaB) in Civil Engineering, RWTH Aachen University, Germany, rose.mankaa@inab.rwth-aachen.de, george.varghese@inab.rwth-aachen.de, marzia.traverso@inab.rwth-aachen.de

[4] Creative Thinking Development (CRETHIDEV), Greece, mdelagram@yahoo.com, manosvak@outlook.com

[5] IECE, Institute for Research in Environment, Civil Engineering and Energy (IECE), North Macedonia, suzana@iege.edu.mk, info@iege.edu.mk

[6] TEMA Research Group, ETS Edificación, Universidad Politécnica de Madrid (UPM), Spain, alejandro.pedreno@upm.es, paola.villoria@upm.es, c.porras@upm.es

[7] CERENA, Instituto Superior Técnico, Universidade de Lisboa, Portugal, mpaulamendes@tecnico.ulisboa.pt

Abstract: Climate change is increasing the vulnerability of cultural heritage buildings through rising temperatures, more frequent and intense heatwaves, changing precipitation patterns, flooding, storms and other extreme weather events. These hazards affect the performance, durability and long-term preservation of heritage assets, requiring conservation strategies that integrate climate adaptation and resilience objectives. While significant progress has been made in understanding climate-related risks to cultural heritage, less attention has been paid to the skills and competencies required of professionals responsible for its conservation, rehabilitation, and management. The ECOHERITAGE Erasmus+ project aims to identify skills gaps, develop a European training programme, and create digital learning resources to support higher education institutions and professionals working in heritage conservation and sustainable construction. It presents the project's rationale, methodology, and expected outcomes, and discusses how educational innovation can contribute to climate adaptation and resilience in the built heritage sector.

Keywords: Cultural Heritage Buildings; Climate Change; Resilience; Higher Education; Skills Development; Sustainable Retrofitting.

1. Introduction

Cultural heritage buildings constitute a significant component of Europe's built environment and play a fundamental role in preserving historical, architectural, cultural and social values. They contribute to the identity of cities and regions, support tourism and local economies, and provide tangible links between past and present generations. Beyond their cultural significance, heritage buildings are increasingly recognised as important assets within sustainable development strategies, contributing to social cohesion, place-making and urban regeneration. However, cultural heritage buildings are becoming increasingly vulnerable to the impacts of climate change (UNESCO, 2007).

Higher air temperatures, more frequent and intense heatwaves, changing precipitation patterns, flooding, storms and other extreme weather events are accelerating the deterioration of historic materials and affecting the performance, durability, and resilience of heritage assets. Climate-related hazards may also compromise the safety, functionality and long-term preservation of buildings with historical and cultural significance. Consequently, heritage conservation can no longer be addressed independently from climate adaptation and resilience strategies.

Over the last decade, several European research and innovation projects have significantly advanced knowledge on climate change impacts on cultural heritage. Projects such as Climate for Culture (FP7), STORM (H2020) and ARCH (H2020) have developed climate-risk assessment methodologies, monitoring systems, resilience frameworks, decision-support tools and adaptation strategies for heritage buildings and historic urban areas. Their results have demonstrated that climate change is increasing the vulnerability of cultural heritage through rising temperatures, heatwaves, flooding, coastal hazards and extreme weather events, while also highlighting the need for preventive conservation and long-term resilience planning. However, despite these advances, relatively limited attention has been given to the development of educational frameworks and professional competencies required to implement climate adaptation measures in practice. This gap between scientific knowledge and professional capacity-building provides the rationale for the ECOHERITAGE project, which focuses on education, skills development and training for climate-resilient cultural heritage buildings.

At the same time, European policies such as the European Green Deal, the Renovation Wave Strategy and the EU Adaptation Strategy encourage the transformation of the built environment towards greater sustainability, energy efficiency and climate resilience (EC, 2019; 2020; EPRS, 2024). While these objectives are widely promoted in the building sector, their implementation in cultural heritage buildings remains particularly challenging. Interventions must balance the need to improve environmental performance with the obligation to preserve authenticity, historical value and architectural integrity. This requires specialised knowledge and multidisciplinary approaches that integrate conservation principles, engineering solutions, sustainability assessment and climate adaptation measures.

Despite growing awareness of these challenges, there remains a significant gap in education and training opportunities specifically addressing climate resilience in cultural heritage buildings. Existing programmes in architecture, engineering, heritage conservation and construction management often address these themes separately, providing limited opportunities for interdisciplinary learning. Furthermore, professionals currently involved in the conservation, rehabilitation and management of heritage assets frequently lack access to continuing education programmes focused on climate risk assessment, sustainable retrofitting strategies, nature-based solutions and resilience planning. Addressing this skills gap is essential to ensure that future professionals are equipped to respond to the complex challenges posed by climate change. Capacity building, knowledge transfer and educational innovation are increasingly recognised as key enablers for the sustainable preservation of cultural heritage. In this context, higher education institutions play a critical role in developing new curricula, training methodologies and learning resources that reflect emerging societal and environmental needs.

The ECOHERITAGE project (Resilient and Bioclimatical Advancement of Cultural Heritage Buildings), funded under the Erasmus+ Programme, was conceived to address these challenges. Bringing together universities and specialised organisations from Portugal, Germany, Spain, Greece and North Macedonia, the project aims to identify educational and professional needs, develop an innovative training framework and create digital learning resources focused on climate-resilient retrofitting of cultural heritage buildings.

This paper presents the rationale, objectives and methodological framework of the ECOHERITAGE project. It discusses the need for new educational approaches in the field of climate resilience and heritage conservation and introduces the training framework that will be developed (during the period 2025-2027) to support students, academics and professionals working with cultural heritage buildings. By linking

climate adaptation, sustainability and educational innovation, the project seeks to contribute to the development of a new generation of professionals capable of preserving Europe's cultural heritage while responding effectively to future environmental challenges.

2. Climate Change and Cultural Heritage Buildings: Current Challenges and Educational Gaps

2.1 Main Climate Threats

Cultural heritage buildings are increasingly exposed to the impacts of climate change, which may accelerate deterioration processes and compromise their long-term conservation. These buildings often include historic materials, traditional construction techniques and architectural features that were not designed to respond to current or future climatic scenarios. As a result, their vulnerability may be higher than that of contemporary buildings (Sesana et al. 2021; Fatorić & Seekamp 2017; EPRS 2024; UNESCO/IPCC/ICOMOS 2021). Among the main climate-related threats, heatwaves and rising temperatures can contribute to thermal stress, material expansion and contraction, changes in indoor environmental conditions and increased cooling demand. These effects may be particularly relevant in historic buildings where passive environmental control strategies are limited or where interventions must respect conservation principles (Pereira et al. 2024). Flooding and heavy precipitation represent another major risk. Increased rainfall intensity and more frequent extreme weather events can affect foundations, walls, façades, roofs and drainage systems. Water infiltration may lead to moisture accumulation, salt crystallisation, biological growth, surface decay and structural deterioration. In heritage buildings, such damage can result not only in technical and functional problems but also in the loss of cultural and historical value.

Moisture-related deterioration is especially relevant in cultural heritage buildings, as many historic materials are highly sensitive to changes in humidity and water movement. The combination of moisture, temperature variation and pollutants may accelerate decay mechanisms in stone, mortar, timber, metals and decorative elements (Liberato & Trigo 2014). Freeze-thaw cycles may also affect heritage materials, particularly in regions where temperature fluctuations around 0 °C are frequent. Water absorbed into porous materials can freeze and expand, causing cracking, scaling and progressive material loss. Although this process is not new, changing climatic conditions may alter its frequency, intensity and geographical relevance (Romero-Gómez et al. 2025).

Extreme events, including storms, droughts, heatwaves and intense rainfall, increase uncertainty in conservation planning. These events may produce sudden damage, overload existing maintenance systems and expose the need for preventive risk assessment and adaptation strategies. Therefore, climate change should be understood not only as an environmental issue but also as a conservation, management and educational challenge for the cultural heritage sector (Mendes & Flores-Colen 2024).

2.2 Challenges for Heritage Conservation

The adaptation of cultural heritage buildings to climate change involves a complex balance between preservation and transformation. On the one hand, heritage buildings must be protected against climate-related risks. On the other hand, any intervention must respect their authenticity, integrity, historical significance and cultural value. This creates a tension between the need for adaptation and the principles of conservation.

Energy efficiency interventions are a particularly relevant example of this challenge. Improving the energy performance of buildings is central to European sustainability objectives, but interventions in heritage buildings cannot follow standard retrofitting approaches. Measures such as insulation, window replacement, ventilation systems or renewable energy integration must be carefully assessed to avoid damaging historic materials, altering architectural character or compromising heritage values.

Material compatibility is another key concern. Retrofitting solutions must be technically effective but also compatible with existing materials and construction systems. The use of inappropriate materials or techniques can accelerate degradation, create moisture imbalances or reduce the reversibility of interventions. This is particularly important when introducing innovative solutions, nature-based strategies, waste-based materials or eco-design approaches in heritage contexts.

Risk management is therefore essential. Cultural heritage buildings require integrated assessment methods that consider climate hazards, material vulnerability, building use, conservation status, social value and long-term maintenance capacity. Risk assessment should support decision-making by helping professionals identify priorities, select suitable adaptation strategies, and plan interventions that are both technically sound and heritage-sensitive.

The ECOHERITAGE project addresses these challenges by promoting an interdisciplinary approach that combines climate adaptation, sustainable retrofitting, conservation principles, energy efficiency and risk assessment. This reflects the need to prepare future professionals to work across disciplinary boundaries and to respond to complex problems in the cultural heritage building sector.

2.3 Current Knowledge Gaps

Although climate change and sustainability are increasingly prominent in debates on the built environment, significant knowledge gaps remain regarding cultural heritage buildings. These gaps can be grouped into technical, professional and educational dimensions.

Over the past decade, several European research and innovation projects have generated valuable knowledge on climate risks and adaptation strategies for cultural heritage. For example, the Climate for Culture project produced extensive climate-risk mapping, climate simulations and impact assessments for historic buildings across Europe, highlighting the vulnerability of heritage assets under future climatic scenarios (Leissner et al., 2015; Climate for Culture, 2014). Similarly, the ARCH project developed resilience frameworks, governance approaches and decision-support methodologies to enhance the capacity of historic urban areas to respond to climate-related and other hazards (ARCH, 2023). The STORM project further contributed by developing monitoring technologies, risk management methodologies and decision-support tools aimed at safeguarding cultural heritage from natural and climate-related threats (STORM, 2021).

Despite these advances, most existing initiatives have primarily focused on technical, environmental and management aspects of climate resilience. Comparatively little attention has been given to the knowledge, skills, and competencies required of professionals responsible for the conservation, rehabilitation, and management of heritage assets (Sesana et al., 2018). Consequently, a disconnect remains between research outcomes and their practical implementation by architects, engineers, conservators, facility managers, planners and public authorities.

From a technical perspective, there remains a need for methods and tools to assess climate risks in heritage buildings and identify appropriate adaptation measures. Professionals require knowledge on climate hazards, building pathology, material behaviour, energy efficiency, environmental performance and sustainable retrofitting solutions. However, these topics are often addressed separately, limiting the development of integrated strategies.

Professional skills gaps are also evident. The conservation and management of cultural heritage buildings require contributions from engineers, architects, urban planners, building managers, facility managers, consultants, public authorities and heritage specialists. However, these professionals may not share the same technical language, priorities or decision-making frameworks. This creates difficulties in interdisciplinary collaboration and in the practical implementation of climate-resilient solutions.

Educational gaps are equally important. Existing higher education and professional training programmes often address heritage conservation, energy efficiency, sustainability and climate adaptation as separate fields. As a result, students and professionals may complete their education without receiving targeted training on adapting cultural heritage buildings to climate change while preserving their cultural significance.

The ECOHERITAGE project was developed in response to these gaps. Its training framework is based on five thematic modules: eco-design and social needs in retrofitting; energy efficiency and economic assessment in heritage buildings; nature-based and waste-based solutions; cultural heritage buildings and climate change; and risk assessment in heritage buildings. Together, these modules aim to provide an integrated educational response to the sector's emerging needs.

3. The Need for New Skills and Competencies

The transition towards climate-resilient and sustainable cultural heritage buildings requires new knowledge, skills, and competencies that are not yet adequately addressed in existing educational and professional training systems. As climate change increasingly affects the built environment, professionals responsible for the conservation, rehabilitation and management of heritage assets must be able to integrate climate adaptation, sustainability and heritage preservation objectives into their decision-making processes. The ECOHERITAGE project is based on the premise that education and capacity building are fundamental enablers of this transition. The project recognises that the challenges associated with cultural heritage buildings cannot be addressed through a single disciplinary perspective. Instead, they require the integration of technical, environmental, social, and management-related competencies that can respond to increasingly complex and interconnected challenges.

3.1 Technical Competencies

One of the main needs identified during the design of the ECOHERITAGE project is the development of technical competencies in climate resilience and the sustainable retrofitting of cultural heritage buildings. Climate risk assessment is becoming an essential competence for professionals involved in heritage conservation and building management. Understanding how climate hazards affect heritage assets and how vulnerability can be assessed is fundamental for the development of adaptation strategies and risk-informed decision-making processes. The ability to identify risks, evaluate exposure and support resilience planning is therefore a key area for future training.

Building pathology and performance assessment also play a critical role. Professionals require a better understanding of deterioration mechanisms, material behaviour and building performance in changing environmental conditions. Knowledge of how climate-related stressors interact with traditional construction materials and systems is increasingly necessary to support conservation and rehabilitation interventions.

Energy efficiency constitutes another important area of competence. While European policies encourage reducing energy consumption and greenhouse gas emissions in buildings, heritage assets present specific constraints and opportunities. Professionals need the ability to evaluate energy performance, identify appropriate improvement measures and balance environmental objectives with conservation requirements.

The project also highlights the importance of nature-based and innovative solutions as part of future professional competencies. These approaches can contribute to climate adaptation, environmental sustainability and improved building performance while supporting broader objectives related to resource efficiency and sustainable development. The integration of such solutions within heritage contexts requires specialised knowledge and critical evaluation skills.

3.2 Cross-Disciplinary Competencies

In addition to technical expertise, the ECOHERITAGE project recognises the growing importance of cross-disciplinary competencies. Heritage conservation increasingly requires collaboration between architects, engineers, planners, conservation specialists, researchers, public authorities and building managers. Professionals must therefore understand not only their own disciplinary field but also the perspectives, priorities and constraints of other stakeholders involved in decision-making processes.

Sustainability assessment represents another emerging competence. Climate resilience and sustainable retrofitting cannot be evaluated solely through technical indicators. Environmental, economic, social and cultural dimensions must be considered simultaneously. Future professionals need to develop the capacity to assess interventions from multiple perspectives and understand their broader impacts on heritage assets and communities.

Digital competencies are also becoming increasingly relevant. The ECOHERITAGE project includes the development of a digital learning platform and online educational resources, reflecting the growing role of digital technologies in knowledge sharing, professional development and lifelong learning. Familiarity with digital tools and online learning environments is, therefore, considered an important component of future skills development.

Stakeholder engagement is another critical competence addressed by the project. Effective adaptation and conservation strategies depend on the participation and cooperation of multiple actors. Professionals must be capable of communicating with diverse audiences, facilitating collaboration, and promoting shared understanding among technical experts, decision-makers, and local communities.

3.3 Educational Challenges

The need for new competencies is closely linked to existing educational challenges. Current educational provision often remains fragmented, with heritage conservation, sustainability, energy efficiency and climate adaptation addressed as separate topics. This fragmentation limits learners' opportunities to develop integrated approaches capable of addressing the complexity of real-world heritage challenges.

The lack of interdisciplinary programmes represents another significant challenge. Many existing curricula focus on specific disciplinary perspectives and offer limited opportunities for cross-disciplinary collaboration across fields such as architecture, engineering, environmental sciences, conservation, and management. As a result, graduates may possess strong technical expertise but limited experience in interdisciplinary problem-solving. Furthermore, opportunities for continuing professional development remain limited in this emerging field. Professionals already working in the sector frequently require access to up-to-date knowledge, specialised training, and flexible learning opportunities that support lifelong learning and adaptation to evolving professional demands.

The ECOHERITAGE project was designed to respond directly to these educational challenges. Through its needs assessment activities, training framework, digital learning platform and pilot courses, the project seeks to establish an integrated educational approach that combines technical knowledge, interdisciplinary collaboration and practical application. The five training modules developed within the project provide a structured response to the identified skills gaps and help strengthen the capacity of higher education institutions and professional communities to address climate resilience in cultural heritage buildings. Ultimately, the project views education and skills development as essential components of climate adaptation strategies, supporting both the preservation of cultural heritage and the sustainable transformation of the built environment.

4. The ECOHERITAGE Project

4.1 Project Objectives

The ECOHERITAGE project was developed in response to the growing need for specialised knowledge and skills in climate resilience and the sustainable retrofitting of cultural heritage buildings, thereby strengthening higher education and professional training capacities in this emerging field. The project is based on the recognition that climate change is creating new challenges for the conservation, management and rehabilitation of heritage assets, while current educational provision remains fragmented and insufficiently adapted to these evolving needs. ECOHERITAGE therefore aims to support the development of innovative educational approaches that address the intersection of heritage conservation, sustainability, climate adaptation, and building performance.

More specifically, the project pursues four complementary objectives; i) to identify emerging educational and professional needs related to climate resilience in cultural heritage buildings through a comprehensive needs assessment involving higher education institutions and relevant stakeholders; ii) to develop a structured training framework and educational resources capable of addressing identified skills gaps; iii) to create a digital learning environment that facilitates access to knowledge, training materials and good practices; and iv) to strengthen cooperation among higher education institutions, researchers and professionals, contributing to the development of a multidisciplinary learning community focused on sustainable heritage conservation. Through these objectives, ECOHERITAGE seeks to contribute to both educational innovation and the broader European transition towards a more sustainable and climate-resilient built environment.

4.2 Partnership

The ECOHERITAGE consortium brings together six partner organisations from five European countries with complementary expertise in cultural heritage, engineering, architecture, sustainability, higher education, digital learning and professional training. The consortium is coordinated by the Instituto Superior Técnico, Universidade de Lisboa (Portugal) and includes RWTH Aachen University (Germany), Universidad Politécnica de Madrid (Spain), the National Technical University of Athens (Greece), the Institute for Entrepreneurship and Economic Development – IECE (North Macedonia), and CRETHIDEV (Greece).

The partnership combines academic institutions with organisations experienced in training, dissemination and stakeholder engagement, ensuring a multidisciplinary perspective throughout the project. This diversity of expertise enables the project to address the technical, educational, and societal dimensions of climate resilience in cultural heritage buildings while promoting international cooperation and knowledge exchange. The consortium structure also supports the development of educational materials that can be adapted and transferred across different European contexts, contributing to the wider impact and sustainability of project outcomes.

4.3 Methodological Approach

The ECOHERITAGE project follows a progressive and interconnected methodology consisting of four main phases. Each phase contributes to the development of the subsequent activities, ensuring that project outputs are grounded in identified needs and validated through practical implementation.

Phase 1 – Needs Assessment

The first phase focuses on the identification of educational and professional needs related to climate-resilient cultural heritage buildings. This activity involves the analysis of existing courses and training programmes, the identification of skills gaps and the collection of information regarding current

educational provision across partner countries. Attention is given to understanding how topics such as climate adaptation, energy efficiency, risk assessment, sustainability and heritage conservation are currently addressed within higher education and professional training programmes. The findings of this phase will provide the evidence base for developing the training framework and educational materials.

Phase 2 – Training Framework Development

The second phase involves designing a comprehensive training framework to address the needs identified during the assessment phase. The framework is organised around five thematic modules that address key aspects of climate resilience and the sustainable retrofitting of cultural heritage buildings. This phase includes defining learning outcomes, curriculum structure, educational content, and training methodologies. The training framework is designed to support both higher education students and professionals seeking to develop specialised competencies in this field. The educational approach adopted by the project promotes interdisciplinarity, combining engineering, architecture, sustainability, heritage conservation and risk management perspectives.

Phase 3 – Digital Platform

The third phase focuses on developing a digital learning environment that will provide access to educational resources and facilitate knowledge exchange among participants. The platform will serve as a repository for project materials, training resources, good practices and dissemination outputs. It will also support the visibility of project activities and provide opportunities for interaction among different stakeholder groups. It represents an important component of the project's strategy to ensure accessibility, scalability and long-term sustainability of the developed educational resources.

Phase 4 – Pilot Courses and Evaluation

The final phase involves implementing and testing the developed training materials through pilot courses, workshops, and learning activities. These pilot actions will allow partners to evaluate the relevance, quality and effectiveness of the educational framework and to collect feedback from participants. The evaluation process will support the refinement of training materials and contribute to the validation of the proposed approach. In addition to supporting quality improvement, the pilot activities will promote stakeholder engagement and facilitate the dissemination of project results among higher education institutions, professionals and other relevant actors involved in cultural heritage conservation and management.

Together, these four phases provide a coherent methodological framework that links needs assessment, educational design, digital innovation, and practical validation, thereby supporting the overall objective of strengthening capacities for climate-resilient cultural heritage buildings across Europe.

5. Proposed Educational Framework

The educational framework proposed within the ECOHERITAGE project was designed (Figure 1) to address the skills gaps identified in relation to climate resilience, sustainability and cultural heritage conservation (UNESCO 2015, Lucchi et al. 2024). The framework adopts an interdisciplinary perspective and seeks to provide learners with the technical, environmental, social and management-related competencies required to address contemporary challenges affecting cultural heritage buildings. It is structured around five complementary modules that collectively cover the main dimensions of climate-resilient retrofitting and heritage conservation. Rather than addressing isolated technical topics, the modules have been conceived as interconnected components of a broader learning pathway, enabling participants to understand the relationships between environmental performance, climate adaptation, social needs, heritage values and risk management.

5.1 Learning Outcomes

The proposed framework aims to equip participants with a set of integrated learning outcomes that combine knowledge acquisition, analytical skills and practical application. At the end of the training programme, participants are expected to:

- Understand the main climate-related challenges affecting cultural heritage buildings.
- Identify and assess climate risks associated with heritage assets.
- Analyse building performance from environmental, technical and conservation perspectives.
- Evaluate energy efficiency measures suitable for heritage contexts.
- Understand the application of nature-based and circular economy approaches in retrofitting interventions.
- Integrate sustainability principles into conservation and rehabilitation strategies.
- Apply risk assessment methodologies to support decision-making processes.
- Develop interdisciplinary approaches to climate adaptation and heritage management.
- Communicate and collaborate effectively with different stakeholder groups involved in heritage conservation and building management.

The framework, therefore, moves beyond purely technical training and seeks to promote holistic problem-solving capabilities.

5.2 Interdisciplinary Approach

One of the defining characteristics of the ECOHERITAGE educational framework is its interdisciplinary nature. The challenges associated with climate resilience in cultural heritage buildings cannot be adequately addressed through a single disciplinary perspective. Effective solutions require the integration of knowledge from architecture, engineering, sustainability sciences, heritage conservation, environmental assessment and management. Module 1 introduces eco-design principles and social dimensions of retrofitting, highlighting the importance of user needs and societal expectations in heritage interventions. Module 2 focuses on the technical and economic dimensions of energy performance improvement. Module 3 explores innovative solutions, including nature-based and waste-based approaches that support sustainability objectives. Module 4 addresses the broader relationship between climate change and cultural heritage buildings, providing a contextual understanding of climate impacts and adaptation needs. Finally, Module 5 focuses on risk assessment methodologies and decision-support processes. Together, the modules create opportunities for learners to develop integrated perspectives and understand how different disciplinary domains contribute to climate-resilient heritage conservation.

5.3 Expected Competencies

The proposed framework aims to strengthen three complementary categories of competencies. The first category comprises technical competencies related to climate risk assessment, building performance evaluation, energy efficiency, sustainable retrofitting and the application of innovative solutions in heritage buildings. The second category includes analytical and decision-making competencies. Participants are expected to develop the ability to assess alternative interventions, evaluate risks and opportunities, and support evidence-based decision-making processes within complex heritage contexts. The third category encompasses transversal competencies, including interdisciplinary collaboration, stakeholder engagement, sustainability thinking and communication skills. These competencies are increasingly recognised as essential for professionals operating in environments characterised by multiple objectives, competing priorities and diverse stakeholder interests.

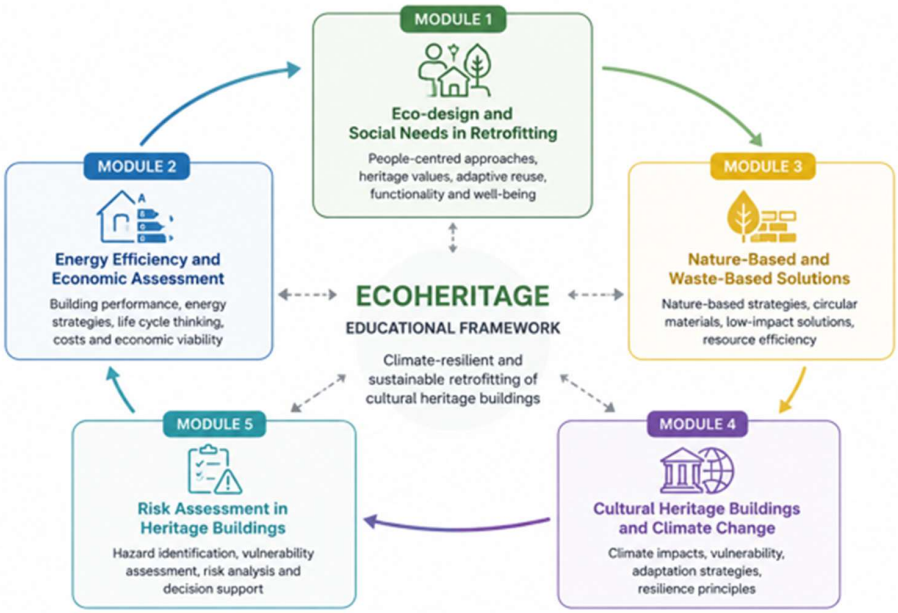


Figure 1 – ECOHERITAGE – Educational Framework – 5-modules

By combining these different dimensions, the framework seeks to contribute to the development of a new generation of professionals capable of addressing climate adaptation challenges while safeguarding the cultural significance and long-term value of heritage buildings (ESA 2020; UNESCO UK 2023; ICOMOS 2019). The educational framework, therefore, represents a structured response to the emerging needs identified by the project and provides a foundation for future training, knowledge transfer and capacity-building activities in the field of climate-resilient cultural heritage conservation.

6. Expected Impact

The ECOHERITAGE project is expected to generate impacts at multiple levels, including higher education, professional practice, the cultural heritage sector and broader sustainability policies. By addressing identified skills gaps and developing innovative educational resources, the project seeks to strengthen capacities for climate-resilient and sustainable management of cultural heritage buildings.

Higher Education

One of the main expected impacts of the project concerns the enhancement of higher education provision in the field of cultural heritage buildings. Through the development of a structured training framework and specialised educational materials, ECOHERITAGE will contribute to the introduction of new curricular content that addresses climate resilience, sustainability, and heritage conservation. The project also promotes innovative teaching and learning methodologies, combining interdisciplinary approaches, digital learning resources, and practical applications to support both academic programmes and lifelong learning initiatives.

Professional Practice

The project is expected to contribute to the development of better-qualified professionals capable of addressing the complex challenges associated with climate change and cultural heritage conservation. By strengthening competencies in climate risk assessment, energy efficiency, sustainable retrofitting, nature-

based solutions, and risk management, the training programme will support more informed decision-making and interdisciplinary collaboration among professionals in the built environment sector.

Cultural Heritage Sector

For the cultural heritage sector, ECOHERITAGE aims to improve the capacity of organisations and professionals to respond to climate-related challenges affecting heritage assets. The project promotes a more integrated understanding of resilience, combining conservation principles with sustainability and adaptation objectives. In the long term, this is expected to contribute to the preservation, functionality and resilience of cultural heritage buildings while supporting their continued social and cultural value.

Policy and Sustainability

The project is also aligned with broader European priorities related to sustainability, climate adaptation and the green transition of the built environment. By supporting capacity building and educational innovation, ECOHERITAGE contributes to the objectives of the European Green Deal and to the implementation of climate adaptation strategies within the cultural heritage sector. Through its educational framework, digital learning platform and dissemination activities, the project seeks to facilitate knowledge transfer and support the adoption of more sustainable and climate-resilient approaches across different European contexts. Overall, ECOHERITAGE views education and professional development as essential components of climate adaptation, providing a foundation for future actions to safeguard cultural heritage buildings in a changing climate.

7. Conclusions

Climate change is creating new and increasingly complex challenges for the conservation, rehabilitation and management of cultural heritage buildings. Rising temperatures, extreme weather events, flooding, moisture-related deterioration and other climate-related hazards may compromise the physical integrity, functionality and cultural value of heritage assets. These challenges require approaches that go beyond conventional conservation and retrofitting practices. The ECOHERITAGE project responds to this need by placing education, capacity building and interdisciplinary cooperation at the centre of climate adaptation for cultural heritage buildings. The project recognises that professionals and students require new competencies that combine heritage conservation, climate risk assessment, energy efficiency, sustainability, nature-based and waste-based solutions, and risk-informed decision-making.

The proposed educational framework, structured around five thematic modules, provides an integrated response to these emerging needs. By combining technical knowledge with cross-disciplinary skills, the framework aims to support learners in understanding the complexity of heritage buildings under climate stress and in selecting appropriate, compatible and sustainable retrofitting strategies. ECOHERITAGE also emphasises the importance of digital learning and international cooperation. The development of a digital training platform, pilot courses, workshops, and dissemination activities will support knowledge transfer among higher education institutions, professionals, and stakeholders across different European contexts.

Overall, the project contributes to strengthening the cultural heritage sector's capacity to respond to climate change. By developing new curricula, training resources and learning methodologies, ECOHERITAGE supports the preparation of a new generation of professionals capable of preserving cultural heritage while contributing to climate adaptation, sustainability and the objectives of the European Green Deal.

Acknowledgments

The authors acknowledge the support of the Erasmus+ Programme through the project ECOHERITAGE – Resilient and Bioclimatical Advancement of Cultural Heritage Buildings (Project No. 2025-1-PT01-KA220-HED-000362842). Funded by the European Union. Views and opinions expressed are however those of the

author(s) only and do not necessarily reflect those of the European Union or the European Education and Culture Executive Agency (EACEA). Neither the European Union nor EACEA can be held responsible for them. The authors acknowledge Fundação para a Ciência e a Tecnologia, I.P. (FCT, https://ror.org/00snfqn58) under the research unit CERIS (UID/6438/2025; DOI:10.54499/UID/06438/2025) and CERENA (UID/04028/2025; DOI: 10.54499/UIDP/04028/2025), and under PhD Scholarship (2025.02906.BDANA) awarded to GB. MPM also acknowledges the FCT through the individual project 2023.08653.CEECIND.

References

ARCH (2023). Advancing Resilience of Historic Areas against Climate-related and other Hazards. Horizon 2020 Project. Available at: https://www.archproject.eu (accessed Jun 2026).

Climate for Culture Project (2014). Climate for Culture: Built Cultural Heritage in Times of Climate Change. European Commission FP7 Project. Available at: https://www.climateforculture.eu

European Commission (2019). The European Green Deal. Brussels, https://commission.europa.eu/strategy-and-policy/priorities-2019-2024/european-green-deal_en / (accessed Jun 2026).

European Commission (2020). A Renovation Wave for Europe – Greening our Buildings, Creating Jobs, Improving Lives. Brussels, https://ec.europa.eu/newsroom/clima/items/690287/ (accessed Jun 2026).

European Commission (2020). European Skills Agenda for Sustainable Competitiveness, Social Fairness and Resilience. Brussels, https://pact-for-skills.ec.europa.eu/community-resources/publications-and-documents/european-skills-agenda-sustainable-competitiveness-social-fairness-and-resilience_en (accessed Jun 2026).

European Parliamentary Research Service (2024). The Impact of Climate Change on Cultural Heritage. European Parliament, Brussels, https://www.europarl.europa.eu/thinktank/en/document/EPRS_BRI(2024)762282 (accessed Jun 2026).

Fatorić, S. & Seekamp, E. (2017). Are cultural heritage and resources threatened by climate change? A systematic literature review. Climatic Change, Springer, vol. 142(1), pages 227-254, May. https://doi.org/10.1007/s10584-017-1929-9

ICOMOS (2019). The Future of Our Pasts: Engaging Cultural Heritage in Climate Action. https://publ.icomos.org/publicomos/jlbSai?html=Pag&page=Pml/Not&base=technica&ref=97C800C028DD1FFC1CE7E96E3E802182 (accessed Jun 2026).

ICOMOS Climate Action Working Group (2024). What We Do – Climate Action Working Group. International Council on Monuments and Sites, https://www.icomos.org/working-group/climate-action/ (accessed Jun 2026).

Leissner, J., Kilian, R., Kotova, L., Jacob, D., Mikolajewicz, U., et al. (2015). Climate for Culture: Assessing the Impact of Climate Change on the Future Indoor Climate in Historic Buildings Using Simulations. Heritage Science, 3(38). https://doi.org/10.1186/s40494-015-0067-9

Liberato, M. L. R., & Trigo, R. M. (2014). Extreme precipitation events and related impacts in western Iberia. Conference: FRIEND-Water 2014, At: Montpellier, France, Proceedings of the IAHS, Publ. 363.

Lucchi, E., Turati, F., Colombo, B. & Schito, E. (2024). Climate-responsive design practices: A transdisciplinary methodology for achieving sustainable development goals in cultural and natural heritage. Journal of Cleaner Production, 472, 142431, 10.1016/j.jclepro.2024.142431.

Mendes, M. P., & Flores-Colen, I. (2024). Greening the deal: Climate change adaptation through circularity and energy efficiency in buildings. In Towards Low and Positive Energy Buildings (pp. 3–23). Springer. https://doi.org/10.1007/978-3-031-70851-0_1.

Pereira, C., Flores-Colen, I., & Mendes, M. P. (2024). Guidelines to reduce the effects of urban heat in a changing climate: Green infrastructures and design measures. Sustainable Development, 32(1), 57–83, https://doi.org/10.1002/sd.2646.

Romero-Gómez, M. I., Flores-Colen, I., Hooper, F., Cardoso, R., Pereira, M. F. C., Bravo, M., & Mendes, M. P. (2025). Testing the durability of hydraulic lime-based renders against extreme weather: Experimental aging tests for compound events in a changing climate. Journal of Building Engineering. https://doi.org/10.1016/j.jobe.2025.114106.

Sesana, E., Gagnon, A.S., Ciantelli, C., Cassar, J. & Hughes, J.J. (2021). Climate change impacts on cultural heritage: A literature review. WIREs Climate Change, 12(4), e710, https://doi.org/10.1002/wcc.710.

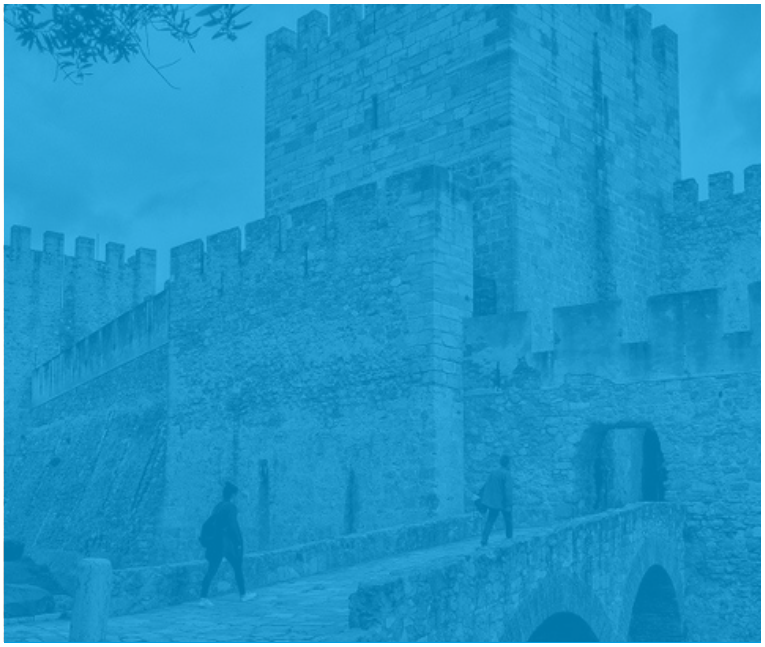
STORM Project (2021). Safeguarding Cultural Heritage through Technical and Organisational Resources Management. Horizon 2020 Project. Available at: https://cordis.europa.eu/project/id/700191

UNESCO (2007). Climate Change and World Heritage: Report on Predicting and Managing the Impacts of Climate Change on World Heritage and Strategy to Assist States Parties to Implement Appropriate Management Responses. UNESCO World Heritage Centre, Paris, https://unesdoc.unesco.org/ark:/48223/pf0000160019 (accessed Jun 2026).

UNESCO (2015). Policy for the Integration of a Sustainable Development Perspective into the Processes of the World Heritage Convention, https://whc.unesco.org/en/compendium/55 (accessed Jun 2026).

UNESCO UK (2023). Bridging the Gaps: Cultural Heritage for Climate Action. UNESCO UK, https://unesco.org.uk/resources/bridging-the-gaps-cultural-heritage-for-climate-action-report (accessed Jun 2026).

UNESCO, ICOMOS & IPCC (2021). International Co-Sponsored Meeting on Culture, Heritage and Climate Change. UNESCO, https://www.icomos.de/data/pdf/final-report-chcc-workshop-july-2021-eng-0530-1619-50.pdf (accessed Jun 2026).



INFRASTRUCTURE



Cinpar 2026
XXII International Conference on Building Pathology and Constructions Repair
15th to 17th July 2026 - Lisboa, Portugal

Surface distress evaluation of interlocking concrete block pavements using the Pavement Condition Index (PCI): a case study in Brazil

Mariana de Araújo LEITE[1], Maria Samira da Silva LIMA[2], José Levi Chaves de SOUSA[3], **Francisco Heber Lacerda de OLIVEIRA**[4]

[1] Universidade Federal do Ceará, *Campus* Fortaleza, Brazil, mariana.leite@det.ufc.br
[2] Instituto Federal de Educação, Ciência e Tecnologia do Ceará (IFCE), *Campus* Quixadá, Brazil, samiramaria20192019@gmail.com
[3] Universidade Federal do Ceará, *Campus* Fortaleza, Brazil, levi.chaves@det.ufc.br
[4] Universidade Federal do Ceará, *Campus* Fortaleza, Brazil, heber@det.ufc.br

Abstract: The use of interlocking concrete block pavements has expanded in Brazilian urban areas, particularly on local and collector roads, due to their ease of maintenance, durability, and associated environmental benefits. However, the functional performance of these pavements is directly related to construction quality and traffic conditions, making periodic evaluations essential to support maintenance planning. In this context, the Pavement Condition Index (PCI) stands out as an objective and standardized tool for assessing pavement surface condition. This study aimed to characterize the functional condition of interlocking concrete block pavements located in the central area of a city in northeastern Brazil using the PCI. The methodology consisted of a case study based on field surveys, in which the study area was subdivided into 23 Sample Units (SUs). In each SU, distress types, severity levels, and extents were identified, enabling the calculation of deduction values and, subsequently, PCI values. The results indicated that approximately 60% of the SUs presented PCI values between 85 and 55, corresponding to conditions classified as Satisfactory or Fair, indicating adequate functional performance under prevailing local traffic conditions. Conversely, approximately 40% of the sample units were classified as Poor or Very Poor, indicating functional deterioration. The most recurrent distresses were depressions, widened joints, and loss of jointing material, mainly associated with construction deficiencies. Overall, the results indicate that, although the evaluated pavements still present acceptable service conditions in most sections, the results highlight the need for localized corrective interventions and preventive actions to avoid accelerated distress progression. The PCI method proved to be effective as a support tool for urban infrastructure management, supporting the prioritization of critical sections and guiding maintenance decision-making compatible with traffic conditions and road use.

Keywords: Surface distresses; Segmental pavement systems; Pavement condition assessment.

1. Introduction

Road infrastructure plays a fundamental role in social and economic development, directly influencing the movement of people, goods, and access to essential services (Santos 2020). In Brazil, the transportation matrix is predominantly road-based, which underscores the need for continuous investment in construction, maintenance, and rehabilitation. According to CNT (2024), 67% of evaluated roads present conditions classified as Fair (40.4%), Poor (20.8%), or Very Poor (5.8%), including pavement-related deficiencies. This scenario underscores the need for appropriate technical solutions and systematic methods for assessing the structural and functional condition of pavements.

Among the alternatives employed in urban paving, interlocking concrete block pavement stands out as a widely adopted solution for low- and medium-traffic roads. This system combines advantages such as ease of maintenance, the possibility of reusing the individual units, thermal comfort, and contributions to sustainable urban drainage management (ABCP 2012). In the state of Ceará, in northeastern Brazil, the use of this pavement type has been increasingly adopted across several municipalities, driven by its operational and environmental benefits (ABCP 2025).

The performance of interlocking concrete block pavement is directly related to the quality of the materials used, the proper construction of the structural layers, and the adequate interlocking of the concrete units. Construction deficiencies or the absence of periodic monitoring may compromise pavement durability and increase maintenance costs (Ferreira Neto 2023). In this context, the application of objective methodologies capable of quantifying pavement functional condition over time becomes essential.

The Pavement Condition Index (PCI), developed by the United States Army Corps of Engineers and standardized through ASTM E2840-11 (ASTM 2024), is one of the most widely applied tools for surface evaluation of pavements. The method relies on the identification of distress types, their severity levels, and extents, yielding a numerical index ranging from 0 to 100 that enables standardized classification and technical support for maintenance prioritization.

In the municipality of Quixadá, state of Ceará, the installation of interlocking concrete block pavements in the central area has been growing since 2019, when urban renewal works carried out in partnership between the State of Ceará and the Municipal Government introduced this solution to streets in the city center (Ceará 2019). However, systematic studies evaluating the functional performance of these roads after their entry into service remain scarce. This gap hinders the consolidation of data-driven preventive maintenance practices grounded in technical and field evidence.

Against this backdrop, the present study aims to characterize the functional condition of interlocking concrete block pavements in the central area of Quixadá, CE, by applying the PCI method, identifying the predominant distresses, and classifying the functional condition of the sample units surveyed. This characterization is intended to contribute to intervention planning and to the improvement of local urban infrastructure management.

2. Technical Background and Regional Context

2.1 Interlocking Concrete Block Pavement in Urban Applications

Interlocking concrete block pavement generally behaves as a flexible pavement whose structure typically comprises a subgrade (foundation), an optional sub-base course, a base course, a bedding sand layer, and a surface course consisting of closely fitted concrete units with sand-filled joints and lateral edge restraints responsible for the interlocking of the system (ABNT 2011). Despite having a concrete block surface, its structural behavior is governed by the redistribution of vertical stresses applied at the surface, with progressive attenuation of loads toward the subgrade, a characteristic feature of flexible pavements (Balbo 2007).

The performance of this system depends on the interaction among three fundamental interlocking mechanisms: horizontal, vertical, and rotational. Horizontal interlock resists acceleration and braking forces; vertical interlock governs the transfer of shear stresses between adjacent units; and rotational interlock prevents eccentric movement under concentrated loads (ABNT 2011; ICPI 2023). The absence or deterioration of these mechanisms may result in horizontal displacement of units, excessive joint widening, and loss of surface stability (ABCP 2022). Figure 1 illustrates the typical cross-section of interlocking concrete pavement and the associated interlocking mechanisms.

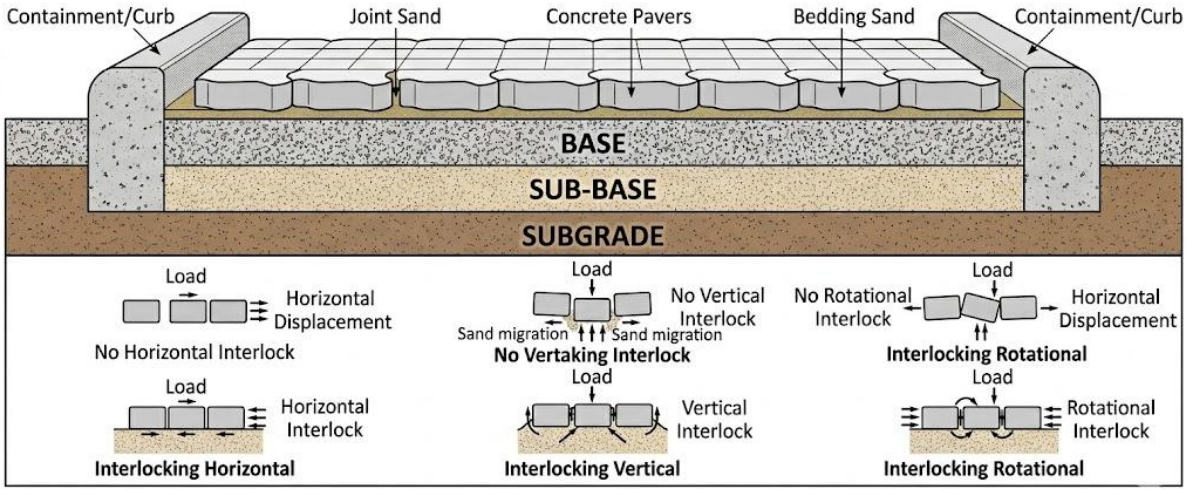


Figure 1 – Typical cross-section of interlocking concrete pavement and load distribution mechanism (adapted from ABCP 2022; ICPI 2023)

Proper construction of the structural layers is critical for system performance. The base course must exhibit sufficient strength and evenness to ensure uniform support for the concrete units, while the bedding sand layer must have controlled gradation and uniform thickness and must not be used to compensate for base course irregularities (ABCP 2010; ABNT 2011). Studies indicate that construction deficiencies, such as inadequate compaction or deficient edge restraints, are among the primary causes of premature distresses in interlocking concrete pavements (Ferreira Neto 2023; Alencar 2024).

In the Brazilian urban context, this pavement type has been employed on local streets, commercial areas, and moderate-traffic zones, owing to its ease of maintenance, potential for unit reuse, and contribution to sustainable urban drainage strategies (ABCP 2012). However, its long-term durability is contingent on the periodic monitoring of functional condition, as distresses such as depressions, loss of jointing material, horizontal displacement, and rutting tend to emerge when construction deficiencies are present or when operational loading exceeds design thresholds (ASTM 2024; Bernucci et al. 2022).

Therefore, while interlocking concrete block pavement offers notable technical and environmental advantages, its long-term performance depends on sound design, construction, and management practices. Systematic assessment of surface condition is thus an essential step towards ensuring system longevity and optimizing maintenance interventions.

2.2 Pavement Condition Index (PCI) Applied to Interlocking Concrete Pavements

The PCI is a standardized functional assessment method based on the systematic visual inspection of existing surface distresses (Páez 2015). Originally developed by the U.S. Army Corps of Engineers and subsequently standardized by the American Society for Testing and Materials, the specific procedure for interlocking concrete pavements is established in ASTM E2840-11 (ASTM 2024).

The method is based on the subdivision of the road segment into sample units, followed by the identification of observed distresses, their classification according to severity level (low, medium, or high), and the measurement of the affected area. From these data, Deduct Values (DVs) are calculated, representing the loss of condition associated with each identified distress. Subsequently, a correction procedure is applied to obtain the Corrected Deduct Value (CDV), enabling the calculation of the final index, which ranges from 0 to 100 (ASTM 2024). On this scale, values approaching 100 indicate pavements in better functional condition, while values approaching 0 represent a critical condition associated with significant loss of surface performance. The operational sequence of the method is summarized in Figure 2, which illustrates the steps from visual inspection through to the determination of the final PCI value.

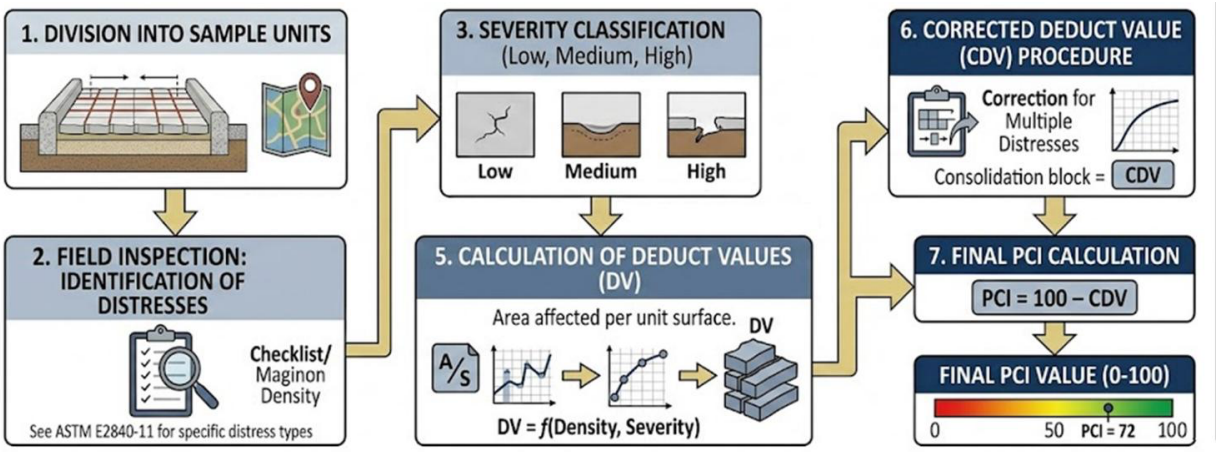


Figure 2 – Simplified flowchart of the PCI calculation procedure according to ASTM E2840-11

As noted by Berbel (2016), the PCI allows the functional state of a pavement to be classified into qualitative categories such as Good, Satisfactory, Fair, Poor, Very Poor, Serious, and Failed, providing a basis for defining preventive or corrective maintenance strategies. Páez (2015) emphasizes that the standardization of the procedure enables comparability across different road segments and constitutes a relevant tool for urban pavement management systems.

For interlocking concrete pavements specifically, ASTM E2840-11 establishes a set of characteristic distress types, including damaged blocks, missing blocks, horizontal displacement, edge restraint damage, excessive joint spacing, rutting, block height difference, and depressions (ASTM 2024; ICPI 2007). The accurate identification of these manifestations is essential, as many are directly associated with construction deficiencies or with the deterioration of the interlocking mechanisms discussed previously.

Studies conducted in municipalities in the interior of Ceará, northeastern Brazil, demonstrate the viability of the PCI as a technical diagnostic tool and a support instrument for municipal management of interlocking concrete pavements (Cunha 2024; Ferreira Neto 2023). Sousa et al. (2025) further reinforce that the adoption of standardized functional evaluation methods contributes to the rationalization of resources and the prioritization of network-level interventions. The PCI therefore constitutes a suitable method for the functional evaluation of the pavements analyzed in this study, enabling the objective quantification of surface condition and the identification of the predominant deterioration mechanisms in the urban context under investigation.

3. Methodology

3.1 Study Area

The study was conducted on interlocking concrete block pavement roads located in the central area of the municipality of Quixadá, CE, in northeastern Brazil, comprising a road network of significance for local urban traffic. Figure 3(a) presents the location of the study area within its urban context, showing its integration within the city's road network. Figure 3(b) provides an enlarged view of the analyzed area, with the boundary delineating the evaluated segments, covering a total area of 5,732.8 m².



(a) (b)

Figure 3 – (a) Location of the study area within the urban context of Quixadá; (b) Enlarged view of the study area (Adapted from Google 2025)

The selection of this area is justified by its strategic importance for urban mobility, characterized by high volumes of vehicles and pedestrians on weekdays. The roads also serve as parking areas, particularly for buses and vehicles from neighboring municipalities and rural zones. On Sundays, although traffic levels are reduced, religious activities sustain continuous use of the parking spaces. Figure 4 presents photographic records illustrating typical road usage conditions. This pattern of use makes the area well suited for evaluating the functional performance of interlocking concrete block pavement under real urban traffic demands.



(a) View of Section A (b) View of Section B (c) View of Sections D and E

Figure 4 – Road usage conditions in the study area on a typical weekday

3.2 Mapping and Definition of Sample Units

For the evaluation, a detailed mapping of the roads comprising the study area was carried out. Given that the study area consists of a compact network of interconnected streets, full coverage was adopted, encompassing all sample units and thereby eliminating the need for the statistical sampling procedure specified by ASTM (2024), since 100% of the sample units were inspected. The roads were subdivided into sections according to the direction of traffic flow and their geometric characteristics. Figure 5 presents the section mapping and the spatial distribution of the 23 sample units.

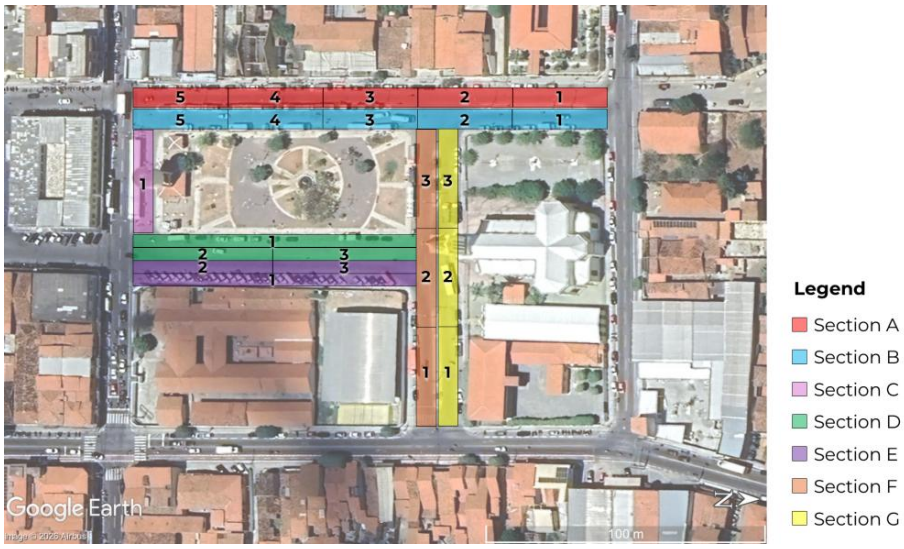


Figure 5 – Mapping of the evaluated segments and sections (Adapted from Google 2025)

The subdivision of sample units complied with the area limits recommended by ASTM (2024), which establishes values of 225 m² ± 90 m² per inspected unit. The dimensions were varied and adjusted to reflect the actual geometric characteristics of each of the 23 sample units analyzed.

3.3 Field Data Collection

Data collection consisted of the identification, classification, and quantification of distresses present in the sample units, in accordance with the criteria established by ASTM (2024). Inspections were conducted through systematic visual assessment and direct field measurements.

Owing to the high traffic volume in the area, inspections were conducted during periods of reduced traffic to ensure greater safety and measurement precision. Preliminary site visits were carried out for area reconnaissance and activity planning. During each inspection, the types of distresses observed, their severity levels (low, medium, or high), and their respective extents were recorded on field data sheets specific to each section. The following instruments were used:

- 50 m tape measure for the demarcation of sample unit boundaries;
- 10 m tape measure for detailed distress measurements;
- wooden straightedge for the severity assessment of depressions and rutting;
- mobile phone for photographic documentation.

3.4 PCI Determination and Data Processing

Following the field survey stage, the collected data were organized and processed using electronic spreadsheets developed to systematize the PCI calculation, in accordance with ASTM (2024) guidelines. The procedure involved converting the affected areas into density values, determining the deduct values, and applying the correction procedure to obtain the PCI for each sample unit.

3.5 Analysis and Interpretation of Results

The PCI values obtained for each sample unit were first analyzed individually. The results were then consolidated by section, enabling assessment of pavement performance at a broader scale. The interpretation was conducted exclusively from a diagnostic perspective, using the PCI as a technical tool for classifying the functional condition of the surveyed roads, without proposing specific interventions or making executive recommendations.

4. Results and Discussion

4.1 PCI Values by Section

The application of the PCI method to the 23 sample units enabled the determination of individual pavement condition values and, subsequently, the mean values by section. Table 1 presents the consolidated results, including the PCI value per sample unit, the corresponding condition classifications, and the mean value obtained for each section analyzed.

Table 1 – PCI values of the sample units and mean value by section

Section	Sample units	PCI per sample unit	Condition	Mean section PCI	Standard deviation	Section condition
A	1	55	Fair	44	20.5	Poor
	2	57	Fair			
	3	57	Fair			
	4	44	Poor			
	5	9	Failed			
B	1	52	Poor	60	7.4	Fair
	2	72	Satisfactory			
	3	59	Fair			
	4	57	Fair			
	5	60	Fair			
C	1	74	Satisfactory	74	-	Satisfactory
D	1	30	Very Poor	44	12.1	Poor
	2	53	Poor			
	3	48	Poor			
E	1	45	Poor	61	18.4	Fair
	2	81	Satisfactory			
	3	56	Fair			
F	1	60	Fair	57	6.4	Fair
	2	50	Poor			
	3	62	Fair			
G	1	81	Satisfactory	53	30.8	Poor
	2	20	Serious			
	3	58	Fair			

The results indicate heterogeneous performance among the evaluated sections. Mean PCI values ranged from 44 (Sections A and D) to 74 (Section C), indicating differences in pavement functional performance

within the same urban area. Section C exhibited the best overall performance, classified as Satisfactory, with a PCI of 74. This section consists of a single sample unit whose surface condition showed a lower incidence of high-severity distresses. Similarly, Section E returned a mean PCI of 61, classified as Fair, albeit with internal variation among its sample units.

By contrast, Section D returned the lowest mean value (PCI = 44), classified as Poor, reflecting a higher level of surface deterioration. This section concentrated sample units with the simultaneous presence of multiple distresses and a greater incidence of medium and high severity levels.

Section A was classified as Poor (mean PCI = 44), a result primarily influenced by Sample Unit 5, whose PCI of 9 characterizes localized functional failure. The presence of extreme values within the same section highlights that pavement condition is not uniform, and localized degradation may occur even when other sample units present intermediate condition ratings. Sections A, E, and G exhibited the highest standard deviations (20.5, 18.4, and 30.8, respectively), indicating considerable internal heterogeneity and reinforcing the need for individual sample unit analysis, since section-level mean values may underestimate localized critical conditions.

Overall, approximately 60% of the sample units presented PCI values between 55 and 85, classified as Fair or Satisfactory, indicating that the majority of the study area still maintains acceptable functional condition. However, approximately 40% of the sample units returned PCI values below 55, evidencing deterioration in specific segments. Three sample units with critical performance are particularly noteworthy:

- Section A – Sample Unit 5 (PCI = 9): characterized by a high concentration of distresses and evident functional impairment;
- Section G – Sample Unit 2 (PCI = 20): associated with construction deficiencies and inadequate repairs;
- Section D – Sample Unit 1 (PCI = 30): located in a parking area, presenting simultaneous occurrence of multiple high-severity distresses.

These extreme values significantly influence section-level mean values and indicate that deterioration does not occur homogeneously, but rather in a localized manner. The analysis of mean values reveals that, although some sections present globally acceptable performance, the existence of critical sample units within the set suggests the need for targeted interventions and continuous monitoring. Consequently, simple mean-based evaluation may underestimate localized severe conditions, reinforcing the importance of individual sample unit analysis. Figure 6 allows a comparative visualization of the mean PCI performance across the evaluated sections.

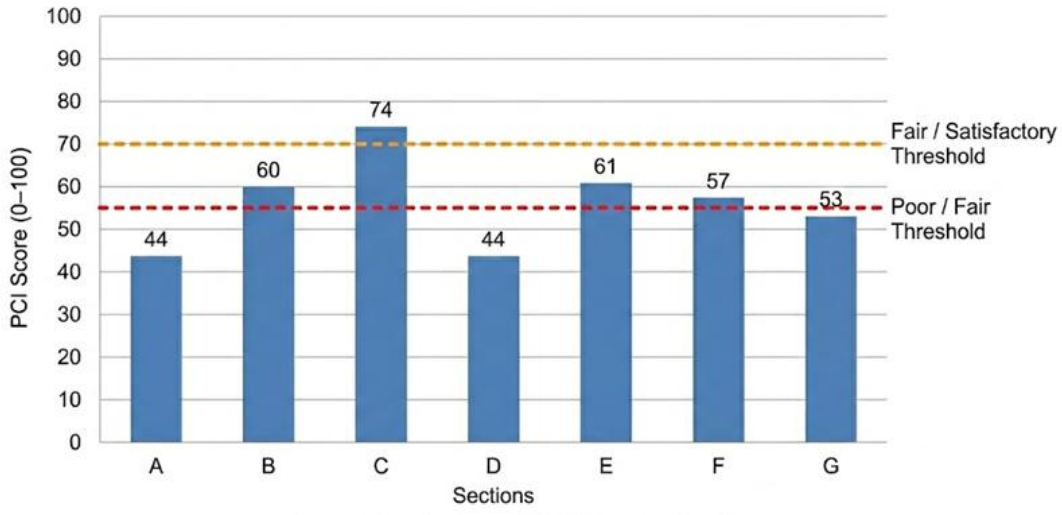


Figure 6 – Mean PCI values by section

Sections A, D, and G are observed to fall below the PCI threshold of 55, indicating Poor condition, while Section C stands out with Satisfactory performance. The remaining sections exhibit intermediate behavior, falling within the Fair range. The quantitative results presented provide the basis for the analysis of predominant deterioration patterns, which will be examined in greater depth in the following subsection, with a focus on the most recurrent distresses and their severity levels.

4.2 Predominant Distresses and Severity Patterns

The analysis of the sample units revealed recurrent deterioration patterns, demonstrating that PCI reduction is more closely related to the nature and severity of distresses than to their frequency of occurrence alone. Figure 7 presents examples of the eight distress types identified during the field inspection, illustrating the manifestations that underpinned the quantitative analysis carried out.



(a) (b) (c) (d) (e) (f) (g) (h)

Figure 7 – Examples of distresses identified during field inspection: (a) Damaged blocks; (b) Depressions; (c) Edge restraint damage; (d) Excessive joint spacing; (e) Block height difference; (f) Loss of jointing material; (g) Missing blocks; (h) Rutting

Table 2 presents the frequency of occurrence of distresses across the 23 sample units, enabling visualization of the overall distribution of manifestations throughout the study area.

Table 2 – Frequency of occurrence of distresses across the 23 sample units

Distress type	Number of occurrences in sample units (n/23)	Impact on PCI value
Damaged blocks	10	Medium
Depressions	23	High
Edge restraint damage	1	High
Excessive joint spacing	23	High
Block height difference	4	Medium
Loss of jointing material	23	Low
Missing blocks	3	High
Rutting	7	High

Of the eight distress types identified, three were present in all evaluated sample units: depressions, excessive joint spacing, and loss of jointing material. Their universal occurrence is indicative of typical behavior of interlocking concrete pavements subjected to urban traffic with repeated loading and prolonged parking, conditions that promote progressive joint widening, pumping of the bedding sand, and the formation of depressions due to differential settlement of the bedding layer (ABCP 2022). It was observed that:

- Depressions occurred in 100% of the sample units (23/23);
- Excessive joint spacing was also present in 100% of the sample units;
- Loss of jointing material likewise occurred in all sample units;
- Damaged blocks were identified in 10 sample units;
- Rutting occurred in 7 sample units;
- Missing blocks and edge restraint damage were less frequent but were associated with the most critical cases.

Despite the high frequency of loss of jointing material, its isolated impact on the PCI proved to be moderate. Across the 23 inspected sample units, this distress covered a total of 4,519.92 m², corresponding to 78.8% of the total inspected area (5,732.8 m²), without a proportional reduction in the index. This indicates that, although the loss of jointing material progressively compromises block interlocking, its immediate effect on functional performance tends to be less severe when compared to structural distresses.

Depressions, on the other hand, exerted a greater influence on PCI reduction, particularly when classified at medium or high severity. Even in areas of limited extent, this distress generated substantial deduct values, significantly affecting the final index. This behavior highlights that surface deformations associated with localized settlement carry greater weight in functional performance assessment.

Distresses such as missing blocks, edge restraint damage, and rutting were directly associated with the sample units presenting the lowest PCI values. In these situations, beyond the structural impact, there is an immediate compromise of pavement functionality and user safety.

The combined assessment of frequency and severity indicates that the deterioration observed in the study area follows two distinct patterns:

- Diffuse pattern, characterized by widely occurring distresses with moderate impact on the index (e.g., loss of jointing material);
- Localized pattern, associated with less frequent distresses but with high impact on PCI reduction (e.g., severe depressions, missing blocks, and edge restraint damage).

This behavior reinforces that distress counting alone is insufficient to characterize pavement functional performance. The severity and the weight assigned to each manifestation in the PCI calculation play a determining role in the final classification. Therefore, the variability observed among sample units stems not merely from the number of distresses present, but from the combination of distress type, severity, and extent, which accounts for the occurrence of extreme values within sections exhibiting intermediate mean ratings.

Although the results obtained are representative of the investigated context, certain methodological limitations should be considered when interpreting the data. The cross-sectional nature of the survey, with inspections conducted at a single point in time, does not allow inferences to be drawn regarding the rate of distress progression over time, which would constrain the development of deterioration models. Furthermore, the evaluation was conditioned by the specific characteristics of the central area of Quixadá, with a mixed-use pattern comprising urban traffic and prolonged parking, which may limit the direct generalization of the PCI values obtained to contexts with distinct loading profiles. Nevertheless, the deterioration patterns identified, particularly the intra-section heterogeneity, the disproportionate influence of localized high-severity distresses, and the universal occurrence of distresses associated with the interlocking system, are consistent with results reported in similar studies conducted in municipalities in the interior of northeastern Brazil (Cunha 2024; Ferreira Neto 2023), suggesting that such patterns may be representative of interlocking concrete pavements installed under analogous urban conditions. In this regard, the methodology employed and the evidence generated contribute to the consolidation of technical references applicable to urban infrastructure management in medium-sized municipalities, particularly those lacking formalized pavement monitoring systems.

5. Conclusions

The application of the PCI method to interlocking concrete block pavements in the central area of Quixadá, CE, demonstrated that surface deterioration does not occur uniformly, but rather in a localized and progressive manner, even within segments presenting apparently acceptable mean performance. This behavior confirms the importance of sample unit-level analysis as a diagnostic instrument more sensitive than aggregate segment-wide assessments.

The results indicate that distresses associated with localized structural capacity loss, such as depressions, rutting, and failures in the interlocking system, exert a disproportionate influence on pavement functional performance compared to more extensive distresses of lower immediate functional severity. This highlights that distress type may be a more decisive factor in pavement condition than frequency of occurrence.

Areas subjected to prolonged parking and vehicle maneuvering were found to be more susceptible to the development of permanent deformations, suggesting that urban loading patterns influence the behavior of interlocking concrete block pavement. This finding reinforces the need to consider actual road use patterns in performance evaluation and maintenance planning.

It is concluded that the PCI is capable of identifying consistent deterioration patterns in urban interlocking concrete pavements, serving as a tool for maintenance prioritization. Beyond classifying road segments, the method enables the recognition of degradation trends and the anticipation of structural failure progression. Consequently, preventive strategies focused on controlling localized settlements and ensuring adequate jointing material maintenance may delay distress progression, thereby contributing to greater pavement durability and improved functional performance throughout the service life.

Acknowledgments

This study was financed in part by the Coordenação de Aperfeiçoamento de Pessoal de Nível Superior – Brasil (CAPES) – Finance Code 001..

References

ABCP. 2010. *Manual de pavimento intertravado*: *Passeio público*. São Paulo: ABCP.

ABCP. 2012. "Pavimento intertravado alia durabilidade e estética." October 31, 2012. Accessed October 21, 2025. https://abcp.org.br/pavimento-intertravado-alia-durabilidade-e-estetica/

ABCP. 2022. *Manual de desempenho – Sistema de piso com peças de concreto (pavimento intertravado)*. São Paulo: ABCP.

ABCP. 2025. "Ceará investe em pavimento intertravado." February 21, 2025. Accessed December 05, 2025. https://abcp.org.br/ceara-investe-em-pavimento-intertravado/

ABNT. 2011. *NBR 15953: Pavimento intertravado com peças de concreto – Execução*. Rio de Janeiro: ABNT.

Alencar, Leonardo Santana de. 2024. *Análise da utilização do pavimento intertravado no município de Lavras da Mangabeira-CE: Um estudo de caso.* Trabalho de Conclusão de Curso, Instituto Federal de Educação, Ciência e Tecnologia da Paraíba, Cajazeiras, PB. Accessed January 15, 2026. https://repositorio.ifpb.edu.br/bitstream/177683/4219/1/TCC%20Leonardo%20Santana%20de%20Alencar.pdf

ASTM. 2024. E2840-11(2024): *Standard Practice for Pavement Condition Index Surveys for Interlocking Concrete Roads and Parking Lots*. West Conshohocken, PA: ASTM International. https://doi.org/10.1520/E2840-11R24.

Balbo, José Tadeu. 2007. *Pavimentação asfáltica: Materiais, projeto e restauração*. São Paulo: Oficina de Textos.

Berbel, Mauê Foloni. 2016. *Aplicação do método PCI – Pavement Condition Index – para determinação de serviços de restauração e manutenção em um trecho da Avenida Tupi de Pato Branco-PR*. Trabalho de Conclusão de Curso, Universidade Tecnológica Federal do Paraná, Pato Branco. Accessed March 15, 2026. https://riut.utfpr.edu.br/jspui/bitstream/1/14499/1/PB_COECI_2016_2_40.pdf

Bernucci, Liedi Bariani, Laura Maria Goretti da Motta, Jorge Augusto Pereira Ceratti, and Jorge Barbosa Soares. 2022. *Pavimentação asfáltica: Formação básica para engenheiros*. 2nd ed. Rio de Janeiro: PETROBRAS/ABEDA.

Ceará. Casa Civil do Governo do Estado do Ceará. 2019. "Governo do Ceará autoriza intervenções de urbanização em Quixadá." December 4, 2019. Accessed March 7, 2026. https://www.casacivil.ce.gov.br/2019/12/04/governo-do-ceara-autoriza-intervencoes-de-urbanizacao-em-quixada/.

CNT. 2024. *Pesquisa CNT de rodovias 2024*. Brasília: CNT.

Cunha, Francisco Tayrones da Silva. 2024. *Aplicação do método ICP na avaliação de pavimentos intertravados: Estudo de caso na Avenida José de Freitas Queiroz no município de Quixadá-CE*. Trabalho de Conclusão de Curso, Instituto Federal de Educação, Ciência e Tecnologia do Ceará, Quixadá.

Ferreira Neto, Silvio Rocha. 2023. *Análise crítica da execução da pavimentação com blocos intertravados no município de Quixeramobim-CE*. Trabalho de Conclusão de Curso, Instituto Federal de Educação, Ciência e Tecnologia do Ceará, Quixadá.

Google LLC. 2025. Google Earth Pro: *Imagem de satélite da região central de Quixadá-CE*. Accessed October 15, 2025. https://earth.google.com/web/.

ICPI. 2007. *Interlocking Concrete Block Pavement Distress Guide*. Toronto: ICPI.

ICPI. 2023. *Tech Spec 4: Structural Design of Interlocking Concrete Pavement for Roads and Parking Lots*. Chantilly, VA: ICPI.

Páez, Edgar Misael Arévalo. 2015. *Índice de condição do pavimento (ICP) para aplicação em sistemas de gerência de pavimentos urbanos*. Master's thesis, Universidade de São Paulo, São Carlos. Accessed January 15, 2026. https://teses.usp.br/teses/disponiveis/18/18143/tde-29072015-095704/publico/DISSERTACAO_2015_emap.pdf

Santos, Pedro Paulo Castro dos. 2020. *Infraestrutura de transporte como estratégia para o desenvolvimento econômico e social regional: Uma análise no contexto do modal rodoviário*. Trabalho de Conclusão de Curso, Universidade Federal do Ceará, Fortaleza. Accessed January 15, 2026. https://repositorio.ufc.br/bitstream/riufc/55591/1/2020_tcc_ppcsantos.pdf

Sousa, José Levi Chaves de, Felipe Silveira Cavalcanti Bezerra, Bruno Reges Almeida de Brito, and Francisco Heber Lacerda de Oliveira. 2025. "Análise comparativa de métodos de avaliação funcional em pavimentos intertravados." In *27º Encontro Nacional de Conservação Rodoviária / 50ª Reunião Anual de Pavimentação*, Belo Horizonte. https://doi.org/10.21526/50rapv.148

Cinpar 2026
XXII International Conference on Building Pathology and Constructions Repair
15th to 17th July 2026 - Lisboa, Portugal

A Computational Tool Based on Artificial Neural Networks for Supporting PCI Evaluation in Interlocking Concrete Block Pavements

Lucas Cavalcante de ALMEIDA[1], Carlos Bruno da Silva FERNANDES[2], Mariana de Araújo LEITE[3], **Francisco Heber Lacerda de OLIVEIRA**[4]

[1] Universidade Federal do Ceará, *Campus* Fortaleza, Brazil, lucascavalcante@det.ufc.br
[2] Instituto Federal de Educação, Ciência e Tecnologia do Ceará (IFCE), *Campus* Quixadá, Brazil, carlosbru0909@gmail.com
[3] Universidade Federal do Ceará, *Campus* Fortaleza, Brazil, mariana.leite@det.ufc.br
[4] Universidade Federal do Ceará, *Campus* Fortaleza, Brazil, heber@det.ufc.br

Abstract: Interlocking concrete block pavements have become a well-established alternative in Brazilian urban roads due to their durability and ease of maintenance. To monitor the performance of this type of pavement, functional evaluation can be performed using the Pavement Condition Index (PCI). However, as the method relies on visual inspections and the interpretation of charts, the results may vary due to evaluator subjectivity. With the increasing use of digital technologies, there is a growing need for tools that make this evaluation process more efficient and standardized. In this context, this study aimed to enhance the application of the Pavement Condition Index (PCI) for the functional condition assessment of interlocking concrete block pavements by means of an Artificial Neural Network–based computational tool. The adopted methodology initially involved the collection and digitalization of data and charts from ASTM E2840-11. Subsequently, the ANN was built and trained, followed by the development of a web-based application for practical use of the tool. Finally, the system was validated using hypothetical data and a field case study. The results showed that the ANN achieved high predictive performance, with an R^2 value of 0.99. The proposed tool correctly reproduced the PCI calculation steps, demonstrating consistency for both hypothetical and field data. In addition, the developed interface enabled the generation of maps and reports for the analysis of sample units. It is concluded that the proposed tool has strong potential to support Pavement Management Systems by contributing to standardized evaluations and reducing interpretation errors.

Keywords: Surface distresses, Computational tools, Pavement condition assessment.

1. Introduction

Road transport is the primary mode of travel in Brazil, accounting for approximately 65% of cargo flow and 95% of passenger transport, making the road network a strategic element for the national economy. Surveys conducted on major Brazilian highways have consistently identified deficiencies in maintenance and signage, reinforcing the need for effective monitoring and management strategies for road infrastructure (CNT 2024).

Among the tools used to assess pavement functional condition, the Pavement Condition Index (PCI) stands out. This methodology is internationally established and applied in Brazil to support pavement management practices (Cunha 2024; Lima 2025). Based on field inspections, the method provides information for maintenance and rehabilitation (M&R) planning, contributing to the efficient use of resources allocated to road infrastructure (ABCP 2022a). The PCI can be applied to different pavement types, including road, airport, and interlocking concrete block pavements. In the context of this work, interlocking concrete block pavement is highlighted as a solution whose use has expanded in Brazil, particularly in small municipalities, due to characteristics such as ease of construction, durability, and simplified maintenance (ABCP 2022b). For this pavement type, the ASTM E2840-11 standard (ASTM 2024), developed by the American

Society for Testing and Materials, is adopted; it systematically establishes distress types, severity levels, and calculation procedures.

Despite the contributions of ASTM (2024), the application of the PCI to interlocking concrete block pavements still presents limitations. The determination of deduct values, carried out through the interpretation of graphical curves, may vary depending on the inspector, introducing subjectivity into the process and compromising the standardization of results. In this context, Artificial Neural Networks (ANN) emerge as an alternative to support pavement condition assessment methodologies, as they are computational models capable of identifying patterns in complex datasets and performing inferences from data with varying levels of uncertainty (Silva et al. 2010).

Given this context, the present study aimed to develop a computational tool based on ANN to support the application of the PCI to interlocking concrete block pavements, seeking to reduce the subjectivity inherent to the procedure. The developed tool, named B-PAVI (*Blocos – Plataforma de Análise de Vias Intertravadas*), was implemented as a web application and validated using both hypothetical and field data.

2. Theoretical Background

The Pavement Condition Index (PCI) is a numerical indicator developed by the United States Army Corps of Engineers (USACE) to assess the surface condition of pavements through the visual identification and quantification of distresses (Shahin 2005). The index ranges from 0 (failed pavement) to 100 (perfect condition), and its rating scale enables categorization into levels ranging from "Failed" to "Good", allowing comparison between pavement sections and rational planning of maintenance and rehabilitation interventions (Shahin 2005). Originally developed for airport pavement evaluation, the method was subsequently adapted for roads and parking lots and standardized by ASTM. In the context of this work, focusing on interlocking concrete block pavements, the PCI method follows the ASTM E2840-11 standard (ASTM 2024). The absence of a specific Brazilian standard for this purpose led to the adoption of American guidelines as reference in national studies.

The significance of the PCI lies in its ability to provide objective, standardized, and low-cost diagnostics based on field visual inspections. By integrating evaluation results into a single interpretable index, the method serves as a tool within Pavement Management Systems (PMS), guiding prioritization decisions for interventions and financial resource allocation (Shahin 2005). It is worth noting that the PCI directly contributes to the development of more effective maintenance strategies, reducing long-term costs associated with accelerated pavement deterioration (Albuquerque 2017).

Despite its contributions, the method presents limitations inherent to its qualitative nature. The primary limitation is its dependence on the inspector's judgment when reading the deduct value (DV) curves, a process that involves the graphical interpretation of continuous values from normative representations. This step tends to introduce variability into results, compromising the reproducibility of assessments across different professionals and over time. Manual pavement condition inspections are slow, labor-intensive, and prone to errors, and inter-rater consistency in distress classification and quantification can be a significant concern. This limitation, inherent to the conventional PCI calculation process, demands technical expertise and is subject to errors arising from the subjectivity of the method, which justifies the development of alternative computational approaches (Attoh-Okine and Adarkwa 2013; Issa, Samaneh, and Ghanim 2022).

The application of the PCI to pavements in the Brazilian context has been gradually documented in urban case studies. Although most studies focus on asphalt pavements, the PCI can serve as a pavement management support tool regardless of the surface type (Berbel 2016).

In the state of Ceará, recent studies have expanded the scope of application of the method to interlocking concrete block pavements. In Quixadá, the evaluation of a section of Avenida José de Freitas Queiroz using the PCI in accordance with ASTM (2024), across ten Sampling Units (SU), indicated a heterogeneous and predominantly degraded structural condition, with four SU classified as Poor, four as Satisfactory, one as

Serious, and one as Failed. The most recurrent distresses, damaged blocks, excessive joint spacing, and loss of joint sand, were present in all units, indicating failures associated with construction quality and the absence of preventive maintenance (Cunha 2024).

In another assessment of streets in downtown Quixadá, approximately 60% of the SU presented PCI values between 55 and 85, with poor construction practice, inadequate design, and lack of preventive maintenance identified as the main deterioration factors (Lima 2025). Comparatively, an evaluation conducted in Quixeramobim across two surveys with a five-month interval recorded a reduction in average PCI from 50 to 34, reinforcing the need for periodic monitoring even in recently maintained sections (Sousa 2025).

Given the limitations inherent to the manual PCI calculation process, researchers have investigated the use of Artificial Neural Networks (ANN) as an alternative to automate and standardize steps that depend on graphical interpretation and technical judgment. In this context, the development of ANN-based predictive models has shown potential for estimating the index from field-observable variables. One example is the Multilayer Perceptron (MLP) model developed to estimate the PCI from distress type and severity in urban roads in Nablus, Palestine, whose results demonstrated the ability of such networks to capture nonlinear relationships between input variables and the condition index (Issa, Samaneh, and Ghanim 2022).

This trend is not limited to isolated studies, being corroborated by broader analyses. A systematic review of 143 papers published over the past three decades identified the main ANN architectures and applications in pavement engineering, along with persistent challenges such as obtaining representative datasets, hyperparameter optimization, and model transferability across different operational contexts (Yang et al. 2021).

The consolidation of the PCI as a reference indicator for interlocking concrete block pavements and the advancement of machine learning techniques thus constitute the context motivating the present work. The developed tool automates the calculation of deduct values from objective inputs, eliminating the graphical curve reading step required by the normative procedure and reducing the variability associated with inspector interpretation. Figure 1 summarizes the complete PCI calculation procedure in accordance with ASTM (2024).

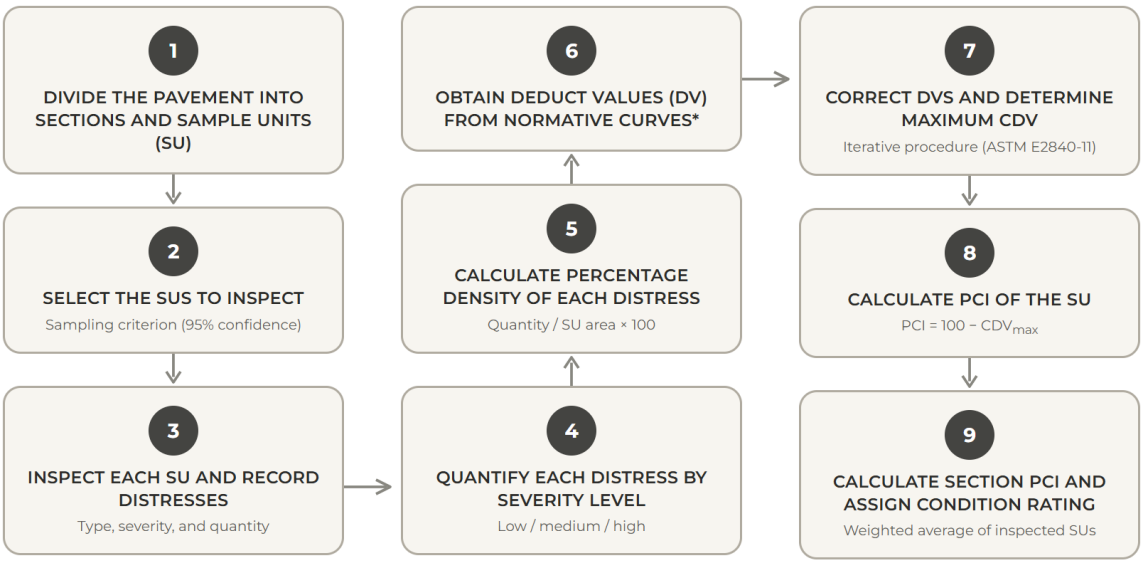


Figure 1 – PCI calculation procedure for interlocking concrete block pavements. (Source: based on ASTM 2024)

3. Methodology

The methodology comprised three stages: (i) data foundation and structuring; (ii) ANN development and training; and (iii) tool implementation and validation. These stages were organized sequentially to ensure consistency between the dataset used, the model construction, and the performance evaluation of the proposed tool.

3.1 Data Foundation and Structuring

The initial stage consisted of converting the deduct value curves, presented in graphical format in ASTM E2840-11, into numerical format. Fixed points were selected along each curve and their coordinate pairs (x-axis: distress density; y-axis: deduct value) were transcribed into spreadsheets, resulting in a structured dataset covering the eleven distress types across the three severity levels, totaling 791 data entries. Table 1 presents an excerpt of the dataset.

Table 1 – Example of data structuring: Distress Corrugation

Distress	Severity	Density (%)	Deduct Value
Corrugation	L	1	3.00
	L	5	6.90
	L	10	10.20
	M	1	12.00
	M	5	26.10
	M	10	34.50
	H	1	34.00
	H	5	44.60
	H	10	53.60

The same procedure was applied to the Corrected Deduct Value (CDV) curves, which relate the Total Deduct Value (TDV) to the coefficient q, defined as the number of distresses whose individual deduct values exceed a minimum threshold stipulated by the standard. For each value of q, a distinct equation is fitted, enabling the iterative calculation of the Maximum Corrected Deduct Value (CDV max).

3.2 ANN Development and Training

For the ANN development, an algorithm was implemented in Python using the TensorFlow library with the Keras API. The dataset is characterized by three input variables: distress type (categorical), severity level (categorical), and percentage density (numerical); and one output variable: the deduct value (numerical). For preprocessing, One-Hot Encoding (binary encoding of categorical variables) was applied to the categorical variables, MinMaxScaler was used for numerical data normalization, and the data were split into an 80% training and 20% testing ratio.

The ANN was structured according to the MLP model, comprising: (a) an input layer with 15 neurons, resulting from the application of One-Hot Encoding to the 11 distress types (11 binary neurons) and to the 3 severity levels (3 binary neurons), plus 1 neuron for the percentage density; (b) a first hidden layer with 32 neurons and ReLU activation (Rectified Linear Unit, a function that retains only positive values); (c) a second hidden layer with 16 neurons and ReLU activation; and (d) an output layer with 1 neuron and linear activation. The number of neurons in each hidden layer was determined through systematic testing, seeking to minimize error and maximize the coefficient of determination (R^2).

3.3 B-PAVI Implementation and Validation

The B-PAVI implementation adopted an architecture divided into backend and frontend. The backend was developed in Python using the FastAPI framework, with endpoints for SU calculation (minimum number of SUs and their positions) and for the PCI calculation of each SU. The frontend was developed with HTML, CSS, and JavaScript, allowing the user to enter road parameters, manage SUs, add distresses, and request PCI calculation. The tool also enables the generation of a georeferenced map in KML format and a technical report in PDF format.

Validation was carried out in two stages. In the first stage, the B-PAVI was tested with hypothetical data covering all eleven distress types across the three severity levels. A hypothetical section of 1,000 m x 5 m was defined, subdivided into 10 SUs of 225 m² each. In the second stage, a field survey was conducted on a real interlocking concrete block pavement section in an urban perimeter measuring 800 m x 7 m (Figure 2). In this section, distresses were manually identified, measured, and classified, and the same data were entered into B-PAVI for comparison of results.



Figure 2 – Analyzed section in urban perimeter

4 Results and Discussion

The results are presented in three parts: the predictive performance of the ANN during training, the tool validation with hypothetical data, and the validation with field data. Together, these analyses allowed for the evaluation of both the generalization capacity of the model and the consistency of B-PAVI under real application conditions.

4.1 ANN Performance

ANN training was performed with 80% of the data reserved for training and 20% for testing. Figure 3 presents the learning curves, showing the evolution of loss (MSE) over the training epochs.

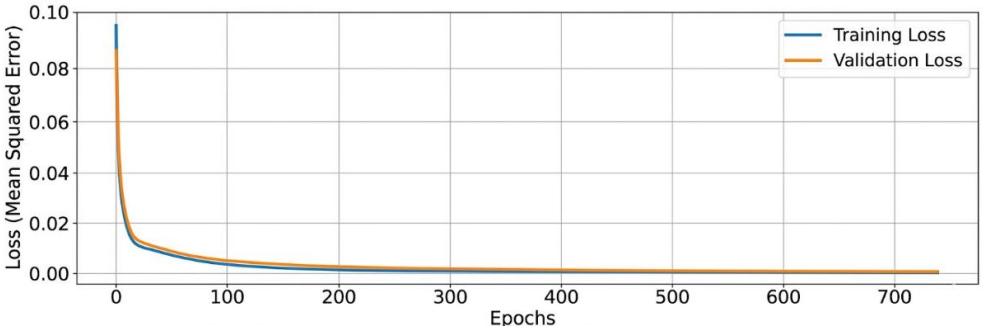


Figure 3 – ANN model learning curves (MSE Loss and Epochs)

The loss decreased from an initial value close to 0.10 to approximately 0.013 within the first 50 epochs, stabilizing gradually from epoch 400 onward. The absence of divergence between the training and validation curves confirms that the model did not suffer from overfitting. Table 2 presents the comparative performance metrics between the training and testing sets.

Table 2 – ANN performance metrics (training and testing sets)

Metric	Training	Test
R^2	0.99	0.99
MAE	0.54	0.91
RMSE	0.86	1.75

The Coefficient of Determination (R^2) reached 0.99 in both the training and testing sets, indicating that the model explains 99% of the variability in deduct values and presents adequate generalization capacity, with no evidence of overfitting. The Mean Absolute Error (MAE) of 0.91 in the testing set means that, on average, the tool produces an error of less than 1 point on the PCI scale, a negligible error for practical purposes of classification and decision-making in pavement management M&R strategies. The Root Mean Square Error (RMSE) of 1.75 confirms that even the largest isolated errors remain below 2 points on the 0-to-100 scale, keeping the tool within an acceptable precision range. The fact that the RMSE is approximately twice the MAE indicates the presence of some more pronounced but isolated deviations, without compromising the overall performance of the model.

Qualitative error analysis also identified that eight of the ten worst predictions belong to two distress types: Block Loss (5 occurrences) and Damaged Blocks (3 occurrences), with a predominance of high severity cases. For Block Loss at high severity, the probable cause is the low representativeness in the dataset (20 samples). For Damaged Blocks at high severity, the greater model uncertainty can be attributed to the inherent variability of this distress type, which represents a limitation to be considered in practical application. From a practical standpoint, these results indicate that predictions associated with these distresses at high severity should be interpreted with caution and, whenever possible, supplemented by direct technical assessment, while also highlighting the need for dataset expansion and balancing to improve model performance.

4.2 Validation with Hypothetical Data

Figure 4 presents the PCI values calculated manually by the standard procedure and those generated by B-PAVI, for each SU and for the average of the hypothetical section. The results demonstrated agreement between the tool and the standard procedure. SUs 1, 7, and 8 produced identical results. The remaining SUs exhibited isolated discrepancies not exceeding 2 PCI points in most cases, with the exception of SU 4 (comprising Damaged Blocks at low severity, Excessive Joint Spacing at high severity, and Loss of Joint Sand at high severity), in which a difference of 4 points resulted in distinct classifications: the manual procedure classified the SU as Serious (PCI = 22), while B-PAVI classified it as Very Poor (PCI = 26). Nevertheless, the validity of the algorithm is confirmed by the overall section average, with a PCI of 47 by the tool and 48 by the standard procedure.

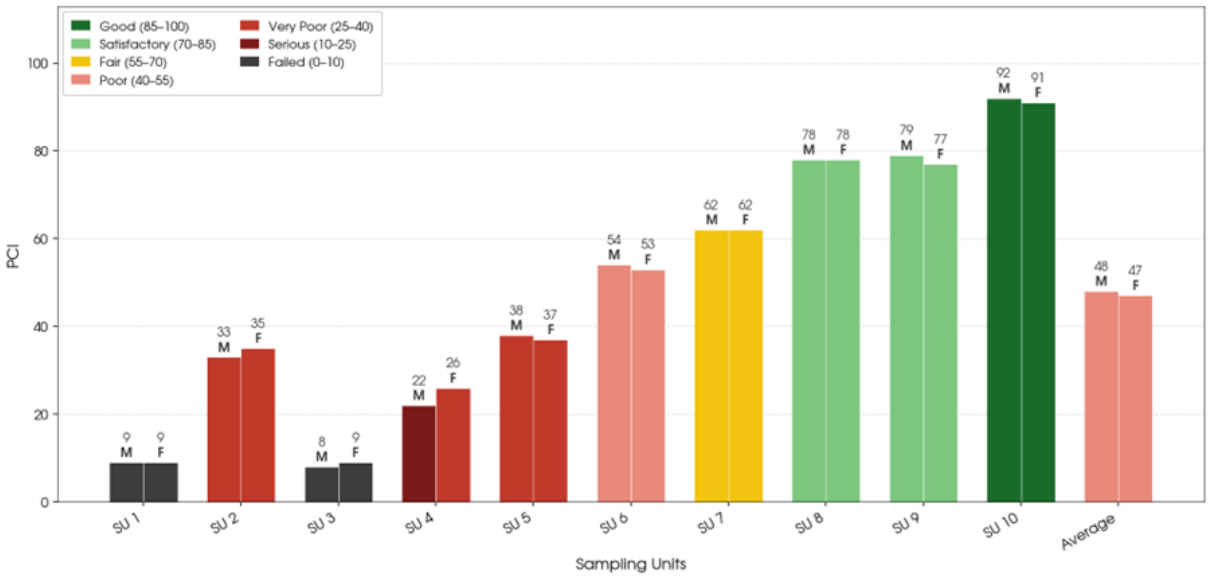


Figure 4 – Comparison between manual procedure and B-PAVI tool results (hypothetical data)

4.3 Field Validation

During the urban section inspection, the most recurrent distresses were Loss of Joint Sand, Excessive Joint Spacing, and Damaged Blocks, observed in all SUs. Figure 5 presents examples of the identified distresses.



Figure 5 – Distresses identified in the section: (a) Loss of joint sand; (b) Excessive joint spacing; (c) Damaged blocks; (d) Depression

Figure 6 presents the comparison between the results of the manual survey and those generated by B-PAVI. Similarities were also observed between the results in most SUs. The differences in SUs 2, 4, 9, and 10 can be attributed both to the subjectivity of the manual method, which depends on the inspector's judgment to select the deduct value from the standard curves (Shahin 2005; Attoh-Okine and Adarkwa 2013), and to the isolated limitations of the ANN for distresses such as Damaged Blocks and Block Loss. The results confirmed

the consistency of the tool, as the manual survey classified the section as Fair with an average PCI of 58, while B-PAVI classified it equally as Fair, with an average PCI of 57.

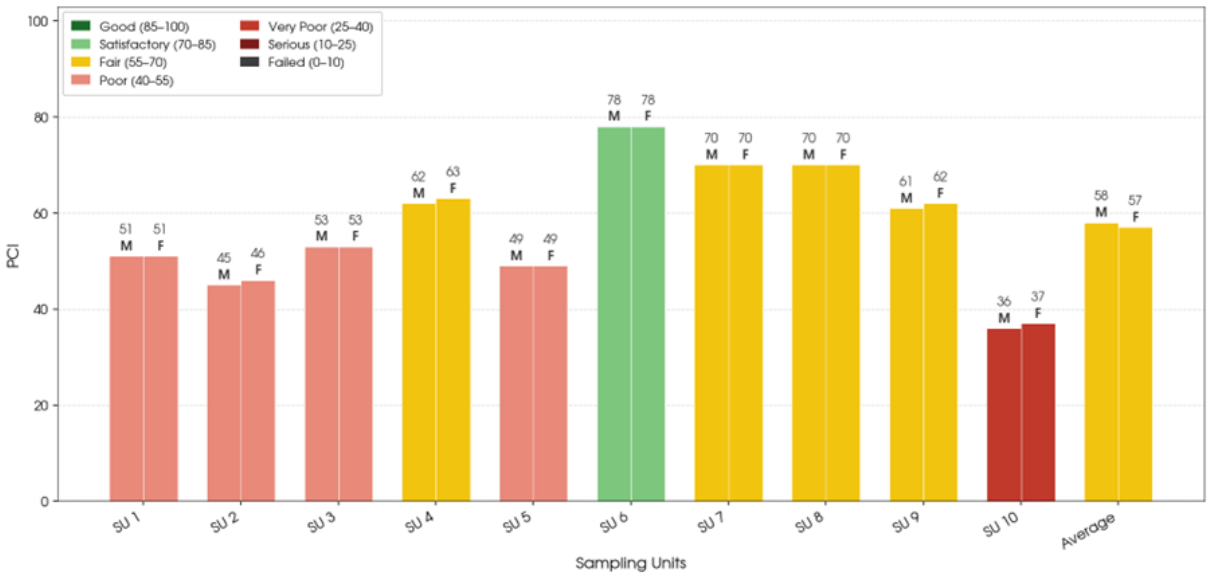


Figure 6 – Comparison between manual procedure and B-PAVI tool results (field data)

Figure 7 presents the geospatial visualization of results in the KML map exported by the tool, with each SU identified by its position and PCI value. Unlike the bar chart, which summarizes results numerically, the georeferenced map allows for the identification of the exact location of sections in worse condition, constituting a direct decision-support resource for maintenance and rehabilitation activities. This functionality represents a distinctive feature of B-PAVI in relation to conventional manual survey approaches, in which results are typically not integrated into spatial visualization systems.

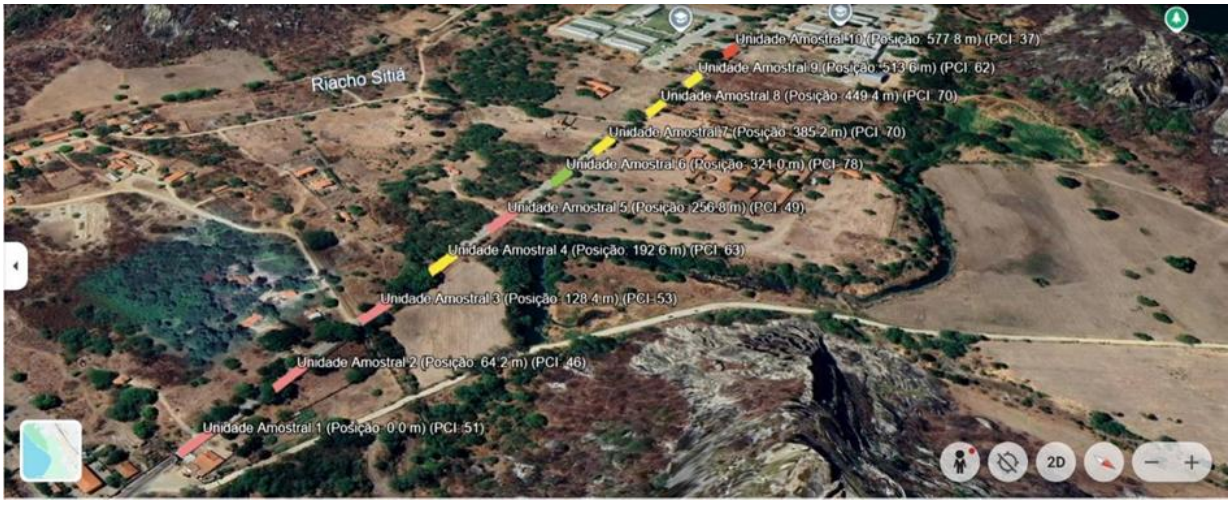


Figure 7 – KML map of the analyzed urban section with the respective PCI values per SU

5 Conclusions

This study showed that PCI calculation can be systematized for interlocking concrete block pavements through an ANN-based computational tool, reducing the dependence on subjective inspector interpretation in the graphical curve reading steps. The developed model presented satisfactory predictive performance, with R^2 of 0.99 in the testing set, and consistently reproduced deduct values for the eleven distress types established by ASTM E2840-11 across the three severity levels. The discrepancies observed for distresses such as Damaged Blocks and Block Loss, although isolated, have traceable causes in the inherent variability of these distress types and did not compromise the overall reliability of the model.

Validation with hypothetical and field data confirmed the consistency of B-PAVI under real application conditions. In the field data, the tool classified the analyzed section as Fair (average PCI of 57), in agreement with the result of the manual procedure (average PCI of 58), with a difference of less than 2% between the methods. Beyond index calculation, B-PAVI integrates complementary functionalities, such as technical report generation in PDF format and georeferenced KML map export, that directly connect field-collected records to the steps of the normative procedure, supporting the communication of results and decision-making in maintenance and rehabilitation activities.

The contribution of this work lies in the consolidation of an approach that transforms a traditionally manual procedure, subject to interpretive variability, into a standardized, reproducible, and operationally applicable process. By integrating predictive modeling, routine automation, and data systematization resources into a single platform, the tool expands the practical applicability of the method and contributes to making interlocking concrete block pavement assessment more consistent and aligned with the demands of a PMS.

Acknowledgments

This study was financed in part by the Coordenação de Aperfeiçoamento de Pessoal de Nível Superior – Brasil (CAPES) – Finance Code 001.

References

ABCP (Associação Brasileira de Cimento Portland). 2022a. *Manual de Intervenção em Pavimento Intertravado*. Prepared by Cláudio Oliveira Silva. São Paulo: ABCP.

ABCP (Associação Brasileira de Cimento Portland). 2022b. *Manual de Desempenho: Pavimento Intertravado*. 1st ed. São Paulo: ABCP/BlocoBrasil.

Albuquerque, T. P. 2017. "Índice de condição baseado em defeitos superficiais para gerência de pavimentos urbanos." Master's thesis, Universidade Federal da Paraíba, João Pessoa.

ASTM International. 2024. *ASTM E2840-11: Standard Practice for Pavement Condition Index Surveys for Interlocking Concrete Roads and Parking Lots*. West Conshohocken, PA: ASTM International.

Attoh-Okine, N. O., and O. Adarkwa. 2013. *Pavement Condition Surveys: Overview of Current Practices*. Newark: University of Delaware, Center for Applied Demography and Survey Research.

Berbel, M. F. 2016. "Aplicação do método do PCI—Pavement Condition Index—para determinação de serviços de restauração e manutenção em um trecho da Avenida Tupi de Pato Branco/PR." Bachelor's thesis, Universidade Tecnológica Federal do Paraná, Campus Pato Branco.

CNT (Confederação Nacional de Transportes). 2024. *Pesquisa CNT de Rodovias 2024*. Brasília: CNT.

Cunha, F. T. da S. 2024. "Aplicação do método ICP na avaliação de pavimentos intertravados: Um estudo de caso na Avenida José de Queiroz Freitas no município de Quixadá." Bachelor's thesis, Instituto Federal de Educação, Ciência e Tecnologia do Ceará, Campus Quixadá.

Issa, A., H. Samaneh, and M. Ghanim. 2022. “Predicting Pavement Condition Index Using Artificial Neural Networks Approach.” *Ain Shams Engineering Journal* 13 (1): 101533.

Lima, M. S. da S. 2025. “Aplicação do Pavement Condition Index (PCI) na avaliação de pavimentos com blocos de concreto intertravado: Estudo de caso no centro de Quixadá/CE.” Bachelor’s thesis, Instituto Federal de Educação, Ciência e Tecnologia do Ceará, Campus Quixadá.

Shahin, M. Y. 2005. *Pavement Management for Airports, Roads, and Parking Lots*. 2nd ed. New York: Springer.

Silva, I. N., D. H. Spatti, and R. A. Flauzino. 2010. *Redes Neurais Artificiais para Engenharia e Ciências Aplicadas: Curso Prático*. São Paulo: Artliber.

Sousa, L. F. L. de. 2025. “Análise comparativa da condição do pavimento de trecho de via com blocos de concreto intertravado na cidade de Quixeramobim/CE por meio do Pavement Condition Index (PCI).” Bachelor’s thesis, Instituto Federal de Educação, Ciência e Tecnologia do Ceará, Campus Quixadá.

Yang, X., Q. Liu, Z. Dong, and X. Zheng. 2021. “Research and Applications of Artificial Neural Network in Pavement Engineering: A State-of-the-Art Review.” *Journal of Traffic and Transportation Engineering (English Edition)* 8 (6): 1000–1021.

Cinpar 2026
XXII International Conference on Building Pathology and Constructions Repair
15th to 17th July 2026 - Lisboa, Portugal

Analysis of the influence of rainfall variability on asphalt pavement deterioration: a case study based on functional condition surveys

Francisco Simeone Matheus Maciel SANTOS[1], Mariana de Araújo LEITE[2], Camila Lima MAIA[3], **Francisco Heber Lacerda de OLIVEIRA**[4]

[1] Universidade Federal do Ceará, *Campus* Fortaleza, Brazil, simeonematheus@gmail.com
[2] Universidade Federal do Ceará, *Campus* Fortaleza, Brazil, mariana.leite@det.ufc.br
[3] Universidade Federal do Ceará, *Campus* Fortaleza, Brazil, camilalima@det.ufc.br
[4] Universidade Federal do Ceará, *Campus* Fortaleza, Brazil, heber@det.ufc.br

Abstract: In the context of climate change, it is relevant to investigate the relationship between rainfall variability and the functional performance of road pavements. This study investigates the relationship between annual average precipitation and the functional condition of the road network in the state of Ceará, northeastern Brazil, from 2012 to 2024, by integrating data from the *Confederação Nacional do Transporte* (CNT) Road Survey and historical precipitation series. The analysis considered the five evaluation classes defined by the CNT (excellent, good, fair, poor, and very poor) across four components: pavement condition, signage, roadway geometry, and overall road condition. Statistical analysis was performed using Pearson's correlation coefficient, adopting a 5% significance level with a two-tailed approach. The results indicated a strong negative correlation between annual average precipitation and the proportion of pavements classified as excellent, both for pavement condition ($r = -0.90$) and overall road condition ($r = -0.71$), indicating a reduction in higher performance levels during wetter periods. Conversely, positive correlations were observed between increased precipitation and the growth of good ($r = 0.73$) and poor ($r = 0.76$) pavement condition classes, suggesting a gradual shift from higher to intermediate and lower condition levels. For road signage, correlations were predominantly moderate, indicating lower direct sensitivity to rainfall variability. Roadway geometry exhibited a distinct behavior, with a positive correlation for the fair condition class ($r = 0.69$) and a negative correlation for the very poor class ($r = -0.67$). Overall, the results indicate an association between rainfall variability and the loss of pavement performance, reflected in the overall condition of the road network. It is concluded that the integration of functional condition surveys and precipitation data contributes to the diagnosis of pavement distresses and to the prioritization of road infrastructure maintenance actions.

Keywords: pavement distresses, rainfall variability, functional condition of pavements, road infrastructure.

1. Introduction

The Brazilian road network constitutes the primary infrastructure supporting the transport of goods and passengers in the country, accounting for more than 60% of total freight volume (CNT 2024). In the context of northeastern Brazil, particularly the state of Ceará, roads play a strategic role in regional connectivity, given the limited capacity of other transport modes. Adequate maintenance of road infrastructure is therefore a fundamental condition for the socioeconomic development of these regions.

The functional performance of asphalt pavements is governed by multiple interacting factors, among which traffic volume and composition, subgrade characteristics, pavement structural materials, and climatic conditions throughout service life are particularly prominent (Bernucci et al. 2022). Among climatic agents, rainfall plays a central role in accelerating deterioration mechanisms. The presence of water can

compromise the load-bearing capacity of the subgrade and promote processes such as infiltration, fatigue cracking, and interlayer debonding (Nazzal et al. 2021; Caro et al. 2008).

In the context of climate change, rainfall variability has been identified as an increasingly relevant factor in pavement design and maintenance. Rising frequency and intensity of extreme precipitation events are projected to shorten the service life of flexible pavement structures (Qiao et al. 2020). In this regard, Stoner et al. (2019) quantified the impacts of climate change on the performance of flexible pavements across the United States, demonstrating that projected increases in precipitation may lead to significant reductions in pavement surface life.

In Ceará, the precipitation regime is characterized by pronounced interannual variability, driven by phenomena such as the El Niño–Southern Oscillation (ENSO) and the Intertropical Convergence Zone (ITCZ) (Da Silva et al. 2020). This climatic irregularity creates favorable conditions for investigating the association between rainfall fluctuations and the functional condition of the road network over time.

Against this background, the present study aims to examine the influence of annual precipitation variability on the functional condition of asphalt pavements in the state of Ceará road network from 2012 to 2024. To this end, data from the *Confederação Nacional do Transporte* (CNT) Road Survey are integrated with historical precipitation series from the *Fundação Cearense de Meteorologia e Recursos Hídricos* (FUNCEME), with statistical analysis based on the Pearson correlation coefficient.

2. Literature Review

Asphalt pavement is a multilayer structure designed to distribute traffic loads so as not to exceed the bearing capacity of the constituent materials (Bernucci et al. 2022). Throughout its service life, this structure undergoes progressive deterioration as a result of the interaction between repeated loading and environmental agents, most notably water.

The principal deterioration mechanisms include fatigue cracking, permanent deformation, surface wear, and disintegration of asphalt layers. Water affects several of these processes: it weakens the adhesive bonds between the asphalt binder and aggregates, reduces subgrade bearing capacity, and promotes the propagation of pre-existing cracks (Caro et al. 2008). At the microscopic scale, moisture induces stripping damage in asphalt mixtures, compromising the internal cohesion of the wearing course, a mechanism that intensifies with prolonged and repeated exposure to precipitation (Nazzal et al. 2021). Figure 1 illustrates the main water-induced deterioration mechanisms in asphalt pavements, highlighting the interactions among precipitation, pavement structure, and functional degradation.

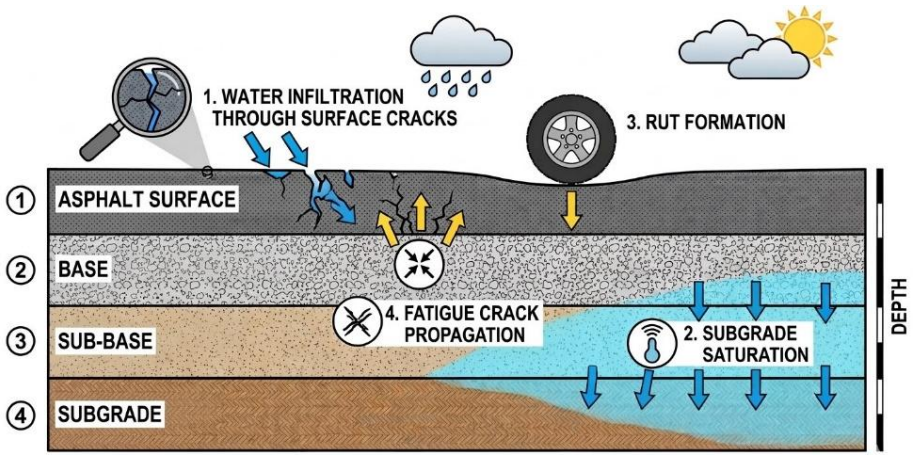


Figure 1 – Schematic cross-section of asphalt pavement deterioration mechanisms induced by water (based on Bernucci et al. 2022; Nazzal et al. 2021)

This vulnerability to water-induced damage becomes more critical in the context of climate change. Extreme precipitation events are projected to increase in both frequency and intensity across numerous regions, with direct impacts on transport infrastructure (IPCC 2023). Higher precipitation levels have been associated with accelerated surface fatigue and increased permanent deformation (Qiao et al. 2020), highlighting the need to incorporate climate projections into pavement design models in order to ensure adequate performance throughout the design life.

At the road network scale, negative correlations between accumulated precipitation and the Pavement Condition Index (PCI) have been identified for urban roads (Llopis-Castelló et al. 2020), corroborating the hypothesis that water acts as an accelerator of pavement degradation. For the North American context, regions facing projected increases in precipitation are expected to record reductions in pavement service life, with direct implications for maintenance and rehabilitation costs (Stoner et al. 2019).

Systematic road condition assessment and climatic monitoring support the diagnosis of road infrastructure and the formulation of pavement maintenance and rehabilitation strategies. In Brazil, various public agencies and sectoral entities conduct periodic surveys of the road network and climatic variables at national, regional, and state scales. Among these initiatives, the CNT Road Survey and the rainfall monitoring network of the FUNCEME are particularly relevant to the present study.

The CNT Road Survey is an annual assessment carried out by the CNT, the representative body of the Brazilian transport sector, which evaluates the condition of the country's paved road network. It constitutes a comprehensive road condition inventory covering federal and state highways, both public and private, across all states, with an assessed extent exceeding 100,000 km per survey cycle (CNT 2024). Due to its regularity, geographic coverage, and methodological standardization, the survey is one of the primary references for diagnosing Brazil's road infrastructure and informing public policies on pavement maintenance and rehabilitation.

The CNT Road Survey methodology considers three dimensions: pavement condition, signage conditions, and road geometric characteristics. Each dimension is classified into five categories (excellent, good, fair, poor, and very poor) with results expressed as a percentage of the assessed extension. The assessment encompasses surface distresses such as cracking, rutting, corrugation, potholes, and patching, as well as longitudinal roughness.

The CNT Road Survey enables the construction of comparable historical time series, facilitating trend analyses and correlation studies with variables of interest such as climatic and socioeconomic indicators. This feature distinguishes the survey from one-off assessments, making it well suited for longitudinal studies on the performance of Brazilian road infrastructure, a context in which the state of Ceará stands out as a particularly relevant unit of analysis for investigating associations between climatic variability and road functional conditions.

Located within the semiarid region of northeastern Brazil, one of the most climatically vulnerable areas on the continent, the state of Ceará is characterized by pronounced interannual rainfall variability and a high frequency of extreme events, including prolonged droughts and intense rainfall episodes. This regime is primarily modulated by the El Niño–Southern Oscillation (ENSO) and the Intertropical Convergence Zone (ITCZ), whose interactions produce years with precipitation well below or well above the historical mean. Mean annual precipitation in the state ranges from less than 400 mm in the driest interior areas to approximately 1,600 mm in the highland zones, with interannual coefficients of variation exceeding 30%, markedly higher than those observed in temperate regions (Da Silva et al. 2020).

This irregularity does not follow a random temporal distribution. Research on the Northeast Brazilian climate identifies the existence of multi-year cycles associated with the warm and cold phases of ENSO, with direct impacts on the intensity and spatial distribution of rainfall: El Niño years tend to produce severe droughts in the semiarid zone, while La Niña years are frequently associated with above-average rainy seasons (Da Silva et al. 2020). This cyclical pattern, in combination with long-term trends and global climate change, creates

a scenario of increasing pressure on the regional road infrastructure. The IPCC (2023) projects that these changes are likely to intensify hydrological extremes in tropical regions.

Systematic monitoring of this climatic behavior in Ceará is carried out by the FUNCEME, a state public agency responsible for maintaining long-term precipitation records for the Ceará territory. These datasets constitute a key reference for climatic studies in the Brazilian semiarid zone. This structural climatic irregularity creates exceptional conditions for investigating how medium-term rainfall oscillations are reflected in the functional performance of road infrastructure. In this context, Ceará presents itself as a case study with the potential to contribute both to regional pavement management and to the broader debate on the adaptation of transport infrastructure to climate change.

3. Research Method

This study is grounded in the integration of secondary data on road functional condition and precipitation. The state of Ceará was adopted as the unit of analysis due to its distinctive climatic characteristics, particularly its pronounced interannual rainfall variability, which makes it a suitable context for investigating associations between precipitation and pavement functional performance. The research was organized into seven sequential steps, summarized in Figure 2 and described in detail below.

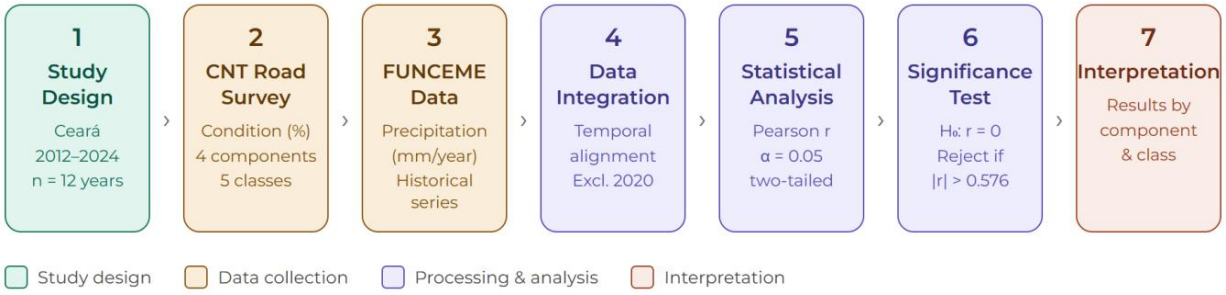


Figure 2 – Methodological framework of the research

Step 1 involved defining the spatial and temporal scope of the study: the state of Ceará over the period from 2012 to 2024. The year 2020 was excluded from the analysis due to the suspension of the CNT Road Survey during the COVID-19 pandemic, resulting in a final sample of 12 annual observations.

Steps 2 and 3 corresponded to the collection of the two datasets employed. The first was the CNT Road Survey (CNT 2024), from which annual data on pavement condition, signage, road geometry, and overall condition, classified as excellent, good, fair, poor, and very poor, were extracted. The results for each category are expressed as a percentage of the assessed extension, comprising the dependent variables of the analysis. The second dataset consisted of historical precipitation series for the state of Ceará, obtained from FUNCEME (2025). Rainfall records, originally provided at daily or monthly resolution, were aggregated into annual averages (mm/year) to enable direct comparison with the annual CNT Road Survey data. The data were subjected to prior outlier screening; all records were retained in the series given the impossibility of precisely determining the collection dates of the CNT Road Survey, which would have precluded any well-founded exclusion. These data constitute the independent variable of the study, representing the mean annual precipitation fluctuations over the period analyzed.

Step 4 organized and aligned the datasets of the two series, ensuring correspondence between the year of road functional assessment and the respective recorded precipitation volume. This allowed the calculation of the Pearson correlation coefficient (r) for each pair formed by annual average precipitation and the percentage of roads in each condition class, across each of the four assessed components, totaling 20 variable pairs (Step 5). The Pearson coefficient ranges from −1 to +1, where values close to −1 indicate strong

negative correlation, values close to +1 indicate strong positive correlation, and values near zero indicate the absence of linear correlation.

Step 6 tested the statistical significance of the obtained correlations. To this end, a significance level of α = 0.05 was adopted with a two-tailed approach, with the null hypothesis defined as H_0: r = 0 — the absence of linear correlation between precipitation and pavement functional condition. The critical value for n = 12 observations is |r| = 0.576, derived from the critical value table for the Pearson correlation coefficient at 10 degrees of freedom (df = n − 2) and a two-tailed significance level of α = 0.05 (Neter et al. 1996), so that correlations with absolute values exceeding this threshold were classified as statistically significant and retained for interpretation in the subsequent step. Finally, Step 7 involved interpreting the results, with analysis of statistically significant and non-significant correlations by component and condition class.

4. Results and Discussion

This section presents and discusses the results across four subsections. The first two separately characterize rainfall variability and the evolution of road functional conditions. The subsequent two integrate both series through Pearson correlation analysis, with interpretation by component and condition class.

4.1 Rainfall Variation in Ceará (2012–2024)

Figure 3 presents the evolution of mean annual precipitation in the state of Ceará between 2012 and 2024, based on FUNCEME data.

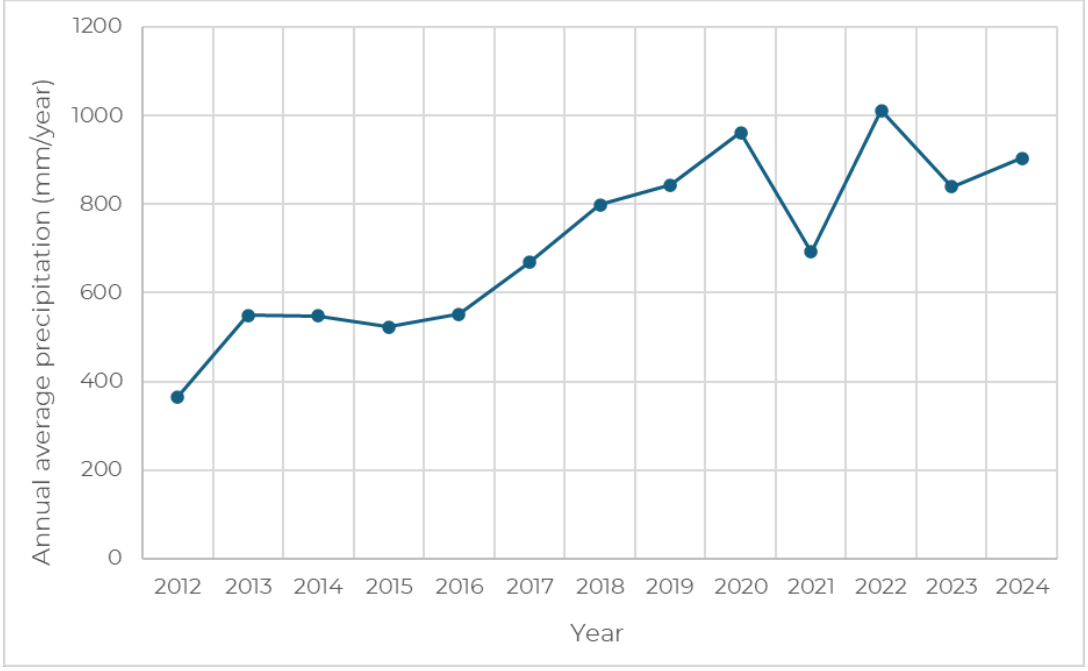


Figure 3 – Annual average precipitation in the state of Ceará, 2012–2024 (adapted from FUNCEME 2025)

The year 2012 recorded the lowest precipitation index of the series (~375 mm/year), associated with an intense El Niño episode that affected the northeastern semiarid zone during that period. From 2013 to 2016, precipitation remained relatively stable, ranging between 510 and 540 mm/year, followed by a rising trend from 2017 onwards. From 2018, an increase in annual rainfall volumes is observed, with greater interannual variability, reaching the highest values in the series in 2020 (~955 mm/year) and 2022 (~1,000 mm/year). This

behavior is consistent with IPCC (2023) projections indicating intensification of hydrological extremes in tropical regions, as well as with the climatic variability patterns associated with ENSO (Da Silva et al. 2020).

4.2 Evolution of Road Functional Conditions — Pavement, Signage, and Geometry

Figure 4 presents the temporal evolution of asphalt pavement conditions in Ceará's road network between 2012 and 2024, by condition class**.** A reduction in the proportion of roads classified as excellent is observed throughout the period, becoming more pronounced from 2018 onwards, coinciding with the period of higher precipitation (Figure 3). Concurrently, a gradual increase in the poor and very poor categories is evident, indicating a progressive shift in pavement condition toward lower performance levels over the historical series.

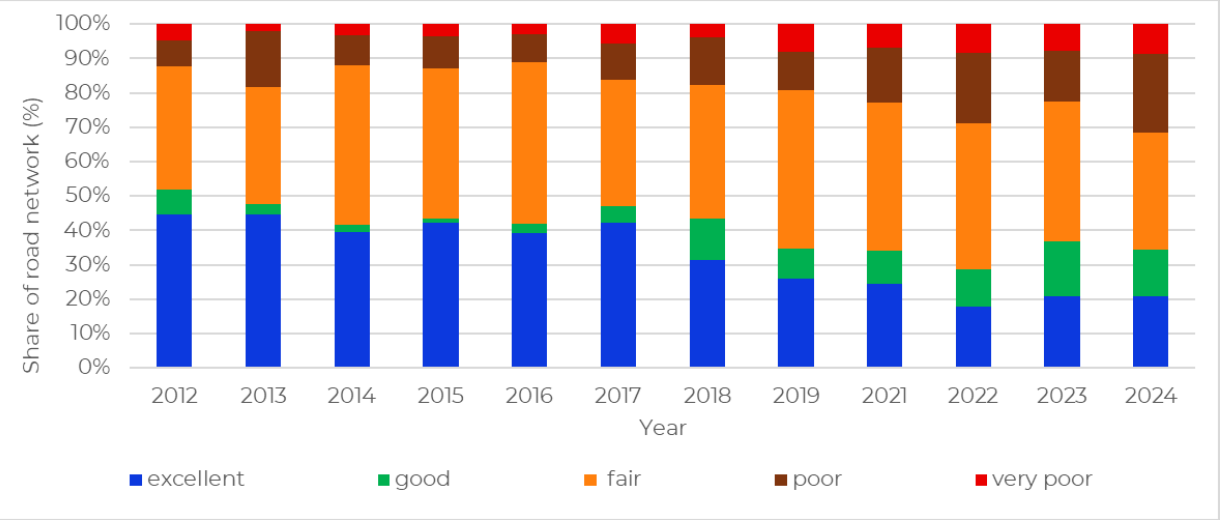


Figure 4 – Pavement condition classification in Ceará road network, 2012–2024 (adapted from CNT 2024)

The fair condition class remained notably stable throughout the entire period. This pattern suggests that this category functions as a transitional zone between higher and lower states, absorbing part of the variation without exhibiting marked oscillations, a behavior consistent with the dynamics of progressive degradation (Bernucci et al. 2022), in which road segments tend to migrate from good to poor conditions while remaining in the fair classification for extended periods. The contemporaneity between increasing precipitation and deteriorating pavement conditions suggests a possible association between the two trends, a hypothesis that is tested statistically and presented subsequently.

Figure 5 presents the temporal evolution of signage conditions in Ceará's road network between 2012 and 2024. Unlike pavement, signage does not exhibit a clear trend of deterioration or improvement throughout the historical series, with the condition classes alternating without a consistent pattern. This behavior suggests that signage is governed by factors distinct from those acting on the asphalt surface, such as periodic maintenance policies and targeted interventions, rather than continuous degradation processes.

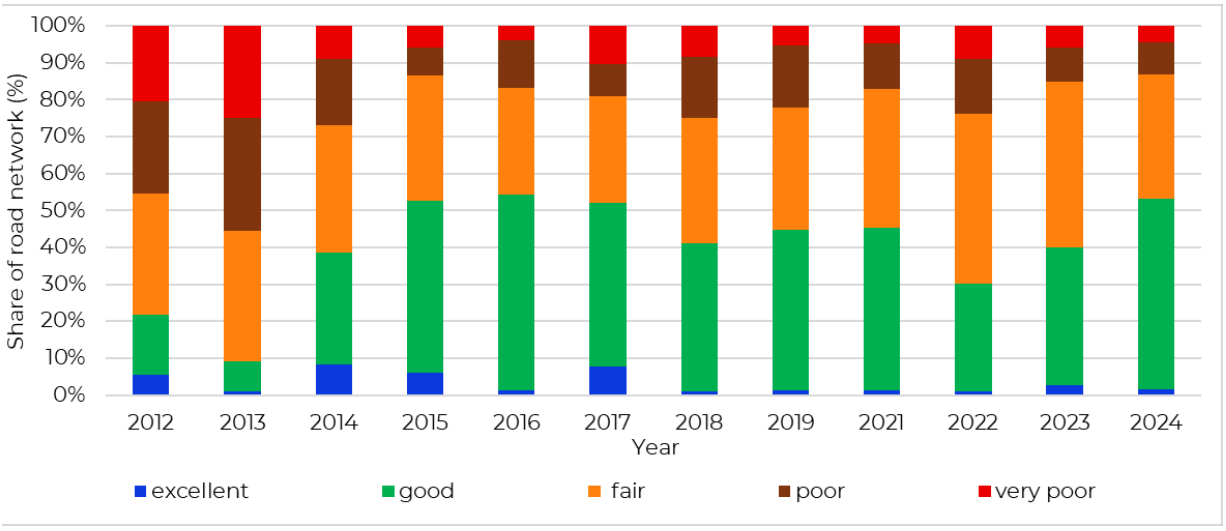


Figure 5 – Signage condition classification in Ceará road network, 2012–2024 (adapted from CNT 2024)

Figure 6 presents the evolution of road geometric conditions over the same period. Road geometric characteristics (such as alignment, carriageway width, curves, and grades) are defined at the design stage and tend to remain stable over time, which explains the lower variability observed compared to pavement. The fluctuations identified primarily reflect localized structural interventions and adjustments carried out on specific road segments, rather than a systematic trend associated with climatic factors.

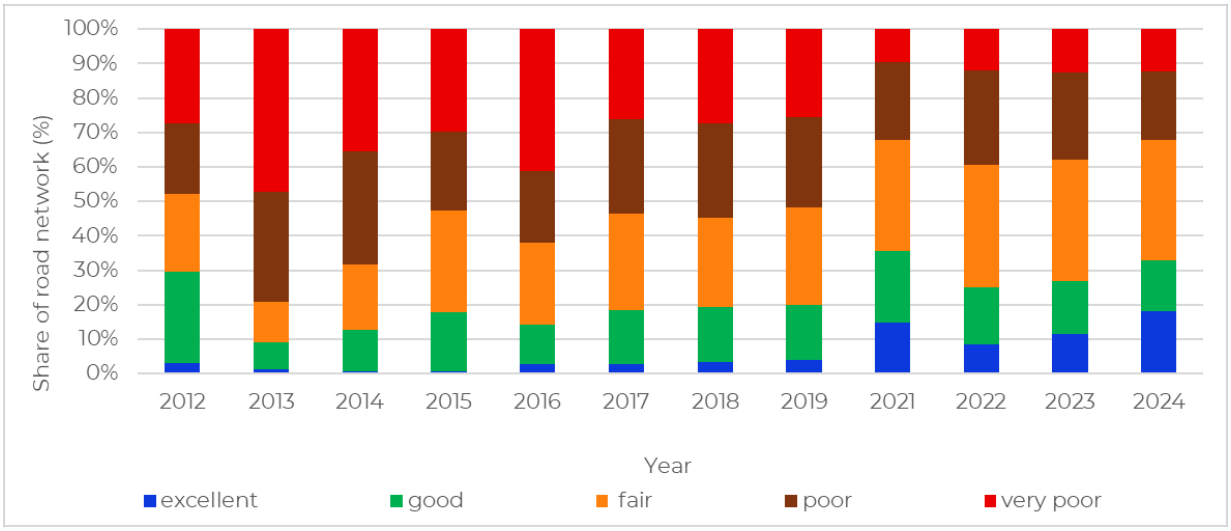


Figure 6 – Road geometry condition classification in Ceará road network, 2012–2024 (adapted from CNT 2024)

4.3 Evolution of Overall Road Condition

Figure 7 presents the evolution of the overall road condition in Ceará between 2012 and 2024. Since it integrates the three assessed components (pavement, signage, and geometry), the overall condition tends to predominantly reflect the behavior of the component with the greatest weight in the global assessment, which, as will be demonstrated, is pavement. A reduction in the proportion of roads classified as excellent is observed throughout the period, accompanied by a growth of intermediate and lower categories, a pattern analogous to that identified in Figure 4 for the pavement component.

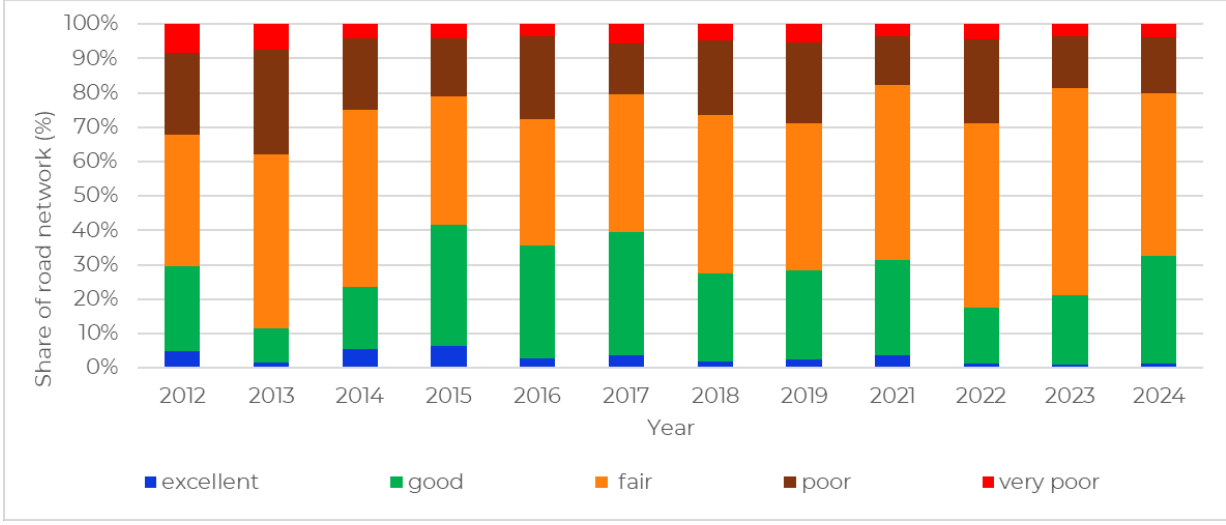


Figure 7 – Overall road condition classification in Ceará road network, 2012–2024 (adapted from CNT 2024)

The similarity between the evolution patterns of overall road condition and pavement reinforces the hypothesis that asphalt surface condition exerts a dominant influence on the global road assessment, representing the most sensitive component to external factors acting during the analyzed period. This observation will be corroborated by the correlation coefficients presented in the following subsection.

4.4Correlation Analysis

Table 1 presents the Pearson correlation coefficients calculated between mean annual precipitation and the condition classes of each component assessed by the CNT Road Survey. Values marked with an asterisk indicate statistically significant correlations ($|r| > 0.576$, $\alpha = 0.05$, two-tailed, $n = 12$).

Table 1 – Pearson correlation coefficients between annual precipitation and CNT condition classes (n = 12, significance level 5%)

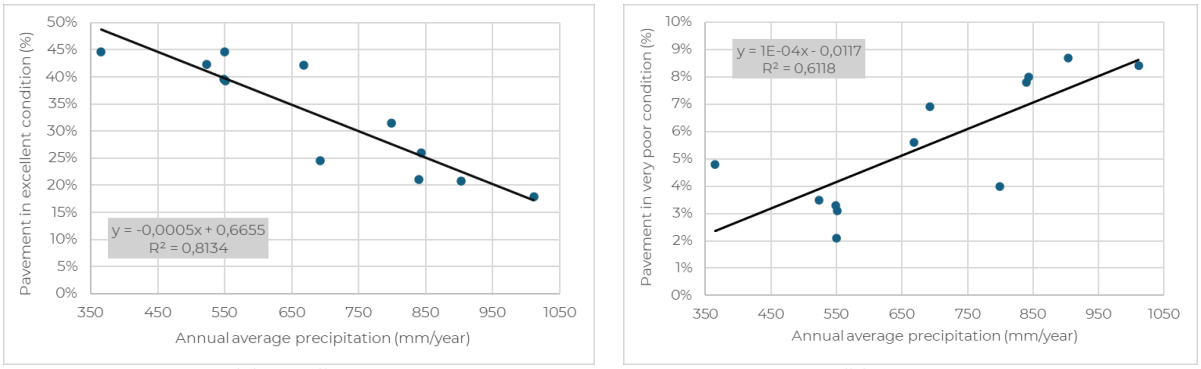
Component	Excellent	Good	Fair	Poor	Very Poor
Pavement	−0.90*	+0.73*	+0.02	+0.76*	+0.78*
Signage	−0.52	+0.34	+0.57	−0.41	-0.50
Geometry	+0.60*	−0.14	+0.69*	+0.06	-0.67*
Overall Condition	−0.71*	−0.11	+0.54	−0.22	-0.47

(*) Statistically significant correlation ($|r| > 0.576$).

Overall, the results indicate that the pavement component is the most sensitive to rainfall variability, followed by overall road condition (which predominantly reflects pavement behavior), while signage and geometry exhibit lower sensitivity to precipitation fluctuations.

The pavement component yielded the most pronounced correlations with annual precipitation. The negative correlation of $r = -0.90$ for the excellent class indicates that, in years of higher precipitation, there is a reduction in the proportional extent of roads in excellent condition, the coefficient with the highest magnitude in the entire analysis. Conversely, the poor and very poor classes presented significant positive correlations ($r = +0.76$ and $r = +0.78$, respectively), indicating a progressive migration of road segments across

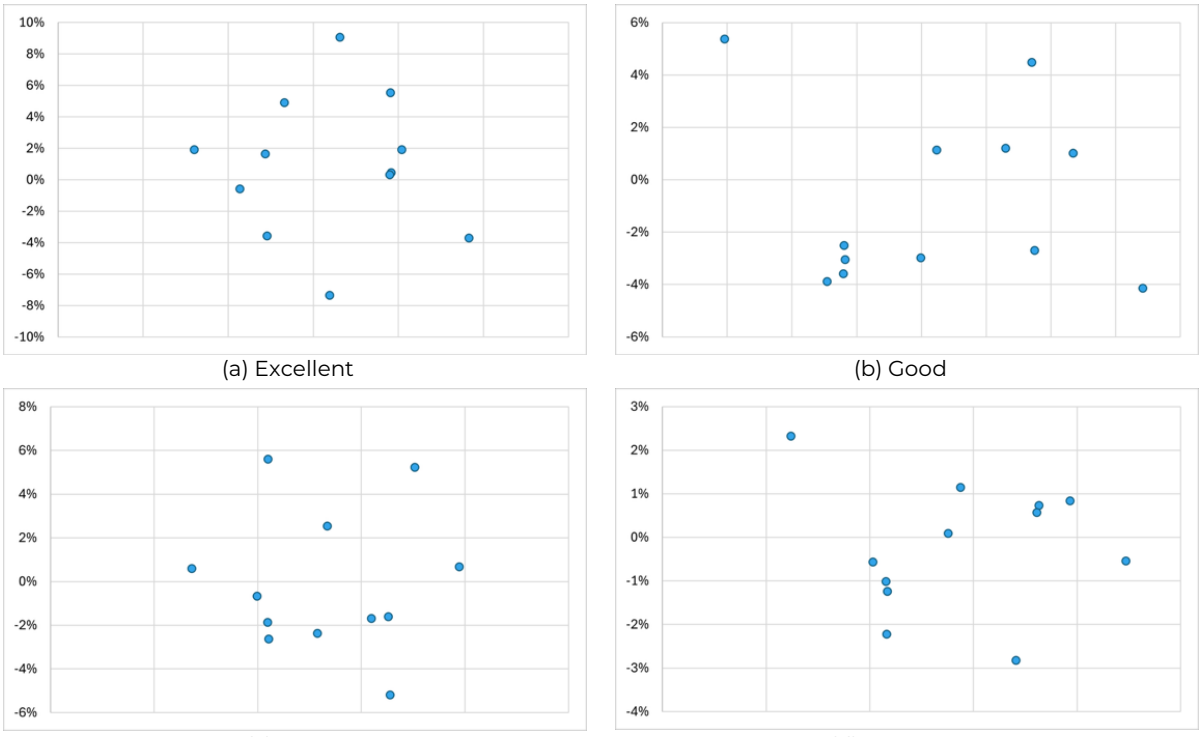
performance categories over time. Figure 8 illustrates this opposite trend between the excellent and very poor classes as a function of rainfall variation, with $R^2 = 0.8134$ and $R^2 = 0.6118$, respectively.



(a) Excellent (b) Very Poor

Figure 8 – Scatter plots of excellent and very poor pavement condition classes versus annual precipitation

The correlation of r = +0.73 for the good class suggests that, as pavements previously classified as excellent degrade, a portion migrates to the good category before reaching the lower classes, a pattern of progressive deterioration consistent with the mechanisms described by Bernucci et al. (2022). An analogous result was reported by Llopis-Castelló et al. (2020) for urban roads, where the Pavement Condition Index (PCI) exhibited a negative correlation with accumulated precipitation. The statistical validity of these correlations is further supported by the residual plots (Figure 9), which display approximately random distributions around zero for the excellent, good, poor, and very poor classes, indicating the absence of systematic patterns that would violate the assumptions of the linear correlation model.



(a) Excellent (b) Good

(c) Poor (d) Very Poor

Figure 9 – Residual plots of pavement condition classes versus annual precipitation, Ceará, 2012–2024

From a management perspective, these results underscore the importance of preventive interventions on road segments still classified as good, to prevent their migration to poor conditions, which require more costly and complex rehabilitation measures. This finding is consistent with the recommendations of Qiao et al. (2020), who emphasize the need to incorporate climate projections into the design and management models of flexible pavements.

The signage component exhibited predominantly moderate and statistically non-significant correlations with annual precipitation, with the highest coefficient being r = +0.57 for the fair class, a value at the threshold of statistical significance. This behavior is explained by two complementary factors: i) the CNT Road Survey is conducted in the second half of the year (the dry season in Ceará), which minimizes the direct effect of rainfall on the observed conditions; and ii) signage degradation is more closely associated with physical wear from traffic and periodic maintenance policies than with climatic variables. The residual plots confirm the inadequacy of linear correlation for most signage classes, reinforcing the limited sensitivity of this component to precipitation.

In turn, the geometry component displayed a distinct behavior, with significant correlations in the fair (r = +0.69) and excellent (r = +0.60) classes, and a significant negative correlation for the very poor class (r = −0.67). This apparently contradictory pattern is explained by the structural nature of road geometry: alignment, carriageway width, curves, and grades are defined at the design stage and tend to remain stable throughout the pavement life cycle, exhibiting low sensitivity to annual climatic fluctuations. The correlations observed in the fair and excellent classes may reflect indirect precipitation impacts, such as shoulder erosion and drainage failures that occasionally affect geometric assessment. The residual analysis for geometry revealed a lack of homoscedasticity across most classes, indicating that linear correlation is not the most appropriate statistical method for this component, a result that reinforces the structural nature of road geometry and its lower responsiveness to climatic factors.

Finally, the overall road condition component displayed a pattern analogous to that of pavement, with a negative correlation of r = −0.71 for the excellent class, the only statistically significant result for this component. This finding confirms the dominant contribution of pavement to the overall condition index and indicates that higher precipitation is associated with a gradual decline in the overall quality of Ceará's roads. The moderate positive correlation of r = +0.54 for the fair class, although not statistically significant, suggests a migration of segments from higher conditions to intermediate levels in wetter years, a behavior consistent with the pavement degradation dynamics described by Qiao et al. (2020).

Taken together, the results demonstrate that precipitation does not act in isolation on road infrastructure but exerts a measurable and statistically verifiable influence on pavement functional performance and, consequently, on the overall condition of roads. These findings provide technical grounds for the incorporation of climatic variables into maintenance and rehabilitation prioritization models for Ceará's road network — an approach that aligns with the IPCC (2023) recommendations for adapting transport infrastructure to climate change.

5. Conclusions

This study has demonstrated that rainfall variability exerts a measurable influence on the functional performance of the road network in the state of Ceará, with impact concentrated in the pavement component and, consequently, in the overall road condition. It was established that the precipitation regime acts as an accelerating factor in functional deterioration, promoting a shift in network conditions toward poor and very poor categories over time. This finding reinforces the importance of incorporating climatic variables into pavement management and maintenance prioritization models, particularly in semiarid regions subject to high interannual precipitation variability.

The lower sensitivity of signage and geometry to precipitation, in turn, suggests that these components are governed by factors of a different nature, such as maintenance policies, structural interventions, and design

adjustments. This distinction may have direct implications for resource allocation in road conservation programs: while pavement maintenance demands climate-sensitive planning, signage and geometry require maintenance cycles independent of the precipitation regime. From a management standpoint, the results reinforce the relevance of preventive interventions on segments still classified as good, anticipating deterioration before the network migrates to conditions requiring higher-cost and more complex interventions.

The integration of the assessed datasets proved feasible and informative for diagnosing road infrastructure conditions, constituting a replicable approach for other Brazilian states. Nevertheless, the absence of information on maintenance history, traffic volume, pavement structural data, and precise collection dates by road segment limits the explanatory power of the adopted model, precluding the isolation of precipitation as an independent causal variable. These limitations do not invalidate the results but rather indicate directions for advancing knowledge in the field.

Acknowledgments

This study was financed in part by the Coordenação de Aperfeiçoamento de Pessoal de Nível Superior – Brasil (CAPES) – Finance Code 001.

References

Bernucci, Liedi Bariani, Laura Maria Goretti da Motta, Jorge Augusto Pereira Ceratti, and Jorge Barbosa Soares. 2022. *Pavimentação asfáltica: Formação básica para engenheiros*. 2nd ed. Rio de Janeiro: PETROBRAS/ABEDA.

Caro, Silvia, Eyad Masad, Amit Bhasin, and Dallas N. Little. 2008. "Moisture Susceptibility of Asphalt Mixtures, Part 1: Mechanisms." *International Journal of Pavement Engineering* 9 (2): 81–98. https://doi.org/10.1080/10298430701792128.

Confederação Nacional do Transporte (CNT). 2024. *Pesquisa CNT de Rodovias 2024*. Brasília: CNT.

Da Silva, Djane Fonseca, Maria José da Silva Lima, Pedro Fernandes de Souza Neto, Heliofábio Barros Gomes, Fabrício Daniel dos Santos Silva, Henrique Ravi Rocha de Carvalho Almeida, Rafaela Lisboa Costa, and Marcos Paulo Santos Pereira. 2020. "Caracterização de eventos extremos e de suas causas climáticas com base no Índice Padronizado de Precipitação para o Leste do Nordeste." *Revista Brasileira de Geografia Física* 13 (2): 449–64. https://doi.org/10.26848/rbgf.v13.2.p449-464.

Fundação Cearense de Meteorologia e Recursos Hídricos (FUNCEME). 2025. *Dados de precipitação média anual do estado do Ceará*. Fortaleza: FUNCEME. http://www.funceme.br.

Intergovernmental Panel on Climate Change (IPCC). 2023. *Climate Change 2023: Synthesis Report. Contribution of Working Groups I, II and III to the Sixth Assessment Report of the Intergovernmental Panel on Climate Change*. Geneva: IPCC.

Llopis-Castelló, David, Tatiana García-Segura, Laura Montalbán-Domingo, Amalia Sanz-Benlloch, and Eugenio Pellicer. 2020. "Influence of Pavement Structure, Traffic, and Weather on Urban Flexible Pavement Deterioration." *Sustainability* 12 (22): 9717. https://doi.org/10.3390/su12229717.

Nazzal, Munir D., Lana Abu Qtaish, Ahmad Al-Hosainat, Sk Abu Talha, Savas Kaya, and Ala R. Abbas. 2021. "Evaluation of Moisture Damage in Asphalt Mixtures at Macro- and Nanoscales." *Journal of Materials in Civil Engineering* 33 (12). https://doi.org/10.1061/(ASCE)MT.1943-5533.0003993.

Neter, John, Michael H. Kutner, Christopher J. Nachtsheim, and William Wasserman. 1996. *Applied Linear Statistical Models*. 4th ed. New York: McGraw-Hill/Irwin.

Qiao, Yaning, Andrew R. Dawson, Tony Parry, Gerardo W. Flintsch, and Wenshun Wang. 2020. “Flexible Pavements and Climate Change: A Comprehensive Review and Implications.” *Sustainability* 12 (3): 1057. https://doi.org/10.3390/su12031057.

Stoner, Anne M. K., Jo Sias Daniel, Jennifer M. Jacobs, Katharine Hayhoe, and Ian Scott-Fleming. 2019. “Quantifying the Impact of Climate Change on Flexible Pavement Performance and Lifetime in the United States.” *Transportation Research Record* 2673 (1): 110–22. https://doi.org/10.1177/0361198118821877.

cinpar2026
XXII International Conference on Building Pathology and Constructions Repair
15th to 17th July 2026 - Lisboa, Portugal

Impact of Structural Pathologies on Property Market Value

Jhennifer Beatriz Bezerra de Souza[1], **João da Costa Pantoja[2]**

[1] Universidade Paulista, Distrito Federal, Brasil, contato@jhennifersouza.com
[2] Universidade de Brasília, Distrito Federal, Brasil, joaocpantoja@gmail.com

Abstract: Building conservation is a determining factor for safety and real estate appreciation; however, the current appraisal methodology in Brazil relies excessively on qualitative classifications and the subjective perception of the appraiser. To fill this gap, this article investigates the influence of structural pathologies on market value and proposes replacing the subjective classification of the state of conservation with a quantifiable index. The proposed methodology integrates the Dutch standard NEN 2767, which qualifies anomalies based on their importance, intensity, and extent, along with adaptations from other researchers, creating a Degradation Index. This technical index is then incorporated into the economic calculation of global depreciation. A demonstrative analysis using a database from a local neighborhood highlighted the limitations of the current system and confirmed the positive elasticity between perceived quality and estimated value. It is concluded that the technical parameterization of the state of conservation establishes a direct and rigorous relationship between physical degradation and property performance, allowing the market value to reflect the actual depreciation caused by pathologies and ensuring greater precision and replicability for expert reports.

Keywords: Structural pathologies; Real estate appraisal; Building condition; Property value appreciation.

1. Introduction

Building conservation is a determining factor for the longevity, safety, and appreciation of real estate assets. ABNT NBR 5674 establishes that building maintenance must be continuous, preventing premature disposability and ensuring adequate conditions of use. ABNT NBR 15575 complements this approach by defining performance requirements throughout the design service life.

However, in Brazil, building maintenance does not always receive due priority, which results in accelerated degradation and the occurrence of structural pathologies, compromising both market value and safety. Data reported by Andrade (2023) indicate that, between January 2014 and July 2023, 540 structural incidents occurred, with approximately BRL 1.75 billion spent on reconstruction works.

During my training as a real estate appraisal expert, I identified an important gap in the databases used to classify the state of conservation: the absence of detailed and standardized criteria. This shortcoming compromises the accuracy of appraisals and may lead to significant distortions in the values assigned to properties. The methodology currently used in the Statistical System of Appraisal Data (SISDEA), based on NBR 14653, uses generic qualitative classifications that depend excessively on the appraiser's subjective perception. This superficiality compromises the accuracy and replicability of reports, generating significant distortions in the values assigned to properties.

This article proposes the combined adoption of the Dutch Standard NEN 2767 and the parameters proposed by Martinatti (2021) and Oliveira (2023) as references for classifying the state of conservation. This approach aims to overcome the current subjectivity by introducing the quantification of degradation through measurable technical parameters. NEN 2767 is an internationally recognized building inspection methodology that allows pathologies to be qualified and quantified based on three fundamental parameters: importance (degree of relevance of the anomaly to performance and safety), intensity (magnitude or severity of the damage), and extent (scope of the affected area).

The dissertation by Martinatti (2021) and the doctoral thesis by Oliveira (2023) advance in this direction by adapting the rigor of NEN 2767 to the Brazilian context and proposing a parameterization of the degradation condition that generates a standardized numerical value. This classification matrix creates a Degradation Index (DI), which establishes a direct and precise relationship between physical degradation and property performance/value. By replacing subjective classification with a quantifiable index, this research offers an original contribution to the Brazilian real estate market. The practical application of this methodology, combined with the Ross-PP (KG) Method for calculating global depreciation, will allow market value to technically reflect the actual depreciation caused by pathologies.

As a methodological contribution, this article proposes transforming the “state of conservation” variable, traditionally treated qualitatively in real estate appraisal databases, into a quantitative variable obtained through a systematized technical inspection. To this end, the assessment by building systems and subsystems is adopted, taking as reference the structure proposed by Silva (2022), who organizes the inspection into systems such as roofing, fire protection and emergency systems, electrical installations, sealing/envelope systems, hydraulic-sanitary installations, and structural systems. In addition, the external environment variable is added, considering that common areas, accesses, facades, sidewalks, and surroundings also influence the perception of conservation, functionality, and market value. Thus, the state of conservation is no longer a general grade assigned subjectively by the appraiser and becomes the result of the technical composition of the conditions observed in each building system.

2. Literature Review

Structural pathologies include manifestations such as cracks, infiltrations, reinforcement corrosion, differential settlements, and construction defects, which affect the integrity, performance, and safety of buildings beyond purely aesthetic problems. They are caused by design failures, execution failures, inappropriate use, or the action of environmental agents.

For an objective analysis of pathologies, several methodologies have been developed to standardize the assessment of building degradation. These methodologies seek to quantify and qualify damage, providing essential data for maintenance and rehabilitation planning.

NEN 2767 offers a systematic approach to determining and recording the condition of building components and systems. The “Condition Assessment” process is an indirect method that quantifies anomalies and contributes to degradation analysis. The standard covers levels ranging from the real estate portfolio to subcomponents, including the assessment of elements, building systems, and defect identification.

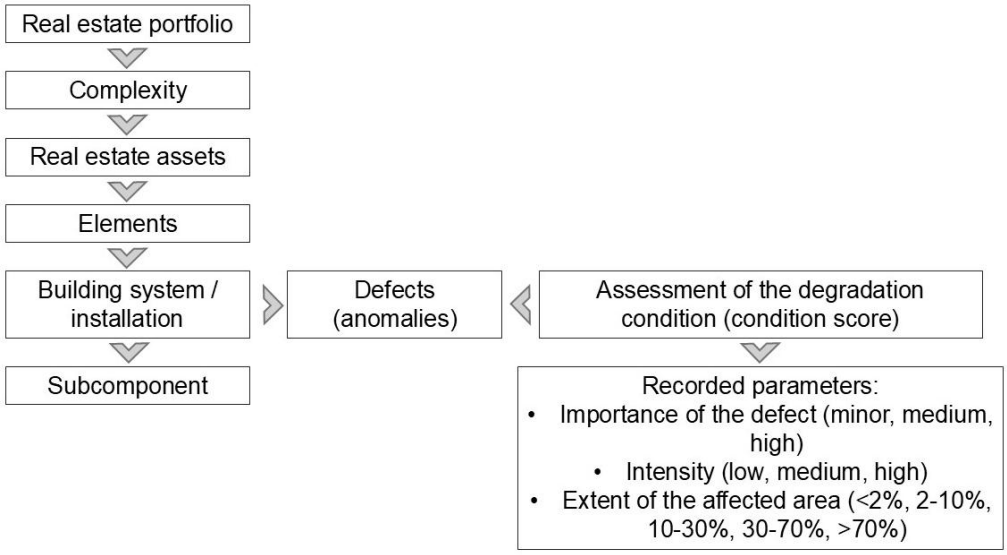
This score is obtained through a detailed inspection during which the anomalies present in each building element are identified, with three fundamental parameters being observed:

- Importance: degree of relevance of the anomaly to the performance and safety of the element;
- Intensity: magnitude or severity of the observed damage;
- Extent: scope of the area affected by the pathology.

Silva (2022) contributes to the operationalization of this assessment by proposing the analysis of the state of conservation by building systems and subsystems, allowing the overall condition of the building to be obtained from the composition of the partial conditions identified in the field. In his dissertation, the author adapts national and international building inspection methodologies, such as NBR 16747, IBAPE, GUT, NEN 2767, MAEC, and GADH, with the objective of calculating the state of conservation of the components and of the building as a whole. This approach is relevant to real estate appraisal because it allows a general and subjective classification to be replaced by a technical reading structured by systems, such as roofing, electrical installations, sealing systems, floors, walls and ceilings, hydraulic-sanitary installations, and structural systems.

The scope of NEN 2767 is hierarchically structured, as represented in Figure 1, starting with the real estate portfolio and progressing to more specific levels: real estate assets, elements, building systems or installations, subcomponents, and, finally, the defects themselves. This model provides a broad and overall view of the construction process, making it possible to assess the performance of a single subcomponent as well as the general condition of the development.

Figure 1 – Simplified flow of the application of NEN 2767 for condition assessment. Source: adapted from NEN 2767:2017 and Martinatti (2021).



Martinatti's dissertation (2021) represents an important adaptation of NEN 2767 to the Brazilian context, proposing the parameterization of the degradation condition based on the combination of these three parameters.

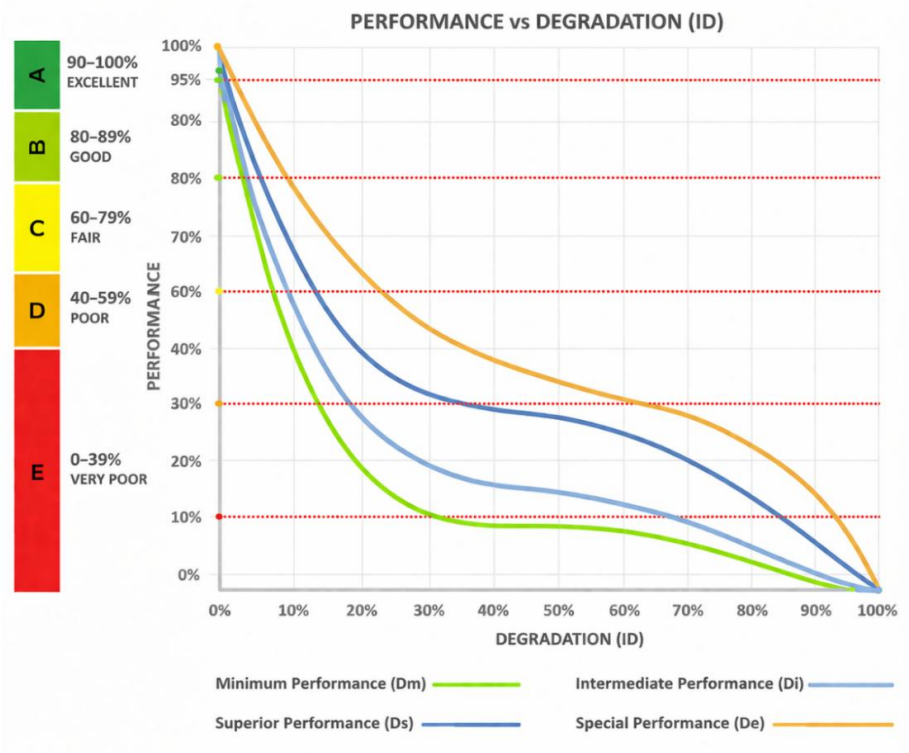
Table 1 – Classification of the parameterized condition. Source: Oliveira (2023) after Martinatti (2021).

Defect	Intensity	Extent				
		<2%	2% - 10%	10% - 30%	30% - 70%	>=70%
Minor	Low	0,17	0,17	0,17	0,17	0,33
	Medium	0,17	0,17	0,17	0,33	0,5
	High	0,17	0,17	0,33	0,5	0,67
Severe	Low	0,17	0,17	0,17	0,33	0,5
	Medium	0,17	0,17	0,33	0,5	0,67
	High	0,17	0,33	0,5	0,67	0,83
Critical	Low	0,17	0,17	0,33	0,5	0,67
	Medium	0,17	0,33	0,5	0,67	0,83
	High	0,33	0,5	0,67	0,83	1

Table 1 presents the classification matrix, in which each intersection between variables generates a standardized numerical value, making it possible to quantify the level of degradation of components and building systems.

This approach reduces subjectivity and enables consistent results among different appraisers. In addition, the method establishes a direct relationship between the degradation index and the overall performance of the property, as shown in Graph 1. In this graph, the lower the degradation index, the higher the performance, and vice versa. The curves are segmented into color ranges (A, B, C, D, and E), which indicate building certification levels by associating physical performance with the classification of the state of conservation.

Graph 1 – Performance x Degradation Index. Source: Oliveira (2023).



Thus, the proposal by Martinatti and Oliveira creates a link between technical assessment and market appraisal, allowing the analysis of the state of conservation to be incorporated more precisely into real estate pricing processes.

Quantifying the impact of pathologies on market value requires a depreciation model that goes beyond simple subjective classification and linear methods. Traditionally, the market uses models such as the Ross-Heidecke Table, but these may be limited when incorporating the complexity of degradation.

In this context, the project adopts the Method for Global Depreciation via the Ross-PP (KG) Method, as detailed by Oliveira (2023). This method presents an improved approach to calculating the physical depreciation of a development, defining the Global Depreciation Factor as a key element in the appraisal.

The KG factor is influenced by the state of conservation of the property. By integrating the Degradation Index (DI), the Ross-PP (KG) model allows depreciation to be calculated objectively and technically, overcoming the limitations of the appraiser's subjective judgment. The detailed formulation of this method will be used in the economic validation stage of the methodology proposed in this study.

3. Methodology

This research adopts as its starting point the methodology currently used for real estate appraisal through the Statistical System of Appraisal Data – SISDEA. This approach will be described in its current configuration and, subsequently, the proposed change will be presented, based on the methodologies and parameters of NEN 2767, Martinatti's dissertation (2021), and Oliveira's doctoral thesis (2023).

3.1 Current Method

For illustrative purposes, a database of apartments located in the Noroeste neighborhood of Brasília is presented, collected from several real estate agencies and brokers. It is important to note that these data are not part of the definitive research sample, being used only to demonstrate how SISDEA works and to show how the system currently deals with the “state of conservation” variable.
Each record contains information such as address, total value, private area, number of bathrooms, view of Burle Marx Park, state of conservation, and number of parking spaces (Table 2).

Table 2 – Database. Source: personal archive

DATABASE

Data Type: Apartamento Noroeste
Objective: Sale Value
City: Brasília
Last Update: 10/07/2024
Prepared by: Jhennifer Souza

ITEM	COLLECTION DATE	CITY	ADDRESS	NEIGHBORHOOD	TOTAL VALUE	PRIVATE AREA	BATHROOMS	VIEW OF PARQUE BURLE MAX	CONDITION	PARKING SPACES
1	10/07/2024	Brasília	SQNW 307, Bloco H	Noroeste	R$ 1.280.000,00	120,00	2	0	3	1
2	10/07/2024	Brasília	SQNW 107, Bloco F	Noroeste	R$ 1.415.000,00	74,00	2	1	4	2
3	10/07/2024	Brasília	SQNW 303, Bloco H	Noroeste	R$ 1.322.930,00	77,00	3	0	5	1
4	10/07/2024	Brasília	SQNW 310, Bloco E	Noroeste	R$ 1.030.000,00	75,00	3	0	4	1
5	10/07/2024	Brasília	SQNW 103, Bloco D	Noroeste	R$ 1.350.000,00	86,00	2	0	5	2
6	10/07/2024	Brasília	SQNW 309, Bloco O	Noroeste	R$ 1.790.000,00	105,00	3	0	4	1
7	10/07/2024	Brasília	SQNW 108, Bloco G	Noroeste	R$ 1.150.000,00	96,00	2	0	3	2
8	10/07/2024	Brasília	SQNW 304, Bloco D	Noroeste	R$ 2.156.474,00	113,00	4	0	4	2
9	10/07/2024	Brasília	SQNW 107, Bloco B	Noroeste	R$ 1.300.000,00	84,00	3	0	4	2
10	10/04/2024	Brasília	SQNW 307, Bloco I	Noroeste	R$ 1.167.000,00	80,00	2	0	5	2
11	10/04/2024	Brasília	CLNW 04/05, Bloco B	Noroeste	R$ 1.023.598,00	75,00	2	0	5	1
12	10/07/2024	Brasília	SQNW 307, Bloco H	Noroeste	R$ 1.120.000,00	84,00	3	0	4	1
13	10/07/2024	Brasília	SQNW 103, Bloco D	Noroeste	R$ 1.736.380,00	86,00	3	1	5	2
14	10/07/2024	Brasília	SQNW 307, Bloco J	Noroeste	R$ 1.189.180,00	84,00	2	0	4	2
15	10/07/2024	Brasília	SQNW 302, Bloco D	Noroeste	R$ 1.150.000,00	89,00	2	0	5	2
16	10/07/2024	Brasília	SQNW 309, Bloco I	Noroeste	R$ 1.500.000,00	103,00	3	0	3	1
17	10/07/2024	Brasília	SQNW 311, Bloco B	Noroeste	R$ 1.180.000,00	86,00	3	0	4	1
18	10/07/2024	Brasília	SQNW 109, Bloco F	Noroeste	R$ 1.300.000,00	83,00	3	0	4	1
19	10/07/2024	Brasília	SQNW 306, Bloco D	Noroeste	R$ 1.240.000,00	83,00	3	0	4	1
20	10/07/2024	Brasília	SQNW 306, Bloco C	Noroeste	R$ 1.170.000,00	64,00	2	0	5	2
21	10/07/2024	Brasília	SQNW 103, Bloco D	Noroeste	R$ 2.271.000,00	168,00	3	1	5	2
22	10/07/2024	Brasília	SQNW 310, Bloco F	Noroeste	R$ 1.970.000,00	172,00	2	0	4	2
23	10/07/2024	Brasília	SQNW 108, Bloco I	Noroeste	R$ 1.060.000,00	75,00	2	0	4	2
24	10/07/2024	Brasília	SQNW 106, Bloco J	Noroeste	R$ 878.315,00	52,00	2	0	5	2
25	10/07/2024	Brasília	SQNW 302, Bloco O	Noroeste	R$ 2.100.000,00	144,00	2	0	4	3
26	10/07/2024	Brasília	SQNW 109, Bloco J	Noroeste	R$ 1.699.000,00	109,00	3	0	5	2
27	10/07/2024	Brasília	SQNW 108, Bloco A	Noroeste	R$ 1.890.000,00	127,00	4	0	4	2
28	10/07/2024	Brasília	SQNW 309, Bloco H	Noroeste	R$ 1.789.000,00	127,00	4	0	3	2
29	10/07/2024	Brasília	SQNW 110	Noroeste	R$ 1.441.090,00	84,00	3	0	4	1
30	10/07/2024	Brasília	SQNW 302, Bloco I	Noroeste	R$ 1.880.000,00	118,00	4	0	5	2

The state of conservation follows the classification provided by NBR 14653, which establishes qualitative concepts assigned to SISDEA numerical codes (Table 3).

Table 3 – State of conservation classification chart. Source: didactic material from the Real Estate Appraisal Expert Course, ConstruMove, 2024.

	CONCEPT	BUILDING	UNIT
6	Under construction or off-plan	Paradigm property / Not yet delivered.	Paradigm property / Not yet delivered.
5	Good (New appearance)	Recently delivered property, with a new appearance.	Recently delivered property, with a new appearance.
4	Good (Used appearance)	Property that does not need repairs, but has a used appearance.	Property that does not need repairs, but has a used appearance.
3	Fair (Minor repairs)	Need for minor repairs, painting, and cleaning.	Need for minor repairs, painting, and cleaning.
2	Fair (Major repairs)	Need for recovery on the facades, watertightness problems; infiltrations, need to redo installations (gas, electrical, fire, plumbing, etc.), need for structural recovery, cumulative or not, within the scope of the common areas.	Need for recovery on the facades, watertightness problems; infiltrations, need to redo installations (gas, electrical, fire, plumbing, etc.), need for structural recovery, cumulative or not, within the scope of the private areas.
1	Poor	Compromised stability and solidity, impaired habitability and/or healthiness, with a high cost of recovery.	Compromised stability and solidity, impaired habitability and/or healthiness, with a high cost of recovery.

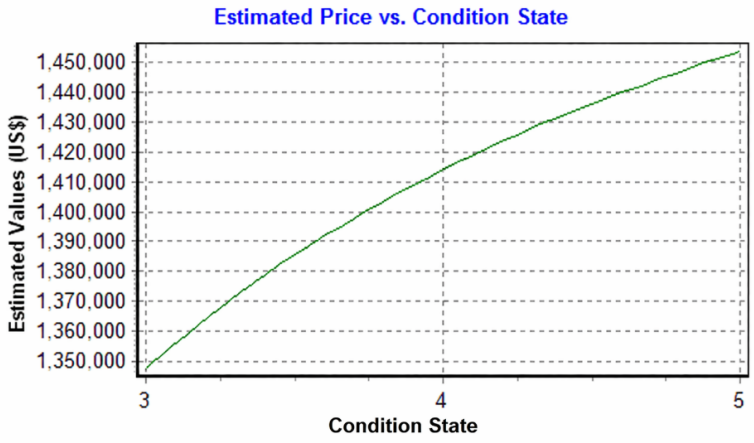
In the system, the “state of conservation” variable is numerically coded for application in statistical models (Table 4), ranging from 1 (Poor) to 6 (Under construction or off-plan).

Table 4 – Description of the variables used in the SISDEA system based on the author's personal database. Source: elaborated by the SISDEA system (2024) based on the author's personal database.

Name	Type	Type	Classification	Variable Description	Enabled
City	Text	Text	Text	Complement to the property address	Yes
Address	Text	Text	Text	Full property address	Yes
Neighborhood	Text	Text	Text	Neighborhood where the property is located	Yes
Informant	Text	Text	Text	Name or identification of the informant	Yes
Informant Phone	Text	Text	Text	Informant's phone or contact number	Yes
Private Area	Numeric	Numeric	Quantitative	Private area of the unit measured in m²	Yes
Bathrooms	Numeric	Numeric	Dichotomous	Bathrooms in service area, Social, and suites	Yes
View of Parque Burle Max	Numeric	Numeric	Dichotomous	View of the park (Has = 1, Does not have = 0)	Yes
Condition	Numeric	Numeric	Qualitative (Assigned Codes)	Property condition (scale based on assigned codes listed as: 1 –Poor 2-Major Repairs 3–Minor Repairs 4–Signs of Use 5–Like New 6–Under Construction)	Yes
Parking Spaces	Numeric	Numeric	Quantitative	Total number of parking spaces including covered, uncovered, and enclosed	Yes
Total Value	Numeric	Numeric	Dependent	Total property value	Yes

The influence of this variable on market value is evidenced in Graph 2, which presents the elasticity of the function at the midpoint of the state of conservation, indicating a positive correlation between perceived quality and estimated value.

Graph 2 – Elasticity of the function at the midpoint. Source: elaborated by the SISDEA system (2024) based on the author's personal database.



3.2 Limitations of the Current Method

Although consolidated and widely used, the current method has a subjective character in the classification of the state of conservation, since the assessment is based mainly on the appraiser's perception and on generic qualitative descriptions. This approach, although fundamental, may result in a superficial analysis, failing to accurately capture the severity and extent of building pathologies.

The example of using the database prepared with properties from the Noroeste neighborhood highlights this limitation, reinforcing the need for more objective criteria.

4. Proposed Improved Methodology

The reformulation of the state of conservation variable in real estate appraisal is proposed by integrating objective technical criteria to improve the Statistical System of Appraisal Data (SISDEA) and the application of NBR 14653. The methodology replaces subjective classification with a quantifiable index, maintaining the numerical compatibility required by SISDEA while increasing the accuracy of the final report.

The inspection proposed in this article will be structured by building systems, adopting as reference the organization presented by Silva (2022), with adaptations to the context of urban real estate appraisal. Initially, the following analysis groups will be considered: roofing; electrical installations; sealing systems, floors, walls and ceilings; hydraulic-sanitary installations; structural systems; and external environment. The fire protection and emergency system may be incorporated when the property typology, the use of the building, or the inspection scope requires such assessment.

Table 5 – Preliminary structure of the inspection form by Building systems for parameterizing the state of conservation. Source: prepared by the author, based on Silva (2022).

System assessed	Examples of components	Urgency level	Parameterization	
			Component condition	System condition
Roofing	Roof covering, structure, gutters, flashings, waterproofing	Classification as priority 1, 2, or 3	Partial component index	Partial system index
Electrical installations	Panels, circuits, finishes, lightning protection system, grounding	Classification as priority 1, 2, or 3	Partial component index	Partial system index
Sealing/envelope systems	Facades, internal walls, frames, ceilings, floors	Classification as priority 1, 2, or 3	Partial component index	Partial system index
Hydraulic-sanitary installations	Reservoirs, water supply, sewage, inspection boxes	Classification as priority 1, 2, or 3	Partial component index	Partial system index
Structural system	Columns, beams, slabs, joints, collapse risk	Classification as priority 1, 2, or 3	Partial component index	Partial system index
External environment	Accesses, sidewalks, common areas, immediate surroundings	Classification as priority 1, 2, or 3	Partial component index	Partial system index

This adaptation is consolidated into four interdependent stages: structuring the inspection form by systems, quantifying degradation, objectively classifying conservation, and incorporating the technical index into the calculation of depreciation and final value. The first stage adopts as reference the organization by building systems and subsystems proposed by Silva (2022), while the subsequent stages use NEN 2767, the works of Martinatti (2021) and Oliveira (2023), and the Ross-PP (KG) Method as their basis.

4.1 Structure of the System-Based Inspection Form

Table 5 presents the preliminary structure of the inspection form proposed for quantifying the “state of conservation” variable. The organization is based on an individual assessment of building systems and their respective components, associating each inspected item with an urgency level and a parameterization of the observed condition. Thus, the condition of the property becomes composed of partial indices, initially calculated by component and subsequently consolidated by system.

For each inspected component, the occurrence of the anomaly, its location, intensity, extent, and degree of impact on performance, safety, functionality, and the perception of property value must be recorded. At the end of the inspection, the partial results of each system will be consolidated to compose the technical conservation index, which may be used as an objective variable in the real estate appraisal process.

4.2 Quantification of Degradation

This stage eliminates the subjectivity of building inspection, providing an exact numerical datum for the state of conservation.

4.2.1 Basis: Application of the Dutch Standard NEN 2767, which proposes a systematic approach to building inspection by quantifying and qualifying anomalies based on technical parameters.

4.2.2 Adaptation: Use of the adaptation by Martinatti (2021), which structures a parameterized condition that relates the intensity and extent of anomalies to different degrees of defects (minor, serious, critical), enabling the attribution of a Numerical Degradation Index (DI).

4.3 Objective Classification of Conservation

The numerical value (DI) is translated into a qualitative classification compatible with the market vocabulary and NBR 14653.

4.3.1 Basis: Consolidation of the Degradation Index (DI) into performance ranges (A-E) by Oliveira (2023), relating degradation percentages to the residual performance of the element or system.

4.3.2 Adjustment: This conversion allows the research to replace subjective descriptions (good, regular, and poor) with measurable technical parameters, without compromising the calculation structure required by SISDEA.

4.4 Depreciation and Final Value

The technical index obtained is inserted into the economic calculation, quantifying its impact on the property value in accordance with the global depreciation calculation.

4.4.1 Calculation Tool: The Method for Global Depreciation via Ross-PP (KG) (Oliveira, 2023) will be employed as an improved approach to calculating the physical depreciation of a development.

4.4.2 Integration: The Degradation Index (DI) from stage 1 will be used as an objective input variable to determine the Global Depreciation Factor (KG) of the Ross-PP Method.

4.4.3 Result: The application of this method will result in a market value that accurately and technically reflects the actual depreciation caused by pathologies, providing support for the economic validation of the methodology.

The new classification structure, to be applied in the next stage of the research, will maintain the numerical compatibility required by SISDEA. The database presented, referring to the Noroeste neighborhood, is used only to exemplify the structure and demonstrate the limitation of the current analysis. The case studies and

practical assessment of this research will be carried out in properties located in another Administrative Region of the Federal District, Brazil.

5. Conclusion

This study presented a proposal to reformulate the state of conservation variable used in the Statistical System of Appraisal Data (SISDEA), seeking to overcome the limitations of the currently employed method, which is predominantly based on subjective descriptions.

The analysis showed that, although the current classification is practical and quick to apply, its qualitative and insufficiently parameterized nature restricts the accuracy of appraisals and makes it difficult to compare properties, especially in contexts of partial or heterogeneous degradation.

The incorporation of consolidated methodologies, such as NEN 2767, the adaptation developed by Martinatti (2021), and the classification by ranges proposed by Oliveira (2023), makes it possible to integrate measurable parameters—intensity, extent, and importance of anomalies—into the field analysis. This approach enables not only a more faithful measurement of the physical condition of the property, but also better integration with statistical appraisal models, as demonstrated by the relationship between state of conservation and estimated value.

The database used in this stage, referring to apartments in the Noroeste neighborhood, served as an example to present how the current method works and to demonstrate its limitations. The proposed methodology will be applied to properties located in other administrative regions, allowing its practical applicability and gain in accuracy to be verified.

It is expected that the adoption of objective technical criteria, combined with the systematic recording of building conditions, will contribute to fairer, more transparent, and more replicable appraisals, in addition to strengthening the reliability of the reports issued.

References

ABNT – Brazilian Association of Technical Standards. NBR 14653-4:2002: Appraisal of assets – Part 4: Developments. Rio de Janeiro, 2002.

ABNT – Brazilian Association of Technical Standards. NBR 14653-1:2019: Appraisal of assets – Part 1: General procedures. Rio de Janeiro, 2019.

OLIVEIRA, IBERÊ PINHEIRO. Certification and appraisal of developments: An approach based on degradation and performance. Doctoral thesis in Architecture and Urbanism – University of Brasília, Federal District, 2023.

SILVA, D. S. T. Management and conservation of Brasília's heritage: a comparative study between Brazilian and international inspection methodologies. Master's dissertation in Architecture and Urbanism, Graduate Program in Architecture and Urbanism, Faculty of Architecture and Urbanism – University of Brasília, Federal District, 2022.

MARTINATTI, D. Development of a multicriteria decision-making model for conservation of the superblocks of the Plano Piloto in Brasília/DF. Master's dissertation in Architecture and Urbanism – University of Brasília, Federal District, 2021.

NEN 2767. Conditiemeting van bouw- en installatiedelen – Deel 1: Methodiek (Condition Assessment of Building and Installation Components – Part 1: Methodology). NEN. Delft. 2006.

NEN 2767. Conditiemeting van bouw- en installatiedelen – Deel 2: Gebrekenlijsten (Condition Assessment of Building and Installation Components – Part 2: List of Faults). NEN. Delft. 2008.

NEN 2767. Conditiemeting van bouw- en installatiedelen – Deel 3: Conditieaggregatie (Condition Assessment of Building and Installation Components – Part 3: Aggregation of Condition Scores). NEN. Delft. 2009.

CONSTRUMOVE. Classification framework for the state of conservation of properties. Course booklet for Real Estate Appraisal Experts. Brasília, 2024.

Personal report. Database and description of variables extracted from the Statistical System of Appraisal Data – SISDEA. Brasília, 2024.

PELLI SISTEMAS. SISDEA – Software para avaliação de imóveis urbanos e rurais. Pelli Sistemas Engenharia. Accessed in 2026.

Cinpar 2026
XXII International Conference on Building Pathology and Constructions Repair
15th to 17th July 2026 - Lisboa, Portugal

Failure mechanisms of the partial collapse of the South Road Axis (*Eixo Rodoviário Sul*) in Brasilia

Yuri BESSA CESARINO[1], José MELO[1], Humberto VARUM [1], Carlos Henrique Linhares Feijão[2]

[1] Construct, Faculty of Engineering, University of Porto, Portugal, up202212113@fe.up.pt, josemelo@fe.up.pt, hvarum@fe.up.pt
[2]NOVACAP Companhia Urbanizadora da Nova Capital do Brasil, Brazil, chlfeijao@gmail.com

Abstract: On February 6th, 2018, part of the South Road Axis viaduct (*Eixo Rodoviário Sul*, known as "*Eixão Sul*") collapsed in Brasilia, Brazil. Although no deaths occurred, the partial failure imposed high costs on the city and its residents, alarming authorities about the safety and maintenance of other essential viaducts and bridges (built during the same construction period as *Eixão*) across the capital. The *Eixão* repair was carried out following detailed investigation and mechanical characterization. However, the type of failure – a sudden shear failure – has not been adequately addressed, even though many other important viaducts have been built with the same structural characteristics as the South Road Axis in the city. This paper presents the full details of the partial collapse of the Eixão, identifying the main components and mechanical sources that led to the brittle failure, particularly regarding the behavior of prestressed concrete members subjected to high shear and cyclic demands. The repair and retrofitting techniques implemented after the disaster are described, and this work concludes with an examination of how this case study can be applied in a broader context to the rehabilitation of similar structures in Brazil's capital.

Keywords: Concrete structures, bridges, maintenance, retrofit, shear failure.

1. Introduction

1.1 Brasilia Historical Context

Brasilia is the capital of Brazil and the 3rd-largest city in the country, with around 3 million people in the city center and about 5 million in the metropolitan area. The city is marketed by its unique set of robust, reinforced and prestressed concrete curved monuments that combine brutalist architectural identity with modernist philosophy. This city is located within the Federal District (DF), serving as the country's administrative center of power, and was designed by the urban planner Lúcio Costa and the famous architects Oscar Niemeyer and Roberto Burle Marx in 1957. Important structural engineers, such as Joaquim Cardoso and Bruno Contarini (among others), made possible many structural challenges imposed by the city concept. Brasilia stands out for its iconic urban plan, a 20th-century modernist city emphasizing functionality, rationality, zoning, open spaces, and a futuristic vision of progress.

The city is considered young (about 66 years old) and was built as part of an ambitious national development program launched in 1956 by the Juscelino Kubitschek administration. The main goal of this program was to rapidly industrialize and modernize Brazil, shifting the capital from the coast to the heart of the country – a known protection strategy dating back to the late 18th century. Construction began in 1956, and the city was inaugurated in 1960, built in an astonishing 41 months with the aid of a massive national labor force, which eventually contributed to the city's social diversity. Initially, the city was planned to support 500,000 people, but it grew 6 times its population in 60 years. The first engineering public company of the city, *Nova Companhia Urbanizadora da Nova Capital* (NOVACAP), was created during this period to participate in the construction of the new Federal District.

The city master plan (today called *Plano Piloto*) designed the city into a plane-like shape, with two main arterial roads (that cross each other at the heart of the city) – the Monumental Axis (*Eixo Monumental via N1*) and the Road Axis (*Eixo Rodoviário DF 002*) – in combination with a hierarchical multi-lane system. This system of roads is integrated with smaller streets, connected by strategic curved access ramps, underpasses and overpasses (called "*tesourinhas*" – cloverleaf ramps) and roundabouts, which effectively increase mobility within the city center, granting (almost) congestion-free automobile circulation. In addition to the absence of traffic lights and the smart function-zoning idea, these decisions promote the 15-minute city concept, which gave the city many elements that helped it earn UNESCO World Heritage status in 1987 as a unique expression of modernist urban principles.

1.2 Rapid Growth of Vehicles and Impact on Viaducts in Brasilia after the Incident

Due to the city's urban planning, which includes large spaces, zoning, and wide roads, the possession of self-owned vehicles is a common demand among city residents. Data from the 2020 Department of Roads and Highways DER/DF (2021) reports an average of 120,000 vehicles per day crossing the capital via the main arterial roads (Monumental Axis and Road Axis), which can be tracked instantaneously using the feature tool available on the DER/DF web page.

Recent public reports from the Department of Roads and Highways state that the city reached over 2 million vehicles in 2024, far exceeding its initial intended design. Some records indicated that the car expectancy was about 1 vehicle per family, which would mean about 125,000 planned vehicles in the 60s (which grew about 16 times according to today's demand).

Lastly, according to NOVACAP, over 96 viaducts were to be retrofitted after the 2018 incident (with investments over USD $ 1.42 million), and 40 strategic viaducts also received investments (over USD $ 30 million) for maintenance, with resources allocated to building 4 extra bridge highways, according to the Brasilia Agency (2019) . In other words, city planning naturally created high demand for car use, which was not expected to reach that many vehicles daily. After the 2018 incident, NOVACAP has inspected more than 360 special structures, the DER/DF inspected over 679 special structures and over 111 of those received immediate requirements, maintenance and strengthening.

1.3 Significance of the Partial Collapse

The sudden partial collapse of the Road Axis Viaduct occurred on February 6th, 2018, around 11:45 am, on a Tuesday, blocking the main road to the city center. It took significant investment and workforce over approximately 2 years to solve the problem. This failure is one of the major examples of bridge highway collapse, due to its complexity and impact. After the structural failure, teams from the public company NOVACAP/DER, in partnership with the Brasilia University Structural team and Engineering Companies, began an in-depth investigation of the collapse by mechanical characterization of debris. This followed a necessary emergency protocol involving structural stabilization, the interruption of traffic, and a traffic detour from the viaduct. Since many other viaducts were built similarly during the city's inauguration and expansion, this investigation marked the beginning of a large maintenance protocol that has been underway ever since, including the creation of a multisectoral committee responsible for managing and monitoring the maintenance of public infrastructural assets in the Federal District.

This proposed work focuses on the forensic analysis of the failure, exploring specific aspects of the shear theory of failure to explain the disaster. This work is an attempt to better understand older structures and hidden structural features that may be part of similar structures built during the same period in the city's capital.

2. South Road Axis Viaduct Engineering Characteristics

The South Road Axis Viaduct (located in the *Galeria dos Estados*) was inaugurated in 1960 and was 58 years old when the incident happened. The viaduct is a critical component of the main road system of the DF 002 highway axis, providing vital access to the central bus station and various commercial, banking, and hospital sectors through the South Wing (*Asa Sul*) of the plan-shape capital.

Its structure was composed of 7 massive delta-shape reinforced concrete column-walls (with cantilevered extensions of 7.4 m prestressed crossbeams) that supported 8 prestressed hollow core slabs (road deck), and two abutments at the viaduct's free ends. The total structure length was about 194 meters, the width about 27 meters, and the distance from the columns about 22 meters. Slabs were about 1 meter-deep with 80 cm-diameter hollow cores, and about 29 ribs, 15 cm thick, spaced 95 cm per slab, with 3 prestressed transversal beams (one at each end and one intermediate). The plan view of the whole viaduct can be seen in Figure 1, while the deck details can be seen in Figure 2.

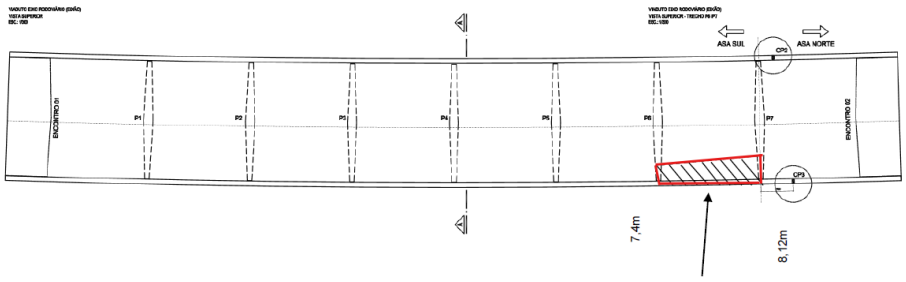
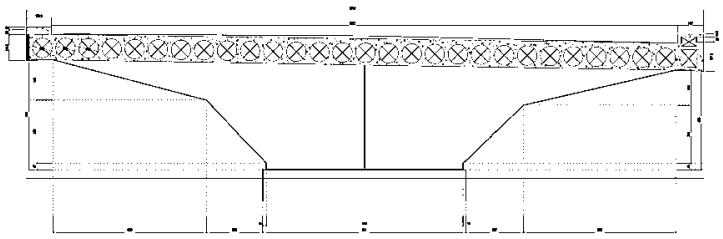
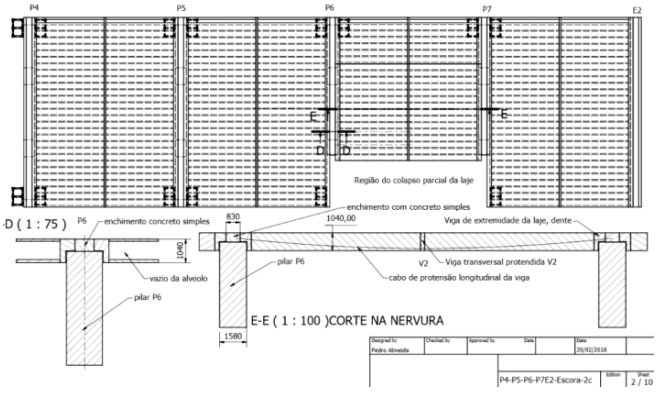


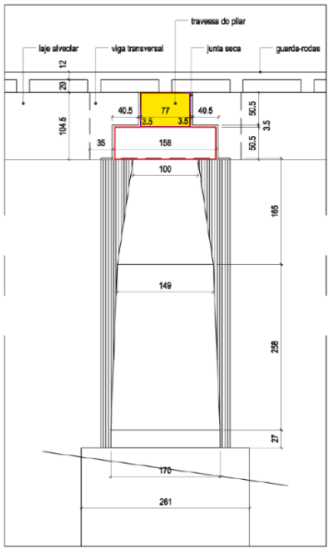
Figure 1 –Plan view of the Road Axis Viaduct in *Galeria dos Estados*, highlighting plan of failure (NOVACAP, Relatório Técnico, 2018).



(a) Delta-wing Column-Wall with hollow deck (section view).



(b) Deck plan view with section cuts.



(c) Delta wing column wall detail highlighting the top crossbeam.

Figure 2 –Structural drawings from the Road Axis Viaduct at *Galeria dos Estados* (NOVACAP, Relatório Técnico, 2018).

Delta wing-shaped column walls were expressively large, 150 to 170 cm thick (varying) section by 27 meters wide (total wingspan) – Figure 2 (a). The top crossbeam of the pillar had an inverted T shape format with 16 prestress cables (containing 12 wires of 5mm, 1500 Mpa in strength – within the red area in Figure 2-c), which was used as support (as a Gerber teeth) for the slabs by bearing pads – Figure 2 (b) and (c). These supporting crossbeams had transverse smooth reinforcements 16 mm in diameter, spaced 8 cm on center. No other longitudinal rebars were used in this section but the prestressing steel.

An important detail of the T inverted shape crossbeam, however, was that it was originally a rectangular section (red rectangle in Figure 2) with a top free space (designed as a center joint on top of the pillars, where there was an 80 cm free space between the faces of the slab and crossbeams for construction purposes used for hydraulic jacking of tendons) that was subsequently filled with plain concrete, forming a 54 cm x 83 cm prismatic bar (highlighted in yellow in Figure 2-c). This element was unreinforced and served to physically isolate the reinforcing from the pavement road in an attempt to prevent water infiltration.

Lastly, the main structural drawings were absent since the city's inauguration in the 60s; however, NOVACAP developed as-built structural drawings (only geometrical properties) in 2013 for information collection, which helped the forensic crew assess debris in 2018. Some older signs of cracking and water infiltration were noted within the bridge main deck and column walls during this period, but reported as "not alarming".

3. South Road Axis Forensics Investigation

3.1 Response Measurements

After the initial partial collapse, the large concrete deck (approximately 7 to 7.8 meters wide) was partially dismantled for investigation. No injuries were reported, and the transportation and fire departments isolated the area and blocked the Road Axis viaduct, creating detours to maintain traffic flow during the emergency protocol. This was only possible because Brasilia's plan was based on large spaces, which wouldn't have been possible if the accident had happened in densely populated areas like the centers of São Paulo or Rio de Janeiro.

Shortly after, engineering teams from NOVACAP and other federal agencies arrived for initial damage assessment. Fire department experts, backed by structural civil engineers from these institutions, recommended emergency structural shoring of the remaining viaduct in locations beneath the delta-shaped column wall extensions, and continuous monitoring of the viaduct (by installing instrumentation to monitor displacements and daily thermal variations to ensure structural stability).

Once the structure was secure and the area was isolated, the Local Government authorized immediate funds for assessment and interventions to ensure the structure's safety and to resolve the problem. Some private engineering companies, aligned with NOVACAP and the structural engineering team from the University of Brasilia, began the forensic investigation of the partial collapse the day after the incident.

3.2 Chronology of Failure

The event is categorized as a "fragile partial collapse" since it occurred suddenly and without prior visible warning signs (excessive deformations or crack development) detectable by visual inspection. Also, there was a restaurant underneath the viaduct, with large kitchen equipment and wall finishes that hid the column-walls. The visual obstruction of parts of the viaduct and the lack of warning signs prevented local authorities from detecting and implementing measures that could have prevented the failure.

The failure started at column wall 7 (P7, the furthest column on the east side of the viaduct), as indicated by shear failure, as shown by the smooth, diagonally shaped section plan in Figure 3(b). All column walls were severely deficient at this time (an endemic problem). Once this element failed, the right portion of the road deck fell, pulling the other support provided by column-wall P6. Since prestressing cables from the hollow core slabs were adhered to the prismatic (plain concrete) element over the prestressed crossbeam on top

of the column walls, the falling of a large section of the deck generated significant kinetic energy, which was partially absorbed by the crossbeam. This immense unbalanced lateral force, in addition to the column wall degradation, exhausted the remaining load-bearing capacity of the cantilever prestressed extension, which fractured in pullout and shear, resulting in concrete spalling (creating a destroyed, unsmoothed surface, seen in Figure 3-a). The last components in trying to self-equilibrate the absence of supporting conditions were the transversal prestressed beams within the deck hollow slab, which also failed under shear, creating a smooth plan of failure (Figure 3-a).



(a) Deck collapse indicating column-wall P6 and transversal beams fractures.

(b) Column-wall P7 fracture.

Figure 3 –Visual inspection of structure fractures right after collapse (NOVACAP, Relatório Técnico, 2018).

3.3 Debris Investigation

The space underneath column-walls P5, P6, and P7 housed an improvised restaurant with utilities and refrigeration equipment fixed directly to the viaduct's pillars and slabs. After the partial collapse and removal of the infill walls, the forensics team was able to assess the structure from different angles. Also, several elements from the failed deck were dismantled by employing jackhammers for visual inspections and reinforcing steel investigation. Drilling core samples and cut steel bar samples were extracted for testing at the University of Brasilia (UnB) structural engineering lab.

During the dismantling of the prestressed crossbeams and prestressed hollow slabs, engineers observed many aspects of the concrete structure: many prestressing wires within cables presented signs of corrosion; some prestressing cables lacked cementitious mortar protection around the steel wires; there were little (if any) non-prestressed steel rebars in the crossbeam over the column-wall, and transversal beams from the slabs; little (if any) transversal reinforcements were observed within the massive cross-section of the wing-shape extensions (cantilevers) from the columns; transversal reinforcements were only noted within the (red rectangular) part of the cross beams (16 mm-diameters, spaced 8 cm on centers); the use of rounded river gravel instead of regular crushed aggregates (like granite or limestone) was detected within the concrete composition; transversal and longitudinal rebars were made of smooth reinforcements; center joint (over the crossbeam, isolating deck cables) as unreinforced and it presented signs of chronic water infiltration, and; the smooth plan section from the diagonal-like crack of the column-wall P7 presented signs of worn out due to cyclic degradation and chronic water infiltrate (descendant from cables). These structural deficiencies (characteristics) from the viaduct concrete elements are indicated in Figure 4 from (a) to (d).

Historical records from Joaquim Cardozo specification notes (from NOVACAP archives) stated that the general concrete strengths employed at the time of construction was between 15 and 18 MPa, with even higher values of 25 MPa for special constructions, like the Alvorada Palace, Planalto Palace, National Congress, and the Cathedral of Brasilia (due to their singularly shaped columns and slender slab systems). For the Road Axis Viaduct at the Galeria dos Estados, concrete specimens were extracted from columns P6 and P7, and their nominal strengths were about 30 MPa after crushing tests conducted at the University of

Brasilia (UnB, 2018). It is believed that the original concrete compressive strength was about 20 MPa or higher at the time, which is similar to the construction period. A similar protocol was used to assess prestressing wires, which had tension strengths of 1500 MPa, typical for the use of high-strength steel in prestressing cables at the time, given the use of normal relaxation wires.



(a) Lack of Cementitious mortar within the cable and use of rounded river gravel aggregates in concrete



(b) Use of smooth rebars



(c) Lack of longitudinal non-prestressed rebars and evidence of water infiltration from the top center joint.



(d) Smooth section cut ("clean" shear) and no transverse reinforcement.

Figure 4 –Debris investigation after the partial collapse (NOVACAP, Relatório Técnico, 2018).

3.4 Standard Recommendations in 1960.

Construction of the viaduct of Galeria dos Estados took place between 1956 and 1960. At this time, the national codes in Brazil for the design of prestressed bridges were absent (only in 1989 did the Brazilian authorities publish the first standard for these structural systems: NBR 7197 - Design of Structures made with Prestress Concrete – ABNT, 1987). Before that, however, engineers would design structures according to NB2 (1941 and 1961 versions — Design and Construction of Concrete Bridges – ABNT, 1960) and NB1 (1940 and 1960 versions — Design of Concrete Structures – ABNT, 1960), which did not address the use of prestressing. Chronologically stating, civil engineers at the time of the viaduct's construction had to follow other international structural design guidelines for designing special structures.

Late records from design guidelines from DNER/DNIT, however, explicitly recommended the use of German Standards in the design of special structures (like bridges) by employing the DIN 1045:1952 "*Beton - und Stahlbetonbau – Bemessung und Ausführung*" (Design and Construction of Concrete and Reinforced

Concrete Structures), DIN 4227:1953 "*Spannbeton – Richtlinien für Bemessung und Ausführung*" (Design of Prestressed Concrete Structures) and DIN 1072:1950 "*Straßen- und Wegbrücken – Lastannahmen*" (Loads on road and pedestrian bridges) and equivalents. Many of these codes at the time were based on admissible stress principles of design, and they served as fundamental guidelines for the development of international recognized codes in the European context (such as the CEB/fib series after the 70s, for example).

Regarding the available Brazilian specifications at the time (NB1 and NB2), shear design was based on principal stresses and checked for the use of required transverse reinforcements, limiting maximum spacing but not the minimum amount of transverse reinforcements. On the other hand, longitudinal reinforcements were determined for tension reinforcing steel using either Rupture Methods (equivalent to USL) or Allowable Stress Method, which could be made of bars or wires (but no mentions are made about minimum non-prestressing steel in avoiding progressive collapse) with minimum amounts of tensions reinforcements varying from 0.15% to 0.2% based on the steel strength type. In addition, these early Brazilian codes had no comments on size effects, cyclic depreciation, nor progressive collapse at the time of the construction of the viaduct, leaving engineers with little technical guidance, in a time when testing is labs was scarce.

4. Failure Anatomy

4.1 Reinforced Concrete Shear Theory

Concrete shear strength of linear prismatic RC elements is essentially sustained by the shear mechanisms of concrete and steel, namely: the concrete intrinsic self-shear strength, aggregate interlocking, dowel action (from longitudinal reinforcing bars), and the transversal strength of stirrups. These mechanisms vary their share on the load-carrying capacity according to the strain state to which the concrete element is subjected. For instance, when shear cracks (characterized by inclined, curved shapes, originating from bending moments and shear forces) start to open, the friction interfaces from concrete interlocking tend to slide and separate as crack width increases, diminishing their contribution. On the other hand, if prestresses are present, the shearing interfaces tend to be squeezed together, increasing their effective shear resistance. If tension is applied or cyclic loading is experienced, the aggregate interlocking tends to wear, decreasing its internal friction resistance.

For regular RC sections, if shear deformations continue to rise, the shear from interlocking action is absorbed by dowel action (through longitudinal steel bars deformation), concrete self-shear strength, and stirrup action. If shear loads continue to increase, the element fails when the transverse reinforcement strains reach their yield limits, and most mechanisms, then, fail simultaneously. Notably, the dowel action, stirrup strength, and concrete shear strength are related to the quantity (in terms of steel area) and quality (concrete and steel strength) of the reinforced concrete specimen. Also, the dowel action is not only a source of shear strength but also a redundant component when failure is reached, since it prevents progressive collapse once elements reach their ultimate capacity by preventing sections from falling as they hang by these bars after concrete fracture (a structural redundancy principle).

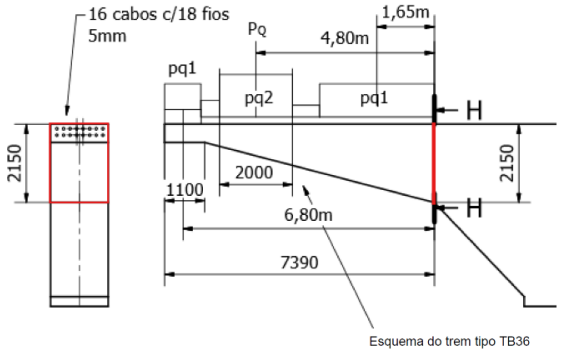
Moreover, the shear strength mechanisms' participation can be affected by cyclic loading, which inherently degrades their mechanical properties (reducing material resistance and increasing microcrack development in concrete and cumulative damage in steel crystals).

However, the behavior of linear prismatic RC elements when subjected to high shear forces is notably different in the absence of transversal reinforcements. The failure mode is predominantly related to the capability of the dowel action to remain elastic. After yielding, the strain deformations are entirely absorbed by the concrete self-shear strength, which can trigger brittle failure. Besides, when linear RC elements lack transverse reinforcement, size effects tend to magnify stress within the section, greatly reducing their apparent strength. This phenomenon does not occur in RC sections with transverse reinforcement (Wight and MacGregor, 2012).

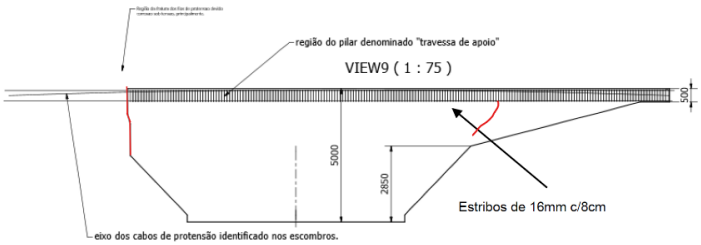
In other words, large concrete sections without transverse reinforcement and few longitudinal rebars are critical to shear loads, as they can produce brittle failure, reduced apparent shear capacity, and little structural redundancy. Even more, cyclic loading in combination with prestress losses can be catastrophic for RC elements.

4.2 Viaduct Failure Explained

The partial collapse was triggered by corrosion under tension of the active (prestressed) reinforcement in the supporting crossbeams at the top of the pillars. This degradation was hidden from sight by the design of the “Gerber” teeth and simple concrete fillings, which obstructed direct visual inspection of the critical support elements. Also, this degradation was aggravated by chronic water infiltration (and cyclic loading) from the road deck cracks and a lack of structural maintenance over the viaduct’s 58-year lifespan. The subsequent collapse was enabled by the lack of passive reinforcement bars (both longitudinal and transverse) and absence of structural redundancy, since steel rebars could have prevented progressive collapse through dowel action. These hidden design flaws were original design vulnerabilities not known to the city authorities, especially given the absence of original drawings, the age of the structure, and outdated code requirements at the time. After the forensic investigation, the observed failure section and reinforcement steel detailing (used in the column-wall extended cross beam) were identified and portrayed in Figure 5.



(a) Column-wall cantilever extension (prestressed crossbeam) indicating its enormous section (without the presence of transversal shear reinforcements).



(b) As-built of the column-wall after collapse, indicating the failed sections in red and the other severely compromised side, with only transversal reinforcements in the crossbeam where prestresses were (absence non-prestressing rebars).

Figure 5 –Structural drawings from the Road Axis Viaduct at Galeria dos Estados indicating the failure sections (2,15 x 1,55 m) and reinforcing steels within the column-wall crossbeam (NOVACAP, Relatório Técnico, 2018).

Lastly, the viaduct collapse was a culmination of long-term systematic flaws, which are emphasized in 5 main points:

1. Notorious lack of structural safety redundancy by the absence of longitudinal reinforcing (non-prestressed) steel within the critical top section of the column-wall (which could have provided dowel action and prevented progressive collapse) and lack of transversal reinforcements in the plan section of the column wing extension (which magnified the size effects in reducing shear resistances);
2. The depreciation of mechanical properties in prestressed reinforcing steel cables due to the development of stress-corrosion (owing to the penetration of moisture through deck cracks, and the deficient cementitious protection within cables) reduced the effective counter-balancing forces

acting at the cantilever section of the delta-wing crossbeam extension, while also reducing the shear resisting mechanisms;

3. Construction and Project obstructions that obscured engineering judgment: presence of architectural features (such as infill walls and drainage gutters from the restaurant), use of permanent concrete joint (preventing the access to the core of the floor system and prestresses), and lack of original structural design drawings, which hid essential signs of distress (opening of cracks and water infiltration) and project deficiencies;
4. Poor quality of materials (compared to today's requirements): use of steel reinforcements made of smooth bars, and poor concrete composition (made with rounded river gravel instead of regular crushed aggregates like granite or limestone). This practice could have substantially altered the performance of sections under high shear loads (by reducing bond strength and thus shear capacity), especially under heavy (unforeseen) vehicle traffic.
5. Large cyclic demands that extrapolated expected demands over time, which were difficult to predict by engineering tools and methods available at the time of construction.

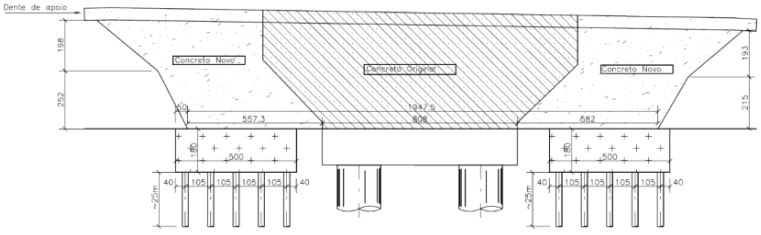
Although time effect decays (like steel relaxation and concrete creep) have not been mentioned, their contributions also impacted the materials performance over time. Their role in the whole failure, although to an extent, was not as significant as cyclic deterioration and shear deficiency.

5. Strengthening and Repairing

Following the emergency stabilization of the viaduct (with shoring and continuous monitoring), long-term structural recovery techniques, such as structural strengthening and repairs, were implemented, focusing on replacing failed components and enhancing the remaining structure to provide adequate performance.

For the column-wall delta-wing cantilever extensions (wings), the prestressed crossbeam was removed and reconstructed to meet current code requirements. The new crossbeams would feature sufficient prestressing and non-prestressing steel, as well as modern bearing pads, to support the road deck. Where the partial collapse occurred, the full deck segment was demolished and a new deck (with similar engineering characteristics, made of prestressed beams and hollow prestressed concrete slab) designed under elastic regime was built.

For the overall column-wall, a section enhancement concrete jacketing with prestressing ties was recommended (to increase its load-bearing capacity greatly). Also, beneath the old wings for columns, it was recommended to add a new section of concrete wall supported by massive foundation blocks over piles, as indicated in Figure 6 (a). Likewise, to create an adequate bond surface between the old and new concrete, reinforcing ties were uniformly distributed around the old column perimeters and attached to it using chemical adhesives.



(a) Column-wall cantilever extension (prestressed crossbeam) indicating its enormous section (without the presence of transversal shear reinforcements).



(a) Final view of the design project once completed.

Figure 6 –Structural drawings from the Road Axis Viaduct at Galeria dos Estados (NOVACAP, Relatório Técnico, 2018).

To prevent the chronic water infiltration that caused the original corrosion, the gap between slabs above the column walls at the crossbeam interface was recommended to be sealed with pre-molded concrete pieces, structural joints, or bolted steel plates, which would permit access for maintenance. This was a key repair requirement that enabled direct visual inspection of the bearing pads and support elements at a reasonable cost, a feature missing in the original 1960 design. The final goal of these combined techniques was to ensure a residual service life of at least 100 years for the recovered structure.

6. Lessons from the Rubble

The challenge of developing Brasilia in 4 years accelerated immensely its construction, putting engineers to the test in a period with limited resources, particularly from a standards perspective. Altogether, the early use of prestressing cable bridges, in addition to the reduced traffic predictability, made many important viaducts in Brasilia vulnerable to shear failures given their non-conforming construction methodologies, as this work indicated by the Road Axis Viaduct collapse forensics investigation. Accordingly, five main points were highlighted in this work regarding the brittle shear failure of the viaduct: absence of structural redundancy in RC details (not required by the codes from the period of construction); depreciation effect in materials over time (infiltration exposure and construction inadequacies); projected and construction obstacles that prevented effective maintenance and early flaw detection; poor quality of materials and methods available at the time of construction (concrete composition, use of smooth bars, absence of cement paste within many prestressing cables), and; unpredicted cyclic demands that extrapolated expected demands over time. Although catastrophic, this partial collapse reveals how older non-conforming heritage structures may be deficient under society's new demands, providing valuable insights and a singular reference for future (similar) engineering challenges within Brazil's capital.

Acknowledgments

This work was financially supported by: UID/04708/2025 and https://doi.org/10.54499/UID/04708/2025, of the CONSTRUCT - Instituto de I&D em Estruturas e Construções - funded by Fundação para a Ciência e a Tecnologia I.P./ MECI, through the national funds. This work was also financially supported by national funds through the FCT/MCTES (PIDDAC), under the project 2022.05721.PTDC with DOI 10.54499/2022.05721.PTDC (https://doi.org/10.54499/2022.05721.PTDC).

References

"Volume Diário De Tráfego - Trechos Rodoviários." Portal de Dados Abertos do Governo do Distrito Federal, 2021, accessed March, 2026, https://www.dados.df.gov.br/dataset/volume-diario-de-trafego-trechos-rodoviarios.

ABNT. *Nb-1/1960: Cálculo E Execução De Obras De Concreto Armado.* Rio de Janeiro: Associação Brasileira de Normar Técnicas, 1960.

———. *Nb-2/1960: Cargas Móveis Em Pontes Rodoviárias.* Rio de Janeiro: Associação Brasileira de Normas Técnicas, 1960.

———. *Nbr 7197: Projeto De Estruturas De Concreto Protendido - Procedimento.* Rio de Janeiro: Associação Brasileira de Normas Técnicas, 1987.

"Gdf Investe 160 Milhões Para Reformar 40 Viadutos E Construir Quatro Novos." Governo do Distrito Federal, 2019, accessed March, 2026, https://www.agenciabrasilia.df.gov.br/w/gdf-investe-r-160-milhoes-para-reformar-40-viadutos-e-construir-quatro.

NOVACAP. *Relatório Técnico - Grupo De Trabalho Conforme Decreto N. 38.841 De 06.02.2018.* Governo do Distrito Federal (Brasília: 2018).

UnB, Universidade de Brasilia. *Relatório Técnico – Dept. Enc/Unb 001. Brasília, 26.02.2018.* . UnB (Brasilia: 2018).

Wight, J. K., and J. G. MacGregor. *Reinforced Concrete Mechanics & Design.* 2012.

cinpar2026
XXII International Conference on Building Pathology and Constructions Repair
15th to 17th July 2026 - Lisboa, Portugal

Procedure for assessing the dynamic resistance of existing bridge structures located in seismically active mining areas

Janusz RUSEK[1], Leszek SŁOWIK[2], Henryk CIUREJ[3]

[1] AGH UST in Cracow, Faculty of Civil Engineering and Resource Management, Poland, rusek@agh.edu.pl
[2] ITB Building, Research InstituteDepartment of Building Structures, Geotechnics, and Concrete, Warsaw, Poland, l.slowik@itb.pl
[1] AGH UST in Cracow, Faculty of Civil Engineering and Resource Management, Poland, hciurej@agh.edu.pl

Abstract: This paper presents the results of computations intended to determine the dynamic resistance of an existing, non-standard Soil Steel Composite Bridge (SSCB) structure to the effects of paraseismic excitations induced by mining tremors. Within the developed method, the dynamic resistance of the structure is defined as the permissible component values of ground motion accelerations at its location. For this reason, it was necessary to conduct numerical dynamic analyses in accordance to the guidelines included in Eurocodes and local regulations concerning the design and erection of structures in mining areas. On this basis, a set of criteria was established that allowed for the determination of the permissible component values of ground accelerations. The range defined by these values, relative to an exceptional combination, can be interpreted as a safety reserve where the dynamic effects generated by a mining tremor can be accepted. It is important to emphasize that the identification of such a safety reserve is essential for existing structures that were designed without taking into account the dynamic effects generated by underground mining operations. Based on available data regarding the existing SSCB bridge structure, a 3D finite element model (FEM) was developed to determine reliable strength intensity measures under static and dynamic loads. Next, in accordance with the methodology used, and considering the design-stage load combinations and the exceptional load combination as separate cases, the allowable values of the component ground vibration accelerations were determined. While working on such an unusual structure, the following methods were adopted for dynamic loading: the response spectrum method for the vertical direction, and, for one of the horizontal directions, an approach based on the physical process of seismic wave propagation in the subsurface. The establishment of this particular research approach was based on the fact that the structure under analysis is sensitive to dynamic excitations, in which inertial effects manifest themselves only in the vertical direction. This approach cannot be applied in the horizontal plane because the inertia of the bridge itself is dominated by the covering layer of ground. Ultimately, the proposed approach made it possible to determine the load-bearing capacity reserve expressed in terms of the permissible values of ground acceleration components. In addition, the computational methods developed for specific directions of dynamic excitation provide guidance on how to proceed with the analysis of non-standard structures such as SSCB structures

.**Keywords:** soil steel composite bridges, bridge structure, structural dynamics, seismic, mining impacts, resistance.

Cinpar 2026
XXII International Conference on Building Pathology and Constructions Repair
15th to 17th July 2026 - Lisboa, Portugal

Thermal behavior of urban pavements under the influence of tree shading: implications for pavement performance and durability

Nayara de Oliveira GURJÃO [1], Lara Sucupira FURTADO [2], Jorge Barbosa SOARES [3]

[1] Federal University of Ceará, Brazil, nayara.gurjao@det.ufc.br
[2] Federal University of Ceará, Brazil, lfurtado@det.ufc.br
[3] Federal University of Ceará, Brazil, jsoares@det.ufc.br

Abstract: The thermal behavior of urban pavements plays a fundamental role in urban microclimate dynamics and in the operational conditions of road infrastructure, especially in cities located in hot climate regions. Different pavement surface courses, such as asphalt mixtures, Portland cement concrete, and alternative surface treatments, exhibit distinct thermal responses as a result of their physical, optical, and thermal properties, influencing solar radiation absorption and heat dissipation. In this context, tree shading emerges as an external factor capable of modifying the energy balance of paved surfaces, with direct effects on roadway surface temperatures. This paper presents a literature review on the thermal influence of tree shading on urban pavements, with emphasis on the thermal response of different pavement surface materials. Studies employing in situ measurements, remote sensing, and thermal modeling are analysed to assess surface temperature variations associated with pavement materials and the presence of trees along the roadway network. The review also presents how reductions in surface temperatures may be associated with pavement performance and durability, related to the emergence of distresses or the need for repairs, considering temperature-sensitive degradation mechanisms. In addition to theoretical advances, the review seeks to analyze the transformation of scientific knowledge into applicable tools, technologies, and computational strategies, such as performance indices and criteria. This knowledge can support decision-making by public administrators and urban planners, aiming to identify applications validated with real data and the transfer of methodologies to different urban scenarios. The available literature suggests the existence of gaps in the integrated analysis of pavement materials, shading conditions, and surface damage, indicating the need for interdisciplinary approaches focused on the climate adaptation of urban infrastructure.

Keywords: Urban pavements; Thermal behavior; Tree shading; Surface materials; Pavement performance.

1. Introduction

Urbanization, population growth, and climate change are reshaping cities worldwide and creating increasingly complex challenges. Transportation infrastructure, in particular, plays a significant role in this context due to its extensive spatial coverage, including the environmental impacts associated with soil sealing, increased surface temperatures, and the intensification of urban heat island (UHI) effects (Santamouris, 2013; Ranagalage, Estoque and Murayama, 2017; Furtado et al., 2025). These challenges are closely aligned with the United Nations Sustainable Development Goals (SDGs), proposed by the United Nations (UN, 2015), particularly SDG 11 (Sustainable Cities and Communities) and SDG 13 (Climate Action), which emphasize the need for resilient, sustainable, and climate-adaptive urban infrastructure.

Among urban infrastructures, pavements represent a substantial portion of the built environment, and their material properties directly influence the absorption, storage, and release of solar radiation, especially in hot tropical cities (Benrazavi et al., 2016; Qin et al., 2022). Parameters such as albedo, emissivity, conductivity, and thermal capacity govern these interactions, affecting surface temperatures, pedestrian thermal comfort, and pavement durability (Ding et al., 2022; Yang et al., 2025).

In addition to thermal effects, elevated pavement temperatures influence the mechanical behavior of asphalt materials. Although thermal effects on the behavior of asphalt materials is well established in the literature, they are not much explored for urban scenarios. High temperatures can accelerate binder oxidative aging, increasing susceptibility to distresses and structural deterioration (McPherson & Muchnick, 2005; Matlack, Khoury and Naik, 2022; Liu et al., 2025).

Urban vegetation has been widely recognized as an effective strategy for mitigating urban thermal impacts and reducing surface temperatures (Speak et al., 2020; Cheela et al., 2021). In Brazil, public policies such as the National Urban Tree Plan (PlaNAU) reinforce its role in mitigating urban heat islands, improving thermal comfort, and enhancing urban resilience (Brazil, 2023).

Through shading and evapotranspiration processes, urban trees reduce the amount of solar radiation reaching paved surfaces and contribute to the cooling of the surrounding microclimate. Consequently, vegetation may also influence the thermal dynamics of pavements and may potentially contribute to reducing material degradation and maintenance demands, although direct evidence regarding long-term pavement performance remains limited. (Underwood et al., 2017; Cheela et al., 2021; Qin et al., 2022).

The literature presents extensive analyses of the thermal properties of urban surface materials and the role of vegetation in microclimate regulation, using approaches such as field monitoring, remote sensing, and numerical modelling (Napoli et al., 2016; Feng et al., 2020; Ahmad, Najar and Ahmad, 2024). However, the interaction between tree shading and the thermal and functional behavior of urban surfaces remains underexplored. Therefore, this study analyses the influence of urban vegetation, particularly tree shading, on surface temperature and its implications for pavement performance through a systematic literature review.

2. Methodology

2.1 Search strategy

An initial search was conducted using specific keyword combinations to identify studies that directly addressed the relationship between vegetation, shading, and the thermal and functional performance of pavements. However, this strategy resulted in a very limited number of studies, with only two articles directly addressing the combined topic.

To overcome this limitation, the scope of the search was broadened by adopting more comprehensive keyword combinations related to urban pavements, vegetation, and thermal behavior. Searches were conducted in the Scopus and Web of Science databases, applying filters to include only articles, review articles, and early access publications between 2000 and 2026. This search resulted in 79 documents in Scopus and 909 documents in Web of Science, which constituted the initial dataset for the screening process (Table 1).

Table 1 – Search strings used in the systematic literature review

List of databases	Search string	Number of documents
Scopus	("pavement" OR "road pavement" OR "road surface" OR "street pavement" OR "sidewalk pavement" OR "urban pavement") AND ("tree shade" OR "tree canopy" OR "urban trees" OR "street trees" OR "urban vegetation") AND ("surface temperature" OR "pavement temperature" OR "land surface temperature" OR "urban heat island" OR "thermal behavior")	79
Web of Science	(pavement OR "road surface" OR asphalt OR concrete) AND (tree OR vegetation OR shade OR shading) AND ("surface temperature" OR thermal OR heat OR "urban heat island")	909

Search strategies were adapted to each database to balance precision and recall, using a more restrictive string in Scopus and a broader approach in Web of Science to ensure sensitivity. Additional relevant studies were identified through reference tracking and prior research by the authors when contributing to the methodological or conceptual discussion.

2.2 Inclusion and exclusion criteria

To ensure the relevance of the selected studies, inclusion and exclusion criteria were established. Studies were included when they:

- addressed urban pavements, road surfaces, or sidewalks. Studies related to land use or urban surfaces that included pavements as part of the analysis were also considered;
- analyzed thermal behavior, surface temperature, or urban heat island effects associated with pavements or urban surfaces;
- investigated vegetation, shading, or environmental factors that influence pavement temperature;
- explored the relationship between vegetation or shading and the thermal and/or functional performance of pavements.

Studies were excluded when they:

- focused exclusively on structural or mechanical pavement performance, without any relation to surface temperature or shading;
- addressed urban heat island effects without reference to pavements, typically focusing only on buildings or urban morphology;
- were not directly related to the thermal and/or functional behavior of urban surfaces.

Studies that presented methodological approaches for analyzing surface materials or modelling the urban thermal environment were also retained when their methods could contribute to the analysis or replication of thermal assessment techniques relevant to pavements.

2.3 Screening process

The selection of articles followed a screening procedure with the following steps: (i) duplicate records from both databases were removed; (ii) the remaining studies were analysed based on their titles, keywords, and a cursory reading of the abstract, when necessary, to identify those aligned with the research scope; (iii) the inclusion and exclusion criteria presented earlier were used to accept, reject, or submit the work to a more in-depth evaluation, in which topics such as introduction and conclusion were explored.

After steps (i) and (ii), 56 articles remained (accepted and subsequently evaluated) to verify their relevance and contribution to the topic. After step (iii), 39 articles were selected, which had open access to the general public or the university. The overall screening process is summarized in Figure 1, which presents the article selection flowchart.

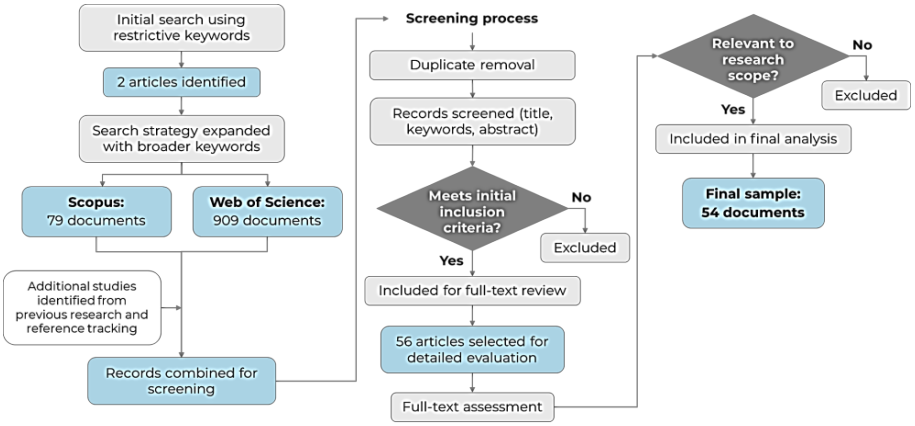


Figure 1 – Flowchart of article selection

Subsequently, 15 supplementary references that were not revealed in the search for scientific articles (including institutional reports and conceptual studies) were incorporated to support the theoretical framework and contextual discussion, resulting in a final corpus of 54 documents.

3. Summary of the systematic literature review

An initial overview of the selected literature is presented in Section 3.1, which provides a classification of the studies according to their main research focus and highlights the distribution of articles across different thematic approaches. Based on the analysis of the selected studies, the literature was organized into three main research themes:

(i) thermal behavior of pavement materials in urban environments;
(ii) the role of vegetation and shading in mitigating pavement surface temperatures and urban heat island effects;
(iii) methods used to analyze pavement temperature and urban microclimates, including spatial analysis, remote sensing techniques, and urban data integration.

The following sections present the main findings of the literature according to these thematic groups.

3.1 Overview and classification of the selected literature

The selected literature highlights a strong predominance of studies focused on thermal aspects (68.5%), while studies integrating functional and thermal performance represented only 13.0%, divided into analyses of pavement behavior (9.3%) and tree shading (3.7%). Although some studies refer to pavement "performance" or "durability", these terms are often used in a general or thermal context, without explicitly addressing the mechanical or structural behavior of pavement materials. Studies investigate the effect of tree shading on pavement surface temperature; however, only two explicitly address its implications for functional (mechanical) performance.

Figure 2 shows the temporal distribution of the analysed documents, including studies selected through the systematic review and complementary references. An increasing publication trend was observed over recent years, indicating growing interest in the topic.

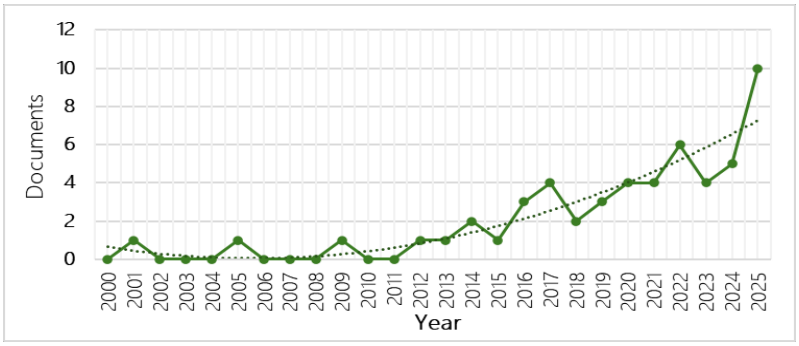


Figure 2 – Historical evolution of the number of documents published per year.

The selected studies were published across a wide range of journals, reflecting the interdisciplinary nature of the topic. Journals such as *Urban Climate* and *Sustainable Cities and Society* highlight the relevance of urban climate and sustainability, while *Building and Environment*, *Energy and Buildings*, and *Renewable & Sustainable Energy Reviews* emphasize thermal performance in the built environment. Additional publications in environmental and infrastructure-related journals further support the integration of climate, vegetation, and pavement research, consistent with the thematic structure of this review.

4. Results from literature analysis

4.1 Thermal and functional behavior of pavements for urban heat mitigation

Published literature highlights urban development characterized by the expansion of large impermeable areas occupied by artificial materials such as concrete and asphalt. The replacement of vegetated surfaces by impervious materials accounts for approximately 30% to 45% of urban areas and represents one of the main drivers of urban heat island (UHI) formation (Santamouris, 2013; Wang et al., 2021; Rouzmehr and Jamshidi, 2025).

These materials exhibit specific properties, such as high thermal absorption rates and varying levels of reflectance, making them both contributors to and affected by climatic variations due to changes in temperature and humidity, the occupation of permeable areas, the absence of surface shading, and the lack of local tree cover (Ibrahim et al., 2018; Ding et al., 2022; Chen et al., 2025; Yang et al., 2025).

Within transportation infrastructure, excessive heat acts as a degrading agent, as increased asphalt pavement temperature accelerates the oxidative aging of the binder. Thus, material characteristics such as albedo (reflectivity), emissivity, and thermal inertia represent key thermophysical properties that directly determine the magnitude of heating of both surfaces and the adjacent air layers (Santamouris, 2013; Qin et al., 2022).

Tsirigoti and Gkyrtis (2026) investigated the use of recycled materials in asphalt mixtures in Greece, which, when combined with high reflectivity properties, can reduce air temperature by up to 1.6 °C. Taleghani and Berardi (2018) specifically analysed pavements and sidewalks in urban environments, demonstrating their significant impact on pedestrian thermal comfort. Dark materials tend to retain more heat during the day and re-emit this heat at night, resulting in high surface temperatures during both periods.

Using climate modelling for California cities, Mohegh et al. (2017) observed that increases in albedo are nearly linearly associated with reductions in air temperature, contributing to urban cooling. Similarly, Qin et al. (2022) identified albedo as the most influential internal factor affecting pavement surface temperature. Due to their low albedo, asphalt pavements absorb shortwave solar radiation and reemit it as longwave radiation, resulting in higher surface temperatures (Cheela et al., 2021; Qin et al., 2022; Engel et al., 2023).

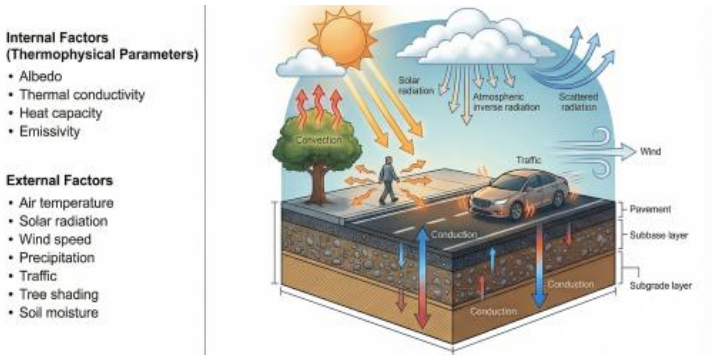


Figure 3 – Typical thermal partitioning at a pavement surface (adapted by authors from Qin et al., 2022)

Light-colored pavements or reflective coatings can reduce surface temperatures by up to 20 °C compared to conventional asphalt (Santamouris, 2013; Cheela et al., 2021; Gong et al., 2023). Thermal properties such as conductivity, albedo, and emissivity influence heat storage and release, although their effects depend on local climatic conditions, which remain difficult to control.

Extreme temperature and humidity conditions not only affect environmental quality and human well-being but also accelerate pavement deterioration, leading to reduced service life, higher maintenance costs, and significant economic impacts, with projections of up to US$ 26 billion in additional costs in the United States by 2040 (Underwood et al., 2017; Guest et al., 2019; Gulzar, Goenaga, and Underwood, 2022; Maadani, Shafiee, and Egorov, 2022).

Reducing asphalt surface temperature can significantly improve pavement performance and durability. Akbari, Pomerantz, and Harvey (2001) showed that a reduction of approximately 10 °C can prevent

permanent deformation from exceeding the failure criterion (12.5 mm), while reductions around 20 °C improve resistance to deformation (McPherson and Muchnick, 2005). Similarly, lower temperatures and thermal amplitudes minimize structural stresses and delay binder aging, reinforcing the potential benefits of shading for pavement performance, particularly in hot climates (Qin et al., 2022; Liu et al., 2025).

4.2 Methods for Evaluating Pavement Temperature and Urban Interactions

Advances in geotechnologies and the availability of urban data have expanded the possibilities for integrated analysis of transportation infrastructure, combining remote sensing, field measurements, and computational simulations (Stathopoulou et al., 2009; Wang et al., 2021; Elmagri et al., 2024).

At the regional scale, satellite data (such as Landsat, MODIS, and ASTER) enable land use characterization, land surface temperature (LST) assessment, and correlation with land cover indices such as the Normalized Difference Vegetation Index (NDVI) and the Normalized Difference Built-up Index (NDBI), revealing that highly impervious areas exhibit significantly higher temperatures (Stathopoulou et al., 2009; Ranagalage et al., 2017; Engel et al., 2023; Ahmad, Najar, and Ahmad, 2024; Façanha and Arantes, 2024).

Studies based on LST and NDVI analyses highlight vegetation as the main factor associated with lower temperatures (Engel et al., 2023; Ahmad, Najar, and Ahmad, 2024; Façanha and Arantes, 2024), whereas other works emphasize that urban materials store more heat and cool more slowly than natural surfaces, and that soil sealing, urban growth, and transport-related areas intensify thermal patterns and should be prioritized for intervention (Stathopoulou et al., 2009; Ranagalage et al., 2017).

At the microscale, unmanned aerial vehicles (UAVs) equipped with thermal cameras enable high-resolution analysis of land use and surface temperature variations, showing that artificial surfaces are major sources of sensible heat, while vegetation-related humidity contributes to cooling (Feng et al., 2020). Additionally, simulation tools such as ENVI-met and Ladybug Tools, along with machine learning approaches, are widely used to model thermal patterns and support urban planning (Choi et al., 2021; Elmagri et al., 2024; Rouzmehr and Jamshidi, 2025; Ye et al., 2025).

Several metrics and indices are used in the literature to characterize material behavior and spatially classify urban areas, including the Leaf Area Index (LAI), Mean Radiant Temperature (MRT), Universal Thermal Climate Index (UTCI), Physiological Equivalent Temperature (PET), evaporation rates, and Standard Effective Temperature (SET*), among others (Sen et al., 2019; Del Serrone et al., 2022; Peluso et al., 2022; Elmagri et al., 2024; Dalla Mora et al., 2025; Lu et al., 2025).

ENVI-met has been widely used to simulate interactions between urban variables and assess their effects on thermal behavior (Tsoka et al., 2020; Choi et al., 2021; Del Serrone et al., 2022; Peluso et al., 2022; Dalla Mora et al., 2025; Ye et al., 2025). For example, Yang et al. (2016) demonstrated that pavement thermal performance in urban canyons is strongly influenced by street geometry and that reflective materials, despite reducing surface temperatures, may increase pedestrian thermal stress. Overall, georeferenced tools support integrated assessments of vegetation, surface temperature, and urban infrastructure, contributing to shading mapping and urban heat mitigation strategies (Figure 4).

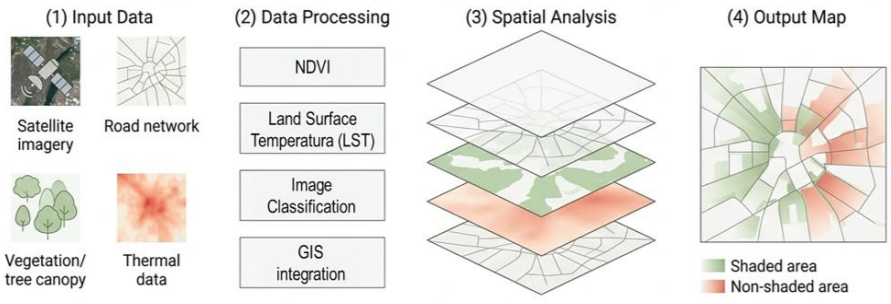


Figure 4 – Conceptual framework for mapping urban shading areas using geospatial data.

4.3 Tree shading effects on pavement thermal and functional performance

The effects of excessive heat on urban surfaces, particularly asphalt pavements, remain an underexplored topic in the literature. Although this issue is often addressed from a thermal performance perspective, it is rarely associated with the functional and mechanical performance of pavements, particularly regarding temperature-related deterioration mechanisms and pavement defects.

Thermoviscoelastic materials, such as Asphalt Concrete (AC), are highly sensitive to temperature variations, and extreme climatic conditions may compromise their mechanical properties and durability (Underwood et al., 2017; Gulzar, Goenaga and Underwood, 2022; Gong et al., 2023; Liu et al., 2025). Elevated temperatures accelerate binder aging, particularly in hot climates where asphalt surface temperatures frequently exceed 60 °C. This condition contributes to the development of pavement defects, such as fatigue cracking and permanent deformation, resulting in increased maintenance demands (Santamouris, 2013; Matlack et al., 2022; Gong et al., 2023; Dehnad et al., 2025).

Several studies address “cool pavements” as strategies to mitigate the effects of high temperatures and urban heat islands, while also contributing to extending infrastructure service life. These strategies include the use of high-reflectance materials and coatings, such as light-colored surfaces and reflective pigments, which increase albedo and reduce solar radiation absorption (Santamouris, 2013; Takebayashi et al., 2014; Wang et al., 2021; Gong et al., 2023). Another approach involves porous pavements or structures capable of retaining water, promoting moisture-based cooling and delaying surface heating (Hendel et al., 2014; Ibrahim et al., 2018; Frere et al., 2024; Dalla Mora et al., 2025). In addition, phase change materials (PCMs) have been employed to regulate pavement temperature through latent heat storage and release, reducing thermal peaks (Santamouris, 2013; Gong et al., 2023; Seifeddine et al., 2023). Most studies prioritize surface temperature reduction, with limited evaluation of long-term structural behavior. For this reason, shading is considered promising for pavement durability, given the influence of temperature on material performance (Wang et al., 2021; Gong et al., 2023).

Urban tree cover acts as an effective thermal mitigation mechanism for pavements through surface shading and evapotranspiration, significantly reducing surface temperatures and associated thermal stresses. Temperature reductions can range from 5 to 25 °C, with experimental evidence reporting reductions of up to 20.9 °C on shaded asphalt surfaces. Although results may vary depending on pavement type, climatic conditions, and tree canopy characteristics, shading stands out as an effective strategy that can provide environmental improvements through the implementation of green areas in cities (Mascaró, 2012; Napoli et al., 2016; Rahman et al., 2019; Kaluarachichi et al., 2020; Speak et al., 2020; Lu et al., 2025; Liu et al., 2025).

Matlack et al. (2022) report that shaded pavements exhibit significantly lower stress levels, from 0.7 to 1.2 MPa, compared to pavements exposed to direct solar radiation, from 1.8 to 5.3 MPa. The authors indicate that stress levels in unshaded areas fall within the range associated with cracking observed in the laboratory. Additionally, it is assumed that tensile stress increases as the pavement ages and stiffens.

Consequently, the protection provided by tree canopies may delay binder aging, potentially reducing defects such as fatigue cracks and permanent deformations, leading to lower maintenance costs and extended service life (Cheela et al., 2021; Matlack et al., 2022; Gong et al., 2023). In particular, McPherson and Muchnick (2005) estimated that shading from large trees can reduce pavement maintenance needs by up to 58% over a 30-year period, corresponding to a cost saving of $7.13 per square meter. However, more empirical evidence is needed to understand these effects on deterioration processes and defect development.

The above-mentioned effect was assessed using the Pavement Condition Index (PCI), which ranges from 0 (poor) to 100 (excellent), and the Tree Shade Index (TSI), defined as the percentage of shaded area, typically equal to or greater than 30% in commercial areas. The results indicated that shaded sections presented significantly higher PCI values, reflecting a lower incidence of cracks and deformations (McPherson and Muchnick, 2005).

Table 2 summarizes the main conclusions regarding tree shading and its thermal and performance effects on pavements. Overall, the studies analysed report substantial reductions in pavement surface temperature under tree shading, but the evidence directly linking these reductions to pavement defects, durability, and long-term performance is still relatively limited.

Table 2 – Synthesis of the literature on tree shading and pavement performance

Study	Method / Strategy	Main findings	Pavement implications	Research gaps
McPherson & Muchnick (2005); Matlack et al. (2022)	Field analysis / modeling – Tree shade	Improved pavement condition; 15–25°C reduction under canopy	Lower thermal stresses and reduced cracking potential. 58% maintenance reduction over 30 years	Limited field validation; need to isolate thermal and biological effects
Gong et al. (2023); Cheela et al. (2021)	Reviews – Shading and cool pavements	Surface temperature reductions of 5–25°C	Potential reduction in rutting, binder aging, softening, and exudation	Limited evidence on long-term mechanical performance
Mascaró (2012); Kaluarachichi et al. (2020)	Modeling + field experiments – Tree canopy	9–10°C reduction depending on canopy and 20.9°C reduction on asphalt	Reduced heat storage and potential pavement preservation benefits	Influence of canopy characteristics remains uncertain
Liu et al. (2025)	Field experiment – Tree shade	Cooling depends on surface properties	Potential urban thermal benefits	Environmental and sensor interactions

Although the thermal benefits are widely validated, authors such as Cheela et al. (2021), Gong et al. (2023), and Matlack et al. (2022) emphasize that the direct relationship between shading-induced cooling and the mechanical/functional response of asphalt still lacks long-term evidence, representing a key research gap in the field. Finally, urban green spaces and street trees are also increasingly recognized as key elements for climate adaptation and public health, contributing to reduced stress, lower incidence of cardiovascular diseases, and decreased overall mortality, while simultaneously mitigating urban heat island effects (Qin et al., 2022; Gurjão et al., 2024; Furtado et al., 2025).

5. Conclusions

This article shows that urban pavements are both contributors to and victims of urban heat, as impervious materials intensify thermal stress while their mechanical performance deteriorates under high temperatures. A second finding is that recent advances in remote sensing, thermal monitoring, simulation, and data-driven methods have significantly expanded the capacity to evaluate pavement temperature and its relationship with urban form, vegetation, and material properties across multiple scales. A third finding is that urban tree shading emerges as a particularly promising strategy because it addresses both sides of the problem at once: it mitigates heat exposure in cities and may also help preserve pavement performance by reducing thermal loading. The contribution of this paper lies in bringing these strands of research together, connecting urban heat mitigation, pavement durability, and green infrastructure within a single analytical perspective (Figure 5). By doing so, it highlights the need to move beyond treating pavements solely as engineering surfaces or urban heat solely as a climatic issue, and instead frames both as interdependent components of urban adaptation. In practical terms, this perspective can support planners, engineers, and local governments in prioritizing tree-based shading strategies, improving pavement design and maintenance decisions, and developing more integrated policies for climate resilience and urban infrastructure management.

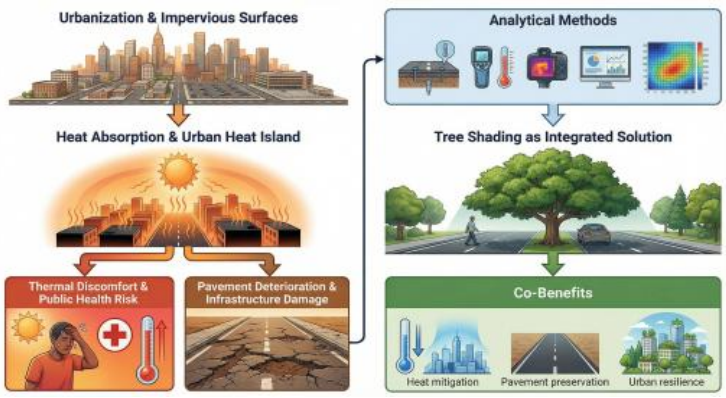


Figure 5 – Literature overview on tree shading and pavement thermal behavior

Acknowledgments

The authors acknowledge the financial support of the Human Resources Program of the Brazilian National Agency of Petroleum, Natural Gas and Biofuels (PRH-ANP), managed by the São Paulo Research Foundation (FAPESP), Brazil. Process n° 2025/03400-7.

References

Ahmad, Bilal, Mohammad Bareeq Najar, and Shamshad Ahmad. 2024. "Analysis of LST, NDVI, and UHI Patterns for Urban Climate Using Landsat-9 Satellite Data in Delhi." Journal of Atmospheric and Solar-Terrestrial Physics 265: 106359. https://doi.org/10.1016/j.jastp.2024.106359

Akbari, Hashem, Melvin Pomerantz, and Haider Taha. 2001. "Cool Surfaces and Shade Trees to Reduce Energy Use and Improve Air Quality in Urban Areas." Solar Energy 70 (3): 295–310. https://doi.org/10.1016/S0038-092X(00)00089-X

Benrazavi, Rezvan Sadat, Kamariah Binti Dola, Norsidah Ujang, and Nour Sadat Benrazavi. 2016. "Effect of Pavement Materials on Surface Temperatures in Tropical Environment." Sustainable Cities and Society 22: 94–103. https://doi.org/10.1016/j.scs.2016.01.011

Brasil. Ministério do Meio Ambiente. 2023. Plano Nacional de Arborização Urbana (PLANAU). Brasília: MMA. Accessed December 27, 2025. https://www.gov.br/mma/pt-br/assuntos/meio-ambiente-urbano-recursos-hidricos-qualidade-ambiental/cidades-verdes-resilientes/areas-verdes-e-arborizacao-urbana/planau

Cheela, Venkata Ravi Sankar, Michele John, Wahidul Biswas, and Prabir Sarker. 2021. "Combating Urban Heat Island Effect: A Review of Reflective Pavements and Tree Shading Strategies." Buildings 11. https://doi.org/10.3390/buildings11030093

Chen, Lu-Ming, Jui-Wen Chen, Timothy J. Lecher, and Paul C. Davidson. 2025. "A Field-Scale Assessment of the Impact of Conventional and Permeable Concrete Pavements on Surface and Air Temperatures." Environments 12: 60192. https://doi.org/10.3390/environments12060192

Choi, Ga Yoon, Hwan Sung Kim, Hyungkyoo Kim, and Jae Seung Lee. 2021. "How Do Paving and Planting Strategies Affect Microclimate Conditions and Thermal Comfort in Apartment Complexes?" International Journal of Climate Change Strategies and Management 13: 97–119. https://doi.org/10.1108/IJCCSM-06-2020-0063

Dalla Mora, Tiziano, Giuseppe Emmi, Paolo Ruggeri, Massimiliano De Bei, and Fabio Peron. 2025. "Mitigation Urban Heat Island by Using Porous and Permeable Block Pavement." Energy and Buildings 346. https://doi.org/10.1016/j.enbuild.2025.116149

Dehnad, Mohammad Hosein, Mohammed Hussein Alwan, Alireza Noory, and Mohab El-Hakim. 2025. “Evaluation of Effective Parameters on Pavement Surface Temperature.” Journal of Road Engineering 5: 313–322. https://doi.org/10.1016/j.jreng.2024.12.008

Del Serrone, Giulia, Paolo Peluso, and Laura Moretti. 2022. “Evaluation of Microclimate Benefits Due to Cool Pavements and Green Infrastructures on Urban Heat Islands.” Atmosphere 13. https://doi.org/10.3390/atmos13101586

Ding, Wei, Wei Feng, Meng Zhen, Qingjiang Zhen, and Ying Liu. 2022. “Experimental Evaluation of the Thermal Performance of Cool Pavement Materials in Cold Regions of China.” Environmental Science and Pollution Research 29 (21): 31121–32. https://doi.org/10.1007/s11356-021-18266-9

Elmagri, Hasna, Tarek M. Kamel, and Hasan Ozer. 2024. “Assessment of the Effectiveness of Cool Pavements on Outdoor Thermal Environment in Urban Areas.” Building and Environment 266. https://doi.org/10.1016/j.buildenv.2024.112095

Engel, Ruth A., Adam Millard-Ball, and V. Kelly Turner. 2023. “Contributions of Roads to Surface Temperature: Evidence from Southern California.” Environmental Research Communications 5. https://doi.org/10.1088/2515-7620/acabb8

Façanha, João Paulo Alves, and Arielle Elias Arantes. 2024. “Análise da Influência da Composição dos Materiais Urbanos nas Temperaturas do Ar e da Superfície para a Cidade de Fortaleza Durante o Biênio 2022/2023.” Revista Brasileira de Sensoriamento Remoto 5 (3): 10–26.

Feng, Li, Huihui Tian, Zhi Qiao, Menmen Zhao, and Yanxia Liu. 2020. “Detailed Variations in Urban Surface Temperatures Exploration Based on Unmanned Aerial Vehicle Thermography.” IEEE Journal of Selected Topics in Applied Earth Observations and Remote Sensing 13: 204–216. https://doi.org/10.1109/JSTARS.2019.2954852

Frere, Maxime, Martin Hendel, Julien Van Rompu, Simon Pouget, and Laurent Royon. 2024. “Pervious Asphalt Pavement and Concrete Wall-Watering for Urban Cooling: Characterization of Surface Cooling Effects at an Outdoor Test Site.” Urban Climate 58. https://doi.org/10.1016/j.uclim.2024.102218

Furtado, Lara Sucupira, Nayara O. Gurjão, Nicolas C. Monteiro, Carlos Matheus Ferreira, Jarbas A. Nunes, Jorge Barbosa Soares, and José A. Macêdo. 2025. “Built to Breathe? Modeling Air Quality with Features of the Built and Natural Environment.” In Anais do Simpósio Brasileiro de Banco de Dados (SBBD), 352–362. [S.l.]: SBC.

Gong, Xing, Quantao Liu, Yang Lv, Shuaichao Chen, Shaopeng Wu, and Hong Ying. 2023. “A Systematic Review on the Strategies of Reducing Asphalt Pavement Temperature.” Case Studies in Construction Materials 18: e01852. https://doi.org/10.1016/j.cscm.2023.e01852

Guest, Geoffrey, Jieying Zhang, Omran Maadani, and Hamidreza Shirkhani. 2019. “Incorporating the Impacts of Climate Change into Infrastructure Life Cycle Assessments: A Case Study of Pavement Service Life Performance.” Journal of Industrial Ecology 24 (2): 356–68. https://doi.org/10.1111/jiec.12915

Gulzar, Saqib, Boris Goenaga, and B. Shane Underwood. 2022. “Novel Index for Vulnerability Assessment of Flexible Pavement Infrastructure to Temperature Rise: Case Study of Developing Countries.” Journal of Infrastructure Systems 28 (1): 1–17. https://doi.org/10.1061/(ASCE)IS.1943-555X.0000669

Gurjão, Nayara de Oliveira, Jorge Luiz Oliveira Lucas Júnior, Lara Sucupira Furtado, and Jorge Barbosa Soares. 2024. “Air Pollution Dynamics in Fortaleza, Brazil: Exploring the Interplay of Traffic and High-Rise Development.” Urban Climate 58: 102176. https://doi.org/10.1016/j.uclim.2024.102176

Hendel, Martin, Morgane Colombert, Youssef Diab, and Laurent Royon. 2014. “Improving a Pavement-Watering Method on the Basis of Pavement Surface Temperature Measurements.” Urban Climate 10: 189–200. https://doi.org/10.1016/j.uclim.2014.11.002

Ibrahim, Siti Halipah, Nurul Izzati Ahmat Ibrahim, Julaihi Wahid, Nurakmal Abdullah Goh, Dona Rose Amer Koesmeri, and Mohd Nasrun Mohd Nawi. 2018. "The Impact of Road Pavement on Urban Heat Island (UHI) Phenomenon." International Journal of Technology 9: 1597–1608. https://doi.org/10.14716/ijtech.v9i8.2755

Kaluarachichi, Thilini Upeksha N., Mark G. Tjoelker, and Sebastian Pfautsch. 2020. "Temperature Reduction in Urban Surface Materials through Tree Shading Depends on Surface Type Not Tree Species." Forests 11. https://doi.org/10.3390/f11111141

Liu, Ting, Peng Xu, Tailong Zhang, Yamei Shen, Yizhou Tao, Feng Qi, and Shaojun Yan. 2025. "Effects of Cloud and Tree Shading on Surface Temperature of Different Pavement Materials for Urban Sidewalks." International Journal of Biometeorology 69: 605–619. https://doi.org/10.1007/s00484-024-02842-y

Lu, Xiaohui, Qiong Li, Peijie Tang, Zining Qiu, Qi Li, and Qing Lin Meng. 2025. "Effect of Pavement Watering under Tree Shade in a Hot and Humid Area: A Case Study in Guangzhou, China." Sustainable Cities and Society 132. https://doi.org/10.1016/j.scs.2025.106818

Maadani, Omran, Mohammad Shafiee, and Igor Egorov. 2021. "Climate Change Challenges for Flexible Pavement in Canada: An Overview." Journal of Cold Regions Engineering 35 (4). https://doi.org/10.1061/(ASCE)CR.1943-5495.0000262

Mascaró, Juan Jose. 2012. "Shaded Pavements in the Urban Environment: A Case Study." Road Materials and Pavement Design 13: 556–565. https://doi.org/10.1080/14680629.2012.657098

Matlack, Glenn Richard, Issam Khoury, and Bhaven Naik. 2022. "Tree Canopy Macrostructure Controls Heating of Asphalt Pavement in a Moist-Temperate Urban Forest." Urban Ecosystems 25: 967–976. https://doi.org/10.1007/s11252-022-01200-3

McPherson, Egbert Gregory, and Jules Muchnick. 2005. "Effects of Street Tree Shade on Asphalt Concrete Pavement Performance." Journal of Arboriculture 31: 303–310. https://doi.org/10.48044/jauf.2005.039

Mohajerani, Abbas, Jason Bakaric, and Tristan Jeffrey-Bailey. 2017. "The Urban Heat Island Effect, Its Causes, and Mitigation, with Reference to the Thermal Properties of Asphalt Concrete." Journal of Environmental Management 197: 522–538. https://doi.org/10.1016/j.jenvman.2017.03.095

Mohegh, Arash, Pablo Rosado, Ling Jin, Dev Millstein, Ronnen Levinson, and George Ban-Weiss. 2017. "Modeling the Climate Impacts of Deploying Solar Reflective Cool Pavements in California Cities." Journal of Geophysical Research: Atmospheres 122: 6798–6817. https://doi.org/10.1002/2017JD026845

Napoli, Marco, Luciano Massetti, Giada Brandani, Martina Petralli, and Simone Orlandini. 2016. "Modeling Tree Shade Effect on Urban Ground Surface Temperature." Journal of Environmental Quality 45: 146–156. https://doi.org/10.2134/jeq2015.02.0097

Peluso, Paolo, Giovanni Persichetti, and Laura Moretti. 2022. "Effectiveness of Road Cool Pavements, Greenery, and Canopies to Reduce the Urban Heat Island Effects." Sustainability 14. https://doi.org/10.3390/su142316027

Qin, Yinghong, Xingyue Zhang, Kanghao Tan, and Junsong Wang. 2022. "A Review on the Influencing Factors of Pavement Surface Temperature." Environmental Science and Pollution Research 29: 67659–67674. https://doi.org/10.1007/s11356-022-22295-3

Rahman, Mohammad A., Astrid Moser, Thomas Roetzer, and Stephan Pauleit. 2019. "Comparing the Transpirational and Shading Effects of Two Contrasting Urban Tree Species." Urban Ecosystems 22: 683–697. https://doi.org/10.1007/s11252-019-00853-x

Ranagalage, Manjula, Ronald C. Estoque, and Yuji Murayama. 2017. "An Urban Heat Island Study of the Colombo Metropolitan Area, Sri Lanka, Based on Landsat Data (1997–2017)." ISPRS International Journal of Geo-Information 6. https://doi.org/10.3390/ijgi6070189

Rouzmehr, Fouzieh, and Saman Jamshidi. 2025. "Pavements and the Urban Heat Island Effect: A Network Analysis of Research Trends and Knowledge Structure." Infrastructures 10. https://doi.org/10.3390/infrastructures10120344

Santamouris, Mat. 2013. “Using Cool Pavements as a Mitigation Strategy to Fight Urban Heat Island: A Review of the Actual Developments.” Renewable and Sustainable Energy Reviews 26: 224–240. https://doi.org/10.1016/j.rser.2013.05.047

Seifeddine, Khaled, Sofiane Amziane, Evelyne Toussaint, and Salah-Eddine Ouldboukhitine. 2023. “Review on Thermal Behavior of Cool Pavements.” Urban Climate 51. https://doi.org/10.1016/j.uclim.2023.101667

Sen, Sushobhan, Jeffery Roesler, Benjamin Ruddell, and Ariane Middel. 2019. “Cool Pavement Strategies for Urban Heat Island Mitigation in Suburban Phoenix, Arizona.” Sustainability 11. https://doi.org/10.3390/su11164452

Speak, Andrew, Leonardo Montagnani, Camilla Wellstein, and Stefan Zerbe. 2020. “The Influence of Tree Traits on Urban Ground Surface Shade Cooling.” Landscape and Urban Planning 197. https://doi.org/10.1016/j.landurbplan.2020.103748

Stathopoulou, Maria, Aikaterini Synnefa, Costas Cartalis, Mat Santamouris, Theoni Karlessi, and Hashem Akbari. 2009. “A Surface Heat Island Study of Athens Using High-Resolution Satellite Imagery and Measurements of the Optical and Thermal Properties of Commonly Used Building and Paving Materials.” International Journal of Sustainable Energy 28: 59–76. https://doi.org/10.1080/14786450802452753

Takebayashi, Hideki, Yutaro Kimura, and Sae Kyogoku. 2014. “Study on the Appropriate Selection of Urban Heat Island Measure Technologies to Urban Block Properties.” Sustainable Cities and Society 13: 217–222. https://doi.org/10.1016/j.scs.2014.01.008

Taleghani, Mohammad, and Umberto Berardi. 2018. “The Effect of Pavement Characteristics on Pedestrians’ Thermal Comfort in Toronto.” Urban Climate 24: 449–59. https://doi.org/10.1016/j.uclim.2017.05.007

Tsirigoti, Dimitra, and Konstantinos Gkyrtis. 2026. “Recycled Pavement Materials and Urban Microclimate: Albedo and Thermal Capacity Effects on Heat Island Mitigation.” Solar 6. https://doi.org/10.3390/solar6010005

Tsoka, Stella, Katerina Tsikaloudaki, Theodoros Theodosiou, and Dimitrios Bikas. 2020. “Urban Warming and Cities’ Microclimates: Investigation Methods and Mitigation Strategies—A Review.” Energies 13. https://doi.org/10.3390/en13061414

Underwood, Benjamin Shane, Zack Guido, Padmini Gudipudi, and Yarden Feinberg. 2017. “Increased Costs to US Pavement Infrastructure from Future Temperature Rise.” Nature Climate Change 7 (10): 704–7. https://doi.org/10.1038/nclimate3390

United Nations Development Programme (UNDP). 2025. “What Is Sustainable Transport and What Role Does It Play in Tackling Climate Change?” Accessed December 27, 2025. https://www.undp.org

United Nations. 2015. “Sustainable Development Goals.” Accessed March 21, 2026. https://sdgs.un.org/goals.

Wang, Chenghao, Zhi-Hua Wang, Kamil E. Kaloush, and Joseph Shacat. 2021. “Cool Pavements for Urban Heat Island Mitigation: A Synthetic Review.” Renewable and Sustainable Energy Reviews 146. https://doi.org/10.1016/j.rser.2021.111171

Yang, Jiachuan, Zhi-Hua Wang, Kamil E. Kaloush, and Heather Dylla. 2016. “Effect of Pavement Thermal Properties on Mitigating Urban Heat Islands: A Multi-Scale Modeling Case Study in Phoenix.” Building and Environment 108: 110–121. https://doi.org/10.1016/j.buildenv.2016.08.021

Yang, Xin, Bowen Li, Nana Li, and Xin Ma. 2025. “A Study of the Cooling Effect of Urban Trees: Influencing Factors, Assessment Methods, Planning Strategies, and Impacts.” Theoretical and Applied Climatology 157 (1): 1–30. https://doi.org/10.1007/s00704-025-05904-2

Ye, Zihao, Jing Liu, and Zhihuan Huang. 2025. “Identifying the Best Combination of Vegetation and Paving Materials to Improve Outdoor Thermal Comfort in a Campus Courtyard.” Scientific Reports 15. https://doi.org/10.1038/s41598-025-05742-2

CINPAR 2026
XXII International Conference on Building Pathology and Constructions Repair
15th to 17th July 2026 - Lisboa, Portugal

CLASSES DE AGRESSIVIDADE DO CONCRETO NO BRASIL: INFLUÊNCIA REGIONAL, PATOLOGIAS E IMPLICAÇÕES EM PROJETO

Stefania Alexina Martins Zebral Silva

Instituto Nova Engenharia, Minas Gerais, Brasil, szengenharaia.eng@gmail.com

Resumo: A durabilidade das estruturas de concreto armado está diretamente relacionada à correta avaliação da agressividade ambiental ao longo da vida útil. No Brasil, a diversidade climática, aliada à intensa urbanização e industrialização, resulta em diferentes níveis de exposição que impactam significativamente o desempenho estrutural. Este trabalho investiga as classes de agressividade ambiental (CAA) definidas pelas normas ABNT NBR 6118:2014 (Projeto de Estruturas de Concreto) e ABNT NBR 12655:2023 (Concreto de Cimento Portland – Preparo, Controle, Recebimento e Aceitação), correlacionando-as com as condições predominantes nas cinco grandes regiões brasileiras: Norte, Nordeste, Centro-Oeste, Sudeste e Sul. A pesquisa adota abordagem qualitativa com base em revisão normativa sistemática e literatura técnico-científica consolidada, integrando análise comparativa internacional com as normas Eurocode 2 (EN 1992-1-1:2023), ACI 318-19 e BS 8500:2019. São discutidas as principais manifestações patológicas associadas a cada classe, as implicações nas fases de projeto, execução e manutenção, e é proposta uma tabela comparativa normativa inédita. Os achados evidenciam a necessidade de critérios de projeto mais rigorosos em ambientes costeiros, industrializados e de elevada umidade tropical, contribuindo para o aumento da vida útil e da confiabilidade das estruturas de concreto armado. Como limitação, a pesquisa não realizou ensaios experimentais, sendo os resultados embasados em revisão da literatura. Estudos quantitativos futuros são recomendados para validação dos padrões de classificação identificados.

Palavras-chave: durabilidade; concreto armado; agressividade ambiental; desempenho estrutural; comparação normativa internacional.

1. INTRODUÇÃO

A durabilidade das estruturas de concreto armado é condição essencial para o desempenho seguro ao longo da vida útil de projeto. Em um país de dimensões continentais como o Brasil, a diversidade climática, o processo de urbanização acelerada e a presença de polos industriais consolidados criam cenários de exposição ambiental extremamente heterogêneos, exigindo uma classificação criteriosa da agressividade ambiental desde a fase de concepção estrutural.

Estudos recentes têm demonstrado que a corrosão de armaduras induzida por carbonatação e por íons cloreto constitui o principal mecanismo de degradação do concreto armado em ambientes urbanos e costeiros (Mumberger et al., 2022; Li et al., 2024). Em áreas litorâneas, os aerossóis marinhos transportam concentrações elevadas de cloretos que penetram na matriz cimentícia, comprometendo de forma irreversível a passivação das barras de aço e reduzindo significativamente a vida útil das estruturas (Rodrigues et al., 2024). A situação é agravada pelo fato de que o Brasil possui uma costa de aproximadamente 7.500 km, com elevada concentração de infraestrutura construída em zonas de influência marinha.

A norma ABNT NBR 6118:2014 (Projeto de Estruturas de Concreto) estabelece quatro classes de agressividade ambiental (CAA I a IV), vinculando-as a parâmetros prescritivos de projeto, como cobrimento nominal das armaduras, resistência característica mínima à compressão e relação máxima água/cimento. A ABNT NBR 12655:2023 (Concreto de Cimento Portland – Preparo, Controle, Recebimento e Aceitação), complementa esses requisitos ao disciplinar o preparo, controle e recebimento do concreto de cimento Portland. Apesar da consistência técnica dessas normas, a simples consulta tabular às classes de agressividade, sem consideração das condições microambientais locais, pode conduzir a projetos insuficientemente conservadores, subestimando o risco real de deterioração.

No plano internacional, normas como o Eurocode 2 (EN 1992-1-1:2023), a ACI 318-19 e a BS 8500:2019 adotam abordagens distintas, em alguns casos baseadas em desempenho que ampliam o ferramental disponível para o projetista e explicitam cenários de exposição com maior granularidade. A comparação entre essas referências e a normatização brasileira revela lacunas e oportunidades de aperfeiçoamento, especialmente quanto à incorporação de modelos de previsão de vida útil e à definição de classes de exposição para ambientes tropicais.

Nesse contexto, o presente artigo tem como objetivo analisar criticamente as classes de agressividade ambiental do concreto armado no Brasil, correlacionando-as com os ambientes típicos das cinco grandes regiões do país, identificando as manifestações patológicas mais recorrentes, discutindo suas implicações no projeto estrutural e propondo uma tabela comparativa normativa inédita entre as principais referências nacionais e internacionais. A pesquisa contribui para a consolidação de uma abordagem regionalizada da classificação ambiental, essencial para a ampliação da confiabilidade e da vida útil das estruturas de concreto no território brasileiro.

2. FUNDAMENTAÇÃO TEÓRICA E NORMATIVA

2.1 Definição normativa das classes de agressividade ambiental

A ABNT NBR 6118:2014 (Projeto de Estruturas de Concreto) classifica a agressividade ambiental em quatro classes progressivas: Fraca (I), Moderada (II), Forte (III) e Muito Forte (IV), com base no risco de deterioração que o ambiente impõe à estrutura ao longo da sua vida útil. Essa classificação considera os principais agentes agressivos ao concreto armado: dióxido de carbono (CO_2), que promove a carbonatação; íons cloreto, transportados por aerossóis marinhos ou por soluções de degelo; sulfatos presentes em solos ou águas subterrâneas; e poluentes industriais gasosos ou líquidos. A ABNT NBR 12655:2023 (Concreto de Cimento Portland – Preparo, Controle, Recebimento e Aceitação), operacionaliza essas classes ao vincular cada nível de agressividade a requisitos mínimos de qualidade do concreto, abrangendo desde o traço e a relação água/cimento até as condições de cura e controle tecnológico da produção.

Segundo Bolina e Tutikian (2016), as normas brasileiras exigem, para estruturas enterradas com vida útil de 75 anos, parâmetros consideravelmente mais restritivos do que os valores mínimos prescritos para a classe II, evidenciando que a simples conformidade normativa básica pode ser insuficiente para garantir o desempenho a longo prazo em condições de agressividade moderada a severa. Mumberger et al. (2022) reforçam essa perspectiva ao proporem parâmetros de durabilidade para vidas úteis entre 50 e 100 anos no Brasil, concluindo que os valores prescritos pela NBR 6118 para as classes I e II são compatíveis com 50 anos de vida útil, mas demandam ajustes para projetos de maior longevidade, especialmente em ambientes costeiros e industrializados.

2.2 Parâmetros de projeto associados às classes de agressividade

Para cada classe de agressividade, as normas brasileiras definem um conjunto articulado de exigências que visam mitigar os mecanismos físico-químicos de degradação. A Tabela 2, apresentada na Seção 4, sistematiza esses parâmetros. O cobrimento nominal das armaduras constitui o principal parâmetro de proteção física do aço, e sua correta especificação depende tanto da classe de agressividade quanto da qualidade do concreto adotado. Estudos de caso conduzidos por Cascudo e colaboradores demonstram que a variabilidade do cobrimento durante a execução é uma das causas mais frequentes de deterioração prematura em estruturas inseridas em ambientes de agressividade moderada a forte.

A relação água/cimento máxima e a resistência característica mínima à compressão atuam em sinergia, reduzindo a porosidade e a permeabilidade da matriz cimentícia e, consequentemente, retardando a penetração de agentes agressivos. A qualidade e o controle tecnológico do concreto completam esse conjunto normativo, estabelecendo diferentes exigências de amostragem, ensaios e controle estatístico conforme a severidade ambiental.

2.3 Mecanismos físico-químicos de degradação

A carbonatação do concreto resulta da reação entre o CO_2 atmosférico e o hidróxido de cálcio presente na pasta de cimento hidratada, produzindo carbonato de cálcio e reduzindo o pH da solução dos poros de valores próximos a 13 para abaixo de 9. Nessa faixa de pH, a camada passivadora que protege as armaduras é destruída, iniciando o processo de corrosão. A taxa de carbonatação é governada pela concentração de CO_2, pela umidade relativa do ambiente com pico de velocidade entre 50% e 70% de UR e pela porosidade do concreto, parâmetro diretamente controlável pela relação água/cimento.

A corrosão por cloretos ocorre por um mecanismo distinto: os íons Cl^- desestabilizam localmente a camada passivadora da armadura sem necessariamente alterar o pH do concreto, deflagrando corrosão por pites altamente localizada. Esse mecanismo é particularmente severo em ambientes marinhos, onde a concentração de cloretos no aerossol pode ser ordens de magnitude superiores às encontradas em zonas continentais. Pesquisas realizadas em estruturas costeiras brasileiras com mais de 40 anos de uso registraram penetração de cloretos muito acima dos limites normativos, resultando em abertura de fissuras superiores a 30 mm e comprometimento estrutural significativo (Rodrigues et al., 2024).

O ataque por sulfatos, predominante em solos argilosos e águas subterrâneas de certas regiões, promove expansão volumétrica da pasta de cimento por formação de etringita secundária e gipsita, levando à fissuração e desagregação do concreto. Em ambientes industriais, a combinação de SO_2, NO_x e outros poluentes gasosos com a umidade superficial cria soluções ácidas que aceleram significativamente todos os mecanismos de degradação descritos.

3. METODOLOGIA

Esta pesquisa adota abordagem qualitativa, de natureza exploratória-descritiva, estruturada em quatro etapas complementares. Na primeira etapa, foi realizada a revisão normativa sistemática das normas ABNT NBR 6118:2014 (Projeto de Estruturas de Concreto) e ABNT NBR 12655:2023 (Concreto de Cimento Portland – Preparo, Controle, Recebimento e Aceitação), com foco na extração dos parâmetros prescritivos associados a cada classe de agressividade ambiental. Essa análise foi estendida às normas internacionais Eurocode 2 (EN 1992-1-1:2023), ACI 318-19, BS 8500:2019 e AS 3600:2018, permitindo a construção de um quadro comparativo inédito.

Na segunda etapa, procedeu-se ao levantamento bibliográfico em bases de dados científicas indexadas, incluindo SciELO, Scopus, Web of Science e Google Scholar, com recorte temporal prioritário entre 2016 e 2024. Os descritores utilizados combinaram termos como 'environmental aggressiveness class', 'concrete durability Brazil', 'chloride-induced corrosion', 'carbonation reinforced concrete', 'service life prediction' e seus equivalentes em português. Foram selecionadas publicações de periódicos científicos com revisão por pares, priorizando estudos com dados empíricos originais ou revisões sistemáticas com evidências robustas.

Na terceira etapa, os dados normativos e os achados da literatura foram integrados em uma análise regionalizada das cinco grandes regiões brasileiras. Para cada região, identificaram-se as condições climáticas e ambientais predominante, temperatura média anual, umidade relativa, proximidade do litoral, presença de polos industriais e agentes agressivos predominantes e correlacionaram-se essas condições com as classes de agressividade mais representativas, conforme a tipologia ambiental definida pela NBR 6118:2014 (Projeto de Estruturas de Concreto). Essa correlação foi sistematizada na Tabela 1.

Na quarta etapa, os resultados da análise regional e da comparação normativa internacional foram consolidados em discussão integradora, identificando implicações para o projeto estrutural, lacunas normativas e recomendações para estudos futuros. O artigo reconhece como limitação estrutural o fato de não ter conduzido ensaios laboratoriais nem levantamentos de campo, sendo os resultados integralmente baseados em revisão da literatura e análise documental. Essa limitação circunscreve as conclusões ao plano qualitativo e sugere a necessidade de estudos experimentais futuros que quantifiquem as taxas de degradação por região e validem os padrões de classificação ambiental propostos.

A metodologia empregada tem como contribuição original a sistematização comparativa até então ausente na literatura nacional entre o sistema normativo brasileiro e quatro referências internacionais de alta relevância técnica, aliada à proposta de uma tabela normativa integradora que pode servir de base para revisões futuras da NBR 6118 (Projeto de Estruturas de Concreto).

4. DISTRIBUIÇÃO REGIONAL DA AGRESSIVIDADE AMBIENTAL NO BRASIL

A heterogeneidade territorial brasileira impõe desafios singulares à classificação da agressividade ambiental. A análise integrada dos fatores climáticos, geográficos e de uso do solo permite identificar padrões regionais de exposição que transcendem a mera consulta tabular às normas e demandam uma leitura contextualizada do microambiente de cada obra. A Tabela 1 sintetiza a distribuição qualitativa das classes de agressividade ambiental predominantes em cada região.

Tabela 1 – Distribuição qualitativa das classes de agressividade ambiental (CAA) nas regiões brasileiras

Região	Classe I (Fraca)	Classe II (Moderada)	Classe III (Forte)	Classe IV (Muito Forte)
Norte	Ausente	Baixa	Alta	Média
Nordeste	Ausente	Baixa	Média	Alta
Centro-Oeste	Alta	Média	Média	Ausente
Sudeste	Baixa	Baixa	Alta	Média
Sul	Baixa	Média	Baixa	Ausente

Fonte: Elaboração própria, com base na ABNT NBR 6118:2014, ABNT NBR 12655:2023 e revisão da literatura.

4.1 Região Norte

Os grandes centros urbanos da Região Norte, como Manaus e Belém, apresentam condições ambientais que enquadram a maioria das estruturas externas nas classes III e IV. A umidade relativa do ar frequentemente supera 80%, as temperaturas médias anuais oscilam entre 26°C e 28°C, e a presença de águas naturais com potencial agressivo, incluindo águas ácidas de igarapés e rios de água preta com pH entre 4 e 5, cria um cenário de degradação acelerada. Esses fatores combinados favorecem a carbonatação e o ataque biogênico da matriz cimentícia, com formação de ácidos orgânicos e inorgânicos por ação microbiológica em ambientes de esgoto e drenagem. Estruturas industriais e de infraestrutura portuária estão sujeitas ainda à ação simultânea de sulfatos e cloretos, caracterizando Classe IV.

4.2 Região Nordeste

A Região Nordeste concentra o maior percentual de estruturas enquadradas na Classe IV no território nacional, em decorrência da extensa linha costeira e da ação intensa de aerossóis marinhos. Capitais como Fortaleza, Recife e Salvador apresentam concentrações de cloretos na atmosfera que chegam a ser dezenas de vezes superiores às registradas em zonas continentais. Em ambientes de até 1 km da orla marítima, o transporte de partículas de sal pelo vento carregador de brisa marinha promove a deposição de cloretos sobre superfícies de concreto, acelerando drasticamente o processo de iniciação da corrosão das armaduras. O estudo de Li et al. (2024) registrou, em edificações costeiras de países tropicais com exposição superior a 40 anos, concentrações de cloreto que excederam em mais de três vezes o limite crítico estabelecido pela norma ACI 318, resultando em fissuração severa do cobrimento. No interior do Nordeste, ambientes semiáridos e solos com elevado teor de sulfatos caracterizam predominantemente as classes II e III.

4.3 Região Centro-Oeste

A Região Centro-Oeste, marcada por regime climático de savana tropical com alternância entre estação seca e chuvosa, apresenta padrão de agressividade predominantemente situado nas classes II e III. Em Brasília, Goiânia e Cuiabá, a baixa umidade relativa na estação seca que pode cair abaixo de 20% em Brasília favorece a fissuração térmica e retração do concreto, fragilizando a barreira física de proteção das armaduras. Na estação chuvosa, os ciclos de molhagem e secagem promovem transporte de íons e carbonatação acelerada. A crescente pressão industrial em alguns polos, como o agronegócio em Mato Grosso, introduz agentes agressivos adicionais que podem elevar localmente a classificação para Classe III.

4.4 Região Sudeste

A Região Sudeste apresenta a maior variabilidade de condições ambientais do país, refletindo sua diversidade geográfica e o intenso processo de urbanização e industrialização. Em São Paulo, a combinação de elevada concentração de CO_2 e poluentes urbanos com umidade moderada resulta em taxas de carbonatação superiores às previstas para ambientes rurais de mesma classe normativa, enquadrando zonas densamente urbanizadas efetivamente na Classe III. No litoral paulista e fluminense, a influência marinha eleva sistematicamente a agressividade para a Classe IV. Belo Horizonte e o Vale do Aço concentram ambientes industriais de alta agressividade, com emissões de SO_2 e outros compostos que potencializam os mecanismos de corrosão. O estudo de Dominicini e Calmon (2017), aplicado às cidades de Vitória (ES) e Florianópolis (SC), demonstrou que a vida útil de estruturas com cobrimento mínimo normativo em ambientes de Classe III costeira pode ser inferior a 20 anos sem adoção de medidas de proteção complementares.

4.5 Região Sul

A Região Sul caracteriza-se por clima subtropical úmido, com invernos frios e verões quentes, e apresenta agressividade predominantemente nas classes II e III. O litoral gaúcho e catarinense, com destaque para Florianópolis e região dos Açores, está sujeito à ação marinha intensa, demandando a aplicação rigorosa dos critérios da Classe III ou mesmo IV em determinados microambientes costeiros. Em áreas continentais como Curitiba e Porto Alegre, os ciclos de molhagem e secagem associados a névoas ácidas em período de inversão térmica elevam localmente o risco de carbonatação. A ausência de ciclos de gelo-degelo na maior parte da região diferencia o Sul brasileiro de países de clima temperado frio, nos quais esse fenômeno constitui mecanismo adicional de degradação a ser normatizado.

5. PARÂMETROS DE PROJETO ASSOCIADOS ÀS CLASSES DE AGRESSIVIDADE

A correta tradução da classificação ambiental em requisitos de projeto é o passo decisivo para garantir a durabilidade estrutural ao longo da vida útil. A Tabela 2 consolida os parâmetros prescritivos estabelecidos pelas normas ABNT NBR 6118:2014 (Projeto de Estruturas de Concreto) e NBR 12655:2023 (Concreto de Cimento Portland – Preparo, Controle, Recebimento e Aceitação) para cada classe de agressividade ambiental, permitindo ao projetista visualizar de forma integrada as exigências que se intensificam progressivamente com o aumento do risco ambiental.

Tabela 2 – Parâmetros de projeto por classe de agressividade ambiental (CAA) segundo ABNT NBR 6118:2014 e ABNT NBR 12655:2023

Parâmetro	CAA I	CAA II	CAA III	CAA IV
fck mín. (MPa)	20	25	30	40
a/c máx.	0,65	0,60	0,55	0,45
Cobrimento nominal — laje (mm)	20	25	35	45
Cobrimento nominal — viga/pilar (mm)	25	30	40	50
Controle tecnológico	Simples	Padrão	Rigoroso	Especial

Fonte: ABNT NBR 6118:2014; ABNT NBR 12655:2023.

O cobrimento nominal é o parâmetro de maior impacto direto na durabilidade, pois representa a principal barreira física à penetração de agentes agressivos. Estudos de Cascudo e colaboradores demonstram que a variabilidade construtiva do cobrimento, frequentemente resultando em valores 20% a 30% inferiores ao especificado, é um dos principais vetores de deterioração prematura. Mumberger et al. (2022) demonstraram que, para vidas úteis de 100 anos em ambientes de Classe II, o cobrimento nominal deveria ser elevado para valores próximos aos exigidos pela norma australiana AS 3600:2018 para 60 anos, sinalizando que os requisitos da NBR 6118 estão calibrados para um horizonte temporal de 50 anos e podem ser insuficientes em projetos de maior longevidade.

A relação água/cimento atua diretamente sobre a porosidade e a permeabilidade do concreto. A redução de 0,65 (Classe I) para 0,45 (Classe IV) representa um salto qualitativo na compacidade da matriz cimentícia, com impactos significativos na resistência à penetração de cloretos e na taxa de carbonatação.

Em ambientes de Classe IV, o emprego de adições minerais como a sílica ativa, a cinza volante e a escória de alto-forno é fortemente recomendado tanto pela literatura técnica quanto pelos documentos de referência do IBRACON, pois essas adições refinam a estrutura dos poros e reduzem a permeabilidade a níveis impossíveis de alcançar apenas com o controle da relação água/cimento.

6. MANIFESTAÇÕES PATOLÓGICAS ASSOCIADAS ÀS CLASSES DE AGRESSIVIDADE

As manifestações patológicas observadas em estruturas de concreto armado apresentam correlação direta com a classe de agressividade do ambiente de exposição. Em ambientes de Classe I, a deterioração tende a ser lenta e confinada a processos de carbonatação superficial, fissuras de retração plástica e eflorescências ocasionais, em geral sem implicações estruturais relevantes nos primeiros ciclos de vida da edificação. A progressão para a Classe II introduz o risco de carbonatação progressiva com redução do pH da solução dos poros ao longo do tempo, favorecendo o início da corrosão das armaduras em elementos com cobrimento insuficiente ou de baixa qualidade.

A Classe III é caracterizada por manifestações mais severas: corrosão generalizada das armaduras com destacamento do cobrimento e manchas de ferrugem na superfície do concreto, ataque por sulfatos em fundações e estruturas enterradas em solos agressivos, e fissuração por expansão das barras corroídas. A Classe IV representa o estágio de maior vulnerabilidade, com corrosão acelerada por íons cloreto, perda de seção transversal das armaduras, desagregação do concreto e, em casos extremos, colapso localizado de elementos estruturais. Estruturas em zonas de respingo marinho classificadas na Classe IV apresentam as

taxas mais severas de deterioração, pois combinam a ação simultânea de ciclos de molhagem e secagem com alta concentração de cloretos.

A literatura internacional consolidada, referenciada por Mehta e Monteiro (2014) e Neville (2016), reforça que o modelo de Tutti, ao separar as fases de iniciação e propagação da corrosão, é essencial para compreender por que estruturas em ambientes de alta agressividade que atingem o fim da fase de iniciação em poucos anos frequentemente menos de 10 anos em zonas de respingo marinho sem proteção adicional progridem rapidamente para deterioração avançada na fase de propagação.

7. COMPARAÇÃO NORMATIVA INTERNACIONAL

A análise comparativa entre a normatização brasileira e as principais referências internacionais revela tanto alinhamentos técnicos quanto diferenças metodológicas relevantes. A Tabela 3 apresenta, de forma inédita, um quadro sinóptico comparativo entre as normas ABNT NBR 6118:2014 (Projeto de Estruturas de Concreto), Eurocode 2 (EN 1992-1-1:2023), ACI 318-19, BS 8500:2019 e AS 3600:2018, abrangendo os aspectos mais relevantes para a classificação da agressividade e o dimensionamento da durabilidade.

Tabela 3 – Comparação normativa internacional: classes de exposição e requisitos de durabilidade para concreto armado

Aspecto	NBR 6118:2014 (Brasil)	Eurocode 2 EN 1992-1-1:2023	ACI 318-19 (EUA)	BS 8500:2019 (Reino Unido)	AS 3600:2018 (Austrália)
N° de classes de exposição	4 (I a IV)	6 grupos (XC, XD, XS, XF, XA, X0)	4 categorias (F, W, S, C)	6 grupos alinhados ao Eurocode	4 (A1–A4) + subclasses
Abordagem metodológica	Prescritiva	Baseada em desempenho	Prescritiva/desempenho	Baseada em desempenho	Prescritiva/desempenho
Cobrimento nominal max. (mm)	50 (CAA IV)	55 (XS3)	75 (estruturas enterradas)	60 (XS3/RC80)	65 (A4)
a/c mínimo (ambiente marinho)	0,45	0,40–0,45 (XS3)	0,40 (C2)	0,40 (XS3)	0,40 (A4)
Vida útil de projeto prevista	50 anos (padrão)	50 ou 100 anos	Não especificado	50 ou 100 anos	50 ou 100 anos (AS)
Modelos de previsão de vida útil	Não normatizados	fib Model Code 2020	Não normatizados	Informativo (BS PD 6349)	Durability design provisions

Fontes: ABNT NBR 6118:2014; EN 1992-1-1:2023; ACI 318-19; BS 8500:2019; AS 3600:2018; Mumberger et al. (2022); Hasan et al. (2025).

A distinção metodológica mais relevante entre a normatização brasileira e as referências europeias reside na abordagem ao dimensionamento para durabilidade. Enquanto o Eurocode 2 e a BS 8500:2019 adotam uma perspectiva baseada em desempenho, articulada com os modelos probabilísticos do fib Model Code 2020, a NBR 6118:2014 (Projeto de Estruturas de Concreto) mantém uma abordagem essencialmente prescritiva. Hasan et al. (2025), em análise comparativa estatística entre ACI 318-19 e EN 1992-1-1:2023, demonstraram que o Eurocode prescreve cobrimentos nominais médios 9,6% superiores aos do ACI para

condições severas de exposição, com as maiores diferenças concentradas em ambientes marinhos, resultado que aponta para maior conservadorismo da norma europeia em ambientes de alta agressividade.

Mumberger et al. (2022) destacam que os parâmetros de durabilidade prescritos pela NBR 6118 (Projeto de Estruturas de Concreto) para as classes I e II são compatíveis com resultados obtidos pela norma australiana AS 3600 para vida útil de 60 anos, mas ficam aquém das exigências da BS 8500 para vidas úteis de 100 anos. Essa constatação é particularmente relevante para o contexto brasileiro de grandes obras de infraestrutura, pontes, túneis, portos que frequentemente demandam vidas úteis de projeto superiores a 50 anos, mas carecem de parâmetros normativos específicos para esse horizonte temporal.

A incorporação de modelos de previsão de vida útil é outro ponto de divergência significativa. O fib Model Code 2020 fornece um arcabouço probabilístico unificado para a previsão do avanço da frente de carbonatação e da penetração de cloretos, parametrizado por dados climáticos e de material. Na normatização brasileira, esses modelos não são normatizados, embora existam estudos nacionais relevantes como os de Possan (2010) e as análises de Dominicini e Calmon (2017) para Vitória e Florianópolis que demonstram a viabilidade de sua aplicação ao contexto tropical brasileiro.

8. IMPLICAÇÕES NO PROJETO ESTRUTURAL E NA GESTÃO DO CICLO DE VIDA

O impacto da classe de agressividade no projeto estrutural vai muito além da consulta às tabelas normativas de cobrimento e resistência mínima. A correta classificação ambiental deve ser entendida como uma decisão estratégica que permeia todas as fases do ciclo de vida da estrutura, desde a concepção até a manutenção preventiva e a eventual intervenção de reparo ou reforço.

Na fase de projeto, a agressividade ambiental determina a escolha do sistema estrutural, dos materiais, dos detalhes construtivos e das especificações de durabilidade. Projetos em ambientes de classes III e IV demandam o emprego de concretos de alto desempenho com adições minerais ativas, a adoção de cobrimentos nominais superiores aos mínimos normativos, o emprego de aditivos inibidores de corrosão em situações de risco extremo e o detalhamento cuidadoso de geometrias que evitem o acúmulo de água e a umidade superficial prolongada. A escolha do cimento em particular, a utilização de cimentos resistentes a sulfatos (RS) em solos agressivos e de cimentos com escória (CPIII) ou pozolânico (CPIV) em ambientes com cloretos tem impacto determinante na permeabilidade e na resistência química do concreto.

Na fase de execução, a garantia do cobrimento nominal especificado em projeto é imperativa. Estudos revisados neste trabalho indicam que desvios de cobrimento da ordem de 20% a 30% abaixo do valor especificado podem reduzir a vida útil de iniciação da corrosão à metade do previsto em projeto, comprometendo de forma irreversível a durabilidade da estrutura antes mesmo do fim da fase de construção. O controle rigoroso da relação água/cimento, a cura adequada por período mínimo de sete dias em ambientes de alta agressividade e a inspeção do cobrimento durante a concretagem são medidas indispensáveis.

Na fase de uso e manutenção, a implantação de planos de inspeção periódica baseados em risco com frequência e escopo determinados pela classe de agressividade ambiental permite a detecção precoce de manifestações patológicas e a intervenção em fase de iniciação da corrosão, quando os custos de reparo são substancialmente inferiores aos das intervenções estruturais avançadas. A relação de Sitter, popularizada por Helene, estabelece que os custos de reparo crescem na razão de 1:5:25:125 conforme se passa das fases de projeto, execução, detecção e intervenção tardia, respectivamente, argumento econômico poderoso para o investimento em classificação ambiental rigorosa desde a concepção.

9. DISCUSSÃO

Os resultados desta pesquisa evidenciam que a correta classificação da agressividade ambiental no contexto brasileiro requer uma abordagem significativamente mais refinada do que a simples consulta às tabelas normativas da NBR 6118:2014 (Projeto de Estruturas de Concreto). A análise regionalizada demonstrou que ambientes urbanos, frequentemente enquadrados na Classe II por critério genérico,

podem apresentar condições de microambiente elevada concentração de CO_2, presença de SO_2 e NO_x, ciclos intensos de molhagem e secagem que os aproximam, na prática, dos requisitos da Classe III. Essa subestimação sistemática do risco pode resultar em especificações de projeto insuficientes e em deterioração prematura de estruturas concebidas para vida útil de 50 anos.

A comparação normativa internacional revelou que o sistema brasileiro apresenta cobertura adequada para o horizonte de 50 anos em condições de agressividade moderada, mas carece de parâmetros específicos para vidas úteis prolongadas de 75 a 100 anos, e, para microambientes de alta agressividade em regiões tropicais úmidas. A introdução de classes de exposição mais granulares, alinhadas à lógica dos grupos de exposição do Eurocode 2 (XC, XD, XS, XF, XA), poderia aprimorar a capacidade do sistema normativo brasileiro de capturar a complexidade dos ambientes tropicais, nos quais a combinação simultânea de alta temperatura, alta umidade e agentes agressivos múltiplos cria sinergias não previstas pelos modelos de deterioração calibrados para climas temperados.

A incorporação de modelos probabilísticos de previsão de vida útil como os calibrados por Mumberger et al. (2022) e os desenvolvidos por Possan (2010) para o contexto brasileiro representa a principal oportunidade de evolução normativa. Esses modelos permitem ao projetista estimar, com base em dados climáticos regionais e parâmetros de material, a probabilidade de corrosão em um dado horizonte temporal, superando as limitações da abordagem prescritiva e habilitando decisões de projeto mais fundamentadas e economicamente eficientes.

Quanto às limitações desta pesquisa, registra-se que a ausência de dados experimentais próprios e de levantamentos de campo limita as conclusões ao plano qualitativo. A classificação regional proposta baseia-se em revisão da literatura e análise normativa, sem validação por meio de medições in situ de concentrações de agentes agressivos ou de taxas de carbonatação em diferentes regiões. Estudos futuros que integrem redes de monitoramento ambiental, ensaios de durabilidade em campo e análise estatística de bancos de dados de patologias estruturais poderão fornecer evidências quantitativas para embasar revisões das normas brasileiras e calibrar modelos de previsão de vida útil adaptados ao contexto tropical.

10. CONCLUSÕES

Este artigo investigou as classes de agressividade ambiental do concreto armado no Brasil, integrando revisão normativa, análise regional e comparação internacional para propor uma visão abrangente e atualizada do tema. As principais conclusões são:

A diversidade climática e ambiental brasileira exige uma abordagem regionalizada da classificação da agressividade, sendo insuficiente a aplicação genérica das classes normativas sem consideração das condições microambientais locais. Ambientes costeiros e industrializados concentram a maior incidência de estruturas em Classes III e IV, com especial criticidade nas regiões Norte e Nordeste.

Os parâmetros de projeto prescritos pelas normas ABNT NBR 6118:2014 (Projeto de Estruturas de Concreto) e NBR 12655:2023 (Concreto de Cimento Portland – Preparo, Controle, Recebimento e Aceitação) são tecnicamente consistentes para o horizonte de 50 anos, mas carecem de valores específicos para vidas úteis prolongadas, lacuna que pode ser suprida pela incorporação de modelos probabilísticos de previsão de vida útil calibrados para o clima tropical brasileiro.

A comparação normativa internacional demonstrou que o Eurocode 2, a BS 8500:2019 e a AS 3600:2018 adotam abordagens baseadas em desempenho que oferecem maior granularidade na classificação dos ambientes e maior cobertura para horizontes temporais superiores a 50 anos. A adoção parcial desses instrumentos em especial os modelos do fib Model Code 2020 pode representar uma evolução significativa na normatização brasileira de durabilidade.

Como contribuição original, este trabalho propõe a primeira tabela comparativa normativa integrando cinco referências nacionais e internacionais (NBR 6118, Eurocode 2, ACI 318, BS 8500 e AS 3600), e apresenta uma distribuição qualitativa revisada e expandida das classes de agressividade ambiental nas regiões brasileiras, incorporando a Classe I à análise e distinguindo os contextos costeiro, urbano e industrial dentro de cada região.

Estudos futuros deverão avançar na direção de validação experimental das classificações propostas, por meio de campanhas de monitoramento ambiental em múltiplas regiões, ensaios de durabilidade em estruturas existentes e desenvolvimento de mapas de agressividade ambiental de maior resolução territorial para o Brasil.

11. REFERÊNCIAS

ABNT – Associação Brasileira de Normas Técnicas. 2014. **NBR 6118: Projeto de Estruturas de Concreto** – Procedimento. Rio de Janeiro: ABNT.

ABNT – Associação Brasileira de Normas Técnicas. 2023. **NBR 12655: Concreto de Cimento Portland – Preparo, Controle, Recebimento e Aceitação**. Rio de Janeiro: ABNT.

ACI – American Concrete Institute. 2019. **ACI 318-19: Building Code Requirements for Structural Concrete and Commentary**. Farmington Hills: ACI.

Bolina, F. L., e B. F. Tutikian. 2016. **"Specification Faced with Durability to Meet Superior Level of Performance in Structural Elements Buried."** Revista IBRACON de Estruturas e Materiais 9 (2): 275–296. https://doi.org/10.1590/s1983-41952016000200008.

BSI – British Standards Institution. 2019. **BS 8500-1: Concrete – Complementary British Standard to BS EN 206**. Londres: BSI.

Dominicini, W. K., e J. L. Calmon. 2017**. "Computational Modeling for Predicting Corrosion Initiation in Reinforced Concrete Structures."** Revista IBRACON de Estruturas e Materiais 10 (6): 1205–1244. https://doi.org/10.1590/s1983-41952017000600006.

EN 1992-1-1. 2023. **Eurocode 2: Design of Concrete Structures – Part 1-1: General Rules and Rules for Buildings. Brussels:** CEN.

Hasan, M., et al. 2025. **"A Comparative Analysis of Concrete Cover Design Methodologies: ACI 318-19 versus EN 1992-1-1:2023."** Journal of Umm Al-Qura University for Engineering and Architecture. https://doi.org/10.1007/s43995-025-00268-0.

Helene, P., e F. Andrade. 2010. **Concreto de Cimento Portland**. In: Isaia, G. C. (ed.). Concreto: Ciência e Tecnologia. São Paulo: IBRACON.

Li, J., et al. 2024. **"A Review of Chloride Transport in Concrete Exposed to the Marine Atmosphere Zone Environment: Experiments and Numerical Models."** Construction and Building Materials 419: 135521. https://doi.org/10.1016/j.conbuildmat.2024.135521.

Mehta, P. K., e P. J. M. Monteiro. 2014. **Concreto: Microestrutura, Propriedades e Materiais.** São Paulo: IBRACON.

Mumberger, F. B., B. F. Tutikian, e F. L. Bolina. 2022. **"Proposed Durability Parameters for Reinforced Concrete Structures with Design Service Life between 50 Years and 100 Years in Brazil."** Revista IBRACON de Estruturas e Materiais 15 (6): e15603. https://doi.org/10.1590/S1983-41952022000600003.

Neville, A. M. 2016. **Properties of Concrete**. 5. ed. Londres: Pearson.

Rodrigues, F. A., et al. 2024. **"Chloride Penetration and Material Characterisation of Carbonated Concrete under Various Simulated Marine Environment Exposure Conditions."** Construction and Building Materials 425: 136046. https://doi.org/10.1016/j.conbuildmat.2024.136046.

Standards Australia. 2018. **AS 3600-2018: Concrete Structures**. Sydney: Standards Australia.

Cinpar 2026
XXII International Conference on Building Pathology and Constructions Repair
15th to 17th July 2026 - Lisboa, Portugal

Impact of Defects on the Deflection Response of Interlocking Pavements

José Levi Chaves de SOUSA[1], Felipe Silveira Cavalcante BEZERRA[2], Webert Brasil Cirilo da SILVA[3], Suelly Helena de Araújo BARROSO[4], Luís Guilherme de Picado SANTOS[5], Francisco Heber Lacerda de OLIVEIRA[6]

[1] Federal University of Ceará, Fortaleza Campus, Brazil, levi.chaves@det.ufc.br
[2] Federal University of Ceará, Fortaleza Campus, Brazil, felipe.silveira@det.ufc.br
[3] Federal University of Ceará, Fortaleza Campus, Brazil, webertbrasil@det.ufc.br
[4] Federal University of Ceará, Fortaleza Campus, Brazil, suelly@det.ufc.br
[5] Instituto Superior Técnico, University of Lisbon, Portugal, luispicadosantos@tecnico.ulisboa.pt
[6] Federal University of Ceará, Fortaleza Campus, Brazil, heber@det.ufc.br

Abstract: Interlocking pavers are widely used on urban roads and in areas with light to moderate traffic due to their ease of installation, localized maintenance, and aesthetic and environmental benefits. However, over their service life, these pavements are susceptible to various defects, such as damaged pavers, rutting, heave, and pumping, which may compromise their structural performance. In this context, deflection measurements are used to evaluate the pavement's bearing capacity and its response to applied loads. Therefore, this study aims to assess whether surface defects influence the deflection values of interlocking pavements by examining the correlation between these variables. An in situ survey was conducted, including defect identification and classification using the Pavement Condition Index (PCI), along with deflection measurements collected on an experimental interlocking pavement section subdivided into five segments with distinct structural configurations. Pearson's correlation coefficient (r) was applied to evaluate the relationships between the analyzed variables. The results indicate an association between deflection values and defects such as rutting, excessive joint spacing, and loss of jointing material. A negative correlation was also observed between deflection and PCI, suggesting that poorer surface conditions are associated with increased structural deformability. These findings demonstrate that integrating functional and structural indicators enhances the understanding of interlocking pavement performance and the interaction between surface defects and load-bearing capacity.

Keywords: Defects; Deflection; Correlation; PCI; FWD.

1. Introduction

Interlocking pavements have been increasingly adopted in urban roads, residential areas, and industrial zones due to their durability and construction versatility (Di Mascio et al. 2019). This solution represents an alternative to conventional asphalt pavements, particularly in regions subjected to extreme climatic conditions and heavy traffic (Rathan & Sunitha, 2021).

Unlike asphalt pavements, interlocking pavements function as an integrated system in which load transfer occurs through the interlock between individual blocks. Their structural stability is ensured by friction within sand-filled joints, which minimizes rotation and displacement of the units. Consequently, interlocking pavements should be analyzed as multilayer systems, where mechanical behavior depends on the interaction between the surface layer, bedding sand, and underlying layers (Lin et al. 2016).

The mechanical performance of this type of pavement is influenced by the laying pattern. Among the available configurations, the herringbone pattern provides better stress distribution and greater resistance to permanent deformation compared to stretcher bond patterns (Lin et al. 2018). Additionally, block

thickness significantly affects structural behavior, influencing both service life and surface deflection control. These parameters are therefore essential for structural evaluation (Di Mascio et al. 2019).

Functional evaluation is typically performed using the Pavement Condition Index (PCI) (Hein et al., 2009), which enables standardized identification of defects such as damaged pavers, depressions, and excessive joint width, providing an overall condition rating (Zoccali et al. 2017). The systematic application of PCI supports performance prediction and decision-making regarding maintenance and rehabilitation (M&R) (Hein et al. 2009).

Despite advances in visual assessment standardization and deflection monitoring (Lin et al. 2016), there remains a need to better understand how surface defects correlate with structural response measured in the field (Singh et al. 2012). Integrating these approaches is essential for optimizing M&R strategies while ensuring user comfort and safety.

Given the above, this study aims to evaluate whether surface defects affect the deflection values of interlocking pavements, based on the correlation between these variables. The study in question was conducted on an experimental section, specifically constructed for research purposes, consisting of different sections with variations in layer materials and low traffic volume. Thus, the results obtained have limitations due to the short length evaluated, which may influence the observed structural response.

2. Literature Review

Interlocking pavements exhibit structural behavior governed by load transfer between blocks, joint friction, and lateral confinement provided by adjacent layers (Panda & Ghosh, 2002). Unlike continuous asphalt pavements, they behave as segmented systems whose equivalent stiffness depends on joint integrity, jointing material quality, and base/subbase conditions (Füssl et al. 2016).

When properly constructed, interlocking pavements can achieve structural performance comparable to asphalt pavements, with efficient stress distribution and controlled vertical deformation (García and Corte, 2021). Instrumented field tests show that stresses transmitted to lower layers depend primarily on the stiffness of the block layer and base (Khanal et al. 2013).

The geometry of paving units and laying patterns, such as the 45° herringbone, also influence resistance to horizontal displacement (Hengl et al. 2018). Furthermore, permeable interlocking pavements have demonstrated effectiveness in reducing runoff while maintaining structural stability under light to moderate traffic (Rathan et al. 2021).

Structural evaluation is essential for understanding the behavior and performance of pavement layers. The use of equipment such as the Heavy Weight Deflectometer (HWD) and the Benkelman Beam enables the measurement of surface deflections, supporting model calibration and the validation of block layer stiffness as a function of its thickness (García and Corte, 2021). In addition, strain and pressure sensors embedded within the structure can continuously monitor the effects of heavy vehicles, enabling load pulses to be correlated with the in situ mechanical response (Khanal et al. 2013; Jones et al. 2016).

One of the primary objectives of functional evaluation, combined with appropriate maintenance practices, is to maximize return on investment while ensuring safe, comfortable, and operational road conditions for users (Fernandes Júnior et al. 1996). Studies adopting integrated approaches indicate that different condition indices, such as the Pavement Condition Index (PCI) and the International Roughness Index (IRI), may yield different classifications for the same road section. In this context, the PCI has been identified as more representative for capturing the specific characteristics of defects in interlocking pavements (Sousa et al. 2024).

These differences are related to the inherent characteristics of this pavement type. The deterioration of interlocking pavements is associated with a reduced ability to transfer forces between blocks, leading to a decrease in the stiffness of the wearing course. Among the main factors contributing to this process are

joint-related defects, particularly the loss of jointing sand, which can reduce pavement service life by up to five years (Bezerra and Oliveira, 2022). In areas subjected to heavy traffic, braking and acceleration further intensify relative displacements between blocks and promote edge breakage when horizontal interlocking is insufficient (Hengl et al. 2018).

It is therefore evident that research correlating field-observed defects with in situ deflection parameters in interlocking pavements remains limited (García and Corte, 2021; Singh et al., 2012). This gap highlights the need for integrated studies that relate functional and structural conditions to better understand whether surface defects influence deflection values and, consequently, the assessment of the structural capacity of interlocking pavements.

3. Methodology

The research methodology was structured in six stages: (i) selection of the study site; (ii) application of the PCI and FWD tests; (iii) tabulation of the data collected in the field; (iv) statistical analysis of the data; (v) preparation of graphs, tables, and figures; and (vi) presentation and interpretation of the results.

The first stage consisted of defining the test section of the interlocking pavement. The section was specifically designed for research purposes, with each segment constructed using different materials in its structural layers. The total area was 175 m² (25 m long × 7 m wide), located at the Pici Campus of the Federal University of Ceará (UFC), in Fortaleza, Brazil (Figure 1).

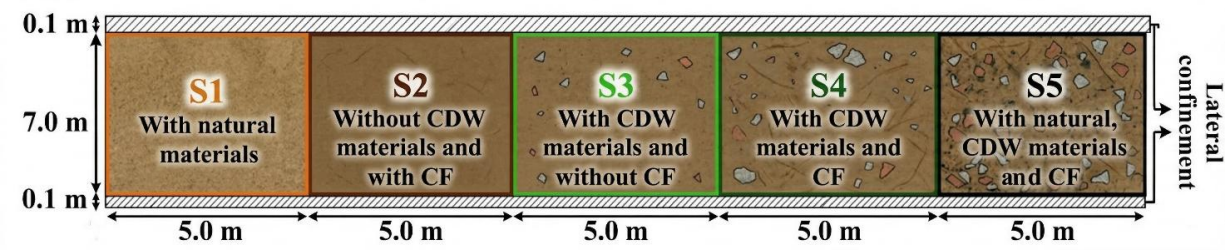


Figure 1 – Experimental concrete interlocking block pavement's sections

The section was divided into five equal experimental segments (S1 to S5), in which natural materials and by-products derived from construction and demolition waste (CDW) were used, along with the incorporation of coconut fibers (CF). The adopted layer thicknesses were 15 cm for the base and subbase, and 0.5 cm, 4.0 cm, and 8.0 cm for the jointing material, bedding layer, and paving blocks, respectively, in accordance with ABNT (2013).

In the second stage, PCI values were determined, ranging from 0 to 100, where 0 represents functional failure and 100 indicates good condition. Defect density and deduction values were also calculated in accordance with ASTM (2024). The entire experimental section was evaluated, covering all five segments, thereby eliminating the need for statistical sampling. Deflections were measured using a Falling Weight Deflectometer (FWD), in accordance with DNER (1996). In the third stage, following field data collection, the results were tabulated in a spreadsheet. In the fourth stage, the dataset was exported to R (version 4.4.0) and analyzed in RStudio. For each pavement section, FWD data were statistically analyzed using Student's t-distribution at a 95% confidence level. Subsequently, Pearson's correlation coefficient was calculated based on defect data and PCI values for each section.

In the fifth stage, graphs and figures were generated in RStudio to visually compare the results and support the interpretation of the functional condition of the interlocking pavement. Finally, in the sixth stage, the results were presented and discussed, enabling an assessment of the performance of the evaluated pavement.

4. Results and Discussions

The PCI graph by section illustrates the variability in functional performance along the evaluated stretch (Figure 2). It presents the PCI value for each sample unit.

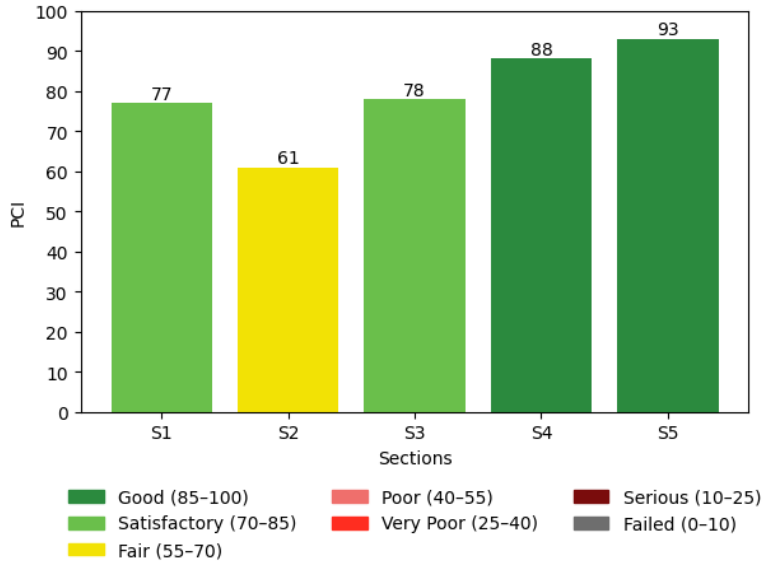


Figure 2 – PCI by Section

The PCI values range from 61 to 93, indicating a functional condition from satisfactory to good, except for Section 2, which is classified as fair. Sections 4 and 5 exhibited the highest indices, suggesting better functional integrity in these stretches. This variation in PCI reflects non-homogeneous pavement behavior, possibly due to differences in materials used across the sections (recycled materials from CDW and CF). Figure 3 relates each section to its respective deduction values and highlights the influence of defect types on the pavement's functional performance.

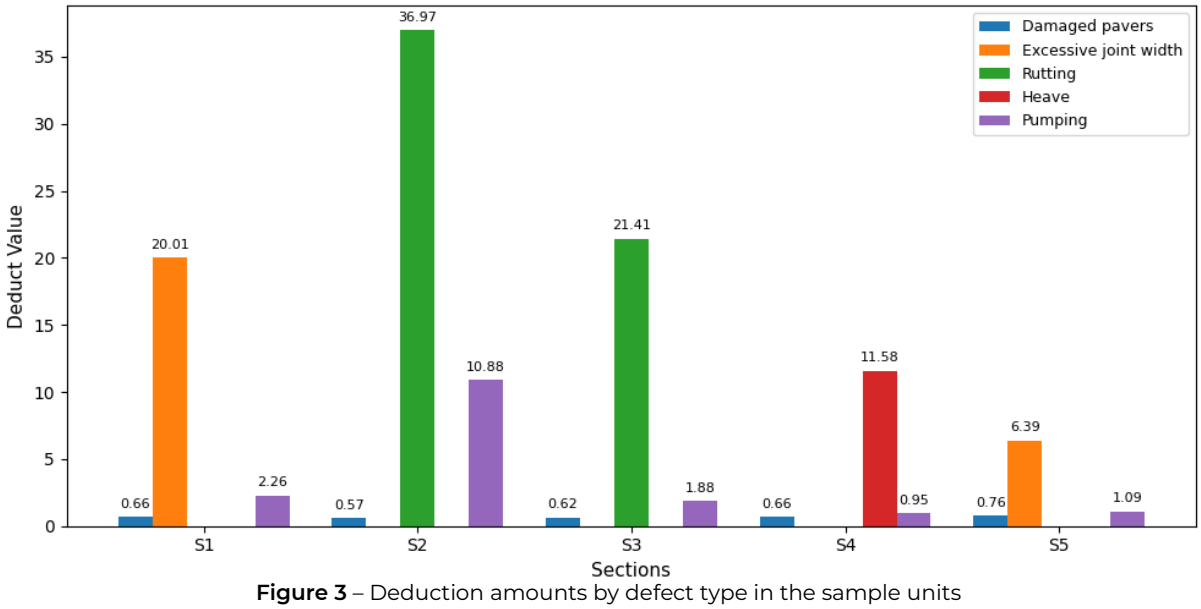


Figure 3 – Deduction amounts by defect type in the sample units

Section 2 exhibits the highest deduction values, primarily due to rutting, which explains its lower PCI compared to the other sections. In general, defects associated with structural deformations have a greater

impact, whereas surface defects, such as damaged pavers, contribute less to index reduction, according to ASTM (2024) tables. Figure 3 also shows that sections with lower deduction values correspond to better functional condition, reinforcing the inverse relationship between the severity and quantity of defects and the performance of the evaluated pavement. The deflection results obtained from the FWD are presented in Table 1.

Table 1 – Statistical Analysis (Deflections)

Round	Deflection (µm)				
	S1	S2	S3	S4	S5
1	461	449	342	445	340
2	415	398	334	396	319
3	423	406	343	406	324
4	412	393	333	394	318
5	425	403	344	399	315
6	416	392	338	388	310
Mean	425	407	339	405	321
Standard Deviation (sd)	18	21	5	21	10
Number of samples	6	6	6	6	6
Value t	2,02	2,02	2,02	2,02	2,02
Characteristic Deflection (µm)	440	424	343	422	330

The largest characteristic deflection was recorded in Section 1, with a value of 440 µm, corresponding to the section with the second-lowest PCI of 77. In contrast, the smallest characteristic deflection was observed in Sample Unit 05, at 330 µm, which had the highest PCI of 93. Thus, the deflection values varied by 110 µm across the analyzed sections. It is also noteworthy that Section 2, which exhibited the lowest PCI, had the second-highest characteristic deflection. Overall, a trend of increasing deflection with decreasing PCI is evident.

Among the analyzed parameters, rutting exhibited the lowest correlation with deflection values (Table 2), with a coefficient of -0.10. However, this result does not align with the expected theoretical behavior, since rutting accumulation is normally associated with a loss of pavement structural capacity, as reported by Bezerra and Oliveira (2022). Therefore, greater rutting would be expected to correspond to higher deflection values, as both variables indicate the progression of pavement deterioration.

Table 2 – Deflection Values vs. Rutting

Deflection × Rutting		
Section	Deflection (µm)	Density (%)
1	440	0
2	424	6
3	343	5,29
4	422	0
5	330	0

The discrepancy between the observed results and the expected behavior may be primarily attributed to the small sample size, consisting of only five observations. This limitation reduces the statistical reliability of the analyses and increases the sensitivity of the correlation coefficient to potential outliers. From a mechanical-structural perspective, rutting represents one of the most significant defects in interlocking pavements. This type of deterioration can cause block displacement and joint opening, reducing lateral friction between the blocks and compromising the interlocking mechanism responsible for proper load distribution within the pavement structure (Bezerra and Oliveira, 2022). Similarly, damaged pavers exhibited a negative correlation of -0.53 with deflections (Table 3).

Table 3 – Deflection Values vs. Damaged Pavers

Deflection × Damaged Pavers		
Section	**Deflection (µm)**	**Density (%)**
1	440	0,54
2	424	0,40
3	343	0,49
4	422	0,54
5	330	0,69

One possible explanation for this result is the low proportion of damaged pavers in the analyzed sample, which diminishes their influence on deflection values compared to other variables. In interlocking pavements, structural performance primarily depends on the transfer of forces between adjacent elements. Therefore, the isolated presence of damaged pavers may be partially offset by the collective behavior of the surrounding elements, reducing the impact of this defect when considered in isolation. Conversely, defects such as heave, excessive joint width, and pumping of jointing material exhibited a positive correlation with deflection values, with coefficients of 0.36, 0.39, and 0.37, respectively (Table 4).

Table 4 – Deflection × Heave × Excessive Joint Width × Pumping

Section	**Deflection (µm)**	**Heave**	**Excessive Joint Width**	**Pumping**
		Density (%)		
1	440	0	17,14	30,86
2	424	12,86	0	31,43
3	343	0	0	26,06
4	422	0	0	10,03
5	330	0	4,29	11,43

An increase in the density of these defects tends to compromise force transfer between panels in the joint regions, reducing the interlocking level of the pavement and increasing the deformability of the structural system, which can result in higher deflection values. However, the moderate correlation strengths indicate that, when analyzed individually, these defects are insufficient to fully explain the variation in observed deflections, suggesting the presence of interactions among multiple factors influencing the pavement's structural performance.

Regarding the PCI, a negative correlation of -0.49 was observed with deflection values (Table 5). This inverse relationship aligns with expected behavior, as lower PCI values indicate poorer pavement surface condition, which may lead to reduced structural stiffness and, consequently, higher deflection values. Furthermore, since the PCI calculation combines multiple defects into a single condition indicator, it provides a more comprehensive representation of the pavement's overall condition, simultaneously accounting for various factors that influence its performance.

Table 5 – Deflection vs. PCI

Deflection × PCI		
Section	**Deflection (μm)**	**PCI**
1	440	77
2	424	61
3	343	78
4	422	88
5	330	93

Finally, it should be noted that the results reflect the specific behavior of the analyzed section; the correlation coefficients cannot be generalized to interlocking pavements in a broader context. The small sample size also limits the precise identification of factors influencing deflection values. Despite this limitation, the analysis allowed the identification of trends between surface defects and the pavement's structural response, contributing to the understanding of this pavement type under real-world field conditions. In small samples, Pearson's correlation coefficient is sensitive to extreme values, so the behavior of a single section can affect the analysis results. Nevertheless, the observed trends provide a foundation for future studies with larger datasets, also incorporating aspects related to ride comfort and user safety.

5. Conclusions

This article analyzed the relationship between defects and the structural response of an interlocking pavement by examining the correlation between Pavement Condition Index (PCI) results and deflection values obtained from the Falling Weight Deflectometer (FWD) test. Despite the limitations presented, the results indicated that some defects, such as heave, excessive joint width, and pumping, showed a positive correlation with deflection values, suggesting that an increase in the occurrence of these defects may contribute to reduced stiffness and greater deformability of the pavement.

On the other hand, defects such as rutting and damaged pavers showed negative correlations, a behavior that may be related to the small sample size and the influence of specific characteristics of the evaluated sections. The analysis also revealed a negative correlation between PCI and deflection values, indicating that poorer pavement functional condition corresponds to greater deformations under load. The importance of functional evaluation as a complementary tool for understanding the structural performance of interlocking pavements is evident. In future studies, incorporating the International Roughness Index (IRI) into interlocking pavements could broaden the functional analysis and allow for an assessment of the relationship between ride comfort and the defects identified in the pavement.

In general, an integrated analysis of functional and structural parameters can provide a more comprehensive assessment of interlocking pavement performance. Although the correlation coefficients obtained cannot be generalized due to the limited number of observations, the identified trends offer

relevant insights into the interaction between surface defects and structural response in interlocking pavements.

Acknowledgments

This study was financed in part by the Coordenação de Aperfeiçoamento de Pessoal de Nível Superior – Brasil (CAPES) – Finance Code 001.

References

Associação Brasileira De Normas Técnicas. NBR 15953:2013: Pavimento intertravado com peças de concreto – execução. Rio de Janeiro: ABNT, 2013.

ASTM. 2024. Standard Practice for Pavement Condition Index Surveys for Interlocking Concrete Roads and Parking Lots. ASTM E2840-11(2024). West Conshohocken, PA: ASTM International.

Bezerra, F. S. C., and F. H. L. Oliveira. 2022. "Effects of Degradation on the Service Life of an Interlocked Pavement." International Journal of Pavement Engineering 23 (13): 4625–35. https://doi.org/10.1080/10298436.2022.2139376.

Di Mascio, Paola, Laura Moretti, and Americo Capannolo. 2019. "Concrete Block Pavements in Urban and Local Roads: Analysis of Stress-Strain Condition and Proposal for a Catalogue." Journal of Traffic and Transportation Engineering (English Edition) 6 (6): 556–65. https://doi.org/10.1016/j.jtte.2018.06.003.

DNER (Departamento Nacional de Estradas de Rodagem). 1996. DNER 273/96: Determinação das deflexões utilizando deflectométrico de impacto tipo "Falling Weight Deflectometer – FWD". Rio de Janeiro: DNER.

Fernandes Júnior, José Leomar, S. A. Margarido, e L. F. Zerbini. 1996. "Priorização em sistemas de gerência de pavimentos urbanos." In Anais da 7ª Reunião de Pavimentação Urbana. São José dos Campos: Associação Brasileira de Pavimentação.

Füssl, J., H. Hengl, L. Eberhardsteiner, W. Kluger-Eigl, and R. Blab. 2016. "Numerical Simulation Tool for Paving Block Structures Assessed by Means of Full-Scale Accelerated Pavement Tests." International Journal of Pavement Engineering 17 (7): 608–21. https://doi.org/10.1080/10298436.2016.1224410.

García, Gabriel, and Nicolás Corte. 2021. "Experimental Study on an In Situ Concrete Block Pavement under Heavy Traffic Loads." International Journal of Pavement Engineering 22 (12): 1548–61. https://doi.org/10.1080/10298436.2021.1902523.

Hein, David K., Brian Aho, and Robert Burak. 2009. "Development of a Pavement Condition Index Procedure for Interlocking Concrete Pavements." In 9th International Conference on Concrete Block Paving, Buenos Aires, Argentina, October 18-21.

Hengl, H. L., W. Kluger-Eigl, M. Lukacevic, R. Blab, and J. Füssl. 2018. "Horizontal Deformation Resistance of Paving Block Superstructures—Influence of Paving Block Type, Laying Pattern, and Joint Behavior." International Journal of Pavement Research and Technology 11 (6): 541–51. https://doi.org/10.1016/j.ijprt.2018.08.001.

Jones, David J., Hui Li, Rongzong Wu, John T. Harvey, and David R. Smith. 2016. "Full-Scale Structural Testing of Permeable Interlocking Concrete Pavement to Develop Design Guidelines." In International Low Impact Development Conference 2016, 212–25.

Khanal, Shila, Susan L. Tighe, and Robert Bowers. 2013. "Pavement Performance Mechanics of Interlocking Concrete Paver Crosswalk Designs." Canadian Journal of Civil Engineering 41 (7): 583–91. https://doi.org/10.1139/cjce-2012-0222.

Lin, Wuguang, Dongkyu Kim, SungWoo Ryu, Han Hao, Ying-En Ge, and Yoon-Ho Cho. 2018. "Evaluation of the Load Dissipation Behavior of Concrete Block Pavements with Various Block Shapes and Construction

Patterns.” Journal of Materials in Civil Engineering 30 (2): 04017291. https://doi.org/10.1061/(ASCE)MT.1943-5533.0002113.

Lin, Wuguang, Yoon-ho Cho, and In Tai Kim. 2016. “Development of Deflection Prediction Model for Concrete Block Pavement Considering the Block Shapes and Construction Patterns.” Advances in Materials Science and Engineering 2016: 5126436. https://doi.org/10.1155/2016/5126436.

Panda, Bikasha Chandra, and Ashok Kumar Ghosh. 2002. “Structural Behavior of Concrete Block Paving. II: Concrete Blocks.” Journal of Transportation Engineering 128 (2): 130–35. https://doi.org/10.1061/(ASCE)0733-947X(2002)128:2(130.

Rathan, Arjun Siva, R. T., and V. Sunitha. 2021. “Development of Design Procedure for Interlocking Concrete Block Pavement.” International Journal of Pavement Engineering 24 (1): 1990290. https://doi.org/10.1080/10298436.2021.1990290.

Rathan, Arjun Siva, V. Aravinda Sai, and V. Sunitha. 2021. “Mechanical and Structural Performance Evaluation of Pervious Interlocking Paver Blocks.” Construction and Building Materials 292: 123438. https://doi.org/10.1016/j.conbuildmat.2021.123438.

Singh, Yendrembam Arunkumar, Teiborlang Lyngdoh Ryntathiang, and Konjengbam Darunkumar Singh. 2012. “An Investigation of Plastic Cell Filled Concrete Block Pavement (PCCBP) Overlay.” Road Materials and Pavement Design 13 (2): 345–59. https://doi.org/10.1080/14680629.2012.676806.

Sousa, José Levi Chaves de, Felipe Silveira Cavalcanti Bezerra, Bruno Reges Almeida de Brito, and Francisco Heber Lacerda de Oliveira. 2024. “Análise Comparativa de Métodos de Avaliação Funcional em Pavimentos Intertravados.” In Anais da 50ª Reunião Anual de Pavimentação (RAPv).

Zoccali, Pablo, Giuseppe Loprencipe, and Andrea Galoni. 2017. “Sampietrini Stone Pavements: Distress Analysis Using Pavement Condition Index Method.” Applied Sciences 7 (7): 669. https://doi.org/10.3390/app7070669.

Cinpar 2026
XXII International Conference on Building Pathology and Constructions Repair
15th to 17th July 2026 - Lisboa, Portugal

Infrastructure, Architecture, and Tourism Urbanization: Digital Modeling of the Impacts of the Sabiaguaba Environmental and Gastronomic Complex, Fortaleza, Ceará, Brazil.

Ricardo Alexandre PAIVA[1], José Lucas Pereira DANTAS[2]

[1] Universidade Federal do Ceará, Fortaleza - CE, Brasil, ricardopaiva@ufc.br
[2] Universidade Federal do Ceará, Fortaleza - CE, Brasil, josedantas@arquitetura.ufc.br

Abstract: In Fortaleza, the capital of Ceará, a significant process of tourism urbanization is underway due to the state's substantial involvement and intervention through: i) ideological frameworks aimed at enhancing the city's image and integrating Fortaleza and Ceará into global economic flows, albeit in a peripheral manner; ii) public tourism policies and urban policies at the federal, state, and municipal levels; iii) and socio-spatial interventions in infrastructure and the construction of large urban projects geared toward tourism. Among these interventions, the creation of the Sabiaguaba Environmental and Gastronomic Complex stands out; it is located within a conservation area at the mouth of the Cocó River. In this context, the objective of this study is to investigate the socio-spatial impacts of the infrastructure and architecture of the Sabiaguaba Environmental and Gastronomic Complex, inaugurated in 2022, in Fortaleza, Ceará. The methodology is grounded in theoretical assumptions related to the concept of tourism urbanization, a phenomenon driven by leisure and consumption; and in practical assumptions, through the use of digital technologies. A practical reality-capture device was adopted through surveys using an Unmanned Aerial Vehicle (UAV) to obtain photos and footage, the information from which was georeferenced. Based on this data, a digital model of the complex was developed using the BIM (Building Information Modeling) platform, enabling a detailed spatial analysis of the project's integration into the local ecosystem. The results demonstrate that the infrastructure, although technically sound, promotes tourism-driven urbanization that leads to tourism gentrification, environmental degradation, and socio-spatial fragmentation and segregation. Finally, the relevance of this work lies in the importance of using digital technologies to produce and generate information on the socio-spatial impacts of tourism-driven urbanization along the Fortaleza coast, thereby contributing to the development of public policies in the areas of tourism, urban planning, and the environment.

Keywords: Tourism Gentrification, Urban Projects, Socio-spatial Fragmentation, Unequal Urbanization, Digital Modeling.

1. Introduction

The Sabiaguaba region, located at the easternmost tip of the coastline of Fortaleza, the capital of the state of Ceará, is characterized by extreme geomorphological and environmental complexity. Consequently, sensitive natural systems, such as fields of shifting and fixed dunes, mangroves, and paleodunes, coexist with the structures and infrastructure resulting from the urban expansion of the capital of Ceará. Historically, these environmental constraints established the parameters for low-impact, low-density human occupation, characterized by spontaneous settlements marked by predominantly vernacular architectural styles that were better suited to the estuary's hydrodynamics, the wind dynamics of the dunes, and the local flora and fauna, maintaining a relative conservation of the ecosystem (Souza et al., 2011). The institutionalization of Sabiaguaba's protection reached a decisive milestone in 2006 with the enactment of Municipal Decrees No. 11,986 and No. 11,987. These instruments formalized the creation of two Conservation Units (UCs): the Sabiaguaba Dunes Municipal Natural Park (PNMDS), aimed at the comprehensive preservation of fragile ecosystems, and the Sabiaguaba Environmental Protection Area (APA da Sabiaguaba), intended for the planning of sustainable land use (Figure 1). From a legal and urban planning perspective, the existence of these provisions establishes the territory as a natural sanctuary in need of preservation. In this sense, these decrees imposed essential regulatory limits for the protection of vital ecosystem functions, such as microclimatic regulation, flood control, and the protection of estuarine

biodiversity, serving as the primary legal instrument against predatory urbanization initiatives and real estate development and speculation in this coastal strip of Fortaleza.

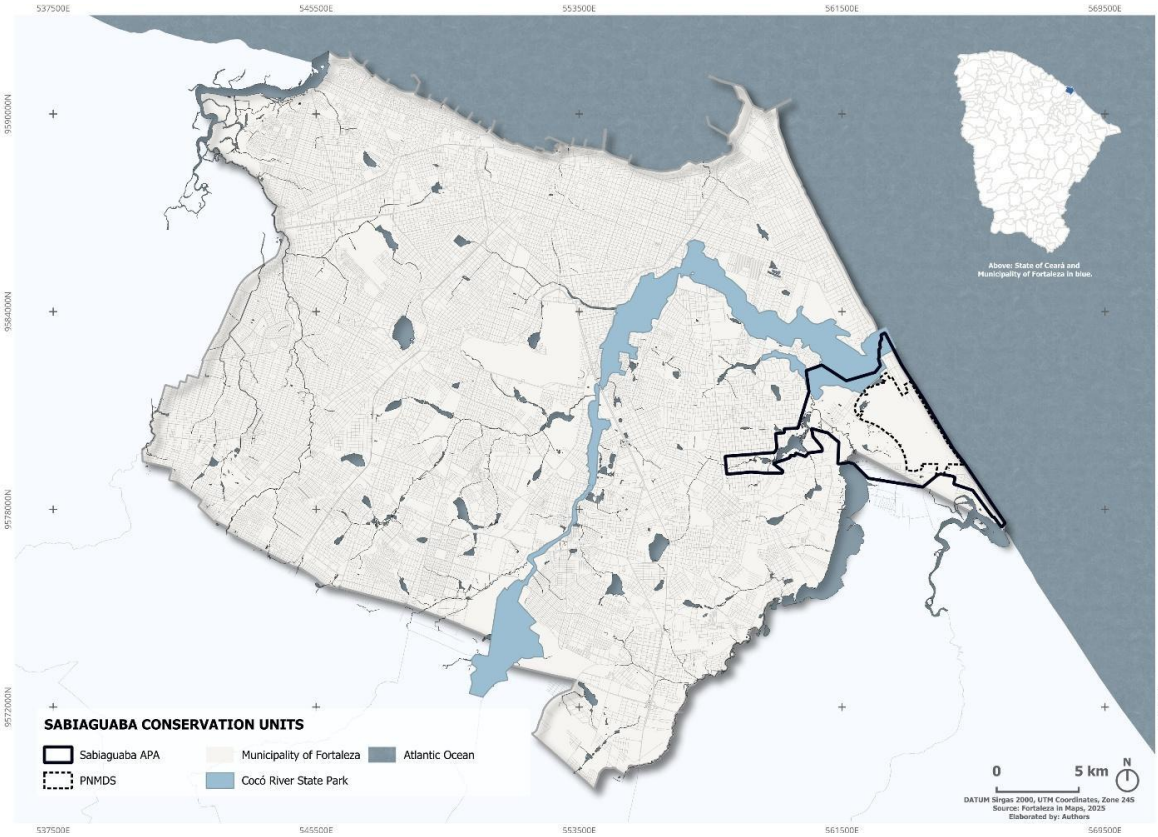


Figure 1 – Geographical location of the Sabiaguaba Conservation Units in the municipality of Fortaleza, Ceará, highlighting the boundaries of the Sabiaguaba Environmental Protection Area (APA) and the Sabiaguaba Dunes Municipal Natural Park (PNMDS). The image allows for a technical assessment of the geographic confinement and spatial friction between the capital's expanding urban fabric and the fragile estuarine ecosystems.
Source: Elaborated by the authors (2026); vectors from the SEFIN-Fortaleza IDE platform; map scale 1:120,000.

However, upon analyzing the historical process, it becomes clear that Sabiaguaba, due in part to the natural barrier of the Cocó River, has transitioned from a state of relative urban isolation to becoming a focal point for real estate and tourism interests in the process of urban spatial development in Fortaleza. As discussed by Paiva (2011), the production of coastal space in Ceará is guided by a dynamic of tourism urbanization that operates by converting the territory's "use value" into real estate "exchange value." This process does not occur naturally, but is induced by the action of the State, which, according to Harvey (2005), acts in the production of space through ideological apparatuses, public policies, and infrastructure. These forms of action materialize in the case under discussion: i) in the mobilization of ideological mechanisms aimed at promoting the urban image and positioning Fortaleza and Ceará within global economic circuits, albeit in a peripheral manner; ii) in the formulation and execution of tourism policies in coordination with urban policies at the federal, state, and municipal levels; iii) in the implementation of socio-spatial interventions manifested in infrastructure and the execution of major urban projects aimed at the enjoyment, consumption, and expansion of tourism. In Sabiaguaba, state actions took the form of large-scale infrastructure projects, notably the bridge over the Cocó River and the CE-010 highway. These transportation infrastructures not only facilitate access to the territory but also function as urban vectors that break down geographical barriers, exposing a fragile ecosystem to the pressure of real estate appreciation and speculation and to the more intense flow of tourism-related activities. It is important to note that the urbanization project for the left bank of the Cocó River, also known as the CE-251 highway project, now consolidated as CE-010, had its environmental licensing process and Environmental Impact Report (EIR)

prepared in 2013; this project constitutes the regulatory framework that anticipated and validated interventions on the left bank of the estuary.

In this regard, according to the assessment by CRZ Projetos (2013), one of the main impacts of the interventions would be a significant increase in tourism demand and the resulting pressure on the ecosystem. In response to this issue, the document highlights the need to relocate local residents and merchants, whose stalls conflicted with the new road layout and new sanitary requirements. Thus, the Sabiaguaba Environmental and Gastronomic Complex (COMAGS) emerges not only as a tourist facility but as the materialization of the relocation solution envisaged in the study, functioning as the technical-legal apparatus that called for some mitigating measures for this problem (Figure 2).

Following this line of thought, the construction of COMAGS in 2022 represented a milestone in this process of induced tourism urbanization; its implementation, within the boundaries of the Sabiaguaba APA, has been the subject of intense controversy and legal battles since its conception (Barros et al., 2024). In this context, the central point of criticism lies in the scale and nature of the intervention: the State introduced a volume of rigid construction (concrete and masonry) into a territory with environmental vulnerabilities. Furthermore, the typological replacement was radical; previously, the area was characterized by the presence of beach huts and thatched huts, ephemeral structures that, although technically simple, were part of the landscape and the communities' ways of appropriating the space. These huts served as subsistence points where the community sold local fish, creating a transitional space where the morphology of the sandy trails dictated land use. By removing these traditional structures to make way for the formal COMAGS project, the intervention severed these socio-spatial ties, creating new ones oriented toward the logic of leisure and tourism consumption (Figure 3).



Figure 2 – A multi-temporal analysis of the Cocó River estuary landscape in 2010, illustrating the pre-intervention scenario before the construction of the CE-010 highway. The image serves as a reference to demonstrate the original morphology, characterized by low-density vernacular beach huts and traditional, spontaneous settlements integrated into the trails.
Source: Elaborated by the authors (2026); historical satellite orthophotos from the SEFIN-Fortaleza platform; capture date: 2010; analytical scale applied: 1:800.



Figure 3 – A multitemporal analysis of the Cocó River estuary landscape in 2023, showing the post-intervention scenario following the implementation of COMAGS. The image provides empirical evidence of tourism-driven urbanization, illustrating the radical typological shift from vernacular structures to rigid concrete and masonry buildings along the riverbank.
Source: Elaborated by the authors (2026); orthophotos from the Fortaleza municipal database; capture date: 2023; analytical scale used: 1:800.

Based on the project description for the Sabiaguaba Environmental and Gastronomic Complex, prepared by the firm Architectus S/S and published on ArchDaily using material submitted by the project team itself, we observe the construction of a narrative that seeks to legitimize the intervention through the interplay of landscape, community memory, environmental preservation, and tourism promotion. It is, therefore, a situated argument, formulated from the perspective of the project's authors, in which architecture is presented as a sensitive and conciliatory response to the demands of the site. In this narrative, the scenic uniqueness of the confluence of the Cocó River and the sea at Sabiaguaba repeatedly emerges as a structuring element of the design concept, transforming the landscape into the project's primary symbolic asset and the foundation for its integration into Fortaleza's leisure, gastronomy, and tourism circuits. By emphasizing the site's visual uniqueness, the discourse shifts the notion of landscape from its role as an ecological and territorial foundation to its instrumentalization as a resource for enhancing value and tourist appeal.

The description also links the development's origins to the historical struggle of Sabiaguaba's traditional families, presenting the complex as a response to local demands for job creation, cultural appreciation, and the harnessing of the region's tourism potential. Although this formulation invokes the idea of community agency and recognition of the so-called "natives," it also produces an effect of consensus-building around the intervention process, obscuring the asymmetries between traditional forms of territorial appropriation and their incorporation into a broader logic of tourist consumption and landscape enjoyment. In other words, the project's discourse tends to frame the community as the legitimizing agent of the operation, while simultaneously reintegrating it into a territorial economy driven by external visitor flows. These changes in the socio-spatial dynamics of the place result in socio-environmental impacts that are not necessarily treated here as positive or negative, but are conditioned by the specific interests of the agents involved, even though the environmental implications point toward the "commodification of the landscape" for the purposes of leisure and tourism consumption (Meneses, 2002).

From an architectural perspective, the narrative emphasizes strategies such as semi-underground construction, the preservation of views, the observation plaza, the suspended platform, and the pier, elements that reinforce the contemplative and experiential dimension of the place. More than just technical resources, such devices highlight an operation in which architecture and infrastructure organize the landscape as a setting for visual, gastronomic, and recreational consumption, aligning with contemporary processes of tourism urbanization that transform environmental and cultural attributes into inputs for

intangible consumption experiences (Paiva, 2013). In this sense, more than a simple gastronomic facility, the complex can be interpreted as infrastructure for the touristification of the landscape and local culture, albeit in a contradictory manner.

2. Methodology

The methodology of this study is based on an analytical and critical approach, structured around the concept of a digital inventory of contemporary architecture, as proposed by Paiva and Medeiros (2024) for the documentation and analysis of significant works in Ceará. The methodological approach utilizes high-precision capture and modeling tools to investigate the dissonance between the space conceived by the State and the impacts of COMAGS on the Sabiaguaba ecosystem. The methodological procedures were organized into three sequential stages: data collection, data processing, and socio-spatial analysis.

The first stage consisted of environmental diagnosis and temporal monitoring, based on the guidelines of Grenier et al. (1993). The authors highlight the need for ongoing research in ecotourism zones to mitigate the phenomenon of "cosmetic greening," a term that defines the use of "green aesthetics" and the language of sustainability merely as a superficial "cosmetic" layer to validate projects that, at their core, ignore the deep ecological and social dynamics of the place. To conduct this monitoring, a DJI Mini 2 Unmanned Aerial Vehicle (UAV) was used. The choice of this sub-250g class equipment is justified by its portability and ability to operate with minimal intrusion in areas of socio-environmental conflict, ensuring that the georeferencing of the information was carried out discreetly. The UAV aerial photography survey was conducted using a pre-programmed flight plan at an altitude of 40 meters, utilizing the 1/2.3" CMOS sensor of the device's native camera to capture oblique and vertical views of the complex and its surroundings. The captured images and georeferenced data were processed and integrated into a GIS (Geographic Information System) environment using QGIS software, referenced to the SIRGAS 2000 / UTM Zone 24S coordinate system, where historical orthophotos from the SEFIN platform were also incorporated.

The integrated use of remote sensors and geographic platforms supports the approach of Rontani et al. 2024, who advocate the use of UAVs and aerial photogrammetry to enrich spatial databases and manage complex territories. In this environment, historical orthophotos from the SEFIN-Fortaleza IDE platform were incorporated, allowing for the observation, with cartographic precision, of vegetation clearance and topographic changes at the mouth of the Cocó River, as well as the verification of the removal of old shacks replaced by the current infrastructure (Figure 4).



Figure 4 – Aerial view of COMAGS obtained by UAV (Unmanned Aerial Vehicle). The image allows us to observe the scale of the architectural intervention at the mouth of the Cocó River and the pressure exerted by the infrastructure on the environmental dynamics.
Source: Elaborated by the authors (2025); Aerial photographic survey using a DJI Mini 2 UAV; date of capture: 2025.

The second phase of the research focused on parametric digital modeling using ArchiCAD 28 software, developed by the Hungarian company Graphisoft. The model was developed based on the original floor plans and technical details provided by the architectural firm in charge. This digital reconstruction enabled the creation of a parametric digital model developed at level of detail 300 (LOD 300), whose informational and geometric density made it possible to reproduce a tridimensional analytical "digital twin" of COMAGS and its immediate surroundings based on its exact metric attributes. This structure served as the fundamental basis for the application of the "think-feel" approach by Carvalho and Ponciano (2021). By transferring COMAGS to the BIM environment, it became possible to compare the project's geometry with reports of technical failures published in local newspapers and media outlets. The modeling served to document and spatialize the reported functional pathologies, such as the complete replacement of the wooden floor in January 2025, just three years after the building's inauguration (SEMA, 2025). The error in material specification given the extremely high salinity reflects a prioritization of immediate visual appeal at the expense of the building's life cycle. Similarly, the critical analysis of the project in the software revealed the absence of exhaust systems in the kitchens and the thermal inadequacy of the awnings, which ultimately create "heat islands" that are hostile to users (Brisa, 2025).

Finally, the socio-spatial dimension was analyzed using the Social Vulnerability Index (IVS), developed in 2015 by the Institute of Applied Economic Research (IPEA). Methodologically, the SVI operates as the inverse of the Human Development Index (HDI): while the HDI measures individual achievements, the SVI maps the deficiencies and absence of services that should be guaranteed by the government. The index consists of 16 indicators structured across three dimensions: Urban Infrastructure, Human Capital, and Income and Work. In Sabiaguaba, the analysis focused on the Urban Infrastructure dimension, which assesses access to basic sanitation and waste collection. This reality, as mapped by the IVS, was compared with the objectives and guidelines outlined in the Management Plan for the Sabiaguaba Conservation Units, approved in 2010, which already anticipated the need to reconcile environmental preservation with social infrastructure for the traditional population. The comparison of these indicators with the high investment in infrastructure for promoting tourism highlights a historical neglect of essential services for the indigenous community in favor of enhancing the urban image for external tourism consumption, revealing social exclusion in the territory.

3. Results and discussion

The results obtained through digital documentation, BIM modeling, and critical analysis of the complex reveal contradictions between the image of landscape enhancement proposed by COMAGS and the actual impacts on the Sabiaguaba area.

Regarding territoriality, the sense of belonging and the identity of the local community were dimensions deeply explored and highlighted by Maciel (2011), who demonstrated how existence in Sabiaguaba is inseparable from daily practices of direct interaction with the ecosystem. For the author, the territory is not merely a physical substrate but a field of meanings, constructed through labor and ancestry. However, this territoriality, based on artisanal fishing and gathering in mangrove areas, is now under threat. Following this line of thought, the urban design and architecture of COMAGS ignore the subjectivity of the place in favor of a space that prioritizes the flow of visitors. By allocating large areas to parking lots and contemplative zones, the project imposes symbolic and physical barriers that disrupt residents' daily lives. The connection of the locals to the sea, the mangroves, and the dunes, explored by Maciel (2011), is sanitized and turned into a "showcase," becoming an institutionalized tourist attraction. This process of "spectacularization" of the urban image, as defined by Paiva (2011), uses architecture as an ideological apparatus to insert Fortaleza into global consumption flows, often at the expense of the decharacterization of local identities (Figure 5).

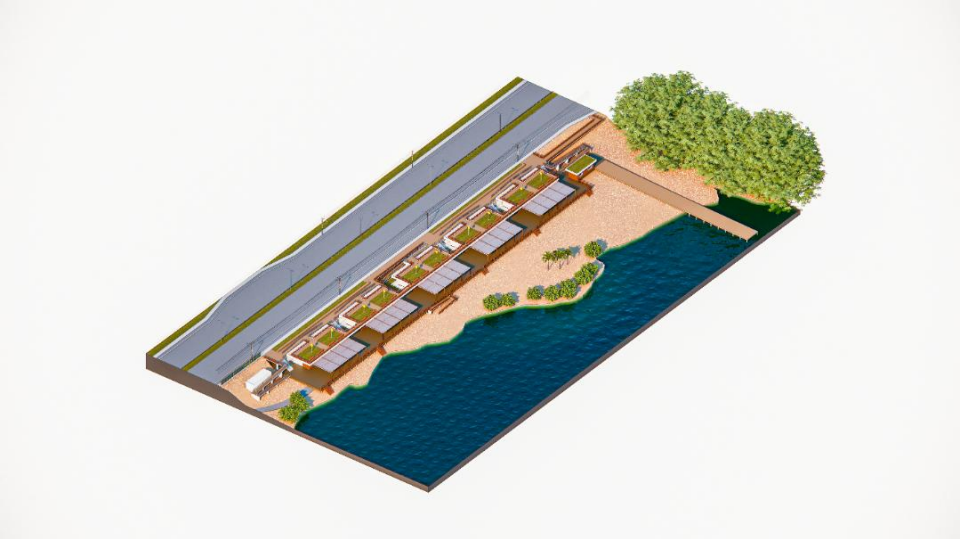


Figure 5 – Spatial relationship between the complex and the Cocó River estuary. The perspective exposes the implementation of the built environment, illustrating the strategies of physical-environmental integration, serving as a basis for analyzing the impact of the infrastructure on the surrounding environment.
Source: Elaborated by the authors (2026); based on the parametric digital twin modeled in ArchiCAD 28 (LOD 300).

From a critical analysis perspective, it is evident that COMAGS exhibits early signs of specification errors that reveal a disconnect between the design and the environment. A striking example occurred in January 2025, just three years after the inauguration, when the complex's wooden flooring required complete replacement (Figure 6). As reported by the local press, the work took place in the middle of the high season, raising serious questions from merchants and highlighting the socioeconomic damage caused by flawed planning. In this context, in an area of extremely high salinity, intense solar radiation, and heavy foot traffic, the choice of a material incapable of withstanding the aggressiveness of the marine environment reveals that the project prioritized immediate visual appeal at the expense of technical performance and the materials' lifecycle. Officially, the Secretariat of the Environment and Climate Change confirmed the completion of this replacement in April 2025. This approach directly conflicts with what Carvalho and Ponciano (2021) advocate, namely that architecture should be a sensitive response to the natural forces of the site, rather than an imposed object that requires immediate corrective maintenance.



Figure 6 – Detail of early pathologies in the COMAGS wooden deck. The accelerated deterioration, manifested in just three years of use, highlights the error in specifying a material with poor performance for the very high salinity, heavy traffic, and high solar radiation conditions of the estuary.
Source: Photographic record of Brisa (2025); date taken: January 2025; detailed close-up photograph.

The modeling performed in ArchiCAD 28 revealed serious deficiencies in environmental comfort that make the space inhospitable. The COMAGS kitchens, which are essential to the operations of local vendors, were designed without adequate exhaust and cross-ventilation, resulting in excessively hot environments that hinder food preparation and degrade work quality (Figure 7). Furthermore, the inappropriate specification of the awning material had an adverse effect: instead of providing shade and coolness, these surfaces create small "heat islands" that, depending on the time of day, make it impossible for visitors and workers to remain in outdoor areas. These functional flaws prove that the intervention ignored local characteristics, requiring constant maintenance funded by the government. The use of UAVs and GIS-based processing, in accordance with the methodology validated by Rontani, Dionizio, and Dezen-Kempter (2024), made it possible to document that such design choices not only fail technically but also generate spatial impacts.

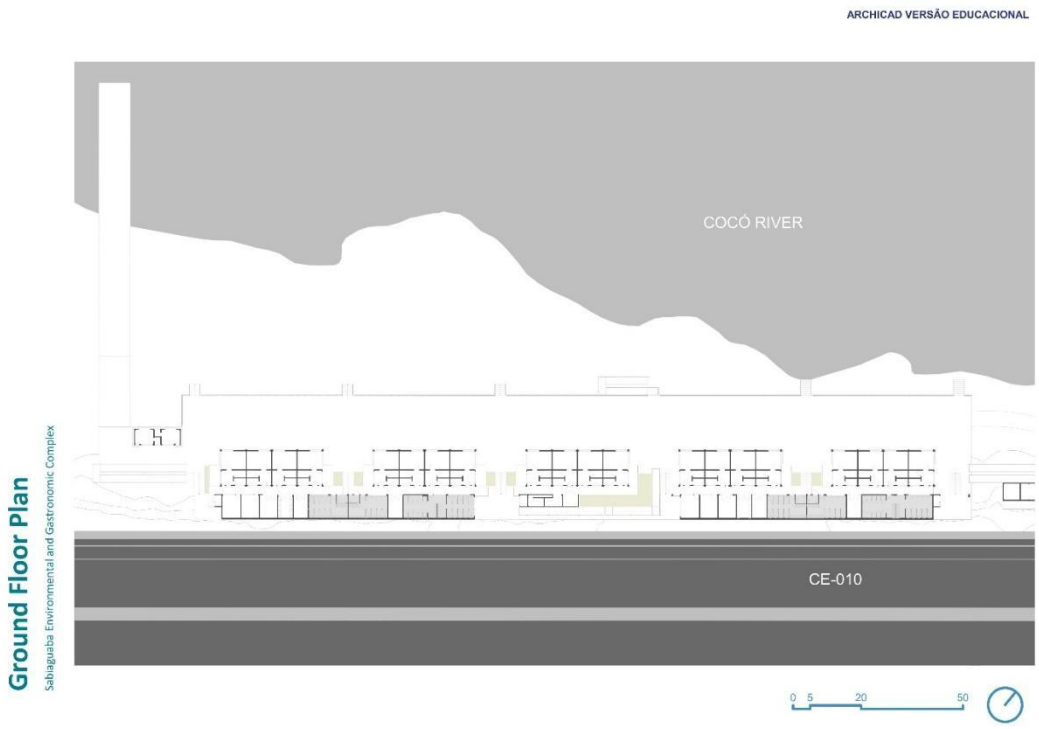


Figure 7 – Floor plan of COMAGS. The project reveals critical deficiencies in natural ventilation strategies, where some kiosks lack effective cross-ventilation and exhaust systems, compromising thermal comfort and the functionality of the kitchen and service areas.
Source: Elaborated by the authors (2026); based on a parametric digital twin modeled in ArchiCAD 28 (LOD 300); scale 1:500.

Thus, this process of aestheticizing the coastline masks severe socio-spatial exclusion: while COMAGS receives investments in scenic lighting, street furniture, and finishing materials, the immediate surroundings, where community life persists, and bonds of identity are formed, remain neglected by urban planning, lacking even basic sanitation and housing infrastructure. From this perspective, the results of this urbanization model become evident when we compare COMAGS' infrastructure with the region's social vulnerability indicators. In this regard, the Social Vulnerability Index (IVS), which in some areas is classified as "high" (Figure 8), reveals that Sabiaguaba is affected by a historical neglect that defies the guidelines established by the Conservation Units Management Plan itself.

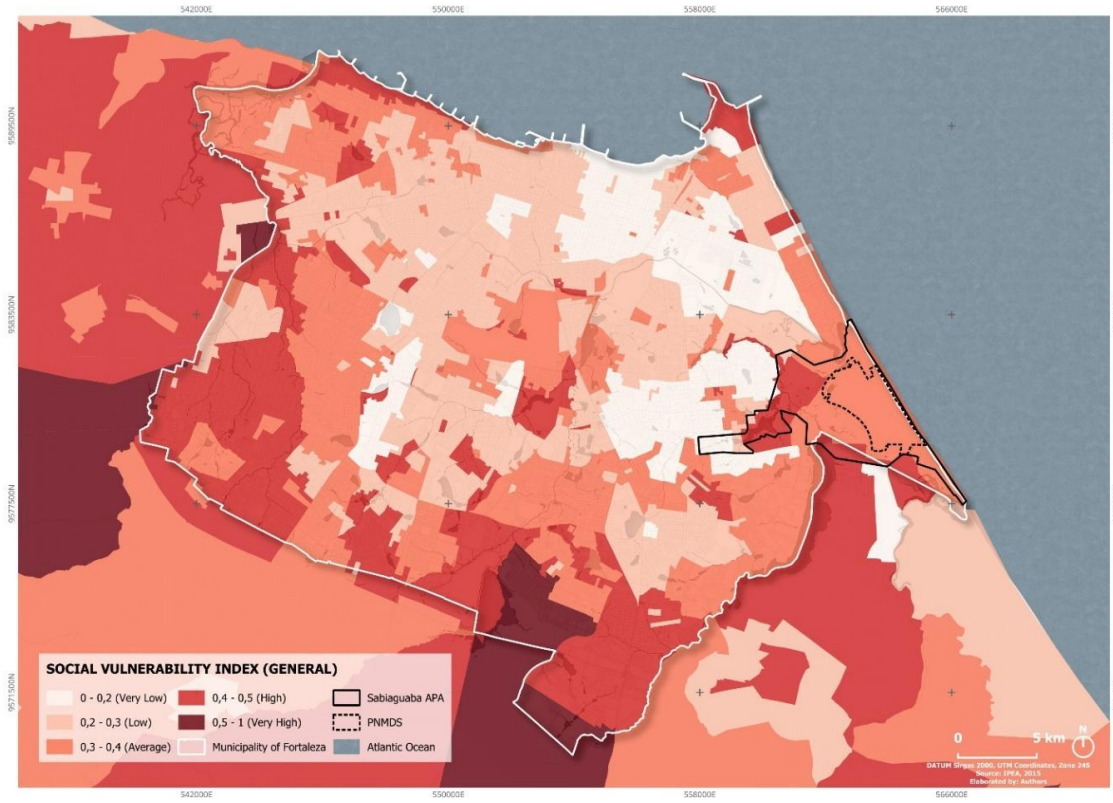


Figure 8 – Map showing the spatial distribution of the Social Vulnerability Index (SVI) in the Sabiaguaba Conservation Units region. The map reveals a serious socio-spatial paradox, demonstrating that areas with "High" social vulnerability directly border the highly commercialized tourist enclave.
Source: Elaborated by the authors using data from IPEA (2015); georeferenced on municipal vectors in QGIS; data processing date: 2026; map scale 1:120,000.

While the technical document clearly outlined the urgent need to assist vulnerable populations through the implementation of ecological sanitation, adequate drainage, and land regularization, what we see today is the opposite. By allocating large investments to raise the construction standards of an area, with leisure and tourism consumption as its sole justification, the state ignores the social welfare goals that the Management Plan designated as priorities. In this sense, this duality creates a "fragment of a city" well-equipped with tourism infrastructure, yet isolated from a periphery where the lack of basic sanitation and waste collection remains neglected.

The chronic ineffectiveness of public authorities in implementing the drainage and sanitation solutions proposed by the Management Plan to mitigate the risks of groundwater contamination and minimize flooding (Figure 9), which is so frequent in the region, leaves the community at the mercy of exclusion and vulnerability. Thus, current public investment does not aim to fulfill the land-use planning and social sustainability advocated by the Management Plan studies, but rather to enhance the city's image for tourism consumption, primarily from abroad. From this perspective, what is witnessed in Sabiaguaba is the conversion of socio-environmental heritage into a real estate asset.



Figure 9 – Photographic record of urban flooding and the lack of basic drainage infrastructure in the residential areas surrounding COMAGS. The image provides evidence of historical socio-spatial fragmentation, confirming that public funds were allocated primarily to improve the region's image as a tourist destination, while vital ecological sanitation solutions guaranteed by the 2010 Conservation Area Management Plan for the indigenous population were neglected.
Source: Photograph by Vieira (2025); date taken: March 2025.

4. Conclusions

The discussion developed in this study does not seek to disqualify the ideas embedded in the project, materialized in a work that, within its own objectives, effectively fulfills the role of producing an urban intervention aimed at enhancing Fortaleza's tourist image, while also providing architectural and tourism-support infrastructure. In fact, the complex has been widely appropriated by the tourism dynamics of Sabiaguaba, contributing to increased visitation of the area. The critiques advanced here, however, are situated within an expanded and broader interpretative framework, aimed at understanding the implications of contemporary architecture and urbanism on pre-existing cultural, territorial, and environmental conditions.

Research on the Sabiaguaba Environmental and Gastronomic Complex reveals that, although state intervention is presented under the guise of promoting the landscape and local culture, its implementation results in a process of exclusionary and technically problematic tourism urbanization. The transition from a low-impact settlement area to a tourist destination has resulted in the replacement of vernacular building types and traditional ties with a logic of "spectacularized" leisure consumption, which prioritizes external visitors at the expense of the local community. The digital modeling methodology and the use of UAVs highlighted the dissonance between the designed space and the environmental reality of the Cocó River estuary. The identified functional pathologies, such as the mis-specification of materials in a high-salinity environment and thermal inadequacy, confirm that the project prioritized immediate aesthetics at the expense of technical sustainability and the project's life cycle.

Furthermore, the contrast between the high investment in tourism infrastructure and the region's high rates of social vulnerability points to a historical neglect of essential services for local residents. It is therefore concluded that COMAGS functions as a tourism infrastructure that promotes tourist gentrification and socio-spatial fragmentation.

Acknowledgments

We would like to thank FUNCAP, the Ceará Foundation for the Support of Scientific and Technological Development, for the financial support provided for the research project “Contemporary Architecture in Ceará [arq.con.ce]: Digital Inventory”, and the research project “ The Social Production of Space in Peripheral Cities: (De)coding Invisible Strategies” and CNPQ for the PIBITI grant awarded in connection with the aforementioned research project.

References

Architectus S/S. 2025. "Complexo Gastronômico da Sabiaguaba / Architectus S/S." *ArchDaily Brasil*, 4 de fevereiro de 2025. https://www.archdaily.com.br/br/1027380/complexo-gastronomico-da-sabiaguaba-architectus-s-s.

Barros, Ana Carla Oliveira de, Francisca Laryssa Feitosa Araujo, Francisco Davy Braz Rabelo, and Edson Vicente da Silva. 2024. "Análise crítica do plano de manejo do Parque Natural Municipal das Dunas e da Área de Proteção Ambiental de Sabiaguaba, Fortaleza, Ceará: à luz da Geoecologia das Paisagens." *Revista Pantaneira* 24 (Edição Especial CIGEPPAM): 181–98.

Brisa, Mateus. 2025. "Complexo da Sabiaguaba: obra durante alta estação é questionada por comerciantes." *O Povo*, 5 de janeiro de 2025. https://www.opovo.com.br/noticias/fortaleza/2025/01/05/complexo-da-sabiaguaba-obra-durante-alta-estacao-e-questionada-por-comerciantes.html.

Carvalho, Francisco Fernando Livino de, and Luiza Ponciano. 2021. "A Arquitetura como Eclosão da Paisagem: Infraestrutura Ecoturística para Unidades de Conservação." *Geograficidade* 11 (especial): 10–25.

CRZ Projetos. 2013. *Relatório de Impacto Ambiental (RIMA): Implantação da Rodovia CE-251 (Trecho Ponte do Rio Cocó – Sabiaguaba)*. Fortaleza: Departamento Estadual de Rodovias (DER/CE).

Fortaleza. 2006a. *Decreto nº 11.986, de 16 de janeiro de 2006. Cria o Parque Natural Municipal das Dunas da Sabiaguaba*. Fortaleza: Diário Oficial do Município.

Fortaleza. 2006b. *Decreto nº 11.987, de 16 de janeiro de 2006. Cria a Área de Proteção Ambiental (APA) da Sabiaguaba*. Fortaleza: Diário Oficial do Município.

Grenier, Dale, Berit C. Kaae, Marc L. Miller, and Roger W. Mobley. 1993. "Ecotourism, Landscape Architecture and Urban Planning." *Landscape and Urban Planning* 25, no. 1-4 (August): 1–16. https://doi.org/10.1016/0169-2046(93)90120-G.

Harvey, David. 2005. *A produção capitalista do espaço*. São Paulo: Annablume.

Ipea (Instituto de Pesquisa Econômica Aplicada). 2015. *Atlas da Vulnerabilidade Social nos Municípios Brasileiros*. Brasília: Ipea. https://ivs.ipea.gov.br/.

Maciel, Maria Laura. 2011. "Demandas ambientais de Sabiaguaba na perspectiva dos marcadores sociais do lugar." Dissertação de mestrado, Universidade Federal do Ceará, Fortaleza.

Meneses, Ulpiano Bezerra. 2002. "A paisagem como fato cultural." In *Turismo e paisagem*, organizado por Eduardo Yázigi, [inserir páginas]. São Paulo: Contexto.

Paiva, Ricardo Alexandre. 2011. "A metrópole híbrida: o papel do turismo no processo de urbanização da RMF." Tese de doutorado, Universidade de São Paulo, São Paulo.

Paiva, Ricardo Alexandre. 2013. "Sobre a relação turismo e urbanização." *PosFAUUSP* 20, no. 33: 126–45. https://doi.org/10.11606/issn.2317-2762.v20i33p126-145.

Paiva, Ricardo Alexandre, and João Victor Frazão de Medeiros. 2024. "Digital Inventory of Contemporary Architecture in Fortaleza (Ceará, Brazil): The Mercado dos Peixes." *Limaq*, no. 14 (novembro): 101–24. https://doi.org/10.26439/limaq2024.n14.6969.

Rontani, Sofia Puppin, Rafael Dionizio, and Eloisa Dezen-Kempter. 2024. "Challenges and Opportunities of the Integrated HBIM-GIS Approach for Urban Cultural Heritage Management." *Emsigradi 2024: Biodigital_intelligent_systems*, 1649–58.

SEMA (Secretaria do Meio Ambiente e Mudança do Clima). 2025. "Complexo Ambiental e Gastronômico da Sabiaguaba conclui a troca do piso." *Portal SEMA*, 10 de abril de 2025.

https://www.sema.ce.gov.br/2025/04/10/complexo-ambiental-e-gastronomico-da-sabiaguaba-conclui-a-troca-do-piso/.

Souza, Lílian Sorele Ferreira, Edson V. Silva, and Fábio Perdigão Vasconcelos. 2011. "As UCs de Sabiaguaba (Fortaleza – Ceará, Brasil): diagnóstico geoambiental e propostas de gestão e manejo." *Revista Geográfica de América Central* 2, no. 47: 1–17.

Vieira, Lara. 2025. "Moradores da Sabiaguaba relatam alagamentos históricos que afetam casas, comércios e trânsito." *O Povo*, 7 de março de 2025. https://www.opovo.com.br/noticias/fortaleza/2025/03/07/moradores-da-sabiaguaba-relatam-alagamentos-historicos-que-afetam-casas-comercios-e-transito.html.

cinpar2026
XXII International Conference on Building Pathology and Constructions Repair
15th to 17th July 2026 - Lisboa, Portugal

Pathological Manifestations in Building Structures: Evaluation of Causes, Impacts on Durability, and Intervention Costs

Bruna Sell[1], Marilia Araújo[2]

[1] Instituto Nova Engenharia, São Paulo, Brazil, brubesell98@gmail.com
[1] Instituto Nova Engenharia, São Paulo, Brazil, marilia_carla10@hotmail.com

Abstract: The presence of pathological manifestations in buildings compromises their durability, safety, and performance over time, in addition to resulting in high costs when proper maintenance becomes necessary. This study aims to analyze, diagnose, and estimate the costs of the main anomalies identified in three buildings located in the city of Joinville, Santa Catarina, Brazil. Among the observed manifestations, infiltration leading to reinforcement corrosion, detachment of coatings, and foundation settlement stand out. The causes of these pathologies were investigated through building inspections and classified using the GUT Matrix methodology, which allowed the prioritization of issues according to their severity, urgency, and tendency to worsen. In Case 1, efflorescence and infiltration were identified as the most critical symptoms, resulting in reinforcement corrosion and requiring immediate corrective actions. In Case 2, the improper application of materials and lack of maintenance obtained high scores in the GUT analysis, indicating compromised façade integrity. In Case 3, the absence of maintenance in hydraulic systems led to soil leaching, resulting in foundation settlement. The cost analysis establishes a relationship between the lack of preventive maintenance and the high costs of corrective interventions. The estimated results reinforce the need for preventive measures and regular inspections to minimize financial impacts and extend the service life of buildings, highlighting the importance of proper structural execution and adequate planning from the design phase.

Keywords: Pathological manifestations. GUT Matrix. Estimate costs.

1. Introduction

Pathological manifestations in buildings constitute a highly relevant topic in civil engineering and are understood as structural and/or functional alterations that result in material degradation and loss of performance of building systems. According to Iantas, such manifestations may be compared to “diseases” of buildings, appearing through cracks, fissures, stains, detachments, deformations, ruptures, corrosion, oxidation, among other anomalies. In general, these occurrences are directly associated with reduced building performance, affecting aspects such as stability, functionality, aesthetics, and, above all, durability under conditions of use and environmental exposure.

In this context, the service life of a building, as defined by ASTM (1982), corresponds to the period during which materials, components, and systems maintain their properties above minimum acceptable performance levels. An element is considered to have reached the end of its service life when its degradation renders it unsafe or economically unfeasible to maintain in operation. Therefore, structural durability may be understood as a function of the performance-versus-time relationship, making it essential that clear criteria regarding expected service life, environmental exposure conditions, and maintenance strategies be established during the design phase in order to ensure the integrity of the building over time.

Several factors contribute to the emergence and progression of pathological manifestations. According to Thomaz (2001), in addition to the natural aging of buildings, major causes include design flaws, execution deficiencies, inappropriate use of materials, and lack of preventive maintenance. Furthermore, the increasing pressure for reduced construction schedules, combined with the use of lighter building systems,

insufficient project detailing, lack of coordination among disciplines, and inadequate construction supervision, directly impacts the final quality of buildings, intensifying the occurrence of anomalies.

Failures resulting from construction defects, lack of maintenance, or improper use of buildings are recurrent and lead to reduced system performance and durability, compromising structural, functional, and economic aspects (Helene; Terzian, 1992). In this regard, Andrade (2012) highlights that approximately 40% of resources invested in the construction sector in developed countries are allocated to structural maintenance, emphasizing the importance of efficient management and conservation strategies throughout the service life of buildings, as can be observed in Figure 1. According to Farias (2023), the most frequent types of degradation are those caused by inadequate operation and maintenance management, and building inspection plays a crucial role in verifying maintenance conditions and usage patterns as a means of ensuring safety, durability, and proper performance.

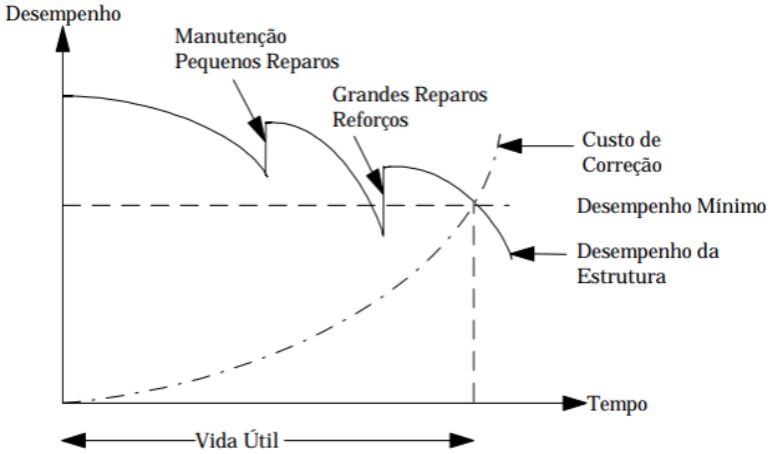


Figure 1 – Performance phases of a structure throughout its service life (adapted from CEB (1992) and Helene (1992))

According to Deutsch (2016), any problem identified at an early stage is easier and significantly less costly to solve. Learning to recognize the symptoms of structural or finishing deterioration makes it possible to avoid or minimize future problems. Ideally, routine inspections should be carried out in order to monitor pathological manifestations affecting the various components of the building under analysis.

The lack of inspections, and consequently the absence of maintenance, leads to severe problems in buildings, which progressively become obsolete and develop construction deficiencies. Negligence and lack of awareness regarding the importance of building inspections make identified repairs more complex and costly (DEUTSCH, 2016). Maintenance of any building aims not only at preserving the asset, but also at preventing performance levels from deteriorating to the point of impairing usability or causing discomfort to occupants. Through proper maintenance, the service life of the building can be extended. Therefore, inspection and maintenance are essential to ensure the safety and service life of the development, in addition to preventing unnecessary repair costs (SARTOR, 2020).

Additionally, climatic conditions and regional characteristics significantly influence building performance. Brazil's climatic diversity, characterized by temperature variations, solar radiation levels, and high rainfall indices in certain regions, requires specific technical knowledge for the proper specification of materials and construction systems. Disregarding these factors — combined with recent climate changes — may intensify degradation processes and compromise building habitability, which should encompass not only aesthetic and functional criteria, but also adequate sanitary and comfort conditions.

Concern regarding building durability gained greater prominence with the publication of the performance standard ABNT NBR 15575 (2013), which establishes parameters for the service life of building systems and reinforces the importance of periodic maintenance. According to Costa (2015), the absence of preventive maintenance can significantly reduce the designed service life of a structural system, potentially resulting in reductions of up to 50%, thereby increasing safety risks and repair costs. Conversely, regular

maintenance associated with small repairs over time contributes to extending service life and maintaining structural performance, as illustrated in Figure 1. Marinho and Mesquita (2020) state that problems arising from pathological manifestations range from minor damage to severe compromise of building safety, potentially leading to structural collapse. According to Sartor (2020), pathological manifestations are increasingly present in buildings, generating risks, occupant discomfort, high repair costs, and property devaluation.

Given this context, the present study aims to analyze three case studies of pathological manifestations in buildings located in Southern Brazil, a region characterized by high humidity and elevated rainfall rates. For this purpose, the Gravity, Urgency, and Tendency (GUT) Prioritization Matrix methodology is applied, enabling the ranking of problems based on qualitative criteria, complemented by failure mode and effects analysis methods, which classify occurrences according to their criticality. In Case 1, efflorescence and infiltration were identified as the predominant manifestations, resulting in reinforcement corrosion processes and requiring immediate intervention. In Case 2, improper material application and lack of maintenance were identified as critical factors, compromising façade integrity and resulting in high repair costs, in disagreement with the guidelines established by ABNT NBR 15575. In Case 3, the lack of maintenance of hydraulic systems caused soil leaching and foundation settlement, aggravated by inadequate palliative interventions. Overall, the analysis demonstrates the direct relationship between the absence of preventive maintenance and the significant increase in corrective intervention costs throughout the service life of buildings.

2. Methodology

The methodology adopted in this study was based on a case study approach, chosen for its ability to thoroughly explore pathological manifestations in real buildings, as well as to analyze solutions applicable to the identified problems. Additionally, a comparison was established between the costs of corrective interventions and those associated with preventive maintenance, highlighting the economic impacts resulting from the lack of proper management throughout the service life of buildings.

For the development of the fieldwork, methodological procedures were defined and structured into six stages, which are schematically presented in Figure 2.

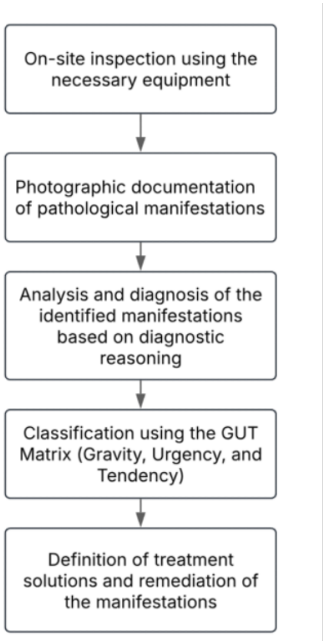


Figure 2 - Flowchart of activities (Author)

These stages ranged from initial data collection to the analysis and interpretation of the obtained results. The surveys carried out provided technical support for understanding the pathological manifestations,

enabling not only the identification of their symptoms but also a more in-depth analysis of their possible causes. This approach contributes to supporting rehabilitation interventions and maintenance strategies, as well as enhancing the understanding of the different stages involved in the construction process, enabling the adoption of more effective preventive measures.

The building inspection was conducted based on the identification and classification of pathological manifestations observed in situ. To prioritize interventions, the GUT Matrix methodology (Gravity, Urgency, and Tendency) was employed, which consists of assigning scores from 1 to 5 for each of these criteria, allowing the ranking of problems according to their level of criticality. According to Kepner and Tregoe (1981), the GUT matrix is a decision-support tool that enables the rational definition of priorities. In this context, as also discussed by Sotille (2014), its application promotes efficient resource allocation and strategic planning of corrective actions.

Each parameter of the GUT matrix was considered as follows: (i) Gravity (G), related to the intensity and extent of potential damage resulting from non-intervention; (ii) Urgency (U), associated with the time available to take action before undesirable consequences occur; and (iii) Tendency (T), which evaluates the progression of the problem over time in the absence of corrective measures. The combination of these factors allowed the establishment of a priority order for the interventions required in each case study.

It is important to note that some limitations were identified in the development of this study, particularly regarding the lack of detailed information on the design and construction stages of the analyzed buildings, as well as the unavailability of formal maintenance records. Furthermore, it was not possible to perform destructive testing or collect material samples, which restricted the analysis primarily to visual and non-destructive methods.

It is also emphasized that this study did not aim to evaluate the qualifications or performance of the professionals and companies involved in the analyzed projects, focusing exclusively on the identification and analysis of pathological manifestations from a symptom-based perspective.

Finally, after conducting the inspections and classifying risks using the GUT matrix, cost estimates were carried out for the repair of the identified pathologies, along with the development of comparative scenarios involving preventive maintenance costs that could have mitigated or prevented the progression of these manifestations. This analysis objectively demonstrated the technical and economic benefits associated with the adoption of systematic maintenance practices throughout the service life of buildings.

3. Headings and Subheadings

The city of Joinville has a humid subtropical climate, characterized by hot summers with high levels of thermal discomfort, mild winters, and high precipitation throughout the year. Average annual temperatures range between 13 °C and 30 °C, with perceived temperatures exceeding 35 °C during the summer due to high relative humidity. Rainfall is significant, with annual averages typically ranging from 1,700 mm to 2,700 mm, according to data provided by the municipal government. These climatic conditions have a direct influence on building performance, particularly with regard to material durability and the occurrence of moisture-related pathological manifestations.

Each case study analyzed refers to a distinct building, with specific construction characteristics, ages, and usage conditions.

3.1 Case 1 - Efflorescence and infiltration

Case 1 corresponds to a public building with more than 26 years of service, comprising several exposed slabs without roofing, such as floor slabs and ramps. In these areas, no effective waterproofing systems were

identified, which favors the occurrence of infiltration due to the porosity of the concrete, allowing water penetration into internal environments, as illustrated in the presented figures. These infiltrations are associated with the failure or absence of waterproofing, resulting in the initiation of reinforcement corrosion processes, as well as incidents such as the detachment of gypsum ceiling panels.

The occurrence of the spalling phenomenon was also observed, characterized by the detachment of concrete due to the expansion of corroded reinforcement. Additionally, the presence of a rainwater drainage system attached to the underside of the beams was identified, lacking proper waterproofing protection, which contributes to the intensification of deterioration processes. This condition is further aggravated by the porosity of the concrete and capillary action, facilitating the ingress of water and aggressive agents.

Based on the application of the GUT Matrix, the analyzed case presents high levels of gravity, urgency, and tendency, as continuous exposure to moisture accelerates the progression of deterioration processes, particularly reinforcement corrosion. The evolution of this condition may compromise the load-bearing capacity of structural elements and, in more critical scenarios, may lead to localized collapse. It is also important to emphasize that, due to the high flow of people in the area, the associated safety risk is significantly increased, requiring priority intervention.be used.



Figure 3 - Exposed reinforcement and attached drainage gutter (Author, 2025)



Figure 4 - Exposed reinforcement and attached drainage gutter (Author, 2025)

Given the current stage of degradation, the recommended corrective measure is the implementation of a complete waterproofing system for all exposed areas, including slabs and ramps, combined with the installation of an efficient drainage system. This system should be composed of appropriate materials, such as properly sized PVC pipes connected to the building's drainage network, ensuring the adequate discharge of rainwater and preventing moisture accumulation in structural elements.

It is important to emphasize that the observed pathological manifestations could have been avoided through the adoption of proper waterproofing and drainage solutions during the design and construction phases. Additionally, the implementation of preventive maintenance and early corrective interventions throughout the building's service life would have contributed to mitigating the progression of reinforcement corrosion processes, significantly reducing the costs and risks associated with the current interventions

3.2 Case 2 - improper material application

Case 2 refers to a building with approximately 8 years of service life, in which pathological manifestations were identified on the façade, notably the detachment of coatings and the significant presence of biological colonization, especially reddish algae. These manifestations indicate unfavorable environmental conditions, characterized by high humidity, insufficient ventilation, and low solar exposure on the analyzed surfaces.

Prolonged exposure to these conditions contributed to the development of efflorescence, resulting from the migration and subsequent crystallization of salts present in cementitious materials. This process promotes substrate degradation, reducing its cohesion and mechanical strength, which in turn leads to coating detachment at various points. Additionally, areas with intense biological colonization and detachment of the finishing layer were observed, as evidenced in the corresponding figures.



Figure 5 - Coating detachment and reddish mold (Author, 2025)

Based on adhesion tests of the coating system, a reduction in the bond strength between the coating and the substrate was identified, indicating weakening of the cementitious material, possibly associated with premature degradation and continuous exposure to moisture.

According to the application of the GUT Matrix, the analyzed case presents high levels of gravity, urgency, and tendency, as the persistence of moisture conditions accelerates façade deterioration mechanisms. The progression of this condition may compromise the integrity of the coating system and, in more critical scenarios, may result in the detachment of fragments, posing risks of material damage and hazards to user safety. It is important to note that, as this is an area with pedestrian circulation, the associated risk level is increased, requiring priority intervention.

As a corrective measure, the complete removal of compromised coating areas is recommended, followed by the restoration of the system using materials suitable and compatible with the exposure conditions. Additionally, the application of water-repellent coatings is suggested to reduce water absorption and enhance system durability. Furthermore, periodic maintenance actions should be implemented, including façade cleaning at intervals of approximately three years and repainting according to manufacturer specifications, in order to mitigate the recurrence of pathological manifestations and ensure adequate performance over time.

3.3 Case 3 - Pipeline failure causing soil leaching and settlement

Case 3 is related to the lack of maintenance of old metallic pipelines, whose oxidation process resulted in sewage leakage into the soil. Over time, these leaks promoted the leaching of fine particles and the consequent erosion of the soil in the foundation support region. As a result, differential settlement was observed, evidenced by inclined cracks at approximately 45° in masonry walls, as well as cracking in structural elements such as columns and beams, as shown in the presented images. This condition highlights the direct relationship between inadequate maintenance of building systems and the impairment of structural performance and stability.



Figure 6 - Diagonal cracks in Masonry Partition Walls (Author, 2025)



Figure 5 - Longitudinal Crack in a Structural Element (Column) (Author, 2025)

From a preventive standpoint, such manifestations could have been avoided through periodic maintenance of the pipelines, including annual inspections and cleaning, as well as the early replacement of compromised sections at the initial stages of leakage. These measures would significantly reduce the risk of soil infiltration and, consequently, the occurrence of leaching and erosion processes responsible for foundation settlement.

At the current stage, the adopted solution required more complex corrective interventions, including foundation reinforcement through the execution of “mega” footings, combined with soil improvement using soil-cement. These measures aim to restore the load-bearing capacity of the ground, mitigate the progression of settlement, and ensure the long-term stability of the structure.

4. Results and Discussions

The analysis of the three case studies clearly demonstrates the direct relationship between the lack of preventive maintenance and the significant increase in the costs of corrective interventions throughout the service life of buildings. In general, it was observed that the costs associated with correcting pathological manifestations can be up to five times higher than those required for implementing preventive measures and proper maintenance.

In Case 1, related to a public building with deficiencies in waterproofing and drainage systems, the estimated cost for corrective interventions—including the removal of the existing pavement and the execution of an adequate waterproofing system using asphalt membrane, as recommended by NBR 9575—is approximately R$ 600,000.00. In contrast, if the waterproofing system had been properly executed during the construction phase, without subsequent interventions compromising its integrity, the estimated cost would have been around R$ 120,000.00. This scenario highlights an increase of approximately five times due to delayed corrective intervention.

In Case 2, associated with the lack of maintenance in hydraulic systems, it was observed that simple preventive measures, such as cleaning and localized replacement of pipes, would have cost approximately

R$ 20,000.00. However, due to the progression of the problem and the occurrence of differential foundation settlement, the initial cost for structural correction reached approximately R$ 95,000.00, in addition to further expenses related to floor replacement and the repair of internal structural elements damaged by the settlement. This case illustrates how seemingly minor issues can evolve into complex pathologies with high repair costs.

In Case 3, it was found that the improper specification of finishing materials—particularly the use of a coating incompatible with the exposure conditions—resulted in the need for complete removal of plaster and façade finishes. The total cost of this intervention exceeded R$ 750,000.00. In contrast, adopting an appropriate solution during the construction phase would have represented an estimated additional cost of only R$ 100,000.00, clearly demonstrating the economic impact of inadequate material selection and lack of technical criteria in the construction process.

Overall, the results indicate that neglecting preventive maintenance practices, as well as deficiencies in design and construction stages, not only reduces the performance and durability of buildings but also leads to significantly higher costs over time. The adoption of preventive measures, combined with proper technical supervision during construction and the implementation of systematic maintenance plans, proves to be substantially more cost-effective and efficient.

Therefore, the importance of an integrated approach is reinforced, encompassing proper specification of materials and construction systems, adequate execution, and continuous monitoring of buildings. Such an approach contributes not only to mitigating pathological manifestations but also to optimizing costs throughout the building life cycle, ensuring greater safety, performance, and durability.

5. Conclusions

This study demonstrated that pathological manifestations in buildings are directly related to deficiencies in the design, construction, and, especially, the lack of preventive maintenance throughout the service life of structures. The analysis of the three case studies showed that factors such as inadequate waterproofing, improper material specification, and neglect in the maintenance of building systems significantly contribute to premature structural degradation and reduced performance.

The application of the GUT Matrix proved to be an effective tool for prioritizing interventions, allowing a systematic evaluation of problems based on their severity, urgency, and tendency to worsen. In all analyzed cases, high levels were identified for these parameters, highlighting the need for immediate corrective actions, particularly in situations involving risks to user safety.

From an economic perspective, the results clearly indicate that the absence of preventive maintenance can significantly increase intervention costs, reaching values up to five times higher than those required during the initial phase or for preventive actions. The analyzed case studies reinforce that simple and low-cost interventions, when carried out early, have the potential to prevent more severe, complex, and costly damages.

Therefore, it is concluded that the adoption of appropriate practices from the design phase—such as proper specification of materials and construction systems—combined with rigorous execution and the implementation of systematic maintenance plans, is essential to ensure the durability, performance, and safety of buildings. Furthermore, the importance of continuous technical supervision and the awareness of managers and users regarding the necessity of preventive maintenance is emphasized.

Finally, this study highlights that investing in construction quality and maintenance should not be seen as an additional cost, but rather as a fundamental strategy to reduce expenses throughout the building life cycle, contributing to the technical, economic, and functional sustainability of the built environment.

References

ANDRADE, J. J. O. Durabilidade das estruturas de concreto. 2012.

ASSOCIAÇÃO BRASILEIRA DE NORMAS TÉCNICAS (ABNT). NBR 15575-1: Edificações habitacionais — Desempenho — Parte 1: Requisitos gerais. Rio de Janeiro, 2013.

AMERICAN SOCIETY FOR TESTING AND MATERIALS (ASTM). Standard definitions of terms relating to durability of materials. 1982.

COMITÉ EURO-INTERNATIONAL DU BÉTON (CEB). Durability of concrete structures. Lausanne, 1992.

COSTA, E. B. Manutenção e durabilidade das estruturas. 2015.

FARIAS, Isabele Silva. Inspeção predial em edificação pública. 2023.

HELENE, P. R. L. Manual para reparo, reforço e proteção de estruturas de concreto. São Paulo, 1992.

HELENE, P. R. L.; TERZIAN, P. Manual de dosagem e controle do concreto. São Paulo, 1992.

IANTAS, L. C. Estudo de caso: análise de patologias estruturais em edificação de gestão pública. 2010. Monografia (Especialização em Construção de Obras Públicas) – Universidade Federal do Paraná, Curitiba.

KEPNER, C. H.; TREGOE, B. B. The new rational manager. Princeton: Kepner-Tregoe, 1981.

MARINHO, J. L. A; MESQUITA, E. F. T. Patologia das edificações: Manifestações nas edificações e no patrimônio histórico. 1ª ed. Editora Leud, São Paulo, 2020.

SENA, G. O. et al. Patologia das Construções. 1ª ed. Editora 2B educação, Salvador, 2020.

SARTOR, A. F. S. Estudo De Caso Sobre Inspeção E Manutenção Predial De Empreendimento Residencial. 2020. 43f. Monografia (Bacharelado em Engenharia Civil) – Universidade Católica de Goiás, Goiânia, 2020

SENE, Thais Sanson; DA COSTA, Lúcia Cortes; SCHEFFER, Sandra Maria. Indicativos de gentrificação na cidade de Ponta Grossa, PR: uma análise a partir da relação entre a legislação urbana municipal e as transformações no espaço urbano. Terr@ Plural, v. 18, p. 1-19, 2024.

SOTILLE, M. A. Gerenciamento de projetos: aplicação da matriz GUT. 2014.

THOMAZ, E. Trincas em edifícios: causas, prevenção e recuperação. São Paulo: Pini, 2001.

cinpar2026
XXII International Conference on Building Pathology and Constructions Repair
15th to 17th July 2026 - Lisboa, Portugal

Analysis of pathological manifestations resulting from prolonged work stoppage in public educational construction: impacts on the execution of coatings.

Vivian Miranda da SIlva[1], Marília Araújo[2]

[1] Instituto Nova Engenharia, São Paulo, Brasil, (engenharia@innovapredial.com.br)
[2] Instituto Nova Engenharia, São Paulo, Brasil, (marilia_carla10@hotmail.com)

Abstract: This study is based on a case study involving a public school building funded by the Federal Government, located in the municipality of Itaperuna, in the state of Rio de Janeiro, Brazil, whose construction cycle was interrupted for approximately four years. During the period of suspension, the reinforced concrete superstructure of the educational facility remained exposed to continuous weathering cycles, without the protection of roofing or enclosure systems. The methodology adopted is grounded in the principles of building pathology and diagnostic engineering, through systematic visual inspection and photographic surveying, with the objective of correlating prolonged environmental exposure with material degradation. The research analyzes the technical consequences resulting from the interruption of the school construction project, demonstrating that the execution of the final finishing layers is technically dependent on the prior treatment of the accumulated pathological manifestations. The study shows that substrate degradation compromises the compatibility and adhesion of finishing systems, requiring restorative interventions to ensure the building's performance and durability requirements.

Keywords: Pathological Manifestations; Diagnostic Engineering; Resumption of Works; Durability of Structures.

1- Introduction

Educational infrastructure plays a fundamental role in ensuring adequate conditions for the teaching and learning process, and the execution of public works aimed at the construction, expansion, and requalification of school units is an essential element to ensure the efficient functioning of these spaces. In this context, the quality and continuity of the works assume direct relevance to the performance and durability of the buildings.

In the social and economic sphere, the high rate of paralysis of educational works directly compromises the expansion of the public education network and the provision of adequate environments for the development of pedagogical activities. The non-completion of these projects implies a waste of public resources, delays in the delivery of essential equipment to the population, and damage to the effectiveness of educational policies. In this context, the data presented reinforce the need for greater technical rigor in the planning, control, and supervision of public works, especially in the educational sector, due to the structural, financial, and social impacts resulting from construction discontinuity.

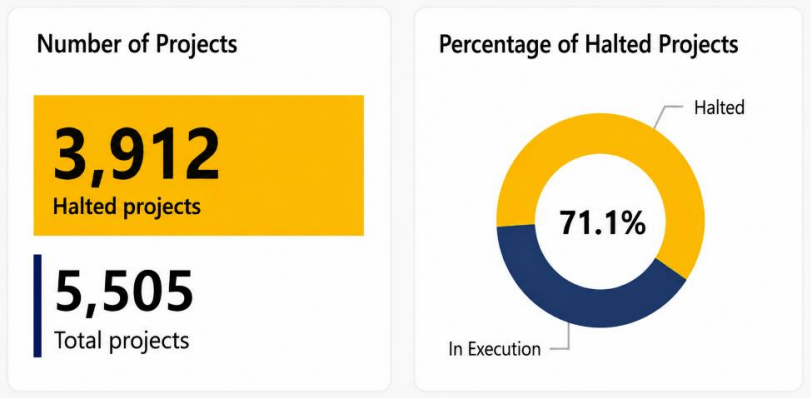


Figure 1: Scenario of Execution and Stoppage of Federal Public Educational Works.
Source: Adapted from the Federal Court of Accounts of Brazil (TCU, 2025).

As shown in Figure 1, it can be observed that, of the 5,505 public educational works monitored by the Federal Court of Accounts (TCU), 3,912 are paralyzed, corresponding to approximately 71.1% of the total projects. The data highlight a critical scenario of construction discontinuity in the education sector, revealing that more than two-thirds of educational works financed with federal public funds are not under construction.

From an engineering perspective, the high rate of paralysis of public educational works represents a technical problem of significant complexity, since the prolonged interruption of executive activities compromises the performance and integrity of the construction systems. In school buildings, the lack of construction continuity exposes structural elements, sealing components, and construction surfaces to weathering actions without proper technical protection, favoring the accelerated development of deterioration processes.

The continuous exposure of materials to climatic variations, associated with the absence of adequate roofing, waterproofing, and rainwater drainage systems, subjects the building components to successive cycles of wetting and drying, intensifying surface degradation and reducing the lifespan of the materials used (SOUZA; RIPPER, 1998). In addition, the stoppage of works interrupts essential executive stages for the proper performance of the building, such as concrete curing, waterproofing procedures, and the application of surface protection mechanisms.

This discontinuity in execution creates favorable conditions for the emergence and spread of pathological manifestations, such as cracking, infiltration, corrosion of the reinforcement, and premature degradation of the building systems. The inadequate interruption of the wet curing of concrete, for example, contributes to the increase in the porosity of the cementitious matrix, facilitating the penetration of aggressive agents and significantly reducing the period of initiation of corrosion of the exposed reinforcement (HELENE, 1993). As a consequence, there is a direct compromise to the structural performance, durability, and safety of buildings, in addition to a significant increase in recovery costs and technical difficulties related to resuming projects.

In this context, the stalled construction ceases to represent merely an unfinished undertaking and becomes a constructive system in continuous physical and functional deterioration (LICHTENSTEIN, 1986). Therefore, it becomes fundamental to understand the relationship between the stoppage of public educational works and the development of pathological manifestations, in order to support more precise technical analyses and contribute to the formulation of strategies aimed at mitigating the damage resulting from construction discontinuity.

Therefore, this research is characterized as an applied study, with a qualitative approach, developed through the case study method, focused on the analysis of pathological manifestations resulting from the prolonged stoppage of the construction of a public daycare center financed by the Federal Government, located in the municipality of Itaperuna, in the state of Rio de Janeiro. It is a larger architectural model within the program, designed to meet the demand for early childhood education in daycare centers and preschools, with a functional structure composed of pedagogical, administrative, and service blocks.

During this period, the reinforced concrete superstructure remained directly subjected to the action of physical, chemical, and biological degradation agents, potentiating the emergence of pathological manifestations and compromising the durability and performance conditions of the construction systems. Given this scenario, the theoretical framework addresses the main pathological manifestations observed in reinforced concrete structures exposed to adverse conditions, highlighting their characteristics, mechanisms of occurrence, and consequences for the building's performance.

2- Theoretical Framework

Prolonged interruptions in public works are a critical factor for the durability and performance of buildings, especially when partially completed structures remain exposed to environmental actions without the adoption of adequate protection measures. From a civil engineering perspective, the halt in the construction cycle involves essential execution stages, such as concrete curing, waterproofing, and surface protection of structural elements, favoring the development and intensification of pathological manifestations over time.

According to the Brazilian Association of Technical Standards, through ABNT NBR 6118:2023, the durability of reinforced concrete structures is directly related to environmental exposure conditions, the quality of materials used, and the correct execution of structural protection systems. The standard highlights that the lack of control of aggressive agents compromises the service life of buildings and accelerates manipulation mechanisms, especially in environments continuously exposed to moisture and weather.In this context, the interruption of construction activities can significantly compromise the concrete curing process. According to ABNT NBR 14931:2023, proper curing is essential to ensure cement hydration, the development of mechanical resistance, and the reduction of concrete permeability. Deficiencies in this process favor the occurrence of plastic and hydraulic shrinkage, resulting in the appearance of surface cracks and reduced structural performance. As highlighted by Thomaz (1989), cracking is one of the most recurrent pathological manifestations in buildings subjected to construction failures or premature exposure to weathering, acting as a preferential pathway for the entry of aggressive agents.

Another relevant mechanism refers to the corrosion of reinforcement bars in reinforced concrete structures. According to Helene (1993), the ingress of moisture, carbon dioxide, and aggressive ions into the pores of the concrete causes the depassivation of the steel, initiating corrosive processes that directly compromise the structural safety and durability of the building. Corrosion promotes volumetric expansion of the steel bars, generating internal stresses capable of causing cracking, detachment of the concrete cover, and reduction of the resistant section of columns, beams, and slabs.

Additionally, prolonged exposure of unfinished structures to wetting, drying, and thermal variations intensifies the physical-chemical deterioration mechanisms of reinforced concrete. According to Helene and Pereira (2007), high surface porosity associated with the absence of structural protection favors the ingress of aggressive agents, such as carbon dioxide, chlorides, and moisture, accelerating the carbonation and corrosion processes of the reinforcement bars.

Carbonation of concrete consists of the reaction between carbon dioxide present in the atmosphere and the alkaline compounds of the cement paste, reducing the hydrogen ion potential (pH) of the concrete and

compromising the passivating layer responsible for protecting the steel. According to Cascudo (1997), the reduction of concrete alkalinity is one of the main factors initiating corrosion in reinforced concrete structures subjected to prolonged environmental exposure.

The persistence of the structure without definitive covering and sealing systems further favors the increase in concrete permeability, intensifying capillary absorption and moisture retention in the structural elements. This phenomenon contributes to the leaching of hydrated cement compounds, loss of surface cohesion, and progressive reduction in the durability of the structure. According to Bauer (2019), the continuous action of water on cementitious materials is one of the main agents of degradation in exposed buildings without adequate protection.

From the perspective of building performance, ABNT NBR 15575:2021 establishes that constructions must meet minimum requirements related to structural safety, watertightness, durability, and design service life. However, in interrupted construction projects, the absence of preventive maintenance and adequate conservation directly compromises these normative parameters, significantly reducing the building's expected service life and increasing future structural recovery costs.

In this scenario, diagnostic engineering plays a fundamental role in evaluating the conditions of stalled buildings. According to Gomide, Pujadas, and Fagundes Neto (2015), the technical diagnosis should consider not only the apparent symptoms of pathological manifestations but also the active mechanisms responsible for the evolution of structural degradation, allowing for more precise, economically viable interventions compatible with the existing state of deterioration.

From this perspective, a stalled construction project ceases to represent merely an unfinished building, becoming a system subjected to continuous processes of physical, chemical, and mechanical degradation. As Souza and Ripper (1998) point out, the evolution of pathological manifestations is directly related to the exposure time and the absence of preventive interventions, significantly increasing rehabilitation costs and compromising the technical viability of resuming the project.

Therefore, understanding the impacts of prolonged interruption on construction systems becomes essential to support more precise technical diagnoses and define appropriate structural recovery strategies. Analyzing pathological manifestations in public educational buildings makes it possible not only to identify the active mechanisms of deterioration, but also to understand how construction discontinuity compromises the performance, safety, durability, and lifespan of buildings over time.

3- Methodology

The study is based on the principles of diagnostic engineering, an area focused on the technical investigation of the performance, durability, and integrity conditions of buildings, with a focus on the identification, characterization, and interpretation of the constructive anomalies present in the analyzed structure. The research concentrated especially on evaluating the effects caused by the continuous exposure of the reinforced concrete superstructure to the elements, considering factors such as humidity, solar incidence, thermal variations, biological agents, and the absence of sealing and roofing systems.

The methodology adopted initially comprised the documentary and historical survey of the work, including information regarding the period of stoppage, the conditions of resumption, and the executive stage of the building. Subsequently, on-site technical inspections were carried out, with systematic procedures of visual observation and photographic recording of the existing constructive conditions.

Figure 2 shows the state of the building at the time of the resumption of work, which occurred in 2023, highlighting the advanced level of exposure of the structural elements and the absence of finishes and protection systems for the construction.



Figure 2: Status of the work at the time of resumption in 2023. Source: Author's own elaboration (2023)



Figure 3: Status of the work at the time of resumption in 2026. Source: Author's own elaboration (2026)

The assessment of pathological manifestations was carried out through a visual technical inspection conducted during the resumption phase of the work, when the building was undergoing the application of

the coatings. The analysis was based on the direct inspection of the constructive elements, with photographic recording and identification of the anomalies observed.

It is noteworthy that the authors had prior knowledge of the building's conditions during the period in which the work remained paralyzed, at which time signs of degradation were already perceptible, characterized mainly by points of superficial darkening, stains associated with the presence of moisture, and initial signs of deterioration in elements exposed to the elements. This knowledge allowed for a comparative analysis between the conditions observed during the stoppage and those verified after the resumption of services.

The records and assessments of the building's conditions were carried out at two distinct times. The first inspection took place in 2023, when construction activities resumed after the period of work stoppage, when the pathological manifestations present in the exposed structure were identified and recorded. The second inspection was carried out in 2026, a period in which the building was in the finishing phase, making it possible to verify the evolution of the conditions observed previously and to evaluate the effects of the interventions carried out during the continuity of the project.

The analysis was based on on-site visual inspections, complemented by photographic records obtained in both stages of evaluation. The comparison between the surveys carried out made it possible to identify the persistence, mitigation or emergence of new pathological manifestations, providing subsidies for the discussion of the impacts resulting from the prolonged stoppage of the work and the measures adopted during its resumption.

4- Analysis and Discussion

Visual inspections carried out on the building allowed the identification of several pathological manifestations associated with the period of work stoppage and the consequent prolonged exposure of the building elements to environmental conditions. The observed anomalies were recorded through photographic documentation and analyzed in light of the degradation mechanisms described in the technical literature and the principles of diagnostic engineering.

In general, occurrences related to the action of moisture, the development of biological agents, the superficial alteration of materials, and deterioration processes resulting from the lack of adequate protection during the interruption of construction activities were observed. The analysis of these manifestations makes it possible to understand the impacts of the prolonged stoppage on the performance and durability of the building, as well as to evaluate the technical implications for the resumption and completion of the work.

The photographic records obtained during the inspections are presented below, accompanied by a description of the identified pathological manifestations, a discussion of their possible causes, and their potential effects on the evaluated construction systems.



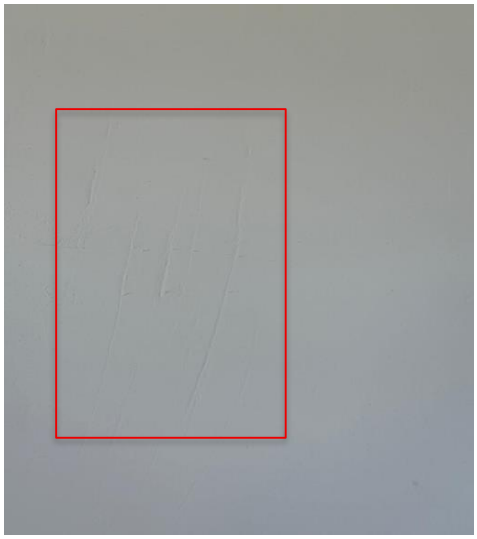
Figure 4 – pathologies found in the walls of the building. Source: Authors' field inspection (2023).

In Figure 4, the severity of the situation is accentuated by prolonged exposure to the elements without the protection of roofs or efficient drainage systems. The continuous dark stain at the base of the walls indicates water saturation of the components, which favors biological colonization (mold and algae), visible by the grayish darkening of the plaster. As pointed out by Santos and Araújo (2022), such pathologies not only compromise aesthetics but also degrade the cohesion of the mortars and reduce the long-term structural and economic performance of the construction.



Figure 5- Dried corrugated conduit. Source: Authors' field inspection (2023).

Figure 5 shows that prolonged pre-exposure degradation of the corrugated conduit results in the phenomenon of polymer drying. Under the action of the sun, the molecular chains of the plastic break, which removes the material's flexibility and makes it extremely brittle.





Figures 6 and 7: Pathological manifestation in the plaster. Source: Authors' field inspection (2026).

The pathological manifestations observed in Figures 6 and 7 comprise mapped cracks in the coating associated, simultaneously, with runoff marks resulting from the action of moisture. These occurrences may be directly related to the set of conditions to which the building was subjected during the period of work stoppage, in which there was prolonged exposure to climatic agents without the proper protection of the construction system.

The mapped cracks are predominantly linked to the mortar shrinkage mechanisms, intensified by inadequate execution and curing conditions. The action of the weather, especially the incidence of solar radiation and ventilation, promoted the accelerated evaporation of the mixing water, generating differential shrinkages and the consequent development of internal stresses in the coating. This scenario favors the emergence of randomly distributed cracks, typical of the mapped pattern.

In parallel, the presence of vertical runoff marks evidences the action of moisture on the surface, indicating possible infiltration or absorption of water by the exposed coating. This process contributes to the surface leaching of mortar and paint components, altering the texture and appearance of the finish, as well as potentially increasing the degradation of the system.

In addition, factors related to the composition and application of the coating such as high fines content, excess cement, multi-layer application, and possible adhesion failures to the substrate act synergistically in intensifying internal stresses and reducing the coating's performance against hygrothermal variations.

Therefore, it is concluded that the identified pathologies do not result from a single isolated agent, but rather from the interaction between material characteristics, execution deficiencies, and adverse environmental conditions, with prolonged exposure to weathering being a determining and aggravating factor for both the development of the mapped cracks and the appearance of the observed signs of moisture.



Figure 8: manifestation of dampness. Source: Authors' field inspection (2026).

In Figure 8, the observed pathological manifestation is characterized by the presence of mold on the surface of the coating, evidenced by greenish stains concentrated at the base of the walls. This type of pathology is directly associated with the continuous presence of moisture, which creates favorable conditions for the proliferation of fungi and microorganisms.

In the case analyzed, the pattern of occurrence indicates a strong relationship with rising damp by capillarity, in which water from the soil is absorbed by porous materials and transported along the masonry. The absence or inefficiency of waterproofing systems at the interface between the soil and the structure contributes significantly to this process.

In addition, the prolonged exposure of the building to the elements during the period of work stoppage acted as an aggravating factor, intensifying the moisture in the building elements. Conditions such as low ventilation and high relative humidity also favor the development of mold, enhancing the degradation of the coating.

Although this manifestation does not directly compromise structural stability, it indicates inadequate building performance conditions, potentially affecting the durability of materials and the healthiness of the environment. Therefore, its occurrence reinforces the need for corrective measures aimed at controlling humidity and adequately protecting building elements.

5- Conclusions

It is concluded that the prolonged exposure of the building during the period of work stoppage is a determining factor for the emergence and intensification of the observed pathological manifestations. The absence of adequate protection allowed the direct action of climatic agents, such as solar radiation, precipitation, and thermal variations, compromising the performance of materials still in the curing process and favoring mechanisms of premature degradation.

In this scenario, not only was the development of mapped cracks and signs of moisture infiltration observed, but also the occurrence of surface disintegration of the coating, evidenced by the powdery ("crumbling") appearance of the wall. This condition stems mainly from the loss of cohesion of the mortar due to inadequate curing, leaching of components, and continuous exposure to moisture, resulting in a weakened substrate.

This degradation significantly compromises the adhesion of new finishing materials, making it difficult to apply fillers, sealers, and paints, in addition to reducing the durability of the system as a whole. Thus, merely superficial interventions become ineffective, making it essential to remove the compromised layers and properly restore the coating.

In this way, it is evident that neglecting the protection of the work not only favors the emergence of pathologies, but also aggravates their complexity and increases recovery costs, directly impacting the final quality of the building. It is therefore reinforced that the adoption of preventive measures during shutdowns, such as surface protection, control of curing conditions, and mitigation of exposure to the elements, is technically indispensable and economically more efficient than subsequent correction.

References

ASSOCIAÇÃO BRASILEIRA DE NORMAS TÉCNICAS. ABNT NBR 15575-1:2021: edificações habitacionais desempenho.

ASSOCIAÇÃO BRASILEIRA DE NORMAS TÉCNICAS. ABNT NBR 6118:2023: projeto de estruturas de concreto. Rio de Janeiro: ABNT, 2023.

ASSOCIAÇÃO BRASILEIRA DE NORMAS TÉCNICAS. ABNT NBR 14931:2023: execução de estruturas de concreto armado, protendido e com fibras — requisitos. Rio de Janeiro: ABNT, 2023.

BRASIL. Tribunal de Contas da União. *Painel de dados*. Available at:

https://paineis.tcu.gov.br/pub/?workspaceId=8bfbd0cc-f2cd-4e1c-8cde-6abfdffea6a8&reportId=013930b6-b989-41c3-bf00-085dc65109de&filterPaneEnabled=false&navContentPaneEnabled=false. Accessed on: April 05, 2026.

BAUER, Luiz Alfredo Falcão. *Materiais de construção*. 6. ed. Rio de Janeiro: LTC, 2019.

CASCUDO, Oswaldo. O controle da corrosão de armaduras em concreto: inspeção e técnicas eletroquímicas. Goiânia: Editora UFG, 1997.

GOMIDE, Tito Lívio Ferreira; PUJADAS, Flávia Zoéga Andreatta; FAGUNDES NETO, Jerônimo Cabral Pereira. Engenharia diagnóstica em edificações. São Paulo: PINI, 2015

HELENE, Paulo. *Patologia, recuperação e reforço de estruturas de concreto*. São Paulo: Pini, 1992.

HELENE, Paulo R. L. Contribuição ao estudo da corrosão em armaduras de concreto armado. 1993. Tese (Livre Docência) – Universidade de São Paulo, São Paulo, 1993. Disponível em: https://teses.usp.br/teses/disponiveis/livredocencia/3/tde-15102025-084830/. Accessed on: May 15, 2026.

HELENE, Paulo; PEREIRA, Fernanda. Manual de reabilitação de estruturas de concreto: reparo, reforço e proteção. São Paulo: RED Rehabilitar, 2007.

LICHTENSTEIN, Norberto Blumenfeld. Patologia das construções. Boletim Técnico do Departamento de Engenharia de Construção Civil, n. 06, 1986Tradução . . Disponível em: https://repositorio.usp.br/directbitstream/2f5de459-e5e4-4a01-8962-1ec0303b3e9a/BT-86_06_251016_082604.pdf. Accessed on: May 15, 2026.

SANTOS, Waldemar Ferreira dos; ARAÚJO, Ítalo Alves de. Building pathology: focus on the emergence of cracks, fissures, splits and gaps in structural masonry walls. Revista Real Conhecer, v. 1, n. 1, 2022. Available at: https://revistas.icesp.br/index.php/Real/article/view/6552. Accessed on: April 08, 2026.

SOUZA, Vicente Custódio Moreira de; RIPPER, Thomaz. Patologia, recuperação e reforço de estruturas de concreto. São Paulo: Pini, 1998. 255 p. ISBN 85-7266-096-8.

THOMAZ, Ercio. Trincas em edifícios: causas, prevenção e recuperação. São Paulo: PINI, 1989.

Cinpar 2026
XXII International Conference on Building Pathology and Constructions Repair
15th to 17th July 2026 - Lisboa, Portugal

Análise da Expansão da Infraestrutura Urbana de Brasília. Aspectos da Reabilitação de Viadutos no Trevo de Triagem Norte

Márcio Augusto Roma BUZAR[1], Paulo Robert MACHADO[2], Leonardo da Silveira Pirillo INOJOSA[3], Stefano GALIMI[4]

[1] FNDE – Fundo Nacional da Educação, Brasília, Brasil, marcio.buzar@gmail.com
[2]DER-DF – Departamento de Estradas de Rodagem do Distrito Federal, Brasília, Brasil, probertsm@gmail.com
[3]UnB – Universidade de Brasília, Brasília, Brasil, leinojosa@unb.br
[4]UnB – Universidade de Brasília, Brasília, Brasil, stefano.galimi@gmail.com

Abstract: A expansão da infraestrutura urbana no Trevo de Triagem Norte (TTN) configura-se como um marco para as estratégias de manutenção do patrimônio da capital federal. A preservação desse acervo moderno exige uma revisão documental rigorosa, que considere desde as diretrizes do projeto original até as intervenções acumuladas ao longo do tempo. Tais transformações culminaram na necessidade de ampliar a capacidade de carga de pontes e viadutos por meio de reforços estruturais, uma vez que o complexo representa uma das principais artérias viárias de Brasília, com alto volume de tráfego no eixo Sul-Norte (MACHADO et al., 2024). O projeto de reabilitação deve garantir segurança, durabilidade e sustentabilidade, integrando a manutenção periódica ao respeito ambiental. O objetivo central é otimizar o desempenho e a vida útil do conjunto estrutural, visando à melhoria da qualidade das construções (Possan & Demoliner, 2013). Ademais, a preservação do patrimônio cultural demanda uma análise das características construtivas originais, das alterações físicas e das patologias decorrentes do envelhecimento dos materiais e da ação antrópica (Formisano & Milani, 2019). Embora o Brasil careça de uma norma específica para essa prática, a ABNT NBR 15575:2013 a define como uma atualização tecnológica voltada à longevidade do bem (Negreiros, 2019). Diante disso, este trabalho utiliza pesquisas históricas e investigações experimentais no TTN para definir um modelo de interpretação qualitativa, visando à intervenção mais adequada à salvaguarda do patrimônio moderno.

Keywords: A maximum of five keywords should be provided. These should accurately describe the content of the paper.

1. Introdução

O patrimônio cultural incorpora a historiografia e a identidade de uma sociedade, detendo um expressivo potencial econômico e social capaz de subsidiar o enfrentamento dos desafios contemporâneos no âmbito das cidades (Matos et al., 2024). Sob essa ótica, torna-se imperativo reposicionar as políticas patrimoniais, integrando-as ao planejamento urbano com ênfase na conservação, manutenção e proteção da infraestrutura urbana moderna. No contexto das infraestruturas rodoviárias, observa-se que as intervenções em Obras de Arte Especiais (OAEs), como pontes e viadutos, têm sido motivadas predominantemente pela obsolescência decorrente da escassez de manutenção preventiva, o que culmina na precarização dos espaços urbanos adjacentes (Galimi et al., 2025).

Essa urgência demanda estudos aprofundados acerca da degradação de elementos estruturais e da avaliação sistêmica do estado de conservação dessas unidades (Lima et al., 2019) A preservação do acervo edificado exige, portanto, uma abordagem multidisciplinar que examine o bem em sua totalidade, harmonizando critérios históricos e estéticos à manutenção do valor patrimonial e à salvaguarda da autenticidade (Peixoto et al., 2022). Nesse cenário, a reabilitação urbana qualifica-se como instrumento de

revitalização capaz de promover melhorias socioestruturais, fundamentando a reutilização de estruturas históricas como centros de renovação cultural e indutores de capital social.

A intervenção em infraestruturas rodoviárias transcende a mera recuperação física; configura-se como uma estratégia de valorização de territórios que, malgrado o estado de degradação, preservam um conteúdo simbólico e histórico relevante. A revitalização busca, portanto, perpetuar a memória e os valores culturais, ressignificando o uso de ativos degradados para reintegrá-los ao tecido social e urbano (Galimi et al., 2025). Tais ações, ao superarem a dimensão estritamente funcional, estabelecem vínculos entre territórios e atividades, otimizando a qualidade do ambiente construído.

Em Brasília, a expansão da infraestrutura urbana e a consequente necessidade de intervenção nas OAEs confrontam-se com as diretrizes de preservação do Conjunto Urbanístico de Brasília (CUB). A reabilitação sustentável surge como o caminho para viabilizar a conservação do patrimônio moderno, onde a intervenção não se limita à recuperação estrutural, mas abrange a refuncionalização e a extensão da vida útil das obras (Negreiros, 2019). O presente trabalho analisa, especificamente, o caso do Trevo de Triagem Norte (TTN), compreendendo o projeto de reabilitação como uma iniciativa de requalificação urbana que visa à reintegração de espaços segregados à malha viária principal, aplicando princípios de reconversão aplicáveis às infraestruturas de transporte (Costa, 2015).

2. Brasília, Patrimônio e Tombamento

A capital brasileira, reconhecida como Patrimônio Cultural da Humanidade pela UNESCO, apresenta desafios ímpares para a preservação de sua infraestrutura modernista. Tal cenário é particularmente crítico em Obras de Arte Especiais (OAEs), que demandam intervenções que conciliem as exigências funcionais contemporâneas à salvaguarda de seu valor histórico-arquitetônico (Galimi et al., 2021). O tombamento de Brasília, enquanto mecanismo de proteção legal, impõe diretrizes rigorosas que visam à preservação da coexistência das quatro escalas urbanísticas concebidas por Lúcio Costa: a monumental, a residencial, a gregária e a bucólica. Qualquer alteração no sistema viário deve, portanto, respeitar a hierarquia dessas escalas, evitando que a expansão da infraestrutura segregue o tecido urbano ou comprometa a visibilidade da linha do horizonte — elemento central da escala bucólica e da concepção de "cidade-parque" (Farret, 2018).

Nesse contexto, a aplicação dos conceitos de autenticidade e integridade às OAEs de Brasília transcende a conservação da matéria original. A integridade refere-se à manutenção da unidade do conjunto urbanístico e da funcionalidade dos eixos, enquanto a autenticidade está vinculada à permanência do espírito do projeto e das soluções estruturais inovadoras que caracterizam a escola carioca de Oscar Niemeyer e Joaquim Cardozo (Peixoto et al., 2022). Intervenções de reabilitação no Trevo de Triagem Norte (TTN) devem, assim, garantir que os reforços estruturais e as ampliações de carga não descaracterizem a leveza e o protagonismo da estrutura, elementos fundamentais da identidade tectônica da capital (Inojosa, 2019)

Os instrumentos normativos decorrentes do tombamento conferem um caráter inalienável à preservação do sítio urbano, estabelecendo que intervenções no sistema viário respeitem uma abordagem integrada dos fenômenos sociais, culturais e ambientais. Nesse sentido, dispositivos como o Decreto n.º 10.829/1987 e a Portaria n.º 314/1992 do IPHAN definem áreas de preservação que englobam não apenas a volumetria edificada, mas o entorno e as infraestruturas que estruturam as quatro escalas de Brasília (Galimi et al., 2021). No caso específico do Trevo de Triagem Norte (TTN), a intervenção exige uma análise aprofundada de seu valor patrimonial, uma vez que a estrutura se insere na zona de amortecimento e visibilidade do Plano Piloto.

Contudo, observa-se que a percepção pública acerca do tombamento muitas vezes restringe-se aos monumentos isolados, em detrimento da compreensão da cidade como um sistema de infraestrutura contínuo. A composição urbanística configura a área de proteção que articula edifícios, espaços livres e vias, constituindo uma totalidade indissociável. Essa complexidade normativa demanda um exame minucioso

das legislações pertinentes para garantir que as intervenções rodoviárias estejam em conformidade com as exigências de proteção (Ficher, 2019).

Embora o tombamento seja ocasionalmente interpretado como um óbice ao desenvolvimento urbano, ele deve ser compreendido como um instrumento de controle e planejamento estratégico. Sua função primordial é balizar o crescimento da metrópole, assegurando que a evolução da infraestrutura não comprometa os valores culturais e históricos que fundamentam a excepcionalidade de Brasília (Farret, 2018

3. Brasília, Infraestrutura Urbana

A capital federal, caracterizada pelo rigor de seu planejamento modernista, apresenta uma infraestrutura urbana complexa e interligada, cuja manutenção e adequação às demandas contemporâneas exigem abordagens metodológicas inovadoras (Alwehab & Juvara, 2018). A gênese morfológica de Brasília fundamenta-se na articulação de dois eixos ortogonais: o Eixo Rodoviário (curvo) e o Eixo Monumental (retilíneo). Esta configuração em "cruz" não apenas organiza o espaço urbano e a mobilidade, mas estabelece a espinha dorsal sobre a qual se assenta a setorização da cidade (Pereira & Avena, 2018).

Nesse sistema, as Obras de Arte Especiais (OAEs) — pontes, viadutos e passagens inferiores — atuam como conectores urbanos essenciais. Elas viabilizam a segregação de fluxos e a continuidade dos eixos sem interrupções por cruzamentos em nível, consolidando a visão de uma cidade planejada para a funcionalidade e para o tráfego de alta fluidez (Oliveira & Sobrinho, 2022). O projeto original (Figura 1) já previa estruturas estratégicas para a conexão das escalas, como exemplificado na Ponte do Braghetto, concebida ainda nos primórdios da construção para viabilizar a saída norte da capital.

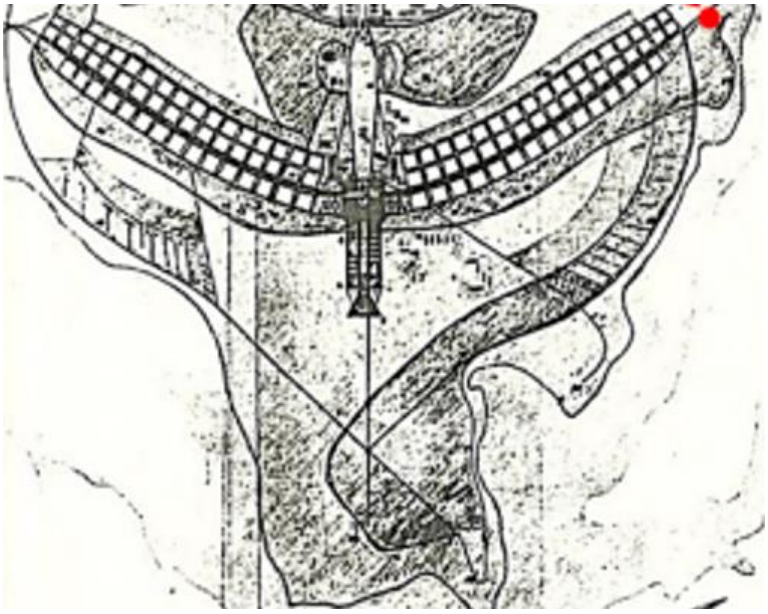


Figura 1 – Esboço do Plano Piloto, com indicação da Ponte do Braghetto em 1956. Fonte: (MACHADO et al., 2024)

Entretanto, após mais de seis décadas de operação, a infraestrutura rodoviária de Brasília enfrenta o desafio do envelhecimento natural dos materiais e da obsolescência tecnológica. O aumento exponencial do volume de tráfego e das cargas rodoviárias, que superam consideravelmente as previsões de cálculo da década de 1960, impõe uma severa degradação às estruturas de concreto armado). Esse cenário exige intervenções de reforço e atualização que equilibrem a necessidade de modernização e segurança estrutural com o respeito absoluto às diretrizes de preservação do patrimônio arquitetônico e urbanístico

(Galimi et al., 2020). A reabilitação destas OAEs, portanto, não é apenas uma demanda de engenharia, mas uma condição para a sustentabilidade da mobilidade urbana no Distrito Federal (Moraes, 2021).

4. O Trevo de Triagem Norte (TTN)

A intervenção no Trevo de Triagem Norte (TTN), que compreende a ampliação e reestruturação do sistema viário na saída norte do Distrito Federal, insere-se num contexto complexo de gestão urbana. O projeto (Figura 2) constitui uma das mais ambiciosas iniciativas de requalificação de infraestrutura rodoviária no Distrito Federal, enfrentando o desafio de expandir a capacidade logística em uma área de sensibilidade patrimonial. O complexo situa-se na extremidade norte do Plano Piloto, articulando o fluxo entre a Asa Norte, a Estrada Parque Indústria e Abastecimento (EPIA) e a Estrada Parque Contorno (EPCT). O projeto foi concebido para mitigar o estrangulamento viário na "Saída Norte", onde a convergência de fluxos das regiões de Sobradinho, Planaltina e condomínios adjacentes gerava congestionamentos crônicos e acelerava a degradação das estruturas pré-existentes (Galimi, 2021). A reabilitação e a modernização desse complexo viário representam, assim, uma resposta fundamental às crescentes demandas de mobilidade e ao desgaste decorrente da intensificação do tráfego, elementos que sobrecarregam as infraestruturas projetadas para um cenário urbano distinto (MACHADO et al., 2024).

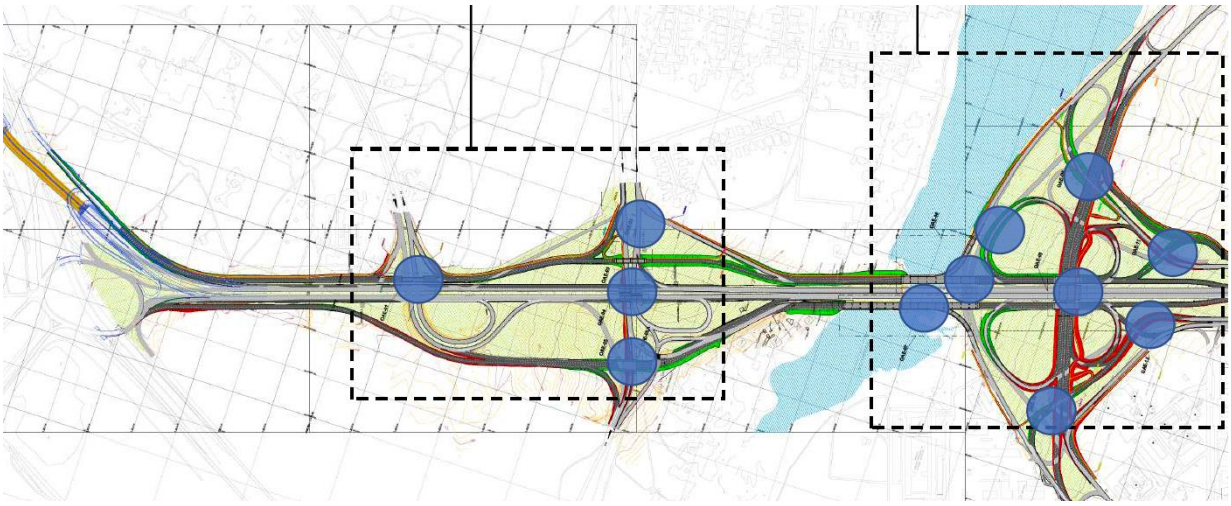


Figura 2 – Conjunto Infraestrutural TTN – Trevo de Triagem Norte. Fonte: (Galimi, 2021)

O Trevo de Triagem Norte é composto por um conjunto de 15 Obras de Arte Especiais, incluindo 13 viadutos e 2 pontes, o retrofit estrutural da Ponte do Braghetto, OEA já existente, além de 9 km de ciclovias, sistemas de drenagem, entre outras adequações como sinalizações e recuperação ambiental. A intervenção, de grande magnitude, visou separar os fluxos locais dos expressos, por meio do conceito de vias marginais para organizar o tráfego que adentra a malha urbana da Asa Norte. A execução, realizada em 2018 pelo DER-DF, adotou padrões modernos de concreto armado e protendido, com vistas a uma vida útil estendida e à redução de custos de manutenção futura por meio de um modelo de retrofit sistêmico (MACHADO et al., 2024).

4.1 A continuidade dos eixos rodoviários principais preservando as vias originais.

A abordagem adotada no TTN priorizou a minimização dos impactos sobre o traçado original, mantendo a coerência com o projeto urbanístico de Lúcio Costa. Brasília foi concebida sob o paradigma modernista, onde a estrutura detém o protagonismo formal e a arquitetura nasce integrada à solução de engenharia (Inojosa, 2019). No entanto, a Ponte do Braghetto, principal componente desse sistema, enfrentava um

cenário de saturação crítica. Antes da intervenção, o volume de tráfego atingia cerca de 100 mil veículos diários, operando muito além da capacidade projetada na década de 1960 (MACHADO et al., 2024).

O desenvolvimento de Brasília foi marcado por um estilo arquitetônico modernista, centrado na expressão artística e na forma. Seu planejamento urbano e paisagístico avançado enfatizava as qualidades espaciais, por meio de abordagens estruturais inovadoras e tecnologias de ponta. Isso impulsionou avanços significativos na construção civil, especialmente em arquitetura e engenharia estrutural, resultando em soluções originais para uma execução eficiente (Inojosa, 2019).

Sendo a primeira ponte construída sobre o Lago Paranoá e figurando nos esboços originais da capital, a Ponte do Braghetto (com 180 m de extensão e 32 m de largura) exigiu um processo de reabilitação que preservasse sua importância simbólica enquanto expandia sua capacidade operacional. O projeto de reabilitação incluiu o retrofit estrutural da obra pré-existente, que apresentava manifestações patológicas decorrentes do envelhecimento natural e da sobrecarga de tráfego. A intervenção não se limitou à estrutura em si, mas reconfigurou toda a região circundante para absorver o fluxo proveniente do Complexo Viário de Torto-Colorado, transformando a antiga passagem em um sofisticado complexo viário, influenciando toda a região circundante (MACHADO et al., 2024). As imagens comparativas de satélite da Figura 3 registram as intervenções entre 2008 e 2020.



Figura 3 – Imagens comparativas de satélite entre 2008 e 2020. Fonte: (MACHADO et al., 2024)

De acordo com Galimi (2021), a complexidade do TTN reside na necessidade de conciliar a preservação do patrimônio moderno com a obsolescência funcional das estruturas originais. A análise das intervenções entre 2008 e 2020 demonstra que, apesar da inserção de novas alças e viadutos, o Eixo Rodoviário manteve sua diretriz original, preservando a leitura das escalas urbanas (Le, 2011). Esta estratégia ratifica a viabilidade de modelos de requalificação que harmonizam a atualização tecnológica — como o uso de concreto de alto desempenho e novas técnicas de reforço — com a salvaguarda do conceito urbanístico original da cidade.

4.2 A adoção de viadutos construídos em trincheiras com preservação da paisagem urbana.

Tal estratégia converge com os princípios de permeabilidade visual e integração ao entorno, característicos do planejamento de Brasília, promovendo a harmonia entre a funcionalidade da infraestrutura e a estética paisagística. Essa metodologia, portanto, reforça o compromisso com a preservação do patrimônio cultural edificado, ao mesmo tempo em que permite a modernização e a otimização da capacidade de fluxo viário em áreas urbanas de alta sensibilidade patrimonial (MACHADO et al., 2024).

A preservação de elementos paisagísticos e o mobiliário urbano, como o uso de calhas para atenuar o impacto visual e ambiental do tráfego, são exemplos de como essas intervenções podem ser integradas ao planejamento urbano, expandindo o uso seguro e esteticamente enriquecedor das infraestruturas (Aflalo, 2020). Adicionalmente, a implementação de transposições e o rebaixamento de certas seções viárias contribuem para mitigar a interferência no tecido urbano e na percepção visual da cidade, alinhando-se com a lógica projetual de transversalidade entre a via e o solo urbano (Moraes, 2021).

No caso específico do TTN, a opção pelas trincheiras em substituição aos elevados convencionais permitiu que o sistema de alças de acesso fosse "ocultado" sob a topografia natural, evitando a fragmentação do horizonte — um dos valores fundamentais do tombamento de Brasília. Essa solução de engenharia responde ao conceito de "cidade-parque", onde a infraestrutura não deve competir com a massa arbórea e os espaços livres, mas sim subordinar-se a eles para manter a fluidez da percepção espacial (Bispo, 2020).

Além disso, o rebaixamento das pistas no TTN favorece o controle da poluição sonora nas áreas residenciais adjacentes da Asa Norte. As paredes das trincheiras, quando tratadas com materiais de absorção e integradas a barreiras vegetais, atuam como atenuadores acústicos, resolvendo um dos maiores desafios de inserir uma via expressa de alta densidade em um contexto urbano consolidado. Essa abordagem transforma a via rodoviária em um componente infraestrutural menos agressivo ao cotidiano da cidade (Moraes, 2022). Além disso, como visto na Figura 4, essa solução preserva o visual do horizonte para o Plano Piloto, mantendo o platô original e a paisagem urbana.



Figura 4 – Perspectiva dos Viadutos 2 ao 5 em nível, preservando o platô original e a paisagem urbana. Fonte: (Galimi 2024)

Por fim, a utilização de passagens inferiores viabiliza a continuidade da rede cicloviária e de pedestres em nível, sem a necessidade de passarelas elevadas que frequentemente descaracterizam a paisagem modernista (Le, 2011,). Ao manter os fluxos de mobilidade ativa na superfície e deslocar o tráfego pesado para o subsolo, o TTN reafirma a premissa de que a modernização da infraestrutura não precisa sacrificar a escala humana e a integridade visual do Plano Piloto.

4.3 Reabilitação das estruturas existentes.

Outra importante intervenção foi a reabilitação estrutural da Ponte do Braghetto, cuja demolição completa constava no projeto original licitado para a obra . Após reunião de equipe técnica, buscou-se a preservação desse patrimônio com a recuperação de sua estrutura e ampliação da capacidade de uso (MACHADO et al. 2024). Na Figura 5, mostra-se a intervenção na Ponte do Braghetto com a recuperação estrutural.



Figura 5 – Vista da recuperação estrutural da Ponte do Braghetto. Fonte: (Machado 2024)

A Ponte do Braghetto, uma das infraestruturas mais conhecidas da capital brasileira, cujo projeto estrutural foi elaborado pelo engenheiro Aderson Moreira da Rocha, foi construída em 1960, pouco antes da inauguração de Brasília. Seu sistema estrutural e construtivo empregou concreto armado protendido por protensão parcial de aderência posterior, com bainhas metálicas, injeção de calda de cimento e ancoragens do tipo Freyssinet, refletindo as tecnologias construtivas da época. Esse tipo de protensão aplica-se a um elemento estrutural de concreto já endurecido, processando a aderência posteriormente.

Em 2018, foram realizadas análises estruturais com o intuito de avaliar o estado de conservação da estrutura e as intervenções necessárias à sua recuperação. As práticas de retrofit estrutural aplicadas na Ponte do Braghetto consistiram na adoção de uma laje de transição com extensão de 6,0 m nas extremidades dos balanços da ponte, na construção de consoles de apoio dessa laje em concreto armado nas extremidades dos balanços, na disposição de armadura de reforço nos apoios para absorver os esforços devidos à laje de transição sobre a face superior do tabuleiro após remoção do capeamento, na adição de armadura de reforço para absorver esforços transversais nos apoios centrais, no tratamento de anomalias como áreas de concreto segregado, armaduras expostas e com baixo cobrimento, além do aumento da seção dos pilares por encapsulamento. Tais intervenções visaram não apenas a recuperação da integridade estrutural, mas também a adaptação da ponte às novas demandas de tráfego, garantindo a longevidade e a segurança da infraestrutura.

4.4Visão crítica do uso atual do Trevo de Triagem Norte.

Apesar das intervenções realizadas para otimização da capacidade de tráfego, observa-se que o Trevo de Triagem Norte, como complexo infraestrutural, ainda apresenta desafios no que tange à integração plena com o tecido urbano circundante. Em uma análise crítica, o TTN ainda não logrou consolidar-se como um "nó-plataforma" (Moraes, 2022) — conceito que define a infraestrutura não apenas como canal de passagem, mas como um espaço de articulação que conecta diferentes modais (transporte coletivo, ciclovias e pedestres) e diversos usos urbanos. Embora a fluidez para o automóvel individual tenha sido priorizada, a barreira física imposta pelas alças de alta velocidade ainda dificulta a permeabilidade para o pedestre e a fruição da orla do Lago Paranoá.

Ademais, a expansão urbana contínua nas regiões adjacentes (Freitas & Anjos, 2016), como o Trecho 2 da Etapa 1 do Setor Habitacional Taquari (Conserva et al., 2019), intensifica uma pressão constante e crescente sobre esta infraestrutura. Esse fenômeno de espraiamento urbano gera um ciclo de demanda que pode, em médio prazo, tornar obsoleta a ampliação recém-concluída, exigindo uma reavaliação permanente de sua capacidade de absorção. A infraestrutura, portanto, deve ser compreendida dentro de uma visão sistêmica de planejamento territorial estratégico do Distrito Federal, e não apenas como uma solução isolada para um gargalo viário específico (Silva & Saboia, 2016).

Outro ponto sensível reside na manutenção do caráter de "cidade-parque". A magnitude do TTN, com sua vasta área de pavimentação e taludes, desafia a escala bucólica projetada por Lúcio Costa. Galimi (2021) pondera que o sucesso do retrofit no patrimônio moderno depende da capacidade da intervenção de regenerar o entorno degradado, transformando "vazios residuais" sob viadutos em espaços públicos qualificados. No estado atual, o TTN ainda carece de uma estratégia de ocupação humana que mitigue a segregação espacial causada pelo sistema de trevos, garantindo que a infraestrutura cumpra sua função social de aproximar, e não apenas de deslocar, os cidadãos (MACHADO et al., 2024).

5. Conclusão

Este artigo analisou a intervenção no Trevo de Triagem Norte, destacando a complexidade envolvida na modernização de infraestruturas rodoviárias em contextos de alto valor patrimonial, como Brasília, e sublinhando a necessidade de se considerar a requalificação urbana sob uma perspectiva multicritério (Galimi et al., 2022).

A análise das intervenções no Trevo de Triagem Norte (TTN) e a reabilitação da Ponte do Braghetto permitem concluir que a reabilitação estrutural se consolida como a alternativa mais sustentável e técnica frente à substituição total das estruturas, a partir do conhecimento detalhado das manifestações patológicas nas estruturas existentes, cruciais para a proposição de diretrizes eficazes de preservação e intervenção, especialmente em obras que constituem patrimônio moderno (Inojosa et al., 2022). Além disso, a requalificação de infraestruturas urbanas, como a proposta para a Ponte do Bragheto, transcende a mera solução de problemas estruturais, abarcando parâmetros ambientais, espaciais e patrimoniais, para uma abordagem holística (Galimi, 2021).

No contexto de Brasília, onde a infraestrutura é parte integrante do valor excepcional do patrimônio, a demolição e substituição de Obras de Arte Especiais (OAEs) representariam uma perda irreparável da autenticidade técnica e histórica da capital. O retrofit, portanto, não apenas estende a vida útil do sistema viário, mas preserva a memória do saber-fazer da engenharia modernista brasileira.

Um fator determinante para o sucesso dessas intervenções é o rigoroso papel da revisão documental e da investigação experimental. Conforme preconizado por Formisano & Milani (2019), a definição de qualquer estratégia de intervenção em estruturas históricas deve ser precedida por um diagnóstico profundo, que combine a análise de projetos originais com ensaios in loco e monitoramento. No TTN, essa investigação permitiu identificar que, embora a Ponte do Braghetto apresentasse sinais de fadiga, sua reserva estrutural e a qualidade do concreto original viabilizavam o reforço em vez da reconstrução, otimizando recursos públicos e tempo de execução.

Para intervenções futuras em OAEs inseridas no patrimônio moderno, as diretrizes, sintetizadas neste estudo apontam para a necessidade de compatibilidade tecnológica, com o uso de materiais e técnicas que respeitem as propriedades físico-químicas do concreto original; mínima intervenção visual, pela adoção de soluções como trincheiras e reforços internos para preservar a silhueta e a linha do horizonte; e abordagem multicritério, com avaliação que considere simultaneamente o desempenho estrutural, o impacto ambiental e a integração espacial.

A complexidade reside em equilibrar a necessidade de adaptação funcional com a preservação da integridade estética e histórica de elementos arquitetônicos e de engenharia que definem a identidade

urbanística da capital (Lima, 2017). A abordagem de requalificação, conforme evidenciado nesse estudo, demonstra a viabilidade de preservar o patrimônio moderno por meio de intervenções que consideram aspectos sociais, culturais, ambientais e econômicos.

O Trevo de Triagem Norte oferece contribuições valiosas para o modelo de gestão de infraestrutura em Brasília. Ele demonstra que é possível modernizar nós logísticos de alta densidade sem descaracterizar o traçado de Lúcio Costa. O TTN serve como um laboratório vivo de como a engenharia diagnóstica pode atuar em favor da preservação, transformando "gargalos" viários em conectores urbanos que respeitam a escala bucólica e monumental da cidade. O desafio remanescente, contudo, é evoluir para uma gestão que transcenda o fluxo automotivo, integrando plenamente a infraestrutura reabilitada ao cotidiano social e aos modais sustentáveis da capital.

Agradecimentos

Os autores agradecem o Programa de Pós-Graduação em Arquitetura e Urbanismo da Faculdade de Arquitetura e Urbanismo da Universidade de Brasília – PPGFAU-UnB.

References

Aflalo, Marcelo. 2020. “A Travessia Facilitada.” Revista LABVERDE 10 (1). University of São Paulo. doi:10.11606/issn.2179-2275.labverde.2020.146744.

Alwehab, A A., and Martina Juvara. 2018. “Planning and Design Attributes of Preplanned Postmodern Capital Cities: A Comparative Study.” KnE Engineering 3 (4). Knowledge E: 208. doi:10.18502/keg.v3i4.2170.

Bispo, Alba Nélida de Mendonça. 2020. “Da Perspectiva Edênica à Concepção Paisagística de Brasília, Cidade-Parque.” PatryTer 3 (6). University of Brasília: 35. doi:10.26512/patryter.v3i6.26965.

Conserva, Cátia dos Santos, Liza Maria Souza de Andrade, Daniel Sant’Ana, Daniela Junqueira Carvalho, Maria Elisa Leite Costa e Sérgio Koide. 2019. “Olhares Sobre a Drenagem Em Brasília: Expansão Urbana e Infraestrutura SOCIoecológica Na Serrinha Do Paranoá, DF.” MIX Sustentável 5 (2). Universidade Federal de Santa Catarina: 149. doi:10.29183/2447-3073.mix2019.v5.n2.149-164.

Costa, Gustavo Sbardelotto da. 2015. “Reconexão de Espaços Degradados à Cidade Por Meio Da Reconversão de Uso de Vazios Industriais : O Caso Do IV Distrito de Porto Alegre.” https://www.lume.ufrgs.br/handle/10183/122532.

Farret, Ricardo. 2018. “BRASÍLIA E O SEU PLANEJAMENTO TERRITORIAL: NOVAS ESCALAS, NOVAS DEMANDAS E NOVOS PARADIGMAS.” Revista Eletrônica Tempo - Técnica - Território / Electronic Magazine Time - Technique - Territory 7 (2). University of Brasília. doi:10.26512/ciga.v7i2.19093.

Ficher, Sylvia. 2019. “BRASÍLIA: LEGISLAÇÃO PATRIMONIAL E GESTÃO URBANA.” Revista Thésis 2 (5). doi:10.51924/revthesis.2018.v2.212.

Formisano, Antonio, and Gabriele Milani. 2019. “Seismic Vulnerability Analysis and Retrofitting of the SS. Rosario Church Bell Tower in Finale Emilia (Modena, Italy).” Frontiers in Built Environment 5 (May). Frontiers Media. doi:10.3389/fbuil.2019.00070.

Freitas, Juvair Fernandes de, e Rafael Sanzio Araújo dos Anjos. 2016. “MONITORAMENTO ORBITAL DA EXPANSÃO URBANA NA CIDADE DE ANÁPOLIS – 1997/2000.” Revista Eletrônica Tempo - Técnica - Território / Electronic Magazine Time - Technique - Territory 1 (1). University of Brasília. doi:10.26512/ciga.v1i1.15881.

Galimi, Stefano. 2021. “Índice De Requalificação Da Infraestrutura Urbana: Uma Proposta Para Avaliação Das Intervenções De Retrofit No Patrimônio Das Obras De Arte Especiais”. Tese (Doutorado em Arquitetura e Urbanismo) – Programa de Pós-Graduação em Arquitetura e Urbanismo, Faculdade de Arquitetura e Urbanismo, Universidade de Brasília, Brasília, DF. 459p.

Galimi, Stefano, Márcio Augusto Roma Buzar, e João da Costa Pantoja. 2022. “Índice de Requalificação Da Infraestrutura Urbana: O Viaduto Central Em Brasília.” Cadernos Metrópole 24 (55). Editora da Pontifícia Universidade Católica de São Paulo: 1097. doi:10.1590/2236-9996.2022-5511.

Galimi, Stefano, Márcio Augusto Roma Buzar, João da Costa Pantoja, e Luiza Teixeira Naili. 2021. “A Conservação Do Patrimônio Moderno Através Das Práticas de Retrofit Na Infraestrutura Urbana de Brasília.” In Tecnologia, Ambiente e Sustentabilidade - Coletânea de Artigos. Universidade de Brasília - UnB.

Galimi, Stefano, João da Costa Pantoja, Márcio Augusto Roma Buzar, and Paulo Robert Santos Machado. 2020. “Retrofit Em Obras Tombadas de Infraestrutura Urbana: O Caso Do Viaduto Sobre a Galeria Dos Estados.” Paranoá Cadernos de Arquitetura e Urbanismo, nº. 26 (May). University of Brasília: 140. doi:10.18830/issn.1679-0944.n26.2020.10.

Galimi, Stefano, João da Costa Pantoja, Márcio Augusto Roma Buzar, and Valmor Cerqueira Pazos. 2025. “Índice de Requalificação Da Infraestrutura Urbana: O Caso Da Ponte San Giorgio Em Génova.” Urbe Revista Brasileira de Gestão Urbana 17 (January). Editora Universitária Champagnat. doi:10.1590/2175-3369.017.e20240283.

Inojosa, Leonardo da Silveira Pirillo. 2019. “O Protagonismo Da Estrutura Na Concepção Da Arquitetura Moderna Brasileira.” Tese (Doutorado em Arquitetura e Urbanismo) – Programa de Pós-Graduação em Arquitetura e Urbanismo, Faculdade de Arquitetura e Urbanismo, Universidade de Brasília, Brasília, DF.

Inojosa, Leonardo da Silveira Pirillo, João da Costa Pantoja, Márcio Augusto Roma Buzar, e Iberê Pinheiro de Oliveira. 2022. “ANÁLISE DE MANIFESTAÇÕES PATOLÓGICAS E DE ESTRUTURAS DE CONCRETO ARMADO PARA PRESERVAÇÃO DO PATRIMÔNIO – MUSEU DA CIDADE – BRASÍLIA-DF.” In Brazilian Journals Editora eBooks, 250. doi:10.35587/brj.ed.0001552.

Le, Xuan Son. 2011. “Places and Models : The Example of the 20th Century New Towns.” HAL (Le Centre Pour La Communication Scientifique Directe), May. Centre National de la Recherche Scientifique. https://theses.hal.science/tel-00647895.

Lima, Henrique Jorge Nery de, Ricardo da Silva Ribeiro, Guilherme S. Melo e Rodolfo de Azevedo Palhares. 2019. “Análise de Manifestações Patológicas do Concreto Em Viadutos Urbanos.” Revista ALCONPAT 9 (2): 247. doi:10.21041/ra.v9i2.308.

Lima, João Pedroso. 2017. “Tem Que Tombar? : Patrimônio Moderno e Forma Alternativa de Conservação.” doi:10.26512/2017.07.t.24446.

MACHADO, Paulo Robert Santos, Leonardo da Silveira Pirillo, INOJOSA, Márcio Augusto, Roma BUZAR, Marcos Aurélio de Sousa, BESSA, e Glaucio de Oliveira Santos. 2024. “Historical Aspects and Rehabilitation of the First Brazilian Bridge with Partial Prestressing – Braghetto Bridge – Brasília-DF.”

Matos, Raulemberde Baia, Anny Karoliny Rodrigues Batista e Eli Conceição de Vasconcelos Tapajós Sousa. 2024. “HISTÓRIA E APRENDIZADO POR MEIO DO PATRIMÔNIO CULTURAL:” Revista de História Bilros. 12 (25). Associação Sul-Rio-Grandense de Pesquisadores em História da Educação (ASPHE). doi:10.52521/bilros.v12i25.14172.

Moraes, Pedro Barreto de. 2021. “Infraestruturas Rodoviárias e Lógicas Projetuais.” Risco Revista de Pesquisa em Arquitetura e Urbanismo (Online) 19 (September). University of São Paulo: 1. doi:10.11606/1984-4506.risco.2021.172202.

———. 2022. “INFRAESTRUTURA RODOVIÁRIA:” Arquitetura Revista 18 (2). University of Vale do Rio dos Sinos: 221. doi:10.4013/arq.2022.182.06.

Negreiros, Iara. 2019. “Retrofit Urbano: Uma Abordagem Para Apoio de Tomada de Decisão.” doi:10.11606/t.3.2019.tde-04022019-091230.

Oliveira, Washington Candido e Fernando Luiz Araújo Sobrinho. 2022. “Usos Del Suelo Urbano y Del Territorio En El Sitio Del Patrimonio Mundial de Brasilia y El Sector Habitacional Jóquei Clube.” PatryTer 5 (10). University of Brasília: 95. doi:10.26512/patryter.v5i10.41187.

Peixoto, Allana de Deus, Flaviana Barreto Lira e Carlos Eduardo Luna de Melo. 2022. “A Integridade Na Conservação Da Arquitetura Moderna: O Caso Do Viaduto Do Eixo Rodoviário Sul Em Brasília.” Pós Revista do Programa de Pós-Graduação em Arquitetura e Urbanismo da FAUUSP 29 (54). University of São Paulo. doi:10.11606/issn.2317-2762.posfauusp.2022.174449.

Pereira, Amneres Santiago de Brito e Biagio Maurício Avena. 2018. “Brasília:” Cenário Revista Interdisciplinar em Turismo e Território 6 (10). University of Brasília: 101. doi:10.26512/revistacenario.v6i10.18904.

Possan, Edna, and Carlos Alberto Demoliner. 2013. “DESEMPENHO, DURABILIDADE E VIDA ÚTIL DAS EDIFICAÇÕES: ABORDAGEM GERAL.” Revista Técnico-Científica 1 (1). http://creaprw16.crea-pr.org.br/revista/Sistema/index.php/revista/article/download/14/10.

Silva, Sued Ferreira da, e Luciana Saboia. 2016. “Paisagens Em Trânsito: O Caso Da Estrada Parque Taguatinga.” Labor & Engenho 10 (3). University of Campinas: 302. doi:10.20396/lobore.v10i3.8646182.

cinpar2026
XXII International Conference on Building Pathology and Constructions Repair
15th to 17th July 2026 - Lisboa, Portugal

Avaliação de vulnerabilidade sísmica de escolas de Lisboa: da priorização à escala urbana à análise estrutural detalhada

Luís FERREIRA[3], João DOUTEL[2], Bruno QUELHAS[1], Sónia STEIGER[4], Cátia SANTANA[5]

[1] NCREP – Heritage Consultancy, Porto, Portugal, bruno.quelhas@ncrep.com
[2] NCREP – Heritage Consultancy, Porto, Portugal, joao.doutel@ncrep.com
[3] NCREP – Heritage Consultancy, Porto, Portugal, luis.ferreiras@ncrep.com
[4] Lisboa SRU – Sociedade de Reabilitação Urbana E.M., Lisboa, Portugal, sonia.steiger@lisboasru.pt
[5] Lisboa SRU – Sociedade de Reabilitação Urbana E.M., Lisboa, Portugal, catia.santana@lisboasru.pt

Resumo: A segurança sísmica dos edifícios escolares constitui uma preocupação central em Lisboa, devido ao seu significativo risco sísmico e elevada densidade populacional. Uma parte considerável do edificado foi construída anteriormente à implementação de regulamentos sísmicos modernos, o que acentua a vulnerabilidade do parque escolar. Neste contexto, a aplicação de metodologias simplificadas à macroescala revela-se fundamental para o apoio à tomada de decisão e à definição de prioridades de intervenção.

Neste âmbito, a pedido da Câmara Municipal de Lisboa, o Laboratório Nacional de Engenharia Civil (LNEC) procedeu à avaliação do parque escolar com base em indicadores de risco, incluindo o estado de conservação e uma estimativa simplificada da resistência sísmica. Posteriormente, no âmbito de trabalhos de investigação do NCREP, foi aplicada uma abordagem alternativa, igualmente à macroescala, baseada em tipologias estruturais, integrando a construção de uma base de dados, a classificação tipológica e a aplicação de métodos de Rapid Visual Screening. Estas metodologias permitem uma priorização preliminar dos edifícios, embora apresentem limitações na caracterização detalhada do seu comportamento estrutural.

No âmbito de intervenções promovidas pela Lisboa SRU, e com base na priorização definida, o NCREP realizou uma análise detalhada de dois edifícios representativos de escolas técnicas construídas entre 1947 e 1962: a Escola Básica Paula Vicente e a Escola Secundária D. Luísa de Gusmão. Para o efeito, foi conduzida uma campanha de inspeção e diagnóstico estrutural, incluindo a caracterização estrutural, a avaliação do estado de conservação e a análise das condições geotécnicas. Com base nesta informação, foram desenvolvidos modelos numéricos detalhados e realizadas análises não lineares, com o objetivo de avaliar o desempenho sísmico e identificar potenciais vulnerabilidades estruturais.

A comparação entre os resultados das abordagens simplificadas e da análise detalhada permite discutir a complementaridade de cada nível de detalhe e as diferenças e limitações associadas a cada metodologia, contribuindo para uma melhor compreensão da sua aplicabilidade na avaliação da vulnerabilidade sísmica de edifícios escolares.

Palavras-chave: Inspeção e diagnóstico estrutural; Vulnerabilidade Sísmica; Escolas Técnicas; Estruturas mistas betão armado e alvenaria.

1. Introdução

A segurança sísmica do parque escolar de Lisboa apresenta-se como um problema simultaneamente técnico, social e político: técnico, porque uma fração significativa do edificado foi construída antes da entrada em vigor da regulamentação sismo-resistente atualmente em vigor e aceite como referência; social, porque a ocupação destes edifícios é elevada e concentrada em horários definidos; político, porque a

definição de prioridades tem implicações orçamentais relevantes e exige sustentação em metodologias de avaliação reprodutíveis e defensáveis.

A fase de maior produção do parque escolar decorreu sob o RBA-1935 e o RSCCS-1958, sem disposições específicas de pormenorização sísmica. O RSA/REBAP (1983) introduziu as primeiras regras explícitas para a ação sísmica; os Eurocódigos estruturais (NP EN 1998-1 e NP EN 1998-3), em vigor desde 2019, constituem o quadro atual de avaliação e reforço de edifícios existentes.

Cerca de 80% das 137 escolas do município de Lisboa foram construídas antes de 1983, das quais um conjunto significativo nunca foi alvo de qualquer intervenção estrutural posterior. Este universo, onde coexistem estruturas de alvenaria, betão armado e estruturas mistas de betão armado e alvenaria, dimensionado de acordo com práticas anteriores à NP EN 1998-1, constitui a população-alvo do processo de avaliação e priorização descrito neste artigo.

O ponto de partida foi o estudo de vulnerabilidade sísmica encomendado pela Câmara Municipal de Lisboa ao LNEC (Carvalho et al., 2021), que avaliou 32 escolas com recurso a metodologia analítica simplificada à macro-escala, permitindo hierarquizar o parque e identificar um conjunto de edifícios prioritários para intervenção estrutural. Com base nessa hierarquização técnica das escolas e nas necessidades particulares de cada escola, a Lisboa SRU identificou escolas prioritárias para intervenção estrutural. Entre as diferentes escolas selecionadas, o NCREP ficou responsável pela análise detalhada de dois edifícios representativos da tipologia das Escolas Técnicas (1947–1962), com estruturas mistas de betão armado e alvenaria, em particular a Escola Básica Paula Vicente (EBPV), em Belém, e a Escola Secundária D. Luísa de Gusmão (ESDLG), na Penha de França.

Paralelamente, no âmbito de uma dissertação de mestrado orientada pelo NCREP (Lezaack, 2025), foi desenvolvido um exercício de triagem por Rapid Visual Screening (RVS) aplicado ao parque escolar de Lisboa, com o objetivo de verificar se este método mais expedito, baseado em tipologias estruturais e inspeção visual exterior, consegue replicar as prioridades identificadas pelo estudo do LNEC para um conjunto de 58 escolas antigas. Este exercício não precedeu nem condicionou a decisão de intervenção; foi antes uma investigação metodológica posterior, orientada para avaliar a rastreabilidade do RVS face a uma avaliação analítica de referência.

O presente artigo compara os resultados das três abordagens aplicadas às mesmas duas escolas: o estudo analítico simplificado do LNEC, que fundamentou a priorização; a análise detalhada do NCREP, que a sustenta tecnicamente e fornece a base para o projeto de reforço; e o exercício RVS, que testa a capacidade de um método de triagem mais expedito em identificar os edifícios de maior risco. O objetivo não é hierarquizar as três abordagens em termos de qualidade absoluta, mas caracterizar a sua função específica, as suas limitações e o grau de convergência ou divergência dos respetivos resultados para um mesmo edifício.

2. Estado da arte

A avaliação da vulnerabilidade sísmica de edifícios existentes recorre a uma hierarquia de métodos de complexidade crescente. No nível mais expedito, os métodos de Rapid Visual Screening, de que o FEMA P-154 (FEMA, 2015) será a referência internacional mais difundida, atribuem a cada edifício uma pontuação a partir da inspeção visual exterior, baseada na tipologia estrutural e em modificadores associados a irregularidades, idade e tipo de solo. Metodologias como o RISK-UE LM1 (Mouroux & Le Brun, 2006) partilham o mesmo princípio com um trade-off entre rapidez de aplicação e profundidade do diagnóstico.

Num nível intermédio, os métodos analíticos simplificados, como o RISK-UE LM2 ou as variantes usadas pelo LNEC (Carvalho et al., 2017), recorrem a modelos de complexidade reduzida e análises não lineares estáticas para estimar curvas de capacidade por tipologia. A Capacity Spectrum Method (CSM) prescrita na NP EN 1998-3:2017 e o método N2 (Fajfar, 2000) constituem o quadro analítico de referência.

No nível mais detalhado, exigido pela NP EN 1998-3 para avaliação individual de edifícios existentes, o desempenho sísmico é avaliado em modelos tridimensionais não lineares com leis constitutivas calibradas com ensaios materiais. A aplicação destes métodos a estruturas mistas de betão armado e alvenaria de meados do século XX coloca dificuldades específicas: armaduras em varão liso, ausência de cintagem nas zonas críticas, presença frequente de pilares curtos e heterogeneidade construtiva entre projeto e execução. Em particular, a representação das paredes de alvenaria, desde modelos de bielas equivalentes até elementos sólidos, é determinante para a previsão dos modos de rotura (Magenes & Penna, 2011; pVanin et al., 2017).

3. Avaliação RVS à escala do parque escolar: validação metodológica

3.1 Enquadramento

A avaliação usando RVS descrita nesta secção foi desenvolvida em (Lezaack, 2025), com o objetivo de verificar se um método de Rapid Visual Screening adaptado ao contexto português, aplicado por tipologias estruturais, consegue replicar as prioridades de intervenção identificadas pelo estudo LNEC (Carvalho et al., 2021) para o conjunto das 58 escolas antigas de Lisboa. Trata-se de um exercício de validação retrospetiva, útil para triagens de parques escolares onde a aplicação do método analítico não é viável para a totalidade dos edifícios.

3.2 Caracterização do parque escolar

O parque escolar gerido pelo município de Lisboa é composto por 137 estabelecimentos públicos, . Não existindo um repositório consolidado da informação relativa a estes edifícios, a sua caracterização foi realizada a partir de diversas fontes municipais (Lisboa Interativa), inventários arquitetónicos (Alegre & Heitor 2019) e arquivos de projeto. Adotando 1985 como ponto de corte regulamentar e 2000 como a data limite de renovações estruturais, o parque divide-se em três grupos: 58 escolas antigas (anteriores a 1985 e sem renovação posterior a 2000), 51 escolas renovadas após 2000 e 28 escolas recentes (posteriores a 1985). As 58 escolas antigas constituem o universo de risco potencial mais elevado e forma a população de partida para a triagem descrita nesta secção.

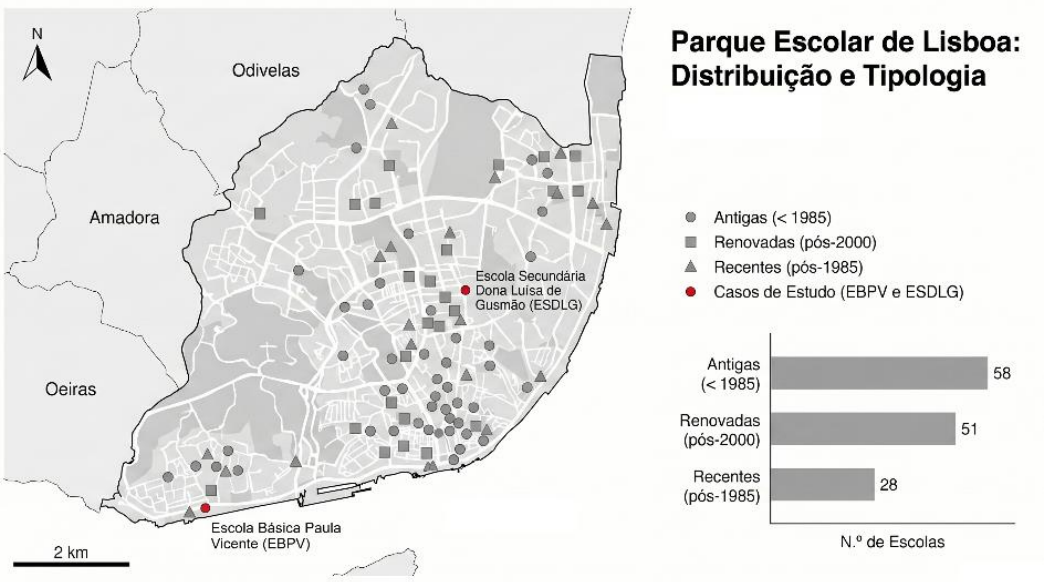


Figura 1 – Mapa de Lisboa com localização das 137 escolas, com identificação da caracterização do parque escolar incluindo EBPV e ESDLG.

3.3 Classificação tipológica e avaliação por RVS

3.3.1 Classificação por tipologia

As 58 escolas antigas foram classificadas em sete tipologias arquitetónicas, Figura 2, com base na aparência exterior, configuração geométrica e contexto histórico-construtivo: Antiga (anterior a 1920, em alvenaria resistente sem normalização), Centenários (1940–1960, do Plano dos Centenários do ensino primário), Técnica (1947–1962, dos planos de ensino técnico), Porticada (1968–1990, em pórticos de betão armado), Bloco 70 - 3×3 (a partir de 1970), Bloco 80 - 3×3 (a partir de 1980) e Outra. A tipologia Técnica - onde se integram a EBPV e a ESDLG - subdivide-se em duas subcategorias: Placa (alvenaria resistente, layout padronizado de 19×62 m) e Porticada-Mista (pórticos de betão armado com paredes de alvenaria de enchimento ou contraventamento). Ambas as escolas alvo do estudo detalhado pertencem a esta segunda subcategoria.

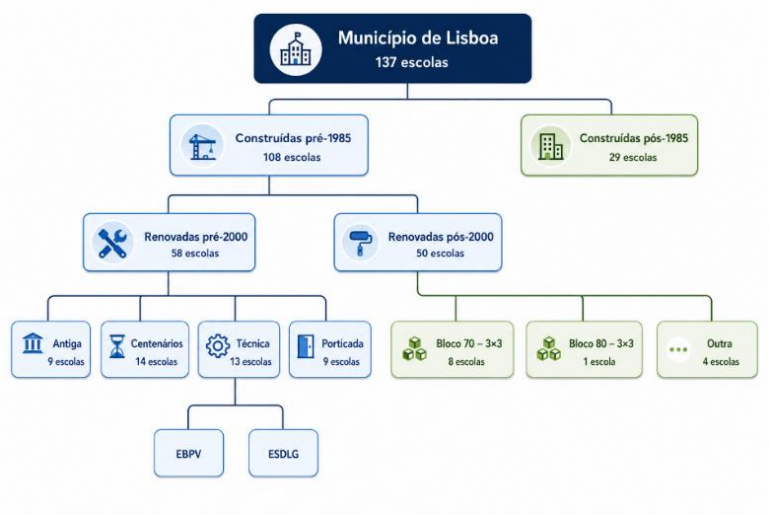


Figura 2 – Classificação das escolas por tipologia.

3.3.2 Avaliação por RVS (Lezaack 2025)

A avaliação RVS aplicou o FEMA P-154 (FEMA 2015), com adaptação ao contexto português. A categoria de sismicidade foi determinada pela aceleração espectral correspondente ao MCE_r, calculada de forma agregada sobre os sismos Tipo 1 (afastado) e Tipo 2 (próximo) da NP EN 1998-1, com fatores corretivos para o período de retorno equivalente. Os valores obtidos ($S_s \approx 1{,}0$ g) colocam Lisboa no limiar entre as classes *High* e *Very High*, optando-se conservadoramente por *High Seismicity*. As escolas técnicas foram classificadas como tipo URM do FEMA (alvenaria não reforçada) por serem as paredes longitudinais de alvenaria a comandar a resposta sísmica, apesar da presença de pórticos de betão armado.

A Figura 3 apresenta a soma média dos modificadores RVS (FEMA P-154) por tipologia estrutural. Valores negativos indicam que os modificadores penalizadores predominam sobre os favoráveis; valores positivos indicam o inverso.

A tipologia Técnica (a vermelho) regista uma soma média de -0.5, coerente com os modificadores negativos na EBPV e na ESDLG. As tipologias Bloco 70-3x3 e Bloco 80-3x3 apresentam os valores mais elevados, refletindo características estruturais mais regulares.

Para a EBPV, foram assinalados sete modificadores penalizadores, dos quais se destacam a presença de *pilotis* e *soft-storey* no piso de cantina, o *plan setback* induzido pela compartimentação por corpos com fundações em socalco e a presença de pilares curtos. Para a ESDLG, foram assinalados seis modificadores, dos quais se destacam o desenvolvimento em encosta, o canto reentrante associado à planta em "L" e a presença de pilares curtos.

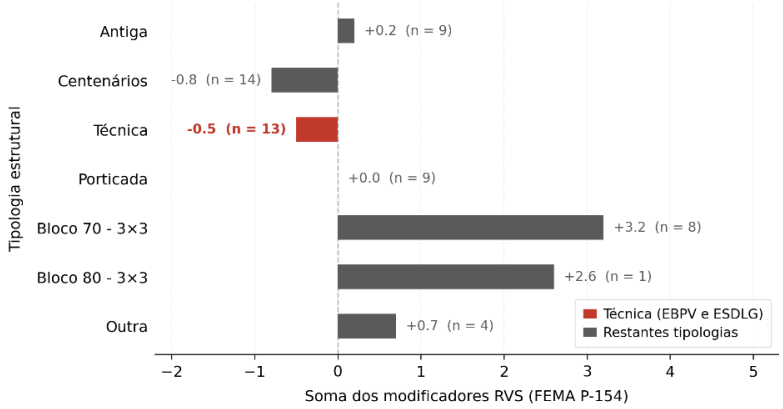


Figura 3 – Resultados da análise RVS por tipologia estrutural: identificação dos grupos prioritários, (Lezaack 2025)

4. Avaliação simplificada: estudo LNEC

4.1 Metodologia

O estudo do LNEC, encomendado pela Câmara Municipal de Lisboa, constitui o instrumento que fundamentou a hierarquização do parque escolar e a identificação das escolas prioritárias para intervenção estrutural. A sua aplicação a 32 escolas de 2.º e 3.º ciclos e secundárias do município (Carvalho et al., 2021) permitiu estimar, para cada edifício, indicadores de risco relativo que sustentaram as decisões de priorização por parte da Câmara Municipal e, subsequentemente, da Lisboa SRU. A EBPV e a ESDLG integram o conjunto de escolas identificadas como prioritárias por este estudo; a decisão de avançar para análise detalhada nestas duas escolas, no âmbito da tipologia Técnica, resultou diretamente dessa priorização.

A metodologia organiza-se em seis passos: (i) tipificação em tipologias estruturais; (ii) caracterização da ação sísmica por cruzamento com o mapa regional de colunas de solo da AML (Campos Costa et al., 2010), sem ensaios geotécnicos específicos; (iii) análise não linear estática (CSM); (iv) avaliação do desempenho face a quatro estados limite; (v) cálculo de perdas esperadas; e (vi) elaboração de ficha individual por escola.

A análise estrutural é realizada em *SeismoStruct*, com elementos de barra de plasticidade distribuída e leis constitutivas de Mander para o betão e Menegotto-Pinto para o aço. Para edifícios mistos, o LNEC adota o modelo do pórtico plano transversal, no qual as paredes de alvenaria são representadas por bielas biarticuladas com módulo de elasticidade de 2,0 GPa, sob o pressuposto de manterem a integridade durante o sismo.

4.2 Resultados para a EBPV e ESDLG

A EBPV é classificada na tipologia “Mista BA” e enquadrada em solo tipo A (rocha sem amplificação, com base no mapa regional do LNEC). Os períodos de retorno globais para os quatro estados limite são, respetivamente, 6 anos (EL1), 14 anos (EL2), 4085 anos (EL3) e 8415 anos (EL4) - sendo os mais baixos para EL1 e EL2 entre as 32 escolas analisadas. O LNEC atribui o desempenho desfavorável ao mecanismo transversal, em que as paredes de alvenaria descarregam apenas verticalmente sobre os pórticos.

A ESDLG é classificada na mesma tipologia, mas em solo tipo H, com amplificação calculada ao nível do substrato rochoso. Os períodos de retorno globais são 88 anos (EL1), 181 anos (EL2), 3110 anos (EL3) e superiores a 10 000 anos (EL4); a perda anual esperada é de 0,09 % e a perda em 50 anos é de 4,06 %, com 18,8 dias de interdição e 621 alunos×mês deslocados. O LNEC sinaliza como vulnerabilidade dominante a ausência de vigas transversais que assegurem o funcionamento em pórtico nessa direção, com os pilares a responder praticamente como consolas, e recomenda reforço focado no aumento de resistência transversal.

4.3 Limitações da abordagem simplificada

A abordagem LNEC é adequada para a hierarquização à escala do parque, mas apresenta limitações que apenas se tornam visíveis face a uma análise de detalhe: (1) a classificação cartográfica atribuiu solo tipo A à EBPV, quando a campanha SPT do NCREP demonstrou tipo C — espetros significativamente mais exigentes; (2) o modelo plano assume alvenaria íntegra, contrariamente ao mecanismo crítico de rotura por corte identificado; (3) materiais genéricos (C16/20, A250) divergem dos experimentais. Os ensaios *in situ* e laboratoriais obtiveram valores distintos em ambas as escolas.

Estas limitações não desqualificam o estudo LNEC no contexto para que foi concebido: hierarquizar o parque à escala municipal e fundamentar decisões de priorização. Indicam, porém, que os resultados não devem ser interpretados como avaliações absolutas de segurança individual.

5. Análise detalhada das escolas EBPV e ESDLG

5.1 Caracterização construtiva das escolas

A EBPV, Figura 4a, na Rua Gonçalves Zarco, em Belém, organiza-se em três corpos interligados: Corpo A - Edifício de Aulas; Corpo B - Ginásio; Corpo C - Intermédio. A estrutura é mista, com pórticos de betão armado, elementos pontuais em betão simples nas fachadas, paredes de alvenaria de pedra calcária e de tijolo cerâmico, e lajes aligeiradas com elementos cerâmicos.

A ESDLG, Figura 4b, com projeto de 1955 e inauguração em 1958, na Rua da Penha de França, organiza-se também em três corpos interligados: Corpo A - Edifício Principal, com planta em "L" e cinco pisos incluindo o desvão da cobertura; Corpo B - Ginásio, com planta retangular e três pisos; Corpo C - Ligação, com formato trapezoidal e dois pisos. A estrutura dos Corpos A, B e C é mista, com pilares de betão armado e simples nas fachadas, paredes de alvenaria de pedra calcária e de tijolo cerâmico, e lajes maioritariamente aligeiradas.



Corpo A e C | Corpo B | Corpo C

(a) Escola EBPV

Corpo A | Corpo B | Corpo C

(b) Escola ESDLG

Figura 4 – Resultados da análise RVS por tipologia estrutural: identificação dos grupos prioritários, (Lezaack 2025)

5.2 Inspeção e diagnóstico

A campanha de inspeção e diagnóstico estrutural foi a primeira fase do trabalho em ambas as escolas, abrangendo: a confrontação dos elementos de arquivo com o edificado existente; a inspeção visual com registo de anomalias e danos; a abertura de janelas de sondagem para caracterização de elementos ocultos; e a realização de ensaios in situ e laboratoriais.



Figura 5 – Ensaios e sondagens de caracterização da estrutura.

A confrontação com os elementos de arquivo da EBPV revelou correspondência global de ~38 %: apenas 16,7 % das secções de pilares correspondem ao projeto, e 50 a 64 % dos elementos horizontais. As discordâncias críticas foram: (i) fundações em alvenaria de pedra, previstas como sapatas de BA; (ii) cobertura em lajes aligeiradas, prevista em madeira.

Em termos gerais, ambas as estruturas apresentam bom estado de conservação, com danos pontuais que não comprometem a estabilidade global. Na EBPV, destacam-se: corrosão de armaduras nos varandins e cornijas; manchas de humidade; e deformação das lajes de cobertura. Na ESDLG, os danos de maior relevância são as manchas de humidade nas coberturas e o ataque por fungos xilófagos na estrutura de madeira.

5.2.1 Caracterização material

A campanha experimental abrangeu, em ambas as escolas, ensaios de compressão em carotes de betão, ensaios de tração em armaduras, ensaios esclerométricos com esclerómetro de Schmidt, ensaios de compressão em provetes de pedra calcária e determinação de densidade e porosidade aberta. A Tabela 1 sintetiza os resultados, com confronto com os valores de referência do RBA-1935 (17.7 MPa para o betão; 363.0 MPa para o aço).

A resistência do betão é próxima do valor regulamentar em ambos os edifícios (EBPV: 18,3 MPa; ESDLG: 16,8 MPa). A resistência das armaduras coloca a EBPV acima da referência (411,0 MPa) e a ESDLG na vizinhança desta (362,5 MPa). A pedra calcária da ESDLG apresenta resistência substancialmente superior à da EBPV, refletindo origens petrográficas distintas, Tabela 1.

Tabela 1 - Caracterização material: EBPV e ESDLG (valores médios).

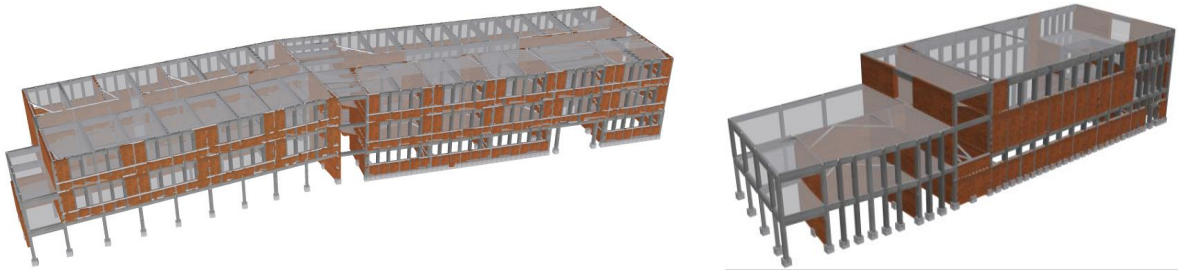
Material	Propriedade	Referência (RBA-1935)	EBPV	ESDLG
Betão armado				
Betão	f_{cm} – resist. compressão [MPa]	17.7	18.3	16.8
Aço (armadura)	f_y – resist. tração [MPa]	363.0	411.0	362.5
Alvenaria de pedra calcária				
Pedra calcária	f_c – resist. compressão [MPa]	-	37.9	62.1
	ρ – densidade aparente [kg/m^3]	-	2348	2239-2557

5.3 Modelação numérica e análise não linear

Ambas as escolas foram analisadas adotando análises estáticas não lineares (*pushover*) integradas com o método N2/CSM da NP EN 1998-3. A ação sísmica foi quantificada para Lisboa (Tipo 1, zona 1.3; Tipo 2, zona 2.3) em solo tipo C, classe de importância III, coeficiente de redução 0.90 (Portaria n.º 302/2019; foi adotado nível de conhecimento normal (KL2) com fator de confiança CF = 1.20). Foram verificados os três estados limite (DL, SD, NC) com duas distribuições de cargas horizontais e excentricidades acidentais.

As escolas foram modeladas no *software SeismoStruct*. Os pilares e vigas em betão armado foram representados por elementos de barra de fibras com modelos de Mander et al. para o betão e Menegotto-Pinto para o aço. As paredes resistentes de alvenaria foram modeladas através elementos de barra (*frame*) que simulam o comportamento no plano de paredes, nembos e lintéis de alvenaria quando sujeitos a forças horizontais (como é o caso dos sismos).

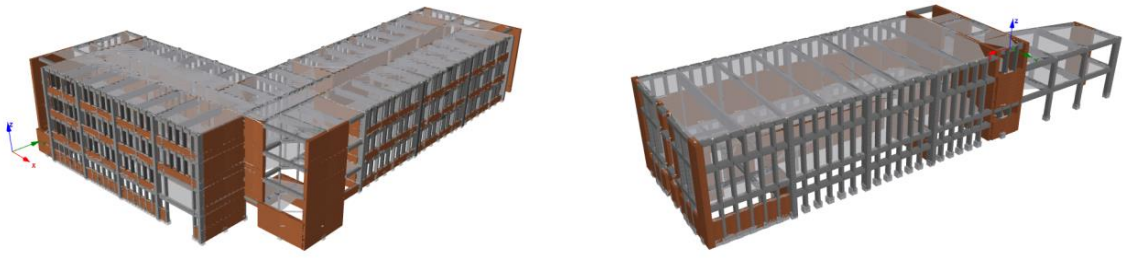
Na escola EBPV, o Corpo B foi modelado isoladamente, enquanto os corpos A e C foram modelados de forma conjunta, Figura 6.



Corpo A e Corpo C Corpo B

Figura 6 – Modelos numéricos para análise da EBPV.

Já na escola ESDLG, o Corpo A foi modelado isoladamente, enquanto os Corpos B e C foram modelados de forma conjunta, Figura 7. As simplificações de ligação de corpos foram assumidas devido à fraca ligação nas zonas de transição entre os corpos.

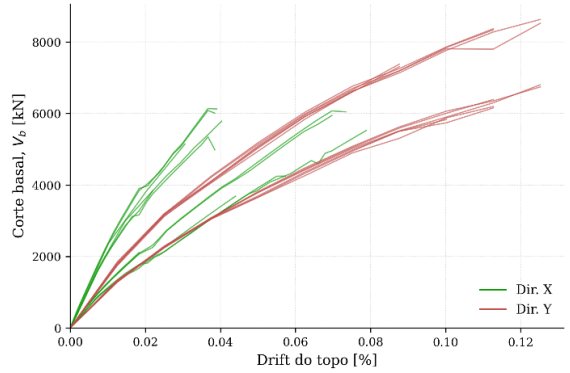


Corpo A Corpo B e Corpo C

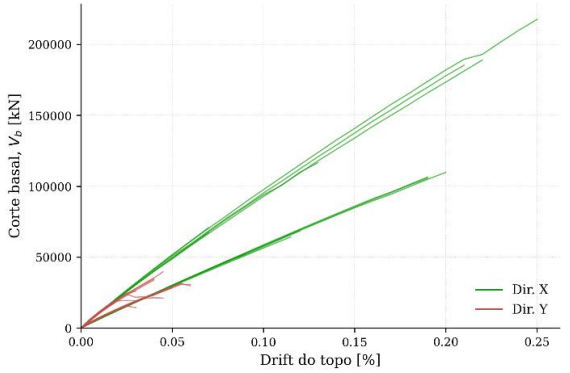
Figura 7 – Modelos numéricos para análise da ESDLG.

Os modelos das escolas anteriormente apresentados permitiram obter as curvas de capacidade das escolas, as quais se apresentam na Figura 8, que posteriormente serviram para a verificação de segurança das estruturas.

EBPV

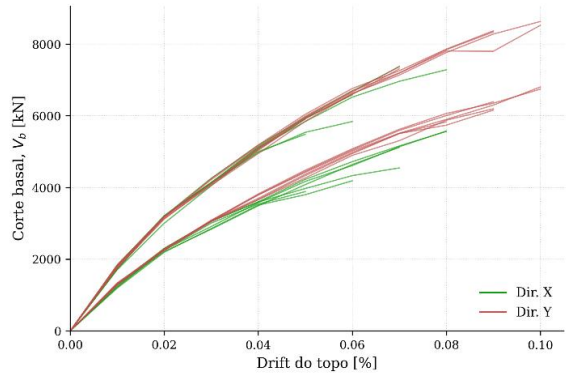


(a) Corpo B (direção X e Y)

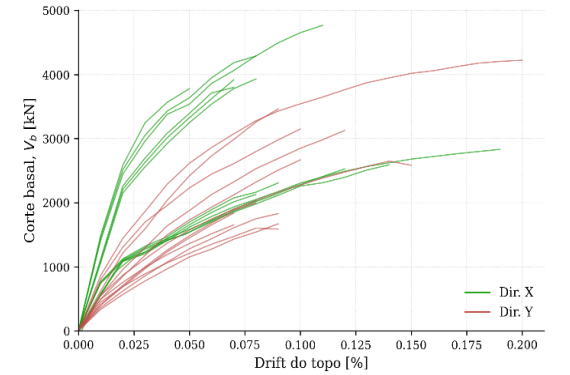


(b) Corpo A e Corpo C (direção X e Y)

ESDLG



(c) Corpo A (direção X e Y)



(d) Corpo B e Corpo C (direção X e Y)

Figura 8 – Curvas de capacidade das escolas.

5.4 Resultados da análise não linear

Em ambas as escolas, a Ação Sísmica Tipo 1 revelou-se condicionante. A Tabela 2 apresenta os *drifts* de capacidade e os *drifts-alvo* para os três estados limite, em cada corpo e direção analisada. O único caso de verificação positiva é o Corpo B - Ginásio da EBPV, quando analisado na direção Y para o estado SD; em todos os restantes casos, a capacidade é significativamente inferior ao alvo regulamentar.

Tabela 2 – Drifts no topo (%): capacidade vs alvo AST1, (estados limite DL, SD e NC).

Corpo	Direção	DL		SD		NC	
		Cap.	Alvo	Cap.	Alvo	Cap.	Alvo
EBPV							
Corpo B	X	0.008	0.042	0.060	0.143	0.080	0.232
Corpo B	Y	0.013	0.019	0.075 ✓	0.065	0.100	0.105
Corpos A + C	X	0.005	0.016	0.086	0.057	0.115	0.092
Corpos A + C	Y	0.005	0.015	0.023	0.138	0.030	0.257

EBPV							
Corpo A	X	0.010	0.068	0.045	0.277	0.060	0.460
Corpo A	Y	0.010	0.056	0.045	0.260	0.060	0.443
Corpos B + C	X	0.020	0.046	0.105	0.165	0.140	0.198
Corpos B + C	Y	0.010	0.051	0.083	0.187	0.110	0.218

✓Estado limite verificado; todos os restantes casos não verificados.

ESDLG - mecanismos de rotura

No Corpo A, o comportamento é predominantemente frágil em ambas as direções, com *drifts* de capacidade (NC) de apenas 0,060%. A planta em `L` introduz excentricidades que mobilizam danos nos elementos transversais à ação, concentrando as roturas por corte nas paredes de alvenaria de maior rigidez e nos pilares das fachadas.

EBPV - mecanismos de rotura

No Corpo B - Ginásio, a direção X é condicionante: a análise regista rotura simultânea por corte em paredes de alvenaria e em pilares de betão armado logo ao nível do estado DL, com *drifts* de capacidade (0,008 %) muito inferiores ao alvo regulamentar (0,042 %). Na direção transversal (Y), este é o único corpo que verifica o estado SD (capacidade 0,075 % vs. alvo 0,065 %), sendo a rotura dominada pelas paredes de alvenaria.

No edifício principal (Corpo A e C) a direção Y é a mais condicionante, os *drifts* de capacidade são de 0,005 % (DL), 0,023 % (SD) e 0,030 % (NC), face a alvos de 0,015 %, 0,138% e 0,257%. Na **Figura 9**, apresenta-se um exemplo dos danos em elementos estruturais que compõem esta escola.

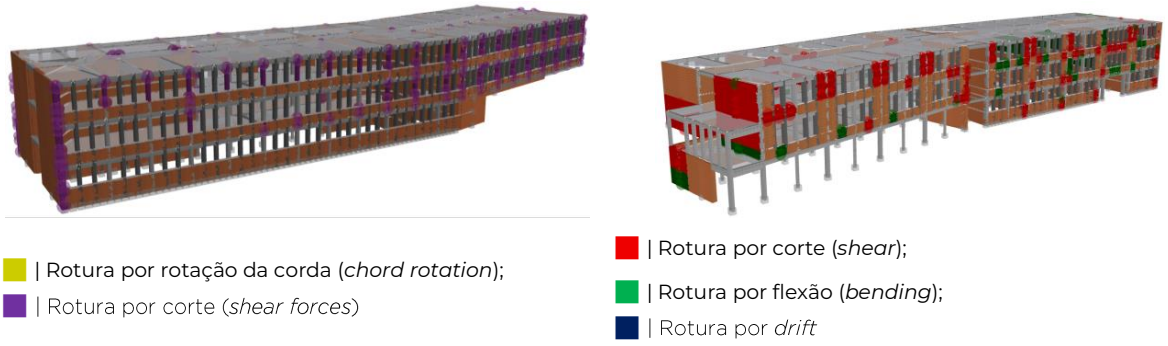


Figura 9 – Danos nos elementos estruturais do Corpo A e C (EBPV) no final da análise pushover (último step antes da rotura) na direção transversal (Y) - AST1.

6. Perspetiva do dono de obra: SRU Lisboa

A Lisboa SRU é uma empresa pública municipal da CML com a missão de promover a reabilitação urbana de equipamentos, habitação e espaço público na Área de Reabilitação Urbana (ARU) de Lisboa.

A intervenção visa adequar as escolas aos padrões de segurança, conforto e funcionalidade definidos pela Carta Educativa da CML e pelo Ministério da Educação.

No âmbito do 5.º Contrato de Mandato – Programa Escolas e Creches, a CML mandatou a Lisboa SRU para intervir em sete escolas do concelho, incluindo a ESDLG e a EBPV. Para cada escola foram elaborados os Relatórios de Inspeção e Diagnóstico Estrutural e de Avaliação da Vulnerabilidade Sísmica (Portaria n.º 302/2019).

Paralelamente, foram lançados concursos de conceção para ambas as escolas. Os projetos, em fase de Estudo Prévio, serão desenvolvidos em BIM; as estratégias de reforço sísmico estão em definição, Figura 10.



(a) EBPV (b) ESDLG

Figura 10 – Projetos em fase de Estudo Prévio.

7. Conclusões

O artigo documentou a avaliação sísmica de duas escolas técnicas de Lisboa (EBPV e ESDLG) com três abordagens: a avaliação simplificada do LNEC (Carvalho et al., 2021), que hierarquizou o parque e fundamentou a seleção para intervenção pela Lisboa SRU; a análise detalhada do NCREP (NCREP, 2025a, 2025b) segundo a NP EN 1998-3 para o projeto de reforço; e RVS por tipologias (Lezaack, 2025) como investigação metodológica.

A comparação principal confronta o estudo simplificado do LNEC com a análise detalhada. Qualitativamente, ambas identificam as escolas como vulneráveis e urgentes; quantitativamente, divergem em três fatores: solo tipo A (cartografia) vs. tipo C (SPT), alvenaria íntegra vs. mecanismo de corte, e pórtico plano sem efeitos torsionais. O LNEC reporta TR(EL3) de 4085 e 3110 anos; o NCREP evidencia rácios capacidade/exigência de 1:5 a 1:10.

O modelo macroescala é adequado para estimar indicadores relativos de vulnerabilidade, mas os seus resultados absolutos não podem fundamentar avaliações individuais de segurança; para os edifícios priorizados, a análise de detalhe é necessária antes de qualquer decisão de intervenção.

A comparação com o LNEC demonstra que o RVS por tipologia identifica os mesmos edifícios prioritários, sugerindo potencial de aplicação a parques mais vastos, sem eliminar a necessidade da análise de detalhe.

Agradecimentos

Os autores agradecem à Lisboa SRU - Sociedade de Reabilitação Urbana E.M., promotora dos estudos de inspeção e diagnóstico estrutural e dos relatórios de avaliação da vulnerabilidade sísmica das duas escolas, pela colaboração ao longo do desenvolvimento dos trabalhos. Agradecem ainda à Câmara Municipal de Lisboa e ao Laboratório Nacional de Engenharia Civil pelo acesso aos resultados do estudo de avaliação da vulnerabilidade sísmica do parque escolar de Lisboa. A contribuição da Eng.ª Alice Lezaack, no âmbito da sua dissertação de mestrado, é igualmente reconhecida.

Referências

Alegre, Alexandra, e Teresa Heitor. 2019. Atlas - School Architecture in Portugal. Lisboa: Instituto Superior Técnico.

Campos Costa, A., et al. 2010. Seismic Hazard Assessment in Portugal. Lisboa: LNEC.

Carvalho, A., Lopes, M., e Coelho, E. 2017. "Risco Sísmico em Portugal Continental." In Atas do 10.º Congresso Nacional de Sismologia e Engenharia Sísmica. Ponta Delgada: SPES.

Carvalho, A., Lopes, M., Candeias, P., et al. 2021. Estudo de Avaliação da Vulnerabilidade Sísmica dos Edifícios das Escolas do Município de Lisboa. Relatório 309/2021 - DE/NESDE. Lisboa: LNEC.

Fajfar, P. 2000. "A Nonlinear Analysis Method for Performance-Based Seismic Design." Earthquake Spectra, 16(3): 573–92.

FEMA. 2015. Rapid Visual Screening of Buildings for Potential Seismic Hazards: A Handbook. FEMA P-154, 3.ª ed. Washington, D.C.: Federal Emergency Management Agency.

Lezaack, A. 2025. Seismic Vulnerability Assessment of School Buildings in Lisbon: A Typological and Rapid Visual Screening Approach. Dissertação de Mestrado.

Magenes, G., e Penna, A. 2011. "Seismic Design and Assessment of Masonry Buildings in Europe." In Proceedings of the 9th Australasian Masonry Conference, Queenstown, New Zealand.

Mouroux, P., e Le Brun, B. 2006. "Presentation of RISK-UE Project." Bulletin of Earthquake Engineering, 4(4): 323–39.

NCREP. 2025a. Relatório de Inspeção e Diagnóstico Estrutural - Escola Básica Paula Vicente. Ref. NCREP_3037P0525_rev02. Porto: NCREP - Heritage Consultancy.

NCREP. 2025b. Relatório de Avaliação da Vulnerabilidade Sísmica - Escola Básica Paula Vicente. Ref. NCREP_3037P0525_EST_RAVS_r02. Porto: NCREP - Heritage Consultancy.

NCREP. 2025c. Relatório de Inspeção e Diagnóstico Estrutural - Escola Secundária D. Luísa de Gusmão. Ref. 3038_LOSRU_L_Gusmao_RID_PE. Porto: NCREP - Heritage Consultancy.

NCREP. 2025d. Relatório de Avaliação da Vulnerabilidade Sísmica - Escola Secundária D. Luísa de Gusmão. Ref. 3038_LOSRU_L_Gusmao_RAVS_rev01. Porto: NCREP - Heritage Consultancy.

NP EN 1998-1. 2010. Eurocódigo 8 - Parte 1: Regras gerais, ações sísmicas e regras para edifícios. Caparica: IPQ.

NP EN 1998-3. 2017. Eurocódigo 8 - Parte 3: Avaliação e reabilitação de edifícios. Caparica: IPQ.

Vamvatsikos, D., e Cornell, C.A. 2002. "Incremental Dynamic Analysis." Earthquake Engineering & Structural Dynamics, 31(3): 491–514.

Vanin, F., Bhowmick, A., e Stojadinovic, B. 2017. "Equivalent Frame Modeling of URM Walls." Bulletin of Earthquake Engineering, 15(10): 4159–87.



DESIGN PROJECTS AND REHABILITATION WORKS



Cinpar 2026
XXII International Conference on Building Pathology and Constructions Repair
15th to 17th July 2026 - Lisboa, Portugal

Decarbonizing Built Heritage: A Technical-Qualitative Assessment of Integrated Retrofit Strategies at the BMCC

Alexandra PEREIRA[1], Mayara Carelli de Paula COSTA[2], Maria Fernanda PEREIRA[3], Maria Teresa Gomes BARBOSA[4]

[1] Federal University of Juiz de Fora, Juiz de Fora, Brazil, alexandra.pereira@estudante.ufjf.br
[2] Federal University of Juiz de Fora, Juiz de Fora, Brazil, eng.mayaracarelli@gmail.com
[3] Federal University of Juiz de Fora, Juiz de Fora, Brazil, mariafernanda.pereira@estudante.ufjf.br
[4] Federal University of Juiz de Fora, Juiz de Fora, Brazil, teresa.barbosa@ufjf.br

Abstract: The climate emergency has repositioned the construction sector at the center of global mitigation strategies, since the built environment accounts for a substantial share of energy consumption and greenhouse gas emissions. Historic buildings, although essential to urban memory, often present limitations in energy performance, requiring solutions that reconcile efficiency, conservation, and reductions in embodied carbon. In this context, retrofit stands out as an environmentally preferable alternative to replacing the existing building stock. This article analyzes the Bernardo Mascarenhas Cultural Center (BMCC), in Juiz de Fora, Minas Gerais, through a technical and heritage diagnosis, intrinsic and extrinsic inspections, and a qualitative matrix of indicators. The adopted approach is technical-qualitative and integrated, rather than a quantitative experimental validation. The results indicate potential for environmental and functional improvement associated with the preservation of the existing structure, the use of reversible solutions, and the maintenance of lower-impact components. The study concludes that retrofit can support the ecological transition of built heritage, provided it is guided by compatibility, reversibility, minimal intervention, and, in future stages, by measurements and simulations capable of quantifying energy and environmental gains.

Keywords: Sustainable retrofit. Case study. Historic buildings. Built heritage. Urban regeneration.

1. Introduction

The climate emergency and the transition toward sustainable cities require the construction sector to contribute effectively to the mitigation of environmental impacts and to the decarbonization of the built environment (IPCC (2022), OECD (2022)). This demand is related to the sector's high energy consumption and greenhouse gas emissions, which represent a substantial share of global energy-related CO_2 emissions (IEA (2023), UNEP (2023)). It is therefore necessary to connect energy efficiency, reductions in embodied carbon, and the preservation of the existing building stock.

Historic buildings, although essential to urban memory, often present energy performance levels below contemporary requirements (Webb (2017), Broström et al. (2022)), forming a relevant field for scientific and technical intervention (Ma et al. (2023)).

In this context, retrofit - understood as the upgrading and modernization of existing buildings through sustainability-oriented interventions - emerges as one of the most responsible strategies for supporting carbon neutrality goals, especially when compared with demolition and new construction (De Wolf et al. (2017), Crawford et al. (2019); Liu et al. (2023)).

The World Economic Forum (WEF, 2023) indicates that adapting an existing building can generate 50% to 75% less carbon than constructing an equivalent building from scratch. This perspective reinforces the idea that the adaptive conservation of existing stock tends to be environmentally preferable to disposal and replacement. Accordingly, studies on embodied carbon argue that existing buildings should be treated as carbon reservoirs whose potential should be preserved whenever possible (Pomponi and Moncaster (2016)).

It must be emphasized, however, that inappropriate interventions can cause irreversible losses to built heritage, both in its material and symbolic dimensions. The main international guidelines recommend that any alteration should observe criteria of compatibility, reversibility, and minimal intervention (McCaig et al. (2018); Luo et al. (2024)), in order to reduce energy demand and improve indoor environmental conditions without compromising the historical integrity of buildings (ICOMOS (2021)).

Lucchi (2022) shows that the combination of non-intrusive monitoring and integrated performance models contributes to safer interventions in heritage buildings. In this field, the systemic reading of the building, or integrated approach, has become consolidated through the Energy Retrofit Hierarchy, which prioritizes the reduction of loads before interventions in the envelope and the adoption of active systems.

Decision-support methods have also expanded in retrofit processes, including multi-criteria assessments (MCDA/MCDM), AHP, TOPSIS, ELECTRE, and SAW, which enable alternatives to be compared according to energy, environmental, heritage, and economic criteria (Zavadskas et al. (2015); UN-HABITAT (2022); Saad et al. (2023)). Although this article does not apply multi-criteria modelling or energy simulations, these references support the organization of indicators and the integrated reading of the case study.

Within this framework, retrofit should be understood as a central strategy for sustainable rehabilitation, capable of articulating technological innovation, energy efficiency, and cultural preservation. In the Brazilian context, this discussion becomes particularly relevant when focused on symbolic buildings such as the Bernardo Mascarenhas Cultural Center (BMCC), located in Juiz de Fora, Minas Gerais, which is the object of this study.

The objective of this paper is to analyze, through a technical-qualitative case study, the potential of retrofit as an instrument for ecological transition in the built environment, relating heritage conservation, environmental performance, and urban sustainability. The analysis seeks to identify opportunities and limitations in the existing interventions, without generalizing the results beyond the evidence observed in the BMCC case.

2. Bernardo Mascarenhas Cultural Center (BMCC)

The Bernardo Mascarenhas Cultural Center (Figure 1) is part of a built complex of high historical, architectural, and symbolic relevance to the city of Juiz de Fora, in Minas Gerais, Brazil. Its origin dates back to the Bernardo Mascarenhas Textile Company, inaugurated on May 7, 1888. The company played a central role in regional industrialization and in the urban consolidation of the municipality at the end of the nineteenth century (Barbosa et al. (2016)).



Figure 1 - Bernardo Mascarenhas Cultural Center (Barbosa et al. (2016)).

Croce (2021) observes that the installation of the factory was decisive for the modernization of Juiz de Fora and enabled the construction of the Marmelos Hydroelectric Power Plant, designed in 1889 and considered the first hydroelectric power plant in Latin America, revealing the connection between industry, technological innovation, and urban expansion.

The BMCC therefore constitutes a heritage asset with expressive historical, architectural, and social materiality. The institutional recognition of the heritage value of the complex occurred in the 1980s through Decree-Law No. 2,866/1983 (JFCH (1983)). In 1984, after the end of industrial activities, the complex underwent several interventions and was protected by municipal listing, which requires the preservation of the façades and original volumetry while allowing internal adaptations compatible with new uses (Barbosa et al. (2016)).

The architectural complex has an approximate area of 12,498 m², in addition to spaces intended for open circulation, civic squares, and urban support areas. It is currently composed of four main buildings (Figure 2): the BMCC (1); the Municipal Market (MM) (2); the Municipal Department of Education, including the library (MDE) (3); and the Youth and Adult Education Center (EC) (4) (JFCH (1983)).

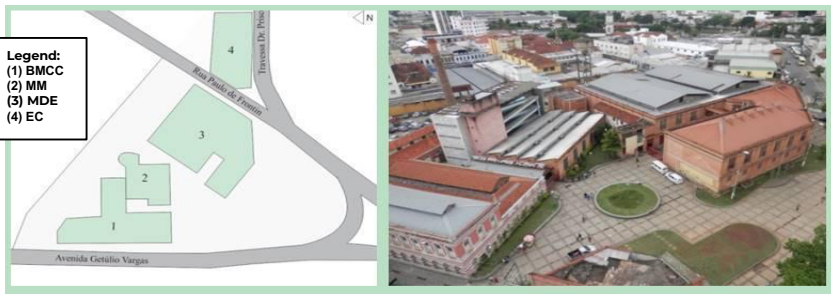


Figure 2 - BMCC sketch (Barbosa et al. (2016)).

The transformation of the former factory complex into a cultural center and public facilities reveals a paradigmatic shift in the understanding of industrial heritage, now recognized not only as a historical remnant but also as active support for contemporary social, educational, and cultural uses. Nevertheless, the intervention stages occurred heterogeneously, resulting in different levels of compliance with sustainability guidelines, environmental comfort, and energy efficiency (Barbosa et al. (2016)).

3. Methodological procedure

Webb (2017) emphasizes that interventions in historic buildings require a holistic reading, because such buildings behave as complex systems in which changes to one element can significantly affect the others. Broström et al. (2022) state that energy-efficiency strategies in historic buildings must balance technical performance and preservation, avoiding risks related to moisture and material degradation.

In this context, the methodological procedure was organized into four stages:

1 - Technical and heritage diagnosis: technical and historical survey of the BMCC architectural project.

2 - Characterization of construction materials and components: carried out in loco through intrinsic inspection (habitability, safety, sustainability, and social responsibility) and extrinsic inspection (anomalies and maintenance services).

3 - Evaluation and prioritization of retrofit: identification of sustainability indicators, including energy efficiency, potential for CO_2 emission reduction, management and maintenance, and the performance of reversible solutions already adopted.

4 - Discussion of the data obtained and indication of more appropriate solutions to strengthen the sustainability of the complex.

The data analysis for stages 1 and 2 was conducted as a technical-qualitative assessment based on building inspection and objective verification of the items evaluated. For the profiles of intrinsic inspection, extrinsic inspection, energy efficiency, potential CO_2 reduction, maintenance, and performance of reversible solutions, yes/no responses were recorded in Tables 1 to 6.

A color-coded classification was then adopted: a green profile for satisfactory performance when more than 90% of the sub-items were met; a yellow profile when 75% to 90% were met, indicating specific imbalances; and a red profile when less than 75% were met, indicating unsatisfactory performance and priority challenges for sustainability (Table 7).

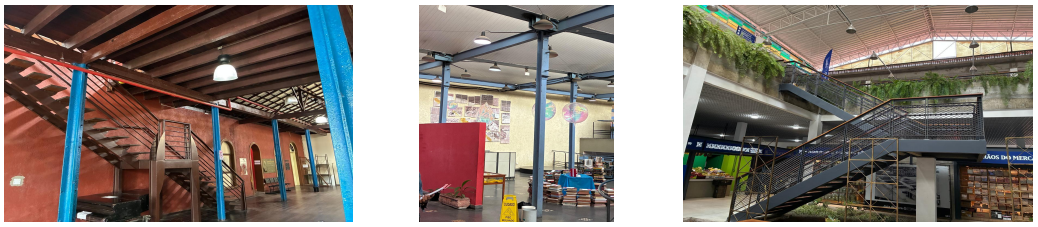
This procedure enabled a preliminary and comparable reading of the sustainable profile of the interventions observed at the BMCC. As a qualitative diagnostic matrix, the results should be understood as support for decision-making and for defining future monitoring priorities, rather than as quantitative proof of energy savings or measured CO_2 reductions.

4. Results and discussion

4.1 Technical and heritage diagnosis:

From an architectural perspective, the BMCC presents a symmetrical composition, a regular rhythm of arched openings, and a language typical of industrial architecture, with exposed solid brick masonry and large spans designed to favor natural lighting and ventilation (Croce (2021)). These characteristics give the building relevant passive potential for environmental comfort.

The restoration carried out in the 1990s, after the partial structural collapse of the building, adopted metal profiles as the main consolidation solution (Figure 3). This strategy is technically appropriate from both heritage and environmental perspectives, since steel offers durability, recyclability, formal distinction from the original structure, and a high degree of reversibility, meeting contemporary principles for the sustainable rehabilitation of historic buildings (Gomide et al. (2019); De Wolf et al. (2020); ICOMOS (2021)).



BMCC MDE MM

Figure 3 - Metal profiles.

Regarding social and cultural indicators, the BMCC stands out for its strong community involvement, consolidating itself as a space for cultural production, education, and access to collective memory, thereby reinforcing its contribution to social sustainability (Croce (2021)). The technical and heritage assessment indicates that, although the building has successfully preserved its historical identity and reactivated its functionality, requalification strategies need to be improved, especially regarding energy efficiency, potential CO_2 reduction, management and maintenance, and the enhancement of reversible solutions already adopted.

4.2. Inspection *in loco*

The technical inspection was based on the integration of intrinsic and extrinsic inspections, as these make it possible to assess the actual conditions of use, conservation, and performance of the building. In accordance with Brazilian standards, such as NBR 16747 (2020), NBR 5674 (2024), and NBR 15575 (2025), the procedure supported the identification of anomalies, the evaluation of the state of conservation of building systems and the envelope, and the

verification of compatibility between use and performance. Extrinsic inspection, based on systematic observation of façades, construction interfaces, and the immediate surroundings, was essential for diagnosing pathological manifestations and defining intervention strategies compatible with existing buildings (Morais and Lordsleem (2019); Hasselmann and Norat (2023); Pereira and Silva (2024); Tavares et al. (2024); Dabous and Hosny (2025)). Tables 1 and 2 present the results.

The analysis of Tables 1 and 2 indicates that the intrinsic and extrinsic inspections recorded satisfactory conditions of habitability, environmental performance, functionality, and structural safety, with no relevant structural anomalies. Thermal comfort through natural ventilation, lighting, indoor air quality, and the reuse of metal profiles from railway tracks stand out positively, demonstrating strategies aligned with durability, material reuse, and the reduction of environmental impacts. The main weaknesses are related to seasonal rising damp, localized detachment of façade coating, and the absence of properly marked escape routes, despite the presence of basic firefighting equipment. Overall, the results indicate favorable conditions for the implementation of sustainable retrofit strategies, provided they are guided by compatibility, reversibility, and the improvement of safety and maintenance management.

Table 1 - Intrinsic inspection.

Requisite	Index	Check parameter	BMCC	MDE	MM
			Inspection		
Habitability	Tightness	Moisture (permeation and air)	No	No	No
		Rising damp (seasonal)	Yes	Yes	No
	Thermal comfort	Cross ventilation	Yes 1	Yes	Yes
		Shading	Yes	Yes	Yes
	Acoustic comfort	Noise insulation	Yes 2	Yes	Yes
	Lighting comfort	Natural	Yes	Yes 4	Yes
		Artificial	Yes	Yes 5	Yes 9
Health	Indoor air quality	Pollutants and microorganisms	No	No	No
Sustainability	Durability	Maintenance service	Yes	Yes	Yes
	Maintainability	Ease of maintenance	Yes	Yes 6	Yes 10
	Environmental impact	Selection of building materials	Yes 3	Yes	Yes
Safety	Structure	Cracks and deformation	No	Yes 7	No
	Fire prevention	Passive protection (fire door, escape route, etc.)	No	No 8	Yes 11
		Active protection (fire extinguishers, sprinklers, etc.)	Yes	Yes	Yes
	Accessibility	Universal criteria	Yes	Yes	Yes

[1]Air-conditioning system in the theater; [2]Limited to the theater; [3]Durable materials and reuse of waste and rejects; [4]Dependence on artificial lighting in the reading room; [5]Suspended artificial lighting, with industrial luminaires distributed along the structure; [6]Periodic maintenance; [7]The coating presents diffuse microcracking with a low degree of severity; [8]There is a risk of entrapment because alternative exit routes are absent and the main door is

the only means of evacuation; [9]The modular grid ceiling allows direct integration with recessed artificial lighting; [10]Execution of maintenance services according to guidelines established in the manual; [11]The signage is legible, contrasting, and well positioned.

Table 2 - Extrinsic inspection.

Requisite	Index	Check parameter	BMCC	MDE	MM
			Inspection		
Durability	Anomalies	Crack (dimension < 0.5 mm)	Yes	No	No
		Crack (0.5 < dimension < 1.5 mm)	No	No	No
		Coating detachment	Yes 1	Yes	No
		Moisture	No	No	Yes

1 Localized coating detachment.

4.3. Sustainability indicators

The evaluation of indicators related to energy efficiency, potential CO_2 emission reduction, management of maintenance services, and performance of reversible solutions is based on contemporary approaches that understand the existing building as an integrated system throughout its life cycle. Recent studies show that retrofit strategies oriented toward energy performance and embodied-carbon mitigation offer significant environmental advantages when compared with replacement of the building stock (Croce (2021); UN-HABITAT (2022)). The literature also shows that maintenance management is essential for the stability of operational performance, while reversible and adaptable solutions contribute to the reduction of future impacts, risk mitigation, and extension of the service life of historic buildings (Opher et al. (2021), IEA (2022); Wu and Shen (2023)). Tables 3 to 6 present the data collected.

The analysis of the requisites presented in Tables 3 to 6 shows an overall performance favorable to sustainable retrofitting, with positive results especially in the potential for CO_2 reduction, in management and maintenance, and in the performance of reversible solutions. The preservation of the existing structure, the adoption of non-invasive interventions, the use of low-carbon materials, and the high reversibility and spatial adaptability of the adopted solutions stand out. In summary, the results indicate that the building has consistent technical conditions for the progressive improvement of its environmental performance, while preserving the principles of compatibility, reversibility, and minimal intervention.

Table 3 - Energy efficiency.

Requisite	Index	Check parameters	BMCC	MDE	MM
			Inspection		
Facade	Performance	Tightness	No	No	No
		Shading	Yes	Yes	Yes
Lighting	Natural	Windows, doors, etc.	Yes	Yes	Yes
		Luminosity	Yes	Yes	Yes
	Artificial	LED	Yes	No	Yes
		Automation	No	No	No

Table 4 - Potential CO_2 emission reduction.

Requisite	Index	Check parameters	BMCC	MDE	MM
			Inspection		
Use	Control	Luminosity	Yes	Yes	Yes
		Air conditioning	No	No	No
		Coating detachment	Yes	No	No
		Moisture	No	No	No
Building materials	Low CO_2	Compatibility	Yes	Yes	Yes
		Conservation	Yes	Yes	Yes
		Reversibility	Yes	Yes	Yes

Table 5 - Management and maintenance services.

Requisite	Index	Check parameters	BMCC	MDE	MM
			Inspection		
Maintenance service	Predictive	Inspection	No	No	No
	Preventive	Inspection	No	No	No
		Repairs	Yes	Yes	Yes

Table 6 - Performance of reversible solutions.

Requisite	Index	Check parameters	BMCC	MDE	MM
			Inspection		
Repair	Reversibility	Fastening system (dry)	Yes	Yes	Yes
		Compatibility	Yes	Yes	Yes
		Removable	Yes	Yes	Yes
Visual	Flexibility	Layout	Yes	Yes	Yes

Finally, an integrated analysis of the BMCC was carried out based on the data evaluated in Tables 1 to 6. For this purpose, a color-coded classification was used, synthesizing performance into three levels: green (satisfactory, with more than 90% of favorable sub-items), yellow (intermediate, with 75% to 90% of favorable sub-items), and red (unsatisfactory, with less than 75% of favorable sub-items). This procedure allows a systemic reading, comparison among indicators, and prioritization of retrofit actions oriented toward sustainability and performance, as shown in Table 7.

The overall performance of the BMCC shows a predominance of green profiles in habitability, health, sustainability, potential CO_2 reduction, management and maintenance services, and performance of reversible solutions. Yellow profiles are concentrated in specific aspects of safety and durability, such as seasonal moisture, localized coating defects, and escape-route limitations. This profile indicates that the building presents favorable technical conditions for sustainable retrofit, allowing the progressive improvement of environmental and functional

performance, provided that future actions are guided by compatibility, reversibility, minimal intervention, and strengthened maintenance management.

Table 7 - BMCC profile.

Indicator	Requisite	BMCC	MDE	MM
		Profile		
Intrinsic inspection	Habitability			
	Health			
	Sustainability			
	Safety			
Extrinsic inspection	Durability			
Energy efficiency	Facade			
	Lighting			
Potential CO_2 reduction	Control			
	Low CO_2			
Management and maintenance	Maintenance			
Reversible solutions	Repair			
	Visual			

4.4. Methodological scope and implications

The results should be read within the scope of the adopted method. The inspection matrix does not replace energy monitoring, dynamic thermal simulation, or life-cycle carbon accounting; rather, it organizes field evidence into a structured diagnostic capable of indicating which aspects of the building already support sustainable retrofit and which aspects require further verification. This distinction is relevant because historic buildings frequently combine architectural value, material heterogeneity, and limitations on intrusive testing. In such contexts, an initial qualitative assessment can reduce decision uncertainty, identify risks, and guide the selection of subsequent quantitative procedures without compromising the heritage fabric.

The contribution of the BMCC case therefore lies in connecting conservation principles with operational performance criteria in a transparent and reproducible manner. The green profiles indicate components and practices that can be maintained or strengthened, such as the preservation of the existing structure, the reuse of materials, and reversible fastening systems. The yellow profiles identify priorities for targeted action, especially moisture control, façade-maintenance routines, and escape-route management. By translating these observations into retrofit priorities, the study supports a gradual intervention strategy compatible with heritage conservation, avoiding overgeneralized claims about decarbonization while still demonstrating how the existing building can act as a platform for environmental improvement.

For future stages, the diagnostic framework should be complemented by quantitative indicators, including pre- and post-intervention energy consumption, indoor temperature and humidity monitoring, envelope-performance assessment, operational-carbon estimates, and embodied-carbon scenarios for alternative retrofit measures. Such data would allow the observed potential for CO_2 reduction to be converted into measurable performance gains and would make the case, more directly comparable with international retrofit studies. The present analysis is therefore positioned as a necessary first step in a broader research sequence, establishing the technical, heritage, and management basis required for more robust environmental evaluation.

5. Conclusions

This study showed that the retrofit of historic buildings can constitute a relevant strategy for the ecological transition of the built environment by reconciling heritage preservation, energy efficiency, potential CO_2 emission reduction, and improved performance in use. The analysis of the Bernardo Mascarenhas Cultural Center (BMCC) indicates that existing buildings, especially those with historical value, should be understood as environmental and cultural assets whose reuse offers substantial advantages when compared with the replacement of the existing building stock.

The integrated application of intrinsic and extrinsic inspections, based on Brazilian standards, made it possible to develop a systemic reading of the building in use, identifying anomalies, weaknesses, and potentialities. The results indicate satisfactory overall performance in habitability, structural safety, functionality, social responsibility, and the performance of reversible solutions, highlighting the reuse of metal profiles from railway tracks, the preservation of the original structure, and the adoption of compatible and non-invasive interventions. With regard to the sustainability indicators analyzed, a particularly positive performance was observed in the potential for CO_2 reduction, associated with the retention of existing components, the use of lower-impact materials, and the extension of the building's service life. Management and maintenance services proved functional, with operational clarity and ease of inspection and repair. Conversely, energy efficiency still presents opportunities for improvement.

It is therefore concluded that the BMCC presents technical and constructive conditions favorable to the consolidation of sustainable retrofit strategies, provided that future interventions are guided by the principles of compatibility, reversibility, minimal intervention, and life-cycle management. The study also demonstrates the need to complement qualitative diagnostic matrices with quantitative procedures in subsequent stages, including energy monitoring, thermal simulation, life-cycle carbon assessment, and scenario analysis, so that the environmental gains associated with retrofit can be measured and compared more robustly.

Acknowledgments

The authors gratefully acknowledge the Brazilian National Council for Scientific and Technological Development (CNPq), the Coordination for the Improvement of Higher Education Personnel (CAPES), the Foundation for the Support and Development of Education, Science and Technology of Minas Gerais (FAPEMIG), and the Federal University of Juiz de Fora (UFJF).

Barbosa, M.T.G. - Bolsista FAPEMIG - CNPq – Brasil (processo BDT-00007-25).

References

Barbosa, Maria Teresa; Paiva, Claudia Dos Reis; Moratori, Daniel de Almeida. 2016. Analysis of the Bernardo Mascarenhas Cultural Complex based on the criteria of sustainable development. In: SBE 16 Brazil & Portugal, Proceedings. Vitória (ES), Brazil.

Associação Brasileira de Normas Técnicas (ABNT). 2020. NBR 16747: Building inspection: guidelines, concepts, terminology and procedures. Rio de Janeiro, Brazil.

Associação Brasileira de Normas Técnicas (ABNT). 2024. NBR 5674: Building maintenance: requirements for the maintenance management system. Rio de Janeiro, Brazil.

Associação Brasileira de Normas Técnicas (ABNT). 2025. NBR 15575: Residential buildings: performance. Rio de Janeiro, Brazil.

Broström, Tor; Leijonhufvud, Gustaf; Eriksson, Petra. 2022. Energy efficiency in historic buildings. In: Routledge Handbook of Sustainable Heritage. London: Taylor and Francis. https://doi.org/10.4324/9781003038955

City of London. 2024. Heritage Building Retrofit Toolkit. London: City of London Corporation. Available at: https://www.cityoflondon.gov.uk/assets/Services-Environment/Heritage-Buildings-Retrofit-Toolkit.pdf. Accessed: Jan. 2026.

Crawford, Robert H.; Stephan, André; Prideaux, Fiona. 2019. Environmental performance in adaptive reuse of buildings. The University of Melbourne, 11. https://doi.org/10.26188/10257728.v11

Croce, Marcus. 2021. Patrimônio industrial e modernização urbana no Brasil. São Paulo: Annablume.

Dabous, Saleh; Hosny, Fatma. 2025. A review of building envelope retrofitting methods for improving energy efficiency, aesthetics, and indoor environmental quality. Energy Nexus, 18. https://doi.org/10.1016/j.nexus.2025.100407

De Wolf, Catherine; Pomponi, Francesco; Moncaster, Alice. 2017. Measuring embodied carbon in buildings: a review. Energy and Buildings, 140, 68-80. https://doi.org/10.1016/j.enbuild.2017.01.075

Gomide, T.; Gullo, M. A.; Fagundes Neto, J.; Flora, S. M. 2019. Inspeção predial. São Paulo: Oficina de Textos.

Hasselmann, Eliza; Norat, Roseane. 2023. Building Inspection as a Tool in the Prevention of Claims in Historic Buildings. CPC, 18(36), 187-209. https://doi.org/10.11606/issn.1980-4466.v18i36p187-209

Historic England. 2022. Energy Efficiency and Historic Buildings. London: Historic England.

IEA. 2022. Technology and Innovation Pathways for Zero-Carbon-Ready Buildings by 2030. Paris: IEA. Available at: https://www.iea.org/reports/technology-and-innovation-pathways-for-zero-carbon-ready-buildings-by-2030. Accessed: Jan. 2026.

Intergovernmental Panel on Climate Change (IPCC). 2022. Climate Change 2022: Mitigation of Climate Change. Cambridge: Cambridge University Press. Available at: https://www.ipcc.ch/report/ar6/wg3/. Accessed: Jan. 2026.

International Council on Monuments and Sites (ICOMOS). 2021. Energy Efficiency and Historic Buildings: Principles and Guidance. Available at: https://icomos.es/wp-content/uploads/2022/10/Guidelines-renewable-energy-related-infrastructures-and-cultural-heritage_ICOMOS-Spain.pdf. Accessed: Jan. 2026.

International Energy Agency (IEA). 2023. Tracking Buildings 2023. Paris: IEA. Available at: https://www.iea.org/reports/world-energy-outlook-2023. Accessed: Jan. 2026.

Juiz de Fora City Hall (JFCH). 1983. Processo de tombamento do Conjunto Arquitetônico Bernardo Mascarenhas - Processo No. 3649/82. Divisão de Patrimônio Artístico e Cultural (DIPAC). Juiz de Fora (MG), Brazil.

Juiz de Fora City Hall (JFCH). 1983. Decreto-Lei No. 2.866, de 1983. Dispõe sobre o tombamento do Conjunto Bernardo Mascarenhas. Juiz de Fora (MG), Brazil.

Liu, Chenfei; Sharples, Stephen; Mohammadpourkarbasi, Hanieyeh. 2023. A Review of Building Energy Retrofit Measures, Passive Design Strategies and Building Regulation for the Low Carbon Development of Existing Dwellings in the Hot Summer-Cold Winter Region of China. Energies, 16, 4115. https://doi.org/10.3390/en16104115

Lucchi, Elena. 2022. Energy Efficiency of Historic Buildings. Buildings, 12(2), 200. https://doi.org/10.3390/buildings12020200

Luo, Shu-Long; Shi, Xing; Yang, Feng. 2024. A Review of Data-Driven Methods in Building Retrofit and Performance Optimization: From the Perspective of Carbon Emission Reductions. Energies, 17, 4641. https://doi.org/10.3390/en17184641

Ma, Zhen; Awan, Muhammad; Lu, Menglong; Li, Shengteng; Aziz, Muhammad; Zhou, Xinlei; Du, Han; Sha, Xinyin; Li, Yixuan. 2023. An Overview of Emerging and Sustainable Technologies for Increased Energy Efficiency and Carbon Emission Mitigation in Buildings. Buildings, 13, 2658. https://doi.org/10.3390/buildings13102658

McCaig, Ian; Pender, Robyn; Pickles, Robyn. 2018. Energy Efficiency and Historic Buildings: How to Improve Energy Efficiency. Historic England Guidance. London: Historic England.

Morais, G. A.; Lordsleem Jr., A. C. 2019. Building maintenance management activity in a public institution. Engineering, Construction and Architectural Management, 26(1). https://doi.org/10.1108/ECAM-01-2018-0024

Opher, Tamar; Duhamel, Mel; Panesar, I.; Brugmann, Rashad; Roy, Adrien; Zizzo, Ryan; Sequeira, Larissa; Anvari, Alireza; MacLean, H. 2021. Life cycle GHG assessment of a building restoration: case study of a heritage industrial building in Toronto, Canada. Journal of Cleaner Production, 270, 123819. https://doi.org/10.1016/j.jclepro.2020.123819

Organisation for Economic Co-operation and Development (OECD). 2022. Building for a Climate, Economic and Social Resilience. Paris: OECD. Available at: https://www.oecd.org/en/about/programmes/net-zero-building-climate-and-economic-resilience.html. Accessed: Jan. 2026.

Pereira, Clara; Silva, Ana. 2024. Operationalisation of building inspections and repair: diagnosis methods and repair techniques for building envelopes. Applied Sciences, 14(16). https://doi.org/10.3390/app14166947

Pomponi, Francesco; Moncaster, Alice. 2016. Embodied carbon mitigation and reduction in the built environment. Journal of Environmental Management, 181, 687-800. https://doi.org/10.1016/j.jenvman.2016.08.036

Saad, Mostafa; Menon, Ramanunni; Eicker, Ursula. 2023. Supporting Decision Making for Building Decarbonization: Developing Surrogate Models for Multi-Criteria Building Retrofitting Analysis. Energies, 16, 6030. https://doi.org/10.3390/en16166030

Tavares, David; Figueiredo, Chenia; Silva, Lenildo; Pantoja, João. 2024. Comparative study of inspection methodologies for assessing the state of degradation of buildings. International Journal of Scientific Management and Tourism, 10(3). https://doi.org/10.55905/ijsmtv10n3-039

Troi, Alexandra; Bastian, Zeno. 2014. Energy efficiency solutions for historic buildings: a handbook. Basel: Birkhäuser.

United Nations Environment Programme (UNEP). 2023. Global Status Report for Buildings and Construction. Nairobi: UNEP. Available at: https://www.unep.org/resources/report/global-status-report-buildings-and-construction. Accessed: Jan. 2026.

United Nations Human Settlements Programme (UN-HABITAT). 2022. World Cities Report 2022: Envisaging the Future of Cities. Available at: https://unhabitat.org/wcr/2022/. Accessed: Jan. 2026.

Zavadskas, Edmundas; Medineckiene, M.; Björk, F.; Turskis, Z. 2015. Multi-criteria decision-making methods in building sustainability assessment/certification. Archives of Civil and Mechanical Engineering, 15(1), 11-18. https://doi.org/10.1016/j.acme.2014.09.001

Webb, Alan. 2017. Energy retrofitting of historic buildings: a review of problems and methods. Renewable and Sustainable Energy Reviews, 77, 748-759. https://doi.org/10.1016/j.rser.2017.01.145

World Economic Forum (WEF). 2023. Building Industry Resilience to Climate Hazards. Available at: https://reports.weforum.org/docs/WEF_Business_on_the_Edge_2024.pdf. Accessed: Jan. 2026.

Wu, Xialu; Shen, Yu-Sheng. 2023. The bibliometric analysis of low carbon transition and public awareness. Atmosphere, 14(6), 970. https://doi.org/10.3390/atmos14060970

cinpar2026
XXII International Conference on Building Pathology and Constructions Repair
15th to 17th July 2026 - Lisboa, Portugal

Improving daylight and energy efficiency in university buildings: A study of the Darcy Ribeiro Campus at the University of Brasilia - Brazil

Joao Francisco Walter COSTA[1], **Eliete de Pinho Araujo[2]**, Claudia Naves David AMORIM[3], Joara Cronemberger Ribeiro SILVA[4]

[1] University of Brasilia, Brazil, jwaltercosta@gmail.com
[2] University of Brasilia, Brazil, eliete.araujo@unb.br
[3] University of Brasilia, Brazil, clamorim.unb@gmail.com
[4] University of Brasilia, Brazil, joaracronemberger@unb.br

Abstract: In educational buildings, particularly universities, energy consumption is linked to needs such as air conditioning, lighting, and equipment use. Approximately, 40% of the total consumption, particularly in warm regions is linked to internal heat gains (high occupancy, equipment, lighting, and solar radiation). Artificial lighting follows as another major consumer, ranging from 20% to 45% of consumption, despite being essential for ensuring environments suitable for teaching and research. In this regard, this study aims to analyze strategies to decrease energy consumption for electric lighting of nine representative buildings inside the Darcy Ribeiro Campus at the University of Brasilia (UnB) in Brazil. The method consisted of selecting 45 buildings inside the campus, sorting them into 3 clusters. Three buildings of each cluster were simulated with the software ClimateStudio to analyze the energy consumption for lighting, considering the addition of external shadings, window film to reduce visible transmission from the windows – from 88% (clear glass) to 62%, and automation of electric lighting. Results demonstrated that passive strategies, of optimizing the sun-shading devices and the addition of the window film were extremely efficient to control daylight entering the room, keeping useful daylight illuminance levels (between 300 and 3000 lux) above 69% in eight of the nine buildings, while reducing areas with disturbing glare in more than 5% of daylit hours. Regarding results of energy consumption for lighting, a decrease between 24% and 52% was observed between the original cases and the optimized ones, with all passive strategies and automation of the lighting systems applied. Therefore, a balance between the luminous comfort and a decrease in the energy consumption for lighting was found in the nine representative buildings inside the Darcy Ribeiro Campus at the University of Brasilia.

Keywords: Zero Energy District. University Buildings. Brasilia. Warm climate. Daylight simulations.

1. Introduction

Buildings account for 36% of the global final energy consumption and 40% of energy-related greenhouse gas emissions, a figure that could reach 50% if no strategy is implemented to reduce these impacts (United Nations, 2023; Zhang et al., 2021). In Brazil, commercial, public, and service buildings accounted for nearly 45% of the national electricity demand in 2024, with 24% for residential, 14.6% for commercial, and 6.3% for the public sector (Ministry of Mines and Energy 2025).

Furthermore, 56% of the world's population lived in cities in 2021, and this figure is projected to rise to 68% by 2050 (United Nations 2025). Consequently, several programs aimed at mitigating the impacts of climate change, coupled with strategies for creating more sustainable cities and communities (Arshad, Haleem, and Nadeem 2025). In the European context, where buildings account for 40% of energy demand and 36% of CO_2 emissions, regulatory frameworks such as the Energy Performance of Buildings Directive (EPBD) have established nearly zero-energy buildings (nZEB) as a mandatory standard for new construction, reflecting

the European Union's commitment to a fully decarbonized building stock by 2050 (European Union 2024). Technically, net-zero and nearly-zero energy buildings are characterized by the ability to meet annual energy demands through renewable self-generation or procurement, achieved in new constructions and comprehensive retrofits involving building envelope optimization, high-efficiency technical systems, and the integration of on-site renewable energy generation (Pless and Torcellini 2009). To achieve the Net-Zero Energy Building (NZEB) standard, three main objectives must be met. First, it is essential to reduce energy waste through improved building envelopes and enhanced HVAC systems. Second, the performance of renewable energy systems must be enhanced using hybrid systems capable of adapting to fluctuations in energy demand. Third, in terms of decarbonization, extensive integration of local renewable energy sources must be implemented in both new and existing buildings (Hainoun et al. 2025). In 2020, the European Union has triggered the transformation of Europe's neighbourhoods into energy districts (Aram, Taherkhani, and Šimelytė 2022; European Union 2024).

In educational buildings, particularly universities, energy consumption is linked to needs such as air conditioning, lighting, and equipment use. Air conditioning is the primary contributor, accounting for up to 40% of total consumption, particularly in hot regions, due to internal heat gain (high occupancy, equipment, lighting, and solar radiation). Artificial lighting follows as another major consumer, ranging from 20% to 45% of consumption (Litardo and Hidalgo-leon 2021). In the Brazilian context, university buildings are categorized into the "public" and "commercial" groups. However, there is no disaggregated information on the energy consumption of this type of building in the National Energy Balance (Garcia 2022). Factors such as the intensive use of equipment, lighting, and solar gain through the building envelope increase the building's thermal load, and consequently, affect the building's overall energy consumption.

Despite its essential role in creating comfortable and productive study and work environments, artificial lighting constitutes a significant source of energy consumption (Quevedo, Geraldi, and Melo 2023). Tests conducted in a full-scale experimental room in Iowa (United States – 40° North/ 93° West) under multiple orientations and sky conditions showed that dynamic shading paired with two glazing options effectively balanced daylight availability, glare control, and thermal performance. The integrated system achieved substantial energy savings, equivalent to 25.4% in cooling and 48.5% in lighting.

In light of this challenge, various approaches can be adopted to improve the energy efficiency and environmental quality of university buildings. Elements such as building morphology, envelope treatment, and internal zoning play a fundamental role in the ability to utilize passive resources, such as natural ventilation and lighting, as they determine the degree of permeability and the possibilities for controlling these flows (Arshad, Haleem, and Nadeem 2025). Furthermore, the adoption of specific technical solutions, such as the modernization of lighting, HVAC, and high-energy-consumption equipment systems, is a relevant strategy (Luo et al. 2022). Studies conducted by Kunwar *et al.* (2020) demonstrated that combining shading devices, different glazing types, and automated lighting controls can significantly reduce a building's energy demand while improving indoor comfort. Additionally, for the well-being of users inside a building, the presence of daylight is of extreme importance and this is linked to a higher productivity as well (Wei et al. 2014; Kokatnur et al. 2025).

In this regard, this study aims to analyze strategies to decrease energy consumption for electric lighting of nine representative buildings inside the Darcy Ribeiro Campus at the University of Brasilia (UnB) in Brazil. This research is inserted into a research project with the main goal of analyzing the feasibility of transforming the Campus into a Zero Energy District (ZED).

2. Method

The object of this study is the Darcy Ribeiro Campus at the University of Brasilia (UnB) in Brazil. The first step of the method was to map the buildings. After that 45 buildings were selected with predominant use of classrooms, professors' rooms, and administrative offices. The second step was to cluster these 45 buildings

by morphological similarities, and 9 were selected for simulation studies. The third step was to gather technical drawings, plans, and collect data regarding electric systems, including the number of computers, lamps, luminaires etc. The fourth step consisted of computer simulations of electric lighting using ClimateStudio software. As there was no separate measurements for the different end uses of electricity in Campus, the energy consumption for lighting was estimated by simulations. Energy consumption for electric office equipment was estimated using DesignBuilder. Figure 1 illustrates the method flowchart. All this process was documented by Soares (2024) and Amorim, and, Cronemberger and Bones (2024).

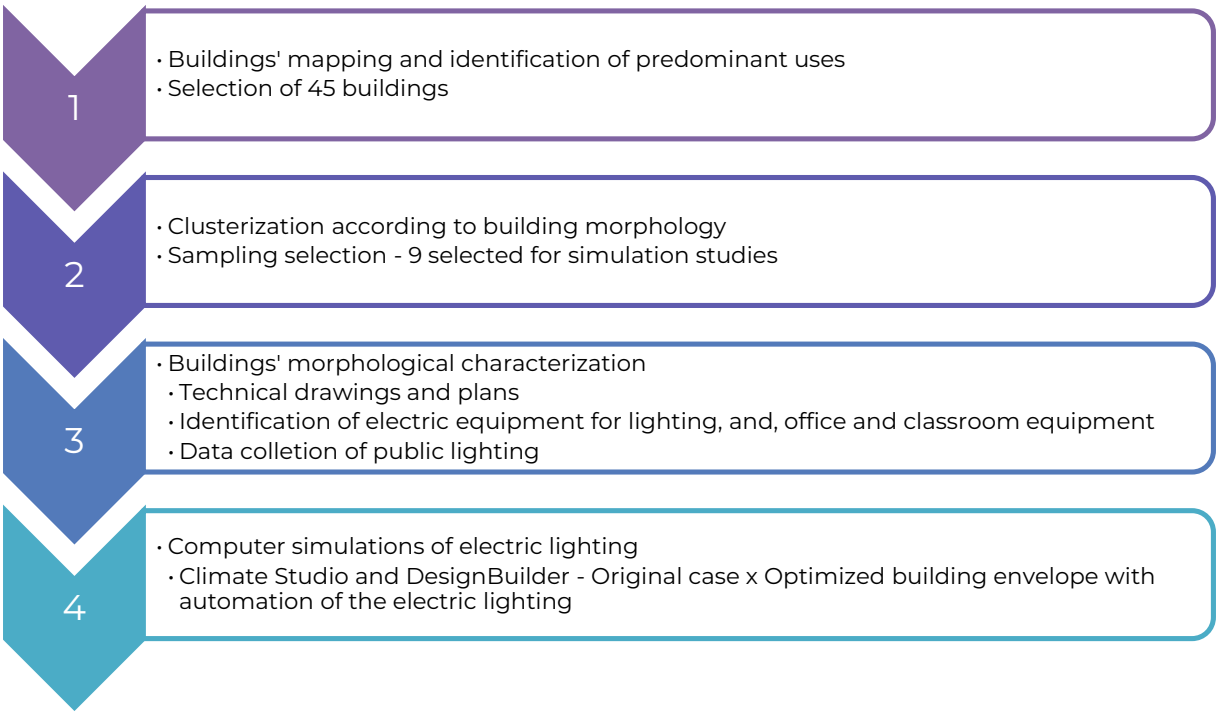


Figure 1 – Method flowchart. Source: The Authors.

The Campus and the selection of buildings are described in the following section.

2.1 The Darcy Ribeiro Campus at the University of Brasilia – Brazil and selection of buildings

The Darcy Ribeiro Campus of the University of Brasília, located in the northern part of the capital, stands out both for its academic significance and for its influence on the urban environment. The campus covers an area of 3,950,579.07 m² and has a built-up area of 552,171.40 m² (CEPLAN/UnB, 2025). In total, there are 93 buildings inside the Campus and the predominant uses are: professors' offices, classrooms, administrative offices, hospital premises and medical uses, laboratories, and residential buildings (Guerreiro *et al*. 2025).

For this study, buildings with the predominant uses of professors' offices, classrooms and administrative rooms were selected. Then, 45 buildings were selected and divided by a cluster analysis, which was carried out based on the homogeneity of use, replicability, the presence of energy monitoring, facades' solar orientation, form factor[1], window-to-wall ratio (WWR) and presence of solar shading devices (Soares 2024).

Guerreiro *et al.* (2025) and Soares (2024) determined that 9 buildings were sufficient to represent the three clusters with an adequate margin of error and confidence interval. Figure 2 shows the selected buildings for the daylight simulation studies. These buildings were chosen to ensure that the simulated buildings served as a representative sample of the different typologies on the campus, assuming that buildings with similar morphological and design characteristics exhibit comparable patterns of environmental impact and energy

[1] Calculated by the ratio between the area of the building envelope in relation to the volume (Inmetro 2021).

consumption. In Cluster 1, the selected buildings were the IPOL/IREL building (Institutes of Political Science and International Relations), the Academic Administration Office (SAA), and the Faculty of Law (FD). In Cluster 2, the selected buildings were the North Classroom Block (BSAN), the Technology Development Support Center (CDT), and João Calmon Pavilion. In Cluster 3, the selected buildings were the Center for Sustainable Development (CDT), Faculty of Technology (FT), SG-10, and CEPLAN.



Figure 2 – Facades of the selected buildings. Source: adapted from adapted from Soares (2024) and Amorim, Cronemberger and Bones (2024).

The climate of Brasilia and the simulation parameters are described in the next sections.

2.2 Climate of Brasilia: present day and in 2050

Brasilia (15° South/47° West) has two distinct seasons marked by a hot-humid period, with a rainy summer, from October to April (with temperatures ranging from 18 °C to 27 °C), and a hot-dry period with a dry winter, from May to September (with temperatures ranging from 15°C to 25°C. Brasilia presents high solar irradiation levels, with a daily average of 467 Wh/m².day. In the hottest months, the means of maximum temperatures reach 30°C (CODEPLAN 2020). The annual daily average of sky cover is 46%, with annual low daily average of 15% and annual high daily average of 83%. Annual averages of global horizontal illumination is 50.358 lux, annual average of daily high, 83.521 lux and annual average of daily low is 20.050 lux. These data were directly extracted from the climate file of Brasilia TMY 2009-2023 (Crawley and Lawrie 2023).

By 2050 the temperature range in the summer (October to April) is expected to vary approximately between 22°C and 28°C, while in the winter (hot and dry season) temperatures will range from about 18 °C to 27 °C. Solar irradiation is projected to increase between 4% and 14% from September to November, resulting in a slightly higher annual daily average of 470 Wh/m² per day. The annual daily average of sky cover remains constant at 50% at every simulated hour in the future climate file of 2050. This is observed as a limitation and does not reflect the sky cover seasonal variations typical of Brasilia's present climate. Annual daily averages of global horizontal illumination remain similar to current values, reaching 51,499 lux, with daily highs of 85,596 lux and daily lows of 11,141 lux. These data were directly extracted from the climate file of Brasilia with prediction models for the year of 2050 (Bracht et al. 2023).

2.3 Workflow of the computer simulations and variables

For the daylight simulations, two climate files were used to represent the climate of Brasilia. The first climate file encompassed the years from 2009 and 2023 and the second one was derived from model projections of the Coordinated Regional Downscaling Experiment, CORDEX project. The details are described in the study of Bracht *et al.* (2023). The inputted climate files were:

- BRA_DF_Brasilia-Kubitschek.Intl.AP.833780_TMYx.2009-2023
- BRA_DF_Brasilia-Kubitschek.Intl.AP.833780_RCP2.6_HadGEM2_regcm_2050s_BrazFuture.zip

The nine buildings were modeled using Rhinoceros v. 7. After this process, ClimateStudio, v. 2.1 was used for daylight calculations and energy consumption of electric lighting (Solemma 2023). Figure 3 shows the workflow of the daylight computer simulations.

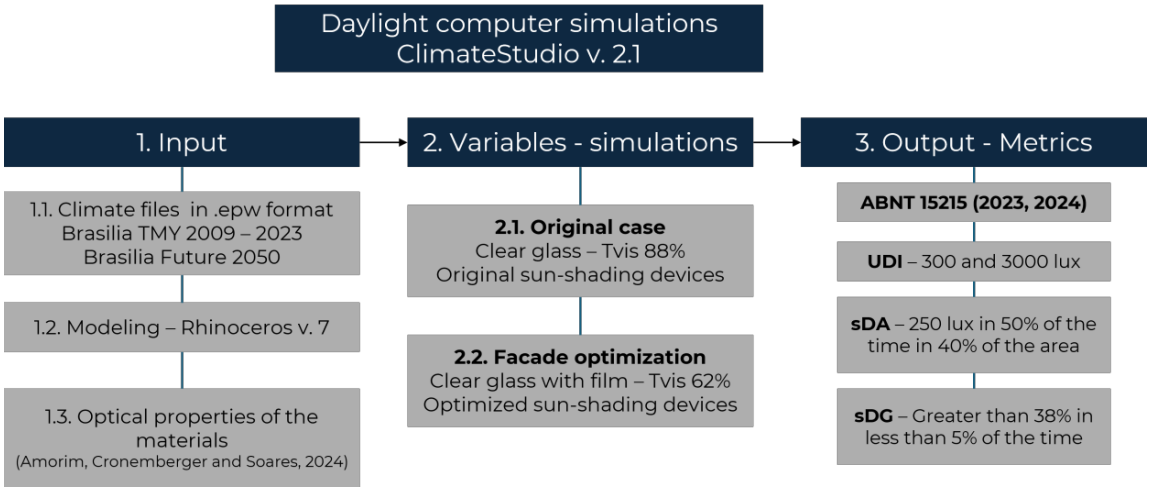


Figure 3 – Workflow of the daylight computer simulations. Source: Adapted from Soares (2024) and Amorim, Cronemberger and Soares (2024).

The nine buildings were modeled as the original case. After that, a facade optimization process was designed in order to add or improve the sun-shading devices and a window film was added to decrease the visible transmissivity of the windows. For all nine buildings in the original case, clear glass with 6 mm was the predominant glass type, with g-value of 0.85 and visible transmittance (Tvis) of 0.88. Regarding the passive strategies, the shading device analysis was carried out by generating a shading mask for each building using the Analysis Sol-AR software, which helps determine the alpha - vertical (α), beta - horizontal (β), shadow angles. For the Glass Type (Film), a gray film was selected with specific characteristics of g-value 0.64 and visible transmittance (Tvis) of 0.62 (Vitro Architectural Glass 2026). A visible transmittance above 40% with a reduced shading coefficient compared to the original condition helps to balance daylight penetration and glare control, improving visual comfort for occupants (Costa, Amorim and Silva 2020; Correia 2024).

The sun-shading devices were individually evaluated for each building, assessing the existing solution and, when inadequate, proposing a new protection angle—either horizontal or vertical—defined on a case-by-case basis. Depending on the buildings' characteristics (such as SG-10 and the School of Technology – FT), or because the existing shading elements did not require modification (as in the Faculty of Law – FD – and the Technology Development Center – CDT), the sun-shading devices were not modified. The sun-shading devices were modelled with a fixed angle. The details regarding the optical properties, including solar absorptance, reflectance, and angles of the sun-shading devices of the nine buildings for each orientation were described by Amorim, Cronemberger and Soares (2024).

The automation of the electric lighting was calculated using DesignBuilder software based on the daylight simulations according to the daylight autonomy levels. DesignBuilder simulates the incidence of daylight throughout the day, and the artificial lighting control system dims or switches off the electric lights when there is sufficient natural light to meet the desired illuminance levels of 500 lux (DesignBuilder Software Ltd., 2024; ABNT, 2013). The strategies for the facade optimization process of the nine buildings are illustrated in Figure 4.

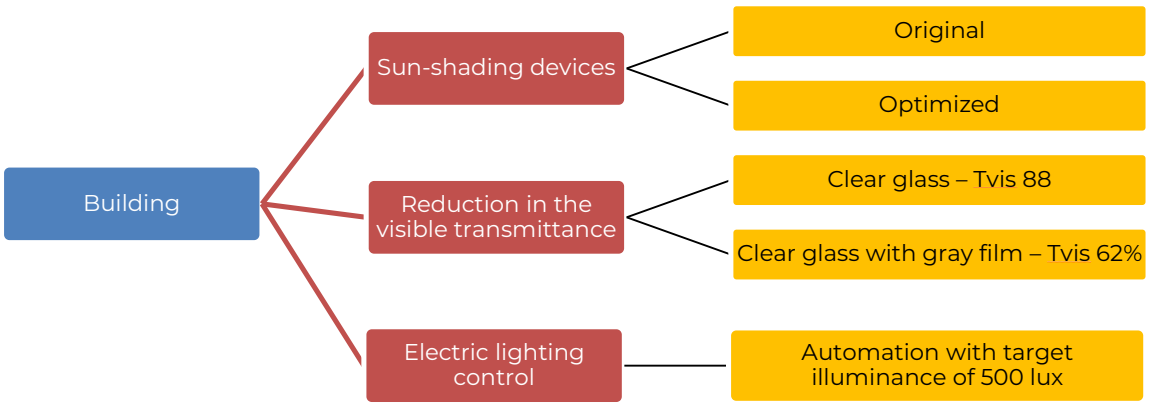


Figure 4 – Strategies for the facade optimization process of the nine buildings. Source: The Author with adaptations from Bones (2024).

The evaluated metrics were, useful daylight autonomy (UDI), spatial daylight autonomy (sDA) and annual glare, which are all climate-based (IES 2023; ABNT 2022; Tregenza and Mardaljevic 2018). To evaluate daylight quality of the indoor environments, such as, classrooms, professors' rooms, and administrative offices, the following parameters were considered between daylit hours, from 8 a.m. and 6 p.m.:

- Useful daylight illuminance (UDI): within the range of 300 to 3000 lux (visual comfort range) for at least 50% of the daylight hours, as recommended by the Brazilian Standard ABNT NBR 15215-4 (2023).
- Spatial daylight autonomy (sDA): with a target illuminance of 250 lux for 50% of the time in 40% of the floor area (Level I), as recommended by ABNT NBR 15215-3 (2024).
- Spatial discomfort glare (sDG): below 5% of the occupied hours: i.e. sDG higher than 38% (disturbing glare) below 5% of the occupied hours, as recommended by ABNT NBR 15215-3 (2024).

The results are presented in the next section.

3. Results and discussion

When combining the morphological variables, form factor (FF) and window-to-wall ratio, with the visual classification of buildings across the three clusters, patterns were observed, as described by Table 1. Cluster 1 buildings (IPOL/IREL, SAA, and FD) show lower form factors (0.32–0.33) and WWR values below 50%. Cluster 2 buildings (BSAN, CDT, and PJC) present similar form factors (0.35–0.38) as cluster 1 buildings, but higher WWR levels, ranging from 50% to over 75%. Cluster 3 buildings (CDS, FT, and SG-10) have the highest form factors (0.44 – 0.48) and higher variations of WWR levels. Results for three of the buildings are presented here by means of example – i.e. one building for each cluster. Following the initial simulations, it was found out that the nine buildings have daylight levels well above those required by the Spatial Daylight Illuminance (sDA) criterion. Consequently, it was decided to analyse them solely using the Useful Daylight Illuminance (UDI) criterion, which covers the range from 300 to 3000 lux, whilst also identifying potential glare issues.

Table 1 - Morphological characteristics related to the form factor and window-to-wall ratio of the simulated buildings. Source: The authors with adaptations from Amorim, Soares and Cronemberger (2024).

Cluster	Buildings	Form factor (FF)	Window-to-wall ratio
1	IPOL/IREL SAA FD	0.32 – 0.33	Equal or less than 50%
2	BSAN CDT PJC	0.35 – 0.38	Between 50% and 75%
3	CDS FT SG-10	0.44 – 0.48	SG-10 - Less than 50% FT: 50% to 75% CDS – Greater than 75%

The results of the daylight simulations are described next.

3.1 IPOL/IREL - Institutes of Political Science and International Relations

The IPOL/IREL building performed well in terms of daylighting, based on the useful daylight illuminance (UDI) criterion, with 74% of its areas falling within illuminance levels between 300 to 3000 lux. Most of the building's spaces are adequately lit for daily activities without causing visual discomfort. However, some specific areas, particularly rooms facing east and west, have illuminance levels exceeding 3000 lux. In the optimized case, with reduction of the visible transmittance, the increase in the average UDI (300 – 3000 lux) was 12%, and for 2050, 4%. Regarding results of sDG (annual glare), approximately 47% of the evaluated views presented more than 5% of the time with disturbing glare (DGP > 38%). In the optimized case, this number dropped by 3.5% and in the future, 3.4%. Figure 5 shows the results of UDI and sDG of IPOL/IREL building.

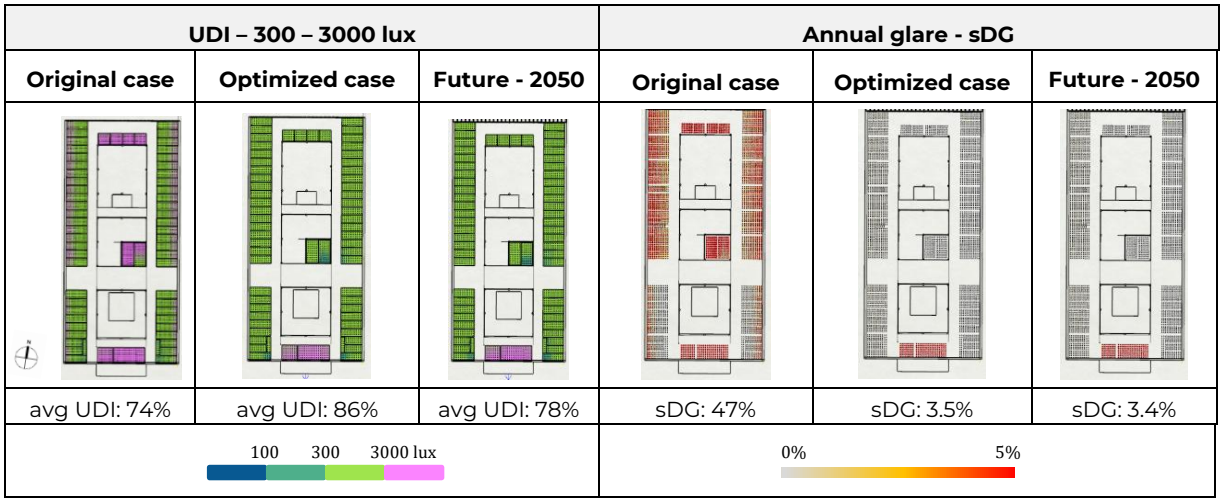


Figure 5 – Results of Useful Daylight Autonomy (UDI) for IPOL/IREL. Source: Climate Studio (2024).

The results of BSAN building are described next.

3.2 BSAN - North Classroom Block

The BSAN building (Figure 6) performed well in terms of daylighting, with 83% of its areas falling within the comfortable illuminance range (300 to 3000 lux). Specific areas, particularly rooms facing north and north-west, have illuminance levels exceeding 3000 lux between 1 p.m. and 5 p.m. This excessive light can be problematic, causing visual discomfort to occupants and indicating the need for adjustments to the solar control devices. In the optimized case, the average UDI dropped from 83% to 78%, and to 72% by 2050.

UDI – 300 – 3000 lux			Annual glare - sDG		
Original case	**Optimized case**	**Future - 2050**	**Original case**	**Optimized case**	**Future - 2050**
					
avg UDI: 83%	avg UDI: 78%	avg UDI: 72%	sDG: 40%	sDG: 1.1%	sDG: 0.8%
					

Figure 6 – Results of Useful Daylight Autonomy (UDI) for BSAN. Source: Climate Studio (2024).

It was observed that BSAN also exhibited a high glare probability index, with 40.3% of views exposed to levels exceeding the ideal threshold for more than 5% of occupied hours. This is caused mainly by the inefficiency of the sun-shading devices, resulting in excessive illuminance levels, thus impairing visual comfort. When the window film was added, causing a drop in the visible transmittance, the sDG dropped from 40% of the area above 5% with disturbing glare, to 1.1% of area, and to 0.8% by 2050, as shown in Figure 6.

3.3 CDS - Center for Sustainable Development

The CDS building (Figure 7) performed well in terms of daylighting, with 74% of its areas falling within the comfortable illuminance range (300 to 3000 lux). Some specific areas, particularly rooms facing north and north-west, have illuminance levels exceeding 3000 lux. In the optimized case, the average UDI increased from 74% to 82%, and by 80% for 2050, with a decrease in the overlit areas.

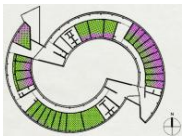
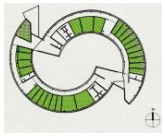
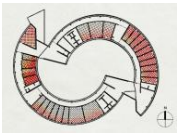
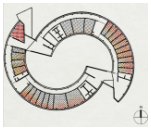
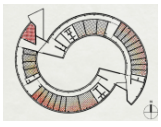
UDI – 300 – 3000 lux			Annual glare - sDG		
Original case	**Optimized case**	**Future - 2050**	**Original case**	**Optimized case**	**Future - 2050**
					
avg UDI: 74%	avg UDI: 82%	avg UDI: 80%	sDG: 42%	sDG: 22%	sDG: 20%
					

Figure 7 – Results of Useful Daylight Autonomy (UDI) for CDS. Source: Climate Studio (2024).

Based on the results of annual glare (Figure 6), it was observed that the building also exhibited a high glare probability index, with 42% of views exposed to levels exceeding the ideal threshold for more than 5% of occupied hours. This is also a high level, caused mainly by the inefficiency of the sun-shading devices and high window-to-wall ratio, resulting in excessive illuminance levels. When the window film and improved sun-shading devices were added, causing a drop in excessive daylight penetrating the room, sDG dropped from 42% of the area above 5% with disturbing glare, to 22% for the optimized case and to 20% by 2050. Nevertheless, compared to the IPOL/IREL and BSAN buildings, CDS presented the worst performance regarding the avoidance of glare. An overview of the results of the daylight simulations are described next.

3.4 Overview of the daylight simulations and energy consumption for electric lighting

When the original buildings (cases) were compared with the optimized ones, the impact of the strategies employed is evident in almost all buildings. Cluster 1 showed the greatest improvement in natural lighting, with an average increase of 9.13% in hours with adequate UDI – between 300 and 3000 lux. The building that saw the greatest improvement in daylighting was SG-10, with almost 24% more hours of comfortable lighting when comparing the original case with the optimized case. It is worth noting that some buildings would face a deterioration in the quality of natural lighting in a future scenario and in the optimized case, indicating that these improvements were punctual and did not work for all cases. For example, a drop of 5.2% was observed for BSAN, as previously observed, PJC – with a drop of 15% and FT, with a drop of 11%. Figure 8 shows the overall results for lighting comfort (quality of natural lighting), based on the percentage of hours with adequate Useful Daylight Illuminance, between 300 and 3000 lux.

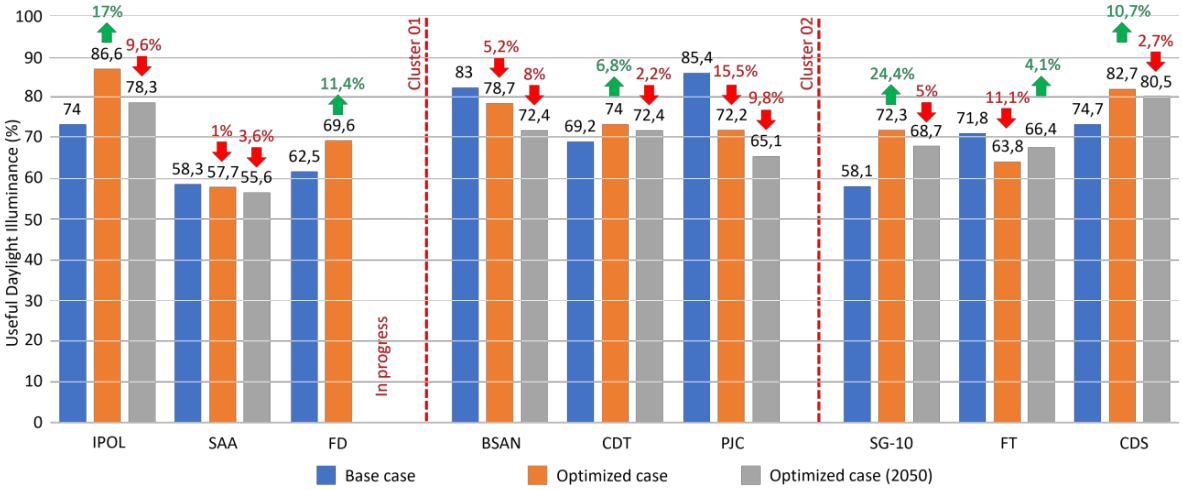


Figure 8 – Summary of Useful Daylight Illuminance results evaluating the quality of daylight of the nine buildings regarding the original buildings (cases), optimized case and future scenario in 2050.

Results showed that for all three clusters, the energy consumption for lighting decreased more than 25% and significant differences were observed, as shown in Table 2. Similar results were seen in clusters 1 and 3. In general, the energy decrease was between 31% and 62%. However, in cluster 2 the decrease in energy consumption for lighting was between 21% and 28%. Besides that, it was possible to verify that the highest energy consumptions for electric lighting was found in the buildings of cluster 2, encompassing BSAN, CDT and PJC.

Results of UDI and annual glare showed improvements in some aspects of daylighting quality inside the indoor environments across all the nine buildings. This is of extreme importance, because the presence of adequate daylighting can increase the productivity of students, professors and other professionals, while increasing the well-being of users inside. Additionally, this was observed in the studies of Wei *et al.* (2014) and Kokatnur *et al.* (2025).

Table 2 – Energy consumption for electric lighting: comparison between the original cases and the optimized cases with all strategies applied. Source: The Authors with adaptations from Amorim, Cronemberger and Soares (2024).

Cluster	Building	Original case (kWh)	Optimized case (kWh)	Change in percentage %
1	IPOL/IREL	107.736,30	66.553,58	-44,27%
1	SAA	86.353,84	50.199,81	-53,21%
1	FD	145.301,05	82.401,31	-47,11%
Avg. decrease				**-48,20%**
2	BSAN	101.901,43	75.868,52	-25,55%
2	CDT	85.994,83	67.936,79	-21,00%
2	PJC	54.868,38	39.282,09	-28,41%
Avg. decrease				**-24,98%**
3	SG-10	18.650,03	7.043,27	-62,23%
3	FT	35.554,70	24.315,76	-31,61%
3	CDS	28.679,75	10.700,52	-62,69%
Avg. decrease				**-52,18%**

The conclusions are presented in the next section.

4. Conclusion

Results demonstrated that passive strategies, of optimizing the sun-shading devices and the addition of the window film were extremely efficient to control daylight entering the room. This was achieved by reducing the visible transmittance from 88% to 62%, and, optimizing the sun-shading devices for each building and window orientation. From the perspective of daylighting, these strategies helped to control glare and improve UDI levels between 300 and 3000 lux inside the evaluated buildings.

Besides that, the passive strategies with the addition of automation in the lighting systems according to daylight autonomy and glare control were efficient strategies to decrease in 24% to 52% the energy consumption for lighting. In general, no relationship was observed among energy consumption for lighting, form factor and window-to-wall ratio, as described in Table 1. Reasons for the differences in the energy consumption decrease are an aspect that is worth further investigation.

Regarding the future scenarios in 2050, despite some deteriorations observed in some cases, UDI levels and annual glare were not significantly different from the optimized cases. Additionally, the climate file for Brasilia in 2050 does not reproduce seasonal variations in sky cover, failing to represent both the hot and dry winter and the hot and rainy summer months. The discussion regarding climate change is more focused on thermal comfort and energy consumption for artificial cooling, but the discussion of future scenarios regarding daylighting and energy consumption for electric lighting in the future is of paramount importance. Different climates and latitudes must be considered as well.

It is concluded, therefore, that a balance between the luminous comfort, with the increase of useful daylight illuminance levels with the reduction of glare, and a decrease in the energy consumption for lighting was found in the nine representative building inside the Darcy Ribeiro Campus at the University of Brasilia. This is extremely important to increase the energy efficiency of the Campus. Among the main limitations of the study, a cost-benefit analysis of the strategies was not included and experimental studies in the Campus' buildings were not conducted. These aspects will be approached in further studies.

Acknowledgments

The authors thank the Research Support Foundation of Distrito Federal (FAPDF) and the Brazilian National Council for Scientific and Technological Development (CNPq) for their support, which made part of this research possible.

References

ABNT - Associação Brasileira de Normas Técnicas. 2013. "NBR ISO – CIE 8995 – 1: Iluminação de Ambientes de Trabalho: Interior." Rio de Janeiro.

ABNT - Associação Brasileira de Normas Técnicas. 2022. "ABNT 15215 - 2: Calculation Procedures for Daylighting and Daylight Spatial Distribution." Rio de Janeiro.

ABNT - Associação Brasileira de Normas Técnicas. 2023. "ABNT NBR 15215 - 4: Experimental Verification of Internal Daylighting Conditions - Measurement Method." Rio de Janeiro.

ABNT - Associação Brasileira de Normas Técnicas. 2024. "ABNT 15215 - 3: Procedures for the Evaluation of Daylighting in Internal Environments." Rio de Janeiro.

Amorim, Cláudia Naves David, Joara Cronemberger, and Marco Túlio Bones Soares. 2024. "Relatório Parcial Do Projeto de Pesquisa: Cenários e Propostas Para Eficiência Energética Em Edifícios e Campus de Balanço Energético Nulo." Brasilia.

Aram, Kimiya, Roohollah Taherkhani, and Agnė Šimelytė. 2022. "Multistage Optimization toward a Nearly Net Zero Energy Building Due to Climate Change." *Energies* 15 (3). https://doi.org/10.3390/en15030983.

Arshad, Md Ozair, Abid Haleem, and Mohd Nadeem. 2025. "Understanding the Energy Retrofit Strategies towards Net Zero Energy Building in Sync with the SDGs: A Review and Bibliometric Analysis." *Journal of Building Engineering* 106 (112574): 1–22.

Bracht, Matheus Körbes, Marcelo Salles Olinger, Amanda Fraga Krelling, André Rodrigues Gonçalves, Ana Paula Melo, and Roberto Lamberts. 2023. "Multiple Regional Climate Model Projections to Assess Building Thermal Performance in Brazil: Understanding the Uncertainty." *Journal of Building Engineering* 88 (109248).

CODEPLAN, Companhia de Planejamento do Distrito Federal. 2020. "Atlas Do Distrito Federal 2020." Brasília. https://www.codeplan.df.gov.br/atlas-do-distrito-federal-2020/.

Correia, Camila Machado de Azevedo, and Positive. 2024. "Positive Energy Schools with Cool Materials and Passive Strategies : Scenarios and Perspectives for the Brazilian Context." University of Brasilia. https://repositorio.unb.br/handle/10482/48514.

Crawley, Drury B, and Linda K Lawrie. 2023. "Development of Global Typical Meteorological Years (TMYx)." https://climate.onebuilding.org/WMO_Region_3_South_America/BRA_Brazil/index.html#IDDF_Distrito_Federal-.

DesignBuilder Software Ltd. 2024. "DesignBuilder Software v. 7.3.0.38." Gloucestershire. https://designbuilder.co.uk/.

Energy, Brasil. Ministry of Mines and. 2025. "Balanço Energético Nacional: Relatório Síntese 2025." *Ben 2025*. Vol. 1. Brasília. https://www.epe.gov.br/pt/publicacoes-dados-abertos/publicacoes/balanco-energetico-nacional-2025.

European Union. 2024. "Energy Performance of Buildings Directive (EPBD) 2024 Implementation." *Structural Survey*. Vol. 23. Brussels. https://doi.org/10.1108/ss.2005.11023aab.001.

Garcia, Marina da Silva. 2022. "Consumo de Energia e Conforto Térmico Em Campus Universitário: Uma

Proposta de Benchmarking." Universidade Federal de Minas Gerais. https://repositorio.ufmg.br/items/af01c972-d7d3-416d-8288-06aa56624278.

Guerreiro, Andiara, Machado Campanhoni Lucas, Júnior Ferreira, Guilherme Oliveira, Mario Emiliano Miskiewiez, Claudia Naves David Amorim, and Joara Cronemberger. 2025. "NZED EM CAMPI UNIVERSITÁRIOS : AVALIAÇÃO DO CONSUMO ENERGÉTICO E POTENCIAL DE EFICIÊNCIA NO CAMPUS DARCY RIBEIRO – UNIVERSIDADE DE BRASÍLIA (UnB)." In *Encontro Latino-Americano e Europeu Sobre Edificações Sustentáveis*, 1–10. Rio de Janeiro: ANTAC.

Hainoun, Ali, Sebastian Stortecky, Daniel Horak, and Ahmed A. Serageldin. 2025. "Monitoring and Evaluation of Integrated Energy Solutions in a Zero-Energy Building (ZEB) in Vienna." *Energy and Buildings* 343 (May): 115906.

Inmetro. 2021. "Instrução Normativa Inmetro Para a Classificação de Eficiência Energética de Edificações Comerciais, de Serviços e Públicas," 139. http://www.inmetro.gov.br/legislacao/rtac/pdf/RTAC002707.pdf.

Kokatnur, Tejas, Fatima Faris, Burak Gunay, William O'Brien, and Elie Azar. 2025. "The WELL Building Standard: A Literature Review and Bibliometric Analysis of a Nascent Field." *Journal of Building Engineering* 103 (112121): 1–23.

Kunwar, N., K. S. Cetin, U. Passe, W. Zhou, and Y. Li. 2020. "Energy Savings and Daylighting Evaluation of Dynamic Venetian Blinds and Lighting through Full-Scale Experimental Testing." *Energy* 197 (117190).

Litardo, Jaqueline, and Ruben Hidalgo-leon. 2021. "Classrooms in Hot and Humid Climates," 1–17.

Luo, Xi, Yongkai Sun, Xiaojun Liu, Yaru Gao, Haili Sun, and Anfeng Liu. 2022. "Course Timetable Optimization for a University Teaching Building Considering the Building Energy Efficiency and Time-Varying Thermal Perception of Students." *Building and Environment* 219 (109175).

Nations, United. 2025. "Global Status Report for Buildings and Construction 2024/2025." *Global Alliance for Building and Construction*. Paris. https://doi.org/10.1049/et.2022.0103.

Pless, Shanti, and Paul Torcellini. 2009. "Getting to Net Zero." *ASHRAE Journal*, no. September 2009: 1–8. https://www.nrel.gov/docs/fy09osti/46382.pdf.

Quevedo, T.C., M.S. Geraldi, and A.P. Melo. 2023. "Applying Machine Learning to Develop Energy Benchmarking for University Buildings in Brazil." *Journal of Building Engineering* 63 (105468).

Soares, Marco Túlio Bones. 2024. "BALANÇO ENERGÉTICO NULO EM EDIFÍCIOS UNIVERSITÁRIOS: O Caso Do Campus Darcy Ribeiro Da Universidade de Brasília." *Dissertação*. Universidade de Brasília. https://www.repositorio.unb.br/handle/10482/51552.

Society, Illuminating Engineering. 2023. "IES LM-83-23 SPATIAL DAYLIGHT AUTONOMY (SDA) AND ANNUAL SUNLIGHT EXPOSURE (ASE)." New York.

Solemma. 2023. "Climate Studio: Advanced Daylighting, Electric Lighting and Conceptual Thermal Analysis." Cambridge, Massachusetts. https://www.solemma.com/climatestudio.

Tregenza, P., and J. Mardaljevic. 2018. "Daylighting Buildings: Standards and the Needs of the Designer." *Lighting Research and Technology* 50 (1): 63–79.

Vitro Architectural Glass. 2026. "Optygray Glass." *Vitro Architectural Glass*, 2026. https://www.vitroglazings.com/products/tinted-glass/gray-bronze-tinted-glass/optigray-glass/.

Costa, Joao Francisco Walter, Amorim, Claudia Naves David, and Silva, Joara Cronemberger Ribeiro. 2020. "Retrofit Guidelines towards the Achievement of Net Zero Energy Buildings for Office Buildings in Brasilia." *Journal of Building Engineering*, August, 101680.

Wei, Minchen, Kevin W. Houser, Brian Orland, Dean H. Lang, Nilam Ram, Martin J. Sliwinski, and Mallika Bose. 2014. "Field Study of Office Worker Responses to Fluorescent Lighting of Different CCT and Lumen Output." *Journal of Environmental Psychology* 39: 62–76.

cinpar2026
XXII International Conference on Building Pathology and Constructions Repair
15th to 17th July 2026 - Lisboa, Portugal

A Resilience Clock for Residential Buildings: Age- and Hazard-Conditioned Fragility and Functional Loss via SFD(t) × UHS(TR)

Hector AROQUIPA[1,3], **Alvaro HURTADO**[2,3], **Urpi BARRETO**[4]

[1]Civil Engineering School, Universidad Nacional Intercultural de la Selva Central Juan Santos Atahualpa, La Merced, Junín, Perú. Email: haroquipa@uniscjsa.edu.pe
[2] Civil Engineering School, Universidad Tecnológica de los Andes, Abancay, Apurímac, Perú. Email: a.hurtado@it-sayari.com
[3] Faculty of Engineering, Universidad Continental, Lima, Perú. Email: haroquipa@continental.edu.pe; a.hurtado@it-sayari.com
[4]Faculty of Engineering, Universidad Continental, Cusco, Perú. Email: ubarreto@continental.edu.pe

Abstract: The residential building stock in Peru accounts for a significant share of the country's seismic exposure and often exhibits progressive functional degradation driven by construction deficiencies, inadequate maintenance, and incremental vertical expansion. Given that seismic demand varies markedly across Peru's distinct hazard zones, "one-size-fits-all" design spectra can mask true vulnerability and lead to suboptimal retrofit strategies. This study proposes a probabilistic framework that couples time-dependent functional degradation, SFD(t), with hazard-consistent seismic demand, UHS(TR), to quantify the evolving likelihood of functionality loss. This evolution is summarized through a practical "resilience clock." The research targets representative 3-, 6-, and 9-story residential buildings located in seismic hazard zones 2, 3, and 4, under three return periods (TR) essential for performance evaluation: 31, 475, and 975 years. Building conditions are characterized via structured field inspections of common building pathologies and, where feasible, in-situ non-destructive testing. These observations are synthesized into SFD as a random variable to explicitly capture uncertainty. Two representative age states are considered (t ≈ 10 and t ≈ 30 years), with SFD distributions estimated by hazard zone and building height. The SFD is mapped to degraded structural capacity, C(t), by penalizing key mechanical properties: stiffness, strength, and ductility. Seismic performance is evaluated through three limit states—Immediate Occupancy (IO), Life Safety (LS), and Collapse Prevention (CP). The probabilistic coupling of demand and capacity produces age-, hazard-, and height-conditioned fragility functions. The primary deliverable is a set of age–risk curves—the resilience clock—enabling the identification of critical ages and supporting risk-informed prioritization of structural interventions before functionality becomes unacceptable.

Keywords: Seismic resilience, Functional degradation, Uniform Hazard Spectrum (UHS), Performance-based assessment, Limit states (IO/LS/CP).

1. Introduction

Peru lies along one of the world's most active subduction margins, where high seismic hazard converges with extensive residential exposure and a highly heterogeneous building stock. In this context, the key question is no longer only whether buildings avoid collapse, but whether they remain functional—habitable, operable, and recoverable within socially acceptable timeframes. Recent research has therefore shifted resilience from a qualitative notion of robustness to a performance-based, recovery-oriented metric defined by functional trajectories, downtime, and restoration pathways. Building-level probabilistic models now account not only for damage, but also for mobilization, repair sequencing, and recovery states. For example, a tall reinforced-concrete core-wall building was reported to require about 3–6 months for functional recovery under service-level shaking, 8–13 months under design-level shaking, and 12–16 months under

maximum-considered shaking, despite no expected collapse. The core message is clear: functionality can be lost well before life safety is compromised, and societal losses are often governed more by downtime than by collapse itself (Terzic *et al.*, 2021; Terzic and Kolozvari, 2022; Kolozvari and Terzic, 2023; Li, Kunnath and Zhao, 2023; Opabola and Galasso, 2024; G *et al.*, 2025; Wu *et al.*, 2025).

This issue is especially critical in Peru because the residential stock is shaped by self-construction, incremental expansion, uneven technical oversight, and strong territorial variability. Evidence from Lima highlights the scale of the problem. In a sample of 120 self-built houses, measured concrete compressive strength ranged from about 110 to 200 kg/cm², over 65% of buildings showed structurally relevant pathologies, and estimated structural functionality degradation reached 3%–38% over 1–30 years, with representative elastic drifts of about 1.2% (Velasquez *et al.*, 2025). These findings show that the Peruvian residential problem is not simply one of vulnerable typologies, but of progressively degraded capacity embedded in a high-hazard environment. Velasquez et al. (2025) further addressed this through an Intelligent Circular Resilience (ICR) framework, linking inspection, materials testing, structural analysis, and functionality estimation through 11 structural evaluation parameters. This was a key conceptual advance, since many resilience approaches implicitly assume an initial functionality of 100%, whereas self-built stock often begins service with non-negligible deficits in stiffness, strength, and ductility. Earlier, Aroquipa and Hurtado (2022) had already proposed a simplified resilience-assessment methodology that incorporated repair time, workforce, and losses into seismic decision-making.

The hazard side is equally important. Modern performance-based assessment has shown that seismic demand must be hazard-consistent, explicitly tied to local hazard, controlling sources, and structural period. In this framework, the Uniform Hazard Spectrum (UHS) derived from Probabilistic Seismic Hazard Analysis (PSHA) remains fundamental because it provides period-specific ordinates associated with a consistent exceedance probability, although recent developments have sought to balance realism and conservatism in target spectra and record selection (Xu and Zhou, 2022; Li, Kunnath and Zhao, 2023; Lai *et al.*, 2024). For Peru, this issue is no longer abstract. A recent PSHA-based study by Aroquipa et al. (2026) computed UHS for 25 Peruvian cities using 22,399 earthquakes, 33 source models, 6 ground-motion prediction models, and five return periods, showing that for some soil classes and periods, UHS ordinates can reach up to about three times the elastic design spectrum prescribed by the Peruvian code. This confirms that future functionality cannot be inferred from typology alone; it must be coupled with local hazard and epistemic uncertainty (Joyner *et al.*, 2021; Ji *et al.*, 2024; Mazumder and Sutley, 2024).

A further dimension is that both vulnerability and functionality are time-dependent. Recent studies on reinforced-concrete systems subject to deterioration have shown that capacity distributions evolve with age, uncertainty widens, and exceedance probabilities can increase substantially when degradation is modelled explicitly rather than treated as background noise (Chen *et al.*, 2024; Otárola *et al.*, 2024; Zhang, Liu and Yu, 2024). In addition, post-earthquake functionality is often governed not only by the structural system, but also by non-structural components and service interdependencies. Utility disruption, acceleration-sensitive elements, and aftershock effects can materially alter downtime and vulnerability, especially in residential occupancies (D'Angela, Magliulo, and Cosenza, 2021; Li, Kunnath, and Zhao, 2023; Mohammadgholibeyki, Koliou, and Liel, 2023; Hosseini *et al.*, 2024). In Peru, where self-construction, uneven quality control, and service dependency are structural features of the housing system, these are not secondary refinements but essential conditions for a defensible resilience assessment.

The main contribution of this study is a unified probabilistic framework that couples condition-based functional degradation, SFD(t), with hazard-consistent seismic demand, UHS(TR), to derive resilience functions simultaneously conditioned on age, hazard level, and building height. Methodologically, unlike conventional functional-recovery studies that assume ideal initial functionality or rely on highly detailed component inventories, the proposed framework treats initial condition as a degraded random variable explicitly linked to losses in stiffness, strength, and ductility. Practically, the resulting resilience is synthesized into a "resilience clock"—age–risk curves and intervention thresholds that identify when functionality

becomes unacceptable under engineering return periods. In doing so, the study closes a critical gap between degradation-informed resilience assessment for self-built housing and hazard-consistent UHS-based demand modelling for Peruvian cities, moving from diagnosis to a hierarchy of actionable resilience metrics for the residential sector (Velasquez *et al.*, 2025; Aroquipa *et al.*, 2026).

2. Methodology

The proposed framework formulates seismic resilience as a time-dependent, hazard-conditioned performance metric by coupling: (i) a hazard-consistent seismic demand represented through Uniform Hazard Spectra, UHS(TR); (ii) a baseline resilience metric expressed through the Simplified Resilience Index (SRI); and (iii) a time-dependent functionality degradation function, SFD(t), which captures the progressive loss of structural functionality due to aging, construction deficiencies, deterioration, and cumulative service-life effects. The final output is a Resilience Clock (RC), defined as an age–risk descriptor that quantifies how the resilience state evolves as a function of both the return period of the seismic action and the age-dependent degradation of the building stock. The workflow is organized into eight sequential steps grouped into four main stages, as illustrated in Figure 1: (1) study definition, (2) hazard characterization through UHS, (3) structural condition assessment and baseline resilience quantification, and (4) time-dependent degradation and resilient-clock synthesis.

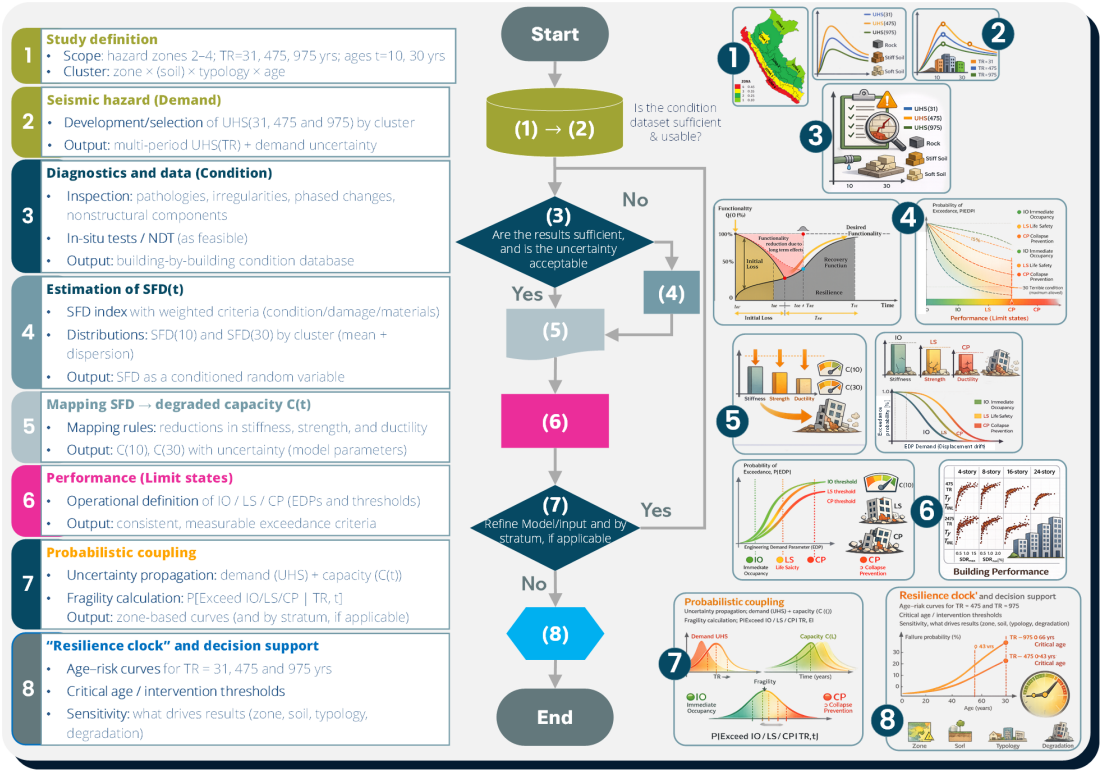


Figure 1 – Flowchart of the proposed methodology for estimating the resilient clock

From a probabilistic standpoint, the methodology extends conventional seismic risk assessment (SRA) by explicitly introducing a time-varying capacity modifier into the resilience estimation. While conventional SRA combines hazard, exposure, and damage to quantify expected consequences, the present approach incorporates the fact that the actual response of residential buildings is not stationary over time. In practical terms, the framework assumes that the resilience state of a building at time t_j, under a seismic demand associated with the return period RP_i, can be expressed as:

$$RC(RP_i, t_j) = SRI(S_a|UHS(RP_i)) \; x \; SFD(t_j) \qquad (1)$$

where $RC(RP_i, t_j)$is the resilient state, $SRI(S_a \mid UHS(RP_i))$is the baseline simplified resilience index conditioned on the spectral acceleration derived from the UHS corresponding to the return period RP_i, and $SFD(t_j)$is the time-dependent structural functionality modifier evaluated at age t_j. Equation 1, therefore, represents a multiplicative coupling between demand-consistent resilience and age-conditioned residual functionality, allowing resilience to be tracked in time under different seismic performance levels.

2.1 Study definition

At this stage, the scope of the assessment shall be established by grouping the building stock into archetypal buildings or taxonomies, followed by identifying their spatial locations to properly define the seismic hazard using the UHS linked to the targeted performance objectives via the return periods. All these factors shall account for aspects related to the representation of actual conditions at the locations where the archetypal buildings are located, while providing a more reliable risk metric for the resilience clock. Also, it should include the status and age of evaluation for incorporating the degradation.

2.2 Uniform Hazard Spectrum (UHS)

The first stage defines the hazard-consistent seismic demand through UHS obtained from PSHA for the target return periods adopted in the study (RP = 31, 475, and 975 years). Unlike generalized code-based spectra, the UHS explicitly reflects local tectonic environment, source predominance, and site effects, and is therefore more suitable for performance-oriented resilience assessment. The estimation follows the procedure proposed by Aroquipa et al. (2026), including seismic source characterization (SM), earthquake catalog processing, ground-motion prediction models, soil classification (ST), and source-dominance thresholds. The resulting spectra provide the period-dependent seismic demand $S_a(T|ST, SM, RP)$ required to evaluate building performance under consistent hazard scenarios and performance objectives correlated via RP.

2.3 Simplified Resilience Index

The second stage defines the baseline resilient condition of each building using the Simplified Resilience Index (SRI) at the damage definition stage proposed by Aroquipa and Hurtado (2022) and modified by Hurtado et al. (2026). The SRI is a reduced-order resilience metric that condenses the conventional elements of seismic risk—damage, losses, repairability, and recovery—into a normalized indicator suitable for comparative evaluation. In the present framework, the SRI is conditioned on the seismic demand extracted from the UHS and interpreted relative to performance objectives such as Immediate Occupancy (IO), Life Safety (LS), and Collapse Prevention (CP). Thus, the SRI provides the reference resilience level assuming nominal structural functionality, prior to introducing the effects of age-dependent degradation. Then, the SRI could be obtained by solving Eq. 2, adapted from Eq. B-6 from Hurtado *et al.* (2026).

$$SRI(im_T = S_a(T|ST, RP, SM)) = 1 - \int_{im}^{im_T} RC(im)dim \Big/ \int_{0}^{im} RC(im)dim \tag{2}$$

where, $SRI(im_T = S_a(T|ST, RP, SM))$ is the SRI for a specific intensity measure (im_T) defined in terms of the $S_a(T|ST, RP, SM)$ which is obtained from the $UHS(RP_i)$ calculated at the previous stage, and $RC(im)$ is the resilience curve, which can be calculated following the step-by-step instructions listed in Appendix B of Hurtado et al. (2026).

2.4 Functional degradation

The third stage incorporates the time-dependent functionality degradation, $SFD(t)$, as a modifier of the baseline resilience state. This term accounts for the progressive reduction in structural functionality resulting from aging, inadequate construction practices, deterioration mechanisms, lack of maintenance, and cumulative in-service effects. The remaining structural functionality is defined as:

$$D(t) = 100\left[1 - P_{\max}\left(1 - e^{-t/f(T_s, C)}\right)\right] \tag{3}$$

where $D(t)$is the remaining structural functionality, $P_{\max}$is the maximum admissible loss, T_s is the structural fundamental period, and C is the global structural quality coefficient. Therefore, the degradation factor is then written as:

$$SFD(t) = \mathrm{D(t)}/100 \tag{4}$$

thereby converting the residual functionality into a dimensionless coefficient ranging from 0 to 1. The coefficient C is obtained through a structural-condition assessment based on geometric, mechanical, constructive, and pathological indicators identified from inspection and, when available, non-destructive or in-situ testing. In this way, $SFD(t)$introduces into the resilience formulation a representation of the actual structural state, rather than assuming invariant capacity throughout the service life.

2.5 Resilient clock

The final stage combines the hazard-conditioned SRI and the time-dependent degradation factor to produce the Resilience Clock (RC). The RC is a synthetic descriptor of resilience evolution over time and hazard intensity and can be represented as age–risk curves, resilience bands, or intervention thresholds. At the end, for each building typology and city, Equation 1 is evaluated at discrete ages $t_j$and return periods RP_i, generating a matrix of resilient states:

$$\mathrm{RC} = \begin{bmatrix} RC(RP_1, t_1) & \cdots & RC\big(RP_1, t_j\big) \\ \vdots & \ddots & \vdots \\ RC(RP_i, t_1) & \cdots & RC\big(RP_i, t_j\big) \end{bmatrix} \tag{5}$$

This matrix is subsequently interpreted in terms of resilience classes and critical thresholds for retrofit prioritization. Because the RC is explicitly conditioned on both local hazard and age-dependent functionality, it provides a more realistic representation of residual resilience than conventional static approaches, particularly for residential stocks where nominal code compliance does not necessarily reflect actual structural condition.

Although the present implementation was developed for residential RC-MRF archetypes, the proposed framework is structurally extensible to other building typologies, provided that the corresponding hazard-consistent demand representation, resilience formulation, and degradation rules are calibrated for the target system. In the same way, the methodology can be expanded to include non-structural and secondary components, particularly when post-earthquake functionality is controlled by acceleration-sensitive or drift-sensitive elements.

3. Results

3.1 Structural archetypes and analytical

The case study was conducted on three representative reinforced-concrete moment-resisting frames (RC-MRF) residential archetypes with 3-, 6-, and 9-story heights, selected to represent the low-, mid-, and relatively high-rise ranges commonly found in the Peruvian residential stock. The three configurations were defined under a common structural logic to isolate the influence of building height on hazard-conditioned resilience. As shown in Figure 2, the structural layouts correspond to regular framed systems with continuous beam-to-column connectivity and repetitive vertical configuration, allowing a consistent comparison of response and degradation effects across building typologies. In the adopted idealization, the estimated fundamental periods were 0.272 s, 0.580 s, and 0.886 s for the 3-, 6-, and 9-story models, respectively. These values place the three archetypes within the short-to-intermediate period range, where the UHS results indicate the highest spectral demand for the analyzed cities. Detailed descriptions of archetypal buildings can be found in Aroquipa Velásquez (2016).

Also, these structural archetypes were intentionally defined with a common structural logic to isolate the effect of building height as the governing parameter within the proposed probabilistic framework. This modelling strategy allows direct comparison of age-conditioned structural performance under different

hazard levels while maintaining typological consistency. Accordingly, the selected building set provides a robust basis for quantifying how the coupled effects of functional degradation SFD(t) and hazard-consistent seismic demand UHS(TR) propagate into age-, hazard-, and height-conditioned resilience functions, and ultimately into the proposed resilience clock for intervention prioritization.

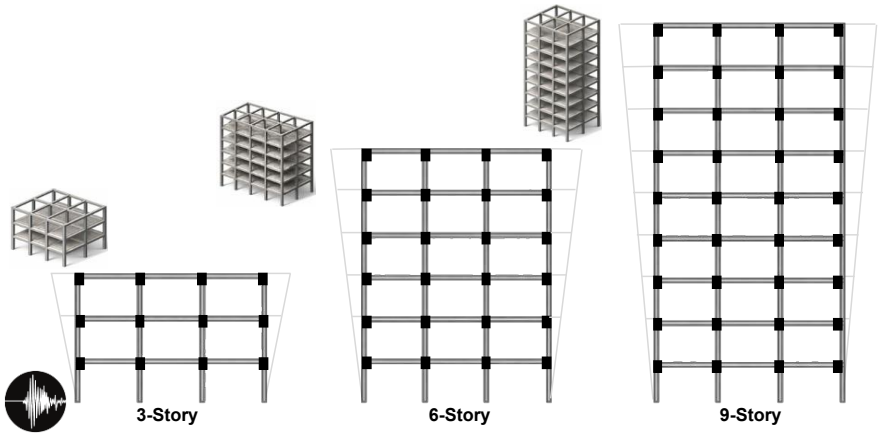


Figure 2 – Building configuration for 3-, 6-, and 9-story

3.2 Uniform Hazard Spectrum (UHS)

In this case study, hazard was considered for three return periods: 32, 475, and 975 years. Each RP is linked to a performance objective of immediate occupancy, life safety, and collapse prevention, respectively. Figure 3 shows the UHS obtained at three representative cities: Lima, Arequipa, and Cusco, associated with seismic zones 4, 3, and 2, respectively. In addition, two soil conditions were assessed within the UHS framework, reflecting the most representative soils in Peru where buildings are built (soft soils, classes D and E, following the NEHRP classification).

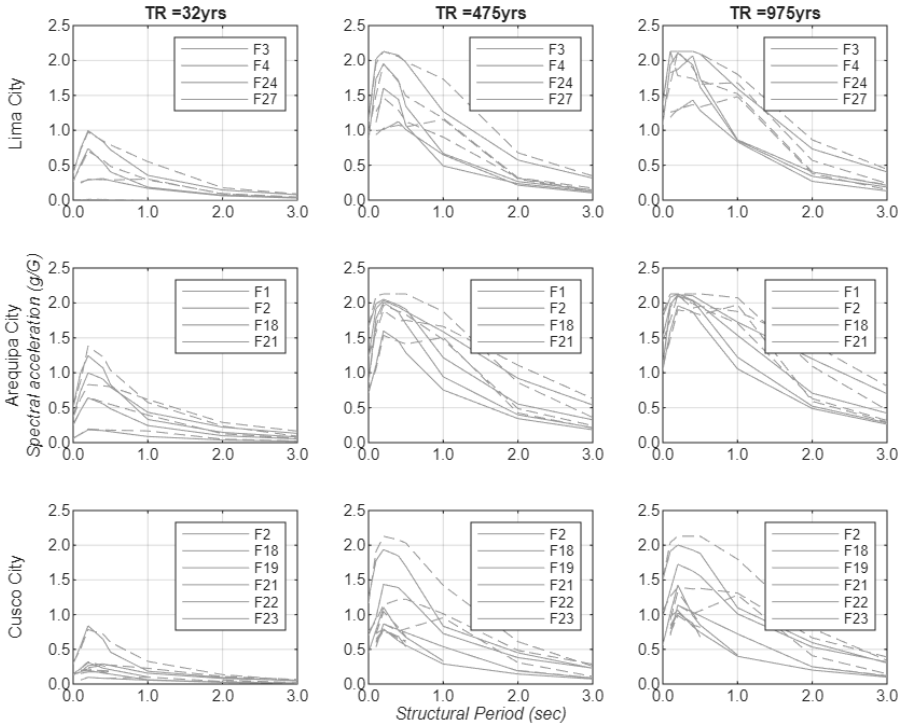


Figure 2 – Results of UHS for seismic Zones 2, 3, and 4

The results indicate a systematic increase in spectral ordinates with return period, together with marked differences in spectral shape and source-to-source variability. For RP = 32 years, the demand is generally moderate and concentrated at short periods, with peak values of about 0.8–1.0 g in Lima, 0.7–1.3 g in Arequipa, and mostly below 0.3 g in Cusco, except for isolated peaks approaching 0.7–0.8 g. For RP = 475 years, the demand rises significantly: Lima and Arequipa reach peak ordinates on the order of 1.7–2.1 g, while Cusco exhibits a wider dispersion, with peaks ranging approximately from 1.0 g to 2.0 g, depending on the controlling fault set. Under RP = 975 years, the most severe spectra in Lima and Arequipa remain close to 2.0–2.1 g, while Cusco also reaches comparable values for specific source scenarios despite belonging to seismic zone 2.

A relevant result is that the highest UHS ordinates are concentrated in the short-to-intermediate period range (approximately 0.2–0.8 s), which directly overlaps the fundamental periods of the three analyzed archetypes. This is particularly critical for the 3- and 6-story buildings, whose periods lie close to the spectral peaks, but it is also relevant for the 9-story system, since the spectral decay toward longer periods is gradual rather than abrupt. In addition, the results reveal strong fault-to-fault dispersion within the same city and return period, particularly for RP = 475 and 975 years, where peak differences between individual spectra are on the order of 0.4–0.7 g in Lima and Arequipa, and even larger in relative terms for Cusco. These findings confirm that generalized code-based spectra are insufficient to represent the actual severity of local seismic demand and justify the use of hazard-consistent $UHS(RP_i)$ as the demand input for resilience assessment.

3.3 Simplified Resilience Index

The baseline resilience assessment indicates that resilience decreases nonlinearly as the intensity measure defined in terms of $S_a(T)$ increases, although the degradation rate differs significantly across scenarios. As shown in Figure 3, the three archetype buildings exhibit similar trends with few differences in the intensity range of $S_a(T)$ between 0.30 and 0.80 g. These results indicate that the same $S_a(T)$ demand may lead to substantially different functional consequences depending on the residual capacity and recovery potential of the system.

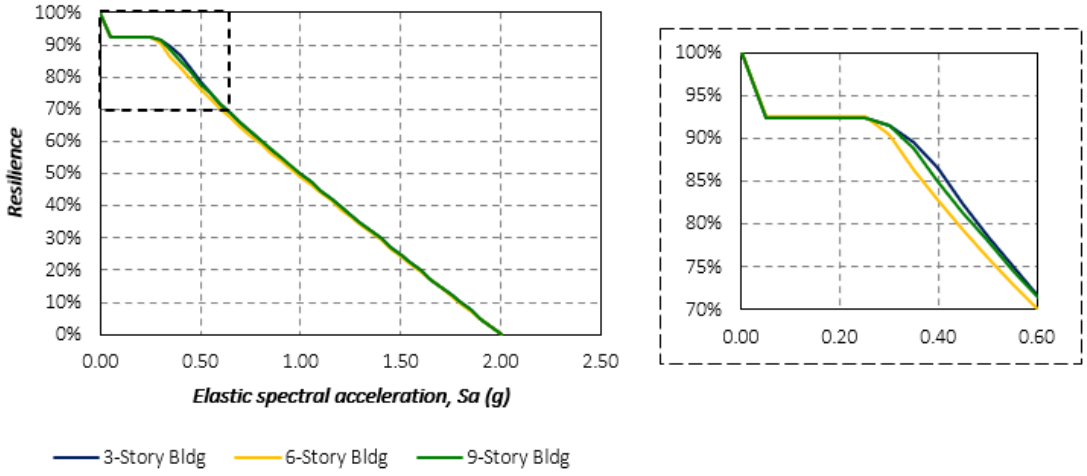


Figure 3 – Resilience curves for buildings assessed

From a performance-based perspective, the most critical reduction in resilience occurs at two points. The first point has a lower $S_a(T)$ of around 0.10g, with a drop of about 8% in resilience, while the second one starts at $S_a(T)$ greater than 0.30g, in which the drop remains constant with almost no noticeable variation among building archetypes. These conditions reflect the influence of the controlling points proposed by the methodological approach used to calculate the SRI. Also, this confirms that $S_a(T)$ is an effective engineering

demand parameter for discriminating resilience loss, but also that the damage–resilience relationship is not unique and must be interpreted in a scenario-dependent manner.

3.4 Time-dependent functionality degradation

Figure 4 presents the evolution of remaining structural functionality, $D(t)$, for the three RC -MRF archetypes. The time-dependent degradation model yields a rapid initial loss of functionality followed by asymptotic stabilization, which is fully consistent with the exponential formulation adopted in Section 2. Using the assumed periods $T_s = 0.272,\ 0.580$, and 0.886s for the 3-, 6-, and 9-story buildings, respectively, the three models start from $D(t = 0) = 100\%$ and decrease to approximately 92.2%, 93.0%, and 93.8% at 5 years, corresponding to losses of about 7.8%, 7.0%, and 6.2%. At 10 years, the curves converge to approximately 92.1%, 92.1–92.2%, and 92.5%, while at 30 years they stabilize near 92.0%, 92.1%, and 92.2%, indicating long-term losses of around 7.8–8.0%.

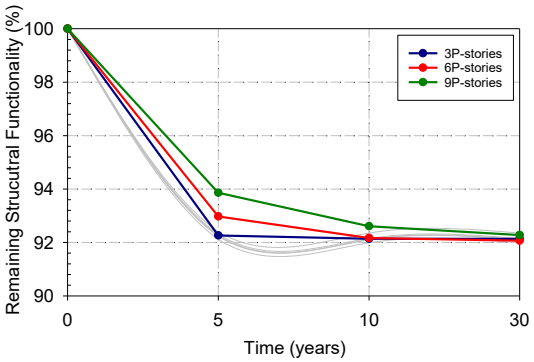


Figure 4 – Functional degradation versus time for the three RC-MRF archetypes. Blue, red, and green curves correspond to the 3-, 6-, and 9-story buildings, respectively

Figure 4 presents the evolution of remaining structural functionality, D(t), for the three RC-MRF archetypes, where the blue, red, and green curves represent the 3-, 6-, and 9-story buildings, respectively. A relevant observation is that, within this formulation, the 9-story archetype exhibits the slowest degradation rate. This does not imply lower seismic vulnerability in absolute terms but rather reflects the role of the degradation-rate function $f(T_s, C)$, which is maximized when the structural period approaches unity. Since the 9-story period ($T_s = 0.886$ s) is closest to that condition, the exponential decay is delayed, and the functionality loss progresses more slowly. Overall, the results indicate that the most significant reduction in functionality occurs within the first 5 years, whereas differences among the three building heights become progressively smaller over time, converging toward a narrow long-term functionality band of approximately 92%.

3.5 Resilient clock

The combined effects of hazard intensity, building height, soil condition, and time-dependent degradation are synthesized in the Resilience Clock shown in Figure 5. The results indicate a consistent reduction in the Seismic Resilience Index (SRI) as building height increases, soil conditions worsen, and the return period becomes more severe. The 3-story buildings generally remain within the high-to-medium-resilience range, the 6-story buildings show an intermediate response, and the 9-story buildings tend to shift toward the low-resilience domain, particularly under adverse soil conditions and higher return periods. This trend is mechanically consistent: taller buildings are more flexible and more sensitive to stiffness degradation and lateral deformation demand, whereas softer soils amplify the response, and larger return periods impose stronger hazard-consistent spectral demand.

The city-specific results show that Lima has the most critical resilience condition, followed by Arequipa, while Cusco generally maintains higher SRI levels, consistent with its location in seismic zones 4, 3, and 2,

respectively. However, the results also show that code-based expectations alone are insufficient: in several cases, especially for taller buildings in Lima and Arequipa under RP = 475 and 975 years, the computed resilience falls below the medium-resilience threshold, despite the normative reference line associated with E.030. This indicates that code compliance does not necessarily guarantee functional resilience, particularly when age-dependent degradation and site-specific hazards are introduced explicitly. Therefore, the Resilience Clock provides a more realistic basis for identifying critical ages, hazard levels, and structural typologies for which intervention becomes necessary.

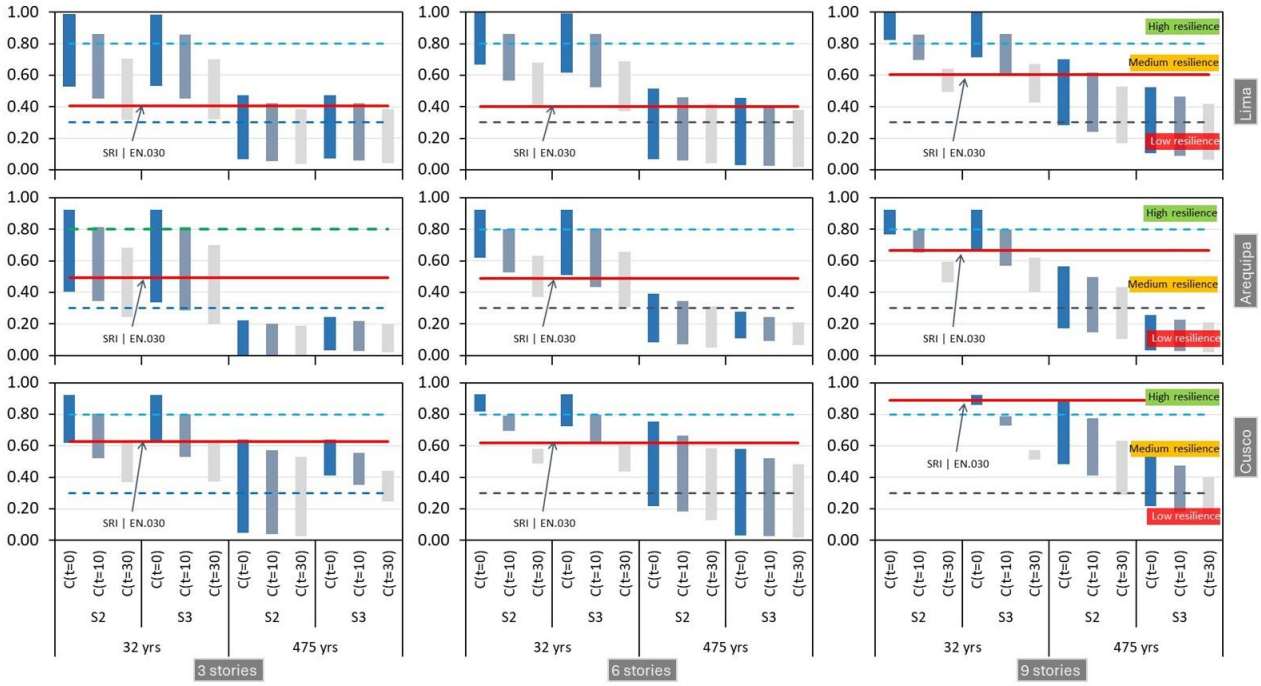


Figure 5 – Results of the resilient clock

4. Discussion

The results show that seismic resilience in residential RC-MRF buildings is governed by the combined effects of local hazard, structural period, and time-dependent functional degradation, rather than by code-based classification alone. The UHS results demonstrate that the spectral demand in Lima (zone 4) and Arequipa (zone 3) reaches peak ordinates on the order of 1.7–2.1 g for RP = 475–975 years, while Cusco (zone 2) may also approach 2.0 g under specific fault scenarios, despite its lower zonation level. Since the fundamental periods of the analysed archetypes (0.272 s, 0.580 s, and 0.886 s) fall within or near the most demanding spectral range, the three building classes are directly exposed to the critical portion of the hazard spectrum. This explains why the resilience loss is more pronounced for taller buildings, softer soils, and larger return periods, and why the E.030 normative reference is not always sufficient to represent actual functional performance. In this regard, the results confirm that hazard-consistent demand models are necessary when the objective extends beyond life safety and includes functionality and recovery.

A second major finding is that incorporating SFD(t) materially improves the realism of resilience estimation. The degradation model shows that the most significant functionality loss occurs during the first years of service, with the three archetypes reaching long-term residual functionality values close to 92% after 30 years, albeit at different decay rates. When this age-dependent condition is coupled with the baseline SRI,

the resulting Resilience Clock clearly distinguishes resilience states by city, height, soil condition, and return period, identifying cases in which resilience drops from medium to low even when a nominal code-based interpretation would suggest acceptable performance. Therefore, the proposed framework bridges the gap between nominal design compliance and actual structural condition, providing a more defensible basis for resilience-based prioritization of retrofit interventions in residential building stocks exposed to variable hazards and progressive degradation.

Taken together, the results confirm that the resilience of residential RC-MRF buildings cannot be adequately described from a static or code-only perspective. The most critical findings are: (i) UHS(RP) reveals local demand levels that may substantially exceed generalized code spectra; (ii) baseline resilience is highly sensitive to Sa(T) demand and structural scenario; (iii) time-dependent degradation causes a non-negligible early functionality loss, even under comparable quality conditions; and (iv) the resulting Resilience Clock clearly differentiates the effect of city, height, soil condition, and age on the transition from acceptable to critical resilience states. Accordingly, the proposed framework provides a technically consistent basis for age-informed retrofit prioritization and hazard-consistent decision-making in residential building stocks.

5. Conclusions

This study proposed a probabilistic resilience framework that couples hazard-consistent seismic demand, represented by UHS(RP), with time-dependent structural functionality degradation, SFD(t), to quantify the evolving resilience of residential reinforced-concrete frame buildings through a Resilience Clock. Based on the results obtained for 3-, 6-, and 9-story archetypes in Lima, Arequipa, and Cusco, the following conclusions can be drawn:

- The use of UHS(RP) reveals a substantially richer and more demanding hazard representation than code-based spectra alone. For RP = 475 and 975 years, Lima and Arequipa reached peak spectral accelerations on the order of 1.7–2.1 g, while Cusco also exhibited values approaching 2.0 g under specific fault scenarios. This confirms that local-source predominance and site effects must be explicitly considered in resilience-oriented assessments.
- The short-to-intermediate spectral range is the most critical for the analyzed residential typologies. The fundamental periods of the assessed archetypes (0.272 s, 0.580 s, and 0.886 s) lie within or near the most demanding UHS band, meaning that low- and mid-rise residential buildings are directly exposed to the highest hazard-consistent demand.
- Resilience decreases systematically with increasing building height, worsening soil conditions, and larger return periods. The Resilience Clock showed that 3-story buildings generally remain in the high-to-medium resilience range, 6-story buildings exhibit intermediate behavior, and 9-story buildings tend to migrate toward low-resilience states, particularly in Lima and Arequipa under RP = 475–975 years.
- Time-dependent degradation is not negligible and must be incorporated explicitly. The functionality model showed that the main degradation occurs in the early service-life stage, while the long-term residual functionality of the three archetypes converges toward approximately 92% after 30 years. This demonstrates that resilience cannot be treated as a static property of the structural system.
- Code compliance alone does not guarantee functional resilience. Several cases fell below the medium-resilience threshold despite the normative reference associated with E.030, indicating that actual resilience depends strongly on the interaction between local hazard, building height, soil condition, and age-dependent structural state.

Overall, the proposed methodology provides a technically consistent and operational tool for linking hazard, degradation, and resilience into a single decision-support framework. Its main practical value lies in

identifying critical ages, hazard levels, and structural typologies for which intervention becomes necessary, thereby supporting risk-informed retrofit prioritization for residential building stocks.

As a limitation, the present study considered simplified structural archetypes and a degradation function calibrated at the building level; therefore, future work should incorporate more refined nonlinear models, broader validation with field data, and explicit treatment of non-structural components and recovery interdependencies.

Beyond its analytical contribution, the proposed framework provides a practical basis for resilience-based decision-making by identifying critical ages, hazard levels, and structural configurations for which intervention becomes necessary.

Acknowledgments

This research did not receive any specific grant from funding agencies in the public, commercial, or non-profit sectors.

References

Aroquipa, H. et al. (2026) "Seismic hazard assessment based on predominance of local earthquake sources: a methodological approach using PSHA applied to the main cities in Peru," Natural Hazards, 122(5), p. 179. Available at: https://doi.org/10.1007/s11069-025-07895-9.

Aroquipa, H. and Hurtado, A. (2022) "Seismic resilience assessment of buildings: A simplified methodological approach through conventional seismic risk assessment," *International Journal of Disaster Risk Reduction*, 77, p. 103047. Available at: https://doi.org/10.1016/j.ijdrr.2022.103047.

Aroquipa Velásquez, H. (2016) *Evaluación de la vulnerabilidad sísmica de edificaciones en concreto reforzado mediante análisis dinámico no lineal simplificado*. Master Thesis. Universidad de los Andes.

Chen, Z. *et al.* (2024) "Time-variant seismic resilience of reinforced concrete buildings subjected to spatiotemporal random deterioration," *Engineering Structures*, 305, p. 117759. Available at: https://doi.org/10.1016/j.engstruct.2024.117759.

D'Angela, D., Magliulo, G. and Cosenza, E. (2021) "Seismic damage assessment of unanchored nonstructural components taking into account the building response," *Structural Safety*, 93, p. 102126. Available at: https://doi.org/10.1016/j.strusafe.2021.102126.

G, M. *et al.* (2025) "Estimation of seismic downtime for building retrofitting decision-making," *Resilient Cities and Structures*, 4(3), pp. 15–29. Available at: https://doi.org/10.1016/j.rcns.2025.07.001.

Hosseini, S.A. *et al.* (2024) "Structural and non-structural fragility curves for low-rise mainshock-damaged buildings subjected to aftershocks," *Structures*, 69, p. 107352. Available at: https://doi.org/10.1016/j.istruc.2024.107352.

Hurtado, A. *et al.* (2026) "Building collapse prediction due to earthquakes through ML algorithm: Hybrid methodology based on past-earthquake damage reports and resilience index," *Resilient Cities and Structures*, 5(1), pp. 102–117. Available at: https://doi.org/10.1016/j.rcns.2026.02.001.

Ji, D. *et al.* (2024) "Generation of spectrum compatible ground motions considering duration," *Soil Dynamics and Earthquake Engineering*, 183, p. 108783. Available at: https://doi.org/10.1016/j.soildyn.2024.108783.

Joyner, M.D. *et al.* (2021) "Recovery-based design of buildings for seismic resilience," *International Journal of Disaster Risk Reduction*, 65, p. 102556. Available at: https://doi.org/10.1016/j.ijdrr.2021.102556.

Kolozvari, K. and Terzic, V. (2023) "Methodology for developing practical recovery-based design requirements for buildings," *Engineering Structures*, 274, p. 115102. Available at: https://doi.org/10.1016/j.engstruct.2022.115102.

Lai, Q. *et al.* (2024) “A novel method for selecting input ground motions in seismic design based on probability,” *Structures*, 61, p. 106133. Available at: https://doi.org/10.1016/j.istruc.2024.106133.

Li, C., Kunnath, S.K. and Zhao, Y. (2023) “A new framework for ground motion selection for structural seismic assessment,” *Engineering Structures*, 285, p. 116055. Available at: https://doi.org/10.1016/j.engstruct.2023.116055.

Mazumder, R.K. and Sutley, E.J. (2024) “A multi-step framework for measuring post-earthquake recovery: Integrating essential infrastructure System’s serviceability in building functionality,” *International Journal of Disaster Risk Reduction*, 114, p. 104929. Available at: https://doi.org/10.1016/j.ijdrr.2024.104929.

Mohammadgholibeyki, N., Koliou, M. and Liel, A.B. (2023) “Assessing building’s post-earthquake functional recovery accounting for utility system disruption,” *Resilient Cities and Structures*, 2(3), pp. 53–73. Available at: https://doi.org/10.1016/j.rcns.2023.06.001.

Opabola, E.A. and Galasso, C. (2024) “A probabilistic framework for post-disaster recovery modeling of buildings and electric power networks in developing countries,” *Reliability Engineering & System Safety*, 242, p. 109679. Available at: https://doi.org/10.1016/j.ress.2023.109679.

Otárola, K. *et al.* (2024) “Simulation-based consequence analysis of reinforced-concrete buildings subjected to earthquake- and environment-induced damage accumulation,” *Engineering Structures*, 317, p. 118554. Available at: https://doi.org/10.1016/j.engstruct.2024.118554.

Terzic, V. *et al.* (2021) “Framework for modelling post-earthquake functional recovery of buildings,” *Engineering Structures*, 246, p. 113074. Available at: https://doi.org/10.1016/j.engstruct.2021.113074.

Terzic, V. and Kolozvari, K. (2022) “Probabilistic evaluation of post-earthquake functional recovery for a tall RC core wall building using F-Rec framework,” *Engineering Structures*, 253, p. 113785. Available at: https://doi.org/10.1016/j.engstruct.2021.113785.

Velasquez, H.A. *et al.* (2025) “Impact of structural degradation on the seismic resilience of self-built housing: an approach based on intelligent circular resilience,” *Journal of Building Pathology and Rehabilitation*, 10(2), p. 123. Available at: https://doi.org/10.1007/s41024-025-00633-5.

Wu, D. *et al.* (2025) “Time-dependent seismic fragility and resilience assessment of a sea-crossing cable-stayed bridge under combined effects of corrosion and scour,” *Engineering Structures*, 340, p. 120702. Available at: https://doi.org/10.1016/j.engstruct.2025.120702.

Xu, L. and Zhou, Z. (2022) “Weighted Average Conditional Mean Spectrum (WACMS): A bridge between common CMS and Uniform Hazard Spectrum (UHS),” *Soil Dynamics and Earthquake Engineering*, 156, p. 107238. Available at: https://doi.org/10.1016/j.soildyn.2022.107238.

Zhang, W., Liu, Y. and Yu, Q.-Q. (2024) “Time-dependent seismic fragility analysis of reinforced concrete columns subjected to chloride-induced corrosion,” *Engineering Structures*, 302, p. 117448. Available at: https://doi.org/10.1016/j.engstruct.2024.117448.

Seismic assessment and strengthening of the Church of Santo Tomás de Aquino in Rondocan, Peru

Elesban NOCHEBUENA-MORA[1], Nuno MENDES[2], Paulo B. LOURENÇO[3]

[1] University of Minho, ISISE, ARISE, Department of Civil Engineering, Guimaraes, Portugal, enochemora@gmail.com
[2] University of Minho, ISISE, ARISE, Department of Civil Engineering, Guimaraes, Portugal, nunomendes@civil.uminho.pt
[3] University of Minho, ISISE, ARISE, Department of Civil Engineering, Guimaraes, Portugal, pbl@civil.uminho.pt

Abstract: The Church of Santo Tomás de Aquino, located in Rondocan (Peru), lies in the Andean highlands of the Cusco region. The building, constructed with thick adobe walls, is representative of the architectural and cultural heritage of the 17th century. In 2016, the church was declared as National Cultural Heritage due to the construction techniques, traditional architecture, and decorative elements, including the wall paintings. Adobe structures are particularly vulnerable to seismic actions because of their brittle behavior. Although the church underwent conservation works in the 1990s, it still exhibits structural vulnerabilities, mainly related to the separation of the walls, especially in the rear façade. A seismic assessment was carried out using a finite element model calibrated with in situ data. Nonlinear pushover analyses revealed a poor seismic performance of the structure. The proposed strengthening strategy includes the construction of adobe buttresses. Timber keys are used to connect the buttresses to the existing walls and to strengthen the wall-to-wall intersections, while geogrids are installed to enhance tensile capacity of the buttresses. The numerical model was subsequently updated to incorporate these interventions. The results of the nonlinear pushover analyses indicate a substantial improvement in structural performance, with an increase in lateral load capacity ranging from 30% to 50% and a reduction in displacements of up to 55% at the Damage Limitation limit state. The proposed intervention reduces the expected damage under frequent seismic events, contributing to the protection of the wall paintings.

Keywords: Adobe building; historic masonry building; strengthening; nonlinear pushover analysis; seismic assessment

1. Introduction

Adobe is a widely used traditional construction material in seismic regions, particularly in the Andean highlands, where historic churches possess high cultural and architectural value. However, adobe structures are highly vulnerable to seismic actions due to their brittle behaviour, low strength, and poor connections between structural elements. These limitations often lead to damage such as wall separation, in-plane shear cracking, and out-of-plane collapse, further exacerbated by the absence of box-like behaviour due to weak connections and flexible diaphragms. To address these challenges, the Getty Conservation Institute (GCI) has developed key initiatives, including Getty Seismic Adobe Project and Seismic Retrofitting Project, aimed at advancing compatible and minimally invasive seismic retrofitting techniques for historic adobe structures (Tolles, Kimbro, and Ginell 2000; Cancino and Lardinois 2012).

This paper presents the seismic assessment and strengthening proposal of the Church of Santo Tomás de Aquino, a 17th century adobe church located in Rondocan, in the Cusco region. The building consists of a single nave with a presbytery and two annexed spaces: a baptistery and a sacristy. Thick adobe walls support

a timber roof system composed of wooden trunks and clay tiles, with some of the walls reinforced with buttresses. The church underwent conservation work between 1995 and 1997. The present study was carried out under the auspices of the GCI, with fieldwork, testing, and numerical analyses conducted by the University of Minho.

The adopted methodology is based on a macro-modelling approach, in which adobe and stone masonry are represented as homogeneous continua, incorporating nonlinear behaviour through a total-strain rotating-crack model. Material properties were derived from in situ testing conducted by the University of Minho and complemented with literature data, while the numerical model was calibrated using ambient vibration test results. The assessment employs nonlinear static (pushover) analysis to identify critical failure mechanisms and to estimate seismic capacity with respect to the demand defined by the Peruvian seismic code. Particular attention is given to the out-of-plane response of walls (Nochebuena-Mora et al. 2025).

Based on the identified vulnerabilities, a strengthening strategy using compatible and reversible techniques is proposed. The intervention includes the addition of new buttresses to enhance out-of-plane resistance, the use of timber keys to improve interlocking at wall intersections and buttress connections, and the incorporation of a polymeric geogrid to increase the flexural and shear capacity of the buttresses. A timber frame is introduced at the top of the walls to improve global behaviour and support a reconstructed roof system, while existing tie beams are repositioned and properly anchored to ensure effective performance under seismic loading. The effectiveness of the proposed intervention is evaluated through comparative nonlinear pushover analyses between the unstrengthened and strengthened configurations. For brevity, the results presented here are limited to a force-based assessment using two performance levels defined by the Italian code, namely the Damage Limitation (DL) and Life Safety (LS) limit states.

2. Building description and current damage state

The Church of Santo Tomás de Aquino is a 17th-century adobe structure located in the Peruvian Andes (Figure 1). The church is situated on a site with an approximate slope of 10% and comprises a single nave with a presbytery, along with a baptistery and a sacristy on the south side (Figure 1b). The interior space defined by the nave and presbytery measures approximately 34.0 m in length and 8.0 m in width.

The structural system consists of a rubble stone masonry bonded with earth mortar in the foundation, which rises above ground level; adobe masonry in walls and buttresses, with the nave walls approximately 2.0 m thick and those of the baptistery and sacristy ranging between 1.0 and 1.2 m; and a gable roof constructed with timber beams in a *par y nudillo* configuration supporting clay tiles. Between 1994 and 1997, the church underwent conservation works, including the replacement of the roof system and adobe units, as well as the addition of timber keys (MINCUL 1998).

The main façade (Figure 1c), oriented west toward the plaza, reaches a height of approximately 11.5 m above the reference level (0.0 m). It is characterized by the principal entrance, consisting of a doorway with stone jambs and a semicircular arch on the exterior face, while the interior face is configured with splayed jambs (embrasures) that support a timber lintel. Above the entrance, a richly decorated choir loft is supported by a timber framework resting on four *quincha* columns and further anchored to the nave walls and the main façade (Figure 1d). The rear façade, located on the east side, rises to approximately 9.7 m above ground level (13.6 m relative to the reference level). This wall features a window with an embrasure with a niche above it (Figure 1d). The triumphal arch is formed by adobe pilasters that carry a *quincha* structure, which constitutes both the arch and its spandrels.

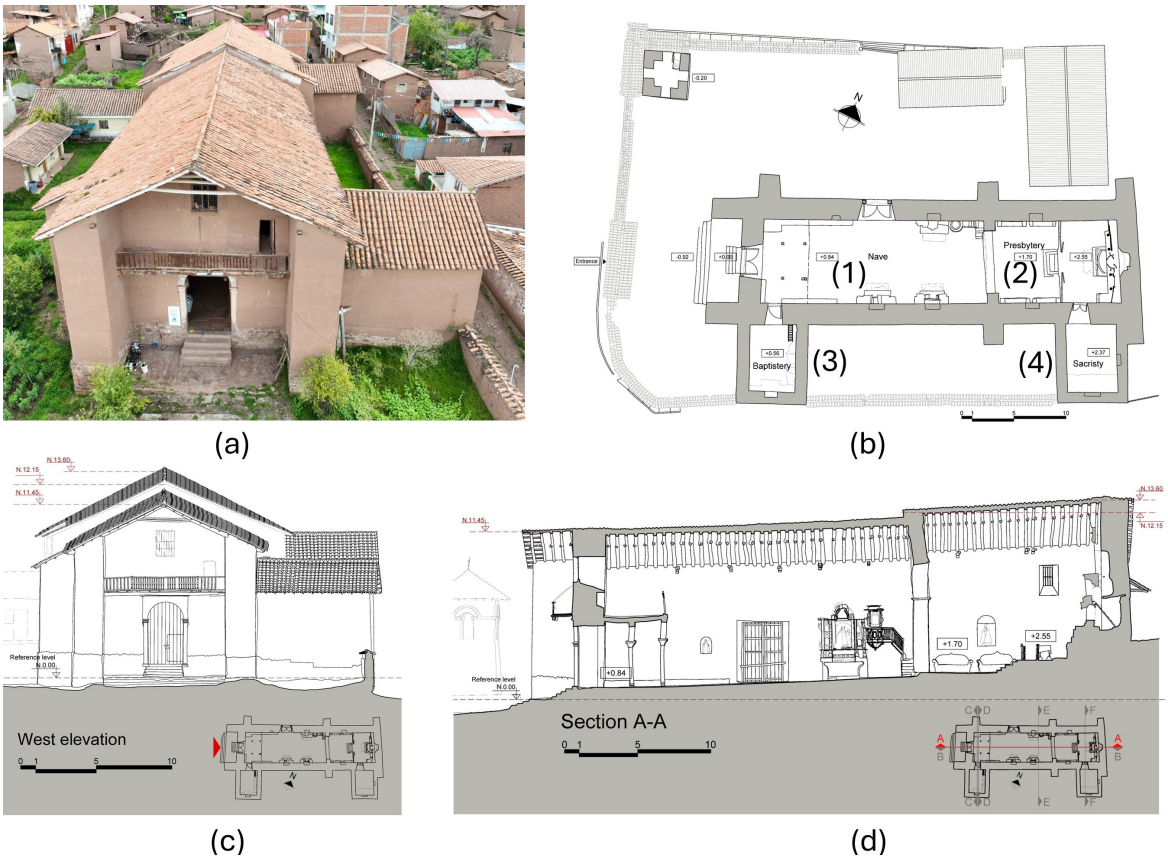


Figure 1 – Church of Santo Tomás de Aquino, in Rondocan, Peru: (a) general view, (b) plan view with North indicated (1-Nave, 2-Presbytery, 3-Baptistery, 4-Sacristy); (c) main façade; and (d) longitudinal section. (Dimensions in meters)

The roof structure is formed by timber trusses made of round wooden members and spaced at intervals of 0.60–0.75 m (Figure 2). Each truss comprises two upper rafters (*sobre pares*) supported on the tops of the lateral walls, two lower rafters (*pares*) resting on an internal timber wall plate, and a collar tie (*nudillo*) connecting the upper ends of the lower rafters. All trusses are linked longitudinally by a continuous ridge beam. The upper rafters extend outward by approximately 0.50 m, forming the eaves and supporting a multilayered roof assembly consisting of canes, an earth–straw mixture, and clay tiles. At wall plate level, nine timber tie beams ensure transverse connectivity between the lateral walls. Additional tie beams are incorporated within the baptistery (two) and the sacristy (two).

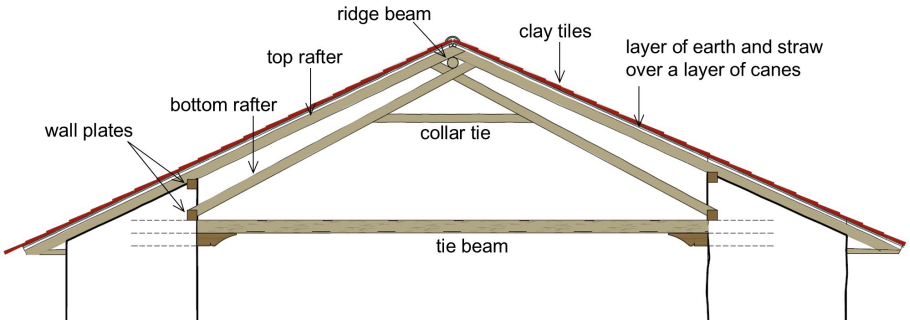


Figure 2 –Roof structure

Mural paintings extend continuously across the interior wall surfaces, covering their full height. In addition, the church contains several movable artworks, many of which are attributed to Bernardo Bitti (Tejada Farfán 2019, 2023). In recognition of its traditional construction techniques, architectural character, and artistic importance, the building was declared a National Cultural Heritage site in 2016 (*Resolución Vice Ministerial Nº 078-2016-VMPCIC-MC* 2016).

An on-site assessment conducted in 2024 documented extensive deterioration and structural damage, despite the conservation works carried out in the 1990s. Cracks were identified at the intersections between the lateral walls and both the main and rear façades, along with separation at the choir loft connections. In the main façade, vertical cracks extending over the full height were observed at its junctions with the nave walls, visible on both the interior and exterior (Figure 3a). The choir loft exhibited partial detachment from the façade and lateral walls, resulting in deformation of its timber components. The most critical damage affected the rear façade, where vertical cracking at the wall intersections (Figure 3b) led to an almost complete loss of connection. Borescopic inspection at a height of 2.0 m revealed crack depths of at least 0.30 m at the south corner and 0.50 m at the north corner. Additional vertical cracking was observed at midspan of the gable walls in the baptistery and sacristy. The spandrels of the triumphal arch exhibited out-of-plane rotation toward the nave, generating cracking at their interfaces with the lateral walls. Moreover, localized material loss was observed at the tops of the walls, primarily associated with water infiltration (Figure 3c).



Figure 3 – Crack as the corners of (a) main façade and (b) rear façade; (c) material loss

3. Strengthening proposal

The proposed strengthening strategy aims to enhance the lateral capacity of the building, particularly its out-of-plane response, using compatible and traditional techniques. Figure 4 illustrates the overall strengthening scheme. The intervention includes the addition of buttresses and timber reinforcement. Seven new buttresses are introduced to improve the lateral capacity of the north and south walls, as well as the rear façade. To ensure effective interlocking, the buttresses are connected to the existing walls using timber keys, primarily designed to resist shear forces (Figure 4a). In addition, a polymeric geogrid is incorporated to enhance both the flexural and shear capacity of the buttresses through horizontal layers embedded within the masonry courses and vertical layers applied to the external surfaces. The proposed buttresses along the lateral walls of the nave were dimensioned and verified through kinematic analysis. Conversely, the buttresses at the rear façade were defined based on architectural criteria.

Timber keys embedded at multiple levels are also proposed to strengthen all building corners and the intersections between the baptistery, sacristy, and nave walls. Additional timber keys are introduced to improve the connection between existing lateral buttresses and the walls. A timber frame (collar beams), embedded at the top of the walls, is designed to support a new roof (constructed using the same *par y*

nudillo system) and to improve the flexural response of the walls (Figure 4b). The existing tie beams will be relocated to have a more uniform distribution along the nave and presbytery, and their anchorage system will be designed to ensure effective performance under both tension and compression during seismic loading. The cross-sections of the new timber elements range from $4 \times 4\ in^2$ to $6 \times 6\ in^2$ (10×10 to $15 \times 15\ cm^2$).

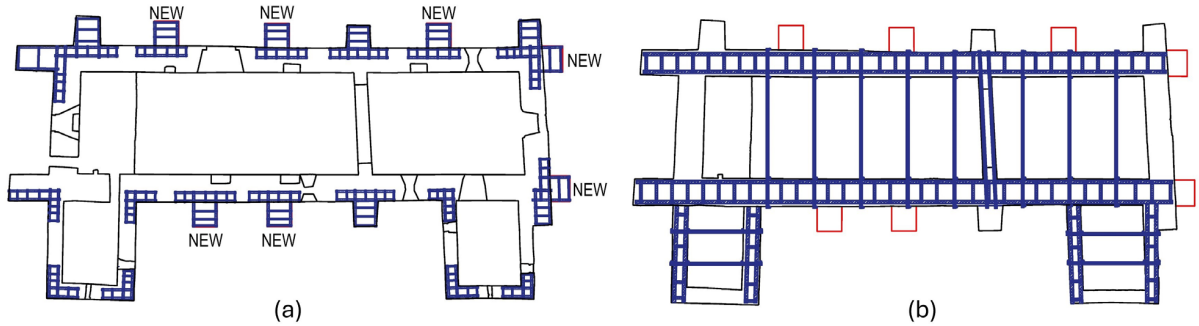


Figure 4 – General strengthening scheme (a) timber keys and buttresses (b) collar beams and tie beams

4. Numerical model

A three-dimensional geometry created in AutoCAD 2024 (Autodesk Inc. 2023) was used to generate the finite element (FEM) model in DIANA 11.0 (DIANA FEA BV 2025). The model comprises the nave, presbytery, baptistery, and sacristy, along with the timber tie beams and the foundation, accounting for elevation changes due to the ground slop (Figure 5a). The choir loft and the spandrels of the triumphal arch were not included, as their contribution to the global structural response of the church was deemed negligible. Boundary conditions were defined by restraining all degrees of freedom at the base of the foundation. The mesh was generated with an average element size of 0.5 m, resulting in four elements across the wall thickness (Figure 5a). The foundation, walls, buttresses, and lintels were represented by twenty-node isoparametric solid elements with quadratic interpolation. The tie beams were modelled as two-node truss elements with an equivalent circular cross-section of 0.20 m in diameter. Stress concentrations at tie–wall connections were minimized by modelling the beam ends as embedded in the walls using reinforcement bar elements continuous with the truss elements and having identical mechanical properties. The roof was omitted from the model as it does not behave as a rigid diaphragm and has a limited contribution to the global seismic response. Instead, its mass contribution was simulated through an equivalent density applied to the upper parts of the walls. Regarding the proposed strengthening strategy, all the timber reinforcement and the polymeric geogrid were incorporated as embedded elements (Figure 5b and c).

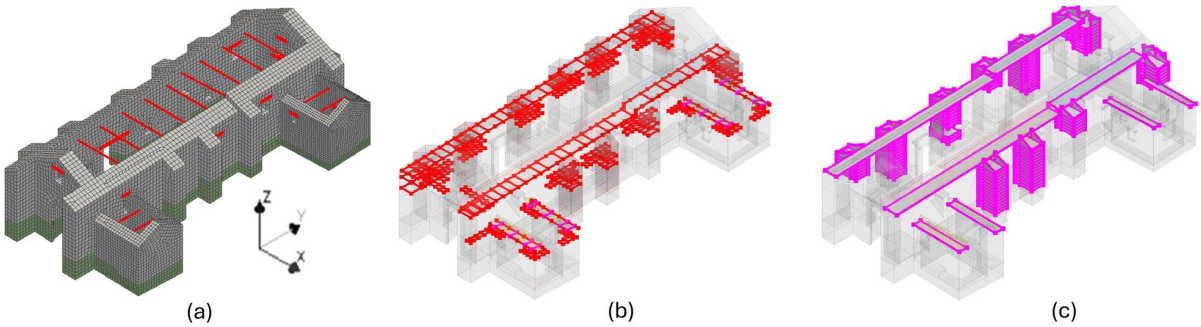


Figure 5 – Numerical model: (a) mesh and material distribution (green-rubble masonry, grey-adobe, red-timber); (b) embedded timber reinforcement; and (c) embedded geogrid reinforcement

4.1 Mechanical properties of the materials

The mechanical properties assigned to the model were defined combining literature data and in situ experimental testing conducted by the University of Minho in April 2024 (Karanikoloudis, Mendes, and Lourenço 2024). The material distribution (Figure 5a) includes rubble stone masonry for the foundation, adobe masonry for the walls, buttresses, and triumphal arch pilasters, and timber for the lintels and tie beams. Adobe and rubble masonry were assumed homogeneous and isotropic, with nonlinear behaviour simulated using a total-strain rotating-crack model. The Young's moduli were obtained from sonic testing and subsequently calibrated by matching the numerical model to ambient vibration test results, using natural frequencies and the Modal Assurance Criterion (MAC) (Allemang and Brown 1982). Compressive response was described by a parabolic hardening–softening law, while tensile response followed an exponential softening relationship (Ferreira 2024). Strength parameters and fracture energies were taken from the literature (Karanikoloudis and Lourenço 2018; Nochebuena-Mora et al. 2025).

Timber elements were modelled as linear elastic materials with properties representative of Eucalyptus species. Existing elements were assigned a density of 420 kg/m³ and a Young's modulus of 5700 MPa (Karanikoloudis, Mendes, and Lourenço 2024), while reinforcement timber was defined with a density of 890 kg/m³ and a Young's modulus of 9316 MPa (Torrealva and Samuel 2025). The geogrid was represented using a perfect plastic law, with a Young's modulus of 538 MPa and a tensile strength of 153 MPa, based on experimental data (Torrealva and Samuel 2025). A summary of the adopted material properties is provided in Table 1.

Table 1 – Mechanical properties

Mechanical properties		**Rubble stone masonry**	**Adobe**	**Existing timber**	**New timber elements**	**Geogrid**
Density	ρ (kg/m³)	1900	1900	420	890	-
Young's modulus	E (MPa)	1400	335	5700	9316	538
Poisson's ratio	v (-)	0.2	0.2	0.3	0.3	-
Compressive strength	f_c (MPa)	0.60	0.45	-	-	-
Tensile strength	f_t (MPa)	0.06	0.05	-	-	153
Compressive fracture energy	G_c (N/mm)	1.80	1.38	-	-	-
Tensile fracture energy	G_f^I (N/mm)	0.01	0.01	-	-	-

5. Seismic assessment of the strengthening proposal

Nonlinear pushover analyses were carried out to evaluate the global performance of the structure and to assess the effectiveness of the proposed strengthening intervention through comparison between the current (unstrengthened) and strengthened states. The model was first subjected to self-weight, followed by incremental monotonic lateral loads simulating seismic inertia using a mass-proportional load pattern (Lagomarsino and Cattari 2015). Due to the irregular geometry, a multidirectional pushover approach was adopted (Kalkbrenner, Pelà, and Sandoval 2019), applying loads along the X and Y axes in both positive and negative directions until ultimate capacity was reached to capture the variability of potential collapse mechanisms. The response was assessed through capacity curves relating load factor (interpreted as

equivalent ground acceleration in g) to control point displacements at the top of the walls. Damage was assessed using principal tensile strain distributions.

For sake of brevity, only the force-based assessment is presented in this work. The reference ground acceleration was defined according to the Peruvian seismic code E.030 (Ministerio de Vivienda Construcción y Saneamiento 2016) for Zone 2 (a_g = 0.25 g), soil type S2 (S = 1.2), and importance factor U = 1.3, resulting in 0.39 g. However, reductions are permitted depending on structural typology. For adobe buildings, code E.080 (Ministerio de Vivienda Construcción y Saneamiento 2017) specifies a lower value of 0.29 g. In line with recommendations for heritage structures, which discourage the use of very high accelerations, a reference value of 0.30 g (a_g = 0.25 g and S = 1.2) was adopted in this study. Two limit states were defined following the Italian code: Damage Limitation (DL, 50-year return period) and Life Safety (LS, 475-year return period). (Ministry of Infrastructure and Transport 2019, 2018). The DL action was obtained by scaling the reference acceleration by 0.47 in accordance with Eurocode 8 (European Committee for Standardization 2004) resulting in 0.14 g. For the LS limit state, the seismic action is divided by a factor q=2 (Ministry of Infrastructure and Transport 2019, 2018), leading to a ground acceleration of 0.15 g. The displacement responses derived from the capacity curves for the unstrengthened and strengthened models were subsequently compared at these two seismic demand levels.

Figure 6 compares the pushover results for the unstrengthened and strengthened conditions in three directions, showing capacity curves and principal tensile strain distributions (corresponding to crack openings ≤ 1.0 mm). As expected, the strengthening intervention improves the global response of the building, increasing both lateral stiffness and load capacity, which results in reduced displacements. In the positive X direction (Figure 6a), the lateral capacity increases by approximately 19%, while displacements at both seismic demand levels are reduced by about 50% in the nave (south wall, also referred to as the Epistle wall). The analysis indicates that, even at 0.15 g, the structure can withstand the seismic action without any damage.

In the negative X direction (Figure 6b), the north wall (also referred to as the Evangelio wall) exhibits a greater increase in lateral capacity, of approximately 30%, together with a reduction in displacements of about 55% in both the nave wall and the existing buttress at the two seismic demand levels. The capacity curves indicate that, in the current condition, the Evangelio wall tends to behave as two distinct segments prior to peak load, with the nave wall being more flexible than the portion adjacent to the buttress. In the post-peak phase, however, the wall transitions into a single rocking mechanism, characterized by diagonal cracking extending from the base toward the corners (Figure 7a). The buttress fails due to shear stress at its connection with the wall. In contrast, the strengthened configuration shows a more uniform response, with the Evangelio wall behaving as a single body throughout the analysis. The damage pattern is characterized by vertical cracking at the corners and the formation of a well-defined hinge along the base, at the interface between the rubble masonry foundation and the adobe wall. For the buttresses connected to the Evangelio wall, failure is governed by crushing of the adobe at the foundation interface, with no evidence of shear damage, indicating the proper functioning of the timber keys.

In the longitudinal direction (positive Y, Figure 6c), the strengthening intervention leads to a significant increase in lateral capacity of approximately 110%, together with a substantial reduction in displacements of up to 90% for both seismic demand levels. In the strengthened configuration, damage localizes at the upper corners of the rear façade, with crack openings not exceeding 1.0 mm and minimal propagation at 0.15 g. In the unstrengthened state, failure is governed by an out-of-plane mechanism that develops under low seismic demand, characterized by corner cracking and the formation of a base hinge, ultimately leading to complete detachment of the façade (Figure 7b). This behaviour is associated with weak wall connections, absence of diaphragm action, and lack of buttresses. In contrast, the strengthened configuration exhibits a more global structural response. The out-of-plane behaviour of the rear façade is coupled with more distributed damage, including shear cracking in the gable walls of the sacristy and baptistery, as well as shear failure in both presbytery walls.

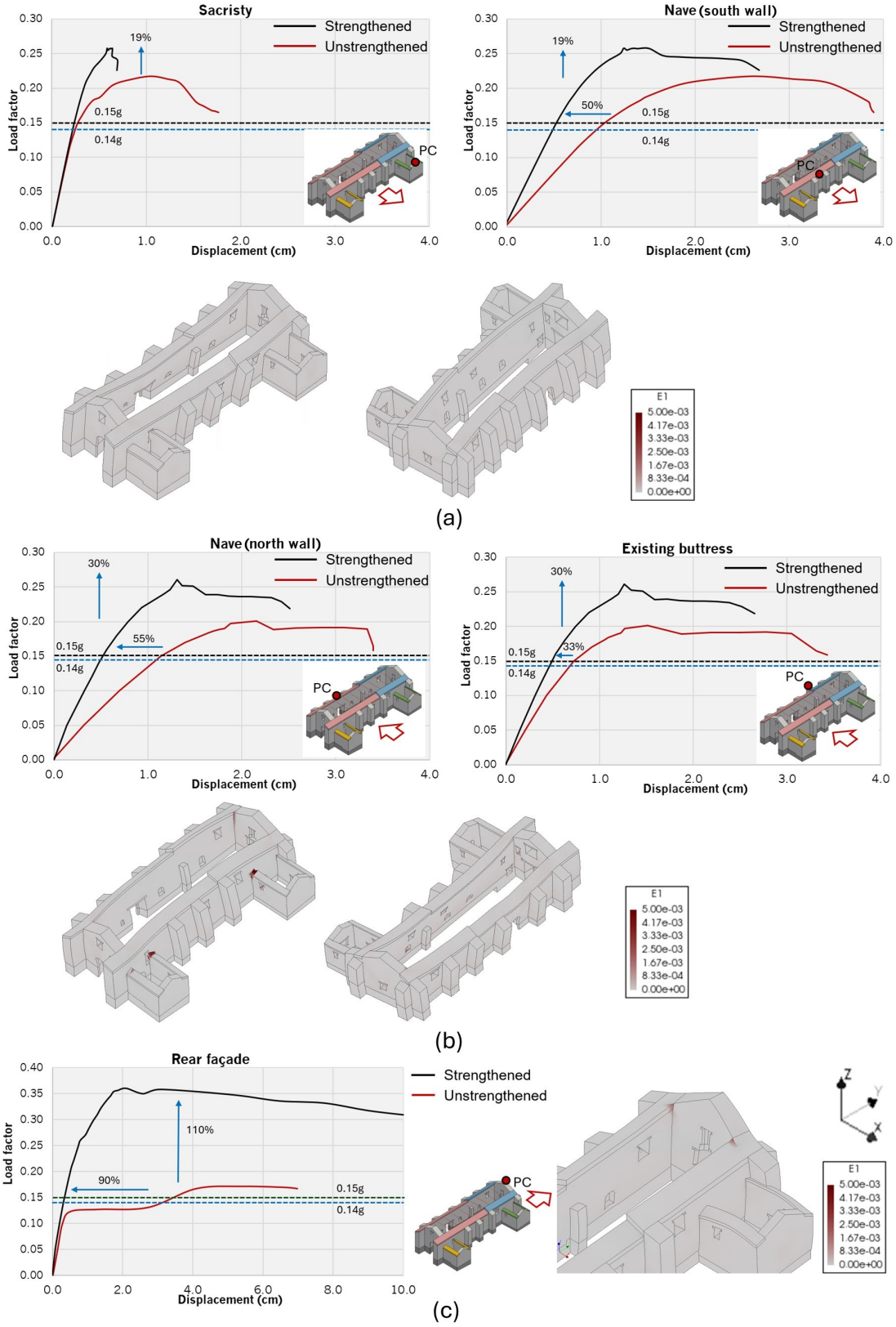


Figure 6 – Capacity curves and principal tensile strains at 0.15 g for: (a) positive X; (b) negative X; and (c) positive Y directions.

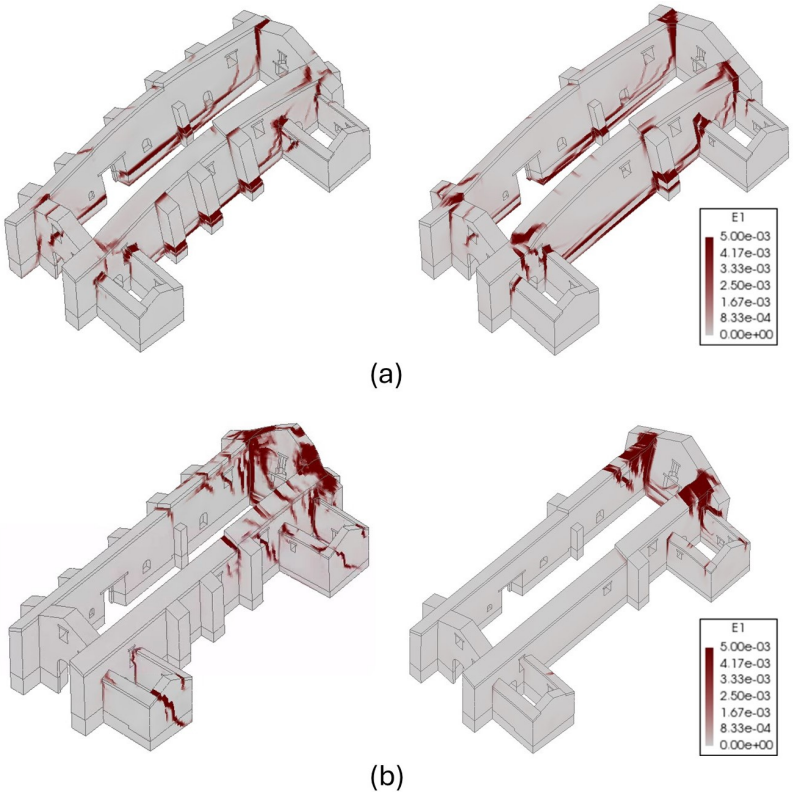


Figure 7 – Damage pattern at ultimate displacement, strengthened (left) and unstrengthened condition (right): (a) negative X and (b) positive Y directions.

6. Conclusions

This study presented the seismic assessment and strengthening proposal for the Santo Tomás de Aquino Church, a 17th century adobe structure representative of Andean earthen heritage. The numerical analyses highlighted the high seismic vulnerability of the building in its current condition, primarily governed by out-of-plane mechanisms of the walls. The results showed that the lateral capacity of the structure is consistently low, with critical deficiencies associated with weak wall connections, absence of diaphragm action, and limited transverse restraint.

The proposed strengthening strategy, based on compatible and reversible techniques, proved effective in significantly improving the seismic performance of the structure. The introduction of additional buttresses, timber keys, timber collar beams, and geogrid reinforcement enhanced both lateral stiffness and load-carrying capacity, while promoting a more global structural response. Nonlinear pushover analyses demonstrated substantial increases in lateral capacity (up to approximately 110% in the longitudinal direction) and significant reductions in displacement demand, reaching up to 90% in some cases. Moreover, the strengthened configuration mitigates localized failure mechanisms, leading to more distributed and controlled damage patterns, particularly in the longitudinal direction, which is the most vulnerable. The comparison between the unstrengthened and strengthened conditions confirms that the intervention effectively addresses the main structural deficiencies, especially by improving wall interconnections and out-of-plane stability.

Overall, the study demonstrates that the proposed intervention significantly enhances the seismic safety of the church, enabling it to better meet the required performance levels for both damage limitation and life safety limit states. This aspect is particularly relevant given the presence of mural paintings within the

interior of the church. Beyond improving safety under strong seismic events, the intervention aims to minimize damage to these artworks during more frequent earthquakes. The results indicate that the reduction in structural displacements contributes to decreasing the risk of damage to the walls and, consequently, to the preservation of the painted surfaces.

The adopted methodology, combining advanced nonlinear numerical modelling, experimental data, and conservation-oriented design, provides a robust framework for the assessment and strengthening of similar adobe heritage structures in seismic regions. In this context, the study contributes by quantitatively demonstrating that compatible strengthening techniques can effectively transform local out-of-plane failure mechanisms into a more global and controlled structural response, while simultaneously improving seismic performance and limiting damage in heritage adobe buildings.

Acknowledgments

This work is partially funded by the Getty Conservation Institute – Seismic Retrofitting Project. The study is also funded by the STAND4HERITAGE project (new STANDards FOR seismic assessment of built cultural HERITAGE) that has received funding from the European Research Council (ERC) under the European Union's Horizon 2020 research and innovation program (Grant No. 833123) as an Advanced Grant. This study is also partially funded by national funds (PIDDAC) under the R&D Unit Institute for Sustainability and Innovation in Structural Engineering (ISISE), under reference UIDB / 04029/2020 (doi.org/https:// doi.org/ 10. 54499/ UIDB/04029/ 2020), and under the Associate Laboratory Advanced Production and Intelligent Systems ARISE under reference LA/P/0112/2020. The opinions and conclusions presented in this paper are those of the authors and do not necessarily reflect the views of the sponsoring organizations.

References

Allemang, Randall J, and David. L Brown. 1982. "A Correlation Coefficient for Modal Vector Analysis." In . https://api.semanticscholar.org/CorpusID:53893454.

Autodesk Inc. 2023. "AutoCAD 2024."

Cancino, Claudia, and Sara Lardinois. 2012. *Seismic Retrofitting Project: Assessment of Prototype Buildings*. Los Angeles, CA, United States of America: Getty Conservation Institute. http://hdl.handle.net/10020/gci_pubs/assess_prototype.

DIANA FEA BV. 2025. "DIANA 11.0."

European Committee for Standardization. 2004. *Eurocode 8: Design of Structures for Earthquake Resistance. Part 1: General Rules, Seismic Actions and Rules for Buildings*. Brussels, Belgium.

Ferreira, Denise, ed. 2024. "DIANA User's Manuals." The Hague, The Netherlands: DIANA FEA.

Gerencia de Obras Division de Puesta en Valor de Monumentos. 1998. "Transcripción informe final de ejecución de obra (1994-1997) Obra Iglesia de Rondoan." Cusco, Peru.

Kalkbrenner, Philip, Luca Pelà, and Cristián Sandoval. 2019. "Multi Directional Pushover Analysis of Irregular Masonry Buildings without Box Behavior." *Engineering Structures* 201 (December): 109534. https://doi.org/10.1016/j.engstruct.2019.109534.

Karanikoloudis, Georgios, and Paulo B. Lourenço. 2018. "Structural Assessment and Seismic Vulnerability of Earthen Historic Structures. Application of Sophisticated Numerical and Simple Analytical Models." *Engineering Structures* 160 (April): 488–509. https://doi.org/10.1016/j.engstruct.2017.12.023.

Karanikoloudis, Georgios, Nuno Mendes, and Paulo B. Lourenço. 2024. "In Situ Inspection and Experimental Testing in the Church of Rondocan, in Peru." Report 2024-DEC/E-10.

Lagomarsino, Sergio, and Serena Cattari. 2015. "PERPETUATE Guidelines for Seismic Performance-Based Assessment of Cultural Heritage Masonry Structures." *Bulletin of Earthquake Engineering* 13 (1): 13–47. https://doi.org/10.1007/s10518-014-9674-1.

Ministerio de Vivienda Construcción y Saneamiento. 2016. *Norma Técnica E.030 "Diseño Sismoresistente."* Lima, Peru.

———. 2017. *Norma E.080 "Diseño y construcción con tierra reforzada."* Lima.

Ministry of Infrastructure and Transport. 2018. *Norme Tecniche per Le Costruzioni, Decreto 17 Gennaio 2018*. Roma, Italy.

———. 2019. *Circolare 2019 Instruction for the Application of the Building Code for Constructions; Aggiornamento delle "Norme tecniche per le costruzioni."* Roma, Italy.

Nochebuena-Mora, Elesban, Nuno Mendes, Matteo Salvalaggio, and Paulo B. Lourenço. 2025. "The Seismic Performance of Earthen Historical Buildings in Seismic-Prone Regions: The Church of Santo Tomás de Aquino in Rondocan as a Complex Example." *Applied Sciences* 15 (13): 7624. https://doi.org/10.3390/app15137624.

Resolución Vice Ministerial Nº 078-2016-VMPCIC-MC. 2016. *Diario Oficial Del Bicentenario El Peruano*. Lima, Peru. https://busquedas.elperuano.pe/dispositivo/NL/1401189-1.

Tejada Farfán, Andrea Giuliana. 2019. "Una Serie de Cuadros de Bernardo Bitti: Del Cuzco a Rondocan a Través de Sus Fuentes Documentales." *Revista Del Archivo General de La Nación* 34 (2): 43–59. https://doi.org/10.37840/ragn.v34i2.94.

———. 2023. "La Oración En El Huerto de Bernardo Bitti S. J. En Rondocan." *Letras (Lima)* 94 (139): 46–60. https://doi.org/10.30920/letras.94.139.4.

Tolles, E. Leroy, Edna E. Kimbro, and William S. Ginell. 2000. "Seismic Stabilization of Historic Adobe Structures: Final Report of the Getty Seismic Adobe Project." Los Angeles, CA, United States of America. http://hdl.handle.net/10020/gci_pubs/seismic_stabilization.

Torrealva, Daniel, and Luna Gremyos Samuel. 2025. "Memoria Descriptiva - Intervención Estructural Del Templo de Santo Tomás de Aquino de Rondocan, Cusco, Perú." Lima, Peru.

Integration of an HBIM Model with Thermographic and Damage Image Analysis Based on Computer Vision

Michael OLIVEIRA[1], Maria Isadora GONÇALVES[2], Francisco Carlos SANTANA[3], Esequiel MESQUITA[4], Mylene VIEIRA[5]

[1] Federal University of Ceara, Brazil; mjackson20@alu.ufc.br
[2] Federal University of Ceara, Brazil; isadoramessias@alu.ufc.br
[3] Federal University of Ceara, Brazil; franciscosantana@alu.ufc.br
[4] Federal University of Ceara, Brazil; emesquita@ufc.br
[5] Federal University of Ceara, Brazil; mylene.melo@ufc.br

Abstract: Buildings of cultural value often present limitations regarding the availability of technical documentation and detailed knowledge of their conservation state. In this context, non-destructive methods become essential to support diagnostic, documentation, and maintenance actions. This study aims to integrate a digital HBIM model with infrared thermography data of the masonry of the Church of São Sebastião, located in the municipality of Russas, Ceará, Brazil. In this works thermograms were interpreted with the support of Computer Vision and Image Processing techniques to detect patterns and map damage in the masonry and roofing systems of the asset. The building geometry was obtained through terrestrial laser scanning, resulting in a three-dimensional point cloud used as the basis for the development of the HBIM model. Infrared thermography surveys were conducted on internal masonry, facades and roof, using both handheld thermal cameras and aerial thermal images acquired by a drone equipped with a thermographic sensor, in order to identify thermal contrasts associated with constructive interfaces, material layers, moisture presence, and other anomalies. The adopted methodology comprised six main stages: (i) geometric survey using mobile laser scanning; (ii) execution of thermographic inspections on the different surfaces of the building; (iii) processing and organization of data obtained from the laser scanner and thermographic images; (iv) development of the digital HBIM model based on the point cloud; (v) analysis of thermographic and damage images using computer vision; and (vi) integration of thermographic information into the HBIM model. The results indicate that the proposed approach enables the integrated organization of geometric, thermographic, and informational data within a unified digital environment. The proposed approach enables the integrated organization of geometric, thermographic, and informational data in a unified digital environment, allowing their association with HBIM elements for technical documentation and systematic recording of the building's conservation condition.

Keywords: Infrared thermography, HBIM, Image Processing, Pathological manifestations, Heritage buildings.

1. Introduction

Historic heritage represents the cultural identity of a society, and its conservation is essential for preserving collective memory. In this context, understanding the current state of degradation of such buildings is fundamental for monitoring conservation conditions and identifying deterioration processes that develop over time, whether caused by natural agents or human action.

Given the need to assess these structures without compromising their physical integrity, investigation techniques that do not damage the original elements become particularly relevant. In this regard, non-destructive testing (NDT) stands out, as it is widely used in the diagnosis of historic structures because it

allows the assessment of materials and construction systems without direct interference with their constitution [1,2]. NDT encompasses different inspection procedures capable of providing information on construction heterogeneities, the presence of moisture, voids, discontinuities, and behavioral changes in masonry and rendering components [3].

Among the various NDT techniques applied to heritage assets, infrared thermography has gained prominence due to its ability to identify thermal anomalies associated with construction defects and superficial or subsurface alterations. It is a non-destructive, non-contact, safe, and rapid data acquisition technique whose interpretation is based on recording the infrared radiation emitted by materials and converting it into thermal images [1,4,5]. Its applications include the identification of moisture, detachments, air pockets behind coatings, hidden elements, and areas with thermal behavior distinct from the surrounding surface [1,6,15]. In historic buildings and rendered façades, thermography has also been used to establish quantitative thermal contrast criteria and to analyze the visibility of anomalies as a function of solar orientation, inspection time, and exposure conditions [15,16].

In the specific case of historic façades and masonry, thermogram interpretation requires attention to factors such as architectural geometry, emissivity, incident radiation, and material heterogeneity, since these variables directly influence the observed thermal distribution [6,7]. Beyond traditional qualitative interpretation, recent studies have expanded the use of thermography for quantitative analyses, including the delimitation of anomalous areas, the evaluation of thermal gradients, and the comparison between regions with different thermal behaviors [15,17,18].

In recent years, non-destructive techniques applied to heritage assets have evolved significantly, particularly through the incorporation of computer vision and Image Processing methods into image processing and interpretation. This advance is associated with the need to automate analytical stages, reduce the subjectivity of manual interpretation, and enhance the ability to identify thermal patterns under different inspection conditions [8,9]. In the specific field of thermography, methods based on machine learning, automated detection, and explainable image processinhave been applied to the analysis of thermal images, yielding promising results in the identification of anomalies in façades and building surfaces [9,19].

At the same time, computer vision has contributed to transforming the thermogram into data that can be segmented, quantified, and geometrically interpreted, extending the use of thermography beyond simple qualitative observation. In this context, digital image processing procedures make it possible to isolate regions of interest, recognize thermal patterns, detect contours, and estimate the extent of anomalous areas, thereby providing more systematic support for diagnostic analysis [17,19]. This type of approach is particularly relevant for heritage surfaces, where the presence of ornamentation, moldings, and material variations may hinder the distinction between geometric effects and actual pathological manifestations [16,19].

This technological development has also fostered the integration of diagnostic results into digital representation and management environments. In this context, approaches based on HBIM (Heritage Building Information Modelling) have become particularly relevant, as they enable geometric, constructive, and diagnostic information to be brought together within a three-dimensional building model [10–12]. The incorporation of data derived from non-destructive inspections into HBIM models has been identified as a relevant strategy for documenting, organizing, and querying information on built heritage, especially when associated with visual records and analytical data [13,20,21].

Thus, the application of computer vision to the interpretation of thermographic images, combined with the insertion of results into HBIM environments, constitutes a line of research directly related to the diagnostic documentation of historic heritage. Although recent advances have expanded the use of digital models in historic buildings, a significant portion of research is still concentrated on geometric representation, indicating the need for approaches that more systematically incorporate inspection and analysis data into the information model [8,14].

In this context, the present study aims to apply computer vision techniques to the interpretation of data derived from infrared thermography surveys, in order to support the detection of thermal patterns and the identification of pathological manifestations in the masonry of a historic building. In parallel, the study proposes the integration of this information into an HBIM environment, with the objective of structuring and centralizing, within a unified digital model, the geometric, imaging, and diagnostic records produced throughout the investigation.

2. Methods and materials

Initially, the Church of São Sebastião, located in Russas, Ceará, was selected due to its historical, cultural, and constructive relevance. Next, the geometric and documentary survey of the building was carried out through the acquisition of a 3D point cloud using terrestrial laser scanning and photogrammetry with an unmanned aerial vehicle, in order to record its architectural configuration and generate the basis for the church's HBIM modelling.

In the following stage, thermographic surveys and photographic records were conducted on the external masonry areas showing the greatest concentration of visible damage, aiming to identify thermal patterns associated with possible pathological manifestations. After acquisition, the thermograms were subjected to digital image processing and computer vision techniques for the segmentation of anomalous regions, recognition of thermal patterns, and quantification of affected areas. Finally, the obtained results were integrated into the HBIM model, as shown in Figure 1, which summarizes the complete methodological workflow of the research.

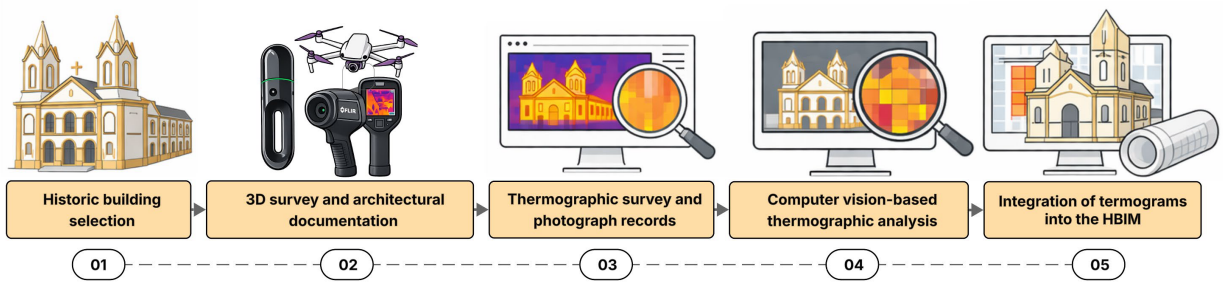


Figure 1 – Workflow of the methodological procedure adopted in the research.

2.1. Historic building selection

O The study was carried out at the Church of São Sebastião, located in Russas, in the state of Ceará. The building was selected due to its relevance to the urban and religious memory of the municipality and for preserving architectural features representative of the local historic construction tradition. In addition to its symbolic importance to the community, the church presents a constructive configuration compatible with the proposed investigation, particularly because of the presence of rendered masonry and surfaces suitable for thermographic analysis.

The consolidation of the church within the local context is associated with the historical formation of devotion to Saint Sebastian in the municipality. Records indicate that, between 1816 and 1817, the region was affected by severe drought and epidemic outbreaks, a context in which popular devotion to Saint Sebastian was strengthened, leading to the idea of constructing a temple dedicated to the saint as part of the local religious imagination [22]. This devotion was later materialized through the construction of the church, completed in 1872, which has since occupied a central role in the city's religious practices and traditional festivities [23].

From a material standpoint, the building is predominantly composed of brick masonry and still preserves architectural elements that retain formal features of its original conception. Over time, however, the building underwent conservation and improvement interventions, with works recorded in different periods, including actions related to the execution of the ceiling structure in the early decades of the twentieth century and later services involving the repair of renderings, repainting, and localized replacement of deteriorated components [22,23]. This history of permanence, continuous use, and partial maintenance provides a relevant condition for investigating thermal patterns associated with superficial alterations and pathological manifestations in its masonry. Figure 2 shows the church in its current condition.



Figure 2 – Photographs of the Church of São Sebastião (2025).

2.2. 3D survey and architectural documentation

Data acquisition for the building was carried out in two complementary stages. The first comprised the geometric and documentary survey through terrestrial laser scanning using the portable Leica BLK2GO device and aerial photogrammetry using a DJI Mavic 3T unmanned aerial vehicle, both adopted as the basis for the three-dimensional modelling of the building.

2.2.1. 3D laser scanning and photogrammetry

Initially, laser scanning of the church was carried out using the portable Leica BLK2GO device, based on LiDAR capture, with the aim of recording the spatial geometry of the architecture and generating a three-dimensional point cloud of the building. The acquisition of the church's internal geometry was performed with the portable scanning sensor, manually operated throughout the interior spaces, and monitored in real time through an iPad Pro tablet connected to the system. During the survey, a reference unit was positioned at a stable location inside the church, while the portable sensor was operated through continuous walking across the surveyed areas. This procedure allowed real-time control of data quality during acquisition and the correction of possible gaps in spatial coverage.

At a later stage, a photogrammetric survey was carried out using a DJI Mavic 3T unmanned aerial vehicle, employed to obtain aerial images of the external regions and difficult-to-access areas, especially the roof, façades, and upper portions of the building. The complementary use of photogrammetry made it possible to expand the geometric documentation of the building and to record areas not fully captured by terrestrial laser scanning. The point cloud obtained from the laser scanning survey was processed in Cyclone Register 360, while the images captured by the drone were processed in RealityScan 2.1.0, which was responsible for generating the building's photogrammetric model. Figure 3a presents the point cloud obtained from mobile laser scanning, used as the geometric basis for the spatial representation of the church, whereas Figure 3b shows the model generated by photogrammetry, providing greater visual detail of the external surfaces and roof.



Figure 3 – Geometric survey and organization of capture points: (a) 3D point cloud of the church; (b) 3D model generated by photogrammetry.

Subsequently, the outputs generated by these two techniques were submitted to the registration and integration stage in CloudCompare, with the aim of constituting a unified geometric basis of the building. This procedure involved the definition of homologous points between the surveys, enabling the spatial alignment between the point cloud obtained by laser scanning and the model generated by photogrammetry. Figure 4a presents the reference points adopted in the laser-scanning model, while Figure 4b shows the corresponding points defined in the photogrammetric model for the alignment process. At the end of this procedure, the unified base was exported to Autodesk Revit, serving as support for the three-dimensional modelling and spatial organization of the analyzed areas.

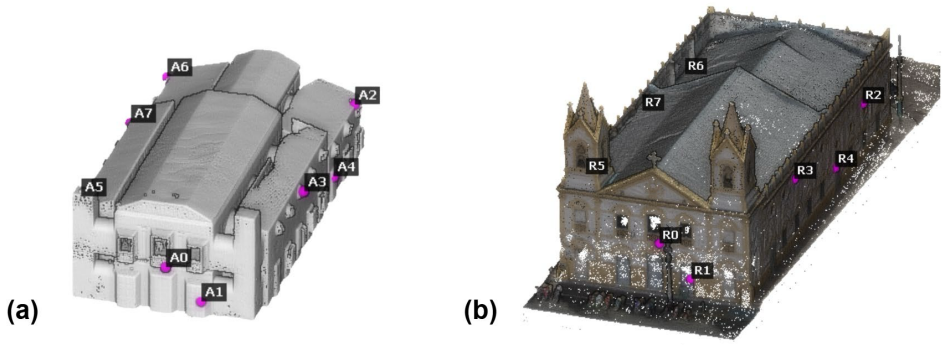


Figure 4 – Definition of homologous points for geometric integration in CloudCompare: (a) reference points in the laser scanning model; (b) corresponding points in the photogrammetric model.

2.2.2 Digital modelling and information structuring

Com With the integrated point cloud completed, the building modelling stage was initiated in Autodesk Revit 2023, using the consolidated geometric base as reference for the construction of the three-dimensional model of the church. The model was structured to represent the architectural configuration of the building and to organize the information produced throughout the research. The masonry elements were defined as the main focus of the investigation and prepared to receive non-geometric attributes associated with the field analyses. For this purpose, the Project Parameters feature in Revit was used, through which parameters linked to the wall category were created, all defined as Text, allowing the standardized insertion of descriptive information into the properties of each analyzed element.

Among the created parameters, the following stand out: ID's, for the individual identification of the wall or analyzed area; Visual inspection, for recording the observations obtained during visual inspection; Thermography analyses, intended to describe the patterns observed in the thermograms; Damage detection, for recording the identified pathological manifestations; Final report, aimed at the final synthesis of the analysis; Digital image, corresponding to the reference of the associated photographic image; and Thermography image, intended for the reference of the corresponding thermogram. Native Revit fields

within the Identity Data group, such as Comments and Mark, were also used to complement the identification of the survey and the building.

In addition to the textual information, the model incorporated the visual records obtained during the research. For this purpose, photographic images and thermograms were inserted over the analyzed elements through decals, a feature used to associate the images with the modelled surfaces according to the investigated region. In this way, the model came to integrate, within a single digital environment, the building geometry, the field records, and the image products generated by the thermographic survey.

2.3 Thermographic survey and photograph records

The thermographic survey was carried out in conjunction with the photographic documentation of the external masonry surfaces of the building, so that each analyzed point included both a visible digital image and its corresponding thermogram. For this purpose, the portable FLIR TG165-X thermal camera, shown in Figure 5a, was used to acquire thermal records of the surfaces with greater exposure to solar radiation. The capture strategy was defined based on passive thermographic analysis, in which solar incidence acts as a natural thermal stimulus, favoring the formation of contrasts on the investigated surfaces. Under this condition, acquisitions were performed during the morning period in order to better exploit solar exposure on the masonry and enhance the visibility of temperature variations associated with possible pathological manifestations. The adopted measurement mode was by reflection, and thermogram interpretation was conducted qualitatively, considering failures in thermal patterns, discontinuities in surface behavior, and their correspondence with anomalies observed in the photographic records.

Throughout the survey, approximately 60 capture points were defined around the perimeter of the church, prioritizing regions with visible indications of pathological manifestations on the external masonry surfaces. As a result, a database composed of 69 color digital images and 69 thermograms was established, corresponding to the same capture locations. The acquisitions were concentrated on the building façades, covering different portions of the external masonry and seeking to include areas with greater solar incidence and higher potential for damage occurrence. The spatial distribution of these points along the building is shown in Figure 5b.

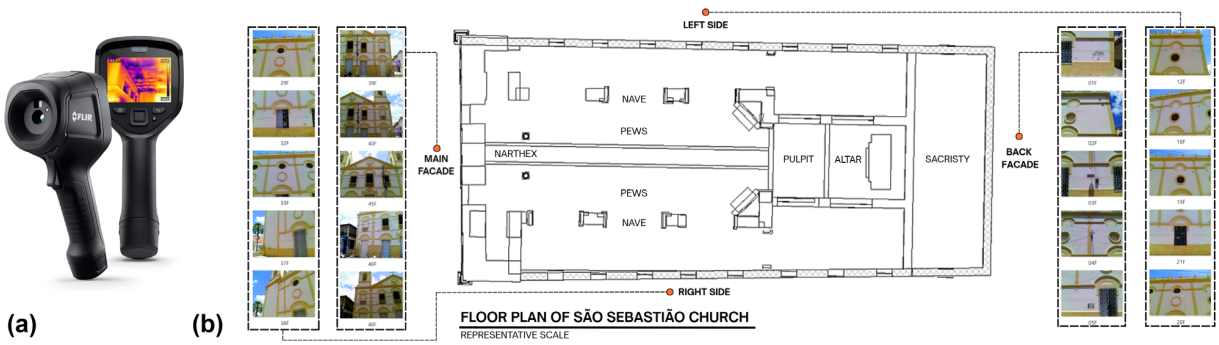


Figure 5 – Thermographic acquisition of the building: (a) FLIR TG165-X thermal camera used in the survey; (b) mapping of the main capture points for photographic images and thermograms.

The organization of the capture points made it possible to relate the location of the records to the apparent surface conditions and the observed thermal patterns. This procedure enabled the formation of a paired dataset composed of corresponding photographic and thermographic images, which was later used in the digital processing and computational analysis of the investigated regions.

2.4 Computer vision-based thermographic and image acquisition

The computational analysis stage of the thermograms was developed in Python, with the integrated use of the OpenCV (cv2), NumPy, and Matplotlib libraries, respectively responsible for image reading and processing, matrix manipulation of the data, and generation of the final analytical visualizations. Initially, the input parameters of the algorithm were defined, including the path of the image to be processed, the number of thermal clusters to be adopted in the segmentation, and the real width of the scene in meters, which was later used for the metric conversion of the detected area. The thermal image was then loaded and converted to the RGB color space, allowing the data to be prepared for the subsequent stages of analysis. At this stage, the Region of Interest (ROI) was also defined by technically cropping the useful portion of the thermogram in order to remove graphical elements external to the analyzed surface, such as scales, logos, and camera interface markers, as summarized in Figure 6.

Import libraries

```
01
1  import cv2
2  import numpy as np
3  import matplotlib.pyplot as plt
```

Test input parameters

```
02
8  caminho_imagem = '/content/drive/MyDrive/VISÃO COMPUTACIONAL/Thermography
   training/FLIR/01.jpg'
9  k_clusters = 3
10 largura_real_metros = 3.5  # Real width of the scene in meters
```

Loading, Initial processing, and K-Means segmentation

```
03
15 img = cv2.imread(caminho_imagem)
16
17 if img is None:
18     print(f"Error: Image not found at {caminho_imagem}")
19 else:
20     img_rgb = cv2.cvtColor(img, cv2.COLOR_BGR2RGB)
21     h, w, _ = img_rgb.shape
22
23     # Scale factor calculation (m² per pixel)
24     fator_conversao_m2 = (largura_real_metros / w) ** 2
25
26     # Define ROI (Technical crop to remove camera interface)
27     roi = img_rgb[40:h-40, 20:w-60].copy()
28     roi_gray = cv2.cvtColor(roi, cv2.COLOR_RGB2GRAY)
```

```
04
33     pixel_values = roi.reshape((-1, 3))
34     pixel_values = np.float32(pixel_values)
35     criteria = (cv2.TERM_CRITERIA_EPS + cv2.TERM_CRITERIA_MAX_ITER, 100, 0.2)
36     _, labels, centers = cv2.kmeans(pixel_values, k_clusters, None, criteria,
       10, cv2.KMEANS_RANDOM_CENTERS)
37     centers = np.uint8(centers)
38     segmented_roi = centers[labels.flatten()].reshape((roi.shape))
```

Detection overlay and Contour-based metric quantification

```
05
43     blur = cv2.bilateralFilter(roi, 9, 75, 75)
44     hsv = cv2.cvtColor(blur, cv2.COLOR_RGB2HSV)
45
46     # Filter for anomalies (Yellow/Orange)
47     lower_warm = np.array([15, 100, 100])
48     upper_warm = np.array([35, 255, 255])
49     mask = cv2.inRange(hsv, lower_warm, upper_warm)
50     mask = cv2.morphologyEx(mask, cv2.MORPH_CLOSE, np.ones((5,5), np.uint8))
51
52     # Create Alert Overlay (Gray background, damage highlighted)
53     alerta_overlay = cv2.cvtColor(roi_gray, cv2.COLOR_GRAY2RGB)
54     alerta_overlay[mask == 255] = [255, 0, 0] # Highlight in Red
```

```
06
59     contours, _ = cv2.findContours(mask, cv2.RETR_EXTERNAL, cv2.
       CHAIN_APPROX_SIMPLE)
60     detecao_final = roi.copy()
61     area_total_pixels = 0
62
63     for cnt in contours:
64         area = cv2.contourArea(cnt)
65         if area > 500:
66             cv2.drawContours(detecao_final, [cnt], -1, (0, 255, 0), 2)
67             area_total_pixels += area
68
69     area_total_m2 = area_total_pixels * fator_conversao_m2
```

Figure 6 – Computational processing workflow applied to the thermograms.

After the Region of Interest (ROI) was defined, a structural segmentation stage was carried out using the K-Means algorithm, adopted to group the image pixels into thermal zones with similar behavior. This operation simplified the interpretation of the thermal field by organizing the surface into transition regions and areas with greater apparent heat concentration. In parallel, for the quantitative extraction of anomalies, the ROI was subjected to a bilateral filter in order to reduce noise without compromising the definition of thermal edges.

Subsequently, the smoothed image was converted from the RGB color space to the HSV color space, a procedure adopted to facilitate the parametric segmentation of the chromatic ranges associated with thermal anomalies. Based on the definition of lower and upper thresholds for the target tones, a binary mask was generated to isolate the regions exhibiting anomalous thermal behavior. Mathematical morphology operations were then applied to this mask, especially morphological closing, in order to fill internal discontinuities and consolidate the segmented region as a continuous body.

Once the final mask was defined, the contours of the segmented areas were detected and a minimum-area filter was applied to remove residual noise and preserve only the regions most relevant for analysis. The areas detected in pixels were then converted into real metric units based on the scale factor calculated from the real width of the scene provided as an input parameter to the algorithm. This procedure allowed the

quantification of the anomalous area in square meters, which was used as a supporting parameter for result interpretation.

Finally, the processing generated an analytical panel composed of different visual products, including the original ROI, the K-Means segmentation, the alert overlay highlighting anomalous areas, the isotherm mapping, and the final image with the quantification of the detected area, as shown in Figure 7. In addition, the algorithm generated a final report containing the reference values of the scene, the number of pixels classified as anomalous, and the total quantified area. To convert the segmented area from pixels into square meters, a real dimensional reference of the analyzed scene was required. In this procedure, the user must provide an estimated dimension of the photographed surface, such as the actual width of the captured masonry panel, allowing the algorithm to establish the scale factor between the image and the corresponding physical dimension. When this information is not incorporated during image acquisition, the metric quantification depends on the dimensional estimate adopted for each image. This set of outputs was used as the basis for the technical interpretation of the thermograms and for the comparison between the thermal patterns observed on the analyzed surfaces.

Results display (5 images)

```
01  74  plt.figure(figsize=(20, 12))
```

Final analyses 1

```
02  76  # 1. Original ROI
    77  plt.subplot(2, 3, 1)
    78  plt.imshow(roi)
    79  plt.title('1. Original ROI (Wall)')
    80  plt.axis('off')
    81
    82  # 2. K-Means
    83  plt.subplot(2, 3, 2)
    84  plt.imshow(segmented_roi)
    85  plt.title(f'2. K-Means Segmentation (K={k_clusters})')
    86  plt.axis('off')
    87
    88  # 3. Alert Overlay
    89  plt.subplot(2, 3, 3)
    90  plt.imshow(alerta_overlay)
    91  plt.title('3. Alert: Damage Localization')
    92  plt.axis('off')
```

Final analyses 2

```
03  94  # 4. Isotherms
    95  plt.subplot(2, 3, 4)
    96  plt.imshow(roi)
    97  plt.contour(roi_gray, levels=10, cmap='magma', linewidths=1.2, alpl
    98  plt.title('4. Isotherms (Thermal Gradient)')
    99  plt.axis('off')
   100
   101  # 5. Final Detection
   102  plt.subplot(2, 3, 5)
   103  plt.imshow(detecao_final)
   104  plt.title(f'5. Quantification: {area_total_m2:.4f} m²')
   105  plt.axis('off')
   106
   107  plt.tight_layout()
   108  plt.show()
```

Final data report

```
01  110  # Terminal Report
    111  print(f"\n{'-'*40}\nQUANTIFICATION REPORT\n{'-'*40}")
    112  print(f"Input reference width: {largura_real_metros:.2f} m")
    113  print(f"Detected area:         {area_total_m2:.4f} square meters")
    114  print(f"Anomalous pixels:      {area_total_pixels} px")
    115  print(f"{'-'*40}")
```

Figure 7 – Results of the computational processing of the thermograms.

2.5 Integration of termograms into the HBIM

After the acquisition and processing of the thermograms, the results of the analyses were incorporated into the building's HBIM model in order to associate the obtained information with the corresponding masonry elements in the digital environment. This stage was carried out in Autodesk Revit, using the previously developed three-dimensional model as the basis for locating the investigated areas. The integration was performed by linking the modelled masonry elements to the data produced during the inspection. Thus, each analyzed section came to store, in its properties, descriptive records related to visual inspection, thermographic interpretation, and the synthesis of the identified damage. In addition to textual information, the visual products obtained in the field, including photographic images and thermograms, were also associated with the model and inserted over the analyzed elements through decals.

In a complementary manner, the results derived from the computational processing of the thermograms, such as the identification of anomalous regions and the quantification of detected areas, were linked to the corresponding elements in the model. In this way, the HBIM environment came to integrate, within a single framework, the building geometry, the photographic records, the thermograms, and the analytical information associated with the investigated masonry surfaces.

3. Results and discussion

3.1 3D survey and HBIM model development

From the integrated processing of laser scanning and photogrammetry, a unified geometric basis of the Church of São Sebastião was obtained and subsequently used for the three-dimensional modelling of the building in Revit. The resulting model represented the architectural configuration of the building in different views, including the main façade, the side façade, and the overall three-dimensional perspective, as illustrated in Figure 8. The modelling included the main volumetric and compositional elements of the church, with emphasis on the external masonry, openings, towers, roof, and decorative mouldings.

In addition to geometry, the model was structured to receive non-graphic data associated with the analyzed masonry. The modelled elements were assigned information related to visual inspection, thermographic analysis, damage identification, and the corresponding photographic and thermal images. This parametrization made it possible to associate the field records with the investigated sections in the digital model, establishing a correspondence between each element, its spatial location, and the analytical information produced.

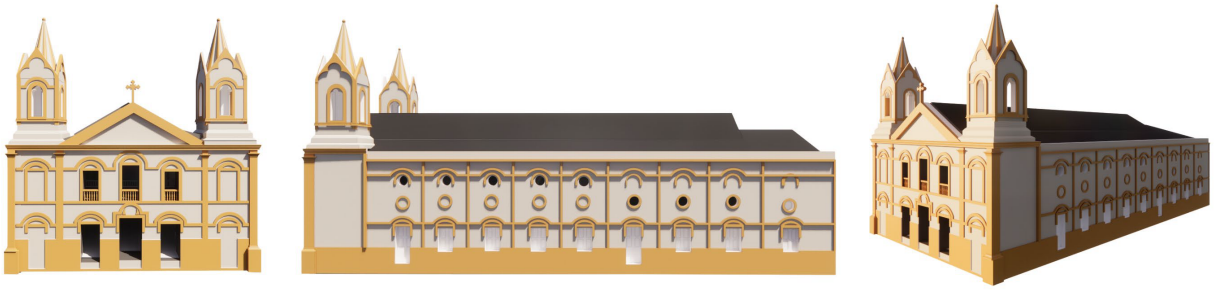


Figure 8 – Architectural 3D digital model of the Church of São Sebastião.

3.2. Thermographic and photographic analysis of masonry surfaces

The integrated analysis of visual inspection, photographic images, and thermograms made it possible to compare the visible expression of damage with the thermal patterns observed in the external masonry of the building. In the areas where the photographic images revealed coating detachment, surface degradation of the mortar, localized exposure of the substrate, and stains associated with moisture, the thermograms showed thermal anomalies spatially compatible with these regions, particularly in the lower bands and central portions of the masonry panels. In these cases, the thermal contrast was more pronounced in zones of adhesion loss and on surfaces showing altered surface behavior of the coating.

In other areas, the photographic images did not clearly reveal coating detachments, cracks, or loss of render, and the thermal behavior appeared more homogeneous. In these situations, temperature variations were concentrated in projecting geometric elements, such as moldings, frames, and opening contours, without direct correspondence to visible surface damage. Areas were also identified in which the thermograms indicated greater thermal heterogeneity than that observed in the photographs, suggesting alterations not clearly perceptible in the visible spectrum, possibly related to internal moisture, discontinuities between layers, or constructive interfaces.

Figure 9 presents, in four cases, the comparison between the photographic and thermographic records of the analyzed surfaces, as well as the processing stages applied to each image. In Cases 1, 2, and 3, the photographs show coating detachment, surface degradation, and localized substrate exposure, while the corresponding thermograms register zones of higher thermal contrast spatially coincident with these areas. In Stages III to VI, K-Means segmentation, damage alert, isotherm analysis, and final quantification allowed the anomalous regions to be isolated and delimited, resulting in estimated areas of 0.494 m^2, 0.296 m^2, and 0.268 m^2, respectively.

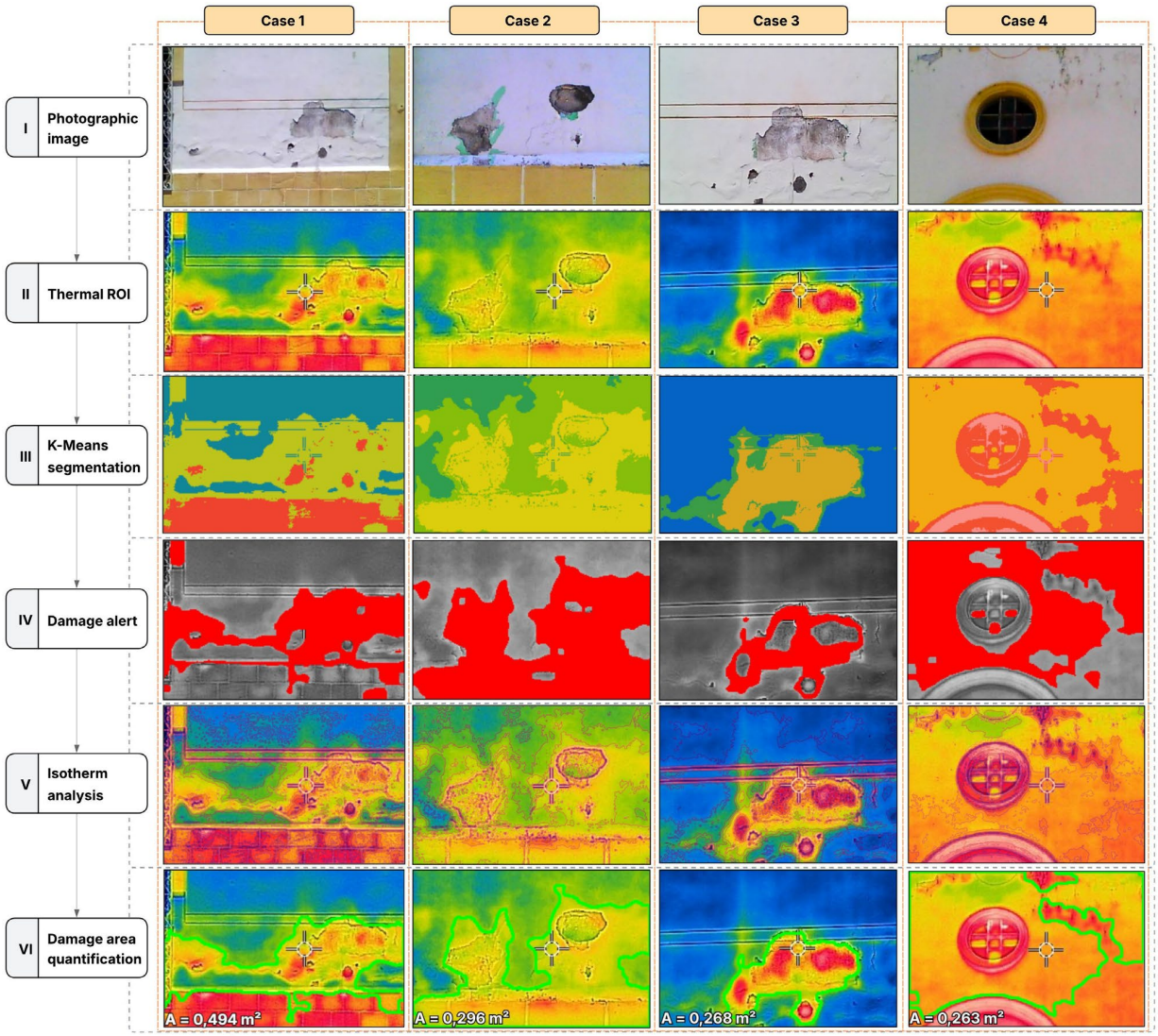


Figure 9 – Processing of four cases for the identification and quantification of surface damage using photographs and thermograms.

In Case 4, the photographic image shows less concentrated visible surface damage; however, the corresponding thermogram indicates a relevant thermal contrast around the circular opening and its immediate surroundings, with an estimated area of 0.263 m². Taken together, the results shown in Figure 9 indicate spatial correspondence between the visible damage identified in the photographic images and the thermal contrasts observed in the thermograms, supporting the applicability of the proposed workflow for inspection purposes while also highlighting areas with anomalous behavior not fully perceptible through visual inspection alone.3.3. Integration of thermo-photographic data into the HBIM environment

After the interpretation of the thermograms and the photographic survey of the damage, the results obtained through visual inspection and computer vision techniques were linked to the corresponding masonry elements in the HBIM model. This integration was carried out by associating each analyzed section with its respective textual and image-based records, bringing together, within the same digital environment, the building geometry, the photographic images, the thermograms, and the analytical information. Figure 10 illustrates this procedure by showing the association between the modelled wall elements, the photographic records of the damage, the thermograms, and the descriptive parameters inserted in the Revit properties palette.

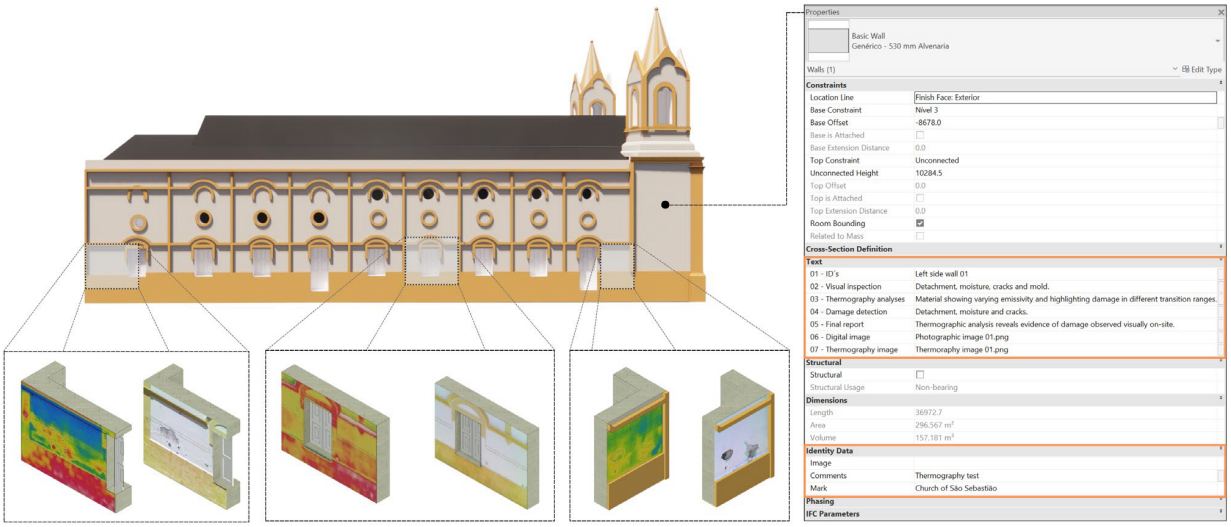


Figure 10 – HBIM model containing data from the thermographic and photographic analyses.

Within the model, the masonry elements were assigned fields for identification, visual inspection, thermographic analysis, damage detection, final report, and references to the image files. In addition, the photographic and thermographic records were applied to the elements by means of decals, allowing each analyzed area to be associated with its spatial location and with the set of information generated during the analytical process.

4. Conclusion

The obtained results show that the integration of geometric survey, thermo-photographic inspection, computer vision, and HBIM modelling enabled the structuring of a technical workflow for the analysis and documentation of the masonry of the Church of São Sebastião. Laser scanning and photogrammetry provided the geometric basis for the digital model, while thermographic and photographic acquisition supported the comparison between visible damage and thermal patterns on the analyzed surfaces. The computational processing of the thermograms allowed the segmentation of anomalous regions, the identification of thermal contrasts, and the quantification of damage areas in metric units. The association of these results with the modelled elements enabled the integration of geometry, inspection images, thermograms, and analytical information within the same digital environment. As a result, the HBIM model concentrated spatial and diagnostic data linked to the investigated masonry, supporting the organization, recording, and updating of inspection information in historic buildings.

References

[1] F. et al. ABDOLLARI-MAMOUDAN, Non-Destructive testing and evaluation of hybrid and advanced structures: a comprehensive review of methods, applications, and emerging trends, Sensors 25 (2025). https://doi.org/10.3390/s25123635.

[2] G. Boccacci, F. Frasca, C. Bertolin, A.M. Siani, Diagnosis of Historic Reinforced Concrete Buildings: A Literature Review of Non-Destructive Testing (NDT) Techniques, in: Procedia Structural Integrity, Elsevier B.V., 2024: pp. 160–167. https://doi.org/10.1016/j.prostr.2024.02.021.

[3] Binda e Saisi, State of the Art of Research on Historic Structures in Italy, Dept. of Structural Engineering, Politecnico of Milan, Italy. (2001).

[4] R. Li, F. Wang, P. Yin, F. Yang, J. Zhao, Z. Yue, L. Liu, S. Sfarra, G.T. Vesala, H. Yue, J. Liu, A review of ultrasonic infrared thermography in non-destructive testing and evaluation (NDT&E): Physical principles, theory, and data processing, Infrared Phys. Technol. 150 (2025). https://doi.org/10.1016/j.infrared.2025.105961.

[5] R.A. OLIVEIRA, Análise de praticas de conservação e reabilitação de edificios com valor pratirmonial, Universidade do Portp, 2003.

[6] J.B. Luz, I. de O. Silveira, M.A.R. Soeiro, Ensaio termográfico de edificação histórica: Igreja de Nossa Senhora da Conceição de Almofala / Thermographic test of historical heritage: Igreja de Nossa Senhora da Conceição de Almofala, Brazilian Journal of Development 7 (2021) 100708–100731. https://doi.org/10.34117/bjdv7n10-401.

[7] J.M. Molines-Cano, A. Almerich-Chulia, J. Llinares Millán, J.L. Vivancos, Constructive Modelling and Structural Analysis of the Church of Santos Juanes: An Approach Using Non-Destructive Techniques, Applied Sciences (Switzerland) 15 (2025). https://doi.org/10.3390/app15179661.

[8] Parente et al., HBIM and Information Management for Knowledge and Conservation of Architectural Heritage: A Review, Heritage 8 (2025). https://doi.org/10.3390/heritage8080306.

[9] S. Peng, S. Addepalli, M. Farsi, Machine Learning in Thermography Non-Destructive Testing: A Systematic Review, Applied Sciences (Switzerland) 15 (2025). https://doi.org/10.3390/app15179624.

[10] Solla et al., Integrating GPR and geomatic data into a Building Information Modelling: The case study of the Monastery of Batalha (Portugal), Def. Univ. Cent (2020). https://doi.org/10.13140/RG.2.2.33925.09447.

[11] COLI et al., 3D HBIM Model and Full Contactless GPR Tomography: An Experimental Application on the Historic Walls That Support Giotto's Mural Paintings, Santa Croce Basilica, Florence—Italy, Heritage 5 (2022) 2534–2546. https://doi.org/10.3390/heritage5030132.

[12] V. Cardinali, A.L. Ciuffreda, M. Coli, M. De Stefano, F. Meli, M. Tanganelli, F. Trovatelli, An Oriented H-BIM Approach for the Seismic Assessment of Cultural Heritage Buildings: Palazzo Vecchio in Florence, Buildings 13 (2023). https://doi.org/10.3390/buildings13040913.

[13] CRUZ et al., Case study: Casa da Câmara de Guimarães. HBIM modeling from non-destructive techniques, Procedia Structural Integrity 64 (2024) 335–342. https://doi.org/10.1016/j.prostr.2024.09.259.

[14] F. Banfi, W. Liu, The State of HBIM in Digital Heritage: A Critical and Bibliometric Assessment of Six Emerging Frontiers (2015–2025), Applied Sciences 16 (2026) 906. https://doi.org/10.3390/app16020906.

[15] COSTA, V. A. S.; BRAZ, V. H. V.; PÓVOAS, Y. V. Análise quantitativa para detecção de descolamento de revestimento de argamassa em fachadas usando termografia infravermelha. XXII International Conference on Building Pathology and Constructions Repair, 2025.

[16] MARTINS, L. L.; LUSTOSA, R. N.; PALMA E SILVA, A. A.; et al. Multi-criteria evaluation of facade degradation using infrared thermography, hygrothermal simulation, and the GUT matrix. XXII International Conference on Building Pathology and Constructions Repair, 2025.

[17] DONATELLI, A.; AVERSA, P.; LUPRANO, V. A. M. Set-up of an experimental procedure for the measurement of thermal transmittances via infrared thermography on lab-made prototype walls. Infrared Physics & Technology, v. 79, p. 135–143, 2016.

[18] SOCOLOSKI, R. F.; MASUERO, A. B. Evaluation of the efficiency of the treatment for rising damp on walls through the insertion of chemical barriers by gravity. Construction and Building Materials, 2019.

[19] WANG, P.; PENG, X.; NIE, Y.; et al. Building facade debonding damage detection method based on explainable artificial intelligence and UAV-thermography in cross scale field of view. Infrared Physics & Technology, 2026.

[20] TAN, Y.; XU, W.; CHEN, P.; ZHANG, S. Building defect inspection and data management using computer vision, augmented reality, and BIM technology. Automation in Construction, v. 160, 105318, 2024.

[21] WANG, T.; GAN, V. J. L. Automated joint 3D reconstruction and visual inspection for buildings using computer vision and transfer learning. Automation in Construction, v. 149, 104810, 2023.

[22] P. de A. ARAÚJO, Capital e Santuário, IOCE, Foraleza, 1986.

[23] Novenário de São Sebastião, (1996).



BUILT HERITAGE



cinpar2026
XXII International Conference on Building Pathology and Constructions Repair
15th to 17th July 2026 - Lisboa, Portugal

Structural Fire Risk in Historic Urban Districts: A Component-Based Analysis of its Relationship with Multidimensional Poverty

Nuria Chiara Palazzi [1], Diego Vásquez [2], Pilar Baquedano-Juliá [3]

[1] Facultad de Arquitectura, Arte, Diseño y Comunicaciones, Universidad Andrés Bello, Santiago, Chile, nuria.palazzi@unab.cl

[2] Facultad de Economía y Negocios, Universidad Andrés Bello, Santiago, Chile, diego.vasquez@unab.cl

[3] Departamento de Arquitectura, Universidad Tecnica Federico Santa Maria, Santiago, Chile, pilar.baquedano@usm.cl

Abstract: Fire risk represents a critical challenge in historic urban districts, where dense building patterns, aging building stock, and limited emergency accessibility coexist with complex socioeconomic conditions. This study examines structural fire risk in the historic district of La Chimba (Santiago, Chile) using a component-based Fire Risk Index (FRI) and its relationship with an adapted Multidimensional Poverty Index (MPI), integrating building-scale indicators with spatial analysis.

The FRI is decomposed into ignition, fire spread, evacuation, and fire suppression components, enabling the identification of distinct risk mechanisms within the historic urban fabric. The results show that overall fire risk is not primarily driven by ignition-related conditions but by constraints associated with fire spread, evacuation performance, and fire suppression capacity, which exhibit greater internal consistency among their underlying indicators and stronger spatial clustering. In contrast, ignition-related conditions display a more fragmented and localized distribution.

The comparison with multidimensional poverty reveals a weak and non-linear relationship at the aggregate level. Poverty shows a moderate positive association with ignition-related conditions, whereas its associations with fire spread and evacuation are moderate and negative, and its association with fire suppression constraints is weak. These findings suggest that poverty acts primarily as a mediating condition that may exacerbate specific fire-risk mechanisms without uniformly increasing overall fire risk.

The results highlight the limitations of fire risk management approaches that focus predominantly on ignition prevention in historic urban districts. Instead, effective fire risk reduction requires integrated strategies addressing evacuation feasibility, fire suppression capacity, and block-scale urban configurations, together with improvements in housing conditions. The proposed component-based framework provides a robust basis for analyzing fire risk in historic urban environments characterized by physical, social, and spatial heterogeneity.

Keywords: Fire risk; Historic urban areas; Multidimensional poverty; Urban vulnerability; Risk governance

XXII International Conference on Building Pathology and Constructions Repair
15th to 17th July 2026 - Lisboa, Portugal

Análise Patológica de Edificação Histórica com Proposta de Reabilitação: Um estudo de caso no Estado do Ceará, Brasil

Gabriele de Sousa RODRIGUES[1]

[1] Fortaleza, Ceará, Brasil, gsr.engcivil@gmail.com

Resumo: O artigo analisa manifestações patológicas e propõe a reabilitação da Casa Juvenal Galeno, prédio histórico em Fortaleza, Ceará. Construída em 1886, foi transformada em espaço cultural em 1919, institucionalizada em 1981 e tombada em 2016 pelo Conselho Estadual do Patrimônio Cultural do Ceará (COEPA), reforçando seu valor histórico (SECULT, 2013). A vistoria técnica identificou manifestações patológicas comuns em edificações históricas e definiu diretrizes de intervenção para garantir segurança, desempenho e preservação. Foi utilizada vistoria não destrutiva, com inspeção visual sistemática, registros fotográficos e consulta à literatura especializada. A avaliação classificou e analisou as anomalias quanto às causas, mecanismos de deterioração e impactos, observando fissuras, infiltrações, umidade, descolamento de revestimentos, deterioração da madeira, oxidação em armaduras, falta de manutenção e deficiências em drenagem e estanqueidade. As recomendações priorizam intervenções mínimas, compatibilidade de materiais, correção de coberturas e drenagem, tratamento da umidade e reforço de elementos comprometidos. A análise destaca a importância da engenharia diagnóstica e da manutenção preventiva, orientando práticas contínuas de conservação e reabilitação para garantir a originalidade e a transmissão do patrimônio histórico. Ressalta a necessidade de preservação, capacitação de profissionais especializados e monitoramento constante, assegurando não apenas a integridade física, mas também a relevância social e cultural da edificação para a comunidade e pesquisadores da história arquitetônica da região.

Palavras-chave: Patologia das construções; Edificações históricas; Manutenção preventiva; Vistoria técnica.

Abstract: The article analyzes pathological manifestations and proposes the rehabilitation of Casa Juvenal Galeno, a historic building in Fortaleza, Ceará. Built in 1886, it was transformed into a cultural space in 1919, institutionalized in 1981, and listed in 2016 by the State Council of Cultural Heritage of Ceará (COEPA), reinforcing its historical value (SECULT, 2013). The technical inspection identified pathological manifestations common in historic buildings and established intervention guidelines to ensure safety, performance, and preservation. A non-destructive inspection was conducted, including systematic visual inspection, photographic documentation, and consultation of specialized literature. The evaluation classified and analyzed anomalies regarding their causes, deterioration mechanisms, and impacts, observing cracks, infiltrations, moisture, detachment of coatings, wood deterioration, reinforcement oxidation, lack of maintenance, and deficiencies in drainage and waterproofing. Recommendations prioritize minimal interventions, material compatibility, correction of roofing and drainage systems, moisture treatment, and reinforcement of compromised elements. The analysis emphasizes the importance of diagnostic engineering and preventive maintenance, guiding continuous conservation and rehabilitation practices to ensure the building's originality and the transmission of its historical heritage. It highlights the need for preservation, training of specialized professionals, and continuous monitoring, safeguarding not only the physical integrity but also the social and cultural significance of the building for the community and researchers of the region's architectural history.

Keywords: Building pathology; Historic buildings; Preventive maintenance; Technical inspection.

1. Introdução

Edificações de valor cultural seguem diretrizes internacionais, como a Carta de Veneza (1964), que orienta a conservação de monumentos e sítios, preservando tanto a obra quanto seu testemunho histórico. No Brasil, essas diretrizes são complementadas pelas normas do IPHAN (Instituto do Patrimônio Histórico e Cultural), que regulam e autorizam intervenções em bens culturais, garantindo autenticidade, integridade e memória coletiva (IPHAN, 2010; IPHAN, 2024).

Na engenharia civil, a reabilitação de edifícios históricos integra normas técnicas atuais, como a ABNT (Associação Brasileira de Normas Técnicas) NBR (Norma Brasileira Registrada) 16747:2020, que estabelece diretrizes para inspeção predial e a ABNT NBR 15575:2013, que trata do desempenho de edificações ao longo de sua vida útil adaptáveis às especificidades do patrimônio. A aplicação criteriosa dessas normas permite identificar anomalias e falhas de manutenção, orientando decisões técnicas que conciliem segurança, funcionalidade, preservação cultural e originalidade.

O estudo focou a Casa Juvenal Galeno, em Fortaleza, Ceará, um marco cultural desde 1919. Realizou-se uma vistoria técnica para identificar manifestações patológicas, resultando em um estudo com recomendações de reparo, reforço e manutenção preventiva, respeitando as características históricas e normativas aplicáveis (ABNT, 2020; Carta de Veneza, 1964; IPHAN, 2010).

O trabalho é relevante por subsidiar intervenções que evitem danos irreversíveis, reduzam custos futuros e assegurem segurança, sem comprometer atributos históricos, integrando a prática e a importância da inspeção predial e conservação do patrimônio para a gestão sustentável da edificação em estudo e podem ser aplicadas a outras edificações.

2. Metodologia

A Casa Juvenal Galeno, construída em 1886, é formada com salão principal, biblioteca, salas múltiplas, banheiros, cozinha, lavanderia, teatro, pátio, depósitos e quintal. Estruturada em alvenaria estrutural de paredes espessas e argamassa, telhado coberto de telhas coloniais, assoalho (piso) de madeira, janelas e portas de madeira trabalhadas, construção típica de edificações da época.

Visita técnica realizada em 1º de julho de 2025, seguindo a norma da ABNT NBR 13752:2024, que orienta para bens históricos, complementada pela ABNT NBR 15575:2013 e orientações do IBAPE:2025 (Instituto Brasileiro de Avaliações e Perícias de Engenharia) e IPHAN:2024, com a objetividade de assegurar clareza e análise das manifestações patológicas existentes.

A vistoria e o laudo foram conduzidos por equipe multidisciplinar, composta por três arquitetos e uma engenheira civil, garantindo cobertura técnica sobre aspectos construtivos e valores históricos e culturais.

A inspeção realizada é do tipo visual e analisou todas as áreas acessíveis, com registro fotográfico e anotações técnicas. Avaliaram-se mobilidade, estanqueidade, acabamento, conservação, integridade estrutural, execução aparente, limpeza e manutenção. Não foram realizados ensaios destrutivos, respeitando restrições de edificações históricas.

A metodologia seguiu quatro etapas: 1) seleção da edificação por relevância histórica e cultural; 2) vistoria detalhada com registro de anomalias; 3) análise técnica com diagnóstico, identificação de causas, prognóstico e indicação de reabilitações compatíveis com normas e diretrizes do IPHAN; 4) confecção de laudo técnico com registro fotográfico das anomalias.

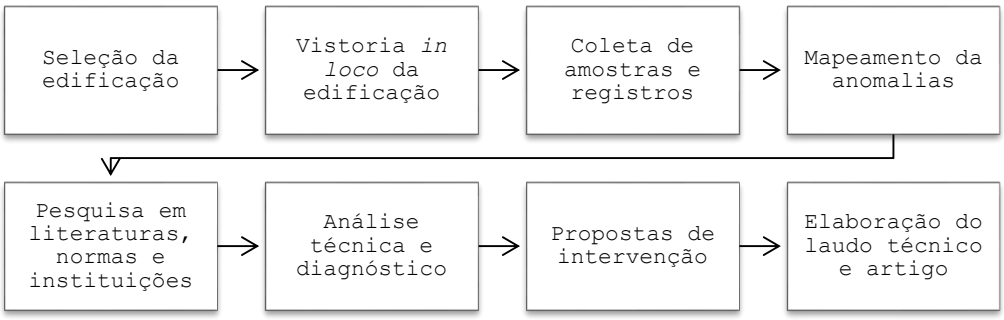
A inspeção identificou fissuras, infiltrações, umidade, bolor, descolamento de revestimentos, deterioração de madeira, oxidação de armadura, obstrução de drenagem e irregularidades elétricas. Cada anomalia foi associada a causas e origem construtiva, permitindo correlacionar mecanismos de deterioração e

sintomas, permitindo diagnóstico e avançando para prognóstico, estimando a evolução dos danos, impactos na segurança e desempenho, e definindo terapias adequadas para mitigação ou reparo.

Após diagnosticar as anomalias, as manifestações patológicas foram classificadas quanto às possíveis causas e origens no sistema construtivo permitindo relacionar causas, mecanismos de deterioração e sintomas, avançando do diagnóstico para o prognóstico. Com base no diagnóstico definiram-se propostas de intervenção técnica adequada para mitigação ou reparo.

O fluxograma, da Figura 1, representa de forma visual o encadeamento das atividades: inspeção detalhada, mapeamento das anomalias confrontadas com normas e diretrizes de conservação, diagnóstico, definição de intervenções e sistematização dos resultados.

Figura 1 – Fluxograma das etapas do trabalho



A falta de documentação arquitetônica ou estrutural limita o conhecimento técnico da edificação, sendo recomendada a elaboração de projeto “as built” para avaliação de armaduras e reforços a implementação de manutenção preventiva sistemática para reduzir falhas recorrentes e garantir a conservação contínua.

As conclusões são preliminares, porém compatíveis com vistoria não destrutiva, e não substituem estudos específicos ou laudos especializados e aprofundados para intervenções complexas. Métodos não invasivos foram privilegiados nesse estudo, aliados às boas práticas de engenharia diagnóstica e conservação de bens culturais.

3. Resultados e Discussão

A metodologia adotada organizou os dados sistematicamente, permitindo síntese das manifestações patológicas mais recorrentes em edificações antigas e identificação de elementos críticos para conservação. Em seguida, discute-se o diagnóstico das principais patologias do estudo de caso, evidenciando sua relevância para a definição de estratégias preventivas e corretivas.

3.1. Principais manifestações patológicas em edificações antigas e históricas

Caporrino (2018) define a Patologia das Edificações como a área que estuda as origens, as manifestações, os mecanismos de evolução e as possíveis soluções para as anomalias que ocorrem em construções, integrando conhecimentos teóricos e práticos.

Fundarò (2018), diz que não se trata apenas de identificar as patologias de uma edificação antiga, mas de garantir que a intervenção siga pilares fundamentais para que a reabilitação seja adequada, considerando o projeto axiológico, o projeto de conservação e o projeto de inovação. Assim, entende-se que o projeto de reabilitação constitui uma combinação equilibrada: inicia-se com um juízo de valor sobre o bem (fase axiológica), seguido pela aplicação de técnicas voltadas à preservação material (fase tecnológica), e culmina na definição de um novo uso ou reuso do bem, adaptado às necessidades contemporâneas (fase de inovação).

Oliveira (2022) apresenta as patologias construtivas observadas na chácara Porangaba, localizada em Fortaleza/CE, datada do final do século XIX (1890-1900). Entre os principais problemas identificados, destacam-se infiltrações provenientes de falhas na cobertura e umidades por capilaridade nas alvenarias. Tais condições evidenciam um processo acelerado de degradação material, comprometendo a durabilidade da edificação e dificultando futuras intervenções de conservação, reabilitação e restauro, sendo essencial a implementação de estratégias preventivas e técnicas apropriadas de preservação para assegurar a integridade estrutural e patrimonial da edificação.

A Casa Juvenal Galeno (1886) e a Chácara de Porangaba evidenciam similaridades nas patologias, destacando infiltrações, umidades ascendentes por capilaridade e manutenção periódica insuficiente, indicando semelhança nos mecanismos de degradação e nos desafios de conservação dessas edificações residenciais históricas.

Coelho e Carvalho (2024), em seu estudo com algumas edificações antigas (Museu Casa de Rui Barbosa – iniciada no século XIX e finalizada 1850 e Pavilhão Mourisco do conjunto da Fundação Oswaldo Cruz foi iniciada por volta de 1905 e concluída em 1918), apesar da diferença temporal das construções, as edificações apresentam padrões comuns de degradação, evidenciando mecanismos de deterioração típicos de edificações históricas brasileiras do século XIX e início do XX.

Como descrito acima, as edificações antigas apresentam anomalias semelhantes, independentemente do ano de construção, do contexto histórico ou dos métodos de conservação adotados. No comparativo entre a Casa Juvenal Galeno (1886), a Chácara de Porangaba (final do século XIX), o Museu Casa de Rui Barbosa (1850) e o Pavilhão Mourisco da Fundação Oswaldo Cruz (1905–1918), observam-se padrões recorrentes de degradação, reforçando a analogia das anomalias entre essas construções: infiltração externa, umidades ascendentes por capilaridade, fissuras em alvenaria, degradação e desplacamento de materiais de acabamento como rebocos, pinturas, pisos e ornamentos, problemas em coberturas e telhados e, principalmente, falhas na manutenção periódica, que intensifica os problemas ao longo do tempo.

Essas similaridades evidenciam que, apesar das diferenças temporais e estruturais, os mecanismos de deterioração em edificações históricas brasileiras seguem padrões comuns, sobretudo ligados à falta de manutenção, reabilitação e a preservação inadequada.

As manifestações descritas a seguir correspondem às mais frequentes em edificações antigas, servindo como introdução e guia ao diagnóstico das patologias observadas na edificação em estudo e se embasa em literatura técnica especializada.

Fissuras, trincas e rachaduras em edificações podem ser causadas por fatores como mudanças térmicas, sobrecargas, deformações estruturais, recalques de fundação e retração de materiais. Em edifícios antigos, esses problemas são mais evidentes devido a métodos construtivos que não utilizavam juntas de dilatação adequadas, favorecendo movimentos descontrolados das estruturas (Thomaz, 2020).

A água pode entrar nas edificações de várias formas, como por precipitação, umidade do terreno, condensação ou falhas em sistemas de abastecimento e drenagem, como caixas d'água e tubulações. Em edifícios antigos, as coberturas são pontos críticos, e a falta de acesso seguro e manutenção periódica favorecem infiltrações e o aparecimento constante de umidade nas paredes, uma das patologias mais comuns (Gomide *et al*., 2021).

A umidade constante nas paredes causa danos progressivos, como manchas, alterações na aparência e condições insalubres, como o crescimento de fungos e bolor. Em edificações antigas, esses efeitos são mais intensos devido à maior porosidade das alvenarias, uso de argamassas menos resistentes e a falta de barreiras de impermeabilização eficientes na época da construção.

O descolamento e desplacamento de revestimentos em edificações antigas ocorrem devido à porosidade das argamassas, que possuem granulometria média a grossa e pouca fração de finos, o que favorece a

perda de aderência entre o revestimento e a alvenaria. Esse problema é agravado pela umidade constante, degradação da argamassa, movimentos estruturais e térmicos, além das incompatibilidades entre revestimentos antigos e materiais modernos, como argamassas ricas em cimento ou pinturas impermeáveis. (VEIGA, 2002).

O descolamento e desplacamento de revestimentos são agravados, ainda mais, pela cristalização de sais solúveis, ação biológica (fungos, algas e raízes), má execução do chapisco, baixa rugosidade da base e uso de areias de baixa fração de finos, comprometendo a aderência. Isso torna o destacamento uma ocorrência comum em fachadas e ambientes internos.

As patologias em estruturas de madeira, segundo Cruz (2001), são causadas por agentes biológicos, físicos e químicos além de fatores atmosféricos e anomalias construtivas, independentemente da época de construção. A falta de manutenção preventiva, combinada com ambientes úmidos e ventilação inadequada, acelera a deterioração, destacando a importância da conservação regular desses elementos.

A degradação da madeira, segundo Brito (2014), vai além desses agentes citados por Cruz (2001) e acrescenta o agente mecânico, dependendo das condições ambientais. Embora seja um processo natural e ecológico, é crítico na engenharia quando afeta elementos estruturais, como coberturas, forros e pisos de edificações antigas por ser mais difícil a restauração e/ou reabilitação e muitas vezes, o elemento tem que ser substituído por completo e com possibilidade de perda de seu *design* original.

3.2. Diagnóstico das principais patologias observadas na Casa Juvenal Galeno.

A matriz-resumo sintetiza as principais manifestações patológicas observadas no objeto de estudo, permitindo identificar padrões recorrentes em edificações antigas ou históricas. Ela evidencia as patologias que apresentam maior frequência e criticidade, servindo como referência para orientar a atenção técnica durante a vistoria *in loco*. Além disso, a matriz contribui para a análise técnica de intervenções preventivas e corretivas, fornecendo uma base sistemática para a análise comparativa de casos e para a implementação de estratégias de conservação, manutenção e reabilitação.

Quadro 1 - Matriz Resumo das principais manifestações Patológicas na Casa Juvenal Galeno

Imagem	Local	Sistema	Manifestações	Diagnóstico	Possíveis Causas	Prognóstico	Recomendações Técnicas
1	Biblioteca	Alvenaria	Fissuras, trincas	Movimentação estrutural	Sobrecarga	Rachaduras	Reparação se houver evolução
2	Hall dos banheiros	Cobertura	Infiltração	Umidade por falta de estanqueidade	Falha no telhado, calhas e vedação.	Evolução de manchas e dano construtivos	Reorganizar telhado e reparar calhas, rufos e vedação
3 e 4	Teatro e depósito	Revestimento	Desagregação	Revestimento degradado por umidade	Umidade e manutenção	Desprendimento do revestimento	Reabilitar com argamassa cimentícia
5 e 6	Depósito	Estrutural	Revestimento	Desplacamento com exposição de armadura	Intempéries, infiltração	Comprometimento estrutural	Reabilitar armaduras
7 e 8	Fiação exposta; Quadro de Força e Luz (QDFL)	Instalações elétricas	Não conformidades elétricas	Falhas de proteção, fixação e segurança	Instalações improvisadas e fora das normas	Risco de choque elétrico e incêndio	Regularizar instalações elétricas, substituindo fiações e conexões inadequadas

Fonte – Dados da pesquisa (2025)

Imagem 01



Imagem 02



Imagem 03



Imagem 04



Imagem 05



Imagem 06



Imagem 07



Imagem 08



As intervenções devem priorizar eficácia, durabilidade e compatibilidade com materiais tradicionais, corrigindo drenagem e impermeabilização em casos de infiltração e aplicando reforços estruturais localizados com resina epóxi ou argamassas cimentícias compatíveis, evitando rigidez excessiva que comprometa o desempenho da edificação.

Para manifestações superficiais, recomenda-se remoção do crescimento fúngico, aplicação de tratamentos antimicrobianos compatíveis com o substrato e controle rigoroso de umidade e ventilação, preservando a integridade física e estética dos materiais originais.

A implementação de intervenções preventivas e corretivas, fundamentadas em diagnósticos detalhados das patologias construtivas, potencializa a segurança estrutural, preservação do valor histórico e longevidade das edificações. Destaca-se a importância de integrar manutenção preventiva sistemática, inspeções periódicas e técnicas compatíveis com o patrimônio histórico, respeitando normas técnicas, critérios de preservação e boas práticas construtivas.

Dois elementos de extrema importância na reabilitação de edificações antigas e históricas são a resina de epóxi e argamassas cimentícias, já citadas aqui. O uso desses elementos permite reforço estrutural, consolidação de elementos deteriorados e proteção contra degradação, assegurando intervenções duráveis, compatíveis e seguras, essenciais para a preservação do patrimônio histórico.

A reabilitação dessa edificação requer técnicas que garantam restauração da integridade estrutural, durabilidade e compatibilidade com os materiais originais. Nesse contexto, o uso combinado de resina epóxi e argamassa cimentícia tem se mostrado estratégico, permitindo restaurar elementos de concreto, alvenaria, pedra e madeira de forma segura e durável (ABNT, 2005a; ASTM INTERNATIONAL, 2023).

A resina epóxi, polímero termoendurecível de alta adesão e baixa viscosidade, é particularmente eficaz para preencher fissuras capilares e macrofissuras, colando internamente os elementos e prevenindo a infiltração de umidade, fator crítico na degradação de estruturas antigas. Suas aplicações incluem consolidação de alvenarias e pedras soltas, reparo e reforço de madeira, ancoragem e fixação de reforços estruturais e proteção contra degradação química e umidade (ASTM C881/C881M-20; ASTM C923-20).

Por outro lado, a argamassa cimentícia desempenha papel complementar, oferecendo resistência mecânica, aderência e durabilidade. É utilizada para preencher fissuras, consolidar alvenarias de pedra ou tijolo e reforçar elementos deteriorados, além de reparos de concreto armado mais recentes (ABNT, 2005b;

ASTM C1713-23, 2023). Contudo, devido à sua rigidez e impermeabilidade, seu uso deve ser criterioso em edificações históricas, pois pode gerar fissuração secundária, retenção de umidade e descolamento de revestimentos. Sempre que possível, recomenda-se o emprego de argamassas à base de cal hidráulica natural (NHL) para garantir flexibilidade e permeabilidade ao vapor de água, assegurando compatibilidade física e química com o substrato histórico.

O planejamento técnico deve envolver: 1. Avaliação estrutural detalhada e identificação de fissuras e patologias; 2. Seleção criteriosa do material, considerando módulo de elasticidade, retração, adesão e compatibilidade mecânica com o substrato; 3. Procedimentos de aplicação controlada, incluindo preparo da superfície, selagem superficial, instalação de bicos de injeção para epóxi, injeção gradual e cura adequada e; 4. Ensaios técnicos conforme normas, garantindo resistência à compressão, tração, aderência e penetração do material (ABNT NBR 13281, NBR 13276, NBR 13277, NBR 13278; ASTM C881/C881M-20; ASTM C923-20; ASTM C1713-23).

A combinação de resina epóxi e argamassa cimentícia, quando aplicada de forma criteriosa e técnica, constitui uma abordagem confiável para reabilitação de edificações antigas, promovendo reforço estrutural, compatibilidade com os materiais originais e conservação em longo prazo do patrimônio histórico.

Para pesquisas futuras o estudo evidencia oportunidades para aperfeiçoamento de materiais e técnicas compatíveis com edificações históricas e para a implementação e/ou melhoramento de estratégias sistemáticas de monitoramento e avaliação de desempenho. Recomenda-se investigação do uso de resinas epóxi para consolidação estrutural e preenchimento de fissuras, considerando aderência, compatibilidade higroscópica, durabilidade e comportamento físico-químico, assim como a avaliação de argamassas cimentícias, incluindo composição, resistência, permeabilidade, retração e compatibilidade com materiais originais, visando à preservação da autenticidade e integridade patrimonial.

4. Conclusão

O presente estudo demonstra que edificações históricas brasileiras apresentam padrões recorrentes de degradação, tais como infiltrações externas, umidades ascendentes por capilaridade, fissuras em alvenaria, desagregação de revestimentos e falhas na manutenção periódica, corroborando os achados de Oliveira (2022) e Coelho & Carvalho (2024). A análise sistemática das manifestações patológicas permitiu a proposição de intervenções compatíveis com os materiais originais e evidenciou a relevância de planos integrados de manutenção preventiva como instrumento estratégico para a preservação estrutural e patrimonial.

A reabilitação de elementos degradados deve contemplar eliminação das fontes de umidade, remoção de revestimentos soltos e preparação criteriosa do substrato, garantindo aderência, compatibilidade higroscópica e integridade estrutural, enquanto a aplicação combinada de resina epóxi e argamassa cimentícia assegura consolidação de fissuras, reforço estrutural localizado, impermeabilização, resistência mecânica e durabilidade, quando controladas espessura, cura e permeabilidade ao vapor d'água.

A integração dessas técnicas, combinada a protocolos rigorosos de inspeção, monitoramento e avaliação do desempenho dos materiais, assegura recuperação funcional, proteção patrimonial e preservação da autenticidade histórica. Recomenda-se a sistematização de procedimentos escaláveis de manutenção preventiva para consolidar boas práticas de conservação, com foco na integridade estrutural e durabilidade dos materiais.

As implicações para práticas profissionais, sobre este estudo, reforça a necessidade de adoção de abordagens integradas e baseadas em evidências no campo da reabilitação patrimonial. Profissionais da engenharia civil, arquitetura e conservação devem priorizar diagnósticos detalhados, planejamento

criterioso e seleção de materiais compatíveis, garantindo intervenções duráveis que respeitem a autenticidade histórica. Além disso, enfatiza-se a importância de protocolos padronizados de manutenção preventiva, permitindo que equipes técnicas programem estratégias replicáveis em diferentes contextos de edificações históricas e antigas.

O estudo aponta a necessidade de pesquisas sobre novos materiais e tecnologias para reabilitação patrimonial, incluindo argamassas modificadas, aditivos impermeabilizantes e resinas de alto desempenho, bem como estudos longitudinais para avaliar desempenho frente a fatores estruturais e ambientais. Ressalta-se a importância de protocolos sistemáticos de monitoramento para detecção precoce de falhas, otimização de intervenções preventivas e preservação da integridade e autenticidade de edificações históricas com suas originalidades.

As literaturas usadas nesse estudo serviram de suporte para embasar narrativas comparativas entre diferentes edificações e criar possibilidades de estratégias de intervenção, podendo subsidiar protocolos de conservação mais eficientes e escaláveis, fortalecendo a base científica para práticas profissionais de preservação patrimonial.

Agradecimentos

Agradeço imensamente aos arquitetos Débora Paz Salles, Grazielle Caldas e Renato Oliveira pela colaboração na elaboração do laudo de inspeção predial, que serviu de base para o desenvolvimento deste artigo, e à minha orientadora, Karol Novaz, por suas valiosas contribuições. Registro também meu reconhecimento aos engenheiros José Soares Teixeira Filho e Jaziel Fernandes pelo aprendizado inicial em engenharia diagnóstica. Agradeço especialmente à minha mãe, dona Nerita, pelo apoio constante, e aos meus irmãos, Jeferson Emídio, Alexandre e Adalberto Júnior, por fazerem parte da minha vida e por serem minha família, junto com seus filhos e esposas.

Referências

ABNT NBR 13281:2005 – Argamassa para assentamento e revestimento de paredes e tetos — Requisitos. ABNT, 2005a.

ABNT NBR 13276:2005 – Argamassa para assentamento e revestimento de paredes e tetos — Preparo da mistura e determinação do índice de consistência. Rio de Janeiro: ABNT, 2005b.

ABNT NBR 13277:2005 – Argamassa para assentamento e revestimento de paredes e tetos — Determinação da retenção de água. Rio de Janeiro: ABNT, 2005c.

ABNT NBR 13278:2005 – Argamassa para assentamento e revestimento de paredes e tetos — Determinação da densidade de massa e do teor de ar incorporado. Rio de Janeiro: ABNT, 2005d.

ABNT NBR 13752:2024 – Perícias de engenharia na construção civil.

ABNT NBR 15526:2012, Versão Corrigida:2016 – Redes de distribuição interna para gases combustíveis em instalações residenciais - Projeto e execução.

ABNT NBR 15575:2013 – Edificações habitacionais – Desempenho.

ABNT NBR 16747:2020 – Inspeção predial – Diretrizes, conceitos, terminologia e procedimentos.

ASTM INTERNATIONAL. ASTM C1713-23 – Standard Specification for Mortars for the Repair of Historic Masonry. West Conshohocken, PA: ASTM International, 2023.

ASTM INTERNATIONAL. ASTM C881/C881M-20 – Standard Specification for Epoxy-Resin-Base Bonding Systems for Concrete. West Conshohocken, PA: ASTM International, 2020.

ASTM INTERNATIONAL. ASTM C923-20 – Standard Specification for Resilient Grout for Structural Crack Injection. West Conshohocken, PA: ASTM International, 2020.

Barbosa, Milena Gonçalves. Reforma em edificações: Um estudo de caso na capela Nossa Senhora das Dores em Monteiro-PB. 2023. Trabalho de Conclusão de Curso (Curso Superior de Tecnologia em Construção de Edifícios) - Instituto Federal de Educação, Ciência e Tecnologia da Paraíba - IFPB campus, Monteiro. “Acessado em 23 de maio de 2026. SUAP: Sistema Unificado de Administração Pública”

Brito, Leonardo Dussarrat. 2014. Patologia em estrutura de madeira: metodologia de inspeção e técnicas de reabilitação. Tese de Doutorado em Engenharia de Estruturas, Escola de Engenharia de São Carlos, Universidade de São Paulo, São Carlos.

Caporrino, Cristiana Furlan. 2018. Patologias em alvenarias. 2. ed. São Paulo: Oficina de Textos.

Carta de Veneza. 1964. Carta Internacional sobre a Conservação e o Restauro de Monumentos e Sítios. Veneza.

COELHO, Carla Maria Teixeira; CARVALHO, Cláudia S. Rodrigues de. Conservação preventiva de edifícios históricos: princípios e práticas. Rio de Janeiro: Mórula Editorial, 2024.

Cruz, H. 2001. Patologia, avaliação e conservação de estruturas de madeira. Lisboa: Laboratório Nacional de Engenharia Civil (LNEC), Núcleo de Estruturas de Madeira. Projeto de pesquisa. Acessado em 28 nov. 2025. https://www.yumpu.com/pt/document/read/12948194/patologia-avaliacao-e-conservacao-de-estruturas-de-madeira.

FUNDARÒ, Mario. Projeto de conservação e de restauro como elementoestruturador de programas de gestão do patrimônio construído: Alguns estudosde casos entre o Brasil e a Itália. Belo Horizonte, 2018. 652 p Tese (Escola dearquitetura) - Universidade Federal de Minas Gerais, Belo Horizonte, 2018.

Gomide, Tito Lívio Ferreira, et al., coords. 2021. Manual de engenharia diagnóstica: desempenho, manifestações patológicas e perícias na construção civil. 2. ed. São Paulo: Leud.

IBAPE (Instituto Brasileiro de Avaliações e Perícias de Engenharia). 2025. Norma de inspeção predial. São Paulo: IBAPE. Acessado em 27 nov. 2025. https://biblioteca.ibape-nacional.com.br.

IPHAN (Instituto do Patrimônio Histórico e Artístico Nacional). 2010. Portaria n.º 420, de 22 de dezembro de 2010: Dispõe sobre as intervenções em bens culturais tombados.

IPHAN (Instituto do Patrimônio Histórico e Artístico Nacional). 2024. Política de Patrimônio Cultural Material. Brasília: IPHAN.

Oliveira, E. C. R. Casa da Cultura parque Porangaba: memória, patrimônio e cidadania. 2022. 136 p. Monografia (Graduação em Arquitetura e Urbanismo) - Centro de Tecnologia, Universidade Federal do Ceará, 2022. “Acessado em 23 de maio de 2026. Repositório Institucional UFC: Casa da Cultura do Parque Porangaba: memória, patrimônio e cidadania”

SECULT (Secretaria da Cultura do Estado do Ceará). 2013. “Casa de Juvenal Galeno.” Acessado em 11 dez. 2025. https://www.secult.ce.gov.br/2013/01/03/casa-de-juvenal-galeno/.

Thomaz, Ercio. 2020. Trincas em edifícios: causas, prevenção e recuperação. 2. ed. revista e ampliada. São Paulo: Oficina de Textos.

Veiga, Maria Rosário. 2002. Argamassas de cal: caracterização, comportamento e durabilidade. Lisboa: LNEC – Laboratório Nacional de Engenharia Civil.

Cinpar 2026
XXII International Conference on Building Pathology and Constructions Repair
15th to 17th July 2026 - Lisboa, Portugal

Desafios na Reabilitação de Edificações no Brasil: a formação acadêmica como elemento-chave para a qualidade das intervenções

Érika Stella Silva Menezes[1], Sara Merhj[2], Ana Clara Matos de Carvalho[3], Márcio Augusto Roma Buzar[4], Valmor Cerqueira Pazos[5]

1 Universidade de Brasília, Brasil, martois.stella@gmail.com
2 Universidade de Brasília, Brasil, saramerhj@gmail.com
3 Universidade de Brasília, Brasil, anaclaramc@hotmail.com
4 Universidade de Brasília, Brasil, buzar@unb.br
5 Universidade de Brasília, Brasil, pazos@unb.br

Resumo: A crescente demanda por intervenções em edificações degradadas evidencia a reabilitação como prática presente na arquitetura contemporânea. Contudo, a pesquisa identificou uma lacuna na formação acadêmica dos arquitetos, os quais, com frequência, concluem a graduação sem a capacitação específica para diagnosticar e intervir em patologias construtivas. Essa limitação afeta a qualidade das intervenções e a atuação técnica dos profissionais diante do patrimônio edificado. Nesse contexto, este estudo analisou os desafios associados à reabilitação de estruturas, com ênfase no papel da formação superior na prevenção de falhas construtivas. Para sustentar a análise, foram examinados dados do Conselho de Arquitetura e Urbanismo do Brasil (CAU/BR), os quais apontam a escassez de disciplinas voltadas ao estudo das patologias construtivas e das técnicas de reparo nas grades curriculares dos cursos de Arquitetura e Urbanismo. Adicionalmente, foram realizadas entrevistas com estudantes de graduação, cujos relatos indicaram percepções críticas quanto à abordagem superficial do tema ao longo da formação. A metodologia adotada permitiu identificar lacunas no ensino e promover reflexões sobre a necessidade de revisão curricular. Os resultados subsidiaram uma análise do modelo vigente de formação, destacando a relevância da inserção de conteúdos específicos sobre patologias e reabilitação de edificações. Concluiu-se que a integração sistemática de conteúdos teóricos e práticos voltados à prevenção e à correção de danos estruturais contribui para a formação de profissionais capacitados a enfrentar os desafios da degradação do ambiente construído, favorecendo maior durabilidade e segurança às edificações. A revisão curricular, nesse sentido, apresenta-se como medida necessária para alinhar a formação acadêmica às exigências atuais do campo profissional e às responsabilidades técnicas e sociais inerentes à prática da arquitetura.

Palavras-chave: Reabilitação de edificações; Patologias construtivas; Formação acadêmica; Arquitetura; Ensino superior.

1. Introdução

O ensino da Arquitetura tem historicamente tratado as disciplinas técnicas e projetuais de maneira fragmentada, o que muitas vezes dificulta a compreensão integrada da estrutura como um elemento essencial no processo criativo. No entanto, o cenário atual exige profissionais capazes de articular técnica, inovação e sustentabilidade de forma coesa. Essa pesquisa nasce da necessidade de repensar os métodos de ensino, propondo uma abordagem mais dinâmica e interdisciplinar, que fortaleça a conexão entre o aprendizado das estruturas e a prática projetual.

A construção curricular no ensino superior deve refletir não apenas as demandas do mercado, mas também as diretrizes pedagógicas e epistemológicas que sustentam a formação crítica e reflexiva dos estudantes. Assim, é essencial adotar concepções de currículos integradores, promovendo um aprendizado situado e contextualizado. No contexto da formação por competências, a construção curricular deve articular saberes

teóricos e práticos, capacitando os estudantes para análises críticas e para a aplicação do conhecimento em contextos reais.

O ensino de estruturas ocupa um papel fundamental, pois a compreensão da lógica estrutural transcende a mera aplicação de cálculos e métodos quantitativos — é um exercício de articulação entre conceito e realidade, capaz de conferir sustentabilidade, segurança e qualidade estética às obras. A simbiose entre forma e estrutura é evidente e necessária, exigindo um retorno às raízes da profissão, onde a responsabilidade pela concepção estrutural volta a ser parte integrante da prática arquitetônica.

Este artigo busca entender como o ensino de Arquitetura e Urbanismo pode evoluir para incluir, de forma mais eficaz, conteúdos sobre reabilitação. A formação acadêmica atual enfrenta desafios que impactam a qualidade das intervenções em edificações existentes. Leite (2005) aponta a falta de disciplinas voltadas para estruturas e sua interação com a arquitetura como uma lacuna que afeta o mercado. Como resultado, arquitetos encontram dificuldades ao lidar com patologias construtivas, devido à falta de conhecimento técnico específico nos currículos universitários. Como destaca Almeida (2008), o desconhecimento sobre as manifestações patológicas mais comuns nas edificações, seus mecanismos de evolução e os métodos adequados de intervenção compromete significativamente a eficiência das soluções aplicadas em projetos de reabilitação. O domínio desses aspectos deve ser considerado um requisito essencial na formação dos profissionais envolvidos com o ambiente construído.

Para Perrenoud (1999), o ensino baseado em competências exige uma abordagem interdisciplinar que articule teoria e prática, proporcionando aos estudantes a capacidade de lidar com desafios reais. No entanto, a realidade mostra que a fragmentação do conhecimento no ensino superior compromete essa integração, levando a dificuldades na atuação profissional. Como aponta Franco (1974), o estudo das estruturas deveria ir além do cálculo matemático, abordando a evolução histórica dos sistemas construtivos para que os futuros arquitetos desenvolvam uma visão mais abrangente das soluções estruturais.

A análise dos dados do Conselho de Arquitetura e Urbanismo do Brasil (CAU/BR), reforça essa percepção. Segundo os registros da entidade, há um número reduzido de projetos de reabilitação estrutural assinados por arquitetos, o que sugere que a formação acadêmica ainda não prepara adequadamente os profissionais para essa área. Esse cenário poderia ser revertido com uma revisão curricular que priorizasse conteúdos sobre diagnóstico de patologias, técnicas de reparo e compatibilização estrutural. Lumi (2003) reforça que a formação em reabilitação arquitetônica exige não apenas o domínio técnico das técnicas de reparo, mas também uma abordagem sensível à preservação da identidade material e simbólica das edificações. A reabilitação eficaz pressupõe uma leitura crítica do edifício existente, integrando conhecimento técnico, histórico e cultural. Como defendem Gamili, Buzar e Pantoja (2022), a transformação do ambiente construído requer profissionais capacitados para compreender a relação entre forma, materialidade e desempenho estrutural, evitando intervenções inadequadas.

Além disso, a falta de comunicação entre arquitetos e engenheiros estruturais compromete a eficiência dos projetos de reabilitação. Carvalho (2003) destaca que a ausência de um vocabulário técnico compartilhado dificulta a colaboração entre as duas áreas, resultando em projetos desarticulados e, muitas vezes, ineficazes. A inclusão de disciplinas que promovam essa interface no ensino superior poderia minimizar esses problemas, preparando os futuros profissionais para uma atuação mais integrada e multidisciplinar.

Portanto, a reformulação curricular se mostra essencial para que o arquiteto seja capaz de compreender e intervir com propriedade no ambiente construído. O fortalecimento das disciplinas voltadas à reabilitação de edificações, aliado a metodologias ativas de ensino, pode contribuir significativamente para a formação de profissionais mais preparados para os desafios da prática contemporânea.

2. Metodologia de obtenção dos dados

A pesquisa adotou duas ações complementares para garantir uma análise mais abrangente e rigorosa dos dados. A primeira ação consistiu na coleta e no tratamento de informações fornecidas pelo CAU/BR, permitindo a identificação de padrões e tendências no campo profissional, com base em dados institucionais amplamente reconhecidos. Essa escolha se justifica pela confiabilidade e pela abrangência das informações disponibilizadas por esse órgão regulador, garantindo uma visão consolidada do cenário atual da profissão.
A segunda ação envolveu a aplicação de formulários direcionados a alunos, visando captar percepções individuais e experiências diretas sobre o tema investigado. Essa abordagem qualitativa permitiu compreender não apenas os dados quantitativos obtidos pelo CAU/BR, mas também interpretar como os estudantes vivenciam e avaliam a formação em patologias construtivas e técnicas de reparo.
Ao final do processo, os resultados das duas metodologias foram confrontados, o que possibilitou avaliar a convergência ou divergência das informações obtidas. Esse cruzamento de dados permitiu uma análise mais aprofundada, garantindo maior robustez às conclusões do estudo e proporcionando uma visão mais holística sobre o tema.

2.1 Coleta de dados do Conselho de Arquitetura e Urbanismo do Brasil (CAU/BR)

Para a obtenção e análise dos dados do CAU/BR, foram coletados 27.785 registros referentes ao período de 2012 a 2024, abrangendo 12 anos de atuação no Distrito Federal. As informações foram organizadas por bairro, região administrativa e tipo de atividade desempenhada, incluindo projeto, execução e gestão. O mapa a seguir ilustra as regiões administrativas mapeadas pelo CAU/BR.

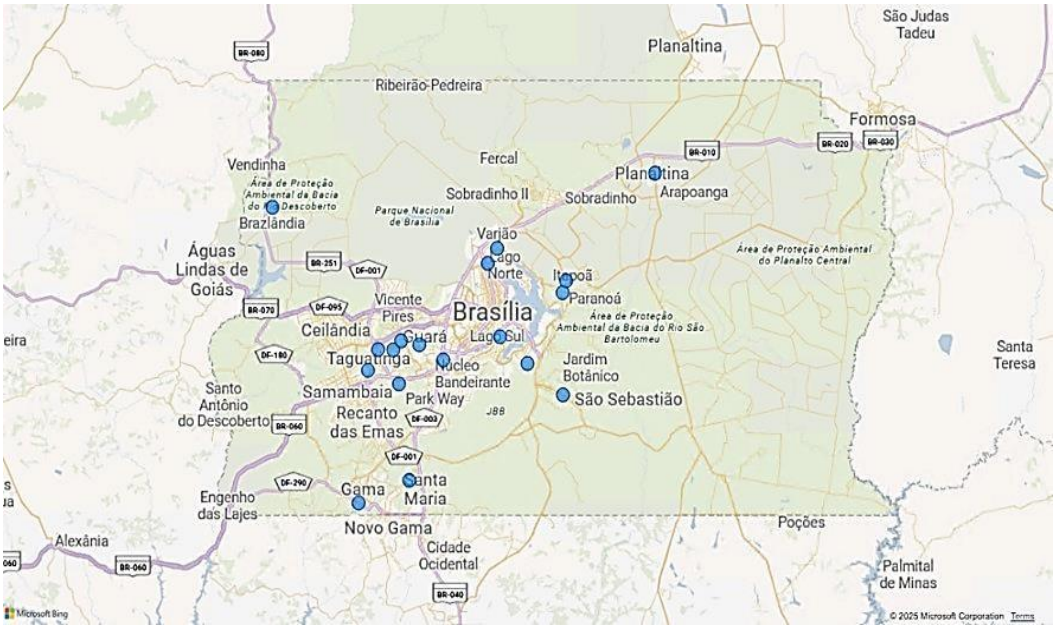


***Figura 1** - Mapa das regiões adminidtrativas do DF mapeadas pela CAU/BR*

O mapa apresentado evidencia a diversidade territorial e a abrangência do levantamento. A inclusão de diferentes áreas do DF é fundamental para compreender as variadas dinâmicas da prática profissional em Arquitetura e Urbanismo, além de reforçar a representatividade dos dados coletados dentro do espaço amostral.

2.1.1 *Tratamento de dados*

O tratamento de dados é uma etapa essencial na pesquisa científica, permitindo a organização, análise e interpretação das informações coletadas. De acordo com Creswell (2014), a forma como os dados são processados impacta diretamente a validade e a confiabilidade dos resultados, tornando indispensável a adoção de métodos adequados para garantir rigor e coerência na análise.

Neste estudo, a etapa de tratamento seguiu um conjunto de procedimentos sistemáticos para transformar as respostas coletadas em informações interpretáveis. Técnicas de categorização e visualização foram aplicadas para identificar padrões e tendências relevantes, enquanto ferramentas estatísticas, conforme recomendações de Hair et al. (2019), foram utilizadas para garantir maior precisão na análise dos resultados.

Os dados CAU/BR, ao serem recebidos, continham dados duplicados e inconsistências que exigiram um processo de refinamento para assegurar sua precisão. Foram aplicados procedimentos de limpeza e padronização, incluindo a remoção de registros duplicados, a verificação de erros e a organização das informações em um formato adequado para análise. Essas etapas foram fundamentais para garantir a qualidade dos dados e uma interpretação confiável dos resultados.

2.2 Questionários aplicados nas turmas de Sistemas Estruturais I e II

No que se refere a abordagem deste trabalho, a aplicação dos questionários para as turmas de sistemas estruturais I e II, oferecido no período noturno da Universidade de Brasília, representou uma estratégia essencial na pesquisa, com o objetivo de compreender a percepção dos estudantes acerca da efetividade e aplicabilidade do currículo em sala de aula. Os questionários aplicados mostram uma aproximação com a realidade da formação, sendo uma forma válida de investigar a percepção sobre ensino e reabilitação. A opinião dos alunos é de grande importância, visto que são os principais receptores do conteúdo acadêmico e podem fornecer informações valiosas sobre a dinâmica das aulas, o processo de aprendizado, as dificuldades enfrentadas, entre outros aspectos relevantes. Os estudantes demonstraram grande receptividade e interesse em responder a todas as questões propostas.

O instrumento foi composto por sete questões, que buscavam captar as opiniões dos alunos sobre diversos aspectos do ensino de Estruturas. As questões abordaram os seguintes tópicos:

1. Em sua opinião, a composição curricular do ensino de Estruturas do seu curso está alinhada com os novos mecanismos e ferramentas tecnológicas recentes?
2. Você percebe alguma dificuldade de comunicação entre arquitetos e engenheiros estruturais?
3. Em sua opinião, a carga horária do ensino de Estruturas é suficiente para um aprofundamento teórico e prático do tema?
4. Você acredita que o ensino de Estruturas poderia ter mais conexões com disciplinas como design arquitetônico, sustentabilidade e construção, ampliando a prática arquitetônica?
5. Você considera que a integração entre teoria e prática poderia fomentar o desenvolvimento de habilidades práticas em projetos reais?
6. O currículo do curso é adequado no que se refere à sustentabilidade, incluindo orientações sobre o uso de recursos de baixo impacto ambiental?
7. Diante das questões abordadas acima, você sugeriria alguma readequação no currículo do seu curso?

Para as sete perguntas, cada aluno podia escolher uma das seguintes opções: Adequado, Pouco adequado, Inadequado e Muito adequado. Em resumo, o objetivo do questionário era realizar uma análise detalhada da percepção dos estudantes em relação à grade curricular. As respostas obtidas forneceram dados valiosos para identificar possíveis lacunas no ensino, além de oferecer sugestões para o aprimoramento do curso.

3. Análise e Resultados

A metodologia dupla desta pesquisa revelou uma lacuna entre as demandas do mercado de trabalho contemporâneo e os resultados da formação acadêmica. A análise dos dados do CAU/BR para a região federal mostrou que apenas 20% dos Registros de Responsabilidade Técnica (RRTs) assinados por arquitetos se referiam a projetos de construção, em comparação com 80% para projetos arquitetônicos tradicionais, conforme ilustrado na Figura 2. Além disso, os projetos de construção representaram apenas 25% dos registros. Essa discrepância quantitativa indica que a formação acadêmica de arquitetos não prioriza adequadamente o ensino de técnicas de construção e reabilitação, levando diretamente a uma diminuição da demanda profissional por esses serviços e ao afastamento gradual dos arquitetos de projetos tecnicamente exigentes. Isso está em consonância com as respostas observadas entre os estudantes na pesquisa; eles percebem essa disciplina como complexa, técnica e inerentemente difícil, o que dificulta sua conexão com o processo criativo de projeto. Ademais, a pesquisa revelou uma distribuição desigual desses projetos. A maioria das Equipes de Resposta Rápida (ERR) está concentrada em áreas densamente povoadas e edifícios antigos, o que reforça a necessidade de treinamento especializado que leve em consideração as características estruturais e a patologia dos edifícios em diversos contextos urbanos, estabelecendo assim uma ligação ainda maior entre teoria e prática.

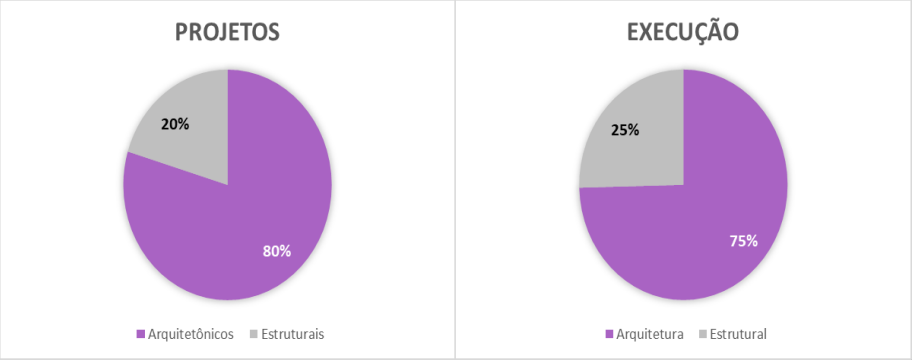


Figura 2 *– RRTs relacionados aos projetos arquitetônicos e estruturais (CAU/BR)*

Em relação aos questionários aplicados aos alunos, os resultados revelaram que 64% concordaram que a carga horária destinada ao ensino da construção civil era insuficiente, enquanto 78% reconheceram dificuldades na comunicação com os engenheiros. A distribuição das respostas entre as quatro opções disponíveis para cada uma das sete perguntas é apresentada na Tabela 1.

Tabela 1 – Resultados dos questionários aplicados

Questionários	Adequado	Pouco adequado	inadequado	Muito adequado	Total
1. Composição Curricular	14	22	4	2	42
2. Comunicação entre engenheiros e arquitetos	11	22	5	4	42
3. Carga horária do Ensino de Estruturas	15	18	5	4	42
4. Ampliação no ensino de Estruturas e conexão com outras áreas	18	2	2	20	42
5. Integração entre Teoria e Prática	16	1	1	24	42
6. Sustentabilidade Estrutural	6	15	17	4	42
7. Necessidade de readequação no currículo	27	5	2	8	42

Para analisar os questionários e fornecer uma visão mais clara das respostas, o diagrama de radar apresentado na Figura 3 exibe as sete questões utilizadas na análise do questionário, ilustrando a distribuição das variáveis, os aspectos proeminentes e os aspectos que necessitam de maior atenção.

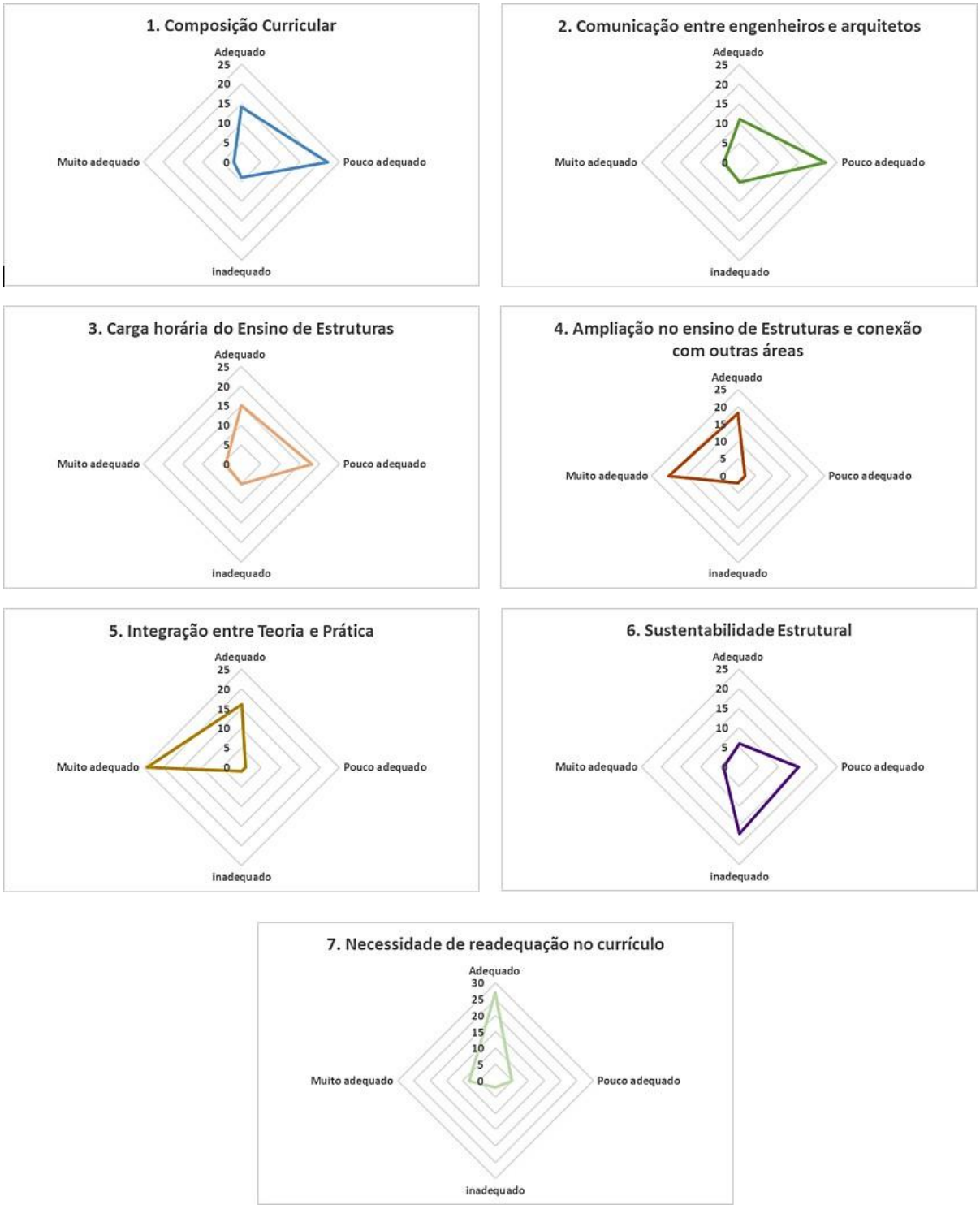


Figura 3 – *Gráficos do tipo radar para os resultados obtidos (CAU/BR)*

Após a análise das respostas dos alunos, os resultados revelaram importantes percepções sobre diversos aspectos do ensino da construção civil no currículo de arquitetura. Em relação ao alinhamento do currículo com os avanços tecnológicos, muitos alunos indicaram que, embora seja parcialmente compatível com as mudanças tecnológicas, ainda requer ajustes para integrar de forma mais eficaz novas ferramentas e desenvolvimentos na área. Quanto à comunicação entre arquitetos e engenheiros civis, uma parcela

significativa dos alunos apontou dificuldades na interação entre essas duas profissões, sugerindo que a formação poderia incorporar mais conteúdo focado na colaboração interdisciplinar para superar esses obstáculos. Em relação ao tempo dedicado ao ensino da construção civil, muitos alunos indicaram que o tempo disponível é insuficiente para uma compreensão profunda dos conceitos e sua aplicação prática, destacando a necessidade de revisar o cronograma do currículo. No que diz respeito à conexão entre o ensino da construção civil e outras áreas do conhecimento, como projeto arquitetônico e sustentabilidade, os alunos manifestaram apoio a uma maior integração dessas disciplinas, o que poderia proporcionar uma formação mais abrangente e alinhada às demandas da prática contemporânea.

Em termos profissionais, os graduados enfatizaram que essas lacunas acadêmicas têm repercussões diretas na prática contemporânea, levando à falta de independência técnica e à baixa qualidade generalizada nas intervenções de reabilitação estrutural. Essa desconexão não só ameaça a integridade estrutural dos edifícios, como também resulta em falhas estruturais que poderiam ter sido evitadas com uma base acadêmica mais coerente. Isso, por sua vez, acarreta consequências econômicas significativas devido à dependência de reparos corretivos dispendiosos em vez de manutenção preventiva. Um aluno expressou esse sentimento, afirmando que se contenta em memorizar equações complexas para passar nas provas, sem ser capaz de traduzi-las em ferramentas para diagnosticar defeitos em edifícios ou avaliar a segurança de estruturas existentes. Isso gera uma ansiedade que os levará a evitar projetos de reabilitação no futuro, temendo a responsabilidade técnica para a qual não foram adequadamente preparados.

Em relação às entrevistas realizadas com membros do corpo docente para analisar o processo educacional, suas declarações revelaram as causas dessa crise e algumas soluções potenciais dentro dos currículos universitários atuais. Os alunos se formam com conceitos básicos, mas carecem da profundidade estrutural necessária para tomar decisões técnicas cruciais. Esse problema foi destacado em uma resposta, que afirmou: "O maior desafio enfrentado pelos alunos não é necessariamente a compreensão dos conceitos estruturais, mas sim a aplicação de fórmulas, devido a deficiências específicas em matemática fundamental". A abundância de cálculos não relacionados ao projeto arquitetônico é um grande obstáculo para os alunos, reforçando a desconexão entre o conteúdo técnico e o processo criativo. Um professor apontou que a ausência de atividades experimentais, como maquetes estruturais e simulações computacionais, dificulta a compreensão dos conceitos. Embora alguns tenham tentado usar modelos de molas e madeira para ilustrar a dinâmica das falhas estruturais, observando que os alunos só compreendem a física da construção quando vivenciam diretamente as limitações e fragilidades dos materiais, esse esforço permanece individualista devido à falta de laboratórios especializados em engenharia estrutural.

4. Conclusão

A ausência de uma formação sólida e direcionada à reabilitação de edificações compromete diretamente a qualidade técnica das intervenções realizadas no ambiente construído. Profissionais que não dominam adequadamente as patologias construtivas e as técnicas de reparo tendem a propor soluções ineficazes, que resultam em falhas recorrentes, comprometendo a durabilidade das obras, a segurança dos usuários e a integridade estrutural dos edifícios. Tais deficiências são especialmente críticas em contextos de reabilitação, nos quais o diagnóstico preciso, a leitura adequada do existente e a compatibilização entre o antigo e o novo são fatores determinantes para o sucesso da intervenção.

Neste cenário, a aproximação entre os conteúdos formativos e as demandas concretas da prática profissional em reabilitação torna-se urgente. Os dados analisados neste estudo reforçam a necessidade de atualização curricular nos cursos de Arquitetura e Urbanismo, com foco explícito em disciplinas voltadas à identificação de patologias, métodos de reabilitação estrutural e intervenções sustentáveis em edificações existentes. Ao mesmo tempo, a integração entre arquitetos e engenheiros, frequentemente fragilizada por falhas de comunicação e formação fragmentada, revela-se como um eixo fundamental para garantir abordagens interdisciplinares mais eficazes.

Embora o currículo atual apresente avanços pontuais, os resultados demonstram que ainda persistem lacunas significativas que comprometem uma formação técnica integrada. É imperativo promover uma reestruturação curricular que preserve o embasamento teórico essencial, mas que também incorpore metodologias ativas, experiências práticas em campo e conteúdos específicos sobre reabilitação de edificações. Só assim será possível preparar arquitetos aptos a atuar com precisão técnica, sensibilidade patrimonial e responsabilidade social.

Além disso, questões como sustentabilidade estrutural, abordagens compatíveis com os desafios ambientais e a ampliação da carga horária dedicada ao ensino de estruturas devem ser trazidas ao centro do debate acadêmico, contribuindo para uma formação mais crítica e conectada às exigências do presente e do futuro da construção civil.

Em síntese, este estudo reforça a urgência de uma formação arquitetônica mais conectada com as práticas contemporâneas de reabilitação, tanto no plano técnico quanto metodológico. Ao defender um ensino que una teoria, prática e interdisciplinaridade, propõe-se não apenas uma revisão curricular, mas um reposicionamento estratégico da formação profissional, capaz de enfrentar os desafios impostos pela crescente demanda por intervenções em edificações degradadas. Fica o convite para que futuras pesquisas explorem novas metodologias pedagógicas voltadas à reabilitação e que políticas públicas e institucionais priorizem a atualização curricular como um passo essencial rumo a uma arquitetura mais qualificada, responsável e transformadora.

Agradecimentos

Este trabalho foi financiado por: Coordenação de Aperfeiçoamento de Pessoal de Nível Superior (CAPES), através da concessão de bolsa de estudos à primeira autora durante seu Mestrado no Programa de Pós-Graduação em Arquitetura e Urbanismo da Universidade de Brasília.

Referências

BAUER, Martin W.; GASKELL, George. Pesquisa qualitativa com texto, imagem e som: um manual prático. Petrópolis: Vozes, 2002.

CAMPANELLI, L. Teoria e prática do restauro. Roma: Laterza, 2009.

CARVALHO, A. Ensino de Arquitetura: uma abordagem crítica. São Paulo: Editora Unesp, 2003.

CRESWELL, J. W. Research Design: qualitative, quantitative, and mixed methods approaches. 4. ed. Los Angeles: Sage, 2014.

FRANCO, M. História das estruturas: uma abordagem didática. Lisboa: Calouste Gulbenkian, 1974.

GAMILI, R.; BUZAR, R.; PANTOJA, J. Transformação do ambiente construído: uma abordagem histórica e social. Brasília: UnB, 2022.

HAIR, J. F. et al. Essentials of business research methods. 4. ed. New York: Routledge, 2019.

HARRIS, R. Information Graphics: a comprehensive illustrated reference. New York: Oxford University Press, 2001.

LUMI, A. A formação em restauro arquitetônico. Firenze: Edizioni ETS, 2003.

PEREZ, F. Arquitetura e ensino: reflexões sobre metodologia. São Paulo: Studio Nobel, 1999.

PERRENOUD, P. Construire des compétences dès l'école. Paris: ESF, 1999.

SANTOS, M. Ensino e aprendizagem no ensino superior. São Paulo: Cortez, 2005.

UNIVERSIDADE DE BRASÍLIA. Diretrizes Curriculares do Curso de Arquitetura e Urbanismo. Brasília: UnB, 2024.

SHARP, D. História em imágenes de la Arquitectura del Siglo XX. Madri: Editorial Gustavo Gili S. A., 1972.

Cinpar 2026
XXII International Conference on Building Pathology and Constructions Repair
15th to 17th July 2026 - Lisboa, Portugal

Semantic Structuring of Generic HBIM Elements for Building Systems

Francisco Carlos SANTANA[1], Rafael Fontenele JÚNIOR[2], Esequiel MESQUITA[3], **Mylene de Melo VIEIRA[4]**

[1]Universidade Federal do Ceará (UFC), Ceará, Brazil, franciscosantana@alu.ufc.br
[2]Universidade Federal do Ceará (UFC), Ceará, Brazil, rafaelfontenelejunior@alu.ufc.br
[3]Universidade Federal do Ceará (UFC), Ceará, Brazil, emesquita@ufc.br
[4]Universidade Federal do Ceará (UFC), Ceará, Brazil, mylene.melo@ufc.br

Abstract: Heritage Building Information Modelling (HBIM) enables the creation of digital models of historic buildings that can be used for strategic information management throughout the asset life cycle. The definition of the Asset Information Requirements (AIR), according to ABNT NBR ISO 19650-1 (2022), plays a central role in delimiting the scope of the model. For maintenance purposes, especially in historic buildings, an AIR oriented toward operational efficiency may prioritize semantically rich models with lower geometric accuracy, in favour of computational performance and model usability. In building systems such as water supply, sanitary sewage, and stormwater drainage, a lower level of geometric detail combined with a higher level of semantic information, related, for example, to maintenance plans, can result in a model that is highly useful for asset management and operation. This study proposes the development of an HBIM maintenance model for the water supply, sanitary sewage, and stormwater systems of the José de Alencar Theatre, a historic building located in the city of Fortaleza, Ceará, Brazil. The methodology is based on field surveys and the creation of HBIM with a grouped structure, in order to incorporate essential maintenance information for inspections, documentation, and component quantification, while maintaining flexibility for targeted interventions, the creation of identification codes (IDs), and the organization format of this information within the model. The results indicate that the parameterization of HBIM model elements with maintenance-related semantic information enables the creation of a tool for the management and conservation of built heritage.

Keywords: Heritage Building Information Modelling, Information Modelling, Building systems, Maintenance, Autodesk Revit.

1. Introduction

Building Information Modelling (BIM) has established itself as a widely used digital methodology to support different activities throughout the building lifecycle, enabling the integration of geometric and semantic information into a shared digital model among various professionals (Rojas et al., 2019). In this context, HBIM emerges as a specialized extension of BIM focused on the survey, documentation, and management of historical buildings, incorporating information related to the construction, historical, and cultural characteristics of architectural heritage (Murphy et al., 2009).

Unlike traditional BIM applications, where the digital model is generally developed from the design and follows the construction process, HBIM operates on existing buildings. In many cases, these structures have undergone centuries of transformations, adaptations, and interventions, which makes the documentation process more complex. Thus, the digital model needs to be built from the existing reality, using surveys such as laser scanning, photogrammetry, and point clouds to digitally reconstruct architectural elements (Bruno & Roncella (2019); Arayici et al., 2017; Roncella, 2019).

The management and conservation of built heritage require a broad set of information about the building, including materials, construction techniques, intervention history, and the state of conservation of elements.

Obtaining this data often involves documentary research, field surveys, and technical analyses, which can demand a significant investment of time and resources (Meseguer et al., 2023). Furthermore, the study of historical buildings involves knowledge that extends beyond the fields of engineering and architecture, requiring the participation of professionals such as historians, archaeologists, conservators, and cultural heritage experts (Maxwell, 2016). In this sense, HBIM is also characterized by its interdisciplinary nature, allowing the integration of different types of knowledge into a shared digital environment (Historic England, 2017).

Despite the potential of the methodology, several studies indicate that a gap still exists between theoretical advances in HBIM and its practical application. A large part of the initiatives focuses mainly on the geometric modelling of buildings, while the informational structuring of the models receives less attention (Parente et al., 2025; Wang et al., 2025). Although processes known as Scan-to-BIM allow converting three-dimensional surveys into digital models, they do not automatically generate the semantic information necessary for building management. Thus, data related to materials, construction pathologies, state of conservation, and intervention history need to be obtained through on-site inspections and complementary documentary research.

Another recurring challenge relates to the efficiency of the modelling process. In HBIM projects, the creation of parametric components often depends on reverse modellingprocedures based on point clouds, which can make the process time-consuming and complex, especially when it involves irregular geometries or ornamental elements characteristic of historical architecture (Wang et al., 2025). In some cases, this process can result in the simplification or even loss of part of the geometric information captured during the digital survey (Delpozzo, Appolonia, Scala, and Adami, 2022).

In this context, the semantic dimension becomes fundamental for the development of HBIM models capable of supporting the management of built heritage. A heritage information model must go beyond the three-dimensional representation of the building, incorporating data related to the materials, construction techniques, state of conservation, and historical value of the elements that make up the building (Historic England, 2017). This information is particularly relevant when considering the integration between HBIM and Facilities Management (FM), as facility management depends on access to structured data that allows planning maintenance, conservation, and operation activities over time Tsay et al. (2023).

However, the use of BIM for Facilities Management still presents important challenges related to the definition and management of information necessary for the building's operation phase. According to Cao et al. (2019), few studies address the problems related to the clear definition of information requirements demanded by asset owners and managers. Furthermore, Tsay et al. (2022) point out that there is still limited knowledge about the application of BIM in facility management, which hinders the proper definition of the information needed to support operational processes.

Matarneh et al. (2019) also highlight that many research initiatives have focused on developing new technologies, while structural issues related to information organization and flow remain underexplored. For BIM to be used more efficiently in facility management, it becomes necessary to ensure the continuity of information flow between BIM and FM systems, create structured repositories of operational data, and develop mechanisms that allow the sharing and updating of this information across different sectors of the organization.

In conventional BIM projects, the transition between the design model and the operation model often involves the exclusion of information considered irrelevant for the maintenance phase (Gao and Pishdad-Bozorgi, 2019). In the case of historical buildings, however, the opposite problem frequently occurs: the scarcity and fragmentation of available information. Records related to renovations, component replacements, or technical specifications are often not available in a systematized way, which compromises decision-making capacity related to the conservation of built heritage (Martinelli, Calcerano, and Gigliarelli, 2022).

In this scenario, HBIM can assume a strategic role in the organization and reconstruction of the building's technical memory, functioning as a digital environment capable of integrating different types of information related to the heritage asset. For this, the proper structuring of data within the model becomes fundamental.

Families in the model play a central role in this process, acting as the main repositories of semantic information within the HBIM model. Through these structures, it is possible to standardize construction elements, assign unique identifiers to components, link external documents, and incorporate data related to maintenance, inspection, and intervention history (Murphy et al., 2017). The definition of these attributes should be guided by pre-established information requirements, such as Organizational Information Requirements (OIR) and Asset Information Requirements (AIR), as established by ABNT NBR ISO 19650-1 (2022).

Given this context, this study proposes an information structuring system in HBIM that begins with on-site surveying and develops through the organization and structuring of generic families for the semantic feeding of data into the digital model. The approach prioritizes the adequate informational input of these families, allowing the generation of quantity takeoffs and supporting analysis and decision-making processes.

Additionally, it seeks to ensure information interoperability through the use of the Dynamo tool, allowing the integration and updating of data related to building maintenance. The method also considers the optimization of the digital model's performance, prioritizing its computational lightness and ease of manipulation.

The application of the proposed system is directed towards the building facilities systems of the José de Alencar Theatre, with the objective of demonstrating the potential of HBIM as a tool to support the management and maintenance of historical buildings. Thus, the developed model is configured not only as a digital repository of the existing architecture but as an instrument capable of supporting the conservation and management processes of built heritage.

2. Methodology

This study proposes an applied methodology for the development of an HBIM model oriented towards the Operations and Maintenance (O&M) management of the plumbing and drainage systems systems of the José de Alencar Theatre , in Fortaleza–CE, Brazil. The approach is based on prioritizing the informational functionality of the model, balancing geometric simplification and semantic enrichment. Modelling with a low Level of Development (LOD) and a high Level of Information (LOI) was chosen, privileging computational performance, organizational clarity, and practical applicability in the context of building maintenance.

The model was conceived so that its elements would act not only as simplified graphic representations but as structured information containers, capable of integrating technical, operational, and heritage data in an associated and hierarchical manner. Figure 1 presents the methodology organised in five main stages: survey, semantic structuring, family development, coding, and information management, which are articulated in a progressive and interdependent way.

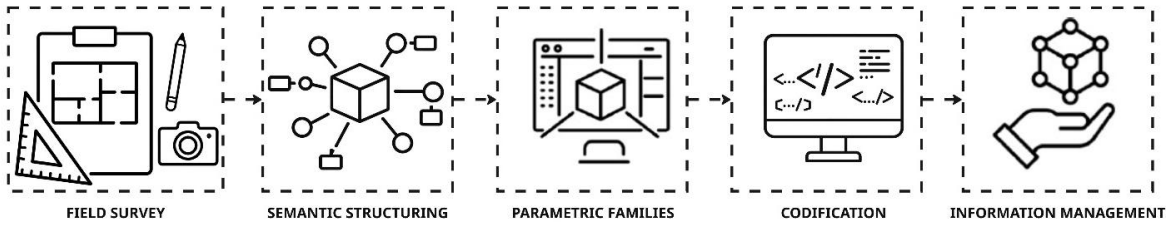


Figure 1 – Methodological process

2.1 Survey and Functional Analysis of the Plumbing and Drainage Systems

The research began with an on-site survey of the building's visible plumbing and drainage systems elements, including washbasins, toilets, faucets, traps, gutters, and other visible components. When available, information regarding brand, manufacturer, model, material, dimensions, colour, system membership, location, installation date, and associated technical documentation was collected.

The survey was complemented by photographic records and the analysis of existing documentation, seeking to consolidate a reliable information base for modelling and semantic enrichment. In parallel, an understanding of the systemic functioning of the hydraulic, sanitary, and stormwater subsystems was developed, recognizing their operational interdependencies.

It was observed that many components operate in an integrated manner within functional assemblies, such as in the case of the washbasin, which brings together elements belonging to different subsystems, but whose performance depends on the articulated functioning of all its components. This finding highlighted the need for constructing associations between elements through information organization, guiding the subsequent semantic structuring.

2.2 Hierarchical Semantic Structuring of the Plumbing and Drainage Systems

Based on the functional analysis, a hierarchical semantic structure was developed at two complementary levels, capable of reflecting both the operational logic of maintenance routines and the technical individuality of the components.

The first level corresponds to the functional assembly, which groups elements located in the same environment and that operate in an integrated manner to perform a specific function. Associated with this level is information related to recurring inspection, cleaning, and preventive maintenance routines, aligning the model with the practice of technical teams.

The second level corresponds to the individual component, to which its own identifiers and specific technical parameters are assigned, enabling asset inventory, quantity takeoffs, and targeted corrective interventions. The coexistence of these two levels allows for hybrid management within the model itself, articulating collective and individual information without redundancies and maintaining organizational coherence, as illustrated in Figure 2.

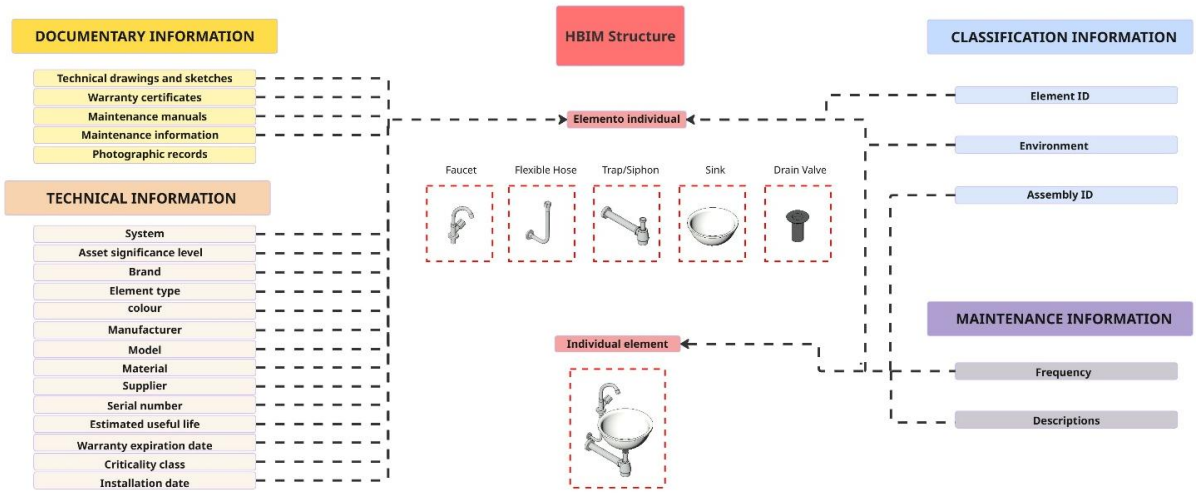


Figure 2 – HBIM Structure for Information Management of Plumbing and Drainage Systems Elements

2.3 Development and Hierarchical Organization of Generic Elements

The implementation of the semantic structure in the HBIM environment occurred through the adaptation and creation of generic elements oriented towards the specific demands of Facility Management (FM). Initially, conventional elements were debugged, with the removal of parameters irrelevant to the operations and maintenance phases. Subsequently, shared parameters were inserted for the incorporation of technical and documentary information, as well as for the creation of new parameters when necessary.

As this is a historic building, some families needed to be custom-developed to ensure coherence with the actual conditions of the construction. Although kept at a generic level and with simplified geometry, these families were adjusted so as not to represent construction typologies incompatible with the existing reality. An example is the case of masonry water tanks, which could not be represented by conventional fiber cement or plastic reservoirs. This adaptation ensured spatial compatibility and interpretive consistency in the model.

To support the hierarchical structure of information, the families were not only debugged or created individually but also organised in a hierarchical manner. Each family is composed of grouped subfamilies, as illustrated in Figure 3 as in the example of the washbasin, which integrates elements such as the faucet, pipes, and trap. These components maintain their individual representation in the model, allowing both the quantification of elements and the insertion of specific information. Simultaneously, the assembly is treated as a single element, enabling the management of collective information, such as cleaning procedures and periodic inspections.

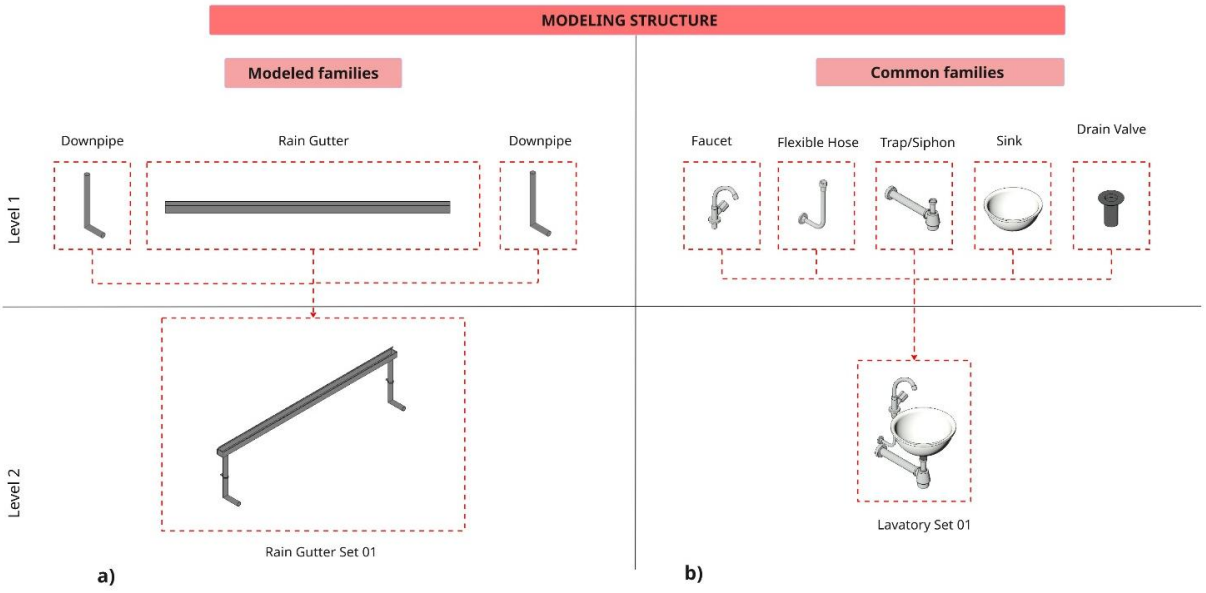


Figure 3 – Illustrates the modelling and hierarchical structuring of elements: (a) geometric modelling process by extrusion in Revit software; (b) generic elements.

Geometric modelling adopted simplified representations, sufficient for the spatial identification of elements, avoiding excessive detailing. This strategy reduced the complexity of the model and optimised its computational performance, while simultaneously promoting semantic enrichment. The proposed structure also ensures adaptability, allowing continuous data updates without the need for remodelling, preserving traceability throughout the entire building lifecycle.

2.4 Hierarchical Coding and Identification System for HBIM Elements

To ensure traceability, standardization, and interoperability with Computerized Maintenance Management Systems (CMMS), a hierarchical coding system was developed that articulates two levels of identification:

Main Code (Assembly ID): identifies a logical grouping of components, which may correspond to a single system or integrated systems. It is used to associate recurring cleaning, inspection, and preventive maintenance routines, as well as general work orders. Its composition includes a prefix referring to the type of assembly (e.g., BAS for toilet) and a sequential numerical suffix that functions as a unique identifier (e.g., BAS01-005).

Sub-code (Element ID): individualizes each component within the assembly, allowing for the recording and control of element-specific information. It is formed by the main code plus a letter for each component (e.g., BAS01-005A for the toilet bowl, BAS01-005B for the seat, BAS01-005C for the flexible hose). When there is more than one identical element, a number is added after the identifying letter. Figure 4 illustrates the implementation of this hierarchical identification system within the model interface.

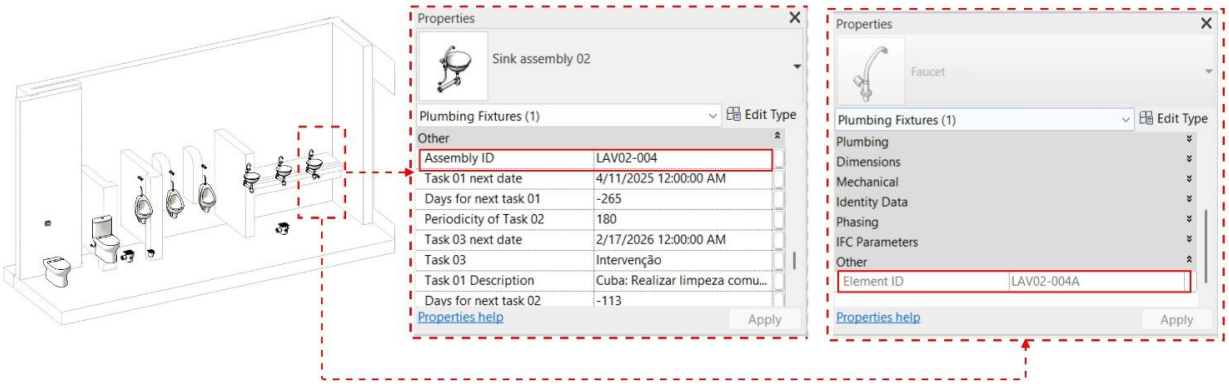


Figure 4 – Implementation of the hierarchical identification system in the model, highlighting the Assembly ID (group level) and Element ID (component level) parameters.

This system guarantees the unambiguous identification of both individual families (components that make up an assembly) and grouped families (the functional assembly as a whole). The structure facilitates data extraction for generating tables and reports, allows direct association with work orders, and enables integration with Excel spreadsheets through Dynamo.

Inserting information into the grouped elements contributes to reducing the informational load of the model, since data related to periodic maintenance, such as cleaning and inspection, is associated directly with the assembly. In practice, these procedures are applied simultaneously to all elements that make up the group, eliminating the need to replicate the same information in each individual component. This approach reflects the actual operations and maintenance flows more faithfully.

Concurrently, the parameters were organised according to their operational purpose, distinguishing information associated with the functional assembly (such as inspection frequency) from that linked to individual components (such as technical specifications and asset data). This organization strengthens the informational logic of the model and expands its compatibility with external management flows, allowing both the visualization of information for a specific element and the monitoring of cleaning routines applied to the group as a whole.

2.5 Hybrid Information Management Strategy

Considering that the BIM environment is not ideal for the extensive storage of voluminous documentation, a hybrid information management strategy was adopted. In this arrangement, only identification, classification, and operational decision-support data remain incorporated into the HBIM model families, while extensive documents, such as technical manuals, detailed reports, photographic records, and complete maintenance histories, are stored in structured external repositories, linked to both the elements and the families depending on the information.

Information related to maintenance, such as cleaning and inspections, is linked to the model through the assembly ID, using routines developed in Dynamo integrated with Excel, according to an approach adapted from Bessa et al. (2025). Unlike conventional approaches, which associate this data with individual elements, in this work the information remains directly linked to the grouped families, reflecting real-world operation and maintenance practices more faithfully (see Figure 5).

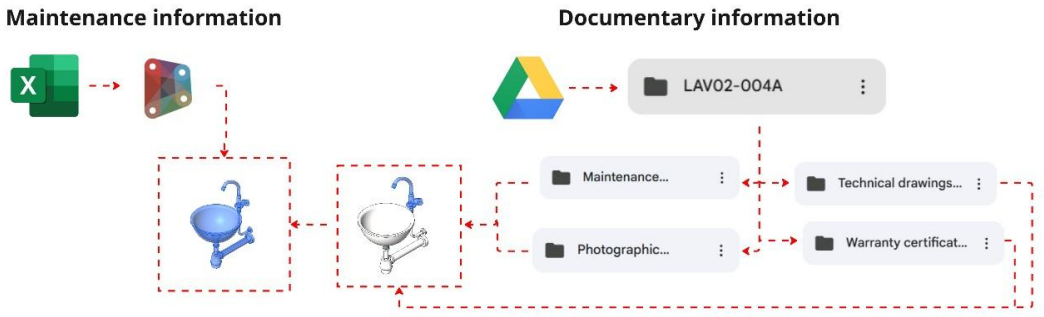


Figure 5 – Hybrid information management workflow: maintenance data integrated into the HBIM model via Excel and Dynamo (left), and documentary information stored in structured Google Drive repositories and linked to the model elements (right).

The connection between the elements represented in HBIM and externally stored documents is established through link parameters or coded references, ensuring a direct association between each element and its corresponding documentation. This approach keeps the model lightweight, navigable, and functional, favours dynamic updates, and expands the potential for interoperability with CMMS systems.

Thus, HBIM is conceived not as an absolute data repository, but as an organizing and visual interface for strategic information, oriented towards the effective support of operation and maintenance activities in historic buildings.

3. Results and Discussion

Regarding the survey of semantic information, this resulted in a considerable amount of data about the elements, such as type, location, colour, material, and manufacturer. However, some information could not be located, either because it was lost over time or because it was never recorded, such as serial number, warranty validity, and installation date. This gap is partly due to the fact that the building is in continuous use, which implies recurring replacements of components over time, whether due to the unavailability of original parts on the market or the need to adapt the system to the building's operation. In Figure 6, it is possible to observe these replacements of plumbing and drainage systems elements.



Figure 6 – Illustrates the replacement of plumbing and drainage system elements over time. (A) Original washbasin with a single operating handle, with the opposite side missing, indicating loss of components. (B) Washbasin after intervention, with the lateral holes sealed and a new faucet installed, demonstrating adaptation to current use conditions.

The installation dates of some elements could be estimated based on the set of characteristics, suggesting they belong to the last major renovation of the building, which took place in 1991. For the remaining elements, the corresponding fields were retained in the model's structure as fillable fields, even though they remained blank at the time of the survey.

Regarding modelling with a low Level of Development (LOD), nine grouped generic elements were developed, structured from grouped generic elements, comprising: one set of inlet valve, two distinct sets of toilets, four lavatories/sinks, one set of urinal, and one set of shower. Some elements remained isolated, bathroom drains, garden faucet, and bathroom valve, as they did not fit into the established grouping categories. For the infrastructure components, two sets of water tanks, thirteen sets of gutters, and seven sets of garden drains were modelled. In Figure 7, it is possible to observe the two generic modelling approaches adopted.

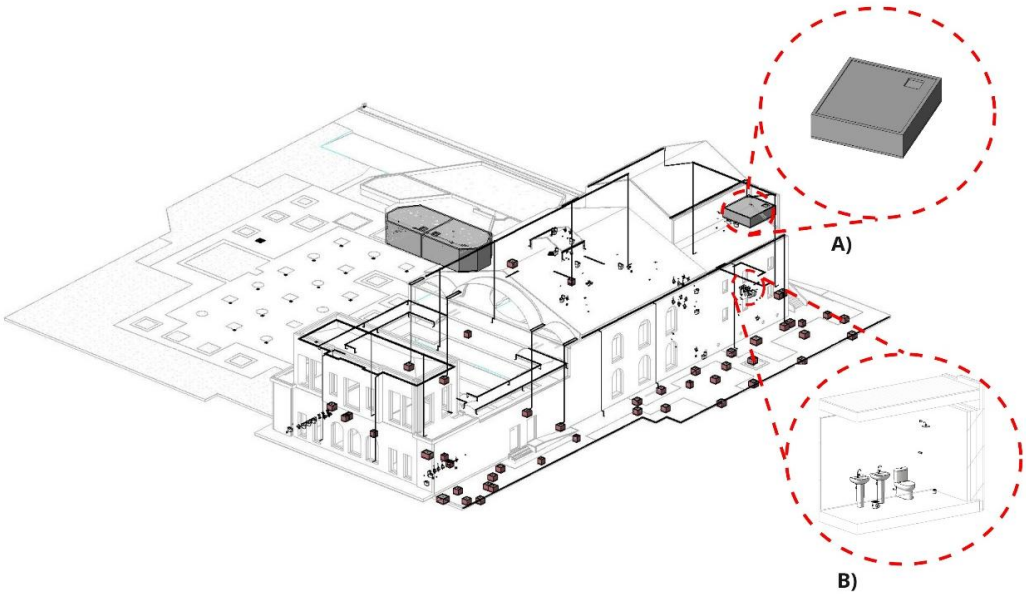


Figure 7 – Illustrates generic modelling approaches with a low Level of Development (LOD). (A) Simplified modelling approach based on minimal geometric representation of elements. (B) Modelling approach

based on aggregation of existing generic elements, which were cleaned, adapted, and combined into unified generic elements.

The strategy of adopting a low LOD associated with generic families allowed for eventual component replacements to be carried out by updating semantic information, without the need for geometric remodelling, an aspect particularly relevant for a building in continuous use, subject to modifications arising from operational needs and the unavailability of original parts on the market.

Regarding coding and integration with external tools, identifiers (IDs) were created for all model elements, enabling their integration with routines developed in Excel and Dynamo. A routine was implemented in Dynamo, as per Bessa (2025), applied to the plumbing and sanitation elements, allowing a maintenance spreadsheet, containing information on inspection, cleaning, and preventive maintenance based on current standards, to be integrated into the model. This integration enabled the functional assemblies to receive such information, as illustrated in Figure 8.

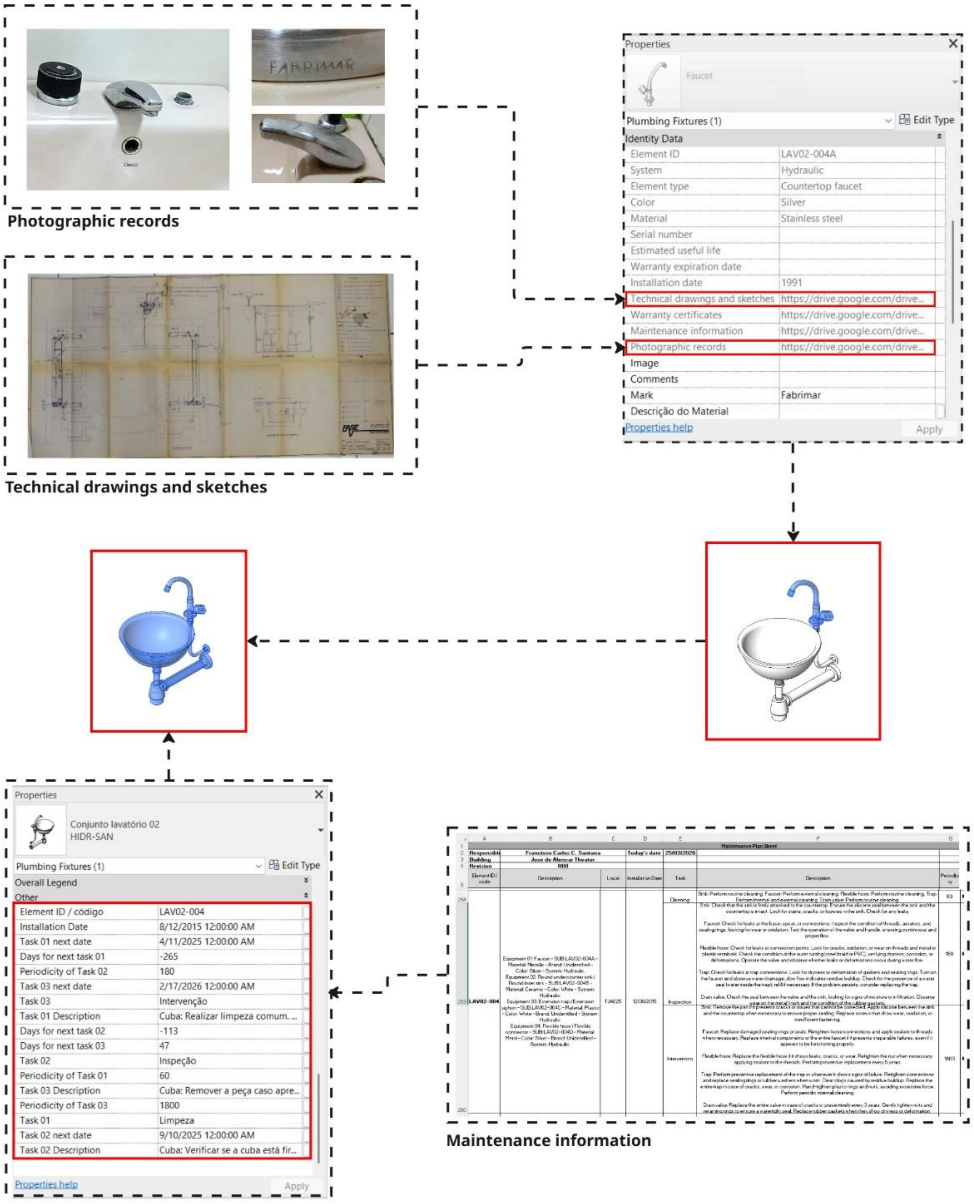


Figure 8 – Bidirectional information flow in the HBIM model. Top-down flow connects documentary and semantic information to the elements through external links and embedded data. Bottom-up flow integrates maintenance information from external spreadsheets into functional assemblies via Dynamo routines.

The coding of Element IDs was applied to a selected set of faucets in order to assess the feasibility of structuring this information. In these cases, both semantic information and the corresponding technical documents, organised in folders on Google Drive and linked to the HBIM model, were associated. This approach allows the maintenance information associated with the assembly (Assembly ID) to be linked with the specific and documentary data linked to the individual elements (Element ID).

Finally, regarding the model structure, the information fields were retained even when left unfilled, ensuring that future documentary discoveries or element replacements can be recorded without requiring a restructuring of the system. This approach gives the model flexibility and the capacity for continuous updating, aligned with the dynamic nature of the building in use.

4. Conclusions

This study presented a methodology for the development of HBIM models oriented toward the operation and maintenance of plumbing and drainage systems in historic buildings, based on the articulation between geometric simplification, hierarchical semantic structuring, and hybrid information management.

Unlike approaches traditionally centered on geometric detailing, the proposed methodology prioritized the informational value of the model, adopting a low Level of Development (LOD) associated with a high Level of Information (LOI). This choice proved adequate for building a lightweight, functional model aligned with real-world building maintenance practices in historic building contexts.

The two-level semantic structure, functional assembly and individual component, proved effective in articulating, within the same HBIM environment, the demands of preventive maintenance (associated with assemblies) and corrective maintenance (linked to individual components), ensuring traceability, standardization, and informational coherence. The hierarchical coding system and the organization of parameters according to operational purpose consolidated this logic, enabling the extraction of structured data and expanding the potential for integration with external management systems such as CMMS.

The adoption of a hybrid information management strategy reinforced the role of HBIM as an organizing hub for digital assets, avoiding model overload and expanding its practical applicability in real-world Facility Management contexts. Linking through identifiers proved sufficient to guarantee the association between modeled elements and extensive documentation stored externally.

The main contributions include: (i) the proposal of objective criteria for FM-oriented geometric simplification in historic buildings; (ii) the development of a two-level hierarchical semantic structure applicable to complex building systems; (iii) the implementation of a coding system that articulates assembly and component identifiers; and (iv) the integration between modeling and operational maintenance logic through routines in Dynamo and Excel.

Among the limitations of the research, it is noted that the model was developed but has not yet been validated under real use conditions with the theater maintenance team. Future work should focus on practical validation of the system through its application in a real context and the use of questionnaires with involved users (such as maintenance technicians and professionals), in order to assess usability, efficiency, and contribution to operational activities. This approach would enable an evidence-based evaluation grounded in real-world use, strengthening the empirical nature of the research.

Additionally, the application was focused on specific plumbing and drainage systems of the José de Alencar Theatre, although these systems are composed of multiple elements and functional interdependencies. Future studies may explore the development of more robust automated integrations between HBIM and CMMS for elements embedded in families; the correlation between technical data of components and cultural information, enabling the establishment of priorities for corrective maintenance based on integrated criteria; and strategies to improve information visualization for both functional assemblies and individual elements.

In summary, the work demonstrates that the effectiveness of HBIM for Facility Management does not lie in increasing geometric complexity, but in the strategic organization of information and its alignment with building operational practices. Thus, it reinforces the transition of HBIM from a predominantly representational tool to a strategic instrument for decision support and operational management, contributing to the consolidation of more efficient, sustainable digital models oriented toward the life cycle of historic buildings.

Acknowledgments

The authors thank the Laboratory of Rehabilitation and Durability of Constructions (LAREB) and Laboratory of Digital Experience (LED) from Federal University of Ceara, Brazil, for their support. The authors acknowledge the Secretaria de Ciência, Tecnologia e Educação Superior do Ceará (Secitece) and FUNCAP (01172921/2022) through financial support to the Scientist Chief Program: Culture and the Secretary of Culture of Ceará (SECULT).

References

ARAYICI, Y. et al. Heritage Building Information Modelling (HBIM): A review of the current state of the art. In: INTERNATIONAL CONFERENCE ON HERITAGE AND DIGITAL TECHNOLOGIES, 2017. Proceedings... 2017.

BESSA, Maycon et al. Customized BIM-Maintenance System for Facilities Management. Cinpar, Brasília, p. 371-382, 2025. Anual. Disponível em: https://zenodo.org/records/16745129. Acesso em: 10 nov. 2025.

BRUNO, N.; RONCELLA, R. HBIM for Conservation: a new proposal for information modeling. Remote Sensing, [S.L.], v. 11, n. 15, p. 1751, 25 jul. 2019.

DELPOZZO, D. et al. Federated HBIM models for cultural heritage: survey model and conceptual model. The International Archives of the Photogrammetry, Remote Sensing and Spatial Information Sciences, [S.L.], v. XLVI-2/W1-2022, p. 191-197, 25 fev. 2022.

GAO, X.; PISHDAD-BOZORGI, P. BIM-enabled facilities operation and maintenance: a review. Advanced Engineering Informatics, [S.L.], v. 39, p. 227-247, jan. 2019.

HISTORIC ENGLAND. *BIM for Heritage: Developing a Historic Building Information Model*. Swindon: Historic England, 2017.

MARTINELLI, L.; CALCERANO, F.; GIGLIARELLI, E. Methodology for an HBIM workflow focused on the representation of construction systems of built heritage. Journal of Cultural Heritage, [S.L.], v. 55, p. 277-289, maio 2022.

MATARNEH, S. T. et al. Building information modeling for facilities management: a literature review and future research directions. Journal of Building Engineering, [S.L.], v. 24, p. 100755, jul. 2019.

MAXWELL, I. COTAC BIM4C Integrating Report Part 1: Conservation Parameters. [S.L.]: COTAC, 2016.

MESEGUER, L. C. et al. Digital Twins: HBIM information repositories to centralize knowledge and interdisciplinary management of architectural heritage. Vitruvio - International Journal of Architectural Technology and Sustainability, [S.L.], v. 8, n. 2, p. 64-75, 21 dez. 2023.

MURPHY, M.; MCGOVERN, E.; PAVIA, S. Historic building information modelling (HBIM). Structural Survey, [S.L.], v. 27, n. 4, p. 311-327, 2009.

MURPHY, M.; MCGOVERN, E.; PAVIA, S. HBIM for the conservation and management of built heritage. Journal of Cultural Heritage, [S.L.], v. 14, n. 3, p. 243-251, 2013.

ASSOCIAÇÃO BRASILEIRA DE NORMAS TÉCNICAS. ABNT NBR ISO 19650-1: Organização e digitalização de informações sobre edificações e obras de engenharia civil, incluindo modelagem da informação da construção (BIM) — Gestão da informação usando modelagem da informação da construção — Parte 1: Conceitos e princípios. Rio de Janeiro: ABNT, 2022.

PARENTE, M.; BRUNO, N.; OTTONI, F. HBIM and Information Management for Knowledge and Conservation of Architectural Heritage: a review. Heritage, [S.L.], v. 8, n. 8, p. 306, 30 jul. 2025.

ROJAS, M. J.; ALARCON, L.; MOURGUES, C. BIM use assessment: A review of the literature. Journal of Construction Engineering and Management, [S.L.], v. 145, n. 5, 2019.

RONCELLA, R. et al. Scan-to-BIM for built heritage: Challenges and opportunities. ISPRS Annals of the Photogrammetry, Remote Sensing and Spatial Information Sciences, [S.L.], v. XLII-2/W11, p. 1019-1026, 2019.

TSAY, G. S. Et a. BIM for Facilities Management: an investigation into the asset information delivery process and the associated challenges. Applied Sciences, [S.L.], v. 12, n. 19, p. 9542, 23 set. 2022.

TSAY, G. S. et al. BIM for FM: understanding information quality issues in terms of compliance with owner's Building Information Modeling Requirements. *Frontiers in Built Environment*, Lausanne, v. 9, 2023. DOI 10.3389/fbuil.2023.1117066.

WANG, X. et al. Bridging Heritage Knowledge and Digital Models: an HBIM integration framework. ISPRS Annals of the Photogrammetry, Remote Sensing and Spatial Information Sciences, [S.L.], v. X-M-2-2025, p. 365-372, 24 set. 2025.

Cinpar 2026
XXII International Conference on Building Pathology and Constructions Repair
15th to 17th July 2026 - Lisboa, Portugal

Caracterização de Chacotas Históricas a partir de Classificação Análoga de Rochas Sedimentares Através de Microscopia por Luz Polarizada

Anne-Mari Pessis[1], Paulo Martin [2], **Maurilio Moraes[3]**, Pablo Góes[4]

1 Fundação Museu do Homem Americano / FUMDHAM, PI, Brasil, annepessis@gmail.com

2 Universidade Federal de Pernambuco/ UFPE, PE, Brasil, paulo.maior@ufpe.br

3 Universidade Federal de Pernambuco/ UFPE, PE, Brasil, maurilio.moraes@ufpe.br

4 Universidade Federal de Pernambuco/ UFPE, PE, Brasil, e-mail: pablo.goes@ufpe.br

Resumo: Este estudo investiga o perfil tecnológico de chacotas de azulejos históricos datados dos séculos XVII e XVIII, provenientes de edificações religiosas localizadas no estado de Pernambuco, Brasil. A pesquisa concentra-se na caracterização das matérias-primas e das condições de processamento envolvidas na produção desses corpos cerâmicos, com ênfase na fração não plástica utilizada como tempero. A metodologia baseia-se na análise petrográfica por Microscopia de Luz Polarizada (MLP) em lâminas delgadas, técnica amplamente empregada em laboratório para a identificação mineralógica e textural de materiais silicáticos. A fração arenosa foi analisada segundo critérios análogos à classificação de rochas sedimentares, permitindo avaliar parâmetros morfológicos como dimensão dos grãos, esfericidade e grau de arredondamento, além da frequência relativa, distribuição e natureza das fases minerais presentes na matriz cerâmica. Os resultados evidenciam a ocorrência de seis perfis tecnológicos distintos entre as amostras analisadas, sugerindo variações nas escolhas de matérias-primas e nas práticas de preparação da pasta cerâmica, independentemente do período estilístico dos azulejos. Entre as fases cristalinas identificadas destaca-se, a presença de akermanita**,** mineral cuja formação é compatível com temperaturas de queima superiores a aproximadamente 950 °C, indicando regimes térmicos relativamente elevados para produções cerâmicas históricas. Do ponto de vista microestrutural, a análise morfológica dos grãos revela predominância de partículas angulares e de baixa esfericidade. Em observação microscópica, esses grãos atuam como concentradores de tensões na matriz vítrea parcialmente sinterizada, favorecendo o desenvolvimento de microfissuras. Tal característica contribui para aumentar a suscetibilidade das chacotas a processos de deterioração, especialmente em ambientes caracterizados por elevada umidade e intensa ação de sais solúveis, condições frequentemente observadas em edificações históricas situadas em áreas litorâneas.

Palavras-chave: Patologia das Construções; Azulejaria Histórica; Microscopia de Luz Polarizada; Petrografia Cerâmica; Perfil Tecnológico.

1. Introdução

A azulejaria histórica em Pernambuco representa um desafio para a patologia das construções devido à sua exposição a ambientes de extrema agressividade (alta salinidade e umidade ascendente) em cidades como Recife e Olinda. Além disso, os perfis tecnológicos revelam que esses azulejos são produto de trabalhos individuais de pequenos grupos, embora houvesse a intensão em controlar a produção manufatureira das Corporações de Ofício em Portugal através das *Casa dos Vinte e Quatro* e historicamente se estabelecessem, em cada período, padrões de tamanhos, cores e temáticas dos vidrados. Levando em consideração que o emprego de revestimento azulejar no interior de edificações religiosas foi uma prática importada de Portugal durante o Período Colonial, deve-se observar que as condições ambientais do país de origem são bem distintas das encontradas no litoral do Nordeste do Brasil, em especial nas cidades de Recife e Olinda, onde se concentram a maioria das igrejas estudadas. e essa circunstância de ordem natural ocorre em todos os edifícios estudados nesta pesquisa. Assim, a proposta de classificação através dos *perfis tecnológicos* possui uma aplicação prática. Isso devido às condições locais extremamente agressivas às peças azulejares, decorrentes do excesso de umidade do solo e do ar, da alta salinidade solúvel e da ineficiência do sistema de drenagem ao redor dos prédios. Essa situação ocorre porque o Recife localiza-se ao nível do mar e é recortado por rios e canais. Caso, por exemplo, da elevada umidade que existe nas paredes do Convento de Santo Antônio, infiltrando-se entre os painéis azulejares. De modo semelhante, Olinda situa-se no alto de uma colina com diversos nascedouros de água. As duas cidades, portanto, possuem situações bem mais agressivas das que se encontram nos países de origem de produção dos azulejos, e são justamente nelas onde se localização a maioria das edificações religiosas com azulejos no interior.

2. Materiais e Métodos

O procedimento analítico por Microscopia de Luz Polarizada (MLP) foi realizado em seis fragmentos cerâmicos previamente selecionados com base em critérios de preservação microestrutural. Foram priorizadas as amostras que apresentava degradação na camada vítrea superficial e integra toda a seção transversal da chacota, para a observação contínua da interface esmalte–corpo cerâmico e para a avaliação integrada da matriz argilosa e da fração arenosa ao longo da espessura do material.

Como suporte metodológico para a aplicação da MLP, adotaram-se como referências clássicas os trabalhos *Pottery Analysis: A Sourcebook*, Rice (1987) e *Ceramic Petrography*: The Interpretation of Archaeological Pottery & Related Artefacts in Thin Section Quinn, (2013).

Essas obras constituem referências consolidadas na literatura ao sistematizarem os procedimentos de análise por microscopia de luz polarizada aplicada a cerâmicas arqueológicas. Além da fundamentação teórica, apresentam estudos de caso que demonstram a eficiência da microscopia com luz polarizada na identificação de matérias-primas, tecnologias de produção e processos de transformação mineral durante a queima.

As amostras utilizadas na preparação das seções delgadas na ordem de 0,03 mm, foram fragmentos de chacotas provenientes das três igrejas localizadas em Recife e Olinda e que são representativas de distintos períodos históricos e estéticos do século XVII e XVII, 0.

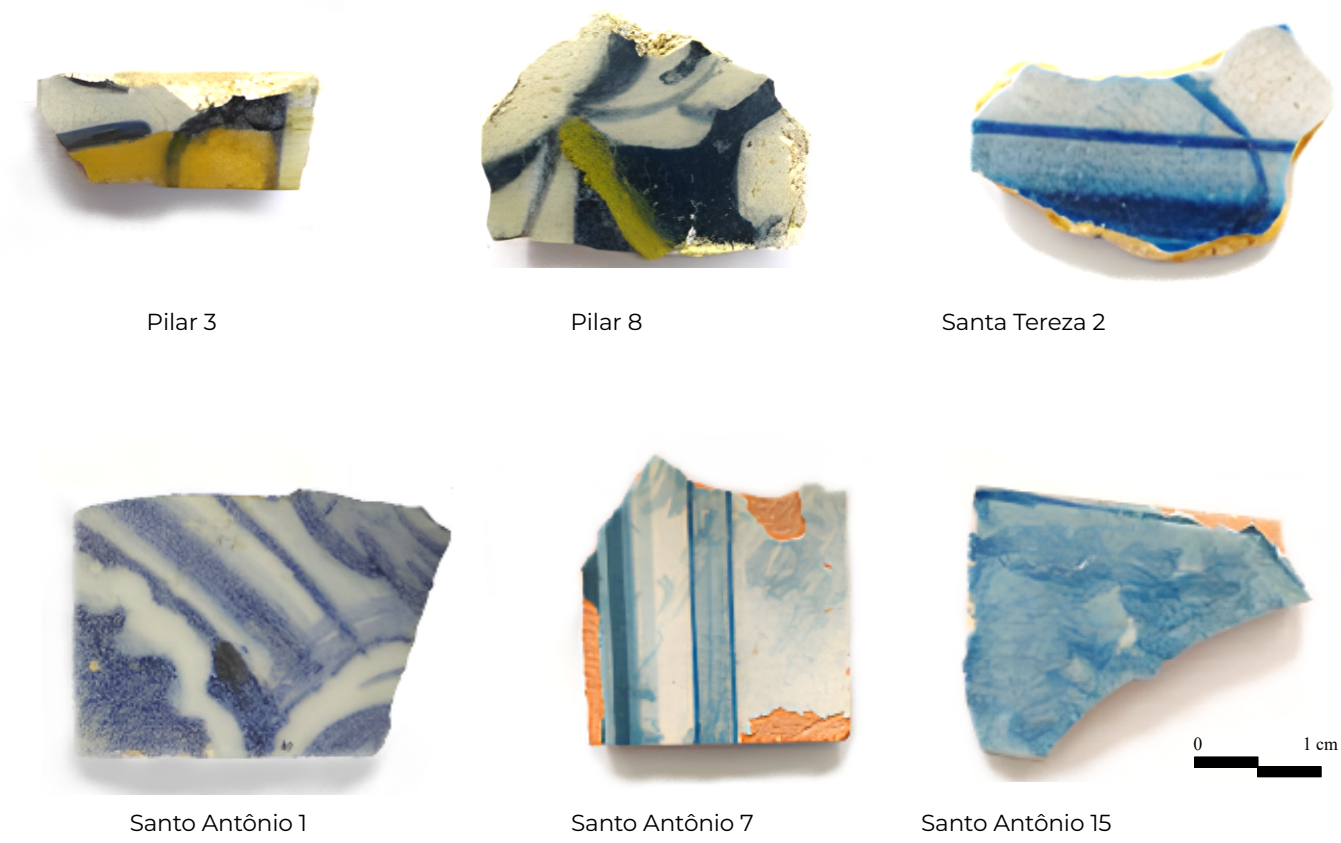


Figura 1 - Conjunto de 6 fragmentos azulejares. Do final da segunda metade do século XVII, proveniente da Igreja Nossa Senhora do Pilar em Recife, (Pilar 3 e 8). Da Primeira Metade do século XVIII, proveniente do Convento e Igreja de Santo Antônio em Igarassu (Santo Antônio 1, 7 e 15) e da metade do século XVIII, proveniente da Igreja Santa Tereza em Olinda.

A metodologia consiste inicialmente em determinar o contexto mineral das chacotas históricas, para tal os seguintes aspectos observáveis são: Morfologia, Fase mineral e Textura. São os dados as serem coletados com o uso da microscopia de luz polarizada. Como propriedades físicas da morfologia é analisado a granulometria, 0, a esfericidade e o arredondamento dos grãos minerais presentes de forma intencional e presentes de forma natural, 0.

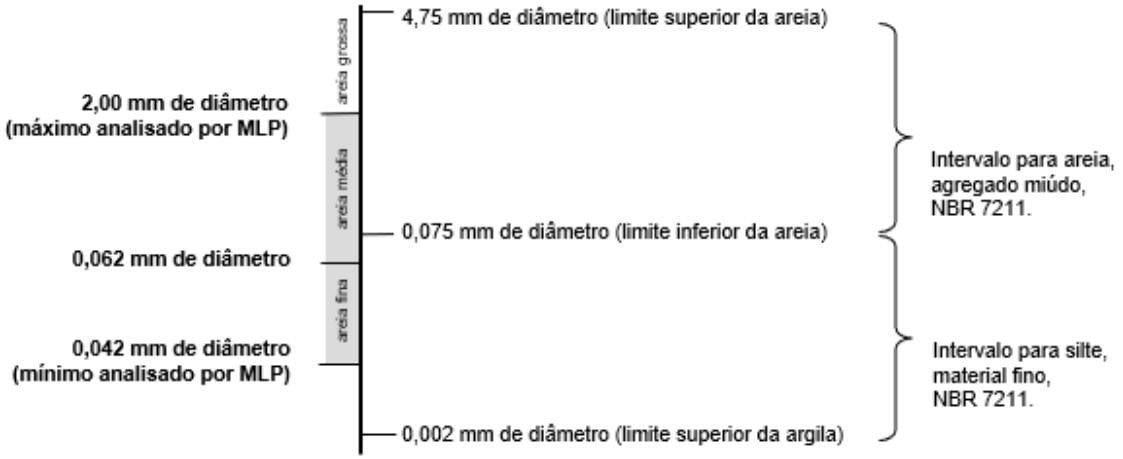


Figura 2 - Parâmetros de granulometria da NBR 7211 e a das rochas sedimentares, adotada para as análises por microscopia por luz polarizada (MLP) nas seções delgadas das amostras de azulejos históricos. O intervalo correspondente à fração areia (agregado miúdo) estende-se entre 0,075 mm a 4,75 mm segundo a norma. Entretanto, o limite inferior da areia fina foi ampliado para 0,042 mm em função da resolução analítica da MLP.

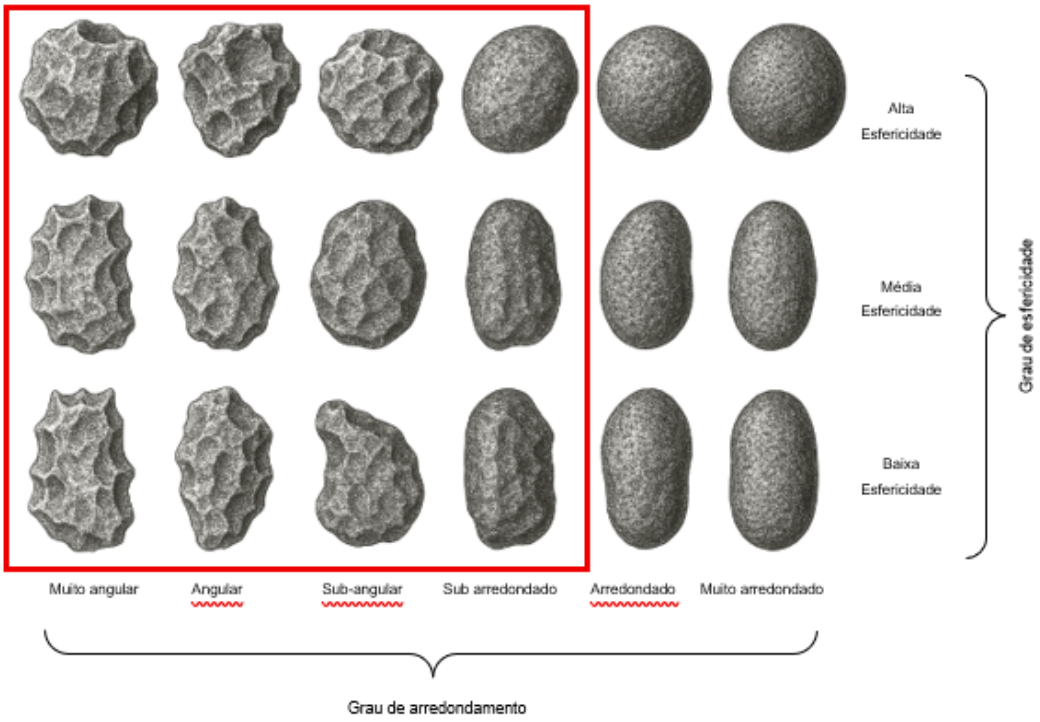


Figura 3 - A comparação visual da granulometria se baseia na medida do grau de agudez de cantos e arestas dos grãos arenosos. Para a esfericidade essa comparação analisa o quanto o grão se assemelha a forma de uma esfera. Uma chacota com grãos muito angulares e baixa esfericidade é mais suscetíveis a ocorrência de microfissuras.

O aspecto observável, fase mineral é definida pelas seguintes propriedades ópticas observáveis: cor, pleocroísmo, relevo, clivagem, partição, hábito, brilho, cor de interferência e ângulo de extinção. Nem sempre é necessário utilizar todas as propriedades, podendo ser escolhidas apenas algumas, 0.

Tabela 1 - Aspectos observáveis como elementos para determinar o contexto mineralógico da chacota, a morfologia e as fases minerais são os primeiros elementos que contribuem para o entendimento das causas das patologias de degradação das chacotas.

Aspectos observáveis	**Propriedades ópticas ou físicas**	**Condições Observáveis**	**Variação**
Morfologia do Tempero (areia)	Granulometria	Dimensão	Fração areia (grossa, média, fina) e fração (argila)
	Esfericidade	Forma	Esfericidade (alta, media, baixa)
	Arredondamento	Geometria das arestas	Angular, sub angular, sub arredondado, arredondado
Fases Minerais	Pleocroísmo	Aspectos da luz Visível	Mudança de cor
	Cor		Incolor, colorido
	Brilho	Refração	Metálico, vítreo, submetálico, adamantino

Já o aspecto observável, textura. permite inferir diretamente informações relacionadas à seleção de matérias-primas, ao preparo da pasta e ao desempenho microestrutural do material. Nesse contexto, a textura é definida neste estudo a partir de duas propriedades físicas: (i) a frequência dos grãos minerais (tempero) e (ii) a distribuição relativa entre a matriz argilosa e a fração areia, cuja interação resulta na organização da pasta cerâmica. A frequência corresponde à proporção volumétrica das fases minerais presentes, sendo um parâmetro fundamental para avaliar o grau de adição de tempero e sua influência na resistência mecânica do corpo cerâmico. Já a distribuição refere-se à forma como esses grãos se encontram dispersos na matriz homogênea ou heterogeneamente, fornecendo indicativos sobre o nível de preparo e homogeneização da pasta, além de sua influência na propagação de tensões e no desenvolvimento de microfissuras, **Error! Reference source not found.** .

Tabela 2 - A quantificação das fases minerais foi realizada por meio do método de contagem de pontos em grade, Stoops (2003). que permite estimativas confiáveis da frequência relativa dos constituintes. Complementarmente, a avaliação da distribuição entre matriz argilosa e tempero foi conduzida a partir da análise de imagens digitais obtidas em diferentes campos da mesma lâmina delgada, posteriormente processadas no software Image J.

Aspectos Observáveis	Subclasse	Condições observáveis	Variação
Textura	Frequência	Grãos minerais	Contagem de pontos em grade em porcentagem
	Distribuição	Concentração matriz argilosa e Tempero (areia)	Proporção entre matriz argilosa e areia (software Image J)

Na ausência de um sistema de referência específico para a classificação de contextos minerais em chacotas históricas, foi desenvolvido neste estudo um **modelo classificatório análogo**, derivado diretamente dos critérios utilizados na classificação de rochas sedimentares. Boggs (2006), Tucker (2001), Winkler (2005).

A adoção desse referencial se justifica pela similaridade estrutural existente entre esses dois materiais no que se refere à presença de uma fração detrítica mineral (areia) dispersa em uma matriz mais fina (argila). Embora as rochas sedimentares sejam produtos de processos naturais de intemperismo, transporte e deposição, enquanto as chacotas resultam de processos antrópicos de preparação de pasta e queima, ambos apresentam organização textural comparável em escala microscópica, o que permite a adaptação dos mesmos parâmetros descritivos. Com base nessa compatibilidade estrutural, os critérios clássicos empregados na sedimentologia particularmente aqueles relacionados à morfologia dos grãos, às fases minerais e às características texturais foram adaptados para a classificação das chacotas históricas 0.

Tabela 3 - Comparativo entre as características básicas utilizadas na classificação de rochas sedimentares e sua analogia para uma classificação das chacotas de azulejos históricos.

Classificação de Rochas sedimentares		**Classificação Análoga de chacotas**
Sandstone Pettijohn et al, (1987)	Areia > 80% granulometria entre 0,062 a 2 mm Esfericidade baixa e alta Arestas subângulosas e subarredondadas	Não identificada nas seções delgadas analisadas.
Quartzo Sandstone Pettijohn et al, (1987)	Quartzo > 90% Granulometria entre 0,042 e 0,062 mm Esfericidade alta Arestas arredondadas	Quartzo entre 80% e 50% da fração areia Granulometria + ou - 0,042 Esfericidade entre média a alta Arestas arredondadas e subarredondadas
Wacke Gilbert et al, (1954)	Argila > 15% Granulometria entre 0,042 a 0,062 mm Esfericidade baixa Arestas subangulosas	Quartzo e feldspato entre 50% e 75% na fração areia Granulometria entre 0,042 a 0,062 mm Esfericidade média a baixa Arestas angulosas a subangulosas
Lithic Sandstone Dott, (1964)	Fragmentos líticos ≥ 25% Granulometria entre 0,042 a 0,062 mm Esfericidade média Arestas subangulosas a subarredondadas	Fragmentos líticos ≥ 10% Areia com cerca de 50% de quartzo e 10% feldspato (tempero) Granulometria + ou - 0,042 Esfericidade entre média a baixa Arestas angulosas

A comparação sistemática das seções delgadas revelou simultaneamente semelhanças e contrastes nos contextos minerais, permitindo reconhecer distintos arranjos tecnológicos associados às matérias-primas empregadas na produção das chacotas. Considerando que um dos objetivos centrais da pesquisa é a definição de perfis tecnológicos capazes de indicar

potenciais manifestações patológicas nos revestimentos cerâmicos, tornou-se necessário extrair informações mineralógicas e texturais confiáveis das matérias-primas.

3. Resultados

Tabela 4 - Comparativo das propriedades físicas ópticas para classificação das amostras de chacotas da igreja do Pilar, da segunda metade do século XVII.

Amostra e classificação análoga	**Morfologia**			**Fases minerais**			**Textura**	
	Granulometria	Esfericidade	Arredondamento	Birrefringência	Cor	Brilho	Frequência	distribuição
Pilar 3: Wacke	Areia média a fina	Grãos subanguloso Esfericidade baixa		Quartzo, feldspato, argila (calcita + dolomita), akermanita			49,5 a 80% de fração argila e 20% a 50,5% de fração de areia	
Pilar 8: Lithic Sandstone	Areia média	Grãos anguloso Esfericidade baixa a média		Quartzo, feldspato, mica, fragmento de rochas, argila (calcita+ óxido de ferro), akermanita			80% a 56% de fração argila e 20% a 444% de fração de areia	

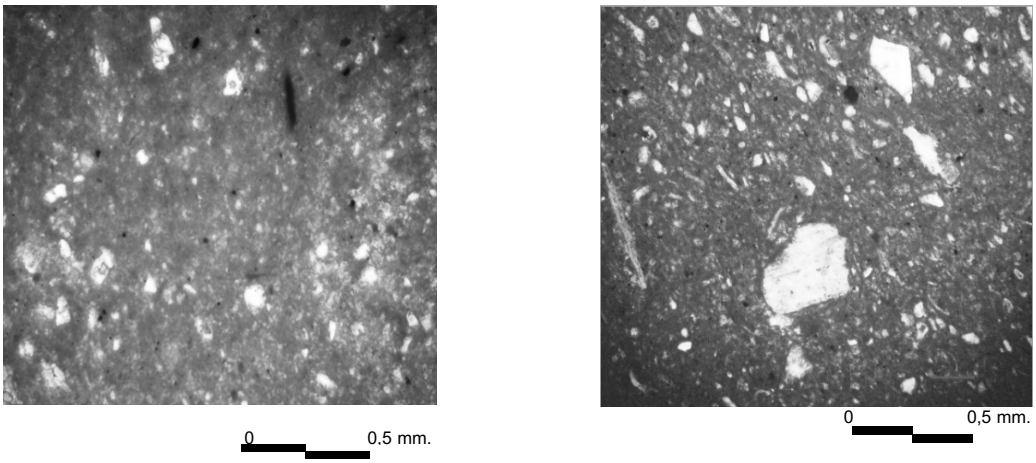


Figura 4 - A esquerda apresenta-se, á imagem micrográfica da amostra Pilar 3, da segunda metade do século XVII. No qual constatou-se que a chacota possui um contexto mineral análogo a classificação Wacke. A direita apresenta-se a imagem micrográfica da amostra Pilar 8, de mesmo período histórico, no qual constatou-se um contexto mineral análogo a classificação Litichic Sandstone.

Tabela 5 - Comparativo das propriedades físicas ópticas para classificação das amostras de chacotas da Igreja Santo Antônio, da primeira metade do século XVIII.

Amostra e classificação Análoga	**Morfologia**			**Fases minerais**			**Textura**	
	Granulometria	Esfericidade	Arredondamento	Birrefringência	Cor	Brilho	Frequência	Distribuição
Santo Antônio 1: Wacke	Areia média a fina	Grãos subanguloso Esfericidade baixa		Quartzo, feldspato, argila (calcita + dolomita), akermanita			75% a 48,5 de argila e 25% a 51,5% de areia	
Santo Antônio 7: Lithic Sandstone	Areia média	Grãos angulosos Esfericidade média		Quartzo, feldspato, fragmento de rocha (biotita) Argila (calcita, óxido de ferro), akermanita			80% a 69% de argila e 20% a 31% de areia	
Santo Antônio 15: Lithic Sandstone	Areia média	Grãos anguloso Esfericidade baixa a média		Quartzo, feldspato, fragmento de rochas (biotita, hematita) argila (calcita+ óxido de ferro), akermanita			60% a 48% de argila e 40% a 52% de areia	

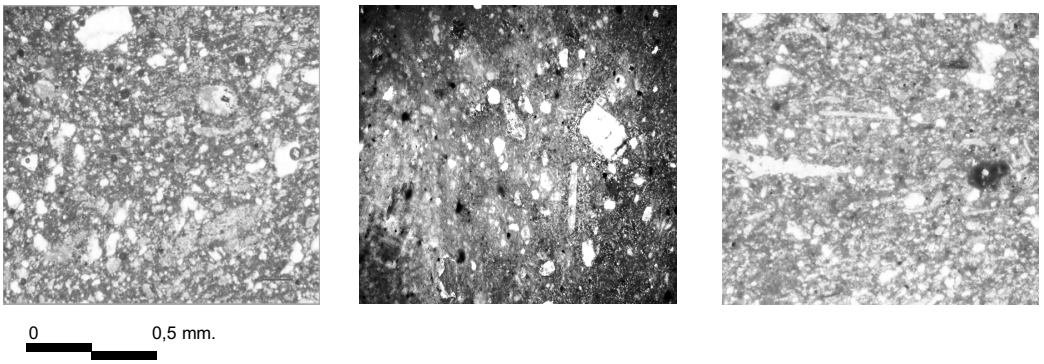


Figura 5- Imagem micrográfica das Amostra da primeira metade do século XVII, Na imagem à esquerda, apresenta-se a amostra Santo Antônio 1, onde constatou-se um contexto mineral análogo a classificação Wacke. Já as Imagens no centro e a direita, apresenta-se as amostras Santo Antônio 7 e Santo Antônio 15, onde constatou se um contexto mineral análogo a classificação Lithic Sandstone.

Tabela 6 - Comparativo das propriedades físicas ópticas para classificação da amostra de chacotas da Igreja Santa Tereza, da segunda metade do século XVIII.

Amostra e classificação Análoga	Morfologia			Fases minerais			Textura	
	Granulometria	Esfericidade	Arredondamento	Birrefringência	Cor	Brilho	Frequência	distribuição
Santa Tereza 2: Lithic Sandstone	Areia média	Grãos anguloso Esfericidade baixa		quartzo, feldspato, fragmentos de rocha (biotita + moscovita +piroxênio), argila (calcita + óxido de ferro), akermanita.			70% a 54% de fração argila e 30% a 46% de fração de areia	

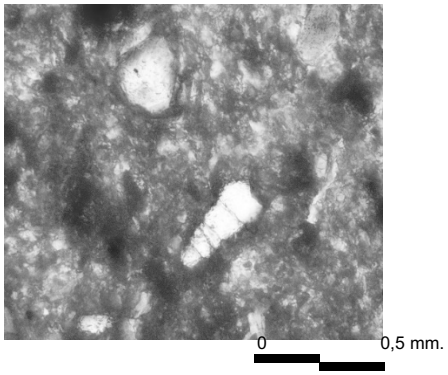


Figura 6- Imagem micrográfica da amostra, da segunda metade do século XVIII, no qual identificão-se um contexto mineral análogo a classificação Litichic Sandstone.

4. Discussão

A singular contribuição deste trabalho reside na aplicação do modelo classificatório análogo baseado em Pettijohn *et al*. (1987), Boggs (2006) e Tucker (2001). Ao classificar as chacotas, mobilizamos conceitos de maturidade textural e empacotamento que são essenciais para prever o comportamento do material frente às patologias de degradação. Essas questões são abordadas de forma intensas nas pesquisas de Mimoso *et al* (2016) especialista em caracterização química, mineralógica e conservação de chacotas e vidrados de azulejos históricos. Uma pasta cerâmica ao se aproxima do padrão análogo wacke, em termos tecnológicos, aponta para uma matriz argilosa pouco depurada e controle limitado do tempero. Do ponto de vista do desempenho, ocorre forte influência da matriz na mecânica do material. Em campo, isso se traduz em peças mais suscetíveis a retração diferencial, microfissuração, difusa e elevada absorção hídrica. Em condições de enterramento ou exposição, essas chacotas tendem a apresentar mobilização de sais, desagregação granular progressiva e perda de coesão superficial. A resistência mecânica, embora suficiente para uso cotidiano, é tipicamente baixa a moderada, com ruptura controlada pela matriz. Por quando uma pasta cerâmica se aproxima do padrão análogo Lithic Sandstone, o cenário muda de forma significativa. Aqui, ainda que a matriz argilosa permaneça presente, há uma participação mais efetiva dos clastos no suporte estrutural. Do ponto de vista tecnológico, o resultado material é uma chacota cerâmica com melhor distribuição de tensões, menor tendência à retração concentrada, acompanhada de vulnerabilidades: microfissuras localizadas, e a heterogeneidade composicional que pode favorecer diferenciais de dilatação térmica, sobretudo em ciclos de aquecimento/resfriamento

contribuindo para desintegração granular e abertura de microcavidades ao longo do tempo. Além disso, a identificação do termômetro mineralógico (akermanita) como marcador térmico superior a 950 °C revela um rigor técnico que remete às discussões de PAULO, B. Lourenço, CARLOS Maia, ARNALDO Sousa Melo, CLARA Pimenta do Vale(2023) , sobre a história das técnicas construtivas e o papel das Corporações de Ofício. Embora os azulejos analisados apresentem variações individuais em seus perfis tecnológicos, eles refletem uma tentativa de controle manufatureiro que atravessou o Atlântico a partir de Portuga.

5. Conclusões

A interpretação dos resultados obtidos para as chacotas de azulejos históricos de Pernambuco fundamenta-se em uma sólida base metodológica que transpõe conceitos da geologia para a arqueometria, ao fazer uso da Microscopia de Luz Polarizada (MLP). Os resultados obtidos neste estudo embora pertencente a uma pequena quantidade de amostras pode servir de ponto de partida para análise de outros conjuntos de chacotas maiores. A analogia com sistemas sedimentares permite mobilizar conceitos consolidados como empacotamento, suporte estrutural e maturidade textural para interpretar materiais antrópicos complexos. Isso eleva o nível de análise da simples descrição microscópica para uma leitura integrada entre tecnologia de produção, desempenho físico e trajetória de degradação. Em resumo, enquanto o padrão análogo **Wacke** foca na relação entre a matriz argilosa e um tempero arenoso rico em quartzo e feldspato, o padrão análogo **Lithic Sandstone** é identificado pela inclusão deliberada ou acidental de fragmentos de rocha e outros materiais complexos que alteram a resistência e a porosidade da cerâmica. O termômetro mineralógico, akermanita funciona como um registro fóssil do rigor térmico e das soluções técnicas aplicadas pelos artesãos nos séculos XVII e XVIII para garantir a durabilidade e a estética dos azulejos. Os critérios de esfericidade, arredondamento e granulometria que definem a morfologia da fração areia (tempero), são indicadores fundamentais para prever a vulnerabilidade de chacotas cerâmicas a manifestações patológicas. A principal patologia desenvolvida em função desses critérios é o surgimento de microfissuras. Enquanto a baixa esfericidade e o arredondamento mais angular promovem a durabilidade ao diminuir espaços vazios, o arredondamento mais arredondado a alta esfericidade agem como gatilhos para falhas estruturais e percolação de fluidos. Dessa forma, o trabalho contribui para a área ao utilizar as técnicas analíticas não apenas como ferramentas de catalogação, mas como indicadores de decisões tecnológicas tomadas pelos artesãos dos séculos XVII e XVIII, preenchendo lacunas sobre a gênese desses materiais e sua trajetória de deterioração no contexto agressivo de Recife e Olinda.

Agradecimentos

Gostaríamos de expressar nossos agradecimentos ao INAPAS (Instituto Nacional de Arqueologia, Paleontologia e Ambiente do Semiárido) pelo financiamento deste projeto, sem o qual esta pesquisa não teria sido possível. Agradecemos também a UFPE (Universidade Federal de Pernambuco) disponibilidade da utilização dos laboratórios e equipamentos utilizados nesta pesquisa, cuja contribuição foi essencial para o desenvolvimento e a conclusão deste estudo.

Referências Bibliográficas

BOGGS, Sam. 2006. *Principles of Sedimentology and Stratigraphy*, Pearson Education, New Jersey, Estados Unidos.

DOTT, Robert Hamilton Junior. 1964. *Wacke, graywacke and matrix – What approach to immature sandstone classification*, Journal of Sedimentary Petrology, Tulsa, Estados Unidos.

Gilbert, Charles M. Williams, Howel, Turner, Francis J. 1954. *Petrografia* - Uma Introdução ao Estudo de Rochas em Lâminas Delgadas. Editor: WH Freeman and Company, San Francisco, California.

PAULO, B. Lourenço, CARLOS Maia, ARNALDO Sousa Melo, CLARA Pimenta do Vale, 2023. 4° Congresso Internacional de História da Construção Luso-Brasileira, *Ambientes em mudança*. Guimarães: Universidade do Minho / Universidade do Porto.

PETTIJOHN, F. J.; POTTER, P. E.; SIEVER, R. 1987. *Sand and Sandstone*. 2nd ed. Springer-Verlag, New York Berlin Heidelberg, London Paris, Tokyo.

QUINN, Sean Patrick. 2013. The Interpretation of Archaeological Pottery & Related Artefacts in Thin Section.

RICE, Prudence M. Pottery . 1987. Analysis: a sourcebook. Chicago: University of Chicago Press, xxiv, 559 p.

STOOPS, Georges.2003. Guidelines for analysis and description of soil and regolith thin sections. Madison: Soil Science Society of America, 184 p.

TUCKER, Maurice Edwin.2001. *Sedimentary Petrology: An Introduction to the Origin of Sedimentary Rocks*, Blackwell Pub., Oxford, Reino Unido.

WINKLER, Erhard Michael. 2005. *Introduction to Clay Minerals: Chemistry, Origin, Uses and Environmental Significance*, Springer, Berlim, Alemanha.

MIMOSO, João Manuel. ESTEVES, Maria de Lurdes, 2016. Uma sistematização do destaque do vidrado em azulejos, III Encontro Luso-Brasileiro de Conservação e Restauro, 9 – 14 p.

Cinpar 2026
XXII International Conference on Building Pathology and Constructions Repair
15th to 17th July 2026 - Lisboa, Portugal

Argumentación en contra del uso de revoques texturados plásticos en fachadas patrimoniales. El caso del Museo Provincial de Bellas Artes de Santa Fe (Argentina)

Manuel Alfredo MINA[1]

[1] Universidad Católica de Santa Fe, Santa Fe, Argentina, manuelmina@ucsf.edu.ar

Resumen: Pese a los enormes avances científicos en el campo de la conservación de edificios de valor patrimonial en general y de sus fachadas en particular, subsisten algunas prácticas erróneas que menoscaban su originalidad, atentan contra su imagen histórica y producen incompatibilidades desde el punto de vista tecnológico que favorecen el surgimiento de lesiones. En este sentido, cabe detenerse en el tratamiento de fachadas provenientes de las primeras décadas del siglo XX, resueltas con revoques conocidos como símil piedra o piedra París que, en oportunidad de su restauración, son intervenidas mediante la aplicación de revoques texturados plásticos. Esta práctica, muy frecuente en la década de 1990 y 2000, favorecida por la novedad de la aparición de estos revestimientos formulados en base a resinas acrílicas, cargas minerales y pigmentos, motivada por su facilidad de aplicación y con las expectativas de impermeabilidad y vida útil, extendió su uso a obras, tanto del patrimonio monumental, como modesto, generando innumerables pérdidas en fachadas de gran valor. Aunque toda la argumentación teórica y los resultados puestos a la vista por el paso del tempo demuestran lo erróneo de este criterio, la práctica no ha sido desterrada por completo y subsiste en intervenciones algunas de ellas sobre ejemplares valiosos del acervo patrimonial de nuestras ciudades. El caso de estudio corresponde a la restauración del Museo Provincial de Bellas Artes Rosa Galisteo de Rodríguez de Santa Fe, fachada construida en 1922 y posteriormente ampliada en 1940, cuyas especificaciones de intervención requieren la aplicación de revoque texturado plástico. El presente trabajo establece la argumentación necesaria para revisar este criterio de actuación, reseña la investigación desarrollada para exponer la constitución original de la fachada y establece lineamientos para intervenir acordes a las buenas prácticas en restauro.

Palabras clave: Patrimonio, fachada, símil-piedra, restauro

1. Introducción

A partir de la necesidad de intervenir en la fachada del Museo Provincial de Bellas Artes Rosa Galisteo de Rodríguez en el contexto de la obra de restauración integral que se está llevando a cabo desde septiembre de 2025, se plantea la oportunidad de basar los criterios y las decisiones técnico - proyectuales en sólidos argumentos que la naturaleza patrimonial del edificio amerita.

En este sentido, existe un vasto marco de actuación referenciado en toda la literatura mundial del restauro, según el cual, previo a cualquier acción de restauración caben ineludibles tareas de investigación y reflexión que garanticen un adecuado criterio que respete el valor patrimonial del edificio o monumento a ser intervenido.

La Carta de Venecia (ICOMOS 1964) constituido en el documento fundante de la restauración moderna, abre su texto señalando en qué punto se ubica el valor de la conservación de los monumentos históricos.

> "Portadoras de un mensaje espiritual del pasado, las obras monumentales de cada pueblo son actualmente el testimonio vivo de sus tradiciones seculares. La humanidad, que cada día toma conciencia de la unidad de los valores humanos, las considera como un patrimonio común, y pensando en las generaciones

futuras, se reconoce solidariamente responsable de su conservación. Ella aspira a transmitirlas con toda la riqueza de su autenticidad." (ICOMOS 1964)

Ahora bien, la misma Carta expresa algunos lineamientos que es imprescindible tener en cuenta a la hora de decidir criterios de intervención. El objetivo de la restauración es salvaguardar tanto la obra de arte como el testimonio histórico que ella constituye y ese cometido se logra, fundamentalmente, basándose en el respeto por el material original y en documentos auténticos.

Por otra parte, cabe señalar que, a lo largo del tiempo, los edificios históricos van siendo objeto de intervenciones, muchas de las cuales no se basan en criterios de consenso internacional y ven menoscabada su imagen a partir de la inclusión de técnicas incompatibles con su originalidad, con su naturaleza técnica y con los criterios estéticos propios del edificio.

Será tarea, por tanto, del restaurador, intentar desandar el camino y devolver al edificio sus valores de originalidad y autenticidad que pudieron perderse (u ocultarse) a lo largo del tiempo.

Centrando específicamente la problemática de la conservación en la cuestión de las fachadas y haciendo foco en los revoques del tipo símil piedra o Piedra París, esta técnica se ha visto, en muchos casos, menoscabada en su tratamiento por criterios desacertados. Las malas decisiones técnicas han desechado las posibilidades de conservar el revoque símil piedra mediante cuidadosas prácticas de limpieza, consolidación y restitución y han optado por recubrirlo con materiales ajenos a la configuración original que han desmerecido gravemente su aspecto estético y han acelerado procesos de deterioros. El caso más elocuente lo constituye la aplicación de pinturas, sean estas a la cal o posteriormente al látex, sobre la superficie del material de frente, técnica que ofrecía una "renovación" del aspecto de la fachada a costa de una irreversible pérdida de originalidad, color, textura y realce de las formas y siluetas de la ornamentación. Esta técnica fue aplicada, tanto sobre fachadas monumentales, como también en obras del patrimonio modesto y reiterada, capa a capa, a lo largo del tiempo tal como se advierte en la Figura 1



Figura 1 – Tratamiento de pintura sobre fachada patrimonial

En las últimas décadas, la aparición en el mercado de un material innovador para el tratamiento de muros exteriores, el revoque texturado plástico, no tardó en desembarcar como técnica de intervención sobre fachadas de valor patrimonial favorecido por una cierta similitud en la textura y coloración y promocionado por su facilidad de aplicación. Este material se difundió con gran rapidez sin que se advirtiera convenientemente sobre su irreversibilidad y sobre una serie de incompatibilidades técnicas tal como se advierte en la Figura 2 y que se abordarán en apartados siguientes.



Figura 2 – Revoque texturado plástico sobre fachada de símil piedra

2. Criterio de intervención en el caso de estudio

2.1 El Museo Rosa Galisteo de Rodríguez

El Museo Provincial de Arte Rosa Galisteo de Rodríguez de la ciudad de Santa Fe (Argentina) constituye un bien de altísimo valor patrimonial por tratarse de un edificio enclavado en la zona fundacional de la ciudad, por ser un referente arquitectónico de la primera mitad del siglo XX de noble factura y rigor estilístico y por ser un referente social del arte pictórico y escultórico para la región. En su interior aloja una valiosísima colección de obras de arte que constituyen un tesoro cultural invaluable para los santafesinos. El museo es también una referencia nacional por sus Salones Anuales, por muestras, conciertos y eventos de renombre en la agenda cultural.

La fachada principal del museo sobre la calle 4 de enero (ver Figura 3) refleja en su configuración las dos etapas de construcción del edificio, el pórtico Norte (sobre la izquierda de la foto) correspondiente a su fundación en 1922 y el resto del frente correspondiente a la ampliación de 1940.



Figura 3 – Revoque texturado plástico sobre fachada de símil piedra

2.2 Análisis del criterio de intervención en fachada

En septiembre de 2025 dieron comienzo las tareas de restauración del edificio del museo en el marco de la licitación pública N° 00601-0056080-6 llevada a cabo por el gobierno provincial sobre un proyecto de la Dirección Provincial de Arquitectura e Ingeniería (DIPAI) con un presupuesto oficial de $ 1.504.159.725,79, lo que representa aproximadamente USD 1.500.000.-

El punto 12-13 del Pliego de Especificaciones Técnicas Particulares PETP titulado “Revestimiento de Material Plástico en Fachadas” (DIPAI 2024) indica la tarea de revestir las fachadas del edificio con el citado material, criterio posiblemente basado en que, en alguna intervención reciente el producto fue aplicado y quizás también en cierta fama de durabilidad e impermeabilidad del material.

Sabido es que los revoques texturados plásticos (“Quimtex” por citar la marca referenciada en el Pliego) son materiales formulados en base a resinas acrílicas (polímero sintético), cargas minerales y pigmentos y cuyo uso se popularizó en nuestra zona en los albores de la década de 1990. Importantes ventajas en su método de aplicación y ciertas expectativas de durabilidad e impermeabilidad hicieron que este material, no solo liderara en poco tiempo las terminaciones de fachadas en arquitecturas nuevas, sino que irrumpiera también en fachadas patrimoniales, en su gran mayoría tratadas con revestimientos símil piedra, dada su similitud cromática y (a cierta distancia) en la textura.

De una lectura temporal del edificio, se sabe que el bloque fundacional del edificio data de 1922 y la ampliación de 1940, datos que hacen descartar, de sentido común, que las fachadas hubiesen tenido en su tratamiento original revoque texturado plástico.

Ahora bien, la pregunta a resolver es cuál fue entonces el tratamiento original del edificio y para esto la tarea debe basarse en tres fuentes: una interpretación epocal en función de las técnicas disponibles y las costumbres al momento de la construcción; una investigación documental y de rescate de información oral y por último el trabajo de campo basado en cateos sobre diversos sectores del muro. Ninguna de las fuentes ha de tener un resultado absolutamente conclusivo por sí sola, sino que, complementándose unas a otras permitirán reconstruir con mayor fidelidad argumental la situación perdida.

En este caso en particular, las tres fuentes de información son absolutamente contundentes y permiten concluir que el Museo fue revestido con revoque símil piedra, técnica que se abordará en el siguiente apartado.

3. La investigación

3.1 Investigación histórica

En las últimas décadas del siglo XIX, una serie de factores se conjugaron para que se ejecutaran en nuestras ciudades los ejemplares edilicios más significativos de nuestro patrimonio arquitectónico. La prosperidad económica devenida del modelo agroexportador imperante, las ideas del iluminismo expresadas en términos estilísticos a través del neoclasicismo, el gusto por los modelos europeos (de Francia e Italia principalmente) y el arribo de numerosos operarios fundamentalmente italianos a partir de las fuertes corrientes inmigratorias del cambio de siglo constituyeron la base sobre la cual se configuró una manera de construir y por tanto una manera de la acabar las fachadas.

Las arquitectas Tarchini y Elías, investigadoras de la Facultad de Arquitectura, Diseño y Urbanismo de la Universidad Nacional del Litoral sostienen:

> "En América Latina, y en Argentina en particular, los revocos de terminación en fachadas históricas son un recurso material indispensable para la interpretación y conservación del patrimonio edificado. Las arquitecturas del academicismo eclecticista realizadas en ciudades tales como Buenos Aires, Rosario y Santa Fe, entre finales del siglo XIX y mediados del siglo XX, recurrieron a la aplicación de revocos y estucos que simulan piedras, debido a la escasez de rocas naturales adecuadas para la construcción, así como por la economía, rapidez y versatilidad que este sistema de revestimiento ofrece y que fue ampliamente difundido por los artesanos y albañiles italianos en la región. Estos morteros y revocos, elaborados a base de cal calcítica aérea y áridos naturales como arenas silíceas, además de rocas metamórficas como mármoles y rocas magmáticas como granitos, aportan no solo textura y coloración, sino también mejoran las características técnicas de las fachadas." (Tarchini y Elías 2024)

Así mismo, el arquitecto e historiador Mario Buschiazzo, considerado el padre de la preservación del patrimonio arquitectónico en la Argentina afirma:

> "Como es sabido, la piedra no es un material que se utilizó para construir en Buenos Aires, salvo como revestimiento o para ejecutar ciertas terminaciones. No obstante su ausencia física, podemos decir que tuvo una amplia presencia visual, ya que el grueso de los edificios académicos ostenta fachadas cuyo revoque imita piedra, de la cual efectivamente estaban hechos los modelos originales que sirvieron para inspirar los detalles estilísticos de aquellos; pero, por supuesto no se trataba en última instancia de piedra sino de argamasa. La auténtica piedra se colocaba en placas de pequeño espesor adheridas al muro de ladrillos, y eso sólo en ciertos lugares, por ejemplo, en los zócalos ejecutados de granito martelinado, que fueron frecuentes a principios de siglo, tanto en obras de importancia como en aquellas carentes de especial lujo..." (Buschiazzo 1971)

Tabla 1 – Composición clásica de los morteros símil piedra de principios del siglo XX

Componente	Función principal	Notas históricas
Cal	Aglomerante	Usada ampliamente antes de la popularización del cemento; aportaba plasticidad y trabajabilidad.
Cemento	Aglomerante	Introducido por inmigrantes italianos; daba mayor resistencia y durabilidad.
Arena	Árido	De granulometría variada; definía textura y compactación del mortero
Mica	Mineral molido	Aportaba brillo superficial y variaciones cromáticas
Dolomita	Mineral molido	Contribuía a tonalidades claras y resistencia.
Calcita	Mineral molido	Generaba tonos ocres y grises

Por otra parte, vale realizar un recorrido imaginario por las obras del patrimonio monumental de la época en la ciudad de Santa Fe y la resolución tecnológica de las fachadas siempre será la misma, revoque símil piedra, también llamado “Piedra París” o más recientemente “Material de Frente”. La Casa de Gobierno, el Teatro Municipal Primero de Mayo, la Escuela Industrial Superior, el Rectorado de la UNL, la Basílica del Cármen y el Hospital Italiano son solo algunos ejemplos que abarcan el abanico de época del museo y exhiben este tratamiento en sus fachadas según puede apreciarse en el collage de fachadas de la Figura 4.



Figura 4 – Edificios emblemáticos de la ciudad de Santa Fe construidos entre 1890 y 1940

En todos los casos, el acabado de los frentes se caracteriza por el uso del símil piedra como material de terminación, generalmente monocromo y la articulación de las superficies mediante el trazado de rehundidos (falsas juntas de distinto ancho y espesor) habitualmente tomadas con un mortero cementicio para enfatizar la idea de mampostería de sillares (bloques) de piedra. En algunas fachadas el material de frente se termina sin más textura que la propia del frataz que utiliza el obrero y en algunos casos más singulares se le da una terminación “peinada” o rayada imitando la impronta que la gradilla dejaba a la piedra natural cuando esta era labrada (Ver Figura 5).



Figura 5 – Texturas al frataz y “peinada”

En el caso de la ornamentación, se combinan dos criterios: por un lado, los ornatos directos, ejecutados sobre la superficie misma de la fachada tal es escaso de molduras, cornisas, guardapolvos y dentículos y por otro, los ornatos aplicados, piezas de molde, elegidos generalmente de catálogos de la época y fijados a la facha con pernos metálicos y mortero (Ver Figura 6). Es habitual que los elementos de molde no coincidan en coloración y textura con el Piedra París de la fachada, situación que en pocas oportunidades se dejaba expuesta componiendo fachadas bitonales, pero que en la mayoría de los casos se resuelve mediante una veladura de las piezas con el símil piedra usado para unificar cromáticamente el conjunto.



Figura 6 - Ornamentación directa y de molde

3.2 Investigación documental

A nivel documental no se han hallado pliegos ni reseñas técnicas de la construcción del edificio de ninguna de sus dos etapas y la fuente más cercana la constituye una escasa cantidad de fotos de épocas que revelan algunos datos útiles.

El documento más antiguo lo constituye una fotografía del acto inaugural del museo ocurrido el 25 de mayo de 1922 y que se reproduce en la Figura 7. La imagen solo aporta la confirmación de que el cuerpo norte de la fachada cuenta con una configuración volumétrica y ornamental idéntica a la actual.

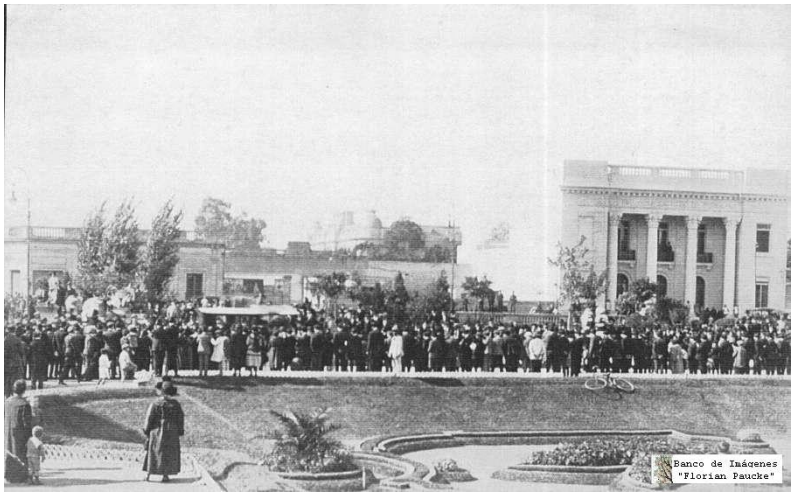


Figura 7 - Inauguración de 1922 – Obtenido de Banco de Imágenes “Florián Paucke”

Otro documento valioso lo constituye la Figura 8 que reproduce una fotografía de 1930 tomada específicamente de la, por entonces, fachada del museo. En la imagen se puede advertir que las columnas de orden corintio y el frontis que aloja las letras labradas “MUSEO ROSA GALISTEO DE RODRIGVEZ” parecen tener un tratamiento cromático diferente al resto de la fachada que amerita ser estudiado en profundidad. Los zócalos evidencian una materialidad diferente al resto de la superficie coherente con las placas de granito gris martelinado que luce actualmente.



Figura 8 - La fachada del Museo en 1930 – Obtenido del Banco de Imágenes Florian Pauke

Observando la foto publicada en la portada del Salón Anual de 1931 (Figura 9) se mantiene la presunción de que las columnas y el frontis pudieron tener un tratamiento cromático diferente al resto de la fachada, pero es evidente que el resto del sistema ornamental está tratado con el mismo criterio de color que los paños de muro.

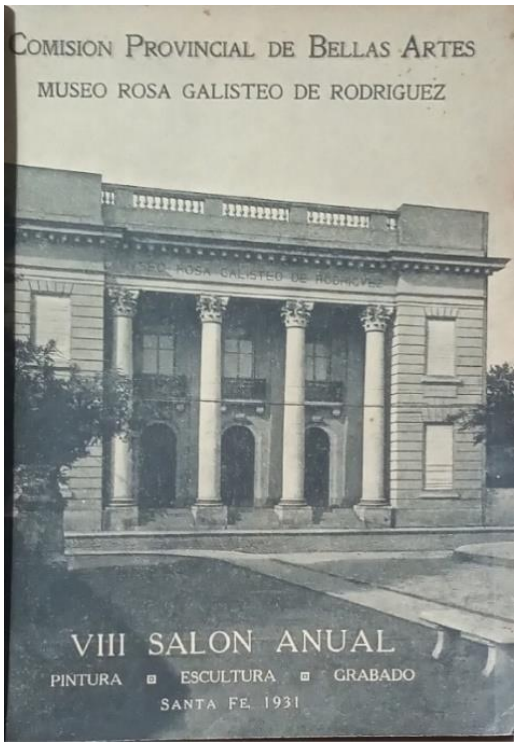


Figura 9 - La fachada del Museo en 1930 – Obtenido del Archivo del Museo Rosa Galisteo

El documento más revelador con el que se cuenta es el afiche de una muestra titulada “Colectivo de Aristas” basado en una fotografía de 1969, la imagen color más antigua que se pudo hallar (Figura 10). En el fondo de una toma familiar efectuada desde calle 3 de febrero se distingue la fachada del Museo, más precisamente el pórtico Sur y el muro de ochava que luce de un color ocre grisáceo característico del Piedra París.



Figura 10 - Afiche de "Colectivo de Artistas" (1969) – Obtenido del Archivo del Museo Rosa Galisteo

Leonardo Scheffer, un destacado miembro del staff del museo, actualmente a cargo del archivo, refirió su constante preocupación por la originalidad del color del edificio, aportando un dato significativo:

"Taverna Irigoyen, director de la Institución durante muchos años, me manifestó que la fachada fue pintada por primera vez a principios de la década de 1980 debido a los numerosos grafitis con leyendas políticas que habían sido estampados con motivo de la agitación de esos años y la cercanía del edificio con la legislatura provincial. El color que se eligió fue rosado, pero antes de eso el edificio fue gris." [1] (Ver Figura 11)



Figura 11 - El frente del Museo pintado de rosado (1981) – Obtenido del Banco de Imágenes Florian Paucke

Reforzando la teoría de que el edificio fue pintado, un artículo periodístico publicado en 2013 en el diario Uno, en oportunidad a las obras de refacción recientemente inaugurados por aquel entonces, refiere que la vuelta a la tonalidad ocre grisáceo de la fachada sería una vuelta a la originalidad de la misma afirmando que el tratamiento en tonos de rosa había sido una intervención de la década de 1980 basada en erráticos criterios de analogías al nombre de la institución o bien buscando similitudes con otros edificios tales como la Casa de Gobierno en la Ciudad Autónoma de Buenos Aires.

[1] Leonardo Scheffer, entrevista personal con el autor, Santa Fe, 6 de febrero de 2026

"Quizás la Intervención que más resalte es el cambio de color del rosa viejo que lucía desde 1982 a este nuevo gris que recupera el verdadero tono que tuvo al ser construido. Es que en una fallida intervención se lo había pintado como tomando a pie juntillas al poema El Golem, en el que Jorge Luis Borges decía *Si (como afirma el griego en el Crátilo) / el nombre es arquetipo de la cosa / en las letras de "rosa" está la rosa/ Y todo el Nilo en la palabra Nilo". Así, creyendo que con ese color se rendía homenaje a la madre del fundador a la vez que se refería directamente al Museo ensimismo, se incurrió en un error histórico. Otros dicen que se hizo para que se pareciera a la Casa Rosada[2] y no para aludir directamente al nombre de pila". (Redacción Diario Uno 2013)

3.3 Investigación de campo

A partir de la realización de cateos en la fachada del Museo, tanto sean en el segmento correspondiente a 1922 como al de 1940, se advierten signos evidentes del tratamiento original de la fachada ejecutada, en ambos casos, con un mortero símil piedra de coloración ocre grisáceo absolutamente congruente con las otras fuentes abordadas en apartados precedentes.

Las calicatas más reveladoras son las ejecutadas en el atrio norte (Figura 12), correspondiente a 1922, en el que asoma nítidamente el símil piedra (aunque con una coloración excesivamente amarronada por estar el tramo afectado por humedades ascendentes por capilaridad) pero dejando expuesto el clásico tratamiento de falsas juntas entre los sillares tomados con mortero de coloración oscura y alta dureza que refieren al uso de cemento portland. El tratamiento de falsas juntas se encuentra tanto en los sillares menores del interior del atrio como tratamiento de superficie, como así también en el fondo de las profundas buñas que configuran el almohadillado a ambos lados del pórtico.



Figura 12 - Calicatas realizadas por el autor en el pórtico de 1922

Dos estratigrafías realizadas en el muro Oeste (Figura 13) revelan datos que vienen a confirmar mucho de lo recabado en la investigación teórica y documental. Por un lado, en la calicata de la figura 11, se puede establecer con precisión la conformación del sistema de revoques previo a las intervenciones de pintura iniciadas entre los ´70 y los ´80. Se advierte la siguiente secuencia:

Mampostería de ladrillos cerámicos macizos / revoque impermeable: de gran dureza y coloración característica del cemento portland como ligante / revoque grueso a la cal: de baja compacidad y evidente presencia de una combinación de arena de sílice y polvo de ladrillo como agregados finos / material de frente: de gran compacidad, en un espesor promedio de 3 a 4mm

[2] Casa Rosada: nombre coloquial con el que se conoce a la Casa de Gobierno de la República Argentina ubicada en la Ciudad Autónoma de Buenos Aires



Figura 13 - Calicatas realizadas por el autor en el muro Oeste de 1940

La cala de la Figura 14 demuestra la presencia del símil piedra como material previo a las intervenciones de pintura (1). Si bien se hace muy difícil establecer la secuencia de al menos, 5 intervenciones de coloración rosa (2), es evidente que la primera intervención sobre el símil piedra fue en esa coloración y que después de sucesivas capas se aplicó un revoque texturado plástico de tonalidad manteca (3) y finalmente un látex más agrisado como tratamiento que hoy exhibe la fachada (4).

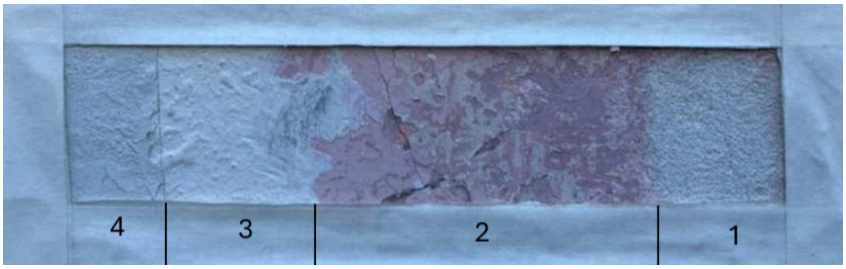


Figura 14 - Estratigrafía de colores realizada por el autor

4. Conclusiones

La coherencia detectada en las tres fuentes de investigación abordada permite afirmar indubitablemente que la fachada del Museo Rosa Galisteo de Rodríguez fue tratada originalmente con mortero símil piedra, tanto en su segmento de 1922 como en el de 1940, con algunas diferencias que se detallaron oportunamente y con un tratamiento monocromo que deberá confirmarse en investigaciones subsiguientes. Cualquier tratamiento de los aplicados sobre la fachada, sean estos de pintura o de revoque texturado plástico han sido intervenciones posteriores y distorsivas tanto de la materialidad del edificio como de su estética.

En un texto de referencia para la disciplina, el reconocido arquitecto restaurador Marcelo Magadán sostiene: que la alteración de los símil-piedra se da masivamente por malas intervenciones de restauración y/o conservación, estas se ejecutan con materiales inadecuados, técnicas incompatibles y al margen de los principios más elementales aceptados en el campo de la restauración. Uno de los errores más frecuentes es la aplicación de pinturas que hace perder irreversiblemente el color y la textura del material original. (Magadán 1999)

Un desacierto muy común es el "re-revocado" de los paramentos mediante la aplicación de una suerte de "enduido" que, modificando la textura, el color y las formas primigenios, transforma negativamente la imagen de los edificios. Existe además una técnica ubicada a mitad de camino entre ésta última y la pintura: se trata de los recubrimientos con carga, que comparten con ambas, no sólo el impacto negativo del que se habló, sino también las deficiencias de comportamiento por fallas en el anclaje entre estos materiales y el sustrato original. Además, no son reversibles mientras que toda intervención con materiales no originales debe poder ser retirada, la naturaleza de anclaje de los texturados plásticos no lo permite, o al menos si lo permite, lo hace a costa de un daño significativo al sustrato. Por otra parte, otorgan una impermeabilidad

excesiva al paramento y sellan los poros a partir de los cuales, estas mamposterías evaporan y eliminan excesos de humedad de distinta procedencia, los texturados plásticos configuran películas que actúan como barreras que favorecen la retención de humedad lo cual redunda en acelerado envejecimiento del símil piedra por la acción de la cristalización de sales solubles que no pueden ser eliminadas por no tener contacto con la atmosfera. La retención prolongada de agua en la masa del mortero endurecido comienza a solubilizar sales consolidantes de los aglomerantes y los disgrega. En algunos casos, la evaporación retenida por detrás del acrílico genera presiones que originan aglobamientos y el posterior decapado del texturado. Esto no solo desmerece largamente la condición estética, sino que abre puntos para el ingreso de humedad al muro tal como se advierte en la Figura 15.



Figura 15 – Diversas patologías desarrolladas por los revoques texturados plásticos

Resuelta la cuestión de la no pertinencia de la aplicación de revestimientos ajenos a la materialidad de la fachada, el desafío es cómo intervenirla para devolver las notas de originalidad perdidas a lo largo del tiempo.

Un criterio absolutamente consensuado a nivel de la literatura de la disciplina y avalado por virtuosas intervenciones de restauro, tanto en el mundo como en Argentina y Santa Fe, establece la necesidad de la vuelta a los materiales originales del edificio. La destacada investigadora Arq. Felicidad Paris Benito de la Universidad Nacional de Mar del Plata sostiene:

"En la restauración, el nuevo material debe cooperar con el original. Esta cooperación sólo está garantizada cuando los materiales son similares. En la reconstrucción del mortero hay que considerar el efecto de envejecimiento que ha sufrido el material original, de manera de poder lograr una imagen semejante. La intervención debe incluir la limpieza del sector, la extracción de sales solubles, la consolidación, la hidrofugación y la reconstrucción de partes perdidas. En cuanto al mortero de reposición, además de ser de similares características del original, se deben cuidar especialmente las técnicas de ejecución, para determinar el color definitivo del revoque. La muestra debe estar totalmente seca, por tanto, es muy importante la ejecución de las muestras en obra y en las diferentes orientaciones que tuvieran las fachadas del edificio."

5. Bibliografía

Buschiazzo, Mario J. *La arquitectura en la República Argentina. 1810-1930.* Buenos Aires: Mac Gaul, 1971.

DIPAI. «Obra: Refacción Museo Provincial de Bellas Artes - PETP.» Santa Fe, 2024.

ICOMOS. *Carta de Vanecia.* Venecia, 1964.

Magadán, Marcelo. «Revoques símil piedra. Pautas para su conservación y restauración.» *Hábitat*, 1999: 11-12.

Redacción Diario Uno. «La Vuelta a la Originalidad.» *Uno*, 17 de Octubre de 2013: 6-7.

Tarchini, María Laura, y María Laura Elías. «Caracterización de Morteros Históricos en Construcciones de Valor Patrimonial de la Ciudad de Santa Fe.» *Técnicas y Estudios de Bienes Patrimoniales*, 2024: 33-47.

cinpar2026
XXII International Conference on Building Pathology and Constructions Repair
15th to 17th July 2026 - Lisboa, Portugal

HBIM-Driven Management of Diagnostic Information: A Proof of Concept

Mariella DE FINO[1], Elena LOZITO[2], Riccardo TAVOLARE[3]

[1] Polytechnic of Bari, Department DICATECh, Italy, mariella.defino@poliba.it
[2] Polytechnic of Bari, Department DICATECh, Italy, e.lozito@studenti.poliba.it
[3] Polytechnic of Bari, Department DICATECh, Italy, riccardo.tavolare@poliba.it

Abstract: Onsite diagnostic investigation related to construction materials and components, including their condition and performance over time, plays a well-established role in knowledge-based management of historic buildings. However, in many practical applications, information is still addressed through traditional approaches based on fragmented data storage, isolated handling, and static representation of outputs. In this context, Historic Building Information Modelling (HBIM) provides an effective framework as an integrative environment capable of structuring and processing diagnostic data beyond their conventional use as supporting documentation. This paper presents a proof of concept for an HBIM-driven framework to diagnostic information management, with specific reference to sonic testing and video-endoscopic inspections applied to masonry structures. The proposed workflow is designed to operate across three complementary levels of integration: (i) incorporation of experimental measurements into the HBIM model by defining parametric diagnostic entities spatially and semantically linked to building elements; (ii) data processing and visualization, implemented via computational workflows based on Visual Programming Language (VPL), in which diagnostic values are filtered, normalized, and elaborated to generate interpretative outputs, including color-coded mappings and parametric representations of masonry stratigraphy; and, (iii) automated extraction and organization of diagnostic reports, conceived as an extension of the HBIM environment to support record-keeping and information reuse. The methodology is validated through its application to a test-bed simulating masonry elements characterized by different orientations, to which stratigraphic configurations and sonic velocity distributions derived from real-case diagnostic investigations were assigned. The proof of concept demonstrates the feasibility and adaptability of HBIM-driven workflows to support structured management of diagnostic information and provides a foundation for future developments toward integrated assessment and control digital strategies.

Keywords: HBIM, VPL, diagnostic testing, masonry structures, historic buildings.

1. Introduction

Onsite diagnostic investigation related to construction materials and components, including their condition and performance over time, plays a well-established role in knowledge-based management of historic buildings (Bolborea et al. 2025; Tejedor et al. 2022; Garrido et al. 2022). However, in many practical applications, information is still addressed through traditional approaches based on fragmented data storage, isolated handling, and static representation of outputs. In this context, Historic Building Information Modelling (HBIM) provides an effective framework as an integrative environment capable of structuring and processing diagnostic data beyond their conventional use as supporting documentation (Fattore et al. 2025; De Fino, Galantucci, and Fatiguso 2023).

As highlighted by a recent comprehensive review on HBIM-based information management (Parente, Bruno, and Ottoni 2025), different approaches can be identified for integrating data derived from diagnostic investigations into BIM environments.

A first approach, commonly referred to as Properties of Elements (PoE), consists in incorporating the results of diagnostic tests directly as properties of the investigated construction components. Within this strategy, numerical outcomes are stored as entity attributes, while images, graphs, and technical reports are generally linked as external documents. Representative examples include the assignment of mechanical resistance derived from double flat jack tests to masonry walls (Croce et al. 2022), as well as the association of resistance drilling profiles with timber beam objects to evaluate the effective resistant cross-section (Santos et al. 2022). In these cases, the precise spatial location of individual tests is not explicitly represented, and the approach proves more suitable for investigations whose results can be meaningfully referred to entire structural components.

A second strategy, known as Symbolic Modeled Objects (SMO), relies on the introduction of custom objects that symbolically represent diagnostic investigations within the HBIM model. These objects are enriched with structured information, such as test typology, execution date, instrumentation, quantitative results, interpretative notes, and links to related documentation. SMO-based solutions have been applied to direct sampling and constructional observations (De Falco et al. 2024), as well as to extensive datasets including reality-based surveys, microscopic analyses, and destructive and non-destructive tests (Garcia-Gago et al. 2022). By decoupling diagnostic information from the construction element, this approach allows for an accurate spatial localization of investigations and facilitates comparisons among multiple tests performed on the same component. However, the semantic integration between symbolic objects and building elements is often implicit, which may limit interoperability at the level of the information model.

A third approach, referred to as Realistic Modeled Objects (RMO), is based on modeling diagnostic investigations through objects that reproduce the actual extent of the investigated area rather than relying on abstract markers. This strategy is particularly suited to diagnostic techniques producing raster-based outputs, such as thermographic images and radargrams, which can be associated with extended surfaces (Cardinali et al. 2023; Coli et al. 2022). In some implementations, diagnostic images are projected directly onto wall objects, not as additional geometries but as new material layers whose properties encode the diagnostic data (Solla et al. 2020). This last solution enables an immediate three-dimensional correlation between investigation results and surface degradation patterns, enhancing visual coherence and supporting element-level contextualization of processed diagnostic outputs, when compared to representations that are limited to reproducing the spatial extent of the investigated area.

Against this background, the paper presents an HBIM-driven proof of concept that advances current SMO-based approaches by shifting the focus from the representation of diagnostic investigations to the computational management of diagnostic information, including its structuring, elaboration, and reuse, while selectively integrating RMO-inspired visualization strategies to project processed results onto building elements and support their direct correlation with surface-related information, particularly conservation conditions. The methodology, demonstrated through sonic testing and video-endoscopic inspections applied to masonry structures, is organized across three complementary levels of integration: (i) the incorporation of experimental measurements into the HBIM model through the definition of parametric diagnostic entities spatially and semantically linked to building elements; (ii) the computational processing and visualization of diagnostic data via Visual Programming Language (VPL) workflows, generating interpretative outputs such as color-coded mappings and parametric representations of masonry stratigraphy; and (iii) the generation and organization of diagnostic outputs within and beyond the HBIM environment, including integrated model-based visualizations and the automated extraction of structured reports to support record-keeping and information reuse.

Accordingly, the paper is structured as follows: Section 2 describes the proposed materials and methods, detailing the testing techniques, the HBIM test-bed, the definition of diagnostic entities, and the computational workflows adopted for data processing and visualization; Section 3 presents the results of the proof of concept, illustrating the implementation of the three levels of integration and the derived diagnostic outputs. Finally, Section 4 discusses the main findings, and current limitations of the approach,

outlining perspectives for future developments toward integrated digital strategies for the assessment and management of historic buildings.

2. Materials and Methods

The proposed proof of concept for an HBIM-driven framework for diagnostic information management is developed on a typological test-bed, conceived as a controlled environment to verify the feasibility and adaptability of the approach prior to its application to real case studies. The test-bed is based on a simplified HBIM model comprising masonry elements with different orientations, each assumed to be investigated through sonic testing and video-endoscopic inspections.

Sonic tests are typically performed by defining two corresponding grids of regularly spaced measurement points on the opposite faces (≈ 1 m^2) of the investigated element. For each homologous pair of points, the time of flight of low-frequency (< 20 KHz) mechanical waves propagating from the emitting probe on one surface to the receiving probe on the opposite surface is measured. Given the known thickness of the element, these measurements allow the calculation of sonic wave velocities, which are commonly used as indicators of material compactness, internal heterogeneity, and the presence of voids or discontinuities. A typical test report includes general information on the building, the execution and processing dates, the name(s) of the operator(s), planimetric localization, the description of the test operating principle and set-up, and the technical specifications of the equipment, a matrix of the acquired velocity values. These data are commonly presented either in point-based form or, by interpolation, as area-based false-color maps.

In parallel, video-endoscopic inspections are carried out through the execution of a transverse micro-drilling (≈ 3 cm diameter) through the masonry element, followed by the insertion of an endoscopic probe equipped with an integrated lighting and recording system. The probe acquires continuous video footage of the internal stratigraphy of the wall, after the introduction of a metric reference that enables the identification and localization of interfaces between adjacent layers. This technique provides qualitative and semi-quantitative information on masonry texture, construction technique, and the thickness and arrangement of internal layers, complementing the results obtained from sonic investigations. In this case as well, the test report includes the previously mentioned general information, together with a sequence of representative frames extracted from the video recording and a stratigraphic section drawing indicating the thickness, material type, and state of conservation of the identified layers.

The proposed BIM-based approach is grounded in the idea that diagnostic information can be treated as structured information entities, semantically and spatially linked to the investigated building elements, according to a logic consistent with the principles of information modelling and with the semantic structure of the IFC (Industry Foundation Classes) data schema. From this perspective, the modelling of diagnostic entities can be interpreted as a process of ontology-based structuring of diagnostic knowledge, in which the results of investigations are formalized as semantic information associated with the objects of the information model. The IFC schema indeed provides an explicit ontological structure based on entities, properties, and relationships, which makes it possible to formally represent knowledge related to the built environment by distinguishing between physical objects (IfcProduct), descriptive properties (IfcProperty), and informative relationships (IfcRelationship). The integration of diagnostic data through Property Sets and semantic relationships therefore makes it possible to enrich the HBIM model through a process of semantic enrichment, in which the information derived from experimental investigations becomes an integral part of the model knowledge base. This approach makes it possible to treat diagnostic data as components of the BIM model knowledge graph (Pauwels, Zhang, and Lee 2017), making them queryable, updatable, and reusable within interoperable information workflows based on open standards.

The methodology adopted in this study is structured into three interrelated operational levels, which define the following workflow:

i. definition and integration of diagnostic entities within the HBIM model through the modelling of parametric information objects associated with the investigated building elements;

ii. computational processing of diagnostic datasets through VPL-based workflows aimed at querying, filtering, and transforming the data contained in the model;

iii. generation and structured extraction of derived information outputs, organized as forms of representation and reusable datasets for the documentation and analysis of diagnostic investigations.

The first level (i) concerns the transformation of experimental measurements into HBIM information entities through the creation of specific parametric families designed to represent the individual diagnostic tests carried out on masonry elements. These entities are configured with parameters capable of recording the main attributes of the test, including, in addition to the general information already mentioned, the numerical values recorded during measurement. From an informational point of view, these data are organized according to a structure consistent with the logic of Property Sets (Psets) provided by the IFC data schema, in which descriptive information is modelled as IfcProperty entities, grouped into IfcPropertySet and associated with model elements belonging to the IfcProduct hierarchy (e.g. IfcWall) through explicit IfcRelDefinesByProperties relationships. The investigated building element is thus interpreted as a product entity (e.g. IfcWall) belonging to the IfcProduct hierarchy, while diagnostic information is structured as informative properties linked to that entity through specific property sets. In this way, the experimental datum is not represented as a simple graphic annotation, but as structured information associated with the investigated building element, while maintaining the distinction between the physical object of the model and the set of properties describing the test results. In addition, each diagnostic entity is characterized by three-dimensional coordinates (X, Y, Z), which make it possible to precisely locate the measurement point on the surface of the investigated masonry element. These coordinates can be manually entered by the operator within the informational parameters, according to a chosen reference system, mainly for descriptive purposes and to support data interpretation. In the subsequent processing phases, these coordinates are automatically acquired and reinterpreted in relation to the geometry of the investigated masonry element through the analysis of the orientation of its axis and its thickness. This makes it possible to reconstruct local spatial relationships that keep explicit the connection between the investigation points and the masonry element under analysis. This approach preserves the relationship between the experimental datum and its position within the three-dimensional space of the building, ensuring the traceability of the measurement within the information model and making explicit the relationship between diagnostic information, building element, and spatial context.

The second level (ii) concerns the computational processing of diagnostic datasets. At this stage, the HBIM model is used not only as an information container, but also as a computational environment capable of supporting processes of querying, processing, and transformation of the data associated with the model objects. To this end, a VPL-based workflow was developed, enabling direct access to the information parameters of the diagnostic entities contained in the model and operations on the datasets associated with the BIM objects. The computational phases first include a model querying stage, in which diagnostic entities are selected by category and their related information parameters are extracted through operations that read the parameters associated with the elements. Subsequently, the data are subjected to a logical filtering stage, which makes it possible to isolate the relevant datasets according to the type of test and the investigated building element, thus allowing different diagnostic investigations contained in the model to be separated and managed distinctly. In the case of sonic testing, once the relevant data have been isolated, the workflow proceeds with the extraction and reorganization of the measured velocity values, which are collected into data structures and subjected to a process of normalization and ordering in order to make them comparable and prepare them for the subsequent visualization and analysis procedures. At the same time, the geometric information related to the position of the different diagnostic points constituting the measurement grid is also extracted, based on the position of the elements within the model coordinate system. Starting from the spatial coordinates of the diagnostic points, the workflow generates a series of

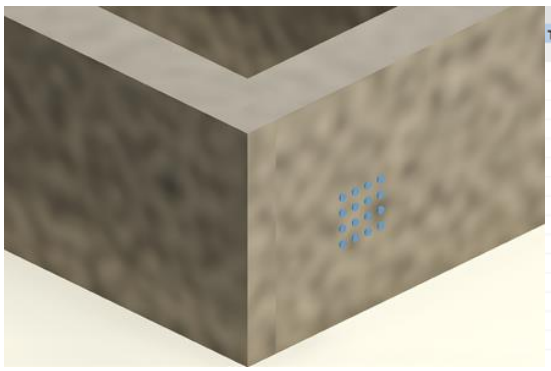
new parametric geometric entities used to support data visualization, by assigning a color coding derived from the recorded values. Similarly, in the case of video-endoscopic inspection, the workflow integrates the generation of parametric entities based on masonry stratigraphic analysis. In this case, the VPL script queries the parameters associated with the diagnostic entities related to the endoscopic test, extracting information on the thickness and type of the different layers identified along the investigated section. These data are subsequently organized into parametric structures, taking into account the position of the diagnostic point and the information related to wall orientation and thickness. The workflow then generates a sequence of appropriately dimensioned three-dimensional geometries representing the different layers detected by the investigation. The resulting geometries are finally integrated into the model as derived information objects, maintaining the association with the original diagnostic entity and making it possible to explicitly visualize the stratigraphic configuration of the investigated masonry within the BIM environment. It is important to emphasize that these representations are not modelled as static objects within the information model. Rather, they are generated dynamically as outputs derived from data processing, thus avoiding the creation of independent geometric objects and maintaining a close relationship between the diagnostic dataset and its visualization. In this sense, diagnostic representation is understood as the result of a computational process applied to the data contained in the model, rather than as a manually modelled element.

The third level (iii) concerns the generation and organization of information outputs derived from the computational workflow. The developed system provides the possibility of automatically extracting the results of the processing steps and organizing them into a series of structured reports, such as false-color maps and summary tables, which can be used for subsequent analyses or documentation.

3. Results

The application of the methodology described was carried out on a simplified parametric model developed in the Autodesk Revit® environment, consisting of perimeter masonry walls and internal partitions. In particular, two orthogonal perimeter walls were used as a simulated test-bed, to which sonic velocity values and stratigraphic configurations derived from real diagnostic investigations carried out by the authors on historic masonry structures were assigned. This choice allowed the workflow to be tested on realistic datasets, producing meaningful diagnostic representations and outputs. In the case of the sonic test (Figure 1), acquisitions on regular grids of points were considered, arranged in a 4×4 pattern, for a total of 16 points distributed over the wall surface, with a constant spacing of 20 cm. In order to integrate sonic velocity data into the model in a structured way, in accordance with the first level of operational integration (i), a dedicated parametric family was developed, conceived as a point-based information object capable of simultaneously representing the spatial position of each measurement within the grid and containing the parameters associated with the test.





A	B	C	D
Tipo_Prova	Muro_Associato	PS_ID_Punto	PS_Velocita_Sonica
sonica	Muro 1	1	1037 m/s
sonica	Muro 1	2	1074 m/s
sonica	Muro 1	3	755 m/s
sonica	Muro 1	4	1136 m/s
sonica	Muro 1	5	808 m/s
sonica	Muro 1	6	863 m/s
sonica	Muro 1	7	1282 m/s
sonica	Muro 1	8	1005 m/s
sonica	Muro 1	9	844 m/s
sonica	Muro 1	10	1050 m/s
sonica	Muro 1	11	1612 m/s
sonica	Muro 1	12	992 m/s
sonica	Muro 1	13	886 m/s
sonica	Muro 1	14	1541 m/s
sonica	Muro 1	15	1019 m/s
sonica	Muro 1	16	1595 m/s

Figure 1 – Real-case sonic test set-up, BIM modelling, and velocity values in the Revit schedule

The parametric structure of the family was defined by introducing a set of custom informative attributes, including both quantitative data (such as sonic velocity and spatial coordinates) and descriptive and management-related information (point ID, test type, associated wall, dates, operators, test operating principle and set-up, and the technical specifications of the equipment used). This configuration made it possible to transform each diagnostic point into a queryable and manageable element within the model, thus supporting the organization, filtering, and subsequent processing of the data.

This initial phase was followed by a sequence of steps (Figure 2) aimed at implementing the second level of operational integration (ii).

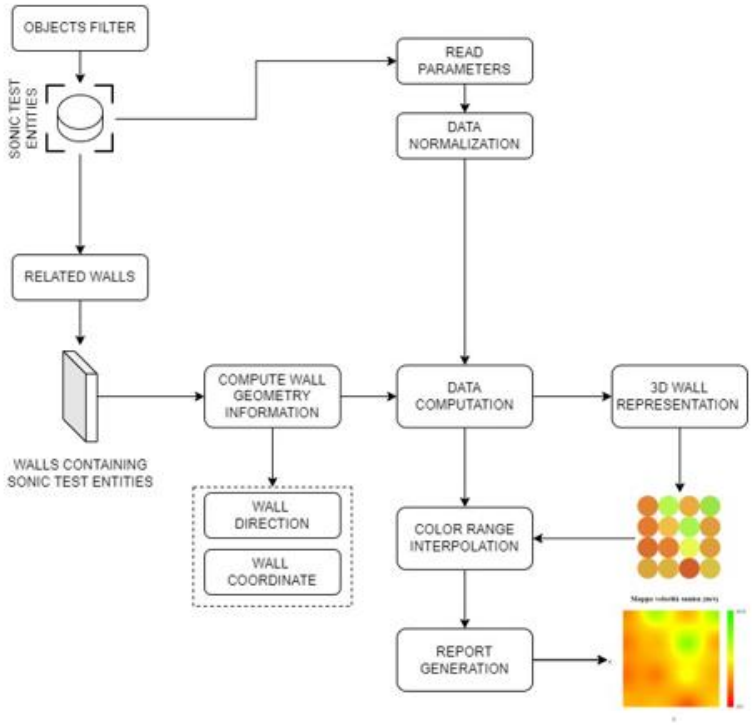


Figure 2 – Sonic test data processing workflow

First, the data filtering phase was performed through the development of a script in Dynamo (Figure 3), a visual programming environment in which users build graphs by connecting nodes, each of which performs a specific operation, while the graph defines the workflow used to read, process, or write data in Revit. More specifically, through the script, all elements belonging to the diagnostic point category were extracted and subsequently filtered according to the parameters Test type and Associated wall. The combined application of these criteria made it possible to obtain a consistent dataset, free from interference, containing only the information entities corresponding to the tests carried out on a specific wall. The sonic velocity values were then extracted and normalized within a user-defined range - 500–2000 m/s in this case, according to the dataset to be represented - thus making them dimensionless and comparable. A continuous red–yellow–green colour scale was then assigned to these values through a Color Range function, in order to progressively highlight variations in the parameter and improve the readability of transitional areas. In addition, the integration of a Python script (Figure 3), based on the Revit API and embedded directly within the VPL workflow, made it possible to automate the association of each diagnostic point with its corresponding wall by exploiting relationship properties and solid intersection checks between the geometric entities (IfcWall and test entity). Subsequently, starting from the wall localization data, the directional vector of the wall face was computed, thus identifying its prevailing orientation within the

workspace. This information proved essential for correctly defining the geometric plane on which the interpolation of the test data was to be performed. Finally, the coordinates of the diagnostic points were used to generate elementary geometries (circular surfaces) positioned in space consistently with the wall orientation. A colour was assigned to each surface according to the normalized sonic velocity value, resulting in a georeferenced point-based representation that is immediately interpretable. Moreover, in order to overcome the discrete nature of the data, an IDW (Inverse Distance Weighting) spatial interpolation was implemented on a regular grid (0.01 m spacing), defined on the plane of the wall according to its orientation (XY or YZ). The interpolated values were calculated as the weighted average of the known points, with weights inversely proportional to distance. The results, normalized within the same reference range, were then converted into a continuous false-colour map, subsequently represented in the model through surfaces and, in parallel, exported in PNG format. Finally, the sonic map can be reintroduced into the model by generating a geometric panel positioned in correspondence with the measurement grid, to which a material using the PNG image as a texture can be assigned. In this way, the visualization could also be extended into the three-dimensional space of the model, allowing for a direct reading of the distribution of values in false colors within the Revit environment.

In the case of the endoscopic test, by contrast, the first level of operational integration (i) involved the creation of an information entity corresponding to a parametric diagnostic point, simulating the video-endoscopic inspection hole (Figure 4). This element acts as an information container including both the test metadata (e.g. ID, investigation type, associated wall, coordinates, etc.) and the stratigraphic parameters resulting from the investigation (layer thicknesses and materials). In this way, the data are structured in a form that is both queryable and integrable within the BIM model. For this purpose, reference was made to the results of a real test performed on masonry investigated through a 20 mm diameter hole to a depth of 90 cm and characterized by an alternation of calcarenite blocks and mortar joints.

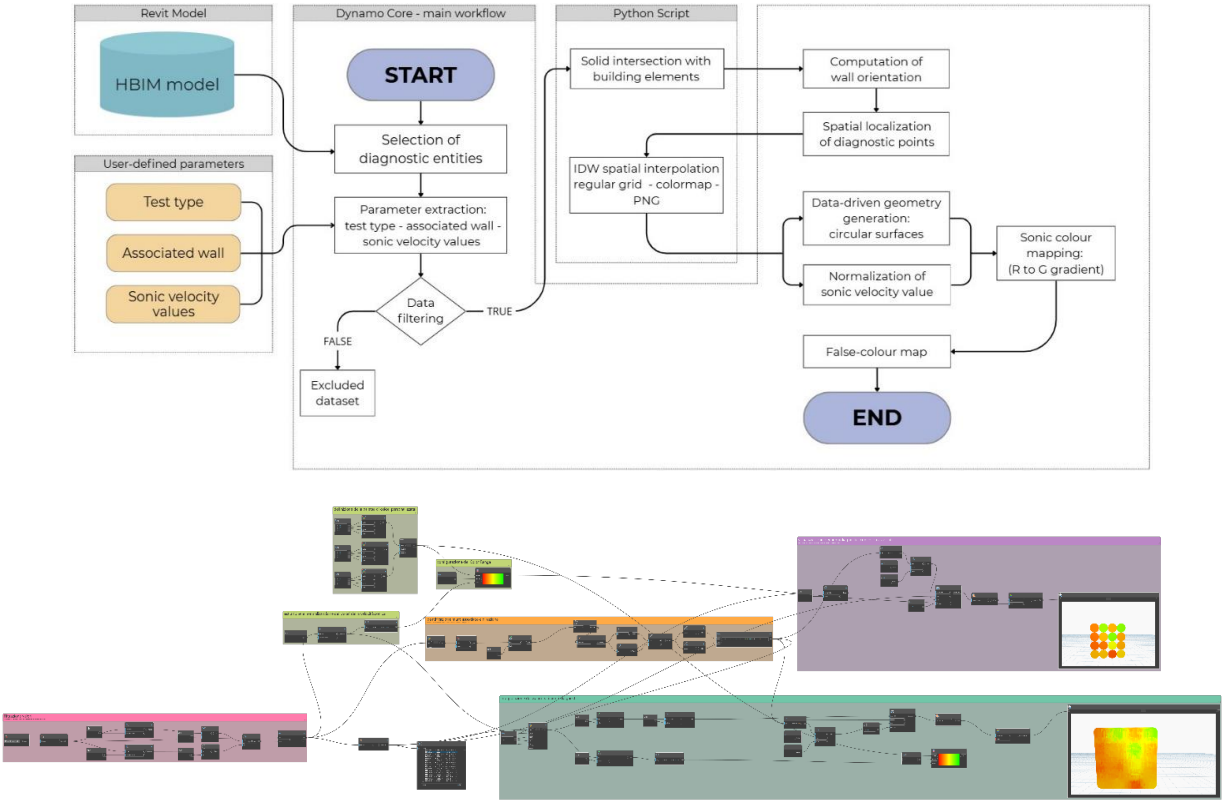


Figure 3 – Integration of the Revit model with user input, Python processing, and Dynamo management: pipeline (top) and script (bottom – full-size version available at: https://github.com/3DMauLAB/HBIM_Diagnostic)

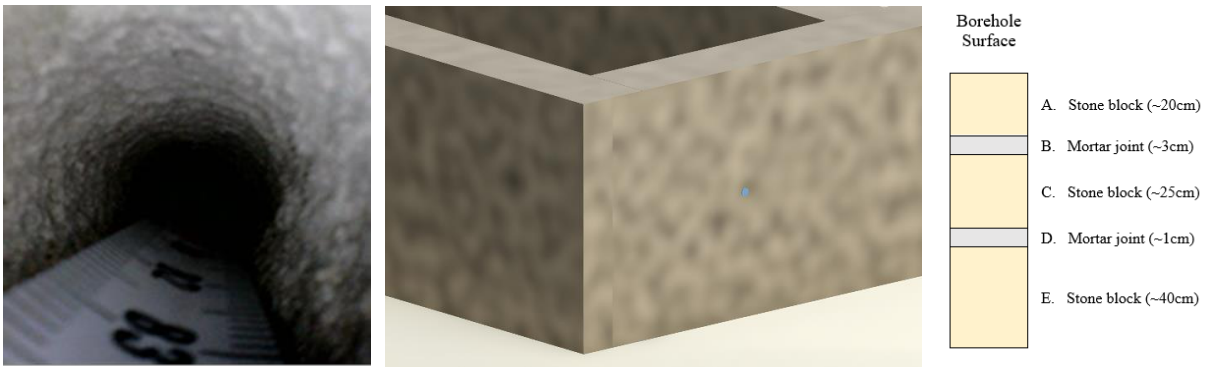


Figure 4 – Real frame from the video-endoscopic investigation, BIM modelling, and stratigraphic scheme

In this case as well, a sequence of phases (Figure 5) corresponding to the second level of operational integration (ii) was implemented through Dynamo (Figure 6).

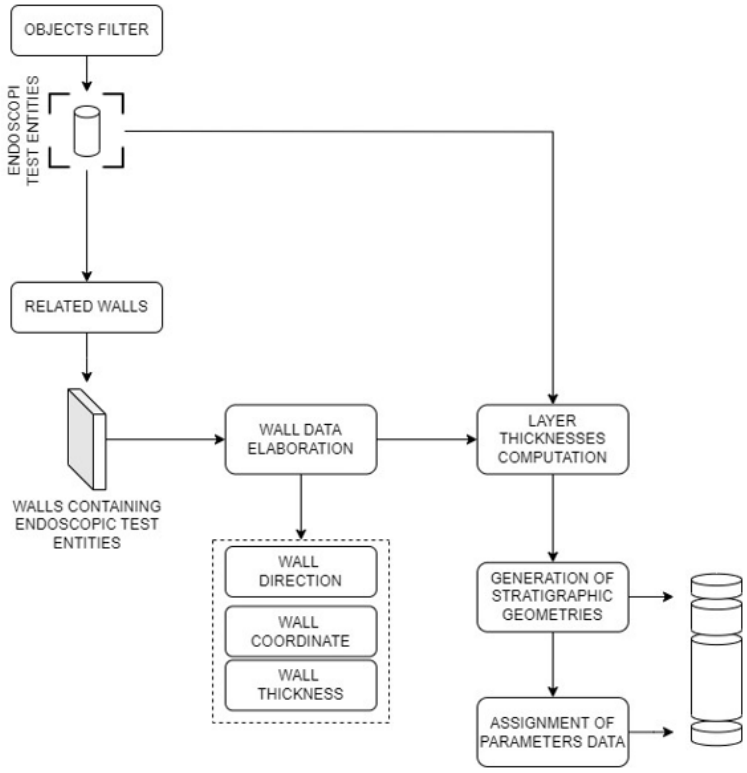
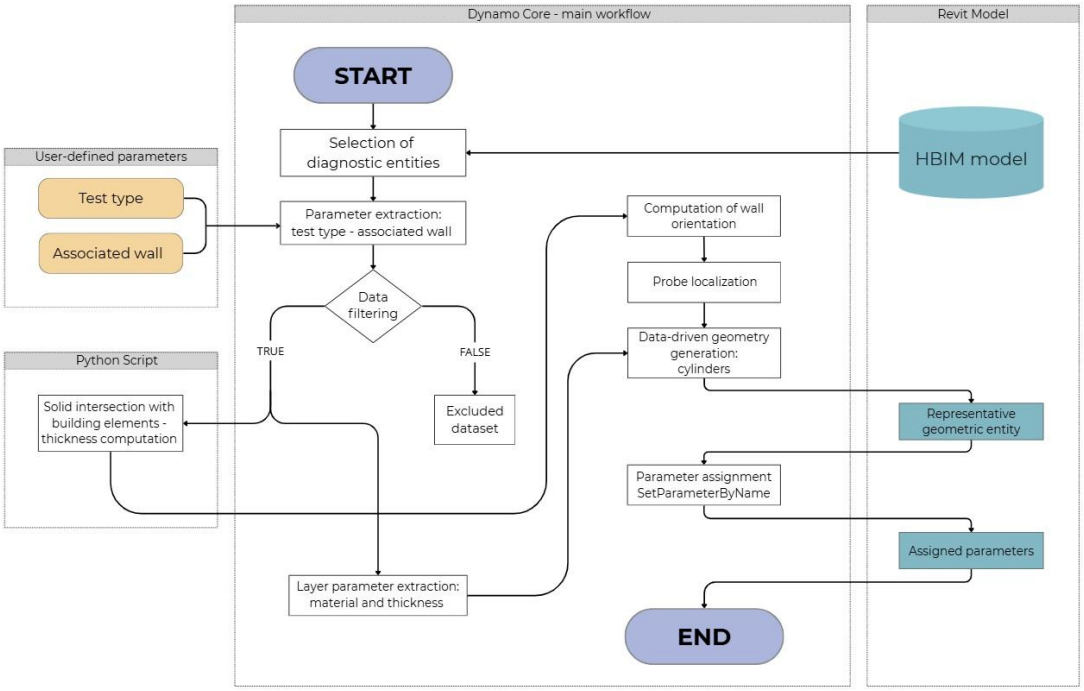


Figure 5 – Videoendoscopy Inspection data processing workflow

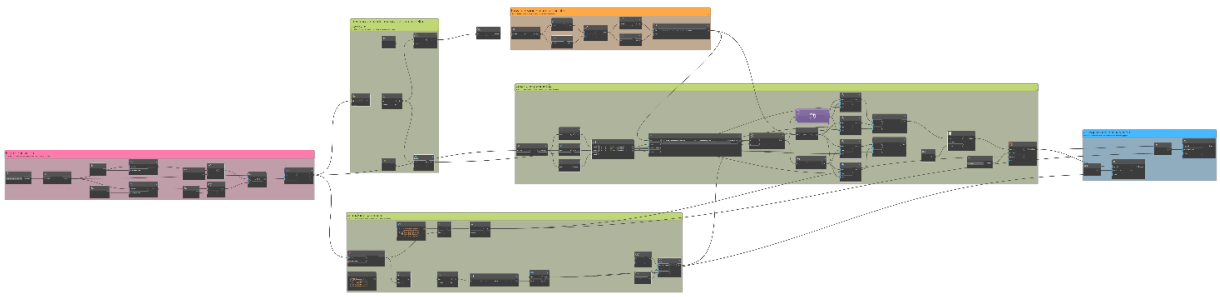
First, the diagnostic points were filtered according to the parameters Test type and Associated wall, thus isolating only those relevant to the endoscopic test. The workflow then proceeded with wall identification and wall data calculation through a Python script, by which each point was associated with the corresponding wall through a geometric intersection check between the diagnostic entity and the IfcWall element. At the same time, the fundamental parameters of the masonry element were extracted, in particular wall thickness and prevailing wall direction. This information is necessary to correctly position the

stratigraphic geometries in space. This was followed by the computation of layer thicknesses, through the extraction and validation of the stratigraphic parameters. The parameters related to the individual layers (materials and thicknesses) were extracted from the diagnostic points in Dynamo through a filtering process designed to exclude null or invalid values, thereby allowing the algorithm to automatically detect the actual number of layers present and correctly assign the corresponding properties to each of them. The stratigraphic data were then translated into three-dimensional geometries in the form of cylinders, each representing a masonry layer. These geometries were generated from the position of the diagnostic point and oriented according to the wall direction, while also taking into account the overall wall thickness in order to reconstruct the correct sequence of layers along the wall section. Finally, the workflow proceeded with the generation of stratigraphic geometries and the assignment of parameter data within the BIM model.



The generated geometries were represented in Revit through the DirectShape function and subsequently enriched with information parameters, including thickness, material, and a representative frame extracted from the video-endoscopic inspection. In this way, each test entity becomes an informative BIM element, directly queryable and consistent with the data acquired in situ.

Figure 6 – Integration of the Revit model with user input, Python processing, and Dynamo management for video-endoscopy inspection: pipeline (top) and script (bottom – full-size version available at: https://github.com/3DMauLAB/HBIM_Diagnostic)



Finally, for both tests, starting from the outputs of the processing stages - namely the sonic map reprojected onto the masonry surface and the stratigraphic entity integrated into the model (Figure 7) - and with reference to the third level of operational integration (iii), a process of automated extraction was implemented to generate structured diagnostic outputs directly from the model. This procedure relies on the interrogation of the parameters associated with the diagnostic entities and on their reorganization into coherent information layouts, including summary tables of recorded values, graphical representations, and exportable datasets. Through the implementation of a Python script, the generation of diagnostic reports from a predefined template was automated. The document is populated by automatically retrieving both the information already embedded in the model and the outputs generated during the processing stages, thus avoiding manual data transcription. The generated report therefore maintains a direct relationship with the BIM model and the queried diagnostic entities, including both descriptive test information and graphical representations derived from the computational workflow (Figure 8). In this way, the correspondence between the information embedded in the model and the derived documentation is preserved, reducing the risk of inconsistencies and ensuring alignment between data processing and output production. Moreover, the parametric nature of the system allows any update in the input data or processing stages to be consistently reflected in the extracted outputs, supporting an incremental and updatable documentation framework. Within this perspective, report generation is not treated as a separate phase, but as a direct extension of the computational workflow, contributing to the consolidation of a structured and reusable information base.

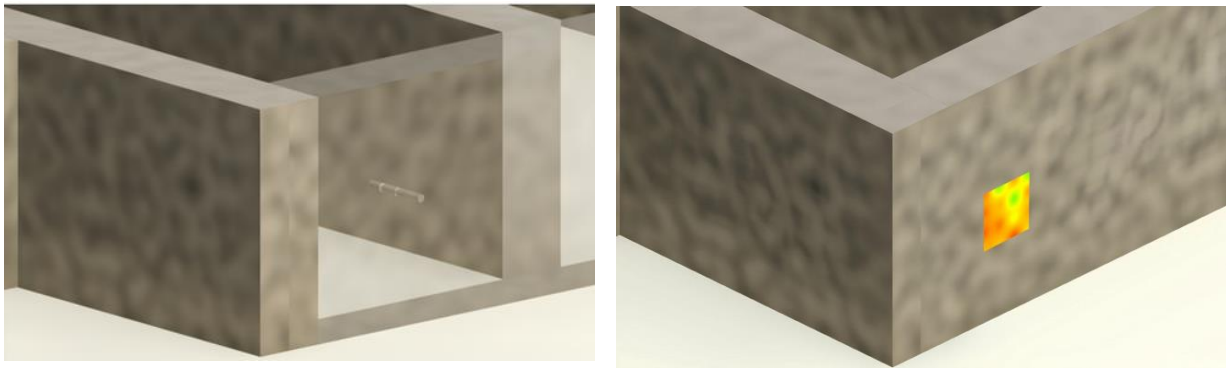


Figure 7 – Output integration in the model

4. Discussion and Conclusions

The proposed demonstration confirms the feasibility of the proof of concept concerning the integration of diagnostic data into BIM models. The resulting information model does not merely represent the geometry and constructional configuration of the building, but also incorporates knowledge related to the materials and performance characteristics of the investigated components. In this sense, the study shows how HBIM can be used not only as a digital repository for survey and documentation purposes, but also as an operational environment for structuring, processing, and reusing diagnostic knowledge.

More specifically, the proposed approach combines the semantic rigour of property-based information structures with the explicit representation of the spatial localization of measurements. This makes it possible to overcome the limitations of approaches that treat diagnostic results either exclusively as attributes of building elements or, conversely, as graphical entities without a formalized semantic structure. The outcome is a model-based environment in which different types of experimental investigations can be consistently associated with individual building components, with clear advantages in terms of information systematization, centralization, and traceability. In this context, a relevant implication lies in the possibility of establishing more structured correlations among diagnostic datasets. The proposed framework supports the comparison of different and complementary investigations performed on the same element, repeated

tests conducted over time on the same component, and equivalent investigations carried out on different elements within the same building. In the case presented here, this means, for example, relating the sonic response - typically associated with material compactness, internal heterogeneity, and the presence of voids or discontinuities - to the localized verification of material consistency and conservation conditions provided by direct endoscopic observation on the same masonry. From this perspective, future developments may exploit the proposed framework to support comparative assessments based on repeated diagnostic acquisitions over time, for example before and after structural consolidation interventions. Likewise, its application to more extensive diagnostic campaigns could enable the comparison of sonic responses across multiple building elements, supporting the investigation of spatially distributed pathologies and more complex deterioration patterns.

With regard to data processing and visualization, the results also demonstrate the usefulness and feasibility of performing interpretative procedures within the same environment used to collect and structure the original information. The automated generation of false-colour maps of sonic velocity distribution and volumetric entities representing masonry stratigraphy shows that the HBIM environment can support not only data storage, but also the production of derived outputs that make diagnostic evidence more immediately readable. This has evident benefits in terms of workflow harmonization, reduced fragmentation of analytical procedures, and a lower risk of operator error, particularly in contexts where users may be experienced in BIM modelling but not necessarily in diagnostic investigation and vice versa.

Another significant outcome concerns the automated extraction and organization of outputs. Integrating diagnostic report production directly into the BIM workflow, in formats such as raster maps, parametric tables, and reusable datasets, facilitates information sharing and promotes continuity between the investigation phase and subsequent phases of interpretation, assessment, and heritage management. In this way, the model can provide a stable and shared reference framework for different operators, different temporal stages, and different categories of data, while also supporting the progressive enrichment of the building knowledge base over time.

Overall, the proposed methodological workflow enables the integration within the HBIM model of three complementary dimensions of diagnostic information management: the semantic structuring of data through parametric entities, their computational processing through VPL-based workflows, and the automated generation of organized information outputs. This integration allows the information model to function not only as an archive of acquired data, but as an operational platform for the management and interpretation of diagnostic knowledge on the built heritage, in line with the principles of interoperability and semantic modelling underpinning the IFC schema.

At the same time, the study presents some limitations that should be acknowledged. The workflow has been tested on a typological test-bed developed as a controlled environment, and the proof of concept has been limited to two diagnostic techniques applied to masonry elements. Although this choice was appropriate for verifying the internal coherence and adaptability of the methodology, further validation on real case studies will be necessary to assess its robustness in relation to more complex geometries, heterogeneous construction conditions, larger datasets, and broader diagnostic campaigns, as well as to support a systematic evaluation of computational performance, scalability, and processing times. In addition, future developments should further investigate the interoperability of the proposed information structure in openBIM environments and its transferability across different software ecosystems.

In all, the proposed framework should be regarded as a starting point that will require further validation before wider generalization can be established, by the integration of additional destructive and non-destructive investigation methods, the implementation of more advanced data querying and comparison procedures, and the connection of diagnostic information with monitoring, assessment, and maintenance-oriented processes. In this broader perspective, the study provides a foundation for the development of integrated digital workflows capable of supporting diagnosis, interpretation, and intervention planning in the knowledge-based conservation and management of historic buildings.

DOCUMENT CODE:	PS/03
CLIENT:	Municipality of Bari
PLACE:	Bari
DATE:	07/06/2025
EQUIPMENT:	Digital ultrasonic detector, model CMS V3HLF-P, with a nominal transmitter frequency of 20 kHz

DIAGNOSTIC REPORT
SONIC TEST

TEST LOCATION (PHOTO):



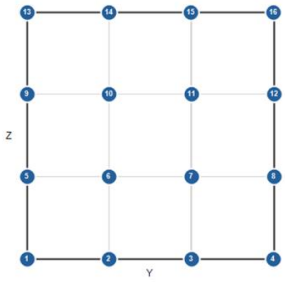
TESTING METHOD:

The sonic investigation was carried out on a ground-floor masonry wall after marking two corresponding grids (4 × 4 nodes with a 20 cm spacing) on the opposite faces of the element. For each pair of corresponding points, five repeated measurements of the sonic wave travel time were acquired and subsequently converted into sonic velocity values based on the known path length. The measurements were then averaged for each node and represented as false-color maps through linear interpolation over the entire grid surface.

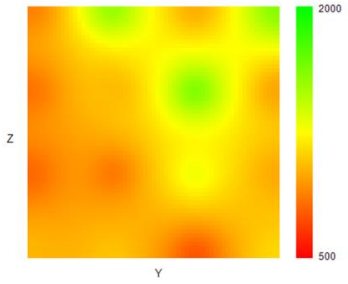
GRID DIAGNOSTIC VALUES:

ID	Sonic Velocity
1	1037 m/s
2	1074 m/s
3	755 m/s
4	1136 m/s
5	808 m/s
6	863 m/s
7	1282 m/s
8	1005 m/s
9	844 m/s
10	1050 m/s
11	1612 m/s
12	992 m/s
13	886 m/s
14	1541 m/s
15	1019 m/s
16	1595 m/s

ACQUISITION GRID LAYOUT:



SONIC MAP:



RESULTS

The grid associated with test PS/03 consists of 16 diagnostic points located on Wall 1. The recorded sonic velocity values range from 755 m/s to 1,612 m/s, with an average value of 1,093.69 m/s. The standard deviation of the measured values is 275.88 m/s.

OPERATOR: NAME SURNAME	**SIGNATURE:** _____

Figure 8 – Automatically generated diagnostic report

References

Bolborea, B, C Baeră, A Gruin, A.-C. Vasile, and A.-M. Barbu. 2025. “A Review of Non-Destructive Testing Methods for Structural Health Monitoring of Earthen Constructions.” *Alexandria Engineering Journal* 114: 55–81. https://doi.org/10.1016/j.aej.2024.11.083.

Cardinali, V, A L Ciuffreda, M Coli, M De Stefano, F Meli, M Tanganelli, and F Trovatelli. 2023. “An Oriented H-BIM Approach for the Seismic Assessment of Cultural Heritage Buildings: Palazzo Vecchio in Florence.” *Buildings* 13 (4). https://doi.org/10.3390/buildings13040913.

Coli, Massimo, Anna L Ciuffreda, Emanuele Marchetti, Davide Morandi, Giammarco Luceretti, and Zeno Lippi. 2022. “3D HBIM Model and Full Contactless GPR Tomography: An Experimental Application on the Historic Walls That Support Giotto’s Mural Paintings, Santa Croce Basilica, Florence—Italy.” *Heritage*. https://doi.org/10.3390/heritage5030132.

Croce, Pietro, Filippo Landi, Benedetta Puccini, Massimiliano Martino, and Alessio Maneo. 2022. “Parametric HBIM Procedure for the Structural Evaluation of Heritage Masonry Buildings.” *Buildings*. https://doi.org/10.3390/buildings12020194.

Falco, Anna De, Francesca Gaglio, Francesca Giuliani, Massimiliano Martino, and Vincenzo Messina. 2024. “An HBIM Approach for Structural Diagnosis and Intervention Design in Heritage Constructions: The Case of the Certosa Di Pisa.” *Heritage*. https://doi.org/10.3390/heritage7040088.

Fattore, C, M Buldo, A Priore, S Porcari, V D Porcari, and M De Fino. 2025. “A Comprehensive Overview of Heritage BIM Frameworks: Platforms and Technologies Integrating Multi-Scale Analyses, Data Repositories, and Sensor Systems.” *Heritage* 8 (7). https://doi.org/10.3390/heritage8070247.

Fino, M De, R A Galantucci, and F Fatiguso. 2023. “Condition Assessment of Heritage Buildings via Photogrammetry: A Scoping Review from the Perspective of Decision Makers.” *Heritage* 6 (11): 7031–66. https://doi.org/10.3390/heritage6110367.

Garcia-Gago, Jesús, Luis Javier Sánchez-Aparicio, Mario Soilán, and Diego González-Aguilera. 2022. “HBIM for Supporting the Diagnosis of Historical Buildings: Case Study of the Master Gate of San Francisco in Portugal.” *Automation in Construction* 141: 104453. https://doi.org/https://doi.org/10.1016/j.autcon.2022.104453.

Garrido, I, M Solla, S Lagüela, and M Rasol. 2022. “Review of InfraRed Thermography and Ground-Penetrating Radar Applications for Building Assessment.” *Advances in Civil Engineering* 2022. https://doi.org/10.1155/2022/5229911.

Parente, Maria, Nazarena Bruno, and Federica Ottoni. 2025. “HBIM and Information Management for Knowledge and Conservation of Architectural Heritage: A Review.” *Heritage*. https://doi.org/10.3390/heritage8080306.

Pauwels, Pieter, Sijie Zhang, and Yong-Cheol Lee. 2017. “Semantic Web Technologies in AEC Industry: A Literature Overview.” *Automation in Construction* 73: 145–65. https://doi.org/https://doi.org/10.1016/j.autcon.2016.10.003.

Santos, David, Manuel Cabaleiro, Hélder S Sousa, and Jorge M Branco. 2022. “Apparent and Resistant Section Parametric Modelling of Timber Structures in HBIM.” *Journal of Building Engineering* 49: 103990. https://doi.org/https://doi.org/10.1016/j.jobe.2022.103990.

Solla, Mercedes, Luisa M S Gonçalves, Gil Gonçalves, Carina Francisco, Iván Puente, Paulo Providência, Florindo Gaspar, and Hugo Rodrigues. 2020. “A Building Information Modeling Approach to Integrate Geomatic Data for the Documentation and Preservation of Cultural Heritage.” *Remote Sensing*. https://doi.org/10.3390/rs12244028.

Tejedor, B, E Lucchi, D Bienvenido-Huertas, and I Nardi. 2022. “Non-Destructive Techniques (NDT) for the Diagnosis of Heritage Buildings: Traditional Procedures and Futures Perspectives.” *Energy and Buildings* 263. https://doi.org/10.1016/j.enbuild.2022.112029.

Cinpar 2026
XXII International Conference on Building Pathology and Constructions Repair
15th to 17th July 2026 - Lisboa, Portugal

Challenges in data collection for the development of maintenance plans for historic buildings for cultural use integrated with HBIM models

Desafios no levantamento de informações para elaboração de planos de manutenção de edificações históricas de uso cultural integrados a modelos HBIM

Geórgia FREIRE[1]; Antonio Gabriel BRITO[2]; Ana Luísa COELHO[3]; Laura Cristina FERREIRA[4]; Francisco Carlos SANTANA[5]; Ana Cecilia VASCONCELOS[6]; Esequiel MESQUITA[7]

[1] Institute of Architecture and Urbanism and Design (IAUD), Federal University of Ceara (UFC), Brazil,
[2] IAUD, UFC, Brazil, gabrielbrito0807@gmail.com
[3] IAUD, UFC, Brazil, analuisalcoelho@gmail.com
[4] IAUD, UFC, Brazil, lauracsferreira20@arquitetura.ufc.br
[5] Laboratory of Rehabilitation and Digitalization of Constructions (LAREB), Federal University of Ceara (UFC), Brazil, franciscosantana@alu.ufc.br
[6] IAUD, UFC, Brazil, anaceciliavas@ufc.br
[7] IAUD, UFC, Brazil, emesquita@ufc.br

Abstract: The preservation of historic buildings for cultural use requires rigorous and up-to-date information on their building systems and technical installations, particularly when the aim is to develop maintenance plans aligned with contemporary management practices. Within this context, Heritage Building Information Modeling (HBIM) has gained prominence due to its capacity to integrate geometric, material, functional, and historical data. However, the application of HBIM to listed heritage buildings faces significant limitations related to the availability and quality of existing information. This paper discusses the challenges encountered during the survey and data acquisition processes required to update the HBIM model of the Theatro José de Alencar, a important cultural facility and listed heritage site in Brazil. The employed research methodology encompasses a literature review, documentary research, semi-structured interviews, and on-site surveys. Consequently, this study provides an analysis of the capture precision levels of the surveying methods utilized within the theater, alongside a critical assessment of the challenges in acquiring data related to building services. Ultimately, a protocol for surveying this specific information is proposed. This protocol structures the data collection activities for building systems, focusing on maintenance management integrated into the heritage asset's HBIM model. This research contributes to the ongoing debate regarding the demand for advanced surveying tools in the built heritage sector, underscoring the necessity for specialized protocols tailored to the assessment of building services in historical structures.

Keywords: Architectural survey; survey protocols; building heritage; maintenance management; HBIM;

1. Introduction

The preservation of historical buildings intended for cultural use demands management frameworks that go beyond episodic restoration interventions. When operational, these assets face intensive and regulatory demands. Under these circumstances, maintenance management assumes a central role, as continuity of use depends on the reliability of the structural systems and building services. Conservation becomes a permanent process, structured by maintenance plans grounded in robust and up-to-date technical information.

The effectiveness of these plans depends on the quality of the available data of the building. In this context, Building Information Modeling (BIM) and Heritage Building Information Modeling (HBIM) integrate geometric, historical, and functional data into a single platform. (Brumana *et al.* 2017; Dore and Murphy 2017; Banfi and Liu 2026; Penjor *et al.* 2024).

However, despite methodological advancements, the application of HBIM to the operation and maintenance (O&M) remains in an emergent stage, exhibiting significant gaps in the structuring of facility

management (FM) data (Oliveira *et al.* 2024; Wojciechowski *et al.* 2024). Most studies focus on capturing and modeling architectural and structural geometry, building services remains underdeveloped (Parente *et al.* 2025).

Technologies such as Terrestrial Laser Scanning (TLS), digital photogrammetry, Unmanned Aerial Vehicle (UAV) imagery, and historical documentary surveys have proven highly effective in documenting the building "envelope" (Froner *et al.* 2024; Vieira et al. 2023). These methods enable high geometric precision and formal detailing, being extensively documented in recent studies. Nevertheless, these methodologies do not automatically capture building services, particularly those embedded within walls, floors, and ceilings. Elements such as plumbing, electrical conduits, cabling, HVAC ducts, drainage networks, and fire protection systems (FPS) are rarely represented in point clouds or models derived exclusively from geometric data. Even when certain components are exposed (e.g., electrical panels, light fixtures, grilles, or exposed pipes), the extraction of relevant technical information is not automatic. The point cloud records their shape and spatial position but does not identify their function, capacity, materiality, conservation status, or connections to other systems. Converting these geometric records into semantically structured data requires technical interpretation, on-site verification, and often, consultation of supplementary documentation. Consequently, both concealed systems and visible elements demand specific procedures for identification, categorization, and informational structuring to be effectively incorporated into the HBIM model.

Current literature reveals that the structuring of specific protocols for the acquisition and modeling of building services data within an HBIM environment remains still in early stages. Studies dedicated to modeling historical architecture (Ribeiro *et al.* 2026), reconstructing construction phases (Castellano-Román and Pinto-Puerto 2019), and analyzing materials predominate (Oliveira Magalhães *et al.* 2025), while building services remain underrepresented or entirely absent from digital models. This limitation underscores the necessity for on-site data collection through targeted inspections, interviews with maintenance teams, analysis of scattered technical documentation, and the application of complementary non-destructive methods, strategies that still lack systematization in recent scientific output.

In light of this scenario, this paper seeks to address the following research question: what are the main challenges in collecting building installation data for the development of maintenance plans in operational historical buildings? This study is based on the hypothesis that current surveying methodologies tailored for HBIM do not systematically encompass building services, thereby requiring the development of specific protocols for their identification, recording, and modeling.

To explore this issue, the Theatro José de Alencar is adopted as a case study. Although the building benefited from architectural surveys produced by the National Institute of Historic and Artistic Heritage (IPHAN) and a point cloud generated via laser scanning, a significant inadequacy in data pertaining to building services was identified. This condition highlighted the need for complementary surveying strategies to update the HBIM model with a focus on maintenance management.

By discussing the challenges encountered throughout this process, this article contributes to the contemporary debate on the digitalization of the built heritage, emphasizing the urgent need for methodologies that systematically integrate geometric data and technical information regarding building installation. Beyond merely amplifying the level of detail of digital models, the objective is to reinforce their role as effective instruments for the preservation and sustainable management of historical buildings intended for cultural use.

2. Data collection and HBIM for FM in built heritage

HBIM supports documentation, analysis, maintenance, and conservation through the integration of geometric and semantic data. Its development has progressively expanded toward facility management (FM) applications.

Several studies have explored HBIM integration in maintenance and conservation processes (Jordan-Palomar et al. 2018; De Fino et al. 2019; Piselli *et al.* 2020; Mora et al. 2021; Khan *et al.* 2022; Matrone *et al.* 2023). Despite this evolution, a critical limitation persists: most HBIM applications remain predominantly focused on geometric and historical representation, while building services systems are systematically underrepresented. This imbalance directly affects the applicability of HBIM in the Operation and

Maintenance (O&M) phase, where decision-making depends on accurate, up-to-date technical information regarding system performance, configuration, and condition.

Maintenance management in heritage buildings assumes particular relevance due to the absence of a demolition phase and the need to ensure the continuity of use (Pishdad-Bozorgi *et al.* 2018). In this context, the Asset Information Model (AIM) becomes a central component, as it integrates geometric, alphanumeric, and documentary data required for lifecycle management.

The distinction between these data types is not merely classificatory but operational. Geometric data enable spatial representation and model construction; alphanumeric data define the technical and functional properties of elements; and documentary data provide contextual and procedural information that cannot be reduced to parametric attributes (Figure 1). The absence of any of these layers compromises the integrity of the AIM and, consequently, the reliability of maintenance planning. This is particularly critical for building services systems, whose performance depends on accurate, detailed, and up-to-date information.

In practice, heritage buildings are often managed through fragmented systems (Tsay *et al.* 2022), limiting interoperability and restricted access to information. This condition reinforces that the main limitation of HBIM for FM is not technological, but informational. Therefore, the effectiveness of HBIM for facility management depends fundamentally on the establishment of systematic data collection processes capable of integrating both geometric and technical information.

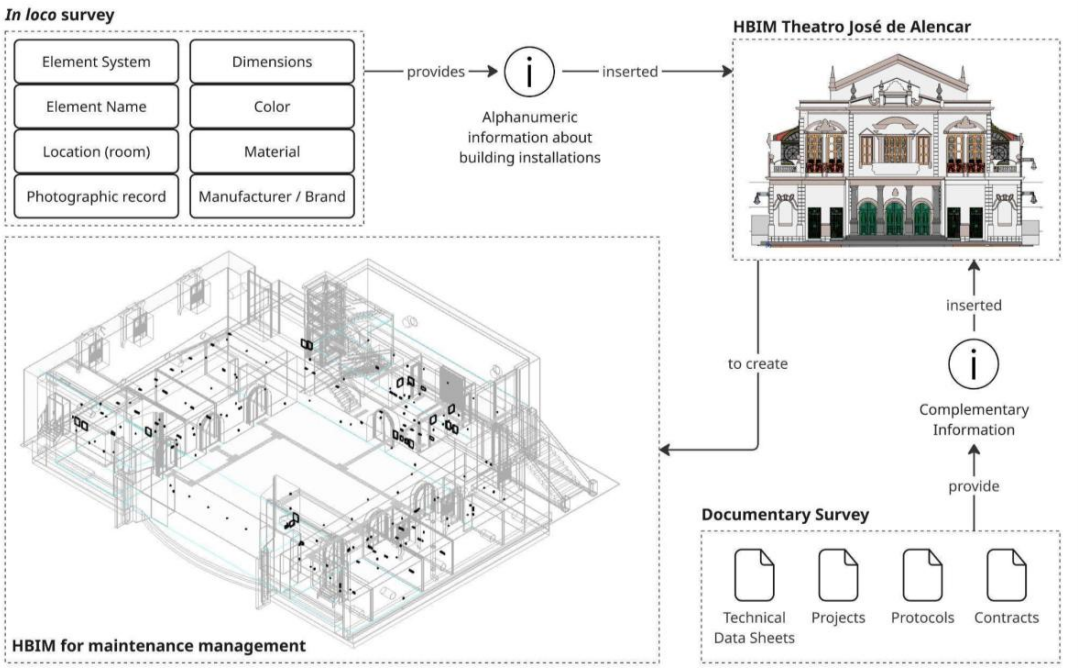


Figure 1 – Workflow for Maintenance Survey.

3. Survey methods and challenges in historic buildings

Survey protocols require alignment between data acquisition methods and the type of information required (Alshawabkeh and Baik 2023). In heritage contexts, four main approaches are typically employed: laser scanning, photogrammetry, documentary research, and visual inspection.

Laser scanning and photogrammetry provide high geometric accuracy and enable detailed three-dimensional representation of the built asset. However, both methods are limited to visible surfaces and are therefore unable to capture embedded building systems. In addition, they do not provide semantic or operational information, which restricts their use in maintenance-oriented applications.

Documentary research contributes to understanding the historical and technical evolution of the building but depends on the availability and reliability of records, which are often incomplete or inconsistent in

heritage contexts. Visual inspection, in turn, enables the identification of materials, construction techniques, and technical systems that cannot be captured digitally, although it depends on accessibility and expert interpretation.

In historic buildings, these limitations are amplified by the absence of reliable “as-built” documentation, the invisibility of embedded systems, and restrictions on invasive inspection methods. As a result, data collection becomes an interpretative process, subject to uncertainty and dependent on multiple sources of information.

These conditions demonstrate that survey methods, when applied in isolation, are insufficient to capture the full range of data required for HBIM-based maintenance. Consequently, integrated approaches combining digital and manual techniques are necessary to bridge the gap between geometric representation and technical information.

4. Methodology

This study adopts a structured methodological approach to investigate the challenges associated with surveying building services systems in historic buildings and to support the development of maintenance plans integrated with HBIM models.

The research process is organized into five stages (Figure 2). The first stage consists of problem formulation based on a literature review, leading to the definition of the research hypothesis. The second stage involves the selection of the case study, the Theatro José de Alencar, based on its historical significance, continuous use as a cultural facility, and the institutional interest in applying HBIM for maintenance management.

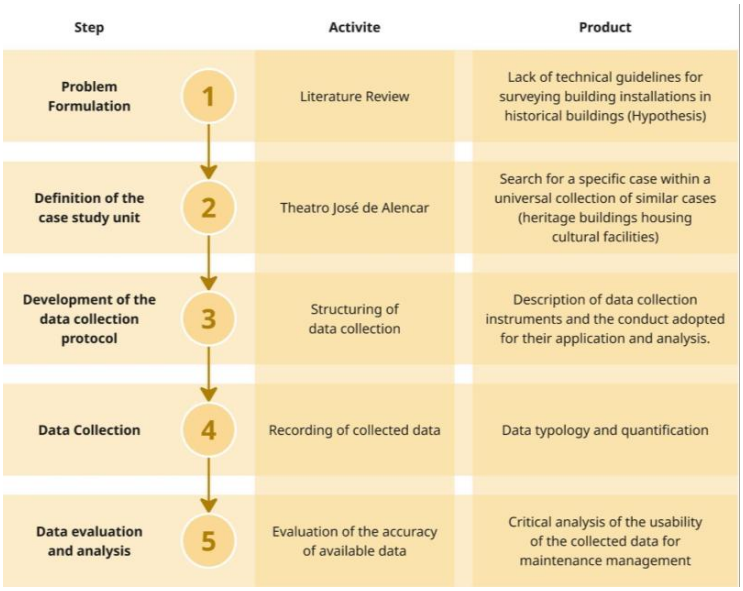


Figure 2 – Research methodology.

The third stage comprises the development of a data collection protocol, defining the procedures, instruments, and analytical strategies for data acquisition. The fourth stage involves data collection, combining documentary research, semi-structured interviews, and in situ surveys. Data were collected between May and July 2025, including ten site visits and the recording of 235 photographs to support system documentation. Finally, the fifth stage consists of evaluating the accuracy and quality of the collected data. This methodological structure ensures that data collection is treated as an analytical and iterative process, directly linked to the reliability and usability of HBIM models in maintenance management.

4.1 Data collection protocol

A multifaceted approach was adopted for data collection, combining different methods to ensure a comprehensive understanding of the building systems and their operational context. Data were collected between May and July 2025, a period during which the building management granted full access to the survey team. This temporal window was critical, as it enabled the observation of maintenance activities under real operating conditions.

The data collection strategy combined documentary research, semi-structured interviews, and on-site surveys of building services systems (Figure 3). Documentary research included the analysis of existing architectural drawings, historical records, point cloud data, a virtual tour of the building, and maintenance management documents. This stage provided a baseline for understanding the building's physical configuration and its documented interventions, although gaps in services-related information were already evident.

Semi-structured interviews were conducted in two formats. The first consisted of an interview with the maintenance manager, focusing on the organizational structure and operational processes of maintenance management. The second involved ten meetings with two maintenance technicians, aimed at documenting daily routines and identifying practical challenges in the execution of maintenance activities. The interview with the maintenance manager was recorded and transcribed. Open-ended questions were used throughout to encourage detailed responses, particularly regarding workflow organization, decision-making processes, and the execution of maintenance tasks.

In parallel, ten on-site visits were carried out to survey building services systems associated with maintenance activities. During these visits, a total of 235 photographs were taken, documenting selected installations and supporting the development of a structured database for system modelling. This empirical dataset played a key role in complementing the limitations identified in existing documentation and digital surveys.

Data collection method	Type of data collected	Data collected	Analysis of the usability of the collected data for FM
Documentary Research	Existing Projects and Surveys	153 digitized documents, including: · 77 related to air conditioning, · 30 to the electrical system, · 16 to the plumbing system, · 30 to the fire prevention system.	Extensive documentation, but outdated in relation to the reality of the building.
	Historical Documentation	Books and historical documents about the theater.	There is no record of the most recent interventions in the theater's building systems.
	Point Cloud and Virtual Tour	1 point cloud of the entire building	Although up-to-date, it does not capture all elements of building installations.
	Maintenance Control Documents	5 contracts with maintenance service providers and 1 maintenance control spreadsheet	Documentation under construction and lacking all the necessary information for each system.
Semi-structured Interviews	Maintenance Manager Maintenance Technicians	· 1 interview with audio recording and transcriptions · 10 interviews with 2 technicians	Provided necessary information for understanding building systems.
On-site Survey	Images of the building's installations and measurements	235 photographs and 47 digital scans of the drawings used in the survey.	Relevant and necessary information for the semantic enrichment of the maintenance model.

Figure 3 – Different methods and types of data collected.

5. Case study: Theatro José de Alencar - Existing documentation and building installations data

The Theatro José de Alencar, located in Fortaleza, Ceará, Brazil, is one of the most significant cultural, historical, and architectural heritage assets in the region. Inaugurated in 1910 and later listed by the Instituto do Patrimônio Histórico e Artístico Nacional (IPHAN) in 1964, the building represents a notable example of

eclectic architecture in Ceará. Its architectural composition is characterized by the integration of imported metallic structures with traditional construction systems, reflecting a combination of French stylistic influences and British structural contributions, particularly in the cast-iron elements fabricated in Scotland (Castro 2010). Beyond its architectural value, the theatre holds strong symbolic and cultural significance, functioning as a continuous space for artistic production, public engagement, and the preservation of collective memory.

Architecturally, the building follows the Italian theatre typology, with a clearly defined and integrated spatial organization. Its material composition, primarily metal, masonry, and wood, combined with the richness of ornamental elements across façades and interior spaces, results in a complex architectural system. This complexity is further intensified by successive maintenance and adaptation interventions carried out over time, reflecting both evolving functional requirements and changing construction practices. From a maintenance perspective, this layered transformation introduces significant challenges, as the current state of the building is the result of cumulative modifications rather than a single, coherent design phase.

The Theatro José de Alencar remains fully operational, hosting performances, events, and guided visits. Field surveys conducted as part of this research indicate that the building retains many of its original characteristics, while also incorporating adaptations driven by functional and regulatory updates. These interventions reveal a process of continuous negotiation between heritage preservation and contemporary use (Figure 4). In terms of building services, updated electrical systems were identified, adapted to meet current demands for lighting and sound. Mechanical systems, such as air conditioning, were introduced after the original construction, requiring integration with the historic structure, alongside fire protection systems. Hydrosanitary installations also show evidence of modernization, particularly in response to current accessibility standards.

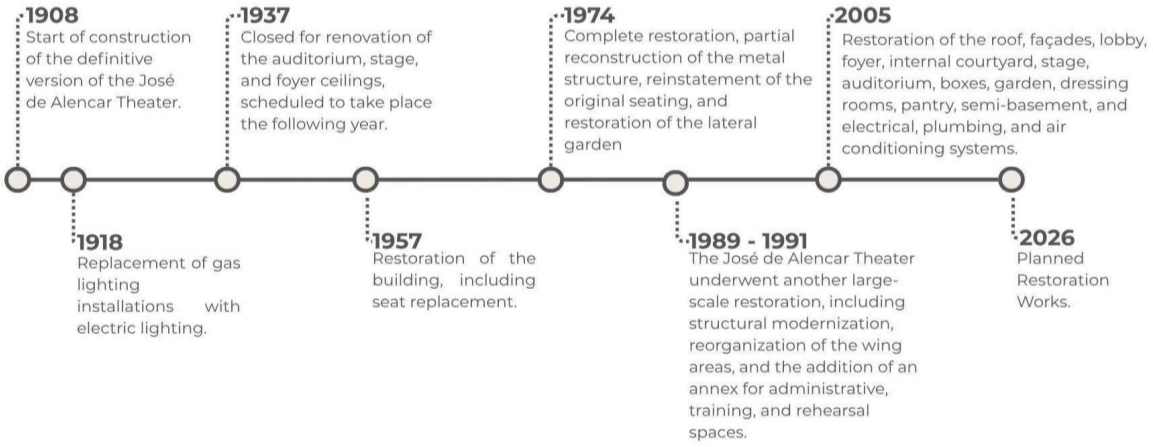


Figure 4 - Timeline of documented maintenance work at the José de Alencar Theatre.

Although the building is supported by architectural documentation, including plans, sections, and elevations, and point cloud data, the analysis revealed substantial inconsistencies and gaps, particularly regarding building services systems. The available documentation reflects different phases of intervention but lacks a comprehensive and reliable record of modifications over time. In several cases, projects associated with renovation works were not executed, and there is no systematic documentation of maintenance interventions. This condition creates a disconnect between the recorded information and the current state of the building.

Point cloud surveys provide a highly accurate representation of visible geometry and support the updating of architectural documentation (Figure 5). However, they do not capture embedded systems, limiting their applicability for maintenance purposes. Consequently, the geometric accuracy of the model does not translate into informational completeness.

The in situ survey identified the presence of electrical, hydrosanitary, HVAC, and fire protection systems; however, no technical documentation was found describing their configuration, layout, or evolution. The

coexistence of obsolete and updated components indicates incremental and undocumented interventions. In several cases, even maintenance staff lacked precise knowledge of system functions and configurations.

This lack of documentation introduces significant uncertainty into maintenance planning, particularly regarding network layouts, system specifications, and intervention history. As a result, the HBIM model risks representing only the visible aspects of the building, without incorporating the infrastructure that supports its operation.

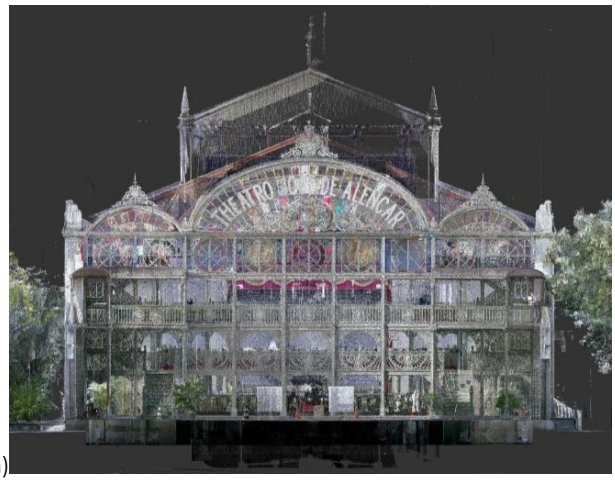
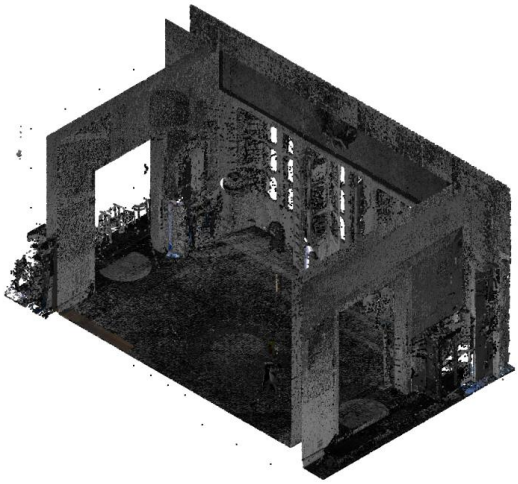
a)  b) 

Figure 5 – a) Point cloud visualization of the facade of the theater's auditorium. b) Point cloud visualization of an interior environment of the theater.

From the case study, it was possible to identify the main challenges in collecting building installation data in historical buildings (Figure 6), which lie not in the absence of geometric data, but rather the lack of structured and reliable information about building installations.

		Systems identified				
		Electrical	Hydrosanitary	Drainage	HVAC	FPS
Challenges in data collection	Difficulty in identifying electrical panels in operation	x				
	Difficulty in identifying inspection boxes that are unregistered and/or unidentified	x	x	x		
	Presence of elements from different eras that perform the same function	x	x	x	x	x
	Lack of plans identifying the elements present in the updated system	x	x	x		x
	Impossibility of identifying the layout of internal piping related to the system	x	x	x	x	x
	Lack of historical records of interventions carried out for system maintenance	x	x	x	x	x

Figure 6 – Summary of the challenges in collecting data from building systems.

Overall, the evidence indicates that interventions in the building systems have occurred progressively over time, responding to functional demands but without the establishment of a comprehensive technical archive encompassing all phases of the building's lifecycle. This fragmented evolution has direct implications for HBIM development. While point cloud data enable accurate geometric representation of visible elements, the absence of reliable technical information regarding embedded systems limits both the modelling process and the incorporation of non-geometric data. As a result, the HBIM model risks remaining

a predominantly geometric representation, failing to adequately capture the infrastructure that supports the building's operation.

From a maintenance planning perspective, the lack of knowledge regarding network layouts, installed components, and intervention history increases uncertainty in decision-making processes. This condition may lead to interventions that are incompatible with the actual state of the building, potentially compromising both its performance and its heritage value. In historic buildings, technical documentation is therefore not merely supportive but essential to ensure user safety and the preservation of the asset.

Consequently, the absence of systematized data on building services in the Theatro José de Alencar constitutes a central challenge for the implementation of integrated heritage management. It also reinforces the need for structured data collection protocols capable of bridging the gap between physical reality and digital representation, thereby enabling HBIM models to function as effective tools for maintenance management rather than as purely descriptive models.

6. Results

The analysis demonstrates that no single technique is capable of capturing the full range of information required for HBIM-based maintenance management (Figures 7 and 8). Instead, each method presents complementary strengths and limitations that directly affect the accuracy, completeness, and usability of the resulting data.

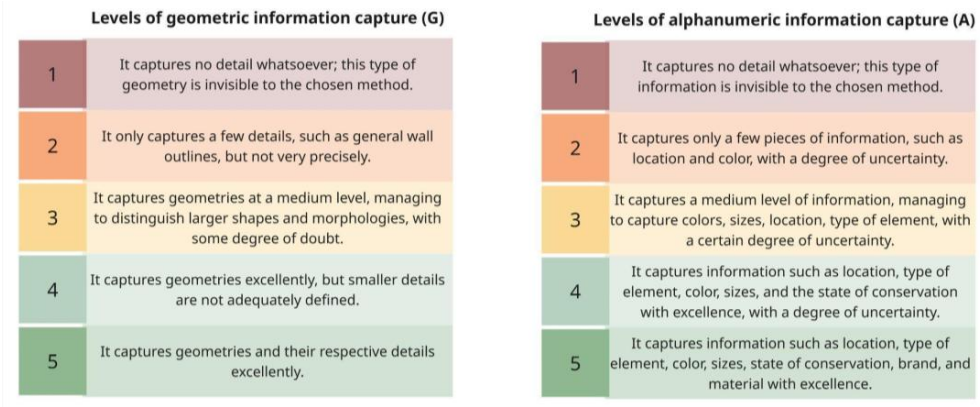


Figure 7 – Levels of precision of surveying methods.

		Elements Surveyed									
		Walls		Windows and Doors		Roofs		Building Systems		Internal Pipes	
	Type of Information Surveyed	G	A	G	A	G	A	G	A	G	A
Survey Method	Laser Scanner	5	4	5	4	1	1	3	4	1	1
	Aerial Photogrammetry	3	3	2	3	5	4	1	3	1	1
	Visual Inspections	4	5	4	5	1	5	4	5	1	1

Figure 8 – Table analyzing the accuracy level of data capture for surveying methods used in theater.

Laser scanning and photogrammetry provide accurate representations of the building. These techniques enable the capture of complex forms with high precision, supporting the development of detailed three-dimensional models. However, both methods are constrained by line-of-sight conditions, as they can only record visible surfaces. Consequently, they are inherently limited in their ability to capture embedded

building services systems. In addition, their capacity to acquire alphanumeric and descriptive information is minimal, restricting their usefulness for maintenance-oriented applications.

Conversely, manual survey methods, particularly visual inspection, play a critical role in capturing semantic and technical data. The in situ survey conducted in this study proved indispensable for identifying building services components located in inaccessible or concealed areas, such as installations beneath fixtures or within enclosed spaces. Moreover, the collection of alphanumeric data, including material, color, brand, and model, was essential for supporting maintenance actions, especially in the context of component replacement and lifecycle tracking. These findings demonstrate that manual surveying should not be regarded as an obsolete practice, but rather as a process of data curation, capable of providing the level of detail required for informed decision-making.

Within the HBIM framework, particularly in FM applications, the integration of geometric and semantic data is a fundamental requirement. Maintenance processes depend on access to reliable information regarding previous interventions, technical specifications, and system configurations. Without this information, maintenance decisions must rely on assumptions or repeated site inspections, reducing efficiency and increasing the risk of inappropriate interventions. In heritage buildings, this issue is further amplified, as replacement actions must be compatible with the original architectural language, preserving both material integrity and historical significance.

Despite the complementary nature of survey methods, significant limitations persist. A key limitation is the absence of systematic documentation over time. The gradual and often undocumented replacement of components, such as electrical fixtures and hydrosanitary elements, results in a heterogeneous accumulation of systems within the building. In such cases, the survey is limited to the observation of existing elements, while previous configurations remain unknown. This lack of historical traceability introduces uncertainty into both the modelling process and maintenance planning.

Another major limitation concerns the invisibility of embedded systems. In historic buildings, invasive inspection methods are generally not permitted, which prevents access to critical information about the layout, materials, and dimensions of internal networks.

To address these challenges, this study proposes a structured protocol for surveying building services systems in historic buildings (Figure 9). The process begins with a preliminary assessment, including the collection and analysis of existing documentation, point cloud data, and interviews with maintenance personnel. This stage establishes the baseline level of available information and identifies data gaps, ensuring that subsequent efforts are strategically targeted.

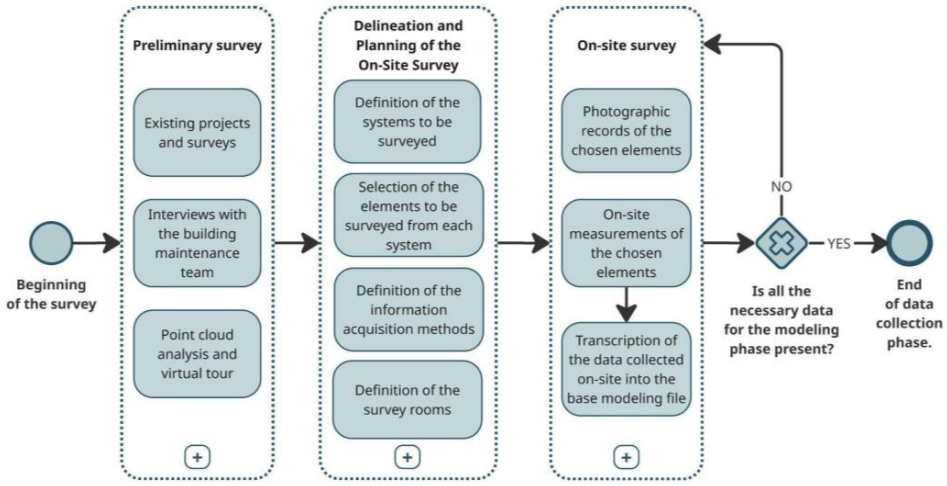


Figure 9 – Protocol for surveying building installation systems in historic buildings.

The second stage involves the planning of the in situ survey, where the systems to be investigated, the data acquisition methods, and the practical conditions for fieldwork are defined. This step is critical, as methodological decisions directly influence the scope and quality of the data collected. The third stage

consists of the survey itself, including measurement, descriptive recording, and photographic documentation of building components. The collected data are then organized and structured for integration into the HBIM model. Finally, a validation stage is conducted to assess data completeness and consistency, ensuring that the information meets the requirements for modelling and maintenance applications.

The proposed protocol addresses a key gap identified in this study: the lack of systematic procedures for collecting alphanumeric and operational data related to building services systems. By formalizing the survey process, the protocol reduces uncertainty, improves data consistency, and enhances the usability of HBIM models for maintenance management. More importantly, it shifts the focus of HBIM workflows from geometry-driven modelling to information-driven processes.

From an analytical perspective, the results indicate that the main challenges in data collection for historic buildings are not solely technical, but also informational and procedural. The absence of documentation, the limitations of non-invasive survey methods, and the lack of standardized workflows collectively hinder the development of reliable HBIM models. Therefore, improving data collection practices is not only a methodological issue but a prerequisite for enabling HBIM to function as an effective tool for Facility Management.

Finally, while the proposed protocol demonstrates potential for improving data collection practices, its applicability across different heritage contexts requires further validation. Future research will test the workflow in additional case studies, allowing for the assessment of its adaptability and robustness. Such validation is essential to ensure that the protocol can support a broader range of heritage assets and operational conditions.

Overall, the findings reinforce that the effectiveness of HBIM in maintenance management is directly dependent on the quality and completeness of the underlying data. Without structured and reliable data collection processes, particularly for building services systems, HBIM models risk remaining descriptive representations rather than operational tools capable of supporting informed decision-making in historic buildings.

7. Discussion and Conclusions

The findings derived from the Theatro José de Alencar case study demonstrate that, despite significant advances in geometric data acquisition through technologies such as laser scanning and photogrammetry, critical gaps persist in the collection and structuring of information related to building services systems. These gaps directly affect the capacity of HBIM models to function as reliable tools for maintenance management, particularly in heritage buildings that remain in continuous use and have undergone successive interventions.

The comparative analysis of survey methods confirms that, while each technique contributes valuable information, none is sufficient when applied in isolation. While laser scanning and photogrammetry provide reliable geometric representation, they fail to capture embedded systems and semantic information. Conversely, manual inspection enables the identification of technical attributes but lacks geometric precision. Therefore, the main challenge is not technological, but related to the integration and systematization of heterogeneous data sources.

From an operational perspective, the study highlights that the effectiveness of HBIM in FM is not determined solely by geometric accuracy, but by the completeness and consistency of the associated semantic data. In this sense, the absence of structured information on building services represents a key limitation, restricting the transition of HBIM models from descriptive representations to decision-support systems.

From a broader perspective, the findings indicate that the effectiveness of HBIM in Facility Management depends fundamentally on data quality and completeness. The transition from geometry-based modelling to information-based management requires a shift in focus from data representation to data acquisition.

As a central contribution, this study highlights the need for structured protocols specifically designed for the collection of building services data in heritage contexts. The proposed protocol addresses this gap by integrating multiple data sources and establishing a systematic workflow for data acquisition and validation. Future research should focus on validating the proposed protocol in different case studies to assess its

adaptability and scalability. Such validation is essential to consolidate its applicability and to support the broader implementation of HBIM in heritage maintenance management.

Acknowledgements

The authors acknowledge the Coordenação de Aperfeiçoamento de Pessoal de Nível Superior (CAPES), and the Secretaria da Cultura do Estado do Ceará (Secult CE) for all support.

This work was financially supported by FUNCAP, Project 01172921/2022 – Cientista Chefe Cultura,; by the National Council for Scientific and Technological Development (CNPq) – Project 302054/2022-7 – PQ2, by the Project - 440926/2024-6 – VISION and Project - 402828/2024-0 – CLIC; CAPES Foundation and Finep 2896/24.

References

Alshawabkeh, Yahya, and Ahmad Baik. 2023. “Integration of Photogrammetry and Laser Scanning for Enhancing Scan-to-HBIM Modeling of Al Ula Heritage Site.” Heritage Science 11 (1): 147.

Banfi, Fabrizio, and Wanqin Liu. 2026. “The State of HBIM in Digital Heritage: A Critical and Bibliometric Assessment of Six Emerging Frontiers (2015–2025).” Applied Sciences 16 (2): 906. https://doi.org/10.3390/app16020906.

Brumana, R., S. Della Torre, D. Oreni, et al. 2017. “HBIM CHALLENGE AMONG THE PARADIGM OF COMPLEXITY, TOOLS AND PRESERVATION: THE BASILICA DI COLLEMAGGIO 8 YEARS AFTER THE EARTHQUAKE (L’AQUILA).” The International Archives of the Photogrammetry, Remote Sensing and Spatial Information Sciences XLII-2/W5 (August): 97–104. https://doi.org/10.5194/isprs-archives-XLII-2-W5-97-2017.

Castellano-Román, Manuel, and Francisco Pinto-Puerto. 2019. “Dimensions and Levels of Knowledge in Heritage Building Information Modelling, HBIM: The Model of the Charterhouse of Jerez (Cádiz, Spain).” Digital Applications in Archaeology and Cultural Heritage 14 (September): e00110. https://doi.org/10.1016/j.daach.2019.e00110.

Castro, José. 2010. “Revista Do Instituto Do Ceará.” O Centenário Do Teatro José de Alencar 1910-2010 (Arquitetura e Consagração) (Fortaleza). https://www.institutodoceara.org.br/revista/Rev-apresentacao/RevPorAno/2010/01_artigos/2010-3-centenarioteatrojosedealencar.pdf.

De Fino, Mariella, Rosella Alessia Galantucci, and Fabio Fatiguso. 2019. “Remote Diagnosis and Control of the Heritage Architecture by Photorealistic Digital Environments and Models.” SCIRES-IT - SCIentific RESearch and Information Technology (IT) 9 (2). https://doi.org/10.2423/i22394303v9n2p1.

Dore, C., and M. Murphy. 2017. “CURRENT STATE OF THE ART HISTORIC BUILDING INFORMATION MODELLING.” The International Archives of the Photogrammetry, Remote Sensing and Spatial Information Sciences XLII-2/W5 (August): 185–92. https://doi.org/10.5194/isprs-archives-XLII-2-W5-185-2017.

Froner, Yacy Ara, Willi De Barros Gonçalves, Luiz Antônio Cruz Souza, et al. 2024. “Data Collection for Cultural Heritage Risk Management: The Damage Map through Heritage Building Information Modeling (HBIM) Project Applied to the Façade of St Francis of Assisi, Ouro Preto, Brazil.” Studies in Conservation 69 (sup1): 98–107. https://doi.org/10.1080/00393630.2024.2379132.

Jordan-Palomar, Isabel, Patricia Tzortzopoulos, Jorge García-Valldecabres, and Eugenio Pellicer. 2018. “Protocol to Manage Heritage-Building Interventions Using Heritage Building Information Modelling (HBIM).” Sustainability 10 (4): 908. https://doi.org/10.3390/su10040908.

Khan, Muhammad, Muhammad Khan, Mushk Bughio, Bushra Talpur, In Kim, and Jongwon Seo. 2022. “An Integrated HBIM Framework for the Management of Heritage Buildings.” Buildings 12 (7): 964. https://doi.org/10.3390/buildings12070964.

Matrone, Francesca, Elisabetta Colucci, Emmanuele Iacono, and Gianvito Marino Ventura. 2023. “The HBIM-GIS Main10ance Platform to Enhance the Maintenance and Conservation of Historical Built Heritage.” Sensors 23 (19): 8112. https://doi.org/10.3390/s23198112.

Mora, Rocío, Luis Javier Sánchez-Aparicio, Miguel Ángel Maté-González, Joaquín García-Álvarez, María Sánchez-Aparicio, and Diego González-Aguilera. 2021. “An Historical Building Information Modelling Approach for the Preventive Conservation of Historical Constructions: Application to the Historical Library of Salamanca.” Automation in Construction 121 (January): 103449. https://doi.org/10.1016/j.autcon.2020.103449.

Oliveira Magalhães, Brendda Karen, Gabriel Souza Duarte, Alice Brasil De Matos Galvão, Ana Cecília Serpa Braga Vasconcelos, and Laís Cristina Barbosa Costa. 2025. “Documentation Strategies for HBIM Model Parameterization: A Case Study of the José de Alencar Theater.” Digital Applications in Archaeology and Cultural Heritage 38 (September): e00443. https://doi.org/10.1016/j.daach.2025.e00443.

Oliveira, Tatiane Cristine Silva Kono De, Angelo Palmisano, and Fábio Friol Guedes De Paiva. 2024. “BIM Para Manutenção e Gestão Pública de Edificações No Brasil: Revisão Sistemática Da Literatura.” Revista Nacional de Gerenciamento de Cidades 12 (87). https://doi.org/10.17271/23188472128720245332.

Parente, Maria, Nazarena Bruno, and Federica Ottoni. 2025. “HBIM and Information Management for Knowledge and Conservation of Architectural Heritage: A Review.” Heritage 8 (8): 306. https://doi.org/10.3390/heritage8080306.

Penjor, Tshering, Saeed Banihashemi, Aso Hajirasouli, and Hamed Golzad. 2024. “Heritage Building Information Modeling (HBIM) for Heritage Conservation: Framework of Challenges, Gaps, and Existing Limitations of HBIM.” Digital Applications in Archaeology and Cultural Heritage 35 (December): e00366. https://doi.org/10.1016/j.daach.2024.e00366.

Piselli, Cristina, Jessica Romanelli, Matteo Di Grazia, et al. 2020. “An Integrated HBIM Simulation Approach for Energy Retrofit of Historical Buildings Implemented in a Case Study of a Medieval Fortress in Italy.” Energies 13 (10): 2601. https://doi.org/10.3390/en13102601.

Pishdad-Bozorgi, Pardis, Xinghua Gao, Charles Eastman, and Alonzo Patrick Self. 2018. “Planning and Developing Facility Management-Enabled Building Information Model (FM-Enabled BIM).” Automation in Construction 87 (March): 22–38. https://doi.org/10.1016/j.autcon.2017.12.004.

Ribeiro, Gilmário C., Mylene M. Vieira, Esequiel Mesquita, Eugenio Moreira, and Grazia Tucci. 2026. “An Integrated HBIM Protocol for Digital Documentation, Management and Reconstruction of Historic Buildings.” Journal of Building Engineering 118 (January): 114920. https://doi.org/10.1016/j.jobe.2025.114920.

Tsay, Gustavo Salles, Sheryl Staub-French, and Érik Poirier. 2022. “BIM for Facilities Management: An Investigation into the Asset Information Delivery Process and the Associated Challenges.” Applied Sciences 12 (19): 9542. https://doi.org/10.3390/app12199542.

Vieira, Mylene M., Gilmário Ribeiro, Renan Paulo, et al. 2023. “Strategy for HBIM Implementation Using High-Resolution 3D Architectural Documentation Based on Laser Scanning and Photogrammetry of the José de Alencar Theatre.” Digital Applications in Archaeology and Cultural Heritage 30 (September): e00287. https://doi.org/10.1016/j.daach.2023.e00287.

Wojciechowski, Anderson Martins, Fábio Kellermann Schramm, and Joshua Zambrano. 2024. “Investigação das aplicações do BIM na gestão da manutenção predial.” October 7, 1–14. https://doi.org/10.46421/entac.v20i1.6381.

cinpar2026
XXII International Conference on Building Pathology and Constructions Repair
15th to 17th July 2026 - Lisboa, Portugal

Residual mechanical properties of masonry materials after exposure to high temperatures

Ema JANKOVIČOVÁ[1], Radek ZIGLER[2]

[1] Czech Technical University, Prague, Czech Republic, jankoema@cvut.cz
[2] Czech Technical University, Prague, Czech Republic, zigler@fsv.cvut.cz

Abstract: The behaviour of historical masonry exposed to high temperatures represents a critical issue in the assessment and preservation of built heritage. Thermal loading can significantly alter the mechanical and physical properties of traditional construction materials, thereby affecting the structural integrity of historic buildings. This study focuses on the response of selected natural stones and fired clay bricks to elevated thermal exposure, with particular emphasis on changes in mechanical performance and material behaviour after cooling.

The investigated specimens were subjected to controlled heating followed by two different cooling regimes, allowing evaluation of the influence of cooling conditions on the resulting material properties. The experimental results revealed a pronounced dependence of mechanical behaviour on both the applied thermal load and the cooling method. Distinct differences were observed among the investigated materials, reflecting their individual mineralogical composition and structural characteristics.

The findings highlight that material response to thermal exposure cannot be generalized and must be assessed individually for each type of masonry. This study contributes to a better understanding of the behaviour of traditional building materials subjected to fire-related damage.

Keywords: Sandstone, fired brick, high temperatures, mechanical properties, colour change

1. Introduction

Historical buildings constitute a fundamental component of cultural heritage, as they embody societal development through their architectural form, construction techniques, and material composition, while frequently holding significant historical importance by virtue of their association with notable figures or events. Masonry has historically represented the predominant construction method, with commonly employed materials encompassing sedimentary rocks such as marlstone, sandstone, and limestone, as well as igneous and metamorphic rocks including granite and trachyte, complemented by fired and unfired clay bricks. Material selection was governed principally by local availability, durability, and workability (Witzany et al. (2024)). Despite their considerable cultural and structural value, these materials are inherently susceptible to fire, which may originate from natural phenomena, human negligence, or ageing infrastructure, and whose severity is exacerbated by high building occupancy and limited firefighting access (Kincaid (2022), (Petrini et al. (2022)). Exposure to elevated temperatures induces water loss, chemical transformations, and microstructural damage in masonry assemblies, resulting in progressive reductions in mechanical strength (Witzany et al. (2024)). Visible post-fire manifestations, including surface blackening, spalling, decomposition, and oxidation, further compromise both the aesthetic integrity and structural performance of stone elements (Dimes (2007)). Although the effects of fire on historical masonry have been the subject of extensive research, the combined influence of material type, construction technique, and thermal exposure on mechanical and physical properties remains insufficiently characterised. This deficiency underscores the necessity for systematic experimental investigations to inform preservation strategies and mitigate risks to cultural heritage assets.

2. State-of-the-art

The effects of elevated temperatures on rock materials of selected lithological types have been previously investigated. High-temperature exposure alters rock microstructure, porosity, mineral composition, and mechanical properties, with important implications for the stability and safety of engineering structures.

Rong et al. (2018) studied the influence of specimen size and temperature on fine-grained marble from Fujian Province, China. Cylindrical specimens (25–100 mm diameter; height-to-diameter ratio 2:1) were heated to 200–600 °C. P-wave velocity decreased significantly with temperature, reaching an approximately 80% reduction at 600 °C due to progressive microcracking. Compressive strength and Young's modulus declined with increasing temperature, with the largest specimens exhibiting the greatest strength reduction. Conversely, deformation at peak stress increased, indicating enhanced ductility.

Guo et al. (2023) investigated sandstone heated to 200–1000 °C. Microcrack development led to a substantial decrease in ultrasonic velocity, which dropped to 29.7% of its initial value at 1000 °C. Bulk density decreased by about 4 %, particularly between 800 °C and 1000 °C.

Franzen et al. (2023) analysed sandstone from Pirna-Neundorf, Germany, exposed to temperatures up to 1250 °C. Ultrasonic velocity remained nearly constant up to 400 °C but decreased progressively at higher temperatures, reaching about 40 % of its original value. Below 400 °C, wet specimens showed lower compressive strength than dry ones; above 500 °C, however, wet samples exhibited strength increases, especially between 600 °C and 800 °C. The highest post-heating strength at 1250 °C was recorded in wet specimens loaded perpendicular to bedding.

Shen et al. (2024) evaluated the combined effects of cyclic loading and elevated temperature on red sandstone. After preloading at different stress levels, specimens were heated to 200–800 °C. P-wave velocity decreased in all cases, most markedly in highly preloaded samples. Compressive strength declined with increasing preloading intensity, while strain capacity increased with temperature.

Wang et al. (2023) investigated fine-grained sandstone heated up to 1200 °C. Bulk density decreased approximately linearly, and mass loss followed a parabolic trend. A slight increase in P-wave velocity at 100 °C was attributed to microcrack closure, followed by progressive deterioration at higher temperatures. Mechanical properties declined significantly above 400 °C, particularly between 400 °C and 600 °C.

Srinivasan et al. (2022) examined granite from the Jalore region, India, subjected to heating (200–600 °C) followed by slow or rapid cooling. Rapidly cooled specimens developed surface cracks at lower temperatures (300 °C) than slowly cooled ones (400 °C). P-wave velocity decreased progressively under both regimes. Compressive strength and Young's modulus declined with temperature, more markedly in rapidly cooled samples; at 600 °C, compressive strength decreased to 38 % (slow cooling) and 21 % (rapid cooling) of the reference value. Tensile strength showed a consistent decrease under rapid cooling, while slowly cooled samples exhibited minor fluctuations. Higher temperatures accelerated fracture development in both cases.

Zhang et al. (2020) studied granite subjected to different cooling regimes. Rapid cooling up to 500 °C slightly increased compressive strength and Young's modulus due to thermal stresses, whereas higher temperatures caused significant reductions, particularly under rapid cooling. Porosity increased with temperature, more sharply in water-cooled samples above 500 °C. P-wave velocity decreased similarly under both cooling conditions.

Han et al. (2019) analysed sandstone exposed to heating up to 800 °C followed by rapid cooling. P-wave velocity decreased by approximately 66 %, and bulk density by about 2 %. Mechanical behaviour evolved in three stages: relative stability up to 200 °C, moderate degradation between 200 °C and 500 °C, and pronounced deterioration above 500 °C. All specimens failed in a brittle manner.

The influence of high temperatures on the mechanical properties of fired bricks was studied by Bošnjak et al. (2020), who investigated the effects of heating up to approximately 1100 °C on calcium–silicate bricks, ceramic bricks, and mortar. For calcium–silicate bricks, an initial increase in compressive strength was followed by a significant decrease after heating to 700 °C, including instances of spontaneous disintegration after cooling. In contrast, ceramic bricks showed minimal change up to 500 °C, after which strength

increased, reaching approximately 5.7 times the reference value at 1100 °C, accompanied by notable changes in volume, colour, and a transition to brittle failure behaviour. Mortars exhibited an approximately linear decrease in compressive strength with increasing temperature, consistent with the expected behaviour of cement-based materials under high-temperature exposure.

In addition to mechanical degradation, elevated temperatures induce visible colour changes due to mineralogical transformations. Iron-bearing minerals oxidize to ferric oxide or hematite Fe_2O_3, producing red to reddish-brown coloration (Ge et al. (2022)).

Pires et al. (2024) investigated two Portuguese limestones (Lioz and Ançã) subjected to elevated temperatures and rapid cooling. CIELab analysis showed temperature-dependent shifts in colour parameters (L*, a*, b*), attributed to mineral decomposition, oxidation, and organic matter transformation.

Hajpál et al. (2004) studied seven sandstones with varying initial hues. Increasing temperature generally led to higher a* values (reddening) and increased b* values (yellowing), although some lithology-specific deviations were observed. Mineral transformations, such as glauconite and chlorite alteration and hematite formation, controlled these colour changes, while lightness (L*) varied depending on mineral composition.

Overall, the reviewed studies consistently demonstrate that increasing temperature leads to progressive microstructural degradation of rock materials, primarily driven by microcrack initiation and propagation, mineral transformations, and thermally induced stresses. These processes result in significant reductions in ultrasonic wave velocity, compressive and tensile strength, and elastic modulus, particularly above critical temperature thresholds commonly observed between 400 °C and 600 °C. Cooling conditions, especially rapid water quenching, further intensify damage and mechanical deterioration. In addition to mechanical weakening, high temperatures induce measurable changes in density, porosity, and colour parameters, reflecting ongoing mineralogical and chemical transformations. Despite lithology-specific differences, the general trend indicates a transition from relatively stable behaviour at low temperatures to accelerated physical and mechanical degradation at higher thermal exposure levels.

However, the findings of individual studies are difficult to generalise due to pronounced variability in mineralogical composition, microstructural properties, and temperature-dependent phase transformations across different material types and provenances. This highlights the need for material-specific investigations, particularly for locally sourced historic building materials, for which systematic thermal characterisation data remain scarce.

3. Materials and methods

3.1 Experimental samples

The materials investigated in this study comprise Hořice sandstone and fired brick. Sandstone became progressively established as a primary construction material in Gothic architecture across the Czech lands from the late fourteenth century onwards, as attested by its prominent use in St. Vitus Cathedral in Prague (Figure 1a). Its application persisted throughout the Baroque period, particularly for sculptural elements and architectural components such as staircases, portals, and window frames. During the second half of the nineteenth century, sandstone was also extensively employed in historicist buildings in Prague, including the National Theatre (Figure 1b), the Rudolfinum, and the National Museum. Building sandstones encompass a range of lithological types, varying from fine- to coarse-grained, with quartz constituting the predominant mineral phase. Intergranular spaces are occupied by primary or secondary cement, which exerts a significant influence on cohesion, porosity, mechanical behaviour, and long-term durability (Kotlík (1999);Hošek (1996)).

For the purposes of the present study, Hořice sandstone was selected as the primary stone material. The quarried deposit is situated in eastern Bohemia, between the towns of Jičín and Hořice in the Podkrkonoší region. The rock is classified as a fine-grained sandstone with a grain size ranging from 0.05 to 0.25 mm,

occurring within the Cenomanian succession of the Bohemian Cretaceous Basin, specifically in the Peruc-Korycany Formation (Korycany beds). The deposits exhibit gentle to sub-horizontal dipping with platy to flaggy bedding and are characterised by sparse, regularly distributed fracturing. Petrographically, the sandstone comprises more than 90% quartz grains, with accessory minerals, including glauconite, feldspars, micas, and heavy minerals, present only in trace amounts. The cement phase consists of a kaolinite–illite mixture with subordinate quartz dust (Rybařík (1996)). A set of 18 cylindrical specimens with a nominal diameter of approximately 35 mm and a height of approximately 70 mm was prepared for mechanical testing (Figure 2a).

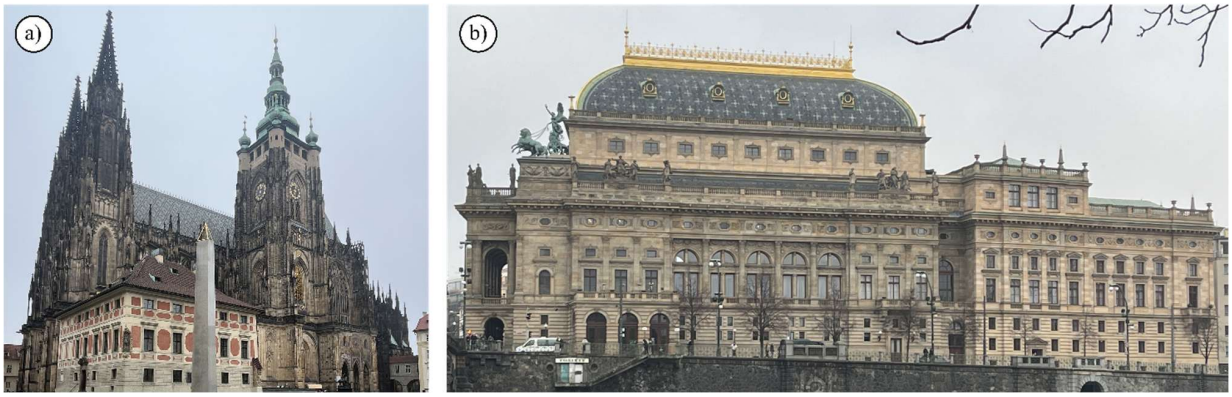


Figure 1 - a) St. Vitus Cathedral in Prague, **b)** The National Theatre in Prague.

Fired brick represents a traditional ceramic building material manufactured from clay rich in clay minerals such as illite, montmorillonite, and kaolinite, commonly containing accessory components including quartz, calcite, mica, and chlorite. During the firing process, clay minerals undergo dehydration at approximately 500–600 °C, followed by the transformation of aluminosilicates into a spinel-type phase and, at higher temperatures, into mullite, accompanied by the concurrent formation of a glassy phase. These mineralogical transformations exert a considerable influence on the microstructure and mechanical properties of the resulting material, the compressive strength of fired bricks typically ranges from approximately 5 MPa to 60 MPa (Witzany et al. (2024); Kotlík (1999)). In this study, a set of 20 cylindrical specimens with a nominal diameter of approximately 35 mm and a height of approximately 60 mm was used. (**Figure 2b**).

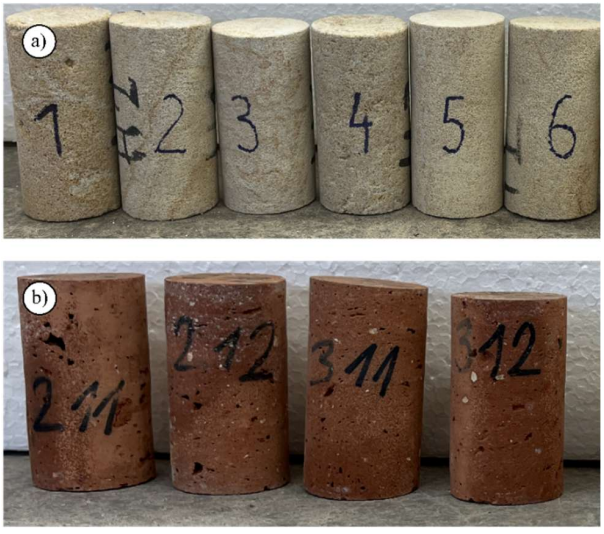


Figure 2 - a) Sandstone samples, **b)** Fired brick samples.

3.2 Experimental procedures and settings

Specimens were heated in an electric muffle furnace (**Figure 3a**) using a two-phase regime: heating to the target temperature at 13–16 °C/min, to minimize thermal shock, followed by a 60 minute isothermal dwell to ensure thermal stabilization Target temperatures were 690 °C, 850 °C, and 1100 °C for sandstone (**Figure 3b**), and 920 °C and 1100 °C for fired brick. After exposure, specimens were cooled either slowly in the furnace or rapidly by water quenching (≈20 °C, 120 s), with rapid cooling applied to samples heated to 850 °C and 1100 °C for sandstone samples and 920 °C and 1100 °C for fired brick samples. Furnace temperature was monitored using two thermocouples.

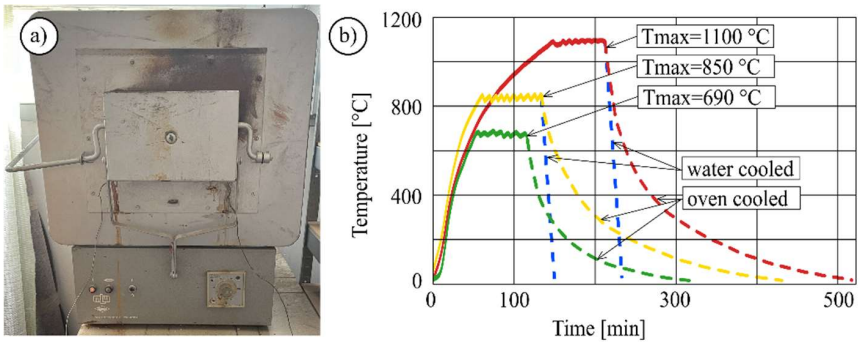


Figure 3 – **a)** Electric muffle furnace, **b)** Heating-cooling curves for Sandstone samples.

Uniaxial compression tests were conducted using a universal testing machine LabTest 4.100.SP1 (maximum load capacity 100 kN) at a loading rate of 0.25 mm/min (**Figure 4**). Stress and strain were derived from force–displacement data, and Young's modulus was determined from the linear elastic region.

Deformation was monitored by digital image correlation (DIC) using an optical extensometer with a 5 Mpx sensor and monochromatic blue illumination optimized for sensor sensitivity. The system included a LaborTech AOX-ONE camera equipped with a 5 Mpx (2448 px × 2048 px) Blackfly BFS-U3-51S5M sensor and a 16 mm lens, complying with EN ISO 9513 accuracy class 0.5 and ASTME 83: Class A. Blue monochromatic LED lighting matched the peak sensitivity of the camera chip used. Data were processed in Alpha® software (version 1.0.377).

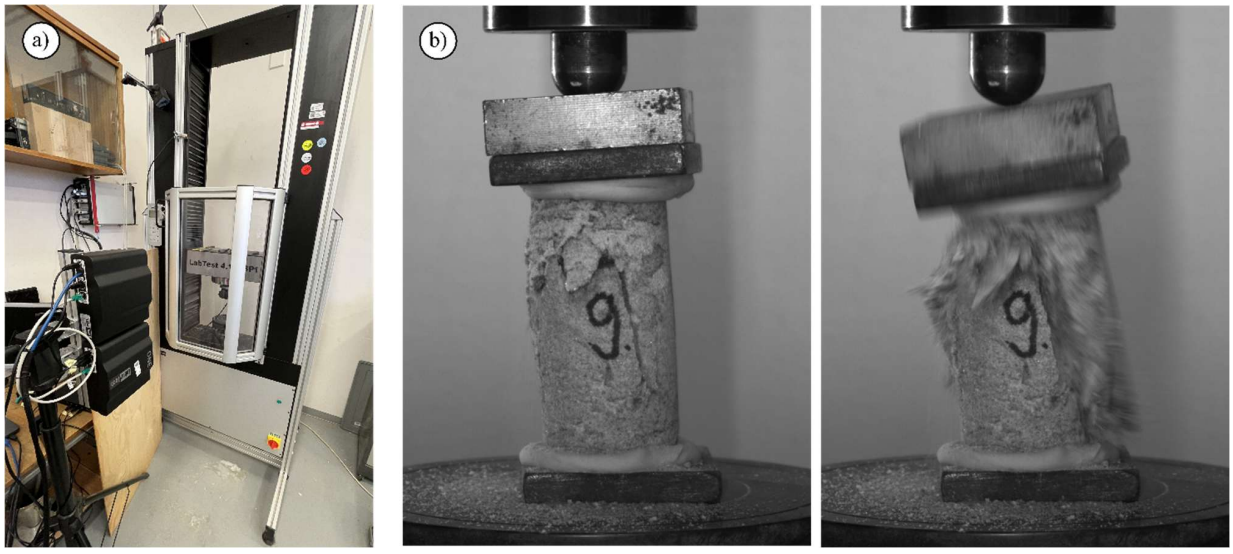


Figure 4 – **a)** Experimental setup, **b)** failure of test specimens under uniaxial compressive loading.

Colour changes were documented using a Canon EOS 60D camera under controlled lighting conditions (two reflectors with diffusers, 5000 K, neutral infinite background). Colour parameters (L*, a*, b*) were

evaluated in the CIELab space from four 100 × 100 px regions of interest per specimen, and the total colour difference (ΔE) was calculated as the Euclidean distance between reference and heated states.

Statistical analysis was conducted in RStudio, including descriptive statistics, Grubbs' test for outliers, and ANOVA followed by Tukey's HSD test ($p < 0.05$).

4. Results and discussion

4.1 Mechanical properties

4.1.1 Sandstone

The reference specimens attained a mean compressive strength of 21.83 MPa (100 %), with individual values ranging from 20.50 to 22.60 MPa (94–104 %). Following heating to 690 °C, mean compressive strength decreased to 19.40 MPa (89 %), with a range of 17.91–20.36 MPa (82–93 %). Specimens heated to 850 °C and cooled slowly in the furnace exhibited a further reduction to 17.66 MPa (81 %), with values between 16.49 and 19.57 MPa (76–90 %), while water-quenched specimens reached 12.30 MPa (56 %), ranging from 8.64 to 14.38 MPa (40–66 %). At 1100 °C, furnace-cooled specimens attained a mean compressive strength of 13.49 MPa (62 %), ranging from 11.43 to 16.79 MPa (52–77 %), whereas water-cooled specimens exhibited the lowest values, with a mean of 7.77 MPa (36 %) and a range of 5.88–10.13 MPa (27–46 %).

The mean strain of the unheated specimens was 0.00150 (100%), with values ranging from 0.00137 to 0.00162 (91–108 %). After heating to 690 °C, mean strain increased to 0.00451 (300 %), with values between 0.00432 and 0.00465 (287–309 %). At 850 °C, furnace-cooled specimens reached a mean strain of 0.00621 (413 %), ranging from 0.00504 to 0.00812 (334–540 %), while water-cooled specimens exhibited a higher mean value of 0.01040 (691 %), with a range of 0.00954–0.01169 (634–777 %). Following exposure to 1100 °C, furnace-cooled specimens exhibited a mean strain of 0.00830 (552 %), ranging from 0.00818 to 0.00853 (544–567 %), while water-cooled specimens attained a mean value of 0.01073 (714 %), ranging from 0.01033 to 0.01151 (687–766 %).

The mean Young's modulus of the unheated specimens was 16.13 GPa (100 %), with values ranging from 15.68 to 16.88 GPa (97–105 %). Following heating to 690 °C, the modulus decreased to 7.52 GPa (47 %), with a range of 6.70–9.03 GPa (42–56 %). At 850 °C, furnace-cooled specimens attained a mean modulus of 4.74 GPa (29 %), ranging from 3.43 to 6.30 GPa (21–39 %), while water-cooled specimens showed a further reduction to 2.42 GPa (15 %), with values between 1.52 and 2.88 GPa (9–18 %). At 1100 °C, the modulus of furnace-cooled specimens was 2.33 GPa (14 %), ranging from 1.79 to 2.84 GPa (11–18 %), and water-cooled specimens exhibited the lowest values, with a mean of 1.17 GPa (7 %) and a range of 0.82–1.70 GPa (5–11 %).

The stress–strain curves for Sandstone specimens are shown in **Figure 5**. Unheated specimens (blue) exhibited an almost linear increase in stress with increasing strain. In thermally exposed specimens, a progressive deviation from linear towards nonlinear, and ultimately exponential, behaviour was observed with increasing temperature. Specimens heated to 690 °C (green) displayed the steepest gradient among all thermally treated groups. For specimens heated to 850 °C (yellow) and 1100 °C (red), the influence of the cooling method was discernible. Furnace-cooled specimens exhibited steeper curve gradients compared to their water-cooled counterparts. Water-cooled specimens were characterized by more pronounced initial strain values and the lowest curve gradients overall.

The observed changes in the slope and shape of the stress–strain curves reflect progressive alterations in the microstructure of the sandstone induced by high-temperature exposure. These include phase and chemical transformations of thermally sensitive minerals, as well as the development of microcracks arising from differential thermal expansion and mineral decomposition, both of which contribute to the degradation of mechanical stiffness and the increasingly nonlinear mechanical response (Franzen et al. (2023); Shen et al. (2024)).

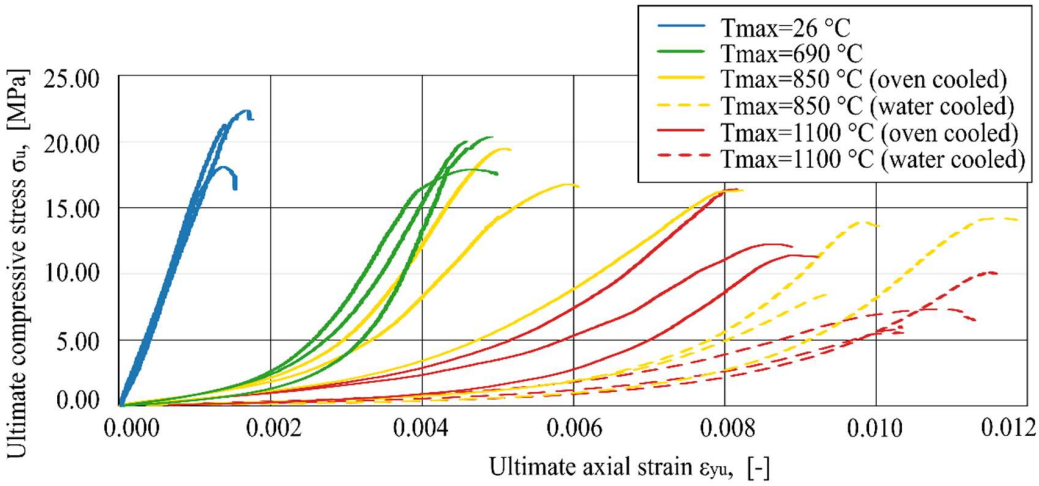


Figure 5 – Stress–strain relationship of Sandstone samples under uniaxial compression.

4.1.2 Fired brick

The unheated specimens exhibited a mean compressive strength of 17.99 MPa (100 %), with values ranging from 14.35 to 24.16 MPa (80–134 %). Following heating to 920 °C and slow furnace cooling, compressive strength decreased to approximately 9.84 MPa (55 %), with values between 8.40 and 11.48 MPa (47–64 %). Specimens subjected to rapid water quenching exhibited a more pronounced reduction, attaining a mean compressive strength of approximately 7.50 MPa (42 %), with values ranging from 6.25 to 9.44 MPa (35–53 %). After heating to 1100 °C and slow furnace cooling, compressive strength increased markedly to approximately 23.18 MPa (129 %), with values between 22.58 and 23.78 MPa (127–132 %). The increase was less pronounced in water-cooled specimens, which attained a mean compressive strength of approximately 12.88 MPa (72 %), with values ranging from 11.22 to 14.97 MPa (62–83 %).

The mean relative strain of the reference specimens was 0.00223 (100 %), with values ranging from 0.00168 to 0.00264 (75–118 %). Following heating to 920 °C and slow furnace cooling, the mean relative strain increased to approximately 0.00330 (148 %), with values between 0.00234 and 0.00493 (105–221 %). Specimens subjected to rapid water quenching exhibited a more pronounced increase, attaining approximately 0.00573 (257 %), with values ranging from 0.00553 to 0.00610 (248–273 %). After heating to 1100 °C and slow furnace cooling, the mean relative strain was 0.00426 (191 %), with values between 0.00325 and 0.00527 (146–236 %), while water-cooled specimens exhibited a mean relative strain of 0.00355 (159 %), ranging from 0.00256 to 0.00498 (115–223 %).

The mean Young's modulus of the unheated specimens was 9.88 GPa (100 %), with values ranging from 8.63 to 11.88 GPa (87–120 %). Following heating to 920 °C and slow furnace cooling, the mean modulus decreased to approximately 3.50 GPa (35 %), with values ranging from 1.88 to 4.83 GPa (51–65 %). In specimens subjected to rapid water quenching, a further reduction was observed, with a mean value of approximately 1.75 GPa (18 %) and a range of 1.28–2.50 GPa (13–25 %). After heating to 1100 °C and slow furnace cooling, the Young's modulus attained a mean value of 7.62 GPa (77 %), with values ranging from 5.22 to 10.02 GPa (53–101 %). Water-cooled specimens exhibited a mean value of 4.05 GPa (41 %), with values between 3.92 and 4.30 GPa (40–44 %).

The stress–strain relationships for Fired brick specimens are presented in **Figure 6**. The steepest curve gradients, characterised by an almost linear increase, were observed in the reference specimens (blue) and in specimens heated to 1100 °C and furnace-cooled (red). Specimens heated to 920 °C and furnace-cooled (yellow) also exhibited an approximately linear trend, however with a lower gradient compared to the reference specimens and those heated to 1100 °C. In the case of water-cooled specimens at both

temperature levels, the stress–strain response approached a nonlinear character, with specimens heated to 1100 °C displaying steeper curve gradients than those heated to 920 °C.

The variations in curve gradient and shape observed across the different thermal and cooling conditions can be attributed to microstructural and compositional changes induced by high-temperature exposure. In fired brick, these include the further sintering of the ceramic matrix, recrystallisation of clay minerals, and thermally driven phase transformations, all of which alter the pore structure and intergranular bonding ((Kotlík (1999); Witzany et al. (2024)).

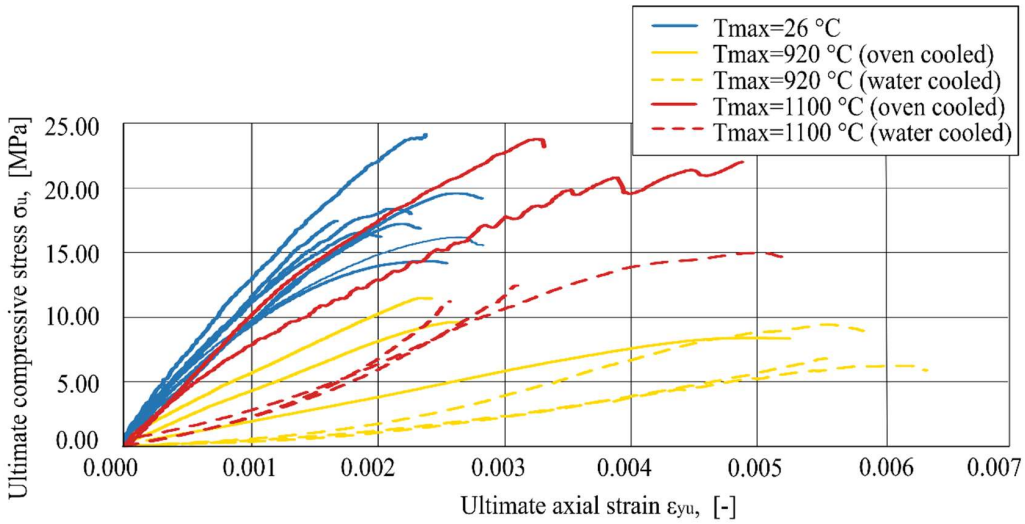


Figure 6 – Stress–strain relationship of Fired brick samples under uniaxial compression.

4.2 Colour change

For the sandstone specimens, colour changes were visible after every temperature treatment (**Figure 7**), chromatic changes were quantitatively evaluated within the CIELab colour space (**Figure 8**). Lightness (L*) decreased slightly with increasing temperature, from the reference value of 52.26 to 48.83 following heating to 690 °C. No statistically significant additional changes in L* were observed at 850 °C or 1100 °C, and the cooling method exerted no discernible influence on this parameter. The a* parameter (red–green axis) increased markedly after heating to 690 °C, from 5.74 to 12.41, indicative of pronounced specimen reddening. At 850 °C, furnace-cooled specimens exhibited a slight decrease to 11.08, while water-cooled specimens attained a value of 12.65. Following heating to 1100 °C, a* decreased under both cooling conditions, to 9.69 for furnace-cooled and 9.55 for water-cooled specimens. For the b* parameter (yellow–blue axis), no substantial change was observed at 690 °C (reference: 17.64; post-heating: 16.74). At 850 °C, furnace-cooled specimens exhibited a decrease to 14.88, whereas water-cooled specimens showed a marginal increase to 17.83. At 1100 °C, b* decreased under both cooling conditions, to 14.26 for furnace-cooled and 14.84 for water-cooled specimens. The total colour difference (ΔE) was 8.11 following heating to 690 °C. At 850 °C, ΔE increased to 8.93 for furnace-cooled specimens and to 8.75 for water-cooled specimens. After heating to 1100 °C, ΔE decreased to 8.08 for furnace-cooled and to 7.49 for water-cooled specimens.

The observed reddening, reflected in the marked increase in a*, is attributable to the oxidation of iron-bearing minerals and the formation of hematite at elevated temperatures. As documented by Hajpál et al. (2004), such mineral transformations, including the alteration of glauconite and chlorite, represent the primary controls on colour change in thermally treated sandstones.

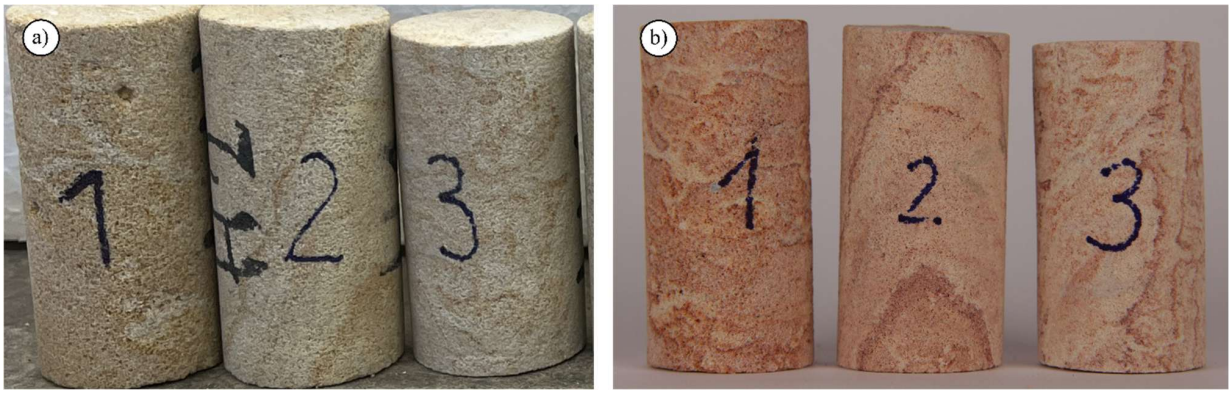


Figure 7 – Sandstone specimens: **a)** unheated reference, **b)** heated to 690 °C.

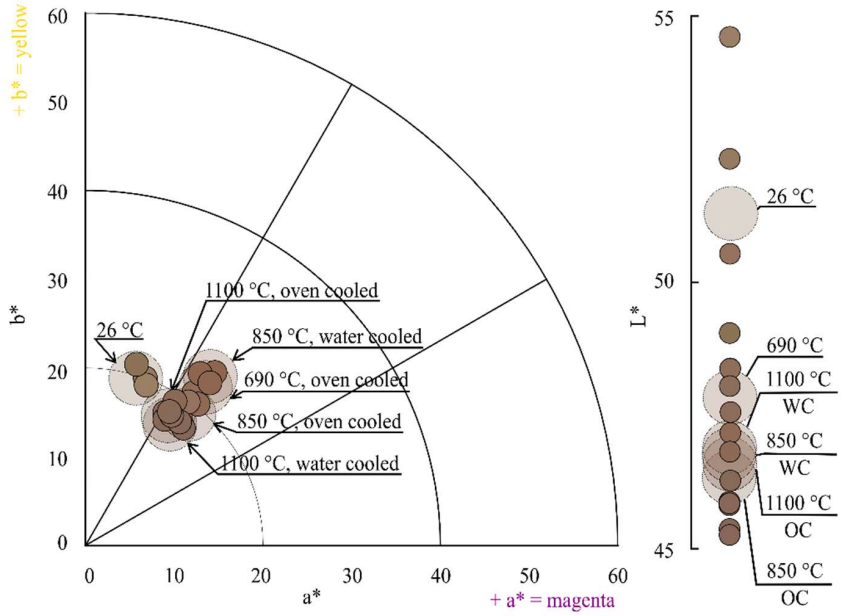


Figure 8 – CIELab colour parameters of Sandstone specimens subjected to elevated temperatures; OC - oven-cooled, WC - water-cooled.

For the fired brick specimens, systematic quantitative evaluation of colour parameters was not performed, owing to the pronounced non-uniformity of coloration across individual specimen surfaces. Specimens heated to 920 °C appeared slightly lighter in colour relative to the reference samples. Following heating to 1100 °C, a marked chromatic contrast was observed between the opposing faces of individual specimens. Rapidly cooled specimens displayed a brown-orange coloration on one face (side a, **Figure 9a**), while the opposing face (side b, **Figure 9b**) appeared dark brown with white spots. Furnace-cooled specimens were characterized by very dark coloration with white spots on side b (**Figure 9b**) and a lighter appearance on side a (**Figure 9a**).

Analogous chromatic changes following high-temperature exposure are reported by Cikrle et al. (2020), in which a markedly dark brown colour corresponds to firing temperatures of approximately 1150 °C, comparable to the appearance of side b in furnace-cooled specimens heated to 1100 °C, while a red-brown coloration is associated with firing temperatures of approximately 1100 °C. These colour shifts are primarily driven by thermally induced oxidation and recrystallisation of iron-bearing mineral compounds within the brick matrix, which produce progressive changes in hue towards red, brown, and dark brown tones as a function of temperature and local thermal conditions (Bošnjak et al. (2020); Kotlík (1999)).



Figure 8 – Fired brick specimens heated to 1100 °C: **a)** side a — first three specimens from the left are furnace-cooled, remaining specimens are water-cooled; **b)** side b — first three specimens from the left are furnace-cooled, remaining specimens are water-cooled.

4.3 Statistical analysis

For the Sandstone specimens, one-way ANOVA confirmed a statistically significant effect of temperature on all mechanical properties for both furnace- and water-cooled specimens ($p \leq 0.004$). Tukey's HSD post hoc test indicated that compressive strength was significantly affected primarily at higher temperatures, particularly at 1100 °C, while relative strain and Young's modulus were significantly influenced across all temperature levels investigated. Two-way ANOVA further demonstrated a statistically significant effect of both temperature and cooling method on compressive strength and Young's modulus, whereas relative strain was less markedly affected by the interaction of these factors. No statistically significant interaction between temperature and cooling method was identified.

For the Fired brick specimen set, one-way ANOVA indicated a statistically significant effect of temperature on all mechanical properties under both cooling regimes ($p < 0.05$). Tukey's HSD test revealed that differences were most pronounced at 920 °C for furnace-cooled specimens, while significant effects were identified at both 920 °C and 1100 °C for water-cooled specimens. Two-way ANOVA confirmed a statistically significant influence of both temperature and cooling method on compressive strength and Young's modulus, whereas relative strain was less consistently affected. A statistically significant interaction between temperature and cooling method was identified exclusively for compressive strength.

5. Conclusion

The present study investigated the effects of elevated temperature and post-exposure cooling method on the mechanical properties and chromatic characteristics of two traditional masonry materials, Hořice sandstone and fired brick, with relevance to the assessment and preservation of historical built heritage.

The experimental results demonstrate that thermal exposure induced progressive and statistically significant degradation of mechanical performance in both materials, albeit with material-specific trends. In sandstone, compressive strength, Young's modulus, and axial strain deteriorated consistently with increasing temperature, with the most pronounced reductions observed at 1100 °C. The cooling method exerted a substantial additional influence, rapid water quenching consistently produced more severe mechanical deterioration than slow furnace cooling at equivalent temperatures, reflecting the damaging effect of thermally induced stress gradients during quenching.

Fired brick exhibited a more complex thermal response. While mechanical properties decreased markedly following heating to 920 °C, specimens heated to 1100 °C and cooled slowly in the furnace displayed a notable recovery in compressive strength, exceeding the reference value by approximately 29 %, attributable to high-temperature mineralogical transformations including mullite formation and glassy phase development. Rapid cooling suppressed this recovery, highlighting the critical role of the cooling regime in governing the final mechanical state of thermally exposed ceramic materials.

Chromatic analysis confirmed measurable colour changes in both materials, most notably progressive reddening in sandstone attributable to iron mineral oxidation, and pronounced surface colour heterogeneity in fired brick at 1100 °C.

Statistical analysis confirmed the significance of both temperature and cooling method on compressive strength and Young's modulus in both materials, with a significant interaction between these factors identified for compressive strength in fired brick.

The findings provide experimentally grounded data to support post-fire damage assessment and conservation of heritage buildings. Future investigations will extend the range of materials and temperature levels examined and address the influence of pre-existing microstructural, mineralogical, petrographic and chemical variability on thermal response, in order to further refine predictive frameworks for the structural assessment of fire-affected heritage structures.

Acknowledgments

This research was funded by internal CTU grants SGS25/010/OHK1/1T/11 “Residual properties of selected building materials after fire” and SGS26/147/OHK1/3T/11 "Analysis of the Dependence of the Physico-Mechanical Properties of Selected Building Materials on Thermal Loading “.

References

Bošnjak, Josipa, Serena Gambarelli, Akanshu Sharma, and Amra Mešković. 2020. ‘Experimental and Numerical Studies on Masonry after Exposure to Elevated Temperatures’. *Construction and Building Materials* 230 (January): 116926. https://doi.org/10.1016/j.conbuildmat.2019.116926.

Cikrle, Petr, Radomír Sokolář, Luboš Topolář, Libor Pazdera, and Ondřej Anton. 2020. ‘Komplexní Metodika pro Nedestruktivní a Šetrnou Semidestruktivní Diagnostiku Fyzikálně-Mechanických Vlastností Historických Pálených Zdících Prvků’. Brno, April 11. http://hdl.handle.net/11012/209227.

Franzen, Christoph, Dana Krause, Heiner Siedel, and Bernd Ullrich. 2023. ‘Heat Effects on Clay-Bearing Building Sandstone’. *Environmental Earth Sciences*, ahead of print. https://doi.org/10.1007/S12665-023-10754-0.

Ge, Shaokun, Bobo Shi, Shuai Zhang, Xiaowei Zhai, and Chunlei Wu. 2022. ‘Thermal Damage and Mechanical Properties of High Temperature Sandstone with Cyclic Heating–Cooling Treatment’. *Bulletin of Engineering Geology and the Environment*, ahead of print. https://doi.org/10.1007/S10064-022-02781-1.

Guo, Jinping, Yanzi Lei, Yang, Ping Cheng, Zhao Wang, and Saisai Wu. 2023. 'Effects of High Temperature Treatments on Strength and Failure Behavior of Sandstone under Dynamic Impact Loads'. *Sustainability*, ahead of print. https://doi.org/10.3390/SU15010794.

Hajpál, M., and Á. Török. 2004. 'Mineralogical and Colour Changes of Quartz Sandstones by Heat'. *Environmental Geology* 46 (3): 311–22. https://doi.org/10.1007/s00254-004-1034-z.

Han, Guansheng, Hongwen Jing, Haijian Su, Richeng Liu, Qian Yin, and Jiangyu Wu. 2019. 'Effects of Thermal Shock Due to Rapid Cooling on the Mechanical Properties of Sandstone'. *Environmental Earth Sciences*, ahead of print. https://doi.org/10.1007/S12665-019-8151-1.

Hošek, J. 1996. 'Stavební Materiály pro Rekonstrukce'. *Vydavatelství ČVUT*, 94–100.

Kincaid, Simon. 2022. 'Fire Prevention in Historic Buildings – Approaches for Safe Practice'. *The Historic Environment: Policy & Practice* 13 (3): 361–80. https://doi.org/10.1080/17567505.2022.2098633.

Kotlík, Petr. 1999. *Stavební Materiály Historických Objektů-Materiály, Koroze, Sanace*. Vysoká škola chemicko-technologická.

Petrini, Francesco, A. Aguinagalde, and Franco Bontempi. 2022. 'Structural Fire Risk for Heritage Buildings by the Performance-Based Engineering Format'. *International Journal of Architectural Heritage*, ahead of print. https://doi.org/10.1080/15583058.2021.2022249.

Pires, Vera, Fabio Sitzia, Carla Lisci, and Licinio Cordeiro. 2024. 'Evaluating Building Stones: Physical-Mechanical Changes from High-Temperature Fire and Water Cooling'. *Heliyon*, ahead of print. https://doi.org/10.1016/J.HELIYON.2024.E36108.

Rong, Guan, Jun Peng, Mengdi Yao, Qinghui Jiang, and Louis Ngai Yuen Wong. 2018. 'Effects of Specimen Size and Thermal-Damage on Physical and Mechanical Behavior of a Fine-Grained Marble'. *Engineering Geology*, ahead of print. https://doi.org/10.1016/J.ENGGEO.2017.11.011.

Rybařík, Václav. 1996. 'Vltavské Mosty'. In *Praha Kamenná*, by D. Březinová, M. Bukovanská, L. Dudková, and Václav Rybařík. Národní muzeum.

Shen, Mingxuan, Yu Zhao, Jing Bi, Chaolin Wang, Tenglong Liu, and Bin Du. 2024. 'Softening Properties and Damage Evolution of the Preloaded Building Sandstone after Exposure to High-Temperature'. *Construction and Building Materials*, ahead of print. https://doi.org/10.1016/J.CONBUILDMAT.2024.134970.

Srinivasan, Vinoth, Haseeb Hasainar, and T. N. Singh. 2022. 'Experimental Study on Failure and Fracturing Attributes of Granite after Thermal Treatments with Different Cooling Conditions'. *Engineering Geology*, ahead of print. https://doi.org/10.1016/J.ENGGEO.2022.106867.

Wang, Pin, Tubing Yin, Xibing Li, and Heinz Konietzky. 2023. 'Evolution of Micro-Damage and Degradation of Macro-Mechanical Properties of Sandstone Due to Thermal Effects'. *Bulletin of Engineering Geology and the Environment*, ahead of print. https://doi.org/10.1007/S10064-023-03094-7.

Witzany, Jiří, Radek Zigler, Klára Kroftová, et al. 2024. *Obnova, Sanace a Rekonstrukce Historických Staveb*. Academia.

Zhang, Fan, Yuhao Zhang, Yu, Dawei Hu, and J. F. Shao. 2020. 'Influence of Cooling Rate on Thermal Degradation of Physical and Mechanical Properties of Granite'. *International Journal of Rock Mechanics and Mining Sciences*, ahead of print. https://doi.org/10.1016/J.IJRMMS.2020.104285.

XXII International Conference on Building Pathology and Constructions Repair
15th to 17th July 2026 - Lisboa, Portugal

From Theory to Practice: Expert Views on Vulnerability of URM Buildings

Antonela MORETIĆ[1], Karlo OŽIĆ[2], Tiago M. FERREIRA[3], Mislav STEPINAC[4]

[1] Faculty of Civil Engineering Zagreb, Croatia, antonela.moretic@grad.unizg.hr
[2] Faculty of Civil Engineering Zagreb, Croatia, karlo.ozic@grad.unizg.hr
[3] Instituto Superior Técnico (IST), University of Lisbon, Portugal, tiago.miguel.ferreira@tecnico.ulisboa.pt
[4] Faculty of Civil Engineering Zagreb, Croatia, mislav.stepinac@grad.unizg.hr

Abstract: Damage observed in recent earthquakes affecting historical unreinforced masonry (URM) buildings has revealed discrepancies between predicted structural performance based on established theoretical models and the behaviour of these structures in practice. These differences raise critical questions regarding the adequacy of current rapid seismic vulnerability assessment methods, particularly when applied to traditional and protected building stock. This paper addresses the gap between existing theoretical frameworks, practical post-earthquake observations, and the perspectives of professionals directly involved in the assessment and rehabilitation of URM buildings.
The study focuses on the role of expert judgment in evaluating the relative importance of parameters influencing the seismic response of historical URM structures. An international survey was conducted to collect expert opinions from professionals with diverse disciplinary backgrounds and regional experience.
The analysis highlights notable differences in parameter prioritization, reflecting variations in professional experience, exposure to real damage scenarios, and interpretative frameworks. These findings demonstrate that theoretical models may not fully capture the complexity of structural behaviour observed in practice and that expert knowledge provides valuable insights into damage mechanisms and vulnerability patterns.
The paper emphasizes the importance of integrating expert perspectives with theoretical foundations to improve the reliability and practical relevance of seismic vulnerability assessments. Such integration is particularly relevant for building pathology and construction repair, where informed decision-making relies on a balanced understanding of theory, observed damage, and professional experience.

Keywords: Expert opinion, Seismic vulnerability, Survey, Heritage, Masonry

1. Introduction

Seismic risk is typically described through three components: hazard, exposure, and vulnerability. Hazard - the likelihood of certain ground motions - depends on location and cannot be controlled, while exposure, tied to population and infrastructure, is also difficult to change. Vulnerability, however, can be reduced. It refers to the *likelihood* of damage at a given seismic intensity and depends on factors such as building age, structural system, materials, design codes, maintenance, and retrofitting, as well as site conditions like soil type and ground stability.
Because of this, assessing seismic vulnerability is essential for reducing risk and predicting potential damage and losses. There is a broad spectrum of assessment methods, which are often tailored to specific regions and building types (Moufid, Mohamed, and Noroozinejad 2020). Their differences reflect variations in construction practices and structural characteristics across countries, as well as specialized focuses on elements like façades or building aggregates. This highlights the need to adapt parameter selection to local conditions to accurately capture building behaviour - an issue that motivated this research. It must be emphasized that this paper presents only a part of the ongoing research, which, in addition to expert opinions, encompasses both empirical and analytical methods. However, this paper itself focuses solely on expert opinions and their significance. The research focuses on the Croatian building stock, specifically traditional unreinforced masonry (URM) buildings from the late 19th and early 20th centuries (Figure 1). These structures were built according to Austrian, German, and Hungarian practices, at a time when seismic

design was not considered. They typically consist of masonry walls with lime mortar, timber floors or shallow vaults at lower levels, and timber roofs. Although their vertical load-bearing capacity generally meets modern standards - evidenced by their long service life exceeding current design expectations - they remain highly vulnerable to earthquakes (Stepinac et al. 2021; Atalić, Novak, and Uroš 2019).

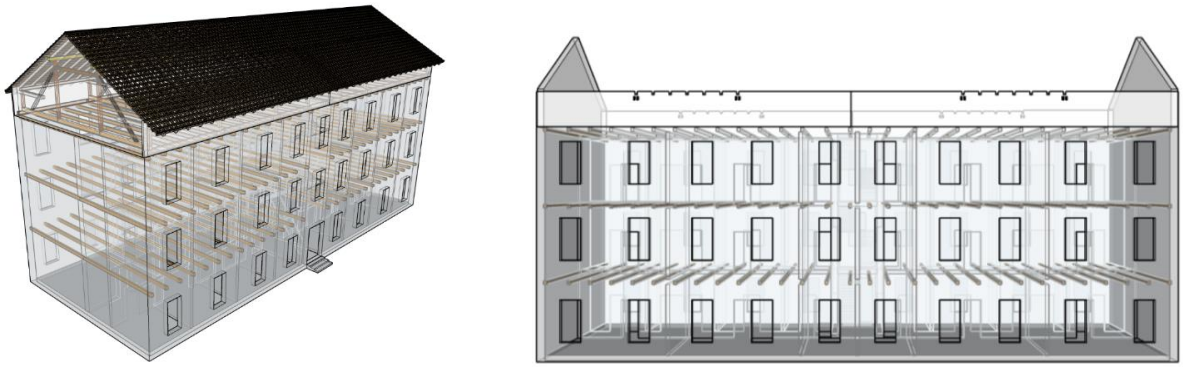


Figure 1 - Characteristic building in Lower Town, Zagreb

The buildings are commonly arranged in urban aggregates (Figure 2), which complicates their seismic behaviour. In Zagreb's Lower Town, these aggregates are fairly uniform in height, usually three to four storeys, but vary in layout. Typical patterns include L-shaped corner buildings, rectangular structures, buildings with plan offsets, and those without adjacent neighbours, alongside occasional reinforced-concrete structures. The interactions among the units lead to two effects: global, involving force redistribution across the whole aggregate, and local, related to pounding between adjacent units with different seismic responses (Torres-Olivares et al. 2024). Key influencing factors include height differences, position within the row, floor misalignment, structural variability, and façade openings (Angiolilli et al. 2021; Schiavoni et al. 2023).



Figure 2 - Aerial view of Zagreb – urban aggregates

A preliminary study of 66 historic masonry buildings in Zagreb's Lower Town, using an Italian-based method, indicated moderate vulnerability but showed notable mismatches with observed damage (Moretić et al. 2022). This highlighted the need to adapt vulnerability parameters to local building characteristics. To address this, a rapid assessment method for unreinforced masonry buildings has been developed, combining analytical models, empirical data, and expert judgment. This paper focuses on the role of expert input in defining parameter weights, which can also be compared with statistically derived values. Expert opinions were collected through a structured international survey, though a reduced number of questions was necessary to ensure participation. The Analytic Hierarchy Process (AHP) was used to convert subjective judgments into quantitative weights.

2. Survey design and data collection

A total of 111 experts in earthquake engineering and masonry structures participated in the survey, mainly based in Europe. The majority of respondents came from academia, including professors, researchers, PhD candidates, and Master's students, while 37% were professionals from the Croatian design and construction sector, contributing practical experience from post-earthquake assessments and reconstruction activities. Participants were also classified according to their professional experience; most had more than three years of experience, and 41% had over ten years, which supports the reliability of the collected responses. In addition, respondents were asked to self-assess their level of expertise on a scale from 1 to 5. The comparison between respondents' years of professional experience and their self-assessed level of expertise indicates a likely positive correlation between these two variables. The majority of respondents reported having between 3 and 20 years of professional experience, while most participants evaluated their expertise at a moderate to high level (levels 3–5). This distribution suggests that respondents with greater professional experience tend to perceive themselves as more knowledgeable and competent in the field of seismic vulnerability and seismic design. Furthermore, lower self-assessment scores (levels 1 and 2) were

represented by a relatively small proportion of respondents, which may indicate that limited expertise is less common among participants with longer professional engagement in the field.
Although most participants were from Croatia, the survey also included experts from other seismically active regions to provide broader perspectives on the seismic behaviour of traditional structures. The participant data is presented in Figure 3.

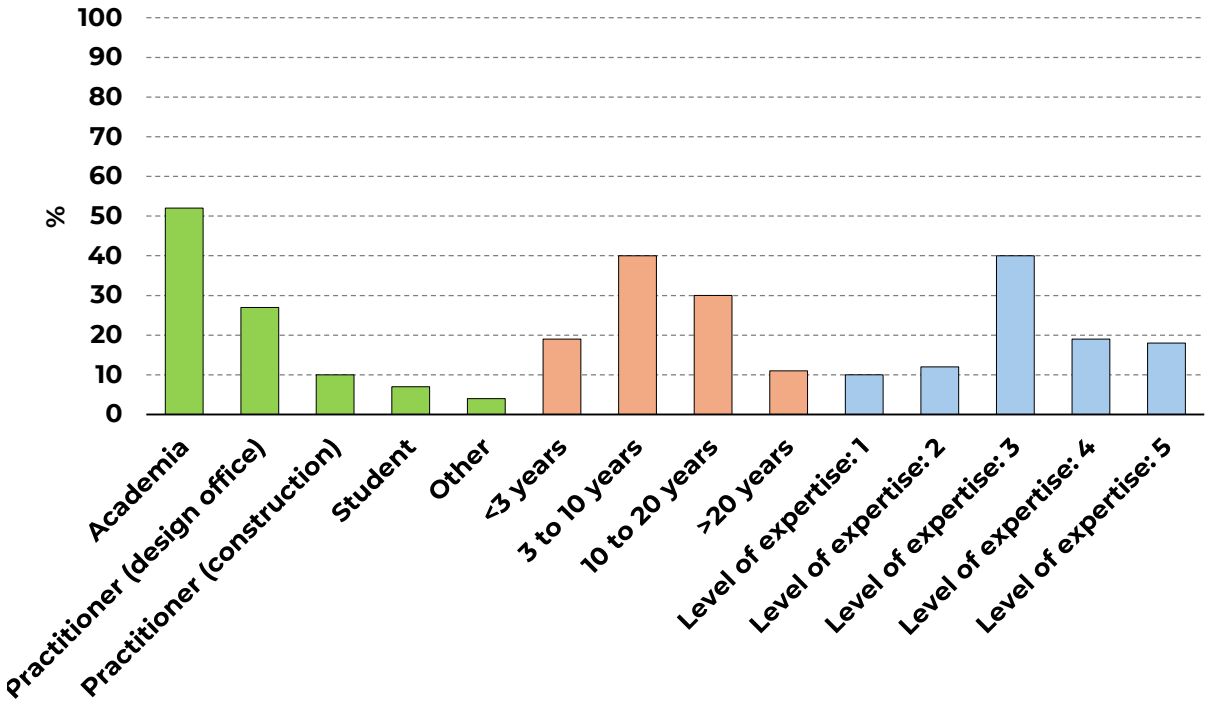


Figure 3 - Participants data

The survey was created using the online platform Fillout and distributed digitally to experts. It was shared through email contacts, direct communication with professionals, social networks such as LinkedIn, WhatsApp groups of post-earthquake building assessment specialists in Croatia, and among participants of the final conference of the ARES project funded by the Croatian Science Foundation.

The questionnaire, which required about 15–20 minutes to complete included the introductory section that collected general participant information and the technical section.

Since the survey included only a limited number of technical questions, the analysed parameters had to be carefully selected. Their choice was guided by damage patterns observed after the 2020 Zagreb earthquake (Novak et al. 2020; Uroš et al. 2021), which helped identify the factors considered most relevant for this study (Figure 4).



Figure 4 - Damage inspected in Zagreb in post-earthquake assessments in 2020

The survey contained three groups of questions. The first asked respondents to rank parameters affecting the seismic behaviour of masonry structures in Croatia and those influencing aggregate vulnerability from most to least important. This produced an average ranking score for each parameter together with qualitative explanations for the most and least influential factors. The second group of questions served as cross-validation. Participants evaluated groups of parameters on a 1–5 scale, where 5 indicated greater influence. The third group of questions also supported cross-validation. First, respondents performed pairwise comparisons, choosing which of two parameters they considered more influential. They then rated their relative importance on a 1–10 scale, where 1 indicated equal importance and 10 indicated extreme dominance of one parameter. These questions referred to both individual masonry buildings and aggregates.

Using different question formats for closely related topics had an important methodological role. It enabled verification of response consistency, reduced systematic bias, and improved data reliability. Varying the phrasing also helped reveal underlying attitudes, supported clearer interpretation by respondents, and reduced fatigue or automatic responses, thereby strengthening the reliability of the measurement scales used in the study.

3. Survey results

Figure 5 shows the results of the key survey question, in which participants ranked 15 parameters according to their influence on building behaviour. The average ranking reflects the mean score across all respondents, with lower values indicating greater influence. The parameters are ordered by perceived importance, with plan regularity identified as the most influential (average score 4.9) and type of roof structure as the least influential (11.5). In addition to the overall results, the respondents' answers were analysed according to their country of origin, as well as with respect to their professional experience and place of employment. These results were later used to calculate weighting factors, which were compared with factors derived from statistical methods (Ožić 2025).

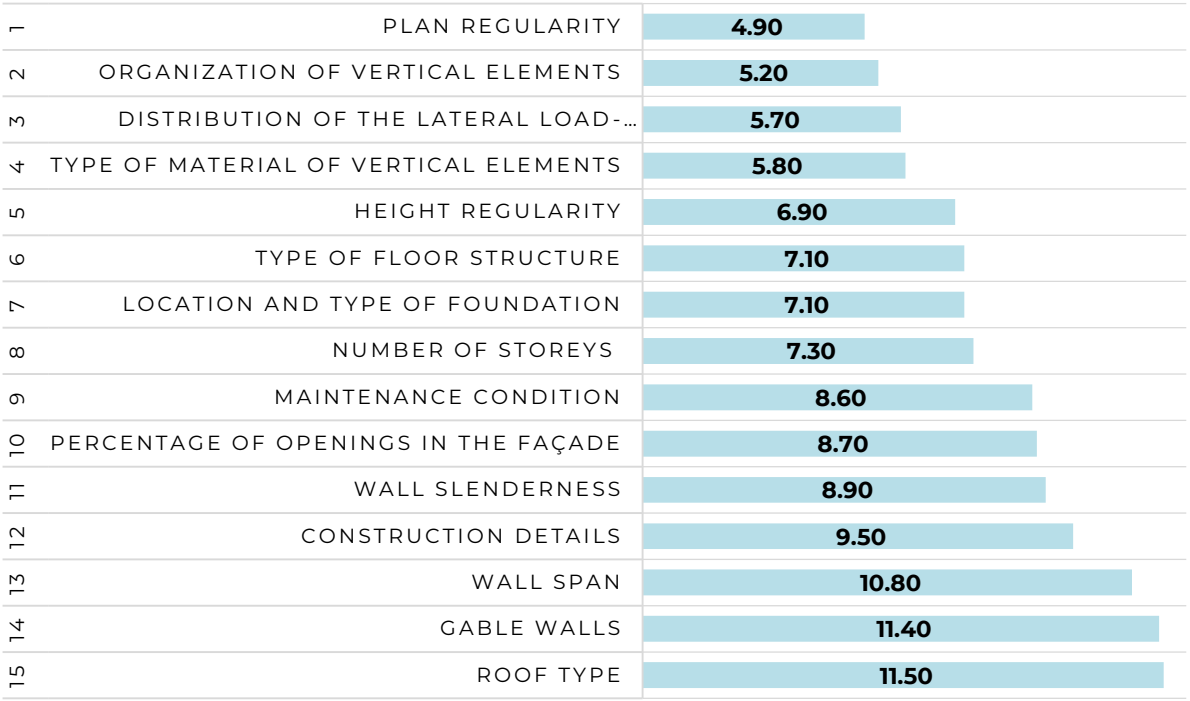


Figure 5 – Investigated vulnerability parameters and their rankings

The average ratings of individual parameters were compared between experts from Croatia and those from the rest of the world. This comparison was intentional, as the objective was to analyse the seismic behaviour of the Croatian building stock. Respondents from Croatia are naturally more familiar with the buildings under assessment, making their input particularly relevant. For most parameters, the ratings are relatively consistent; however, a notable difference is observed for the parameter related to foundation location and type. Croatian experts likely consider this parameter less important, which may be attributed to the relatively uniform soil and foundation conditions in the city of Zagreb. Interestingly, domestic experts assigned greater importance to parameters such as wall slenderness and wall span, both of which are associated with out-of-plane failure mechanisms. Although such mechanisms were not dominant during the Zagreb earthquake, this observation may reflect specific perceptions or experiences among Croatian experts regarding the potential vulnerabilities of masonry structures.

A comparison between academic and professional participants reveals a clear divergence in opinions. Academics tend to emphasise regularity and structural organisation, while practitioners prioritise practical aspects, such as wall span. A pronounced difference is observed for wall slenderness (parameter 11), which practitioners consider less influential, possibly because of the similar configurations of buildings in Zagreb.

Differences are also evident for the type of floor structure (parameter 6), indicating varying priorities in assessing its impact on seismic behaviour.

The results were also compared according to years of professional experience. The most pronounced differences are observed among participants with the least experience, whose responses deviate considerably from those of more experienced respondents. This suggests that less experienced participants may lack sufficient practical insight to evaluate certain aspects accurately. In contrast, participants with more than 10 years of experience show greater consistency in their assessments. Some differences remain between the most experienced group and those with medium levels of experience (3–10 years), which may indicate a transitional stage of professional development in which opinions gradually align with increasing expertise.

A separate classification was also performed based on participants' self-assessed level of expertise in the field, measured on a scale from 1 to 5 (where 1 indicates no expertise and 5 indicates a high level of expertise). This subjective assessment does not necessarily correspond to years of professional experience but provides additional insight into how participants perceive their own expertise and how this perception influences their evaluation of the parameters. Differences are observed across all categories, with the most pronounced contrast between participants who do not consider themselves experts and those who identify as experts. These findings suggest that self-perceived knowledge and expertise can significantly influence how the importance of individual parameters is assessed.

When it comes to parameters related to the behaviour of buildings within an aggregate, the comparison of responses from Croatian experts with those from the rest of the world (Figure 6) reveals the most notable difference regarding the influence of adjacent buildings of varying heights. Croatian respondents rated this parameter as less influential, whereas international experts considered it the most significant. This discrepancy reflects the characteristics of the Croatian building stock, which is relatively uniform in both height and number of stories. Consequently, while Croatian experts recognize the relevance of this parameter, they assign it a lower influence, likely due to limited experience with building stocks where such variations are more pronounced.

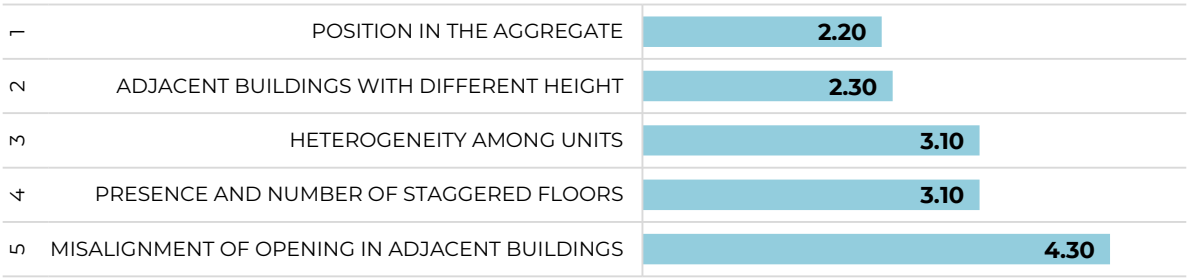


Figure 6 – Investigated aggregate vulnerability parameters and their rankings

In second group of questions, participants rated each group of parameters on a scale from 1 to 5, where 1 indicated low influence and 5 high influence. This question served as a consistency check for the first question. The results show that parameters related to building regularity were considered the most influential, aligning with the findings from the first question and reflecting participants' confidence in their evaluations. The agreement between these independent questions supports the reliability of the collected data and highlights the importance of consistency when assessing the influence of various parameters on the seismic behaviour of buildings.

The final part of the survey comprised nine pairwise-comparison questions, in which participants selected the more influential parameter and assessed its relative importance. As with the previous question, this section acted as a consistency check, given the practical limitations on the total number of questions. The results confirm the hierarchy of parameter influence established in the first question. All compared pairs follow the same ranking, except for the pair Percentage of openings and Maintenance condition, where 55% of participants rated Percentage of openings as more influential, contrary to the initial ranking. This discrepancy is minor, as the two parameters were ranked consecutively in the first question.

Based on the average ratings presented in Figure 5 and Figure 6, the ranking and influence of each parameter were analysed, with their consistency confirmed through responses to the remaining survey questions. To enable direct comparison with parameter influence rankings derived from empirical data using statistical methods, the average scores were normalised and converted into weighting factors (

Table **1**). A similar approach has been applied in related civil engineering studies requiring parameter weighting based on expert judgment (Ortega et al. 2021). Vulnerability index methods (Pinheiro et al. 2015; Ferreira, Vicente, and Varum 2014) typically assign parameter weighting factors ranging from 0.50 to 1.50 in increments of 0.25. Accordingly, weighting coefficients were defined by approximating the normalised regression coefficients to multiples of 0.25. The primary criterion was rounding normalised average scores to the nearest multiple of 0.10, with normalisation limits set between 0.055 (minimum) and 0.085 (maximum). In this study, the methodology was applied inversely: higher average ratings correspond to lower weighting factors, and lower average ratings correspond to higher weighting factors.

Table 1 – *Weight factors according to the survey results*

Number	Parameter	Average rating	Normalized rating	Weight factor
1	Plan regularity	4.9	0.0410	1.50
2	Organization of vertical elements	5.2	0.0436	1.50
3	Distribution of the lateral load-resisting system	5.7	0.0477	1.50
4	Type of material of vertical elements	5.8	0.0486	1.50
5	Height regularity	6.9	0.0578	1.25
6	Type of floor structure	7.1	0.0595	1.25
7	Location and type of foundation	7.1	0.0595	1.25
8	Number of storeys	7.3	0.0611	1.25
9	Maintenance condition	8.6	0.0720	1.00
10	Percentage of openings in the façade	8.7	0.0729	1.00
11	Wall slenderness	8.9	0.0745	1.00
12	Construction details	9.5	0.0796	0.75
13	Wall span	10.8	0.0905	0.50
14	Gable walls	11.4	0.0955	0.50
15	Roof type	11.5	0.0963	0.50
1	Position in the aggregate	2.2	0.1467	1.50
2	Adjacent buildings with different heights	2.3	0.1533	1.50
3	Heterogeneity among units	3.1	0.2067	1.10
4	Presence and number of staggered floors	3.1	0.2067	1.10
5	Misalignment of opening in adjacent buildings	4.3	0.2867	0.50

A notable dispersion is observed among the methods regarding the relative influence of individual parameters. For instance, parameter P2 (material type of vertical elements) is considered highly significant by most methods yet ranked as least important by (Petrini and Benedetti 1984). Similarly, for parameter P4 (configuration of the lateral load–resisting system), methods such as (Ožić 2025; Ortega et al. 2021) and the present survey assign high weights (1.25–1.50), while (Vicente, Varum, and Mendes da Silva.; Ortega et al. 2021) report lower influence. For P10 (maintenance condition), (Petrini and Benedetti 1984)and (Vicente, Varum,

and Mendes da Silva) classify it as highly influential, whereas (Ferreira, Vicente, and Varum 2014; Ožić 2025) assign much lower weights (0.50–0.75).

Some parameters, such as the number of stories, appear only in selected methodologies (Ferreira, Vicente, and Varum 2014; Ortega et al. 2021) and are omitted elsewhere. Wall span shows greater agreement, with most methods assigning medium importance, except Petrini and Benedetti 1984. Conversely, parameter Z1 (gable walls) receives the highest weight (1.25–1.50) in Ožić 2025 but is excluded from several other methodologies.

These findings demonstrate that different approaches attribute unequal significance to the same parameters, highlighting that the choice of method can substantially affect the final assessment. The omission of specific parameters (e.g., gable walls, staircases) indicates that methodologies are not universally applicable but tailored to particular construction typologies or regional conditions. Consequently, selecting a vulnerability assessment method requires careful consideration of the building characteristics and the purpose of the analysis to ensure reliable seismic vulnerability estimation.

Experts' opinions on the relative importance of aggregate vulnerability parameters differ from the weighting factors used defined by existing methods. Existing methodologies are primarily based on Italian or Portuguese building stocks and urban aggregates, where buildings typically share a common wall—a condition not generally present in Croatian buildings. Therefore, the observed differences were expected. For the Croatian context, the presence of adjacent units of different heights carries greater significance than in the Italian case, although in both contexts the position of a building within the row is considered the most influential parameter. Heterogeneity among units holds similar importance in both cases. Additionally, the survey results in the presence of adjacent units with different heights and number of staggered floors being equally important, whereas existing methodologies rank number of staggered floors as one of the least influential parameters. Conversely, the misalignment of openings between adjacent buildings is considered the least influential by the survey participants. These differences primarily reflect the structural distinctions between the building stocks: in Italy, adjacent units commonly share walls, whereas in Croatia, units typically lean against each other without structural interconnection

4. Conclusion

Numerous methodologies have been proposed for assessing the seismic vulnerability of historical URM buildings, all of which carry inherent advantages and limitations.This study aimed to identify key parameters influencing the seismic vulnerability of Croatian historic URM buildings and determine their relative importance through expert judgment. Although methods from other regions, particularly Italy, have been applied due to typological similarities, post-earthquake observations revealed discrepancies between predicted and observed damage. Croatian URM buildings exhibit unique features, and limited local earthquake data make empirical vulnerability functions underdeveloped, highlighting the need for region-specific assessment.

An online survey with 111 experts in earthquake engineering and masonry structures provided quantitative insight into parameter importance. Results showed high consistency among experienced experts and across academic and industry groups. Differences between Croatian and international respondents reflected regional variations in aggregate configuration and structural connectivity.

Still, these findings demonstrate that expert opinion is a valuable complement to empirical and analytical data in defining parameter weights for rapid assessment tools tailored to Croatian URM buildings. While the proposed weighting scheme provides a consistent expert-based framework, future work should also address its calibration against alternative weighting approaches and observational evidence. In this context, the derived weights could serve as an initial basis for calibrating existing vulnerability assessment methodologies, ensuring their adaptation to the specific characteristics of Croatian URM buildings and improving the reliability of rapid assessment tools through data-driven refinement of parameter

importance. Future work should further focus on systematic post-earthquake data collection and the development of national databases to support empirically grounded, locally adapted fragility functions and more robust vulnerability assessments.

Acknowledgments

This research is funded by the Institutional project POTEPUH, Vulnerability Assessment of Traditional Unreinforced Masonry Buildings in Aggregates in Croatia, project leader: Mislav Stepinac.

References

Angiolilli, Michele, Sergio Lagomarsino, Serena Cattari, and Stefania Degli Abbati. 2021. "Seismic Fragility Assessment of Existing Masonry Buildings in Aggregate." *Engineering Structures* 247 (August): 113218. https://doi.org/10.1016/j.engstruct.2021.113218.

Atalić, Josip, Marta Šavor Novak, and Mario Uroš. 2019. "Seismic Risk for Croatia: Overview of Research Activities and Present Assessments with Guidelines for the Future." *Gradjevinar* 71 (10): 923–47. https://doi.org/10.14256/JCE.2732.2019.

Ferreira, Tiago Miguel, Romeu Vicente, and Humberto Varum. 2014. "Seismic Vulnerability Assessment of Masonry Facade Walls: Development, Application and Validation of a New Scoring Method." *Structural Engineering and Mechanics*.

Moretić, Antonela, Nicola Chieffo, Mislav Stepinac, and Paulo B. Lourenço. 2022. "Vulnerability Assessment of Historical Building Aggregates in Zagreb: Implementation of a Macroseismic Approach." *Bulletin of Earthquake Engineering*, no. 0123456789. https://doi.org/10.1007/s10518-022-01596-5.

Moufid, Moustafa, Fadzli Mohamed, and Ehsan Noroozinejad. 2020. "The Seismic Vulnerability Assessment Methodologies : A State-of-the-Art Review." *Ain Shams Engineering Journal* 11 (4): 849–64. https://doi.org/10.1016/j.asej.2020.04.001.

Novak, Marta Šavor, Mario Uroš, Josip Atalić, Marijan Herak, Marija Demšić, Maja Baniček, Damir Lazarević, Nenad Bijelić, Milan Crnogorac, and Mario Todorić. 2020. "Zagreb Earthquake of 22 March 2020 – Preliminary Report on Seismologic Aspects and Damage to Buildings." *Građevinar* 72 (10): 843–67. https://doi.org/10.14256/JCE.2966.2020.

Ortega, Javier, Graça Vasconcelos, Hugo Rodrigues, Mariana Correia, and Tiago Filipe Da Silva Miranda. 2021. "Development of a Numerical Tool for the Seismic Vulnerability Assessment of Vernacular Architecture." *Journal of Earthquake Engineering* 25 (14): 2926–54. https://doi.org/10.1080/13632469.2019.1657987.

Ožić, Karlo. 2025. "An Expeditious Seismic Vulnerability Assessment Method for Essxisting Unreinforced Masonry Buildings."

Petrini, Vincenzo, and Duilio Benedetti. 1984. "A Method for Evaluating the Seismic Vulnerability of Masonry Buildings."

Pinheiro, Marisa, Sara Sanches, Tiago Miranda, Adriana Neves, Joaquim Tinoco, Alexandra Ferreira, and António Gomes Correia. 2015. "A New Empirical System for Rock Slope Stability Analysis in Exploitation Stage." *International Journal of Rock Mechanics and Mining Sciences* 76 (June): 182–91. https://doi.org/10.1016/j.ijrmms.2015.03.015.

Schiavoni, Mattia, Ersilia Giordano, Francesca Roscini, and Francesco Clementi. 2023. "Advanced Numerical Insights for an Effective Seismic Assessment of Historical Masonry Aggregates." *Engineering Structures* 285 (April): 115997. https://doi.org/10.1016/j.engstruct.2023.115997.

Stepinac, Mislav, Paulo B. Lourenço, Josip Atalić, Tomislav Kišiček, Mario Uroš, Maja Baniček, and Marta Šavor Novak. 2021. "Damage Classification of Residential Buildings in Historical Downtown after the ML5.5 Earthquake in Zagreb, Croatia in 2020." *International Journal of Disaster Risk Reduction* 56 (April). https://doi.org/10.1016/j.ijdrr.2021.102140.

Torres-Olivares, Sebastian, Beatriz González-Rodrigo, Erick I. Saavedra-Flores, and Juan Carlos Mosquera-Feijoo. 2024. "Seismic Behaviour of Reinforced-Masonry Aggregate under Different Types of Interaction between Adjacent Dwellings." *Bulletin of Earthquake Engineering* 22 (2): 583–609. https://doi.org/10.1007/s10518-023-01782-z.

Uroš, Mario, Marta Šavor Novak, Josip Atalić, Zvonko Sigmund, Maja Baniček, Marija Demšić, and Sanja Hak. 2021. “Post-Earthquake Damage Assessment of Buildings - Procedure for Conducting Building Inspections.” *Građevinar* 72 (12): 1089–1115. https://doi.org/10.14256/JCE.2969.2020.

Vicente, Romeu, Humberto Varum, and J.A.R. Mendes da Silva. n.d. “Estratégias e Metodologias Para Intervenções de Reabilitação Urbana Avaliação Da Vulnerabilidade e Do Risco Sísmico Do Edificado Da Baixa de Coimbra.”

Cinpar 2026
XXII International Conference on Building Pathology and Constructions Repair
15th to 17th July 2026 - Lisboa, Portugal

INTEGRATION OF AN HBIM DIGITAL MODEL WITH GPR DATA INTERPRETED USING MACHINE LEARNING

Maria Isadora GONÇALVES[1], Francisco Carlos SANTANA[2], Michael OLIVEIRA[3], Esequiel MESQUITA[4], Mylene VIEIRA[5]

[1] Universidade Federal do Ceará, Russas, Brasil, isadoramessias@alu.ufc.br
[2] Universidade Federal do Ceará, Russas, Brasil, franciscosantana@alu.ufc.br
[3] Universidade Federal do Ceará, Russas, Brasil, mjackson20@alu.ufc.br
[4] Universidade Federal do Ceará, Russas, Brasil, emesquita@ufc.br
[5] Universidade Federal do Ceará, Russas, Brasil, mylene.melo@ufc.br

Abstract: Historic buildings represent a fundamental part of cultural heritage, as they reflect cultural, economic aspects and construction techniques characteristic of different historical periods. The preservation of these assets largely depends on knowledge of their construction characteristics, which can be achieved through the application of non-destructive testing, enabling the investigation of these structures without compromising their integrity and thereby supporting documentation, diagnosis, and maintenance actions. Furthermore, the integration of different diagnostic data becomes essential for a more comprehensive and reliable understanding of these structures. In this context, the use of artificial intelligence techniques has become increasingly relevant, as it optimizes processes and stages that require time and specialized interpretation, making analyses more efficient and systematic. Thus, this study aims to integrate a digital model based on a point cloud with radargram data interpreted through machine learning techniques. The study was carried out at the Church of São Sebastião, located in the municipality of Russas, Ceará, Brazil. Ground Penetrating Radar (GPR) surveys were conducted on internal and façade masonry, with the objective of identifying interfaces, construction layers, moisture presence, and other anomalies. The methodology was structured into five main stages: (i) selection of the building under study; (ii) data acquisition using GPR, laser scanning, and photogrammetry; (iii) development of the HBIM digital model based on the point cloud; (iv) application of machine learning techniques for the automatic detection of patterns in radargrams; and (v) integration of GPR data into the digital model. The results indicate the potential of the proposed approach for understanding the construction systems of historic buildings, highlighting the importance of integrating these data into a digital environment as a supporting tool for heritage conservation and management.

Keywords: Non-destructive testing; GPR; HBIM; Machine learning; Cultural heritage.

1. Introduction

Historic buildings represent a cultural heritage of great relevance to society, reflecting architectural, historical, and social characteristics over time. The proper preservation of these structures largely depends on technical knowledge of their construction features and the availability of historical documentation. However, this task represents a significant challenge, mainly due to the complexity of the construction techniques employed and the limited or nonexistent technical records (Binda e Saisi, 2001; Mesquita et al., 2016).

In this context, non-destructive testing (NDT) techniques are the most suitable for diagnosing historic heritage, as they consist of methods that do not cause physical or chemical alterations to the analyzed asset (Binda e Saisi, 2001). Among these techniques, three-dimensional laser scanning has been widely used to obtain accurate geometric data, enabling the generation of point clouds and digital models that faithfully represent the building geometry. This geometric representation is fundamental for heritage

documentation, as it serves as a basis for broader conservation-related processes (Parente et al., 2025). However, although this technique is effective for surface geometry, it does not provide information about the internal composition of structural elements. To overcome this limitation, several non-destructive techniques have proven effective in characterizing internal features, among which Ground Penetrating Radar (GPR) stands out as one of the most advanced technologies in civil engineering, with increasing application in the conservation of historic monuments (Annan, 2003; Jasieńko, Raszczuk e Frąckiewicz, 2024).

GPR is a geophysical method based on the propagation of electromagnetic waves in natural (geological) and artificial environments (masonry and concrete), detecting contrasts between materials with different dielectric properties. The equipment operates using transmitting antennas, which emit pulses, and receiving antennas, which capture signals reflected by embedded components. The results of these tests are two- or three-dimensional images of the captured reflections, known as radargrams (Carrik, 2017; Alvarado et al., 2025).

Despite its potential, the interpretation of GPR data is complex, especially in historic structures characterized by high material heterogeneity and a wide variety of construction patterns (Parente et al., 2025). The analysis requires operator expertise and careful definition of acquisition parameters, making the process time-consuming and labor-intensive (Pérez-Gracia et al., 2012; Ludeno et al., 2020). In this regard, Parente et al. (2025) highlight the need for process automation in the field of cultural heritage through the use of artificial intelligence, given the increasing volume and complexity of diagnostic data (Parente et al., 2025).

In recent years, advances in computational techniques have driven the application of machine learning models for radargram interpretation. These approaches enable the automatic recognition of disturbance patterns, construction interfaces, and structural anomalies, reducing subjectivity and optimizing the analysis workflow (küçükdemirci e sarris, 2022; Banfi e Liu, 2026; Li, Chiabrando e Sammartano, 2026). However, recent studies indicate that artificial intelligence applications in GPR data are predominantly focused on signal processing and the recognition of hyperbolic patterns in B-scans, typically associated with the detection of objects or localized discontinuities (Küçükdemirci e Sarris, 2022). Furthermore, most research focuses on AI applications for detecting thickness variations and pavement damage (Gao *et al.*, 2020; Li et al., 2021), archaeological investigations (Küçükdemirci e Sarris, 2022), detection of buried elements (Qiu et al., 2022), and concrete structures (Küçükdemirci e Sarris, 2022; Yuan, Yuan e He, 2024; Banfi e Liu, 2026). The exploration of more complex construction patterns, particularly in masonry and flooring systems of historic structures, remains limited.

At the same time, Historic Building Information Modeling (HBIM) has emerged as a relevant tool for digital heritage documentation, enabling the organization of geometric, historical, and diagnostic information within an integrated environment. Recent studies by Banfi (2026) demonstrate that HBIM has experienced a significant technological shift since 2019, evolving from a focus primarily on geometric surveying to encompassing intelligent heritage management (Banfi e Liu, 2026). In this context, several studies have explored HBIM as an interdisciplinary tool for integrating historical, geometric, and non-destructive testing data. In some cases, NDT techniques and artificial intelligence approaches have been associated with digital models to enrich building information (Solla et al., 2020; Coli et al., 2022; Cardinali *et al.*, 2023).

Despite the advances observed in recent decades, both in HBIM development and in the application of artificial intelligence techniques for GPR data processing, significant gaps remain in these approaches, particularly regarding the lack of standardized methods for structured information storage (Celli e Ottoni, 2023; Parente et al., 2025). Moreover, Parente (2025) highlights that most HBIM research focuses on the geometric definition of models (75.8%), while the characterization of internal structural elements remains one of the least explored areas (18.2%). This imbalance highlights the need for approaches that integrate diagnostic investigations into HBIM environments in a structured manner (Banfi e Liu, 2026), such as those provided by GPR testing.

In this context, the present research proposes an HBIM-based approach focused on the collection and organization of information regarding internal composition and potential pathologies in historic masonry structures. To this end, it integrates three-dimensional geometric surveying obtained through laser scanning with internal characterization performed using GPR testing, combined with machine learning techniques for the automatic identification of disturbance patterns in radargrams. The results are georeferenced within the digital model generated from the point cloud, enabling precise localization of the investigations and the association of diagnostic information with the corresponding structural elements. Thus, the HBIM model evolves beyond a purely geometric representation to incorporate internal information that supports analysis, conservation, and decision-making processes in the context of built heritage.

2. Materials and Methods

Initially, laser scanning surveys were carried out over the entire architecture of the church, with the aim of obtaining the building geometry. This survey enabled the generation of a three-dimensional model, serving as the basis for modeling and integrating the remaining investigative data.

Following the geometric survey, GPR tests were performed to identify construction patterns, characterize internal interfaces, and detect potential pathologies in the investigated areas. Subsequently, the data obtained from GPR underwent processing and the application of machine learning techniques, aiming to support the automated identification of internal features.

After completing the data acquisition and processing stages, the next step consisted of integrating the GPR data into the three-dimensional model of the building. The methodological process was carried out as shown in Figure 1.

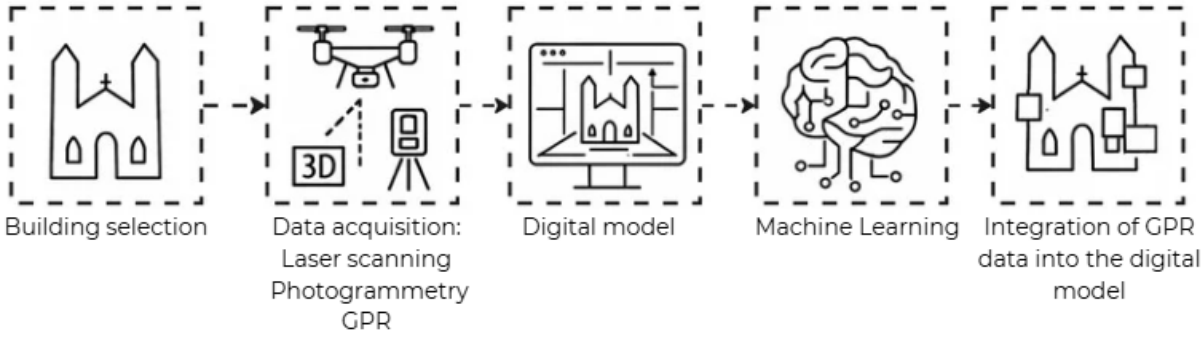


Figure 1: Methodological workflow adopted in the research

2.1 Building selection

The São Sebastião Church, located in the municipality of Russas, in the state of Ceará, Brazil, was selected as the case study for this research due to its significant historical, cultural, and religious value for the region, being considered an important part of the local heritage. In addition, the building preserves architectural elements characteristic of its construction period, particularly its internal space defined by structural arches, the presence of an altar, and ornamental features that retain original characteristics, allowing for a better understanding of the construction techniques employed.

Its origin dates back to the 19th century and is directly associated with significant historical events of that period, during which the region experienced severe drought and epidemic outbreaks, leading to the emergence of popular devotion to Saint Sebastian. In this context, the church was built in 1872 and has since played a central role in the religious and cultural expressions of the community, particularly during festivities dedicated to its patron saint (Araújo, 1986; Novenário de São Sebastião, 1996).

he church is constructed of brick masonry and has undergone localized maintenance and improvement interventions over time. Records indicate that the building has been subject to renovations over the years, including plaster restoration, replacement of deteriorated elements, and improvements to both interior and exterior finishes (Araújo, 1986; Novenário de São Sebastião, 1996). Figure 2 presents the church in its current condition, including its location, façade, and internal environment.



Figure 2: Church of São Sebastião – Russas/CE

2.2 Data acquisition

2.2.1 Laser Scanning and Photogrammetry Survey

The geometric survey of the building was carried out in two distinct stages, starting with laser scanning and subsequently using an unmanned aerial vehicle (drone), both of which served as the basis for the building modeling.

The laser scanner used was the portable Leica BLK2GO, a lightweight and wireless device with a height of 279 mm, a diameter of 80 mm, and an approximate weight of 775 g. It presents a relative accuracy ranging from 6 to 15 mm and an absolute accuracy of approximately 20 mm. The acquisition system consists of three main components: a portable LiDAR scanning sensor, a fixed reference unit, and a mobile device used for real-time visualization and monitoring of the data acquisition.

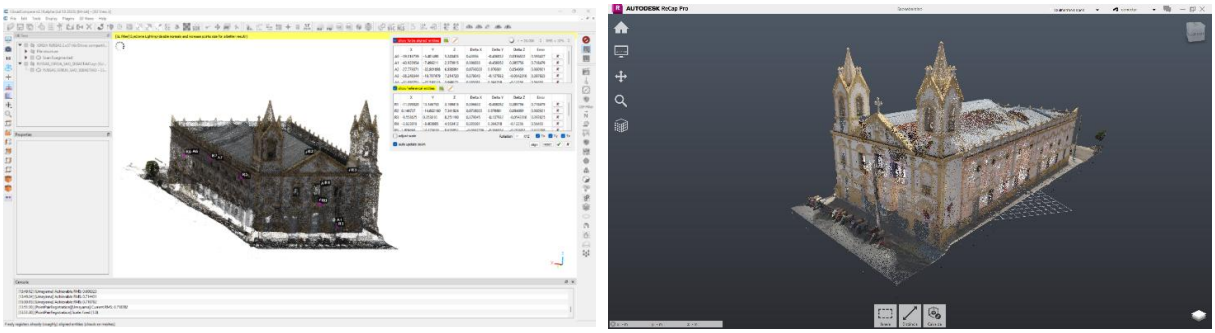


Figure 3: Integration of point cloud and photogrammetry data in CloudCompare software

During the survey, the fixed unit was positioned at a strategic location inside the building and remained stably mounted throughout the acquisition process. The portable BLK2GO sensor was manually operated through continuous walking along the building, while the mobile device connected to the system enabled real-time visualization of the generated point cloud, allowing for monitoring of data quality and adjustments to the acquisition path when necessary.

Following this stage, photogrammetry was performed using an unmanned aerial vehicle (UAV), specifically the DJI Mavic 3T, equipped with an integrated camera, to capture aerial images of areas with difficult access, such as the roof and façade of the church.

The processing of the point cloud obtained from the laser scanner was carried out using Cyclone Register 360 software. The photogrammetric processing using the UAV was conducted in RealityScan 2.1.0, which generated a point cloud from the captured images. After generating the internal and external point clouds of the building, both datasets were integrated using CloudCompare software (Figure 3). Finally, the complete model of the church was exported to Autodesk Revit software to initiate the modeling process and the creation of parameters for data integration into the HBIM model.

2.2.2 GPR Data Acquisition

The investigation of the internal characteristics of the church masonry was carried out using a Proceq GP8000 GPR system, a portable and wireless device with approximate dimensions of 22.1 × 18 × 14 cm and a weight of 1.5 kg, suitable for handling on vertical surfaces. The equipment operates with a central frequency antenna of 2000 MHz, appropriate for the investigation of shallow structures and for achieving high spatial resolution, allowing the identification of internal construction details (Elkarmoty et al., 2024; Jasieńko, Raszczuk e Frąckiewicz, 2024).

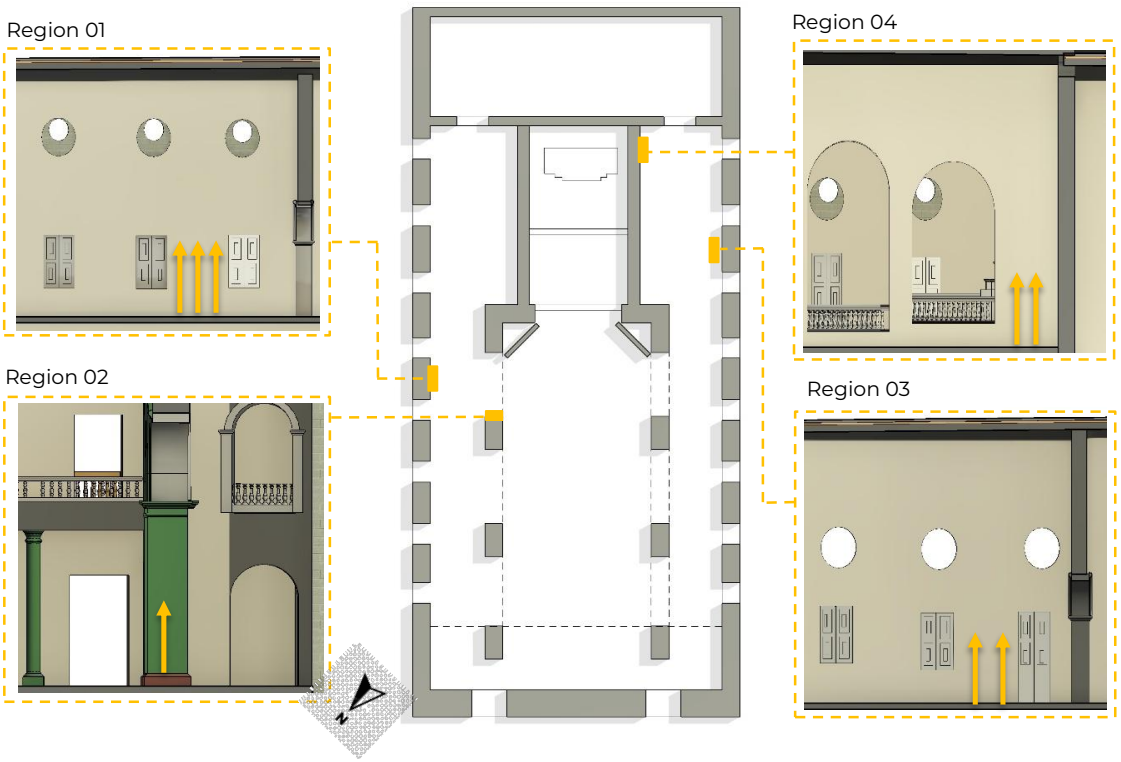


Figure 4: Floor plan showing the locations of GPR data acquisition on the church walls

Prior to data acquisition, the locations to be investigated were defined in order to cover different areas of the church. Four distinct regions of walls and pillars were selected with the aim of identifying construction patterns, interfaces between materials, and potential internal anomalies. In total, nine data acquisitions were performed, comprising three tests in Region 01, teste in Region 2 and two tests in each of Regions 03 and 04, as shown in Figure 4.

During data acquisition, the equipment was moved continuously and in a controlled manner along the surfaces, maintaining a uniform speed and consistent contact with the surface. The scanning profiles were carried out along vertical lines, starting from the base of the walls and extending up to approximately 1.60 m in height. This limit was defined based on the operator's reach and the area of interest, particularly with respect to the analysis of possible moisture-related phenomena at the base of the walls.

Subsequently, the raw signals were processed using Proceq GPR software through procedures such as noise filtering and depth adjustment based on the assumed dielectric constant, with the aim of reducing interference and noise while enhancing the received signal.

2.3 Digital Model

The modeling stage began with the import of the point cloud in RCP format into Revit, which served as the basis for the construction of the building's geometric model. Within the modeling environment, the simultaneous use of different views, plans, sections, and elevations, was adopted, allowing greater accuracy in the interpretation and modeling process based on the point cloud. Through this approach, it was possible to reconstruct the architectural elements while respecting their actual shape, position, and proportions. Part of the structural elements was represented using system families available in the software, while specific elements characteristic of the church and not included in the standard libraries were modeled using custom families.

The adopted level of development can be classified as LOD 300, in which elements are represented with correct dimensions, morphology, position, and orientation, enabling direct measurements within the model and the integration of non-graphical data (Cardinali *et al.*, 2023). According to Celli and Ottoni (2023), this level of detail is appropriate for HBIM models focused on data integration, where the objective is not to fully replicate the building geometry, but rather to maintain an adequate level of detail to distinguish individual architectural elements (Celli e Ottoni, 2023). Figure 5 illustrates the three-dimensional model of the building developed in Revit.

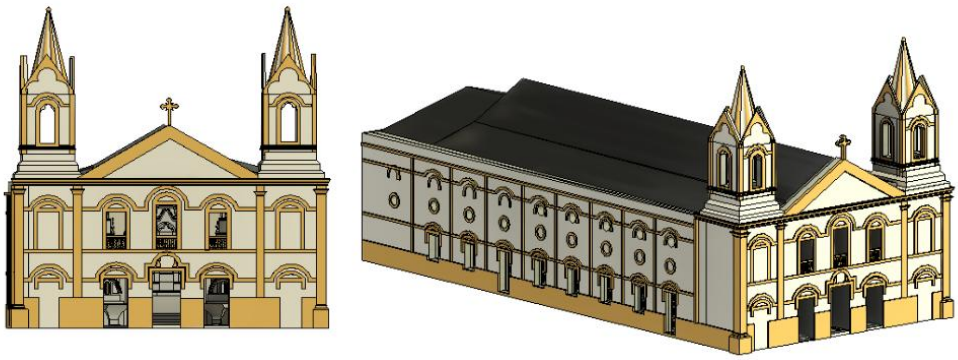


Figure 5: 3D modeling of the church in Revit software

2.4 Machine Learning

The methodology was based on the application of the YOLO (You Only Look Once) algorithm for the automatic detection of patterns in images. Initially, the computational environment was configured in Python, and an image dataset was constructed using images selected from open-source platforms such as Flickr, Unsplash, and Pexels. The images were annotated using the LabelImg tool, considering three main classes: interfaces between layers, regions associated with moisture, and potential voids (Figure 6a). The annotations were exported in .xml format and subsequently converted into a format compatible with the YOLO model within the Python environment.

The training process was carried out using a dataset of 174 annotated images, enabling the model to learn visual patterns associated with the defined classes. After training, a preliminary validation was performed

using the annotated images themselves, in which the model demonstrated consistent detections aligned with the manual annotations (Figure 6b).

Finally, the trained model was applied to radargram images from the São Sebastião Church that were not included in the training dataset.

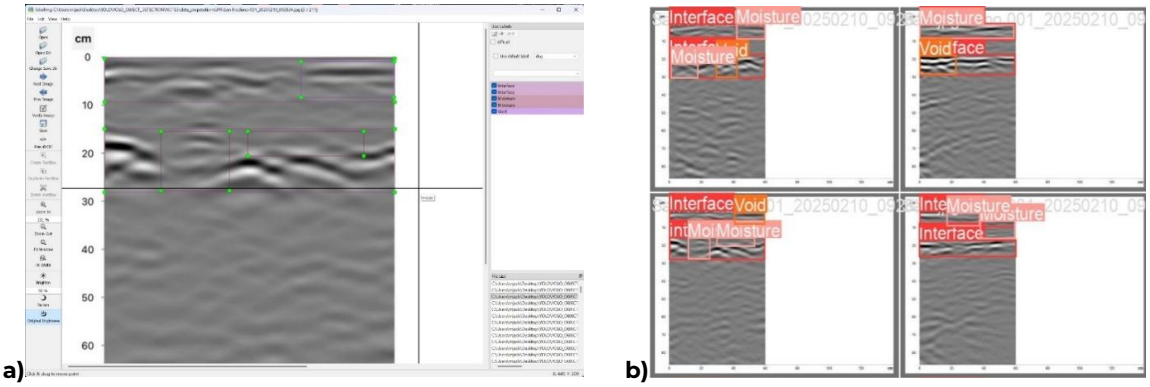


Figure 6: (a) Annotation of patterns using bounding boxes; (b) Model validation.

2.5 Integration of GPR Data into the Digital Model

The creation of informational content begins with the insertion of GPR test data into the HBIM model, respecting the actual size and location of the test execution within the structure.

The workflow starts with the modeling of a generic model component using the extrusion tool in Revit. This element was modeled according to the dimensions of the investigated section, where the height of the extrusion corresponds to the extent of the scanning line, the width corresponds to the signal penetration depth obtained from the test, and a representative thickness of 2 cm was adopted to avoid excessive interference with the model.

Once the geometric base was established, the insertion of GPR data was carried out using the *decal* tool. This command allows 2D images, such as radargrams, to be applied directly onto model surfaces. Through scale and rotation adjustments, the radargram is manipulated so that its boundaries exactly match the edges of the created object, ensuring the real scale of both the signal depth and extent (Figure 7). This process eliminates distortions in spatial interpretation and ensures that the detected anomalies are represented in their actual positions.

Finally, the element composed of both geometry and radargram is positioned within the overall geometry of the church, being inserted precisely at the location where the test was performed.

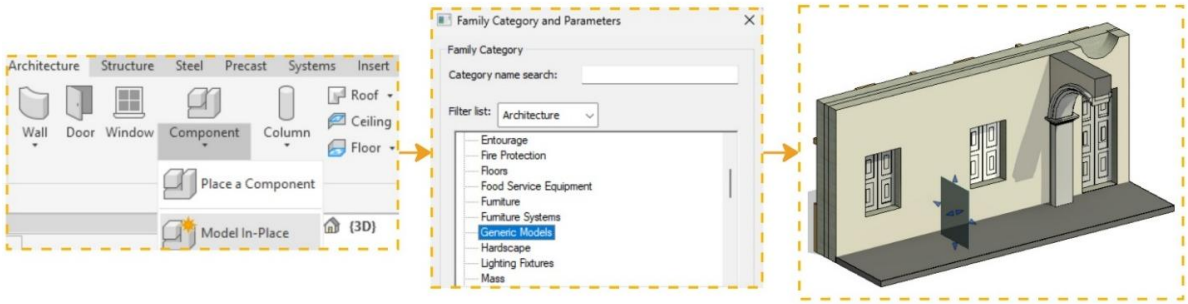


Figure 7: Modeling process of the generic model for radargram placement

3. Results

3.1 Machine Learning

Figure 8 presents the main radargrams obtained across the different investigated surfaces. In Figure 8a, in the near-surface region (0–10 cm), continuous high-amplitude reflections can be observed, associated with interfaces between masonry construction layers. Below this region, at depths between approximately 10 and 40 cm, a more heterogeneous pattern is identified, characterized by irregular reflections, possibly related to the presence of moisture.

When GPR is applied to materials with high moisture content, two main behaviors may be observed. In the first, the electromagnetic wave propagates through a highly conductive medium, undergoing strong attenuation and a consequent significant reduction in signal amplitude. Under this condition, the ability to detect internal interfaces is reduced, and some anomalies may become imperceptible in the radargram. In the second behavior, an increase in reflection amplitude is observed, which occurs when there is contrast between regions with different moisture contents, such as interfaces between dry and wet zones. The greater the difference in dielectric constant between these media, the stronger the reflection intensity (Pérez-Gracia et al., 2022).

The application of the machine learning model in Figure 8a enabled the identification of the near-surface interface with high reliability, correctly highlighting its continuity along the profile. In addition, regions associated with moisture near the surface were detected and highlighted by the bounding boxes generated by the model. However, the model showed limitations in interpreting deeper regions, as indicated by the white and orange arrows. The region marked by the orange arrow presents isolated disturbances without continuity, likely associated with the transition between wetter and drier zones. In contrast, the region indicated by the white arrow exhibits typical patterns of highly saturated zones, with significant signal attenuation, resulting in an area with no visible reflections.

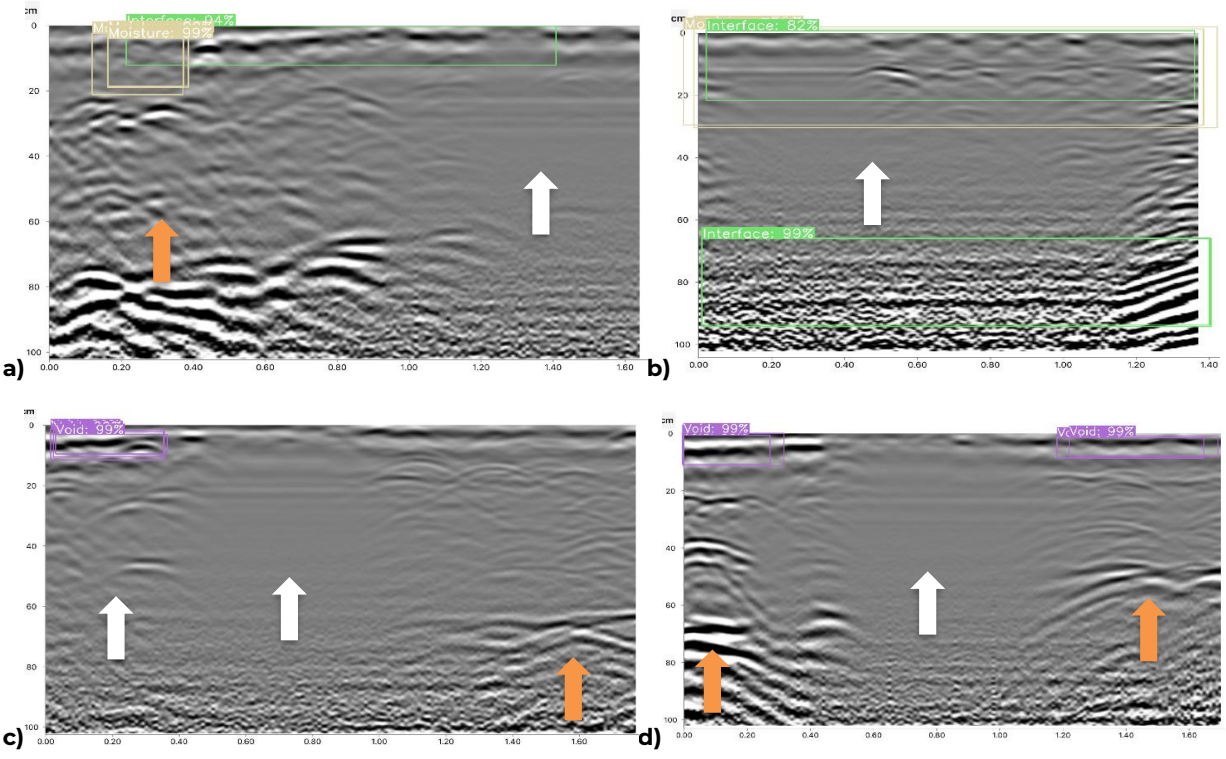


FigurE 8: Detection of radargram reflection patterns using YOLO. (a) Radargram from Region 01; (b) Radargram from Region 02; (c) Radargram from Region 03; (d) Radargram from Region 04.

In Figure 8b, the near-surface region shows continuous reflections of low to medium amplitude, associated with the outer masonry layer. In the intermediate zone, a reduction in signal amplitude is observed, possibly related to the presence of moisture. The machine learning model performed well in identifying the main interfaces, successfully detecting the near-surface interface and indicating moisture-related regions, as highlighted by the bounding boxes in the radargram. However, it did not explicitly identify the intermediate zone characterized by signal attenuation associated with high moisture content (white arrow).

At greater depths, the machine learning model indicated the presence of a new interface in this region. However, analysis of the radargram suggests that this response is associated with signal energy loss during propagation rather than a real physical interface, as incorrectly detected by the model.

The radargrams presented in Figures 8c and 8d show, in the near-surface portion (approximately 0–15 cm), medium- to high-amplitude reflections associated with the outer masonry layer. In Figure 8c, a region in the upper left area stands out, characterized by high-amplitude reflections and strong contrast, associated with the presence of voids or internal discontinuities. In Figure 8d, two regions at the edges of the profile exhibit similar characteristics, also consistent with the presence of shallow voids.

In the intermediate zone of both figures (8c and 8d), a pattern of low amplitude is observed, indicating strong signal attenuation (white arrows), possibly associated with high moisture content. In some portions of this layer, more pronounced reflections can be identified, suggesting the presence of multiple interfaces and internal variations within the structure, although these are not clearly defined due to signal loss in adjacent regions (orange arrows).

3.2 Integration of GPR Data into the Digital Model

Figure 9 presents the insertion of radargrams into the digital model, associated with their corresponding regions of the masonry. It can be observed that each test was represented by an individual element, positioned according to its actual location within the building.

The radargrams were incorporated into the model including the markings of the detected features, allowing direct visualization of the classified regions along the profiles. Detections associated with interfaces, zones of signal attenuation, and potential voids, identified through machine learning, are displayed on the surface of the created generic model, facilitating the visual identification of these characteristics within the context of the building.

In addition to the graphical representation, each radargram inserted into the model contains a set of associated information. These data can be accessed directly through the Revit properties panel by selecting the corresponding element. Among the available information are: profile identification, acquisition date, and the model and frequency of the equipment used.

To enhance the visualization of radargrams within the model, the “Hide in View” command can be applied to the masonry elements, allowing the test-representative object and its associated information to be clearly visualized without interference from other structural components.

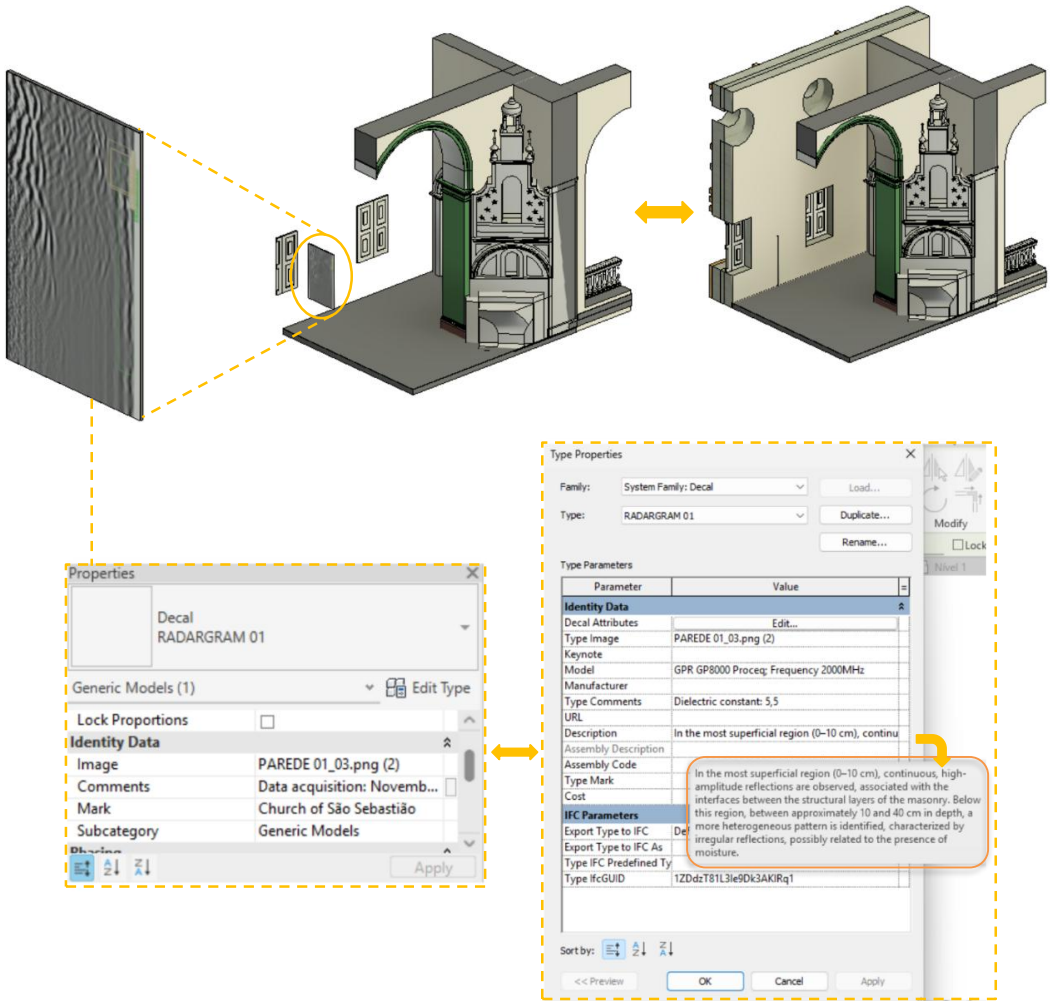


FigurE 9: Data Integration in the HBIM Environment

4. Conclusion

The present research aimed to apply machine learning techniques for the automatic detection of interfaces, moisture zones, and potential voids in GPR tests applied to historic masonry structures. Additionally, the obtained data were integrated into a digital environment, in which the building geometry was reconstructed from point cloud data, enabling the spatial representation of the test results.

The results obtained from GPR tests demonstrated the high capability of the method to identify internal interfaces and reflections, even in structures characterized by high complexity, such as historic masonry. Factors such as operator expertise, type of equipment used, and signal processing procedures are fundamental to achieving more reliable results.

The incorporation of machine learning techniques, through the YOLO model, proved to be effective in the automated detection of the analyzed features, enabling the identification of relevant patterns in radargrams with greater speed and consistency. However, it was observed that the model performance is directly influenced by the quality, diversity, and representativeness of the training dataset, as well as by the complexity of the investigated medium. In scenarios characterized by high material heterogeneity and overlapping reflections, limitations in the detection process were identified, with the occurrence of regions in the radargrams not recognized by the model.

These results highlight the need to improve the dataset and adopt more robust training strategies to enhance detection capability and accuracy in complex contexts. Despite these limitations, the model demonstrated promising performance, indicating that machine learning techniques can serve as a reliable support tool for the interpretation of GPR data in masonry structures.

The integration of results into the HBIM environment proved to be highly effective, allowing the association of geometric data with diagnostic information in a unified digital model. Furthermore, the data insertion process was found to be simple and easy to implement, not requiring complex procedures, which reinforces the practical feasibility of the proposed methodology. The georeferenced insertion of radargrams and their interpretations enabled the spatial visualization of the identified anomalies, promoting a more intuitive and integrated understanding of the building. This approach expands the role of HBIM as an informational platform capable of storing, organizing, and communicating complex technical data, contributing to more efficient heritage conservation processes.

As future perspectives, the need to expand and diversify the dataset used for training machine learning models is highlighted, aiming to improve their generalization capability and performance in more complex scenarios. Additionally, the potential for integrating data from different non-destructive testing techniques into the HBIM environment is emphasized, allowing the incorporation of multiple layers of diagnostic information into a unified model, which can contribute to more comprehensive, reliable, and management-oriented analyses of historic heritage.

5. Acknowledgements

This work was financially supported by FUNCAP, Project 01172921/2022 – Cientista Chefe Cultura, Project 10581391/2022 – International collaboration FUNCAP/INSA Rouen Normandie; by the National Council for Scientific and Technological Development (CNPq) – Project 302054/2022-7 – PQ2, by the Project - 440926/2024-6 – VISION and Project - 402828/2024-0 – CLIC, CAPES Foundation and Finep 2896/24

6. References

ALVARADO et al. (2025) “Non-destructive testing and kinematic limit analysis applied to a historic masonry church early intervened with RC elements”, *Engineering Failure Analysis*, 169. https://doi.org/10.1016/j.engfailanal.2024.109205.

ANNAN, A.P. (2003) *Ground penetrating radar applications, principles, procedures*, *Sensors and Software*. Mississauga, Canada: Sensors and Software.

ARAÚJO, P. de A. (1986) *Capital e Santuário*. IOCE. Foraleza.

Banfi, F. e Liu, W. (2026) “The State of HBIM in Digital Heritage: A Critical and Bibliometric Assessment of Six Emerging Frontiers (2015–2025)”, *Applied Sciences*, 16(2), p. 906. https://doi.org/10.3390/app16020906.

BINDA, L. e e SAISI, A. (2001) “State of the Art of Research on Historic Structures in Italy”, *Dept. of structural engineering, Politecnico of Milan, Italy.* [Preprint].

Cardinali, V. *et al.* (2023) “An Oriented H-BIM Approach for the Seismic Assessment of Cultural Heritage Buildings: Palazzo Vecchio in Florence”, *Buildings*, 13(4). https://doi.org/10.3390/buildings13040913.

CARRIK, E. (2017) *Ground Penetrating Radar: Theory and Practice*. Butterworth-Heinemann.

Celli, S. e Ottoni, F. (2023) “Managing Information to Improve Conservation: The HBIM of the Wooden Chain of Santa Maria del Fiore”, *Sensors*, 23(10). https://doi.org/10.3390/s23104860.

COLI, M., CIUFFREDA, A.L. e DONIGAGLIA, T. (2022) “Technical Analysis of the Masonry of the Bargello’ Palace, Florence (Italy)”, *Applied Sciences (Switzerland)*, 12(5). https://doi.org/10.3390/app12052615.

ELKARMOTY et al. (2024) “Georadar Survey and Simulation for Subsurface Investigation at Historical Mosque of Sorghatmesh, Cairo, Egypt”, *Buildings*, 14(11). https://doi.org/10.3390/buildings14113653.

Gao, J. *et al.* (2020) “Autonomous pavement distress detection using ground penetrating radar and region-based deep learning”, *Measurement: Journal of the International Measurement Confederation*, 164. https://doi.org/10.1016/j.measurement.2020.108077.

JASIEŃKO et al. (2024) “Areas of GPR application in researches of historical masonry structures”, *Research Square* [Preprint]. https://doi.org/10.21203/rs.3.rs-4022334/v1.

KÜÇÜKDEMIRCI, M. e SARRIS, A. (2022) “GPR Data Processing and Interpretation Based on Artificial Intelligence Approaches: Future Perspectives for Archaeological Prospection”, *Remote Sensing*. MDPI. https://doi.org/10.3390/rs14143377.

Li et al. (2021) “Detection of concealed cracks from ground penetrating radar images based on deep learning algorithm”, *Construction and Building Materials*, 273. https://doi.org/10.1016/j.conbuildmat.2020.121949.

Li, X., Chiabrando, F. e Sammartano, G. (2026) “Machine Learning and Deep Learning for Cultural Heritage Conservation: A Bibliometric and Task-Oriented Review”, *Remote Sensing*, 18(4), p. 628. https://doi.org/10.3390/rs18040628.

LUDENO et al. (2020) “On the Combined Use of Ground Penetrating Radar and Crack Meter Sensors for Structural Monitoring: Application to the Historical Consoli Palace in Gubbio, Italy”, *Surveys in Geophysics*. Springer, p. 647–667. https://doi.org/10.1007/s10712-019-09526-y.

MESQUITA et al. (2016) “ALCONPAT-Boletim técnico 11-Caracterização, avaliação e recuperação estrutural de construções históricas”. https://doi.org/10.13140/RG.2.1.1445.1606.

Parente, M. et al. (2025) “HBIM and Information Management for Knowledge and Conservation of Architectural Heritage: A Review”, *Heritage*. Multidisciplinary Digital Publishing Institute (MDPI). https://doi.org/10.3390/heritage8080306.

Pérez-Gracia, V., GONZALEZ-DRIGO, R. e SALA, R. (2012) “Ground-penetrating radar resolution in cultural heritage applications”, *Near Surface Geophysics*, p. 77–87. https://doi.org/10.3997/1873-0604.2011015.

Perez-Gracia, V., Solla, M. e Fontul, S. (2022) “Analysis of the GPR signal for moisture detection: application to heritage buildings”, *International Journal of Architectural Heritage*, 18(2), p. 230–253. https://doi.org/10.1080/15583058.2022.2139652.

QIU et al. (2022) “Research on Real-Time Automatic Picking of Ground-Penetrating Radar Image Features by Using Machine Learning”, *Horticulturae*, 8(12). Disponível em: https://doi.org/10.3390/horticulturae8121116.

SOLLA, M. et al. (2020) “Integrating GPR and geomatic data into a Building Information Modelling: The case study of the Monastery of Batalha (Portugal)”, *Def. Univ. Cent* [Preprint]. https://doi.org/10.13140/RG.2.2.33925.09447.

Yuan, S., Yuan, Z. e He, K. (2024) “Image Recognition of Concrete Electromagnetic Flaw Detection Based on Improved YOLOv7”, *Proceedings of the 2024 7th International Conference on Image and Graphics Processing*, 2024, p. 153–158. https://doi.org/10.1145/3647649.3647675.

“Novenário de São Sebastião”, (1996)

Cinpar 2026
XXII International Conference on Building Pathology and Constructions Repair
15th to 17th July 2026 - Lisboa, Portugal

Lime Mortars with Fibres and Residues for the Sustainable Rehabilitation of Wattle and Daub Walls

Kátia SOARES[1], Isabel TORRES[2,3], Ana VELOSA[4]

[1] Faculty of Science and Technology of Coimbra University, Coimbra, Portugal.
katia.soares@student.dec.uc.pt
[2] University of Coimbra, CERIS, Civil Engineering Department.
[3] ITECONS, Coimbra, Portugal. itorres@dec.uc.pt
[4] Institution, University of Aveiro, Civil Engineering Department, Aveiro, Portugal, avelosa@ua.pt

Abstract: This study evaluates the impact of the simultaneous incorporation of waste glass grinding powder (WGP) and *bracejo* fibres (Stipa gigantea) in hydraulic lime mortars (NHL 3.5) for the rehabilitation of wattle and daub walls. The research was based on the hypothesis that combining the pozzolanic nature of WGP with the fibrous structure of *bracejo* (BCJ) could balance the requirements for strength, deformability, and hygrothermal behavior. Matrices with 10% and 30% binder replacement by WGP (by mass) were analyzed, with and without the addition of 2.5% BCJ (by volume). The mortars were characterized regarding workability, open porosity, bulk density, capillary absorption, water vapor permeability, and mechanical strength at 28 days. The results demonstrate that the matrix with 30% WGP showed better rheological compatibility with the fibres, resulting in a more interconnected porous network that enhanced vapor permeability and drying efficiency. Although the fibres reduced compressive strength, the 30% WGP mortars showed the lowest relative loss in flexural strength (only 7%), indicating a superior fibre-matrix interface. It is concluded that the combination of 30% WGP and 2.5% BCJ provides a sustainable and technically viable solution, ensuring substrate "breathability" and the mechanical compatibility required for the conservation of wattle and daub heritage.

Keywords: Lime mortars; Wattle and daub walls; Vegetal fibres; Waste glass grinding powder; Heritage rehabilitation.

1. Introduction

Bracejo (*Stipa gigantea* or *Celtica gigantea*) is a perennial grass with a reduced cross-section, common in dry terrains and medium-altitude areas in Portugal. This plant resource is traditionally exploited through artisanal craftsmanship in basketry and matting, and its use in wattle and daub is part of a vernacular logic as a fibrous filling material, without a primary structural function.

Studies report that the incorporation of plant fibres into lime mortars tends to reduce mechanical strength, although it improves shrinkage and cracking control, strain energy dissipation capacity, and porosity regulation, facilitating the "breathability" of the substrate. In contrast, literature on the incorporation of ground flat glass waste highlights, under certain conditions, strength gains primarily associated with its pozzolanic activity and, complementarily, to filler effects.

In this framework, it is hypothesized that the combination of *bracejo* (BCJ) and waste glass grinding powder (WGP) can generate a synergy capable of balancing conflicting requirements in rehabilitation mortars. The objective is not the maximization of strength, but rather the establishment of a compromise between load-bearing capacity, cracking control, and deformable compatibility with wattle and daub walls.

Thus, the present study analyzed hydraulic lime mortar mixes with 10% and 30% binder replacement (by mass) with WGP, and mixes with the addition of 2.5% BCJ (by volume). The mechanical performance of these

compositions was evaluated, as well as open porosity, bulk density, capillary water absorption, permeability, and drying index. The results indicate the compatibility of the mortars with regulatory requirements, contributing to the development of sustainable and technically suitable solutions for the conservation of wattle and daub heritage.

1.1 State of the Art

Lime mortars have been widely used in the rehabilitation of traditional construction systems, particularly in vernacular techniques such as wattle and daub walls, due to their mechanical compatibility, high vapor permeability, and deformation capacity (Ayat et al., 2022; Soares et al., 2021). In recent decades, there has been a growing interest in improving the performance of these mortars through the incorporation of industrial waste and bio-based materials, aiming for both sustainability and compatibility with historical substrates (Ruffolo et al., 2025; Rubio-Aguinaga et al., 2025).

The use of finely ground glass powder as a partial binder replacement has been the subject of several studies. Literature indicates that, when properly processed, glass exhibits pozzolanic activity, contributing to the formation of additional cementitious compounds and the increase of mechanical strength. Additionally, glass particles act as a filler material, promoting the refinement of the pore structure. However, the magnitude of these effects depends on particle size, replacement ratio, and curing conditions, with replacement levels between 10% and 30% frequently identified as ideal for balancing mechanical performance and durability (Aliabdo et al., 2016; Tironi et al., 2012; Velosa et al., 2009).

Nevertheless, the incorporation of waste specifically from the flat glass grinding process (WGP) remains poorly explored. In a recent study, Santos et al. (2024) observed that partial replacement of Portland cement with up to 10% WGP does not compromise compressive strength and may even increase it when the material replaces the aggregate, in addition to reducing capillary absorption and shrinkage.

Parallelly, the inclusion of lignocellulosic materials, such as BCJ, has been explored to confer toughness to lime matrices. These materials are characterized by low density and a flexible structure, although their incorporation generally results in an increase in porosity and a reduction in compressive strength due to the introduction of less rigid phases and weaker interfaces. In contrast, they offer critical advantages in shrinkage control and strain dissipation capacity, while also favoring vapor permeability and drying efficiency (Arizzi and Cultrone, 2012).

From a microstructural perspective, the distribution and connectivity of pores play a decisive role. In systems combining dense mineral additions (such as WGP) and absorbent plant inclusions (such as BCJ), the pore network may become less connected, influencing water and vapor transport differently from total porosity (Soares et al., 2025; Poyet, 2021).

Despite the individual potential of these materials, their combined use in lime mortars for rehabilitation is still incipient. This combination may originate synergistic or competing effects: while mineral additions refine the structure, plant materials expand it (Zicarelli et al., 2025). The present study contributes to filling this gap by analyzing hydraulic lime mortars with the simultaneous incorporation of WGP and BCJ. The objective is to sustain that the performance of these hybrid mortars results from a complex equilibrium that prioritizes compatibility with the original wattle and daub system, ensuring permeability, compatible strength, and reduction of cracking.

2. Experimental Campaign

The investigation was carried out in the laboratories of the Institute for Research and Technological Development in Construction, Energy, Environment and Sustainability (ITeCons), with the support of the Departments of Civil Engineering and Geosciences at the University of Aveiro. The study was structured into two main phases:

2.1 Preparation of Materials and Characterizations

The waste used (R3) consists of the powder obtained from the dehydration of the residual sludge generated during the industrial grinding of flat glass (including tempered, laminated, and common glass). The material was collected in a wet state directly from the sedimentation basins of the company Beiraglass (Oliveira de Frades, Portugal). Although the industrial process uses the flocculant FLOC AC 9S for water clarification, its volatile nature, combined with the rigorous laboratory drying process, ensures the integrity of the final material. This condition is corroborated by the low Loss on Ignition values (LOI < 3.6%) obtained in the chemical characterization, indicating the absence of significant organic residues in the precursor.

To obtain the powder, the sludge was oven-dried at 70°C ± 5°C. until constant mass. Due to the high fineness intrinsic to the grinding process, the material did not require laboratory grinding and was used directly after drying. The characterization of R3 included X-ray Fluorescence (XRF), Laser Diffraction Particle Size Analysis, and the determination of chemical reactivity through the Modified Chapelle Test.

The BCJ employed was provided by the Historical Villages of Portugal Tourism Development Association. The material was initially fragmented into lengths of less than 3 cm and subsequently subjected to an immersion treatment in a saturated calcium hydroxide solution [$Ca(OH)_2$] for 24 h in an airtight container. This procedure aims to remove impurities and extractables from the leaf surface, promoting modifications that favor the interface between the fibrous phase and the lime matrix (Siouta et al., 2024). After treatment, the BCJ was washed with running water, oven-dried at 70°C ± 5°C until constant mass and characterized by XRF and water absorption tests following a standard operating procedure (SOP) specifically developed for this study.

The binder used was a natural hydraulic lime (NHL 3.5), certified according to the EN 459-1 standard. As an aggregate, natural pit sand (Miranda do Corvo) was adopted in accordance with EN 13139, characterized through sieve-based particle size analysis.

To ensure the workability of the mixtures, a third-generation polycarboxylate-based (PCE) superplasticizer, Sika® ViscoCrete®-3003, was used. This admixture acts through surface adsorption and steric hindrance, allowing for a high reduction in mixing water and the maintenance of consistency without the introduction of chlorides.

2.2 Characterization of Mortars – Fresh and Hardened State

The molding of the prismatic specimens (40 ± 1) mm × (40 ± 1) mm × (160 ± 1) mm was performed in standardized metallic molds according to the EN 1015-11 standard. Workability was adjusted through the flow table test (EN 1015-3), ensuring consistency suitable for application in wattle and daub. Four distinct formulations were produced, organized into two series:

- **R3 Series (Mineral Matrices):** Mortars with partial replacement of hydraulic lime (NHL 3.5) by glass waste (R3) at levels of 10% and 30% (by mass), without fibre addition.
- **BCJ Series (Hybrid Mortars):** Produced by adding 2.5% (by volume) of BCJ to the matrices of the previous series. In these mixtures, an additional amount of water was included to compensate for the intrinsic absorption of the fibres, as previously determined by the SOP procedure, thus keeping the matrix workability constant.

Due to the slow initial hardening kinetics of natural hydraulic lime, demolding occurred after 48 h, a procedure provided for in the EN 1015-11 standard to ensure the physical integrity of the specimens. The total curing regime lasted 28 days, comprising an initial period of 7 days in hermetically sealed plastic bags (favoring the hydration of hydraulic phases), followed by 21 days in a controlled environment with a temperature of (20 ± 2) °C and relative humidity of (65 ± 5) %, conditions that promote the progressive carbonation of the lime.

The reported results correspond to the average values obtained from three specimens for the mechanical strength tests, four specimens for the water vapor permeability tests, and six specimens for the remaining tests.

The symbology used for specimen identification was as follows: SUS corresponds to the project abbreviation; R3 refers to the sludge glass residue; L indicates that the substitution was applied to the binder; and B indicates the use of *bracejo* fibers.

For example, SUS-R3LB-10% corresponds to a mortar containing sludge glass residue, with a 10% binder substitution and the incorporation of *bracejo* fibers.

3. Preliminary Results and Analysis

3.1 X-Ray Fluorescence (XRF)

The elemental chemical composition of both WGP-R3 and BCJ was determined by XRF, with the main mineral oxides presented in Figure 1. The tests were conducted following the protocols of the Materials and GeoResources Laboratories (I and II) at the University of Aveiro.

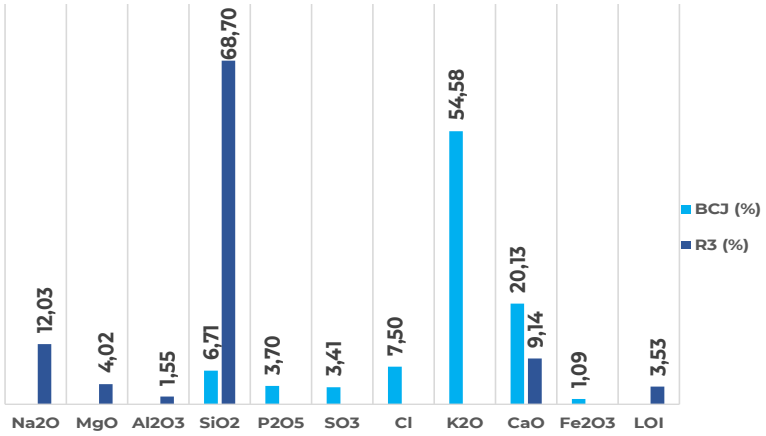


Figure 1 - Chemical Composition of Materials

Regarding R3, the results confirm a predominance of silica (SiO_2 = 68.70%), which may be a key element for the expected pozzolanic reactivity, if it is in the amorphous state. Furthermore, Na_2O (12.03%) and CaO (9.14%), contents were identified, which are characteristic of common soda-lime glasses. The low Loss on Ignition value (LOI = 3.53%) corroborates the effectiveness of the previous thermal treatment in eliminating volatiles, ensuring the integrity of the mineral precursor.

As for the BCJ, chemical analysis reveals that the residual mineral phase is primarily composed of potassium oxide (K_2O = 54.58%) and calcium oxide (CaO = 20.13%). It is essential to emphasize that these values represent the normalized distribution of oxides within the inorganic fraction, which typically constitutes a small percentage (usually <20%) of the total lignocellulosic fiber mass. Since Loss on Ignition (LOI) was not performed for this specific sample to quantify the organic/inorganic ratio, these results should be interpreted as a qualitative indicator of the mineral species present in the fibre's structure.

3.2 Pozzolanic Activity of WGP (R3)

The pozzolanic activity of the WGP-R3 residue was evaluated through the Modified Chapelle test, following the internal procedure LabCIVIL.MAT.PE004 (based on the French standard NF P 18-513).

This method quantifies the initial (rapid) reactivity of the material through its capacity to fix calcium hydroxide [$Ca(OH)_2$].

The obtained value was 814.60 mg of $Ca(OH)_2$ per gram of residue. According to the criteria established by Raverdy et al. (1980) and the guidelines of the NF P 18-513 standard, materials that fix more than 330 mg of $Ca(OH)_2$/g are classified as high reactivity pozzolans. The achieved result, being significantly higher than the normative limit, confirms the high potential of R3 to react with hydraulic lime, contributing to the reinforcement of the matrix through the formation of new cementitious compounds (C-S-H).

3.3 Particle Size Distribution of Aggregate and WGP (R3)

The particle size distribution of the sand (Figure 2) was determined according to the EN 933-1 standard, using the wet sieving method followed by drying and dry sieving. The sand exhibits a continuous and well-graded distribution, falling entirely within the limits specified by EN 13139 for aggregates intended for mortar production.

The particle size characterization of R3 (Figure 3) was obtained by laser diffraction using the Mastersizer 2000 (Malvern) equipment, based on Mie theory. The measurements, performed in triplicate, revealed the following statistical parameters: D_{10} = 2.063 µm, D_{50} = 13.181 µm and D_{90} = 43.283 µm, with a Span of 3.127 e Bulk Density = 716 Kg/m³.

A Span value greater than 2 indicates a broad and diversified particle size distribution. The curve shows an asymmetrical distribution with significant dispersion of particle sizes. The fact that the D_{50} is below 45 µm is a strong indicator of pozzolanic activity potential. This effect is reinforced by the D_{10} value (between 1.9 and 3.7 µm) which confirms a relevant presence of ultra-fine particles, increasing the specific surface area and, consequently, the chemical reactivity of the residue.

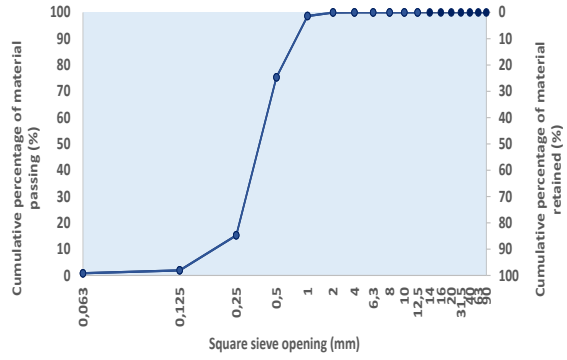


Figure 2 - Sand Particle Size Distribution Curve

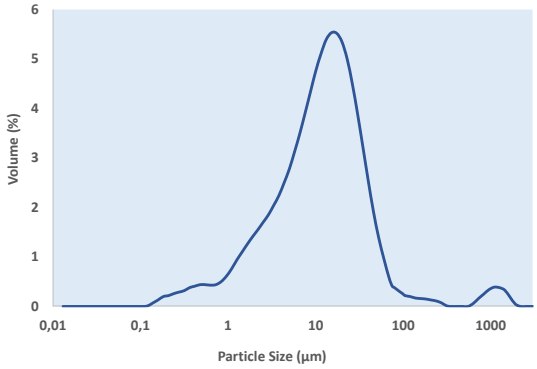


Figure 3 – R3 Laser Diffraction Particle Size Distribution Curve

3.4 Bulk Density

The determination of the bulk density of the materials was carried out in accordance with the EN 1097-3 standard, and the results are presented in Table 1. For contextual purposes, the literature indicates expected ranges between 1,500 and 1,600 kg/m³ for dry sand; between 700 and 800 kg/m³ for natural hydraulic lime (NHL 3.5); and between 740 and 1,250 kg/m³ for ground glass.

Table 1 - Bulk density of materials

MATERIALS	BULK DENSITY $\rho_{b\ (kg/m^3)}$
Fine sand	1509
Hydraulic lime NHL 3.5	700
R3	854

The values obtained highlight significant contrasts between the mixture's constituents. Fine sand exhibits the highest bulk density (1509 kg/m³), which is consistent with its granular nature and particle arrangement. In contrast, the hydraulic lime NHL 3.5 presents the lowest value (700 kg/m³), a characteristic associated with the high fineness of its particles and the larger volume of inter-particle voids in the uncompacted state.

The value observed for WGP-R3 (854 kg/m³) is at an intermediate level, being higher than that of the lime. This difference suggests that the partial replacement of the binder with R3 will promote a change in the overall particle size distribution of the matrix, positively influencing the packing density. Consequently, this variation is expected to impact the water demand for workability, the final porosity, and the mechanical performance of the resulting mortars.

3.5 Flow Spread Consistency

The determination of consistency by flow spread was performed in accordance with the EN 1015-3 standard. The results obtained are systematized in Table 2.

Table 2 - Water-to-binder ratio and Flow spread

Simple	Water-to-binder ratio (w/b) (%)			Flow spread (mm)
	$w_{(R3LP)}/b$	$w_{(BCJ)}/b$	w/b	
SUS-R3LP-10%	52			173
SUS-R3LPB-10%	52	1.25	53.25	157
SUS-R3LP-30%	55			177
SUS-R3LPB-30%	55	1.25	56.25	179

It is observed that all reference formulations (without fibres) presented flow spread values within the target range (175 ± 10 mm). However, the incorporation of BCJ resulted in distinct rheological behaviors depending on the binder matrix.

In the SUS-R3LPB-10% mix, the flow spread was lower than the normative range and the value of its respective reference. In contrast, the SUS-R3LPB-30% mix maintained a consistency practically identical to that of the fibre-free matrix. Since the BCJ underwent rigorous prior conditioning (saturation and drying) and laboratory conditions remained constant, these variations stem from the specific interaction between the fibres and the paste composition.

In the mix with 10% R3, the higher proportion of hydraulic lime (90% of the binder) results in a matrix with a higher specific surface area and inter-particle porosity, which increases the water demand of the matrix. Under these conditions, the introduction of BCJ fibres, even with compensation water, appears to reduce the overall mobility of the system due to the greater entrapment of free water within the lime's porous network.

On the other hand, in the mix with 30% R3, the higher presence of glass powder—a non-absorbent material with a less irregular surface—favors greater availability of free water in the system. This water acts as a lubricant at the fibre-matrix interface, mitigating the internal friction effect caused by the BCJ and maintaining the mortar's fluidity. Thus, it is concluded that the effect of plant fibres on workability is conditioned by the binder matrix's ability to maintain available water for the lubrication of solid inclusions.

3.6 Open Porosity and Apparent Density

The determination of apparent density and open porosity was performed in accordance with the EN 1936 standard. Apparent density is defined as the ratio of the mass of the dry specimen to its apparent volume, while open porosity corresponds to the volumetric percentage of interconnected pores relative to the total volume. The results are presented in Figure 4 and Figure 5, respectively.

The results show that the incorporation of BCJ led to a slight and consistent increase in open porosity across both series (average increment of 3%). Regarding apparent density, a reduction of approximately 2% was observed in the 10% R3 series after the introduction of the fibres, whereas in the 30% R3 series, the values remained practically unchanged.

A combined analysis of these datas with the consistency tests allows for a microstructural interpretation of the system. In the SUS-R3LP-10% series, the introduction of BCJ caused a loss of workability (reduction in flow spread), which hindered compaction and the rearrangement of particles during molding. This phenomenon resulted in less efficient packing, leading to increased porosity and a consequent reduction in density.

In contrast, in the SUS-R3LP-30% series, maintaining fresh-state consistency facilitated molding, allowing the density to remain stable even in the presence of fibres. In these compositions, the increase in porosity (from 20.61% to 21.25%) does not stem from poor compaction, but rather from the intrinsic nature of the plant material and the creation of potentially more porous Interfacial Transition Zones (ITZ) between the fibre and the mineral matrix.

Thus, the results suggest that the impact of BCJ on the microstructure is mediated by the rheology of the binder matrix: matrices with a higher R3 content prove to be more tolerant of fibre incorporation, preserving the density of the hardened material.

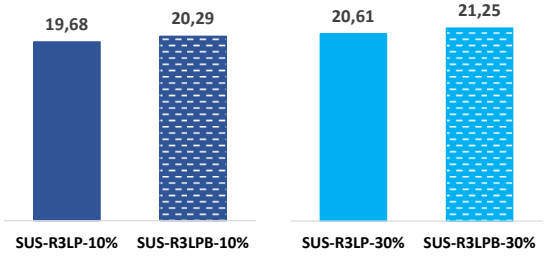


Figure 4 - Open Porosity (%)

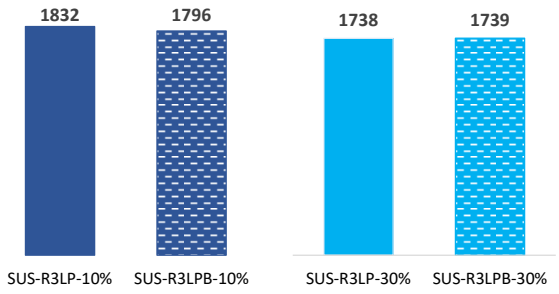


Figure 5 - Apparent Density (Kg/m³)

3.7 Water and Vapor Transport Behavior

The water absorption coefficient by capillarity (A_w) defines the rate of mass absorption per unit area as a function of the square root of time when the material face is in partial contact with water. The tests were performed in compliance with the ISO 15148 standard, and the results are systematized in Figure 6.

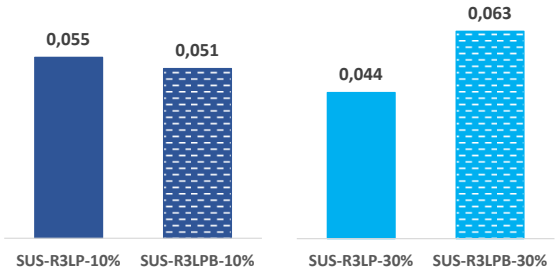


Figure 6 - Water Absorption by Capillarity [kg/(m^2.s$^{0.5}$)]

Data analysis reveals that the incorporation of BCJ influences capillary behavior in contrasting ways depending on the binder matrix. In the 10% R3 series, a slight reduction in the absorption coefficient was observed after the introduction of fibres. In contrast, in the 30% R3 series, the presence of BCJ resulted in a significant increase in this parameter (from 0.044 to 0.063 [kg/(m^2.s$^{0.5}$)]).

It is important to highlight that the reduction in workability observed in the SUS-R3LPB-10% mix is a direct consequence of the adopted methodology, which prioritized maintaining the original matrix's water-to-binder (w/b) ratio by adding only the strict compensation water for the BCJ. It is assumed that if the consistency had been fixed as an invariant parameter (through free adjustment of the mixing water), the microstructural and capillary behavior of this mixture might have resembled that observed in the 30% R3 mix. However, the choice to keep the mix proportions fixed allowed for the identification that the matrix with lower glass content is intrinsically more sensitive to the introduction of plant fibres regarding the maintenance of its internal mobility.

Thus, the results suggest that BCJ alters the connectivity of the porous network differently in each system. In the 10% R3 mix, the lower fluidity of the paste may have induced greater tortuosity or partial blockage of capillary channels by mechanical compression of the particles. Conversely, in the 30% R3 mix, maintaining consistency allowed for a fibre distribution that favored the creation of preferential transport paths. Under these conditions, the fibre-matrix interface and the internal channels of the BCJ appear to act as water conduits, facilitating capillary rise. This effect is particularly relevant for rehabilitation mortars, where moisture transport management is a determining factor for the conservation of wattle and daub substrates.

Water vapor permeability (δ_m) tests were conducted according to the EN 1015-19 and ISO 12572 standards, with results systematized in Figure 7. This property defines the rate of vapor transport through the material per unit of time, area, and pressure gradient, characterizing the "breathability" of the mortar.

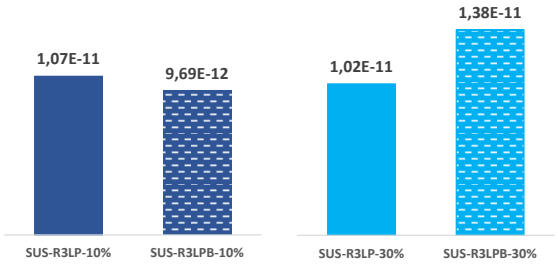


Figure 7 - Water vapor permeability (kg/(m·s·Pa))

The results show distinct behaviors consistent with the capillary absorption observations. In the 10% R3 series, BCJ incorporation resulted in a slight reduction in permeability (from 1.07x10^{-11} to 9.69x10^{-12} kg/(m·s·Pa)). In contrast, the 30% R3 series showed a significant increase in this parameter, reaching 1.38x10^{-11} kg/(m·s·Pa).

.

These data reinforce the previously presented microstructural interpretation: in the mix with lower glass content (10% R3), the porous structure became less connected or more tortuous due to lower matrix workability during molding. Inversely, in the 30% R3 mix, the presence of BCJ and the better fluidity of the paste favored the formation of a more interconnected porous network that is less resistant to diffusion. In this case, the interfaces between the fibres and the mineral matrix seem to function as preferential channels not only for liquid water but also for vapor flow, optimizing the hygrothermal performance of the mortar in wattle and daub systems.

Drying tests were performed following the RILEM II.5 recommendation and the EN 16322 standard to evaluate water evaporation kinetics. The Drying Index (I_s), presented in Figure 8, quantifies the material's

overall resistance to moisture loss, while the Knick Point (Table 3) identifies the transition between the constant drying rate period (surface evaporation) and the falling rate period (internal transport).

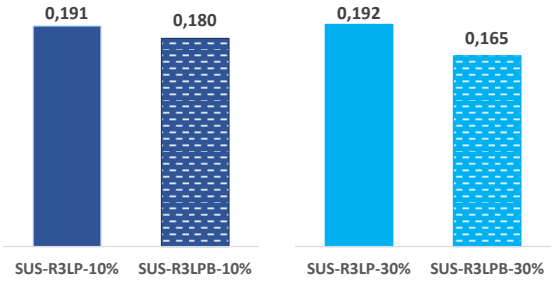


Figure 8 - Drying Index

Table 3 - Knick Point

Sample	Knick Point (H)
SUS-R3LP-10%	13,54
SUS-R3LPB-10%	19,40
SUS-R3LP-30%	9,25
SUS-R3LPB-30%	18,30

Analysis of the results reveals that BCJ incorporation promoted a decrease in I_s in both series, with this reduction being more pronounced in the 30% R3 mix (dropping from 0.192 to 0.165). This behavior indicates greater drying efficiency, which is consistent with the previously observed increase in open porosity and vapor permeability.

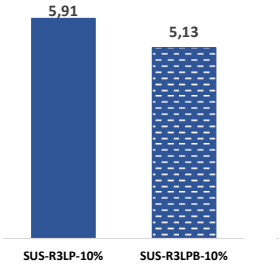
Regarding the Knick Point, a significant prolongation of the initial drying phase was verified in both fibre-containing compositions (nearly doubling the time in the 30% R3 mix). This phenomenon suggests that BCJ acts as an internal reservoir that feeds the evaporation surface for a longer duration, maintaining a high drying rate during the initial period.

Integrally, the results for capillarity (A_w), vapor permeability δ_m), and drying kinetics (Is) demonstrate that BCJ incorporation significantly influences the hygrothermal behavior of the mortars, acting differently depending on the WGP dosage. In the system with lower glass powder incorporation (10% R3), matrix rheology induced the formation of a less connected and more tortuous porous network, restricting water transport in both liquid and vapor phases. In contrast, in the system with higher glass powder content (30% R3), better workability allowed BCJ to promote a more open and interconnected structure. Under these conditions, the fibres and their interfaces function as preferential channels, favoring capillary absorption, vapor diffusion, and drying efficiency simultaneously.

This duality highlights that WGP acts not only as a pozzolanic precursor but as a rheological compatibilization agent, which is essential to ensure that the introduction of plant fibres results in a material with high moisture management capacity—a vital characteristic for the preservation of traditional wattle and daub buildings.

3.8 Compressive and Flexural Strength

The mechanical strengths were determined at 28 days of curing, in accordance with the EN 1015-11 standard, using 40×40×160 mm prismatic specimens and an Instron 5900R5884 universal testing machine. The results for compressive and flexural strength are systematized in Figure 9 and Figure 10, respectively.



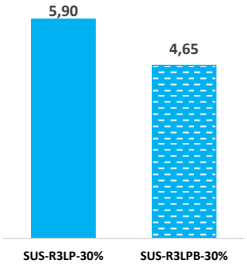
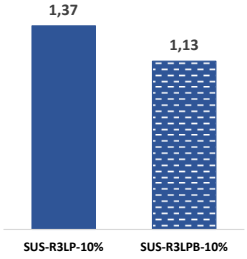


Figure 9 - Compressive Strength (MPa)



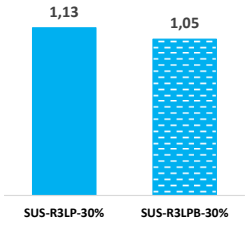


Figure 10 - Flexural Strength (MPa)

In general, the incorporation of BCJ resulted in a reduction in mechanical performance, an expected behavior due to the increase in open porosity previously discussed. Regarding compressive strength, a decrease of 13% was observed for the 10% R3 series and 21% for the 30% R3 series. However, the flexural behavior revealed important nuances: while the 10% R3 mix suffered a 17% drop, the 30% R3 mix presented the lowest relative reduction (only 7%).

This discrepancy between compressive and flexural stress reinforces the integrated analysis of the physical properties. In the 10% R3 mix, the loss of workability hindered compaction, generating macrostructural defects that impaired both stress regimes. Conversely, in the 30% R3 mix, the maintenance of fresh-state fluidity allowed for a more homogeneous distribution of the fibres and a better fibre-matrix interface (bond strength). Although the more open and connected structure (confirmed by capillarity and permeability tests) reduced the compressive load capacity, the fibres were able to act more effectively as "stress-transfer bridges" (crack-bridging) under flexion. This phenomenon mitigates the brittleness of the pozzolanic glass matrix, providing the mortar with a greater deformation capacity before failure—a fundamental characteristic for compatibility with deformable wattle and daub substrates.

4. Conclusion

The present study evaluated the impact of the simultaneous incorporation of waste glass grinding powder (WGP) and *bracejo* (BCJ) in hydraulic lime mortars for the rehabilitation of wattle and daub. The main conclusions are:

- **Matrix-Fibre Synergy:** The performance of the BCJ is strictly dependent on the WGP content. The replacement of 30% of lime with glass powder optimized the rheology, allowing for better fibre incorporation and a more efficient porous structure than in the mixes with only 10% WGP.
- **Hygrothermal Behavior:** The introduction of BCJ into matrices rich in glass powder (30% R3) promoted a more connected porous network, increasing vapor permeability and capillary absorption. Combined with the reduction of the Drying Index (I_s), this system demonstrated a superior moisture management capacity, essential for the preservation of historical substrates.
- **Mechanical Performance and Ductility:** Although fibre incorporation reduced compressive strength, the 30% R3 mix showed high retention of flexural strength (only 7% drop). This suggests a better fibre-matrix interface and a greater capacity for stress redistribution, favoring compatibility with deformable supports.
- **Sustainability and Applicability:** The combination of 30% WGP and 2.5% BCJ proved to be the most balanced solution. WGP acts not only as a pozzolanic precursor but as a rheological compatibilization agent, resulting in a sustainable mortar that prioritizes "breathability" and flexibility over mechanical stiffness.

5. Acknowledgements

This work was developed within the scope of the project "Sustainability of innovative **wattle and daub** mortars" (**COMPETE2030-FEDER-00845500**), co-funded by the European Regional Development Fund (ERDF) through the Support System for the Creation of Scientific and Technological Knowledge, under the Innovation and Digital Transition Program (COMPETE 2030). The authors would like to thank the Foundation for Science and Technology (FCT) for financial support through research grant **2022.13467/BD**, and the **CERIS** research unit (funding **UIDB/04625/2020**). Special recognition is also extended to **ITECONS** and the **Department of Geosciences at the University of Aveiro** for providing laboratory infrastructure, as well as

to the companies **Beiraglass** and **Secil**, and the **Historical Villages of Portugal Tourism Development Association**, for the essential supply of materials and waste for the experiments.

6. Bibliography

Ayat, Amira, Hamoudi Bouzerd, Tahar Ali-Boucetta, Antonia Navarro, and Mohamed Larbi Benmalek, 2022." Valorisation of waste glass powder and brick dust in air-lime mortars for restoration of historical buildings: Case study theatre of Skikda (Northern Algeria)." Construction and Building Materials, Volume 315, 125681. https://doi.org/10.1016/j.conbuildmat.2021.125681

Soares, Kátia, Isabel Torres, and Inês Flores Collen. 2021. "Argamassas e soluções térmicas de isolamento [Mortars and thermal insulation solutions]." Construção Magazine, no. 106 (Novembre/Dezember): 8–13.

Ruffolo, Silvestro Antonio Maria Antonietta Zicarelli, Regina Adomako, , Nicola Schiavon, Francesca Giordano, Andrea Macchia, Mauro Francesco La Russa, 2025. "The use of powdered olive stone in lime-based mortars for the conservation of cultural heritage: A performance evaluation." Construction and Building Materials, Volume 499, 144137. https://doi.org/10.1016/j.conbuildmat.2025.144137

Rubio-Aguinaga, A., L. Kyriakou, J. M. Fernández, I. Navarro-Blasco, S. Pavia, and J. I. Álvarez. 2025. "Sustainability of PCM-Lime Mortars for Heritage Retrofitting: Carbon Footprint and Impact on Energy Demand across Climates." Case Studies in Construction Materials 23: e05294. https://doi.org/10.1016/j.cscm.2025.e05294

Aliabdo, Ali A., Abd Elmoaty M. Abd Elmoaty, and Ahmed Y. Aboshama, 2016." Utilization of waste glass powder in the production of cement and concrete." Construction and Building Materials, Volume 124, 866-877. https://doi.org/10.1016/j.conbuildmat.2016.08.016

Tironi, A., M. A. Trezza, A. N. Scian, and E. F. Irassar. 2012. "Kaolinitic Calcined Clays: Factors Affecting Their Performance as Pozzolans." Construction and Building Materials, 28, 276–281. https://doi.org/10.1016/j.conbuildmat.2011.08.06

Donatello, S., M. Tyer, and C. R. Cheeseman. 2010. "Comparison of Test Methods to Assess Pozzolanic Activity." *Cement and Concrete Composites* 32 (2): 121–127. https://doi.org/10.1016/J.CEMCONCOMP.2009.10.008.

Velosa, A. L., F. Rocha, e M. R. Veiga. 2009. "Influence of Chemical and Mineralogical Composition of Metakaolin on Mortar Characteristics." *Acta Geodynamica et Geomaterialia* 6 (1): 121–126

Shi, Caijun and Kejin Zheng. 2007. "A Review on the Use of Waste Glasses in the Production of Cement and Concrete." *Resources, Conservation and Recycling* 52 (2): 234–247. https://doi.org/10.1016/j.resconrec.2007.01.013

Santos, Emerson Anchieta, Giovanna Victória do Nascimento Araújo, Guilherme Menezes Fonseca, Vanessa Gentil de Oliveira Almeida, Herbert Alves de Oliveira, Luciano de Melo, and Fernanda Martins Cavalcante de Melo. 2024. "Influência da incorporação de resíduo de lapidação de vidro nas propriedades da argamassa de cimento Portland." Revista Matéria 29 (2). https://doi.org/10.1590/1517-7076-RMAT-2023-0330

Arizzi, Andrea and Daniela Cultrone. 2012. "Air Lime-Based Mortars Blended with a Pozzolanic Additive and Different Admixtures: A Mineralogical, Textural and Physical-Mechanical Study." *Construction and Building Materials* 31: 135–143. https://doi.org/10.1016/j.conbuildmat.2011.12.069

Soares, Kátia, Isabel Torres, Inês Flores-Colen, and Dora Silveira. 2025. "The Influence of Traditional Substrates on the Behaviour of Lime Mortars." *International Journal of Architectural Heritage* 19 (3): 346–69. doi:10.1080/15583058.2023.2286503

Poyet, Stéphane. 2021. "Water Transport Properties of Virtual Fractal Porous Media: Implications for the Unsaturated Transport Properties of Cement-Based Materials." Cement and Concrete Research 150: 106613. https://doi.org/10.1016/j.cemconres.2021.106613

RATO, Vasco Nunes da Ponte Moreira, 2006. “Influência da microestrutura morfológica no comportamento de argamassas”. Ficheiro do Repositório da Universidade Nova de Lisboa Faculdade de Ciências e Tecnologia: VNPMR, 2006

Zicarelli, Maria Antonietta, Regina Adomako, Silvestro Antonio Ruffolo, Nicola Schiavon, Francesca Giordano, Andrea Macchia, and Mauro Francesco La Russa. 2025. “The Use of Powdered Olive Stone in Lime-Based Mortars for the Conservation of Cultural Heritage: A Performance Evaluation.” Construction and Building Materials 499: 144137. https://doi.org/10.1016/j.conbuildmat.2025.144137

Siouta, Louiza, Maria Apostolopoulou, and Asterios Bakolas. 2024. "Natural Fibers in Composite Materials for Sustainable Building: A State-of-the-Art Review on Treated Hemp Fibers and Hurds in Mortars" *Sustainability* 16, no. 23: 10368. https://doi.org/10.3390/su162310368

Raverdy, M., E. Prudhomme, J. M. Montel, and J. Devaux. 1980. “Study of Pozzolanic Activity of Industrial and Natural Pozzolans by Means of the Modified Chapelle Test.” In *Proceedings of the 7th International Congress on the Chemistry of Cement*, vol. 3, III-35–III-41. Paris

CEN (European Committee for Standardization). 1999. *EN 1015-3: Methods of Test for Mortar for Masonry - Part 3: Determination of Consistence of Fresh Mortar (by Flow Table)*. Brussels: CEN.

CEN (European Committee for Standardization)**.** 2000. *EN 933-1: Tests for Geometrical Properties of Aggregates - Part 1: Determination of Particle Size Distribution - Sieving Method*. Brussels: CEN.

CEN (European Committee for Standardization). 2008. *EN 1015-19: Methods of Test for Mortar for Masonry - Part 19: Determination of Water Vapour Permeability of Hardened Rendering and Plastering Mortars*. Brussels: CEN.

CEN (European Committee for Standardization)**.** 2008. *EN 1936: Natural Stone Test Methods - Determination of Real Density and Apparent Density, and of Total and Open Porosity*. Brussels: CEN.

CEN (European Committee for Standardization). 2013. *EN 13139: Aggregates for Mortar*. Brussels: CEN.

CEN (European Committee for Standardization). 2013. *EN 16322: Conservation of Cultural Heritage - Test Methods - Determination of Drying Properties*. Brussels: CEN.

CEN (European Committee for Standardization). 2014. *EN 932-5: Tests for General Properties of Aggregates - Part 5: Common Equipment and Calibration*. Brussels: CEN.

CEN (European Committee for Standardization). 2019. *EN 1015-11: Methods of Test for Mortar for Masonry - Part 11: Determination of Flexural and Compressive Strength of Hardened Mortar*. Brussels: CEN.

ISO (International Organization for Standardization). 2002. *ISO 15148: Hygrothermal Performance of Building Materials and Products - Determination of Water Absorption Coefficient by Partial Immersion*. Geneva: ISO.

ISO (International Organization for Standardization). 2016. *ISO 12572: Hygrothermal Performance of Building Materials and Products - Determination of Water Vapour Transmission Properties - Cup Method*. Geneva: ISO.

LabCIVIL (Universidade de Aveiro). 2025. *Procedimento LabCIVIL.MAT.PE004: Ensaio de Chapelle Modificado*. Aveiro: UA.

RILEM. 1980. *Recommended Test No. II.5: Evaporation Capacity of Water*. Paris: RILEM.

CINPAR 2026
XXII International Conference on Building Pathology and Constructions Repair
15th to 17th July 2026 - Lisboa, Portugal

O Sítio Histórico de Sobral, Brasil: A importância do tombamento pelo IPHAN na requalificação de edificações e espaços urbanos

The Historic Site of Sobral, Brazil: The importance of its listing by IPHAN in the requalification of buildings and urban spaces.

Eder Paulus Moraes GUERRA[1] Marlene Elias LEITE[2]

[1] **Prof. Msc, Universidade Estadual Vale do Acaraú, Sobral, Brasil, eder_paulus@uvanet.br**

[2] Profa, Msc, Secretaria Municipal de Educação, Sobral, Brasil, marleneea28@gmail.com

Resumo: A requalificação de edificações representa um instrumento balizador desenvolvido pelos gestores urbanos no processo de tombamento do patrimônio histórico. A cidade de Sobral mantém preservado um sítio histórico composto de 2.500 edificações tombadas, a maioria contida numa área de aproximadamente 1,484 km². Dentre as diversas edificações situadas na área tombada estão marcos como o Paço Municipal, a Catedral da Sé e, com destaque analítico neste estudo, o Teatro São João. Construído entre 1875 e 1880 e tombado pelo Estado do Ceará (decreto nº 16237-1983) e posteriormente pelo Instituto do Patrimônio Artístico e Histórico Nacional (IPHAN), o teatro é referência por sua riqueza arquitetônica e erudição artística. Os objetivos deste trabalho foram apresentar aspectos referentes ao tombamento e à requalificação urbana em Sobral, as intervenções feitas no Teatro São João e o estado de conservação atual deste. A metodologia baseou-se em pesquisas bibliográficas e documentais, além de registros fotográficos e uso de fissurômetro. O processo de tombamento em Sobral considerou não apenas o valor arquitetônico, mas a dinâmica morfológica atual, refletida em projetos de mobilidade no entorno protegido. A edificação teatral foi submetida a quatro intervenções (1875-1885, 1940, 1973 e 2003), de modo que atualmente seu pavimento subterrâneo apresenta estado de conservação que compromete a segurança estrutural, contrastando com a beleza preservada de sua fachada e interiores.

Palavras-Chave: Patrimônio Histórico; Requalificação Urbana; Sobral; Teatro São João; Tombamento.

Abstract: The requalification of buildings represents a guiding instrument developed by urban managers in the process of listing historical heritage. The city of Sobral maintains a preserved historical site composed of 2,500 listed buildings, most of which are contained within a polygon of 5.33 km in an area of approximately 1.484 km², extending from the banks of the Acaraú River to Cel. Monte Alverne Street. This architectural and urban complex was listed as a national heritage site in 1999 by the National Institute of Historic and Artistic Heritage – IPHAN, leading the public authorities to carry out large planned investments in the requalification of its buildings, some of which date back to the 18th century, such as the São João Theater (neoclassical), a group of houses in the Art Nouveau style, townhouses decorated with Greco-Roman motifs, several religious buildings, such as the Sé Church (Sertanejo Baroque) and Nossa Senhora do Rosário Church (built by slaves), the Captain-Major's House (colonial) and the post office (Art Deco). The development of action plans for the restoration of these buildings was carried out through architectural surveys, damage mapping, and proposed interventions. Numerous difficulties were encountered, such as a lack of knowledge about the materials used at the time of construction and the construction techniques employed, with the maintenance of facades and total destruction of interiors being common. The objectives of this work were to present aspects related to the listing of historical heritage in the city of Sobral, the renovations carried out on its buildings,

and their current state of conservation. The methodology used was based on bibliographic research, laws, the study of heritage preservation, books, and documents, as well as photographic records. The listing process in Sobral took into account the artistic and architectural value of the buildings.

Keywords: Historical Heritage, Urban Redevelopment, Listing as a Heritage Site, Sobral, São João Theatre.

1. Introdução

A preservação do patrimônio cultural no Brasil transita, historicamente, entre o ideal de salvaguarda da memória e os desafios operacionais impostos pela dinâmica urbana contemporânea. o ato de tombar uma edificação ou um conjunto arquitetônico não se encerra na homologação de decretos; trata-se, na verdade, do início de um processo contínuo — e frequentemente conflituoso — de gestão, manutenção e requalificação. à medida que as políticas patrimoniais superam a visão estritamente monumentalista em favor de uma compreensão integrada da cidade como organismo vivo (Fonseca 2017), o sítio histórico da cidade de Sobral, no estado do Ceará, desponta como um laboratório a céu aberto para a análise das políticas de preservação no país. nele, evidenciam-se as tensões cotidianas entre a modernização das infraestruturas viárias e a perpetuação da identidade cultural.

A cidade mantém preservado um polígono histórico rigorosamente delimitado que abriga cerca de 2.500 edificações tombadas, concentradas em uma área de aproximadamente 1,484 km². essa expressiva densidade patrimonial não é fruto do acaso, mas o reflexo direto da opulência econômica vivida pela região no século XIX. impulsionada pelo ciclo do algodão e da carne de charque, uma elite sertaneja emergente financiou a construção de praças, templos e equipamentos culturais (Ponte 2014). diferentemente de núcleos coloniais formados de maneira puramente orgânica, o traçado e as construções sobralenses foram fortemente moldados por uma sociedade que buscava espelhar os ideais civilizatórios europeus no semiárido nordestino. o resultado é um conjunto arquitetônico coeso, que transita com fluidez entre o neoclassicismo e o ecletismo, marcando o espaço público com uma estética burguesa singular. Nesse cenário consolidado, edificações de caráter religioso e administrativo ancoram a leitura visual e a dinâmica funcional do território. O Teatro São João, construído entre 1875 e 1880, consolida-se como um dos maiores símbolos da influência europeia no interior nordestino. Mais do que um mero edifício de espetáculos, o teatro representava o ápice do refinamento de uma época ansiosa por modernidade e, atualmente, atua como um dos principais pontos focais das políticas de fomento e restauro na região.

Contudo, a proteção legal e a refuncionalização de bens dessa magnitude suscitam debates complexos no campo da arquitetura e do urbanismo. Autores de referência na teoria do restauro, como Kühl (2018), alertam que a requalificação urbana, quando excessivamente focada na valorização cenográfica das fachadas e na estética dos espaços de fruição, corre o risco de negligenciar degradações invisíveis, criando uma falsa sensação de preservação. É precisamente essa dicotomia — o descompasso entre a requalificação de superfície e a integridade construtiva — que instiga a presente investigação.

Diante desse contexto, o presente artigo tem como objetivo analisar o impacto do tombamento realizado pelo Instituto do Patrimônio Histórico e Artístico Nacional (IPHAN) na requalificação dos espaços urbanos de Sobral (Figura 1), articulando as recentes ações de urbanismo na malha histórica com um estudo de caso focado no Teatro São João (Figura 2). Ao evidenciar o contraste entre a beleza conservada das áreas de

convivência e a vulnerabilidade latente nas fundações da edificação teatral, este trabalho propõe uma reflexão crítica sobre os limites dos projetos contemporâneos de revitalização e a urgência da adoção de planos de manutenção preventiva contínua no patrimônio edificado brasileiro.

Figura 1: Espaço urbano



Fonte: Arquivo do autor

Figura 2: Teatro São João



Fonte: Arquivo do autor

1.1 O Tombamento como Instrumento de Requalificação Urbana

O debate sobre a proteção de sítios históricos ganhou novos e complexos contornos nas últimas décadas, refletindo um amadurecimento nas doutrinas de preservação no Brasil. Se no início do século XX a tônica das políticas patrimoniais recaía quase exclusivamente sobre a monumentalidade isolada — priorizando as grandes obras de "pedra e cal" do período colonial —, hoje a compreensão abrange a dinâmica funcional e morfológica dos espaços sociais como um todo (Chuva 2012). Essa mudança de paradigma reconhece que a cidade não é um mero suporte físico para construções antigas, mas um organismo vivo cujas relações sociais, trânsito e economia local são intrínsecos à memória do lugar. Assim, a proteção patrimonial contemporânea exige metodologias que articulem a preservação do passado com as demandas habitacionais e viárias do presente. Essa transição teórica é fundamental para mitigar os riscos inerentes aos processos de tombamento descontextualizados. Como adverte Choay (2001), a fetichização do monumento pode esvaziá-lo de sua função social autêntica, transformando-o em um corpo estranho na malha da cidade. Quando um edifício histórico é tratado apenas como um artefato intocável de contemplação, ele tende a sofrer um processo de museificação que afasta a população local, gerando áreas urbanas cenográficas, porém esvaziadas de vitalidade cotidiana.

Em Sobral, o processo de tombamento municipal, estadual e federal adotou, de maneira convergente, uma perspectiva de conjunto arquitetônico e urbanístico. Castriota (2019) argumenta que a requalificação urbana em centros históricos deve atuar primordialmente como um mediador entre o ímpeto do desenvolvimento contemporâneo e a salvaguarda inegociável da memória coletiva. Em vez de congelar o centro da cidade, a gestão sobralense buscou delimitar um polígono de proteção rígida que permitisse a leitura clara de sua evolução histórica, ao mesmo tempo em que incentivava intervenções capazes de modernizar a infraestrutura de suporte aos cidadãos e ao comércio local.

A justificativa para essa tutela em larga escala encontra respaldo na singularidade da formação urbana do município. O traçado e a volumetria das edificações sobralenses materializam o apogeu econômico vivenciado no século XIX, impulsionado pelas rotas comerciais do algodão e pela indústria do charque (Ponte 2014). Esse capital excedente foi traduzido na construção de casarões de porão alto, igrejas majestosas e equipamentos culturais de grande porte, conformando uma paisagem onde o ecletismo e o neoclassicismo predominam. Preservar a dinâmica morfológica desse traçado significa, portanto, manter legível a história de uma elite sertaneja que buscou mimetizar os hábitos europeus no interior do semiárido nordestino. A materialização prático-espacial dessa premissa de integração é visível nos projetos recentes de intervenção viária, com destaque para as ações que integram o projeto conhecido como "Sobral Novo Centro". Essa

iniciativa buscou resolver o crônico conflito entre a matriz urbana do século XIX e o volume de tráfego motorizado do século XXI. A requalificação das vias adjacentes aos monumentos históricos incluiu a substituição criteriosa da pavimentação asfáltica tradicional por blocos intertravados (Figura 3). Além de reduzir a velocidade dos veículos (traffic calming), esse tipo de piso favorece a drenagem das águas pluviais, mitigando alagamentos que frequentemente ameaçam as alvenarias de fundação dos casarões seculares ao longo da malha tombada e contribui para a melhoria do conforto térmico.

Figura 3: blocos intertravados



Fonte: Arquivo do autor

Outro acerto urbanístico dessa requalificação foi o ambicioso projeto de internalização da fiação elétrica e de telecomunicações no polígono central. Historicamente, o emaranhado de cabos aéreos atua como uma poluição visual severa, fragmentando a leitura estética das fachadas e desvalorizando os detalhes ornamentais das platibandas e beirais. Com o enterramento de uma grande parte das redes, recuperou-se o cone visual de marcos estruturantes da cidade. O pedestre contemporâneo passou a vivenciar a escala real da Praça de Cuba e a apreciar a verticalidade das torres da Catedral da Sé, promovendo uma reapropriação afetiva e estética do espaço público por parte da população (Fonseca 2017).

Contudo, a gestão de um conjunto com tamanha densidade impõe severos e constantes desafios de conservação preventiva. É fundamental que a academia e os órgãos de fiscalização mantenham um olhar crítico sobre as obras de revitalização. O verniz do planejamento urbano de superfície — traduzido no embelezamento de praças, na nova iluminação cênica e nas vias repavimentadas — é indubitavelmente crucial para a apropriação do espaço pela população. No entanto, essa maquiagem urbana muitas vezes oculta fragilidades estruturais agudas nas infraestruturas seculares.

A introdução de novas infraestruturas em centros históricos, ainda que benéfica do ponto de vista urbanístico, exige intervenções no subsolo que frequentemente alteram o microclima do terreno. Valas para fiação subterrânea ou novas redes de drenagem podem modificar a acomodação do lençol freático, refletindo diretamente nas fundações de pedra ou tijolo maciço das edificações antigas. Ribeiro e Oliveira (2021) destacam que a incompatibilidade de materiais em restauros e intervenções viárias — como o uso excessivo de concreto armado e cimento Portland ao redor de alvenarias tradicionais que precisam "respirar" — é uma das maiores causas de patologias silenciosas, resultando em umidade ascendente e fissuras estruturais crônicas.

Portanto, conclui-se que o impacto do tombamento e das subsequentes requalificações em Sobral é amplamente positivo no que tange à preservação da morfologia e ao uso social do espaço. Entretanto, para que essa salvaguarda seja sustentável a longo prazo, o planejamento urbano deve transcender a camada visual da paisagem. Requer-se a implementação de análises prediais mais criteriosas e contínuas, garantindo que o sucesso estético e funcional de edificações de ponta, como a Casa da Cultura (Figura 4) e

o Musel Dom José Tupinambá da Frota (Figura 5), sejam acompanhados por um rigoroso controle de saúde estrutural, evitando que os monumentos colapsem por trás de suas fachadas recém-restauradas.

Figura 4: Casa da Cultura



Fonte: Arquivo do autor

Figura 5: Museu Dom José



Fonte: Arquivo do autor

1.2 O Caso do Teatro São João: Erudição, Intervenções e Patologias

Referência máxima de requinte no tecido urbano sobralense, o Teatro São João evidencia o grau de erudição artística e o poderio econômico alcançados no final do século XIX. A construção do edifício, erguido entre 1875 e 1880, não foi uma obra isolada ou um capricho estético aleatório, mas a materialização de um projeto de classe. Conforme aponta Ponte (2014), a emergente elite local, enriquecida pelos ciclos do algodão e da carne de charque, necessitava de equipamentos urbanos que legitimassem seu status e aproximassem a urbe sertaneja dos padrões civilizatórios europeus. Assim, o teatro nasce como um marco de distinção social, encravado no centro de uma cidade que passava por intensas transformações urbanísticas e econômicas.
Do ponto de vista morfológico e arquitetônico, a fachada principal do Teatro São João funciona como um imponente cartão de visitas neoclássico com flertes no ecletismo. A frente do edifício é ritmada por uma sucessão de arcos de volta inteira no pavimento térreo. Esses vãos não apenas facilitavam a ventilação cruzada, essencial para o conforto térmico no semiárido, mas também conferiam leveza a uma estrutura de alvenaria autoportante robusta. Coroando essa composição, a fachada culmina em um frontão curvo majestoso que abriga um óculo central vazio, um detalhe tipicamente europeu que anunciava aos transeuntes o luxo e a grandiosidade das dependências internas.

Ao ultrapassar o saguão de entrada, o visitante é imediatamente inserido na clássica configuração de palco à italiana e plateia em formato de ferradura. Essa tipologia espacial, amplamente difundida na Europa dos séculos XVIII e XIX, foi perfeitamente adaptada à realidade cearense. A disposição em "U" das varandas curvas, sustentadas por delgadas colunas de ferro fundido, foi projetada não apenas para otimizar a acústica do recinto, mas para atender à dinâmica social do "ver e ser visto" (Ponte 2014). A burguesia local ocupava os camarotes superiores, exibindo suas vestimentas e joias, enquanto o espetáculo ocorria simultaneamente no palco e na própria platéia.

É na materialidade de seus interiores que o edifício consolida sua aura de Belle Époque sertaneja. A mobília original, composta por elegantes assentos com encosto e assento em palhinha indiana, demonstra uma notável inteligência projetual. Diferente dos pesados estofados de veludo usados na Europa, a palhinha permitia a transpiração dos espectadores frente às altas temperaturas de Sobral. Em contrapartida, o palco permaneceu emoldurado por densas e tradicionais cortinas vermelhas, mantendo o peso cenográfico e a

ambiência dramática exigida pelas óperas e operetas da época. Esse hibridismo material atesta a sofisticação de um projeto que soube fundir o cânone internacional com as exigências climáticas locais.

No entanto, a compreensão contemporânea de uma edificação tão singular exige ir além da contemplação de sua beleza pretérita. Choay (2001) adverte que a fetichização do monumento — ou seja, o apego excessivo apenas à sua imagem gloriosa do passado — pode transformá-lo em uma alegoria vazia, descolada da realidade estrutural presente. O Teatro São João, sob a chancela do tombamento, transcendeu sua função original de mero local de entretenimento aristocrático para se converter em um bem cultural de apropriação coletiva. Contudo, manter essa monumentalidade viva e operante no século XXI impõe desafios técnicos que a simples fruição visual muitas vezes ignora.

A erudição estética que admiramos hoje não chegou até nós de forma inalterada; ela é o resultado direto de sucessivas campanhas de restauro e modernização. Castriota (2019) argumenta que o patrimônio histórico não é uma entidade cristalizada no tempo, mas um instrumento dinâmico que sofre contínuas reelaborações. No caso específico do teatro de Sobral, a edificação foi submetida a grandes intervenções, notadamente nas décadas de 1940, 1970 e no início dos anos 2000. Tais ações buscaram adequar o edifício às novas normas de segurança, acessibilidade e climatização, garantindo que o teatro não fosse reduzido a um museu inerte, mas permanecesse como um equipamento cultural ativo e vibrante.

Além desses dados históricos, houve outras modificações que foram feitas com a finalidade de deixar o Teatro São João como era originalmente. Dessa forma, ressalta-se:

> O desenho original da curva da alvenaria que delimita o bordo do procênio, foi encontrado sob o aterro existente e reconstruido em seu desenho original mais elegante e equilibrado.
> A boca de cena visivelmente alterada em sua largura e fechamento superior com elementos construtivos retilíneos de concreto armado, foi recomposta com o fechamento em arco abatido de desenho original, conforme registro fotográfico.
> Foram removidos elementos de concreto – escadas e plataformas – na área do palco, elementos esses aposto em data recente e inadequados às necessidades técnicas e ao sistema de movimentação da mecânica cênica.
> As aberturas de vãos de acesso ao palco e nichos encontrados sob emparedamento, foram reabertos ou deixados à mostra como registro.
> As escadas de acesso até então existentes interligando a plateia aos dois balcões e visivelmente estranhas aos níveis e às aberturas dos vãos das portadas laterais, foram removidas e substituidas por escadas novas metálicas de desenvolvimento helicoidal, reasgatando a solução de acesso anteriormente existente. (Rodrigues, 2005)

As Figuras 6 e 7 mostram antes e depois da substituição dos dois níveis de camarotes pela solução concebida no desenho original, ou seja, apenas um nível.

Figura 6: Linhas de camarotes antes da prospecção de 2003 **Figura 7**: Depois da prospecção de 2003



Fonte: Arquivo Ricardo Rodrigues



Fonte: Arquivo do autor

Apesar da inegável importância dessas intervenções para a sobrevida funcional do teatro, a história das políticas de preservação revela um descompasso estrutural severo. Historicamente, os órgãos de tutela patrimonial voltaram suas energias muito mais para a homologação legal (a chancela do bem) e para a recuperação das fachadas do que para a manutenção estrutural profunda (Chuva 2012). Fonseca (2017) corrobora essa visão ao apontar que a preservação federal no Brasil muitas vezes tratou o edifício como uma "casca esteticamente perfeita", negligenciando o monitoramento contínuo das infraestruturas invisíveis, como os telhados ocultos, os porões e as fundações.

É exatamente nessa lacuna de gestão preventiva que emergem as patologias críticas do Teatro São João. Avaliações recentes demonstraram que, em total oposição ao deslumbramento proporcionado pelo salão de espetáculos, o pavimento subterrâneo da edificação clama por socorro. Esse espaço inferior, originalmente concebido para a movimentação de maquinários cênicos e ventilação do assoalho, apresenta hoje um quadro crônico de degradação. Fissuras de origem diferencial mapeiam as alvenarias de embasamento, evidenciando o sofrimento da estrutura original perante acomodações do solo e flutuações do lençol freático.

Esse cenário de risco é potencializado por equívocos técnicos cometidos nas próprias campanhas de intervenção do passado. Ribeiro e Oliveira (2021) destacam que as obras de consolidação estrutural realizadas nas décadas de 1970 e 1980 no Brasil padecem, frequentemente, da incompatibilidade mecânica e química de materiais. No afã de "salvar" as ruínas, utilizou-se massivamente o concreto armado e o cimento Portland (de alta rigidez e baixíssima porosidade) diretamente sobre alvenarias históricas de tijolo maciço e argamassas de cal. O resultado desse choque tecnológico é a retenção implacável da umidade no interior das grossas paredes antigas, que perdem sua capacidade de transpirar.

No Teatro São João, essas cicatrizes de intervenções passadas cobram um alto preço na base da edificação. A umidade ascendente, sem poder evaporar pelas paredes agora impermeabilizadas por argamassas incompatíveis, migra verticalmente, carreando sais e promovendo a desagregação lenta e silenciosa dos aglomerantes históricos. Esse processo não é apenas uma "falha estética" restrita a um porão oculto, mas um vetor de risco contínuo que ameaça diretamente a estabilidade global do palco e das pesadas arquibancadas em ferradura que se apoiam sobre essa superestrutura. Portanto, o estudo das patologias do Teatro São João desnuda um alerta crucial para o futuro da salvaguarda arquitetônica. A beleza arrebatadora de suas cortinas vermelhas e a nostalgia de sua plateia em palhinha criam uma ilusão de integridade definitiva. Contudo, a verdadeira preservação de um ícone da Belle Époque sertaneja não pode se sustentar apenas na manutenção de sua vitrine visual. É urgente que os paradigmas contemporâneos de gestão do patrimônio incorporem a conservação curativa e a engenharia diagnóstica como eixos inseparáveis do restauro, garantindo que o requinte do passado repouse sobre fundações seguras no presente.

De fato, a sala de espetáculos e a fachada principal apresentam um excelente estado estético, fruto direto dos esforços das últimas intervenções governamentais. A pintura impecável do frontão, a restauração minuciosa das poltronas e varandas de ferradura, aliadas à requalificação do entorno com a bela pavimentação externa de blocos intertravados, transmitem uma imediata sensação de dever cumprido por parte das polí-

ticas públicas. Castriota (2019) reconhece que essas ações de embelezamento e integração urbana são instrumentos válidos para mediar a relação entre a sociedade e a memória, promovendo a apropriação do bem. Todavia, essa mesma maquiagem cenográfica acaba por gerar uma perigosa anestesia em relação à manutenção profunda, criando uma narrativa de preservação que se encerra na camada mais superficial do edifício histórico. O esforço municipal, embora louvável do ponto de vista do planejamento viário e da mobilidade no centro expandido, frequentemente desconsidera as repercussões hidrogeológicas de suas trincheiras e novas pavimentações no microclima do subsolo histórico. Trata-se do clássico paradoxo da gestão urbana patrimonial: investimentos volumosos na urbanização do entorno enquanto o núcleo estrutural do próprio monumento padece de uma negligência orçamentária para a conservação curativa preventiva de suas infraestruturas ocultas.

Nesse diapasão, a realidade diagnosticada no Teatro São João serve como um contundente estudo de caso para desmistificar a eficácia isolada dos instrumentos legais de proteção. O tombamento pelo IPHAN ou pelas instâncias estaduais não imuniza a edificação contra a degradação silenciosa provocada pelas acomodações do solo e pela umidade estrutural persistente. Como argumentam Chuva (2012) e Fonseca (2017), a chancela de patrimônio é um marco declaratório vital que reconhece o valor cultural, mas que carece de eficácia prática se não for sucedida de políticas perenes de financiamento para manutenção diária.

Conclui-se, portanto, que a sobrevivência do Teatro São João e da integridade física do próprio sítio histórico de Sobral depende de uma reestruturação imediata nos paradigmas de intervenção urbana. É imperativo transitar de um modelo de revitalização focado no impacto da imagem turística para uma gestão técnica que valorize a engenharia diagnóstica e a manutenção contínua das áreas invisíveis aos olhos do público. O esplendor dos lustres da sala de espetáculos e a vivacidade neoclássica das fachadas só terão significado duradouro se a base subterrânea que as sustenta for tratada com o mesmo rigor científico, garantindo que o edifício resista ao tempo de forma verdadeiramente integral.

2. Metodologia

De acordo com Chaves (2015), os métodos para avaliação e análise de edifícios revelam-se importantes ferramentas utilizadas para tomada de decisão, onde seu estudo e compreensão constitui o primeiro passo para o desenvolvimento de metodologias adequadas às exigências atuais. A partir de uma abordagem qualitativa, fundamentada em levantamentos bibliográficos, análise documental e inspeção física in loco com o uso sistemático de registros fotográficos e fissurômetro, busca-se discutir como as intervenções de requalificação estética e urbana dialogam com a necessidade de conservação estrutural profunda. Foram analisados inventários de bens e registros históricos realizados nas diferentes épocas das intervenções construtivas do Teatro São João, localizado na cidade de Sobral-Ce.

A avaliação contemporânea da integridade de bens patrimoniais exige o distanciamento da mera contemplação estética, adentrando o rigor do diagnóstico técnico. Nesse escopo, os registros realizados por meio de inspeção visual sistemática, utilizando câmera fotográfica de alta resolução, e a medição das patologias ativas com o auxílio de fissurômetro de precisão revelaram dados alarmantes e profundamente contrastantes no Teatro São João. A metodologia de prospecção adotada buscou ultrapassar a superfície visível que frequentemente engana o observador leigo ou o turista circunstancial. Como alerta Choay (2001), a alegoria construída em torno do monumento tende a ocultar sua materialidade vulnerável, fetichizando a sua imagem pública em detrimento de sua substância física. A investigação demonstrou que, enquanto as áreas de grande circulação ostentam um apuro visual irretocável, o miolo construtivo da edificação padece de um processo de arruinamento contínuo.

3. Resultados e Discussões

Os dados apresentados evidenciam um paradoxo profundo no modelo brasileiro de gestão patrimonial, perfeitamente ilustrado na dinâmica do Sítio Histórico de Sobral. Ao proteger legalmente cerca de 2.500 edificações e promover ações de infraestrutura como o projeto "Sobral Novo Centro", a gestão urbana demonstra notável maturidade na valorização macroespacial do patrimônio. Como argumenta Fonseca (2017), a trajetória das políticas de preservação no Brasil superou a visão de isolamento do bem, passando a compreender o território como uma paisagem cultural viva. Em Sobral, essa evolução é inegável: a liberação visual das fachadas da Casa da Cultura e do Musel Dom José Tupinambá da Frota, agora livres do emaranhado de fios elétricos e valorizadas por pavimentações adequadas, comprova um esforço ímpar de reintegração da memória à paisagem e ao usufruto cotidiano.

Esse sucesso macroespacial reflete o amadurecimento das próprias diretrizes institucionais de proteção no país. Chuva (2012) relembra que as políticas de tombamento do IPHAN, em sua gênese, carregavam um viés fortemente monumentalista, focado na chancela de bens coloniais isolados. Hoje, o entendimento abrange a complexidade da malha urbana. Castriota (2019) corrobora essa perspectiva ao afirmar que a requalificação urbana contemporânea deve atuar como um mediador ativo entre o desenvolvimento da cidade e a salvaguarda da memória. Ao adaptar o entorno para pedestres e modernizar as vias sem descaracterizar a morfologia do século XIX — período de opulência econômica fundamentada no algodão e no charque Ponte (2014) —, Sobral evita a cristalização de seu centro, mantendo-o como um espaço de governança e fé pulsantes.

A trajetória de uma edificação histórica transcende o momento de sua inauguração, configurando-se como um palimpsesto arquitetônico onde diferentes épocas inscrevem suas necessidades, tecnologias e visões de mundo. Como postula Choay (2001), o monumento histórico raramente chega aos dias atuais em sua pureza original; ele é moldado pelas sucessivas apropriações e pelos esforços de salvaguarda ou modernização que sofre ao longo do tempo. Compreender a saúde estrutural de um bem tombado exige, portanto, uma análise diacrônica de suas modificações. No caso de edifícios de uso coletivo e contínuo, as intervenções não são apenas estéticas, mas operacionais, visando adequar a estrutura se secular às exigências contemporâneas de segurança, conforto e habitabilidade.

Nesse sentido, ao longo de seus mais de 140 (cento e quarenta) anos de existência, o Teatro São João passou por diversas modificações arquitetônicas e estruturais para se adequar a novas normativas de uso e resolver falhas crônicas de manutenção. Conforme levantamento documental realizado nos arquivos públicos e nos registros dos órgãos de proteção patrimonial, a edificação foi submetida a quatro grandes ciclos de intervenção. Para facilitar a compreensão temporal e metodológica dessas campanhas de obras, a Tabela 1 sintetiza o cronograma, os objetivos e o caráter principal dessas ações modificativas.

Tabela 1 – Resumo das intervenções estruturais e arquitetônicas realizadas no Teatro São João ao longo de sua história:

Ano(s) da Intervenção	Objetivo Principal / Procedimentos Adotados
1875 a 1885	Período de edificação e conclusão de acabamentos finos da fachada e interiores
1940	Reformas pontuais para modernização e adaptações funcionais de maquinário.
1973	Intervenção de consolidação estrutural liderada por órgãos estaduais de proteção.
2003	Projeto contemporâneo de requalificação, focando em acessibilidade e climatização.

A adaptação para o conforto contemporâneo de 2003 exigiu um alto preço técnico. A instalação de pesados sistemas de ar-condicionado central introduziu novas cargas dinâmicas (vibrações contínuas) na estrutura centenária. No Teatro São João, a união de um ambiente interno artificialmente frio com o calor externo do Ceará potencializou a formação de microclimas úmidos, especialmente nas áreas menos ventiladas, como o pavimento subterrâneo.

Ao se inspecionar os níveis inferiores do teatro, constatou-se que o foco crítico e emergencial da edificação reside em seu pavimento subterrâneo. Originalmente concebido no século XIX para servir como câmara de ventilação natural e espaço de acomodação para os maquinários cênicos primitivos (Ponte 2014), esse porão encontra-se atualmente em um estado de insalubridade e degradação estrutural severa. A ausência de luz natural e a drástica redução da circulação de ar — agravada pelo selamento das aberturas durante as reformas para climatização moderna — transformaram esse espaço em um ambiente propício à proliferação de agentes biodeterioradores e à acumulação de patologias mecânicas que ameaçam todo o conjunto superior.

E uma negligência estrutural é, paradoxalmente, agravada por equívocos técnicos cometidos nas próprias tentativas de salvaguarda ao longo do tempo. O diagnóstico do subsolo do teatro revela que as intervenções das décadas de 1970 e de 2003 introduziram sérias incompatibilidades construtivas. Ribeiro e Oliveira (2021) enfatizam que o uso indiscriminado de cimento Portland e elementos de concreto armado em estruturas históricas tradicionais altera a permeabilidade das alvenarias, aprisionando a umidade do lençol freático e gerando até manifestações patológicas estruturais (Figuras 8 e 9). Foram realizadas vistorias no início de março e ao final de maio de 2026 observando-se a evolução destas manifestações patológicas. Sabe-se que a parte inferior da viga é a região tracionada, e o aço sendo principal responsável por suportar os esforços de flexão. Neste caso, com a utilização do fissurômetro observou-se que a camada de concreto afetada deslocou-se para fora em relação ao alinhamento original 0,6mm. A intervenção padrão propõe o escoramento da estrutura, escareação com a remoção de todo o concreto solto e deteriorado, limpeza da armadura com a substituição das barras comprometidas, aplicação do primer anticorrosivo e argamassa estrutural, respeitando o cobrimento mínimo exigido pelas normas técnicas. Uma fissura de 0,5mm, classificada como trinca moderada e também observada em uma parede próxima, sugere que a estrutura comprometida da viga continua sob forte tensão e espalhando o esforço para outras áreas.

Figura 8: Corrosão de armaduras



Fonte: Arquivo do autor

Figura 9: Corrosão de armaduras



Fonte: Arquivo do autor

Dessa forma, as patologias hoje observadas nas fundações do Teatro São João não são apenas fruto da ação do tempo, mas também o resultado de restauros passados que ignoraram a fisiologia original dos materiais construtivos do século XIX.

A umidade proveniente do lençol freático, que antes evaporava naturalmente pela base das paredes, agora é forçada a subir por capilaridade até encontrar áreas de reboco tradicional para escapar. Esse fenômeno de umidade ascendente causa o descolamento crônico das pinturas, a eflorescência de sais e a degradação acelerada dos tijolos maciços localizados no porão da edificação (Figuras 10 e 11).

Figura 10: Infiltrações e umidade



Fonte: Arquivo do autor

Figura 11: Infiltrações e umidade



Fonte: Arquivo do autor

Por conseguinte, conclui-se que as requalificações urbanas contemporâneas não podem prescindir de uma engenharia diagnóstica contínua. O modelo de intervenção baseado em grandes reformas esporádicas e no embelezamento de fachadas deve ceder espaço para a cultura da manutenção preventiva. É imperativa a exigência de laudos estruturais permanentes e a aplicação de tecnologias não destrutivas (como termografia e georadar) visando antecipar colapsos antes que eles ameacem a integridade do bem e a segurança do público.

4. Conclusões

As principais descobertas deste trabalho indicam que o Sítio Histórico de Sobral é um exemplo de vanguarda no reconhecimento da dinâmica urbana. Projetos contemporâneos de pavimentação e zeladoria revitalizaram o entorno de equipamentos vitais, como o Museu Dom josé Tupinambá da Frota e os espaços religiosos, fomentando a vitalidade cultural da cidade.

Portanto, a sobrevivência do Teatro São João e da integridade física do próprio sítio histórico de Sobral depende de uma reestruturação imediata nos paradigmas de intervenção urbana. É importante transitar de um modelo de revitalização focado no impacto da imagem turística para uma gestão técnica que valorize a engenharia diagnóstica e a manutenção contínua das áreas invisíveis aos olhos do público. O esplendor dos lustres da sala de espetáculos e a vivacidade neoclássica das fachadas só terão significado duradouro se a base subterrânea que as sustenta for tratada com o mesmo rigor científico, garantindo que o edifício resista ao tempo de forma verdadeiramente integral.

A contribuição inédita desta análise, contudo, reside no diagnóstico crítico da assimetria das requalificações. No caso do Teatro São João, apesar das quatro grandes campanhas de intervenção (1875-1885, 1940, 1973 e 2003), a eficácia foi predominantemente estética e funcional. A requalificação garantiu a fruição visual e o conforto do público, mas negligenciou aspectos vitais de engenharia em sua superestrutura.

Como implicação prática, conclui-se que é imperativa a elaboração de um Plano de Manutenção Preventiva para os monumentos do Sítio Histórico. Somente através da superação da cultura das "reformas estéticas de superfície" em favor de uma engenharia de "conservação estrutural contínua" será possível assegurar que o patrimônio tombado sobreviva com segurança e autenticidade.

Referências

Castriota, Leonardo Barci. 2019. Patrimônio Cultural: Conceitos, Políticas, Instrumentos. São Paulo: Annablume.

Choay, Françoise. 2001. A Alegoria do Patrimônio. São Paulo: Estação Liberdade.

Chuva, Márcia. 2012. Os Arquitetos da Memória: A construção do patrimônio histórico e artístico nacional no Brasil. Rio de Janeiro: Editora UFRJ.

Fonseca, Maria Cecília Londres. 2017. O Patrimônio em Processo: trajetória da política federal de preservação no Brasil. Rio de Janeiro: Editora UFRJ.

Inventário de Bens Arquitetônicos, IBA. 2005. Teatro São João. Sobral, Instituto do Patrimônio Histórico e Artístico Nacional – IPHAN.

Ponte, Sebastião Rogério. 2014. Sobral: História e Memória. Fortaleza: Edições UFC.

Ribeiro, Carlos, e Ana Oliveira. 2021. "Patologias em estruturas históricas: incompatibilidade de materiais em restauros do século XX". Revista Brasileira de Arqueologia e Conservação 12 (3): 45-62.

Rodrigues, A. R. B. 2005. Prêmio IAB Jornalismo: Teatro São João – Sobral - Ce. Fortaleza.

Tavares, A. et al. 2010. Manual de Reabilitação e Manutenção de Edifícios**.** Faculdade de Engenharia Civil, Universidade de Aveiro Inovadomus, Portugal.

Cinpar 2026
XXII International Conference on Building Pathology and Constructions Repair
15th to 17th July 2026 - Lisboa, Portugal

Componentes pré-fabricados de argamassa armada: quadro analítico dos danos em um CAIC em Goiânia

Gabriel Lopes MONTANINE[1], Vanda Alice Garcia ZANONI[2]

[1] Universidade de Brasília, Brasília, Brasil, gabriel.montanine@aluno.unb.br
[2] Universidade de Brasília, Brasília, Brasil, vandazanoni@unb.br

Resumo: A argamassa armada é uma tecnologia construtiva definida como uma variante do concreto armado, diferenciando-se pelas propriedades, composição e processo de produção. Caracterizada por uma malha de aço difusa, alto teor de cimento e agregado miúdo, a argamassa armada possibilita a execução de elementos de grande dimensão e pequena espessura. Apesar da sua invenção no século XIX, foi experimentada e aprimorada na segunda metade do século XX. No Brasil, o arquiteto João Filgueiras Lima, o Lelé, adotou a pré-fabricação de componentes em argamassa armada como solução construtiva para seus edifícios escolares e equipamentos urbanos. Os Centros de Atenção Integral à Criança e ao Adolescente – CAICs, complexos escolares pré-fabricados em argamassa armada projetados por Lelé e construídos na década de 90, atualmente tornaram-se objetos de estudos e debates sobre seu estado de conservação, principalmente pelas intervenções inadequadas à sua preservação como patrimônio cultural. Os processos de degradação da argamassa armada são semelhantes aos do concreto armado, no que se refere aos agentes, mecanismos de degradação e manifestações patológicas, conforme as condições de exposição ambiental dos edifícios. Nesse sentido, o objetivo deste artigo é estabelecer um quadro analítico de suporte às ações de inspeção e diagnóstico de edificações em argamassa armada. Para tanto, foram realizadas inspeções visuais e levantamento fotográfico em um CAIC, identificando, classificando e analisando as principais manifestações patológicas nos componentes da cobertura, apontando os possíveis agentes e mecanismos de degradação. Os resultados permitiram constatar que os danos presentes nos componentes do sistema de cobertura ocorrem principalmente em função das condições de exposição ambiental e reduzido cobrimento das armaduras da argamassa armada. O estudo pretende contribuir para as ações de manutenção e conservação, cujas intervenções dependem do entendimento dos processos de envelhecimento desse material, considerando suas especificidades.

Palavras-chave: mapeamento de danos; sistema de cobertura; manifestações patológicas; estado de conservação; manutenção.

1. Introdução

A argamassa armada foi desenvolvida por Jean Louis Lambot na segunda metade do século XIX, sendo inicialmente aplicada em pequenas embarcações que, devido à alta impermeabilidade do material, tornavam-se capazes de resistir à ação da umidade. O engenheiro civil italiano Pier Luigi Nervi (1891-1980) foi um dos expoentes pela difusão da argamassa armada, reconhecido pelo uso do material em suas formas estruturais fluídas e sistemas de coberturas leves pré-moldadas. Nervi acreditava no potencial econômico do material, conferindo rigidez e leveza às estruturas por meio de nervuras.

De acordo com Hanai (1981) e Librório (1989), a argamassa armada é caracterizada por elementos de pequena espessura, limitando-se a 40 mm, composta por um arranjo de malhas de aço distribuídas por toda a seção do elemento. De acordo com a NBR 11173 (ABNT, 1990), o cobrimento de argamassa varia de acordo com as condições de exposição, considerando a espessura de 4 mm para ambientes protegidos e

6 mm em ambientes não protegidos. Lajaj *et al.* (2015) apontam que o tipo de malha e sua configuração influenciam no comportamento e resistência da argamassa armada.

A argamassa armada representa a gênese do concreto armado e, segundo Hanai (1981), ambos pertencem à mesma família com pequenas distinções de processos de produção e composição, caracterizando-se como uma extensão da tecnologia do concreto armado.

João Filgueiras Lima, o Lelé, foi um dos arquitetos precursores da tecnologia da argamassa armada no Brasil, por meio da aplicação do material na pré-fabricação de componentes leves. Os Centros Integrados de Atendimento à Criança e ao Adolescente – CIAC (1990-1992) compõem o conjunto de escolas projetadas por Lelé utilizando a tecnologia. Implantados por todo o território brasileiro, os CIACs passaram, por razões políticas, a ser denominados Centros de Atenção Integral à Criança e o Adolescente – CAICs.

Lelé concebeu o projeto-piloto das escolas com componentes padronizados e pré-fabricados, prevendo uma substituição periódica dos componentes como uma estratégia de conservação. O arquiteto acreditava que sua execução simplificada e seu custo operacional inferior ao de peças de concreto armado representariam a solução construtiva adequada à incipiente industrialização do país (Nobre, 2010). No entanto, a rede de fábricas idealizada por Lelé não se consolidou devido à desarranjos no programa governamental, o que comprometeu a efetividade da construção das escolas e o controle da produção dos componentes. Além disso, a desativação das fábricas de argamassa armada e a falta de cuidados periódicos nas escolas dificultaram os processos de conservação (Vilela e Ficher 2025).

Após 30 anos de existência, alguns autores têm discutido o estado de conservação dessas unidades escolares. Nos levantamentos realizados por Pereira *et al.* (2022), foram identificados que das 269 unidades remanescentes do programa, 85% estão ativas e 15% inativas, demonstrando que a maioria das escolas ainda permanecem em uso, cumprindo sua função social, enquanto a outra parcela encontra-se em estado de vulnerabilidade e abandono.

Alguns fatores como a falta de manutenções periódicas em seus sistemas, a descaracterização por substituições e intervenções inadequadas, além da incipiente atuação das instituições de preservação, têm prejudicado a permanência desse conjunto arquitetônico (Vilela 2018). Com a falta de manutenção e ações que priorizam a conservação preventiva, os componentes e elementos construtivos ficam sujeitos à degradação, afetando a durabilidade, principalmente daqueles que compõem a envoltória, como o sistema de cobertura. Nos cenários de conservação dos CAICs, o sistema de cobertura é o mais afetado, devido à constante exposição às intempéries, à falta de manutenção e substituições por novas coberturas metálicas (Pereira e Oliveira 2023 e Vilela 2018).

Librório (1989) destaca em seus estudos que não é possível determinar o comportamento global e definir parâmetros de durabilidade do material, pois é necessário considerar os diversos ambientes e microrregiões de implantação dos edifícios. Nas inspeções realizadas pelo autor em componentes de argamassa armada, foram identificados que os elementos expostos à ação das chuvas, molhagem e secagem frequentes ou em contato com substâncias agressivas, devem receber em sua superfície uma camada de tratamento de proteção. A argamassa armada é um material poroso e a remoção da camada superficial pode potencializar essa condição de exposição aos agentes de degradação, levando à despassivação da armadura e eventual deterioração da malha de aço pela ação da corrosão.

Segundo Zanoni (2015), as ações externas de origem climática constituem um dos principais agentes de degradação que reduzem o desempenho ao longo da vida útil das edificações. Esse processo de degradação da cobertura ocasiona um conjunto de prejuízos funcionais e estéticos, que podem ser mitigados mediante a adoção de um plano de manutenção continuada e inspeções periódicas (Zanoni 2015 e Santos 2025).

O Documento de Madrid – Nova Deli (2017) aponta que as condições de deterioração dos materiais do século XX devem ser analisadas cuidadosamente, identificando e compreendendo os danos visíveis para delinear procedimentos adequados de intervenção. Por essa, entre outras razões, é essencial compreender

o comportamento dos materiais diante da influência dos agentes de degradação e condições de exposição.

Nesse contexto, este artigo tem o objetivo de elaborar um quadro analítico das manifestações patológicas dos componentes de argamassa armada do sistema de cobertura a partir dos levantamentos físicos *in loco* e das análises das causas, mecanismos e agentes de degradação. Para isso, foi realizada uma inspeção predial em uma unidade remanescente do CAIC (atualmente ocupada pela Unidade Universitária de Goiânia – Laranjeiras, da Universidade Estadual de Goiás - UEG).

Busca-se compreender e identificar, por meio da inspeção predial no conjunto arquitetônico, quais as manifestações patológicas mais recorrentes no sistema de cobertura em argamassa armada, considerando as condições de exposição ambiental. O estudo justifica-se pela necessidade de aprofundar as pesquisas sobre as manifestações patológicas presentes nos componentes de argamassa armada, bem como pelo cenário de vulnerabilidade observado na conservação de algumas unidades dos CAICs. Dessa forma, o trabalho oferece uma base referencial e ilustrativa dos danos para os responsáveis pela gestão da manutenção, auxiliando no planejamento futuro das ações de conservação.

2. Método

O estudo tem caráter exploratório e a análise das manifestações patológicas nos componentes pré-fabricados em argamassa armada configura-se de natureza qualitativa, apoiada em inspeção predial, conforme diretrizes indicadas na NBR 16747 (ABNT 2020). Para o desenvolvimento do quadro analítico, foram adotados os seguintes procedimentos: I - Levantamento de campo e aquisição de imagens aéreas do sistema de cobertura do CAIC; II – Identificação e classificação dos danos; III – Classificação do nível de gravidade.

Após sistematização dos dados coletados, elaborou-se um quadro analítico (Quadro 1) que sintetiza a avaliação do estado de conservação da cobertura do CAIC Laranjeiras. Cada manifestação patológica identificada durante a inspeção *in loco* é ilustrada por meio de imagem, classificada, associada à descrição das possíveis causas, agentes e mecanismo de degradação e classificada quanto ao nível de gravidade. Ressalta-se que a investigação e análise foi realizada sem o suporte de testes laboratoriais e instrumentos de medição da extensão dos danos, fundamentando-se na inspeção visual e sensorial e em referências bibliográficas.

2.1 Levantamento de campo e aquisição de imagens aéreas do sistema de cobertura do CAIC

O levantamento de campo foi realizado na unidade do CAIC - a atual Unidade Universitária de Goiânia – Laranjeiras da UEG (Figura 1). Localizado na cidade de Goiânia, no Estado de Goiás, região centro-oeste do Brasil, o complexo educacional encontra-se em ambiente urbano, e por esta condição, de acordo com a NBR 6118 (ABNT 2023), enquadra-se na Classe de Agressividade Ambiental (CAA) do tipo moderada com risco pequeno de deterioração da estrutura. A unidade ainda preserva sua cobertura original em argamassa armada, permitindo inspecionar o estado de conservação do sistema.

Foram inspecionados os cinco componentes que compõem o sistema de cobertura do CAIC: telha- capa; telha-canal; telha de borda (presente nas extremidades do edifício); placa de cobertura; e sheds. O levantamento de campo foi realizado de forma sistemática e sensorial e as imagens foram adquiridas por um drone (DJI Air 2s) com câmera acoplada. Em algumas regiões, foram realizadas inspeções mais detalhadas, utilizando um dispositivo móvel para registro fotográfico das manifestações patológicas.

Figura 1 – Unidade Universitária de Goiânia – Laranjeiras, da Universidade Estadual de Goiás (UEG)

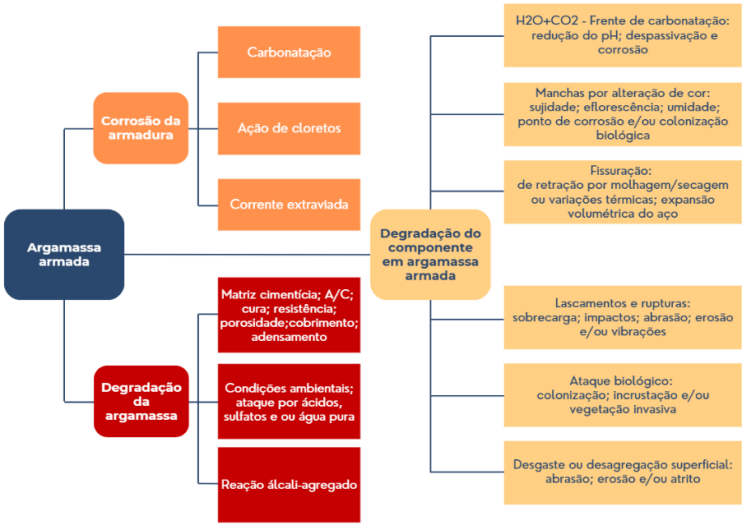


Fonte: Os autores, 2025.

2.2 Identificação e classificação dos danos

Após o levantamento de campo, foi realizada a identificação e classificação das manifestações patológicas. Os critérios para classificação e interpretação dos danos foram baseados em Librório (1989), Helene (1989) e Bertolini *et al.* (2013). A análise de cada manifestação patológica considerou as prováveis causas e mecanismos de degradação, a partir dos fatores de degradação da argamassa armada e processos de corrosão da armadura, conforme Figura 2.

Figura 2 – Causas e mecanismos



Fonte: Os autores (2026), baseado em Helene (1989), Librório (1989) e Bertolini *et al.* (2013)

2.3 Classificação do nível de gravidade

O nível de gravidade abrange a análise do risco oferecido aos usuários, ao meio ambiente e ao bem edificado. Para indicar o nível de gravidade dos danos registrados nos componentes, foi definido uma escala de classificação, por meio de uma régua graduada de cores em 5 níveis com os diferentes critérios - desprezível, mínima, moderada, crítica e altamente crítica -, conforme representado na Figura 3. A

definição dos níveis foi baseada nos critérios de classificação apresentados por Carvalho (2018) e Zanoni *et al.* (2023). As réguas graduadas com cores foram inseridas e demarcadas no quadro analítico.

Figura 3 – Critérios de classificação do nível de gravidade

Nível de gravidade	Cor padrão	Critério de classificação
Desprezível		Risco de impacto ao patrimônio edificado geralmente reversível, sem prejuízo À saúde e segurança dos usuários ou ao meio ambiente. Alterações na argamassa armada que não se enquadram nas condições das outras categorias, com ocorrência eventual e não sistêmica.
Mínima		Risco de causar prejuízos menores à aparência estética do patrimônio edificado, sem prejuízo ao usuário ou ao meio ambiente. Danos de baixa gravidade, com causas bem definidas, que não interferem na estanqueidade do sistema e se limitam ao componente, eventualmente afetando outras camadas.
Moderada		Risco de provocar a perda parcial de desempenho e funcionalidade por afetar a estanqueidade do sistema, podendo resultar em sua degradação precoce. Danos de pequeno grau de gravidade quanto a saúde e segurança do usuário, mas que ao gerar pontos de vulnerabilidade no sistema, podem evoluir para consequências mais graves no futuro, para um ou mais componentes do sistema.
Crítica		Risco para o patrimônio edificado e para o meio ambiente, com perda de desempenho e funcionalidade que compromete a vida útil do sistema e a segurança e a saúde do usuário. Danos resultantes de outros processos de degradação, de modo sistêmico ou não, e que podem afetar um ou mais componentes do sistema.
Altamente crítica		Danos graves do ponto de vista da saúde e segurança do usuário, afetando também o patrimônio edificado e o meio ambiente, resultantes de outros processos de degradação, de modo sistêmico ou não, e que afetam mais de um componente.

Fonte: Os autores (2026), baseado em Carvalho (2018) e Zanoni *et al.* (2023).

3. Resultados e Discussões

Durante a inspeção do sistema de cobertura do CAIC Laranjeiras, foram identificadas diversas manifestações patológicas, tais como: manchas de sujidade, manchas de umidade, variação cromática, exposição e corrosão da armadura, desgaste superficial, fissuras geométricas, lascamentos nas extremidades das telhas, desbotamento, fraturas dos apoios da telha, desplacamento da argamassa armada e infiltração.

A Figura 4 mostra o estado de conservação dos componentes da cobertura. Na Figura 4(a), observa-se que a superfície dos componentes de telha possui manchas de sujidade e umidade. A Figura 4(b) ilustra a superfície após processo de limpeza e proteção efetuado recentemente. O mapeamento dos danos foi realizado nos dois casos: sem limpeza e com limpeza.

Figura 4 – Registro com drone das áreas da cobertura com potencial de análise



(a) (b)

Fonte: Os autores, 2025.

Os sheds, no momento da inspeção, apresentavam-se em bom estado de conservação, embora com sinais de envelhecimento próprios do tempo de vida útil em serviço e das condições de exposição. Foram identificados desbotamento da pintura azul e algumas manchas de sujidade, principalmente na parte externa superior dos componentes.

As telhas-capa são apoiadas sobre as telhas-canal por meio de abas laterais. Esse sistema de montagem permite deslocamentos das telhas no sentido do eixo longitudinal (Figura 5). Durante a vistoria foram identificadas fraturas nos apoios e lascamentos nas extremidades do componente. A maior concentração de argamassa nas extremidades da peça, em decorrência do processo de produção, torna a região mais suscetível a lascamentos e desgaste. Causas mecânicas de impacto e vibrações ou sobrecarga de equipamentos instalados na cobertura podem condicionar aos lascamentos, o que afeta o aspecto físico do painel e a integridade dos apoios laterais. Dependendo da dimensão e profundidade do lascamento, ocorre também a exposição da armadura.

Figura 5 – Deslocamentos no eixo longitudinal das telhas-capa



Fonte: Os autores, 2025.

Foi identificado nas telhas-canal, telha-capa e telha de borda que o desgaste superficial, manchas de sujidade, mancha de umidade e fissuração geométrica são as manifestações patológicas mais recorrentes. Devido à reduzida espessura de cobrimento da argamassa armada, o desgaste superficial contribui para o aumento da porosidade do material e a diminuição da camada de proteção da malha de aço. Consequentemente, o desgaste superficial potencializa uma ação mais agressiva da frente de carbonatação pela exposição constante da superfície às intempéries e à poluição urbana. Fatores intrínsecos relacionados à produção da argamassa armada - como a qualidade da matriz cimentícia e a variabilidade do cobrimento nominal -, podem acelerar a corrosão das armaduras. Além disso, o cobrimento insuficiente em contato com a umidade por meio dos ciclos de molhagem e secagem aceleram os mecanismos de retração superficial da pasta, propiciando a entrada de agentes de degradação pelas fissuras.

Manchas de sujidade são provenientes de partículas atmosféricas, poeira, poluição e dejetos animais que se depositam na superfície dos componentes expostos às intempéries, afetando o aspecto físico e a variação cromática da superfície. Manchas de sujidade podem ocasionar retenção de umidade, pois favorecem o empoçamento de água.

As manchas de umidade em coberturas planas ocorrem pela retenção das águas pluviais, em situações de escoamento inadequado, insuficiência dos sistemas de drenagem, obstruções ou presença de vegetação ou sujeira acumulada. A umidade constante pode resultar na colonização biológica e desenvolvimento de fungos, bolor e microorganismos. De acordo com Librório (1989), as superfícies infectadas e constantemente úmidas promovem a redução do pH da argamassa e a desagregação superficial, tornando a superfície porosa e favorecendo a despassivação da armadura.

Foram identificadas fissuras geométricas de padrão reticulado na região das armaduras. A fissuração pode estar relacionada às variações higrotérmicas dos componentes ou associada às tensões internas provocadas pela expansão do volume da armadura com corrosão. De acordo com Souza e Ripper (1998),

as fissuras localizadas na região das armaduras são mais nocivas, pois permitem a infiltração direta de agentes de degradação, facilitando a corrosão das armaduras.

As vigas-calhas possuem dupla função: estrutural e de canal para escoamento das águas pluviais até os tubos de queda embutidos nos pilares. Nas áreas voltadas para as fachadas, foram identificados acúmulos de umidade decorrentes de falhas na inclinação de escoamento, comprometendo o desempenho do sistema de drenagem. Além disso, desplacamentos da camada de argamassa armada foram identificados nessas áreas, resultando na exposição das armaduras. Esta condição favorece o processo de corrosão, uma vez que a perda da proteção superficial permite o contato direto do aço com os agentes de degradação.

Observa-se na Figura 5 a presença de sujeira e folhas no fundo da viga-calha, dificultando o escoamento das águas e o acúmulo de umidade no bocal de entrada do tubo de queda nos pilares. A umidade constante nesse local provoca processos corrosivos no tubo de descida, o que facilita a infiltração no teto das salas.

As placas de cobertura localizadas abaixo dos componentes de telhas desempenham a função de laje de forro. Entre as placas e os painéis de telha existe um espaço ventilado e vazio, onde foram identificadas manchas de sujidade e acúmulo de entulhos provenientes de serviços anteriores de manutenção.

As superfícies internas estavam em bom estado de conservação, porém em algumas regiões foram detectadas infiltrações causando manchas de umidade e sujidades. Foi identificado empolamento e formação de bolhas na pintura da superfície interna das vigas-calhas decorrente da infiltração de água na interface entre a laje e viga-calha.

3.1 Quadro analítico

Por meio da identificação e análise das principais manifestações patológicas constatadas, o Quadro 1 apresenta uma síntese dos dados, composta por imagens exemplificativas registradas no momento da inspeção, classificação e descrição de cada manifestação patológica. O quadro relaciona essas ocorrências às condições de exposição, agentes e mecanismos de degradação envolvidos.

Quadro 1 – Quadro analítico das manifestações patológicas.

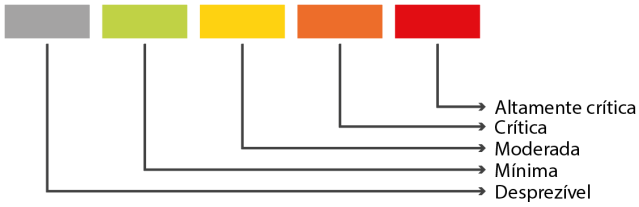
Classificação da manifestação patológica	Imagem	Descrição
Manchas de sujidade 		Presença de sujidades na superfície da telha decorrentes da deposição de partículas atmosféricas, poeira, poluição e dejetos animais. As telhas com superfícies mais porosas propiciam maior impregnação de sujeira. Esta condição pode afetar o aspecto físico da superfície e causar variação cromática.
Deposição de sujeira na superfície da placa de cobertura 		O espaço para a camada de ar existente entre a telha e a placa de cobertura torna-se um lugar favorável para o acúmulo de sujidade e detritos provenientes de serviços de manutenção. A água da chuva pode direcionar esses detritos para as calhas e chegar aos tubos de queda, entupindo a entrada dos coletores. O acúmulo de entulho pode causar danos à superfície da placa, por ações mecânicas, além de favorecer pontos de infiltração.

Empolamento da tinta 		Infiltrações na laje provenientes das águas pluviais da cobertura escoam para as vigas e danificam a pintura. Possíveis falhas no tratamento e proteção adequada das superfícies podem ter provocado o empolamento da tinta.
Obstrução do bocal do tubo de queda por acúmulo de sujidade e folhas 		Deposição de folhas no bocal do tubo de queda devido à existência de árvores de grande porte próximas ao edifício. A falta de manutenção e acúmulo desses detritos vegetais provocam o entupimento dos coletores de água pluvial. Além disso, entulhos e restos de construção costumam ser depositados inadequadamente sobre as lajes e, em períodos chuvosos, são carreados para as calhas e tubos de queda, ocasionando obstruções e novos entupimentos.
Manchas de umidade 		Manchas de umidade provenientes de empoçamento, acúmulo de sujeira e escoamento inadequado, quando persistentes, tendem a escurecer e podem indicar a presença de colonização biológica por fungos, bolores e outros microorganismos. A ocorrência dessas manchas também pode sinalizar ciclos repetitivos de molhagem e secagem, responsáveis por provocar variações volumétricas no material e acelerar os mecanismos de retração superficial da pasta.
Desgaste superficial 		Perda gradual da pasta devido à exposição contínua da argamassa armada às intempéries, somada ao desgaste natural provocado pela ação do tempo ou por falhas no processo de produção. Esse desgaste resulta em porosidade excessiva e na degradação da camada de pasta responsável pela estanqueidade do componente, tornando-o vulnerável à ação e à penetração de agentes agressivos que podem atingir as armaduras.

(Continua)

Corrosão da malha de aço 		Corrosão eletroquímica ocorre pela despassivação do aço, resultante da interação destrutiva das armaduras com agentes de degradação, como a umidade e o gás carbônico que penetram pela porosidade superficial, processo favorecido pelo desgaste superficial ou por falhas no cobrimento de argamassa.
Fissuração geométrica 		Fissuras localizadas na região da malha podem estar associadas às tensões internas provocadas pela expansão volumétrica da armadura com corrosão. O reduzido cobrimento de argamassa favorece o mapeamento das fissuras geométricas que acompanham a posição das barras na malha de aço.
Lascamento nas extremidades do componente 		Perda de seção da telha por lascamento da argamassa armada. A região afetada localiza-se na extremidade onde ocorre a concentração de pasta de argamassa durante o processo de produção. Nesse ponto, não há presença de armadura. A causa pode estar relacionada a fatores de origem mecânica, como impacto na região.
Fratura nos apoios laterais 		Deslocamentos horizontais da telha, impactos e sobrecargas podem provocar lascamentos nos apoios laterais, fragilizando a estruturação do componente. As movimentações estruturais e térmicas dos painéis também podem favorecer a fratura dos apoios laterais.

(Continua)

Deslocamento da telha capa 		Nas regiões onde foram realizadas a limpeza das telhas-capa foram identificados deslocamentos horizontais dos pontos de apoios. As movimentações podem ocorrer por ações humanas devido às falhas de operação durante a manutenção, instalação de equipamentos e/ou reparos.
Desplacamento do cobrimento de argamassa armada 		Desplacamento do cobrimento de argamassa armada devido ao acúmulo de umidade por falhas no sistema de drenagem, possíveis deficiências na matriz cimentícia ou problemas no processo de produção. A dificuldade de adensamento do material nas regiões onde os coletores são posicionados costuma resultar em pontos com menor aderência e maior porosidade, favorecendo a degradação precoce.
Legenda: 		

Fonte: Os autores, 2026.

Com a inspeção verificou-se que os componentes de argamassa armada da cobertura são acometidos por manifestações patológicas relacionadas a diversas naturezas e causas. Dentre as manifestações patológicas identificadas, as manchas de umidade e manchas de sujidade ocorrem devido a falhas nos escoamentos das águas pluviais e ausência de manutenções periódicas, sendo considerado mínimo o seu nível de gravidade.

A retenção de umidade na telha pode levar a ocorrência de outras manifestações patológicas como a colonização biológica, afetando as características físicas da superfície, favorecendo o desgaste superficial e consecutivamente o aumento da porosidade superficial da argamassa. Esta condição, quando não tratada, pode levar a exposição das armaduras, permitindo o contato de agentes de degradação, resultando na corrosão das armaduras. Com isso, a relevância de manutenções periódicas, recuperação da camada de cobrimento, limpeza e aplicação de camadas impermeabilizantes podem reduzir os riscos de exposição das armaduras e prolongar a vida útil do componente.

Os lascamentos e fraturas laterais dos apoios das telhas não representam uma manifestação patológica predominante, porém quando acometem os componentes podem afetar sua integridade estrutural. As fissuras geométricas em torno da malha de aço representam um risco para sua durabilidade e desempenho, podendo evoluir para consequências mais graves se os agentes de degradação atingirem as armaduras.

Os desplacamentos de argamassa identificados nas vigas-calhas representam as manifestações patológicas com nível de gravidade crítico, pois ocorre o risco de perda de desempenho com a exposição das armaduras, comprometendo a vida útil do sistema. Esta condição ocorre devido às falhas no escoamento de água que resultam no acúmulo de umidade nas extremidades da viga. A falta de manutenção, ausência de inspeção e falta de limpeza dos tubos de queda das águas pluviais podem potencializar a corrosão das armaduras e diminuir o desempenho estrutural do elemento, além de prejudicar esteticamente o conjunto arquitetônico, pois localizam-se em regiões visíveis nas fachadas.

A ausência de manutenções periódicas e de sistemas de escoamento eficientes tornam a retenção de umidade e sujidade como o principal agente de degradação. Durante a vistoria não foram detectadas manifestações patológicas com nível de gravidade altamente crítica.

4. Conclusões

Por meio da inspeção predial realizada no CAIC foi possível analisar e compreender as manifestações patológicas presentes nos componentes de argamassa armada, bem como suas causas, agentes e mecanismos. Passados mais de 30 anos de existência depois de sua construção, os resultados demonstram que a cobertura do CAIC, considerando as condições de exposição e agressividade ambiental de Goiânia, apresenta um estado de conservação razoável. Os procedimentos metodológicos adotados podem ser utilizados e adaptados nos CAICs implantados em outros contextos regionais para analisar e avaliar o estado de conservação, de modo a propor práticas corretivas e delinear os procedimentos de manutenção e intervenção para cada região.

A dificuldade de reposição dos componentes com o mesmo padrão original, devido a desativação das fábricas de argamassa armada propostas por Lelé, tornam as manutenções preventivas e corretivas essenciais para garantir a durabilidade e a integridade do edifício. Ainda assim, este estudo exploratório e qualitativo evidência que, os mecanismos, causas e agentes de degradação da argamassa armada são semelhantes com os presentes no concreto armado, embora possuam características e composição material distintas.

O quadro analítico sintetiza as manifestações patológicas detectadas na vistoria e apresenta o nível de gravidade como indicativos do risco e grau de degradação, com o propósito de orientar as atividades de inspeção, de reparo e manutenção nos componentes pré-fabricados em argamassa armada, servindo como base referencial para os profissionais responsáveis e gestores das edificações. A formatação adotada que associa a cor para a correspondência do nível de gravidade da manifestação patológica auxilia na priorização dos procedimentos de intervenção. Portanto, trata-se de um instrumento que contribui para a preservação do conjunto arquitetônico escolar pré-fabricado de Lelé, de modo a assegurar a continuidade de sua função social e suporte físico para a educação de diversas crianças e adolescentes no Brasil.

Agradecimentos

À Universidade de Brasília (UnB), à Coordenação de Aperfeiçoamento de Pessoal de Nível Superior (CAPES) e à Fundação de Apoio à Pesquisa do Distrito Federal (FAPDF) pelo apoio financeiro recebido.

Referências

ABNT. 2023. *NBR 6118: Projeto de Estruturas de Concreto – Procedimento*. Rio de Janeiro: ABNT.

ABNT. 2020. *NBR 16747: Inspeção predial – diretrizes, conceitos, terminologia e procedimento*. Rio de Janeiro: ABNT.

ABNT. 1990. *NBR 11173: Projeto e execução de argamassa armada*. Rio de Janeiro: ABNT.

Bertolini, Luca, Bernhard Elsener, Pietro Pedeferri, Elena Redaelli, e Rob B. Polder. 2013. *Corrosion of Steel in Concrete: Prevention, Diagnosis, Repair*. Weinheim, Germany: Wiley-VCH Verlag GmbH & Co.

Carvalho, Geovanna Brasil de. 2018. *Proposta para representação gráfica de mapas de danos em fachadas modernistas de concreto armado aparente*. Dissertação de Mestrado, Universidade de Brasília. http://repositorio.unb.br/handle/10482/34857

Hanai, João Bento de. 1981. *Construções de argamassa armada; situação, perspectivas e pesquisas*. Tese de Doutorado, Escola de Engenharia de São Carlos da Universidade de São Paulo. https://doi.org/10.11606/T.18.1982.tde-20250609-141250

Helene, Paulo. 1989. "Envelhecimento das superfícies de concreto aparente e produtos de proteção". In *Anais Simpósio Nacional de Tecnologia da Construção: Reforços, Reparos e Proteção das Estruturas de Concreto,* 175-208. São Paulo.

ICOMOS – ISC20C. 2017. Documento de Madrid – Nova Deli: Abordagens para a conservação do Patrimonio Cultural do Século XX.

Lalaj, Ornela, Yavuz Yardım, e Salih Yılmaz. 2015. "Recent perspectives for ferrocement". *Res. Eng. Struct. Mat.*, no. 1. http://dx.doi.org/10.17515/resm2015.04st0123

Liborio, Jefferson Benedicto Libardi. 1990. *Estudo patológico de construções de argamassa armada existentes no Brasil*. Tese de Doutorado, Escola de Engenharia de São Carlos da Universidade de São Paulo. https://doi.org/10.11606/T.18.1990.tde-06122024-105934.

Pereira, Ivanilson Santos, Alcília Afonso, e Claudia Terezinha de Andrade Oliveira. 2022. "Gestão do patrimônio arquitetônico: inventário digital dos CAICs no brasil". In *Anais do 5° Simpósio Científico ICOMOS Brasil e 2° Simpósio Cientifico ICOMOS/LAC*. Belo Horizonte: UFMG. https://www.even3.com.br/anais/5-icomos-2-icomos-lac/573785-gestao-do-patrimonio-arquitetonico--inventario-digital-dos-caics-no-brasil.

Pereira, Ivanilson Santos, e Claudia Terezinha de Andrade Oliveira. 2023. "Modelagem Paramétrica aplicada à documentação de pré-fabricados produzidos por Lelé: o caso dos CAICs". In *Ecos da Modernidade no norte e Nordeste brasileiro*, editado por Alcília Afonso e José Antonio Viana Lopes, 62-87. São Luís: Centro Universitário UNDB. https://docomomobrasil.com/ebook-docomomo-brasil/

Santos, Lara Monalisa Alves dos. 2025. *Inspeção predial em cobertura plana: uso de tecnologias digitais de aquisição de imagens e processos automatizados*. Tese de Doutorado, Universidade de Brasília. http://repositorio.unb.br/handle/10482/52368

Souza, Vicente Custódio Moreira de, e Thomaz Ripper. 1998. *Patologia, recuperação e reforço de estruturas de concreto*. São Paulo: PINI.

Vilela, Adalberto, e Sylvia Ficher. 2025. "Vestígios de uma modernidade em aço: a sede do TCU/AL e a degradação da arquitetura pré-fabricada de Lelé no Brasil". *Revista VIS: Revista do Programa de Pós-Graduação em Artes Visuais*, [S. l.], no. 1. https://periodicos.unb.br/index.php/revistavis/article/view/58075/42873

Vilela, Adalberto. 2018. *Architecture without Applause: The Manufactured Work of João Filgueiras Lima, Lelé*. Tese de doutorado, ETH Zurich.

Zanoni, Vanda Alice Garcia. 2015. *Influência dos agentes climáticos de degradação no comportamento higrotérmico de fachadas em Brasília*. Tese de Doutorado, Universidade de Brasília. http://repositorio.unb.br/handle/10482/19579

Zanoni, Vanda A. G., org., Flaviana B. Lira, Oscar L. Ferreira, Keila N. T. Frazão, Juliana Gehlen, Tatiana R. P. Jucá, Ana E. de A. Medeiros, Carlos E. L. de Melo, Letícia N. C. Mishina, Cláudio H. de A. F. Pereira, Rafael B. Rios, and Amanda V. Santos. 2023. *Programa de Conservação e Manutenção Continuada para as Edificações da Universidade de Brasília: Da Concepção ao Delineamento de Programas e Planos. Relatório Geral – Módulo I | Módulo II | Módulo III*. Brasília: Universidade de Brasília, Faculdade de Arquitetura e Urbanismo.

Cinpar 2026
XXII International Conference on Building Pathology and Constructions Repair
15th to 17th July 2026 - Lisboa, Portugal

Architectural Documentation of the San Sebastian Church

Daiane Oliveira da SILVA[1], Francisco Carlos SANTANA[2], Ana Cecília Serpa Braga VASCONCELOS[3], Mylene de Melo VIEIRA[4], Esequiel Fernandes Teixeira MESQUITA[5]

[1] UFC, Russas, Brasil, daianeoliveira@alu.ufc.br
[2] UFC, Russas, Brasil, franciscosantana@alu.ufc.br
[3] UFC, Fortaleza, Brasil, anaceciliavas@ufc.br
[4] UFC, Russas, Brasil, mylene.melo@ufc.br
[5] UFC, Fortaleza, Brasil, emesquita@ufc.br

Abstract: The architectural documentation of built heritage is a fundamental step in preserving cultural memory, providing a basis for future interventions, and enabling the proper management of these assets. In the Brazilian context, many historic buildings present documentary gaps resulting from the absence of systematized technical records over time. This research addresses the architectural documentation of the San Sebastian Church, located in the municipality of Russas, Ceará, Brazil, built in 1872, whose historical trajectory includes significant interventions throughout the 20th century, such as the first recorded renovation in 1922 and the complete repainting carried out in 1995. The study aims to survey and systematize the architectural and historical data of the building and to incorporate this information into a digital model of the historic asset. The methodology comprised three main stages: a bibliographic and documentary survey of existing sources; laser scanning to obtain the geometry of the building through the generation of a point cloud; and the integration of historical information into the digital model. As a result, relevant historical documents were identified, and a digital model was developed based on the point cloud, incorporating information on the transformations that have occurred over time and the current condition of the church. The research highlights the importance of integrating documentary data and field survey data with digital technologies as strategies for conservation and information organization, supporting future restoration and preservation efforts.

Keywords: Architectural heritage; Architectural documentation; Point cloud; Digital survey

1. Introduction

Historic buildings constitute an important component of cultural heritage, as they preserve architectural, social, and historical values across generations. These assets represent material records of the evolution of construction techniques, social dynamics, and local identities, playing a fundamental role in understanding the urban and cultural development of communities (Tan et al., 2026). Furthermore, such buildings contribute to the construction of collective memory, functioning as physical landmarks that connect past and present. In this sense, their preservation goes beyond material conservation, encompassing the maintenance of their historical and cultural meanings. The valorization of these assets directly contributes to strengthening local identity and promoting culture (Atik et al., 2023). Therefore, built heritage assumes a strategic role both in academia and in society.

However, the long-term preservation of these structures is directly conditioned by the existence of technical and historical records that allow understanding their original configuration, transformations, and current state (Hussein et al., 2024). The absence or insufficiency of documentation significantly compromises the preservation of built heritage memory, hindering the analysis of past interventions and the proposal of future actions (Salah et al., 2025). Moreover, it limits the production of scientific knowledge related to built heritage, as it restricts access to essential information about its evolution. This scenario highlights the need for systematic processes of data recording and organization. Thus, architectural documentation emerges as an essential element for heritage safeguarding, as it enables the recording, interpretation, and transmission of information over time.

Architectural documentation is, therefore, one of the fundamental pillars for the preservation of built heritage (Merzhiievska et al., 2026). Through it, it is possible to systematically record the physical, constructive, and historical characteristics of buildings, allowing the understanding of their evolution over time. This process enables the identification of transformations, degradation, and interventions that affect the integrity of heritage assets (Li et al., 2023). Additionally, it provides essential technical support for historical studies, conservation projects, and valorization actions. In contexts where consolidated technical records are lacking, documentation becomes even more relevant, acting as a tool for reconstructing the construction history of buildings. In this way, it contributes both to the preservation of material memory and to the advancement of scientific knowledge (Moyano et al., 2025).

With the advancement of digital technologies, new approaches have been incorporated into architectural documentation processes, significantly enhancing their accuracy, reliability, and capacity for data integration. Among these approaches, the use of three-dimensional digital models stands out, as they allow a more faithful representation of the geometric characteristics of buildings (Penjor et al., 2024). In addition, these technologies enable the organization of large volumes of information within structured digital environments. As a result, there has been a transformation in how heritage is documented, analyzed, and managed. This technological progress has driven the development of new methodologies for recording and interpreting built heritage, incorporating dimensions that were previously less explored, such as the integration of geometric and informational data (Cardinali et al., 2023).

In this context, Historic Building Information Modeling (HBIM) has emerged as a relevant tool for the documentation and management of historic buildings. Unlike conventional Building Information Modeling (BIM), HBIM seeks to integrate geometric, constructive, and historical data into digital models, enabling a more comprehensive representation of heritage. This approach allows not only the three-dimensional modeling of the building, but also the incorporation of information about the historical and cultural value associated with its elements. Recent studies have expanded this discussion by introducing different levels of information applied to HBIM. The Level of Information (LOI) emphasizes the incorporation of technical and historical data (Brumana et al., 2019), while the Level of History (LOH) focuses on the inclusion of historical narratives (Stefano Brusaporci et al., 2021). Complementarily, the Level of Knowledge (LOK) proposes dynamic and continuously updated models (Korro Bañuelos et al., 2021).

At the same time, reality capture technologies have played a central role in the evolution of architectural documentation. Terrestrial laser scanning (TLS) stands out as one of the main techniques used in this context (Kubacka et al., n.d.). This technology enables the acquisition of highly accurate geometric data through the generation of three-dimensional point clouds (Fellas & Demosthenous, 2025). The process is based on the emission of laser beams capable of capturing millions of points in space, accurately recording building geometry. As a result, complex and hard-to-access elements can be represented with a high level of detail. In addition, TLS offers advantages such as rapid data acquisition and error reduction (Merzhiievska et al., 2026). Therefore, it is considered a highly suitable tool for heritage documentation.

Despite these technological advances, there is still a significant gap in the integration of geometric data and systematically organized historical information (Fernandes Dionizio et al., 2025). In many cases, digital models focus primarily on geometric representation, neglecting the historical dimension that characterizes heritage. This limitation compromises the development of more complete and informative models and reduces their analytical potential over time. In this sense, there is a clear need for approaches that combine digital surveying with documentary analysis. The integration of these dimensions enables the creation of richer and more representative models, enhancing the understanding of architectural heritage (Moral Saiz et al., 2021).

In recent years, digital heritage documentation has significantly advanced, driven by the integration of reality capture techniques and information modeling. Since 2020, studies have emphasized the combination of HBIM, photogrammetry, and laser scanning, enabling the generation of detailed and semantically structured three-dimensional models (Cardinali et al., 2023). At the same time, collaborative

platforms for point cloud annotation and digital twin applications for heritage management have been developed (Medjdoub et al., 2026). These approaches allow not only documentation but also continuous monitoring of buildings. As a result, the potential applications of digital models have expanded (Atik et al., 2023), reinforcing the importance of integrating multiple technologies in architectural documentation (Lewińska et al., 2022).

More recently, advances in artificial intelligence, machine learning, and extended reality technologies have further expanded the possibilities for analyzing and managing built heritage (Martinenko et al., 2025). These tools enable the automation of data interpretation processes, the identification of degradation patterns, and support decision-making in interventions. Additionally, they allow the creation of immersive environments for visualization and analysis (Carvalho Ottoni & Cordeiro Ottoni, 2025). This trend reflects a transformation in how heritage is studied and preserved. The integration of these technologies with HBIM points to new perspectives in architectural documentation, consolidating a scenario of increasing digitalization of cultural heritage.

Despite these advancements, studies that consistently integrate historical information into digital models are still scarce. Such data are essential for understanding the trajectory of buildings, their meaning, and the context in which they were constructed and transformed over time (Lukito, 2025). Furthermore, they enable the identification of interventions, renovations, and spatial changes. The absence of this historical dimension limits heritage interpretation and reduces the informational value of digital models. Therefore, it is necessary to develop approaches that integrate historical and geometric data in a structured manner. This integration enriches heritage representation and enhances its cultural, historical, and scientific value (Ribeiro et al., 2026).

In this context, this study aims to perform the architectural documentation of the San Sebastian Church, located in the municipality of Russas–CE, Brazil, through the integration of digital surveying and documentary analysis. The research seeks to systematize geometric, architectural, and historical information about the building, contributing to the organization of knowledge related to this heritage asset. Furthermore, it aims to provide support for historical studies and to enhance the understanding of the building's transformation process over time. To this end, reality capture technologies are employed, particularly terrestrial laser scanning, enabling the generation of a three-dimensional point cloud and the development of a digital model. Thus, this study contributes to advancing practices in built heritage documentation.

2. Historical Building – San Sebastian Church

The present study focuses on the San Sebastian Church, a religious building located in the municipality of Russas, in the Jaguaribe Valley, state of Ceará, Brazil. The selection of this case study is justified by its historical, cultural, and architectural relevance within the regional context, as well as its significant level of preservation when compared to other religious buildings in the semi-arid region of Ceará that have undergone more extensive transformations over time. In this sense, the church represents an important example of local built heritage, allowing an integrated analysis of historical, constructive, and architectural aspects.

The origin of the building is directly related to the socio-environmental context of the 19th century in the interior of Ceará, marked by severe droughts and epidemics such as cholera and bubonic plague, which strongly affected the population (Araújo, 1986). In this scenario, popular religiosity played a central role as a form of collective coping, resulting in the construction of devotional spaces. The San Sebastian Church thus emerged from a vow made by the local community and was dedicated to the saint traditionally associated with protection against diseases, highlighting the strong relationship between faith, territory, and social memory.

The construction of the temple was led by the parish priest Lino Deodato Rodrigues de Carvalho and was completed around 1872 (Araújo, 1986). Since then, the building has maintained its original layout and presents relative spatial integrity, despite interventions carried out over time. In addition to its material value, the church preserves its religious and symbolic function, serving as a venue for cultural expressions and festivities that remain active. This continuity of use, combined with its historical relevance and the potential for analyzing constructive transformations, reinforces its suitability as a study object, particularly in research focused on architectural documentation and heritage information modeling. Figure 1 presents an external view of the San Sebastian Church.

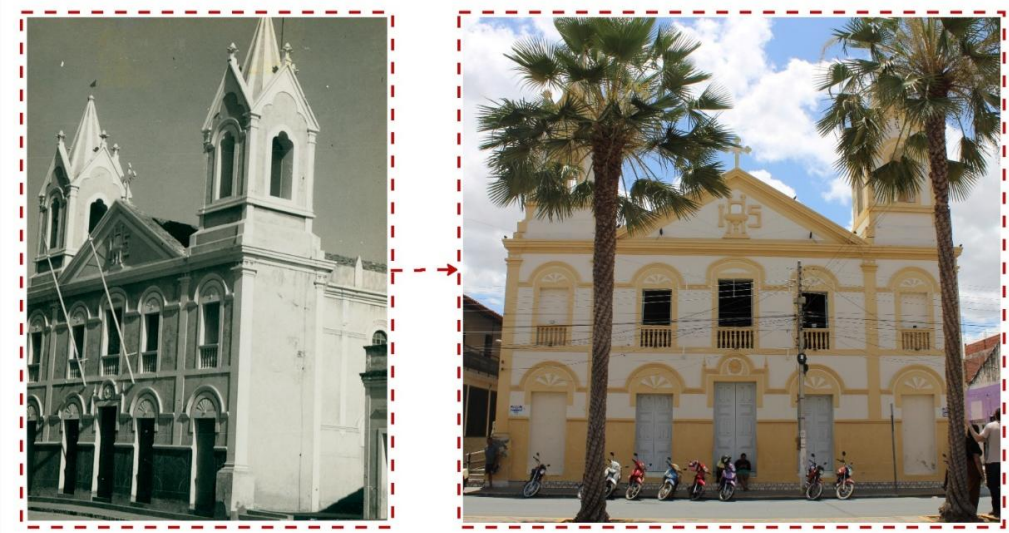


Figure 1 – Comparative external views of the San Sebastian Church in 1951 and 2026.

3. Methodology

3.1 Documentary and historical survey

The historical and documentary survey of the San Sebastian Church was conducted using an exploratory approach, aiming to identify buildings of relevance in the municipality of Russas with potential for research development. Initially, consultations were carried out in the local museum archive, where the church was selected as the study object due to its historical value and its relatively high level of preservation, especially when compared to other religious buildings in the region.

After defining the case study, contact was established with the parish priest, through whom authorization was obtained to access the church's documentary archive. The analyzed material includes a variety of primary sources, such as written records, historical photographs, administrative documents, and materials related to religious festivities. Among these, notebooks and booklets used during the celebrations of San Sebastian stand out, as they contain information on the organization of festivities, community fundraising, and interventions carried out in the building.

The document analysis was conducted systematically, allowing the indirect identification of different stages of maintenance, renovation, and adaptation of the church over time. These data were organized into a timeline and subsequently correlated with the geometric information obtained from the digital survey. This procedure enabled the development of a consistent basis for understanding the building's evolution, highlighting the importance of integrating local historical sources with digital technologies in architectural heritage documentation. Figure 2 presents examples of the historical documentation collected during the research.

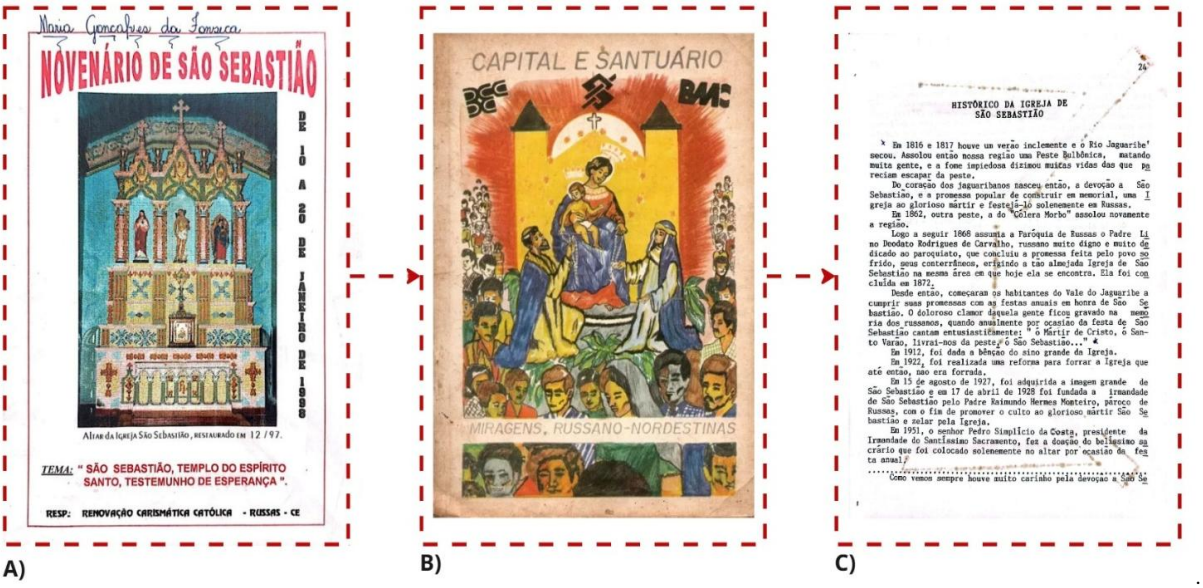


Figure 2 – Historical documents collected: (a) novena booklet cover; (b) cover of a historical publication on the San Sebastian Church; (c) excerpt from the novena booklet containing historical descriptions and records of interventions.

3.2 Laser scanning survey

The geometric survey of the San Sebastian Church was carried out using terrestrial laser scanning with the portable Leica BLK2GO scanner (Leica Geosystems), based on SLAM (Simultaneous Localization and Mapping) technology, which enables continuous acquisition of three-dimensional data without the need for fixed stations. Data collection was performed through a continuous path inside the building, covering all interior spaces, with real-time monitoring to ensure data quality and coverage. After acquisition, the point cloud was processed using proprietary Leica Geosystems software, resulting in a detailed three-dimensional model that served as the basis for digital modeling and the integration of historical information.

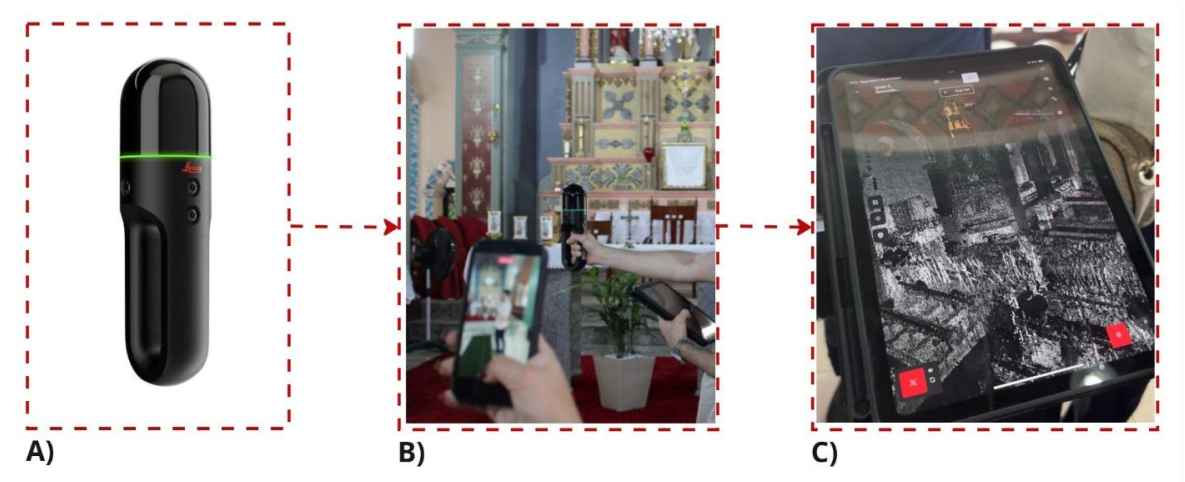


Figure 3 – Architectural survey using the BLK2GO laser scanner: (a) BLK2GO device; (b) in situ data acquisition process; (c) real-time monitoring of point cloud generation on a tablet during scanning.

3.3 Point cloud processing and digital modelling

After acquisition, the point cloud was processed and imported into Autodesk Revit, where it served as the basis for the digital modeling of the building. The data were previously organized and verified for geometric

consistency, enabling the construction of a parametric three-dimensional model representing the main architectural features of the San Sebastian Church, including walls, openings, and roof elements. The modeling process followed the BIM logic, allowing the structuring and association of information, with the incorporation of historical data related to interventions over time. Thus, the resulting model acts as an integrated information repository, aligned with HBIM principles and oriented toward the historical analysis of the building. Figure 4 presents the simplified flowchart of the methodological steps adopted in this research.

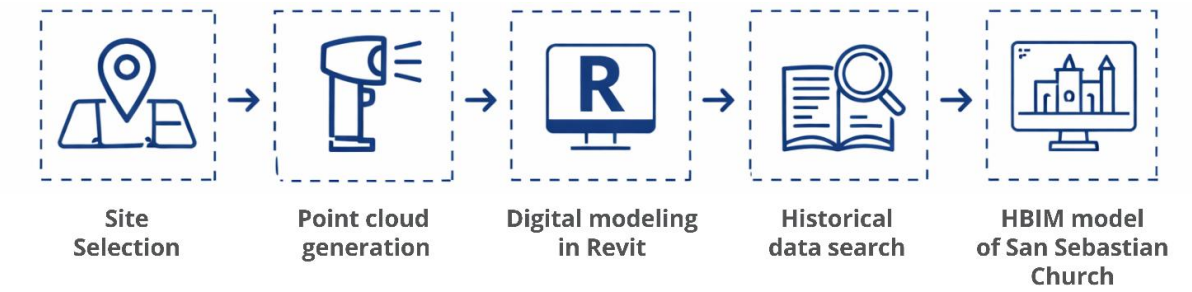


Figure 4 – Flowchart of the methodological workflow for the documentation of the San Sebastian Church.

4. Results and Discussion

4.1 Digital model based on point cloud

The digital modeling process resulted in a parametric three-dimensional representation of the Church of São Sebastião, accurately capturing its main architectural elements, such as walls, openings, and roof structures. Based on the point cloud, the model presents high geometric fidelity, ensuring consistency and alignment with the existing building. The rendered façade reinforces the reliability of the model in representing the built reality. In addition to its geometric accuracy, the model is structured parametrically, allowing the integration of historical and semantic data within the HBIM framework. Thus, it constitutes a comprehensive digital asset for documentation, visualization, and future analyses. Figure 6 illustrates the process of point cloud generation, integration, and application, as well as the resulting model.

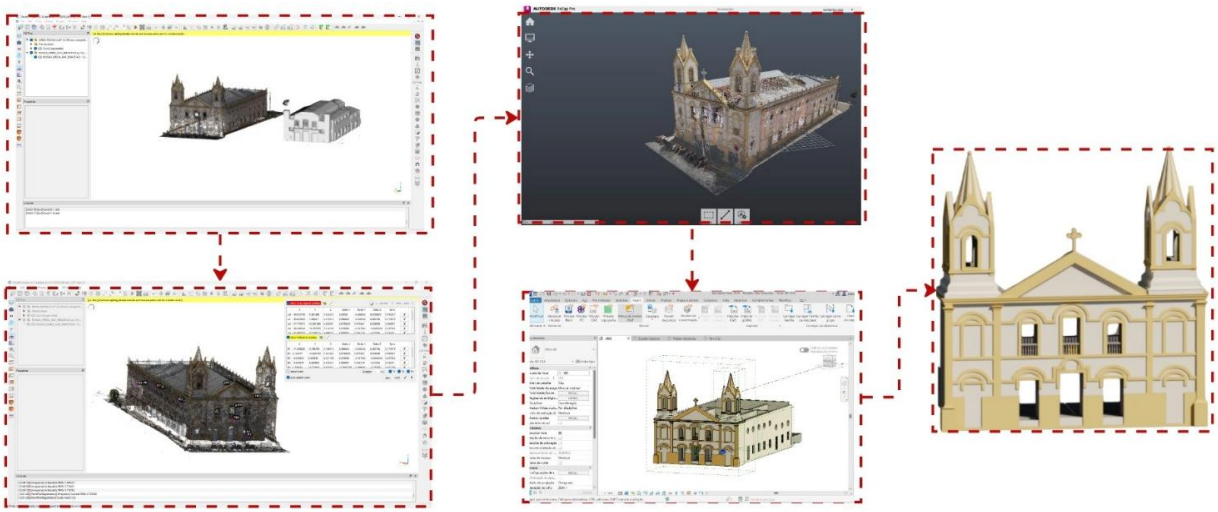


Figure 6 – Representation of point cloud processing and subsequent architectural modeling.

4.2 Historical documentation

The documentary survey conducted within the archive of the San Sebastian Church parish enabled the identification of a relevant set of historical sources related to the building. Among the analyzed materials, religious booklets used in local festivities stand out, as they contain descriptive records about the church's history, as well as information regarding interventions carried out over time. Additionally, excerpts from the book Imagem e Santuário were identified, contributing to the understanding of the building's origin, its constructive aspects, and the context of its implementation. These sources, combined with complementary searches, allowed the consolidation of a consistent historical overview of the study object.

The analyzed documents reveal different interventions carried out on the building, including renovations, restorations, and acquisitions of liturgical elements. In addition to written records, historical photographs were identified, visually documenting these transformations, such as changes to the altar, restoration works, and roof replacement. It is also noteworthy that some changes were not formally recorded in written documents but were inferred through comparative image analysis. This is the case of the replacement of the original flooring—previously hydraulic tile—with ceramic covering, as evidenced by photographic records from different periods.

The systematization of this information enabled the construction of a timeline of interventions carried out on the San Sebastian Church, presented in Table 1, which summarizes the main modifications identified over time. Additionally, Figure 5 illustrate the evolution of the building, facilitating the understanding of the transformations that occurred. Together, these elements contribute to the organization of the building's historical knowledge and serve as a basis for its integration into the HBIM model, allowing the association of historical data with the digital representation of the heritage asset.

Table 1 – Summary of the interventions carried out at the San Sebastian Church over time. Source: Authors' elaboration based on documentary survey (2025).

Year / Period	Type of Intervention	Description of Modification	Technical Characterization
1868–1872	Construction	Construction of the church under the coordination of the parish priest Father Lino Deodato Rodrigues de Carvalho, in fulfilment of a vow made by the local population after epidemics	Original implementation of the building at the current site; traditional construction system
1912	Acquisition	Blessing and installation of the main bell	Addition of a liturgical and functional element to the tower
1922–1924	Renovation	Installation of the church's internal ceiling	Intervention in the upper enclosure element (ceiling), previously non-existent
1927	Acquisition	Acquisition of the image of Saint Sebastian	Addition of an artistic and symbolic element to the interior
1951	Acquisition	Donation and installation of the tabernacle on the altar	Incorporation of a fixed liturgical element into the main altar
1991	Cleaning and Restoration	General cleaning, plaster repairs, termite removal, and renewal of the Stations of the Cross	Conservation intervention and recovery of finishes and decorative elements

1992	Construction and Renovation	Construction of restrooms, sacristy, and lateral arches; new interior painting	Expansion of the building and updating of interior finishes
1993	Acquisition	Installation of a sound system and new altar elements	Functional modernization and liturgical adaptation
1994	Restoration and Acquisition	Restoration of side altars and acquisition of fans and benches	Intervention in artistic elements and improvement of environmental comfort
1995	External Renovation and Restoration	Façade painting and partial ceiling recovery with wood replacement	Maintenance of the external envelope and localized structural repair
1996	Electrical Renovation	Replacement and expansion of the electrical system and lighting improvements	Update of the building's electrical system
1997	Artistic Restoration	Restoration of the Saint Sebastian altar with artistic painting	Intervention in a historical-artistic element
2020	Renovation	Replacement of the roof with a metal structure	Significant modification of the roofing system (material and performance)



Figure 5 – Historical records of interventions at the San Sebastian Church: (a) altar restoration in 1997; (b) roof renovation process in 2020; (c) installation of the new metal roofing system.

4.3 Digital model and integration of historical information

The stage of integrating historical information consisted of incorporating into the digital model the previously cataloged data (Table 1), including records of interventions, dates, and documentary evidence. The information was integrated according to its availability: interventions with photographic records had the images linked to the corresponding elements of the model (Figure 7), while those with limited data were represented through temporal annotations.

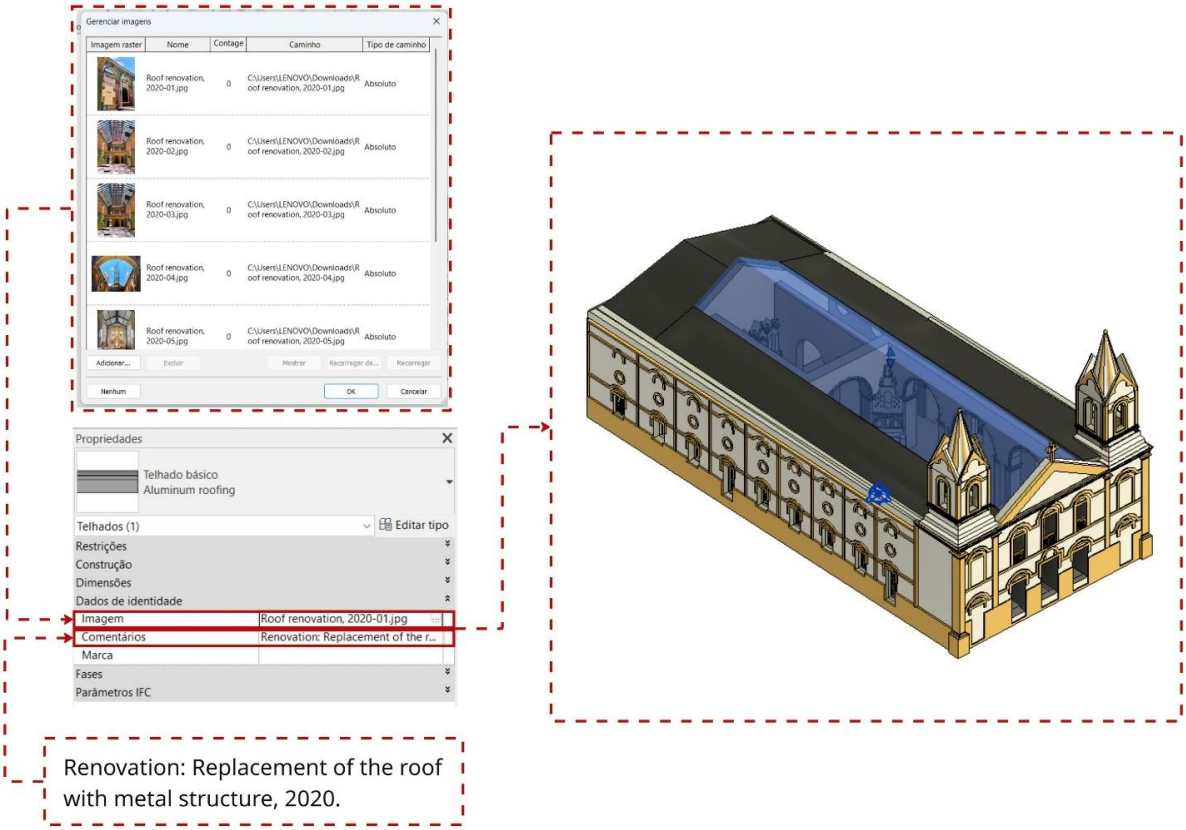


Figure 7 – Illustration of the integration of documentary information into the model, incorporating images and semantic data derived from literature and personal records.

Additionally, the chromatic changes of the building were modeled through the creation of different model states, allowing the faithful representation of distinct moments over time. In this context, two main scenarios were developed: the current model, in which the building is represented in yellow, and the model corresponding to the year 2006, represented in green, as evidenced by the historical records (Figure 8).

This approach enabled the development of an enriched HBIM model, in which geometric and historical information are integrated within a single digital environment. The resulting model not only represents the physical configuration of the building but also systematizes its evolution over time, serving as a tool to support historical analysis, heritage documentation, and decision-making in future interventions.



Figure 8 – Representation of the façade color changes over time (A–2005; B–2026).

5. Conclusions

This study demonstrated the potential of integrating terrestrial laser scanning and HBIM methodologies for the documentation and analysis of built heritage, using the San Sebastian Church as a case study. The results highlight the importance of generating an accurate geometric survey through point cloud acquisition and its subsequent conversion into a parametric digital model, particularly in contexts where no prior technical documentation, such as architectural drawings or plans, is available. In this sense, the developed model not only represents the current physical configuration of the building but also establishes a reliable digital record of the asset.

The main contribution of this research lies in the integration of historical information into the digital model, based on documentary sources, photographic records, and institutional materials. The association between geometric data and historical evidence enabled the identification and interpretation of interventions carried out over time, including constructive and chromatic changes. This approach reinforces the role of HBIM as a comprehensive tool for heritage documentation, allowing the systematization of dispersed information within a structured and accessible environment.

Furthermore, this work highlights the importance of maintaining continuous and organized records of interventions in historic buildings. The absence of formal documentation, observed in the case study, reflects a common reality in many contexts, while also demonstrating how informal records, such as photographs and notes, can be essential in supporting future conservation actions. In this regard, the adoption of systematic documentation practices by religious institutions and heritage management bodies can significantly contribute to heritage preservation. As a future perspective, the expansion of the model through the incorporation of additional temporal layers, the improvement of information standardization,

and the application of the methodology to other historic buildings are highlighted, strengthening digital heritage documentation practices.

Acknowledgments

The authors would like to thank the parish priest, Father Pedro, for his availability and authorization to conduct this research at the San Sebastian Church. The authors also extend their gratitude to the entire team of the Nossa Senhora do Rosário Parish for their hospitality, cordiality, and support throughout the development of this study. Special thanks are given for providing access to historical records, documents, and personal archives, which were essential for the development and consolidation of the results presented.

References

Atik, M. E., Duran, Z., Yanalak, M., Seker, D. Z., & Ak, A. (2023). 3D modeling of historical measurement instruments using photogrammetric and laser scanning techniques. *Digital Applications in Archaeology and Cultural Heritage*, *30*. https://doi.org/10.1016/j.daach.2023.e00286

Brumana, R., Banfi, F., Cantini, L., Previtali, M., & Della Torre, S. (2019). Hbim level of detail-geometry-Accuracy and survey analysis for architectural preservation. *ISPRS Annals of the Photogrammetry, Remote Sensing and Spatial Information Sciences*, *42*(2/W11), 293–299. https://doi.org/10.5194/isprs-Archives-XLII-2-W11-293-2019

Araújo, P. de A. (1986). *Capital e Santuário: Miragens Russano-Nordestinas*. Imprensa Oficial do Ceará (IOCE).

Cardinali, V., Ciuffreda, A. L., Coli, M., De Stefano, M., Meli, F., Tanganelli, M., & Trovatelli, F. (2023). An Oriented H-BIM Approach for the Seismic Assessment of Cultural Heritage Buildings: Palazzo Vecchio in Florence. *Buildings*, *13*(4). https://doi.org/10.3390/buildings13040913

Carvalho Ottoni, A. L., & Cordeiro Ottoni, L. T. (2025). A deep learning approach for cultural heritage building classification using transfer learning and data augmentation. *Journal of Cultural Heritage*, *74*, 214–224. https://doi.org/10.1016/j.culher.2025.06.010

Hussein, K. A., Abrahim, A. R., Mohammed, A. S., & Ali, K. A. (2024). Digital preservation of heritage urban facades: An integrated approach using historic building information modeling and shape grammar analysis. *Digital Applications in Archaeology and Cultural Heritage*, *35*, e00383. https://doi.org/10.1016/j.daach.2024.e00383

Fellas, A., & Demosthenous, M. (2025). Enhancing Sustainable Heritage Documentation: Integrating Remote Sensing and HBIM. *IOP Conference Series: Earth and Environmental Science*, *1558*(1). https://doi.org/10.1088/1755-1315/1558/1/012056

Fernandes Dionizio, R., Murphy, M., & Dezen-Kempter, E. (2025). Multi-Scale Documentation of Modern Brazilian Architecture: An HBIM-HGIS Approach. *International Journal of Architectural Heritage*, *19*(12), 3307–3324. https://doi.org/10.1080/15583058.2025.2492243

Korro Bañuelos, J., Rodríguez Miranda, Á., Valle-Melón, J. M., Zornoza-Indart, A., Castellano-Román, M., Angulo-Fornos, R., Pinto-Puerto, F., Acosta Ibáñez, P., & Ferreira-Lopes, P. (2021). The role of information management for the sustainable conservation of cultural heritage. *Sustainability (Switzerland)*, *13*(8). https://doi.org/10.3390/su13084325

Kubacka, E., Kotarski, A., Gapiński, A., Pilarski, J., Woźniak, S., Wójcik, J., & Zychowicz, Ł. (n.d.). *INTERNATIONAL JOURNAL OF CONSERVATION SCIENCE ANALYSIS OF EFFECTIVENESS OF USING 3D SCANNERS IN PREPARATION OF ARCHITECTURAL AND CONSTRUCTION DOCUMENTATION: CASE STUDY OF HISTORIC BUILDING*. Retrieved www.ijcs.ro

Lewińska, P., Róg, M., Żądło, A., & Szombara, S. (2022). To save from oblivion: Comparative analysis of remote sensing means of documenting forgotten architectural treasures – Zagórz Monastery complex, Poland. *Measurement: Journal of the International Measurement Confederation*, *189*. https://doi.org/10.1016/j.measurement.2021.110447

Li, Y., Zhao, L., Chen, Y., Zhang, N., Fan, H., & Zhang, Z. (2023). 3D LiDAR and multi-technology collaboration for preservation of built heritage in China: A review. *International Journal of Applied Earth Observation and Geoinformation*, *116*. https://doi.org/10.1016/j.jag.2022.103156

Lukito, Y. N. H. (2025). Documenting vernacular heritage with 3D scanning technology: The case of Wae Rebo village, Manggarai, Indonesia. *Digital Applications in Archaeology and Cultural Heritage*, *37*. https://doi.org/10.1016/j.daach.2025.e00416

Martinenko, A., Pejić, M., Obradović, M., & Ristić, N. D. (2025). Advancing 3D reconstruction: Evaluating surveying techniques for medium-sized heritage objects. *Measurement: Journal of the International Measurement Confederation*, *256*. https://doi.org/10.1016/j.measurement.2025.118596

Medjdoub, B., Shakmak, B., Chalal, M., Khosravi, M., Sajad, R., Bezai, N., & Illangakoon, A. (2026). Restoring Pugin: Toward Predictive Conservation of Historical Buildings Using a Digital Twin Approach. *Sustainability (Switzerland)*, *18*(3). https://doi.org/10.3390/su18031516

Merzhiievska, N., Dunaievskyi, Y., Dunaievska, A., Chaban, A., & Andrieieva, Y. (2026). A novel educational model for architectural heritage preservation in Ukraine: Digital tools amidst wartime challenges. *Digital Applications in Archaeology and Cultural Heritage*, *40*. https://doi.org/10.1016/j.daach.2026.e00507

Moral Saiz, S., Oliver-Faubel, I., & Jordán Palomar, I. (2021). Implementación de HBIM en patrimonio arquitectónico. Estudio del caso de La iglesia de la Sang de Llíria. *EGE-Expresión Gráfica En La Edificación*, (15), 4–26. https://doi.org/10.4995/ege.2021.16075

Moyano, J., Martínez, E., Nieto-Julián, J. E., & Fernández-Alconchel, M. (2025). Integrating wooden altarpieces into H-BIM: Geometric profiling, complex artworks, and digital heritage mapping. *Automation in Construction*, *175*. https://doi.org/10.1016/j.autcon.2025.106213

Penjor, T., Banihashemi, S., Hajirasouli, A., & Golzad, H. (2024). Heritage building information modeling (HBIM) for heritage conservation: Framework of challenges, gaps, and existing limitations of HBIM. *Digital Applications in Archaeology and Cultural Heritage*, *35*. https://doi.org/10.1016/j.daach.2024.e00366

Ribeiro, G. C., Vieira, M. M., Mesquita, E., Moreira, E., & Tucci, G. (2026). An integrated HBIM protocol for digital documentation, management and reconstruction of historic buildings. *Journal of Building Engineering*, *118*. https://doi.org/10.1016/j.jobe.2025.114920

Salah, R., Károlyfi, K. A., Szép, J., & Géczy, N. (2025). A structured framework for HBIM standardization: Integrating scan-to-BIM methodologies and heritage conservation standards. In *Digital Applications in Archaeology and Cultural Heritage* (Vol. 37). Elsevier Ltd. https://doi.org/10.1016/j.daach.2025.e00420

Stefano Brusaporci, Alessandra Tata, & Pamela Maiezza. (2021). The “LoH - Level of History” for an Aware HBIM Process. In *42th INTERNATIONAL CONFERENCE OF REPRESENTATION DISCIPLINES TEACHERS. CONGRESS OF UNIONE ITALIANA PER IL DISEGNO. PROCEEDINGS 2020. LINGUAGGI, DISTANZE, TECNOLOGIE*. FrancoAngeli srl. https://doi.org/10.3280/oa-693.117

Tan, X., Xie, H., Xia, C., Ying, Y., Hokoi, S., & Li, Y. (2026). Artificial intelligence in five key phases of architectural heritage conservation: A systematic review. In *Journal of Building Engineering* (Vol. 117). Elsevier Ltd. https://doi.org/10.1016/j.jobe.2025.114862

Cinpar 2026
XXII International Conference on Building Pathology and Constructions Repair
15th to 17th July 2026 - Lisboa, Portugal

Integração entre tradição e inovação: desafios para aplicação da madeira laminada colada em patrimônios edificados

Mônica NICOLAU[1], Ricardo DIAS SILVA[2]

[1] Centro Universitário Cidade Verde, Maringá, Brazil, monicanicolau.engenharia@gmail.com
[2] Universidade Estadual de Maringá, Paraná, Brazil, rdsilva@uem.br

Abstract: This study aims to evaluate the potential of glued laminated timber (Glulam) as a solution for the structural rehabilitation of a historic building located in the city of Viseu, Portugal, through a qualitative and analytical approach based on a case study. The methodology applied in this research is grounded in the need to develop an integrated understanding of the existing structural behavior, the identified pathological manifestations, and the compatibility between the original construction systems and contemporary solutions, such as engineered timber. For the development of the study, an architectural and structural characterization of the building was carried out, including a dimensional survey, identification of the original construction systems, and technical inspections. The structural diagnosis was supported by systematized visual inspections aimed at assessing the state of conservation and the load-bearing capacity of the structural elements. Based on the data obtained, this article presents a proposal for structural rehabilitation using Glulam, founded on the principles of mechanical compatibility, durability, reversibility, and minimal intervention, in accordance with heritage preservation guidelines. The study thus discusses the importance of harmonizing tradition and innovation, highlighting its decisive role in durability, structural safety, and the preservation of the cultural values of the built heritage.

Keywords: Glued Laminated Timber, structural behaviour, heritage, wood structures, engineered wood

1. Introdução

A preservação do patrimônio edificado representa um campo de atuação complexo e multidisciplinar, no qual se articulam valores históricos, culturais, sociais e técnicos. As edificações históricas constituem testemunhos materiais de técnicas construtivas, modos de vida e contextos tecnológicos específicos de seu tempo, sendo, portanto, fundamentais para a construção da memória coletiva e da identidade urbana. Intervir nesses bens exige uma abordagem criteriosa, capaz de assegurar a integridade material e simbólica das construções, ao mesmo tempo em que se atendem às exigências contemporâneas de segurança estrutural, funcionalidade e durabilidade. Nas últimas décadas, a reabilitação do patrimônio cultural construído tem se consolidado como uma alternativa sustentável à substituição do edificado existente, alinhando-se a diretrizes internacionais de conservação e às políticas de redução de impactos ambientais no setor da construção civil. Nesse contexto, a reabilitação estrutural assume papel central, uma vez que muitas edificações históricas apresentam manifestações patológicas decorrentes do envelhecimento natural dos materiais, de intervenções inadequadas ao longo do tempo ou de alterações nas solicitações de uso. A escolha das soluções estruturais torna-se, portanto, um ponto crítico, exigindo compatibilidade entre os materiais originais e os sistemas introduzidos (Tavares, 2010). Paralelamente, observa-se um avanço significativo no desenvolvimento de materiais e sistemas construtivos inovadores, especialmente no campo da madeira engenheirada (Delfino; Silva, 2025). Entre esses, a madeira laminada colada (MLC) destaca-se por suas elevadas propriedades mecânicas, estabilidade dimensional, possibilidade de vencer grandes vãos e flexibilidade arquitetónica. Além disso, a MLC apresenta vantagens ambientais relevantes, associadas ao uso de matéria-prima renovável e ao seu potencial como sumidouro de carbono, fatores que reforçam seu

alinhamento com os princípios da construção sustentável. A aplicação da MLC na reabilitação estrutural tem ganho destaque, sobretudo em edifícios históricos com sistemas em madeira ou alvenaria tradicional associada à madeira. A introdução da MLC em patrimônios edificados envolve desafios técnicos, normativos e conceituais, incluindo compatibilidade de materiais, comportamento estrutural, reversibilidade e respeito aos princípios da conservação. Diretrizes como a mínima intervenção, a distinguibilidade entre o novo e o antigo e a reversibilidade das ações, impõem limites e condicionantes à adoção de soluções estruturais inovadoras. Nesse sentido, a utilização da MLC deve ser precedida por um diagnóstico rigoroso do estado de conservação da edificação, pela compreensão aprofundada dos sistemas construtivos originais e por uma avaliação crítica da adequação da solução proposta ao contexto patrimonial específico. O artigo analisa a integração entre tradição e inovação na reabilitação patrimonial, avaliando o potencial da MLC, seu desempenho e compatibilidade com os princípios de conservação, por meio de um estudo de caso em Viseu. A metodologia aplicada baseia-se na necessidade de compreender, de forma integrada, o comportamento estrutural existente, as manifestações patológicas identificadas e a compatibilidade entre os sistemas construtivos originais e soluções contemporâneas, como a madeira engenheirada. Para o desenvolvimento do trabalho, procedeu-se à caracterização arquitetónica e estrutural do edifício, incluindo levantamento métrico, identificação dos sistemas construtivos originais e inspeções técnicas. O diagnóstico estrutural baseou-se em inspeções visuais sistematizadas para avaliar o estado de conservação e a capacidade resistente. Com base nos dados, propõe-se a reabilitação com MLC, orientada pelos princípios de compatibilidade mecânica, durabilidade, reversibilidade e mínima intervenção, alinhada à preservação patrimonial. Destaca-se a importância de conciliar tradição e inovação para garantir durabilidade, segurança estrutural e preservação cultural.

2. Identificação do Edifício

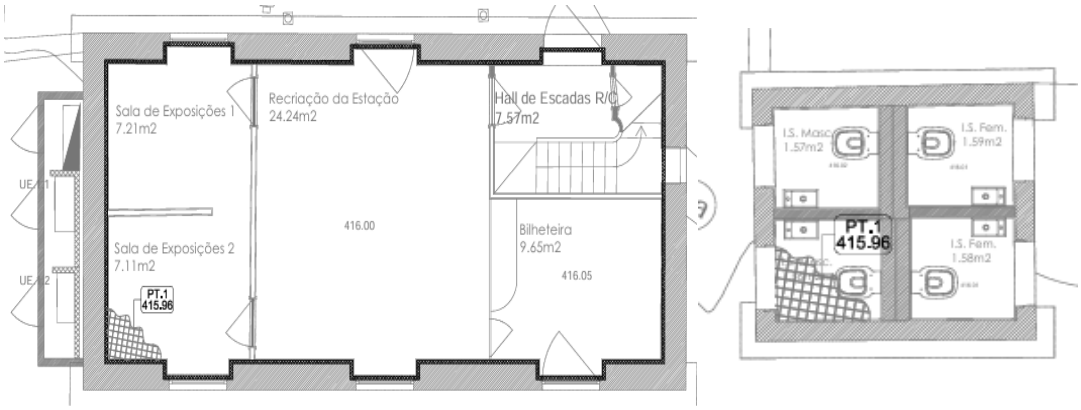
Trata-se de um edifício originalmente classificado como apeadeiro, localizado na freguesia de Torredeita (Figura 1), no concelho de Viseu, Portugal, caracterizado como uma infraestrutura ferroviária de pequena escala, concebida para atender paragens locais ao longo da linha férrea. A sua concepção arquitetónica assenta na simplicidade construtiva e operacional, destinando-se predominantemente ao embarque e desembarque de passageiros, sem incorporar os serviços e a complexidade funcional inerentes a uma estação ferroviária convencional. A intervenção analisada neste estudo refere-se a uma obra de reabilitação, cujo objetivo consistiu na adaptação do Apeadeiro de Torredeita para uso museológico e sanitários como infraestruturas de apoio (Lopes, M), assegurando a compatibilização entre a preservação das características originais do edifício e a introdução de novas funções, em consonância com os princípios da conservação e reabilitação do património edificado.



Figura 1: Apeadeiro da Estação Ferroviária

2.1 Caracterização arquitetónica e estrutural do edifício

Do ponto de vista arquitetónico e construtivo, originalmente o edifício é composto por um volume único, de planta retangular, desenvolvido em dois pavimentos, com área total de 107,15 m² (Figura 2), implantado paralelamente à via-férrea. Originalmente, as paredes exteriores portantes foram executadas em alvenaria de pedra, ligadas por argamassas à base de cal, solução que confere ao edifício robustez estrutural e elevada inércia térmica. Estas paredes apresentam, de modo geral, bom estado de conservação, não sendo observadas deformações estruturais percetíveis. Os paramentos exteriores são revestidos com reboco tradicional, de acabamento simples, compatível com a função original do edifício e com as práticas construtivas correntes à época da sua construção.



a) Piso Térreo b) Instalações Sanitárias

Figura 2: Plantas Arquitetónicas (Lopes, M)

A cobertura era do tipo inclinada, executada com asnas tradicionais, possuindo estrutura em madeira maciça, constituída por vigas principais e elementos secundários. O telhado é realizado com telha cerâmica tradicional, solução construtiva amplamente utilizada no período histórico em que o edifício foi construído. Os pavimentos térreos assentam diretamente sobre o solo, sem a presença de soluções de impermeabilização ou de isolamento térmico, refletindo as práticas construtivas vigentes à época da sua execução. Esta configuração construtiva favorece a ocorrência de fenómenos de umidade ascensional, com potenciais repercussões negativas na durabilidade dos materiais e no desempenho higrotérmico dos espaços interiores. No que se refere às paredes interiores, estas são executadas em tabique, técnica amplamente difundida no período, caracterizada por uma estrutura leve de madeira preenchida com argamassa tradicional (Nicolau, 2023). Tal sistema construtivo revela-se coerente com a lógica construtiva do edifício, embora apresente vulnerabilidade acrescida à ação da umidade e à ausência de manutenção continuada. As aberturas conservam elementos em madeira, nomeadamente portadas e balcões, executados de acordo com as técnicas da época, com recurso a carpintaria artesanal. Estes elementos apresentam não apenas valor funcional, associado à proteção solar, à ventilação natural e ao controle da iluminação, mas também valor simbólico e patrimonial, contribuindo para a autenticidade do conjunto. Adicionalmente, a sua permanência permite a leitura das soluções originais de sombreamento e ventilação passiva, fundamentais para o conforto ambiental antes da introdução de sistemas mecânicos. A preservação destes componentes assume, assim, relevância no contexto de intervenções de reabilitação, devendo ser privilegiadas estratégias de conservação e reforço compatíveis com os materiais e técnicas originais. O diagnóstico do estado de conservação evidenciou a presença de patologias construtivas recorrentes em edifícios ferroviários históricos, fortemente associadas à ação da umidade e à ausência de manutenção continuada. Verificaram-se manifestações de umidade ascensional nas paredes, com degradação progressiva dos rebocos, eflorescências salinas e destacamento superficial dos revestimentos. Adicionalmente, foram identificadas infiltrações provenientes da cobertura, responsáveis por manchas de umidade persistentes e pela deterioração localizada de elementos estruturais e não estruturais. A exposição

prolongada à água favoreceu ainda o aparecimento de fenómenos de biodeterioração, como o desenvolvimento de fungos e bolores, com impacto negativo na salubridade dos espaços interiores. Nos elementos de madeira observaram-se apodrecimento, fissuração e ataque de insetos xilófagos, comprometendo a resistência e durabilidade. A ausência de drenagem e impermeabilização agravou as patologias e sua disseminação. Esse quadro exige uma reabilitação integrada, baseada em diagnóstico rigoroso, que corrija os danos e elimine suas causas, garantindo a conservação do património edificado. As intervenções estruturais e construtivas foram concebidas de modo a minimizar a remoção de material original, recorrendo a técnicas de consolidação compatíveis com a alvenaria e a madeira existentes. A adaptação museológica implicou a introdução de infraestruturas contemporâneas, como sistemas elétricos, iluminação expositiva, condições mínimas de conforto ambiental e dispositivos de segurança, integrados de forma discreta e não intrusiva. O projeto procurou preservar a legibilidade histórica do edifício, valorizando seus elementos construtivos originais e reforçando seu caráter identitário.

3. Inspeções Técnicas

O edifício existente caracterizava-se por apresentar um estado de degradação significativo, evidenciando um baixo nível de conservação geral, compatível com um prolongado período de ausência de manutenção sistemática. Foram identificados diversos danos de natureza construtiva e estrutural, comprometendo parcialmente o desempenho global do edifício e a sua capacidade de resposta às solicitações de uso. Verificou-se a ocorrência de percolação de águas para o interior, tanto ao nível da cobertura como dos pisos, resultando em manifestações patológicas visíveis em diferentes elementos construtivos, como manchas de umidade, destacamento de revestimentos e degradação de materiais sensíveis à água. Ao nível dos pavimentos, observaram-se deformações localizadas, associadas à ação prolongada da umidade e ao envelhecimento natural dos materiais, bem como a presença de elementos de revestimento em avançado estado de degradação. Em algumas áreas, estas deformações indiciam perda de rigidez e comprometimento da estabilidade local, exigindo avaliação técnica mais aprofundada. Adicionalmente, foram identificados sinais de deterioração em elementos estruturais e não estruturais adjacentes, agravados por infiltrações recorrentes e pela exposição a agentes bióticos e abióticos. Este conjunto de patologias (Figura 3), evidencia a necessidade de uma intervenção de reabilitação integrada, fundamentada em diagnóstico técnico rigoroso. O diagnóstico do estado de conservação evidenciou as manifestações de umidade ascensional nas paredes, acompanhadas de degradação dos rebocos, eflorescências salinas e destacamento superficial dos revestimentos, sobretudo nas zonas inferiores dos paramentos. Adicionalmente, foram identificadas infiltrações provenientes da cobertura, responsáveis pelo aparecimento de manchas de umidade e pela degradação localizada de elementos de madeira, nomeadamente na estrutura de suporte da cobertura e em componentes secundários.



Figura 3: Conjunto de patologias - Estado de conservação do edifício

Nestes elementos, constataram-se indícios de biodeterioração, com ocorrência de ataques de insetos xilófagos e deterioração associada à exposição prolongada à umidade, comprometendo parcialmente o desempenho estrutural de alguns componentes. Apesar das patologias identificadas, não se verificaram, à observação visual, indícios evidentes de colapso iminente, nem deformações excessivas ou abatimentos generalizados da cobertura, o que sugere que, no momento da inspeção, o edifício apresentava um desempenho estrutural global ainda satisfatório, embora carecendo de intervenções de conservação e reabilitação adequadas para assegurar a sua estabilidade e durabilidade a médio e longo prazo, face ao aumento da sobrecarga exigida pela nova funcionalidade do edifício.

4. Identificação dos Sistemas Construtivos

Os métodos construtivos adotados nas construções históricas refletem um conjunto de soluções técnicas desenvolvidas a partir do conhecimento empírico, da disponibilidade de materiais locais e da necessidade de adequação às condições climáticas e funcionais de cada época. Estes sistemas caracterizam-se, de modo geral, pela utilização de materiais naturais, por processos construtivos artesanais e por uma lógica estrutural claramente legível. Entre os sistemas construtivos mais representativos encontrados no edifício, destaca-se o tabique, amplamente utilizado em paredes interiores e, em alguns casos, em divisórias leves (Fernandes, 2015; Padrão et al., 2021a; Padrão et al., 2021b). Este método baseia-se numa estrutura de madeira maciça, composta por montantes, travessas e ripas, preenchida e revestida com argamassas à base de terra e/ou cal, frequentemente reforçadas com fibras vegetais (Figura 4). O tabique apresenta vantagens associadas à leveza, à flexibilidade construtiva e à boa adaptação às compartimentações interiores, além de contribuir para o comportamento higrotérmico do edifício. Do ponto de vista estrutural, este sistema revela um desempenho satisfatório quando adequadamente conservado, permitindo uma distribuição eficiente das cargas próprias e uma resposta favorável a pequenas deformações. No entanto, a sua durabilidade está condicionada à proteção contra a umidade, uma vez que a madeira e as argamassas tradicionais são particularmente sensíveis à ação da água. A ausência de ventilação adequada e a presença de infiltrações podem conduzir à degradação dos elementos de madeira, ao apodrecimento biológico e à perda de coesão dos revestimentos. Observam-se, com frequência, fissurações, destacamentos do reboco e deformações localizadas, frequentemente associadas a variações higrométricas e a intervenções incompatíveis realizadas ao longo do tempo. Acresce que a substituição das argamassas tradicionais por materiais cimentícios rígidos pode agravar patologias existentes, comprometendo a capacidade de respiração das paredes. Neste contexto, a compreensão aprofundada do funcionamento do tabique é essencial para a definição de estratégias de reabilitação compatíveis, que respeitem a lógica construtiva original, garantam a reversibilidade das soluções adotadas e promovam a melhoria do desempenho térmico, acústico e estrutural do edifício, sem comprometer o seu valor histórico e patrimonial.



Figura 4: Estrutura de madeira existente no interior do Apeadeiro

As estruturas de madeira maciça desempenham um papel central no sistema construtivo original do edifício, sendo empregadas em pavimentos, coberturas e elementos de escoramento, assumindo simultaneamente funções estruturais e construtivas. As ligações eram, maioritariamente, realizadas por meio de encaixes, cavilhas de madeira ou elementos metálicos simples, garantindo um comportamento estrutural compatível com as solicitações da época e com os conhecimentos técnicos então disponíveis. Este tipo de solução evidencia um elevado grau de racionalidade construtiva, assente na utilização eficiente dos recursos materiais e na mão de obra especializada. A madeira utilizada, geralmente proveniente de espécies locais, apresentava secagem natural e seções dimensionadas de acordo com critérios empíricos, mas eficazes, de resistência e durabilidade (Appleton, 2023). O sistema estrutural revela ainda uma conceção flexível, permitindo acomodar pequenas deformações sem perda imediata de estabilidade, característica relevante em edifícios antigos. Contudo, a ação prolongada de agentes bióticos e abióticos, como umidade, fungos e insetos xilófagos, pode comprometer significativamente a integridade destes elementos ao longo do tempo. A inexistência de tratamentos de proteção adequados agrava este processo. A cobertura era complementada por beirados portugueses (Figura 10-b2). Para além da sua função técnica, assumem também um papel relevante na leitura arquitetónica característica das construções tradicionais, conferindo identidade formal ao edifício. As portadas de madeira, associadas aos vãos envidraçados, constituíam outro elemento recorrente nas edificações, característico das construções históricas do período, integrando-se de forma coerente no sistema construtivo e na expressão arquitetónica do edifício. Para além do seu valor estético e patrimonial, desempenhavam funções fundamentais no controle da iluminação natural, na regulação da ventilação e na proteção térmica dos espaços interiores, contribuindo para estratégias passivas de conforto ambiental. Estes elementos permitiam a adaptação do edifício às variações climáticas diárias e sazonais, reduzindo a incidência direta da radiação solar e favorecendo a ventilação cruzada. A sua execução seguia técnicas artesanais, com recurso a madeiras de espécies locais, selecionadas pela sua durabilidade e resistência mecânica. As portadas eram geralmente articuladas por ferragens simples, também de produção artesanal, que asseguravam o seu correto funcionamento. De forma complementar, destacam-se as escadas de madeira como elementos estruturais e funcionais relevantes na organização espacial do edifício, assegurando a circulação vertical entre pisos. Executadas com madeira maciça e sistemas de encaixe tradicionais, estas escadas refletiam soluções construtivas ajustadas às limitações técnicas e espaciais da época. Tal como as portadas, as escadas de madeira encontram-se particularmente expostas aos efeitos do uso continuado, da umidade e do envelhecimento natural dos materiais, apresentando desgaste nos degraus, folgas nas ligações e perda de rigidez estrutural. Assim, a sua conservação e eventual reabilitação exigem uma abordagem criteriosa, que preserve a autenticidade construtiva e garanta condições adequadas de segurança, funcionalidade e integração patrimonial. As argamassas tradicionais à base de cal são fundamentais em construções históricas, devido à sua permeabilidade, compatibilidade com a alvenaria e capacidade de acomodar deformações, contribuindo para a durabilidade e evitando patologias decorrentes de materiais incompatíveis.

5. Proposta de reabilitação estrutural com MLC

Em particular, todos os elementos introduzidos, nomeadamente novas estruturas e/ou novos materiais, foram devidamente avaliados de forma a não danificarem, ou alterarem o funcionamento, ou estabilidade física e química dos elementos existentes, quer estruturais, quer de revestimento.

5.1 Pavimento

A solução de intervenção passa pela execução de um piso de madeira, com a substituição dos elementos existentes, para também fazer face ao aumento da sobrecarga prevista para o edifício, recorrendo a vigas de madeira laminada colada de pinho nórdico (Pinus Sylvestris) da classe resistente GL24h com a execução de tarugos em vigas de madeira maciça de pinho nacional (Pinus Pinaster) da classe resistente C18 (Figura 5). Todos receberam um tratamento prévio contra agentes bióticos.

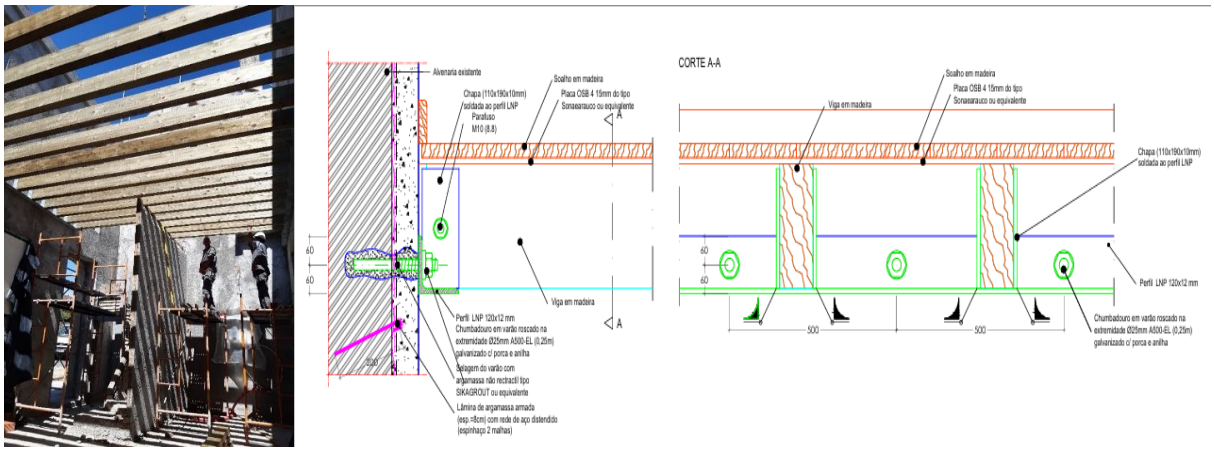


Figura 5: Pavimento de madeira – Interface entre Pav. 01 e Pav. 02 e Detalhe – Piso 1 - Apoio das vigas novas (Lopes, M)

A introdução da chapa metálica soldada e ancorada à alvenaria existente do edifício revelou-se necessária para corrigir as irregularidades geométricas das aberturas originais, uma vez que a parede, executada em alvenaria de pedra natural, apresentava variações significativas de alinhamento, prumo e espessura. Estas irregularidades inviabilizavam a fixação direta e rigorosa dos elementos estruturais em madeira, comprometendo o correto posicionamento das vigas e a regularidade do sistema construtivo. Assim, a chapa metálica (Figura 6), foi chumbada na alvenaria por meio de varões roscados, fixados com porcas e anilhas, garantindo uma ligação mecânica eficiente e controlada. A ancoragem foi complementada com selagem em argamassa não retrátil, assegurando a correta transferência de esforços, a eliminação de folgas e a durabilidade da ligação ao longo do tempo. Esta solução permitiu a criação de um plano regular e contínuo de apoio, funcionando como elemento de transição entre a alvenaria existente e a nova estrutura em madeira. Desta forma, tornou-se possível a fixação das vigas de madeira com seções uniformes e previamente dimensionadas, assegurando a padronização das peças, o correto alinhamento estrutural e a adequada distribuição das cargas. A chapa metálica desempenhou, portanto, um papel fundamental na calibragem da parede, conciliando as imperfeições do suporte original com as exigências geométricas e construtivas da nova solução estrutural, em conformidade com os princípios de compatibilidade e reversibilidade aplicáveis às intervenções em patrimônio edificado. As vigas de madeira laminada colada, com dimensões nominais de 21 × 136 × 3600 mm, constituíram o principal elemento estrutural do sistema de pavimento, tendo sido dimensionadas de modo a garantir a capacidade resistente, a rigidez adequada e a compatibilidade com o edifício existente (Figura 8). Sobre estas vigas foi executado o sistema de piso, concebido a partir de uma solução multicamada, visando o desempenho estrutural, acústico e de conforto de utilização.



Figura 6: Piso 1 – Chapa metálica chumbada na alvenaria

O acabamento final é composto por assoalho de madeira de pinho, acabado com verniz de proteção semimate, conferindo resistência ao desgaste superficial, facilidade de manutenção e adequada valorização estética do espaço. O assoalho foi aplicado por colagem sobre uma manta resiliente em aglomerado de borracha, com espessura de 4,5 mm, cuja função principal é a atenuação da transmissão de ruídos de impacto e a melhoria do isolamento acústico entre os pavimentos.

5.2 Cobertura

A cobertura em madeira maciça encontrava-se degradada, com perda de secção resistente devido à umidade e a agentes bióticos, provocando deformações, instabilidade e infiltrações, além de baixo desempenho térmico, o que justificou sua substituição integral (Lopes, Mário – Projetos Estruturais). A nova cobertura inclinada, em madeira laminada colada, foi concebida para garantir compatibilidade com o edifício e melhorar a estanqueidade e o desempenho térmico. Adotou-se um sistema multicamada, conciliando soluções tradicionais e contemporâneas, respeitando os princípios de mínima intervenção e reversibilidade. A estrutura inclui asnas, cumeeira e madres em MLC de pinho nórdico (GL24h) e varas em pinho nacional (C18), todos tratados contra agentes bióticos.

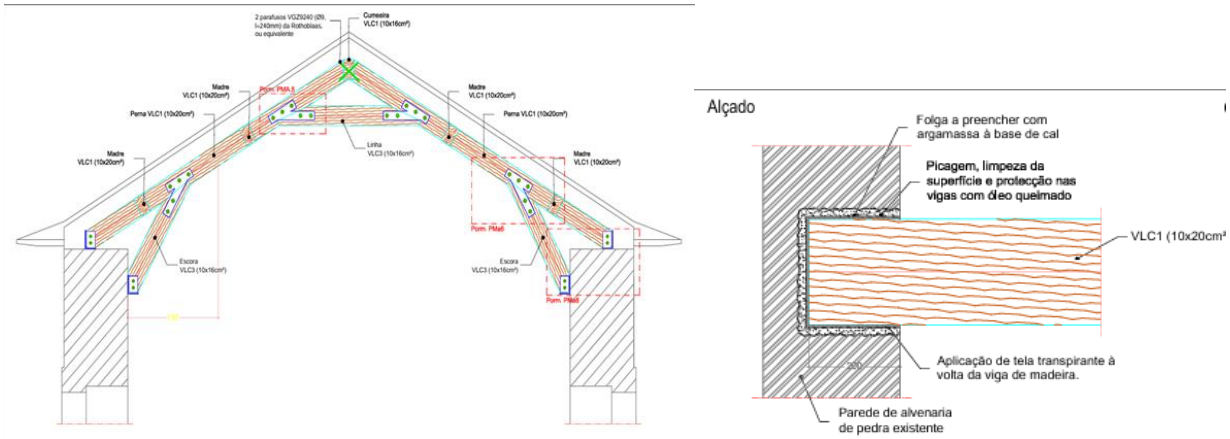


Figura 7: Alçado da estrutura da cobertura e detalhe do encastre da viga - (Lopes, M)

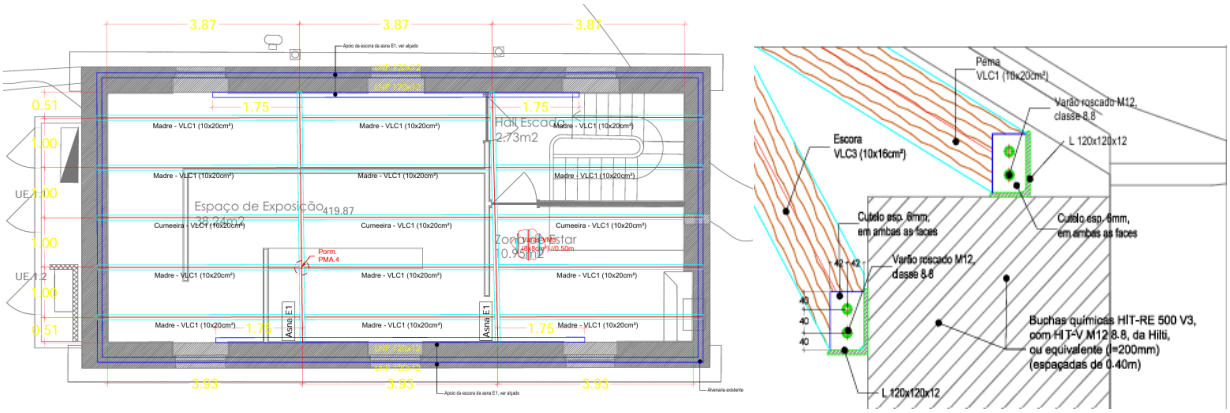


Figura 8: Planta estrutural da cobertura e pormenor apoio nas paredes de alvenaria - (Lopes, M)

Tomou-se o cuidado de garantir que o encastramento da viga de madeira à alvenaria de pedra portante recebesse tratamentos específicos, compatíveis com os materiais originais da edificação, de forma a assegurar a preservação dos elementos construtivos existentes. Inicialmente procedeu-se à picagem das zonas degradadas, seguida da limpeza cuidadosa da superfície de contacto e da aplicação de proteção nas

vigas por meio de óleo queimado, visando a redução da absorção de umidade (Figuras 7 e 8). Em seguida, realizou-se a colocação de uma tela transpirável envolvente à extremidade da viga, com o objetivo de permitir a difusão do vapor de água e evitar a retenção de umidade no contacto madeira–alvenaria. Posteriormente, o preenchimento da folga existente foi efetuado com argamassa à base de cal, garantindo compatibilidade físico-química e higrotérmica com os materiais tradicionais. Esta solução contribui para a durabilidade da madeira, minimiza o risco de patologias associadas à umidade e assegura a correta transmissão de esforços à alvenaria portante. (Figura 9)



Figura 9: Estrutura da Cobertura – Detalhe das ligações

5.2.1 Suporte da Cobertura

O suporte da cobertura é descontínuo e constituído por painéis de madeira, placas de OSB com espessura de 18 mm, devidamente fixadas às vigas de madeira laminada colada, assegurando a distribuição uniforme das cargas, assegurando a rigidez global do sistema e a adequada distribuição das cargas. Sobre este suporte foi aplicado isolamento térmico em poliestireno extrudido (XPS), com espessura de 80 mm, visando a redução das perdas térmicas e a melhoria do comportamento higrotérmico do edifício. Esta configuração multicamada contribui para a limitação das variações térmicas no interior, promovendo maior conforto ambiental (Figura 10). Adicionalmente, a utilização de materiais com estabilidade dimensional adequada permite acomodar deformações e variações higroscópicas da estrutura em madeira. A solução adotada revela-se compatível com intervenções em edifícios existentes, assegurando desempenho técnico e durabilidade adequada ao sistema de cobertura.



a) Execução da claraboia e placas de OSB b) XPS e DRS BT 50 c) Beirado português

Figura 10: Revestimentos da cobertura

A claraboia em edifícios históricos melhora iluminação e ventilação, mas sua introdução exige compatibilizar desempenho funcional com a preservação da cobertura, avaliando a estrutura existente e respeitando os princípios de mínima intervenção e reversibilidade. A sua localização e dimensão devem ser cuidadosamente estudadas, de modo a minimizar o impacto visual e a garantir a legibilidade da intervenção, em conformidade com os princípios de mínima intervenção e reversibilidade preconizados pelas cartas internacionais de conservação do patrimônio.

5.2.2 Impermeabilização da Cobertura

A impermeabilização foi garantida pela aplicação de placa subtelha asfáltica do tipo DRS BT 50, integrante do sistema ONDULINE, fixada mecanicamente ao suporte por meio de pregos apropriados, assegurando a continuidade da barreira impermeável e a proteção contra infiltrações. Este sistema contribui ainda para a durabilidade da estrutura de madeira, ao permitir uma adequada ventilação da cobertura. Trata-se de manta resiliente aplicada sobre a base contínua em placas de OSB. Esta base intermédia permite ainda uma correta interface entre a estrutura portante e o revestimento final, reduzindo tensões localizadas e acomodando pequenas deformações. A solução adotada alia eficiência estrutural, desempenho acústico e compatibilidade construtiva. Desta forma, garante-se não apenas a funcionalidade e durabilidade do pavimento, mas também a integração coerente entre técnicas construtivas contemporâneas e o contexto do patrimônio edificado.

5.2.3 Revestimento Final

O revestimento final foi executado com telhas cerâmicas do tipo lusa aba canudo, na cor vermelha, com dimensões de 43 × 26 cm, fixadas com massa de poliuretano, garantindo a estabilidade das peças face às ações climáticas. Foram igualmente previstos elementos de remate em madeira nas zonas de beirados e laterais, assegurando a proteção dos painéis e a coerência formal da solução adotada. A formação de beirado decorativo integrou-se na solução da cobertura, desempenhando simultaneamente funções técnicas e arquitetónicas, nomeadamente a proteção dos paramentos verticais contra a ação direta da chuva e a valorização da leitura arquitetónica do edifício. A solução adotada evidencia a viabilidade da integração entre sistemas construtivos contemporâneos e técnicas tradicionais.

5.3. Escada

A escada de madeira foi tratada, com substituição de revestimentos e limpeza dos elementos estruturais, incluindo reforços pontuais e tratamento contra agentes biológicos. Foram ainda verificadas as ligações e condições de segurança, visando garantir estabilidade, funcionalidade e preservação do seu valor histórico.



Figura 11: Escada de acesso ao pavimento superior antes das intervenções

6. Demais intervenções

As paredes de alvenaria de pedra existentes, foram alvo de picagem de rebocos, execução de lâmina de argamassa armada com 6cm de espessura pelo interior para consolidação e regularização do paramento, regularização e consolidação do coroamento das paredes de alvenaria de pedra existentes e contraventamento das paredes na direção fora-do-plano, através da melhoria da ligação aos pavimentos e coberturas. No nível do térreo, foi executado um novo piso, foram adotados o concreto C25/30 para pavimentos térreos, e o aço A500NR em armaduras ordinárias. tanto no edifício da estação quanto no edifício das instalações sanitárias.

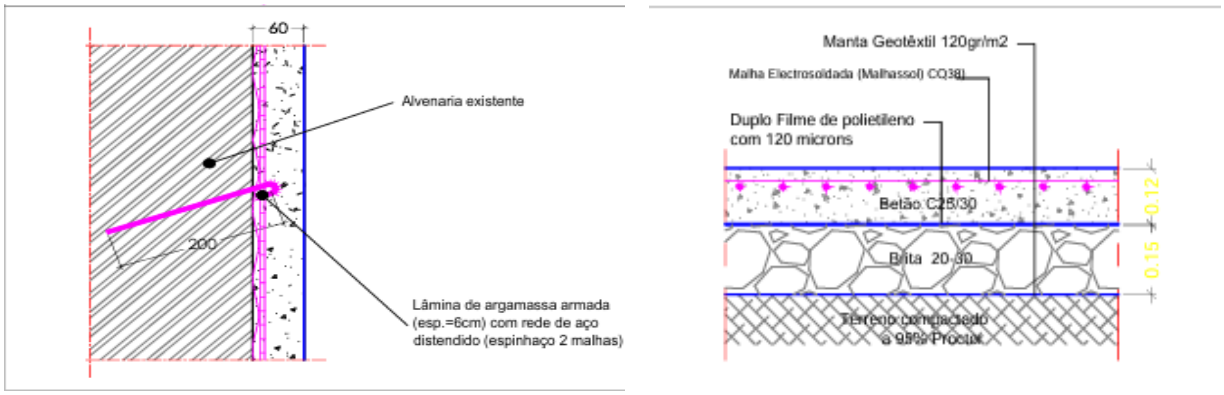


Figura 12: Pormenor do pavimento térreo e lâmina de argamassa armada (Lopes, M)

7. Materiais

As estruturas metálicas foram fabricadas em aço do tipo S275JR (EN 10025-2). As estruturas de madeira foram de madeira de pinho nacional (Pinus Pinaster) da classe resistente C18 e de madeira laminada colada de pinho nórdico (Pinus Sylvestris) da classe resistente GL24h. Todos os elementos novos receberam um tratamento contra insetos e fungos xilófagos. As características adotadas para cada um dos materiais são as especificadas no REBAP (Regulamento de Betão Armado e Pré-Esforçado) e no EC2 (EN 1992-1-1: Projecto de Estruturas de Betão), no EC3 (EN1993-1: Projecto de Estruturas de Aço), no EC5 (NP EN 1995-1-1 - Projecto de Estruturas de Madeira. Parte 1.1: Regras gerais e regras para edifícios) e na norma EN 338 (Structural timber - Strength classes). As ligações realizadas entre elementos de madeira apresentam características mecânicas e de resistência com especificação Rothoblaas®. As ligações foram realizadas com parafusos, todo roscado com ponta auto perfurante e suportes metálicos.

8. Conclusão

A madeira laminada colada (MLC), adotada pelo Engenheiro Calculista (Lopes, M0, afirma-se, neste estudo, como um material protagonista e estratégico no contexto da reabilitação de edifícios históricos, ao conjugar as vantagens inerentes à madeira enquanto material renovável com um desempenho estrutural superior e maior fiabilidade dimensional. A sua elevada relação resistência/peso e o controle industrial do processo de fabrico permitem responder de forma eficaz às exigências estruturais contemporâneas, sem comprometer a integridade dos sistemas construtivos tradicionais. A resposta favorável da MLC às variações térmicas e higrométricas, aliada à possibilidade de conceção de elementos estruturais de grandes vãos e geometrias controladas, revela-se particularmente relevante em intervenções sobre o edificado existente. Quando devidamente protegida contra agentes de degradação, nomeadamente a umidade e a ação biológica, e corretamente integrada em contacto com materiais históricos, a MLC demonstra um comportamento compatível do ponto de vista físico-mecânico e higrotérmico. Os resultados evidenciam que a utilização da madeira laminada colada contribui não apenas para a melhoria do desempenho estrutural, mas também

para a redução do peso próprio das estruturas e, consequentemente, das ações transmitidas às alvenarias portantes existentes. Adicionalmente, a sua aplicação favorece princípios fundamentais da conservação do património, como a reversibilidade das soluções, a legibilidade da intervenção e a minimização de impactos sobre os elementos originais. Conclui-se, assim, que a MLC constitui uma solução tecnicamente robusta e ambientalmente sustentável para intervenções de reabilitação estrutural, permitindo conciliar a preservação da autenticidade histórica com as exigências atuais de segurança, durabilidade e sustentabilidade. A sua adoção, quando sustentada por diagnóstico rigoroso e por critérios de compatibilidade material, reforça o papel da madeira engenheirada como elemento-chave na salvaguarda e valorização do património construído.

9. Referências Bibliográficas

APPLETON, J. Reabilitação de edifícios antigos: patologias e técnicas de intervenção. Lisboa: LNEC, 2003.

DELFINO, D. S.; SILVA, R. D**.** "Metodologias de Projeto para Arquitetura em Madeira Engenheirada: uma perspectiva híbrida". In: XVIII Ebramem, 2025, Curitiba. XVIII EBRAMEM - Encontro Brasileiro em Madeiras e em Estruturas de Madeira. Recife: Even3, 2025. v. 1.

Fernandes, C. R. 2015. "Avaliação Experimental do Comportamento Mecânico de Paredes de Tabique." Dissertação de Mestrado. Instituto Politécnico de Viseu. Portugal.

Lopes, M - Eng. Civil – OE nº 64157 – Portugal – Projetos Estruturais.

Nicolau, M. (2023). "Caracterização *in situ* dos elementos estruturais em madeira de um edifício situado no centro histórico de Viseu." Dissertação de Mestrado. Instituto Politécnico de Viseu. Portugal.

Padrão, J. Guedes, J., Pinto, J., Arêde, A. (2020). "As paredes de tabique em Viseu – Detalhes construtivos e caracterização material." Revista Portuguesa de Engenharia de Estruturas. Ed. LNEC. Série III. n. º14. ISSN 2183-8488. pp.71-84.

Padrão, J., Guedes, J., Pinto, J., Arêde A. 2021a. "Tabique walls, a light timber structure – constructive details and material characterization." Architecture, Structures and Construction Journal. Ed. Springer Nature. https://doi.org/10.1007/s44150-021-00010-z.

Padrão, J., Silva, R., Arêde, A., Guedes, J. 2021b. "Paredes de tabique submetidas à compressão vertical – proposta de ensaio *in situ* e interpretação dos resultados obtidos." Revista Portuguesa de Engenharia de Estruturas. Ed. LNEC. Série III. n.º 17. ISSN 2183-8488 pp. 39-48.

SILVA, R. D. "VEDAÇÃO EM CONSTRUÇÕES DE MADEIRA E DERIVADOS". Escola de Engenharia de São Carlos – EESC-USP).

TAVARES, M.; COSTA, A. Reabilitação estrutural do património edificado. Coimbra: Imprensa da Universidade de Coimbra, 2010.

Cinpar 2026
XXII International Conference on Building Pathology and Constructions Repair
15th to 17th July 2026 - Lisboa, Portugal

Benchmarking Traditional Earthen Construction Technologies for Sustainable and Affordable Housing in Tanzania

Tuba TATAR[1], Sarah PHOYA[2], Rehema MONKO[3], Geoffey MBATA[4] Alvin RUJWEKA[5]

[1] Sakarya University, Sakarya, Türkiye, ttatar@sakarya.edu.tr
[2] Ardhi University, Dar Es-salaam, Tanzania, sarah.phoya@aru.ac.tz
[3] Ardhi University, Dar Es-salaam, Tanzania, rehema.monko@aru.ac.tz
[4] Ardhi University, Dar Es-salaam, Tanzania, geofrey.mbata@aru.ac.tz
[5] Dar es salaam Institute of Technology, Dar Es-salaam, Tanzania, alvinrujweka@gmail.com

Abstract: Traditional earthen construction technologies represent a significant yet increasingly underutilized resource for sustainable and affordable housing development in Sub-Saharan Africa. This paper presents the outcomes of the PURSUE Project inception study, which benchmarks vernacular housing systems through detailed field investigations conducted in Mbulu District (Manyara Region) Kondoa District (Dodoma Region) and Makumbusho village Dar es salaam Tanzania. The study documents and analyses a range of indigenous dwelling typologies, including Mwera, Iraqw, Hehe, Bembe, and Nyakyusa houses, focusing on their spatial organization, which based on daily activities such as food preparation, livestock management, and communal living, material composition, construction techniques, and environmental performance. These housing systems are predominantly built using locally available materials such as earth, timber, bamboo, grass, stone, lime, and ash, resulting in structures with low embodied energy, high thermal mass, and strong climatic responsiveness. The findings highlight how traditional construction practices integrate architectural form, material selection, and settlement patterns with landscape, climate, and cultural knowledge, achieving durable and resource-efficient housing solutions. The paper also examines the ongoing transition from earthen and thatched construction to burnt clay brick masonry and corrugated metal roofing, driven by urbanization, market accessibility, and changing socio-economic aspirations. While this transition often retains traditional spatial layouts, it signifies a gradual shift away from vernacular building wisdom toward standardized materials perceived as more modern and permanent. By systematically documenting traditional earthen housing technologies and their contemporary transformations, this study establishes a technical and cultural knowledge base to inform future research, capacity building, and the development of sustainable construction and rehabilitation strategies rooted in local contexts.

Keywords: Earthen construction; Sustainable housing; Sub-Saharan Africa; Tanzania; Cultural landscape

1. Introduction

Green building materials and construction techniques are coming to the forefront whereas the impact of building materials on global warming frequently discussed these days (Mehra, ve diğerleri 2022). Structural green materials such as; bamboo, soil, recycled steel, engineered timber have been promoted more all over the world while traditional construction techniques and materials have been also gotten attention by end-users, architects and engineers. Vernacular building traditions refers to buildings created by local communities, where design choices are shaped by cultural traditions. It differs significantly across regions due to variations in climate, landscape, and cultural context. These technologies are grounded in the use of locally available materials and indigenous knowledge systems, resulting in building forms characterized by low embodied energy and high contextual suitability with minimal cost (Matos, Milheiro-Oliveira ve Varum

2025). The main factor influencing the development of the vernacular construction practices is depending on geographical location, climatic conditions, cultural practices, and the accessibility of locally available building materials such as adobe (i.e., mud blocks, whole walls), masonry (i.e., stone, clay) and timber (Sassu 2002). Over time, vernacular dwellings have adapted to environmental conditions, resource availability, and societal needs. These traditions emerged through long-term trial and error, guided by the practical expertise of local builders who possess deep, place-specific knowledge, an asset that is increasingly diminishing in today's era of globalization and remote practices. Therefore, studying and integrating the principles of traditional vernacular architecture into contemporary design holds considerable value. Building layout, like circular, rectangular and linear plans, is another factor usually related to cultural, historical, and urban planning traditions.

Vernacular building traditions fall under sustainable construction which emphasizes on reducing environmental impacts while ensuring economic and social viability. The structures align remarkably well with contemporary environmental goals. Their reliance on local materials reduces transportation impacts, while their typically low energy consumption and capacity for reuse or natural decomposition make them environmentally sensitive solutions. The study done by Mora-Ruiz et al., (2025) confirm that such construction practices significantly lowers greenhouse gas emissions compared to cement-based materials and supports circular construction practices. In addition, the study by Fouad et al., (2025) affirmed that vernacular construction practice offers a low-carbon alternative suitable for sustainable housing delivery. In this sense, vernacular architecture is not merely a record of past creativity but also a valuable source of inspiration for developing resilient and sustainable construction practices today. On the contextual of spatial studies also show that vernacular structures maintain strong links with cultural identity and local livelihoods, reinforcing their relevance in sustainable development discourse (Zhang et al., 2024). These practices symbolize an extremely refined intelligence that branches not from formal design rules but from the lived experiences accumulated over generations. By utilizing local materials and construction techniques, such as natural ventilation in warm climates or thermal mass in arid regions that perfectly adapt to regional climates, these structures are inherently sensitive to their surroundings. This enables the construction of buildings that typically achieve high levels of energy efficiency without relying on mechanical systems.

Furthermore, vernacular building traditions e reflects the identity, values, and social practices of the communities that build and inhabit it; it creates spaces that are not only functional but also meaningful. The construction process typically fosters community participation and knowledge transfer, thereby strengthening social cohesion and continuity. The characteristics and scale of buildings vary according to their region, geographical context, climatic conditions which differ considerably across locations and the availability of local resources. Despite their low cost and excellent thermal and acoustic performance, these buildings are associated with several challenges, particularly related to wall erosion caused by water and wind. Additional issues arise from vegetation growth and the presence of termites and other insects. Most structural deficiencies are linked to the foundations, which are typically constructed as shallow trenches, approximately 30-40 cm deep, from which the walls are erected. These foundations are often inadequate, as the erosive action of water can undermine the walls to greater depths. As a result, erosion at the base leads to a loss of cohesion among the wall components, causing gradual yet continuous structural deterioration (Fumo ve Di Nardo 2015).

In recent years, processes such as globalization and rapid urbanization, obvious by the growth of urban populations, have increasingly challenged the continuity of vernacular building traditions and urban forms specifically in Africa. These include increasing pressure on the environment, existing infrastructure, and urban building stock, as well as limited time and insufficient access to appropriate construction materials for new housing and services. At the same time, a more deeply rooted pattern in African development is the prioritization of non-African architectural models over vernacular traditions. Formal architectural practices across the continent have long been shaped by European influences, reflecting broader historical processes in which African societies were compelled to adopt European languages, governance systems, and cultural

norms during the colonial period. Although African cities existed and functioned effectively prior to colonization, their forms and structures did not align with European definitions of urbanity. Western concepts of urban form and building typologies continue to be regarded as superior, even when they conflict with local environmental conditions and cultural practices. Ones of the best examples of vernacular structures can be observed in Tanzania which is located on the Eastern coast of Africa and its population is over 61 million and one of the fastest growing countries in Africa. The total number of buildings is more than 14 million according to the CENSUS 2022 (The United Republic of Tanzania National Bureau of Statistics 2022). Urban population in Tanzania is 36% according to the World Bank data in 2024 (World Bank 2024). In Tanzania, homes are also built through self-help and/or community-based approaches. Most homes in the country do not comply with engineering standards, and informal settlements remain a major problem in the country. The 2011/12 National Population and Housing Census revealed that among more than 9 million households, the primary wall materials were cement bricks (20.3%), sun-dried bricks (26.3%), fired bricks (26.3%), and posts and mud (23.5%) (The United Republic of Tanzania National Bureau of Statistics 2022). The most common building types in Tanzania are traditional houses, unreinforced masonry structures made of adobe bricks, unreinforced masonry structures made of fired brick/concrete blocks, and reinforced concrete structures. The vast majority of residential buildings are vulnerable to damage and prone to collapse due to natural disasters (Silva, Tatar ve Henshaw 2021). Table 1 lists the common local building materials in Tanzania based on the region. Bamboo, grass, and mud are the most communal structural material in the country.

Table 1 - Tanzanian vernacular construction materials *(Runyoro 2020)*

Ethnic Group in Tanzania	Housing construction elements
Western Tanzania	Poles, sticks, bamboo, mud & grass, elephant grass roofing
South East Tanzania	Poles, sticks, bamboo, soil and grass
Southern Highlands	Bamboo (extensive), mud & grass
Coastal areas	Sticks, soil, palm leaves, mud & poles, grass thatch (common)
Central Tanzania	Bush poles, grass and soil
Inter lacustrine region	Poles, bamboo, sticks and grass
Nilo-Hamitics	Poles, sticks, grass and soil
Kosain&Luo	Mud and grass

This paper investigates the common vernacular building structures in Tanzania as a part of an EU funded project, PURSUE (PURSUE, PURSUE 2025). The PURSUE project aims to promote the usage of locally available, eco-friendly, and affordable construction materials, fostering collaboration among higher education institutions, professionals, and communities in Sub-Saharan Africa (SAR). The project involves collaboration between universities in Türkiye, Portugal, Mozambique, Tanzania, and Somalia, focusing on supporting sustainable development goals such as industry innovation, sustainable cities, responsible consumption, climate action, and partnerships for development. The main objectives of this study are:

- To document and benchmark traditional earthen construction technologies in Tanzania.
- To analyze the material systems and construction techniques used in vernacular dwellings.
- To evaluate the environmental and cultural significance of these housing systems.
- To identify lessons for sustainable and affordable housing development.

2. Vernacular Constructions in Tanzania

2.1 Cultural and Environmental Context

Traditional housing systems in Tanzania have evolved through long-term adaptation to climate, available resources, and social organization. Settlements often respond to topography, agricultural activities, and environmental conditions. In Mbulu District, for example, settlements are located in the Mbulu Highlands, characterized by undulating hills, volcanic soils, and seasonal water systems that influence building location and materials. Traditional communities such as the Iraqw people develop housing forms closely integrated

with their agricultural landscapes and collective settlement patterns. The main challenge the users face is the regular maintenance of dwellings, such as reapplying mud plaster to the walls three or more times per year to prevent the structural failure. Moreover, the rectangular plan of the dwelling may cause problems with wall separation at the corner and connections and out-of-plane collapse under lateral loading such as a strong wind or earthquake.

2.2 Traditional Building Materials

Natural materials such as stone, timber, straw, sheep's wool, plant-based fibers (e.g., hemp), cork, and clay have long formed the basis of traditional construction practices. However, over the past fifteen years, particularly in Europe and the United States, there has been a renewed and growing interest in both natural and unconventional building materials.

Traditional (natural) materials can generally be categorized according to their function within a building system. As structural components, materials such as timber, stone, rammed earth, straw bales, and clay bricks are commonly employed in load-bearing construction. For insulation purposes, materials like sheep's wool, hemp fibers, and cork are widely used due to their favorable thermal properties. Additionally, natural materials also serve complementary roles in finishing applications, including plastering, painting, and flooring, where clay and cork are frequently utilized (Spišáková ve Mačková 2015).

Among these materials, stone remains one of the most prominent. It is a highly durable and low-maintenance option, characterized by its significant thermal mass. Stone is also highly versatile, available in a wide range of shapes, sizes, colors, and textures, making it suitable for applications such as flooring, walls, arches, and roofing. Furthermore, it integrates harmoniously with the natural environment and can be readily reused or recycled for various construction purposes. Stone is often incorporated at the base of walls or within foundations. Its primary function is to protect earthen walls from moisture ingress and erosion, thereby enhancing the durability and longevity of the structure. Earth serves as the primary material for wall construction in many vernacular buildings (Matos, Milheiro-Oliveira ve Varum 2025). It is typically used either in the form of compacted mud or shaped into sun-dried blocks, providing both structural capacity and thermal mass. Timber is commonly employed for structural elements such as frames and roof beams. It is generally sourced from nearby forests, making it a locally available and renewable material that supports the overall framework of the building. Grass and thatch are widely used in roofing systems. These materials not only offer effective protection against rainfall by shedding water efficiently but also provide natural insulation, helping to regulate indoor temperatures. Lime and ash are occasionally added as stabilizing agents in construction. These materials improve the strength and resistance of earth-based mixtures, contributing to better performance against environmental effects. These materials offer:

- low embodied energy
- strong thermal performance
- environmental compatibility
- Often mixed with cow dung to improve cohesion and durability

Table *2* shows the comparison of the building materials in Tanzania based on labor, cost, time consumption, and distance to transport material. The locally available materials do not require laboring, have the minimum cost, necessitate less the construction time with limited needs of transportation in comparison with the other structural materials in the country.

Table 2 - Comparison of the building materials in Tanzania *(Buccellato ve Reineccius 2013)*

Type	Building Materials	Labor	Cost (0-$$$)	Time of Construction	Distance to Transport Material
Wattle and Daub	Mud with ash or manure as binding agent	Local, not hired	0	2 days	0
	Sisal poles	Local, not hired	0	5 days (to strip bark & trim)	Up to 15 km on foot

	Sisal split stalks for holding together walls	Local, not hired	0	5 days to prepare, 1 day to put in place	Up to 15 km on foot
	Corrugated metal with lumber wood trusses	Local, hired	$$ (for labor and material)	1 week	45 km by vehicle
Concrete Masonry Units	Concrete block units	Not local, hired	$$$ (for labor and material)	2 to 5 years (based on funding)	15 to 45 km by vehicle
	Poured concrete foundation	Not local, hired	$$$ (for labor and material)	1 week (depends on funding)	15 to 45 km by vehicle
	Corrugated metal and lumber wood trusses	Local, hired	$$ (for labor and material)	1–2 weeks (usually larger, complex structures)	45 km by vehicle
Compressed Earth Bricks	Walls: Soil (40% sand, 25% gravel, 25% clay, 10% silt and water), Concrete & mortar, Rebar (not always)	Local, hired	$$	Up to 2 years (based on funding)	0 (soil), 15 to 45 km by vehicle (concrete)
	Poured concrete foundation	Not local, hired	$$$	1 week (depending on funding and size)	15 to 45 km by vehicle
	Corrugated metal roof with wood trusses	Local, hired	$$$	1–2 weeks (usually larger, complex structures)	45 km by vehicle

3. Methodology

3.1 Research Design

This study adopts a qualitative multiple case study design to benchmark traditional earthen construction technologies across different geographical and cultural contexts in Tanzania. The case study approach is appropriate for investigating complex, context-dependent phenomena such as vernacular architecture, where boundaries between the phenomenon and context are not clearly defined (Yin, 2018). The qualitative approach allows for an in-depth understanding of material use, construction techniques, and socio-cultural influences that cannot be adequately captured through purely quantitative methods (Creswell, 2014). This design is widely applied in studies of traditional construction systems and sustainable architecture.

3.2 Study Areas

Field investigations were conducted in Mbulu District, Kondoa District, and Makumbusho Village. These sites were purposively selected to capture climatic and cultural diversity, as well as well-preserved vernacular housing systems. This purposive selection is justified in qualitative research aiming for information-rich cases rather than statistically representative samples (Patton, 2015).

3.3 Sampling Strategy and Sample Size

A purposive sampling strategy was employed to select between 15 and 24 dwelling units, with approximately 5–8 houses examined per study site. Purposive sampling is appropriate for studies that focus on specific characteristics, such as vernacular housing typologies and traditional material use, as it enables the selection of information-rich cases relevant to the research objectives (Patton, 2015). The chosen sample size is consistent with qualitative research standards, where depth of analysis is prioritized over statistical generalization (Creswell, 2014). This approach ensured the inclusion of representative housing typologies, variations in construction techniques, and different levels of structural condition. In Mbulu District and Kondoa District, Tembe houses were selected as the dominant vernacular typology. In contrast, at Makumbusho Village, a broader range of indigenous housing types was examined, including Mwera, Iraqw,

Hehe, Bembe, and Nyakyusa houses, reflecting the site's role as a cultural repository of diverse Tanzanian architectural traditions.

3.4 Selection Criteria

Selection criteria, guided by methodological rigor and relevance to research objectives, included: typological representation of dominant vernacular forms (Oliver, 2006); material authenticity focusing on traditional earthen systems (Houben & Guillaud, 1994); state of conservation for assessing durability; environmental context capturing climatic and geographical variations; and accessibility for detailed documentation.

3.5 Data collection methods

Data collection combined field and desk research: direct observation of construction, materials, and structural conditions; photographic surveys of building elements; measured sketches of spatial organization and construction systems; informal interviews with builders and occupants regarding construction practices and cultural context; and a literature review of earthen construction technologies and performance.

3.6 Analytical framework

This study uses a multi-criteria framework to holistically assess vernacular housing performance by integrating material (thermal, structural, durability), environmental (climatic responsiveness, embodied energy), socio-cultural (spatial organization, cultural practices), and construction technique (methods, adaptability) considerations. Multi-criteria analysis is a common method in sustainable construction research for evaluating complex systems (Kibert, 2016).

4. Vernacular Housing Typologies in Tanzania

4.1 Mwera (Banda) House

Mwera (Banda) House is traditionally built in a rectangular layout using natural, locally sourced materials, reflecting both environmental adaptation and cultural craftsmanship. Construction begins by digging small holes and placing sturdy wooden poles approximately two meters apart to form the main structural framework. Thinner miombo sticks are then woven horizontally between these poles at intervals of about 30 cm, creating a tight lattice that strengthens the walls and supports the clay render. Wet red clay mixed with water and sometimes small amounts of grass or cow dung for binding is applied over this woven frame to form thick, durable walls. A small window is intentionally left near the roofline to ensure sufficient ventilation and allow daylight into the interior without compromising security or heat control. The roof is supported by a network of wooden rafters and is meticulously thatched with layers of elephant grass. This type of thatching is not only lightweight but also provides excellent thermal performance, keeping the interior cool during hot seasons and warm during cold nights. The sloped form of the roof helps shed rainwater effectively, which is essential in the region's tropical climate. Figure 1 illustrates a typical Mwera house in Tanzania.

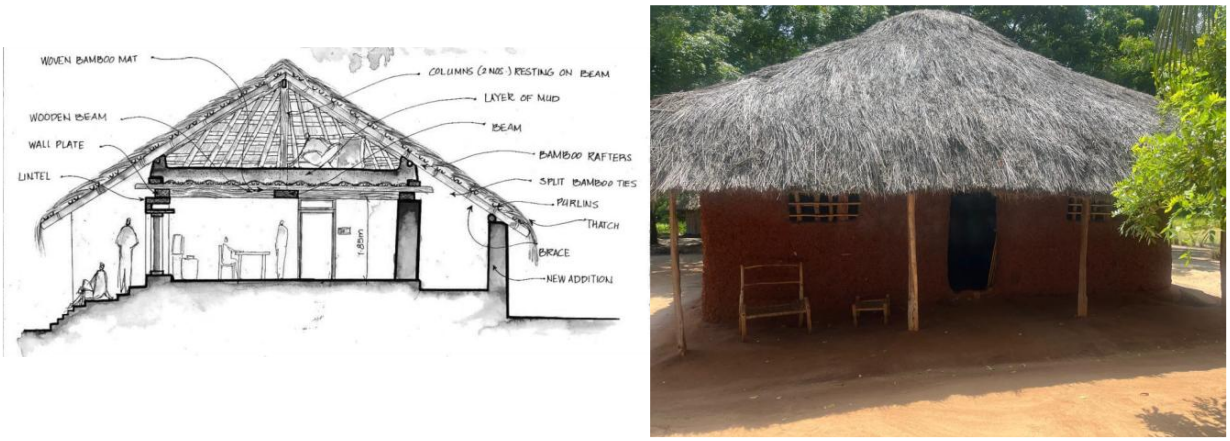


Figure 1 - Typical Mwera house in Tanzania

4.2 Iraqw House (Tembe)

Wa-Iraq Houses (Tembe) are traditionally rectangular dwellings characterized by their thick mud walls and distinctive flat earthen roofs. Built entirely from natural, locally available materials such as mud, clay, timber and cow dung. These houses demonstrate an efficient and sustainable architectural system well adapted to the Iraq tribe's environment. The walls are constructed either from sun-dried mud bricks or by applying layers of mud plaster over a simple wooden framework. This results in dense, thermally efficient walls that help keep the interior cool during the day and warm during cold nights. Cow dung is often mixed into the mud as a binding agent, improving the material's strength, durability and resistance to cracking. A defining feature of the house is its flat roof. Supported by strong timber beams laid across the main walls, the roof is topped with layers of compacted earth. This earthen roof is carefully tamped to enhance waterproofing and stability, allowing it to withstand wind, heat, and occasional rainfall. In some cases, grass or small branches are integrated beneath the mud layer to improve structural cohesion. Figure 2 displays a great example about Iraqw house in Tanzania.



Figure 2 - Typical Iraqw house in Tanzania

4.3 Hehe House

Hehe Houses (Tembe) are traditional rectangular or slightly oval structures built using wattle-and-daub techniques and natural local materials. Their construction begins with arranging strong wooden poles vertically into the ground to create the main frame of the house. Between these poles, smaller flexible sticks are woven horizontally to form a tight lattice that supports the wall structure. This woven framework is then plastered with layers of wet mud mixed with grass or cow dung, producing thick, sturdy walls that provide

excellent insulation against heat and cold. The walls are often smoothened by hand and left to dry naturally in the sun. The roof is typically constructed from wooden rafters covered with dense thatching made of long grasses, often elephant grass or similar locally available varieties. This thatched roof is designed with a gentle slope to shed rainwater efficiently and maintain a cool interior temperature. Figure 3 shows a sketch and one existing Hehe house in Tanzania.



Figure 3 - Typical Hehe house in Tanzania

4.4 Bembe House

Bembe House (Msonge houses) are traditionally constructed using a flexible framework that forms a rounded, dome-like structure. The building process begins with bending slender poles and securing them together to create a curved skeletal frame. This arched framework provides both strength and resilience, enabling the house to withstand heavy rains and shifting weather conditions. Once the main frame is set, the walls are woven with reeds, banana fibres, or other flexible plant materials to create a tight lattice.

This woven surface acts as a supportive base for the wall covering. Layers of mud are then applied over the lattice, forming a firm, smooth exterior that strengthens the structure and provides effective protection against rain and wind. The roof is traditionally thatched with bundles of dried grass or overlapping banana leaves. These materials are carefully arranged in thick layers to ensure water flows off easily, preventing leaks and maintaining a cool, well-insulated interior. Figure 4 displays a typical bembe house in Tanzania.



Figure 4 - Typical Bembe house in Tanzania

4.5 Nyakyusa House

Nyakyusa houses (Bamboo House) are traditionally constructed using bamboo as the primary structural material, reflecting the tribe's close connection to the forested landscapes of the Southern Highlands.

Building a house is a communal activity, where relatives and neighbors gather to assist, reinforcing social unity and cooperation. The construction process begins by assembling strong bamboo poles to form the main framework of the house. These poles are arranged vertically and horizontally, then tied securely to create a stable skeleton. Additional bamboo pieces are woven or lashed into the structure to strengthen the walls and support the roof. Because bamboo is lightweight yet durable, the completed structure remains flexible an advantage in areas prone to heavy rain or strong winds. A distinctive cultural characteristic of Nyakyusa housing is the attention given to decoration and finishing. Significant effort is spent smoothing the surfaces, arranging bamboo neatly, and sometimes embellishing entrances or edges to showcase craftsmanship. The quality of finishing often reflects pride, skill, and social identity within the community. Figure 5 illustrates Nyakyusa houses in Tanzania.



Figure 5 - Typical Nyakyusa house in Tanzania

The comprehensive comparative analysis of vernacular housing typologies in Tanzania is summarized in Table 3.

Table 3 - Comparative analysis of vernacular housing typologies in Tanzania

Typology	Structural System	Main Materials	Roof Type	Strength	Weakness	Environmental Performance
Mwera House	Timber frame + wattle and daub	Wooden poles, woven sticks, mud, grass, cow dung	Sloped thatched roof (elephant grass)	Lightweight structure; good airflow; adaptable construction	Vulnerable to erosion; weak wall cohesion; low durability against moisture	Good thermal insulation; effective ventilation; suitable for tropical climate
Iraqw House	Load-bearing earthen walls	Mud, clay, timber, cow dung, stone (foundation)	Flat earthen roof	Thick walls provide strength and insulation; compact layout	Poor resistance to water infiltration; heavy roof load;	High thermal mass; stable indoor temperature (day-night balance)

					foundation erosion risk	
Hehe House	Wattle and daub system	Wooden poles, sticks, mud, grass, cow dung	Sloped thatched roof	Flexible structure; easy to construct; low-cost materials	Weak structural integrity; prone to biological degradation (termites, vegetation)	Good thermal performance; efficient rainwater drainage
Bembe House	Flexible curved frame (dome-like)	Bent poles, reeds, banana fibers, mud	Thatched (grass/banana leaves)	Aerodynamic form improves resistance to wind; structural flexibility	Limited load-bearing capacity; high maintenance of organic materials	Good climatic adaptation; efficient rain shedding; stable internal environment
Nyakyusa House	Bamboo frame structure	Bamboo, grass, earth (foundation)	Thatched roof	Flexible and resilient to environmental loads; community-based construction	Low durability; susceptible to decay, insects, and moisture	Good ventilation; lightweight; suitable for humid environments

5. Results and Discussion

Cross-case comparison across typologies and regions evaluated using standardized indicators for thermal performance, durability, structural stability, and material efficiency via comparative benchmarking.

5.1 Thermal Performance of Earthen Materials

The findings indicate that traditional earthen construction systems across the study areas exhibit strong thermal performance due to their high thermal mass. Materials such as compacted earth walls and mud-plastered roofing systems absorb heat during the day and release it gradually at night, thereby moderating indoor temperature fluctuations.

In semi-arid environments such as Kondoa District and Mbulu District, this thermal behavior contributes significantly to indoor comfort by reducing daytime overheating and maintaining warmth during cooler nights. Similarly, in the coastal context of Dar es Salaam, earthen walls help buffer high ambient temperatures, although ventilation plays a more critical role due to humidity. These findings confirm that earthen materials provide an effective passive cooling strategy, reducing dependence on mechanical systems and supporting climate-responsive housing design.

5.2 Durability Performance and Degradation Mechanisms

Despite their environmental and thermal advantages, earthen structures are susceptible to several durability challenges. The most common form of deterioration observed across the case studies is surface erosion, primarily caused by rain impact, surface runoff, and wind action. This results in gradual material loss and weakening of wall sections over time.

Another critical issue is foundation-related failure, particularly in structures lacking adequate plinth protection. In several cases, direct contact between earthen walls and the ground led to moisture ingress through capillary action, causing rising damp, material disintegration, and eventual structural instability.

However, buildings incorporating stone foundations or raised plinths demonstrated improved resistance to moisture and longer service life. This highlights the importance of integrating basic protective measures to enhance the durability of earthen construction.

5.3 Structural Performance and Failure Modes

The structural assessment revealed several inherent weaknesses in traditional earthen construction systems, particularly in relation to lateral stability and wall integrity. These vulnerabilities are primarily attributed to the low tensile strength of earthen materials and the absence of effective reinforcement mechanisms.

5.4 Out-of-Plane Failure:

Out-of-plane wall failure was identified as a major structural risk, especially in buildings constructed with unreinforced earthen walls and weak roof-to-wall connections. Under lateral loads, such as wind pressure, walls tend to bulge and may eventually collapse outward due to insufficient tensile resistance and lack of proper anchorage. This type of failure is particularly evident in structures with large unsupported wall spans and inadequate structural integration between wall and roof elements.

5.5 Corner Separation:

Corner separation and cracking at wall junctions were also commonly observed across the case studies. These failures are typically associated with poor bonding between intersecting walls, often resulting from construction techniques that do not ensure adequate interlocking or continuity at corners. The absence of reinforcement elements, such as tie beams or corner strengthening, further exacerbates this weakness. Over time, progressive cracking at these junctions compromises the structural integrity and stability of the entire building. Overall, these findings highlight the need for incorporating simple and effective reinforcement strategies such as improved bonding techniques, timber ring beams, and corner stabilization methods. These will enhance the structural performance of earthen construction systems without undermining their sustainability advantages.

6. Conclusions

The findings of this study demonstrate that traditional earthen construction technologies in Tanzania embody a highly efficient and context-responsive approach to housing, shaped by centuries of adaptation to local climatic, environmental, and socio-cultural conditions. The investigated vernacular typologies, Mwera, Iraqw, Hehe, Bembe, and Nyakyusa houses, reveal a sophisticated integration of locally available materials, construction techniques, and spatial configurations, resulting in structures that are not only affordable and resource-efficient but also environmentally sustainable. These systems exhibit low embodied energy, strong thermal performance, and a high degree of compatibility with their surrounding landscapes, confirming their relevance within contemporary sustainability discourse.

However, the study also highlights a significant ongoing transition toward modern construction materials such as burnt bricks and corrugated metal roofing, driven by urbanization, changing socio-economic aspirations, and perceptions of durability and modernity. While this shift often preserves certain spatial and cultural characteristics, it simultaneously risks the gradual loss of valuable vernacular knowledge and practices. In this context, the results emphasize the necessity of adopting a balanced and integrative approach that does not disregard traditional systems but rather enhances them through scientific validation and technological innovation.

The PURSUE project provides a critical framework for this transition by bridging traditional knowledge with modern engineering practices through education, capacity building, and technology transfer. By equipping stakeholders with the necessary tools and knowledge to improve the performance of local materials, the project supports the development of resilient, affordable, and sustainable housing solutions tailored to regional needs. Ultimately, this research underlines that the future of housing in Sub-Saharan Africa lies not in the replacement of vernacular systems, but in their informed transformation, ensuring that cultural heritage, environmental sustainability, and technical advancement are effectively aligned.

7. References

Buccellato, A., and M. Reineccius. "Exploring Vernacular East African Architecture: Lessons for the Modern World." *Vernacular Traditions, ASCA*, 2013: 55-64.

Fumo, M, and L Di Nardo. "Constructive Tradition becomes Future - Design an educational and professional training establishment in Africa - Tanzania." *The Fifth Asian Conference on Sustainability, Energy and the Environment*. Osaka, 2015.

Matos, A.M., P. Milheiro-Oliveira, and H. Varum. "New Technologies for Earth Construction: 3D Printing, a Reality or a Mirage?" In *Sustainable Materials for the Built Environment*. Springer Series in Materials Science, 2025.

Mehra, S., M. Singh, G. Sharma, S Kumar, and Navishi Chadha, P. "Impact of Construction Material on Environment." In *Ecological and Health Effects of Building Materials*, by J.A. Malik and S Marathe. Springer, Cham, 2022.

Munoz, N.S., and S. Moriset. "Building vernacular, building sustainable. Case studies of contemporary architecture." *SOStierra2017, UPV*. Valencia, 2018.

PURSUE. *PURSUE*. 2025. https://pursue.sakarya.edu.tr/ (accessed 03 31, 2026).

—. *PURSUE*. n.d. https://pursue.sakarya.edu.tr/ (accessed 03 31, 2026).

Runyoro, Aileen. *The Role of Vernacular Architecture in Adaptive reuse, A case of the Old Boma Building, Bagamoyo, Tanzania*. Hasselt: University of Hasselt (Master's Thesis), 2020.

Sassu, Mauro. "VERNACULAR HOUSING CONSTRUCTION." Pisa, 2002.

Silva, V., T. Tatar, and P. Henshaw. *METEOR: definition of taxonomy for multi-peril vulnerability. Report M5. 1/P*. British Geological Survey, 2021.

Spišáková, M., and D. Mačková. "The use potential of traditional building materials for the realization of structures by modern methods of construction." *Journal of Civil Engineering* 10, no. 2 (2015): 127-138.

The United Republic of Tanzania National Bureau of Statistics. 2022. https://sensa.nbs.go.tz/ (accessed 03 2026, 25).

World Bank. *World Bank*. 2024. https://data.worldbank.org/indicator/SP.URB.TOTL.IN.ZS?locations=TZ (accessed 03 30, 2026).

Zhai, Z. J., and J. M. Previtali. "Ancient vernacular architecture: characteristics categorization and energy performance evaluation." *Energy and buildings* 42, no. 3 (2010): 357-365.

Zhang, Y., Li, X., & Wang, L. (2024). Vernacular architecture and climate adaptation: Lessons for sustainable design. Sustainable Cities and Society, 102, 105230.

CINPAR 2026
XXII International Conference on Building Pathology and Constructions Repair
15th to 17th July 2026 - Lisboa, Portugal

Underground Intervention in a Historic Building: Structural Compatibility and Heritage Preservation at the Museu Paulista

Gabriel Juliani MENTONE[1], Drª Fabiana Lopes OLIVEIRA[2]

[1] Universidade de São Paulo, Brazil, gabriel.mentone@usp.br
[2] Universidade de São Paulo, Brazil, floliveira@usp.br

Abstract: Contemporary interventions in historic buildings often pose significant technical challenges, especially when involving pre-existing pathological conditions, strict heritage constraints, and the need for functional expansion. In this context, this paper presents a case study of the intervention carried out at the Museu Paulista in São Paulo, focusing on the structural connection between the historical load-bearing masonry building and an underground reinforced concrete extension constructed beneath its foundations. The objective is to critically analyze the design and construction solutions adopted to enable this interface, considering the risks related to settlement, vibration, and cracking, further aggravated by the presence of works of art integrated into the masonry and by pathological conditions resulting from previous interventions. The methodology is based on a case study, with the analysis of project documentation, construction records, field observations and a critical comparison with guidelines from international heritage charters, especially regarding the use of contemporary techniques and the functional adaptation of cultural assets. The results show that the initial planned execution had to be revised due to soil behavior and observed settlements, leading to the adoption of solutions such as micropiles, jet grouting, tunnel excavation using the NATM method, and continuous geotechnical monitoring, allowing safe excavation while preserving the structural and material integrity of the monument. The interventions resulted in controlled settlements, without inducing cracks in the historic masonry or damage to the artworks, although with significant impacts on the schedule. It is concluded that contemporary extensions to historic buildings are technically feasible when guided by criteria of minimal intervention, structural compatibility, reversibility, and rigorous risk management, demonstrating that techniques usually associated with large-scale projects can be fundamental for mitigating pathologies and supporting the preserving built heritage

Keywords: Foundation reinforcement, historic building, contemporary intervention, underground excavations, containment techniques

1. Introduction

The Museu Paulista building, located in the city of São Paulo and popularly known as the Ipiranga Museum, is one of the most significant architectural and symbolic landmarks of Brazil's cultural heritage. Designed by the Italian engineer and architect Tommaso Gaudêncio Bezzi and constructed between 1885 and 1890, the building was originally conceived as a monument commemorating the Independence of Brazil. It was later adapted to house a scientific and educational museum, consolidating its role throughout the twentieth century as an important cultural institution.

As is common in many historic buildings, the structure gradually developed pathological manifestations resulting from material aging, previous interventions, and the evolving functional and technical requirements associated with contemporary museum use. In 2013, following the worsening of structural and construction-related problems, the museum was closed to the public, initiating an extensive process of technical studies and planning aimed at its restoration, modernization, and functional expansion.

Within this context, the University of São Paulo launched, in 2017, a National Architectural Competition for the rehabilitation, restoration, and expansion of the Museu Paulista complex. The winning proposal,

developed by H+F Arquitetos (Hereñú + Ferroni Arquitetos), adopted an approach based on reconciling heritage conservation with the functional upgrading of the museum.

Construction works began in October 2019 and were carried out under conditions of considerable technical complexity, further intensified by the stringent restrictions imposed by heritage protection authorities. The Museu Paulista building and the Independence Park are protected simultaneously at the federal, state, and municipal levels, requiring that every intervention be carefully planned in order to preserve the material integrity and symbolic significance of the listed heritage property.

Among the principal design strategies adopted were improvements in functionality and accessibility, modernization of technical infrastructure systems, and, most notably, the construction of a new underground extension intended to accommodate reception facilities, temporary exhibition spaces, and visitor support areas. This extension was implemented beneath the front esplanade and connected directly to the historic building through vertical circulation cores constructed adjacent to the existing foundations.

The implementation of this intervention posed particularly complex technical challenges, primarily due to the need to carry out deep excavations and construct new structural elements in close proximity to the foundations of a historic load-bearing masonry building subject to strict heritage constraints and containing artistic elements integrated into the masonry fabric. In this context, balancing heritage conservation, structural safety, and construction feasibility became a central aspect of both the design and execution phases of the project.

Against this background, the present paper aims to analyze the planning and execution of the vertical connection between the historic Museu Paulista building and the underground extension, discussing the structural and geotechnical solutions adopted to enable interventions of this nature in sensitive historic buildings. In doing so, the study seeks to contribute to the technical discussion on underground excavations and complex structural interfaces between historic constructions and contemporary additions.

2. Construction System of the Museu Paulista

The building of the Paulista Museum presents a construction system characteristic of the late 19th century, predominantly based on load-bearing masonry made of solid ceramic bricks. Vertically, the building consists of four levels, including a continuous basement extending beneath its entire footprint, as well as additional levels within the towers. Horizontally, it is divided into three sectors. The central sector consists of a single tower that receives and distributes the flow of visitors to the upper floors and to the two lateral exhibition sectors. The lateral sectors, east and west, each comprise a side tower connected to the central one through a wing. Each lateral tower contains a wooden helical staircase that provides vertical circulation to the upper floors. The wings are composed of exhibition rooms connected by *loggias*[1]. Figure 1 presents the ground floor plan of the monument building, highlighting the sectioning axis that separates the front façade from the rest of the building body due to the intervention carried out in the basement.

The structural walls have variable thicknesses, approximately 50 cm in internal partitions and reaching up to 1.40 m in external façades or in areas subjected to higher structural demands. The floor systems are heterogeneous, including solutions in concrete, ceramic hollow blocks, and timber structures. Ceilings are made of either wood or stucco, while internal finishes consist of lime-and-sand mortars applied directly onto the masonry or onto vegetal fibre lath made from juçara palm.

[1] loggia is an architectural space typical of historic buildings, particularly widespread in Renaissance Italy, characterized as a covered gallery integrated into the body of the building. Unlike a projecting balcony, it is recessed and defined by columns or pillars, forming a laterally open area that enhances natural lighting and ventilation while providing protection from sun and rain. Derived from classical and medieval traditions, it constitutes a transitional element between interior and exterior, widely used in palaces and public buildings as a space for social interaction, circulation, and contemplation, while also contributing rhythm, lightness, and depth to façades.

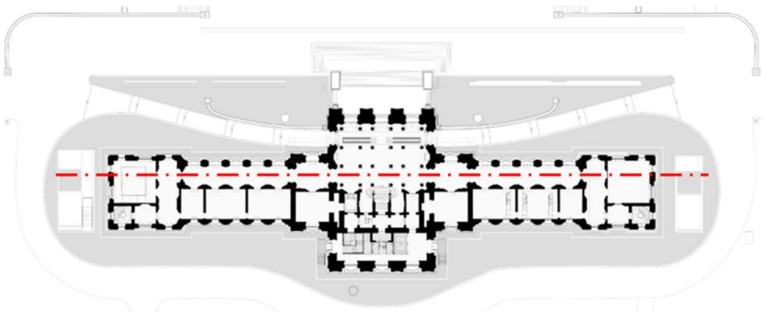


Figure 1 – Ground floor plan of the monument building Source: H+F Aquitetos (available at: https://hf.arq.br/projeto/museu-paulista/, accessed on April 5, 2026)

The foundations are composed of continuous strip footings in stone masonry bonded with mortar, approximately 2.00 m in height, consistent with the construction techniques of the period. Originally, the basement functioned as a ventilation and moisture-regulation space for the foundations, playing an important role in the hygrothermal balance of the building.

However, during a series of localized interventions in the 1990s, the basement was excavated and adapted for functional uses, coming to house sanitary facilities and administrative areas. This intervention led to the sectioning of the foundations along the front façade, particularly in the region beneath the loggias, resulting in structural movements and the emergence of cracks, especially in the front façade of the building.

This pre-existing condition constitutes a key factor in understanding the structural behavior of the monument within the context of contemporary interventions, revealing a history of modifications that have directly impacted its stability.

3. The Proposed Intervention

The architectural intervention proposed for the Paulista Museum was based on reconciling the preservation of the historic building with the need for functional expansion of the complex. In this context, a new underground volume was conceived beneath the front esplanade, with dimensions comparable to those of the monument building. The underground design strategy aimed to avoid interference with the monumental character of the historic structure, preserving its position and visual perspectives from all sides with minimal impact.

Figure 2 illustrates how the volumes relate within the landscape, without overlapping one another and with minimal intervention in existing elements. The intervention is only perceptible through the openings created in the existing granite balustrade, as no new architectural volume obstructs the pre-existing views or landscape.

The underground expansion was designed to accommodate visitor reception and welcoming functions, as well as exhibition spaces and support areas, establishing a direct connection with the monument through vertical accesses implemented adjacent to its foundations. This solution made it possible to preserve the volumetric integrity and the landscape reading of the complex, avoiding the insertion of visible elements that could compromise its historical perception. Figure 3 illustrates the scale of the reception hall proposed in the underground expansion, designed to distribute visitors throughout the cultural facility.



Figure 2 – Photograph of the façade of the extension and the monument building. Photo: Nelson Kon. Source: H+F Aquitetos (available at: https://hf.arq.br/projeto/museu-paulista/, accessed on April 4, 2026)

The connection between the underground structure and the historic monument was initially conceived through two main axes. The first, intended for primary circulation, consists of escalators installed beneath the former carriage access of the historic building, known as the via dos coxos. The via dos coxos was the monumental access route used by visitors attending events hosted in the building. It consists of two curvilinear ramped arms that enter through the sides of the central tower beneath the Noble Hall, as shown in Figure 1. In this way, carriages could stop inside the building itself, in a covered and protected area, for the boarding and disembarking of visitors.



Figure 3 – Photograph of the reception hall and ticketing area of the extension building. Photo: Nelson Kon. Source: H+F Aquitetos (available at: https://hf.arq.br/projeto/museu-paulista/, accessed on April 4, 2026)

With the intention of providing museum visitors with a sensory experience analogous to the historical arrival by carriage, this connection is composed of galleries that wrap around a soil mass responsible for supporting the loads of the monumental staircase, aligning beneath the axis of the via dos coxos. In this interpretation, the escalator functions as the “carriage” that transports visitors into the monument, directly to the ground-floor hall. Figure 4 presents a section along the axis of the via dos coxos, where the ramped accesses used by carriages and the underground intervention guiding visitors to the hall via escalators can be clearly observed.

The second axis, dedicated to elevator access, originates from the escalator axis and advances toward the interior of the building, crossing several foundation lines that support the main hall and the Noble Hall, which houses the painting Independência ou Morte.

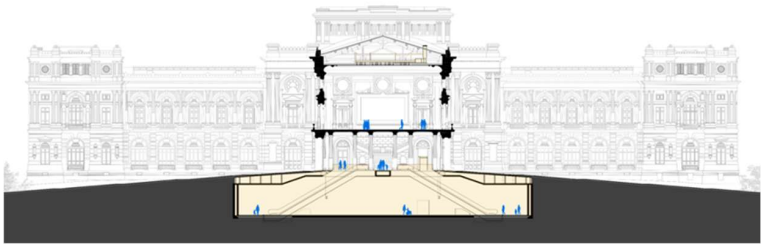


Figure 4 – Section of the main axis connecting the underground building to the monument. Source: H+F Arquitetos (available at: https://hf.arq.br/projeto/museu-paulista/, accessed on April 4, 2026)

The execution of these connections required excavations approximately 10.0 m deep in regions characterized by high concentrations of structural stresses, particularly near the central tower and the front façade. Furthermore, the proposed solutions involved the direct interaction between contemporary reinforced concrete structures and the historic load-bearing masonry system in stone. This was compounded by the structural fragility of the area due to previous interventions in the foundations carried out to adapt the basement for functional uses.

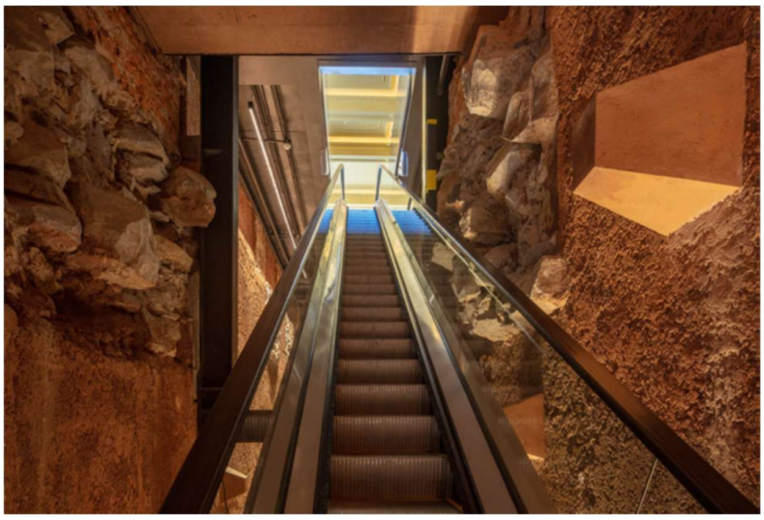


Figure 5 – Photograph of the reception hall and ticketing area of the extension building. Photo: Nelson Kon. Source: H+F Aquitetos (available at: https://hf.arq.br/projeto/museu-paulista/, accessed on April 4, 2026)

From a technical standpoint, the intervention posed significant challenges, mainly related to settlement control, soil stability, and vibration mitigation. These challenges were further intensified by the presence of artworks such as the portraits applied using the marouflage[2] technique on the central marble staircase, integrated into the masonry, whose integrity depended on extremely strict deformation limits.

Figure 5 materially illustrates the connection between the two buildings through the escalator emerging in the via dos coxos. It is possible to observe, in the lower part of the image, the pigmented concrete structures that form the anchored retaining walls at the levels of the underground expansion. Above, at the center of the figure, the rock masses that were demolished and originally composed the continuous foundation of the monument can be seen, along with soil nailing systems. Additionally, part of the vertical steel profile forming a metallic ring used to ensure continuity in load transfer within the shallow foundation system is visible, extending up to the emergence point within the ground-floor hall.

[2] *Marouflage* is a technique in which a painting executed on canvas is permanently adhered to a rigid support, such as a wall or panel, causing it to lose its mobility and become an integral part of the building's architecture.

Thus, the feasibility of the proposal depended not only on the adequacy of the adopted structural solutions but also on rigorous execution control and on strategies capable of reconciling technical requirements with the constraints imposed by heritage preservation.

4. Implemented Solution

The execution of the interventions was carried out based on a plan that incorporated continuous geotechnical monitoring and the adoption of progressive excavation and retaining strategies. As an initial measure, a line of micropiles with a diameter of 30 cm, spaced at 1.20 m intervals, was installed along the perimeter of the interface between the monument building and the extension, including both sides of the connection corridors. The primary function of this micropile line was to restrain potential movements of the sectioned foundation line of the basement and, consequently, of the front façade supported on it.

Simultaneously, the excavations were monitored through daily topographic surveys in order to detect any soil or structural movements. Preliminary geotechnical investigations, carried out under restrictions to avoid vibrations, indicated the presence of fill material in the area.

During the early excavation stages, still within the initial phases of the retaining system, differential settlements were identified in the region where the wing meets the west tower of the building. These displacements were associated with variations in the groundwater table level, which was found to be higher than initially indicated in the surveys.

In response to this scenario, excavation activities within the central area were suspended and the executive design was revised in order to mitigate the risks associated with excavation works in the most sensitive portion of the intervention.

As a result of this revision, the originally planned solution for the elevator access corridor—also based on excavation and anchored retaining walls—was replaced by the construction of a tunnel using the NATM (New Austrian Tunneling Method)[3], allowing for a more efficient redistribution of stresses within the soil mass and reducing the need for rigid retaining systems.

In addition, supplementary reinforcement was implemented through steel-cased micropiles (Schedule 80 steel pipes) installed side by side along the escalator corridor walls, the tunnel crown (see Figure 6), and the perimeter of the elevator shaft. These micropiles were interconnected by structural beams, providing additional stability to the system.

Figure 6 presents the cross-section of the tunnel excavated using the New Austrian Tunnelling Method (NATM), illustrating the stabilization system adopted to enable excavation beneath the foundations of the historic building. The scheme shows the semicircular arrangement of self-drilling steel-cased micropiles installed along the tunnel crown to provide pre-support of the soil mass prior to excavation advance.

The system was designed to reduce deformations around the excavation and control stress redistribution induced by material removal, thereby minimizing differential displacements in the foundations of the historic monument. The micropiles function as temporary retaining and ground-reinforcement elements, forming a resistant arch capable of transferring part of the loads to more stable zones of the ground.

The section also illustrates the sequential excavation procedure characteristic of the NATM, in which excavation advances are carried out in small increments and immediately followed by the application of shotcrete. This approach allows the reinforced ground itself to participate in the structural stabilization of

[3] The NATM (New Austrian Tunneling Method) is a tunnel construction methodology based on the principle that the excavated ground itself (soil or rock) should be mobilized as a structural support element. Instead of relying on immediate rigid linings, the method employs sequential excavation with continuous monitoring of deformations and the progressive application of flexible support systems—such as shotcrete, anchors, and steel ribs—adjusting the support measures according to the behavior of the ground

the tunnel, reducing the need for large rigid support structures and enabling progressive control of deformations.

In addition to the micropiles installed at the tunnel crown, lateral reinforcement elements can be observed in the support zones of the tunnel, contributing to the overall stability of the excavated section. The system was further complemented by soil nails, self-drilling spiles, and jet grouting reinforcement, installed according to excavation progress and the results obtained through continuous geotechnical monitoring.

The adoption of the ntion, as it provided greater constructior encountered during execution, especially uctural sensitivity of the historic building.

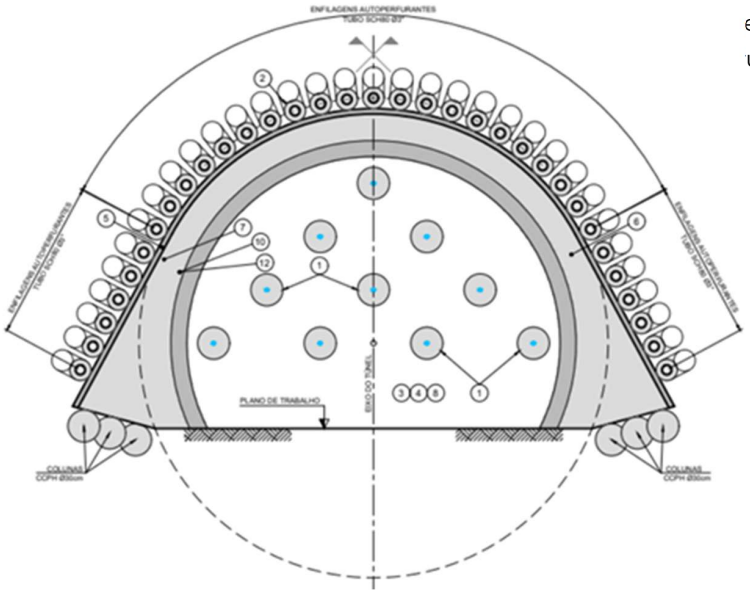


Figure 6 – Construction detail of the NATM tunnel design. Source: Maffei Engenharia e Consultoria Ltda.

Excavation activities in the central area resumed only after the completion of these reinforcement measures, including the simultaneous installation of jet grouting columns and the micropiles surrounding the elevator shaft. Subsequent excavation works were carried out in stages between April and September 2021, combining soil nailing and anchored retaining wall systems according to excavation depth and local ground conditions.

Construction of the NATM tunnel commenced only after stability conditions had been fully established, including the installation of self-drilling spiles and reinforced soil nails, and was completed by the end of November 2021. Continuous monitoring made it possible to assess the behavior of the soil–structure system throughout all stages of the intervention. A total of twelve settlement monitoring pins were installed on the lateral columns of the Via dos Coxos within the historic building to track displacements during the excavation process. In addition, fifteen monitoring pins were installed along five cross-sections of the NATM tunnel following the commencement of tunnel excavation works.

Figure 7 shows the location of the settlement monitoring pins installed along the side of the Via dos Coxos within the historic Museu Paulista building. These instruments were used for the continuous monitoring of vertical displacements induced by excavation activities and retaining interventions carried out during construction. The monitoring points identified as PR-44 to PR-55 were strategically distributed in areas considered particularly sensitive from a structural perspective, especially near the interface between the historic monument and the new underground connections.

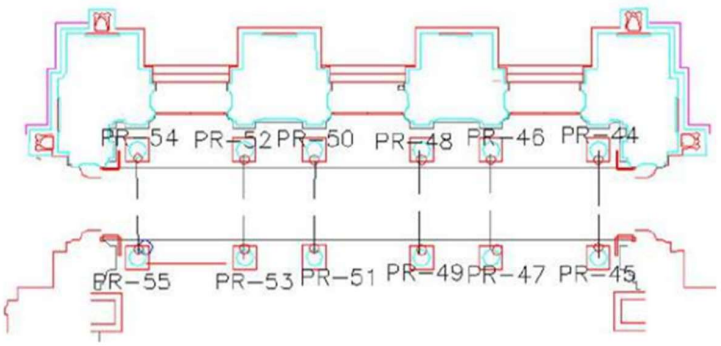


Figure 7 – Layout of settlement monitoring pins PR-44 to PR-55 installed along the side of the Via dos Coxos. Source: Museu Paulista Instrumentation Monitoring Report.

For the analysis of structural behavior, particular attention was given to monitoring points PR-52, PR-53, PR-54, and PR-55, located near the NATM tunnel portal and in regions subjected to the most significant changes in the stress state of the soil mass. These points exhibited a greater potential for differential displacements due to the combined effects of deep excavations, the presence of previously weakened historic foundations, and the execution of successive retaining structures within a confined area.

The monitoring system made it possible to track the temporal evolution of settlements throughout the various construction stages, providing essential data for assessing the stability of the historic structure and supporting decision-making during the execution of the works. Systematic analysis of the instrumentation readings enabled the identification of changes in soil–structure interaction during the early phases of excavation, allowing the revision of the originally proposed solutions before more significant displacements could compromise the integrity of the monument.

Beyond its role as a safety control measure, the monitoring program was instrumental in validating the effectiveness of the adopted reinforcement techniques, including steel-cased micropiles, jet grouting, and the NATM tunnel. The instrumentation data demonstrated that, following the implementation of the supplementary stabilization measures, displacement rates progressively decreased and the structural behavior of the monitored area became stabilized.

Therefore, Figure 7 not only illustrates the distribution of the monitoring instruments but also highlights the importance of continuous geotechnical monitoring as an essential risk management tool for underground interventions carried out beneath sensitive historic structures.

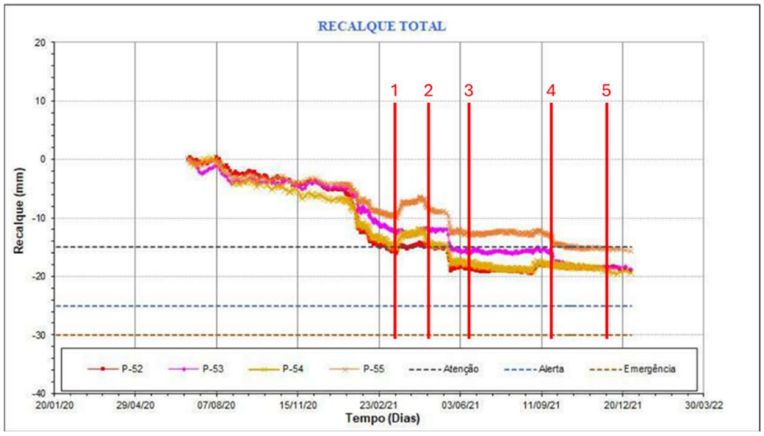


Figure 8 – Graphical record of the monitoring results for points PR-52, PR-53, PR-54, and PR-55 during the excavation and retaining works at Museu Paulista. Source: Museu Paulista Instrumentation Monitoring Report

The records presented in Figure 8 illustrate the progressive development of settlements throughout the various stages of excavation and structural reinforcement. During the initial phases of excavation for the underground extension, monitoring points PR-52 to PR-55 exhibited gradual vertical displacements, reaching an accumulated settlement of approximately 10 mm by Point 1 on the graph.

This initial behavior indicates the direct influence of deep excavations on both the redistribution of stresses within the soil mass and the response of the foundation system, which had previously been weakened by interventions carried out in the basement during the 1990s. Despite the occurrence of measurable displacements, the observed values remained within acceptable limits for historic masonry structures, and no new cracks or deterioration of existing pathological manifestations were identified.

From Point 1 onward, corresponding to the commencement of excavation works for the escalator corridor, a more pronounced increase in the slope of the settlement curves can be observed, indicating a greater sensitivity of the building's front section to the underground works carried out along the axis of the Via dos Coxos. This behavior prompted a revision of the originally proposed construction solutions and the adoption of additional stabilization measures.

At Point 2 on the graph, corresponding to the beginning of the underground works associated with the escalator corridor and the implementation of supplementary reinforcement measures, a gradual reduction in displacement rates can be observed. The progressive stabilization of the settlement curves following the installation of steel-cased micropiles, self-drilling spiles, and jet grouting reinforcement demonstrates the effectiveness of the adopted measures in controlling ground movements and redistributing stresses within the soil mass.

The monitoring results indicate that the combination of construction solutions adopted was effective in controlling differential settlements despite the considerable geotechnical and structural complexity of the intervention, which involved deep excavations adjacent to sensitive historic foundations and artistic elements integrated into the masonry fabric. Continuous monitoring proved essential in guiding design revisions and allowing construction strategies to be adapted to the actual behavior of both the structure and the ground during execution.

During specific stages of construction, some monitoring points reached threshold values classified as an "attention level," requiring increased caution during excavation and enhanced monitoring procedures. However, no interruption of construction activities was required. Temporary cross-bracing systems were installed between the excavation sides to relieve lateral earth pressures and reduce settlement levels, ensuring that none of the monitoring points reached the established "alert level," which would have required suspension of activities and could potentially have led to cracking within the historic masonry.

The temporary bracing system proved effective in stabilizing the settlement process. It can be observed that during excavation at the deeper levels, where anchored retaining walls had already been installed, ground movements became virtually negligible. Point 3 on the graph indicates the beginning of the construction of the anchored retaining walls, consisting of two levels of anchors. The interval between Points 4 and 5 corresponds to the construction period of the NATM tunnel.

Following the commencement of the horizontal excavation of the NATM tunnel, monitoring data indicate displacements of approximately 2 mm at points PR-53 and PR-55, both located near the tunnel portal. Nevertheless, no significant movements were recorded during tunnel excavation, demonstrating the effectiveness of the stabilization measures that had been implemented.

Monitoring of the horizontal tunnel excavation was carried out by measuring the distances between three monitoring pins installed along the tunnel crown at five monitoring sections distributed throughout the excavation advance. The pins were located at the highest point of the crown (P1) and at its lateral extremities (P2 and P3). The monitored distances between these points were designated C1–2, C1–3, and C2–3, as illustrated in Figure 9.

Figure 9 presents the monitoring results for sections S1, S3, and S5. With the exception of Section S3, all sections exhibited similar behavior. During the initial stages of excavation, compressive effects caused convergence between the monitoring points until structural stabilization was achieved. In other words, the tunnel opening tended to close slightly as stresses were redistributed.

In Section S1, the greatest displacements occurred between points P2 and P3 relative to P1, indicating that vertical displacement at the crown was more significant than horizontal displacement at the side points. This behavior is attributed to the proximity of the anchored retaining wall system. In contrast, Section S5 exhibited its greatest displacement through convergence between the lateral points P2 and P3, indicating that lateral earth pressures had a greater influence on tunnel closure than the direct vertical loading acting on point P1.

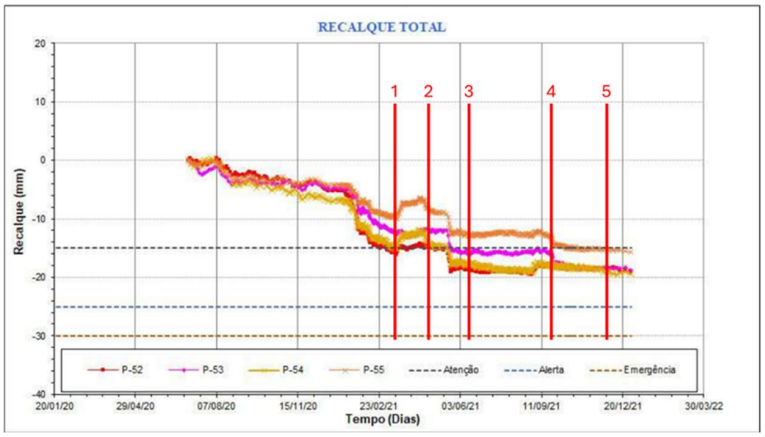


Figure 9 – Superimposed convergence monitoring data for NATM tunnel sections S1, S3, and S5. Source: Museu Paulista Instrumentation Monitoring Report.

The behavior observed in Section S3, however, differed from that of the other monitored sections. In this case, the distances between the monitoring points increased until stabilization was achieved, with the largest displacement occurring between lateral points P2 and P3. This behavior is opposite to that observed in Section S5, indicating that, at this location, the tunnel section experienced vertical compression that tended to induce lateral expansion prior to stabilization.

By correlating the monitoring data obtained from the tunnel sections with the measurements recorded at the monitoring points located directly above them, as presented in Figure 8, it can be observed that most of the deformations occurring within the tunnel did not directly affect the historic building. Instead, these movements resulted primarily from the redistribution and re-equilibration of stresses within the surrounding soil mass.

The revision of the original design and the implementation of the solutions described above had a significant impact on the project schedule, extending the duration originally planned for the retaining works in the central area by approximately one year. Nevertheless, the construction schedule was adjusted to allow progress on other work fronts, thereby minimizing the impact on the overall completion time of the project.

5. Results and Discussion

The design revisions and solutions adopted throughout the execution proved to be essential for enabling the proposed intervention, ensuring the preservation of the structural and material integrity of the historic building.

Although settlements occurred during the excavation process, they remained within controlled limits and did not result in cracking of the masonry or damage to the artworks integrated into the monument. The

impact on the construction schedule was significant; however, it was mitigated through adjustments in the execution planning and the reorganization of work fronts.

In light of international heritage charters, the intervention can be analyzed from two main perspectives: the use of contemporary techniques and the functional adaptation of the historic building.

Regarding the use of new materials and techniques, an evolution can be observed in the interpretation of heritage guidelines over time. The Athens Charter adopts a more permissive stance, encouraging the use of modern techniques as a means to prevent the degradation of historic elements. The Venice Charter, in turn, takes a more cautious position, recommending their use only when traditional techniques prove inadequate and provided that their effectiveness is well established.

This understanding is reinforced by later documents, such as the Amsterdam Declaration and the Nairobi Recommendation, which emphasize the importance of maintaining traditional techniques and preserving intangible knowledge, while also recognizing the need for systematic studies on the application of contemporary methods.

The Burra Charter consolidates this approach by accepting the use of modern techniques, provided that they effectively contribute to the preservation of the cultural value of the asset, while also emphasizing the importance of reversibility whenever possible.

In the case analyzed, the adoption of techniques such as micropiles, jet grouting, and excavation using the NATM method can be understood as a response to the limitations of traditional techniques when faced with the complexity of the intervention. These solutions were employed with the objective of minimizing vibrations, controlling deformations, and ensuring the overall stability of the system, in accordance with preservation principles.

With regard to functional adaptations, heritage guidelines converge in recognizing functionality as a key condition for the preservation of cultural assets. The maintenance of the exhibition use within the historic building, combined with the relocation of incompatible functions to the underground extension, demonstrates alignment with these principles.

The adopted solution allowed for the preservation of the spatial configuration and significant elements of the monument, while simultaneously enabling its adaptation to contemporary demands.

The combined analysis of these aspects indicates that the design and construction decisions sought to balance technical and functional requirements with the principles of heritage preservation, even though revisions and adjustments were necessary throughout the process.

6. Conclusion

The analysis of the intervention carried out at Museu Paulista demonstrates that the construction of underground extensions beneath historic load-bearing masonry buildings is technically feasible, provided that it is guided by rigorous criteria for risk management, structural compatibility, and the preservation of the cultural significance of the heritage asset.

The case study shows that the adoption of contemporary engineering and construction techniques may be not only appropriate but also necessary in situations of high technical complexity, particularly when pre-existing instability conditions or severe intervention constraints are present.

The design revisions implemented throughout the construction process highlight the importance of flexible and adaptive approaches capable of responding to actual site conditions without compromising conservation objectives. As a result of these adjustments, the maximum monitored displacements remained below the thresholds generally considered critical for crack initiation in historic masonry structures, ensuring the structural and artistic integrity of the monument throughout all stages of construction.

Finally, it is important to emphasize that the successful integration of heritage conservation and contemporary intervention depends not only on technical solutions but also on a critical understanding of the principles that guide the conservation of cultural heritage, allowing them to be applied in a contextualized and informed manner.

In light of the foregoing, and in accordance with the principles established by international heritage charters, it can be concluded that the incorporation of contemporary construction technologies into restoration projects is not only possible but may also be essential for safeguarding the physical, functional, and symbolic integrity of cultural heritage assets. As demonstrated by the Museu Paulista case study, the use of solutions such as micropiles, jet grouting, and controlled excavation techniques showed that, when guided by the principles of minimum intervention, compatibility, reversibility, and respect for authenticity, such technologies do not compromise the values that justified the heritage designation of the property. On the contrary, they contribute to the rehabilitation and continued use of the building, enabling its adaptation to contemporary requirements without altering its original character. Thus, this study reaffirms that a balanced integration of tradition and innovation constitutes both a legitimate and necessary approach to the conservation of built heritage, ensuring its continuity and relevance for future generations.

Acknowledgments

The authors would like to express their gratitude to Carlos Eduardo Moreira Maffei, from Maffei Engenharia e Consultoria Ltda., for providing access to technical materials related to the foundation reinforcement project of the Paulista Museum (Ipiranga Museum), including soil analysis data, design calculations, and monitoring records. Access to this material was essential for the development of this research.

The authors also thank the Paulista Museum of the University of São Paulo for authorizing and supporting this study, thereby making a significant contribution to its development. Due acknowledgment and proper credit are given to the aforementioned firm for the project and the materials utilized.

References

Escritório Internacional dos Museus das Nações. 1931. “Carta de Atenas.” Atenas.

ICOMOS – International Council on Monuments and Sites. 1964. “Carta de Veneza.” Veneza.

ICOMOS – International Council on Monuments and Sites. 2013. “Carta de Burra.” Austrália.

Congresso do Patrimônio Arquitetônico Europeu. 1975. “Declaração de Amsterdã.” Amsterdã.

UNESCO – United Nations Educational, Scientific and Cultural Organization. 1976. “Recomendações de Nairóbi.” Quênia.

Costa, A., A. V. Fonseca, J. Guedes, N. Raposo, and E. Paupério. 2009. “Reconstrução do baluarte do cavaleiro da muralha de Chaves.” Portugal.

Marques, D. O., and J. L. Borges. s.d. “Aterros sobre solos moles reforçados com colunas de jet grouting encabeçadas por tecido geossintético.”

H+F Arquitetos. s.d. “Projeto Executivo do Museu Paulista.” https://hf.arq.br/projeto/museu-paulista/

.ArchDaily Brasil. 2023. “Modernização e Restauro do Museu do Ipiranga / H+F Arquitetos.” https://www.archdaily.com.br/br/994350/modernizacao-e-restauro-do-museu-do-ipiranga-h-plus-f-arquitetos

Cinpar 2026
XXII International Conference on Building Pathology and Constructions Repair
15th to 17th July 2026 - Lisboa, Portugal

Modelagem digital do Museu da Imagem e do Som a partir de nuvem de pontos

Gabriel DUARTE[1] Ana Cecília VASCONCELOS[2], Esequiel MESQUITA[4], Eugênio MOREIRA[3], e Mylene VIEIRA[5]

[1] Universidade Federal do Ceará, Ceará, Brasil, gabrielsouzaduarte52@gmail.com
[2] Universidade Federal do Ceará, Ceará, Brasil, anaceciliavas@iaud.ufc.br
[3] Universidade Federal do Ceará, Ceará, Brasil, emesquita@ufc.br
[4] Universidade Federal do Ceará, Ceará, Brasil, eugeniomoreira@daud.ufc.br
[5] Universidade Federal do Ceará, Ceará, Brasil, mylene.melo@ufc.br

Resumo: No contexto do desenvolvimento da tecnologia em todos os setores da atualidade, muito se discute acerca do potencial da aplicação de estratégias de modelagem digital no patrimônio histórico edificado no âmbito nacional e internacional. Em contrapartida, os cenários de desaparecimento da materialização da cultura brasileira são cada vez mais recorrentes. Dessa forma, essa pesquisa surge dentro dos esforços para desenvolver e aplicar metodologias inovadoras que cruzem dados geométricos com informações construtivas, históricas e de gestão, num modelo integrado, objetivando a documentação digital do acervo arquitetônico cearense por meio da aplicação dos princípios do *Heritage Building Information Modeling* (HBIM) e levantamento com *laser scanner* terrestre. Buscou-se refletir sobre o processo de aplicação da metodologia e novas perspectivas, visando fazer uma reconstrução digital que facilite a tomada de decisões para a gestão e a manutenção. O método, que adota a abordagem do estudo de caso no edifício anexo do Museu da Imagem e do Som Chico Albuquerque em Fortaleza, Ceará, permite a execução dos processos de captura da edificação aplicados a geometria e particularidades individuais do objeto arquitetônico, promovendo uma análise focada e pontual do processo. A metodologia foi dividida nas etapas de: levantamento com nuvem de pontos, modelagem digital, integração de informações adicionais como detalhes construtivos e revestimentos aplicados. Como produto final, obteve-se material de documentação técnica da edificação para auxiliar na gestão e manutenção do bem, além de resultados que confirmam a eficiência dos métodos e sua aplicabilidade para o registro das demais obras do acervo arquitetônico cearense, mantendo um memorial do processo de digitalização e modelagem do Museu da Imagem e do Som Chico Albuquerque. Por fim, conclui-se que o levantamento através da nuvem de pontos para modelagem digital mostrou-se eficiente e aplicável para demais bens.

Palavras Chave: HBIM. Modelagem digital, Nuvem de pontos.

1. Introdução

O patrimônio histórico edificado e edifícios de uso cultural e turístico nas cidades são alvos de diversas discussões no âmbito acadêmico e social, principalmente no que tange às estratégias de conservação, manutenção e gestão. Em contrapartida, os cenários de desaparecimento da materialização da cultura brasileira são cada vez mais recorrentes, estes, muitas vezes agravados por fatores naturais, mudanças climáticas e até geopolíticas (Kuroczyński e Argasiński 2025; Fatorić e Seekamp 2017). Meios que divulguem e apoiem a tomada de decisão do ponto de vista construtivo para a conservação desses bens exigem trabalhos custosos e enfrentam desafios em manter as documentações existentes de fácil acesso e organizadas. Para além disso, as instituições e órgãos de proteção do patrimônio enfrentam diversas limitações que levam a atuação no visível e urgente, deixando de lado planos e alternativas estratégicas que identifiquem riscos e ameaças de forma preventiva (Campos e Corrêa 2021), o que evidencia a necessidade de estratégias que identifique prioridades e alinhe custos a um processo otimizado (Freire 2026). Assim, os esforços para o desenvolvimento e implementação de meios de representação eficientes que atendam as particulares dos edifícios para fins de documentação, são fundamentais.

Com o desenvolvimento de tecnologias, novas ferramentas como a fotogrametria e o *laser scanner* surgiram para dar suporte ao processo de documentação do patrimônio construído, inclusive no cenário brasileiro, a exemplo dos trabalhos de Gonçalves e Inojosa (2022), Vieira et al. (2024), Ribeiro et al (2025), que por meio de nuvem de pontos alcançam níveis elevados de detalhamento, seja para simulação estrutural, modelagem de objetos e arquitetura. Além disso, outra metodologia consolidada que auxilia no processo de documentação é o *Building Information Modeling* (BIM), que possibilita a criação de modelos compatíveis para diversas disciplinas e inserção de informações paramétricas, o que vem constituindo um paradigma para o processo de projeto de novos edifícios com maior precisão. A inclusão da dimensão informacional e paramétrica na metodologia BIM permite anexar informações de materiais e custos num ambiente colaborativo e multidisciplinar, além de possibilitar, se usado de forma contínua, o monitoramento e gestão com dados atualizados (Rubens 2023) e (Freire 2026). Entretanto, a documentação de edifícios já existentes, seguindo a metodologia BIM, encontra restrições ao analisar geometrias complexas e com documentação dispersa ou inexistente (Ribeiro 2025).

Contornando esta problemática, o *Heritage Building Information Modeling* (HBIM) proposto por Murphy *et al.* (2009) diferente do BIM, se desenvolve com o objetivo de documentar e preservar o patrimônio histórico edificado, surgindo para levantar estruturas já existentes, unificar e sistematizar informações ao modelo, sejam elas históricas ou de construção, permitir o acompanhamento da obra ao longo do tempo e monitorar manifestações patológicas (Monteiro 2024). O HBIM possibilita que estratégias de conservação, manutenção e restauro sejam mais agilizadas e eficientes num ambiente integrado, por meio de uma modelagem digital 3D gerada por engenharia reversa que, segundo Yang *et al.* (2020) pode ser sistematizado em 4 tipos, sendo eles: o modelo geométrico, que reconstroi a entidade original numa forma holística; o semântico, que atribui significado; o paramétrico que permite modificação dos elementos com base em parâmetros; e o informacional que constroi um banco de dados com os atributos, materiais e demais informações dos componentes. Ou seja, para além de um modelo geométrico, o HBIM funciona como um repositório de informações que podem ser úteis para intervenções, reformas e restauros.

Aliado a tecnologias otimizadas de levantamento já amplamente utilizadas como o laser scanner e a integração com software de modelagem BIM, esse trabalho visa aplicar os princípios da metodologia HBIM na modelagem digital do edifício anexo do Museu da Imagem e do Som Chico Albuquerque em Fortaleza, Ceará. O objetivo é registrar o processo de reconstrução, fortalecer o método e avaliar sua aplicabilidade, além de manter a documentação do acervo arquitetônico cearense, atendendo a demanda da Secretaria de Cultura do Estado do Ceará (Secult CE) para gestão e manutenção do ativo. Essa pesquisa se mostra relevante ao partir de uma demanda real e integrar tecnologias digitais de levantamento, modelagem e processamento para a manutenção dos edifícios cearenses de uso turístico e cultural.

2. Metodologia

2.1 Estudo de caso: Museu da Imagem e do Som Chico Albuquerque

O Museu da Imagem e do Som Chico Albuquerque (MIS), atualmente localizado na Avenida Barão de Studart, 410, na cidade de Fortaleza, Ceará é um instrumento da Secretaria de Cultura do Estado do Ceará (Secult-CE) e funciona na antiga residência Fausto de Cabral (Figura 1a), prédio tombado em âmbito estadual definitivamente desde 2016 (Secult 2016). Datado de 1951 e com projeto atribuído a José Barros Maia, “Mainha”, a construção de traços ecléticos foi executada para ser a casa do senador Fausto Cabral, o edifício já abrigou a residência oficial do Governo do Estado em 1963, o Museu Histórico e Antropológico do Estado em 1972, a sede do Departamento de Patrimônio Histórico (Depac) e desde 1996 passou a ser a sede do Museu da Imagem e do Som (Governo do Estado 2015) e (Azevedo 2012). Durante o ano de 2018 o MIS passou por uma grande reforma e restauros, onde ganhou um prédio anexo de 5 andares, com mais salas de exposição, laboratórios de mixagem, áudio, e imagem, centros de pesquisa e biblioteca. Chamado agora de Complexo do Museu da Imagem e do Som, o prédio antigo e o novo, além da praça que existe entre eles, compõem um importante atrativo cultural e turístico para a cidade.

Este trabalho aplicou o processo de modelagem e estudo para o prédio novo anexo do museu (Figura 1b e 1c). Com as obras finalizadas em 2022 e projeto assinado pelo arquiteto portugês José Manuel Carvalho Araújo, o edifício já se consagra como importante marco turístico e arquitetônico da cidade. A obra priorizou

o afastamento do edifício para o limite posterior do terreno e a criação de uma generosa praça com arquibancadas para assistir apresentações ao ar livre e projeções que ocorrem na grande fachada de concreto aparente do edifício, possibilitando uma relação de plateia e tela entre o prédio e a cidade (Archdaily 2023). O programa sofisticado aliado a tecnologia de ponta coloca o museu em níveis excepcionais de qualidade em serviços e exibições. São cinco pisos, sendo um o térreo e dois no subsolo, o prédio conta com sala imersiva, laboratórios de audiovisual, salas de exposição e biblioteca.

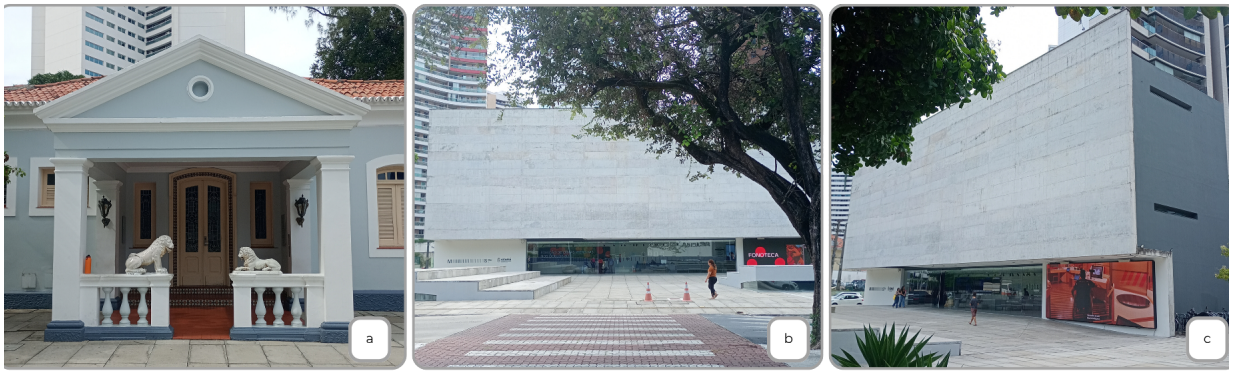


Figura 1. Museu da Imagem e do Som Chico Albuquerque

2.2 Levantamento e modelagem digital

O levantamento para captura de dados geométricos foi feito usando *laser* scanner terrestre visando chegar ao *Scan-to*-BIM, processo que visa a obtenção de um modelo BIM preciso e de alta qualidade a partir de uma nuvem de pontos (León 2018). Em seguida, os *setups* de cada captura realizados por um *scanner* Leica® BLK360 foram processados e unidos para gerar um modelo 3D da nuvem de pontos, a fim de se incorporar ao ambiente BIM para modelagem dos elementos construtivos. Na etapa de levantamento também foram coletadas fotos 360 para montagem de passeios interativos pelo edifício de forma virtual disponibilizados no site do DocumentaCe (www.documenta.com.br).

O processo de modelagem digital utilizou o formato protocolado pela prática do Documenta CE, grupo em rede ligado ao projeto Cientista Chefe da Cultura da Secult-CE que já conta com exemplares de bens digitalizados com métodos validados e publicados, como a Casa José de Alencar (Rubens *et al.* 2023) a Igreja Matriz de Nossa Senhora do Rosário (Ribeiro 2023) o Theatro José de Alencar (Vieira *et al.* 2023), e o Sobrado Doutor José Lourenço (Ribeiro 2025). O protocolo de modelagem HBIM sistematizado por Ribeiro (2025) busca uma uniformização de processos e linguagens de representação, reunindo todos os processos de modelagem em cinco etapas: o plano de execução BIM (PEB), que visa organizar ferramentas, prazos, nível de detalhes e objetivos; a modelagem digital, que modela os elementos construtivos; a precisão geométrica, que garante coerência dimensional entre o levantado e modelado; o enriquecimento semântico, que atribui significado e informações aos elementos; e a documentação e reconstrução digital que visa a produção de material gráfico arquitetônico e de divulgação.

O software de modelagem BIM adotado foi o Autodesk® Revit®, permitindo uma visualização tridimensional detalhada do modelo e uma variedade de funcionalidades que auxiliam no gerenciamento de dados. Segundo Penjor *et al.* (2024) é o software mais utilizado para criação de modelos HBIM com cerca de 60% de uso, consagrando suas ferramentas como as que melhor se adequam na construção digital. A nuvem de pontos foi importada e deu-se início a modelagem dos elementos primários como pisos, paredes, forros, escadas, cobertura e platibanda, em seguida, elementos construtivos secundários como portas, janelas, guarda-corpo, canteiros, arquibancadas e revestimentos foram incorporados. A Figura 2 ilustra de forma esquemática as etapas do processo da captura do edifício à modelagem final.

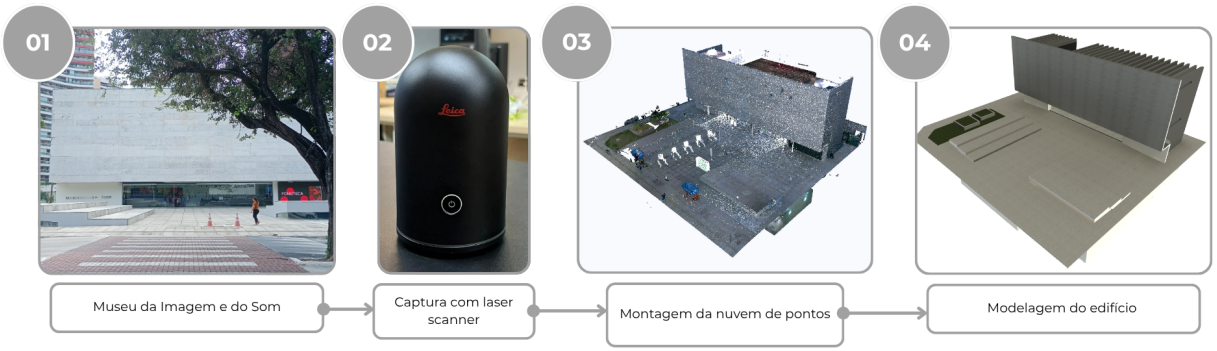


Figura 2. Esquema do processo de captura à modelagem final

2.3 Enriquecimento semântico

A etapa de enriquecimento semântico visa agregar informações dos elementos construtivos ao modelo, por meio de considerações de acabamento, nível de ornamentação, particularidades construtivas, camadas, dentre outros, seguindo o proposto por Magalhães *et al.* (2024) no HBIMPath. O HBIMPath é um protocolo de documentação desenvolvido para otimizar e organizar o levantamento de informações acerca de materiais, acabamentos e ornamentação que muitas vezes são característicos de edifícios históricos e que nem sempre são contempladas em modelos tridimensionais convencionais. Seu objetivo, em diálogo com o aspecto semântico e informacional de Yang *et al.* (2020), é complementar os modelos geométricos com informações como: acabamento, questões de aspecto e superfície, espessura de camadas, quando disponível essa informação, além de demais comentários e acréscimos que se julgue necessário ser incluído ao modelo na forma de texto ou imagem. Essa metodologia permite acrescentar informações especialmente nos casos em que o nível de detalhe exigido da representação não seja tão rigoroso ou necessário, ou seja, um alto nível de ornamentação de um elemento pode ser somente descrito, enquanto seu modelo geométrico é simplificado.

As informações foram levantadas *in loco* e por meio de *tours* virtuais disponíveis na plataforma DocumentaCE (www.documenta.com.br) posteriormente organizadas em fichas de catalogação externas por elemento construtivo para depois serem integradas nos atributos de materiais e componentes no modelo geométrico, assim, o enriquecimento semântico se dá na transformação de dados documentais ou de texto alfanumérico em informação paramétrica no modelo (Ribeiro 2025). Por se tratar de uma construção recente e de arquitetura contemporânea, essa etapa é facilitada, afinal, os métodos construtivos são os usuais e existem registros de construção, além disso os materiais de revestimento são facilmente reconhecíveis.

2.4 Reconstrução digital e documentação

A reconstrução digital propõe a criação de imagens a partir do modelo, de forma a recriar seu contexto, gerando uma ambientação sensível ao entendimento e apropriação do espaço para leigos. Essa etapa se utiliza de qualidades fotográficas para a apresentação e comunicação de iluminação, materiais de revestimento, acabamentos e superfícies de uma forma geral. Ribeiro (2025) afirma que a renderização de imagens é o recurso mais direto e rápido para entender a aparência atual ou histórica de um edifício e Miao (2021) aponta para o uso de renderização como meio de divulgação do edifício pelo seu alto nível de detalhes e alcance de imagens para milhares de pessoas.

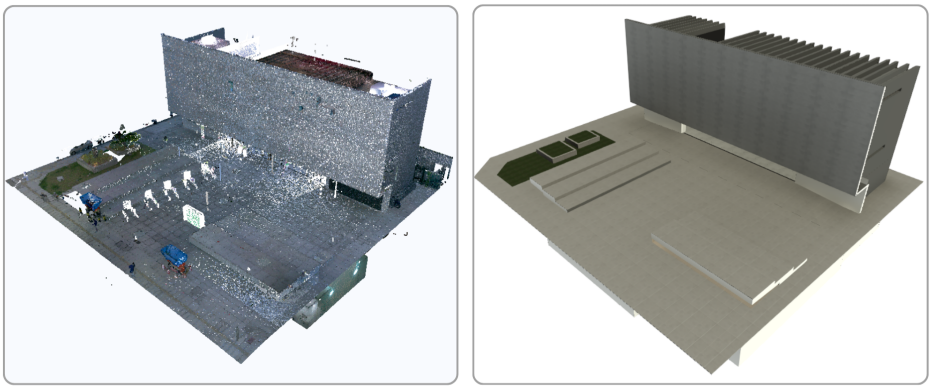
Visando criar imagens de renderização de modo otimizado, este trabalho propõe o uso de inteligência artificial para melhoramento e refinamento de imagem diretamente a partir do modelo tridimensional, por mais que ainda pouco usual, esse cenário é promissor e vem sendo cada vez mais estudado dentro da representação em arquitetura (Muslo e Koçyiğit 2024 e Nabizadeh Rafsanjani e Nabizadeh 2023). Foi usado o ChatGpt® e o Gemini® para renderizações gerais e a Inteligência Artificial do D5 Render® para criação de mobiliário a partir de imagens. Os prompts foram estruturados de modo a especificar o nível de qualidade da Imagem e estilo de renderização, adicionar contexto urbano semelhante ao entorno do edifício do MIS, presença humana para efeitos de escala e iluminação externa ou interna conforme fosse necessário.

Já a etapa de documentação visa a elaboração de pranchas técnicas da arquitetura do edifício contendo as informações e desenhos de: implantação, planta dos pisos, planta de cobertura, cortes, elevações, tabelas entre outros. A modelagem na metodologia BIM permite que os desenhos técnicos sejam construídos de forma concomitante ao modelo tridimensional, dessa forma, após a modelagem finalizada, as vistas são salvas e configuradas de acordo com os padrões gráficos desejados e exportadas para formatos de documento, como PDF.

3. Resultados e Discussões

3.1 Levantamento e modelagem digital

A aplicação da metodologia proposta permitiu a criação da modelagem digital a partir da estrutura existente do prédio anexo do Museu da Imagem e do Som Chico Albuquerque em Fortaleza, Ceará, com enfoque nos elementos captados pela nuvem de pontos. A Figura 3 ilustra o resultado dos dados do levantamento da edificação com o *laser scanner* terrestre formando a nuvem de pontos completa do edifício e o paralelo com a modelagem geral finalizada, ou seja, a inserção de pisos, paredes, escadas, revestimentos e demais componentes construtivos na interface BIM do Revit. Do ponto de vista geométrico o resultado mostrou-se fiel à nuvem de pontos, atendendo de forma precisa o nível de detalhes exigido e as dimensões do objeto arquitetônico.



Nuvem de pontos | Modelagem do edifício

Figura 3. Perspectiva da nuvem de pontos e do modelo HBIM

3.2 Enriquecimento semântico

O enriquecimento semântico que objetiva agregar informações alfanuméricas ao modelo BIM mostrou-se de fundamental importância para a integração de dados construtivos, e que muitas vezes não estão disponíveis na nuvem de pontos. Dessa forma, o uso de *tours* virtuais e visitas presenciais complementaram a aquisição de informações ao permitirem uma análise mais detalhada dos materiais e acabamentos empregados nos elementos construtivos. A Figura 4 mostra os resultados da aplicação da ficha de catalogação para a esquadria de acesso à biblioteca do museu, partindo do preenchimento das informações da planilha à inserção das informações no modelo. Ao final da análise da esquadria, foi possível adicionar por texto o tipo de abertura, posição da maçaneta, forma de fixação, materialidade, acabamentos e cor dos caixilhos. Ficou evidente a relação entre o HBIMPath e a linguagem arquitetônica da edificação. Diferentemente do estudo de Magalhães et al. (2024), desenvolvido no edifício eclético do Theatro José de Alencar, caracterizado pela maior variedade de materiais e acabamentos, o MIS apresenta uma arquitetura com menor diversidade material, o que simplificou o estudo dos componentes e de suas superfícies. Vale ressaltar que estudos futuros mais aprofundados esperam uma caracterização mais ampliada utilizando ensaios não destrutivos que determinem constituição de camadas e composição dos elementos construtivos com maior exatidão.

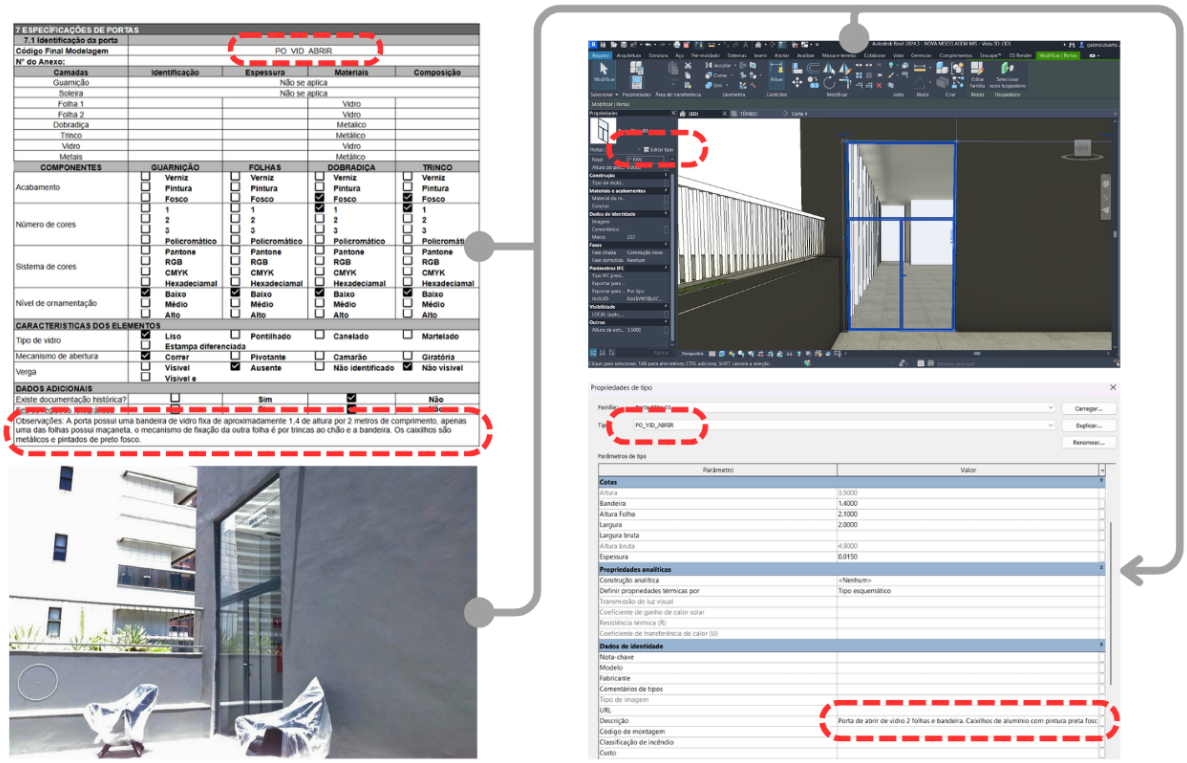


Figura 4. Fluxo de aquisição de dados para enriquecimento semântico

3.3 Reconstrução digital e documentação

Como produto final da etapa de reconstrução digital e documentação obteve-se os *renders* para fins de divulgação e ambientação e a elaboração das pranchas técnicas da arquitetura do museu contendo plantas, vistas, cortes, elevações e detalhes construtivos, permitindo uma leitura atualizada das condições do edifício. A Figura 5 reúne as imagens para reconstrução digital geradas com inteligência artificial (ChatGPT® e Gemini®) a partir do modelo tridimensional do museu. Para ambientação do espaço interno na Figura 5b utilizou-se a inteligência artificial do D5 Render® que permitiu a recriação do mobiliário 3D a partir de fotos. Já na Figura 5e, o mobiliário do espaço interno foi sugerido pelo ChatGPT® para simular uma possível exposição. Os resultados mostraram-se consistentes e fiéis as proporções originais da nuvem de pontos e do edifício, além de ter sido considerado um método fácil, rápido, replicável e muito eficiente.

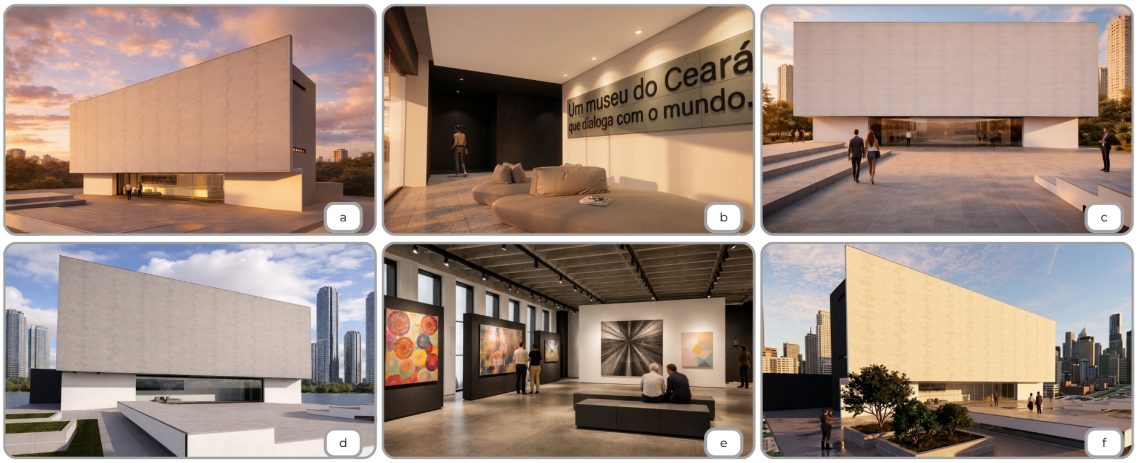


Figura 4. Renderizações externas e internas do museu

A Figura 5 sistematiza os prompts utilizados para geração das imagens e as modificações dos resultados obtidos, de modo a facilitar reproduções e documentar o processo.

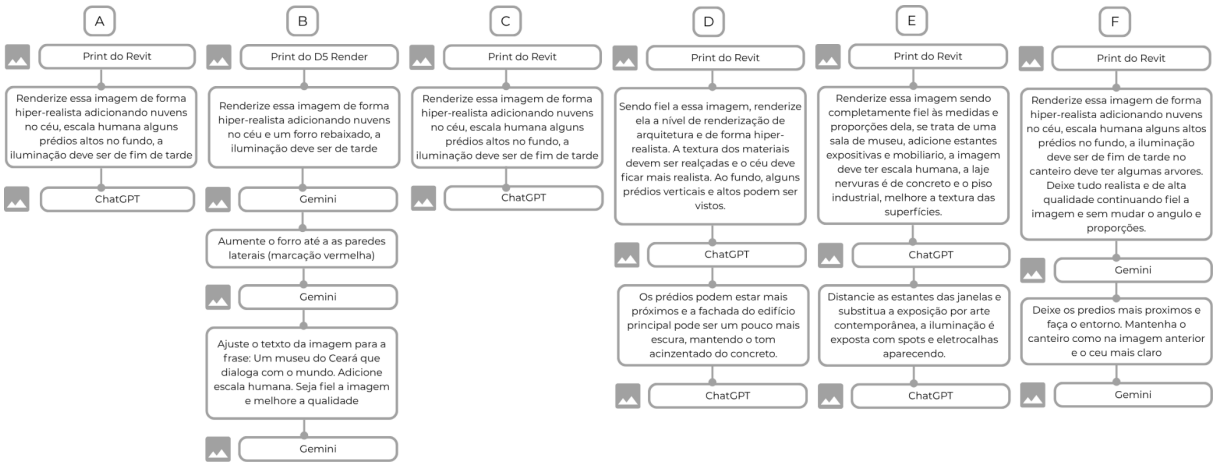


Figura 5. Sistematização dos prompts referentes a Figura 4.

Do ponto de vista da documentação técnica, a Figura 6 exemplifica os resultados ao apresentar a prancha de elevações do museu, contendo os desenhos da fachada norte, sul, leste e oeste. Devido o sistema BIM, a montagem de documentos técnicos mostrou-se otimizada, visto que uma vez tendo o modelo completo, a extração de vistas no *software* acontece de forma automática, além disso, possibilita o uso de diferentes gráficos de modo instantâneo, permitindo personalização e padronização dos esquemas de representação.

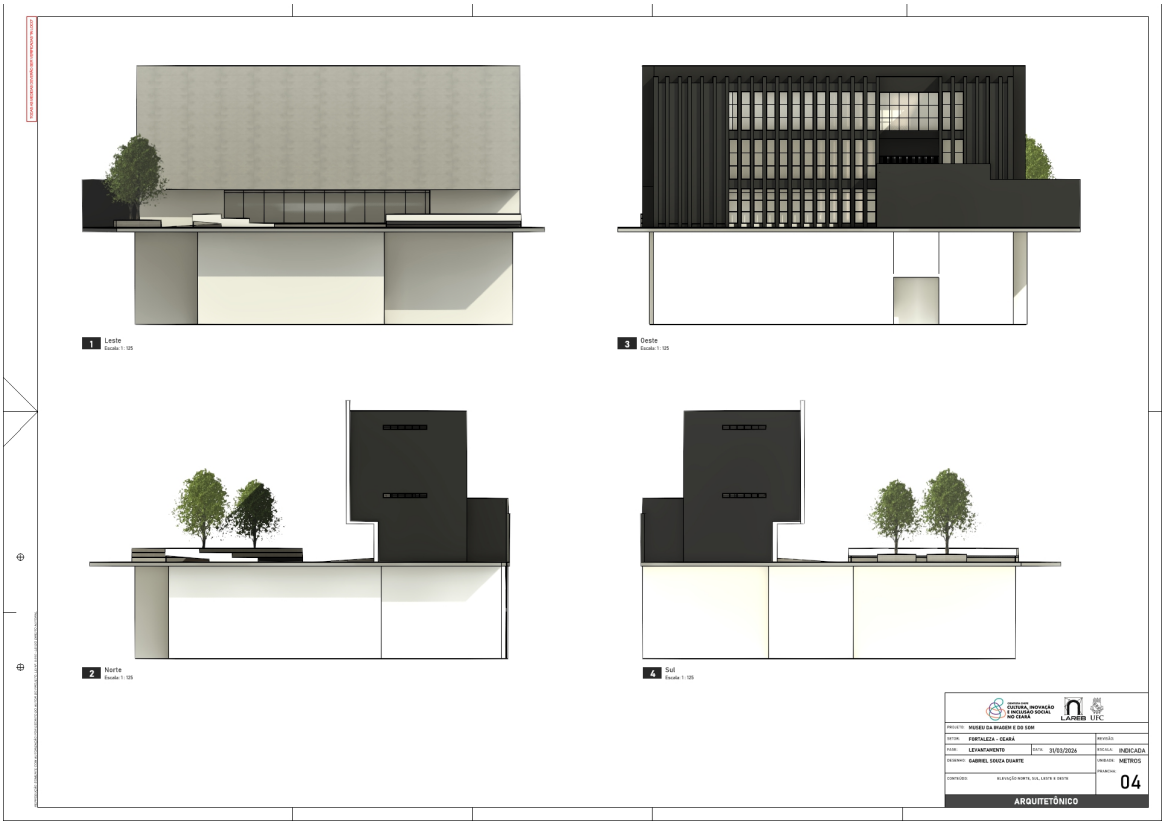


Figura 6. Prancha de elevações do museu

4. Conclusão

O trabalho realizado no edifício anexo do Museu da Imagem e do Som Chico Albuquerque em Fortaleza, Ceará, propôs e validou a aplicação dos princípios da metodologia HBIM a partir de levantamento com nuvem de pontos esperando discutir e produzir material acerca de métodos inovadores, precisos e eficientes de documentação de edifícios históricos de uso cultural e turístico para o desenvolvimento da cidade. A utilização do software Revit como ferramenta capaz de integrar os dados levantados por nuvem de pontos com a construção do modelo geométrico pela adição dos elementos construtivos, mostrou-se de alta eficiência chegando a níveis de representação de alta qualidade, além da otimização na criação de material técnico de arquitetura como plantas, cortes e vistas. O levantamento de dados que atribuiu significado ao modelo geométrico mostrou-se fundamental para a inserção de informações que auxiliem na gestão e manutenção do ativo, como se propõe o HBIM. Nesse momento, observou-se que o preenchimento das planilhas de catalogação pela visualização dos elementos no *tour virtual* tornou o processo fácil e intuitivo, além disso, a transposição das informações no software de modelagem permitiu o agrupamento de dados textuais descritivos sobre o observado nos elementos do edifício. As renderizações realizadas com inteligência artificial (ChatGPT®, D5IA® e Gemini®) apontaram para um método novo e promissor de geração de imagens de alta qualidade, com o tempo otimizado quando comparado aos processos tradicionais de renderização e que mostraram resultados muito satisfatórios.

Vale ressaltar as dificuldades e limites da pesquisa, a começar pela etapa de levantamento que requer dispositivos de alto processamento para operação dos dados, além de limites no âmbito de caracterização e composição de sistemas, que exigem estudos mais aprofundados. Quanto a expectativas para trabalhos futuros, espera-se superar os limites deste e avançar com o modelo à nível de modelagem de sistemas complementares, protocolos de gestão, detalhamentos de componentes construtivos, simulações térmicas, monitoramento de estruturas entre outros.

Por fim, a modelagem digital desenvolvida neste estudo validou o processo de reconstrução virtual de edifícios de uso cultural e turístico para fins de documentação, usando tecnologia de ponta e métodos de alta precisão geométrica. A metodologia abre caminho para ferramentas futuras de gestão, integrando e agilizando processos num ambiente virtual colaborativo. O estudo de caso no Museu da Imagem e do Som confirma o processo e demonstra a replicabilidade para outros contextos, abrindo caminho para novas experiências de implementação.

Agradecimentos

Este trabalho foi financiado pela FUNCAP, Projeto 01172921/2022 – Cientista Chefe Cultura, Projeto 10581391/2022 – Colaboração Internacional FUNCAP/INSA Rouen Normandie; Conselho Nacional de Desenvolvimento Científico (CNPq) – Project 302054/2022-7 – PQ2, pelo Projeto - 440926/2024-6 – VISION e Projeto - 402828/2024-0 – CLIC, Fundação CAPES e Finep 2896/24.

Referências

ArchDaily Brasil. 2023. “MIS - Sound and Image Museum of Ceará / Carvalho Araújo”. Acessado em 25 de março de 2026. https://www.archdaily.com/999434/mis-sound-and-image-museum-of-ceara-carvalho-araujo

Azevedo, Miguel Ângelo de. 2012. “Datas e fatos para a História do Ceará (1996 - 1997)”. Revista do Instituto do Ceará.

Campos, Luana, Corrêa, Sandra. 2021. “Políticas Públicas de Gestão de Risco ao Patrimônio Cultural Frente aos Efeitos das Mudanças Climáticas”. Habitus: 78-92. https://doi.org/10.18224/hab.v19i1.8997.

Fatorić, S., and Seekamp, E. 2017. “Are cultural heritage and resources threatened by climate change? A systematic literature review”. Climatic Change, 142(1–2), 227–254. https://doi.org/10.1007/s10584-017-1929-9.

Freire, G., Vieira, M., & Mesquita, E. 2026. “HBIM protocol for supporting the management and maintenance of historic buildings”. Journal of Building Engineering, 124. https://doi.org/10.1016/j.jobe.2026.116053

Governo do Estado do Ceará. 2015. “Prédio do Museu da Imagem e do Som é tombado provisoriamente pelo Coepa”. Acessado em 25 de março de 2026. https://www.ceara.gov.br/2015/07/15/predio-do-museu-da-imagem-e-do-som-e-tombado-provisoriamente-pelo-coepa/

Gonçalves, L. L., & Inojosa, L. S. P. 2022. “BIM Methodology applied to Structural Analysis of the Built Heritage”. Proceedings of the joint XLIII Ibero-Latin-American Congress on Computational Methods in Engineering, CILAMCE.

Kuroczyński, P., & Argasiński, K. 2025. “Implementing HBIM for Cultural Heritage Preservation From Documentation to Sustainable Management”. ISPRS Annals of the Photogrammetry, Remote Sensing and Spatial Information Sciences, *X-M-2–2025*, 175–184. https://doi.org/10.5194/isprs-annals-x-m-2-2025-175-2025.

León, Daniel Forero. 2018. “Mejora del modelo Historic Building Information Modeling (HBIM) para la gestión de fases histórico-constructivas. Aplicación al caso de la nave de la iglesia de San Juan del Hospital en Valencia”. Trabajo Final de Máster, Universidad Politecnica de Valencia.

Magalhães, Brenda *et al*. 2025. “Documentation strategies for HBIM model parameterization: A case study of the José de Alencar Theater”. Digital Applications in Archaeology and Cultural Heritage, *38*. https://doi.org/10.1016/j.daach.2025.e00443.

Miao, Scarlett. 2021. "A renderização como ferramenta de preservação do patrimônio na China". ArchDaily Brasil. (Trad. Libardoni, Vinicius) Acessado 11 Abr 2026. <https://www.archdaily.com.br/br/960246/a-renderizacao-aplicada-a-preservacao-do-patrimonio-historico-na-china> ISSN 0719-8906

Monteiro, Mychayanny de A. Santiago. 2024. “Historic Building Inoformation Modeling (HBIM): Desempenho, Vida Útil, Degradação e Patologia em Edificações Históricas”. Revista Foco, *17*(8), e6047. https://doi.org/10.54751/revistafoco.v17n8-157.

Muslu, O. & Koçyiğit, R. G. 2025. “Artificial intelligence in the context of photorealism in architectural visualization”. CONTEXTO, Revista de la Facultad de Arquitectura de la Universidad Autónoma de Nuevo León. https://orcid.org/0000-0002-9748-7913

Nabizadeh Rafsanjani, H., & Nabizadeh, A. H. 2023. “Towards human-centered artificial intelligence (AI) in architecture, engineering, and construction (AEC) industry”. In Computers in Human Behavior Reports (Vol. 11). Elsevier B.V. https://doi.org/10.1016/j.chbr.2023.100319

Penjor, T. *et al*. 2024. “Heritage building information modeling (HBIM) for heritage conservation: Framework of challenges, gaps, and existing limitations of HBIM”. Digital Applications in Archaeology and Cultural Heritage, 35. https://doi.org/10.1016/j.daach.2024.e00366.

Ribeiro, Gilmário da Costa. 2025. “Representação Digital do Patrimônio Histórico: Protocolo de Modelagem HBIM e Semiautomação de Geometrias Complexas.” Dissertação de mestrado, Universidade Federal do Ceará, Campus Russas.

Ribeiro, Gilmário da Costa. 2023. “A Aplicação de Tecnologia de Captura e da Metodologia BIM na Elaboração do Projeto do Museu de Arte Sacra da Igreja Matriz de Nossa Senhora do Rosário em Aracati/CE”. Trabalho de Conclusão de Curso, Universidade Federal do Ceará, Campus Russas.

Rubens, T. *et al*. 2023. “Digitalization based on high-resolution scanning and HBIM tools for damage assessment of the José de Alencar house”. Journal of Building Pathology and Rehabilitation, 8(1). https://doi.org/10.1007/s41024-023-00275-5.

Secretaria da Cultura do Estado do Ceará. 2016. “Conselho Estadual de patrimônio aprova tombamento definitivo da casa de Fausto Cabral, onde funciona o MIS CE”. Acessado em 25 de março de 2026. https://www.secult.ce.gov.br/2016/06/22/conselho-estadual-de-patrimonio-aprova-tombamento-definitivo-da-casa-de-fausto-cabral-onde-funciona-o-mis-ce/

Vieira, M. M., *et al*. 2023. “Strategy for HBIM implementation using high-resolution 3D architectural documentation based on laser scanning and photogrammetry of the José de Alencar theatre”. Digital Applications in Archaeology and Cultural Heritage, 30. https://doi.org/10.1016/j.daach.2023.e00287.

Vieira, M. M. *et al*. 2024. “Semi-automatic scan-to-BIM procedure applied to architectural ornaments of Nossa Senhora do Rosário Church, Aracati-CE”. Springer, *9*(1). https://doi.org/10.1007/s41024-024-00436-0.

Yang, X. et al. 2020. “Review of built heritage modelling: Integration of HBIM and other information techniques”. In Journal of Cultural Heritage (Vol. 46, pp. 350–360). Elsevier Masson s.r.l. https://doi.org/10.1016/j.culher.2020.05.008.

cinpar2026
XXII International Conference on Building Pathology and Constructions Repair
15th to 17th July 2026 - Lisboa, Portugal

Social Tourism and Modern Heritage: Digital Documentation and Conservation of the SESC Garanhuns Holiday Camp (1956), Brazil

Ricardo Alexandre PAIVA[1], Francisco Canuto LINS NETO[2]

[1] Federal University of Ceará, Fortaleza-CE, Brazil, ricardopai@gmail.com
[2] Federal University of Ceará, Fortaleza-CE, Brazil, canutolins@arquitetura.ufc.br

Abstract: Social tourism in Brazil gained strong momentum through state action, particularly with the creation of the Social Services in the 1940s—employer-funded institutions aimed at promoting vocational training and the health, culture, and leisure of workers. In this context, infrastructures aligned with the principles of modernism were conceived, among which holiday camps stand out as important spatial manifestations of social tourism. The initiatives of the Social Service of Commerce (SESC) in providing leisure and tourism facilities for the working class are exemplary, such as the SESC Garanhuns Holiday Camp in Pernambuco, designed by architect José Armando Farias (1927–1974) and inaugurated in 1956. However, socio-spatial transformations over time have compromised the complex's material and immaterial integrity, as it has undergone successive alterations and expansions that have affected its original architectural characteristics. Thus, this paper investigates how the digital modeling of the original SESC Garanhuns Holiday Camp building, through HBIM (Heritage Building Information Modeling) processes, can support actions for documentation, conservation, and management of modern heritage. The methodology is grounded in the theoretical and practical assumptions of digital redrawing in historical research, articulating the use of HBIM with the concept of the Digital Twin, understood as strategic platforms for the documentation, conservation, and analysis of the built heritage. As a main result, the study highlights a parametric HBIM model conceived as a virtual matrix capable of integrating analog and digital data and information, as well as multiple representations and analyses. Finally, this model constitutes a relevant instrument for the documentation, management, and conservation—albeit in a digital environment—of the building, contributing to the preservation of the memory of social tourism and modern heritage in Brazil.

Keywords: Heritage Building Information Modeling, BIM model, HBIM, Heritage, Digital Twin

1. Introduction

The establishment of Social Services throughout the 1940s stimulated social tourism activities across the country, primarily by creating institutions dedicated to improving health, culture, and recreation for the working class. Against this backdrop, various structures were designed in accordance with the principles of the modern movement, notably the summer camps, which exemplify an architectural program crucial to the consolidation of social tourism in Brazil. The Social Service of Commerce (SESC), through its initiatives aimed at promoting leisure and tourism, was one of the key drivers behind the development of facilities that contributed to the spread of modernism in the country. Among these facilities, the SESC Garanhuns Holiday Camp stands out, designed by Ceará-born architect José Armando Farias (1927–1974) and inaugurated in 1956.

However, successive socio-spatial changes have compromised the physical and intangible integrity of the building, given the gradual alterations and expansions carried out over time, which ultimately led to the loss of the original design's distinctive character. This scenario reflects a lack of awareness regarding the heritage, historical, and cultural value of works with modernist attributes, both on the part of society and of the agencies responsible for safeguarding and preserving them (PAIVA; DIÓGENES, 2018). The SESC

Garanhuns holiday camp is one of countless examples that, due to a lack of awareness of its intrinsic values, result in what is known as “architectural death,” understood as the total disappearance when the building is completely destroyed, or partial, when the building loses the original characteristics that gave it its architectural identity (AMORIM, 2007).

Within this scenario, heritage documentation, conservation, and management activities are often rendered impossible or compromised due to the lack of a systematic architectural inventory. The body of information available regarding a site of cultural and heritage interest tends to be lost over time and in the face of constant physical alterations, reflecting the inability to manage and integrate data related to architectural heritage. According to Simeone et al. (2014), a large volume of information is lost in isolated files, such as 2D CAD technical drawings and photographic surveys, generating a set of data that is not integrated and limited to various unconnected “islands of knowledge.”

An effective strategy for dealing with this issue is the application of BIM technology combined with the concept of a Digital Twin (a precise virtual replica of a physical object, system, or environment) to develop a parametric three-dimensional digital model capable of capturing, organizing, and systematizing information related to cultural heritage in an integrated manner. This approach enables the implementation of management and conservation actions—even in a digital environment—for a heritage site. Thus, the use of BIM for heritage recording, conservation, and management—referred to as Heritage Building Information Modeling (HBIM)—enables the creation of a reliable and unified inventory of a subject of study, allowing different users to consult, update, and manage information related to the architectural asset (SIMEONE et al., 2014).

Accordingly, this study investigates how the digital modeling of the original SESC Garanhuns holiday camp building, through the application of HBIM, can support heritage documentation, conservation, and management efforts. The theoretical framework is based on the principles of HBIM, linked to the concept of the Digital Twin, for the documentation and redrawing of the building. The practical assumptions, on the other hand, refer to the process of parametric digital modeling, based on a documentary survey comprising original architectural drawings, 2D CAD drawings, and historical photographs, which enabled the creation of an integrated digital inventory and a three-dimensional model, contributing to the memory of social tourism and modern heritage in Brazil.

2. The SESC Garanhuns Holiday Camp

Institutions such as the Social Service of Commerce (SESC) were pioneers in promoting social tourism in Brazil around the 1940s, an activity that was new at the time, given that taking annual vacations was a rare practice among retail workers (SESC DEP. PERNAMBUCO, 1965). The inauguration of the SESC Bertioga Vacation Center in 1948, considered the first facility of its kind in the country, marked the institution’s initial effort to promote the well-being of its beneficiaries through activities focused on education, health, leisure, culture, and assistance (CHEIBUB, 2011).

Similarly, the SESC Regional Department in Pernambuco was working to consolidate plans to establish a holiday camp in the municipality of Garanhuns, located in the Agreste region of Pernambuco, initially through lease and lodging agreements with local hotels. This strategy proved advantageous for the institution’s activities, as it enabled the organization of a vacation program focused on collective social service. Thus, the initiative was not limited to traditional recreational activities but also served as a means to promote the physical and mental well-being of the beneficiaries, while fostering a stronger sense of community among the participants (SESC DEP. PERNAMBUCO, 1965).

Throughout the 1950s, the holiday camp established itself as one of SESC’s most successful and widely promoted activities in Pernambuco. However, the need arose to install the service in its own building. Given the years of experience gained through lease and lodging agreements, the SESC Regional Department in Pernambuco launched, in 1952, a design competition for the headquarters of the SESC Garanhuns Holiday

Camp (Figure 1), with the winner being the then-recently graduated architect from Ceará, José Armando Farias (1927–1974), who had obtained his degree in Recife.



Figure 1 – SESC Garanhuns Holiday Camp
Source: José Armando Farias Memorial

Inaugurated on May 6, 1956, the SESC Garanhuns Holiday Camp stands as a striking example of Modernist architecture in northeastern Brazil. The building is situated on a slightly undulating site, seeking to establish a direct relationship between the built space and the outdoors, with a focus on the natural landscape. Its primary geometric composition consists of a gentle curve that follows the topography of the lot and opens to the exterior through a system of pilotis, creating a continuous veranda. The most striking visual element of the structure is a large panel of *"cobogós"* in a trapezoidal shape, which follows the curvature of the building. The Holiday Camp had an initial capacity to accommodate 82 people distributed across 12 apartments. It featured a library, game room, meeting room, auditorium for theatrical performances and cinema, as well as a large garden of tropical plants with a pond (SESC DEP. PERNAMBUCO, 1965).

Over the course of its nearly 70 years, the complex has undergone numerous renovations and expansions that have almost completely altered the original design, with the construction of new apartment buildings (Figure 2). According to Amorim (2007), there are several types of architectural deaths, among them death by "external architectural parasites," which occurs with the incorporation of elements extrinsic to the original compositional concept of the architectural design, introduced due to new demands of human activities. Given this, even though the building retains its original use and activities, its compositional logic has been completely altered, compromising its material and immaterial integrity and rendering it almost unrecognizable.



Figure 2 – Current Status of the SESC Garanhuns Holiday Camp
Source: www.sescpe.org.br

In addition, active public participation is a key factor in the preservation of heritage assets, given that when the public lacks a connection to the building or its surroundings—a reflection of a lack of identification—the preservation process becomes more difficult and complex, especially when it comes to architectural works of the Modern Movement (DOĞAN, 2020). From this perspective, the SESC Garanhuns Holiday Camp stands as a clear example of the invisibility of Modern Movement works, reflecting a lack of recognition by society and the agencies responsible for safeguarding and preserving their heritage and cultural value.

The original building underwent successive renovations and expansions (Figure 3) driven by SESC's need to expand the facilities of the former Holiday Camp, due to partnerships established by the Pernambuco department with other regional units in neighboring states (SESC DEP. PERNAMBUCO, 1965). Currently, the complex has 101 apartments, with eight times as many beds as the original building. In addition, the former garden has given way to new annexes, which house a variety of recreational activities, such as swimming pools, a restaurant, a convention center, and a gym, among other facilities.

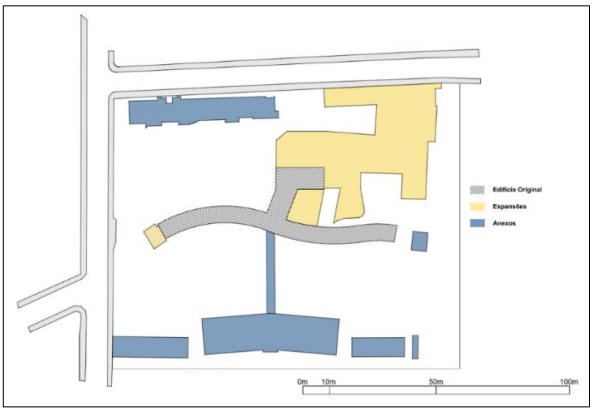


Figure 3 – Expansions and Additions to the Original Building
Source: Produced by the authors

3. Methodology

3.1 Theoretical Assumptions: Redrawing and Documentation in a BIM Environment

The development of documentation for an architectural object is a complex process that draws upon various fields of knowledge within the disciplines of architecture and urban planning to compile, clarify, and supplement the historical, formal, and structural characteristics of a building (Waisman, 2013). In this context, redrawing establishes itself as a fundamental methodology in the documentation of historical and cultural heritage, as it enables an in-depth analysis of the building and contributes to the systematization and transmission of knowledge regarding its materiality and significance over time.

The use of redrawing as a method of historical research and analysis is not a recent practice. It is a technique that gained prominence during the Renaissance, when artists and architects used representational media —such as drawings and other iconographic records—to document the legacy of classical architecture, conducting studies, research, and the construction and reconstruction of works that no longer existed or were disappearing. This approach ensures a deeper connection with the architectural work, allowing the creation of documentation to go beyond a mere collection of data about a project, becoming a means of transmitting knowledge (VÁZQUEZ RAMOS, 2016).

The redrawing of documentation has become one of the most important tools for preserving the memory of a heritage site, whether through traditional methods or new resources. From this perspective, even if a building disappears entirely or partially, its visual record can be restored, albeit with limitations, access to the work, perpetuating its legacy and the way in which human beings connect to it (OLIVEIRA, 2008).

In addition, digital technologies open up new possibilities for documentation, particularly through the creation of parametric 3D models capable of emulating specific aspects of the architectural object. Among these technologies, BIM (Building Information Modeling) has been driving significant changes in representation methods in Architecture and Urban Planning, marking a gradual transition from traditional analog methods to an integrated data environment. According to López et al. (2018), BIM has been expanding its scope of application to the field of cultural heritage, enabling its representation in a virtual environment to contribute to documentation and management activities.

HBIM (Heritage Building Information Modeling)—where "Historical" has recently been replaced by "Heritage"—has emerged as a branch of BIM that is not limited to the design process for new buildings, but extends to initiatives involving the digital redesign and documentation of existing structures. In HBIM, it is possible to create interactive parametric elements that represent the historic structure, developed based on documentary sources and other historical records (MURPHY; MCGOVERN; PAVIA, 2013).

Thus, the concept of the Digital Twin reinforces this approach by enabling the creation of a realistic model of a physical object through a dynamic virtual representation, capable of continuously aggregating updated data and reflecting its characteristics, behaviors, and transformations throughout its life cycle (MADNI; MADNI; LUCERO, 2019). Concerning architectural objects, the digital twin of a heritage site allows for the integration of construction and historical information associated with this digital model, fostering a deeper understanding of the physical space, encompassing aspects such as materiality, construction techniques, and progressive modifications, such as expansions and renovations, in addition to guiding potential decision-making regarding heritage management (MESEGUER; VALLDECABRES, 2023).

3.2 Practical Assumptions: Parametric 3D Modeling

To create the 3D model, it was first necessary to conduct iconographic research, given that, in order to build a parametric model faithful to the original building, as much information as possible must be gathered (original technical drawings (Figure 4), photographic records (Figure 5), texts, etc.). Only through this survey is it possible to adequately understand the building under study. In this work, sources and documents provided by the family of architect José Armando Farias were used; the family preserves a large part of his collection, which contributed to the creation of a memorial housed in the architect's former office. The "José Armando Farias Memorial" brings together personal objects (furniture, drawing boards, drawing materials, books); photographs of works and travels; paintings and engravings created by him; as well as some originals and heliographic copies of studies and working drawings of projects, as well as perspectives (PAIVA; DIÓGENES, 2014).

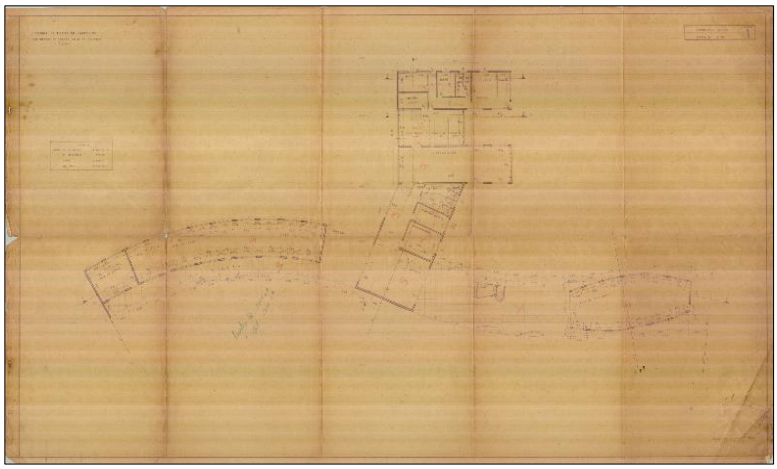


Figure 4 – Original Technical Floor Plan Drawing
Source: José Armando Farias Memorial



Figure 5 – Photo Gallery of the recently inaugurated Holiday Camp
Source: José Armando Farias Memorial

The modeling process for the SESC Garanhuns Holiday Camp was carried out using Graphisoft Archicad 28 BIM software. Following an initial analysis, the modeling began by importing the original technical drawings—which had already been digitized in .pdf format—into the software and organizing them into different worksheets that served as a guide for creating the model using the vectorization tool. In total, there were five digitized drawings, containing floor plans, sections, elevations, and construction details. During data collection, 2D CAD drawings of the most recent renovation of the SESC Garanhuns Tourism and Leisure Center (the current name of the former holiday camp) were made available, which served to fill in some information gaps, such as the absence of certain metric data.

In Archicad, the architectural model was created using parametric elements already available in the platform (walls, slabs, beams, columns, window frames, etc.), adapted to the specific requirements of the original project, which contributed to a more efficient development of the model. It was necessary to individually model some more complex elements, such as the *"cobogó"* curtain on the upper floor (Figure 6). During this process, it was found that using the original technical drawings would not be sufficient to vectorize the project in a way that would ensure an accurate reconstruction, given the distortions the drawings had undergone during digitization. To resolve this issue, .dwg files containing the 2D CAD drawings of the building's current configuration were used. These files were transferred from Autodesk AutoCAD to Archicad.



Figure 6 – 2D CAD technical drawings of the building's current configuration
Source: PROJEBRÁS LTDA

Although the original technical documents for the project were readily available in excellent condition—thanks to the architect's family's efforts to preserve his work—no information regarding the site's topography was found. Topographic data proved essential to the modeling process, since the way the building is situated on the lot reveals the architect's concern with creating a volumetry that respects the existing surroundings. To generate a topographic approximation, the Quantum Geographic Information System (QGIS) software was used to obtain the contour lines with their elevations in .dxf file format. Following this procedure, it was possible to transfer this information to Archicad and model the lot according to its topography, using the mesh element associated with the generated file.

Furthermore, by comparing the 2D CAD technical drawings, photographs of the project as it was newly completed in the 1950s and 1960s, and the original drawings, it was possible to determine that certain changes were made during construction. The original design called for a flat slab waterproofed with an asphalt membrane, which was later replaced by a low-slope tile roof concealed by a small parapet, in addition to some windows with different numbers of panes.

4. Results and Discussion

The main product is the three-dimensional parametric model, provided in .pln format, which compiles the data and information from the historical documentation inventoried for the preparation of this study. In conjunction with this product, digital documentation was developed, consisting of redrawn floor plans (Figure 7), sections, and elevations (Figure 8) of the Holiday Camp reconstruction. Furthermore, using the features provided by Archicad itself, it was possible to create rendered perspectives (Figure 9). This set of traditional information, combined with the graphic representations produced, contributes to the architectural analysis of the building, enabling a better understanding of aspects such as zoning, the building's layout on the site, floor distribution, enclosures (window frames and "*cobogó*" panels), and, above all, spatiality, serving as a foundation for future initiatives in education, research, and heritage intervention.

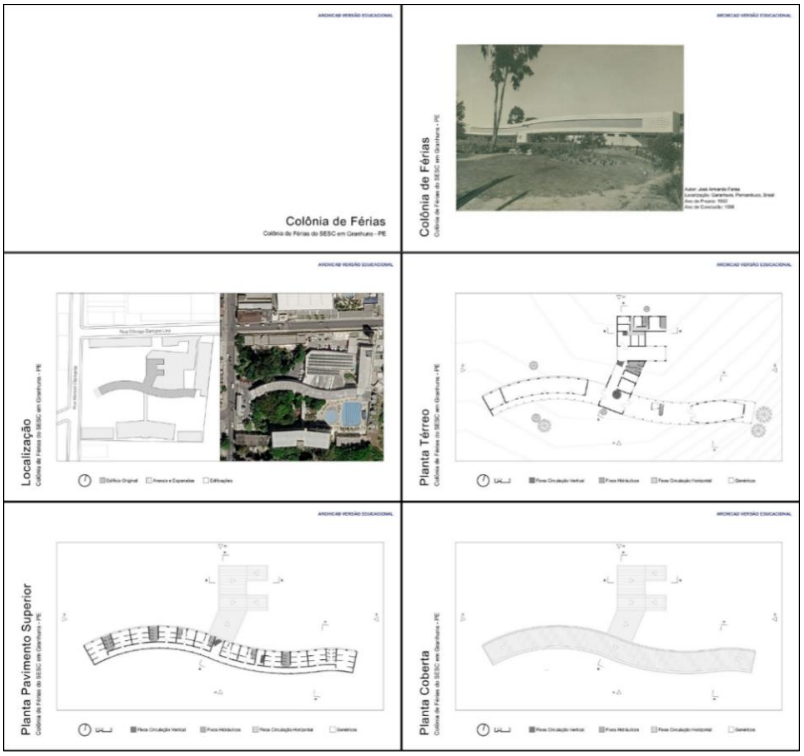


Figure 7 – Digital documentation
Source: Produced by the authors

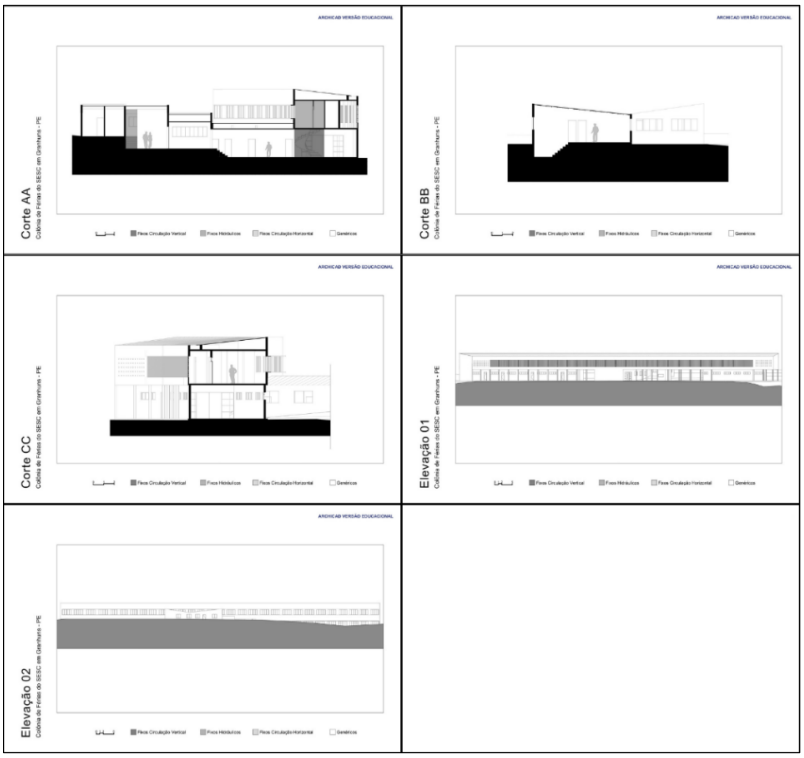


Figure 8 – Digital documentation
Source: Produced by the authors

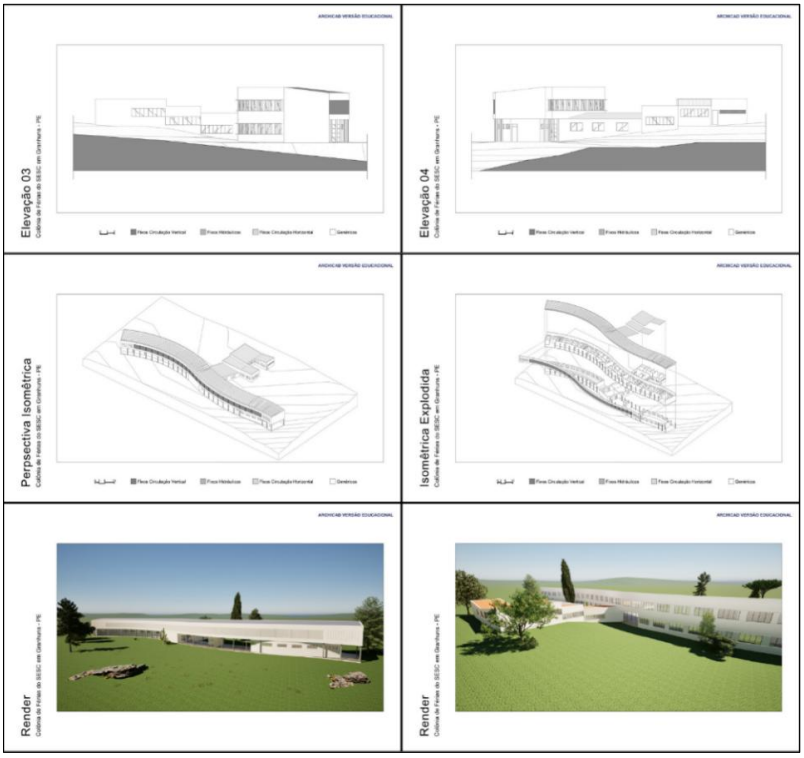


Figure 9 – Digital documentation
Source: Produced by the authors

This process, aimed at creating a digital twin using BIM as a tool, reaffirms the versatility and ability of this methodology to integrate data from different sources, such as photographic records, digitized documents, and files based on various programming languages. Such integration helps streamline operations, making them more agile and reliable. In this specific context, the application of HBIM strengthens the use of new technologies aimed at preserving the legacy of buildings that have undergone processes of historical erasure, as well as at enhancing their potential as cultural heritage.

5. Conclusions

This study sought to demonstrate how the digital reconstruction of the SESC Garanhuns Holiday Camp (1956), through the application of BIM combined with the Digital Twin concept, can support architectural documentation, heritage conservation, and information management. The results confirm that the integration of original drawings, historical photographs, CAD files, and topographic data into a single parametric three-dimensional model made it possible to reconstruct the spatial, formal, and structural logic of José Armando Farias's modernist design, despite the profound alterations that compromised its integrity over time.

The research demonstrates that HBIM goes beyond the realm of mere graphic representation, serving as an effective methodological tool for organizing, systematizing, and preserving scattered documentary information that would otherwise remain fragmented across isolated archives. In this sense, the resulting digital model functions simultaneously as a heritage inventory and a digital obituary, capable of safeguarding the architectural memory of a modern work subjected to processes of partial "architectural death" resulting from successive expansions and parasitic additions. Beyond its documentary function, the model also offers a consistent foundation for preservation strategies, educational activities, critical historical interpretation, and potential restoration or redevelopment efforts.

From a broader perspective, the study contributes to the debate on the preservation of modern heritage linked to the history of social tourism in Brazil, highlighting how digital technologies can revitalize the cultural significance of buildings that have been physically altered or rendered socially invisible, bridging the fields of architectural and urban theory and history with technology. The case of SESC Garanhuns thus reinforces the relevance of the HBIM as a link between memory, management, and conservation, especially in contexts where the original project survives only partially. As a corollary, possibilities are identified for expanding this digital twin to interactive management platforms, allowing for continuous data updates, maintenance protocols, and greater public dissemination of the legacy of Brazilian modern architecture.

Acknowledgments

The authors would like to thank CNPq (the National Council for Scientific and Technological Development) for the financial support provided for the research project "Social Tourism and Modern Architecture in Brazil," as well as for the PIBIC fellowship also awarded by CNPq as part of that project.

References

Amorim, Luiz Manuel do Eirado. 2007. Obituário arquitetônico: Pernambuco modernista. Recife: Editora UFPE.

Cheibub, Bernardo Lazary. 2011. "Ponderações sobre o turismo social a partir da história institucional do Serviço Social do Comércio (SESC) e da produção acadêmica brasileira." In International Conference on Tourism & Management Studies. Algarve.

Cortés Meseguer, Luis, and Jorge García Valldecabres. 2023. "Digital twins: HBIM information repositories to centralize knowledge and interdisciplinary management of architectural heritage." VITRUVIO –

International Journal of Architectural Technology and Sustainability 8 (2): 64–75. https://doi.org/10.4995/vitruvio-ijats.2023.20534.

Doğan, Huriye Armağan. 2020. “Modernist architectural heritage as a place-making element: the case of Ankara.” Miasto i Kultura (City and Culture).

López, Francisco, et al. 2018. “A review of heritage building information modeling (H-BIM).” Multimodal Technologies and Interaction 2 (21). https://doi.org/10.3390/mti2020021

Madni, Azad M., Carla C. Madni, and Scott D. Lucero. 2019. “Leveraging digital twin technology in model-based systems engineering.” Systems 7 (1): 7. https://doi.org/10.3390/systems7010007.

Murphy, Maurice, Eugene McGovern, and Sara Pavia. 2013. “Historic building information modelling: adding intelligence to laser and image-based surveys of European classical architecture.” ISPRS Journal of Photogrammetry and Remote Sensing 76: 89–102. https://doi.org/10.1016/j.isprsjprs.2012.11.006.

Oliveira, M. M. 2008. A documentação como ferramenta de preservação da memória. Brasília: Programa Monumenta/IPHAN.

Paiva, Ricardo Alexandre, and Beatriz Helena Bezerra Nogueira Diógenes. 2014. “Caminhos da arquitetura moderna em Fortaleza: a contribuição do arquiteto José Armando Farias.” In Anais do 5° Seminário Docomomo Norte/Nordeste. Fortaleza: Núcleo Docomomo Ceará/UFC. https://doi.org/10.5281/zenodo.19293895

Paiva, Ricardo Alexandre, and Beatriz Helena Nogueira Diógenes. 2018. “Dinâmica imobiliária e preservação da arquitetura moderna em Fortaleza: o passado, o presente e o futuro em questão.” Arquitextos 19 (223.02). https://vitruvius.com.br/revistas/read/arquitextos/19.223/7243.

Serviço Social do Comércio (SESC-PE). n.d. Comentários sobre dezessete anos de colônia de férias: oito anos em convênios com hotéis e nove anos em ambiente próprio. Recife: Administração Regional no Estado de Pernambuco.

Simeone, Davide, Stefano Cursi, and Ilaria Toldo. 2014. “BIM and knowledge management for archaeological heritage.” In Proceedings of the 34th Annual Conference of the Association for Computer Aided Design in Architecture (ACADIA). Los Angeles. https://doi.org/10.52842/conf.acadia.2014.681.

Vázquez Ramos, Fernando Guillermo. 2016. “Redesenho: conceitos gerais para compreender uma prática de pesquisa histórica em arquitetura.” Arquitextos 17 (195.09). https://vitruvius.com.br/revistas/read/arquitextos/17.195/6181.

Waisman, Marina. 2013. O interior da história: historiografia arquitetônica para uso de latino-americanos. São Paulo: Perspectiva.

cinpar2026
XXII International Conference on Building Pathology and Constructions Repair
15th to 17th July 2026 - Lisboa, Portugal

Integrating Computer Vision and Machine Learning for Detection of Damage in Historic Buildings

Michael OLIVEIRA[1], Esequiel MESQUITA[2], Mylene VIEIRA[3]

[1] Federal University of Ceara, Brazil; mjackson20@alu.ufc.br
[2] Federal University of Ceara, Brazil; emesquita@ufc.br
[3] Federal University of Ceara, Brazil; mylene.melo@ufc.br

Abstract: The inspection and diagnosis of pathological manifestations in historic buildings, fundamental for planning conservation and maintenance actions and are traditionally based on manual visual assessments. Although widely adopted, this approach presents limitations related to evaluating subjectivity, inconsistency of records, and difficulties in systematizing the collected information. In this context, this study proposes the application of Computer Vision (CV) and Machine Learning (ML) techniques for the automated detection of pathological manifestations in structural and architectural elements of the historic asset José de Alencar Teatre (TJA), located in Fortaleza, Brazil. The research was based on the construction of an image dataset obtained during inspection campaigns carried out at the TJA. The images were organized, pre-processed, and manually labeled according to damage classes associated with structural and architectural components, including cracks, corrosion, moisture stains, coating detachment, and surface degradation. Based on this dataset, an image classification model was developed using supervised learning techniques and implemented on the Microsoft Custom Vision platform, which applies Convolutional Neural Network (CNN) architectures for visual pattern recognition. The methodological procedure comprised image acquisition and preprocessing, definition of damage classes, iterative model training, validation, and performance evaluation using classification metrics. The results indicated satisfactory model performance in identifying the analyzed damage classes, with accuracy values above 85%. In the application stage, the probabilistic responses generated by the model showed correspondence with the visible damage patterns observed in the submitted images, indicating consistency between automated classification and field inspection records. The proposed method showed technical applicability as a support tool for damage mapping, organization of diagnostic information, and incorporation of image-based analysis into digital documentation environments for historic building maintenance and conservation.

Keywords: Computer vision; Machine learning; Pathological manifestations; Built heritage; Building inspection.

1. Introduction

The conservation of historic buildings depends directly on the proper identification of damage manifestations affecting their architectural and structural elements over time. These assets are subject to the combined effects of natural aging, environmental exposure, moisture, inadequate interventions, and lack of maintenance, factors that contribute to the occurrence of cracks, detachments, superficial losses, oxidation processes, and other forms of material deterioration [1,2]. For this reason, the inspection stage plays a central role in diagnosis and intervention planning, especially in buildings whose historical and cultural value requires procedures compatible with the preservation of their physical and documentary integrity [1,3].

Although widely employed, conventional visual inspection still presents limitations related to evaluator subjectivity, variability between records, the high time required, and the difficulty of systematizing information collected in the field [4,5]. On extensive surfaces with complex geometries, ornamentation, and

the coexistence of multiple pathological manifestations, exclusive reliance on manual observation tends to hinder the comparison between inspection campaigns and to compromise the standardization of diagnoses [4,6]. This issue becomes even more critical in historic buildings, where the assessment of pathological conditions must be technically consistent and compatible with documentation and long-term monitoring processes [2,3].

In this context, computer vision has been established as a promising alternative for the systematic processing of inspection images, allowing photographic records to be treated not only as visual documentation, but also as data suitable for segmentation, pattern recognition, classification, and automated tracking [3,4]. In the field of damage detection, methods based on machine learning and deep learning have been applied to the identification of cracks, surface defects, localized degradation, and the classification of failure types in several materials and components [7–10]. These advances demonstrate that the automation of visual interpretation can reduce dependence on manual assessment and increase objectivity in anomaly evaluation [7,8].

In the context of historic heritage, the application of these techniques is of particular interest, as it allows photographic surveys to be used as the basis for the construction of labeled image datasets and for the training of models aimed at recognizing pathological manifestations in façades and building elements. Recent studies have shown that systems based on artificial intelligence can support the production of deterioration maps from façade images and assist in monitoring the evolution of cracks and other damage in heritage buildings [2,11]. In addition, the quality and diversity of training images, the definition of classes, and the consistency of labeling directly influence model performance, especially when different types of damage present similar morphological characteristics [12].

Similar methods have been applied to the automated identification of damage in underwater concrete [8], steel cables [7], internal equipment profiles [9], drilling components [10], and aquaculture nets [16], as well as to damage monitoring in civil infrastructure [13–15]. Although developed in different contexts, these studies demonstrate the applicability of classification and detection algorithms to reduce inconsistencies in manual inspection and support image-based assessments [8,13].

At the same time, computer vision has been increasingly incorporated into broader building inspection and management workflows. Approaches based on three-dimensional reconstruction, association between 2D images and digital models, augmented reality, and BIM integration have been used to locate defects, record their position, and structure inspection data in digital environments [4–6]. This type of integration is particularly relevant in technical documentation strategies, as it enables the results of automated visual analysis to be related to the spatial representation of the building and to information storage and retrieval systems [5,6].

In the field of civil construction, there is also evidence of the practical application of supervised classification platforms to building inspection tasks. Staffa et al. [17] demonstrated the feasibility of using Microsoft Custom Vision for the automated identification of nonconformities in building roofs, based on an image dataset collected with an unmanned aerial vehicle. This type of application is particularly relevant to the present research, as it demonstrates the possibility of employing an accessible supervised learning platform for the classification of damage recorded during technical inspections [17].

Despite these advances, a gap still remains between the development of computational models and their systematic application to the inspection of historic buildings, especially in assets with high architectural complexity, material diversity, and the need for continuous documentation [1,2]. A significant portion of existing studies is focused on civil infrastructure, industrial components, or specific surfaces, whereas historic buildings require models capable of dealing with diverse pathological manifestations, overlapping damage, ornamental interference, and variations resulting from material aging [1,2,11].

In this context, the present study proposes the application of computer vision and machine learning (ML) techniques for the automated detection of pathological manifestations in structural and architectural elements of the Teatro José de Alencar, located in Fortaleza, Ceará. The research is based on the construction of an image dataset obtained during inspections of the building, followed by the organization, preprocessing, labeling, and supervised training of the algorithm on the Microsoft Custom Vision platform. The study investigates the feasibility of automated damage classification as a support tool for technical inspection activities, damage mapping, and the systematization of diagnostic records in historic buildings.

2. Methods and materials

The methodological procedure adopted in this research was structured into five sequential stages, comprising the selection of the heritage building, data acquisition through field inspections and photographic records, the development of the image dataset for training the Machine Learning (ML) model, the supervised training and validation of the computer vision model, and the application of the validated model for automated damage detection. This workflow was defined to support the organization, classification, and interpretation of the pathological manifestations identified in the architectural and structural elements of the Teatro José de Alencar, as summarized in Figure 1.

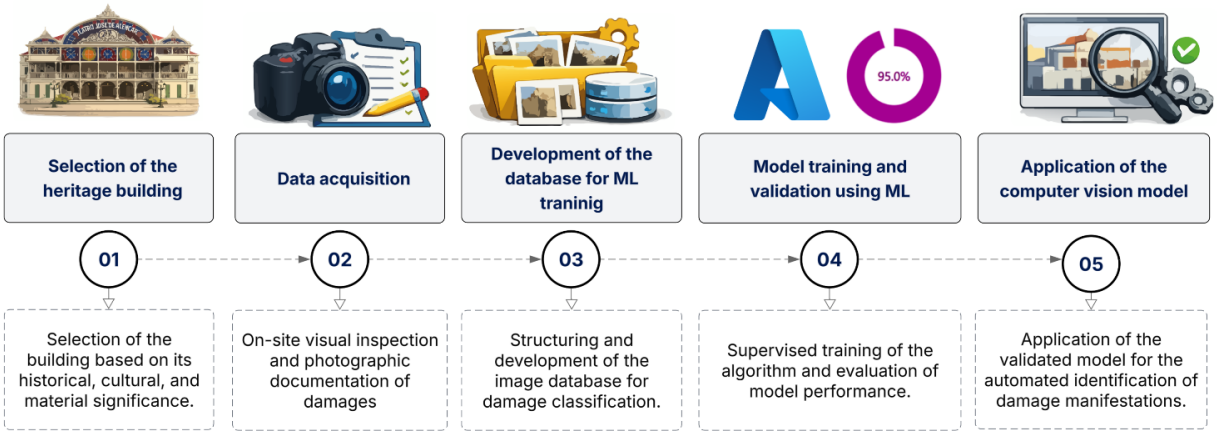


Figure 1 – Workflow of the methodological procedure adopted in the research.

2.1. Selection of the heritage building

The Teatro José de Alencar (TJA), located in Fortaleza, Ceará, was defined as the object of study of this research due to its historical, cultural, and architectural relevance, as well as its material and constructive complexity. It is a listed building, inaugurated in 1910, whose configuration combines masonry elements, ornamental cast-iron metallic components, and characteristics associated with the neoclassical and art nouveau styles, giving the asset a high degree of uniqueness for studies focused on inspection, documentation, and conservation.

The selection of the TJA is also justified by the existence of an HBIM model previously developed by Vieira et al. (2023), based on digital documentation strategies using scan-to-BIM, with terrestrial laser scanning and aerial photogrammetry [18]. This model already constitutes a consolidated geometric and informational basis for the asset, which favors the expansion of analyses related to maintenance and diagnosis. In this context, the application of computer vision to the TJA is inserted as a direct complement to the workflow under development for the building, contributing to the organization of the image dataset, the automated identification of damage, and the improvement of the analysis tools applied to its architectural and structural elements.



Figure 2 – 3D digital model of the Teatro José de Alencar developed by Vieira et al. (2023).

2.2. Data acquisition

The data acquisition stage was developed from visual inspections carried out at the Teatro José de Alencar, with a focus on the systematic photographic documentation of the conditions observed in the architectural and structural elements of the building. Image capture was carried out strategically, prioritizing areas with a greater concentration of visible damage, different exposure conditions, and a variety of constructive elements, in order to provide a broader visual reading of the condition of the building.

As a result, an archive of approximately 1,200 digital photographs was established, obtained in the field and organized as the basis for the damage mapping of the building. These records were used to identify, locate, and document the damage observed during the inspection, supporting the enrichment of the 3D digital model of the Teatro José de Alencar under development. For this purpose, the mapping information was structured through parameters inserted in Autodesk Revit, using the Project Parameters feature in the Manage tab, allowing the creation of specific fields for associating the data with the analyzed elements. From this set, a specific selection of images corresponding to the masonry elements was carried out, defined as the focus of interest for subsequent submission to the computer vision analysis stages. After the analysis, the corresponding images and results were intended to be inserted into and mapped within the model according to their respective locations, allowing the photographic record, damage identification, and its spatial position to be associated within the digital environment.

2.3. Development of the database for Machine Learning

The development of the database for model training was based on the collection of images with visual patterns representative of recurring damage on masonry surfaces, following the stages of collection, screening, and labeling presented in Figure 3. To compose this dataset, both images obtained during the surveys carried out on the asset and complementary images available on the web were used, selected in order to enrich the visual variability of the classes and increase the model's generalization capacity. This strategy made it possible to gather different lighting conditions, textures, scales, framings, and damage intensities, contributing to the formation of a more consistent basis for supervised training.



Figure 3 – Workflow for image database preparation.

After the initial constitution of the dataset, a database of approximately 500 images was structured for training the algorithm to recognize seven damage classes: mold, efflorescence, detachment, degradation, cracks, dampness, and spalling. From this set, a data cleaning stage was carried out, aimed at screening and refining the images by excluding redundant records, images with low sharpness, inadequate framing, or low visual representativeness. Subsequently, the data labeling stage was performed, in which the selected images were organized and labeled according to their respective classes, allowing each visual pattern to be associated with its corresponding diagnostic category.

This process was necessary to provide the model with a base set of previously classified visual examples, from which the algorithm could learn to recognize regularities, differences, and characteristic patterns of each type of damage. In this way, the database was structured not only as an image repository, but also as a supervised training base prepared to support the development of automated damage classification in digital images.

2.4. Model training and validation using AI

The training of the computer vision model was carried out on the Microsoft Custom Vision (Azure AI) platform, adopted as a supervised learning environment for the automatic classification of damage in digital images. The methodological workflow used at this stage comprised the phases of platform configuration, image submission, model training, metric evaluation, performance validation, and final application of the algorithm, as presented in Figure 4. This structure was defined to allow the learning process to occur sequentially, from the initial organization of the project to the obtaining of a model capable of classifying the submitted images.

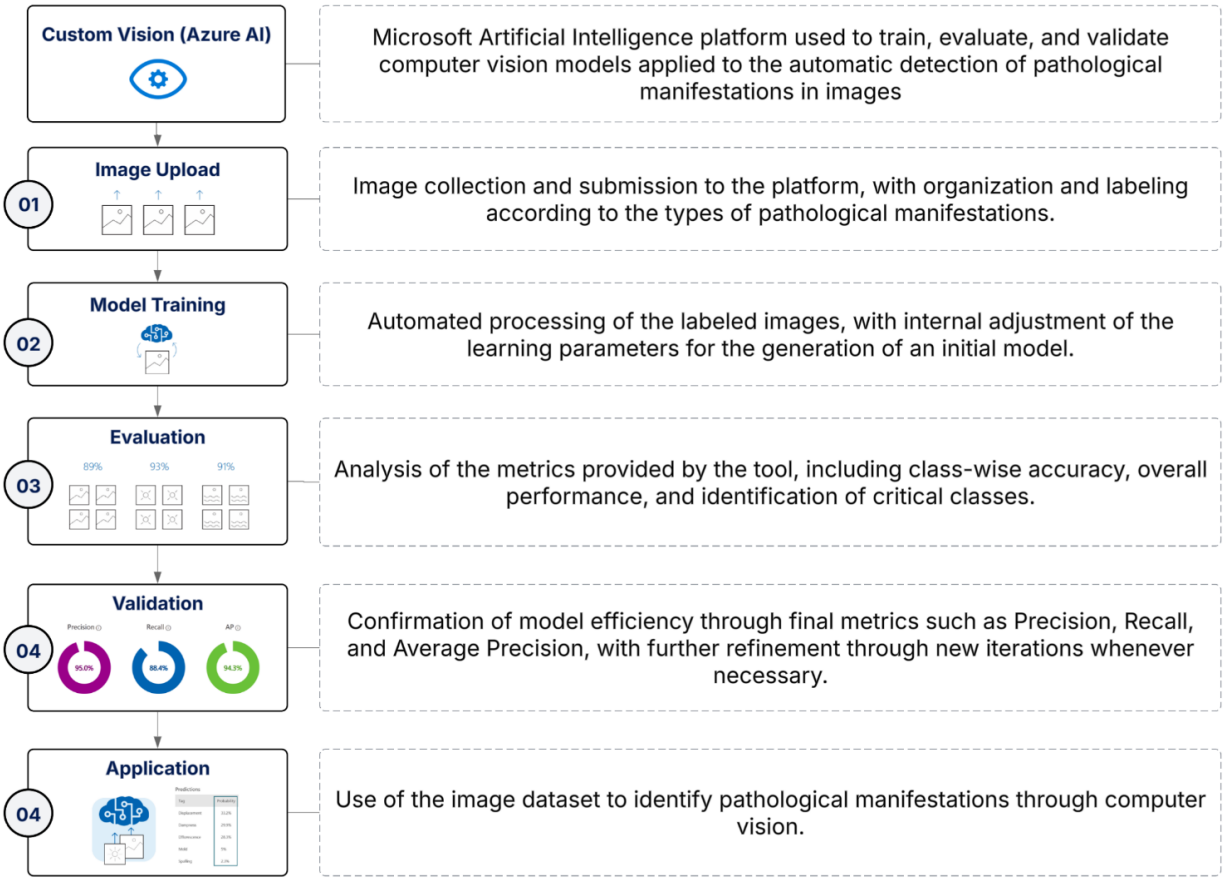


Figure 4 – Workflow of model training, evaluation, and validation.

Initially, a specific project was created on the platform, configured for the classification of masonry damage images. At this stage, the project name, the description of the analysis scope, and the classification domain to be used in the Custom Vision environment were defined, in addition to the type of classification adopted for the training. Next, the previously structured image database was submitted, with the samples organized according to their respective pathological classes. After the image upload, supervised training of the model was initiated. At this stage, the algorithm began to process the visual patterns present in each labeled class, seeking to recognize regularities, morphological differences, and recurring characteristics among the analyzed damage types. This processing occurred automatically on the platform itself, based on the provided examples, allowing the internal adjustment of the learning parameters and the generation of an initial classification model.

In the following stage, the metrics produced by the system were analyzed to verify the performance of the trained model. This evaluation considered the indicators presented by the platform for each class and for the model as a whole, making it possible to observe the behavior of the algorithm in relation to the learned patterns and to identify possible critical classes, with greater visual overlap or lower distinction between them. Based on this assessment, new refinement iterations were carried out whenever necessary, with the aim of improving training consistency and reducing ambiguities in classification. Figure 5 illustrates the project configuration and the visual organization of the training images according to their respective damage classes.

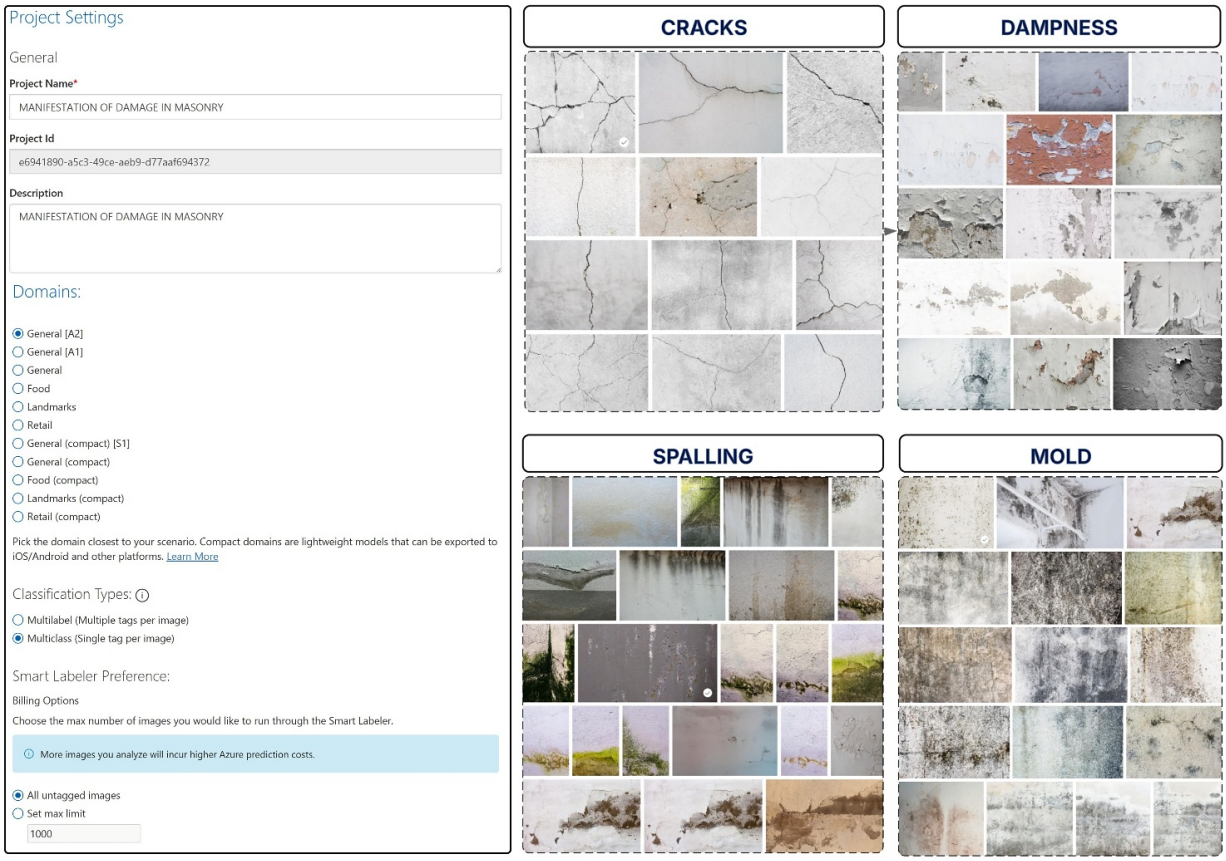


Figure 5 – Project configuration and organization of damage classes.

Model validation was carried out based on the final metrics provided by the platform, with emphasis on Precision, Recall, and Average Precision, adopted as parameters to confirm the efficiency of the algorithm. These indicators made it possible to verify the model's capacity to correctly recognize the visual patterns associated with each damage class, as well as to assess the balance between sensitivity and precision in

classification. Once satisfactory performance was achieved, the validated model proceeded to the final application stage.

Finally, the trained and validated model was used for the automated analysis of digital images, allowing the identification of pathological patterns based on the classes learned during training. At this stage, the algorithm began to function as a support tool for the technical interpretation of images, providing classificatory outputs based on the previously structured database. In this way, the use of Custom Vision made it possible to operationalize the supervised classification of damage in masonry images, establishing a continuous methodological workflow between database development, training, validation, and model application.

2.5. Application of Computer Vision model

After the training, evaluation, and validation stages, the computer vision model was applied to the automated analysis of digital images, with the aim of identifying visual patterns associated with the previously defined damage classes. At this stage, the images submitted to the algorithm were processed on the Microsoft Custom Vision platform, which began to provide, for each analyzed record, the probabilities of association between the image and the classes trained in the model. The application was carried out on representative images of the architectural and structural elements of the building, allowing verification of the algorithm's ability to recognize damage patterns under real inspection conditions.

The analysis of the results was performed based on the classification probabilities assigned to each class, making it possible to identify the predominance of certain damage patterns and to analyze the coherence between the model's output and the visual characteristics observed in the images. After the computer vision analysis stage, the information resulting from damage classification was added to the building's 3D digital model, allowing the photographic records, the identified damage patterns, and their spatial location to be associated within the same representational environment.

Thus, the methodology was concluded with the application of the validated model to the photographic records, establishing a continuous workflow between data acquisition, image database organization, supervised training, and automated analysis. This procedure made it possible to structure a methodological sequence aimed at identifying damage in digital images, based on the recognition of visual patterns learned from the previously developed dataset.

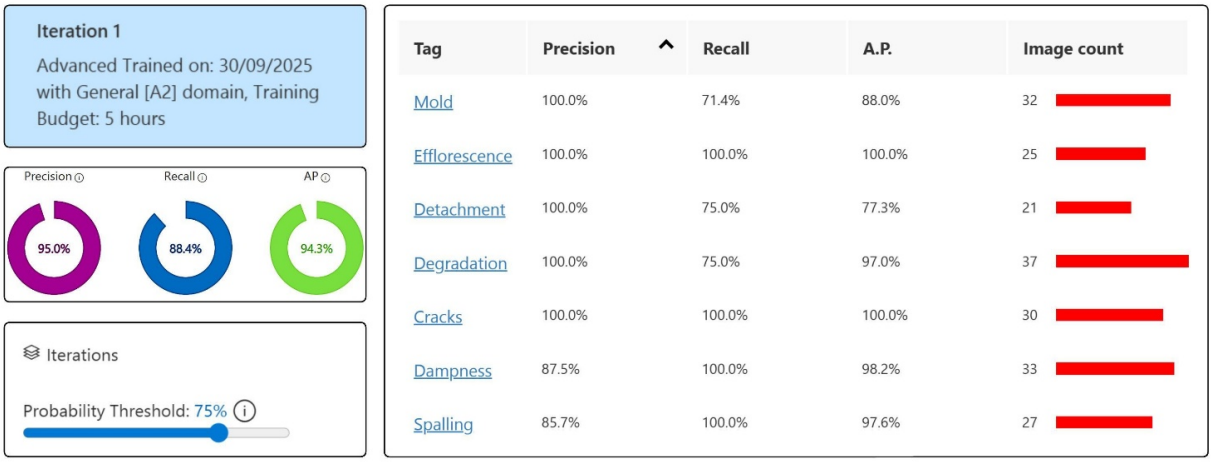
3. Results and discution

3.1. Image database development and model training

The image database structured for model training enabled the development of a first iteration of supervised classification on the Microsoft Custom Vision platform, using the General [A2] domain. Training was completed in approximately 5 hours, with a probability threshold set at 75%, resulting in global metrics of 95.0% precision, 88.4% recall, and 94.3% average precision (AP). These results indicate that the model presented satisfactory performance in identifying the trained classes, with a high success rate in positive classifications and a good overall balance between sensitivity and precision (Figure 6).

The class-by-class analysis (Figure 6) showed consistent performance for most of the evaluated damage patterns. The efflorescence and cracks classes presented the best results, with 100.0% precision, 100.0% recall, and 100.0% AP, indicating a high visual distinction of these patterns in the training set. The degradation, dampness, and spalling classes also showed high performance, with AP values of 97.0%, 98.2%, and 97.6%, respectively. On the other hand, the mold and detachment classes presented the lowest recall values, at 71.4% and 75.0%, respectively, although they maintained 100.0% precision. This behavior indicates that, for these classes, the model correctly classified the recognized images but still showed lower sensitivity in recovering all available examples in the analyzed set. In terms of sample distribution, the database used

in training showed moderate variation among classes, with counts ranging from 21 to 37 images per tag, suggesting that the model was trained with a relatively balanced dataset, although still subject to the influence of visual variability and the number of examples available in certain categories.



Tag	Precision	Recall	A.P.	Image count
Mold	100.0%	71.4%	88.0%	32
Efflorescence	100.0%	100.0%	100.0%	25
Detachment	100.0%	75.0%	77.3%	21
Degradation	100.0%	75.0%	97.0%	37
Cracks	100.0%	100.0%	100.0%	30
Dampness	87.5%	100.0%	98.2%	33
Spalling	85.7%	100.0%	97.6%	27

Figure 6 – Evaluation of model performance by damage class.

3.2. AI-Based Computer Vision for Damage Detection in Masonry

The application of the computer vision model to images of the external façades of the Teatro José de Alencar showed correspondence between the probabilistic outputs provided by the platform and the visible damage patterns on the analyzed surfaces. The photographs submitted to the algorithm correspond to sections of masonry with visible damage identified by visual inspection, allowing comparison between automated classification and the condition observed in the field (Figure 7).

In Figure 7a, the highest probability was assigned to the detachment class (64.7%), compatible with the localized loss of coating observed at the base of the wall. In Figure 7b, the predominant class was dampness (78.8%), consistent with the presence of continuous dark stains and surface alteration associated with moisture. In Figure 7c, the model indicated the highest association with spalling (34.2%), followed by degradation (30.8%) and detachment (30.0%), a result compatible with the simultaneous presence of material loss, surface degradation, and coating detachment. In Figure 7d, the highest probability was attributed to dampness (40.3%), followed by efflorescence (24.5%) and detachment (22.7%), reflecting the overlap of distinct visual patterns on the same analyzed surface.

The images submitted to the model present variations in natural lighting, texture heterogeneity, surface alterations, geometric elements, and coexistence of damage, conditions that directly influence the classification process. Even so, the outputs provided by the algorithm-maintained correspondence with the predominant visual patterns identified on the external façades of the building. In addition to indicating the class with the highest probability, the model also presented secondary classes with relevant percentages, allowing the simultaneous presence of more than one damage pattern in the same image to be recorded.

The results obtained in this stage show that probabilistic classification made it possible to identify visible damage patterns in the masonry based on the classes trained in the model. In the analyzed examples, the classes with the highest probability assigned by the system coincided with the predominant patterns visible in the images. The interpretation of the probabilities provided a hierarchy among competing classes and allowed comparison between the automated output and the visual records obtained during inspection. In this way, the application of the model to the TJA photographs established an analytical stage based on supervised classification, using real façade images for the recognition of visual patterns associated with the mapped damage.

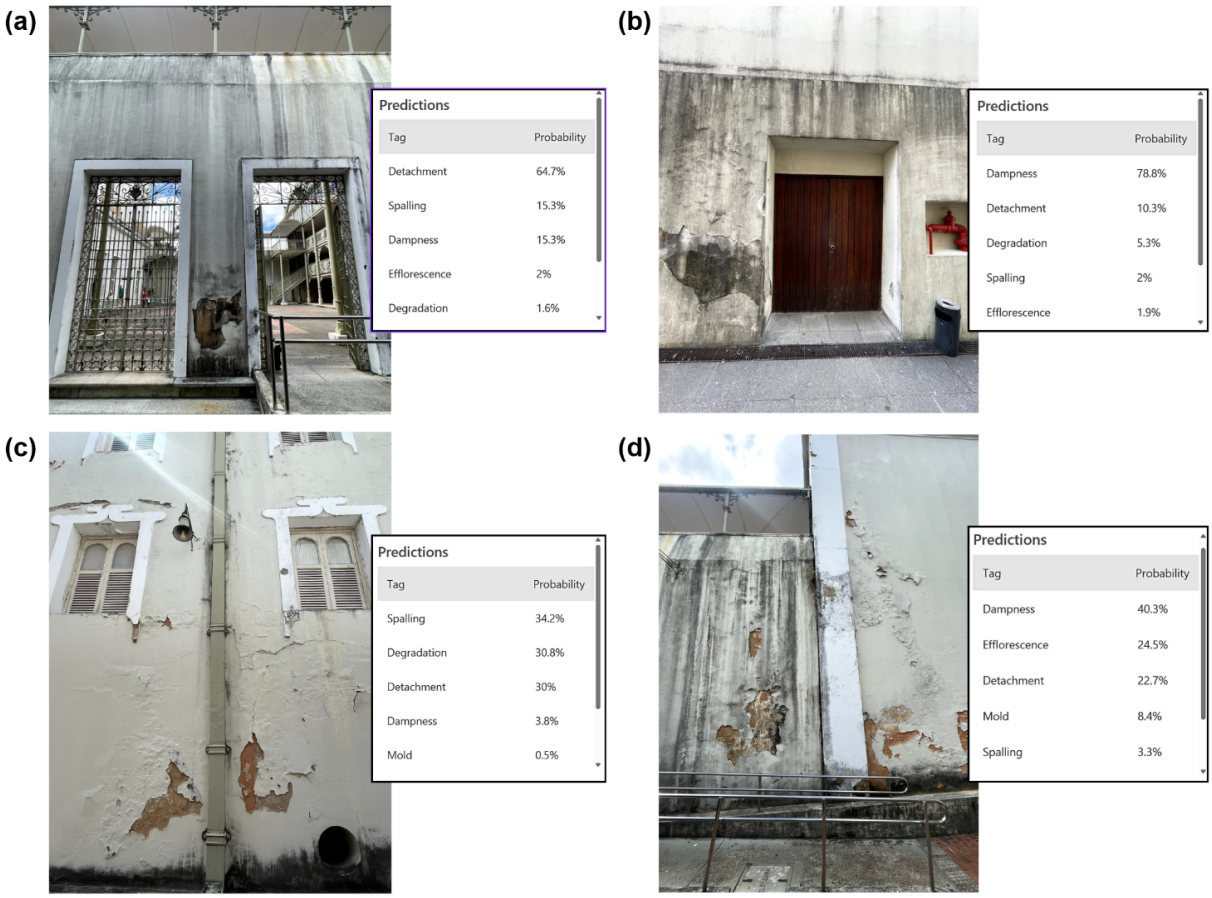


Figure 7 – Predictions of damage manifestations in masonry using computer vision.

3.3. Integration of Damage Data into the 3D Digital Model

The analyzed sections of the façades and internal environments were linked to the respective elements of the model, enabling the visual mapping of damaged regions and the organization of the information obtained during inspection and automated classification. In this process, the data were inserted through parameters associated with the modelled elements, allowing the recording of information such as visual inspection description, element code, location, and reference to the corresponding image.

The insertion of this information into the digital model made it possible to structure a visual and informational basis linked to the analyzed architectural elements, bringing together in the same environment the field-observed damage records, the images used in the analysis, and the data resulting from computer vision classification. In this way, the model came to concentrate not only the geometric representation of the building, but also the location and identification of the mapped damage, establishing a direct correspondence between the modelled element, the photographic evidence, and the associated diagnostic information. This procedure consolidated the workflow developed in the study, integrating photographic survey, supervised classification, and spatial organization of the data in the 3D digital model of the Teatro José de Alencar.

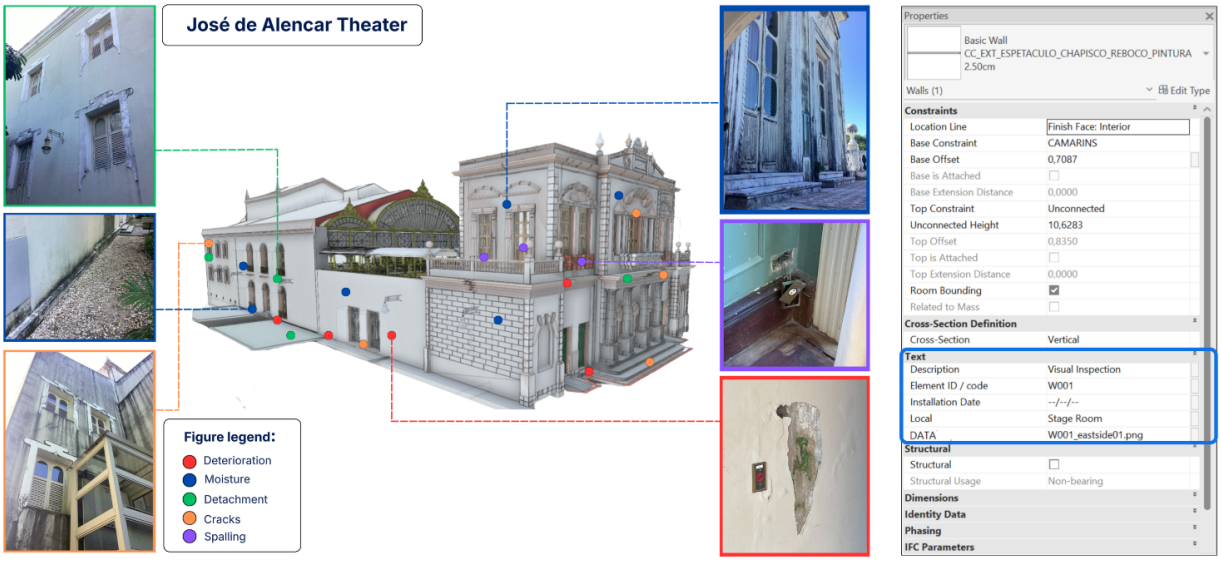


Figure 8 – Damage mapping and data insertion into the 3D digital model.

4. Conclusion

This study investigated the application of Computer Vision (CV) and Machine Learning (ML) techniques for the automated detection of damage patterns in structural and architectural elements of the Teatro José de Alencar, a historic building located in Fortaleza, Ceará. The methodological workflow comprised field photographic survey, the development of a labeled image dataset, the supervised training and validation of a classification model on the Microsoft Custom Vision platform, and the subsequent insertion of the resulting information into a 3D digital model. The trained model presented satisfactory performance, with global metrics of 95.0% precision, 88.4% recall, and 94.3% average precision, indicating adequate recognition capability for the damage classes adopted in the research.

The application of the validated model to façade images of the building showed correspondence between the probabilistic outputs provided by the algorithm and the visible damage patterns identified during field inspection. In addition to the classification of the predominant damage in each image, the model also indicated secondary classes with relevant probabilities, allowing the overlap of visual patterns on the same masonry surface to be recorded. The subsequent insertion of this information into the 3D digital model made it possible to associate photographic records, identified damage types, and mapped building elements within the same representational environment. The obtained results show that the proposed workflow is technically applicable as a support tool for damage mapping, the organization of diagnostic information, and the integration between automated image classification and digital documentation processes for historic buildings.

Funding

This work was financially supported by FUNCAP, Project 01172921/2022 – Cientista Chefe Cultura, Project 10581391/2022 – International collaboration FUNCAP/INSA Rouen Normandie; by the National Council for Scientific and Technological Development (CNPq) – Project 302054/2022-7 – PQ2, by the Project - 440926/2024-6 – VISION and Project - 402828/2024-0 – CLIC, CAPES Foundation and Finep 2896/24.

References

[1] Sanchez-Aparicio, L. J., F. L. del Blanco-García, D. Mencias-Carrizosa, et al. 2023. “Detection of Damage in Heritage Constructions Based on 3D Point Clouds: A Systematic Review.” Journal of Building Engineering 77: 107440. https://doi.org/10.1016/j.jobe.2023.107440.

[2] Ararat, M. B., and T. K. Yenice. 2026. “The Use of Artificial Intelligence in Damage Assessment of Historical Buildings.” Frontiers of Architectural Research 15: 554–565. https://doi.org/10.1016/j.foar.2025.06.008.

[3] Ye, C., Z. Yan, Z. Xu, et al. 2026. “Crack Detection and Evolution Monitoring for Heritage Buildings: A Systematic Computer Vision-Based Approach.” Journal of Infrastructure Intelligence and Resilience. https://doi.org/10.1016/j.iintel.2026.100207.

[4] Tan, Y., W. Xu, P. Chen, and S. Zhang. 2024. “Building Defect Inspection and Data Management Using Computer Vision, Augmented Reality, and BIM Technology.” Automation in Construction 160: 105318. https://doi.org/10.1016/j.autcon.2024.105318.

[5] Wang, T., and V. J. L. Gan. 2023. “Automated Joint 3D Reconstruction and Visual Inspection for Buildings Using Computer Vision and Transfer Learning.” Automation in Construction 149: 104810. https://doi.org/10.1016/j.autcon.2023.104810.

[6] Zhou, X., X. Li, Y. Zhu, and C. Ma. 2025. “Towards Building Digital Twin: A Computer Vision Enabled Approach Jointly Using Multi-Camera and Building Information Model.” Energy and Buildings. https://doi.org/10.1016/j.enbuild.2025.115523.

[7] Huang, X., Z. Liu, X. Zhang, et al. 2020. “Surface Damage Detection for Steel Wire Ropes Using Deep Learning and Computer Vision Techniques.” Measurement 161: 107843. https://doi.org/10.1016/j.measurement.2020.107843.

[8] Cui, B., C. Wang, Y. Li, et al. 2024. “Application of Computer Vision Techniques to Damage Detection in Underwater Concrete Structures.” Alexandria Engineering Journal 104: 745–752. https://doi.org/10.1016/j.aej.2024.08.020.

[9] Zhou, Y., R. Cao, P. Li, et al. 2022. “A Damage Detection System for Inner Bore of Electromagnetic Railgun Launcher Based on Deep Learning and Computer Vision.” Expert Systems with Applications 202: 117351. https://doi.org/10.1016/j.eswa.2022.117351.

[10] Yang, X., X. Feng, C. Cheng, et al. 2025. “Automatic Detection and Classification of Drill Bit Damage Using Deep Learning and Computer Vision Algorithms.” Natural Gas Industry B. https://doi.org/10.1016/j.ngib.2025.03.004.

[11] Cheng, M.-Y., M. N. Sholeh, and A. Kwek. 2024. “Computer Vision-Based Post-Earthquake Inspections for Building Safety Assessment.” Journal of Building Engineering 94: 109909. https://doi.org/10.1016/j.jobe.2024.109909.

[12] Chen, F., Y. Li, H. Sun, et al. 2025. “Petal Damage and Bent Flower Detection Method of Rose Cut Flowers Based on Computer Vision.” Scientia Horticulturae. https://doi.org/10.1016/j.scienta.2024.113927.

[13] Feng, D., and M. Q. Feng. 2018. “Computer Vision for SHM of Civil Infrastructure: From Dynamic Response Measurement to Damage Detection—A Review.” Engineering Structures 156: 105–117. https://doi.org/10.1016/j.engstruct.2017.11.018.

[14] Wu, T., L. Tang, F. Zhou, et al. 2024. “Damage Detection Based on Accelerometers and Computer Vision Measurements of Moving Load-Induced Structural Responses.” Mechanical Systems and Signal Processing 211: 111246. https://doi.org/10.1016/j.ymssp.2024.111246.

[15] Cha, Y.-J., J. G. Chen, and O. Büyüköztürk. 2017. “Output-Only Computer Vision Based Damage Detection Using Phase-Based Optical Flow and Unscented Kalman Filters.” Engineering Structures 132: 300–313. https://doi.org/10.1016/j.engstruct.2016.11.038.

[16] Labra, J., M. D. Zuniga, J. Rebolledo, et al. 2023. “Robust Automatic Net Damage Detection and Tracking on Real Aquaculture Environment Using Computer Vision.” Aquacultural Engineering 101: 102323. https://doi.org/10.1016/j.aquaeng.2023.102323.

[17] Staffa, L. B. Jr., L. S. V. Sá, M. I. S. C. Lima, and D. B. Costa. 2020. “Uso de Técnicas de Processamento de Imagem para Inspeção de Estruturas de Telhados de Edificações para Fins de Assistência Técnica.” ENTAC 2020. https://doi.org/10.46421/entac.v18i.1178.

[18]Vieira, Mylene M., et al. 2023. “Strategy for HBIM Implementation Using High-Resolution 3D Architectural Documentation Based on Laser Scanning and Photogrammetry of the José de Alencar Theatre.” Digital Applications in Archaeology and Cultural Heritage 30: e00287. https://doi.org/10.1016/j.daach.2023.e00287.

cinpar2026
XXII International Conference on Building Pathology and Constructions Repair
15th to 17th July 2026 - Lisboa, Portugal

Electromechanical Self-Sensing Behavior of Lime Mortars with Carbon Nanotubes and Microfibers

Ryan **ARAÚJO**[1], Antonella D'ALESSANDRO[2,*], Andrea MEONI[3], Filippo UBERTINI[4], Esequiel MESQUITA[5]

E-mail: *antonella.dalessandro@unipg.it*

[1] Department of Civil and Environmental Engineering, University of Perugia, Perugia, Italy, ryan.araujodematos@dottorandi.unipg.it
[2] Department of Civil and Environmental Engineering, University of Perugia, Perugia, Italy, antonella.dalessandro@unipg.it
[3] Department of Civil and Environmental Engineering, University of Perugia, Perugia, Italy, andrea.meoni@unipg.it
[4] Department of Civil and Environmental Engineering, University of Perugia, Perugia, Italy, filippo.ubertini@unipg.it
[5] Laboratory of Digital Experience, Institute of Architecture and Urbanism and Design, Federal University of Ceara, Fortaleza, Brazil, emesquita@ufc.br

Abstract: This study investigates the electromechanical self-sensing behavior of lime mortars modified with carbon nanotubes (CNTs) and carbon microfibers (CMFs) for potential Structural Health Monitoring (SHM) applications in heritage-compatible materials. A hydrated lime mortar was produced with CNT contents of 0.20 and 0.40 wt.% of binder and CMF contents of 0.05, 0.10, and 0.20 wt.% of binder, in addition to a reference mixture. The mortars were evaluated for workability, compressive strength, electrical resistance, and electromechanical response under cyclic compressive loading using a biphasic measurement method. As expected, the incorporation of conductive additions reduced the workability of the fresh mixtures, with a more pronounced effect observed in mortars containing CMF. The mechanical performance improved in mixtures with both CNT and CMF, with optimal contents identified at 0.20 wt.% CNT and 0.05 wt.% CMF. Electrical resistance decreased in all modified mortars, with CMFs proving more effective in reducing the resistance of the lime matrix within the investigated range of filler content. Under cyclic compression, the mixtures exhibited different levels of piezoresistive behavior. The mortar containing 0.20 wt.% CNT showed the highest electromechanical sensitivity, while the mixture with 0.20 wt.% CMF also demonstrated a stable and significant response. In contrast, the reference mortar and the mixture containing 0.10 wt.% CMF exhibited limited self-sensing performance, as indicated by λ values of 4.52 and 6.41 and R^2 values of 0.01 and 0.12, respectively, although the latter showed one of the lowest electrical resistance values among the investigated mixtures. The results indicate that the self-sensing performance of lime mortars depends not only on increased electrical conductivity but also on the balance between filler dispersion, matrix integrity, and the sensitivity of the conductive network to deformation.

Keywords: Lime mortars; Carbon nanotubes; Carbon microfibers; Self-sensing materials, Structural health monitoring

1. Introduction

Historic buildings are frequently subjected to risks associated with the development of damage over time, resulting from actions such as earthquakes, settlements, the introduction of additional loads, usage conditions not foreseen in the original design, and deficiencies in maintenance, factors that may compromise their structural integrity and, consequently, the safety of users (Matos et al., 2025; Oliveira, 2015; Pringopoulos et al., 2024). In this context, the early identification of damage, combined with the timely adoption of safety measures, can prevent or mitigate the progression of structural pathologies. Although periodic inspections remain essential for assessing the performance of these buildings, Structural Health Monitoring (SHM) stands out as an effective tool for continuous or quasi-continuous detection and diagnosis of damage at early stages, as well as for assessing structural risks (E. F. T. Mesquita, 2019).

In recent decades, the development of SHM systems has been closely linked to advances in sensing technologies, particularly those based on electrical, mechanical, and optical measurements. Devices such as strain gauges (Biswal et al., 2016), linear variable differential transducers (Andreades et al., 2020), and optical sensors (Liao et al., 2020) have been widely applied in the instrumentation of different types of structures, enabling the continuous acquisition of data related to their in-service behavior (Gao et al., 2018; Kot et al., 2021; Mesquita et al., 2023; Sakiyama et al., 2019). However, the application of these sensors presents several challenges, including installation difficulties in hard-to-access locations, the need for numerous wired connections, costs, and long-term operational limitations.

Considering these limitations, the development of smart sensing materials has emerged as a promising alternative for SHM applications. These materials consist of structural composites that become electrically conductive and exhibit piezoresistive properties through the incorporation of carbon-based fillers, such as carbon microfibers (CMFs), carbon nanotubes (CNTs), and graphite, which enable variations in electrical resistivity in response to mechanical deformations (Meoni et al., 2018; Nalon et al., 2020; Ubertini et al., 2018). Studies reported in the literature have predominantly focused on developing self-sensing cementitious mortars for SHM applications (Cholker, 2021; Ding et al., 2021; Meoni et al., 2021; Rao et al., 2020). However, in the context of heritage conservation and sustainable construction practices, lime-based mortars play a fundamental role due to their physical and mechanical compatibility and greater affinity for the materials used in historical buildings (Dalalbashi et al., 2025). Despite this relevance, the application of lime-based matrices with self-sensing properties remains in the early stages of development.

Based on recent literature, although still in an early stage of development, studies investigating lime-based matrices with self-sensing properties are increasing. Dimou et al. (2020) demonstrated that the addition of 0.15 wt.% of CNTs promoted an approximately 12% reduction in the electrical resistivity of lime-based pastes. Xu et al. (2021) observed that the incorporation of CMFs at the highest investigated dosage (1 wt.% by volume) allowed the preservation, or even slight improvement, of mechanical properties, with increases of 11.24% in compressive strength and 3.69% in tensile strength. In addition, Drougkas et al. (2023) highlighted the effectiveness of incorporating CNTs into lime mortars, showing that adding 0.4 wt.% CNTs reduced electrical resistivity. Moreover, the incorporation of graphite and CMFs resulted in reductions in electrical resistivity of approximately 50% and 70%, respectively, along with a slight increase in flexural and compressive strengths, thereby reinforcing the potential of these materials for SHM applications.

Despite recent advances, additional studies are still needed to investigate the effectiveness of lime-based matrices in the context of SHM, particularly in developing analyses that correlate states of mechanical deformation, the occurrence of damage, and variations in the electrical parameters of these matrices. In this regard, the present study aims to contribute to enabling the effective use of self-sensing lime mortars for the monitoring and preservation of historical heritage. To this end, lime mortars were produced with different concentrations of CNTs and CMFs. The mixtures were evaluated for workability and mechanical properties. The electrical and electromechanical capabilities were evaluated using the biphasic measurement method.

2. Materials and methods

2.1 Materials

A commercial hydrated lime (CL 90-S) with a density of 2.24 g/cm³ was used as a binder. According to the manufacturer's chemical analysis (non-volatile basis), the combined CaO + MgO content exceeded 90%, CO_2 was below 10%, and unhydrated oxides were negligible, as indicated in EN 459-1 (2015). The aggregate used was a siliceous sand with a nominal particle size distribution of 0–3 mm. It presented a density of 2.63 g/cm³, a maximum grain size of 2.36 mm, and a fineness modulus of 2.71. Tap water was used and CNTs functionalized with carboxyl (-COOH) groups via acid treatment were incorporated into the mortar mixtures. The CNTs were supplied as a powder by Nanoview® Nanotecnologia, with diameters ranging from 10 to 30 nm and lengths between 1 and 10 µm. The CMFs used in this study presented a diameter of 7 µm and a length of 6-8 mm.

2.2 Experimental design and production of specimens

Mortars were prepared following EN 196-1 (2005) mixing procedures, according to conservation and masonry practice. Although the standard specifies the binder-to-aggregate proportion by weight, the dry components were mixed at a 1:3 volume ratio, a common practice in the production of mortars for masonry and conservation applications (Drougkas et al., 2023). This adoption results in a mortar with a lower binder content compared with that specified by the standard. Nevertheless, this proportion remains suitable for application as a repointing mortar in conservation contexts. The water-to-binder ratio was fixed at w/b = 1.00 (considering the total water, including the water used for CNT dispersion). Six mixes were produced, including a reference mortar and mortars modified with CNTs or CMFs, with the filler contents and mix proportions summarized in Table 1. The selected contents were defined within ranges commonly investigated in the literature (Dalalbashi et al., 2025; Danoglidis et al., 2016; Dimou et al., 2022).

Table 1 – Mix proportions of lime mortars with CNT and CMF additions.

Filler type	Filler content (wt.% of binder)	Lime (g)	Sand (g)	Water (g)	CNT (g)	CMF (g)
REF	0.00	443.52	1562.22	439.08	-	-
CNT	0.20	443.52	1562.22	439.08	0.89	-
CNT	0.40	443.52	1562.22	439.08	1.77	-
CMF	0.05	443.52	1562.22	439.08	-	0.22
CMF	0.10	443.52	1562.22	439.08	-	0.44
CMF	0.20	443.52	1562.22	439.08	-	0.89

Prismatic specimens (40x40x160 mm) were cast in triplicate, incorporating four metallic electrodes embedded within the samples and spaced 4 cm apart in the central region, following the configuration of strain gauges used in structural monitoring (Materazzi et al., 2013). These specimens were used for electrical and electromechanical tests. In addition, cubic specimens (40x40x40 mm) were prepared for compressive strength tests. The fresh mixture was poured into molds previously coated with oil, in two layers, each layer being compacted with 30 strokes of a metallic rod. Finally, the specimens remained in the molds for 72 h at 24°C under controlled conditions.

To reduce agglomeration and promote homogeneous distribution, the CNTs were previously dispersed in deionized water following methodological procedures like those reported by Vasconcelos et al. (2024). A fixed ratio of 0.033 g of CNT per mL of water was used. The suspension was sonicated for 15 min using a probe sonicator (VCX 750 Sonics®, 750 W) operating in cyclic mode (20% amplitude), with temperature

control maintained at 24°C, providing adequate dispersion in the aqueous solution, as reported by Matos et al. (2025), prior to incorporation into the mixtures. Figure 1 illustrates the experimental process flow, covering the stages from material dispersion to specimen casting.

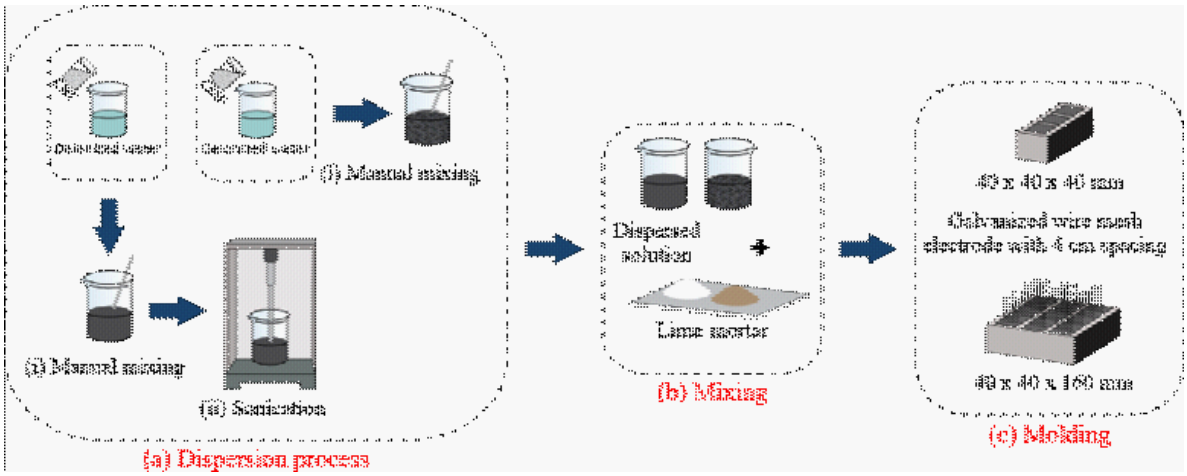


Figure 1 – Schematic representation of the process from dispersion to specimen casting.

2.3 Experimental tests

2.3.1 Workability

The consistency of the mortars was evaluated using a flow table test with a Kantro cone, in accordance with NBR 13276 (2016), similar to EN 1015-3 (1999).

2.3.2 Compressive strength

Compressive strength was determined using cubic specimens (40x40x40 mm) at 56 days, employing a universal testing machine (EMIC, model GR048, Instron, Norwood, USA), following procedures equivalent to EN 196-1 (2005), with adaptations for the present study.

2.3.3 Biphasic measurement

Electrical tests were performed to investigate the percolation threshold and characterize the material's electrical properties. For this purpose, a biphasic electrical measurement approach proposed by Downey et al. (2017) was used, which applied an alternating square signal. In the present study, a square wave signal with an amplitude of ±10 V, a frequency of 1 Hz, and a peak-to-peak voltage of 20 V was applied using a function generator. The experimental setup was configured in a four-electrode system, in which the external electrodes were responsible for applying the electrical current to the specimen, while the internal electrodes were used to measure the potential difference (V_{in}), following the reading scheme illustrated in Figure 2. Furthermore, a reference resistor (Rg) was connected in series with the sample, allowing the indirect determination of the electrical current through Ohm's law, according to Eq. (1), based on the voltage drop (V_{Rg}) monitored across (Rg). Finally, the sample's electrical resistance was obtained using Eq. (2) from the voltage measured between the internal electrodes. The measurements were taken when the specimens were 56 days old.

$$i = \frac{V_{Rg}}{Rg} \quad (1)$$

Thus, the electrical resistance of the specimen was calculated according to:

$$R = \frac{V_{in}}{i} \quad (2)$$

where i is the electrical current, V_{Rg} is the voltage drop across the reference resistor Rg, V_{in} is the voltage measured between the internal electrodes, and R is the electrical resistance of the specimen.

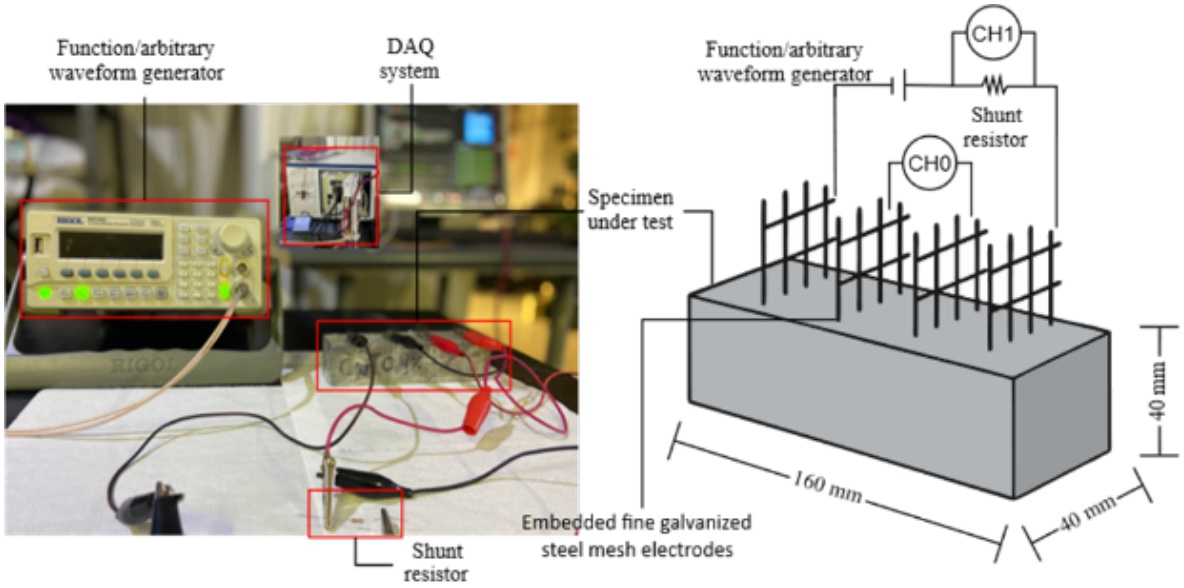


Figure 2 – Experimental setup adopted for the determination of electrical resistance using the biphasic measurement method.

2.3.4 Electromechanical test

For the electromechanical test, prismatic specimens were subjected to cyclic compressive loading, with two cycles at each stress level. Maximum stress levels of 0.125 MPa, 0.1875 MPa, and 0.25 MPa were adopted, with a minimum stress of 0.0125 MPa, as illustrated in Figure 3, with a loading and unloading rate of 50 N/s.

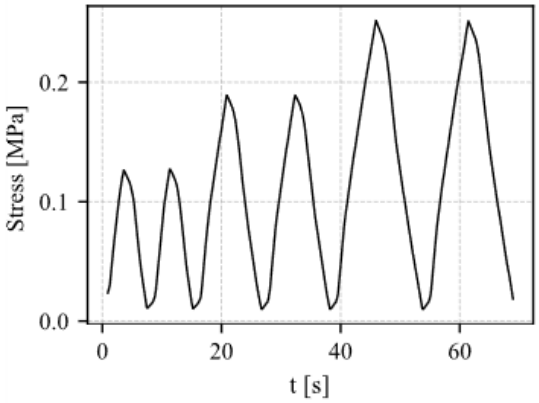


Figure 3 – Cyclic compressive loading protocol for electromechanical tests.

During the test, the electrical resistance was monitored simultaneously using the biphasic electrical measurement system previously described to correlate the imposed deformation with the material's electrical response. Thus, the electrical response was quantified through the fractional change in resistance (FCR), defined by Eq. 3:

$$\frac{\Delta R}{R_0} = \frac{R - R_0}{R_0} \tag{3}$$

where R is the measured electrical resistance and R_0 is the reference resistance, taken before the beginning of cyclic loading (or at the initial instant of the analyzed segment). The gauge factor (λ), used as a parameter of electromechanical sensitivity, was calculated according to Eq. 4:

$$\lambda = \frac{\Delta R/R_0}{\varepsilon} \quad (4)$$

Where ε is the axial strain, estimated from the axial displacement recorded by the testing machine and normalized by the initial specimen height (160 mm), corresponding to nominal strain. Gauge factor λ was determined as the slope coefficient of a linear fit of the FCR vs ε relationship, applied to the selected data segment used for analysis. Thus, the experimental setup of the electrical and mechanical tests is illustrated in Figure 4.

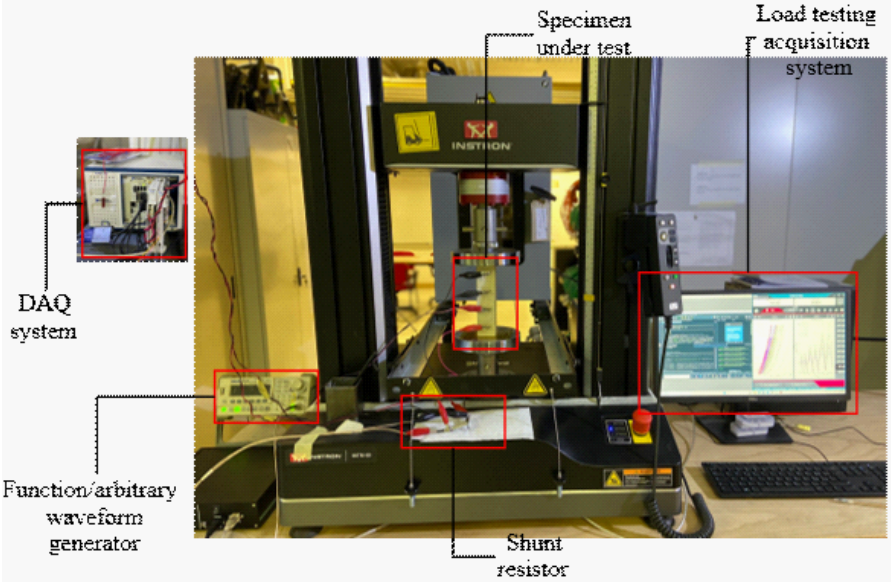


Figure 4 – Schematic overview of the experimental setup used for electromechanical testing.

3. Results and discussion

The incorporation of conductive additions modified the fresh-state behavior, mechanical performance, electrical properties, and electromechanical response of the lime mortars. As observed in previous studies, linear behavior was not observed: instead, the results indicated the existence of optimal contents, defined by the balance between dispersion, matrix integrity, and the formation of a conductive network within the material (Dalalbashi et al., 2025; Drougkas et al., 2023).

The workability analysis of lime mortars with varying CNT and CMF contents showed a reduction in the flow diameter of the fresh mixtures, as illustrated in Figure 5. The REF mixture exhibited high fluidity, with a spread of 290 ± 2 mm, whereas the mortars containing CNTs showed a reduction to 257 ± 7 mm at 0.20 wt.%, followed by a partial recovery to 282 ± 5 mm at 0.40 wt.%. This behavior indicates a strong influence of the dispersion state. The results suggest that the rheological response is highly sensitive to both the dispersion state and the high specific surface area introduced by the nanotubes in the lime matrix, which may lead to changes in the degree of agglomeration and in the microstructural organization of the system depending on the addition content (Nalon et al., 2024).

In contrast, the incorporation of CMF led to a notable reduction in workability, with the most pronounced effect observed at 0.10 wt.% (234 ± 3 mm), while 0.05 wt.% and 0.20 wt.% reached 241 ± 4 mm and 244 ± 3 mm, respectively. This behavior is generally associated with increased internal friction and the mechanical interlocking effect resulting from the fibrous morphology, which tends to restrict the relative mobility of particles (D'Alessandro et al., 2024; Safiuddin et al., 2018). Nevertheless, a consistent reduction in workability with increasing CMF content was not observed, which may be attributable to factors such as variations in

dispersion and homogenization, localized agglomerate formation, and non-uniform fiber distribution within the mixture. These aspects can alter the rheological response even when the mass content is increased.

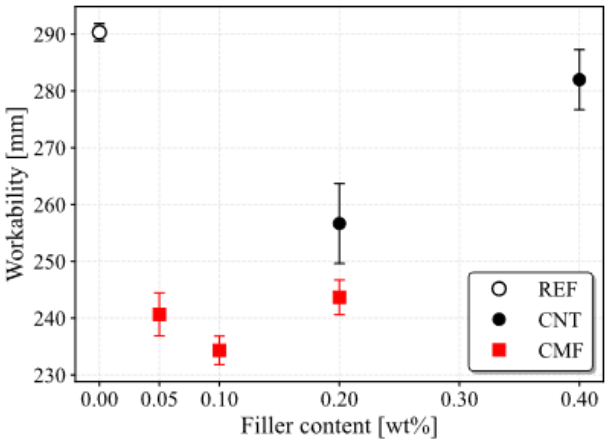


Figure 5 – Workability values of lime-doped mortars.

The results presented in Figure 6 show that this modification in the fresh state affects the mechanical performance, although not in a directly proportional manner to the flow spread. While the REF sample exhibited a compressive strength of 0.86 MPa, the mixtures containing CNTs showed their best performance at 0.20 wt.%, with a nearly twofold increase in mechanical strength, reaching a value close to 1.70 MPa. Increasing the CNT content to 0.40 wt.%, although still higher than the reference mixture, resulted in a strength of 1.15 MPa. This behavior suggests the existence of an optimal incorporation content, possibly associated with the balance between adequate dispersion and the onset of nanotube agglomeration, which may generate discontinuities or stress concentrations within the matrix (Konsta-Gdoutos et al., 2010; Thomoglou et al., 2023). Similarly, the mortars containing CMF exhibited significant strength gains, particularly at a content of 0.05 wt.%, reaching approximately 2.10 MPa, corresponding to an increase of 143% compared with the reference mixture. A progressive reduction in strength is observed with increasing fiber content (0.10 wt.% and 0.20 wt.%), which may be related to the greater difficulty in achieving adequate dispersion and to the possible formation of voids or fiber concentration zones at higher contents (D'Alessandro et al., 2024).

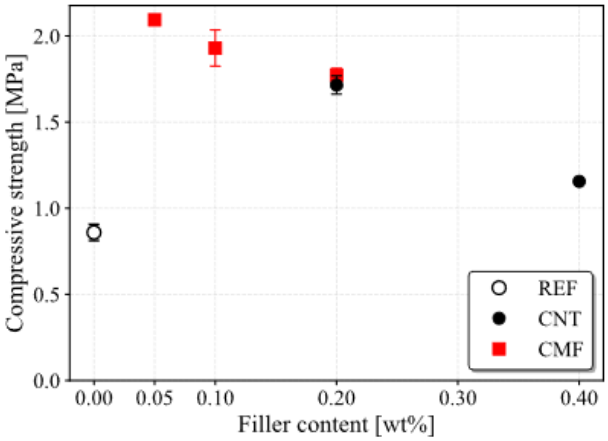


Figure 6 – Compressive strength results of lime mortars with CNTs and CMFs.

Figure 7 shows that incorporating conductive additions reduced the electrical resistance of the lime matrix, confirming the formation of internal conductive pathways. For the CNT series, the electrical resistance decreased

from 16.88 MΩ in the reference mixture to 10.09 MΩ at 0.20 wt.%, representing a reduction of approximately 40 wt.%, but increased again to 15.91 MΩ at 0.40 wt.%, corresponding to a decrease of 5.75% relative to the reference. This behavior indicates that the 0.20 wt.% content provided a more efficient conductive network, whereas the increase to 0.40 wt.% likely impaired effective connectivity due to less homogeneous dispersion and a greater tendency toward agglomeration (Dimou et al., 2022).

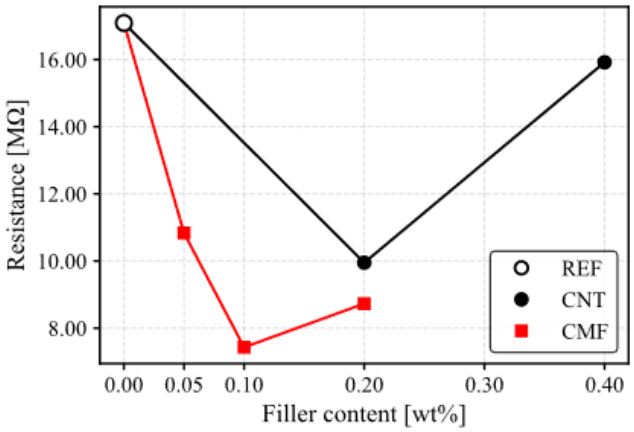


Figure 7 – Electrical resistance variation of lime mortars with different CNT and CMF contents.

In the case of mortars containing CMFs, a greater reduction in electrical resistance was observed, particularly in the samples with 0.10 wt.% and 0.20 wt.% microfibers. The 0.10 wt.% content reached 7.30 MΩ, followed by a slight increase at 0.20 wt.% to 8.59 MΩ, corresponding to reductions of 56.75% and 49.11%, respectively. Moreover, even the lowest evaluated content, 0.05%, already reduced electrical resistance to 10.84 MΩ, equivalent to a 35.72% decrease. These results indicate that, in terms of electrical performance, CMFs were more efficient than CNTs. This behavior may be associated with the geometry and dimensions of the microfibers, whose length favors the formation of more extended conductive pathways throughout the matrix (Drougkas et al., 2023). This behavior shows partial coherence with the mechanical results, since this series exhibited the highest compressive strength among the contents studied. Therefore, these contents combine mechanical improvement with reduced electrical resistance. In addition, CMF-modified mortars exhibited satisfactory mechanical performance relative to the reference mixture, despite a progressive reduction in strength with increasing fiber content. Thus, the incorporation of conductive functionality through CMF did not compromise mechanical performance.

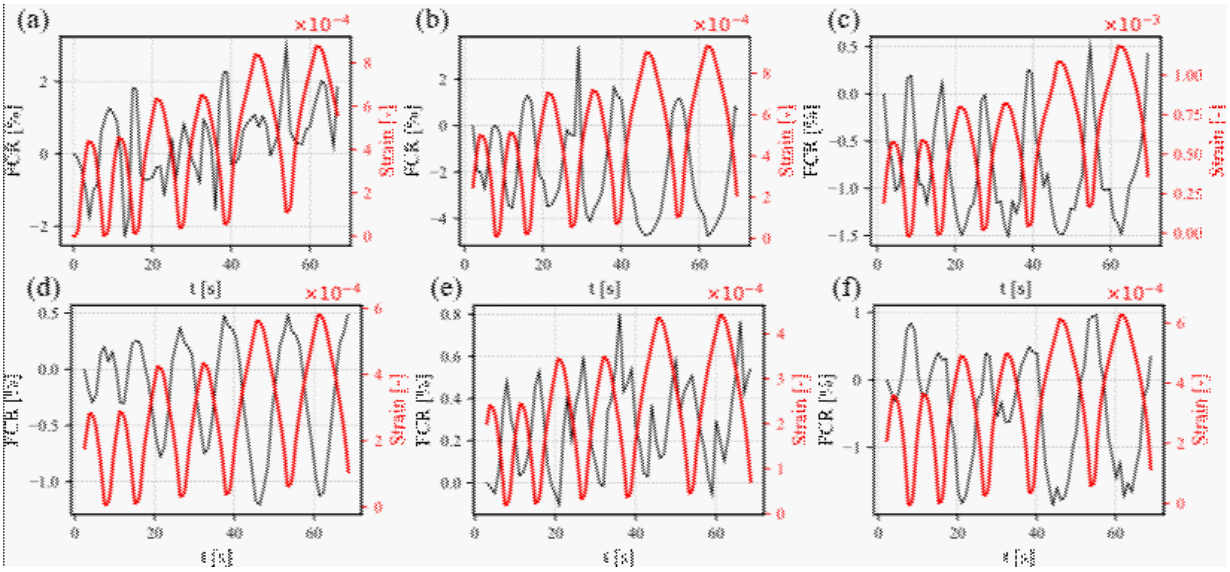


Figure 8 – Time-dependent FCR and Strain response of lime mortars under cyclic compressive loading: (a) REF, (b) CNT 0.20 wt.%, (c) CNT 0.40 wt.%, (d) CMF 0.05 wt.%, (e) CMF 0.10 wt.%, and (f) CMF 0.20 wt.%.

Figure 8 presents the electromechanical behavior of the mortars, monitoring the variation in electrical resistance during the application of compression cycles, thereby enabling evaluation of their sensing performance. The mixtures containing 0.20 wt.% CNT, 0.40 wt.% CNT, 0.05 wt.% CMF, and 0.20 wt.% CMF, corresponding to graphs (b), (c), (d), and (f), exhibited FCR oscillations that generally followed the strain cycles, indicating a higher sensitivity to the applied loading. In contrast, the reference mixture (a) and the mixture containing 0.10 wt.% CMF (e) showed more scattered signals with lower and less regular amplitudes, suggesting a weaker and less stable electromechanical response, as also indicated by their R^2 values of 0.01 and 0.12, respectively.

The results of the electromechanical tests are summarized in Table 2, which presents the main associated parameters, including sensitivity and fitting quality. The reference mortar (a) showed $\lambda = 4.52$ and $R^2 = 0.01$, indicating that the lime matrix without conductive additions did not develop a reliable electromechanical response under the evaluated conditions. This behavior is consistent with the observed scattered signal, indicating low sensitivity to the applied load. The mixture containing 0.20 wt.% CNT (b) showed the highest absolute sensitivity value ($\lambda = 74.77$), associated with $R^2 = 0.78$, representing the best performance among the compositions evaluated. This result shows a trend similar to that reported by Drougkas et al. (2023), who, despite using a different matrix based on natural hydraulic lime (NHL 3.5), also observed higher sensitivity at lower CNT contents, followed by a reduction in performance as the reinforcement fraction increased. Consistently, the composition with 0.40 wt.% CNT (c) maintained piezoresistive behavior, but with significantly lower sensitivity ($\lambda = 18.56$), suggesting the formation of a conductive network that was less responsive to loading-induced variations.

Table 2 – Electromechanical parameters.

Filler type	Filler content (wt.% of binder)	λ [-]	R^2
REF	0.00	4.52	0.01
CNT	0.20	74.77	0.78
CNT	0.40	18.56	0.68
CMF	0.05	29.79	0.85

CMF	0.10	6.41	0.12
CMF	0.20	45.80	0.78

Among the mixtures containing CMF, the best performance was obtained for 0.20 wt.% (f), with λ = 45.80 and R^2 = 0.78, followed by 0.05 wt.% (d), with λ = 29.79 and R^2 = 0.85. In contrast, the composition with 0.10 wt.% CMF (e), despite showing one of the lowest average electrical resistance values among the investigated mixtures, resulted in λ = 6.41 and R^2 = 0.12, indicating limited sensing performance. Although Figure 8 indicates a response to load application, despite the scattered signal observed for this mixture, Figure 9 shows that the CMF 0.1 wt.% mixture presents less defined hysteresis loops, with less consistent trajectories throughout the loading cycles. This behavior reinforces the instability of the electromechanical response, in agreement with the low λ and R^2 values. Results reported by Dalalbashi et al. (2025) using hydraulic lime matrices (NHL 5) indicate a similar trend, with good performance at CMF contents, although the best result was observed at 0.10 wt.%. In addition, this set of results demonstrates that higher electrical conductivity does not necessarily imply greater electromechanical sensitivity, showing that self-monitoring performance depends not only on the formation of conductive pathways but also on the ability of the network to respond effectively to strain variations, in line with the trend observed by these authors.

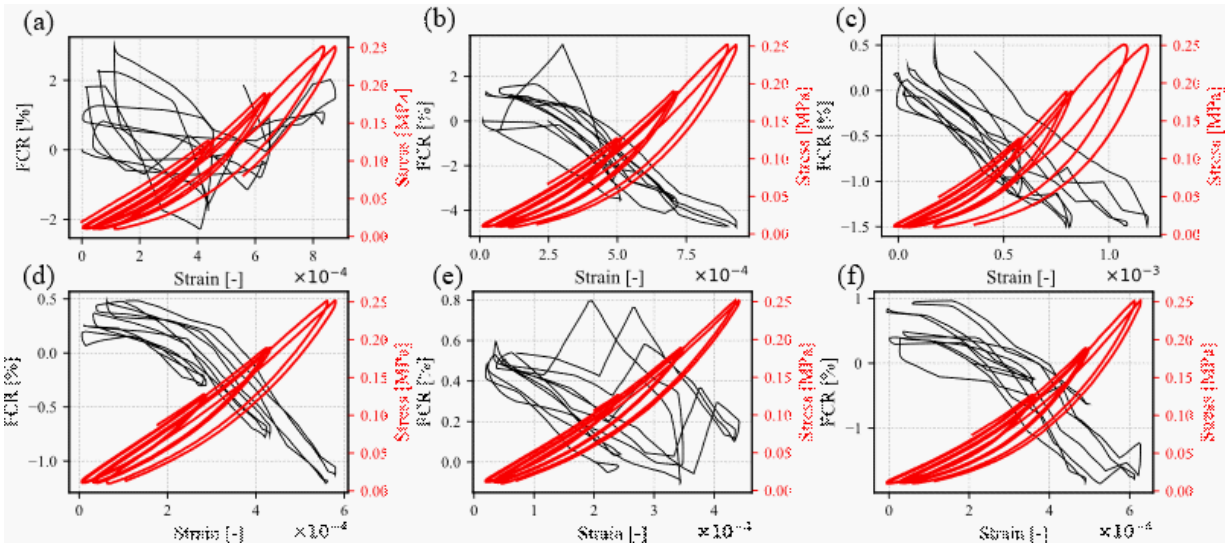


Figure 9 – Fractional change in electrical resistance (FCR) as a function of strain for lime mortars under cyclic compressive loading: (a) REF, (b) CNT 0.20 wt.%, (c) CNT 0.40 wt.%, (d) CMF 0.05 wt.%, (e) CMF 0.10 wt.%, and (f) CMF 0.20 wt.%.

4. Conclusion

The incorporation of CNTs and CMFs altered the fresh-state, mechanical, electrical, and electromechanical behavior of lime mortars, confirming the potential of these additions to develop self-sensing materials. The results showed that the performance of the mixtures did not evolve monotonically with increasing filler content, indicating the existence of optimal formulations that balance dispersion, matrix integrity, and conductive network configuration. Among the mixtures containing CNTs, the 0.20 wt.% content exhibited the best overall performance, combining increased mechanical strength, reduced electrical resistance, and greater electromechanical sensitivity. Among the mixtures containing CMF, the 0.05 wt.% content showed the best mechanical performance, while 0.20 wt.% exhibited the best electromechanical response. From an electrical perspective, CMFs were more effective at reducing the matrix's overall electrical resistance.

In general, mortars containing conductive additives have shown promise for their enhanced mechanical and sensing performance. This result is particularly relevant for retrofitting applications on existing structures, in which the objective is to combine additional functionality with compatibility with the original matrix to be restored. As a future perspective, studies will focus on evaluating the evolution of these properties over time, particularly relevant for verifying the stability of the mechanical, electrical, and electromechanical behavior of the developed formulations. Furthermore, complementary microstructural analyses may contribute to a deeper understanding of how these inclusions influence the matrix's internal structure and performance. Such advances may consolidate the development of lime mortars with potential application as sensing materials for monitoring historical heritage structures.

Acknowledgments

The authors gratefully acknowledge the support from the Italian Ministry of University and Research (MUR) through the FIS-2021 Advanced Grant project “Smart Masonry enabling SAFEty-assessing STructures after earthquakes (SMS SAFEST)” (Project code FIS00001797). This work was financially supported by FUNCAP; by the National Council for Scientific and Technological Development (CNPq) - Project 302054/2022-7 - *PQ2*, by the Project - 440926/2024-6 - *VISION* and Project - 402828/2024-0 - *CLIC*, CAPES Foundation and *Finep 2896/24*.

References

Andreades, C., Malfense Fierro, G. P., & Meo, M. (2020). A nonlinear ultrasonic SHM method for impact damage localisation in composite panels using a sparse array of piezoelectric PZT transducers. *Ultrasonics*, *108*, 106181. https://doi.org/10.1016/j.ultras.2020.106181

Biswal, S., & Ramaswamy, A. (2016). Measurement of existing prestressing force in concrete structures through an embedded vibrating beam strain gauge. *Measurement*, *83*, 10–19. https://doi.org/10.1016/J.MEASUREMENT.2016.01.031

British Standards Institution. (2005). *Methods of testing cement : part 1 : determination of strength*. British Standard.

Cholker, A. K. (2021). Incorporation of Smart Concrete in Large-Scale RC Beams for Evaluating Self-Sensing and structural Properties. *Arabian Journal for Science and Engineering 2021 46:11*, *46*(11), 10695–10710. https://doi.org/10.1007/s13369-021-05517-7

Dalalbashi, A., Mendizabal, V., Drougkas, A., & Sarhosis, V. (2025). Electromechanical and piezoresistive behaviour of hydraulic lime mortar incorporating carbon microfibers for self-sensing applications. *Construction and Building Materials*, *497*, 143933. https://doi.org/10.1016/j.conbuildmat.2025.143933

D’Alessandro, A., & Ubertini, F. (2024). Mechanical and Durability Investigation of Composite Mortar with Carbon Microfibers (CMF). *Applied Sciences 2024, Vol. 14, 14*(7). https://doi.org/10.3390/app14072773

Danoglidis, P. A., Konsta-Gdoutos, M. S., Gdoutos, E. E., & Shah, S. P. (2016). Strength, energy absorption capability and self-sensing properties of multifunctional carbon nanotube reinforced mortars. *Construction and Building Materials*, *120*, 265–274. https://doi.org/10.1016/J.CONBUILDMAT.2016.05.049

Dimou, A. E., Charalampidou, C. M., Metaxa, Z. S., Kourkoulis, S. K., Karatasios, I., Asimakopoulos, G., & Alexopoulos, N. D. (2020). Mechanical and electrical properties of hydraulic lime pastes reinforced with carbon nanomaterials. *Procedia Structural Integrity*, *28*, 1694–1701. https://doi.org/10.1016/j.prostr.2020.10.144

Dimou, A. E., Metaxa, Z. S., Kourkoulis, S. K., & Alexopoulos, N. D. (2022). Piezoresistive Properties of Natural Hydraulic Lime Binary Pastes with Incorporated Carbon-Based Nanomaterials under Cyclic Compressive Loadings. *Nanomaterials 2022, Vol. 12, 12*(20). https://doi.org/10.3390/nano12203695

Ding, Y., Li, D., Ma, Y., Liu, G., Song, S., Zhang, D., & Ding, G. (2021). Self-localization of the flexural cracks of fiber reinforced concrete beams. *Construction and Building Materials*, *302*, 124364. https://doi.org/10.1016/j.conbuildmat.2021.124364

Downey, A., D'Alessandro, A., Baquera, M., García-Macías, E., Rolfes, D., Ubertini, F., Laflamme, S., & Castro-Triguero, R. (2017). Damage detection, localization and quantification in conductive smart concrete structures using a resistor mesh model. *Engineering Structures*, *148*, 924–935. https://doi.org/10.1016/j.engstruct.2017.07.022

Drougkas, A., Sarhosis, V., Basheer, M., D'Alessandro, A., & Ubertini, F. (2023). Design of a smart lime mortar with conductive micro and nano fillers for structural health monitoring. *Construction and Building Materials*, *367*, 130024. https://doi.org/10.1016/j.conbuildmat.2022.130024

European Committee for Standardization (CEN). (1999). *Methods of test for mortar for masonry - Part 3: Determination of consistence of fresh mortar (by flow table)*.

European Committee for Standardization (CEN). (2015). *lime - Part 1: Definitions, specifications and conformity criteria*.

Gao, W., Huo, L., Li, H., & Song, G. (2018). Smart concrete slabs with embedded tubular PZT transducers for damage detection. *Smart Materials and Structures*, *27*(2), 025002. https://doi.org/10.1088/1361-665X/AA9C72

Henrique Nalon, G., Lopes Ribeiro, J. C., Gonçalves Pedroti, L., Marcio da Silva, R., Nery Duarte de Araújo, E., & Emilio Soares de Lima, G. (2024). Smart laying mortars for masonry structures: effects of lime/cement ratio and carbon nanomaterials content on self-sensing behavior. *Cement and Concrete Composites*, *145*, 105351. https://doi.org/10.1016/j.cemconcomp.2023.105351

Konsta-Gdoutos, M. S., Metaxa, Z. S., & Shah, S. P. (2010). Highly dispersed carbon nanotube reinforced cement based materials. *Cement and Concrete Research*, *40*(7), 1052–1059. https://doi.org/10.1016/j.cemconres.2010.02.015

Kot, P., Muradov, M., Gkantou, M., Kamaris, G. S., Hashim, K., & Yeboah, D. (2021). Recent Advancements in Non-Destructive Testing Techniques for Structural Health Monitoring. *Applied Sciences 2021, Vol. 11, 11*(6). https://doi.org/10.3390/app11062750

Liao, W., Zhuang, Y., Zeng, C., Deng, W., Huang, J., & Ma, H. (2020). Fiber optic sensors enabled monitoring of thermal curling of concrete pavement slab: Temperature, strain and inclination. *Measurement*, *165*, 108203. https://doi.org/10.1016/j.measurement.2020.108203

Materazzi, A. L., Ubertini, F., & D'Alessandro, A. (2013). Carbon nanotube cement-based transducers for dynamic sensing of strain. *Cement and Concrete Composites*, *37*(1), 2–11. https://doi.org/10.1016/j.cemconcomp.2012.12.013

Matos, R. A., Santos, M. S., Cruz de Araújo, A. J., Mesquita, E., Triana-Camacho, D. A., D'Alessandro, A., & Ubertini, F. (2025). Physico-mechanical and electrical characterization of mortars enhanced with carbon nanotubes and microfibers. *Construction and Building Materials*, *494*(4), 143537. https://doi.org/10.1016/j.conbuildmat.2025.143537

Meoni, A., D'Alessandro, A., Downey, A., García-Macías, E., Rallini, M., Materazzi, A. L., Torre, L., Laflamme, S., Castro-Triguero, R., & Ubertini, F. (2018). An Experimental Study on Static and Dynamic Strain Sensitivity of Embeddable Smart Concrete Sensors Doped with Carbon Nanotubes for SHM of Large Structures. *Sensors 2018, Vol. 18, 18*(3). https://doi.org/10.3390/S18030831

Meoni, A., D'Alessandro, A., Mancinelli, M., & Ubertini, F. (2021). A Multichannel Strain Measurement Technique for Nanomodified Smart Cement-Based Sensors in Reinforced Concrete Structures. *Sensors 2021, Vol. 21, 21*(16). https://doi.org/10.3390/s21165633

Mesquita, E. F. T. (2019). *Engenharia do Patrimônio* (1st ed.). [s.n.].

Mesquita, E., Sousa, I., Vieira, M., Matos, A. M., Santos, L. P. M., Silvestro, L., Salvador, R., D'Alessandro, A., & Ubertini, F. (2023). Investigation of the electrical sensing properties of cementitious composites produced with multi-wall carbon nanotubes dispersed in NaOH. *Journal of Building Engineering*, *77*(11), 107496. https://doi.org/10.1016/j.jobe.2023.107496

Nalon, G. H., Ribeiro, J. C. L., Araújo, E. N. D. de, Pedroti, L. G., Carvalho, J. M. F. de, Santos, R. F., & Aparecido-Ferreira, A. (2020). Effects of different kinds of carbon black nanoparticles on the piezoresistive and mechanical properties of cement-based composites. *Journal of Building Engineering*, *32*, 101724. https://doi.org/10.1016/j.jobe.2020.101724

Oliveira, M. A. N. (2015). *A multi-physics approach applied to masonry structures with non-hydraulic lime mortars*. Universidade do Minho (Portugal).

Pringopoulos, T. A., Thomoglou, A. K., Fantidis, J. G., Thysiadou, A. A., Metaxa, Z. S., Pringopoulos, T. A., Thomoglou, A. K., Fantidis, J. G., Thysiadou, A. A., & Metaxa, Z. S. (2024). Advanced Lime Mortars for Historical Architectural Structures. *Engineering Proceedings 2024, Vol. 70, 70*(1). https://doi.org/10.3390/ENGPROC2024070058

Rao, R. K., & Sasmal, S. (2020). Smart nano-engineered cementitious composite sensors for vibration-based health monitoring of large structures. *Sensors and Actuators A: Physical*, *311*, 112088. https://doi.org/10.1016/j.sna.2020.112088

Safiuddin, M., Abdel-Sayed, G., & Hearn, N. (2018). Effects of Pitch-Based Short Carbon Fibers on the Workability, Unit Weight, and Air Content of Mortar Composite. *Fibers 2018, Vol. 6, 6*(3). https://doi.org/10.3390/fib6030063

Sakiyama, F. I. H., Lehmann, F., & Garrecht, H. (2019). Structural health monitoring of concrete structures using fibre-optic-based sensors: a review. *Magazine of Concrete Research*, *73*(4), 174–194. https://doi.org/10.1680/jmacr.19.00185

Técnicas, A. B. D. N. (2016). NBR 13276: Argamassa para assentamento e revestimento de paredes e tetos–Determinação do índice de consistência. *Rio de Janeiro*.

Thomoglou, A. K., Falara, M. G., Voutetaki, M. E., Fantidis, J. G., Tayeh, B. A., & Chalioris, C. E. (2023). Electromechanical properties of multi-reinforced self-sensing cement-based mortar with MWCNTs, CFs, and PPs. *Construction and Building Materials*, *400*, 132566. https://doi.org/10.1016/j.conbuildmat.2023.132566

Ubertini, F., & D'Alessandro, A. (2018). Concrete with self-sensing properties. *Eco-Efficient Repair and Rehabilitation of Concrete Infrastructures*, 501–530. https://doi.org/10.1016/B978-0-08-102181-1.00018-6

Vasconcelos, A. R. C., Matos, R. A., Silveira, M. V., & Mesquita, E. (2024). Applications of Smart and Self-Sensing Materials for Structural Health Monitoring in Civil Engineering: A Systematic Review. *Buildings*, *14*(8), 2345. https://doi.org/10.3390/buildings14082345

Xu, W., Jalal, M., Zakira, U., & Wang, L. (2021). Study on the Mechanical Properties and Durability of Carbon Fiber Reinforced Lime-Based Mortar. *IOP Conference Series: Earth and Environmental Science*, *719*(3), 032032. https://doi.org/10.1088/1755-1315/719/3/032032

XXII International Conference on Building Pathology and Constructions Repair
15th to 17th July 2026 - Lisboa, Portugal

GEOPHYSICAL CHARACTERIZATION OF HISTORIC MASONRY USING GROUND-PENETRATING RADAR (GPR)

Maria Isadora GONÇALVES[1], Renan Nogueira PAULO[2], Lucas Gomes MENDES[3], Eugenio MOREIRA[4], Mylene de Melo VIEIRA[5], Esequiel MESQUITA[6]

[1]Federal University of Ceará, Russas, Brasil, isadoramessias@alu.ufc.br
[2]Università Degli Studi di Perugia, Perugia, Italy, renan.nogueirapaulo@dottorandi.unipg.it
[3]Federal University of Ceará, Fortaleza, Brasil, lucasmendes@arquitetura.ufc.br
[4]Federal University of Ceará, Fortaleza, Brasil, eugeniomoreira@iaud.ufc.br
[5] Federal University of Ceará, Russas, Brasil, mylene.melo@ufc.br
[6] Federal University of Ceará, Russas, Brasil, emesquita@ufc.br

Abstract: Historic constructions constitute an architectural and cultural heritage of inestimable value, reflecting cultural and economic aspects that are essential to the history of a society. The preservation of historic monuments depends primarily on knowledge of their construction techniques; however, this task proves to be a major challenge, as most of these monuments exhibit complex and poorly documented construction methods. Unlike modern constructions, whose composition, geometry, and behavior are well known, historic buildings are composed of thick masonry with heterogeneous internal material distribution and a wide variety of techniques, configurations, and construction typologies. In this context, deepening the understanding of these structures becomes essential through the development of technical records and documentation that allow for an accurate characterization of their construction features. Accordingly, the main objective of this study is the application of Ground-Penetrating Radar (GPR) for the non-destructive investigation of the internal structure of the masonry of the Church of Almofala, located in the municipality of Itarema, Ceará, Brazil. GPR surveys were carried out on internal masonry elements of the building, aiming to identify construction patterns, interfaces, voids, moisture presence, and internal anomalies. The adopted methodology was structured into four main stages: (i) characterization of the building, (ii) GPR data acquisition (iii) signal processing and (iv) interpretation and analysis of the results. The results demonstrate the effectiveness of GPR in detecting internal interfaces and characterizing construction heterogeneities, highlighting its potential as a supporting tool for diagnostic, rehabilitation, and preservation actions of built cultural heritage.

Keywords: Non-destructive testing; GPR; Historic heritage.

1. Introduction

Ground-Penetrating Radar (GPR) is a non-destructive geophysical technique based on the propagation of electromagnetic waves in natural media, such as geological formations, and artificial media, such as masonry and concrete. The method enables the identification of contrasts between materials with different dielectric properties through the analysis of reflected signals. The system operates by means of transmitting antennas, responsible for emitting electromagnetic pulses, and receiving antennas, which record the signals reflected by internal elements of the structure (Annan, 2003; Alvarado et al., 2025). The signal is generated at the boundary between two or more materials and is reflected when the electromagnetic properties of the materials change. Thus, the radar is capable of detecting materials as long as there is a contrast in the electromagnetic properties between the investigated media. (Utsi, 2017).

GPR data acquisition is performed through the continuous movement of the equipment along linear profiles, enabling the sequential recording of reflected signals. After processing, these data are converted into two- or three-dimensional images, known as radargrams or echograms, which represent the internal characteristics of the analyzed structure (Solla *et al.*, 2020; Alvarado et al., 2025; Grzyb et al., 2025).

Over the past decades, GPR has been widely applied in several fields, including archaeology, glaciology, geology, civil engineering, and, more recently, in the conservation of historic heritage (Solla, 2024; Balasubramani, 2025; Brandes et al., 2025; Hatem et al., 2025). Its increasing use in this field is associated with its ability to provide rapid and detailed information about the interior of structures, often inaccessible through conventional methods. Unlike other testing techniques that require longer processing and interpretation times, GPR provides near-immediate results, making it advantageous for preliminary diagnostics and field inspections.

Recent studies highlight a wide range of applications in historic heritage, among which the following stand out: the characterization of masonry, enabling the analysis of composition, thickness, and arrangement of construction layers (Cruz et al., 2024; Grzyb et al., 2025), the location and identification of ancient foundations, often absent from historical records (García-Nieto *et al.*, 2024; Parnow et al., 2024), the detection of corrosion in metallic reinforcements ((Solla, 2024)); the identification of voids and hidden cavities within walls (Cruz et al., 2024), the distinction of construction materials and overlapping layers within the masonry (Alvarado et al., 2025), and the assessment of the structural condition, including the presence of cracks, deterioration, and moisture (Perez-Gracia, Solla and Fontul, 2022; Elkarmoty et al., 2024).

The application of GPR in historic masonry presents high potential, considering that these structures are characterized by significant heterogeneity resulting from the use of different materials and multiple construction phases. Pioneering studies, such as that of Binda (1998), demonstrated the effectiveness of the method in detecting voids, inclusions, and defects, as well as in assessing wall conditions and identifying moisture and internal layers (Binda et al., 1998).

Historic masonry is composed of a combination of different materials, mainly stone, brick, and blocks. It is also possible to identify the presence of natural components such as lime, earth, and, in some cases, residues of materials available at the construction site (De Almeida, 2013; Carlos and Domingues, 2017). These structures may be bonded with mortar, being referred to as mortared masonry, or, in many cases, simply assembled without binders, characterizing dry-joint masonry (ICOMOS, 2006; Carlos and Domingues, 2017). In addition, they exhibit significant variability in thickness and internal configurations, and may consist of single or multiple layers depending on the construction typology and structural function (Rosa, 2013; Jorne et al., 2015).

This diversity is related to the way technical knowledge was transmitted. According to Mateus (2002), construction techniques were disseminated through model buildings used as references and later adapted to local conditions. This process contributed to the formation of structures with high internal variability and a lack of construction standardization, characteristics that increase the difficulty of their investigation (Mateus, 2002).

Given this complexity, the use of non-destructive techniques becomes essential for the characterization of these structures. However, the interpretation of GPR radargrams still represents a significant challenge, as it depends directly on the experience of the operator and interpreter and is influenced by factors such as the properties of the investigated medium, acquisition parameters, the equipment used, and data processing conditions (Fernandes, 2006; Martini, 2019; Bevan. B, 2020)

Despite the advances observed in the application of GPR in historic masonry, there are still limitations related to signal interpretation in highly heterogeneous media, especially in buildings with poorly documented construction techniques. The complexity of radargrams, combined with material variability, makes the accurate identification of interfaces and internal anomalies difficult, highlighting the need for applied studies aimed at improving interpretative criteria.

In this context, the Church of Almofala, located in the municipality of Itarema, Ceará, Brazil, stands out as an important example of historic heritage, characterized by traditional masonry construction techniques, making it a relevant object for GPR investigation. Therefore, the present study aims to apply the GPR method to investigate the masonry of the Church of Almofala, seeking to identify construction patterns and

possible internal anomalies, such as voids and moisture, thereby contributing to non-destructive diagnostics and the preservation of built cultural heritage.

2. Methodology

The study began with the delimitation of the investigation area, defined based on the selection of the Church of Almofala, a building of significant historical and religious value to the region. Subsequently, GPR surveys were carried out on the masonry of the church, aiming to identify construction interfaces, the presence of hidden elements, cracks or debonding between layers, and moisture.

After the data acquisition stage, signal processing was performed, including the application of filters and the definition of parameters compatible with the characteristics of the investigated medium. Finally, the analysis of the obtained responses was conducted based on the interpretation of reflection patterns observed in the radargrams. The methodological process was carried out as presented in Figure 1.

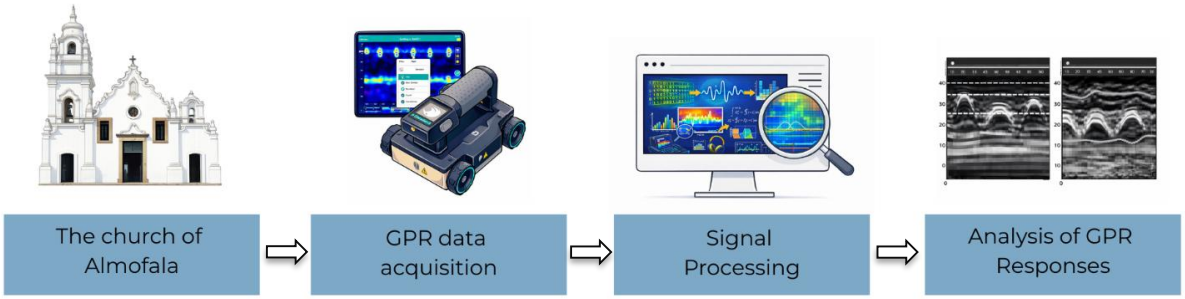


Figure 1: Stages of the methodological process.

2.1 The church of Almofala

The Church of Immaculate Conception, popularly known as the Church of Almofala, is located in the district of Almofala, in the municipality of Itarema, on the coast of Ceará. The church is listed by the National Institute of Historic and Artistic Heritage (IPHAN) under registration number 652-T-62 and is recognized as an important cultural and historical landmark of the region. (Carvalho *et al.*, 2013).

he construction of the church dates back to the early 18th century, having been built between 1712 and 1758, replacing an earlier chapel made of wattle and daub and thatch. The church is composed of brick and stone masonry, with walls approximately 77 cm thick. The materials used include large bricks, weighing around 5 kg, lime- and clay-based mortar, as well as the incorporation of natural elements such as seashells from the coast. The original structure also made use of wood, such as Brazilian cedar, used in elements like the roof and frames, which were later replaced due to degradation over time.

(Carvalho *et al.*, 2013; Luz, Silveira and Soeiro, 2021).

One of the most remarkable aspects of the church's history refers to its burial by a migrating sand dune, which began around 1897 as a result of changes in the region's wind patterns. The building remained covered by sand for approximately four decades, being progressively uncovered from the 1930s and completely excavated around 1943. This event contributed to the deterioration of several construction elements, especially those more susceptible to moisture and the weight of the sand overburden, such as the roof and wooden componentes (IPHAN, 1980; Carvalho *et al.*, 2013).

Throughout the 20th century and the early 21st century, the church underwent several restoration and maintenance interventions. The first actions took place between the 1940s and 1950s and were carried out by the local community without adequate technical rigor.

Subsequently, more structured interventions were conducted by preservation agencies, such as those promoted by SPHAN/Pró-Memória in the 1980s, which included the restoration of the roof, plaster, frames,

and architectural elements. Other relevant interventions occurred in 1997, focusing on the recovery of structural elements, and in 2005, aimed at preventive maintenance, especially in the treatment of infiltration and efflorescence (Carvalho *et al.*, 2013).

Currently, the church is in regular use for religious activities and is in good overall condition. However, it presents pathological manifestations mainly associated with environmental agents, such as marine aerosol (salt spray), moisture, and the natural aging of materials.

Among the main observed issues are the presence of infiltration, salt efflorescence, degradation of wooden elements, peeling of coatings, and plaster detachment. Additionally, inappropriate interventions carried out over time, involving the use of materials incompatible with the original construction, have contributed to the emergence of new anomalies (Carvalho *et al.*, 2013; Luz, Silveira and Soeiro, 2021).

In this context, the Church of Almofala represents a relevant case study for the application of non-destructive techniques, such as GPR, contributing to the investigation of construction characteristics in heterogeneous media and to the understanding of wave reflection behavior in complex built environments with the presence of anomalies.



Figure 2: Church of Almofala, Itarema, Ceará, Brazil: (a) Re-emergence of the church after the removal of the sand volume (Carvalho, 2013); (b) External view of the church in its current state; (c) Internal view of the church in its current state.

2.2 GPR data acquisition

The GPR equipment used in the tests was the Proceq GP8000 model, characterized as a handheld, wireless, and lightweight device, suitable for investigations on both vertical and horizontal surfaces. The equipment operates with a central frequency antenna of 2000 MHz, which provides more detailed images but with reduced penetration depth, making it appropriate for the study of shallow structures such as masonry, concrete, and architectural elements (Elkarmoty et al., 2024; Jasieńko, Raszczuk and Frąckiewicz, 2024).

The regions selected for the study encompassed masonry areas defined based on a preliminary inspection of the building, prioritizing locations that exhibited visible pathological manifestations, such as cracks and moisture presence, as well as zones of structural interest and construction uncertainty.

GPR data acquisition was performed by moving the antenna along the surface of the masonry, following previously defined linear and continuous trajectories, with lengths varying according to the extent required

or each investigated area. In total, four acquisitions were carried out, distributed across different points of the church (Figure 3).

Subsequently, the data were processed using the Proceq GPR application, with the application of filters and the definition of parameters compatible with the analyzed material.

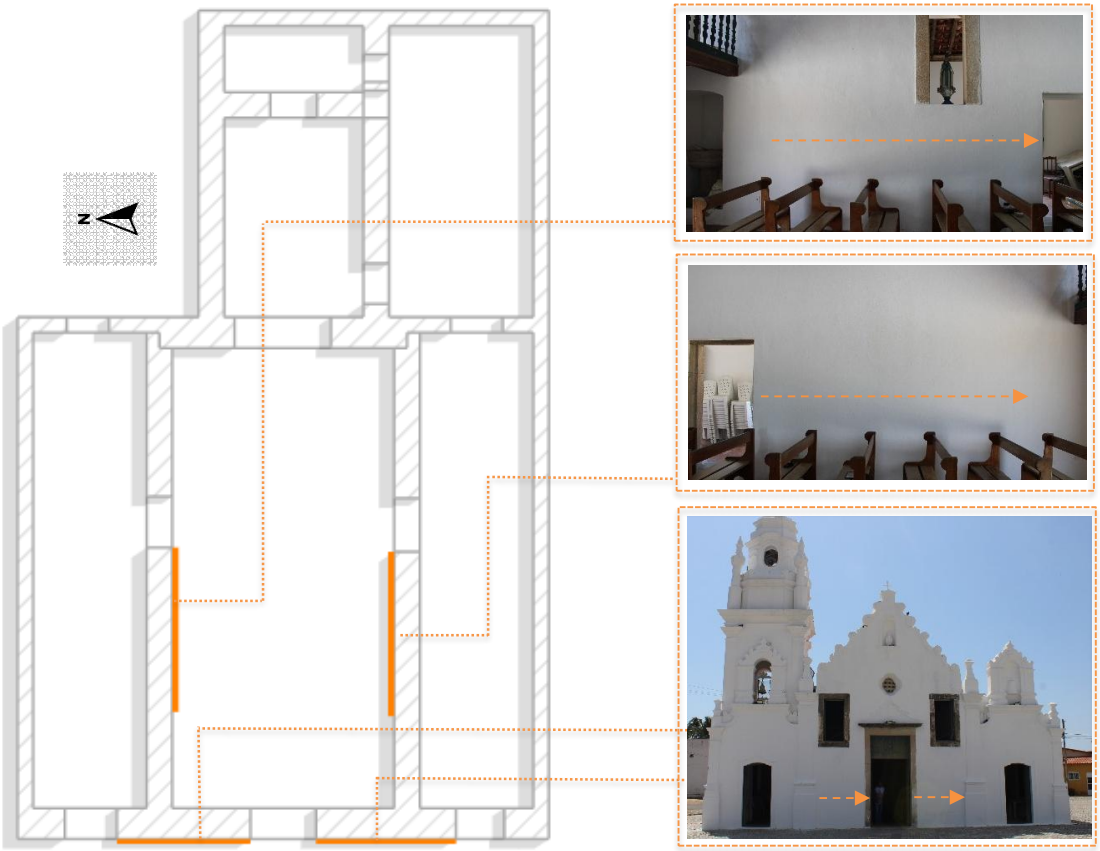


Figura 3: Data acquisition locations

2.3 Signal Processing

Data processing was carried out using the GPR's own application, which includes the main parameters for analyzing the results. The primary objective of this stage is to improve the quality of the acquired signal to enhance the interpretation of reflections, avoiding distortions or the loss of relevant targets. Figure 3 illustrates the difference between a raw radargram and the same radargram after processing. Processing techniques vary according to the equipment, and there are no fixed rules for parameter selection; these are defined based on the operator's experience and the level of detection required (Utsi, 2017).

First, the dielectric constant of the investigated medium was defined. According to Carvalho, the church is mainly composed of clay-based bricks, with inclusions of mortar and regional elements such as seashells. In this context, clayey materials exhibit a wide range of dielectric constant values, which may vary between 8 and 40 for moist clays, while under dry conditions these values typically range between 2 and 5 (Reynolds, 2011). In heterogeneous masonry, defining this parameter becomes even more challenging, and the adoption of representative average values is common. Thus, for GPR analysis purposes, a weighted average can be adopted, considering the volumetric contribution of the different constituent materials, such as

bricks, mortar, and possible infill materials, resulting in an average value of approximately 7.0 for the overall structure (Qian *et al.*, 2026).

For the visualization of radargrams, a grayscale color scale was adopted, as it provides better perception of signal amplitude variations and enhances the identification of reflection continuity, even in regions where signal intensity is reduced. Although chromatic scales may be visually more appealing, they can lead to overinterpretation of the data or make it difficult to identify low-amplitude targets. In this sense, as discussed by Erik Utsi, the grayscale scale is a more appropriate alternative for analysis, allowing for a more accurate and consistent representation of the patterns present in radargrams (Utsi, 2017).

Other processing procedures were also applied to improve the quality of the radargrams and assist in data interpretation. Among these, noise cancellation stands out, used to reduce interference and improve the signal-to-noise ratio, and background removal, applied to eliminate reflections associated with the homogeneous medium and highlight internal discontinuities. Additionally, gain adjustments were applied, including linear gain and time gain compensation (TGC), aiming to compensate for signal attenuation with depth. The definition of the time window allowed the establishment of the investigation limit, while A-scan analysis was used to support the interpretation of individual signals. The adopted spatial sampling rate directly influenced the resolution of the obtained data, and a repetition rate of 1 scan/cm provided adequate spatial resolution for identifying variations along the profiles. Furthermore, the adoption of a 1:1 aspect ratio ensured proper geometric representation of the radargrams, preventing distortions in the interpretation of features (Utsi, 2017). The adopted processing parameters are presented in Table 1, and the comparison between the raw radargram and the processed radargram can be observed in Figure 4.

Filtering	**2000MHz**
Dielectirc constant (εr)	7
Noise Cancellation	Activated
Background Removal	6 ns
Linear Gain	16-20 dB
TGC (Time Gain Compensation)	3-4 dB/ns
Time Window	16 ns
Repetition Rate	1 scan/cm
Viewing scale	Grayscale
Aspect Ratio	1:1

Table 1: GPR processing parameters.

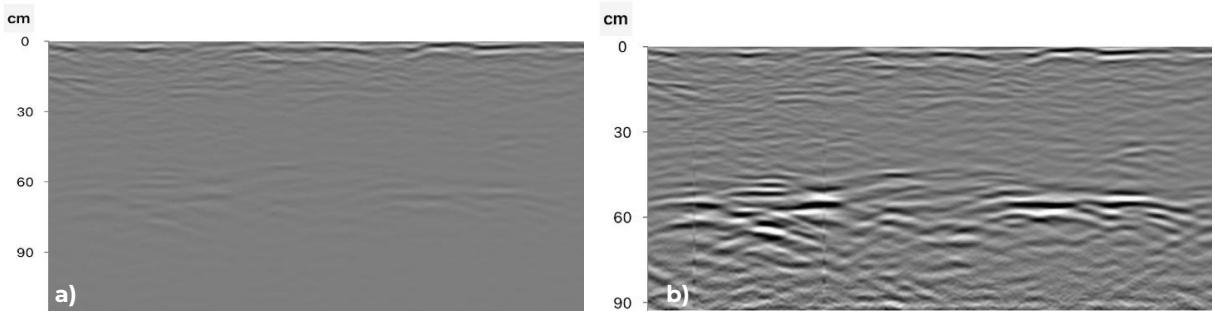


Figure 4: Difference in radargram processing: (a) Raw radargram; (b) Processed radargram.

2.4 Analysis of GPR Responses

The interpretation of GPR data in historic masonry presents inherent limitations due to the heterogeneity of the medium, which results in complex and non-uniform dielectric contrasts. This condition may lead to multiple reflections, signal scattering, and variable attenuation, contributing to ambiguity in the identification of internal features.

The analysis of GPR responses was structured based on interpretative criteria applied to radargrams, aiming to identify internal features of the masonry through the evaluation of electromagnetic signal reflection patterns. For this purpose, parameters such as continuity, amplitude, and geometry of the reflections were considered.

Initially, continuous (linear) reflection patterns were used to identify possible interfaces between materials, bedding joints, and extensive discontinuities, such as cracks or fractures. It is important to note that GPR does not directly detect the opening of these discontinuities, but rather the variations in electromagnetic properties associated with them, such as the presence of air, moisture, or changes in material composition.

(Fernandes, 2006; Utsi, 2017).

Subsequently, responses with hyperbolic geometry were associated with the presence of point targets or small-sized features, such as voids, inclusions, or localized discontinuities. The occurrence of multiple overlapping hyperbolas was interpreted as an indication of heterogeneous or degraded media, possibly related to intense cracking, internal voids, delamination, or fragmented materials (Fernandes, 2006; Utsi, 2017)

In the specific case of air-filled voids, these tend to exhibit high reflection coefficients, resulting in high-amplitude signals. However, in voids with irregular or asymmetric geometry, increased signal scattering may occur, reducing the accuracy in defining their boundaries (Qian *et al.*, 2026).

Additionally, regions with significant signal attenuation were analyzed as possible indicators of moisture presence. Under high moisture conditions, the energy of the electromagnetic signal may dissipate, resulting in radargrams with a low presence of reflections, characterizing a highly moist medium. On the other hand, the interface between dry and moist regions generates high-amplitude reflections (Perez-Gracia *et al.*, 2021).

3. Results

3.1 Analysis and Interpretation of GPR Responses

The analysis of the radargrams allowed the identification of different reflections within the masonry, mainly interfaces between construction layers, voids, and moisture. The obtained radargrams reveal distinct reflection patterns directly associated with the internal heterogeneity of the investigated masonry. In general, the presence of well-defined interfaces, homogeneous zones, regions with strong signal attenuation, and areas with high structural complexity can be observed.

The blue arrows indicate the superficial layer, characterized by continuous linear reflections, interpreted as the interface between the external plaster and the beginning of the brick masonry. This type of response is typical of planar boundaries between materials with different dielectric properties, highlighting the transition between construction layers.

Similarly, the white rectangles, highlighted in Figures 4a and 4b, show continuous sub-horizontal reflectors associated with internal interfaces within the masonry. These features may be related to the arrangement of bricks and bedding joints, reflecting variations in material composition and possible distinct construction phases.

The red arrows indicate high-amplitude reflections associated with more pronounced dielectric contrasts within the medium. These responses are typically related to the presence of air-filled voids or localized discontinuities, as air presents a high contrast relative to the surrounding materials, resulting in stronger

reflections. Such features are particularly evident in Figure 4a and may indicate internal detachment or zones with loss of cohesion.

The light blue arrows, observed in Figure 4c, are interpreted as transitions between regions with different moisture contents, such as the interface between dry zones and areas with higher water presence. As discussed by Utsi (2017), variations in moisture content significantly influence the electromagnetic response due to the increase in dielectric permittivity and electrical conductivity, resulting in amplitude contrasts and signal distortions. Alternatively, these responses may also be associated with heterogeneous regions filled with different materials.

The orange rectangles highlight areas with low reflectivity or absence of reflections, characterized by a "cleaner" appearance in the radargram. This behavior is consistent with the attenuation of the electromagnetic signal, generally associated with the presence of moisture, which promotes the dissipation of signal energy and reduces the visibility of internal interfaces. This phenomenon makes interpretation more difficult and may mask relevant features.

Finally, the region highlighted in green presents a highly heterogeneous pattern, characterized by multiple overlapping reflections, irregular geometries, and significant amplitude variation. This behavior indicates a complex internal medium, possibly associated with degradation processes, the presence of voids, material fragmentation, or irregular infill. This type of response is related to signal scattering, typical of non-homogeneous media and frequently observed in historic masonry.

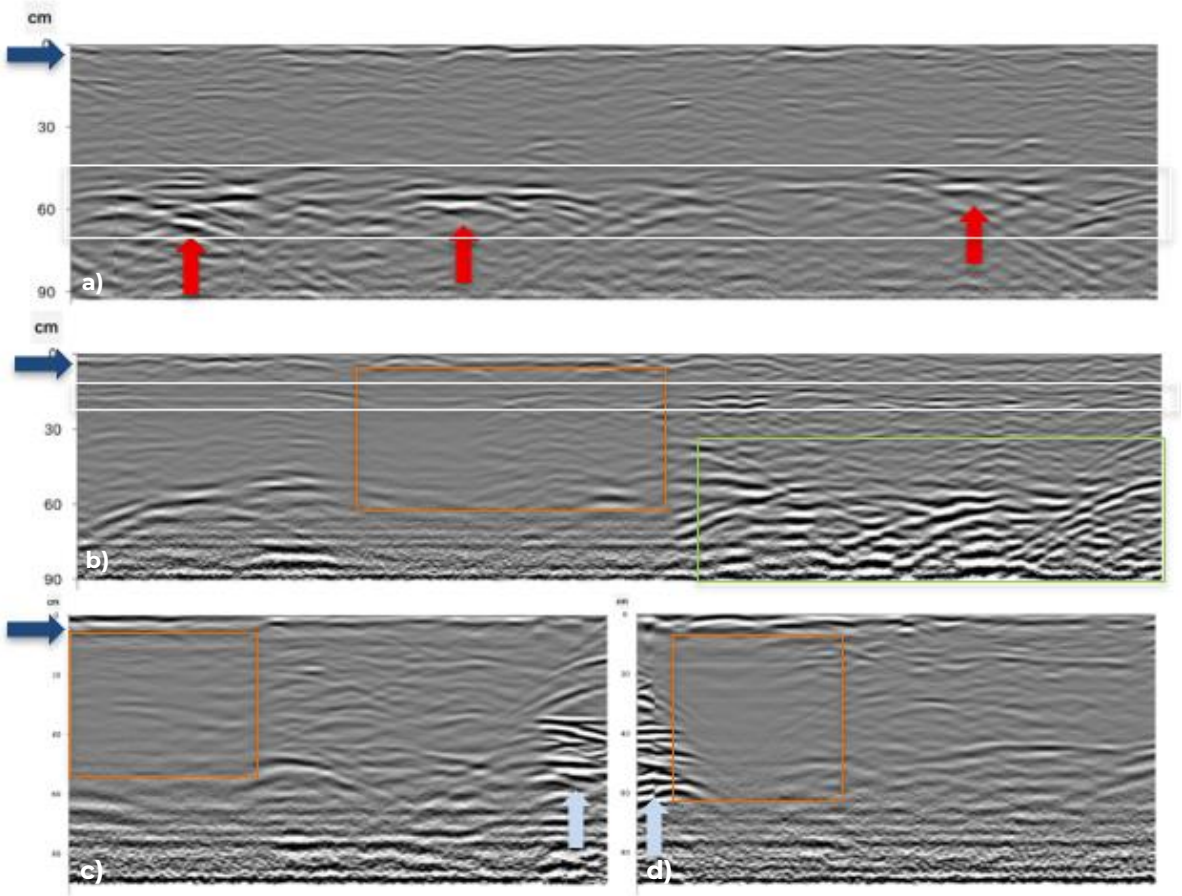


Figure 5: Radargrams obtained in the investigated masonry: (a) Presence of interfaces between layers and strong reflections indicative of voids; (b) Presence of interfaces between layers and regions of signal attenuation indicative of moisture, along with strong reflections indicating high heterogeneity; c) and d) Presence of interfaces between layers, signal attenuation possibly indicative of moisture, and strong reflections demonstrating heterogeneity.

4. Conclusion

Based on the obtained results, the following conclusions can be highlighted:

· The application of GPR proved to be effective in identifying internal features in historic masonry, contributing to the non-destructive analysis of these structures;

· The careful definition of processing parameters was essential for improving radargram quality and increasing the reliability of interpretations;

· The use of filters, such as noise removal, background removal, and gain compensation, made it possible to highlight relevant reflection patterns without compromising data integrity;

· The appropriate selection of the dielectric constant, combined with the use of a grayscale scale, facilitated the identification of signal continuity and the distinction between different internal features;

· The interpretation of radargrams enabled the identification of interfaces between construction layers, regions with possible voids, zones of attenuation associated with moisture presence, and areas with high internal heterogeneity;

· The obtained results reinforce the potential of GPR as an efficient tool for investigating historic masonry, even considering the limitations imposed by the heterogeneous nature of these materials;

· The interpretation of GPR data remains dependent on the operator's experience and prior knowledge of signal behavior in heterogeneous media.

Therefore, the application of the method requires rigorous analysis and interpretation criteria in order to minimize ambiguities and ensure greater reliability of the results.

5. Acknowledgements

This work was financially supported by FUNCAP, Project 01172921/2022 – Cientista Chefe Cultura, Project 10581391/2022 – International collaboration FUNCAP/INSA Rouen Normandie; by the National Council for Scientific and Technological Development (CNPq) – Project 302054/2022-7 – PQ2, by the Project - 440926/2024-6 – VISION and Project - 402828/2024-0 – CLIC, CAPES Foundation and Finep 2896/24.

6. References

DE ALMEIDA, C.M.N. V. (2013) *Paredes de alvenaria do Porto. Tipificação e caracterização experimental*. Tese de Doutorado. Universidade do Porto, Portugal.

ALVARADO et al. (2025) "Non-destructive testing and kinematic limit analysis applied to a historic masonry church early intervened with RC elements," *Engineering Failure Analysis*, 169. Available at: https://doi.org/10.1016/j.engfailanal.2024.109205.

Annan (2003) *Ground penetrating radar applications, principles, procedures*, *Sensors and Software*. Mississauga, Canada: Sensors and Software.

BALASUBRAMANI, D.P. (2025) "Applications of Geophysical techniques in geotechnical engineering," *Indian Geotechnical Journal*, 55(4), pp. 2477–2491. Available at: https://doi.org/10.1007/s40098-025-01343-y.

BEVAN, B.W. et al (2020) "Ground-penetrating radar at Chaco Canyon, USA, 1974 - 1976." Available at: https://doi.org/10.13140/RG.2.2.20527.66729.

BINDA, L., LENZI, G. and SAISI, A. (1998) "NDE of masonry structures: use of radar tests for the characterisation of stone masonries," *Ndt & e International*, 31(6), pp. 411–419.

BRANDES et al. (2025) “Lithological control on the geometry of strike-slip faults – insight from ground-penetrating radar (GPR) survey and analogue modelling,” *Tectonophysics*, p. 230944. Available at: https://doi.org/10.1016/j.tecto.2025.230944.

CARLOS, J. and DOMINGUES, M. (2017) *Caracterização tipológica e mecânica de paredes de alvenaria de pedra em centros urbanos antigos — Caso de estudo de Viseu*. Universidade de Coimbra.

Carvalho, F. *et al.* (2013) *ASPECTOS HISTÓRICOS E ESTADO DE CONSERVAÇÃO DA IGREJA DE ALMOFALA-CEARÁ (BRASIL)*.

CRUZ et al. (2024) “Case study: Casa da Câmara de Guimarães. HBIM modeling from non-destructive techniques,” *Procedia Structural Integrity*, 64, pp. 335–342. Available at: https://doi.org/10.1016/j.prostr.2024.09.259.

Elkarmoty et al. (2024) “Georadar Survey and Simulation for Subsurface Investigation at Historical Mosque of Sorghatmesh, Cairo, Egypt,” *Buildings*, 14(11). Available at: https://doi.org/10.3390/buildings14113653.

FERNANDES, F.M.C.P. (2006) *Part II NDT in masonry using Ground Penetrating Radar*.

García-Nieto, M.C. *et al.* (2024) “A Geophysical Investigation in Which 3D Electrical Resistivity Tomography and Ground-Penetrating Radar Are Used to Determine Singularities in the Foundations of the Protected Historic Tower of Murcia Cathedral (Spain),” *Remote Sensing*, 16(21). Available at: https://doi.org/10.3390/rs16214117.

GRZYB et al. (2025) “Preliminary assessment of structural masonry damage in Malbork Castle,” *Case Studies in Construction Materials*, 22. Available at: https://doi.org/10.1016/j.cscm.2024.e04166.

HATEM et al. (2025) “Geophysical Exploration for Archaeological Ruins North of Senusret I Pyramid, El-Lisht Area, Giza, Egypt,” *Pure and Applied Geophysics*, 182(4), pp. 1673–1695. Available at: https://doi.org/10.1007/s00024-024-03613-x.

ICOMOS (2006) *Recomendações para a análise, conservação e restauro estrutural do patrimônio aruitetonico*.

Jasieńko, J., Raszczuk, K. and Frąckiewicz, P. (2024) “Areas of GPR application in researches of historical masonry structures,” *Research Square* [Preprint]. Available at: https://doi.org/10.21203/rs.3.rs-4022334/v1.

JORNE, F., SILVA, V. and ROSA, C. (2015) “Caracterização de alvenarias antigas: levantamento tipológico, análise das secções e caracterização dos materiais.” Lisboa: CONPAT 2015. Available at: https://www.researchgate.net/publication/281651944.

Luz, J.B., Silveira, I. de O. and Soeiro, M.A.R. (2021) “Ensaio termográfico de edificação histórica: Igreja de Nossa Senhora da Conceição de Almofala / Thermographic test of historical heritage: Igreja de Nossa Senhora da Conceição de Almofala,” *Brazilian Journal of Development*, 7(10), pp. 100708–100731. Available at: https://doi.org/10.34117/bjdv7n10-401.

MARTINI R (2019) *Caracterização de Alvenarias de Granito Baseada em Técnicas Geofísicas, Mecânicas e Redes Neuronais*. Tese de Doutorado,. Universidade do Porto (Portugal).

Mateus, J.M. (2002) *Técnicas tradicionais de construção de alvenarias - A literatura técnica de 1750 a 1900 e o seu contributo para a conservação de edifícios históricos*. Lisboa.

PARNOW et al. (2024) “Roman stone masonry walls: The application of Ground Penetrating Radar to ancient structures,” *E3S Web of Conferences*. EDP Sciences. Available at: https://doi.org/10.1051/e3sconf/202457901003.

Perez-Gracia, V. *et al.* (2021) “Assessment of humidity damage in cultural heritage,” *2021 11th International Workshop on Advanced Ground Penetrating Radar, IWAGPR 2021* [Preprint]. Available at: https://doi.org/10.1109/IWAGPR50767.2021.9843177.

Perez-Gracia, V., Solla, M. and Fontul, S. (2022) “Analysis of the GPR signal for moisture detection: application to heritage buildings,” *International Journal of Architectural Heritage*, 18(2), pp. 230–253. Available at: https://doi.org/10.1080/15583058.2022.2139652.

Qian, W. *et al.* (2026) “Advanced GPR signal processing for void detection in historic masonry structures: Application to the Ming Great Wall,” *Measurement: Journal of the International Measurement Confederation*, 268. Available at: https://doi.org/10.1016/j.measurement.2026.120629.

REYNOLDS, J.M. (2011) *An Introduction to Applied and Environmental Geophysics*. Available at: www.wiley.com/go/reynolds/introduction2e.

ROSA, C. (2013) *Caracterização de alvenarias de pedra antigas*. Faculdade Nova Lisboa.

Solla, M. *et al.* (2020) “A building information modeling approach to integrate geomatic data for the documentation and preservation of cultural heritage,” *Remote Sensing*, 12(24), pp. 1–24. Available at: https://doi.org/10.3390/rs12244028.

SOLLA, M., PÉREZ-GRACIA, V. and FONTUL, S. (2024) “Corrosion Assessment of Reinforced Concrete Structures using Ground-Penetrating Radar,” *Proceedings of the World Congress on New Technologies*. Avestia Publishing. Available at: https://doi.org/10.11159/icceia24.130.

UTSI, E.CARRIK. (2017) “Ground penetrating radar.” Available at: https://books.google.com/books/about/Ground_Penetrating_Radar.html?hl=pt-BR&id=JSK2DQAAQBAJ (Accessed: November 8, 2025).

IPHAN (1980) “IPHAN.”

Cinpar 2026
XXII International Conference on Building Pathology and Constructions Repair
15th to 17th July 2026 - Lisboa, Portugal

Damage mapping of a 50's building as a strategy for maintenance.

Bruna VALE[1], Francisco Carlos SANTANA[2], Oscar NETO[3], Esequiel MESQUITA[4]

[1] Federal University of Ceará, Fortaleza, Brazil, brunahigino@alu.ufc.br
[2]Federal University of Ceará, Fortaleza, Brazil, franciscosantana@alu.ufc.br
[3]Federal University of Ceará, Fortaleza, Brazil, oscardequeiroz@alu.ufc.br
[4]Federal University of Ceará, Fortaleza, Brazil, emesquita@ufc.br

Abstract: The conservation of built historical heritage requires strategies that go beyond the preservation of memory and collective identity, incorporating technical actions focused on maintenance to ensure the long-term integrity of buildings. In this context, the use of technologies for the maintenance of built heritage has been widely discussed within the scientific community and has become a fundamental strategy for the conservation of these assets. The use of drones for surveying pathological manifestations in historic buildings has become increasingly common and contributes to the development of more accurate diagnoses. With the aim of contributing to the preservation and documentation of historic buildings, this paper analyzed the pathological manifestations identified in one of the earliest residential condominium complexes in Fortaleza/CE, the Dona Bela Building, a residential complex composed of three blocks. Based on the photogrammetric survey, on-site measurements, and photographic data acquisition, a set of detailed damage maps of the apartments and facades was produced, as well as a technical report on the identified pathologies. These outputs contribute to the strengthening of maintenance and management strategies for historical heritage.

Keywords: Damage mapping; Drone surveying; Historic Buildings; Maintenance strategies; Pathological manifestations.

1. Introduction

The first notion of urban historical heritage emerged in the 18th century and became consolidated through the accelerated modernization processes of major European cities, when preservation gained prominence and came to be recognized as an asset of irreplaceable value for society, whose loss is considered irreparable (Choay, 2011). Since then, historical heritage has played a crucial role in understanding the past, contributing to the cultural identity and collective memories of societies. However, these assets are constantly exposed to environmental changes, natural hazards, and other factors, leading to their gradual deterioration over time. (Hajirasouli and Banihashemi, 2020)

In the contemporary context, the documentation of historic buildings face frequent challenges, as records are often incomplete, fragmented between interventions, or even nonexistent, which compromises their long-term preservation (Godinho *et al.,* 2020). In this scenario, documentation becomes essential not only to preserve building information over time but also to support decision-making and maintenance processes, highlighting the importance of incorporating recently available technologies. *(*Rubens *et al.,* 2022*)* Damage mapping stands out as a strategic tool in this process, as it enables not only systematic recording but also the classification of pathological manifestations, supporting the identification of the causes of alteration and deterioration of architectural surfaces (Scandurra and Luggo, 2023).

With the progressive aging of buildings, structures undergo changes over time due to the interaction between the built environment and external conditions, resulting in a gradual reduction of their service life (De Moura Junior *et al.,* 2022). Pathological manifestations such as cracks, infiltrations and oxidations commonly found in historical buildings are further aggravated by environmental and climatic conditions, while in older constructions, structural problems caused by material degradation are among the main

causes. The identification and analysis of these pathologies through technical reports and damage maps are essential steps in understanding the conservation state of building, and should be conducted through survey of existing damages (Xavier *et al.,* 2022). However, traditional inspection techniques are based on in situ measurements, which may present limitations in terms of spatial accessibility, operator safety, and the level of precision and detail obtained, especially in buildings under continuous use.

In this context, advances in digital technologies have enabled greater accuracy in the diagnostic documentation of built heritage through in situ surveys.. Murphy *et al.,* (2009) define Historic Building Information Modelling (HBIM) as a methodology for the development of parametric models based on Building Information Modelling (BIM) for historical buildings, incorporating historical data and information captured through laser scanning and photogrammetry. Currently, laser scanning and photogrammetry are considered highly accurate and non-invasive methods for acquiring geometric data in historical buildings. (Aricò *et al.,* 2024). The integration of these methods allows for the generation of point clouds derived from on-site data acquisition, a process known as Scan-to-BIM (Brumana *et al.,* 2019). The use of these techniques, combined with Unmanned Aerial Vehicle (UAV), which have become accessible tools for heritage data acquisition, has proven advantageous in improving surveys, particularly for capturing hard-to-reach areas such as tall buildings, roofs and upper facades (Sun *et al.,* 2015).

The combined use of photogrammetry, laser scanning and UAVs constitutes a technological approach capable of enhancing the development of accurate and efficient damage maps, enabling the analysis, classification and identification of pathologies with greater rigor. In parallel, thematic mapping within HBIM models has been widely discussed in recent years. While some researchers focus on geometric representation of damage through ultra-thin layers overlaid onto model elements, others encode such information as parameters associated with each component of the model. Additionally, the use of standardized hatching to represent different types of deterioration has become an effective strategy for identifying pathologies with greater scientific rigor, promoting the adoption of internationally shared terminology and contributing to the standardization of diagnostic processes (Delpozzo *et al.,* 2022).

Thus, this study aims to analyze the pathological manifestations identified in the Dona Bela Residential Complex, built in the 1950s and one of the first multifamily residential buildings in the city of Fortaleza, Ceará, Brazil. The selection of this case study is justified by its historical relevance in the process of urban verticalization, as well as by its current condition of continuous use, highlighting the real limitations associated with conducting inspections in inhabited historical buildings. Through the integration of UAVs surveys, photogrammetry, in situ measurements, and photographic records, it was possible to develop a technical report of the identified pathologies, as well as thematic damage maps of both the building facades and floor plans. As a scientific contribution, this study proposes an integrated technological approach for damage mapping in inhabited historical buildings under conditions of restricted access. In this sense, the research reinforces the potential of digital technologies as fundamental tools for the documentation and management of historic buildings in continuous use.

2. Case Study

The Dona Bela Residential Complex, located on Coronel Ferraz Street in the city of Fortaleza, state of Ceará, constitutes an important architectural landmark in the context of vertical multifamily residential use. During this period, a New Urban Code for the municipality of Fortaleza (1952) was established, regulating the so-called “apartment houses”:

Art. 339° – When multiple dwellings are grouped within the same building, sharing a common main entrance connected to all units and a properly installed concierge, this configuration shall be defined as an apartment house. (Prefeitura de Fortaleza, 1952)

According to Cavalcante (2015), apartment buildings began to be constructed in residential areas in the second half of the 1950s, following the city’s urban expansion towards the Centro-Aldeota axis, also known as the Outeiro district, where the case study of this research is located. In a context marked by verticalization and the predominance of mixed-use buildings, with emphasis on commercial and institutional activities, Dona Bela stands out as the first apartment complex designed exclusively for residential use built in the 1950s.

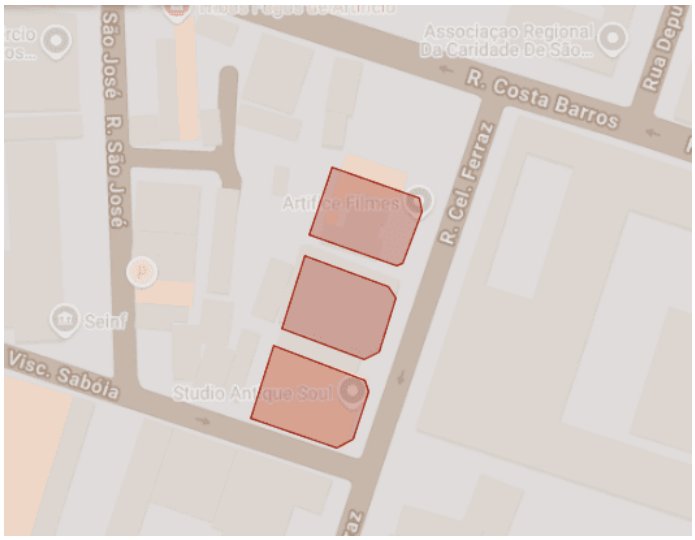


Figure 1 – Dona Bela urban complex location.

Constructed in the second half of the 1950s, the Dona Bela Building (Figure 2) features a reinforced concrete structure and consists of three apartment blocks (A, B and C), each comprising three floors with two units per floor, totaling 18 units in the complex. Cavalcante (2015) states that although the authorship of the projects is unknown, the real estate company responsible for the development, Imobiliária Pedro Philomeno, presents aesthetic similarities with other buildings, such as the São Pedro Building (Figure 3), which was demolished in 2024, suggesting the possibility of a common designer across different projects.



Figure 2 – Dona Bela Building.



Figure 3 – São Pedro Building.

Each residential unit includes four bedrooms, one social bathroom, a kitchen with dining area, living and dining rooms, as well as a service area and bathroom (Figure 5). Vertical circulation is organized through two staircases: one for service and another for social access. (Cavalcante and Paiva, 2019)

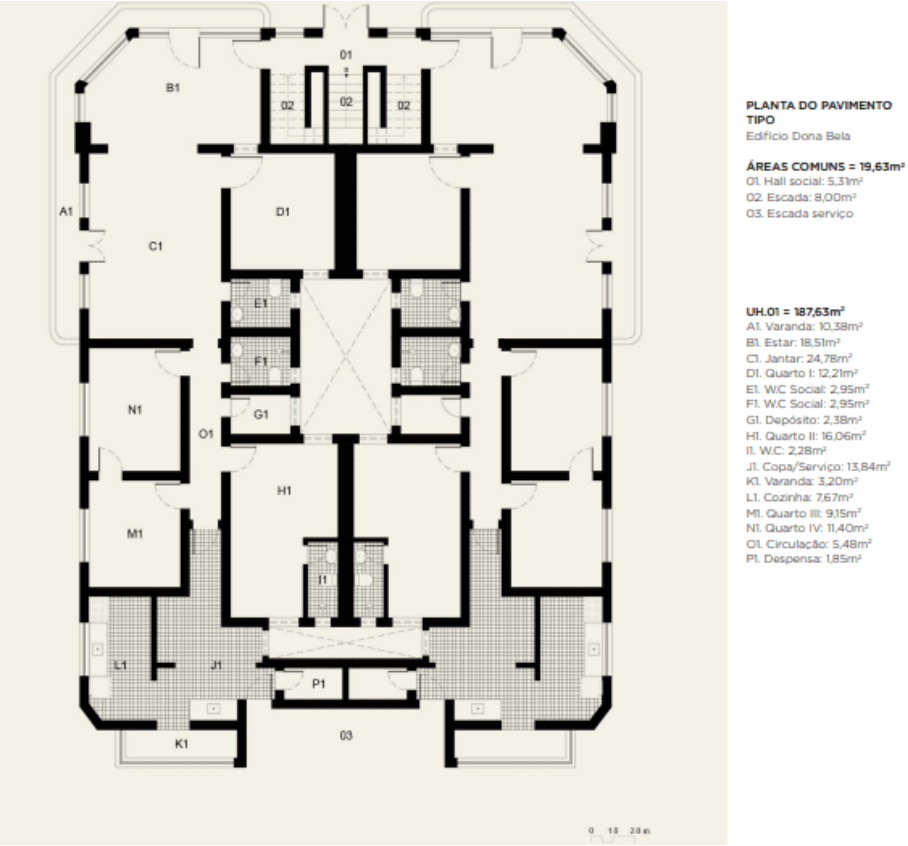


Figure 4 – Typical floor plan of the Dona Bela Building designed by Marcia Cavalcante

The complex stands out for reflecting architectural features associated with Mediterranean-influenced modernism (Secultfor, 2015), characterized by straight lines and parapets, slabs resembling canopies, rounded balconies, and monochromatic finishes, predominantly in white tones, with wooden louvered window frames and facade ornaments (Figure 5).



Figure 5 – Dona Bela building facades.

Due to its importance not only for Ceara's modernist architecture but also as one of the few remaining inhabited examples of early multifamily residential buildings, the Dona Bela Complex was listed as a protected heritage site in 2015 by the Secretariat of Culture of Fortaleza. This designation was motivated by its pioneering architectural production in reinforced concrete, particularly associated with developments

by entrepreneur Pedro Philomeno Gomes. Furthermore, the complex is located near the first protected urban architectural ensemble in the city, reinforcing its historical significance in the context of Fortaleza's urban development (Secultfor, 2015).

Currently, the Dona Bela Complex remains inhabited, although its occupancy profile has changed over time. Unlike its original residential population, the complex now accommodates residents engaged in cultural and creative economy activities, such as artists, music producers, filmmakers, and young adults interested in the reoccupation and revitalization of Fortaleza's downtown area. Some residents have transformed their units into collaborative and cultural spaces which, especially on weekends, activate Coronel Ferraz Street and have become symbols of resistance against the urban decline that has affected the neighborhood in recent decades.

However, these new uses and forms of occupation have led to transformations within the residential units, including the construction of independent annexes on the rooftops of each block and localized interventions carried out by residents, such as the subdivision of existing units to accommodate additional occupants. These actions, combined with the aging of construction materials, exposure to regional climatic conditions, and the lack of proper maintenance, contribute to the progression of pathological manifestations within the Dona Bela Complex.

In this context, the Municipality of Fortaleza launched in 2025 the Call for Proposals to Promote the Cultural Heritage of the City of Fortaleza, through which 16 architectural assets were selected to undergo technical assessments conducted by architects, engineers and specialized professionals to evaluate their current condition. The Dona Bela Complex was among the selected properties.

Given this scenario, an in situ survey and a technical report on pathological manifestations were carried out with the aim of documenting, identifying and mapping the damages present in the residential complex. This process sought to understand the current state of conservation of the building and to support strategies for maintenance and preservation of the existing heritage.

3. Methodology

This research adopts a case study approach focused on the diagnosis of pathological manifestations supported by innovative technologies to enhance the maintenance and management of a historic residential building. The process was divided into five stages (Figure 6) and combined digital surveying technologies, in situ inspections for data acquisition, and the development of a technical report for the identification of pathologies through damage mapping.

It is important to emphasize that the methodology was adapted due to the building's condition of continuous use, which imposes limitations on access and data acquisition in certain residential units. Therefore, complementary strategies were implemented to ensure comprehensive data collection.

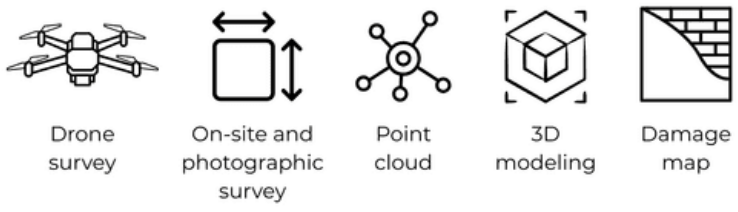


Figure 6 – Methodological workflow

3.1 Drone Survey

An Unmanned Aerial Vehicle (UAV), mode DJI Mavic 3T Thermal, was used to capture high resolution images of facades and upper areas of the building complex that were not accessible through conventional inspection methods (Figure 7). The aerial survey enabled precise documentation of upper areas while minimizing physical intervention, Additionally, thermographic data were acquired using the UAV's thermal camera (Figure 8).

However, some limitations were identified during the process, particularly related to the presence of exposed electrical wiring and surrounding vegetation, resulting from the continuous use of the building. These factors affected image quality, especially at ground and first-floor levels. As a result, complementary in situ photographic records were required to support visual data acquisition.



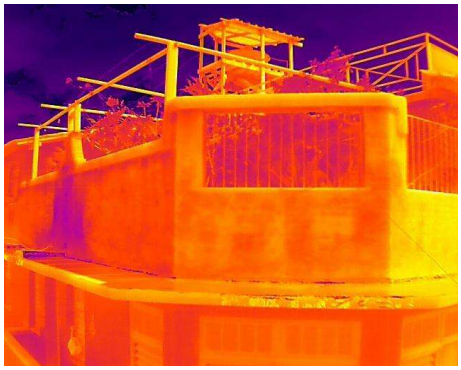


Figure 7 – Image captured by UAV. **Figure 8** – Thermography by a UAV's thermal camera.

3.1.1 On-site and photographic survey

For the in situ survey, both digital laser measuring devices and steel measuring tapes were used to obtain dimensional data for each apartment. Photographic records were also collected for all units where access was granted, documenting not only deviations from the original layout but also pathological manifestations relevant for future maintenance.

The acquisition of photographic data from both internal and external areas enabled systematic documentation of the current condition of the buildings, as well as the modifications carried out over time (Figure 09 and 10).





Figure 9 Staircase built by residents. **Figure 10** – Exposed Rebar.

3.1.2 Point Cloud

Based on the data obtained from UAV and in situ surveys, a point cloud of the Dona Bela building complex was generated (Figure 11). This dataset served as the basis for the development of the three-dimensional model and for the identification of pathological manifestations. This approach aligns with recent HBIM implementation strategies, which integrate multiple data acquisition techniques to support heritage conservation processes (Vieira *et al.,* 2023).

It was observed that the quality of the point cloud varied throughout the building. Higher accuracy was achieved in upper areas, such as the roof and second floor, where external interferences, such as electrical wiring and vegetation, were absent. In contrast, ground and first-floor levels presented lower data quality due to these obstructions, which limited visibility and data capture.

Despite these constraints, the point cloud enabled the identification of several facade pathologies and supported the development of the building's 3D model (Figure 12).

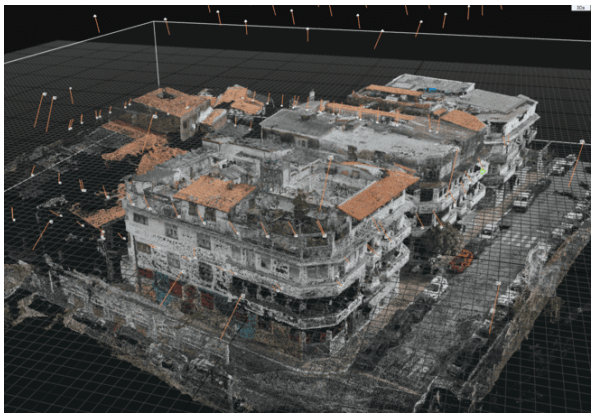


Figure 11 Dona Bela point cloud.



Figure 12 Pathologies detected on the facade.

3.1.3 3D modelling

Based on the collected data, an information model was developed using BIM software (Figure 13). The Dona Bela complex was modeled on Revit®, and subsequently exported to the Industry Foundation Classes (IFC) format to allow interoperability with other platforms and collaborative data enrichment among the research team.

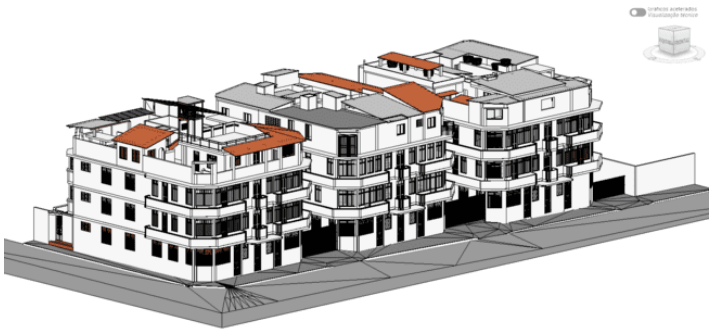


Figure 13 Dona Bela 3D modelling

The BIM model supported the development of damage maps for both facades and floor plans, which were incorporated into the technical pathology report.

3.1.4 Damage map

A technical report of pathological manifestation was developed, integrating all documented processes, in situ photographic records, and the categorization of pathologies by type, building, block, and apartment unit. The identification and classification of pathological manifestations were guided by established criteria from construction pathology studies.

Images captured by the UAV served as the basis for identifying and recording the detected pathologies. Additionally, the BIM model created in Revit enabled the creation of damage maps for both the facades and the floor plans of the Dona Bela Complex.

Pathological manifestations were modeled in the BIM environment using generic model families. During this process, challenges were encountered regarding the geometric representation of pathologies, particularly in defining their shapes and in cases where multiple pathologies overlapped within the same area. For larger and continuous pathologies, linear demarcations were adopted to represent their spatial propagation across extended surfaces.

Following the modeling process, specific parameters were assigned to each pathology, including location data such as building name, block, facade or internal view, and floor level. In addition, visual coding

strategies, such as color differentiation and graphical markings, were applied to enhance identification and to ensure consistency with the damage mapping system.

Furthermore, an image parameter was implemented to associate photographic records with each modeled pathology, enabling the integration of visual documentation and facilitating the identification and classification of pathological manifestations within the BIM environment.

4. Results and Discussion

The results of this study are focused on the identification of pathological manifestations affecting both facades and internal environments of the residential units within the Dona Bela Complex. The main damages identified include coating detachment, cracks, infiltration, loss of elements, moisture-related deterioration, oxidation, and surface soiling, indicating different stages of degradation over time, combined with material aging and exposure to environmental conditions. These findings reinforce the need for a systematic maintenance plan for the historic building.

The development of the technical pathology report enabled the visualization of damages in each residential unit by block, as well as the categorization of pathologies and the corresponding damage maps. This structured systematization supports both documentation and future decision-making processes related to maintenance and management.

The categorization of pathologies was carried out using an alphanumeric coding system designed to ensure traceability and systematic data organization, contributing to the informational enrichment of the damage maps. The identification was structured by block, location (internal or external), and floor level. For example, in Block C, facade images were labeled with the code CF followed by a numerical identifier (Figure 14), while ground-floor units were labeled with codes beginning with C followed by numbering (Figure 15). For instance, C101 refers to Block C, ground floor, unit 1. This standardization enabled the structured organization of photographic records and identified pathologies, facilitating analysis and comparison across different areas of the building.

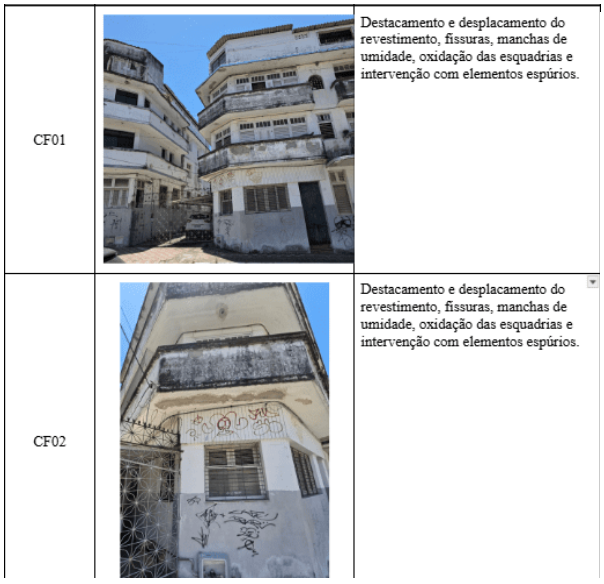


Figure 14 Categorization of block C facades.

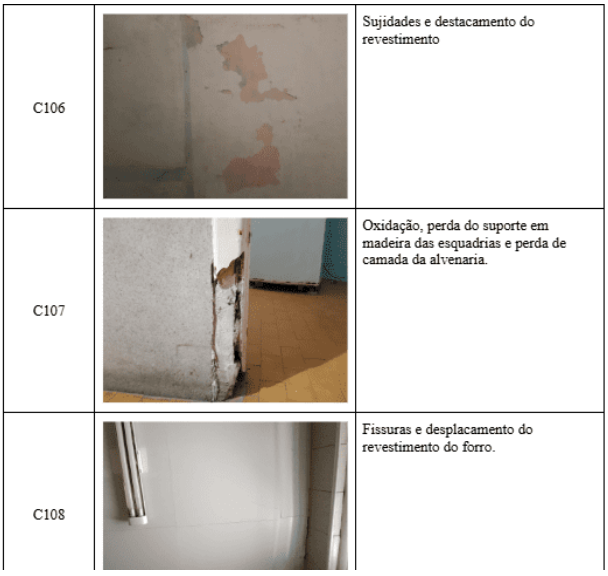


Figure 15 Categorization ground floor block C.

Based on this categorization, damage maps were developed for both facades (Figure 16) and residential units in floor plan representation (Figure 17). These maps enabled a systematic visualization of the spatial distribution of pathologies, as well as the identification of damage concentration in specific areas, particularly those exposed to weather conditions and water accumulation, such as the building facades.

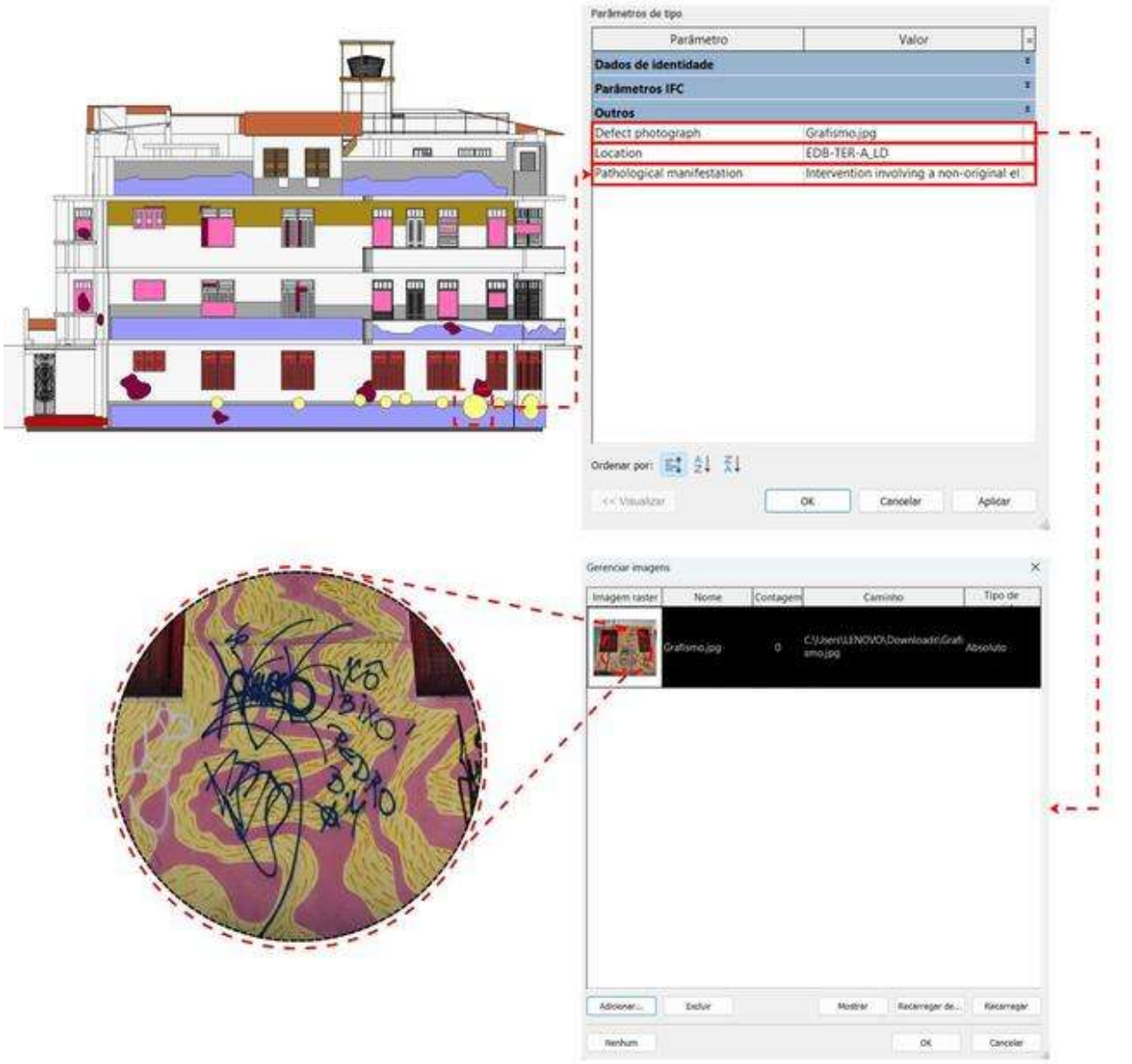


Figure 16 Damage map Block A facade.



Figure 17 Damage map housing unit

The analysis of internal environments revealed significant modifications to the original layout due to interventions carried out by residents, These changes include the creation or removal of spaces within each unit, reflecting spatial adaptations to contemporary needs. Additionally, a greater variability of pathological manifestations was observed, indicating the combined influence of the lack of systematic maintenance and interventions performed without proper technical supervision over time.

The results demonstrated a predominance of pathologies related to humidity. Among the manifestations identified, 19.8% correspond to infiltration stains, 19.1% to coating detachment, 13.5% to cracks, 11.5% to coating flaking, 7.6% to dirt, while other pathologies such as yellowing, oxidation, and loss of elements accounted for lower percentages.

On the facades, for example, the most recurrent pathological manifestations were coating detachment, cracks, surface soiling, and oxidation process. These areas exhibited a higher concentration of pathologies when compared to the internal environments, a condition associated with continuous exposure to solar radiation, rainfall, and humidity variations. These results corroborate studies that relate climatic exposure to the aging and progressive degradation of historical buildings. (Xavier et al., 2022)

Furthermore, the analysis indicated significant differences in the concentration of pathologies among the blocks of the complex. Block C, for instance, presented fewer internal modifications when compared to the others blocks, preserving the original spatial configuration of the floor plan in several residential units and exhibiting a lower incidence of interventions carried out by residents. In contrast, substantial alterations were observed in the roof areas of all three blocks over time. Originally intended for laundry and service functions, these spaces have gradually been adapted to accommodate new uses and annexes constructed by residents. Such interventions not only altered the original spatial typology but also directly influenced the conservation conditions of the building, particularly due to the overlap of constructions materials, successive architectural adaptations, and the lack of adequate technical supervision throughout the years.

The condition of continuous use of the building, combined with ongoing modifications, proved to be a determining factor in the heterogeneous distribution of pathologies. Furthermore, restricted access to certain units limited data collection, highlighting a common challenge in studies involving inhabited historical buildings. This condition reinforces the need for integrating multiple survey techniques, as adopted in this study, as well as flexible methodologies capable of addressing operational constraints and ensuring reliable data acquisition in contexts of continuous occupation.

5. Conclusion

Through the integration of technologies applied to data acquisition for assessing the current state of conservation of Dona Bela Complex, it was possible to identify and analyze the various pathological manifestations present in the building. Based on these data, an updated technical diagnosis was developed, supported by the production of damage maps to assist decision-making processes, enabling a more comprehensive understanding of the current conditions of the complex.

Furthermore, the results revealed that pathological manifestations are heterogeneously distributed across both residential units and facades, being directly associated with material exposure to environmental factors, as well as the lack of systematic maintenance and the absence of technical supervision over interventions carried out over time.

The integrated use of UAV systems, photogrammetry, point cloud generation, and three-dimensional modelling proved to be effective for the documentation and diagnosis of the identified pathologies. Even within a context marked by visual and spatial constraints, the combination of these tools enabled the acquisition of accurate findings to reinforce the potential of damage mapping and systematic data organization as key tools to support decision–making in maintenance and conservation processes.

Overall, this study highlights the importance of integrating these technologies, as well as the need for developing protocols that enable continuous monitoring of conservation conditions in inhabited historic buildings. In this sense, the integration of digital technologies and technical diagnosis represents a promising approach for the conservation and preservation of built historical heritage.

Acknowledgments

This work was financially supported by FUNCAP, Project 01172921/2022 – Cientista Chefe Cultura, Project 10581391/2022 – International collaboration FUNCAP/INSA Rouen Normandie; by the National Council for Scientific and Technological Development (CNPq) – Project 302054/2022-7 – PQ2, by the Project - 440926/2024-6 – VISION and Project - 402828/2024-0 – CLIC, CAPES Foundation and Finep 2896/24.

References

Aricò, Manuela, Claudia Ferro, Marcello La Guardia, Mauro Lo Brutto, Germana Taranto, and Gaspare Massimo Ventimiglia. “Scan-to-BIM Process and Architectural Conservation: Towards an Effective Tool for the Thematic Mapping of Decay and Alteration Phenomena.” *Heritage* 7, no. 11 (November 6, 2024): 6257–81. https://doi.org/10.3390/heritage7110294.

Brumana, Raffaella, Daniela Oreni, Luigi Barazzetti, Branka Cuca, Mattia Previtali, and Fabrizio Banfi. “Survey and Scan to BIM Model for the Knowledge of Built Heritage and the Management of Conservation Activities.” In *Research for Development*, 391–400, 2019. https://doi.org/10.1007/978-3-030-33570-0_35

Cavalcante, Márcia Gadelha. “Edifícios De Apartamentos Em Fortaleza: Universalidades E Singularidades,” Novembro 1, 2021. https://repositorio.ufc.br/handle/riufc/61980.

Cavalcante, Márcia, Paiva, Ricardo Alexandre. “O edifício de apartamentos no Centro de Fortaleza (1935-1959): Signos da modernidade arquitetônica. Janeiro 1, 2019. https://www.researchgate.net/publication/338456104_O_EDIFICIO_DE_APARTAMENTOS_NO_CENTRO_DE_FORTALEZA_1935-1959_signos_da_modernidade_arquitetonica#fullTextFileContent

Choay, Françoise. 2011. A alegoria do patrimônio. Brasil: Estação Liberdade.

Delpozzo, D., D. Treccani, L. Appolonia, A. Adami, and B. Scala. “HBIM AND THEMATIC MAPPING: PRELIMINARY RESULTS.” *the International Archives of the Photogrammetry, Remote Sensing and Spatial Information Sciences/International Archives of the Photogrammetry, Remote Sensing and Spatial Information Sciences* XLVI-2/W1-2022 (February 25, 2022): 199–206. https://doi.org/10.5194/isprs-archives-xlvi-2-w1-2022-199-2022.

De Moura Júnior, José Maria, Lydia Marques Barreto, Willames De Albuquerque Soares, Eliana Cristina Barreto Monteiro, and Thulio Roberto Silva Do Nascimento. “Manifestações Patológicas E Mapa De Danos Em Patrimônio Histórico: Estudo De Caso Da Basílica E Convento De Nossa Senhora Do Carmo Em Recife-PE.” *Research Society and Development* 11, no. 8 (June 28, 2022): e53511831484. https://doi.org/10.33448/rsd-v11i8.31484.

Godinho, Márcia, Rita Machete, Madalena Ponte, Ana Paula Falcão, Alexandre B. Gonçalves, and Rita Bento. “BIM as a Resource in Heritage Management: An Application for the National Palace of Sintra, Portugal.” *Journal of Cultural Heritage* 43 (December 27, 2019): 153–62. https://doi.org/10.1016/j.culher.2019.11.010.

Hajirasouli, Aso, and Saeed Banihashemi. “The Unfolding Tragedy of Kandovan: The Loss of the Last Inhabited Cone-shaped Settlement in the World.” *Habitat International* 102 (July 20, 2020): 102211. https://doi.org/10.1016/j.habitatint.2020.102211.

Murphy, Maurice, Eugene McGovern, and Sara Pavia. “Historic Building Information Modelling (HBIM).” *Structural Survey* 27, no. 4 (August 27, 2009): 311–27. https://doi.org/10.1108/02630800910985108.

Penjor, Tshering., Saeed Banihashemi, Aso Hajirasouli, and Hamed Golzad. Heritage building information modeling (HBIM) for heritage conservation: Framework of challenges, gaps, and existing limitations of HBIM, December 2024.
https://www.sciencedirect.com/science/article/pii/S2212054824000511.

Prefeitura Municipal de Fortaleza. Código Urbano do Município de Fortaleza. Lei n° 188, de 16 de maio de 1950, Decreto de 29 de novembro de 1952.

Rubens, Tallis, Gilmário Ribeiro, Renan Paulo, Maycon Bessa, Eugênio Moreira, Mylene Vieira, and Esequiel Mesquita. “Digitalization Based on High-resolution Scanning and HBIM Tools for Damage Assessment of the José De Alencar House.” *Research Square (Research Square)*, December 13, 2022. https://doi.org/10.21203/rs.3.rs-2361581/v1.

Scandurra, S., and A. Di Luggo. “BSDD TO DOCUMENT STATE OF PRESERVATION OF ARCHITECTURAL HERITAGE IN OPEN-HBIM SYSTEMS.” the International Archives of the Photogrammetry, Remote Sensing and Spatial Information Sciences/International Archives of the Photogrammetry, Remote Sensing and Spatial Information Sciences XLVIII-M-2–2023 (June 26, 2023): 1427–34. https://doi.org/10.5194/isprs-archives-xlviii-m-2-2023-1427-2023.

Secultfor. “Parecer Técnico N. 260/2015 da Coordenação de Patrimônio Histórico e Cultural da Secretaria de Municipal de Cultura de Fortaleza: 1938/2015.

Sun, Z., and Y. K. Cao. “Data Processing Workflows From Low-cost Digital Survey to Various Applications: Three Case Studies of Chinese Historic Architecture.” *the International Archives of the Photogrammetry, Remote Sensing and Spatial Information Sciences/International Archives of the Photogrammetry, Remote Sensing and Spatial Information Sciences* XL-5/W7 (August 13, 2015): 409–16. https://doi.org/10.5194/isprsarchives-xl-5-w7-409-2015.

Vieira, Mylene M., Gilmário Ribeiro, Renan Paulo, Maycon Bessa, Francisca R. Sousa, Eugênio Moreira, and Esequiel Mesquita. “Strategy for HBIM Implementation Using High-resolution 3D Architectural Documentation Based on Laser Scanning and Photogrammetry of the José De Alencar Theatre.” *Digital Applications in Archaeology and Cultural Heritage* 30 (August 5, 2023): e00287. https://doi.org/10.1016/j.daach.2023.e00287.

Xavier, Edemar Dias, Junior, Adriane Borda, Mauren Aurich, and Ariela Da Silva Torres. “Técnicas Visuoespaciais Para a Detecção De Manifestações Patológicas Em Fachadas Argamassadas.” *Research Society and Development* 11, no. 5 (April 17, 2022): e59711528810. https://doi.org/10.33448/rsd-v11i5.28810.

Cinpar 2026
XXII International Conference on Building Pathology and Constructions Repair
15th to 17th July 2026 - Lisboa, Portugal

Digital documentation of cultural heritage based on high-resolution scanning

Oscar de Queiroz Holanda NETO[1], Bruna Higino VALE[2], Francisco Carlos da Cunha SANTANA[3] and Esequiel MESQUITA[4]

[1] Universidade Federal do Ceará, Fortaleza, Brazil, oscardequeiroz@alu.ufc.br1
[2] Universidade Federal do Ceará, Fortaleza, Brazil, brunahigino@alu.ufc.br2
[3] Universidade Federal do Ceará, Fortaleza, Brazil, franciscosantana@alu.ufc.br3
[4] Universidade Federal do Ceará, Fortaleza, Brazil, emesquita@ufc.br4

Abstract: The use of digitization technologies has become a highly valuable tool in the documentation of built heritage. Equipment such as drones and laser scanners enables more accurate building mapping, facilitating the creation of HBIM (Heritage/Historic Building Information Modeling) models. This paper aims to detail the 3D modeling process for the Dona Bela building, a modernist structure of historical significance in the city of Fortaleza, Brazil. For this process, digital surveys were conducted using photogrammetry and thermography with drones, as well as traditional surveying methods. As a result, a point-cloud-based 3D model was generated that presents in detail the characteristic elements of the façades, as well as their pathologies. Thus, the effectiveness of these technologies in the documentation and preservation of built heritage is evident.

Keywords: Point-cloud, HBIM, Digital documentation, Digitization, Built heritage.

1. Introduction

Historical heritage is fundamental to the culture and identity of a people. For both tangible and intangible heritage, the documentation of the asset is essential, as it is through such documentation that we comprehend the history and relevance of the heritage, and enable actions for its preservation and protection (Cardellicchio et al., 2024). However, we emphasize here the importance of documenting built heritage, which encompasses construction methods, structural and architectural elements, and condition assessment reports, among other aspects. Evidently, the process of acquiring and preparing this documentation requires a high degree of precision and data processing (Ribeiro et al., 2025). In the case of in loco data acquisition, such as the technical surveying of the building or the preparation of a report on its state of conservation, the acquisition process becomes a challenge. The methodology of acquisition using tape measures, sketches, and photographs, although still common, entails inaccuracies and is more time-consuming. In cases involving the detailing of façades, balconies, and roofs, access is often unfeasible, and it also poses risks to the professional in charge, especially when dealing with historical buildings, which frequently exhibit an advanced state of deterioration (Fidelis et al., 2024).

Given this fact, the use of digitization equipment, such as laser scanners and photogrammetry, greatly assists the data acquisition process, serving as an efficient and safe alternative with greater informational richness. Through these technologies, it is possible to produce three-dimensional models with a high degree of fidelity (Rubens et al., 2023) that, in addition to serving as heritage documentation (Merzhiievska et al., 2026), also allow for the management and maintenance of the building (Aroquipa et al., 2025), as well as serving as an instrument for heritage education, whether through its use in educational institutions or by making digital models available on the internet, enabling access to both researchers and the general public worldwide (Kilis et al., 2025).

It is important to emphasize that when it comes to the digitization of built heritage, the management of this data constitutes a multidisciplinary field that requires the participation of specialists from the areas of architecture, engineering, conservation and restoration, computer science, and many others (Vieira et al.,

2023). Furthermore, for a multidisciplinary team to manage this quantity of data throughout the entire life cycle of the heritage asset, the use of an integrated information system that allows for interoperability between all its agents is necessary (Allegra et al., 2020; Apollonio et al., 2019). Information modeling software acts in this space by providing the necessary instrumental and methodological subsidies for this demand (Dionizio and Dezen-Kempter, 2025).

First introduced by Murphy et al. (2013), Heritage/Historic Building Information Modelling (HBIM) consists of an approach for constructing parametric models in a BIM (Building Information Modelling) environment for existing buildings, based on historical data and captures via photogrammetry and laser scanning. Since then, much has been contributed to the field, whether in the proposal of protocols (Ribeiro et al., 2025), in the definition of methodologies (Rubens et al., 2023), or in the digitization of buildings of historical relevance (Fidelis et al., 2023), which has facilitated the establishment of the HBIM approach as a current practice in the documentation, preservation, management, and accessibility of built heritage.

Based on this, the objective of this paper is to present the high-resolution aerial photogrammetry and thermography acquisition process for the production of a three-dimensional model of the Dona Bela building, a historical construction located in the center of Fortaleza-CE. With the use of a drone and the RealityScan® tool, the captured images were converted into a three-dimensional model and a point cloud of the building.

2. Dona Bela Building — historical and architectural details

Erected in the second half of the 1950s, the Dona Bela building is the first in the city of Fortaleza intended exclusively for residential purposes (Cavalcante, 2021). Located at Rua Coronel Ferraz, nos. 26-76, in the *Centro* neighborhood, it features rounded-corner balconies that surround its façades and extend over the sidewalks in composition with its generally straight corners. Such characteristics, combined with marquee-type slabs, monochromatic finishes, and wooden shutter frames, evidence the stylistic appreciation of the developments by Imobiliária Pedro Philomeno, responsible not only for the Dona Bela Building but for other emblematic architectural projects in Fortaleza: the Lord Hotel (1956), also located in the city center, and the Iracema Plaza Hotel (1951), commonly known as the Edifício São Pedro, which achieved the distinction of being the first luxury hotel built on the Fortaleza coastline (Gomes, 1988). All three developments present architectural characteristics of a clear modernist tendency — something considered innovative at the time, the style of which only officially began in the capital in the late 1950s[1].

Designed as 3 apartment blocks, each with 3 floors, with 2 apartments per floor, totaling 18 apartment units[2], the building — which can be seen in Figure 1 — had its provisional heritage listing opened on June 30, 2016 (Secultfor, 2016). According to the technical opinion issued on November 18, 2015, the architectural relevance of the Dona Bela building and its sister buildings "represents visionary attitudes in the city" (Secultfor, 2015). Beyond the architectural level, the building also plays an important role in the city's cultural identity, as it hosts various cultural projects, such as *Casa Sônica*—a space dedicated to musical realization and a laboratory for sound performances (Secult, 2025)—and the *Salão das Ilusões*, which has inhabited the space for 16 years and is an important catalyst for cultural projects in the areas of visual arts, fashion, music, scenography, and gastronomy (O Povo, 2018). Such historical relevance reinforces the importance of its preservation, both physically and documentally.

[1] It is only in the late 1950s that the first moment of modern architecture in Fortaleza emerges, when newly graduated architects from Ceará, such as José Liberal de Castro, José Neuson Braga, Ivan Brito, and others, return to the capital and bring debates about the trend practiced in Rio and Recife (Paiva and Diógenes, 2017).

[2] Over the years, the morphology and use of the spaces have been altered, so that, currently, the upper floor, originally intended for laundry rooms, has been re-adapted to accommodate new apartment units, just as some lower apartments have undergone reconfigurations.



Figure 1 – Dona Bela Building. Source: Authors, 2025.

Today, ten years after the issuance of the provisional heritage listing, the building still remains without definitive listing, suffering from a process of progressive deterioration and undergoing small renovations exclusively at the initiative of the tenants, which reinforces the importance of urgent heritage safeguarding actions.

Given this, due to the *Edital de Fomento ao Patrimônio Cultural Edificado*, carried out by the *Secretaria Municipal da Cultura de Fortaleza* (Secultfor), with funding from the *Política Nacional Aldir Blanc de Fomento à Cultura* (PNAB), a new survey of the building was carried out to prepare a technical report on the current state of conservation of the building, for the purpose of forwarding to the definitive heritage listing registration of the building. The present work is part of the actions of this project.

3. Materials and methods

The digitization process of the Dona Bela building follows the HBIM protocol (Figure 2) and ranges from the gathering of technical documentation and historical information of the building to the equipment and tools to be used and the level of detail necessary for the documentation (Rubens et al., 2023). This complete protocol is divided into four stages: planning, acquisition, processing, and BIM modeling. Since the scope of the present work was to collect data on the pathologies of the roof and upper floors, as well as to produce a low-density point cloud, only for the purposes of complementation and compatibility with the technical survey of the internal areas of the building, this work will be limited to the first three stages of the protocol, which will result in the construction of the building's point cloud.

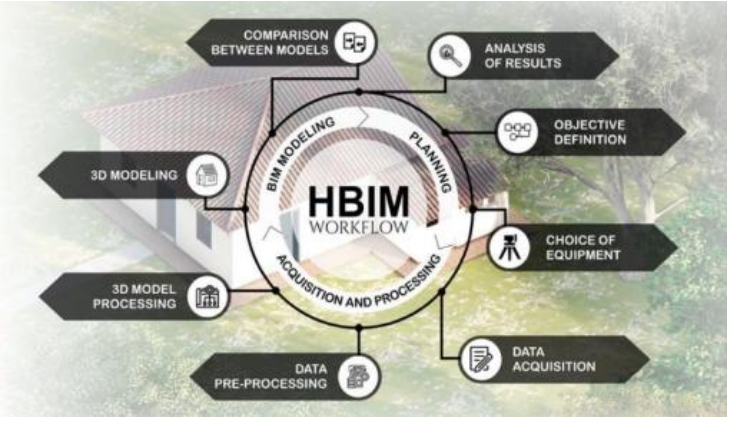


Figure 2 – HBIM procedural workflow. Source: Rubens *et al.*, 2023.

3.1 Planning

Before starting the building data acquisition, it is necessary to conduct a preliminary study based on the construction's historical and archival documentation. This stage is fundamental for us to know the past of the building and understand its present state (Bruno and Roncella, 2018). Consequently, it is necessary to establish some definitions: what is the objective of the model and what are the acquisition equipment. These prior definitions are important because the product to be generated and the equipment to be used must be aligned with the purpose of the model. Along with this, it is also necessary to define the mode of acquisition, the level of precision, and the form of data storage. For the case of the Dona Bela building survey, documentary research was carried out in the literature, newspaper reports, and official documents that present information regarding the history of the building, original plans, and construction methods, in addition to reports from tenants about changes made over the years. Such information was valuable for us to have a general scope of the construction and thereby guide our approach regarding our objective.

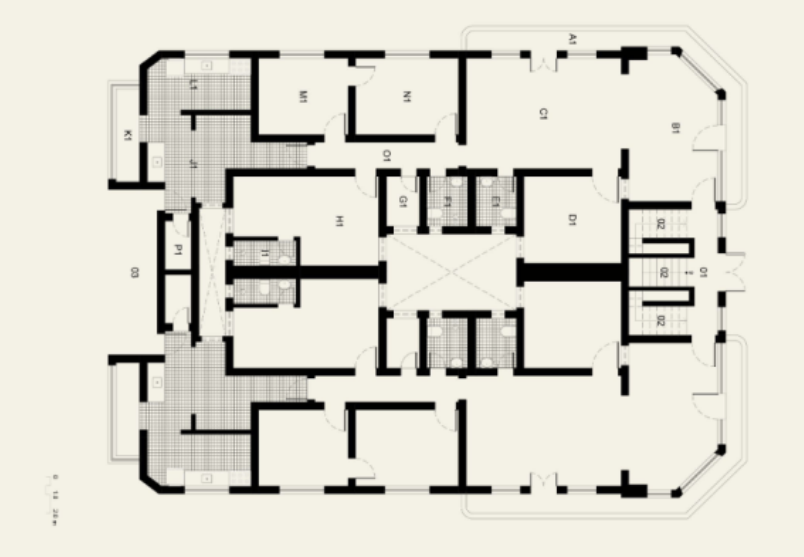


Figure 2 – Typical floor plan. Source: Cavalcante, 2021.

3.2 Data acquisition and processing

Following the planning stage, the data acquisition and processing phase begins. This moment is subdivided into three instances: capture, pre-processing, and point cloud processing. In the capture phase, it is necessary to analyze the building's surroundings and identify which elements may cause visual obstruction to the equipment. Conditions such as the weather, vegetation, and public utility wiring can compromise or even make the capture unfeasible. In the survey in question, the presence of vegetation and public utility wiring on the building's front façade was observed, which compromised captures at the first and second-floor levels, conditioning the flight to favor top and upper-floor captures. It is important to emphasize that, as it is a public area and a residential building owned by third parties, it is necessary to request flight permission. As this survey comprises an action that integrates a public notice, such requests, both from the city government and the tenants, were already granted in advance.

The equipment used was a DJI Mavic 3T Thermal drone model (Figure 3), which performed an overflight over the roof and in front of the façades of the 3 apartment blocks.



Figure 3 – DJI Mavic 3T Thermal. Source: Authors, 2025

Equipped with three high-resolution cameras—a 48MP wide lens with 1/2-inch CMOS, a 12MP telephoto lens with 1/2-inch CMOS and hybrid zoom capacity of up to 56x, and a thermal lens that provides data on point and area temperature, high-temperature alerts, color palettes, and isotherms. 204 images of 4000 x 3000 pixels (Figure 4) and 204 thermal images of 640 x 512 pixels (Figure 5) were captured, with a 2-second interval between each capture. This interval between captures is important to ensure corresponding texture and volumetric elements between images, enabling overlap, a factor necessary for producing a detailed 3D model of the building. Only one day was necessary for the acquisition of the aerial photogrammetry of the building.



Figure 4 – Façade and rooftop of Dona Bela building captured with DJI Mavic 3T high res lens. Source: Authors, 2025.

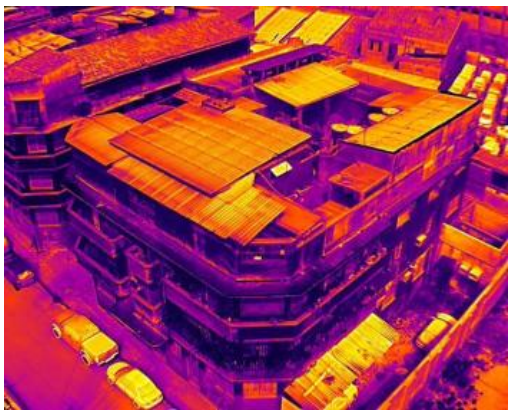


Figure 5 – Façade and rooftop of Dona Bela building captured with DJI Mavic 3T termal lens. Source: Authors, 2025.

The pre-processing phase consists of the preparation of the three-dimensional model. The software used was RealityScan®, which allows aligning and converting the photogrammetry of the building into a 3D model mesh (Figure 6) and a point cloud (Figure 7). The intent of this 3D model is to document the pathologies of the roof and façades of the building, as well as those of its architectural elements, while the point cloud provides the volumetric data of the building.

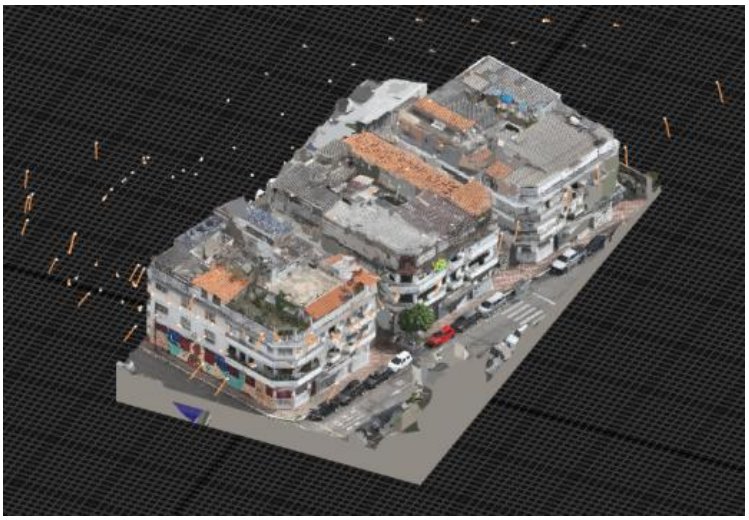


Figure 6 – 3D Model of Dona Bela building on RealityScan®. Source: Authors, 2025.



Figure 7 – Point cloud-based model on RealityScan®. Source: Authors, 2025.

4. Results and discussions

The photogrammetry performed with the drone allowed for the generation of a three-dimensional model of the building with practicality, efficiency, and safety, making it possible to represent both the architectural elements and the pathologies present on the façades and roof, both with a high level of detail, which is impractical through traditional survey techniques. The details of the façade and the pathologies can be observed in Figure 8.



Figure 8 – Façade details and pathologies on 3D model. Source: Authors, 2025.

The aerial thermography captured allowed us to analyze the heat distribution in the building. When this type of mapping is performed, the temperature difference can be visualized in the images, allowing for the identification of infiltrations without the use of invasive methods, an intervention not recommended in historical buildings (Cruz et al., 2024). Such analysis enables the immediate conclusion of some causes of pathologies. For example, in Figure 9, we can identify the region of lower temperature (in violet), which indicates the occurrence of infiltration as the cause of the pathology, as indicated in Figure 10.

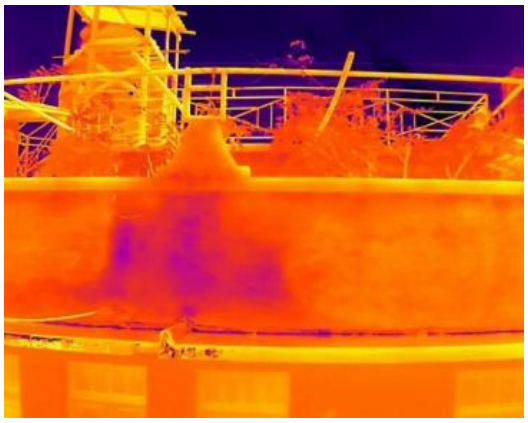


Figure 9 – Humidity detected with thermal camera. Source: Authors, 2025.



Figure 10 – Pathology related to detected humidity. Source: Authors, 2025.

The level of detail obtained with the 3D model allowed for the construction of a point cloud with 536,725 points. An analysis carried out in the RealityScan® software showed that the quality level of the top captures was superior compared to the captures perpendicular to the ground, especially of the façades at the first and second-floor levels, which corroborates the flight plan carried out by the drone. However, the quality level obtained meets the expectations of the work, since the model complements the data collected by the traditional survey method. The result of the analysis can be seen in Figures 11 and 12.

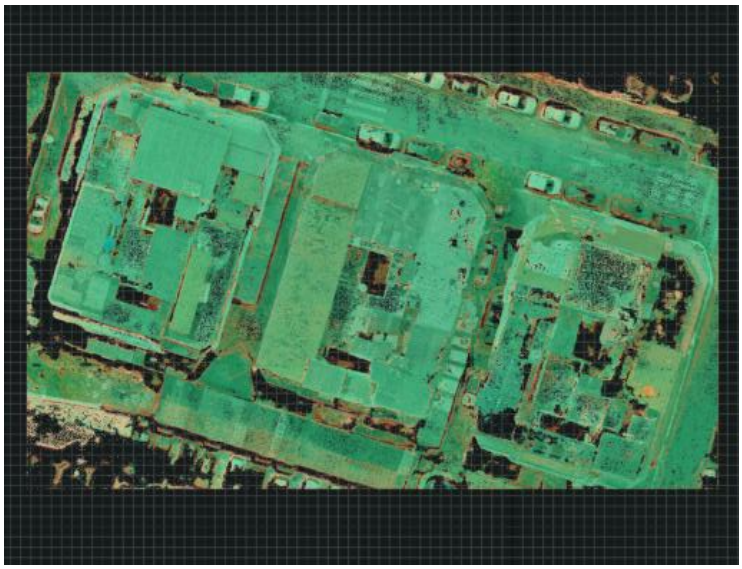


Figure 11 – Mesh quality analysis of top view captures. Source: Authors, 2025.

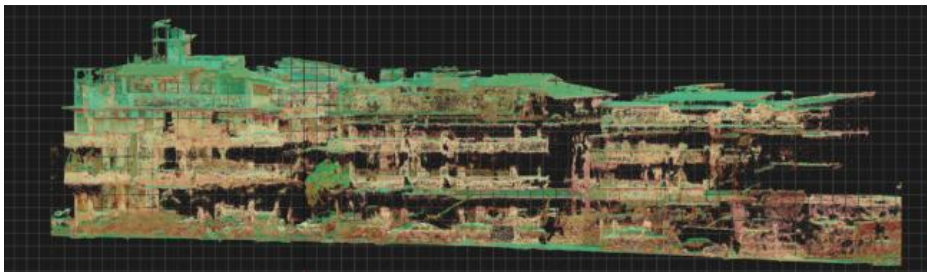


Figure 12 – Mesh quality analysis of side view captures. Source: Authors, 2025.

All data collected in this survey, especially the model built through aerial photogrammetry, are vital for the creation of an HBIM model of the building. Such data allow for the construction of parametric families and the mapping of the building's structural and pathological elements, which enables not only the updating of heritage documentation but also its preservation and management and re-adequation actions of the property in more efficient and precise ways.

5. Conclusions

Through the study conducted on the Dona Bela Building, it was verified that the use of aerial photogrammetry and thermography proved to be an efficient and promising method for surveying built heritage. Therefore, it can be concluded that:

- Aerial photogrammetry provided dimensional, aesthetic, and pathological manifestation information necessary for the construction of an adequate 3D model of the building, serving as both a source of geometric data and documentation of the built heritage;
- Thermography provided conclusive data on the heat distribution in the building, enabling a quick and efficient diagnosis of pathologies associated with humidity, without the need for invasive interventions in the structure, ensuring its integrity.
- The point-cloud-based model reached the expected quality level, providing reliable geometric data for the preparation of a BIM model.
- The study showed that the use of digitization technologies is a good ally for mapping pathologies and technical surveying of historical buildings, providing precise data efficiently and safely.
- Situations in which it is not possible to carry out a complete flight plan around the building, due to visual obstructions, impose the use of complementary capture techniques to improve the level of

detail of the model, which can be terrestrial photogrammetry or laser scanner survey. Such approaches need to be evaluated during the planning stage.

6. References

Allegra, V., F. Di Paola, M. Lo Brutto and C. Vinci. 2020. "Scan-to-BIM for the management of heritage buildings: the case study of the castle of Maredolce (Palermo, Italy)." The International Archives of the Photogrammetry, Remote Sensing and Spatial Information Sciences 43: 1355–1362. https://doi.org/10.5194/isprs-archives-XLIII-B2-2020-1355-2020.

Apollonio, Fabrizio. I., Gaiani, Marco and Bertacchi, Silvia. 2019. "Managing cultural heritage with integrated services platform." The International Archives of the Photogrammetry, Remote Sensing and Spatial Information Sciences 42: 91–98. https://doi.org/10.5194/isprs-archives-XLII-2-W11-91-2019.

Aroquipa, Hector, Alvaro Hurtado, and Christiam Angel. 2025. "Methodological framework for integrating structural health monitoring and digital-twin models for seismic assessment of heritage buildings: Case study of Basilica Maria Auxiliadora, Lima, Peru." Structures. Vol. 80. Elsevier. https://doi.org/10.1016/j.istruc.2025.110115.

Bruno, Nazarena, and Riccardo Roncella. 2018. "A restoration oriented HBIM system for cultural heritage documentation: The case study of Parma Cathedral." The International Archives of the Photogrammetry, Remote Sensing and Spatial Information Sciences 42: 171-178. https://doi.org/10.5194/isprs-archives-XLII-2-171-2018.

Cardellicchio, Luciano, Paolo Stracchi, and Anastasia Globa. 2024. "Digital heritage construction: Testing the heritage value of construction documentation and building processes through Virtual Reality." Frontiers of Architectural Research 13.5: 1039-1055.

Cavalcante, Márcia Gadelha. 2021. “Edifícios de apartamentos em Fortaleza: universalidades e singularidades”. Impresa Universitária.

Cruz, Yago, et al. 2024. "Case study: Casa da Câmara de Guimarães. HBIM modeling from non-destructive techniques." *Procedia Structural Integrity* 64 (2024): 335-342. https://doi.org/10.1016/j.prostr.2024.09.259.

Dionizio, Rafael Fernandes, and Eloisa Dezen-Kempter. 2025. "HBIM-HGIS for a Multi-Level Knowledge-Based Approach." Digital Applications in Archaeology and Cultural Heritage: e00461. https://doi.org/10.1016/j.daach.2025.e00461.

Fideles, Bruna Tayna Macedo, et al. 2024. "Levantamentos digitais como suporte à inspeção em edificações: uma aplicação no Acquário Ceará." CONCRETO & Construções-ISSN 1809-7197 114.114.

Fideles, Bruna Tayna Macedo, et al. 2023. "Assessment of metric accuracy on data acquisition using point cloud: an application to the José de Alencar Theater." Journal of Building Pathology and Rehabilitation 8.1: 55. https://doi.org/10.1007/s41024-023-00300-7.

Gomes, F. A. Philomeno. 1988. “Centenário de Nascimento de Pedro Philomeno Ferreira Gomes (1888-1988)”.

Kilis, Nikolaos, et al. 2025 "AI tools for generating Digital Heritage Twins enhancing storytelling in educational games." Digital Applications in Archaeology and Cultural Heritage: e00451. https://doi.org/10.1016/j.daach.2025.e00451.

Merzhiievska, Natalia, et al. 2026. "A Novel Educational Model for Architectural Heritage Preservation in Ukraine: Digital Tools amidst Wartime Challenges." Digital Applications in Archaeology and Cultural Heritage: e00507. https://doi.org/10.1016/j.daach.2026.e00507.

Murphy, Maurice, Eugene McGovern, and Sara Pavia. 2013. "Historic Building Information Modelling–Adding intelligence to laser and image based surveys of European classical architecture." /SPRS journal of photogrammetry and remote sensing 76: 89-102. https://doi.org/10.1016/j.isprsjprs.2012.11.006.

Paiva, Ricardo Alexandre, and Beatriz Helena Nogueira Diógenes. 2017. "Dinâmica imobiliária e preservação da arquitetura moderna em Fortaleza: o passado, o presente e o futuro em questão." Seminário Docomomo Brasil: Anais 12.

Ribeiro, Gilmário C., et al. 2025. "An Integrated HBIM Protocol for Digital Documentation, Management, and Reconstruction of Historic Heritage Structures." Journal of Building Engineering: 114920. https://doi.org/10.1016/j.jobe.2025.114920.

Rubes, Tallis, et al. 2023. " Digitalization based on high-resolution scanning and HBIM tools for damage assessment of the José de Alencar house." Journal of Building Pathology and Rehabilitation 8.1: 30. https://doi.org/10.1007/s41024-023-00275-5

Rubens, Tallis, et al. 2023. "Digitization of historical heritage: Nossa Senhora do Rosário Church, Aracati-CE." Journal of Building Pathology and Rehabilitation 8.2: 71. https://doi.org/10.1007/s41024-023-00320-3.

Viana, Carlos Negreiros. 2008. “A vida empresarial de Pedro Philomeno: um longo e fundamental capítulo da história industrial do Ceará”. *R*evista do Instituto do Ceará, 214.

Vieira, Mylene M., et al. 2023. "Strategy for HBIM implementation using high-resolution 3D architectural documentation based on laser scanning and photogrammetry of the José de Alencar theatre." Digital Applications in Archaeology and Cultural Heritage 30: e00287.

Secult, " Apoiado pela Secult, Projeto Mina realiza pesquisa e produção na música e da arte sonora feita por mulheres", Secretaria Estadual da Cultura do Ceará, January 9, 2025, https://www.secult.ce.gov.br/2025/01/09/apoiado-pela-secult-projeto-mina-realiza-pesquisa-e-producao-na-musica-e-da-arte-sonora-feita-por-mulheres/.

Secultfor. 2015. “Parecer Técnico N. 260/2015 da Coordenação de Patrimônio Histórico e Cultural da Secretaria Municipal de Cultura de Fortaleza”: 1938/2015.

Secultfor. 2016. “Processo de Tombamento do Imóvel Conjunto Dona Bela”. Portaria N° 38/2016. https://cultura.fortaleza.ce.gov.br/images/Portaria_38-2016.pdf.

O Povo, “Salão das Ilusões”, Jornal O Povo, September 29, 2018, https://mais.opovo.com.br/jornal/vidaearte/2018/10/o-som-da-resistencia.html.

Cinpar 2026
XXII International Conference on Building Pathology and Constructions Repair
15th to 17th July 2026 - Lisboa, Portugal

Point Clouds Beyond BIM: Aesthetic Composition and Montage Techniques for Immersive Room Films in Heritage Education.

Diego RICCA[1], Marcelo AGUIAR[2], Lucas SOUZA[3] , Eugenio MOREIRA[4], Esequiel MESQUITA[5], **Vitória FONTENELE**[6]

[1] Laboratory of Digital Experience - Federal University of Ceara, Brazil, Diegoricca@daud.ufc.br
[2] State University of Campinas, Brazil, Marceloaguiar.arq@gmail.com
[3] Laboratory of Digital Experience - Federal University of Ceara, Brazil, lucasbaptista@me.com
[4] Laboratory of Digital Experience - Federal University of Ceara, Brazil, eugeniomoreira@iaud.ufc.br
[5] Laboratory of Digital Experience - Federal University of Ceara, Brazil, emesquita@ufc.br
[6] Laboratory of Digital Experience - Federal University of Ceara, Brazil, vitorianfontenele@arquitetura.ufc.br

Abstract: Currently, the digitalization of architectural heritage through photogrammetry and 3D scanning has established itself as a fundamental strategy for preservation and documentation, with the point cloud of buildings as its central product. Although frequently used as a reference for Building Information Modeling (BIM), point clouds also possess aesthetic and informative potential, allowing them to be manipulated as visual material in immersive exhibitions focused on heritage education. In this sense, this work systematizes production techniques and design decisions for an immersive experience based on point clouds within a museum context. The research reports on the development of the exhibition “Do Ponto ao Patrimônio” (From Point to Heritage), presented at the Museum of Image and Sound of Ceará (MIS-CE) in an immersive environment known as “Tear da Experiência” (Experience Loom), as part of the Chief Scientist Program for Culture of Ceará, held in 2024 in a room equipped with a Computer Assisted Virtual Environment (CAVE) system. The main objective is to evaluate the effectiveness of this immersive approach in fostering heritage awareness. The methodology involved an empirical assessment with 14 visitors, triangulating semi-structured interviews with Likert-scale questionnaires. Point clouds were processed and stylized in Blender, with an emphasis on procedures via Geometry Nodes for composing camera movements, density and opacity variations, dissolution and distortion effects, and the construction of visual rhythms consistent with the narrative. Results indicate that the immersive experience acts as a mediator of memory, facilitating affective engagement and critical awareness regarding heritage loss, particularly in the case of the demolished São Pedro Building. Finally, the set of language and performance strategies that sustained the readability and artistic character of the CAVE experience are discussed, pointing out limitations and recommendations for future exhibition designs involving point clouds.

Keywords: PointCloud, Heritage, VR, CAVE, Museum.

1. Introduction

As cities expand, the conflict between urban growth and the preservation of cultural heritage becomes a complex management challenge. Policies fail to protect architectural heritage and its historic buildings from wars, uncontrolled tourism, and unregulated urbanization (UNESCO, WHC. World Heritage in Danger, 2021), a scenario that often results in demolitions and the disfigurement of monuments, especially in the southern hemisphere. In this context, the adoption of participatory approaches — which recognize the local community as a central agent in protection policies — becomes essential. Engaging and raising public awareness through formal and non-formal educational experiences (FRULLO; Mattone, 2024) can serve as a tool to strengthen the sense of belonging and the urgency regarding the preservation of built heritage.

The use of museums as spaces that promote heritage education is widely advocated by Van Boxtel, Grever, and Klein (2016), since these institutions offer objects and narratives capable of connecting the public to their own history. Recently, the digitization of architectural heritage through photogrammetry and 3D laser

scanning has become a fundamental strategy for preservation and technical documentation (Penjor et al., 2024). The main product of this process is the "point cloud": a dense set of three-dimensional coordinates that captures the geometry and appearance of a structure with high precision.

Although point clouds are often used only as a reference for modeling in Heritage Building Information Modeling (HBIM), they have an intrinsic aesthetic and informative potential, and can be manipulated as primary visual material in immersive exhibitions, functioning as an alternative to involve technological advances and heritage education in the same context. Gabellone (2023) presents the Virtual Neapolis project, which aims to promote heritage sites and the history of the city of Naples through a Virtual Reality (VR) experience. To build the tour, tools such as photogrammetry (which can generate a point cloud and a mesh), 3D modeling, virtual restoration, among others, were used.

In this sense, this work aims to present the production techniques and design decisions involved in the development of an immersive experience based on point clouds. The article reports on the development of the exhibition "From Point to Heritage," presented at the Museum of Image and Sound of Ceará (MIS-CE) in 2024. To explore the exhibition as a tool for public awareness, this study conducted an empirical evaluation with 14 participants. The methodology adopted a mixed-methods approach, triangulating semi-structured interviews with a Likert-scale questionnaire. This phase indicates how immersion influences public perception of heritage and willingness to engage in preservation.

From a scientific point of view, the article contributes in four fronts: (1) it systematizes a workflow for transposing point clouds into immersive audiovisual narratives; (2) it discusses point clouds not only as a technical support for modeling, but also as a visual, aesthetic, and educational language; (3) it proposes an interpretation of the experience based on the relationships between heritage mediation, narrative, and attention; and (4) it indicates empirical insights regarding the potential of immersive technologies in promoting heritage awareness.

2. Theoretical Framework: The Aesthetics of Point Clouds and Heritage Education

Three-dimensional documentation through laser scanning and photogrammetry is often reduced to its metric utility in engineering and architecture, traditionally being used as a basis for digital modeling in the Scan-to-BIM and HBIM workflows. In this field, the point cloud serves as a support for geometric recording, documentation, analysis, and modeling of historical buildings, although important challenges persist regarding interoperability, process automation, and the translation of complex geometries, deformations, and irregularities of the built heritage into consistent parametric models (Vieira et al., 2023; Cotella, 2023; Penjor et al., 2024).

However, beyond this technical use, the point cloud can also be understood as an expressive medium, endowed with aesthetic, narrative, and educational potential. Recent studies show that its discontinuous, translucent, and spectral visuality can be explored as its own visual language, both in artistic practices and in immersive applications aimed at heritage mediation. In this sense, the point cloud ceases to operate merely as an intermediate step in modeling and begins to be used directly as a rendering asset, interactive storytelling, and museum experience, favoring sensitive ways of approaching landscapes, buildings, and processes of historical transformation (Gabellone, 2023; Ivsic, McCormack, and Dziekan, 2023; Lei, Fiorillo, and Fassi, 2024; de Kleijn et al., 2024).

In the debate on motivation and learning in museums, Csikszentmihalyi and Hermanson (1995) offer a central contribution to this research by understanding the museum experience not as a simple transmission of information, but as an expanded form of learning, involving cognitive, sensory, and emotional dimensions. Starting from the idea that attention is a scarce and contested resource, the authors argue that the visitor's experience depends on the environment's ability to mobilize curiosity, interest, and engagement through qualities such as novelty, surprise, complexity, and ambiguity. These elements function as stimuli capable of attracting and sustaining the subject's psychic energy, favoring exploratory behaviors and paving the way for states of intrinsic motivation. In this context, the concept of flow becomes especially relevant, as it designates a condition of deeper engagement, in which there is a balance between the challenges proposed by the experience and the visitor's willingness to face them.

This understanding directly dialogues with the perspective adopted in this research and with the **Experience Loom** model, developed by Ricca (2023), in which design is conceived from the articulation between different attentional layers and their transitions. In the thesis, the author proposes the so-called attention-based design as a means of structuring experiences capable of guiding the subject from more peripheral and automatic levels to more focused and reflective levels, with everyday education as a horizon of mediation. From this perspective, the experience depends not only on the content presented, but on the way stimuli, rhythms, forms, and relationships of interest are organized over time, constituting a true narrative of attention. This formulation is particularly fruitful for the field of heritage education, as it allows us to understand the immersive experience as a mediation that not only informs about heritage, but also seeks to capture, guide, and sustain the public's engagement with its memory, its symbolic dimension, and its cultural permanence.

From this perspective, the visitor's brain is prompted to fill in the "gaps" between the bright points of the cloud, making a cognitive and perceptual effort that can favor states of greater engagement with the historical object. The point cloud then ceases to operate merely as a technical record and begins to function as a visual and narrative language, capable of articulating estrangement, curiosity, contemplation, and reflection. It is within this framework that the exhibition From Point to Heritage is situated, a work of the subproject "Technology and Innovation of the Cultural Heritage of Ceará," linked to the Chief Scientist of Culture Program. Conceived as an immersive audiovisual heritage education experience, the exhibition uses the deconstruction of the point cloud to guide the viewer on a journey among buildings that are part of the history of Ceará. The following details the methodological procedures and technical choices that enabled the transposition of the point cloud into the immersive environment.

3. Methodology

This work is characterized as applied research, with a qualitative approach, with exploratory and descriptive objectives, developed through a case study of the immersive exhibition From Point to Heritage (Gil, 2002; Creswell and Poth, 2018; Yin, 2018). The investigation systematizes the technical workflow and design decisions involved in transforming point clouds into an audiovisual exhibition narrative, encompassing the stages of data collection, processing, optimization, and animation.

In the field of design, the study approaches the Research through Design perspective, since the conception and materialization of the exhibition artifact also operate as a means of producing knowledge about processes, visual strategies, and heritage mediation (Frayling, 1994; Zimmerman, Forlizzi, and Evenson, 2007). From a practical point of view, the transformation of point clouds into a fluid exhibition narrative requires interaction between professionals from various fields: architecture, engineering, design, visual arts, and digital media systems. As analytical corpus, the script, storyboard, and decisions regarding capture, processing, deciphering, animation, and audiovisual editing of the exhibition were considered, understood as design evidence of the case study. The analysis focused on identifying how these technical and narrative decisions contributed to: (a) the visual legibility of the point clouds, (b) the construction of an immersive environment, and (c) heritage mediation through strategies of attention, contemplation, and reflection. Therefore, the workflow was divided into four phases, presented below.

3.1 Building Survey Process:

The digitization encompassed eight emblematic buildings of Ceará's heritage, with different typologies, construction materials, and states of conservation, namely the José de Alencar Theater, the Pinacoteca do Ceará, the MIS-CE, the School of Arts and Crafts, the São Pedro Building, the São Luiz Cinema-Theater, the Church of Our Lady of the Rosary of Black Men, and the Parish Church of Our Lady of the Rosary. Of the eight buildings mentioned above, the first six are located in Fortaleza/CE, while the last two are in the city of Aracati/CE. The survey adopted a hybrid approach so that the buildings could be scanned with the greatest possible coverage:

- **Terrestrial Laser Scanner (Leica BLK 360)**: Responsible for capturing external terrestrial and internal environments of the buildings, scanning the geometry through point clouds and the colors through panoramic photographs.

- **Aerial Photogrammetry (DJI Phantom 4)**: Used to record roofs, domes, and upper facades, completing the building's volumetry through a point cloud generated from digital photographs, the base files for performing photogrammetry.

In addition, some strategies were used to maximize information capture and reduce noise in the point clouds. One of the main strategies for a good survey is to have a well-defined planning phase, which is fundamental when considering the size of these buildings, which increases the number of captures required. By aligning schedules and agendas, it is possible to avoid rework by reducing the circulation of people and capture noise generated by sunlight (Vieira et al., 2023). However, even with good planning, some noise was still generated in the captures, such as people and objects, which were used as elements for the construction of the environment when interacting with the lights used in Blender.

3.2 Point Cloud Processing

After scanning the buildings, the data is extracted from the aforementioned tools and processed on computers. The laser scanner captures are processed in the Leica Cyclone Register 360 software, while the drone photographs undergo data analysis in the Reality Capture operating system, shown, respectively, in Figure 1 and Figure 2. After individual processing of the obtained data, CloudCompare is used to combine the two point clouds, resulting in the complete building represented by millions of points.

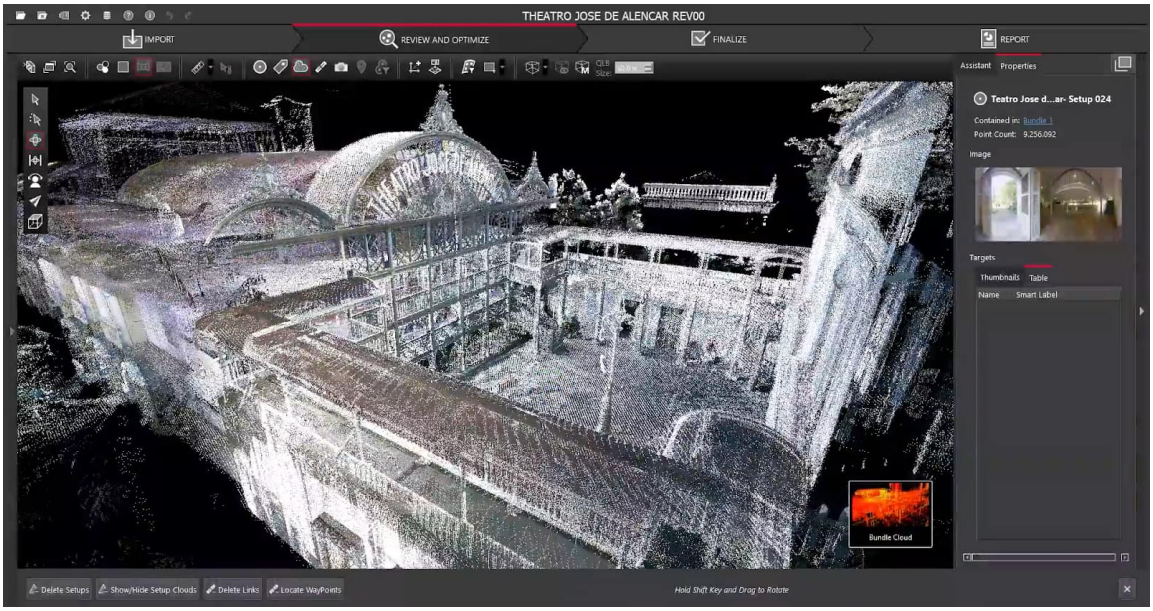


Figure 1 – Processing of the José de Alencar Theater in Leica Cyclone Register 360

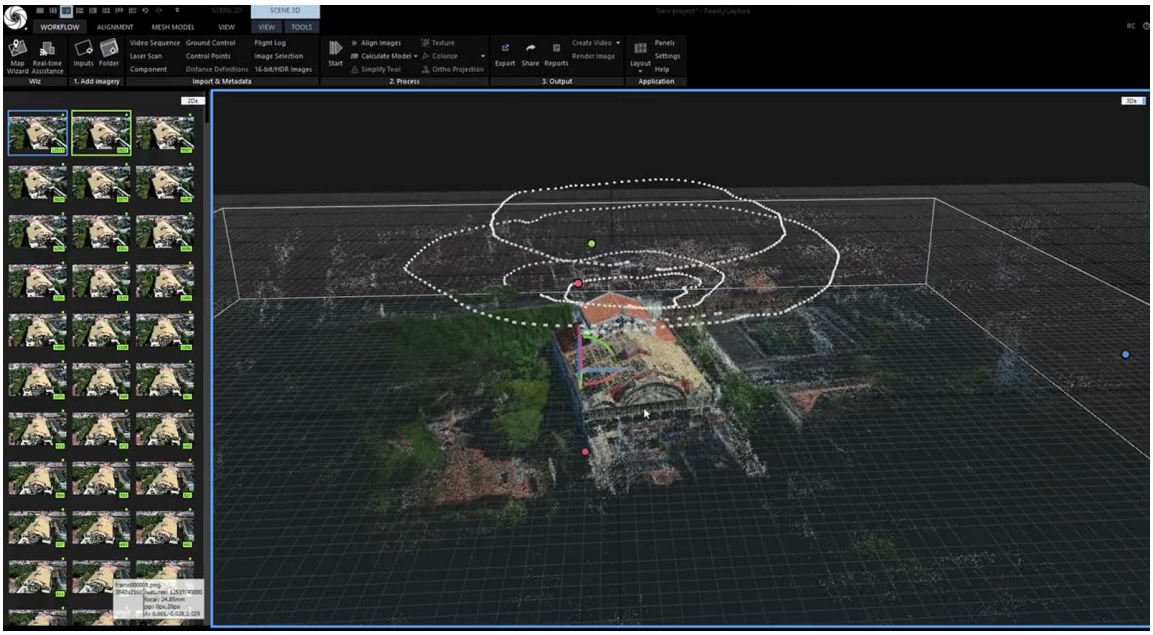


Figure 2 – Processing of the José de Alencar Theater in Reality Capture

3.3 Decimation and Optimization Strategies

To achieve the fluidity required for an immersive film, the original point clouds, containing billions of coordinates, needed to be drastically reduced while maintaining the legibility of the structural form. The Spatial Subsampling algorithm in the CloudCompare software was used. Unlike random decimation, which could destroy edges and fine architectural details, spatial subsampling ensures a constant minimum distance between points (e.g., 1 point every 5 millimeters), eliminating noise and unnecessary overlap, reducing the density to approximately 6 to 10 million points per cloud. However, in scenes with more than one point cloud, the ideal cloud density was between 1 and 3 million points, so the difference in density between clouds was used as a resource to generate contrast and highlight elements.

3.4 The Point Cloud Animation Process

To construct the immersive narrative, data from the eight digitized buildings were imported from CloudCompare into Blender software in PLY format. The structuring of the experience was based on a pre-defined script and storyboard, conceived as a contemplative and philosophical journey about the importance of historical heritage in consolidating the cultural identity of Fortaleza.

The technical configuration of the virtual environment consisted of implementing a rig of five synchronized cameras, whose proportions and fields of view replicate the projection surfaces (four walls and floor) of the immersive room at MIS-CE, which were named T1, T2, T3, T4, and T5. This setup step was important to ensure the absence of spatial distortions and to facilitate real-time visualization of the transitions between the point clouds.

With the point cloud in Blender and the camera setup ready, the camera movement to be performed is programmed, which uses angles and effects that make the film more dynamic, with the aim of providing new points of view of the heritage. Furthermore, light points are used in the recorded scenes to highlight volume and provide an atmosphere in the virtual space by simulating the real light points of buildings in the digital environment. To enhance cognitive engagement and the feeling of immersion, visual effects of fireflies and distortion were added to the point clouds. The noises that were kept in the point clouds interacted with the firefly, acquiring its brightness and color upon touch.

After rendering all the scenes, the videos were then compiled in the sequence established by the storyboard and edited in After Effects, which was responsible for adding subtitles and transitions. The finalization was

done by inserting an original soundtrack and diegetic sound effects, captured and mixed in the museum's audio laboratory and with tests in the immersive room as shown in Figure 3, consolidating the complete sensory experience.



Figure 3 – Sound production and video testing process.

4. Storytelling of the exhibition

4.1 Development in the immersive classroom

The immersive room at MIS-CE is composed of five synchronized projection surfaces (four perimeter walls and the floor). To achieve this, the vanishing points of the video had to be adjusted so that the spatial continuity of the buildings was not interrupted at the edges of the room. In addition, spatialized audio was used so that, when the visitor enters the projection, there is a collective and shared experience as shown in Figure 4.



Figure 4 – People's interaction with the exhibition.

4.2 Narrative Structure

More than organizing an exhibition sequence, the narrative structure of the show was conceived as a mediation strategy, in which decisions regarding form, rhythm, spatialization, and transition guide the visitor through different regimes of attention and symbolic engagement with the heritage. The immersive experience was structured in four main narrative acts. The first presents the point as the fundamental unit and starting point of the exhibition, demonstrating the genesis of form: how sets of points structure lines, which evolve into planes and grids until they consolidate the buildings (Figure 5). In the second act, the viewer is invited on a contemplative journey, in which the point clouds of the eight scanned buildings float in an ethereal space (Figure 6). This stage uses smooth camera movements and an atmospheric soundtrack,

allowing the public to appreciate the scale and typological diversity of Fortaleza's heritage without the distractions of the real urban environment.

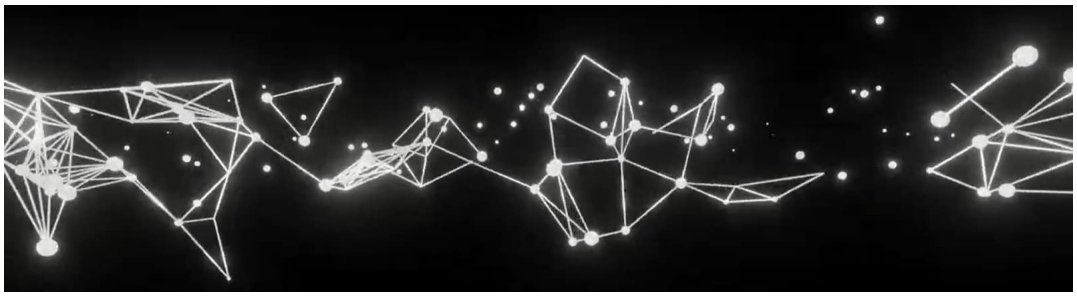


Figure 5 –The point as a representation of the beginning.



Figure 6 – Valley of the buildings.

In the third act, the narrative transitions from external visualization to the exploration of the interior of selected monuments, a journey made possible by the inherent transparency of the point cloud, which allows for a unique perception of internal spatiality (Figure 7) (FIgure 8). Finally, the narrative culminates in the São Pedro Building (Figure 9), the first building with more than 3 floors to be constructed on Iracema Beach and an icon of Ceará architecture (Government of the State of Ceará, 2023), which was demolished in 2024. In this segment, the point cloud takes on a critical documentary character. The visual transition uses distortion and fragmentation effects to symbolize the vulnerability of heritage in the face of urban neglect. By concluding the exhibition with a building that no longer physically exists but survives digitally, the narrative reinforces the urgency of preservation policies and the role of 3D documentation as a guardian of collective memory.



Figure 7 – Virtual tour of the José de Alencar Theater.



Figure 8 – Virtual tour of the Museum of Image and Sound of Ceará.



Figure 9 – Representation of the valley of buildings with the São Pedro building in the center.

The organization of these four acts suggests that the exhibition's storytelling is not limited to the sequential presentation of digitized buildings, but operates as a progressive construction of attention, engagement, and awareness. By starting from the abstraction of the point, moving towards the constitution of architectural forms, guiding the viewer through a contemplative journey among the buildings, and finally concentrating the experience on the São Pedro Building as the symbolic and critical apex of the narrative, the work structures different layers of discovery, permanence, and reflection. In this process, elements such as spatial continuity, sound ambience, smoothness or tension of camera movements, and fragmentation effects act as strategies of sensitive mediation, guiding the gaze and intensifying the relationship between visitor and heritage.

Thus, the narrative seeks not only to inform about the buildings represented, but to create conditions for a deeper engagement with their memory, approaching the notion of flow discussed by Csikszentmihalyi and Hermanson (1995) and which can be interpreted, in light of Ricca (2023), as a narrative of attention, in which the experience articulates initial capture, contemplative permanence and reflective deepening in immersive contexts of heritage awareness.

5. Results and Impact

To understand the impact of the exhibition on users, an empirical evaluation of the "From Point to Heritage" exhibition was conducted with 14 participants. The methodology was based on a mixed-methods approach, involving semi-structured interviews and a five-point Likert scale, structured into blocks of negative and positive aspects (Table 1 and 2).

The quantitative results suggest a positive reception of the immersive experience. In the block regarding negative aspects (Table 1), the majority of participants disagreed with the statements, suggesting that the exhibition was not perceived as repetitive or visually uncomfortable. Regarding positive aspects (Table 2), there was a strong consensus on the engaging character of the immersive room (12 out of 14 responses in

the maximum agreement category), which points to the effectiveness of the proposed decimation and animation workflow. Furthermore, there was a high level of motivation for physically (re)visiting the buildings (12 out of 14 responses in the maximum agreement category), indicating the technology's potential as a driver for heritage tourism and urban awareness.

Qualitatively, the analysis of the reports suggests that the exhibition acted as a memory mediator, allowing visitors to revisit affective experiences related to the presented spaces. The confrontation with the three-dimensional nature of the point clouds facilitated the immediate recognition of unique architectural elements — such as the patio of the Theatro José de Alencar or the auditorium of the Cine São Luiz — enabling visitors to access prior experiences. This mediation element was particularly notable in the case of the São Pedro Building; upon encountering the digital representation of a demolished monument, participants highlighted this moment throughout the interviews, with the term "São Pedro" being repeated 11 times across the 12 interviews. Thus, the exhibition may be understood as an important tool for raising awareness regarding heritage loss and the permanence of collective memory in the face of urban neglect.

Table 1 – Likert Scale: Negative Aspects

NEGATIVE ASPECTS					
SENTENCES	LINKERT SCALE (NUMBER OF RESPONSES)				
	1	2	3	4	5
The changes in angle and perspective during the experience caused me discomfort.	10	2	1	1	1
The scenes were too fast; I could not observe the buildings as I wished.	11	0	0	3	0
The soundtrack and sound effects did not seem connected to the visuals.	7	3	2	2	0
The sound distracted or overloaded my perception of the experience.	11	1	2	0	0
The experience is repetitive.	10	2	2	0	0

Table 2 – Likert Scale: Positive Aspects

POSITIVE ASPECTS					
SENTENCES	LINKERT SCALE (NUMBER OF RESPONSES)				
	1	2	3	4	5
The experience influenced my opinion on the preservation of the city's historical buildings.	0	1	1	5	7
I learned something new about the city's architectural heritage through the experience.	0	1	2	2	7
The experience motivated me to contribute to the preservation of architectural heritage.	0	0	4	7	8
The experience made me feel an emotional connection with the historical buildings presented.	0	1	1	5	7
I will talk about my experience of watching the exhibition with colleagues and family members.	0	0	0	7	7

I recognized all or most of the buildings represented.	1	1	1	7	3
I have previously read, heard, or watched materials or news about the built heritage of Ceará.	2	2	1	5	4
The immersive room provided an engaging experience.	0	0	0	2	12
After watching the experience, I am more interested in personally (re)visiting the presented buildings.	0	0	1	1	12

6. Conclusions

This work aimed to present the production techniques and design decisions involved in developing an immersive experience based on point clouds. From the exhibition "From Point to Heritage," it was possible to highlight that the digitization of heritage buildings has a potential that goes beyond the Scan-to-BIM workflow. By reinterpreting the point cloud, this work demonstrates the feasibility of using it as a means of public communication and heritage education, fundamental dimensions for the appreciation and preservation of heritage. The incorporation of these buildings into museum environments through immersive systems, such as the immersive room, expands the possibilities of bringing society and heritage closer together, by transforming the monument into a sensory and informative experience. This approach reinforces the role of museums in promoting a deeper historical understanding through engagement with heritage.

By visualizing the building through its points, transparencies, and overlays, the public is prompted to make a cognitive effort that, as suggested by Csikszentmihalyi and Hermanson (1995), can favor engagement conditions close to what they describe as flow, which can enhance intellectual and emotional engagement with the historical object. This strategy reinforces the idea that 3D surveying can generate products that transcend technical modeling, serving as a basis for narratives capable of democratizing access to heritage. Furthermore, community participation in non-formal educational experiences proves relevant for activating cultural protection policies and expanding the social reach of these actions. In this sense, technology allows buildings that are difficult to access, closed off, or have already materially disappeared to be visited virtually, making heritage knowledge more inclusive and accessible.

It is also possible to understand the narrative structure of the exhibition in light of the Loom of Experience, insofar as the immersive path organizes a progression between different attentional levels (Ricca, 2023). The initial impact of the point cloud visuality, the sound environment, and the spatialization of the content function as elements that capture and guide attention; then, the contemplative journey between forms, transparencies, and scales favors the permanence and deepening of the experience; finally, the arrival at the case of the São Pedro Building shifts the visitor to a more reflective layer, in which memory, loss, and the urgency of preservation are articulated in a critical way. In this sense, the exhibition not only presents information about the heritage but also constructs a narrative of attention, in which visual, sound, and spatial stimuli are organized to lead the public from an initial sensory perception to a deeper symbolic implication.

The case of the São Pedro Building powerfully exemplifies the urgency of this approach, consolidating 3D documentation as a safeguarding practice and also as a critical gesture of memory. Even in the face of physical demolition, its digital permanence in the museum acts as a historical record and as a manifestation against the loss of collective memory. In summary, this work demonstrates that digital technology, when articulated with educational processes in museums, can transform public perception of heritage and strengthen cultural identity through the recognition, awareness, and appreciation of historical structures.

Although this study is limited to a single case study, it presents not only the production methodology but also research findings regarding public reception. The collected data suggest the effectiveness of the proposed approach. Thus, this work not only validates the developed design workflow but also establishes technical parameters for future investigations and new applications of immersive technologies in heritage education.

Acknowledgments

This work was financially supported by FUNCAP, Project 01172921/2022 – Cientista Chefe Cultura, Project 10581391/2022 – International collaboration FUNCAP/INSA Rouen Normandie; by the National Council for Scientific and Technological Development (CNPq) – Project 302054/2022-7 – PQ2, by the Project - 440926/2024-6 – VISION and Project - 402828/2024-0 – CLIC, CAPES Foundation and Finep 2896/24.

References

Casacivilsuzetenocrato. "Histórico Em Fortaleza, Edifício São Pedro Vai Abrigar Distrito Criativo." Governo Do Estado Do Ceará, March 17, 2022. www.ceara.gov.br/2022/03/17/historico-em-fortaleza-edificio-sao-pedro-vai-abrigar-distrito-criativo/.

Cotella, Victoria Andrea. "From 3D Point Clouds to HBIM: Application of Artificial Intelligence in Cultural Heritage." *Automation in Construction* 152 (2023): 104936. https://doi.org/10.1016/j.autcon.2023.104936.

Creswell, John W., and Cheryl N. Poth. *Qualitative Inquiry and Research Design: Choosing Among Five Approaches*. 4th ed. Los Angeles: Sage, 2018.

Csikszentmihalyi, Mihaly. *Flow: The Psychology of Optimal Experience*. New York: Harper & Row, 1990.

Csikszentmihalyi, Mihaly, and Kim Hermanson. "Intrinsic Motivation in Museums: Why Does One Want to Learn?" In *Public Institutions for Personal Learning: Establishing a Research Agenda*, edited by John H. Falk and Lynn D. Dierking, 67–77. Washington, DC: American Association of Museums, 1995.

De Kleijn, Maurice, Krien Clevis, Jesús García González, Marco Roling, Jorne Jongsma, Rens de Hond, Henk Scholten, and Eric M. Moormann. "Art and Archaeology in an Interactive Time-Traveling Online and Museum Experience: A Case Study on the Via Appia Antica." *Digital Applications in Archaeology and Cultural Heritage* 33 (2024): e00342. https://doi.org/10.1016/j.daach.2024.e00342.

Frayling, Christopher. "Research in Art and Design." *Royal College of Art Research Papers* 1, no. 1 (1994).

Frullo, Nadia, and Manuela Mattone. "Preservation and Redevelopment of Cultural Heritage through Public Engagement and University Involvement." *Heritage* 7, no. 10 (2024): 5723–5747. https://doi.org/10.3390/heritage7100269.

Gabellone, Francesco. "Development of an Immersive VR Experience Using Integrated Survey Technologies and Hybrid Scenarios." *Heritage* 6, no. 2 (2023): 1169–1186. https://doi.org/10.3390/heritage6020065.

Gil, Antonio Carlos. *Como Elaborar Projetos de Pesquisa*. 4th ed. São Paulo: Atlas, 2002.

Ivsic, Lucija, Jon McCormack, and Vince Dziekan. "The Point Cloud Aesthetic: Defining a New Visual Language in Media Art." *Virtual Creativity* 13, no. 2 (2023): 213–229. https://doi.org/10.1386/vcr_00085_1.

Lei, Y., F. Fiorillo, and F. Fassi. "3D Survey Point Cloud Data as Direct Rendering Assets for Visualising Complex Heritage in Virtual Applications." *The International Archives of the Photogrammetry, Remote Sensing and Spatial Information Sciences* XLVIII-2/W4-2024 (2024): 279–286. https://doi.org/10.5194/isprs-archives-XLVIII-2-W4-2024-279-2024.

Penjor, Tshering, Saeed Banihashemi, Aso Hajirasouli, and Hamed Golzad. "Heritage Building Information Modeling (HBIM) for Heritage Conservation: Framework of Challenges, Gaps, and Existing Limitations of HBIM." *Digital Applications in Archaeology and Cultural Heritage* 35 (2024): e00366. https://doi.org/10.1016/j.daach.2024.e00366.

Ricca, Diego Enéas Peres. "Tear da Experiência: Design Baseado na Atenção para a Educação Cotidiana em Realidade Estendida." PhD diss., Universidade de São Paulo, 2023.

UNESCO World Heritage Centre. 2021. “World Heritage in Danger.” UNESCO. https://whc.unesco.org/en/danger/.

Van Boxtel, Carla, Maria Grever, and Stephan Klein. "Introduction: The Appeal of Heritage in Education." In *Sensitive Pasts: Questioning Heritage in Education*, edited by Maria Grever and Carla Van Boxtel, 1–18. New York: Berghahn Books, 2016. https://doi.org/10.1515/9781785333057-002.

Vieira, Mylene M., Gilmário Ribeiro, Renan Paulo, Maycon Bessa, Francisca R. Sousa, Eugênio Moreira, and Esequiel Mesquita. "Strategy for HBIM Implementation Using High-Resolution 3D Architectural Documentation Based on Laser Scanning and Photogrammetry of the José de Alencar Theatre." *Digital Applications in Archaeology and Cultural Heritage* 30 (2023): e00287. https://doi.org/10.1016/j.daach.2023.e00287.

Yin, Robert K. *Case Study Research and Applications: Design and Methods*. 6th ed. Los Angeles: Sage, 2018.

Zimmerman, John, Jodi Forlizzi, and Shelley Evenson. "Research through Design as a Method for Interaction Design Research in HCI." In *Proceedings of the SIGCHI Conference on Human Factors in Computing Systems*, 493–502. New York: ACM, 2007. https://doi.org/10.1145/1240624.1240704.

Cinpar 2026
XXII International Conference on Building Pathology and Constructions Repair
15th to 17th July 2026 - Lisboa, Portugal

Adaptive vs. Uniform Decimation: A Quantitative Analysis of 3D Mesh Optimization for HBIM

Dárcio Matheus de O. SILVA[1], Eugênio MOREIRA[2], Mylene VIEIRA[3], **Esequiel MESQUITA**[4]

[1] Laboratory of Rehabilitation and Durability of Constructions - Federal University of Ceara, Brazil, darciodfx@alu.ufc.br
[2] Laboratory of Digital Experience - Federal University of Ceara, Brazil, eugeniomoreira@iaud.ufc.br
[3] Laboratory of Rehabilitation and Durability of Constructions - Federal University of Ceara, Brazil, mylene.melo@ufc.br
[4] Laboratory of Digital Experience - Federal University of Ceara, Brazil, emesquita@ufc.br

Abstract: The integration of complex 3D meshes into Heritage Building Information Modeling (HBIM) platforms is often limited by computational bottlenecks. This paper proposes and validates a workflow to quantitatively evaluate mesh optimization techniques using uniform and adaptive decimation. The methodology involves generating multiple Levels of Detail (LODs) in SideFX Houdini and then analyzing them in Python, with a focus on geometric accuracy and error distribution. The results demonstrate that adaptive decimation, although computationally more expensive, preserves critical details with greater fidelity and achieves a lower mean error. The protocol validates the adaptive approach as the superior strategy for optimizing digital assets in HBIM, offering a robust balance between efficiency and geometric fidelity.

Keywords: 3D mesh optimization; adaptive decimation; uniform decimation; geometric accuracy.

1. Introduction

The documentation and management of historic buildings constitute a central challenge for the preservation of cultural heritage. The Heritage Building Information Modeling (HBIM) approach has emerged as an advanced paradigm for this purpose, overcoming the limitations of traditional BIM in handling irregular geometries and the absence of original technical documentation. As noted by Noardo (2018), HBIM representations demand an exceptional level of detail and geometric accuracy to faithfully represent the as-is condition of the built heritage. In this context, three-dimensional reconstruction from point clouds has become a pillar of the HBIM workflow, providing the basis for accurate and information-rich digital models (Cotella 2023).

The acquisition of high-density point clouds is predominantly performed through photogrammetry and laser scanning (LiDAR). These technologies, frequently combined to optimize survey fidelity (Pepe et al. 2020; Pirotti et al. 2022), produce a massive set of points that requires processing to generate a continuous surface. The conversion of the point cloud into a polygonal mesh is a critical step, performed by surface reconstruction algorithms (Xu et al. 2021; Morel et al. 2018).

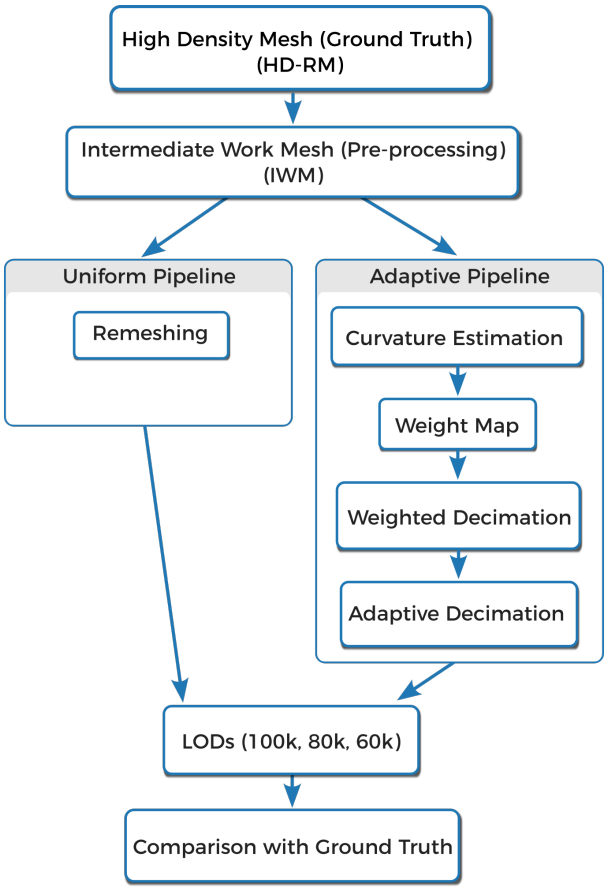
The result, however, is typically a very high-density mesh, whose data volume imposes severe computational bottlenecks, rendering its integration into HBIM platforms inefficient (Ismail et al. 2023). To overcome this limitation, optimization techniques such as mesh decimation are employed (Dunyach et al. 2013). Decimation strategies can be uniform or adaptive, preserving details based on curvature criteria (Wang et al. 2019). Although the literature describes these techniques in isolation, there is a gap in the systematic, comparative evaluation of their results in the context of HBIM. There is a lack of quantitative protocols to compare the impact of different decimation methods on the trade-off between geometric accuracy and polygonal density, especially when applied to complex elements such as architectural ornaments.

To address this gap, this study proposes and evaluates a methodological workflow for generating and optimizing 3D mesh models from point clouds for integration into HBIM platforms. The methodology comparatively investigates two polygonal decimation techniques implemented in the Houdini software: adaptive and uniform. The quantitative evaluation is performed through automated analyses, considering two main metrics: execution time and geometric accuracy. Therefore, the work aims to establish a protocol for optimizing digital assets in the context of built heritage documentation and to determine the advantages and limitations of each processing approach.

2. Methodology

This study employed an experimental workflow to comparatively evaluate two 3D mesh optimization strategies for HBIM applications. The methodology comprises six main stages: i) identifying the case study and input data; ii) specifying the hardware and software; iii) pre-processing and generating an intermediate working mesh; iv) generating three Levels of Detail (LODs) via uniform decimation; v) generating three LODs via curvature-based adaptive decimation; and vi) performing a quantitative comparative analysis of the results. The core processing workflow, from the input reference mesh to the final comparative analysis, is visually represented in Figure 1.

Figure 1 – Methodological workflow flowchart, from the input point cloud to the comparative analysis of the six generated LODs.



2.1 Object of Study and Input Data

The case study focuses on a pair of porcelain lion sculptures from Porto, Portugal, dating from the early 20th century. These pieces are distinctive architectural elements on the facade of the historic building that currently houses the Museum of Image and Sound of Ceará (MIS-CE), as illustrated in Figure 2. The high-

density polygonal meshes of both sculptures, generated via photogrammetry and comprising approximately 50 million polygons each, served as the 'ground truth' and primary data for the experiments.

Figure 2 – Facade of MIS-CE, highlighting the lions (case study): (1) left and (2) right. Source: Adapted from MIS-CE (2024).



2.2 Hardware and Software Specifications

All experiments were conducted on a workstation with the following specifications: an Intel Core i5-12450H processor; 16 GB of RAM (DDR5, 4800 MHz); an NVIDIA GeForce RTX 2050 GPU (4 GB GDDR6); and the Windows 11 operating system. The following software and libraries were used: MeshLab (v. 2023.12) for normal computation and reference mesh generation; SideFX Houdini (v. 20.5.445) to implement the uniform and adaptive decimation workflows; and Python (v. 3.11.6) with the PyVista (v. 0.45.2) and VTK (v. 9.4.2) libraries for geometric distance computation, NumPy (v. 2.3.1) for numerical operations, Pandas (v. 2.3.0) for data manipulation, and Matplotlib (v. 3.10.3) / Seaborn (v. 0.13.2) for plot generation.

2.3 Reference Mesh Generation

The High-Density Reference Mesh (HD-RM), which served as the ground truth for the accuracy analyses, was generated using the MeshLab software. In this environment, the point cloud was initially processed with the Compute Normals for Point Sets function, setting the neighbors parameter to 20 to ensure a consistent vector orientation. Subsequently, with the normals computed, the surface was reconstructed using the Surface Reconstruction: Screened Poisson algorithm, where the octree depth was set to 11 to guarantee the capture of fine details. This process yielded a closed and geometrically faithful polygonal mesh, which was fundamental for the validation of the optimized models.

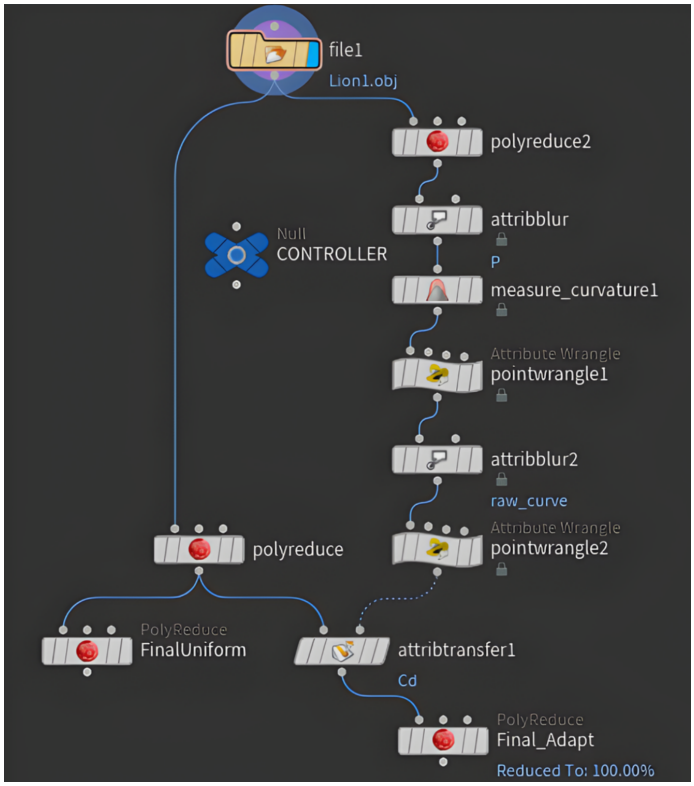
2.4 Intermediate Working Mesh Generation (IWM)

Due to the high density of the HD-RM, which imposed computational constraints, an Intermediate Working Mesh (IWM) was generated. The 50-million-polygon HD-RMs were imported into SideFX Houdini and subjected to an initial decimation using the PolyReduce node. The target was set to 35% of the original polygon count, resulting in more manageable IWMs. These IWMs served as the common starting point for the two subsequent optimization pipelines.

2.5 Optimization and Generation of Levels of Detail (LODs) in Houdini

Starting from the IWMs, two distinct workflows, detailed in Figure 3, were applied to generate three LODs for each method, with target polygon counts of 100,000, 80,000, and 60,000.

Figure 3 – The complete node graph of the workflow implemented in Houdini.



For the optimization, two distinct pipelines were applied. The first, uniform decimation, processed the Intermediate Working Mesh (IWM) with the Remesh node, aiming for a homogeneous topological reorganization. The polygon density was controlled by the "Element Sizing" parameter, which was iteratively adjusted to generate three distinct meshes for each sculpture, corresponding to the target LODs of 100,000, 80,000, and 60,000 polygons.

In contrast, the adaptive method implemented a selective decimation strategy to preserve geometric details. The process began with the creation of a weight map: the mesh was first smoothed with an AttribBlur node (15 iterations) to mitigate noise, and subsequently, the Measure Curvature node computed the curvature at each point. The resulting attribute was then processed with the AttribBlur and Attribute Wrangle nodes to generate the final map. Once created, this weight map was transferred to the IWM via the AttribTransfer node, and the mesh, now enriched with the attribute, was subjected to a final PolyReduce node. The operation of this final node was controlled by the map, forcing the algorithm to remove polygons from flat areas while preserving the topology in regions of high curvature. This procedure was repeated to generate the three corresponding LODs for each element.

2.6 Quantitative Analysis and Evaluation Metrics

To quantitatively assess the performance of each optimization method, the six generated Level of Detail (LOD) models were compared against the IWM. The analysis was conducted using a set of Python scripts, which implemented the following procedures.

Geometric deviation was computed using the PyVista (v. 0.45.2) library, which invokes the vtkImplicitPolyDataDistance function from the VTK (v. 9.4.2) toolkit. This method computed the signed Euclidean distance from each vertex of the optimized mesh to the closest point on the surface of the

reference mesh. From the resulting distance vector for each LOD, a set of statistical metrics was calculated in order to characterize the deviation. These include the Mean Absolute Error (MAE), defined as the average of the absolute distance values and indicating the overall mean deviation, and the Standard Deviation (σ), which measures the dispersion and variability of the signed errors. In addition, the Maximum Error was determined as the largest absolute deviation value found on any vertex of the mesh, while the 95th Percentile of Absolute Error represents the error value below which 95% of the vertices are found.

Additionally, an analysis was performed to compare the spatial concentration of inaccuracies. This procedure, executed at the face (polygon) level, followed these steps: 1) the mean absolute error was calculated for each face of a given LOD, defined as the average of the absolute errors of its constituent vertices; 2) an error threshold was established based on the performance of the mesh generated by the adaptive method, defined as the 95th percentile error value of its polygons, thereby isolating the 5% of faces with the greatest deviations; and 3) this same threshold value was subsequently applied to the mesh generated by the uniform method in order to quantify the percentage of its faces that exceeded this error standard. This approach allows for a direct comparison of the prevalence of high-error areas between the two methods, using a quality standard derived from the adaptive method. To ensure the transparency and reproducibility of the research, the SideFX Houdini project, the Python analysis scripts, and the generated 3D models were made available in a public repository github.com/darciodfx/HBIMAnalysis.

3. Results

The application of the optimization methodologies yielded six Level of Detail (LOD) models with distinct characteristics in terms of polygonal density and geometric accuracy. The quantitative results are presented sequentially below.

The two methodologies were applied to generate LODs with target polygon counts of 100,000, 80,000, and 60,000. Table 1 summarizes the final polygon counts and the processing times required by each pipeline in SideFX Houdini. It was observed that the adaptive method consistently required a longer processing time than the uniform method for all analyzed LODs.

Table 1 – Comparison of processing times for each generated LOD per model

	Target LOD (Polygons)	Method	Final Polygons	Processing Time(s)
Lion 1	100 000	Uniform	100 720	200
		Adaptive	100 000	274
	80 000	Uniform	80 401	174
		Adaptive	80 000	227
	60 000	Uniform	60 020	138
		Adaptive	60 000	171
Lion 2	100 000	Uniform	100 210	198
		Adaptive	100 000	271
	80 000	Uniform	81 201	172
		Adaptive	80 000	216
	60 000	Uniform	60 802	140
		Adaptive	60 000	167

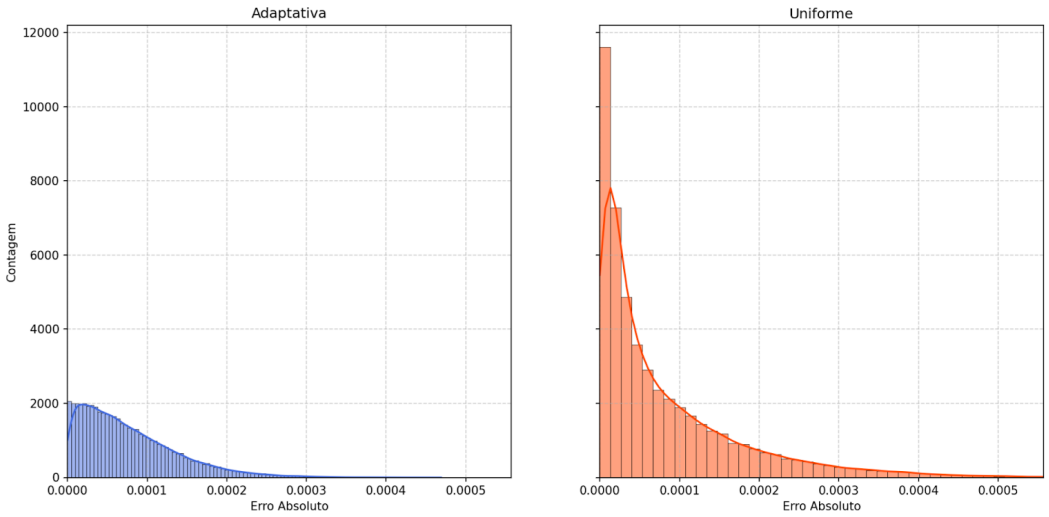
The comparison of the optimized models with the high-density reference mesh revealed significant differences in geometric accuracy. Table 2 presents the key error metrics for each LOD. The results indicate that, across all levels of detail, the adaptive decimation method consistently produced lower values for Mean Absolute Error (MAE), Standard Deviation (σ), Maximum Error, and the 95th Percentile.

Table 2 – Geometric accuracy statistics (units in meters) for the LODs generated for models 1 and 2

	Target LOD (Polygons)	Method	MAE	Standard Deviation (σ)	Maximum Error	95th Percentile
Lion 1	100,000	Uniform	0,00008275	0,00012731	0,00133629	0,00028494
		Adaptive	0,00007679	0,00009769	0,00046900	0,00019432
	80,000	Uniform	0,00009573	0,00014666	0,00114182	0,00032849
		Adaptive	0,00009040	0,00011477	0,00058602	0,00022870
	60,000	Uniform	0,00011633	0,00017671	0,00141270	0,00039383
		Adaptive	0,00011175	0,00014131	0,00069942	0,00028392
Lion 2	100,000	Uniform	0,00008002	0,00011852	0,00100580	0,00026333
		Adaptive	0,00006762	0,00008483	0,00046347	0,00016772
	80,000	Uniform	0,00009331	0,00013730	0,00144706	0,00030580
		Adaptive	0,00007943	0,00009935	0,00055832	0,00019751
	60,000	Uniform	0,00011504	0,00016848	0,00150104	0,00037435
		Adaptive	0,00009818	0,00012219	0,00069595	0,00024404

The analysis of the absolute error distribution corroborates the findings in Table 2, albeit with important nuances. Figure 4 presents the error histograms for the 100k-polygon LOD. The histogram for the uniform method (right) is characterized by an extremely sharp and elevated peak at error values near zero, indicating that a vast majority of its vertices possess a very low geometric deviation. In contrast, the histogram for the adaptive method (left) exhibits a considerably lower peak and a broader distribution, with a tail that tapers off more gradually than that of the uniform model. This pattern was observed consistently across all analyzed LODs.

Figure 4 – Comparative histograms of the absolute error distribution for the adaptive (left) and uniform (right) methods, for the 100,000-polygon LOD



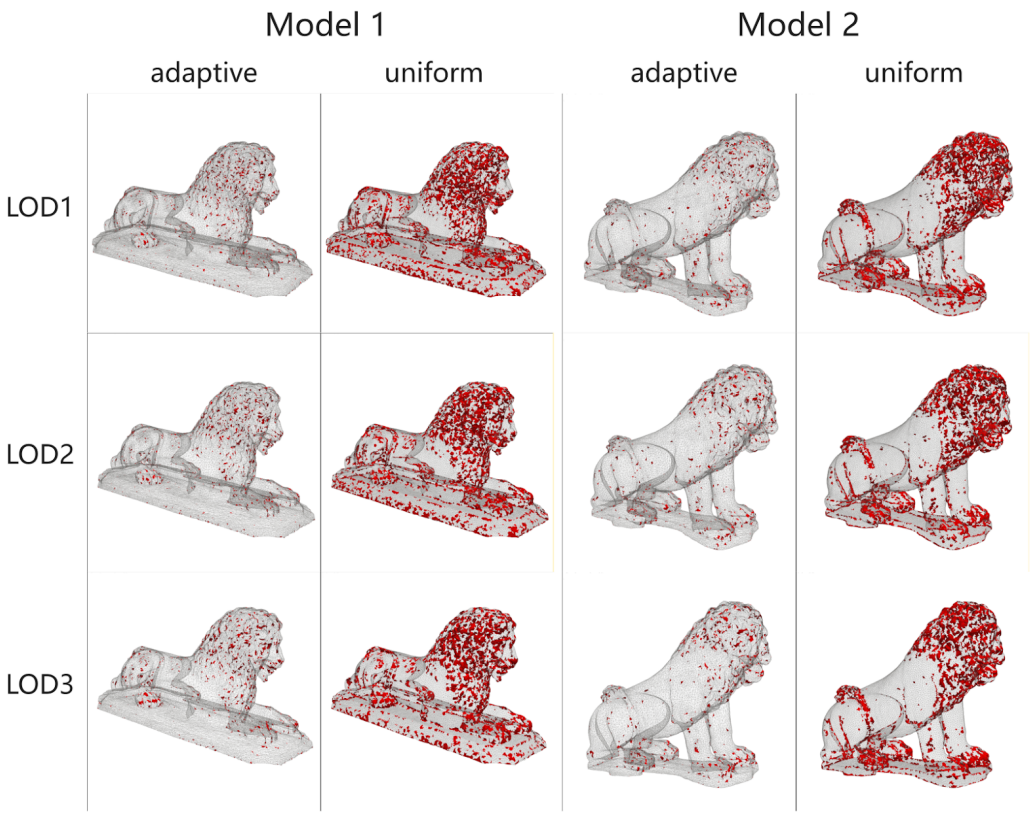
The error prevalence analysis, which uses a threshold derived from the 5% of polygons with the highest error on the adaptive mesh, quantified the disparity in performance. Table 3 details the results for each LOD. For the 100,000-polygon LOD, with an error threshold of 0.00013079, it was found that 19.88% of the polygons on the uniform mesh exceeded this value, compared to 5.00% for the adaptive mesh.

Table 3 – Error prevalence analysis, using a common threshold derived from the adaptive mesh for each LOD

	Total polygons	Polygons (Adaptive)	Error Threshold	Polygons (Uniform)
Lion 1	100,000	5%	0,00014811	18.44%
	80,000	5%	0,00017367	18.08%
	60,000	5%	0,00021414	17.44%
Lion 2	100,000	5%	0,00013079	19.88%
	80,000	5%	0,00015324	19.73%
	60,000	5%	0,00018950	19.91%

This quantitative difference is visually confirmed in Figure 5, where the polygons exceeding the defined error threshold are shown in red.

Figure 5 – Spatial visualization of polygons with an error exceeding the threshold for all generated LODs



4. Discussion

The quantitative and visual results presented demonstrate the clear superiority of the adaptive decimation method over the uniform one for optimizing 3D meshes with complex geometries. The principal finding of this study lies in the relationship between error distribution and the overall model accuracy. As indicated in Table 2, the adaptive method consistently achieved a lower Mean Absolute Error (MAE). This is due to its ability to intelligently allocate the "polygon budget," preserving topological density in high-curvature areas—such as the lion's mane and facial contours—that are crucial to the object's visual identity.

In contrast, the uniform method, by reorganizing the mesh homogeneously, generates significantly larger errors in these same critical areas. This phenomenon explains the apparent paradox observed in the error histograms (Figure 4). The sharp peak in the uniform method's histogram signifies that it produces many polygons with near-zero error on flat surfaces, but at the cost of over-smoothing the details. The adaptive method, in turn, accepts a small, more distributed error across the entire surface to ensure the preservation of complex shapes, resulting in superior average performance. The error prevalence analysis (Table 3) quantifies this shortcoming compellingly: when using the same quality standard, the uniform mesh exhibited nearly four times as many "high-error" polygons.

Finally, the longer processing time of the adaptive method (Table 1) represents a classic trade-off between performance and quality. The additional computational cost stems from the extra steps of curvature calculation and attribute processing, an investment justified by the superior accuracy of the final model.

4.1 Implications for HBIM and Contribution to Knowledge

This study addresses the gap identified in the literature (Section 1.2) by providing a quantitative protocol for the comparative evaluation of mesh optimization techniques within the HBIM context. While studies such

as Wang et al. (2019) describe the theoretical benefits of adaptive decimation, our research provides empirical validation and concrete metrics that demonstrate its practical effectiveness.

The primary implication for HBIM practice is the validation of a workflow that enables the generation of significantly lighter and more efficient digital assets without compromising the geometric fidelity of complex ornamental elements. This directly addresses interoperability and performance bottlenecks in BIM software (Ismail et al. 2023), enabling the integration of richer, more detailed as-is models. Thus, a conceptual model is proposed for mesh optimization in HBIM that balances three factors: Geometric Accuracy, Computational Efficiency, and Detail Preservation. Our findings position adaptive decimation as the strategy that best balances these three pillars.

5. Conclusions

This study presented a quantitative workflow for the evaluation of 3D mesh optimization techniques in the context of Heritage Building Information Modeling (HBIM). The results consistently demonstrate the superiority of the adaptive decimation method over the uniform approach, particularly in terms of geometric accuracy and error distribution. By preserving critical high-curvature features while efficiently reducing polygonal density, the adaptive method achieved lower Mean Absolute Error (MAE), reduced variability, and fewer high-error regions across all Levels of Detail (LODs) analyzed.

The primary contribution of this work lies in the establishment of a reproducible and quantitative protocol for comparing mesh simplification strategies, addressing a gap in the HBIM literature. This protocol enables a more rigorous assessment of the trade-off between geometric fidelity and computational efficiency, which is essential for the integration of complex 3D assets into BIM environments.

From a practical perspective, the findings support the adoption of adaptive decimation as a more reliable strategy for optimizing high-resolution meshes of architectural heritage elements. This has direct implications for improving interoperability, reducing computational costs, and enabling the use of detailed as-is models within HBIM platforms.

Despite the consistent findings, some limitations should be acknowledged. Firstly, the study focused on a single type of object: an organic sculpture with high surface complexity. The magnitude of the adaptive method's superiority may vary for architectural elements with distinct characteristics, such as predominantly flat facades. Finally, the methodology was implemented in a specific commercial software (SideFX Houdini); although the principles are universal, the exact replication of the workflow on other platforms, particularly open-source ones, may present challenges.

Based on the identified limitations, the following directions for future work are suggested. First, the application and validation of the methodological protocol proposed herein to a broader range of architectural heritage typologies. Second, the investigation of analogous workflows using open-source software, such as Blender, to democratize access to the technique. The most promising avenue of research, however, would be to extend the pipeline beyond geometric optimization, exploring semi-automated methods for converting the optimized mesh into parametric and semantically rich objects, thereby completing the Scan-to-HBIM cycle.

Acknowledgments

This work was financially supported by FUNCAP, Project 01172921/2022 – Cientista Chefe Cultura, Project 10581391/2022 – International collaboration FUNCAP/INSA Rouen Normandie; by the National Council for Scientific and Technological Development (CNPq) – Project 302054/2022-7 – PQ2, by the Project - 440926/2024-6 – VISION and Project - 402828/2024-0 – CLIC, CAPES Foundation and Finep 2896/24.

References

Cotella, V. 2023. "From 3D point clouds to HBIM: Application of artificial intelligence in cultural heritage." Automation in Construction. https://doi.org/10.1016/j.autcon.2023.104936

Dunyach, M., D. Vanderhaeghe, L. Barthe, and M. Botsch. 2013. "Adaptive remeshing for real-time mesh deformation." In Eurographics 2013 – Short Papers, edited by M.-A. Otaduy and O. Sorkine, 29–32. The Eurographics Association. https://doi.org/10.2312/conf/EG2013/short/029-032

Ismail, F., S. Shukor, N. Rahim, and R. Wong. 2023. "Surface reconstruction from unstructured point cloud data for building digital twin." International Journal of Advanced Computer Science and Applications. https://doi.org/10.14569/ijacsa.2023.0141075

Morel, J., A. Bac, and C. Véga. 2018. "Surface reconstruction of incomplete datasets: A novel Poisson surface approach based on CSRBF." Computer Graphics 74: 44–55. https://doi.org/10.1016/j.cag.2018.05.004

Noardo, F. 2018. "Architectural heritage semantic 3D documentation in multi-scale standard maps." Journal of Cultural Heritage. https://doi.org/10.1016/J.CULHER.2018.02.009

Pepe, M., D. Costantino, and A. Garofalo. 2020. "An efficient pipeline to obtain 3D model for HBIM and structural analysis purposes from 3D point clouds." Applied Sciences 10, no. 4: 1235. https://doi.org/10.3390/app10041235

Pirotti, F., M. Piragnolo, A. Vettore, and A. Guarnieri. 2022. "Comparing accuracy of ultra-dense laser scanner and photogrammetry point clouds." In The International Archives of the Photogrammetry, Remote Sensing and Spatial Information Sciences 43(B1): 353–359. Presented at XXIV ISPRS Congress, 6–11 June 2022, Nice, France. https://doi.org/10.5194/isprs-archives-XLIII-B1-2022-353-2022

Wang, Y., J. Zheng, and H. Wang. 2019. "Fast mesh simplification method for three-dimensional geometric models with feature-preserving efficiency." Scientific Programming 2019: 4926190. https://doi.org/10.1155/2019/4926190

Xu, Z., C. Xu, J. Hu, and Z. Meng. 2021. "Robust resistance to noise and outliers: Screened Poisson surface reconstruction using adaptive kernel density estimation." Computers & Graphics 97: 19–27. https://doi.org/10.1016/j.cag.2021.04.005

Cinpar 2026
XXII International Conference on Building Pathology and Constructions Repair
15th to 17th July 2026 - Lisboa, Portugal

HBIM for modeling a cultural heritage asset using a hybrid scan-to-BIM workflow: Challenges and Insights from the Pinacoteca do Ceará

Antônio Gabriel BRITO[1], Eugênio MOREIRA[2], Mylene VIEIRA[3], Esequiel MESQUITA[4], **Vitória FONTENELE**[5]

[1] Laboratory of Digital Experience - Federal University of Ceara, Brazil, antoniogabriel@arquitetura.ufc.br
[2] Laboratory of Digital Experience - Federal University of Ceara, Brazil, eugeniomoreira@iaud.ufc.br
[3] Laboratory of Rehabilitation and Durability of Constructions - Federal University of Ceara, Brazil, mylene.melo@ufc.br
[4] Laboratory of Digital Experience - Federal University of Ceara, Brazil, emesquita@ufc.br
[5] Laboratory of Digital Experience - Federal University of Ceara, Brazil, vitorianfontenele@arquitetura.ufc.br

Abstract: The conservation of historic buildings requires comprehensive data regarding their construction systems, geometries, and the degradation state of their components. The development of a Heritage Building Information Model (HBIM) is established as a methodology capable of integrating all the architectural information of a building into a single file, providing the necessary inputs for developing a maintenance plan. This article analyzes the modeling process and the challenges encountered regarding the Pinacoteca do Ceará—a building within the Complexo Cultural Estação das Artes in Fortaleza, a cultural and heritage facility of notable relevance to the city. The workflow adopted a Scan-to-BIM approach, utilizing a hybrid data capture strategy. The architectural survey was conducted using Laser Scanning for horizontally accessible areas, complemented by UAV-based digital aerial photogrammetry with SfM-MVS processing. Data processing involved the use of Leica Cyclone Register 360 software for TLS data and RealityScan for processing the UAV imagery. The final integration of the point clouds was performed in the CloudCompare software, resulting in a unified point model with millimeter-scale precision, an indispensable baseline for parametric modeling faithful to the geometric reality. During the process, overlaying the point cloud onto previous historical records revealed significant discrepancies, such as a lack of orthogonality in structural walls, alongside dimensional and typological variations in window and door frames that were absent from the original documentation. Identifying these asymmetries is crucial for the precise diagnosis of structural deformations and for planning custom-made components during restoration. In conclusion, mapping these inconsistencies through HBIM constitutes an essential digital representation for heritage safeguarding, overcoming the uncertainties inherent in traditional surveying methods.

Keywords: HBIM; Pinacoteca do Ceará; Scan-to-BIM; Heritage; Point Cloud.

1. Introduction

The maintenance and preservation of built cultural heritage has found in advanced digitalization a fundamental method for safeguarding buildings, as evidenced by **Ni et al. (2024)**. In this regard, Heritage Building Information Modeling (HBIM) establishes itself as more than just a three-dimensional modeling tool, but also a complex information management system. Unlike conventional BIM, which focuses on the design of new constructions, HBIM is based on the documentation of pre-existing buildings, integrating geometric, historical, and conservation status information into a parametric model that enables optimized preventive maintenance and future restoration interventions.

However, the effectiveness of this method faces a recurring logistical barrier: the inaccuracy of existing traditional data surveys. Frequently, the existing physical documentation of historical buildings does not correspond to the actual constructed geometry, as manual measurements can lead to cumulative errors and result in significant discrepancies with reality **(Barrile; Bernardo; Bilotta, 2022)**. Furthermore, these documents often ignore structural deformations, settlements, or modifications that occurred throughout the building's existence. This gap between the documentary record and the actual state of the building can compromise the planning of restoration and maintenance interventions, leading to quantitative errors and technical incompatibilities during construction.

Although technologies such as Laser Scanning have revolutionized architectural surveying by capturing geometries with millimeter precision, total capture still faces limitations in large-scale or volumetrically complex buildings. Laser Scanning, despite its pivotal role in geometric data capture, is still limited to the terrestrial scale and cannot achieve highly precise results for urban-scale equipment or hard-to-reach areas, such as roofs and elevated parapets. Frequently, these geometric gaps result in incomplete point clouds due to occlusions. This scenario mandates the adoption of a hybrid data capture strategy, combining distinct forms of secondary data capture to ensure the integrity and reliability of the Digital Twin, as seen in **Salah, Géczy, and Károlyfi (2026)**.

Given this context, the development of the HBIM model of the Pinacoteca do Ceará is detailed—a building of notable relevance to the built cultural heritage of the state of Ceará and part of the Complexo Cultural Estação das Artes in Fortaleza. The analysis documents the modeling strategies adopted in light of the building's available documentary collection and its eventual discrepancy with the geometry captured in situ, highlighting a comparison between pre-existing manual geometric records and the high-precision survey obtained via Laser Scanning and photogrammetry, as well as the recording of data provenance within the model elements.

2. Case Study

The Pinacoteca do Ceará, the central building of the Estação das Artes Cultural Complex, is characterized as a landmark of industrial railway heritage in Fortaleza, dating from the early 20th century. The pinacoteca, managed through a partnership between the Ceará Secretariat of Culture and the Mirante Institute, consists of seven warehouses remaining from the former Rede Ferroviária Federal S.A. (RFFSA). The building's relevance extends beyond its monumental scale, establishing itself as a center for cultural and artistic dissemination whose preservation is guaranteed by significant legal frameworks: municipal listing, which occurred on April 24, 1980, and state listing, on October 30, 1983, under Law No. 16,237.

Figure 01 - Main Facade of the Pinacoteca do Ceará



Source: Government of the State of Ceará

The recent intervention and restoration project, carried out by the Carvalho Araújo firm, adopted a design approach that values and highlights the pre-existing railway industrial elements to house a contemporary program. This requalification established the building as one of the most ambitious

architectural-urban regeneration processes in the capital of Ceará, transforming the railway architecture into a safeguarding device for the state's artistic and cultural memory. From a morphological and geometric standpoint, the warehouses are characterized by wide clear spans and exposed metallic structures. In contrast, the service and connection blocks exhibit contemporary languages that establish a dialogue with the pre-existing load-bearing masonry, while the facades present a highly complex rhythmic composition, marked by the repetition of frames and ornamental relief moldings.

The development of the Pinacoteca's HBIM representation required the synthesis of a heterogeneous range of data. As primary sources, a high-precision digital survey was used, obtained through TLS (fundamental for the metric capture of internal spaces and ornamental details) and aerial photogrammetry, employed here to fill the occlusion gaps in roofs and elevated parapets. Complementarily, secondary sources consisting of the Pinacoteca's archives of previous interventions in 2D CAD format were utilized. The overlay of these sources revealed significant geometric discrepancies, particularly regarding the orthogonality and alignment of the main structural walls, evidencing the accumulation of errors inherent to the manual and analog surveying methods previously used.

The documentary workflow was structured to minimize such inconsistencies and ensure the fidelity of the final digital model. The processing of the collected data followed a rigorous sequence of interoperability among a specific series of software programs:

- **Leica Cyclone Register 360:** Used here for the registration, consolidation, and assembly of point cloud files originating from Laser Scanning.
- **Reality Scan:** Employed in processing the images captured by UAV for the generation of point clouds of the roofs through Structure-from-Motion/Multi-View Stereo processing.
- **CloudCompare:** Acted as the geometric fusion environment, enabling the registration of TLS and photogrammetry data into a single file.
- **Autodesk Recap:** Applied in the refinement, segmentation, and cleaning stage of the unified point cloud.
- **Autodesk Revit:** Final modeling platform, where the synthesis between the point clouds (primary data) and historical documentation (secondary data) is carried out.

3. Methodology

3.1 Data Collection

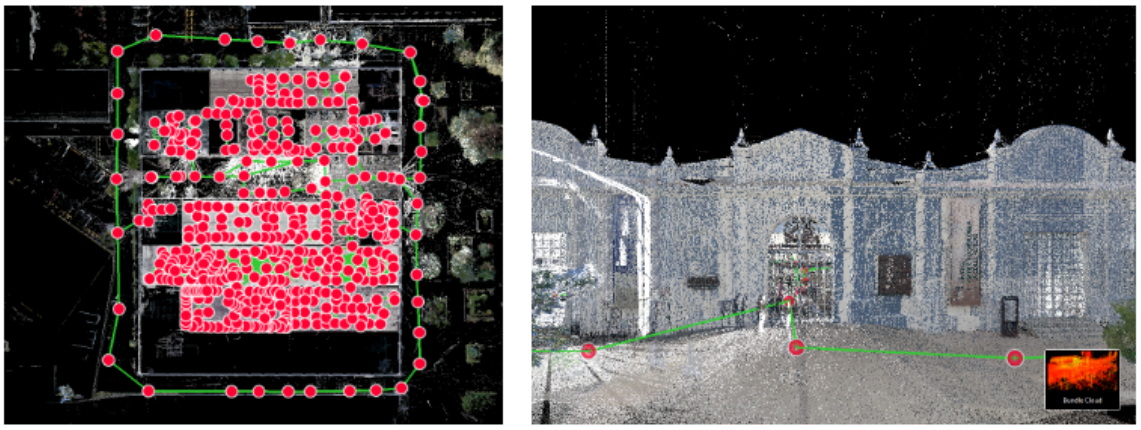
The methodological workflow followed for the Pinacoteca do Ceará was structured under a Scan-to-BIM approach, a process characterized by the transposition of real geometric data into a parametric digital environment. This transposition was divided into interdependent and consecutive stages, beginning with the field survey (data collection), progressing through computational processing, and ultimately culminating in the development of the HBIM representation.

3.1.1 Terrestrial Geometric Survey: Laser Scanning

The primary survey stage took place over a period of 15 days of technical visits to the Pinacoteca do Ceará, using the Leica BLK360 laser scanning equipment.

Taking into account the monumental scale of the building, the rhythmic succession of the industrial warehouses, and the complexity of its ornaments, the laser capture strategy was designed to mitigate occlusion zones. To this end, 601 setups (scanner positions) were carried out, strategically spaced across the interior of the warehouses, accessible service areas, and the external perimeter. Each capture cycle, set to a medium point density, required approximately 5 minutes, providing a detailed sampling of the masonry, metallic structural systems, and ornaments (Figure 02).

Figure 02 - Pinacoteca do Ceará viewed in the Cyclone Register 360 software with visible setups



Source: By the authors

3.1.2 Aerial Photogrammetry

Parallel to the terrestrial scanning, a photogrammetric survey was conducted using an Unmanned Aerial Vehicle (UAV), model DJI Mavic 3T Enterprise, during a single day of fieldwork at the study site.

This technique was essential for documenting the roofs and elevated parapets, areas invisible to the terrestrial laser scanner. High-quality photogrammetric images with adequate overlap were acquired (Figure 3), which were subsequently processed in the Reality Scan software. This process generated a triangle mesh in approximately 47 minutes, providing the fundamental geometric baseline for the building's roofs.

Figure 3 - Aerial photographs of the Pinacoteca do Ceará captured by drone



Source: By the authors

3.1.3 Documentary Survey and Secondary Data (CAD Base)

Beyond active reality captures, the methodology required the collection of secondary data. The use of pre-existing CAD documentation—composed of floor plans from complementary projects, such as hydraulic and electrical installations—was motivated by the impossibility of fully covering the building through laser scanning, due to the survey team's restricted access to specific areas of the Pinacoteca. Consequently, sectors such as service cores, restrooms, and pantries presented gaps in

the resulting point cloud, necessitating the collection and utilization of these secondary sources to subsequently ensure the completeness and volumetric integrity of the BIM model.

3.2 Data Processing and Integration

3.2.1 Registration, Photogrammetric Processing, and Unification

The initial processing of the laser scanning (TLS) data was carried out in the Leica Cyclone Register 360 software. The raw point cloud, resulting from the union of multiple scans, totaled 2,098,098,135 points, presenting a root mean square (RMS) error of 0.007 m. Due to the repetitive modularity of the Pinacoteca do Ceará's railway architecture, the purely automatic alignment algorithm was susceptible to incorrect geometric overlaps between homologous geometries. Thus, the manual registration of the setups was adopted. The procedure consisted of a visual pre-alignment, followed by an automatic mathematical refinement using the software's native Cloud-to-Cloud (C2C) algorithm. This process ensured the preservation of geometric fidelity and prevented spatial distortions and the propagation of errors along the succession of warehouses.

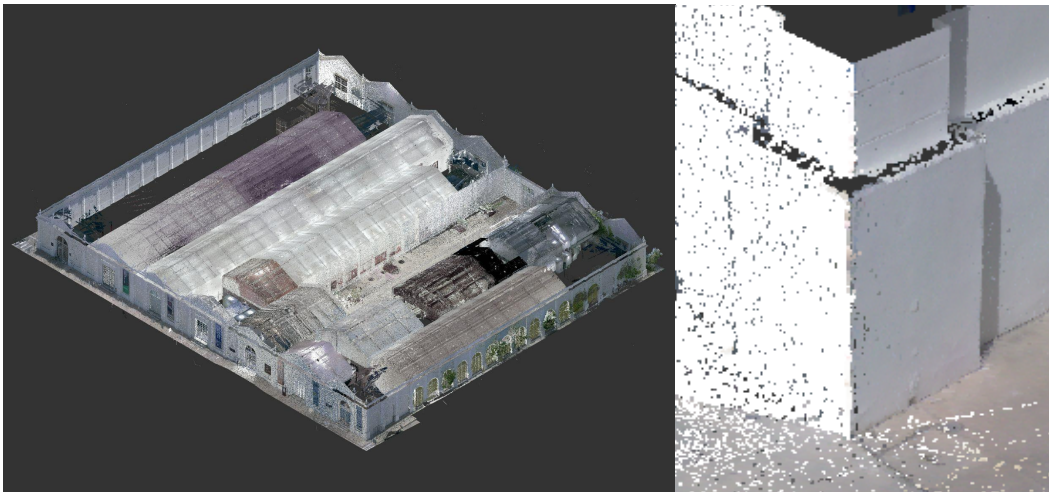
Concurrently, the data captured by the UAV was processed in the Reality Capture software to generate the aerial photogrammetric model. The processing was executed on a workstation equipped with an AMD Ryzen 9 7900X (4.70 GHz) processor, 32 GB of RAM, and an NVIDIA GeForce RTX 4070 (12 GB) graphics card. The photogrammetric reconstruction resulted in the generation of the point cloud in approximately 47 minutes, providing the fundamental geometric baseline for the building's roofs.

The consolidation of these multimodal datasets was performed in the CloudCompare software. To align the different scales and coordinate systems, the TLS point cloud was adopted as the absolute reference (spatial anchor), since its sub-centimeter precision is guaranteed in the surveying of interiors and facades. The photogrammetric cloud was imported and subjected to an initial alignment by selecting homologous points (point-pair picking), followed by a fine adjustment of translation, rotation, and scale using the Iterative Closest Point (ICP) algorithm. The final unified cloud, composed of the 601 terrestrial laser stations and the aerial survey, mitigated the individual visual restrictions of each method, consolidating an integral and highly reliable geometric base for the object of study.

3.2.2 Refinement, Segmentation, and Interoperability

Before beginning the modeling process, the unified point cloud was imported into Autodesk ReCap, an environment dedicated to the manipulation and cleaning of spatial data. During this stage, "slicing" and the removal of noise and captured elements that do not add geometric value to the object of study—such as vegetation, vehicles, pedestrians, and adjacent buildings—were carried out. This cleaning process is vital for the computational optimization of the model, preventing the loading of unnecessary data and ensuring an unobstructed view of the building's geometry (Figure 4).

Figure 4 - On the left, the complete point cloud of the Pinacoteca. On the right, segmentation of the cloud, highlighting a single pillar to capture more specific details in a more optimized manner.



Source: By the authors

A fundamental aspect of this stage was the segmentation of the point cloud. The robust file was preserved for future use, while a copy was fragmented into smaller subsets with specific characteristics, enabling the diagnosis and isolated observation of elements such as facade ornaments, frames, and internal compartments. This division allowed the computer to process only the geometric fragment required for each modeling stage. With the point cloud refined, segmented, and optimized, the data constituted an ideal substrate for import into Autodesk Revit, the platform where parametric modeling commenced.

3.3 HBIM Representation

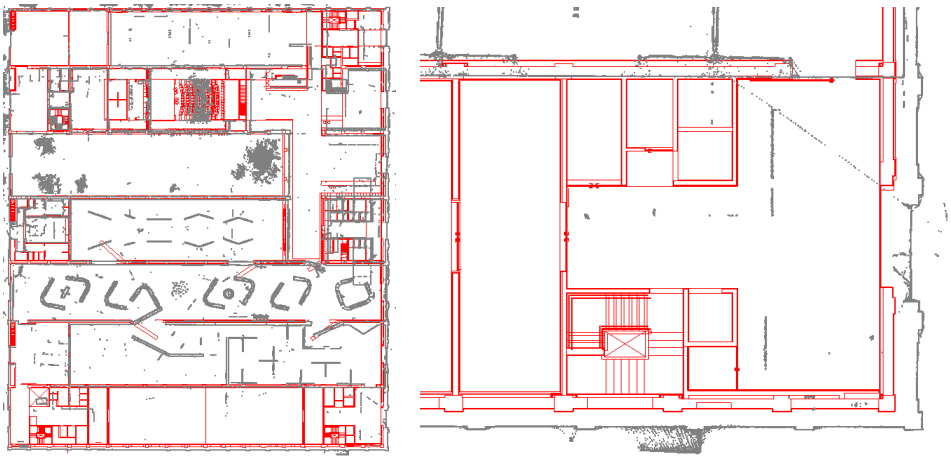
The development of the HBIM model for the Pinacoteca do Ceará was founded on the premise of achieving a more accurate modeling of the built reality, aiming to consolidate a precise database for the management and safeguarding of the heritage asset. To ensure the integrity and completeness of the model, a hybrid strategy was adopted, integrating direct reality capture via the Scan-to-BIM workflow with the use of secondary documentary sources (CAD) for areas with restricted access or incomplete capture coverage.

3.3.1 Definition of hybrid strategy (point cloud + CAD)

Upon overlaying the pre-existing CAD documentation onto the point cloud, significant geometric and dimensional divergences were identified, such as variations in the thickness of structural walls, discrepancies in usable areas, and alterations in the internal spatial configuration (Figure 5).

Considering the typology of the Pinacoteca do Ceará (characterized by wide open warehouses with peripheral service cores), a hybrid modeling strategy was adopted. The point cloud, obtained through laser scanning and aerial photogrammetry, was established as the primary geometric reference for large alignments and facades. For the service blocks, where access for reality capture was restricted, the CAD base was utilized with local adjustments anchored to reliable references from the point cloud. This decision is based on the premise that cumulative errors in traditional surveys tend to be more critical over large expanses, whereas smaller environments exhibit greater precision.

Figure 5 - Overlay of the CAD model (in red) onto the Point Cloud



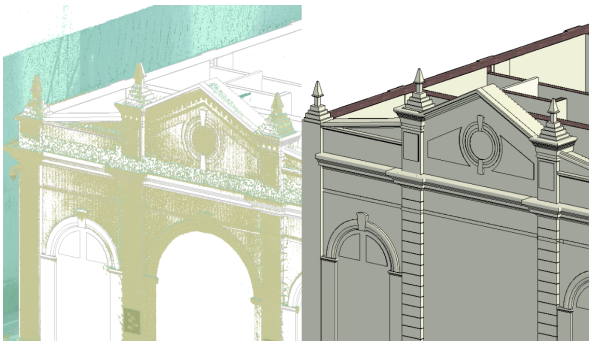
Source: By the authors

3.3.2 Parametric Modeling by Elements

After the consolidation of the point cloud and the definition of the integration guidelines with secondary data, the workflow focused on the BIM environment, using Autodesk Revit as the modeling software. The point cloud, linked to the project, served as a three-dimensional guide for geometry extraction. To enable technically precise modeling, section boxes and multiple transverse and longitudinal sections were systematically generated. These features allowed the tracing of baselines for walls and structural elements directly over the point cloud sections, ensuring that the model incorporated the asymmetries and the lack of orthogonality detected in the survey.

Unlike conventional modeling based on schematic plans, the process prioritized the creation of native geometries and Revit families that reflected the actual state of the heritage asset (Figure 6).

Figure 6 - Modeling of the Pinacoteca do Ceará's main facade captured via Laser Scanner overlaid on the Point Cloud.



Source: By the authors

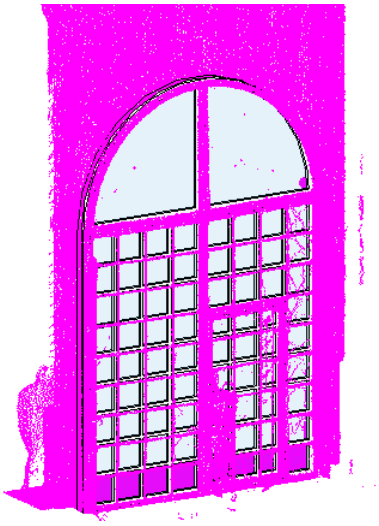
In the process of representation by categories of constructive elements, the modeling workflow was segmented into distinct strategies, adapted to the geometric complexity and nature of each component of the Pinacoteca.

The walls were identified through the analysis of the voids between the captures of internal and external faces in the point cloud. The modeling strategy consisted of subdividing each wall into three distinct layers: two fixed finishes of 2.0 cm and a structural core of variable thickness, adjusted

according to the actual dimension detected in the cloud. This method allowed for the precise documentation of thickness variations throughout the building.

In the case of the frames, the procedure consisted of isolating specific cutouts from the original point cloud using Autodesk ReCap software. These cutouts were processed in CloudCompare to ensure format compatibility within the Revit family editing environment. From this, these cloud segments were used to base the modeling of the different types of frames (Figure 7).

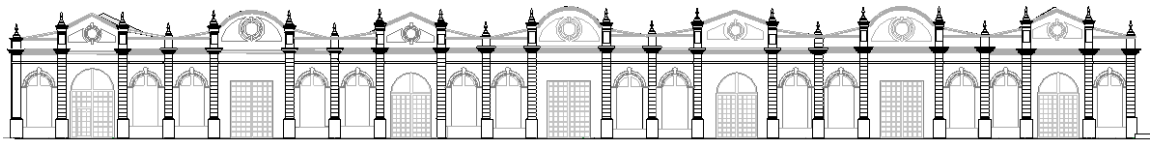
Figure 7 - Window and Door Modeling Process in Revit Using the Point Cloud



Source: By the authors

Regarding the ornaments, due to their singular and non-standardized geometry, Revit's in-place modeling tool was utilized. The process was supported by sections, views, and floor plans extracted directly from the point cloud, complemented by the visual aid of panoramic images captured by the laser scanner. Access to the 360° images recorded during the captures allowed for a detailed visual verification of textures and reliefs which, at times, are difficult to interpret solely through the point cloud.

Figure 8 - Modeling of the Main Facade of the Pinacoteca do Ceará in Revit



Source: By the authors

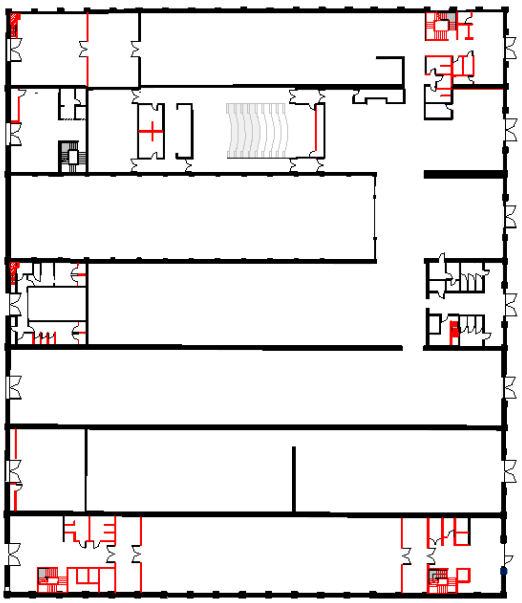
3.3.3 Characterization of Data Origin and Informational Reliability

To ensure the reliability of the information and the HBIM model, an intrinsic parameter was applied to the wall elements to characterize the provenance of each component. Thus, the origin of the element is recorded, safeguarding the precision of the point cloud survey process.

The use of this data field enabled the implementation of graphic override filters within the BIM environment, facilitating the visual identification of each geometry's origin in floor plans and sections. This methodological decision is fundamental for future asset management, as it allows researchers and managers to promptly identify which areas possess greater precision and which present higher

informational uncertainty due to access restrictions during the survey. Consequently, the model establishes itself not only as a geometric representation but as a technical record regarding the reliability of the Pinacoteca survey.

Figure 9 - Differentiation of Modeling Provenance between CAD (in red) and Point Cloud (in black)



Source: By the authors

Figure 10 - Modeling Provenance Property extracted from CAD

Dados de identidade	
Imagem	
Comentários	CAD
Marca	
Aprovado	☑
Reprovado	☑

Source: By the authors

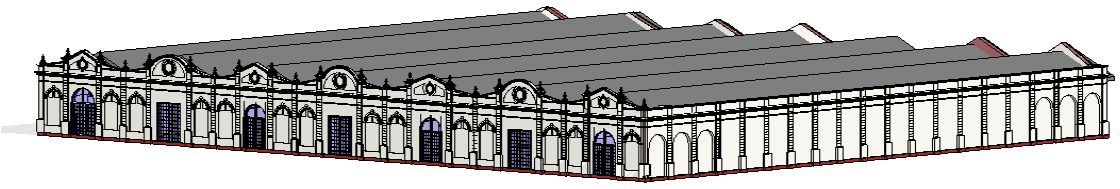
4. Results

The Scan-to-BIM workflow of the Pinacoteca do Ceará resulted in an HBIM model that is geometrically more precise and, unlike traditional surveys, allows for the inclusion of information intrinsic to the elements.

By overlaying the point cloud—generated by the integration of Laser Scanning and aerial photogrammetry—onto the CAD records, critical discrepancies were identified, such as the lack of orthogonality in structural walls and millimeter-scale variations in door and window openings. While imperceptible in conventional surveys, these are decisive for diagnosing pathologies and planning conservation interventions.

The effectiveness of the adopted hybrid strategy is manifested in the ability to fully represent the object, even in the face of access restrictions in certain sectors. To ensure the intellectual integrity of the model, the application of a data provenance filter was fundamental. This approach allowed each parametric component to be categorized according to its source of origin (point cloud or secondary documentation), granting the model the character of a historical and scientific record.

Figure 11 - General View of the Model in Revit



Source: By the authors

5. Final Considerations

The process of digitization and HBIM representation of the Pinacoteca do Ceará, using the Scan-to-BIM methodology, proved to be more than just an exercise in spatial representation; it also establishes itself as a rigorous protocol for the protection and safeguarding of built cultural heritage. The results obtained indicate that reality capture through Laser Scanning and photogrammetry is of paramount importance in overcoming the geometric inconsistencies typically found in traditional manual surveys. The resulting model is more than a mere visual representation; it is also a repository of deformities, misalignments, and real metrics that characterize the object's material identity accumulated over time (Alshawabkeh and Baik, 2024).

One of the central factors addressed in this research was the inconsistency of pre-existing documentation when faced with the complexity of a historical building. Over time, 2D CAD records or manual analog sheets tend to "idealize" the space, imposing orthogonalities and symmetries that very rarely survive the construction phase or the passing of years. In the case of the Pinacoteca, the identification of structural walls outside of orthogonal alignment demonstrated that old documentation, while valuable from a historical and documentary standpoint, is insufficient as a geometric database for interventions and management.

In this context, the article proposes that historical records be approached as complementary and secondary sources, useful for understanding internal materials, hidden systems, or smaller, specific areas. The primacy of point clouds over drawing ensures that the analysis of pathologies and restoration components is performed with the aid of a base that is millimetrically faithful to the original building. The union of active and passive sensors filled data gaps caused by occlusions, culminating in a model that ranges from the detail of facade ornaments to the complex volumes of parapets and roofs. Unlike BIM models generated for new constructions, where precision is assumed by the design, in HBIM, parametric elements possess their own provenance configuration. The introduction of parameters in the Pinacoteca model—characterizing elements modeled through laser scanning, aerial photography, or a historical plan—is a technical advancement. Such a distinction makes it explicit to heritage managers where the information is a faithful capture of reality and where it is merely a documentary inference. This clarity is fundamental for decision-making in maintenance and restoration works.

The produced HBIM representation transcends pre-existing passive documentation. By integrating non-orthogonalities and temporal deformations, the file transforms into an input for structural analysis. Unlike models generated through standard plans, which simulate ideal equilibrium

scenarios, the Digital Twin of the Pinacoteca allows for simulations that take real geometric deviations into account, enabling monitoring over time.

Furthermore, for the entities managing the facility, the model can also become a tool for asset management, building maintenance, and logistical information. The ability to aggregate conservation data into specific elements optimizes the planning of events such as painting cycles, roof cleaning, and component replacement, in addition to streamlining resources and ensuring the longevity of the Pinacoteca do Ceará.

As a next step, the study points to the need for standardizing the provenance parameters of the modeled data. The segmentation of recording methods across different buildings and contexts ultimately hinders comparisons between models. Therefore, it is proposed to develop a recording confidence metric to be applied universally to HBIM models created for the same purpose, even by different teams. This metric would enable researchers and maintenance agencies to quantitatively and qualitatively assess the degree of precision and reliability of entire digital collections.

Acknowledgments

This work was financially supported by FUNCAP, Project 01172921/2022 – Cientista Chefe Cultura, Project 10581391/2022 – International collaboration FUNCAP/INSA Rouen Normandie; by the National Council for Scientific and Technological Development (CNPq) – Project 302054/2022-7 – PQ2, by the Project - 440926/2024-6 – VISION and Project - 402828/2024-0 – CLIC, CAPES Foundation and Finep 2896/24.

References

NI, Zhongjun et al. **Parametric Digital Twins for Preserving Historic Buildings**: A Case Study at Löfstad Castle in Östergötland, Sweden. Norrköping: Linköping University, 2024. Acesso em: 28 mar. 2026.

SALAH, Rnin; GÉCZY, Nóra; KÁROLYFI, Kitti Ajtayné. **Predictive hybrid scan-to-BIM method improves heritage building documentation completeness and accuracy**. Scientific Reports, v. 16, n. 1, 2026.

Barrile, V., Bernardo, E., & Bilotta, G. (2022). An Experimental HBIM Processing: Innovative Tool for 3D Model Reconstruction of Morpho-Typological Phases for the Cultural Heritage. Remote Sensing, 14(5), 1288.

ALSHAWABKEH, Yahya; BAIK, Ahmad; MIKY, Yehia. **HBIM for Conservation of Built Heritage**. ISPRS International Journal of Geo-Information, [s. l.], v. 13, n. 7, p. 231, jul. 2024. Disponível em: https://doi.org/10.3390/ijgi13070231. Acesso em: 28 mar. 2026.

Cinpar 2026
XXII International Conference on Building Pathology and Constructions Repair
15th to 17th July 2026 - Lisboa, Portugal

A Multi-Sensor Acquisition Framework for Built Heritage Documentation: Application at the Church of Nossa Senhora da Conceição de Almofala

José L. G. MENDES[1], Guilherme L. de Oliveira[2], Renan Nogueira Paulo[3], Eugênio MOREIRA[4], **Esequiel MESQUITA**[5]

[1] Laboratory of Digital Experience - Federal University of Ceara, Brazil, lucasmendes@arquitetura.ufc.br
[2] Laboratory of Digital Experience - Federal University of Ceara, Brazil, guilhermeoliveira@arquitetura.ufc.br
[3] Laboratory of Digital Experience - Federal University of Ceara, Brazil, eugeniomoreira@iaud.ufc.br
[4] SHMeeLAB - University of Perugia, Italy, renanpaulo2712@gmail.com
[5] Laboratory of Digital Experience - Federal University of Ceara, Brazil, emesquita@ufc.br

Abstract: The preservation of built cultural heritage is frequently hindered by a lack of precise technical documentation, which is essential for restoration interventions and heritage management. Given the limitations of conventional methods in capturing complex geometries, this paper proposes and validates an operational multi-sensor acquisition framework for high-fidelity geometric documentation. The protocol is structured around the integration of reality-capture technologies to overcome challenges related to occlusion and scale, and was tested and validated at the Church of Nossa Senhora da Conceição de Almofala (Itarema/CE, Brazil), a nationally listed landmark characterized by demanding environmental and morphological conditions. The framework's methodology is organized into stages of pre-survey planning, technological zoning, and the integration of data from three complementary sensors: terrestrial laser scanning (TLS), mobile mapping (SLAM), and aerial photogrammetry via unmanned aerial vehicles (UAV). This workflow enabled the consolidation of a dense point cloud comprising approximately 639 million points with a residual metric error of only 0.003 m, ensuring the geometric completeness of both complex interiors and inaccessible roof structures. The results demonstrate that the proposed framework is effective in eliminating occlusion zones and generating a metrically reliable digital representation suitable for supporting Heritage Building Information Modeling (HBIM) processes. The primary contribution of this study lies in defining a systematized, transferable workflow that transforms raw multi-sensor geometric data into high-precision geometric information for the safeguarding and management of built heritage.

Keywords: HBIM, Multi-scanner Digitization, Digital Safeguarding

1. Introduction

Built cultural heritage documentation is a fundamental component of conservation, restoration, management, and long-term knowledge transmission, since interventions on historic buildings depend on reliable records of their geometry, materials, condition, and spatial organization (ICOMOS 1964; Antonopoulou and Bryan 2017; ICOMOS 2007). Traditional documentation methods based on manual survey, 2D drawings, photographic records, and descriptive reports remain valuable, but they are often insufficient when high geometric completeness, metric reliability, three-dimensional representation, and data reusability are required (Boardman and Bryan 2018; Oliveira 2008).

Recent advances in reality-capture technologies have significantly expanded the possibilities for heritage documentation. Terrestrial laser scanning (TLS), digital photogrammetry based on Structure-from-Motion (SfM), and mobile mapping systems based on Simultaneous Localization and Mapping (SLAM) can generate dense three-dimensional datasets with different balances of accuracy, speed, coverage, and operational flexibility, making them especially useful in complex historic environments. However, none of these technologies is universally sufficient on its own. Their performance depends on object scale, accessibility, surface properties, lighting conditions, occlusions, and the intended level of geometric detail, which makes methodological planning and sensor selection critical steps in the documentation process (Sammartano

and Spanò 2018; Remondino et al. 2014; Bedford 2017; Boardman and Bryan 2018). This issue is particularly relevant in historic buildings, where irregular geometries, inaccessible roof structures, narrow interiors, highly reflective surfaces, and environmental constraints frequently limit the effectiveness of single-sensor workflows (Themistocleous et al. 2015). For this reason, current best practice increasingly favors hybrid acquisition strategies in which different technologies are assigned to different zones or documentation tasks according to their technical suitability, and later integrated into a common spatial reference framework (ICOMOS 2007; Argasiński and Kuroczyński 2023).

Although Heritage Building Information Modeling (HBIM) has become an important framework for the structured representation and management of historic buildings, the quality of any future HBIM model depends directly on the reliability and completeness of the survey data from which it is derived (López et al. 2018). Accordingly, this research focuses on the preceding stage: the definition and application of a multi-sensor acquisition protocol capable of generating a consolidated point cloud suitable for supporting future scan-to-HBIM developments. This paper proposes a multi-sensor protocol for the geometric documentation of built heritage, organized into four articulated stages: pre-survey planning, technological zoning and field acquisition, multi-source registration and consolidation, and quality-oriented preparation of the final point cloud. The protocol is applied and discussed through the case of the Church of Nossa Senhora da Conceição de Almofala in Ceará, Brazil, a historic building whose morphology and environmental conditions provide a demanding testbed for hybrid acquisition. The paper's contribution lies in demonstrating how a structured acquisition protocol can support complete, metrically consistent, and operationally viable documentation in a complex heritage context.

2. Multi-sensor acquisition protocol

The documentation of built heritage through digital reality-capture technologies requires more than simply selecting appropriate sensors. It requires a structured operational workflow capable of ensuring geometric completeness, metric consistency, and traceability of results across successive stages. Based on current best practice in heritage survey (Antonopoulou and Bryan 2017; Boardman and Bryan 2018; Bedford 2017), the protocol proposed here is organized into four sequential and interdependent macrophases: (1) pre-survey planning and requirements definition; (2) technological zoning and sensor assignment; (3) field acquisition; and (4) multi-source registration, consolidation, and quality control. Each phase conditions the quality of the next, making them interdependent rather than merely sequential. (figure 1)

2.1 Pre-survey planning and requirements definition

Before any field operation begins, the documentation requirements must be formally defined. This includes establishing the expected geometric level of detail (LOD), the spatial extent of the survey, the sensors available, and the intended use of the resulting data (Groetelaars 2015; Bedford 2017). In the context of heritage documentation, the LOD determines the acceptable point spacing and the minimum positional accuracy of the final dataset, which in turn guides sensor selection and field strategy. For example, LOD 300 (compatible with intervention projects and standard HBIM) typically requires point spacing between 3 and 10 mm and a metric precision in the order of 5–10 mm, while LOD 400 (detail and ornament documentation) may require sub-3 mm resolution (Boardman and Bryan 2018; Bedford 2017).

A critical component of pre-survey planning is defining the geodetic control strategy. Georeferencing through a network of ground control points (GCPs) measured with a total station or GNSS equipment is the recommended practice, as it enables the dataset to be placed in an absolute spatial reference system, supports integration with cartographic data, and makes the results verifiable against independent measurements (Fryskowska 2017). The geometry of the GCP network matters more than the number of points alone: well-distributed control points across the building's vertical and horizontal extents are essential for constraining systematic errors in both TLS registration and SfM photogrammetric adjustment (Page et al. 2017).

However, a georeferenced control network is not always operationally feasible, due to access constraints, regulatory restrictions, budget limitations, or time pressures in the field. In such cases, it is still possible to produce a metrically reliable and internally consistent multi-sensor dataset by adopting a relative

registration strategy: one acquisition is designated as the fixed reference, and all others are aligned to it. The sensor chosen as the reference must have the highest intrinsic metric precision. Among the technologies typically used in heritage documentation, terrestrial laser scanning (TLS) has consistently demonstrated the highest internal metric accuracy, with point-positioning errors generally in the range of 1–6 mm, depending on distance and scanner model (Fryskowska 2017). As a consequence, when absolute georeferencing is unavailable, the consolidated TLS point cloud should be established as the fixed reference cloud, and all other datasets should be aligned to it. The TLS cloud should not be scaled or transformed; it remains the geometric ground truth of the relative coordinate system.

This two-tier approach preserves metric integrity in both scenarios while honestly acknowledging the difference between absolute accuracy (position in a global reference system) and relative accuracy (internal geometric consistency of the dataset). For most conservation, documentation, and HBIM-preparation purposes, high relative accuracy is the primary requirement (Antonopoulou and Bryan 2017).

2.2 Technological zoning and sensor assignment

A key methodological decision in multi-sensor survey design is the spatial assignment of each technology to the building zones for which it is best suited. This technological zoning approach is grounded in the complementary nature of the available sensors: each technology has specific strengths and limitations regarding range, accuracy, occlusion tolerance, accessibility, and operational speed.

TLS is the most appropriate technology for zones requiring high metric accuracy at close to medium range: interior spaces, façades, and structurally significant elements where precise dimensional data is essential (Boardman and Bryan 2018; Bedford 2017). SLAM mobile scanning is best deployed for general volumetric capture of circulation spaces, interior-exterior transitions, and areas where speed is operationally critical but millimetric precision is not the primary requirement (Sammartano and Spanò 2018). UAV photogrammetry (SfM) is a viable technology for inaccessible zones such as roof surfaces, tower tops, and upper cornices, while also providing important chromatic and textural information (Themistocleous et al. 2015; Remondino et al. 2014). Table 1 summarizes the technology–zone assignment logic that informs the protocol.

Table 1 – Technology–zone assignment matrix for multi-sensor heritage documentation: recommended sensor allocation by spatial zone, documentation priority, and acquisition strategy.

Zone	Priority	Assigned technology
Interior spaces (general)	Speed, continuity	SLAM
Interior details, altars, ornaments	Metric accuracy	TLS
Façades and exterior walls	Metric accuracy, color	TLS
Roof surface and upper coverage	Coverage, accessibility	UAV (SfM)
Tower tops and inaccessible upper zones	Coverage, accessibility	UAV (SfM)
Interior–exterior transitions	Geometric continuity	SLAM

The occlusion zones specific to each building (defined by its morphology, height, and spatial organization) must be identified during pre-survey reconnaissance and explicitly addressed in the zoning plan. The fundamental principle is that the limitations of each technology must be compensated by the strengths of another, so that the composite dataset achieves spatial continuity without relying on any single sensor to cover the entire building.

2.3 Field acquisition

The field acquisition sequence follows the zoning plan, but should also be ordered to maximize the value of each step. The recommended sequence is: SLAM first, to establish a rapid global volumetric context; UAV second, to capture the inaccessible upper zones; and TLS last, to provide the metric ground-truth layer for registration.

SLAM acquisition should begin with a closed-loop trajectory that connects interior and exterior spaces in a single continuous pass. Closed-loop trajectories are essential for SLAM-based systems because they allow the algorithm to detect the return to a previously mapped location and use that constraint to correct drift errors accumulated during the scan (Sammartano and Spanò 2018). The SLAM output is a dense, continuous but less precise point cloud that serves primarily as a volumetric connector between the higher-accuracy datasets.

UAV photogrammetric acquisition should be planned in two complementary flight modes: nadir (gimbal at 90°) for systematic roof coverage and accurate orthorectification, and orbital (oblique, 45°–60°) for upper façade areas, cornices, eaves, and tower surfaces that neither ground sensors nor the nadir pass can capture. To ensure reliable SfM convergence, a minimum frontal overlap of 75–80% and a lateral overlap of at least 60% are recommended; higher overlaps are particularly important in orbital flight modes around complex architectural volumes, where surface texture variability and convergent viewing angles increase the risk of keypoint-matching failures (Bedford 2017). If GCPs are available, they should be distributed to cover the full vertical extent of the building, not just the ground plane, to constrain photogrammetric distortions across all elevations (Fryskowska 2017). When operating under challenging illumination conditions (such as strong solar radiation on highly reflective surfaces), acquisition should be planned according to sun position to mitigate overexposure and keypoint-detection failures in SfM/MVS processing (Remondino et al. 2014).

TLS acquisition should follow a station plan that ensures a minimum 30% overlap between adjacent scans, which is necessary for reliable scan-to-scan registration and error minimization (Boardman and Bryan 2018). Stations should be positioned to provide redundant coverage of structurally and architecturally significant zones, and to include areas already captured by SLAM and UAV, enabling cross-sensor validation. Where reflective surfaces challenge laser return quality, HDR scanning (multiple exposure intensities per station) can help recover surface detail.

2.4 Multi-source registration, consolidation, and quality control

The processing stage transforms heterogeneous raw data into a single, geometrically coherent and quality-assessed point cloud. This is the most methodologically sensitive stage because systematic errors in any dataset propagate into the final product if not detected and corrected.

TLS registration and consolidation should be performed first, as this dataset forms the metric backbone of the final model. Individual scans can be aligned through several methods, depending on available resources and field conditions: (a) target-based registration, using artificial retro-reflective markers or natural reference objects placed at known positions to establish geometric correspondences between scans; (b) automatic cloud-to-cloud registration, where algorithms detect and match geometric features across overlapping scans without the need for physical markers, reducing field setup time but requiring sufficient geometric complexity in the scene (Shao et al. 2019); and (c) hybrid registration, combining a manual or visual coarse pre-alignment (in which the operator positions scans into approximate spatial correspondence using identifiable architectural features) with a subsequent ICP-based fine adjustment that iteratively minimizes point-to-point or point-to-surface distances to convergence. Regardless of the method used, a global bundle adjustment should follow individual scan pairing to distribute residual errors across all scan positions rather than accumulating them sequentially. The output should be assessed using a quality report that documents per-scan overlap, link strength, and maximum registration error; an RMS registration error below 5 mm is generally acceptable for LOD 300 documentation.

SfM photogrammetric processing should include bundle adjustment of camera positions and orientations, followed by dense multi-view stereo (MVS) reconstruction. If GCPs are available, they are introduced at this stage to constrain the photogrammetric model to the absolute or relative reference system. If GCPs are not available, the photogrammetric model is processed in its own coordinate system and subsequently aligned to the TLS reference cloud.

Multi-sensor integration is performed by aligning SLAM and SfM outputs to the fixed TLS reference cloud. The alignment should follow a progressive three-step strategy: coarse manual alignment, semi-automatic point-pair picking using unambiguous architectural features (corners, ridge lines, eave edges), and fine iterative closest point (ICP) refinement. The TLS cloud is kept fixed at all stages; only the SLAM and SfM clouds are transformed. Post-fusion cleaning includes spatial subsampling to remove redundant points at zones of overlap, topological filtering to eliminate disconnected islands, and statistical outlier removal (SOR). The consolidated point cloud should be evaluated with respect to three quality criteria: (a) registration accuracy, expressed as maximum and mean registration error; (b) spatial coverage, assessed visually and by identification of residual occluded zones; and (c) point density consistency, to ensure homogeneous coverage across zones surveyed by different sensors.

The final product is a georeferenced (or TLS-anchored) multi-source point cloud with documented provenance, verified registration metrics, and explicit notation of any residual limitations. This dataset constitutes the primary input for subsequent semantic segmentation and HBIM representation workflows (Dore and Murphy 2017).

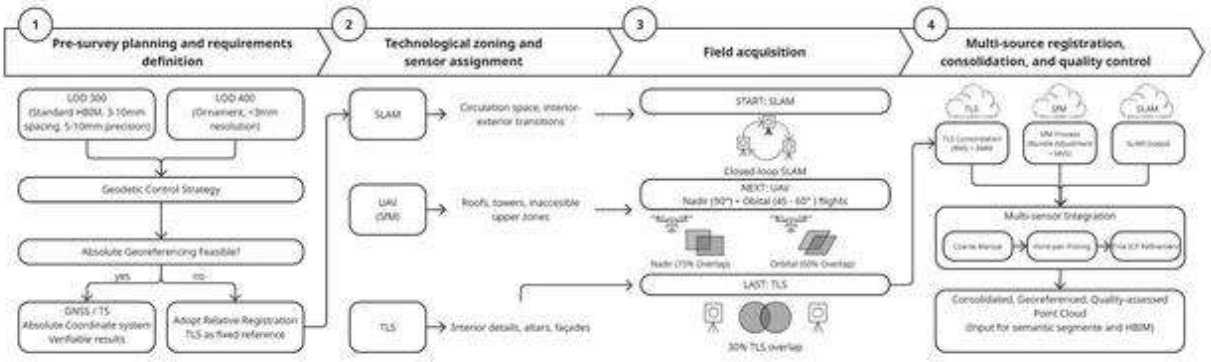


Figure 1 – Multi-sensor acquisition protocol diagram Source: Author

3. Case study: Church of Nossa Senhora da Conceição de Almofala

The Church of Nossa Senhora da Conceição de Almofala, located in Itarema, Ceará, Brazil, was erected in 1712 and is listed as national heritage by the Instituto do Patrimônio Histórico e Artístico Nacional (IPHAN, process no. 1000-T-79, 1980) (figure 2). The building is notable for having been buried under mobile coastal dunes between 1897 and the 1940s, a process that subjected the masonry fabric to exceptional geomorphological stress and contributes to its ongoing significance as both an architectural and cultural landmark. The church follows a colonial plan composed of a single nave, a lateral sacristy, and a bell tower rising above the main façade, with a two-pitch ceramic tile roof that is structurally complete but partially degraded. The exterior surfaces are finished in whitewashed lime render, producing characteristically high surface reflectance.

As a validation environment for the proposed protocol, Almofala concentrates several categories of constraint that are representative of difficult heritage survey conditions. Morphologically, the vertical mass of the bell tower creates significant occlusion zones for any ground-based sensor, while the sloped roof surface and its upper cornices are entirely inaccessible to terrestrial instruments. Internally, the transition between the nave, the altar, and the sacristy generates spatial continuity challenges that fixed-station sensors cannot easily resolve without a high number of setups. Environmentally, the coastal setting introduces persistent aeolian instability that limits UAV operational windows, and the combination of intense solar radiation and high surface albedo on the whitewashed façades creates overexposure conditions that challenge both photogrammetric keypoint detection and laser intensity homogeneity. The convergence of these morphological and environmental constraints, which affect all three sensor families in distinct ways, makes the Church of Almofala a demanding yet representative testbed for verifying the

practical applicability, robustness, and complementarity of the multi-sensor acquisition protocol described in Section 2. (figure 2)



Figure 2 – The Church of Nossa Senhora da Conceição de Almofala today. Source: Project archive.

4. Application of the protocol at Almofala

4.1 Pre-survey decisions

Prior to fieldwork, the scope of documentation was defined in alignment with the project team's conservation and research objectives. The target level of detail was established at LOD 300 for the architectural body as a whole, with localized LOD 400 coverage for the altar's high-complexity interior elements and carved wooden ornamentation (Figure 3). The survey was designed to produce a geometrically complete, chromatically accurate, and metrically consistent point cloud of the entire building, including all façades, the roof surface, the bell tower, and the interior nave, suitable to serve as the primary geometric input for future HBIM development. A georeferenced geodetic control network was not established during this campaign due to operational constraints. Accordingly, the consolidated TLS point cloud was designated as the fixed metric reference, and all other datasets were aligned to it, following the relative registration strategy described in Section 2.2. The three sensors mobilized were the Leica BLK360 (TLS), the Leica BLK2GO (SLAM), and the DJI Mavic 3T Enterprise (UAV photogrammetry, SfM). (Figure 4)



Figure 3 – the altar's high-complexity interior elements and carved wooden ornamentation



Figure 4 – (a) BLK 2Go, (b) BLK 360 e (c) Drone DJI Mavic 3T Enterprise. Source: Project archive

4.2 Technological zoning

The morphological and environmental constraints identified in Section 3 directly informed the sensor-to-zone assignment. The interior nave was assigned to SLAM for rapid volumetric capture, while the altar-mor and carved ornamental elements were assigned to TLS at maximum resolution density, given the priority of metric accuracy for these architecturally significant components. All exterior façades were assigned to TLS, with HDR scanning mode activated to compensate for the high albedo of the whitewashed lime render under direct solar radiation; façade capture was concentrated during periods of oblique natural light to preserve shadow detail in relief elements such as cornices and portals. The roof surface and the upper

sections of the bell tower, both inaccessible to ground sensors, were assigned exclusively to UAV photogrammetry. Interior-to-exterior spatial transitions were covered by SLAM as a geometric connector between the TLS interior and exterior setups.

4.3 Field acquisition sequence

Phase 1 — SLAM (BLK2GO). The SLAM acquisition was conducted as the first field operation to establish the building's global volumetric context. The operator followed a continuous closed-loop trajectory that began and ended at the same physical point, circling the exterior perimeter and passing through the interior nave via the main entrance. The closed-loop constraint allowed the SLAM algorithm to detect and correct accumulated drift errors at closure. The full trajectory was completed in approximately 15 minutes, yielding a continuous but moderate-density point cloud covering both interior and exterior volumes. (Figure 5)



Figure 5 – Performing SLAM (BLK2GO). Source: Research archive.

Phase 2 — UAV photogrammetry (DJI Mavic 3T Enterprise). The aerial acquisition was organized in two complementary flight modes. A nadir flight (gimbal at 90°) provided systematic coverage of the roof surface, yielding precise orthometric data on the condition of the ceramic tiles and the exact building footprint. An orbital flight executed three 360° passes around the church at varying altitudes, with the gimbal inclined between 45° and 60°, plus three additional focused passes at tower height to capture the bell tower faces, eave edges, and upper cornices. Flight operations were concentrated during meteorological calm windows to mitigate aeolian instability. A total of 470 images were captured, of which 466 were successfully aligned. Despite planning for favorable lighting conditions, the high albedo of the façades produced homogeneous textures and localized overexposure in sections of the orbital imagery, resulting in insufficient keypoint detection for SfM convergence. These areas were corrected by manually introducing control points tied to identifiable surface features (microfissures, weathering marks, and tile boundaries), thereby ensuring correct triangulation and restoring geometric continuity in the affected zones. (figure 6)



Figure 6 – Sample of nadir flight images (left); Sample of orbital flight (right). Source: Research archive.

Phase 3 — TLS (Leica BLK360). Fixed-station TLS scanning was performed last, providing the metric reference layer for the entire registration workflow. A stations were deployed, distributed across two fronts: interior stations concentrated on the altar and ornamental woodwork at maximum density, and exterior stations covering all façades at high resolution. Station placement ensured a minimum inter-scan overlap of 30%, sufficient for reliable scan-to-scan registration. HDR mode was applied at all exterior stations to balance the radiometric response between the intensely lit lime-render surfaces and the deep shadows at corbels and portals. (figure 7)(figure 8)



Figure 7 – PerformingTLS (Leica BLK360). Source: Research archive.

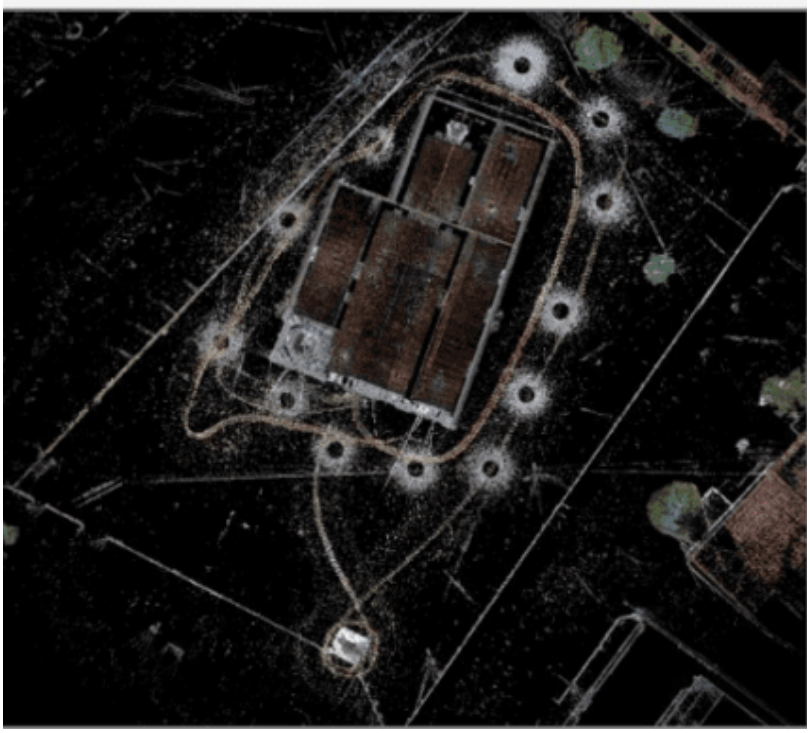


Figure 8 – TLS path (Leica BLK360). Source: Research archive.

4.4 Processing, registration, and consolidation

TLS and SLAM consolidation: The 26 TLS setups and 2 SLAM trajectories (all captured with Leica ecosystem equipment) were imported into Leica Cyclone REGISTER 360, which enabled native interoperability between the two sensor types within a single project environment. The registration workflow followed three steps: manual visual pre-alignment using overlapping geometric features; automatic ICP-based fine registration, generating per-link quality reports; and global bundle adjustment to minimize cumulative error across all connections. The consolidated terrestrial cloud exhibited approximately 430 million points, with a mean scan overlap of 69% and a maximum registration error of 0.003 m. (figure 9)

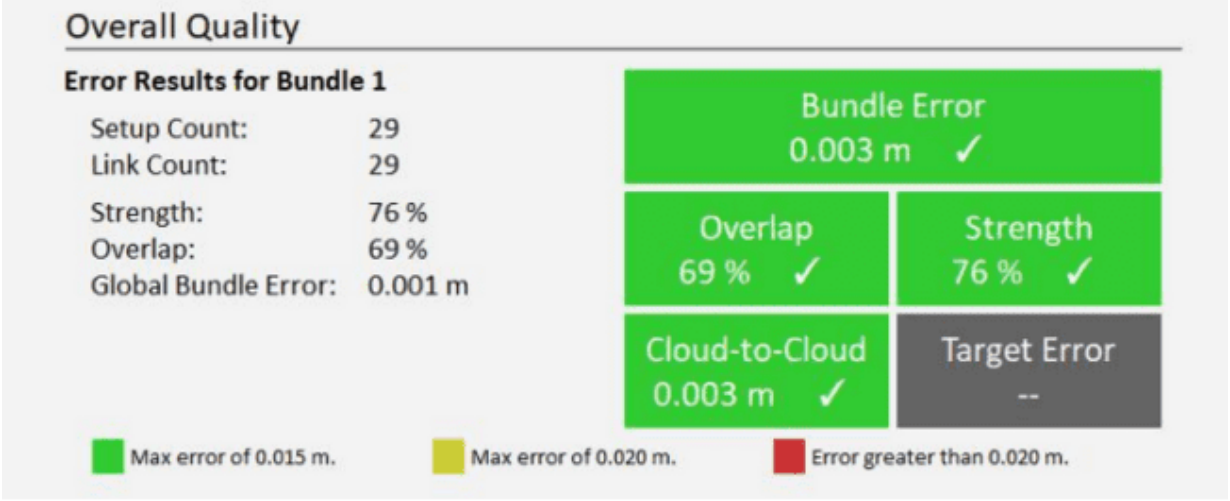
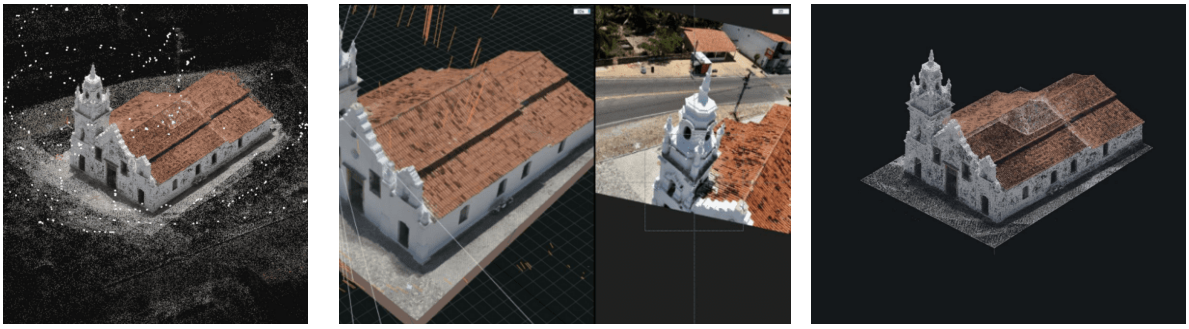


Figure 9 – Excerpt from the report generated by Cyclone REGISTER 360 for the terrestrial scan clouds. Source: Developed by the authors.

SfM photogrammetric processing: The 466 aligned images were processed in RealityScan using a standard SfM/MVS pipeline: SIFT-based keypoint detection, tie-point matching, bundle adjustment for camera orientation, and dense MVS reconstruction. A bounding box was applied prior to dense reconstruction to exclude surrounding elements. The resulting photogrammetric cloud contained approximately 288 million points, covering the roof surface, the bell tower, and the upper portions of all façades, with dense chromatic information. (figure 10)



(a) (b) (c)

Figure 10 – (a) Sparse cloud with tie-points and camera positions; (b) Process of manual control point insertion in RealityScan software; (c) Aerial photogrammetry result. Source: Developed by the authors.

Multi-sensor integration: Final fusion of the terrestrial and aerial datasets was performed in CloudCompare 2.13.1. The consolidated TLS cloud was established as the fixed reference. The SfM cloud was aligned using the hybrid three-stage strategy described in Section 2.5: coarse manual positioning, semi-automatic point-pair picking at six unambiguous architectural features (tower corners, ridge lines, eave extremities), and ICP fine refinement configured with a target RMS tolerance of 1.0×10^{-5} and a random sampling of 50,000 points per iteration. Post-fusion homogenization was performed using spatial subsampling at a 10 mm minimum inter-point distance, followed by topological filtering (Label Connected Components), statistical outlier removal (SOR), and manual trimming of residual artifacts. The final consolidated point cloud comprises approximately 639 million points, with smooth spatial transitions between the terrestrial and aerial layers and no identified residual occlusion zones in architecturally significant areas (Figure 11).

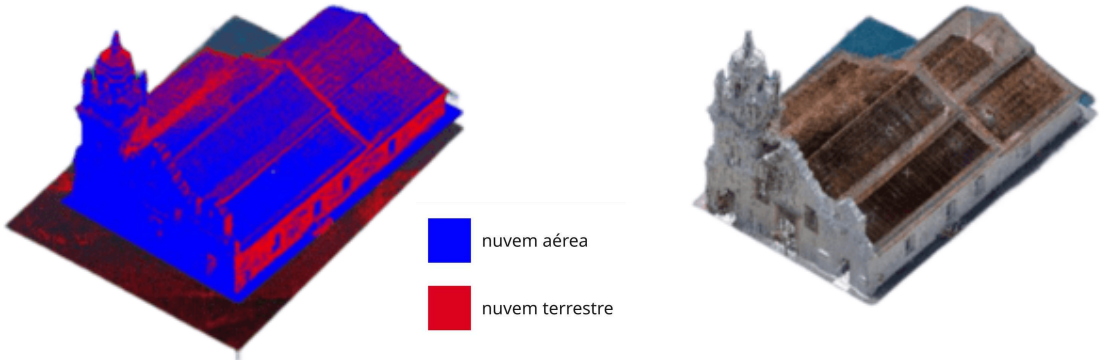


Figure 11 – Consolidated cloud. On the left, color-coded by source (terrestrial cloud/aerial cloud); on the right, with RGB coloring.

4.5 Results and quality assessment

The application of the protocol at the Church of Almofala produced a geometrically continuous, multi-source point cloud of the complete building in its current state of conservation. The maximum registration error of 0.003 m confirms metric consistency within the consolidated dataset at a level appropriate for LOD 300 documentation and compatible with the precision requirements for future parametric HBIM

representation. The sequential sensor deployment (SLAM for volumetric context, UAV for inaccessible upper zones, TLS for metric ground truth) demonstrated effective complementarity: the occlusion zones specific to each sensor were systematically compensated for by the coverage strengths of the others, and no single technology would have been capable of producing equivalent spatial completeness independently. Limitations acknowledged include the absence of absolute georeferencing, which restricts the dataset to a relative coordinate system and prevents direct integration with cartographic or topographic datasets without a subsequent alignment operation; and the manual correction required in the SfM photogrammetric model due to surface overexposure, which introduces a degree of interpretive intervention in the aerial point cloud that should be documented as part of the survey paradata (Bentkowska-Kafel and Denard 2016).

5. Conclusion

This paper proposed a structured multi-sensor acquisition protocol for the geometric documentation of built cultural heritage, organized around four interdependent stages: pre-survey planning and requirements definition, technological zoning and sensor assignment, sequential field acquisition, and multi-source registration with quality-oriented consolidation. The protocol was applied to the Church of Nossa Senhora da Conceição de Almofala, a nationally listed heritage building in Ceará, Brazil, whose morphological complexity and demanding coastal environment provided a representative and rigorous context for validation.

The results show that the structured combination of TLS, SLAM-based mobile scanning, and UAV photogrammetry, each assigned to the building zones for which it is technically most appropriate, can produce a metrically consistent and spatially complete dataset under conditions in which any single-sensor strategy would produce significant coverage gaps. The final consolidated cloud of approximately 639 million points, with a maximum registration error of 0.003 m, confirms that the workflow is operationally viable and produces data at a quality level compatible with LOD 300 heritage documentation requirements.

Two limitations must be explicitly acknowledged. First, the absence of a georeferenced geodetic control network restricts the dataset to a relative coordinate system, sufficient for documentation and conservation purposes but requiring a subsequent alignment operation before integration with absolute cartographic references. Second, the manual introduction of control points during SfM processing, which is necessary due to surface overexposure, constitutes an interpretive intervention that must be recorded as part of the survey paradata to ensure scientific transparency and reproducibility. Both limitations are consistent with real-world operational constraints and do not invalidate the protocol; rather, they illustrate the importance of explicit quality reporting and honest documentation of methodological decisions.

The primary contribution of this work is not the documentation of a specific building, but the definition of a transferable acquisition framework applicable to other heritage structures that present similar challenges of occlusion, inaccessibility, and environmental constraints. The resulting point cloud constitutes a geometrically reliable and traceable dataset suitable to serve as the primary input for future scan-to-HBIM workflows, in which the raw geometry produced here would be progressively enriched with semantic, material, historical, and conservation data to support the long-term management of the built heritage asset. Future research should address integrating a georeferenced control network from the first campaign stage, systematically quantifying per-zone coverage completeness, and defining explicit acceptance criteria for each sensor's contribution to the consolidated dataset.

6. Acknowledgments

This work was financially supported by FUNCAP, Project 01172921/2022 – Cientista Chefe Cultura, Project 10581391/2022 – International collaboration FUNCAP/INSA Rouen Normandie; by the National Council for Scientific and Technological Development (CNPq) – Project 302054/2022-7 – PQ2, by the Project - 440926/2024-6 – VISION and Project - 402828/2024-0 – CLIC, CAPES Foundation and Finep 2896/24.

References

Antonopoulou, Sofia, and Paul Bryan. 2017. *BIM for Heritage: Developing a Historic Building Information Model*. Historic England.

Argasiński, K., and P. Kuroczyński. 2023. "PRESERVATION THROUGH DIGITIZATION - STANDARDIZATION IN DOCUMENTATION OF BUILD CULTURAL HERITAGE USING CAPTURING REALITY TECHNIQUES AND HERITAGE/HISTORIC BIM METHODOLOGY." *The International Archives of the Photogrammetry, Remote Sensing and Spatial Information Sciences* XLVIII-M-2–2023 (June): 87–94. https://doi.org/10.5194/isprs-archives-XLVIII-M-2-2023-87-2023.

Bedford, Jon. 2017. *Photogrammetric Applications for Cultural Heritage: Guidance for Good Practice*. Historic England.

Bentkowska-Kafel, Anna, and Hugh Denard, eds. 2016. *Paradata and Transparency in Virtual Heritage*. 0 ed. Routledge. https://doi.org/10.4324/9781315599366.

Boardman, Clive, and Paul Bryan. 2018. *3D Laser Scanning for Heritage: Advice and Guidance on the Use of Laser Scanning in Archaeology and Architecture*. Historic England.

Dore, C., and M. Murphy. 2017. "CURRENT STATE OF THE ART HISTORIC BUILDING INFORMATION MODELLING." *The International Archives of the Photogrammetry, Remote Sensing and Spatial Information Sciences* XLII-2/W5 (August): 185–92. https://doi.org/10.5194/isprs-archives-XLII-2-W5-185-2017.

Fryskowska, A. 2017. "ACCURACY ASSESSMENT OF POINT CLOUDS GEO-REFERENCING IN SURVEYING AND DOCUMENTATION OF HISTORICAL COMPLEXES." *The International Archives of the Photogrammetry, Remote Sensing and Spatial Information Sciences* XLII-5/W1 (May): 161–65. https://doi.org/10.5194/isprs-archives-XLII-5-W1-161-2017.

Groetelaars, Natalie Johanna. 2015. "Criação de modelos BIM a partir de 'nuvens de pontos': estudo de métodos e técnicas para documentação arquitetônica." Tese de Doutorado, Universidade Federal da Bahia.

ICOMOS. 1964. "International Charter for the Conservation and Restoration of Monuments and Sites (Venice Charter)." Chartetr. IInd International Congress of Architects and Technicians of Historic Monuments. https://admin.icomos.org/wp-content/uploads/2025/03/Venice_Charter_EN.pdf.

ICOMOS. 2007. *International Heritage Documentation Standards*. RecorDIM TG16. Atenas.

Oliveira, Mário Mendonça De. 2008. *A Documentação Como Ferramenta De Preservação Da Memória: Cadastro, Fotografia, Fotogrametria E Arqueologia*. Cadernos Técnicos 7. IPHAN.

Page, Chris, Pascal Sirguey, Richard Hemi, et al. 2017. "Terrestrial Laser Scanning for the Documentation of Heritage Tunnels: An Error Analysis." *Proceedings of the FIG Working Week, Helsinki, Finland* 29.

Remondino, Fabio, Maria Grazia Spera, Erica Nocerino, Fabio Menna, and Francesco Nex. 2014. "State of the Art in High Density Image Matching." *The Photogrammetric Record* 29 (146): 144–66. https://doi.org/10.1111/phor.12063.

Sammartano, Giulia, and Antonia Spanò. 2018. "Point Clouds by SLAM-Based Mobile Mapping Systems: Accuracy and Geometric Content Validation in Multisensor Survey and Stand-Alone Acquisition." *Applied Geomatics* 10 (4): 317–39. https://doi.org/10.1007/s12518-018-0221-7.

Shao, Jie, Wuming Zhang, Nicolas Mellado, et al. 2019. "Automated Markerless Registration of Point Clouds from TLS and Structured Light Scanner for Heritage Documentation." *Journal of Cultural Heritage* 35 (January): 16–24. https://doi.org/10.1016/j.culher.2018.07.013.

Themistocleous, K., M. Ioannides, A. Agapiou, and D. G. Hadjimitsis. 2015. "The Methodology of Documenting Cultural Heritage Sites Using Photogrammetry, UAV, and 3D Printing Techniques: The Case Study of Asinou Church in Cyprus." Edited by Diofantos G. Hadjimitsis, Kyriacos Themistocleous, Silas Michaelides, and Giorgos Papadavid. https://doi.org/10.1117/12.2195626.

Wilkinson, Mark D., Michel Dumontier, IJsbrand Jan Aalbersberg, et al. 2016. "The FAIR Guiding Principles for Scientific Data Management and Stewardship." *Scientific Data* 3 (1): 160018. https://doi.org/10.1038/sdata.2016.18.

cinpar2026
XXII International Conference on Building Pathology and Constructions Repair
15th to 17th July 2026 - Lisboa, Portugal

Wattle and daub (tabique) mortars in Northern Portugal

Ana VELOSA[1], Kátia SOARES[2], Albino COSTA[3], Isabel TORRES[4,5]

[1] University of Aveiro, CERIS, Civil Engineering Department, Aveiro, Portugal, avelosa@ua.pt
[2] University of Coimbra, Civil Engineering Department, Coimbra, Portugal, katia.soares@student.dec.uc.pt
[3] Património Cultural IP, albinoestelita@patrimoniocultural.gov.pt
[4] University of Coimbra, CERIS, Civil Engineering Department.
[5] ITECONS, Coimbra, Portugal, itorres@dec.uc.pt

Abstract: Wattle and daub (tabique) structures are widespread throughout the country and have particular relevance in the North of Portugal, in which they are used in all regions and type of buildings.

These wooden-based structures, nailed with horizontal wooden laths, constitute the basis for interior compartment division in bourgeois urban buildings, palace houses and vernacular architecture. The type of wood and care in construction of these elements differs accordingly and variations are also encountered, such as the use of braided plant fibres as a structural element. Often, as a lateral façades or attics (less commonly as main façades), *tabiques* were also employed, with a rendering or, most frequently, schist slates as a final finishing.

The interest of this paper is, however, to provide information on the mortars that filled the space between laths and acted as a render providing a uniform finishing for these walls. For this purpose, a series of samples were taken from the various regions of northern Portugal, encompassing rural and urban areas. Sampling also considered both external and internal structures.

The analysis of the samples implied fragmentation and removal of fibres, division between binder and aggregate and determination of the composition of binder and aggregate fractions.

Results showed a variety of solutions linked to the availability of local materials and also to the possibility of incorporating air lime, when this product wasn't accessible locally. The use of these findings is of particular interest for the preservation of *tabique* structures in the present intervention actions.

Keywords: Lime mortars; Earth Mortars; Tabique walls; Preservation

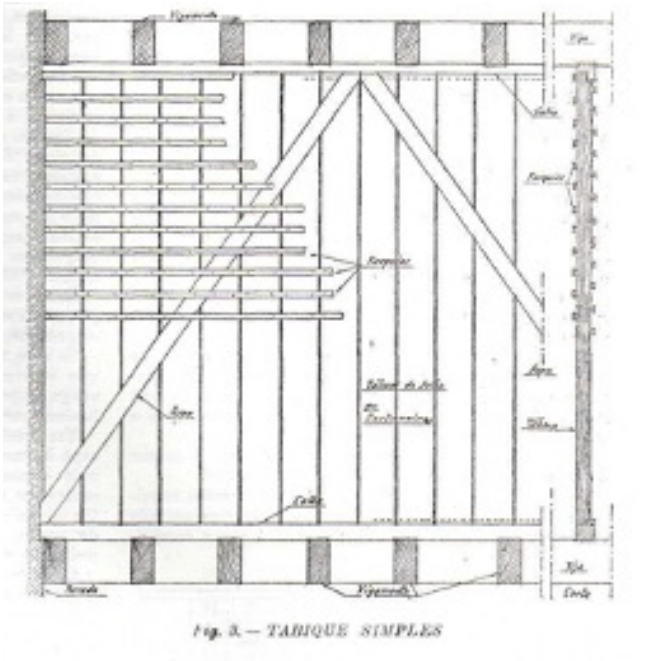
1. Introduction

Wattle and daub (*tabique* – Figure 1) systems are common in Portugal, with extensive use throughout the whole country, but with special predominance in the north and centre as well as in all urban areas. These partitions have a long history, and their use encompasses rural dwellings and urban houses, mainly in interior divisions, but also, less often, as external walls.

This building element combines a lightweight timber framework with an infill of interwoven wooden strips (wattle), typically made from local wood species. The structural frame, often composed of vertical posts and horizontal members, provides stability, while the wattle lattice acts as a support for the daub (Figure 1). The daub is a composite material traditionally made from a mixture of earth, clay, sand, straw, or, otherwise, a lime-based mortar, and left to dry, forming a solid wall infill. This technique is valued for its use of locally available, low-cost materials and its adaptability to regional climates. Mortars play a crucial role in both the filling and rendering stages: earth-based mortars are locally sourced and provide compatibility with the timber structure and breathability, while lime-based mortars are often linked to more relevant buildings (or

urban) and structures and/or applied as external renders to improve durability and weather resistance, maintaining relevant characteristics such as vapour permeability. Mortars in *tabique* elements have the purpose of helping to protect the structure while maintaining its ability to regulate moisture.

Figure 1 – Simple *tabique* wall (Leitão, 1896)



2. Historical observations on Tabique mortars in Portugal

Inside the built spaces, lime was applied as an element of filling and finishing partitions, which is the main type of partition inside the houses. In these elements, it is possible to find several examples of the use of fibres in the composition of the lime coating. To fill the slats between the partitions, a mortar of lime and sand was used in a 1:1 ratio (Leitão, 1896) that needed to be spooned in order to ensure its adhesion to the wooden structure. As a finish, various techniques – *fresco, fingido, escaiola* – were employed by specialized artisans.

The same author mentions earth-based mortars (Figure 2), stating that: "*Além das argamassas citadas,...,, que são as de que se faz mais vulgar applicaçào, ha também as argamassas de terra, que podem ser empregadas em casas pobres de campo*." Regarding the choice of the earth to be used in these mortars, Leitão infers that it shouldn't be too clayey, for fear of subsequent cracking (due to shrinkage). Furthermore, he explains that the earth shouldn't be too sandy either, or this could result in the lack of necessary cohesion. In terms of the execution procedure, he goes on to state that earth should be mixed with water to form a homogeneous paste after a thorough removal of stones and fibres. Proportions of earth versus sand are given as 3:1, presumably in terms of volume.



Figure 2 – *Tabique* wall with earth mortars (filling and rendering)

3. Further results of current studies

Although research on these partitions has been performed (Cardoso, 2013; Cepeda et al, 2010; Pinto et al, 2011), there was a definite knowledge gap concerning a more extensive overview in terms of the composition and characteristics of filling and rendering mortars, signifying the generation of doubts in conservation/rehabilitation actions.

In order to address this issue, recently, a Master thesis, Costa, 2021, produced as outcome research on the traditional plastering mortars used as wall coatings on *tabique* walls in Northern Portugal, aiming to support compatible conservation and rehabilitation of vernacular built heritage. This work encompassed a survey on existing buildings, including on-site sampling and documentation, complemented by bibliographic research and interviews with craftsmen to capture empirical know-how.

As a further complement, Soares et al, 2024, presented a series of results regarding studies of *tabique* mortars. The study was based on 49 samples and the results indicated mortars with earth or air lime as the main binders; considering the air lime mortars, some also incorporated clayey sand,

In continuity, a recent study on the porosity of *tabique* mortars in Portugal conducted by Soares et al, 2024, concluded that earth mortars usually present more porosity than lime mortars and the addition of fibres (vegetable fibres, mainly straw) increases this porosity, especially in terms of larger pores. This has a direct influence on the behaviour of renders, generating higher permeability.

4. Composition of tabique mortars in Northern Portugal

The results expressed in this paper encompass a set of two sampling and testing campaigns. The first campaign, exclusive to Northern Portugal was executed by Costa in 2021 and resulted in a Master Thesis (Costa, 2021). The second campaign is part of the PhD Thesis of Soares, which embraces the whole national territory and the results of which have already been partially published (Soares et al, 2024(1); Soares et al, 2024(2)). The junction of these two campaigns allows for a more extensive overview of *tabique* mortars in Northern Portugal.

4.1. Sampling

Sampling encompasses the work carried out by Costa, 2021 and Soares. Costa, 2021, collected 30 mortar samples and another 40 samples were subsequently sampled by Soares. The sampling area was delimited to the north of Portugal, including mortars from: Porto, Lamego, Guiães, Boassas, Fermentãos, Salzedas, Aveiro, Guimarães, Cinfães, Vila Real, Alfândega de Fé, Mondim de Basto, Braga, Mogadouro, Póvoa de Varzim, Esposende, Vila do Conde, Espinho.

These samples were collected from both interior and exterior *tabique* walls. The size of the samples collected varied according to the state of conservation of the building (Figure 3). A complete set of testing procedures was performed incorporating physical and mechanical characteristics and composition. In some cases, the sample size was small and therefore testing procedures were adapted. For the specific purpose of this paper, mortar composition tests and results will be described and analysed.



Figure 3 – External *tabique* in need of conservation

4.2 Testing procedures

The characterization tests of the samples were carried out in the laboratories of Itecons and the University of Aveiro (UA), in accordance with the applicable rules and procedures.The employed methodology took into account current methods for the testing of historical mortars (Velosa et al, 2010).

To characterise the sampled mortars, the following analytical methods and tests were used:

Acid dissolution was performed based on ASTM-C 25-11e1 and by the methodology suggested by some authors (Alvarez et al, 1999; Jedrzejewska, 1960) to dissolve carbonates (calcite, magnesite and dolomite) and create a residue composed by the aggregate fraction. Hydrochloric acid was used to guarantee a residue composed mainly by siliceous sand. Results give an approximate value of binder/aggregate ratio, as the used acid dissolution technique dissolves carbonates and partially dissolves soluble silica. The obtained residue was dried until constant mass was achieved. Particle size distribution by dry sieving was performed on the residue obtained from acid dissolution according to standard BS 3406-2.

X-Ray Diffraction (XRD) provided qualitative information on the crystalline mineral phases existent in the samples. For this analysis, mortars were crushed and dried at a low temperature. This analysis was performed on the fraction below 75µm to allow a more thorough analysis of the binder. The equipment used was a Panalytical X-Pert Pro X-Ray Diffractometer.

4.3 Results and discussion

Results indicate a predominance of lime-based mortars, either composed by pure lime or a lime/earth mix (Table 1). In the first sampling procedure (Costa, 2021), lime-based mortars presented a most common mass ratio of 1:3, with aggregates mainly in the fine sand to medium sand range. A smaller set of earth-based mortars, some incorporating straw, occurs mainly inland; in these mortars the fine fraction (below 63µm) is significant. XRD/XRF results point to the widespread use of locally available materials (siliceous aggregates derived from granitic and metamorphic sources), while interviews confirmed traditional mixes and adjustments to modify setting and workability.

Table 1 – Binder fraction in analysed mortars

Sampling	Number samples	Lime	Earth	Lime and Earth
Costa, 2021	30	13	9	8
Soares, 2024	40	17	18	5

The second campaign produced distinct results, due to the amount of earth mortars encountered. However, similarly to the first campaign it is evident that earth filling and rendering plasters are more common inland. The use of lime follows a similar pattern, with pure lime mortars and lime/earth mixes, most probably due to the type of sand (*saibro*) used for these purposes.

According to Figure 4, which shows the soluble percentage of mortars and their insoluble residue, great differences can be found in these mortars. Clearly, very low solubility is linked to earth mortars. Mortars with lime have solubility ranges that can also be quite low when small amounts of air lime were used, mostly coupled with the use of clayey sand. High solubility ranges, of over 25%, corresponding to lime:sand ratios (in mass) richer than 1:3, which are less common.

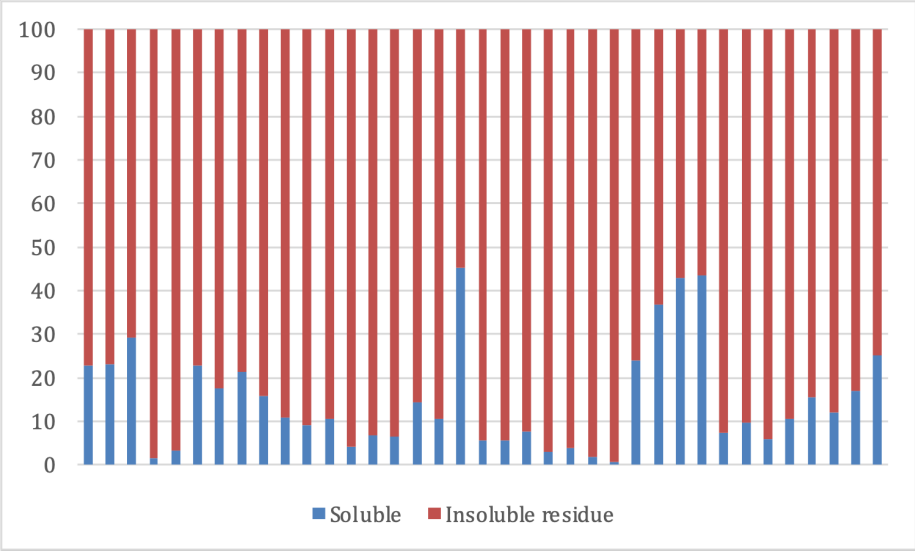


Figure 4 – Soluble and insoluble residue of mortars

The amount of earth mortars found in a very good conservation state demands a closer look at these materials. Although not common to all earth mortars, vegetable fibres, usually straw, are often found. Figure 4 shows two samples taken from Salzedas (filling of external partition) and Fermentãos (filling of internal partition).



Figure 5 – Earth and straw mortars (Salzedas and Fermentãos)

Chemical composition (XRF) results of earth mortars from the second campaign, shown in Figure 6 and the corresponding particle size division, portrayed in Figure 7, provide further information on these materials.

Although it is clear that the same type of composition corresponds to specific locations, linking locally sourced materials to the analysed buildings, it is curious that this is not completely reflected in terms of particle size, opening the possibility for sieving of earth prior to execution, in some cases.

The amount of clay can also be quite high, a few times over 60%. In these cases XRD results showed the predominance of kaolinite, which may attend to the adequate behaviour of filling materials and renders. The use of fibres, however, doesn't seem to have a direct link to either clay percentage or its mineralogical composition.

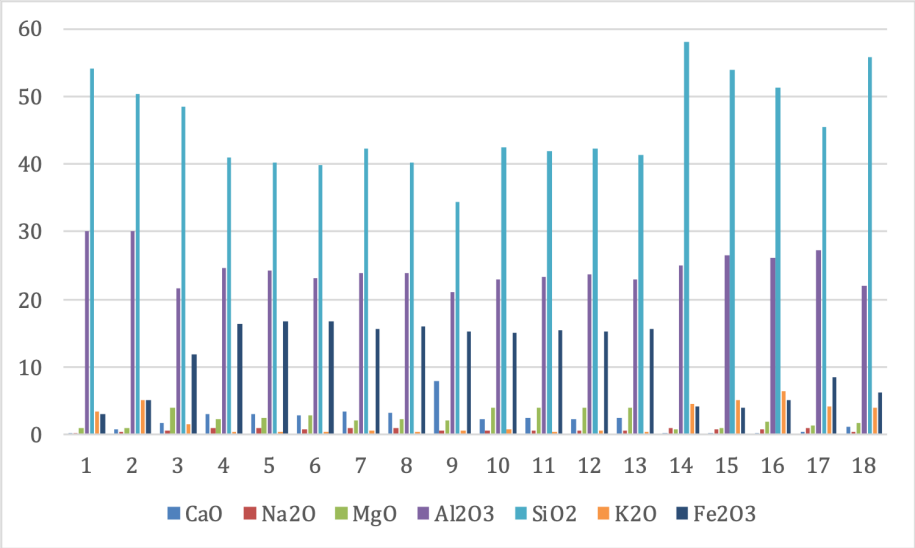


Figure 6 -Chemical composition of earth mortars

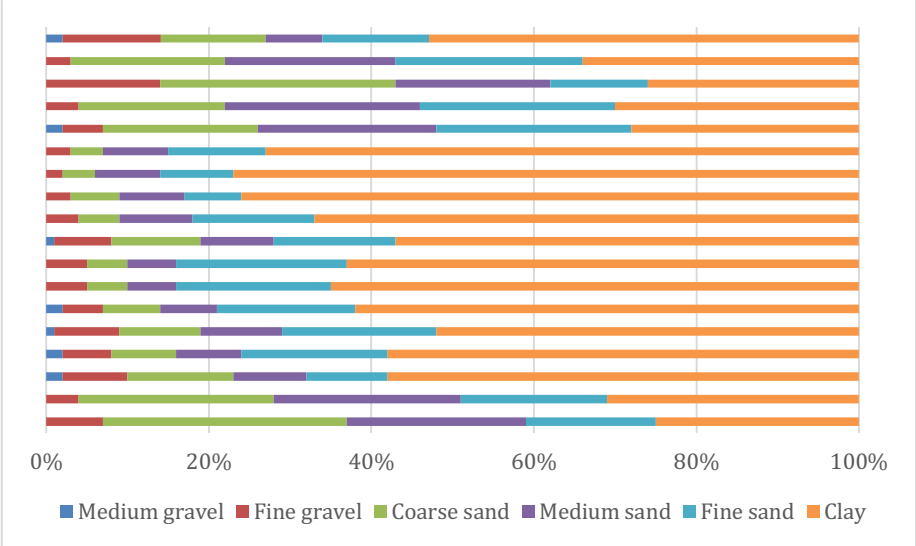


Figure 7 – Particle division of earth mortars

Conclusion

Tabique filling and rendering mortars in Northern Portugal are mainly lime based or comprised by earth as binding materials. In the case of lime-based mortars, there is a high variation in the percentage of lime used, but there is a predominance of 1:3 mass ratio. In terms of earth mortars, these are more common in interior regions and may contain fibres. Earth seems to be locally sourced and, sometimes, sieved. Mostly, mortars, whichever composition, were found in a very good conservation state. Workmanship may be a clue towards this conclusion.

Overall, the findings corroborate written and oral knowledge and highlight these mortars as low-impact, largely reversible solutions, informing heritage-compatible repair strategies and potential development of pre-dosed mixes.

Acknowledgments

This work was developed within the scope of the project "Sustainability of innovative wattle and daub mortars" (COMPETE2030-FEDER-00845500), co-funded by the European Regional Development Fund (ERDF) through the Support System for the Creation of Scientific and Technological Knowledge, under the Innovation and Digital Transition Program (COMPETE 2030). The authors would like to thank the Foundation for Science and Technology (FCT) for financial support through research grant 2022.13467/BD, and the CERIS research unit (funding UIDB/04625/2020).

References

Alvarez, J.I., Martín, A., Casado, P., García, J., Navarro, I., Zornoza, A., 1999. Methodology and validation of a hot hydrochloric acid attack for the characterization of ancient mortars, *Cement and Concrete Research* 29:1061-1065.

ASTM C25-11e1, Standard Test Methods for Chemical Analysis of Limestone, Quicklime, and Hydrated Lime, ASTM International, West Conshohocken, PA, 2011.

BS 3406-2 Methods for determination of particle size distribution, Recommendations for gravitational liquid sedimentation methods for powders and suspensions, British Standard Institute, London, 1986.

Cardoso R. Caracterização da Construção em Tabique de Lamego e Alto Douro. Tese de Doutoramento Universidade da Beira Interior. Covilhã; 2013. https://doi.org/10.1002/stc.1988.

Cepeda, A., Lousada, J., Vieira, J., Varum, H., Tavares, P., Fernandes, L., Pinto, J. Estudo do material terra aplicado na construção de tabique existente no Alto Tâmega. Artigo 6º ATP / 9º SIACOT. Coimbra; 2010. http://hdl.handle.net/10773/7181.

Costa, A. Argamassas de Revestimento de Tabiques no Norte de Portugal. Dissertação de mestrado. Universidade de Aveiro, Aveiro; 2021.

Jedrzejewska, H. 1960. Old Mortars in Poland: A New Method of Investigation, Studies in Conservation 5 (4):132-138.

Leitão, L., Curso Elementar de Construções, Imprensa Nacional, Lisboa (1896)

Pinto J; Cardoso R; Paiva A; Cunha S; Cruz D; Vieira B; Louzada J; Varum H. Caracterização de Paredes Tradicionais de Tabique. Aveiro; 2011. http://hdl.handle.net/10773/8010.

Soares K., Torres I., Velosa, A. Análise da porosimetria de argamassas de tabique, V Simpósio Argamassas e soluções térmicas de revestimento, 11 e 12 de julho de 2024 - Coimbra

Soares K., Torres I., Velosa, A. Characterization of traditional mortars used in wadding and rendering on walls of wattle and daub in Portugal, Construction Pathology, Rehabilitation Technology and Heritage Management, May 07-10, 2024. Gijon, Spain

Velosa, A.L., Veiga, R, Coroado, J., Ferreira , V.M., Rocha, F. Characterization of ancient mortars from Roman times to the nineteenth century' in Compatibility issues of new mortars with substrates and ancient mortars, Materials, Technologies and Practice in Historic Heritage Structures, Bostenaru Dan, Maria; Prikryl, Richard; Török, Ákos (eds.), Springer, Berlin, ISBN: 978-90-481-2683-5, 235-257, 2010.

Cinpar 2026
XXII International Conference on Building Pathology and Constructions Repair
15th to 17th July 2026 - Lisboa, Portugal

Framework for Assessing and Mapping Degradation Risks in Historic Building Facades

Ricardo M.S.F. ALMEIDA[1], Eva BARREIRA[2], Raquel SEBASTIÃO[3], Romeu VICENTE[4]

[1] Department of Civil Engineering, Polytechnic Institute of Viseu, Portugal, ralmeida@estgv.ipv.pt
[2] Department of Civil Engineering, University of Porto – Faculty of Engineering, Portugal, barreira@fe.up.pt
[3] Department of Informatics, Polytechnic Institute of Viseu, Portugal, raquelsebastiao@estgv.ipv.pt
[4] CERIS, Department of Civil Engineering, University of Aveiro, Portugal, romvic@ua.pt

Abstract: Historical facades exhibit complex degradation patterns strongly influenced by external environmental factors. The preservation of these structures has traditionally relied on visual inspections and qualitative assessments, which often lack scalability, generalization, and real-time monitoring capabilities. Recent advances in digital technologies, particularly machine learning (ML), artificial intelligence (AI), and building information modelling (BIM), bring forward new opportunities for more accurate, efficient, and quantitative approaches for façade assessment and mapping.

A significant portion of the historic built environment is made of stone, with granite being the predominant material in northern Portugal. Historic stone facades are affected by physical, chemical, and biological degradation mechanisms, namely salt crystallisation, biocolonisation, and, in colder regions, freeze-thaw cycles. Moisture content plays a critical role in these processes, as it governs many of the weathering mechanisms responsible for long-term material deterioration, posing substantial challenges to conservation strategies.

This paper presents the framework of a research project aimed at developing a tool for assessing and mapping the degradation state of historical building facades through AI-based analysis of photographic and thermal imaging data. Computer vision techniques are used to extract relevant features from visible and infrared images, which are then integrated into machine learning models for a comprehensive assessment of the conservation state of facades.

An experimental campaign was setup using small-scale wall specimens with embedded and fully characterised defects. Preliminary results are presented and discussed under different setups and environmental conditions. The analysis focuses on temperature evolution within regions of interest and on thermal contrast between defective and flawless areas. The results demonstrate the potential of thermal imaging not only as a non-destructive diagnostic technique, but also as a source of structured data for advanced models aimed at the automated detection of façade degradation.

Keywords: Infrared thermography; façade inspection; defect detection; image segmentation; heritage conservation.

1. Introduction

The assessment of degradation in building façades, particularly in historical constructions, remains a complex and largely manual process. Inspection campaigns typically rely on visual surveys and expert judgement, which, although effective in many cases, are inherently subjective, difficult to reproduce, and not easily scalable to large building stocks.

Infrared thermography (IRT) has been widely adopted as a non-destructive technique capable of revealing subsurface anomalies such as moisture accumulation, delamination, voids, and thermal bridges. Its ability

to provide rapid, full-field measurements makes it particularly attractive for façade diagnostics (Maldague, 2001; Grinzato *et al.*, 2002). However, in most practical applications, thermographic inspection is still based on qualitative interpretation of thermograms, which limits its objectivity and integration into systematic assessment frameworks.

In recent years, several studies have explored the use of quantitative thermographic approaches for defect detection in building envelopes (Bauer *et al.*, 2016; Garrido *et al.*, 2022). These methods typically rely on the analysis of temporal temperature evolution and the extraction of features such as thermal contrast, phase delay, or cooling rates. Such methods aim to reduce subjectivity and improve robustness under varying environmental conditions. However, their application is often limited to controlled scenarios, and the integration of these indicators into automated workflows remains a challenge.

At the same time, computer vision techniques have been increasingly applied to the inspection and condition assessment of building façades and masonry structures. These approaches enable the automated detection and classification of defects based on image data, reducing the need for manual interpretation. Recent studies have demonstrated the potential of both traditional image processing and machine learning techniques for identifying cracks, detachments, and surface degradation in building elements (Wang *et al.*, 2019; Wang *et al.*, 2024).

In the context of heritage conservation, digital and image-based methodologies have also been explored to support preventive maintenance and monitoring strategies (Masciotta et al., 2019). However, the application of these techniques to thermographic data remains limited, particularly in approaches that combine physically-based thermal analysis with image-based segmentation within a unified framework. The RiskMap project is developed within this context, aiming to create a framework for assessing and mapping degradation risks in building façades using visual and thermal data. A central requirement of this framework is the ability to detect and localise defects based on image-derived features automatically.

Within the project the framework proposes a thermography-driven workflow for automated façade defect detection that bridges thermal feature analysis with image-based segmentation. The approach is demonstrated on a controlled experimental dataset with embedded defects, enabling a systematic evaluation of thermal features and their suitability for automated detection. By linking feature extraction to segmentation, the work provides a step towards the integration of thermography into scalable façade risk mapping systems.

2. RiskMap framework

The RiskMap project is conceived as an integrated framework for the assessment and mapping of degradation risks for building façades, combining multi-source data acquisition with advanced processing and analysis techniques.

The framework is designed to support the transition from isolated inspections to continuous, data-driven assessment workflows. It integrates information from different methods, including visible imagery, infrared thermography, and contextual building data, to generate spatially explicit representations of façade condition and associated degradation risks.

The overall workflow can be structured into the following steps:

- Data acquisition – collection of visual and thermal data using appropriate sensing technologies, either in controlled environments or in real-world conditions. This step includes fixed sensors, mobile platforms, and aerial systems;
- Pre-processing – correction and normalization of raw data to account for environmental effects, sensor characteristics, and acquisition conditions. This step ensures the comparability and consistency of the data;

- Feature extraction – derivation of relevant indicators from the acquired data, capturing patterns associated with degradation mechanisms. This includes both spatial and temporal thermal and visible features;
- Automated detection and segmentation – identification and delineation of anomalous regions based on extracted features. This step transforms raw data into actionable information by highlighting areas of potential concern;
- Risk mapping – aggregation of detected anomalies and defects into a spatial framework, enabling the generation of condition maps and supporting decision-making processes. This stage may be linked to BIM or digital twin platforms.

Within this pipeline, thermographic data plays a critical role in detecting subsurface defects that are not visible in standard imagery. However, its effective integration into automated workflows depends on the definition of robust and transferable features, as well as on the development of reliable segmentation methods. Figure 1 shows the pipeline and the highlighted section represents the focus of this work, where thermographic data are processed through feature extraction and image-based segmentation to support automatic defect detection.

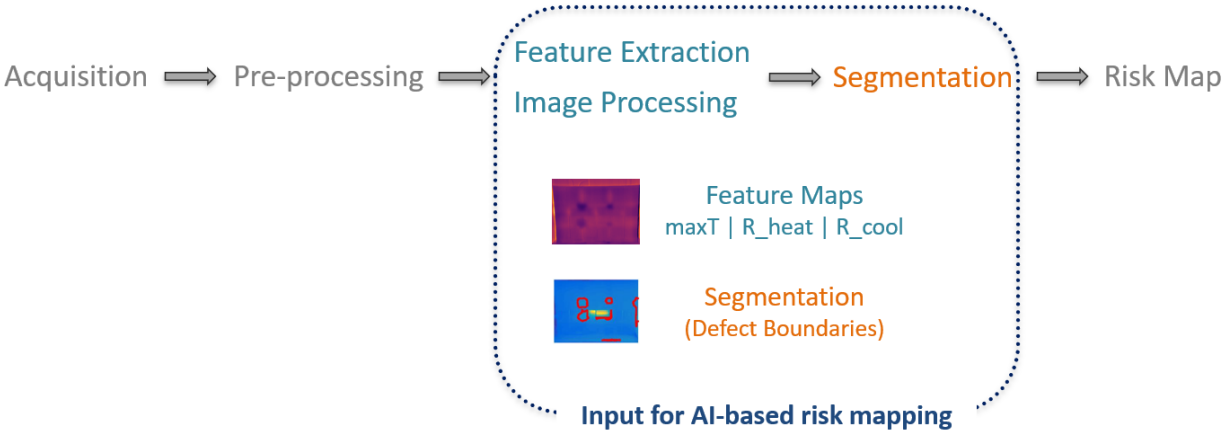


Figure 1 – Conceptual workflow of the RiskMap framework

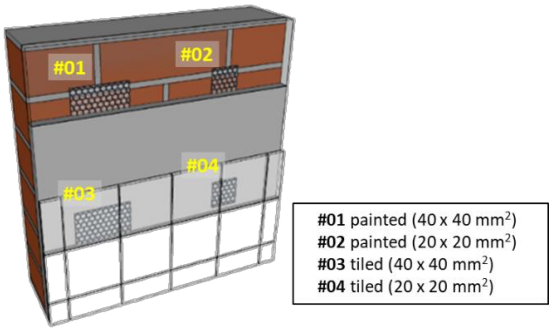
The present work focuses on the intermediate stages of this framework, namely the extraction of thermographic features and their use in automated defect segmentation. These stages are essential for enabling the transition from data acquisition to meaningful risk mapping outputs.

3. Experimental dataset

To support the development and validation of the proposed workflow, an experimental dataset was obtained using a laboratory-scale wall specimen (0.90 x 0.60 m^2) specifically designed to include subsurface defects with known geometry, size, and location.

The specimen was constructed to reproduce typical façade configurations and includes two distinct surface finishes: a painted surface (top half of the wall) and a ceramic-tiled surface (bottom half of the wall). This configuration also enables the evaluation of the influence of surface properties on thermal behaviour and defect detectability.

Artificial defects were embedded within the wall during construction using bubble wrap, providing a controlled reference for validation. These defects simulate common façade anomalies, such as voids or detachments, and allow a direct comparison between detected and actual defect locations (Figure 2).

a) 

b) 

Figure 2 – Experimental setup: a) wall specimen scheme with the defects; b) infrared thermographic recording setup

Active infrared thermography was employed to generate measurable thermal contrasts. An external infrared heat source was used to induce a controlled heating phase, followed by a natural cooling phase. Thermal images were acquired at regular intervals throughout both phases, resulting in time-resolved thermographic sequences.

In this experimental campaign, the following devices were used: (i) an infrared camera, to capture thermal images, (ii) an emissometer, to determine the emissivity of the surfaces, (iii) a 2500 W infrared lamp as external heat source.

The acquisition protocol was designed to ensure repeatability and comparability between experimental runs. All data were recorded in radiometric format, enabling quantitative analysis at the pixel level.

The resulting dataset is particularly suitable for the objectives of this work for two main reasons: controlled conditions allow the systematic evaluation of thermal features and their sensitivity to different factors, such as surface finish and heating configuration; known and reliable reference data that enables the validation of segmentation results and the assessment of detection accuracy.

In the context of this study, the dataset is used not only to analyse thermographic behaviour but also to support the development of two complementary approaches: (i) the extraction of thermal indicators for quantitative analysis, and (ii) the application of an image-based segmentation pipeline for automatic defect detection.

4. Thermal data analysis and feature extraction

To characterise the thermal behaviour of the wall specimen and support the interpretation of defect-related anomalies, a quantitative analysis of the thermographic data was performed. The acquired thermal images were organised into a three-dimensional dataset T(x,y,t), where *x* and *y* represent spatial coordinates and *t* the acquisition time. This representation enables the analysis of both spatial and temporal thermal variations.

To enhance defect-related thermal signals and remove noise, a baseline normalization procedure was applied. The thermographic image acquired before the heating phase was used as a reference and subtracted from all subsequent images:

$$T'(x,y,t) = T(x,y,t) - T_{baseline}(x,y) \quad (1)$$

This normalization process reduces the influence of initial temperature distributions and highlights transient thermal effects associated with heat transfer. Based on the normalized data, a set of pixel-wise thermal indicators was computed to capture different aspects of the thermal response.

The computed indicators reveal distinct thermal patterns between defective and non-defective regions. Figure 3 presents representative maps of the maximum thermal contrast (maxT) and cooling rate (R_cool) obtained from the experimental dataset. Maximum thermal contrast highlights pixels exhibiting the strongest thermal response, which are expected to correspond to subsurface defects and is defined as the maximum measured temperature in each pixel throughout the entire experiment; cooling rate is defined in equation (2) and estimated using linear regression over the corresponding time intervals.

$$R_cool\ (x,y) = dT'(x,y,t)/dt) \tag{2}$$

Defective regions are visible as localized anomalies, particularly in the painted surface finishing (top half of the specimen), where higher thermal contrast can be observed.

During the heating phase, the thermal response is strongly influenced by the spatial distribution of the heat source, leading to marked thermal patterns. As a result, indicators such as maximum thermal contrast and heating rate may be affected by global gradients unrelated to subsurface defects. In contrast, during the cooling phase, the thermal response becomes primarily governed by intrinsic material properties. Defective regions typically exhibit slower cooling rates due to differences in heat transfer, resulting in improved contrast relative to intact areas. This behaviour is consistent with previous findings reported in the literature (Freitas et al., 2014).

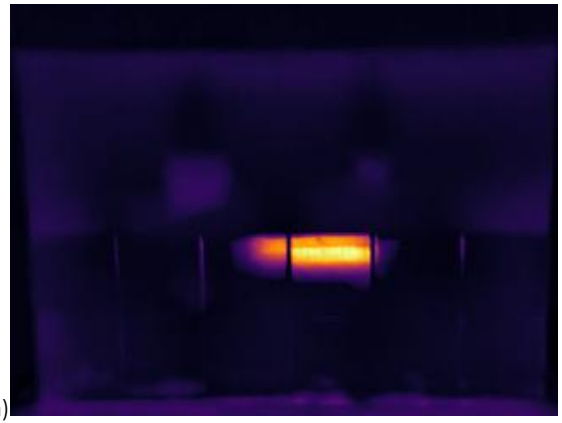
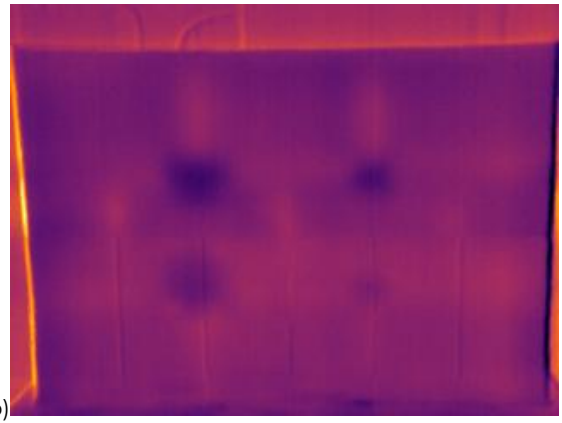
a)  b) 

Figure 3 – Pixel-wise thermal indicators derived from the experimental dataset: (a) Maximum thermal contrast (maxT); (b) Cooling rate (R_cool)

The influence of surface properties is also evident in the results. In the painted surface, defects are more clearly distinguishable due to higher thermal contrast. On the other hand, the ceramic-tiled surface presents lower contrast and increased variability, which can be attributed to differences in surface reflectivity and thermal properties. Despite these surface-related challenges, cooling-based indicators still allow the identification of defective regions, confirming their robustness under different surface conditions.

The extracted thermal indicators provide quantitative insight into the thermal behaviour of façade elements and support the interpretation of degradation mechanisms. Although these indicators are not directly used in the segmentation procedure presented in this work, they can play an important role in understanding the physical basis of defect detectability and in guiding the selection of relevant processing strategies in future work.

5. Automatic defect segmentation

While the analysis of thermal indicators provides important insight into the physical behaviour of defective and intact regions, the implementation of automated detection requires complementary processing strategies. To enable the automated identification of defective areas, an image-processing-based segmentation approach was developed.

5.1 Segmentation pipeline for defect detection in thermographic images

The developed pipeline operates directly on thermographic images, exploiting chromatic and spatial information to map and outline anomalous regions, and consists of three main stages: (i) preprocessing, (ii) threshold-based segmentation, and (iii) morphological post-processing.

The segmentation pipeline begins with image preprocessing to enhance defect-related patterns, while reducing noise and illumination inconsistencies. At first, image contrast was enhanced based on histogram equalization using Contrast Limited Adaptive Histogram Equalization (*Zuiderveld*, 1994). This method operates on small regions (ceramic tiles dimension), increasing local contrast, while mitigating noise amplification in homogeneous areas. Thus, it allows for normalizing the frequency distribution and compensating for non-uniform illumination. To further reduce stochastic fluctuations introduced during contrast enhancement, a median filter was applied. This filtering step reduces noise while preserving edges and smoothing the image texture, improving the robustness of subsequent segmentation. Threshold-based segmentation was performed using Otsu's method (*Otsu*, 1979), which automatically determines the optimal threshold by minimising intraclass variance between background and foreground (regions of interest). This results in a binary mask highlighting candidate regions of interest. The use of a global threshold ensures computational efficiency while maintaining robustness across frames with similar thermal conditions.

To improve the spatial coherence and structural integrity of the segmented regions, a sequence of morphological operations was applied:

- Noise removal: elimination of small isolated regions;
- Morphological closing: filling of internal gaps and merging of neighbouring regions;
- Dilation: expansion of the boundaries of the segmented regions to ensure complete coverage of defect areas.

Additionally, a margin near the image borders was excluded to avoid artifacts caused by background elements and edge effects. This ensures that segmentation is restricted to the relevant wall-specimen area and improves the reliability of the results.

A key component of the proposed pipeline is the selection of the most appropriate colour space and the most representative channel. For thermographic images associated with the heating phase, the segmentation process was applied in two steps:

1) Removal of the heating source: the chromatic component of the Red (R) channel in the RGB colour space was used to identify and mask the region corresponding to the heating lamp. This step reduces the influence of the external heat source and enhances the contrast between defective and non-defective areas, preventing false detection.

2) Defective region detection: the defective regions were segmented using the Hue (H) channel of the HSV colour space. The use of the H channel is particularly advantageous, as it separates chromatic information from luminance and saturation effects. This allows the identification of defects based on colour variations associated with thermal gradients due to heterogeneities.

As a result, defective regions can be identified as localized variations in the chromatic signature, often corresponding to thermal hotspots.

This approach was observed to produce consistent segmentation results across multiple frames and experimental runs, as discussed in Section 5.2.

5.2 Segmentation results

The consistency and robustness of the proposed segmentation pipeline was evaluated when applied to multiple thermographic sequences acquired under similar experimental conditions as described in section 2.

Figure 4 presents a sequence of segmentation results obtained during the heating phase for a representative experimental run. The detected regions show a stable spatial correspondence with the known location of the embedded defects. Although some variability is observed across frames, the main defective areas are consistently identified throughout the sequence.

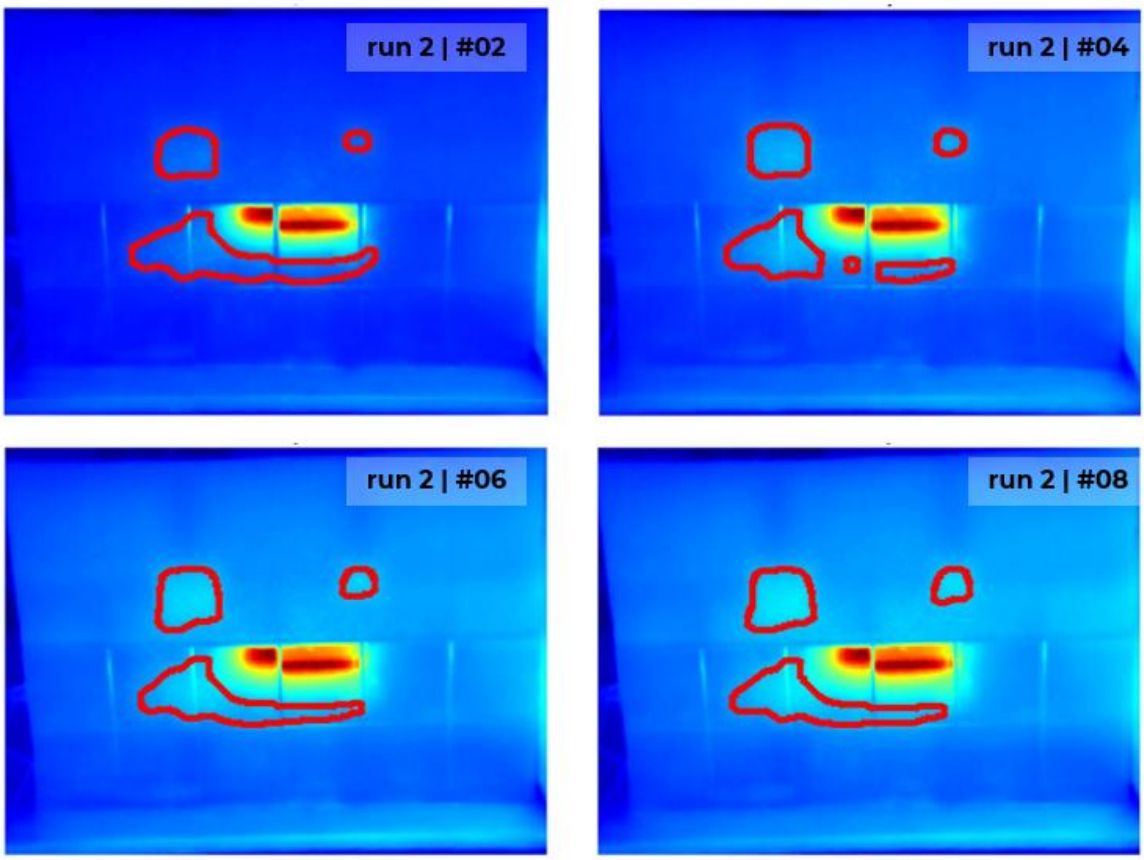


Figure 4 – Temporal evolution of segmentation results during the heating phase

To further assess repeatability, Figure 5 compares segmentation results obtained from two independent experimental runs under similar conditions. Overall, the results demonstrate a good level of agreement in terms of defects localization and general shape, confirming the robustness of the proposed approach. Moreover, it can be noticed that across different experimental runs, the segmentation results reliably indicate higher defect detectability on the painted surface than on the ceramic-tiled surface. These findings confirm that the nature of the wall surface finishing material may pose an additional challenge to the application of the proposed methodology, potentially requiring future adaptations to the experimental protocol and/or data processing strategy according to the material under analysis.

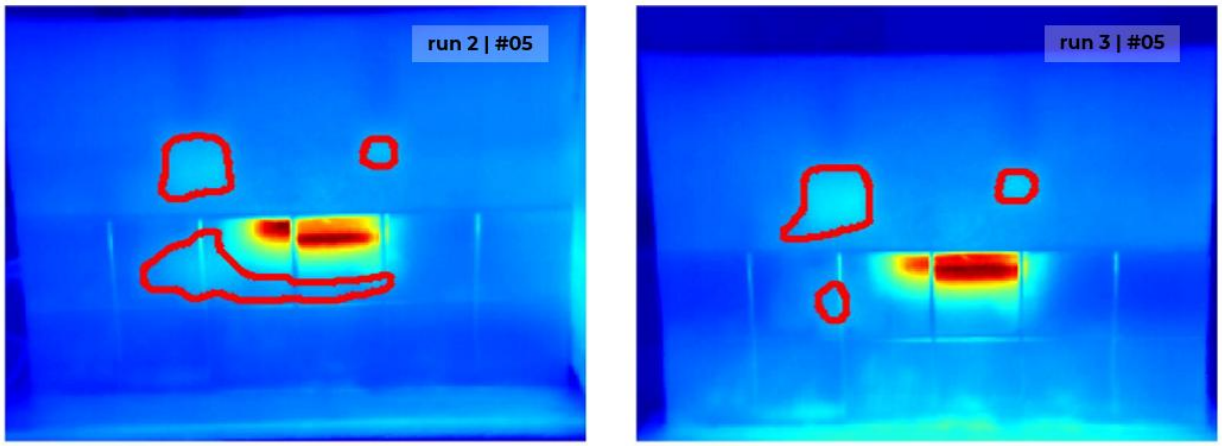


Figure 5 – Comparison of segmentation results between independent experimental runs

Despite these positive results, some limitations can be observed. In particular, small false-positive regions may appear, especially in areas with low thermal contrast or influenced by boundary effects. Additionally, slight variations in the extent of the segmented regions are observed across time and between runs, reflecting the sensitivity of the method to thermal conditions and surface properties.

Overall, the results demonstrate the feasibility of integrating image-based segmentation into thermography-driven workflows for automated façade assessment.

6. Discussion

The results presented in this study highlight the relevance of combining thermographic analysis with image-based segmentation for the automated detection of façade defects. The observed differences in defect detectability between surface types can be explained by their distinct surface reflectivity and thermal properties, which is particularly observable in the ceramic-tiled area reducing defect identification and segmentation performance.

Moreover, the analysis of thermal indicators (Section 4) provides a clear physical interpretation of defect detectability. Cooling-based indicators were shown to offer improved robustness under non-uniform heating conditions, as they are primarily governed by intrinsic material properties rather than external excitation. This finding is consistent with previous studies and reinforces the importance of considering temporal thermal behaviour in façade diagnostics.

On the other hand, the segmentation approach (Section 5) demonstrates that chromatic information in thermographic images can be effectively exploited for automated defect detection. The use of the HSV colour space, and particularly the Hue channel, enables the separation of chromatic variations associated with thermal gradients from luminance effects, improving robustness under non-uniform heating conditions. This confirms the suitability of colour-based representations for thermographic image analysis in controlled scenarios. Moreover, the results obtained across multiple frames and independent experimental runs indicate that the method is robust with respect to temporal variability and acquisition conditions. The consistent localisation of defects supports the applicability of the approach in controlled environments and suggests potential for extension to more complex scenarios.

However, some limitations must be acknowledged. The presence of false-positive detections in areas with low thermal contrast indicates sensitivity to noise and to local thermal variability due to differences in the surface properties. Additionally, the extent of the segmented regions varies slightly across time and between

runs, reflecting the dynamic nature of heat transfer processes and the influence of environmental conditions.

Another important limitation is the reliance on controlled heating conditions and known experimental configurations. In real-world applications, factors such as solar radiation, wind, and material heterogeneity may introduce additional variability, requiring further adaptation of the methodology.

These limitations suggest that further developments are required to improve robustness and generalisation. In particular, the integration of adaptive thresholding strategies, multi-temporal analysis, or ML-based approaches may enhance detection accuracy under more variable conditions. Despite these limitations, the proposed approach represents a step towards the integration of thermographic data into automated façade assessment frameworks. The combination of physically meaningful indicators and image-based segmentation provides a complementary perspective that can support more robust and scalable analysis.

7. Conclusions

This paper presented a thermography-driven workflow for the analysis and automated detection of defects in building façades, within the context of the RiskMap project framework. The proposed approach integrates thermal data analysis with an image-based segmentation pipeline, enabling the direct identification of defective areas in thermographic imagery.

The main contribution of this work regards the combination of quantitative thermographic analysis and automated defect detection. A segmentation pipeline based on contrast enhancement, thresholding, morphological operations, and colour space selection is proposed. Thus, relying on the physical interpretability of thermal indicators gathered/allied with a segmentation strategy based on chromatic information, the proposed workflow provides a structured and reproducible approach for façade condition assessment. An experimental campaign conducted on a wall specimen with induced and controlled defects was used to generate a dataset for evaluating both the thermal behaviour of the specimen and the performance of an image-based segmentation approach. The analysis of thermal indicators showed that cooling-related features provide more robust information for defect detection, particularly under non-uniform heating conditions, while the segmentation pipeline enables consistent and spatially coherent defect localisation across time and independent experimental runs. In particular, higher defect detectability was observed in painted surfaces compared to ceramic-tiled surfaces.

Although some limitations were identified, particularly regarding false positives and sensitivity to thermal variability, the proposed approach shows strong potential for the integration of thermographic data into automated façade inspection/assessment workflows.

Future work should focus on extending the proposed methodology to real-world scenarios, integrating combined multi-modal data sources and ML techniques to improve defect detection reliability and generalisation.

Acknowledgments

This work was financially supported by: COMPETE 2030, by Portugal 2030, and by the European Union, within the framework of the project “RiskMap - AI-based tool for buildings degradation risk mapping”, with number 14828 and operation code at the Funds Platform COMPETE2030-FEDER-00831700, and UID/04708/2025 and https://doi.org/10.54499/UID/04708/2025, of the CONSTRUCT - Instituto de I&D em Estruturas e Construções - funded by Fundação para a Ciência e a Tecnologia, I.P./ MECI, through the national funds.

References

Bauer, E., Elier Pavón, Eva Barreira, Eliane Kraus De Castro. 2016. “Analysis of building facade defects using infrared thermography: Laboratory studies”. Journal of Building Engineering 6: 93-104. https://doi.org/10.1016/j.jobe.2016.02.012.

Freitas, Sara S., Vasco Peixoto de Freitas, Eva Barreira. 2014. “Detection of façade plaster detachments using infra-red thermography – A nondestructive technique”. Construction and Building Materials 70: 80-87. https://doi.org/10.1016/j.conbuildmat.2014.07.094.

Garrido, I., Eva Barreira, Ricardo M.S.F. Almeida, Susana Lagüela. 2022. “Introduction of active thermography and automatic defect segmentation in the thermographic inspection of specimens of ceramic tiling for building façades”. Infrared Physics & Technology 121, 104012. https://doi.org/10.1016/j.infrared.2021.104012.

Grinzato, E., Paolo Giulio Bison, Sergio Marinetti. 2002. “Monitoring of ancient buildings by the thermal method”. Journal of Cultural Heritage, 3(1), 21–29. https://doi.org/10.1016/S1296-2074(02)01159-7.

Maldague, X.P.. 2001. “Theory and Practice of Infrared Technology for Nondestructive Testing”. Wiley.

Otsu, N.. 1979. "A Threshold Selection Method from Gray-Level Histograms". IEEE Transactions on Systems, Man, and Cybernetics, 9(1), 62-66. Wang, N., Xuefeng Zhao, Peng Zhao, Yang Zhang, Zheng Zou, Jinping Ou. 2019. “Automatic damage detection of historic masonry buildings based on mobile deep learning”. Automation in Construction 103: 53-66. https://doi.org/10.1016/j.autcon.2019.03.003.

Wang, P., Jianzhuang Xiao, Xingxing Qiang, Rongwei Xiao, Yi Liu, Chang Sun, Jianhui Hu, Shijie Liu. 2024. “An automatic building façade deterioration detection system using infrared-visible image fusion and deep learning”. Journal of Building Engineering 95, 110122. https://doi.org/10.1016/j.jobe.2024.110122.

Zuiderveld, K.. 1994 "Contrast Limited Adaptive Histogram Equalization". Graphic Gems IV, Academic Press Professional, 474–485.

Cinpar 2026
XXII International Conference on Building Pathology and Constructions Repair
15th to 17th July 2026 - Lisboa, Portugal

Incorporation of Eggshell Residues in Lime Mortars for Rehabilitation of Wattle and Daub Walls

Isabel TORRES[1,2] ,Jessika CAHINO[3], Kátia SOARES[4], Gina MATIAS[5], Ana VELOSA[6]

[1] University of Coimbra, CERIS, Civil Engineering Department.
[2] ITECONS, Coimbra, Portugal, itorres@dec.uc.pt
[3] University of Coimbra, Civil Engineering Department, Coimbra, Portugal, jessikacahino@gmail.com
[4] University of Coimbra, Civil Engineering Department, Coimbra, Portugal, katia.soares@student.dec.uc.pt
[5] CERIS, ITECONS, Coimbra, Portugal, ginamatias@itecons.uc.pt
[6] University of Aveiro, CERIS, Civil Engineering Department, Aveiro, Portugal, avelosa@ua.pt

Abstract: Wattle and daub is a traditional construction system characterised by a timber framework infilled and coated with mortars based on earth, lime, and natural aggregates, exhibiting good thermal performance. Nevertheless, its susceptibility to moisture, biological degradation of timber elements, and inadequate past interventions has led to significant deterioration of this type of construction.

The rehabilitation of wattle and daub walls plays a crucial role in the preservation of traditional built heritage and should be guided by the principles of compatibility, reversibility, and minimal intervention.

The use of compatible mortars formulated with traditional binders and materials of natural or recycled origin is essential for rehabilitation interventions. Several studies have shown that the incorporation of waste materials into rehabilitation mortars can enhance their mechanical and environmental performance, thereby contributing to sustainability. Thus, the rehabilitation of wattle and daub walls should be regarded not only as a heritage conservation action but also as an opportunity for the development of sustainable and technically appropriate construction solutions.

This study is part of an ongoing research project focused on the development of lime-based mortars incorporating waste materials for the rehabilitation of wattle and daub walls.

The present paper reports the results of an experimental campaign carried out to characterise lime mortars incorporating eggshell waste to assess their suitability for application in the rehabilitation of wattle and daub walls.

Keywords: Lime mortars; Wattle and Daub Walls; Eggshell Residues; Heritage rehabilitation

1. Introduction

Wattle and daub construction represents one of the most widespread traditional building techniques across various regions of the world, particularly in rural and vernacular architecture. This system, typically composed of a timber framework (wattle) infilled with an earthen or lime-based mixture, reflects the use of locally available materials and low-energy construction methods. Despite its historical significance and environmental advantages, this type of construction is highly susceptible to degradation due to moisture, biological activity, and mechanical damage, which poses significant challenges for conservation and rehabilitation efforts.

Lime mortars have long been recognized as compatible materials for the repair of traditional structures, owing to their vapor permeability, flexibility, and chemical compatibility with original substrates. In recent decades, increasing attention has been given to improving the performance of lime-based materials while maintaining their sustainability and compatibility. This has led to the exploration of alternative additives and

waste-derived materials that can enhance mechanical properties and durability without compromising the ecological footprint of the construction process.

In this context, a research project is currently under development within the scope of a collaboration between the University of Aveiro and Itecons, funded by the Foundation for Science and Technology (FCT). The main objective of this project is the formulation of sustainable mortars for the rehabilitation of wattle and daub walls. One of the key strategies to enhance the sustainability of these mortars is the incorporation of waste materials as partial replacements for either the binder or the aggregates. This approach contributes, on the one hand, to reducing the volume of waste sent to landfills and, on the other hand, to decreasing the consumption of non-renewable natural resources. By promoting the valorization of residues within construction materials, this research aligns with the principles of circular economy and sustainable development in the built environment.

Eggshell residues emerge as a promising secondary raw material. Generated in significant quantities by the food industry, eggshell waste is primarily composed of calcium carbonate ($CaCO_3$), similar to limestone, which is the main constituent of lime. The reuse of eggshells in construction materials aligns with circular economy principles by diverting waste from landfills and reducing the demand for virgin raw materials. Previous studies have indicated that finely ground eggshell powder can influence the microstructure, setting behaviour, and mechanical strength of cementitious and lime-based systems.

Although eggshell production is very high and its characteristics are very interesting, there is still limited use of this waste product. In Portugal, some use is observed in agriculture, namely as an alkalizing corrective (to correct the pH of acidic soils), as a component in agricultural fertilizer, and as a source of calcium for laying hens (increasing egg production and shell quality).

In other countries other applications have been found:

- The powder resulting from the prior dissolution of the bark in acetic acid is indicated as a remedy for osteoporosis and other diseases of the human joints, King'ori (2011)

- Calcium carbonate for fertilizers, animal feed, heavy metal removal and paper treatment with membrane separation; use of calcium oxide (CaO) as a catalyst in biodiesel production; purification of calcium carbonate; production of hydroxyapatite. Oliveira et al. (2013).

The incorporation of eggshell residues into lime mortars for the rehabilitation of wattle and daub walls presents a novel approach that combines heritage conservation with sustainable material innovation. However, the effects of such incorporation on the physical, mechanical, and durability properties of lime mortars, particularly in the context of traditional earthen-lime systems, remain insufficiently understood.

Therefore, this study aims to investigate the feasibility of using eggshell residues as a partial replacement or additive in lime mortars intended for the rehabilitation of wattle and daub constructions. The research focuses on evaluating the influence of eggshell incorporation on key performance indicators, including workability, mechanical strength, porosity, and durability, while ensuring compatibility with traditional materials and techniques.

The present study reports the preliminary findings of an experimental campaign aimed at the development of hydraulic lime mortars incorporating waste-derived materials

2. Experimental campaign

2.1 Compositions analysed

To assess the feasibility of replacing part of the sand with eggshell waste (ES) in hydraulic lime (NHL 3.5) mortars, four mortars were formulated. The selected mix ratio for all formulations was 1:4 (lime:sand). Two different types of sand (S1 and S2) were used. Thus, two reference mortars without waste were prepared, and two mortars were formulated in which the waste was introduced as a replacement for 25% of the sand.

Table 1 shows the compositions and proportions of the prepared mortars.

Table 1 – Components and proportions of the mortars

Designation	Hydraulic lime	Sand S1	Sand 2	Eggshell	Proportion
H_S1	X	X			1:4:0
H_S1_ES	X	X		X	1:3:1
H_S2	X		X		1:4:0
H_S2_ES	X		X	X	1:3:1

2.2 Characterization of raw materials

Before being incorporated into the mortars, the eggshell residues, that came from the food industry, did not undergo any prior treatment; they were not washed, nor was the organic membrane removed; they were simply oven-dried at a controlled temperature of 100 °C ± 5 °C until all moisture was completely removed.

After this process, the dried eggshells were ground in a jaw crusher equipped with a 4 mm sieve, aiming to obtain particles with suitable granulometry for incorporation into the mixtures.

Following this treatment, the eggshells and the other raw materials were characterized.

2.2.1 Particle size analysis

The particle size analysis of the sands and eggshells was performed in accordance with the standard EN 933-1:2012 - Tests on the geometric properties of aggregates - Part 1. Figure 1 shows the particle size distribution curves obtained.

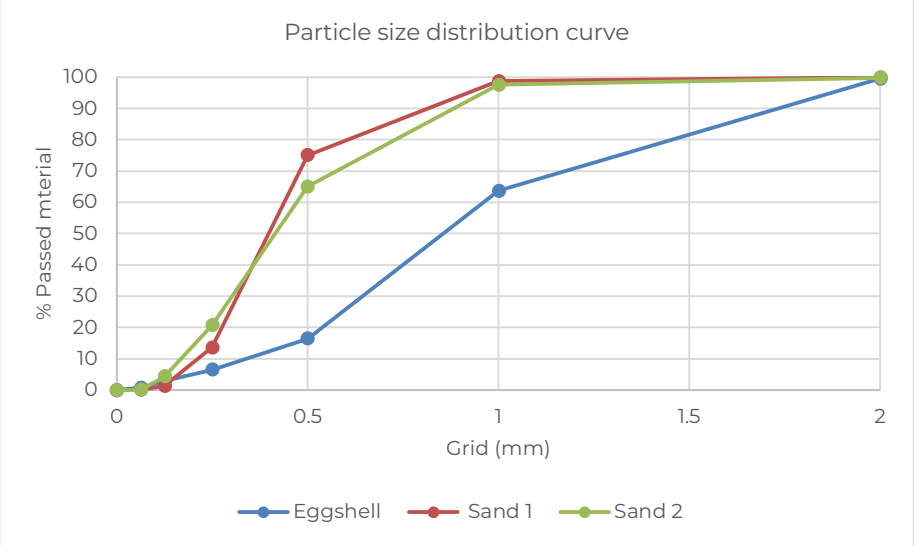


Figure 1 – Granulometric curves of sand and eggshell

2.2.2 Loose bulk density of the constituents

To determine the density of the aggregates (sand and eggshells), the method described in standard EN 1097-3:1998 - Tests on the mechanical and physical properties of aggregates - Part 3: Determination of density and void volume was used.

Table 2 presents the results obtained for the density of the various components.

Table 2 – Loose bulk density of the constituents

	Sand S1	Sand S2	Eggshell	Lime
Loose bulk density (kg/m³)	1487.22	1389.05	854.21	750

2.2.3 Determination of the density and water absorption of aggregates

The determination of bulk density and water absorption of the aggregates was carried out in accordance with the EN 1097-6:2022 standard (IPQ, 2024), which establishes the test methods for evaluating the physical properties of aggregates intended for use in mortars, concrete, and other construction materials.

Table 3 presents the results obtained for the bulk density and water absorption of the various components.

Table 3 – Bulk density and water absorption of the constituents

	Sand S1	Sand S2	Eggshell
Bulk density (kg/m³)	2636	2601	2336
Water absorption (%)	0.138	1.309	3.211

As can be observed from the obtained results, the shell residues are significantly lighter and exhibit higher water absorption capacity, which is expected to influence the properties of mortars incorporating them, particularly regarding their porous structure.

2.3 Mortar Preparation

For the development of the laboratory tests, 24 (twenty-four) prismatic specimens with dimensions of 40 × 40 × 160 mm were cast, in accordance with the applicable standard recommendations. Six specimens were produced for each formulation. After casting, the specimens were subjected to a curing period of 28 days under suitable controlled environmental conditions.

After the curing period, the specimens were used to perform laboratory tests aimed at determining open porosity, apparent bulk density by immersion, water absorption by capillarity. For the water vapour permeability test, in accordance with ISO 12572:2016 – Hygrothermal performance of building materials and products – Determination of water vapour transmission properties, sixteen cylindrical specimens were prepared with a diameter of 106 mm and a thickness of 15 mm.

These tests were carried out to characterize the performance and durability of the different mortar formulations, allowing a comparative analysis between them and contributing to the evaluation of their technical feasibility in lime mortars intended for the rehabilitation of wattle and daub constructions

2.4 Properties of mortars in the fresh state

2.4.1 Consistence of Fresh Mortar

For the characterization of fresh mortars, the standard EN 1015-3:1999 (IPQ, 1999): Methods of test for mortar for masonry - Part 3: Determination of consistency of fresh mortar (by flow table), was used, which specifies the method for determining consistency by spreading. This test aims to evaluate the fluidity and workability of the mortar, essential parameters to ensure proper application and performance in the laying and coating process.

The results obtained for the consistency of all mortars are presented in table 4.

Table 4 – Consistency of the mortars

Mortar	Consistency (mm)
H_S1	167.68
H_S1_ES	177.92
H_S2	179.17
H_S2_ES	176.14

It is observed that all formulations presented flow spread values within the target range (175 ± 10 mm).

2.5 Properties of mortars in the hardened state

2.5.1 Open porosity and apparent density

Apparent density translates the simple direct relationship between the dry mass of a specimen and the volume it occupies, while open porosity represents the relationship between the volume of pores in the sample and the total volume. The determination of these properties was carried out in accordance with the procedures established in the standard EN 1936:2006 – Test methods for natural stone – Determination of real and apparent density and total and open porosities.

The results for apparent specific gravity are presented in Figure 2 and for open porosity are presented in Figure 3.

Based on the obtained results, it can be concluded that the incorporation of eggshell waste into the mortar mixtures resulted in a reduction in bulk density. This behaviour is consistent with the physical properties of the constituent materials, as the bulk density of processed eggshell residues is significantly lower than that of conventional natural sand aggregates. Consequently, the partial replacement of sand with eggshell-derived material results in a lighter composite matrix, reflecting its lower specific mass.

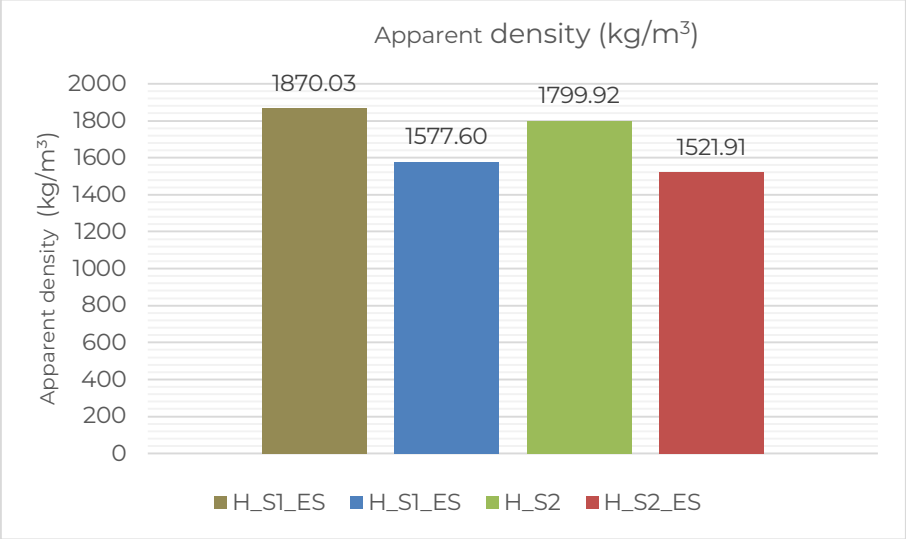


Figure 2 – Apparent density of the mortars

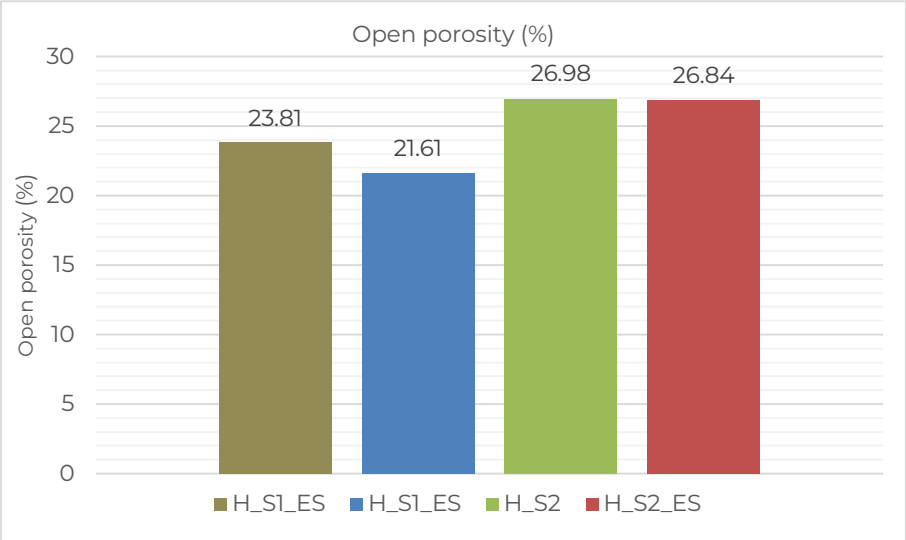


Figure 3 – Open porosity of the mortars

2.5.2 Water absorption by capillarity

The capillary absorption coefficient gives us an indication of the water absorption capacity of a mortar when placed in contact with a layer of water. The determination of water absorption by capillarity was carried out in accordance with the procedures established in the standard EN 1015-18:2002 – Methods of test for mortar for masonry - Part 18: Determination of water absorption coefficient due to capillary action of hardened mortar.

The results for water absorption curves are presented in Figure 4 and for water absorption coefficients of the mortars are presented in Table 4.

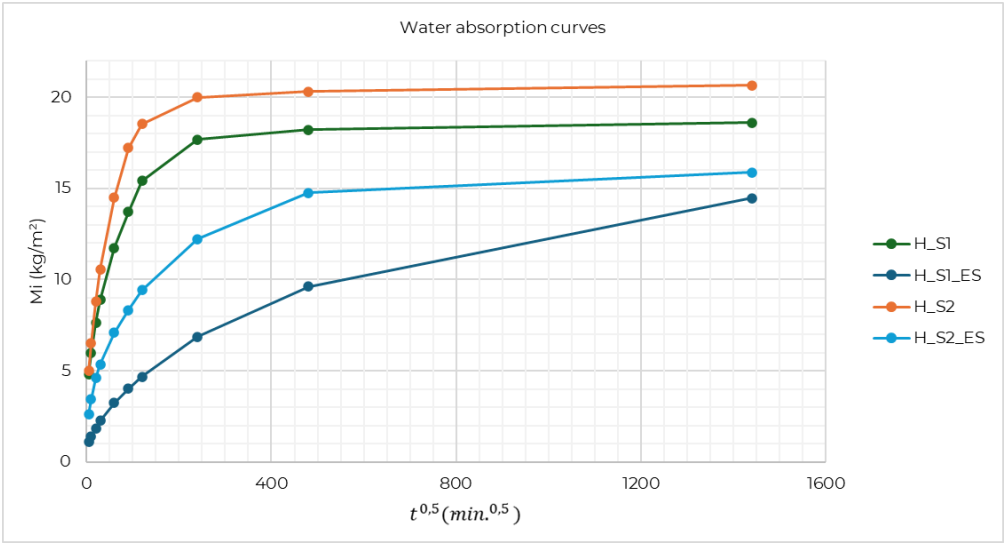


Figure 4 – Water absorption curves of the mortars

Table 4 – Water absorption coefficients of the mortars

Mortar	Water absorption coefficients [kg/(m².min^{0,5})]
H_S1	1.244
H_S1_ES	0.418
H_S2	1.750
H_S2_ES	0.769

The incorporation of eggshell waste into the mortar formulations resulted in a significant reduction in the water absorption coefficient. This behaviour agrees with the observed trends in open porosity, which likewise exhibited a decrease with the introduction of eggshell-derived material. Such findings suggest that the inclusion of this residue contributes to a densification of the pore structure and a reduction in capillary connectivity within the matrix. Consequently, the diminished absorptive capacity can be attributed to the modification of the microstructural characteristics of the mortar, leading to a less accessible pore network and enhanced resistance to water ingress.

2.5.3 Water vapour permeability

The determination of water vapour permeability was carried out in accordance with the procedures established in the standard ISO 12572:2016 – Hygrothermal performance of building materials and products – Determination of water vapour transmission properties. This parameter reflects a material's ability to allow water vapor to pass through it, was determined in accordance with the aforementioned standard, and the wet cup method was used.

The results for water vapour permeability coefficients are presented in Figure 5.

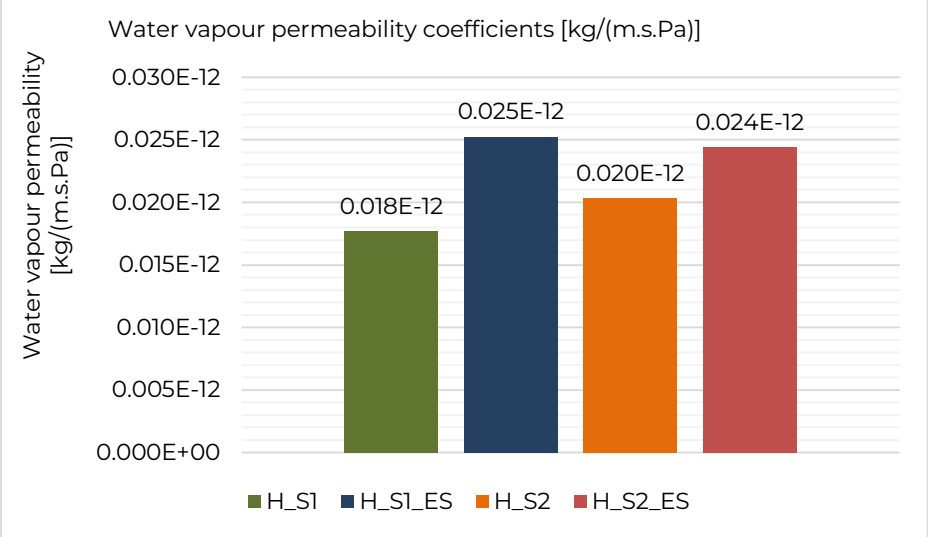


Figure 5 – Water vapour permeability coefficients of the mortars

The results indicate that the incorporation of the residues promoted an increase in water vapor permeability. This outcome was not initially anticipated, particularly considering the reductions observed in both water absorption and open porosity. However, this apparent discrepancy can be attributed to modifications in the structure and distribution of pores within the mortar matrix. Specifically, while total open porosity and

capillary absorption may decrease, the connectivity and morphology of the finer pores may be altered to facilitate vapor diffusion. Such microstructural changes are not fully elucidated by conventional porosity or absorption measurements and would require more detailed characterization techniques, such as mercury intrusion porosimetry, to provide a comprehensive understanding of pore distribution and size.

3. Conclusions

Eggshell waste has attracted considerable interest in the scientific community due to its chemical and physical properties. The fact that its composition is primarily calcium carbonate makes this byproduct appealing as a substitute for some of the mineral calcium carbonate used in the manufacture of many materials, thus making them more sustainable.

This paper presents the characterization of hydraulic lime mortars intended for the rehabilitation of partition walls. Two reference mortars were analysed without the introduction of residues and with two different types of sand, and two other mortars with the introduction of residues replacing 25% of the each sand.

In this study, it was possible to conclude that the introduction of eggshells into mortars, in general, was advantageous, as it allows for a reduction in the amount of aggregate while maintaining the required functional characteristics. The characterization performed allowed us to conclude that the introduction of eggshells reduced bulk density, porosity and the capillarity coefficient, while increasing vapor permeability.

For a more complete characterization, it will still be necessary to carry out some more tests, namely:

- determination of the mechanical strengths;

- determination of the dynamic modulus of elasticity (through measurement of the fundamental resonance frequency) which corresponds to the rate of change of deformation of a given material when subjected to stress;

- determination of the drying index which indicates the rate at which water is lost over time — essentially, it describes its drying kinetics.

- determination of adhesion to the substrate which indicates the ability of the mortar to adhere to and remain bonded to the substrate.

- determination of thermal conductivity which reflects the ability of the mortar to allow a flow of heat to pass through it.

Acknowledgments

This work was developed within the scope of the project "Sustainability of innovative wattle and daub mortars" (COMPETE2030-FEDER-00845500), co-funded by the European Regional Development Fund (ERDF) through the Support System for the Creation of Scientific and Technological Knowledge, under the Innovation and Digital Transition Program (COMPETE 2030). The authors would like to thank the Foundation for Science and Technology (FCT) for financial support through research grant 2022.13467/BD, and the CERIS research unit (funding UIDB/04625/2020).

References

King'ori *"A review of uses of Poultry Eggshells and Shell Membranes*", International Journal of Poultry Science, Vol. 10, Ed.11, pgs 908-912, 2011

Oliveira, D.A., Benelli, P.; Amante, E.R. "*A literature review on adding value to solid residues: eggs shells*", Journal of Cleaner Production, vol. 46, pp. 42-46, 2013

CEN (European Committee for Standardization)**.** 2012. EN 933-1: Tests for Geometrical Properties of Aggregates - Part 1: Determination of Particle Size Distribution - Sieving Method. Brussels: CEN.

CEN (European Committee for Standardization). 1998. EN 1097-3: Tests for mechanical and physical properties of aggregates - Part 3: Determination of loose bulk density and voids. Brussels: CEN.

CEN (European Committee for Standardization). 2022. EN 1097-6: Tests for mechanical and physical properties of aggregates - Part 6: Determination of particle density and water absorption. Brussels: CEN.

ISO (International Organization for Standardization). 2016. ISO 12572: Hygrothermal Performance of Building Materials and Products - Determination of Water Vapour Transmission Properties - Cup Method. Geneva: ISO.

CEN (European Committee for Standardization). 1999. EN 1015-3: Methods of Test for Mortar for Masonry - Part 3: Determination of Consistence of Fresh Mortar (by Flow Table). Brussels: CEN.

CEN (European Committee for Standardization). 2006. EN 1936: Natural Stone Test Methods - Determination of Real Density and Apparent Density, and of Total and Open Porosity. Brussels: CEN.

CEN (European Committee for Standardization). 2002. EN 1015-18:2002: Methods of test for mortar for masonry - Part 18: Determination of water absorption coefficient due to capillary action of hardened mortar. Brussels: CEN.

Cinpar 2026
XXII International Conference on Building Pathology and Constructions Repair
15th to 17th July 2026 - Lisboa, Portugal

Mapping technical façade elements under low-intensity seismicity to support risk-informed urban decision-making

Elena CANTATORE[1], Fabio FATIGUSO[2]

[1] Politecnico di Bari, Bari, Italy, elena.cantatore@poliba.it
[2] Politecnico di Bari, Bari, Italy, fabio.fatiguso@poliba.it

Abstract: Building façades constitute a critical spatial interface between urban open spaces and their users, where technical façade elements (TFEs) directly mediate everyday safety conditions. This is especially evident in historic urban areas, where tourist exposure is higher. Despite growing evidence from recent earthquakes, façade-related components remain largely underrepresented in conventional seismic risk frameworks, particularly under low-intensity and low-to-moderate seismicity, where cumulative damage processes and environmental degradation can increase outdoor vulnerability. This study proposes an operational framework for the systematic characterisation, qualification and spatialisation of façade-related TFEs, to support preventive decision-making. The methodology is grounded in two complementary knowledge sources: (i) the critical integration of regulatory and technical references, used to define a unified taxonomy and catalogue of façade elements; and (ii) the comparative analysis of real damage patterns observed during recent seismic events. This empirical analysis supports the identification of prevalent vulnerability patterns across different TFEs, and specifically elements exhibiting early sensitivity under low-intensity seismic actions. The classified TFEs and their associated attributes are structured into a minimum dataset for implementation within a GIS-based environment, enabling georeferenced mapping and aggregation of façade-related vulnerabilities. Therefore, element typologies, relative importance and prevalent damage classes are combined into a coherent qualitative classification system. This enables the rapid identification of potential critical façade elements without reliance on complex numerical modelling. Furthermore, the spatialised information provides a valuable decision-support layer for policymakers, facilitating the identification of urban open sub-areas characterised by reduced safety levels for users in outdoor. Overall, the systematisation and assessment of outcomes from façade to district scale offer a scalable and transferable tool for urban surveys, supporting the prioritisation of recurring vulnerability classes within façade element taxonomies. The framework is finally tested in a historic urban context, demonstrating its capability to capture differentiated vulnerability patterns across façade fronts.

Keywords: Technical Façade Elements (TFEs), Low-intensity seismicity, GIS-based mapping, Vulnerability, Urban open space safety.

1. Introduction

Building façades represent a critical spatial boundary between urban open spaces and their users, where Technical Façade Elements (TFEs), typically designed to serve interior functions, may significantly affect the everyday safety conditions of outdoor occupants. This interaction becomes particularly relevant in historic urban contexts, characterised by dense built fabrics, narrow streets, and highly frequented public spaces, where user exposure to potential hazards is significantly increased (Bernabei et al. 2021).

Within this interface, TFEs—such as balconies, cornices, parapets—constitute elements whose failure may directly affect users occupying adjacent open spaces, including streets and squares. Their role is therefore not limited to building performance but extends to the broader dimension of urban safety (Cheraghi and Behnam 2026; Mannucci *et al.* 2022; Lu *et al.* 2019). Traditional seismic risk assessments have predominantly

focused on structural behaviour and, more generally, on the seismic response of entire façades. However, increasing evidence from post-earthquake observations highlights the vulnerability of façade elements, particularly under low-intensity and low-to-moderate seismicity. In these contexts, cumulative damage processes, material ageing, and environmental degradation can progressively reduce damage activation thresholds, leading to early failure mechanisms even in the absence of significant structural distress (Rodgers *et al.* 2025; Miranda *et al.* 2012; Perrone *et al.* 2019; Merino *et al.* 2023).

Despite this evidence, façade-related elements remain marginal within conventional risk assessment frameworks, which rarely consider their interaction with user exposure in urban open spaces. This limitation is particularly critical in historic centres, where the spatial morphology of the built environment amplifies the consequences of localised failures. In such contexts, urban policymakers are required to ensure the safe use of public open spaces while also supporting effective spatial reorganisation and emergency evacuation planning (Cantatore *et al.* 2023; Ruggiero *et al.* 2021).

Given the relevance of façades and the scale of streets and squares as public open spaces, the management of façade vulnerability requires a multi-dimensional approach capable of collecting, assessing, and managing detailed information on TFEs, as well as capturing the broader system of buildings and blocks shaping urban open areas. The integration of façade-scale observations with spatial analysis tools represents a key opportunity. Geographic Information Systems (GIS) enable the organisation, aggregation, and visualisation of TFE-related data, supporting the identification of spatial vulnerability patterns across urban open spaces. This facilitates the transition from element-based observations to district-scale interpretations, providing a robust basis for preventive decision-making and risk-informed urban management.

1.1 Recent experiences and regulatory framework in managing Façade Technical Elements

The role of non-structural elements in seismic risk has progressively gained attention in both technical guidelines and scientific literature.

Eurocodes and the Italian Technical Standards for Construction (NTC 2018) acknowledge the relevance of architectural and façade components for building occupant safety (Audisio *et al.* 2026). This aspect is further emphasised in CARTIS-based applications, where non-structural elements play a significant role in building vulnerability assessment and support large-scale post-event data collection and interpretation (Del Carlo *et al.* 2025; Zuccaro *et al.* 2015). However, these regulatory frameworks mainly address classification, design, and assessment from a building-oriented perspective, with a primary focus on indoor conditions rather than providing operational tools for outdoor safety management.

A complementary line of research is represented by post-earthquake observational studies (O'Reilly *et al.* 2024; Baird and Ferner 2017; Sheshov *et al.* 2022), which analyse damage to façade elements through the interpretation of debris, cracks, and failure mechanisms generated by seismic events. These studies extend the understanding provided by regulatory frameworks, particularly for buildings not originally designed according to seismic criteria, such as historic constructions. As such, they provide valuable insights that require further systematisation to effectively support outdoor user safety management.

Moreover, studies conducted in areas characterised by recurrent low-magnitude seismicity, such as the Campi Flegrei, highlight the role of cumulative damage processes in progressively reducing the reliability of façade elements. These analyses often focus on sub-components of TFEs (e.g., plasters and decorative elements), emphasising how their state of decay contributes to the overall vulnerability of façades. In these contexts, the concept of damage threshold becomes particularly relevant, as certain elements may exhibit early sensitivity to seismic actions well below those typically considered in structural design (Liberotti *et al.* 2026; Castelluccio *et al.* 2021; Gaudiosi *et al.* 2020).

1.2 Work aim

Building on the above considerations, existing approaches remain predominantly building-oriented and

focused on high-intensity seismic scenarios, leaving the indoor–outdoor interface only partially explored, particularly in terms of outdoor effects induced by secondary debris. In particular, the combined role of element classification, its relevance (in terms of potential consequences), and damage thresholds (in terms of activation conditions) is rarely formalised within simplified assessment frameworks suitable for the rapid management of outdoor urban safety. This gap highlights the need for approaches capable of integrating qualitative classification systems with spatial analysis tools, enabling the transition from façade-level observations to urban- and district-scale vulnerability mapping. Such approaches can support policymakers in managing outdoor user safety under both ordinary and extraordinary use of outdoor open areas.

Within this context, the present work aims to address this gap by proposing a GIS-based tool for the collection and systematisation of TFEs and their main attributes, enabling the spatial management of vulnerability information and outdoor safety conditions. To achieve the aim, two preliminary activities are developed: (i) the classification of TFEs, based on the integration of thematic guidelines and normative frameworks; and (ii) the definition of a simplified qualification matrix based on relevance and observed damage patterns, to identify vulnerability classes of TFEs and supporting decision-making processes.

Accordingly, Section 2 presents the methodological framework; Section 3 illustrates the results, including the classification of TFEs (Section 3.1), the vulnerability qualification matrix (Section 3.2), the GIS-based data model for TFE codification and qualification (Section 3.3), and its application to a real case study (Section 3.4). Finally, Section 4 discusses the main outcomes and conclusions.

2. Methodology for the Characterisation and Qualification of Façade Elements

To achieve the outlined objectives, the study adopts a three-phase methodology, each phase addressing a specific sub-objective of the research. In detail:

- Phase 1 focuses on the identification and codification of Technical Façade Elements (TFEs) associated with building façades, based on national and international regulatory frameworks addressing non-structural elements. Specifically, the Italian Technical Standards for Construction (NTC 2018) and the CARTIS form (sub-section 3.2 of the form) (Reluis and Protezione Civile, n.d.) are analysed and systematised to derive a synthetic and consistent list of TFEs, accounting for façade-specific characteristics. In addition, the American FEMA E-74 guidelines (Federal Emergency Management Agency (FEMA) 2012) are included to extend the analysis beyond the national context. Each TFE class is assigned a specific code, contributing to the definition of a unified taxonomy.
- Phase 2 aims to develop a simplified tool for assessing the prevalent intrinsic vulnerability patterns of TFEs. The tool is structured as a two-dimensional matrix that classifies the codified TFEs according to: (i) their relevance to user safety (Relevance Index – R-index), and (ii) their prevalent damage behaviour (Prevalent Damage Index – PD-index). The R-index is derived from design prescriptions and criteria embedded in the adopted regulatory frameworks (CARTIS, NTC, FEMA), while the PD-index is defined based on literature and grey sources documenting observed damage to TFEs under seismic and low-intensity events. The attribution of the R-index was based on the primary consequences associated with the failure of each TFE. Elements whose failure may directly threaten users occupying adjacent public spaces were classified as High relevance, whereas elements mainly associated with service interruption or localised functional impacts were assigned to the Medium relevance class. Similarly, the PD-index was derived from the comparative interpretation of observed damage patterns across the analysed case studies. Elements repeatedly exhibiting instability, detachment, or damage under low-to-moderate seismic actions were classified as Early-sensitive, while those predominantly activated under stronger shaking conditions were assigned to the High-threshold class. The empirical basis includes: the 2016 Central Italy seismic sequence (Norcia–Amatrice) (Pagan 2021; Perrone *et al.* 2019), the bradyseismic activity in Campi Flegrei (2009–2023) (Castelluccio *et al.* 2025) —also supported by photographic evidence from daily newspapers—and the Christchurch earthquakes

(2010–2011) (Commission 2012), where façade-related failures caused significant casualties in outdoor spaces. For each index, two qualitative levels are defined, resulting in a simplified matrix describing the prevalent vulnerability of TFEs in relation to damage activation thresholds.

- Phase 3 builds upon the results of the previous phase by integrating the TFE codification and the vulnerability matrix into a GIS-based model. This phase enables the spatial representation of TFEs and their distribution along façades, supporting the development of a synthetic and queryable decision-support system for policymakers. In this context, TFEs are analysed according to their spatial characteristics (point, linear, or areal), allowing the definition of a minimum dataset for GIS implementation that extends the information associated with their codification. The resulting data structure is organised at the façade level, linking the geographical position of façades with their associated TFE attributes.

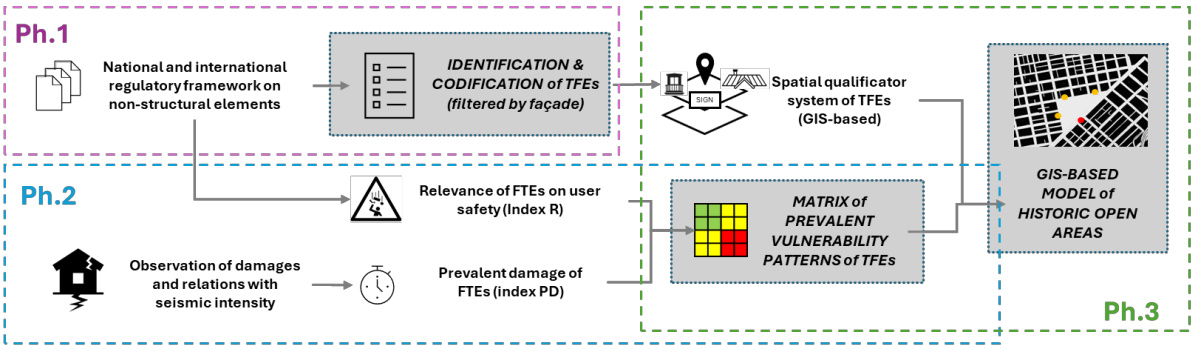


Figure 1 – Schema of activities involved in the pursued method, defined for each sub-aim (grey blocks) and phase

To illustrate the outcomes of the methodology, Section 3 presents the results of the three phases, with particular emphasis on the third phase through its application to a representative area of the historic centre of Bari (Southern Italy).

3. Results

The results of the methodology are structured according to the three phases described in Section 2, leading to a coherent system for the classification, qualification, and synthesis of Technical Façade Elements (TFEs).

3.1 Classification of façade elements

The first outcome consists of a unified taxonomy of TFEs derived from the integration of CARTIS forms, NTC 2018, and FEMA E-74 guidelines.

As shown in Table 1, the classification includes non-structural elements identified within the regulatory frameworks, grouped into architectural (A), mechanical (M), and content-related (C) categories. The codification of TFE types is limited to elements that exhibit a direct interaction with façades. Accordingly, a filtering process is applied to identify only those components that interact with the building envelope and may pose a risk to adjacent public spaces.

Each element is therefore assessed in terms of façade admissibility, and only the admissible subset is retained for subsequent analyses (Tables 2–3, Figure 2).

The integration of multiple sources enables the extension of the classification beyond purely architectural components, incorporating systems and elements that influence both safety and functionality.

Table 1 – Codification of Technical Façade Elements and associated source

Code	Element name	Source	Façade admissibility	Code	Element name	Source	Façade admissibility
-	Non-structural partitions	CARTIS / NTC	No	A11	Emergency stairs / walkways	NTC	Yes**
A02	Roof covering (tiles)	CARTIS	Yes*	A12	Canopies / signs	NTC	Yes
A03	Chimneys / vertical protrusions	CARTIS	Yes	M01	Façade systems (gutters, AC units)	NTC	Yes
A04	Balconies	CARTIS	Yes	-	Internal systems	NTC	No
A05	Cornices	CARTIS	Yes	M03	Elevators	NTC	Yes**
A06	Parapets	CARTIS	Yes	M04	HVAC systems	FEMA	Partial***
-	Light suspended ceilings	CARTIS	No	M05	Escalators	FEMA	Yes**
-	Heavy suspended ceilings	CARTIS	No	-	Fire protection systems	FEMA	No
-	Light false vaults	CARTIS	No	-	Equipment (medical/industrial)	FEMA	No
-	Heavy false vaults	CARTIS	No				

* included only when interacting with façade edges, **included only if external, ***included only when externally mounted

3.2 Qualification of TFEs according to relevance R-index and PD index towards the definition of the synthetic matrix of TFEs vulnerability

The second result concerns the definition of the simplified matrix to describe the vulnerability of the identified FTEs.

First of all, the Relevance Index (R-index) is derived from regulatory frameworks. As summarised in Table 2, each TFE is assigned a qualitative level of importance (High or Medium), based on its potential impact on user safety and building functionality.

Architectural elements directly exposed to public spaces (e.g., balconies, cornices, parapets) are consistently classified as high relevance due to their direct life-safety implications. Conversely, most mechanical systems are classified as medium relevance, as their failure generally affects functionality rather than immediate safety. This classification provides a simplified yet robust interpretation of regulatory prescriptions, translating them into an operational assessment tool.

Then, the definition of the Prevalent Damage Index (PD-index) follows, deriving it from the comparative analysis of real seismic events. Table 3 summarises the main damage mechanisms identified across the case studies of Central Italy (2016), Campi Flegrei, and Christchurch. The analysis highlights two main behavioural patterns:

- Early-sensitive elements (PD = E), which exhibit damage under low-to-moderate seismic actions (e.g., balconies, cornices, façade systems);
- High-threshold elements (PD = H), which are activated only under stronger shaking or after cumulative damage processes. This distinction confirms the importance of considering not only the severity of damage but also the activation threshold, especially in low-intensity seismic contexts.

Table 2 – Classification of the Identified TFEs in coherence with the R-index classes (High or Medium)

Code	Element name	R class	Code	Element name	R class
A04	Direct exposure and high risk of falling elements	High	A11	Critical for evacuation safety	High
A05	High mass elements prone to detachment	High	A12	Local hazard, limited extension	Medium
A06	Overturning risk toward public space	High	M01	Limited mass, localized risk	Medium
A03	Local collapse with direct hazard	High	M04	Functional relevance, limited direct hazard	Medium
A02	Falling elements affecting pedestrians	High			

Table 3 – Classification of the Identified TFEs in coherence with the PD-index classes (Early sensitive=E or High-threshold=H)

Code	Source	Explanation	PD class	Code	Source	Explanation	PD Class
A04	Campi Flegrei + Christchurch	Early activation under low shaking	E	A03	Norcia + Christchurch	Collapse at higher intensity	H
A05	All cases	Frequent early detachment	E	A02	Norcia	Damage after cumulative effects	H
A06	Campi Flegrei	Instability at moderate intensity	E	A11	Christchurch	Damage only in strong events	H
A12	Campi Flegrei	Early localized failures	E	M04	Christchurch	Moderate-to-high activation threshold	H
M01	Campi Flegrei	Detachment at moderate acceleration	E	A03	Norcia + Christchurch	Collapse at higher intensity	H

This distinction emphasises the importance of considering not only damage severity but also activation thresholds, particularly in low-intensity seismic contexts.

The integration of the R-index and PD-index results in a four-class qualitative matrix, presented in Figure 2. This matrix represents the core outcome of the methodology, enabling the identification of distinct vulnerability patterns, defined as follows:

- High R – Early PD: elements with high impact and early damage activation (most critical – Vulnerability Class A);
- High R – High PD: elements with severe consequences but higher activation thresholds (critical under higher seismic intensity – Vulnerability Class B);
- Medium R – Early PD: elements with frequent damage but limited consequences (low impact but rapid activation – Vulnerability Class C);
- Medium R – High PD: elements with limited relevance and higher resistance (low impact and high activation threshold – Vulnerability Class D).

Overall, the matrix provides a simplified yet effective decision-support tool, enabling the rapid identification of vulnerability patterns associated with façade elements.

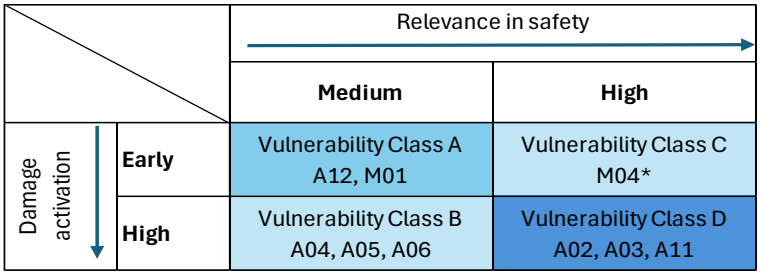


Figure 2 – Simplified matrix of the identified TFEs in coherence with R-index and DP-index qualification and distributed in coherence with the identified Vulnerability Classes

3.3 Census structuring and GIS-oriented data model

In continuity with the methodological framework described in Section 2, the set of Technical Façade Elements (TFEs), previously classified and qualified, is further processed through a data abstraction procedure aimed at enabling their systematic census and spatial implementation. Rather than introducing new descriptive categories, this phase translates the previously defined TFEs into a structured data model, ensuring consistency with the classification system and the associated indices (R-index and PD-index).

As a first requirement, the codified TFEs are characterised according to:

- geometric abstraction, whereby each TFE is associated with a simplified spatial typology (areal, linear, or point-like), enabling a homogeneous representation of heterogeneous elements. Table 4 summarises the adopted approach.
- relational structuring, through which TFEs are organised into a dataset linking spatial references, typological attributes, and vertical distribution (storey levels).

Within this framework, TFE contents associated with each façade are interpreted as a spatial interface, discretised both horizontally (façade units) and vertically (storey levels), allowing multiple TFEs to be assigned to the same spatial entity.

Table 4 – Set of minimum data for geometric abstraction of the identified TFEs

Type of TFE	Geometric content n.1	Geometric content n.2	Geometric content n.3
Punctual	n. of elements for each floor [*TFECode_n*]		
Linear	n. of elements for each floor [*TFECode_n*]	length/height of the element in each floor [*TFECode_l*]	
Aereal	n. of elements for each floor [*TFECode_n*]	length of the element in each floor [*TFECode_l*]	depth/height of the elements in each floor [*TFECode_h*]

Regarding spatial referencing, the organisation of metadata within the GIS environment follows a hierarchical “one-to-many” structure:

- each building, typically identified through a cadastral open-source layer (polygon), is assigned a unique Building_ID;
- each Building_ID is associated with a set of façades, represented through point or line geometries and uniquely identified by a Façade_ID;

- for each façade (Façade_ID), attribute tables are structured to collect TFE-related data (Table 4) for each storey level.

With reference to vulnerability-related information, each spatial unit (Point_ID) within the district is enriched with an aggregated attribute derived from the vulnerability matrix, corresponding to the highest vulnerability class among the TFEs identified on the associated façades. This enables the direct spatial representation of alert levels within the GIS environment.

3.4 Application on the ancient core of Bari

To demonstrate the applicability of the proposed approach, the methodology is implemented in a representative area of Bari's historic core. This context is characterised by high tourist activity and narrow streets, increasing exposure and risk for outdoor users. Its historical development results in recurring building typologies and limited variability in TFE distribution. The case study is further supported by the local seismic classification, characterised by predominantly low-intensity events. Figure 3 illustrates the extent of the analysed area. The dataset covers the southern portion of the historic core, including more than 200 façades, typically developed over three to four storeys above ground. Besides, Figure 4 shows the structure of FTEs metadata collected at the scale of each façade, highlighting the granularity at the floor scale.

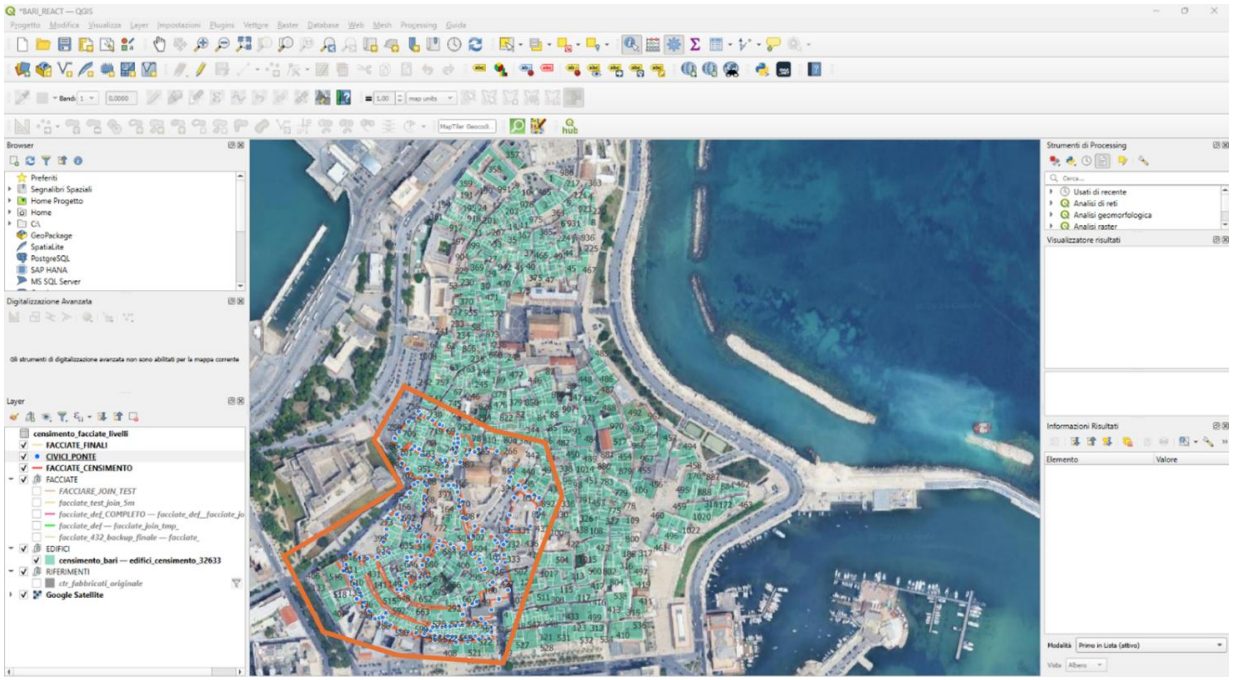


Figure 3 – Perimetration of the sub-area of the ancient core of Bari (orange polygon), analysed with the described approach

A more detailed focus is provided in Figure 5 for Piazza dell'Odegitria, a key open space within the investigated area. This square represents a highly polarised urban space, characterised by the presence of the Cathedral and multiple commercial activities, which significantly increase pedestrian flows and tourist presence. The analysis shows that most façades surrounding the square are characterised by Vulnerability Class C elements (low impact but early activation), mainly due to the widespread presence of parapets, typically located in the upper portions of façades.

At the same time, the georeferenced classification highlights localised exceptions, including façades characterised by Vulnerability Class A elements. These differentiated vulnerability patterns provide relevant

insights for urban safety management. In particular, the presence of higher vulnerability classes along specific edges of the square suggests the need for targeted planning strategies, including the optimisation of evacuation routes and the management of pedestrian flows during both ordinary conditions and emergency scenarios. This is especially relevant in the context of low-intensity seismic events, where early damage activation of TFEs may still pose significant risks to outdoor users.

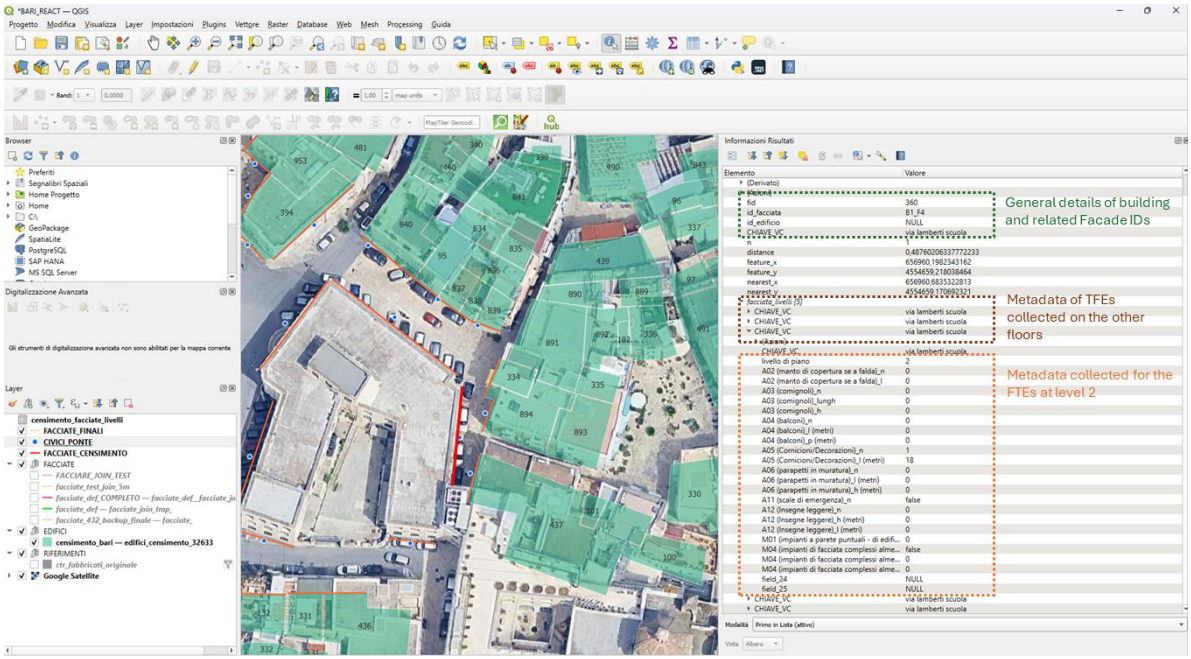


Figure 4 – Overview of TFEs contents gathered in the GIS-Based environment and details of multi-dimensional scale of the collected metadata

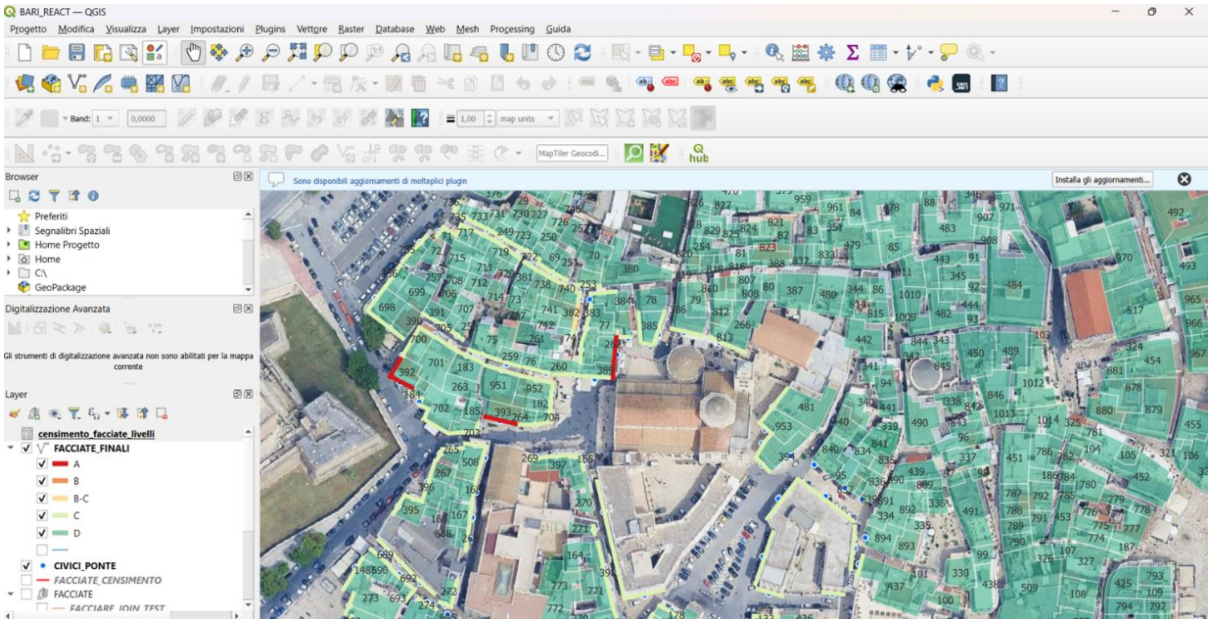


Figure 5 – Distribution of Vulnerability Classes of TFEs in facades distributed along the borders of Piazza dell'Odegitria

4. Discussion and Conclusions

The proposed framework highlights the relevance of Technical Façade Elements (TFEs) as interface components in the assessment of outdoor urban safety, particularly under low-intensity seismic conditions. By focusing on non-structural elements as conceived in national and international regulatory frameworks, the study addresses a dimension of seismic risk that is often overlooked in conventional approaches yet directly affects users in everyday urban environments.

The adoption of a qualitative and screening-level methodology, based on the combined use of the Relevance Index (R-index) and the Prevalent Damage Index (PD-index), enables the rapid qualification of TFEs. This approach allows the translation of façade-level observations into structured information, supporting consistent and scalable assessments without the need for complex modelling tools. As a screening-oriented approach, the proposed framework intentionally simplifies the complexity of façade behaviour by two qualitative indices and four vulnerability classes. The resulting classification does not explicitly account for factors such as material degradation, connection details, maintenance conditions, or local amplification effects, which may influence the actual performance of TFEs. Moreover, the vulnerability classes were derived from the interpretation of regulatory references and recurring damage observations rather than from statistically calibrated fragility functions. Therefore, they should be interpreted as relative indicators supporting prioritisation and preventive decision-making rather than as quantitative measures of failure probability.

The integration of the dataset within a GIS-based environment represents a key advancement of the proposed framework. The spatialisation of vulnerability levels (A–D) allows the identification of clusters of critical conditions and supports the interpretation of façade-related vulnerability in relation to urban open spaces, particularly streets and squares characterised by high levels of user exposure. Thus, the methodology enables a shift from building-scale analysis to a more comprehensive district-scale perspective.

The application to the historic urban context of Bari confirms the capability of the framework to capture differentiated vulnerability patterns across façade fronts, highlighting the role of both element typology and spatial configuration in defining safety conditions. In particular, higher vulnerability levels are frequently associated with elements characterised by both high relevance and low damage thresholds, located in areas of intense pedestrian use.

From an operational perspective, the proposed approach provides a useful decision-support tool for public administrations, facilitating the prioritisation of interventions and the identification of urban sub-areas characterised by reduced safety conditions. The possibility of aggregating data from the façade scale to the district scale enhances its applicability within urban survey and monitoring processes. In this context, the framework can support not only emergency planning but also promote local suggestions in preventive maintenance strategies to private owners and organize different levels of priority of interventions for public buildings aimed at reducing long-term exposure to façade-related risks.

Although tested in a historic Mediterranean context, the methodology is designed to be transferable to other urban environments, provided that local regulatory references and context-specific TFE characteristics are appropriately integrated.

Finally, the integration of façade-related vulnerability with the spatial configuration of urban open spaces opens further perspectives for the analysis of user exposure and movement patterns. In this sense, future developments may include the incorporation of geometric and morphological parameters, as well as dynamic data related to pedestrian flows, supporting more advanced applications in evacuation planning and the design of safer pedestrian mobility strategies.

In line with validation purposes, future activities may take into account the opportunity to investigate the validation of the proposed classes through post-event damage inventories and broader urban case studies. At the same time, the relevance of the users' safety in outdoor environments, future research can take

advantage of these synthetic results to combine the analysed seismic-induced vulnerability on outdoor users with other kinds of hazards, such as heatwaves, to reflect the opportunity to test multi-safe places.

Acknowledgments

This work has been supported by the funding from the “National Recovery and Resilience Plan (PNRR)", Mission 4 “Education and Research” – Component 2 “From Research to Business” – Investment 1.3 “Extended partnerships among universities, research centres, and companies for the funding of basic research projects”, funded by the European Union – NextGenerationEU – under the Call issued by Ministerial Decree No. 341 of March 15, 2022. Project “Multi-Risk sciEnce for resilienT commUnities undeR a changiNg climate (RETURN)” – Project Code PE0000005 – CUP E63C22002000002, funded through Ministerial Decree No. 1552 of October 11, 2022. CASCADE CALL Spoke 5 TS1 “Urban and Metropolitan Settlements” – Project “Modeling and simulation of multi-risk scenarios in urban and metropolitan areas considering the interactions between physical systems and the population in emergency situations” (ReACT), funded through Grant Award Decree DR/2025/107 dated 13/01/2025 issued by the University of Naples Federico II in its capacity as Spoke.

References

Audisio, Lorenzo, Matteo Tatangelo, Michele D’Amato, and Rosario Gigliotti. 2026. “Floor Response Spectra for Seismic Design of Non-Structural Elements According to the Italian NTC 2018.” *Procedia Structural Integrity* 78: 1277–84. https://doi.org/10.1016/j.prostr.2025.12.163.

Baird, Andrew, and Helen Ferner. 2017. “Damage to Non-Structural Elements in the 2016 Kaikōura Earthquake.” *Bulletin of the New Zealand Society for Earthquake Engineering* 50 (2): 187–93.

Bernabei, Letizia, Giovanni Mochi, Gabriele Bernardini, and Enrico Quagliarini. 2021. “Seismic Risk of Open Spaces in Historic Built Environments: A Matrix-Based Approach for Emergency Management and Disaster Response.” *International Journal of Disaster Risk Reduction* 65 (November): 102552. https://doi.org/10.1016/j.ijdrr.2021.102552.

Cantatore, Elena, Dario Esposito, and Alberico Sonnessa. 2023. “Mapping the Multi-Vulnerabilities of Outdoor Places to Enhance the Resilience of Historic Urban Districts: The Case of the Apulian Region Exposed to Slow and Rapid-Onset Disasters.” *Sustainability* 15 (19): 14248. https://doi.org/10.3390/su151914248.

Carlo, Federica Del, Silvia Caprili, and Tiago Miguel Ferreira. 2025. “Development and Validation of a New Approach to Assess the Seismic Vulnerability of Masonry Structures Based on the CARTIS Form.” *International Journal of Architectural Heritage* 19 (10): 2299–2316. https://doi.org/10.1080/15583058.2024.2421296.

Castelluccio, Roberto, Diego Di Martire, Luigi Guerriero, and Veronica Vitiello. 2021. “Methods for Assessing the Vulnerability of Non-Structural Components. Monitoring for Risk Managment.” *Sustainable Mediterranean Construction*, 156.

Castelluccio, Roberto, Veronica Vitiello, Rossella Marmo, and Mariacarla Fraiese. 2025. “Damage to Technical Elements of the Building Envelope in the Typical Multi-Risk Scenario of the Campi Flegrei Area.” In , 162–79. https://doi.org/10.1007/978-3-031-71863-2_11.

Cheraghi, Siamak, and Behrouz Behnam. 2026. “Probabilistic Assessment of Factors Influencing Façade Fire Formation and Extension.” *Architectural Science Review* 69 (1): 16–49. https://doi.org/10.1080/00038628.2025.2455955.

Commission, Canterbury Earthquakes Royal. 2012. “Volume 4: Earthquake-Prone Buildings.” *Canterbury Earthquakes Royal Commission, Wellington*.

Federal Emergency Management Agency (FEMA). 2012. “FEMA E-74 - Reducing the Risks of Nonstructural Earthquake Damage – A Practical Guide.”

Gaudiosi, Germana, Giuliana Alessio, Rosa Nappi, Valentina Noviello, Efisio Spiga, and Sabina Porfido. 2020. “Evaluation of Damages to the Architectural Heritage of Naples as a Result of the Strongest Earthquakes of the Southern Apennines.” *Applied Sciences* 10 (19): 6880. https://doi.org/10.3390/app10196880.

Liberotti, Riccardo, Mattia Schiantella, Federico Cluni, and Vittorio Gusella. 2026. “Architectural Non-Structural Elements (NSEs) and Heritage Safety: Restoration Interventions for the Seismic Vulnerability Reduction.” *Procedia Structural Integrity* 78: 1919–26. https://doi.org/10.1016/j.prostr.2025.12.244.

Lu, Xinzheng, Zhebiao Yang, Gian Paolo Cimellaro, and Zhen Xu. 2019. “Pedestrian Evacuation Simulation under the Scenario with Earthquake-Induced Falling Debris.” *Safety Science* 114 (April): 61–71. https://doi.org/10.1016/j.ssci.2018.12.028.

Mannucci, Simona, Federica Rosso, Alessandro D’Amico, Gabriele Bernardini, and Michele Morganti. 2022. “Flood Risk of Open Spaces: From Microscale Factors of Built Environment to Risk Reduction Strategies.” In , 159–69. https://doi.org/10.1007/978-981-16-6269-0_14.

Merino, Roberto J., Daniele Perrone, Roberto Nascimbene, and Andre Filiatrault. 2023. “Performance-based Seismic Classification of Acceleration-sensitive Non-structural Elements.” *Earthquake Engineering & Structural Dynamics* 52 (13): 4222–44. https://doi.org/10.1002/eqe.3973.

Miranda, Eduardo, Gilberto Mosqueda, Rodrigo Retamales, and Gokhan Pekcan. 2012. “Performance of Nonstructural Components during the 27 February 2010 Chile Earthquake.” *Earthquake Spectra* 28 (1S1): 453–71. https://doi.org/10.1193/1.4000032.

O’Reilly, Gerard J., Kan Hasegawa, Davit Shahnazaryan, José Poveda, Yu Fukutomi, Akihiro Kusaka, and Masayoshi Nakashima. 2024. “On the Fragility of Non-structural Elements in Loss and Recovery: Field Observations from Japan.” *Earthquake Engineering & Structural Dynamics* 53 (3): 1125–44. https://doi.org/10.1002/eqe.4066.

Pagan, Kelly. 2021. “Analisi Di Vulnerabilità Sismica Della Basilica Di San Benedetto a Norcia Dopo Il Terremoto Del 2016: Indagini Strutturali, Modellazione Numerica e H-BIM.” UNIVERSITÀ DEGLI STUDI DI PADOVA. https://www.collegioingegnerivenezia.it/upload/collegioingegnerivenezia_whoihma2vg/media/eventi_2/2024/2024_04_20_PremioIngEccellenti/Tesi-Abstract/06-Pagan_Kelly-TESI.pdf.

Perrone, Daniele, Paolo Calvi, Roberto Nascimbene, Erica C. Fischer, and Gennaro Magliulo. 2019. “Seismic Performance of Non-Structural Elements during the 2016 Central Italy Earthquake.” *Bulletin of Earthquake Engineering* 17 (10): 5655–77. https://doi.org/10.1007/s10518-018-0361-5.

Reluis and Protezione Civile. n.d. “Scheda CARTIS.” https://www.protezionecivile.gov.it/static/09c8499fe4acaa014adf2f86539fc720/allegato-b-scheda-cartis-comparto.pdf.

Rodgers, Casey J., Nathaniel Levine, and Billie F. Spencer. 2025. “Quantitative Post-Earthquake Building Condition Inference from Exterior Drift-Sensitive Nonstructural Damage Observations.” *Engineering Structures* 336 (August): 120348. https://doi.org/10.1016/j.engstruct.2025.120348.

Ruggiero, Giovanni, Rossella Marmo, and Maurizio Nicolella. 2021. “A Methodological Approach for Assessing the Safety of Historic Buildings’ Façades.” *Sustainability* 13 (5): 2812. https://doi.org/10.3390/su13052812.

Sheshov, Vlatko, Roberta, Apostolska, Zhivko, Bozinovski, Marija Vitanova, Blagojce Stojanoski, Kemal Edip, Aleksandra Bogdanovic, et al. 2022. “Reconnaissance Analysis on Buildings Damaged during Durres Earthquake Mw6.4, 26 November 2019, Albania: Effects to Non-Structural Elements.” *Bulletin of Earthquake Engineering* 20 (2): 795–817. https://doi.org/10.1007/s10518-021-01271-1.

Zuccaro, Giulio, Mauro Dolce, Daniela De Gregorio, Elena Speranza, and Claudio Moroni. 2015. “La Scheda CARTIS per La Caratterizzazione Tipologico-Strutturale Dei Comparti Urbani Costituiti Da Edifici Ordinari. Valutazione Dell’esposizione in Analisi Di Rischio Sismico.” *Proceedings of the GNGTS*.

Cinpar 2026
XXII International Conference on Building Pathology and Constructions Repair
15th to 17th July 2026 - Lisboa, Portugal

Large-Scale Seismic Vulnerability Assessment of Masonry Buildings: A Critical Appraisal of Index-based Methods

Letizia MANCINI[1], Maria Giovanna MASCIOTTA[1,2], Giorgia CIANCHINO[1], Tiago Miguel FERREIRA[3], Giuseppe BRANDO[1,2]

[1] Department of Engineering and Geology, "G. d'Annunzio" University of Chieti-Pescara, Pescara, Italy, letizia.mancini@phd.unich.it
[2] UdA-TechLab, Research Center, "G. d'Annunzio" University of Chieti-Pescara, Chieti, Italy
[3] CERIS, Instituto Superior Técnico (IST), University of Lisbon, Lisbon, Portugal

Abstract: Ex ante seismic vulnerability assessment plays a central role in preventing damage to exposed assets and becomes particularly relevant when intended to support public administrations in the large-scale planning of seismic risk mitigation strategies. In such contexts, the large number of buildings to be analysed requires the adoption of rapid assessment approaches that, while forgoing advanced and time-consuming analyses, allow the evaluation of extensive building portfolios through a limited set of structural and typological parameters capable of capturing their expected seismic behaviour.

By applying and comparing two large-scale seismic vulnerability assessment methods for masonry buildings, both based on the Vulnerability Index, this study highlights the operational potential of these tools while critically examining the inherent sources of error and uncertainty embedded in their formulation. The objective is to raise awareness of the need for a careful and informed interpretation of the results, especially when they serve as a basis to support decision-making processes and prioritize mitigation interventions.

The analysis focuses on a sample of masonry buildings located in the municipality of Campotosto, a small town in the province of L'Aquila (Central Italy) severely affected by the 2016–2017 seismic sequence. The work contributes to a broader effort toward the progressive refinement of large-scale assessment methodologies, ultimately enhancing the reliability and robustness of territorial-scale seismic vulnerability analyses.

Keywords: Seismic risk management, Vulnerability index methods, Historic centres, Uncertainty quantification

1. Introduction

Large-scale vulnerability assessment represents a fundamental tool for supporting seismic risk mitigation policies and territorial emergency planning, especially in historic urban areas characterized by vulnerable masonry building stocks (Blyth, et al. 2020). In this context, the need to analyse a large number of structures within limited timeframes has promoted the widespread use of rapid assessment procedures based on simplified and empirical approaches. Among them, Vulnerability Index methods are currently recognised as one of the most effective and operational solutions for territorial-scale applications due to their simplicity, reduced data requirements and ability to provide damage scenarios useful for decision-making processes.

Despite their extensive application and validation in the literature, large-scale vulnerability assessment methods remain intrinsically affected by different sources of error and uncertainties. These may derive from the adopted analytical formulations, the engineering judgment of data, as well as the assumptions related to seismic input parameters. Since the outcomes of these methodologies are often used to prioritise mitigation strategies and allocate economic resources, understanding their limitations becomes essential for a correct interpretation of the results.

Within this framework, the present study focuses on the identification and critical appraisal of the main sources of uncertainty affecting large-scale seismic vulnerability assessment methods for masonry buildings. This objective is pursued through the comparison of two well-known and widely validated VI-based approaches proposed by (Ferreira, Vicente, et al. 2013) and (Brando, et al. 2017) with application to a sample of buildings located in the municipality of Campotosto (L'Aquila, Italy).

This work presents a synthesis of the main results from a broader study on the analysis of the main sources of error and uncertainties affecting large-scale seismic vulnerability assessment approaches. A more comprehensive discussion and additional results are provided in (Masciotta, Mancini, et al. 2025).

The paper is organised as follows. Section 2 outlines the methodologies adopted to estimate the seismic vulnerability of the historic centre under investigation. Section 3 presents the case study of Campotosto along with the results from the vulnerability assessment. Finally, Section 4 discusses the sources of errors and uncertainties associated with the adopted methods, and Section 5 summarises the main conclusions of the study.

2. Materials and Methods

As highlighted by (Baquedano-Juliá, et al. 2024), index-based methodologies have experienced significant development over the last years. Their simplicity, cost-effectiveness and time-efficiency make them particularly suitable for large-scale risk analysis, especially in developing contexts where economic and skilled human resources for heritage protection are limited. In light of these advantages and considering the need to analyse a large building sample while investigating the inherent sources of uncertainty affecting large-scale methods, two widely validated approaches are selected, namely the methodologies proposed by (Ferreira, et al. 2013) and by (Brando, et al. 2017). Although developed in different contexts and calibrated using post-earthquake damage data from distinct regions, both approaches share a common methodological framework for the seismic vulnerability assessment of masonry buildings. They are based on the computation of a Vulnerability Index (VI) obtained through the evaluation of the main structural features and seismic-related deficiencies of buildings, typically collected via rapid in situ surveys. The VI provides a quantitative representation of the physical and structural characteristics of each building and is subsequently used to estimate expected damage levels through vulnerability functions. A detailed description of the two methodologies is provided below.

2.1 Vulnerability index method by Ferreira et al.

The method proposed by (Ferreira, et al. 2013) builds upon the (GNDT 1994) II level approach originally developed for Italian masonry structures. It was subsequently adapted to the Portuguese traditional building stock by (Vicente, et al. 2011) and later refined and calibrated by (Ferreira, et al. 2013) according to the damage observation from the 1998 Azores earthquake (Ferreira, et al. 2017). The method allows for the estimation of a seismic vulnerability index for each building through the weighted evaluation of 14 parameters, each representing a key aspect influencing the global seismic response of the structure. As reported in **Table 1**, these parameters are grouped into four categories to highlight their differences and relative importance. For each parameter, a class C_{vi} of growing vulnerability (A, B, C and D) is assigned, along with a corresponding weight, varying from 0.5 for less influential parameters up to 2.5 for the most significant ones. A comprehensive description of the classification criteria and weighting scheme of the method is provided in (Eudave, et al. 2022).

Finally, the seismic vulnerability index (I_{vf}^*) is computed according to Eq. 1, yielding values in the range of 0 to 750, which are subsequently normalised (I_v) as reported in Eq. 2.

$$I_{vf}^* = \sum_{i=1}^{14} C_{vi} \cdot p_i \tag{1}$$

$$I_v = \frac{I_{vf}^* \cdot 100}{750} \quad (2)$$

For each building, I_v is then used to derive the vulnerability factor (V) (Eq. 3) and consequently estimate the mean damage grade (μ_D) (Eq. 4), which also depends on the macroseismic intensity (I) – defined according to EMS-98 scale, and on the ductility factor (Q) – which accounts for the structural typology of buildings and is assumed equal to 3.0. The resulting μ_D value ranges from 0 (no damage) to 5 (complete or near-collapse damage).

$$V = 0.592 + 0.0057 \cdot I_v \quad (3)$$

$$\mu_D = 2.5 + \left[3 \times tanh\left(\frac{I + 6.25 \cdot V - 12.7}{Q}\right)\right] \quad (4)$$

Table 1 – Parameters, classes and weights associated with the vulnerability index *(Ferreira, et al. 2013)*

Parameter	Class C_{vi}				Weight p_i	Relative weight over the I_v
	A	B	C	D		
Group 1. Structural building system						50/100
BP1. Type of resisting system	0	5	20	50	2.50	
BP2. Quality of the resisting system	0	5	20	50	2.50	
BP3. Conventional strength	0	5	20	50	1.00	
BP4. Maximum distance between walls	0	5	20	50	0.50	
BP5. Number of floors	0	5	20	50	0.50	
BP6. Location and soil conditions	0	5	20	50	0.50	
Group 2. Irregularities and interactions						20/100
BP7. Aggregate position and interaction	0	5	20	50	1.50	
BP8. Plan configuration	0	5	20	50	0.50	
BP9. Height regularity	0	5	20	50	0.50	
BP10. Wall façade openings and alignment	0	5	20	50	0.50	
Group 3. Floor slabs and roofs						18/100
BP11. Horizontal diaphragms	0	5	20	50	0.75	
BP12. Roofing system	0	5	20	50	2.00	
Group 4. Conservation status and other elements						12/100
BP13. Fragilities and conservation status	0	5	20	50	1.00	
BP14. Non-structural elements	0	5	20	50	0.75	

2.2 Vulnerability index method by Brando et al.

Similarly to the previous approach, the method proposed by (Brando, et al. 2017) aims to estimate the potential earthquake-induced damage in masonry buildings by evaluating 14 key parameters (**Table 2**) associated with their main sources of vulnerability. Each parameter is initially assessed through two distinct scores: a fragility score (v_{kf}), representing its contribution to increasing seismic vulnerability, and a protection score (v_{kp}), accounting for features that mitigate vulnerability. These scores are combined with a weighting coefficient that reflects the relative influence of each parameter on the structural response to seismic actions, as expressed in Eq. (5). Both the scoring system and the weighting coefficients were calibrated based on observed damage to traditional masonry buildings following the 2009 L'Aquila earthquake. Further details can be found in (Brando, et al. 2017) and (Rapone, et al. 2018).

In this case, the seismic vulnerability index (i_v), ranging from 0 (no vulnerability) to 1 (maximum vulnerability), is computed for each building according to Eq. 5. The value is then converted into the vulnerability factor (V) using the polynomial function expressed in Eq. 6. Finally, V is used to estimate the mean damage grade (μ_D)

according to Eq. 7, which is defined based on the formulation proposed by (Lagomarsino and Giovinazzi 2006).

Table 2 - Parameters and respective weights associated with the vulnerability index *(Brando, et al. 2017)*

Vulnerability Parameter (P_k)	Vulnerability type	Weight (ρ_k)
P1	Position	1.5
P2	Number of stories	1.5
P3	1st mode mechanism	1.5
P4	2nd mode mechanisms	1.0
P5	Arches	1.0
P6	Vaults	1.0
P7	Slabs	1.0
P8	Thrusting forces	0.8
P9	Presence of added structures	0.5
P10	Stairs	1.0
P11	Irregularities	0.8
P12	Non-structural elements	0.5
P13	Site effects	1.5
P14	Non-seismic external hazard	0.3

This formulation relates the expected damage to the seismic input (I), expressed in terms of macroseismic intensity (I) – defined according to MCS scale, as well as to the vulnerability factor (V) and the ductility coefficient (Q), which is assumed equal to 2.3 unlike Ferreira's approach. In line with empirical large-scale vulnerability assessment methods, the μ_D value ranges from 0 (no damage) to 5 (collapse or near-collapse).

$$i_v = \frac{1}{6} \cdot \frac{\sum_{k=1}^{14} \rho_k \cdot (v_{kf} - v_{kp})}{\sum_{k=1}^{14} \rho_k} + 0.5 \tag{5}$$

$$V = a + b \cdot i_v + c \cdot {i_v}^2 + d \cdot {i_v}^3 = 0.53 + 1.16 \cdot i_v - 4.00 \cdot {i_v}^2 + 4.21 \cdot {i_v}^3 \tag{6}$$

$$\mu_D = 2.5 \cdot \left[1 + tanh\left(\frac{I + 6.25 \cdot V - 13.1}{Q}\right)\right] \tag{7}$$

The application of the aforementioned methodologies to a selected sample of buildings enabled their comparative evaluation and provided the basis for investigating the sources of error and uncertainty inherent in large-scale vulnerability assessment methods, which are further discussed in Section 4.

3. Seismic vulnerability assessment of the historic centre of Campotosto

3.1 Description of the case study

Campotosto is a small town located in the central Italian Appenine, in the province of L'Aquila. The historic centre was severely affected by the 2009 and 2016-2017 earthquakes, leaving the community struggling to return to normal, particularly after the seismic event of 18 January 2017. The municipality was chosen as the case study due to its high seismic risk, resulting from both its geographical setting and the vulnerability of its building stock, factors that have been also highlighted in previous studies (Cocco, et al. 2019), (Brando, et al. 2020), (Masciotta, et al. 2024).

Following the 2009 L'Aquila earthquake, the urban centre of Campotosto was subdivided into three areas (A, B and C) according to their different lithological features, in accordance with the reconstruction plan. Due to the condition of the historic centre at the time of the survey, which was affected by extensive demolition and reconstruction activities, the analysis focused on Zone B, for which 60 buildings were selected to ensure a good representativeness of the different building typologies within the case study area.

(Figure 1A). The seismic vulnerability assessment was performed based on the data collected during the survey. The investigated building stock is relatively homogeneous in terms of structural and construction features. As can be seen in (Figure 1B), it mainly consists of aggregate poor-quality masonry built with local sandstone. The structural units have an elongated rectangular plan and develop over two- or three- storeys above the ground. The external walls have an average thickness of approximately 0.70 m and are typically characterised by a three-leaf arrangement. The internal core is unstable and composed of filling material, while the external leaves are made of irregular size stones bonded with weak mortar. Inadequate transverse connections are also frequently observed. In addition, the poor interlocking between orthogonal walls and the absence of seismic devices encourage independent wall behaviour. Concerning the floors, they mainly consist of flexible or semi-rigid systems weakly connected to the vertical walls, thus hindering the effective redistribution of horizontal seismic forces. Additional vulnerability factors observed include misalignment of floors and roofs between adjacent structural units, enlargement of openings, and plan or elevation modifications carried out over time using materials different from the original ones.

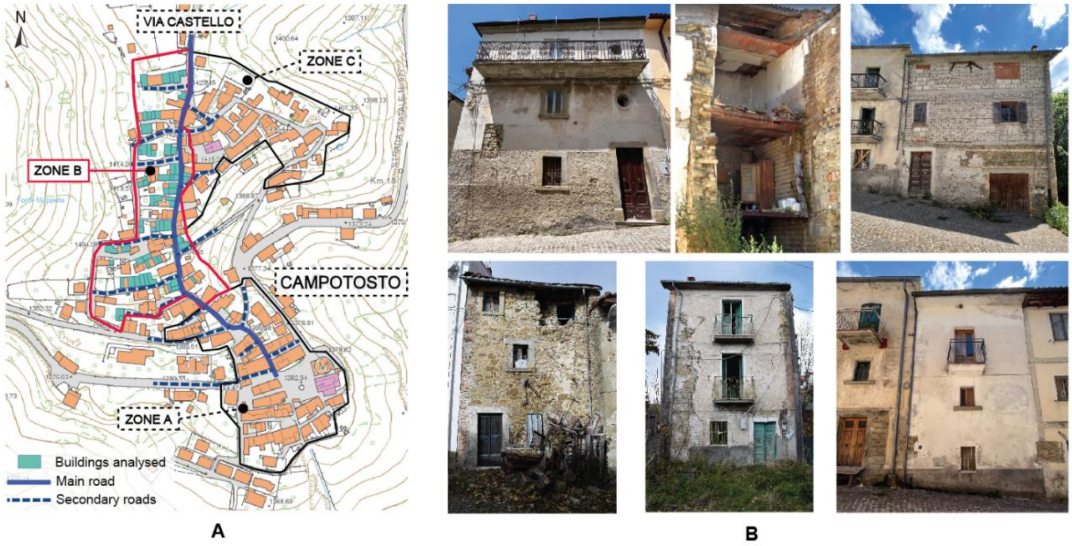


Figure 1 - Subdivision of the municipal area into zones according to the reconstruction plan following the 2009 L'Aquila earthquake. Identification of the area of interest with the buildings analysed (A). Structural features of the buildings in the historic centre

3.2 Seismic vulnerability assessment and comparison with observed damage

The vulnerability assessment of the 60 masonry buildings selected in the historic centre of Campotosto was carried out using the two VI methods outlined in Section 2. First, the vulnerability index and the mean damage grade were evaluated according to the different formulations, taking into account the seismic intensity (I) recorded during the 18th January 2017 seismic event, which INGV rated as VIII. Afterwards, the estimated damage was compared with that observed during the fieldwork and classified according to the five damage levels of the EMS-98 macroseismic scale (Grünthal 1998). To enable this comparison, the observed discrete damage grades (D_i) were converted into mean damage grades (μ_D) by applying the correspondence proposed by (Bramerini , et al. 1995).

For visualisation purposes, two graphs are produced to easily compare observed and estimated damage for each building as a function of its vulnerability index, each representing one of the two adopted methods (Figure 2). For each building, the observed damage is expressed in terms of mean damage grade (μ_D), defined as the average between the upper and lower bounds of the range associated with the assigned damage level. It should be noted that, in Figure 2A and B, the points representing the observed damage exhibit a variation along the abscissa because they are related to the vulnerability index computed according to the specific method considered. Figure 2 reveals that the two approaches exhibit different

trends in terms of damage estimation. While Ferreira's method shows a gradual increase in mean damage with increasing vulnerability index, Brando's method yields μ_D values that remain approximately constant for $i_v < 0.5$.

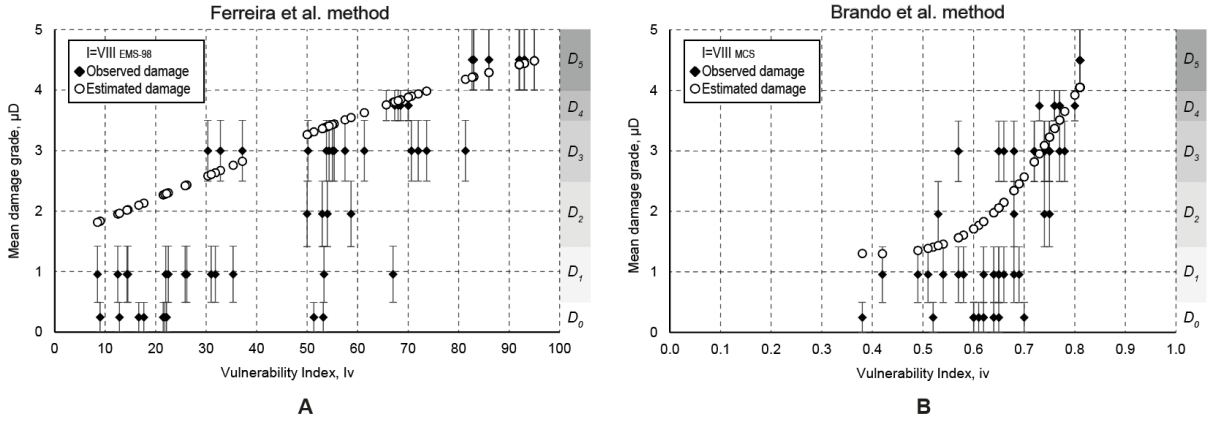


Figure 2 - Observed mean damage grades versus estimated damage grades: comparison between VI methods proposed by Ferreira et al. (A) and Brando et al. (B)

A more detailed comparison between observed and estimated damage shows that Ferreira's method tends to overestimate lower damage grades (D_0, D_1 and D_2) while providing more accurate predictions for higher damage levels (D_3, D_4 and D_5). This behaviour can be attributed to limitations in the analytical formulation (Eq. 4). For example, even for $I_v = 0$ and $I_{EMS98} = VIII$, the resulting $\mu_D = 1.54$ exceeds the upper bound of the D1 range ($D_1 = \{0.5 \leq \mu_D < 1.42\}$), thereby preventing the correct identification of D_0 and D_1. As a consequence, damage tends to shift toward higher classes, particularly D_2. A better agreement between observed and predicted damage is found for $I_v > 30$. A similar tendency is observed for Brando's method, which also overestimates low damage grades (D_0 and D_1), due to the inherent limitations of the formulation (see Eq. 7). However, a good agreement is achieved for $i_v > 0.7$, which corresponds approximately to the threshold between damage levels D_2 and D_3, indicating higher reliability in predicting moderate-to-severe damage (D_3, D_4 and D_5). As can be seen in Figure 3 the spatial distribution of the results indicates that both methods provide the same damage level for approximately half of the analysed buildings. More specifically, Ferreira's approach provides damage predictions consistent with the observed damage for 47.7% of the analysed buildings, while the remaining cases are characterized by damage overestimation. By contrast, Brando's method shows agreement with the observed damage for 50% of the buildings, whereas overestimation occurs in 38.3% of cases and underestimation in 11.7%.

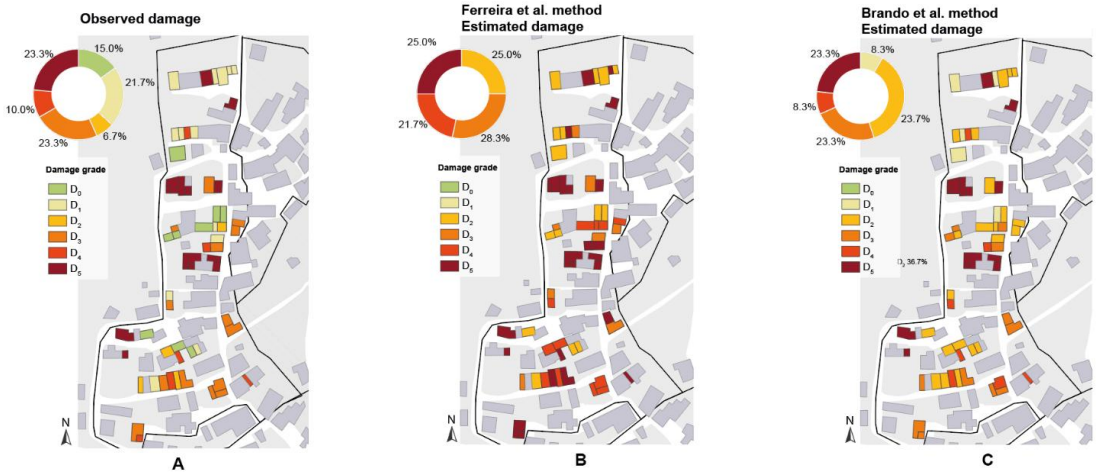


Figure 3 - Comparison between the spatial distribution of the observed discrete damage grades (A) and the estimated discrete damage grade obtained from Ferreira's (B) and Brando's (C) methods.

4. Analysis of uncertainties and sources of error

The effectiveness of vulnerability index-based methods as a decision-support tool in large scale evaluations is nowadays widely recognised (Baquedano Juliá and Ferreira 2021). Nevertheless, these approaches are inherently affected by various sources of error and uncertainty. These mainly arise from the subjective evaluation of building parameters, which depends on data quality and on the expertise of the surveyors, as well as from the use of empirically calibrated weights that may vary depending on the reference dataset. Additional uncertainty is related to the selection of representative building samples in large-scale analyses, which can be difficult to define accurately and may lead to biased assessments of the overall building stock. In this work, particular attention is given to the investigation and discussion of uncertainties associated with the analytical formulations of the methodologies described above (Eqs. 4 and 7). Specifically, the influence of seismic intensity (I), ductility factor (Q) and vulnerability factor (V) is analysed.

4.1 Influence of macroseismic intensity (I) and site effects

Both Ferreira's and Brando's methodologies estimate the mean damage grade (μ_D) as a function of a predefined macroseismic intensity. However, the two approaches rely on different macroseismic scales. Brando's method adopts the Mercalli-Cancani-Sieberg scale (MCS), widely used, particularly in Italy, for the assessment of historical earthquake effects, whereas Ferreira's method employs the more recent EMS-98 scale. Unlike the MCS scale, which was primarily developed for masonry buildings and does not explicitly distinguish between structural typologies, the EMS-98 introduces a classification based on building vulnerability, including also structures designed according to modern codes and categorising them into six vulnerability classes. Despite these differences, a previous study (Del Mese, et al. 2023) showed good agreement between the MCS and EMS-98 scales for buildings featuring a vulnerability class A, which includes structures made of rubble stone and fieldstone masonry. Since the building stock in Campotosto is predominantly composed of such typologies, it can be reasonably assumed to fall within class A, allowing the two macroseismic scales to be considered compatible for the purposes of this study.

Nevertheless, the assumed compatibility between the MCS and EMS-98 scales still represents a potential source of uncertainty, particularly considering the simplified correspondence adopted between the two intensity measures and the conversion of observed discrete damage levels into mean damage grades. These aspects may contribute to discrepancies between observed and predicted damage and should therefore be considered when interpreting the results.

To investigate further the influence of seismic intensity on damage estimation, the damage function of either method (Eqs 4 and 7) is plotted for both intensity levels VII and IX (Figure 4), i.e. for the macroseismic intensities closest to those recorded during the 2017 Campotosto earthquake.

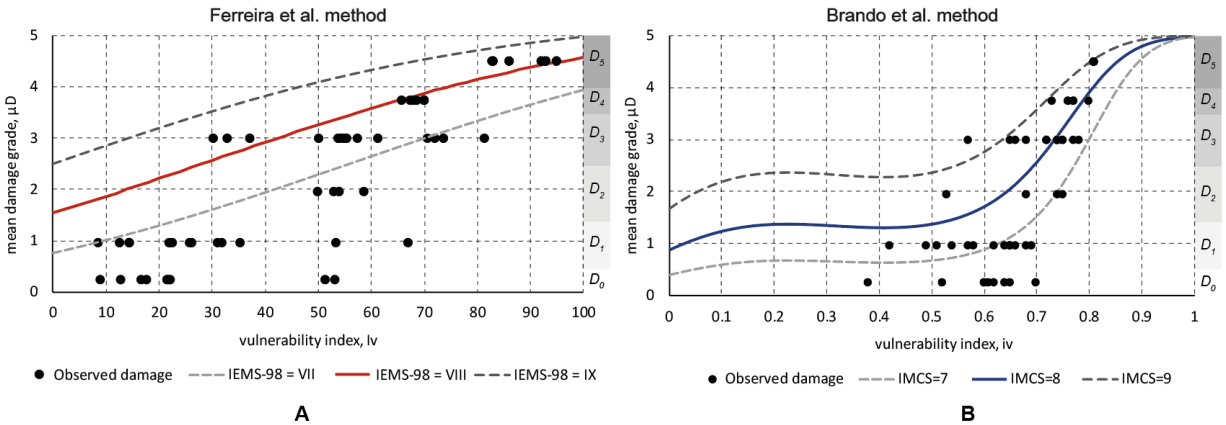


Figure 4 - Vulnerability curves according to Ferreira's (A) and Brando's (B) methods as a function of the macroseismic intensity.

The plots highlight several relevant trends related to the influence of seismic intensity on damage estimation.

- None of the considered formulations adequately capture damage level D0.
- Damage level D1 is better reproduced for intensity VII than for higher intensity values in both approaches, due to the downward shift of the curves, which results in lower μ_D values. However, Ferreira's method tends to overestimate D1 for $I_v > 25$.
- As for D2, Ferreira's formulation provides good agreement with observations for intensity VII, whereas Brando's method distributes predictions between intensities VII and VIII.
- Damage D3 is best captured by Brando's method with intensity VIII, while predictions with I=VII require i_v values greater than 0.75. In Ferreira's approach, D3 is reproduced across a wider range of vulnerability values, reflecting a greater dispersion in the dataset.
- Concerning D4, intensity VIII yields the most accurate predictions in both methods. In contrast, intensity VII generally leads to an underestimation of damage.
- Finally, with regard to damage level D5, Ferreira's method shows a better overall agreement with observed data, accurately capturing all corresponding damage cases.

As highlighted by the previous results, the adoption of a single seismic intensity value may constrain the accurate prediction of damage scenarios, due to uncertainties affecting this parameter, particularly local site effects. As noted by (Brando, et al. 2020), different zones within Campotosto exhibit varying amplification levels related to soil conditions. To underline the consequences of this phenomenon, two structurally similar buildings located in areas with different amplification factors (AFs) are selected for comparison: building 140 located in a low-amplification zone (AF=1.1–1.5) and building 215 sited in a high-amplification zone (AF=1.5–2.0) (Figure 5). Both are three-storey rubble stone masonry structures with comparable geometric and structural features, leading to similar damage grade values in the two approaches ($\mu_{D_215} = 2.06$; $\mu_{D_140} = 2.15$ with Brando's formulation and $\mu_{D_215} = 2.82$; $\mu_{D_140} = 2.43$ with Ferreira's formulation).

However, observed damage differs significantly: building 140 shows almost no damage (D_1), while building 215 is classified as D3. This discrepancy is likely due to different local amplification conditions, highlighting the critical role of site effects and the limitations of assuming uniform seismic intensity.

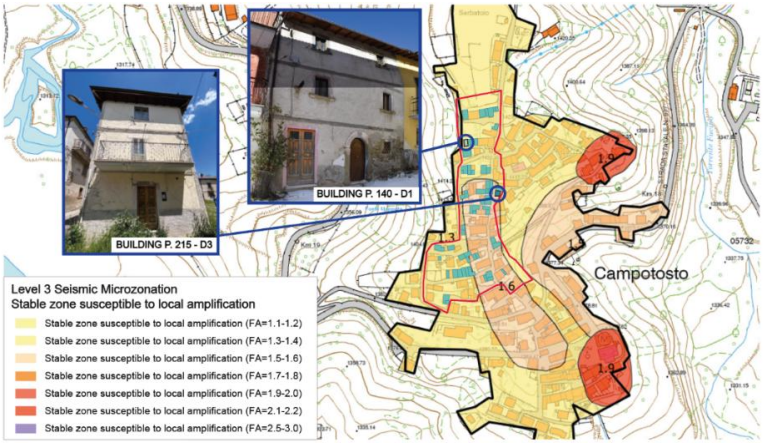


Figure 5 - Selection of two structurally similar buildings located in areas with different amplification factors, according to Level III microzonation studies.

4.2 Epistemic uncertainties associated with the ductility factor (Q)

Another source of uncertainty in the analytical formulation of analysed methods lies in the ductility factor (Q). With values ranging from 1 to 4, this parameter represents the capacity of the structure to undergo inelastic deformation while maintaining its load bearing capacity.

The two selected methodologies adopt different reference values: Brando's method assumes $Q = 2.3$, representative of masonry buildings not designed for ductile behaviour – according to (Lagomarsino and Giovinazzi 2006), whereas Ferreira's method adopts $Q = 3.0$, following the original formulation calibrated by (Bernardini, et al. 2007), which is associated with moderately ductile masonry structures. These values are derived from different calibration processes and case studies, highlighting the influence of methodological assumptions on the results.

To further investigate this source of uncertainty, a parametric analysis is conducted by varying Q from 1.5 to 4.0, revealing how this factor significantly affects the shape of the vulnerability curves (Figure 6).

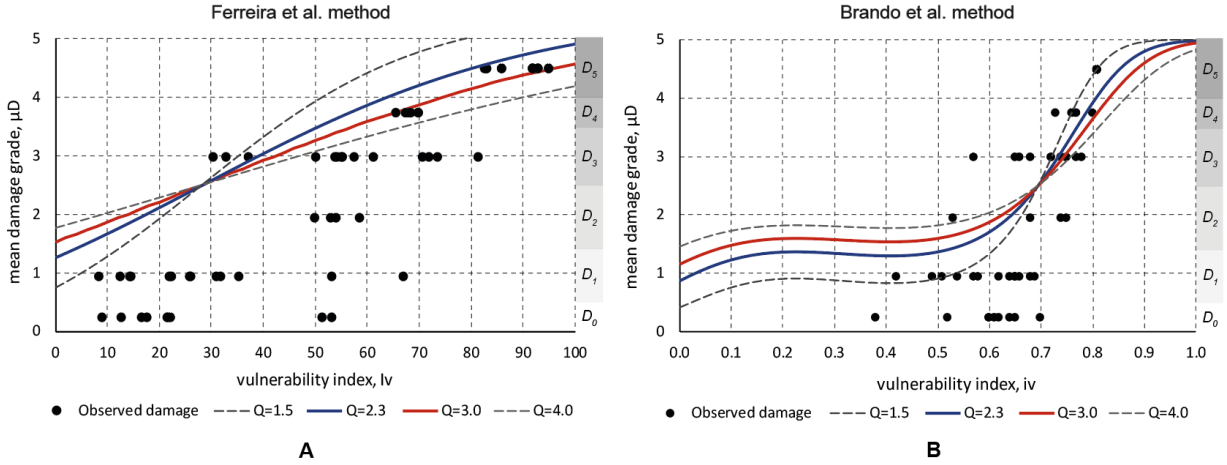


Figure 6 - Vulnerability curves according to Ferreira's (A) and Brando's (B) methods, as a function of the ductility factor.

In both methods, increasing ductility factors produce a rotation of the curves, altering the predicted damage levels. This results into different responses: in Brando's method, the variability is more pronounced for low vulnerability values, allowing a partial capture of lower damage levels, but reducing accuracy for higher damage grades. In contrast, Ferreira's method shows limited sensitivity for low damage levels and improved predictive capability for higher damage grades.

This behaviour reflects the different calibration strategies of the two methods. Since Q is intrinsically building-dependent, assigning a single representative value for an entire building stock introduces epistemic uncertainty. While this uncertainty can be reduced through detailed structural knowledge, such refinement is generally not feasible in large-scale analyses, making it an inherent limitation of VI-based approaches.

4.3 Influence of the vulnerability factor (V)

The vulnerability factor (V) represents another critical source of uncertainty, as it directly governs the relationship between the vulnerability index and the expected damage. The two methods compared in this study adopt different formulations for this parameter: a linear function in Ferreira's approach (Eq. 3) and a cubic function in Brando's (Eq. 6). These formulations were originally calibrated using distinct datasets and structural typologies, thus leading to different shapes of the resulting vulnerability curves and, consequently, to different damage predictions. In both cases, the availability of additional information could be used to refine the analytical formulations by modifying the respective coefficients. For example, (Mosoarca, et al. 2019) used a linear equation for the vulnerability factor, but with coefficients different than those proposed by (Ferreira, et al. 2013).

To better analyse the influence of V, a comparative analysis is performed between the original curves, derived from the equations presented in Section 2, and the modified curves obtained by reversing Eq. 3 and Eq. 6 (Figure 7). For comparative purposes, the following relationship is assumed: $I_v = 100 i_v$.

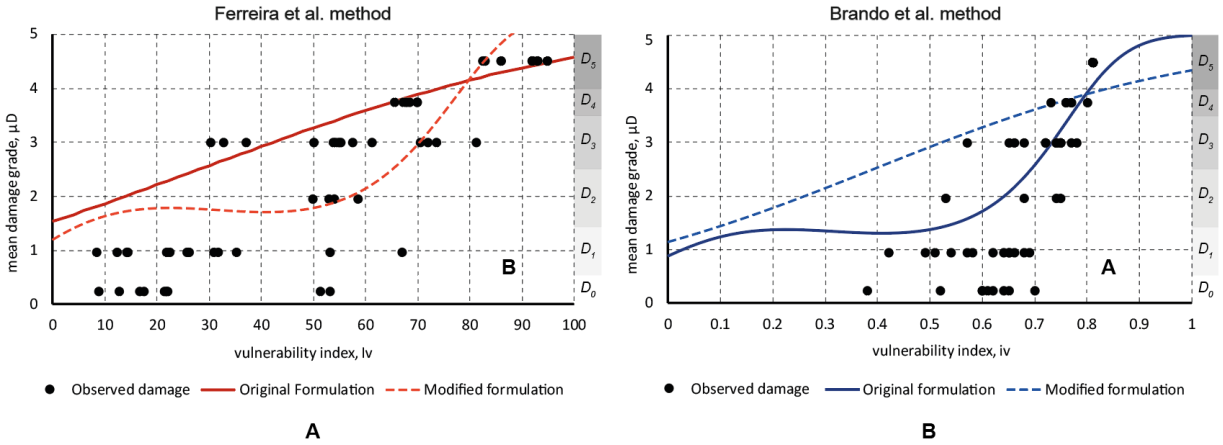


Figure 7 - Vulnerability curves according to the Ferreira's (A) and Brando's method (B), as a function of vulnerability factor.

The analysis shows that modifying the V functions alone does not improve the accuracy of the results. Indeed, the modified formulations lead to increased discrepancies between observed and predicted damage. This confirms that the calibration process plays a fundamental role: the reliability of the results strongly depends on the similarity between the analysed building stock and the one used to derive the original vulnerability functions. Therefore, the vulnerability factor introduces uncertainties not only due to its analytical formulation but also due to its dependence on the representativeness of the calibration dataset.

To provide a quantitative comparison between the predictive performance of the investigated methods, Figure 8 summarises the distribution of coherent (C), overestimated (O), and underestimated (U) damage predictions obtained for all the analysed cases associated with the investigated uncertainty sources, namely the macroseismic intensity (I), the ductility factor (Q), and the vulnerability factor (V).

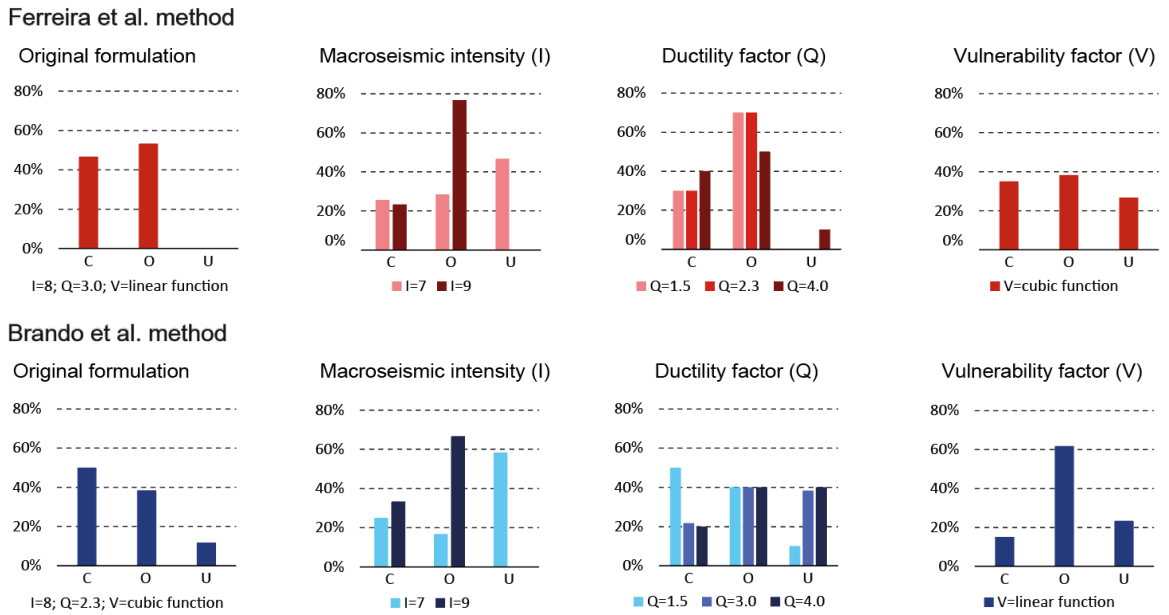


Figure 8 - Distribution of coherent (C), overestimated (O), and underestimated (U) damage predictions obtained with Ferreira's and Brando's methods for the different uncertainty sources analysed, namely macroseismic intensity (I), ductility factor (Q), and vulnerability factor (V).

5. Conclusions

This paper investigates and compares two widely used seismic vulnerability index methods. By applying both approaches to a sample of 60 buildings in the historic centre of Campotosto (AQ), Central Italy, the main sources of error and uncertainty affecting large-scale methods are identified and discussed.

The results show that the choice of the methodology itself represents a primary source of uncertainty. The two approaches, although conceptually similar, produce different damage distributions: Brando's method provides a more balanced prediction across damage levels, while Ferreira's method tends to overestimate damage but performs better for higher damage grades.

Particular attention is given to the analytical formulations adopted in the two methods for estimating the mean damage grade, focusing on the impact of macroseismic intensity (I), vulnerability factor (V) and ductility factor (Q), on the results.

The analyses highlighted that:

- The assumption of uniform seismic intensity (I) over a large area neglects local effects, such as soil amplification, which can potentially lead to significantly different damage scenarios even for structurally similar buildings
- The ductility factor (Q) influences the shape of the damage curves but is typically assigned as an average value for the building stock. Its variability at the building level introduces epistemic uncertainty that is difficult to reduce in large-scale applications
- The analytical formulation of the vulnerability factor (V) strongly depends on the reference dataset used for calibration. When applied to building stocks with different structural features, this may lead to inconsistencies in damage prediction.

Overall, the study confirms that large-scale vulnerability assessment methods, while efficient and widely applicable, are inherently affected by multiple sources of uncertainty. These should be explicitly acknowledged and carefully considered when interpreting results and supporting decision-making processes.

References

Baquedano Juliá, Pilar, e Tiago Miguel Ferreira. 2021. "From single- to multi-hazard vulnerability and risk in Historic Urban Areas: a literature review." *Natural Hazards* (Springer) 108: 93-128. doi:10.1007/s11069-021-04734-5.

Baquedano-Juliá, Pilar, Tiago Miguel Ferreira, Camilo Arrigada-Luco, Cristián Sandoval, Nuria Chiara Palazzi, e Daniel Oliveira. 2024. "Multi-vulnerability analysis for seismic risk management in historic city centres: an application to the historic city centre of La Serena, Chile." *Natural Hazards* 120: 9223–9266. doi:https://doi.org/10.1007/s11069-023-06008-8.

Bernardini, A., S. Giovinazzi, S. Lagomarsino, e S. Parodi . 2007. "Vulnerability and damage prediction at the territorial scale according to a macroseismic methodology consistent with the EMS-98 scale." *Proceedings of the 12th Conference of Italian National Association of Earthquake Engineering.* Pisa.

Blyth, A., B. Di Napoli, F. Parisse, Z. Namourah, E. Anglade, A. M. Giatreli, H. Rodrigues, e T. M. Ferreira. 2020. "Assessment and mitigation of seismic risk at the urban scale: an application to the historic city center of Leira, Portugal." *Bulletin of Earthquake Engineering* 18: 2607-2634. doi:https://doi.org/10.1007/s10518-020-00795-2.

Bramerini , F., G. Di Pasquale , G. Orsini, A. Pugliese, R. Romeo, e F. Sabetta. 1995. "Rischio sismico del territorio italiano: studio di una metodologia e risultati preliminari." *7° Convegno Nazionale di Ingegneria Sismica in Italia.* Italia. 1099-1108.

Brando, Giuseppe, Alessandro Pagliaroli, Giulia Cocco, e Francesco Di Buccio. 2020. "Site effects and damage scenarios: the case study of two historic centers following the 2016 Central Italy earthquake." *Engineering Geology* 272. doi:https://doi.org/10.1016/j.enggeo.2020.105647.

Brando, Giuseppe, Gianfranco De Matteis , e Enrico Spacone. 2017. “Predictive model for the seismic vulnerability assessment of small historic centres: Application to the inner Abruzzi Region in Italy.” *Engineering Structures* 153: 81-96. doi:10.1016/j.engstruct.2017.10.013.

Cocco, G., A. D'Aloisio, E. Spacone, e G. Brando. 2019. “Seismic Vulnerability of Buildings in Historic Centers: From the "Urban" to the "Aggregate" Scale.” *Frontiers in Built Environment* 5. doi:10.3389/fbuil.2019.00078.

Del Mese, S., L. Graziani, F. Meroni, V. Pessina, e A. Tertulliani. 2023. “Considerations on using MCS and EMS-98 macroseismic scales for the intensity assessment of contemporary Italian earthquakes.” *Bulletin of Earthquake Engineering* 21: 4167–4189. doi:https://doi.org/10.1007/s10518-023-01703-0.

Eudave, Rafael Ramírez, Tiago Miguel Ferreira, e Romeu Vicente. 2022. “Parameter-based seismic vulnerability assessment of Mexican historical buildings: Insights, suitability and uncertainty treatment.” *International Journal of Disaster Risk Reduction* 74. doi:https://doi.org/10.1016/j.ijdrr.2022.102909.

Ferreira, T. M., N. Mendes, e R. A. Silva. 2019. “Multiscale Seismic Vulnerability Assessment and Retrofit of Existing Masonry Buildings.” *Buildings* 9(4). doi:DOI: 10.3390/buildings9040091.

Ferreira, T. M., Romeu Vicente, J. A. R. Mendes da Silva, Humberto Varum, e Anibal Costa . 2013. “Seismic vulnerability assessment of historical urban centres: case study of the old city centre in Seixal, Portugal.” *Bulletin of Earthquake Engineering* 11: 1753-1773. doi:https://doi.org/10.1007/s10518-013-9447-2.

Ferreira, T.M., R. Maio, e R. Vicente. 2017. “Seismic vulnerability assessment of the old city centre of Horta, Azores: calibration and application of a seismic vulnerability index method.” *Bulletin of Earthquake Engineering* 15: 2879-2899. doi:https://doi.org/10.1007/s10518-016-0071-9.

GNDT. 1994. “Exposure Sheet and Vulnerability Assessment of Damage of the First and Second Level for Masonry and Reinforced Concrete.” Rome: Gruppo Nazionale per la Difesa dai Terremoti .

Grünthal, G. 1998. “European Macroseismic Scale 1998 Cahiers du Center Europeen de Grodynamique et de Seismologie. Conseil de l'Europe, Luxembourg.”

Lagomarsino, Sergio, e Sonia Giovinazzi. 2006. “Macroseismic and mechanical models for the vulnerability and damage assessment od current buildings.” *Bulletin of Earthquake Engineering* 4: 415-443. doi:https://doi.org/10.1007/s10518-006-9024-z.

Masciotta, Maria Giovanna, Letizia Mancini, Giorgia Cianchino, Tiago Miguel Ferreira, e Giuseppe Brando. 2024. “ENHANCING SEISMIC RESILIENCE IN HISTORICAL CENTRES THROUGH VULNERABILITY ASSESSMENT AND RETROFITTING.” *18th World Conference on Earthquake Engineering*. Milan.

Masciotta, Maria Giovanna, Letizia Mancini, Giorgia Cianchino, Tiago Miguel Ferreira, e Giuseppe Brando. 2025. “Sources of errors and uncertainties in large-scale seismic vulnerability assessment methods.” *Journal of Building Engineering* 111. doi:https://doi.org/10.1016/j.jobe.2025.113477.

Mosoarca, M., I. Onescu, E. Onescu, B Azap, N. Chieffo, e M. Szitar-Sirbu. 2019. “Seismic vulnerability assessment for the historical areas of the Timisoara city, Romania.” *Engineering Failure Analysis* 101: 86-122. doi:https://doi.org/10.1016/j.engfailanal.2019.03.013.

Rapone, D., G. Brando, E. Spacone, e G. De Matteis. 2018. “Seismic vulnerability assessment of historic centers: description of a predictive method and application to the case study of Scanno (Abruzzi, Italy).” *International Journal of Architectural Heritage* 18-19. doi:DOI: 10.1080/15583058.2018.1503373.

Vicente, R. , S. Parodi, S. Lagomarsino, H. Varum, e M. Silva. 2011. “Seismic vulnerability and risk assessment: case study of the historic city centre of Coimbra, Portugal.” *Bulletin of Earthquake Engineering* 9: 1067–1096. doi:DOI 10.1007/s10518-010-9233-3.

Cinpar 2026
XXII International Conference on Building Pathology and Constructions Repair
15th to 17th July 2026 - Lisboa, Portugal

Retrofitting techniques applied to Chilean masonry towers: a preliminary typological survey of four case studies

Marco BARRIENTOS[1], Tania HINOSTROZA[2], Wilson TORRES[3], **Cristián SANDOVAL**[4]

[1] Universidad de Santiago de Chile, Escuela de Arquitectura, Santiago, Chile, marco.barrientos.m@usach.cl
[2] Pontificia Universidad Católica de Chile, Departamento de Ingeniería Estructural y Geotécnica, Santiago, Chile, tania.hinostroza@uc.cl
[3] Universidad de la Frontera, Departamento de Ingeniería en Obras Civiles, Temuco, Chile, wilson.torres@ufrontera.cl
[4] Pontificia Universidad Católica de Chile, Departamento de Ingeniería Estructural y Geotécnica, Santiago, Chile, cristian.sandoval@uc.cl

Abstract: This work presents preliminary insights into an ongoing research project that aims to identify, represent, and analyze the retrofitting techniques applied to masonry towers following the 8.0 Mw Algarrobo (1985) and 8.8 Mw Maule (2010) earthquakes in Chile. In this work, four towers are qualitatively analyzed in detail, demonstrating the heterogeneity of the criteria and the types of retrofitting techniques applied, including rigid frames, walls, tie rods, and diaphragms, across reinforced concrete, steel, and mixed systems. The latter is cross-referenced with the typological analysis of the temple (basilica, Latin cross, single-nave, and three-nave layouts), and the categorization of the towers by location, number of bodies, and architectural style. The preliminary conclusions point the study towards an integrated architectural and qualitative structural analysis, which allows for the identification of criteria and methods for retrofitting techniques that balance seismic performance with respect for heritage values and attributes, in accordance with contemporary criteria on the matter.

Keywords: Masonry tower, unreinforced masonry, earthquake damage, retrofitting techniques.

1. Introduction

Unreinforced masonry (URM) bells and clock towers represent a key component of architectural heritage worldwide. However, due to typological features such as geometrical configuration, slenderness, regularity, and mechanical properties, among others, they are extremely prone to suffering damage and local or global collapses under seismic demands (Augenti et al. 2013; Di Tommaso and Casacci 2013; Preciado et al. 2015; Valente and Milani, 2016; Palazzi et al., 2020; Nuzzo and Faella 2021; Valente and Milani 2016; Masciotta and Lourenço 2022). In fact, URM towers rank among the most seismically vulnerable macro-elements in the well-known 28 collapse mechanisms catalog of URM historic churches (Dipartimento della Protezione Civile 2006). Therefore, conducting research in this field is essential not only for a better understanding of these complex structural issues but also for the preservation of these valuable constructions. Several works have addressed this matter, primarily to investigate structural stability and crack patterns associated with specific morphological features. However, few studies have focused on the seismic retrofit interventions, criteria, and techniques used in existing URM towers.

In this regard, Sepe (2008) proposed a large-scale vulnerability assessment method for ancient towers and 4 possible tower positions within a building: isolated, corner, included, and projecting. In line with the damage mechanisms of the abacus, Di Tomasso and Casacci (2013) identified 8 local-specific seismic damage mechanisms for isolated towers, related to crack patterns and out-of-plane collapse. In addition, different analytical models and/or numerical analysis techniques have been applied, such as the work by Bartoli et al. (2017) and linear static analysis using a simple finite element model (Ceroni et al., 2007; Montoya and Barrero, 2017). The studies on historic tower retrofitting interventions are limited. De la Torre et al. (2004) analyzed a set of cases in Mexico and concluded that the local steel-stressed strengthening technique has

demonstrated satisfactory seismic performance. Di Tomasso and Cassaci (2013) analyzed cases of FRP- and steel-rigid-frame strengthening techniques in Italy. Binda et al. (2010) conducted a case study in which a brick-repair, replacement, and mortar-joint-repair retrofitting technique was found to be efficient for a specific case in Monza, Italy. Foti et al. (2016) suggested, for a specific case study, the introduction of a wood structure in the tower's upper area and a system of rods and/or reinforced perforations in the lower area, in addition to grouting and sealing interventions on uneven mortar joints. Milani et al. (2017) investigated a specific case in northern Italy and proposed using the mortar-and-steel-frame technique to improve seismic performance. Despite the brief overview of different research approaches presented here, historic URM towers must be studied on a case-by-case basis due to the numerous variables.

The seismic strengthening of masonry towers remains one of the most challenging tasks in earthquake engineering and heritage preservation. These structures exhibit significant variability in their seismic response due to the inherent heterogeneity of their constituent materials, including different types of masonry units, mortars, main structural elements, and materials introduced during previous repair campaigns. In addition, masonry towers display a broad range of geometric configurations, including variations in height-to-width ratios, wall thicknesses, internal arrangements, openings, and connections between structural components, all of which strongly influence their dynamic behavior and collapse mechanisms under seismic loading. In this scenario, selecting strengthening strategies is further complicated by the need to reconcile seismic safety objectives with conservation requirements. While modern seismic design principles often favor interventions that maximize structural performance and mitigate damage, conservation-oriented approaches seek to preserve historical authenticity through minimal, reversible, and compatible interventions (Palazzi et al., 2026). As a result, the seismic assessment and retrofit of masonry towers require case-specific solutions that account for structural vulnerability, expected seismic demand, material degradation, and compliance with contemporary conservation principles, thereby limiting the applicability of standardized strengthening methodologies.

This work describes and qualitatively analyzes strengthening interventions carried out in four Chilean masonry towers. The study demonstrates the heterogeneity of the criteria and the types of retrofitting techniques applied, including rigid frames, walls, tie rods, and diaphragms, across reinforced concrete, steel, and mixed systems.

2. Cases of study

This work presents 4 case studies of unreinforced masonry (URM) buildings with single towers (Figure 1): 1 civil building and 3 historic churches. The cases are the Historic National Museum (HNM) clock tower and the bell towers of the San José (SJ), Santísimo Sacramento (SS), and San Francisco de Barón (SFB) churches. The NHM is a 2-story, continuous neoclassical façade, secular building arranged around an interior central patio, with a tower over the main façade. SJ and SS have a Latin cross and single-nave layout, with the tower centered in front of the main façade, aligned with the central axis and over the narthex. Both churches are eclectic in the neo-Romanesque and neo-Gothic styles. SFB is a Neobaroque 3-nave church with an apse and a lateral chapel, and the bell and clock tower are over the narthex, aligned with the central axis. NHM, SJ, and SS cases are constructed with URM firebrick box walls, while SFB has an adobe-and-wood system around the box walls, except for the narthex and the tower, which are URM firebrick masonry structures.

As will be seen, the retrofitting techniques employed vary in the materials and structural criteria they use. Some solutions can be described as invasive and irreversible, while others could be considered more in line with modern conservation criteria. In some cases, the reinforcement elements are anchored at specific points in the existing masonry structure, while in others, they are partially embedded within the masonry. The latter highlights the great heterogeneity of the solutions adopted and the lack of guidelines to address this problem.

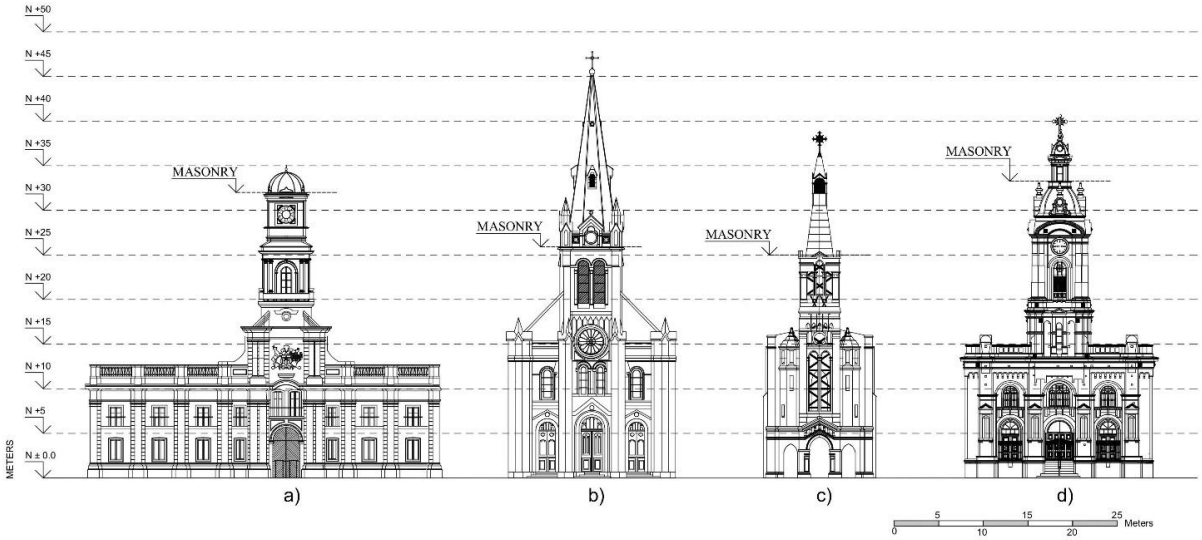


Figure 1 – Front view of the URM towers under study: a) National Historic Museum; b) San José church; c) Santísimo Sacramento church; d) San Francisco de Barón church.

2.1 National Historic Museum (ex Real Audiencia Palace), Santiago

The NHM is in the middle of Santiago's downtown historic core, the capital city of Chile, and is surrounded by the Central Chilean Postal Office building on the west and Santiago's Municipal Headquarters on the east. The MHN building, also known as the Real Audiencia Palace due to its colonial-era construction and functions, was designed by the Chilean architect Juan José de Goycoolea. It was built between 1804 and 1808, before the Republic of 1818's independence from the Spanish Empire, and is one of the few colonial buildings currently conserved in Santiago. It was declared a Historic National Monument in 1969 (Decreto N° 12392 1969). It has historic, urban, architectural, social, artistic, technical, and cultural heritage values. 8 modules compose the 2-story main façade (22 m long side and 12 m in height), where the access and the clock tower are in the fifth west-to-east module, forming an anomalously asymmetrical neoclassical architectural composition.

The clock tower has 3 free-standing bodies with progressively diminishing story heights and is settled across the 5th front-side module and the transverse façade width. From the ground floor to the top of the wall of the last module, it is 32 m high, with 7 interior levels of variable height. From the ground floor to the 5th interior level, the tower's layout is 5.5 m on the front and back sides and 7.85 m on the lateral sides. The next-to-the-last body is inscribed in a 5.2 m square, and the top free-standing body has a 4.0m square layout. The 3 free-standing bodies are 21 m high. The main façade and the lower tower's body were built in 1808, while the other 2 upper bodies were built between c. 1865 and 1875. Except for specific interventions (such as architectural transformations to the front windows), the tower's exterior architectural features have been preserved. In contrast, at least 2 main structural strengthening interventions were carried out after the 1985 (8.0 Mw) Algarrobo and 2010 (8.8 Mw) Maule earthquakes.

2.1.1 1978-1982 phase

Due to the setting up of the National Historic Museum, an architectural project was carried out between 1978 and 1982, consisting, among some new extensions, of the main façade, clock tower, central patio, and roof architectural restoration, which also included the wooden second-floor structure replacement for a reinforced concrete (RC) slab along the south and main façade's building side. This intervention changed its original structure and increased its horizontal rigidity.

2.1.2 1982-2010 phase

The clock tower sustained serious damage during the 1985 Algarrobo earthquake (8.0 Mw). A critical assessment was carried out, which identified extended crack pattern damage along the interior tower's east and west façades in the lower and middle stages. The upper body registered crack patterns around the 4 exterior façades. Based on it, a retrofitting project was carried out in 1986. The main structural criteria and techniques considered were internal and continuous reinforced concrete (RC) columns, and beam-strengthening insertions within URM walls. Figure 2 shows the retrofit project carried out in the NHM.

The columns and beams inserted into masonry walls have variable sections and are shown from the ground floor to the upper body of the tower. A column-and-beam semi-embedded structure inside the interior was also displayed on the ground-floor access walls, with isolated foundations. A continuous RC rigid frame rises from this level up to the 6th interior floor. Except for the 7th level, which has a steel-structured floor, the others are wooden-structured. The free-standing upper tower's 2 bodies focus on major RC retrofit elements, including short walls and beams. It is important to underline the increasingly diminishing dimensions observed in the 3 free-standing body layouts, which consequently imply variations in the walls' width and axial axes, and thus in the geometrical RC retrofitting elements as well. Between the 5th and 6th floors, the rigid RC frames have been fitted with in-plane RC struts in the interior façades, increasing their vertical rigidity.

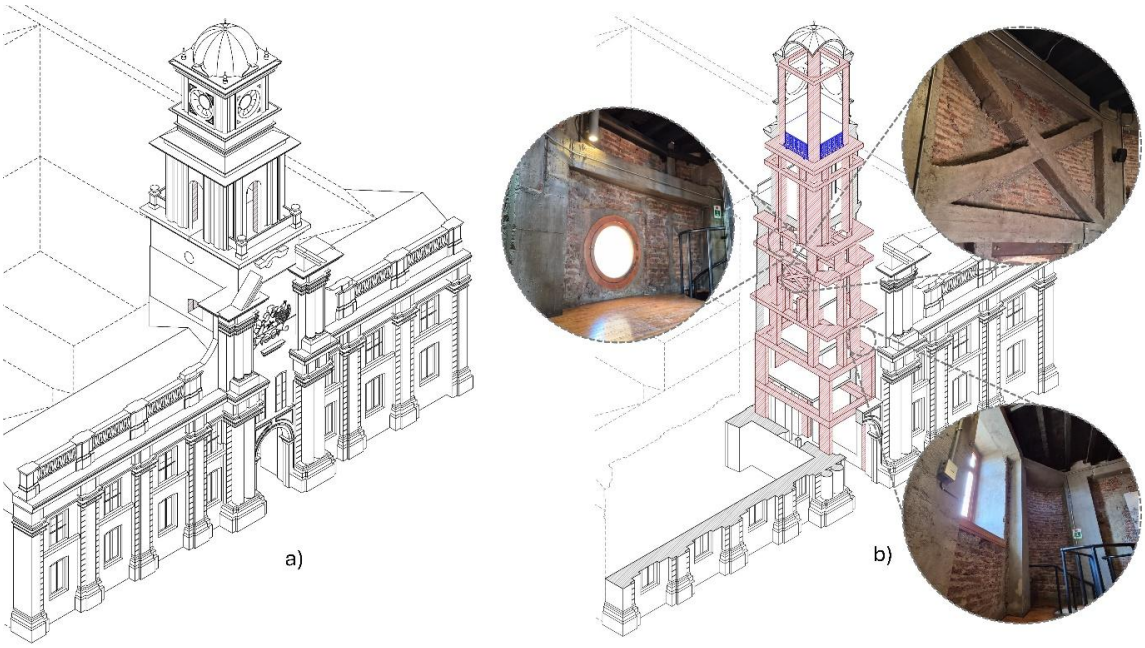


Figure 2 – Strengthening intervention applied to NHM tower: a) exterior view; b) axonometric section with internal RC retrofitting elements (red: RC structure; blue: steel structure).

2.2 San José church, Santiago

The San José church was designed by the French architect Eugène Joannon and built between 1903 and 1909. It is located in the historic Yungay neighborhood, near Santiago's downtown, and is a key building in a historic urban complex block. The church is legally protected as a heritage building by the local Pinteresque Zone (Decreto N°43 2009; Decreto N°13 2019) and as a Historic Conservation Building under the Historic Conservation Building ordinances (Ficha 30, 2005-6). Historic, urban, architectural, artistic, social, and religious values highlight their relevance to heritage. The main façade is preceded by the narthex and the bell tower, which rises 26.5 m to the top's masonry walls, has 4 interior wooden structure floors, and is a 12

m free-standing body high with a 5.5 m front side to 6.4 m lateral sides layout. Two main recent intervention stages have been identified.

2.2.1 1985 - ~2010 phase

After the 1985 Algarrobo earthquake, the bell tower sustained concentrated seismic damage to the upper free-standing body. After a visual on-site inspection, ring RC embedded beams around the inner top masonry walls were identified. Due to the lack of historical information and difficult access, its dimensions and execution data are unknown.

2.2.2 ~2010 – 2026 phase

After the 2010 Maule earthquake, shear damage was identified in the masonry walls' bodies from the ground floor to the middle bell tower. A mixed rigid RC and steel column-and-beam frames within interior walls retrofitting intervention was carried out between 2012 and 2013. The ground and second floors were strengthened with RC columns and beams, and the upper levels were strengthened with steel frames, as shown in Figure 3. The intermediate floors and the spire are wood-structured. An on-site visual inspection identified a lack of continuity in structural retrofitting. However, due to limited access, some areas could not be assessed, specifically at the RC and steel frame connections. The RC columns and beams have an average section of 0.3x0.3 m and are embedded in most masonry walls. The columns, beams, and strut steel elements have a 150x150mm regular section with welding unions. The steel structure is connected to the masonry walls via a plate-and-bolt connection, likely crossing the exterior façade. As shown in Figure 3, the intermediate heights of the steel frame structure vary from level to level.

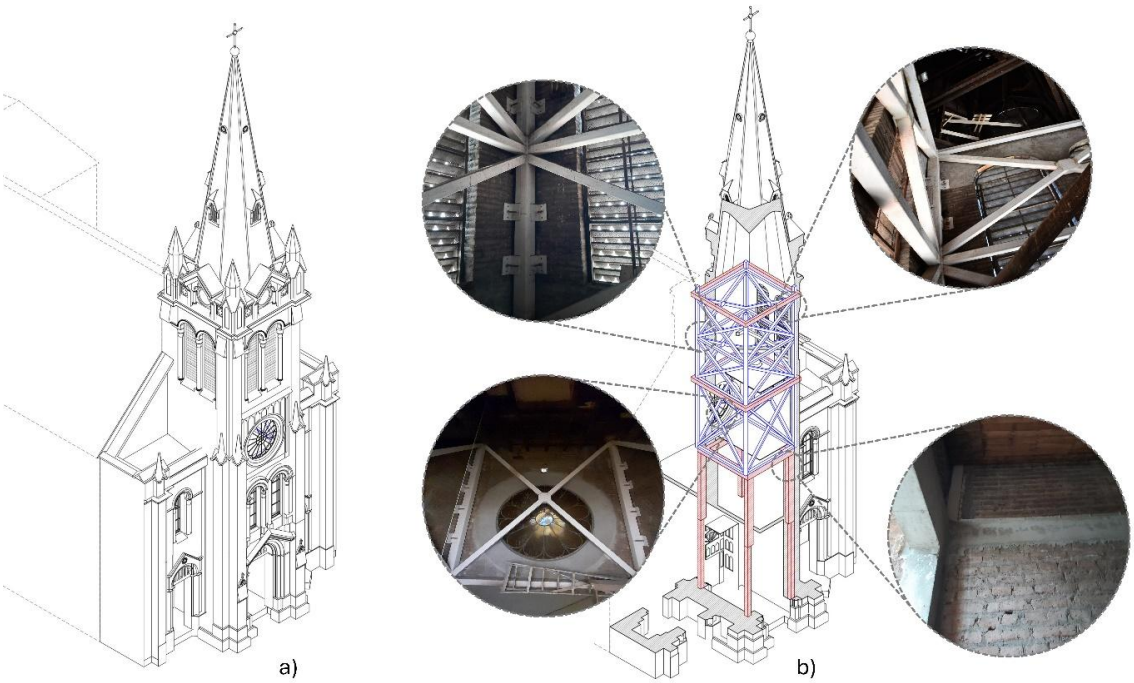


Figure 3 – Strengthening intervention applied to the tower of the San José church: a) exterior view; b) axonometric section view of internal retrofitting internal skeleton (red: RC structure; blue: steel structure).

2.3 Santísimo Sacramento church, Santiago

This church was designed by the French architect Emilio Doyère and built between 1891 and 1896. It was declared a Historic Monument in 1986 (Decreto 132 1986). Its heritage values are historic, architectural, artistic, religious, and technical. The bell tower is centered in front of the main façade, over the prominent 3-

arch narthex, which has 2 lateral semi-octagonal turrets. The entire façade of the building is of exposed brick masonry, including the narthex and bell tower, which facilitated identification of previous structural exterior repair interventions. Its slenderness underlines a particular feature of this case. The tower's average dimensions are inscribed within a 4.7 m square section, and the masonry structure rises 25 m from the base of the spire, which is steel-structured. The tower has 10 wooden structures that make up the interior floors. The study identified 4 retrofitting intervention phases:

2.3.1 1965-1979 phase

Although there is no historical evidence about probable seismic damages after the 1965 La Ligua (7.4Ms) and the 1971 Illapel (7.5Ms) (Servicio Sismológico Nacional) earthquakes, a retrofitting project (1979) with RC columns and beams strengthening elements around the whole masonry structure -including the bell tower- led to supposed eventual local and/or global seismic damages. This project was not executed.

2.3.2 1979-1996 phase

Due to the likely accumulation of damage, in addition to that from the 1985 Algarrobo earthquake, a retrofitting project was carried out in 1996. The structural execution considered an inner steel frame as a mesh that overlapped across the interior bell tower's walls, extending from the choir floor to the top of the masonry wall structure. The ground floor has RC columns and beams, with soil foundations inserted within the columns and arcs. The RC elements are connected to the steel retrofitting internal skeleton and receive the axial vertical loads. The steel frame is connected to the masonry walls by double interior and exterior plates and bolts, probably extending to the exterior façade.

2.3.3 1996-2012 phase

After the 2010 Maule earthquake, seismic damage around the church's box URM walls was repaired in 2012. There is no historical evidence of the details of the retrofitting intervention. However, based on on-site visual inspection and historical photographs, it is possible to identify crack patterns that appear to have been repaired with a concrete technique. In addition, there were no records of local and/or global seismic damage in the bell tower, which the 1996 retrofitting intervention can partially explain. However, for a stronger hypothesis formulation, a major volume of evidence is needed.

2.3.4 2022-2026 phase

The last documented retrofitting intervention was carried out in 2022. The intervention considered external double-tilted columns (Figure 10), connected to the masonry walls by an exterior platen and bolts. Each steel column has soil foundations. The intervention also included interior architectural restoration. However, due to the lack of recent relevant seismic events, it is not yet possible to analyze the church's seismic behavior.

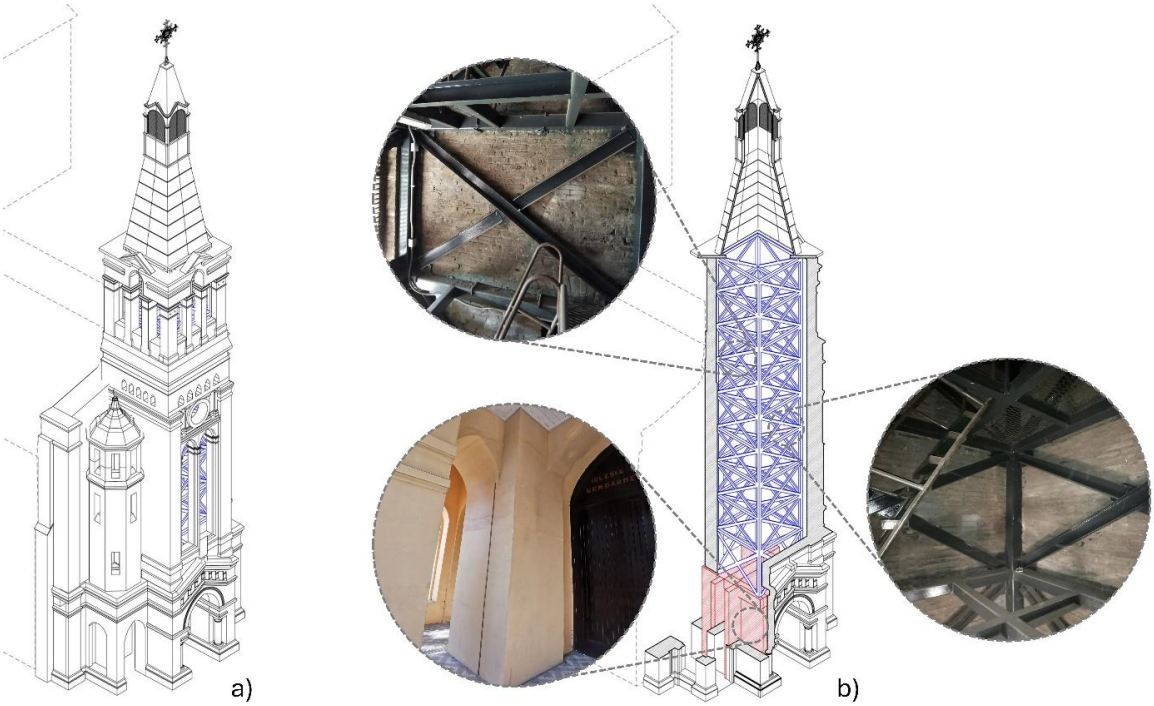


Figure 4 – Strengthening intervention applied to the tower of the Santisimo Sacramento church: a) exterior view; b) axonometric section view of internal retrofitting internal skeleton (red: RC structure; blue: steel structure).

2.4 San Francisco de Barón church, Valparaíso

The SSB temple and monastery are in the seaside city of Valparaíso, 120km from the capital, Santiago. The urban complex is located on the Barón Hill and is a visual landscape icon. The 3-nave (adobe and wooden structure) church was built between 1845 and 1863, and the URM narthex, built between 1890 and 1892, was designed by the Italian architect Eduardo Provasoli in a neo-Baroque style. The complex is a National Monument (Decreto 687, 1983). The church's heritage values are historic, architectural, urban, artistic, religious, social, and technical ones. The current state of the main façade shows a firebrick structure with no stucco finishing, and the bell and clock tower is on the central module's narthex with 2 free-standing bodies and a dome at the top. The church has suffered 3 burning episodes (1983, 2010, and 2013) and several earthquake shocks, such as Valparaíso, 1906 (8.2 Mw); La Ligua, 1965 (7.4 Mw); Illapel, 1971 (7.5 Mw); Algarrobo, 1985 (8.0 Mw); Maule, 2010 (8.8 Mw); and Illapel, 2015 (8.3 Mw) (Servicio Sismológico Nacional). The 3-nave interior structure was rebuilt in 2021, and despite the historic seismic sequence, the church is still standing, which is uncommon. A 3-front-side arcade, URM lateral and rear walls, and dome ceilings structure the URM narthex. The narthex is 21 m long on the side, 9 m wide, and 11.5 m high to the upper cornice of the façade. The wall thickness varies from 0.8 to 1.5 m. The bell and clock tower rises 19.7 m from the cornice base to the dome's top line and 31.2 m from the base ground floor to the top. The tower's average octagonal layout is inscribed on a 7.1 m front-side and 6.6 m lateral-side rectangle. 3 main interventions have been identified.

2.4.1 1984-2009 phase

The 1984 fire destroyed the interior 3-nave wooden structure, arcades, vaults, and roof, and affected the adobe and brick-stone masonry structure. Despite the lack of documentary evidence, it is possible to infer seismic damage after the 1985 Algarrobo earthquake. Between 2007 and 2008, the Mar Vasto study proposed a structural emergency retrofitting intervention using vertical steel tensile bars from the tower's top to the ground floor's narthex, and horizontal steel tensile bars across the perimetral URM-free-standing bodies' walls. However, there is no evidence of the proposed structural design, nor of whether it was finally

executed. In 2009, another non-executed architectural restoration and structural retrofitting project was developed, which included vertical tensile bars in the URM narthex.

2.4.2 2009-2013 phase

2 catastrophes affected the temple in 2010: the Maule earthquake in March, and a fire in September that once again destroyed the 3-nave wooden structure, arcades, vaults, and roof. The masonry structure was affected as well. To repair the church, a restoration initiative was carried out in 2011, during which horizontal steel bar strengthening techniques were applied to the free-standing URM walls, as shown in Figure 5. The steel bars are displayed across the perpendicular walls and extend to the inner wall sides. Outside the URM walls, an RC device was installed as an intermediate connector between the steel reinforcement bars and the masonry structure. To support the steel bells, a set of 2 parallel double-T steel beams per side, anchored to the masonry walls at the interior top of the second free-standing body, was added. In 2013, another fire event burned the building, except for the narthex and the bell and clock tower masonry structure.

2.4.3 2013-2026 phase

In 2021, an integral reconstruction, restoration, and structural strengthening intervention was carried out on the church and the ancient monastery, which are now in their current state. The interior 3-nave was rebuilt with a completely wooden structure and interior finishing. Masonry block repairs and replacement of damaged blocks were performed on the exterior and interior tower façades. Existing steel strengthening elements were repaired, and internal wooden floors were rebuilt.

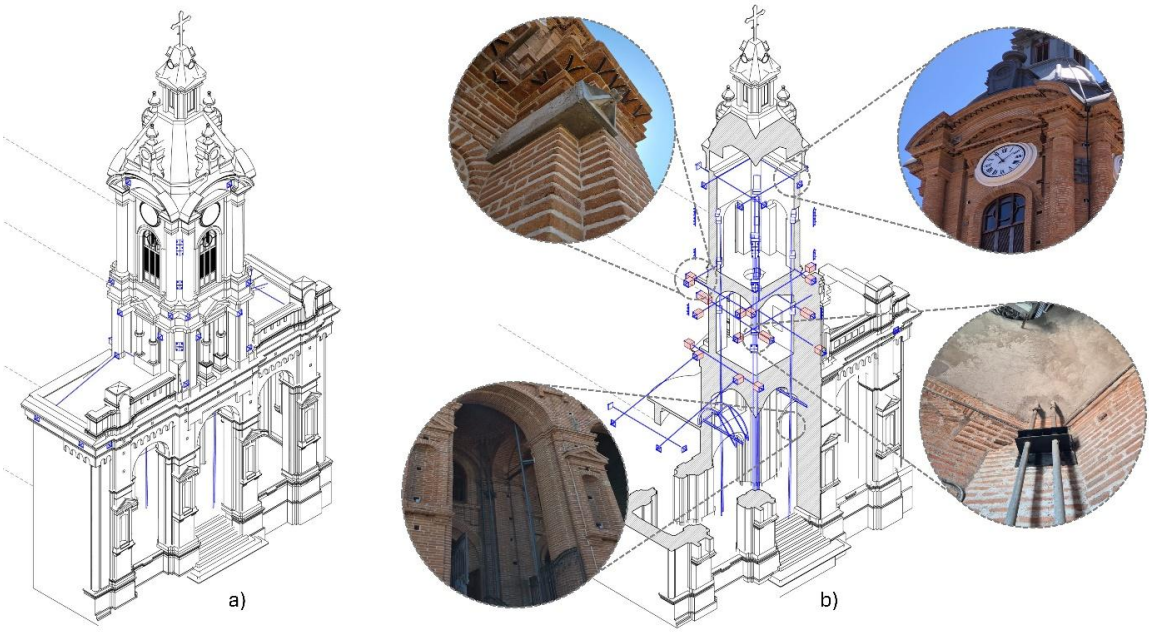


Figure 5 – SFB axonometric southeast view sequence: a) exterior view; b) ~~exploded~~ axonometric section view of internal RC retrofitting internal skeleton. (red: RC structure; blue: steel structure).

The main retrofitting intervention included continuous steel tensile bars from the top of the bell and clock tower to the ground floor along the central narthex module addition (Figure 5b). The bars are anchored to the masonry walls through steel plates and bolts on both the inner and outer sides, and their vertical continuity is provided by steel connectors at intervals. Due to insufficient information, the active tensile strength of the vertical steel bars is uncertain. In addition, horizontal steel bar strengthening techniques

were applied to the walls of the free-standing URM bodies. The steel bars are displayed across the perpendicular walls and extend to the inner wall sides. Outside the URM walls, an RC device was installed as an intermediate connector between the steel reinforcement bars and the masonry structure. Connecting the border sides to the tower's base free-masonry walls, combined with a similar setting at the main façade top to the back longitudinal wall against an out-of-plane mechanism.

3. Conclusions and future research directions

Historic URM towers are valuable architectural structures worldwide. However, they are the most seismically vulnerable structures and may concentrate major seismic damage, local and/or global collapses, impacting society, the economy, and cultural heritage. This study examined 4 architectural-historical bell and clock tower types (3 in Santiago and 1 in Valparaíso), each with different strengthening criteria and techniques, most executed over the past 4 decades following the 1985 Algarrobo and 2010 Maule megathrust earthquakes. From 2010 to the present, no serious seismic events have shaken the area around their location; thus, it is not yet possible to determine their seismic behavior and the effectiveness of the retrofitting interventions. The study identified clear heterogeneity in the variety of architectural bell and clock towers, as well as in the retrofitting and strengthening criteria and techniques used across different chronological periods and circumstances.

3.1 Architectural type diversity

The 4 study cases have 1 single (clock bell and/or clock) tower in front of the main façade. In SJ, SS, and SFB churches, the tower is aligned with the central façade's axis and the narthex of the arcade. SJ and SS temples have a Latin-cross layout, and SFB has a 3-nave layout. Despite its neoclassical style, the HNM clock tower is on the main building's access but in an asymmetrical position on the façade. The towers' height (from the ground floor to the top URM structure) is round, from 25 m (SS) to 32 m (NHM) and 8.5 m (SS) to 21 m (NHM) along the free-standing tower's bodies with a 4.7 m per side averaged layout (SS) to 7.1 m on the front side and 6.6 m on the lateral sides (SFB). Most of the cases registered seismic damage after the 1985 (8.0 Mw) and 2010 (8.8 Mw) earthquakes concentrated on free-standing bodies, as expected according to the literature. Furthermore, the masonry tower's walls have diminishing thickness and vertical-axis variations from the bottom to the top, with vertical load continuity. Finally, all cases have a wooden structure on an intermediate floor, except for the NHM, which has a steel horizontal frame on its upper floor. The total slenderness of the cases is MHN 6,7; SJ 4.8; SS 5.3, and SFB 4.7. Moreover, the slenderness of the free-standing tower is MHN 4.4; SJ 2.2; SS 1.8, and SFB 3.0. Thus, the MHN clock tower represents the slenderest case of study considering the total height and the partial free-standing height.

3.2 Seismic retrofitting intervention criteria and techniques

Despite some geometrical configuration similarities between the cases of study, such as the number of free-standing bodies (2 or 3), morphological regularity, the presence of openings, progressive diminishing width from base walls to the upper ones, and the crack patterns registered after the past 2 earthquakes, the retrofitting techniques applied are all different. Conversely, all interventions were carried out along the inner walls of the masonry structure, thereby diminishing the impact on the heritage attributes. 4 retrofitting intervention types were identified: a) the NHM case has rigid, monolithic, and continuous RC columns and beams embedded and semi-embedded in the masonry structure frames and displayed from the ground floor (with isolated soil foundations) to the top; b) The SJ church has a mixed RC columns and beams embedded frame around the prominent narthex arcades with isolated soil foundations, which acts as the base support for free vertical steel rigid columns, beams, and struts with variable height and connected by platen and bolts to the 4 masonry internal walls' sides; c) The SS church has a mixed RC columns and beams embedded frame around the prominent narthex arcades with isolated soil foundations. Over it, steel

columns, beams, and struts are vertically displayed to the masonry walls' top line. The steel structure is embedded within a double interior and exterior plate and bolt components traversing the masonry width walls; d) the SFB church strengthening technique applied is based mainly on horizontal and vertical steel stress bars. The horizontal ones are freely set along each inner masonry wall, extending to the exterior façades and connected by a RC device on each side of both free-standing towers' bodies. In addition, the longitudinal masonry wall planes (the façade and back wall's narthex) are connected through steel stressed bars set on each lateral side next to the tower. Along with the intrados, narthex arcades were inserted with steel strengthening plates and horizontal bars between the arch's imposts.

The heterogeneous strengthening techniques applied to the examined cases indicate a lack of unified seismic retrofitting criteria, which can be partially explained by differences in execution periods, earthquake shock characteristics, and crack patterns and damage. Except for the SFB church, the strengthening interventions identified in the other cases can be classified as a 'tower in tower' retrofit, with a variety of techniques applied. It is not possible to evaluate their seismic performance at this time. Moreover, to preserve the tower and its valuable heritage and architectural type, the diversity-applied techniques highlight the need for a common set of criteria and an intervention approach.

The research methodology has involved a first stage of on-site data collection to address information gaps arising from historical data on the church construction process, historical seismic performance, executed intervention works, and visual on-site surveys. Then, as in the research carried out by Alvarado et al. (2025), the work will integrate different non-destructive tests (NDT), such as terrestrial laser scanning (TLS), photogrammetry with unmanned aerial vehicles (UAVs), ground penetration radar (GPR), ultrasonic pulse velocity measurement, Schmidt hammer, pendulum hammer, and penetration tests. In addition, an experimental campaign to estimate the modal properties of the masonry towers under study will be conducted using the same method as that used for the Metropolitan Cathedral of Santiago, Chile (Torres et al., 2017).

Acknowledgments

This work was supported by the Agencia Nacional de Investigación y Desarrollo (ANID), under FONDECYT Grant No. 11241325, Chile.

References

Alvarado, R., Barrientos, M., Suazo, A., Menanno, G., Pérez-Pinedo, L., Palazzi, N. C., & Sandoval, C. (2025). Non-destructive testing and kinematic limit analysis applied to a historic masonry church early intervened with RC elements. *Engineering Failure Analysis*, *169*, 109205.

Augenti, N., Nanni, A., & Parisi, F. (2013). Construction failures and innovative retrofitting. *Buildings*, *3*(1), 100-121.

Bartoli, G., Betti, M., & Monchetti, S. (2017). Seismic risk assessment of historic masonry towers: comparison of four case studies. *Journal of Performance of Constructed Facilities*, *31*(5), 04017039.

Binda, L., Saisi, A., & Tiraboschi, C. (2010). El comportamiento a largo plazo de torres y estructuras de fábrica. El Campanario de la Catedral de Monza. *Loggia, Arquitectura & Restauración*, (22-23), 108-121.

Ministerio de Educación. 1969. Decreto N° 12392: Declara Monumento Histórico el Templo San José del Barrio Yungay. Santiago: Diario Oficial de la República de Chile, January 11, 1969.

Ministerio de las Culturas, las Artes y el Patrimonio. 2019. Decreto N° 13: Reglamento sobre Monumentos Nacionales. Santiago: Diario Oficial de la República de Chile.

Ministerio de Vivienda y Urbanismo. 2009. Decreto N° 43: Fija diseño estructural para edificios en zonas sísmicas y modifica Decreto N° 61. Santiago: Diario Oficial de la República de Chile.

Torre Rangel, O., López Vázquez, R., Salazar Hernández, A., & Roldán Cabrera, J. C. (2004). Evaluación estructural y comportamiento de las reparaciones efectuadas a edificaciones históricas.

Di Tommaso, A., & Casacci, S. (2013). Sopravvivenza di torri e campanili in ambiente sismico. In *Proceedings of the CIAS Conference Evoluzione nella sperimentazione per le costruzioni, Creta* (Vol. 95118).

Dipartimento della Protezione Civile. 2006. "Approvazione dei modelli per il rilevamento dei danni, a seguito di eventi calamitosi, ai beni appartenenti al patrimonio culturale." Gazzetta Ufficiale della Repubblica Italiana, March 7, 2006.

Formisano, A., & Milani, G. (2019). Seismic vulnerability analysis and retrofitting of the SS. Rosario church bell tower in Finale Emilia (Modena, Italy). *Frontiers in Built Environment*, *5*, 70.

Foti, D., Diaferio, M., & Venerito, M. (2016). Non-Destructive Damage Detection and Retrofitting Techniques on a Historical Masonry Tower. In Proceedings of the 3rd International Balkans Conference on Challenges of Civil Engineering (3-BCCCE), 429–38. Tirana, Albania: Epoka University.

Masciotta, M. G., & Lourenço, P. B. (2022). Seismic analysis of slender monumental structures: current strategies and challenges. *Applied Sciences*, *12*(14), 7340.

Milani, G., Shehu, R., & Valente, M. (2017). Seismic vulnerability reduction of masonry churches: a case study. *Procedia engineering*, *199*, 272-277.

Montoya, J. O., & Barrero, R. A. (2017). Análisis tridimensional por premallado de la torre del templo Santa Lucía, por medio de macroelementos. Esempi di Architettura (EdA), no. 1: 1–12.

Nuzzo, M., & Faella, G. (2021). The carmine maggiore bell tower: An inclusive and sustainable restoration experience. *Sustainability*, *13*(3), 1445.

Palazzi, N. C., Alvarado, R., Sandoval, C., & Roca, P. (2026). Integration of structural requirements and conservation criteria in masonry wall interventions: A pilot study considering five in-plane strengthening methods. *Construction and Building Materials*, *520*, 146060.

Palazzi, N. C., Rovero, L., De La Llera, J. C., & Sandoval, C. (2020). Preliminary assessment on seismic vulnerability of masonry churches in central Chile. *International Journal of Architectural Heritage*, *14*(6), 829-848.

Preciado, A., Bartoli, G., & Budelmann, H. (2015). Fundamental aspects on the seismic vulnerability of ancient masonry towers and retrofitting techniques. *Journal of Civil Engineering and Management* 21 (1): 1–15.

Sepe, V., Speranza, E., & Viskovic, A. (2008). A method for large-scale vulnerability assessment of historic towers. *Structural Control and Health Monitoring: The Official Journal of the International Association for Structural Control and Monitoring and of the European Association for the Control of Structures*, *15*(3), 389-415.

Torres, W., Almazán, J. L., Sandoval, C., & Boroschek, R. (2017). Operational modal analysis and FE model updating of the Metropolitan Cathedral of Santiago, Chile. *Engineering Structures*, *143*, 169-188.

Valente, M., & Milani, G. (2016). Seismic assessment of historical masonry towers by means of simplified approaches and standard FEM. *Construction and Building Materials*, *108*, 74-104.

cinpar2026
XXII International Conference on Building Pathology and Constructions Repair
15th to 17th July 2026 - Lisboa, Portugal

Material Parameter updating Based on Operational Modal Analysis (OMA): Application to the Sciri Tower

Renan PAULO[1], Filippo UBERTINI[1], Marco BRECCOLOTTI[1], Jerfson LIMA[2], Esequiel MESQUITA[3]

[1] University of Perugia, Perugia, Italy, renan.nogueirapaulo@dottorandi.unipg.it

[2] Federal University of Ceará, Russas, Brazil, jerfson.lima@ufc.br

[3] Federal University of Ceará, Fortaleza, Brazil, emesquita@ufc.br

Abstract:

Structural Health Monitoring (SHM) has become a key tool for the preservation of historical heritage, particularly in medieval constructions. The use of sensors enables real-time acquisition of structural responses, such as accelerations, which can be employed for damage detection. In this context, Operational Modal Analysis (OMA) emerges as a non-destructive technique for identifying the dynamic properties of such structures. This study presents the calibration of the mechanical properties of the Sciri Tower, a medieval masonry structure located in the historic center of Perugia, which has been previously investigated by the University of Perugia. The main objective is to improve the model's geometry based on point cloud data and carry out a new material calibration. An iterative manual calibration procedure was performed by comparing the natural frequencies obtained from numerical simulations with the first four vibration modes identified through OMA. As a result, four distinct material sets were defined and calibrated. This type of analysis represents a fundamental step toward the development of predictive models, including nonlinear analyses for seismic scenarios and pushover analyses.

Keywords: Operational Modal Analysis, Medieval tower, Point cloud, Finite elements method, Structural health monitoring

1. Introduction

Masonry structures constitute a significant portion of the world's architectural heritage, encompassing a large number of historical and medieval buildings that remain in service today. These structures, however are particularly vulnerable to seismic actions due to their low tensile strength, brittle behavior, and often limited structural redundancy. This vulnerability is especially relevant in countries such as Italy, where seismic events frequently threaten the preservation of historic centers and monuments. Among recent examples, the 2012 Emilia earthquake as showed in Tiberti, Acito, and Milani (2016) which highlighted the susceptibility of masonry towers and heritage constructions to earthquake-induced damage, emphasizing the necessity of preventive conservation strategies and reliable assessment methodologies.

The structural assessment of historical masonry buildings, however, presents unique challenges when compared to modern constructions. Centuries of modifications, material degradation, construction irregularities, and the use of vernacular building techniques often result in significant uncertainties regarding both geometry and material properties. Furthermore, the historical value of such structures generally prevents the execution of extensive destructive tests, making the direct characterization of their mechanical properties difficult. Consequently, the development of reliable numerical models capable of predicting structural behavior remains a complex task.

In recent decades, vibration-based Structural Health Monitoring (SHM) has emerged as a valuable tool for the preventive conservation of historic structures. Through the continuous or periodic acquisition of dynamic response data, SHM systems enable the identification of structural changes and provide relevant

information regarding the global behavior of buildings (Alvandi and Cremona 2006; Ubertini et al. 2018; Ramos et al. 2010; Masciotta, Ramos, and Lourenço 2017). In this context, Operational Modal Analysis (OMA) has gained considerable attention due to its ability to extract modal parameters under ambient excitation conditions, eliminating the need for artificial loading systems that may be impractical in heritage structures.

Beyond structural monitoring purposes, experimentally identified modal parameters can be employed in finite element model updating procedures, allowing the indirect estimation of mechanical properties through the calibration of numerical models. Such approaches have been successfully applied to several historical masonry structures and are currently recognized as effective non-destructive techniques for reducing uncertainties associated with material characterization (Salachoris et al. 2024; C. Gentile and Saisi 2006; Carmelo Gentile, Saisi, and Cabboi 2015). Nevertheless, the reliability of the updated mechanical parameters strongly depends on the accuracy of the numerical model adopted. Since modal properties are governed by both mass and stiffness distributions, inaccuracies in the geometric representation of the structure may significantly affect the stiffness matrix and consequently the calibration process, potentially leading to non-unique or physically inconsistent solutions.

Recent advances in terrestrial laser scanning and digital photogrammetry have enabled the generation of highly detailed three-dimensional geometric surveys, allowing the accurate reconstruction of complex historical structures. These technologies provide dense point clouds capable of capturing geometric irregularities, deformations, and construction details that are often neglected in conventional survey techniques. Therefore, integrating high-fidelity geometric acquisition methods with finite element model updating procedures represents a promising strategy for improving the reliability of structural assessment methodologies for heritage masonry buildings.

Previous studies have investigated the dynamic behavior of the Sciri tower through Operational Modal Analysis and finite element model updating. However, the influence of high-fidelity geometric reconstruction obtained from terrestrial laser scanning and aerial photogrammetry on the calibration of the mechanical properties has not yet been thoroughly investigated. Considering that the accuracy of numerical model updating procedures strongly depends on the quality of the geometric representation, this study aims to develop a finite element model of the Sciri tower based on an integrated point-cloud survey and to calibrate its mechanical properties using experimentally identified modal parameters. The results are compared with those available in the literature to assess the influence of geometric fidelity on the estimation of masonry mechanical properties.

1.1 Sciri tower

The Sciri tower is a historic masonry structure located along Via dei Priori in the historic center of Perugia, Italy. The tower was constructed during the 13th century and reaches a height of approximately 41 m. It is surrounded on three sides by adjacent masonry buildings approximately 17 m high, while its front façade remains fully exposed. The tower belonged to the noble Oddi family until 1488, when ownership was transferred to the Sciri family following violent conflicts between rival noble clans that forced the Oddi family into exile. In 1680, the tower and the adjacent building were donated to the Third Franciscan Order, which remained the owner until 2011, when the entire complex was transferred to the Municipality of Perugia.

Regarding its construction materials, the masonry is homogeneous and regular, consisting of squared white limestone blocks (García-Macías and Ubertini 2020). The tower has an approximately rectangular cross-section measuring 7.15 × 7.35 m and can be ideally divided into two structural portions: a lower section and an upper section. The lower section, extending up to a height of 8.4 m, is characterized by masonry walls approximately 2.1 m thick, containing a limited number of small openings, and by a stone masonry vaulted slab located above the rooms of a former chapel (Vaiano et al. 2019). The upper section, extending to the full height of 41 m, consists of slender continuous masonry walls with thicknesses varying between 1.6 m and 1.4 m. Four brick masonry vaulted floors, each approximately 1.5 m wide, are located at different elevations throughout the tower. In addition, a brick masonry roof vault closes the structure at the top. Figure 1a

presents an aerial view of the tower and the surrounding building complex, while Figure 1b shows the ground-floor plan of the tower-house complex.

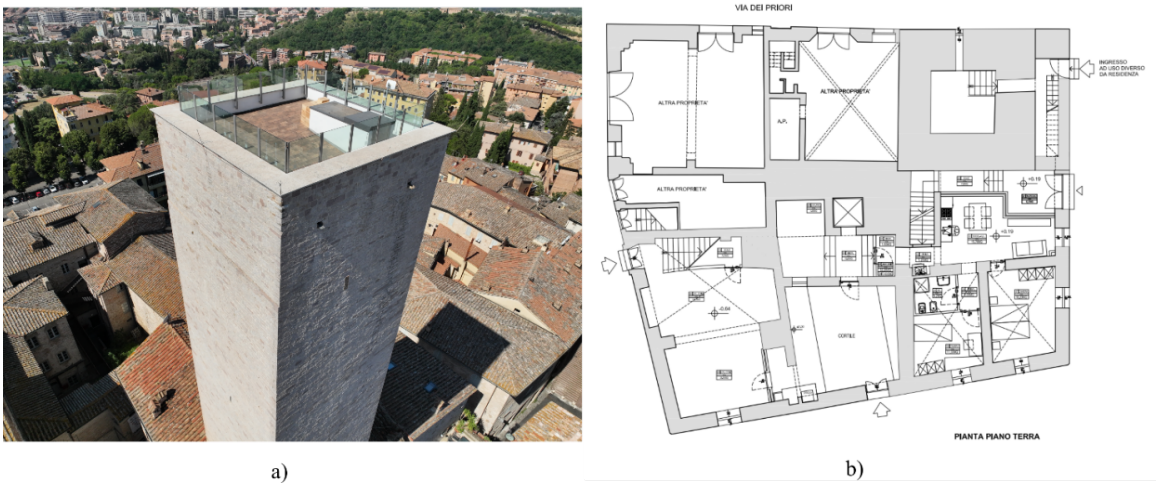


Figure 1 – Sciri tower: (a) aerial view; (b) ground-floor plan.

1.2 Operational Modal Analysis

The Sciri tower was previously investigated by researchers from the University of Perugia through an Ambient Vibration Test (AVT) conducted in May 2017. Details of the experimental campaign can be found in (García-Macías e Ubertini 2020; Venanzi et al. 2020). A total of twelve high-sensitivity uniaxial accelerometers (10 V/g), model PCB 393B12, were installed throughout the tower to measure ambient vibrations induced by environmental actions such as wind and traffic. The sensor layout is shown in Figure 2**Error! Reference source not found.**. The accelerometers, identified as A1 to A12, were installed at Levels 1, 3, 4, and 5 of the tower, while the data acquisition unit was positioned at Level 2. Following signal processing, seven vibration modes were identified within the frequency range between 0 and 11 Hz (Table 1). The identified modes consisted of two bending modes in the northwest direction (x-direction), denoted as Fx1 and Fx2, two bending modes in the southwest direction (y-direction), denoted as Fy1 and Fy2, one torsional mode (Tz1), and two higher-order bending modes (Fx3 and Fy3). The first four identified mode shapes are presented in Figure 3.

Table 1 – Natural frequencies and vibration modes. Adapted from Venanzi et al. (2020).

Vibration mode	1	2	3	4	5	6	7
Mode type	Fx1	Fy1	Fx2	Fy2	Tz1	Fx3	Fy3
Natural Frequency [Hz]	1.722	1.925	5.615	6.006	8.399	9.896	10.928

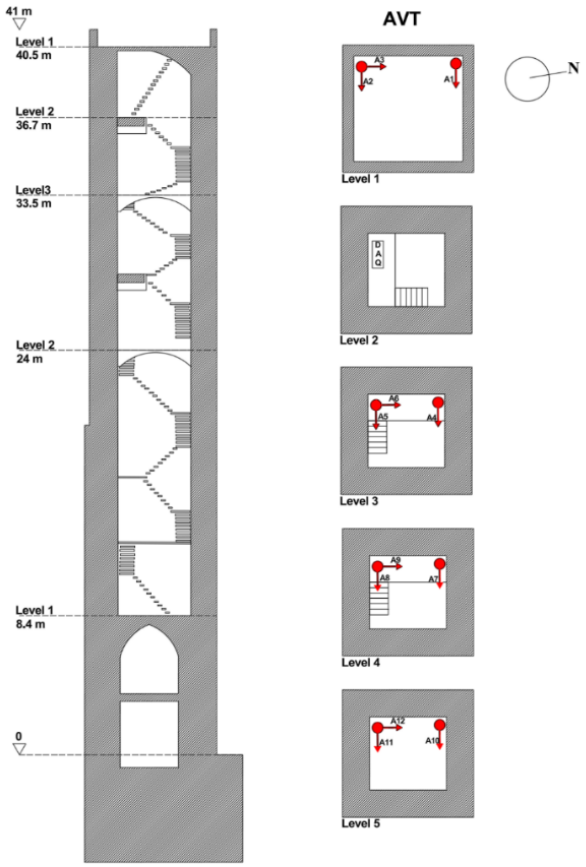


Figure 2 – Sensors layout for AVT Adapted from Venanzi et al. (2020).

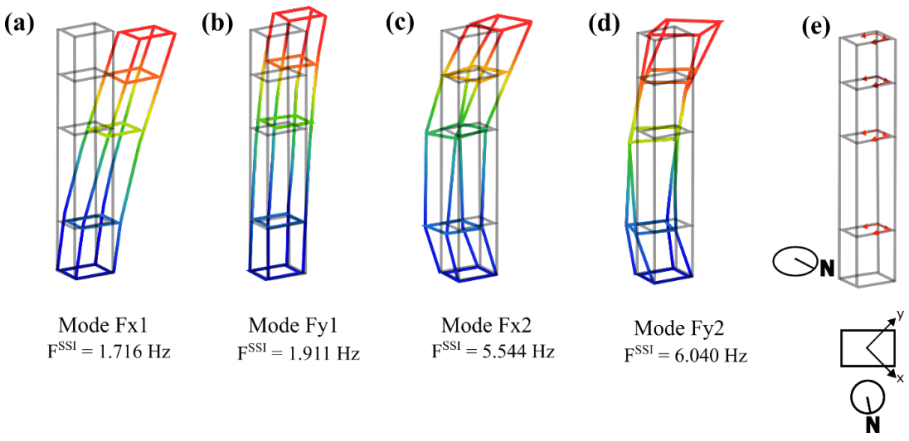


Figure 3 - First four experimentally identified mode shapes Adapted from Venanzi et al. (2020).

The modal parameters identified through the Operational Modal Analysis constitute the experimental benchmark adopted for the calibration of the finite element model developed in this study. To evaluate the structural behavior of the Sciri tower, a three-dimensional finite element model was developed in ABAQUS. The modeling procedure included point-cloud-based geometric reconstruction, geometry simplification,

material definition, loadings, boundary conditions and mesh convergence analysis. The methodology adopted for the generation and calibration of the numerical model is described in the following sections.

2. Metodology

2.1.1 Point cloud and 3D geometry

The geometric representation of the Sciri tower was obtained through an integrated survey combining terrestrial laser scanning and aerial photogrammetry. A Leica RTC360 laser scanner (Figure 4a) was employed to capture the inner parts and construction details of the structure at ground level in exterior areas. To ensure complete coverage of regions inaccessible from terrestrial viewpoints, the survey was complemented by an aerial photogrammetry campaign using a DJI Mavic 3 Enterprise drone (Figure 4b). The point clouds generated from both acquisition techniques were merged and registered in CloudCompare®, producing a unified high-density three-dimensional dataset. The combined point cloud was subsequently exported in .RCP format and imported into Revit® software, where the geometric model of the structure was reconstructed. The integration of terrestrial laser scanning and photogrammetry enabled the generation of a high-fidelity geometric representation, reducing uncertainties associated with geometric idealization and providing a reliable basis for numerical analyses.



Figure 4 - Point cloud data acquisition process: a) Terrestrial laser scanner RTC360; b) Drone DJI Mavic 3 Enterprise.

To improve computational efficiency while preserving the global structural response, secondary architectural features such as ornamental elements, roof components, and the roof slab were excluded from the numerical model and replaced by equivalent boundary conditions when appropriate. The resulting geometry was exported in .SAT format and imported into ABAQUS®, where it was discretized as a single homogeneous deformable solid. Additional geometric partitions were introduced to separate the tower from the adjacent buildings, allowing independent material calibration during the model updating procedure. Figure 4 summarizes the adopted workflow, from point cloud acquisition and processing to the generation of the finite element model used in the subsequent analyses. The Figure 5 summarizes the workflow adopted for the generation of the finite element model, from point cloud acquisition and processing to geometric reconstruction and finite element discretization.

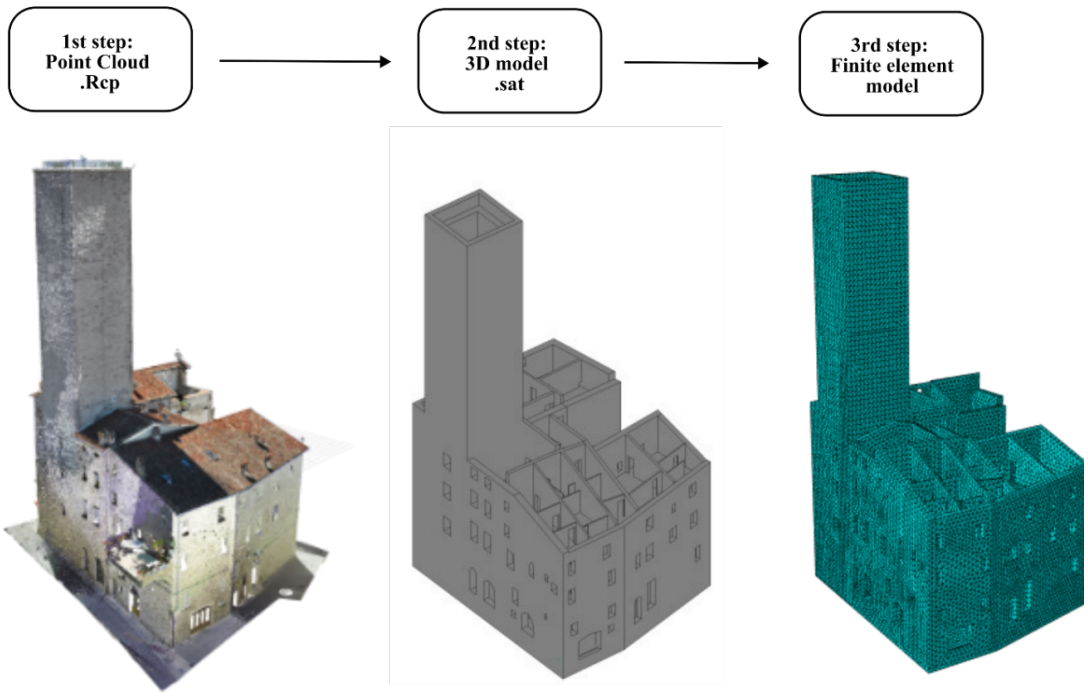


Figure 5 - Geometric modeling workflow of the Sciri tower: (a) acquired point cloud; (b) three-dimensional model developed in Revit®; (c) finite element model.

2.1.2 Material Properties

The initial mechanical properties adopted in the numerical model were selected according to the ranges recommended by the Italian Building Code (*Ministero delle Infrastrutture e dei Trasporti, 2009)*, as summarized in Table 2. Two masonry typologies were considered: squared stone masonry, representing the tower, and solid brick masonry with lime mortar, representing portions of the surrounding buildings.

The tower and the adjacent structures were assigned independent material definitions. Furthermore, the surrounding buildings were subdivided into two distinct regions, initially assigned identical mechanical properties but allowed to vary independently during the calibration process as described by Figure 6. This strategy was adopted to better capture possible differences in stiffness distribution and structural interaction between the tower and its surrounding environment.

The calibration procedure was performed manually through successive adjustments of the elastic modulus, material density and Poisson's ratio. The objective was to minimize the discrepancies between the numerical and experimental modal properties obtained from the Operational Modal Analysis, particularly the first four natural frequencies, which were adopted as calibration targets due to their relevance to the global dynamic behavior of the structure.

Table 2 – Inicial material mechanical parameters

Type of masonry	Fm (N/cm^2)	τ0 (N/cm^2)	E (N/mm^2)	G (N/mm^2)	W (KN/m^3)
Masonry of squared stone blocks	800	12	3200	940	22
Masonry of solid bricks with lime mortar	400	9.2	1800	600	18

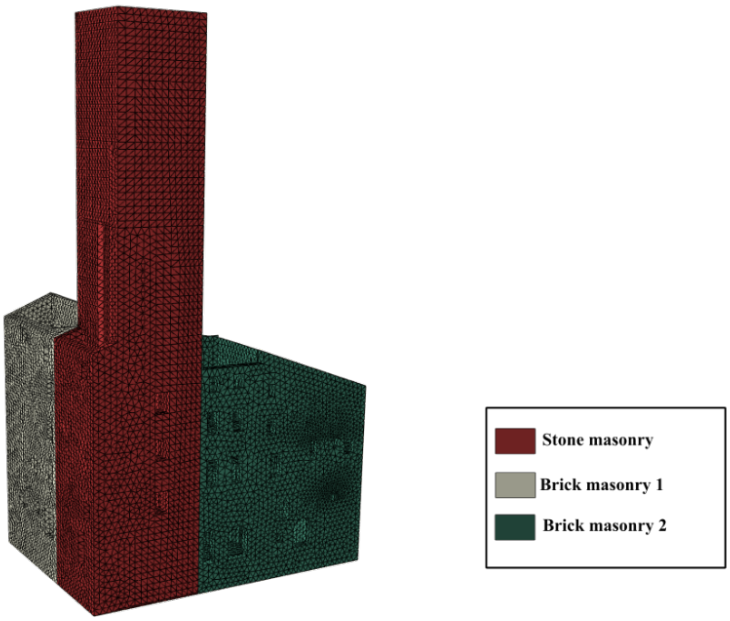


Figure 6 - Material configuration.

2.1.3 Loadings and boundary conditions

Regarding the loading conditions, the self-weight of the structure was automatically considered through the gravity load. Since the roof systems were not explicitly included in the numerical model, their contribution was represented through equivalent external loads applied to the corresponding supporting walls. Based on the estimated weight of the omitted structural components, equivalent loads of 350 kN, 112 kN, and 330 kN were assigned to Roofs 1, 2, and 3, respectively, as represented in Figure 7. Concerning the boundary conditions, the base of the model was assumed to be fully fixed.

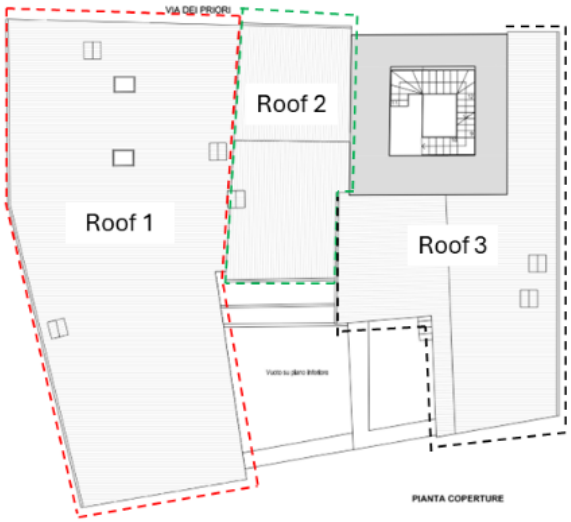


Figure 7 – Roof load distribution.

2.1.4 Mesh and element type

Before the material calibration, a mesh convergence study was conducted to evaluate the influence of mesh refinement on the estimated natural frequencies of the structure. The finite element model was discretized using second-order tetrahedral elements (C3D10), and four characteristic element sizes were investigated, which are 0.8 m, 0.6 m, 0.5 m, and 0.4 m. The corresponding results are presented in Table 3.

For the present model, mesh refinement resulted in a gradual increase in the estimated natural frequencies, indicating convergence of the numerical solution. The variation between successive mesh refinements progressively decreased, particularly for the first four natural frequencies, which were selected as the primary targets of the subsequent model updating procedure.

The final mesh size was selected by balancing computational efficiency and numerical accuracy. Based on the results obtained for the first four natural frequencies, the 0.5 m mesh provided a better result between solution accuracy and computational cost and was therefore adopted for all subsequent analyses. The resulting finite element model consisted of 495,523 nodes and 291,872 C3D10 tetrahedral elements.

Table 3 - Mesh Convergence Study

Mesh size	Natural frequencies [Hz]			
	1st	2nd	3rd	4th
0.8 m	1.209	1.286	4.193	4.339
0.5 m	1.211	1.289	4.202	4.349
0.4 m	1.215	1.291	4.211	4.359
0.3 m	1.224	1.299	4.243	4.392

Table 4 presents the results obtained from the initial numerical model prior to calibration, compared with the experimental modal properties identified through the Operational Modal Analysis. It can be observed that the first two natural frequencies presented errors exceeding 40%, indicating a significant discrepancy between the stiffness of the numerical model and the actual structural behavior of the tower.

Table 4 – Natural frequencies comparison before calibration

Vibration mode	1	2	3	4
Natural Frequency F^{SSI} [Hz]	1.722	1.925	5.615	6.006
Natural Frequency $F^{FEM}{}_0$ [Hz]	1.211	1.289	4.202	4.349
Error %	-42.20	-49.34	-33.63	-38.10

3. Results and discussion

As a result of the manual calibration procedure, after approximately 15 iterations, the material properties presented in Table 5 were obtained. It can be observed that the Young's modulus assigned to the stone masonry increased from 2400 MPa to 4200 MPa. For the surrounding brick masonry, the calibrated Young's modulus values increased from 1200 MPa to 3500 MPa and 4800 MPa for regions 1 and 2, respectively. In particular, the value obtained for Brick Masonry 2 exceeded that assigned to stone masonry. This result likely reflects the need to compensate for structural stiffness contributions that were not explicitly represented in the numerical model, such as local connections. Consequently, higher elastic modulus values were required to reproduce the experimentally identified dynamic behavior.

Table 5 – Material Properties after calibration

Material		Young's Modulus [MPa]	Poisson's Ratio	Mass density [kg/m³]
Before tuning	Stone masonry	2,400	0.25	2,200
	Brick masonry	1,200	0.25	1,800
After tuning	Stone masonry	4,200	0.25	2,000
	Brick masonry 1	3,500	0.2	2,000
	Brick masonry 2	4,800	0.2	2,000

Despite these adjustments, the calibrated parameters produced satisfactory agreement with the experimental modal data, as shown in Table 6. The first two natural frequencies presented relative errors of 4.56% and -1.27%, respectively, indicating that the adopted material properties can reproduce the fundamental dynamic behavior of the structure with good accuracy. The third and fourth vibration modes also presented relatively small frequency discrepancies, with errors of -2.42% and -5.76%, respectively.

Table 6 - Comparison between experimental and numerical modal parameters after calibration

Vibration mode	1	2	3	4
Natural Frequency F^{SSI} [Hz]	1.722	1.925	5.615	6.006
Natural Frequency F^{FEM} [Hz]	1.801	1.901	5.479	5.660
Error	4.56%	-1.27%	-2.42%	-5.76%

According to the modal analysis results, the first two vibration modes exhibited the same deformation patterns identified through the Operational Modal Analysis conducted by the University of Perugia, corresponding to bending in the x- and y-directions, respectively. For the third and fourth modes, however, although the natural frequencies remained close to the experimental values, differences were observed in the associated mode shapes. In the numerical model, the third mode corresponded to bending in the y-direction and the fourth mode to bending in the x-direction, whereas the opposite sequence was identified experimentally during the OMA campaign.

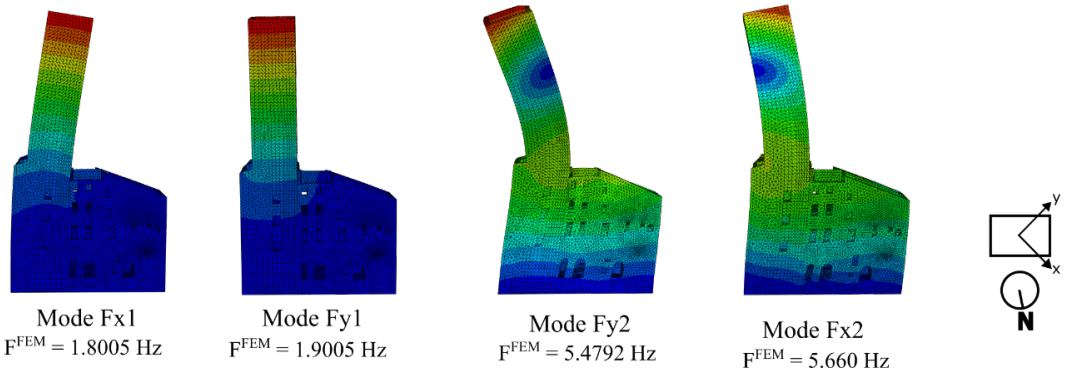


Figure 8 – Natural frequencies and modal shapes FEM model.

4. Conclusions

This study presented the development and calibration of a finite element model of the Sciri tower, a 13th-century masonry tower located in the historic center of Perugia, Italy. The proposed methodology combined a geometric model obtained through terrestrial laser scanning and aerial photogrammetry with an Operational Modal Analysis (OMA)-based model updating procedure. The geometric survey data was processed in Revit® and subsequently imported into ABAQUS®, where the numerical model was generated and discretized using second-order tetrahedral elements (C3D10).

The dynamic characterization of the structure was based on experimental modal parameters previously identified by the University of Perugia. These data served as reference values for the calibration of the elastic mechanical properties of the masonry. The updated model showed good agreement with the experimental results for the first two natural frequencies and their associated mode shapes, with relative errors of 4.56% and −1.27%, respectively. These results indicate that the proposed model was able to reproduce the global dynamic behavior of the tower with satisfactory accuracy. For the subsequent vibration modes, although the discrepancies in natural frequencies remained relatively small, differences were observed between the numerical and experimental mode shapes.

Despite these limitations, the study demonstrates the potential of integrating point-cloud-based geometric reconstruction with vibration-based identification techniques for the structural assessment of heritage masonry buildings. The methodology provides a robust framework for the calibration of numerical models and contributes to the development of more reliable tools for conservation, monitoring, and seismic vulnerability assessment of historic structures. Future developments should focus on creating more partitions and try more different materials in the analysis to better represent the global stiffness of the tower.

Furthermore, automated model updating strategies based on optimization algorithms or surrogate models could be employed to improve parameter identification.

5. Acknowledgments

The authors gratefully acknowledge the support from the Italian Ministry of University and Research (MUR) through the FIS-2021 Advanced Grant project “Smart Masonry enabling SAFEty-assessing STructures after earthquakes (SMS SAFEST)” (Project code FIS00001797).

The present work was carried out with the support of CNPq, National Council for Scientific and Technological Development – Brazil.

6. References

Alvandi, A., and C. Cremona. 2006. “Assessment of Vibration-Based Damage Identification Techniques.” *Journal of Sound and Vibration* 292 (1–2). Academic Press: 179–202. doi:10.1016/j.jsv.2005.07.036.

García-Macías, Enrique, and Filippo Ubertini. 2020. “Automated Operational Modal Analysis and Ambient Noise Deconvolution Interferometry for the Full Structural Identification of Historic Towers: A Case Study of the Sciri Tower in Perugia, Italy.” *Engineering Structures* 215 (July). Elsevier Ltd. doi:10.1016/j.engstruct.2020.110615.

Gentile, C., and A. Saisi. 2006. “Ambient Vibration Testing of Historic Masonry Towers for Structural Identification and Damage Assessment.” *Construction and Building Materials*, October.

Gentile, Carmelo, Antonella Saisi, and Alessandro Cabboi. 2015. “Structural Identification of a Masonry Tower Based on Operational Modal Analysis.” *International Journal of Architectural Heritage* 9 (2). Taylor and Francis Inc.: 98–110. doi:10.1080/15583058.2014.951792.

Masciotta, Maria Giovanna, Luís F. Ramos, and Paulo B. Lourenço. 2017. “The Importance of Structural Monitoring as a Diagnosis and Control Tool in the Restoration Process of Heritage Structures: A Case Study in Portugal.” *Journal of Cultural Heritage* 27 (October). Elsevier Masson SAS: 36–47. doi:10.1016/j.culher.2017.04.003.

Ministero delle Infrastrutture e dei Trasporti, NTC. 2009. *Istruzioni per l’applicazione Delle Nuove Norme Tecniche per Le Costruzioni Di Cui al Decreto Ministeriale 14 Gennaio 2008*. Circolare.

Ramos, L. F., L. Marques, P. B. Lourenço, G. De Roeck, A. Campos-Costa, and J. Roque. 2010. “Monitoring Historical Masonry Structures with Operational Modal Analysis: Two Case Studies.” *Mechanical Systems and Signal Processing* 24 (5): 1291–1305. doi:10.1016/j.ymssp.2010.01.011.

Salachoris, Georgios Panagiotis, Gianluca Standoli, Michele Betti, Gabriele Milani, and Francesco Clementi. 2024. “Evolutionary Numerical Model for Cultural Heritage Structures via Genetic Algorithms: A Case Study in Central Italy.” *Bulletin of Earthquake Engineering* 22 (7). Springer Science and Business Media B.V.: 3591–3625. doi:10.1007/s10518-023-01615-z.

Tiberti, Simone, Maurizio Acito, and Gabriele Milani. 2016. “Comprehensive FE Numerical Insight into Finale Emilia Castle Behavior under 2012 Emilia Romagna Seismic Sequence: Damage Causes and Seismic Vulnerability Mitigation Hypothesis.” *Engineering Structures* 117 (June). Elsevier Ltd: 397–421. doi:10.1016/j.engstruct.2016.02.048.

Ubertini, Filippo, Nicola Cavalagli, Alban Kita, and Gabriele Comanducci. 2018. “Assessment of a Monumental Masonry Bell-Tower after 2016 Central Italy Seismic Sequence by Long-Term SHM.” *Bulletin of Earthquake Engineering* 16 (2). Springer Netherlands: 775–801. doi:10.1007/s10518-017-0222-7.

Vaiano, G., I. Venanzi, A. Formisano, and F. Ubertini. 2019. “Seismic Behaviour of Isolate and Aggregate Masonry Towers: The Case Study of the Sciri Tower in Perugia.” In *COMPDYN Proceedings*, 1:1441–59. National Technical University of Athens. doi:10.7712/120119.7010.19301.

Venanzi, Ilaria, Alban Kita, Nicola Cavalagli, Laura Ierimonti, and Filippo Ubertini. 2019. *CONTINUOUS OMA FOR DAMAGE DETECTION AND LO-CALIZATION IN THE SCIRI TOWER IN PERUGIA, ITALY*.

———. 2020. “Earthquake-Induced Damage Localization in an Historic Masonry Tower through Long-Term Dynamic Monitoring and FE Model Calibration.” *Bulletin of Earthquake Engineering* 18 (5). Springer: 2247–74. doi:10.1007/s10518-019-00780-4.

Cinpar 2026
XXII International Conference on Building Pathology and Constructions Repair
15th to 17th July 2026 - Lisboa, Portugal

Metodologia Digital Integrada para a Conservação do Património Construído: da Reconstrução Virtual ao Fabrico Aditivo

Inês BOURGEOIS[1], Guilherme ASCENSÃO[2], Victor FERREIRA[3], Hugo RODRIGUES[4]

[1] CERIS, Departamento de Engenharia Civil da Universidade de Aveiro, Campus Universitário de Santiago, Aveiro, 3810-193, Portugal, inescbourgeois@ua.pt
[2] CERIS, Departamento de Engenharia Civil da Universidade de Aveiro, Campus Universitário de Santiago, Aveiro, 3810-193, Portugal, guilhermeascensao@ua.pt
[3] CERIS, Departamento de Engenharia Civil da Universidade de Aveiro, Campus Universitário de Santiago, Aveiro, 3810-193, Portugal, victorf@ua.pt
[4] CERIS, Departamento de Engenharia Civil da Universidade de Aveiro, Campus Universitário de Santiago, Aveiro, 3810-193, Portugal, hrodrigues@ua.pt

Resumo: Na presente investigação é apresentada uma metodologia digital integrada inovadora para o restauro de elementos do património construído, combinando reconstrução digital e fabrico aditivo. Num primeiro momento estabelece um fluxo de trabalho otimizado de reconstrução digital, incorporando digitalização 3D através de fotogrametria, modelação e reconstrução computacional de elementos ornamentais danificados. Foram produzidas próteses através de impressão 3D em polímero (PLA) – para prototipagem rápida e validação geométrica – e impressão 3D com pastas à base de cal otimizadas (NHL) – para uma compatibilidade melhorada com os substratos históricos. A fidelidade dos elementos reproduzidos utilizando PLA e formulações de pasta NHL foram avaliadas através de um método de comparativo dos modelos digitais das peças impressas. Foram ainda incorporados sensores de temperatura, humidade relativa e CO_2 para monitorização de condições ambientais locais. Os processos de reconstrução digital, materiais de impressão, tecnologias de fabrico e métodos de monitorização propostos foram validados num estudo de caso localizado num monumento com classificação de Património Mundial da UNESCO, demonstrando um fluxo de trabalho inovador para a conservação de edifícios patrimoniais.

Palavras-chave: Património construído; Reconstrução digital; Fabrico aditivo; Monitorização

1. Introdução

Os edifícios patrimoniais requerem frequentemente ações extensivas de conservação e reabilitação devido a uma ampla variedade de patologias, que podem resultar da passagem do tempo, de danos induzidos pela ação humana, de condições ambientais a que estão sujeitos, ou, ainda, de efeitos meteorológicos extremos. Os métodos tradicionais de conservação e reabilitação são morosos e dependem fortemente de trabalho manual altamente especializado; contudo, o setor enfrenta atualmente sérias dificuldades na contratação de mão de obra qualificada, o que provoca atrasos nos projetos e aumenta os custos.

Nos últimos anos, as tecnologias digitais têm vindo a ser introduzidas na conservação de edifícios patrimoniais, sobretudo para o levantamento e a documentação digital de estruturas e elementos construtivos com relevância histórica e cultural. Entre as tecnologias digitais, a fotogrametria tem-se destacado como uma ferramenta altamente eficaz e economicamente eficiente para documentar com precisão espaços e objetos tridimensionais (De Fino et al., 2023; Sugiyama et al., 2025). Esta permite recolher informação geométrica e textural, possibilitando a criação de modelos digitais de alta resolução para análise detalhada e avaliação do estado de conservação. Deste modo, permite uma análise geométrica eficaz e o planeamento de ações de conservação a longo prazo. Além disso, através dos modelos digitais obtidos com

esta tecnologia, é possível aplicar processos de reconstrução virtual de elementos danificados ou perdidos (Bourgeois, Ascensão, et al., 2024; Bourgeois et al., 2025); baseando-se quer em elementos de referência bem preservados com características semelhantes, quer recorrendo a evidências historicamente documentadas. Em paralelo, desenvolvimentos recentes das tecnologias de fabrico aditivo (ou impressão 3D) têm vindo a demonstrar as possibilidades de aplicação para a recuperação de elementos patrimoniais, ao permitirem a produção de réplicas físicas precisas de artefactos e ornamentos arquitetónicos. Até ao momento, a impressão 3D tem sido utilizada sobretudo para enriquecer experiências educativas e interpretativas destinadas a visitantes e educadores em contextos de património cultural (Arapakopoulos et al., 2022; Balletti et al., 2018; Balletti & Ballarin, 2019). Ainda assim, a sinergia entre a documentação digital precisa e o fabrico digital oferece novas perspetivas para a reabilitação patrimonial, particularmente na criação de próteses para elementos ornamentais danificados de elevado valor artístico e cultural, nos quais a autenticidade e compatibilidade são princípios de base (Bourgeois, Ascensão, et al., 2024). Neste sentido, a técnica de fotogrametria tem um papel fundamental, ao fornecer a estrutura de aquisição digital necessária para a documentação de geometria e de texturas de alta resolução – permitindo a obtenção de *digital twins* que podem ser eficazmente utilizados para orientar processos precisos de impressão 3D e o fabrico de próteses de alta resolução. Avanços adicionais podem incluir sensores embutidos nas próteses arquitetónicas – nomeadamente sensores de temperatura, humidade e CO_2 – os quais tem demonstrado ser uma mais-valia, ao permitir a monitorização em tempo real de condições ambientais e as suas consequências (Bansal et al., 2022; Blanco et al., 2018; Bourgeois, Pereira, et al., 2024; Parida et al., 2024; Pereira et al., 2024).

Através do caso de estudo aplicado no Mosteiro da Batalha, classificado como Património Mundial da UNESCO, foram examinadas preliminarmente a execução prática e os desafios associados à implementação de um fluxo de trabalho integrado de reconstrução digital e fabrico aditivo, sendo os resultados aqui discutidos. O fluxo de trabalho e as potenciais linhas de investigação a explorar em futuros desenvolvimentos deste trabalho são ilustrados na Figura 1. Os avanços futuros poderão incluir a integração em ambiente BIM, a adoção de automação e de fabrico orientado por inteligência artificial, bem como o desenvolvimento de materiais inovadores imprimíveis em 3D e de tecnologias de fabrico, todos com o objetivo de agilizar a tomada de decisão, otimizar os processos de fabrico e melhorar a qualidade e a relação custo-eficácia das próteses arquitetónicas funcionalizadas, contribuindo para melhores práticas de conservação e reabilitação.

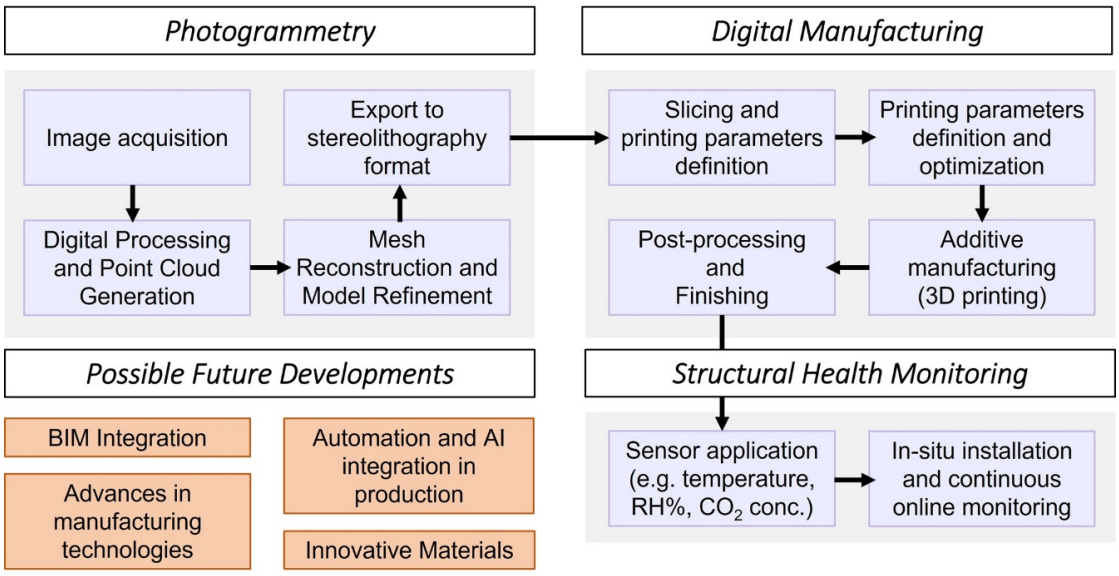


Figura 1 – Fluxo de trabalho

2. Caso de Estudo

O Mosteiro da Batalha (ver Figura 2) é um dos exemplos mais notáveis da arquitetura gótica em Portugal, estando classificado como Património Mundial da UNESCO desde 1983. A sua construção foi requisitada pelo rei D. João I, após a vitória portuguesa na Batalha de Aljubarrota, que garantiu a independência do país.

Ao longo dos séculos, o mosteiro resistiu a dois grandes sismos, em 1755 e 1962, e às invasões francesas, entre 1807 e 1810, acontecimentos que aumentaram drasticamente as necessidades de conservação do mosteiro e aceleraram a degradação natural de muitos dos seus elementos estruturais e ornamentais. Há registos de trabalhos de conservação desde o século XIX; contudo, o complexo monástico é vasto e rico em elementos de elevado valor estético e cultural que ainda necessitam de restauro, bem como em muitos elementos decorativos em falta que faziam parte da ornamentação original.

Em trabalhos anteriores, os autores reportaram levantamentos detalhados que identificaram vários elementos ornamentais como potenciais candidatos à aplicação experimental da metodologia de restauro digital aqui proposta (Bourgeois, Ascensão, et al., 2024; Bourgeois et al., 2025; Sugiyama et al., 2025). Neste trabalho, foram selecionados como caso de estudo os pináculos – elementos muito presentes nas zonas de cobertura – uma vez que se identificou danos locais em diversos elementos que necessitam de intervenção. A Figura 2 apresenta um exemplo do elemento num bom estado de conservação, destacando um elemento que constitui o pináculo e que foi selecionado para reprodução.

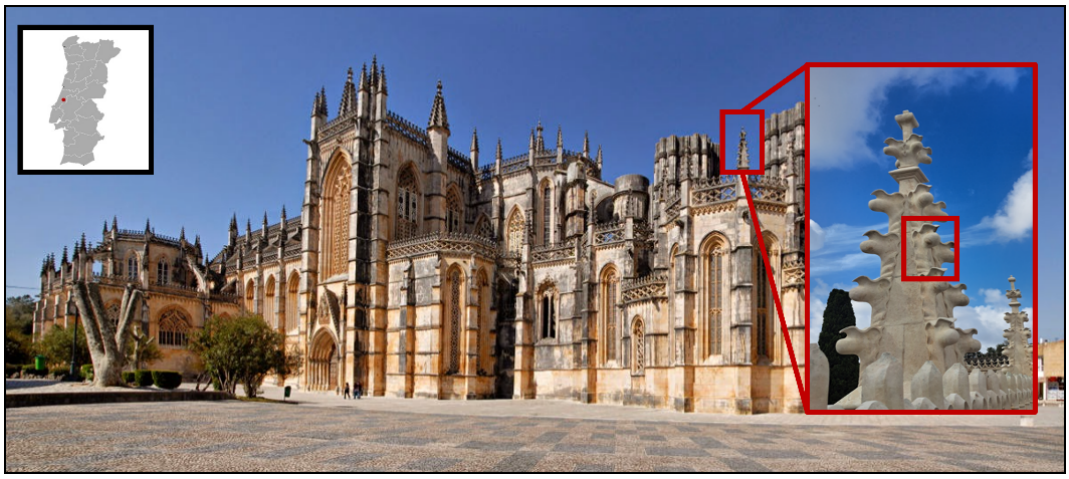


Figura 2 – Fachada principal do Mosteiro de Batalha. A imagem inserida no canto superior esquerdo mostra a localização geográfica do Mosteiro de Batalha em Portugal e, à direita, uma imagem em grande plano de um pináculo e do elemento ornamental a reproduzir.

3. Materiais e Métodos

Foram utilizadas técnicas de fotogrametria, modelação paramétrica e reconstrução computacional para criar modelos digitais do elemento ornamental a reproduzir. Para o levantamento de imagem, foi utilizada uma câmara digital Sony A6100 para captar fotografias de ambos elementos deteriorados e elementos bem conservados. O software Agisoft Metashape foi utilizado para realizar o processo de fotogrametria e obter nuvens de pontos dos mesmos. Com a informação digital destes elementos, foi realizada a modelação computacional recorrendo ao software Blender. Durante o processo de modelação, foram aplicados processos para garantir a compatibilidade entre os modelos e os respetivos suportes do elemento danificado. Uma vez assegurada a compatibilidade adequada, os modelos finais foram convertidos para o

formato de estereolitografia (.stl), para processamento em software de fatiamento e geração de ficheiros G-code para impressão.

Para a prototipagem rápida e o refinamento dos modelos, foram produzidas próteses poliméricas utilizando filamento de ácido polilático (Polylite PLA Pro, Polymaker). Neste caso, o software Bambu Studio foi utilizado como plataforma de fatiamento, e a impressora Bambu Lab X1E foi utilizada para a impressão. A impressão foi realizada a velocidades entre 50 e 150 mm/s para a camada inicial e para a parede interior, respetivamente. Foi definida uma altura de camada de 0,12 mm para melhorar a precisão e a resolução. Foi utilizado um padrão de enchimento com 10% de densidade, bem como suportes do tipo árvore para sustentar cavidades internas (3,0 cm x 5,0 cm x 2,5 cm) concebidas durante a fase de modelação para a colocação de sensores (ver

Figura **3** e Figura 4). Após a impressão, os suportes temporários foram facilmente removidos manualmente, sem provocar quaisquer defeitos nas próteses impressas. Não foi necessário qualquer pós-processamento adicional.

Foi desenvolvido, validado e embutido um sensor Arduino SCD40 nas próteses para monitorizar as condições ambientais, incluindo temperatura, humidade relativa e níveis de CO_2. A funcionalização das próteses impressas em 3D visa estabelecer correlações entre as condições ambientais e a progressão de determinadas patologias construtivas, perspetivando o desenvolvimento futuro de um sistema de sensorização simples, não intrusivo e contínuo, suportado por próteses inteligentes de elevada fidelidade. Antes da colocação do sensor, foram perfurados pequenos orifícios nas próteses para permitir a circulação de ar e possibilitar a medição precisa dos dados ambientais (ver Figura 5).

Para uma maior compatibilidade estética com os substratos históricos, foram desenvolvidas pastas de cal hidráulica natural (NHL) para *robocasting*. O fatiamento para *robocasting* foi realizado utilizando o software Simplify3D. Foi utilizada uma impressora 3D Delta Wasp 40100 equipada com um extrusor WASP 3.0 e um bocal circular com 2 mm de diâmetro, operando a 1250 mm/min e com uma altura de camada de 1,8 mm. Neste caso, foi utilizado um padrão de enchimento retilíneo, embora com uma densidade de enchimento superior, de 50%, em comparação com as impressões em PLA.

As pastas de NHL utilizadas para impressão foram previamente desenvolvidas pelos autores, sendo compostas por cal hidráulica natural comercial NHL 3.5, de acordo com a norma EN 459–1 (Secil®, Pataias, Portugal), argila caulinítica (A130S, MotaCeramic Solutions®, Oiã, Portugal) e água destilada. Nanoclay (Myta, Zaragoza, Espanha), um agente modificador de viscosidade à base de celulose (Walocel, DOW, Estarreja, Portugal) e um superplastificante de elevado desempenho (Master Ease 3530, BASF Portugal, Porto, Portugal) foram utilizados como aditivos modificadores da reologia, de modo a tornar as pastas compatíveis com os requisitos reológicos das tecnologias de impressão 3D. Uma descrição detalhada das formulações das pastas, das proporções de mistura, dos aditivos utilizados e do método de preparação é apresentada noutro trabalho (Bourgeois, Ascensão, et al., 2024; Bourgeois et al., 2025).

Todas as próteses foram impressas em condições ambiente (20 °C ± 5 °C e HR 65% ± 5%). Após a impressão, as próteses em PLA foram armazenadas em condições ambiente, enquanto as próteses à base de NHL foram curadas em ambiente controlado (20 °C ± 5 °C e HR 95% ± 5%) durante 7 dias, de modo a minimizar a retração, sendo posteriormente também armazenadas em condições ambiente.

4. Resultados e Discussão

A metodologia aplicada permitiu demonstrar a viabilidade da reconstrução digital de elementos ornamentais danificados com base na tecnologia da fotogrametria. A aplicação desta técnica possibilitou a

obtenção de uma representação tridimensional suficientemente detalhada dos elementos existentes, evidenciando que a qualidade do modelo final depende fortemente da resolução, quantidade e consistência das imagens recolhidas, bem como do desempenho do software utilizado no processamento fotogramétrico. A aquisição de um conjunto alargado de imagens de alta resolução, com elevado grau de sobreposição, revelou-se essencial para gerar uma nuvem de pontos robusta e um modelo preliminar coerente do pináculo (Bourgeois, Ascensão, et al., 2024). A justaposição da nuvem de pontos do elemento danificado com o modelo reconstruído permitiu avaliar e ajustar a compatibilidade geométrica entre a prótese digital e a estrutura existente, assegurando um encaixe mais adequado no suporte original. Este processo evidenciou a relevância da integração entre levantamento digital e modelação computacional para minimizar discrepâncias geométricas antes da fase de fabrico. Além disso, a incorporação de uma cavidade interna para alojamento do possibilitou compatibilizar os requisitos estéticos da reconstrução ornamental com funcionalidades adicionais de monitorização. A

Figura **3** apresenta uma vista lateral do modelo 3D otimizado, bem como a cavidade concebida para a colocação do sensor.

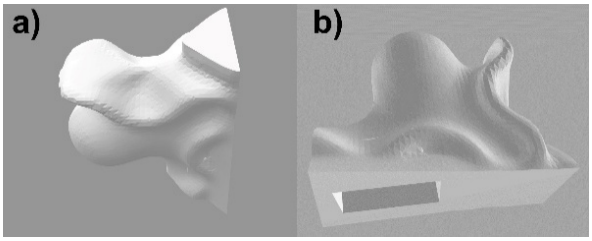


Figura 3 – Modelo do elemento ornamental: a) vista lateral e b) cavidade para a instalação do sensor.

Para prototipagem rápida, foram inicialmente produzidas próteses em PLA. A Figura 4 a) ilustra o processo de fatiamento e o percurso de impressão, enquanto a Figura 4 b) mostra a cavidade interna e as estruturas de suporte temporárias utilizadas durante a impressão. Dada a natureza termoplástica do PLA, o processo de impressão revelou-se altamente fiável, decorrendo sem constrangimentos ou dificuldades técnicas. Não foi necessário qualquer pós-processamento além da remoção manual dos materiais de suporte. A Figura 4 c) mostra a prótese impressa final, enquanto a Figura 4 d) apresenta a sua fidelidade ao modelo digital gerado por fotogrametria. Como se pode observar, as próteses impressas foram capazes de replicar com precisão o modelo digital, com desvios inferiores a -0,2%. A distribuição gráfica da exatidão geométrica não revela áreas críticas, indicando uma distribuição homogénea de erros mínimos de impressão. Assim, as próteses em PLA demonstram um potencial significativo para aplicações em edifícios patrimoniais, nomeadamente ao permitirem a prototipagem rápida, o ajuste de modelos e a criação de réplicas manuseáveis de baixo custo para experiências culturais e educativas imersivas.

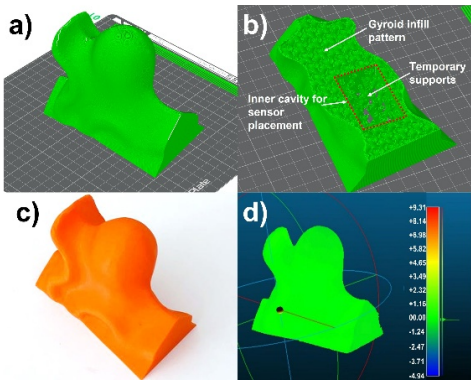
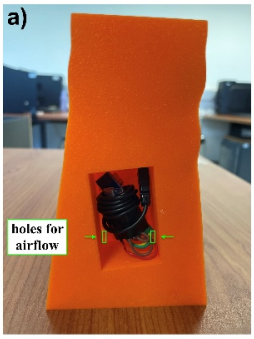


Figura 4 – a) Visualização do percurso de corte e impressão, b) pré-visualização do padrão interno e do preenchimento, c) prótese em PLA impressa, e d) análise da fidelidade do modelo e distribuição gráfica da precisão geométrica. Escala de cores — verde-azulado escuro: redução de volume > 2%; verde-claro: desvio de volume < 2%, e laranja-avermelhado: aumento de volume > 5%.

A Figura 5 a) mostra a integração do sensor nas próteses em PLA e destaca as localizações específicas das aberturas para circulação de ar. As leituras ambientais do sensor SCD40 foram recolhidas ao longo de um período de 12 dias, num ambiente laboratorial controlado, para validação do sistema. As medições de temperatura, humidade relativa e CO_2 foram realizadas em intervalos regulares de 1 hora, sendo os dados transmitidos para uma base de dados online. Os resultados de temperatura refletiram com precisão a temperatura média no interior da sala de ensaio, sendo também capazes de acompanhar as variações dia-noite (ver Figura 5 b). As medições de humidade relativa permaneceram estáveis ao longo do período de monitorização e em boa concordância com as condições ambientais (ver Figura 5 c). Por sua vez, as medições dos níveis de concentração de CO_2 mostraram-se capaz de captar picos de concentração coincidentes com períodos de maior ocupação da sala (Figura 5 d), nunca excedendo o limiar recomendado de 1000 ppm, prescrito pela maioria das normas europeias para espaços públicos interiores. Em conjunto, estes resultados preliminares demonstram que o sistema de sensorização desenvolvido, incorporado em próteses inteligentes, pode ser eficazmente utilizado para monitorizar dados ambientais em edifícios patrimoniais e, por conseguinte, poderá ser explorado para otimizar o planeamento da manutenção e a conservação a longo prazo.



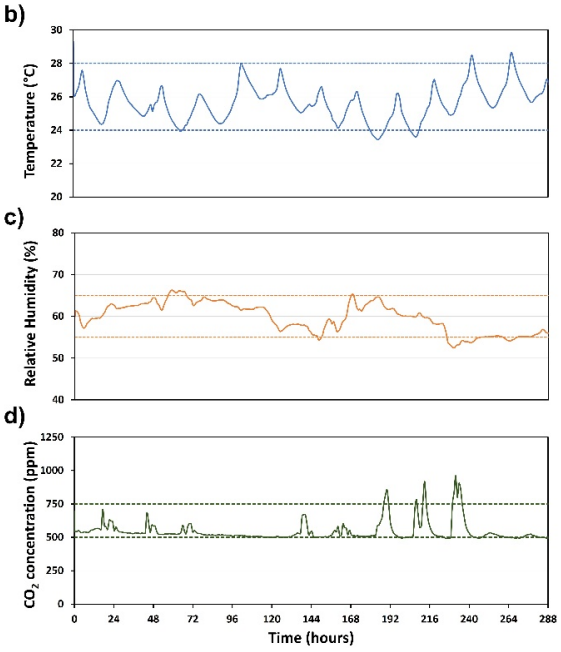


Figura 5 – Localização do sensor no interior da prótese de PLA a) e dados ambientais recolhidos: b) temperatura (°C), c) humidade relativa (%) e d) concentração de CO_2 (ppm).

A Figura 6 a) mostra o processo de fatiamento e o percurso de impressão das próteses em NHL. Embora tenha sido utilizado software diferente, a modelação digital nesta fase foi muito semelhante ao processo descrito para as próteses em PLA. As pastas de NHL foram previamente desenvolvidas e otimizadas para impressão em estudos anteriores (Bourgeois, Ascensão, et al., 2024; Bourgeois et al., 2025), não tendo ocorrido entupimentos nem bolhas de ar significativas que comprometessem o processo de impressão. Foi alcançada uma extrusão bastante consistente, sendo apenas necessários ajustes mínimos de pressão e de velocidade de impressão durante o processo. A Figura 6 b) apresenta uma amostra de uma prótese de pináculo produzida com pastas de NHL, evidenciando a consistência do produto impresso.



Figura 6 – a) Visualização do percurso de corte e impressão, b) prótese NHL impressa e c) análise da fidelidade do modelo e distribuição gráfica da precisão geométrica. Escala de cores: verde-azulado escuro:

redução de volume > 10%; amarelo-verde claro: desvio de volume < 10% e laranja-vermelho: aumento de volume > 10%.

À semelhança da metodologia seguida para as próteses em PLA, as próteses produzidas com pastas de NHL foram digitalizadas após a impressão e cura, e justapostas ao modelo digital para avaliar a sua exatidão e fidelidade. Os resultados mostram que, embora as próteses impressas em 3D com NHL tenham, de um modo geral, replicado a geometria original, apresentaram desvios significativamente superiores aos das suas congéneres em PLA, variando aproximadamente entre -5% e +25% (ver Figura 6 c). A análise volumétrica indica que tais desvios se caracterizaram predominantemente por aumentos de volume, e não por reduções, estando muito provavelmente associados à deformação plástica do filamento no estado fresco, mais do que à redução dimensional decorrente de fenómenos de retração durante a cura.

As próteses em PLA demonstraram uma fidelidade geométrica visivelmente superior relativamente aos modelos digitais, beneficiando de um comportamento térmico mais previsível durante a impressão e de uma deformação plástica e retração pós-impressão mínimas. Em resultado da sua maior capacidade para reproduzir características complexas dos elementos ornamentais, as próteses em PLA parecem vantajosas quando é exigida uma correspondência geométrica rigorosa. Contudo, embora as próteses poliméricas possam destacar-se na reprodução de detalhes morfológicos finos, a sua compatibilidade química e física com substratos históricos é limitada, levantando questões de compatibilidade mecânica e química com o suporte original, bem como à durabilidade a longo prazo. Neste contexto, as próteses em NHL, embora ainda apresentem desafios em termos de fidelidade dimensional – que poderão ser ultrapassados através do refinamento dos parâmetros de impressão, do ajuste das formulações dos materiais, da compensação por escala ou da exploração de estratégias de fabrico híbridas – demonstraram potencial para futura otimização e aplicação em projetos de conservação e reabilitação.

5. Conclusões

Este trabalho apresenta um fluxo de trabalho digital inovador para a reabilitação do património contruído, integrando reconstrução virtual e fabrico aditivo avançado. Através do caso de estudo de um elemento ornamental de um monumento classificado como Património Mundial da UNESCO, o Mosteiro da Batalha, foi demonstrado o valor da tecnologia de fotogrametria no levantamento digital detalhado que permite uma base sólida para a reconstrução digital de ornamentos patrimoniais danificados e perdidos, sendo posteriormente explorado para produzir próteses de reabilitação precisas.

As próteses de reabilitação foram produzidas utilizando materiais poliméricos, nomeadamente PLA, e materiais de base mineral, nomeadamente NHL, tendo a sua qualidade de impressão e fidelidade geométrica sido avaliadas. Os resultados mostram que as próteses em PLA oferecem maior controlo sobre o processo de fabrico e superior estabilidade dimensional, enquanto as próteses à base de NHL apresentam níveis mais baixos de fidelidade geométrica e precisão de impressão. Ainda assim, as próteses em NHL foram produzidas com uma precisão razoável, demonstrando um valor promissor para futura otimização e aplicação em projetos de reabilitação que priorizem a autenticidade cultural e a compatibilidade material.

Assim, verificou-se que a seleção do material depende das prioridades de conservação e dos requisitos específicos de utilização pós-impressão de cada projeto, devendo considerar fatores como a eficiência de impressão, o desempenho físico e a compatibilidade a longo prazo com a estrutura original. A integração bem-sucedida de sensores incorporados nas próteses impressas revelou-se também viável, evidenciando um potencial valor acrescentado para a monitorização em tempo real e in situ do estado de conservação estrutural. Com desenvolvimentos futuros deste trabalho, poderão ser concebidas soluções de

monitorização economicamente eficientes e não intrusivas, visando contribuir para o desenvolvimento de práticas de conservação preventiva baseadas em dados.

Agradecimentos

Esta investigação foi financiada pela Fundação para a Ciência e a Tecnologia (FCT), ao abrigo do financiamento UID/6438/2025 (https://doi.org/10.54499/UID/06438/2025) da unidade de investigação CERIS. Este trabalho foi também apoiado pela FCT no âmbito do projeto de investigação 2024.14274.PEX – 3D Printing for the Conservation and Recovery of Built Heritage Elements – PRINTHERITAGE (https://doi.org/10.54499/2024.14274.PEX).

Referências

Arapakopoulos, A., Liaskos, O., Mitsigkola, S., Papatzanakis, G., Peppa, S., Remoundos, G., Ginnis, A., Papadopoulos, C., Mazis, D., Tsilikidis, O., & Yighourtakis, Y. (2022). 3D Reconstruction & Modeling of the Traditional Greek Trechadiri: "Aghia Varvara." *Heritage*, *5*(2), 1295–1309. https://doi.org/10.3390/heritage5020067

Balletti, C., & Ballarin, M. (2019). An application of integrated 3D technologies for replicas in cultural heritage. *ISPRS International Journal of Geo-Information*, *8*(6). https://doi.org/10.3390/ijgi8060285

Balletti, C., Ballarin, M., & Vernier, P. (2018). Replicas in cultural heritage: 3D printing and the museum experience. *International Archives of the Photogrammetry, Remote Sensing and Spatial Information Sciences - ISPRS Archives*, *42*(2), 55–62. https://doi.org/10.5194/isprs-archives-XLII-2-55-2018

Bansal, T., Talakokula, V., Rama Jyosyula, S. K., Vicente, R., & Ascensão, G. (2022). Embedded Piezo-Sensor-Based Automatic Performance Monitoring of Chloride-Induced Corrosion in Alkali-Activated Concrete. *Sustainability (Switzerland)*, *14*(19). https://doi.org/10.3390/su141912917

Blanco, H., Boffill, Y., Lombillo, I., & Villegas, L. (2018). An integrated structural health monitoring system for determining local/global responses of historic masonry buildings. *Structural Control and Health Monitoring*, *25*(8), e2196. https://doi.org/10.1002/stc.2196

Bourgeois, I., Ascensão, G., Ferreira, V., & Rodrigues, H. (2024). Methodology for the Application of 3D Technologies for the Conservation and Recovery of Built Heritage Elements. *International Journal of Architectural Heritage*, 1–12. https://doi.org/10.1080/15583058.2024.2341327

Bourgeois, I., Pereira, L., Antunes, P., Ferreira, V., & Rodrigues, H. (2024). Non-intrusive monitoring of historic structures using fibre Bragg gratings – Application at the monastery of Batalha. *Journal of Building Engineering*, *94*, 109879. https://doi.org/10.1016/j.jobe.2024.109879

Bourgeois, I., Sugiyama, G., Capistrano, J., Ascensão, G., Ferreira, V., & Rodrigues, H. (2025). Smart 3D printed elements for conservation of damaged heritage structures. *Journal of Building Engineering*, *112*. https://doi.org/10.1016/j.jobe.2025.113595

De Fino, M., Galantucci, R. A., & Fatiguso, F. (2023). Condition Assessment of Heritage Buildings via Photogrammetry: A Scoping Review from the Perspective of Decision Makers. *Heritage*, *6*(11), 7031–7067. https://doi.org/10.3390/heritage6110367

Parida, L., Moharana, S., Vicente, R., & Ascensão, G. (2024). A proof of concept study on reliability assessment of different metal foil length based piezoelectric sensor for electromechanical impedance techniques. *Scientific Reports*, *14*(1). https://doi.org/10.1038/s41598-023-49762-2

Pereira, L., Bourgeois, I., Rodrigues, H., Varum, H., & Antunes, P. (2024). Fiber Bragg grating based displacement sensors with low visual impact for structural health monitoring applications – Monastery of Batalha case. *Sensors and Actuators A: Physical*, *368*. https://doi.org/10.1016/j.sna.2024.115117

Sugiyama, G., Bourgeois, I., & Rodrigues, H. (2025). A holistic methodology for the assessment of Heritage Digital Twin applied to Portuguese case studies. *Digital Applications in Archaeology and Cultural Heritage*, *36*. https://doi.org/10.1016/j.daach.2024.e00390

XXII International Conference on Building Pathology and Constructions Repair
15th to 17th July 2026 - Lisboa, Portugal

Porto Historical Heritage – Digital Twins and Underground Excavation Works

João PINTO[1], Hélder SILVA[2], Emanuel FERREIRA[3], João LIGUORI[4], António ARÊDE[5], José M. CASTRO[6], João POÇAS MARTINS[7], Luís SANHUDO[8]

[1]Faculdade de Engenharia, Universidade do Porto, Rua Dr. Roberto Frias s/n, 4200-465 Porto, Portugal, jmpinto@fe.up.pt
[2] Associação BUILT CoLAB – Colaborative Laboratory for the Future Built Environment, Porto, Portugal, helder.silva@builtcolab.pt
[3] Faculdade de Engenharia, Universidade do Porto, Rua Dr. Roberto Frias s/n, 4200-465 Porto, Portugal, Emanuelferreira.eng@gmail.com
[4] Faculdade de Engenharia, Universidade do Porto, Rua Dr. Roberto Frias s/n, 4200-465 Porto, Portugal, jmcruzliguori.ec@gmail.com
[5] CONSTRUCT, Faculdade de Engenharia, Universidade do Porto, Rua Dr. Roberto Frias s/n, 4200-465 Porto, Portugal, aarede@fe.up.pt
[6] CONSTRUCT, Faculdade de Engenharia, Universidade do Porto, Rua Dr. Roberto Frias s/n, 4200-465 Porto, Portugal, miguel.castro@fe.up.pt
[7] CONSTRUCT, Faculdade de Engenharia, Universidade do Porto, Rua Dr. Roberto Frias s/n, 4200-465 Porto, Portugal, jppm@fe.up.pt
[8] Associação BUILT CoLAB – Colaborative Laboratory for the Future Built Environment, Porto, Portugal, luis.sanhudo@builtcolab.pt

Abstract: The Metro of Porto (MdP) service, in Porto, Portugal, is presently expanding its network. Part of that expansion, namely the new Pink Line, which will connect “Casa da Música” (Music Hall in Boavista zone) to the São Bento train station, is fully underground and at least half of its extension runs underneath important built historical heritage assets in Porto downtown.

Following a risk analysis of all buildings within the project's influence area, the MdP administration requested that the Faculty of Engineering of the University of Porto (FEUP) support the structural assessment and survey of a set of historical landmarks to identify potential issues and effects arising from underground excavation works. This includes iconic Porto monuments, namely the Clérigos Church-Museum-Tower, the São Bento train station, the adjacent Congregados Church and the Boavista Obelisk, where possible settlements, rotations, vibrations, and crack openings are continuously measured by installed sensors and data acquisition systems.

This paper describes the development and implementation of digital twins of monuments that have been subjected to continuous monitoring of structural response during the construction works. The monitoring system is briefly described, followed by a summary of the architecture of the computational framework responsible for data collection and transformation. The paper continues with the presentation of the BIM models of the historical buildings. The implementation of the digital twins in a web-based framework is then discussed, with a focus on the developed interface that enables the dynamic exchange and contextualized visualization of data between the monitoring system and the geometric layer of the digital twin.

Keywords: Digital Twins, Historical buildings. Structural monitoring, Underground excavation effects

1. Introduction

The integration of emerging technologies across various professional sectors has accelerated remarkably in recent decades, driven by significant advances in computing, automation, and data management. In the field of civil engineering, the incorporation of these innovations represents a strategic opportunity to enhance the efficiency, safety, and sustainability of built structures. However, this transition also poses a considerable challenge due to the traditionally conservative nature of the sector and the high degree of responsibility associated with structural integrity, where potential failures can have severe consequences.

In this context, Structural Health Monitoring (SHM) has established itself as a multidisciplinary technology, serving as a powerful tool to raise the standards of maintenance and intelligent infrastructure management. Supported by mathematical analysis techniques, SHM systems enable engineers to track structural conditions, detect anomalies, and assess safety based on long-term data acquired through a strategic sensor network (Farrar and Worden, 2007; Cunha, Caetano and Magalhães, 2007). These non-destructive and non-invasive methodologies allow for the collection of vast volumes of data concerning accelerations, velocities, displacements, rotations, settlements, as well as environmental variables such as temperature. However, as infrastructure complexity increases, the autonomous, accurate, and robust processing of these monitoring data has become a primary concern for the SHM technical community.

The rapid development of simulation, data acquisition, and communication technologies has fostered unprecedented interactions between the physical and virtual spaces. To bridge the gap between raw data collection and intuitive interpretation, the concept of the Digital Twin (DT) has emerged as a transformative solution. A DT is developed by combining real-time data with a virtual representation of the structure, functioning as a dynamic digital mirror that integrates physical and virtual data throughout the entire lifecycle of the asset. This synergy generates a massive volume of data that can be processed by advanced analytics, providing a cyber-physical system with precise insights into the operational state and real-world structural response.

Beyond the capabilities of traditional monitoring methods, a DT can combine real-time sensor data with historical datasets, enabling the analysis of trends, patterns, and correlations that might otherwise go undetected. Despite these benefits, implementing DTs in infrastructure monitoring faces challenges related to scalability and computational demands. The complex nature of civil structures frequently requires high processing capacity, which can limit the efficiency of real-time monitoring.

Typically developed within a Building Information Modeling (BIM) environment and linked to physical sensors, the Digital Twin (DT) architecture developed in this study facilitates real-time remote monitoring and lifecycle management. This approach is particularly vital in complex urban environments, where the preservation of architectural heritage must be balanced with the expansion of modern infrastructure. By ensuring automated synchronization and spatial contextualization of monitoring data, this paper presents a functional framework designed to enhance the decision-making process, contributing to the mitigation of potential damage and the preservation of structural integrity in critical projects, such as the Metro of Porto infrastructure works.

2. Brief state of art overview

2.1 SHM and Damage in Built Heritage

Safeguarding structures of high heritage value within consolidated urban environments constitutes a complex challenge in contemporary structural engineering, exacerbated by the need for underground transportation infrastructure. The preventive conservation of these assets is governed by the principles of minimum intervention and the preservation of material authenticity (Flah *et al.*, 2021). Consequently, SHM systems have established themselves as indispensable non-destructive methodologies for the continuous diagnosis and behavioral prognosis of structures (Bao and Li, 2021).

Throughout its lifecycle, historical built heritage accumulates damage resulting from material degradation/fatigue phenomena, cyclic actions, and successive rehabilitation interventions that introduce mechanical heterogeneity and modify the original load paths (Cimino *et al.*, 2022; Clementi *et al.*, 2021). In terms of structural mechanics, damage manifests as alterations in the geometric or constitutive properties of the system that adversely affect structural stiffness and/or load-bearing capacity. SHM systems operate by detecting these anomalies through continuous comparative analysis between the baseline state and subsequent states, aiming at mitigating catastrophic risks and optimizing lifecycle costs through condition-based predictive maintenance strategies (Farrar and Worden, 2007; Magalhães, Cunha and Caetano, 2012).

2.2 Data Streams, IoT, and Sampling Rates

The effectiveness of a SHM system critically depends on the data acquisition architecture and the topology of the sensor network within the Internet of Things (IoT) ecosystem. Contemporary smart sensors integrate analog transducers, local microprocessors for preliminary signal processing, and wireless communication modules (Pinto, 2023). From an analytical perspective, the collected data support four levels of diagnostic maturity: descriptive (statistical characterization), exploratory (identification of correlations and outlier filtering), predictive (stochastic trend modeling), and prescriptive (direct decision-making support in risk management).

A fundamental design parameter in monitoring engineering is the sampling rate. Excessively high sampling rates introduce high-frequency noise and overburden storage layers, whereas undersampled frequencies may prevent the detection of critical kinematic features (da Silva, 2022).

To manage the high volume of generated data, the architecture can implement gateways as edge computing nodes. These devices act in the local aggregation and pre-processing of the signal, performing a preliminary downsampling prior to remote transmission. This approach reduces system latency and optimizes network bandwidth.

2.3 Digital Twin Paradigm and Semantic Modeling Challenges

The concept of the Digital Twin (DT) represents the evolution of static information models into dynamic, synchronous representations characterized by a continuous, bidirectional flow of information between the physical asset and its virtual counterpart (Grieves and Vickers, 2016). In civil engineering, and particularly within historical heritage, creating a DT faces severe constraints due to morphological asymmetry, geometric irregularities, and the lack of standardization among ancient constructive elements.

Different taxonomies have been proposed to classify virtual representations of infrastructure. In particular, models have been classified as Digital Shadows rather than Digital Twins when they simply transfer data from the physical asset to its digital representation via a one-way, automated data flow. This taxonomy has been widely accepted by industry and academia, but the current standard, EN 18162, for DTs applied to the built environment does not explicitly include these categories as steps towards a fully compliant DT.

Although Heritage BIM (HBIM) methodologies, supported by photogrammetric surveys and Laser Scanning, offer high geometric fidelity through point clouds, scientific practice validates the adoption of simplified modeling strategies when developing DTs oriented towards risk management. By removing or neglecting non-critical building components (such as roof structures), processing efficiency and graphical rendering of the three-dimensional model are optimized. This controlled geometric simplification preserves the rigor of the structural domain while ensuring the responsiveness required for real-time simulation and visualization of physical interactions.

2.4 Time Series Management and Dedicated Storage Architecture

The continuous nature of SHM systems dictates the generation of massive data streams structured chronologically, where each record is strictly linked to a timestamp. Conventional relational databases

demonstrate computational inefficiency and horizontal scalability issues when subjected to this type of load. For this reason, advanced SHM systems utilize time series databases.

InfluxDB (InfluxData, 2026a) stands out in this category as a storage engine optimized for write-intensive operations and concurrent analytical reads. Structuring data into *measurements* (physical variables), *fields*, and *tags* provides high efficiency for historical data querying and compression. Through the Flux analytical query language (InfluxData, 2026b), the system executes automated aggregation routines and retention policies directly within the data layer. This technical infrastructure enables the dynamic feeding of interactive dashboards seamlessly integrated into the three-dimensional environment of the DT. Consequently, the end user benefits from a unified platform where time series are spatially contextualized within the geometry of the monument, allowing short-term deformation peaks to be correlated with the physical progress of adjacent infrastructure works.

3. Case study: Porto Historical Buildings and the Metro of Porto expansion works

3.1 Framework

The application of the developed methodology is based on a SHM campaign of high-value heritage assets integrated within the direct zone of influence of the Porto Metro network expansion works. The project focuses on the construction of the Pink Line (Line G), an underground infrastructure approximately 3 km in length with double tracks, connecting the São Bento intermodal hub to the Boavista Roundabout. Given that the alignment is executed entirely in a tunnel and within a dense urban environment, the Faculty of Engineering of the University of Porto (FEUP) was requested to program, implement, and monitor a strategic plan for continuous observation to mitigate risks associated with ground stress relief and potential settlements induced by the advancing excavation fronts.

The core of this analysis focused on four highly vulnerable monuments: the São Bento Railway Station, the Church of Santo António dos Congregados, the Clérigos Church and Museum, and the Monument to the Peninsular War Heroes (also called Boavista Obelisk), three of which are identified and located in an aerial plan view shown in Fig. 1.

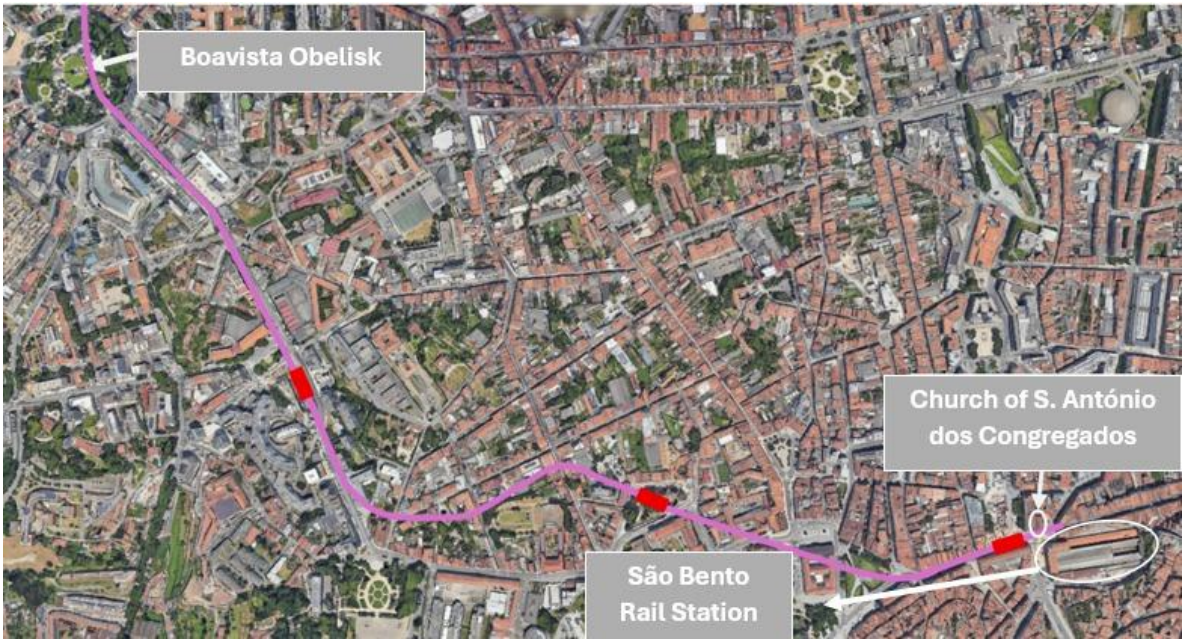


Figure 1 – Alignment of the new Pink Line (in the final construction stages), highlighting the three monuments considered in the case study: the Boavista Obelisk, the Church of Santo António dos Congregados and the São Bento Railway Station

3.2 Structural Characterization and Sensor Network Configuration

Each of the monuments highlighted in Fig. 1 was object of study, under which a monitoring sensor system was installed to characterize its structural behavior during the construction works in the surrounding area. The instrumentation was spatially distributed across critical zones and levels, utilizing five sensor typologies parameterized by standardized coding: crack meters (FS) for monitoring the opening and closing of cracks, clinometers (CL) for recording in-plane and out-of-plane wall rotations, temperature sensors (T) for monitoring temperature variations, level sensors (SN) for settlement control, and accelerometers (VB) for dynamic recording.

4. Prototype Architecture and System Development

4.1 System Architecture and Data Engineering

The developed prototype consists of a web-based Digital Twin (DT) platform designed for real-time Structural Health Monitoring (SHM) of heritage monuments within the influence zone of the Porto Metro expansion works. The system integrates three-dimensional geometric models, IoT sensor networks, and time-series databases into a unified, browser-accessible environment, aimed at providing a robust decision-support tool.

The solution adopts a decoupled client-server topology modularized via Docker containers, ensuring portability, operational stability, and the elimination of software dependency conflicts. Within the storage core, InfluxDB was selected for its native support of the Flux query language, executing filtering, aggregation, and downsampling processes directly within the data layer, thereby mitigating frontend latency when querying extensive historical datasets.

Communication is mediated by an Express.js (Node.js) proxy server. Data is hierarchically organized into isolated repositories (*buckets*) assigned to each monument. Inside each bucket, measurements are segmented by tagged fields (*tags* and *fields*), mapping each physical transducer to its respective engineering quantity (rotation, displacement, temperature, or acceleration). This modeling approach, based on JSON metadata, provides system scalability since accommodating new monuments or expanding the sensor network requires no source-code modifications or database migrations.

4.2 Automated Querying and Adaptive Processing

The automated query engine is based on an intelligent mapping logic structured across three functional dimensions:

- **Configuration Management:** The system automatically identifies the location of each sensor within the database, eliminating the need for rigid, hard-coded programming for newly deployed equipment.
- **Adaptive Processing:** Queries are dynamically adjusted based on the time frame selected by the user (e.g., minute-by-minute data for daily analyses or daily averages for monthly trends), optimizing both graphical clarity and computational effort.
- **Data Abstraction:** The strict separation between the interface logic and the database layer ensures system scalability, enabling the seamless integration of new monuments or sensors in the future without modifying the core codebase.

4.3 Semantic Interoperability via IFC Standard

The conversion of static geometric models into dynamic representations leverages the neutral IFC 4.3 format. Crucially, this updated standard provides significantly enhanced semantic definitions for sensor entities and dynamic property sets compared to legacy versions, natively streamlining the logical

connection between real-time IoT time-series streams and specific structural components of each monument (Jiang *et al.*, 2022). To link time-series data to the IFC geometry, a layer of interactive markers (*digital anchors*) was implemented with two relevant properties:

- **Selective Visibility:** A dedicated rendering technique based on 2D markers implemented with Three.js was developed to ensure that sensor references remain visible even when located behind opaque structural components such as walls, columns, slabs, and roofs. This capability enables the instantaneous localization of sensors installed in concealed zones or embedded deep within the structure.
- **Semantic Identification:** Each marker is bound to a unique ID that establishes a direct mapping to the corresponding tags and fields within the database (InfluxDB), encompassing spatial coordinate properties (X, Y, Z) and the respective physical metric being monitored.

4.4 User interface and result browsing

4.4.1 General layout and features

The primary value of this Digital Twin is to grant the user immediate access to monitoring data directly within the spatial context of the 3D model. The interface was engineered to bridge the abstraction gap typical of conventional technical reports. As shown in the platform's homepage (Figure 2), the user is greeted with an integrated visualization environment that structurally contextualizes each asset, establishing an intuitive gateway for real-time remote inspection.



Figure 2 – Homepage interface of the digital twin platform for historical structures

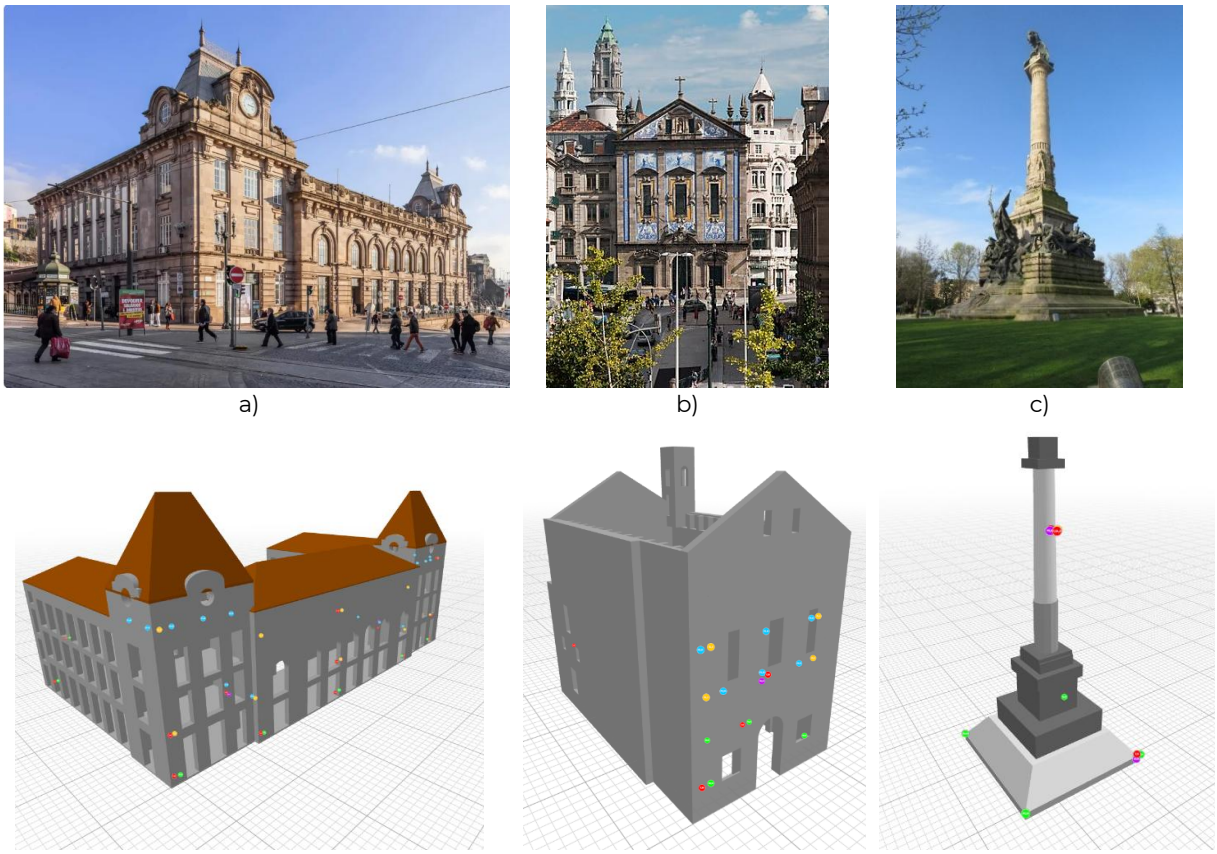


Figure 3 – Views of the three historical buildings and corresponding digital twin models: a) and d) São Bento Railway Station, b) and e) Church of Santo António dos Congregados, c) and f) Boavista Obelisk

Upon clicking a 2D marker, the system recognizes the sensor ID, extracts its historical dataset from InfluxDB, and automatically identifies the geometrically closest temperature sensor via a proximity algorithm (Fig. 4). By concurrently rendering both mechanical and temperature parameters within a floating panel, the platform enables the user to analyze the influence of cyclic environmental effects from any baseline shifts potentially induced by the adjacent construction works.

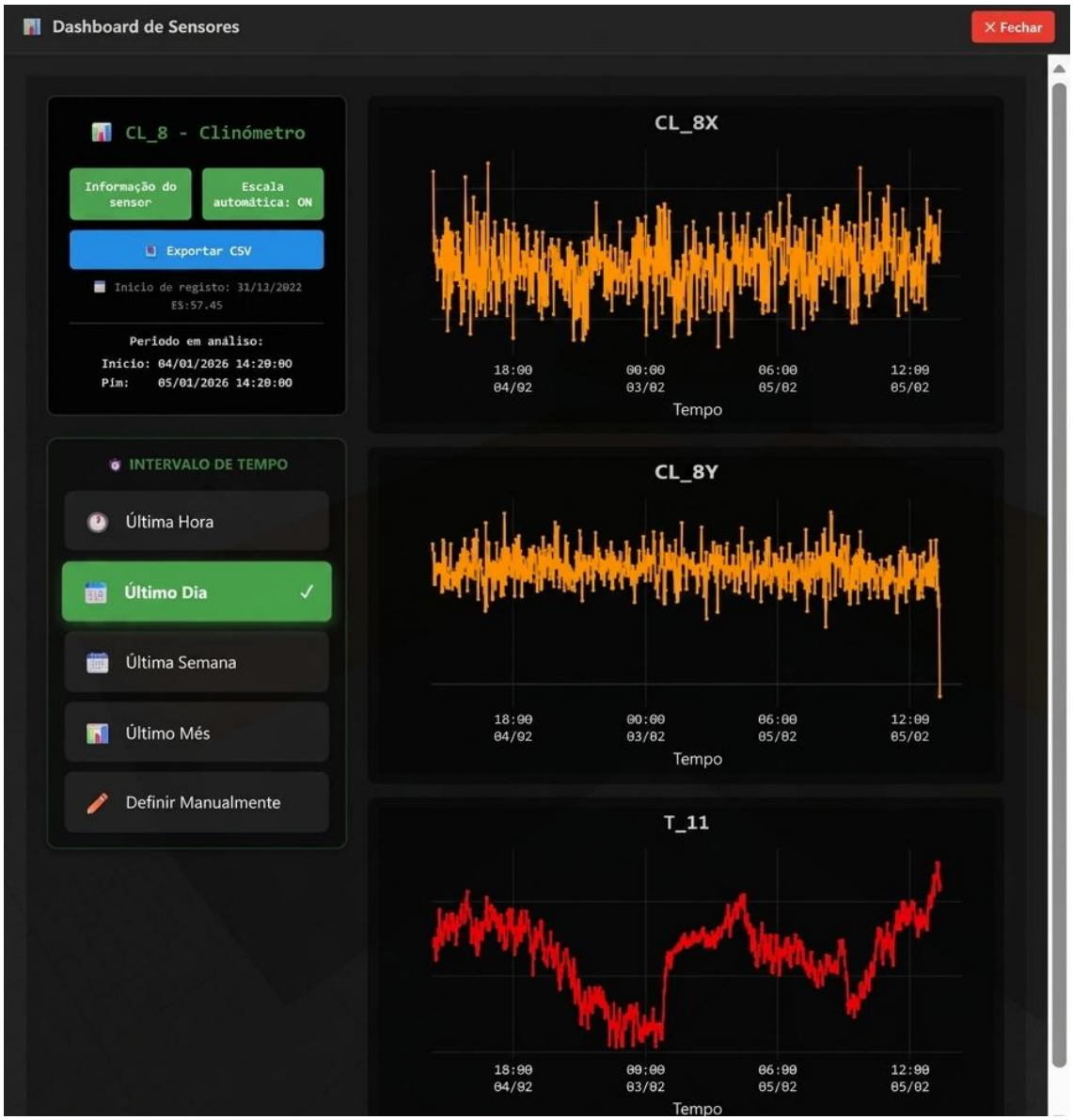
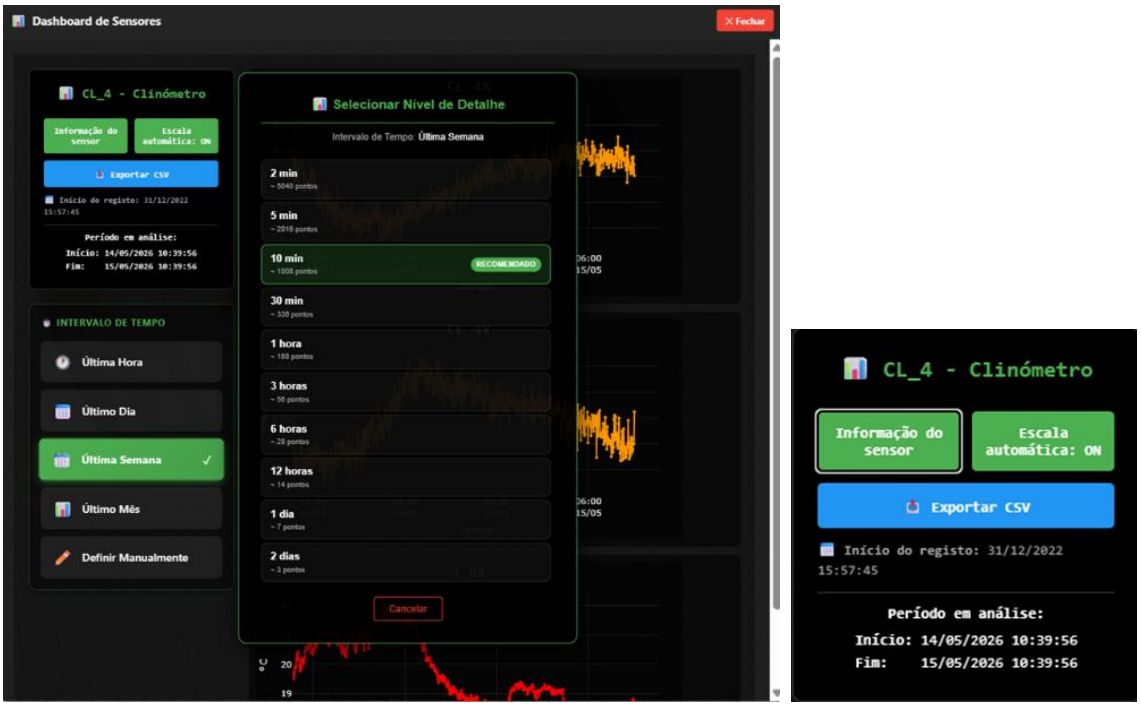


Figure 4 – Clinometer CL_8 with its respective associated temperature sensor, T_11

4.4.2 Temporal filtering and results' management

To streamline the analytical process, some filtering mechanisms were integrated:

- **Specific Period Selection:** Users can choose predefined intervals or specify dates on a dynamic calendar, allowing monitoring data to be analyzed during relevant construction phases or specific operational milestones of the project (Fig. 5a). In addition, the interface provides an estimate of the number of data points and the corresponding data volume associated with each aggregation period, enabling users to anticipate query complexity and facilitating more efficient data retrieval.
- **Data Export:** All queried data can be exported in .csv format, enabling users to extract clean datasets tailored to the selected analysis and aggregation window for further use in external specialized software (Fig. 5b).



a) b)

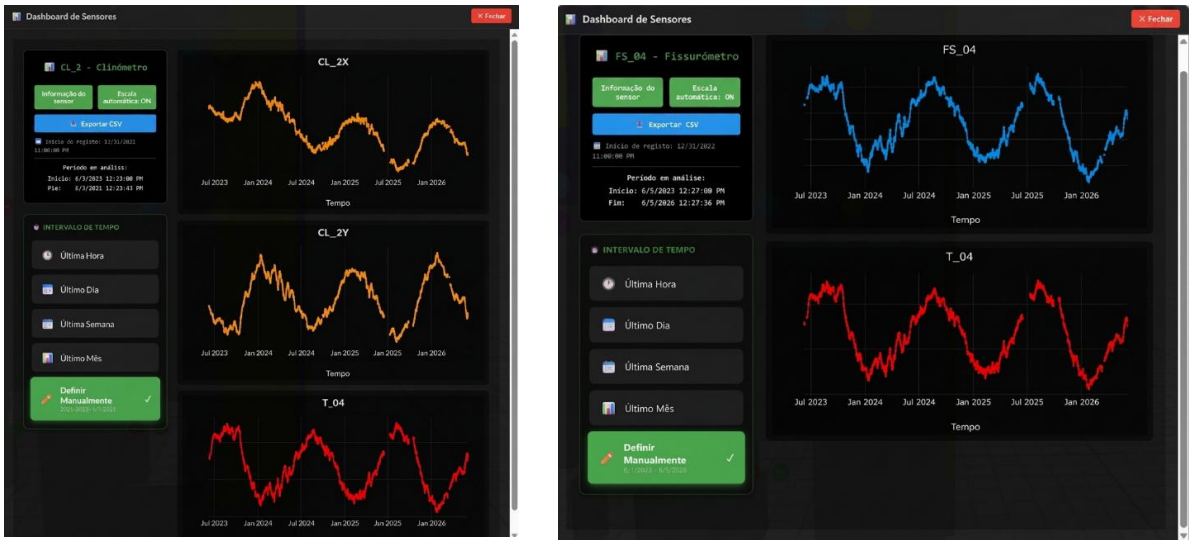
Figure 5 – a) Selection window for the data aggregation period; b) Export window for the .csv format file

4.4.3 Exemplification of results

The primary objective of this section is to show practical results obtained from the multi-sensor network installed across the historical monuments, focusing on the datasets retrieved from one clinometer and one crackmeter shown in Fig. 6. To evaluate the long-term structural behavior and validate the data handling capacity of the platform, a comprehensive dataset spanning an extended period of approximately three years was selected for analysis.

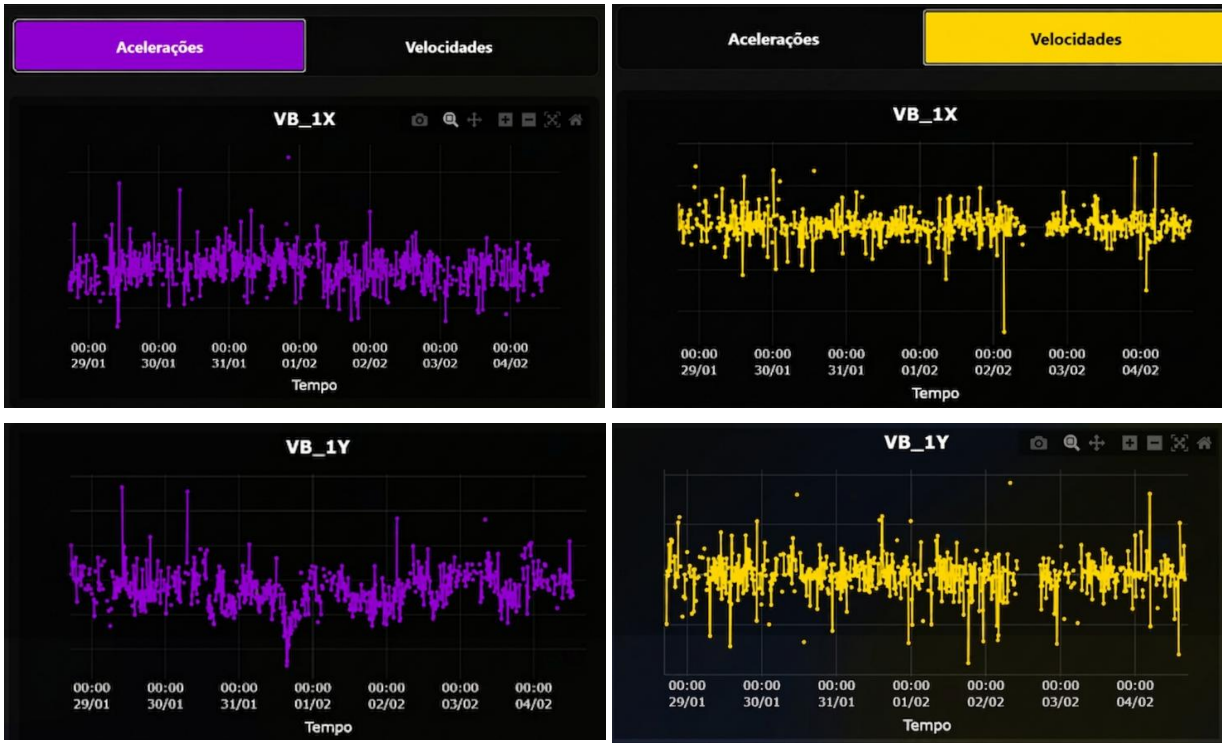
As illustrated in the retrieved records, the structural variations and displacements closely follow the cyclical patterns of ambient temperature fluctuations. This high correlation between the physical deformations and thermal actions indicates that these structural responses are directly related to ambient temperature variations. Thus, the visualization of these continuous, long-term trends suggests that the structural integrity of the monitored assets has not been adversely affected by the adjacent underground excavation works. Furthermore, the seamless rendering of this massive three-year time-series underscores the efficiency of the developed Digital Twin framework in transforming raw, continuous sensor readings into clear, actionable structural health indicators.

Additionally, Figures 7 and 8 present the experimental records captured by one sensor of the accelerometer network. These datasets illustrate the acceleration and velocity profiles over time, serving as continuous indicators of the structural vibration levels and providing a general baseline to monitor the overall dynamic behavior of the monument during the construction works.



a) b)

Figure 6 – Long-term structural health monitoring data spanning a three-year monitoring period: (a) clinometer CL_2 results for X and Y components correlated with temperature sensor T_04; (b) crackmeter FS_04 displacement results correlated with temperature sensor T_04.



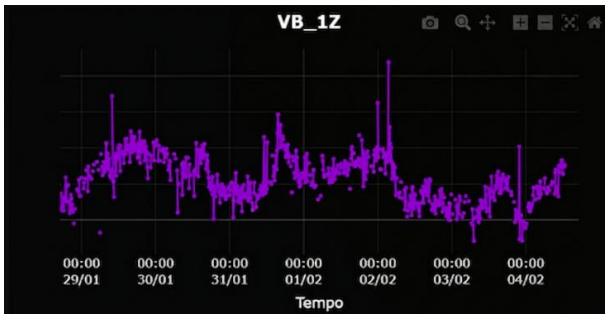


Figure 7 – Layout of the acceleration records (m/s^2), highlighted in purple, across the three components X, Y, and Z

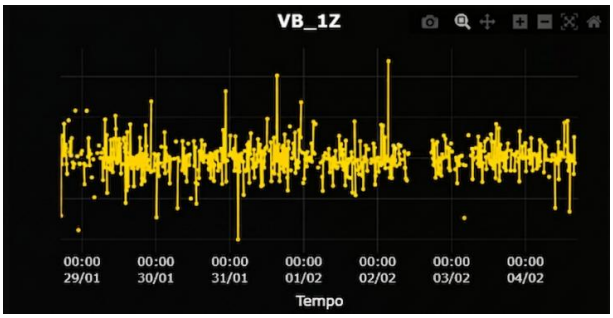


Figure 8 – Layout of the velocity records (mm/s), highlighted in yellow, across the three components X, Y, and Z

5. Conclusions

This paper sought to briefly describe the development process of a web-based Digital Twin (DT) platform as a useful and robust tool for real-time Structural Health Monitoring (SHM) of monuments prone to be affected by adjacent construction works or other type of anthropogenic or natural action sources. The transition from static geometric models to a dynamic digital ecosystem resolved critical data engineering challenges, namely the management of massive volumes of readings and the mitigation of latency.

The key developments of the prototype refer to the spatial contextualization of the information, overcoming the paradigm of analyzing readings in abstract graphs or isolated tables, since the automated query engine and the 3D interactive markers eliminate this barrier. Through selective visibility, the user instantaneously localizes sensors installed in concealed zones. Furthermore, the addition of the closest temperature sensor to the sensor under analysis allows the user to perceive the effects of thermal variations in the records, by distinguishing reversible cyclic deformations from eventual anomalous movements caused by other adjacent sources.

The development criteria granted the platform the necessary robustness to support decision-making and monument management. The structuring based on JSON metadata ensures that the inclusion of new sensors or structures can be achieved immediately and autonomously. Moreover, the current architecture provides a straightforward migration path towards relational database solutions, enabling the ecosystem to scale in terms of users, sensors, monitored structures, and data sources and schemas. The ecosystem thus establishes a robust, interoperable, and reproducible methodological framework, useful for the preservation and deformation control of built heritage under the influence of adjacent complex urban infrastructure interventions or other external action sources.

Future developments may further extend the capabilities of the platform beyond monitoring functions. In particular, control and automation mechanisms based on Shelly devices could be integrated into the Digital Twin environment, enabling the remote switching and management of routers and gateways according to their spatial location within the monitored infrastructure. In addition, the capabilities offered by available communication libraries open the possibility of remotely managing sensor configurations directly through the platform, paving the way for adaptive monitoring strategies. Such developments would allow the proposed framework to evolve from a monitoring-oriented system towards a more active and interactive cyber-physical ecosystem.

Acknowledgements

This study was partially financially supported by: UID/04708/2025 and https://doi.org/10.54499/UID/04708/2025, of the CONSTRUCT - Instituto de I&D em Estruturas e Construções - funded by Fundação para a Ciência e a Tecnologia, I.P./ MECI, through the national funds.

References

Bao, Yuequan, and Hui Li. 2021. "Machine Learning Paradigm for Structural Health Monitoring." *Structural Health Monitoring* 20 (4): 1353–1372. https://doi.org/10.1177/1475921720918545.

Cimino, Mario G. C. A., Gualtiero Fantoni, Francesco Lazzeri, Alessandro Stefanini, and Tommaso Inguaggiato. 2022. "Deep Learning of Structural Changes in Historical Buildings: The Case Study of the Pisa Tower." *Advanced Engineering Informatics* 52: 101601. https://doi.org/10.1016/j.aei.2022.101601.

Clementi, Francesco, Stefano Lenci, and Antonella Saisi. 2021. "Structural Health Monitoring of Architectural Heritage: From the Past to the Future Advances." *International Journal of Architectural Heritage* 15 (11): 1558–3058. https://doi.org/10.1080/15583058.2021.1912243.

Cunha, Álvaro, Elsa Caetano, and Filipe Magalhães. 2007. "Output-Only Modal Identification of Civil Engineering Structures: A Case Study." *Structural Control and Health Monitoring* 14 (5): 717–742. https://doi.org/10.1002/stc.176

da Silva, Hélder Alexandre Martins. 2022. "Desenvolvimento de Um Digital Twin no Contexto da Monitorização de Estruturas." Dissertação de Mestrado, Faculdade de Engenharia da Universidade do Porto (FEUP).

Farrar, Charles R., and Keith Worden. 2007. "An Introduction to Structural Health Monitoring." *Philosophical Transactions of the Royal Society A: Mathematical, Physical and Engineering Sciences* 365 (1851): 303–315. https://doi.org/10.1098/rsta.2006.1928.

Flah, Majdi, Issam Nser, Noureddine Benasla, and Tarek Zayed. 2021. "Machine Learning Algorithms in Civil Structural Health Monitoring: A Systematic Review." *Archives of Computational Methods in Engineering* 28 (4): 2621–2643. https://doi.org/10.1007/s11831-020-09471-x.

Grieves, Michael, and John Vickers. 2016. "Digital Twin: Mitigating Unpredictable, Undesirable Emergent Behavior in Complex Systems." In *Transdisciplinary Perspectives on Complex Systems: New Findings and Approaches*, edited by N. Kotiadis and A. A. Tsatsaronis, 85–113. Cham: Springer.

InfluxData. 2026a. "Flux Language Reference." *InfluxData Documentation*. Accessed June 5, 2026. https://docs.influxdata.com/flux/.

InfluxData. 2026b. "InfluxDB Documentation (Version 2.4)." *InfluxData Platform*. Accessed June 5, 2026. https://www.influxdata.com.

Jiang, Fadi, Ling Ma, and Xiangyu Wang. 2022. "Digital Twin for Building Lifecycle Management: A Systemic Review and Future Research Agenda." *Automation in Construction* 142: 104526. https://doi.org/10.1016/j.autcon.2022.104526.

Magalhães, Filipe, Álvaro Cunha, and Elsa Caetano. 2012. "Vibration Based Structural Health Monitoring of an Arch Bridge: From Automated OMA to Damage Detection." *Mechanical Systems and Signal Processing* 28: 212–228. https://doi.org/10.1016/j.ymssp.2011.06.011.

Pinto, G. 2023. "Como funcionam os sensores inteligentes em soluções de IoT?" *V2COM* (blog), December 23, 2023. https://v2com.com/2023/12/23/iot-sensores-inteligentes/.

Cinpar 2026
XXII International Conference on Building Pathology and Constructions Repair
15th to 17th July 2026 - Lisboa, Portugal

Unveiling hybrid two-way out-of-plane response of existing unreinforced masonry structures through extensive shake-table testing

Dario VECCHIO[1], Babar ILYAS[2], Paulo X. CANDEIAS[3], Nuno MENDES[4], Paulo B. Lourenço[5]

[1] University of Minho, ISISE, ARISE, Guimarães, Portugal, dariovecchio4@yahoo.it
[2] University of Minho, ISISE, ARISE, Guimarães, Portugal, babarilyas7@gmail.com
[3] LNEC, NESDE, Lisbon, Portugal, pcandeias@lnec.pt
[4] University of Minho, ISISE, ARISE, Guimarães, Portugal, nunomendes@civil.uminho.pt
[5] University of Minho, ISISE, ARISE, Guimarães, Portugal, pbl@civil.uminho.pt

Abstract: The 2030 Agenda for Sustainable Development has set the objectives to reduce the risk of disasters. In the context of Sustainable Cities (Goal 11), the promotion of planning and management of human settlements in disaster-prone areas is stressed. Nearly 50% of the global built heritage stock is represented by unreinforced masonry structures (URM), historically built in seismic-active regions. URMs are highly vulnerable to strong ground motions, particularly when they lack wall-to-wall and wall-to-diaphragm connections, which reduce the box-behaviour and increase the likelihood of out-of-plane (OOP) deformations.

Current code-oriented assessments for the OOP response of URMs due to strong ground motions are based on simplified kinematic or pushover analyses. On the one hand, assuming a rigid deformation up to collapse, these methods lead to reasonable estimates of the yielding and ultimate capacity of buildings and monumental structures. On the other hand, these methods do not incorporate the highly non-linear response associated with rocking and non-smooth contacts, as well as the influences of different seismic signals.

This contribution presents two shake-table campaigns addressing these gaps for the upcoming Second Generation of Eurocodes. Using dry-stack masonry to replicate the behaviour of existing URM structures, extensive dynamic testing was conducted on half- and full-scale specimens between the University of Minho (PT) and LNEC, Lisbon (PT). Experimental outcomes revealed complex OOP responses dependent on boundary conditions, as well as varying geometry and input signals. A hybrid two-way bending collapse mechanism was identified, providing the first evidence on a still limited literature topic. Experimental data were post-processed and made publicly available to support the calibration and validation of numerical models. The work was developed within the Stand4Heritage project that, in line with the 2030 Agenda Goals, aims at introducing new standards for safeguarding built cultural heritage.

Keywords: Unreinforced masonry, out-of-plane, shake-table test, dry-stack, hybrid two-way bending.

1. Background and motivation

On September 25, 2015, 193 United Nations Member States adopted the 2030 Agenda for Sustainable Development through the implementation of 17 Sustainable Development Goals (UN (2015)). Among all, Goal 11 promotes sustainable urban development and the resilience of human settlements to the threat of natural hazards. In this context, particular attention should be paid to unreinforced masonry structures (URMs), which account for more than 50% of the existing built heritage and are highly present in earthquake-prone areas. Despite extensive research in recent times, full comprehension of the URMs' capacity when subjected to ground motions (GMs) excitation is still limited due to uncertainties in material and boundary conditions (Parisi and Augenti (2012), Roca *et al.* (2010), Rota *et al.* (2014)). URMs are known to withstand horizontal actions if the so-called box-behaviour is available (Lourenço *et al.* (2010)). During a seismic event, two stiffnesses are activated: the in-plane (IP) and the out-of-plane (OOP). While the former is higher and usually associated with damage accumulation and crack openings (Inzunza Araya *et al.* (2024)), the latter is lower due to limited tensile and shear strength-to-mass ratio (Ferreira *et al.* (2015)) and poor wall-to-wall and wall-to-diaphragm connections.

The current version of the Eurocodes provides guidelines regarding the OOP response for newly designed and existing URMs. The former is based on global ductility (capacity-design approach) and prescriptive rules to prevent any OOP mechanism (European Committee for Standardization (2005, a)). The latter acknowledges that existing URMs may not meet the prescriptive rules (European Committee for Standardization (2005, b)) and suggests the estimation of design flexural strength and overburden values, while limiting vertical slenderness (height-to-thickness ratio). However, Griffith *et al.* (2007) provided evidence in their campaign that, if an adequate degree of connections is met, URM walls may sustain displacements above their flexural capacity. The upcoming Second Generation of the Eurocode has markedly improved the assessment of the OOP response, suggesting the use of an equivalent Single-Degree-of-Freedom (SDOF) system and pushover analyses (CEN/TC 250 (2004)). Nevertheless, dynamic effects have not been accounted for. In fact, due to rocking and non-smooth contacts in extremely narrow events, URMs might dissipate internal energy differently than what is assumed in rigid-body deformations (Lagomarsino (2015)). In addition, interactions between IP-OOP mechanisms may arise, forming hybrid two-way bending (Vaculik *et al.* (2014)), which was observed in a static campaign (Restrepo Vélez *et al.* (2014)).

To address these gaps, this paper details the design and presents preliminary outcomes from two extensive shake-table testing campaigns conducted between the University of Minho (PT) and LNEC, Lisbon (PT). The dynamic OOP response of URM assemblies was investigated by testing reduced-scale and full-scale specimens. Because mortar usually ages in existing URMs, the specimens were built using dry-stack configurations. All the specimens featured a U-shaped configuration, tested under varying geometries, input signals and wall-to-diaphragm connections. Several tests and repetitions demonstrated hybrid two-way bending, the non-linear behaviour of rocking structures, and the role of the wall-to-diaphragm connection in the OOP collapse mechanisms. Experimental data were collected into an open-access dataset (Vecchio *et al.* (2026)) for future validations of refined numerical models and probabilistic analyses targeting adequate Intensity Measures (IMs) and the construction of Fragility Curves (FCs). Both experimental campaigns were conducted within the Stand4Heritage project (STAND4HERITAGE (2020)) funded by the EU through the European Research Council (Advanced Grant No. 833123), with the ambitious goal of improving the next generation of code-based guidelines for the preservation of the existing built heritage.

2. Shake-table campaigns

This section describes the design, including material and specimens' geometry, instrumentation, choice of the input signals, and loading protocol of both experimental campaigns. While the reduced-scale specimens were tested at the University of Minho, a full-scale specimen was tested at LNEC.

2.1 Reduced-scale specimens

The reduced-scale campaign was conducted on the 1-Degree-of-Freedom (DoF) shake table of the University of Minho, having operational ranges: (i) ± 5 g in acceleration, (ii) ± 85 cm/s in velocity, (iii) ± 125 mm in displacement, (iv) 0-50 Hz in frequency, and (v) 3 tons as maximum payload. Two specimens were constructed using hard granite blocks typical of the *Iberian Peninsula* built heritage stock, with the following dimensions: (i) 300 mm x 150 mm x 150 mm and (ii) 150 mm x 150 mm x 150 mm (length, height, and width). The material characterisation, including density ρ, compressive strength f_c, elastic modulus E, normal k_n and tangential interface stiffness k_n, friction coefficient μ, and hysteretic damping ξ, were available prior to the start of the campaign (Colombo (2025)). The values are listed in **Table 1**.

Table 1 – Material and interface properties adopted in the experimental program

ρ	f_c	E	k_n	μ	k_s	ξ
(kg/m^3)	(MPa)	(GPa)	(MPa/mm)	(MPa/mm)	(-)	(%)
2580	139	73.9	10^1-10^4	10^1-10^2	0.48	2.0-5.5

The U-shaped configuration featured a central façade (orthogonal to the direction of the loading), and two sidewalls (in the direction of the loading). The geometry was based on constant height and length of the sidewalls, with an aspect ratio (façade span-to-height ratio) of 0.8 for Specimen A and 1.4 for Specimen B. The total weight of the specimens did not exceed the shake-table maximum payload, with total weights of 2.1 and 2.8 tons, respectively. The reduced-scale campaign focused on the insufficient wall-to-diaphragm connection. Therefore, the design boundary conditions included fixed base support, moment connection due to corner interlocking, and vertical restraint at the end of the sidewalls. The fixed base support was achieved by drilling and anchoring the first masonry course with M18 bolts to base steel plates, which were connected to the shake-table through M27 threaded bolts. Corner interlocking was provided with a typical toothing texture, overlapping half of the blocks' length in each masonry course. Finally, a system of extension springs was used to apply precompression at the end of the sidewalls, to avoid undesired deformation of the sidewalls, leaving the façade free to deform in the OOP direction and the sidewalls to detach.

Unlike conventional shake-table tests, the reduced-scale campaign took advantage of Digital Image Correlation (DIC) techniques. The six cameras installed along the perimeter of the shake table were initially paired and calibrated with speckle patterns glued on the visible blocks. This strategy allowed recording and spatial reconstruction of the specimens' deformation during the dynamic loading. The DIC software Istra4D (Dantec Dynamics (2022)) was used to estimate the coordinate and displacement time histories of any points detected on the visible surfaces. In addition to the DIC cameras, the shake-table accelerometer and Linear Variable Differential Transducer (LVDT) were used to monitor the input acceleration and displacement time histories. The vertical precompression was monitored with four conventional load cells.

A preliminary numerical investigation on a contact-based model (Vecchio *et al.* (2025)) showed collapse due to overturning when the model was subjected to two near-fault ground motions (GMs). These GMs were selected from the European Strong Motion Database (ESM) (Luzi *et al.* (2020)). To avoid disintegration due to high-frequency content (Indirli *et al.* (2013), Vlachakis *et al.* (2020)), Butterworth and Fourier bandpass filters were applied to the original GMs. The original GMs represented the 1998 Fajal (PT) and one of the 2016 Central Italy (IT) seismic events (NRC station). Both events induced in several URMs buildings and monumental structures collapses due to overturning of structural and non-structural elements.

The loading protocol followed an Incremental Dynamic Analysis (IDA) (Vamvatsikos and Cornell (2004, 2005)) protocol through scaling of the input signals from low intensity up to the shake-table limits. Incremental scale factors of 20% and 25% were tuned with dummy masses against the shake table prior to the start of the campaign, resulting in maximum increments of 200% and 320% for Signal 1 (filtered Fajal 1998) and Signal 2 (filtered NRC 2016), respectively. The IDA was performed with multiple repetitions at high-

displacement and collapses areas, to assess the randomness of the response, obtain sufficient data for the fitting of empirical FCs and observe the variability of the OOP collapses. To avoid any biased responses, the specimens were constantly reconstructed upon separation or damage before each seismic test. Four testing batches were conducted, featuring 54 tests for Batch I (Specimen A under Signal I), 54 for Batch II (Specimen A under Signal II), 53 for Batch III (Specimen B under Signal 1), and 50 for Batch IV (Specimen B under Signal II). **Figure 1** shows the specimens, including plan and elevation views, direction of the loading, and details of the boundary conditions. **Table 2** reports the main characteristics of the chosen inputs.

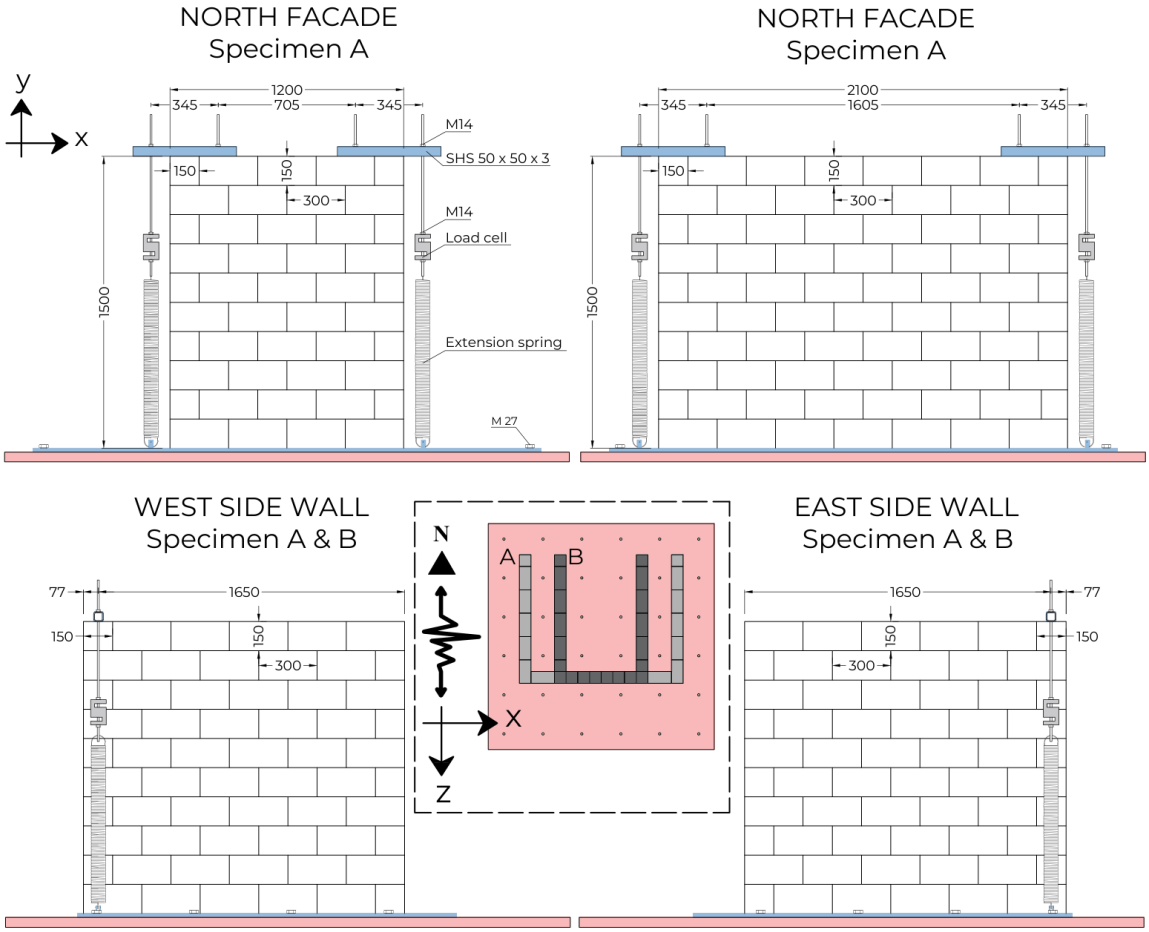


Figure 1 – Plan, elevation views and instrumentation details of the reduced-scale campaign

Table 2 – Characteristics of the input signals of the reduced-scale campaign

Signal	PGA |g|	PGV |cm/s|	PGD |mm|	Incremental scale factors (%)	IDA range (%)
1	0.368	34.7	37	25	0-200
2	0.236	22.7	33	20	0-320

2.2 Full-scale specimen

The full-scale campaign was conducted at LNEC Lisbon, which hosts a 3-DOF platform of with dimensions of 6400 mm x 5600 mm that can operate within the following operational ranges: (i) maximum acceleration of ±1 g, (ii) maximum velocity of 65 cm/s, (iii) maximum displacement of ±200 mm, (iv) frequency range of 0-40 Hz, (v) and maximum payload of 40 tons. The U-shaped specimen was made of granite blocks (see 2.1) with two dimensions: (i) 600 mm x 300 mm x 300 mm and (ii) 300 mm x 300 mm x 300 mm (length, height,

and width). The geometry featured 3000 mm-high walls, 900 mm-long sidewalls, and 4200 mm-long façade, resulting in an aspect ratio of 1.4. The campaign was designed to observe the hybrid two-way bending with a wall-to-diaphragm connection condition. Therefore, the boundary condition system included: (i) fixed base support, (ii) moment connection given by interlocking at the corners, (iii) vertical restraint at the end of the sidewalls, and (iv) rotational restraint on the façade, allowing only uplift. The fixed base support was achieved by encasing the first masonry course in perimetral UPNs 300x100 steel profiles, whose bottom flat flanges were drilled with chemical anchors into the 200-mm thick reinforced concrete base, while the profiles were stiffened at each 500 mm along the perimeter. Corner interlocking was provided with a typical toothing texture (see 2.1) while two steel rods were prestressed up to 10 kN to restrain the ends of each sidewall against undesired deformations. A more complex system was required to implement the rotational restraint. First, an HEB 300 was anchored to the additional top masonry course, which in turn was left unconnected to the bottom course. The HEB 300 was used to distribute uniformly a vertical overburden representing the weight of a parapet with a system of eight extension springs. Next, the web and the top flange of the HEB 300 were connected horizontally to a rear retaining frame, using two horizontal channel profiles to counteract coupled forces. A pair of rollers was provided at the end of each horizontal profile, allowing only sliding on the vertical flange surface of the steel column belonging to the retaining frame.

The instrumentation adopted for the full-scale campaign included: (i) ENDEVCO and PCB accelerometers, (ii) LVDTs, (iii) JX-P420 wire potentiometers, (iv) Hamamatsu C5949 optical potentiometers, and (v) 101BH load cells. The accelerometers were placed to monitor acceleration amplification according to the expected deformation, at the reinforced concrete base, and on the web of the HEB 300. The LVDTs were located at the mid-height and mid-length in the external side of the façade, at 1/3 and 2/3 of the height in the internal side of the façade, and on the sliding connections. Wire potentiometers were used to monitor displacements under the boundary conditions, while Hamamatsu optical displacement transducers measured 2D displacements at the end of the HEB 300. Finally, load cells were employed to monitor the vertical overburden in the extension spring system and the precompression level in the steel rods.

Only one signal (1-DoF) was selected for the present campaign. The GM representing the 1999 Düzce (TK) was employed as it represents a far-field event, and with different characteristics from the signals used in the reduced-scale campaign. Because the peak displacement exceeded the LNEC shake-table capacity, a Butterworth bandpass filter was applied to the GM.

Due to facility and material restrictions, fewer tests were conducted in this campaign. Prior to and after the application of 50% incremental scale factors, dynamic identification tests were conducted to assess the reduction in frequency. This campaign featured a total of 11 seismic tests and 10 dynamic identifications. **Table 3** reports the main characteristics of the selected input. **Figure 2** shows the plan and elevation views for the geometry, direction of the loading, details of the boundary conditions, and the adopted instrumentation.

Table 3 – Characteristics of the input signal of the full-scale campaign

Signal	PGA |g|	PGV |cm/s|	PGD |mm|	Incremental scale factors (%)	IDA range (%)
1999 Düzce	0.16	22.3	39.8	50	0-250

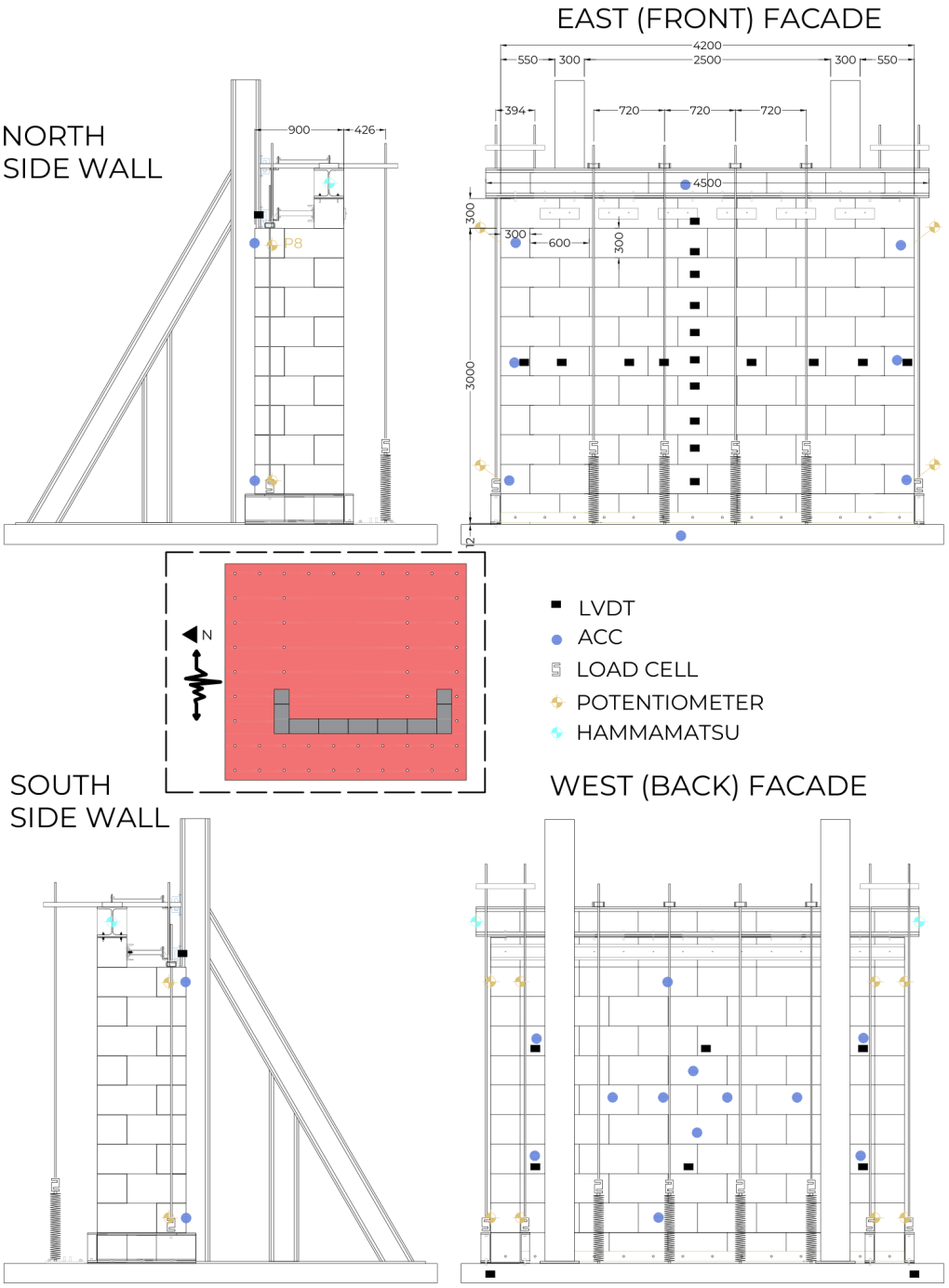


Figure 2 – Plan, elevation views and instrumentation details of the full-scale campaign

3. Experimental results

3.1 Evidence of hybrid two-way bending

Preliminary outcomes showing the presence of hybrid two-way bending can be observed by plotting the experimental IDAs. The adopted Engineering Demand Parameter (EDP) is the maximum Absolute Vector Magnitude computed in the x-z plane between the x- and the z-displacements of the blocks sitting at the top course of the specimens (**Figure 1**), against the Peak Ground Acceleration (PGA) of the seismic input.

While the blocks' numbers and locations, according to the open-access database (Vecchio *et al.* (2026)), are depicted in **Figure 3**, **Figure 4** shows the experimental IDAs for each testing Batch. Note that the red dashed horizontal line at 300 mm is used only to separate collapse from non-collapse events.

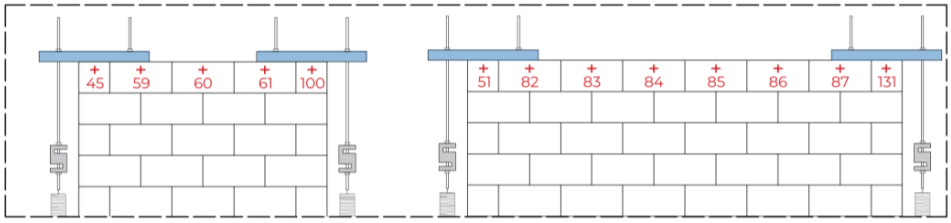


Figure 3 – Location of the points and blocks adopted to compute the absolute vector magnitude

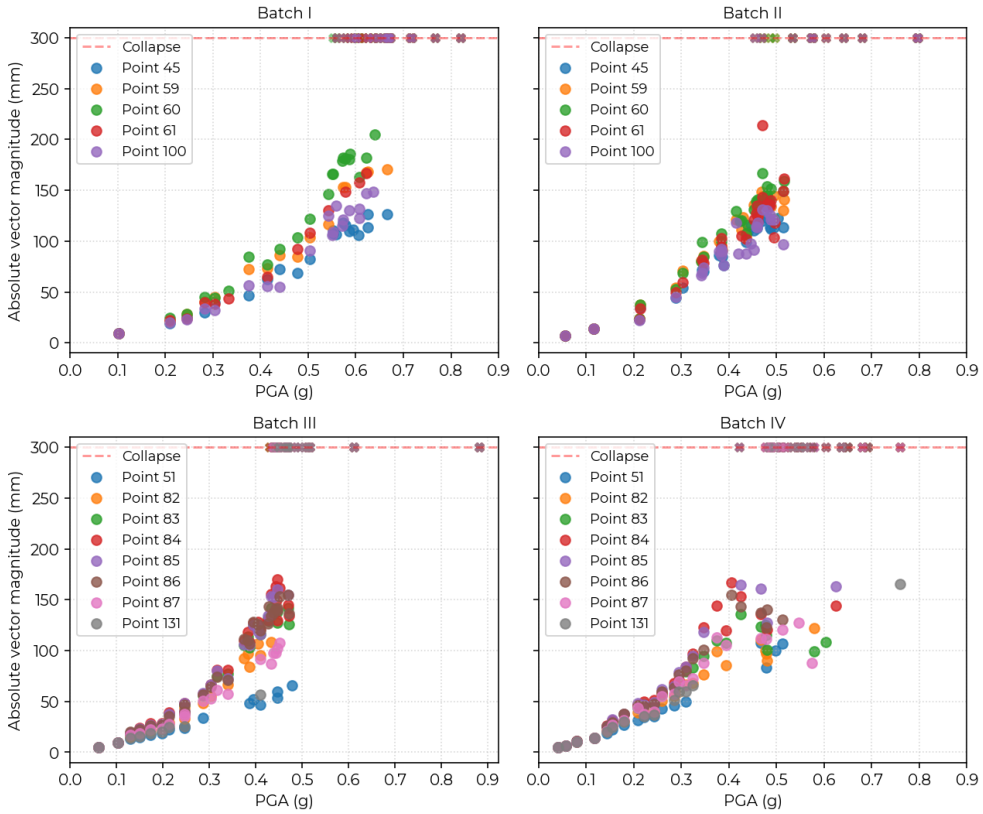


Figure 4 – Experimental Incremental dynamic analyses (IDAs) of the reduced-scale campaign: absolute vector magnitude vs PGA (Peak Ground Acceleration)

Evidence of hybrid two-way bending can be observed in the displacement magnitude exhibited by the central façade when compared to the corners. Excluding the collapse events, the central blocks exhibit larger displacements in the OOP direction, while the corner blocks show significant lateral deformation. The behaviour is attributed to torsional rotation at the corners, while the central façade tends to bend and form a typical arching mechanism (horizontal arching mechanism). Despite a slight asymmetry due to the dry-stack configuration, the corners follow similar trends. The influence of the geometry can be observed in earlier collapse events and pronounced randomness (larger dispersion) for Batch III and Batch IV due to the higher aspect ratio. Also, different signal inputs influence the response. For example, Signal 1 produces higher displacement of the central blocks and steeper IDAs (less dispersion).

The displacements' components for two corner blocks, P41 and P51, for Batches I-II and Batches III-IV, respectively, are compared in **Figure 5** to validate the abovementioned. Note that here, collapse events are

disregarded. The comparison is useful to verify that the specimens are deforming both in the OOP direction (z-axis) and laterally (x-axis). While the OOP direction is linked to rigid overturning, the lateral deformation is converted to torsional rotation of the corner. This response confirms the participation of the sidewalls and the hybrid two-way bending characterised by horizontal arching of the façade and rotation due to frictional behaviour at the interfaces.

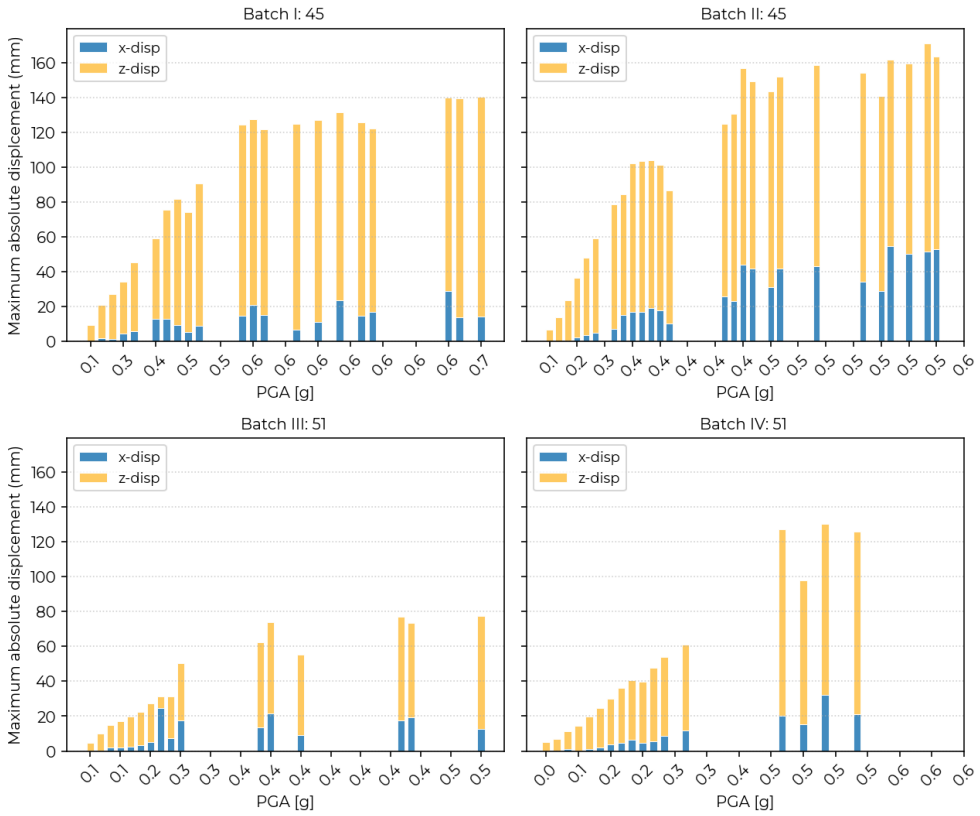


Figure 5 – Maximum absolute displacements and corresponding x- and z-axis components

3.2 The role of the wall-to-diaphragm connection

The importance of the wall-to-diaphragm connection is observed in the comparison between the reduced-scale specimens' and the full-scale specimen's responses. Note that the top boundary condition for the latter (rotational restraint and uplifting) is a possible configuration of existing URMs, in particular for one-way spanning walls (Vlachakis *et al.* (2025)). Due to that and to the presence of corner interlocking, interaction between vertical and horizontal bending was expected, leading to hybrid two-way bending with participation of sidewalls.

Figure 6 shows the OOP collapse mechanism observed in the reduced-scale specimens. The absence of an adequate wall-to-diaphragm connection between the façade and the sidewall led to the overturning of the façade with the participation of the sidewalls. The participation of the sidewalls was observed to increase at larger intensities. The influence of the input signal can be observed by comparing Batches I-III vs Batches II-IV, in particular knowing that Signal 1 is characterised by a dominant velocity pulse in the time history, while Signal 2 resembles more a cyclic behaviour. As a result, greater dispersion is observed in the OOP collapses of Batches II-IV. Not only that, but other OOP collapse mechanisms were also observed throughout the campaign. Nevertheless, the hybrid two-way bending occurred frequently, approximately 65% of the total observed collapse events.

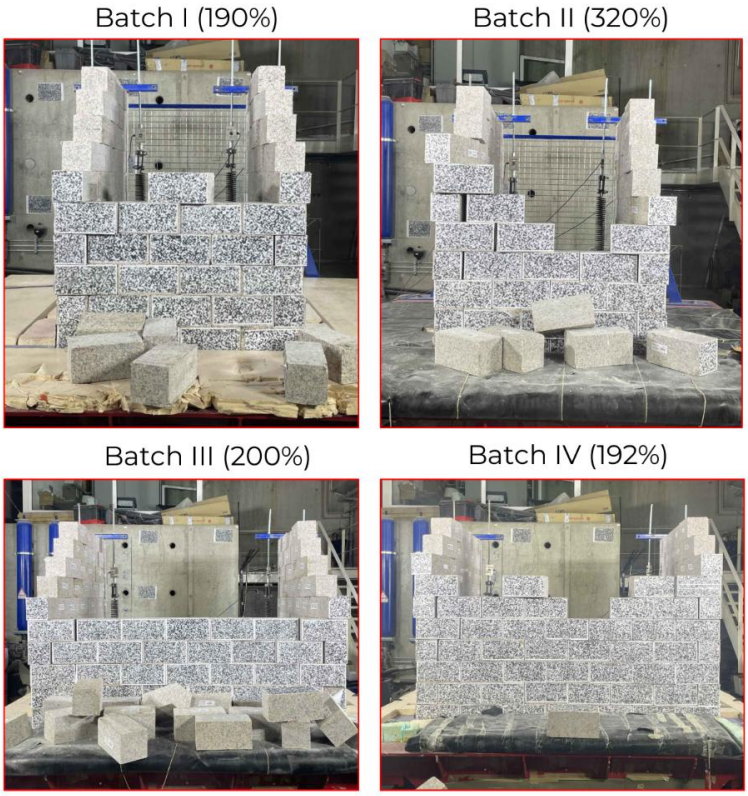


Figure 6 – OOP collapses observed in the reduced-scale campaign due to the insufficient wall-to-diaphragm connection

Figure 7 shows the OOP collapse mechanism experienced by the full-scale specimen. On the left, the picture depicts the expected OOP mechanism composed of horizontal and vertical bending (rigid two-way bending) (Graziotti *et al.* (2019), whereas the right side displays the observed OOP collapse mechanism at the 250% scale factor of the 1999 Düzce GM. In both pictures, the red dashed lines represent the separation of the interfaces, and the arrows indicate the direction of the expected (untested configuration) and observed (tested configuration) rotations. First, the frictional dissipative behaviour at the interfaces (corner interlocking) influenced the response, creating a non-vertically symmetric cracking pattern in both corners. In addition, the applied vertical overburden was not sufficient to prevent the OOP deformation of the façade, which experienced an arching mechanism, with a collapsed block at the mid-length. Nevertheless, the overburden was sufficient in preventing collapse in the sidewalls and in limiting vertical bending of the façade, which behaved as a cantilever. As a result, the test confirmed the hybrid two-way bending composed by horizontal bending of the façade together with the participation of the sidewalls, while providing experimental evidence on the influence of the wall-to-diaphragm connection.

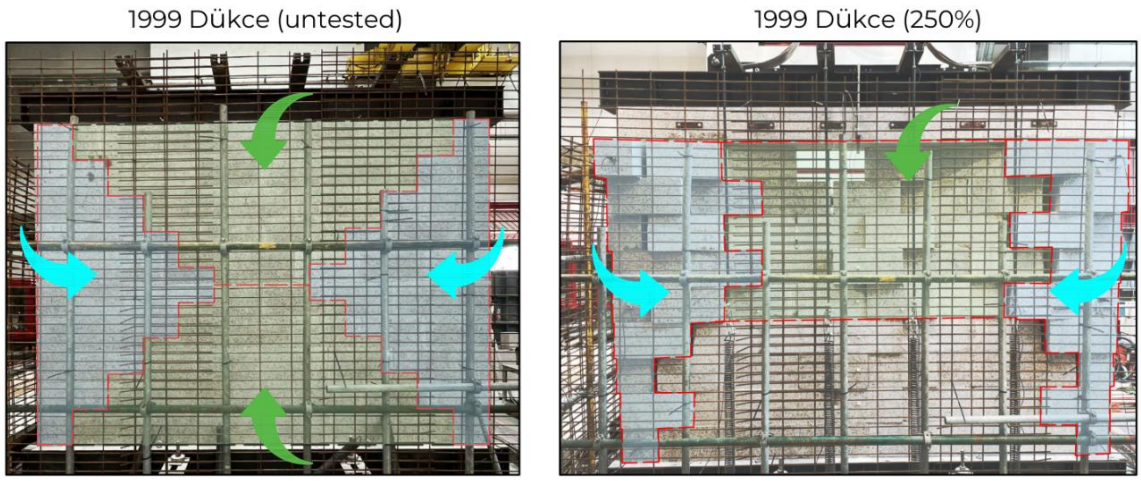


Figure 7 – OOP collapses observed in the full-scale campaign due to insufficient wall-to-diaphragm connection. On the left, the expected response, on the right, the obtained collapse mechanism. Note that the green and light blue colours are used for the rotation over the horizontal and vertical axis, respectively

4. Conclusions and future works

This paper has discussed the preliminary outcomes obtained from two extensive shake-table campaigns on the seismic OOP response of URM specimens. URMs are vulnerable to natural hazards such as earthquakes, and for that, are considered in the objectives defined by Goal 11, Sustainable Cities, which is part of the 2030 Agenda for Sustainable Developments. Research is needed to enhance knowledge of existing URM buildings and monumental structures when subjected to natural hazards such as earthquakes. Dynamics affects the OOP response and the influence of geometry, boundary conditions, and different inputs, but it still lacks adequate comprehension. Also, the next generation of Eurocodes does still not account for complex non-linear behaviour due to rocking, energy dissipation, and mechanisms' coupling leading to mixed collapses. The campaigns described in this paper have taken advantage of dry-stack masonry to conduct several tests and repetitions. One of the major outcomes was the experimental evidence of hybrid two-way bending, featured by simultaneous bending/overturning of the façade together with participation of the sidewalls. The second major objective of collecting the experimental data (reduced-scale specimens) into a reliable and open-access database was also achieved. Based on that, future works will focus on the calibration and validation of refined numerical models to simulate the dynamic response of URMs under varying geometry, input signals and boundary conditions. Also, future research will be carried out in probabilistic frameworks, including analyses on adequate intensity measures and the final construction of fragility curves.

Acknowledgments

This work was financed by national funds through FCT (*Fundação para a Ciência e a Tecnologia*) under agreement 2023.03854.BDANA (first author) and 2024.01310.BD (second author). The experimental campaigns were fully funded by the STAND4HERITAGE project (New STANDard FOR seismic assessment of built cultural HERITAGE) that has received funding from the European Research Council (ERC) under the EU Horizon 2020 research and innovation program through the Advanced Grant No. 833123. This study was also partly funded by FCT/MECI through project 2022.05425.PTDC (RESISTANCE) and project national funds (PIDDAC) under the R&D Unit Institute for Sustainability and Innovation in Structural Engineering (ISISE), under reference UIDB/04029/2020, and under the Associate Laboratory Advanced Production and Intelligent Systems ARISE under reference LA/P/0112/2020.

References

CEN/TC 250. 2024. Draft: “Eurocode 8 – Design of structures for earthquake resistance – Part 1 -1: General rules and seismic action.”

Colombo Carla. 2025. “Experimental evaluation of the static and dynamic out-of-plane response of block-type masonry structures.” University of Minho.

Dantec Dynamics. 2022. “Software Manual Q-4xx System.” Nova Instruments.

European Committee for Standardization. 2005a. “Eurocode 6 – Design of masonry structures – Part 1 -1: General rules for reinforced and unreinforced masonry structures (EN 1996-1-1).”

European Committee for Standardization. 2005b. “Eurocode 8 – Design of structures for earthquake resistance– Part 3: Assessment and retrofitting of building (EN 1998-3).

Ferreira Tiago Miguel, Costa Alexadre Anibal, Costa Anibal. 2015. “Analysis of the Out-of-Plane Seismic Behavior of Unreinforced Masonry: A Literature Review.” International Journal of Architectural Heritage 9 (8): 949-972. https://doi.org/10.1007/s10518-025-02116-x.

Graziotti Francesco, Tomassetti Umberto, Satyadhrik Sharma, Grottoli Luca, Magenes Guido. 2019. “Experimental response of URM single leaf and cavity walls in out-of-plane two-way bending generated by seismic excitation.” Construction and Building Materials 195: 650-670. https://doi.org/10.1016/j.conbuildmat.2018.10.076.

Griffith Michael Craig, Vaculik Jaroslav, Nelson Lam, Wilson John, Lumantarna Elisa. 2007. “Cyclic testing of unreinforced masonry walls in two-way bending.” Earthquake Engineering and Structural Dynamics 36 (6): 801-821. https://doi.org/10.1002/eqe.654.

Indirli Maurizio, Leonidas Alexandros Kouris, Formisano Antonio, Borg Ruben Paul, Mazzolani Federico. 2013. “Seismic damage assessment of unreinforced masonry structures after the Abruzzo 2009 earthquake: The case study of the historical centers of L’Aquila and Castelvecchio Subequo.” International Journal of Architectural Heritage 7 (5): 536-578. https://doi.org/10.1080/15583058.2011.654050.

Inzunza Araya Ernesto, Saloustrous Savas, Beyer Katrin. 2024. “Influence of the Horizontal-to-Vertical Compressive Strength of Hollow Clay Bricks on the In-Plane Drift Capacity of Unreinforced Masonry Walls.” 18th International Brick and Block Masonry Conference.

Lagomarsino Sergio. 2015. “Seismic assessment of rocking masonry structures.” Bulletin of Earthquake Engineering 13 (1): 97-128. https://doi.org/10.1007/s10518-014-9609-x.

Lourenço Paulo Brandão, Mendes Nuno, Ramos Luis, Oliveira Daniel Vitorino. 2011. “Analysis of masonry structures without box behavior.” International Journal of Architectural Heritage 5 (4): 369-382. https://doi.org/10.1080/15583058.2010.528824.

Luzi Lucia, Lanzano Giovanni, Felicetta Chiara, D’Amico Maria Clara, Russo Emiliano, Sgobba Sara, Pacor Francesca, ORFEUS Working Group 5. 2020. “Engineering Strong Motion Database (ESM) (Version 2.0).” Istituto Nazionale di Geofisica & Vulcanologia.

Parisi Fulvio, Augenti Nicola. 2012. “Uncertainty in Seismic Capacity of Masonry Buildings.” Buildings 2 (3): 218-230. https://doi.org/10.3390/buildings2030218.

Restrepo-Vélez Luis Fernando, Magenes Guido, Griffith Michael Craig. 2014. “Dry stone masonry walls in bending-Part I: Static tests.” International Journal of Architectural Heritage 8 (1): 218-230. https://doi.org/10.1080/15583058.2012.663059.

Roca Pere, Cervara Miguel, Gariup Giuseppe, Pelà Luca. 2010. “Structural analysis of masonry historical constructions. Classical and advanced approaches.” Archives of Computational Methods in Engineering 17 (3): 299-325. https://doi.org/10.1007/s11831-010-9046-1.

Rota Maria, Penna Andrea, Magenes Guido. 2014. “A framework for the seismic assessment of existing masonry buildings accounting for different sources of uncertainty.” Earthquake Engineering and Structural Dynamics 43 (7): 1045-1066. https://doi.org/10.1002/eqe.2386.

STAND4HERITAGE. 2020. *https://stand4heritage.org/.*

United Nations. (2015). “Transforming Our World: The 2030 Agenda for Sustainable Development.”

Vaculik Jaroslav, Griffith Michael Craig, Magenes Guido. 2014. “Dry stone masonry walls in bending-Part II: Analysis.” International Journal of Architectural Heritage 8 (1): 29-48. https://doi.org/10.1080/15583058.2012.663060.

Vamvatsikos Dimitrios, Cornell Allin. 2002. “Incremental dynamic analysis.” Earthquake Engineering and Structural Dynamics 31 (3): 491-514. https://doi.org/10.1002/eqe.141.

Vamvatsikos Dimitrios, Cornell Allin. 2004. “Applied Incremental dynamic analysis.” Earthquake Spectra 20 (2): 523-553. https://doi.org/10.1193/1.1737737.

Vecchio Dario, Ilyas Babar, Mendes Nuno, Lourenço Paulo Brandão. 2025. “A discontinuous model for selecting ground motion records for the out-of-plane shake table campaign on masonry structures”. Structural Analysis of Historical Constructions: SACH 2025 1 (64).

Vecchio Dario, Ilyas Babar, Mendes Nuno, Lourenço Paulo Brandão. 2026. “Dataset from shake table testing of U-shaped dry stack unreinforced masonry structures subjected to out-of-plane seismic action.” Built Environmental Data. https://doi.org/10.60756/uminho-c554.

Vlachakis Georgios, Colombo Carla, Vecchio Dario, Anastasios Giouvanidis, Lourenço Paulo Brandão. 2025. “Appraisal of the overburden mass and boundary conditions on the rocking behaviour of the vertical spanning strip wall.” Meccanica 60 (7): 2047-2068. https://doi.org/10.1007/s11012-024-01910-2.

Vlachakis Georgios, Vlachaki Evangelia, Lourenço Paulo Brandão. 2020. “Learning from failure: Damage and failure of masonry structures, after the 2017 Lesvos earthquake (Greece).” Engineering Failure Analysis 117. https://doi.org/10.1016/j.engfailanal.2020.104803.



MANAGEMENT AND STANDARDS



XXII International Conference on Building Pathology and Constructions Repair
15th to 17th July 2026 - Lisboa, Portugal

Conceptual Model of Resilient Decision-Making for PDHR in Critical Zones

Carlos OLIVEIRA CRUZ[1], **Ahmed ASHOUR**[2]

[1] CERIS, Institute of Superior Técnico, University of Lisbon, Portugal, oliveira.cruz@tecnico.ulisboa.pt
[2] CERIS, Institute of Superior Técnico, University of Lisbon, Portugal, ahmed.ashour@tecnico.ulisboa.pt

Abstract: Post-Disaster Housing Reconstruction (PDHR) in critical zones remains insufficiently addressed within existing reconstruction theories and decision-support approaches. Most current frameworks prioritize technical optimization, cost efficiency, and sustainability under relatively stable operational assumptions, while providing limited consideration for contextual feasibility under conditions of uncertainty, instability, and constraints. Consequently, reconstruction alternatives that appear technically optimal in stable conditions may become operationally infeasible in critical zones.

Therefore, this paper proposes a resilience-oriented conceptual framework for PDHR decision-making in critical zones. The framework introduces contextual feasibility as a preliminary screening mechanism prior to technical and economic optimization. The proposed model consists of three sequential analytical layers, starting with feasibility assessment (filter), then goes to the second layer of performance evaluation, and last layer of economic evaluation. The framework integrates hybrid Multi-Criteria Decision-Making (MCDM) approaches and Cost–Benefit Analysis (CBA) to support trade-off analysis between contextual operability, technical performance, sustainability, and long-term economic value in order to enhance the decision-making.

Keywords:

Contextual Feasibility; Critical Zones; Decision-Making; Post-Disaster Housing Reconstruction (PDHR); Resilience.

1. Introduction

Post-disaster housing reconstruction (PDHR) represents a critical phase of disaster recovery that extends beyond rebuilding damaged structures to influencing long-term social recovery, economic stability, institutional legitimacy, and community resilience (Johnson, 2007). Over recent decades, significant progress has been made in developing reconstruction frameworks emphasizing cost efficiency, sustainability, structural resilience, and rapid recovery through approaches such as “Build Back Better” (BBB), Sendai Framework, and resilience-based design methods (Kennedy et al., 2008; Lizarralde et al., 2010). Emerging technologies including modular construction, prefabrication, and 3D-printing systems have further expanded opportunities for accelerating reconstruction while reducing material waste and lifecycle costs.

However, many existing reconstruction frameworks remain implicitly grounded in assumptions of operational stability and predictable recovery conditions. This limitation becomes increasingly problematic in what this paper conceptualizes as “critical zones”: environments characterized by persistent uncertainty, instability, and operational constraints that continue beyond the initial disaster event. Such conditions may emerge from recurring natural or human disasters, political instability, forced displacement, institutional fragility, sanctions, economic collapse, disrupted supply chains, or restricted site accessibility (Tierney, 2023). Unlike conventional recovery environments, reconstruction in critical zones occurs under continuously evolving disruptions that directly affect implementation feasibility and decision-making processes.

In such contexts, reconstruction failure is often linked not to the technical inadequacy of reconstruction systems, but to the inability of decision-making frameworks to adapt to contextual realities. Reconstruction alternatives that appear technically optimal under normal conditions may become operationally infeasible due to governance fragmentation, logistics disruption, insecurity, or resource shortages. Experiences from post-earthquake Haiti and the Middle East conflict-affected regions (Ex, Syria and Yemen) demonstrate how institutional fragility, disrupted logistics, and political instability can fundamentally constrain reconstruction implementation despite substantial technical and financial support (Barakat & Zyck, 2011; Schuller, 2016).

Although existing PDHR literature increasingly recognizes complexity and uncertainty in disaster recovery, resilience is still predominantly conceptualized as a characteristic of reconstruction outcomes rather than of the decision-making process itself. Existing frameworks largely focus on how resilient, sustainable, or cost-effective reconstruction outputs may be, while comparatively limited attention has been given to whether the decision-making architecture itself remains adaptive, feasible, and robust under persistent disruption. In critical zones, the central challenge is often not identifying the theoretically “best” solution, but identifying solutions capable of surviving contextual constraints while maintaining acceptable performance outcomes.

Accordingly, this paper argues that resilience in PDHR should be reconceptualized as a property of the reconstruction decision-making process itself. To address this gap, the study proposes a resilience-oriented conceptual framework for PDHR decision-making in critical zones. The framework introduces contextual feasibility as a preliminary screening mechanism prior to technical and economic optimization. It integrates feasibility assessment, performance evaluation, and economic assessment through the combined application of hybrid MCDM approaches and Cost–Benefit Analysis (CBA). The novelty of the framework lies in integrating contextual feasibility within a sequential resilience-oriented decision architecture where feasibility precedes performance. The study therefore contributes a conceptual foundation for future empirical research and practical application in highly constrained reconstruction environments.

2. Theoretical Grounding

2.1 Defining the Critical Zone Construct: Characteristics and Context

Post-disaster housing reconstruction (PDHR) has traditionally been examined within relatively stable recovery environments, where reconstruction activities are assumed to progress through sequential phases of emergency response, recovery, rebuilding, and eventual normalization (Alexander, 2014). However, an increasing number of contemporary disasters occur within critical zones. The expression of “Critical Zones” in this paper is used as a metaphor to refer to a spatial-operational framework for protracted crisis zones,

where it is mainly characterized by persistent uncertainty, instability, and contextual constraint. This criticality varies in degree depending on the origin. It can originate from natural, human-made or hybrid sources. Furthermore, it usually witnesses one or more of socio-economic fragility, political unrest, governance fragmentation, and repeated disruptions that continuously affect reconstruction processes, making the predictable recovery trajectories no longer reliably apply. Such environments challenge the assumptions embedded in conventional post-disaster recovery models and require a broader conceptualization of reconstruction dynamics that extends beyond traditional recovery conditions (Tierney, 2023).

Examples include conflict-affected regions, politically unstable territories, areas under sanctions, regions experiencing repeated climate-related disasters, displacement environments, economically collapsed states, or territories suffering from long-term infrastructure degradation (Wisner, 2004). In such contexts, reconstruction challenges extend beyond physical damage and involve dynamic socio-political and operational disruptions (Lewis, 1999). Unlike conventional post-disaster settings, where disruption is often temporary and recovery pathways are comparatively linear, critical zones are characterized by recurrent disruptions that alter the assumptions upon which traditional reconstruction models are based (Olshansky et al., 2012). and made the reconstruction decision-making and its implementation in such zones is a challenging task.

2.2 Limitations of Existing Theories and Decision-Support Approaches in PDHR at Critical Zones

Several influential theories and frameworks have shaped PDHR planning and reconstruction policy over recent decades. These include the disaster management cycle, the “Build Back Better” concept, the Sendai Framework for Disaster Risk Reduction, sustainability-oriented reconstruction models, and various optimization-based decision-support tools such as MCDM and the traditional project management “Iron Triangle.” While these frameworks have significantly improved reconstruction planning in many contexts, their isolated applicability within critical zones remains inefficient.

2.2.1 Limitations of the Disaster Management Cycle

The traditional disaster management cycle conceptualizes disasters through sequential stages including mitigation, preparedness, response, recovery, and reconstruction (Alexander, 2014). Although widely adopted, this framework assumes that disasters represent temporary disruptions followed by progressive stabilization.

However, recovery processes in critical zones rarely follow linear trajectories. Olshansky et al. (2012) argue that post-disaster recovery processes are often nonlinear, compressed, and deeply shaped by uncertainty. In conflict-affected or politically unstable environments, reconstruction may occur simultaneously with ongoing crises, making conventional stage-based recovery models insufficient.

The reconstruction experience following Hurricane Katrina illustrates this limitation. Despite extensive technical and financial resources, recovery was significantly complicated by governance fragmentation,

institutional failures, and social inequalities that traditional disaster frameworks failed to adequately address (Comfort, 2006).

2.2.2 Limitations of the "Build Back Better" Approach

The "Build Back Better" (BBB) paradigm emphasizes improving resilience, sustainability, and development outcomes during reconstruction processes (Kennedy et al., 2008). While conceptually valuable, BBB often assumes that institutional systems, governance mechanisms, and reconstruction resources remain sufficiently functional to support long-term rebuilding strategies.

In highly constrained environments, however, immediate operational feasibility may become more critical than optimization-oriented rebuilding objectives. Reconstruction priorities may shift toward adaptability, accessibility, and rapid deployability rather than idealized long-term redevelopment goals.

The post-2010 Haiti reconstruction process demonstrates this limitation. Despite extensive international promotion of sustainable reconstruction principles, implementation was severely constrained by institutional fragmentation, land tenure conflicts, weak governance coordination, and heavy dependence on imported systems and external actors (Schuller, 2016). As a result, many reconstruction initiatives struggled to achieve intended recovery outcomes.

2.2.3 Limitations of the Sendai Framework

The Sendai Framework for Disaster Risk Reduction emphasizes resilience-building, risk governance, preparedness, and sustainable recovery (UNDRR, 2015). However, the framework primarily operates at the strategic policy level and provides limited operational guidance for reconstruction decision-making under persistent instability and constrained implementation conditions.

While Sendai strongly promotes resilience-oriented recovery, it does not sufficiently address how reconstruction decisions should adapt when governance systems are fragmented, logistics are disrupted, or operational feasibility continuously changes.

2.2.4 Limitations of the Short-Term versus Long-Term Approach

PDHR literature frequently distinguishes between short-term emergency shelter and long-term permanent reconstruction. However, this distinction becomes increasingly blurred within critical zones where temporary settlements may persist for years or even decades due to prolonged instability and displacement conditions (Quarantelli, 1995).

In many conflict-affected regions, temporary housing systems have evolved into semi-permanent environments because political and operational conditions prevented transition toward conventional long-term reconstruction. Such realities challenge simplified temporal distinctions embedded within traditional recovery models.

2.3 Limitations of Traditional Decision-Support Tools

2.3.1 The Iron Triangle

The traditional “Iron Triangle” framework evaluates project success primarily through cost by tools such as LCCA and CBA, in addition to time duration, and output quality dimensions. Although useful for conventional project management, this approach inadequately captures contextual uncertainty, institutional fragility, political instability, and operational feasibility challenges present in critical zones.

2.3.2 Multi-Criteria Decision-Making (MCDM)

MCDM approaches have become increasingly popular in reconstruction planning because they allow simultaneous evaluation of multiple criteria. However, many MCDM applications prioritize performance optimization without sufficiently accounting for whether reconstruction alternatives remain feasible under unstable operational conditions.

Therefore, a technologically advanced reconstruction solution may rank highly according to sustainability or cost-efficiency metrics while remaining impossible to implement due to material shortages, border restrictions, security risks, or institutional collapse.

The reconstruction experience in Syria provides an illustrative example. Several technically sophisticated reconstruction proposals were proposed during the conflict period, yet implementation remained severely constrained by political fragmentation, sanctions, infrastructure destruction, restricted logistics, and governance instability (Barakat & Zyck, 2011). Similarly, reconstruction efforts following Hurricane Katrina revealed how social inequality, governance fragmentation, and institutional failures complicated recovery implementation despite substantial technical and financial resources (Vale & Campanella, 2005).

These examples collectively demonstrate that existing PDHR theories and decision-support tools remain insufficient for critical zones because they continue to prioritize reconstruction performance without adequately integrating contextual feasibility into the decision-making process itself.

Accordingly, this paper argues that resilient PDHR decision-making in critical zones requires a conceptual integration of feasibility measures into the performance ones to guarantee the resilience of the decision-making architecture operating under persistent uncertainty and operational disruption.

3. Research Methodology

3.1 Research Design

This study adopts a conceptual research design aimed at developing a theoretically grounded framework for resilient decision-making in Post-Disaster Housing Reconstruction (PDHR) within critical zones. Conceptual research is particularly appropriate for addressing emerging or insufficiently theorized phenomena where existing models fail to adequately explain complex realities (Jaakkola, 2020). In the context of PDHR, existing reconstruction theories and decision-support approaches remain largely grounded in assumptions of operational stability, creating limitations when applied to environments characterized by persistent uncertainty, instability, and/or constraints.

Accordingly, the purpose of this study is not to empirically test a predefined hypothesis, but to construct a new conceptual understanding of resilient decision-making under constrained operational conditions. The research, therefore, focuses on theory synthesis, conceptual integration, and analytical abstraction derived from existing literature.

The methodological process consisted of two sequential phases:

1. Systematic identification and synthesis of relevant decision-making variables from the literature;
2. Conceptual abstraction and framework development based on identified theoretical patterns.

This structure was adopted to ensure methodological transparency and theoretical rigor during the framework development process.

3.2 Literature Review and Knowledge Synthesis

3.2.1 Literature Review Strategy

The first phase of the study involved a structured literature review aimed at identifying the principal concepts, variables, and theoretical gaps associated with PDHR decision-making in unstable and constrained environments.

The review process was informed by Preferred Reporting Items for Systematic Reviews and Meta-Analyses (PRISMA) principles to improve transparency in article selection and thematic synthesis. Relevant literature was collected from two major academic databases; Scopus, Web of Science. The search strings were developed using Boolean operators and combinations of four core thematic clusters, as explained in "Table 1".

Table 1 - Research Clusters

Cluster	Keywords
Decision-making	Decision-making OR "MCDM" OR "multi-criteria decision analysis" OR "decision framework"
Disaster consequences	Post-disaster OR destruction
Housing reconstruction	"Housing reconstruction" OR "residential rebuilding" OR "Shelter" OR housing
Critical zones	Restriction OR uncertainty OR disruption OR "disaster-prone regions" OR instability

Peer-reviewed journal articles, books, institutional reports, and international policy frameworks were reviewed to ensure interdisciplinary coverage of the topic.

3.2.2 Inclusion and Exclusion Criteria

To improve relevance and conceptual consistency, the review prioritized studies that:

- Addressed PDHR or reconstruction decision-making;

- Discussed resilience, uncertainty, or operational constraints;
- Examined governance, logistics, or implementation challenges;
- Applied evaluation or prioritization approaches in disaster recovery contexts.

Studies focused exclusively on structural engineering performance without decision-making relevance were excluded. Similarly, purely technical construction optimization studies without contextual constraints, instability, uncertainty, or disruptions were not prioritized.

3.3 Analytical Approach

The collected literature was analyzed using thematic synthesis and conceptual categorization techniques. The objective of this phase was to identify recurring patterns, relationships, and gaps within existing PDHR decision-making approaches.

Particular attention was given to:

- Variables influencing reconstruction implementation;
- Criteria used in reconstruction evaluation;
- Limitations of existing decision-support frameworks;
- Operational causes of reconstruction failure in unstable contexts.

Through iterative comparison and abstraction, the analysis revealed that existing PDHR literature often prioritizes performance-related evaluation criteria, while contextual feasibility-related conditions are less presented without sufficient integration between them under persistent disruption. This observation became central to the conceptual development process. Figures 1 and Table 2 represent this review.

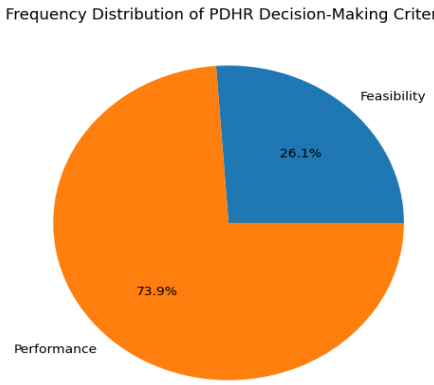


Figure 1 - Frequency distribution of PDHR decision-making criteria in the literature

Table 2 - Frequency distribution of PDHR decision-making criteria in the literature

Criterion	Performace Vs. Fesability	Frequency of Studies	
Cost effectiveness (total costs)	Performance	13	(Gaspari et al., 2025), (Frangedaki & Lagaros, 2025), (Indrawan et al., 2025),(Deria et al., 2024), (Garcia-Ruiz

Criterion	Performace Vs. Fesability	Frequency of Studies	
			et al., 2024), (Khaddour et al., 2024), (Bazli et al., 2023), (Archer et al., 2023), (Martins et al., 2023),(Leonard et al., 2023), (Begic & Krstic, 2022), (Sojobi & Liew, 2022), (Ghannad et al., 2020)
Maintenance cost	Performance	6	(Gaspari et al., 2025), (Frangedaki & Lagaros, 2025), (Archer et al., 2023), (Sojobi & Liew, 2022), (Shahzad et al., 2022), (Ghannad et al., 2020)
Financing availability/budget	Feasbility	2	(Feng & He, 2025), (Gaspari et al., 2025)
Time efficiency(in general)	Performance	9	(Deria et al., 2024), (Bazli et al., 2023), (Archer et al., 2023), (Martins et al., 2023), (Begic & Krstic, 2022), (Feng & He, 2025), (Indrawan et al., 2025), (Leonard et al., 2023), (Sojobi & Liew, 2022)
Sustainability (in general)	Performance	3	(Feng & He, 2025), (Moreno-Sierra et al., 2020), (Zea Escamilla & Habert, 2017)
Carbon footprint / gases emissions	Performance	5	(Feng & He, 2025), (Islam et al., 2026), (Khaddour et al., 2024), (Barreca et al., 2022), (Kuittinen & Takano, 2017)
Energy efficiency	Performance	3	(Khaddour et al., 2024), (Begic & Krstic, 2022), (Kuittinen & Takano, 2017)
Waste reduction	Performance	2	(Bazli et al., 2023), (Sojobi & Liew, 2022)
End-of-life disposal/Recycling	Performance	2	(Feng & He, 2025), (Frangedaki & Lagaros, 2025)
Lightweight construction materials	Performance/ Fesability	5	(Indrawan et al., 2025) , (Feng & He, 2025), (Sojobi & Liew, 2022), (Barreca et al., 2022), (Li & Deng, 2019)
Structural design/resilience	Performance	6	(Indrawan et al., 2025), (Rahmayati & Altassan, 2025),(Choorapulakkal et al., 2024), (Bazli et al., 2023), (Archer et al., 2023), (Maqsood et al., 2019)
Material manufactring and quality	Performance	3	(Gaspari et al., 2025), (Sojobi & Liew, 2022), (Frangedaki & Lagaros, 2025)
Construction code compliance	Feasibility	1	(Gaspari et al., 2025)
On-site labor demand/ Productivity	Performance	2	(Shahzad et al., 2022), (Ghannad et al., 2020)
Skilled labour necessity/Avilability	Performance/ Fesability	2	(Frangedaki & Lagaros, 2025), (Bazli et al., 2023)
Indoor thermal performance(Comfort)	Performance	3	(Feng & He, 2025), (Leonard et al., 2023), (Moreno-Sierra et al., 2020)
Social (in general)	Feasbility	4	(Frangedaki & Lagaros, 2025), (Gaspari et al., 2025), (Maqsood et al., 2019), (Kuittinen & Takano, 2017)
Cultural appropriateness	Feasbility	2	(Frangedaki & Lagaros, 2025), (Bazli et al., 2023)
Constructor participantion and knowledge	Feasbility	2	(Frangedaki & Lagaros, 2025), (Bazli et al., 2023)
Community engagement	Feasbility	2	(Frangedaki & Lagaros, 2025), (Bazli et al., 2023)
Transportation /mobility	Feasbility	6	(Ghannad et al., 2020), (Frangedaki & Lagaros, 2025), (Feng & He, 2025), (Leonard et al., 2023), (Maqsood et al., 2019), (Li & Deng, 2019)
Building typology	Feasbility	2	(Gaspari et al., 2025), (Rahmayati & Altassan, 2025)
Construction Flexibility	Performance	2	(Bazli et al., 2023), (Feng & He, 2025)

Criterion	Performace Vs. Fesability	Frequency of Studies	
location of the reconstructed houses	Feasbility	1	(Garcia-Ruiz et al., 2024)

4. The Proposed Conceptual Model

This study proposes a resilience-oriented conceptual framework for Post-Disaster Housing Reconstruction (PDHR) decision-making in critical zones characterized by uncertainty, instability, governance fragility, supply-chain disruption, and operational constraints. Unlike conventional reconstruction approaches that primarily focus on technical optimization and performance efficiency, the proposed framework argues that reconstruction suitability in critical zones must first satisfy contextual feasibility conditions before technical and economic evaluation can be meaningfully conducted.

The framework begins with identifying potential reconstruction alternatives such as traditional construction systems, modular housing, prefabricated structures, hybrid systems, and emerging technologies including 3D printing. Rather than assuming all reconstruction systems are equally deployable across different contexts, the model recognizes that reconstruction feasibility depends heavily on environmental, institutional, logistical, political, and socio-economic conditions.

The first analytical layer consists of a contextual feasibility filter, representing the primary conceptual contribution of the framework. This layer evaluates whether reconstruction alternatives can realistically operate under critical-zone constraints. Feasibility criteria include institutional capacity, supply-chain stability, labor accessibility, political conditions, financing availability, and social acceptance. The framework proposes the use of Multi-Criteria Decision-Making (MCDM) methods to evaluate alternatives according to weighted contextual criteria. Alternatives that fail to satisfy minimum feasibility conditions are excluded from subsequent evaluation stages.

Reconstruction alternatives that pass the feasibility stage proceed to the second analytical layer: performance evaluation. This stage assesses technical and operational performance using criteria such as construction speed, structural resilience, flexibility, sustainability, and long-term adaptability. Because reconstruction priorities may vary significantly across disaster contexts, the framework allows adaptive weighting of performance criteria using hybrid MCDM approaches.

The third analytical layer consists of economic evaluation through Cost–Benefit Analysis (CBA). This stage evaluates lifecycle implications, affordability, maintenance requirements, and long-term recovery value. The integration of MCDM and CBA enables the framework to balance contextual feasibility, technical performance, and economic sustainability within a unified decision-support structure.

Finally, the framework synthesizes feasibility assessment, performance evaluation, and economic analysis into an integrated trade-off decision process aimed at supporting resilient reconstruction strategies under persistent uncertainty and operational disruption. The novelty of the framework lies not in the isolated use of MCDM or CBA methods, but in integrating them within a sequential resilience-oriented decision architecture where contextual feasibility precedes optimization.

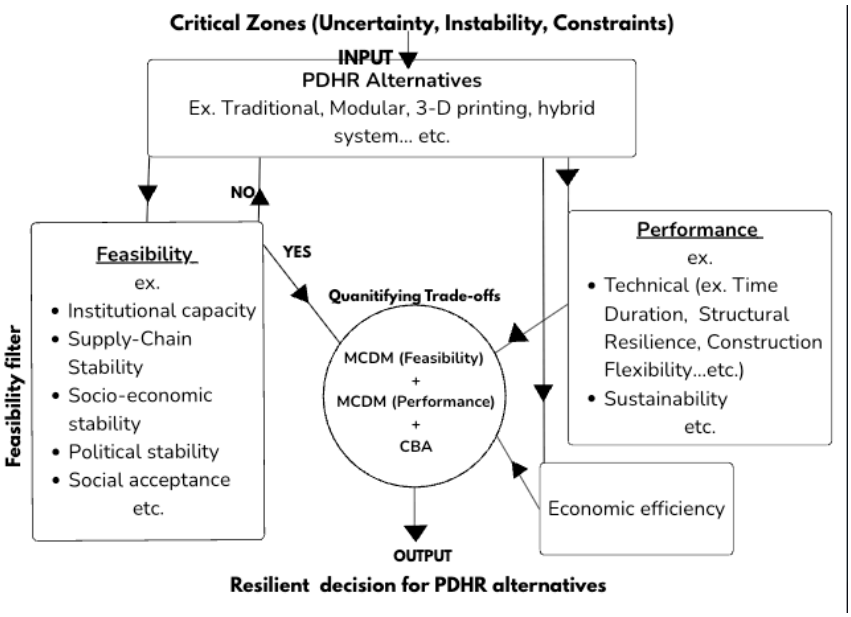


Figure 2 - Model for PDHR decision making in critical zones

5. Discussion

The findings of this study suggest that reconstruction decision-making in critical zones cannot rely solely on conventional performance-oriented approaches. Although criteria such as cost efficiency, sustainability, construction speed, and structural resilience remain important, reconstruction success in unstable environments is often determined by contextual feasibility rather than technical superiority alone. In such conditions, reconstruction systems that appear optimal theoretically may become impractical due to disrupted supply chains, governance fragility, labor shortages, financing limitations, or political instability.

The proposed framework therefore emphasizes that resilient PDHR decision-making requires integrating contextual feasibility alongside technical and economic evaluation. Existing reconstruction models frequently prioritize optimization-based performance criteria while underrepresenting operational constraints that directly affect implementation capability. However, experiences from conflict-affected and disaster-prone regions demonstrate that institutional capacity, logistics continuity, material accessibility, and social acceptance can fundamentally determine reconstruction success or failure in practice.

The study further argues that reconstruction priorities are not universally fixed across all disaster contexts. Different critical zones may require different evaluation priorities depending on operational realities. Consequently, the integration of hybrid Multi-Criteria Decision-Making (MCDM) approaches and Cost–Benefit Analysis (CBA) provides greater flexibility for balancing contextual feasibility, technical performance, and long-term economic sustainability.

The primary theoretical contribution of this study lies in reframing resilience from an outcome-oriented concept toward a process-oriented perspective. The framework shifts reconstruction logic from identifying the theoretically optimal solution toward identifying the most contextually survivable and operationally adaptable solution under persistent uncertainty and disruption.

6. Conclusion and Future Research

This paper proposed a resilience-oriented conceptual framework for Post-Disaster Housing Reconstruction (PDHR) decision-making in critical zones characterized by instability, uncertainty, and operational disruption. Unlike conventional approaches that primarily emphasize technical optimization, the framework introduces contextual feasibility as a preliminary filter prior to performance and economic evaluation. The study argues that resilient reconstruction depends not only on resilient housing outcomes, but also on resilient decision-making processes capable of adapting to unstable conditions.

The framework integrates feasibility assessment, performance evaluation, and Cost–Benefit Analysis (CBA) through hybrid Multi-Criteria Decision-Making (MCDM) approaches to support adaptive reconstruction planning under constrained environments.

However, the framework remains conceptual and requires empirical validation. Future research should test the model through case studies, expert evaluation, simulation modelling, or Delphi methods in conflict-affected and disaster-prone regions. Further studies may also explore the integration of digital technologies and real-time data systems to improve operational decision support in critical zones.

References

Alexander, David. (2014). *Principles of emergency planning and management*. Dunedin Academic Press Ltd.

Archer, R., Choi, H., Vasconez, R., Najm, H., & Gong, J. (2023). Adaptive coastal construction: designing amphibious homes to resist hurricane winds and storm surges. *Journal of Ocean Engineering and Marine Energy*, *9*(2), 273–290. https://doi.org/10.1007/s40722-022-00267-6

Barakat, S., & Zyck, S. A. (2011). Housing Reconstruction as Socio-economic Recovery and State Building: Evidence from Southern Lebanon. *Housing Studies*, *26*(1), 133–154. https://doi.org/10.1080/02673037.2010.512750

Barreca, F., Arcuri, N., Cardinali, G. D., Fazio, S. Di, Rollo, A., & Tirella, V. (2022). A Highly Sustainable Timber-Cork Modular System for Lightweight Temporary Housing. *Civil Engineering Journal (Iran)*, *8*(10), 2336–2352. https://doi.org/10.28991/CEJ-2022-08-10-020

Bazli, M., Ashrafi, H., Rajabipour, A., & Kutay, C. (2023). 3D printing for remote housing: Benefits and challenges. *Automation in Construction*, *148*, 104772. https://doi.org/10.1016/j.autcon.2023.104772

Begic, H., & Krstic, H. (2022). View of Possibilities of Using Prefabricated Modular Panels for Building NZEB Buildings in Earthquake-Affected Areas in Croatia – Case Study. *International Journal of Sustainable Construction Engineering and Technology*.

Choorapulakkal, A. A., Madandola, M. G., Al-Kandari, A., Furlan, R., Bayram, G., & Mohamed, H. A. A. (2024). The Resilience of the Built Environment to Flooding: The Case of Alappuzha District in the South Indian State of Kerala. *Sustainability*, *16*(12), 5142. https://doi.org/10.3390/su16125142

Comfort, L. K. (2006). Cities at Risk. *Urban Affairs Review*, *41*(4), 501–516. https://doi.org/10.1177/1078087405284881

Deria, A., Ghannad, P., & Lee, Y. (2024). Dynamic Real-Time Optimization of Modular Unit Allocation to Off-Site Facilities in Postdisaster Reconstruction Using Deep Reinforcement Learning. *Journal of Management in Engineering*, *40*(4). https://doi.org/10.1061/JMENEA.MEENG-5900

Feng, X.-T., & He, B.-J. (2025). Sustainability vision for low-carbon, comfortable, inclusive, and recyclable temporary buildings. *Energy and Buildings*, *328*, 115213. https://doi.org/10.1016/j.enbuild.2024.115213

Frangedaki, E., & Lagaros, N. D. (2025). *Sustainable and Resilient Earthen Post-disaster Shelters* (pp. 58–68). https://doi.org/10.1007/978-3-031-92754-6_6

Garcia-Ruiz, A., Díez-Minguito, M., Verichev, K. S., & Carpio, M. (2024). Bibliometric Analysis of Urban Coastal Development: Strategies for Climate-Resilient Timber Housing. *Sustainability (Switzerland)*, *16*(4). https://doi.org/10.3390/su16041431

Gaspari, M., Galasso, C., & Gentile, R. (2025). Unveiling vulnerabilities: Integrating socioeconomic and physical dimensions in residential exposure modelling. *International Journal of Disaster Risk Reduction*, *125*. https://doi.org/10.1016/j.ijdrr.2025.105557

Ghannad, P., Lee, Y.-C., & Choi, J. O. (2020). Feasibility and Implications of the Modular Construction Approach for Rapid Post-Disaster Recovery. *International Journal of Industrialized Construction*, *1*(1), 64–75. https://doi.org/10.29173/ijic220

Indrawan, S. E., Purwanto, L. M. F., Hermawan, & Ch'ng, M. (2025). Adaptive Structural Models for Post-Flood Housing Construction on South Kalimantan's Peatland. *Civil Engineering and Architecture*, *13*(4), 3129–3143. https://doi.org/10.13189/cea.2025.130421

Islam, A. H. M. S., Barua, A., & Alam, M. R. (2026). Sustainable timber-concrete composite housing for the coastal region of Bangladesh: a comparative study. *Journal of Building Pathology and Rehabilitation*, *11*(1). https://doi.org/10.1007/s41024-025-00699-1

Jaakkola, E. (2020). Designing conceptual articles: four approaches. *AMS Review*, *10*(1–2), 18–26. https://doi.org/10.1007/s13162-020-00161-0

Kennedy, J., Ashmore, J., Babister, E., & Kelman, I. (2008). The Meaning of 'Build Back Better': Evidence From Post-Tsunami Aceh and Sri Lanka. *Journal of Contingencies and Crisis Management*, *16*(1), 24–36. https://doi.org/10.1111/j.1468-5973.2008.00529.x

Khaddour, L. A., Osunsanmi, T., Olawumi, T. O., & Bradly, L. (2024). Multi-Attribute Analysis for Sustainable Reclamation of Urban Industrial Sites: Case from Damascus Post-Conflict. *IOP Conference Series: Earth and Environmental Science*, *1363*(1), 012087. https://doi.org/10.1088/1755-1315/1363/1/012087

Kuittinen, M., & Takano, A. (2017). The energy efficiency and carbon footprint of temporary homes: a case study from Japan. *International Journal of Disaster Resilience in the Built Environment*, *8*(4), 326–343. https://doi.org/10.1108/IJDRBE-08-2015-0039

Leonard, J., Pang, W., Stoner, M. W., & Albright, D. (2023). *Deployable Wood Structures for Disaster Relief and Military Use*. *6*, 3518–3525. https://doi.org/10.52202/069179-0458

Lewis, J. (1999). *Development in Disaster-Prone Places*.

Li, S., & Deng, K. (2019). Lightweight reconfigurable structure system (LRSS): Rethinking temporary buildings. *WIT Transactions on the Built Environment*, *183*, 101–112. https://doi.org/10.2495/ARC180101

Maqsood, T., Wehner, M., Dale, K., & Edwards, M. (2019). Reduction of flood vulnerability through the implementation of mitigation strategies. *Proceedings of the International Conference on Natural Hazards and Infrastructure*.

Martins, R., Carmo, R. N. F., Costa, H. S. S., & Júlio, E. N. B. S. (2023). A review on precast structural concrete walls and connections. *Advances in Structural Engineering*, *26*(14), 2600–2620. https://doi.org/10.1177/13694332231191073

Moreno-Sierra, A., Pieschacón, M., & Khan, A. (2020). The use of recycled plastics for the design of a thermal resilient emergency shelter prototype. *International Journal of Disaster Risk Reduction*, *50*(7), 101885. https://doi.org/10.1016/j.ijdrr.2020.101885

Olshansky, R. B., Hopkins, L. D., & Johnson, L. A. (2012). Disaster and Recovery: Processes Compressed in Time. *Natural Hazards Review*, *13*(3), 173–178. https://doi.org/10.1061/(ASCE)NH.1527-6996.0000077

Quarantelli, E. L. (1995). Patterns of sheltering and housing in US disasters. *Disaster Prevention and Management: An International Journal*, *4*(3), 43–53. https://doi.org/10.1108/09653569510088069

Rahmayati, Y., & Altassan, N. (2025). Reviewing the Design of Flood Emergency Shelters in Indonesia and Bangladesh in Response to the Climate Change Impacts. *IOP Conference Series: Earth and Environmental Science*, *1488*(1). https://doi.org/10.1088/1755-1315/1488/1/012127

Schuller, Mark. (2016). *Humanitarian aftershocks in Haiti*. Rutgers University Press.

Shahzad, W. M., Rajakannu, G., & Kordestani Ghalenoei, N. (2022). Potential of Modular Offsite Construction for Emergency Situations: A New Zealand Study. *Buildings*, *12*(11). https://doi.org/10.3390/buildings12111970

Sojobi, A. O., & Liew, K. M. (2022). Multi-objective optimization of high performance bio-inspired prefabricated composites for sustainable and resilient construction. *Composite Structures*, *279*, 114732. https://doi.org/10.1016/j.compstruct.2021.114732

Tierney, Kathleen. (2023). *The Social Roots of Risk Producing Disasters, Promoting Resilience*. Stanford Business Books.

UNDRR. (2015). *Sendai Framework for Disaster Risk Reduction 2015-2030*.

Vale, L. J., & Campanella, T. J. (2005). *The Resilient City: How Modern Cities Recover from Disaster*.

Wisner, Ben. (2004). *At risk : natural hazards, people's vulnerability, and disasters*. Routledge.

Zea Escamilla, E., & Habert, G. (2017). Method and application of characterisation of life cycle impact data of construction materials using geographic information systems. *International Journal of Life Cycle Assessment*, *22*(8), 1210–1219. https://doi.org/10.1007/s11367-016-1238-y

Cinpar 2026
XXII International Conference on Building Pathology and Constructions Repair
15th to 17th July 2026 - Lisboa, Portugal

Heritage Management and the Progressive Deterioration of an Earthen *Troje* in Mexico City

Pilar ESPINOZA VÁZQUEZ[1], Gerardo SALAZAR[2], Humberto VARUM[3], Luz Olivia DOMINGUEZ PRIETO[4], Tarsicio PASTRANA SALCEDO[5]

[1] School of Engineering and Architecture (ESIA), National Polytechnic Institute (IPN), Tecamachalco, Mexico, pespinozav2300@alumno.ipn.mx
[2] CONSTRUCT, Faculty of Engineering University of Porto, Porto, Portugal, gsalazar@fe.up.pt
[3] CONSTRUCT, Faculty of Engineering University of Porto, Porto, Portugal, hvarum@fe.up.pt
[4] School of Engineering and Architecture (ESIA), National Polytechnic Institute (IPN), Tecamachalco, Mexico, ludominguezp@ipn.mx
[5] School of Engineering and Architecture (ESIA), National Polytechnic Institute (IPN), Tecamachalco, Mexico, tpastranas@ipn.mx

Abstract: The conservation of earthen masonry heritage is conditioned by technical considerations as well as by administrative procedures and regulatory frameworks that govern intervention practices. This study is motivated by the need to understand how management decisions can either mitigate or accelerate structural vulnerability in earthen buildings. The research focuses on a rare and culturally significant earthen *troje* located in the dense urban context of Mexico City, within the former Hacienda de San Nicolás Tolentino Buenavista. By correlating archival records (1970–2009) with fieldwork documentation, the study establishes a direct link between institutional processes and physical decay. The analysis shows that cumulative management failures contributed to the progressive structural weakening of the *troje*, ultimately leading to severe deterioration. Rather than resulting from a single technical failure, the case demonstrates how management practices can themselves present systemic threats to earthen heritage. Three key patterns are identified: delayed responses to documented structural threats, the use of incompatible materials, and external interventions that altered the building's structural and spatial integrity. Additionally, the case exposes limitations in current regulatory frameworks, particularly their insufficient consideration of earthen construction systems and challenges in enforcement. Consequently, the study highlights the need for integrated approaches that align technical knowledge, clear regulatory instruments, and effective institutional coordination to prevent administrative processes from becoming drivers of earthen heritage deterioration in urban contexts.

Keywords: earthen masonry heritage, heritage management, administrative decision-making, structural deterioration, urban heritage.

1. Introduction

Earthen architectural heritage represents a specialized and increasingly rare category of the built environment, particularly within dense urban contexts such as Mexico City. While traditional construction techniques such as adobe and rammed earth remain widely represented in rural areas of Latin America, their presence in large metropolitan environments is exceptional, making their conservation a matter of urgent cultural priority. While environmental factors are commonly recognized as primary agents of decay, the survival of these rare urban earthen structures is increasingly threatened by human and institutional actions. Recent research has significantly advanced the technical understanding of earthen materials, including their structural behavior and conservation needs, as illustrated by Sánchez-Calvillo *et al.* (2024).

However, comparatively less attention has been paid to how administrative processes fail to address the specific complexities of earthen architecture, particularly within urban systems. In many cases, unclear intervention protocols, lack of coordination between institutions or insufficient technical knowledge among stakeholders contribute significantly to the progressive deterioration of heritage structures, as noted by Abad Rodas and Idrovo Carpio (2016), Guerrero Baca and Esteba Ávalos (2022), and Robles García and Corbett (2017).

In Mexico, the conservation of architectural heritage is regulated under the Federal Law on Archaeological, Artistic and Historical Monuments and Zones (1972, latest amendment April 1, 2024) and its Regulations (1975, latest amendment January 5, 2024) (DOF, 1972; DOF, 1975; Rotondaro *et al.,* 2024, 56). This legal framework establishes institutional responsibilities and authorization procedures, through the National Institute of Anthropology and History (INAH). Although it provides a formal basis for protection, its application often reveals limitations when addressing the specific complexities of earthen architecture. Despite international efforts to standardize earthen construction since the early 2000s, as documented by Rotondaro *et al.* (2024), most notably through the PROTERRA network and technical standards such as Mexico's NMX-C-508-ONNCCE-2015 regarding Compressed Earth Blocks, regulatory frameworks specifically tailored for the intervention of historic earthen structures remain insufficient. While these efforts have transitioned from academic initiatives into formal technical documents, their application within heritage conservation practice, particularly under institutional frameworks, continues to face significant challenges.

This paper examines the case of an earthen *troje* located within the former Hacienda de San Nicolás Tolentino Buenavista in Iztapalapa, Mexico City. The building, originally constructed between the 18th and early 19th centuries, has undergone a series of administrative processes, interventions, and periods of neglect that have significantly altered its structural condition over time. The availability of archival documentation makes this case particularly relevant for analyzing the relationship between management decisions and material deterioration. In light of this, the aim of this study is to identify how administrative actions, authorization processes, and institutional coordination have influenced the progressive deterioration of this historically significant building. By highlighting the interaction between regulatory frameworks, technical practices, and material performance, this study contributes to a broader understanding of heritage management as a critical factor in the conservation, or deterioration, of earthen architecture.

2. Methodology

The methodology is based on three complementary components. First, an archival research process was conducted in the INAH historical archives, *Archivo Histórico y Planoteca Jorge Enciso (AHP-JE)* of the *Coordinación Nacional de Monumentos Históricos (CNMH)*, where administrative records, technical reports, or official letters (1970–2009) related to the case study were identified and analyzed. Second, fieldwork was carried out with authorization from the local authorities, including photographic documentation, architectural survey, and on-site identification of construction systems, materials, and deterioration patterns. Finally, a comparative analytical approach was developed, consisting of the chronological correlation between documented administrative actions and the current physical condition of the building. This allowed the identification of causal relationships between management decisions, intervention practices, and observed deterioration processes.

3. Study Case

This research examines an 18th-century earthen *troje* located within the San Lorenzo Tezonco civil cemetery in Iztapalapa, Mexico City (see Figures 1 and 2). According to INAH (1989; 1990), this structure is officially protected under Mexican heritage law (DOF, 1972) and is registered in the National Catalog of Historic

Monuments (ID: I-0014100021). Its 16th–19th century chronology, specifically identified as the Troje of San Nicolás Tolentino Buenavista, meets the required legal criteria for national protection.



Figure 1 – General (east) view of the *Troje* in 1975. Source: INAH (1989)



Figure 2 – West façade view of the Troje in 1975. Source: INAH (1989)

The building originally belonged to the Hacienda de San Nicolás Tolentino Buenavista, a historic agricultural estate founded in 1580 (Nazario Cruz 2014, 34), and located adjacent to the indigenous town (*pueblo originario*) of San Lorenzo Tezonco. The hacienda's development benefited from its strategic location near streams and the former Lake Xochimilco, where access to essential roads, local ranches, and indigenous labor settlements was further enhanced by its proximity to Mexico City, the primary commercial and demographic center of New Spain. Its main economic activity centered on the cultivation of alfalfa and oats (Gómez and Villasana 2021). Throughout its history, it had several owners, including the Jesuits, who acquired it in 1705 and retained ownership until 1767. This period is considered the hacienda's time of greatest prosperity, as it experienced no economic losses and reached an extension of approximately five thousand hectares. However, in comparison with other Jesuit properties, it remained relatively small.

By 1792, there are records documenting the *troje* as part of the hacienda complex, indicating that, in addition to a masonry house with arches, there was also a two-level *troje* described as large and capable of storing the agricultural production of the hacienda (Nazario Cruz 2014, 39–40). In 1812, another document describes the hacienda as having a *troje* composed of three bays with 20 masonry pilasters supporting 20 wooden columns, with both levels connected by a vaulted staircase (Lara Paredes 2017, 33). The building's current state aligns with these historical descriptions: a two-story structure with adobe walls and stone buttresses. Records indicate that the buttresses were early 20th-century interventions, designed to align with the architectural rhythm and spacing of the original perimeter walls (INAH, 1994b; 1994e). Currently, 16 masonry columns are preserved on the ground floor, with four others documented as collapsed. In 1908, the owners established the *Compañía Agrícola de San Nicolás, Sociedad Anónima* with the aim of draining and irrigating the land to improve productivity. Due to limited economic returns, the property was gradually subdivided and sold in lots during the first half of the 20th century. At the same time, part of the land was granted to the town of San Lorenzo Tezonco, with which there had been longstanding conflicts since the hacienda's foundation over land appropriation. In 1970, the government expropriated the remaining hectares to establish what is now the San Lorenzo Tezonco Civil Cemetery (Gómez and Villasana 2021).

The *troje* currently features a foundation of irregular stone masonry bonded with lime–sand mortar. Ground-floor walls are constructed of adobe bricks (approximately 40 × 15 × 10 cm) with 5-cm joints. The structural system includes columns with stone masonry bases and fired-clay brick shafts. The floor system is supported by wooden beams resting on capitals atop the columns; this assembly consists of timber joists and wooden

planks embedded into the walls, topped with a layer of earthen fill (*terrado*), a lime–sand leveling bed, and a brick floor finish. Upper-level walls exhibit mixed construction, preserving original adobe masonry in some sections while introducing fired-brick masonry with cement–sand mortar in others. Between these walls, buttresses of mixed stone and fired-brick masonry are bonded with lime–sand mortar. These are topped by reinforced concrete posts that support a roof structure of steel trusses and galvanized metal sheets (see Figure 3).

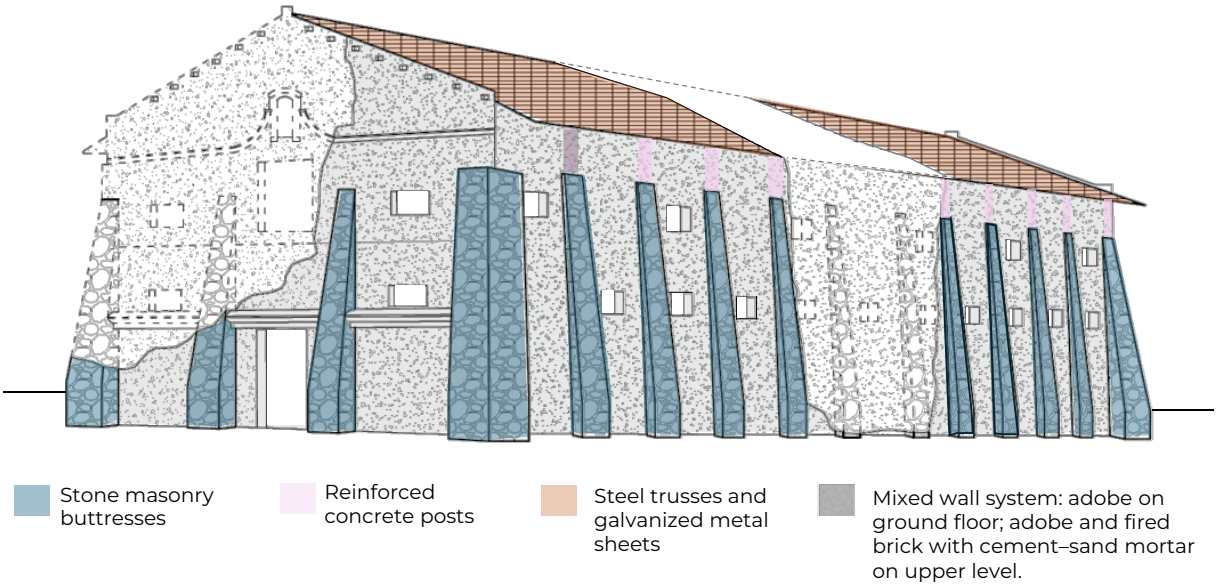


Figure 3 –Schematic exterior volumetry of the southeast façade indicating some materials and the collapsed vertical supports (dashed lines) at the time of survey (2025). Created by P. Espinoza Vázquez

4. Results: administrative timeline and deterioration processes

This section contextualizes the actions performed on the *troje* by examining the administrative and physical records of the hacienda found in the historical archive AHP-JE of the CNMH-INAH. At the time of this research (2024), these documents were preserved under the original name of the former hacienda (*Ex-Hacienda* de San Nicolás, currently the San Lorenzo Civil Cemetery). The records cover the period from 1970, when the remaining hacienda lands were expropriated by the Department of the Federal District (DDF), to 2009. The earliest documentation from this period corresponds to a formal report submitted to INAH regarding unauthorized restoration works (INAH 1970a). This indicates that the institution became aware of ongoing interventions at that time, which prompted administrative actions through on-site inspections. This early documentation also makes it possible to establish the original condition of the *troje*, which at that time still preserved its traditional materials and structural system (INAH 1970c). Table 1 presents the chronological records of administrative actions during 1970, as well as the associated deterioration processes and their consequences. This initial phase is particularly relevant, as it documents both the original state of the building and the first administrative responses to unauthorized interventions.

Table 1 – Administrative actions and deterioration recorded in 1970

Date / Reference	Administrative action	Type of deterioration
February 11, 1970 (INAH, 1970b)	Site inspection and testimony from the works supervisor regarding structural changes (Reported Nov 24)	Demolition of 15 rooms and stone-and-mud masonry of the formerly Hacienda; replacement with incompatible modern materials (brick/concrete) despite preservation of the chapel's Ex-hacienda (*troje* unaffected at the time of reporting)
February 18, 1970 (INAH, 1970a)	Formal report to INAH regarding arbitrary 'restoration' works	Alteration of architectural integrity of the urban setting by destroying original fabric of historic buildings within the *Ex-hacienda* (*troje* unaffected at the time of reporting)
December 7, 1970 (INAH, 1970c)	Site inspection and formal summons for rehabilitation plans following the detection of unauthorized and incompatible interventions	Assessment of the *troje* as well-preserved stone-and-mud masonry with original timber roofing; potential risk identified due to proposed conversion into a chapel without approved technical drawings
December 14, 1970 (INAH, 1970d)	INAH requested a formal technical briefing with DDF supervisors to address the intervention actions	Although there were institutional attempts to mitigate improper interventions through technical alignment on restoration methods, the resulting preventive mechanisms failed to achieve effective conservation

While the 1970 records document the initial condition of the *troje* and early administrative actions, the following documentation shown in Table 2 reflects the long-term effects of these processes, including structural deterioration, delayed interventions, and increasing risk of collapse. The documents shown in Table 1 and Table 2 provide an overview of the transformations experienced by the *troje* over a period of nearly four decades. Following the expropriation of the hacienda, the site was repurposed as a civil cemetery, and the existing structures began to be modified without prior notification to INAH. As a result, institutional inspections were conducted, confirming that demolition works had already taken place in the *Ex-hacienda*. At the time of the initial inspections in 1970, the *troje* itself had not yet been intervened. However, it was described as having a well-preserved timber roof structure. This contrasts with later documentation from 1989, which reports a metal roof, increased wall heights, and structural instability in the lateral walls (INAH 1989; 1990). Due to the absence of documentation between 1970 and 1989, these modifications were most likely carried out between 1970 and 1975, as supported by photographic evidence from 1975 (see Figure 1 and Figure 2). Despite requests for clarification from those responsible for the works in 1970, there is no record indicating that proper coordination or compliance was achieved. By 1990, technical assessments identified severe deterioration, including diagonal cracks (45°), settlements, and wall tilting, and even included a cost estimate for restoration. However, there is no evidence that any intervention was carried out.

Four years later, according to INAH (1994a), a partial collapse of the *troje* was reported, which is illustrated in Figure 4. Considering this, a new technical assessment was made, which confirmed differential settlements that likely produced the collapse of the south façade. The report concluded that, due to the damage state that can be observed in Figure 5, urgent intervention was required, including structural shoring and the development of an integral restoration project. Although an intervention proposal was prepared shortly after, no action was implemented.

By May 1995, local authorities formally requested authorization for either the demolition or rescue of the building due to the imminent risk of collapse. One year later, in June 1996, the CNMH-INAH denied

authorization for a proposed intervention project submitted by a private company, citing non-compliance with conservation criteria. Beyond this period, there is no record of restorative work. Aside from a 2009 permit for a water treatment plant next to the west façade, the building has not undergone formal intervention, leading to the progressive deterioration shown in Figure 6, Figure 7 and Figure 8.

Table 2 – Chronological record of administrative actions and associated deterioration processes (1989–2009)

Date / Reference	Administrative action	Type of deterioration
April 4, 1989 (INAH, 1989)	Official report documenting spatial alterations and structural instability	Evidence of early structural failure; height increase to accommodate a gabled roof; documented instability in the front and right lateral walls; building's original 16th-century proportions compromised by its conversion into a warehouse
January 30, 1990 (INAH, 1990)	Technical memorandum and restoration cost estimate providing a detailed structural diagnostic	Progressive material degradation; active structural instability including a 20cm stair separation, diagonal cracking (45°), and a wall tilt caused by soil settlement between the 4th and 5th axes; presence of biological growth (lichens) and moisture; despite façade decay and makeshift galvanized roof, the original 18th-century timber mezzanine remained in good condition
September 20-22, 1994 (INAH, 1994a; 1994b)	Urgent decree for structural shoring and integrated restoration planning	Increased risk of total collapse; differential settlements caused by a nearby artesian well (20m distance) resulting in severe fractures (45°), masonry fragmentation, and wall tilts; failure of the metal roof and identification of historical but structurally detached buttresses
October10-21, 1994 (INAH, 1994c; 1994d; 1994e)	Rapid emergency response sequence (commission, inspection, and formal proposal) triggered by a public report of structural collapse (in coordination with local authorities in Iztapalapa)	Confirmation of ongoing differential settlements requiring specialized soil studies; identification of early 20th-century buttresses as insufficient to stabilize the earthen walls; proposal (but not implemented solutions) to consolidate adobe masonry with brick tie-ins and treat timber with pentachlorophenol to combat biological decay
May 12-29, 1995 (INAH, 1995a; 1995b)	Formal petition for demolition authorization issued by the Iztapalapa Delegation to INAH	Advanced structural decay leading to the total restriction of access; local authorities prioritize public safety over heritage value, citing the "danger of collapse" of the earthen masonry walls
June 10, 1996 (INAH, 1996)	Official rejection of the intervention project submitted by a private firm	Prolonged exposure of the compromised structure due to inadequate project proposals; administrative refusal to authorize works that did not comply with conservation principles
March 23-27, 2009 (INAH, 2009a; 2009b)	Conditional feasibility granted for the construction of an adjacent Water Treatment Plant	Partial demolition of historic stone-and-mud boundary walls; transformation of the monument's setting despite "safeguarding" claims by the developers



Figure 4 – South façade of the Troje in 1995, showing the structural collapse of the wall. Source: INAH (1995b)



Figure 5 – Main (east) façade of the Troje in 1995, showing visible structural cracking and material decay. Source: INAH (1995b)



Figure 6 – North façade of the Troje showing the collapse of the roof trusses and metal sheeting. Photograph by P. Espinoza Vázquez, May 3, 2024.



Figure 7 – Main (east) façade of the Troje, showing the structural decay and vegetation growth. Photograph by P. Espinoza Vázquez, June 4, 2023.



Figure 8 –Aerial roof view. Photograph by P. Espinoza Vázquez, December 14, 2024

5. Discussion

This section interprets these findings to identify underlying patterns, systemic issues, and broader implications for heritage management.

5.1 Management-Driven Patterns of Decay

The analysis of archival documentation and field observations reveals that the deterioration of the *troje* cannot be attributed to a single technical failure, but rather to a sequence of administrative decisions, omissions, and interventions carried out over several decades. The chronological correlation between documented actions and the building's physical condition allows for the identification of three main patterns in which management processes directly contributed to structural and material degradation.

5.1.1 Deterioration driven by delayed actions and institutional fragmentation

One of the most significant factors identified is the lack of timely intervention despite clear evidence of structural damage. As early as 1989 and 1990, official documents reported instability in the walls, presence of moisture, cracking, and differential settlement. However, no effective intervention was implemented following these assessments. This delay allowed existing pathologies to evolve into more severe structural problems, ultimately leading to partial collapses reported in 1994. This pattern suggests a disconnection between technical diagnosis and administrative response, likely influenced by fragmented institutional responsibilities and unclear coordination between authorities and stakeholders. The absence of prompt action in response to known risks has transformed manageable deterioration processes into critical structural failures. In this sense, deterioration was not only the result of material vulnerability, but also of inaction within the management system.

5.1.2 Incompatible interventions and lack of technical coherence

A second key factor is the introduction of incompatible materials and construction systems during earlier interventions, particularly those carried out around the 1970s. Archival evidence and current building analysis indicate that original earthen masonry was modified through the addition of reinforced concrete elements, steel roofing systems, and masonry using cement-based mortars. These changes introduced significant differences in stiffness, weight, and mechanical behavior between the original and new materials. In earthen architecture, such incompatibility can lead to stress concentrations, cracking, and loss of structural continuity. The observed fissures and failures in the *troje* are consistent with these phenomena (Pilar Vázquez, 2025). This situation reflects not only a lack of technical knowledge, but also the historical promotion of inadequate intervention criteria. As noted in restoration guidelines from the 1970s and 1980s, cracks in adobe walls were often treated using methods developed for stone materials, such as injections of lime–sand mortars with added cement (SEDUE 1984, quoted in Guerrero Baca and Uviña Contreras 2020, 146-147). Such approaches failed to consider the specific mechanical behavior of earthen systems, introducing material incompatibilities that could accelerate structural deterioration rather than mitigate it. Although contemporary conservation practices have advanced significantly, the case illustrates how earlier decisions, taken without adequate technical criteria, can have long-term negative consequences on structural stability.

5.1.3 External interventions and the loss of cultural and spatial integrity

The construction of new infrastructure in the immediate surroundings of the *troje*, particularly the water treatment plant authorized in 2009, represents a third form of impact linked to management decisions. While the project included certain measures intended to mitigate its effect on the historic structure, documentation indicates that construction activities had already begun prior to full authorization, and that elements of the original site, such as perimeter walls, were partially demolished (INAH, 2009). Beyond

physical damage, this type of intervention alters the spatial configuration, visual perception, and cultural significance of the heritage asset. The insertion of contemporary infrastructure within the historic context compromises the integrity of the architectural ensemble and reflects a prioritization of functional needs over heritage conservation. This highlights the absence of regulatory instruments capable of adequately protecting not only the building itself, but also its surrounding cultural landscape.

5.2 Regulatory and institutional challenges in earthen heritage conservation in Mexico

As noted in Section 3, Mexican heritage legislation (DOF, 1972) primarily bases its cataloging criteria on the time of construction, as well as on location within designated heritage zones or proximity to historically significant contexts, thereby overlooking construction materials and techniques in the legal protection process. This creates a contradiction, as earthen buildings of exceptional value may be legally protected due to their historical classification, yet receive insufficient attention if they are isolated, located outside recognized heritage areas, or simply overlooked, as is the case of the *troje* of San Nicolás Tolentino Buenavista. Since restoration projects are regulated by the INAH, which operates within this legal framework, interventions involving earthen construction systems tend to receive consistent oversight only when they are visible and formally recognized. In practice, this process often depends on the willingness of property owners or practitioners to request permits, as official supervision typically begins with this administrative step.

If a building is isolated and no permit is requested, INAH is often unaware of interventions until irreversible changes have already occurred. Furthermore, current legislation does not adequately address the specific complexities of earthen construction systems, and lacks clear technical guidelines tailored to their conservation. As a result, poorly conceived interventions, particularly those involving incompatible materials, can themselves become a source of deterioration. Such cases are common, as the introduction of rigid materials into systems such as adobe or rammed earth frequently leads to structural incompatibilities, especially in seismic regions. When materials with significantly different mechanical behavior are combined, the weaker system, typically the earthen structure, tends to fail, leading to progressive damage caused by the intervention itself.

In practice, few construction companies assume full responsibility for the design of restoration projects. Most interventions rely on contemporary materials that can negatively affect the original structure, and they are frequently carried out without adequate supervision, further aggravating the problem. While it is important to provide technical guidance to practitioners, it is equally necessary to raise awareness about the value of earthen heritage, which is often associated with perceptions of precariousness that hinder its conservation. Awareness efforts should extend beyond professionals to include workers and, most importantly, property owners, who ultimately make the key decisions regarding intervention and preservation.

5.3 Community participation and indigenous stakeholders in heritage management

The role of indigenous communities in heritage conservation processes remains a critical yet often overlooked dimension within heritage management frameworks. In the case of the *troje* of San Nicolás Tolentino Buenavista, its proximity to the *pueblo originario* of San Lorenzo Tezonco highlights the relevance of considering local stakeholders not only as passive observers, but as active participants in decision-making processes. This perspective is also supported by contemporary legal frameworks, such as the Cultural, Natural and Biocultural Heritage Law of Mexico City (GOCM, 2020), which establishes the obligation to consult indigenous communities (i.e., *pueblos originarios*) in decisions affecting their heritage and territory. However, the limited implementation of such frameworks in practice reveals a gap between regulatory intent and actual heritage management processes.

Consultation with indigenous communities in restoration projects should be understood as a fundamental principle, both from an ethical standpoint and within the broader framework of sustainable cultural management. Heritage sites are not merely architectural objects with historical or aesthetic value, they are

embedded within living social, symbolic, and territorial networks, where communities maintain ongoing relationships of memory, identity, and everyday use. In this sense, the exclusion of these communities from decision-making processes represents not only a technical omission, but also a form of cultural dispossession that reproduces historical patterns of marginalization. When restoration is approached solely as a material intervention, there is a risk of stripping heritage assets of their cultural meaning by neglecting their social and symbolic dimensions.

Incorporating community perspectives allows for the recognition of local knowledge, traditional practices, and culturally embedded meanings that cannot be fully understood through a purely technical lens. These forms of knowledge not only enrich the historical interpretation of heritage buildings, but can also contribute practical criteria for their conservation, use, and reinterpretation in the present. From this perspective, consultation is closely linked to the recognition of indigenous communities as rights-bearing subjects, in accordance with existing legal frameworks that establish their right to participate in decisions affecting their environment and cultural heritage. Moreover, community participation fosters processes of social appropriation, strengthening long-term conservation and reducing conflicts derived from interventions perceived as external or imposed.

6. Conclusions

This study demonstrates that the deterioration of the *troje* of San Nicolás Tolentino Buenavista cannot be understood solely as a consequence of material vulnerability, but rather as the result of long-term interactions between technical conditions and heritage management processes. By correlating archival documentation (1970–2009) with field observations, the research identifies a clear relationship between administrative decisions and progressive structural degradation.

Three key findings emerge from this analysis. First, delayed responses to documented structural risks allowed minor pathologies to evolve into critical failures, including partial collapses. Second, the introduction of incompatible materials, particularly rigid systems within earthen construction, generated mechanical imbalances that accelerated deterioration. Third, external interventions, such as the construction of nearby infrastructure, contributed not only to physical damage but also to the loss of spatial and cultural integrity. Together, these factors confirm that deterioration was cumulative and closely linked to management practices rather than to a single technical failure.

A central contribution of this study is the identification of heritage management itself as a potential risk factor. In contexts where coordination is lacking, protocols are unclear, or authorization processes are delayed, management may act as a threat rather than as a protective mechanism. This shifts the perspective from viewing conservation as a purely technical challenge to understanding it as a multidimensional process involving administrative efficiency, regulatory clarity, and technical knowledge. The case also highlights structural limitations within existing legal frameworks in Mexico, particularly the lack of specific guidelines for historic earthen constructions. This underscores the need for more integrated regulatory approaches that incorporate technical, administrative, and social dimensions of conservation. In parallel, the findings emphasize the importance of strengthening awareness among stakeholders, including local communities, practitioners and property owners, to ensure informed decision-making and appropriate interventions.

Finally, although no documents explicitly report seismic damage to the historic *troje*, the documented impact of the 1985 and 2017 earthquakes on earthen structures in Mexico suggests that such effects may have been underreported or overlooked. This points to gaps in documentation and damage assessment, reinforcing the need for more comprehensive evaluation methods that combine archival research with structural analysis. Overall, this study contributes to a broader understanding of how misaligned management systems can actively drive the deterioration of earthen heritage, highlighting the urgency of developing coordinated, technically informed, and context-sensitive conservation frameworks.

Acknowledgments

The authors gratefully acknowledge the *Consejo Nacional de Humanidades, Ciencias y Tecnologías* (CONAHCYT) for the Master's scholarship awarded under CVU 756259, and the CNMH-INAH for the access provided to its archives. The authors also acknowledge the support by Funding – UID/04708, http://doi.org/10.54499/UID/04708/2025, of the CONSTRUCT – Instituto de I&D em Estruturas e Construções – funded by Fundação para a Ciência e a Tecnologia, I.P./ MCTES through national funds.

References

Abad Rodas, María de Lourdes, and Diana Idrovo Carpio. 2016. *"La conservación de la arquitectura de tierra de inmuebles con valor ambiental"* 16° Seminario Iberoamericano de Arquitectura y Construcción con Tierra, Paraguay.

DOF. 1972. "*Ley Federal sobre Monumentos y Zonas Arqueológicos, Artísticos e Históricos*." Originally published in the *Diario Oficial de la Federación* on May 6, 1972. Latest amendment published on April 1, 2024.

DOF. 1975. *"Reglamento de la Ley Federal sobre Monumentos y Zonas Arqueológicos, Artísticos e Históricos*." Originally published in the *Diario Oficial de la Federación* on December 8, 1975. Latest amendment published on January 5, 2024.

Espinoza Vázquez, Pilar. 2025. *"Método de intervención de edifícios patrimoniales de tierra cruda en entornos urbanos. El caso de la Troje de la Antigua Hacienda de San Nicolás Tolentino Buenavista del siglo XVIII en la Ciudad de México."* MSc Thesis, ESIA-IPN, Tecamachalco.

GOCM. 2020. "*Ley de patrimonio cultural, natural y biocultural de la Ciudad de México"*. Published in the *Gaceta Oficial de la Ciudad de México* on October 29, 2020.

Gómez, Ruth, and Carlos Villasana. 2021. *"La antigua hacienda de San Lorenzo Tezonco que hoy es un panteón."* El Universal 4.

Guerrero Baca, Luis Fernando, and Francisco Uviña Contreras. 2020. *"Integración de tierra y cal en restauraciones arquitectónicas."* Gremium, 7 (14): 137–150. https://doi.org/10.56039/rgn14a11

Guerrero Baca, Luis Fernando, and Esteban Ávalos Beltrán. 2022. *"Condicionantes de la salvaguardia de estructuras prehispánicas de tierra en México."* Gremium, 9 (18): 59–72. https://doi.org/10.56039/rgn18a06

INAH, Archivo Histórico y Planoteca Jorge Enciso de la CNMH. 1970a. "*La Troje (Ex Hacienda de Sn. Nicolás) (Hoy Panteón civil de San Lorenzo).*" Official Letter 7004-11-488. Mexico City, February 18.

———. 1970b. "*La Troje (Ex-Hacienda de Sn. Nicolás)(Hoy Panteón civil de San Lorenzo).*" Official Letter 5042-3389. Mexico City, November 24.

———. 1970c. *"La Troje (Ex-Hacienda de Sn. Nicolás)(Hoy Panteón civil de San Lorenzo)."* Report dated December 07, 1970. Mexico City, December 07.

———. 1970d. *"La Troje (Ex-Hacienda de Sn. Nicolás)(Hoy Panteón civil de San Lorenzo)."* Official Letter dated December 14, 1970. Mexico City, December 14.

———. 1989. *"La Troje (Ex-Hacienda de Sn. Nicolás) (Hoy Panteón civil de San Lorenzo)."* Official Letter 401-39-116. Mexico City, April 04.

———. 1990. *"La Troje (Ex-Hacienda de Sn. Nicolás) (Hoy Panteón civil de San Lorenzo)."* Memorandum 10. Mexico City, January 30.

———. 1994a. *"La Troje (Ex-Hacienda de Sn. Nicolás) (Hoy Panteón civil de San Lorenzo)."* Memorandum 113. Mexico City, September 20.

———. 1994b. *"La Troje (Ex-Hacienda de Sn. Nicolás) (Hoy Panteón civil de San Lorenzo)."* Official Letter dated September 22, 1994. Mexico City, September 22.

———. 1994c. “La Troje (Ex-Hacienda de Sn. Nicolás) (Hoy Panteón civil de San Lorenzo).” Official Letter 133/94. Mexico City, October 10.

———. 1994d. *“La Troje (Ex-Hacienda de Sn. Nicolás) (Hoy Panteón civil de San Lorenzo).”* Official Letter 401-39C-833. Mexico City, October 17.

———. 1994e. *“La Troje (Ex-Hacienda de Sn. Nicolás) (Hoy Panteón civil de San Lorenzo).”* Memorandum 116. Mexico City, October 21.

———. 1995a. *“La Troje (Ex-Hacienda de Sn. Nicolás)(Hoy Panteón civil de San Lorenzo).”* Official Letter dated May 12, 1995. Mexico City, May 12.

———. 1995b. *“La Troje (Ex-Hacienda de Sn. Nicolás) (Hoy Panteón civil de San Lorenzo).”* Official Letter dated May 29, 1995. Mexico City, May 29.

———. 1996. *“La Troje (Ex-Hacienda de Sn. Nicolás) (Hoy Panteón civil de San Lorenzo).”* Official Letter 401-22-191. Mexico City, June 10.

———. 2009a. *“La Troje (Ex-Hacienda de Sn. Nicolás) (Hoy Panteón civil de San Lorenzo).”* Official Letter dated March 23, 2009. Mexico City, March 23.

———. 2009b. *“La Troje (Ex-Hacienda de Sn. Nicolás) (Hoy Panteón civil de San Lorenzo).”* Official Letter dated March 27, 2009. Mexico City, March 27.

Lara Paredes, Edgar Allan. 2017. *“La imagen de pueblo se perdió: La lucha por la tierra en San Lorenzo Tezonco de zona Lacustre a zona industrial (1904-1949).”* Mexico City: UNAM.

Nazario Cruz, Luis Fernando. 2014. *“El título primordial de San Lorenzo Tezonco.”* Mexico City: *Asamblea Legislativa VI Legislatura*.

Robles García, Nelly and Jack Corbett. 2018.“From Archaeological Site to World Heritage Site: The Emergence of Social Management at Monte Alban, Mexico.” In: Makuvaza, S. (eds) Aspects of Management Planning for Cultural World Heritage Sites. Springer. https://doi.org/10.1007/978-3-319-69856-4_4

Rotondaro, Rodolfo, Yolanda Aranda-Jiménez, and Ariel González, eds. 2024. “Marcos normativos de la arquitectura y construcción con tierra en Iberoamérica.” 1st ed. Buenos Aires: Red Iberoamericana PROTERRA.

Sánchez-Calvillo, Adrià, Lidia Rincón, Erwan Hamard and Paulina Faria. 2024. "Bibliometric Analysis on Earthen Building: Approaches from the Scientific Literature and Future Trends". Buildings 14 (12): 3870. https://doi.org/10.3390/buildings14123870

SEDUE. 1984. “*Especificaciones generales de restauración*.” Mexico City: SEDUE.

cinpar2026
XXII International Conference on Building Pathology and Constructions Repair
15th to 17th July 2026 - Lisboa, Portugal

Proposed Adaptation of the GUT Criticality Matrix for the Maintenance Management of Concrete Pavements in Fuel Stations: A Comparative Approach between Mechanical Damage and Chemical Attack

Larissa GUIMARÃES[1], Marília ARAÚJO[2]

[1] Instituto Nova Engenharia, Brazil, englpcarneiro@gmail.com
[2] Instituto Nova Engenharia, Brazil, marilia@construpat.com.br

Abstract: The maintenance management of concrete pavements in fuel station networks requires rigorous prioritization of interventions within a context characterized by the simultaneous occurrence of pathological manifestations, operational risks, and budgetary constraints. The absence of hierarchical assessment tools specifically tailored to this type of infrastructure often results in delayed corrective actions, with significant technical, environmental, and economic impacts throughout the service life of the pavement system.

This study proposes the adaptation of the GUT Criticality Matrix (Gravity, Urgency, and Trend) for the maintenance management of pavements in fueling areas, integrating the assessment of mechanical damage and deterioration associated with chemical attack.

The methodology is based on a multi-case study conducted at 16 fuel stations, using a systematized visual inspection protocol that included the mapping of cracking, abrasion-induced wear, surface disintegration, and failures in joint sealing systems.

The research establishes differentiated weighting parameters capable of distinguishing operational safety risks from environmental risks and evaluates the effectiveness of the adapted matrix as a decision-support tool for defining preventive maintenance strategies.

The findings are applicable to concrete pavements in service subjected to highly aggressive environments, contributing to the improvement of maintenance management practices in infrastructures exposed to the combined action of cyclic loads and chemical agents.

Keywords: Maintenance Management; GUT Criticality Matrix; Concrete Pavements; Building Pathology; Fuel Stations.

1. Introduction

The deterioration of concrete pavements in operational areas represents a significant issue in infrastructure engineering, particularly when these systems are simultaneously subjected to intense mechanical loading and chemically aggressive environments (ACI 2013; FHWA 2015; Neville 2011). In fuel stations, this condition is especially critical, as fueling lanes are exposed to cyclic traffic from heavy vehicles and frequent contact with hydrocarbons and petroleum derivatives, creating a scenario conducive to the progressive degradation of concrete (Neville 2011; FHWA 2015).

The interaction between mechanical stresses and physicochemical processes promotes the development of pathological manifestations such as cracking, joint spalling, surface wear, and chemical contamination, compromising both the structural performance and durability of the pavement (Neville 2011; FHWA 2015, ASTM 2020). Furthermore, discontinuities such as joint sealing failures act as preferential pathways for the infiltration of aggressive fluids, intensifying deterioration mechanisms and potentially causing environmental impacts associated with subgrade contamination (FHWA 2015; DNIT 2004a).

In this context, the systematic identification and classification of pathological manifestations constitute fundamental steps for assessing pavement condition and planning effective maintenance strategies (ASTM 2020; DNIT 2004b). Methods based on standardized visual inspection, such as those established by ASTM

(ASTM D6433) and procedures from Departamento Nacional de Infraestrutura de Transportes (DNIT), enable the characterization of damage extent and severity, providing a consistent technical basis for decision-making (ASTM 2020; DNIT 2004b).

Concurrently, the maintenance management of infrastructure assets requires the incorporation of criticality and risk criteria in order to prioritize interventions under budgetary and operational constraints (ISO 2014). Decision-support tools such as the GUT matrix (Gravity, Urgency, and Trend) are widely used for problem prioritization, allowing not only the assessment of damage severity but also the urgency of intervention and the potential for deterioration over time (Kepner and Tregoe 1981; Seleme and Stadler 2010).

However, the traditional application of the GUT matrix in engineering systems presents limitations related to subjectivity in parameter assignment, especially when based solely on the evaluator's perception (Kepner and Tregoe 1981; Seleme and Stadler 2010). This limitation becomes even more critical in pavements exposed to combined deterioration mechanisms, in which the isolated assessment of physical severity may not adequately reflect the associated functional and environmental risks.

Given this context, this study proposes an adaptation of the GUT matrix for the maintenance management of concrete pavements in fuel stations, incorporating measurable physical parameters and objective technical criteria for criticality assessment. The developed methodology integrates the analysis of pathological manifestation severity with functional and risk aspects, aiming to reduce subjectivity in the decision-making process and to improve the prioritization of interventions in environments subjected to the combined action of mechanical loads and chemical agents.

2. Theoretical Framework

The deterioration of concrete pavements results from the interaction between physical, mechanical, and chemical mechanisms that progressively affect their structural and functional performance (ACI 2013; Neville 2011). Discontinuities such as cracks, joint failures, and surface degradation facilitate the infiltration of water and aggressive substances, contributing to the progression of deterioration and the reduction of pavement service life (ACI 2013; ABNT 2014). In operational areas subjected to cyclic traffic from heavy vehicles and exposure to hydrocarbons, such as fuel stations, damage associated with mechanical loading coexists with processes related to infiltration and chemical degradation of concrete (ACI 2013; Neville 2011). The simultaneous action of these mechanisms may intensify deterioration and compromise the structural integrity and durability of the pavement over time.

Repeated exposure to fuels and petroleum derivatives may promote chemical attack processes within the cementitious matrix. Although hardened concrete exhibits relative stability when exposed to pure mineral oils, commercial fuels often contain organic compounds capable of reacting with cement hydration products, particularly under oxidative conditions or in the presence of acidic fractions associated with biodiesel blends (Neville 2011). These reactions may lead to partial dissolution of the cement paste, increased capillary porosity, and reduced surface strength, thereby favoring progressive degradation of the concrete (ACI 2013).

In this context, a combined deterioration mechanism is established, in which physicochemical processes and mechanical loading act synergistically. Surfaces previously weakened by chemical attack become more susceptible to abrasion and spalling when subjected to stresses induced by heavy vehicle traffic (FHWA 2015). Additionally, structural discontinuities such as cracks or poorly sealed joints may act as preferential pathways for infiltration, facilitating the percolation of aggressive fluids and contributing to support loss phenomena, such as fines pumping (DNIT 2004a; Neville 2011).

The evaluation of rigid pavement condition is based on the systematic identification and classification of pathological manifestations, constituting a fundamental step in characterizing its structural and functional state. Technical standards such as ASTM D6433 and Departamento Nacional de Infraestrutura de Transportes (DNIT 061/2004) establish standardized criteria for visual inspection and defect classification

based on their extent and severity, recognizing these parameters as key indicators of pavement condition (ASTM 2020; DNIT 2004b). The application of these criteria enables an objective characterization of the physical state of the structure and provides a consistent technical basis for maintenance planning.

Beyond physical condition, infrastructure asset maintenance management requires consideration of functional criticality and the risk associated with deterioration progression. The guidelines of International Organization for Standardization (ISO 55000) establish that maintenance decisions should integrate asset condition assessment with operational impact and risk level, aiming to ensure performance and reliability (ISO 2014).

In this context, prioritization tools are frequently employed to support decision-making processes in maintenance management. Among these, the GUT matrix (Gravity, Urgency, and Trend) stands out, as its structure enables the ranking of problems based on damage severity, urgency of intervention, and the trend for deterioration over time, constituting a widely used tool in management and criticality analysis processes (Kepner and Tregoe 1981; Seleme and Stadler 2010).

3. Methodology

3.1 General Structure of the Proposed Method

The proposed method consists of adapting the GUT matrix (Gravity, Urgency, and Trend) for the classification of the criticality of pathological manifestations in concrete pavements, based on the integration of measurable physical deterioration parameters, operational criteria, and risk-related aspects. The structure of the method was developed with the objective of reducing the subjectivity associated with the traditional application of the GUT matrix, establishing objective and reproducible technical criteria for prioritizing maintenance interventions, in accordance with the asset management principles established by International Organization for Standardization (ISO 55000) (ISO 2014).

The proposed adaptation is based on the introduction of the Pathological Condition Index (ICP), defined as the product of three independent parameters that characterize the observed condition of the pathological manifestation: extent (E), intensity (I), and functional impact (F). The extent parameter represents the proportion of the affected area relative to the analyzed functional area, while intensity describes the level of observed physical degradation, and functional impact represents the influence of the pathological manifestation on pavement performance and functionality.

The Pathological Condition Index (ICP) is determined according to Equation (1):

$$ICP = E \times I \times F \tag{1}$$

The ICP does not replace the normative severity classification defined by ASTM D6433; rather, it constitutes a complementary index specifically developed to support prioritization processes in asset management by integrating physical and functional parameters into a single metric.

In the proposed method, Gravity (G) is not assigned directly through qualitative judgment, as in the traditional application of the GUT matrix. Instead, Gravity is derived from the Pathological Condition Index (ICP), establishing a correspondence between the measurable physical condition of the pathological manifestation and the severity level used in the matrix.

The relationship between the Pathological Condition Index and Gravity is defined through a discrete classification function, as represented in Equation (2), in which G corresponds to the assigned gravity level and ICP represents the index calculated based on measurable physical parameters.

$$G(ICP) = \begin{cases} 1, & \text{if } 1 \leq ICP \leq 5 \\ 2, & \text{if } 6 \leq ICP \leq 15 \\ 3, & \text{if } 16 \leq ICP \leq 30 \\ 4, & \text{if } 31 \leq ICP \leq 60 \\ 5, & \text{if } 61 \leq ICP \leq 125 \end{cases} \tag{2}$$

Based on the obtained values, gravity can be classified according to Table 1.

Table 1 – Gravity (G) Classification as a Function of the Pathological Condition Index (ICP)

Pathological Condition Index (ICP)	Gravity (G)	Classification
1 to 5	1	Very Low
6 to 15	2	Low
16 to 30	3	Moderate
31 to 60	4	High
61 to 125	5	Very High

The final criticality of the pathological manifestation is obtained as the product of the three parameters of the GUT matrix, as presented in Equation (3):

$$\text{Criticality} = G \times U \times T \tag{3}$$

where G represents the severity of the pathological manifestation, derived from the Pathological Condition Index; U represents the urgency of intervention; and T represents the trend of deterioration progression, considering the physical mechanisms and exposure conditions that influence its evolution.

The proposed structure has a heuristic nature and was developed based on risk engineering principles and the operational logic of the GUT matrix. The adoption of a multiplicative formulation for the Pathological Condition Index is grounded in the interdependent nature of the parameters extent, intensity, and functional impact, in which the combination of high values results in a non-linear increase in severity, reducing compensation effects between variables that are common in additive approaches. Similarly, the criticality defined as the product of Gravity, Urgency, and Trend maintains consistency with the classical structure of the GUT matrix, preserving the combined influence of the factors that govern the prioritization of interventions.

The adopted scales reflect the nature of the evaluated parameters: extent, intensity, and functional impact represent discrete states of observable physical condition and were defined in four levels, in order to balance discrimination capability and field reproducibility. In turn, the parameters Urgency and Trend, associated with decision-making and damage progression, were defined in five levels, allowing greater sensitivity in differentiating operational scenarios and deterioration regimes.

The conversion of the Pathological Condition Index into Gravity levels was established through increasing ranges that preserve the hierarchy of observed deterioration and allow its compatibility with the GUT matrix scale. The final classification of criticality was structured into four priority levels, aiming to simplify the application of the method in maintenance management while enabling clear definition of intervention strategies, without compromising the model's sensitivity, which is ensured by the preceding calculation stages.

3.2 Pathological Manifestations and Condition Assessment Parameters

The pathological manifestations considered in this study were selected based on systematized visual inspections carried out on concrete pavements in fuel stations, identifying the most relevant occurrences in terms of frequency and functional impact. The identification and classification of these manifestations were

based on the terminology and criteria established by Departamento Nacional de Infraestrutura de Transportes (DNIT 060/2004), which defines the main defects in rigid pavements and their associated mechanisms (DNIT 2004a).

Based on these criteria and on field-observed conditions, the following pathological manifestations were considered: joint sealant failure, joint spalling, cracking, corner break and localized failures, surface wear, and superficial chemical contamination.

The characterization of the physical condition of each pathological manifestation was performed through the classification of the parameters extent (E), intensity (I), and functional impact (F), as defined in Section 3.1.

The extent parameter (E) was defined as the relative proportion of the element affected by the pathological manifestation, in accordance with deterioration assessment criteria based on damage extent established by ASTM (ASTM D6433) (ASTM 2020). The adopted classification is presented in Table 2.

Table 2 – Classification of the Extent Parameter (E)

Classe	Relative extent of the affected element
1	Up to 10% of the affected element
2	Between 10% and 30%
3	Between 30% and 60%
4	Greater than 60%

The intensity parameter (I) represents the level of observed physical degradation and is defined based on measurable characteristics such as crack width, depth of material loss, and degree of surface deterioration, in accordance with the severity criteria established by ASTM (ASTM D6433) and concrete durability guidelines (ACI 2013; ASTM 2020). The adopted criteria are presented in Table 3.

Table 3 – Classification Criteria for the Intensity Parameter (I)

Pathological Manifestation	Low (1)	Moderate (2/3)	Critical (4)
PM 01 – Joint Sealant Deficiency	Sealant with superficial cracks, still adhered	Dried sealant or partial loss of adhesion / Sealant with continuous failures	Sealant absent
PM 02 – Joint Spalling	Depth less than 5 mm	Depth less than 5 mm / Between 5 mm and 20 mm	Depth greater than 20 mm
PM 03 – Cracking	Crack width < 0.3 mm	0.3–1.0 mm / 1.0–3.0 mm	> 3,0 mm
PM 04 – Corner Break and Localized Failure	Depth < 10 mm	Depth between 10 mm and 25 mm / Between 25 mm and 50 mm	Severe loss, depth > 50 mm or affecting a large portion of the slab thickness
PM 05 – Surface Wear	No significant aggregate exposure	Partial aggregate exposure / Generalized exposure	Significant loss of surface thickness

Pathological Manifestation	Low (1)	Moderate (2/3)	Critical (4)
PM 06 – Superficial Chemical Contamination	Staining without texture alteration	Visible with slight alteration / Impregnation with surface texture alteration	Severe impregnation with signs of concrete degradation

The functional impact parameter (F) represents the influence of the pathological manifestation on pavement performance, considering aspects such as infiltration, loss of support, and impairment of load transfer. This parameter allows the incorporation of functional effects associated with the observed damage into the physical assessment (ACI 2013; Neville 2011). The adopted criteria are presented in Table 4.

Table 4 – Classification Criteria for the Functional Impact Parameter (F)

Pathological Manifestation	Low (1)	Moderate (2/3)	Critical (4)
PM 01 – Joint Sealant Deficiency	No evidence of infiltration / Potential infiltration	Visible infiltration / Presence of fines or contamination within the joint	Evidence of loss of support, pumping, or associated structural degradation
PM 02 – Joint Spalling	No significant functional impact	Minor interference in load transfer / Significant interference	Evident functional loss or structural impairment of the joint
PM 03 – Cracking	Superficial crack without immediate functional impairment	Visible infiltration / Presence of associated degradation	Structural impairment or slab instability
MP 04 – Corner Break and Localized Failure	Potential impact without instability	Onset of local integrity loss / Compromise of slab corner stability	Significant structural impairment or risk of progressive failure
PM 05 – Surface Wear	Potential impact on durability	Increased surface permeability / Impairment of surface strength or texture	Significant functional impairment with associated structural risk
PM 06 – Superficial Chemical Contamination	Potential impact on surface durability	Localized functional alteration / Impairment of surface durability	Significant degradation with risk of progressive deterioration

The combined classification of the extent, intensity, and functional impact parameters enables an objective characterization of the physical condition of pathological manifestations, providing a consistent technical basis for the calculation of the Pathological Condition Index and the subsequent evaluation of criticality according to the proposed method.

3.3 Urgency and Trend Classification

In addition to the physical severity of the pathological manifestation, the prioritization of interventions must consider operational factors and the likelihood of deterioration progression. In this context, the Urgency (U)

and Trend (T) parameters were defined based on observable technical criteria, incorporating functional, regulatory, and environmental aspects into the criticality assessment, in accordance with the asset management principles established by International Organization for Standardization (ISO 55000) (ISO 2014).

In this adaptation, the Urgency parameter does not represent the relative importance of the assessed area, since fueling lanes present a homogeneous intrinsic operational criticality. Instead, it represents the available time window for intervention before the evolution of the pathological mechanism to functionally or environmentally critical degradation states, in line with condition-based maintenance and asset management principles established by ISO 55000.

The Trend parameter (T) represents the rate and likelihood of future deterioration progression and is defined based on the active pathological mechanisms and exposure conditions. This parameter is defined independently of the current severity level and reflects the intrinsic kinetic behavior of the degradation mechanism under prevailing environmental and operational conditions, in accordance with durability and deterioration principles established by the American Concrete Institute (ACI 201.2R-13) and the classical literature on construction pathology. The technical criteria adopted for assigning these parameters are presented in Table 5.

In the present model, aspects related to environmental risk are not treated as an independent variable but are incorporated into the Urgency (U) and Trend (T) parameters. Urgency reflects the need for intervention in view of the potential for short-term functional and environmental impairment, while trend incorporates the progression dynamics of deterioration associated with exposure to aggressive agents, such as hydrocarbons. Thus, manifestations with potential for infiltration or contamination tend to assume higher values in these parameters, reflecting their greater environmental impact. In this way, environmental risk is considered in an integrated manner within the criticality assessment process, in accordance with a risk-based management approach.

Table 5 – Measurable Criteria for the Urgency (U) and Trend (T) Parameters

Parameter	Low Range (Scores 1–2)	Moderate Range (Score 3)	Severe/Critical Range (Scores 4–5)
Urgency (U) *(Context, Timeframe, and Standards)*	Long term: Damage with slow progression, with no expectation of functional, structural, or environmental impairment in the short term	Medium term (serviceability limit state reached): Damage with potential to evolve into functional or environmental impairment in the medium term	Immediate action (zero timeframe): Damage with a high probability of rapidly evolving into functional, structural, or environmental impairment
Trend (T) *(Kinetics under Traffic)*	Stabilized / Slow: Inactive progression (e.g., old shrinkage cracks) or long-term natural wear.	Linear: Continuous mechanical degradation, progressing proportionally to traffic volume	Exponential: Accelerated dynamics (e.g., fines pumping, or continuous chemical dissolution)

The final criticality is determined as the product of Gravity, Urgency, and Trend, as defined in Equation (3). Based on the obtained values, criticality was classified into priority levels for intervention, as presented in Table 6, enabling the consistent application of the method in maintenance management.

Table 6 – Criticality Classification

Criticality Range	Classification
1 – 15	Low
16 – 40	Moderate
41 – 80	High
81 – 125	Critical

3.4 Field Application of the Method

The proposed method was applied to concrete pavements in sixteen operating fuel stations located in the state of Bahia (Feira de Santana, Candeias, Lauro de Freitas, Imbassaí, and Camaçari), a region with a tropical climate characterized by high temperatures and a seasonal rainfall regime. The stations were selected based on the operational representativeness of fueling areas subjected to mixed traffic and exposure to potentially aggressive agents.

The analyzed pavements consist of cast-in-place concrete slabs with distribution reinforcement (welded wire mesh) and a typical thickness of 20 cm. It was observed that four units are between 5 and 10 years old, while the remaining ones are over 10 years old. It is noteworthy that no structured record of recent maintenance was available for the analyzed pavements.

The inspections were conducted in February by more than one evaluator with a background in civil engineering, using a standardized inspection form in accordance with the procedures established by ASTM (ASTM D6433) (ASTM 2020).

For each occurrence, the parameters extent (E), intensity (I), and functional impact (F) were determined, enabling the calculation of the Pathological Condition Index and Gravity. Subsequently, the Urgency (U) and Trend (T) parameters were assigned, allowing the calculation of criticality. The data were organized into a structured database, enabling comparative analysis between manifestations and evaluated units.

4. Results and Discussion

4.1 Database Structuring

The application of the proposed method resulted in the structuring of a database containing records of the pathological manifestations identified during the inspections carried out on the evaluated pavements. For each occurrence, the parameters extent (E), intensity (I), and functional impact (F) were organized according to the criteria defined in Section 3, enabling an objective characterization of the physical condition and the calculation of severity and criticality indices.

Table 7 presents an example of the data structure used for the classification of pathological manifestations in one of the evaluated pavements.

Table 7 – Database structure for the classification of pathological manifestations

Station	Pathological Manifestation	Extent (E)	Intensity (I)	Functional Impact (F)
S011	Joint Sealant Deficiency	4	4	3
S011	Joint Spalling	1	1	2

4.2 Calculation of the Pathological Condition Index and Gravity

Based on the structured data, the Pathological Condition Index (ICP) was calculated for each identified pathological manifestation using the parameters extent (E), intensity (I), and functional impact (F). From the ICP value, Gravity (G) was assigned, followed by the determination of the Urgency (U) and Trend (T) parameters, enabling the calculation of criticality according to the proposed method.

The adoption of maximum criticality values as an analytical parameter is grounded in a conservative asset management approach. In infrastructures susceptible to environmental liabilities and structural failures, the prioritization of interventions must necessarily be guided by the highest operational risk scenario (worst case), ensuring that acute manifestations are not underestimated or diluted by global statistical averages of the pavement.

The parametric conversion of physical degradation into discrete numerical indices ensures that pathological manifestations of different natures are assessed under a unified risk metric, mitigating the subjective biases inherent to purely visual inspection. Table 8 presents the structure used for determining these parameters in one of the evaluated pavements.

Table 8 – Example of ICP and criticality calculation

Station	Pathological Manifestation	E	I	F	ICP	G	U	T	Criticality
S011	Joint Sealant Deficiency	4	4	3	48	4	3	3	36 (Moderate)
S011	Joint Spalling	1	1	2	2	1	1	3	3 (Low)
S011	Superficial Chemical Contamination	3	3	4	36	4	3	4	48 (High)

4.3 Criticality Classification of Pathological Manifestations

The application of the proposed method enabled the classification of the criticality of pathological manifestations identified in the evaluated pavements, allowing for comparative analysis among different types of deterioration. The results revealed variations in criticality as a function of the deterioration mechanism and the associated functional impact.

Preliminary analysis of the calculated criticality values indicates that manifestations associated with surface deterioration and chemical exposure tended to present higher criticality levels than those predominantly related to mechanical deterioration. This behavior suggests that the proposed method is capable of distinguishing different deterioration mechanisms according to their potential impact on pavement performance and durability.

Table 9 presents the consolidation of the obtained results, considering the maximum criticality values observed for each type of pathological manifestation.

Table 9 – Criticality classification by type of pathological manifestation

Pathological Manifestation	Maximum Observed Criticality	Classification
Joint Sealant Deficiency	36	Moderate
Joint Spalling	12	Low
Cracking	27	Moderate
Corner Break and Localized Failure	18	Moderate
Surface Wear	48	High
Superficial Chemical Contamination	60	High

The results reveal variations in criticality levels as a function of the nature of the manifestation and its associated functional impact, showing that certain manifestations reached high classifications, while others remained predominantly within low to moderate levels. The obtained classification demonstrates that the method enables the discrimination of different deterioration patterns based on objective criteria, establishing a consistent technical basis for the interpretative analysis presented in the subsequent section.

4.4 Comparative Analysis between Mechanical Damage and Chemical Attack–Related Deterioration

The consolidation of the results presented in Table 9 highlights distinct patterns of behavior between predominantly mechanical manifestations and those associated with loss of watertightness and exposure to aggressive chemical agents. Mechanical-type manifestations exhibited maximum criticalities classified between low and moderate. Although such pathologies may compromise local structural performance, their progression was shown to be primarily linked to mechanical loading imposed by cyclic traffic, with evolution conditioned by stress redistribution and the integrity of slab support, as described in the technical literature on rigid pavements.

In contrast, manifestations associated with joint sealant failure and superficial chemical contamination reached higher criticality levels, including high classifications. A greater influence of these mechanisms was observed on the Urgency (U) and Trend (T) parameters, particularly when associated with the risk of infiltration of aggressive fluids and the acceleration of concrete degradation processes. This behavior is consistent with durability principles established by the American Concrete Institute (ACI), according to which the ingress of aggressive agents is a determining factor in intensifying deterioration and reducing the service life of the material.

From a pathological perspective, the inherently aggressive environment of fuel stations amplifies the criticality of these surface anomalies. Chronic spillage of hydrocarbons, especially commercial mixtures containing biodiesel fractions, induces oxidation reactions that release organic acids onto the pavement surface. These compounds react directly with portlandite (calcium hydroxide) in the cementitious matrix, leading to dissolution and softening of the hardened paste. Consequently, the concrete exhibits reduced abrasion resistance and increased capillary porosity, becoming a highly permeable medium. This irreversible degradation cycle increases the Trend (T) parameter in the adapted matrix, highlighting the severity of chemical exposure.

The comparison between the groups indicates that, while mechanical damage is predominantly related to immediate structural performance, manifestations associated with chemical attack present a greater potential for progression and cumulative impact on system durability. This distinction reinforces the importance of considering the dominant deterioration mechanism when interpreting the obtained criticality levels, validating the adoption of management protocols that prioritize the restoration of system watertightness as a primary conservation premise.

4.5 Applicability of the Method for Intervention Prioritization

The application of the adapted method enabled the systematic classification of the criticality of the observed pathological manifestations, allowing the prioritization of interventions based on objective technical criteria.

The analysis of the set of evaluated manifestations across the 16 fuel stations indicates that, although most occurrences present criticality levels ranging from low to moderate, the highest values are concentrated in specific manifestations, particularly those associated with surface wear and superficial chemical contamination.

When analyzing the maximum criticality per pavement, as presented in Table 10, it is observed that all evaluated units fall within moderate to high priority levels, indicating that the presence of these higher-impact manifestations is a determining factor in defining overall criticality.

Table 10 – Criticality classification by pavement

Station	Maximum Criticality	Priority Classification	Station	Maximum Criticality	Priority Classification
S001	36	Moderate	S009	36	Moderate
S002	36	Moderate	S010	36	Moderate
S003	36	Moderate	S011	48	High
S004	18	Moderate	S012	36	Moderate
S005	60	High	S013	36	Moderate
S006	36	Moderate	S014	36	Moderate
S007	36	Moderate	S015	36	Moderate
S008	60	High	S016	36	Moderate

The consolidated results reinforce the distinction previously observed between assessments based solely on physical severity and those grounded in an integrated risk analysis. The practical relevance of the proposed methodological adaptation is evidenced by the reallocation of intervention priorities when considering combined environmental and mechanical risk. From the perspective of a traditional GUT matrix, manifestations with high visual impact, such as cracking, would tend to be prioritized. However, the obtained results indicate that manifestations associated with loss of watertightness and chemical contamination assume greater relevance in intervention prioritization, highlighting a divergence from conventional approaches predominantly based on visual severity.

This behavior is attributed to the direct influence of these manifestations on the Urgency (U) and Trend (T) parameters. The absence of adequate sealing not only constitutes the root cause for the onset of pumping phenomena and the consequent loss of slab support, but also acts as a direct pathway for subgrade contamination by hydrocarbons.

From a maintenance management perspective, the proposed method may also support the optimization of maintenance planning by directing available resources toward manifestations with greater deterioration potential and associated environmental risk. This approach enables more efficient allocation of maintenance budgets and may contribute to reducing the need for extensive corrective interventions through earlier and more targeted preventive actions.

The results are consistent with established technical practice in pavements subjected to aggressive operational environments, reinforcing the applicability of the method as a robust decision-support tool aligned with durability principles and risk-based management.

5. Conclusion

This study presented an adaptation of the GUT matrix for the maintenance management of concrete pavements in fuel stations, grounding the Gravity (G) parameter in a Pathological Condition Index based on measurable physical parameters. The proposed structure reduced the subjectivity inherent in the traditional application of the tool and improved the consistency and reproducibility of criticality classification.

The application of the method in sixteen operational units demonstrated its feasibility under real service conditions and enabled a comparative assessment of predominantly mechanical damage and manifestations associated with loss of watertightness and chemical attack. The results indicated that, while mechanical damage tends to produce localized structural effects governed by traffic loading, manifestations related to infiltration and chemical contamination exert a greater influence on urgency and deterioration trend, reflecting a higher potential for long-term degradation.

The findings demonstrate that integrating physical severity, operational context, and deterioration potential provides a more comprehensive assessment of pavement condition than approaches based solely on visible damage. The proposed model therefore constitutes a robust technical framework for intervention prioritization in environments exposed to the combined action of cyclic loads and chemical agents, consistent with asset management and concrete durability principles. Although the method demonstrated applicability under real operating conditions, the study was limited to sixteen fuel stations within a specific geographic context. Future studies involving larger datasets, different climatic conditions, and long-term monitoring may contribute to further validating and refining the proposed classification framework.

{References

American Concrete Institute. 2013. *ACI 201.2R-13: Guide to Durable Concrete*. Farmington Hills, MI: American Concrete Institute.

Associação Brasileira de Normas Técnicas. 2014. *ABNT NBR 6118: Projeto de Estruturas de Concreto – Procedimento*. Rio de Janeiro: ABNT.

ASTM International. 2020. *ASTM D6433-20: Standard Practice for Roads and Parking Lots Pavement Condition Index Surveys*. West Conshohocken, PA: ASTM International.

Departamento Nacional de Infraestrutura de Transportes. 2004a. *DNIT 060/2004 – PRO: Defeitos nos Pavimentos Rígidos – Terminologia*. Rio de Janeiro: DNIT.

Departamento Nacional de Infraestrutura de Transportes. 2004b. *DNIT 061/2004 – PRO: Avaliação Objetiva de Pavimentos Rígidos – Procedimento*. Rio de Janeiro: DNIT.

Federal Highway Administration. 2015. *Pavement Maintenance Manual*. Washington, DC: U.S. Department of Transportation.

International Organization for Standardization. 2014. *ISO 55000: Asset Management – Overview, Principles and Terminology*. Geneva: ISO.

Kepner, Charles H., and Benjamin B. Tregoe. 1981. *The New Rational Manager*. Princeton, NJ: Princeton Research Press.

Neville, A. M. 2011. *Properties of Concrete*. 5th ed. Harlow, UK: Pearson Education Limited.

Seleme, Robson, and Humberto Stadler. 2010. *Controle da Qualidade: Ferramentas Essenciais*. Rio de Janeiro: Elsevier.

XXII International Conference on Building Pathology and Constructions Repair
15th to 17th July 2026 - Lisboa, Portugal

Data structuring and systemic failure analysis in built asset management: application to fire detection and suppression system maintenance

Maycon Handerson de Oliveira BESSA[1], Luiz Carlos Magalhães OLIMPIO[2], Gilmário Da Costa RIBEIRO[3], Esequiel Fernandes Teixeira MESQUITA[4], Mylene de Melo VIEIRA[5]

[1] LAREB, Federal University of Ceara, Russas, Brazil, mayconbessa@alu.ufc.br
[2] LAREB, Federal University of Ceara, Russas, Brazil, olimpio@ufc.br
[3] LAREB, Federal University of Ceara, Russas, Brazil, gilmariocosta@alu.ufc.br
[4] LED, Federal University of Ceara, Fortaleza, Brazil, emesquita@ufc.br
[5] LAREB, Federal University of Ceara, Russas, Brazil, mylene.melo@ufc.br

Abstract: This paper proposes a data structuring framework for as-built BIM models, focusing on asset management and risk mitigation in fire protection systems. The research advances the transition from geometry-centric to systems-centric models, enabling the visualization of functional interdependencies among components. The methodology utilizes the Navistools plugin to establish a link between Autodesk Navisworks and an external SQL-based database. This integration facilitates the management of extensive metadata, including asset hierarchies, unique identifiers (GUIDs), and dependency parameters. Validation was conducted at the José de Alencar Theater, a landmark public building in Brazil requiring precise Operation and Maintenance (O&M) strategies. Results demonstrate the effectiveness of visual management in simulating failure scenarios, highlighting cascade effects within detection and suppression loops. Through color-coded viewpoints and status tables, it becomes possible to instantaneously identify zones affected by the inoperability of specific elements, such as pumps or control valves. This data structuring approach enhances decision-making in both emergency and maintenance contexts, promoting operational efficiency and proactive risk mitigation.

Keywords: BIM; SQL; Navisworks; Risk Management; Fire Protection Systems

1. Introduction

Construction asset information must be properly structured to support decision-making during the operation and management phase (Nicał and Wodyński, 2016). In this context, a common database is required to store the information needed throughout the various stages of Architecture, Engineering, and Construction (AEC) and Operation and Maintenance (O&M) (Spilling, 2016). Building Information Modeling (BIM) can enable this information to be stored within a single digital model (Love et al., 2015). However, several difficulties are observed, such as fragmented information, inadequacies in building management (Tsay, Staub-French, and Poirier, 2022), and the slow issuance of work orders (Gao and Pishdad-Bozorgi, 2019). Other challenges relate to the lack of clear roles within the organizational team and the exchange of information between the BIM model and the facility management system (Matarneh et al., 2019).

Nevertheless, BIM remains a transformative technology in the field of facility management (Salzano et al., 2023; Peng, Au-Yong, and Myeda, 2024). A BIM model works as a shared knowledge tool, forming a reliable basis for decision-making during the facility's life cycle (Farghaly et al., 2018). The information required for Asset Management (AM) can be extracted from the model and linked to a database that stores information related to the built asset to form the Asset Information Model (AIM) (Kivits and Furneaux, 2013). The AIM becomes a set of information containers related to the operational phase (ABNT NBR ISO 19650-1, 2022), providing a fundamental basis for improving its management.

Studies by Harode, Ensafi, and Thabet (2022) propose a framework for defining the documentation, requirements, and procedures necessary to establish a systems-centric as-built BIM model. A model with multi-level building system classification allows the maintenance team to visualize components and their

system information in emergency situations. To mitigate fire damage in buildings, proactive management, prevention, and response activities are essential. In the stages preceding incident response actions, the inspection and monitoring of installation elements—such as sprinkler and alarm systems—are fundamental to effective facility management (Bae, Cha, and Jiang, 2025). However, the integration between BIM models and asset management faces semantic and taxonomic barriers (Pärn, Edwards, and Sing, 2017).

To address this issue, this study proposes a four-level structuring utilizing a SQL environment to direct data flows for fire protection system management. The objective is to develop an Asset Information Model (AIM) for smoke detection and fire protection systems to support maintenance management. The model is prepared to deliver the necessary information for critical operations and to address operational challenges, aiming at both safety and efficiency.

2. Theoretical Background

2.1 Information management on buildings

Building information models has the potential to support quick access to relevant data during emergency situations (Schönfelder et al., 2024). The semantic richness of elements and the information flow among project stakeholders characterize the application maturity (Succar, 2009). These flows must be perceived and designed, as their properties will define the characteristics of the databases and the platforms for access, input, and exchange. Thus, the definition of containers and their semantic structures are crucial stages for information and project management. Some approaches include the Information Container for Linked Document Delivery (ICDD) (ABNT NBR ISO 19650-1, 2022; Hagedorn et al., 2022) and its integration into a Common Data Environment (CDE) (Karlapudi, Prathap, and Menzel, 2021), incorporating languages such as SPARQL or SQL into asset information management (Kim et al., 2024) and guiding the choice of compatible platforms.

Leveraging the potential of computerized models requires properly structured information to mitigate interpretation errors and reduce response times. At the core of this data structure is the ontological definition, which assigns meaning to the labels of each element. This grouping task is vital for simplification; establishing systems and subsystems defines meaning based on interrelationships, breaking down complexity into smaller, more comprehensible clusters (Succar, 2009). This process can be defined as taxonomy, which is the description of terms and their relationship within a specific knowledge domain. Developing an object taxonomy can provide a common terminology that facilitates knowledge sharing, helps identify knowledge gaps in the field, and supports decision-making (Usman et al., 2017).

Data structuring plays a fundamental role in ensuring that building information models remain accessible and comprehensible for asset management teams (Ensafi, Harode, and Thabet, 2022). Modern buildings frequently incorporate highly complex and interconnected systems, including mechanical, electrical, security, and automation systems. In such environments, specialized teams are typically responsible for the operation and maintenance of individual systems. Given this multidisciplinary nature, organizing information requires distinct semantic frameworks tailored to the specific needs of each technical specialty.

The implementation of unique identifiers underpins data consistency, interoperability, and traceability throughout the facility life cycle, facilitating the integration of dynamic information flows (Kim et al., 2024) across web-based platforms (Hagedorn et al., 2023) and relational databases (Bae, Cha, and Jiang, 2025). Such methods for information allocation and organization are well-established within the field of data science. Specifically, Structured Query Language (SQL) serves as the industry-standard tool for developing and managing relational databases, offering robust logical frameworks for storing complex, interrelated datasets (Silberschatz, Korth, and Sudarshan, 2020). Integrating relational databases with digital building has become increasingly feasible through advancements in BIM. Such integration allows for the management of complex metadata tied to assets, streamlining hierarchical organization, dependency mapping, and life cycle monitoring (Wong and Lee, 2022; Hagedorn et al., 2023). As a result, BIM models are

shifting from geometric representations toward comprehensive information repositories that empower decision-making throughout the facility's operational life.

2.2 Fire Safety System Management

The incorporation of automated and intelligent approaches has expanded the role of BIM as a critical infrastructure for managing operational data, supporting essential maintenance activities (Wang et al., 2025) and improving process quality (Leygonie, Motamedi, and Iordanova, 2022). This is particularly relevant for Fire Safety Equipment (FSE), where long life cycles and high costs often lead to deficiencies in inspection and maintenance (Liu, Zhang, and Zhu, 2012). Since irregular inspections and outdated layouts can compromise protection and increase fire risks (Shafiq et al., 2022), the recurrence of discrepancies between management platforms and actual equipment status remains a significant challenge. Consequently, implementing automated structures for status verification within a BIM-based framework is essential to enhance the efficiency and reliability of fire safety systems (Lin et al., 2025; Pishdad-Bozorgi et al., 2018).

Maintenance management based on the individual identification and precise location of each equipment is essential in FSE. To this end, technologies such as GPS (Ergen, Akinci and Sacks, 2007), RFID (Elghamrawy and Boukamp, 2010), UWB (Teizer, Venugopal and Walia, 2008), and 3D LiDAR (Wang et al., 2022) are commonly used. However, these solutions may require additional devices, leading to increased costs (Brilakis, Park and Jog, 2011). In this context, BIM models derived from point clouds enable the representation of the built environment and the linkage of physical elements to their associated data, supporting both design and maintenance management.

Thus, BIM-FSE models contribute to improving the efficiency and effectiveness of inspections by providing structured equipment inventories, supporting navigation to the components, and enabling the systematic updating of information associated with fire system assets (Aziz et al., 2023). Complementarily, digital twins extend these capabilities by enabling the real-time representation of the conditions of physical systems, distinguishing themselves from traditional BIM models and supporting dynamic processes for decision-making and operational optimization (Opoku et al., 2021; Tuhaise, Tah and Abanda, 2023).

3. Methodology

Based on the As-Is model developed by Bessa, M. et al. (2025) (Figure 1), this methodology integrates document review, on-site technical diagnosis, and semantic enrichment to ensure a Level of Development (LOD) consistent with Operation and Maintenance (O&M) requirements. The study, conducted on the Fire Protection System of the José de Alencar Theater, focuses on a high-complexity section of the building. This approach facilitates the transition from a predominantly geometric representation to a systems-oriented Asset Information Model (AIM), specifically engineered for risk management and operational efficiency.

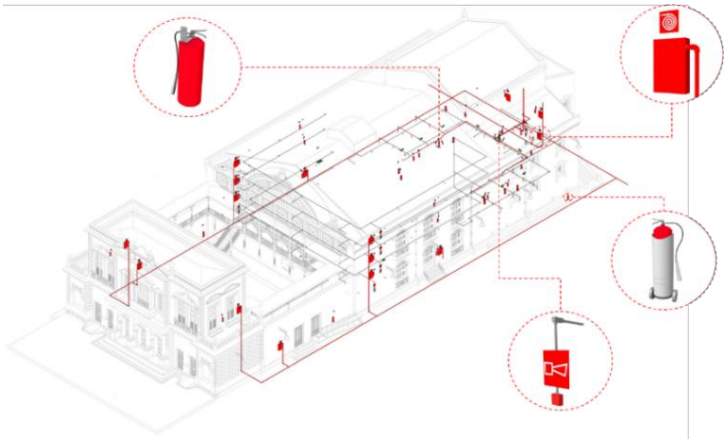


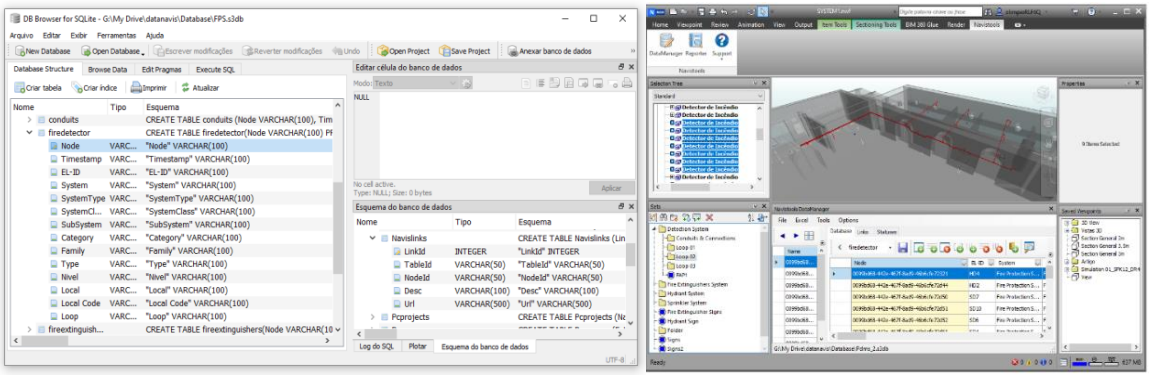
Figure 1 - BIM model of the fire protection system

The BIM model served as geometric and informational framework for the structuring and integration of data critical to O&M. This digital repository encompasses the primary fire protection subsystems: manual suppression (including portable and wheeled fire extinguishers); automatic water-based suppression (the sprinkler network); the Standpipe and Hose System (comprising hydrants and sectional control valves); and the detection and alarm systems.

3.1 Database Organization and Management

The implementation of a relational database linked to model elements enhances the flexibility and accessibility of system information, enabling the management of semantic richness and the selective sharing of data among stakeholders, with access control based on user profiles. This approach contributes to information security and improves communication throughout the building lifecycle. The adoption of SQL allows data and embedded intelligence to be structured and captured in an organized manner, facilitating queries, ensuring data integrity, and maintaining persistence beyond geometric files. The use of a unique primary key (GUID) mitigates errors and optimizes the processing and updating of records.

The database (Figure 2a) was developed in the .s3db format using DB Browser for SQLite (DB4S, 2024), adopting SQL version 3.0 due to constraints of the DataManager and Reporter plugin (Codemil, 2025), also known as NavisTools, which visually integrates data into Autodesk Navisworks. Figure 2b presents a section of the database (index “firedetector”) and the database schema, highlighting the linkage established by NavisTools through the “navislinks” table.



(a) (b)

Figure 2 - (a) Database structure interface in DB Browser for SQLite (b) Navisworks interface illustrating the NavisTools DataManager and Reporter visual platform.

3.2 Fire Protection System Taxonomy

The implementation of BIM for asset management necessitates a paradigm shift, transitioning from purely geometric requirements to the identification of data critical for operational success. Such information should be structured according to a pyramidal classification that spans from early project stages to the Operation and Maintenance (O&M) data gathered during the facility's lifecycle (Becerik-Gerber et al., 2012). To manage this complexity, taxonomies are employed to categorize system attributes and document portfolios, utilizing hierarchical classifications that prioritize spatial location, unique identifiers, and technical specifications (Farghaly et al., 2018). For critical systems like fire protection, a robust taxonomy is essential to ensure data management that supports rapid and accurate decision-making in high-occupancy venues, such as theaters and cinemas.

The taxonomic structure for the fire protection systems in this study follows the iterative ontology development process outlined by Noy and McGuinness (2001). After defining the domain and scope, the focus shifted from geometric data to critical non-geometric requirements. A four-level class hierarchy was then established, extending from the macro-system level (Fire Protection System) to element-specific

attributes (SubSystem Name). This structure ensures a distinct separation between broader domain knowledge and practical operational data.

3.3 Scenario Simulation

The creation of the loop property was intended to capture interdependencies within suppression and detection systems. By defining the LOOP parameter in SQL, the model facilitates the visualization of the "scale effect," allowing, for example, the identification of which sprinkler heads or detectors will be deactivated if a valve is isolated for maintenance (Figure 4). This approach is critical for risk mitigation, as it enables "what-if" analyses prior to any physical intervention. Mapping these loops ensures that the fire protection system is not indiscriminately deactivated, allowing preventive risk measures to be implemented in the affected zones during downtime while maintaining adequate protection in areas not impacted by maintenance activities.

3.4 Visual Management

The developed model provides an accurate graphical representation of the components and building systems. To achieve its informational role, the geometry, spatial orientation, and three-dimensional coordinates of the elements reflect as-is conditions, meeting appropriate Level of Development (LOD) and Level of Accuracy (LOA). The correct representation of in situ conditions enables O&M teams to locate, identify, and inventory assets across the entire building portfolio, reducing uncertainties and rework. In particular, for elements concealed behind walls, ceilings, or floors, reliable BIM models prevent unnecessary destructive interventions during corrective maintenance, renovations, or retrofits.

Within the Lean Construction framework, visual management—or Mieruka—is a fundamental principle for rendering complex information immediately accessible, thereby accelerating effective decision-making (Nguyen, 2009). By eliminating ambiguities and reducing the cognitive load required to interpret vast datasets, Mieruka transforms abstract information into intuitive, actionable visual cues. In this study, visual management serves as the interface that bridges the complexity of SQL-structured data with the Autodesk Navisworks coordination environment. This approach involves pre-configuring the model with specific viewpoints and operational scenarios designed to optimize Facility Management (FM) response. Consequently, highlighting a detection or suppression loop within the model, coupled with the identification of affected zones, allows for an instantaneous situational diagnosis.

4. Results

4.1 Database Management and Taxonomy

The database structuring ensured that the fire system's semantics were preserved independently of the original authoring platform. In this example application, 14 parameters were associated with the automatic sprinkler system (Table 1). Leveraging a database language contributes to both organization and customization, allowing each category—as defined by the management team—to receive a structure tailored to its intended use.

Among the associated parameters is the GUID (Globally Unique Identifier), which serves as the Primary Key for the SQL database. This ensures the semantic richness and information persistence advocated by Succar (2009). From an ontological perspective, the GUID functions as the defining attribute for the identity of the 'concept' (the fire asset), ensuring that the relationship between the geometric object in Navisworks and the non-geometric data in SQL remains unambiguous and imperishable.

Regarding structural adjustments for database management, the GUID is configured within the Navistools plugin as the 'Key Property.' This configuration enables a link (via DataManager) that automates data synchronization between the visual platform and the relational database. This eliminates information

redundancy and inconsistency—common challenges in delivering As-Built models for O&M—resulting in a model that supports updates without losing functional interdependencies."

Table 1 – Parameters, description and objectives in the cluster sprinkler (Level 4).

Parameter	Description	Objective
GUID	Permanent identifier that ensures the bidirectional link and integrity between the 3D geometry and the SQL database.	Data preserving
EL-ID	Secondary asset identifier based on the authoring software's native ID (e.g., Revit ID) for audit traceability.	Identification
SYSTEM	Level 1: Defines the building macro-system to which the asset belongs (e.g., Fire Protection).	System Property
SYSTEMTYPE	Level 2: Classifies the system by its primary function and functional grouping (e.g., Automatic Suppression)	System Property
CLASSIF	Level 3: Details the technology or operating method of the subsystem (e.g., Hydraulic Suppression).	System Property
SYSTEM NAME	Level 4: Identifies the specific technical name of the subsystem or network (e.g., Sprinkler System).	System Property
Category	Native object category in the BIM environment, used for standardizing filters and automatic groupings.	Class Property
Family	Identifies the technical template or design "family" that defines the object's graphical and functional properties.	Class Property
Type	Concise technical specification of the asset's model or variant within its family.	Class Property
Name	Human-readable description for rapid asset identification by field and management teams.	Communication
Local	Identification of the floor or physical location area of the asset within the building.	Rastreability
Local Code	Unique code of the environment (room/space) according to the project's official numbering plan.	Rastreability
***Loop* (Laço)**	Defines the operational "loop" or ring to which the asset is connected, allowing for the tracking of dependencies	Fail Analysis Impact
Installation Date	Historical record of the installation date for warranty control, service life, and technical depreciation..	Life Cycle
Days next task	Predictive parameter that calculates the remaining time until the next preventive maintenance, mitigating failure risks.	Risk Mitigation

The hierarchical structuring of the fire system serves as an ontological foundation that transitions the BIM model from a purely geometric representation to a systems-centric one. This hierarchy acts as a meaning-making mechanism, transforming isolated components into cohesive information clusters that make interdependencies explicit and reduce the cognitive load in asset management. In practice, this 'taxonomic understanding' allows facility managers at José de Alencar Theater to query the SQL database by functional classes rather than generic IDs—searching for 'Detection System - Loop 01' instead of an isolated element. This operational context facilitates rapid fault isolation and enables the automated creation of Selection Sets in Navisworks based on these defined levels (Figure 6a).

The 'Loop' parameter acts as a logical cluster that replicates the physical topology of the fire protection network. This allows the system to identify not only an equipment’s location but also its functional 'ring,' making explicit the interdependencies that cause cascade effects in maintenance or failure scenarios. The results demonstrate more agile and secure data handling, where access to technical information no longer requires physical manuals but occurs directly within the Navisworks.

Furthermore, a natural convergence exists between BIM and Data Science when efforts are directed toward creating a digital ecosystem with integrated data flows. Native parameters—such as category, family, and Element-ID—act as identity anchors, while SQL serves as an expansion medium, establishing a strategic decoupling between geometry and metadata. This architecture allows for the systemic enrichment of the asset without compromising the integrity of the original model, simplifying the complexity inherent in

overlapping maintenance data, standards, and performance metrics. Thus, database management acts as an algorithm for taxonomic organization, ensuring that information flows in a structured and persistent manner, transforming raw data into actionable intelligence for the building's life cycle.

4.2 Scenario Simulation

This section presents two scenarios demonstrating the practical application of a systems-centric BIM model in supporting emergency maintenance. To facilitate operational interpretation, the model employs a color-coded graphical representation (Figure 3), where each system and its respective operational loops are visually distinct. This configuration enables the immediate identification of systems and circuits involved in each simulated event, streamlining the analysis of the functional scope and impact of each occurrence.



Figure 3 - Integrated visualization of fire protection systems, with color coding to distinguish different systems and their respective operational loops

4.2.1 Emergency Simulation – SKP13 Activation (Room C DR4)

Using the viewpoints previously configured in the “Sprinkler System – Loop 02” folder, it was possible to automatically identify the components of the sprinkler system associated with Room C DR4, including pipes, fittings, sectional control valves, and terminal devices (Figure 4). To validate the system-oriented model, an emergency scenario was simulated involving the unintended activation of device SPK13, with the aim of evaluating the model’s capability to support the identification of the affected subsystem, the delimitation of the impact area, and the definition of hydraulic isolation actions.

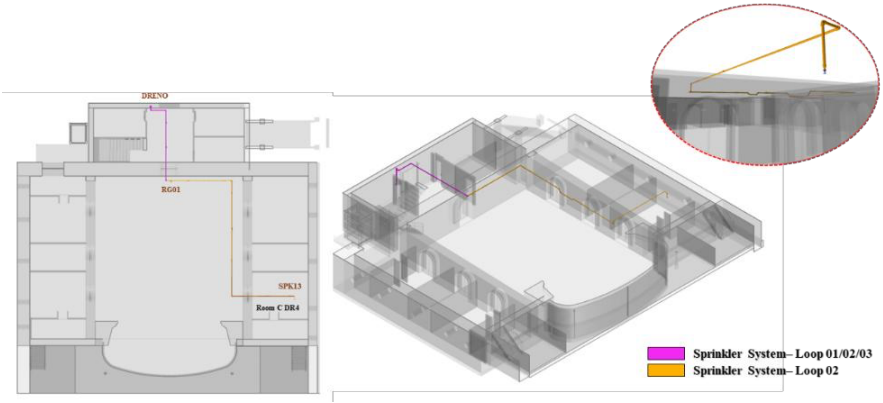


Figure 4 - Emergency simulation with activation of SPK13 and isolation of Loop 02 of the sprinkler system, including spatial tracking of the hydraulic network and identification of the sectional control valve.

In the analyzed scenario, SPK13 was identified as part of Loop 02, which serves devices SPK03 through SPK13. This loop-based organization allowed the automatic isolation—via the corresponding viewpoint—of all hydraulic circuit components, including branch lines, risers, fittings, and control valves, thereby clarifying the functional extent of the event. The analysis identified RG01 as the critical element for the complete

hydraulic isolation of Loop 02, where its closure isolates sprinklers SPK03 to SPK13. Post-isolation, the model facilitated spatial tracking of the piping route to SPK13, enabling the verification of critical network sections during leakages or localized failures (Figure 4). This functionality is vital for the targeted inspection of fittings, directional changes, vertical segments, and interfaces with other building systems.

4.2.2 Emergency Simulation – SD14 Activation (Room D DR1)

In this second emergency simulation, a fire event was triggered by detector SD14 within the building's detection and alarm system. During operation, the alarm control panel signaled an activation without immediate visual confirmation, necessitating the rapid identification of the triggered device, its associated room, the communication loop, and the specific addressing panel. Utilizing the pre-configured viewpoints for the detection system, the model automatically identified detector SD14, its precise spatial coordinates, and its corresponding location within Room D DR1.

Analysis indicated that SD14 belongs to Addressable Loop 03, enabling the operational response to be directed precisely to its corresponding control panel. This loop-based organization allowed for the automatic isolation of all devices within the circuit, facilitating the verification of potential communication failures or infrastructure degradation. Furthermore, the model enabled the tracking of Loop 03's conduit routing, from main segments to individual detector branches. This capability is essential for identifying critical points—such as directional changes, junctions, and shared segments—thereby supporting rapid on-site inspections during actual fire events (Figure 5).

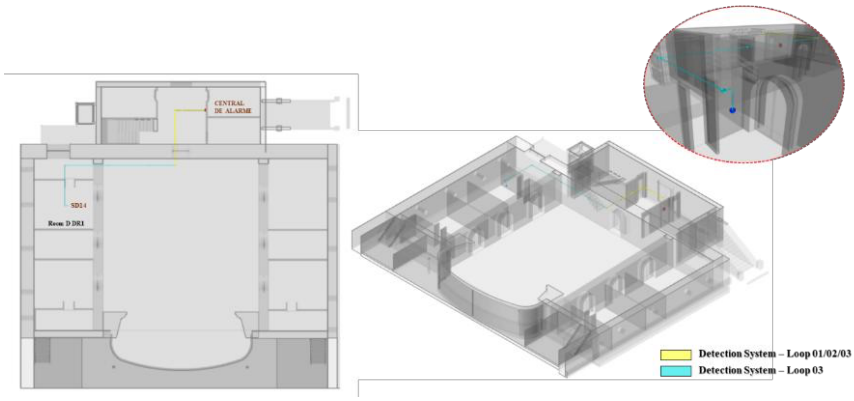


Figure 5 - Emergency simulation with activation of SD14 and isolation of Loop 03 of the detection system, including spatial tracking of the infrastructure.

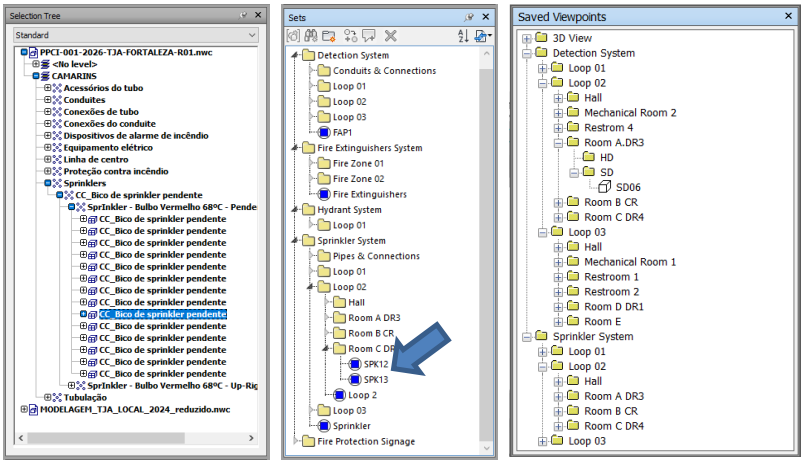
4.3 Visual Management

A systems-centric BIM model configured for O&M enables the application of rule-based filters to functional and relational attributes, allowing for the precise identification, isolation, and selective visualization of components during emergency events. By storing these dynamic visualizations as hierarchical viewpoints, *the model reorganizes navigation and supports rapid decision-making, aligning visual representations* directly with the building's operational logic (Figure 6b). This structure further highlights the interdependencies between multi-disciplinary components, facilitating cross-impact analysis and allowing facility management teams to instantaneously assess the relationships between technical systems, spatial configurations, and occupied areas during an incident.

The filters and search rules required to generate selection sets and viewpoints are defined during the model preparation phase for delivery to the owner, ensuring that, at the start of operation, the model is ready to support emergency response. In addition, new viewpoints can be incorporated throughout the building lifecycle to address operational demands or emerging risk scenarios. In this study, the viewpoints were hierarchically organized to support emergency maintenance, enabling navigation both by operational loop

and by the served space, facilitating the identification of circuits and the visualization of associated assets, such as smoke detectors (SD), heat detectors (HD), and infrastructure elements.

Each space is subdivided into asset-specific folders containing viewpoints that integrate the corresponding subsystem with the architectural model. In this way, viewpoints are simultaneously categorized by loop, space, and equipment type, providing multiple pathways to access operational information. It should be noted that, as this hierarchical structure is directly linked to the physical and functional configuration of the analyzed building, it is project-specific and must be adapted when applied to other facilities, as illustrated in Figure 6b.



(a) (b)

Figure 6 – (a) Selection Tree window, representing the logical structure of the native source program; (b) Sets window for asset management; Viewpoints window for hierarchical organization by loops and spaces.

5. Conclusions

The study demonstrated that the integration between the BIM model and the SQL database, enabled by the NavisTools plugin, overcomes the Level 3 semantic interoperability challenges pointed out by Pärn et al. (2017). The use of GUID as a primary key ensured the persistence of the “semantic richness” encouraged by Succar (2009), allowing critical maintenance and lifecycle information to remain undamaged despite the volatility of geometric files. This decentralized data architecture proved to be an effective solution for managing complex assets, avoiding the overload of native models and facilitating the flow of information among stakeholders.

The application of a four-level functional taxonomy, combined with the methodology proposed by Noy and McGuinness (2001), enabled the transformation of the geometric model into a systems-centered AIM. The clustering of elements into operational loops simplified the inherent complexity of the fire protection system of the José de Alencar Theater. The results demonstrated that organizing data into clusters not only structures the asset inventory but also assigns functional meaning to assets, allowing the management team to instantly visualize interdependencies and impact zones in failure scenarios.

The structuring of viewpoints integrated with automated selection sets demonstrated the potential of Visual Management as a decision-support tool. The transition to an interface that associates non-geometric data (such as “Days to next task”) with 3D spatial representation optimizes response time in O&M activities. It is concluded that the proposed methodology transforms BIM from a static resource into a dynamic data ecosystem, essential for the proactive safeguarding of cultural assets of high social and artistic relevance, where technical accuracy is inseparable from heritage preservation.

Finally, this study contributes to the field of construction management by proposing a data science–driven approach that decouples geometry from information. This flexibility allows the database to be continuously expanded without interfering with the original BIM model, offering a viable and scalable pathway for managers to implement efficient digital asset management.

References

ABNT NBR ISO 19650-1 (2022) Organização da informação acerca de trabalhos da construção — Gestão da informação usando a modelagem da informação da construção. Rio de Janeiro.

Aziz, A. et al. (2023) FULLY AUTONOMOUS FIRE SAFETY EQUIPMENT INSPECTION MISSIONS ON A LEGGED ROBOT PREPRINT PRESENTED AT I3CE 2023 CORVALLIS, OREGON. Available at: https://cocodataset.org/.

Bae, S., Cha, H. and Jiang, S. (2025) "IFC-BIM–Based Fire Information System for Enhancing Preventive Building Maintenance," Journal of Performance of Constructed Facilities, 39(3). Available at: https://doi.org/10.1061/JPCFEV.CFENG-4778.

Becerik-Gerber, B. et al. (2012) "Application Areas and Data Requirements for BIM-Enabled Facilities Management," Journal of Construction Engineering and Management, 138(3), pp. 431–442. Available at: https://doi.org/10.1061/(asce)co.1943-7862.0000433.

Bessa, M. et al. Customized BIM-Maintenance System for Facilities Management. In: 2025.

Brilakis, I., Park, M.-W. and Jog, G. (2011) "Automated vision tracking of project related entities," Advanced Engineering Informatics, 25(4), pp. 713–724. Available at: https://doi.org/10.1016/j.aei.2011.01.003.

Chae, S. and Yoshida, T. (2010) "Application of RFID technology to prevention of collision accident with heavy equipment," Automation in Construction, 19(3), pp. 368–374. Available at: https://doi.org/10.1016/j.autcon.2009.12.008.

DIN SPEC 91391-2 (2019) DIN SPEC 91391-2:2019 Common data environments (CDE) for BIM projects – Function sets and open data exchange between platforms of different vendors – Part 2: Open data exchange with common data environments. Berlin.

Eastman Chuck et al. (2014) Manual de BIM: um guia de modelagem da informação da construção para arquitetos, engenheiros, gerentes, construtores e incorporadores. 2nd ed. Porto ALegre: Bookman Editora.

Elghamrawy, T. and Boukamp, F. (2010) "Managing construction information using RFID-based semantic contexts," Automation in Construction, 19(8), pp. 1056–1066. Available at: https://doi.org/10.1016/j.autcon.2010.07.015.

Ensafi, M., Harode, A. and Thabet, W. (2022) "Developing systems-centric as-built BIMs to support facility emergency management: A case study approach," Automation in Construction, 133, p. 104003. Available at: https://doi.org/10.1016/j.autcon.2021.104003.

Ergen, E., Akinci, B. and Sacks, R. (2007) "Tracking and locating components in a precast storage yard utilizing radio frequency identification technology and GPS," Automation in Construction, 16(3), pp. 354–367. Available at: https://doi.org/10.1016/j.autcon.2006.07.004.

Farghaly, K. et al. (2018) "Taxonomy for BIM and Asset Management Semantic Interoperability," Journal of Management in Engineering, 34(4). Available at: https://doi.org/10.1061/(ASCE)ME.1943-5479.0000610.

Gao, X. and Pishdad-Bozorgi, P. (2019) "BIM-enabled facilities operation and maintenance: A review," Advanced Engineering Informatics, 39, pp. 227–247. Available at: https://doi.org/10.1016/j.aei.2019.01.005.

Hagedorn, P. et al. (2022) "ams-icdd-usecases: Use cases for employing ICDD containers for infrastructure asset management ."

Hagedorn, P. et al. (2023) “BIM-Enabled Infrastructure Asset Management Using Information Containers and Semantic Web,” Journal of Computing in Civil Engineering, 37(1). Available at: https://doi.org/10.1061/(ASCE)CP.1943-5487.0001051.

Halder, S. and Afsari, K. (2023) “Robots in Inspection and Monitoring of Buildings and Infrastructure: A Systematic Review,” Applied Sciences, 13(4), p. 2304. Available at: https://doi.org/10.3390/app13042304.

Harode, A., Ensafi, M. and Thabet, W. (2022) “Linking BIM to Power BI and HoloLens 2 to Support Facility Management: A Case Study Approach,” Buildings, 12(6), p. 852. Available at: https://doi.org/10.3390/buildings12060852.

Hu, D., Gan, V.J.L. and Yin, C. (2023) “Robot-assisted mobile scanning for automated 3D reconstruction and point cloud semantic segmentation of building interiors,” Automation in Construction, 152, p. 104949. Available at: https://doi.org/10.1016/j.autcon.2023.104949.

Karlapudi, J., Prathap, V. and Menzel, K. (2021) “An explanatory use case for the implementation of information container for linked document delivery in common data environments.” . Proceedings of the EG-ICE 2021 Workshop on Intelligent Computing in Engineering.

Kim, Y.-J. et al. (2024) “Advanced fire emergency management based on potential fire risk assessment with informative digital twins,” Automation in Construction, 167, p. 105722. Available at: https://doi.org/10.1016/j.autcon.2024.105722.

Kivits, R.A. and Furneaux, C. (2013) “BIM: Enabling Sustainability and Asset Management through Knowledge Management,” The Scientific World Journal, 2013(1). Available at: https://doi.org/10.1155/2013/983721.

Leygonie, R., Motamedi, A. and Iordanova, I. (2022) “Development of quality improvement procedures and tools for facility management BIM,” Developments in the Built Environment, 11, p. 100075. Available at: https://doi.org/10.1016/j.dibe.2022.100075.

Lin, F. et al. (2025) “Efficient visual inspection of fire safety equipment in buildings,” Automation in Construction, 171. Available at: https://doi.org/10.1016/j.autcon.2025.105970.

Liu, R. and Issa, R.R.A. (2013) “Issues in BIM for Facility Management from Industry Practitioners’ Perspectives,” Computing in Civil Engineering. Reston, VA: American Society of Civil Engineers, pp. 411–418. Available at: https://doi.org/10.1061/9780784413029.052.

Liu, X., Zhang, H. and Zhu, Q. (2012) “Factor Analysis of High-Rise Building Fires Reasons and Fire Protection Measures,” Procedia Engineering, 45, pp. 643–648. Available at: https://doi.org/10.1016/j.proeng.2012.08.216.

Love, P.E.D. et al. (2015) “A systems information model for managing electrical, control, and instrumentation assets,” Built Environment Project and Asset Management, 5(3), pp. 278–289. Available at: https://doi.org/10.1108/BEPAM-03-2014-0019.

Matarneh, S.T. et al. (2019) “Building information modeling for facilities management: A literature review and future research directions,” Journal of Building Engineering, 24, p. 100755. Available at: https://doi.org/10.1016/j.jobe.2019.100755.

Nicał, A.K. and Wodyński, W. (2016) “Enhancing Facility Management through BIM 6D,” Procedia Engineering, 164, pp. 299–306. Available at: https://doi.org/10.1016/j.proeng.2016.11.623.

Oh, S.-W. et al. (2004) “An Application of PDA and Barcode Technology for the Improvement of Information Management in Construction Projects.” Available at: https://doi.org/10.22260/ISARC2004/0090.

Opoku, D.-G.J. et al. (2021) “Digital twin application in the construction industry: A literature review,” Journal of Building Engineering, 40, p. 102726. Available at: https://doi.org/10.1016/j.jobe.2021.102726.

Pärn, E.A., Edwards, D.J. and Sing, M.C.P. (2017) “The building information modelling trajectory in facilities management: A review,” Automation in Construction, 75, pp. 45–55. Available at: https://doi.org/10.1016/j.autcon.2016.12.003.

Peng, Y., Au-Yong, C.P. and Myeda, N.E. (2024) “Knowledge graph of building information modelling (BIM) for facilities management (FM),” Automation in Construction, 165, p. 105492. Available at: https://doi.org/10.1016/j.autcon.2024.105492.

Pishdad-Bozorgi, P. et al. (2018) “Planning and developing facility management-enabled building information model (FM-enabled BIM),” Automation in Construction, 87, pp. 22–38. Available at: https://doi.org/10.1016/j.autcon.2017.12.004.

Salzano, A. et al. (2023) “Existing assets maintenance management: Optimizing maintenance procedures and costs through BIM tools,” Automation in Construction, 149. Available at: https://doi.org/10.1016/j.autcon.2023.104788.

Schönfelder, P. et al. (2024) “Enriching BIM models with fire safety equipment using keypoint-based symbol detection in escape plans,” Automation in Construction, 162, p. 105382. Available at: https://doi.org/10.1016/j.autcon.2024.105382.

Shafiq, I. et al. (2022) “Recommendations on Firefighting System Design, Erection, and Safe Operation,” Journal of Pipeline Systems Engineering and Practice, 13(1). Available at: https://doi.org/10.1061/(ASCE)PS.1949-1204.0000592.

Silberschatz, A., Korth, H.F. and Sudarshan, S. (2020) Database System Concepts. McGraw-Hill Education. McGraw-Hill Education. Available at: https://books.google.com.br/books?id=5xbQuwEACAAJ.

Spilling, M. (2016) “Asset management surveying practice.” , Bishop’s Stortford, U.K, p. 26.

Succar, B. (2009) “Building information modelling framework: A research and delivery foundation for industry stakeholders,” Automation in Construction, 18(3), pp. 357–375. Available at: https://doi.org/10.1016/j.autcon.2008.10.003.

Teizer, J., Venugopal, M. and Walia, A. (2008) “Ultrawideband for Automated Real-Time Three-Dimensional Location Sensing for Workforce, Equipment, and Material Positioning and Tracking,” Transportation Research Record: Journal of the Transportation Research Board, 2081(1), pp. 56–64. Available at: https://doi.org/10.3141/2081-06.

Tsay, G.S., Staub-French, S. and Poirier, É. (2022) “BIM for Facilities Management: An Investigation into the Asset Information Delivery Process and the Associated Challenges,” Applied Sciences, 12(19), p. 9542. Available at: https://doi.org/10.3390/app12199542.

Tuhaise, V.V., Tah, J.H.M. and Abanda, F.H. (2023) “Technologies for digital twin applications in construction,” Automation in Construction, 152, p. 104931. Available at: https://doi.org/10.1016/j.autcon.2023.104931.

Usman, M. et al. (2017) “Taxonomies in software engineering: A Systematic mapping study and a revised taxonomy development method,” Information and Software Technology, 85, pp. 43–59. Available at: https://doi.org/10.1016/j.infsof.2017.01.006.

Wang, B. et al. (2022) “Vision-assisted BIM reconstruction from 3D LiDAR point clouds for MEP scenes,” Automation in Construction, 133, p. 103997. Available at: https://doi.org/10.1016/j.autcon.2021.103997.

Wang, X. et al. (2025) “Enhancing building fire safety inspections with cognitive ergonomics-driven augmented reality: Impact of interaction modes,” Automation in Construction, 170, p. 105939. Available at: https://doi.org/10.1016/j.autcon.2024.105939.

Wetzel, E.M. and Thabet, W.Y. (2015) “The use of a BIM-based framework to support safe facility management processes,” Automation in Construction, 60, pp. 12–24. Available at: https://doi.org/10.1016/j.autcon.2015.09.004.

Wong, M.O. and Lee, S. (2022) “IFC-based information exchange for multi-agency response to indoor fire emergencies,” Automation in Construction, 144, p. 104623. Available at: https://doi.org/10.1016/j.autcon.2022.104623.

cinpar2026
XXII International Conference on Building Pathology and Constructions Repair
15th to 17th July 2026 - Lisboa, Portugal

Leveraging Data Analytics to Manage Visitor Flows in Heritage Sites

Enrico QUAGLIARINI[1], Gabriele BERNARDINI[1], **Alessandro CEPPETELLI**[2], Chiara MARIOTTI[1], Paola RUGGIERI[3]

[1] Department of Construction, Civil Engineering and Architecture, Polytechnic University of Marche, Ancona, Italy, e.quagliarini/g.bernardini/chiara.mariotti@staff.univpm.it
[2] Department of Science of Antiquities, Sapienza University of Rome, Rome, Italy, alessandro.ceppetelli@uniroma1.it
[3] Department of Architecture, Uffizi Galleries, Florence, Italy, paola.ruggieri@cultura.gov.it

Abstract: This paper presents a data-driven methodological workflow for the analysis of visitor flows, applied to the architectural and landscape system of Pitti Palace and Boboli Gardens in Florence (Italy). This heritage site combines the periodic monitoring of stone façades – prone to deterioration and detachment – with high visitor pressure, as millions of people visit its five museums each year. The method relies exclusively on raw data already available to site managers, namely tabular records from the ticketing system, thereby ensuring transferability and privacy protection without visual user tracking. The analysis covers 18 months in 2024-2025 and begins with the selection and filtering of relevant variables, including entry times to the museums and ticket categories. The resulting dataset is processed through big data approaches combining unsupervised Machine Learning and statistical analysis, with a focus on identifying homogeneous clusters by overall attendance, seasonality, and user categories. For each cluster, temporal distribution analyses enable the identification of trends and outliers. The workflow can then be extended to infer visit sequences and dwell times by integrating on-site measurements of access durations and travel times among the site's museums, enabling the reconstruction of flow dynamics across the complex. The proposed workflow is intended to support site managers in decision-making processes to optimise visitor flows and address heritage conservation issues, while enhancing user safety and comfort.

Keywords: use of heritage; preventive conservation; people-centred approach; time-series analysis; crowding assessment

1. Introduction

The management of heritage site is increasingly recognised as a multidimensional challenge that extends well beyond the conservation of historical materials (UNESCO et al. 2013; UNESCO et al. 2026). People-centred and human-centred approaches to heritage conservation seek to balance the relationships between people, buildings, and landscapes, recognizing that the physical presence of users within heritage spaces constitutes a variable that shapes conservation outcomes (Wells 2020) and should be integrated into monitoring and preservation activities. The first core of these concepts relies on the Declaration of Amsterdam (ICOMOS 1975) and on the idea of integrated conservation, as an effort to adapt existing conservation approaches to the ever-changing challenges of the human environment (Houbart 2016). Within this framework, managing these dynamics becomes a structural component of preventive conservation and of strategies aimed at assessing risks, ensuring long-term preservation alongside safety and comfort (Vandesande and Balen 2018; Della Torre 2021; Moioli 2023).

This need is particularly urgent in high-attendance heritage sites such as large museum complexes, historic gardens, and architectural systems, where the requirements of physical conservation of both collections and buildings must be continuously reconciled with visitor experience, comfort and safety, managing

overcrowding conditions and heterogeneous visitor profiles. In such contexts, maintenance actions, monitoring campaigns and conservation works cannot be planned independently of visitor flows, since attendance regimes and circulation patterns directly influence operational feasibility of the work and the quality of the visitor experience. For instance, the impact of visitor density on material deterioration of collections and buildings represents a challenging area, with number of studies investigating the correlation between visitor presence and indoor microclimatic conditions (Camuffo 2019). More broadly, estimates of visitor intensity and visit duration provide practical exposure proxies for preventive planning, supporting the identification of critical time windows and sensitive areas where conservation measures and operational strategies should be prioritised. From this perspective, when visitor numbers reach the scale typical of major heritage sites, the relevant system extends beyond indoor museum rooms to include outdoor spaces, entrances, and connecting paths that structure flows across the site and its immediate surroundings. A systemic approach that looks beyond the museum threshold and encompass the urban public spaces is therefore not optional, but necessary.

The scale of this challenge is widely recognised, and major museums have begun to place visitor reception and spatial decongestion at the centre of their institutional strategies. A significant example is the Louvre Nouvelle Renaissance project, an ambitious redesign of one of the world's most visited museums, which focuses on improving the outdoor spaces, including the main square and the areas surrounding the complex (Louvre Museum 2026). Currently, research on visitor flow management in heritage sites has evolved along a distinct trajectory, drawing on technologies and methods primarily derived from urban mobility research and retail analytics within different scales. Bluetooth data (Versichele et al. 2014; Yoshimura, Krebs, and Ratti 2017), Wi-Fi sensors (Gao and Schmöcker 2021), GPS tracking, and video-based computer vision systems (Huang et al. 2020; Ding et al. 2023) have been used to reconstruct the spatial and temporal distribution of visitors across a range of heritage sites. At the urban scale, user-generated content and georeferenced reviews have supported the analysis of visitor behaviour in historic city centres (Girardin et al. 2008; Barrena-Herrán, Modrego-Monforte, and Grijalba 2025), while at a territorial scale, open-source data from platforms have been used to map tourism distribution and identify patterns of spatial concentration (Bishop et al. 2025; Paliska, Brezovec, and Sedmak 2026). More recent methodological frameworks have moved toward integrated, time-dependent assessments of user exposure and vulnerability in historic urban environments. These recognise that the comfort and risk profile of a heritage space changes continuously as a function of who is present, when, and in what numbers (Bernardini et al. 2024; Sparvoli et al. 2026; Quagliarini et al. 2026), offering insightful tools of assessing spatio-temporal variations of exposure and vulnerability of users. These approaches have generated valuable insights, but typically they require dedicated sensing infrastructure, reliance on third-party platforms, visual tracking systems that raise privacy concerns, and often involve qualitative assumptions that treat users as evenly distributed across outdoor spaces. In contrast, official museums' ticketing systems generate continuous, high-resolution records of admissions and represent a widely available source that can support visitor-flow analysis without additional tracking infrastructure, giving precise information on their spatio-temporal distribution.

In this perspective, the historic city centre of Florence, a UNESCO World Heritage site since 1982 (UNESCO 1982), provides a relevant context. The city is among the most affected by overtourism in Italy (ISTAT 2026), and the density of museums, together with documented co-visitation patterns within the local cultural network, significantly amplifies visitor flows throughout the city (Oliva et al. 2020). Within this framework, The Uffizi Galleries complex is one of the city's principal attractors (Giusti 2024), and has implemented measures to decongest the public circulation spaces connecting museums, particularly those surrounding the Uffizi Gallery museum. For this, ticketing data have been used for specific optimization tasks, such as the predictive modelling of queue formation at Uffizi Square (Attanasio et al. 2022). Within the Uffizi Galleries complex, the Pitti Palace and Boboli Gardens system represents a paradigmatic case, combining high and seasonally variable attendance with ongoing conservation and maintenance needs across both indoor museum and extensive outdoor areas. The system requires continuous maintenance and monitoring

activities, especially in areas near historical architectures constructed with Pietraforte sandstone, the typical Florentine historical construction material characterised by an intrinsic propensity to delaminate and detach (Salvatici et al. 2020; Mariotti et al. 2026), and the wide green heritage in the Boboli Gardens, as living heritage. This condition makes the reconciliation between material conservation and visitor-flow management not merely operational but safety-critical, and ticketing data can inform tailored campaigns that reduce the impacts on the visit.

2. Research Aim and Contribution

The research aims to improve the coexistence of conservation needs related to historical materials, the human efforts required to preserve them, and the variable pressure generated by visitors. This paper proposes a data-driven methodological workflow that transforms raw ticketing records into a structured representation of visitor flow within the Pitti-Boboli system in Florence, enabling heritage managers to integrate user-presence data into conservation planning, maintenance scheduling, and operational decision-making. The novelty lies in the use of museum ticketing data which, despite being routinely collected by institutions, have received limited attention in the visitor-flow management as a primary resource for reconstructing visitors' spatio-temporal distribution and visit sequences across a complex heritage site. The resulting outputs can enable professionals to plan actions that optimise accessibility and usage patterns, mitigate potential negative impacts from conservative activities, enhance the use of built heritage, and support the valorisation of cultural heritage places.

3. Materials and Methods

3.1 Study area: the Pitti Palace and the Boboli Gardens system within the Uffizi Galleries complex

Pitti Palace and the Boboli Gardens, which are part of the Uffizi Galleries museum system, have significantly impacted the number of visitors to Florence. The Uffizi Galleries complex – comprising three primary sites: the Uffizi Gallery, the Pitti Palace, and the Boboli Gardens – attracted more than 5.2 million visitors in 2024 (Italian Ministry of Culture 2025). This articulated museum complex extends across the city centre on both sides of the Arno River, with Pitti Palace and the Boboli Gardens situated in the Oltrarno district. The three sites are historically connected by the Vasarian Corridor, which was recently re-opened following a restoration programme.

From a cultural, functional and spatial perspective, the Pitti Palace and the Boboli Gardens are intrinsically connected (Figure 1). The palace's Renaissance core was constructed using Pietraforte, which exemplifies a fundamental technique of rusticated ashlar construction, thereby contributing to the consolidation of Florentine building traditions. For the original construction and subsequent expansions over the following centuries, Pietraforte was sourced from the Boboli hill, one of the main quarries that supplied building material to the city. From 1549, the Boboli Gardens were designed on the slope behind the palace, featuring a geometric and regular arrangement of trees and flowerbeds. It is therefore possible to interpret the transformations of the palace and the garden as the evolution of a single, integrated architectural–landscape system. In its current state, the Pitti-Boboli system functions as a unified visitor system, characterised by flexible access and non-linear visitation patterns. Visitors are able to access Pitti Palace from Piazza Pitti and select from a variety of curated itineraries within the building. Additionally, the Boboli Gardens are accessible from within the palace and via supplementary entrances located throughout the city. These characteristics contribute to the system's particular suitability for the investigation of visitor flow as a spatio-temporal phenomenon, which cannot be confined to a single indoor museum environment. For the purposes of the visitor-flow analyses presented in this paper, the system is operationally represented through five admission-controlled nodes: the Boboli Gardens and four museums within the Pitti Palace,

namely the Palatine Gallery, the Gallery of Modern Art, the Museum of Fashion and Costume, and the Treasury of the Grand Dukes.

From the perspectives of conservation and operations, the case study is also paradigmatic, as both the palace and the garden require continuous care. The garden's green heritage is inherently "living", while the indoor museum spaces demand ongoing attention to preserve historic collections. Furthermore, the external façades built in Pietraforte are exposed to pressures related to time, environment, climate change, and human-induced factors that affect conservation conditions. In this context, the coexistence of high visitor volumes and ongoing conservation needs represents a central management challenge. Since 2018, the Uffizi Galleries have conducted periodic monitoring campaigns of the Pietraforte sandstone façades (Landi et al. 2019) to respond to these challenges. The scheduling of maintenance actions and site operations is therefore contingent upon a clear understanding of the temporal and spatial distribution of visitor presence across the system, with the dual objectives of ensuring safety and comfort while maintaining compatibility with conservation requirements (Mariotti et al. 2023; Quagliarini et al. 2025; Mariotti et al. 2026).



Figure 1 – View of Pitti Palace (a), Boboli Gardens (b) and the representation of the system entrance and exits (c) over the study period (photos and graphics by Alessandro Ceppetelli, 2025)

3.2 Multi-source data

In accord with the research scope, the analysis is based on quantitative data in the form of raw tabular records, which are already available to site managers via the ticketing system. This choice facilitates the investigation of visitor flow without the deployment of additional tracking infrastructure and supports the transferability of the workflow to comparable sites. The observation period extends over an 18-month timeframe, from January 2024 to June 2025, and involved two datasets. The initial dataset is a daily record of the total number of visitors to both the Pitti Palace and the Boboli Gardens, with daily entries divided into primary ticket categories – regular, reduced, and free admission – in line with the Italian regulatory framework for admission fees to state-owned cultural sites. These categories are recognised as management-relevant descriptors. In the case of the Pitti-Boboli system, the ticketing offer encompasses regular, reduced, and free-admission single tickets, which are issued for either the Pitti Palace or the Boboli Gardens, as well as combined single tickets, which grant access to both sites. Moreover, a range of additional ticket categories are available, including those that grant access to the broader Uffizi Galleries system or other combinations associated with specific cards valid in the historic city centre.

The second is an entry-level dataset with hourly timestamps, organised on a per-entry basis. For each day, records are kept of individual entrances to the nodes under consideration in the study. The records encompass a unique ticket identifier, the timestamp of the entrance, the category of the ticket, and the accessed node. The employment of a numerical code as the identifier ensures that it cannot be associated with a specific individual, thereby ensuring the privacy of the subject.

3.3 Method and workflow

The research method follows a data-driven workflow, based on data presented in 3.2, to analyse visitor flow in the complex heritage site of Pitti-Boboli system. The procedure is applied over the entire observation window and is designed to be replicable across other sites and observation periods. The workflow combines statistical analysis (Attanasio et al. 2022) and unsupervised Machine Learning with the aim of producing management-oriented indicators and outputs suitable for the site-manager to integrate user-presence data into conservation planning. Workflow consisting of the following steps:

- **Cluster-based characterization of typical visiting days through daily raw data analysis**
  - *General characterization and descriptive statistics*: the analysis begins with the main daily dataset, as presented in 3.2. Daily entrance records are aggregated into time series. Descriptive statistics are computed to characterise the dataset and its variability over the selected period. Time series and frequency distributions of entrances are analysed to quantify the temporal concentration of visitors and to provide a first representation of attendance patterns.
  - *Seasonality characterization and selection of representative periods based on unsupervised clustering*: to identify homogeneous attendance regimes within the observation window, k-means clustering is applied to the processed dataset. Clusters are interpreted in relation to overall attendance levels, seasonal dynamics, and ticket categories, enabling the definition of comparable demand profiles. In parallel, seasonality is characterised through the analysis of temporal patterns in the daily entrance time series, framing clusters within broader seasonal phases. Based on these outputs, representative periods are selected for more detailed analysis at higher temporal resolution.
- **Typical visitors' flow characterization through hourly raw data analysis**
  - *Selection of the variables and of the period of study*: selection and filtering of the variables required to describe visitor flow and definition of the period of study.
  - *Visit sequences and mean time of visit:* the workflow can be extended to reconstruct visit sequences across the five admission-controlled nodes by linking successive admissions recorded for the same ticket. Time differences between consecutive admissions provide time-related indicators describing inter-node transitions. To support interpretation, inter-node travel times are measured on-site by timing representative pedestrian paths between nodes.

The workflow has been designed to be generalisable across multi-venue heritage sites because it requires only standard ticketing fields. In scenarios where entry-level timestamps are not available, the pipeline can still be applied at daily scale for seasonality identification, while higher-resolution analyses become possible whether per-entry records are provided.

4. Results

Results are organized according to the workflow phases as defined in Section 3.3.

4.1 Cluster-based characterization of typical visiting days

4.1.1 General characterization and descriptive statistics

Starting from the main daily dataset, all ticket categories included in the Uffizi Galleries daily report were considered, namely regular, reduced, and free-admission tickets. Descriptive statistics were computed to characterise the dataset and its variability over time. Daily entrance records were then aggregated into time series (Figure 2), and frequency distributions were computed to quantify the temporal concentration of visitors and provide a first representation of attendance patterns.

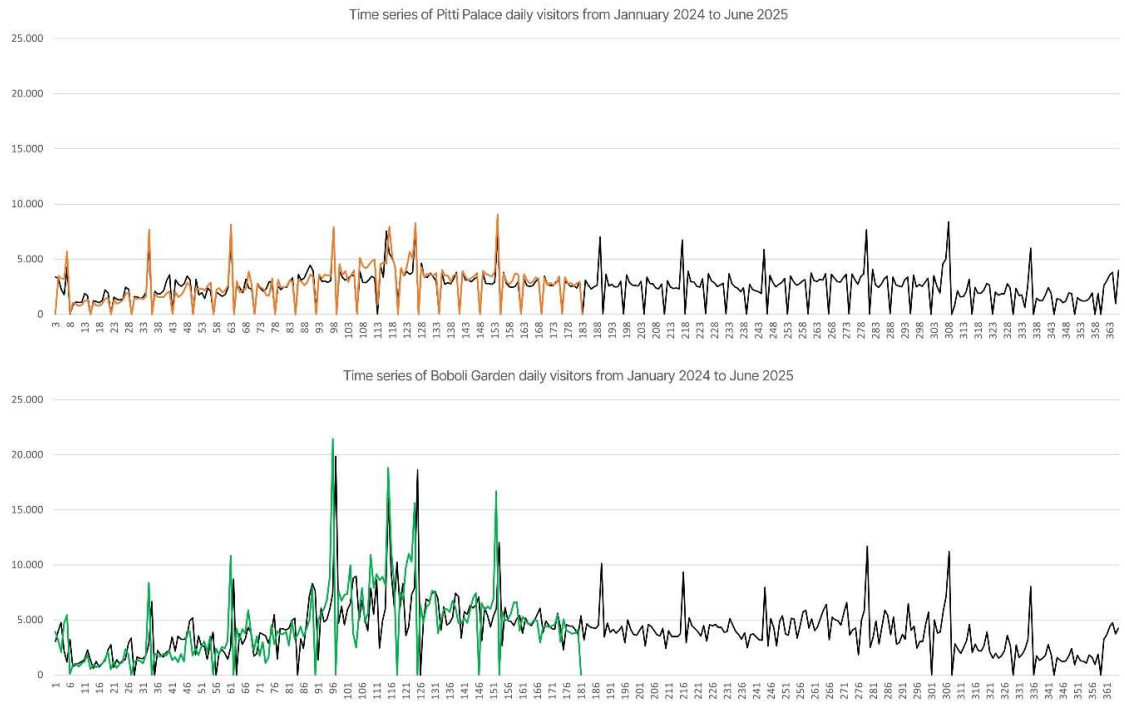


Figure 2 – Time series of entrances for both Pitti Palace and Boboli Gardens during the period from 1st of January 2024 to 30th of June 2025. The black lines refer to 2024, while the coloured lines refer to 2025

Overall, the two time series show both differences and similarities. The weekly pattern of the Pitti Palace is generally more stable over the year, with lower attendance in January–February and November–December. Peaks systematically occur on free-admission days. The weekly peak also varies across the year: during lower-attendance months, the highest values are typically observed on weekends, whereas during the rest of the year, the weekly peak is often observed on Tuesday. Moreover, all museums within the Pitti Palace are closed on Mondays in order to facilitate the regular maintenance of the exhibition spaces. The time series for the Boboli Gardens is more variable, suggesting a stronger sensitivity to external conditions. Compared with Pitti Palace, the overall pattern is wider and less predictable, whereas Pitti Palace visitors appear more

evenly distributed across the observation period. With respect to ticket categories, excluding free-admission days, free-admission tickets represent a significant percentage of daily entrances, equal to 19.32% for the Pitti Palace (540 mean visitors per day) and 17.10% for the Boboli Gardens (688 mean visitors per day). A general increase in total attendance is observed in the first semester of 2025 compared with the same period of 2024. The overall distribution remains similar, but peaks on weekends and free-admission days become more pronounced.

4.1.2 Seasonality characterization and selection of representative periods based on unsupervised clustering

In order to identify homogeneous attendance regimes within the observation window, the k-means clustering algorithm was applied to the dataset that had been processed. The results of this study are presented in Figure 3. The interpretation of clusters was undertaken in relation to overall attendance levels, seasonal dynamics, and ticket categories, thereby enabling the definition of comparable demand profiles. Concurrently, seasonality was characterised through the analysis of temporal patterns in the daily entrance time series, with the resultant clusters being framed within broader seasonal phases (Figures 4-5).

The clustering workflow was implemented in Python, utilising the pandas and numpy libraries for data management, the scikit-learn library for preprocessing and clustering, and the matplotlib library for visualisation. The K-means algorithm was applied to three daily admission features, namely total daily entrances to the Pitti Palace, total daily entrances to the Boboli Gardens, and the overall daily total for the system. The standardisation of inputs was achieved through the implementation of the StandardScaler method. Operationally, the clusters define four categories of daily visitors' affluence: low attendance-days (cluster 1), medium attendance-days (cluster 0), high to very high attendance-days (cluster 3), and exceptional attendance-days (cluster 2). The number of clusters was evaluated through the use of silhouette analysis, whereby the average silhouette score was computed from k=2 to k=10. In this assessment, the highest score was achieved by k=3 (0.531), while the second-best result was provided by k=4 (0.481). Despite the marginal reduction in the resultant score, the k=4 model was primarily selected because it allows the separation of medium attendance-days to high/very high attendance-days, that would otherwise have been grouped together. Moreover, the system-level behaviour demonstrates that Pitti manifests a more dispersed distribution in comparison to the more compact and linear pattern exhibited by Boboli, who functions as the primary driver of system attendance over the 18-month period (Figure 3).

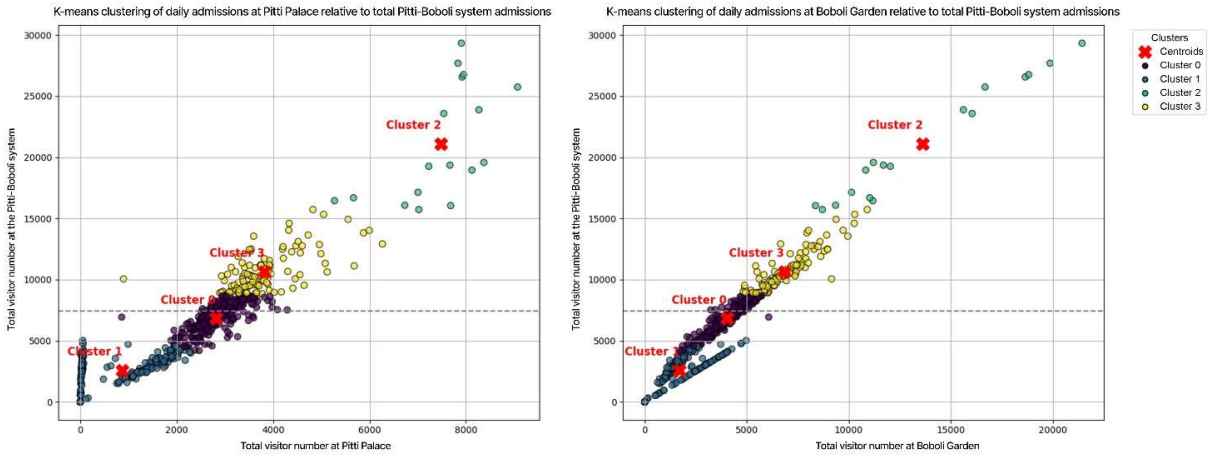


Figure 3 – Scatter plot of the k-means clustering of daily admissions. The left panel shows the results for Pitti Palace, and the right panel shows the results for Boboli Gardens

A monthly histogram representation (Figure 4) synthesises the distribution of days per month by cluster membership and supports the identification of distinct seasonal phases. For the Pitti–Boboli system, the results indicate three main periods: a low-to-medium attendance phase including January, February, November, and December; a medium-to-high attendance phase including March, June, July, August, and

October; and an exceptional-attendance phase including April, May, and September. Outliers are present and are largely associated with free-admission days, during which attendance increases sharply even during lower-attendance months (Figure 5).

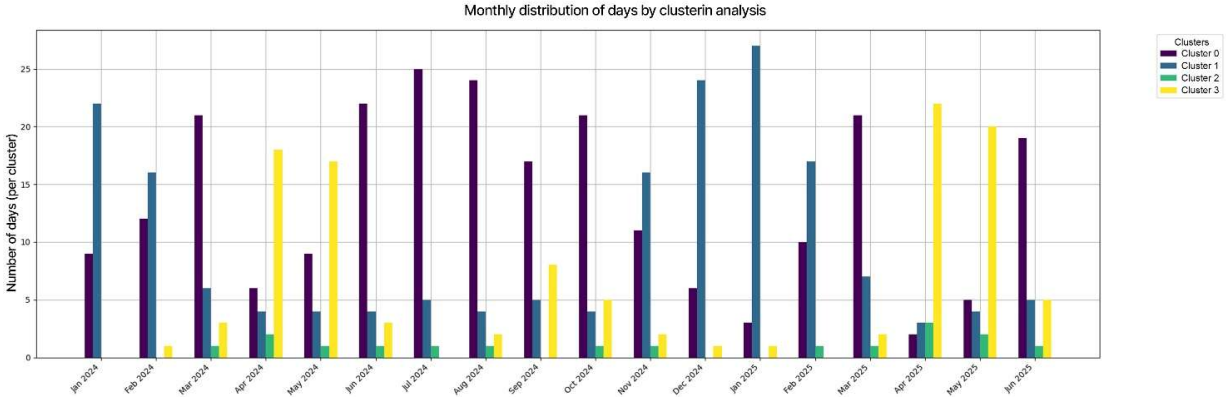


Figure 4 – Monthly distributions of days across attendance cluster for the identification of the seasonal phases

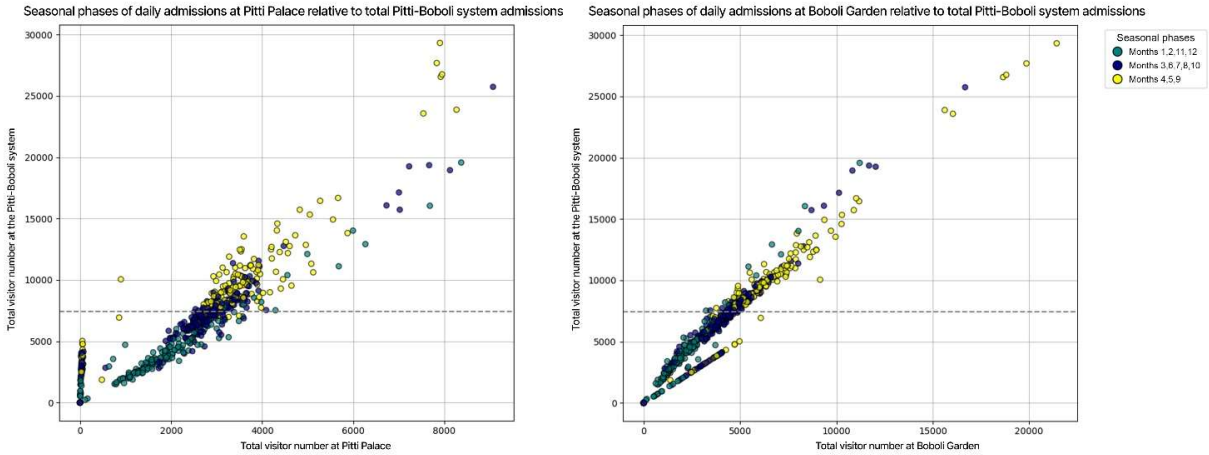


Figure 5 –Scatter plots showing the three main periods of visiting identified from the results of Figure 4: low-to-medium (petrol green), medium-to-high (violet) and exceptional (yellow) daily admissions. he left panel shows the results for Pitti Palace, and the right panel shows the results for Boboli Gardens

4.2 Typical visitors' flow characterization

4.2.1 Selection of the variables and the period of study

To study intra-day fluctuations in visitors' spatio-temporal distribution, entrance timestamps to each venue are required for a sample of visitors. The hourly dataset is composed of tables reporting the list of tickets used to enter each venue, including the entrance time. For the analyses presented here, a representative sample was selected within the medium-attendance regime previously identified. The sample includes six weeks: 16–23 June 2024, 12–18 August 2024, 02–08 September 2024, 23–29 September 2024, 07–13 October 2024, and 17–22 June 2025. These weeks were selected because their statistics are the closest to the representative values of the medium-attendance regime.

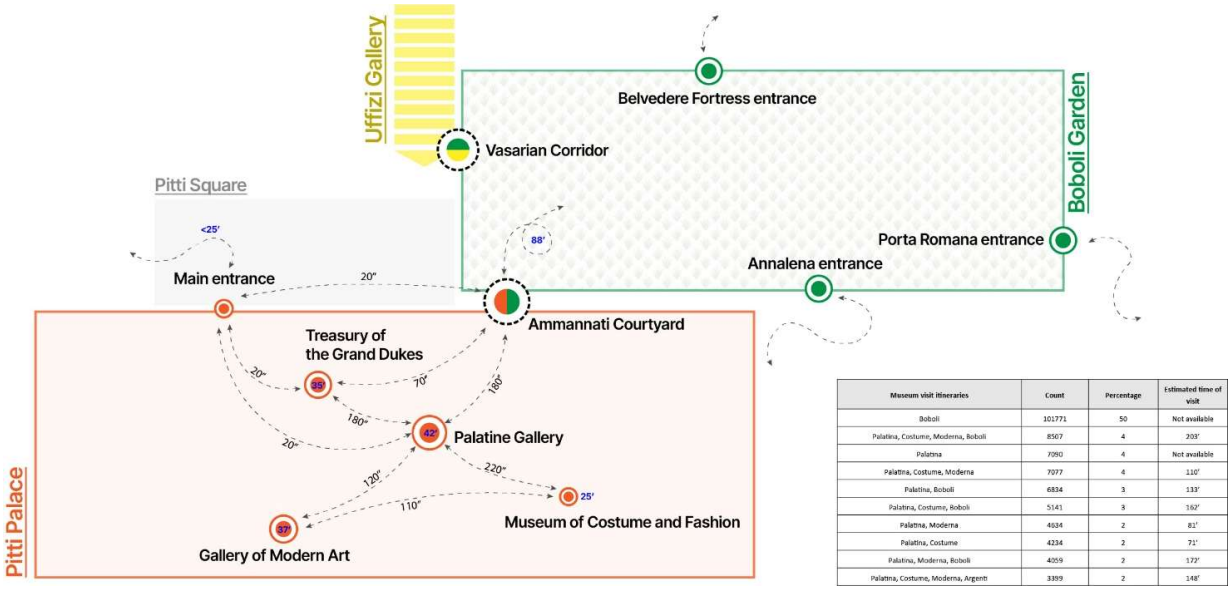
4.2.2 Sequence of visit and mean time of visit

The workflow can be extended to reconstruct visit sequences across venues and to estimate mean visit times, based on admission records and subsequent integration steps. By linking the entrance time and the visited venue for the same ticket, it is possible to describe transitions across the system and derive time-

related indicators. Figure 6 provides a schematic representation of the main venues within the Pitti–Boboli system and their main access points.

Within the selected sample period, the Boboli Gardens represent the main attractor, accounting for 50% of total entrances. The second venue by attendance is the Palatine Gallery, which is frequently the first museum visited within the system.

For each observed visit sequence, mean visit times were derived by computing the time difference between consecutive entrances. To support interpretation, inter-venue travel times were also measured on-site by timing the most direct pedestrian routes, excluding elevator use and assuming typical walking conditions. Based on these results, visit duration within the system ranges from approximately 70 minutes to over three hours, depending on individual preferences and visit composition. These results do not include combined itineraries involving the Uffizi Gallery and the Vasarian Corridor.



Museum visit itineraries	Count	Percentage	Estimated time of visit
Boboli	101771	50	Not available
Palatina, Costume, Moderna, Boboli	8567	4	203'
Palatina	7090	4	Not available
Palatina, Costume, Moderna	7077	4	110'
Palatina, Boboli	6834	3	133'
Palatina, Costume, Boboli	5141	3	162'
Palatina, Moderna	4634	2	81'
Palatina, Costume	4234	2	71'
Palatina, Moderna, Boboli	4059	2	172'
Palatina, Costume, Moderna, Argenti	3399	2	148'

Figure 6 – Schematic representation of the possible flows within the Pitti-Boboli system, showing mean venue visit times (blue) and mean inter-venue travel times (dashed arrows). The Ammannati Courtyard and the Vasarian Corridor act as the main hinges connecting Pitti Palace, Boboli Gardens and the Uffizi Gallery across the Arno River. The table summarises the main visit itineraries and provides an estimated total visit duration, excluding waiting time at the entrances

5. Conclusions and future works

The present paper proposes and tests a data-driven workflow that transforms raw ticketing records into management-oriented information on visitor flow in a complex indoor–outdoor heritage site. The workflow integrates daily time-series analysis and descriptive statistics with unsupervised clustering to identify homogeneous attendance regimes and seasonal phases. It then employs entry-level admissions to characterise flows' dynamics, reconstructing visit sequences across museums within the system.

Applied to the Pitti Palace–Boboli Gardens system, the analyses produced several useful results in line to the objectives of the research. Initially, the implementation of clustering facilitated the identification of varied attendance patterns, outliers, and a seasonality structure. Secondly, the distribution of visitors within the study period revealed stable profiles and recurrent weekly patterns. This finding supports the identification of predictable high-demand time slots and a data-drive preventive planning of interventions. Thirdly, sequence-based analysis indicated that the Boboli Gardens act as the primary attraction in the selected

sample and that the Palatine Gallery is the main museum visited in the Pitti Palace; the results provide empirical ranges for overall visit duration, from approximately 70 minutes to over three hours depending on visit composition.

These findings demonstrate that ticketing data can be structured into actionable indicators to support preventive planning and operational decisions. This includes the scheduling of maintenance and monitoring activities, as well as the mitigation of flow-related criticalities affecting visitor safety and comfort. For instance, maintenance actions could be deployed, in each building area, during those days and daytime with minimum visitors' attendance, focusing their priority also depending on space fruition levels. Visitors' flow monitoring could be recommended in critical attendance days and areas to prevent possible problems in their movement in the building, as well as to increase movement comfort levels or positively manage emergency and evacuation conditions. Visitors' flow can be optimized depending on their effective visiting plans, by creating alternative museum paths towards which visitors can be addressed (potentially reducing overcrowding). Safety and emergency planning can be managed by using dynamic conditions in building fruition, thus moving towards "dynamic" and scenario-based plans rather than static assumptions. In particular, these data can also inform evacuation assessment through simulation models, since this work provides basis for realistic distribution of users (by number and position) over space and time. This can also create benefits in the best, ideal localization of emergency staff members depending on crowding levels. Temporary solutions for outdoor comfort improvement (e.g. temporary sunsails and waiting areas) can be positioned in public open spaces depending on the use and crowding conditions. Finally, these analyses may prove crucial for designing monitoring strategies for the external façades of the complex, constructed from Pietraforte stone – particularly the Pitti Palace. Regular inspections conducted throughout the year can be coordinated with visitor flows, ensuring high safety standards without compromising the quality of the visitor experience.

The workflow proposed is transferable and scalable. The process is transferable due to the absence of a requirement for additional tracking infrastructure, and it can be applied in any context where admission systems provide comparable records. Furthermore, it is scalable due to the capacity for the extension of the same pipeline to longer time period and additional venues sites.

Future works will prioritise the integration of these findings with systematic qualitative evidence concerning visitor movement in outdoor spaces, the implementation of results in dynamic maps and three-dimensional models for immediate decision support, and the extension of the framework towards an integrated risk-oriented perspective. This will be achieved by coupling spatio-temporal exposure patterns with conservation information on material criticalities and monitoring outcomes. Such development will enable a more mutualistic, heritage- and people-centred planning of preventive interventions, thereby reducing disruption to the visit while supporting long-term conservation.

Acknowledgments

The authors gratefully acknowledge Dr. Simone Verde, Director of the Uffizi Galleries, and the Office of *Servizi Aggiuntivi* of the Uffizi Galleries, with special thanks to Angela Rossi and Simone Cianfanelli for their support. Doctoral scholarship funding for Arch. Eng. Alessandro Ceppetelli was provided by the European Union – Next Generation EU, Mission 4, Component 1, CUP B53C23003570006.

References

Attanasio, Alessandro, Maurizio Maravalle, Henry Muccini, Fabrizio Rossi, Gianluca Scatena, and Francesco Tarquini. 2022. "Visitors Flow Management at Uffizi Gallery in Florence, Italy." *Information Technology & Tourism* 24 (3): 409–34. https://doi.org/10.1007/s40558-022-00231-y.

Barrena-Herrán, Mikel, Itziar Modrego-Monforte, and Olatz Grijalba. 2025. "Mapping the Spatiotemporal Urban Footprint of Residents and Tourists: A Data-Driven Approach Based on User-Generated Reviews." *ISPRS International Journal of Geo-Information* 14 (12). https://doi.org/10.3390/ijgi14120456.

Bernardini, Gabriele, Tiago Miguel Ferreira, Pilar Baquedano Julià, Rafael Ramírez Eudave, and Enrico Quagliarini. 2024. "Assessing the Spatiotemporal Impact of Users' Exposure and Vulnerability to Flood Risk in Urban Built Environments." *Sustainable Cities and Society* 100 (January 2024): 105043. https://doi.org/10.1016/j.scs.2023.105043.

Bishop, Michaël Virgil, Rannveig Ólafsdóttir, Tracy Michaud, and Colleen Metcalf. 2025. "Crowdsourced Mapping of Tourism Distribution and Dynamics in Iceland Using Flickr." *Scandinavian Journal of Hospitality and Tourism* 25 (4): 330–46. https://doi.org/10.1080/15022250.2024.2355905.

Camuffo, Dario. 2019. *Microclimate for Cultural Heritage: Measurement, Risk Assessment, Conservation, Restoration, and Maintenance of Indoor and Outdoor Monuments*. Elsevier.

Della Torre, Stefano. 2021. "Italian Perspective on the Planned Preventive Conservation of Architectural Heritage." *Frontiers of Architectural Research* 10 (1): 108–16. https://doi.org/10.1016/j.foar.2020.07.008.

Ding, Shaogang, Ruishan Zhang, Yingying Liu, Pan Lu, and Minnan Liu. 2023. "Visitor Crowding at World Heritage Sites Based on Tourist Spatial-Temporal Distribution: A Case Study of the Master-of-Nets Garden, China." *Journal of Heritage Tourism* 18 (5): 632–57. https://doi.org/10.1080/1743873X.2023.2214680.

Gao, Yuhan, and Jan-Dirk Schmöcker. 2021. "Estimation of Walking Patterns in a Touristic Area with Wi-Fi Packet Sensors." *Transportation Research Part C: Emerging Technologies* 128 (July 2021): 103219. https://doi.org/10.1016/j.trc.2021.103219.

Girardin, Fabien, Filippo Dal Fiore, Carlo Ratti, and Josep Blat. 2008. "Leveraging Explicitly Disclosed Location Information to Understand Tourist Dynamics: A Case Study." *Journal of Location Based Services* 2 (1): 41–56. https://doi.org/10.1080/17489720802261138.

Giusti, Serena. 2024. "Museums after the Pandemic, from Resilience to Innovation: The Case of the Uffizi." *International Journal of Cultural Policy* 30 (1): 67–80. https://doi.org/10.1080/10286632.2023.2167986.

Houbart, Claudine. 2016. "Towards an 'Integrated Conservation' : The Contribution of R.M. Lemaire and Piero Gazzola during the First Decade of ICOMOS (1965-1975)." Paper presented at "HERITAGE IN TRANSFORMATION. HERITAGE PROTECTION IN THE 21ST CENTURY - PROBLEMS, CHALLENGES, PREDICTIONS." 2016. https://orbi.uliege.be/handle/2268/183441.

Huang, Xiaoting, Minxuan Li, Jingru Zhang, Linlin Zhang, Haiping Zhang, and Shen Yan. 2020. "Tourists' Spatial-Temporal Behavior Patterns in Theme Parks: A Case Study of Ocean Park Hong Kong." *Journal of Destination Marketing & Management* 15 (March 2020): 100411. https://doi.org/10.1016/j.jdmm.2020.100411.

ICOMOS. 1975. The Declaration of Amsterdam. Amsterdam, ICOMOS.

ISTAT. 2026. Official website. https://www.istat.it/comunicato-stampa/i-flussi-turistici-anno-2024/, last accessed 09/03/2026.

Italian Ministry of Culture. 2025. Minicifre della cultura. Edizione 2025. Una raccolta di dati statistici sulla cultura. Rome, Italian Ministry of Culture. https://pubblicazioni.fondazionescuolapatrimonio.it/Minicifre-della-cultura-Edizione-2025/

Landi, Stefano, Teresa Salvatici, Carlo Alberto Garzonio, Paola Ruggieri, and Angela Pintore. 2019. "Monitoraggio Dei Paramenti Lapidei Dei Prospetti Del Cortile Di Palazzo Pitti Di Bartolomeo Ammannati." *Lo Stato Dell'Arte* 17 (2019). https://www.torrossa.com/gs/resourceProxy?an=5172249&publisher=F53057#page=663.

Louvre Museum. 2026. Official website. https://presse.louvre.fr/louvre-nouvelle-renaissance-cinq-groupements-retenus-pour-le-concours-international-darchitecture/, last accessed 09/03/2026.

Mariotti, Chiara, Paola Ruggieri, Elena Pozzi, Teresa Salvatici, Irene Centauro, Alessandro Ceppetelli, and Carlo Alberto Garzonio. 2023. *Governare l'emergenza progettando la cura, tra conservazione*

materiale e fruizione in sicurezza. Approcci predittivi per Palazzo Pitti a Firenze. Roma. https://iris.uniroma1.it/handle/11573/1707268.

Mariotti, Chiara, Paola Ruggieri, Teresa Salvatici, and Alessandro Ceppetelli. 2026. "Preventive and Planned Conservation: A Knowledge-Based Tool to Manage Heritage at Risk. Strategies for the Pitti Palace in Florence." *International Journal of Architectural Heritage* 20 (2): 150–77. https://doi.org/10.1080/15583058.2025.2524758.

Moioli, Rossella. 2023. *La conservazione preventiva e programmata: una strategia per il futuro: premesse, esiti e prospettive degli interventi di Fondazione Cariplo sul territorio*. Nardini editore.

Oliva, Stefania, Francesco Capone, Luciana Lazzeretti, and Alessandra Petrucci. 2020. "Managing Visitors' Flows in Museums. The Case of Firenze Card." *Il Capitale Culturale. Studies on the Value of Cultural Heritage*, no. 22 (December 2020): 369–93. https://doi.org/10.13138/2039-2362/2379.

Paliska, Dejan, Aleksandra Brezovec, and Gorazd Sedmak. 2026. "Image-Based Analysis of Tourist Destination Perceptions: A Deep Learning and Spatial–Temporal Study in Slovenia." *Tourism and Hospitality* 7 (2). https://doi.org/10.3390/tourhosp7020052.

Quagliarini, Enrico, Alessia Freddo, Caterina Alighieri, Maud Natalucci, and Gabriele Bernardini. 2026. "A Novel Dynamic Disaster Risk Assessment of Urban Built Environments: An Application to Flood and Earthquake." *International Journal of Disaster Risk Reduction*, February 24, 2026, 106072. https://doi.org/10.1016/j.ijdrr.2026.106072.

Quagliarini, Enrico, Chiara Mariotti, Paola Ruggieri, and Alessandro Ceppetelli. 2025. "Consolidating Stone Architectural Heritage: A Spatio-Temporal Analysis of Restoration Practices at the Pitti Palace in Florence." In *Mechanics of Masonry Structures Strengthened with Composite Materials*, edited by Giovanni Castellazzi and Cristina Gentilini, 126–46. Cham: Springer Nature Switzerland. https://doi.org/10.1007/978-3-032-05032-8_11.

Salvatici, Teresa, Sara Calandra, Irene Centauro, Elena Pecchioni, Emanuele Intrieri, and Carlo Alberto Garzonio. 2020. "Monitoring and Evaluation of Sandstone Decay Adopting Non-Destructive Techniques: On-Site Application on Building Stones." *Heritage* 3 (4): 1287–301. https://doi.org/10.3390/heritage3040071.

Sparvoli, Gessica, Elena Bosi, Gabriele Bernardini, Enrico Quagliarini, and Tiago Miguel Ferreira. 2026. "How Much Do Users Matter? An Integrated Method for Building Flood Vulnerability and Exposure Assessment in Historic Urban Areas." *Sustainable Cities and Society* 136 (January 2026): 107084. https://doi.org/10.1016/j.scs.2025.107084.

Uffizi Galleries. 2026. Official website. https://www.uffizi.it/, last accessed 09/03/2026.

UNESCO. 1982. Official website. https://whc.unesco.org/en/list/174/, last accessed 09/03/2026.

UNESCO, ICCROM, ICOMOS and IUCN. 2013. Managing Cultural World Heritage. Paris, UNESCO.

UNESCO, ICCROM, ICOMOS and IUCN. 2026. Managing World Heritage. Paris, UNESCO.

Vandesande, A., and K. Van Balen. 2018. "Preventive Conservation Applied to Built Heritage: A Working Definition and Influencing Factors." In *Innovative Built Heritage Models*. CRC Press.

Versichele, Mathias, Liesbeth de Groote, Manuel Claeys Bouuaert, Tijs Neutens, Ingrid Moerman, and Nico Van de Weghe. 2014. "Pattern Mining in Tourist Attraction Visits through Association Rule Learning on Bluetooth Tracking Data: A Case Study of Ghent, Belgium." *Tourism Management* 44 (October 2014): 67–81. https://doi.org/10.1016/j.tourman.2014.02.009.

Wells, Jeremy C. 2020. "The Affect of Old Places: Exploring the Dimensions of Place Attachment and Senescent Environments." In *Place Meaning and Attachment*. Routledge.

Yoshimura, Yuji, Anne Krebs, and Carlo Ratti. 2017. "Noninvasive Bluetooth Monitoring of Visitors' Length of Stay at the Louvre." *IEEE Pervasive Computing* 16 (2): 26–34. https://doi.org/10.1109/MPRV.2017.33.

cinpar2026
XXII International Conference on Building Pathology and Constructions Repair
15th to 17th July 2026 - Lisboa, Portugal

Study of strategies for the evaluation of metal structures under fire action

María de las Nieves GONZÁLEZ GARCÍA[1], Alberto LEAL MATILLA[2], María Isabel PRIETO BARRIO[3], Fernando Israel OLMEDO ZAZO[4], Alfonso COBO ESCAMILLA[5]

[1] Universidad Politécnica de Madrid, Madrid, Spain, mariadelasnieves.gonzalez@upm.es
[2] Universidad Politécnica de Madrid, Madrid, Spain, alberto.leal.matilla@upm.es
[3] Universidad Politécnica de Madrid, Madrid, Spain, mariaisabel.prieto@upm.es
[4] Universidad Politécnica de Madrid, Madrid, Spain, fi.olmedo.zazo@upm.es
[5] Universidad Politécnica de Madrid, Madrid, Spain, alfonso.cobo@upm.es

Abstract: In many cases, the most economically viable option for building rehabilitation consists of making minimal structural interventions and changing their use. When the buildings being worked on have a metal structure and belong to older periods, it is very common for the structure to have many exposed parts and for fire protection precautions not to have been taken when they were initially designed. In addition, these structures often have a high plastic potential, and both designers and property owners wish to leave elements visible, without fire protection. In the fire evaluation of structures, a decisive parameter is the time during which they must be able to withstand the action of the fire, which can be assessed in various ways. The mandatory regulations in Spain, the Technical Building Code, offer two procedures to evaluate the fire exposure time of a structure. These two procedures are also included in the Eurocodes. In this work, these two procedures are analysed and compared. The first is the most commonly used and is based on the direct application of a table. The second is rarely used and is somewhat more laborious; it is an analytical procedure that employs expressions taking into account various factors that influence the behaviour of the fire. The results show that the first of the procedures often provides structural fire resistance time values that are much higher than those obtained with the second. It is concluded that the use of the analytical procedure, present in both the Technical Building Code and the Eurocodes, constitutes a viable alternative in many cases.

Keywords: Fire; Steel; Equivalent fire for fire exposure; Fire curve.

1. Introduction

The effects of fires can significantly reduce the load-bearing capacity and stiffness of isolated elements and compromise the mechanical safety of the entire structure (Faghihi et al. - 2023; Randaxhe et al. - 2021). From a purely structural perspective, the statistics conducted by the European Convention for Constructional Steelwork (ECCS) for decades regarding collapses occurring in steel structures (ECCS - 1974), fire is one of the main agents of these collapses. The effects produced on recent collapses such as those that occurred in September 2001at the World Trade Centers (Usmani - 2005) or the Plasco building in Tehran in January 2017 (Behnam - 2019) only confirm what has been pointed out since the 1970s. Moreover, when the fire is caused by earthquakes, the consequences are greater (Chandra et al. - 2021) (Norouzi et al. - 2018). This highlights that the safety of the structure against collapse in the event of a fire must be properly studied.

The European codes of the 1970s (ECCS - 1978) establish the socially acceptable level of the probability of structural failure in a fully developed fire to be similar to that of seismic action. In both cases, not only are the actions not increased, but a certain reduction in their value is also allowed. This amounts to assuming a

higher probability of structural failure than that calculated under normal conditions, which is logical for accidental actions.

Since 1981, the basic Spanish fire protection standards NBI CPI 82 "Conditions for fire protection in buildings" have adopted the classic system of classifying structural elements based on their "Fire Resistance" measured in minutes to define the safety of a structure against fire.

Thus, "fire resistance time" is mentioned when one wants to express its behaviour in the event of a fire. This method has been used in Europe for many years since the 1980s and has its roots in the classical level of structural theory, purely experimental and empirical, of analysis through furnace tests of structural elements subjected to a conventional law of temperature variation over time defined by the ISO 834 standard (ISO - 834).

In this work, the results obtained through both procedures will be compared to assess the suitability of using each one. To do this, first, the fire action is presented; next, both procedures are outlined, and finally, a case will be resolved to analyse the results obtained.

2. Fire lesson

According to the recommendations of the European Convention for Constructional Steelwork (1978), a fire should be considered as an accidental situation during which it is necessary to ensure the load-bearing capacity and integrity of the structure for a sufficient period of time in order to:

- Allow the evacuation of the occupants of the building.
- Establish appropriate safety conditions for the provision of firefighting services.
- Limit the spread of the fire within the building itself and towards adjacent structures.
- To prevent, to some extent, the probable material damage resulting from the deterioration or collapse of the structure.

In general, it is considered that a structural element loses its load-bearing or functional capacity under the action of fire as a consequence of the loss of:

- Characteristics of load-bearing capacity.
- Thermal insulation capacity.
- Flame-tightness capacity.

In metal structures, only the load-bearing capacity is considered.

This limit state can be established with three conditions:

- Collapse criterion.
- Excessive strain rate criterion.
- Excessive deformation criterion.

Usually, only the collapse criterion is considered. According to this criterion, the limit state of exhaustion is considered to occur when the piece or structure subjected to temperature increases due to fire exposure and requested by the rest of the concomitant actions exhausts its load-bearing capacity as a result of any of the following phenomena:

- Transformation of the structure into a mechanism.
- Elastic or inelastic instability.

The critical temperature of a steel element is defined as the temperature of the steel at which the collapse criterion under fire action of the standards is reached, assuming the elastic limit of the material as a function of the temperature reached.

The validity of the design is based on verifying that the temperature reached by the element is below the critical temperature. The value of the temperature reached by the structural element largely depends on

the exposure time during the fire. In the regulations, there are two procedures to calculate this time. the use of them often leads to very different results.

3. Increase in temperature during a fire

One of the fundamental parameters for evaluating a structure against fire action is determining the evolution of the temperature in the fire compartment over time.

The first works carried out with the intention of standardising the value of the temperature rise that occurs during a fire bore fruit in 1975, with the publication of the ISO 834 standard, and in 1981, in Spain, with the UNE 23093, currently EN 1363 (EN 1363:2012). At the international level, the publication of the ISO 834 standard was fundamental in the regulation of fire safety in buildings, defining criteria such as mechanical stability, airtightness, and thermal insulation. The standard. The most well-known contribution of the standard is the definition of a logarithmic expression to determine the temperature reached in an enclosure where a fire has fully developed, based on the elapsed time. Figure 1 shows the curve of the ISO 834 standard.

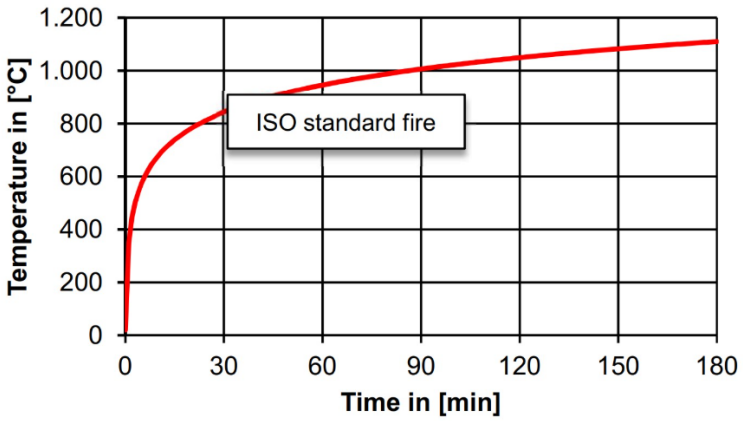


Figure 1 – Value of the temperature as a function of time. Image of the curve in the ISO 834

The image in Figure 1 is the graphical representation of the normalised time-temperature curve, a nominal curve currently defined in the UNE EN 1363-1:2015 standard to represent a fully developed fire model in a fire compartment (equation 1).

$$\theta_g = \theta_o + 345 \cdot \log_{10}(8t + 1)\ (^{\circ}C) \quad (1)$$

Being:

θ_g Gas temperature in the sector [°C]

θ_o Ambient temperature

t Time since the fire started [min]

In addition to using Equation 1 to obtain the temperature reached in a fire, other models can be employed, which have been developed since the 1970s and are more accurate. The results of the tests conducted by Arnault and published in 1974 (Arnault et al. - 1974) represented a significant advance in understanding the influence of various variables on the behaviour of a real fire. The test programs were based on the study of the influence on a real fire of the following three parameters:

- Fire load
- Open ventilation surface
- Nature of the walls that delimit the fire sector.

From these results, real fire curves were obtained that reflect the variation in ambient temperature over real time in the analysed fire compartment.

In the development of a real fire, the following factors influence it:

- Amount of heat energy potentially released during the combustion of the materials present in the enclosure.
  Porosity, shape, and distribution of the combustible materials.
- Ventilation conditions.
- Geometry and thermal characteristics of the enclosure walls.

Once the temperature in the enclosure has been obtained, either with the standardised ISO 834 curve or with more realistic models, the temperature that the structural elements will reach can be calculated. In the case of metal structures, the procedure for evaluating their response to fire action is based on obtaining the critical temperature that the structure can reach depending on the actions it must withstand and its geometric and mechanical characteristics.$(\theta_{s,cr})$ and compare it with the temperature it will reach as a consequence of the fire ($\theta_{s,max}$), which in turn is a function of the temperature reached in the chamber, which depends on the exposure time (equation 2).

$$\theta_{s,max} \leq \theta_{s,cr} \tag{2}$$

4. Time of fire exposure that a structure must withstand: Technical Building Code

According to the Technical Building Code, Basic Document SI on fire safety (Ministry of Housing and Urban Agenda – 2025), the fire resistance of a main structural element of a building (including floor slabs, beams and supports) is sufficient if either of the following two conditions is met: i) it achieves the class indicated in Table 1, which represents the time in minutes of resistance to the action represented by the standardised time-temperature curve, or ii) it withstands said action for the equivalent duration of exposure to fire obtained using an analytical procedure contained in Annex B of the document. Thus, CTE-DB-SI provides two distinct procedures for determining the necessary duration during which the structure must be capable of withstanding the fire action.

4.1 First procedure. Fire resistance table for structural elements

CTE-DB-SI provides a table setting out the minimum fire resistance requirements for structural elements, depending on the building's use and the evacuation height conditions

Table 1 – Sufficient fire resistance of structural elements

Use of the fire compartment in question	**Basement floors**	**Above-ground floors**		
		Building evacuation height		
		≤15m	**≤28m**	**>28m**
Detached house	R 30	R 30	-	-
Residential Housing, Public Housing, Teaching, Administrative	R 120	R 60	R 90	R 120
Commercial, Public sector, Healthcare	R 120	R 90	R 120	R 180
Car park (building used exclusively for this purpose or situated on land zoned for another use)	R 90			
Car park (located under a different use)	R 120			

4.2 Second procedure. Analytical procedure

This annex sets out the procedure for determining the equivalent fire exposure time which, as specified in CTE-DB-SI, may be used as an alternative to the fire duration to be withstood, for both structural and compartmentalisation purposes. The equivalent fire exposure time cannot be applied to timber or composite structures. The equivalent time is obtained by considering the geometric and thermal characteristics of the area, as well as the design fire load value.

This annex also sets out the expression of the standardised time-temperature curve defined in standard UNE EN 1363-1:2015, which is used as the fire curve in the methods for determining resistance described in this CTE-DB-SI. The Eurocode relating to fire action (CEN - 2002) specifies other nominal fire curves.

The expression provided by CTE-DB-SI is valid for structural elements made of reinforced concrete or steel. The design value of the equivalent time, $t_{e,d}$, in minutes is obtained based on the thermal properties of the building envelope, the ventilation of the space, the type of material constituting the structure, and the fire load present in the sector (expression 3).

$$t_{e,d} = k_b \cdot w_f \cdot k_c \cdot q_{f,d} \quad (3)$$

Being:

k_b, conversion factor based on the thermal properties of the building envelope; this may be taken as 0.07. Annex F of standard UNE EN 1991-1-2:2004 provides more precise values.

w_f, ventilation coefficient depending on the shape and size of the sector.

k_c, correction factor based on the structural material.

$q_{f,d}$, calculated value of the fire load density based on the use of the sector, in MJ/m^2.

The ventilation coefficient wf is calculated as follows (Equation 4):

$$w_f = (6/H)^{0.3}[0.62 + 90(0.4 - \alpha_v)^4/(1 + b_v \cdot \alpha_h)] \geq 0.5 \quad (4)$$

Being:

$\alpha_v = A_v/A_f$ the ratio of the area of the openings in the façade to the floor area of the sector, within the limits $0{,}025 < \alpha_v < 0{,}25$.

$\alpha_h = A_h/A_f$ the ratio of the area of the roof openings, A_h, to the floor area of the sector.

$b_v = 12{,}5\ (1 + 10\ \alpha_v - \alpha_v^2) \geq 10$

H height of the fire compartment (m)

Openings in facades or roofs include voids, skylights, windows (whether openable or not), glazed surfaces and, in general, any area likely to allow air to enter the area where the fire is taking place.

The correction coefficient K_c depending on the structural material, is obtained from Table 2 included in the CTE.

Table 2 – K_c correction factor values according to the structural material

Cross-sectional material	k_c
Reinforced concrete	1
Coated steel	1
Uncoated steel	13.7 · O

where O (Equation 5) is the aperture coefficient with the limits $0.02 \leq O \leq 0.2\ (m^{\frac{1}{2}})$

$$O = \frac{A_v\sqrt{h}}{A_t} \quad (5)$$

A_t is the total surface area of the building envelope (walls, floor and ceiling), including openings (m^2).

h is the average height of the vertical openings (m)

The design value of the fire load density, $q_{f,d}$, is determined on the basis of the characteristic fire load value for the sector, $q_{f,k}$, as well as the probability of ignition and the foreseeable consequences of the fire, as shown in (Equation 6):

$$q_{f,d} = q_{f,k} \cdot m \cdot \delta_{q,1} \cdot \delta_{q,2} \cdot \delta_n \cdot \delta_c \quad (6)$$

m is a combustion coefficient that takes into account the proportion of the fuel that burns in the fire. Where the burning material is of a cellulosic nature (wood, paper, textiles, etc.), m may be taken as 0.8. In the case of other types of material where the combustion coefficient is unknown, m may be taken as 1 to err on the side of caution.

δ_{q1} is a coefficient that takes into account the risk of initiation based on the size of the sector.

δ_{q2} a coefficient that takes into account the risk of ignition due to the type of use or activity.

δ_n a coefficient that takes into account existing voluntary active measures (Equation 7),

$$\delta_n = \delta_{n,1} \cdot \delta_{n,2} \cdot \delta_{n,3} \quad (7)$$

δ_c correction factor based on the consequences of the fire

The values of δ_{q1} are given in Table 3, contained in CTE DB SI; intermediate values can be obtained by linear interpolation.

Table 3 – Values of the coefficient δ_{q1} for the risk of initiation due to sector size

Area of sector A_t (m^2)	Risk of initiation δ_{q1}
< 20	1.00
25	1.10
250	1.50
2500	1.90
5000	2.00
<10000	2.13

The values of δ_{q2} are given in Table 4, which is contained in CTE DB SI.

Table 4 – Values of the δ_{q2} coefficient for the risk of onset due to use or activity

Activity	Risk of initiation δ_{q2}
Housing, Administrative, Residential, Educational	1.00
Commercial, Car parks, Healthcare, Public access	1.25
Premises with low special risk	1.25
Premises with medium special risk	1.40
Premises with high special risk	1.60

The values of the coefficient δ_n based on existing active measurements are given in Table 5, contained in CTE DB SI.

Table 5 – Values of the coefficient δ_n depending on the active measures in place

Automatic detection δ_{n1}	Automatic fire brigade alert δ_{n2}	Automatic expiry δ_{n3}
0.87	0.87	0.61

The values de δ_c for the potential consequences of a fire, depending on the building's evacuation height, are given in Table 6, contained in CTE DB SI.

Table 6 – Values of the coefficient δ_c due to the potential consequences of the fire

Discharge height	δ_c
Buildings with a downward evacuation height of more than 28 m or an upward evacuation height of more than one storey	2.0
Buildings with a downward evacuation height of between 15 and 28 m or an upward evacuation height of up to 2.8 m. Car parks beneath other uses	1.5
Buildings with a downward evacuation height of less than 15 m or used exclusively as a car park	1.0

In the case of buildings where it is unacceptable for them to be rendered out of service, or where there could be a high number of casualties in the event of a fire—such as hospitals—the values given must be multiplied by 1.5.

The characteristic value of the fire load density, $q_{f,k}$, is obtained by adding the characteristic value of the permanent fire load density, estimated by its average or expected value, and the characteristic value of the variable fire load density, estimated as the value that is exceeded in only 20% of cases.

The permanent fire load density corresponds to the cladding and other permanent combustible elements included in the design. It can be obtained from the specific values provided by the manufacturer of each product or, failing that, from tables of values for generic materials.

The variable fire load density can be assessed element by element, as indicated in standard UNE EN 1991-1-2: 2004, in which case protected loads may be taken into account, or it may be obtained from Table 7, for areas where fire load accumulations do not exceed those typical of the intended use, such as storage areas, intensive document archives, book depositories, etc. The fire load densities in Table 7 are on the safe side and are valid provided that the actual use of the building is as intended in the design. However, where the designer considers that, in a particular case, the fire loads will be significantly lower, they may avail themselves of the option provided for in the article and assess it themselves element by element, bearing in mind that, in such a case, the designer is responsible for that assessment and for reflecting in the final construction documentation the specific conditions of use that make it applicable, whilst the operator of the activity shall be responsible for compliance with those specific conditions of use.

Table 7 – Characteristic values for variable fire load density depending on the intended use

Intended use	Characteristic value of variable fire load density (MJ/m²)
Commercial	730
Residential	650
Hospital/Public Care Homes	280
Administrative	520
Educational	350
Public venues (theatres, cinemas)	365
Car parks	280
Premises classified as high-risk	160

5. Case study

In order to compare the differences in the assessment of a structure's fire resistance, a space used for teaching purposes will be studied. This is a classroom located on the first floor with an evacuation height of 4.00 m.

Determining the fire exposure time of the structure

In this case, the building is used for educational purposes, is situated on the first floor and has an evacuation height above ground level of 4 m (≤15 m).

Using the first procedure and these values, Table 1 indicates R 60; that is, the structure must withstand the effects of a fire for 60 minutes.

Using the second procedure, the equivalent fire exposure time is obtained from:

$$t_{e,d} = k_b \cdot w_f \cdot k_c \cdot q_{f,d}$$

Conversion factor depending on the thermal properties of the building envelope, k_b.

k_b = 0.07

Ventilation coefficient w_f:

$$w_f = (6/H)^{0.3}[0.62 + 90(0.4 - \alpha_v)^4/(1 + b_v \cdot \alpha_h)] \geq 0.5$$

H = 3.50 m

A_v = 48.00 m^2

α_v = 240 m^2

$\alpha_v = 0.2$

$\alpha_v = 0.0$

b_v = 37

Replacing:

$$w_f = (6/3.50)^{0.3}[0.62 + 90(0.4 - 0.2)^4/(1 + 37 \cdot 0)] = 0.9 \geq 0.5$$

Correction coefficient, Kc:

In this case, it is bare, unprotected steel:

$$K_c = 13.7 \cdot O$$

Being O = 0.088

$$K_c = 13.7 \cdot 0.088 = 1.12$$

Calculation value for fire load density, $q_{f,d}$.

$$q_{f,d} = q_{f,k} \cdot m \cdot \delta_{q,1} \cdot \delta_{q,2} \cdot \delta_n \cdot \delta_c$$

For educational purposes, the characteristic value of the fire load density, $q_{f,k}$. is taken directly from Table 7

$q_{f,k}$ = 350 MJ/m^2

m = 0.8 (all the materials present are of the cellulose type)

$\delta_{q,1} = 1.48$ (depending on the floor area of the section)

$\delta_{q,2} = 1.00$ (risk of ignition due to use)

A coefficient that takes into account existing voluntary active measures, δ_n

$\delta_n = \delta_{n,1} \cdot \delta_{n,2} \cdot \delta_{n,3}$ (existing voluntary measures)

$\delta_{n,1}$ = 0.87 (automatic detection)

$\delta_{n,2} = 0.87$ (automatic fire alarm)

$\delta_{n,3}$ = 0.61 (automatic shutdown)

$$\delta_n = \delta_{n,1} \cdot \delta_{n,2} \cdot \delta_{n,3} = 0.87 \cdot 0.87 \cdot 0.61 = 0.46$$

A factor that takes into account the potential consequences of the fire, δ_c

$\delta_c = 1.0$ (downpipe height of less than 15.0 m.)

Replacing:

$$q_{f,d} = q_{f,k} \cdot m \cdot \delta_{q,1} \cdot \delta_{q,2} \cdot \delta_n \cdot \delta_c = 350 \cdot 0.8 \cdot 1.48 \cdot 1.00 \cdot 0.46 = 190.6\, MJ/m^2$$

The equivalent fire exposure time is calculated as:

$$t_{e,d} = k_b \cdot w_f \cdot k_c \cdot q_{f,d} = 0.07 \cdot 0.9 \cdot 1.12 \cdot 190.6 = 13.45\, min$$

Thus, this second procedure results in a fire exposure time of 13.45 minutes, compared with 60 minutes using the first (standard) procedure in the table 1

The temperature reached by the gases in the enclosure after these times would be (Figure 1 and equation 1):

$$\theta_g = \theta_0 + 345 \cdot \log_{10}(8t + 1)$$

Substituting the times given above into this expression yields gas temperatures of 945 °C and 722.36 °C for 60 minutes and 13.45 minutes, respectively.

To verify the structural impact of the times obtained using both procedures, a 10.0 m span beam subjected to a uniformly distributed load corresponding to its permanent load and the teaching-use surcharge is examined; this consists of an HEB-240 section made of S 275 JR steel that is embedded in the floor slab to half its depth. Under these conditions, the shape factor is A_m/V=65 and the oversizing coefficient is μ_{fi}=2.58, assuming that the structure was initially designed under elastic and linear conditions and has been verified under plastic conditions. If the verification had also been carried out under elastic and linear conditions, μfi=1.76.

The temperatures reached by the steel, depending on its massiveness factor and the temperature reached by the gas in the enclosure, are 907 °C for a duration of 60 minutes and 349 °C for a duration of 13.45 minutes.

As a result of reaching these temperatures, the elastic limit of the steel drops to an extraordinarily low value of 16.5 MPa for a duration of 60 minutes. However, for an exposure time of 13.45 minutes, the elastic limit retains its initial value. It follows that, in the case of 60 minutes, it is necessary to provide protection for the structure; however, when the structure's exposure time to fire is 13.45 minutes, the structure does not need to be protected against the effects of fire. Table 8 summarises the above values.

Table 8 – Summary of the results obtained in the case study

Methods	Exposure time (minutos)	Gas temperature (ºC)	Steel temperature (ºC)	Yield Strenght (MPa)
Simplified method	60	945	907	16.5
Analytic method	13.45	722.36	349	275

6. Conclusions

This study has analysed two procedures included in the Eurocode and the CTE DB SI to determine the duration for which a structure must be capable of withstanding the effects of a fire. The analysis of the two methodologies and the resolution of a case study have led to the following conclusions.

- The mandatory regulations in Spain for calculating the time a structure must withstand the effects of a fire provide for two very different analysis procedures: one based on the application of a table and another analytical procedure.

- These two procedures are also covered by the Eurocode, which is not a mandatory regulation in Spain but is a reference standard.
- When these two procedures are applied, the times obtained yield very different values.
- Applied to a real-world case, the use of the table-based procedure results in a temperature in the structural steel that necessitates its protection, whereas with the analytical procedure the temperature reached is low enough that the elastic limit is not altered, making protection unnecessary.
- The above cannot be generalised to all situations. The values obtained for equivalent fire exposure time depend on multiple factors, and the value of the steel's elastic limit depends on the temperature reached within the enclosure and the massiveness factor of the cross-section.

References

Faghihi, Faranak, Mehmed Numanović, and Markus Knobloch. 2023. "The Effect of Thermal Creep on the Fire Resistance of Steel Columns." Fire Safety Journal 137: 103750. https://doi.org/10.1016/j.firesaf.2023.103750

Randaxhe, Jérôme, Nicoleta Popa, Olivier Vassart, and Nicola Tondini. 2021. "Development of a Plug-and-Play Fire Protection System for Steel Columns." Fire Safety Journal 121: 103272. https://doi.org/10.1016/j.firesaf.2020.103272

European Convention for Constructional Steelwork. 1974. Fire Safety in Construction Steelworks, ECCS-III-74-2E.

Usmani, A. S. 2005. "Stability of the World Trade Center Twin Towers Structural Frame in Multiple Floor Fires." Journal of Engineering Mechanics 131 (6): 654–657. https://doi.org/10.1061/(ASCE)0733-9399(2005)131:6(654)

Behnam, Behrouz. 2019. "Fire Structural Response of the Plasco Building: A Preliminary Investigation Report." International Journal of Civil Engineering 17: 563–580. https://doi.org/10.1007/s40999-018-0332-x

Chandra, Amit, Anjan Bhowmick, and Ashutosh Bagchi. 2021. "Performance of Steel Moment-Resisting Frames in Post-Earthquake Horizontally Traveling Fire." Journal of Structural Fire Engineering 12 (4): 541–566. https://doi.org/10.1108/JSFE-09-2020-0028

Norouzi, Anahita, Ashoutosh Bagchi, Anjan Bhowmick, and Amit Chandra. 2018. "Parametric Study on Post-Earthquake Fire Behavior of Steel Moment Resisting Frames." In Proceedings of the CSCE Annual Conference, Fredericton, Canada, June 13–16. https://legacy.csce.ca/elf/apps/CONFERENCEVIEWER/conferences/2018/pdfs/Paper_ST70_0611014000.pdf

European Convention for Constructional Steelwork. 1978. European Recommendations for Steel Construction, ECCS-EG-77-2E.

ISO. 2025. ISO 834-1:2025: Fire-Resistance Tests—Elements of Building Construction—Part 1: General Requirements. Geneva.

European Committee for Standardization. EN 1363:2012,"Fire resistance test (Part 1 General requeriments)". Bruxelles, 2012.

Arnault, P., H. Ehm, and J. Kruppa. 1974. "Essais d'incendies naturels." Construction Métallique, no. 3: 5–17.

Ministerio de Vivienda y Agenda Urbana. 2025. Código Técnico de la Edificación (CTE). Documento Básico SI: Seguridad en caso de incendio. Madrid. https://www.codigotecnico.org/DocumentosCTE/SeguridadEnCasoDeIncendio.html

European Committee for Standardization (CEN). 2002. EN 1991-1-2: Eurocode 1: Actions on structures – Part 1-2: General actions – Actions on structures exposed to fire. Brussels. https://www.une.org/encuentra-tu-norma/busca-tu-norma/norma?c=norma-une-en-1991-1-2-2019-n0061459



RESEARCH AND RECENT DEVELOPMENTS



cinpar2026
XXII International Conference on Building Pathology and Constructions Repair
15th to 17th July 2026 - Lisboa, Portugal

Corrosion Assessment for prestressed steel strands based on experimental data and numerical analysis

Thamara TOFETI LIMA[1*], Ralf JÄNICKE[1], Roland KRUSE[1], Boso SCHMIDT[2], Vincent OETTEL[2]

[1] Technische Universität Braunschweig, Institute of Applied Mechanics, Braunschweig, Germany

[2] Technische Universität Braunschweig, Institute of Building Materials, Concrete Construction and Fire Safety (iBMB), Braunschweig, Germany

*Corresponding author, e-mail: t.tofeti-lima@tu-braunschweig.de

Abstract: The deterioration of prestressed bridges is often caused by corrosion of reinforcement and prestressing tendons. This study evaluates the effects of different corrosion morphologies – uniform and pitting – on prestressing steel strands with diameters of 12.5 and 15.7 mm exposed to a salt-spray humid chamber for up to five weeks. Visual inspections revealed predominantly uniform corrosion in the smaller-diameter strands and non-uniform pitting corrosion in the larger-diameter strands. Tensile testing quantified reductions in ductility as functions of strand diameter and exposure duration. Although the 12.5 mm strands exhibited greater mass loss, the 15.7 mm strands experienced a more rapid reduction in ductility under identical exposure conditions, attributed to the presence of corrosion pits. To interpret these experimental observations, a finite-element model was developed in COMSOL Multiphysics® using specimen geometries obtained from the tests. Parametric simulations investigated the influence of friction coefficients and pit locations on stress distribution, deformation, and contact pressure. Results demonstrate that, beyond cross-sectional loss, pit location – particularly on inner wires or on the inner side of outer wires – induces significant local von Mises stress concentrations and increased deformation. These findings provide new insights into corrosion-induced mechanical degradation mechanisms in prestressing steel strands.

Keywords: corrosion; prestressed strands; pit corrosion; ductility; stress distribution

1. Introduction

Over the past decades, the European highway network has expanded significantly, leading to a substantial increase in bridge infrastructure (Wilkening et al. 2024). In Germany alone, statistics from the Federal Highway Research Institute (2023) indicate that nearly 69% of the more than 40,000 highway bridges are constructed using prestressed concrete. The structural performance of these bridges relies primarily on prestressing tendons composed of multiple high-strength steel strands. As the main load-carrying component, deterioration of prestressing steel can critically affect the structural behaviour and safety. Among deterioration mechanisms, corrosion is considered the most prevalent cause of damage in prestressed concrete structures (Nguyen et al. 2011). In particular, chloride-induced corrosion – caused by the ingress of contaminated water or de-icing brine, insufficient grout filling, or inadequate protection of anchorage zones – poses a major threat. Prestressing steel is especially sensitive to localized damage due to its high strength. Even moderate cross-sectional loss can result in disproportionate reductions in structural capacity; for example, Poston et al. (2003) reported that a strength reduction of approximately 25% in strands may lead to live-load capacity losses exceeding 50%. A further concern is that corrosion in prestressing tendons often develops without visible external signs, increasing the risk of sudden brittle failure. However, early detection and reliable quantification of corrosion remain challenging because the internal

arrangement of twisted wires prevents direct inspection and complicates the evaluation of corrosion severity and spatial distribution.

Research on the mechanical behaviour of corroded prestressing strands remains relatively limited, and experimental procedures are not yet fully standardized. Accelerated corrosion is commonly induced using electrochemical techniques; however, the resulting damage morphology may differ from natural corrosion processes (Darmawan and Stewart 2007; Enright and Frangopol 1999; Tu, Dong, and Fang 2019). Alternative methods, such as salt spray or climate chamber exposure, have been proposed to better simulate progressive chloride attack and wet–dry cycles, producing corrosion patterns closer to those observed in practice (Wang et al. 2020). Nevertheless, most experimental programs focus primarily on overall mass loss rather than on detailed characterization of uniform and localized pitting corrosion and its mechanical consequences. Several approaches have been used to quantify corrosion-induced cross-sectional loss. Mass loss can be estimated using Faraday's law based on electrochemical principles, as prescribed in ASTM standards, whereas localized pitting corrosion can be evaluated through pit-depth measurements using instruments such as pit-depth gauges. In the latter case, an idealization of the damaged cross section is required to estimate the effective loss of area, and the adopted methodology may influence the interpretation of corrosion damage and its mechanical implications.

The influence of corrosion on the mechanical properties of prestressing wires is also not yet fully understood. Li et al. (2022) reported negligible effects on elastic modulus and yield strength but significant reductions in ultimate strain, while Vu et al. (2009) observed degradation in on the same factors. For multi-wire strands, the mechanical response becomes even more complex due to stress redistribution, inter-wire contact, and friction effects. Consequently, numerical modelling is often required to complement experimental observations and to investigate internal stress mechanisms that cannot be directly measured. Several studies have combined experimental investigations with numerical modelling. Lu et al. (2016) conducted tests on corroded seven-wire strands and proposed a micromechanical damage model to explain failure mechanisms in prestressed concrete structures. Jeon et al. (2019) developed an equivalent material model based on a spring analogy to represent different corrosion geometries derived from experimentally measured pit depths. Giriraju et al. (2022) proposed analytical models for predicting the mechanical behaviour of corroded strands using tensile test results and a pitting factor to represent corrosion severity. Although these approaches provide valuable insights, further investigation is required to better understand the influence of corrosion location and inter-wire interaction on strand behaviour.

To address these limitations, the present study proposes an integrated experimental and numerical investigation of chloride-induced corrosion in prestressing steel strands. Corrosion was induced using controlled salt spray exposure for periods of two, three, four, and five weeks. Mass loss measurements, corrosion rate calculations, and photographic documentation of corroded cross sections were combined with tensile testing to evaluate the degradation of strength and ductility. Based on the experimental observations, a numerical model was developed to simulate stress distribution within corroded strands, incorporating both cross-sectional loss due to pitting corrosion and inter-wire friction with varying coefficients and spatial corrosion configurations. The main objective of this study is therefore to establish a relationship between corrosion-induced section loss, contact stress redistribution, and the resulting degradation of mechanical performance in prestressing steel strands. By linking experimental observations with physically based numerical modelling, this work aims to contribute to a more reliable assessment of corrosion damage in prestressed concrete structures.

2. Materials and Methods

2.1 Exposure Conditions

A prestressing steel strand is made from a number of wires twisted together in the same direction and with nearly the same lay length. The strand is then subjected to a finishing thermo-mechanical treatment. BEKAERT high strength, low relaxation, seven-wire strands (ST 1670/1860) with nominal diameters of 12.5 and 15.7 mm and length of 950 mm were used for this study. These strands are commonly used in the construction of prestressed concrete bridges and were therefore selected for testing. Technical specifications from the strands were measured in 12 specimens and are given in Table 1.

First, the geometry and initial mass of all prestressing strands were measured. For the corrosion investigation, three specimens of the same diameter were prepared for each exposure duration, while three uncorroded specimens of identical diameter served as reference samples. Corrosion was accelerated using a salt spray chamber, in which the temperature was maintained between 39 and 42 °C and the relative humidity was 100 %. A 3 % sodium chloride (NaCl) solution was continuously sprayed onto the specimens in the form of a fine mist. These aggressive environmental conditions enabled significant corrosion levels to develop within a relatively short period. The strands were exposed in the chamber for 2, 3, 4, and 5 weeks. Naming of the samples is as follows: non corroded (NC), 2 weeks (2W), 3 weeks (3W), 4 weeks (4W) and 5 weeks (5W). The tests were conducted in accordance with DIN EN ISO 9227:2022-02 (2022). After removal from the chamber, the specimens were covered with corrosion products (rust). Prior to further examination, photographic documentation and mass measurements were carried out. Since the corrosion products hindered the evaluation of the actual corrosion damage, the strands were untwisted and cleaned by sandblasting. After cleaning, the wires were reassembled into strands, and their mass was measured again, followed by photographic documentation and visual inspection.

Table 1 – Material properties of the strand

Nominal Diameter (mm)	Average Cross Section Area (mm^2)	Average Maximum Tensile Force (kN)	Average Yield Strength (MPa)	Average Elastic Modulus (GPa)	Weight per meter (g/m)
12.5	94.1	177	1708	190	726.3
15.7	152.2	280	1733	188.8	1172

2.2 Tensile Tests

Tensile tests were conducted on both uncorroded and corroded prestressing steel strands to assess the degradation of their mechanical properties. The tests were performed in accordance with DIN EN ISO 15630-1:2019-05 (2019). To prevent premature failure of the strands at the clamping points during testing due to the applied gripping force, the strand ends were first sheathed with aluminium tubes and secured with adhesive. The total specimen length was 950 mm. The strands were marked at 100 mm intervals, and a gauge length of 100 mm was defined for strain measurement. Strain was determined from the crosshead displacement of the testing machine, which was continuously recorded during the test and normalized by the defined gauge length. The prepared specimens were subsequently mounted in the tensile testing machine and loaded at a displacement rate of 5 mm/min until failure occurred. After testing, the specimens were removed from the testing apparatus, visually inspected and photographed for documentation..

2.3 Corrosion Assessment

To assess corrosion, the chosen method was the calculation of corrosion rates through the obtained values of mass loss. The specimens were weighed before and after exposure in the salt spray chamber and, after cleaning. Then, through simple subtraction of the values the mass loss can be obtained. The calculated mass loss represents the total loss over the entire length and cross section of the test specimen. In order to obtain more information corrosion rates (CR) were also calculated using the chemical characteristics of the steel and the mass loss, by Equation 1, which follows the principles of the Faraday Laws and is fully detailed on the

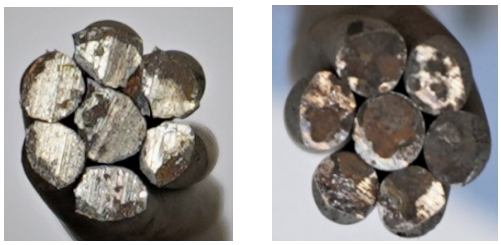
standard ASTM G102-89 (2015), where W is the weight loss (mg), D is the steel density (g/cm³), A is the cross-sectional area (cm²) and T is the time (hours).

$$CR = (87.6 \times W)/(D \times A \times T) \quad (1)$$

3. Experimental Results

3.1 Visual Inspection

Visual inspection of the specimens revealed that the corrosion morphology varied with both exposure duration and strand diameter. Figure 1 presents specimens of 12.5 mm and 15.7 mm strands after rust removal following 5 weeks of exposure. For the 12.5 mm strands, corrosion pits were observed to be relatively uniformly distributed along the outer wire surfaces. In addition, corrosion was present on the contact interfaces between individual wires, indicating that the aggressive environment was able to penetrate between the wires of the strand. For 15.7 mm strands, they exhibited significantly deeper pits at the same exposure duration. Notably, corrosion was also detected on the inner wire, suggesting that the corrosive environment can reach internal components of the strand even under the tested conditions. These observations challenge simplifications adopted in previous studies. For example, Jeon et al. (2019) assumed in their numerical analysis that corrosion of the inner wire could be neglected, arguing that such damage occurs rarely and is difficult to examine experimentally. However, the results obtained in the present study indicate that both inner and outer wires are susceptible to corrosion, even for similar exposure durations. Consequently, neglecting inner-wire corrosion may lead to an underestimation of the overall deterioration of prestressing strands, and its potential influence should therefore be considered in analytical and numerical investigations.



a) b)

Figure 1 – Photos of strands after 5 weeks of exposure to the salt chamber for a) 12.5mm and b) 15.7mm strands

3.2. Mass Loss and Corrosion Rate

Figure 2 a) illustrates the relationship between average mass loss and exposure time for the 12.5 mm and 15.7 mm strands. The average value calculated among the three samples was chosen for better visualization of results. As expected, the mass loss increases with increasing exposure duration for both strand diameters, indicating a progressive development of corrosion under the accelerated salt spray conditions. At early exposure stages (2 weeks), the difference in mass loss between the two strand diameters is relatively small. However, as the exposure time increases, the divergence between the two trends becomes more pronounced. The 12.5 mm strands consistently exhibit higher mass loss values than the 15.7 mm strands for comparable exposure durations. Furthermore, the results show an approximately linear increase in mass loss with exposure time, as indicated by the high coefficients of determination (R^2 = 0.9843 for 12.5 mm strands and R^2 = 0.9747 for 15.7 mm strands). This suggests that, within the investigated exposure period,

the corrosion process progresses at a nearly constant rate. The greater mass loss observed in the smaller-diameter strands may be attributed to their higher surface area to volume ratio.

Concerning corrosion rates, Figure 2 b) shows the corrosion rate for the 12.5 mm and 15.7 mm strands over the exposure period. The corrosion rates fluctuate slightly but generally remain between approximately 1.2 and 2.0 mpy (mils per year) for both diameters. Notably, the corrosion rates for the 12.5 mm strands are consistently marginally higher than those of the 15.7 mm strands, which aligns with the observed mass loss trends. The relatively stable corrosion rates over time correspond with the approximately linear increase in mass loss for both strand sizes, indicating a near-constant corrosion progression under the accelerated salt spray conditions. This consistency reinforces the interpretation that corrosion advances at a steady rate during the investigated exposure period.

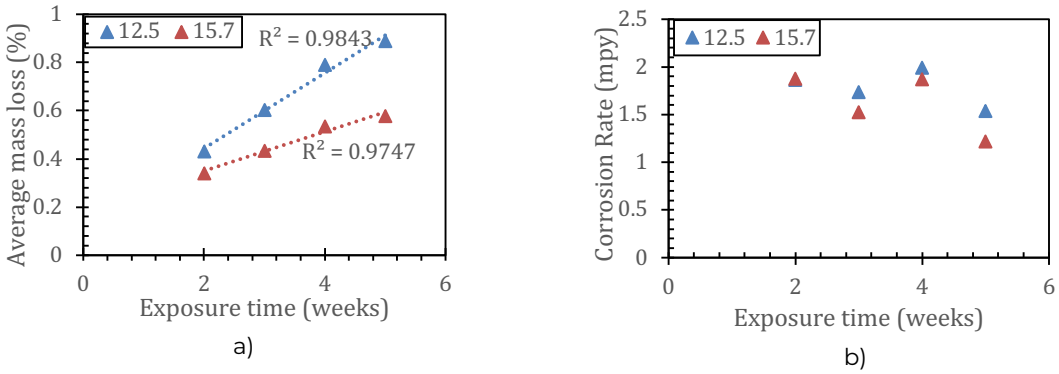


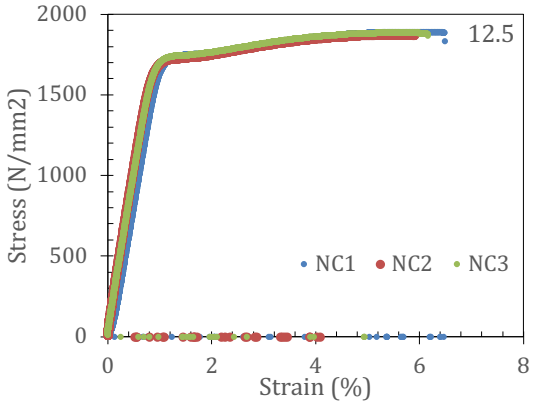
Figure 2 – Corrosion progression according to the exposure time in terms of a) mass loss and b) corrosion rate

3.3. Tensile Tests

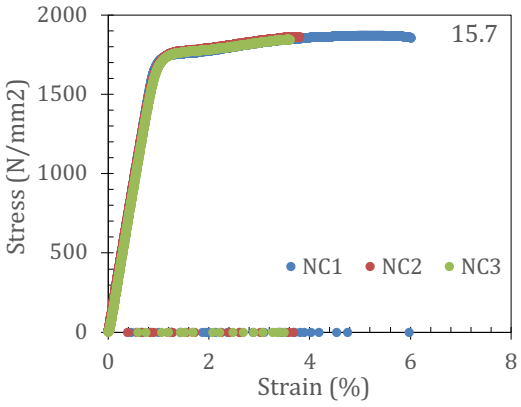
Figure 3 presents the tensile test results for the two strand diameters over different exposure periods. The data indicate that ductility decreases with longer exposure times and increasing mass loss. For the smaller 12.5 mm strands, significant plastic deformation is still observed after 2–4 weeks of exposure, whereas the larger 15.7 mm strands exhibit only a limited plastic region, suggesting brittle failure shortly after yielding, particularly noticeable after 5 weeks of exposure. Figure 4 a) quantifies ductility loss by showing the average maximum deformation for each sample set. The analysis and error bars show that the 12.5-mm strands exhibit virtually no variation, while the 15.7 mm strands exhibit considerable variability, even within the same set.

Interestingly, although 12.5 mm strands experience greater overall mass loss (see Section 3.2), the larger 15.7 mm strands lose ductility more rapidly under equivalent exposure conditions. This difference arises from corrosion morphology. Small-diameter strands corrode more uniformly, causing gradual thinning and a proportional reduction in ultimate elongation. In contrast, larger strands often develop deep, localized pits, which act as stress concentrators and crack initiation sites. This behaviour is likely linked to the strand geometry: 15.7 mm strands have larger interstices and occluded cells, where chloride-laden moisture can accumulate, promoting deep pitting. Smaller strands shed corrosion products more easily, favouring uniform, shallower attack. Post-test visual inspections confirmed these observations. All wires failed in the smaller strands, whereas in the larger strands, the most corroded wires failed first after exposure periods longer than 2 weeks. This supports the hypothesis that the failure of individual wires governs the behaviour of larger strands. This also explains the bigger variation within the same dataset for bigger bars, since then the individual characteristics play a bigger role, while for smaller, the “bulk” properties tend to be more prominent.

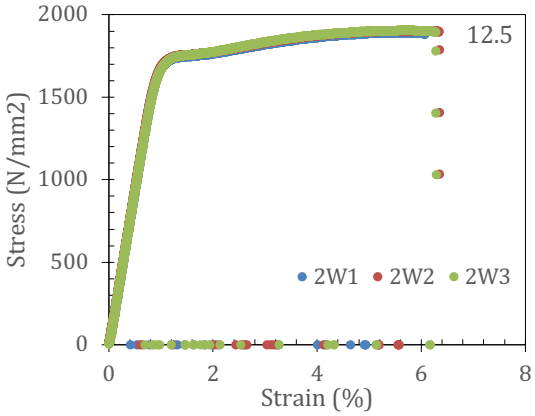
Despite the pronounced changes in ductility, elastic properties such as yield strength show only slight reductions with corrosion (Figure 4 b). Surface micro-cracks propagate slowly under small strains, minimally affecting bulk stiffness. After yielding, deformation accelerates crack propagation, reducing overall ductility. It is worth noting that field conditions, such as stress-corrosion cracking or hydrogen embrittlement, could produce more severe micro-cracks and may degrade elastic properties more than observed in these controlled tests.



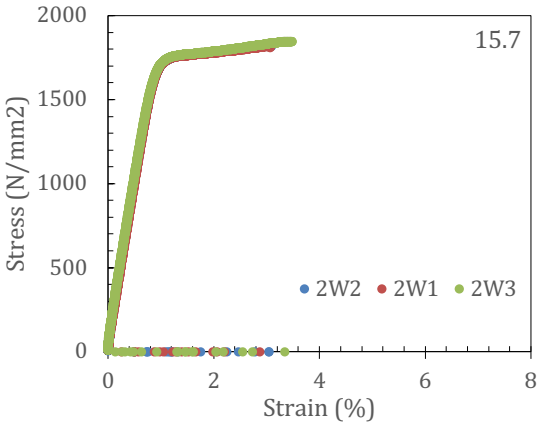
a)



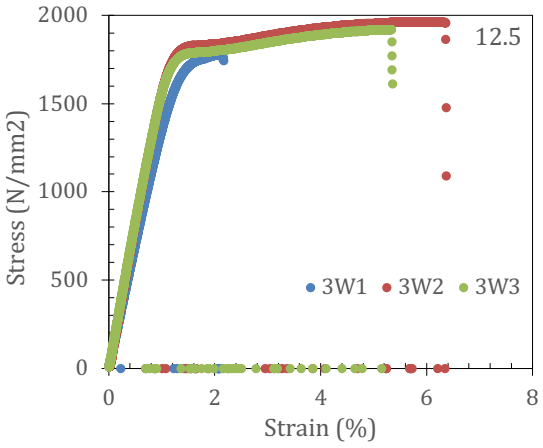
b)



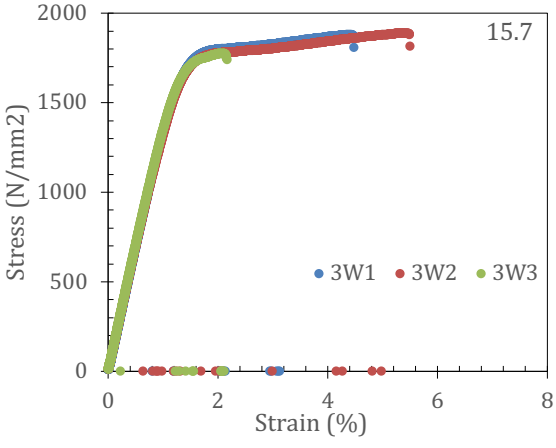
c)



d)



e)



f)

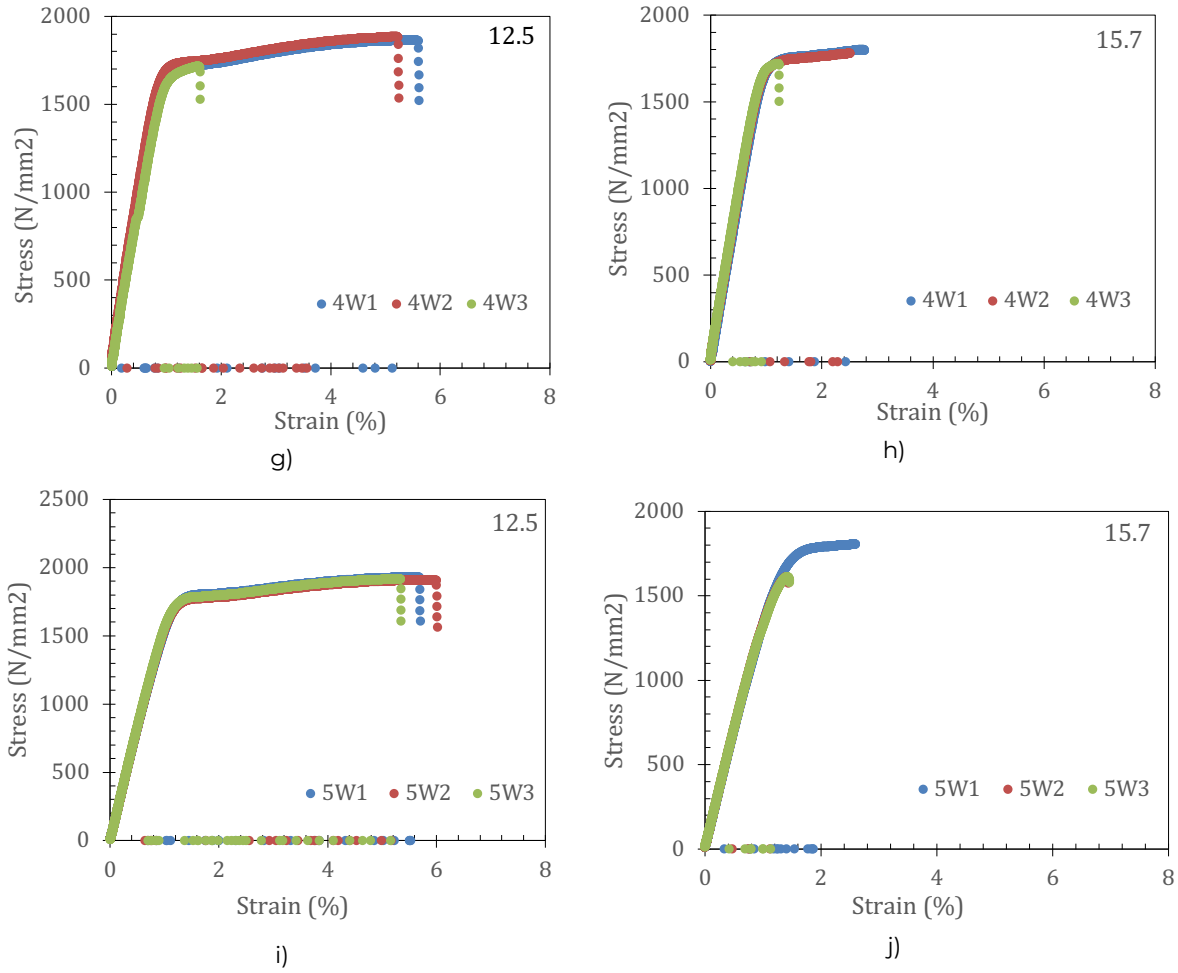


Figure 3 –Stress–strain curves from tensile tests of prestressing strands after different durations of salt-chamber exposure. 12.5 mm strands: (a) non-corroded (NC), (c) 2 weeks (2W), (e) 3 weeks (3W), (g) 4 weeks (4W), (i) 5 weeks (5W). 15.7 mm strands: (b) non-corroded, (d) 2 weeks, (f) 3 weeks, (h) 4 weeks, (j) 5 weeks.

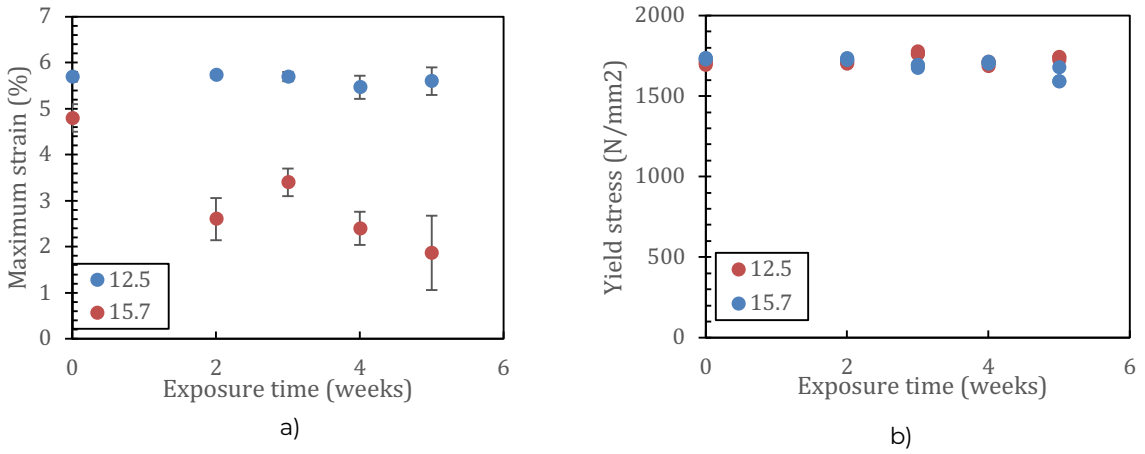


Figure 4 – Effect of salt-chamber exposure time on tensile properties of prestressing strands: (a) maximum deformation; (b) yield stress

4. Numerical Analysis

Because experimental results can be strongly influenced by testing conditions, a numerical model was developed to better understand the stress distribution within corroded prestressing strands. The model accounts for cross-sectional loss due to pitting corrosion – identified as a major influencing factor – as well as inter-wire friction by considering different friction coefficients and spatial corrosion configurations within the strand cross-section. Unlike previous approaches, the proposed framework explicitly investigates the effect of corrosion-induced reductions in contact stresses on the global mechanical behaviour of the strand and evaluates how the location of corrosion damage influences stress distribution among the wires.

The numerical model was implemented in COMSOL Multiphysics® (version 5.6) and developed following the modelling approaches presented by Utting and Jones (1987), Huang (1978), and Kumar et al. (1997). Wire friction was represented using the Coulomb friction coefficient μ. The material properties were taken from the software structural steel database and adjusted according to manufacturer data: density 7810 kg/m^3, Young's modulus 195.9 GPa and Poisson's ratio of 0.30. A linear elastoplastic material model was assumed. The strand geometry consists of seven wires: one straight inner wire surrounded by six outer helical wires. The model dimensions were defined using the mean values obtained from the measured geometry of the 12.5 mm diameter strands, assuming identical diameters for all wires. The outer wires are symmetrically arranged around the inner wire with a 60° angular spacing, and the total modelled strand length was set to 100 mm. The geometric parameters used in the model are summarized in Table 2. Figure 5 a) illustrates the geometry.

To define the corrosion configurations used in the simulations, the failure classification proposed by Remitz and Empelmann (2020) was adopted. Cross-sectional loss due to corrosion was calculated using the hemispherical pit model proposed by Val and Melchers (1997). For simplicity, only strands with a nominal diameter of 12.5 mm were considered here. Pit geometry was idealized as a circular cross-sectional loss; therefore, corrosion in the inner wire was represented as a cylindrical pit. To ensure comparable cross-sectional loss among the outer wires, corrosion was also applied along the helical geometry of the wires. Using the difference function in COMSOL, the damaged volume was subtracted from the original wire geometry to obtain the residual cross section. Figure 5 b) shows how the damaged area was subtracted from the strand and modelled.

For simplification, the pit height was assumed to be 5 mm in all cases. Pit depths of 1.00 mm, 2.00 mm, and 3.00 mm were considered for some configurations, while depths of 0.486 mm, 0.935 mm, and 1.300 mm were used for others. These values were selected so that the resulting reductions in cross-sectional area were comparable across different corrosion configurations. Regarding friction parameters, previous studies such as Erdönmez (2020) suggest that a Coulomb friction coefficient of 0.115 very well represents inter-wire friction. To evaluate the influence of friction on stress distribution, two additional values close to this reference value (μ=0.10 and μ=0.14) were also considered for both non-corroded and corroded strands. In total, 21 numerical cases were analysed (Figure 6). Cases 1–3 represent non-corroded strands analysed with different friction coefficients, while cases 4–6 correspond to corroded strands subjected to the same friction parameters. The reference value 0.115 was subsequently used for cases 7–21. Cases 7–18 investigate four different corrosion configurations with increasing pit depth. Finally, cases 19–21 consider identical total cross-sectional loss as in the previous cases but distributed among multiple wires, representing combinations of the four failure types. This approach allows the evaluation of how identical overall strand section loss may lead to different stress distributions depending on how corrosion damage is distributed among the wires.

Table 2 - Geometric parameters of the strands used in the model

Inner wire	Outer wires

Length(mm)	Radius (mm)	Number of turns	Major radius(mm)	Minor radius (mm)	Axial pitch (mm)	Radial pitch (mm)
100	2.08	100/197.67	4.16	2.08	197.67	0

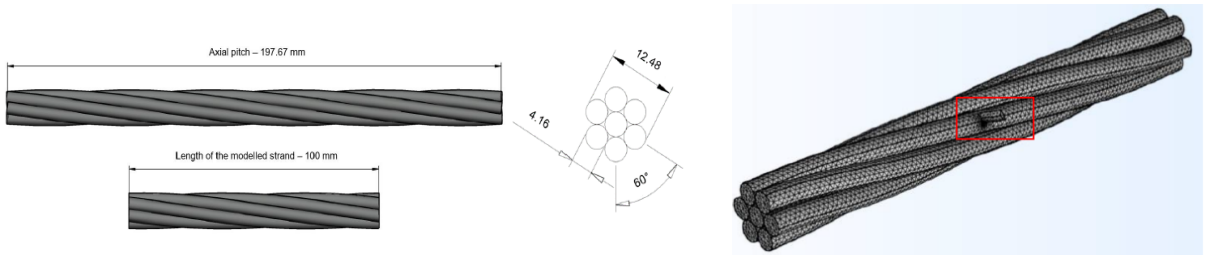


Figure 5 –a) Geometry of the strand and b) Example of a mesh for strands on cases 4-7 showing the subtraction of the corroded area

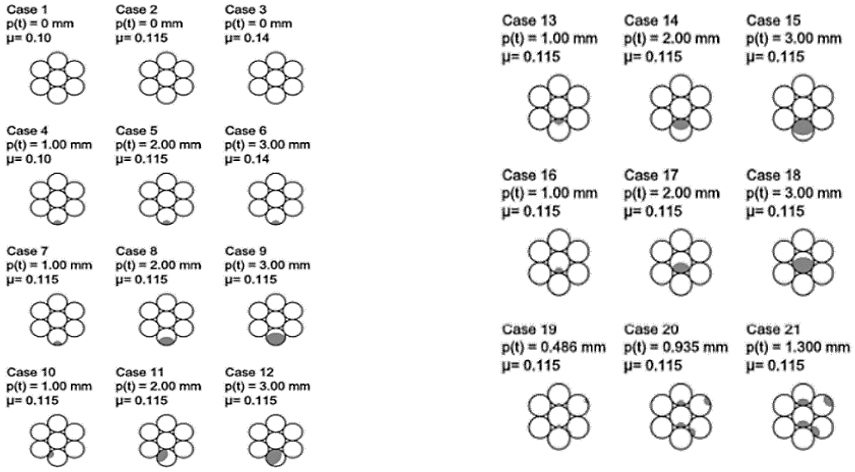


Figure 6 – Overview of studied cases

4.1 Results

The following section presents and discusses the results of the simulations for a tensile test with a force of 100 kN. It compares the maximum deformation, the maximum von Mises stress, and the contact pressure related to non-corroded and corroded strands with different friction coefficients and different distributions of the pits.

4.1.2 Influence of friction coefficients

Simulations indicated that strand deformation decreases with increasing frictional force as expected irrespective of corrosion. Regarding contact pressure, the highest values occur at the wire contact points, particularly near the strand ends where wire displacement intensifies due to elongation during testing, as illustrated in Figure 7 a). Stress distributions show little variation when comparing similar friction conditions within the non-corroded and corroded groups. However, under the same load, corroded strands exhibit generally higher stress levels than non-corroded ones. For uncorroded strands (cases 1 to 3), the maximum

von Mises stress increases with higher friction coefficients, whereas for corroded strands, it decreases as friction increases. These trends are summarized in Figure 7 b).

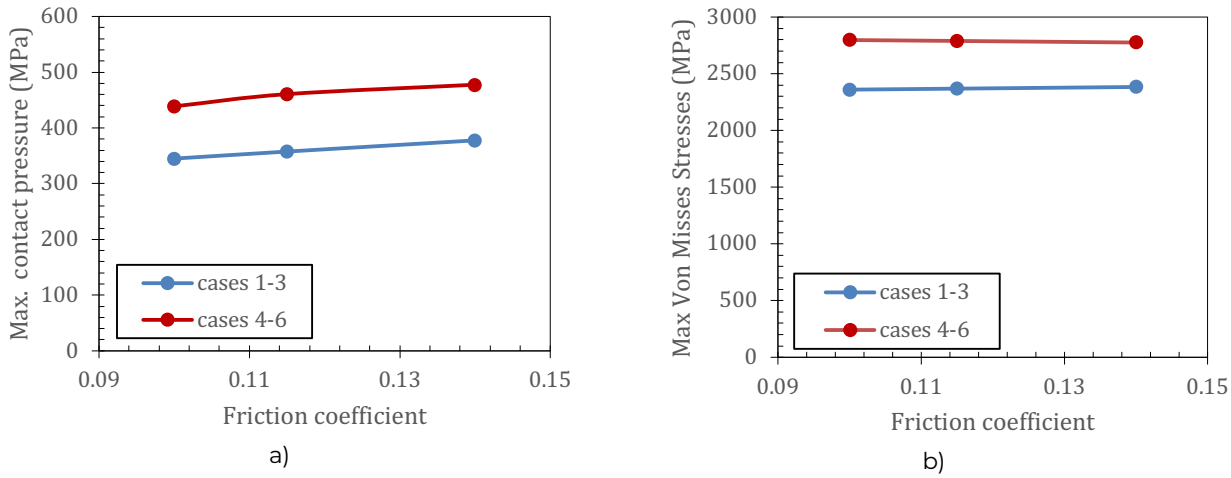


Figure 7 -Influence of the friction coefficient on a) the contact pressure and b) the stress distribution

4.1.2 Variation of section loss versus deformation, contact pressure and stress distribution

Figure 8 a) shows the relationship between deformation and cross-sectional loss for a constant friction coefficient of μ=0.115. As expected, deformation increases with increasing section loss. For mild corrosion (1.33% section loss), deformation remains relatively consistent across all cases. However, for severe corrosion (9.66% section loss), the deformation varies significantly depending on the corrosion location. When corrosion occurs on the external surface of the outer wires (cases 7–9), deformation changes only slightly, a trend also observed when corrosion is distributed among several wires (cases 19–21). In contrast, corrosion located on the inner surfaces of the outer wires (cases 10–15) produces a noticeable increase in deformation, particularly when the pits are in contact with the inner wire (cases 13–15). The largest increase occurs when corrosion affects the inner wire (cases 16–18), highlighting the critical influence of internal damage. Compared with the non-corroded strand (case 2), the severe corrosion case of the inner wire (case 18) results in an increase in deformation of approximately 0.8 mm.

Regarding the stress distribution, in all cases, higher stresses occur within the inner wires and along the inner surfaces of the outer strands. Local stress concentrations develop at the corrosion pits due to the reduction in cross-sectional area, except when corrosion occurs on the outer surface of the strand (cases 7–9), where stress peaks are minimal. When corrosion affects the inner surfaces of the outer wires or the inner wire, the maximum stresses occur near the damaged region. The relationship between section loss and maximum Von Mises stress is shown on Figure 8 b) and indicates good agreement with experimental observations, as failure tends to initiate at stress concentrations located at the corroded areas. For mild corrosion, pit location has a limited effect on stress levels. However, for severe corrosion, pits located on the inner surfaces of the outer wires (cases 12 and 15) or on the inner wire (case 18) produce significantly higher stresses compared with distributed corrosion, with case 18 exhibiting the highest stress concentration.

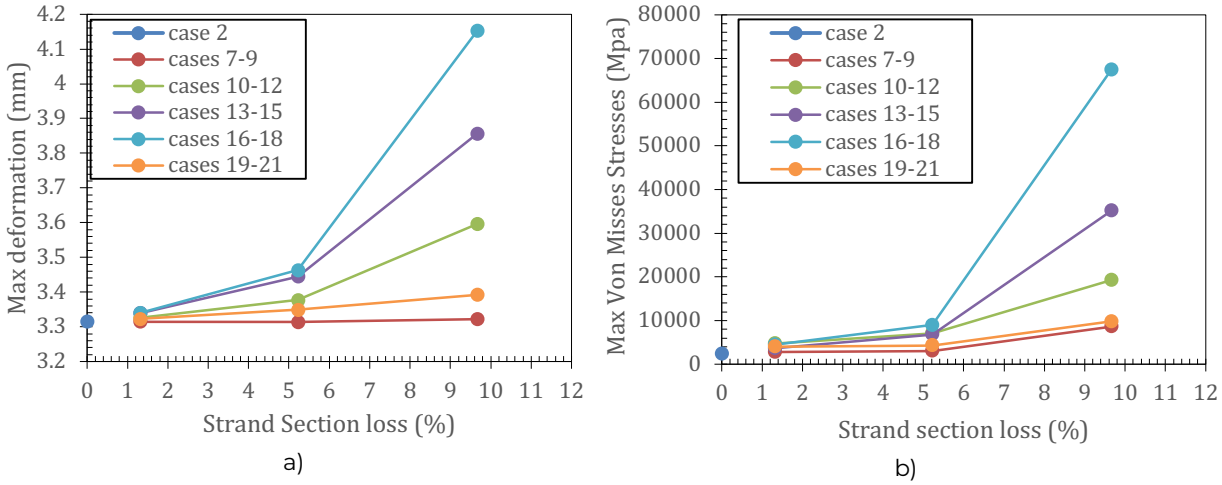


Figure 8 – Influence of varying section loss for studied cases on a) Maximum deformation and b) Stress distribution

5. Conclusions

This paper evaluates and discusses the influences of corrosion on the mechanical behaviour of steel strands used for prestressed concrete. Seven-wire prestressed steel strands with nominal diameters of 12.5 mm and 15.7 mm were subjected to aggressive conditions in a salt spray chamber for periods of 2, 3, 4 and 5 weeks. Tensile tests were conducted to assess the impact of corrosion on the mechanical properties and with the help of numerical simulations the following conclusions were obtained:

- Exposure in salt spray caused clear diameter-dependent corrosion morphology: 12.5 mm strands tended to corrode more uniformly (including at wire interfaces), while 15.7 mm strands developed deeper localized pits, and corrosion was observed on the inner wire – showing that internal corrosion can occur and should not be neglected in modelling.
- Mass loss increased linearly with exposure time for both diameters, with 12.5 mm strands showing higher mass loss overall and slightly higher corrosion rates, consistent with a higher surface area to volume ratio.
- Corrosion mainly reduced ductility rather than elastic properties: yield strength changed only slightly, but maximum deformation dropped markedly with exposure. Despite lower mass loss, 15.7 mm strands lost ductility faster because deep localized pits acted as stress concentrators, leading to earlier, more brittle failure; in these strands, failure was often governed by the most corroded individual wires.
- Simulations confirmed that corrosion location strongly controls mechanical response for severe damage: outer-surface corrosion had limited effect while inner-surface and especially inner wire corrosion produced the largest deformation increases and the highest stress concentrations, matching observed failure initiation at corroded regions.

References

ASTM International. 2015. *Standard Practice for Calculation of Corrosion Rates and Related Information from Electrochemical Measurements (ASTM G102-89).* West Conshohocken, PA: ASTM International.

BEKAERT. n.d. *Prestressing 7-Wire Strand prEN 10138-3: Datasheet.* Accessed October 15, 2023. https://www.bekaert.com/es/test-description.

Darmawan, M. S., and M. G. Stewart. 2007. “Spatial Time-Dependent Reliability Analysis of Corroding Pretensioned Prestressed Concrete Bridge Girders.” *Structural Safety* 29 (1): 16–31. https://doi.org/10.1016/j.strusafe.2005.11.002.

ISO – International Standard. 2019. *Steel for the Reinforcement and Prestressing of Concrete –Test Methods – Part 1: Reinforcing Bars, Wire Rod and Wire (EN ISO 15630-1:2019-05)*. Switzerland: ISO.

ISO – International Standard. 2022. *Corrosion Tests in Artificial Atmospheres – Salt Spray Tests (EN ISO 9227:2022-02)*. Switzerland: ISO.

Enright, M. P., and D. M. Frangopol. 1999. “Reliability-Based Condition Assessment of Deteriorating Concrete Bridges Considering Load Redistribution.” *Structural Safety* 21 (2): 159–195. https://doi.org/10.1016/S0167-4730(99)00015-6.

Erdönmez, C. 2020. “Analysis and Design of Compacted IWRC Meshed Model under Axial Strain.” Int. Journal of Mechanical and Materials Design 16 (3): 647–661. https://doi.org/10.1007/s10999-019-09481-x.

Giriraju, R., A. K. Sengupta, and R. G. Pillai. 2022. “Tensile Behaviour of Corroded Strands in Prestressed Concrete Systems.” *Journal of the Institution of Engineers (India): Series A* 103 (3): 867–879.

Huang, N. C. 1978. “Finite Extension of an Elastic Strand with a Central Core.” *Journal of Applied Mechanics* 45 (4): 852–858. https://doi.org/10.1115/1.3424431.

Jeon, C.-H., J.-B. Lee, S. Lon, and C.-S. Shim. 2019. “Equivalent Material Model of Corroded Prestressing Steel Strand.” *J. Mater. Res. Technol.* 8 (2): 2450–2460. https://doi.org/10.1016/j.jmrt.2019.02.010.

Kumar, K., J. E. Cochran, and J. A. Cutchins. 1997. “Contact Stresses in Cables Due to Tension and Torsion.” *Journal of Applied Mechanics* 64 (4): 935–939. https://doi.org/10.1115/1.2789002.

Li, J., T. Miki, Q. Yang, and M. Mao. 2022. “Experimental Study on Prestressing Force of Corroded Prestressed Concrete Steel Strands.” *Journal of Advanced Concrete Technology* 20 (9): 550–563.

Lu, Z.-H., F. Li, and Y.-G. Zhao. 2016. “An Investigation of Degradation of Mechanical Behaviour of Prestressing Strands Subjected to Chloride Attacking.” In *Proceedings of the 5th International Conference on the Durability of Concrete Structures*.

Nguyen, V.-S., M. C. Jeong, T. S. Han, and J. S. Kong. 2011. “Reliability-Based Optimisation Design of Post-Tensioned Concrete Box Girder Bridges Considering Pitting Corrosion Attack.” *Structure and Infrastructure Engineering*, 1–19. https://doi.org/10.1080/15732479.2010.524653.

Poston, R. W., K. H. Frank, and J. S. West. 2003. “Enduring Strength.” *Civil Engineering* 73 (9): 58.

Remitz, J., and M. Empelmann. 2020. “Cyclic Tensile Tests on Prestressing Strands Embedded in Concrete.” Materials and Structures 53 (3). https://doi.org/10.1617/s11527-020-01484-x

Tu, B., Y. Dong, and Z. Fang. 2019. “Time-Dependent Reliability and Redundancy of Corroded Prestressed Concrete Bridges at Material, Component, and System Levels.” *Journal of Bridge Engineering* 24 (9). https://doi.org/10.1061/(ASCE)BE.1943-5592.0001461.

Utting, W. S., and N. Jones. 1987. “The Response of Wire Rope Strands to Axial Tensile Loads—Part I: Experimental Results and Theoretical Predictions.” *International Journal of Mechanical Sciences* 29 (9): 605–619. https://doi.org/10.1016/0020-7403(87)90033-6.

Val, D. V., and R. E. Melchers. 1997. “Reliability of Deteriorating RC Slab Bridges.” Journal of Structural Engineering 123 (12): 1638–1644. https://doi.org/10.1061/(ASCE)0733-9445(1997)123:12(1638)

Vu, N. A., A. Castel, and R. François. 2009. “Effect of Stress Corrosion Cracking on Stress–Strain Response of Steel Wires Used in Prestressed Concrete Beams.” *Corrosion Science* 51 (6): 1453–1459.

Wang, L., T. Li, L. Dai, W. Chen, and K. Huang. 2020. “Corrosion Morphology and Mechanical Behavior of Corroded Prestressing Strands.” *Journal of Advanced Concrete Technology* 18 (10): 545–557.

Wilkening, M., L. Joachim, V. Oettel. 2024. “Investigations on the fatigue loading of thin-walled and resource-efficient UHPFRC segmental bridges.” *Eng. Struct.* 306. https://doi.org/10.1016/j.engstruct.2024.117858

Cinpar 2026
XXII International Conference on Building Pathology and Constructions Repair
15th to 17th July 2026 - Lisboa, Portugal

Optimising resource value extraction in demolition and rehabilitation: A digital twin-transition approach - EU Horizon DISCOVER project

Jorge de Brito [1], José Dinis Silvestre [1], João Gomes Ferreira [1], João Pacheco [1], Rui Silva [1], Miguel Bravo [1], Renato Neves [1], **Isobel Andrews [1]**

[1] CERIS, Departamento de Engenharia Civil, Arquitectura e Ambiente, Instituto Superior Técnico (IST), Universidade de Lisboa, Lisboa Portugal.

Abstract: The construction and demolition sector generates approximately 38% of all waste annually in the EU. The resulting impact of around 820 million tonnes of waste from demolition and rehabilitation projects requires careful management. While it is recognised that there is value in construction materials extracted from demolition and rehabilitation sites via selective deconstruction strategies, recovery and reuse of such materials remains limited due to organisational and logistical challenges which currently render full selectivity infeasible during the end-of-life phase of buildings.

The DISCOVER consortium brings together 14 project partners from research and industry institutions across the EU, combining expertise on robotics and artificial intelligence with deconstruction techniques, waste management, and lifecycle assessment. The project partners are working together to address the challenge of increasing sustainable deconstruction strategies for optimised material recovery, with the goal of preserving the value contained in construction materials for secondary uses. The project integrates the findings and developed models into an automated robotic inspection system, feeding into digital twin BIM tools to build interactive pathways to the decision-makers in industry. Engagement with stakeholders in the industry and interaction with live demolition projects are continuously being utilised to build life cycle assessment models for demolition processes and outcomes for recovered materials and to train robotic inspection prototypes throughout the four-year project. Doing so is expected to lead to a reduction of construction and demolition waste by 55% and greenhouse gas emissions in the sector by 20%, improving overall circular practices in the construction life cycle.

This paper presents the DISCOVER proposals and methodologies for improving the sustainable management of building deconstruction, material extraction and circular treatment of construction and demolition waste (CDW) in the EU.

Keywords: Deconstruction, sustainability, digitalisation, inspection, materials

1. Introduction

Annually, the construction and demolition sector accounts for about 38% of the total amount of waste generated in Europe (Eurostat 2023). and about 24% of global extractions of raw materials (Bribián et al., 2011), making this sector the largest resource consuming and waste producing one in the EU (Luciano et al. 2022). Rehabilitation, including renovation, retrofitting and maintenance projects are estimated to be the second largest contributor to the total quantity CDW generated in the EU after demolition (Zhang et al. 2021). Rehabilitation is a necessary tool for conserving buildings and structures key cultural importance and is logically recognised as being more sustainable than new construction in infrastructure management generally, due to lower resource requirements (Popescu et al., 2024). However, with the ageing building stock in the majority of European cities, renovation works, including rehabilitation and maintenance, are estimated to be responsible for around 30% of the associated CDW generated by a building during its life (Sáez et al. 2018). While it is good news that efforts in the EU are resulting in an increase in rehabilitation of existing infrastructure, it is also necessary to consider the question of waste management from these projects, as removal of existing materials sometimes generates more waste in the short term than new construction projects.

The European Green Deal aims for a carbon neutral economy by 2050 (European Commission 2019). The construction and demolition (including rehabilitation and maintenance) sector also currently accounts for almost 40% of carbon emissions in society, with 11% related to material production, transportation and implementation

(United Nations and International Energy Agency 2019). Since construction materials also account for 24% of global extractions of raw materials (Bribián et al., 2011), it is reasonable to continue to pursue progress on the management of CDW.

The EU Horizons DISCOVER project was launched with the aim of reducing CDW in the EU by 55%, thereby reducing construction related emissions by 15%. This project is currently being undertaken, employing a combination of methods. The first stage involves the automation of pre-demolition or rehabilitation inspections processes using robotic innovations. Two prototypes, known within the project as Oliwall and Pokeye, are currently undergoing testing for this purpose. This involves laser scanning of the site to provide spatial information and automatic identification of the materials encountered on the site. This information is then linked to building information modelling (BIM) tools to allow industry professionals to have easy access to the information gathered. The model will be programmed to provide deconstruction methodology recommendations and end of life options for extracted materials to enable material recovery for circular reuse, with associated environmental and cost impacts.

The project also encompasses life cycle assessment (LCA) and life cycle costing (LCC) to consider and compare deconstruction and extraction strategies for the most valuable materials. The end result is an identification of the optimal deconstruction and recovery options for identified materials. Of key importance is that the outputs of the project will be made accessible to industry professionals via BIM plugin tools, which will assist with decision-making in the industry. This is an essential step in building effective change as approximately 70% of industry professionals currently use BIM tools to execute their professional activities (Hasek, 2021).

2. Objectives

The DISCOVER project addresses shortcomings in deconstruction processes by integrating robotics and digital technology to assist in sustainable assessments. This is structured into 6 key objectives, which combine to contribute to advancements in the field of sustainable deconstruction, firstly by developing intelligent learning models for material and component identification, integrating this into an autonomous inspection system and combining with environmental and cost analyses as follows:

Objective 1: To create a set of autonomous and synchronous robotics systems for the precise, fast and less labour-intensive analysis, identification and digitisation of materials and construction components from existing built works, based on mobile manipulators and new data fusion approaches.

Objective 2: To achieve fully automatic understanding of data coming from cameras, ground-penetrating radar (GPR), laser-induced breakdown spectroscopy (LIBS), etc., using sensor fusion techniques and machine learning algorithms, rapidly analysing the properties and characteristics of elements and materials (e.g. composition, dimensions, mass, technical properties, identification of asbestos, fixing and repair needs, etc.).

Objective 3: To create an integrated digital framework to synchronously process and visualise the data brought by the system, leveraging on the wealth of information on the Building Information Modelling (BIM) digital twin.

Objective 4: To enhance the circularity of construction and building elements and materials by an improved identification and management of deconstruction methods.

Objective 5: Development of a sustainability assessment framework to guide demolition methods, considering reuse and recycling of demolition assets and improvement of the sustainability of demolition activities.

Objective 6: To foster the adoption of robotic systems and collaborative BIM tools within the work processes of stakeholders in the construction industry, in special for the deconstruction process, to increase safety and productivity.

Together the objectives embody a system of progressive autonomy in building inspections and integrate digitisation of sustainable assessments in the planning and execution of deconstruction works.

3. State of the art

Robotics and AI are emerging technologies that have been identified as having a significant role to play in building deconstruction and promoting circularity of materials. The potential of robotics in enabling component reuse in the deconstruction sector has been found to be significant in its ability to assist in the transition to circular deconstruction via pre-works inspections in disassembly projects (Thakuri et al., 2024). This is supported by the opinion of industry professionals including engineers, architects, managers, manufacturers, suppliers, contractors, facility managers and circular economy experts worldwide, who, when asked about the challenges of implementing circular practices, indicate that they expect that AI, vision-based robotics and digital twin technologies will play a crucial role in scaling up the adoption of CE practices in the future. In addition, "Complexity in handling and managing CDW materials" was identified as one of the top three barriers to successful implementation of CE practices in the management of CDW (Swarnakar et al., 2025). This indicates strong industry support for innovative developments in this field, such as those the DISCOVER project is intending to achieve.

In the project works phase, whereby the demolition or rehabilitation works are taking place, material separation in combination with waste reuse and recycling has been found to reduce the environmental impact of CDW when compared with disposal of landfill, with around 77% reduction in climate impact (Coelho and de Brito, 2012). These findings are supported by case studies in both Spain and Italy, where selectivity of demolition processes was identified as being a key step in the reduction of carbon associated with the deconstruction stage (Mercante et al., 2011), (Vitale et al., 2017). **Examination of the environmental impacts of demolition processes and waste reuse often involves life cycle assessment.** LCA studies have observed a significant reduction of the environmental impacts associated with diverting CDW from landfill and treating it in a circular manner. One study quantifies this as a reduction of 36% in environmental impacts in person equivalent (PE) when waste is downcycled or recycled rather than landfilled, a figure which rises to 59% in environmental impact savings when recycling after selective demolition is employed, DISCOVER intends to increase this practice. Landfilling was also found by LCC analysis to be the most expensive end-of-life solution (Di Maria et al., 2018).

Meanwhile, the end-of-life phase and deconstruction processes is noted as being a phase that tends to be overlooked or given insufficient consideration in most LCA studies on building life cycle and that this stage should be further investigated to achieve the EU circular economy goals (Ivanica et al., 2022). Additionally, further study is needed on analysing the differences in the impacts of recycling and downcycling of recovered waste streams from deconstructed elements in LCA studies (Bayram and Greiff 2023), which is also something that DISCOVER intends to address.

When considering the digital integration of processes and analyses in the context of circular management of deconstructed infrastructure, BIM has been identified as being a critical industry tool and that the successful implementation of digital technologies in the management of end-of-life processes facilitate reuse of materials within a circular economy model (Thakuri et al., 2023). The authors indicate that the hypothesis could be usefully supported by the implementation of further research involving case studies to test the premise. This is further highlighted by an increasing number of construction professionals, who use BIM or other digital tools in their activities, currently estimated to be around 70% of construction professionals in the EU (Hasek, 2021), indicating that this is a reliable platform on which to convey knowledge and decision support tools.

4. Methodology

The DISCOVER project involves a multidisciplinary expert team from 14 research and industry institutions, across 7 EU countries working together to address the issues of material identification, spatial assessment and management of deconstruction scenarios and recovered materials with the goal of reducing

environmental impact of demolition activities and improving human safety for those involved. The methodology involves careful collaboration between partners.

4.1. Automated pre-demolition inspection

The first stage of the project, both for DISCOVER and in terms of any demolition or rehabilitation project is the pre-works inspection. The DISCOVER project aims to automate this phase of the project via robotic inspection. The robotic system will act as a substitute for human labour in the high-risk situations of pre-demolition or renovation sites, which often comprise potentially unstable situations or exposure to hazardous substances. It will have the capacity to scan buildings and infrastructure to gather data on geospatial elements, materials and building components, both visible as well as complex and concealed components. Two robotic prototypes are developed to perform these tasks - Oliwall and Pokeye. The goal of the robots is to act autonomously within deconstruction sites, performing spatial mapping of the works area and subsequent element and material identification via AI recognition, based on the geometric information supplied by Oliwall, and the subsequent testing of materials where necessary, via samples gathered by Pokeye.

An analysis of expected components and materials, based on the typical characteristics of the building stock in the EU, contributes to the robotic identification system. This key information is used to train the algorithm to identify these elements via the robotic scanning and minimally invasive testing. The integration of artificial intelligence algorithms will contribute to the rapid analysis of spaces set for demolition or renovation works as well as strong supporting indications of the building elements and characteristics of the materials, both visible and concealed. The robots are equipped with laser scanning, ground penetration radar (GPR) for identifying hidden elements in walls and floors and in the case of Pokeye, drilling and sampling apparatus.

4.2. Building Information Modelling (BIM) - the digital twin

The digitalisation phase of the project intends to integrate the geospatial and material information identified in the automated pre-works inspection phase of the project into a BIM Model. Additionally at this stage, optimal strategies and recommendations for deconstruction techniques are integrated, with varying degrees of selectivity and waste management, taking into account the environmental impacts and potential material value and costs.

This phase involves three key tasks:

1. Definition and implementation of a methodology for the conversion of the data collected by the robotic analysis of the works area into semantic BIM objects, including the definition of data formats and pipeline workflow as well as a python script for processing information and converting it into semantic BIM objects;
2. Development of a database containing building information, including the standard material list and the live data collected by the robotic inspections. This is programmed to facilitate subsequent data exploitation and interoperability in such a way that the information can be accessed by external industry operators and entities to inform decision-making in real life projects. This is an advanced stage that incorporates the information contributed by the robotic inspections and AI models with detailed analysis of deconstruction options and techniques, material extraction potential, associated costs and life cycle impact assessment for material recovery paths as well as material traceability throughout their multiple secondary use lives;
3. Construction of a user-friendly digital interface to facilitate use for industry professionals. This includes the development of a visually interactive model characterised by the creation of an open dataset of construction material textures for the machine learning which enables a user-friendly visual interface to facilitate access to the information supplied by the development of step 2 above.

The digitally integrated decision-making support tool will be continually optimised throughout the project by input from existing stakeholders in the industry and via the validation and testing of assumptions from the pilot case studies for different building types and policy contexts.

4.3. Recovery pathway modelling

A key phase of the project methodology involves reducing the environmental impact of deconstruction and disassembly projects by analysing different selectivity scenarios for deconstruction whereby buildings or components are taken apart piece by piece with the key aim being extraction of materials for recovery and reuse, with consideration of the cost of doing so and the resale value of materials. This involves detailed analysis of deconstruction scenarios and methods in terms of techniques, equipment, cost, time and labour with the goal of understanding the optimal strategies for extracting the maximum amount of recovered material, while retaining a feasible deconstruction timeline and budget.

The relevant techniques are studied, considering equipment energy use and emissions, water use, labour and time associated with each option. This information contributes to a detailed life cycle assessment of different deconstruction scenarios that assists in comparing available options for disassembly of buildings or building elements. Following from this, multi-life-cycle assessment and cost life cycles are considered for the materials recovered based on the selected deconstruction scenarios. The reuse and recycling options for each material studied will be considered and the environmental impacts and costs associated with different waste management strategies for each material stream will be compared for the optimal outcome. With input from the on-site robotic inspection system, a secondary material database will be maintained for the recovered materials as a key solution at this stage, with emphasis on material traceability to keep track of the multiple life cycle uses of extracted materials and the associated environmental and cost savings associated with each service life.

This data collected from the LCA of different demolition scenarios and material recovery paths and market value will be included as part of the digital plugin tool to allow this information to be accessible to decision-makers and project managers in the industry.

4.4. Data acquisition from live case studies

The robotic system, AI model and digital integration will be tested on live case studies from four sites across the EU, each representing different infrastructure types and policy backgrounds. The robotic prototypes will be employed to test the geospatial and laser scanning system, material identification, material sampling and integration into BIM to create a visual model. The case studies will also be used to test assumptions made about the feasibility of selective deconstruction recommendations as well as the LCA and LCC models and to assess the conditions created by different policy contexts.

The four pilot studies comprise one historic masonry-based structure in Lisbon, one mixed material, concrete framed structure in Brussels, a reinforced concrete infrastructure project in Warsaw and a mixed materials industrial structure in Barcelona. Each selected project is already marked for demolition. The same methodology can be also applied to renovation works or rehabilitation projects, considering materials to be removed. The robotic scanning aids in building BIM tools, assessment of materials to be removed and cost and environmental analysis of the extracted materials, helping to improve the current shortcoming and main area of criticism associated with renovation and rehabilitation projects - the management of extracted waste - and the case study pilot sites will help to support the project implementation.

5. Project progress

5.1. Robotic prototypes

The robot prototypes, Oliwall and Pokeye are the first of their kind to perform the task of pre-works inspection in existing buildings. Oliwall is operational and ready to be tested on site at the first case study site. Currently testing of Oliwall's capabilities within the laboratory is ongoing. Oliwall can gather geometric

data and correctly identify building elements and objects. It travels autonomously with the successful functioning of the safety feature which enables it to stop when encountering humans in its path for added safety. The prototype of Oliwall undergoing training can be seen in Figure 1 and testing of the mobile abilities in Figure 2.



Figure 1 - Oliwall in training (Universitat Politècnica de Catalunya, 2026)

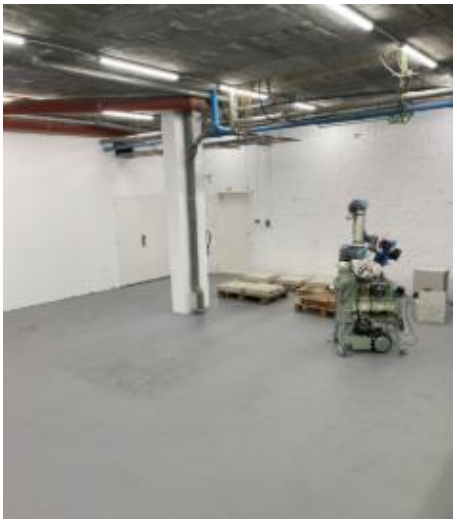


Figure 2 - Oliwall in motion testing (Universitat Politècnica de Catalunya, 2026)

Pokeye is also ready to be tested on a case study site. Currently, the definition of specifications for the autonomous invasive identification system, the development of portable analyser system for material inspection and robotic drilling for material extraction for further analysis are complete and the prototype of Pokeye is being finalised with the coordination tool and user interface almost complete.

5.2. Material list development

Expert analysis of materials commonly identified in older buildings and infrastructure has been carried out to contribute information to the training of Oliwall in the identification of the materials and elements. The material list has been divided into categories and indicators of the ease of extraction. These materials are methodically laid out and categorised by identification difficulty, reuse potential and commercial value as well as the likely risk of hazardous substances contained within them, as seen in Table 1.

5.3. AI algorithms in progress

Currently the AI algorithms are undergoing development and have contributed to the learning of the robot to correctly identify elements and objects. So far, the algorithm has been trained to visually identify objects and elements with 88784 images used in training.

5.4. Industry survey results regarding current best practices in demolition and motivations

Detailed surveys regarding current practices by active stakeholders in the demolition industry have been shared with companies and professionals in the industry across the EU and UK. The survey covers questions on the principal strategies currently employed in the industry considering different building types, current pre-demolition practices, general deconstruction techniques applied, the uptake of selectivity in deconstruction projects and incentives for increasing this practice as well as waste management strategies. The results of the survey have been analysed to determine the general status quo of the approach of different companies across Europe in regard to demolition activities. General insights include 31 survey results so far:

- The most identified pre-works inspection was visual expert inspection with identification of hazardous materials being the highest priority.

- Companies were asked to identify which incentives would encourage them to increase their selective practices in demolition projects. Figure 4 indicates that the most identified incentive was financial or fiscal benefits or penalties and policy requirements.

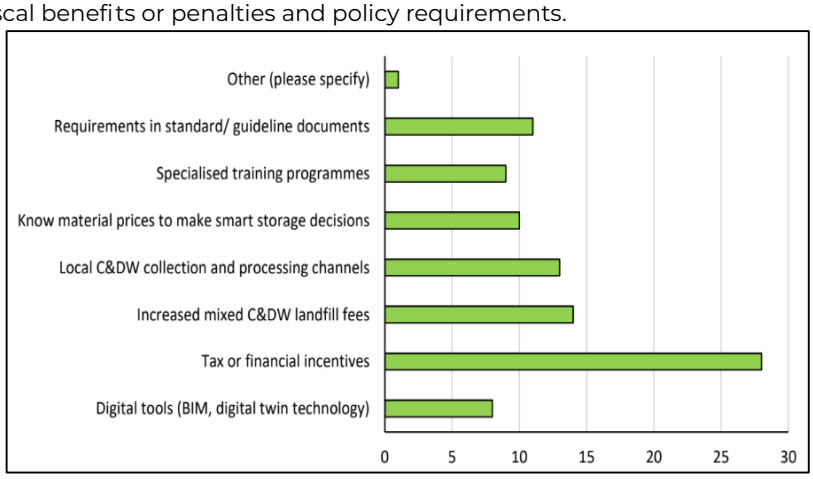


Figure 3 - Encouragement to apply selective demolition in the EU, as reported by demolition companies (Instituto Superior Técnico 2026)

- Generally, the findings showed that demolition companies most frequently use mechanical demolition with specialist equipment as a primary technique across a variety of building types. This indicates an associated promising versatility with this technique. Secondary techniques employed vary significantly across different building types. In many building types, manual demolition was identified as being the second-most employed option, which does indicate feasibility of increased selectivity processes;
- Insights on waste management from demolition projects indicated that currently in the EU 70% of CDW was reused onsite or sold to recycling facilities. Meanwhile nearly 30% of waste emitted from demolition sites is still being sent to landfill. If this is fully representative, this comprises about 238 million tonnes of CDW still ending up in landfill across the EU each year. This is evidenced in Figure 5 showing the survey results on outcomes of demolition waste.

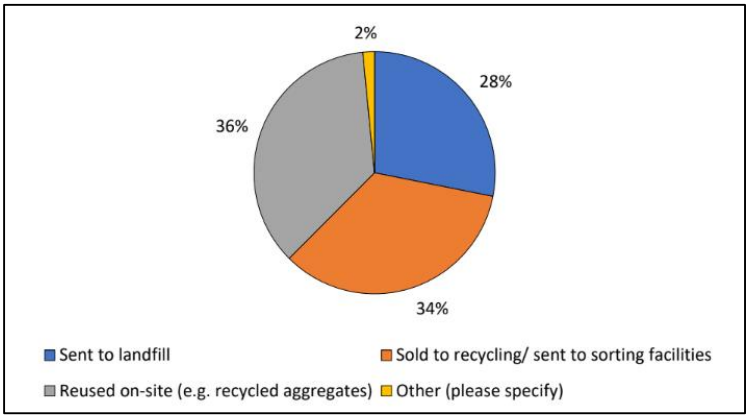


Figure 4 - Survey results showing current outcomes of demolition waste (Instituto Superior Técnico 2026)

5.5. LCI progress

Input from sister projects and project industry partners, as well as survey data, are being used for the development of a life cycle inventory to inform the LCA and LCC phase of the project. Detailed data collected will contribute inputs on energy and water use associated with most commonly used equipment for

deconstruction as well as labour hours, cost and risk exposure. This information will be used to analyse and compare different techniques for their relative environmental and cost impacts including the energy and water use as well as the output of recovered materials and their environmental savings and financial value.

Table 1 - Material list for the consideration of the AI algorithm training and scanning tools and consideration in the LCA and LCC analyses and material database (Universitat Politècnica de Catalunya, 2026)

Group	Material	Identification difficulty	Separation difficulty#	Reuse/recycling potential	Commercial value*	Possibility of hazardous substances	Remarks
Hazardous waste	Asbestos-containing materials	Hard	Normal/Hard	-	None	Asbestos	Highly varied applications ; visual recognition or (mostly) lab.
	Tar asphalt	Hard	Normal	-	None	Tar	Can be tested with PAK spray or lab analysis.
	Tar roofing	Hard	Hard	-	None	Tar	Can be tested with PAK spray or lab analysis.
	WEEE containing CFCs/HCFCs/HFCs	Normal	Normal	-	None	CFCs/HCFCs/HFCs	e.g. refrigeration, freezing and air-conditioning installations
	WEEE: fluorescent lamps	Easy	Easy	-	None	Mercury	Easy to identify, manual measurement is time-consuming.
	WEEE: ionising smoke detector	Easy	Easy	-	None	Radioactive	Easy to identify, manual measurement is time-consuming.
	WEEE / other materials containing PCBs	Normal	Normal	-	None	PCBs	e.g. transformers and capacitors.
	Gases in pressure containers	Easy	Easy	-	None	Dangerous substances	e.g. fire extinguisher, manual measurement is time-consuming
	oil tanks	Normal	Normal	-	None	Mineral oil	In plastic or metal; sometimes underground.
	Materials contaminated by fire	Easy	Normal	-	None	Soot	-
	Contaminated treated wood	Normal	Normal	-	None	Toxic chemicals	e.g. train sleepers, garden wood.
Others	Textile	Easy	Normal	Reuse + Recycling	Normal	-	e.g. carpet flooring.
	Light bulbs	Easy	Easy	-	Low	Small doses of mercury	Easy to identify, manual measurement is time-consuming.
	Gypsum and lime plaster	Normal	Hard	-	Low	Gypsum: sulphate + can contain asbestos	Interfering substances in stony material but selective removal is time-intensive - Future: possible sulphate norm for recycled aggregates (gypsum vs lime plaster).
	Porcelain	Easy	Normal	Reuse	Normal	-	Currently, no separate recycling pathway.
	Fibre cement board	Normal	Normal	Recycling	Normal	-	Similar looking to asbestos-containing fibre cement (high risk for contamination).
	Types of floor-insulation	Normal	Hard	-	Low	-	e.g. (1) concrete with expanded clay aggregates; (2) insulating screed/mortar (EPS beads) - (1) disposed of with debris, aggregates can be interfering substances (2) mixed waste.
	Composite and/or non-separable materials	Normal	Normal/Hard	Sometimes	Normal	-	e.g. sandwich panels, sectional doors, concrete slab with epoxy floor.

Note: WEEE = Waste Electrical and Electronic Equipment; *Commercial Value should not be the main criterion, given the variability. If an extended producer responsibility (EPR) is/will be implemented for a material, it has a significant impact on the price. #Indication of the easiness for a material to be dismantled (including the required equipment and taking into account the fixing method).

1404

6. Expected outcomes

Results of the DISCOVER project are pending its conclusion. Expected outcomes and impacts of the project include technical innovations in robotics and artificial intelligence-based inspection, digital integration for management of secondary recovered assets for increased circularity, site safety and reduction of environmental impact. Figure 6 highlights the expected impact pathways for the output of the project based on the DISCOVER objectives.



Figure 6 - Expected Impact pathways of the output of the DISCOVER project

6.1. Technical expectations and industry level impact

The robotic system represents an innovation in the industry that fills a gap in the current approach to deconstruction in terms risk to human life and end of life management for buildings and materials. The robotic inspections will interact with artificial intelligence models developed in the project to allow for fast paced analysis of the components and material characteristics identified on site, which effectively replace expert individual inspection systems in high-risk situations. The data gathered from the AI integrated robotic inspections will feed into a BIM plugin tool. The BIM model provides an interactive tool for decision makers with a visual interface and information on materials and components present. It offers additional input regarding selective deconstruction recommendations based on a multi-criteria analysis including the material characteristics, cost, time and environmental impact comparison. This digital twin will work effectively for demolition and/or rehabilitation sites in different building types with varying material composition, historical and policy context across the EU. The BIM model, with input from the robotic model and AI inspection tools, will provide the user with:

- Visual interface of the works area;
- Building elements and material composition and quantities, both visible and concealed;
- Best practices and recommendations for selective deconstruction based on inputs of time, labour, cost and outputs of extracted materials;
- LCA and LCC analyses associated with different deconstruction scenarios and with material recovery scenarios to provide insights into environmental impacts and potential savings and material value within a circular management strategy.

The obtained materials extracted from the works projects will be traceable to facilitate the maximisation of circularity for materials extracted from project areas.

6.2. Environmental expectations

The goals of the DISCOVER project relate to the reduction of environmental impact of demolition of buildings and building elements as well as the associated human cost. Overall, the expectations following from the successful implementation of the methodologies described to develop the innovative approach to circularity in deconstruction include the following:

- Lower construction sector emissions by 15%;
- Increase reused components by up to 20% and reduce construction and demolition waste in the EU by 55%. (m.kat 2025).

7. Conclusions

DISCOVER is an EU initiative involving research and industry partners working on an innovative solution to reduce the impact of and realise the potential of the currently under-exploited resource of waste materials generated annually in the EU, originating from the deconstruction of infrastructure. DISCOVER intends to transform attitudes to waste in the deconstruction sector via innovative solutions in the field of robotics and artificial intelligence to accelerate automation of pre-works inspections, reducing the need for human involvement in high-risk environments and increasing the availability of spatial and material mapping of works areas via integration to a digital twin. The digital twin will provide a user interface for industry professionals whereby support tools are offered to aid in circular decision-making regarding techniques and methods for deconstruction and extraction of valuable materials for re-circulation and repeated use. The DISCOVER project is currently underway, having achieved several milestones and with expected outcomes at the end of 2028 to include advancements in the field of robotics and AI in deconstruction for improved circularity and sustainability in the management of CDW.

Acknowledgements

This project has received funding from the European Union's Horizon Europe research and innovation programme under grant agreement No101129909 (DISCOVER)

This research was funded in whole or in part by the Fundação para a Ciência e a Tecnologia, I.P. (FCT, https://ror.org/00snfqn58) under Grant UID/6438/2025 of the research unit CERIS. For the purpose of Open Access, the authors have applied a CC-BY public copyright license to any Author's Accepted Manuscript (AAM) version arising from this submission.

References

Eurostat. 2023. "Waste Statistics." Ec.europa.eu. January 2023. https://ec.europa.eu/eurostat/statistics-explained/index.php?title=Waste_statistics.

m.kat. 2025. "ABOUT DISCOVER - Discover Horizon." Discover Horizon. January 29, 2025. https://discover-horizon.eu/project/.

Bribián, Ignacio Zabalza, Antonio Valero Capilla and Alfonso Aranda Usón. 2011. "Life Cycle Assessment of Building Materials: Comparative Analysis of Energy and Environmental Impacts and Evaluation of the Eco-Efficiency Improvement Potential." *Building and Environment* 46 (5): 1133–40. https://doi.org/10.1016/j.buildenv.2010.12.002.

Luciano, A., L. Cutaia, P. Altamura and E. Penalvo. 2022. "Critical Issues Hindering a Widespread Construction and Demolition Waste (CDW) Recycling Practice in EU Countries and Actions to Undertake: The Stakeholder's Perspective." *Sustainable Chemistry and Pharmacy* 29 (October): 100745. https://doi.org/10.1016/j.scp.2022.100745.

Zhang, Chunbo, Mingming Hu, Benjamin Sprecher, Xining Yang, Xiaoyang Zhong, Chen Li and Arnold Tukker. 2021. "Recycling Potential in Building Energy Renovation: A Prospective Study of the Dutch Residential Building Stock up to 2050." *Journal of Cleaner Production* 301 (June): 126835. https://doi.org/10.1016/j.jclepro.2021.126835.

Popescu, Elena, Carlos Silva and Baht Hassan. 2024. “Benefits of Rehabilitation vs. Replacement: Environmental Considerations.” September 25, 2024. https://www.researchgate.net/publication/384328270_Benefits_of_Rehabilitation_vs_Replacement_Environmental_considerations.

Sáez, Paola Villoria, Jaime Santa, Mercedes, Pilar Mercader-Moyano and Antonio García Sánchez. 2018. “Estimation of Construction and Demolition Waste in Building Energy Efficiency Retrofitting Works of the Vertical Envelope” 172 (January): 2978–85. https://doi.org/10.1016/j.jclepro.2017.11.113.

European Commission. 2019. “The European Green Deal.” European Commission. European Commission. 2019. https://commission.europa.eu/strategy-and-policy/priorities-2019-2024/european-green-deal_en.

United Nations and International Energy Agency. 2019. “2019 Global Status Report for Buildings and Construction: Towards a Zero-Emissions, Efficient and Resilient Buildings and Construction Sector.” *Unep.org*. https://doi.org/978-92-807-3768-4.

Hasek, Alexandra. 2021 “BIM Adoption in Europe: 7 Countries Compared.” *PlanRadar*. Last modified March 5, 2026. https://www.planradar.com/bim-adoption-in-europe/

Thakuri, Prabhat Kiran, Lauri Alkki and Leena Aarikka-Stenroos. 2024. “Digital Technologies Enabling Component Reuse in Circular Value Chains: Using Digital Twin, Internet of Things and Robots in Construction and Manufacturing Sectors.” *R and D Management*, December. https://doi.org/10.1111/radm.12744.

Swarnakar, Vikas, Abdelrahman E. E. Eltoukhy, Mohammed Omar, Adolf Acquaye, Khaled Alawadi and Malik Khalfan. 2025. “Unlocking Circular Economy Potential in Construction and Demolition: An Empirical Analysis of Success Factors, Failure Drivers, Benefits, and Emerging Technologies.” *Smart and Sustainable Built Environment*, July 1–21. https://doi.org/10.1108/sasbe-01-2025-0044.

Coelho, André and Jorge de Brito. 2012. “Influence of Construction and Demolition Waste Management on the Environmental Impact of Buildings.” *Waste Management* 32 (3): 532–41. https://doi.org/10.1016/j.wasman.2011.11.011.

Mercante, Irma T., María D. Bovea, Valeria Ibáñez-Forés and Alejandro P. Arena. 2011. “Life Cycle Assessment of Construction and Demolition Waste Management Systems: A Spanish Case Study.” *The International Journal of Life Cycle Assessment* 17 (2): 232–41. https://doi.org/10.1007/s11367-011-0350-2.

Vitale, Pierluca, Noemi Arena, Fabrizio Di Gregorio and Umberto Arena. 2017. “Life Cycle Assessment of the End-of-Life Phase of a Residential Building.” *Waste Management* 60 (February): 311–21. https://doi.org/10.1016/j.wasman.2016.10.002.

Di Maria, Andrea, Johan Eyckmans and Karel Van Acker. 2018. “Downcycling versus Recycling of Construction and Demolition Waste: Combining LCA and LCC to Support Sustainable Policy Making.” *Waste Management* 75 (May): 3–21. https://doi.org/10.1016/j.wasman.2018.01.028.

Ivanica, Raphaela, Michael Risse, Gabriele Weber-Blaschke, and Klaus Richter. 2022. “Development of a Life Cycle Inventory Database and Life Cycle Impact Assessment of the Building Demolition Stage: A Case Study in Germany.” *Journal of Cleaner Production* 338 (March): 130631. https://doi.org/10.1016/j.jclepro.2022.130631.

Bayram, Berfin and Kathrin Greiff. 2023. “Life Cycle Assessment on Construction and Demolition Waste Recycling: A Systematic Review Analyzing Three Important Quality Aspects.” *The International Journal of Life Cycle Assessment*, February. https://doi.org/10.1007/s11367-023-02145-1.

Instituto Superior Técnico. 2026. *Deliverable 4.1: Demolition Methods Impacts*. Zenodo. https://doi.org/10.5281/zenodo.18339267

Universitat Politècnica de Catalunya. 2026. *Deliverable 1.3: Oliwall*. Zenodo. https://doi.org/10.5281/zenodo.18338695

Universitat Politècnica de Catalunya. 2026. *Deliverable 1.2: Navi-Wall*. Zenodo. https://doi.org/10.5281/zenodo.18338562

Cinpar 2026
XXII International Conference on Building Pathology and Constructions Repair
15th to 17th July 2026 - Lisboa, Portugal

Análise Química por Fluorescência de Raios X Portátil em Metal do Passado

Portable X-Ray Fluorescence Chemical Analysis of Ancient Metal

Adolpho Guido de ARAÚJO[1], Eudes de Arimatéa ROCHA[2], Arnaldo Manoel Pereira CARNEIRO[3], Pablo Borba de Barro GÓES[4], Marcos David dos SANTOS[5], Paulo Martin Souto MAIOR[6]

[1] Escola Politécnica da Universidade de Pernambuco, Recife, Brasil, adolpho.guido@upe.br
[2] Escola Politécnica da Universidade de Pernambuco, Recife, Brasil, eudes.rocha@upe.br
[3] Universidade Federal de Pernambuco, Recife, Brasil, arnaldo.carneiro@ufpe.br
[4] Universidade Federal de Pernambuco, Recife, Brasil, pablo.goes@ufpe.br
[5] Universidade Federal de Pernambuco, Recife, Brasil, marcos.david@ufpe.br
[6] Universidade Federal de Pernambuco, Recife, Brasil, pmsmaior@yahoo.com

Resumo: A utilização de instrumentos portáteis de fluorescência de raios X foi essencial para investigações de análises multielementares no campo da arqueometalurgia. O objetivo desta pesquisa foi investigar a aplicação da fluorescência de raios X em um artefato metálico do sítio histórico Baluarte Porta da Terra. O arcabouço metodológico foi desenvolvido em seis etapas: atividade preliminar, análise de fluorescência de raios X, procedimentos de limpeza, análise de fluorescência de raios X, preparação metalográfica e análise de fluorescência de raios X. Foram identificados 14, 16, 14 e 13 elementos químicos, com percentual de Fe de 50,87%, 70,15%, 96,08% e 96,00% para as quatro condições: artefato bruto, limpo, amostra longitudinal e amostra transversal, respectivamente. Os metais do passado em grau de deterioração carecem de metodologias específicas para a obtenção de informações assertivas e bem-sucedidas no contexto da arqueometalurgia. Difundir teorias e práticas da fluorescência de raios X portátil pode criar, ampliar, acelerar e aprofundar informações necessárias para gerar análises conjuntas direcionadas à elucidação das informações dos materiais de construção dos patrimônios históricos.

Palavras chaves: Fluorescência de Raios X Portátil; Análises Composicionais; Procedimentos; Metal histórico.

Abstract: The use of portable X-ray fluorescence instruments was essential for multielement analyses in the field of archaeometallurgy. The objective of this study was to investigate the application of X-ray fluorescence to a metallic artifact from the Baluarte Porta da Terra historical site. The methodological framework was developed in six stages: preliminary activity, X-ray fluorescence analysis, cleaning procedures, X-ray fluorescence analysis, metallographic preparation, and X-ray fluorescence analysis. A total of 14, 16, 14, and 13 chemical elements were identified, with Fe percentages of 50.87%, 70.15%, 96.08%, and 96.00% for the four conditions: raw artifact, cleaned artifact, longitudinal sample, and transverse sample, respectively. Ancient metals in advanced stages of deterioration require specific methodologies to obtain accurate and successful information within the context of archaeometallurgy. The dissemination of theories and practices related to portable X-ray fluorescence may create, expand, accelerate, and deepen the information necessary to generate integrated analyses aimed at elucidating the construction materials of historical heritage sites.

Keywords: Portable X-Ray Fluorescence; Compositional Analyses; Procedures; Historical Metal.

1. Introdução

As investigações sobre os materiais metálicos representaram informações que ampliaram a compreensão da evolução da metalurgia (Hernandez-Escampa et al. 2010). O registro material do passado teve um papel importante no mundo (Wayman 2000), pois permitiu a datação e o controle do contexto espacial dos dados (Levy et al. 2008), reconstituindo aspectos pouco conhecidos da história, em razão da escassez de relatos escritos, da falta de fontes primárias arquivísticas e das lacunas da historiografia disponível (Campos and Granato, 2015). Logo, uma melhor compreensão do passado tornou-se cada vez mais importante, à medida que nossas vidas e nosso futuro se tornaram mais complexos (Wayman, 2000). Os registros arqueológicos dos materiais metálicos foram de grande importância para a compreensão das redes sócio-políticas existentes (Hsu et al. 2020), e a determinação da composição química de objetos individuais ajudou a localizar a origem do metal e, potencialmente, a data de produção (Alipour et al. 2021).

Os instrumentos de campo portáteis, baseados na tecnologia de energia dispersiva por fluorescência de raios X, reportaram as concentrações elementares dos materiais analisados (Bruker, 2025). As análises da composição de elementos metálicos por espectrometria de fluorescência de raios X por dispersão de energia (FRX-ED) requereram uma discussão prévia mais extensa (Llorens and Ruiz, 2018). Os instrumentos portáteis de fluorescência de raios X e suas aplicações ganharam considerável atenção na comunidade arqueológica nos últimos anos (Frahm and Doonan, 2013), mas a aplicação das técnicas nas amostras arqueológicas foi frequentemente limitada pela dificuldade na preparação das amostras (Hiller and Wess, 2006). Os arqueólogos históricos recorreram cada vez mais à química arqueológica para construir narrativas sobre colonialismo, escravidão, economias políticas, inovações tecnológicas e uma série de outros tópicos (Greer *et al.*, 2025), e a análise composicional global multielementar, realizada pela fluorescência de raios X, ajudou a aprofundar os conhecimentos químicos do passado.

O Laboratório de Perfil Técnico (Lapet), no Núcleo de Metrologia Arqueológica da Universidade Federal de Pernambuco, possui uma numerosa coleção de vestígios de materiais metálicos advindos de escavações arqueológicas, extraídos/coletados na região metropolitana de Recife-PE. Foram resgatados inúmeros artefatos metalúrgicos de escavações arqueológicas nos sítios históricos da cidade do Recife e depositados no Laboratório de Perfil Técnico, sofrendo um processo contínuo e avançado de corrosão (Souto Maior and Souza, 2019). Alguns artefatos metálicos não resistiram ao tempo, pois os estados mínimos de conservação para estudos arqueometalúrgicos não foram atendidos. Os pesquisadores ressaltaram que a deterioração de artefatos antigos dependeu de vários fatores, tais como composição dos materiais, processos de fabricação e ambientes aos quais foram expostos (Dwivedi and Mata, 2019). Portanto, a preservação do patrimônio cultural foi de importância fundamental para o desenvolvimento e o enriquecimento cultural de um povo, bem como guardou informações e registros da história humana, das crenças, dos costumes, do conhecimento tecnológico e das condições sociais, econômicas e políticas de um grupo em determinada época (Asfora, 2010). Urge incentivar, desenvolver e executar pesquisas científicas de ordem experimental para a obtenção de respostas analíticas sobre o passado desses artefatos metálicos.

2. Metodologia

O planejamento experimental da pesquisa foi dividido em seis etapas. A primeira etapa, denominada atividade preliminar, consistiu no resgate dos artefatos metálicos e na caracterização macroscópica. A segunda etapa foi a análise de fluorescência de raios X (FRX) do artefato nas condições iniciais (antes de qualquer manipulação ou tratamento). A terceira etapa foi destinada aos procedimentos de limpeza (manuais, mecânicos e químicos). Em seguida, foram realizadas as análises de fluorescência de raios X (FRX) dos artefatos nas condições limpas (menor incidência de contaminações e/ou impurezas). A quinta etapa foi a preparação da lâmina (amostra), composta pelo corte metalográfico e embutimento. Finalmente, a sexta etapa foi destinada à análise de fluorescência de raios X (FRX) do núcleo metálico (seções longitudinal e transversal). A Figura 1 apresenta o fluxograma do planejamento experimental.

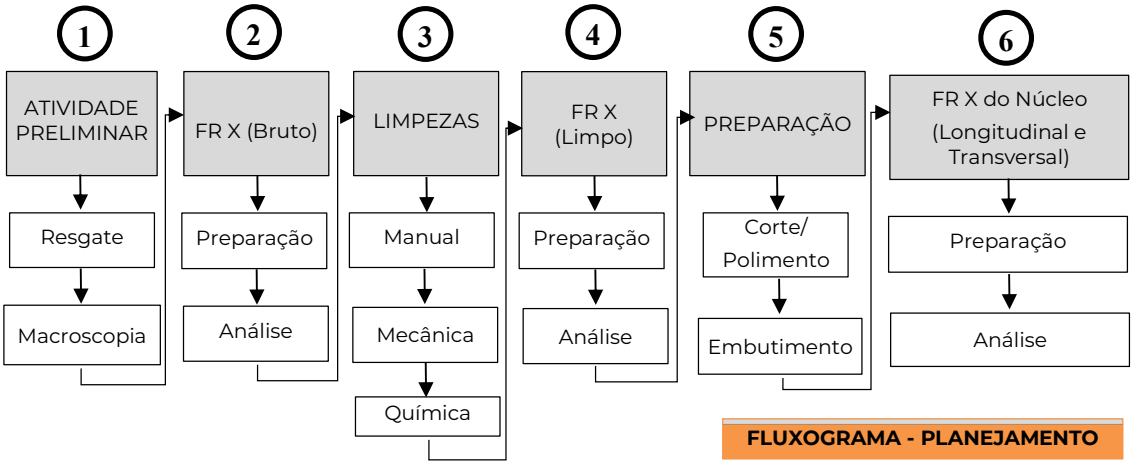


Figura 1 – Planejamento Experimental

2.1 Atividade preliminar

O artefato metálico foi resgatado das ruínas das construções do sítio histórico Baluarte Porta da Terra e etiquetado com a numeração nº 2553, contendo as seguintes informações: nível: DEC.06; município: Recife; UF: PE; quadrícula: A3; setor: A. O artefato foi resgatado em 18 de agosto de 2004 e identificado visualmente como matéria-prima metálica. As características macroscópicas realizadas no laboratório indicaram dimensão longitudinal de 10,99 cm e peso de 0,058 kg.

O sítio histórico Baluarte Porta da Terra fica localizado na área central, denominada Ilha do Recife no período colonial, e foi um dos primeiros lugares em Pernambuco onde foi registrada a ocupação de colonos europeus (Souto Maior and Souza, 2019). Os trabalhos arqueológicos tiveram início no canteiro do baluarte com um levantamento fotográfico, a locação da estação topográfica, a divisão interna em setores (A, B, C e D) e, finalmente, o procedimento de escavações e resgates dos artefatos (Medeiros, 2005). A Figura 2 apresenta uma planta de localização dos setores de escavações do sítio histórico Baluarte Porta da Terra.



Figura 2 – Setor de escavação do Baluarte Porta da Terra

Fonte: (Medeiros, 2005).

2.2 Fluorescência de raios X do artefato bruto

O equipamento portátil de fluorescência de raios X foi utilizado no artefato bruto, com tempo de aplicação de 60 segundos, realizando três leituras no mesmo ponto. O equipamento identificou os elementos químicos e estabeleceu a média das três leituras das concentrações em partes por milhão (ppm), posteriormente transformadas em porcentagens. O procedimento de análise consistiu na aplicação direta do instrumento de fluorescência de raios X no artefato bruto (Figura 3).



Figura 3 – Artefato metálico bruto nº 2553

2.3 Limpezas

O primeiro desafio para o estudo do artefato metálico foi o procedimento de limpeza, pois as concreções e as oxidações dificultaram o reconhecimento do tipo de fragmento metálico. Logo, foram realizadas limpezas em etapas sequenciadas para obter um resultado significativo. Nesta pesquisa, foi utilizada uma sequência dividida em três fases: limpeza manual, limpeza mecânica e limpeza química (**Erro! Fonte de referência não encontrada.**).

Tabela 1 – Tipos de limpezas realizadas no artefato metálico

Limpeza manual	Limpeza mecânica	Limpeza química
Utilizaram-se escovas de aço com água destilada para a remoção das partículas de concreções e oxidações encontradas na superfície da peça metálica.	Utilizou-se uma micro-retífica multiuso com brocas de cerâmica para a remoção profunda das partículas mais duras de concreções e oxidações agregadas à superfície da peça metálica.	Por meio de um processo eletrolítico com uma bateria de automóvel, cabos de 6 mm, água destilada, sal marinho e uma peça metálica sacrificada, foi realizada a limpeza química final.

2.4 Fluorescência de raios X do artefato limpo

O procedimento de análise de fluorescência de raios X portátil na amostra limpa foi similar ao procedimento realizado na amostra bruta, no qual houve aplicação direta do instrumento de fluorescência de raios X no artefato, no tempo de 60 segundos, realizando três leituras no mesmo ponto. A Figura 4 apresenta o artefato metálico após os procedimentos de limpeza.



Figura 4 – Artefato metálico limpo nº 2553

2.5 Preparação metalográfica

A preparação das lâminas requereu cuidados especiais. O tamanho da amostra foi fundamental para a análise de fluorescência de raios X, bem como a qualidade do corte, a regularização, a planicidade e o polimento superficial. Com a utilização de uma serra diamantada portátil, com um líquido refrigerante especial para cortes metalográficos, foram realizados cortes, fatias, secções e pedaços das partes longitudinal e transversal do artefato metálico (Figura 5).



Figura 5 – Serra de corte diamantada portátil para corte metalográfico

Após as extrações dos pedaços das amostras, as lâminas receberam lixamento na superfície da camada superficial com a utilização das lixas n° 500, 1500 e 3000. O procedimento de lixamento utilizou uma sequência de lixas com movimentos repetidos de ida e volta, na direção de cima para baixo da face da amostra, por 1 minuto. Em seguida, o procedimento consistiu em girar em 90° o sentido da face e realizar o lixamento por mais 1 minuto. Esse procedimento foi repetido 4 vezes e, finalmente, foi realizado o polimento com feltro verde e pasta diamantada de 1 e 1,4 µm na politriz (Figura 6).



Figura 6 – Regularização, polimento e acabamento da lâmina metálica

A última etapa de preparação das lâminas consistiu na impregnação com resina e no acabamento da superfície. Nesta fase, foi selecionado um molde padrão circular de policloreto de vinila (PVC), com altura de um centímetro. Em seguida, a resina foi preparada e lançada no molde para a criação da primeira camada de impregnação. Na sequência, a amostra foi depositada no molde e coberta com resina epóxi (Figura 7).



Figura 7 – Embutimento da lâmina metálica na resina Epoxi

2.6 Fluorescência de raios X do núcleo

A fluorescência de raios X foi aplicada no núcleo metálico da amostra (seções longitudinal e transversal) para identificar e quantificar os elementos químicos da matriz metálica, isenta de contaminações e pátinas agregadas à superfície durante as análises anteriores. O tempo de leitura foi de 60 segundos, com calibração para metais, utilizando instrumento de fluorescência de raios X modelo S1 TITAN, tensão de 15 kV e corrente de 13,9 µA. Os procedimentos de utilização do instrumento de fluorescência de raios X foram idênticos aos procedimentos utilizados nas duas oportunidades anteriores (Figura 8).

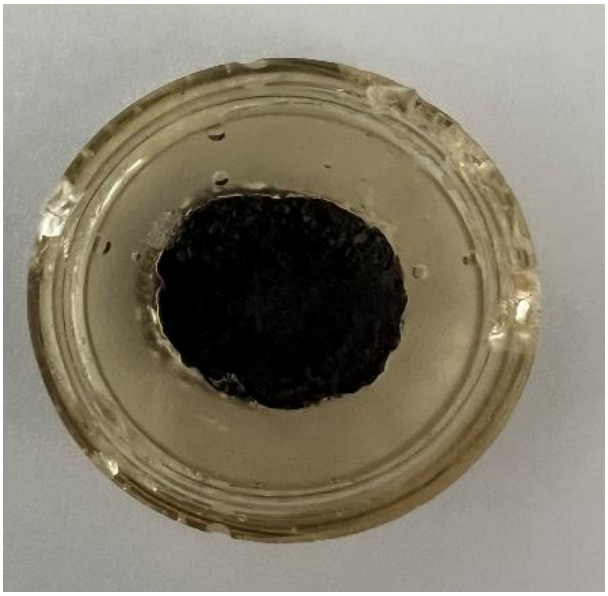


Figura 8 – Núcleo metálico embutimento na resina Epoxi

3. Resultados e discussão

Os resultados foram divididos em três subitens: 3.1 Artefato metálico bruto e limpo; 3.2 Amostras metálicas (seções longitudinal e transversal); e 3.3 Análise conjunta.

3.1 Artefato metálico bruto e limpo

As análises de fluorescência de raios X no artefato foram obtidas tanto na situação do artefato bruto quanto na do artefato limpo, apresentando análises multielementares de 14 e 16 elementos químicos, respectivamente (Tabela 2). Segundo Rogan *et al.* (2019), a fluorescência de raios X portátil foi baseada no princípio de que os elementos detêm uma energia de ligação única dos elétrons, associada ao elemento correspondente, capaz de detectar vários elementos químicos.

Tabela 2 – Resultados da fluorescência de raios X nos artefatos bruto e limpo

EQ	Fe	Ca	Co	Si	Cu	Al	Ti	Mn	Cr	Rb	Sn	Ba	Sd	Pd	Sr	Zr	Cd
AB (%)	50,87	14,02	*n.i*	26,59	*n.i*	7,98	0,17	0,04	*n.i*	0,01	0,05	0,04	0,02	0,08	0,17	0,03	0,01
AL (%)	70,15	1,28	0,08	28,32	0,01	0,71	0,05	0,07	0,01	0,01	0,04	0,03	0,01	0,06	0,02	*n.i*	0,01
MÉDIA	60,51	7,65	0,04	27,46	0,01	4,35	0,11	0,06	0,01	0,01	0,05	0,04	0,02	0,07	0,10	0,02	0,01
DP	13,63	9,01	0,06	1,22	0,01	5,14	0,08	0,02	0,01	0,00	0,01	0,01	0,01	0,01	0,11	0,02	0,00
CV (%)	22,53	117,76	141,42	4,46	141,42	118,31	77,14	38,57	141,42	0,00	15,71	20,20	47,14	20,20	111,65	141,42	0,00

Nota: EQ: Elementos químico; AB: Artefato bruto; AL: Artefato limpo; DP: Desvio padrão; CV: Coeficiente de variação; *n.i.:* não identificado.

A análise do artefato bruto foi comprometida pela pátina, concreção e oxidação. Conforme Llorens and Ruiz (2018), a corrosão do metal criou, na maioria dos casos, uma camada superficial de compostos (pátina), na qual encontraram-se todos os elementos químicos do metal saudável, mas com proporções de peso e/ou percentual muito diferentes das do próprio metal. Os resultados apresentaram informações imprecisas sobre a matriz metálica, observadas mediante a comparação dos resultados da fluorescência de raios X no artefato bruto versus o artefato limpo, como, por exemplo: quantidade significativa de Ca e Al no artefato bruto e quantidade desprezível desses mesmos elementos químicos na análise do artefato limpo; ausência de Co, Cu e Cr no artefato bruto, em contraponto com a presença desses elementos químicos no artefato limpo. De acordo com Handheld XRF (2024), dependendo da distância de aplicação e do tipo da dose (profunda ou rasa), o feixe pode atingir diferentes profundidades.

O problema observado durante a execução do programa experimental foi a investigação do artefato metálico bruto, pois a quantidade de contaminações, pátinas e concreções dificultou a manipulação e a obtenção de resultados sobre a composição global e multielementar do metal. Para Carl and Young (2016), a fluorescência de raios X na peça bruta permitiu estudos de superfície do artefato metálico, fornecendo benefícios para futuros estudos. O estado de conservação do artefato bruto foi crítico, estando totalmente coberto de pátinas e restos de construção, dificultando a identificação, manipulação e investigação. Segundo Aranda-Contamina *et al.* (2021), o estado de conservação dos objetos metálicos foi um ponto importante, e, como boa prática, a escolha de artefatos menos comprometidos permitiu melhor manipulação para eliminar a pátina superficial durante a limpeza.

3.2 Amostras metálicas (seções longitudinal e transversal)

As análises de fluorescência de raios X nas amostras foram obtidas para as seções longitudinal e transversal, resultando em análises multielementares de 14 e 13 elementos químicos, respectivamente (Tabela 3). Conforme Llorens and Ruiz (2018), os ensaios de fluorescência de raios X foram desenvolvidos para analisar a superfície do objeto, extraindo informações até uma profundidade de algumas dezenas de micrômetros.

Tabela 3 – Resultados da fluorescência de raios X das amostras seção longitudinal e seção transversal

EQ	Fe	Co	Ta	Cu	Ti	Mn	Sn	Pd	Zr	Bi	Pb	W	Rh	V	Se
ASL (%)	96,08	3,26	0,19	0,05	0,03	0,05	0,14	0,02	0,01	0,05	0,05	0,03	*n.i*	0,03	0,02
AST (%)	96,00	3,25	0,23	0,06	0,03	*n.i*	0,16	0,03	0,01	0,04	0,09	*n.i*	0,03	0,03	0,02
MÉDIA	96,04	3,26	0,21	0,06	0,03	0,03	0,15	0,03	0,01	0,05	0,07	0,02	0,02	0,03	0,02
DP	0,06	0,01	0,03	0,01	0,00	0,04	0,01	0,01	0,00	0,01	0,03	0,02	0,02	0,00	0,00
CV	0,06	0,22	13,47	12,86	0,00	141,42	9,43	28,28	0,00	15,71	40,41	141,42	141,42	0,00	0,00

Nota: EQ: Elementos químico; AB: Artefato bruto; AL: Artefato limpo; DP: Desvio padrão; CV: Coeficiente de variação; *n.i*: não identificado.

Não foram observadas grandes alterações dos elementos químicos e de suas quantidades nas análises da amostra da seção longitudinal, quando comparadas às análises da amostra transversal. Os principais elementos químicos identificados foram Fe, Co e Ta, perfazendo 99,53% na amostra longitudinal e 99,48% na amostra transversal. Conforme Llorens and Ruiz (2018), os ensaios de fluorescência de raios X foram desenvolvidos para analisar a superfície do objeto, extraindo informações até uma profundidade de algumas dezenas de micrômetros. Este resultado reforçou a precisão da análise de fluorescência de raios X, quando realizadas nas regiões profundas e protegidas das amostras.

3.3 Análise conjunta

Foi realizada a aplicação da fluorescência de raios X no metal em quatro condições distintas, a saber: a primeira, no artefato metálico bruto (condições originais do artefato resgatado); a segunda, no artefato metálico limpo, após os procedimentos de limpeza manual, mecânica e química (eletrólise); e, finalmente, no núcleo metálico (seções longitudinal e transversal), produzido após os cortes metalográficos, nos quais foram identificados 14, 16, 14 e 13 elementos químicos, respectivamente. De acordo com Kaufman *et al.* (2016), a espectroscopia portátil de fluorescência de raios X permitiu análises rápidas, não destrutivas e minimamente invasivas, que serviram simultaneamente para caracterizar o metal.

O metal foi resgatado das ruínas do sítio histórico Baluarte Porta da Terra, coberto de terra e restos de construções. Durante as análises de FRX, foi identificado e quantificado o elemento Ca, sendo observado um grande percentual na amostra bruta e um pequeno percentual na amostra limpa. Em contraponto, quando analisado o núcleo metálico, esse elemento químico (Ca) não foi identificado. Possivelmente, o Ca foi resultado da contaminação por quartzo contido nos materiais de construção, tais como reboco e cimento, aderidos à superfície do artefato metálico. De acordo com María Gómez De Salazar and Soria (2000), materiais metálicos enterrados apresentaram elementos contaminantes, como o quartzo, agregados à superfície deles. Segundo Rogan *et al.* (2019), a otimização das configurações do FRX portátil para um elemento impediu a análise quantitativa de vários outros elementos de interesse. Por exemplo, para elementos como Ca e Fe, quando a quantificação pareceu aceitável, diferentes tipos de solo e faixas elementares alteraram significativamente a precisão da abordagem.

Aconteceram tentativas frustradas durante a fase de preparação da amostra para investigação do núcleo, como, por exemplo, a dificuldade do corte metalográfico para extrair uma amostra com área mínima capaz de receber o diâmetro total do feixe de raios X do instrumento. Conforme Kaufman *et al.* (2016), o ponto de detecção da FRX na amostra foi um quesito importante, pois, em algumas regiões pequenas, quando o diâmetro do feixe de FRX foi maior, a fluorescência produzida foi absorvida pelo material e, posteriormente, pelo ar, resultando na quantificação total menor que 100% dos elementos químicos. De acordo com Colpaert (2008), os elementos químicos intervieram diretamente na composição dos metais, como nos aços comuns definidos pelas percentagens de carbono, silício, manganês, fósforo e enxofre. O metal estudado apresentou o ferro como elemento majoritário presente nas quatro situações e outros elementos secundários (Tabela 4).

Tabela 4 – Resultado conjunto da fluorescência de raios X

EQ	AB (%)	AL (%)	ASL (%)	AST (%)	MÉDIA	DP	CV (%)
Fe	50,87	70,15	96,08	96,00	78,28	21,97	28,07
Ca	14,02	1,28	*n.i.*	*n.i.*	3,83	6,82	178,39
Co	*n.i.*	0,08	3,26	3,25	1,65	1,86	112,68
Si	26,59	28,32	*n.i.*	*n.i.*	13,73	15,87	115,58
Ta	*n.i.*	*n.i.*	0,19	0,23	0,11	0,12	116,51
Cu	*n.i.*	0,01	0,05	0,06	0,03	0,03	98,13
Al	7,98	0,71	*n.i.*	*n.i.*	2,17	3,89	178,88
Ti	0,17	0,05	0,03	0,03	0,07	0,07	96,19
Mn	0,04	0,07	0,05	*n.i.*	0,04	0,03	73,60
Cr	*n.i.*	0,01	*n.i*	*n.i.*	0,00	0,01	200,00
Rb	0,01	0,01	*n.i.*	*n.i.*	0,01	0,01	115,47
Sn	0,05	0,04	0,14	0,16	0,10	0,06	62,88
Ba	0,04	0,03	*n.i.*	*n.i.*	0,02	0,02	117,80
Sd	0,02	0,01	*n.i.*	*n.i.*	0,01	0,01	127,66
Pd	0,08	0,06	0,02	0,03	0,05	0,03	57,97
Sr	0,17	0,02	*n.i.*	*n.i.*	0,05	0,08	173,07
Zr	0,03	*n.i.*	0,01	0,01	0,01	0,01	100,66
Cd	0,01	0,01	*n.i.*	*n.i.*	0,01	0,01	115,47
Bi	*n.i.*	*n.i.*	0,05	0,04	0,02	0,03	116,89
Pb	*n.i.*	*n.i.*	0,05	0,09	0,04	0,04	124,54
W	*n.i.*	*n.i.*	0,03	*n.i.*	0,01	0,02	200,00
Rh	*n.i.*	*n.i.*	*n.i.*	0,03	0,01	0,02	200,00
V	*n.i.*	*n.i.*	0,03	0,03	0,02	0,02	115,47
Se	*n.i.*	*n.i.*	0,02	0,02	0,01	0,01	115,47
TOTAL	*100*	*100*	100	*99,98			

Nota: *n.i.*: não identificado; EQ: Elemento químico; AB: Artefato bruto; AL: Artefato limpo; ASL: Amostra seção longitudinal; AST: Amostra seção transversal; DP: Desvio padrão; CV: Coeficiente de variação; *AST de dimensões pequenas não obtendo 100% da identificação e quantificação multielementar.

As quantificações totais das análises de fluorescência de raios X do artefato bruto, do artefato limpo, da amostra longitudinal e da amostra transversal representaram o percentual total de 100%, com exceção da amostra transversal, que totalizou 99,98%. De acordo com Handheld XRF (2024), o diâmetro mínimo do feixe dos instrumentos de fluorescência de raios X portáteis, na distância mínima de 1,50 cm, correspondeu a 1,20 cm. Por isso, a amostra transversal, com diâmetro menor que 1,20 cm, apresentou resultado incompleto da quantificação total dos elementos químicos. Alguns elementos identificados e quantificados com pequenas porcentagens nas quatro análises ocorreram devido à contaminação ou às limitações na configuração do instrumento. Rogan *et al.* (2019) identificaram que mudanças simples nas configurações, como alterar a tensão emitida pelo FRX portátil, ampliaram a sensibilidade do instrumento para análises de elementos como, por exemplo, Cu.

A pesquisa confirmou que o artefato metálico foi uma liga ferrosa e teve como elemento principal o ferro, perfazendo um quantitativo de 50,87% no estado bruto, 70,15% no estado limpo, 96,08% no núcleo (ASL) e 96,00% no núcleo (AST). Corroborado por Jr. Callister and Rethwisch (1940), que afirmou que as ligas ferrosas foram aquelas em que o ferro foi o componente principal, mas o carbono e os outros elementos de ligas metálicas, provocaram mudanças bastante drásticas no diagrama de fases binário ferro-carbono. Conforme Llorens and Ruiz (2018), os instrumentos de fluorescência de raios X não identificaram elementos químicos

com número atômico pequeno, como, por exemplo, o carbono, com número atômico 6. Tal limitação reduz a possibilidade de identificação de algumas ligas, como, por exemplo, aquelas compostas pelo elemento químico carbono.

O cobalto não foi identificado na amostra bruta, possivelmente porque a quantidade de pátinas, concreções e oxidações limitou a sua identificação pelos raios X emitidos na superfície. No entanto, o cobalto foi identificado e quantificado nas duas outras análises (limpa e núcleo), e as evidências apontaram que provavelmente foi inserido intencionalmente para produzir uma liga ferrosa com características específicas. Dehaine *et al.* (2021) afirmaram que o cobalto forneceu propriedades físicas únicas, incluindo resistência ao calor, força e propriedades magnéticas, e teve uma ampla variedade de aplicações nas ligas metálicas.

A Tabela 5 apresentou a matriz de identificação dos elementos químicos com diferentes resultados nas análises de FRX aplicadas ao mesmo material em quatro condições distintas, a saber: artefato bruto, artefato limpo, amostra da seção longitudinal e amostra da seção transversal, tanto nos aspectos qualitativos (tipo de elemento químico identificado) quanto no aspecto quantitativo (quantidade em percentual). A análise conjunta sugeriu as seguintes observações: o único elemento químico identificado nas quatro condições foi o Fe, definido como elemento químico majoritário; Ca, Si, Al, Ti e Sr foram identificados no artefato bruto e limpo, mas ficaram ausentes nas análises das amostras longitudinal e transversal, podendo corresponder a contaminações aderidas ou tratamentos na superfície do artefato; Co, Ta e Sn foram identificados nas amostras longitudinal e transversal, fazendo parte do núcleo metálico, e podem ter sido inseridos para fornecer características específicas da liga; os demais elementos (Cu, Mn, Cr, Rb, Ba, Sd, Pd, Zr, Cd, Bi, Pb, W, Rh, V e Se) não foram identificados e/ou obtiveram quantidades irrelevantes/desprezíveis. De acordo com Llorens and Ruiz (2018), os problemas de análises de superfície por fluorescência de raios X foram inerentes às transformações que ocorreram entre o material original e o material analisado, como, por exemplo, o efeito da corrosão nos metais.

Tabela 5 – Matriz de identificação dos elementos químicos

EQ	Fe	Ca	Co	Si	Ta	Cu	Al	Ti	Mn	Cr	Rb	Sn	Ba	Sd	Pd	Sr	Zr	Cd	Bi	Pb	W	Rh	V	Se
AB																								
AL																								
ASL																								
AST																								

Legenda:

Elemento Químico Presente	
Elemento Químico (<0,09%)	
Elemento Químico Ausente	

4. Conclusão

O instrumento portátil de fluorescência de raios X possibilitou, de forma prática, simples e precisa, a determinação qualitativa e quantitativa multielementar dos artefatos metálicos. A técnica foi baseada na excitação dos elétrons do átomo de um material por uma fonte de radiação (raios X primários), na qual foi liberada uma radiação secundária (fluorescência), com uma energia característica de cada elemento químico. Os raios X fluorescentes, ao atingirem o detector (placa de silício), identificaram e quantificaram os elementos químicos presentes nas amostras, pois cada elemento químico emitiu uma energia única. Os instrumentos mais modernos evoluíram e tiveram sua fonte de excitação composta por um tubo de raios X com ânodo de ródio, ideal para elementos químicos com número atômico entre 12 e 92. Por isso, alguns elementos, como carbono, oxigênio e sódio, entre outros com número atômico fora desse intervalo, não foram identificados.

A utilização da fluorescência de raios X permitiu confirmar os elementos químicos presentes na superfície do metal (contaminações), verificar a composição elementar em pontos estratégicos do artefato metálico e determinar, qualitativa e quantitativamente, a composição elementar do metal. Ficou comprovado que o artefato metálico foi constituído majoritariamente de ferro, apresentando uma pequena quantidade de cobalto no núcleo. As evidências iniciais foram claras quanto ao nível de tecnologia na produção de ligas metálicas utilizadas na construção do sítio histórico Baluarte Porta da Terra, desenvolvido pelos europeus.

Os resultados revelaram o potencial do FRX portátil no suporte a pesquisas na área de arqueologia, bem como a simplicidade da utilização e da realização do programa experimental, incentivando pesquisadores de áreas distintas das ciências exatas e da natureza. Ficou evidente que as análises por instrumentos portáteis de fluorescência de raios X serviram para encurtar as investigações sobre determinados materiais, agregando ou descartando a continuidade do programa experimental, economizando tempo, recursos financeiros e esforço humano nas pesquisas na área da arqueometalurgia.

Referencias

Alipour, R., Rehren, T. and Martinón-Torres, M. (2021) "Chromium crucible steel was first made in Persia," *Journal of Archaeological Science*, 127. Available at: https://doi.org/10.1016/j.jas.2020.105224.

Aranda-Contamina, P. *et al.* (2021) "Mediterranean and atlantic. archaeometallurgy of the late bronze age and early iron age from the settlement El Morredón (Fréscano, Zaragoza)," *Zephyrus*, 87, pp. 105–124. Available at: https://doi.org/10.14201/ZEPHYRUS202187105124.

Asfora, V.K. (2010) *Fluorescência De Raios X Por Dispersão De Energia Aplicada À Caracterização De Tijolos De Sítios Históricos De Pernambuco*, *CLIO Arqueológica*. Dissertação. Universidade Federal de Pernambuco.

Bruker (2025) *Manual de Referência S1 TITAN*.

Campos, G. de N. and Granato, M. (2015) "Ornamento em bronze, com formato de voluta e ornamento em florão, luminária de metal dourado, prédio sede do MAST (Foto: Jaime Acioli, 2010). 269," pp. 269–296.

Carl, M. and Young, M.L. (2016) "Complementary analytical methods for analysis of Ag-plated cultural heritage objects," *Microchemical Journal*, 126, pp. 307–315. Available at: https://doi.org/10.1016/j.microc.2015.12.019.

Colpaert, H. (2008) *Metalografia dos produtos siderúrgicos comuns*. 4ª. Edited by A.L.V. da C. e Silva. São Paulo: Edgard Blucher.

Dehaine, Q. *et al.* (2021) "Geometallurgy of cobalt ores: A review," *Minerals Engineering*. Elsevier Ltd. Available at: https://doi.org/10.1016/j.mineng.2020.106656.

Dwivedi, D. and Mata, J.P. (2019) "Archaeometallurgical investigation of ancient artefacts' degradation phenomenon," *npj Materials Degradation*. Nature. Available at: https://doi.org/10.1038/s41529-019-0097-y.

Frahm, E. and Doonan, R.C.P. (2013) "The technological versus methodological revolution of portable XRF in archaeology," *Journal of Archaeological Science*. Academic Press, pp. 1425–1434. Available at: https://doi.org/10.1016/j.jas.2012.10.013.

Greer, M.C. *et al.* (2025) "Archaeological Chemistry and Historical Archaeology: Reviewing 50 Years of Analyses on Sixteenth- to Twenty-First-Century Materials," *International Journal of Historical Archaeology* [Preprint]. Available at: https://doi.org/10.1007/s10761-025-00809-2.

Handheld XRF (2024). Manual de Referência MODEL 900 MODEL 800 MODEL 600 MODEL 500 MODEL 300 MODEL 200.

Hernandez-Escampa, M., Gonzalez, J. and Uruchurtu-Chavarin, J. (2010) "Electrochemical assessment of the restoration and conservation of a heavily corroded archaeological iron artifact," *Journal of Applied Electrochemistry*, 40(2), pp. 345–356. Available at: https://doi.org/10.1007/s10800-009-0003-3.

Hiller, J.C. and Wess, T.J. (2006) “The use of small-angle X-ray scattering to study archaeological and experimentally altered bone,” *Journal of Archaeological Science*. Academic Press, pp. 560–572. Available at: https://doi.org/10.1016/j.jas.2005.09.012.

Hsu, Y.K. *et al.* (2020) “Discerning social interaction and cultural influence in Early Iron Age Mongolia through archaeometallurgical investigation,” *Archaeological and Anthropological Sciences*, 12(1). Available at: https://doi.org/10.1007/s12520-019-00952-y.

Jr. Callister, W.D. and Rethwisch, D.G. (1940) *Materials science and engineering an introduction*. Eighth. Edited by Wiley. Versailles.

Kaufman, B. *et al.* (2016) “Ferrous metallurgy from the Bir Massouda metallurgical precinct at Phoenician and Punic Carthage and the beginning of the North African Iron Age,” *Journal of Archaeological Science*, 71, pp. 33–50. Available at: https://doi.org/10.1016/j.jas.2016.04.002.

Levy, T.E. *et al.* (2008) “High-precision radiocarbon dating and historical biblical archaeology in southern Jordan,” *PNAS*, 105(43), pp. 16460–16465. Available at: www.pnas.org/cgi/content/full/.

Llorens, S.R. and Ruiz, I.M. (2018) “The archaeometallurgical project of the Iberian Peninsula (1982-2017),” *Trabajos de Prehistoria*, 75(2), pp. 223–247. Available at: https://doi.org/10.3989/tp.2018.12213.

María Gómez De Salazar, J. and Soria, A. (2000) *Estudio arqueometalúrgico de un hacha de hierro encontrada en la villa de “La Olmeda” Falencia, España*, *Rev. Metal. Madrid*. Available at: http://revistademetalurgia.revistas.csic.es.

Medeiros, E.G. de M. (2005) *O povoado dos arrecifes e o baluarte holandês do século XVII*. Dissertação. Universidade Federal de Pernambuco.

Rogan, G. *et al.* (2019) “Optimization of portable X-ray fluorescence spectrometry for the assessment of soil total copper concentrations: application at an ancient smelting site,” *Journal of Soils and Sediments*, 19(2), pp. 830–839. Available at: https://doi.org/10.1007/s11368-018-2091-3.

Souto Maior, P.M. and Souza, R. (2019) “Marcos cronológicos e identificação dos usos de vestígios arqueológicos metálicos de quatro sítios históricos em Pernambuco,” *FUMDHAMentos*, XVI(2019), pp. 19–53.

Wayman, Michael L. (2000) “Archaeometallurgical contributions to a better understanding of the past,” *Materials Characterization*, 45(4–5), pp. 259–267. Available at: https://doi.org/10.1016/S1044-5803(00)00108-X.

cinpar2026
XXII International Conference on Building Pathology and Constructions Repair
15th to 17th July 2026 - Lisboa, Portugal

Proposal for an optimal timing for maintenance and rehabilitation strategies on interlocking pavements

Adailson Araújo dos SANTOS[1], Felipe Silveira Cavalcanti BEZERRA[2], **Francisco Heber Lacerda de OLIVEIRA**[3]

[1] Federal University of Ceara, Ceara, Brazil, adailson.araujo@det.ufc.br
[2] Federal University of Ceara, Ceara, Brazil, felipesilveiracb@hotmail.com
[3] Federal University of Ceara, Ceara, Brazil, heber@det.ufc.br

Abstract: The Interlocking Concrete Block Pavement (ICBP) has been used in many countries as a sustainable paving alternative due to its durability, ease of maintenance, and improved drainage. However, the combined effects of traffic and climate lead to pavement deterioration over its service life. Maintenance and rehabilitation (M&R) interventions help delay this degradation process when properly applied, although they require financial resources and time. This study aims to evaluate whether it is possible to establish the optimal timing for M&R activities based on performance assessment and associated costs. The study was conducted on an 1,880 m road section, divided into ten homogeneous segments. Based on deflection data obtained from the Benkelman Beam Test, a back-analysis of the ICBP was performed to determine the stiffness of the block layer. Subsequently, a mechanistic-empirical elastic analysis was carried out using the AEMC software. From this, the service life, expressed as the number of Equivalent Single Axle Loads that the structure can still withstand, and the Residual Requests (RR) of the ICBP were determined. Four different scenarios for M&R activities were analyzed, and the costs of each scenario were estimated over the projected service life. It was observed that sections with lower stress absorption capacity in the block layer presented higher M&R costs. Furthermore, prioritizing preventive maintenance (RR = 60%), even at earlier stages and with higher frequency, results in lower costs over the service life. This methodology serves as a useful decision-making tool for establishing M&R strategies aimed at extending the service life of ICBP.

Keywords: Deflection, Performance assessment, Costs, Back-analysis, Elastic analysis.

1. Introduction

Compared to other types of pavements, the Interlocking Concrete Block Pavement (ICBP) presents several advantages, such as lower maintenance costs, greater ease in performing repairs, and improved stormwater drainage (Jamshidi et al. 2019; Mora et al. 2025; Sain et al. 2025). Additionally, this type of pavement shows better performance and cost-effectiveness compared to asphalt pavements for low- and medium-traffic roads (Gogoi 2019). Although the use of ICBP has been expanding worldwide, there are still gaps related to its management (Gogoi and Dutta 2019). This highlights the need for rational strategies to ensure safety, comfort, and performance throughout its service life.

Environmental factors and traffic contribute to the degradation of the ICBP structure, reducing its service life (Bezerra and Oliveira 2022). To mitigate this process, maintenance and rehabilitation (M&R) activities are required, usually planned through Pavement Management Systems (PMS). These systems are decision-support tools aimed at defining more efficient strategies to preserve adequate pavement conditions (Xiao et al. 2026). For this purpose, it is necessary to characterize structural conditions, which reflect the remaining load-bearing capacity (Jeon et al. 2025). In the case of ICBP, this characterization is performed using non-destructive methods such as the Benkelman Beam Test (BBT) and the Falling Weight Deflectometer (FWD) (Rathan and Sunitha 2021).

The typical ICBP structure consists of a surface layer made of concrete blocks supported by a bedding layer, as well as base, sub-base, and subgrade layers. Although the surface layer is composed of rigid elements, the structural behavior of ICBP is similar to that of flexible pavements (Rathan et al. 2021). Applied loads are

distributed among the layers, reducing stresses transmitted to the subgrade (Bezerra 2023). As a result, the layers respond elastically, generating recoverable deflections on the pavement surface. These deflections are used as indicators of the structural performance of ICBP (García and Corte 2021), as they express system deformability and support the design of reinforcements, as well as the definition of M&R strategies.

Laboratory determination of the elastic modulus (EM) for the block layer is complex and not yet standardized. An alternative approach is to perform a back-analysis (Rathan and Sunitha 2022). This process uses pavement deflections to estimate layer stiffness. With this, it is possible to conduct elastic analyses of ICBP and define management parameters. The structural condition of the pavement is related to its ability to withstand traffic loads, reflecting the current state of the structure compared to its initial condition. In this context, this condition can be quantified using RR, understood as a fraction of the design service life (Mikolaj et al. 2025). For ICBP, RR is directly related to vertical strain at the top of the subgrade. Therefore, its estimation is based on structural results obtained from mechanistic-empirical analysis (Rahman et al. 2018).

The management of ICBP based on structural parameters that indicate the remaining performance of the structure is characterized as a Condition-Based Maintenance approach. This approach is recognized as one of the main strategies for efficient transport infrastructure management (Gou and Liang 2026). Defining the optimal timing for M&R activities is essential to reduce costs and maximize pavement performance. Recent studies have sought to support this decision-making process: Gogoi et al. (2023) developed a multicriteria decision tool to establish a hierarchical maintenance plan for ICBP roads. Anitha et al. (2021) developed the concept of critical time to assess environmental performance and assist in scheduling interventions. These studies demonstrated effectiveness in improving the selection of M&R strategies.

Therefore, this study aims to analyze whether there is an impact on determining the optimal timing for M&R activities in ICBP, based on structural performance and intervention costs. The results are expected to contribute to the development of a decision-support tool, promoting more efficient use of resources and ensuring proper M&R of pavement structural conditions over time.

2. Methodology

Initially, the study area was defined, and structural data of the ICBP were collected (material characterization and deflection measurements). Subsequently, a back-analysis process was performed to determine the stiffness of the surface layer (block layer + bedding layer). Using these data, an elastic analysis of the structure was conducted, and RR was determined. After that, scenarios for M&R activities were proposed, and the costs of each scenario were established over the projected service life of the ICBP. Finally, the most technically and economically efficient strategy was defined. The Figure 1 summarizes the methodological structure of this study.

The study was carried out on a dual carriageway with a length of 1,880 m and a width of 7.2 m. The analysis was conducted in the 4th year of ICBP operation, with an estimated Equivalent Single Axle Load (ESAL) of 9.52×10^6. A service life horizon of 20 years was considered. The section is located in a port region, which justifies the robustness of the structure (Figure 2), designed to support heavy traffic with granular material in the lower layers over a sandy subgrade. The concrete blocks used were Unistein-shaped and laid in a herringbone pattern.

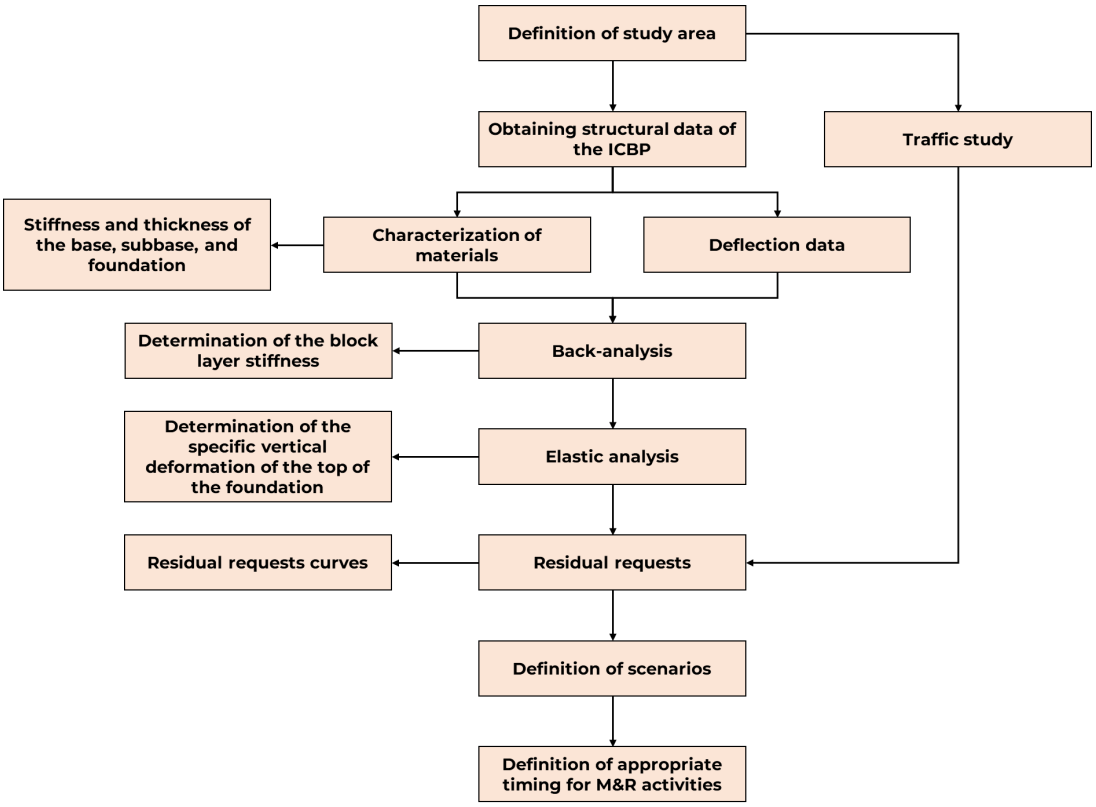


Figure 1 – Study structure (Authors 2026)

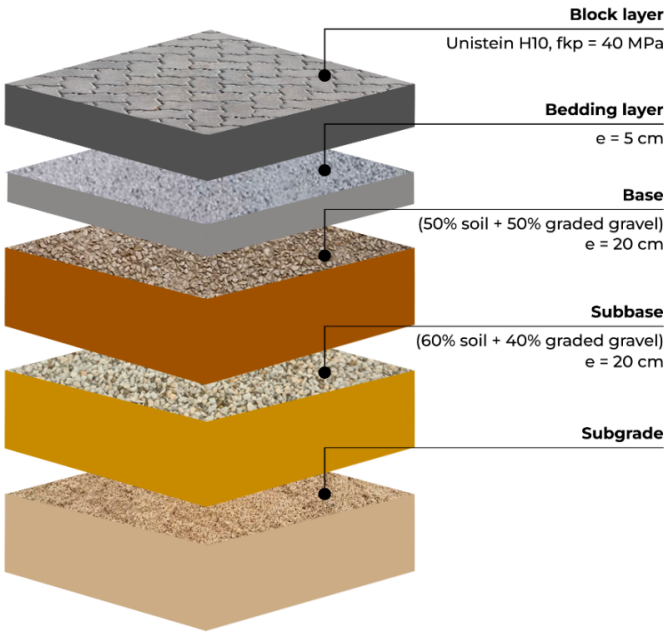


Figure 2 – ICBP structure (Authors 2026)

The section was divided into 10 homogeneous segments (ASTM 2019), with one section every 6 stations. The materials of the structure, except the bedding layer, were tested in the laboratory to obtain the stiffness of each layer. For this study, Shackel (1990) parameters were adopted for the bedding layer due to the difficulty of sampling and testing. Table 1 presents the geotechnical data for the materials used in the structure.

Table 1 – Geotechnical data of the materials

Layer	RM (MPa)	Poisson's ratio	Density (g/cm³)	Optimal humidity (%)	Composite RM model			
					K1	K2	K3	R^2
Bedding layer	15	0.30	1.65	-	-	-	-	-
Base	515	0.35	2.14	9.20	1124.65	0.46	- 0.22	0.82
Subbase	276	0.35	1.89	12.20	1281.95	0.56	0.01	0.92
Subgrade	235	0.40	1.79	11.00	696.05	0.44	-0.13	0.80

2.1 Traffic study

Based on vehicle counts at the study site, ESAL was calculated. The section presented an Average Daily Traffic (ADT) of 800 vehicles. Based on the American Association of State Highway and Transportation Officials method (AASHTO 1993), ESAL was projected over the 20-year service life of the ICBP (Table 2). These data were used to define RR for each section.

Table 2 – Traffic study

Year	ESAL	ADT	Year	ESAL	ADT
0	1.72×10^6	800	**11**	2.74×10^7	1369
1	3.53×10^6	840	**12**	3.05×10^7	1437
2	5.43×10^6	882	**13**	3.38×10^7	1509
3	7.43×10^6	927	**14**	3.72×10^7	1584
4	9.52×10^6	973	**15**	4.08×10^7	1664
5	1.17×10^7	1022	**16**	4.45×10^7	1747
6	1.40×10^7	1073	**17**	4.85×10^7	1834
7	1.65×10^7	1126	**18**	5.26×10^7	1926
8	1.90×10^7	1182	**19**	5.70×10^7	2022
9	2.17×10^7	1242	**20**	6.15×10^7	2123
10	2.45×10^7	1304			

2.2 Back-analysis

For this study, deflections were obtained using the BBT. However, it is important to note that this method was developed and calibrated for continuous surface pavements. Therefore, joints between the blocks may introduce variability in the measured results, and the deflection response may not accurately reflect the behavior of the flexible structure.

To address this, a statistical treatment based on the student's t-distribution was applied, considering a 95% confidence level (one-tailed), in order to determine the characteristic deflections of each section. The back-analysis was conducted using the BackCAP software (version 1.6.0), developed by Barroso et al. (2022). This software allows the definition of variation ranges for the resilient modulus (RM) of the materials, providing more representative results.

The equipment used in the measurements recorded deflections only at the center of the applied load (D0) and at a distance of 25 cm (D25), which made it impossible to determine the deflection basin of the ICBP. The material characterization data — RM, Poisson's ratio, and layer stiffness — together with the deflection values, were used as input data in the back-analysis software. The deflection results are presented in Table 3. Section 8 was excluded from the analysis due to inconsistencies in the deflection data collection.

Table 3 – Traffic study

Section	Station		Do (0,01mm)			D25 (0,01mm)		
	Start	End	Average	Standard deviation	Characteristic deflection	Average	Standard deviation	Characteristic deflection
1	0	6	43.00	3.83	**47.51**	8.50	1.91	10.75
2	8	14	37.50	3.42	**41.52**	7.50	3.42	11.52
3	16	22	39.00	5.03	**44.92**	5.50	1.91	7.75
4	24	30	41.00	3.46	**45.08**	7.50	3.00	11.03
5	32	38	41.00	2.00	**43.35**	7.00	8.27	16.74
6	40	46	47.50	17.84	**68.49**	10.50	6.81	18.51
7	48	54	42.00	12.65	**56.88**	10.00	4.32	15.08
9	64	70	91.33	9.87	**10.97**	16.67	5.77	26.40
10	72	78	92.00	2.83	**95.33**	9.50	2.52	12.46

For the back-analysis, the RM values obtained from laboratory tests were adopted. However, for the subgrade, free variation of RM was allowed, acknowledging that several factors may influence its mechanical behavior. For the base, subbase, and bedding layer, a variation of ±10% around the reference RM values was considered, aiming to achieve better agreement with the obtained results.

Regarding the surface layer, the blocks and the bedding layer were treated together as a segmented layer, due to the distinct mechanical properties and structural responses that characterize these materials (Kim et al. 2024). The linear RM constitutes a parameter equivalent to the EM, which is the property used in the back-analysis process.

2.3 Elastic analysis

After obtaining the elastic properties of each layer, an elastic analysis of the ICBP was carried out. For this analysis, the base, subbase, and subgrade materials were considered non-linear elastic. For the ICBP surface layer (block layer + bedding layer), a linear behavior was assumed, considering the EM obtained from the back-analysis. The AEMC software v.2.4.6 (DNIT 2021) was used. The applied load was 8.2 tf, corresponding to the Brazilian standard axle load (single axle with dual wheels). Full bonding between layers was assumed, since elastic results tend to be more critical under bonded conditions (Bezerra et al. 2024).

In the elastic analysis, a Cartesian coordinate system with orthogonal axes was considered, where the z-axis is aligned with the direction of load application, the y-axis corresponds to the direction of traffic movement, and the x-axis is perpendicular to the y-axis. For this analysis, two points were defined at the top of the subgrade: (x = 0; y = 0; z = 42.01 cm) and (x = 16.2 cm; y = 0; z = 42.01 cm). As a result of the analysis, the vertical strain at the top of the subgrade (εz) was obtained at both points, and the highest value was considered. This approach was adopted because, near the ICBP surface, stresses are higher at the tire–pavement contact area (x = 16.2 cm). However, with increasing depth, the overlap of stress bulbs occurs, leading to higher stresses at the center of the standard axle (x = 0).

2.4 Service life

Subsequently, a mechanistic-empirical verification was performed in order to estimate the number of standard axle load repetitions that the structure can withstand (service life). This analysis was based on the limiting criterion of vertical strain at the top of the subgrade (Rahman et al. 2018), applied through Equation 1. From this approach, it was possible to estimate the percentage of service life consumed by the structure in each analysis period.

$$ESAL_{sl} = \left(\frac{28000}{\varepsilon_z}\right)^4 \times 10^{-2} \quad (1)$$

where, $ESAL_{sl}$ is the number of admissible repetitions of the standard axle load and ε_z is the vertical strain at the top of the subgrade (m/m).

2.5 Residual requests

The service life of the ICBP is directly associated with the vertical strain at the top of the subgrade, and RR is derived from the structural results obtained through mechanistic-empirical analysis. For its calculation, Equation 2 was used, which incorporates the reduction in service life as a function of the degradation caused by traffic, based on the ESAL previously determined by Equation 1.

$$RR_i(\%) = \frac{ESAL_{sl} - ESAL_i}{ESAL_{sl}} \times 100 \quad (2)$$

where, RR_i is the residual service life for year i, $ESAL_{sl}$ is the number of admissible repetitions of the standard axle load under current conditions, and $ESAL_i$ is the number of equivalent single axle load for year i.

2.6 Definition of optimal timing for M&R strategies

For each ICBP section, RR was calculated and a curve representing the structural degradation over the service life was developed. Each curve generated an equation, which was used to define time (variable y) for each level of degradation (variable x). Based on this, scenarios for different M&R strategies in the ICBP were proposed, and the costs over the 20-year design life were calculated. The optimal timing for M&R was defined as the strategy that resulted in the lowest cost. Thus, four distinct scenarios were considered:

a) performing only preventive maintenance at RR = 60%;
b) performing only corrective maintenance at RR = 40%;
c) performing only reinforcement at RR = 20%;
d) performing only reconstruction at RR = 0%.

For each ICBP section, the number of M&R cycles required for the pavement to reach its design service life was determined. After each cycle, it was assumed that the pavement's initial functional and structural conditions were fully restored. Table 4 presents the M&R strategies and costs according to the RR classification, as well as their cost per square meter. The costs were obtained from Brazilian reference tables for the base year 2025 and converted into US dollars.

Table 4 – M&R strategies and costs according RR classification

RR classification (%)		M&R strategy	Specification	Cost/m², in dollar
Very good	80 ≤ RR < 100	Do nothing	No intervention required	-
Good	60 ≤ RR < 80	Preventive maintenance	Grouting with or without vegetation removal	$ 0.64
Fair	40 ≤ RR < 60	Corrective Maintenance	Replacement of damaged blocks, replacement of curbs, correction of finishes, and repair of specific depressions.	$ 28.31
Poor	20 ≤ RR < 40	Reinforcement	Replacement of the block layer and an increase in the block layer thickness.	$ 45.94
Very poor	0 ≤ RR < 20	Reconstruction	Demolition of pavement structure with complete reconstruction	$ 52.28

3. Results and discussion

In this section, the results of the back-analysis and the elastic analysis are first presented. This process results in the estimation of how many repetitions of the standard axle load each ICBP section can withstand at the end of the 20-year service life. Subsequently, the Residual Requests (RR) results for each section are presented. Finally, the cost results for each adopted M&R strategy are presented.

3.1 Back-analysis and elastic analysis

Table 5 presents the Elastic Modulus (EM) values obtained for the block layer in each ICBP section, as well as the relative errors resulting from the back-analysis. In addition, it presents the results obtained from the elastic analysis performed using the AEMC software and number of standard axle load repetitions that the structure can withstand (service life).

Table 5 – Results of back-analysis and elastic analysis

Back-analysis (Blocks layer)			Specific vertical deformation at the top of the subgrade (m/m)	ESAL (service life)
Section	Elastic Modulus (MPa)	Relative error		
1	2778	0,0000	-3.34×10^{-4}	4.94×10^{7}
2	4583	0,0005	-2.96×10^{-4}	8.01×10^{7}
3	3433	0,0007	-3.18×10^{-4}	6.01×10^{7}
4	3391	0,0005	-3.19×10^{-4}	5.94×10^{7}
5	3927	0,0001	-3.08×10^{-4}	6.83×10^{7}
6	432	0,0002	-4.55×10^{-4}	1.43×10^{7}
7	1286	0,0002	-3.90×10^{-4}	2.66×10^{7}
9	10	0,0007	-5.24×10^{-4}	8.15×10^{6}
10	15	0,0050	-5.23×10^{-4}	8.22×10^{6}

Table 5 shows a strong dependence between the increase in deformations and the reduction in ICBP durability. This behavior is mainly associated with the low EM values of the block layer obtained from the back-analysis. In the case of Sections 9 (10 MPa) and 10 (15 MPa), the results indicate low stiffness of this layer, compromising its ability to absorb and redistribute the applied stresses, which increases the demand on the underlying layers and reduces the service life. This performance is also related to the deflection values, as these same sections exhibited the highest vertical displacements, reinforcing the indication of lower structural capacity.

In contrast, Section 2 stood out for presenting the lowest value of vertical deformation at the top of the subgrade and, consequently, the highest service life. This result can be attributed to lower deflection combined with a high EM value of the block layer, indicating greater stiffness and efficiency in dissipating loading stresses, thereby reducing stress propagation to the underlying layers.

Considering the projected traffic over the 20-year design life (ESAL of 5.70×10^{7}), it is observed that Sections 1, 6, 7, 9, and 10 exhibited degradations before reaching the design service life, indicating structural inadequacy under the applied loading. It is worth noting that the AEMC software was developed for asphalt pavements and may not fully represent the elastic analysis. The software assumes homogeneous layers, which constitutes a simplification in the analysis of ICBP.

3.2 Residual requests

After obtaining the results of the vertical strain at the top of the subgrade and the ESAL of service life, it was possible to calculate the RR for each section. Figure 3 shows the deterioration curves for each section.

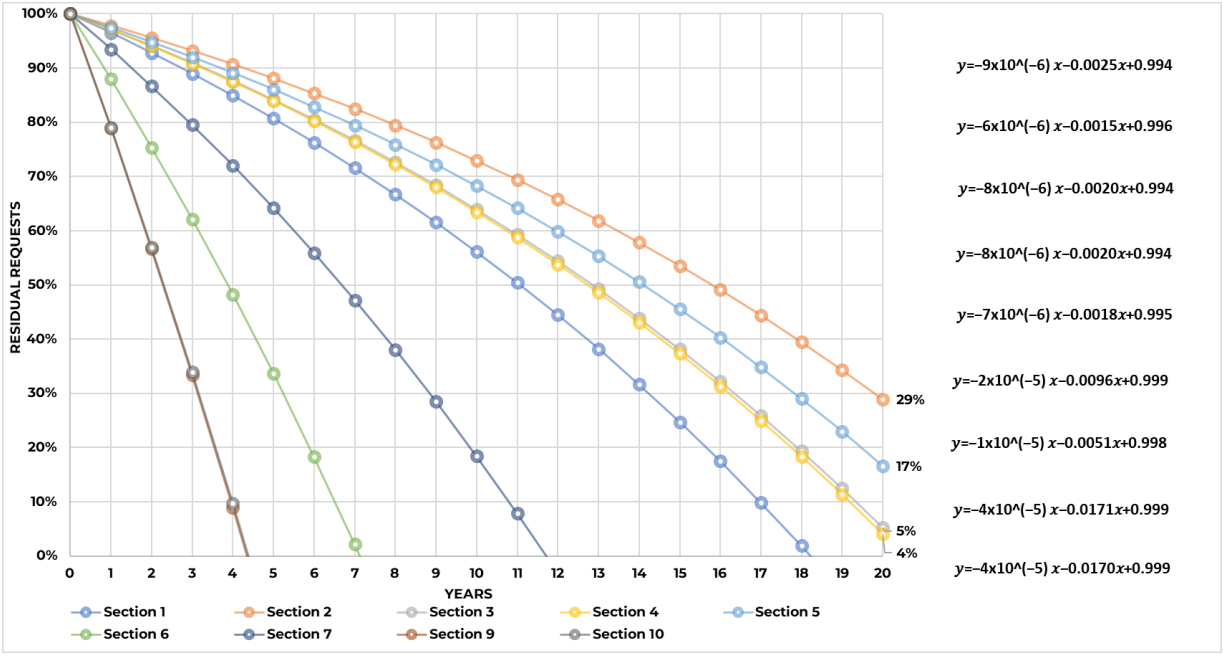


Figure 2 – Results of the residual requests (Authors 2026)

Sections 1, 6, 7, 9, and 10 reach RR values of 0%, indicating that these structures fail before the end of the ICBP design service life. Sections 9 and 10 stand out, as they showed the greatest reductions in RR over the analyzed period, reaching failure conditions approximately four years and four months after the structural evaluation. This behavior is consistent with the low EM values of the block layer in these sections, as well as the high vertical strains observed at the top of the subgrade. As a result, a rapid loss of structural capacity is observed, since the block layer provides limited contribution, transferring most of the stresses to the granular layers.

In contrast, Section 2 presented the highest RR value at the end of the design period (29%). Additionally, Sections 5, 3, and 4 did not reach failure conditions within the analyzed interval, although they were classified as being in very poor condition at the end of the 20 years. These results are associated with lower levels of vertical strain at the top of the subgrade, indicating better structural performance. In general, it is observed that sections with greater capacity to attenuate stresses transmitted to the subgrade exhibited higher service life.

Initially, it is observed that the R^2 values indicate an excellent fit of the models to the deterioration curves. Sections 9 and 10 present higher coefficients associated with x (linear) and x^2 (quadratic), in absolute terms. This indicates a more pronounced deterioration rate. This behavior confirms the previously discussed results, highlighting a rapid loss of RR and, consequently, a shorter service life for these structures. On the other hand, Section 2 presents the lowest coefficients, reflecting a slower degradation rate.

3.3 Definition of optimal timing for M&R strategies

Table 6 shows the M&R timing for each scenario in each section. In addition, it presents the number of M&R cycles required for each section over the 20-year service life, as well as the costs associated with each scenario.

Table 6 – M&R timing, the number of M&R cycles and the costs for each section

RR	M&R strategies	M&R time, in month (cicles of M&R)									Cost, in dollar
		Sections									
		1	2	3	4	5	6	7	9	10	
60%	PM	112 (2.1)	161 (1.5)	130 (1.8)	130 (1.9)	141 (1.7)	38 (6.2)	69 (3.5)	22 (10.8)	22 (10.7)	1,736,171.60
40%	CM	153 (1,6)	214 (1.1)	175 (1.4)	175 (1.4)	190 (1.3)	56 (4.3)	98 (2.4)	33 (7.4)	33 (7.3)	10,776,993.80
20%	RF	189 (1.3)	260 (1.0)	214 (1.1)	214 (1.1)	232 (1.0)	69 (3.5)	126 (1.9)	43 (5.6)	43 (5.6)	13,743,621.10
0%	RC	220 (1.1)	299 (1.0)	247 (1.0)	249 (1.0)	268 (1.0)	87 (2.8)	151 (1.6)	52 (4.6)	52 (4.6)	12,919,322.50

The PM strategy, applied at 60% RR, involves earlier interventions—especially in the most critical sections, such as 9 and 10, which require action as early as 22 months—yet results in the lowest total cost (approximately $1.74 million). This demonstrates that early interventions are more economically efficient over the pavement life cycle. On the other hand, as the RR level decreases, the time to intervention increases, but so do the associated costs. CM, RF, and RC strategies present higher costs compared to the PM strategy (521%, 694%, and 656%, respectively). This behavior indicates that delaying interventions is not economically advantageous. It is worth noting that RF costs were higher than RC, due to the small difference in unit cost and the higher frequency of RF interventions.

Variability in performance among sections is also observed: Sections 6, 7, 9, and 10 require more frequent interventions across all scenarios, confirming their lower structural capacity. In contrast, Section 2 stands out for its higher durability. Furthermore, preventive strategies involve a higher frequency of interventions but result in lower cumulative costs, whereas corrective strategies reduce intervention frequency but increase the cost per intervention.

4. Conclusions

This study aimed to evaluate whether it is possible to define the optimal timing for M&R strategies in ICBP, considering structural performance and the costs associated with interventions. The analysis revealed a strong relationship between the stiffness of the block layer, the vertical strains at the top of the subgrade, and the service life, enabling the identification of sections with critical structural performance and accelerated degradation behavior. The results indicate that, for the analyzed period and considering the imposed constraints and comfort conditions, structures in which stresses are absorbed by the surface layer (block layer + bedding layer) are more suitable for heavy traffic.

From a techno-economic perspective, it was found that preventive strategies, applied at RR = 60%, result in lower life-cycle costs, even with a higher frequency of interventions. In contrast, delaying M&R actions leads to significant cost increases and accelerated loss of structural capacity. It is concluded that the integration of structural analysis, deterioration modeling, and economic evaluation provides a consistent approach to support decision-making in Interlocking Pavement Management Systems. The results reinforce the importance of adopting rational, performance-based strategies, contributing to more efficient use of resources and to the expansion of knowledge on ICBP management, which is still underexplored in the literature.

Acknowledgments

Acknowledgments to the Brazilian Portland Cement Association (ABCP) for the financial support provided for conducting the structural tests.

References

American Association of State Highway and Transportation Officials (AASHTO). (1993). Guidefor Design of Pavement Structures. AASHTO, Washington, DC.

Anitha, Arya Chandralal, Muhammed Siddik Abdul Samad, and George K. Varghese. 2021. “Environmentally Useful Life of Interlocking Concrete Block Pavements: Critical Time Period Concept.” Journal of Sustainable Water in the Built Environment 7 (2). https://doi.org/10.1061/jswbay.0000939.

ASTM C136. Standard Test Method for SieveAnalysis of Fine and Coarse Aggregates. American Society for Testing andMaterials, West Conshohocken, 2019.

Barroso, E.S.;Oliveira, J.L.F.; Parente Jr.., E.; Babadopulos, L.F.A.L.; Bastos, J.B.S. Efficient backcalculation procedure forasphalt pavements using the Finite Element Method. In: Ibero-Latin-AmericanCongress on Computational Methods in Engineering, 43., 2022, Foz do Iguaçu. Proceedings [...].Foz do Iguaçu: ABMC, 2022. Available at: https://publicacoes.softaliza.com.br/cilamce2022/article/view/5584/4650.Accessed on: 20 Oct. 2025.

Bezerra, F. S. C., and F. H. L. Oliveira. 2022. “Effects of Degradation on the Service Life of an Interlocked Pavement.” International Journal of Pavement Engineering 24 (2). https://doi.org/10.1080/10298436.2022.2139376.

Bezerra, F. S. C. Avaliação dodesempenho de pavimentos intertravados em função da abertura das juntas,diferentes bases e defeitos na camada de rolamento. 2023. f 91. Dissertação(Mestrado em Engenharia de Transportes) - Centro de Tecnologia, UniversidadeFederal do Ceará, Fortaleza, 2023.

Bezerra, F.S.C., F.L.C. Sousa, S.H.A. Barroso, and F.H.L. Oliveira. 2024. “ANÁLISE de SENSIBILIDADE DA ADERÊNCIA E DO COMPORTAMENTO RESILIENTE DOS MATERIAIS EM PAVIMENTOS INTERTRAVADOS.” Proceedings.science. https://proceedings.science/anpet/anpet-2024/trabalhos/analise-de-sensibilidade-da-aderencia-e-do-comportamento-resiliente-dos-materiai?lang=pt-br.

DNIT IS–247. Studies for the Development ofImplementation Projects using the National Design Method – MeDiNa. NationalTransport Infrastructure Department, Brasilia, 2021 (in Portuguese).

García, Gabriel, and Nicolás Corte. 2021. “Experimental Study on an in Situ Concrete Block Pavement under Heavy Traffic Loads.” International Journal of Pavement Engineering 23 (10): 3467–80. https://doi.org/10.1080/10298436.2021.1902523.

Gogoi, Ripunjoy. 2019. “Cost Effectiveness of Interlocking Concrete Block Pavements for Low Volume Traffic Roads.” International Journal of Engineering and Advanced Technology 8 (6): 1239–44. https://doi.org/10.35940/ijeat.f8382.088619.

Gogoi, Ripunjoy, and Bhupali Dutta. 2019. “Maintenance Prioritization of Interlocking Concrete Block Pavement Using Fuzzy Logic.” International Journal of Pavement Research and Technology, November. https://doi.org/10.1007/s42947-019-0098-9.

Gogoi, Ripunjoy, Bhupali Dutta, P. Mahakavi, and Prince Akash Nagar. 2023. “Analytical Hierarchy Process in the Maintenance Decision-Making of Interlocking Concrete Block Pavements.” Lecture Notes in Civil Engineering, 103–14. https://doi.org/10.1007/978-981-99-1886-7_9.

Guo, Chunhui, and Zhenglin Liang. 2026. “Meta-Predictive Maintenance for Rapid Adaptation across Diverse Infrastructure Maintenance Tasks.” Reliability Engineering & System Safety 272 (August): 112493. https://doi.org/10.1016/j.ress.2026.112493.

Jamshidi, Ali, Kiyofumi Kurumisawa, Gregory White, Tatsuo Nishizawa, Toshifumi Igarashi, Toyoharu Nawa, and Jize Mao. 2019. “State-of-The-Art of Interlocking Concrete Block Pavement Technology in Japan as a Post-Modern Pavement.” Construction and Building Materials 200 (March): 713–55. https://doi.org/10.1016/j.conbuildmat.2018.11.286.

Jeon, Jihun, Younghwan Son, Taejin Kim, and Sangbeom Jo. 2025. “Life Cycle Greenhouse Gas Assessment of Permeable Concrete Block Pavements with Industrial By-Products.” Waste Management 204 (June): 114968. https://doi.org/10.1016/j.wasman.2025.114968.

Kim, Inhyun, Choong-Ki Chung, and Jung-Hyun Ryu. 2024. “Evaluation of Interlocking Block Pavement Performance under Varying Construction Conditions by Model Chamber Tests.” Case Studies in Construction Materials 22 (December): e04067. https://doi.org/10.1016/j.cscm.2024.e04067.

Mikolav, Ján; Lubos, Remek ; Kozel, Matúš; et al. Maximizing Pavement Service Life: A Comprehensive Process Model Based on Structural Life Extension, Serviceability Deterioration Processes, and Asset Value. Applied Sciences, v. 15, n. 16, p. 8782–8782, 2025.

Mora, Tiziano Dalla , Giuseppe Emmi, Paolo Ruggeri, Massimiliano De Bei, and Fabio Peron. 2025. “Mitigation Urban Heat Island by Using Porous and Permeable Block Pavement.” Energy and Buildings 346 (July): 116149. https://doi.org/10.1016/j.enbuild.2025.116149.

Rahman, M.M.; Beecham, S.; Mcintyrem, E.; Iqbal, A.. Mechanistic designof concrete block pavements. In: Victorian Symposium – Geotechnics andTransport Infrastructure, 3., 2018, Melbourne. Proceedings [...]. Melbourne:AGS, 2018. Available at: https://geomechanics.org.au/papers/mechanistic-design-of-concrete-block-pavements/.Accessed on: 2 Oct. 2025.

Rathan, Arjun Siva , Aravinda Sai V, and Sunitha V. 2021. “Mechanical and Structural Performance Evaluation of Pervious Interlocking Paver Blocks.” Construction and Building Materials 292 (July): 123438. https://doi.org/10.1016/j.conbuildmat.2021.123438.

Rathan, Arjun Siva, and V. Sunitha. 2021. “Development of Deflection Prediction Model for Interlocking Concrete Block Pavements.” Transportation Research Record: Journal of the Transportation Research Board 2676 (3): 292–314. https://doi.org/10.1177/03611981211051339.

Sain, Amit, Arun Gaur, and Partha Pratim Sarkar. 2025. “Assessment of Infiltration in Modified Block Pavements: Integrating Pervious Concrete for Innovative Pavement Construction.” Journal of Structural Design and Construction Practice 30 (3). https://doi.org/10.1061/jsdccc.sceng-1690.

Shackel, B. Designand Construction of Interlocking Concrete Block Pavements. 2 ed. London and NewYork: Elsevier Applied Science, 1990.

Xiao, Feng, Qianhong Song, Jie Gao, Shunxin Yang, and Huapeng Chen. 2026. “Anomaly Detection and Correction Framework for Pavement Maintenance and Rehabilitation Data Based on LSTM.” Journal of Transportation Engineering, Part B: Pavements 152 (2). https://doi.org/10.1061/jpeodx.pveng-1967.

cinpar2026
XXII International Conference on Building Pathology and Constructions Repair
15th to 17th July 2026 - Lisboa, Portugal

Influence of Construction and Demolition Waste as Fine Aggregate Replacement on the Performance of Self-Compacting Mortars

Fernando Augusto de Almeida JORGE[1], Valquíria Claret SANTOS[2], Regina Mambeli BARROS[3]

[1] Universidade Federal de Itajubá (UNIFEI), Itajubá, Brazil, fe_jorge98@hotmail.com
[2] Universidade Federal de Itajubá (UNIFEI), Itajubá, Brazil, valquiria@unifei.edu.br
[3] Universidade Federal de Itajubá (UNIFEI), Itajubá, Brazil, mambeli@unifei.edu.br

Abstract: The increasing generation of construction and demolition waste (CDW) and the depletion of natural resources have driven the development of more sustainable cementitious materials. This study evaluates the feasibility of partially replacing natural sand with CDW as fine aggregate in self-compacting mortars (SCM). Four mixtures were produced with replacement levels of 0%, 10%, 20%, and 30% by mass. The materials were characterised through particle size distribution and specific gravity tests. The fresh-state properties were assessed using mini-slump-flow and mini-V-funnel tests, while hardened-state performance was evaluated by measuring compressive strength and estimating the modulus of elasticity at 28 days. All mixtures exhibited adequate self-compactability, maintaining satisfactory flowability and stability. The results indicated that the mixture with 10% CDW replacement achieved the highest compressive strength, slightly outperforming the reference mixture. Higher replacement levels (20% and 30%) resulted in moderate reductions in mechanical performance. The maximum compressive strengths observed were 47.45 MPa (0%), 47.93 MPa (10%), 44.68 MPa (20%), and 39.80 MPa (30%). An increasing trend in stiffness was observed with higher CDW content. The results suggest that partial replacement of natural sand with CDW up to 10% is technically viable, providing environmental benefits without compromising mechanical performance. The findings also highlight the importance of controlling the physical properties of recycled aggregates to ensure consistent performance in self-compacting mortars.

Keywords: self-compacting mortar; construction and demolition waste; recycled aggregates; compressive strength; sustainability.

1. Introduction

The rapid growth of construction activities has significantly increased the consumption of natural resources and the generation of construction and demolition waste (CDW). The extraction of natural aggregates, particularly sand, has led to severe environmental impacts, including river degradation, ecosystem disturbance, and depletion of non-renewable resources (Frazao 2015; John 2000).

At the same time, the accumulation of CDW has become a major environmental challenge, especially in urban areas, necessitating sustainable waste management strategies and material reuse. In this context, the incorporation of CDW as recycled aggregate in cementitious materials has emerged as a promising solution to reduce environmental impacts and promote circular economy practices in the construction industry (Hansen 1992; Leite 2001; Ferreira 2013).

However, the use of recycled aggregates introduces technical challenges, such as higher porosity, increased water absorption, and variability in physical properties, which can directly affect the fresh and hardened behaviour of cementitious composites (Nedeljkovic *et al.* 2021; Han *et al.* 2023; Peiris *et al.* 2025).

In the specific case of self-compacting mortars (SCM), maintaining adequate rheological properties is essential to ensure flowability, stability, and resistance to segregation without mechanical compaction.

Previous studies indicate that moderate replacement levels of natural aggregates with recycled materials can preserve or even improve certain properties, while higher replacement levels tend to reduce mechanical performance due to microstructural changes and weaker interfacial transition zones (ITZ) (Singh *et al.* 2020; Guessoum *et al.* 2023; Zhang *et al.* 2023).

Although recycled aggregates have been widely investigated, most existing studies focus on coarse recycled aggregates in structural concrete. Systematic evidence on the use of CDW as a *fine* aggregate specifically in *self-compacting* mortars remains comparatively scarce, particularly regarding the link between fresh-state behaviour and mechanical performance. Addressing this gap is the central motivation of the present work.

Therefore, this study aims to evaluate the effect of partially replacing natural sand with CDW on the rheological and mechanical properties of self-compacting mortars. Four replacement levels (0%, 10%, 20%, and 30%) were investigated, focusing on flowability, viscosity, compressive strength, and modulus of elasticity. The main original contribution of this work is the identification of an optimal fine-CDW replacement level for self-compacting mortars, at which mechanical performance is enhanced relative to the reference while rheological stability is preserved. The results contribute to advancing the understanding of sustainable cementitious materials and support the development of more environmentally responsible construction practices.

2. Materials and Methods

2.1 Materials and CDW characterisation

The construction and demolition waste (CDW) used in this study was collected from two construction sites in Taubaté, Brazil. The waste originated from structural and non-structural masonry and internal plastering activities; consequently, it consisted predominantly of hardened cementitious mortar and fired-clay (ceramic) fragments, with minor amounts of fine concrete debris. No glass, metal, wood, gypsum, or organic contaminants were retained. The material was manually pre-selected on-site to remove contaminants and coarse particles, transported to the Civil Engineering Laboratory of the Federal University of Itajubá (UNIFEI), and processed in accordance with the applicable Brazilian standard for recycled aggregates from CDW (NBR 15116:2021).

Because masonry- and render-derived CDW is dominated by porous ceramic and adhered mortar, it is expected to exhibit higher water absorption and intra-particle porosity than natural siliceous sand. These compositional features are known to govern the fresh- and hardened-state response of the resulting mortars and are therefore central to interpreting the results reported below. It should be noted that the present characterisation is based on the origin, visual-manual composition, and physical properties of the CDW; a quantitative mineralogical or chemical characterisation was outside the scope of this study and is identified as a limitation in Section 5.

The other materials used in this study were Portland cement (CP II-F-32), metakaolin as a supplementary cementitious material, a polycarboxylate-based superplasticiser (SP), natural river sand, and potable water. The physical characterisation of the aggregates, including particle size distribution and specific gravity, was performed to ensure compatibility between natural and recycled materials and to minimise variability in mixture behaviour.

2.2 Mix design and proportions

The mix design was based on the methodology proposed by Gomes, Gettu, and Agulló (2003), which considers the separate optimisation of the paste phase and the granular skeleton to achieve self-compacting behaviour. This approach is widely adopted in the design of self-compacting cementitious materials due to its effectiveness in balancing flowability and stability. The mix proportions of the four mixtures are summarised in Table 1.

Table 1 – Mix proportions of the evaluated mixtures

Mixture	Cement (g)	Metakaolin (g)	SP (g)	Sand (g)	CDW (g)	Water (g)
B	1201	60.5	13	2022.0	0.0	540
T1	1201	60.5	13	1819.8	202.2	540
T2	1201	60.5	13	1617.6	404.4	540
T3	1201	60.5	13	1415.4	606.6	540

A reference mixture (B) was defined and used as the basis for all compositions. The water-to-cement ratio (w/c) was kept constant at 0.45, and the metakaolin and superplasticiser contents were held constant to isolate the effect of CDW incorporation. Four mixtures were produced with CDW replacement levels of 0%, 10%, 20%, and 30% by mass of natural sand, identified as B, T1, T2, and T3, respectively. Replacement was carried out by mass to ensure direct comparability between mixtures, avoiding distortions arising from differences in material density.

2.3 Test methods

Fresh-state properties were evaluated using the mini-slump-flow and mini-V-funnel tests, which are commonly applied to assess flowability and viscosity in self-compacting systems (EFNARC 2005). The density of the fresh mixtures was also determined. Due to the self-compacting nature of the materials, no mechanical compaction was applied during casting.

For the hardened state, cylindrical specimens 50 mm in diameter and 100 mm in height were moulded. After 24 hours, the specimens were demoulded and cured under water until testing at 28 days. Compressive strength tests were performed to evaluate mechanical performance, and the modulus of elasticity was estimated from the stress-strain relationships obtained during testing. Statistical analysis was carried out using mean values, standard deviations, coefficients of variation, and 95% confidence intervals to assess the consistency and reliability of the experimental results.

3. Results and Discussion

3.1 Particle size distribution

The particle size distribution of the natural sand and CDW is presented in Figure 1. Both materials exhibited similar grading characteristics, with fineness modulus values of 2.24 and 2.26, respectively, indicating that both are classified as medium sand. This similarity indicates that partial replacement of natural sand with CDW does not significantly alter the overall grading of the mixture, which is essential for maintaining adequate packing and workability.

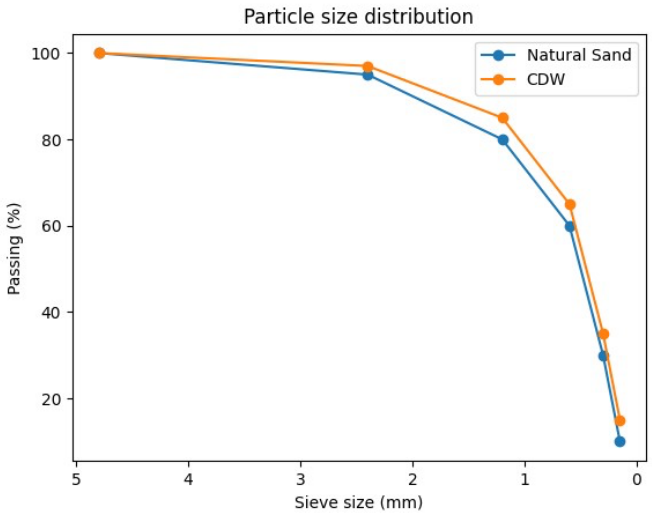


Figure 1 – Particle size distribution of natural sand and construction and demolition waste (CDW)

A slightly higher content of fine particles was observed in the CDW, particularly in the lower sieve sizes. This behaviour is commonly associated with adhered mortar and the intrinsic heterogeneity of recycled materials, in which crushing processes and residual cement paste generate additional fines (Leite 2001; Hansen 1992).

3.2 Fresh-state properties

All mixtures exhibited adequate self-compacting behaviour, maintaining satisfactory flowability and stability. The mini-slump-flow results are presented in Figure 2, with spread values ranging from 300 mm to 310 mm, indicating that the incorporation of CDW did not significantly compromise the flowability of the mixtures.

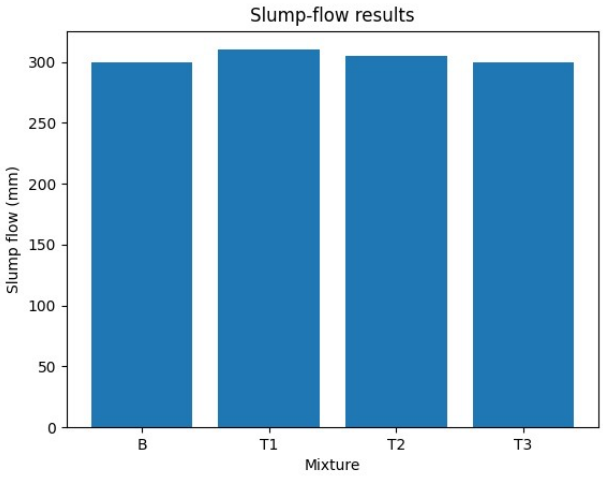


Figure 2 – Mini-slump-flow results for the evaluated mixtures

The mini-V-funnel results are shown in Figure 3, with flow times ranging from 7 to 15 seconds, demonstrating acceptable viscosity levels for self-compacting mortars. A slight increase in flow time was observed with

increasing CDW content, suggesting higher internal friction and viscosity, which can be attributed to the rougher surface texture and higher absorption capacity of the recycled aggregate.

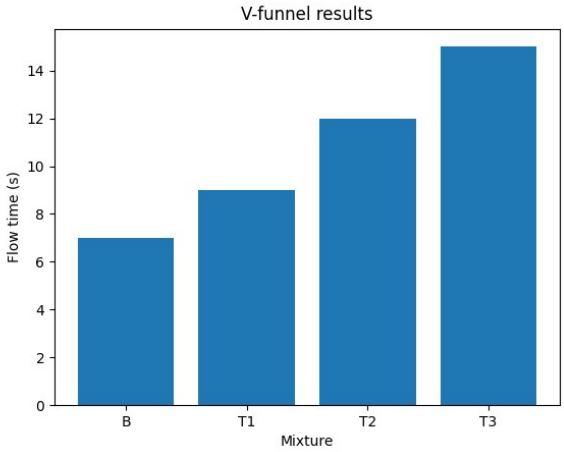


Figure 3 – Mini-V-funnel flow time for the evaluated mixtures

These findings are consistent with previous studies indicating that recycled aggregates can increase the viscosity of cementitious mixtures due to their porous structure and irregular morphology (Nedeljkovic *et al.* 2021; Singh *et al.* 2020).

3.3 Compressive strength

The compressive strength results at 28 days are presented in Figure 4. The reference mixture (B) achieved a maximum strength of 47.45 MPa, while the mixture with 10% CDW replacement (T1) reached 47.93 MPa, representing a slight increase in mechanical performance.

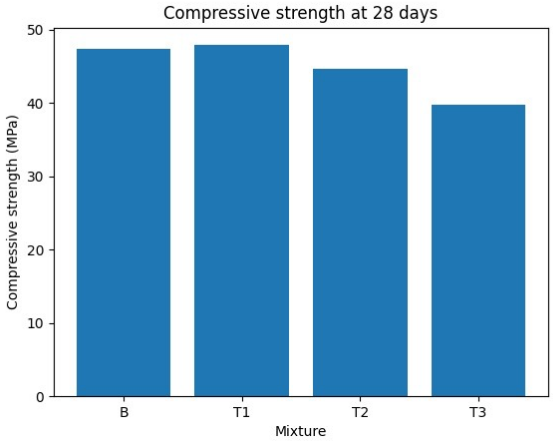


Figure 4 – Compressive strength of mixtures at 28 days

For higher replacement levels, a reduction in compressive strength was observed. The T2 and T3 mixtures presented maximum strengths of 44.68 MPa and 39.80 MPa, corresponding to reductions of approximately 6.8% and 16.1%, respectively, relative to the reference mixture. The microstructural interpretation of this trend is developed in Section 3.5.

3.4 Modulus of elasticity

An increasing trend in the modulus of elasticity was observed with higher CDW content, as shown in Figure 5. Although higher replacement levels reduced compressive strength, the increase in stiffness suggests a change in the mechanical behaviour of the material towards a more rigid, and potentially more brittle, response.

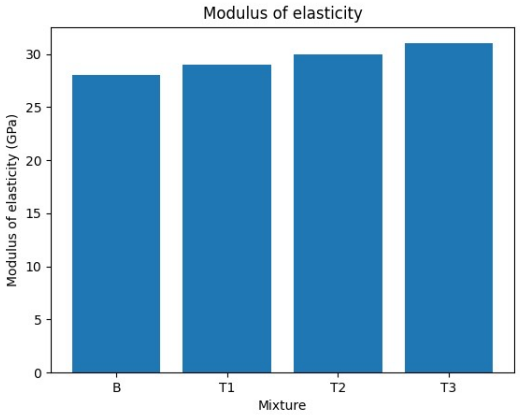


Figure 5 – Modulus of elasticity of the evaluated mixtures

This apparently counter-intuitive combination of decreasing strength and increasing stiffness is consistent with the dual role of recycled fine particles reported in the literature. The rigid ceramic and residual-paste fragments in the CDW raise the overall stiffness of the granular skeleton, increasing the composite modulus, while at the same time the porous, weaker ITZ that they introduce reduces the peak load that the matrix can sustain (Han *et al.* 2023; Zhang *et al.* 2023). Strength and stiffness are therefore governed by different mechanisms and need not vary in the same direction.

3.5 Microstructural interpretation

The strength results can be explained by two competing microstructural mechanisms. At the 10% replacement level, the additional fine fraction supplied by the CDW acts as a micro-filler, improving particle packing, reducing the volume of capillary voids, and densifying the matrix; this filler effect enhances load transfer and accounts for the slight strength gain of T1 over the reference (Zhang *et al.* 2023; Guessoum *et al.* 2023).

At 20% and 30% replacement, the detrimental effects of the recycled aggregate become dominant. The higher porosity and water absorption of the ceramic and adhered-mortar particles weaken the interfacial transition zone (ITZ) between aggregate and cement paste, which is typically the limiting region for crack initiation in cementitious composites. The adhered mortar also introduces a more porous, less homogeneous microstructure, lowering the overall load-bearing capacity. This behaviour is widely reported for cementitious composites containing recycled aggregates (Han *et al.* 2023; Peiris *et al.* 2025; Nedeljkovic *et al.* 2021). The transition from a beneficial filler effect to a dominant ITZ-weakening effect therefore explains the existence of an optimal replacement level near 10%.

Figure 6 shows the variation in compressive strength as a function of CDW replacement level, with an initial increase at 10% followed by a progressive reduction at higher levels. This non-monotonic trend reinforces the interpretation that the interaction between recycled particles and the cementitious matrix, mediated by packing density and ITZ quality, governs both the mechanical and rheological response of the material.

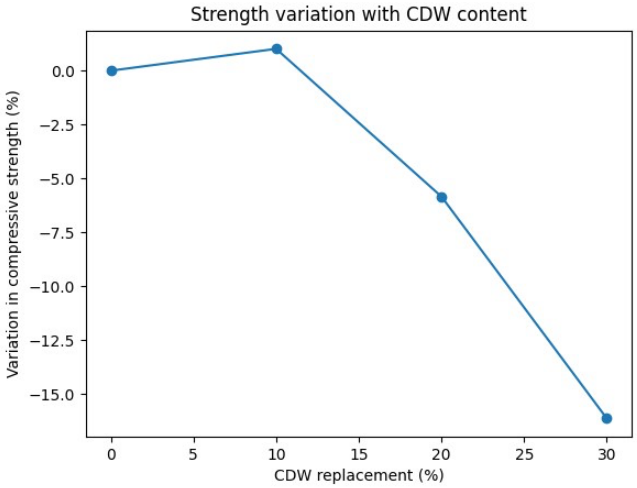


Figure 6 – Variation in compressive strength as a function of CDW replacement level

4. Limitations and Future Work

The present study has limitations that should be acknowledged and that define clear directions for future research. First, the mechanical characterisation was based solely on 28-day results; testing at earlier ages (e.g., 7 and 14 days) would provide a more complete picture of strength development and of how CDW affects the hydration kinetics of the matrix. Second, the microstructural mechanisms invoked here to explain the results, particularly the densification at 10% and the ITZ weakening at higher contents, were inferred from macroscopic behaviour and the literature rather than directly observed; scanning electron microscopy (SEM) and porosity measurements would allow these mechanisms to be confirmed and quantified.

Third, the CDW was characterised in terms of its origin, visual-manual composition, and physical properties, but not through quantitative mineralogical or chemical analysis. Given that the heterogeneity of CDW is a recognised source of variability, a more detailed compositional characterisation, combined with assessment of multiple batches, would strengthen the reliability and generalisability of the findings. Future work will therefore incorporate multi-age testing, SEM-based microstructural analysis, and a fuller characterisation of the recycled aggregate, as well as durability-oriented tests.

5. Conclusions

This study evaluated the use of construction and demolition waste (CDW) as a partial replacement for natural sand in self-compacting mortars. All mixtures maintained adequate self-compacting behaviour, with satisfactory flowability and viscosity, even at higher replacement levels. Among the evaluated compositions, the mixture with 10% CDW replacement presented the best overall performance, achieving slightly higher compressive strength than the reference mixture, an effect attributed to improved particle packing and a filler effect that densifies the cementitious matrix.

Increasing the replacement level to 20% and 30% reduced compressive strength by approximately 6.8% and 16.1%, respectively, mainly due to the higher porosity and water absorption of the recycled aggregate and the consequent weakening of the interfacial transition zone. In contrast, the modulus of elasticity increased with CDW content, indicating a shift towards a stiffer mechanical response governed by the rigidity of the recycled particles.

Overall, the partial replacement of natural sand with CDW up to 10% is technically viable, enabling the production of more sustainable self-compacting mortars without compromising mechanical performance. The novel contribution of this work is the identification of this optimal fine-CDW content for SCM and the mechanistic explanation of the strength-stiffness trade-off observed at higher contents. Given the inherent variability of CDW, controlling the physical properties of the recycled aggregate remains essential for consistent and reliable behaviour in practical applications.

Acknowledgments

The authors would like to thank the Federal University of Itajubá (UNIFEI) for providing the infrastructure and laboratory facilities necessary for this research, and gratefully acknowledge the support of the Civil Engineering Laboratory staff. The authors also acknowledge the financial support provided by CAPES (Coordination for the Improvement of Higher Education Personnel) through the PROAP programme.

References

EFNARC. 2005. *The European Guidelines for Self-Compacting Concrete: Specification, Production and Use*. Farnham: EFNARC.

Ferreira, L. 2013. “Reuse of Construction and Demolition Waste in Cementitious Composites.” *Construction and Building Materials* 40: 1102–11.

Frazao, E. B. 2015. *Areia para construção civil no Brasil: produção, consumo e impactos ambientais*. São Paulo: Oficina de Textos.

Gomes, P. C. C., R. Gettu, and L. Agulló. 2003. “Optimization of High-Performance Self-Compacting Concrete by the Use of Packing Models.” *Cement and Concrete Research* 33 (6): 789–95.

Guessoum, H., A. Boukendakdji, and E. Kadri. 2023. “Effect of Recycled Fine Aggregates on the Rheological and Mechanical Properties of Self-Compacting Mortars.” *Materials Today Communications* 34: 105123.

Han, T., X. Li, J. Zhang, and Y. Wang. 2023. “A Review on the Treatment and Utilization of Recycled Concrete Aggregates in Cementitious Materials.” *Construction and Building Materials* 363: 129831.

Hansen, T. C. 1992. *Recycling of Demolished Concrete and Masonry.* London: CRC Press.

John, V. M. 2000. “Reciclagem de resíduos na construção civil: contribuição para metodologia de pesquisa e desenvolvimento.” PhD diss., Escola Politécnica, Universidade de São Paulo.

Leite, M. B. 2001. “Avaliação das propriedades mecânicas de concretos produzidos com agregados reciclados de resíduos de construção e demolição.” PhD diss., Universidade Federal do Rio Grande do Sul.

Nedeljkovic, M., G. Visser, T. Nijland, and J. Valcke. 2021. “Physical and Mechanical Properties of Recycled Aggregate Concrete: A Review.” *Materials* 14 (13): 1–23.

Peiris, C., K. Mallawaarachchi, and A. Gallage. 2025. “Mechanical and Durability Properties of Concrete with Recycled Construction Waste: A Review.” *Journal of Building Engineering* 95: 108000.

Singh, N., S. Kumar, and S. Kumar. 2020. “A Review on Properties of Recycled Aggregates and Their Influence on Concrete Performance.” *Construction and Building Materials* 262: 120767.

Zhang, P., Q. Li, and Y. Wang. 2023. “Influence of Recycled Fine Aggregates on the Mechanical Properties and Microstructure of Cementitious Materials.” *Journal of Cleaner Production* 384: 135512.

Cinpar 2026
XXII International Conference on Building Pathology and Constructions Repair
15th to 17th July 2026 - Lisboa, Portugal

Durabilidade da cor em concretos pigmentados pretos: avaliação do comportamento cromático sob envelhecimento acelerado

Vanessa Monteiro da SILVA [1], Elton Belarmino de SOUSA [2], Fabiana Lopes de OLIVEIRA [3]

[1] Faculdade de Arquitetura e Urbanismo e de Design (FAUUSP), São Paulo, São Paulo, Brasil, vanessamonteiro@usp.br
[2] Faculdade de Arquitetura e Urbanismo e de Design (FAUUSP), São Paulo, São Paulo, Brasil, eltonbeslousa@usp.br
[3] Faculdade de Arquitetura e Urbanismo e de Design (FAUUSP), São Paulo, São Paulo, Brasil, floliveira@usp.br

Abstract: O concreto pigmentado tem se consolidado como uma solução relevante na arquitetura contemporânea, ao permitir a incorporação da cor diretamente à matriz cimentícia, eliminando a necessidade de revestimentos superficiais. No entanto, a durabilidade cromática desses materiais, especialmente em condições de exposição ambiental, ainda constitui um desafio. Neste contexto, o presente estudo teve como objetivo avaliar o comportamento cromático de concretos autoadensáveis de coloração preta, produzidos com pigmentos à base de magnetita (Fe_3O_4) submetidos ao envelhecimento acelerado por radiação ultravioleta. Foram produzidas três misturas: concreto de referência (sem pigmento), concreto com pigmento A (fabricante A) e concreto com pigmento B (fabricante B), com e sem aplicação de hidrofugante. As amostras foram submetidas a ensaios de envelhecimento acelerado em câmara de radiação ultravioleta (CUV), com ciclos alternados de radiação e condensação. A exposição totalizou aproximadamente 4553 horas de exposição, tempo equivalente a 15 anos de intemperismo natural, considerando que cada 150 horas na câmara representam 6 meses de exposição em condições naturais. A avaliação cromática foi realizada por espectrofotometria, utilizando o sistema CIELAB e o parâmetro ΔE para quantificação das variações de cor ao longo do tempo. Adicionalmente, foram realizados ensaios de resistência à compressão, absorção de água, índice de vazios e capilaridade. Os resultados indicaram baixa variação cromática das amostras, evidenciando boa estabilidade da cor, com desempenho superior dos pigmentos inorgânicos sintéticos. Observou-se que o uso de hidrofugante contribuiu para a redução das variações de luminosidade. Do ponto de vista físico e mecânico, a incorporação de pigmentos resultou em redução da resistência à compressão, especialmente em idades iniciais, além de pequenas alterações nas propriedades de absorção e porosidade. Conclui-se que o uso de pigmentos pretos em concretos autoadensáveis é tecnicamente viável.

Keywords: concreto pigmentado; envelhecimento acelerado; degradação cromática; durabilidade; Fe_3O_4.

1. Introdução

O concreto pigmentado tem se consolidado como uma estratégia relevante na arquitetura contemporânea, especialmente em soluções que exploram o concreto aparente como elemento expressivo. Ao permitir a incorporação da cor diretamente à matriz cimentícia, elimina a necessidade de revestimentos superficiais e amplia as possibilidades projetuais, associando desempenho estrutural e qualidade estética.

Entre os pigmentos utilizados, destacam-se os óxidos de ferro, amplamente empregados devido à sua estabilidade química, disponibilidade e resistência a agentes ambientais. Ainda assim, a manutenção da estabilidade cromática ao longo do tempo permanece como um desafio, sobretudo em elementos expostos à radiação ultravioleta, variações térmicas e ciclos de umidade, que podem provocar alterações perceptíveis na cor. Essa questão é particularmente relevante em concretos de tonalidade escura, como aqueles produzidos com pigmentos à base de magnetita (Fe_3O_4).

Apesar do crescente uso do concreto pigmentado, ainda são limitados os estudos voltados à avaliação sistemática da durabilidade cromática desses materiais, especialmente sob condições de envelhecimento acelerado. Soma-se a isso a ausência de metodologias normatizadas específicas para esse tipo de análise.

Diante desse cenário, este estudo tem como objetivo avaliar o comportamento cromático de concretos pigmentados pretos produzidos com pigmentos inorgânicos de Fe_3O_4, com ênfase na variação de cor sob envelhecimento acelerado por radiação ultravioleta, comparando seu desempenho ao concreto de referência e analisando a influência do tipo de pigmento na estabilidade cromática ao longo do tempo.

2. Fundamentação Teórica

Na arquitetura contemporânea, o concreto pigmentado alia desempenho técnico e valor estético, permitindo a exploração de diferentes tonalidades e superfícies, além de contribuir para a redução de custos de manutenção ao longo da vida útil da edificação (HELENE; TERZIAN, 1992; NEVILLE, 2012; RUSSO, 2024). Sua aplicação reforça a identidade visual dos projetos e estabelece relações com o contexto urbano e paisagístico (MEHTA; MONTEIRO, 2014; CHING, 2024; CONSANI, 2022).

No contexto brasileiro, a Praça das Artes, em São Paulo, destaca-se como exemplo da aplicação do concreto pigmentado em larga escala, evidenciando seu papel na integração entre volumes e na mediação entre o novo e o existente. De forma semelhante, projetos residenciais, como a Casa Terra (MARQUEZ, 2015; ARCHDAILY BRASIL, 2021) e a Residência Montagnola (SYED, 2017), demonstram o uso do concreto pigmentado como elemento estruturador da linguagem arquitetônica, e não apenas como acabamento superficial (Figura 1).

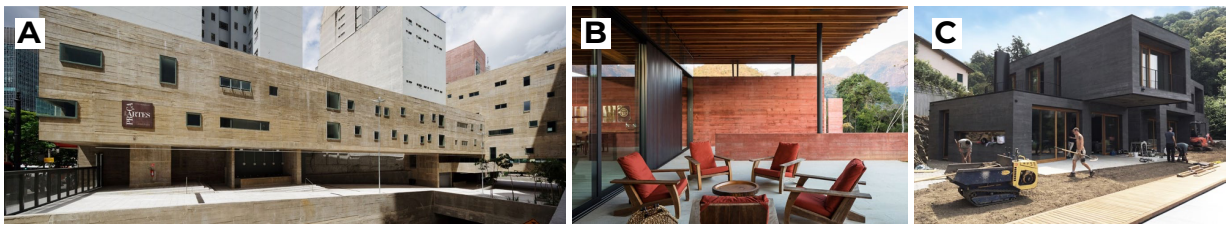


Figura 1 – A, Praça das Artes, Brasil Arquitetura, São Paulo, Brasil; B, residencia Casa Terra, Bernardes Arquitetura, Itaipava, Rio de Janeiro, Brasil; C, Residência Montagnola, Attilio Panzeri & Partners, Lugano, Suíça

Fonte: A, Archdaily Brasil (2012); B, Archdaily Brasil (2021); C, Syed (2017)

A durabilidade estética do concreto pigmentado, entretanto, depende da estabilidade cromática ao longo do tempo. A exposição a agentes ambientais, como radiação ultravioleta, variações térmicas e ciclos de umidade, pode provocar alterações na aparência superficial, resultando em mudanças perceptíveis de cor (NEVILLE, 2016; MEHTA; MONTEIRO, 2014).

Os pigmentos utilizados na coloração de materiais cimentícios podem ser classificados, de forma geral, em orgânicos e inorgânicos, cujas propriedades dependem de sua composição química (PFÄFF, 2022). Os pigmentos orgânicos apresentam cores mais intensas e maior variedade cromática, porém tendem a apresentar menor estabilidade frente à radiação ultravioleta e às condições ambientais, podendo sofrer desbotamento ao longo do tempo, já os pigmentos inorgânicos apresentam maior estabilidade química e térmica, além de menor toxicidade. (BONDIOLI et al., 1998).

3. Metodologia

A metodologia do estudo foi iniciada com a realização de um levantamento bibliográfico de literatura científica e normas técnicas brasileiras, com ênfase no uso de pigmentos pretos e em suas propriedades físico-mecânicas e cromáticas.

3.1 Produção dos concretos e moldagem das amostras

Durante o desenvolvimento da pesquisa, foram acompanhadas as etapas iniciais do processo de produção do concreto pigmentado, que compreenderam a preparação das fôrmas de madeira plastificada, dimensionadas para garantir resistência à umidade, facilitar o desmolde e assegurar adequada distribuição dos agregados (Figura 2).

Na etapa experimental, foram produzidos corpos de prova cilíndricos de concretos autoadensáveis pigmentados, além de um concreto de referência, sem adição de pigmento. A produção das misturas, bem como os ensaios no estado fresco, foi realizada em parceria com a empresa Engemix. Também foram moldados seis corpos de prova prismáticos, com dimensões de 9 × 9 × 4 cm, destinados aos ensaios de envelhecimento acelerado. Adicionalmente, os corpos de prova também foram utilizados para a realização de ensaios de caracterização no estado endurecido.



Figura 2- Formas desenvolvidas para a confecção dos corpos de prova (Fonte: autores)

Em paralelo, foi acompanhado o cálculo do volume de concreto necessário para a moldagem dos corpos de prova, conforme as recomendações técnicas. O traço de referência, definido em parceria com a Engemix, foi composto por cimento CP II E 40, sílica, agregados miúdos e graúdos, aditivo superplastificante e relação água/cimento de 0,5. Para a produção dos concretos pigmentados, foi incorporado 10% (máximo permitido pela norma) de pigmento preto à base de Fe_3O_4, em relação à massa de cimento, resultando em três misturas distintas: concreto de referência (sem pigmento), concreto com pigmento A e concreto com pigmento B (Tabela 1). os valores apresentados correspondem à dosagem laboratorial proporcional.

Tabela 1 – Traços dos concretos de referência e coloridos

Amostra	Água (g)	CP II E 40 SH (g)	Sílica (g)	Brita 0 (g)	Brita 1 (g)	Areia de quartzo (g)	Areia de brita (g)	Aditivo super-plastifi-cante (%)	Pig-mento A (%)	Pig-mento B (%)
Concreto de referência (sem pigmento)	1850	3590	110	7630	850	3940	6230	27.41	-	-
Concreto com Pigmento A	1850	3590	110	7630	850	3940	6230	48.53	10	-
Concreto com Pigmento B	1850	3590	110	7630	850	3940	6230	38.25	-	10

(Fonte: autores)

Neste estudo, foram empregados dois pigmentos de Fe_3O_4 provenientes de fornecedores distintos, os quais foram caracterizados no IPT- Instituto de Pesquisas Tecnológicas por meio de espectrometria de fluorescência de raios X, com leitura direta na superfície do material. (ABNT NBR 14656:2023) - Tabela 2:

Tabela 2 – Composição química dos pigmentos A e B

Determinação	Pigmento A	Pigmento B
Óxido de Ferro (Fe3O4)	74,1	97,3
Óxido de Titânio (TiO2)	3,9	Não detectado
Dióxido de Silício (SiO2)	4,4	1,5
Óxido de Cálcio (CaO)	7,2	0,1
Óxido de Alumínio (Al2O3)	0,9	0,1
Trióxido de Enxofre (SO3)	3	Não detectado
Óxido de Magnésio (MgO)	4,6	Não detectado
Óxido de Zinco (ZnO)	0,1	< 0,1
Óxido de Estrôncio (SrO)	0,1	Não detectado
Óxido de Manganês (MnO)	0,6	0,2
Óxido de Cromo (Cr2O3)	0,1	0,1
Óxido de Fósforo (P2O5)	0,8	0,4
Óxido de Zircônio (ZrO2)	< 0,1	Não detectado
Óxido de Rubídio (Rb2O)	< 0,1	Não detectado
Óxido de Níquel (NiO)	< 0,1	< 0,1
Óxido de Nióbio (Nb2O5)	< 0,1	Não detectado
Óxido de Cobre (CuO)	< 0,1	0,2
Óxido de Molibdênio (MoO3)	Não detectado	< 0,1
Óxido de Potássio (K2O)	0,2	Não detectado
Óxido de Chumbo (PbO)	Não detectado	< 0,1
Óxido de Vanádio (V2O5)	0,2	Não detectado

(Fonte: autores)

Segundo a composição química observada e a classificação de Bondioli et al., os dois pigmentos analisados podem ser considerados inorgânicos, pois não possuem carbono em sua composição. O pigmento A pode ser classificado como inorgânico natural, por apresentar menor grau de pureza, enquanto o pigmento B corresponde a um pigmento inorgânico sintético, obtido por meio de processamento químico. Em ambos os casos, o principal componente identificado é o Fe_3O_4, óxido de ferro (II, III), embora o pigmento A apresente maiores teores de outros óxidos em comparação ao pigmento B.

Após a concretagem, os corpos de prova foram submetidos à cura inicial em tanque de imersão por 24 horas, assegurando hidratação adequada e preservação da cor superficial. Em seguida, foram desformados e mantidos em ambiente controlado para cura posteriormente, parte das placas recebeu aplicação de hidrofugante à base de silano/siloxano no canteiro experimental da FAU, aplicado em três demãos, com a finalidade de avaliar comparativamente o desempenho estético e a durabilidade de superfícies protegidas e não protegidas (Figura 3).



Figura 3 – Corpos de prova de concreto pigmentado preto sendo aspergidos com hidrofugante (Fonte: autores)

3.2 Caracterização dos materiais

A caracterização do concreto no estado fresco foi realizada conforme as normas ABNT NBR 15823-2:2017 (cone de Abrams), NBR 15823-3:2017 (anel J), NBR 15823-4:2017 (caixa L), NBR 15823-5:2018 (funil V) e NBR 16887:2020 (teor de ar) (Figura 4)

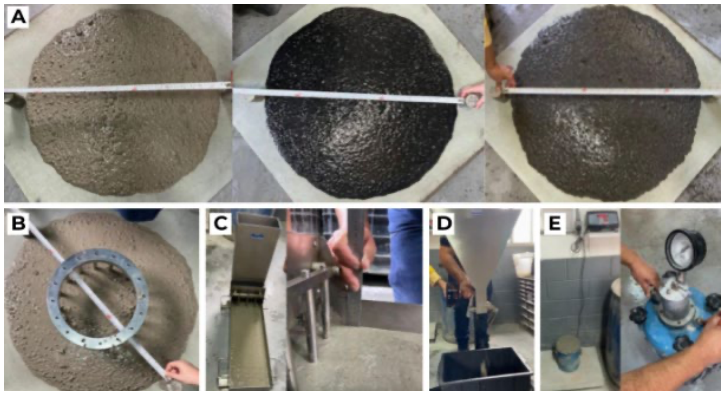


Figura 4 – Caracterização do concreto produzido em estado fresco. A, cone de Abrans; B, anel J; C, Caixa L; D, funil V; E; análise do teor de ar incorporado. (Fonte: autores)

No estado endurecido, foram realizados ensaios de compressão axial aos 7 e 28 dias, conforme a NBR 5739:2018, além de ensaios de absorção de água, índice de vazios e massa específica (NBR 9778:2005) e absorção por capilaridade (ABNT NBR 9779:2012) (Figura 5).

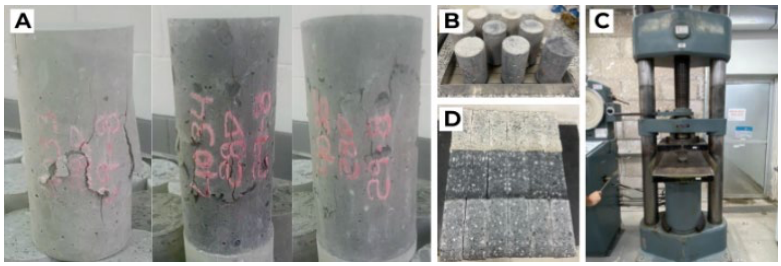


Figura 5 –Caracterização do concreto no estado endurecido: A) corpos de prova rompidos aos 28 dias; B) ensaio de absorção por capilaridade; C) ensaio de compressão diametral; D) corpos de prova após ruptura diametral e linha limite de distribuição. (Fonte: autores)

3.3 Estudo do envelhecimento acelerado e avaliação cromática das amostras

O ensaio de envelhecimento acelerado foi realizado em câmara de radiação ultravioleta (CUV), com o objetivo de simular, em intervalo reduzido, os efeitos da radiação solar e da umidade sobre o concreto pigmentado. O procedimento seguiu a ABNT NBR 15.380:2015, com ciclos alternados de quatro horas de radiação UVB e quatro horas de condensação, em câmara c-UVB, no LMCC/IPT. Os corpos de prova foram submetidos a ciclos de 150 horas, sendo retirados ao final de cada ciclo para estabilização térmica em ambiente protegido da luz e posterior análise por espectrofotometria. A duração total do ensaio foi de

aproximadamente 4553 horas, equivalente a cerca de 15 anos de degradação (Figura 6), permanecendo as amostras ainda em monitoramento.

A avaliação cromática foi realizada por espectrofotometria, utilizando o sistema CIE L*a*b* (CIELAB)[1], com quantificação da variação de cor por meio do parâmetro ΔE. As medições foram realizadas com espectrofotômetro da marca 3nh, operando com o software SQCX Color Quality Control, utilizando observador padrão CIE de 10° e iluminante D65, sem consideração do componente de reflexão especular (SCE) (Figura 6).



Figura 6 – A, placas dispostas na câmara de radiação ultravioleta (CUV), LMCC/IPT; B, Espectrofotômetro 3nh executando medição de placa; C, gabarito empregados nas aferições das placas de concreto com o espectrofotômetro (Fonte: autores)

4. Resultados e Discussões

Com relação ao ensaio de *slump-flow,* o concreto de referência apresentou classe SF2 (750 mm), enquanto os concretos pigmentados atingiram SF3 (≥ 760 mm), conforme a ABNT NBR 15823-1:2017.

Tabela 3 – Média de espalhamento, em mm, e quantidade de aditivo superplastificante, em ml, em cada mistura de concreto

Amostra	Slump flow (mm)			t500 (s)	VSI *		Amostra	Espalhamento médio (mm)	Dosagem de superplastificante (mL)	Classe de espalhamento
	Ensaio 1	Ensaio 2	Média do espalhamento							
Concreto de referência (sem pigmento	730	770	750	4	0		Concreto de referência (sem pigmento)	750	93,3	SF2
Concreto com Pigmento A	760	760	760	3	0		Concreto com Pigmento A	760	165,2	SF3
Concreto com Pigmento B	780	770	775	4	0		Concreto com Pigmento B	775	130,2	SF3

* VSI - sigla em inglês para *Visual Stability Index*, correspondente ao Índice de Estabilidade Visual (Fonte: autores)

Apesar da maior fluidez, todos os concretos apresentaram IEV igual a 0, indicando elevada estabilidade, sem segregação ou exsudação, evidenciando adequado equilíbrio entre fluidez e coesão. No ensaio de

[1] L* (Luminosidade): Controla o claro/escuro. Vai de (0) (preto absoluto) a (100) (branco perfeito); a*: Controla o espectro verde-vermelho. Valores negativos indicam tons de verde e valores positivos indicam tons de vermelho. b*: Controla o espectro azul-amarelo. Valores negativos representam azul e valores positivos representam amarelo.

viscosidade, todas as misturas foram classificadas como VS2, indicando que a incorporação dos pigmentos não alterou significativamente o comportamento reológico global (Tabela 4).

Tabela 4 – Resultados do ensaio de espalhamento e estabilidade visual do concreto autoadensável.

Amostra	Média de espalhamento (mm)	Classe de espalhamento/ *Slump-flow*	t500 (s)	Funil V (s)	Classe de viscosidade plástica	IEV
Concreto de referência (sem pigmento)	750	SF 2	4	12:11	VS 2/VF 2	0
Concreto com Pigmento A	760	SF 3	3	-	VS 2	0
Concreto com Pigmento B	775	SF 3	4	-	VS 2	0

(Fonte: autores)

Os ensaios de habilidade passante realizados no concreto de referência (anel J e caixa L) indicaram bom desempenho (PJ1 e PL2) conforme a Tabela A.3 da NBR 15823-1:2017, sugerindo adequada capacidade de escoamento em meios confinados. Considerando a similaridade reológica, infere-se comportamento semelhante para os concretos pigmentados.

A análise do teor de ar incorporado (Tabela 5) evidenciou diferenças relevantes, com destaque para o concreto com pigmento A, que apresentou teor de ar de 6,5% e redução da massa específica. Esse resultado indica possível interferência do pigmento na estabilidade das bolhas de ar, o que pode impactar propriedades no estado endurecido. Já o pigmento B apresentou comportamento mais próximo ao concreto de referência.

Tabela 5 – Massa específica e teor de ar do concreto fresco (método pressométrico)

Amostra	Média de espalhamento "*Slump-flow*" (mm)	Amostra ensaiada – Teor de Ar Aparente (A1)	Massa específica (kg/m³)
Concreto de referência (sem pigmento)	750	SF 2	4
Concreto com Pigmento A	760	SF 3	3
Concreto com Pigmento B	775	SF 3	4

(Fonte: autores)

A Tabela 6 apresenta os resultados dos ensaios de resistência à compressão dos corpos de prova cilíndricos, bem como os valores de massa específica, absorção de água e índice de vazios. Aos 7 dias, o concreto de referência apresentou resistência média de 48,2 MPa, enquanto os concretos pigmentados apresentaram valores inferiores, sendo 37,0 MPa para o concreto com pigmento A e 41,9 MPa para o concreto com pigmento B, evidenciando redução mais acentuada na mistura com pigmento A. Aos 28 dias, observa-se o ganho de resistência em todas as misturas, com o concreto de referência atingindo 66,5 MPa, enquanto os concretos com pigmento A e B apresentaram resistências médias de 54,3 MPa e 54,6 MPa, respectivamente, indicando aproximação entre os concretos pigmentados nessa idade.

De modo geral, os resultados demonstram que a incorporação de pigmentos reduz a resistência à compressão em relação ao concreto de referência, especialmente em idades iniciais, embora essa diferença diminua ao longo do tempo, sugerindo tendência de estabilização do desempenho mecânico.

Tabela 6 – Propriedades mecânicas e físicas do concreto endurecido”

a) Resistência à compressão aos 7 e 28 dias.

Ensaio	Amostra	CP	Resistência à compressão (MPa)	Média (MPa)
Compressão axial 7 dias	Concreto de referência (sem pigmento)	1	47,7	48,2
		2	48,7	
		3	48,2	
	Concreto com pigmento A	4	38,8	37
		5	37	
		6	36,6	
	Concreto com pigmento B	7	41,1	41,19
		8	42,1	
		9	41,9	
Compressão axial 28 dias	Concreto de referência (sem pigmento)	10	66,4	66,5
		11	66,5	
		12	67,9	
	Concreto com pigmento A	13	54,3	54,3
		14	53,2	
		15	54,8	
	Concreto com pigmento B	16	54,4	54,6
		17	54,6	
		18	55,2	

b) Absorção de água, índice de vazios e massa específica

Amostra	CP	Massa específica			Absorção de água (%)	Índice de vazios (%)
		Seca (ρs)	Saturada (ρsat)	Real (ρr)		
Concreto de referência (sem pigmento)	1	2,42	2,49	2,61	2,90	7,10
	2	2,44	2,50	2,60	2,5	6,20
	Média	**2,43**	**2,50**	**2,61**	**2,70**	**6,70**
	Desvio	0,01	0,01	0,01	0,28	0,64
Concreto com pigmento A	1	2,35	2,44	2,56	3,50	8,20
	2	2,38	2,45	2,56	3,00	7,20
	Média	**2,37**	**2,45**	**2,56**	**3,30**	**7,70**
	Desvio	0,02	0,01	0,0	0,40	0,70
Concreto com pigmento B	1	2,44	2,51	2,62	2,90	7,10
	2	2,43	2,50	2,60	2,70	6,50
	Média	**2,44**	**2,51**	**2,61**	**2,80**	**6,80**
	Desvio	0,01	0,01	0,01	0,10	0,40

(Fonte: autores)

Com relação a absorção de água e índice de vazios dos corpos de prova, observa-se que os valores de massa específica foram semelhantes entre as misturas, com cerca de 2,61 g/cm³ para o concreto de referência e com pigmento B, e 2,56 g/cm³ para o concreto com pigmento A. Em relação à absorção de água e ao índice de vazios, o concreto com pigmento A apresentou os maiores valores (3,30% e 7,70%), enquanto o concreto com pigmento B apresentou comportamento próximo ao concreto de referência (2,80% e 6,80% contra 2,70% e 6,70%). De modo geral, os resultados indicam que o pigmento A promoveu leve aumento da porosidade, enquanto o pigmento B manteve comportamento semelhante ao concreto de referência.

Os resultados do ensaio de absorção de água por capilaridade indicaram comportamento semelhante entre os concretos analisados, com aumento progressivo da absorção ao longo do tempo. Para o concreto de referência, os valores médios variaram de 0,13 g/cm² (3 h) a 0,33 g/cm² (72 h), com altura média de ascensão capilar de 3,54 cm. O concreto com pigmento A apresentou valores ligeiramente inferiores nas primeiras idades, variando de 0,12 g/cm² (3 h) a 0,36 g/cm² (72 h), e altura média de 3,21 cm. Já o concreto com pigmento B apresentou os maiores valores de absorção, variando de 0,17 g/cm² (3 h) a 0,44 g/cm² (72 h), com altura média de 3,57 cm. De modo geral, observou-se que o concreto com pigmento A apresentou

menor absorção de água, enquanto o concreto com pigmento B apresentou maior capilaridade. Apesar dessas diferenças, os valores obtidos foram próximos, indicando comportamento compatível entre as misturas. Adicionalmente, verificou-se maior variabilidade nos resultados do concreto com pigmento A, com desvio de aproximadamente 0,5 cm na altura de ascensão capilar, enquanto o concreto com pigmento B apresentou comportamento mais uniforme.

Embora não tenham sido aplicados testes estatísticos inferenciais, os valores médios e os desvios obtidos permitem avaliar a tendência de comportamento das misturas. Nos ensaios de compressão, observou-se baixa dispersão entre os corpos de prova de uma mesma composição, o que reforça a consistência dos resultados. A redução da resistência à compressão nos concretos pigmentados foi mais expressiva aos 7 dias, correspondendo a aproximadamente 23% para o pigmento A e 13% para o pigmento B em relação ao concreto de referência. Aos 28 dias, essa diferença diminuiu, com reduções próximas de 18% para ambos os concretos pigmentados, indicando maior aproximação do desempenho mecânico com o avanço da idade.

Conforme apresentado na Figura 7, são ilustradas as placas de concreto utilizadas na análise colorimétrica, correspondentes às amostras avaliadas, incluindo o concreto de referência e os concretos pigmentados com pigmentos A e B, com e sem aplicação de hidrofugante, após os ciclos de envelhecimento acelerado.

Os resultados foram analisados por média e desvio padrão, não sendo aplicados testes estatísticos inferenciais devido ao número reduzido de amostras.



Figura 7 – Placas durante o ensaio de envelhecimento acelerado (com pigmento A, referência e com pigmento B, com e sem hidrofugante, respectivamente e da esquerda para a direita) (Fonte: autores)

4.1 Análise dos resultados cromáticos pelo sistema CIELAB e da diferença de cor (ΔE)

Os resultados obtidos a partir do sistema CIELAB permitiram avaliar a evolução cromática das amostras ao longo do envelhecimento acelerado, considerando os parâmetros L* (luminosidade), a* (eixo verde–vermelho), b* (eixo azul–amarelo) e a diferença total de cor ΔE*. A análise comparativa entre as amostras com e sem hidrofugante demonstrou que o envelhecimento acelerado influenciou principalmente os parâmetros L* e b*, enquanto o parâmetro a* permaneceu relativamente estável durante todo o período experimental.

4.1.1 Análise das amostras sem hidrofugante

O concreto de referência apresentou os maiores valores de luminosidade (L*) entre todas as amostras, variando aproximadamente de 59,7 a 65,2 ao longo do envelhecimento acelerado. Observa-se tendência gradual de aumento de L*, especialmente após aproximadamente 3000 horas de exposição UVB, indicando clareamento superficial progressivo da matriz cimentícia.

No parâmetro b*, os valores permaneceram positivos e elevados, variando aproximadamente entre 6,4 e 8,0, indicando predominância de tonalidade amarelada característica da pasta cimentícia. Nota-se redução gradual do parâmetro b* ao longo do tempo, sugerindo diminuição da componente amarela superficial devido à exposição à radiação ultravioleta e aos ciclos de condensação.

O parâmetro a* apresentou pequenas variações próximas da neutralidade cromática, mantendo-se entre aproximadamente 0,3 e 0,6, evidenciando baixa influência do envelhecimento sobre o eixo verde–vermelho.

Quanto à diferença total de cor (ΔE*), o concreto de referência sem hidrofugante apresentou aumento progressivo ao longo do envelhecimento, partindo de aproximadamente 0,5 e atingindo valores próximos de 4,2 ao final de 4553 horas. Esse comportamento demonstra que, mesmo sem pigmentação, a matriz cimentícia sofre alterações cromáticas perceptíveis ao longo do envelhecimento acelerado.

O concreto contendo pigmento A apresentou os menores valores de luminosidade (L*), permanecendo predominantemente entre 32,5 e 34,8 durante todo o ensaio, caracterizando superfície visualmente mais escura e com menor tendência ao clareamento quando comparado às demais amostras.

O parâmetro a* apresentou valores muito próximos da neutralidade cromática, oscilando discretamente em torno de 0,0, indicando baixa alteração no eixo verde–vermelho ao longo do envelhecimento.

Já o parâmetro b* apresentou valores negativos, aproximadamente entre -0,5 e 0,0, indicando tendência à tonalidade azulada. Observam-se oscilações mais acentuadas nesse parâmetro quando comparadas ao concreto de referência e ao pigmento B, sugerindo maior instabilidade cromática superficial.

A análise da diferença total de cor (ΔE*) demonstra comportamento relativamente estável nas primeiras etapas do envelhecimento, com valores entre aproximadamente 1,3 e 2,1 até cerca de 3000 horas de exposição. Entretanto, após esse período, observa-se aumento progressivo de ΔE*, atingindo valores próximos de 3,0 ao final do ensaio. Esse comportamento indica que as alterações cromáticas se tornam mais significativas nos estágios mais avançados do envelhecimento acelerado.

O concreto produzido com pigmento B apresentou comportamento intermediário de luminosidade, com valores de L* variando aproximadamente entre 36,5 e 44,5. Observa-se redução inicial significativa de L* nos primeiros ciclos de envelhecimento, seguida de relativa estabilização e posterior aumento gradual da luminosidade ao longo do tempo.

O parâmetro a* permaneceu praticamente constante, com valores próximos de 0,3 a 0,5, indicando elevada estabilidade no eixo verde–vermelho.

No parâmetro b*, os valores permaneceram próximos da neutralidade cromática, variando aproximadamente entre 0,0 e 1,0. Comparativamente ao pigmento A, o pigmento B apresentou menores oscilações no eixo azul–amarelo, evidenciando maior estabilidade cromática superficial.

Em relação à diferença total de cor (ΔE*), o concreto com pigmento B apresentou os maiores valores iniciais entre os concretos pigmentados, atingindo aproximadamente 7,8 nas primeiras 500 horas de envelhecimento. Contudo, observa-se redução progressiva de ΔE* ao longo do tempo, alcançando valores próximos de 3,0 ao final do ensaio. Esse comportamento sugere que as alterações cromáticas iniciais foram mais intensas, seguidas de estabilização gradual da superfície pigmentada.

4.1.2 Análise das amostras com hidrofugante

Nas amostras protegidas com hidrofugante, o concreto de referência apresentou aumento contínuo do parâmetro L*, variando aproximadamente de 65 para 69, indicando clareamento superficial mais pronunciado quando comparado às amostras sem proteção.

O parâmetro b* apresentou redução gradual de aproximadamente 6,6 para valores próximos de 5,3, demonstrando diminuição da componente amarela ao longo do envelhecimento.

O parâmetro a* permaneceu estável, com pequenas oscilações próximas de 0,3.

Quanto à diferença de cor ΔE*, observa-se crescimento contínuo durante o envelhecimento acelerado, atingindo valores próximos de 4,1 ao final do ensaio, comportamento semelhante ao observado nas amostras sem hidrofugante.

O concreto com pigmento A protegido com hidrofugante apresentou valores de L* entre aproximadamente 34 e 38, com leve aumento de luminosidade ao longo do envelhecimento acelerado.

O parâmetro a* permaneceu próximo da neutralidade cromática, enquanto o parâmetro b* manteve valores negativos, variando aproximadamente entre -1,6 e -0,8, indicando persistência da tonalidade azulada superficial.

Em relação ao ΔE*, observa-se comportamento relativamente estável durante grande parte do envelhecimento, com valores inferiores a 2,0 até aproximadamente 3000 horas de exposição. Entretanto, após esse período, ocorre aumento gradual dos valores, atingindo aproximadamente 2,9 ao final do ensaio. Comparativamente às amostras sem hidrofugante, não se observa redução significativa das alterações cromáticas totais, indicando limitada eficiência do tratamento superficial nesse sistema pigmentado.

O concreto contendo pigmento B e protegido com hidrofugante apresentou o comportamento cromático mais estável entre todas as amostras analisadas.

Os valores de L* permaneceram relativamente estáveis, variando aproximadamente entre 41 e 46, com menores oscilações ao longo do envelhecimento quando comparados às amostras sem proteção superficial.

O parâmetro a* apresentou elevada estabilidade próximo da neutralidade cromática, enquanto o parâmetro b* permaneceu entre aproximadamente -0,1 e 0,4, indicando mínima alteração no eixo azul–amarelo.

A diferença total de cor ΔE* apresentou redução progressiva ao longo do envelhecimento acelerado, passando de aproximadamente 3,8 nas primeiras 500 horas para valores próximos de 1,1 ao final do ensaio. Esse comportamento evidencia elevada estabilidade cromática superficial e demonstra que a aplicação do hidrofugante contribuiu significativamente para minimizar as alterações cromáticas do concreto pigmentado com pigmento B.

4.1.3 Análise comparativa geral

A análise integrada dos resultados demonstra que o envelhecimento acelerado afetou principalmente os parâmetros L* e b*, enquanto o eixo a* permaneceu relativamente estável em todas as misturas.

O concreto de referência apresentou tendência de clareamento progressivo da superfície, com aumento de luminosidade e redução gradual da componente amarela ao longo do tempo. Entre os concretos pigmentados, o pigmento A apresentou maior instabilidade cromática no parâmetro b* e maiores oscilações superficiais durante o envelhecimento.

Por outro lado, o pigmento B apresentou o comportamento cromático mais estável, especialmente quando associado à aplicação do hidrofugante. A redução progressiva dos valores de ΔE* ao longo do envelhecimento indica maior estabilidade óptica e menor susceptibilidade às alterações superficiais induzidas pela radiação UV e pela umidade.

De forma geral, os resultados demonstram que a durabilidade cromática dos concretos pigmentados depende da interação entre composição mineralógica do pigmento, estabilidade dos parâmetros CIELAB, porosidade da matriz cimentícia e eficiência da proteção superficial. Entre os materiais analisados, o sistema contendo pigmento B associado ao hidrofugante apresentou o melhor desempenho global quanto à estabilidade cromática e resistência às alterações superficiais provocadas pelo envelhecimento acelerado (Figura 8).

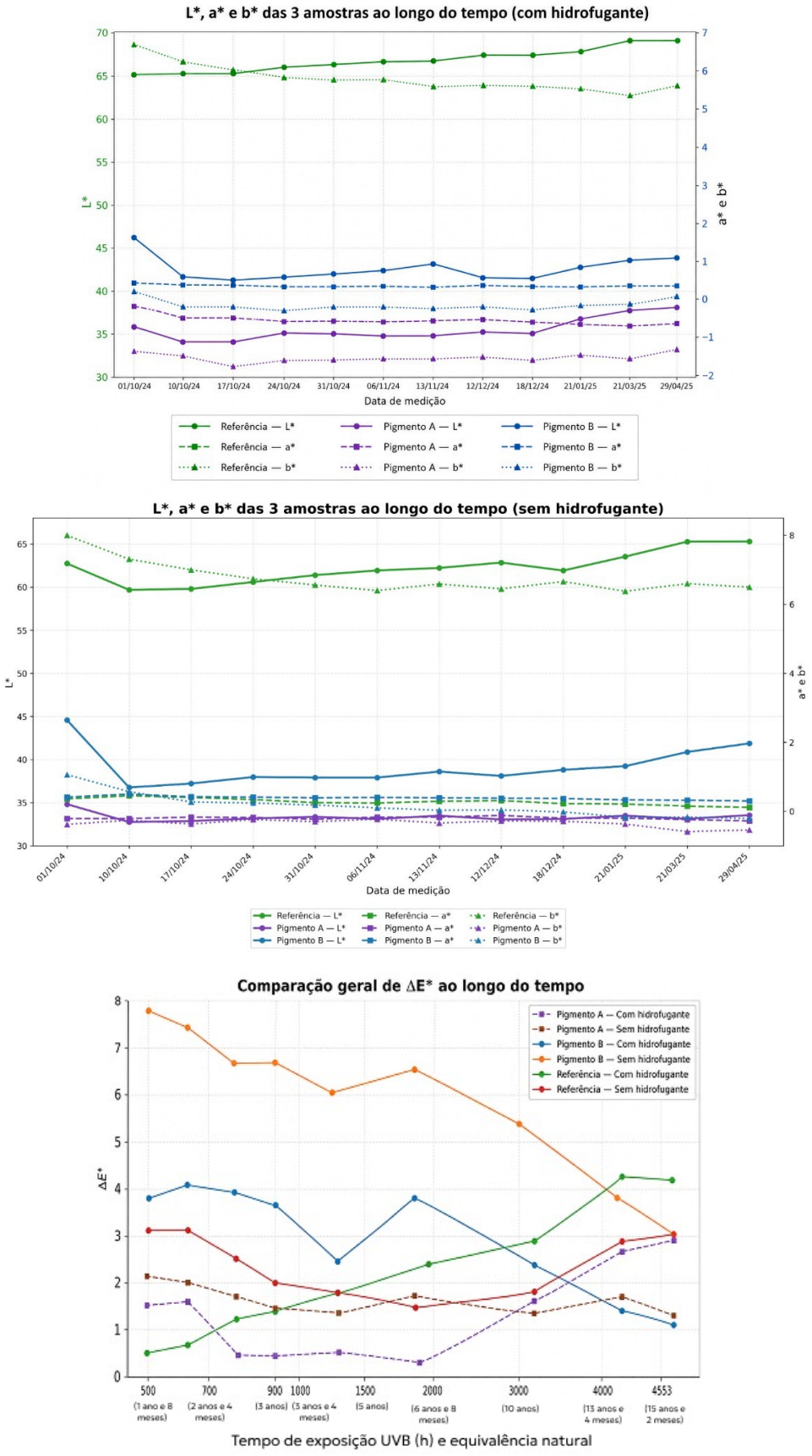


Figura 8 – Análise do envelhecimento acelerado das placas de concreto. (Fonte: autores)

5. Conclusões

Conclui-se que a incorporação de pigmentos pretos à base de Fe_3O_4 em concretos autoadensáveis apresentou desempenho satisfatório quanto à durabilidade estética e viabilidade tecnológica para aplicações arquitetônicas aparentes expostas ao intemperismo. Os ensaios de envelhecimento acelerado, realizados durante aproximadamente 4553 horas em câmara UV - equivalentes a cerca de 15 anos de exposição natural simulada - demonstraram que as alterações cromáticas variaram conforme a composição química dos pigmentos e a aplicação do hidrofugante.

A análise pelo sistema CIELAB indicou que os parâmetros mais afetados pelo envelhecimento foram L* e b*, enquanto o parâmetro a* permaneceu relativamente estável em todas as amostras, com variações inferiores a aproximadamente ±0,5. O concreto de referência apresentou aumento gradual da luminosidade (L*), variando aproximadamente entre 59,7 e 69,1, associado ao clareamento superficial da matriz cimentícia, enquanto o parâmetro b* reduziu de aproximadamente 7,8 para 5,3, indicando diminuição da componente amarelada ao longo do envelhecimento.

Entre os concretos pigmentados, o pigmento A apresentou os menores valores de luminosidade, com L* variando aproximadamente entre 32,5 e 38,2, além de maior instabilidade no parâmetro b*, cujos valores oscilaram entre -1,6 e 0,0. Já o pigmento B apresentou comportamento cromático mais estável, com L* variando entre aproximadamente 36,5 e 46,3 e b* próximo da neutralidade cromática, entre -0,1 e 1,0.

A análise da diferença total de cor (ΔE*) demonstrou comportamentos distintos entre os sistemas analisados. O concreto com pigmento B sem hidrofugante apresentou os maiores valores iniciais de ΔE*, atingindo aproximadamente 7,8 nas primeiras 500 horas de envelhecimento, porém com redução progressiva até cerca de 3,0 ao final do ensaio. Nas amostras contendo pigmento B com hidrofugante, o ΔE* reduziu de aproximadamente 3,8 para 1,1, evidenciando elevada estabilidade cromática e maior eficiência da proteção superficial. Em contrapartida, o concreto com pigmento A apresentou ΔE* relativamente estável até aproximadamente 3000 horas, seguido de aumento gradual até valores próximos de 3,0, independentemente da aplicação do hidrofugante.

As diferenças de desempenho observadas estão associadas à composição química dos pigmentos. O pigmento B apresentou teor de Fe_3O_4 de 97,3%, enquanto o pigmento A apresentou 74,1% e maior presença de óxidos secundários, o que provavelmente contribuiu para maior instabilidade óptica e maior susceptibilidade às alterações cromáticas superficiais.

Do ponto de vista mecânico, os concretos pigmentados apresentaram redução da resistência à compressão em relação ao concreto de referência. Aos 7 dias, as resistências médias foram de 48,2 MPa para o concreto de referência, 37,0 MPa para o concreto com pigmento A e 41,9 MPa para o concreto com pigmento B. Aos 28 dias, os concretos pigmentados atingiram aproximadamente 54 MPa, enquanto o concreto de referência apresentou 66,5 MPa.

Os ensaios físicos indicaram maior absorção de água e índice de vazios no concreto com pigmento A (3,5% e 8,2%) em comparação ao concreto de referência (2,7% e 6,7%), enquanto o concreto com pigmento B apresentou desempenho intermediário, com absorção próxima de 3,0% e índice de vazios de 7,2%.

De forma geral, os resultados demonstram que o concreto produzido com pigmento B associado ao hidrofugante apresentou o melhor desempenho global, combinando menores variações de ΔE*, maior estabilidade dos parâmetros L*, a* e b*, menor absorção de água e comportamento mecânico mais próximo ao concreto de referência, demonstrando maior potencial para aplicação em concretos arquitetônicos aparentes submetidos à exposição ambiental prolongada.

Referências

ABNT – ASSOCIAÇAO BRASILEIRA DE NORMAS TÉCNICAS**. ABNT NBR 16887:2020 – Determinação do teor de ar em concreto fresco. Método pressométrico**. Rio de Janeiro. ABNT, 2020.

ABNT – ASSOCIAÇAO BRASILEIRA DE NORMAS TÉCNICAS. **ABNT NBR 5739:2018 - Ensaio de compressão de corpos de prova cilíndricos.** Rio de Janeiro. ABNT, 2018.

ABNT – ASSOCIAÇAO BRASILEIRA DE NORMAS TÉCNICAS**. NBR 15380:2015 - Tintas para construção civil — Método para avaliação de desempenho de tintas para edificações não industriais — Resistência à radiação UV e à condensação de água pelo ensaio acelerado.** Rio de Janeiro. ABNT, 2015.

ABNT – ASSOCIAÇAO BRASILEIRA DE NORMAS TÉCNICAS. **NBR 15823-2:2017 – Ensaio de determinação do espalhamento pelo Método do Cone de Abrams**. Rio de Janeiro. ABNT, 2017.

ABNT – ASSOCIAÇAO BRASILEIRA DE NORMAS TÉCNICAS**. NBR 15823-3:2017 – Concreto autoadensável. Parte 3: Determinação da habilidade passante – Método do anel J.** Rio de Janeiro. ABNT, 2017.

ABNT – ASSOCIAÇAO BRASILEIRA DE NORMAS TÉCNICAS**. NBR 15823-4:2017 – Concreto autoadensável. Parte 4: Determinação da habilidade passante – Métodos da caixa L e da caixa U.** Rio de Janeiro. ABNT, 2017.

ABNT – ASSOCIAÇAO BRASILEIRA DE NORMAS TÉCNICAS**. NBR 15823-5:2018 – Concreto Autoadensável - Parte 5: Determinação da viscosidade - Método do funil V.** Rio de Janeiro. ABNT, 2018.

ABNT – ASSOCIAÇAO BRASILEIRA DE NORMAS TÉCNICAS**. NBR 16846:2020 – Cimento Portland e outros materiais em pó– Determinação da cor e a diferença de cor por medida instrumental.** Rio de Janeiro. ABNT, 2020.

ABNT – ASSOCIAÇAO BRASILEIRA DE NORMAS TÉCNICAS**. NBR 9778:2009 – Ensaio de determinação da absorção de água, índice de vazios e massa específica (MAV)**. Rio de Janeiro. ABNT, 2009.

ABNT – ASSOCIAÇAO BRASILEIRA DE NORMAS TÉCNICAS**. NBR 9779:2013 – Ensaio de determinação da absorção de água por capilaridade.** Rio de Janeiro. ABNT, 2013.

ARCHDAILY BRASIL. **Casa Terra - Bernardes Arquitetura**. ArchDaily Brasil, 2021. Disponível em: <https://www.archdaily.com.br/br/895001/casa-terra-bernardes-arquitetura>.Acesso em: 24 mar. 2026

ARCHDAILY. **Praça das Artes / Brasil Arquitetura**, 2012. Disponível em: <https://www.archdaily.com.br/br/626025/praca-das-artes-brasil-arquitetura>. Acesso em: 22 fev. 2026

BONDIOLI, F.; MANFREDINI, T.; OLIVEIRA, A. P. N. Pigmentos inorgânicos: projeto, produção e aplicação industrial. **Cerâmica Industrial**, v. 3, n. 4-6, p. 13-17, 1998.

CHING, F. D. K. *Arquitetura: forma, espaço e ordem*. 5. ed. São Paulo: Martins Fontes, 2024

CIE – Commission Internationale de l'Éclairage. *Colorimetry*. 4rd ed. Vienna, 2018

CONSANI, C. P. **Concreto pigmentado**: técnica, cromática e durabilidade. 2022. Dissertação (Mestrado) – Universidade de São Paulo, São Paulo, 2022.

EZZELDIN, Y. **Properties of pigmented concrete**. Cairo: The American Institute of Cairo, 2021.

HARTMANN, C.; BENINI, H. Concreto Arquitetônico e Decorativo. In.: ISAIA, G. (Ed.). **Concreto: Ciência e Tecnologia**. São Paulo: Ibracon, 2011.

HELENE, P.; TERZIAN, P. *Manual de dosagem e controle do concreto*. São Paulo: PINI, 1992.

MARQUEZ, A. **Casa Terra**. Galeria da Arquitetura, 2015. Disponível em: <https://www.galeriadaarquitetura.com.br/projeto/bernardes-arquitetura/casa-terra/4571?utm_source=chatgpt.com>. Acesso em: 22 mar. 2026

MEHTA, P. K.; MONTEIRO, P. J. M. *Concrete: microstructure, properties and materials*. 4th ed. New York: McGraw-Hill, 2014.

NEVILLE, A. M. *Properties of concrete*. 5th ed. London: Pearson, 2012

RUSSO, M.M. **Proteção de superfície a base de dióxido de titânio aplicada em concretos pigmentados: eficiência, durabilidade e cromaticidade.** 2024, 243f. Dissertação (Mestrado em Arquitertura e Urbanismo) – Faculdade Arquitetura e Urbanismo, Universidade de São Paulo, São Paulo, 2024.

SYED, S. Concreto preto: Como Attilio Panzeri cria contraste com uma receita especial. Arcahdail Brasil, 2017. Disponível em: <https://www.archdaily.com.br/br/879095/concreto-preto-como-attilio-panzeri-cria-contraste-com-uma-receita-especial>. Acesso em: 20 mar. 2026.

cinpar2026
XXII International Conference on Building Pathology and Constructions Repair
15th to 17th July 2026 - Lisboa, Portugal

Band Gap Tuning of 1D Phononic Crystals for Subway Vibration Mitigation: A Parametric Study of Periodic Foundations and Barriers

Lucas L. SANTOS[1], Carlos H. COSTA[2]

[1] Federal University of Ceará, Russas, Brazil, lucasls.engcivil@gmail.com
[2] Federal University of Ceará, Russas, Brazil, carloshumberto@ufc.br

Abstract: Increasing urban expansion has intensified the challenges associated with subway-induced vibrations, which compromise human comfort and the structural integrity of adjacent buildings. As an innovative solution, one-dimensional phononic crystals (1D-PnCs) have been applied as periodic foundations and barriers, leveraging their ability to block elastic wave propagation within specific frequency ranges known as band gaps. This paper presents a parametric study of 1D-PnCs composed of alternating layers of concrete and rubber for structural vibration mitigation. Using the Transfer Matrix Method (TMM), the dispersion relations and the Frequency Response Function (FRF) of the system were analytically modeled. The methodology investigated the sensitivity of the band gaps to variations in elastic properties and geometric parameters. For practical application purposes, the optimized design was evaluated against real-world experimental Vibration Acceleration Level (VAL) spectra from two distinct subway lines. The results reveal that the dynamic behavior is predominantly governed by the impedance of the flexible inclusion and the unit cell dimensions. Calibrating the lattice constant to 0.48 m demonstrated efficacy in mitigating global low-frequency peaks below 30 Hz. Additionally, adjusting the rubber's elastic modulus enabled targeted spectral modulation: stiffening the material isolated the 6.3 Hz and 12.5 Hz peaks in Line 3, whereas reducing its stiffness optimized the blockage of a highly energetic 16 Hz peak in Line 5. It is concluded that the parametric manipulation of 1D-PnCs enables customized isolation designs, ensuring efficient vibration attenuation in civil engineering applications.

Keywords: Transfer Matrix Method; Bragg Scattering; Acoustic Impedance Contrast; Elastic Wave Propagation; Ground-Borne Vibration.

1. Introduction

Structural integrity and human comfort in civil buildings are frequently compromised by anthropogenic vibrations, particularly those induced by subway and railway traffic (Erkal; Kocagöz, 2020). With the rapid expansion of transit-oriented development (TOD) and the growing construction of buildings over or adjacent to subway stations, the control of secondary indoor vibrations has become a critical challenge in urban engineering (Xing, Zhu and Chen, 2025). Operating predominantly in low-frequency ranges from 4 to 20 Hz, these vibrations can cause issues ranging from progressive structural fatigue and material damage to severe occupant discomfort and direct interference with sensitive equipment (Jakubczyk-Galczynska; Jankowski, 2014; Zhu et al., 2014).

Over the last three decades, phononic crystals (PnCs) have emerged as a revolutionary solution for the control and manipulation of mechanical wave propagation, whether acoustic waves in fluids or elastic waves in solids (Fabro et al., 2021; Jin et al., 2025). PnCs can be defined as artificial periodic structures characterized by the spatial periodic variation of their material properties, such as density and elastic modulus (Liu; Guo; Wang, 2020). According to Maldovan and Thomas (2009) the fundamental characteristic of PnCs is the existence of acoustic band gaps (ABGs) or phononic band gaps. These ABGs consist of forbidden spectral ranges where the propagation of mechanical waves is completely suppressed, a phenomenon analogous

to the photonic band gaps (PBGs) observed in photonic crystals (Laude et al., 2009). Outside these stop bands, elastic waves can propagate freely, allowing the periodic structure to act as a natural harmonic filter (De Lima et al., 2025).

The physics behind the formation of these forbidden bands allows distinguishing two main categories of periodic structures: conventional phononic crystals and acoustic metamaterials. In conventional PnCs, band gaps are physically induced by the Bragg scattering effect. This phenomenon occurs due to the coupling between waves propagating in opposite directions, which are resonantly excited when the wave vector satisfies the Bragg condition. This leads to destructive interference in specific frequency ranges. For this mechanism to be effective, the wavelength (λ) must be comparable to the lattice constant (a), meaning $\lambda \approx 2a$. In contrast, acoustic metamaterials operate in the subwavelength regime, where $\lambda \gg a$. In these structures, the formation of gaps does not depend on spatial periodicity at the wavelength scale, but rather on local resonances within the scatterers, causing the material to exhibit effective negative properties in certain frequency ranges (Liu; Guo; Wang, 2020).

The width and position of the ABGs depend intrinsically on the geometry of the structure and, crucially, on the acoustic impedance contrast ($Z=\rho \cdot c$) between the constituent materials (Liu; Guo; Wang, 2020). Impedance is a fundamental concept that describes a material's resistance to acoustic or elastic waves (Geng; Zhu; Chong, 2018). The greater the impedance mismatch between the matrix and the scatterer, the more intense the reflections at the interfaces, functioning on the principle of destructive interference of multiple reflected waves that prevent wave transmission (Jain; Pujari; Laskar, 2021; Li et al., 2023). In this context, Kee et al. (2000) highlight that both mass density contrast and elastic constant contrast play vital roles in the formation of ABGs, as the modulation of these properties scatters the waves and impedes their transmission, resulting in sound absorption and vibration isolation effects.

Unlike traditional base isolation systems, which rely fundamentally on energy dissipation through damping or on increasing the structure's natural period, periodic foundations and barriers function as geometric filters acting at the building's base or directly within the soil (Xiong; Shi; Xiang, 2012).

However, the effectiveness of this advanced protection system relies strictly on the precise alignment (tuning) between the designed band gap frequencies and the predominant excitation frequencies of the vibration source. This tuning is achieved by manipulating the geometric and elastic properties of the unit cell (Jia; Shi, 2010).

Within this context, this paper presents an analytical-parametric study for band gap modulation in 1D-PnCs designed as periodic foundations and barriers for subway vibration mitigation. The dynamic response and dispersion relations of the periodic structure, composed of a rigid concrete matrix and flexible rubber inclusions, are analytically modeled using the Transfer Matrix Method (TMM). To validate the efficacy and practical applicability of the proposed geometric and material optimization, the design of these foundations and barriers is directly applied and evaluated against real-world experimental Vibration Acceleration Level (VAL) spectra. These spectra were recorded on Lines 3 and 5 of a subway system analyzed by Xing, Zhu and Chen (2025) demonstrating how the manipulation of internal parameters can be efficiently tuned to block critical frequencies and acceleration peaks generated by passing trains.

2. Methodology and Theoretical Model

This research adopts an analytical-parametric approach for the design of one-dimensional phononic crystals (1D-PnCs) applied as periodic foundations and barriers. The main objective is to determine, through a parametric study, the optimal combination of materials and geometries capable of mitigating subway-induced vibrations, as illustrated by the practical conceptual scheme in Figure 1(a).

The methodological procedure is divided into four main stages: (1) definition of the physical model; (2) mathematical formulation of wave propagation; (3) evaluation of the reference model against experimental spectra; and (4) parametric study for band gap tuning.

2.1 Physical Model Conception

The system was modeled as a 1D-PnC, which is characterized by the periodic spatial repetition of two layers of homogeneous solid materials: a rigid matrix (Concrete, Material A) and a flexible inclusion (Rubber, Material B). This periodic arrangement defines a fundamental unit cell of lattice constant a ($a = d_A + d_B$), as detailed in Figure 1(c). The geometric and theoretical configuration of this system is detailed in Figure 1(b).

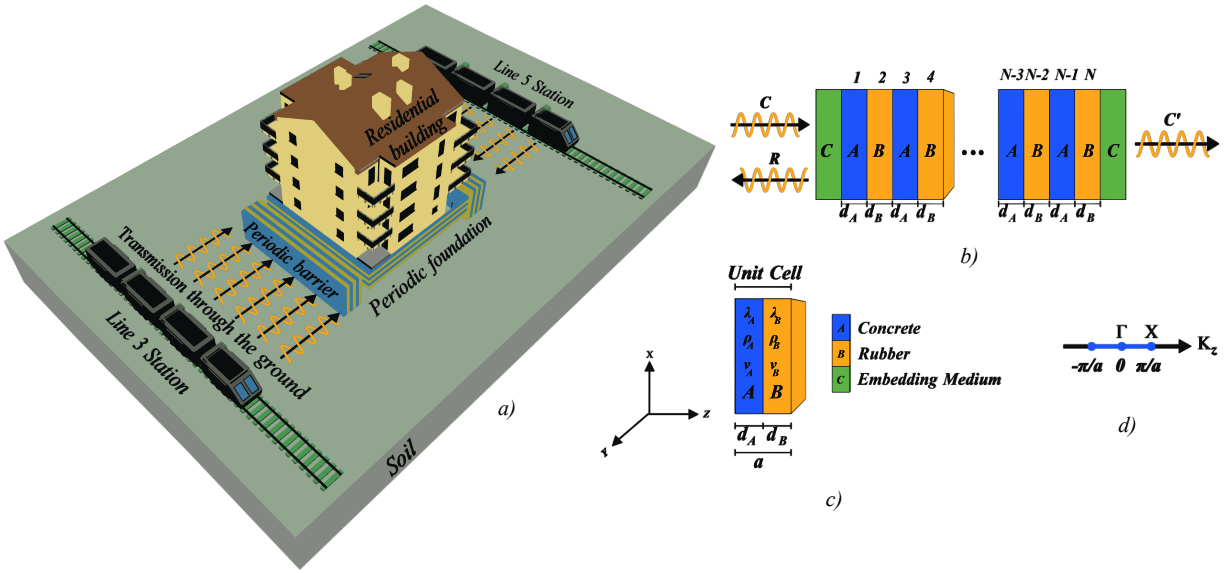


Figure 1 – Conceptual application and theoretical modeling of one-dimensional phononic crystals (1D-PnC) in civil engineering: (a) Conceptual scheme illustrating their use as periodic barriers and foundations for mitigating subway vibrations; (b) Multilayered periodic structure subjected to incident waves; (c) Fundamental two-component unit cell (concrete and rubber) highlighting material properties; (d) First irreducible Brillouin zone representation.

The performance of this system in blocking normal or oblique incident elastic waves is based on the acoustic impedance mismatch ($Z=\rho \cdot c$) between the two media, where ρ is the density and c is the wave propagation velocity in the respective material. This dynamic behavior is mapped in the first Brillouin Zone (Figure 1(d)). The velocities $c_T = \sqrt{\mu/\rho}$ and $c_L = \sqrt{(\lambda+2\mu)/\rho}$, at which transverse and longitudinal elastic waves propagate, are determined by the mechanical properties of the solid materials in question. Here $\lambda = E\nu/((1+\nu)(1-2\nu))$ and $\mu = E/(2(1+\nu))$ are the Lamé constants, where E is the Young's Modulus and ν is the Poisson's ratio, which describe the mechanical properties of the homogeneous solid material.

2.2 Transfer Matrix Method (TMM)

The dynamic response of the 1D-PnC was analytically modeled using the Transfer Matrix Method (TMM), which relates the amplitudes of elastic waves along continuous periodic media.

For the propagation of longitudinal (L) or transverse (T) waves along the z-direction, the displacement dynamics ψ in a medium j is described by the wave equation (De Lima et al., 2025).

$$\nabla^2 \psi_{\gamma,j} = \frac{1}{{c_{\gamma,j}}^2} \frac{\partial^2 \psi_j}{\partial t^2} \quad (1)$$

here $\gamma \in \{L, T\}$ and the velocity $c_{\gamma,j}$ depends on the density (ρ_j), and Lamé constants (λ_j, μ_j) of the material. The general solution superimposes the transmitted wave and the reflected wave in medium j, with amplitudes ϕ_j and $\overline{\phi}_j$.

$$\psi_j(x,y,z) = (\phi_j e^{ik_{zj}z} + \overline{\phi}_j e^{-ik_{zj}z})\, e^{i(k_{xj}x - 2\pi f t)} \quad (2)$$

The TMM establishes the continuity conditions for displacement and the stress tensor at the material interfaces, given by $\tau_{\gamma,j}(z) = \Lambda_{\gamma,j} \frac{\partial \psi_j}{\partial z}$. The term $\Lambda_{\gamma,j}$ depends on the propagation mode, where $\Lambda_{L,j} = \lambda_j + 2\mu_j$ for longitudinal waves and $\Lambda_{T,j} = \mu_j$ for transverse waves. For the transition from layer A to layer B, the interface transmission matrix (M_{AB}) is defined as:

$$\begin{pmatrix} \phi_B \\ \overline{\phi}_B \end{pmatrix} = M_{AB} \begin{pmatrix} \phi_A \\ \overline{\phi}_A \end{pmatrix} \tag{3}$$

$$M_{AB} = \frac{1}{2} \begin{pmatrix} 1 + \frac{\Lambda_{\gamma,A} K_{zA}}{\Lambda_{\gamma,B} K_{zB}} & 1 - \frac{\Lambda_{\gamma,A} K_{zA}}{\Lambda_{\gamma,B} K_{zB}} \\ 1 - \frac{\Lambda_{\gamma,A} K_{zA}}{\Lambda_{\gamma,B} K_{zB}} & 1 + \frac{\Lambda_{\gamma,A} K_{zA}}{\Lambda_{\gamma,B} K_{zB}} \end{pmatrix} \tag{4}$$

Within layer j of thickness d_j, the geometric phase shift is governed by the homogeneous propagation matrix (M_j):

$$\begin{pmatrix} \phi'_j \\ \overline{\phi'}_j \end{pmatrix} = M_j \begin{pmatrix} \phi_j \\ \overline{\phi}_j \end{pmatrix} = \begin{pmatrix} e^{-ik_{zj}d_j} & 0 \\ 0 & e^{ik_{zj}d_j} \end{pmatrix} \begin{pmatrix} \phi_j \\ \overline{\phi}_j \end{pmatrix} \tag{5}$$

The global transfer matrix of the finite structure (M) is constructed by the sequential product of the matrices representing each layer and interface. When evaluating a finite 1D-PnC with N unit cells embedded in a medium C, the boundary conditions at the entrance and exit must be accounted for. For a single unit cell (N=1), the wave transmits from medium C into layer A, propagates through layers A and B, and emerges back into medium C, yielding the global matrix $M_1 = M_{CA} M_A M_{AB} M_B M_{BC}$. For a periodic structure composed of N unit cells, the internal reflections and transmissions repeat. This periodic repetition is analytically generalized by raising the transfer matrix of the internal interfaces to the power of N-1. Thus, the generalized global transfer matrix M_N for any number of cells is defined as:

$$M_N = M_{CA} M_A M_{AB} M_B (M_{BA} M_A M_{AB} M_B)^{N-1} M_{BC} \tag{6}$$

The relationship between the wave amplitudes propagating through the entire finite structure is governed by the global transfer matrix M_N. Assuming the wave is incident from medium C, passes through the periodic structure, and exits into a semi-infinite medium C, there is no backward-propagating wave at the exit boundary. Thus, the state vectors comprising the forward (ϕ) and backward ($\overline{\phi}$) wave amplitudes at the entrance and exit are related as:

$$\begin{pmatrix} \phi'_c \\ 0 \end{pmatrix} = M_N \begin{pmatrix} \phi_c \\ \overline{\phi}_c \end{pmatrix} = \begin{pmatrix} M_{11} & M_{12} \\ M_{21} & M_{22} \end{pmatrix} \begin{pmatrix} \phi_c \\ \overline{\phi}_c \end{pmatrix} \tag{7}$$

By expanding this matrix equation, the boundary condition at the exit (0) allows us to solve for the reflected wave amplitude at the entrance as $\overline{\phi}_c = -(M_{21}/M_{22})\,\phi_c$. Substituting this relation back into the upper equation eliminates the reflected component, yielding the absolute ratio of the transmitted (ϕ'_c) to the incident (ϕ_c) wave amplitude:

$$\left| \frac{\phi'_c}{\phi_c} \right| = \left| M_{11} - \frac{M_{12} M_{21}}{M_{22}} \right| \tag{8}$$

Finally, to evaluate the vibration attenuation levels in practical engineering terms, the Frequency Response Function (FRF) is calculated in decibels (dB), following the methodologies of Cheng et al. (2020) and Zhao et al. (2021). The FRF represents the transmission loss and is defined as the logarithmic ratio of these amplitudes:

$$FRF = 20log\left(\left| \frac{\phi'_c}{\phi_c} \right| \right) = 20log \left| M_{11} - \frac{M_{12} M_{21}}{M_{22}} \right| \tag{9}$$

A negative FRF value indicates that the periodic material successfully attenuates the dynamic response, whereas a positive value represents a response amplification.

To analyze the behavior of an infinite structure, the Bloch-Floquet theorem is applied to the global matrix of a single unit cell (M'). Unlike the finite model, this matrix does not account for the external host medium, but rather the internal wave propagation cycle from one cell to the adjacent one. It encompasses the

propagation through both layers and the crossing of their internal interfaces, mathematically expressed by the product $M'= M_A M_{AB} M_B M_{BA}$. The relationship between the state vectors of adjacent cells is given by:

$$\begin{pmatrix} \phi_{l+1} \\ \dot{\phi}_{l+1} \end{pmatrix} = M' \begin{pmatrix} \phi_l \\ \dot{\phi}_l \end{pmatrix} = \begin{pmatrix} M'_{11} & M'_{12} \\ M'_{21} & M'_{22} \end{pmatrix} \begin{pmatrix} \phi_l \\ \dot{\phi}_l \end{pmatrix} \quad (10)$$

Here M' represents the global transfer matrix of a single unit cell. Therefore, the dispersion relation is obtained by applying Bloch's theorem:

$$cos(ka) = 1/2\, Tr[M'] \quad (11)$$

The dynamic spectrum of the structure is evaluated by Equation (11) at frequencies where $|1/2Tr[M']| \leq 1$, the wave vector k is real, indicating free propagation (passbands). Conversely, when $|1/2Tr[M']|>1$, k assumes a complex value, rendering the wave evanescent. These spectral regions constitute the band gaps, resulting in the blockage of vibrations.

2.3 Definition of the Reference Model

A reference unit cell model was established to evaluate the initial performance of the periodic structure against a real-world excitation scenario. The material properties adopted for the concrete and rubber are summarized in Table 1.

Table 1 – Material properties of 1D-PnC

Material	Young's Modulus	Poisson's ratio	Density
	E (Pa)	ν	ρ (kg/m³)
Concrete	25 x 10^9	0.33	2300
Rubber	0.147 x 10^6	0.463	1300

Geometrically, the reference unit cell was modeled with identical thicknesses for both layers, where d_A=d_B=0.2 m, resulting in a lattice constant a=0.4 m. To evaluate the effectiveness of this configuration, the band structures for S and P waves were calculated, and the results are illustrated in Figure 2.

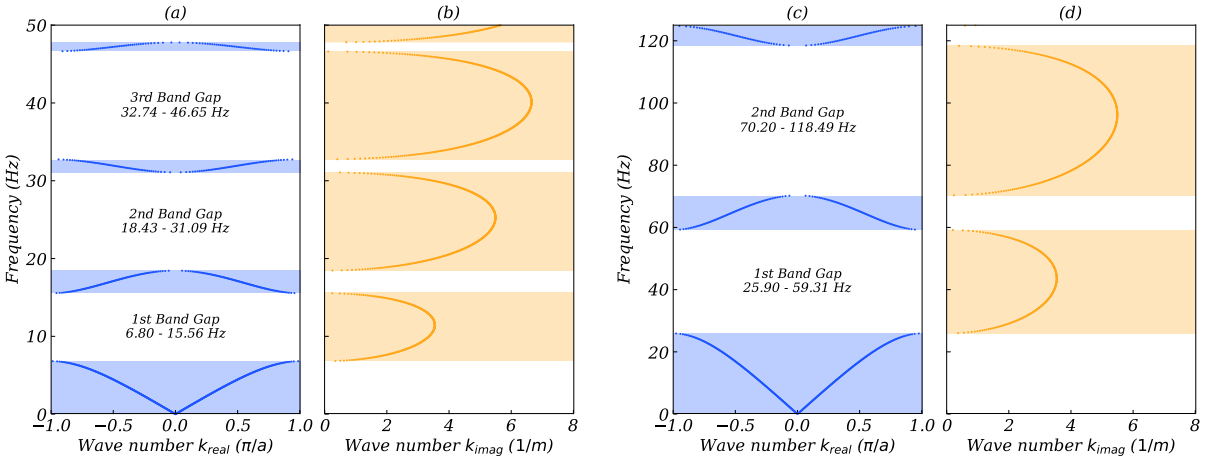


Figure 2 – Dispersion relations of the 1D phononic crystal: (a) real part (k_{Real}) and (b) imaginary part (k_{Imag}) of the wavenumber for S-waves; (c) real part (k_{Real}) and (d) imaginary part (k_{Imag}) of the wavenumber for P-waves

The objective of this evaluation was to verify whether the limits of the first two theoretical S-wave band gaps were capable of covering the predominant excitation frequencies as solution for the vibration problem. For this purpose, the experimental Vibration Acceleration Level (VAL) spectra obtained by Xing, Zhu and Chen (2025), measured on Lines 3 and 5 of a subway system in Chengdu, China, were used as the mitigation target. According to Xing, Zhu and Chen (2025), for Line 3, two peaks were observed in the vertical direction near 6.3 Hz and 12.5 Hz, with amplitudes of 85.4 dB and 84.7 dB, respectively. In the longitudinal direction, the peak occurs at 6.3 Hz with 84.8 dB, and in the horizontal direction at 8 Hz with an amplitude of 80.2 dB. For

Line 5, when the train enters the station, the highest vibration amplitude is found in the 4 Hz to 20 Hz range, reaching a peak of 86.6 dB at 16 Hz. In the 1-4 Hz and 20-80 Hz ranges, the maximum level is 70.9 dB, with a peak at 3.15 Hz.

Comparing these predominant excitation frequencies with the theoretical dispersion relations of the reference model as seen in Figure 2(a) and (b), it is observed that the initial configuration is only partially effective. The first S-wave band gap, spanning from 6.80 Hz to 15.54 Hz, successfully encompasses the horizontal peak at 8 Hz and the vertical peak at 12.5 Hz from Line 3, theoretically providing attenuation for these specific components. However, the reference structure fails to cover some critical frequency ranges. The peaks at 3.15 Hz from the Line 5 and 6.3 Hz fall entirely within the first propagation band, meaning they would pass through the structure without mitigation. Consequently, while the reference 1D-PnC demonstrates foundational potential for vibration mitigation, its band gaps are not adequately tuned to completely block the most severe train-induced vibrations. This gap in performance highlights the necessity of the proposed optimization.

2.4 Parametric Study and Target Frequency Tuning

Considering the limitations of the reference model, the core stage of the methodology consisted of a parametric study to tune the frequency ranges of the band gaps. The objective was to investigate the sensitivity of the band gaps to variations in the physical and geometric parameters. The procedure was carried out in two stages. Initially, keeping the unit cell geometry fixed (a=0.4 m), the influence of the elastic properties (E, ν) and the density (ρ) of the constituent materials was investigated. Subsequently, the internal geometric configuration of the structure was analyzed, evaluating the impact of varying the layer thickness ratio ($r = d_{Rubber}/d_{Concrete}$), the lattice constant ($a = d_{Concrete}+d_{Rubber}$), and the filling fraction ($f = d_{Rubber}/a$).

3. Results and discussion

3.1 Sensitivity Analysis of the Band Gaps to Parametric Variations

To understand how the material properties govern the behavior of the band gaps, this section presents a parametric study similar to those conducted by Jia and Shi (2010), Li et al. (2023), Witarto et al. (2016). In Figure 3, it is observed that as the value of E_{Rubber} increases, there is an upward shift in the lower and upper frequency limits of both band gaps. This occurs because an increase in E_{Rubber} raises the Lamé constants (λ e μ), consequently increasing the wave velocities c_T and c_L and the wave propagation frequencies.

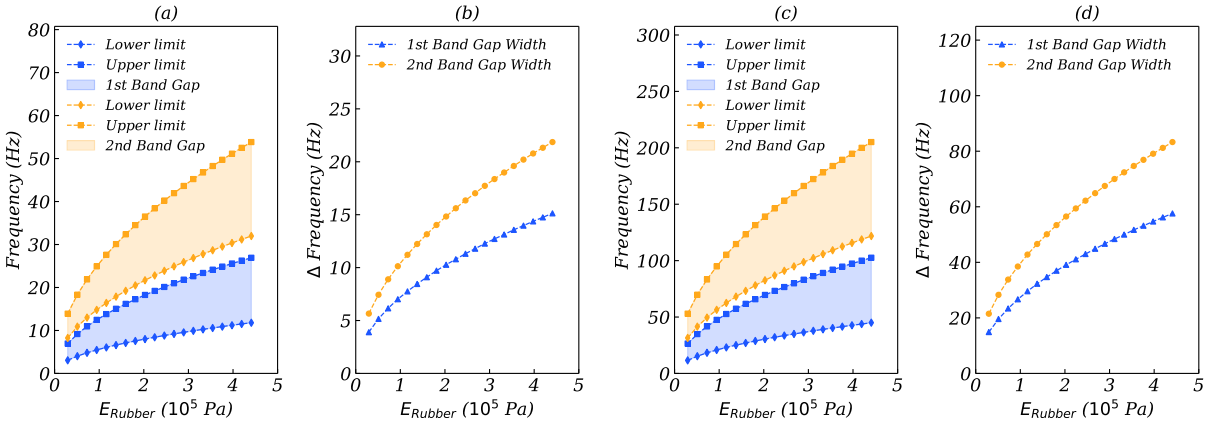


Figure 3 – Influence of the rubber Young's modulus (E_{Rubber}) on the band gap properties. (a) Frequency limits and (b) band gap width for S-waves; (c) frequency limits and (d) band gap width for P-waves

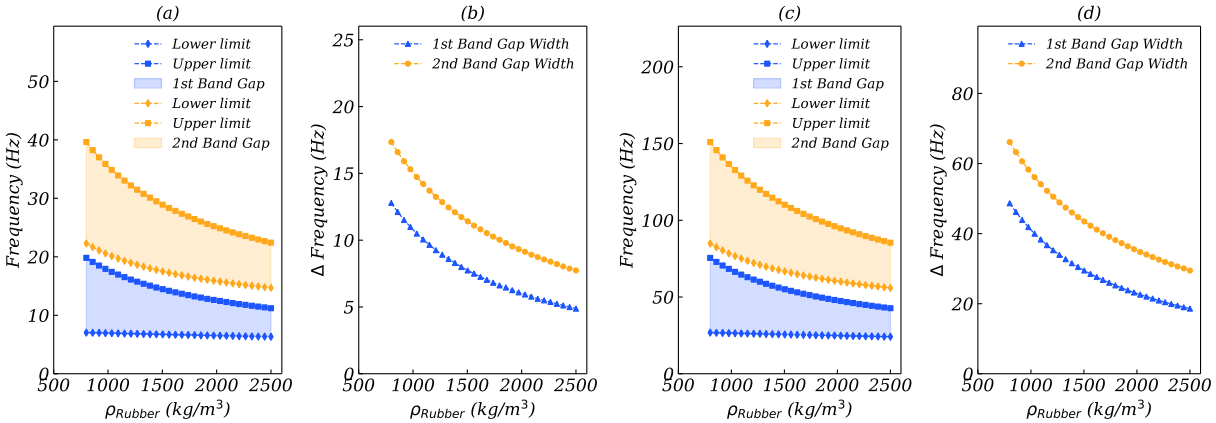


Figure 4 – Influence of rubber density (ρ_{Rubber}) on the band gap properties. (a) Frequency limits and (b) band gap width for S-waves; (c) frequency limits and (d) band gap width for P-waves

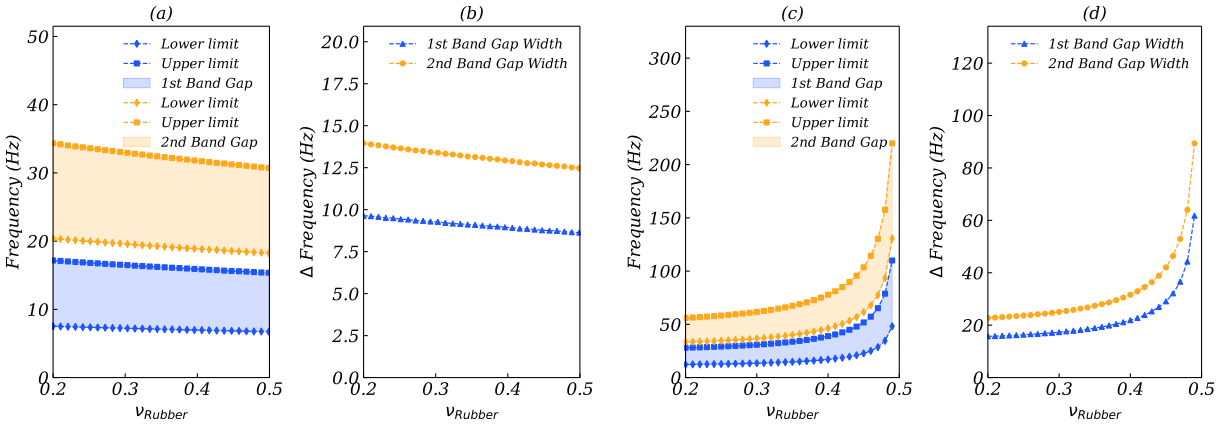


Figure 5 – Influence of rubber Poisson's ratio (ν_{Rubber}) on the band gap properties. (a) Frequency limits and (b) band gap width for S-waves; (c) frequency limits and (d) band gap width for P-waves

Increasing ρ_{Rubber} shifts the band gaps to lower frequencies (Figure 4). This occurs because an increase in ρ_{Rubber} decreases the wave velocities c_T and c_L thereby reducing the propagation frequencies. For S-waves, the influence of ν_{Rubber} is relatively small, causing a slight reduction in both the lower and upper boundary frequencies (Figure 5a).

On the other hand, for P-waves, the sensitivity is extremely high as ν_{Rubber} approaches the incompressibility limit of rubber at 0.5. As illustrated in Figure 5(c), both the frequencies and the band gap width increase exponentially.

When varying the Young's modulus of the concrete ($E_{Concrete}$), the upper and lower limit frequencies, as well as the widths of the first two band gaps, remained constant for both S-waves and P-waves (Figure 6). The same behavior was observed in the analysis of the Poisson's ratio (Figure 8) which demonstrates that the elastic properties of the rigid layer (concrete) exert less influence on the limits and widths of the band gaps than the properties of the inclusion material (rubber). Conversely, increasing the concrete density ($\rho_{Concrete}$), lowers the frequency ranges of the band gaps (Figure 7).

As shown in Figure 9, and increase in the thickness ratio ($r = d_{Rubber}/d_{Concrete}$), shifts both the lower and upper frequency limits to lower values, but results in narrower band gaps.

Figure 10 demonstrates an inversely proportional relationship between the unit cell size (a) and the band gap position. This behavior is intrinsic to the diffraction physics in PnCs, where the condition for destructive interference (Bragg reflection) is met when the wavelength becomes comparable to the spatial periodicity of the structure ($\lambda \approx 2a$) (Jin; Djafari-Rouhani; Torrent, 2019).

Figure 11 shows that as the filling fraction $f = d_{Rubber}/a$ approaches 1, the band gap width tends to zero, since the periodic structure and the impedance contrast cease to exist.

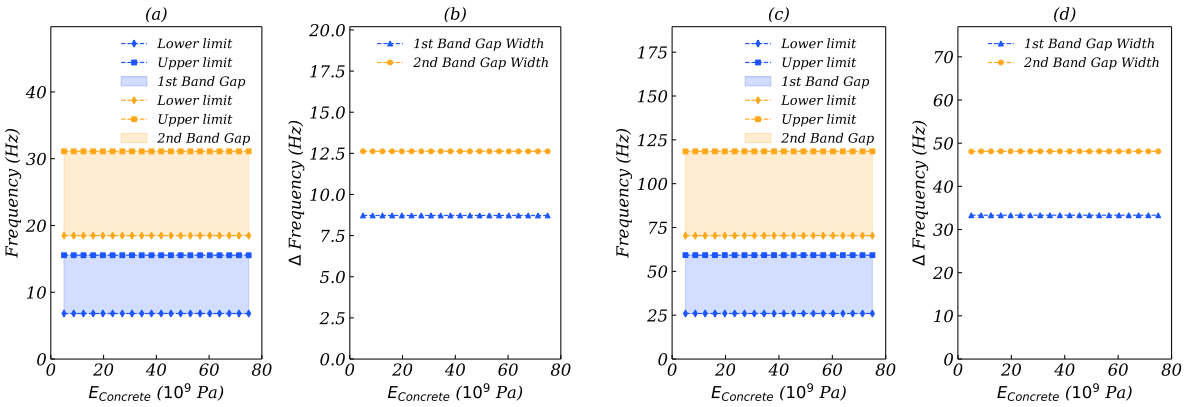


Figure 6 – Influence of the concrete Young's modulus ($E_{Concrete}$) on the band gap properties. (a) Frequency limits and (b) band gap width for S-waves; (c) frequency limits and (d) band gap width for P-waves

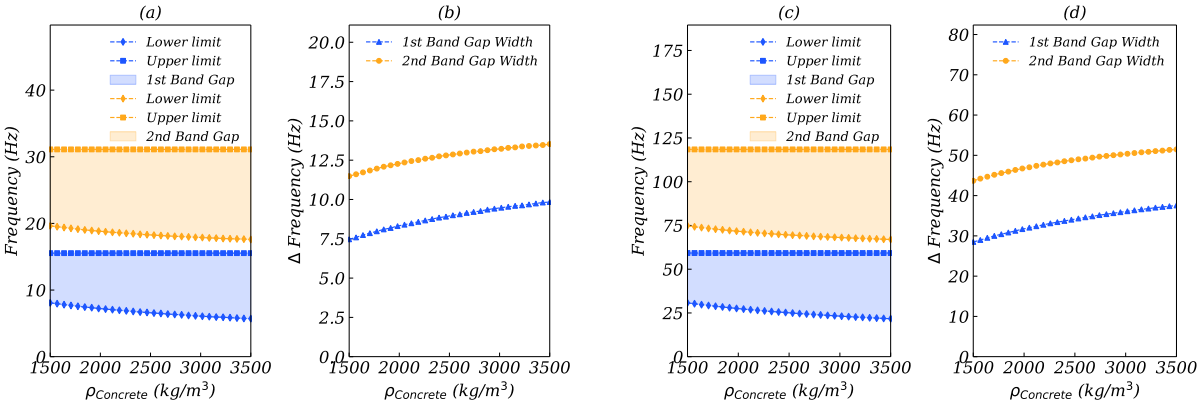


Figure 7 – Influence of the concrete density ($\rho_{Concrete}$) on the band gap properties. (a) Frequency limits and (b) band gap width for S-waves; (c) frequency limits and (d) band gap width for P-waves

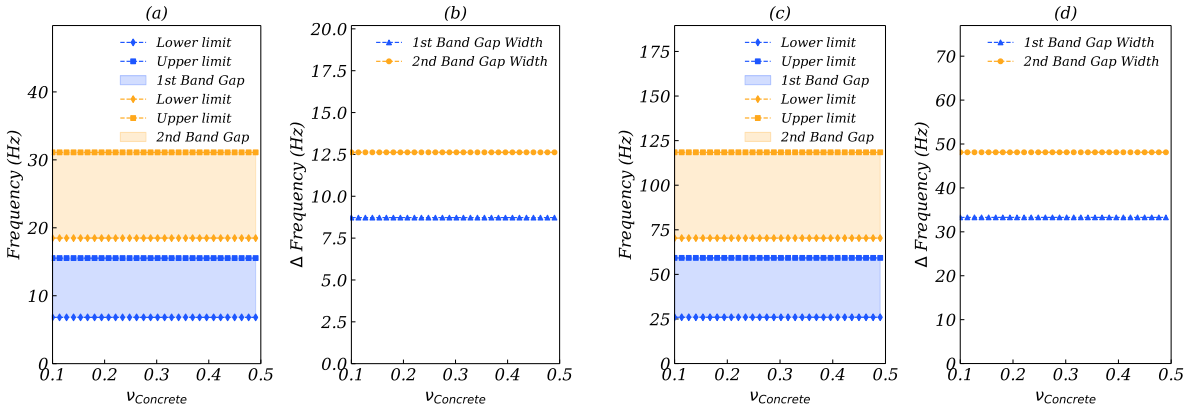


Figure 8 – Influence of the concrete Poisson's ratio ($\nu_{Concrete}$) on the band gap properties. (a) Frequency limits and (b) band gap width for S-waves; (c) frequency limits and (d) band gap width for P-waves

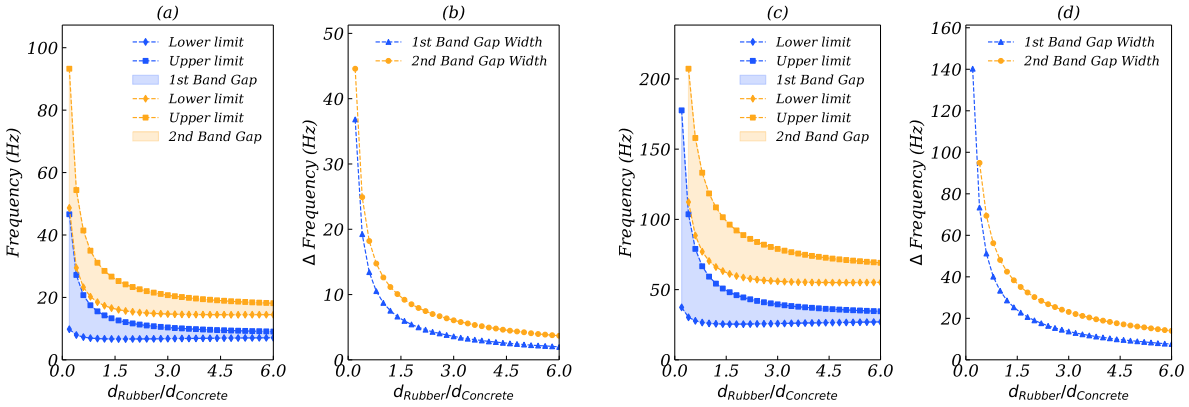


Figure 9 – Influence of the thickness ratio (r=$d_{Rubber}/d_{Concrete}$) on the band gap properties. (a) Frequency limits and (b) band gap width for S-waves; (c) frequency limits and (d) band gap width for P-waves

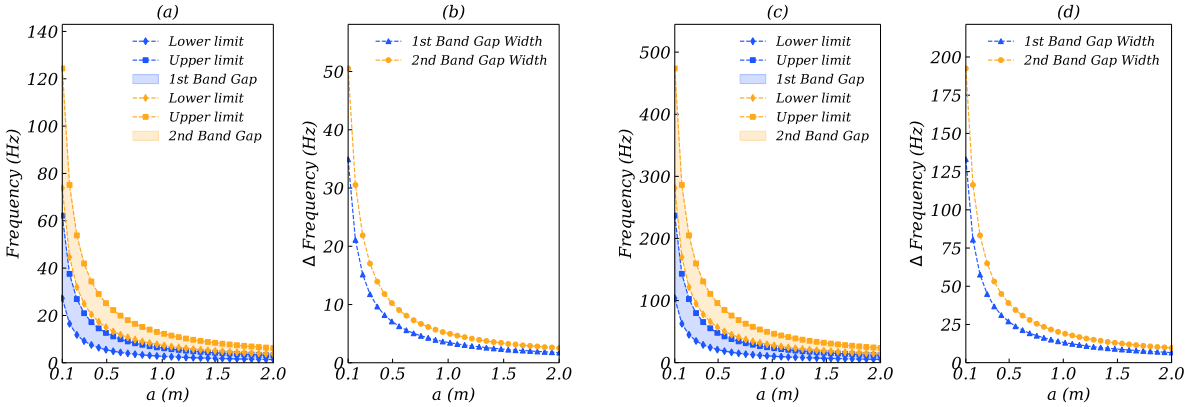


Figure 10 – Influence of lattice constant (a=$d_{Concrete}$+ d_{Rubber}) on the band gap properties. (a) Frequency limits and (b) band gap width for S-waves; (c) frequency limits and (d) band gap width for P-waves

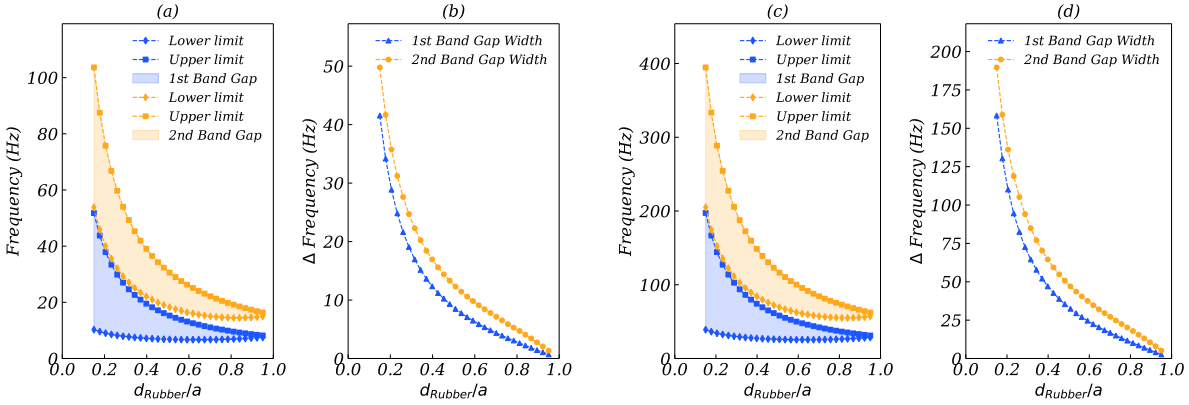


Figure 11 – Influence of the filling fraction (f=d_{Rubber}/a) on the band gap properties. (a) Frequency limits and (b) band gap width for S-waves; (c) frequency limits and (d) band gap width for P-waves

3.2 Design of the Optimized Periodic Structures and Optimal Tuning for Lines 3 and 5

Figure 12 illustrates the behavior of the periodic foundation after optimizing the geometric lattice parameter to a = 0.48 m. The band structure analyzed for S and P waves, represented in Figure 12(b) and (d), shows the formation of the band gaps. In Figure 12(a) and (c), it is possible to observe that significant transmission drops occur exactly within the theoretically predicted band gap frequencies. The arrangement with four unit cells exhibits deeper attenuation levels compared to the two unit cell arrangement.

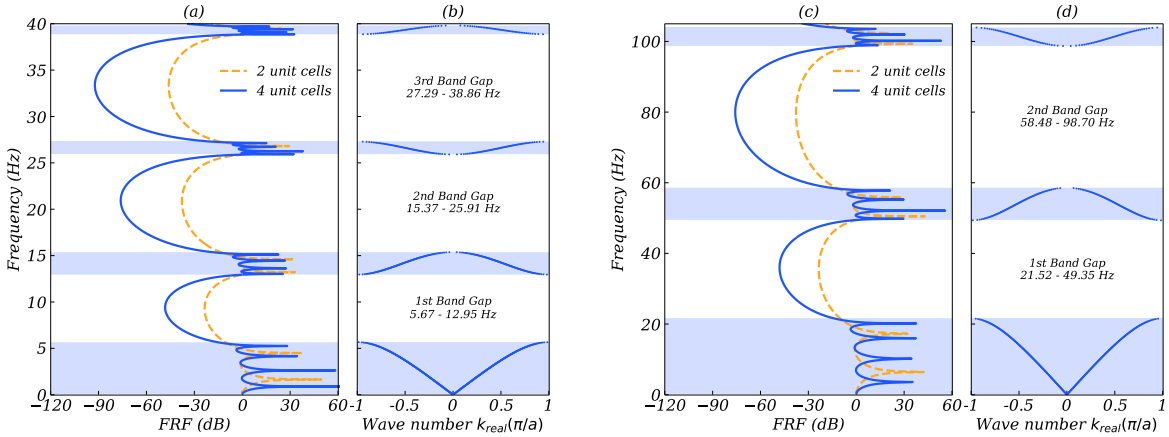


Figure 12 – Dynamic properties of the optimized unit cell (adjusted lattice constant a = 0.48 m). The behavior for S-waves is presented on the left: (a) Frequency Response Function (FRF) for finite arrangements; (b) band structure. The corresponding behavior for P-waves is detailed on the right: (c) FRF; (d) band structure

It was observed that the first band gap, which extends from 5.67 to 12.95 Hz, effectively encompasses the low-frequency peaks, such as those observed around 6.3 Hz and 12.5 Hz in all directional components. Furthermore, the second band gap, ranging from 15.37 to 25.91 Hz, covers the secondary excitation peaks. This is evident for Line 5, where the Periodic Foundation (PF) successfully isolates the peak occurring at 16 Hz. Figure 13 presents the dynamic response of the periodic barrier after adjusting E_{Rubber} = 1.16 x 10^5 Pa.

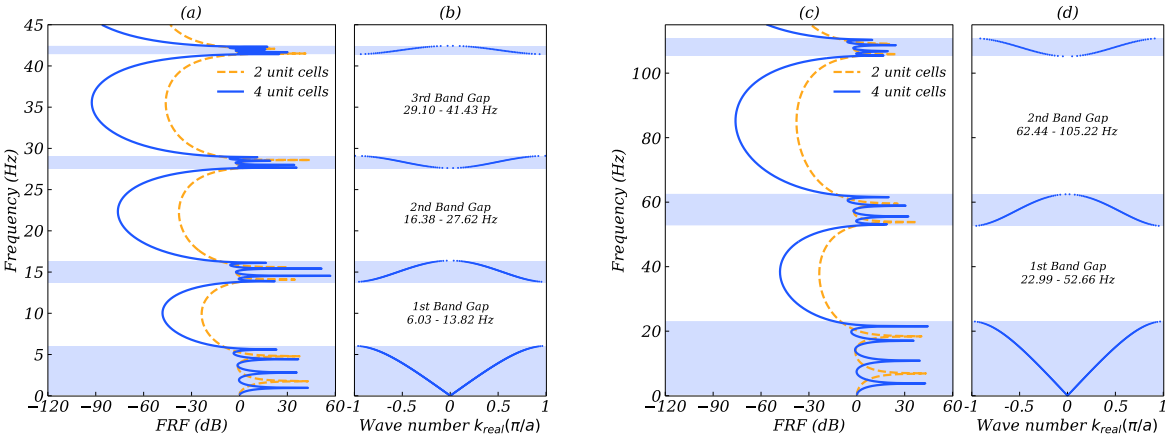


Figure 13 – Dynamic properties of the optimized unit cell (adjusted rubber Young's modulus E_{Rubber} = 1.16 x 10^5 Pa). The behavior for S-waves is presented on the left: (a) Frequency Response Function (FRF) for finite arrangements; (b) band structure. The corresponding behavior for P-waves is detailed on the right: (c) FRF; (d) band structure

As illustrated by the band structure graph Figure 13(b) and (d) and confirmed by the FRF Figure 13(a) and (c), the new band gap zones are shifted to slightly higher frequencies.

The first band gap, ranging from 6.03 to 13.82 Hz, can effectively mitigate the frequency peaks at 6.3 Hz and 12.5 Hz present in Line 3. For Line 5, the second band gap, in the range of 16.38 to 27.62 Hz, was shifted to the right. Consequently, the secondary energetic peak occurring exactly at 16 Hz in the longitudinal direction falls outside the attenuation zone. Thus, this limitation directly motivates the subsequent optimization step, which aims to perform a new adjustment in the material properties to encompass this 16 Hz peak once again. The next objective was to identify a configuration that could offer targeted isolation specifically for Line 5. Figure 14 presents the behavior of the periodic structure when the rubber's elastic modulus is reduced to E_{Rubber} = 0.94 x 10^5 Pa.

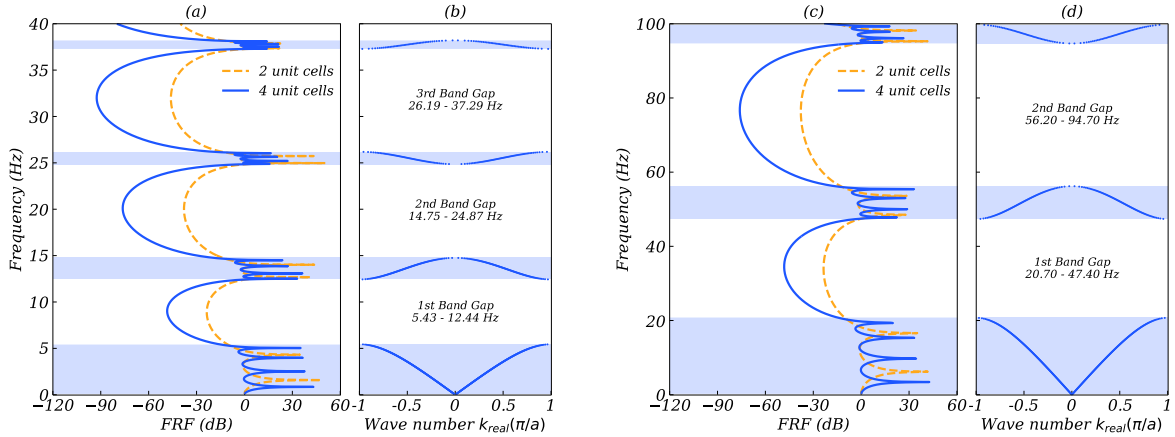


Figure 14 – Dynamic properties of the optimized unit cell (adjusted rubber Young's modulus E_{Rubber} = 0.94 x 10^5 Pa). The behavior for S-waves is presented on the left: (a) Frequency Response Function (FRF) for finite arrangements; (b) band structure. The corresponding behavior for P-waves is detailed on the right: (c) FRF; (d) band structure

As observed in the FRF (Figure 14(a) and (c)) and the band structure (Figure 14(b) and (d)), this reduction in stiffness shifts the band gap frequencies downward. This modification, when superimposes the adjusted band gaps onto the VAL spectra of (a) Line 3 and (b) Line 5, exhibits varying performance depending on the specific railway line. For Line 5, this adjustment proves to be effective. The resulting second band gap successfully encompasses the main peaks occurring at 12.5 and 16 Hz in the longitudinal direction. However, when applied to Line 3 although the first band gap manages to cover the 6.3 Hz peak, the second peak at 12.5 Hz falls outside the attenuation range.

4. Conclusions

This paper demonstrated the feasibility and effectiveness of applying one-dimensional phononic crystals (1D-PnCs) as periodic foundations and barriers for mitigating subway-induced vibrations. Through an analytical-parametric approach based on the Transfer Matrix Method (TMM), it was possible to map the dynamic response of the structure and strategically modulate the attenuation ranges (band gaps). The sensitivity analysis revealed that the dynamic behavior of the system is predominantly governed by the unit cell dimensions and the impedance contrast imposed by the rubber inclusion. It was found that geometry dictates the overall position of the attenuation bands. Adjusting the lattice constant to 0.48 m proved highly efficient in encompassing the global energy peaks concentrated at low frequencies, below 30 Hz, which are typical of the railway excitations studied. Furthermore, calibrating the elastic properties of the rubber layer enabled targeted spectral optimization, validated against real-world Vibration Acceleration Level (VAL) spectra. Stiffening the rubber proved ideal for isolating the critical peaks at 6.3 Hz and 12.5 Hz recorded on Line 3. Conversely, reducing its elastic modulus reconfigured the mechanical filter, precisely blocking the energetic 16 Hz peak characteristic of Line 5. It is concluded that the design of 1D-PnCs should not be generic, but rather customized to the vibrational signature of each specific site. The predictive methodology proposed herein provides civil engineering with a tool for designing tailor-made passive isolation systems.

Acknowledgments

This study was financed in part by the Coordenação de Aperfeiçoamento de Pessoal de Nível Superior - Brasil (CAPES) - Finance Code 001.

References

Cheng, Zhibao, et al. 2020. "Seismic Vibrations Attenuation via Damped Layered Periodic Foundations." Engineering Structures 211 (May).

De Lima, P. D. S., et al. 2025. "Transmission Properties of Kolakoski Aperiodic Phononic Crystals." Wave Motion 136 (June).

Erkal, Aykut, and Muhammed Şerif Kocagöz. 2020. "Interaction of Vibrations of Road and Rail Traffic with Buildings and Surrounding Environment." Journal of Performance of Constructed Facilities 34, no. 3 (June).

Fabro, Adriano T., et al. 2021. "Wave and Vibration Analysis of Elastic Metamaterial and Phononic Crystal Beams with Slowly Varying Properties." Wave Motion 103 (June).

Geng, Qian, Songye Zhu, and Ken P. Chong. 2018. "Issues in Design of One-Dimensional Metamaterials for Seismic Protection." Soil Dynamics and Earthquake Engineering 107 (April): 264–78.

Jain, Saumitra, Sumiran Pujari, and Arghadeep Laskar. 2021. "Investigation of One Dimensional Multi-Layer Periodic Unit Cell for Structural Base Isolation." Structures 34 (December): 2151–63.

Jakubczyk-Galczynska, Anna, and Robert Jankowski. 2014. "Traffic-Induced Vibrations: The Impact on Buildings and People." In Dept. of Mathematical Modelling.

Jia, Gaofeng, and Zhifei Shi. 2010. "A New Seismic Isolation System and Its Feasibility Study." Earthquake Engineering and Engineering Vibration 9, no. 1 (March): 75–82.

Jin, Yabin, Bahram Djafari-Rouhani, and Daniel Torrent. 2019. "Gradient Index Phononic Crystals and Metamaterials." Nanophotonics 8, no. 5: 685–701.

Jin, Yabin, et al. 2025. "The 2024 Phononic Crystals Roadmap." Journal of Physics D: Applied Physics 58, no. 11 (March).

Kee, Chul Sik, et al. 2000. "Essential Role of Impedance in the Formation of Acoustic Band Gaps." Journal of Applied Physics 87, no. 4: 1593–96.

Laude, V., et al. 2009. "Evanescent Bloch Waves in Phononic Crystals." In SPIE (February).

Li, Z. C., et al. 2023. "Locally Resonant Bandgap and Dynamic Responses of Meta-Sandwich-Like Plate with L-Shaped Beam–Mass Resonators." International Journal of Dynamics and Control 11, no. 4 (August): 1445–64.

Liu, Junyi, Hanbei Guo, and Ting Wang. 2020. "A Review of Acoustic Metamaterials and Phononic Crystals." Crystals 10, no. 4 (April).

Maldovan, Martin, and Edwin L. Thomas. 2009. Periodic Materials and Interference Lithography. Weinheim: Wiley-VCH.

Witarto, Witarto, et al. n.d. "Analysis and Design of One Dimensional Periodic Foundations for Seismic Base Isolation of Structures." Journal of Engineering Research and Applications. www.ijera.com.

Xing, Mengting, Juxiang Zhu, and Dingqing Chen. 2025. "Assessing Train-Induced Building Vibrations in a Subway Transfer Station and Potential Control Strategies." Buildings 15, no. 7 (April).

Xiong, Chen, Zhifei Shi, and Hongjun Xiang. 2012. "Attenuation of Building Vibration Using Periodic Foundations." Advances in Structural Engineering 15, no. 8: 1375–88.

Zhao, Chunfeng, et al. 2021. "Isolation Performance of a Small Modular Rectangular Reactor Using 1D Periodic Foundation." Engineering Structures 244 (October).

Zhu, Songye, et al. 2014. "Impact of Construction-Induced Vibration on Vibration-Sensitive Medical Equipment: A Case Study." Advances in Structural Engineering 17: 907–20.

Cinpar 2026
XXII International Conference on Building Pathology and Constructions Repair
15th to 17th July 2026 - Lisboa, Portugal

Discrete element-based particle modelling optimization for stone masonry wall's structural assessment

M. MARQUES[1], N. MONTEIRO AZEVEDO[2], I. CISMASIU[3], **F. PINHO**[4]

[1] Civil Engineering Department, Faculdade de Ciências e Tecnologia, Universidade NOVA de Lisboa, Caparica, Portugal, mmr.marques@campus.fct.unl.pt
[2] LNEC – National Laboratory for Civil Engineering, Lisboa, Portugal, nazevedo@lnec.pt
[3] Civil Engineering Department, Faculdade de Ciências e Tecnologia and CERIS, Universidade NOVA de Lisboa, Caparica, Portugal, ildi@fct.unl.pt
[4] Civil Engineering Department, Faculdade de Ciências e Tecnologia and CERIS, Universidade NOVA de Lisboa, Caparica, Portugal, ffp@fct.unl.pt

Abstract: The structural assessment of rubble stone masonry is inherently complex because its constituent materials, stones and mortar, exhibit significant heterogeneity and uncertain properties, along with well-known variability in stone geometry, size, and positioning. A micro-modelling strategy based on a detailed particle model (PM) that follows a discrete element method (DEM) has been applied in the modelling and evaluation of traditional stone masonry unreinforced walls, transversally confined walls and walls reinforced with sprayed micro-concrete layers with external steel mesh and transverse confinement. Simulations of axial and shear–compression loading show that DEM-based PMs accurately reproduce the behaviour of ancient masonry, albeit at high computational demand. In this work the proposed DEM-based PM has been optimized to reduce computational cost. Coarser mortar particle representations are adopted to assess its impact on the overall predicted response. The results, including uniaxial compression and compression-shear tests, show that the adopted micro-modelling approach can be optimized without compromising its predictive capability and overall performance.

Keywords: Rubble-stone masonry; particle model; optimization.

1. Introduction

In Portugal, ancient buildings represent nearly 50% of the built heritage and their structural walls are mostly constructed using rubble stone masonry. Moreover, these masonry buildings were built before the existence of structural safety codes and regulations, and were designed to solely resist vertical loads, and therefore are particularly vulnerable to seismic actions. The structural assessment of rubble stone masonry is inherently complex because its constituents, the filler material such as limestones, and a binder such as lime, exhibit significant heterogeneity and uncertain properties, along with well-known variability in stone geometry, size, and arrangement, Pinho and Lúcio (2017). Traditional continuum-based methods often fail to capture key failure mechanisms such as cracking, sliding and progressive collapse, Roca et.al (2010), particularly under seismic loading. To address this limitations, micro-modelling strategies have been increasingly adopted, with Discrete Element Method (DEM) approaches proving particularly effective for masonry. Lemos (2017) showed that DEM is particularly well suited for capturing nonlinear behaviour and collapse mechanisms in masonry under static and dynamic loading conditions. Similarly, Gobin et al. (2021) demonstrated that DEM is capable of effectively capturing the behaviour of masonry under seismic action, with crack patterns and resulting collapse mechanisms emerging directly from the analysis.

A micro-modeling strategy based on a detailed particle model (PM) that follows a discrete element method (DEM) has been applied to the modelling and evaluation of traditional unreinforced stone masonry walls Azevedo et al. (2022), transversally confined walls Cismaşiu et al. (2023) and walls reinforced with sprayed micro-concrete layers with external steel mesh and transverse confinement, Azevedo et al. (2025). The studies have shown that the 2D DEM-based PMs reliably reproduced the response of the ancient masonry under uniaxial compression and compression-shear loading conditions, though they entail high computational demand. Devanand et al. (2025) adopted a similar DEM-based particle micro-modelling approach for brick masonry and demonstrated that it can accurately reproduce masonry behaviour under compression-loading conditions. Chen et al. (2024) modelled rubble masonry walls using a coupled finite–discrete element micro-modelling approach employing a coarser masonry representation when compared to those adopted in this paper.

In this work the DEM-based PM has been optimized to reduce its known computational cost. Coarser mortar particle representations were adopted to assess their impact on the overall predicted response. The results presented, namely uniaxial compression and monotonic compression-shear tests, show that the adopted micro-modelling approach can be optimized without compromising its predictive capability and overall performance. Ongoing work is focused on an optimization strategy based on a hybrid finite element/discrete element algorithm as proposed by Azevedo and Lemos (2022) that reduces the number of particles and contacts required to properly represent the stone behaviour by replacing the internal particle discretization with a coarser finite element mesh and retaining only the boundary particles.

2. Discrete Element-Based Particle Model (PM)

2.1 Fundamentals

The masonry elements (stones and mortar) are represented by rigid circular particles with three degrees of freedom (two translations and one rotation) that interact at the point of contact (Figure 1). At the contact point normal (k_n) and shear stiffness (k_s) springs are assigned which allow elastic deformations. Complex macroscopic nonlinear responses can be obtained if brittle or simple contact softening-based laws are adopted at the contact level. The calculation cycle of a discrete element algorithm is based on two principles: the force–displacement law, the forces acting on each particle are related to the particle's displacement relative to neighboring particles, and the law of motion, given the forces applied to the centroid of the particle, the new position of the particle is determined by applying Newton's second law, that are sequentially applied, see Cundal and Stark (1979) and Azevedo *et al.* (2010).

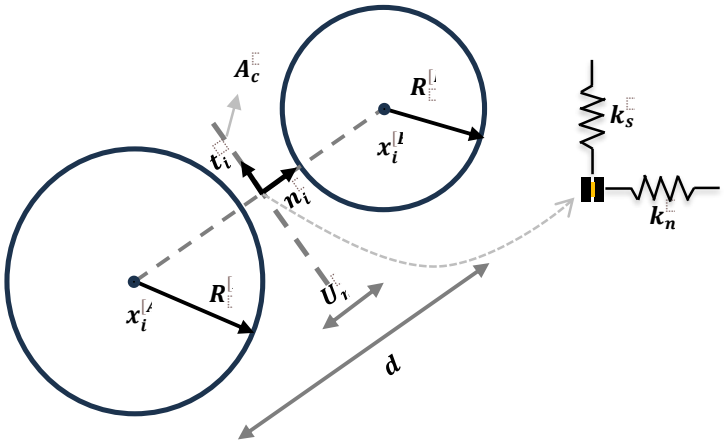


Figure 1 – PM contact model

At a given time increment, the contact normal force ($\Delta F_n\ (t)$) and the shear contact force ($\Delta F_s\ (t)$) increments are defined based on a linear force–displacement relationship, given the contact normal ($\Delta x_n\ (t)$) and shear ($\Delta x_s\ (t)$ displacement increments and the contact stiffnesses:

$$\Delta F_n\ (t) = -k_n\ \Delta x_n\ (t) \tag{1}$$

$$\Delta F_s\ (t) = -k_s\ \Delta x_s\ (t) \tag{2}$$

2.2 Contact stiffness and contact strength

The normal and shear contact stiffnesses are defined using the following expressions:

$$k_n\ = A_c\ \frac{\bar{E}}{d} \tag{3}$$

$$k_s\ = \alpha\quad k_n \tag{4}$$

where $\bar{E}$ is the modulus of elasticity of the equivalent continuous material; d is the distance between the centers of gravity of the circular particles in contact (Figure 1); A_c is the contact area (Figure 1) and α is the shear stiffness to the normal stiffness ratio.

The total tensile strength ($F_{n.max}$), the maximum cohesion (C_{max}), the maximum shear strength ($F_{s.max}$) and the total compressive strength ($F_{nc.max}$) are defined given the maximum tensile stress ($\sigma_{n.t}$), the maximum cohesive stress (τ), the normal force acting on the contact (F_n), the friction term (μ_c), the maximum compressive stress, ($\sigma_{n.c}$) and the contact area, it is possible to define, as shown in Equations (5)–(8):

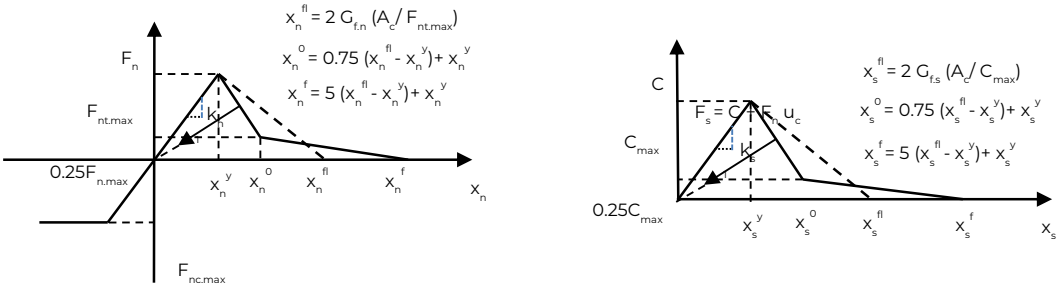
$$F_{n.max} = \sigma_{n.t}\ A_c \tag{5}$$

$$C_{max} = \tau\ A_c \tag{6}$$

$$F_{s.max} = C_{max} + F_n\ \mu_c \tag{7}$$

$$F_{nc.max} = \sigma_{n.c}\ A_c \tag{8}$$

A bilinear softening damage model is adopted for the contact point in the normal (tensile) and shear directions, see Azevedo *et al.* (2010) and Azevedo *et al.* (2022), Figure 2.



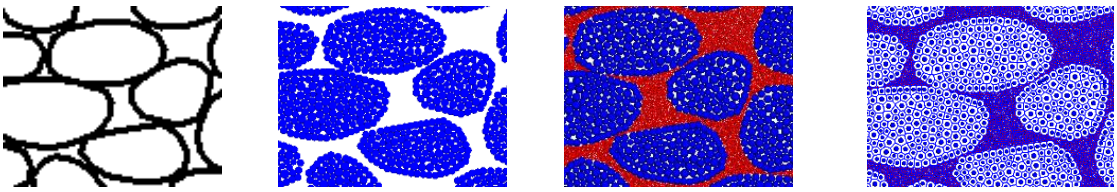
a) Normal direction b) Shear direction

Figure 2 – Contact model: Bilinear softening damage model in the normal (tensile) and shear directions and a yield plateau in compression, Azevedo et al. (2010) and Cismaşiu et al. (2023)

In this constitutive model, the maximum values of tensile strength and cohesion are reduced according to the total damage value, which is defined by the sum of tensile and shear damage. The contact damage value at a given direction is defined as a function of the maximum contact displacement in that direction. In the normal direction, the maximum contact displacement is defined given the adopted contact fracture energy in the normal direction ($G_{f.n}$), similarly, the maximum shear displacement is defined given the contact fracture energy in the shear direction ($G_{f.s}$). For stone masonry walls modelling it is necessary to adopt a yield plateau in the normal direction (compression), Azevedo *et al.* (2022) and Cismaşiu *et al.* (2023).

2.3 Model generation

The arrangement and geometry of the stones in the masonry wall are determined through a mapping process of the stone units (Figure 3a). Following, each stone unit is discretized with particles (Figure 3b). Subsequently, the void space surrounding each stone, representing the mortar, is also discretized with circular particles (Figure 3c). The mortar particle size distribution was chosen to match the material's granular structure; however, this led to high computational demand. Nevertheless, computational constraints may require the adoption of coarser particle distributions. The contacts are established using the Voronoi-Laguerre tessellation of the gravity centers of each circular particle (Figure 3d). Three types of contacts are present in a PM model of a rubble-masonry wall: mortar-mortar (m-m), mortar-stone (m-s) and stone-stone (s-s).



a) Masonry specimen b) Stone discretization c) Mortar discretization d) Particle contacts

Figure 3 – Rubble stone masonry wall model generation, Azevedo et al. (2022) and Cismaşiu et al. (2023)

3. PM Parameter Calibration

One particular feature of PMs is that the elastic and strength contact properties cannot be assigned directly from laboratory test results. Instead, these parameters are calibrated at the assembly level so that the particle system reproduces the macroscopic behaviour of the material they represent in known experimental tests such as uniaxial tensile and compression tests, and biaxial or triaxial tests. In the absence of experimental test results, the strength parameters of the m–s contacts are adopted as 50% of the calibrated m–m contact strength parameters., Azevedo et al. (2022); Cismaşiu et al. (2023).

The macroscopic elastic response of a PM is related to the adopted Young's modulus of the equivalent continuous material ($\bar{E}$) and to the adopted stiffness factor (α) that relates the shear stiffness and normal stiffness. The macroscopic strength response of a PM is controlled by six contact parameters, namely the maximum tensile stress ($\sigma_{n.t}$), the maximum cohesion stress (τ), the friction coefficient (μ_c), the tensile contact fracture energy ($G_{f.n}$), the shear contact fracture energy ($G_{f.s}$), and to the maximum compression stress value ($\sigma_{n.c}$) that defines the yield plateau in the normal direction under compression.

A simple trial and error calibration procedure based on user experience is carried. The elastic contact parameters are initially set to match the macroscopic Young modulus and Poisson coefficient, followed by setting the contact strength parameters to match the known macroscopic parameters, such as the tensile and the compression strength of the masonry element (mortar, stone) being calibrated. Research efforts on

the automation of the calibration of the micro-mechanical parameters, Kibriya et. al (2024) make PMs more appealing, as some experimental data may not be available for existing masonry structures.

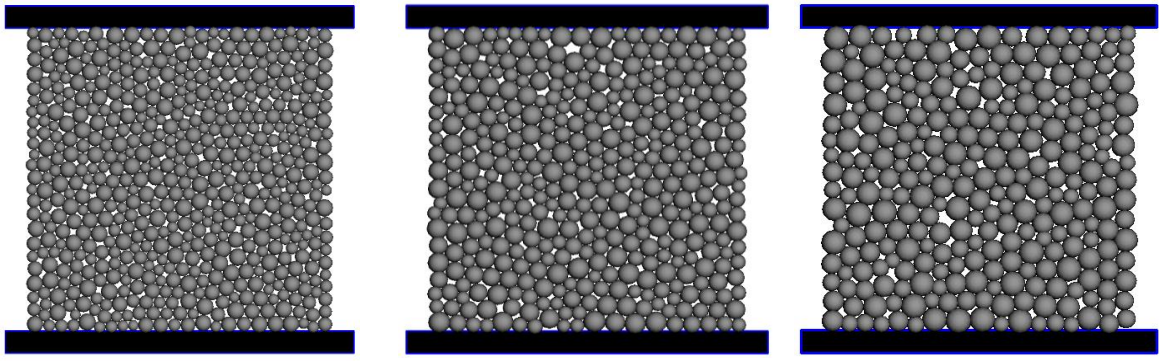
The contact properties of the stone and mortar were calibrated based on the experimental tests carried out for stones and mortar, Pinho (2007), see Table 1. Other authors have also provided experimental values for the mechanical properties of the stone masonry components, which could be used for calibration purposes of the mortar and stone contacts properties, see D'Altri et al. (2020) and Saloustros et al. (2023). It is worth mentioning that databases compiling results from experimental studies on the mechanical properties of stone masonry walls can provide significant support for PM parameter calibration, Murano et al. (2020).

Table 1 – Elastic and strength macroscopic values: experimental values, Pinho (2007)

Material	$\mathbf{E}$ (GPa)	υ	σ_c (MPa)
Stone	6.0	0.29	47.8
Mortar	0.075	0.16	0.65

The properties of the s–s contacts, representative of stone, were calibrated on 0.20 m × 0.20 m numerical models. The properties of the m–m contacts, representative of mortar, were calibrated on 0.04 m × 0.04 m numerical models. The model size should be chosen to match the size adopted in the experimental tests. The numerical models were subjected to pure compression and pure tension tests using the Parmac2d PM implementation.

For the stone units with an average dimension of 16.7 cm, a PM model with a uniform radius distribution between 0.003 m and 0.005 m was adopted in all models. In the reference model (R), PM model with a uniform radius distribution between 0.000714 m and 0.00119 m was adopted for the mortar, Azevedo et al. (2022). Note that the adopted maximum radius value corresponds to the maximum size of the sand used in the laying mortar, Pinho (2017). To assess the impact of mortar particle size on the overall predicted response, different coarser mortar particle representations are adopted, namely: PM model (M2) with a uniform radius distribution between 0.0008568 m and 0.001428 m; and PM model (M3) with a uniform radius distribution between 0.0009996 m and 0.001666 m. Figure 4 presents the developed mortar PMs adopted for the calibration of the contact properties for uniaxial compression and tensile strength. When compared with the reference PM model, in the PM model M2 a radius multiplier of 1.2 was adopted for the minimum and maximum radius distributions, whereas a radius multiplier of 1.4 was adopted in the PM model M3.



a) PM model R c) PM model M2 d) PM model M3

Figure 4 – Uniaxial compression PMs - 0.04 m × 0.04 m

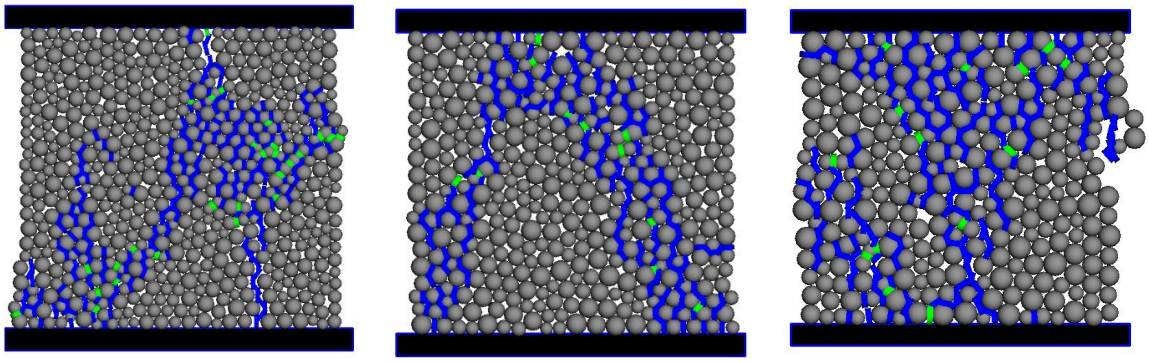
Table 2 presents calibrated PMs contact properties obtained through a trial and error procedure. The s-s and m–m (R) contacts were calibrated as part of the work presented in Azevedo et al. (2022). In all PMs

representing the mortar, a maximum compression value of 0.80 MPa was adopted in the normal direction, close to the maximum uniaxial compression value of the laying mortar, Pinho (2007). The m–m (M2) and m–m (M3) contacts were calibrated within the framework of this work. As shown in Table 2 the calibrated contact properties values for PM models with different particle assemblies, see Figure 4, are very similar. The similarity is mainly due to the fact that the contacts areas and the contact interactions are established using the Voronoi-Laguerre tessellation of the circular particle gravity centers (Figure 3d).

Table 2 – Elastic and strength PMs contact calibrated properties

Contacts	$\bar{E}$ (GPa)	α	$\sigma_{n.t}$ (MPa)	τ (MPa)	μ_c	$G_{f.n}$ (N/m)	$G_{f.s}$ (N/m)
s-s	8.6	0.11	8.9	35.7	1.0	0.3838	56.1403
m-m (R)	0.090	0.43	0.171	0.171	1.0	0.0014	0.0033
m-m (M2)	0.0905	0.40	0.179	0.179	1.0	0.0019	0.0046
m-m (M3)	0.0910	0.39	0.169	0.169	1.0	0.0019	0.0049

Figure 5 presents the final contact cracking distribution predicted in uniaxial compression for the different assessed mortar PM models. The obtained final crack patterns are the expected failure patterns when the loading plates have zero friction. Figure 6 presents the stress-deformation for the uniaxial compression test for the calibrated m-m contact properties. It can be observed that the PM models representing mortar have a very similar behaviour close to the observed in hydrated air lime mortar.



a) PM model R c) PM model M2 d) PM model M3

Figure 5 – Uniaxial compression - PM cracking distribution in uniaxial compression

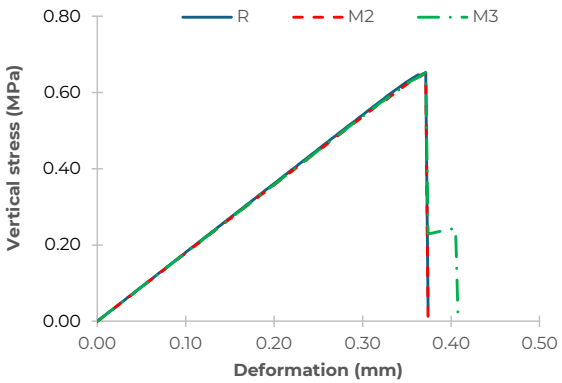
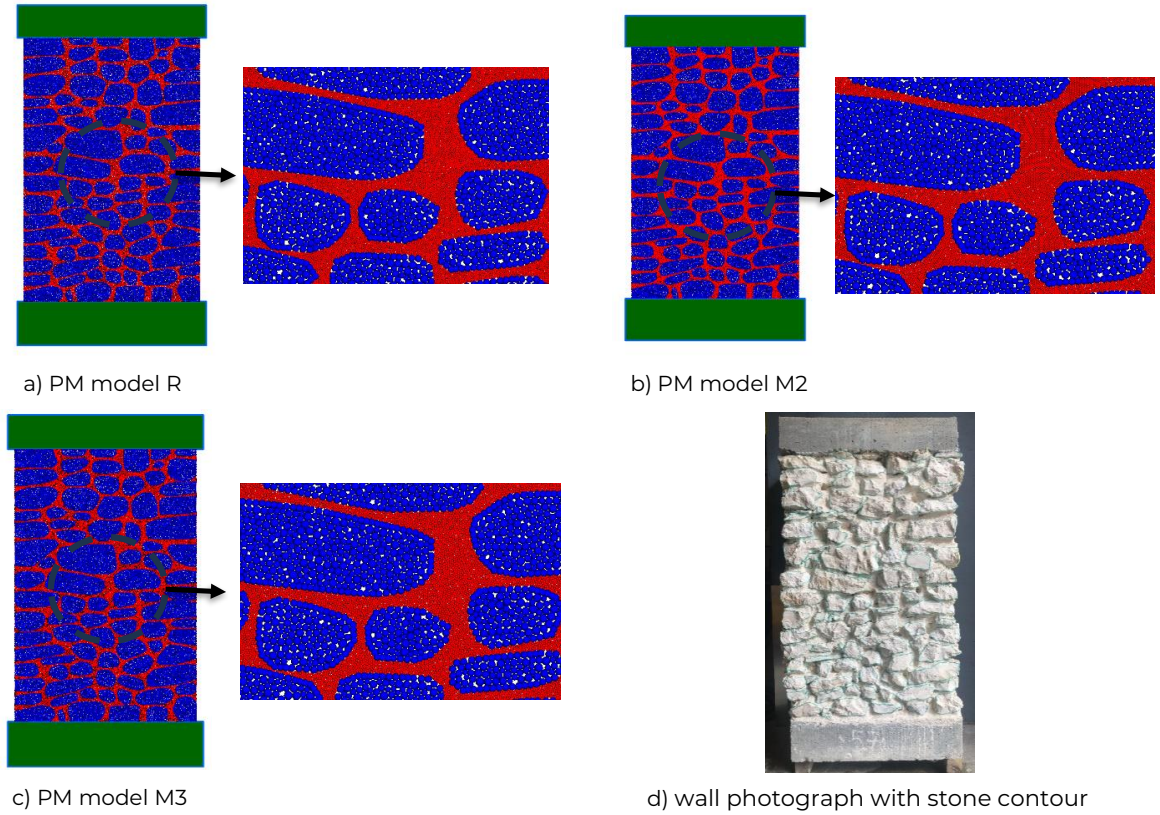


Figure 6 – Stress-displacement diagram for compression tests

4. Numerical uniaxial compression and shear-compression tests of the specimen M57

4.1 Experimental setup

The PM numerical models developed in this work are built based on the experimental studies conducted by Pinho (2007) which evaluated the effectiveness of different strengthening techniques by subjecting several rubble-stone masonry specimens to two specific testing conditions: axial compression and shear-compression tests. The 2D PM numerical models are defined from the frontal faces of the tested walls with 0.40 m width, Pinho (2007). In this work one unreinforced rubble-stone masonry specimens: M57 with dimensions 1.20 m x 0.80 m x 0.40 m is adopted, Figure 7.



a) PM model R

b) PM model M2

c) PM model M3

d) wall photograph with stone contour

Figure 7 – Frontal wall PMs and photograph with stone contour of specimen M57

Table 3 presents, for the different mortar adopted, mortar particle size distributions, the total number of particles and contacts used in the discretization of specimen M57.

Table 3 – PMs number of particles and number of contacts

Model	Particles		Contacts		
	Stone	Mortar	s-s	m-m	s-m
M57 (R)	14997	94131	39842	264660	21338
M57 (M2)	14822	65747	39545	182094	18801
M57 (M3)	14650	48542	39205	132323	16919

As shown the PM model based on a M2 mortar discretization, M57 (M2), enables when compared with the reference mortar discretization, M57 (R), a 31% reduction in the total number of particles and contacts, whereas, the PM model based on a M3 mortar discretization, M57 (M3), enables when compared with the reference mortar discretization, M57 (R), a 50% reduction in the total number of particles and contacts.

4.2 Results and discussion

4.2.1 Uniaxial compression tests

The numerical prediction of the uniaxial compression test for models M57 (R), M57 (M2), and M57 (M3), along with the experimental results, is shown in Figure 8. The m–m and s–s contact parameters for each PM model are presented in Table 2, while the m–s contact parameters are defined as 50% reduction of the m-m calibrated contact strength. As shown in Figure 8an excellent agreement with the experimentally observed behaviour is predicted, both in terms of peak strength and residual strength, for all the adopted mortar discretizations.

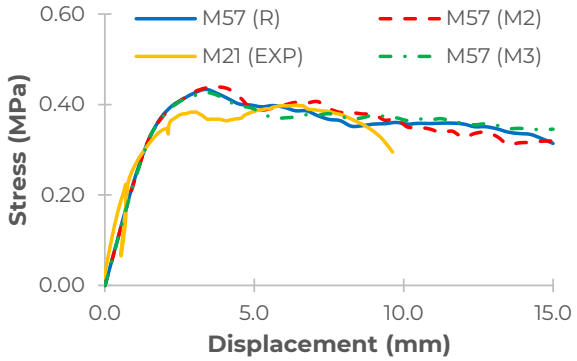


Figure 8 – Vertical Stress-Vertical displacement curve of model 57 (PM Numerical models) and experimental response of tested specimen M21 with similar geometry, Pinho (2007)

Figure 9 presents the damage evolution throughout the uniaxial compression test for the PM's with different mortar discretizations. All PMs predict a similar behaviour, meaningful damage initiates at around 40% of the peak strength with a steady growth up to the peak strength, after peak strength the damage evolution is slightly more restrained.

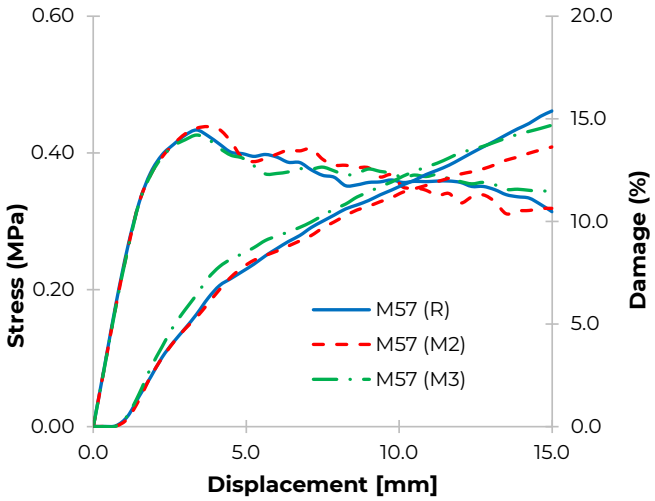
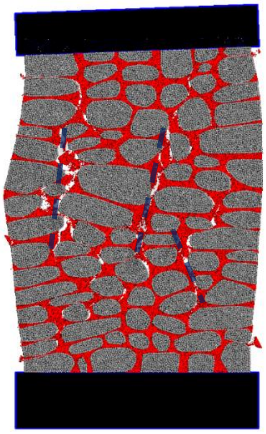
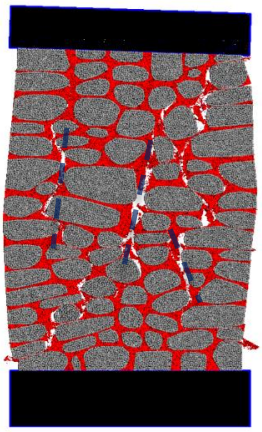


Figure 9 – PMs predicted Stress-displacement curve of model M57 including damage evolution

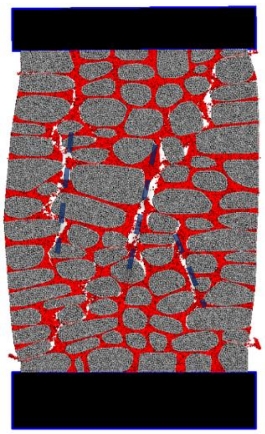
Figure 10 presents the PMs predicted failure modes along with the failure mode observed experimentally for a wall with similar geometry (M43), Pinho (2007). As shown, the PMs predicted failure modes are very similar to each other, with the principle macroscopic cracks having similar locations and extensions, and to the failure mode observed experimentally.



a) PM M57 (R)



b) PM M57 (M2)



c) PM M57 (M3)



d) M43 Experimental model

Figure 10 – Uniaxial compression failure mode - PMs Numerical prediction versus experimental observation

The running time of the PM M57 (R) is approximately 65 hours on a 12th Gen Intel ® Core i9-12900 KF–3.19Hz. The PM M57 (M2) enables a 25% reduction cost, whereas the PM M57 (M3) enables a 50% reduction cost, with similar predictions under uniaxial loading.

4.2.2 Monotonic shear-compression tests

The M57 based PM models were also evaluated under shear-compression. A vertical pre-compression stress of 0.23 MPa, identical to the experimental value adopted by Pinho (2007). Note that, in the experimental program carried out by Pinho (2007) only the walls with dimensions 1.20 m x 0.80 m x 0.40 m were assessed under shear-compression. As shown in Figure 11, the PM models with different mortar discretizations predict similar responses under a shear-compression loading condition. With the M57 (M3) PM the peak strength value is 6% higher than that predicted with the M57 (R) PM model. The M57 (M2) PM predicts an even closer peak strength value, only 2% higher than that predicted with the reference model, M57 (R).

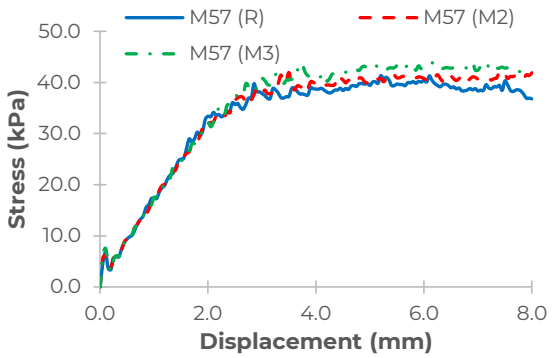
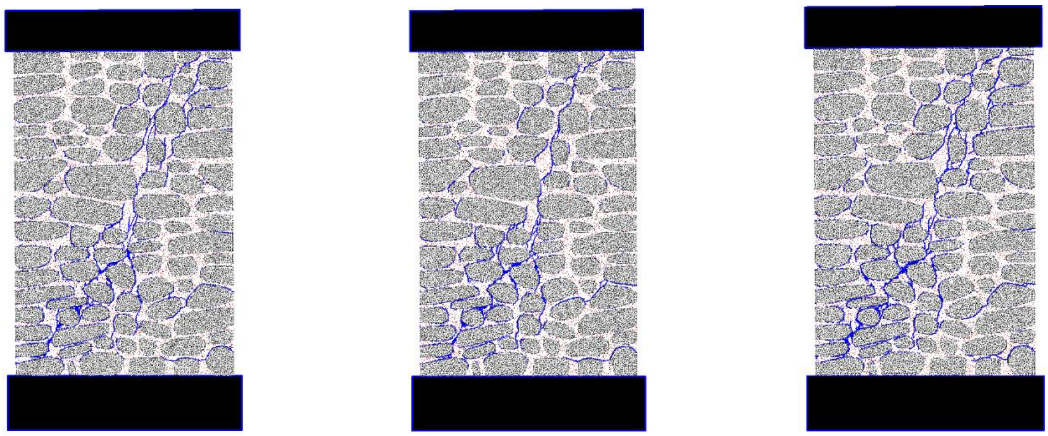


Figure 11 – Horizontal stress-horizontal displacement curve of M57 PM numerical models

Figure 12 presents the PMs predicted final contact damage distribution. As shown, the PMs predicted contact damage distributions are similar to each other. Figure 12 also shows that damage initially occurs at the s-m contacts, latter propagating to form the final macroscopic final cracks.



a) PM model M57(R) c) PM model M57(M2) d) PM model M57(M3)

Figure 12 – Shear-compression PMs predicted final contact damage distribution

The running time of the PM M57 (R) is approximately 50 hours on a 12th Gen Intel ® Core i9-12900 KF–3.19Hz. The PM M57 (M2) enables a 27% reduction cost, whereas the PM M57 (M3) enables a 44% reduction cost, with similar predictions under shear-compression loading.

5. Conclusions

The results presented show that the adopted 2D micro-modelling approach can be optimized without compromising its predictive capabilities and overall performance by coarsening the mortar discretization. The coarsened mortar PMs have an excellent agreement with the reference PM that adopts a finer discretization. The maximum strength, the failure mode, and the overall mechanical behaviour observed experimentally in rubble-stone masonry walls under uniaxial compression and under shear-compression are well predicted with the coarsened mortar discretizations. Work is underway to replace the particle discretization adopted in the stone discretization with a coarser finite element mesh adopting only the boundary particles.

Acknowledgments

This work is part of the research activities of the second author within the research project StepDam: A step forward for the ability to anticipate and prevent failures of concrete dam foundations, supported by LNEC. This work is also part of the research activities of the third and fourth authors under research grant NOVAID-B273 funded by NOVA.ID - Association for Innovation and Development of NOVA School of Science and Technology. This research was funded in whole or in part by the Fundação para a Ciência e a Tecnologia, I.P. (FCT, https://ror.org/00snfqn58) under Grant UID/6438/2025 (https://doi.org/10.54499/UID/06438/2025) of the research unit CERIS.

References

Azevedo, Nuno Monteiro, José V. Lemos; João Rocha de Almeida. 2010. “A discrete particle model for reinforced concrete fracture analysis”. Struct. Eng. Mech., 36, 343–361. https://doi.org/10.12989/sem.2010.36.3.343.

Azevedo, Nuno Monteiro, and José V. Lemos. 2022. "A Hybrid Particle/Finite Element Model with Surface Roughness for Stone Masonry Analysis" *Applied Mechanics* 3, no. 2: 608-627. https://doi.org/10.3390/applmech3020036.

Azevedo, Nuno Monteiro, Fernando F. S. Pinho, Ildi Cismaşiu, and Murilo Souza. 2022. "Prediction of Rubble-Stone Masonry Walls Response under Axial Compression Using 2D Particle Modelling" Buildings 12, no. 8: 1283. https://doi.org/10.3390/buildings12081283.

Azevedo, Nuno Monteiro, Ildi Cismaşiu, Fernando F. S. Pinho, and Filipe Neves. 2025. "Numerical Modeling of Reinforcement Solutions in Traditional Stone Masonry Using a Particle Model" *Buildings* 15, no. 7: 1058. https://doi.org/10.3390/buildings15071058.

Chen, Xudong, Zigong Liang, Andrew H.C. Chan. 2024. “Simulating the damage of rubble stone masonry walls using FDEM with a detailed micro-modelling approach” Comput. Part. Mech. 11, 2839–2855. https://doi.org/10.1007/s40571-024-00757-4.

Cismaşiu, Ildi, Nuno Monteiro Azevedo, and Fernando F. S. Pinho. 2023. "Numerical Evaluation of Transverse Steel Connector Strengthening Effect on the Behavior of Rubble Stone Masonry Walls under Compression Using a Particle Model" *Buildings* 13, no. 4: 987. https://doi.org/10.3390/buildings13040987.

Cundall, P. A., and O. D. L. Strack. 1979. “Discrete Numerical Model for Granular Assemblies.” *Géotechnique* 29 (1): 47–65. https://doi.org/10.1680/geot.1979.29.1.47.

D’Altri, Antonio Maria, Vasilis Sarhosis, Gabriele Milani, Jan Rots, Serena Cattari, Sergio Lagomarsino, Elio Sacco, Antonio Tralli, Giovanni Castellazzi & Stefano de Miranda. 2020. "Modeling Strategies for the Computational Analysis of Unreinforced Masonry Structures: Review and Classification" Arch. Comput. Methods Eng. 27, 1153–1185. https://doi.org/10.1007/s11831-019-09351-x.

Devanand, Kanaeshvarr, Bahman Ghiassi, Asaad Faramarzi, Moura Mehravar. 2025. "Particle-Based DEM to Assess Masonry Behaviour Under Compression.” In 18th International Brick and Block Masonry Conference; Milani, G., Ghiassi, B., Eds.; IB2MaC 2024. Lecture Notes in Civil Engineering; Springer: Cham, Switzerland, Volume 613. https://doi.org/10.1007/978-3-031-73314-7_19.

Pinho, Fernando F. S.. 2007. Ordinary Masonry Walls – Experimental study with unstrengthened and strengthened specimens. Ph.D. Thesis. Civil Engineering. NOVA FCT, Lisbon, Portugal. (In Portuguese).

Pinho, Fernando F. S. and Válter J. G. Lúcio. 2017. “Rubble stone masonry walls. Material properties, carbonation depth and mechanical characterization”. International Journal of Architectural Heritage. 2017; 11(5), 685-702.

Gobbin, Francesca, Gianmarco de Felice, Jose V. Lemos. 2021. “Numerical procedures for the analysis of collapse mechanisms of masonry structures using discrete element modelling”. Engineering Structures, 246, 113047. https://doi.org/10.1016/j.engstruct.2021.113047

Kibriya, Ghulam, János Botzheim, Ákos Orosz, Katalin Bagi. 2024. “Automatic calibration of a discrete element model of a masonry arch by swarm intelligence methods” Computers &Structures, 299, 107401, doi.org/10.1016/j.compstruc.2024.107401

Murano, Antonio, Javier Ortega, Hugo Rodrigues, Graça Vasconcelos. 2021. "Updating mechanical properties of two-leaf stone masonry walls through experimental data and Bayesian inference" Constr. Build. Mater. 298, 123626. https://doi.org/10.1016/j.conbuildmat.2021.123626.

Roca, Pere, Miguel Cervera, Giuseppe Gariup and Luca Pela’. 2010. “Structural Analysis of Masonry Historical Constructions. Classical and Advanced Approaches” Arch Computat Methods Eng 17, 299–325, https://doi.org/10.1007/s11831-010-9046-1

Saloustros, Savvas, Andrea Settimi, Andrea Cabriada Ascencio, Julien Gamerro, Yves Weinand & Katrin Beyer. 2023. "Geometrical digital twins of the as-built micro-structure of three-leaf stone masonry walls with laser scanning". Sci. Data 10, 533. https://doi.org/10.1038/s41597-023-02417-3.

XXII International Conference on Building Pathology and Constructions Repair
15th to 17th July 2026 - Lisboa, Portugal

The Role of the CIB Student Chapter IST/UL: Perspectives on Research and Cooperation

Jéssica Deise BERSCH[1], Giovanna Schäfer BARTELS[2], Jorge DE BRITO[3], Inês FLORES-COLEN[4]

[1] CERIS, Instituto Superior Técnico, Universidade de Lisboa, Av. Rovisco Pais 1, 1049-001, Lisboa, Portugal, jessica.d.bersch@tecnico.ulisboa.pt
[2] CERIS, Instituto Superior Técnico, Universidade de Lisboa, Av. Rovisco Pais 1, 1049-001, Lisboa, Portugal, giovanna.schafer@tecnico.ulisboa.pt
[3] CERIS, Instituto Superior Técnico, Universidade de Lisboa, Av. Rovisco Pais 1, 1049-001, Lisboa, Portugal, jorge.brito@tecnico.ulisboa.pt
[4] CERIS, Instituto Superior Técnico, Universidade de Lisboa, Av. Rovisco Pais 1, 1049-001, Lisboa, Portugal, ines.flores.colen@tecnico.ulisboa.pt

Abstract: This paper presents the CIB Student Chapter of Instituto Superior Técnico (IST), University of Lisbon, affiliated with the Research Group "Studies on Construction", of the Civil Engineering Research and Innovation for Sustainability (CERIS) research unit. Originally established in 2004 as the first CIB Student Chapter in Portugal, it was relaunched in 2025 to foster international exchange and research excellence among students, especially those in PhD programs. By aligning academic research with innovation, the Chapter intends to prepare future leaders in the construction sector. This article describes the internal organization of the Chapter and outlines its action plan based on the scope of CIB Working Commissions addressing: Heat and Moisture Transfer in Buildings; Facilities Management and Maintenance; Prediction of Service Life of Building Materials and Components; and Building Pathology. The importance of engaging with this Student Chapter is discussed through testimonies from former and current members, highlighting the initiative's impact on their academic and professional development.

Keywords: CIB Student Chapter, PhD Students, International Cooperation, Research and Innovation, Built Environment.

1. Introduction

Global challenges require international collaboration in research, benefiting from multiple perspectives, players (Haley *et al.*, 2024) and approaches. In this context, research networks are expanding and increasingly including emerging research economies (Adams, 2012). In Civil Engineering, combining efforts with researchers, policymakers and industry stakeholders is fundamental to pursuing sustainable construction practices, seeking environmental responsibility and social well-being (Khan, McNally, 2023).

Aligned with these needs, the International Council for Research and Innovation in Building and Construction (CIB) is a worldwide network created in 1953 that currently comprises more than 40 Technical Commissions. The Council fosters international cooperation to improve the quality and impact of research and innovation in the building and construction sector. CIB scope covers technical, economic, environmental and organizational aspects across all stages of the built environment life cycle, from research to implementation.

Within the CIB structure, there are several Student Chapters, representing organized groups of students enrolled at CIB Member universities having common interests in the work of CIB Commissions and Priority Themes: sustainable construction, integrated design and delivery solutions and resilient urbanization. These students are envisioned as future leaders of building research and innovation, participating in an environment that fosters engagement and inspiration while promoting international cooperation.

Following this educational framework, the CIB Student Chapter from Instituto Superior Técnico (IST), University of Lisbon (UL), was originally inaugurated in 2004, being the first CIB Student Chapter in Portugal (Flores-Colen, de Brito, 2004). After more than a decade of activities that lasted until 2020, the Student Chapter IST/UL was officially relaunched in 2025. The Chapter is associated with Research Group 5 (RG5), "Studies on Construction", of Civil Engineering Research and Innovation for Sustainability (CERIS).

The objective of this paper is to share perspectives on research and collaboration under the scope of the CIB Student Chapter IST/UL. This Chapter is structured around the United Nations Sustainable Development Goals (SDGs), mainly SDGs 4 (Quality Education), 9 (Industry, Innovation and Infrastructure), 11 (Sustainable Cities and Communities) and 17 (Partnerships for the Goals). Furthermore, it is devoted to priorities highlighted during the 26th United Nations Climate Change Conference (COP26), such as the urgent need for resilience and action against climate change impacts in the built environment.

The internal organization of the Chapter is detailed, together with its action plan and promoted activities. The thematic framework that characterizes the core pillars of expertise of the Chapter are outlined, combined with their alignment with CIB Working Commissions. Finally, the importance of engaging in the CIB Student Chapter IST/UL regarding academic and professional development is reported based on information shared by former and current members. The purpose of the discussion is to introduce our Chapter under the scope of the CIB Community, contributing to the CIB Vistas Program foundational values: people, the planet, global collaboration and the future.

2. Internal organization

Figure 1 illustrates the categories of participants involved in the management and benefiting from the actions of the CIB Student Chapter IST/UL. The dashed arrows represent an open line for communication and contribution among the different levels, allowing for cooperation, exchanges and collaborative inputs.

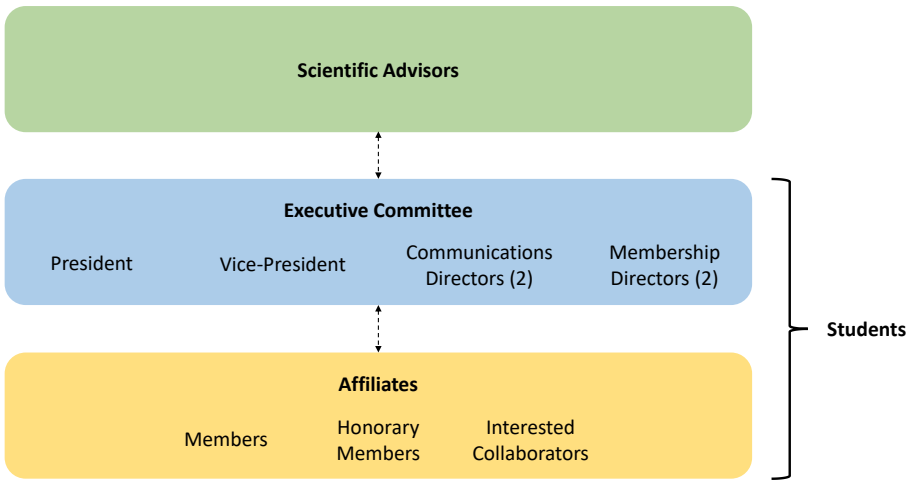


Figure 1 - Internal organization of the CIB Student Chapter IST/UL

The Scientific Advisors are faculty members from the Department of Civil Engineering, Architecture and Environment (DECivil) at IST who provide institutional and scientific support to the Chapter. Their names and contact details are communicated to the CIB General Secretariat, thereby ensuring the continuity of the Chapter, the formal connection with the university and the official point of contact between the Student Chapter and CIB.

Regarding the governance of the Chapter, the Executive Committee is composed of students who take on internal management responsibilities. The positions made available in the relaunch of the group are President, Vice President, two positions for Communications Directors and two positions for Membership

Directors, with the possibility of adding others in the future as needed.

Student president and Vice-President duties include the overall coordination of the Chapter, the strategic definition of activities and institutional representation within CIB and the academic community. The Communications Directors are responsible for the internal and external dissemination of the Chapter's activities, ensuring the maintenance of communication channels and the visibility of initiatives among students and the scientific community. The Membership Directors are responsible for supporting the recruitment of new participants and implementing strategies to ensure their continued and active participation within the Chapter.

The members of the CIB Student Chapter IST/UL are master's students with research grants, PhD students and researchers from RG5 of CERIS who actively collaborate on the initiatives organized. Honorary members are former students who participated as a member from the Chapter during their period at CERIS. Finally, interested collaborators are students and researchers willing to participate in the Chapter, but unable to become members due to their affiliation with research areas or institutions other than CERIS RG5.

The relaunch of the CIB Student Chapter IST/UL relies on Professors Inês Flores-Colen and Jorge de Brito as Scientific Advisors, whose experience is particularly relevant as they participated in the founding of this first CIB Student Chapter in Portugal and have since remained active members of CIB. Presidency and Vice-Presidency positions are currently held by Jéssica Bersch and Giovanna Bartels; Renato Neves and Nicollas Moreira serve as Communications Directors, while Isobel Andrews and Fernanda Magalhães are the Membership Directors.

3. Action plan and activities

An Action Plan was defined upon the relaunch of the CIB Student Chapter IST/UL for the upcoming years. For this purpose, the main actions planned by the group were distributed as yearly or continuous activities, as illustrated in Figure 2.

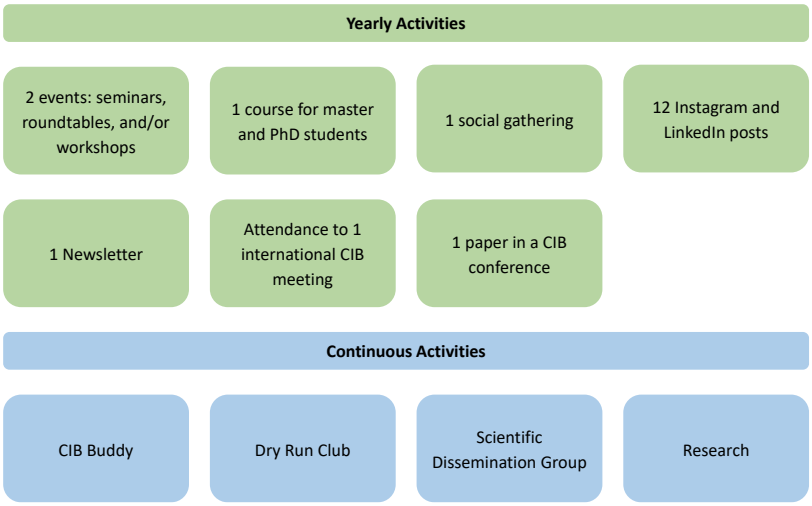


Figure 2 - Action plan of the CIB Student Chapter IST/UL

Regarding yearly tasks, seminars, workshops and roundtables are envisioned to disseminate the activities carried out within the scope of the CIB Student Chapter and promote knowledge sharing and transfer among its members, considering the associated thematic framework, themes of interest for the affiliates and research developed by students. The first seminar was held in October 2025 and was attended by more than 30 participants. In addition to the presentation of the Chapter, the event featured a keynote titled "Decarbonization in the construction sector: Educational approaches in the Netherlands," by Thais Varella, MSc in Environmental

Studies and Lecturer in Environmental Science at Avans University of Applied Sciences, Netherlands.

Courses for master's and PhD students are structured as training sessions planned to cover topics of interest to the Chapter. The objective for the sessions is for members to share their expertise with one another. Training on the development and presentation of graphs, machine learning, or specific Civil Engineering software is considered relevant, for example.

At least at the end of each academic year, CIB Student Chapter members who are pursuing their PhD studies are invited to a social gathering, beginning with a pitch-style presentation on the status of their theses, followed by networking and social activities. This event is designed to foster collaboration and friendship among students.

The digital presence of the Student Chapter is maintained through Instagram (@cibstudentist), YouTube (https://www.youtube.com/channel/UCqh9u2cKfn1eHC7xmL0oKnA) and its own website (https://cibsc.wordpress.com/). Additionally, an annual newsletter synthesizes the outputs of the Chapter to be sent to the affiliates. For the digital presence of the Chapter, a custom logo was developed within the Communications Directory, based on the CIB and IST logos, as presented in Figure 3.



Figure 3 - Logo of the CIB Student Chapter IST/UL

As part of the international engagement, opportunities for integration with other CIB Student Chapters throughout the world are pursued during Chapter members' attendance at national and international conferences, especially those supported by CIB, through the presentation of activities and discussions of potential collaborations. Knowledge dissemination is planned through paper publications and presentations at CIB partner events, such as the International Conference on the Durability of Building Materials and Components (DBMC).

Regarding the Chapter's ongoing activities, the CIB Buddy program intends to support students of DECivil/IST within the academic environment in Lisbon. International or new students may connect with the Student Chapter and receive support from members, who are responsible for highlighting opportunities to engage in research, sharing PhD experiences and assisting with contact with professors.

The Dry Run Club's purpose is to provide scheduled meetings whenever the members need to present their papers at conferences or for thesis and dissertation defences. These sessions allow practicing the presentation of scientific work to colleagues in a peer-based environment, contributing to the improvement of the work and the development of confidence.

Research is a core activity of the CIB Student Chapter, enabling the development of innovations that address resilience and climate change impacts in the built environment. Each member pursuing a master's or PhD conducts research with potential impact, seeking, where possible, collaboration with the CIB Commissions considered in this work, such as Hygrothermal Science, Facilities Management, Service Life Prediction or Building Pathology.

Finally, the scientific dissemination group is an open communication channel operating through the Student Chapter mailing list to disseminate scientific papers, events and other materials that contribute to the knowledge and development of the group. The pieces of news shared by the cibstudent@tecnico.ulisboa.pt e-mail address are those perceived as relevant by the members, Scientific Advisors and other academic or industry professionals.

4. Thematic framework

The CIB Student Chapter IST/UL was relaunched with a focus on the themes approached by the CIB Commissions “W040 - Heat and Moisture Transfer in Buildings”, “W070 - Facilities Management and Maintenance”, “W080 - Prediction of Service Life of Building Materials and Components” and “W086 - Building Pathology”, mainly due to the Executive Committee and Scientific Advisors expertise. Table 1 summarizes the thematic framework of the Chapter.

Table 1 - Thematic framework of the CIB Student Chapter IST/UL

Alignment with CIB Commission	Expertise	Focus
W040	Hygrothermal Science	Heat, moisture, air and salt transfer
W070	Facilities Management	Asset management, relationship between technical, financial and sociological aspects of building facilities
W080	Service Life Prediction	Durability design and service life prediction methodologies
W086	Building Pathology	Inspections, diagnosis and rehabilitation

Beyond addressing the individual scope presented by each commission of interest, the Chapter promotes an integrated approach to the built environment. Within the scope of W040, the focus respects the physical laws governing heat and moisture transfer to optimize building performance. Hygrothermal assessments in walls contribute to building resilience and adaptability to a changing climate, long-term sustainability and more efficient costs (Palani *et al.*, 2023). Hygrothermal simulations can even be used to predict and prevent mould growth (Sukop, Ostrý, 2025). Therefore, the focus on W040’s topics is complemented by W086 under the Student Chapter framework, where systematic pathology surveys provide diagnostic data necessary for sustainable rehabilitation and maintenance. Building pathology refers to the causes, mechanisms and consequences of failures that compromise structural integrity, hygrothermal performance and indoor air quality (Freitas, 2021).

Furthermore, the Chapter explores durability and service life (W080) and the socioeconomic challenges of asset management (W070). As service life is the period during which construction can meet changing performance requirements without reaching unacceptable levels (Silva *et al.*, 2021) and facility services intend to ensure better condition, quality and durability of building assets (Baniya, 2023), the focus on the operational phase is crucial for optimizing strategies for circularity, resilience and global cost prediction in buildings.

By fostering collaboration between academia and industry, the group seeks to translate theoretical models into practical maintenance strategies that enhance the long-term value and resilience of construction. For that purpose, the integrated thematic framework adopts a life cycle perspective of the built environment and building materials, envisioning reduced environmental impacts during their construction, use and end of life phases (Pedroso *et al.*, 2022). In this context, reliable reference service life datasets of building materials become crucial to contribute to reducing uncertainties (Sadeghi *et al.*, 2025).

Deriving from the expertise shown in Table 1, when approaching the themes, the Chapter seeks to expand by including current and pressing trends. The role of digital transformation in these fields is recognized, thereby encouraging the integration of artificial intelligence (AI) and digital tools in the promoted activities to enhance inspection, management and maintenance (Torres-Gonzáles *et al.*, 2023, Valença *et al.*, 2024). By structuring and gathering data generated throughout the whole life cycle of buildings, AI can improve construction processes (Abioye *et al.*, 2021).

Moreover, climate change effects on buildings need to be addressed (Barrelas *et al.*, 2023, Lacasse *et al.*, 2020) and, for that purpose, the Chapter seeks to contribute to the understanding of these impacts, the decarbonization of the construction sector (Bartels *et al.*, 2025) and the promotion of sustainable rehabilitation practices (Rucha *et al.*, 2026), in line with global sustainability agendas. Circular economy is also under the scope of the Student Chapter, including concerns over bio-based (Bellei *et al.*, 2025, Moreira *et al.*, 2024), innovative (Bersch *et al.*, 2023) and recycled (Neves *et al.*, 2025) materials, especially in areas at risk (Magalhães *et al.*, 2024).

5. Engagement and professional growth

Figure 4 shows a word cloud developed based on a survey answered by six members belonging both to the current Executive Committee of the CIB Student Chapter IST/UL or that were its former Presidents. The responses corresponded to the five words that the experience on the Chapter reminded them of. In summary, the Chapter appears to connect students to a global scientific ecosystem, thus working as expected from its foundational objectives. Beyond technical expertise, terms like 'Engagement', 'Motivation' and 'Friendship' suggest that the Chapter also fosters a sense of belonging and soft skills development.



Figure 4 - Word cloud for engaging in the CIB Student Chapter IST/UL

Concerning the skills developed during active participation in the Executive Committee of the Chapter, as shown in Figure 5, leadership and team management were highlighted. Organizing projects and events, combined with the communication associated to them appeared second.

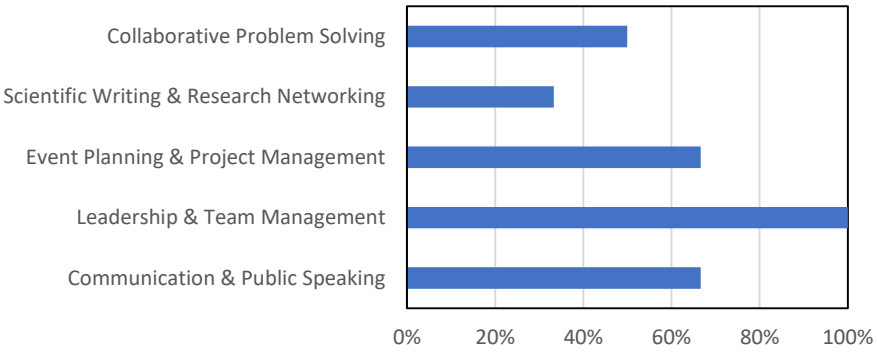


Figure 5 - Skills developed during active participation in the Executive Committee of the CIB Student Chapter IST/UL

The active functioning of the Chapter also involves challenges. These are related to recruiting new members, keeping them motivated over time and inspiring them to collaborate with the team. Identifying opportunities for international cooperation and research fields were also raised by the survey participants. Furthermore, organizing high-impact technical events and balancing the Chapter activities with PhD and research workloads are part of the more demanding tasks.

The engagement in the CIB Student Chapter IST/UL is reported by its members as a transformative experience for both academic and professional development. Participation in the Chapter facilitates the creation of national and international research networks, expanding beyond the academic sphere. Moreover, it provides scientific exposure and interactions between PhD students from different fields, allowing them to share their journeys. For leadership roles, the experience is particularly impactful, fostering the development of soft skills, such as strategies to keep members active and motivated.

Ultimately, the Chapter serves as a bridge to the global CIB Community, introducing the members to its structure and experts. When discussing how to foster international cooperation in science, members emphasized the importance of seeking connections with other institutions and Student Chapters, CIB Working Commissions and Task Groups and foreign peers in innovative research topics. For some respondents, participating in the Student Chapter allowed them to join Working Commissions meetings, collaborate in reports and understand the challenges and demands in specific CIB areas.

6. Conclusions

The relaunch of the CIB Student Chapter IST/UL in 2025 reaffirms its role as an educational platform for international cooperation in building and construction research. The thematic framework fosters an integrated research approach that aligns traditional construction, including hygrothermal behaviour and building pathology, with service life prediction and facilities management. This synergy tackles the built environment's life cycle, essential for addressing climate change and promoting technological and sustainable rehabilitation.

Qualitative evidence from members highlights that the Chapter goes beyond technical training, allowing the development of leadership skills for members, especially those involved in the Executive Committee, including team management, strategic communication and institutional representation. The Chapter can open the doors to the CIB international community through synergies with Working Commissions and other Student Chapters. Besides academia-industry interactions, belonging to the group allows sharing of PhD research journeys, resulting in an active, collaborative and friendly environment.

The benefits in terms of networking, scientific exposure and soft skills development outweigh the challenges of maintaining engagement within the group. Future efforts will focus on expanding digital integration and strengthening partnerships, ensuring that the CIB Student Chapter IST/UL continues to prepare leaders for the construction sector who are committed to people, the planet, global collaboration and the future.

Acknowledgments

This research was funded in whole by the *Fundação para a Ciência e a Tecnologia*, I.P. (FCT, https://ror.org/00snfqn58) under Grant UID/6438/2025 (https://doi.org/10.54499/UID/06438/2025) of the research unit CERIS. The authors appreciate the FCT grant number 2023.05316.BD (DOI: https://doi.org/10.54499/2023.05316.BD) and the Ministry of Science, Technology and Higher Education (MCTES), under the researcher employment stimulus funded by the Portuguese State Budget, by ATE - *Aliança para a Transição Energética* (56) co-financed by PRR - *Plano de Recuperação e Resiliência da União Europeia*. The authors thank the International Council for Research and Innovation in Building and Construction (CIB) for the support.

References

Abioye, Sofiat O., Lukumon O. Oyedele, Lukman Akanbi, Anuoluwapo Ajayi, Juan Manuel Davila Delgado, Muhammad Bilal, Olugbenga O. Akinade, and Ashraf Ahmed. 2021. “Artificial intelligence in the construction industry: A review of present status, opportunities and future challenges”. Journal of Building Engineering 44: 103299. https://doi.org/10.1016/j.jobe.2021.103299.

Adams, Jonathan. 2012. “The rise of research networks”. Nature 490: 335-336. https://doi.org/10.1038/490335a.

Baniya, Bishal. 2023. “Circularity in facility management: conceptualisation and potential areas for circularity-oriented actions”. Sustainability 15 (11): 8460. https://doi.org/10.3390/su15118460.

Barrelas, Joana, Ana Silva, Jorge de Brito, and António Tadeu. 2023. “Effects of climate change on rendered façades: expected degradation in a progressively warmer and drier climate—A review based on the literature”. Buildings 13(2): 352. https://doi.org/10.3390/buildings13020352.

Bartels, G. S., M. Martinho, I. Flores-Colen, J. D. Silvestre, R. Gomes, and J. Fernandes. 2025. “Integrating embodied emissions data into retrofit decision-making: a methodological approach for building decarbonisation”. IOP Conference Series: Earth and Environmental Science 1568: 012022. https://doi.org/10.1088/1755-1315/1568/1/012022.

Bellei, Poliana, Manuel Francisco Costa Pereira, Isabel Torres, Genevieve Foray, and Inês Flores-Colen. 2025. “Re-Valorizing oyster-shell waste in natural hydraulic lime-based mortars for brick substrate applications: Performance and Durability”. Materials 19(1): 27. https://doi.org/10.3390/ma19010027.

Bersch, Jéssica D., Inês Flores-Colen, Angela B. Masuero, and Denise C. C. Dal Molin. 2023. “Photocatalytic TiO_2-based coatings for mortars on facades: A review of efficiency, durability, and sustainability”. Buildings 13(1): 186. https://doi.org/10.3390/buildings13010186.

Haley, Aimee, Sintayehu Kassaye Alemu, Zenawi Zerihun, and Liisa Uusimäki. 2024. “Internationalisation through research collaboration”. Educational Review 76 (4): 675–690. https://doi.org/10.1080/00131911.2022.2054958.

Flores-Colen, Inês, and Jorge de Brito. 2004. “O CIB Student Chapter no DECivil do Instituto Superior Técnico” (in Portuguese) [The CIB Student Chapter at DECivil of Instituto Superior Técnico]. Paper presented at 2° Congresso Nacional de Construção, Porto, December 13-15. 2004.

Freitas, Vasco Peixoto. 2021. “The vision of building pathology professionals”. In Publication 422 - CIB W086 - Building Pathology - New Trends on Building Pathology, edited by J. de Brito and Inês Flores-Colen. CIB.

Khan, Mehran, and Ciaran McNally. 2023. “A holistic review on the contribution of civil engineers for driving sustainable concrete construction in the built environment”. Developments in the Built Environment 16: 100273. https://doi.org/10.1016/j.dibe.2023.100273.

Lacasse, Michael A., Abhishek Gaur, and Travis V. Moore. 2020. “Durability and climate change—Implications for service life prediction and the maintainability of buildings”. Buildings 10(3): 53. https://doi.org/10.3390/buildings10030053.

Magalhães, Fernanda Caroline, Poliana Bellei, Inês Flores-Colen, and Eduarda Marques da Costa. 2024. “Blue circular economy—Reuse and valorization of bivalve shells: The case of Algarve, Portugal”. Recycling 9 (2): 27. http://dx.doi.org/10.3390/recycling9020027.

Moreira, Nicollas, Poliana Bellei, Fernanda Magalhães, and Inês Flores-Colen. 2024. "Incorporação de resíduos de cascas de ostra em blocos de betão sustentáveis" (in Portuguese) [Incorporation of oyster shell waste into sustainable concrete blocks]. Paper presented at 5° Congresso Luso-Brasileiro de Materiais de Construção Sustentável - Congresso Construção 2024, Lisboa, November 6-8, 2024.

Neves, Renato, Jorge de Brito, and Miguel Bravo. “Performance of concrete produced with binders obtained through alkali-activation of different construction and demolition wastes”. Construction and Building Materials 473: 141060. https://doi.org/10.1016/j.conbuildmat.2025.141060.

Palani, Hevar, Hamed Khaleghi, Parisa Salehi, and Aslihan Karatas. 2023. “Assessing hygrothermal performance in building walls engineered for extreme cold climate environments”. Sustainabiliy 15 (24): 16597. https://doi.org/10.3390/su152416597.

Pedroso, Pedro Frazão, José Dinis Silvestre, Giovanni Borsoi, and Inês Flores-Colen. 2022. “Life cycle assessment of protection products for external thermal insulation composite systems”. Sustainability 14(24): 16969. https://doi.org/10.3390/su142416969.

Rucha, M., S. Piçarra, A.P. Ferreira Pinto, M. F. Montemor, and B. Sena da Fonseca. 2026. “Superficial and in-depth effects of novel water-based fluorinated alkoxysilanes formulations for stone materials”. Journal of Building Engineering 117: 114801. https://doi.org/10.1016/j.jobe.2025.114801.

Sadeghi, Sara, Marzieh Riahinezhad, Elnaz Esmizadeh, and Michael A. Lacasse. 2025. “Service life dataset for non-structural building envelope materials”. National Research Council Canada. Construction Research Centre. https://doi.org/10.4224/40003877.

Silva, Ana, Jorge de Brito, and Pedro Lima Gaspar. 2021. “Service life: Concepts and definitions”. In Publication 423 - CIB W080 - Prediction of Service Life of Building Materials & Components, edited by Jorge de Brito and Ana Silva. CIB.

Sukop, Lukáš, and Milan Ostrý. 2025. “Hygrothermal performance of structures with diffusion-open and semi-diffusion-open internal insulation systems: A literature review”. Journal of Building Engineering 108: 112954. https://doi.org/10.1016/j.jobe.2025.112954.

Torres-Gonzáles, Marta, Jónatas Valença, Bruno O. Santos, Ana Silva, and Maria Paula Mendes. 2023. “StainView: A fast and reliable method for mapping stains in facades using image classification in HSV and CIELab colour space”. Remote Sensing 15(11): 2895. https://doi.org/10.3390/rs15112895.

Valença, Jónatas, Killian Morin, Nathan Jouen, Nathália Olivo, Marta Torres-Gonzalez, Maria Paula Mendes, and Ana Silva. 2024. “Feeling-BIM: A digital model to support maintenance decisions, based on automatic inspection and dwellers’ feelings”. Journal of Building Engineering 87: 108937. https://doi.org/10.1016/j.jobe.2024.108937.

For More Information

https://cinpar2026.tecnico.ulisboa.pt/

cinpar2026@tecnico.ulisboa.pt

@cinpar2026

Cinpar 2026
XXII International Conference on Building Pathology and Constructions Repair
15th to 17th July 2026 - Lisboa, Portugal

#CINPAR2026CONFERENCE



CINPAR 2026

XXII International Conference on Building Pathology and Constructions Repair
15th to 17th July 2026 - Lisboa, Portugal

